nature

Vol 298 No 5869 1–7 July 1982 £1.60 $4.00

CUK-H06882-29A-RP424

Lei NO 5870-5871 5873

STRATIGRAPHY AND FAUNA OF MIDDLE AWASH VALLEY, ETHI[redacted]PIA

BRITISH GAS

ENGINEERING RESEARCH AWARDS

British Gas has established a new scheme for postgraduate engineering awards for research in areas of value to British Gas. Up to 3 Engineering Research Awards will be made each year to support Ph.D or D.Phil research in engineering in universities or polytechnics in the U.K. This scheme is complementary to the existing British Gas Research Scholarships.

Of the Awards to be made in 1982, one will be for research in the general field of **HIGH DENSITY DIGITAL TAPE RECORDING.** This is an area in which British Gas has stimulated some important developments in recent years.

British Gas interests in this field include: –

1. Investigation of facets which influence the recording process; tape system dynamics, tape emulsion, head drive, design and properties of recording heads, wrap angle, head gap.
2. Consideration of data coding methods, data deskewing, data recovery, data compaction.
3. Data formatting, error detection and correction, data reduction.

Specific proposals are invited from university or polytechnic staff, which either relate directly to one or more of the above topics, or associated fields of interest in magnetic tape recording technology.

Attractive financial aspects of the Award include: a maintenance allowance comparable to a fully "topped-up" Science and Engineering Research Council CASE award (currently £3,830 for a student living in London); an equipment allowance for the Department of £1,000 adjusted annually to take account of inflation; a book allowance of up to £200; and an opportunity for the holder of an Award to make one technical visit abroad.

Proposals should be sent to the Manager, External Affairs, Research & Development Division, British Gas Corporation, 326 High Holborn, London WC1V 7PT, from whom further information may be obtained. Closing date for applications is 26th July 1982.

BRITISH GAS

Circle No.01 on Reader Service Card.

Journal of Microcomputer Applications

Editors in Chief: J.L. Alty and M.J. Taylor

Publication: Quarterly
Subscription: Volume 5, 1982
Full Rate: £30.00 (UK) / $ 79.00 (overseas)
Personal Rate: £15.00 (UK) / $ 39.50 (overseas)

From 1982 Academic Press will take over from Liverpool University Computer Laboratory the publication of the Journal of Microcomputer Applications. This international quarterly journal will provide a forum for all those involved in the applied areas of microcomputing, in university, industrial and commercial environments. It will report work carried out in the design, production and testing of microcomputer applications in all fields – computer control, data processing, telecommunications, networks, medical systems and others.
A novel approach of the journal will be its coverage of previously neglected software aspects, such as design techniques and the application of high-level languages on microcomputer systems. Papers on hardware will also be welcomed, for example on design, integration and testing of systems, interfacing problems and new devices. The journal will also include tutorial papers, letters and book reviews, and special sections will be planned to cover applications in particular fields, or investigate particular problem areas. Long or short contributions of the highest quality will be sought, and all papers carefully refereed. As it is very important that papers in this fast-moving field are published quickly, rapid publication will be a key aspect of this journal.

Sample copies available on request from ***Jane Lawrence, Academic Press Inc. (London) Ltd, 24-28 Oval Road, London NW1 7DX. Please quote reference JL/06.82/A108.***

Academic Press
A Subsidiary of Harcourt Brace Jovanovich, Publishers
London New York Toronto Sydney San Francisco
24-28 Oval Road, London NW1 7DX, England
111 Fifth Avenue, New York, NY 10003, USA

Circle No.13 on Reader Service Card.

nature
is available in Microform.

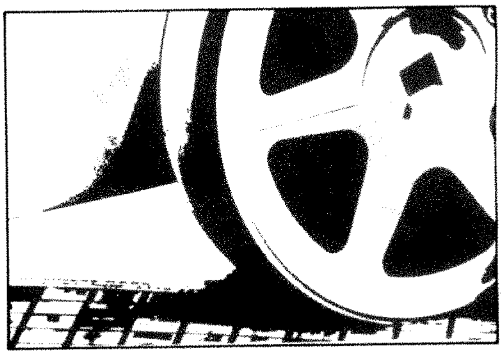

University Microfilms International

Please send additional information
for ______________________
(name of publication)
Name ______________________
Institution ______________________
Street ______________________
City ______________________
State __________ Zip __________
300 North Zeeb Road, Dept. P.R., Ann Arbor, Mi. 48106

Circle No.25 on Reader Service Card.

nature

Vol. 298 No. 5869 1 July 1982

Should the Atlantic be widened? 1
Private funds matter 2
Riding for a fall? 2

NEWS

Waste in research services damned
New prospectus for European lab
Industrial secrets still in demand
Chemical weapons treaty
French universities
Argonne prepares for change
Franco-Soviet space-flight
French science *loi*
Laboratory animal welfare
US science societies 3

CORRESPONDENCE

Falklands/Cosmology/IQ/
Nucleic acid sequence library 8

NEWS AND VIEWS

Atmospheric chemists *in flagrante*? (P Campbell)
A corona around the Milky Way (J N Bregman)
Sons and daughters (T H Clutton-Brock)
***Decapentaplegic* — hopes held out** (G Struhl)
Synthetic peptides as the basis for future vaccines (J Beale)
The internal evolution of Venus and the galilean satellites (S C Solomon) 9

BOOK REVIEWS

The Mind's I (*arranged by* D R Hofstadter and D C Dennett) Marie Jahoda; **Violent Phenomena in the Universe (*by* J V Narlikar)** William H Press; **Basics of Electron–Positron Collisions (*by* F M Renard)** Maurice Jacob; **Photosynthesis (G Akoyunoglou, *ed.*)** M C W Evans; **Medical Thinking (*by* L S King)** W F Bynum; **Membrane Physiology of Invertebrates (R B Podesta, *ed.*)** R B Moreton; **Inorganic Stereochemistry (*by* D L Kepert)** M G B Drew 103

MISCELLANY

100 years ago 16
New on the market ix
Classified advertising xi

Cover

rchaic *Homo sapiens* from Bodo, Middle Awash alley, Afar, Ethiopia (photograph by Assefa Mebrate). Stratigraphy and fauna of the Middle Awash Valley are discussed on pages **17** and **25**

ARTICLES

Geology and stratigraphy of Neogene deposits, Middle Awash Valley, Ethiopia J E Kalb, E B Oswald, S Tebedge, A Mebrate, E Tola & D Peak 17
Fossil mammals and artefacts from the Middle Awash Valley, Ethiopia J E Kalb, C J Jolly, A Mebrate, S Tebedge, C Smart, E B Oswald, D Cramer, P Whitehead, C B Wood, G C Conroy, T Adefris, L Sperling & B Kana 25

Less-no 70,71,73

Protection against foot-and-mouth disease by immunization with a chemically synthesized peptide predicted from the viral nucleotide sequence J L Bittle, R A Houghten, H Alexander, T M Shinnick, J G Sutcliffe, R A Lerner, D J Rowlands & F Brown 30
Transcript secondary structures regulate transcription termination at the attenuator of *S. marcescens* tryptophan operon I Stroynowski & C Yanofsky 34
Superattenuation in the tryptophan operon of *Serratia marcescens* I Stroynowski, M van Cleemput & C Yanofsky 38

294

LETTERS TO NATURE

Optical identification of X-ray source H0139–68 with an AM Herculis-type system N Visvanathan & A Pickles 41
Zonal harmonic model of Saturn's magnetic field from Voyager 1 and 2 observations J E P Connerney, N F Ness & M H Acuña 44
Macroscopic evidence of molecular chirality in columnar mesophases J Malthête, J Jacques, N H Tinh & C Destrade 46
Electron density images from imperfect data by iterative entropy maximization D M Collins 49
Structure of the Red Sea at 20°N from gravity data and its implication for continental margins C Brown & R W Girdler 51
Significance of $^{87}Sr/^{86}Sr$ ratios in the Merensky cyclic unit of the Bushveld Complex F J Kruger & J S Marsh 53
Age constraints on the proposed Plio–Pleistocene boundary stratotype at Vrica, Italy J D Obradovich, C W Naeser, G A Izett, G Pasini & G Bigazzi 55
Brown adipose tissue thermogenesis is 'suppressed' during lactation in mice P Trayhurn, J B Douglas & M M McGuckin 59
Relationship of β-adrenoreceptor density to fitness in athletes J Butler, M O'Brien, K O'Malley & J G Kelly 60
Visual pigments in the four-eyed fish, *Anableps anableps* J A Avery & J K Bowmaker 62
Serotonin alters the phosphorylation of specific proteins inside a single living nerve cell J R Lemos, I Novak-Hofer & I B Levitan 64

Nature® (ISSN 0028-0836) is published weekly on Thursday, except the last week in December, by Macmillan Journals Ltd and includes the Directory of Biologicals (mailed in December) and Annual ndex (mailed in February). Annual subscription for USA and Canada US $198.50 (for subscription prices elsewhere, see next page). Orders (with remittance) and change of address labels to: Macmillan ournals Ltd, Brunel Rd, Basingstoke RG21 2XS, UK. Second class postage paid at New York, NY10010 and additional mailing offices. US Postmaster send form 3579 to: *Nature*, 15 East 26 treet, New York, NY 10010.

0028-0836/82/26000C-02$01.00

Contents continued overleaf

Amersham supplies an extensive range of high quality oligodeoxynucleotides for use as

- linkers and adaptors
- probes and primers
- model substrates for restriction enzymes
- reference compounds in HPLC analysis or sequencing experiments

Please call Amersham or your local representative for a brochure describing these products and their applications.

Amersham International plc, Amersham, England Telephone 024 04 4444
In the U.S.A. and Canada, Amersham Corporation, Illinois 60005 Telephone 312-364-7100
and 800-323-9750 (Tollfree)
In W. Germany, Amersham Buchler GmbH & Co KG, Braunschweig Telephone 05307-808-0

Amersham

Circle No.16 on Reader Service Card.

Science in France
Science in West Germany

Copies of these special supplement issues are still available.

Prices (including postage): UK, £2.50 each; USA & Canada, US $6.00 (surface), US $9.00 (air); Rest of World, £3.00 (surface), £4.00 (air).

Orders (with payment) to:
Nature, Macmillan Journals Ltd,
Brunel Road, Basingstoke, Hants
RG21 2XS, England.

Annual Subscription including Index (51 issues)

UK & Eire		£85
USA & Canada		US$198.50
Belgium	Airspeed only	BF7450
West Germany	Airspeed only	DM450
Netherlands	Airspeed only	G505
Switzerland	Airspeed only	SF395
Rest of Europe	Airspeed only	£100
Rest of World	Surface	£100
Rest of World*	Airmail	£150

**(not USA, Canada & Europe)*

Personal subscription rates are available in some countries to subscribers paying by personal cheque or credit card.

Details can be obtained from:
UK: *Nature* Promotion Department,
Canada Road, Byfleet, Surrey KT14 7JL.
Telephone: Jonathan Earl: Byfleet (09323) 41459
USA: *Nature*, 15 East 26 Street, New York, NY 10010
Credit card orders only (in USA & Canada):
Call toll-free: (800) 824-7888 (Operator 246)
In California: (800) 852-7777 (Operator 246)

All other circulation enquiries concerning existing subscriptions please contact:
Nature Circulation Department, Macmillan Journals Ltd., Brunel Road, Basingstoke, Hants RG21 2XS, UK
Telephone: (0256) 29242 Telex: 858493

Back issues: (Post-paid) UK, £2.50; USA & Canada, US$6.00 (surface), US$9.00 (air); Rest of World, £3.00 (surface), £4.00 (air).

***Nature* Binders:**
Single Binders: UK, £4.00; Rest of World, $10.00
Set(s) of 3 Binders: UK, £10.00; Rest of World, 25.00

***Nature* First Issue Facsimile:**
UK, 75p; Rest of World (surface), $1.50, (air), £2.00

***Nature* Annual Indexes (1971-1981):**
Price (post-paid):
UK, £5.00 each; Rest of World, $10.00

***Nature* Directory of Biologicals:**
(Hardcover edition)
UK, £22.50; Rest of World, $45.00

***Nature* Wallcharts:**
How Britain Runs its Science; How the US Runs its Science; UK, £3.50; USA, $7.95 each

***Nature* in Microform:**
For Information:
UK: UMI, 18 Bedford Row, London WC2R 4EJ
USA: 300 North Zeeb Road, Ann Arbor, Mi 48106

Orders (with remittance) to:
Nature, Macmillan Journals Ltd.,
Brunel Road, Basingstoke, Hants RG21 2XS, UK
Tel: (0256) 29242 Telex: 858493

MACMILLAN JOURNALS

Neuropeptide coexistence in human cortical neurones S R Vincent, O Johansson, T Hökfelt, B Meyerson, C Sachs, R P Elde, L Terenius & J Kimmel 65

Fission-spectrum neutrons at reduced dose rates enhance neoplastic transformation C K Hill, F M Buonaguro, C P Myers, A Han & M M Elkind 67

Malignant transformation of human embryo retinoblasts by cloned adenovirus 12 DNA P Byrd, K W Brown & P H Gallimore 69

Circulating immune complexes in infants fed on cow's milk R D'Amelio, R Seminara, E Galli, G Antoniazzi, L Businco & F Aiuti 72

Binding of C3b proceeds by a transesterification reaction at the thiolester site M K Hostetter, M L Thomas, F S Rosen & B F Tack 72

Translation of mRNA for human granulocyte-macrophage colony stimulating factor A J Lusis, D W Golde, D H Quon & L A Lasky 75

A common mechanism for the synthesis of membrane and secreted immunoglobulin α, γ and μ chains W Cushley, B E H Coupar, C A Mickelson & A R Williamson 77

Production of colony-stimulating factors by murine T cells in limiting dilution and long-term cultures F G Staber, L Hültner, F Marcucci & P H Krammer 79

Japanese wild mouse, *Mus musculus molossinus*, has duplicated immunoglobulin γ2a genes A Shimizu, Y Hamaguchi, Y Yaoita, K Moriwaki, K Kondo & T Honjo 82

Monoclonal antibodies show that neurofibrillary tangles and neurofilaments share antigenic determinants B H Anderton, D Breinburg, M J Downes, P J Green, B E Tomlinson, J Ulrich, J N Wood & J Kahn 84

A model for the molecular requirements of immunoglobulin heavy chain class switching K B Marcu, R B Lang, L W Stanton & L J Harris 87

Complete amino acid sequence and maturation of the mouse submaxillary gland renin precursor J-J Panthier, S Foote, B Chambraud, A D Strosberg, P Corvol & F Rougeon 90

Prostatic steroid binding protein: gene duplication and steroid binding M Parker, M Needham & R White 92

Inverted repeats surround the ribitol–arabitol genes of *E.coli* C C D Link & A M Reiner 94

LexA protein inhibits transcription of the *E. coli uvrA* gene *in vitro* A Sancar, G B Sancar, W D Rupp, J W Little & D W Mount 96

The *uvrD* gene of *E. coli* enclodes a DNA-dependent ATPase K Oeda, T Horiuchi & M Sekiguchi 98

A relationship between replicon size and supercoiled loop domains in the eukaryotic genome M Buongiorno-Nardelli, G Micheli, M T Carrī & M Marilley 100

Nature in Poland

Readers wishing to subscribe to a weekly copy of *Nature* on behalf of a colleague in Poland (where hard currency is scarce) should send a cheque for £50 (or the equivalent in any currency), accompanied by their name and address and that of the proposed recipient, to the *Nature* office in London or New York (see addresses opposite page 1). For further details, readers are referred to *Nature* 3 June, p.354.

Reading this book is a biological necessity.

The Growth of Biological Thought

Diversity, Evolution, and Inheritance
Ernst Mayr

This controversial, epic work is the first book ever to integrate biological thought with Western intellectual tradition.

Beginning with Aristotle, Mayr traces the development and maturation of the three central concepts of biology – classification of life forms, evolution of the species, and inheritance and variation of characteristics.

"No other book tells in such a lucid and critical way the evolution of ideas that led to modern biology." – François Jacob

"A masterly analytical and synthesizing history of biological ideas by a master biologist."
– Robert K. Merton

"This great book should be required reading for every biologist and for everyone interested in the history and philosophy of science." – I. Bernard Cohen

"It is a wonderful thing when the world's leading evolutionary biologist and a top historian collaborate on a book of such breadth and depth. In this case, they are both the same man, Ernst Mayr, and the result is wonderful." – Stephen Jay Gould

"Truly an extraordinary book."
– René Dubos

4014

RP424

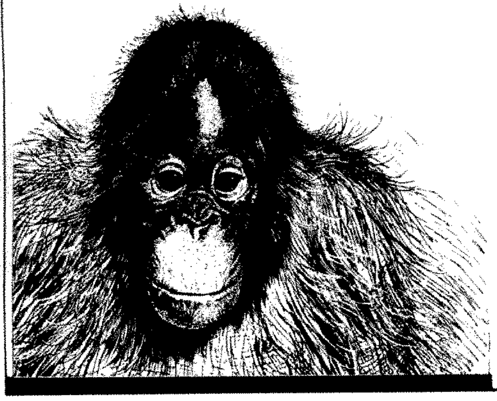

Published June 1982, £21.00

Harvard University Press

126 Buckingham Palace Road
London SW1W 9SD

Circle No.03 on Reader Service Card.

EDITORIAL OFFICES

London
4 Little Essex Street, WC2R 3LF
Telephone: (01) 836 6633 Telex: 262024

Editor: John Maddox

Deputy Editor: Peter Newmark

Alun Anderson
Philip Campbell
Isobel Collins
Tim Lincoln
David Millar
Naomi Molson
Sara Nash
Geoffrey North
Peta Pickering
Judy Redfearn
Miranda Robertson
Robert Walgate
Charles Wenz
Nigel Williams

Washington
991 National Press Building, DC 20045
Telephone: (202) 737-2355 Telex: 64280
Washington Editor: Deborah Shapley
Stephen Budiansky

Publisher: Elizabeth Hughes

Marketing Director: Ray Barker

International Advertising Manager:
Andy Sutherland
Features Advertising Manager: Marion Delaney
Classified Sales Manager: Jean Neville
Telephone: (01) 240 1101
Promotion Manager: Jonathan Earl

New York
15 East 26 Street, New York, NY 10010
Telephone: (212) 689-5900

American Publisher: Robert Ubell

American Advertising Manager: Henry Dale

Marketing Services Manager: Sheila Kane

USA Classified Advertising:
Cathy Moore

Canadian Display and Classified
Peter Drake, 32 Front Street West,
Suite 200 Toronto, Ontario M5J IC5
(416) 364-1623

Display Advertising Representatives
USA
Nature New York Office—(212) 689-5900
Roy McDonald Associates, Inc.
Dallas—(214) 941-4461
Roy McDonald Associates, Inc.
Houston—(713) 988-5005
Didier & Broderick, Inc. Chicago—
(312) 498-4520
Jobson/Jordan/Harrison/Schulz, Inc.
San Francisco (415) 392-6794
Los Angeles & Pasadena (213) 796-9200
Daniel Adams Associates, Inc.
Philadelphia—(215) 353-6191
CEL Associates Boston—(617) 848-9306
Brinker & Brinker Fort Lauderdale
(305) 771-0064
Mary Grunmeier, New Jersey
(201) 572 9018
Donald E. Northup Associates,
Dalton, PA (717) 563 2145
West Germany and Austria
Franz Schrecklinger
TMW Top Media Werbegesellschaft GmbH
Frankfurt (611) 726046
Holland and Belgium
Kevin Ward
G. Arnold Teesing BV
Amsterdam (020) 2636 15
Switzerland
Verena Hugi
Agentur Iff AG
Schaffhausen (053) 45821
Scandinavia
Andrew Karnig
Andrew Karnig & Associates AB
Stockholm (08) 51 68 70
Japan
Mashy Yoshikawa
Orient Echo Inc
Tokyo 541-4923

Nature®
ISSN 0028-0836
Registered as a newspaper at
the British Post Office

Vol. 298 No. 5869 1 July 1982

nature

Vol. 298 No. 5872 22 July 1982

Who sells to the Soviet Union? 313
Muddle about universities 313
Pity the luckless British 314

NEWS

JPL takes on classified research
France ponders biotechnology
British Telecom
Britain's nuclear power
Whales' Waterloo
Badger gassing
British academic industry
Britain is odd-man-out on 2,4,5-T
Synthetic fuels
High-energy physics
Franco-Soviet space flight 315

CORRESPONDENCE

Nuclear risk/SI units/German universities/Gould's book 320

NEWS AND VIEWS

New branches for old roots (B Cox)
Chaos, randomness and dimension (T Geisel)
Do mitochondria share enzymes with the rest of the cell? (T Fox)
Bone in the cartilaginous fishes (B Hall)
Hipparcos: space-age astrometry (A Cruise)
Monoclonal antibodies to human malignant melanoma (R Reisfeld)
What limits photosynthesis? (C Foyer, R Leegood & D Walker)
New views of the immunoglobulin heavy chain switch (K Marcu & M Cooper) 321

BOOK REVIEWS

Social Anthropology (*by* E Leach) R D Attenborough; **Cancer: A Comprehensive Treatise, 2nd Edn, Vol. 1 (F F Becker, *ed.*)** Peter Alexander; **Fusion, Vol. 1 (E Teller, *ed.*)** R S Pease; **Biomedical Innovation (E B Roberts *et al.*, *eds*)** John P Bunker and Jinnet Fowles; **Polyatomic Molecules (*by* R S Mulliken and W C Ermler)** W G Richards; **DNA Tumor Viruses, 2nd Edn (J Tooze, *ed.*)** Peter W J Rigby 403

MISCELLANY

100 years ago 322
Classified advertising xvi

Cover

Monoclonal antibodies against human T lymphocytes label Purkinje neurones in many species (see p.375)

Structure and variation of human α_1-antitrypsin (a review) R W Carrell, J-O Jeppsson, C-B Laurell, S O Brennan, M C Owen, L Vaughan & D R Boswell 329

ARTICLES

Internal rotation and gravitational quadrupole moment of the Sun D O Gough 334
The thermal springs of Bath J N Andrews, W G Burgess, W M Edmunds, R L F Kay & D J Lee 339
T24 human bladder carcinoma oncogene is an activated form of the normal human homologue of BALB- and Harvey-MSV transforming genes E Santos, S R Tronick, S A Aaronson, S Pulciani & M Barbacid 343
Synthesis and assembly of hepatitis B virus surface antigen particles in yeast P Valenzuela, A Medina, W J Rutter, G Ammerer & B D Hall 347

LETTERS TO NATURE

Evidence for an oblique magnetic solar rotator D O Gough 350
VHF Faraday polarization fluctuations and strong *L*-band amplitude scintillations near Appleton anomaly crests A Das Gupta, M C Lee & J A Klobuchar 354
Is the olivine–spinel phase transformation martensitic? P J Vaughan, H W Green II & R S Coe 357
Noise in chaotic systems J Guckenheimer 358
Natural production of tritium in permeable rocks J N Andrews & R L F Kay 361
Role of Mn (IV) oxide in abiotic formation of humic substances in the environment H Shindo & P M Huang 363
Is the CH_4, H_2 and CO venting from submarine hydrothermal systems produced by thermophilic bacteria? J A Baross, M D Lilley & L I Gordon 366
Evidence that patterning mechanisms in developing and regenerating limbs are the same K Muneoka & S V Bryant 369
Selective collateral elimination in early postnatal development restricts cortical distribution of rat pyramidal tract neurones B B Stanfield, D D M O'Leary & C Fricks 371
Glycogenolysis induced by serotonin in brain: identification of a new class of receptor T T Quach, C Rose, A M Duchemin & J C Schwartz 373
Monoclonal antibodies against human T lymphocytes label Purkinje neurones of many species J A Garson, P C L Beverley, H B Coakham & E I Harper 375

Nature® (ISSN 0028-0836) is published weekly on Thursday, except the last week in December, by Macmillan Journals Ltd and includes the Directory of Biologicals (mailed in December) and Annual Index (mailed in February). Annual subscription for USA and Canada US $198.50 (for subscription prices elsewhere, see next page). Orders (with remittance) and change of address labels to: Macmillan Journals Ltd, Brunel Rd, Basingstoke RG21 2XS, UK. Second class postage paid at New York, NY10010 and additional mailing offices. US Postmaster send form 3579 to: *Nature*, 15 East 26 Street, New York, NY 10010.

0028-0836/82/29000C-02$01.00

Contents continued overleaf

Get the complete package...

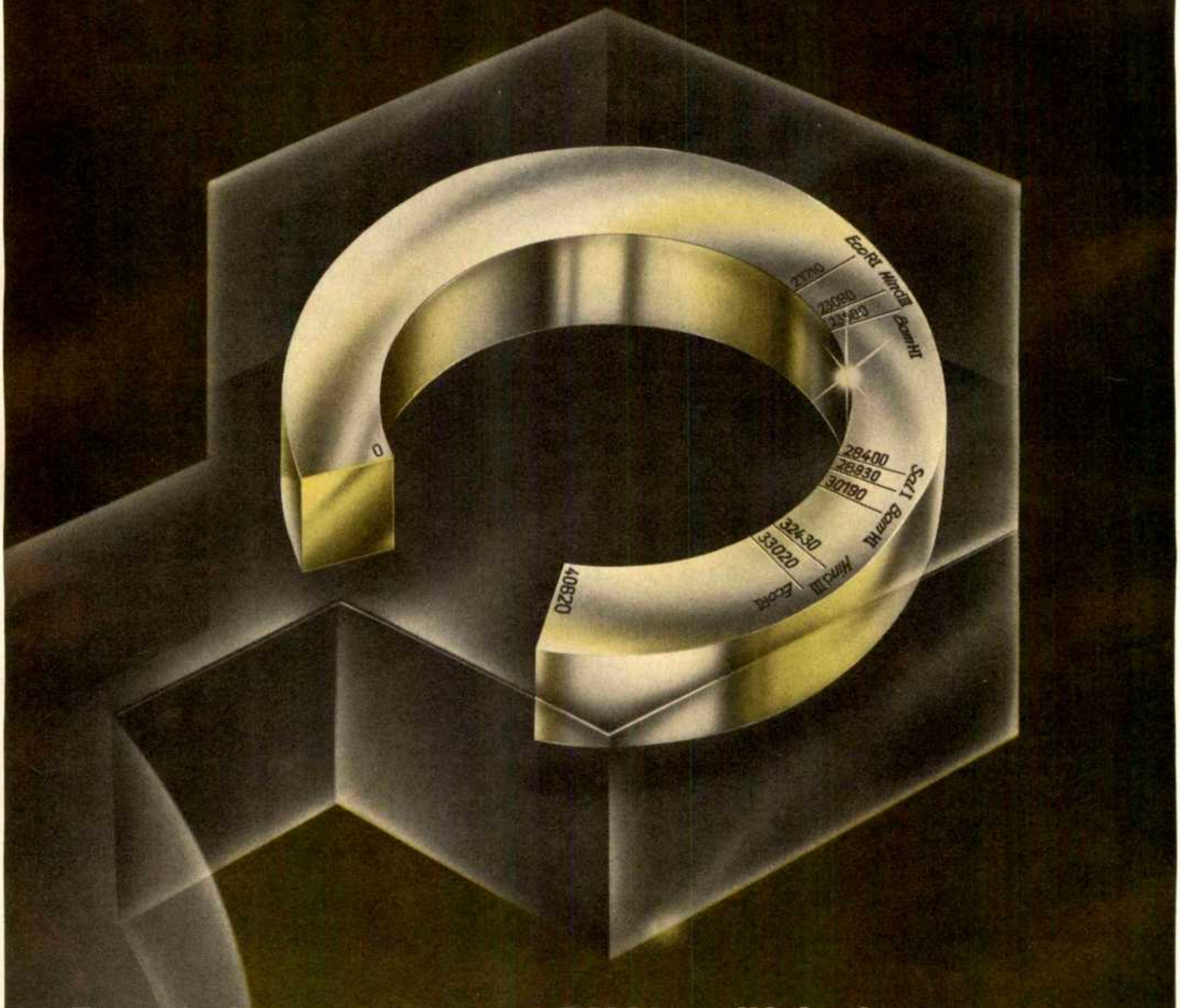

- **Restriction enzymes**
- **Cloning vectors**
- **DNA 'modifying' enzymes**
- **Lambda *in vitro* packaging kit**

now available to complement our wide range of radiolabelled products

Amersham - for products you know you can trust

Please call Amersham or your local representative for a booklet describing these products and their applications

Amersham International plc
Amersham England HP7 9LL
telephone Little Chalfont (024 04) 4444

Amersham

Amersham Australia PTY Limited Sydney **Amersham Belgium SA/NV** Brussels **Amersham Buchler GmbH & Co. KG** Braunschweig W Germany **Amersham Corporation** Arlington Heights Illinois USA **Amersham France SA** Paris **Amersham Japan** Tokyo **Amersham Nederland BV** Utrecht

Circle No. 10 on Reader Service Card

Science in France Science in West Germany

Copies of these special supplement issues are still available.

Prices (including postage): UK, £2.50 each; USA & Canada, US $6.00 (surface), US $9.00 (air); Rest of World, £3.00 (surface), £4.00 (air).

Orders (with payment) to:
Nature, Macmillan Journals Ltd,
Brunel Road, Basingstoke, Hants
RG21 2XS, England.

Annual Subscription including Index (51 issues)

UK & Eire		£85
USA & Canada		US$198.50
Belgium	Airspeed only	BF7450
West Germany	Airspeed only	DM450
Netherlands	Airspeed only	G505
Switzerland	Airspeed only	SF395
Rest of Europe	Airspeed only	£100
Rest of World	Surface	£100
Rest of World*	Airmail	£150

**(not USA, Canada & Europe)*

Personal subscription rates are available in some countries to subscribers paying by personal cheque or credit card.

Details can be obtained from:
UK: *Nature* Promotion Department,
Canada Road, Byfleet, Surrey KT14 7JL.
Telephone: Jonathan Earl: Byfleet (09323) 41459
USA: *Nature*, 15 East 26 Street, New York, NY 10010
Credit card orders only (in USA & Canada):
Call toll-free: (800) 824-7888 (Operator 246)
In California: (800) 852-7777 (Operator 246)

All other circulation enquiries concerning existing subscriptions please contact:
Nature Circulation Department, Macmillan Journals Ltd., Brunel Road, Basingstoke, Hants RG21 2XS, UK
Telephone: (0256) 29242 Telex: 858493

Back issues: (Post-paid) UK, £2.50; USA & Canada, US$6.00 (surface), US$9.00 (air); Rest of World, £3.00 (surface), £4.00 (air).

***Nature* Binders:**
Single Binders: UK, £4.00; Rest of World, $10.00
Set(s) of 3 Binders: UK, £10.00; Rest of World, 25.00

***Nature* First Issue Facsimile:**
UK, 75p; Rest of World (surface), $1.50, (air), £2.00

***Nature* Annual Indexes (1971-1981):**
Price (post-paid):
UK, £5.00 each; Rest of World, $10.00

***Nature* Directory of Biologicals:**
(Hardcover edition)
UK, £22.50; Rest of World, $45.00

***Nature* Wallcharts:**
How Britain Runs its Science; How the US Runs its Science; UK, £3.50; USA, $7.95 each

***Nature* in Microform:**
For Information:
UK: UMI, 18 Bedford Row, London WC2R 4EJ
USA: 300 North Zeeb Road, Ann Arbor, Mi 48106

Orders (with remittance) to:
Nature, Macmillan Journals Ltd.,
Brunel Road, Basingstoke, Hants RG21 2XS, UK
Tel: (0256) 29242 Telex: 858493

MACMILLAN JOURNALS

Germinal centre B cells: antigen specificity and changes in heavy chain class expression	G Kraal, I L Weissman & E C Butcher	377
Somatic variants of murine immunoglobulin λ light chains	A L M Bothwell, M Paskind, M Reth, T Imanishi-Kari, K Rajewsky & D Baltimore	380
Mapping class I gene sequences in the major histocompatibility complex	L R Pease, S G Nathenson & L A Leinwand	382
Reactivation of latent feline leukaemia virus infection	J L Rojko, E A Hoover, S L Quackenbush & R G Olsen	385
Culture of macrophage cell lines from normal mouse bone marrow	J Činátl, E Paluska, V Chudomel, V Malasková & M Elleder	388
Biosynthesis of membrane factor B by mouse peritoneal macrophages	Y M Ooi & B S Ooi	389
A bifunctional gene product involved in two phases of the yeast cell cycle	J R Piggott, R Rai & B L A Carter	391
Ligation of oligonucleotides by pyrimidine dimers — a missing 'link' in the origin of life?	R J Lewis & P C Hanawalt	393
Potential Z-DNA forming sequences are highly dispersed in the human genome	H Hamada & T Kakunaga	396
Receptor-rich intracellular membrane vesicles transporting asialotransferrin and insulin in liver	M T Debanne, W H Evans, N Flint & E Regoeczi	398

MATTERS ARISING

Dielectric constant of ice	J F Nagle Reply: D J Adams	401
Body temperature changes during the practice of G Tum-mo yoga	J M Pasachoff M A Strassburg Reply: H Benson	402

GUIDE TO AUTHORS

Authors should be aware of the diversity of *Nature*'s readership and should strive to be as widely understood as possible.

Review articles should be accessible to the whole readership. Most are commissioned, but unsolicited reviews are welcome (in which case prior consultation with the office is desirable).

Scientific articles are research reports whose conclusions are of general interest or which represent substantial advances of understanding. The text should not exceed 3,000 words and six displayed items (figures plus tables). The article should include an abstract of about 50 words.

Letters to *Nature* are ordinarily 1,000 words long with no more than four displayed items. The first paragraph (not exceeding 150 words) should say what the letter is about, why the study it reports was undertaken and what the conclusions are.

Matters arising are brief comments (up to 500 words) on articles and letters recently published in *Nature*. The originator of a Matters Arising contribution should initially send his manuscript to the author of the original paper and both parties should, wherever possible, agree on what is to be submitted.

Manuscripts may be submitted either to London or Washington (decisions being made only in London). Manuscripts should be typed (double spacing) on one side of the paper only. Three copies are required, each accompanied by copies of lettered artwork. No title should exceed 80 characters in length. Reference lists, figure legends, etc. should be on separate sheets, all of which should be numbered. Abbreviations, symbols, units, etc. should be identified on one copy of the manuscript at their first appearance.

References should appear sequentially indicated by superscripts in the text and should be abbreviated according to the *World List of Scientific Periodicals*, fourth edition (Butterworth 1963–65). The first and last page numbers of each reference should be cited. References to books should clearly indicate the publisher and the date and place of publication. Unpublished articles should not be formally referred to unless accepted or submitted for publication, but may be mentioned in the text.

Each piece of artwork should be clearly marked with the author's name and the figure number. Original artwork should be unlettered. Suggestions for cover illustrations are welcome. Original artwork (and one copy of the manuscript) will be returned when manuscripts cannot be published.

Requests for permission to reproduce material from Nature *should be accompanied by a self-addressed (and, in the case of the UK and USA, stamped) envelope.*

New from Napco®:

An autoclave engineered for the biotechnologist.

Step-saving convenience.
Completely portable unit goes anywhere. Plugs in standard 20 amp. outlet, requires no plumbing.

Timer measures only actual sterilization cycle.
New automatic precision timer starts running only after sterilization temperature is reached.

Fully automatic precision performance.
No attention is required by the operator through the complete sterilizing cycle.

Slow or fast exhaust cycle.
Switch to slow or fast exhaust cycle with the flip of a switch.

There's much more. Send for the new Napco autoclave brochure for complete information.

napco

National Appliance Company
Subsidiary of
Heinicke Instruments Company
10855 S.W. Greenburg Road,
Portland, Oregon 97223
800-547-2555
or (503) 639-3161
Telex: 151144

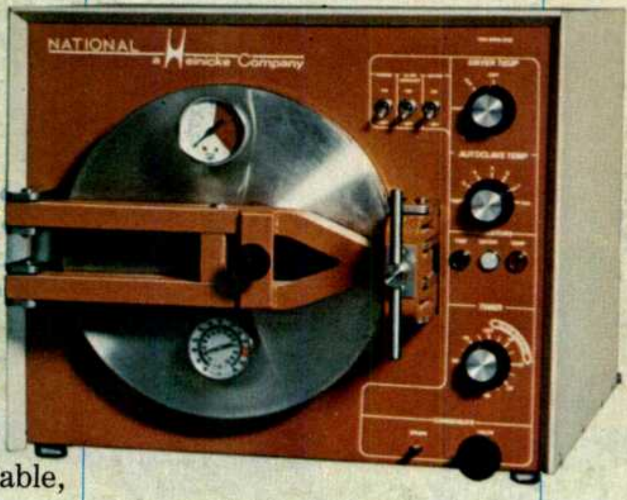

Napco instruments are designed to work. But if you should ever have an equipment problem, Napco technical service assistance is available, dial toll-free 800-547-2555.

Ask your dealer's salesman today:
American Scientific Products,
Curtin-Matheson,
Fisher Scientific Co., Preiser,
Sargent-Welch, S.G.A. Scientific,
Arthur H. Thomas Co.,
In Canada:
Fisher Scientific Co., Ltd.

Circle No.01 on Reader Service Card.

nature

Vol. 298 No. 5874 5 August 1982

James Watt and biotechnology 501
Talks, guns and butter 502

NEWS

Gandhi puts India's claim to USA
France to supply Tarapur fuels
Electronics industry
Balancing the francs
British biotechnology
Entrepreneurship
Signs of hope
US employment
Anthrax island
UK research councils
Telecommunications
UK higher education
Nuclear aftermath
Repression in Guatemala
Plea from a Soviet refusnik 503

CORRESPONDENCE

Prions/parasites/Poland/etc. 510

NEWS AND VIEWS

The NK cell: a phagocyte in lymphocyte's clothing? (B Babior & D Parkinson)
The fifth major D/V *Challenger* operation in central equatorial waters (Leg 85 Staff)
Protein folding by numbers (R Pain)
Measuring competition in plant communities (P Moore)
Lysosome proton pump identified (M Geisow)
The end of the message (N Proudfoot)
Two different viral transforming proteins bind the same host tumour antigen (D Lane & E Harlow)
The beginnings of solar-terrestrial studies (D Hughes)
Air pollution in the Arctic (B Ottar) 511

BOOK REVIEWS

Koestler: A Biography (*by* I Hamilton) Nicholas Wade; **Sky Atlas 2000.0 (*by* W Tirion) *and* Sky Catalogue 2000.0, Vol 1 (A Hirshfeld and R W Sinnott, *eds*)** David W Hughes; **Plurality of Worlds (*by* S J Dick)** A Rupert Hall; **The Clocks That Time Us (*by* M C Moore-Ede *et al.*)** Arthur T Winfree; **The Soul of a New Machine (*by* T Kidder)** Simon Lavington 587

Cover

The present-day mantle of the Earth's crust is made up of three chemically independent components (see p.519). The cover illustration is derived from Fig. 2 on p.521

ARTICLES

Nd, Sr and Pb isotopic systematics in a three-component mantle A Zindler, E Jagoutz & S Goldstein 519
Palaeolimnology and archaeology of Holocene deposits north-east of Lake Turkana, Kenya R B Owen, J W Barthelme, R W Renaut & A Vincens 523
Expression of murine H-2K^b histocompatibility antigen in cells transformed with cloned *H-2* genes A L Mellor, L Golden, E Weiss, H Bullman, J Hurst, E Simpson, R F L James, A R M Townsend, P M Taylor, W Schmidt, J Ferluga, L Leben, M Santamaria, G Atfield, H Festenstein & R A Flavell 529
Formation of transmembrane tubules by spontaneous polymerization of the hydrophilic complement protein C9 J Tschopp, H J Müller-Eberhard & E R Podack 534

LETTERS TO NATURE

Spontaneous generation of density perturbations in the early Universe M Crawford & D N Schramm 538
The peculiar variable star R Aquarii and its jet M Kafatos & A G Michalitsianos 540
Magnetostrictive control of coercive force in multidomain magnetite J P Hodych 542
Langmuir–Blodgett films of long-chain amines G L Gaines Jr 544
Photoreduction of methyl viologen in aqueous neutral solution without additives T W Ebbesen, G Levey & L K Patterson 545
Air hydrate inclusions in fresh ice core H Shoji & C C Langway Jr 548
Major ion chemistry of some large Chinese rivers H Ming-hui, R F Stallard & J M Edmond 550
Dynamic uplift of the Himalaya C Wang, Y Shi & W Zhou 553
Analysis of interspecific interactions in a coastal plant community — a perturbation approach J A Silander & J Antonovics 557
Inhibition of experimental ascending urinary tract infection by an epithelial cell-surface receptor analogue C S Edén, R Freter, L Hagberg, R Hull, S Hull, H Leffler & G Schoolnik 560
A stem cell for stem cells in murine haematopoiesis D I Burton, J D Ansell, R A Gray & H S Micklem 562
Analysis of fibroblast proteins from patients with Duchenne muscular dystrophy by two-dimensional gel electrophoresis E Rosenmann, C Kreis, R G Thompson, M Dobbs, J L Hamerton & K Wrogemann 563

Nature® (ISSN 0028-0836) is published weekly on Thursday, except the last week in December, by Macmillan Journals Ltd and includes the Directory of Biologicals (mailed in December) and Annual *Index* (mailed in February). Annual subscription for USA and Canada US $198.50 (for subscription prices elsewhere, see next page). Orders (with remittance) and change of address labels to: Macmillan Journals Ltd, Brunel Rd, Basingstoke RG21 2XS, UK. Second class postage paid at New York, NY10010 and additional mailing offices. US Postmaster send form 3579 to: *Nature*, 15 East 26 Street, New York, NY 10010.

0028-0836/82/31000C-02$01.00

Contents continued overleaf

NIKON VISIONS

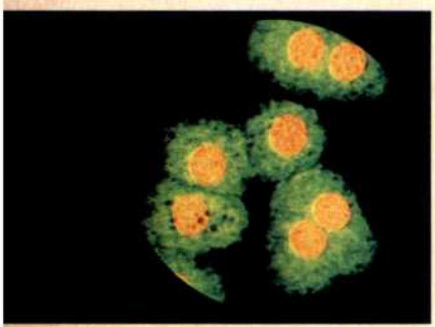

NIKON REVOLUTIONIZES OPTICAL PERFORMANCE WITH THE FX PHOTOMICROGRAPHY SYSTEMS.

CF UV-F 40X Rat liver cells

INSTRUMENTATION
Nikon's advanced UFX, HFX, AFX automatic exposure camera systems and PFX manual system.

SIGNIFICANCE
Nikon's exclusive FX direct projection design increases light transmission efficiency to greatly reduce exposure times, enhance lowlight metering sensitivity and dramatically improve image quality.

SPECIFICS
Nikon's remarkably affordable FX camera systems speed and simplify the photomicrographic process. High light transmission efficiency reduces typical exposure times by up to a factor of five. This is especially important for darkfield and fluorescence techniques.

To aid ease of operation, the models UFX, HFX, and AFX offer fully automatic microprocessor exposure control and LED digital exposure readout. Model UFX features a highly sensitive photomultiplier system with choice of 1% spot or integrated average metering, exposure memory and motorized 35mm film advance. Models HFX and AFX employ Silicon Photo Diode metering.

All Nikon FX Camera Systems adapt to 35mm, Polaroid, and 4×5 formats.

Extend *your* vision. Write:
NIPPON KOGAKU K.K.,
Fuji Bldg., 2-3, Marunouchi
3-chome, Chiyoda-ku, Tokyo
100, Japan.

Nikon
Extending Man's Vision

Circle No.32 on Reader Service Card.

Science in France
Science in West Germany

Copies of these special supplement issues are still available.

Prices (including postage): UK, £2.50 each; USA & Canada, US $6.00 (surface), US $9.00 (air); Rest of World, £3.00 (surface), £4.00 (air).

Orders (with payment) to:
Nature, Macmillan Journals Ltd,
Brunel Road, Basingstoke, Hants
RG21 2XS, England.

Annual Subscription including Index (51 issues)

UK & Eire		£85
USA & Canada		US$198.50
Belgium	Airspeed only	BF7450
West Germany	Airspeed only	DM450
Netherlands	Airspeed only	G505
Switzerland	Airspeed only	SF395
Rest of Europe	Airspeed only	£100
Rest of World	Surface	£100
Rest of World*	Airmail	£150

**(not USA, Canada & Europe)*

Personal subscription rates are available in some countries to subscribers paying by personal cheque or credit card.

Details can be obtained from:
UK: *Nature* Promotion Department,
Canada Road, Byfleet, Surrey KT14 7JL.
Telephone: Jonathan Earl: Byfleet (09323) 41459

USA: *Nature*, 15 East 26 Street, New York, NY 10010
Credit card orders only (in USA & Canada):
Call toll-free: (800) 824-7888 (Operator 246)
In California: (800) 852-7777 (Operator 246)

All other circulation enquiries concerning existing subscriptions please contact:

Nature Circulation Department, Macmillan Journals Ltd., Brunel Road, Basingstoke, Hants RG21 2XS, UK

Telephone: (0256) 29242 Telex: 858493

Back issues: (Post-paid) UK, £2.50; USA & Canada, US$6.00 (surface), US$9.00 (air); Rest of World, £3.00 (surface), £4.00 (air).

***Nature* Binders:**
Single Binders: UK, £4.00; Rest of World, $10.00
Set(s) of 3 Binders: UK, £10.00; Rest of World, 25.00

***Nature* First Issue Facsimile:**
UK, 75p; Rest of World (surface), $1.50, (air), £2.00

***Nature* Annual Indexes (1971-1981):**
Price (post-paid):
UK, £5.00 each; Rest of World, $10.00

***Nature* Directory of Biologicals:**
(Hardcover edition)
UK, £22.50; Rest of World, $45.00

***Nature* Wallcharts:**
How Britain Runs its Science; How the US Runs its Science; UK, £3.50; USA, $7.95 each

***Nature* in Microform:**
For Information:
UK: UMI, 18 Bedford Row, London WC2R 4EJ
USA: 300 North Zeeb Road, Ann Arbor, Mi 48106

Orders (with remittance) to:
Nature, Macmillan Journals Ltd.,
Brunel Road, Basingstoke, Hants RG21 2XS, UK
Tel: (0256) 29242 Telex: 858493

MACMILLAN JOURNALS

Recognition of a polymorphic monocyte antigen in HLA — A van Leeuwen, A Termijtelen, S Shaw & J J van Rood — 565

Immunotherapy in nude mice of human hepatoma using monoclonal antibodies against hepatitis B virus — D Shouval, D A Shafritz, V R Zurawski Jr, K J Isselbacher & J R Wands — 567

Oxygen intermediates are triggered early in the cytolytic pathway of human NK cells — J C Roder, S L Helfand, J Werkmeister, R McGarry, T J Beaumont & A Duwe — 569

Adenosine-induced slow ionic currents in the *Xenopus* oocyte — I Lotan, N Dascal, S Cohen & Y Lass — 572

Presence of cyclic nucleotide-Ca^{2+} independent protein kinase in bovine brain coated vesicles — A Pauloin, I Bernier & P Jollès — 574

Injection of subunits of cyclic AMP-dependent protein kinase into cardiac myocytes modulates Ca^{2+} current — W Osterrieder, G Brum, J Hescheler, W Trautwein, V Flockerzi & F Hofmann — 576

The DNase I sensitivity of *Xenopus laevis* genes transcribed by RNA polymerase III — J Coveney & H R Woodland — 578

Is avian adeno-associated virus an endogenous virus of chicken cells? — G J Dawson, V J Yates, P W Chang & J J Oprandy — 580

Evolutionary selection for perfect hairpin structures in viral DNAs — U R Müller & W M Fitch — 582

Evolution of early mechanisms of translation of genetic information into polypeptides — H Kuhn & J Waser — 585

GUIDE TO AUTHORS

Authors should be aware of the diversity of *Nature*'s readership and should strive to be as widely understood as possible.

Review articles should be accessible to the whole readership. Most are commissioned, but unsolicited reviews are welcome (in which case prior consultation with the office is desirable).

Scientific articles are research reports whose conclusions are of general interest or which represent substantial advances of understanding. The text should not exceed 3,000 words and six displayed items (figures plus tables). The article should include an abstract of about 50 words.

Letters to *Nature* are ordinarily 1,000 words long with no more than four displayed items. The first paragraph (not exceeding 150 words) should say what the letter is about, why the study it reports was undertaken and what the conclusions are.

Matters arising are brief comments (up to 500 words) on articles and letters recently published in *Nature*. The originator of a Matters Arising contribution should initially send his manuscript to the author of the original paper and both parties should, wherever possible, agree on what is to be submitted.

Manuscripts may be submitted either to London or Washington (decisions being made only in London). Manuscripts should be typed (double spacing) on one side of the paper only. Three copies are required, each accompanied by copies of lettered artwork. No title should exceed 80 characters in length. Reference lists, figure legends, etc. should be on separate sheets, all of which should be numbered. Abbreviations, symbols, units, etc. should be identified on one copy of the manuscript at their first appearance.

References should appear sequentially indicated by superscripts in the text and should be abbreviated according to the *World List of Scientific Periodicals*, fourth edition (Butterworth 1963–65). The first and last page numbers of each reference should be cited. References to books should clearly indicate the publisher and the date and place of publication. Unpublished articles should not be formally referred to unless accepted or submitted for publication, but may be mentioned in the text.

Each piece of artwork should be clearly marked with the author's name and the figure number. Original artwork should be unlettered. Suggestions for cover illustrations are welcome. Original artwork (and one copy of the manuscript) will be returned when manuscripts cannot be published.

Requests for permission to reproduce material from Nature *should be accompanied by a self-addressed (and, in the case of the UK and USA, stamped) envelope.*

BEAT THE WATER SHORTAGE!

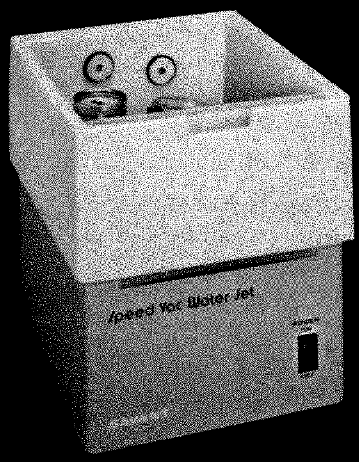

SPEED VAC WATER JET — An efficient vacuum source created by a high pressure pump forcing water through a jet. The preferred method for removing organic solvent vapors since Hi-Vac oil pumps can easily be ruined by condensed organic solvents.

- Vacuum Chambers
- Distillation Apparatus
- Filtering Flasks
- Dessicators
- Fume & Vapor Removal
- Dialysis Devices

SPEED VAC
WATER
JET

SPEED VAC "NO BUMP" CONCENTRATOR

"NO BUMP" Evaporation System for concentrating samples by volume reduction prior to analysis by Gas Chromatography (GC), High Pressure Liquid Chromatography (HPLC), Electrophoresis, TLE or TLC. 100% sample recovery with Eluates, Hydrolysates, Extracts, and Dialized Solutions ... separate volatile organic solvents from Aqueous Solvents in one instrument.

"NO BUMP" means no losses and considerable savings if the sample is a valuable one. We guarantee that your isolation technique will yield incomparable results when you use a Speed Vac Concentrator.

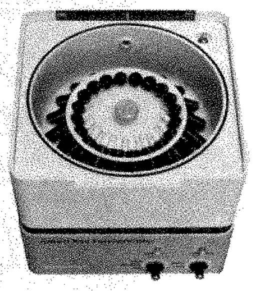

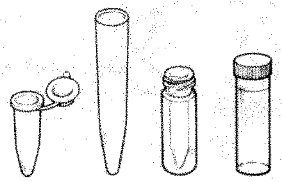

U.S. Pat. #422669

Send for literature today.

Savant
SAVANT INSTRUMENTS, INC.
221 Park Ave., Hicksville, NY 11801 ● (516) 935-8774.

Circle No.01 on Reader Service Card.

OPPORTUNITIES IN BIOTECHNOLOGY

for those with chemical, biochemical and molecular biology backgrounds

Vital information for anyone interested in biotechnology, whether BS, MS, or PhD. Genetic engineering company and career directory — a comprehensive, up-to-date summary of trends and employment opportunities in biotechnology. The Biotechnology Directory contans detailed, multifaceted information covering over 200 US and foreign firms. It includes names and addresses of contacts, descriptions of areas of research and projected research goals, summaries of past and present hiring trends, and the qualifications required for employment by each company. The Directory also provides concise background information on every company, from the largest public corporation to the smallest privately held firm.

Organized according to fields of application, the directory is divided into five sections: agriculture/animal health, chemicals/energy, human health, hybridomas, and pharmaceuticals. $25/section or $100 for all five. A more detailed financial and scientific directory will also be made available. For more information call (617) 734-8428 or write to:

Information Resources
P.O. Box 1734 GMF
Boston, MA 02205

Circle No.05 on Reader Service Card.

nature

Vol. 298 No. 5874 12 August 1982

Disunited nations in outer space 593
Gamekeeper turned poacher 593
Jumpiness of bankers 594

NEWS

More trouble for Stanford's patent
Space wars at UN conference
India's space hopes
US astronomy
Fields Medal awards
British academic pay
US drug regulation
Arthritis drug proscribed in Britain
FDA regulations
Venture capital investment
Polish students abroad
Nature guide to bio-riches 595

CORRESPONDENCE

Celltech and MRC/Numbers/Carcinogens 600

NEWS AND VIEWS

What are quarks made of? (L Lyons)
Proteins containing nickel (A J Thomson)
Remote operation of telescopes (M Penston)
The biogeography of the Pacific Basin (J M Diamond)
Warts and all (M Saveria Campo)
Antigenic variation in the trypanosome (M Turner)
Anilides and the Spanish toxic oil syndrome (A Pestaña & E Muñoz) 601

BOOK REVIEWS

Vision (*by* **D Marr**) Stuart Sutherland; **NMR in Molecular Biology** (*by* **O Jardetzky and G C K Roberts**) Alfred G Redfield; **Solar Flare Magnetohydrodynamics (E R Priest,** *ed.***)** Robert Rosner; **Biological Energy Transduction: The Uroboros** (*by* **R F Fox**) Robert M Macnab; **The Channels of Mars** (*by* **V R Baker**) Lionel Wilson 691

MISCELLANY

100 years ago 607
Announcements 690
Classified advertising ix

Cover

A new marker is used to show that aspartate and glutamate may be involved as neurotransmitters in photoreceptors of the cone (p.**657**)

ARTICLES

Aspherical Earth structure from fundamental spheroidal-mode data	G Masters, T H Jordan, P G Silver & F Gilbert	609
Sm-Nd, Rb-Sr and U-Th-Pb systematics of granulite facies rocks from Fyfe Hills, Enderby Land, Antarctica	D J DePaolo, W I Manton, E S Grew & M Halpern	614
An inter-laboratory comparison of radiocarbon measurements in tree rings	International Study Group	619
***De novo* methylation and expression of retroviral genomes during mouse embryogenesis**	D Jähner, H Stuhlmann, C L Stewart, K Harbers, J Löhler, I Simon & R Jaenisch	623
Single base substitution in an intron of oxidase gene compensates splicing defects of the cytochrome *b* gene	G Dujardin, C Jacq & P P Slonimski	628

LETTERS TO NATURE

Is our vacuum metastable?	M S Turner & F Wilczek	633
A search for evidence of superheavy-element fission in chondritic metal	R K Bull & P Mold	634
Detection of nitrogen at {100} platelets in diamond	S D Berger & S J Pennycook	635
Reconstruction of past ice conditions in a Hudson Bay estuary using tree rings	G C Jacoby & L D Ulan	637
Isotope evidence for Pleistocene climatic changes in Kashmir, India	R V Krishnamurthy, M J DeNiro & R K Pant	640
An anomalous Suess effect above Europe	A F M de Jong & W G Mook	641
Triassic bedded cherts in central Japan are not pelagic	R Sugisaki, K Yamamoto & M Adachi	644
Mid-Palaeozoic travels of Arctic-Alaska	J F Sweeney	647
A mutation in *Drosophila* alters normal connectivity between two identified neurones	J B Thomas & R J Wyman	650
Cross-species neural grafting in a rat model of Parkinson's disease	A Björklund, U Stenevi, S B Dunnett & F H Gage	652
Associated amacrine cells could mediate directional selectivity in pigeon retina	A P Mariani	654
Glycine receptor alteration in the mutant mouse *spastic*	W F White & A H Heller	655
Aspartate aminotransferase-like immunoreactivity as a marker for aspartate/glutamate in guinea pig photoreceptors	R A Altschuler, J L Mosinger, G G Harmison, M H Parakkal & R J Wenthold	657

Nature® (ISSN 0028-0836) is published weekly on Thursday, except the last week in December, by Macmillan Journals Ltd and includes the Directory of Biologicals (mailed in December) and Annual Index (mailed in February). Annual subscription for USA and Canada US $198.50 (for subscription prices elsewhere, see next page). Orders (with remittance) and change of address labels to: Macmillan Journals Ltd, Brunel Rd, Basingstoke RG21 2XS, UK. Second class postage paid at New York, NY10010 and additional mailing offices. US Postmaster send form 3579 to: *Nature*, 15 East 26 Street, New York, NY 10010.

0028-0836/82/32000C-02$01.00

Contents continued overleaf

Take a closer look at what you get with a Philips gamma counter

- Spectrum scan and plot.
- Automatic recalibration.
- Sample capacity of 310, 480 or 620.
- RIA curve plot for single and dual label.
- Individually programmable sample trays (pioneered by Philips).
- Multi-user capability.
- Choice of detectors.
- User-oriented keyboard.
- Sample trays can be used in a centrifuge.
- Priority interrupt measurements.
- 15 Different measurement and calculation programmes (30 with optional personal computer).
- Sophisticated RIA data processing, including 4 parameter dose response models, outlier detection, region of interest selection and weighted regression.
- Choice of lead shields.
- Highly competitive price.
- Small, medium or large volume samples.
- Refrigerated and ambient systems.
- Service and spares availability guaranteed for at least 10 years.
- Remote control and additional data processing through the use of an optional personal computer.*

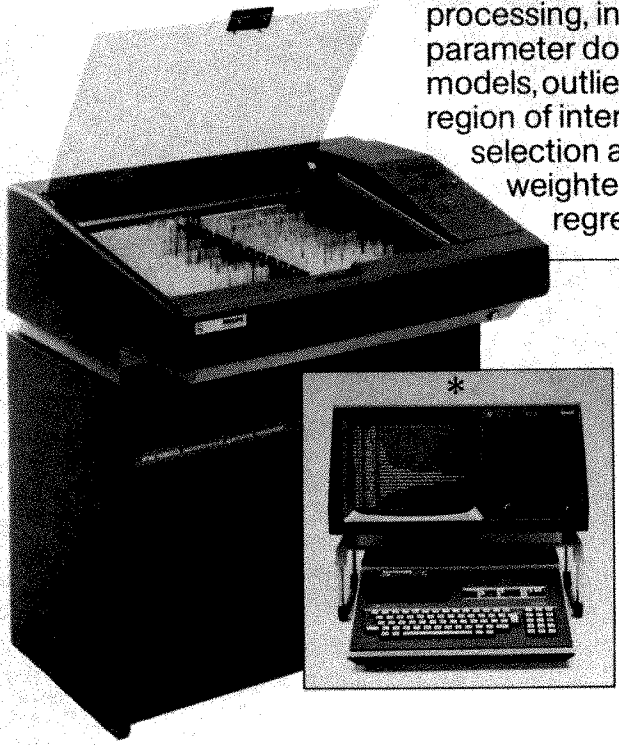

And that's just an introduction to the Philips AGC. Full details are described in our brochure. Contact your sales representative or drop us a line and we'll gladly send you a free copy.

Nuclear Analysis Manager,
Philips Industries, Science and Industry,
Lelyweg 1, 7602 EA ALMELO, The Netherlands.
Telephone (05490) - 1 82 91, Telex 36591.

PHILIPS

Circle No.07 on Reader Service Card.

Science in France Science in West Germany

Copies of these special supplement issues are still available.

Prices (including postage): UK, £2.50 each; USA & Canada, US $6.00 (surface), US $9.00 (air); Rest of World, £3.00 (surface), £4.00 (air).

Orders (with payment) to:
Nature, Macmillan Journals Ltd,
Brunel Road, Basingstoke, Hants
RG21 2XS, England.

Annual Subscription including Index (51 issues)

UK & Eire		£85
USA & Canada		US$198.50
Belgium	Airspeed only	BF7450
West Germany	Airspeed only	DM450
Netherlands	Airspeed only	G505
Switzerland	Airspeed only	SF395
Rest of Europe	Airspeed only	£100
Rest of World	Surface	£100
Rest of World*	Airmail	£150

**(not USA, Canada & Europe)*

Personal subscription rates are available in some countries to subscribers paying by personal cheque or credit card.

Details can be obtained from:
UK: *Nature* Promotion Department,
Canada Road, Byfleet, Surrey KT14 7JL.
Telephone: Jonathan Earl: Byfleet (09323) 41459
USA: *Nature*, 15 East 26 Street, New York, NY 10010
Credit card orders only (in USA & Canada):
Call toll-free: (800) 824-7888 (Operator 246)
In California: (800) 852-7777 (Operator 246)

All other circulation enquiries concerning existing subscriptions please contact:
Nature Circulation Department, Macmillan Journals Ltd., Brunel Road, Basingstoke, Hants RG21 2XS, UK
Telephone: (0256) 29242 Telex: 858493

Back issues: (Post-paid) UK, £2.50; USA & Canada, US$6.00 (surface), US$9.00 (air); Rest of World, £3.00 (surface), £4.00 (air).

***Nature* Binders:**
Single Binders: UK, £4.00; Rest of World, $10.00
Set(s) of 3 Binders: UK, £10.00; Rest of World, 25.00

***Nature* First Issue Facsimile:**
UK, 75p; Rest of World (surface), $1.50, (air), £2.00

***Nature* Annual Indexes (1971-1981):**
Price (post-paid):
UK, £5.00 each; Rest of World, $10.00

***Nature* Directory of Biologicals:**
(Hardcover edition)
UK, £22.50; Rest of World, $45.00

***Nature* Wallcharts:**
How Britain Runs its Science; How the US Runs its Science; UK, £3.50; USA, $7.95 each

***Nature* in Microform:**
For Information:
UK: UMI, 18 Bedford Row, London WC2R 4EJ
USA: 300 North Zeeb Road, Ann Arbor, Mi 48106

Orders (with remittance) to:
Nature, Macmillan Journals Ltd.,
Brunel Road, Basingstoke, Hants RG21 2XS, UK
Tel: (0256) 29242 Telex: 858493

M MACMILLAN JOURNALS

Origin of lignans in mammals and identification of a precursor from plants M Axelson, J Sjövall, B E Gustafsson & K D R Setchell **659**

Fibronectin in adhesion, spreading and cytoskeletal organization of cultured fibroblasts I Virtanen, T Vartio, R A Badley & V-P Lehto **660**

Evidence for contractile flexing of the gliding bacterium *Flexibacter* FS-1 R P Burchard **663**

X-ray scattering by myosin S-1: implications for the steric blocking model of muscle control R Mendelson **655**

Insulin stimulates tyrosine phosphorylation of the insulin receptor in a cell-free system M Kasuga, Y Zick, D L Blithe, M Crettaz & C R Kahn **667**

Insertion of diphtheria toxin into and across membranes: role of phosphoinositide asymmetry J J Donovan, M I Simon & M Montal **669**

Genetic recombination and directional selection for DDT resistance in *Drosophila melanogaster* P B Flexon & C F Rodell **672**

Maintenance of broad host range plasmid RK2 replicons in *Pseudomonas aeruginosa* C M Thomas, A A K Hussain & C A Smith **674**

Point mutations during generation of expression-linked extra copy of trypanosome surface glycoprotein gene A C Rice-Ficht, K K Chen & J E Donelson **676**

Amplification of endogenous *myc*-related DNA sequences in a human myeloid leukaemia cell line S Collins & M Groudine **679**

Sequences on the human Y chromosome homologous to the autosomal gene for argininosuccinate synthetase S P Daiger, R S Wildin & T-S Su **682**

Initiator tRNAs from archaebacteria show common unique sequence characteristics Y Kuchino, M Ihara, Y Yabusaki & S Nishimura **684**

Mechanism of C-terminal amide formation by pituitary enzymes A F Bradbury, M D A Finnie & D G Smyth **686**

Effect of an allozyme polymorphism on regulation of cell volume T J Hilbish, L E Deaton & R K Koehn **688**

Nature in Poland

Readers wishing to subscribe to a weekly copy of *Nature* on behalf of a colleague in Poland (where hard currency is scarce) should send a cheque for £50 (or the equivalent in any currency), accompanied by their name and address and that of the proposed recipient, to the *Nature* office in London or New York (see addresses opposite page **593**). For further details, readers are referred to *Nature* 3 June, p.354.

The world's leading scientists get it every week and so should you... at ½ price.

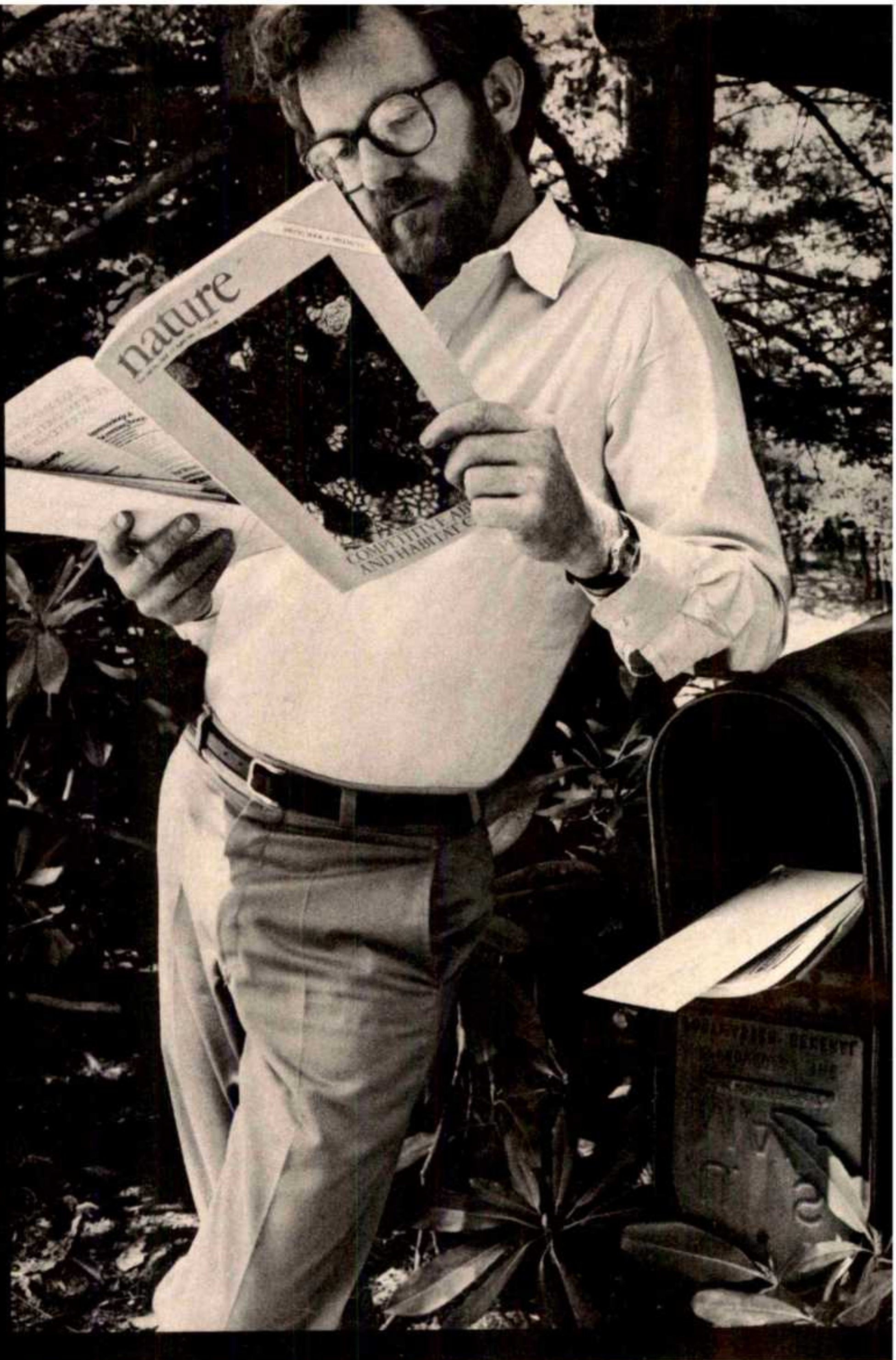

Scientists who are leaders in their ield and who get to reap the rewards of their achievements are among Nature's most eager readers.

And they are renewing their subscriptions to *Nature* in record numbers.

If, like them, you keep searching or ways to speed up your research, or if you're looking for advancement where you work, or are thinking of moving on to something more stimuating, how can you afford to be without your own personal subscription o *Nature?*

It's the most certain and consistent way to get the research results, news, opinion, and analysis you need, while hey're still fresh and can be applied most usefully to your own work.

With your own *Nature*, you'll be well ahead of the monthly journals whose reports often lag a year or more behind ours. And there isn't a science weekly anywhere that covers research developments in as many parts of the world, as fully and authoritatively, as *Nature* does.

The good news is that we've cut *Nature's* personal subscription rate n half and, to top it off, if you subscribe for a full year, we'll send you, free, a copy of *Nature's* new, annual *Directory of Biologicals*. Planned for all 1982, the *Directory* will be the first truly worldwide buyers' guide to biological products. It will be available only to yearly subscribers (or, for $45, to buyers of the hardcover version, in bookstores).

A personal subscription to *Nature* has never been more attractive. We urge you to clip and mail the coupon today. For credit-card orders only, **call toll-free now: (800) 824-7888. Ask for operator 130.**

In California: (800) 852-7777.
Ask for operator 130.

Now: Nature at ½ price – plus a bonus book, free

NAT 22

To: **Nature** 15 East 26th Street,
New York, N.Y. 10010

☐ Please send me a year of *Nature* at ½ price, **$99.25**, plus my free *Directory of Biologicals*

☐ I enclose my *personal* check

☐ Please bill my credit card account

Account No.:

☐ Visa ☐ Master ☐ Amer. Ex. Exp. Date

Name

Address

City State Zip

Orders *must* include personal check or credit card data. Offe good in the U.S. and Canada and is subject to change without notice. In the U.K. send personal check for £42.50, c credit card data, to: Nature, 4 Little Essex St., London WC2

nature

Nuclear LUAncy or sensible choice? 695
An almighty crash 696

NEWS

Japan reaches for the stars
Remote sensing for all at UN
Remote sensing satellites
South African funds
French Comité National
US computer industry
US biotechnology
Biotechnology centre
New sights for Land 697

CORRESPONDENCE

Coal costs/Ball of fire/Badgers/etc. 702

NEWS AND VIEWS

Mitochondrial mosaics — maturases on the move (L A Grivell & P Borst)
Where has that Moon been? (K Lambeck)
From CoA to complement: thioesters as the spring in the molecular mouse trap (J Fothergill)
Focus on filaments: embryology to pathology (B Lane & B Anderton)
Do steroid receptors recognize DNA sequences? (J R Tata)
Molecular heterogeneity and the nervous system (C J Barnstable)
BIRPS: deep seismic reflection profiling around the British Isles (D H Matthews) 703

BOOK REVIEWS

Risk and Culture (*by* M Douglas and A Wildavsky) Dorothy Nelkin; **The Expanding Universe: Astronomy's 'Great Debate' 1900–1931 (*by* R W Smith)** Owen Gingerich; **The Theory of Vibrational Spectroscopy and Its Application to Polymeric Materials (*by* P C Painter *et al.*)** Warner L Peticolas; **Gene Cloning in Organisms Other than *E. coli* (P H Hofschneider and W Goebel, *eds*)** Noreen Murray; **Principles of Pollution Control (*by* F Sandbach)** Eirene White 775

Cover

Illustration of DNA and cro repressor in its presumed DNA-binding conformation (see p.718). The various DNA bases and amino acids of the protein are indicated by different colours. (Figure drawn with an Advanced Electronics Design Inc. 512CTR color graphics terminal by Mr David Bacon, using the program written by Mr Colin Broughton whom we thank for their assistance.)

ARTICLES

A pregalactic Population III: primordial helium and heavy elements and the microwave background P W Tarbet & M Rowan-Robinson 711
Vitrification of pure liquid water by high pressure jet freezing E Mayer & P Brüggeller 715
The molecular basis of DNA-protein recognition inferred from the structure of cro repressor D H Ohlendorf, W F Anderson, R G Fisher, Y Takeda & B W Matthews 718
Complete nucleotide sequence and identification of membrane components of the histidine transport operon of *S. typhimurium* C F Higgins, P D Haag, K Nikaido, F Ardeshir, G Garcia & G Ferro-Luzzi Ames 723

LETTERS TO NATURE

Character of 'prolate' galaxies D O Richstone & M D Potter 728
Composition-dependent glass-transition temperatures and copolymers P R Couchman 729
Gold deposition at low temperature on sulphide minerals G M Bancroft & G Jean 730
Layered convection and crystal layers in multicomponent systems R C Kerr & J S Turner 731
Lithospheric thinning associated with rifting in East Africa R F Wendlandt & P Morgan 734
Oligo-Miocene rift of Sardinia and the early history of the Western Mediterranean Basin A Cherchi & L Montadert 736
High rock stresses as a consequence of glaciation A Carlsson & T Olsson 739
Evidence for $^{13}C/^{12}C$ fractionation between tree leaves and wood S W Leavitt & A Long 742
Oxic diagenetic products as indicators of past oceanic algal populations and diversity F T Gillan & R B Johns 744
Age of the Lufeng, China, hominoid locality L J Flynn & Q Guo-qin 746
Natural selection on body size and proportions in house sparrows R C Fleischer & R F Johnston 747
Genetic differences in individual behaviour associated with shell polymorphism in the snail *Cepaea nemoralis* J S Jones 749
Pluripotent embryonic stem cell lines can be derived from t^{w5}/t^{w5} blastocysts T Magnuson, C J Epstein, L M Silver & G R Martin 750
Plasminogen activator-plasmin system and neuronal migration G Moonen, M P Grau-Wagemans & I Selak 753
Transformation of fast fibres to slow prevented by lack of activity in developing lobster muscle C K Govind & K S Kent 755

Nature® (ISSN 0028-0836) is published weekly on Thursday, except the last week in December, by Macmillan Journals Ltd and includes the Directory of Biologicals (mailed in December) and Annual Index (mailed in February). Annual subscription for USA and Canada US $198.50 (for subscription prices elsewhere, see next page). Orders (with remittance) and change of address labels to: Macmillan Journals Ltd, Brunel Rd, Basingstoke RG21 2XS, UK. Second class postage paid at New York, NY10010 and additional mailing offices. US Postmaster send form 3579 to: *Nature*, 15 East 26 Street, New York, NY 10010. ©1982 Macmillan Journals Ltd.

0028-0836/82/33000C-02$01.00

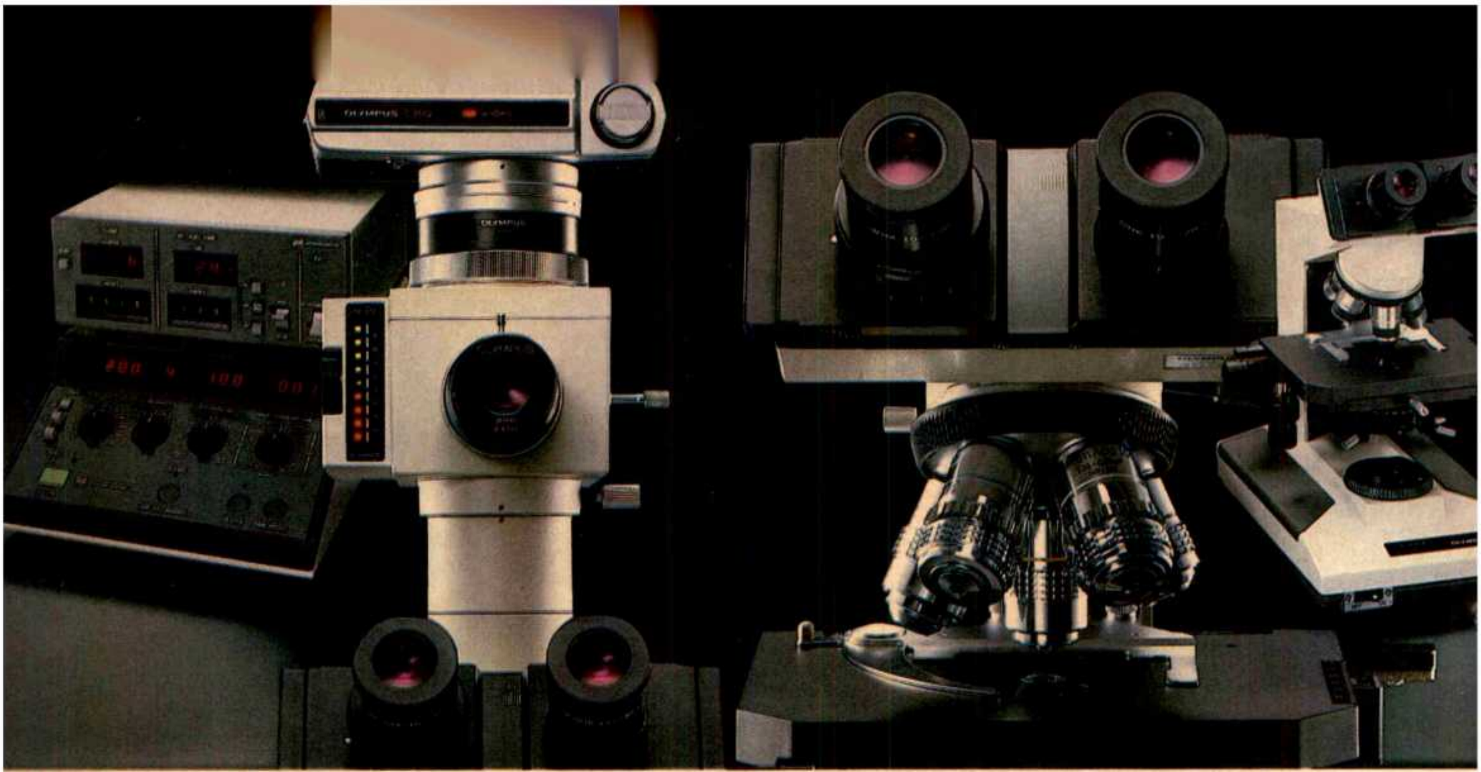

Two Outstanding Solutions From A Well-Known Name, Synonymous With Precision

In microscopy, what we see is of utmost importance. The sharper the detail, the better. And our findings should not only be visible through the viewing eyepiece.
We should be able to document them quickly, easily and accurately on photographic film. Olympus, a well-known name in precision instruments, now offers outstanding solutions to both needs. The BH-2 System Microscope and the PM-10AD Photo and Cinemicrographic System. A superb combination that features the latest optical, mechanical and electronic advances. And best answers the diverse requirements of microscopy and photomicrography today.

BH-2 MICROSCOPES

The Modern Scientists' Choice.

To satisfy different user applications, the new BH-2 System Microscope is available in three different configurations.

Model BHS microscope is best suited for research and demanding clinical applications. It accepts a wide variety of modular accessories to ensure the highest system performance possible. A highly sophisticated model, it is perfect for photomicrography.

Model BHT microscope is suitable for research and training purposes. Space-saving and easy-to-handle, it features the same choice of accessories as the BHS.

Model BHTU microscope is especially effective for routine laboratory applications where observation of numerous specimens is required. It assures smooth handling and marking of all specimens.

LB OBJECTIVES

Indispensable Value That Makes The BH-2 Top-Of-The-Line.

Olympus is proud to offer a newly-computed series of LB (long barrel) objectives which offer increased working distance and the utmost in resolution, contrast, image clarity and flatness of field. In conjunction with the new 10x viewing eyepiece, these objectives provide a visual field of 20, the largest available for a conventional microscope.

What's more, a completely new and unique illuminating system permits Köhler illumination, even with 1x and 2x objectives.
In addition, 1x and 2x objectives are parfocal with 4x and higher power objectives.

PM-10AD

It Leaves Nothing To Chance.

The beauty of the PM-10AD Photomicrographic System is that it leaves no room for error. A built-in microcomputer ensures quick, accurate and fully automated photographic and cinematographic documentation. Exposure, 35mm film transport and compensation for reciprocity failure are completely automatic. A complete selection of film formats and other advanced features are provided. Thanks to the clearly readable LED digital display the programming and monitoring of various functions, e.g. time-lapse photography, can be performed with a minimum of effort and experience.

OLYMPUS®

OLYMPUS OPTICAL CO.,LTD.
San-Ei Building, 22-2, Nishi Shinjuku 1-chome, Shinjuku-ku, Tokyo, Japan
OLYMPUS OPTICAL CO. (EUROPA) GMBH.
Postfach 104908, Wendenstrasse 14-16, 2 Hamburg 1, West Germany
OLYMPUS CORPORATION OF AMERICA
4 Nevada Drive, New Hyde Park, N.Y. 11042, U.S.A.

Circle No.20 on Reader Enquiry Card.

Science in France
Science in West Germany

Copies of these special supplement issues are still available.

Prices (including postage): UK, £2.50 each; USA & Canada, US $6.00 (surface), US $9.00 (air); Rest of World, £3.00 (surface), £4.00 (air).

Orders (with payment) to:
Nature, Macmillan Journals Ltd,
Brunel Road, Basingstoke, Hants
RG21 2XS, England.

Annual Subscription including Index (51 issues)

UK & Eire		£85
USA & Canada		US$198.50
Belgium	Airspeed only	BF7450
West Germany	Airspeed only	DM450
Netherlands	Airspeed only	G505
Switzerland	Airspeed only	SF395
Rest of Europe	Airspeed only	£100
Rest of World	Surface	£100
Rest of World*	Airmail	£150

**(not USA, Canada & Europe)*

Personal subscription rates are available in some countries to subscribers paying by personal cheque or credit card.

Details can be obtained from:
UK: *Nature* Promotion Department,
Canada Road, Byfleet, Surrey KT14 7JL.
Telephone: Jonathan Earl: Byfleet (09323) 41459
USA: *Nature*, 15 East 26 Street, New York, NY 10010
Credit card orders only (in USA & Canada):
Call toll-free: (800) 824-7888 (Operator 246)
In California: (800) 852-7777 (Operator 246)

All other circulation enquiries concerning existing subscriptions please contact:
Nature Circulation Department, Macmillan Journals Ltd., Brunel Road, Basingstoke, Hants RG21 2XS, UK
Telephone: (0256) 29242 Telex: 858493

Back issues: (Post-paid) UK, £2.50; USA & Canada, US$6.00 (surface), US$9.00 (air); Rest of World, £3.00 (surface), £4.00 (air).

***Nature* Binders:**
Single Binders: UK, £4.00; Rest of World, $10.00
Set(s) of 3 Binders: UK, £10.00; Rest of World, 25.00

***Nature* First Issue Facsimile:**
UK, 75p; Rest of World (surface), $1.50, (air), £2.00

***Nature* Annual Indexes (1971-1981):**
Price (post-paid):
UK, £5.00 each; Rest of World, $10.00

***Nature* Directory of Biologicals:**
(Hardcover edition)
UK, £22.50; Rest of World, $45.00

***Nature* Wallcharts:**
How Britain Runs its Science; How the US Runs its Science; UK, £3.50; USA, $7.95 each

***Nature* in Microform:**
For Information:
UK: UMI, 18 Bedford Row, London WC2R 4EJ
USA: 300 North Zeeb Road, Ann Arbor, Mi 48106

Orders (with remittance) to:
Nature, Macmillan Journals Ltd.,
Brunel Road, Basingstoke, Hants RG21 2XS, UK
Tel: (0256) 29242 Telex: 858493

MACMILLAN JOURNALS

Kainic acid stimulates excitatory amino acid neurotransmitter release at presynaptic receptors J W Ferkany, R Zaczek & J T Coyle 757

An opioid benzodiazepine D Römer, H H Büscher, R C Hill, R Maurer, T J Petcher, H Zeugner, W Benson, E Finner, W Milkowski & P W Thies 759

A novel intercistronic regulatory element of prokaryotic operons C F Higgins, G Ferro-Luzzi Ames, W M Barnes, J M Clement & M Hofnung 760

Identification of a centriole-associated protein by antibodies present in normal rabbit sera K Turksen, J E Aubin & V I Kalnins 763

***Mycoplasma pneumoniae* adhesin localized to tip structure by monoclonal antibody** J Feldner, U Göbel & W Bredt 765

A multicopy insertion sequence in the bovine genome with structural homology to the long terminal repeats of retroviruses R E Streeck 767

DNA synthesis in purified DNA-membrane complexes extracted from a *Bacillus subtilis* pol A mutant P Benjamin, P Strumph, M Kenny & W Firshein 769

***In vivo* aminoacylation of brome mosaic and barley stripe mosaic virus RNAs** L S Loesch-Fries & T C Hall 771

Differential scattering of circularly polarized light by the helical sperm head from the octopus *Eledone cirrhosa* M F Maestre, C Bustamante, T L Hayes, J A Subirana & I Tinoco Jr 773

MISCELLANY

100 years ago 710
Classified advertising xii

Nature in Poland

Readers wishing to subscribe to a weekly copy of *Nature* on behalf of a colleague in Poland (where hard currency is scarce) should send a cheque for £50 (or the equivalent in any currency), accompanied by their name and address and that of the proposed recipient, to the *Nature* office in London or New York (see addresses opposite page **593**). For further details, readers are referred to *Nature* 3 June, p.354.

The world's leading scientists get it every week and so should you... at ½ price.

Scientists who are leaders in their field and who get to reap the rewards of their achievements are among *Nature's* most eager readers.

And they are renewing their subscriptions to *Nature* in record numbers.

If, like them, you keep searching for ways to speed up your research, or if you're looking for advancement where you work, or are thinking of moving on to something more stimulating, how can you afford to be without your own personal subscription to *Nature*?

It's the most certain and consistent way to get the research results, news, opinion, and analysis you need, while they're still fresh and can be applied most usefully to your own work.

With your own *Nature*, you'll be well ahead of the monthly journals whose reports often lag a year or more behind ours. And there isn't a science weekly anywhere that covers research developments in as many parts of the world, as fully and authoritatively, as *Nature* does.

The good news is that we've cut *Nature's* personal subscription rate in half and, to top it off, if you subscribe for a full year, we'll send you, free, a copy of *Nature's* new, annual *Directory of Biologicals*. Planned for fall 1982, the *Directory* will be the first

Now: Nature at ½ price – plus a bonus book, free

logical products. It will be available only to yearly subscribers (or, for $45, to buyers of the hardcover version, in bookstores).

A personal subscription to *Nature* has never been more attractive. We urge you to clip and mail the coupon today. For credit-card orders only, **call toll-free now: (800) 824-7888. Ask for operator 130.**

In California: (800) 852-7777.

NAT-23

To: **Nature** 15 East 26th Street,
New York, N.Y. 10010

☐ Please send me a year of *Nature* at ½ price, $99.25, plus my free *Directory of Biologicals*

☐ I enclose my *personal* check

☐ Please bill my credit card account

Account No.:

☐ Visa ☐ Master ☐ Amer. Ex. Exp. Date

Name

Address

City State Zip

Orders *must* include personal check or credit card data. Offer good in the U.S. and Canada and is subject to change without notice. In the U.K. send personal check for £42.50, or

nature

Vol. 298 No. 5876 26 August 1982

Life as a wonderful one-hoss shay 779
Language of love 780

NEWS

Vienna accord on remote sensing
Few winners in Australian budget
Canada's array poised
Wanted under martial law
US plant patent disputed
Australian patents bill
German nuclear power
Belgian nuclear fuel
Language of science
Astronomer on fast
Drug promotion 781

CORRESPONDENCE

Patents and plant breeding 786

NEWS AND VIEWS

Man the exterminator (J M Diamond)
Twinkle, twinkle quasi star . . . (M Abramowicz)
Opioids at Cape Cod (B M Cox)
Do antigen-presenting cells distinguish self from non-self? (M C Raff)
Iron-sulphur interconversions and the activation of aconitase (R Cammack)
Evolution and molecular biology (A Leigh Brown) 787

Detectors in astronomy

Optical astronomy (A Boksenberg)
Infrared astronomy (E T Young)
X-ray astronomy (B Taylor) 795

BOOK REVIEWS

Darwin to DNA, Molecules to Humanity (*by* G L Stebbins) J S Jones; **Cell Biology of Physarum and Didymium, Vol.1 (H C Aldrich and J W Daniel, *eds*)** Michael Carlile; **Foraminifera (*by* J R Haynes)** John W Murray; **Gene Amplification (R T Schimke, *ed.*)** Joseph G Gall; **Meteorites: A Petrologic–Chemical Synthesis (*by* R T Dodd)** John A Wood; **Gauge Theories in Particle Physics (*by* I J R Aitchison and A J G Hey)** P V Landshoff 873

Cover

A simulation of the density contours of the Universe when it was a million years old (produced by J. Silk, A. Szalay and Ya. B. Zeldovich). This distribution, produced if adiabatic fluctuations survive the earlier stages of the big bang, later evolves into a large-scale distribution of galaxies in good agreement with recent observations. The early Universe is reviewed on page 801. This week's issue also contains articles on optical, IR and X-ray detectors in astronomy (see page 795)

The inflationary Universe — birth, death and transfiguration (a review) J D Barrow & M S Turner 801

ARTICLES

Phase transitions and dynamics of the Universe V Petrosian 805
Trace elements in orogenic lherzolites reveal the complex history of the upper mantle M Loubet & C J Allègre 809
Reversion of a promoter deletion in yeast S Scherer, C Mann & R W Davis 815
Chemical evidence for the capsomeric structure of phage Qβ H Takamatsu & K Iso 819

LETTERS TO NATURE

Is there a local source of magnetic monopoles? S Dimopoulos, S L Glashow, E M Purcell & F Wilczek 824
Interstellar scintillation and pulsar velocities A G Lyne & F G Smith 825
Inclinations of the uranian rings R G French, J L Elliot & D A Allen 827
An example of induced centrifugal force in general relativity J M Cohen, W J Sarill & C V Vishveshwara 829
Space shuttle ice nuclei R P Turco, O B Toon, R C Whitten & R J Cicerone 830
The Earth's early hydrosphere A Henderson-Sellers & J G Cogley 832
Optimized anomalous dispersion crystallography: a synchrotron X-ray polychromatic simultaneous profile method U W Arndt, T J Greenhough, J R Helliwell, J A K Howard, S A Rule & A W Thompson 835
Australian seismic refraction results, isostasy and altitude anomalies P Wellman 838
Vertical distribution and isotopic fractionation of living planktonic foraminifera from the Panama Basin R G Fairbanks, M Sverdlove, R Free, P H Wiebe & A W H Bé 841
Trans-sexually grafted antennae influence development of sexually dimorphic neurones in moth brain A M Schneiderman, S G Matsumoto & J G Hildebrand 844
Exaggerated salt appetite of spontaneously hypertensive rats is decreased by central angiotensin-converting enzyme blockade R DiNicolantonio, J S Hutchinson & F A O Mendelsohn 846
Interphotoreceptor retinol-binding proteins: possible transport vehicles between compartments of the retina Y L Lai, B Wiggert, Y P Liu & G J Chader 848
Detection of K^+ and Cl^- channels from calf cardiac sarcolemma in planar lipid bilayer membranes R Coronado & R Latorre 849

Nature® (ISSN 0028-0836) is published weekly on Thursday, except the last week in December, by Macmillan Journals Ltd and includes the Directory of Biologicals (mailed in December) and Annual Index (mailed in February). Annual subscription for USA and Canada US $198.50 (for subscription prices elsewhere, see next page). Orders (with remittance) and change of address labels to: Macmillan Journals Ltd, Brunel Rd, Basingstoke RG21 2XS, UK. Second class postage paid at New York, NY10010 and additional mailing offices. US Postmaster send form 3579 to: *Nature*, 15 East 26 Street, New York, NY 10010.

0028-0836/82/34000C-02$01.00

Contents continued overleaf

No other image analyser offers so much research capability in such a compact unit.

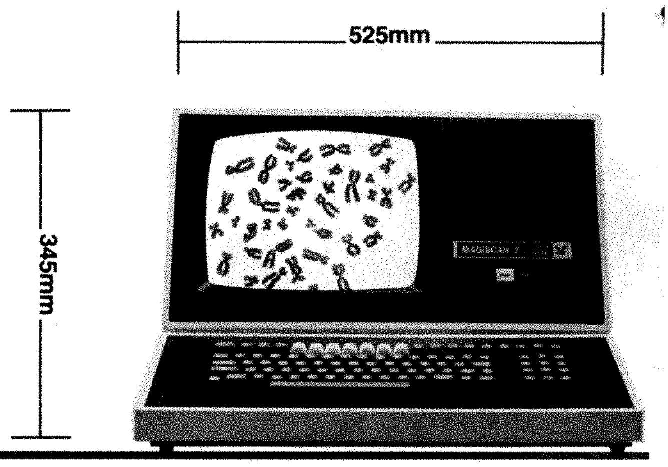

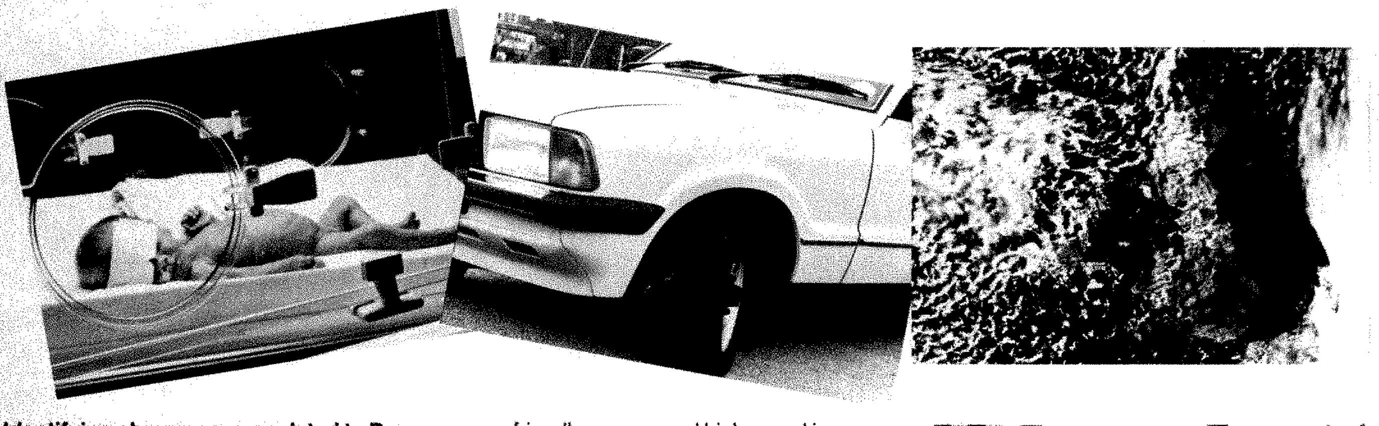

Identifying chromosomes related to Downs Syndrome in unborn babies . . . helping research into safer, more efficient tyres and brakes for the motor industry . . . analysing satelite photographs to help predict earthquakes . . .
. . . just three examples of the power and flexibility of the Magiscan 2 image analysis system.
The integrated hardware/software design of Magiscan 2 not only provides an extra large image store; ease of operation via interactive, user friendly menus, and high speed image and data processing, it also enables the complete package to fit into a desk-top unit, which occupies the minimum of valuable laboratory space.

If you want to count, measure or analyse images from optical or electron microscopes, photographs, films or real life objects, Magiscan 2 has the power and flexibility to provide reliable results . . . without taking over your laboratory.

Joyce-Loebl
A Vickers Company

Joyce-Loebl - Team Valley - Gateshead - Tyne & Wear - NE11 0QW - ENGLAND - Tel: (0632) 822111 - Telex: 53257.

USA - Vickers Instruments, Inc. - PO Box 99 - Riverview Business Park No 27 - Malden - Massachusetts 02148 - Tel: (617) 324-0350 - Telex: 949413. **W. Germany** - Joyce-Loebl GmbH - Emanuel-Leutz - Strasse 1 - 400 Dusseldorf 11 - Tel: 0211/594091-4 - Telex: 8581998.

MAGISCAN 2

Circle No.13 on Reader Service Card.

Science in France
Science in West Germany

Copies of these special supplement issues are still available.

Prices (including postage): UK, £2.50 each; USA & Canada, US $6.00 (surface), US $9.00 (air); Rest of World, £3.00 (surface), £4.00 (air).

Orders (with payment) to:
Nature, Macmillan Journals Ltd,
Brunel Road, Basingstoke, Hants
RG21 2XS, England.

Annual Subscription including Index (51 issues)

UK & Eire		£85
USA & Canada		US$198.50
Belgium	Airspeed only	BF7450
West Germany	Airspeed only	DM450
Netherlands	Airspeed only	G505
Switzerland	Airspeed only	SF395
Rest of Europe	Airspeed only	£100
Rest of World	Surface	£100
Rest of World*	Airmail	£150

**(not USA, Canada & Europe)*

Personal subscription rates are available in some countries to subscribers paying by personal cheque or credit card.

Details can be obtained from:
UK: *Nature* Promotion Department,
Canada Road, Byfleet, Surrey KT14 7JL.
Telephone: Jonathan Earl: Byfleet (09323) 41459
USA: *Nature*, 15 East 26 Street, New York, NY 10010
Credit card orders only (in USA & Canada):
Call toll-free: (800) 824-7888 (Operator 246)
In California: (800) 852-7777 (Operator 246)

All other circulation enquiries concerning existing subscriptions please contact:
Nature Circulation Department, Macmillan Journals Ltd., Brunel Road, Basingstoke, Hants RG21 2XS, UK
Telephone: (0256) 29242 Telex: 858493

Back issues: (Post-paid) UK, £2.50; USA & Canada, US$6.00 (surface), US$9.00 (air); Rest of World, £3.00 (surface), £4.00 (air).

***Nature* Binders:**
Single Binders: UK, £4.00; Rest of World, $10.00
Set(s) of 3 Binders: UK, £10.00; Rest of World, 25.00

***Nature* First Issue Facsimile:**
UK, 75p; Rest of World (surface), $1.50, (air), £2.00

***Nature* Annual Indexes (1971-1981):**
Price (post-paid):
UK, £5.00 each; Rest of World, $10.00

***Nature* Directory of Biologicals:**
(Hardcover edition)
UK, £22.50; Rest of World, $45.00

***Nature* Wallcharts:**
How Britain Runs its Science; How the US Runs its Science; UK, £3.50; USA, $7.95 each

***Nature* in Microform:**
For Information:
UK: UMI, 18 Bedford Row, London WC2R 4EJ
USA: 300 North Zeeb Road, Ann Arbor, Mi 48106

Orders (with remittance) to:
Nature, Macmillan Journals Ltd.,
Brunel Road, Basingstoke, Hants RG21 2XS, UK
Tel: (0256) 29242 Telex: 858493

MACMILLAN JOURNALS

Macrophage binding of *Staphylococcus albus* is blocked by anti-I-region alloantibody — J Stewart, E J Glass & D M Weir — 852

A molecular basis for the two locus model of human complement component C4 — M H Roos, E Mollenhauer, P Démant & C Rittner — 854

Nucleotide sequence of the rat skeletal muscle actin gene — R Zakut, M Shani, D Givol, S Neuman, D Yaffe & U Nudel — 857

Structure of the human immune interferon gene — P W Gray & D V Goeddel — 859

DNA precursors in chemical mutagenesis: a novel application of DNA sequencing — M D Topal, C A Hutchison III & M S Baker — 863

Antifreeze effect of thermal hysteresis agents protects highly supercooled insects — K E Zachariassen & J A Husby — 865

***E. coli* F_1-ATPase interacts with a membrane protein component of a proton channel** — J E Walker, M Saraste & N J Gay — 867

Evidence for hydrogen bonding of bound dioxygen to the distal histidine of oxycobalt myoglobin and haemoglobin — T Kitagawa, M R Ondrias, D L Rousseau, M Ikeda-Saito & T Yonetani — 869

Myosin phosphorylation, agonist concentration and contraction of tracheal smooth muscle — P de Lanerolle, J R Condit Jr, M Tanenbaum & R S Adelstein — 871

MISCELLANY

100 years ago 794
Product review xix
Classified advertising xxi

Nature in Poland

Readers wishing to subscribe to a weekly copy of *Nature* on behalf of a colleague in Poland (where hard currency is scarce) should send a cheque for £50 (or the equivalent in any currency), accompanied by their name and address and that of the proposed recipient, to the *Nature* office in London or New York (see addresses opposite page **779**). For further details, readers are referred to *Nature* 3 June, p.354.

MONOCLONAL ANTIBODIES

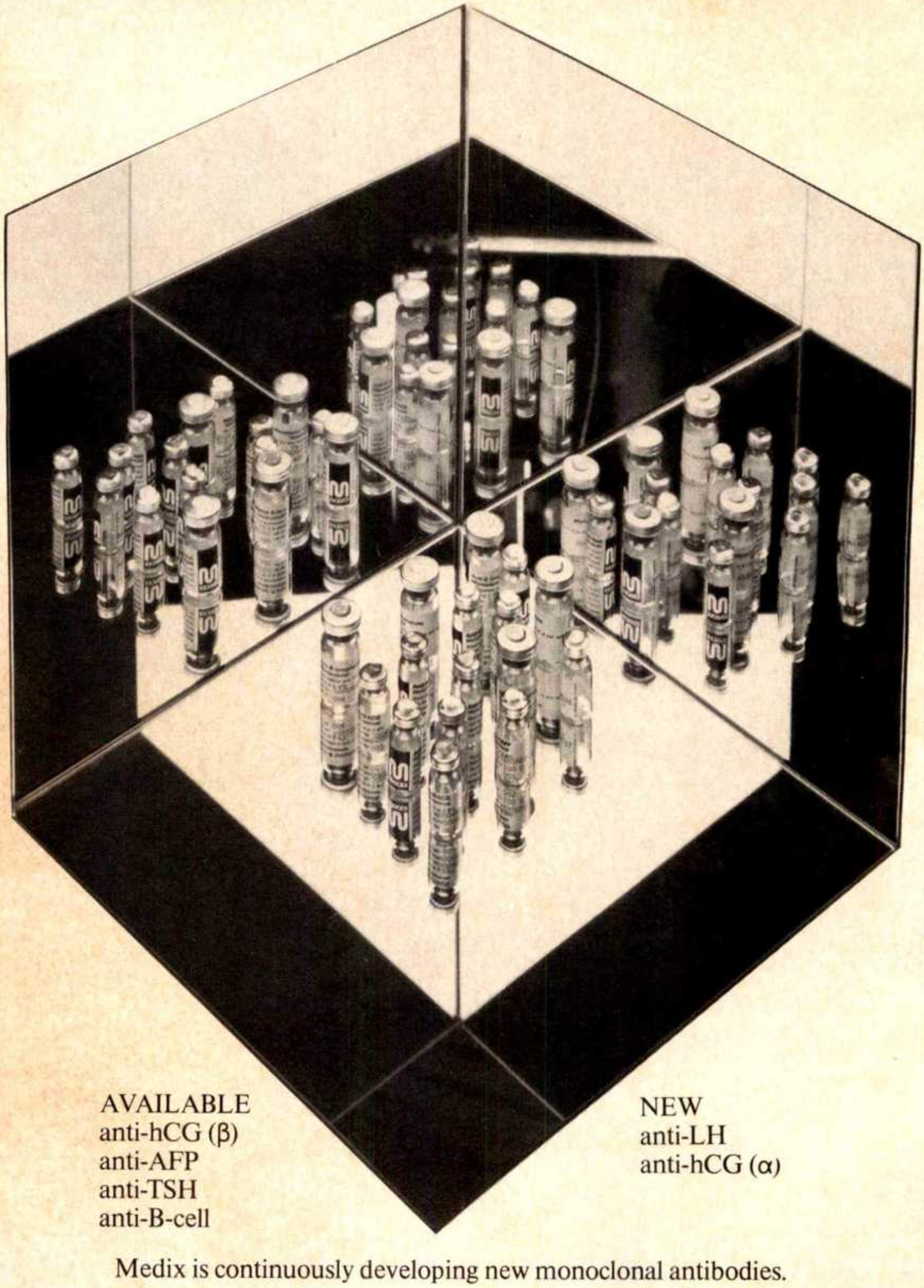

AVAILABLE
anti-hCG (β)
anti-AFP
anti-TSH
anti-B-cell

NEW
anti-LH
anti-hCG (α)

Medix is continuously developing new monoclonal antibodies.

For further information:

MEDIX

OY MEDIX AB, PB 819, SF-00101 HELSINKI 10, FINLAND
tel. 358-0-5050155, telex 123367 medix sf

Circle No. 15 on Reader Service Card.

nature

1 July 1982

Should the Atlantic be widened?

Mr Alexander Haig's replacement as United States Secretary of State is not in itself remarkable; his successor's task is to head off the growing estrangement of the United States from Western Europe.

The departure of Mr Alexander Haig as United States Secretary of State will not be widely mourned; his vanity and impulsiveness ensured that even those governments elsewhere whose causes he supported were uneasy about his essays in diplomacy. But Mr Haig could hardly have chosen a more momentous time to resign. This week has seen the beginning of the Geneva talks on strategic arms between the United States and the Soviet Union, perhaps the most cheerful development on the international scene for a decade. But the meeting of the heads of governments of the European Community in Brussels this week will also have served to emphasize that relations between the United States and Western Europe are fast running towards the rocks. If Mr George P. Schultz, Mr Haig's successor, can find the time from what is bound to be his immediate preoccupation with the Middle East, he will put Western Europe at the top of his pile of problems. And he will conclude that there are two important conditions that his government must satisfy — that it must acquire a better understanding of what the European problem is and a literally more coherent way of dealing with it.

There are three main groups of issues to be ironed out — one military, one economic and one a mixture of economics and politics. The first, difficult enough, is the simplest. The United States resents what it considers to be the underspending by European governments on conventional forces and the unwillingness of some of them to provide hospitality for the intermediate-range nuclear missiles due to be installed from the end of 1983. The first complaint has substance and should be met, preferably by better planning of the mutual defence of Western Europe. The second complaint, understandable enough, overlooks the delicacy of the domestic politics of those Western European governments, perhaps all of them, dependent to some extent for their survival on voters who are unwilling to give house-room to other people's missiles without something in return. The United States is right to ask that those in Western Europe whom it is willing to help defend should share some of the risks but wrong to expect a favourable response while it was dragging its own feet on arms control. Mercifully, that stumbling block may now have been removed. Much will depend on what happens in Geneva. But the needless delay in embarking on these talks may already have helped to undermine Chancellor Helmut Schmidt's West German government (which, admittedly, has other than nuclear problems on its plate). The need all along has been for a fuller sense in Western Europe of having been consulted in the planning of mutual defence. Mr Schultz and Mr Caspar Weinberger, the United States Secretary of Defense, should bend their energies to that goal.

The economic problem is much less tractable, derived as it is from the pact between Congress and the Administration that the budget deficit should be allowed to run at $80,000 million or, probably, even more. The strictly domestic consequences of this development are predictable, but will be delayed. The inflation rate, now dramatically reduced to about 6 per cent a year, will either shoot up again within a year or the flickering promise of economic revival will be extinguished. Meanwhile, the United States is meeting its huge budget deficit by borrowing funds from overseas — the effect of the prevailing high interest rate that underpins the banking system, one of whose consequences is the strength of the dollar against other currencies. What is happening is the opposite of what happened in the late 1960s, when the Johnson Administration paid for the Vietnam war by printing dollar bills and thus exporting inflation. Now, by sucking in funds from the international banking system, the Reagan Administration is exporting deflation.

The consequences for the economies of Western Europe are already serious and much resented. But why should not the United States manage its financial affairs in the way that suits it best, putting up with the domestic consequences as they fall? For two reasons. First, it is no longer possible to separate international financial relationships from international relations generally. With the best will in the world, states in Western Europe thrown into recession by exported deflation will be less able than otherwise to modernize their armed forces and shoulder a full part in their own defence. But they will also be less easily persuaded to other desired goals if they are struggling to deal with domestic difficulties they believe with reason to be caused by the eccentric economic policies of the United States. And it cuts no ice to say that the US Federal Reserve, whose decisions determine interest rates, is constitutionally autonomous. Everybody knows that. But everybody also knows that the Administration is responsible for the budget deficit that makes the Federal Reserve behave the way it does. Second, and more sinister, there is mounting evidence that the United States is seeking the best of both worlds — the right to export deflation but also the right to avoid the consequences that should follow by restraining international trade. Congress and the Administration have embarked on a host of protectionist projects whose result could be to destroy the international monetary and trade system that has sustained us all these past several decades. Europeans in their present mood will go off on their own. Mr Schultz would be well advised to head them off.

The presenting symptom of the third group of urgent issues is the Soviet pipeline for the sale of natural gas to Western Europe (see *Nature,* 3 June, p.349). Arguments about this project have rumbled on for several months. The declared customers for the pipeline's product (France, West Germany and neutral Switzerland) have agonized about the strategic implications of buying Soviet gas, and have publicly decided that they should sign up. The United States, since the accession of Mr Reagan and the appointment of Mr Haig, has blown hot and cold about the implications. Washington has made no secret of its view that they were unwelcome, but has occasionally said that they must be stopped. Mr Haig appears to have made his way at the Versailles summit last month with his expressions of sympathy for the dilemma of European governments placed in this cleft stick. The Administration's decision on Wednesday last week that United States corporations must instruct their subsidiaries and licensees in Europe (and elsewhere) not to supply advanced equipment for the construction of the pipeline is nevertheless unseemly — and a sufficient cause for Mr Haig's resignation.

It is beyond belief that a government so well provided with lawyers can have perpetrated such a gaffe. Corporations registered as such in the United States do not set up overseas subsidiaries for the fun of it, but (rightly) for self-advantage. At some point in the development of their business, they calculate that the time has come when an autonomous overseas corporation would be a better source of revenue than a force of travelling salesmen living

0028-0836/82/260001 02$01.00

out of suitcases. Qualitatively, the benefits of separate incorporation vary. Sometimes there is tax to be saved. Sometimes, local incorporation provides access to public purchasing that would otherwise be denied. Whatever the reasons for separation, however, the subsidiary corporation becomes a legal entity in the locality in which it is incorporated, and thus subject to local laws. But what if the local laws do not allow that an overseas subsidiary of a United States corporation should tear up a contract because of some instruction from its head office sent retrospectively at the behest of the State Department? This is what is now being required of those with contracts for the Soviet pipeline. The chief result, of course, will be a rash of law-suits and of compensation payments (ironically in convertible currency of the kind that the Administration wishes to deny to the Soviet Union). Further ahead but longer lasting will be the impression left in the minds of Western European governments (and/or their voters) that the United States has slipped into the habit of behaving as if Washington's writ is unconstrained.

Thus the events of the past few days have cast a pall over Western Europe. For the past several years, it has been customary (but not always easy) to say that the defects of the then-current foreign policy of the United States were the consequences of the division of responsibility between the White House and the State Department that seems at last to have been the indignity that Mr Haig could not stomach. Each time this recurrent crisis has come round, another tranche of transatlantic loyalists has been lost to doubt, but European governments have usually buckled to and have been able to hold the line. Always, in the past thirty years, transatlantic cultural cohesion has proved to be a powerful cement. And in any case there has been no alternative to United States hegemony. But now the wind is changing.

Private funds can matter

The legend that foundations are now too small to exert an influence has been shown to be false.

Private foundations have become financially so much smaller than public sources of research funds that it is customary to disregard them. For what, the argument tends to be, can foundations hope to accomplish with their meagre funds when the more immediate threat is to the survival of institutions, the annual running costs of which tend to outstrip the capital resources of foundations? Fortunately, that gloomy inference is not as valid as simple arithmetic would suggest. The lie is neatly given to this canard by the imaginative grant announced last week by the Wolfson Foundation to the two British centres for research in tropical diseases, the London School of Hygiene and Tropical Medicine and the Liverpool School of Tropical Medicine. The circumstances are worth remarking.

Both institutions are relics of the days of what the British used to call Empire, founded as they were to safeguard overseas servants of the Crown from unfamiliar infections by insect-borne parasites of various kinds. Almost by accident, they became places at which physicians, following the precept that prophylaxis is preferable to cure, sought to work out ways of dealing with tropical diseases at their source. Inevitably, they became prominent among the centres, mostly outside the tropics, at which an understanding of tropical diseases was cultivated and cherished. With the passage of time and the collapse of Empire (or colonialism), they have been increasingly supported by agencies concerned above all that physicians and paramedical people from the tropics should have a sufficient training in the diagnosis and treatment of these infections.

From here on, the tale is muddied. It happens (again by accident) that the London and Liverpool centres are parts of the British university system, and that the British government has recently decreed that new overseas students should pay such outrageous tuition fees that they cannot afford to be educated. So, earlier in this academic year, it seemed as if the tropical medicine schools in London and Liverpool would be in serious trouble, deprived of students and then robbed of funds with which to pay members of their faculties.

The Wolfson grant to the two schools jointly will in the circumstances have a marvellous effect. At a cost of £3 million over five years ("chicken-feed" will say the public research councils) it should be possible to keep the core of each research faculty in being and to arrange that the research they do is at once more imaginative and more closely coordinated than in the past. There is talk of using genetic manipulation to make parasitic antigens, and of understanding the human genetics of susceptibility to parasitic infection. But the prospectus is open-ended. Plainly, it would have been impossible for any public research council to have made such a grant. Yet the chances are high that it will succeed, and that two distinguished centres of research will remain productive. If, anomalously, it should turn out that research in tropical medicine continues to be centred partly in developed countries such as the United Kingdom and the United States, what harm will be done by that? Last month, the European Parliament gave the European Commission a hard time because it had proposed spending part of its meagre research budget earmarked for development in developed countries. The Commission has a longer purse than the Wolfson Foundation, but is less well advised.

Riding for a fall?

The French minister for science and technology may be about to overreach himself.

M. Jean-Pierre Chevènement, minister of science and technology in the Mitterrand government, seems seriously to have blotted his copy-book. For the best part of a year M. Chevènement's inclinations towards the left of his party have been hidden by his devotion to the cause of social transformation by the beneficent, even lavish, support of research and development, but last week he chose to exceed his brief by speaking in public about the war in Lebanon. Worse still, he gave it as his opinion that President François Mitterrand should invite the leader of the Palestine Liberation Organization, Mr Yassir Arafat, to Paris. For his pains, M. Chevènement has been rebuked in the most humiliating way, by means of a statement issued through the President's press secretary to the effect that the President and his foreign minister, M. Claude Cheysson, have no immediate need of Chevènement's assistance. Even Chevènement's friends must be wondering what he is about, alienating his colleagues in the French government just when the final decisions are being made about the budget for next year.

First, the good news. Such is the commitment of the President and the government as a whole to the cause of science and technology as the harbingers of innovation and thus of the prosperity that will buy social transformation that the immediate consequences of M. Chevènement's little lapse are unlikely to be serious. With Chevènement's *loi* now through the Assembly, (see page 6), the chances are good that next year's budget will be protected. Whether the same can be said of Chevènement himself is another question.

While ambition is inseparable from politics, ambition that shows too openly is, paradoxically, mistrusted. In the past year, M. Chevènement has been admired in the true Latin sense of the word (*admirare* = "to wonder at") for the clarity and certainty of his promises and envied because nobody expects them to be delivered for several years, let alone during the reasonable tenure by a bright young minister of a single office. During the past few months, Chevènement has succeeded as well as he could have hoped in carrying his *loi* through the French Parliament, but not without making enemies. Now there is some anecdotal evidence that his attention has begun to wander. His recent speeches have been repetitive; during the debate on his bill in the Assembly last week, he confined himself to what he called "laconic remarks". M. Chevènement seems to be preparing himself for other pastures. He may find that they are less hospitable than he would like if he continues to alienate the Elysée and the rest of the leadership.

0028-0836/82/260002-01$01.00

Waste in research services damned

UK laboratories lack incentive to save costs

A damning indictment of peripheral waste in British government research establishments was published earlier this week by Sir Derek Rayner, one of the Prime Minister's favourite businessmen and her special adviser on efficiency in government. The report, based on surveys of 19 establishments and concerned exclusively with services for the support of research, suggests that savings of about a fifth in annual budgets would be possible without jeopardizing quality.

The survey is one of several being carried out of efficiency in different parts of the government's business. It consists of a summary of the several separate reports linked together by Sir Derek's own generalizations. One of his central complaints is that in government establishments the cost of support services, ranging from cleaners and doormen to specialist workshops, is lumped together as a central overhead and not apportioned to separate research projects.

The essential failure, says the report, is that neither the provider nor the user of laboratory support services has clear authority and accountability for judging value for money. Rayner says that research establishments should be reorganized in such a way that identifiable research managers are responsible for the whole cost of their projects.

In passing, the survey has uncovered a variety of memorable sources of waste. One establishment was found to have ten deliveries of internal mail each day while the National Physical Laboratory near London maintained eight vehicles that each made less than one journey a month. At the government's Building Research Establishment, a staff of six storemen handled an average of 10 transactions each a day, while the Royal Signals and Radar Establishment was found to have a stock of 17,500 items of scientific equipment with an average age of 8.7 years.

The Central Veterinary Laboratory is reported to have been breeding rats at a cost of £30 a head when suitable animals could have been bought in for about £2 each. The Royal Aircraft Establishment at Farnborough provides itself with an air taxi service at a cost a third greater than commercial charges.

The report on the coordinated survey complains that the government research establishments hold that outside suppliers should be used only when the establishment is too busy or cannot meet the technical need. This, the report says, “is wrong and costly”.

Establishments also tend to be extravagant of land and buildings. The report says that the National Physical Laboratory could save £635,000 a year by giving up 200,000 square feet of floor space and that the Central Veterinary Laboratory should dispose of 245 acres of land now used for breeding animals uneconomically. The report points out that establishments as at present organized have no incentive to make savings of this kind.

The Rayner report also complains that establishments charge too little for services provided to outside users and so “give away . . . public money”. Some establishments provide research reports free of charge when they have a “commercial value”, others sell products whose cost of production has been underestimated and others undercharge for services “in order to win contracts”.

The cost of the bureaucracy itself seems to be substantial. In four establishments covered by the survey on which the report is based, the cost of checking invoices externally doubled the real cost of all the items purchased. But the gravamen of the report's complaint is that “the individual manager of a scientific project is not aware of or responsible for the actual costs of the support he consumes”. The report recommends that responsibility should be transferred to project managers.

The suggested savings on annual costs amount to 14 per cent of the budget now spent on support services within the 19 laboratories and would be made chiefly by shedding 1,518 support staff, or 19 per cent of the total now employed. The report also recommends the disposal of 270 acres of land, 450,000 square feet of accommodation and 200 vehicles, thus raising £6.65 million.

Ministers responsible for the laboratories concerned have apparently agreed in principle to the report's recommendations. Government departments will be performing similar scrutinies of other laboratories in the hope of finding similar savings elsewhere. The plan is to draw up “action plans” for streamlining the support services of individual laboratories by the end of the year. Much remains to be settled, however, not least the questions of how to shed posts and how to change the jobs of researchers so as to encompass greater management responsibility. The reactions of laboratories and staff unions will be eagerly awaited. **Judy Redfearn**

New prospectus for European lab

Substantial changes in the direction and style of research at the European Molecular Biology Laboratory (EMBL) in Heidelberg were being put to the laboratory's council earlier this week by Dr Lennart Philipson, the director-general chosen by the council to succeed Sir John Kendrew's inaugural seven-year reign.

The plans are the outcome of consultation between Philipson and the staff of EMBL and of an almost total lack of contact between the incoming and the outgoing directors-general — ending in a most unknightly deed by Sir John. There have inevitably been clashes within the scientific advisory committee on the extent to which EMBL should pursue a structural approach to biology.

In essence, Philipson's plans call for a shift in emphasis from structural biology towards cell biology, for concentration on fewer areas of research and for better integration of the costly instrumentation division with the laboratory's biological programme. Philipson also says that EMBL's outstations at Hamburg and Grenoble should grow and become more autonomous, and that the laboratory should increase its role as an international training centre, offering more technical courses and eventually a PhD programme.

Another of Philipson's plans is to replace the system of indefinite tenure for a few of the 250 of his staff with one of rolling tenure for up to a quarter of them. In practice, this will mean that those with tenure will always be on five years' notice. Philipson believes this to be the best way of retaining flexibility while attracting good scientists for short periods. Philipson says that in part this proposal is a response to an unexpected legacy inherited from Kendrew. As soon as he was named director-general in November 1980, he says, he asked that no additions be made to the four tenured staff without consultation either with himself or with the chairman of this council. Kendrew, however, afterwards endowed eight staff members with tenure, five of them within his last three months, without consultation. He was, it appears, quite within his rights to do so (but when asked earlier this week about his reasons refused to comment).

The intended difference in style of research in the next five years reflects a change in both time and directors-general. Whereas Kendrew encouraged certain biological themes at the laboratory, he was prepared to back individuals whose research was not closely allied to any one of them. Philipson, however, tends to the view that backing individuals was even then an outdated approach, and says that the modern need is for a team approach to major problems in biology. Philipson thus intends to concentrate the biological research of EMBL on membranes and on the process of differentiation. Membrane biology is the one area of research in which

0028-0836/82/260003-02$01.00

the laboratory has a high reputation. The work, however, has been mostly on mechanisms of transport across membranes, and Philipson plans to supplement this with a structural approach. As a start, he claims to have recruited a specialist Rosenbush from Basle, who has recently obtained some of the first ever crystals of a membrane protein, the structure of which will be worked out at EMBL.

The laboratory has much less of a reputation in differentiation, and Philipson's plans depend upon the recruitment of new staff. There may soon be a major project on the terminal differentiation of blood cells and later another on growth factors, but competition with other laboratories on differentiation in *Drosophila* is all ruled out. Other projects ruled out or resisted during planning include mobility within protein molecules, chromatin structure and protein folding.

Inevitably the emphasis on some areas of research will be at the expense of others. Whereas Kendrew felt it essential to have a foot in the door of neurobiology, Philipson will close the door. But Philipson, like Kendrew, is committed to instrumentation as a key to the success of EMBL, believing, however, that it should be better integrated into the research projects. About half of the laboratory's budget is spent on instrumentation, with the most advanced project that on low temperature electron microscopy designed to minimize damage to specimens.

The instrumentation division has also been essential to the unquestioned success of the synchrotron radiation outstation at DESY in Hamburg, where EMBL staff have been chiefly involved with building equipment for use by external collaborators. Philipson hopes to succeed where Kendrew failed by persuading the council to increase the staff at Hamburg from 17 to 25. He plans a similar increase at its neutron diffraction out station at Grenoble.

These plans are based on Philipson's appraisal that the outstations have done more than any other part of EMBL to justify its existence as a European laboratory able to engage in research that cannot be mounted nationally.

Both Kendrew and Philipson admit that such a description cannot be applied to much that goes on in Heidelberg, but Philipson emphasizes the increased role he intends for EMBL as a unique centre for training in molecular biology. It remains a manifest disappointment for many observers that the programme of research at Heidelberg is still much as it might be in any large well-funded national laboratory. And it could only justifiably be for that reason, monetary considerations apart, that Philipson might fail at the end of this year to get the 10 per cent budget increase needed to bring EMBL up to its full strength. **Peter Newmark**

Chemical weapons treaty

Talking again

Washington

The Soviet Union may be willing to accept some provisions for on-site inspections in a treaty banning chemical weapons. The first hint of Soviet movement on this issue — which has been the chief obstacle in US–Soviet negotiations on chemical arms — came in a speech on 15 June by Soviet Foreign Minister Andrei Gromyko to the United Nations special session on disarmament.

The United States broke off negotiations in 1980 on a treaty that would ban not only the use of chemical weapons, which is already prohibited by international treaty (the Geneva Protocol of 1925), but also their development, production or stockpiling. Soviet refusal to accept any on-site inspections and the Soviet invasion of Afghanistan were cited at the time as the reasons for suspending the talks.

In his speech, Gromyko said that a chemical arms treaty should provide for "a possibility of carrying out systematic international on-site inspections", of the destruction of existing weapons and of the continued limited production of toxic chemicals that would be permitted for defensive research purposes under a treaty.

The US State Department is officially saying only that it is studying the proposal and that it is too early to comment. The State Department is apparently wary of showing any favourable response until it can assess the substance of Gromyko's statement. The Soviets may elaborate on their proposal at the international disarmament conference which convenes on 20 July in Geneva.

A State Department official did say, however, that the Soviet proposal appears to address at least two of the three concerns the United States has been pressing — inspection of stockpile destruction and inspection of the permitted research production. The third area is inspection of the shut-down and elimination of existing chemical arms facilities.

James Leonard, who was the US representative at the Geneva disarmament

Industrial secrets still in demand

Washington

The arrest of 18 Japanese businessmen in the United States last week on charges of conspiracy to steal confidential computer information from International Business Machines Corporation may really have been just the latest instalment in a long tradition of international technical espionage. According to Professor Alfred Gollin, a historian at the University of California at Santa Barbara, it now appears that at least two self-appointed spies kept tabs on Wilbur and Orville Wright and reported to the British military.

One was C. S. Rolls (of the automobile company) who in 1908 wrote to the British Committee of Imperial Defence offering to go to France and "draw out" the Wright Brothers. Rolls also bought a Wright biplane, which he offered to put at the disposal of the government. For several years before, the Wrights had negotiated with the British on a sale of their planes, but the deals repeatedly fell through.

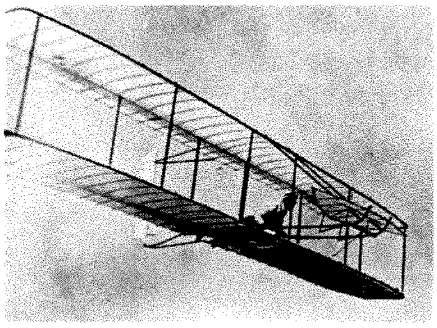

The other unofficial spy was Patrick Alexander, an active member of the Royal Aeronautical Society. He first visited the Wrights in 1902, a full year before their first powered flight, and apparently became quite friendly with them. Professor Gollin found that, for a private citizen, Alexander did have unusual entrée into government circles. This included a close working relationship with the secret Balloon School and with a key figure in the British army's aeronautical programme.

But Alexander also demonstrated the pitfalls of leaving the job to amateurs. He was actually invited by the Wrights to Kitty Hawk to witness their first flight on 17 December 1903, but went instead to the St Louis Exhibition — this was when world's fairs were still worth going to, no doubt.

The Wrights later became convinced that Alexander was in fact a spy. But by that time, the Wrights were embroiled in a patent fight and, according to Dr Tom Crouch of the National Air and Space Museum in Washington, "they thought everyone was spying on them".

In fact, says Dr Crouch, "they developed a conspiratorial mentality themselves", going so far as to send their younger brother, Lorin Wright, to spy on Glenn Curtis, their rival. In what became another amateur performance, Lorin simply marched into Curtis's factory and began taking pictures until he was discovered and had his film forcibly and prematurely exposed by a Curtis employee.

Dr Crouch suggests that any spying that did go on was motivated more by the commercial interests of individuals than the military interests of governments. On the other hand, Edwardian England clearly did have its worries about the Wrights' invention. "The story is not that man can fly", said a British newspaper publisher at the time, "but that Britain is no longer an island". **Stephen Budiansky**

0028-0836/82/260004-02$01.00

conference from 1969 to 1971 and who is now with a pro-arms control group called the Committee for National Security, says that although the Soviets are clearly making political hay out of the proposal, it is nonetheless more than just words if experience is any guide. "They know that if they make a statement like this, they will eventually be called on it", he says.

Stephen Budiansky

French universities

More change

Paris

The French universities are to be reformed — again. A couple of years ago, the then President Giscard D'Estaing's minister of universities, Mme Alice Saunier-Seïté, set about the universities with a hatchet, amputating this and that to academic screams of "Fascist!" and worse. But now, more quietly and more carefully, the present socialist government of France is setting about a similar task. According to present analysis, Mme Saunier-Seïté was right about many things — it was only her draconian methods that were wrong.

The socialist idea is to base change on a 130-point questionnaire sent out a few months ago to presidents of universities, engineering schools and other such establishments by M. Claude Jeantet, cabinet member at the ministry of national education. The questionnaire was very far-reaching: it encouraged respondents to redefine the role of higher education in France. Jeantet has just analysed the results of that questionnaire — and he will use them to prepare the text of a new law on French higher education for his minister, M. Alain Savary. The new law is promised for the autumn. Although Jeantet will not publish the figures until then, it is already emerging that the government's task will be aided by a remarkable and sudden change in social outlook in the universities — one that has surprised even Jeantet. Now, university staff, often regarded in France as left-wing, see the government and even industry as partners, rather than enemies as appeared to be the case under Giscard d'Estaing. Now, it seems from the questionnaire, the universities are ready to forge links with industry and to run more courses aimed at training students for productive employment — an area in which they have previously been weak. It seems that one remnant of the 1968 university rebellion — a horror of the market-place, and of all government control — is being replaced by a nationalistic commitment to help France escape from the present economic crisis. According to Alain Geismar, one of the revolutionaries of 1968 and now vice-president of the University of Paris VII, the universities are now preparing to consider the provision of continuing education, post-retirement courses and science shops on the Netherlands model.

Behind a broad willingness to change in the universities, however, a number of difficult issues lurk. For example, one of the hottest and perhaps most important for French science is the reform of the French PhD system, presently a two-step exercise which is both weaker and stronger than an American PhD. The weak step is the more contentious: the troisième cycle (essentially a two- or three-year MSc course). A good result in the troisième cycle is enough to get a graduate an effectively tenured post as a researcher (assistant at a university, or attaché in a government laboratory). The second step — the major thesis, leading to a doctorat d'état — can take seven years.

Science minister Jean-Pierre Chevènement's law for research and technology, in its present form, contains a commitment to change the system, but no details about how it is to be done; that is up to Jeantet and Savary.

Tenure is, however, a very closely regarded right in France, and the unions, whose influence over the government is strong, will defend it vehemently. One University of Paris professor, whose left-wing leanings combined with a desire to see France do good research perhaps make him typical, said last week that he was "schizophrenic" over the issue. The French system leaves a large pool of relatively untalented researchers at work in France, half of whom would not be in research if they were in the United States.

Robert Walgate

Argonne prepares for change

Washington

Argonne National Laboratory is renouncing a 16-year old agreement with a consortium of some 30 universities that has governed the laboratory ever since its principal machine, the Zero Gradient Synchrotron (ZGS), was built.

The laboratory outside Chicago is one of several, large, multipurpose energy laboratories whose fate is being deliberated by the White House and the Energy Research Advisory Board of the Department of Energy (DoE) (see *Nature* 6 May, p.3). Rumours that Argonne was to be closed helped prompt the move to change and streamline the laboratory's management. The ZGS itself was turned off a few years ago, leaving the laboratory to carry out other energy studies and nuclear physics, as well as some biology and other basic research.

Back in the heyday of building machines for high-energy physics, many colleges in the middle of the country wanted to have a big machine. When it was decided to put it near Chicago, a compromise was effected, in which other universities in the region could make input, and help get their scientists onto the machine, through a management group, the Argonne Universities Association (AUA). AUA's main job was to coordinate the high-energy physics programme at Argonne, but it also had management responsibility in other areas. The University of Chicago was also involved in management, through a tripartite agreement involving the university, AUA and DoE, which provides 90 per cent of the laboratory's budget of $200 million.

Without the ZPG, however, there is no need for regional high-energy physics co-ordination at Argonne. As one scientist formerly at the laboratory says, the AUA structure is also potentially divisive, allowing almost anyone who wants to do something to Argonne to get into the act.

So Argonne's management will gradually be streamlined. AUA will bow out and the University of Chicago will become the manager. Regional universities can still participate through an advisory steering committee. DoE will continue to fund the laboratory.

The laboratory seems unlikely to go out of business, according to DoE, but it may be substantially redirected. For instance, Senator Charles Percy wants to bolster the laboratory's flagging mission by transferring civilian research activities now at Los Alamos and Livermore laboratories to Argonne.

Deborah Shapley

Franco-Soviet space-flight

Up and away

The space-flight of the Frenchman Jean-Loup Chrétien, the first West European in orbit, has been hailed as a triumph for détente and cooperation in both France and the Soviet Union. Although events in Poland had moved a number of French scientists to sign petitions advocating withdrawal from the flight, the Centre National d'Etudes Spatiales (CNES) says that Chrétien's is merely the logical next step in a cooperation programme that has been flourishing for fifteen years.

The coincidence of Chrétien's flight and the final test-run of the US shuttle prompted *Le Monde* to draw a contrast between the French approach and the "cold-war" aspects of *Columbia.* (The fact that, in spite of frequent official denials, the Soviets also appear to be working on a shuttle with, presumably, a similar military potential, was overlooked.)

In their run-up to the flight, the French have exercised considerable tact, even coining the word "spacionaute" to avoid using either the American or the Russian terminology. In return, the Soviet side has permitted a degree of openness about the preparations for the flight that has not been seen since the preparations for the Soyuz-Apollo flight in 1975. While some of this

0028-0836/82/260005-02$01.00

must have been unavoidable, some revelations seem to have been made purely as an exercise in détente. Five days before the flight, for example, Professor Igor Konstantinovich Bazhinov, the deputy chief of flight ballistics, admitted on Moscow radio that Salyut-7 had undergone unexpected orbital drift, and that a special correction had been necessary to ensure the successful docking of the "international" crew — a degree of intimacy with his audience that is unusual by Soviet standards.

The French experimental programme for the flight was, in fact, outlined in the CNES annual reports for 1980, and includes sensory physiology (including the vestibular, visual and kinaesthesic systems) and the effects of soft radiation on the developmental capacities of unicellular and multicellular organisms. The biological experiments are a continuation of previous Franco-Soviet work using unmanned probes.

Little has been said, however, about the type of space station to be visited by the "spacionaute". Although all CNES releases spoke cautiously of a "Salyut" station, without giving it a number, they were illustrated by a schematic diagram of Salyut-6. Only after the launch this spring of Salyut-7 was it stated that Chrétien would pass his historic week in space aboard what the Soviets say is a more advanced and more confortable space station. **Vera Rich**

French science *loi*

Who will lose?

Paris

The long-awaited French law for science and technology, which guarantees a 17.8 per cent annual real growth in government civil research spending until 1985, is now almost on the statute books. At present, it lies under the harsh light of an inter-house committee of the French Parliament, which is attempting to reconcile the differences between the views of the Senate (which all but overturned the law) and the Assembly (which supported it). Second readings are to take place next week but it appears that the law will sail through much as planned by M. Jean-Pierre Chevènement and his team, even if those most affected will be reading its provisions with a magnifying glass to see exactly what has, and what has not, been left in.

One thing that was left out is causing the more cautious of French scientists to pause for thought. The law is divided into three sections: an introduction, the law proper (which is quite short) and an annexe. The full force of law attaches only to the law proper, so one question has been what is to go into the law, and what into the annexe? In the research ministry version, fundamental science is mentioned only in the annexe — where there is talk of 13 per cent growth (less than the 17.8 per cent total growth, reflecting the fact that the Chevènement plan mostly concerns technology). Some deputies at the Assembly, briefed by university researchers, pushed for the 13 per cent to be inscribed into the law proper, but the government refused.

Does this mean that basic research is going to be less well protected against the current French financial crisis than technology? Some French scientists fear so. The question is how far should Chevènement's technological imperatives, outlined in seven major investment programmes from space to biotechnology, encroach on and influence the whole of science. It is beginning to look as if they will be very pervasive.

For example, new accounting methods are to be applied to the big government research organizations, such as the Centre National de la Recherche Scientifique (CNRS), which means that they will be controlled from the ministry, programme by programme, rather than by total budget. The organizations will also be given explicit new tasks, such as the application of their research to profitable ends.

Even the small protection given to basic science by the ministry of national education may be being eroded, as the ministry appears to be adopting the same priorities as the ministry of research. (In distributing its research money, which amounts to perhaps a fifth of the total obtained by universities, the ministry of national education recently asked universities to favour groups already supported through the ministry of research and technology.)

Nevertheless, the fears may be misplaced if French research is compared with the situation of research in other countries. If the 13 per cent figure is respected — and ministry of research officials insist that although only in the annexe, the figure has force — French scientists will be doing far better than their foreign colleagues. For the sum includes a 4.5 per cent annual increase in the number of salaries, and salaries amount to more than two-thirds of basic research costs. The result is that next year's true research budget — what a laboratory director will have in his pocket to spend — would be up by more than 25 per cent in real terms, an increase so large that one senior researcher said last week that it would be "frankly a problem" working out how to spend the money.

For the ministry, the next problem will be how to raise the money promised, against a sombre French economic background (although the promised figures are only averages to 1985) and then how to put into effect certain structural changes outlined in the law. Not least of these is the reform of CNRS and related organizations which will be given new statutes allowing them to make profitable links with industry. CNRS will also get new rules for electing its internal review body, the Comité National. These new rules are themselves contentious. It appears that the Comité will exclude university lecturers not at present or previously associated with the organization, thus, according to some, deepening the rift between the universities and CNRS. **Robert Walgate**

Laboratory animal welfare

Congress in sight of compromise

Washington

After months of negotiation between animal welfare groups and representatives of the biomedical research community, a bill that would tighten up standards for the treatment of laboratory animals has reached the House of Representatives Science and Technology Committee.

This compromise proposal (HR 6245) is now the only serious contender among the several animal welfare bills filed with the House. It will be taken up by the committee later this month when the House returns from its Independence Day recess. The bill avoids some of the extreme measures that some animal groups had pressed for, such as setting aside up to 50 per cent of the National Institutes of Health (NIH) funds now going to work involving animals used for research into non-animal substitutes. But it would impose strict requirements on the care of animals used in federally-supported research. Researchers would have to justify any distress caused to a research animal and ensure that pain was minimized (through the use of tranquillizers and anaesthetics, for example). No animal could be used in more than one major operative procedure, except in special circumstances.

The legislation grew out of hearings held last autumn by a House subcommittee in response to considerable public pressure. At that time legislation for the protection of laboratory animals was not serving the interests of anyone very well. Under the present law, the Animal Welfare Act of 1966, the responsibility for enforcement falls on the Department of Agriculture (USDA), which critics say is understaffed and cannot do a proper job.

Last autumn, for instance, USDA inspectors found only minor violations in Dr Edward Taub's laboratory just weeks before he was indicted under Maryland's animal cruelty law for causing pain and suffering to monkeys. Although Dr Taub protested that he was the victim of a public relations stunt by a group called People for Ethical Treatment of Animals, which had infiltrated one of its members into Dr Taub's Institute for Behavioral Research in Silver Spring, Maryland, he was convicted of the charges and also had a $200,000 NIH grant taken away from him. Dr Taub appealed against the conviction, and his case is now being heard.

In an effort to obtain the widest possible support for new legislation, the subcom-

0028-0836/82/260006-02$01.00

mittee staff consulted groups such as the American Physiological Society and the Association of American Medical Colleges when drafting the bill, as well as animal welfare groups such as the Humane Society of America. The bill was reported out of the subcommittee on 9 June by a 14–1 vote.

Universities still have two strong objections, however, that may be raised in the full committee and may prevent any action being taken. One is that the standards set by the bill are quite high. For one thing, the new legislation would apply to rats and mice, which were exempted from the Animal Welfare Act. (Farm animals would continue to be exempt under the new bill.) Research facilities would also have to be accredited by an organization such as the American Association for the Accreditation of Laboratory Animal Care (AAALAC), which since 1965 has certified about 400 facilities under a voluntary programme. Universities claim that it would cost $500 million to bring the remaining NIH-supported universities up to the very high AAALAC standards.

This objection may be answered in part by a 10-year phase-in provision, which the subcommittee staff says should allow much of the upgrading (installation of new ventilation equipment, for example) to be done in the course of routine laboratory modernization and repair.

The second objection is that research facilities will have to set up animal studies committees and in particular will have to appoint one member from outside the university who is "primarily responsible for representing community concerns regarding the welfare of animal subjects". The committees would act much as human experimentation review committees do.

Balancing these possible objections, however, is an apparently growing recognition by the research community of the benefits that mandatory regulations will bring in terms of public reassurance — much as the recombinant DNA guidelines provided what one scientist calls an "umbrella of trust". This may be especially important now that the effectiveness of the Animal Welfare Act and the essentially voluntary system have been called into question.

Stephen Budiansky

US science societies

Women's rights boycott shadow

St Louis

Although the Equal Rights Amendment (ERA) to the US Constitution has now failed, many states will continue to be deprived of important scientific conferences for years to come. And it is possible that some societies will continue to boycott the fifteen states that dragged their heels on the amendment.

The amendment would have added to the constitution an interdiction of discrimination on the grounds of sex. By the extended deadline of 30 June, however, only 35 of the required 38 states had ratified the amendment, which thus becomes a dead letter.

The boycott was first organized in 1977 by the National Organization for Women (NOW), the most prominent feminist organization in the United States. Convention promoters in non-ratifying states have admitted they lost millions of dollars' worth of business during the ERA boycott. Convention sites in ratified states and Canada benefited.

How societies will respond to the lapsing of ERA is not yet clear. Some have abandoned the boycott, but others with large numbers of women members or which are otherwise committed to equal rights for women and minorities are ambivalent about giving their convention business to non-ratifying states.

The scientific societies that adopted the NOW boycott, and avoided Missouri, Illinois and some southern states none of which ratified ERA (see box), include the American Association for the Advancement of Science (AAAS), the American Society for Cell Biology, the Society for Neuroscience, the Society for Developmental Biology, the Endocrine Society, the American Astronomical Society and the Biophysical Society. But AAAS stresses that its policy on meetings is independent of NOW's boycott.

No complete list of boycotting societies exists, but if the experience of Professional Associates of St Louis is typical, fewer than half of all scientific organizations supported the boycott. Professional Associates handles convention planning for nine science groups, of which three supported the boycott. Of those three, two decided to drop the boycott in booking meeting sites after 30 June.

NOW itself has not decided whether to keep the boycott going past the deadline, but the question is likely to come up at its board meeting in July. Even if NOW formally ends the boycott, it will affect where organizations hold meetings for several years if only because many societies make their meeting plans years in advance.

AAAS, the Society for Neuroscience and the American Psychiatric Association are booked only in ratified states until the end of 1986, the Biophysical Society until 1985 and the American Society for Cell Biology until 1984. The boycott excluded some of the most popular convention sites in the United States such as Atlanta, Chicago, New Orleans, St Louis, Kansas City and Las Vegas.

Some other societies did not honour the boycott only because it was logistically too difficult. The Federation of American Societies for Experimental Biology (FASEB), for example, says it would have liked to have supported the boycott but "The federation's meetings are so large — 15,000 to 20,000 people — we require 50-60 simultaneous meeting rooms. Only one or two cities in ratified states can provide that." The FASEB meeting was held this year in New Orleans in Louisiana, which like most other southern states has not ratified ERA. But two of the six member societies of FASEB, the American Society of Biological Chemists and the American Association of Immunologists, do honour the boycott when they meet as separate groups.

AAAS acknowledges that it has been inconvenienced by its stand, especially when it switched its 1979 meeting from Chicago to Houston in order to hold the meeting in a ratified state. "It's always inconvenient to move a meeting in less than a year's time. We had to be in several different places in Houston." AAAS meetings can draw 4,000 to 8,000 people.

Non-ratifying states

The 15 states that did not ratify ERA are: **Alabama, Arizona, Arkansas, Florida, Georgia, Illinois, Louisiana, Mississippi, Missouri, Nevada, North Carolina, Oklahoma, South Carolina, Utah, Virginia.**

Germal Sanderson, vice-president for sales of the Chicago Convention and Tourism Bureau, acknowledged that cancellation of business meetings had caused "significant losses". He estimated that 23 groups cancelled previously scheduled meetings, costing the city more than $11 million. The effect of the ERA boycott could last until 1989, he said.

Nobody knows if the boycott helped or hurt the movement to ratify ERA. People representing boycotted convention areas agree that it did not help the ratification effort and may have hurt it.

Jim Hutchinson, director of convention sales for the New Orleans Convention Bureau, says "It was ridiculous to begin with. It inconvenienced a lot of people and not another state has ratified since it started". NOW itself does not know if the boycott swung any legislators' votes its way. "It certainly was effective in terms of dollars lost" says Judy Murphy, NOW press secretary. "But if it helped, it was just one or many things we did."

Karen Freeman

0028-0836/82/260007-01$01.00

CORRESPONDENCE

Falklands story

SIR — The history given by Asociacion Argentina Para el Progreso de las Ciencias (*Nature* 10 June, p.450) is in error.

The islands were discovered by the English navigator John Davis, inventor of the backstaff and double quadrant, in 1592. Hawkins was there in 1594.

Commodore Byron took the islands for England in 1765 on the basis of this prior discovery and when the naval garrison was withdrawn in 1774 it left a plaque claiming full sovereignty and allowing Spain to maintain its settlement until 1806.

In 1816 the new United Province of Rio de la Plata having overthrown the Spanish yoke claimed to succeed Spain and a local governor was installed by them in the Falklands in 1828. In 1833 Britain expelled the Argentine soldiers and again raised the Union Jack in the Falklands.

The British prime minister said in 1834 that the British were not prepared to permit any other state to exercise a right as derived from Spain that Britain had denied to Spain herself.

The present conflict does not have its origin in Grytviken, but in the recent naked aggression by Argentina. What was said in 1834 by the British prime minister still stands.

F.W. COUSINS

Westminster, London SW1, UK

Burning question

SIR — Most cosmologists feel that the evidence currently available suggests that the Universe originated with a big bang and is now in an expansion phase. One of the more important questions presented by such a scenario is whether or not the Universe will recontract to its primordial super-massive germ. The physical evidence required for resolution of this issue is not yet available.

There is, however, a source which provides the answer clearly and unequivocally. In II Peter 3; 10 it is stated: "But the day of the Lord will come as a thief in the night; in the which the heavens shall pass away with a great noise, and the elements shall melt with fervent heat, the earth also and the works that are therein shall be burned up."

ALEX HARVEY

Department of Physics,
Queens College, New York, USA

Whence high IQs?

SIR — In *Nature* of 20 May, A.M. Anderson in his comments[1] on the article in the same issue by R. Lynn entitled "IQ in Japan and the United States shows a growing disparity"[2], refers to the increase in educational opportunities in Japan since the 1930s, perhaps implying that this increase might be partly responsible for "the Japanese IQ increase", even though Lynn argues against it. While agreeing with Anderson that no intelligence test can be totally culture-free and, therefore, the performance in any such test cannot be unreservedly taken as a true measure of a person's intelligence[3], I suggest that what has been found in Japan may indeed be true of all countries where a large proportion of the population has been deprived educationally and socially, over many generations and where people have overcome this deprivation through rapid democratization of education.

Where opportunities for education and access to knowledge and information, have been limited, education (or lack of it) tends to run in families, with only an extremely small proportion of either class (the educated or the educationally deprived) changing over to the other class. In India, for example, I estimate that education is a hereditary prerogative of between 12 and 20 million persons (2–3 per cent of the population) representing less than 4 million small families and half-a-million "large" families — large in the sense of Indian "joint" families[4]. Probably, less than 10,000 persons every year (out of a total population of 680 million) enter the educationally privileged class from the under-privileged, changing the complexion of neither class.

For those who are educated, the day-to-day problems of survival are lessened. The survival of the uneducated, on the other hand, depends on their possessing abilities which would allow them to cope with the adverse environment in which they must live. Thus the uneducated of today would, as a result of evolutionary pressures, come to possess more "native" (that is inherited) intelligence, than the educated ones on whom by and large these pressures have not operated.

Since the intelligence tests cannot give a true indication of the native intelligence of a person who has been socially, culturally and economically deprived in early childhood, when the cultural patterns are often irrevocably fixed, the above-mentioned difference between the native intelligence of the long-deprived and the long-privileged would show up only when the two groups have had equal opportunities and a comparable environment to live in from the very beginning. A consequence of such a situation would be an apparent rise in the average intelligence of a population where there has been educational deprivation of a large population for a long period, as such deprivation disappears — as has happened in Japan since the 1930s.

If what I have said above is true, one could make two predictions: (1) what has been found in Japan should be found to be also true of other countries and populations where there has been democratization of education on a large scale in a relatively short time; and (2) the average IQ of those who have moved up from a traditionally educationally deprived state should be higher than of those who have been educationally privileged for generations due to circumstances of birth. We must, in that case also, conclude that in the United States, real democratization of educational and related opportunities has not occurred to the extent to which it has in Japan. The fact that the differences in IQ were found by Lynn even at the age of 6 could be merely an indication of the improved environment in Japan, in which the children were brought up to that age, as a consequence of the true educational status of the parents having improved across the population in the earlier generation(s).

P.M. BHARGAVA

Centre for Cellular and Molecular Biology,
Hyderabad, India

---

1. Anderson, A.M. *Nature* **297**, 181-182 (1982).
2. Lynn, R. *Nature* **297**, 222-223 (1982).
3. Bhargava, P.M. *Bull. Atomic Sci.* **26**, 40 (1976).
4. Bhargava, P.M. *New Quest* **15**, 147 (1979).

Sequence software

SIR — In the article "Europe leads on sequences" (*Nature* 15 April, p.596), the problem of the collection of nucleic acid sequences is discussed. While it is a crucial problem, it is not the only one. Once collected, the sequences should be easily and quickly accessible to a large number of users, the mode of interrogation of the data base should be manifold, flexible and selective, and the answers should be immediate. Otherwise, the enormous effort required to set up a sequence library would be partly nullified by its limited use. At present, access to the data by most European users occurs by means of magnetic tapes, requested and sent by mail, containing all the sequences and related information stored in the library. The recipient of the tape then needs to read the entire tape on his own computer before the required information can be extracted. This procedure is time consuming and inefficient.

We have developed, on a computer Digital VAX/VMS 11-780 (Physics Institute, GNCB, Bari), an interactive software system for the retrieval and analysis of nucleic acid sequences. This system, which works in real time, offers a large number of options both for perusing and for analysing the data. No specific computer knowledge is required since the users, connected with remote terminals through telephone lines, are guided throughout their work. The main novel feature of the system is the mechanism of data retrieval, which is accomplished through the use of forty keys. Each key can be used alone or in combination with others. Among the available keys are: sequence code, bibliographic citations (journal, year of publication, personal communication), date of entry into the library, number of base pairs, function and biological source. Among eukaryotes, the selection can be made by kingdom, phylum or division, class, genus and species. An analogous selection is offered for prokaryotes. Viral nucleotide sequences can be retrieved by using the virus name, the genus, the family or the host. Biological groups of particular interest can also be selected, for example protozoa, bacteria, algae, fungi, lichens, higher plants, invertebrates and vertebrates. The outputs can be tailored to specific needs, through a choice of what to print and on which output device.

To test our software, we used sequences from a collection of about five hundred, kindly given to us by Dr Greg Hamm (European Molecular Biology Laboratory, Heidelberg) and by Dr Kurt Stüber (Genetics Institute, Cologne). These data were reorganized in order to make them compatible with our software. In planning the system, we took into consideration the fact that precise requirements and standards for a nucleic acid sequence library do not yet exist. Therefore, we incorporated into the software design provisions for great flexibility in terms of additions, deletions and changes.

This system is available to the scientific community upon request and without cost. We hope that it will become a useful research tool.

CECILIA SACCONE, CECILIA LANAVE,
MARCELLA ATTIMONELLI, GIULIA SIMPSON

Institute of Biological Chemistry,
University of Bari, Italy

NEWS AND VIEWS

Atmospheric chemists *in flagrante*?

from Philip Campbell

OVER the past decade or so, the problems associated with the chemistry of the troposphere (the lowest 10 km of the atmosphere) have attracted increasing attention. The ecological effects of acidic rain and climatic effects of carbon dioxide have both generated many conferences and much media coverage. It was something of a change — even a relief — to see these topics recede (if only temporarily) within the general chemical perspective of a recent discussion meeting*. The organizers' declared aim was to assess the chemistry of the troposphere, particularly as influenced by biota and by the hydrosphere and lithosphere. Fundamental chemical questions were apparent. For instance, free hydroxyl radicals are now thought to be the most significant oxidizers in the troposphere, yet they can barely be detected using current techniques. With such problems being highlighted, the impression left by the meeting is that atmospheric chemists have been caught *in flagrante ignorantia* by their increasingly industrialized planet.

Apart from their chemical production in the atmosphere itself, tropospheric gases originate from volcanoes, oceans, man and his by-products and from biota and their detritus. Much attention at the meeting was focused on biogenic emissions, which represent virtually the sole source of such important trace constituents as ammonia and methane. Biological processes occur both on land and in the oceans of course, but the former, being arguably less homogeneous, present more problems.

A characteristic problem is: how representative are emission measurements of nitrous oxide from a particular site? That is, how reliably can they be extrapolated towards a global budget? Given the significant dependence of emission rates on crop and soil types, for example, and the influence of fertilizers, the need for comprehensive measurements is obvious — doubly so when temporal variations arise due to temperature dependence. More generally, given that compositions of many important trace species are in the parts per trillion (10^{-12}) by volume range, there were strong pleas for quality control of measurements and for accompanying background data on ambient UV and visible radiation for example. The latter are important because of the photodependence of important oxidation processes discussed below.

The source regions of the biosphere can be split into the oxic (containing free oxygen) and anoxic. The former include the upper layers of the ocean and of soils. As well as such fully oxidized species as carbon dioxide, oxic regions also produce such relatively reduced species as nitrous and nitric oxides from bacterial processes and ammonia from the decay of animal excreta. The anoxic environment (lower soil regions, and the interiors of animals for example) harbours the production of reduced species such as hydrogen sulphide (by sulphate-reducing bacteria) and methane (primarily by anaerobic bacteria in waterlogged soils and in termites).

As well as the specific uncertainties associated with such emission processes, participants highlighted the problems of modulation and transport in the biosphere. This problem is well illustrated by hydrogen sulphide. Bacterial reduction of continental shelf sediments is thought to result in a billion (10^9) tons of H_2S being produced every year, yet only a few million tons reach the atmosphere. The balance is taken up by oxidation in the upper layers of the oceans or, more to the point, by biological oxidation by sulphur bacteria which, in this manner, consume the gas with extreme efficiency. Similar processes have been observed with nitrous oxide.

As layers of bacteria only fractions of a millimetre thick can have a significant role, participants emphasized the care required when measuring fluxes between environmental 'compartments'. In contrast, rarer volatiles such as carbonyl sulphide and dimethyl sulphide (DMS) slip through the bacterial net. DMS is a very important carrier in the global sulphur cycle, being produced by marine algae and having a strong ocean–atmosphere flux. Investigation into possible continental sources of this and other volatile sulphur compounds was placed high on the conference shopping list.

It is now clear that the tropospheric chemical fates of virtually all the important trace gases are governed by free hydroxyl radicals. As R. J. Cicerone (National Center for Atmospheric Research, Boulder) remarked, this statement would have been ridiculed a decade or so ago when few believed that electrically neutral free radicals could exist in the troposphere. In 1971, however, H. Levy suggested that excited oxygen atoms produced by the well known UV photolysis of tropospheric ozone would react with water to produce free hydroxyl radicals. These highly reactive species, present in minute (and at present barely detectable) quantities, oxidize important trace species such as methane, carbon monoxide, hydrogen sulphide, ammonia and a host of others.

It is obviously important, therefore, that the temporal and spatial behaviour of tropospheric ozone be well understood. An important source is downward diffusion from the stratosphere. However, hydroxyl radicals also play an important part in determining tropospheric ozone concentrations, because they fill the role of active catalysts both in its production (permitting the oxidation of carbon monoxide by oxygen) and its destruction (where ozone oxidizes carbon monoxide to produce carbon dioxide and oxygen). These processes require reaction sequences which involve NO and NO_2 and produce the intermediate species HO_2. Thus, it was strongly recommended that the atmospheric distributions of these species and of O_3 and OH be intensively investigated. Such work will require the further development of experimental techniques due to the minute quantities of some of the species concerned. Also essential will be the continuation of laboratory kinetic studies since a knowledge of rate constants is central to atmospheric chemical modelling.

The hydroxyl radicals are one example of the significant role of gas-phase catalysis, where minute quantities of a trace species will significantly affect not only the chemical but also the thermal balance of the atmosphere. Thus, those currently concerned about the effects of chloro-

---

*The Dahlem Workshop on Atmospheric Chemistry was held in Berlin on 2-7 May 1982.

Philip Campbell is Physical Sciences Editor of Nature.

0028-0836/82/260009-02$01.00

fluorocarbons on stratospheric ozone (another example of such catalysis) may broaden their attention downwards as the very complex tropospheric pathways become better understood.

Although the oxidation processes described above are important, others may be equally so and are equally ill defined at present. An important example is that of SO_2. The concentrations of SO_2 and C_2H_2 observed in the remote troposphere are roughly the same although their emissions from combustion are in the ratio of 100:1. Their gas-phase oxidation rates by hydroxyl radicals are similar, so some other mechanisms for SO_2 removal exist. One of these is wet-phase oxidation.

It was remarked that atmospheric aqueous chemists appear to be at the stage reached by their gas-phase colleagues a decade or so ago, with islands of information in a sea of uncertainty. Although the chemical components in atmospheric water are moderately well known, their reactions are still very uncertain. The main oxidizing agents are thought to be H_2O_2, O_3 and O_2, and the best (or least poorly) understood process probably the aqueous oxidation of SO_2 to sulphate, of obvious relevance to acidic rain. Aqueous kinetics are strongly pH dependent and depend also on the presence of catalysts such as manganese ions and graphite. There are unpublished observations that indicate that H_2O_2 may be much more prevalent in rainwater than previously thought. Complications include photochemical effects and the fact that equilibrium may not be reached in raindrops.

The probable importance of transition metals for aqueous catalysis was emphasized together with the uncertainties concerning their chemical form. For instance, organic complexes of transition metals have been observed to drastically enhance oxidation of reduced sulphur compounds, while complexation of reduced iron and manganese inhibits their catalytic abilities. The need for laboratory studies of such problems is urgent, together with field identification of complexes in rainwater, aerosols, and so on.

Other uncertainties in the aqueous phase are associated with gas solubilities. G. Ayers (CSIRO, Mordialloc) reported measurements of ammonia in rainfall that indicated considerably lower solubilities than expected. Whether the difficulties lie with the earlier measurements of the Henry's Law constant or with unknown processes peculiar to rainwater is not known. Given ammonia's importance in providing atmospheric alkalinity, such problems (which may also become apparent for other trace species) would appear to be fundamental.

Although the topic of the conference was chemical, the problems of aqueous chemistry are closely linked with the physics of the water cycle itself (for instance, repeated condensation and evaporation within clouds). Moreover, the means by which atmospheric constituents are incorporated into raindrops, snow and aerosols require detailed investigation, because they not only affect the chemical transformation of species but also represent an important atmospheric sink in global budgets. As an example, and in a memorable display of technical bravura, W.G.N. Slinn (Battelle-Pacific NW Labs, Richland) demonstrated the cleansing action of rain through its depletion of in-flight insect populations.

Given the wide range of outstanding but clearly identified problems associated with the chemistry of today's atmosphere, it would seem presumptuous to consider tackling the equivalent problems of the past, where only a few species have so far been directly identified (as opposed to inferred). Nevertheless, one group of participants was allotted the task of assessing the records of past atmospheric composition. Ice cores, lake and marine sediments and tree-rings can together provide information over the Quaternary period (the past two million years or so), the tree-ring interpretations being dependent on models of leaf uptake and transfer and so on. Ice-cores from Greenland and Antarctica offer the most direct record of composition, stretching back 10^5 years or more, but practitioners are the first to acknowledge that considerable work is required before the full potential of this resource is realized. Further back in time, the geological record requires a considerable degree of inference to yield compositional information. Past carbon dioxide concentrations are of obvious importance to the climatologists owing to their attendant greenhouse tendencies, and climatic change is more directly documented in sediments than composition.

This has necessarily been a selective review of a wide-ranging meeting, concentrating, for instance, on the inorganic gaseous constituents of the troposphere. But considerable attention was also given to the sources and fates of organic species (for which data are scarce) and of metalloid compounds [such as $(CH_3)_4Sn$]. Another extremely important set of atmospheric constituents is the aerosols, whose impact on the chemical balance of the troposphere is profound, and whose composition, physical characteristics and chemical and physical evolution (nucleation and transport) need extensive investigation. □

A corona around the Milky Way

from Joel N. Bregman

MANY new observations in the UV, X-ray and radio wavelength regions indicate that a multi-component corona of hot and cool gas surrounds the disk of our Galaxy. Unlike the disk itself, which is rich in relatively easily studied neutral and ionized gas and cosmic rays, the components of the surrounding region have proved difficult to investigate. Attempts are now being made to fit the new observations to coronal models in which the activity of the disk gives rise to the corona and the heating and cooling processes naturally cause phase changes in the gas, resulting in a complex corona.

Evidence that clouds of gas exist above the disk first came from observations of the Ca II absorption lines against the optical continua of stars, by Münch and Zirin[1]. The optical absorption lines are produced by cool ($<10^{3.5}$K) clouds of gas but Münch and Zirin[1], in studies of stars far above the disk, discovered more absorption lines than could be accounted for by gas clouds in the disk alone. Several recent studies, in which UV spectra of hot, distant stars were obtained with the International Ultraviolet Explorer (IUE), support and greatly extend the earlier optical work. Absorption lines of Si IV and C IV, commonly seen in these UV spectra, originate in either collisionally ionized gas at 10^5K or photoionized gas at 10^4K. It is not yet possible to measure directly the distance to individual clouds, but distances can be calculated by interpreting the absorption line velocities with a model for galactic rotation. The clouds probably lie within 30,000 light yr of the galactic disk[2–4] (while, for comparison, the half-thickness of the disk is only 600 light yr).

X-ray observations reveal that another component of the corona is gas considerably hotter than that responsible for optical or UV absorption lines. The Wisconsin X-ray group find an X-ray background flux (1 keV), some of which is associated with the Galaxy and probably originates above the disk in a flattened corona[5]. Unfortunately, they are unable to distinguish between emission from point sources (stars) and diffuse gas, nor do they directly measure the distance to their emitters. Nevertheless, these observations at least are consistent with a hot diffuse corona ($\sim 3\times10^6$K, $n\sim10^{-3}$ cm^{-3} if the height of the corona is that suggested from optical studies).

Radio observations complete our current understanding of the corona. Observations of the 21 cm hyperfine transition of neutral hydrogen show many

---

Joel N. Bregman is at the Department of Physics, New York University, 4 Washington Place, New York, New York 10003.

0028-0836/82/260010-02$01.00

cool clouds ($< 10^3$K) with high velocities[6]. Because these velocities cannot arise from galactic rotation of ordinary disk gas, several investigators have suggested that the clouds reside in the corona and may be falling towards the disk[7-10]. Radio measurements of pulsars show that the pulsed radiation is dispersed by electrons of mean density $0.025\ \text{cm}^{-3}$ and scale height greater than 1,500 light yr (ref. 11). Finally, a weak low-frequency radio continuum background[12] that is probably synchrotron emission from cosmic rays interacting with the coronal magnetic field is observed. These observations are consistent with the model if there are significant cosmic ray intensities at distances greater than 3,000 light yr from the disk[13]. The galactic disk thus seems surrounded by a thick corona composed of thermal gas at several temperatures ($< 10^4$K, 10^4–10^5K, $\geq 10^6$K) as well as cosmic rays and magnetic fields.

Although no single theory explains the presence of all these components, progress has been made in linking some of the components together. Spitzer[14] pointed out that if million degree gas could escape the disk, it would surround the Galaxy with a corona several tens of thousands of light years thick. This corona would lose thermal energy through radiation in a process such that cooling condensations of gas would grow quickly and form into clouds much cooler ($\leq 10^4$K) than the rest of the corona[7-10]. These clouds may fall into the disk, merge with the interstellar disk gas and eventually re-emerge as hot gas again, in a cycle that has been termed a 'galactic fountain'. For certain temperatures and densities of the hot coronal gas, the theoretical velocity pattern of the cool clouds roughly reproduces that of the high-velocity clouds of neutral hydrogen[9]. While the interior of these cool clouds is probably neutral, their surface may be photoionized by soft X rays, or by photons from hot stars. The ionized surface layer would be the site of the Si IV and C IV absorption lines seen in the UV spectra. Although this model links together the various phases of the thermal gas, it is not without problems, one being that cosmic rays are not included.

As a first step towards remedying this omission Hall[15] has considered the connection between a hot turbulent corona, and the propagation of cosmic rays and the structure of the magnetic field. In this model, the cosmic rays occupy approximately the same volume as the hot corona and large-scale turbulence in the hot gas causes magneto-hydrodynamic instabilities which result in small-scale density fluctuations and magnetic field irregularities in the gas. Consequently, cosmic rays are scattered as they propagate through the corona in such a way that the size of the cosmic ray corona and the diffusion coefficient within it can be accounted for. □

---

1. Münch, G. & Zirin, H. *Astrophys. J.* **133**, 11 (1961).
2. Savage, B. & de Boer, K. *Astrophys. J.* **243**, 460 (1981).
3. York, D.G. *A. Rev. Astr. Astrophys* (in the press).
4. Pettini, M. & West, K.A. *Astrophys. J.* (in the press).
5. Nousek, J.A., Fried, P.M., Sanders, W.T. & Kraushaar, W.L. *Astrophys. J.* (in the press).
6. Giovanelli, R. *Astrophys. J.* **85**, 1155 (1980).
7. Shapiro, P.R. & Field, G.B. *Astrophys. J.* **205**, 762 (1976).
8. Chevalier, R.A. & Oegerle, W.R. *Astrophys. J.* **227**, 398 (1979).
9. Bregman, J.N. *Astrophys. J.* **238**, 577 (1980).
10. Habe, A. & Ikeuchi, S. *Prog. theor. Phys.* **64**, 1995 (1980).
11. Falgarone, E. & Lequeux, J. *Astr. Astrophys.* **25**, 253 (1973).
12. Webster, A. *Mon. Not. R. astr. Soc.* **185**, 507 (1978).
13. Higdon, J.C. *Astrophys. J.* **232**, 113 (1979).
14. Spitzer, L. *Astrophys. J.* **124**, 20 (1982).
15. Hall, A.N. *Mon. Not. R. astr. Soc.* **199**, 355 (1982).

Sons and daughters

from T.H. Clutton-Brock

In some species of invertebrates, the sex ratios of emerging adults can vary from nearly 100 per cent males to nearly 100 per cent females[1,2]. Although the immediate causes of sex ratio variation are diverse — in some species, sex ratios are controlled by environmental conditions during growth while in haplo-diploid organisms they depend on the proportion of fertilized to unfertilized eggs laid — the evidence that they represent adaptive strategies of reproduction is overwhelming[2]. But can diploid organisms such as birds and mammals, where sex is chromosomally determined, vary the sex ratio of their progeny in an adaptive fashion, too? The traditional view is that they can't[3] but several recent studies have challenged this position.

The most sensational of these claims, made by Nancy Burley of the University of Illinois, is that coloured leg rings fitted to the legs of zebra finches not only affected their attractiveness as mates but also influence the sex ratio of the progeny they produce[4]. According to Burley, pairs generally bias the sex ratio of their offspring towards the sex of the more attractive parent; for example, those in which the male wears an 'attractive' ring and the female an 'unattractive' one tend to produce male-biased sex ratios. This arrangement, Burley argues, will increase parental fitness.

Not surprisingly, the publication of these claims evoked a strong response. Many laboratory and field studies of social behaviour in birds use colour rings. How many effects might have been obscured — or produced — by the colour of the rings used? How many population explosions — or crashes — could coloured leg rings have caused? Two critiques of Burley's paper have been recently published in *Science*[5,6] and although Burley rebuts some of the criticisms in the same issue, the small size of her sample and the absence of any relationship between the reproductive success of males and the sex ratio of their offspring in other bird species[7,8] indicate a strong need for her experiments to be replicated before their generality is accepted.

What of other cases of variation in secondary (birth or hatching) sex ratios in birds and mammals? In many cases, suggested effects do not approach statistical significance[9-11]. In addition, a proportion of significant trends are likely to be fortuitous: sex ratios have universal interest and it is probable that few biologists with access to breeding data fail to look for consistent trends, publishing only if significant effects are found. Since there is no way of estimating the number of those looking for variation in sex ratios, it is impossible to tell what proportion of significant trends could have arisen by chance. There are certainly many data sets in which no sex ratio bias is evident[8,11-13]; in particular, the search for genetic variance in the sex ratio among outcrossed vertebrates has been largely unsuccessful[14]. Where genetic effects have been implicated, they are typically very small indeed; for example, an analysis of 150,000 births sired by 107 bulls found significant differences in the sex ratio of progeny sired by different fathers but, after correcting for the expected binomial variation, the standard deviation of the proportion of males produced was only 1.5 per cent[15].

Nevertheless, a growing number of studies suggest that secondary sex ratios can and do vary among birds and mammals. Birth sex ratios not uncommonly differ from unity in mammals: female-biased ratios are uncommon while a considerable number of sexually dimorphic mammals, including man, show male-biased birth sex ratios which differ significantly from unity in large samples[16,17]. Exceptions include two species of lemmings which produce around twice as many daughters as sons, apparently because a proportion of females are of XY karotype with an X chromosome that causes its bearer to be a female and to produce mainly or exclusively X-bearing eggs[18-20].

Secondary sex ratios also vary within species. In laboratory mice maintained on low-fat diets, birth sex ratios fell from 50 per cent male in a control group to 24 per cent among experimental animals[21], while a group of female white-tailed deer maintained on a low plane of nutrition produced 70 per cent sons compared with

---

T.H. Clutton-Brock is at the Department of Zoology, University of Cambridge, Cambridge CB2 3EJ.

0028-0836/82/260011-03$01.00

Table 1 Relationship between fawn sex ratio and the temporal interval between onset of oestrus and insemination in white-tailed deer (from ref. 25)

	Hours in oestrus					
	13–24	25–36	37–48	49–96	Total	$\bar{x}$
Male fawns	4	12	25	21	62	
Female fawns	24	19	15	5	63	
Per cent males	14.3	38.7	62.5	80.8		49.6
No. of does	15	15	21	16	67	
Fawns/ mother	1.87	2.07	1.90	1.69		1.88

47 per cent among females reared on a high plane of nutrition[22]. Significant associations between birth sex ratios and the timing of insemination relative to ovulation[23,24] have been demonstrated in several studies of human data and in a recent experiment with white-tailed deer (see Table 1). More males are born early in the breeding season in some seals[26-29] as well as in red-winged blackbirds[8] while this trend is reversed in some other birds[30]. Two recent studies of baboons and macaques show that socially dominant females produce more daughters than sons while subordinates produce more sons than daughters (Table 2). And in several ungulate species there is evidence that more males are produced at high population density[33] while research on rodents indicates that birth sex ratios vary significantly with the population cycle[34,35]. In none of these cases is the mechanism responsible for the variation in sex ratio yet known but the effects should not be lightly dismissed on this score. Both male- and female-biased mortality can occur during gestation[36-43] and the possibility of variation in the sex ratio at conception cannot be excluded (see refs 44–46).

A central question is whether variation in secondary sex ratios is adaptive — as is clearly the case in haplo-diploid organisms.

Table 2 Sex ratios in relation to maternal dominance rank in macaques and baboons

Species	Maternal rank		
Papio cynocephalus	High		Low
(Wild population: ref.31)			
Females	19		7
Males	10		15
Per cent males	29		22
Macaca mulatta			
(Captive group: ref. 32, Simpson, unpublished)			
1972–1981	High	Medium	Low
Females	20	12	13
Males	9	19	20
Per cent males	31	61	61
Pre-1972	High		Others
Females	18		7
Males	6		15
Per cent males	25		68

Trivers and Willard[47] argued that in species where reproductive success varies more widely among males than females and parental investment influences the success of offspring, females should produce more sons at times when they are in superior body condition (and so can afford to invest heavily in each offspring) and more daughters when in inferior condition, perhaps adjusting the sex ratio of their progeny through sex-differential mortality among their offspring. Their theory was subsequently disputed[10] but has since been shown to be robust[8,48], though the evidence cited in support of it is unconvincing[10].

Some cases appear to agree with the predictions of Trivers and Willard's theory. The low proportion of males produced by mice reared on poor diets[21] fits Trivers and Willard's predictions and so, too, may the female-biased sex ratios produced by early breeding grackles[30]. Other studies have shown that under circumstances of food shortage male neonates are less likely to survive[49,50], though an alternative explanation is that increased mortality is one of the costs of faster growth rates, higher metabolic rates and reduced fat deposition among growing males in dimorphic species[51].

However, there are as many trends that apparently contradict the predictions of Trivers and Willard's theory, including the tendency for female white-tailed deer maintained on a low plane of nutrition to produce male-biased sex ratios[22] and for dominant baboons and macaques to produce female-biased ones[31,32]. These results could still be fitted within the framework of the theory if breeding success proved to vary more widely in females than males. Alternatively, parental investment may sometimes have a greater *effect* on females than males — for it is the effects of parental investment on variance in the reproductive success among male and female offspring rather than the amount of variance *per se* that will determine which sex a parent should invest in most. A difference of this kind has been invoked by Altmann[31] to account for the female-biased sex ratios produced by dominant baboons: in this species, as well as in rhesus macaques, the reproductive success of females is related to the rank of the matriline to which they belong and dominant mothers may be able to influence the reproductive success of their daughters more than that of their sons. But it is important to remember that neither variation in lifetime reproductive success nor the effects of parental investment on success have yet been measured in both sexes in any wild vertebrate.

Other functional relationships may also be involved. The tendency for late inseminations to produce male-biased progeny could allow individuals to bias the sex ratio of their offspring towards the rarer sex[35] — an effect which has been experimentally demonstrated in guppies[52]. In species where females remain in their natal area while males disperse, sisters may compete with each other for food and male-biased sex ratios may be favoured[53], especially when population density is high. Conversely, where populations are divided into small inbreeding populations, competition between brothers for mates may favour female-biased ratios — which could explain the occurrence of female biases among lemmings[54]. Where males are more likely to die before the termination of parental investment, an excess of males may be produced at birth[16,55] — an argument originally produced by R. A.

---

1. Hamilton, W. D. *Science* **156**, 477 (1967).
2. Charnov, E. L., Hartogh, R. L. L., Jones, W. T. & van der Assem, J. *Nature* **289**, 28 (1981).
3. Maynard Smith, J. *Behav. Ecol. Sociobiol.* **7**, 247.
4. Burley, N. *Science* **211**, 721 (1981).
5. Immelman, K., Hailmann, J. P. & Baylis, J. R. *Science* **215**, 422 (1982).
6. Thissen, D. & Martin, E. *Science* **215**, 423 (1982).
7. Patterson, C. B. & Emlen, J. M. *Am. Nat.* **115**, 743 (1980).
8. Fiala, K. L. *Evolution* **35**, 898 (1981).
9. Caughley, G. *J. Reprod. Fert.* **25**, 145 (1971).
10. Myers, J. H. *Am. Nat.* **112**, 381 (1978).
11. Williams, G. C. *Proc. R. Soc.* **B205**, 567 (1979).
12. Vickers, A. *J. Reprod. Fert.* **13**, 375 (1967).
13. Kaufman, M. H. *J. Reprod. Fert.* **35**, 67 (1973).
14. Maynard Smith, J. *The Evolution of Sex* (Cambridge University Press, 1978).
15. Bar-Anan, R. & Robertson, A. *Theor. appl. Genet.* **46**, 63 (1975).
16. Fisher, R. A. *The Genetical Theory of Natural Selection* (Oxford University Press, 1930).
17. Clutton-Brock, T. H. & Albon, S. D. in *Current Problems in Sociobiology* (ed. King's College Sociobiology Group) (Cambridge University Press, 1982).
18. Hasler, J. F. & Banks, E. M. *Can. J. Zool.* **53**, 777 (1975).
19. Fredga, K., Gropp, A., Winking, H. & Frank, F. *Hereditas* **85**, 101 (1977).
20. Bengtsson, B. O. in *Measuring Selection in Natural Populations* (eds Christiansen, F. & Fenchel, T.) (Springer, New York, 1977).
21. Rivers, J. P. W. & Crawford, M. A. *Nature* **252**, 297 (1974).
22. Verme, L. J. *J. Wildl. Mgmt* **33**, 881 (1969).
23. James, W. H. *Lancet* **i**, 112 (1971).
24. Guerrero, R. *Stud. Famm. Plann.* **6**, 367 (1975).
25. Verme, L.J. & Ozoga, J.J. *J. Wildl. Mgmt* **45**, 710 (1981).
26. Coulson, J.C. & Hickling, G. *Nature* **109**, 281 (1961).
27. Boyd, J. M. & Campbell, R. N. *J. Zool.* **164, 469** (1971).
28. Stirling, I. *Austr. J. Zool.* **19, 267** (1971).
29. Stirling, I. *J. Mammal.* **52, 842** (1971).
30. Howe, H. *Science* **198, 744** (1977).
31. Altmann, J. *Baboon Mothers and Infants* (Harvard University Press, 1980).
32. Simpson, M. J., Simpson, A., Hooley, J. & Zunz, M. *Nature* **290, 49** (1981).
33. McCullough, D. R. *The George River Deer Herd* (University of Michigan Press, Ann Arbor, 1979).
34. Nanmov, S. P., Gibet, L. A. & Shatlova, S. P. *Zh. Obshch. Biol.* **30**, 673 (1967).
35. Werren, J. H. & Charnov, E. L. *Nature 272*, 349 (1978).
36. Weisner, B. P. & Sheard, N. M. *Proc. R. Soc. Edinburgh* **55**, 1 (1935).
37. Trivers, R.L., Seger, J. & Hare, H. Unpublished data.
38. Chapman, A. B., Casida, L. E. & Cote, A. *Proc. Am. Soc. Anim. Prod.* **1938**, 303 (1938).
39. Craft, F. A. E. *Am. Nat.* **71**, 529-559 (1937).
40. Sackett, G. P., Holm, R. A., Davis, A. E. & Fahrenbach, C. E. *Symp. 5th Congr. Int. Primat.*, 186 (1974).
41. McMillen, M. M. *Science* **204**, 89 (1979).
42. Howard, A., McLaren, A., Michie, D. & Sander, G. *J. Gene.* **55**, 200 (1955).
43. Gosling, L. M. & Petrie, M. in *Physiological Ecology* (eds Townsend, C. R. & Calow, P.) (Blackwells, Oxford, 1981).
44. Beatty, R. A. *Phil. Trans. R. Soc.* **B259, 3** (1970).
45. Roberts, A. M. *J. Biosoc. Sci.* **10**, 169 (1978).
46. Roberts, A. M. *J. Biosoc. Sci.* **10**, 169 (1978).
47. Trivers, R. L. & Willard, D. E. *Science* **179, 90** (1973).
48. Okansen, L. *Am. Nat.* **117**, 109 (1981).
49. Howe, H. F. *Ecology* **57**, 1195 (1976).
50. McClure, P. A. *Science* **211**, 1058 (1981).
51. Glucksman, A. *Biol. Rev.* **49**, 423 (1974).
52. Geodakian, V. A., Kosobutsky, V. I. & Bileva, D. S. *Genetika* **9**, 154 (1967).
53. Clark, A. B. *Science* **201**, 163 (1978).
54. Stenseth, N. C. *Oikos* **30**, 83 (1978).
55. Taylor, P. D. *Nature* **291, 64** (1981).
56. Dittus, W. P. J. *Behaviour* **63**, 281 (1977).
57. Dittus, W. P. J. *Behaviour* **69**, 265 (1979).
58. Silk, J. B., Samuels, A. & Rodman, P. S. *Behaviour* (in the press).

Fisher to explain the existence of male-biased birth sex ratios in man[16].

Alternatively, sex ratio variation may sometimes be a non-adaptive consequence of an adaptive mechanism. For example, in baboons and macaques, females are likely to remain in the troop where they are born throughout their lives and mothers may be able to increase the reproductive success of their offspring by removing as many potential competitors as possible[56]. In several species, there is evidence that female juveniles are more likely to be attacked or threatened by conspecifics than males[57,58], and one study has even suggested that this effect may extend to females pregnant with female fetuses[40], possibly increasing the likelihood that subordinates will abort if they have conceived daughters.

However, the basis for adaptive explanations of sex ratio variation in vertebrates is weak because we know virtually nothing about the extent to which parental investment affects the reproductive success of sons and daughters in wild populations or the environmental factors that modify its influence. In addition, the very flexibility of adaptive arguments undermines their credibility since there are few trends to which a plausible, adaptive explanation could not be fitted. Before accepting such arguments, we need to know considerably more about the distributions of the effects they claim to explain. How is maternal rank related to the sex ratio in primates where daughters do not inherit their mother's rank? Is high population density associated with female-biased birth sex ratios in species where daughters disperse and sons remain in their natal area? Do species which show particularly biased birth sex ratios also show especially strong sex differential mortality during early growth? And how is sex ratio variation achieved? Until these questions have been examined, we shall continue to be left with some interesting data, a plethora of stimulating ideas and few firm conclusions.

Decapentaplegic — hopes held out

from Gary Struhl

FRUIT flies are composed of around a million cells arranged in a miraculously complex pattern. Each eye, for example, contains about 700 facets arranged in a crystalline lattice; each facet is itself a precise hexagonal array of specialized receptor, pigment and accessory cells. How such intricate patterns arise is a central problem in developmental biology. In the case of the eye, it was once thought that each facet arose independently as the descendent of a single cell. But this simple lineage model fell by the wayside with the discoveries that facets are not clones[1], and that any two cells in a cluster of neighbouring facets can arise as daughters from the same mother cell[2]. Thus, in the eye, as in most other tissues of the adult epidermis, cell patterns are not dictated by cell ancestry, but rather by interactions between cells. And in order for such interactions to give rise to the coherent cell patterns of organs and appendages, there must be mechanisms for organizing and interpreting spatial information in large populations of cells.

At present, we can only speculate about how cells know where they are in a developing tissue, and how they use this information to decide what to do. Whatever the mechanism, however, its components must be molecules encoded by genes, and this fact provides one of the few approaches to understanding how cell patterning occurs. In principle, it should be possible to identify the particular genes whose products are responsible for organizing and interpreting spatial information, and, once identified, it should be possible to isolate such genes, purify their products and determine their mode of action at the molecular level.

Unfortunately, there is at least one serious flaw in this golden scenario — how does one identify the relevant genes? There are of the order of 10^4 genes in the *Drosophila* genome, of which only a few are probably integral components of the cell patterning mechanism. At present, the only criterion for finding these few needles buried in the genomic haystack is mutant phenotype. But here is a catch-22: without a clear understanding of the mechanism in question, it is difficult to predict the phenotypes of mutations which eliminate its component parts. So choosing the right genes is a difficult business, depending as much on chance and intuition as on objective arguments. And unfortunately, an error in judgement may go undetected for several years.

In a recent paper[3], Spencer *et al.* have described a complex genetic locus in *Drosophila*, *decapentaplegic* (*dpp*; otherwise called *held out*[4]), which they suggest encodes a series of related gene products involved in positional signalling. If their suggestion is correct, understanding how the products of this locus work will be of fundamental importance. What is their evidence? Briefly, they have obtained a series of mutations in this locus which result in the absence of specific parts of the adult appendages. The mutations fall into several discrete classes which can be arranged in an order such that low-class mutations remove only a few distal structures in each appendage, whereas progressively higher-class mutations remove more and more proximal structures (the highest-class mutations appear to kill the embryo). In addition, the functional genetic units defined by the different classes of mutation are arranged on the chromosome in an order that corresponds directly with their phenotypic hierarchy. On the basis of these results, the authors "presume that the functional units in the *decapentaplegic* complex correspond to a series of structural genes encoding activities in morphogenetic positional signalling".

Because this work may comprise the foundation of a detailed genetic and molecular analysis, it is well to ask how good this presumption is. At its basis lies the assumption that loss of distal structures results from absence of positional signalling along the proximo-distal axis. As Spencer *et al.* note, there is no easy way to assess the validity of this assumption. Consequently, one must bear in mind that there may be other less interesting explanations for the preferential loss of distal portions of adult appendages. For example, distal portions of most imaginal disks may proliferate more rapidly than proximal portions; it is possible that in the absence of the *decapentaplegic* gene(s), rapidly proliferating cells may accumulate a toxic metabolite, or run out of an essential metabolite, thereby leading to cell death and consequent loss of structures.

It may help to compare the phenotypes of *decapentaplegic* mutations with the phenotypes of other mutations thought to be primary defects in the cell patterning mechanism. For example, homeotic mutations, exemplified by mutations of the *bithorax* complex[5], result in particular parts of the animal developing like other parts (for example, some of the abdominal segments developing like the second thoracic segment). That is, they result in the replacement of one cell pattern by another. In addition, such mutations transform the cell pattern of both the larval and

---

Gary Struhl is in the MRC Laboratory of Molecular Biology, Hills Road, Cambridge CB2 2QH.

1. Ready, D.F., Hanson, T.E. & Benzer, S. *Devl Biol.* **53**, 217 (1976).
2. Lawrence, P.A. & Green, S.M. *Devl Biol.* **71**, 142 (1979).
3. Spencer, F.A., Hoffmann, F.M. & Gelbart, W.M. *Cell* **28**, 451 (1982)
4. Lindsley, D.L. & Grell, E.L. *Carnegi Instn Wash. Publ. No.* **627** (1968).
5. Lewis, E.B. *Nature* **276**, 565 (1978).
6. Kornberg, T. *Proc. natn. Acad. Sci. U.S.A.* **78**, 1095 (1981).
7. Nusslein-Volhard, C. & Wieschaus, E. *Nature* **287**, 795 (1980).

0028-0836/82/260013-02$01.00

adult epidermis in a corresponding fashion. A second example is that of mutations such as *engrailed*[6] and the segmentation mutations isolated and described by Nusslein-Volhard and Wieschaus[7] which alter the pattern of all segments in a homologous fashion. These mutations affect all segments of the embryo, and in a few cases all segments of the adult. Moreover, they generally result in deletion of a particular portion of the segment and in mirror image duplication of the remaining portion. Again, as in the case of homeotic mutations, these mutations result in phenotypes which may be described as the replacement of one cell pattern by another. Also, like the homeotic mutations, they alter the cell pattern of the embryo, and hence affect cells which have not undergone extensive proliferation.

Whether mutations which result in the replacement of one cell pattern by another are more likely to be relevant to the process of positional signalling than mutations which simply eliminate homologous portions of cell pattern is anybody's guess. Similarly, it is difficult to assess whether mutations which alter cell pattern in precise ways in the absence of extensive proliferation are of more interest than mutations which cause the elimination of proliferating cells. In the case of the *decapentaplegic* complex, further descriptions of mutant phenotypes at the cellular level may help to bolster the argument that this gene complex plays a specific part in positional information. But ultimately, the validity of this argument, or lack thereof, may only be apparent after all the hard work is done — when we understand the molecular roles of the *decapentaplegic* gene products. □

Synthetic peptides as the basis for future vaccines

from John Beale

MOST antigenic determinants of proteins are thought to be conformational rather than sequential; they depend upon the three-dimensional folding of the molecule rather than on the linear sequence of amino acids. Jim Bittle and his colleagues provide in this issue of *Nature*, p.30, an example of the importance of the primary amino acid sequence for foot-and-mouth disease virus (FMDV). They synthesized peptides corresponding to several regions of the virus polypeptide VP1 and found that one of them, corresponding to amino acids 141–160, when coupled to keyhole limpet haemocyanin (KLH) and given with an adjuvant, produced neutralizing antibodies to FMDV and protection against challenge in animals. Another peptide, containing amino acids 201–213 of VP1, also produced neutralizing antibodies. This is an exciting result for both theoretical and practical reasons.

The fact that alteration of conformation by denaturation or enzymatic digestion greatly changes antigenicity suggests that most antigenic determinants of proteins are conformational rather than sequential. For foot-and-mouth disease, for example, the viral peptides derived from either infected cells or disrupted virus have lost most of their immunogenicity; genetically engineered VP1 is also of low immunogenicity[1]. However, several recent lines of evidence suggest that small synthetic peptides having the sequence of antigenic determinants on a protein will, in fact, react with antibody to the intact native antigen and in some instances will neutralize its biological activity.

Langbeheim, Arnon and Sela[2], for example, found that a 20 amino acid peptide corresponding to amino acids 89–108 of the coat protein of MS2 phage, when coupled to a carrier, induced antibodies in animals which neutralized the phage and were as effective as antibody to the intact phage or the coat protein. The neutralization test involved the use of goat antiglobulin which may have produced neutralization without the primary antibody binding to a specific neutralizing site. Peptides representing other regions of the coat protein were ineffective. Similar results come from synthetic peptides corresponding to the antigenic determinant regions of diptheria toxin[3] and the natural cyanogen bromide immunizing fragment of the M protein of type 24 *Streptococcus pyogenes*[4]. Success with hepatitis B virus has also been achieved by several groups, although protection in chimpanzees has not yet been reported (see A. Zuckerman *News & Views* **295**, 98; 1982). Attempts to reproduce the native conformation of the antigenic determinant by producing a cyclic peptide[5] did not yield an antigen clearly superior to the linear peptides[6].

The situation with influenza virus is more confused. Studies of variants using monoclonal antibodies and X-ray crystallography[7] have provided very precise information about the amino acid sequences and the antigenic sites, so the effectiveness of synthetic peptides would be confidently predicted. In the event, although antibodies raised against several KLH-linked synthetic peptides could react with influenza haemagglutinin, they did not react with the previously delineated antigenic sites[8]. Moreover, antibodies raised against the haemagglutinin did not react with the synthetic peptides. These results suggest conformation of the molecule is important.

A key question is whether synthetic peptides can form the basis for a practical vaccine. The results so far obtained have great promise. Peptides with differing specificities might even be coupled to a single carrier protein to give a multivalent vaccine. Problems still remain to be solved, however, some applicable to all vaccine candidates and others more specific to particular vaccines. For foot-and-mouth disease, a synthetic vaccine would have to compete with existing vaccines which are produced by highly developed technology and are very efficient and cheap. Nonetheless, existing vaccines have some problems. First, safety: a number of outbreaks of foot-and-mouth disease have been associated with failures of the inactivation process. The most recent outbreaks in Jersey, and on the Isle of Wight, almost certainly derived from such an accident, as was shown by careful analysis of the molecular characteristics of the virus which showed striking identity between vaccine strains and strains isolated from outbreaks (ref.9 and see J. Brooksby *News & Views* **293**, 431; 1981). Clearly, a synthetic peptide overcomes these problems, but in truth, safety is not a problem if formalin is avoided as an inactivating agent. This chemical has well established limitations for viral inactivation but when acetyl ethyleneimine is substituted there are no problems with inactivation of FMDV. A second consideration is effectiveness. There are several problems for existing vaccines; first, antigenic variability. One of the reasons for suspecting that the two regions on VP1 would be effective immunogens was that they vary in amino acid sequence from strain to strain. New synthetic peptides will be required for each strain but the process of cloning and sequencing the VP1 in order to identify new peptides to synthesize should be simple. Indeed, a number of new peptides might be made ahead of time. Some strains grow poorly in cell culture and are poor vaccine strains for this reason, whilst others are very unstable or are poor strains for less clearly defined reasons. These problems may well be solved by the use of synthetic peptides. Similarly, all foot-and-mouth disease virions are relatively unstable, especially at below *p*H 5.0 and at ambient temperatures; again synthetic peptides are likely to be superior because they are more stable. The existing vaccines are effective after a single dose when given with an adjuvant, usually absorption to aluminium hydroxide and saponin for cattle and an oily adjuvant for pigs. So far, the vaccines prepared from VP1 produced

---

John Beale is at The Wellcome Research Laboratories, Langley Court, Beckenham, Kent BR3 3BS.

0028-0836/82/260014-02$01.00

in *Escherichia coli* have proved less effective than existing vaccines. Thus, even after two doses, antibody levels are much lower than after a single dose of conventional whole-virus vaccines. Synthetic peptides are reported by Bittle *et al.* to be far more effective than VP1 but this comparison is a bit unreal for two reasons: first, the VP1 they used was prepared by SDS treatment and polyacrylamide gel electrophoresis which is a denaturing step and may hide the sites in VP1 reacting with anti-peptide sera or with native virions. Also, VP1 is a relatively small protein, whereas the synthetic peptide was coupled to KLH, one of the most immunogenic carrier proteins in the immunologist's repertoire. The results of coupling VP1 produced by genetic engineering to a similar immunogenic carrier would have been a more valid comparison. Perhaps the most encouraging feature, however, was the almost equally good results they obtained from a single dose using aluminium hydroxide compared with Freunds adjuvant. The dose schedule and duration of immunity are important aspects of vaccine development. As noted earlier for foot-and-mouth disease vaccine, because of the difficulty of mustering animals for vaccination, protection is required from a single dose, but two to three doses may be given each year. For many other vaccines a two-dose primary schedule can be followed by booster doses over a period of years. The performance of vaccines based on synthetic peptides in these respects will need study, but there is no reason to suppose they will prove less efficient than existing killed vaccines.

The feasibility and economics of synthetic peptide vaccines are difficult to judge. The situation for foot-and-mouth disease, where there is an existing relatively cheap vaccine, is very different from that of hepatitis B, for example, where the vaccine is very expensive and can be made only on a limited scale. Another key factor will be the degree of purity of the peptides required. Lerner and his colleagues did not make any special efforts to purify the peptides that are produced by the Merriefield solid-phase synthesis. Plainly it will be essential to establish that the effects are due to a peptide truly of the sequence deduced from DNA sequencing. The degree of purity ultimately required will doubtless vary according to the application. It will be necessary to have a synthetic process that consistently produces the same product — no doubt the spur of a practical application will lead to improved methods and reduced costs. The size of the peptide to be made will be a key factor. Another important element requiring more research is the carrier. In the present experiments with FMDV, KLH was used but it seems certain to be superseded because of supply problems. The addition of a carrier such as KLH negates some of the advantages of a defined synthetic vaccine and problems of hypersensitivity to the carrier may occur when repeated injections are necessary. Clearly there are alternative carriers, such as tetanus toxoid or poly-DL-lysine, and this is an important matter for more research.

Similarly, there will be a need for an adjuvant. Aluminium hydroxide is a clinically acceptable adjuvant for man and it is encouraging that it worked for FMDV. The question of the adjuvant is linked to the requirement for a carrier and the best combination will need to be reassessed. Knowledge about adjuvants is at present a dark area of immunology.

The work of Bittle *et al.* is a significant step along the road to synthetic vaccines. It opens up exciting possibilities for vaccine development which should be vigorously pursued. □

1. Kleid, D G *et al. Science* **214**, 1125 (1981)
2. Langbeheim, H , Arnon, R & Sela, M *Proc natn Acad Sci U S A* **73**, 4636 (1976)
3. Audibert, F *et al Nature* **289**, 593 (1981)
4. Beachey, E H *et al Nature* **292**, 452 (1981)
5. Dreesman, G.R. *et al Nature* **295**, 158 (1982)
6. Lerner, R A. *et al Proc natn. Acad Sci U S A* **78**, 3403 (1981)
7. Wiley, D.C., Wilson, I H & Skehel, J J *Nature* **289**, 373 (1981)
8. Green, N *et al. Cell* **28**, 477 (1982)
9. King, A.M Q *et al. Nature* **293**, 479 (1981)

The internal evolution of Venus and the galilean satellites

from Sean C. Solomon

THE solid planets and satellites of this Solar System display a great diversity of surface features. The Moon and Mercury and many of the icy satellites of Jupiter and Saturn have heavily cratered terrains that have been little altered for billions of years. Jupiter's moon Io has been continuously resurfaced over periods of millions of years by vigorous volcanic eruptions fuelled by the dissipation of huge solid-body tides. The Earth has a lithosphere underlying the ocean basins that is recycled by plate tectonics over a period of about 100 million years. Despite their differences, all these bodies have been shaped by common physical processes during their formation and subsequent evolution. A continuing challenge, made evident by the many new results on the internal and surface evolution of planets and satellites presented at the 13th Lunar and Planetary Science Conference*, is to understand how these common processes have produced the observed diversity of Solar System objects.

Particular interest at the conference was focused on Venus and the galilean satellites of Jupiter, all objects of recent scrutiny by US and Soviet spacecraft.

Dramatic new results have come from Venera 13 and 14 which landed on Venus on 1 and 15 March respectively (V.L. Barsukov and Yu. A. Surkov, Vernadsky Institute of Geochemistry and Analytical Chemistry; and see *News and Views* **296**, 607; 1982). Most notable are the chemical analyses of compositions of Venus soils, derived by X-ray fluorescence, that indicate similarities to a high-potassium alkali basalt at Venera 13 and a terrestrial oceanic tholeiite at Venera 14. On Earth tholeiites, because they comprise the upper igneous crust of all ocean basins, are the most common volcanic rock type. Discovery of such basalts on Venus supports the hypothesis that the major-element compositions of the two planets and their respective mechanisms for the formation and eruption of basaltic magma are similar.

Detailed comparisons of Venus and Earth with respect to planetary composition, mechanical properties and tectonic evolution were also presented. The bulk density of Venus, after correcting for the effects of compression, is generally estimated to be about one per cent less than that of the Earth[1]. The difference is often explained in terms of a slightly different composition for the two planets[1,2]. K.A. Goettel (Washington University) suggested that Venus may have a bulk density at standard conditions equal to or greater than that of the Earth. Such a result would hold if internal temperatures are significantly higher for Venus than for Earth at comparable depths and if Venus has a thicker layer of basaltic crust[3]. The required higher temperatures may occur, however, only if Venus has no analogue to terrestrial plate recycling[4]. If Goettel's suggestion is correct, then cosmochemical models for inner planet formation will require revision.

There is much debate over whether some version of plate tectonics operates on Venus. The issue has broad implications for our understanding of heat transfer and surface evolution on silicate planets. H. Spetzler, I.C. Getting (CIRES, University of Colorado) and H. Mizutani (University of Nagoya) have made a new contribution in a theoretical formulation for brittle failure in silicate planets based on stress corrosion theory and the interaction of growing cracks. Including the effects of

---

*The 13th Lunar and Planetary Science Conference was held at the Lyndon B Johnson Space Center, Houston, Texas on 15–19 March 1982

Sean C. Solomon is an Associate Professor of Geophysics in the Department of Earth and Planetary Sciences, Massachusetts Institute of Technology, Cambridge, Massachusetts 02139.

0028-0836/82/260015-02$01.00

water on the rate of crack growth, they have calculated the effective failure strength as a function of depth in each of the terrestrial planets. For Venus, assuming the partial pressure of H_2O in near-surface rocks to equal that in the lower atmosphere, they calculate a very low value of crustal strength (about 10 MPa) and conclude that plate subduction on Venus would be unlikely.

This author and J.W. Head (Brown University) took a different view. Venus must lose an amount of heat per mass roughly comparable to that known for the Earth[5]. Solid planets and satellites transfer internally generated heat to the surface by plate recycling, as on Earth[6], lithospheric conduction, as on the Moon, and hotspot volcanism, as on Io. Each has been suggested as the dominant mechanism for lithospheric heat transfer on Venus[6–8] and we argued that none can be ruled out given our present knowledge of the venusian surface. In particular, plate recycling cannot be excluded once it is recognized that the characteristics of plate divergence and convergence zones on Venus and Earth will be different because of the different surface temperatures (740K on Venus) and surface abundances of water. Whatever the dominant mechanism of lithospheric heat transfer, however, given a global heat loss per mass comparable to that for the Earth, we must conclude that most of the large-scale topographical features on Venus are young compared with the surface ages of the smaller terrestrial planets.

The galilean satellites, because their surfaces are cold and are composed of unusual materials, display landforms and surface histories that are difficult to understand simply by extrapolation from the known outcomes of processes on the terrestrial planets. Europa, for instance, has a high-albedo icy surface criss-crossed by numerous darker lineations of great length and probably of tectonic origin[9]. T.B. McCord (University of Hawaii) and colleagues reported on a new spectral unit map of Europa derived from Voyager multispectral images. At least four distinguishable units occur; the darker lineations are spectrally similar to other dark units. E. Schonfeld (Johnson Space Center) proposed that the brown colour of the lineations and the low reflectance of the satellite at 3–4 μm may be due to the presence of organic molecules erupted from Europa's interior during episodes of aqueous volcanism. Interpreting the lineations as lithospheric fractures, P. Helfenstein (Brown University) showed that they may be the result of tidal stresses, although the details of such an explanation are considerably more complicated than in earlier versions[10].

The galilean satellites Ganymede and Callisto are similar in size and bulk density, yet their surfaces differ markedly[9]. Callisto displays a surface that has been little altered since an era of heavy impact bombardment. Ganymede, however, preserves heavily cratered units but also contains younger and more lightly grooved terrain, thought to be of extensional tectonic origin, suggesting the hypothesis that Ganymede has undergone greater global expansion than Callisto since the period of high impact flux. P.Y. Huang (MIT) and this author tested this idea by calculating the lithospheric thermal stress that would accumulate from global thermal evolution, including the effects of subsolidus convection and phase changes in H_2O ice, and concluded that Ganymede and Callisto would have had similar stress histories if their initial conditions were similar. If, however, Ganymede began at higher temperatures because of thermal gradients in the proto-jovian nebula[11], the difference in stress histories can account for the different surface characteristics. New estimates of lithospheric thermal gradients versus time in Ganymede and Callisto were reported by Q.R. Passey (Caltech) and E.M. Shoemaker (US Geological Survey) from the distribution of viscously relaxed craters of various diameters and by W.B. McKinnon (University of Arizona) from the widths of concentric ring scarps, interpreted as graben, in impact basin structures. Both studies indicate higher thermal gradients on Ganymede than on Callisto in the period 3 to 4 billion years ago.

The detailed tectonics of grooved terrain formation on Ganymede continue to receive special study. M.T. Zuber (Brown University) estimated the displacement that has occurred between large units of cratered terrain on Ganymede under the assumption that concentric arcs of ring structures in different units were formed by a single event; different locations of the centres of curvature for different units suggest displacements of up to 40 deg arc. M.P. Golombek (Lunar and Planetary Institute) derived a limit of one per cent on the increase in satellite radius associated with extension in the grooved terrain on the assumptions that the grooves are graben and that the dip angles of the bounding normal faults are 60° or greater. This limit agrees with that of McKinnon[11] based on the lack of tectonic disruption of Galileo Regio. S.K. Croft (Lunar and Planetary Institute) proposed that grooved terrain is formed by hydraulic fracturing driven by overpressured water during the final phases of global freezing following early differentiation.

Many of the icy satellites of Saturn show extensional features broadly similar to those of Ganymede[12]. S.W. Squyres, R.T. Reynolds, P. Cassen (Ames Research Center) and S.J. Peale (University of California, Santa Barbara) drew particular attention to Enceladus, which shows features similar to the grooves of Ganymede and large areas of low crater density. Resurfacing of such younger areas could occur either by extrusion of fresh material or by complete relaxation of topography due to a high thermal gradient. A new model by D.J. Stevenson (Caltech) for magma migration by crack propagation through the lithosphere, when applied to Enceladus, suggests that volcanism may occur by comparatively infrequent eruptions of large volumes of H_2O–NH_3 fluids, lending support to the volcanic resurfacing hypothesis. Squyres and his colleagues showed that tidal dissipation is an adequate heat source for volcanism on Enceladus as long as a forced eccentricity several times higher than the current value existed continuously or episodically through a substantial part of its history.

As the data from Pioneer, Venera and Voyager missions continue to be analysed, hypotheses for the evolution of Venus and of the outer planet satellites will be refined. To test these hypotheses will require new spacecraft observations. The US Galileo mission to Jupiter will help provide data for the jovian satellites, and the Soviet Union has announced plans for additional landers to be sent to the Venus surface to conduct further chemical analyses and imaging experiments. A major gap in our knowledge of Venus, however, is a global map of the surface at sufficiently fine resolution to distinguish among the proposed hypotheses for the tectonic evolution of the planet. While the proposed Venus Orbital Imaging Radar mission has fallen victim to reductions in the NASA planetary programme budget, a less ambitious and less costly Venus radar mapping mission is currently being considered to fill this gap. Completion of such a mission would provide a major step towards a full understanding of the evolution of Earth-like planets. ☐

---

1. Ringwood, A.E. & Anderson, D.L. *Icarus* **30**, 243–253 (1977).
2. Goettel, K.A., Shields, J.A. & Decker, D.A. *Proc. lunar planet. Sci.* **12B**, 1507–1516 (1981).
3. Anderson, D.L. *Geophys. Res. Lett.* **7**, 101–102 (1980).
4. Turcotte, D.L., Cooke, F.A. & Willemann, R.J. *Proc. 10th lunar planet. Sci. Conf.*, 2375–2392 (1979).
5. Sclater, J.G., Jaupart, C. & Galson, D. *Rev. Geophys. Space Phys.* **18**, 269–312 (1980).
6. Phillips, R.J. *et al. Science* **212**, 879–887 (1981).
7. Head, J.W., Yuter, S.E. & Solomon, S.C. *Am. Scient.* **69**, 614–623 (1981).
8. Phillips, R.J. & Malin, M.C. in *Venus* (eds Hunten, D.M., Colin, L. & Donahue, T.M.) (University of Arizona Press, in the press).
9. Smith, B.A. *et al. Science* **204**, 951–972 (1979); **206**, 927–950 (1979).
10. Helfenstein, P. & Parmentier, E.M. *Proc. 11th lunar planet. Sci. Conf.*, 1987–1998 (1980).
11. McKinnon, W.B. *Proc. lunar planet. Sci.* **12B**, 1585–1598 (1981).
12. Smith, B.A. *et al. Science* **212**, 163–191 (1981); **215**, 504–537 (1982).

Corrigendum

In the *News and Views* article on 'Cause and treatment of atherosclerosis' by C.T. Dollery (*Nature* **297**, 286; 1982), the sentence "C.T. Dollery (Royal Postgraduate Medical School, London) described a new method for measuring plasma 6-oxo-PGF, the hydrolysis product of PGI_2, which uses gas chromatography–negative ion chemical ionization mass spectrometry and has a sensitivity limit of 500 pg ml^{-1}" should read ". . . a sensitivity limit of 500 cg ml^{-1}".

ARTICLES

Geology and stratigraphy of Neogene deposits, Middle Awash Valley, Ethiopia

Jon E. Kalb*, Elizabeth B. Oswald†, Sleshi Tebedge‡, Assefa Mebrate§, Emmanuel Tola‖ & Dennis Peak¶

* Vertebrate Paleontology Laboratory, Texas Memorial Museum, Balcones Research Center, The University of Texas, 10100 Burnet Road, Austin, Texas, USA
† Bureau of Land Management, Albuquerque, New Mexico 87107, USA
‡ Department of Systematics and Ecology, The University of Kansas, Lawrence, Kansas, 66044, USA
‖ Ethiopian Geological Survey, Ministry of Mines, Addis Ababa, Ethiopia
¶ 3521 21st Street, San Francisco, California 94114, USA

The Middle Awash Valley, Afar, Ethiopia, contains a sedimentary sequence that is >1 km thick, spans much of the Neogene, and contains vertebrate fossils throughout . Newly defined formations described here are older and younger than the hominid-bearing Hadar Formation. The Awash deposystem reflects deposition in an evolving triple junction.

THE Awash River Valley in the Afar Depression (Fig. 1) is unique for containing a 'triple junction river'[1], and, as reported here, a sedimentary record >1 km thick (Fig. 2) that spans much of the Neogene history of the region, including the final breakup of Afro-Arabia. Fossil remains occur throughout the sequence, including those of early hominids. Either hominid fossils or artefacts occur throughout >0.5 km of strata, from the lower Pliocene levels at Hadar[2] to Pleistocene strata at Bodo[3,4] and Andalee[5] (Fig. 2).

This report is based on six seasons of fieldwork with intervening studies by the Rift Valley Research Mission in Ethiopia[1,3–9] (RVRME), under the direction of one of us (J.K.), from early 1975 to mid-1978. Geological investigations are reported below. The accompanying article[10] will report palaeontological and archaeological findings as well as the age of the deposits.

The area studied lies between volcanic plateaus within the Middle Awash Valley (delimited at Awash Station and Tendaho) between Gewani village and Hadar (Fig. 1). Previous geological work in the area is limited to preliminary geological mapping along the SE margin of the area[11,12], observations near Gewani[13], studies at Hadar[1,14,15] and photogeology[13,14,16].

The area studied by the RVRME extends from Gewani to 10°57'N (Fig. 3). The area was geologically mapped from 1:60,000 air photos. This includes the area north to Hadar (from studies by J.K. and D.P. in 1972–73 and traverses by J.K. and A.M. in 1975–76). Extensive base map preparation (aided by H. Mosca and W. Singleton) preceded field surveys. Some 120 geological profiles taken in the map area are referred to in Figs 4 and 5 and in the text by profile numbers (P.1,2,3, and so on); elevations are estimated from published sources[17]. Geographical names are from Afar inhabitants (those in quotation marks are provisional).

The map area (Fig. 3*a*, *b*) lies within a northeastward-drained trough bounded to the west by the Ethiopian Escarpment made up largely of the Miocene 'Fursa basalts'[18], and to the east by a basalt plateau comprised of the Pliocene 'Upper' Afar Stratoid Series[19,20] (UASS). The south-central area (Fig. 3*a*) is capped by basalts of the 'Lower' Afar Stratoid Series (LASS). This central area is complexly faulted and referred to as the Central Awash Complex (CAC) (Fig. 3*a*); it contains the 'Hatowie Graben', bounded by the 'West Hatowie Horst' (WHH) and the 'East Hatowie Horst' (EHH).

The map area forms a northward-dipping structure (due to greater subsidence towards the triple junction) with margins blockfaulted towards the central part of the basin and to the north: older strata crop out to the south along basin margins and the CAC (Figs 3, 5). Dips are greatest at basin and graben margins (or zones of maximum uplift), generally in older strata, and are least pronounced in Pleistocene deposits. Fault trends generally conform to the NW–SE Ethiopian (East African) Rift trend (Fig. 1). Closer inspection reveals the NW trend becomes generally more westerly to the north, and the NE trend more easterly to the south (Figs 3*a*, *b*), a reflection of the rotational movements of the Arabian and East African plates (see refs 21, 22).

Typical badland topography in the area forms exposures up to 20–40 m along basin margins to the south, up to 15–20 m on the EHH, and 90–100 m to the north, where strata are deeply incised by the Awash River.

Stratigraphy (Awash Group)

Stratigraphical studies to date are contained in reports to the Ethiopian Government, in regional, site or faunal descriptions[1,4–9], or will shortly appear in monographic form[23]. Below we summarize the studies and provide the first regional stratigraphical framework for the Middle Awash, as well as briefly describe individual stratigraphical units. [For reference, the Mio-Pliocene boundary is established at 5 Myr (ref. 24), the Plio-Pleistocene boundary at about 1.6 Myr (ref. 25) and the middle Pleistocene boundaries at about 700,000 yr and 125,000 yr (ref. 26).]

The Awash Group is defined here as all late Cenozoic continental sedimentary strata within the catchment of the Awash River. As described below, its known thickness is >1 km thick, and includes the late Miocene Chorora Formation[27] on the SW Hararghe Escarpment (Fig. 1) and the Pliocene Hadar Formation[2], and the presently-described Adu-Asa, Sagantole, Matabaietu and Wehaietu Formations (Fig. 2).

Adu-Asa Formation: Estimated to be late Miocene to early Pliocene[8,10], with a minimum thickness of 145 m; it is best exposed in the SW map area (Fig. 3*a*), between 725 and 825 m a.s.l. (above sea level), and in the CAC from ~640–660 m a.s.l. Adu refers to Adu Dora (white place stream); Asa refers to Asa Koma (red hill). Units comprising the formation (from bottom to top) are the Adu, Asa,and Kuseralee Members (Fig. 2).

Adu Member: At least 40 m of strata either in fault contact or unconformable with the 'Fursa basalts'[18] (P.2,3). The lower unit, especially prominent at upper Ananu and Adu Dora N. (P.3,4), consists of up to 30 m of variegated, predominantly pinkish clays and silts with some variable, cross-bedded sands (up to 2.5 m) and yellow-green clays. The upper unit consists of 12 m or more of massive diatomites (up to 2–3 m), white,

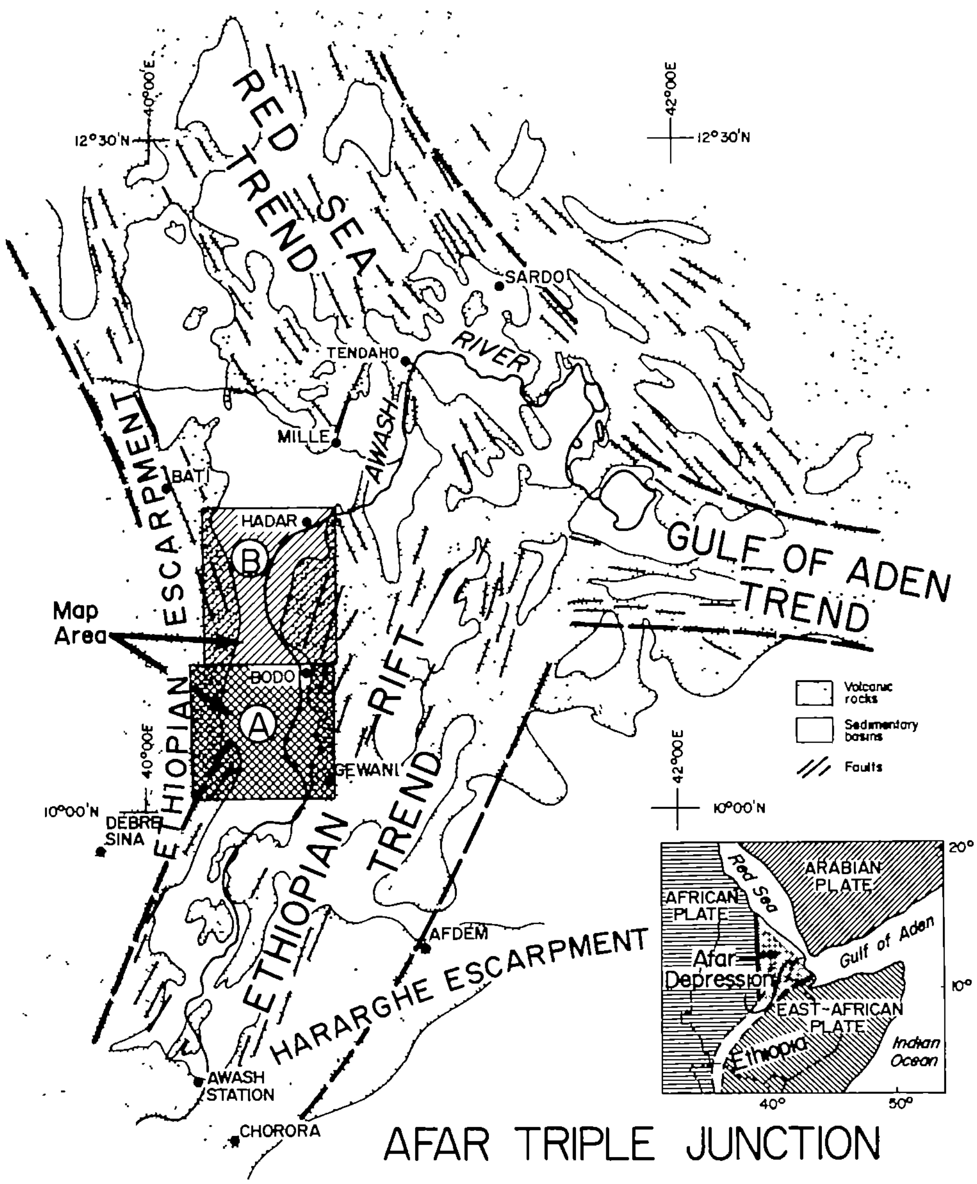

Fig. 1 Study area location map.

indurated clay with some fish bones, reddish-brown clay, and some grey, laminated tuffs.

Asa Member: At least 75 m of strata overlying the Adu Member. The base of the lower unit is marked by either an erosional surface containing distorted bedding and gravel lenses (P.4,6) and/or prominent tuffs. At Asa Hill (P.5), this unit consists of up to 33 m of waterlain well-stratified tuffs (1–3.5 m thick), reddish-brown clays, some coarser layers and minor diatomite lenses. At Adu Dora N. (P.7), the upper unit consists of 30–40 m of predominantly reddish-brown clay, with discontinuous sand (up to 1.2 m), silt and thin tuff layers. Elsewhere, this unit may be overlain by (LASS?) basalts or unconformable alluvium. Fossiliferous strata that may be equivalent to this member exist at Saitune Dora (Fig. 3*a*).

Kuseralee Member: Up to 30 m of strata beneath the LASS basalts, especially at Kuseralee and elsewhere along the margins of the Hatowie Graben (Fig. 3*a*). The stratigraphical position of this unit to the Asa Member is based on its downfaulted lower altitudinal, central position in the basin (P.9,13) and by its more derived fauna. Between Kuseralee and Koba-ah Streams (P.12,13) are up to 30 m of mauve to pinkish tan, sometimes grey, clays with some silts and channel sands and sandstones (up to 3.5 m). Clays form a baked contact zone subjacent to the basalts. Equivalent strata may occur in the eastern Awash between Asaberi and As Streams (Fig. 3*a*), beneath thick (LASS?) basalts (P.61).

Sagantole Formation: Estimated to be early Pliocene[8,10], with a thickness of 210–226 m (Fig. 2) overlying the LASS basalts. Best exposed in the eastern CAC between 757 and 660 m a.s.l. (Fig. 3*a*, 5). We divide this formation into the Haradaso and Aramis Members and two informal units, the Beearyada and Kalaloo beds (Fig. 2).

Haradaso Member: From 71 to 76 m. The lowest strata preserved on the LASS basalts may be in down-faulted structures on the EHH at Haradaso (P.14) and elsewhere. Here are 10–15 m of predominantly reddish-brown and grey clays, with some silts, sands and vertebrate remains[10]. The main unit is in depositional (locally conformable?) or fault contact with the eastern CAC basalt margin and extends 1–2 km eastward between Aramis and Sagantole S. Streams (P.16,17). Here up to 61 m of strata consist of four sand and clay units. Sands are 2.5–6.5 m thick, dominantly fine- to medium-grained, may be laminated or contain coarser lenses, but are commonly homogeneous and interdigitated with tan, reddish-brown or grey clays, silt and shale (with fish remains). At mid-sequence, a lignitic or carbonaceous shale (5–10 m) (P.16,17) exists within a grey (partly tuffaceous?) clay. Upper sands are brown, contain coarser layers, and are associated with brown clays and silts. Equivalent strata in the eastern Awash may exist between Sibabi and Asaberi (P.62,64) overlying (LASS?) basalts, and at lower Wẹe-ee (P.65).

Aramis Member: At least 50 m of strata unconformable or in fault contact (?) with the Haradaso Member (P.18,20). This unit is distinguished by the first major appearance of tuff, which occurs throughout this (and overlying) units. At Sagantole S. are at least 50 m of: (1) tan silts (12.5 m) with siltstones and tuffs (up to 1.75 m); (2) tan, orangish silt (24 m) with sand and tuff layers—upward becomes increasingly sandy (up to 88 m) with gravel lenses; (3) light tan silt (11 m) with sandstone lenses. Equivalent beds in the eastern Awash may exist at lower Wee-ee (P.65).

Beearyada beds: Thickness ~75–85 m (exact values are unknown owing to faulting). Between Aramis S. and Sagantole N. (P.20,23), these beds conformably overlie the Aramis Member and consist of: (1) well-bedded yellow tuffs (4 m+) (P.20); (2) pinkish to tan silts with grey, well-stratified, laterally continous tuffs (2 cm–1.5 m), and some sand, sandstone and clay (30–40 m); (3) at Beearyada, tan silt and sand below and coarsening upward sand and conglomerate above (11.5 m); (4) repeat of (2) above (5.3 m); (5) brown clay, silt and some sands, tuff and brown mudstone (15–18 m). These beds are capped by laterally continuous, gastropod limestone layers (P.23). Strata possibly equivalent to the upper part of this unit in the eastern Awash lie below a widespread gastropod limestone between Kalaloo and Bodo Streams nearest the basalt (P.24,25), and south (Fig. 3*a*).

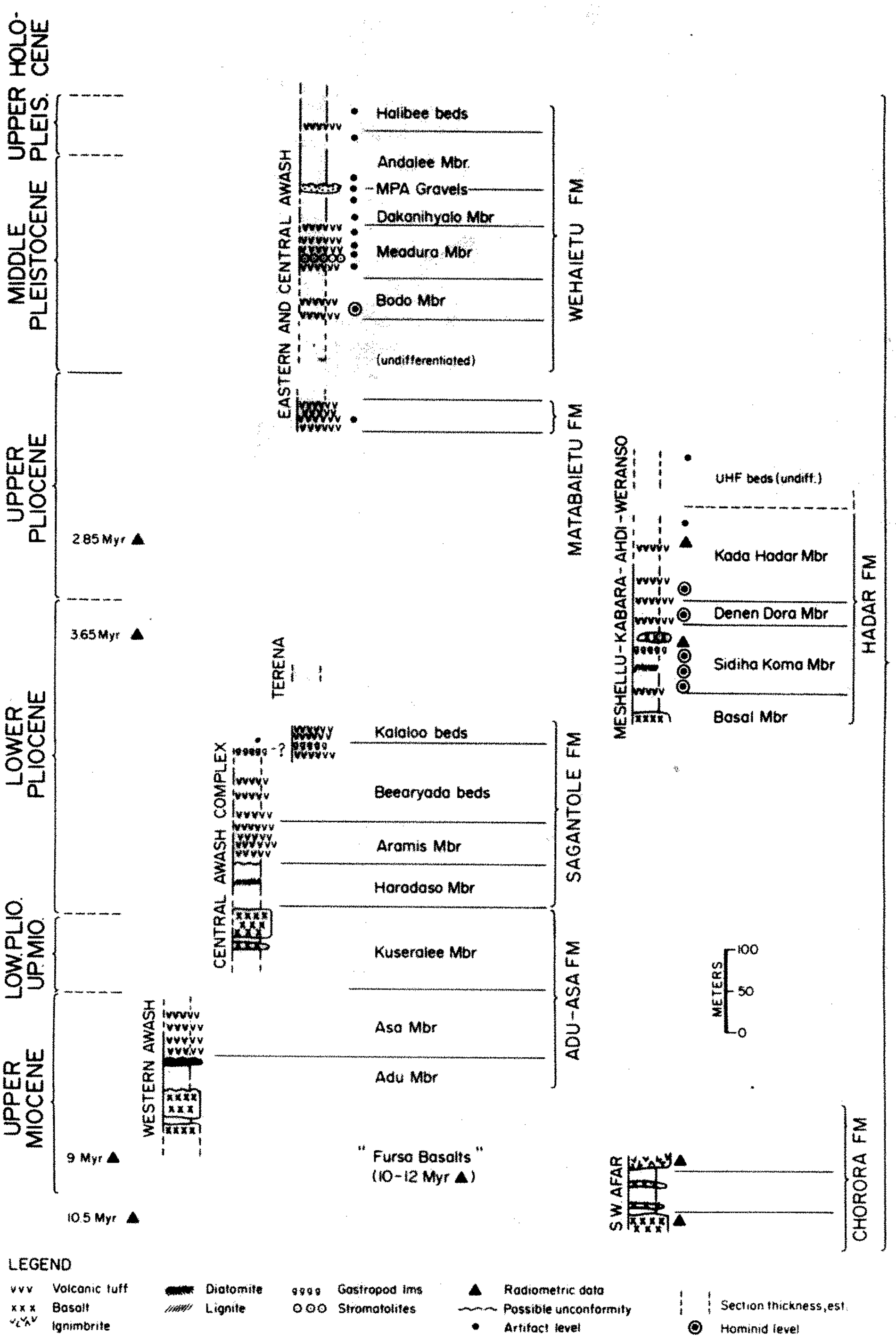

Fig. 2 Stratigraphy of the Awash Group.

a

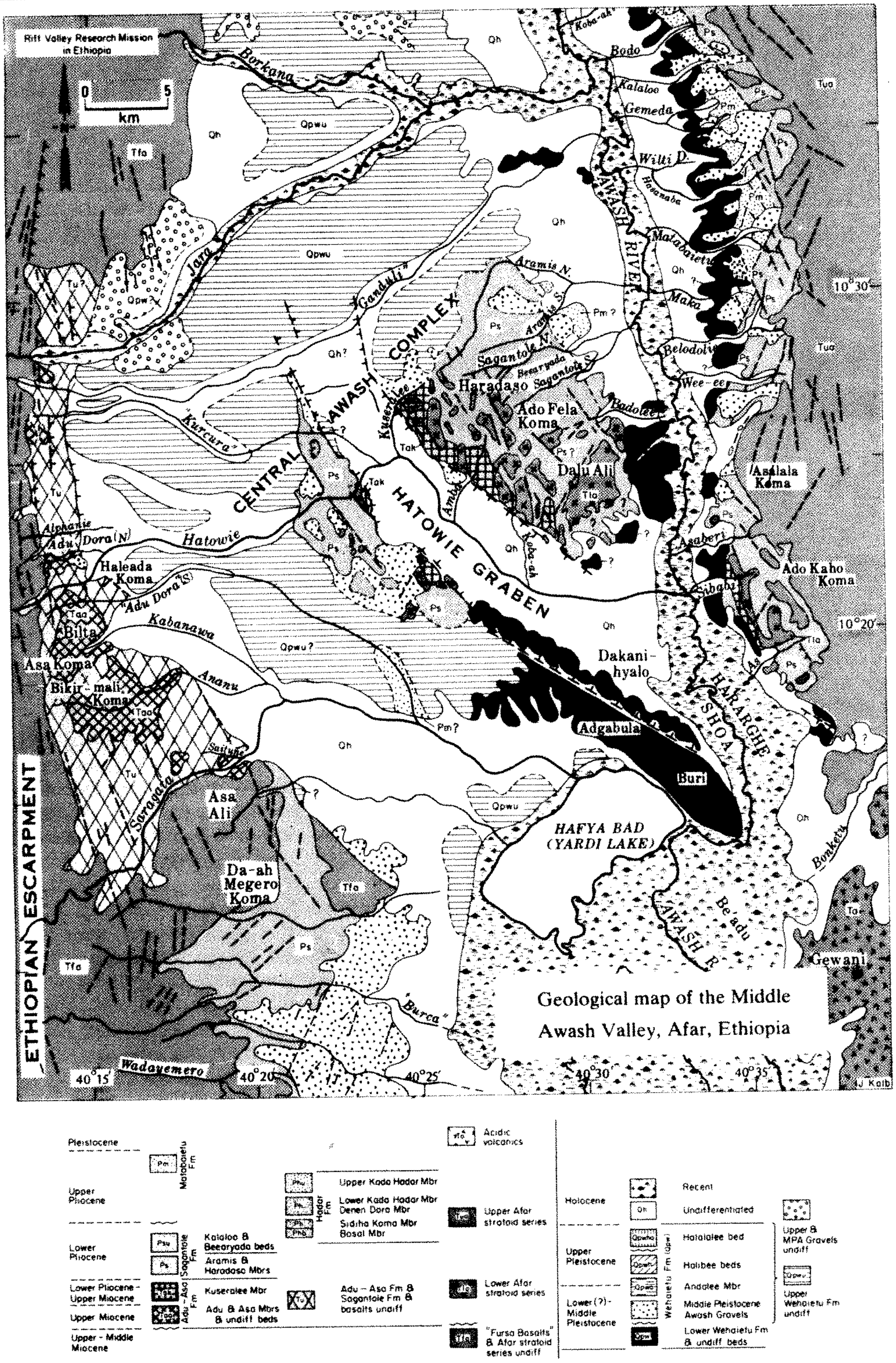

Fig. 3 *a*, Geological map of the Central Middle Awash Valley (southern sector). *b*, Geological map of the Central Middle Awash Valley (northern sector).

Kalaloo beds: A minimum of 14–15 m of strata. Overlying the gastropod limestone (P.24–26)/between Kalaloo and Bodo Streams, the base is marked by a widely traceable coarse or lapilli tuff (10–35 cm), followed by a variable sequence of tan silts with siltstone, sand, and microconglomerate lenses, with grey and brown clay upwards. Several tan, silty tuff layers (0.5 m to 3.5 m in a channel at mid-sequence) are present. Some disconformable strata may exist in the upper portion.

Hadar Formation: Predominantly middle Pliocene[10,28,29], and up to 270 m thick, this unit crops out well north of the Sagantole Formation (Fig. 3*b*), and, because of regional subsidence, at lower elevations (P.40,48). If physical correlation is possible betweeen the Hadar and Sagantole Formations, it would probably require tracing the Kada Damoumou basalt[30] (P.46) to basalts further south that intercalate the Sagantole Formation. The Kada Damoumou basalt seems to correlate with basalt to the SE; correlation further south is complicated by erosion of overlying beds, and intervening faults and younger beds. Basalt in a stream-bed ~5 km SW of the Ounda Meshellu–Awash confluence appears to lie at the base of the Hadar Formation (P.40) (Fig. 2).

Upper Hadar Formation (UHF) beds, undifferentiated: At least 50 m thick, these beds crop out north of Hadar in the drainages of Ledi, Geraru and Weranso Streams and the Mile River[14,15]. These beds, first surveyed in 1971–74 by three of us (J.K., D.P., E.O.), and in part by Taieb[14,15], occur downdip to

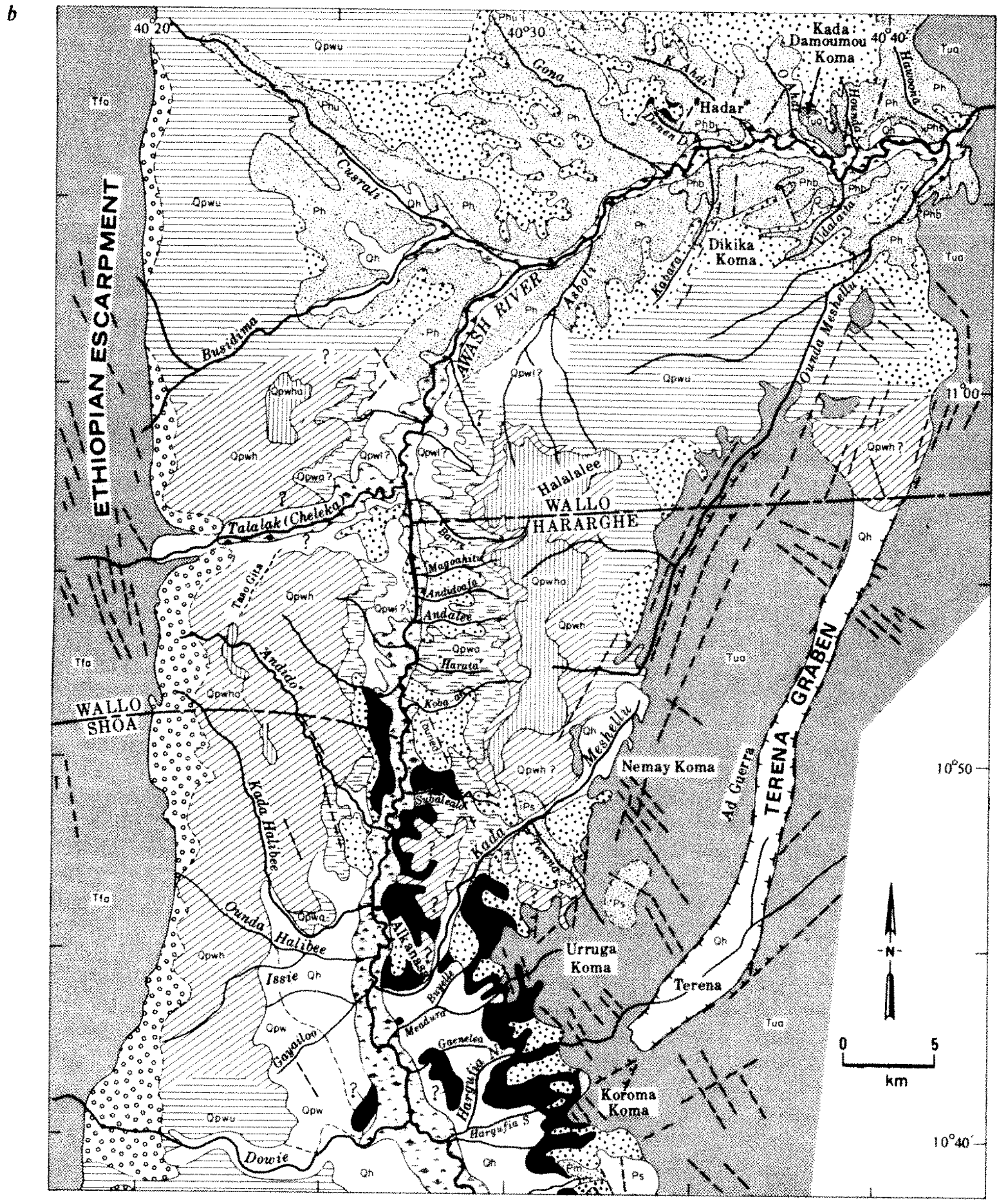

Fig. 3 (*cont.*)

or are downfaulted in relation to the Hadar Formation (P.48). They are broadly similar to the described strata in the upper Hadar Formation, but contain fauna associated with younger units[10].

Matabaietu Formation: Late Pliocene[10], at least 52–57 m thick (Fig. 2), and best exposed in the eastern Awash (Fig. 3*a*). In fault contact or unconformable with the Sagantole Formation (P.70,73). At Matabaietu, the lower unit consists of 34–39 m of up to three variable, discontinuous, cyclic units of clay, sand and tuff deposition. At the base are predominantly reddish-brown clays (23–28 m thick), with some mottled darker clay. Sands (up to 2 m) are irregularly bedded, calcareous and contain gravel lenses, cross-beds and plant casts. Tuffs are up to 2.5 m, sandy or silty, reworked, well-weathered and contain gravels, plant casts and limestone concretions. The upper tuff, from which an Oldowan chopper was recovered[10], is referred to as the 'chopper tuff'. The upper unit (14 m) outcrops west and updip from the chopper tuff, which it appears directly to overlie, although a fault contact is possible. Strata consist of: tan and grey clays (12 m) with small concretions and plant casts; argillaceous tuffs with plant casts; and some microconglomerate lenses. The unit is capped by up to 4 m of (unconformable?) pebble conglomerate and minor brownish-grey clay. Similar strata exist in the uppermost levels of Hadar and in the UHF beds. Based on faunal considerations, the upper UHF beds may be of similar age[10].

Bikirmali beds: Up to 30–40 m or more of poorly-sorted tuffaceous alluvium truncate the Asa Member at Bikirmali Hill (P.6) (Fig. 2*a*) and elsewhere. The stratigraphical position of these beds is uncertain; however, a late Pliocene age is inferred by fragmentary vertebrate remains (*Hexaprotodon*, progressive *Elephas recki*)[10]. Basic basalts (7–8 m) cap the sequence.

Lower Pleistocene (?) Awash conglomerate: It may be that only minor deposits document the period between the Matabaietu Formation and the Bodo Member (Wehaietu Formation). Their faunas clearly show the age difference between these two units[10]. Missing strata may be explained by faulting, and in part by erosional episode at the end of Matabaietu deposition, which may possibly be recorded by uppermost conglomerates at Matabaietu and Bodo; north of Hadar, conglomerates cap the UHF beds at various localities, perhaps the most prominent being at As Hill, 15 km NW of Hadar. Here massive (4–6 m thick), resistant conglomerates, some 35–45 m above the surrounding plain, truncate the UHF beds,

Lower (?) to Middle Pleistocene beds, undifferentiated: At Wilti Dora, a 3–4 m waterlain tuff overlies the Matabaietu Formation unconformably and is downthrown to the west by a normal fault. This tuff contains some fossils, including: *Kolpochoerus* sp., hypsodont *Hippopotamus* sp. and *E.* cf. *recki*, and the first appearance of *Equus* in the Awash Group. West of and apparently overlying the 'Equus tuff' are >14 m of largely unfossiliferous brown clays, with some conglomerate layers that extend southward and may be the same as sediments (estimated at 20–30 m thick) west of the conglomerates capping the Matabaietu Formation at Matabaietu. At Bodo, as at Wilti Dora, a thick tuff (Equus tuff?) appears to overlie the Matabaietu Formation unconformably and is offset by faults. Fossils from this tuff are *Equus* and a large *Theropithecus* (similar to a robust form from the Bodo Member) (C. Jolly, personal communication).

Wehaietu Formation: Early (?) to late Pleistocene[10], with an estimated thickness of 200–250 m. Exposed throughout the map area (Fig. 3*a*, *b*), between 500–650 m a.s.l. (Fig. 5). Wehaietu is a name in the Afar language used interchangeably for the Awash River. This formation is divided into (from bottom to top): the Bodo, Meadura, and Dakanihyalo Members, the MPA Gravels, the Andalee Member, and the informal Halibee beds (Fig. 2). The MPA gravels divide the formation into two readily distinguishable larger units, the lower and upper Wehaietu Formation.

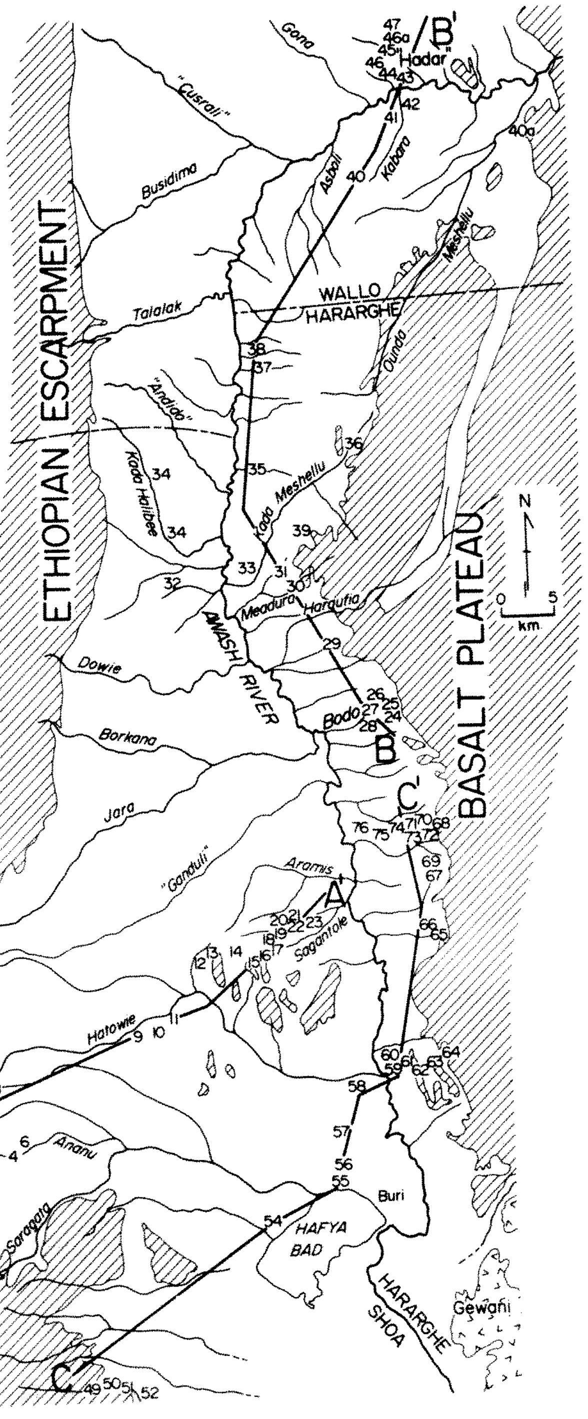

Fig. 4 Geological profile index map.

Bodo Member: At least 16–19 m of strata between the Bodo and 'Koba-ah' Streams (Fig. 3*a*, *b*). The base of the member, as presently defined, consists of the previously-described Upper Bodo Sand Unit[4] (UBSU) (P.28) that unconformably overlies thick, reddish-brown clays (Matabaietu Formation). Acheulian artefacts and fossils, including an archaic *Homo* cranium[3], are abundant throughout the lower half of the unit[10]. North of Bodo, the USBU is overlain by brown clays containing (barring any intervening faults) tuff lenses that wedge out to the west.

Meadura Member: A minimum of 45–50 m of strata between Hargufia and Meadura Streams (Fig. 3*b*). These strata have not been correlated directly with the Bodo Member because of intervening alluvium; however, because of lithological differences, the northward regional dip (almost certainly placing the Meadura beds higher stratigraphically) and faunal distinctions[10], these strata are treated as a separate unit. At Meadura, the lowermost strata may be those to the far east, altitudinally higher than the main (downfaulted?) outcrop areas to the west, in marginal grabens, and in adjacent areas to the south. To the west, a minimum of 35 m strata lie unconformably against basalts, or are downfaulted. Lithologies exhibit considerable lateral facies variation and are dominantly brown (sometimes mottled grey) and tan clays, tuffaceous silts and tuffs (0.6–1 m); fine- to coarse-grained sands (1–4.6 m) with gravel lenses; and poorly-sorted sandstone conglomerates (0.7–1.4 m). Tuffaceous deposits are concentrated in the upper sequence, as is abundant calcium carbonate material. The latter includes spheroidal stromatolite boulders (up to 1.5 m in diameter) with laminations and micro-structure similar to bacterial stromatolites (R. L. Folk, personal communication); these can be traced southwards to Hargufia[4]. Strata are broadly similar at Hargufia but may extend lower stratigraphically (P.29,30).

Middle Pleistocene beds, undifferentiated: Estimated 25–35 m of strata. At Buyelle (P.31), the Meadura Member is overlain by at least 15 m of predominantly orangish-brown, fine-grained sediments that abut basalts (Fig. 3*b*). Between 'Alkanasa' (P.33) and 'Subalealo' (P.35) are a minimum of 10–15 m predominantly sandy sediments with tuff layers. Thick, well-bedded tuffs, tan silts and clays occur at the base of the Subalealo sequence; to the north, these beds appear truncated by the MPA Gravels; immediately south, they may be overlain unconformably by the upper Wehaietu Formation (?). Fauna from Subalealo is consistent with that in the Meadura Member. In the Hadar area, terraces wedged between the Hadar Formation and the MPA Gravels, bearing Acheulian tools[31,32] (P.46a), may be assigned to the lower Wehaietu Formation.

Dakanihyalo Member: At least 15–20 m of strata that occupy the SE portion of the WHH (Fig. 3*a*). The higher stratigraphical position of this unit relative to the Meadura Member is inferred by its central and generally lower altitudinal position (P.56,57) in the Awash basin, and its associated fauna[10]. At Dakanihyalo and to the west, sediments are commonly buff and reddish-brown discontinous beds dominated by medium to very coarse, cross-bedded sandstones (locally up to 5 m thick), and pebble conglomerates, with silt and clay interbeds.

Middle Pleistocene Awash Gravels: 1–4 m thick, these gravels are ubiquitous in the Middle Awash[31] (Figs 2, 3*a*, *b*) truncating the lower Wehaietu Formation or older units. They are named the MPA Gravels to distinguish them from late Pleistocene and Holocene gravels[33] as well as from older gravels. Their relationship to surrounding units is best seen between Ounda Meshellu and 'Barre' Streams (Fig. 3*b*).

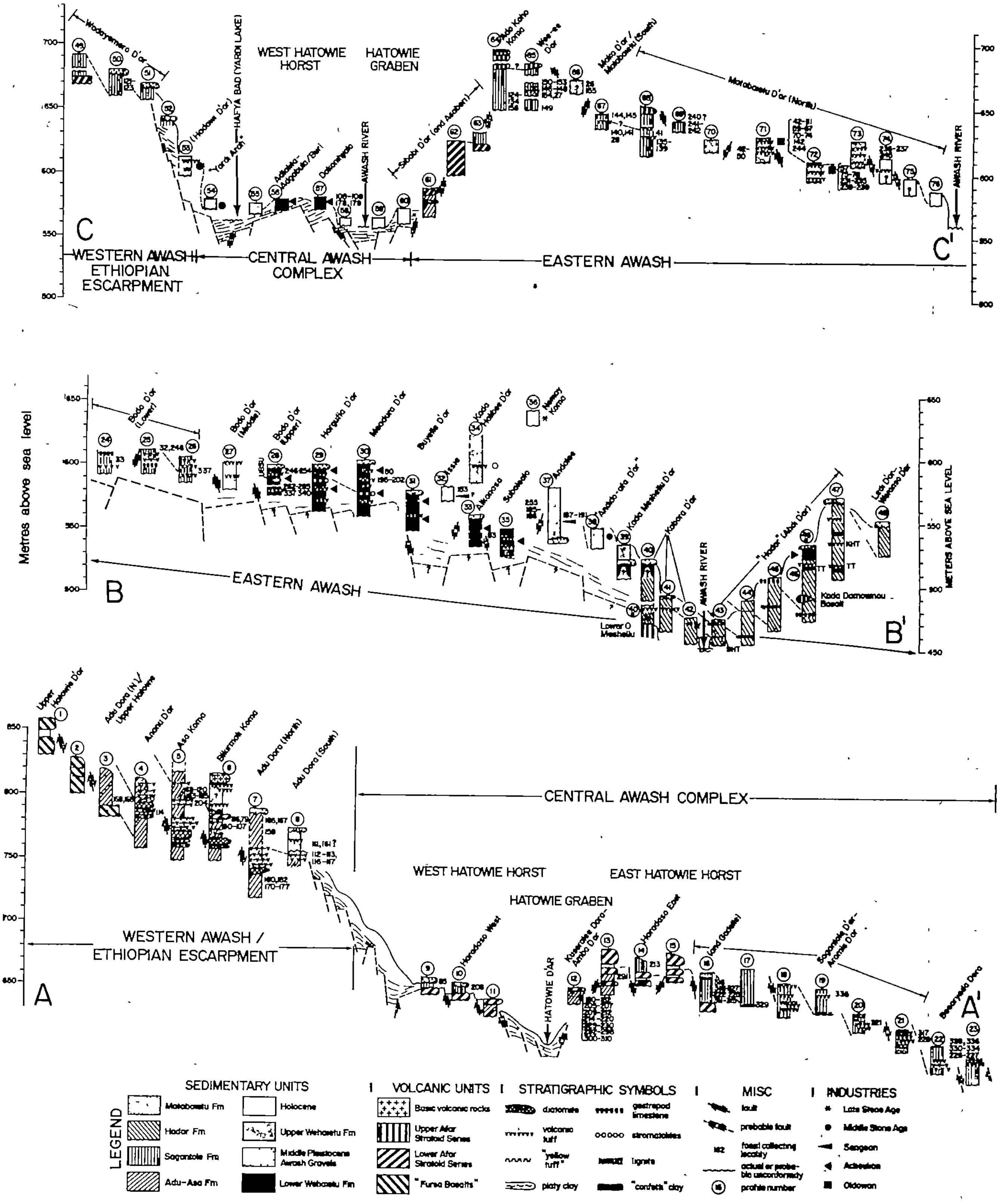

Fig. 5 Composite geological profiles of the Middle Awash Valley.

Andalee Member: Estimated to be a minimum of 55–60 m thick. In the northern map area (Fig. 3*b*), these strata appear to onlap progressively the northward-dipping MPA Gravels, forming an unconformable wedge that thickens to the north (and in the central part of the basin). At Andalee, a preliminary assessment of the local geology has been made[5]. The lower sequence rests on the MPA Gravels (P.37) and consists of 6–8 m of sand, silt and clay interbeds with calcified concretions, microconglomerate lenses, and a rich concentration of very small- to medium-sized vertebrates, associated with a Sangoan-like tool industry[5,10]. The upper sequence is >34 m thick and consists of massive brown clay and silt with cross-bedded sands and gravel lenses.

At Issie, in beds that appear to lie just below the basal tuff (?) of the Halibee beds, is another locality rich in very small- to medium-sized vertebrates associated with a diverse tool industry[5,10]. These are contained within 2–3 m of tan loosely-consolidated silts and clays with minor sands.

Halibee beds: Estimated to be up to 35–45 m of strata conformable with the Andalee Member (P.34), as best observed between Kada Halibee Stream and the Talalak River (Fig. 3*b*). These beds are undifferentiated and informally defined. Generally, at the base seems to be a widely traceable tuff layer, overlain by predominantly light-coloured, fine-grained, loosely-consolidated sediments containing some tuffs and darker clay, sand and gravel layers.

Halalalee bed: Mantling the Halalalee plain (Fig. 3*b*), at the top of the Halibee beds, is 1–2 m of unconformable, dark-brown and grey clayey layer that may be a palaeosol. Only remnant patches of this bed occur in the western Awash, overlaying the upper Halibee beds.

Holocene beds: Deposits that postdate the Halibee beds, and contain late Stone Age artefacts[10] and vertebrate remains, occur throughout the Middle Awash (Fig. 3*a*, *b*) at progressively lower altitudes, between ~645 and 490 m a.s.l. At Nemay Koma, in the uppermost catchment of Kada Meshellu Stream (Fig. 3*b*) (P.36), between ~630 and 645 m a.s.l., are at least several metres of predominantly tan fine-grained sediments unconformably overlying Pliocene basalt and strata. Along the SE margin of the map area near Gewani (Fig. 3*a*) are 4–8 m of deposits that represent a lake terrace at least 575 m a.s.l. These deposits are diatomaceous and rich in calcium carbonate and stromatolitic material[13]. At Mero Buri, south of Hafya Lake some 14–16 km, are 3–4 m of light-brown silts and sands occurring several metres above the modern Awash floodplain.

Palaeoenvironments

The base of the late Miocene Adu-Asa Formation is marked by fluvio-lacustrine deposition in the lower Adu Member. Massive diatomite formation in the upper Adu Member indicates distinct lake development. The end of the Adu period is marked by erosion (localized?) and an abrupt onset of massive tuff deposition in the Asa Member, probably associated with widespread volcanic (and hydrothermal) activity, regional subsidence and an eastward migration of lacustrine deposition. This period may have coincided with or slightly preceded one of widespread tectonism and renewed spreading in the southern Red Sea in the late Miocene[35].

The thickness and stratification of the tuffs in the Asa Member combined with minimal diatomite formation and fluvial layers, indicate that the Adu-Asa lake environment probably entered a period of instability, decreasing depth and increasing fluvial influences. The upper Asa Member suggests a return to alluvial conditions and a tapering off of volcanic activity. The Kuseralee Member indicates predominantly fluvial deposition; this was interrupted, and the Adu-Asa Formation sealed, by massive extrusion of LASS basalt lavas during the latest Miocene to earliest Pliocene[10].

Strata comprising the bulk of the Haradaso Member suggest a dominantly progradational depositional pattern (lake margin, marsh, stream) that may reflect adjustments to regional subsidence. The Aramis Member and Beearyada beds appear dominated by shallow and marginal lacustrine environments, with episodes of fluvial and fluvio-deltaic deposition; the Kalaloo beds indicate predominantly lake margin and alluvial deposition. Tuffs throughout these units indicate continuous volcanic activity, as do intercalated UASS basalts.

The Hadar Formation generally reflects a northeastwards migration of the Awash deposystem during the Pliocene, indicated by a pattern of basin expansion at Hadar during the middle Pliocene, and progradation in the late Pliocene (cf. ref. 28). This accompanied the well-documented period of extensive graben development and subsidence in the central Afar during the Pliocene (see refs 21, 22).

The predominantly fluvial deposits in the upper Hadar Formation also appear dominant in the UHF beds and the Matabaietu Formation (and the Bikirmali beds) and point to a prolonged period of alluviation and some downcutting in the late Pliocene, accompanying a change in base level, tectono-volcanic activity, an eastward migration of lacustrine deposition (especially evident at Geraru[15]) and generally drier conditions. This period may have been followed by a major episode of clastic deposition and erosion in the early Pleistocene.

It is clear that by the time of deposition of the lower Wehaietu Formation in the early (?) to middle Pleistocene, the Middle Awash had undergone major structural and geomorphic changes with deposition concentrated at distinctly lower elevations and further north. Whereas the fluvial deposits at Bodo[4] and the Acheulian tool-bearing terraces at Hadar indicate alluviation and downcutting, the calcium carbonate-rich deposits and stromatolites stretching from Hargufia to Meadura indicate a period of widespread transgressive lacustrine deposition. The texture of the stromatolites suggests bacterial growth enhanced by geothermal waters (see, for example, ref. 36); their spheroidal shape suggests a lacustrine setting similar to that described for stromatolites near Lake Turkana[37]. Strata overlying the Buyelle–Alkanasa beds, including the Dakanihyalo Member, suggest predominatly fluvial deposition. Associated tuffs throughout the lower Wehaietu Formation indicate continued volcanic activity, probably from silicic centres near Gewani[19,20] and elsewhere; likewise, faults and tilted strata indicate tectonic activity.

The MPA Gravels indicate major peneplanation and extensive downcutting during an apparently prolonged and major dry period, probably during the late-middle Pleistocene[38]. At this time, strata were heavily eroded, and an extensive, northward-sloping pediment was created, such that the upper Wehaietu Formation onlapped the MPA Gravels from north to south. The lower Andalee Member (and its associated fauna) suggests deposition initially occurred in a sub-arid environment much like the modern Awash Valley[5]. Following deposition of the Halibee beds and continued tectono-volcanic activity, the Awash was again subjected to regional downcutting. This began apparently at the end of the Pleistocene and continued during successive dry periods during the Holocene (compare with refs 33, 34, 38). Intervening wetter periods seem to be indicated by (lacustrine?) deposits at Nemay Koma and near Gewani. Those near Gewani are equivalent in age to transgressive lake deposits described in the central Afar[13,33]. An early Holocene lake in the Gewani area would extend possibly over much of the depressed area extending from Sibabi to the basalt plateau 44 km to the south (Fig. 3*a*).

The palaeogeography of the Middle Awash indicates a deposystem that has continuously migrated towards lower and more northeasterly positions from the late Miocene to the present. Basin development was in concert with subsidence and rotation of host structures controlled by crustal attentuation and plate movements in the triple junction. This interaction of deposition with tectonics is reflected in the movement of lake basins to the NE, as well as by major changes in base level that amplified the effects of erosion and downcutting during dry periods.

J.K. acknowledges assistance from: FORGE, the Wenner-Gren Foundation for Anthropological Research, the Explorer's Club, and the Office of International Geology, USGS. J.K., S.T., A.M. appreciate assistance from the Vertebrate Paleontology Laboratory, Texas Memorial Museum. We thank the following Ethiopian institutions: Ministry of Culture and Sports Affairs, Ministry of Mines, Addis Ababa University, Commissions for Higher Education and Science & Technology and the Development through Cooperation Campaign, also colleagues and associates of RVRME, especially Dejene Aneme and Ketema Kidane; also the late Alfred Kelleher, Lita Osmundsen, Karl Butzer and Sharon McKern, and C. J. Jolly, Wann Langston Jr, J. A. Wilson and W. A. Muehlberger for helpful comments.

Received 9 February; accepted 6 April 1982.

1. Kalb, J. E. *Sinet: Eth. J. Sci* **1,** 87–98 (1978).
2. Taieb, M., Johanson, D. C., Coppens, Y. & Aronson, J. L. *Nature* **260,** 289–293 (1976).
3. Conroy, G., Jolly, C., Cramer, D. & Kalb, J. *Nature* **276,** 67–70 (1978).
4. Kalb, J. E. *et al. Palaeogeogr. Palaeoclimatol., Palaeoecol.* **30,** 107–120 (1980).
5. Kalb, J. E., Jaeger, M., Jolly, C. J. & Kana, Berhane. *J. Archaeol. Sci.* (in the press).
6. Kalb, J. E. (ed.) *Rift Valley Research Mission in Ethiopia, Report 8, Annual Report 1975–1976* (Ethiopian Ministry of Culture and Sports Affairs, Addis Ababa, 1976).
7. Kalb, J. E. (ed.) *Rift Valley Research Mission in Ethiopia, Report 23, Annual Report 1976–77* (Ethiopian Ministry of Culture and Sports Affairs, Addis Ababa, 1976).
8. Kalb, J. E. & Jolly, C. J. *Garyounis Sci. Bull.* (in the press).
9. Tebedge, Sleshi, thesis, Univ. Texas at Austin (1981).
10. Kalb, J. E. *et al. Nature* **298,** 25–29 (1982).
11. Gortani, M. & Bianchi, A. in *Missione Geologia dell'Azienda Generale Italiana Petroli, (A.G.I.P.) nella Dancalia Meridionale e Sugli Altipiani Hararini (1936–1938): Illustrazione Geologica.* Vol.1, 132–133 (Accademia Nazionale dei Lincei, Roma, 1943) (reprinted 1973).
12. Gortani, M. & Bianchi, A. in *Missione Geologia dell'Azienda Generale Italiana Petroli (A.G.I.P.) nella Dancalia Meridionale e Sugli Altipiani Hararini (1936–1938): Atlante Geologico* Vol. 1 (Accademia dei Lincei, Roma, 1943) (reprinted 1973).
13. Taieb, M. thesis, Univ. Paris VI (1974).
14. Taieb, M., Coppens, Y., Johanson, D. C. & Kalb, J. *C. r. hebd. Séanc. Acad. Sci., Paris* **275D,** 819–822 (1972).
15. Taieb, M., Coppens, Y., Johanson, D. C., Bonnefille, R. & Kalb, J. *C. r. hebd. Séanc. Acad. Sci., Paris* **279D,** 735–738 (1974).
16. United Nations *Investigations of Geothermal Resources for Power Development: Geology, Geochemistry, and Hydrology of Hot Springs of the East African Rift System within Ethiopia* (U.N.P.D., New York, 1973).
17. U.S. Army Topographic Command, Joint Operations Graphic (Ground) (1/250,000), Series 1501, Sheets NC 37-3 and 4, NC 17-7 and 8, NC 37-11 and 12 (Defense Mapping Agency, Topographic Centre, Washington, D.C., 1972).
18. Zanettin, B. & Justin-Visentin, E. in *Afar Depression of Ethiopia* (eds Pilger, A. & Rösler, A.) 300–309 (Schweizerbart'sche, Stuttgart, 1975).
19. Varet, J. *Geology of Central and Southern Afar,* 19–27 (C.N.R.S, Paris, 1978).
20. *Geological Map of Central and Southern Afar,* 1/500,000 (C.N.R.S-C.N.R, Paris 1975).
21. Tazieff, H., Varet, J., Barberi, F. & Giglia, G. *Nature* **235,** 144–147 (1972).
22. Barberi, F., Ferrara, G., Santacroce, R. & Varet, J. in *Afar Depression of Ethiopia* (eds Pilger, A. & Rösler, A.) 28–54 (Schweizerbart'sche, Stuttgart, 1975).
23. Kalb, J. E., Oswald, E. B., Mebrate, A., Tebedge, S. & Jolly, C. J. *Newsl. Stratig.* (in the press).
24. Berggren, W. A. & Van Couvering, J. A. *Palaeogeogr. Palaeoclimatol. Palaeoecol.* **16,** 1–216 (1974).
25. Haq, B. U., Berggren, W. A. & Van Couvering, J. A. *Nature* **269,** 483–488 (1977).
26. Butzer, K. W. & Isaac, G. L. in *After the Australopithecines: Stratigraphy, Ecology, and Cultural Change in the Middle Pleistocene* (eds Butzer, K, W, & Isaac, G. L.) 901–903 (Mouton, The Hague, 1975).
27. Sickenberg, O. & Schönfeld, M. in *Afar Depression in Ethiopia* (eds Pilger, A. & Rösler, A.) 277–284 (Schweizerbart'sche, Stuttgart, 1975).
28. Aronson, J. L. & Taieb, M. in *Hominid Sites: Their Geologic Settings* (eds Rapp, G. Jr & Vondra, C. F.) 165–195 (Westview, Colorado, 1981).
29. Taieb, M., Johanson, D. C., Coppens, Y. & Tiercelin, J. J. *C. r. hebd. Séanc. Acad. Sci., Paris* **287,** 259–461 (1978).
30. Aronson, J. L. *et al. Nature* **267,** 323–327 (1977).
31. Corvinus, G. *Nature* **256,** 468–471 (1975).
32. Corvinus, G. *Nature* **261,** 571–572 (1976).
33. Gasse, F. & Street, F. A. *Palaeogeogr. Palaeoclimatol., Palaeoecol.* **24,** 279–325 (1978).
34. Butzer, K. W., Isaac, G. L., Richardson, J. L. & Washbourn-Kamau, C. *Science* **175,** 1069–1076 (1972).
35. Girdler, R. W. & Styles, P. *Nature* **247,** 7–11 (1974).
36. Folk, R. L. & Chafetz, H. S. *Geol. Soc. Am., Ann. Meet. Abstr.* **428** (1980).
37. Johnson, G. D. *Nature* **247,** 520–523 (1974).
38. Hays, J. D., Imbrie, J. & Shackleton, N. J. *Science* **194,** 1121–1132 (1976).

Fossil mammals and artefacts from the Middle Awash Valley, Ethiopia

Jon E. Kalb[*], C. J. Jolly[†], Assefa Mebrate[‡], Sleshi Tebedge[§], Charles Smart[‖], E. B. Oswald[¶], Douglas Cramer[#], Paul Whitehead[**], C. B. Wood[††], G. C. Conroy[‡‡], Tsrha Adefris[†], Louise Sperling[§§], & Berhane Kana[‖‖]

[*] Vertebrate Paleontology Laboratory, Balcones Research Center, The University of Texas, 10100 Burnet Road, Austin, Texas 78758, USA
[†] Department of Anthropology, New York University, New York, New York 10003, USA
[‡] Department of Systematics & Ecology, The University of Kansas, Lawrence, Kansas 66044, USA
[§] Department of Geological Sciences, The University of Texas, Austin, Texas 78712
[‖] Department of Vertebrate Zoology, Academy of Natural Sciences, Philadelphia, Pennsylvania 19103, USA
[¶] Bureau of Land Management, Albuquerque, New Mexico 87107, USA
[#] Department of Cell Biology, New York University Medical Center, New York, New York 10003, USA
[**] Osborn Memorial Laboratory, Department of Biology, Yale University, New Haven, Connecticut 06511, USA
[††] Providence College, Providence, Rhode Island 02918, USA
[‡‡] Division of Biology and Medicine, Brown University, Providence, Rhode Island 02912, USA
[§§] Department of Anthropology, McGill University, Montreal, Quebec, Canada H3A 2K6
[‖‖] Department of Biology, Addis Ababa University, Addis Ababa, Ethiopia

A review of fossil mammalian faunas from the Middle Awash indicates they span most of the later Neogene and document evolutionary change in several mammalian groups, especially Primates, Proboscidea and Artiodactyla. Oldowan artefacts first appear in the late Pliocene, while Acheulian and later industries and apparent occupation sites occur in Pleistocene beds.

INVESTIGATION of the Middle Awash deposits by the Rift Valley Research Mission in Ethiopia[1,2] (RVRME) resulted in the documentation of 333 fossil localities and hundreds of archaeological occurrences. Fossil and artefact localities were plotted on air photographs (1 : 60,000) and/or site maps (1 : 6,000) and in stratigraphical sections that permitted them to be precisely located geographically and inserted in the regional geological sequence. Detailed locality maps and reports were submitted to the Ethiopian Government[3,4].

Approximately 2,500 fossils were collected and studied in the Ethiopian National Museum and the Paleobiology Research Laboratory at Addis Ababa University. Only limited samples of artefacts were recovered. Fossils and artefacts are stored in the Ethiopian National Museum. Many additional fossil specimens, especially skulls of large ungulates that were too bulky to be collected with the resources at hand, were left *in situ* (and often photographed) for future collection. When added to the previously described data from the Hadar Formation, these collections provide a biostratigraphical sequence that documents long stretches of the evolutionary history of the Middle Awash fauna since the late Miocene.

Fauna and biostratigraphy

Mammalian taxa identified in the collections are systematically listed in Table 1 and are designated according to stratigraphical unit. Table 2 provides the distribution of major taxa according to the order of their first appearance in the regional sequence, inclusive of taxa from the Chorora[5] and Hadar Formations[6,7]. Most work has been carried out on the primates, Proboscidea and Artiodactyla. Previous accounts of the various vertebrate taxa are contained in reports to the Ethiopian Government[3,4], regional summaries[1,8], site reports[9,10], and studies of individual taxa[11–13]. More detailed treatment will be reported elsewhere[14].

Table 1 Systematic faunal list, Awash Group (newly described units only)

- **Mammalia**
  - Chiroptera indet. (As)
- **Primates**
  - Cercopithecidae
    - Cercopithecus cf aethiops (An, Ani)
    - Cercopithecus sp. ('Ha', Me)
    - Papio (=Dinopithecus cf. ingens) (MA)
    - Papio cf. hamadryas (Bo)
    - Theropithecus oswaldi ('Ka', MA, Bo, An)
    - Parapapio sp. (Ka)
    - cf Papionini indet. (small) (Ku, Ha)
    - Colobus cf. guereza (An, Ani)
    - cf. Paracolobus chemeroni (As, Ku)
    - Paracolobus chemeroni (MA)
    - Colobinae indet. (cf. Libypithecus) (Ku)
    - Colobinae indet. (MA)
  - Hominidae
    - Homo sapiens cf. rhodesiensis (Bo)
- **Rodentia**
  - Muridae
    - Murinae indet. (An, Ani)
  - Cricetidae
    - Gerbillinae indet. (An)
    - cf. Dendromurinae (An)
  - Thryonomyidae indet (Bo)
    - cf Thryonomys sp. (An)
  - Hystricidae
    - cf. Hystrix sp. (MA, An)
  - Rodentia indet (As, Ku, 'Ha', MA, Bo, Me, An, Ani)
- **Carnivora**
  - Canidae
    - gen. et sp. indet. (An)
  - Mustelidae
    - Lutrinae indet. (An)
  - Felidae
    - Megantereon sp. (MA)
    - Dinofelis sp. (MA)
    - gen. et sp. indet. (Ku)
  - Hyaenidae
    - Crocuta crocuta ultra (MA)
    - Crocuta sp. (An)
    - gen et sp. indet ('As')
  - Carnivora indet (Ku, Ha, Bo, An)
- **Proboscidea**
  - Gomphotheriidae
    - Anancus sp. (Ad, As, Ku, Ha, Ar/Be, Be, Ka)
  - Elephantidae
    - Stegotetrabelodon cf. orbus (As)
    - 'Stegodibelodon schneideri' (Ad)
    - Primelephas cf. gomphotheroides (AA)
    - aff. Mammuthus subplanifrons (Ku)
    - Mammuthus subplanifrons (Ar/Be)
    - Loxodonta adaurora (Ar/Be)
    - Elephas cf. ekorensis (Be, Ka)
    - Elephas recki (MA, Et, Bo, Me, Da, An)
- **Deinotherioidea**
  - Deinotheriidae
    - Deinotherium bozasi (SA, MA)
    - Deinotherium sp. (small) (As, Ku)
- **Perissodactyla**
  - Equidae
    - Hipparion cf. primigenium (As)
    - Hipparion cf. afarense (MA)
    - Hipparion sp. (AA, SA, Bo, An)
    - Equus cf. numidicus (Et)
    - Equus sp. (Bo, Da, An)
  - Rhinocerotidae
    - Diceros bicornis ('As')
    - Ceratotherium cf. praecox (Ku)
    - Ceratotherium cf. simum (MA, Bo, 'Me')
    - gen. et sp. indet (AA, SA, Bo, Me, Ani)
- **Artiodactyla**
  - Suidae
    - Phacochoerus aethiopicus (Me, An, Ani)
    - Kolpochoerus sp 'A' (Ad, As)
    - Kolpochoerus sp. 'B' (cf. K. 'majus') (Bo, An)
    - Kolpochoerus olduvaiensis (Da)
    - Kolpochoerus afarensis (Ar/Be, MA)
    - Kolpochoerus limnetes (MA, Bo, 'Me')
    - Metridiochoerus jacksoni (MA)
    - Metridiochoerus cf. jacksoni (Bo)
    - Notochoerus euilus (MA)
    - Notochoerus cf. euilus ('Be')
    - Notochoerus scotti (MA)
    - Nyanzachoerus kanamensis (Ku, SA)
    - Nyanzachoerus jaegeri (Ar/Be, Be)
    - Nyanzachoerus cf. tulotos (Ad, As)
  - Hippopotamidae
    - Hippopotamus sp. (MA, Et, Me, Da)
    - Hippopotamus cf. gorgops (Bo)
    - Hexaprotodon cf. harvardi (AA, SA)
    - Hexaprotodon sp (small) (MA)
  - Giraffidae
    - Giraffa cf. pygmaea (MA)
    - Giraffa cf. jumae (An)
    - Giraffa sp. (Bo)
    - Sivatherium maurusium (As, 'Ha', Ar/Be, MA)
    - gen. et sp indet. (Ku)
  - Bovidae
    - cf Ugandax gautieri (Ku)
    - cf. Pelorovis sp (Bo, An)
    - Bovini indet. (small) (An)
    - Bovini indet. (large) (Me, Da, Ani)
    - Miotragocerus sp. (As)
    - cf. Mesembriportax acrae (Ku)
    - Boselaphini indet. (AA, Be)
    - ?Caprini ('Me')
    - Tragelaphus sp. (Lothagam type) (As, Ku)
    - Tragelaphus sp. ('pre-nakuae') (Ku, Ha, 'Ka')
    - Tragelaphus cf nakuae (MA)
    - Tragelaphus cf. scriptus (An, Ani)
    - Tragelaphus sp (large) (Da, An)
    - Redunca sp. (Me, An, Ani)
    - Kobus cf. subdolos (As)
    - Kobus sp. (MA)
    - Kobus cf. ellipsiprymnus (Bo)
    - cf. Kobus leche (Bo)
    - Reduncini indet (AA, MA, Ani)
    - Hippotragini indet. (Ku, Ar/Be)
    - Aepyceros sp. (MA)
    - Aepyceros cf. melampus (Bo, An)
    - Alcelaphus cf. buselaphus (Bo)
    - Connochaetes sp. (Da)
    - Alcelaphini indet. (Ku, Ar/Be, MA, An)
    - Gazella sp. (Ar)
    - cf Gazella (Ku, MA, 'Me')

Formations: AA, Adu-Asa (inclusive), SA, Sagantole (inclusive); MA, Matabaietu. Sub-units. Ad, Adu; As, Asa, Ku, Kuseralee; Ha, Haradaso; Ar, Aramis; Be, Beearyada beds; Ka, Kalaloo beds, Et, Equus tuff; Bo, Bodo; Me, Meadura, Da, Dakanihyalo, An, Andalee; Ani, Andalee (Issie). Other· Provisionally assigned units in quotation marks.

The age of the Middle Awash units and their relationship to the wider African late Neogene biostratigraphical sequence can be estimated from their stratigraphical relationships and the composition of their faunas. These data are compatible with the few radiometric dates presently available from the Middle Awash. We anticipate that additional radiometric and palaeomagnetic data will provide a stronger chronological framework in the region.

The Chorora Formation is bracketed by radiometric dates of 10.5 and 9 Myr[5], and its fauna bears resemblances to that of the Ngorora Formation[15]. The Fursa basalts, which underlie the Adu-Asa Formation, are dated at 10–12 Myr[16]. The Lower Afar Stratoid Series (LASS) basalts[2], which immediately overlie the same formation, are as yet undated, but they (and the underlying Adu-Asa Formation) are clearly older than the Upper Afar Stratoid Series (UASS) basalts, whose maximum age is 4.4 Myr[17]. The Adu-Asa fauna is comparable with assemblages from late Miocene units in the Baringo basin—the Mpesida beds (±7 Myr), the Lukeino Formation (±6.5 Myr) and the Kaperyon Formation (±5 Myr)—and to the fauna from the Lothagam-1 beds[18–23]. The latter is conventionally dated to ±5.5 Myr[20]. More precise affinities of each member can be suggested, particularly based on Suidae and Probosicidea, although these must be regarded as hypothetical.

The faunas of the Adu and Asa Members both include a very primitive nyanzachoerine that has been referred to by Harris and White[23] as *Nyanzachoerus tulotos* and by A. F. Wilkinson (personal communication) as resembling *Bunolistriodon* (=*Kubanochoerus*) *massai*. This suid, together with the presence of *Stegotetrabelodon*, '*Stegodibelodon*', *Primelephas* and *Miotragocerus* suggests that the lower levels of the Adu-Asa Formation may be at least as old as the late Miocene Lothagam-1 beds or perhaps the Lukeino Formation. A late Miocene age is supported by a primitive *Anancus*—the first of four evolutionary stages for this genus in the lower Awash Group—similar to that found in Lothagam-1 (V. J. Maglio, personal communication), *Kobus* cf. *subdolus*, known from Langebaanweg[24], and indirectly by a primitive *Sus*-like suine identified as 'early' *Kolpochoerus* (H. B. S. Cooke, personal communication).

Stegotetrabelodonts are absent in the Kuseralee Member while an apparently more advanced *Primelephas* is present, as well as a primitive elephant retaining features of both *Mammuthus subplanifrons* and *Primelephas*. A more advanced form of *Anancus*, similar to *A. kenyensis*, has replaced that from the Asa Member, while *Nyanzochoerus kanamensis* has replaced *N.* cf. *tulotos*. A bovine similar to *Ugandax gautieri* from the lower Kaiso Formation[25] is present, as is *Mesembriportax*, known from 'E' Quarry, Langebaanweg[24]. A colobine monkey has similarities to *Libypithecus*, known from North Africa[26]. Overall, the Kuseralee fauna suggests a date later than Lothagam-1, but distinctly earlier than Lothagam-3, and very close to the Mio-Pliocene boundary (5 Myr[27]).

Fauna in the Sagantole Formation, which overlies the LASS basalts, is comparable with that of early Pliocene units in the Baringo Basin (lower Chemeron Formation, Aterır beds)[19,23,28], in the Lake Turkana basin (the Lothagam-3[23], Ekora and Kanapoi[20] beds, the Mursi Formation[29]) and, in South Africa, Langebaanweg[13,23,30,31]. Again, some tentative correlations within this span are suggested by the phylogenetically active pigs and elephants. The Haradaso fauna is probably older than Kanapoi, itself capped by a 4-Myr basalt[20]. The fauna of the Aramis Member and Beearyada beds is similar to that of Kanapoi itself, in particular in the combination of an early *Notochoerus* with *Nyanzachoerus jaegeri*, and the first appearance of *Loxodonta*, together with primitive *Elephas*. The Kalaloo beds incorporate more derived forms of two proboscidean lineages, a *Mammuthus* exhibiting features intermediate between *M. subplanifrons* and *M. africanavus* and a very advanced *Anancus* (unlike described species). The cercopithecoid monkey, *Theropithecus oswaldi*, is apparent for the first time, represented by a small and evidently primitive form. Very similar forms of *Theropithecus* and *Mammuthus* are also seen at Hadar (personal communications from E. Delson, and M. Beden).

The age of the Hadar Formation can be estimated at between ~4 and 2.5 Myr on the basis of included basalt and tuffs[32]. Its fauna has been compared with that of the Laetolil Formation (3.7–3.5 Myr), Members A–C in the Shungura Formation (3.0–2.4 Myr), the lower units at East Turkana and the Kaiso Formation[7,23,32–41].

Fauna in the Matabaietu Formation includes many forms absent from the Hadar Formation, and suggest a moderately younger age, and is generally comparable with that of Members D–F of the Shungura Formation (2.4–2.0 Myr)[29,32–39], the Chemoigut beds at Baringo[42], collecting unit 3 in the Koobi Fora Fm, Olduvai below the Lemuta Member[28,35,41] and the upper Kaiso Formation[23,43]. The UHF beds[2] are broadly similar in stratigraphical position and the fauna that they contain.

The Wehaietu Formation is clearly Pleistocene in age. The fauna of the lower units (Equus tuff; Bodo, Meadura and Dakanihyalo Members) may be comparable with Olduvai above the Lemuta Member[23,44], and Olorgesailie[45], while a combination of faunal, stratigraphical and archaeological evidence[2,10] suggests that the upper Wehaietu Formation above the Andalee Member is late Pleistocene, perhaps synchronic with the Abhe I beds of the central Afar[46]. A single ^{14}C date of 8,955±yr BP from the Holocene beds near Gewani[47] suggests that these beds are equivalent in age to lake sediments deposited in the central Afar between 5,000 and 11,000 yr BP[46].

Archaeology

We now provide a regional overview of the RVRME archaeological sites whose individual descriptions or stratigraphical contexts have been presented, or will shortly appear, elsewhere[1,2,9,10,48–50]. An Oldowan-like industry occurs in the lower Matabaietu Formation at Matabaietu[49] and Wilti Dora, where it is associated with large mammals, especially elephants.

Table 2 Distribution of major taxa in the Awash Group

Awash Group		Adu-Asa Fm			Sagan-tole Fm						Wehaietu Fm					
Taxa	Chorora Fm	Adu Mbr	Asa Mbr	Kuseralee Mbr	Haradaso Mbr	Aramis Mbr/Bee. beds	Kalaloo beds	Hadar Fm	UHF beds	Matabaietu Fm	Bodo Mbr	Meadura Mbr	Dakanihyalo Mbr	Andalee Mbr (Andalee)	Andalee Mbr (Issie)	Present (Middle Awash)
Colobus guereza														o	o	x
Cercopithecus aethiops														x	x	x
Tragelaphus cf. scriptus														x		x
Kolpochoerus cf. olduvaiensis													x			
Connochaetes sp													x			
Phacochoerus sp.												x			x	x
Kobus cf ellipsiprymnus												x			x	x
Elephas recki (stages 3-4)											x	x	x	o		
Theropithecus oswaldi aff. leakeyi											x			x		
Alcelaphus cf. buselaphus											x					x
Equus sp.											x	x	x	x		x
Thryonomys sp.											x			x		
Kolpochoerus sp. B ('majus')											x			x		
cf. Pelorovis sp.											x			x		
Paracolobus chemeroni										o						
Theropithecus oswaldi cf. oswaldi										x						
Notochoerus scotti										x						
Giraffa cf. pygmaea										x						
Kolpochoerus limnetes									o	x	x					
Hippopotamus sp									x	x	x	o	x			x
Metridiochoerus sp.									o	x	x					
Elephas recki (stage 2-3)									x	x						
Tragelaphus cf. nakuae									x	x						
Ceratotherium simum								x	x	o	o	o				
Giraffa jumae								x						o		
Kobus sp. A (Hadar type)								x								x
Aepyceros sp.								x	x	x	x			x		
Dinofelis sp.								x		x						
Crocuta sp.								x		x				o		x
Megantereon sp.								x		x						
Hipparion afarense								x		o						
Elephas recki (stages 1-2)								x								
Colobinae indet								x	x	x						
Parapapio sp.							x	x								
Anancus sp. ('stage D')							x									
Mammuthus sp. nov. ('Hadar type')							x	x								
Notochoerus euilus						o		x	o	x						
Deinotherium bozasi						x	x	x	x	x						
Kolpochoerus afarensis						x		x	o	x						
Loxodonta adaurora						o		x								
Nyanzachoerus jaegeri						x										
Elephas cf. ekorensis						o	o	x								
Anancus sp. ('stage C')						x										
cf. Papionini (small)				x	x											
Anancus sp. ('stage B')				x	x											
Ceratotherium of praecox				x				x								
Gazella sp.				o				o		o				x		x
Ugandax sp.				o				x								
cf. Mesembriportax acrae				o												
Mammuthus subplanifrons				o		x										
Cercophithecinae				x	x	x	x	x	x	x	x	x		x	x	x
Nyanzachoerus kanamensis				x	x	x	x	x								
Tragelephus sp. ('pre-nakuae')				x	x			x								
Colobinae indet. (cf. Libypithecus)				x												
Sivatherium maurusium			x			x	x	x	x	x						
Miotragocerus sp.			x													
Kobus cf. subdolus			x													
Deinotherium sp. (small)			x	x												
cf. Paracolobus chemeroni			x	x												
Primelephas gomphotheroides		o	x	x												
Anancus sp. ('stage A')		o	x													
Stegotetrabelodontinae		x	x													
Nyanzachoerus sp. A ('tutolos')		x	x													
Kolpochoerus sp. A		x	x													
Hexaprotodon sp.		x	o	x		x		x	x	x						
Hipparion cf. primigenium	x		x													
Hipparion sp.	x	x	x	x	x	x		x	x	x	o					
Dicerorhinus aff. leakeyi	x															
?Palaeotraginae	x															
?Gomphotherium sp.	x															
		Late Miocene		Late Miocene–Early Pliocene		Early Pliocene			Late Pliocene			Middle Pleis.			Late Pleis.	Present

×, Present; o, most similar or probable form present. Fm, Formation; Mbr, Member.

An early lithic site has also been reported in the upper Kada Hadar Member of the Hadar Formation[51], and two of us (J.K., E.O.) have recorded a diverse Oldowan assemblage in the UHF beds. Archaeological sites in the Wehaietu Formation document middle and late stages in the development of the Acheulian Industrial Complex[1,9,10,48,50]. In numerous localities, artefact assemblages occur in clusters in apparent primary association with the remains of single large- or medium-sized mammals, suggesting butchery sites. At other localities, the occurrence of both tools and debitage suggest tool manufacture. Tools are generally made of basalt, usually identifiable as of local derivation.

Assessment of the total early (?) to Middle Pleistocene Acheulian sequence in the lower Wehaietu Formation reveals that the Acheulian Complex is represented throughout >100 m of stratigraphical section, in an area of >25 km^2. From Hargufia to Subalealo alone, a distance of 20 km, individual tool occurrences are virtually continuous and number in the hundreds, with artefacts in the tens of thousands. In this area, at Bodo, and in the area surrounding Dakanihyalo and Adgabula, there are at least eight separate levels of Acheulian tools representing several distinct stages in the development of the Acheulian Complex. At all levels, tools are associated with faunal remains, often in direct context, suggesting butchery sites or living floors. At least one quarry/factory site is present (at Meadura), and the apparent occurrences of burned bone associated with tools [at Meadura (?), Adgabula] may prove to be among the earliest records for fire use known.

The MPA Gravels are associated with three distinct sets of artefacts. Within the gravels are highly rolled and weathered tools derived from older, Acheulian- (and Oldowan- ?) bearing deposits. Later artefacts occur on the surface of the gravels, derived as lag from the erosion of overlying sediments—a fact that has caused confusion about the age of this deposit[52,53]. Corvinus[54], working at Hadar, was the first to demonstrate clearly the stratigraphical relationship of these gravels to underlying *in situ* Acheulian tool-bearing deposits. Artefacts *in situ* on the surface and, reportedly, also within the MPA Gravels[54] may bear similarities to those from Andalee.

Artefacts from the lower sequence at Andalee represent one of the rare occurrences of an *in situ* 'Sangoan' industry and are associated primarily with very small- to medium-sized mammals[10]. Finally, the assemblage from Issie contains a diversity of retouched, well-formed tools that suggest later industrial influences. Middle Stone Age tools predominate in assemblages elsewhere in the upper Wehaietu Formation. Late Stone Age microlithic tools made from silicic materials occur throughout the Holocene beds, especially at Nemay Koma and Mero Buri. Ceramics occur at several localities on or adjacent to the Awash floodplain.

Discussion

When added to the previously-described Hadar Formation, the stratigraphical sequence running from the Adu-Asa Formation through the Wehaietu Formation provides one of the longest and most complete records of land vertebrate evolution yet recognized in the African Neogene. In particular, the formations and faunas newly described here document faunal evolution immediately preceding the well-known middle Pliocene of Hadar, and provide a uniquely continuous record of faunal, cultural and environmental change during the last half of the Pleistocene.

The faunas of the latest Miocene to earliest Pliocene and Middle to late Pleistocene of Africa are known from scattered sites that in most cases cannot be unambiguously arrayed against a single stratigraphical and chronological scale. Hopefully such a scale should be significantly improved now that the essentials of the stratigraphy of the Middle Awash deposits are known, intercalated as they are with volcanic materials. The collections reported here have already contributed to knowledge of the history of major taxa during this period. Among the Bovidae, for example, are a combination of genera (*Miotragocerus*, *Mesembriportax*, *Ugandax*) known separately from North, South and East Africa[24]. Among the Suidae, the succession of species in the genus *Nyanzachoerus* is documented, as is that for *Kolpochoerus*. The latter includes what may be the earliest African suine in the Adu and Asa Members, a primitive *Sus*-like form which tends to confirm Cooke's hypothesis about the origins of this genus[55]. Advanced kolpochoeres in the Wehaietu Formation provide insights into what may be among the latest representatives of this genus.

The Proboscidea include material that documents extensively some hitherto poorly known taxa. The gomphotheriid *Anancus* occurs throughout the Adu-Asa and Sagantole Formations, throughout >350 m of section. This occurrence is more extensive than any previously described from trans-Saharan Africa, and will ultimately form the basis of a full revision of the group, one of major biostratigraphical importance. At present, the Awash anancines are grouped into evolutionary stages, in the course of which molars become larger and more complex. Stages in the series serve to link sites such as Langebaanweg, Sahabi and Lothagam. Similarly, all recognized genera of Elephantidae are present in the Middle Awash. These include stegotetrabelodonts, as well as a variety of true elephantines that particularly document early stages of diversification of this subfamily. The biogeographical implications of the presence of elephantines in the late Miocene of East Africa, and their absence from the post-Messinian of Libya, are discussed elsewhere[8].

At least seven cercopithecid genera are recognized in the Middle Awash. Those accorded the most attention, species close to the modern *Cercopithecus* and *Colobus* monkeys, are exceptionally well-represented in the Andalee Member[10]. The excellent preservation and abundance of monkeys of these forms and age are unknown elsewhere. *Theropithecus* (*Simopithecus*) is also abundantly represented, in almost all known forms of *T. oswaldi*[56] (including, as a subspecies, *T. darti*). These range from a primitive form from Wee-ee (Kalaloo beds?), similar to material known throughout the Hadar Formation, to derived forms from the Wehaietu Formation that recall *T. o. mariae* and *T. o. leakeyi* from East Africa[56].

The recognition of extensive, highly fossiliferous strata antedating the Hadar Formation raises the possibility of documenting the earlier stages of hominid evolution. The hominid remains from the Hadar Formation have been vigorously touted as representatives of a single, thoroughly plesiomorphous hominid species ancestral to all known later forms[37]. This view is not unchallenged, others (see, for example, ref. 57) seeing representatives of two lineages in the collection. In any case, there is evidence that bipedal hominids were present earlier than 4 Myr at Kanapoi[58], and a hominid-like hominoid of uncertain affinities and unknown locomotor type is known from Lothagam-1[59]. It is hoped that the Adu-Asa Formation, which contains abundant fauna and apparently overlaps both Lothagam-1 and Kanapoi, will in time yield hominid specimens sufficiently complete to be assignable to an unambiguous position within the hominid clade, and thus to throw light on the timing and circumstances of the initial radiation of the family.

Like other East African sites, the Middle Awash sees the first appearance of clearly recognizable human artefacts in the late Pliocene (Matabaietu and upper Hadar Formations). When analysed more fully, the many occurrences of artefacts together with the remains of animals in this and the Wehaietu Formation will permit the testing of hypotheses about the relative importance of hunting, scavenging and fortuitous association in producing such archaeological sites in the Plio–Pleistocene. The hominid skull recovered from the base of the Wehaietu Formation at Bodo[11] not only provides critical evidence on archaic *Homo sapiens*; it also provides an unequivocal relationship between the morphological grade of tool-maker with a specific 'grade' in Acheulian technology. Overlying Acheulian tool-bearing units may yield other hominids of potentially more derived forms. Most significantly, the presence of ample tuffs throughout the Acheulian sequences allows for construction of a chronometric framework for both changing technologies and technicians, in what may well be the single most extensive Acheulian deposits described.

The diversified lithic 'Sangoan' industry at Andalee may document that transitional period between the longstanding conservatism of the Acheulian and the relative cultural diversity that characterizes the late Pleistocene[7]. The Andalee industry and its predominantly smaller fauna stand in marked contrast to the association of large tools and large game animals found in the Acheulian sites. Kalb *et al.*[9] speculate this may reflect adjustments to faunal turnover and changing man–land relationships following a prolonged arid period at the end of the Middle Pleistocene. Further studies at Andalee will elucidate this question, as will work at nearby Issie.

Overall, the succession of Acheulian, Sangoan and MSA industries in the Wehaietu Formation may provide a reasonable picture of man–land relationships during the middle and late Pleistocene during such crucial events as the first appearance of artificial fire in the region, the Acheulian–Sangoan transition, and thence to the MSA and LSA, and the appearance of modern humankind.

Conclusions

The Middle Awash Valley contains a largely complete record of mammalian evolution spanning at minimum the past 5–6 Myr. This record is contained within a stratigraphical sequence >1 km thick, making it one of the most extensive fossil sequences in the African Neogene. Evidence of hominid habitation, in the form of hominid fossils or artefacts, is found here in >0.5 km of beds, extending over ~4 Myr, from the lower levels of the Hadar Formation[37] to the Matabaietu Formation, through the Wehaietu Formation and the Holocene beds. The Middle Awash contains one of the most continuous records of hominid habitation in the Old World. Likewise, the stone tool occurrences extending throughout over 300 m of the Awash sequence, encompassing of the order of 2–2.5 Myr, from the upper Hadar Formation and the Matabaietu Formation to the Recent, documents one of the most continuous records of human cultural change known.

The present work and that in our previous paper, should lay a firm foundation for a coherent and orderly programme of research in the Middle Awash in the years to come.

We acknowledge assistance from: Fund for Overseas Research Grants and Education (to J.K., S.T., A.M. and T.A.); Wenner-Gren Foundation (to C.S., J.K., D.C., C.W. and G.C.); the L. S. B. Leakey Foundation (to C.J., C.S., C.W., D.C., G.C.); Explorer's Club (to D.C., J.K. and P.W.); the Departments of Anthropology, Southern Methodist (to C.S., C.W. and J.K.), New York (to C.J., G.C., T.A.), and Rutgers Universities (to D.C.); Boise Fund, Oxford University (to D.C.); Bache Fund, US National Academy of Sciences (to C.W.); Museum of Comparative Anatomy, Harvard University (to C.W.); Austin Gem & Mineral Society (to S.T.); Sigma Xi Fund (to P.W.); and the Vertebrate Paleontology Laboratory, Texas Memorial Museum (to J.K., S.T. and A.M.). We thank the following Ethiopian institutions: Ministry of Culture and Sports Affairs, Ministry of Mines, Addis Ababa University, Commissions for Higher Education and Science and Technology, and the Development Through Cooperation Campaign. We thank the following for assistance on faunal identifications: D. Torre (Carnivora), D. A. Hooijer and A. Azzaroli (Perissodactyla), H. B. S. Cooke (Suidae), D. Geraads (Giraffidae), Rodentia (Mesfin Asnake), and especially V. J. Maglio (Proboscidea); also, those who assisted on archaeological surveys and identifications, H. Mosca, W. Singleton, P. A. Larson, Jr, Saladin Abubaker, and especially Fred Wendorf. Special thanks to Karl Butzer, Lita Osmundson, V. J. Maglio, and Sharon McKern.

Received 9 February, accepted 4 May 1982

1 Kalb, J E *Sinet Eth. J Sci* **1,** 87–98 (1978).
2 Kalb, J E. *et al Nature* **298,** 17–25 (1982)
3 Kalb, J. E (ed.) *Rift Valley Research Mission in Ethiopia, Report 8, Annual Report 1975–1976* (Ethiopian Ministry of Culture and Sports Affairs, Addis Ababa, 1976).
4. Kalb, J. E (ed) *Rift Valley Research Mission in Ethiopia, Report 23, Annual Report 1976–1977* (Ethiopian Ministry of Culture and Sports Affairs, Addis Ababa, 1976)
5 Sickenberg, O & Schonfeld, M in *Afar Depression of Ethiopia* (eds Pilger, A. & Rosler, A) 277–284 (Schweizerbart'sche, Stuttgart, 1975).
6 Taieb, M., Johanson, D C., Coppens, Y & Aronson, J L *Nature* **260,** 289–293 (1976).
7. Beden, M *Bull Soc Géol Fr.* **21,** 271–276 (1979)
8. Kalb, J E & Jolly, C. J *Garyounis Sci. Bull* (in the press)
9. Kalb, J E *et al. Palaeogeogr. Palaeoclimatol Palaeocol.* **30,** 107–120 (1980).
10 Kalb, J E , Jaeger, M , Jolly, C J & Kana, B *J. Archaeol Sci* (in the press)
11 Conroy, G , Jolly, C., Cramer, D. & Kalb, J *Nature* **276,** 67–70 (1978)
12. Tebedge, Sleshi, thesis, Univ Texas at Austin (1981)
13. Mebrate, Assefa, & Kalb, J E. *Sinet· Eth. J. Sci* (in the press)
14. Kalb, J E. *et al.* (in preparation).
15. Pickford, M. in *Geological Background to Fossil Man* (ed. Bishop, W W) 237–262 (Scottish Academic, Edinburgh, 1978)
16. Zanettin, B & Justin-Visentin, E. in *Afar Depression of Ethiopia* (eds Pilger, A & Rosler, A.) 300–309 (Schweizerbart'sche, Stuttgart, 1975)
17 Varet, J. *Geology of Central and Southern Afar,* 19–27 (CNRS, Paris, 1978)
18. Chapman, G R & Brooke, M. in *Geological Background to Fossil Man* (ed. Bishop, W W) 207–224 (Scottish Academic, Edinburgh, 1978).
19 Bishop, W W in *Calibration of Hominoid Evolution* (eds Bishop, W W. & Miller, J A) 219–246 (Scottish Academic, Edinburgh, 1972).
20. Behrensmeyer, A. K in *Earliest Man and Environments in the Lake Rudolf Basin* (eds Coppens, Y., Howell, F C., Isaac, G & Leakey, R. E. F) 163–170 (University of Chicago Press, 1976).
21. Pickford, M in *Geological Background to Fossil Man* (ed. Bishop, W. W) 263–278 (Scottish Academic, Edinburgh, 1978)
22. Smart, C in *Earliest Man and Environments in the Lake Rudolf Basin* (eds Coppens, Y., Howell, F C., Isaac, G. L & Leakey, R E F) 361–369 (University of Chicago Press, 1976)
23. Harris, J. M & White, T D. *Trans Am philos. Soc* **69,** 1–128 (1979)
24. Gentry, A W. *Ann S Afr. Mus* **79,** 213–337 (1980)
25. Coryndon, S. in *The Evolution of African Mammals* (eds Maglio, V J & Cooke, H B S.) 483–495 (Harvard University Press, 1978)
26. Simons, E. L & Delson, E. in *The Evolution of African Mammals* (eds Maglio, V J & Cooke, H B. S.) 100–119 (Harvard University Press, 1978)
27 Berggren, W A & Van Couvering, J A. *Paleogeogr Paleoclimatol Paleoecol* **16,** 1–216 (1974).
28. Cooke, H B S. & Maglio, V. J in *Calibration of Hominoid Evolution* (eds Bishop, W W. & Miller, J A.) 303–329 (Scottish Academic, Edinburgh, 1972)
29. Coppens, Y. & Howell, F. C in *Earliest Man and Environments in the Lake Rudolf Basin* (eds Coppens, Y , Howell, F C , Isaac, G L & Leakey, R E F) 177–192 (University of Chicago Press, 1976)
30 Coppens, Y., Maglio, V J., Madden, C. T. & Beden, M. in *The Evolution of African Mammals* (eds Maglio, V. J & Cooke, H. B S.) 336–367 (Harvard University Press, 1978).
31 Hendey, Q. B *Ann. S Afr Mus* **75,** 1–24 (1978)
32 Aronson, J. L & Taieb, M. in *Hominid Sites· Their Geologic Settings* (eds Rapp, G., Jr & Vondra, C. F.) 165–195 (Westview, Colorado, 1981).
33 Harris, J M in *Koobi Fora Research Project· The Fossil Hominids and an Introduction to their Context 1968–1974* (eds Leakey, M. G & Leakey, R. E. F) 32–63 (Clarendon, London, 1978).
34 Cooke, H. B. S. *Kirtlandia* **29,** 1–63 (1978)
35 Beden, M. *Géobios.* **13**(6) 891–901 (1980)
36 Beden, M *Bull Soc Géol Fr 8*ᵉ, 32 (1980)
37 Johanson, D C & White, T. D *Science* **209,** 321–330 (1979)
38. Howell, F C in *The Evolution of African Mammals* (eds Maglio, V. J & Cooke, H. B. S) 154–248 (Harvard University Press, Cambridge, 1978).
39. Brown, F H & Shuey, R. T in *Earliest Man and Environments in the Lake Rudolf Basin* (eds Coppens, Y , Howell, F. C , Isaac, G. L. & Leakey, R. E F) 64–78 (University of Chicago Press, 1976)
40 Coppens, Y , Gray, B T. & Johanson, D C in *Actes de 8*ᵉ *Congrés Panafrican de Prehistoire et des Études du Quaternaire,* Nairobi (eds Leakey, R. E F & Ogot, B. A) 56–57 (1981).
41. Beden, M in *Actes du 8*ᵉ *Congrés Panafrican de Prehistoire des Etudes du Quaternaire,* Nairobi (eds Leakey, R. E F. & Ogot, B. A) 72–76 (1981)
42 Bishop, W. W , Hill, A & Pickford, M in *Geological Background to Fossil Man* (ed. Bishop, W. W.) 309–328 (Scottish Academic, Edinburgh, 1978)
43. Cooke, H B S. & Coryndon, S. C. *Fos. Vert. Afr* **3,** 107–224 (1970)
44 Leakey, M. D *Olduvai Gorge, 3· Excavations in Beds I and II,* 1–306 (Cambridge University Press, 1972)
45 Isaac, G. L. in *Geological Background to Fossil Man* (ed. Bishop, W W.) 173–206 (Scottish Academic, Edinburgh, 1978)
46. Gasse, F. & Street, F. A. *Palaeogeogr Palaeoclimatol Palaeoecol* **24,** 279–325 (1978).
47. Taieb, M. thesis, Univ. Paris VI (1974).
48. Singleton, W L. in *Rift Valley Research Mission in Ethiopia, Report 23, Annual Report 1976–1977* (ed Kalb, J E.) (Ethiopian Ministry of Culture and Sports Affairs, Addis Ababa, 1977)
49 Larson, P Jr *Nyame Akuma* **11,** 6–10 (1977)
50 Singleton, W. L. in *Rift Valley Research Mission in Ethiopia, Report 23, Annual Report 1976–1977* (ed. Kalb, J E.) (Ethiopian Ministry of Culture and Sports Affairs, Addis Ababa, 1977).
51 Johanson, D C., Taieb, M., Coppens, Y & Roche, H *C r. Acad hebd Séanc Sci , Paris* **287**D, 237–240 (1978)
52. Taieb, M. in *Afar between Continental and Oceanic Rifting* (eds Pilger, A. & Rosler, A.) 80–88 (Schweizerbart'sche, Stuttgart, 1976).
53. Corvinus, G. *Nature* **256,** 468–471 (1975).
54 Corvinus, G *Nature* **261,** 571–572 (1976).
55 Cooke, H B. S *Science* **201,** 460–463 (1978)
56. Jolly, C J. *Bull Br. Mus. nat. Hist* **22,** 1–23 (1972)
57. Olson, T. R *Symp Soc. Study Hum. Biol* **21,** 99–128 (1981).
58 Patterson, B. & Howells, W W. *Science* **156,** 64–66 (1967).
59. Patterson, B., Behrensmeyer, A. K & Sill, W D. *Nature* **226,** 918–921 (1970)

Protection against foot-and-mouth disease by immunization with a chemically synthesized peptide predicted from the viral nucleotide sequence

James L. Bittle, Richard A. Houghten, Hannah Alexander, Thomas M. Shinnick, J. Gregor Sutcliffe & Richard A. Lerner

Committee for the Study of Molecular Genetics, Research Institute of Scripps Clinic, La Jolla, California 92037, USA

David J. Rowlands & Fred Brown

Animal Virus Research Institute, Pirbright, Surrey GU24 0NF, UK

Chemically synthesized peptides corresponding to two different regions of the VP1 polypeptide of foot-and-mouth disease virus (FMDV) produced high levels of serotype-specific virus neutralizing antibody in cattle, guinea pigs and rabbits. A single inoculation of one of these peptides protected guinea pigs against subsequent challenge with the virulent virus.

FOR at least four centuries foot-and-mouth disease has been one of the world's major animal plagues[1]. The virus affects both domestic and wild ruminants and swine. Its ease of dissemination, coupled with the loss of productivity of the animals following infection, usually estimated at 25%, make it a disease of major concern. The problem is worldwide as the disease is present in every continent except Australia and North America. The disease is controlled by slaughter in those countries where it does not normally occur but vaccination is used where it is endemic. The extent of the problem is such that over 1,000 million doses of vaccine are used each year but, although vaccines have been available for the past 40 years, the disease is still widespread. The vaccines are produced by inactivation of virus harvests produced in cultures of baby hamster kidney cells or in bovine tongue epithelium fragments. Although these vaccines are generally effective, there are certain drawbacks to their use. For example, several strains of the virus cannot be grown to a titre high enough to provide sufficient antigenic mass for effective vaccination. In addition, the virus particle is very unstable, particularly below *p*H 7, so it is necessary to store vaccines under refrigeration to retain their potency. This is clearly a major limitation, particularly in tropical climates. The recent association of outbreaks of the disease in Europe with improperly inactivated virus[2] illustrates another disadvantage of this type of vaccine, particularly in those regions of the world where the disease has been virtually eradicated. These disadvantages have prompted continuing studies on the structural features of the virus particle that are necessary for immunogenic activity with a view to developing alternative vaccines.

The virus, which belongs to the aphthovirus genus of the family Picornaviridae, contains one molecule of infectious single-stranded RNA of molecular weight (M_r) $\sim 2.6 \times 10^6$ and 60 copies of each of four polypeptides VP1–VP4 (ref 3). An important antigenic role for VP1 is indicated by the fact that treatment of the virus particle with trypsin results in the cleavage of only this polypeptide, with a concomitant decrease in infectivity and, depending on the virus strain, a loss of immunizing activity[4]. Indeed, VP1 isolated from virus particles has some, albeit very low, immunizing activity[5–8], whereas the other three viral polypeptides have no such activity. Based on this observa-

Table 1 Antibody response of rabbits to different peptides of VP1 of FMDV, type 0, strain Kaufbeuren

Rabbit no.	Peptide	Anti-peptide antibody titre	Neutralization index ($\log_{10}$)*
1	9–24	80–160	≤ 0.3
2	9–24	40–80	≤ 0.3
3	17–32	80–160	≤ 0.5
4	17–32	20–40	≤ 0.9
5	25–41	40–80	≤ 0.5
6	25–41	640–1280	≤ 0.9
7	1–41	320–640	≤ 0.9
8	1–41	320–640	≤ 0.7
9	141–160	320–640	≥ 3.9
10	141–160	320–640	≥ 3.7
11	151–160	80–160	2.9
12	151–160	160–320	1.1
13	200–213	>1280	3.5
14	200–213	160–320	3.1

In the second column, numbers refer to the amino acid, starting at the amino-terminus. Rabbits were immunized with peptide-coupled KLH inoculating 200 μg in complete Freund's adjuvant (1:2) s.c. in the footpad on day 0; 200 μg in incomplete Freund's adjuvant s.c. on day 14; 200 μg with 4 mg of aluminium hydroxide intraperitoneally (i.p.) on day 21 and day 50 and were then bled on day 57. The enzyme-linked immunosorbent assay (ELISA) was used to test all antisera for their ability to react with the peptide used for immunization. Antibody was bound to antigen immobilized on polystyrene plates and the antigen–antibody complex was detected using an enzyme-labelled goat anti-rabbit IgG. Five pmol of antigen in 0.1% bovine serum albumin (BSA) phosphate-buffered saline (PBS) were added to each well of a 96-well microtitre plate and dried overnight at 37 °C. The dried antigen was then fixed to the plates with 50 μl per well of methanol for 5 min at room temperature. Before adding the antibodies, the plates were coated for 4 h with 3% BSA/PBS to block nonspecific adsorption of antibodies to the plate. Twofold serial dilutions of each antiserum were prepared in minimal essential medium containing 10% fetal calf serum, 25 μl of the serum dilution were added per well and the plates were incubated overnight at room temperature. Unbound antibody was then washed off with water. The antigen–antibody complex was reacted with 25 μl per well of 1:100 dilution of goat anti-rabbit IgG coupled to glucose oxidase. Excess goat anti-rabbit antibody was washed off with water and the reaction was developed by adding 50 μl per well of developing solution [25 ml 0.1 M Na-phosphate buffer, *p*H 6.0, 3 ml 20% glucose, 200 μl 0.1% horseradish peroxidase, 200 μl of chromogen (2,2′-amino-di-[3-ethylbenzthiazolin-sulphonate]) at 20 mg ml^{-1} in Na-phosphate buffer, *p*H 6.0]. The plates were read in a Titertek Multiskan at 414 nm, and the values presented are the reciprocal of the serum dilution binding to 50% of 5 pmol of antigen.

* Equal volumes of virus dilutions and undiluted sera were inoculated i.p. into suckling mice. The values give the difference between the titre of the virus plus normal serum and the virus plus antiserum.

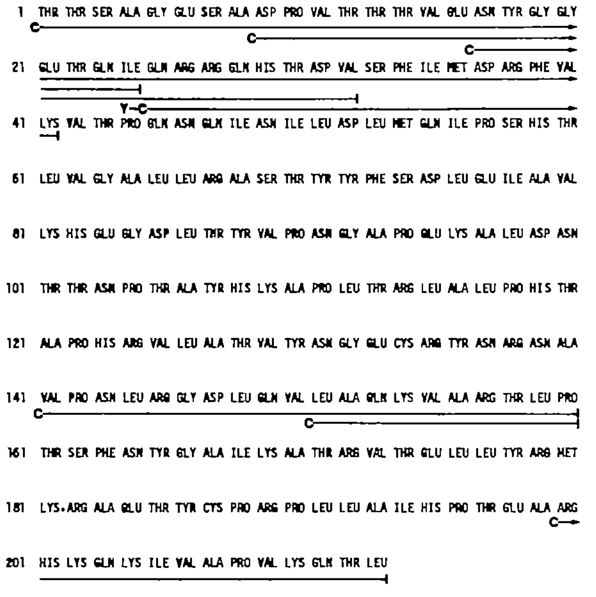
1 THR THR SER ALA GLY GLU SER ALA ASP PRO VAL THR THR THR VAL GLU ASN TYR GLY GLY
C
C
C
21 GLU THR GLN ILE GLN ARG ARG GLN HIS THR ASP VAL SER PHE ILE MET ASP ARG PHE VAL
Y–C
41 LYS VAL THR PRO GLN ASN GLN ILE ASN ILE LEU ASP LEU MET GLN ILE PRO SER HIS THR
61 LEU VAL GLY ALA LEU LEU ARG ALA SER THR TYR TYR PHE SER ASP LEU GLU ILE ALA VAL
81 LYS HIS GLU GLY ASP LEU THR TYR VAL PRO ASN GLY ALA PRO GLU LYS ALA LEU ASP ASN
101 THR THR ASN PRO THR ALA TYR HIS LYS ALA PRO LEU THR ARG LEU ALA LEU PRO HIS THR
121 ALA PRO HIS ARG VAL LEU ALA THR VAL TYR ASN GLY GLU CYS ARG TYR ASN ARG ASN ALA
141 VAL PRO ASN LEU ARG GLY ASP LEU GLN VAL LEU ALA GLN LYS VAL ALA ARG THR LEU PRO
C
C
161 THR SER PHE ASN TYR GLY ALA ILE LYS ALA THR ARG VAL THR GLU LEU LEU TYR ARG MET
181 LYS.ARG ALA GLU THR TYR CYS PRO ARG PRO LEU LEU ALA ILE HIS PRO THR GLU ALA ARG
C
201 HIS LYS GLN LYS ILE VAL ALA PRO VAL LYS GLN THR LEU

Fig. 1 The 213-amino acid sequence of VP1 as translated by Kurz *et al.*[13] from the nucleic acid sequence. Regions of the protein chosen for synthesis are indicated by bold underlining. C or Y at the end of such a line indicates the addition of cysteine or tyrosine not found in the primary sequence. Peptides were synthesized by the solid phase method[17–19] using a Beckman Model 990B peptide synthesizer. The initial amino acid resin was prepared by esterification of Boc-(MeoBzl)-Cys-OH (2.0 g of the anhydrous caesium salt. 4.3 mequiv) to chloromethylated resin (polystyrene–1% divinylbenzene, bio-beads S.X -1, 200–400 mesh, 0 70 mmol g^{-1}) in 25 ml anhydrous dimethylformamide (DMF) by stirring for 24 h at 50 °C. A threefold excess of caesium salt over active chloride polymer was found to give almost complete substitution. Substitution was determined to be 0.55 mequiv g^{-1} by the picric acid test and amino acid analysis, and 0.53 mequiv g^{-1} following HCl-propionic acid hydrolysis. For each synthesis, 1 0 g (0.53 mequiv) of Boc-(MeoBzl)-Cys resin was used The following side-chain protecting groups were used. *O*-Br-Z for lysine and tyrosine; *O*-benzyl for threonine, serine, aspartic acid and glutamic acid; tosyl for arginine; *N*-formyl for tryptophan; and *N*-dinitrophenyl for histidine. Protected amino acids (from Vega Biochemicals or Peninsula Laboratories) were recrystallized from the appropriate solvent to give single spots on TLC (chloroform/acetic acid = 15:1 or chlorofrom/methanol = 10:1) All couplings were carried out using a 10-fold excess of Boc-AA-OH. For asparagine and glutamine, an equimolar amount of *N*-hydroxy benzotriazole was added to the protected amino acid and dimethyl formamide was used as the solvent. All coupling reactions were ≥99% complete by the picric acid test. The removal of dinitrophenyl from histidine-containing peptides was accomplished with *N*-methyl mercaptoacetamide[20] in DMF by mixing with the resin-bound peptide for 15 min. Removal was >95%. The protected peptide polymers (500 mg to 2.5 g, 0 12–0 60 mequiv) were treated with twice their weight of anisole and with 40 times their volume (relative to weight) of anhydrous HF at 4 °C for 1 h. For peptides containing glutamic acid, 5% v/v pyridine was added to the HF to prevent anisylation. After evaporating the HF with a stream of N_2, the red residue was mixed with anhydrous ether (50×, w/v) and stirred vigorously for 15 min; after repeating the ether extraction three times, the white residue was filtered and dried *in vacuo*. This dried resin–peptide mixture was generally extracted with 5% HOAc, lyophilized and amino acid analysis performed (approximately 90% removal of the peptide from the resin was accomplished in this manner). For peptides containing tryptophan, the *N*-formyl protecting group was removed from the peptide by treatment for 1.5 min at *p*H 11.5 (NaOH) in the presence of hydrazine. If the amino acid analysis was acceptable (±5% of theory), the peptides prepared in the above manner were used directly, if not, they were purified to the desired extent by CM-cellulose chromatography, partition chromatography, or HPLC as needed. Yields ranged from 20–60% depending on the given peptide, and the purity needed The peptides were coupled to a protein carrier, KLH, through the cysteine of the peptide, using *N*-maleimidobenzoyl-*N*-hydroxysuccinimide ester (MBS) as a coupling agent, as described by Liu *et al.*[21].

tion, workers in Europe and the USA[9–11] have investigated the possibility of producing the protein by recombinant DNA technology, and Kleid *et al.*[11] have produced by this means 1–2 × 10^6 copies of VP1 per *Escherichia coli* cell. However, the expressed protein appears to be no more active weight for weight than VP1 produced from virus particles and it is clear that much remains to be learned about the structural features necessary for effective immunization before VP1 can be considered a realistic alternative to killed virus particles.

Application of recombinant DNA technology has also allowed nucleotide sequences of the virus genome to be determined, from which the primary amino acid sequence of VP1 can be deduced. Sequences are now available for two strains of serotype A[11,12] and one of type O[13]. In addition, Strohmaier and his colleagues[14] have provided evidence, by measuring the immunogenic activity of enzymatically or chemically derived fragments of VP1 of the type 0 strain, that sites eliciting neutralizing antibody are located in the carboxy-terminal half of the molecule. We have chemically synthesized peptides corresponding to several regions of VP1 of this strain of virus and report here that some of these induce neutralizing and protective antibodies against the disease.

Chemically synthesized peptides induce neutralizing antibodies in rabbits

Previous studies[14] indicated that the carboxy-terminal region was important in inducing neutralizing antibody. In addition, nucleic acid sequencing of the two strains of type A[11,12] and one of type 0[13] demonstrated that there was considerable variability between positions 130–160 and 190–213. We reasoned that this variability was due to the availability of these regions for interaction with neutralizing antibody and their consequent subjection to high selective pressure. To study the molecule further, we also selected a series of N-terminal peptides for synthesis. Seven peptides from VP1 of type 0 virus (strain Kaufbeuren), corresponding to four regions near the amino-terminus (1–41), one at the carboxy-terminus (200–213) and two near the centre of the molecule (141–160 and 151–160) were synthesized, coupled to keyhole limpet haemocyanin (KLH) and inoculated into rabbits (see Fig. 1). The KLH-coupled peptides elicited anti-peptide antibody titres as assayed by ELISA (Table 1). However, a virus neutralizing antibody response was elicited only by the peptides in the middle region and at the carboxy-terminus.

The serotype specificity of the antibodies produced in the rabbits by the peptides spanning regions 141–160 and 200–213 was determined in neutralization tests using the homologous virus and viruses of types A and C. Although there was some cross-neutralization, the level was considerably lower than that of the homotypic reaction (Table 2). These results show that the serotype specificity of the sera produced by inoculation of the synthetic peptides mimicks that found with sera against whole virus. The cross-neutralization may reflect the limited sequence homology among the different serotypes.

Guinea pigs immunized with synthetic peptides are protected against foot-and-mouth disease

Having established that peptides 141–160 and 200–213 produced high levels of neutralizing antibodies on multiple inoculation into rabbits, we tested the effectiveness of a single inoculation of the antigens in producing neutralizing antibodies in guinea pigs and in providing protection against challenge. Guinea pigs were inoculated subcutaneously (s.c.) with 20 or 200 μg of either of the two peptide conjugates, mixed with

Table 2 Serotype specificity of the anti-peptide antibodies

Antibody to peptide region:	Neutralization index ($\log_{10}$)* against		
	0 Kaufbeuren	C Indaial	A-61
141–160 (rabbit 9)	4.3	−0.1	1.1
141–160 (rabbit 10)	≥6.3	1.9	2.3
200–213 (rabbit 13)	2.9	−0.1	1.5
200–213 (rabbit 14)	3.3	0.3	1.5

C Indaial belongs to serotype C, subtype 3; A-61 belongs to serotype A, subtype 10.

* See Table 1 legend.

Freund's complete adjuvant or aluminium hydroxide gel. Parallel groups of animals were inoculated with either 1 or 10 μg of purified inactivated virus particles mixed with either of the same two adjuvants. After 35 days, the animals were bled by heart puncture to determine the level of neutralizing antibody and then challenged by inoculating one hind footpad with 10^4 ID_{50} (50% infectious dose) of the homologous virus which had been passaged once in guinea pigs. The results, summarized in Table 3, demonstrate the effectiveness of peptide 141–160 in producing neutralizing antibody and protecting the animals against infection. As little as 200 μg provided complete protection and even 20 μg provided substantial protection, in view of the severity of the challenge. There was good correlation between the level of neutralizing antibody and the response to challenge. Those animals whose sera had a neutralizing index of ~1.5 or greater were protected.

In contrast, inoculation of guinea pigs with a similar amount of VP1, prepared by SDS-polyacrylamide gel electrophoresis (SDS-PAGE) gave a much lower neutralizing antibody response. We have observed this for several different preparations of VP1 from viruses of types 0 and A.

Biochemical characterization of the virus components reacting with the anti-peptide sera

The rather surprisingly superior neutralizing antibody response of the animals to inoculation with the synthetic peptides, compared with that observed in studies using VP1, prompted us to explore the basis for this difference. As only the antisera to peptides 141–160 and 200–213 had neutralizing activity, we confined our experiments to these and we have characterized the reactivities of these novel reagents in a variety of assays commonly used in this virus system. First, the antisera were tested for their ability to precipitate purified ^{35}S-methionine-labelled virus antigens (Table 4). Intact 146S virus particles were precipitated by (1) the anti-peptide sera, (2) a rabbit antiserum prepared against purified VP1, (3) convalescent guinea pig serum and (4) guinea pig serum prepared against 146S particles. With the exception of the serum against the 146S particles, the same antisera also precipitated the 12S virus protein subunit, which is a pentamer of VP1–3, produced by heating 146S particles to 60°C. The lack of reaction between antisera to 146S particles and the 12S subunit has been described previously[15]. Disruption of the 146S particle into its constituent polypeptides by treatment with 8M urea at 37 °C, followed by dilution to reduce the urea concentration, led to a loss of reactivity with the anti-146S serum and a considerable reduction in its reaction with the convalescent serum. However, there was less reduction with three of the four anti-peptide sera. The anti-VP1 serum precipitated the denatured protein efficiently.

Table 3 Protection of guinea pigs against challenge with FMDV by inoculation with inactivated virus particles, VP1 or synthetic peptides 141–160 and 200–213

Antigen	Dose (μg)	Adjuvant	Neutralization index ($\log_{10}$)*	No. protected/ No. challenged
Virus	1	$Al(OH)_3$	2.7(1.1–2.3)	1/4
	10	$Al(OH)_3$	≤4.9(3.4–≤4.5)	2/2
	1	Freund's	2.5(1.3–2.9)	2/2
	10	Freund's	≤5.3(≤4.5)	4/4
VP1	20	$Al(OH)_3$	0.5(0.1–0.9)	ND
141–160	20	$Al(OH)_3$	2.1(0.9–2.7)	3/4
	200	$Al(OH)_3$	2.7(1.7–≤3.7)	3/3
	20	Freund's	2.1(0.1–2.5)	1/4
	200	Freund's	≤3.3(1.5–≤3.3)	4/4
200–213	20	$Al(OH)_3$	1.1(ND)	1/3
	200	$Al(OH)_3$	0.7(ND)	2/4
	20	Freund's	1.1(ND)	0/4
	200	Freund's	0.5(ND)	0/4

* Neutralizing activity of pooled serum from eight animals. Values in parentheses give the range of activity in the individual animals that were challenged. ND, not done.

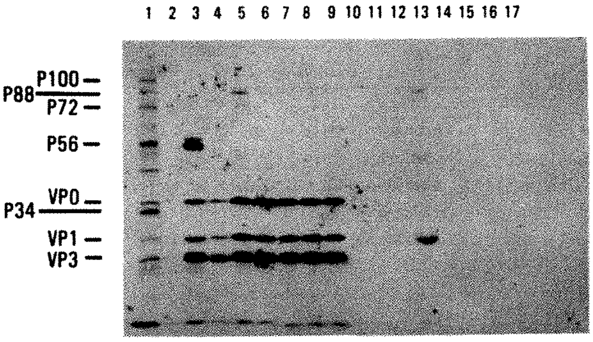

Fig. 2 Comparison of immune precipitation of viral proteins by different antisera. FMDV-infected BHK 21 cells were labelled with ^{35}S-methionine from 2.5 to 3 h post-infection, when host cell protein synthesis was almost completely halted. The cells were then lysed by treatment with 1 ml of 1% NP-40, 0.5% DOC in 0.15 M NaCl, 50 mM Tris-HCl, *p*H 7.5 and the nuclei pelleted in a microfuge for 5 min. Aliquots (20 μl) of the supernatant were diluted with 1 ml of NETS (0.15 M NaCl, 5 mM EDTA, 50 mM Tris-HCl, *p*H 7.5 and 0.5% NP40) immediately, or after adding SDS to 1% and heating at 100 °C for 2 min. The appropriate antiserum (30 μl) was added to each sample and complexes allowed to form at 4°C overnight. Washed, inactivated *Staphylococcus aureus* ghosts (Pansorbin) were then added to adsorb IgG molecules and separated by centrifuging for 5 min in a microfuge. The pellets were washed twice with NETS and the adsorbed IgG and complexed antigens eluted by suspending the pellets in Laemmli disruption buffer[22]. The proteins were denatured by heating at 100 °C for 2 min and separated on an 11% Laemmli gel[22]. The gels were prepared for fluorography[23] and exposed to X-ray film. Lane 1, total cell extract; lanes 2–9, immune precipitates of undenatured extracts; lanes 10–17, immune precipitates of SDS-denatured extracts. Lanes 2 and 10, control rabbit serum; lanes 3 and 11, convalescent guinea pig antiserum; lanes 4 and 12, guinea pig antiserum to 146S particles; lanes 5 and 13, rabbit antiserum to VP1; lanes 6 and 14, antiserum 9 to peptide 141–160; lanes 7 and 15, antiserum 10 to peptide 141–160; lanes 8 and 16, antiserum 13 to peptide 200–213; lanes 9 and 17, antiserum 14 to peptide 200–213.

The same antisera were then tested for their ability to precipitate the virus-specfic antigens in infected BHK 21 cells. The antigens were extracted in their native state by disrupting the cells with deoxycholate (DOC) and Nonidet P-40 (NP40)[16] and used either directly or after denaturation by heating at 100 °C in the presence of 1% SDS. The immunoprecipitated proteins were separated by PAGE (Fig. 2); all the antisera precipitated both the virus structural proteins and their precursor, P88 (lanes 3–9). The convalescent antiserum also precipitated some of the non-structural polypeptides. As the structural proteins are present as complexes when extracted from cells in these conditions, antisera reactive with VP1 also precipitate the other structural polypeptides.

After denaturation of the proteins with SDS, only the rabbit anti-VP1 serum precipitated VP1 and the structural protein precursor P88 (Fig. 2, lane 13); VP1 was precipitated neither by the control rabbit serum (lane 10), by convalescent serum (lane 11) nor by the anti-146S serum (lane 12). The antisera against peptides 141–160 (lanes 14, 15) and 200–213 (lanes 16, 17) precipitated very little of the SDS-denatured antigens; a very faint VP1 band could be seen in the 200–213 precipitates on the original autoradiograph.

The reactivity of the various antisera for denatured molecules was further examined by the Western blotting technique, whereby the proteins from purified denatured virus particles were separated by SDS-PAGE, transferred to nitrocellulose, probed with antiserum and the reaction visualized by autoradiography after binding ^{125}I-labelled protein A. The results (Fig. 3) again show a lack of reaction between VP1 and the convalescent and anti-146S sera (lanes 2 and 3) and a strong reaction with anti-VP1 serum (lane 4). Reaction between the 200–213 antisera and VP1 (lanes 7, 8) was more obvious than in the immunoprecipitation experiment (Fig. 2); only a weak reaction with the two anti-141–160 sera (lanes 5, 6) was seen.

Taken together, these data indicate that the anti-peptide sera react with the protein species containing the appropriate sequence, including precursor molecules, and that they resemble anti-viral anti-sera in reacting well with native components. Because of their propensity to bind to native VP1, these sera also precipitate other protein species which, in non-denaturing conditions, are bound to the primary target by virtue of the protein–protein interactions important in the structure of this virus. On the other hand, it is clear that the activity of the anti-VP1 serum is directed primarily against denatured protein, an observation easily understandable in view of the fact that this serum was prepared against SDS-denatured protein. VP1 isolated by other means has been an equally poor antigen for generating an anti-viral response (D.J.R. and F.B., unpublished work).

Discussion

Table 4 Precipitating activity of different antisera against the 146S virus particle, 12S subunit and viral polypeptides

		Amount of antigen precipitated (counts per 20 min)		
Serum	Animal	146S particle	12S subunit	Viral polypeptides
Normal	Rabbit	667	616	637
Convalescent	Guinea pig	2,692	1,833	742
146S particle	Guinea pig	2,889	668	646
VP1	Rabbit	3,231	2,457	1,553
141–160	Rabbit 9	3,123	2,212	774
141–160	Rabbit 10	3,174	2,312	1,047
200–213	Rabbit 13	3,434	2,259	1,070
200–213	Rabbit 14	3,215	2,266	1,127

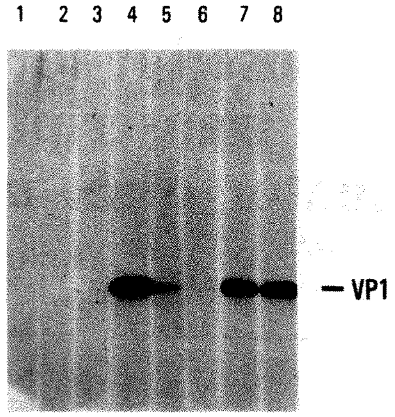

Fig. 3 Comparison of the reaction of different antisera with separated viral polypeptides. Purified FMDV 146S particles were denatured with Laemmli disruption buffer[22] at 100 °C for 2 min and the proteins separated on a 10% polyacrylamide gel slab. The proteins were electrophoretically transferred to a nitrocellulose sheet which was then cut into strips. The strips were immersed in a solution of 10 mg ml^{-1} haemoglobin containing the different antisera. After thorough washing, the strips were immersed in a solution of ^{125}I-labelled *S. aureus* protein A. The washed, dried strips were then exposed to X-ray film to visualize the binding of protein A to IgG molecules immobilized on the strips. Lane 1, control rabbit serum; lane 2 convalescent guinea pig antiserum; lane 3, guinea pig antiserum to the 146S particle; lane 4, rabbit antiserum to VP1; lanes 5 and 6, rabbit antisera 9 and 10 to peptide 141–160; lanes 7 and 8, rabbit antisera 13 and 14 to peptide 201–213.

Our results show that a single inoculation of the synthetic peptide 141–160 elicits sufficient neutralizing antibody to protect guinea pigs against subsequent challenge with FMDV. Although we have not yet accumulated sufficient data to allow a precise comparison, the results obtained so far indicate that, on an equal weight basis, a single peptide has from one to as much as 10 per cent of the activity of the inactivated virus particle. Furthermore, the neutralizing antibody titre elicited by the peptide is several orders of magnitude greater than the best results obtained by immunization with the capsid protein VP1, irrespective of whether this is produced by disruption of virus particles[5–8] or by expression in *E. coli* cells[11]. Indeed, in several of our own experiments (for example, see Table 3) and in other studies[5–8], the level of neutralizing antibody response to one inoculation of the capsid protein was negligible. The reason for this difference may be that the antibody induced by the synthetic peptide is more closely related qualitatively to that induced by virus particles than to that induced by VP1. It is possible that the separated VP1 does not fold properly when deprived of the scaffolding provided by the other capsid proteins. Thus the immunodominant site presented to the immune system by free VP1 may be largely irrelevant to neutralization. In contrast, a small free peptide may be able to adopt a conformation approximating that which it assumes in the virus particle, a situation that is unlikely when it is constrained by the neighbouring amino acids in an improperly folded VP1.

One clear advantage of the synthetic 141–160 peptide is its activity in eliciting a protective antibody response after a single inoculation. This good response to a single inoculation is important, because successful immunization against foot-and-mouth disease in the field depends on the vaccines being sufficiently active to produce a protective response with one inoculation. Indeed, preliminary work in cattle and pigs shows that the synthetic peptide 141–160 can elicit an antibody response sufficient to protect these species against the disease. Thus the prospects for a totally synthetic vaccine against foot-and-mouth disease are encouraging.

We thank David Morrell for the Western blot experiment and Janet Haresnape for the anti-VP1 serum.

Note added in proof: Since the submission of this article, we have obtained evidence that synthetic peptides corresponding to amino acids 141–160 of the VP1 of two subtypes of serotype A of FMDV (subtype 10, strain 61 and subtype 12, strain 119) also elicit the production in rabbits of levels of neutralizing antibody similar to those described here.

Received 19 April; accepted 4 May 1982.

1. Fracastorius, H. *De Contagione et Contagiosis Morbis et Curatione* Vol. 3 (1546).
2. King, A. M. Q., Underwood, B. O., McCahon, D., Newman, J. W. I. & Brown, F. *Nature* **293**, 479–480 (1981).
3. Cooper, P. D. *et al. Intervirology* **10**, 165–180 (1978).
4. Wild, T. F., Burroughs, J. N. & Brown, F. *J. gen. Virol.* **4**, 313–320 (1969).
5. Laporte, J., Grosclaude, J., Wantyghem, J., Bernard, S. & Rouze, P. *C. r. hebd. Séanc. Acad. Sci., Paris* **276**, 3399–3401 (1973).
6. Bachrach, H. L., Moore, D. M., McKercher, P. D. & Polatnick, J. *J. Immun.* **115**, 1636–1641 (1975).
7. Kaaden, O. R., Adam, K.-H. & Strohmaier, K. *J. gen. Virol.* **34**, 397–400 (1977).
8. Meloen, R. H., Rowlands, D. J. & Brown, F. *J. gen. Virol.* **45**, 761–763 (1979).
9. Kupper, H. *et al. Nature* **289**, 555–559 (1981).
10. Boothroyd, J. C. *et al. Nature* **290**, 800–802 (1981).
11. Kleid, D. G. *et al. Science* **214**, 1125–1129 (1981).
12. Boothroyd, J. C., Harris, T. J. R., Rowlands, D. J. & Lowe, P. A. *Gene* **17**, 153–161 (1982).
13. Kurz, C., Forss, S., Kupper, H., Strohmaier, K. & Schaller, H. *Nucleic Acids Res.* **9**, 1919–1931 (1981).
14. Strohmaier, K., Franze, R. & Adam, K.-H. *J. gen. Virol.* **59**, 295–306 (1982).
15. Cowan, K. M. *Adv. Immun.* **17**, 195–253 (1973).
16. Harris, T. J. R., Brown, F. & Sangar, D. V. *Virology* **112**, 91–98 (1981).
17. Marglin, A. & Merrifield, R. B. *A. Rev. Biochem.* **39**, 841–866 (1970).
18. Houghten, R. A., Chang, W. C. & Li, C. H. *Int. J. Peptide Protein Res.* **16**, 311–320 (1980).
19. Sutcliffe, J. G. *et al. Nature* **287**, 801–805 (1980).
20. Houghten, R. A. & Li, C. H. *Analyt. Biochem.* **98**, 36–46 (1979).
21. Liu, F., Zinnecker, M., Hamaoka, T. & Katz, D. H. *Biochemistry* **18**, 690–697 (1979).
22. Laemmli, U. K. *Nature* **227**, 680–685 (1970).
23. Bonner, W. M. & Laskey, R. A. *Eur. J. Biochem.* **46**, 83–88 (1974).

Transcript secondary structures regulate transcription termination at the attenuator of *S. marcescens* tryptophan operon

I. Stroynowski* & C. Yanofsky

Department of Biological Sciences, Stanford University, Stanford, California 94305, USA

We have analysed the regulatory behaviour of deletion mutants lacking different segments of the leader region of the tryptophan operon of Serratia marcescens. *Our results support the model in which a particular RNA structure, the terminator, is recognized during transcription as a transcription termination signal, and an alternative RNA structure, the anti-terminator, prevents formation of the terminator. It appears that the role of translation, ribosome stalling and shifts between alternative RNA secondary structures, is simply to regulate formation of the terminator.*

SEVERAL bacterial operons encoding amino acid biosynthetic enzymes are regulated by attenuation (for reviews see refs 1–3). This regulatory mechanism involves controlled transciption termination at a site, the attenuator, located in the leader region, the segment of the operon between the transcription start site and the first structural gene. Comparison of the sequences of the leader regions of the six-amino acid biosynthetic operons known to be regulated by attenuation[4–7] reveals considerable similarities. Each operon has a potential peptide-coding region in the leader transcript which, if used, would specify a small peptide rich in the regulatory amino acid. Immediately beyond, there is a site of transcription termination, an attenuator. This site consists of an A + T-rich sequence preceded by a G + C-rich sequence exhibiting dyad symmetry. The segment of the transcript corresponding to the G + C-rich region in each operon can potentially form a stable hydrogen-bonded stem and loop structure. Transcription termination at the attenuator of each of these operons is controlled by the extent of charging of appropriate transfer RNAs with the regulatory amino acid, implicating leader peptide synthesis in the regulation of termination.

A model attempting to explain attenuation was proposed by Lee and Yanofsky[4] for the *trp* (tryptophan) operon of *Escherichia coli*. It was suggested that a G + C-rich secondary structure forms in the transcript just before RNA synthesis stops and serves as the recognition signal for transcription termination at the attenuator. An alternative secondary structure in the transcript was also predicted. If this structure, located in the earlier segment of the leader transcript, formed, it could prevent formation of the presumed transcription termination signal. It was hypothesized that this alternative secondary structure would eliminate transcription termination at the attenuator and thereby increase expression of the operon. The switch between the alternative RNA secondary structures was proposed to be regulated by ribosome movement along the transcript during translation of the coding region for the leader peptide. Specifically, ribosome stalling at the tandem Trp codons of the transcript—a consequence of the unavailability of charged tRNA^{Trp}—was thought to mask a critical segment of the transcript, thus favouring formation of the RNA stem and loop mutually exclusive with the formation of the termination secondary structure. This interpretation is consistent with the results of subsequent studies on attenuation performed with the *trp* operons of *E. coli* and other enteric bacteria[4–7]. The model has been applied to other amino acid biosynthetic operons; it has been used to explain attenuation in the *phe*[8], *his*[9], *thr*[10], *leu*[11] and *ilv*[12,13] operons.

Many features of the proposed model have not been verified by studies with any of the operons mentioned. We report here the results of experiments designed to test the fundamental hypothesis that alternative RNA secondary structures are involved in the regulation of transcription termination at the *trp* attenuator.

A model for attenuation in the *trp* operon of *S. marcescens*

Mutational and physiological studies with *Serratia marcescens* indicate that the *trp* genes of this enterobacterium are coordinately regulated in response to changes in tryptophan concentration[14–16]. The regulatory region of the *S. marcescens trp* operon is organized identically to those of *Escherichia coli* and *Salmonella typhimurium*[17]. There is a promoter–operator used to regulate transcription initiation and a leader region within which transcription termination is controlled.

Figure 1 gives the alternative RNA secondary structures of *S. marcescens* analogous to those of the *E. coli* leader transcript, and Fig. 1*a* shows the secondary structures that could be predicted to form *in vitro*. On the basis of studies with the *trp* operon of *E. coli*, the *in vivo* studies described here, and the results of *in vitro* transcription experiments to be presented elsewhere, we believe that the stem and loop structure labelled 3:4 in the figures is the structure recognized by the transcribing polymerase as a transcription termination signal; for example, deletion mutants that can only form structure 3:4 efficiently terminate transcription at the attenuator *in vivo* and *in vitro*. In view of these findings, structure 3:4 will henceforth be designated the 'terminator'[11]. When cells are starved of tryptophan, the ribosome translating the peptide-coding region is believed to stall over either of the adjacent Trp codons, thereby masking transcript segments A1, 1B and 2B. In these conditions, secondary structure 2A:3 could form before the synthesis of segment 4, and thereby preclude formation of the terminator. Substantial *in vivo* and *in vitro* evidence indicates that structure 2A:3 has an important role in preventing termination. We shall designate a structure such as 2A:3 in Fig. 1*b* as an anti-terminator. The stalled ribosomes shown in Fig. 1*b* are centred over the His and Arg codons of the peptide-coding region. Ribosomes stalled at these positions would block pairing of 1A with 2A, and 1B with 2B, but would not interfere with pairing of 2A with 3. These schematic representations are based on the findings in Table 1 showing that starvation for His, Trp or Arg relieves transcription termination at the *trp* attenuator of *S. marcescens*. Starvation for proline, a residue not present in the leader peptide, has no effect. These observations support the conclusion derived from comparable studies performed with *E. coli*[6] and suggest that attenuation is regulated through ribo-

---

* Present address: Division of Biology, California Institute of Technology, Pasadena, California 91109, USA.

0028-0836/82/260034—05$01.00

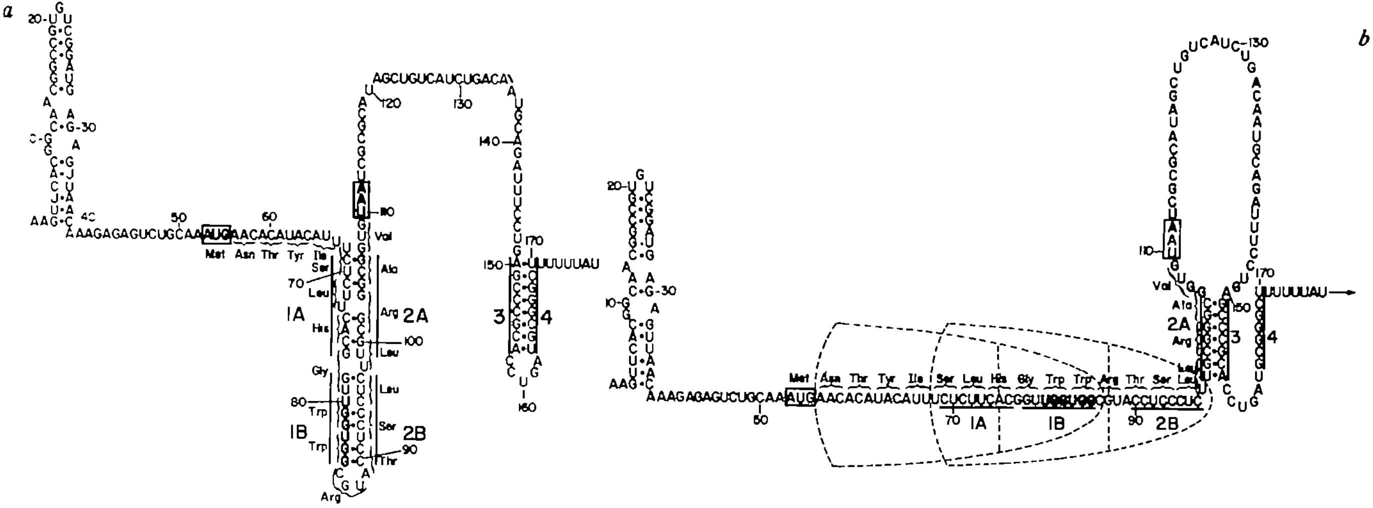
a
b
AGCUGUCAUCUGACA
AAAGAGAGUCUGCAAAUGAACACAUACAUU
Met Asn Thr Tyr Ile Ser Leu His Gly Trp Trp Arg Thr Ser Leu
Val
Ala
Arg
1A
1B
2A
2B
3
4
UUUUUUAU
Met Asn Thr Tyr Ile Ser Leu His Gly Trp Trp Arg Thr Ser Leu
AAAGAGAGUCUGCAAAUGAACACAUACAUUUCUCUUCACGGUUGGUGGCGUACCUCCCUC
UUUUUUAU

Fig. 1 . Secondary structure alternatives in the *S. marcescens trp* leader transcript. Numbering is from the presumed 5′ nucleotide of the transcript. The likely leader peptide initiation and termination codons are enclosed in boxes and the predicted amino acid sequence of the transcript is as reported[17] except for an additional A residue at position 150 The numbered RNA segments are those thought to participate in the various secondary structures that either cause or prevent transcription termination at the attenuator. The structures in *a* are predicted to form *in vitro*; hairpin loop 3:4 is believed to be the signal responsible for transcription termination. When the transcript is translated *in vivo* coincident with transcription of the *trp* leader region, structure 3·4 is thought to form and cause transcription termination. *b* Shows an alternative secondary structure. This structure, 2A.3, is believed to form in cells starved of His, Gly, Trp or Arg because the translating ribosome (schematically represented as dashed bullets stalled over His and Arg codons) stalls in the critical region of the transcript. Formation of structure 2A·3 prevents formation of structure 3·4, thereby preventing transcription termination. The various structures have the following calculated free energies of formation[19]· 1:2, $\Delta G = -4$ kcal mol^{-1} (see text for discussion); 2·3, $\Delta G = -19.6$ kcal mol^{-1}, 3.4, $\Delta G = -21.6$ kcal mol^{-1}. The hypothetical structure formed by pairing of nucleotides 3–19 with 23–27 has a theoretical $\Delta G = -1.8$ kcal mol^{-1}. To simplify discussion of potential secondary structures we have assumed that this structure forms We know of no function for such a structure

some stalling over a crucial segment of the transcript and not by the tryptophan deficiency *per se*.

If the role of the ribosome is simply to mask appropriate segments of the *trp* transcript, we could simulate such masking by deleting the corresponding segment of the transcript. Accordingly, we produced a set of overlapping deletions having both termini within the leader region. We selected those deletions that also removed the leader peptide ribosome-binding site and translation start codon to avoid the complication of translation. We describe here the *in vivo* analysis of the effects of these deletions on attenuation.

Analysis of deletion mutants lacking segments of the *trp* leader region of *S. marcescens*

Deletions around the *Hpa*I site, nucleotides 32–37, in the *trp* leader region were produced *in vitro* by exonuclease digestion, as described in the accompanying paper[18]. Each deletion mutant was characterized by DNA sequence analysis to determine the deletion junction. The leader regions containing deletions were then introduced into the chromosome in single copy form for operon expression studies. The recipient for these studies was an *E. coli* strain that lacked the *trp* repressor and had a deletion of *trpE* (*trpR* Δ *trpLE1413*). This deletion removes the *E. coli trp* attenuator and *trpE*, resulting in the production of sufficiently high levels of the *trpD* protein of *E. coli* to activate a broad range of levels of *S. marcescens trpE* protein. Cultures were either grown with excess tryptophan or starved of this amino acid. As the translation start codon of the leader transcript was deleted in all the deletions analysed, the +Trp values are most relevant to considerations of operon expression.

Figure 2*a* summarizes expression data for four deletions that remove the leader translation start codon. With the exception of deletion 221, operon expression, and presumably transcription readthrough, is reduced to 8–18% of the value obtained with the wild-type leader region. As documented in the accompanying paper[18], deletions that prevent translation of the peptide-coding region cause increased termination, or superattenuation. Presumably, in such strains secondary structure 1A–1B:2A–2B forms and prevents pairing of 2A with 3. Thus, 3:4, the terminator, forms at high frequency. In this explanation it is assumed that when the coding region is translated in wild-type, structure 2A:3, the anti-terminator, forms occasionally, leading to a moderate level of transcription readthrough. Deletion mutant 221 requires additional explanation. The sequence created by the deletion in this strain, CGGCC.AACAC (nucleotides 16–18 fused to nucleotides 56–58), is complementary to the 1A–1B junction (nucleotides 78–83, Fig. 2*a*) and conceivably could pair with this segment and thereby reduce the frequency of 1A–1B pairing with 2A–2B. Free 2A–2B would thus be available to generate the anti-terminator. Mutant 307, which differs from 221 by only one base pair (C is substitued by G at position 18), has fourfold lower expression. In agreement with this result, it can be calculated that this C→G substitution considerably reduces the theoretical estimate of the free energy of the potential secondary structure (from $\Delta G = -5.6$ to $\Delta G = +1.6$ kcal mol^{-1}).

The importance of segments 1A and 1B in the regulation of transcription termination is evident from analyses of deletions having endpoints in these segments (Fig. 2*b*). In general, as more of segment 1A–1B is removed, the level of observed *trpE* expression increases until it reaches values of ~400%, reflecting the absence of termination at the attenuator. Mutant 206 is an

Table 1 The effect of starvation for various amino acids on readthrough transcription in the *S. marcescens trp* operon

Growth conditions	% Of pulse-labelled RNA annealed to *S marcescens trpE* DNA	Relative *trpE* mRNA levels
Non-starved	0.13	(100%)
Trp-starved	0.62	476
Arg-starved	0.53	410
His-starved	0.46	353
Pro-starved	0.15	115

The numbers in the last column indicate the average structural gene *trpE* mRNA level expressed by λSm4 derivatives in *E. coli* starved for the particular amino acid, relative to the value obtained with a non-starved culture (100%). The results are averaged from six experiments. The error of the measurement is 20% of the number given. The non-starved λSm4 lysogen (*E coli* background, LS993 *trpR* Δ*trp ED24 argE his pro ilv*) was grown in minimal medium containing 0.05% casein hydrolysate, 0.2% glucose and 50 μg ml^{-1} of required amino acids. Samples of this culture were filtered, washed and starved of individual amino acids for 5 min before being pulse-labelled for 30 s at 30 °C with ^{3}H-uridine. The labelled RNA was hybridized in duplicate to plasmid pITS 9, which carries *S. marcescens trpE*, and the vector plasmid pACYC184 (ref. 24) The difference between these two values is indicated in the second column as a net per cent of the added label which was bound to filters It is taken as a measure of readthrough transcription beyond the attenuator.

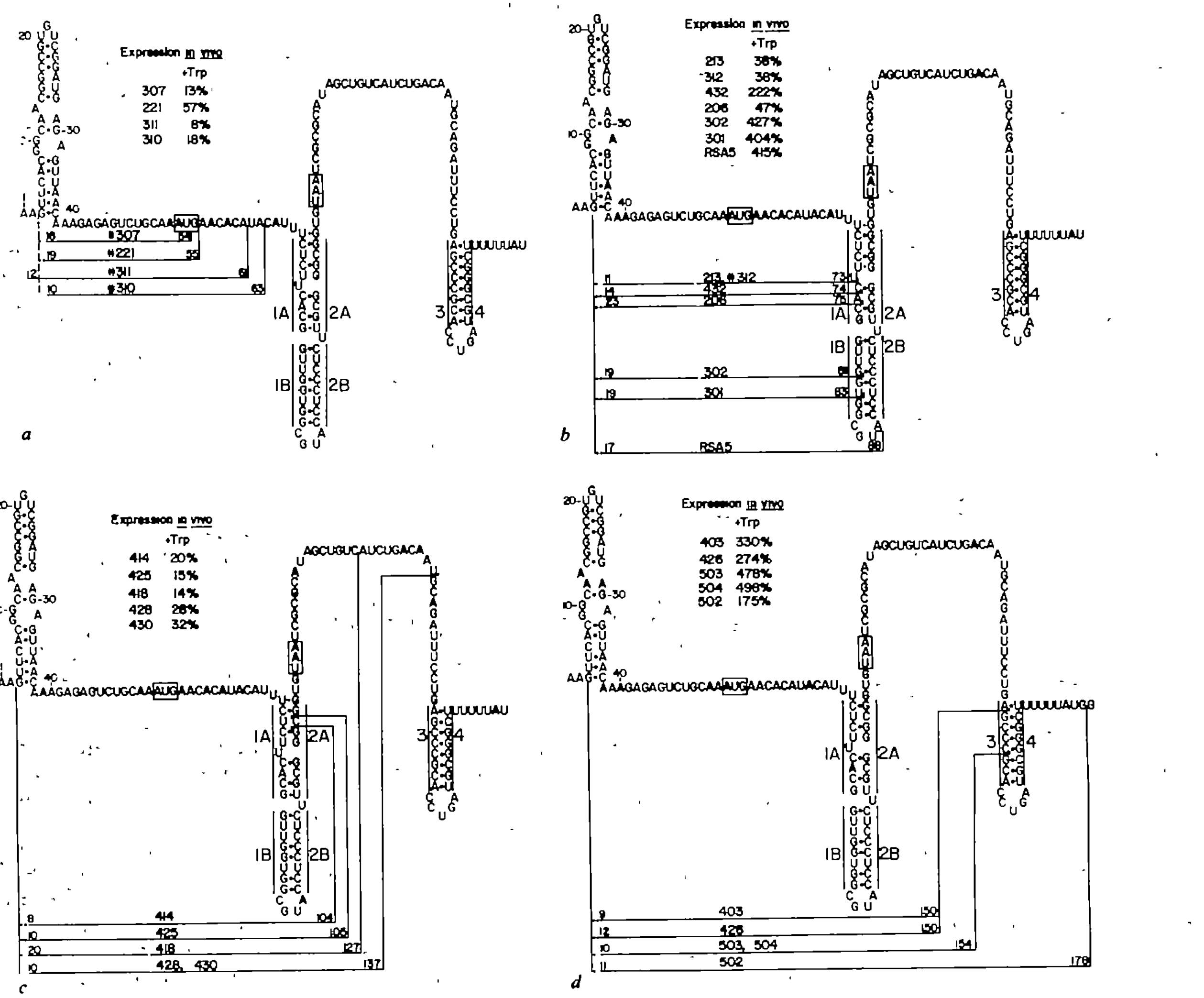

Fig. 2. Deletions in the *S. marcescens trp* leader region that remove the putative translation start codon and regions beyond, increase or decrease transcription termination at the attenuator. Small numbers at the end of the deletion bars indicate the outermost positions of the deleted nucleotides. Deletions are grouped according to the position of the right-hand endpoints. Expression *in vivo* represents the level of *trpE*-encoded anthranilate synthetase produced in *E. coli* strains carrying a single copy of the mutant *S. marcescens trp* leader region followed by an intact *trpE* gene. The numbers correspond to the per cent of the wild-type (*S. marcescens*) *trpE* expression in the same strain (W3110 *trpR* Δ*trpLE1413 tnaA2*/λgtSm4 wild type) grown with an excess of tryptophan. The results are averaged from at least three separate experiments. The experimental error is 20% of the values shown. For the determination of *trpE* enzyme levels the strains were grown at 30 °C in minimal medium[25] supplemented with 0.1% glucose, 0.05% acid-hydrolysed casein and 50 μg ml^{-1} of L-tryptophan. Cells were collected at a density of 6×10^8–7×10^8 per ml, washed with saline, resuspended in 0.1 M Tris-HCl (*p*H 7 8) and disrupted by sonication. Cell debris was removed by centrifugation and the levels of anthranilate synthetase component I were determined in the ammonia assay[26]. DNA sequence analyses were carried out by the method of Maxam and Gilbert[27]. *a*, Deletions which end before segment 1 cause superattenuation (see accompanying paper)[18]. *b*, Deletions which end in or near segment 1B generally cause high readthrough. *c*, Deletions which end between segments 2 and 3 cause increased termination. *d*, Deletions which remove all of segment 2 and part or all of segments 3 and 4 cause high readthrough.

exception to this pattern. Note, however, that the deletion in 206 allows nucleotides 17–20 (CCGU) to pair with segment 2A at positions 104–107 (GCCG), thereby conceivably restoring hydrogen bonding between segments 1 and 2.

The free energy of formation for the wild-type base-paired 1:2 structure, calculated by currently recommended rules[19], is $\Delta G = -4$ kcal mol^{-1}. We believe that this value may be a gross underestimate of the true stability of this structure. We feel that the theoretical bases for stability predictions do not take into account the unusual sequences present in structure 1:2. In particular, the high pyrimidine content of the interior loops and the possible contribution of tertiary interactions may markedly influence stability. From our observations we tentatively conclude that structure 1:2 is moderately stable. An alternative hypothetical structure can be deduced for 1:2, and will be discussed below.

Deletions which remove segments 1 and 2 result in superattenuation—*trpE* expression four- to sevenfold lower than that in wild-type (Fig. 2*c*). The behaviour of this class of deletions establishes that the terminator, 3:4, is the only secondary structure signal necessary to cause transcription termination at the attenuator. Deletion of increasing portions of the loop region separating segments 2 and 3 confirm this conclusion; the extent of termination in mutants of this class is essentially the same as in deletion mutants that simply remove the translation start codon. Thus, superattenuation is observed whether or not 1:2 exists and can form.

The final set of deletions are those having endpoints in region 3 or beyond 4 (Fig. 2*d*). These result in high levels of operon expression, suggesting that there is little or no termination. Surprisingly, deletions 403 and 426 largely eliminate termination yet they disrupt only one base pair of structure 3:4 (A–U, nucleotides 150 and 170). These deletions change the calculated ΔG for 3:4 from −21.6 kcal mol^{-1} to −19.4 kcal mol^{-1}. We do not know why these mutations have such a profound effect. In *E. coli*, the predicted stability of structure 3:4 in termination-deficient mutants that show two- to fourfold increased expression of the operon *in vivo* is reduced by ~50% (refs 5, 20). All these mutations, unlike the *S. marcescens* deletions, affect the central GC pairs of the terminator. Deletion 502 removes the entire terminator but the observed expression in this mutant is not as high as in deletion 503. Studies *in vitro* indicate that there is no transcription termination on templates with this deletion (I.S. and C.Y., unpublished). We hypothesize that as this deletion ends 26 nucleotides upstream from the *trpE* structural gene, it interferes with ribosome binding and initiation of translation of *trpE* mRNA.

A curious effect of tryptophan starvation

All the deletions described here remove the start codon for the leader peptide and consequently eliminate translation of the peptide-coding region. Nevertheless, we have found that every deletion mutant in which there is transcription termination at the attenuator responds to tryptophan starvation by exhibiting a 1.5–2-fold increase in anthranilate synthetase levels (data not shown). In contrast, deletion mutants that do not terminate transcription at the attenuator have identical anthranilate synthetase levels whether starved of tryptophan or not. The explanation for this observation is unknown. Perhaps the small increase is due to some general effect of starvation on transcription termination; this effect is being investigated further.

Alternative RNA secondary structures in the regulation of attenuation

We have examined the effects on gene expression of 21 deletions with endpoints entirely within the leader region of the *trp* operon of *S. marcescens*. Although our functional analyses were carried out in *E. coli*, we have shown that in this heterologous system the wild-type *trp* operon of *S. marcescens* is regulated by attenuation in a qualitatively identical manner to the *trp* operon of *E. coli*. We find that deletions within the *S. marcescens* leader region which remove the leader peptide start codon and different segments of the region beyond may increase, decrease or have no effect on transcription termination at the attenuator. The positions of the deletion endpoints and their effect on gene expression are summarized in Fig. 3. It is apparent that as the right-hand endpoint extends further into the leader region, transcription termination increases, then decreases, then increases again and finally is eliminated entirely compared with the wild-type. These findings are most readily explained in terms of the alternative secondary structure models schematically represented in Fig. 1.

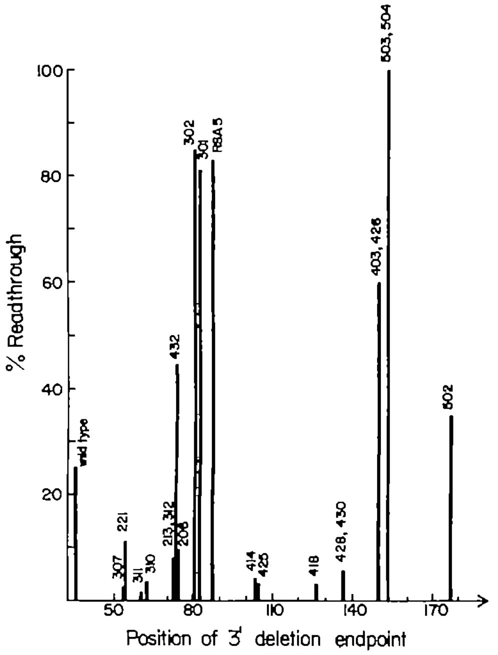

Fig. 3 Positions of right-hand deletion endpoints in *S. marcescens trp* leader mutants and the effect on *trpE* expression. The height of each bar represents the level of anthranilate synthetase produced during growth with tryptophan relative to the level observed in deletion mutants 503 and 504 (set at 100). The range of *S. marcescens trp* operon expression varies 30–60-fold in different deletion mutants. Maximum transcription termination is observed in the translation-defective deletion mutant, 311, in which readthrough occurs at ~10% that in wild type. By comparison, in the *E coli* initiation codon point mutant, *trpL29*, readthrough is ~25% that in wild type[20]

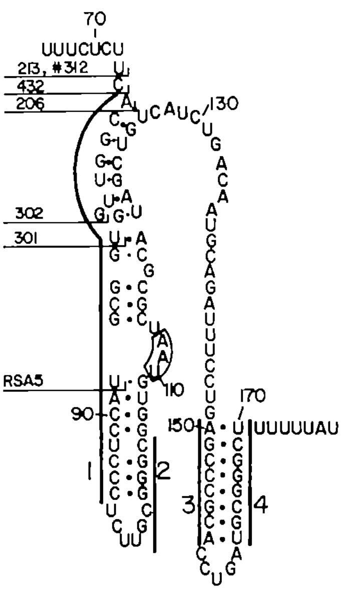

Fig. 4 An alternative potential secondary structure in the *S. marcescens trp* leader transcript The secondary structure labelled 1:2 is formed by the pairing of segments of the transcript other than those paired in the structures depicted in Figs 1 and 2 Note that segment 2 is identical in all the structures and can pair with either segment 1 or segment 3. The endpoints of the deletions described in Fig. 2*b* are indicated. Some of these deletions reduce termination at the attenuator (see text). The calculated ΔG value for the hypothetical structure shown involving nucleotides 75–126 is −23 kcal mol^{-1}, and for the portion of the structure involving nucleotides 88–109, −13 kcal mol^{-1}. In making these estimates it was assumed that a G · U base pair is equivalent to an A · U base pair.

Another potential 1:2 RNA secondary structure exists (Fig. 4); this structure is predicted to be more stable than structure 1:2 as drawn in Figs 1 and 2. However, the effect of deletions 432, 302 and 301 is inconsistent with the structure in Fig. 4, for these deletions should not reduce termination if structure 1:2 in Fig. 4 is correct, but should relieve termination according to structure 1:2 in Figs 1 and 2. In view of our findings, we prefer the secondary structure presented in Figs 1 and 2.

Several studies on attenuation in the *trp*[5–7,20,21] and *his*[22,23] operons support the assumption that changes in the secondary structure of the leader transcript mediate the regulatory response. The experiments described here were designed to test this assumption. The results obtained are in agreement with the secondary structure model and the expected consequences of deleting specific RNA segments that can participate in base pairing. Thus, we believe that the ribosome translating the leader transcript has no role other than sterically to prevent base pairing by the segment of RNA with which it is in contact. This conclusion is supported by the results of *in vitro* transcription studies with restriction fragments bearing the *Serratia* deletions described here (I.S. and C.Y., in preparation). In these studies we have found that in a minimal transcription system consisting of restriction fragments and RNA polymerase, the same pattern of increased termination and termination relief seen *in vivo* with our deletion mutants is reproduced *in vitro*. We conclude, therefore, that when the RNA terminator forms, the transcribing RNA polymerase molecule recognizes that structure and transcription termination occurs. The role of translation, ribosome stalling and alternative RNA secondary structure formation, is simply to regulate formation of the terminator.

These studies were supported by grants from the USPHS, the NSF and the American Heart Association. I.S. was a postdoctoral fellow of the American Cancer Society. C.Y. is a Career Investigator of the American Heart Association. We thank Magda van Cleemput for help with DNA sequence analyses and Roberto Kolter for stimulating discussions and a critical reading of the manuscript.

Received 16 February; accepted 23 April 1982.

1 Crawford, I. P. & Stauffer, G. V *A Rev. Biochem.* **49**, 163–195 (1980)
2. Yanofsky, C *Nature* **289**, 751–758 (1981).
3. Platt, T. *Cell* **24**, 10–23 (1981)
4. Lee, F. & Yanofsky, C. *Proc. natn Acad. Sci. U S A.* **74**, 4365–4369 (1977)
5. Stauffer, G. V., Zurawski, G. & Yanofsky, C. *Proc. natn. Acad. Sci U S.A.* **75**, 4833–4837 (1978).
6 Zurawski, G , Elseviers, D., Stauffer, G V & Yanofsky, C., *Proc natn. Acad Sci. U.S A* **75**, 5988–5992 (1978).
7. Oxender, D., Zurawski, G. & Yanofsky, C. *Proc natn. Acad Sci. U.S A.* **76**, 5524–5528 (1979)
8. Zurawski, G., Brown, K., Killingly, D. & Yanofsky, C. *Proc. natn Acad. Sci U S.A* **75**, 4271–4275 (1978)
9. Johnston, H M , Barnes, W. M , Chumley, F. G., Bossi, L. & Roth, J. R. *Proc natn Acad Sci. U S A* **72**, 508–512 (1975)
10. Gardner, J. F *Proc. natn. Acad. Sci U S.A* **76**, 1706–1710 (1979).
11 Gemmill, R. M , Wessler, S. R., Keller, E B. & Calvo, J. R *Proc natn Acad Sci U S A* **76**, 4941–4945 (1979)
12. Lawther, R P. & Hatfield, G. W. *Proc. natn. Acad Sci. U.S A* **77**, 1862–1866 (1980)
13 Nargang, F. E., Subrahmanyam, C S. & Umbarger, H. E. *Proc. natn Acad. Sci U S.A.* **77**, 1823–1827 (1980)
14. Manson, M & Yanofsky, C *J Bact.* **126**, 679–689 (1976).
15. Hutchinson, M A. & Belser, W L *J. Bact* **98**, 109–115 (1969)
16. Largen, M. & Belser, W L *Genetics* **75**, 19–22 (1973)
17 Miozzari, G. F & Yanofsky, C *Nature* **276**, 684–689 (1978).
18 Stroynowski, I , van Cleemput, M & Yanofsky, C *Nature* **298**, 38–41 (1982)
19. Tinoco, I *et al Nature new Biol.* **246**, 40–41 (1973)
20. Zurawski, G. & Yanofsky, C *J molec Biol* **142**, 123–129 (1980)
21. Winkler, M. E , Mullis, K., Barnett, J., Stroynowski, I T. & Yanofsky, C *Proc natn. Acad Sci. U.S.A* **79**, 2181–2185 (1982).
22. Johnston, H. M. & Roth, J R. *J. molec. Biol.* **145**, 713–734 (1980)
23. Johnston, H. M & Roth, J. R. *J. molec Biol.* **145**, 735–756 (1980)
24. Chang, A C Y. & Cohen, S. *J. Bact* **134**, 1141–1156 (1978).
25. Nogel, H. & Bonner, D. M *J biol. Chem* **218**, 97–106 (1956).
26 Zalkin, M & Ching, D. *Biochemistry* **7**, 3566–3573 (1968)
27. Maxam, A. & Gilbert, W. *Proc natn Acad Sci U S.A* **74**, 560–564 (1977)

Superattenuation in the tryptophan operon of *Serratia marcescens*

Iwona Stroynowski*, Magda van Cleemput & Charles Yanofsky

Department of Biological Sciences, Stanford University, Stanford, California 94305, USA

Deletions were generated in vitro *in the leader region of the tryptophan operon of* Serratia marcescens *and subsequently incorporated into the* Escherichia coli *chromosome in single copy form. Deletions which removed the translation start codon for the leader peptide or which ended in the ribosome recognition region preceding the leader peptide coding segment, caused superattenuation, that is, increased transcription termination at the attenuator. Apparently, the capacity to initiate translation of this coding region modulates expression of the operon.*

THE tryptophan (*trp*) operon of each of the six enterobacterial species that have been studied (refs 1–5 and M. Blumenberg and C.Y., in preparation) is controlled at the level of transcription termination by a mechanism called attenuation. In each *trp* operon, translation of a short peptide coding region in the initial, leader segment of the transcript seems to regulate the formation of alternative secondary structures, one of which is recognized by RNA polymerase as a transcription termination signal. It has been proposed that in cells which have an adequate supply of Trp-$\mathrm{tRNA}^{\mathrm{Trp}}$, translation proceeds to the end of the coding region, thereby favouring formation of the RNA secondary structure that serves as the termination signal. However, when most of the cellular $\mathrm{tRNA}^{\mathrm{Trp}}$ is uncharged, the ribosome translating the peptide coding region of the transcript stalls at one of two adjacent Trp codons, generating an alternative RNA secondary structure that excludes formation of the termination structure.

Studies with *Escherichia coli* mutants defective in the regulation of transcription termination at the *trp* operon attenuator[6] suggest that translation of the peptide coding region is utilized for two purposes. First, translation mediates the regulatory response to changes in the level of charged $\mathrm{tRNA}^{\mathrm{Trp}}$. Second, translation establishes the moderate level of transcription read-through that is characteristic of cultures growing with excess tryptophan. Thus, there is fourfold increased transcription termination at the attenuator of a leader mutant in which the start codon for the leader peptide has presumably been inactivated. This observation suggests that attenuation is modulated by the ability to initiate translation as well as by tryptophan availability.

Here we describe the production of deletions within the *trp* leader region of *Serratia marcescens* and analyse the effects of those that alter RNA segments believed to be essential for initiation of synthesis of the leader peptide. Our findings indicate that elimination of translation initiation results in increased transcription termination at the attenuator, or superattenuation.

Directed *in vitro* deletion mutagenesis in the *trp* leader region of *S. marcescens*

Deletions were generated around the *Hpa*I site at position 34/35 of the leader region by limited digestion with *Bal*31 exonuclease[7] (Fig. 1*a*). This exonuclease acts quasi-processively at both 3′ and 5′ termini of double-stranded DNA to release 5′ mononucleotides; digestion predominantly produces blunt ends[7]. There are two *Hpa*I sites in the *trp* regulatory region; *trp* repressor was added to protect the *Hpa*I site in the promoter. However, as *Bal*31 digestion of the promoter would inactivate it, strains with such deletion plasmids would not be detected in the subsequent step requiring *trpE* expression. Following *Bal*31 digestion, ligation and transformation, plasmids were isolated from individual transformants and screened for deletions in the desired region by examining the size of the single *Eco*RI fragment that contains the *trp* regulatory region, and by mapping restriction sites within the fragment. The distribution of deletion endpoints in the mutants was further characterized by DNA sequence analysis[8] and is shown in Fig. 2. There is asymmetry in the length of the segment deleted on either side of the *Hpa*I site, presumably because deletions extending into the *trp* promoter are not recovered.

Expression of deletion mutants

The effect of the deletions on attenuation was determined after introducing each deletion into the chromosome, in single copy form, as outlined in Fig. 1*b*. Briefly, phage $\lambda gtSm4Cm^r$ was grown in a bacterium with each deletion plasmid and the lysate obtained was used to transduce a *trpR trpE* deletion strain to Trp$^+$. Control experiments showed that lysogens prepared with a homologous phage that has *trpE*$^+$ and the 22 base pairs

---

* Present address: Division of Biology, California Institute of Technology, Pasadena, California 91109, USA.

0028-0836/82/260038—04$01.00

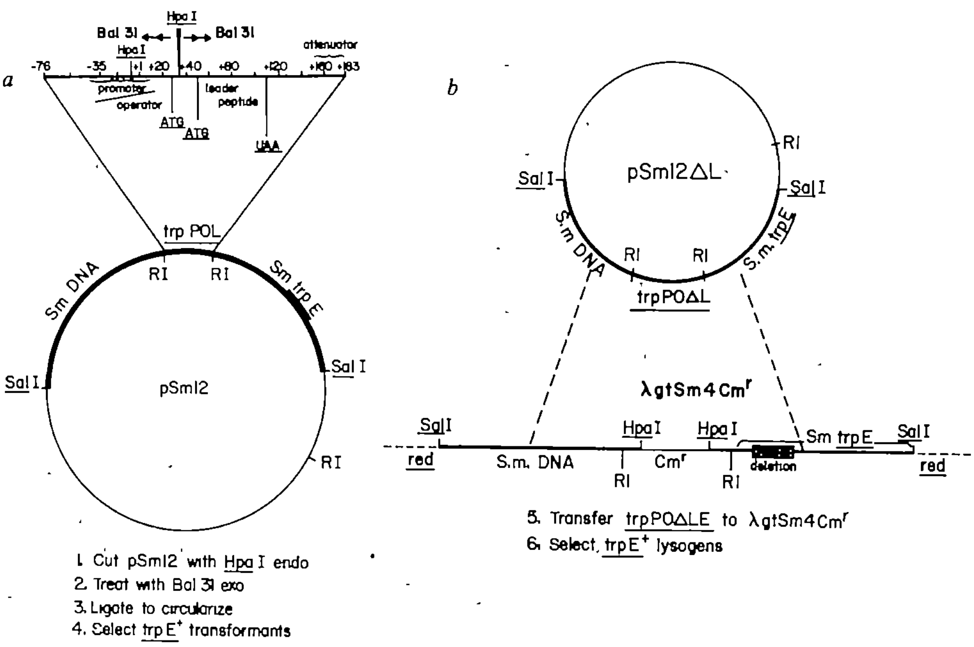

Fig. 1 Deletion mutagenesis of the *trp* leader region of *S. marcescens* (*a*) and introduction of deletions into the *E. coli* chromosome (*b*). Deletions were generated in plasmid pSM12[4]. The *EcoRI* fragment containing the regulatory region of the *S marcescens trp* operon is shown enlarged at the top of the figure (*a*). Number +1 corresponds to the presumed site of transcription initiation The 'in-phase' AUG and UAA codons indicate the potential coding region for the leader peptide. Deletions were generated around the *Hpa*I site at position 34/35. To ensure preferential cutting at this site, partial digestion with *Hpa*I was done in the presence of *E. coli trp* repressor, which is known to protect the *Hpa*I site at postion −11/−12 from cleavage[4]. 20 μg of partially digested DNA was treated with *Bal*31 exonuclease in a reaction mixture containing 20 mM Tris-HCl *p*H 8.1, 200 mM NaCl, 12 mM $CaCl_2$, 12 mM $MgSO_4$ and 1 mM Na_2EDTA in a 300 μl total volume. The reaction mixture was incubated on ice and samples were taken after 1 and 15 min, the mixture was transferred to room temperature, and samples were taken after an additional 1, 4 and 6 min The reactions were stopped by adding 10 mM EDTA *p*H 8 and the DNA precipitated with ethanol. 1 μg of DNA from each sample was resuspended in 200 μl of ligation buffer (60 mM Tris-HCl *p*H 7.6, 10 mM $MgCl_2$, 1 mM ATP). The mixtures were incubated in the presence of T4 DNA ligase for 2–4 h at room temperature and used directly to transform *E. coli* strain JA221 (C600 r^-m^+ Δ *trpE5 thr leu recA*) to Trp^+. The plasmid DNA from the transformants was analysed by digestion with *Eco*RI and *Hin*fI restriction enzymes. Approximately 25% of the plasmids carried a deletion of the *Hin*fI site at postion 43/47 and preserved the integrity of the *Eco*RI sites bordering the *trppoL* region These plasmids were used to transform W3110 *trpR* Δ *trpE5 tnaA2* to Trp^+ and were analysed further by sequencing[8]. The regulatory region containing each deletion was transferred to phage λ and then into the *E coli* chromosome by general recombination and lysogenization as shown schematically in *b*. To promote recombination, *E. coli recA*⁺ strains containing the mutant plasmids were infected lytically with bacteriophage λgtSm4Cmʳ. The lysates were used to lysogenize strain W3110 *trpR* Δ *trpE5 tnaA2* at a permissive temperature (30 °C). The recombinants were identified as Trp^+ prototrophs, temperature sensitive and unable to grow in the presence of 25 μg ml^{-1} of chloramphenicol To ensure single copy lysogeny the infections were performed at low multiplicity (<0.001). Bacteriophage λgtSm4Cmʳ was constructed by recombinant DNA techniques using DNA from λgt4 (Ron Davis, personal communication), pSM12[4] and pACYC184[17].

preceding it intact, but lacks the *S. marcescens trpPOL Eco*RI fragment, have less than 0.1% of the wild-type level of anthranilate synthetase (*trpE*⁺) activity and are phenotypically Trp^-. Thus, *trpE*⁺ expression from our leader deletion lysogens must originate at the *trp* promoter in the *Eco*RI segment. This conclusion was substantiated by introducing *trpR*⁺ into some of these strains and showing that *trpE* expression was under *trp* repressor control.

In Fig. 3 we indicate the sequence of the leader transcript segment containing each deletion junction. Also shown is *trpE* expression relative to that of a control culture containing the unaltered wild-type leader region. The first four deletion mutants, 204–208, have the wild-type sequence in the ribosome binding region for leader peptide synthesis[9]. These strains exhibit wild-type levels of anthranilate synthetase and respond to tryptophan starvation by a four- to five-fold increase in synthetase levels. The fifth deletion mutant, 102, has half the wild-type levels both in the presence of and following starvation for, tryptophan. Note that the sequence in the ribosome binding region is altered although homologous GAG sequences are located slightly earlier than in wild type. We interpret the findings with this mutant as indicating that translation initiation does occur at the 102 AUG start codon but is somewhat reduced in frequency relative to that of the wild type.

The second group of deletions, represented by seven independently isolated deletion plasmids, have a considerably different effect. Strains with these deletions have 8–10-fold reduced anthranilate synthetase levels compared with the wild type;

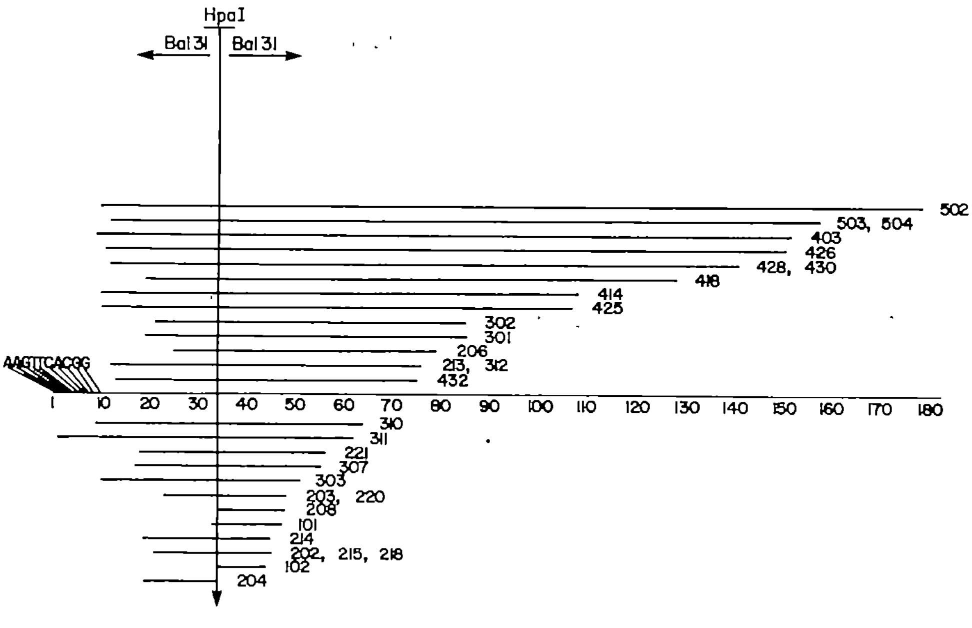

Fig. 2 Distribution of deletion endpoints in the *S. marcescens trp* operon leader region Numbering is from the presumed site of transcription initiation. The site of *Hpa*I cleavage and direction of *Bal*31 digestion are indicated by arrows The nucleotide sequence of the first 10 residues is shown on the left.

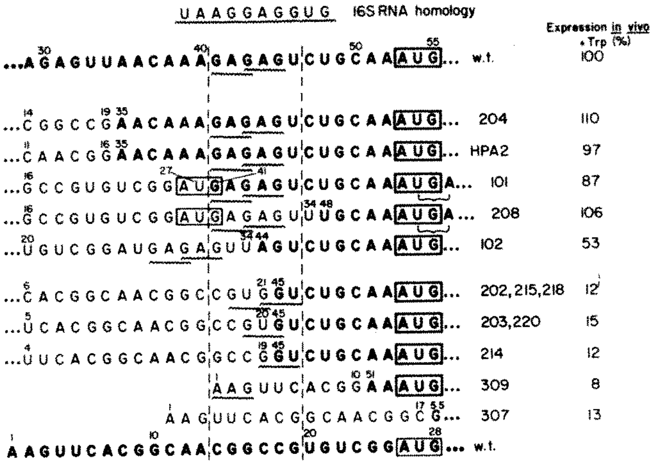
UAAGGAGGUG 16S RNA homology
Expression in vivo +Trp (%)
...AGAGUUAACAAAGAGAGUCUGCAAAUG... w.t. 100
...CGGCCGAACAAAGAGAGUCUGCAAAUG... 204 110
...CAACGGAACAAAGAGAGUCUGCAAAUG... HPA2 97
...GCCGUGUCGGAUGAGAGUCUGCAAAUGA... 101 87
...GCCGUGUCGGAUGAGAGUUUGCAAAUGA... 208 106
...UGUCGGAUGAGAGUUAGUCUGCAAAUG... 102 53
...CACGGCAACGGCCGUGGUCUGCAAAUG... 202,215,218 12
...UCACGGCAACGGCCGUGUCUGCAAAUG... 203,220 15
...UUCACGGCAACGGCCGGUCUGCAAAUG... 214 12
AAGUUCACGGAAAUG... 309 8
AAGUUCACGGCAACGGCG... 307 13
AAGUUCACGGCAACGGCCGUGUCGGAUG... w.t.

Fig. 3 The nucleotide sequence of the segments of the leader transcript containing deletion junctions. The former positions of the fused nucleotides are indicated by small numbers. The mutant sequences are aligned at wild-type position 55 and compared with the wild-type sequence at the top and bottom of the figure. The presumed initiation codon is boxed by a heavy line, while the AUG which is thought not to function as a translation initiation codon is boxed by a thin line. Nonsense UGA codons which are in phase with AUG codons are bracketed. Complementarity to 16S rRNA is underlined by wavy lines. Vertical broken lines show the region thought to be important in ribosome binding and initiation of leader peptide synthesis. Numbers referring to expression *in vivo* refer to per cent of wild-type *trpE* expression measured in the same strain containing the wild-type region. Growth conditions and assays of *trpE* enzyme activity are described in Fig. 2 legend of the accompanying paper.

these levels are increased only slightly when the strains are starved of tryptophan (see accompanying paper[10]). These deletions have in common changes in the nucleotide sequence of the ribosome binding region. However, in each case we can indicate some new sequence that is complementary to the 3′ end of 16S rRNA. We interpret these findings as indicating that in these deletions there is little or no translation initiation at the normal AUG start codon, and that the absence of translation is responsible for reduced *trpE* expression. The final mutant, 307, deletes through the start codon; it behaves indistinguishably from the preceding group of seven.

At the bottom of the Fig. 3 we present the sequence of the first 28 nucleotides of the transcript. There is a potential AUG start codon at positions 26–28 that is in-phase with the AUG at 53–55. We believe that this AUG codon is not used as a site of translation initiation, for the following reasons. First, deletions which remove this region are phenotypically indistinguishable from wild type. Second, fusion of this region in deletions 101 and 208 places the first AUG out of phase with the second AUG, but in-phase with a UGA stop codon that overlaps that second AUG. If the first AUG were used as a site of translation initiation we would expect that translation from this site would interfere with in-phase translation of the tryptophan codons, which must occur in view of the tryptophan starvation response. Thirdly, if translation were initiated in wild type at the first AUG, several amino acid residues including Arg would be added at the amino-terminal end of the leader peptide. Yet arginine starvation relieves transcription termination at the attenuator[10], implying that in the absence of this amino acid a ribosome can reach—and stall at—the Arg codon located immediately following the tandem Trp codons. Finally, there are no sequences resembling a Shine–Dalgarno sequence in the appropriate segment of the transcript (Fig. 3).

Significance of reduced operon expression in mutants with altered leader peptide translation initiation regions

The increase in transcription termination at the attenuator in deletion mutants implies that in wild type there is some mechanism responsible for establishing a moderate level of transcription readthrough and hence operon expression in cultures growing with excess tryptophan. The superattenuating deletions have in common changes in the sequence of nucleotides believed to be required for efficient ribosome binding; these changes presumably result in reduced initiation of synthesis of the leader peptide.

Alternatively, the leader segments could contribute to an RNA secondary structure involved in regulation. However, as deletions 204, HPA2, 101 and 208 lack segments of the same region yet exhibit wild-type expression and response, it seems likely that a defect in translation initiation is responsible for the observed reduction of expression. This interpretation leads to the conclusion that normal translation of the leader peptide coding region proceeds concomitantly with transcription and that ribosome movement or position is responsible for the moderate level of expression seen in wild type. In accordance with the model proposed previously[2] and supported by the findings in the accompanying paper[10], we conjecture that the anti-termination secondary structure, 2:3 forms occasionally when a ribosome translates the peptide coding region. This could occur by transitory masking of segment 1 by a sluggish ribosome, occasional pairing of segments 2 and 3 as the ribosome dissociates from the stop codon, or masking of segment 1 by a second ribosome on the transcript. The role of transcriptional pausing[11] in the synchronization of transcription with translation must be investigated before these or other explanations can be realistically distiguished.

Regardless of the basis for the moderate expression in wild type, our findings indicate that superattenuation could be used by the bacterium to achieve a level of *trp* operon expression well below that characteristic of cultures growing in the presence of excess tryptophan. Thus, if a cell were incapable of initiating

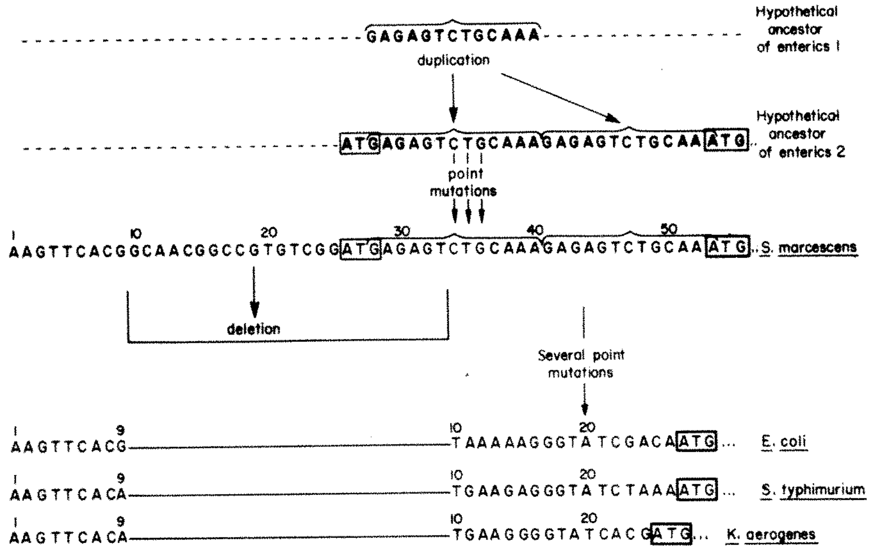
GAGAGTCTGCAAA
Hypothetical ancestor of enterics 1
duplication
ATGAGAGTCTGCAAAGAGAGTCTGCAAATG
Hypothetical ancestor of enterics 2
point mutations
1 10 20 30 40 50
AAGTTCACGGCAACGGCCGTGTCGGATGAGAGTCTGCAAAGAGAGTCTGCAAATG.. S. marcescens
deletion
Several point mutations
1 9 10 20
AAGTTCACG TAAAAAGGGTATCGACAATG... E. coli
AAGTTCACA TGAAGAGGGTATCTAAAATG... S. typhimurium
AAGTTCACA TGAAGGGGTATCACGATG... K. aerogenes

Fig. 4 A sequence of possible evolutionary events leading to the present-day nucleotide sequences of the *trp* leader regions of various enterics. In reality the postulated deletion event would have taken place in a common ancestor of the Enterobacteria, which could have had a nucleotide sequence somewhat similar to that of *S. marcescens.*

translation of the leader coding region, for whatever reason—a deficiency of formylating activity, lack of an initiation factor or a drastic decrease in the number of available ribosomes—this would be recognized as a signal to superattenuate. If this feature is common to all instances of attenuation control of amino acid biosynthetic operons, it is apparent that attenuation may be used generally to attain a greater range of operon expression than had previously been thought possible. Two mutations of the *his* operon leader region support this hypothesis[12,13]. They are phenotypically similar to our superattenuating deletions and are altered in the region potentially involved in translation initiation in *his* leader peptide synthesis. Studies on *trp* mRNA synthesis in *trpR* strains of *E. coli* following a nutritional or carbon source shift-up suggest that superattenuation may occur naturally in the wild-type operon[14].

Tryptophan starvation in strains with either the *E. coli* or *S. marcescens* wild-type *trp* operon results in operon expression approaching the level seen in leader deletion mutants that lack the attenuator. This finding suggests that in tryptophan starvation conditions translation initiation must be so efficient that virtually every *trp* mRNA molecule has a ribosome stalled over the Trp codons of the leader transcript. The view that the leader ribosome binding site is efficient is supported by *in vivo* and *in vitro* studies[15,16].

Possible duplication in the *S. marcescens* leader region

Comparison of the initial segment of the *trp* leader regions of several enterobacteria (Fig. 4) reveals that *S. marcescens* seems to have a 25-base pair insert. This region in *S. marcescens* contains a putative start codon that is in phase with the functional start codon at 53–55 (Fig. 2). The role, if any, of this extra segment is brought into question by the findings discussed earlier that deletions that remove this segment have no detectable effect *in vivo* on attenuation and its regulation. The RNA segment bases 3–19 can form a weak secondary structure with segment base 23–37 (see accompanying paper[10]); however, we know of no functional role for this pairing. We must consider the possibility, therefore, that the insert is a remnant of an ancestral sequence that once had a function. The sequence of a segment of the insert is strikingly similar to a proximal sequence, suggesting that the insert arose as a consequence of duplication. Presumably, a portion of one of the duplicated segments was deleted in the evolution of leader regions of the *E. coli* type. A sequence of possible evolutionary events is depicted in Fig. 4. One might imagine that the duplication arose initially in response to selection for a more efficient ribosome binding site or a requirement for simultaneous translation by two ribosomes. Some time thereafter the weaker of the two ribosome binding sites was inactivated to give the present-day sequence of *S. marcescens*, or deleted to produce the *E. coli* arrangement. In this regard it is of interest that *trpG* and *trpD* are separate, adjacent genes in *S. marcescens*[4] whereas in *E. coli* and other enterobacteria these genes are fused in what seems to be a more advantageous arrangement. Both this instance and the existence of the apparent non-functional insert in the *S. marcescens trp* leader region suggest that the *trp* operon of *S. marcescens* may be more primitive than its counterpart in *E. coli*. Support for this view awaits specific tests of the functional significance of the different genetic arrangements.

These studies were supported by grants from the USPHS, the NSF and the American Heart Association. I.S. was a Postdoctoral fellow of the American Cancer Society. C.Y. is a Career Investigator of the American Heart Association. We thank our colleagues for critical reading of this manuscript.

Received 16 February; accepted 23 April 1982.

1. Jackson, E. & Yanofsky, C. *J. molec. Biol.* **76,** 89–101 (1973).
2. Lee, F. & Yanofsky, C. *Proc. natn. Acad. Sci. U.S.A.* **74,** 4365–4369 (1977).
3. Lee, F., Bertrand, K., Bennett, G. & Yanofsky, C. *J. molec. Biol.* **121,** 193–217 (1978).
4. Miozzari, G. F. & Yanofsky, C. *Nature* **276,** 684–689 (1978).
5. Miozzari, G. F. & Yanofsky, C. *Proc. natn. Acad. Sci. U.S.A.* **75,** 5580–5584 (1978).
6. Zurawski, G., Elseviers, D., Stauffer, G. V. & Yanofsky, C. *Proc. natn. Acad. Sci. U.S.A.* **75,** 5988–5992 (1978).
7. Gray, H. B. *et al.* in *Gene Analysis and Amplification* Vol. 2 (eds Chinkjain, J. G. & Papas, T. S.) (North Holland, Amsterdam, 1981).
8. Maxam, A. M. & Gilbert, W. *Proc. natn. Acad. Sci. U.S.A.* **74,** 560–564 (1974).
9. Shine, J. & Dalgarno, L. *Proc. natn. Acad. Sci. U.S.A.* **71,** 1342–1346 (1974).
10. Stroynowski, I. & Yanofsky, C. *Nature* **298,** 34–38 (1982).
11. Winkler, M. E. & Yanofsky, G. *Biochemistry* **20,** 3738–3744 (1981).
12. Johnston, H. M. & Roth, J. R. *J. molec. Biol.* **145,** 713–734 (1980).
13. Johnston, H. M. & Roth, J. R. *J. molec. Biol.* **145,** 735–756 (1980).
14. Rose, J. K. and Yanofsky, C. *J. molec. Biol.* **69,** 103–118 (1972).
15. Schmeissner, V., Ganem, D. & Miller, J. H. *J. molec. Biol.* **109,** 303–326 (1977).
16. Miozzari, G. F. & Yanofsky, C. *J. Bact.* **133,** 1457–1466 (1978).
17. Chang, A. C. Y. & Cohen, S. *J. Bact.* **134,** 1141–1156 (1978).

LETTERS TO NATURE

Optical identification of X-ray source H0139−68 with an AM Herculis-type system

N. Visvanathan & A. Pickles

Mount Stromlo and Siding Spring Observatories,
Research School of Physical Sciences, Australian National University,
Private Bag, Woden Post Office, ACT 2606, Australia

We report here the identification of the soft X-ray source H0139−68 with a star at RA = 01 h 39 min 37.5 s, dec = −68° 08′ 32″ (1950). Time-resolved spectrophotometry of the star over 3 h shows a V magnitude variation between 14.9 and 16.4 with a period of ~110 min. The spectra are dominated by emission lines of neutral hydrogen, neutral helium and singly ionized helium throughout the period. The line ratios of the Balmer lines H_γ/H_β and the He I lines are flatter relative to case B recombination values, while the He II ratios are consistent with optically thin recombination. The mean radial velocity of the emission lines varies with the photometric period roughly sinusoidally from 340 to −150 km s^{-1}. The continuum is very red at maximum light, flat at minimum and shows strong polarization. These optical characteristics of the candidate star are similar to those of the magnetic cataclysmic variable AM Herculis.

The candidate star is marked X in Fig. 1, along with the X-ray source error circle of radius 36 arc s (ref. 1). Spectrophotometric observations of the candidate star were obtained on the night of 6 October 1981, with the 1DPCA[2] at the $f/8$ cassegrain focus of the Mount Stromlo Observatory 1.9-m telescope. We obtained 17 spectra of the candidate star in the time interval 15 h 20 min UT to 18 h 20 min UT, with a

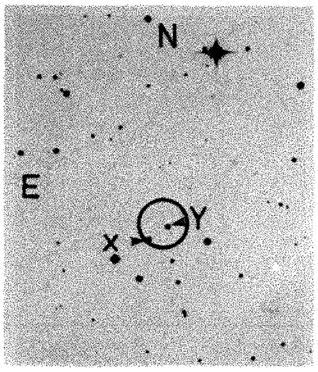

Fig. 1 The circle of diameter 72 arc s defines the X-ray source location, and X marks the optical identification with H0139−68. The coordinates of X are RA = 01 h 39 min 37.5 s, dec = −68° 08′ 32″ (1950). The star marked Y shows a late-type spectrum with no variability.

Table 1 *Line ratios in H0139 − 68*

Brightness phase	H_γ/H_β	He I $\lambda 5,016/\lambda 4,471$	He I $\lambda 5,876/\lambda 4,471$	He II $\lambda 5,411/\lambda 4,686$
Minimum	0.81	0.70	1.16	0.08
Rising	0.87	0.76	1.12	0.05
Maximum	0.83	0.64	1.24	0.05
Falling	0.78	0.67	1.21	0.04

time resolution of 10 min. The spectra cover the wavelength region 4,000–6,100 Å with a resolution of 3.2 Å. The star and sky apertures used had dimensions 3 × 7 arc s with a separation of 160 arc s. The absolute energy distribution of each sky-subtracted, wavelength-calibrated scan was computed by calibration of standard stars[3] observed in the same way as the candidate star. The sky transparency and seeing were good during the night, and the mean relative error in absolute flux is estimated to be 5%. Star Y in Fig. 1 was also observed, and found to have a late-type stellar spectrum, with no evidence for variability.

The apparent magnitude in the conventional *V* band has been computed for each scan, and is plotted as a function of time in Fig. 2*a*, where both universal time (UT) and Julian day (JD) of observation are given; 2σ error bars and the observational dwell time are also indicated. Figure 2*b* shows the corresponding variation with time of the fluxes computed in the lines of H I, He I and He II.

The significant feature in the visual light curve (Fig. 2*a*) is the deep minimum observed which is as much as 1.5 mag in amplitude and appears to repeat after ~110 min. Recent observations of the star[4] support the reality of this period. The emission line fluxes (Fig. 2*b*) also show variation with time, though with smaller amplitudes. Furthermore, the radial velocity of the emission lines (Fig. 4) shows a sinusoidal variation with a period about 110 min.

The above behaviour reveals that Star X is an eclipsing system where the deep minimum in the light curve corresponds to the mid-point of the primary eclipse. The unusual length of the primary eclipse (about 0.5 period) as well as the domination of the spectra during this period by emission lines indicate that the change of light that we see during the eclipse is not due to the primary star but mostly from a heated region a few radii from the primary. AM Herculis exhibits a similar light curve with a period of 186 min (ref. 5).

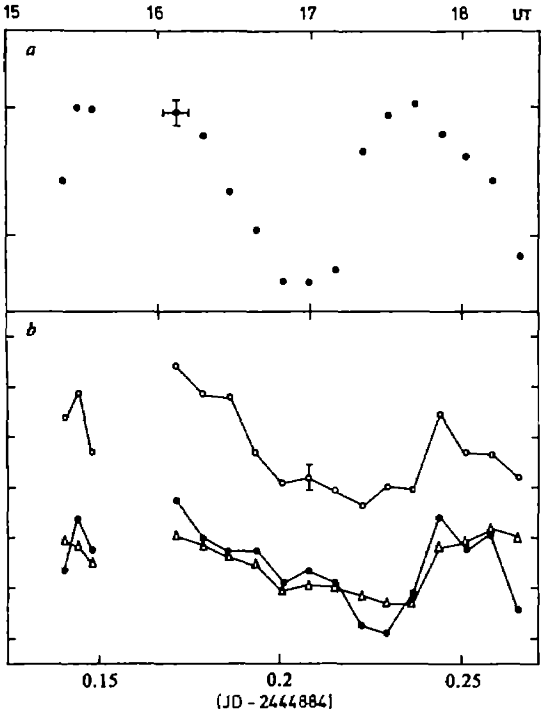

Fig. 2 *a*, The spectrophotometrically derived apparent *V* magnitude light curve for the star X: 2σ error bars, and observation dwell times are shown. A period of ~110 min is apparent. *b*, The emission line fluxes as a function of time of observation: 2σ error bars are shown. ○, H I; ●, He I; △, He II.

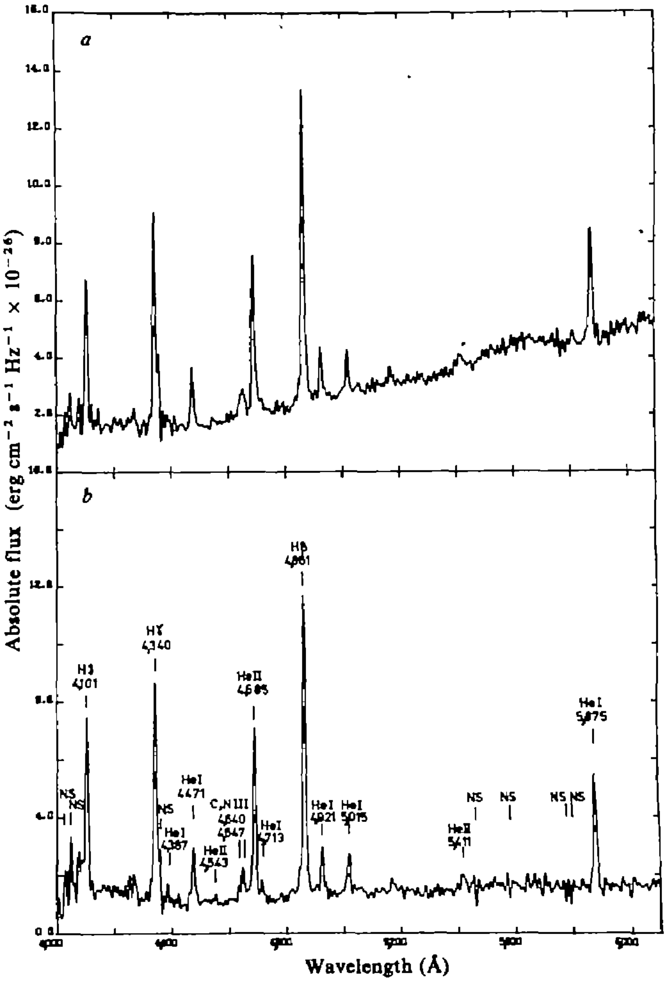

Fig. 3 The spectrum of star X at maximum (*a*) and minimum (*b*). Each spectrum is the average of four 10-min observations, and the spectra have been Fourier filtered to remove high-frequency noise. Emission lines due to H I, He I, He II, C III and N III are marked, residual night-sky features are labelled NS. The continuum is very red at maximum, and flat at minimum. The line-widths are smaller at minimum, as indicated by the resolved N III (λ4,640), C III (λ4,647) feature.

Figure 3 shows the absolute energy distribution of star X during its maximum and minimum brightness phases. Each spectrum shown is the average of four 10-min scans selected from the light curve at appropriate phases. It can be seen that the spectra are dominated by emission lines of H I, He I and He II: a feature due to N III (λ4,640) and C III (λ4,647) which is commonly seen in X-ray counterparts, is also apparent and is resolved at minimum. A detailed look at all the spectra indicates the presence of emission lines throughout the binary period (Fig. 2*b*).

The line ratio of the Balmer lines H_γ/H_β, given in Table 1, is found to vary little with phase. It is flatter relative to the case B recombination value for an optically thin gas[6]. This is true also for the He I lines and indicates that the emission regions observed are optically thick in these lines. Also the high value of 0.8 for the ratio of H_γ/H_β is suggestive of collisional excitation as well and implies an electron density as high as 10^{13} cm^{-3} in the line emitting regions[7].

Thus the emission spectrum of H I and He I reveal the presence of regions in the system which are optically thick and collisionally dominated. On the other hand, He II line ratios (Table 1) are consistent with optically thin recombination radiation indicating stratification of the line emitting regions.

Note that we do not see any stellar absorption features in the spectra at any phase. We deduce that any underlying stellar continuum contribution is <10% of the measured flux implying an apparent V_{mag} of 19 or fainter for any unseen stellar system.

More information on the line-emitting region can be obtained from the radial velocity data. The stronger H I, He I and He II lines have been fitted with gaussians to determine the line centres and line widths for each line of each scan separately. The measured line widths (σ of the fitted gaussian, expressed as velocity dispersion) have been corrected for instrumental broadening by quadratically subtracting the measured arc line width of 130 km s^{-1}. We are unable to detect any multiple components in the lines at any phase, but the instrumental resolution is insufficient to detect the presence of sharp components as seen in AM Herculis[8]. The radial velocity curve given in Fig. 4*a* shows a roughly sinusoidal variation with mean amplitude of $2K = 490$ km s^{-1}, asymmetrically distributed about velocity zero (with respect to the Sun). The line widths of the emission lines (Fig. 4*b*) also change with phase, with both maximum recessional velocity and maximum line width occurring near maximum light. The higher ionization species He I, He II display higher maximum recessional velocity and higher broadening at maximum than do the H I lines. These differences are significantly greater than the mean errors for single velocity or width determinations, which are indicated in Fig. 4*b*.

Part of the asymmetry in the radial velocity curve may be due to the unknown systemic velocity, but the large amplitude and variation in the line width with phase imply the presence of a gas stream. The radial velocity of the system is then dominated by streaming motions of a single mass transfer stream directed towards the primary. The orbital notion component for a typical system (with a red dwarf of mass ~0.2 $M_\odot$ and a white dwarf of mass 0.3 $M_\odot$) is derived as 80 km s^{-1}, with a maximum of 170 km s^{-1} for a white dwarf mass of ~1.4 $M_\odot$. Higher orbital velocities imply the presence of a large mass secondary which would be too luminous not to be seen. This mass transfer stream is consistent with models of AM Herculis[9,10] and VV Puppis[11] in which a single mass transfer stream from a late-type star overflowing its Roche Lobe, is funnelled down onto a magnetic white dwarf primary, with the magnetic field lines constraining the mass flow. In this model the velocity width would be due to the line-of-sight sampling of a range of velocities along the falling gas stream. The varying angle between the line-of-sight and the gas stream would account for the variation in line width with phase. The higher maximum recessional velocity and larger width of the higher ionization species, indicates that they originate closer to the primary, where the velocities are higher.

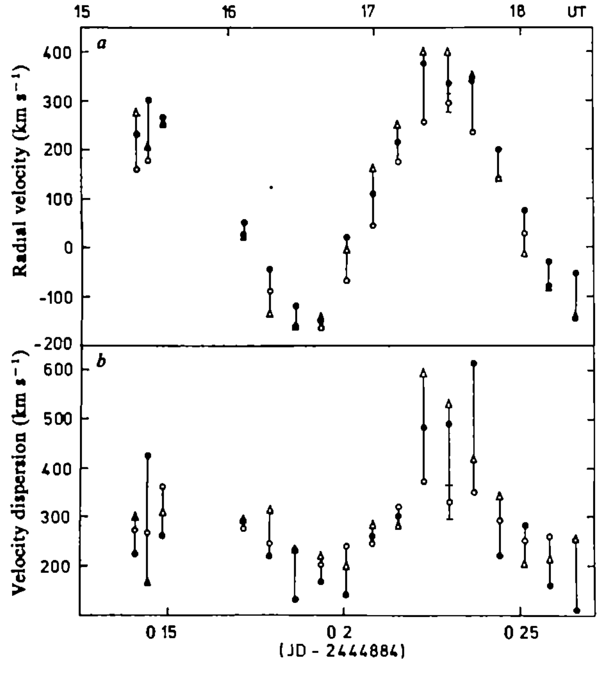

Fig. 4 *a*, The emission line radial velocities (w.r.t. Sun) of H I (○), He I (●) and He II (△) as a function of time of observation: 2σ error bars for a single observation are shown. *b*, The velocity dispersion (σ of fitted gaussian) of the emission lines as a function of time of observation. The instrumental broadening measured on arc lines has been quadratically subtracted. This figure shows that both maximum radial velocity and maximum velocity dispersion are higher for higher ionization species. There is some indication of phase shift between the different species.

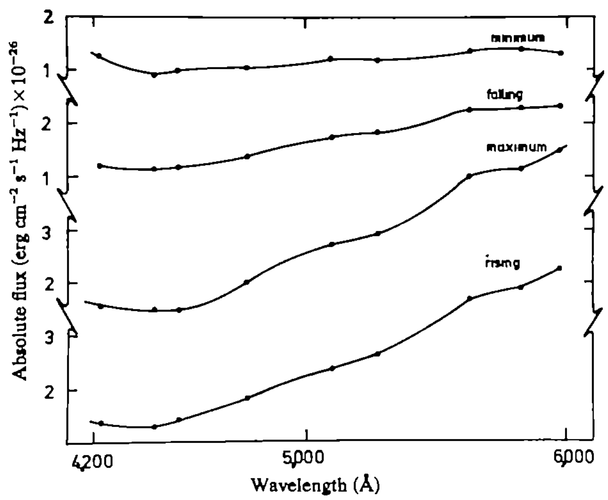

Fig. 5 The continuum flux as a function of phase. The marked points are the mean fluxes in regions away from emission lines, with freehand fits to the points shown. There is indication of cyclotron absorption troughs at maximum, at λ4,500 and λ5,400.

The absolute energy distribution in the continuum between 4,200 and 6,000 Å has been computed by averaging the line-free regions of each spectral scan, and plotting these points against wavelength for four different parts of the light curve (Fig. 5). It can be seen that the continuum is reddest during the rising and bright phases of the system, while it is flat during the faint and falling phases. This variation of the continuum is also seen in AM Herculis[10] and VV Puppis[11].

If we accept the model of matter transfer onto a magnetic white dwarf primary, then we might expect to see both linear and circular polarization in the optical continuum, due to the presence of cyclotron radiation at optical frequencies. Note that there is a suggestion of cyclotron absorption harmonics at 4,500 and 5,400 Å in the continuum at maximum (Fig. 5) and preliminary linear polarization observations indicate that the continuum is polarized as high as 7% close to maximum[12].

In summing up the evidence for this optical identification, we note that periodic variation of the continuum, line emission, and radial velocity of the candidate star reveals that the star is an eclipsing system. The spectra have bright emission lines of H I and He I originating in optically thick and high density regions in the system. The nearly sinusoidal radial velocity and velocity width variations with phase indicate the presence of a gas stream falling into the primary. The continuum colour varies with phase. Linear polarization of the continuum supports the cyclotron origin for the continuum observed, implying the presence of a magnetic white dwarf in the system[12]. Fast photoelectric photometry of the Star X indicates flickerings on a time scale of 100 s or less[4]. All these observed characteristics of the candidate star are seen in the binary system AM Herculis[10] which has been identified with a soft X-ray source[13]. Within 36 arc s of the Star X there is the X-ray source H0139−68 (ref. 1), a source originally detected with the low energy detectors of HEAO A-2 experiment and found to be highly variable over periods as short as 3 h. No flux was detected above 0.4 keV indicating a soft spectrum. Observations with the image proportional counter of the Einstein observatory confirmed the variability of the source and the presence of flickering on a time scale of 20 s or less.

Thus, the remarkable similarity between Star X and AM Herculis and the presence of the variable X-ray source H0139−68 very near to Star X, establish the Star X, a new AM Herculis type system, as the optical counterpart of H0139−68.

We thank P. C. Agarwal and G. R. Riegler for intimating the position of the variable X-ray source in advance of its publication. A. J. P. acknowledges the support of an Australian National University postgraduate scholarship.

Received 21 January; accepted 9 March 1982

1 Agarwal, P C., Rao, A. R , Riegler, G. R., Pickles, A. J. & Visvanathan, N *IAU Circ.* No 3649 (1981)
2 Stapinski, T. E , Rodgers, A. W. & Ellis, M J *Adv Electron Electron Phys* **52**, 389 (1979).
3. Oke, J. B. *Astrophys. J. Suppl.* **27**, 21–35 (1974).
4. Pickles, A. & Visvanathan, N. (in the press)
5. Szkody, P. & Brownlee, D. E *Astrophys. J. Lett.* **212**, L113–L116 (1977)
6 Osterbrock, D E *Astrophysics of Gaseous Nebulae* (Freeman, San Francisco, 1974)
7 Adams, W. M & Petrosian, V. *Astrophys. J* **192**, 199–205 (1974).
8. Greenstein, J. L , Sargent, W L W., Boroson, T A. & Boksenberg, A *Astrophys. J. Lett* **218**, L121–L127 (1977).
9. Chanmugam, G & Wagner, R L. *Astrophys J Lett.* **213**, L13–L16 (1977).
10. Stockman, H. S. *et al* *Astrophys J.* **217**, 815–831 (1977)
11. Visvanathan, N & Wickramasinghe, D T. *Mon Not R. astr Soc.* **196**, 275–288 (1981).
12. Visvanathan, N , Hillier, J & Pickles, A *IAU Circ.* No. 3658 (1982).
13 Hearn, D., Richardson, J & Clark, G. W *Astrophys. J. Lett.* **210**, L23–L26 (1976)

Zonal harmonic model of Saturn's magnetic field from Voyager 1 and 2 observations

J. E. P. Connerney, N. F. Ness & M. H. Acuña

Laboratory for Extraterrestrial Physics, NASA/Goddard Spaceflight Center, Greenbelt, Maryland 20771, USA

An axisymmetric octupole model of Saturn's planetary magnetic field is proposed here. This three parameter model, characterized by the Schmidt-normalized spherical harmonic coefficients $g_1^0 = 21{,}535$ nT, $g_2^0 = 1{,}642$ nT and $g_3^0 = 2{,}743$ nT, is extremely efficient in representing the main magnetic field of Saturn and reconciling the *in situ* magnetic field observations obtained by Pioneer 11 with those obtained by the Voyager 1 and 2 spacecraft. Saturn's unique magnetic field configuration is thus not that of a simple displaced dipole but rather appears to be the axisymmetric part of a complex dynamo field. This result is consistent with Stevenson's model of the interior of Saturn[1], in which the differential rotation of a metallic fluid shell above the active dynamo region attenuates all non-axisymmetric components of the dynamo field.

The first *in situ* observations of the magnetic field of Saturn were obtained by the Pioneer 11 spacecraft in September 1979[2,3]. Charged particle and magnetic field data both revealed a near perfect alignment of Saturn's magnetic dipole and rotational axes. Subsequent spherical harmonic analyses of the Pioneer 11 vector helium magnetometer observations[4] led to a model of Saturn's magnetic field ('Nominal 79 dipole') characterized by a dipole of 0.2 $G-R_S^3$ (where 1 Saturn radius R_S is 60,000 km) aligned with Saturn's rotation axis and offset to the north along the rotation axis by 0.05 R_S. [The units $G-R_S^3$ are dimensionally equivalent to standard units of magnetic dipole moment, the numerical value having been divided by the cube of the planetary radius.] Acuña *et al.*[5] considered an axisymmetric potential expansion of Saturn's magnetic field to order $n=2$ (quadrupole) and obtained from the Pioneer 11 fluxgate observations a g_2^0 coefficient of 1,500 nT, equivalent to a northward displacement of the dipole by ~0.04 R_S.

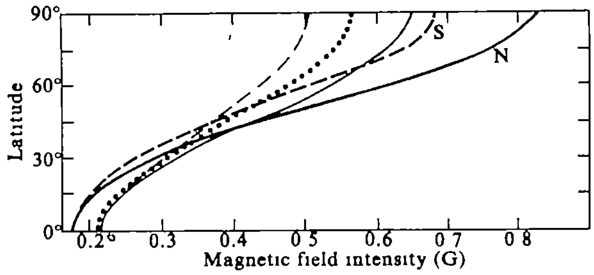

Fig. 1 Magnetic field intensity as a function of latitude on Saturn's oblate (flattening = 10.6) surface. Bold solid (dashed) line is the field intensity at north (south) latitudes corresponding to the Z_3 model (see text). Light lines indicate the field intensity of the offset (~0.04 R_S) dipole model and the dotted line corresponds to a simple centred dipole with 0.21 $G-R_S^3$ moment.

The Voyager 1 encounter with Saturn in November 1980[6] presented a second opportunity to study Saturn's planetary magnetic field. Voyager 1 approached to within 3.07 R_S of Saturn and obtained the first observations of Saturn's magnetic field at high latitudes (to 41°S). Analyses of the Voyager 1 observations confirmed many aspects of Saturn's main field deduced from the Pioneer 11 observations but did not confirm the inferred northward displacement of the dipole[6,7]. The near-equatorial Pioneer 11 approach to within 1.35 R_S yielded observations confined to a more limited range of latitude (±6°). The recent Voyager 2 encounter with Saturn (periapsis: 2.69 R_S) in August 1981[8] provided additional observations of Saturn's field at both high northern and southern latitudes (±30°). We now report the first internal field analyses to include the Voyager 2 vector magnetic field observations.

Our analysis of the magnetic field observations at Saturn uses the traditional spherical harmonic expansion of a scalar potential V from which the magnetic field is obtained through $B = -\nabla V$ (ref. 9). This representation requires that no sources be present within the minimum spherical shell enclosing the observations, and/or the region of representation, that is, that the volume of space $r_{\min} < r < r_{\max}$ contains no electrical currents ($\nabla \times B = 0$). The planetary field is characterized by the Schmidt-normalized coefficients g_n^m, h_n^m associated with the terms in V which decrease with increasing r. The external field is approximated by the first-order expansion corresponding to a uniform external field (G_1^0, G_1^1 and H_1^1). The external field is due primarily to an equatorial azimuthal ring current of ~7×10^6 A flowing between ~8 and 16 R_S (ref. 10). We therefore confine our analysis and modelling to observations obtained inside of 8 R_S. We use 48-s averages of the vector magnetic field data

Table 1 Model fits of Saturn's magnetic field from Voyager 1 and 2 observations

	Unconstrained ($n_{\max}=2$)			Axisymmetric ($n_{\max}=3$)		
	V1	V2	V1+V2	V1	V2	V1+V2
g_1^0	21,302	21,912	21,439	21,576	21,433	21,535
g_1^1	455	23	−143	–	–	–
h_1^1	343	−176	143	–	–	–
g_2^0	535	1,908	1,882	1,715	1,643	1,642
g_2^1	318	−1,452	−515	–	–	–
g_2^2	1,016	1	500	–	–	–
h_2^1	−815	−551	−433	–	–	–
h_2^2	851	351	−36	–	–	–
g_3^0	–	–	–	2,686	2,583	2,743
G_1^0	−9	−10	−9	−11	−8	−10
G_1^1	0	−2	−1	0	−1	−1
H_1^1	2	−1	0	0	−2	0
r.m.s.	1.9	2.4	3.1	3.0	2.5	3.2
Equivalent offsets (R_S):						
Δx	+0.0093	−0.0384	−0.0137			
Δy	−0.0222	−0.0142	−0.0120			
Δz	+0.0125	+0.0436	+0.0439			

All entries are in nT.

0028–0836/82/260044—03$01 00

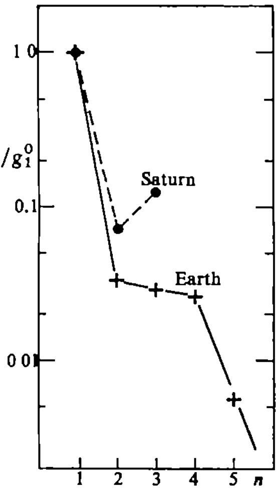

Fig. 2 Relative magnitude of the zonal harmonic (g_n^0) terms of the Earth's magnetic field and the Z_3 zonal harmonic model of Saturn's magnetic field.

obtained at 60-ms intervals to obtain least-squares model fits to the observations, with one exception. Data obtained by Voyager 2 during two brief roll manoeuvres performed near closest approach are included as field magnitude observations only, as the orientation of the spacecraft during these manoeuvres is uncertain (~2°). All of the models were obtained assuming equal weights for the individual observations and using the nonlinear inversion techniques described previously[11].

Our search for an appropriate physical model for Saturn's internal magnetic field can be traced through the model fits tabulated in Table 1. The notation *IjEk* denotes a spherical harmonic expansion with internal (*I*) coefficients to degree and order *j* and external (*E*) coefficients to degree and order *k*. Analyses of the Voyager 1 and 2 observations individually in terms of a physical model including dipole ($n = 1$) and quadrupole ($n = 2$) terms only leads to best fit parameters which, with the exception of the main dipole g_1^0 term, show little reproducibility from one spacecraft encounter to another. In particular, the expected north polar offset (g_2^0) obtained from the Pioneer 11 observations[3,4] is not to be found in the Voyager 1 (V1) *I2E1* model fit, but it does appear in the Voyager 2 (V2) *I2E1* fit (the spatial offsets of an equivalent tilted dipole derived from the *I2* coefficients are listed at the bottom of Table 1). An *I2E1* model fit to all of the Voyager observations results in reduced non-axisymmetric terms ($m \neq 0$) and a g_2^0 appropriate to a northward offset.

These results, and inferences on the axisymmetry of Saturn's magnetic field drawn from the charged particle observations at Saturn[12,13], and current models of Saturn's interior[1], motivated a conceptual model and inversion technique which favours zonal ($m = 0$) harmonics over tesseral ($n > m > 0$) and sectorial ($n = m$) harmonics. We accomplish this by introducing a renormalization of the model parameters $\bar{g}_n^m = g_n^m/100$ ($m \neq 0$). This is equivalent, in our search for a minimum length solution to the least-squares minimization, to *a priori* knowledge of the uncertainties of the parameter estimates[14]. This technique has the advantage that it allows non-axisymmetric components ($m \neq 0$) of the model to be introduced after the zonal harmonics to assess their importance. Details regarding the method of constructing solutions by sequential introduction of (independent) parameters can be found in refs 11, 15.

The results of these 'constrained' model fits are summarized in Table 1. Each solution uses only 3 of the 15 internal field parameters of an *I3E1* spherical harmonic expansion since we found that inclusion of non-axisymmetric internal field terms offered minimal improvement in the model fits. Analysis of the V1 and V2 observations individually in terms of a physical model consisting of zonal harmonics to the order of $n = 3$ leads to very consistent results. That is, the V1 model does an excellent job of predicting the magnetic field observed by V2 in a very different region of space, and vice versa. Thus, this third-order zonal harmonic model behaves as a proper model whereas models including dipole and quadrupole terms only do not.

We therefore propose as a model of Saturn's planetary magnetic field the third-order zonal harmonic model fitted to both V1 and V2 observations, listed in Table 1 and hereafter designated as the 'Z_3' model (zonal of order 3). No equivalent offsets are listed for the axisymmetric models because the relative magnitudes of the derived g_n^0 terms are inconsistent with a simple axially offset of the dipole. The ratio g_3^0/g_2^0 is too large by a factor of ~30 to be attributed to a dipole offset.

The Z_3 model is an extremely efficient representation of Saturn's planetary field, requiring only three parameters. It fits the combined V1 and V2 observations with little more than half the r.m.s. residual of a best-fitting axially offset dipole. Inclusion of a (small) fourth-order zonal harmonic (g_4^0) does not significantly improve the fit to the observations nor does it alter appreciably the values of the Z_3 model parameters. Much of the remaining difference (~3 nT r.m.s.) between the Z_3 model magnetic field and the V1 and V2 observed field is due to external sources (in addition to and distinct from the ring current, which itself varied between V1 and V2 observations) which are not well modelled by the uniform external field approximation used here.

The Voyager 1 observations suggest the presence of a large-scale current system, the exact geometry of which is as yet undetermined but is thought to involve $\sim 6 \times 10^6$ A of polar current flowing into Saturn's south pole. The unmodelled external field observed during the Voyager 2 encounter appears to be attributable to solar wind induced time variations in Saturn's magnetosphere. A better understanding of these external sources will probably be required before the Z_3 model can be improved, perhaps with the inclusion of (relatively small) non-axisymmetric terms. In its present form, however, the Z_3 model is consistent with the Pioneer 11, Voyager 1 and Voyager 2 magnetic field observations as well as the charged particle micro-absorption feature observed by the Voyager 2 CRS investigation[13] and identified with the satellite Tethys.

The Z_3 model leads to significantly enhanced polar surface field intensities on Saturn as shown in Fig. 1. Compare the surface field intensity of the Z_3 model as a function of latitude with that of an offset dipole model obtained by setting g_3^0 of the Z_3 model to zero, and that of a centred aligned dipole of moment $0.21\,G-R_S^3$. The maximum polar intensities in the north and south are ~0.84 and ~0.65 G, comparable with the Earth's ~0.7 G polar intensities. Note also that the equatorial surface field magnitude is reduced to ~0.18 G by the large g_3^0 term of the Z_3 model. The relative magnitude of the Z_3 model g_n^0 coefficients is compared in Fig. 2 with the relative magnitude of the Earth's axisymmetric g_n^0 terms[16]. Saturn's g_n^0 are larger in magnitude than those of the Earth.

Cowling's theorem[17] excludes the possibility of maintaining a steady state axisymmetric dynamo by fluid motions. It is possible, though improbable, that Saturn's highly axisymmetric field configuration is reflective of the decay phase of a magnetic field reversal[18]. More appealing is the suggestion that the dynamo itself is not axisymmetric[1] but only outwardly appears as such. If what we observe at Saturn is but the axisymmetric part of a complex Earth or Jupiter-like dynamo, the magnitude of Saturn's g_n^0 terms may be the only available observable relevant to Saturn's dynamo. The differential rotation of the metallic conducting shell above Saturn's dynamo in Stevenson's model[1] leads to an increase in the axisymmetric toroidal field deep within Saturn's interior. Some form of flux expulsion must inevitably occur to relieve the ever-increasing magnetic pressure. Could the process of flux expulsion result in a relatively short-lived and localized magnetic field anomaly unobserved by more distant spacecraft but sufficient to modulate Saturn's radio emission[19]? The lack of any detectable departure from axial symmetry remains the most enigmatic aspect of Saturn's unique magnetic field.

We thank our Voyager colleagues and our colleagues at the NASA Goddard Space Flight Center for useful discussions, also R. Thompson, F. Hunsaker, L. White, and the data processing and technical support staff at GSFC for their assistance.

Received 19 April, accepted 24 May 1982.

1 Stevenson, D. J. *Science* **208**, 746–749 (1980).
2. Smith, E. J. *et al. Science* **207**, 407–410 (1980)
3. Acuña, M. H & Ness, N. F. *Science* **207**, 444–446 (1980).
4. Smith, E J. *et al J. geophys Res.* **85**, 5655–5674 (1980).
5. Acuña, M H. *et al. J. geophys Res.* **85**, 5675–5678 (1980).
6. Ness, N F. *et al. Science* **212**, 211–217 (1981).
7 Acuña, M. H. *et al Nature* **292**, 721–724 (1981)
8. Ness, N. F *et al. Science* **215**, 558–563 (1982).
9. Chapman, S. J. & Bartels, J *Geomagnetism* (Oxford University Press, 1940)
10. Connerney, J. E P. *et al. Nature* **292**, 724–726 (1981).
11. Connerney, J. E. P. *J. geophys. Res* **86**, 7679–7693 (1981).
12. Simpson, J. A. *et al. J. geophys. Res.* **85**, 5731–5762 (1980).
13 Vogt, R E. *et al Science* **215**, 577–582 (1982)
14 Lawson, C. L & Hanson, R. J. *Solving Least Squares Problems* (Prentice-Hall, New Jersey, 1974).
15. Connerney, J. E. P. *et al. J. geophys. Res* **86**, 3623–3627 (1982)
16. Langel, R. A. *et al. Geophys Res. Lett.* **7**, 793–796 (1980).
17. Cowling, T. G. *Mon. Not. R. astr. Soc* **94**, 39–48 (1934).
18. Hide, R. *Nature* **293**, 728–729 (1981).
19. Kaiser, M L & Desch, M. D. *J. geophys Res.* (in the press).

Macroscopic evidence of molecular chirality in columnar mesophases

Jacques Malthête & Jean Jacques

Laboratoire de Chimie des Interactions Moléculaires, Collège de France, 11 place Marcelin Berthelot, 75231 Paris Cedex 05, France

Nguyen Huu Tinh & Christian Destrade

Centre de Recherche Paul-Pascal, Domaine Universitaire,
33405 Talence Cedex, France

Besides the classical liquid crystals observed with rod-like molecules (nematic and smectic mesophases) and plastic crystals obtained in the case of globular compounds, two new classes of thermotropic mesophases consisting of two-dimensional aromatic flat molecules have been investigated[1–3]: D columnar mesophases (columns of disk-like molecules in regular two-dimensional periodic array) and N_D nematic mesophase (disk-like molecules parallel to an average plane). We report here two examples of molecular chirality directly observable in D mesophases of a resolved disk-like compound.

Some hexasubstituted benzene[1], triphenylene[4–10], truxene[11–14] or anthraquinone[15,16] derivatives (Fig. 1) exhibit highly viscous and birefringent mesophases between the solid state and the isotropic liquid, which correspond to a columnar arrangement of diskoid molecules.

These columnar structures, denoted D in Fig. 2*a* legend, differ from one another by the symmetry group of the two-dimensional lattice and by the stacking, regular or not, of disk-like molecules in the columns[2]: hexagonal two-dimensional lattices (Fig. 2*b*) with order (D_{ho}) or disorder (D_{hd}) of the molecules in each column, rectangular two-dimensional lattice (Fig. 2*c*) with disorder of the molecules in each column (D_{rd}). The columns can be upright or tilted with respect to the molecular reference plane. A single example of strongly tilted columnar phase (D_t) has been observed (tilt angle ~55°)[9].

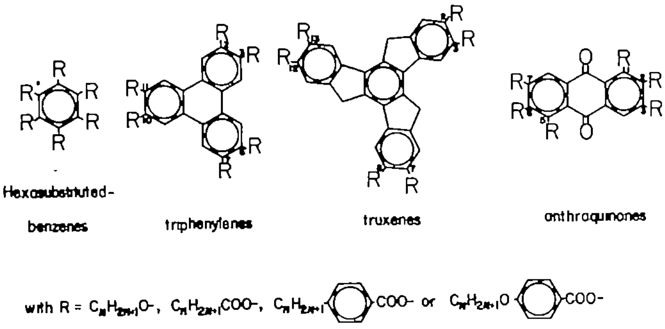
R
Hexasubstituted-benzenes
triphenylenes
truxenes
anthraquinones
with R = $C_nH_{2n+1}O-$, $C_nH_{2n+1}COO-$, $C_nH_{2n+1}-C_6H_4-COO-$ or $C_nH_{2n+1}O-C_6H_4-COO-$

Fig. 1 Mesogenic disk-like cores.

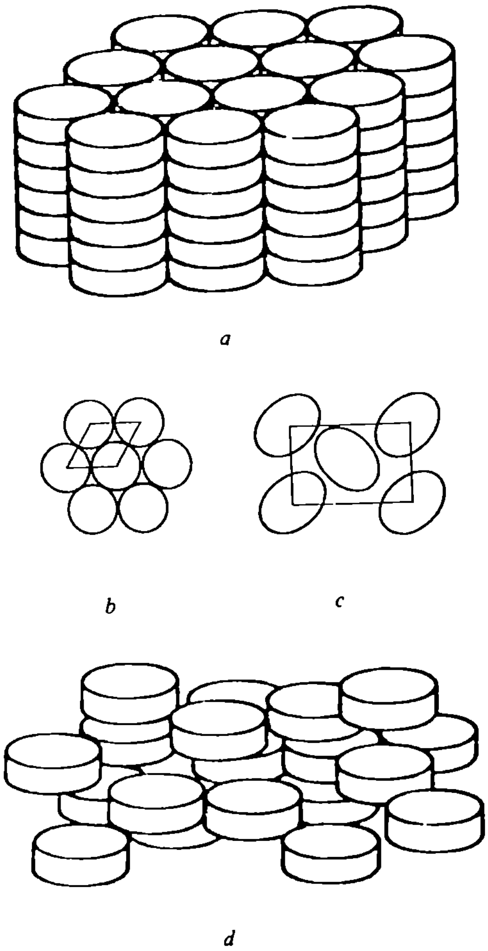

Fig. 2 *a*, Structure of columnar phase (with ordered disks). Schematic representation of hexagonal (*b*) and rectangular (*c*) phase lattices. D_{rd} phases are generally of the Pgg symmetry[17], but one example of Pmg symmetry has been described[15,16]. *d*, Structure of N_D nematic phase. The nematic nature of this phase has been checked by X-ray diffraction measurements[9].

A fluid phase (N_D) with optical schlieren texture, in any point similar to the classical nematic one, forms the second class of mesophases exhibited by disk-like compounds. This N_D nematic phase, in which the only order is a parallelism between flat cores (Fig. 2*d*), is observed with several hexa (*p*-alkyl or alkoxy) benzoyloxytriphenylenes[7–10] or truxenes[14] and with some hexaalkanoyloxytruxenes[11–13]. The chiral variant, cholesteric (N_D^*)[18,19], is obtained with optically active diskoid molecules.

We have recently described the two mesogenic enantiomers of the hexasubstituted triphenylene (*I*)[18]. Our first observations of the two successive thermotropic columnar mesophases of (+) or (−) (*I*) mounted between two glass slides and viewed under a polarizing microscope did not reveal any chirality in the medium. Nevertheless, we have shown that these substances could easily twist the N_D nematic phase of some hexabenzoyloxytriphenylenes as might be expected. Furthermore, we recently reported the existence of a N_D^* cholesteric phase for a pure disk-like compound[19].

The large analogy between columnar and smectic phases had given us an inkling of the existence of a twisting induced by

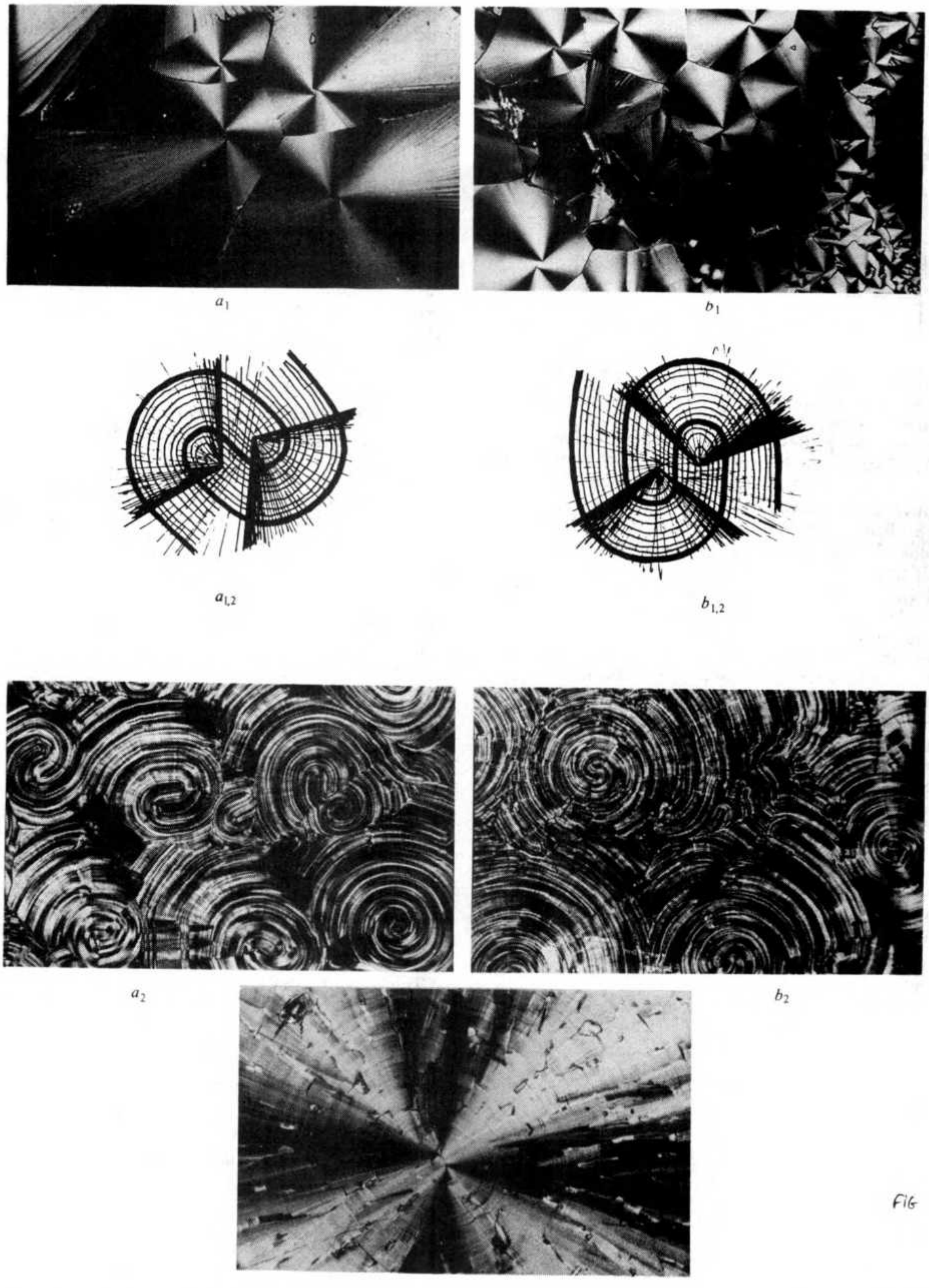

FIG

Fig. 3 *a*, (+)-(*I*); *b*, (−)-(*I*); *c*, (±)-(*I*). a_1 and b_1, enantiomorphic 'opposite points' in the D_{r1} phase (×100). $a_{1,2}$ and $b_{1,2}$, enantiomorphic 'opposite points' and spirals at $D_{r1} \rightarrow D_{r2}$ transition (schematic representations). a_2 and b_2, enantiomorphic spirals in the D_{r2} phase (×100). *c*, Racemic texture at $D_{r1} \rightarrow D_{r2}$ transition (detail). The two columnar phases of (*I*) were first identified with D_{rd} and D_{hd} owing to their textures and the miscibility of the low-temperature mesophase with some D_{rd} phases of hexaalkanoyloxytriphenylenes. But recent X-ray diffraction results on one enantiomer point out that the high-temperature columnar phase is, in fact, another rectangular phase with different symmetry. Pending more refined X-ray diffraction measurements we shall name the high temperature phase: D_{r1} and the low temperature one: D_{r2} (A. M. Levelut provided these preliminary data). (+)-(*I*) and (−)-(*I*) were purified by thin-layer chromatography on silica gel (using 10% acetone/hexane mixture as eluant) and recrystallized from ethanol/ether mixture. (+)-(*I*): $[\alpha]^{25}_{278} = +12.4°$ (c, 1 in chloroform) (Found: C, 74.70; H, 9.71; $C_{78}H_{120}O_{12}$ requires C, 74.96; H, 9.68). (−)-(*I*): $[\alpha]^{25}_{278} = -11.6°$ (c, 1 in chloroform) (Found: C, 74.81; H, 9.84; $C_{78}H_{120}O_{12}$ requires C, 74.96; H, 9.68). IR (neat) 1,770; 1,515; 1,255; 1,200; 1,125; 920 cm^{-1}. ^1H NMR ($CDCl_3$)δ 0.9 (*s*, 18 H), 1.1 (*d*, $J = 6.3$ Hz, 18 H), 1.35 (*s*, 60 H), 2.1 (*m*, 6 H), 2.5 (*m*, 12 H), 8.2 (*s*, 6 H).

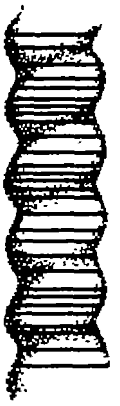

Fig. 4 Spiral column (with disordered optically active molecules).

optically active molecules in a tilted columnar phase (D_t) [18], as was the case with biaxial tilted smectics (S_C, S_F, S_I) composed of rod-like molecules[20,21].

The two columnar phases of (*I*) were first described as upright D_{rd} and D_{hd} phases[18]; consequently the absence of twisting with optically active solute molecules looked 'normal'. But some recent optical observations—in the case, for example, of (*I*) with R = *n*-alkanoyl chain (P. Oswald, personal communication)—seem to favour a slight tilt of the columns, and so we have made new observations on free droplets.

A careful re-examination of the two columnar mesophases of compound (*I*) allowed us to observe an evident chirality and to prove the existence of new chiral mesophases.

The transition temperatures (°C) of (+) or (−)-(*I*) are:

K 59 D_{r2} 64.5 D_{r1} 97.5 I (K, crystal; I, isotropic liquid).

The racemic mixture (±)-(*I*) melts at 47.5 °C and the isotropic phase appears at 95.5 °C.

On cooling isotropic free droplets, one can see—between crossed polarizers—near 96 °C, a fan-shaped texture consisting of only one type of pairs with 'opposite points'. Both enantiomers exhibit similar non-superposable figures, each one being the reflection image of the other (Fig. 3a_1, b_1). On further cooling, near the $D_{r1} \rightarrow D_{r2}$ transition, a spiralization of the medium is evident: some spirals are generated around the pairs of opposite points as shown in Fig. 3$a_{1,2}$, $b_{1,2}$. On heating immediately after the spiralization takes place, the effect remains up to the clarification point, but if the temperature is maintained for a few minutes a progressive change in the spiral figures can be seen. Once more we observe two antipodal figures (Fig. 3a_2, b_2). In addition the spirals reveal a periodicity of the oily streaks (note that, in all the figures, 'opposite points' and spirals are visible—but less clearly—between uncrossed polarizers).

In the case of an equimolecular mixture of (+)-(*I*) and (−)-(*I*), we observe, as expected, non-chiral figures resembling concentric rings (D_{r2}) or face-to-face 'opposite points' (D_{r1}) (Fig. 3*c*). We have noticed that many achiral disordered columnar phases ((*I*) with R = *n*-alkanoyl chain) consist of a statistical mixture of right- or left-handed spirals or opposite points in addition to some perfect achiral figures.

3-Methylnonanoic acids (R)-(+)-(*IV*) and (S)-(−)-(*IV*) have been prepared by a convenient adaptation of a procedure described by Prout *et al.*[22] from (S)-(+) and (R)-(−)-2-octanols (via the *p*-toluenesulphonates). Hexaesters (+)-(*I*) and (−)-(*I*) were obtained by interaction of the 3-methylnonanoyl chlorides (respectively from (R)-(+)-(*IV*) and (S)-(−)-(*IV*) with 2, 3, 6, 7, 10, 11-hexahydroxytriphenylene (*II*) prepared by heating the corresponding hexamethoxy derivative (*III*) with pyridine hydrochloride[23]. Compound (*III*) was prepared by treating veratrole with *p*-chloranil in sulphuric acid[24].

We have presented the first evidence of two rectangular columnar mesophases which form examples of a directly observable molecular chirality. Nevertheless, the chiral molecular packing in these media raises several questions:

- Why are the enantiomorphic figures clearly visible only on free droplets?
- Is each column chiral—as, for instance, one of the enantiomorphic spiral columns of St Peter's high altar in the Vatican City (Fig. 4)?
- Or is this phenomenon connected to a peculiar chiral packing on the surface of the mesomorphic droplet?

We are now carrying out optical studies and X-ray diffraction measurements to understand more closely the structure of these two mesophases.

We thank Dr J. Prost for cooperation, Dr A. M. Levelut and Professor Y. Bouligand for interest, discussions and some preliminary X-ray measurements.

Received 19 January; accepted 26 April 1982

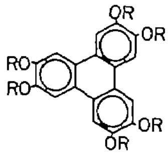

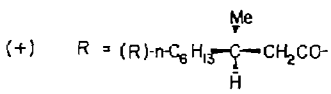

$(+)\quad R = (R)\text{-}n\text{-}C_6H_{13}\text{—}\overset{Me}{\underset{H}{C}}\text{—}CH_2CO\text{-}$ (*I*)

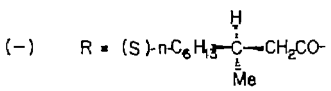

$(-)\quad R = (S)\text{-}n\text{-}C_6H_{13}\text{—}\overset{H}{\underset{Me}{C}}\text{—}CH_2CO\text{-}$ (*I*)

R = H (*II*)

R = Me (*III*)

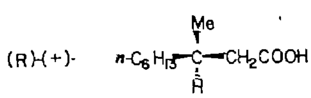

$(R)\text{-}(+)\text{-}\quad n\text{-}C_6H_{13}\text{—}\overset{Me}{\underset{H}{C}}\text{—}CH_2COOH$ (*IV*)

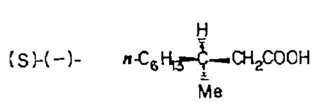

$(S)\text{-}(-)\text{-}\quad n\text{-}C_6H_{13}\text{—}\overset{H}{\underset{Me}{C}}\text{—}CH_2COOH$ (*IV*)

1. Chandrasekhar, S , Sadashiva, B. K. & Suresh, K A *Pramāna* **9**, 471–480 (1977).
2 Destrade, C., Nguyen Huu, Tinh, Gasparoux, H., Malthête, J. & Levelut, A. M *Molec. Cryst. Liq Cryst.* **71**, 111–135 (1981).
3. Billard, J. *Springer Series in Chemical Physics*, 383–395 (Springer, Berlin, 1980)
4. Billard, J., Dubois, J. C., Nguyen Huu, Tinh & Zann, A. *Nouv. J. Chim* **2**, 535–540 (1978).
5. Destrade, C., Mondon, M. C. & Malthête, J *J. Phys* **40C3**, 17–21 (1979)
6. Cotrait, M., Marsau, P., Destrade, C. & Malthête J *J Phys* **40**, L519–L522 (1979)
7 Nguyen Huu, Tinh, Bernaud, M C., Sigaud, G & Destrade, C *Molec Cryst. Liq Cryst.* **65**, 307–314 (1981)
8. Nguyen Huu, Tinh, Destrade, C & Gasparoux, H. *Phys. Lett* **72A**, 251–254 (*1979*)
9. Levelut, A M , Hardouin, F , Gasparoux, H , Destrade, C. & Nguyen Huu, Tinh *J. Phys.* **42**, *147–152* (*1981*)
10 Nguyen Huu, Tinh, Gasparoux, H & Destrade, C *Molec Cryst. Liq Cryst* **68**, 101–111 (1981)
11. Destrade, C., Malthête, J , Nguyen Huu, Tinh & Gasparoux, H *Phys Lett* **78A**, 82–84 (1980).
12. Destrade, C , Gasparoux, H., Babeau, A., Nguyen Huu, Tinh & Malthête, J. *Molec Cryst Liq. Cryst.* **67**, 37–48 (1981)
13. Nguyen Huu, Tinh, Malthête, J & Destrade, C. *Molec. Cryst Liq Cryst Lett*, **64**, 291–298 (1981)
14. Nguyen Huu, Tinh, Malthête, J & Destrade, C. *J Phys Lett* **42**, *L417–L419* (1981)
15 Queguiner, A., Zann, A., Dubois, J C. & Billard, J *Proc int. Liq. Cryst Conf*, Bangalore, *35–40* (Heyden, *London, 1980*)
16. Billard, J., Dubois, J C , Vaucher, C. & Levelut, A M *Molec. Cryst Liq Cryst.* **66**, 115–122 (1981).
17 Levelut, A M. *Proc int. Liq Cryst Conf*, Bangalore, 21–27 (Heyden, London, 1980).
18 Destrade, C , Nguyen Huu, Tinh, Malthête, J. & Jacques, J *Phys Lett* **79A**, 189–192 (1980).
19. Malthête, J., Destrade, C , Nguyen Huu, Tinh & Jacques, J. *Molec Cryst Liq. Cryst. Lett.* **64**, 233–238 (1981).
20 Keller, P , Jugé, S., Liébert, L. & Strzelecki, L *C.r Acad. Sci. hebd séanc*, *Paris* **282**C, 639–641 (1976)
21 Keller, P., Zann, A , Dubois, J. C & Billard, J *Springer Series in Chemical Physics*, 57–61 (Springer, Berlin, 1980)
22. Prout, F. S., Dickson, D. E & Klimkowski, R J *J org Chem.* **24**, 826–829 (1959)
23 Royer, R. & Demerseman, P. *Bull Soc. Chim Fr* 2633–2648 (1968)
24. Musgrave, O. C. & Webster, C J. *J. chem Soc C* 1397–1401 (1971)

Electron density images from imperfect data by iterative entropy maximization

Douglas M. Collins

Department of Chemistry, Texas A & M University,
College Station, Texas 77843, USA

Information theory provides a uniquely powerful apparatus for reconstructing an image from imperfect data in its dual space. An iterative procedure based on constrained entropy maximization is presented here for reconstruction of electron density from imperfect single-crystal X-ray diffraction data. In the ideal situation, continuous electron density, its periodicity given by the lattice, is the Fourier transform of an infinite set of structure factors whose squared moduli are observables. An ideal electron density is unattainable from experiment because of the common experimental inadequacies of incomplete and noisy data discussed by Gull and Daniell[1]. These inadequacies are partially overcome in the present procedure which yields true super-resolution and is economical even for protein crystal structures as illustrated.

Although Gull and Daniell[1] focused on radioastronomical applications, their maximum entropy solution for a best map of radio intensity from experimental data is quite general, and its formalism is appropriate to the X-ray crystallographic problem. Nevertheless, the formalism is unsatisfactory for many crystallographic applications on two counts. First, convergence properties are not characterized and appear to be undesirable as recourse to partial sums was required for convergence in the reported application[1]. Second, the formalism fails in the absence of noise; this is a common difficulty with many spectral analyses based on entropy maximization[2]. It could be argued that artificial introduction of noise is possible in the presumably few applications for which the naturally occurring noise level is inadequate. However unlikely, such a state of affairs in experiments carefully designed to minimize or offset natural noise constitutes a dilemma to be avoided.

A formalism, designed from the outset to result in an iterative procedure, for a maximum-entropy mapping of electron density can be readily composed with the aid of an approximation for the natural logarithm. We assume that the corresponding inexactness for the most part becomes immaterial on iteration as in any successive approximation procedure. It also will be assumed that the density functions and the experimental data are discrete samplings on regular grids appropriate to discrete Fourier transform algebra[3].

Consider that there is a positive definite trial electron density τ obtained from the transform of experimental structure factors $\hat{F}$ (experimental modulus, model-based phase); the scale of $\hat{F}$ is set to make $\hat{F}_{\mathbf{k}=0}$ equal the number of electrons in a unit cell. Within the range of observations it is desired that F the transform of ρ differs from $\hat{F}$ as little as possible subject to maximization of the entropy which measures the difference between ρ and τ, ρ constrained to be positive definite. After the pattern of Gull and Daniell[1] maximize

$$Q(\lambda) = -\sum_{\mathbf{x}} \rho'_{\mathbf{x}} \ln[\rho'_{\mathbf{x}}/\tau'_{\mathbf{x}}] - \frac{\lambda}{2} \sum_{\mathbf{k}\in K} |F_{\mathbf{k}} - \hat{F}_{\mathbf{k}}|^2/\sigma^2_{\mathbf{k}}$$

by setting

$$\partial Q(\lambda)/\partial \rho_{\mathbf{x}} = 0$$

where the sum over $\mathbf{x}$ includes a complete unit cell, the entropy formula[4] uses $\rho' = \rho/\sum \rho_{\mathbf{x}}$ and $\tau' = \tau/\sum \tau_{\mathbf{x}}$, λ is a disposable constant to be evaluated, K denotes the set of reciprocal lattice points for which there are useful observations, and σ is the standard deviation of $\hat{F}$. Evidently

$$-\ln \rho_{\mathbf{x}} + \ln \tau_{\mathbf{x}} + A + \hat{F}_{\delta}\lambda \sum_{\mathbf{k}\in K} \frac{1}{\sigma^2_{\mathbf{k}}} (\hat{F}_{\mathbf{k}} - F_{\mathbf{k}}) \exp\{-2\pi i \mathbf{k}\cdot\mathbf{x}\} = 0 \quad (1)$$

for which the relationship $\hat{F}_0 = \sum(\text{volume/grid point})\rho_{\mathbf{x}}$ has been used, it is assumed that $-\mathbf{k}\in K\ \forall \mathbf{k}\in K$, and A is given by

$$A = (\sum \rho_{\mathbf{x}})^{-1} \sum \rho_{\mathbf{x}} \ln[\rho_{\mathbf{x}}/\tau_{\mathbf{x}}]$$

If as desired the agreement between $\hat{F}$ and F is good, then A which measures the scale disparity between ρ and τ is small. Neglect of A and rearrangement of equation (1) result in

$$\rho_{\mathbf{x}} = \exp\left[\ln \tau_{\mathbf{x}} + \hat{F}_0\lambda \sum_{\mathbf{k}\in K} \frac{1}{\sigma^2_{\mathbf{k}}} (\hat{F}_{\mathbf{k}} - F_{\mathbf{k}}) \exp\{-2\pi i \mathbf{k}\cdot\mathbf{x}\}\right] \quad (2)$$

which forms the basis for the reconstruction procedure presented here. Note that equation (2) certainly satisfies one of the two earlier mentioned problems of convergence and (possibly) noise-free data. Disappearance of the latter problem is trivially evident, for if the modelled density should ever transform to $F_{\mathbf{k}} = \hat{F}_{\mathbf{k}}$, $\forall \mathbf{k}\in K$, then $\rho = \tau$ and cannot be changed by use of equation (2). Although neglect of A may bias the entropy term, a formalism results which, as desired, does not fail in the absence of noise. On the other hand, use of $A = 0$ means the convergence question must await an empirical answer as initially provided in the illustration.

Equation (2) may be rearranged to yield

$$\ln[\rho_{\mathbf{x}}/\tau_{\mathbf{x}}] = \hat{F}_0\lambda \sum_{\mathbf{k}\in K} \frac{1}{\sigma^2_{\mathbf{k}}} (\hat{F}_{\mathbf{k}} - F_{\mathbf{k}}) \exp\{-2\pi i \mathbf{k}\cdot\mathbf{x}\}$$

For good agreement of ρ and τ the logarithm may be approximated as

$$\ln x \approx x - 1$$

to give

$$(\rho_{\mathbf{x}} - \tau_{\mathbf{x}}) = \tau_{\mathbf{x}}\hat{F}_0\lambda \sum_{\mathbf{k}\in K} \frac{1}{\sigma^2_{\mathbf{k}}} (\hat{F}_{\mathbf{k}} - F_{\mathbf{k}}) \exp\{-2\pi i \mathbf{k}\cdot\mathbf{x}\}$$

which permits a formal estimation of λ at $\tau_{\max}$. Correspondence with standard crystallographic difference map formalism[5] implies for λ the evaluation

$$\lambda = (V\tau_{\max}\hat{F}_0)^{-1} \left(\frac{1}{n_K} \sum_{\mathbf{k}\in K} \frac{1}{\sigma^2_{\mathbf{k}}}\right)^{-1} (2 - \delta_{\bar{1}})$$

where V is the volume of a unit cell, n_K is the number of terms in the sum, and $\delta_{\bar{1}} = 1$ or 0 according to the presence or absence of a centre of symmetry. For constant errors, $\lambda = (V\tau_{\max}\hat{F}_0)^{-1}\sigma^2(2 - \delta_{\bar{1}})$. It follows that the standard crystallographic difference synthesis may be interpreted as an approximate difference between unit-weighted maximum-entropy representations of experimental and modelled electron densities.

Deterministic interpretation of the logarithm of equation (2) suggests the form

$$\ln \rho_{\mathbf{x}} = \ln \tau_{\mathbf{x}} + \text{corrective terms}$$

or

$$\ln(\rho_{\mathbf{x}}/\tau_{\mathbf{x}}) = \text{corrective terms}$$

For a formal difference of <10% between τ and ρ, the left-hand side may be approximated within 0.1% as

$$\ln(\rho/\tau) = (\rho - \tau)/\tfrac{1}{2}(\rho + \tau) \approx \Delta\rho/\rho$$

Evidently this would be an accurate deterministic form for the

Table 1 The course of reconstruction

	At the start	After four iterations
R	0.22	0.14
$\langle\lvert\alpha_{\mathrm{IR}} - \alpha_{\mathrm{MEM}}\rvert\rangle^*$	0 (0)	25 (32)
$\langle\lvert\alpha_{\mathrm{LS}} - \alpha_{\mathrm{MEM}}\rvert\rangle^*$	36 (44)	31 (38)

Tabulated quantities are explained in the text.

* Modulus weighted averages are given; the corresponding unweighted averages are given in parentheses. All values are in degrees.

0028-0836/82/260049—03\$01.00

corrective terms. With λ evaluated at $\tau_{\max}$, the maximum entropy solution for corrective terms as given in equation (2) differs from the deterministic form only as the values for ρ move down from their highest levels. This fortuitously corresponds with the experimental situation in which the lowest levels of a density function are usually rather less significant than the highest levels. Relative to accurate deterministic corrections, the maximum-entropy corrections down-weight the significance of the lowest density levels through absence of the ρ^{-1} dependence. Moreover, because the highest density levels contribute most to the value for F, and because the maximum entropy corrections place functional emphasis on correcting the highest density levels, it is expected that repeated application of equation (2) quite generally will constitute a stable, convergent, iterative reconstruction of electron density. Although in the presence of error the resulting density may never be better than an asymptotic approximant, it will be positive definite, well behaved, and in good agreement with the observations by the criterion of a constrained maximum of configurational entropy.

'Super-resolution' is a term used[1,2] to denote the fact that maximum-entropy methods can yield functions of resolution higher than that which corresponds to the band limits of the data. The term is sometimes used to indicate that the presence of noise in a set of data can lead to apparent but improperly high resolution. Super-resolution of the proper sort is highly desirable and can be understood to arise in the present case through imposition of a (perfectly general) model for electron density. While the maximum-entropy formalism yields a result which is maximally non-committal with regard to missing or unavailable data[6,7], it does require an exponential representation for the density function. Because the sampling of the density may be made arbitrarily dense, the exponential representation corresponds to a function which is not only positive definite and well behaved, but also continuous and consequently possessed of an infinite transform with unlimited resolution. There is no general way to know how well the implied transform samples for $\mathbf{k} \notin K$ agree with the unavailable observations or even that they agree at all. But in crystallographic application maximum-entropy formalisms can lead to density maps at more than twice the resolution expected for straightforward Fourier synthesis of structure factors[8]. As we now show, iterative reconstruction based on equation (2) does in fact produce real super-resolution.

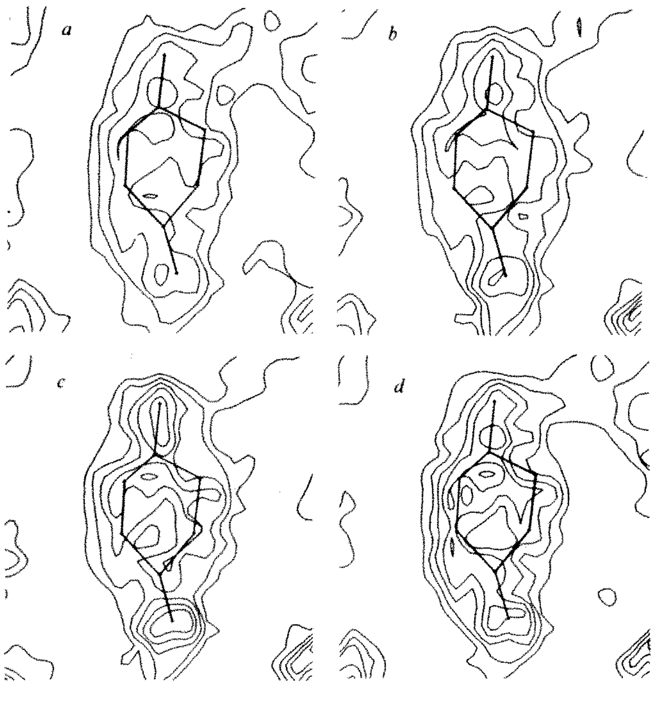

Fig. 1 *a*, Tyrosine-11 based on 2.0 Å data and isomorphous replacement phases. *b*, Tyrosine-11 based on 2.0 Å data and least-squares phases. *c*, Tyrosine-11 based on 1.5 Å data and least-squares phases. *d*, Tyrosine-11 in a maximum entropy reconstruction iteratively developed from the data and phases used in *a*.

The rubredoxin of *Clostridium pasteurianum* has been studied in single-crystal X-ray diffraction experiments and its noncentrosymmetric structure reported[9] at a resolution of 1.5 Å (minimum interplanar spacing). A structure model was fitted to the 1.5 Å experimental data by least squares and the structure-factor phases computed from this model, the experimental structure-factor moduli, and the atom coordinates of the model are all given in the structure report[9]. Phases which had been determined by isomorphous replacement methods at 2.0 Å resolution were provided by Dr Sayre with permission from Professor Jensen. The reconstruction procedure used for the present illustration may be outlined as follows. (1) Compute an electron density τ using $\hat{F}$ the experimental structure moduli and phases from isomorphous replacement, all at 2.0 Å resolution, and to ensure a positive definite density at the start replace τ by the larger of $(\tau, \tau_{\max}/100)$ for each position $\mathbf{x}$. Compute and file $\ln \tau$ and the transform of (modified) τ as initial F. (2) Computation of equation (2) with the phase of F assigned to $\hat{F}$ gives ρ whose transform is a new F and logarithm is a new $\ln \tau$. (3) Scale $|F|$ so it is on the same scale as $|\hat{F}|$ and compute

$$R = \sum_{\mathbf{k}\in K} ||\hat{F}_{\mathbf{k}}| - |F_{\mathbf{k}}|| / \sum_{\mathbf{k}\in K} |\hat{F}_{\mathbf{k}}|$$

(4) Repeat steps (2) and (3) until the improvement in R is judged to be not significant.

Although 1.5 Å data are available for rubredoxin, only the 2.0 Å subset together with initial isomorphous-replacement phases were used in the reconstruction. This allows for demonstration of super-resolution by comparison of the reconstructed density function with a reference density using about twice as much data. The reference density was obtained by standard Fourier synthesis of a complete 1.5 Å structure-factor set obtained as experimental moduli and phases calculated from the refined atomic model; these calculated phases are considered to be correct for this illustration.

The course of the calculation through four iterations is summarized in Table 1. Each iteration is based on a forward and reverse Fourier transformation[10] of samples on a grid of 64 points per cell edge. Computing time for each complete iteration was ~30% more than required for the Fourier syntheses alone. For the 2,812 unique data used, the average magnitude of difference between the phases from the maximum entropy method α_{MEM} and the phases from the atomic model, the so-called least-squares phases α_{LS}, is given in Table 1. A companion entry gives the average magnitude of difference between α_{MEM} and the phases from isomorphous replacement α_{IR}. These average phase deviations taken together show that the maximum entropy method yields a result which in some sense concerning phases lies between the sets from isomorphous replacement and least-squares refinement. The value for $R = \sum ||\hat{F}| - |F|| / \sum |\hat{F}|$ is amenable to more definite interpretation. A first significance of R is as a criterion of convergence for the reconstruction procedure. An analytical discussion of this point is lacking but it is easy to see that the procedure will stop if and only if $R = 0.0$. Yet if R stops changing between iterations, then clearly in some average sense no further desirable change is occurring. A second use for R or its value at convergence is as a preliminary indicator of global error in a data set. Because the exponential model for electron density is perfectly general, error-free data ideally should yield $R = 0.0$ at the conclusion of a maximum-entropy reconstruction. Of course, data are not error-free and random data errors correspond to an uncorrelated, necessarily zero-mean process which is not representable by an exponential model. The maximum entropy procedure may, nevertheless, offset some error effects, but in unpredictable ways because the exponential representation of density plus error destroys the additive relationship. With reservation in this regard and also concerning the possibility of false entropy maxima, it seems that the asymptotic value of R should approximate $\sum|\varepsilon|/\sum|\hat{F}|$, ε being the true experimental error in $|F|$.

Quality of image is demonstrated in Fig. 1 by comparison of different representations of the tyrosine-11 residue of rubredoxin[9]. Tyrosine-11 was chosen on the joint grounds of its planarity and previous use as an example[9,11]. Figure 1*a–d* shows interpolated sections of density maps in the least-squares plane of the reported coordinates for atoms in the planar tyrosine group. Contour levels begin at 0.0 and increase in steps of 0.30 electrons $Å^{-3}$; the line segment ends correspond to reported atomic positions. Figure 1*a* is based on 2.0 Å data with phases from isomorphous replacement and represents the starting point for all further structure description and refinement. Figure 1*b*, *c* are based on the least-squares phases calculated from the atomic model. Although the reported atomic model and associated phases are being used here as a kind of standard, note that in the original report they were considered subject to improvement. Clearly, Fig. 1*b* which is based on 2.0 Å data and least-squares phases gives a better representation of tyrosine than does Fig. 1*a*. Figure 1*c* which is based on least-squares phases and the complete 1.5 Å data set is even better and of obviously higher resolution. The maximum-entropy reconstruction is given in Fig. 1*d* which is more similar to Fig. 1*c* than to the others. In fact one could reasonably argue from their appearance that Fig. 1*d*, if anything, is of higher resolution than Fig. 1*c*. Clearly, the maximum entropy reconstruction based on only 2.0 Å data and isomorphous–replacement phases shows real super-resolution as it is of obviously greater true resolution than the classical representation of the same data given in Fig. 1*a*.

Maximum-entropy methods for image reconstruction potentially yield the best image model derivable from the available data[2]. This does not refer to a best image model in an absolute sense, but in the sense of being the model least likely to need correction on measurement and consideration of additional data[2]. While the virtues of maximum entropy analysis are claimed for the present procedure, the approximations used mean that its details could be improved on. In connection with the rubredoxin illustration, note that individual standard errors for structure moduli were not used and the default unit values are not commensurate with optimum results from the calculations. Even so, in contrast to other types of image enhancement[8,12], the present procedure seems to be exceptionally stable and requires no special adaptation for dominating atoms or groups as, for example, the iron–sulphur group of rubredoxin. While no evidence has been developed in specification of a radius of convergence, it seems that the outlined procedure is applicable without further modification in every case for which there are structure moduli and corresponding initial phases of the quality normally attained by isomorphous replacement methods.

I thank J. Skilling for help with formulation of the entropy expression. This work has been supported in part by the Robert A. Welch Foundation through grant A-742 and by the Research Corporation through a Cottrell Research Grant.

Received 9 February; accepted 4 May 1982.

1. Gull, S. F. & Daniell, G. J. *Nature* **272**, 686–690 (1978).
2. Benjamin, R. *IEE Proc.* **F127**, 341–353 (1980).
3. Oppenheim, A. V. & Schafer, R. W. *Digital Signal Processing*, Ch. 3 (Prentice-Hall, New Jersey, 1975).
4. Jaynes, E. T. *IEEE Trans.* **SSC-4**, 227–241 (1968).
5. Ramachandran, G. N. & Srinivasan, R. *Fourier Methods in Crystallography* (Wiley-Interscience, New York, 1970).
6. Ables, J. G. *Astr. Astrophys. Suppl.* **15**, 383–393 (1974).
7. Jaynes, E. T. *Phys. Rev.* **106**, 620–630 (1957).
8. Collins, D. M. *Acta crystallogr.* **A34**, 533–541 (1978).
9. Watenpaugh, K. D., Sieker, L. C., Herriott, J. R. & Jensen, L. H. *Acta crystallogr.* **B29**, 943–956 (1973).
10. Hubbard, C. R., Quicksall, C. O. & Jacobson, R. A. *The Fast Fourier Algorithm and the Programs ALFF, ALFFDP, ALFFPROJ, ALFFT, and FRIEDEL* (Ames, Iowa, 1971).
11. Collins, D. M., Cotton, F. A., Hazen, E. E. Jr, Meyer, E. F. Jr & Morimoto, C. N. *Science* **190**, 1047–1053 (1975).
12. Collins, D. M., Brice, M. D., la Cour, T. F. M. & Legg, M. J. *Crystallographic Computing Techniques* (eds Ahmed, F. R., Huml, K. & Sedláček, B.) 330–335 (Munksgaard, Copenhagen, 1976).

Structure of the Red Sea at 20° N from gravity data and its implication for continental margins

C. Brown* & R. W. Girdler

School of Physics, The University, Newcastle upon Tyne
NE1 7RU, UK

Recent gravity data have enabled a gravity profile extending 1,500 km over Nubia, the Red Sea and Arabia to be compiled. Using a modal value of −48 mGal for the Bouguer anomaly over Africa away from regions of rifting we have determined the way in which the lithosphere thins and breaks to form the Red Sea. We find that nearly the whole of the Red Sea from coast to coast is probably underlain by oceanic crust and the regions of thinning extend for ~120 km landwards of the Nubian coast and 180 km landwards of the Arabian coast. This implies that for continental margins similar to those of the Red Sea, the vast thicknesses of sediments might be underlain by early oceanic lithosphere rather than by thinned and downfaulted continental lithosphere.

The Red Sea is a critical region for studying the breakup of the continents, the evolution of continental margins and new oceanic crust. The presence of large positive Bouguer gravity anomalies over the deep axial trough suggested that the trough might be underlain by dense oceanic crust[1]. This was confirmed in the 1960s when high seismic velocities and large magnetic anomalies were found[2]. The magnetic anomalies were interpreted in terms of seafloor spreading[3] and a model constructed in which the deep axial trough was underlain by oceanic crust formed over the past few million years and the main trough and shelves were underlain by downfaulted shield rocks covered by large thicknesses of sediments[4,5]. In 1970 McKenzie *et al.*[6] applied plate tectonics and fitted the remarkably parallel shorelines (previously noticed by Wegener). This stimulated much new work on the nature of the crust underlying the vast thicknesses of sediments to the sides of the axial trough. In particular, magnetic surveys showed remarkable lineations and the suggestion was made that the Red Sea may have formed in at least two stages of seafloor spreading[7]. Further studies[8] showed magnetic lineations over the margins of the Red Sea to be widespread. Recently, a very detailed aeromagnetic survey (R. Horn, personal communication) has been carried out between Sudan and Arabia on behalf of the Red Sea Commision. This shows extensive lineations with remarkable symmetry. The magnetic anomalies thus suggest the presence of oceanic crust beneath the sediments and extending approximately to the coasts at least in the southern two thirds of the Red Sea. This is also supported by the interpretation of the gravity anomalies.

Gravity data from a recent geotraverse across northern Africa[9] enable a long profile to be constructed across the Red Sea and its neighbouring Nubian and Arabian plates. The location of the profile is shown in Fig. 1. The coordinates of the stations in Nubia and Arabia were projected onto a line with azimuth N56° passing through Port Sudan. For Nubia, 32 stations obtained on the geotraverse provided simple Bouguer anomalies and heights at an average spacing of 16 km. For the Red Sea, Bouguer anomalies and depths on a N56° line from Port Sudan to Jeddah were obtained from charts with contour intervals 10 mGal and 100 m respectively[10]. For Arabia, Bouguer anomalies and heights for 21 stations[11] eastwards from the Red Sea Arabian coast at an average spacing of 15 km were used. The complete profile (Fig. 2*a*) shows that the whole of the Red Sea from coast to coast is associated with positive

---

* Present address: Applied Geophysics Unit, University College, Galway, Ireland.

0028–0836/82/260051—03$01.00

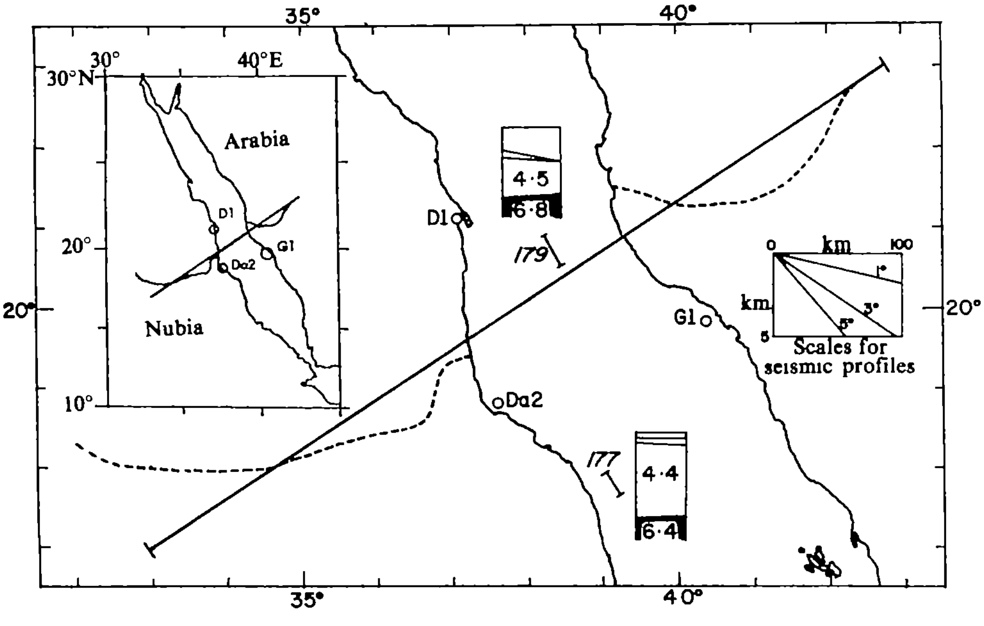

Fig. 1 The location of the profile and its projection on to the line N56°. The locations of the boreholes Dungunab-1 (D-1), Durwara-2 (Da-2) and Ghawwas-1 (G-1) and seismic refraction lines 177 and 179 are also shown.

Bouguer anomalies which reach a maximum of more than +100 mGal. Landwards from the coasts the anomalies become negative reaching values of −50 mGal on the Nubian side and −100 mGal on the Arabian side.

To interpret the profile we need to make assumptions concerning the thickness and structure of the lithosphere away from the regions of rifting and to estimate the regional gravity anomaly. For the continental US, isostatic response data[12] seem to be incompatible with density anomalies below ~80 km but in Canada observations of the wavelength and amplitude of bending in the vicinity of supercrustal loading[13] give estimates of ~110 km for lithospheric thickness. For unrifted Africa, the simple assumption is made that the lithosphere is 100 km thick and is associated with a Bouguer anomaly of −48 mGal derived from a statistical study of 1°×1° means[14]. The structure of the African lithosphere based on seismic studies[15] with the velocities converted to densities using the Nafe–Drake curve[16] is shown in Fig. 2*a* and the more detailed structure of the crustal part in Fig. 2*b*.

For the continental part of the profile it is necessary to compute geological corrections for the light volcanics and sediments near Harrat Rahat and Harrat al Kishb at ~22.5° N, 41°E. A uniform specific gravity (SG) of 2.3 was assumed with the volcanic pile underlain by PreCambrian basement at sea level. It is also necessary to correct for the light sediments on the Nubian and Arabian coastal plains. These were assumed to have a uniform SG of 2.2 with thicknesses taken from the Tectonic Map of Africa[17].

For the Red Sea, there are three boreholes in the neighbourhood of the profile[19], two on the Nubian side and one on the Arabian side (Fig. 1). All are close to the coasts. On the west side, the borehole to the north, at 21.10° N, 37.10° E (Dungunab-1) has 1,563 m of sediment and the borehole to the south at 18.81° N, 37.64° E (Durwara-2) has 4,152 m of sediment. Both then penetrated basalt. The borehole on the east side at 19.84° N, 40.37° E (Ghawwas-1) has a sediment thickness >3,446 m. There are also two reversed seismic refraction profiles[2] which constrain the velocity structure to the top of the oceanic layer 3 in the main trough (line 177) and axial trough (line 179). The velocities were converted to specific gravities using the Nafe–Drake curve[16] giving values of 2.00 (equivalent to 2.3 km s^{-1}) for the sediments, 2.45 (4.4 km s^{-1}) for the evaporites and 2.80 (6.45 km s^{-1}) for oceanic layer 3. The Mohorovičić discontinuity was not detected on these lines and a depth of 11 km was assumed. If it is assumed that isostatic compensation is complete at 100 km (the depth assumed for the base of the African lithosphere[14]), a simple calculation shows that the average specific gravity of the oceanic mantle beneath line 177 in the main trough is ~3.25. The details of the Red Sea structure used in the interpretation of the gravity profile are shown in Fig. 2*b*

With these constraints the lithospheric structure was adjusted until the Bouguer anomaly was fitted to within ±10 mGal over the whole length of the profile (Fig. 2*a*).

The resulting structure shows the following features from west to east: (1) As the western margin of the Red Sea is approached, the lithosphere begins to thin rapidly. (2) The continent–ocean boundary is only 7 km seaward of the Nubian coast at this latitude. (3) A crustal intrusive zone about 90 km wide exists beneath the centre of the Red Sea. Its top is at a depth of 4 km and it has a SG of 2.88 corresponding to the 6.76 km s^{-1} layer observed on seismic line 179. (4) The ocean–continent boundary coincides with the coastline on the Arabian side. (5) The region of lithospheric thinning has a slightly different form on the eastern side. (6) The 'normal' lithosphere is reached between 120 and 180 km from the coasts.

The model demonstrates that nearly all of the Red Sea at 20° N is underlain by oceanic crust but note that the exact demarcation of its boundaries depends critically on the specific gravities and thicknesses of the sediments and evaporites forming the marginal shelves.

A similar result has been obtained by Gettings[19] for a gravity survey of the Arabian margin between 16.3° N and 17.3° N, which includes the Tihamah Asir Coastal plain. Here, an extremely steep gradient (4–5 mGal km^{-1}) is observed at the Tihamah-shield boundary. Gettings interprets this as indicating the presence of oceanic crust beneath the Tihamah as well as beneath the Red Sea shelf.

Independent support for the presence of oceanic crust beneath the Red Sea shelves (apart from the magnetic lineations discussed earlier) comes from the fact that the whole of the Red Sea is a region of high heat flow[20]. It has been shown[21] that the heat flow values from boreholes on the Sudan coastal plain are considerably higher than would be expected from the radioactive heat production of granitic continental crust.

Although our results are based primarily on the gravity profile across the Red Sea, they are consistent with other geophysical data for this region.The conclusion that the whole of the Red Sea at 20° N, including the vast thicknesses of sediments on the shelves is underlain by oceanic crust agrees with results from the westernmost Gulf of Aden[22] where seismic reflection and gravity data require the ocean–continent boundary to be between the 183 m contour and the coast. In these regions, attenuation of the lithosphere, such as there is, seems to be landward of the coasts. Other passive continental margins similar to those of the Red Sea and Gulf of Aden might have

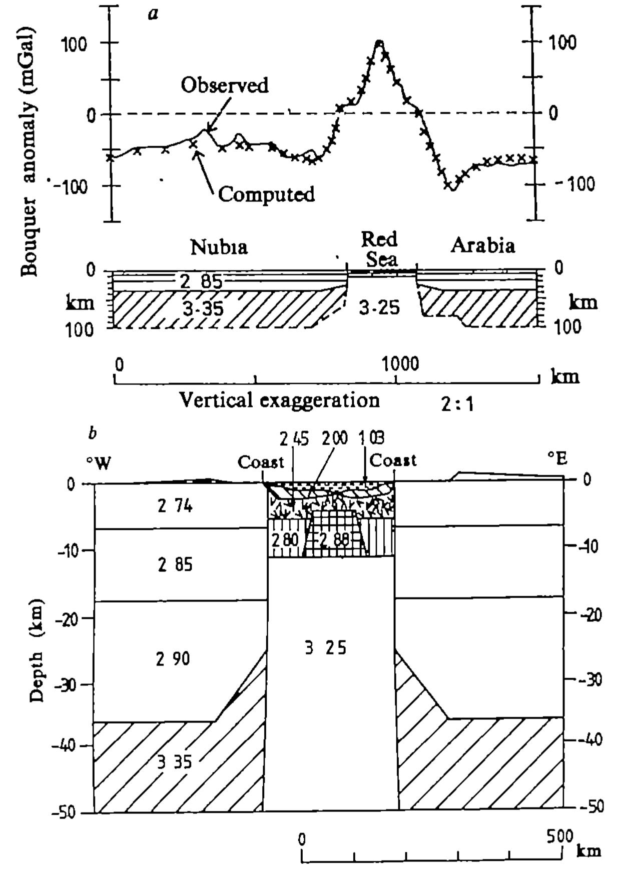

Fig. 2 *a*, The Bouguer gravity anomaly profile with the lithospheric structure used to fit the observed values. Details of the crustal structure of the Red Sea and the neighbouring continental lithosphere are shown in Fig. 2*b*. The positive anomaly over the Red Sea is due to the intrusive zone penetrating upper parts of the lithosphere giving a positive density contrast. The sharp boundaries between the anomalous mantle beneath the Red Sea and the normal mantle beneath the continents have been introduced to facilitate the gravity computations and should not be construed to represent an abrupt transition between geologically distinct regions in the mantle. *b*, Details of the structure of the crust and upper mantle used in the interpretation of the gravity profile shown in *a*. The attraction of each layer has been computed using a reduced specific gravity $\rho' = \rho - 2.67$ where ρ takes the following values: 2.00 (sediments); 2.45 (evaporites); 2.80 (oceanic layer 3); 2.88 (crustal intrusion); 3.25 (anomalous mantle) for the Red Sea and 2.74 (upper crust), 2.85 (middle crust); 2.90 (lower crust), 3.35 (normal mantle) for the continental lithosphere. The attraction of the mantle layers have been computed to a depth of 100 km.

oceanic crust underlying their shelves and we suggest that theories for the evolution of such 'continental margins' should consider this possibility.

We thank Dr Peter Styles for helpful comments and C.B. is indebted to the NERC for a research studentship.

Received 5 February, accepted 26 April 1982.

1. Girdler, R W. *QJl geol. Soc Lond* **114**, 79–105 (1958)
2. Drake, C L. & Girdler, R. W *Geophys J.R. astr. Soc.* **8**, 473–495 (1964).
3. Vine, F. J *Science* **154**, 1405–1415 (1966)
4 Girdler, R W *Proc geol. Ass.* **78**, 165–178 (1967).
5 Lowell, J. D & Genik, G. J. *Bull Am Ass petrol Geol.* **56**, 247–259 (1972)
6. McKenzie, D P , Davies, D & Molnar, P. *Nature* **226**, 243–248 (1970)
7. Girdler, R W. & Styles, P *Nature* **247**, 7–11 (1974)
8. Hall, S. A. thesis, Univ Newcastle upon Tyne (1976). *U.S Geol Surv. Saudi Arabian Proj Rep.* **275**, 1–260 (1979)
9. Brown, C., Girdler, R W & Renner, R. G. B *J. geophys. Res.* **85**, 6436–6442 (1980)
10 Allan, T D. & Morelli, C *The Sea* Vol 4 (ed Maxwell, A E) 493–542 (Wiley, New York, 1970)
11 Sowerbutts, W. T. C. thesis, Univ Newcastle upon Tyne (1972)
12. Banks, R. J , Parker, R. L & Huestis, S P. *Geophys. J R. astr. Soc.* **51**, 431–452 (1977).
13. Walcott, R. I. *J. geophys. Res* **75**, 3941–3954 (1970)
14. Brown, C. & Girdler, R W *J. geophys Res* **85**, 6443–6445 (1980).
15 Grumper, F. & Pomeroy, P. W. *Bull seism Soc. Am.* **60**, 651–688 (1970).
16 Nafe, J. E. & Drake, C L *The Sea* Vol 3 (ed. Hill, M B) 794–815 (Wiley, New York, 1963)
17. *International Tectonic Map of Africa at* 1 5,000,000 (UNESCO, 1968)
18. Coleman, R. G. *Geological Map of the Red Sea* (US Geological Survey, 1973).
19. Gettings, M. E *Red Sea Research* 1970–1975. *Miner Resour. Bull.* **22-K**, 1–11 (Kingdom of Saudi Arabia, 1977).
20. Girdler, R. W. & Evans, T. R. *Geophys. J.R astr. Soc.* **51**, 245–251 (1977).
21. Evans, T. R. & Tammemagi, H. Y. *Earth planet. Sci. Lett.* **23**, 349–356 (1974).
22. Girdler, R. W., Brown, C., Noy, D. J. M & Styles, P. *Phil Trans. R Soc* **A298**, 1–43 (1980).

Significance of $^{87}Sr/^{86}Sr$ ratios in the Merensky cyclic unit of the Bushveld Complex

F. J. Kruger & J. S. Marsh

Department of Geology, Rhodes University,
Grahamstown, 6140 South Africa

In a number of mafic layered intrusions, layers with platinum group element (PGE) mineralization coincide with breaks in cumulus mineral composition and isotopic variation trends through the layered sequence[1,2]. For example, in the Bushveld Complex in South Africa, abrupt increases in initial $^{87}Sr/^{86}Sr$ ratios occur at the UG-2 and Merensky pegmatoid (or 'reef') horizons, both of which are exploited for PGEs. We report here the results of a detailed Sr-isotope study across the Merensky unit and its immediate foot- and hangingwall-rocks which, when considered together with new ideas on processes operating in magma chambers[3–5], suggest that magma mixing and post-cumulus infiltration of liquids displaced from below were important during crystallization of the Merensky pegmatoid.

In the Bushveld Complex the PGE-bearing Merensky pegmatoid is part of the Merensky cyclic unit which occurs at the base of the main zone (subdivision after Willemse[6]—Fig. 1). Above the Merensky unit lies the lithologically similar Bastard cyclic unit. Both these units consist of a basal layer of orthopyroxenite which grades upwards through mela- and leuconorite into anorthosites with sporadically developed poikilophitic orthopyroxene crystals ~5 cm across, known as 'mottled anorthosites'. Thin stringers of chromitite usually occur at the base of each unit. In the case of the Merensky unit a layer of pegmatoid consisting mainly of large orthopyroxene crystals with interstitial plagioclase occurs at the base—this is the PGE-bearing Merensky pegmatoid.

As part of a detailed study of the Merensky unit at Rustenburg Platinum Mines in the western lobe of the Bushveld Complex, we have determined $^{87}Sr/^{86}Sr$ ratios (Table 1) on a suite of whole rocks and plagioclase collected from these two cyclic units and the immediate footwall to the Merensky pegmatoid. The variation of initial Sr-isotope ratios with height (Fig. 1) indicates a step-like pattern which confirms, in general, the results of Hamilton[1].

Plagioclase separates from the Footwall unit and the Merensky pegmatoid and pyroxenite have a constant initial $^{87}Sr/^{86}Sr$ which, significantly, is identical to that for rocks from the same stratigraphic interval in the eastern lobe[1]. With height through the Merensky unit we find a dramatic increase in $^{87}Sr/^{86}Sr$ for both whole rocks and plagioclase. In a 60-m section through the overlying Bastard unit the initial ratios are more uniform, but not constant, between 0.70749 and 0.70803, which is within the range found by Hamilton for the main zone of the eastern lobe.

This pattern of initial $^{87}Sr/^{86}Sr$ ratio variation can help constrain processes occurring at this level during the crystallization of the Bushveld Complex. In general, two main models can be envisaged. First, the increase in $^{87}Sr/^{86}Sr$ through the Merensky cyclic unit and the high values (for mafic rocks) for main zone samples might reflect *in situ* contamination of the existing magma by its wall rocks. Alternatively, the main zone rocks might have crystallized from an influx of new magma (with

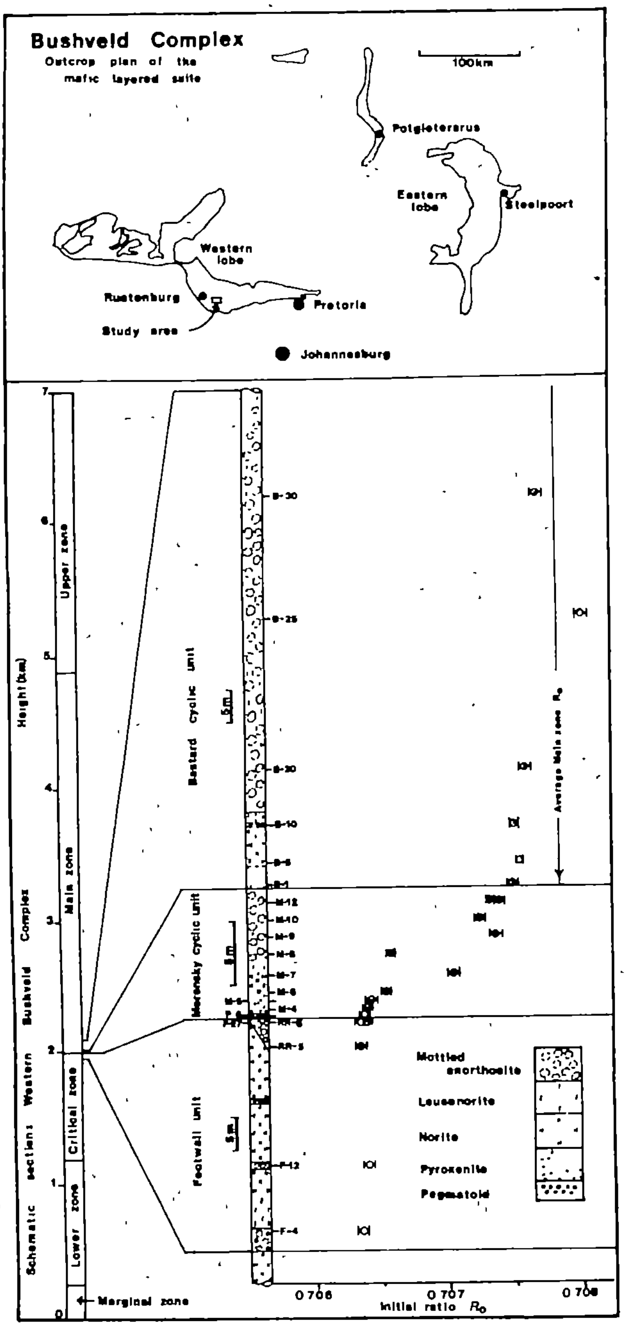

Fig. 1 Location map and stratigraphical positions for samples for which initial $^{87}Sr/^{86}Sr$ ratios have been determined. Note the differences in scale between the Merensky and Bastard and Footwall units. The average main zone initial $^{87}Sr/^{86}Sr$ (R_0) ratio is from ref. 1. O, Plagioclase; ●, whole rocks.

$^{87}Sr/^{86}Sr > 0.7075$) into the chamber and the Sr-isotope variation in the Merensky unit reflects the interaction of this new magma, or its crystallization products, with existing material in the magma chamber.

For the case of *in situ* contamination, magma with $^{87}Sr/^{86}Sr = 0.7064$ crystallized to produce the footwall sequence. At the start of accumulation of the Merensky unit, the existing magma became contaminated with more radiogenic Sr, presumably by mixing with partial melts generated in the roof and walls of the intrusion. The increasing $^{87}Sr/^{86}Sr$ ratio in the Merensky cyclic unit would therefore reflect progressive contamination of the magma and the increasing incorporation of more radiogenic Sr into cumulus minerals that build the cyclic unit. Contamination ceased at the level of the base of the Bastard cyclic unit and crystallization proceeded to produce rocks of the main zone, which has elevated and more uniform $^{87}Sr/^{86}Sr$ ratios.

Most of the data necessary for evaluating the feasibility of this model are unavailable, but considerations presented below suggest that *in situ* contamination is an unlikely explanation for the Sr-isotope variations. It seems unlikely that the contamination process was as short-lived as would be suggested by the thinness of the Merensky unit, and that it ceased abruptly, as indicated by the more uniform ratios in the Bastard unit. During the short contamination interval the magma must have been rapidly and efficiently mixed because rocks at this level in both the eastern and western lobes of the complex have similar Sr-isotope compositions (see Table 1 and ref. 1). If contamination occurred at the roof of the intrusion, transport of the contaminating Sr to the crystallization front at the base implies whole-magma convection. Although this possibility cannot be excluded, it seems more likely that contamination at the roof would cause self-stratification of the magma with convection cells confined to several layers[5], thus inhibiting thorough mixing of the magma. In the Rustenburg area the Merensky unit is orders of magnitude thinner than the main zone, and, using the principle of balancing the heat budget by assuming that the amount of melting in the wall rocks is roughly equivalent to the amount of crystallization, we conclude that a very small proportion of contaminant, much less than 1%, would be mixed in with the main zone. To produce the significant elevation of $^{87}Sr/^{86}Sr$ from 0.7064 to 0.7075 the contaminant must have very high Sr and/or $^{87}Sr/^{86}Sr$. Transvaal supergroup sediments that host the complex have low $^{87}Sr/^{86}Sr$ ratios[1,7]. Felsites of the Rooiberg group which form the roof of the intrusion have low Sr concentrations (average 70 p.p.m.; ref. 8) although no Sr-isotope data are available. Assuming that the precontaminated magma had Sr = 250 p.p.m. (calculated from Sr-concentration of cumulus plagioclase crystals in the Footwall unit) and that the extent of contamination was 1%, then the contaminant must have $^{87}Sr/^{86}Sr > 1.0$. This reduces to > 0.78 for 5% contamination. These ratios are high for felsites with $Rb/Sr \sim 2.5$ that were erupted shortly before emplacement of the Bushveld Complex and whose crustal or mantle precursors had very much lower Rb/Sr ratios.

The formation of main zone rocks from one or more new influxes of gabbroic magma is favoured by several workers[1,9–11].

Table 1 Results of Rb/Sr analysis

Sample	$^{87}Sr/^{86}Sr$*	Rb (p.p.m.)†	Sr (p.p.m.)†	Rb/Sr	$^{87}Sr/^{86}Sr$)‡
Bastard cyclic unit					
B-30CPL§	0.70872±4	4.7	398	0.0118	0.70771
B-25CPL	0.70849±4	2.2	403	0.0054	0.70803
B-20CPL	0.70819±4	2.7	392	0.0070	0.70760
B-10CPL	0.70787±3	1.7	407	0.0041	0.70752
B-5PL	0.70806±2	2.4	416	0.0059	0.70756
B-1IPL	0.70806±4	2.6	385	0.0067	0.70749
Merensky cyclic unit					
M-12WR	0.70776±3	1.7	403	0.0042	0.70740
M-12CPL	0.70757±3	1.2	419	0.0029	0.70732
M-10WR	0.70789±2	2.9	386	0.0075	0.70725
M-9CPL	0.70765±4	1.4	425	0.0033	0.70737
M-8WR	0.70699±2	1.9	394	0.0047	0.70659
M-7CPL	0.70731±4	1.2	392	0.0030	0.70705
M-6WR	0.70696±2	1.4	322	0.0044	0.70655
M-5IPL	0.79723±4	4.4	469	0.0094	0.70643
M-4IPL	0.79733±2	4.9	457	0.0108	0.70641
P-6IPL	0.70665±2	1.7	497	0.0033	0.70637
Footwall unit					
RR-6PL	0.70661±3	1.3	477	0.0027	0.70638
RR-5CPL	0.70672±4	2.1	483	0.0044	0.70634
F-27CPL	0.70653±5	1.1	482	0.0022	0.70634
F-12CPL	0.70663±4	1.3	486	0.0027	0.70640
F-4CPL	0.70665±4	1.6	479	0.0034	0.70636

* Present day $^{87}Sr/^{86}Sr$ ratio ± 2 s.e.m NBS-987 = 0.71026 ± 2 during this study.

† Rb and Sr concentrations were determined by high precision Wd-XRF.

‡ Initial $^{87}Sr/^{86}Sr$ ratio calculated using an age of 2,100 Myr and $\lambda = 1.42 \times 10^{-11}\ yr^{-1}$ for ^{87}Rb

§ PL, plagioclase, WR, whole rock, CPL, cumulus plagioclase chadacrysts hosted by orthopyroxene, IPL, intercumulus plagioclase.

Thermal and density contrasts between existing and new liquids and the nature of intrusion of the new magma would cause convective or turbulent mixing[12–15] of a presently unpredictable nature, as the exact properties of the magmas, the shape of the magma chamber, the rate of intrusion, and the position and shape of the conduits are unknown. Our detailed mineral and whole-rock composition data suggest that the new magma was compositionally similar to the existing magma, except that $^{87}Sr/^{86}Sr$ was >0.7075 and possibly >0.7086, as available data for the main zone (Table 1; ref. 1) vary between these limits.

The pattern of Sr-isotope variation (Fig. 1) precludes a behaviour suggested by some experiments[3,12] whereby the new magma flows to the bottom of the chamber displacing the existing magma upwards and after crystallizing a layer of crystals, mixes with it by convection. A more compelling model involves mixing of the magmas as the new influx enters the chamber. One possibility is that the deposition of the Merensky cyclic unit was concomitant with progressive influx and efficient mixing of the new magma into the existing liquid. The increasing $^{87}Sr/^{86}Sr$ ratios would therefore reflect the increasing proportion of new magma in the crystallizing mixture. The isotope data require that the influx ceased at the time the base of the Bastard unit was accumulating but the development of cyclic units and the similarity of mineral composition variations through the Merensky and Bastard units are difficult to reconcile with this restriction.

The possibility we prefer is one where the new magma entering the chamber mixes with the existing liquid and the Merensky and succeeding cyclic units form by accumulation of crystals precipitating from the blended magmas. This model would presumably result in a sharp step-like increase in $^{87}Sr/^{86}Sr$ at the base of the Merensky unit, contrary to what is observed. However, we suggest that whole-rock $^{87}Sr/^{86}Sr$ ratios in the Merensky unit were subsequently modified by infiltration of intercumulus liquid from the Footwall unit, a process described elsewhere[3,16]. This upward migrating liquid would displace or mix with that in the Merensky unit and the proportion of Sr with the isotopic signature of the footwall would decrease with height through the overlying crystal pile. The $^{87}Sr/^{86}Sr$ of the intercumulus material would therefore vary with the proportion of Sr introduced from the footwall, and the pattern depicted in Fig. 1 could result.

Although we have not been able to demonstrate directly the mixed isotopic character of Merensky cyclic unit rocks, comparison of data for M-7CPL with M-8WR (Table 1) is suggestive. Sample M-7CPL is of plagioclase primocrysts separated from enclosing orthopyroxene oikocrysts and these have $^{87}Sr/^{86}Sr = 0.70705$, approaching values typical of the main zone. The whole-rock sample M-8 comprises plagioclase primocrysts and intercumulus plagioclase and orthopyroxene and has $^{87}Sr/^{86}Sr = 0.70659$ which is close to values typical of the Footwall unit despite its higher stratigraphical position. Three intercumulus plagioclase separates for the basal pyroxenites and the pegmatoid of the Merensky unit have $^{87}Sr/^{86}Sr$ ratios that are almost identical, within error, to the Footwall unit initial ratio. We recall that Hamilton[1] found similar ratios in pyroxenites from the lower part of the Merensky unit; this is consistent with our data because in these rocks most of the Sr is contained in the intercumulus phases.

Our data support a role for a new magma influx, magma mixing and the process of infiltration metasomatism in the genesis of the Merensky pegmatoid. At this stage the implication for the origin of the associated PGE mineralization is unclear, as isotopic variations across the PGE-mineralized UG-2 layer have yet to be documented. If our interpretation of the Sr-isotope data for the Merensky unit is valid, models for PGE mineralization in layered igneous rocks should consider these processes.

The CSIR, Pretoria, and Johannesburg Consolidated Investment Co. provided financial support. Isotopes were determined at the Open University, UK and J.S.M. thanks Chris Hawkesworth and Professor Ian Gass for hospitality.

Received 4 January, accepted 28 April 1982.

1 Hamilton, J. *J Petrol.* **18,** 24–52 (1977)
2 Keith, D W, Todd, S. G., Schissel, D. J. & Irvine, T N. *Abstr Soc Econ. Geol. 3rd int Platinum Symp., S. Afr* (1981).
3 Irvine, T. N in *Physics of Magmatic Processes* (ed. Hargraves, R B.) 325–383 (Princeton University Press, 1980).
4 McBirney, A. R. & Noyes, R M *J. Petrol* **20,** 487–554 (1979)
5 Rice, A. *J geophys Res.* **86,** 405–417 (1981).
6 Willemse, J. *Econ Geol Monogr* **4,** 1–22 (1969)
7. Davies, R. D, Allsopp, H L, Erlank, A. J. & Manton, W. I. *Geol. Soc. Afr Spec. Publ.* **1,** 576–593 (1970)
8 Lenthall, D. H. & Hunter, D R *Precambr Res.* **5,** 359–400 (1977).
9 Sharpe, M R *J geol. Soc.* **138,** 307–326 (1981)
10. Coertze, F J *Geol Surv. S Afr. Mem* **66,** 148 (1974).
11 McCarthy, T. S. & Cawthorn, R G. *J Petrol.* **21,** 245–264 (1980).
12. Huppert, H. E & Turner, J S. *Earth planet. Sci Lett* **54,** 144–152 (1981).
13 Turner, J S & Chen, C. F. *J. Fluid Mech* **63,** 577–592 (1974).
14 Germeles, A E. *J Fluid Mech* **71,** 601–623 (1975).
15. Sparks, R S J., Meyer, P. & Sigurdsson, H *Earth planet Sci Lett.* **46,** 419–430 (1980).
16. Lauder, W. R. *Nature* **227,** 365–366 (1971).

Age constraints on the proposed Plio–Pleistocene boundary stratotype at Vrica, Italy

John D. Obradovich*, Charles W. Naeser*, Glen A. Izett†, Giancarlo Pasini‡ & Giulio Bigazzi§

* US Geological Survey, Denver Federal Center, Denver, Colorado 80225, USA
† US Geological Survey, National Center, Reston, Virginia 22092, USA
‡ Istituto di Geologia Marina del Consiglio Nazionale delle Ricerche, Bologna, Italy
§ Istituto di Geocronologia e Geochimica Isotopica del Consiglio Nazionale delle Ricerche, Pisa, Italy

Estimates[1–4] of the age of the stratotype Plio–Pleistocene boundary in Italy range from 1.65 to 2.5 Myr. We aim here to clarify this dating confusion, and we present new radiometric data on ashes from the proposed stratotype section, Vrica, Italy which indicate that the Plio–Pleistocene boundary must be less than 2 Myr old. Biostratigraphical criteria—the first appearance datums (FADs) and last appearance datums (LADs) of planktonic foraminifera and calcareous nannoplankton tied to the magnetic reversal chronology—suggest that this boundary may be nearer to 1.7 Myr. Attempts to make the boundary far older than this are without basis.

Haq *et al.*[1] have applied the calcareous nannoplankton and planktonic biochronological framework established from palaeomagnetically-dated deep sea cores to the section at Le Castella, southern Italy and estimated an age of 1.6 Myr for the Plio–Pleistocene boundary. (This age is now revised to 1.65 Myr based on the use of the newly adopted decay constants for ^{40}K (ref. 5).) Note that although the section at Le Castella was proposed at the Seventh INQUA Congress as a section suitable for defining the Plio–Pleistocene boundary stratotype

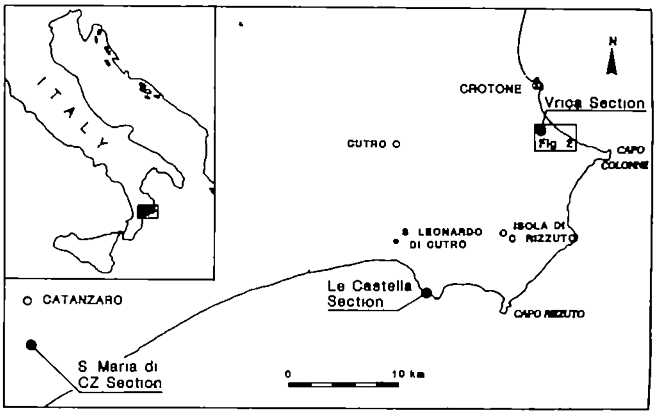

Fig. 1 Location of the Plio–Pleistocene sections at Vrica and Le Castella, and sampling localities (Calabria, Italy).

0028–0836/82/260055—05$01 00

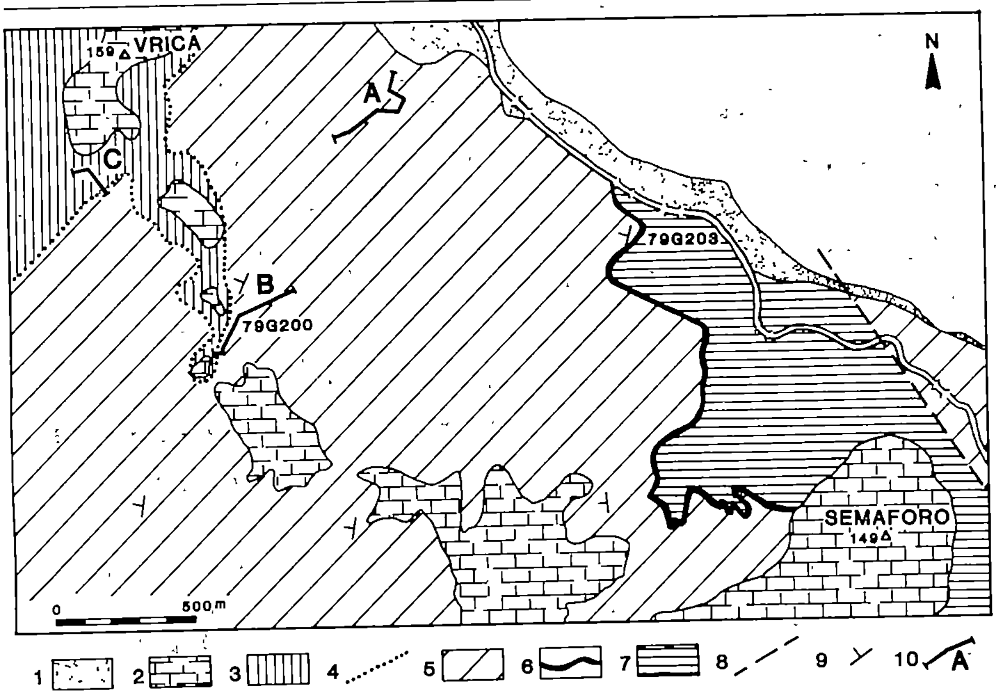

Fig. 2 Geological sketch map of the Vrica area, modified from Selli *et al.*[3]. 1, Beach sand and dunes; 2, calcarenites and sands of the marine terrace ('Milazzian'); 3, grey marly silty clays with sapropelic intercalations (early Pleistocene); 4, first appearance of *Hyalinea baltica*, 35 m above the *m* marker bed ash (<1.99 Myr); 5, grey marly silty clays with sapropelic intercalations (early Pleistocene, upper and middle Pliocene; the terminology for the Pliocene follows that of Italian workers); 6, lower volcanic ash horizon (2.22 Myr); 7, grey clays (middle Pliocene); 8, faults; 9, dip; 10, intervals sampled for the reconstruction of the columnar section going from the base of unit X to the top of unit Z (see Fig. 3, after ref. 16.).

this recommendation has never been officially accepted. Moreover, Colalongo *et al.*[6] have demonstrated the presence of a hiatus at the height of the 'marker bed' of Emiliani *et al.*[7] (considered by many to coincide practically with the Plio–Pleistocene boundary) at the Le Castella section[8,9]. Selli *et al.*[3] proposed that a new boundary stratotype at the Vrica section (Figs 1, 2) be accepted because of the continuity of section, better exposures, a thicker interval above and below the boundary, and an equally good fossil record. They reported several age determinations on a volcanic ash, termed the *m* marker bed, and a pumice block immediately above it in the short interval where the Plio–Pleistocene boundary would fall (Fig. 3): These ages, based on the K–Ar (Savelli in ref. 3) and fission-track, F-T (Bigazzi and Bonadonna in ref. 3) methods, ranged from 2.0 to 2.2 Myr. An even older age of 2.5 Myr has been determined by Boellstorff[4] using the F-T method on glass shards from the *m* marker bed. All of these ages, however, are far older than the age suggested by Haq *et al.*[1]. Given these divergent results we collected ash samples at Vrica and other localities where volcanic tephra are associated with sediments of late Pliocene or early Pleistocene age. At Vrica we collected the *m* marker bed ash and a Pliocene ash that is 280 m lower in the section.

Collecting the Pliocene ash was comparatively easy as the ash is thick (20 cm) and its lower part is relatively coarse. This ash is characterized by the presence of hornblende, plagioclase, and zircon. We obtained concordant ages of 2.22±0.03 Myr (K–Ar, hornblende); 2.0±0.16 Myr (F-T, zircon), and 2.2±0.2 Myr (F-T glass) (Tables 1*a* and 2). However, these results are: (1) in disagreement with the ages of 3.1 and 3.4 Myr previously determined by Dymond (in Selli[10]) using the K–AR method on glass shards from separate samples of the same Pliocene ash bed. One of these samples comes from the same locality where we collected our sample (79G203 in Fig. 2), the other comes from the environs of St Leonardo di Cutro (ref. 10 and R. Selli, personal communication); (2) younger than the 2.5 Myr age reported by Boellstorff[4] for the *m* marker bed ash which is 280 m higher in the section at Vrica; (3) the same as the 2.2±0.2 Myr age determined by Savelli[3] for glass shards from the *m* marker bed ash, though recalculation based on the data given in ref. 3 indicates an age of 2.27 Myr; and (4) almost the same age for the *m* marker bed ash of 2.07±0.33 Myr determined by Bigazzi and Bonadonna on glass shards (in ref. 3). Clearly something was wrong.

It was found that the sample of ash dated by Bigazzi and Bonadonna inadvertently had two labels attached to it, one indicating the sample to be the Pliocene ash and the other the *m* marker bed ash. Instrumental neutron activation analysis (INAA) of the glass dated by Bigazzi and Bonadonna and that of the Pliocene ash we collected in 1979 indicate that they are indeed the same ash. That is, the supposed *m* marker bed ash dated by Bigazzi and Bonadonna is actually the Pliocene ash and their result of 2.07±0.33 Myr agrees with our determinations.

Table 1 Analytical data for the K–Ar age determinations

DKA no.	Sample no.	Mineral	%K	Moles ^{40}Ar* g^{-1} (×10^{-11})	% Rad. Ar	Age (Myr)±1σ
a, **Pliocene ash**						
3864	79G203	Hornblende	0.805 (FL)	0.311	40.8	2.22±0.05
3936	79G203	Hornblende	0.781 (ID)	0.301	32.9	2.22±0.04
b, *m* **Marker bed ash**						
3861	79G201 (−80m)	Biotite (S)	7.21 (FL)	3.250	33.5	2.60±0.05
3935	79G201 (+80m)	Biotite (S)	7.21 (FL)	2.882	32.1	2.30±0.05
3965	79G200 (−80m)	Biotite (P)	7.03 (FL)	2.601	23.3	2.13±0.05
4128	79G200 (+80m)	Biotite (P)	6.99 (ID)	2.410	12.5	1.99±0.08
c, **Vrica pumice**						
4201		Hornblende	0.377 (ID)	0.154	7.6	2.35±0.16

Decay constants for ^{40}K (ref. 5): $^{40}K/K = 1.167\times10^{-2}$ atom %; $\lambda_\beta = 4.962\times10^{-10}\ yr^{-1}$; $\lambda e + e' = 0.581\times10^{-10}\ yr^{-1}$. ID, isotope dilution; FL, flame photometry.

Table 2 Analytical data for the F-T age determination

Sample no.	Mineral	Correction method[17]	D^S/D^I or Temperature	$\rho_s \times 10^5$ tracks cm^{-2}	$\rho_i \times 10^{15}$ tracks cm^{-2}	$\Phi \times 10^{15}$ n cm^{-2}	App. age (Myr)	Corr. age (Myr)	$\pm 1\sigma$ (Myr)	Grains	$r, \bar{s}$
79G203	Zircon	—	—	3.21 (95)	94.8 (1404)	1.01	2.0	—	0.16	12	0.98 (r)
79G203	Glass	size	0.83	0.0281 (316)	0.235 (1046)	0.190	1.37	1.9	0.2	200/130	3.8% ($\bar{s}$)
79G203	Glass	plateau	200 °C	0.0272 (307)	0.144 (560)	0.190	—	2.2	0.2	230/100	4.8% ($\bar{s}$)

D^S/D^I, size ratio of spontaneous to induced tracks, shown for the size corrected age only. Temperature, heating temperature for the plateau age. ρ_s, ρ_i, Spontaneous and induced track densities respectively. (), Number of tracks counted. Φ, Neutron fluence, referred to the standard SRM 962 of the NBS. App. age, apparent age before any correction. Corr. age, corrected age. Grains, the number of glass grains used for counting the spontaneous and induced tracks respectively are shown; for zircon the total number of grains counted using the external detector method. $\bar{s}$, Experimental standard deviation, in per cent, of the induced track counting; r, correlation coefficient. Decay constant for the spontaneous fission of ^{238}U $= 7.03 \times 10^{-17}$ yr^{-1}: although the Denver and Pisa F-T groups routinely use slightly different values for the decay constant the same value is used here for consistency. The glass irradiations were performed in the Pavia University (Italy) reactor and the zircons were irradiated at the USGS reactor, Denver, Colorado.

J. Dymond (personal communication) revealed that unpublished ^{40}Ar/^{39}Ar stepwise heating data for the sample of Pliocene ash at St Leonardo di Cutro indicates that the glass shards contain excess radiogenic argon. We believe that this is also true of the other ash sample from Capo Colonne.

With respect to Savelli's determination of 2.27 Myr (revised) for the *m* marker bed ash we can only stress that K–Ar ages based on total fusion of glass shards are to be viewed with caution[11]. Without independent criteria such as Dymond's ^{40}Ar/^{39}Ar stepwise heating approach or dating of a more reliable uncontaminated mineral phase of the ash, there is no way to appraise the results.

We think that Boellstorff probably dated the Pliocene ash but we have not been able to verify this point. However, his age of 2.5 Myr, whether for the Pliocene ash or the *m* marker bed ash, is inconsistently old compared with our radiometric data and current biostratigraphic data. The calcareous nannoplankton *Gephyrocapsa aperta* appears 17 m below the Pliocene ash at Vrica[13]. In deep sea cores *G. aperta* makes its first appearance at 2.36 Myr (ref. 2) but in the Mediterranean its appearance could be younger. With these constraints Boellstorff's result is too old for the Pliocene ash and particularly the *m* marker bed ash.

Collection of the *m* marker bed ash proved difficult because it is at most 2–3 thick and is quite lenticular. Two samples of the ash were collected. A primary sample of about 1 kg was collected very carefully to avoid any extraneous material. The exterior surface of each solid fragment of ash was removed with a knife to avoid possible contamination. A much larger secondary sample was collected with less caution. This ash is characterized by the presence of biotite and plagioclase. Unfortunately the absence of zircon prevented dating by the F-T method as the glass shards from this particular ash are not suited to dating by this method.

Our efforts to date the *m* marker bed ash have been only partially successful. Biotite from the secondary sample yielded an age of 2.6 Myr, older than that of the underlying Pliocene ash (see Table 1*b*). We concluded that the biotite sample is contaminated and separated the secondary and primary samples into two size fractions, +80 mesh and −80+100 mesh. Contamination is probably greater in the finer fraction and that fraction should yield the older age. The results in Table 1*b* indicate that this is so. The coarser fraction of the primary sample yielded the youngest age: 1.99 Myr.

Electron microprobe analysis for potassium, iron, magnesium, titanium, and calcium were performed on each of the four biotite separates to determine, if possible, the level of contamination. Two distinct classes of detrital biotite are evident. These are characterized by (1) higher Fe, slightly higher K, and lower Mg, (2) lower Fe, slightly lower K, and higher Mg contents than the normal population of primary biotite. Several grains which showed lowered levels for all of the elements examined were excluded from the tabulation as it was

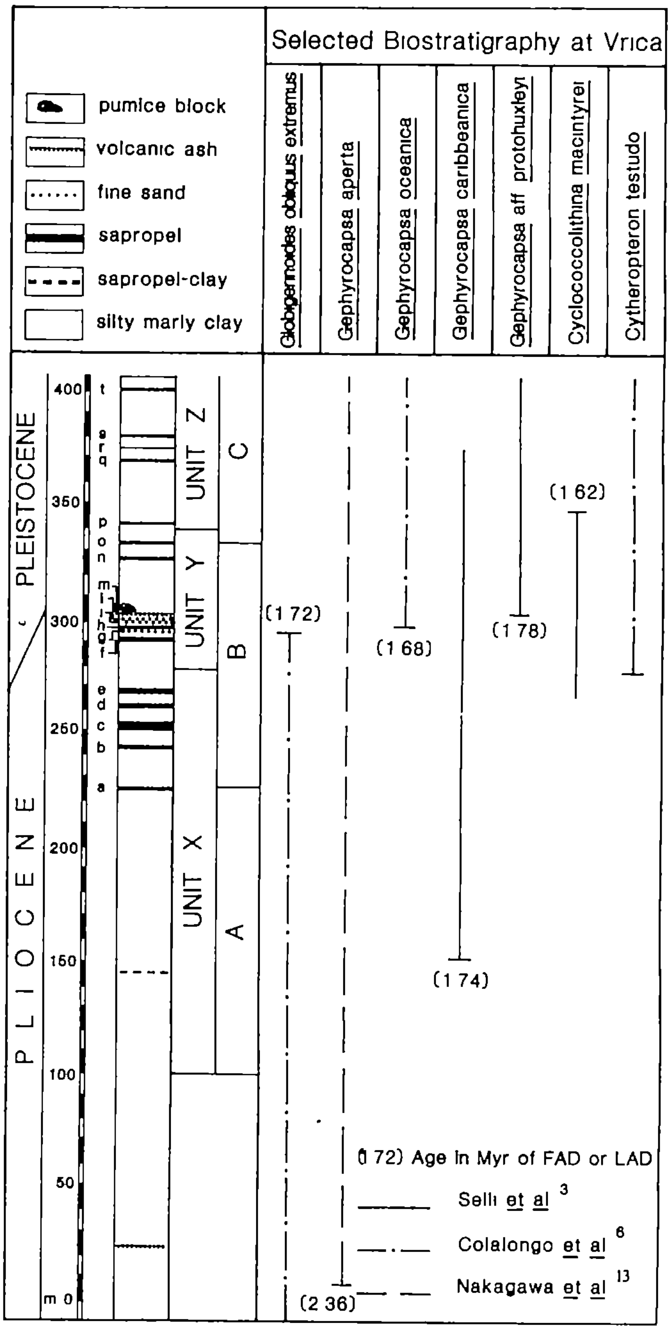

Fig. 3 Selected biostratigraphical data at Vrica. The columnar section is taken from ref. 3 (from the boundary of unit X upwards) and ref. 13 (below the lower boundary of unit X, simplified).

thought that they probably represented leached biotite grains. The detrital grains can be listed as follows:

Primary	(+80 mesh)	2 grains out of 102
	(−80+100 mesh)	6 grains out of 127
Secondary	(+80 mesh)	1 grain out of 110
	(−80+100 mesh)	6 grains out of 132

The limited number of grains examined may not give a realistic appraisal of the true level of contamination but these samples are definitely contaminated.

In retrospect, then, the age of the *m* marker bed and the proposed Plio–Pleistocene boundary-stratotype which should be placed close to this level should be younger than 1.99 ± 0.08 Myr.

Savelli and Mezzetti[12], Selli *et al.*[3], and Colalongo *et al.*[6] have repeatedly stressed the importance of the presence of a block of 'perfectly preserved pumice' immediately above the *m* marker bed ash at Vrica. This statement needs to be clarified.

First, one might infer from these reports that the pumice was actually collected at Vrica. However, the pumice block was collected from a quarry west of the city of Crotone some 4 km north of the Vrica section. One of us (G.P.), however, is convinced that the level at which the pumice block was found can be correlated to a level located ~1 m above the *m* marker bed at the Vrica section. Second, there is a large dissimilarity in the mineralogy and chemistry of the pumice and the *m* marker bed ash. The pumice contains phenocrysts of hornblende and plagioclase while the ash contains biotite and plagioclase. INAA of the glass fraction indicates that the pumice block is very similar to but not an exact equivalent of the Pliocene ash.

Approximately 250 g of the pumice was sent to Denver and sufficient hornblende for a single analysis was recovered. The K–Ar age of 2.35 ± 0.16 Myr (Table 1*c*) obtained was interpreted as indicating that the pumice block has been reworked from an older pumice layer and thus has no relevance to the age of the *m* marker bed.

The question really is just how much younger than 1.99 ± 0.08 Myr might the actual age of the *m* marker bed be? Selli *et al.*[3] used the sparsely available radiometric data and drilling efforts near Semaforo (Fig. 2) to propose rates of sedimentation of 35–48 cm kyr^{-1} for the 1,250 m between the top of the Messinian which they assumed to be 6 or 7 Myr old and the Pliocene ash previously dated at 3.4 Myr. If we use the more commonly accepted age of 5 Myr for the Miocene–Pliocene boundary and the 2.2 Myr age for the Pliocene ash we get an average rate of 45 cm kyr^{-1}. This rate is still in agreement with Selli *et al.*[3] because of the change in age of ~1 Myr at each end of the stratigraphical section. Assuming continuous sedimentation and applying this rate to the 280 m between the Pliocene ash and the *m* marker bed gives an age of ~1.6 Myr for the *m* marker bed. However, average rates of sedimentation must be used with caution.

Ultimately the resolution of the problem of the age of the *m* marker bed and, of course, the age of the Plio–Pleistocene boundary may rest on biostratigraphical and palaeomagnetic criteria. Nakagawa *et al.*[13] have presented a preliminary version of the magnetostratigraphy of the Vrica section, but later circulated results and interpretations quite different and conflicting: therefore the treatment of this topic is at present impractical. Thus we give here only a brief treatment of the relevant biostratigraphy at Vrica.

Berggren *et al.*[2] have summarized the numerous first appearance datums (FADs) and last appearance datums (LADs) of certain planktonic foraminifera and calcareous nannoplankton which have been recognized in deep sea cores and related to the magnetic reversal time scale. In using FADs and LADs one must keep in mind that the first appearance datum at any specific geographical locality may not coincide in time and may be younger than the first evolutionary appearance datum just as the last appearance datum may simply represent the disappearance of a particular species from a certain locality or region and so may be older than the true world-wide extinction of that species. Among the FADs and LADs mentioned by Berggren *et al.*[2] and by Haq *et al.*[1] the following have been recognized at Vrica (see Fig. 3 for the distribution within the section).

Planktonic foraminifera: (1) LAD of *Globigerinoides obliquus* occurs in deep sea cores at the top of the Olduvai normal polarity event with an interpolated age of 1.72 Myr (ref. 2). At Vrica *G. obliquus* is recognized at the subspecific level as *G. obliquus extremus* but this is in the same concept of *G. obliquus* recognized by Haq *et al.*[1], mentioned by Berggren *et al.*[2] and confirmed by Berggren (personal communication).

Calcareous nannoplankton: (1) LAD of *Cyclococcolithina macintyrei* occurs in deep sea cores above the Olduvai normal polarity event and has an interpolated age of 1.62 Myr (ref. 2, p. 285). (2) FAD of *Gephyrocapsa oceanica* in deep sea cores occurs just above the top of the Olduvai normal polarity event and has an interpolated age of 1.68 Myr (ref. 2, p. 284). (3) FAD of *Gephyrocapsa caribbeanica* in deep sea cores occurs just below the top of the Olduvai normal polarity event and has an interpolated age of 1.74 Myr (ref. 2, p. 285). The utility of the FAD of this species may be reduced because of conflicting concepts of it held by various investigators (ref. 14, p. 19). If the FAD of *G. caribbeanica* at Vrica section really occurs 73 m below sapropel layer a as indicated by Selli *et al.*[3] (Fig. 3), then we are faced with a troublesome fact. The FADs of *G. oceanica* and *G. caribbeanica* are separated by some 140 m of sediment. according to Berggren *et al.*[2] this interval would represent ~60,000 yr giving an average rate of sedimentation of ~230 cm kyr^{-1}, an inordinately high rate for this part of the section. (4) FAD of *Gephyrocapsa protohuxleyi* in deep sea cores is within the top of the Olduvai normal polarity event but occurs slightly before the FAD of *G. caribbeanica* (ref. 1, Fig. 5). If we adopt for the Olduvai the age limits proposed by Berggren *et al.*[2] (1.72–1.88 Myr), the FAD of *G. protohuxleyi* has an interpolated age of 1.78 Myr. At Vrica *G.* aff *protohuxleyi* has been recognized and occurs ~10 m above the FAD of *G. oceanica*. (5) FAD of *Gephyrocapsa aperta* occurs in deep sea cores below the Olduvai normal polarity event and has an interpolated age of 2.36 Myr (ref. 2, p. 284). At Vrica *G. aperta* makes its first appearance 17 m below the Pliocene ash whose age is 2.22 Myr.

Figure 3 shows the age assignments for the various FADs and LADs in parentheses. Despite the qualifications cited above an age of ~1.7 Myr for the *m* marker bed would be consistent with the biostratigraphical data.

According to the recent resolution of the joint meeting of the INQUA Subcommission 1 − *a* (= ICS Working Group N/Q Boundary) and the IGCP Project 41 made during the International Geological Congress in Paris (July 1980), "the N/Q boundary should be placed in the Vrica section taking into account the FAD of the early cold guest *Cytheropteron testudo* (whatever its palaeoclimatic significance could be), which occurs in Vrica 10 m above Sapropel *e*. [Colalongo *et al.*[6,9], and Colalongo and Sartoni[15], have demonstrated that in the Vrica section the FAD of *C. testudo* is accompanied by palaeontological events (FADs and LADs of planktonic foraminifera and calcareous nannofossils) that are useful for long-distance correlations.] On the other hand, there are alternative possibilities for selecting a level as the N/Q boundary stratotype in the Vrica section, within the stratigraphical interval between level *e* and the volcanic ash level *m*, which are closely related with the FAD of *C. testudo*, within a reasonably short time range."

Taking this resolution into account, it is apparent that the proposed Plio–Pleistocene Boundary stratotype in the Vrica section will fall close to 1.7 Myr and that all other published estimates suggesting an age of 2 Myr or more are inappropriate.

We thank W. Berggren, D. Hopkins, K. MacDougall, K. Pierce, and G. M. Richmond for their critical comments, Professor Jack Dymond for allowing us to cite his unpublished ^{40}Ar/^{39}Ar results, also G. Cebula, J. Groen, H. Mehnert, and K. Futa for technical assistance. J.D.O., C.W.N and G.A.I. are indebted to the National Geographic Society for financial assistance.

Received 20 January; accepted 22 April 1982

1. Haq, B. U., Berggren, W. A & VanCouvering, J. A. *Nature* **269**, 483–488 (1977).
2. Berggren, W. A. *et al. Quat. Res.* **13**, 277–302 (1980)
3. Selli, R. *et. al G. Geol.* **42**, 181–204 (1977)
4. Boellstorff, J. *Science* **202**, 305–307 (1978).
5. Steiger, R. H. & Jager, E. *Earth planet. Sci Lett.* **36**, 359–362 (1977).
6. Colalongo, M. L., Pasini, G & Sartori, S *Boll Soc. Paleontol. Ital.* (in the press).
7. Emiliani, C., Mayeda, T & Selli, R *Bull. geol. Soc. Am* **72**, 679–688 (1961).
8. Raffi, I. & Rio, D. *Paleontol. stratigr. Evoluz.* **1**, 181–186 (1980).
9. Colalongo, M. L. *et al., Geografia Fis. Dinam. Quat* (in the press)
10. Selli, R. *G. Geol.* **35**, 51–59 (1970)
11. Naeser, C. W., Briggs, N. D., Obradovich, J. D & Izett, G A in *Tephra Studies* (eds Self, S. & Sparks, R. S. J.) 13–48 (Reidel, Dordrecht, 1981)
12. Savelli, C. & Mezzetti, R. *X INQUA Congress*, Birmingham, 400 (1977)
13. Nakagawa, H. *et al., Proc. 2nd Symp. on the N/Q Boundary, USSR*, 1977 (in the press).
14. Gartner, S. *Mar Micropaleont* **2**, 1–25 (1977)
15. Colalongo, M. L. & Sartori, S *G Geol* **42**, 205–220 (1977)
16. Pasini, G *et al., G Geol* **41**, 446–456 (1977).
17. Arias, C., Azzaroli, A , Bigazzi, G. & Bonadonna, F. P. *Nucl. Tracks* **5**, 129–136 (1981).

Brown adipose tissue thermogenesis is 'suppressed' during lactation in mice

Paul Trayhurn, Jenny B. Douglas & Martina M. McGuckin

Dunn Nutritional Laboratory, University of Cambridge and
Medical Research Council, Milton Road, Cambridge CB4 1XJ, UK

Brown adipose tissue is considered to be the main site of thermoregulatory non-shivering thermogenesis in the newborn of many mammalian species, in arousing hibernators, and in adult cold-adapted rats and mice[1–4]. Several recent studies have now suggested that the tissue may also be important in the regulation of energy balance. Evidence has been obtained indicating that the ability of genetically obese (*ob/ob* and *db/db*) mice to become obese on a normal energy intake is mainly due to reduced brown adipose tissue thermogenesis[5–7], and a reduction in the activity of the tissue has also been observed in rats made obese by lesions of the ventromedial hypothalamus[8]. In contrast, increases in thermogenesis in brown adipose tissue have been implicated in the immediate thermic effect of food[9] and in cancer cachexia[10], and a substantial augmentation of the activity of the tissue has been demonstrated in rats and mice exhibiting regulatory diet-induced thermogenesis as a response to chronic voluntary over-feeding[11–14]. Whether or not brown adipose tissue thermogenesis changes in other, more physiological, states where energy flux and metabolic efficiency are altered (independently of environmental temperature) has not been established. We now report that the thermogenic activity of brown adipose tissue is suppressed in mice during the 'physiological hyperphagia' of lactation, and show that this probably results in a substantial reduction in the energy requirement for maintenance of the lactating animal.

The animals used in this study were mice of the 'Aston' variety[15], aged between 2½ and 4 months. Pregnant and lactating animals were taken during their first or second litter, and each litter contained between 6 and 10 pups. Virgin females, housed in pairs, were used as controls. The temperature of the animal house was maintained at 21 ± 2 °C, and the mice were subject to a 12 h light/12 h dark cycle (light period from 07.00 h). All mice were given free access to both water and a low-fat commercial breeding diet (Spillers–Spratts Rodent Breeding Diet 1).

In the first experiments the weight, total protein content and cytochrome oxidase activity (E.C.1.9.3.1) of brown adipose tissue from the readily accessible interscapular site were determined for virgin mice and for mice at mid-lactation (days 9–12 post partum). A comparison was also made with mice during late pregnancy (see Table 1). The total amount of interscapular brown adipose tissue was greater in both the lactating and pregnant animals than in the virgin mice. This increase is probably due to increased lipid deposition, as the total protein content of the tissue was lower in both the pregnant and lactating animals. The cytochrome oxidase activity in brown adipose tissue of the lactating mice was reduced to half the level in the virgin animals, indicating that during lactation there is a substantial decrease in the overall oxidative capacity of the tissue. The cytochrome oxidase activity was also reduced in late pregnancy, to a value between that of the virgin and lactating animals.

Table 1 Weight, protein content and cytochrome oxidase activity of interscapular brown adipose tissue from virgin and lactating mice

	Virgin	Pregnant	Lactating
Tissue weight	68.5 ± 3.8	102.6 ± 8.8‡	93.7 ± 3.5‡
(mg)	(17)	(6)	(12)
Total protein	11.7 ± 0.5	9.6 ± 0.4*	8.2 ± 0.4‡
content (mg)	(17)	(6)	(12)
Total cytochrome			
oxidase activity	17.5 ± 0.8	13.2 ± 0.6†	8.8 ± 1.1‡
(μmol cytochrome	(15)	(6)	(10)
c oxidized per min)			

Mice were killed by cervical dislocation and the interscapular brown adipose tissue rapidly removed, and trimmed free of other tissues. The cytochrome oxidase activity of brown adipose tissue was measured spectrophotometrically[28], and the total protein content assayed by a modified Lowry method[29] using BSA as a standard. The results are given as mean ±s.e.m., with the numbers of animals shown in parentheses.

* $P < 0.05$; † $P < 0.01$; ‡ $P < 0.001$, compared with the virgin animals (Student's *t*-test).

The principal mechanism for thermogenesis in brown adipose tissue is via a proton conductance pathway across the inner mitochondrial membrane, which results in the uncoupling of respiration from ATP synthesis[16]. The proton conductance pathway can be blocked by purine nucleotides, such as GDP, which bind to a specific 'uncoupling' protein of molecular weight 32,000 (refs 17, 18). The activity of the proton conductance pathway is generally assessed from the extent to which radioactively labelled purine nucleotides bind to brown adipose tissue mitochondria[19–22]. Table 2 shows the results of a GDP-binding study of virgin, pregnant and lactating mice. Compared with the virgin mice, GDP binding was much lower in both early (days 1–3 post partum) and mid-lactation; it was also low during late pregnancy. Binding was lowest at mid-lactation and was not significantly increased 24 h after the pups had been abruptly weaned. These results suggest that the activity of the thermogenic proton conductance pathway is substantially reduced during pregnancy and lactation in mice.

The full extent of the reduction in brown adipose tissue thermogenesis in lactating mice was assessed by reference to the level of GDP binding in virgin animals acclimated for 3 weeks at an environmental temperature (33 °C) where there is

Table 2 GDP binding to brown adipose tissue mitochondria from virgin and lactating mice

	GDP bound (pmol per mg mitochondrial protein)
Virgin	249.4 ± 24.7 (10)
Pregnant	88.0 ± 7.4 (7)*
Lactating (early)	93.3 ± 14.6 (6)*
Lactating (mid)	56.2 ± 5.5 (8)*
Abruptly weaned at mid-lactation	65.5 ± 5.0 (6)*
Virgin, adapted at 33 °C	55.1 ± 5.0 (9)*

Mice were killed by cervical dislocation and brown adipose tissue rapidly removed from the interscapular, subscapular and dorso-cervical sites. Mitochondria were then prepared as described by Cannon and Lindberg[30]. GDP binding was measured by incubating the mitochondria with 10 μM ^{3}H-GDP at 20 °C, *p*H 7.1, for 7 min, as described previously[7,14]. (^{3}H-GDP and ^{14}C-sucrose were obtained from Amersham.) The results are given as mean ±s.e.m., with the number of observations shown in parentheses. For each assay, mitochondria were obtained from 1–2 mice.

* $P < 0.001$, compared with the virgin animals (Student's *t*-test).

0028–0836/82/260059—02$01.00

Table 3 Respiration rates in brown adipose tissue mitochondria from virgin and lactating mice

Additions	Mitochondrial respiration (nmol O_2 per min per mg mitochondrial protein)	
	Virgin	Lactating (mid)
–	110.7 ± 18.9	53.3 ± 9.0*
BSA (2.5 mg ml^{-1})	308.2 ± 15.3	188.2 ± 13.4†
GDP (1 mM)	131.1 ± 10.8	149.4 ± 10.3(NS)
Change in rate with GDP	-177.2 ± 18.6	-38.8 ± 8.7†

Brown adipose tissue mitochondria were prepared as described in Table 2 legend. Respiration was measured at 25 °C in a Yellow Springs YSI model 53 oxygen electrode, using medium (pH 7.1) containing 100 mM sucrose, 10 mM glycylglycine and 5 μM rotenone, with 10 mM α-glycerophosphate as substrate[24]. The results are mean ±s.e.m. for 6 groups of virgin and 6 groups of lactating mice (each group consisted of mitochondria obtained from 2 mice).

* $P < 0.05$; † $P < 0.001$, compared with the virgin animals (Student's t-test). NS, not significant ($P > 0.05$).

no requirement for non-shivering thermogenesis[23]. The results obtained with mice in these conditions (Table 2) were almost identical to those observed at mid-lactation. A Scatchard analysis of binding data showed that the reduced GDP binding in lactating mice was due to a reduction in the number of binding sites, and not to any change in affinity; the apparent dissociation constant (K_D) was approximately 3 μM at pH 7.1 for both virgin and lactating animals.

The GDP-binding assay is a physicochemical index of the proton conductance pathway. To obtain a more direct physiological measure of the thermogenic activity of brown adipose tissue mitochondria during lactation, mitochondrial respiration was determined (with α-glycerophosphate as substrate) in the presence and absence of exogenous GDP. The results in Table 3 show that in the presence of bovine serum albumin (BSA), which removes the inhibitory effects of endogenous fatty acids on the activity of α-glycerophosphate dehydrogenase[24,25], the mitochondrial respiration rate was significantly higher in virgin than in lactating mice. Following the addition of GDP, to recouple the mitochondria and restore respiratory control, the respiration rate fell much more in the virgin than in the lactating mice, and there was no longer any significant difference between the two groups. The difference between the respiration rates before and after adding GDP was almost 5 times higher for the virgin than for the lactating mice; thus, brown adipose tissue mitochondria from lactating mice seem to be much more fully 'coupled' than those from virgin animals.

The results presented here clearly demonstrate that thermogenesis in brown adipose tissue is suppressed in lactating mice, and the suppression is such that the thermogenic activity is similar to that of mice adapted to thermoneutral conditions. Alterations in the metabolism of brown adipose tissue in lactation have been observed previously by Agius and Williamson[26,27] in studies on lipogenesis. Not only is thermogenesis for thermoregulatory purposes inhibited in brown adipose tissue during lactation, but the increased food intake of the lactating animal does not result in a dietary-induced stimulation of the tissue—in contrast to the response invoked during overfeeding in normal, non-lactating, rats and mice[11-14]. This is, of course, a rational response as substrates which would otherwise be dissipated in brown adipose tissue as heat are available for the synthesis of milk[26,27].

The inhibition of brown adipose tissue thermogenesis would be expected to have a significant energy sparing effect on the lactating animal. To obtain an estimate of the possible (maximum) quantitative importance of such an effect, we have measured the energy intake of virgin mice, aged 3 months, adapted at 21 °C and at 33 °C (thermoneutrality); the difference should reflect the normal energy flux through brown adipose tissue and those tissues (for example, heart) which have a supportive role in thermogenesis[3,4,6,13]. At 21 °C the gross energy intake of the virgin mice was 76 kJ per day, while at 33 °C it was 45 kJ per day, giving a figure of 31 kJ per day for the energy expenditure on thermogenesis at 21 °C. Thus, if *in vitro* experiments on mitochondrial respiration and GDP binding accurately reflect the activity of brown adipose tissue *in vivo*, the suppression of brown adipose tissue thermogenesis in the lactating mouse could conserve as much as 31 kJ per day, and this is equivalent to 40% of the maintenance energy requirement of the normal, non-lactating, animal.

The most likely explanation for the results obtained here is either that during pregnancy and lactation there is a distinct physiological adaptation for energy conservation (mediated by prolactin?), or that the increased metabolic heat production which results from fetal growth and milk synthesis is sufficient to obviate the need for any specific thermoregulatory heat production. Whichever explanation is correct, the inhibition of brown adipose tissue thermogenesis would be expected to have a significant effect on the overall energy expenditure and energy requirement of the lactating mouse. Whether there are implications from the observations presented here for other (larger) species, including man, is not clear. In conclusion, our results, together with a previous study on lipogenesis following intragastric feeding[26], indicate that the lactating animal may be a valuable model in which to investigate the regulation of thermogenesis in brown adipose tissue.

We thank Drs W. A. Coward and D. Isler for valuable discussions, and Mr A. Kimmerling for technical assistance.

Received 15 March; accepted 10 May 1982.

1. Smith, R. E. & Horwitz, B. A. *Physiol. Rev.* **49,** 330–425 (1969).
2. Jansky, L. *Biol. Rev.* **48,** 85–132 (1973).
3. Foster, D. O. & Frydman, M. L. *Can. J. Physiol. Pharmac.* **56,** 110–122 (1978).
4. Foster, D. O. & Frydman, M. L. *Can. J. Physiol. Pharmac.* **57,** 257–270 (1979).
5. Himms-Hagen, J. & Desautels, M. *Biochem. biophys. Res. Commun.* **83,** 628–634 (1978).
6. Thurlby, P. L. & Trayhurn, P. *Pflügers Arch. ges. Physiol.* **385,** 193–201 (1980).
7. Goodbody, A. E. & Trayhurn, P. *Biochem. J.* **194,** 1019–1022 (1981).
8. Seydoux, J., Rohner-Jeanrenaud, F., Assimacopoulos-Jeannet, F., Jeanrenaud, B. & Girardier, L. *Pflügers Arch. ges. Physiol.* **390,** 1–4 (1981).
9. Glick, Z., Teague, R. J. & Bray, G. A. *Science* **213,** 1125–1127 (1981).
10. Brooks, S. L., Neville, A. M., Rothwell, N. J., Stock, M. J. & Wilson, S. *Biosci. Rep.* **1,** 509–517 (1981).
11. Rothwell, N. J. & Stock, M. J. *Nature* **281,** 31–35 (1979).
12. Brooks, S. L., Rothwell, N. J., Stock, M. J., Goodbody, A. E. & Trayhurn, P. *Nature* **286,** 274–276 (1980).
13. Rothwell, N. J. & Stock, M. J. *Pflügers Arch. ges. Physiol.* **389,** 237–241 (1981).
14. Trayhurn, P., Jones, P. M., McGuckin, M. M. & Goodbody, A. E. *Nature* **295,** 323–325 (1982).
15. Thurlby, P. L. & Trayhurn, P. *Br. J. Nutr.* **39,** 397–402 (1978).
16. Nicholls, D. G. *Biochim. biophys. Acta* **549,** 1–29 (1979).
17. Nicholls, D. G. *Eur. J. Biochem.* **62,** 223–228 (1976).
18. Heaton, G. M., Wagenvoord, R. J., Kemp, A. & Nicholls, D. G. *Eur. J. Biochem.* **82,** 515–521 (1978).
19. Rafael, J. & Heldt, H. W. *FEBS Lett.* **63,** 304–308 (1976).
20. Desautels, M., Zaror-Behrens, G. & Himms-Hagen, J. *Can. J. Biochem.* **56,** 378–383 (1978).
21. Desautels, M. & Himms-Hagen, J. *Can. J. Biochem.* **57,** 968–976 (1979).
22. Sundin, U. & Cannon, B. *Comp. Biochem. Physiol.* **65B,** 463–471 (1980).
23. Trayhurn, P. & James, W. P. T. *Pflügers Arch. ges. Physiol.* **373,** 189–193 (1978).
24. Nicholls, D. G. *Eur. J. Biochem.* **49,** 573–583 (1974).
25. Bukowiecki, L. J. & Lindberg, O. *Biochim. biophys. Acta* **348,** 115–125 (1974).
26. Agius, L. & Williamson, D. H. *Biochem. J.* **190,** 477–480 (1980).
27. Agius, L. & Williamson, D. H. *Biochem. Soc. Trans.* **8,** 590–591 (1980).
28. Yonetani, T. & Ray, G. S. *J. biol. Chem.* **240,** 3392–3398 (1965).
29. Schacterle, G. R. & Pollack, R. L. *Analyt. Biochem.* **51,** 654–655 (1973).

Relationship of β-adrenoreceptor density to fitness in athletes

J. Butler, M. O'Brien, K. O'Malley & J. G. Kelly

Departments of Clinical Pharmacology and Anatomy, Royal College of Surgeons in Ireland, St Stephens Green, Dublin 2, Eire

Physical training in man results in a decreased heart rate at rest[1,2], associated with an apparent decrease in the activity of the sympathetic nervous system[1,3]. One possible mechanism for this would be alterations in β-adrenoreceptor density with training. Exercise produces large increases in plasma catecholamine concentrations[4,5]. Moreover, lymphocyte β-adrenoreceptor density in man is inversely correlated with plasma and urinary noradrenaline concentrations and is positively correlated with cardiac sensitivity to isoprenaline[6]. Thus,

0028-0836/82/260060—03$01.00

alterations in β-adrenoreceptor density in the cardiovascular system might be reflected in changes in lymphocyte β-adrenoreceptor density. We have now measured lymphocyte β-adrenoreceptor density in a group of athletes of varying degrees of fitness before and after they embarked on an intensive training programme. Our results show clear correlations between degree of physical fitness and receptor density and we conclude that decreases in sympathetic nervous system responsiveness following physical training are related to decreases in β-adrenoreceptor density.

Observations were made on 16 male swimmers aged 14–24 yr. The subjects were of varying fitness and were about to embark on a 2-month intensive training programme. A venous blood sample (30 ml) was obtained from each subject at 10.30 a.m. Lymphocytes were isolated using the method of Boyum[7] and β-adrenoreceptor density was measured by a radioligand binding method similar to that of Williams *et al.*[8]. At 11 a.m. on the same morning, each subject underwent submaximal exercise on a Monarch bicycle ergometer and fitness levels were then assessed using predicted aerobic capacity (maximal oxygen intake, max VO_2) from the Astrand–Rhyming nomogram[9]. Results for max VO_2 and adrenoreceptor densities were only correlated at the completion of the study. No subject was receiving any drugs.

Pre-training max VO_2 was 24–61 ml per kg per min (mean, 49.6±2.3 s.e.m.) and pre-training β-adrenoreceptor density varied over 1,538–385 receptors per lymphocyte (mean, 1,062±97 s.e.m.) (Fig. 1*a*). There was a complex inverse relationship between max VO_2 and β-adrenoreceptor density (Spearman's $\rho = 0.75$, $P < 0.001$). At low to average levels of fitness, β-adrenoreceptor density was in the region of 1,000–1,500 sites per cell, in good agreement with values previously reported by us in young people of average physical fitness[10]. At higher levels of fitness, however, represented by max VO_2 values greater than 45–50 ml per kg per min, receptor density decreased sharply.

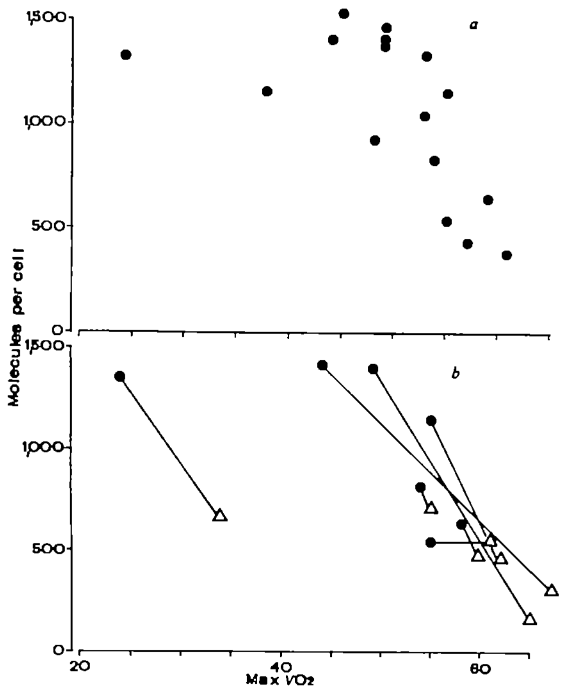

Fig. 1 *a*, Relationship between maximal oxygen intake (max VO_2 in ml per kg per min) and lymphocyte receptor density (as molecules of dihydroalprenolol specifically bound per cell), in 16 swimmers of varying fitness before embarking on a training programme. Lymphocyte β-receptor density was estimated by a method similar to that of Williams *et al.*[8]. Lymphocyte membranes (0.1 ml) equivalent to 2×10^6 cells were incubated with ^{3}H-dihydroalprenolol (102 Ci mmol^{-1} Amersham) at concentrations of 0.5–5.5 nM. The final volume was 0.2 ml. After incubation for 15 min at 37 °C the reaction was terminated by the addition of 2 ml ice-cold buffer (50 mM Tris, 2 mM $MgCl_2$, *p*H 7.6). Membranes were separated by immediate filtration through Whatman GFC filters which were then washed with three 2-ml volumes of buffer. Nonspecific binding was estimated in the presence of 10^{-5} M alprenolol. Numbers of specific dihydroalprenolol binding sites were calculated using Scatchard plots. *b*, Maximal oxygen uptake (ml per kg per min) plotted against lymphocyte receptor density (as molecules of dihydroalprenolol specifically bound per cell) in seven swimmers before (●) and after (△) a 2-month training programme.

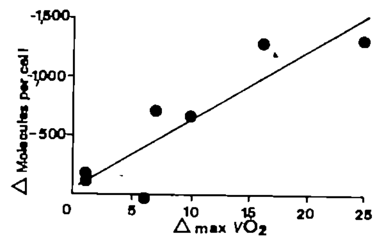

Fig. 2 Relationship between change in receptor density (as decrease in the number of molecules of dihydroalprenolol specifically bound per cell) and change in maximum oxygen intake (as increase in max VO_2, ml per kg per min) in the seven swimmers who underwent a 2-month training programme. The line of best fit, determined by linear regression analysis, is shown (correlation coefficient = −0.89, $P < 0.01$).

Seven subjects completed their training schedule satisfactorily and were reassessed. Figure 1*b* plots pre- and post-training values for max VO_2 and receptor density for each of these subjects. Training increased max VO_2 in every case, the mean pre-training value being 48.7±4.5 ml per kg compared with a mean post-training value of 58.1±4.1 ml per kg ($P < 0.05$, Student's *t*-test for paired data). After training, lymphocyte β-adrenoreceptor density in these seven subjects decreased from a mean of 1,074±152 receptors per cell to a mean of 458±78 ($P < 0.05$) and in all but one subject, receptor density decreased. The single exception showed an insignificant change in receptor density from 547 to 554 sites per cell. Those subjects showing the greatest increase in fitness also tended to show the greatest fall in lymphocyte β-adrenoreceptor density and there was a significant linear correlation between change in receptor density and change in max VO_2 (Fig. 2).

Our results show a clear, inverse relationship between physical fitness and lymphocyte β-adrenoreceptor density. Physical training can further reduce β-adrenoreceptor density and this reduction is proportional to changes in fitness. The most likely explanation involves changes in concentrations of circulating catecholamines, although effects of other exercise-related metabolic processes such as metabolic acidosis cannot be excluded. Exercise results in large increases in plasma catecholamine concentrations. These increases are slightly lower in trained subjects but are still substantial[5]. High concentrations of sympathomimetic amines in man, whether from exogenous or endogenous sources, result in a decreased responsiveness of lymphocytes to stimulation by these agents[11], associated with decreases in receptor density[12,13]. The reductions in receptor density at higher levels of physical fitness seen in the present study probably result from regular exposure to high concentrations of catecholamines. Fraser and colleagues[6] recently found evidence that these reductions could result in decreased sympathetic nervous system responsiveness and showed that low lymphocyte β-adrenoreceptor densities were associated with low cardiac sensitivity to isoprenaline.

We suggest that the decreased sympathetic nervous system responsiveness seen in athletes is due to a decreased β-adrenoreceptor density resulting from chronic exposure to high concentrations of catecholamines. Teleologically, this could represent a protective mechanism against chronic sympathetic nervous system stimulation. Physical fitness should be taken into account in studies involving measuring β-adrenoreceptor density or responsiveness.

This work was supported by the MRC of Ireland.

Received 2 February; accepted 10 May 1982

1. Le Blanc, J *et al. J appl. Physiol* **42**, 166–173 (1977).
2. Adams, T. D *et al Circulation* **64**, 958–965 (1981)
3 Ekblom, B., Kilbom, A. & Soltysiak, J *Scand J clin. Lab Invest.* **32**, 251–256 (1973)
4 Bannister, E W. & Griffiths, J. *J appl Physiol* **33**, 674–680 (1972)
5 Johnston, R H., Park, D M., Rennie, M J & Sulaiman, W R. *J Physiol, Lond.* **241**, 23P–25P (1974).
6. Fraser, J, Nadeau, J, Robertson, D. & Wood, A J J *J clin Invest.* **67**, 1777–1784 (1981)
7. Boyum, A *Scand J. clin Lab Invest.* **21**, Suppl. 97, 77–79 (1968)
8. Williams, L. T., Snyderman, R. & Lefkowitz, R. J. *J. clin Invest* **57**, 149–155 (1976)
9 Astrand, P O. & Rhyming, I. *J appl. Physiol.* **7**, 218–222 (1954)
10. Doyle, V. M, Kelly, J. G. & O'Malley, K *Br J. clin. Pharmac.* **12**, 265p–266p (1981)
11. Greenacre, J. K. & Conolly, M E. *Br. J. clin Pharmac.* **5**, 191–197 (1978).
12. Galant, S. P., Duriseti, L, Underwood, S. & Insel, P. A. *New Engl J. Med* **299**, 933–936 (1978).
13 Krall, J. F., Connolly, M. & Tuck, M. L. *J. Pharmac. exp. Ther.* **214**, 554–560 (1980).

Visual pigments in the four-eyed fish, *Anableps anableps*

J. A. Avery & J. K. Bowmaker

Department of Zoology and Comparative Physiology,
Queen Mary College, University of London, Mile End Road,
London E1 4NS, UK

The retinae of terrestrial and marine vertebrates generally contain the visual pigment, rhodopsin, whereas those of freshwater vertebrates contain porphyropsin[1,2]. The latter pigment absorbs light at longer wavelengths than rhodopsin and therefore has increased red sensitivity, which is possibly beneficial to animals living in water containing suspended particles since these may cause image degradation due to light scattering at short wavelengths. Many fish and amphibians have both types of pigment, and in some fish, the proportion of rhodopsin to porphyropsin is greater in the dorsal half of the retina[3]. In the bullfrog, *Rana catesbeiana*, the ventral retina contains only rhodopsin, whereas the dorsal retina has appreciable amounts of porphyropsin[4]. This may be attributable to the fact that the bullfrog often has only its eyes and nose protruding above the water surface, thus the dorsal part of the retina is used for aquatic vision and the ventral part for aerial vision. The 'four-eyed' fish, *Anableps*, is able to see simultaneously in air and water; it normally swims so that the eye is bisected by the water meniscus. Each eye has a single retina, but the dorsal part receives images from the water, and the ventral region receives aerial images[5,6]. Thus it has been suggested that the dorsal region should show more red dominance[7], with porphyropsins being restricted to this area. We have measured the absorbance spectra of the photoreceptors, and report here that the same visual pigments are present in the dorsal and ventral regions of *Anableps* retina.

A visual pigment molecule consists of a protein moiety, opsin, and a chromophore, based on either vitamin A_1 or A_2. Rhodopsins, generally found in the retinae of terrestrial and marine vertebrates, are based on vitamin A_1, whereas porphyropsins, found in freshwater vertebrates, are based on vitamin A_2. Using the same opsin, a vitamin A_2 pigment absorbs light at longer wavelengths than a vitamin A_1 pigment, hence porphyropsin has increased red sensitivity compared with rhodopsin.

Live specimens of *Anableps anableps* (obtained from a tropical fish supplier in London) were maintained in brackish water (specific gravity 1.005, pH 7–8, temperature 22–24 °C). The fish were dark-adapted overnight before an experiment. All procedures were then carried out under dim red light (Kodak safelight no. 2).

The fish were decapitated, and the eyes removed and stored in the dark at 4 °C until required. Each eye was cut into dorsal and ventral sections with a razor blade, using as a guide the horizontal corneal pigment band which marks externally the division between the two halves of the eye. The retina was removed from each section and placed in freshwater teleost Ringer's solution. A small piece of retina (~1 mm²) was cut from one of the retinal halves and prepared using a method similar to that described elsewhere[8]. Briefly, the tissue was cut into fragments with razor blades and squashed between two coverslips, which were sealed with paraffin wax to avoid evaporation. Microspectrophotometric measurements were made using a modified Leibman microspectrophotometer[9,10] under computer control, as described elsewhere[11]. The microspectrophotometer was programmed to step from 750 nm to 390 nm in 2-nm steps, taking in data at even-numbered wavelengths, and to return, taking in data at odd-numbered wavelengths.

In both regions of the retina, four distinct cell types were identified: rods, single cones and two different classes of double cone. The rods contained a visual pigment having a wavelength of maximum absorbance (λ_{max}) 506 nm (Fig. 1), which is in

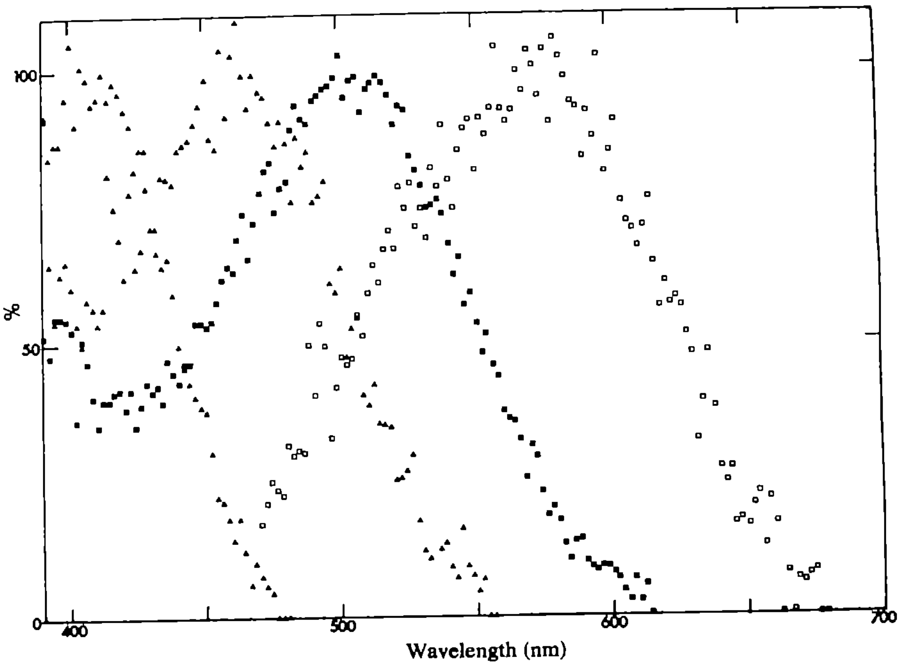

Fig. 1 Mean absorbance spectra for four classes of photoreceptor from dorsal and ventral retinal samples for three individual fish. The maximum absorbance (λ_{max}) values of the four classes are: single cone, 409 nm ($n = 13$); rod, 506 nm ($n = 9$); middle-wave-sensitive member of double cone, 463 nm ($n = 4$); long-wave-sensitive member of double cone, 576 nm ($n = 6$). Each point represents the average of values obtained at two adjacent wavelengths, one value recorded in the descending scan, the other in the ascending scan. The mean spectra have been normalized to a maximum of 100%. For each absorbance spectrum, the approximate wavelength of peak absorbance was estimated and each of 25 individual values on either side of the provisional peak was referred to the appropriate nomogram to estimate the wavenumber of peak sensitivity; this operation involves determining where the nomogram must be located on the wavenumber abscissa to yield the absorbance value under consideration. The nomograms used were the Dartnall A_1 nomogram[13] for the rods, the frog green rod nomogram[10] for the single cones and the P463 cones, and the rhesus monkey red cone spectrum[17] for the P576 cones. For the short wave-sensitive cones, the maximum absorbance was estimated using 20 points on the right-hand side only of the provisional peak.

0028–0836/82/260062—03$01 00

agreement with that given by Schwanzara[12] for an extract of the visual pigment of *Anableps*. The single cones contained a pigment maximally sensitive to short wavelengths (λ_{max} = 409 nm), while the double cones contained two pigments absorbing at longer wavelengths, with maximum absorbances of 463 nm and 576 nm. One class of double cone contained only the long-wave-sensitive pigment in both members, whereas the other class contained both the middle- and long-wave-sensitive pigments (Fig. 1). The shape of the absorbance spectra of the rods was well fitted by a Dartnall nomogram[13], which suggests that the pigment was probably based on vitamin A_1.

Ellipsosomes similar to those described by MacNichol *et al.*[14] but termed 'oil droplets' by Borwein and Hollenberg[5] were found in the ellipsoid region of the inner segment of the cones. The ellipsosomes in the double cones did not contain carotenoids, as found in birds and reptiles[15], but contained a pigment whose spectrum closely resembled that of reduced cytochrome *c*, with an intense short-wavelength absorbance band (λ_{max} = 415 nm) and two less intense absorbance bands at longer wavelengths (519 and 549 nm) (Fig. 2). The ellipsosomes of the double cones in which both members contained the 576-nm pigment (P576) were identical, with the short-wave absorbance band having a maximum density of ~0.3. A similar absorbance spectrum was measured for the ellipsosomes of the long-wave-sensitive member of the other class of double cone, but in the spectrum of the ellipsosomes of the members containing the P463, the density of the pigment was considerably greater, with a short-wave absorbance of ~0.5. Ellipsosomes were visible in the inner segments of the single cones sensitive to short wavelengths, but contained no detectable pigment.

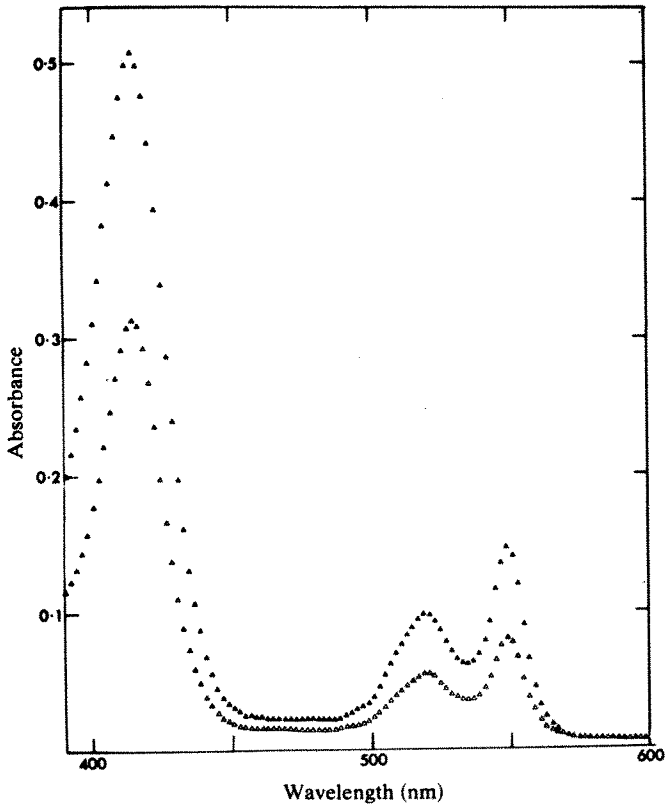

Fig. 2 ▲, Mean absorbance curve of six ellipsosomes from the P463 members of double cones and △, mean absorbance curve of seven ellipsosomes from the P576 members of double cones. The wavelengths of peak absorbance are 415, 519 and 549 nm.

As light must pass through the ellipsosomes to reach the photosensitive outer segment, it has been suggested that the ellipsosome acts as an intracellular colour filter[14]. The principal effect would be to filter a narrow band of violet–blue light (400–430 nm) from the outer segment. Making reasonable assumptions for the end-on absorbance of the cone outer segments, it is possible to construct relative spectral sensitivity functions for the different cone types (Fig. 3). It is clear that the filtering by the ellipsosomes narrows the short-wave limb of the visual pigment spectrum, particularly that of the P463 member of the double cone. This results in the P463 member of the double cone having a rapidly decreasing sensitivity from 460 nm to 420 nm, whereas the P409 single cones have a rapidly increasing sensitivity in the same region of the spectrum. This invites speculation as to possible neural interaction between these cone types which would confer increased wavelength discrimination in the short-wave region of the spectrum.

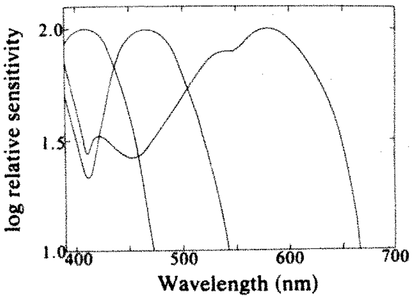

Fig. 3 Log relative sensitivity functions for the three classes of cone. These were derived by determining the absorptance spectrum for each class of cone and subtracting from this the mean absorbance spectrum of the ellipsosomes found in the inner segments of the corresponding cone type. In the case of the single cones, the sensitivity function is the same as the absorptance spectrum, as the ellipsosomes in these receptors are spectroscopically clear. The absorbance spectrum of a given class of cone (that is, the ratio of absorbed to incident light for a beam passing axially through the receptor) was calculated assuming an end-on absorbance of 0.25. The cone outer segments were ~6–10 µm long but appeared to be broken at the tips, and we have taken the true outer segment length to be ~15 µm. The specific absorbance of the cells was ~0.15, similar to values reported for other cones containing pigments based on vitamin A_1 (ref. 10).

The Cyprinodontidae (flagfish, minnows) and the Poecilidae (mollies, guppies) are closely related to the Anablepidae, all being members of the Order Microcyprini. The visual pigments of these families are very similar to those of *Anableps*; they too have violet-sensitive single cones, middle- and long-wave-sensitive double cones, and ellipsosomes in the double cone inner segments[16]. They also occupy a similar habitat in that they are all found very close to the surface in freshwater, and they are strongly diurnal and primarily surface feeders.

Although there seems to be no difference in the visual pigments in the two halves of the retina in *Anableps*, it cannot be excluded that the dorsal region may be more red-sensitive than the ventral region, either as a result of an uneven distribution of the various cone types in the two halves of the retina, or due to neural interaction giving prominence to the long wave-sensitive double cones.

Received 17 February; accepted 6 May 1982.

1. Wald, G. *Documenta ophth.* **3,** 94–134 (1949).
2. Crescitelli, F. in *Handbook of Sensory Physiology* Vol. 7/1 (ed. Dartnall, H. J. A.) 245–363 (Springer, Berlin, 1972).
3. Muntz, W. R. A. & Northmore, D. P. M. *Vision Res.* **11,** 551–561 (1971).
4. Reuter, T., White, R. H. & Wald, G. *J. gen. Physiol.* **58,** 351–371 (1971).
5. Borwein, B. & Hollenberg, M. J. *J. Morph.* **140,** 405–442 (1973).
6. Schwassmann, H. O. & Kruger, L. *Vision Res.* **5,** 269–281 (1965).
7. Easter, S. S. Jr in *Vision in Fishes* (ed. Ali, M. A.) 609–617 (Plenum, New York, 1975).
8. Bowmaker, J. K., Dartnall, H. J. A. & Mollon, J. D. *J. Physiol., Lond.* **298,** 131–143 (1980).
9. Leibman, P. A. & Entine, G. *J. opt. Soc. Am.* **54,** 1451–1459 (1964).
10. Knowles, A. & Dartnall, H. J. A. *The Photobiology of Vision* (Academic, New York, 1977).
11. Jacobs, G. H., Bowmaker, J. K. & Mollon, J. D. *Nature* **292,** 541–543 (1981).
12. Schwanzara, S. A. *Vision Res.* **7,** 121–148 (1967).
13. Wyszecki, G. W. & Stiles, W. S. *Colour Science* (Wiley, New York, 1967).
14. MacNichol, E. F. Jr, Kunz, Y. W., Levine, J. S., Harosi, F. I. & Collins, B. A. *Science* **200,** 549–551 (1978).
15. Leibman, P. A. & Granda, A. M. *Nature* **253,** 370–372 (1975).
16. Levine, J. S. & MacNichol, E. F. Jr *Sensory Processes* **3,** 95–131 (1979).
17. Bowmaker, J. K., Dartnall, H. J. A., Lythgoe, J. N. & Mollon, J. D. *J. Physiol., Lond.* **274,** 329–348 (1978).

Serotonin alters the phosphorylation of specific proteins inside a single living nerve cell

José R. Lemos, Ilse Novak-Hofer & Irwin B. Levitan*

Friedrich Miescher-Institut, PO Box 273, CH-4002 Basle,
Switzerland

The large size and ready identifiability of molluscan neurones have made it possible to investigate the hypothesis[1,2] that cyclic AMP-dependent protein phosphorylation may regulate neuronal electrical properties. For example, it has been found recently that intracellular application of the catalytic subunit of cyclic AMP-dependent protein kinase can alter the electrical activity of various molluscan neurones (refs 3, 4; J. De Peyer, H. Reuter and I.B.L., unpublished). We have recently demonstrated[5] that injection of a specific protein kinase inhibitor into identified *Aplysia* neurone R15 blocks the increase in K^+ conductance normally elicited in R15 by serotonin[6], implicating protein phosphorylation in the regulation of a specific ion channel by a neurotransmitter. We report here attempts to identify phosphoproteins which may be involved in such regulation, by measuring protein phosphorylation in R15 following the intracellular injections of $\gamma[-^{32}P]$ATP. The results indicate that we can indeed measure protein phosphorylation inside an individual living nerve cell, and that the extent of phosphorylation of several proteins in R15 is influenced by serotonin.

Previous attempts to measure protein phosphorylation in individual molluscan neurones have been carried out by incubating ganglia with $^{32}P_i$, then isolating nerve cell bodies and analysing the radioactive phosphoproteins[7–11]. These studies suffer from the major disadvantage that the cell body of interest can never be isolated entirely free of glia and portions of neighbouring neuronal cell bodies which contribute to the labelling pattern. Furthermore, only the cell body, and not the axonal and dendritic processes in the neuropile, is sampled by this procedure. We have circumvented these problems by developing techniques for the injection of 10^5–10^6 c.p.m. of $[\gamma-^{32}P]$ATP into neurone R15, and have analysed the radioactive phosphoproteins produced. To examine the distribution of the radioactivity in the abdominal ganglion, we have fixed and sectioned ganglia following such injections, and have examined the sections by autoradiography. The results (not shown) demonstrate that all the radioactivity is restricted to R15. Thus, when the entire abdominal ganglion is analysed by gel electrophoresis, all the radioactive phosphoproteins originate from R15's soma and neuropile processes. R15 is voltage-clamped throughout the labelling period, so changes in the phosphorylation profile in the cell can be related to changes in membrane conductance. In addition, voltage-clamping assures that changes in phosphorylation are due directly to the effects of serotonin rather than to changes in the cell's spontaneous activity induced by serotonin.

Of the total radioactivity injected into neurone R15, ~2% was incorporated into trichloroacetic acid-insoluble, chloroform/methanol-washed material during the following 50 min ($1.9 \pm 0.6\%$ in control ($n = 14$) cells, $2.1 \pm 0.8\%$ in serotonin-treated ($n = 12$) cells; not significantly different). Analysis of this material, after partial acid hydrolysis, using two-dimensional high-voltage thin-layer electrophoresis[12] shows that only two amino acid residues are phosphorylated, the major one being phosphoserine and the minor one phosphothreonine. This further substantiated that the extracted material was phosphoprotein. The polyacrylamide gel autoradiogram in Fig. 1 and the densitometric scans in Fig. 2

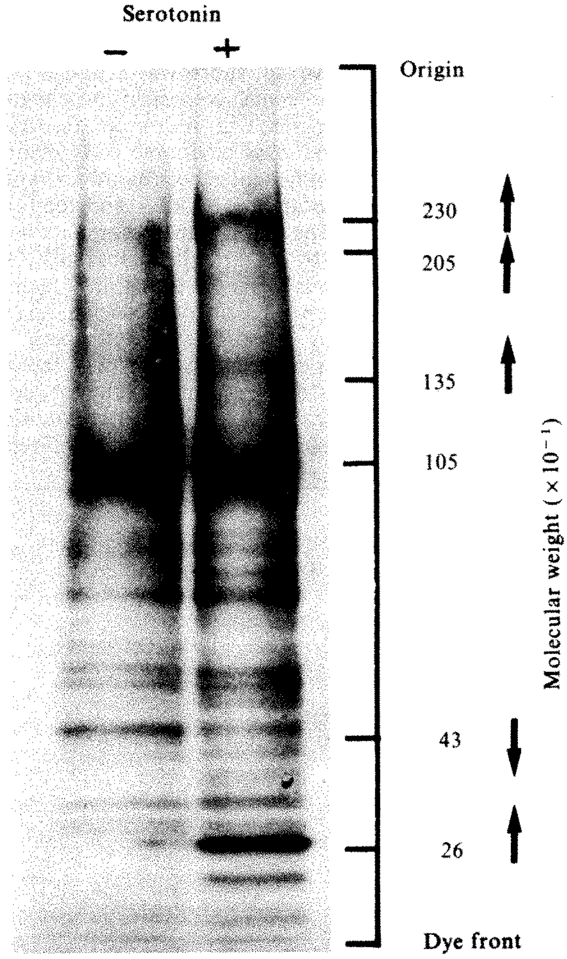

Fig. 1 Analysis of proteins phosphorylated in living neurone R15. Immediately before each experiment, $[\gamma-^{32}P]$ATP (Amersham; >5,000 Ci $mmol^{-1}$) was concentrated in an Eppendorf microfuge tube, using a rotary evaporator, to a final concentration of 1 $\mu Ci\ nl^{-1}$. For storage the $[\gamma-^{32}P]$ATP was rediluted to a concentration of 50 $mCi\ ml^{-1}$ in H_2O and was kept at −20 °C. With this protocol the ATP preparation could be used several times without substantial radiolytic decay. Using a Hamilton syringe, ~50 nl of the concentrated ATP solution were placed in the tip of a microelectrode pulled from 'Microstar' capillary tubing (Radnoti Glass). Electrodes were used within minutes of filling, again to avoid substantial radiolytic decay and/or blockage of the electrode tip. ATP solution (0.5–2.0 nl; estimated by movement of the meniscus in the electrode tip) was injected into voltage-clamped neurone R15 (estimated cell body volumes 20–60 nl) under pressure. Analysis of the material remaining in the electrode tip after the injection indicated that >85% of the radioactivity was still in ATP. The total amount of ATP injected (0.1–0.4 pmol) was ≤1% of the endogenous level in R15 (D. Weinreich, personal communication). These ATP injections did not alter the current–voltage relationship of R15. The ganglion was first perfused with normal *Aplysia* saline for 30 min and then with either normal *Aplysia* saline or saline containing 5 μM serotonin for an additional 20 min. Serotonin produces a large increase in K^+ conductance in this time[5,6]. Cells were voltage-clamped throughout, and only those exhibiting normal current–voltage characteristics and normal responses to serotonin were taken for analysis. Fifty minutes after injection the entire abdominal ganglion was frozen in liquid N_2, and homogenized in 1 ml of ice-cold stop buffer (50 mM MOPS, *p*H 7.0, 20 mM EDTA, 10 mM NaF, 1 mM ATP). The connective tissue sheath remained essentially intact and was discarded. Two ml of 20% trichloroacetic acid (TCA) was added to the homogenates at 4 °C. The resulting precipitates were collected by centrifugation, washed twice with 10% TCA, then twice with chloroform/methanol (1:2 then 2:1, v:v) to extract phospholipids. The pellets were redissolved in 100 μl of sample buffer (100 mM dithiothreitol, 80 mM Tris-HCl, *p*H 6.8, 2% SDS, 10% glycerol). Samples were boiled for 2 min and run on an SDS-polyacrylamide gradient (5–17.5% acrylamide) slab gel[13]. In this experiment, the control (−serotonin) track was loaded with 11,600 c.p.m., incorporated following an injection of 360,000 c.p.m. of $[\gamma-^{32}P]$ATP into R15; the +serotonin track contained 18,000 c.p.m. (600,000 c.p.m. injected). Following electrophoresis the gel was dried and autoradiographed using Kodak X-Omat X-ray film for 7 days. The resulting autoradiogram exhibits at least 15 phosphoprotein bands originating from within R15. ↑↓, Bands whose phosphorylation state was significantly increased or decreased, respectively, by serotonin (see Table 1).

---

*Present address: Graduate Department of Biochemistry, Brandeis University, Waltham, Massachusetts 02254, USA.

Table 1 Relative incorporation into individual phosphoprotein bands

M_r	% Of total radioactivity Controls ($n = 8$)	Serotonin ($n = 8$)	Mean % change
230,000	4.1±0.3	6.9±1.0	+69*
205,000	7.5±0.5	10.3±1.1	+41*
135,000	8.2±0.5	10.6±0.7	+29*
105,000	19.7±1.5	20.2±1.6	+2
82,000	8.7±0.6	8.6±0.7	−1
68,000	11.8±0.8	13.1±1.1	+12
50,000	8.8±0.5	8.8±0.3	0
43,000	5.0±0.2	4.1±0.2	−21*
36,000	4.4±0.5	4.2±0.6	−5
31,000	3.9±0.8	2.7±0.3	−30
26,000	3.5±0.3	5.9±0.5	+55*
22,000	5.8±1.2	3.6±0.4	−31

Densitometric scans of autoradiograms (for example, Fig. 2) were used to quantify the relative amount of radioactivity in individual phosphoprotein bands. Areas under each peak were computed as a percentage of the total area of the scan; thus, the numbers in the table represent the radioactivity in each band as a percentage (means ± s.e.m.) of the total radioactivity in the gel. Experiments performed on the same day were paired and Student's t-test used to evaluate the differences (expressed here as mean % change) between control and serotonin-treated ganglia. Although the 31,000- and 22,000-M_r proteins showed large mean per cent changes, they also exhibited large variability (see, for example, Fig. 2) and thus these changes were found not to be significant ($P > 0.6$).

*Changes induced by serotonin which were significant ($P <$ 0.02–<0.007).

demonstrate that at least 15 phosphoproteins, of molecular weights (M_rs) 22,000–230,000, were labelled in R15 during the 50 min following injection of [γ-^{32}P]ATP. When serotonin was added to the medium bathing the abdominal ganglion during the last 20 min of the labelling period, there was a large increase in K^+ conductance in R15[5,6], and a change in the extent of labelling of several phosphoproteins. This number of changes is not surprising because serotonin increases cyclic AMP levels in this cell[6] and this could lead to a variety of changes in the phosphorylation state of many intracellular proteins. The phosphorylation of several high molecular weight proteins (M_rs 230,000; 205,000; 135,000) and of a 26,000-M_r protein was increased significantly in the presence of serotonin (Figs 1, 2; Table 1). In addition, there was a decrease in the phosphorylation of a 43,000-M_r band (Figs 1, 2; Table 1).

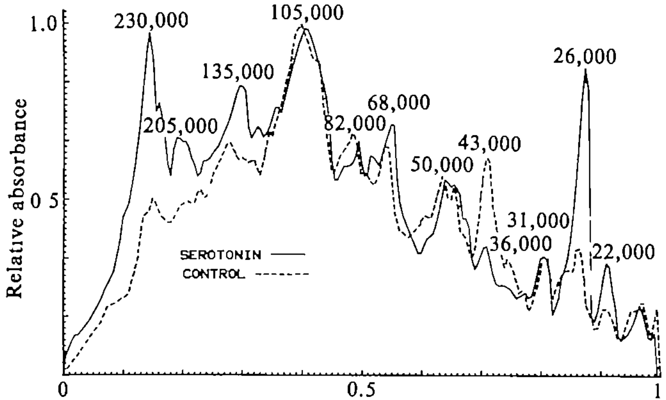

Fig. 2 Densitometric scans of the autoradiograms shown in Fig. 1. Autoradiograms were scanned using a Joyce-Loebl densitometer. The scanner was centred on each gel track, and the scan width was set at maximum to average the density across the entire track. Because the 105,000-M_r peak was not affected by serotonin (see Table 1), we normalized the scans to the height of this peak to facilitate visualization of the specific effects of serotonin. This analysis permits the evaluation of changes in labelling of specific phosphoproteins independent of differences in total incorporation from one cell to another ———, Serotonin; · · · · · ·, control.

There is only limited information on protein phosphorylation in the *Aplysia* nervous system. Although our early studies[7,8] (recently confirmed by Paris *et al.*[10]) indicated that serotonin could influence the phosphorylation state of a high molecular weight protein, it is not clear whether it is related to the 135,000-M_r protein described here. The present experiments indicate that, in addition to this phosphoprotein, the phosphorylation of several other proteins in R15 can be influenced by serotonin. This *in vivo* approach should permit an analysis of the possible role of these phosphoproteins in the regulation of K^+ conductance in this cell.

We thank Dr A. Matus and Mr M. Ackermann for help with the sectioning and autoradiography, Mr J. Maeder for computer programming and Dr J. Martin-Pérez for analysing the phosphoamino acids.

Received 28 September 1981, accepted 28 April 1982

1. Kuo, J. & Greengard, P *Proc natn Acad Sci U S A* **64**, 1349–1355 (1969)
2. Greengard, P *Fedn Proc* **38**, 2208–2217 (1979)
3 Kaczmarek, L K *et al Proc natn Acad Sci U S.A* **77**, 7487–7491 (1980)
4 Castellucci, V *et al Proc natn Acad Sci U S A* **77**, 7492–7496 (1980)
5 Adams, W B & Levitan, I B *Proc natn Acad Sci U.S A* (in the press)
6 Drummond, A H , Benson, J A. & Levitan, I B. *Proc natn Acad Sci. U.S.A* **77**, 5013–5017 (1980)
7 Levitan, I. B. & Barondes, S H. *Proc natn Acad Sci U S A* **71**, 1145–1148 (1974)
8. Levitan, I. B , Madsen, C J & Barondes, S. H *J Neurobiol* **5**, 511–525 (1974)
9 Jennings, K R , Kaczmarek, L K. & Strumwasser, F *Soc Neurosci Abstr* **5**, 249 (1979)
10. Paris, C. G , Kandel, E R & Schwartz, J H *Soc Neurosci Abstr* **6**, 844 (1980)
11 Neary, J T , Crow, T & Alkon, D L *Nature* **293**, 658–660 (1981)
12 Sefton, B M , Hunter, T., Beemon, K & Eckhart, W *Cell* **20**, 807–816 (1980).
13 Laemmli, U K *Nature* **227**, 680–685 (1970)

Neuropeptide coexistence in human cortical neurones

S. R. Vincent*, O. Johansson*, T. Hökfelt*,
B. Meyerson†, C. Sachs‡, R. P. Elde§,
L. Terenius|| & J. Kimmel¶

* Department of Histology, Karolinska Institutet, Stockholm, Sweden
† Departments of Neurosurgery and ‡ Neurology, Karolinska Hospital, Stockholm, Sweden
§ Department of Anatomy, University of Minnesota, Minneapolis, Minnesota 55455, USA
|| Department of Pharmacology, Uppsala University, Uppsala, Sweden
¶ McIlwain Laboratory, University of Kansas Medical Center, Kansas City, Kansas 66044, USA

The growth hormone release-inhibiting factor somatostatin was originally isolated and characterized from hypothalamic extracts[1]. Avian pancreatic polypeptide (APP) was first isolated from chicken pancreas[2]. Using antibodies raised against these peptides, both somatostatin-like[3–5] and APP-like[6,7] immunoreactivities have been found in many regions of the nervous system, and the peptides have been shown to coexist with catecholamines or other neuropeptides in certain neuronal systems[8–11]. In particular, we have recently reported that some neurones in the rat telencephalon contain both somatostatin- and APP-like immunoreactivities[12]. We present here immunohistochemical evidence that in the human cerebral cortex also, some neurones contain both immunoreactivities.

Specimens of human frontal, temporal and cingulate cortex were obtained from patients undergoing lobe resection as a treatment for glial tumours. Small pieces (about 10 × 5 × 2 mm) of cortex of normal appearance were taken from cortical areas, located as far as possible from the pathological area, immediately after the lobe was resected. The specimens were immersed in ice-cold 10% formalin in 0.1 M phosphate buffer for 2–6 h. The time between occlusion of the blood supply to the cortex and the immersion of the tissue was ~30 min. After fixation

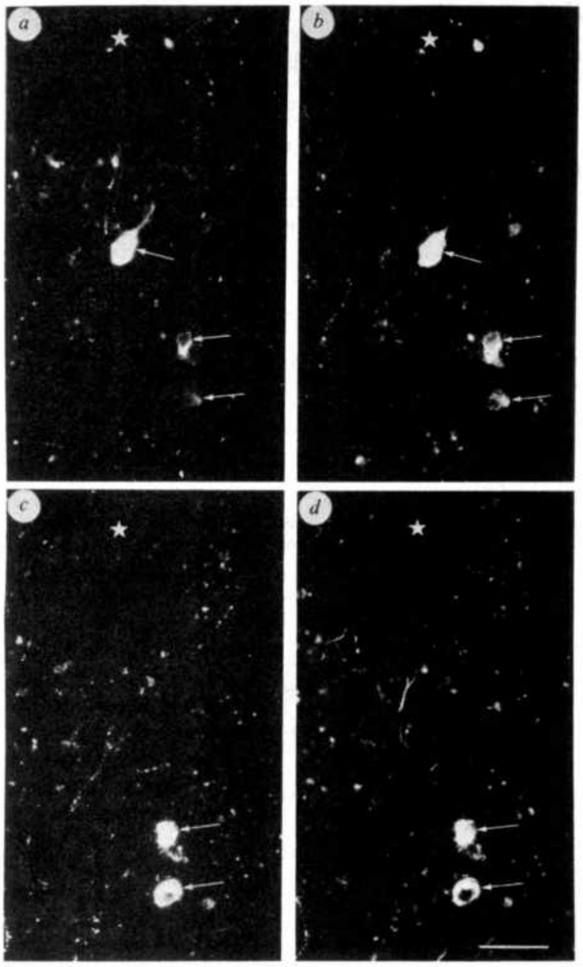

Fig. 1. *a–d*, Immunofluorescence micrographs of 10 μm thick sections of the human neocortex after incubation with antisera to somatostatin (*a*, *d*) or APP (*b*, *c*). *a* and *b*, The same section stained initially for somatostatin (*a*), then eluted according to Tramu *et al.*[16] and restained with antibodies against APP (*b*). *c*, *d*, The same section, which is adjacent to that shown in *a* and *b*, first stained for APP-like immunoreactivity (*c*), then eluted[16] and restained for somatostatin (*d*). Arrows indicate neurones that contain both somatostatin- and APP-like immunoreactivities, in either the serial section or the restaining experiments. ☆, A blood vessel. Scale bar, 50 μm for *a–d*.

the tissues were rinsed in 0.1 M phosphate buffer containing 5% sucrose for at least 24 h. Sections were then cut on a cryostat (Dittes) and processed according to the indirect immunofluorescence technique of Coons and collaborators[13,14].

Alternate 10 μm thick sections of cortex were incubated overnight at 4 °C with antisera raised in rabbits against APP[7,12] or somatostatin[15]. Both sera were diluted 1:100 in 0.1 M phosphate buffer containing 0.3% Triton X-100. After rinsing, the sections were incubated with fluorescein isothiocyanate (FITC)-conjugated swine anti-rabbit IgG (Dako), rinsed, coverslipped and examined in a Zeiss fluorescence microscope.

In further experiments, sections that had been stained for one neuropeptide were photographed, then the initial antiserum was eluted with 0.1% $KMnO_4$ in 0.2% $H_2S_2O_4$ for 30 s and the sections decolorized in 0.5% $Na_2S_2SO_5$ for 15 s (ref. 16). The sections were then incubated in the FITC-conjugated IgG and examined in the fluorescence microscope. If no staining was observed at this stage, indicating that the first antibody had been successfully eluted, the sections were then incubated with antibody to the other neuropeptide, followed by the FITC-conjugated IgG and once more examined in the microscope and photographed. Using this procedure the same section could be sequentially stained for somatostatin- and APP-like immunoreactivities.

Antisera incubated with an excess of the respective neuropeptide (50 μg of synthetic somatostatin or APP per ml antiserum diluted 1:10) served as controls. Preabsorption of the somatostatin antibody with APP or of the APP antibody with somatostatin had no effect on the resultant staining pattern. This indicates that none of the sera used in these experiments recognizes both peptides.

In sections incubated with antisera to APP, we observed a dense network of immunoreactive fibres. In specimens cut perpendicular to the cortical surface, a definite pattern of fibres could be discerned. In cortical layers II–VI, most of the APP-positive fibres appeared to run vertically out from the deeper layers towards the surface, although many fibres branched laterally as well. In contrast, in layer I, most of the APP-positive fibres ran parallel to the cortical surface; however no fibres were seen in the outer 50 μm of cortex. This staining pattern was observed in frontal, temporal and cingulate cortex specimens.

In sections incubated with anti-somatostatin antisera, the pattern of fibres observed was similar to that described for APP. The somatostatin-positive fibres fluoresced much more weakly, however, and, in particular, the fibres running parallel to the cortex in layer I were much less heavily stained.

Many immunoreactive cell bodies were observed in the cortex following incubation of the sections with either APP or somatostatin antisera. The cells were scattered throughout layers II–VI, and were also commonly found in the subcortical white matter. The cells were pyramidal, bipolar, round or multipolar in shape, with dendrites spreading out in all directions.

In serial sections stained alternatively for APP or somatostatin, we often found that one portion of a cell was positive for APP in one section while in a second section, the other portion was positive for somatostatin (Fig. 1*a*,*c*). This indicates that a single cell can contain both neuropeptides. Examples of this were found in all cortical layers except layer I.

The coexistence of somatostatin- and APP-like immunoreactivities in a cortical neurone was also frequently demonstrated in the elution–restaining experiments. Using this protocol, we found neurones that first stained for somatostatin (Fig. 1*a*) and then, after elution, restained for APP (Fig. 1*b*), and cells that were first shown to be APP positive (Fig. 1*c*) and, after elution and restaining, also seen to contain somatostatin immunoreactivity (Fig. 1*d*).

The occurrence of more than one neuroactive substance in a single neurone has recently been reviewed[17,18]. The phenomenon was first observed in invertebrates, but has since also been observed in mammalian neurones, and now in human brain.

We have shown that the coexistence of somatostatin and APP reported here is not due to cross-reactivity of the antisera. Also, larger presumed precursor molecules have been found for both peptides[19–22] and they seem quite distinct. This and the clear differences in the distribution of the peptides in other brain regions[12] suggests that they do not have a common precursor and that their coexistence is a special property found only in certain cell types.

The coexistence of somatostatin- and APP-like peptides within a selective population of neurones suggests that they both may function as transmitters or modulators of neural information. In this regard, somatostatin has been found to have potent electrophysiological effects on cortical neurones[23–25] and both calcium-dependent release[26,27] and high-affinity binding[28] of somatostatin have been demonstrated in mammalian brain. APP has also been found to have postsynaptic actions[29]. Thus the presence of these two neuroactive substances in a single cortical neurone may allow the cell to transmit more than one message to its postsynaptic targets.

Recently somatostatin levels have been found to be reduced in the cerebrospinal fluid of patients with Huntington's disease[30]. Also, cortical somatostatin levels are markedly reduced in Alzheimer's disease and in senile dementia of Alzheimer type[31,32]. This suggests that a loss of forebrain somatostatin neurones may be a symptom of these diseases. As an APP-like peptide is contained in many forebrain somatostatin cells, these diseases are probably also associated with a loss of APP-like immunoreactivity. The role of cortical neurones containing both somatostatin- and APP-like immunoreactivity in these conditions remains to be determined.

We thank Ms Annika Edin, Ms Anne Peters and Ms Waldtraut Hiort for technical assistance and Ms Birgit Frideen for secretarial help. This work was supported by grants from the Swedish MRC (04X-2887), Magnus Bergvalls Stiftelse and Knut and Alice Wallenbergs Stiftelse. S.R.V. is a fellow of the Canadian MRC.

Received 16 February; accepted 23 April 1982

1 Brazeau, P *et al. Science* **179,** 77–79 (1973).
2 Kimmel, J R, Hayden, L J & Pollock, H G *J biol Chem.* **250,** 9369–9376 (1975)
3 Hokfelt, T, Efendić, S, Johansson, O., Luft, R & Arimura, A *Brain Res* **80,** 165–169 (1974)
4. Bennet-Clarke, C, Romagnano, M A & Joseph, S. A. *Brain Res* **188,** 473–486 (1980).
5. Fley, J. C. W, Maderdrut, J L, Roger, L J & Petrusz, P *Neuroscience* **6,** 2173–2192 (1981).
6 Lorén, I, Alumets, J, Håkanson, R. & Sundler, F *Cell Tissue Res* **200,** 179–186 (1979)
7. Hokfelt, T, Lundberg, J M, Terenius, L, Jancsó, G. & Kimmel, J. *Peptides* **2,** 81–87 (1980).
8 Hokfelt, T *et al Proc. natn. Acad Sci U.S.A* **74,** 3587–3591 (1977).
9. Schultzberg, M *et al. Neuroscience* **5,** 687–744 (1980).
10 Lundberg, J. M. *et al Acta physiol scand* **110,** 107–109 (1980)
11 Hunt, S P, Emson, P C, Gilberg, R, Goldstein, M & Kimmel, J *Neurosci Lett* **21,** 125–130 (1981).
12 Vincent, S R. *et al Neuroscience* **7,** 439–446 (1982)
13 Coons, A H in *General Cytochemical Methods* (ed Danielli, J F) 399–422 (Academic, New York, 1979)
14 Hokfelt, T, Fuxe, K, Goldstein, M & Joh, T H *Histochemie* **33,** 231–254 (1973)
15 Arimura, A *et al Metab clin Exp* **24,** Suppl 1, 1139–1149 (1978)
16. Tramu, G, Pillez, A & Leonardelli, J *J Histochem Cytochem.* **26,** 322–324 (1978)
17. Hokfelt, T. *et al.* in *Neural Peptides and Neuronal Communication* (eds Costa, E. & Trabucchi, M.) 1–23 (Raven, New York, 1980).
18. Hokfelt, T, Johansson, O, Ljungdahl, Å., Lundberg, J. M. & Schultzberg, M *Nature* **284,** 515–521 (1980).
19. Hobart, P., Crawford, R., Shen, L. P., Pictet, R. & Rutter, W. J. *Nature* **288,** 137–141 (1980).
20. Pradayrol, L., Jornvall, H, Mutt, V. & Ribet, A. *Eur. biochem. Soc. Lett.* **109,** 55 (1980).
21 Schally, A V. *et al. Proc. natn Acad. Sci. U.S.A.* **77,** 4489–4493 (1980).
22. Schwartz, T. W. & Tager, H. S. *Nature* **294,** 589–591 (1981).
23 Renaud, L P., Martin, J. B. & Brazeau, P. *Nature* **255,** 233–235 (1975).
24. Ioffe, S., Havlicek, V., Friesen, H. & Chernick, V. *Brain Res.* **153,** 414–418 (1978).
25. Dodd, J. & Kelly, J. S *Nature* **273,** 674–675 (1978).
26. Iversen, L. L. *et al. Nature* **273,** 161–163 (1978).
27. Lee, C.-M. & Iversen, L. L. *Brain Res.* **219,** 355–361 (1981).
28. Sikant, C B. & Patel, Y. C. *Proc. natn. Acad. Sci. U.S.A* **78,** 3930–3934 (1981).
29. Lundberg, J. M., Änggård, A., Hökfelt, T. & Kimmel, J. *Acta physiol. scand.* **110,** 199–201 (1980).
30. Cramer, H., Kohler, J., Oepen, G., Schomburg, G. & Schroter, E. *J. Neurol.* **225,** 183–187 (1981)
31. Rossor, M. N, Emson, P. C, Mountjoy, C. Q, Roth, M. & Iversen, L. L. *Neurosci. Lett.* **20,** 373–377 (1980)
32. Davies, P, Katzman, R & Terry, R D. *Nature* **288,** 279–280 (1980).

Fission-spectrum neutrons at reduced dose rates enhance neoplastic transformation

C. K. Hill, F. M. Buonaguro*, C. P. Myers*, A. Han & M. M. Elkind*

Mammalian Cell Biology Group, Division of Biological
and Medical Research, Argonne National Laboratory, Argonne,
Illinois 60439, USA

We have studied the effect of reduced dose rates of radiation on neoplastic transformation using the C3H/10T1/2 mouse embryo-derived cell line developed by Reznikoff *et al.*[1]. In this cell system, transformation can be measured by scoring the foci of piled-up cells that occur after the loss of contact inhibition of growth. We report here that reduction of the dose rates of fission-spectrum neutrons (of mean energy 0.85 MeV) from 38.5 or 10.3 to 0.43 and 0.086 rad min^{-1} has no effect on cell killing but increases transformation frequency. These data are in contrast to previously published results obtained with ^{60}Co γ rays where reduction of the dose rate resulted in a marked reduction in transformation frequency[2,3]. Although cancer induction in man involves many factors besides those at the cellular level, the implication from our findings is that the risk of cancer induction due to work-related exposure to neutrons in the nuclear power industry may be greater than previously thought.

Cell cultures were grown at 37 °C in plastic T-flasks, or in plastic 100-mm Petri dishes, in Eagle's basal medium (Gibco) supplemented with 10% heat-inactivated fetal calf serum (Reheis Chemical Co., Illinois) according to methods previously described[2–5]. The JANUS reactor of the Division of Biological and Medical Research, Argonne National Laboratory, was used to expose cells to fission-spectrum neutrons[5]. A special incubator, made of light plastic and styrofoam to minimize any changes in the quality of the neutron beam, was used for the low dose rate exposures at 0.43 and 0.086 rad min^{-1}, and the cells were kept at 37 °C while attached in plastic T-flasks containing Eagle's supplemented medium. In all experiments, irradiated cells were removed from the incubator after exposure, trypsinized, plated out in Petri dishes and placed in conventional incubators for the 6 weeks necessary for transformed foci to develop[1,5]. In a control experiment, cells were grown in the special incubator without irradiation. No transformed colonies were observed for these controls; that is, the transformation frequency per surviving cell was $<8.7\times10^{-5}$. Dosimetry was performed inside the incubator at the position of the cells[5]. High-dose rate irradiations (38.5 or 10.3 rad min^{-1}) were carried out at room temperature[5]. Transformed foci were scored as previously described[1,5] and transformation frequencies per surviving cell were calculated according to Han and Elkind[5].

Consistent with the earlier results of Sinclair[6] with V79 Chinese hamster cells, the data in Fig. 1 show no significant variation in cell killing after a reduction in the fission-spectrum neutron dose rate from 38.5 to 0.086 rad min^{-1} (5.2 rad hr^{-1}) even though the cells were irradiated in optimal growth conditions. The lowest dose rate used here was 20-fold less than that previously reported[6,7]. At 0.086 rad min^{-1}, cells undergo one

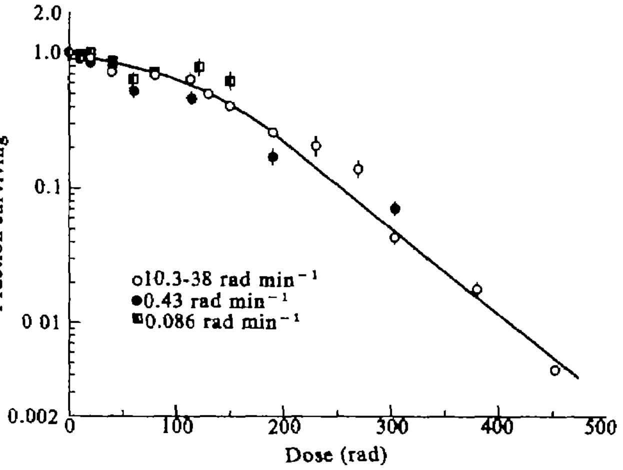

Fig. 1 The survival of 1OT1/2 cells exposed to fission-spectrum neutrons from the JANUS reactor at the Argonne National Laboratory. The line is drawn through the average surviving fractions from all experiments performed over a 3-yr period. The individual data points shown at high and at low dose rates were obtained concurrently as part of this study; the doses refer to the integrated exposures of populations of cells. Cells in growth medium were exposed at 37 °C and immediately after exposure were suspended by trypsinization and plated for survival. Plating efficiency = 21–42%, multiplicity ~ 1. Bars represent standard errors[5].

---

* Present addresses Istituto di Patologia Generale, Sant'Andrea delle Dame, 2 Napoli 80138, Italy (F M B), Department of Therapeutic Radiology, V A. Hines Hospital, Hines, Illinois 60141, USA (C P M), Department of Radiology and Radiation Biology, Colorado State University, Fort Collins, Colorado 80523, USA (M M.E)

Table 1 Transformation of 1OT1/2 cells by fission-spectrum neutrons

Dose (rad min^{-1})	Surviving fraction	No. surviving cells per dish*	No. of dishes	No. of foci†	No. dishes without foci	λ	Transformation frequency per viable cell ($\times 10^{-4}$)
Controls	1.0	242	2,409	6	2,403	0.0025	0.103
10.3–38.0							
10	0.970	135	173	2	171	0.0116	0.86
21	0.957	212	165	5	160	0.0308	1.4
41	0.753	200	119	8	113	0.0517	2.6
76	0.709	176	112	17	97	0.143	8.2
114	0.651	404	19	7	12	0.379	9.4
151	0.412	108	15	5	10	0.405	37.5
189	0.269	223	68	71	22	1.13	50.6
227	0.172	536	16	16	3	1.67	31.2
303	0.0421	107	19	9	12	0.460	42.9
378	0.0178	299	56	91	12	1.54	51.5
454	0.00450	250	20	23	4	1.61	64.4
0.43							
10	0.920	150	166	34	146	0.128	8.6
21	0.864	167	356	45	322	0.10	6.0
41	0.831	170	262	31	232	0.122	7.1
62	0.540	281	19	8	12	0.459	16.3
114	0.462	203	144	43	108	0.287	14.1
189	0.171	90	103	40	74	0.331	36.3
303	0.070	129	83	54	41	0.588	110.0
0.086							
10	0.941	145	188	19	172	0.089	6.1
21	0.961	136	228	24	205	0.106	7.8
41	0.869	169	164	28	139	0.165	9.7
62	0.655	187	141	26	121	0.152	8.2
80	0.716	173	12	4	8	0.405	23.4
121	0.823	195	17	11	10	0.531	27.2
150	0.647	170	9	10	4	0.811	47.6

A survival curve based on averages of the data from all experiments (Fig. 1) was used to estimate surviving fractions for the exposures at 10.3–38.0 rad min^{-1}. For the low-dose rate exposures, surviving fractions are those determined from the same population used to estimate the transformation frequency. Details of the λ calculation and its standard error are given in ref. 5. λ, The average number of transformed foci per dish, was computed from the proportion of dishes free of transformed colonies, f, by $\lambda = -\ln f$. Transformation frequency = λ/number of surviving cells per dish. Controls, that is, unirradiated cells, represent the cumulative data from the transformation experiments reported for this and other studies[2–5].

* Number corrected for plating efficiency of unirradiated cells and surviving fraction per 90-mm plastic Petri dish.

† Total number of type 2 and 3 transformed foci[1,5].

or two divisions during exposure, depending on the length of exposure. However, flow cytofluorographic analyses of the DNA content of the cells in each sample, using an Ortho Instruments 2150 system, indicated that no significant perturbation in distribution of cell cycles occurred until 150 rad had accumulated at 0.43 rad min^{-1}, or 100 rads at 0.086 rad min^{-1}. Thus, it is unlikely, especially at the smaller doses, that our results were significantly affected by changes in cell-cycle distributions during exposure.

There was no apparent reduction in transformation frequency when the dose rate of fission-spectrum neutrons was reduced by a factor of 200 (38.5 to 0.086 rad min^{-1}). Indeed, whereas at higher doses the high and protracted dose rates seemed to induce the same transformation frequency, at 10–70 rad there was a significant enhancement of transformation frequency for dose rates of 0.43 and 0.086 rad min^{-1}. The data for transformation at high dose rates in Fig. 2 are a combination of those previously published[5] and those obtained in the present series of experiments; the two sets of results did not differ significantly and therefore were pooled. Table 1 summarizes the results plotted in Figs 1 and 2.

Although cells apparently are unable to repair sublethal damage when exposed to the JANUS reactor beam at reduced dose rates, consistent with earlier studies performed with the same beam using fractionation of high dose-rate exposures[8,9], the enhanced transformation shown in Fig. 2 is unexpected. Han and Elkind[5] showed that the fractionation of high dose-rate exposures of neutrons from the JANUS reactor had little if any effect on transformation frequency per surviving cell. Figure 2 shows that reduced dose rates significantly enhance transformation in the low dose region from 10–70 rad, with no concomitant effect on survival (Fig. 1).

To illustrate further the qualitatively unexpected nature of our transformation results, Fig. 3 compares the ratios of transformation frequencies per survivor at low to high dose rates for neutrons from the JANUS reactor and for ^{60}Co γ rays[3]. Clearly, the reduced dose rates of γ-ray irradiation, in the 0–100 rad region, are less effective than high dose rates, while for the same dose interval, low dose rates of fission-spectrum neutrons are appreciably more effective than high dose rates. Furthermore, few if any of the changes in transformation frequency can be attributed neither to differential cell killing, in view of the small amount, and dose rate independence of lethality in this dose range (Fig. 1), nor to parasynchronous effects as already noted.

There are some indications, primarily from results obtained with *in vivo* systems[10–13], that low dose rates of fission-spectrum neutrons may be more effective at producing tumours than high dose rates. However, interpretation of the results following whole-body exposures is complicated by the interactions among different tissue and organ systems (for example, see Fry[12] in reference to the induction of Harderian gland tumours). Our results, obtained with actively growing mammalian cells in culture, show that enhanced induction rates of neoplastic transformation could be due to intracellular events in the target cells themselves. A similar specificity applies to the observation that reduced transformation frequencies due to low dose rates of ^{60}Co γ rays result from repair processes in the target cells[3].

Finally, we may draw from our data several inferences about mechanisms. Compared with γ rays, fission-spectrum neutrons may be considered a high linear energy transfer (LET) radiation. The shoulder on the neutron survival curve indicates that accumulation of sublethal damage contributes to cell killing and that such damage is not repaired, in contrast to the repair of sublethal damage from γ rays observed for prolonged exposure[3]. As an acute dose of fission-spectrum neutrons does not prevent the repair of the damage that is additive to X-ray-induced sublethal damage[8], we infer that different targets are affected by high as opposed to low LET radiation and that the damage (or the target) responsible for neutron-induced killing cannot be repaired. With respect to transformation, we note that, at reduced dose rates of γ rays, survival increases but transformation per surviving cell decreases, both relative to high dose rate exposure, and that transformation is reduced even in the dose region where cell killing is minimal. In similar exposure conditions, reduced dose rates of fission-spectrum neutrons result in enhanced transformation. Thus we infer that the repair of γ-ray-induced transformation damage has a net error-free component of repair, and that the increase in neutron-induced transformation results from a net error-prone component of repair independent from sublethal damage in view of the dose rate independence of the latter. Further experiments are in progress to determine whether the same targets are involved in transformation induced by high- compared with low-LET radiations.

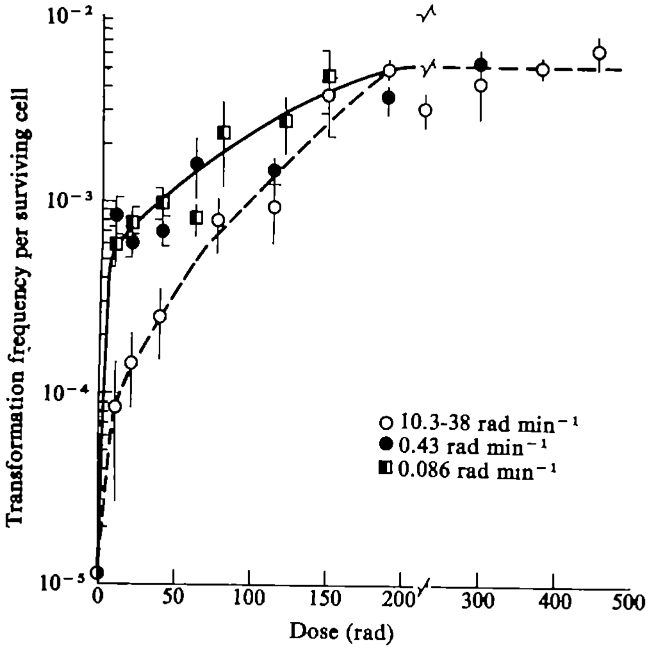

Fig. 2 Transformation frequency per surviving cell for 1OT1/2 cells exposed to fission-spectrum neutrons (data given in Table 1). The broken line represents the acute dose rate curve and the solid line indicates the data from both low dose rates used. Other details as for Fig. 1.

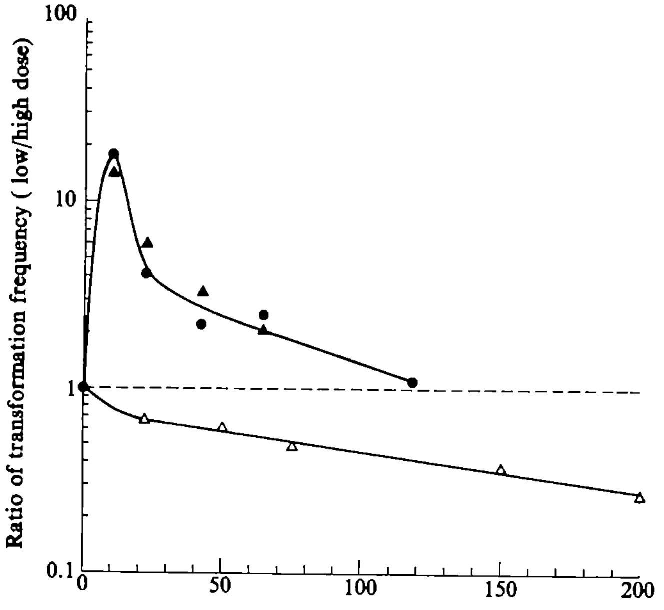

Fig. 3 The ratio of transformation frequency per surviving cell for low compared with high dose rates, obtained for 1OT1/2 cells, as a function of dose. For both fission-spectrum neutrons and ^{60}Co γ rays, the doses refer to the integrated exposures of populations of cells. Dose rate independence would plot as the broken line shown. ●, ▲ = 0.43 and 0.086 rad min^{-1}, respectively, of JANUS neutrons. △, 0.1 rad min^{-1} ^{60}Co γ rays.

This research was supported by the US Department of Energy under contract no. W-31-109-ENG-38. We acknowledge the assistance of E. Buess and J. Dainko. We also thank G. Holmblad, J. Trier, Gerry Fox and Art Shirvin for dosimetry and for the smooth running of the reactor.

Received 5 February, accepted 26 April 1982

1. Reznikoff, C A, Brankow, D W & Heidelberger, C *Cancer Res* **33**, 3231–3238, 3239–3249 (1973).
2 Han, A, Hill, C K. & Elkind, M M *Int J Radiat Biol* **37**, 585–589 (1980).
3 Han, A., Hill, C K. & Elkind, M. M *Cancer Res* **40**, 3328–3332 (1980)
4 Han, A. & Elkind, M M. *Radiat. Res* **74**, 88–100 (1978)
5 Han, A. & Elkind, M M. *Cancer Res* **39**, 123–130 (1979)
6 Sinclair, W. K. *Division of Biological and Medical Research, A Rep.*, 29–31 (Argonne National Laboratory, 1970)
7 Sinclair, W. K *Division of Biological and Medical Research, A Rep*, 152 (Argonne National Laboratory, 1973)
8 Ngo, F Q. H., Han, A., Utsumi, H. & Elkind, M. M *Int J Radiat Oncol Biol Phys* **3**, 187–193 (1977)
9 Ngo, F Q. H, Utsumi, H, Han, A. & Elkind, M M. *Int J. Radiat Biol* **36**, 521–530 (1979).
10 Thomson, J F, Williamson, F S., Grahn, D & Ainsworth, E J *Radiat Res.* **86**(3), 559–572, 572–588 (1981)
11. Vogel, H. H & Dickson, H. W *Abstr. 29th a. Meet Radiation Research Society*, Minneapolis (1981); *Radiat Res.* **87**(2), 453 (1981).
12 Fry, R. J M. *Int J. Radiat Oncol. Biol. Phys* **3**, 219–226 (1977)
13. Ullrich, R L. & Storer, J. B *Abstr 29th a Meet Radiation Research Society*, Minneapolis (1981); *Radiat Res* **87**(2), 454 (1981)

Malignant transformation of human embryo retinoblasts by cloned adenovirus 12 DNA

P. Byrd, K. W. Brown & P. H. Gallimore

Cancer Research Campaign Laboratories, Department of Cancer Studies, University of Birmingham, The Medical School, Birmingham B15 2TJ, UK

Human adenoviruses can morphologically transform rodent cells *in vitro*. The transforming gene(s) resides in the early region 1 (E1) transcription unit (0–11.2 map units) at the left end of the conventional adenovirus genome[1–4]. The only adenovirus-transformed human cell line reported so far, the 293 cell line, was isolated from cell cultures transfected with sheared DNA of the non-oncogenic subgroup C adenovirus type 5 (Ad 5)[5,6]. The ability of this line to complement the growth of Ad 5 E1 mutants has facilitated the isolation of transformation-defective Ad 5 mutants[7,8]. As no oncogenic subgroup A adenovirus type 12 (Ad 12) transformed human cell lines were available for the selection of Ad 12 E1 mutants, we attempted to isolate such lines by transfecting cell cultures with a recombinant plasmid (pAsc2) which contained the Ad 12 *Eco*RI-C DNA fragment (0–16.5 map units) inserted at the *Eco*RI site of pAT153 (ref. 9). We describe here the isolation of a pAsc2-transformed human embryo retinoblast cell line that contains many copies of the Ad 12 transforming region, expresses virus-specified proteins and, following inoculation into athymic mice, forms tumours which resemble retinoblastomas.

The suggestion that Ad 12-induced rodent tumours originate specifically from primitive neural epithelium[10], together with the discovery that this virus induces retinal tumours following intraocular inoculation of rats and baboons[11,12], prompted us

0028-0836/82/260069—03$01 00

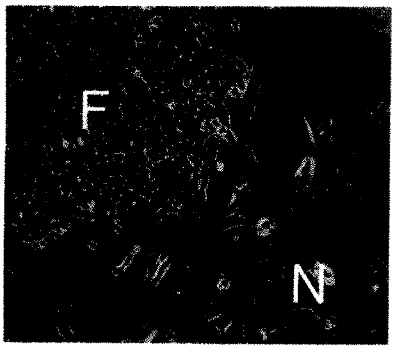

Fig. 1 An edge of a pAsc2-transformed human embryo retinoblast focus. The retinas from the eyes of an 18-week-old male fetus (therapeutically aborted) were distributed in six 50-mm tissue culture dishes and grown in RPMI medium containing 20% fetal calf serum (FCS) and antibiotics (penicillin and streptomycin, 100 units ml^{-1}). Ten days after seeding, the cultures (containing $\sim 1\times10^6$ cells per dish) were transfected with pAsc2 (10 μg per dish) using the calcium phosphate precipitation technique[25] with the glycerol boost[26]. Seventeen hours after transfection, each culture, including two control cultures which were transfected with pAT153 alone (10 μg per dish), was subcultured to four 50-mm dishes. The cells were then grown in RPMI medium containing 5% FCS and antibiotics. Only one PAsc2-transformed focus (F) was identified against the background of normal (N) cells; the experiment was terminated 10 weeks after transfection. This focus was isolated and established in a 35-mm dish and after 14 days the transformed cells were transferred to a 50-mm dish. This transformed cell line (Ad 12 HER1) was subsequently grown and passaged in 90-mm dishes at a split ratio of 1:15; the cells are maintained in RPMI containing 10% FCS and antibiotics. ×75.

to attempt to transform human embryo retinoblasts (HER cells) *in vitro* with pAsc2. Primary cultures of human retinoblasts were transfected with pAsc2, and one transformed focus, identified 45 days after transfection (Fig. 1), was isolated and established as a continuous cell line. This cell line has been designated Ad 12 HER 1 and is the first reported Ad 12-transformed human cell line. Cytogenetic analysis revealed a pseudotetraploid human karyotype. We have grown the Ad 12 HER1 cell line beyond the 36th tissue culture passage level and at no time has its growth entered a crisis phase. This is in contrast to the establishment of the 293 cell line[6].

Human embryo retinoblasts are the only human cell type we have been able to transform reproducibly with pAsc2. In two recent experiments, 10 transformed cell foci were identified in seven dishes of pAsc2-transfected HER cells (10 μg pAsc2 per 1×10^6 cells per dish); 4 of these foci were isolated and established as cell lines. The low specific transforming activity of pAsc2 on HER cells, which is an order of magnitude lower than on cultures of primary rat cells[9], is >100-fold higher than that on human embryo kidney (HEK) cells. The isolation and biological properties of the pAsc2-transformed HEK cell lines and additional pAsc2-transformed HER cell lines will be reported elsewhere (J. Whittaker, P.B. and P.H.G. in preparation).

When Ad 12 HER1 cell DNA was digested with the restriction endonucleases *Bgl*II or *Sst*I and subjected to Southern blotting analysis[13] using ^{32}P-labelled Ad 12 *Eco*RI-C DNA fragment as probe, Ad 12 sequences were found on many DNA fragments (Fig. 2, tracks 3 and 4, respectively) whose sizes

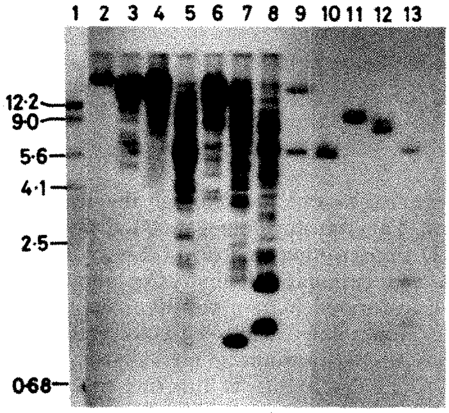

Fig. 2 Detection of Ad 12 DNA sequences in Ad 12 HER1 cell DNA. Samples (5 μg) of Ad 12 HER1 DNA were digested with restriction endonucleases, electrophoresed in a 0.8% agarose gel and subjected to Southern blotting analysis as described previously[9]. Track 1, 5 μg normal HEK cell DNA and 20 pg Ad 12 DNA (equivalent to ~0.64 copies per cell) digested with *Eco*RI; track 2, high molecular weight Ad 12 HER1 DNA; tracks 3, 4, 5, 6, 7, 8, Ad 12 HER1 DNA digested with *Bgl*II, *Sst*I, *Eco*RI, *Bam*HI, *Xba*I and *Hin*dIII respectively: tracks 9, 10, 11, 12, 13, 5 μg normal HEK cell DNA and 20 pg pAsc2 (equivalent to 2.4 copies per cell) digested with *Bgl*II, *Eco*RI, *Bam*HI, *Xba*I and *Hin*dIII respectively. Track 1 was hybridized with ^{32}P-labelled Ad 12 DNA; tracks 2–13 were hybridized with ^{32}P-labelled Ad 12 *Eco*RI-C DNA fragment. The sizes of the Ad 12 DNA *Eco*RI fragments (in kilobase pairs) are indicated. Summation of the autoradiographic bands and their intensities indicates that each Ad 12 HER1 cell contains the equivalent of ~50 copies of the Ad 12 *Eco*RI-C DNA fragment.

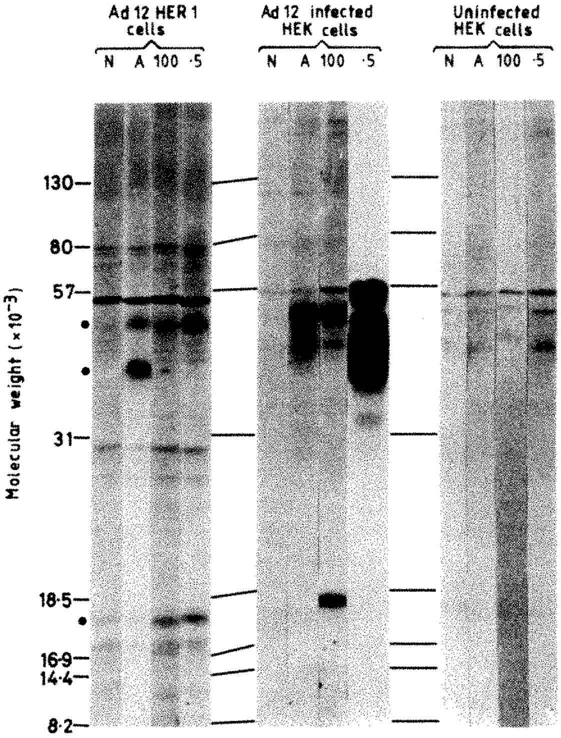

Fig. 3 Immunoprecipitation of Ad 12-specific proteins. Ad 12 HER1 cells, HEK cells or Ad 12-infected HEK cells (15 h after infection at M.O.I. of 400 plaque-forming units per cell) were preincubated in 9-cm dishes for 1 h in 3 ml of methionine-free modified Eagle's medium, containing 2% (v/v) FCS, and then labelled for 2 h in the same medium containing 100 μCi L-^{35}S-methionine (>600 Ci mmol^{-1}, Amersham). Cleared extracts were made from the labelled cells and aliquots were immunoprecipitated with normal rat serum or Ad 12 tumour-bearer serum (pAsc2 HLBRK1, Ad 12/LP/100-1 or 0.5J4) essentially as described elsewhere[27]. Immunoprecipitates were run on 10–15% gradient SDS-polyacrylamide gels[28] and ^{35}S-labelled proteins were detected by fluorography[29]. The cell extracts and tumour bearer sera are identified above the tracks; normal rat serum and rat sera raised against pAsc2 HLBRK1, Ad 12/LP/100-1 or 0.5J4 are identified as N, A, 100 and ·5 respectively. ●, Ad 12-specific proteins expressed in Ad 12 HER1 cells. The positions and sizes of molecular weight standards are indicated to the left of the tracks containing extracts of Ad 12 HER1 cells; their positions in the tracks containing extracts of uninfected and Ad 12-infected HEK cells are indicated by lines connecting to the Ad 12 HER1 tracks.

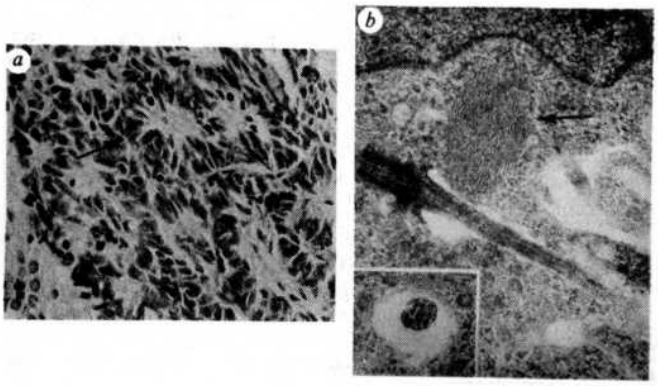

Fig. 4 *a*, Section through a cerebral tumour produced in a nude mouse following intracranial inoculation of Ad 12 HER1 cells. The arrow indicates a Homer–Wright rosette. The tumour was fixed in FAM (formaldehyde, acetic acid and methanol (1:1:8), paraffin sectioned and stained with haematoxylin–eosin. ×650. *b*, Electron micrograph of part of an Ad 12 HER1 cell showing a longitudinal section through a cilium and a multilamellar structure (arrow) which is reminiscent of the outer segment of a photoreceptor cell (×31,250). Inset, transverse section of an Ad 12 HER1 cilium showing 9+0 microtubule configuration (×75,000). Cells were fixed in 1% glutaraldehyde and post-fixed with 1% osmium tetroxide. Sections were stained with uranyl acetate and lead citrate.

ranged from >12 kilobase pairs (12 kb) to 2.2 kb. As these enzymes cleave host DNA sequences only, each fragment represents a separate insert of pAsc2 sequences. DNA fragments which co-migrated with the Ad 12 *Eco*RI-C DNA fragment and linear pAT153 DNA (data not shown) following digestion of Ad 12 HER1 DNA with *Eco*RI (Fig. 2, track 5) produced intense autoradiographic bands. This suggests that Ad 12 HER1 cells contain intact, integrated copies of the viral and vector sequences and it is likely that some of the inserts contain tandem repeats of the entire recombinant plasmid. The Ad 12 and Ad 12–pAT153 DNA fragments expected from digestion of pAsc2 by *Eco*RI, *Bam*HI, *Hin*dIII or *Xba*I were all identified in Ad 12 HER1 DNA following digestion with these enzymes (Fig. 2, tracks 5, 6, 7, 8). In addition, other fragments were identified which contained both Ad 12 DNA and pAT153 or these DNA species independently. The structures of these fragments, ranging in size over >12–0.63 kb, have not been determined.

^{35}S-methionine-labelled extracts from Ad 12 HER1 cells or HEK cells collected 18 h after infection by purified Ad 12 virus were immunoprecipitated using Ad 12 tumour-bearer rat sera. The sera were raised against tumorigenic cell lines that expressed proteins from Ad 12 early region 1 and other early regions (0.5J4)[14] or from E1 only (Ad 12/LP/100–1 (ref. 15) and pAsc2 HLBRK1 (ref. 9)). Polypeptides with molecular weights of 52,000 (52K), 41K and 18K were detected (Fig. 3) and as they were not immunoprecipitated from extracts of uninfected HEK cells, must be authentic Ad 12-specified proteins. Therefore, Ad 12 HER1 cells express proteins which are known to be encoded within the Ad 12 E1 transcription unit[16,17].

The tumorigenic potential of Ad 12 HER1 cells has been ascertained by inoculating 6–10-day-old congenitally athymic nude mice. Subcutaneous inoculation of 5×10^6 Ad 12 HER1 cells at the fifth, sixth and seventh tissue culture passage levels resulted in tumours at the site of inoculation in 1/7, 1/5 and 1/6 injected animals respectively, with latent periods of 73–89 days. However, all animals (4/4) injected intracranially with as few as 1×10^4 cells at the eighth passage died from cerebral tumours with a mean time to death of 75 days. Thus, Ad 12 HER1 cells are highly tumorigenic when inoculated intracranially. Histological analysis of Ad 12 HER1-induced tumours showed them to consist of clusters of small cells with many mitotic figures. Homer–Wright rosettes and incomplete rosettes were frequently seen (Fig. 4*a*); these rosettes and Flexner–Wintersteiner rosettes are characteristic of poorly differentiated human retinoblastomas[18].

Electron microscopic analysis occasionally revealed cilia with 9 + 0 microtubule configuration on Ad 12 HER1 cells (Fig. 4*b* and inset). This configuration is characteristic of cilia of normal human retinal photoreceptor cells and retinoblastoma cells[19] and has also been observed in cilia of Ad 12 virus-induced retinal tumours of the rat and baboon[11,12]. In Ad 12 HER1 cells we also observed oval membranous structures adjacent to the cilia (Fig. 4*b*). Although we have been unable to identify these bodies with certainty, they are reminiscent of the outer segments of photoreceptor cells; similar disk-like membranous structures have been found in human retinoblastoma cells[19].

Ad 12 HER1 cells are completely permissive for Ad 12 virus replication and we are attempting to isolate Ad 12 E1 mutants by complementation on this cell line. However, recombination between transfecting mutated viral genomes and the abundant Ad 12 sequences in this cell line, may preclude the isolation of E1 mutants. Therefore, we are also attempting to isolate mutants on other pAsc2-transformed HER and HEK lines which contain low copy numbers of integrated Ad 12 early region 1.

Whereas the use of liquid-phase saturation-hybridization with radiolabelled adenovirus DNA to screen DNA and RNA from a large number of human cancers failed to detect adenovirus-specific sequences[20–23], it has been claimed that adenovirus-related mRNA can be detected by *in situ* hybridization of radiolabelled adenovirus DNA onto cryostat sections of human neurogenic tumours[24]. Although many adenovirus serotypes cause eye infections, the only circumstantial evidence that Ad 12 may cause ocular diseases is derived from animal models of retinoblastoma[11,12]. The evidence presented here demonstrates that cloned Ad 12 E1 region can transform human cells, and as Ad 12-transformed human embryo retinoblasts produce tumours which resemble poorly differentiated retinoblastomas, we believe that further study of retinoblastomas for adenovirus nucleic acids is warranted.

We thank Professor D. G. Harnden for his encouragement throughout this study and for helpful discussion of the manuscript, Dr D. R. Barry for help with the tumour pathology, Val Nash and Paul Reeve for technical assistance, Sue Williams for printing the illustrations and Debbie Williams for typing the manuscript. This study was supported by the Cancer Research Campaign (CRC). P.H.G. is a CRC Fellow.

Received 11 March; accepted 30 April 1982.

1. Van der Eb, A. J. *et al. Cold Spring Harb. Symp. quant. Biol.* **44,** 383–399 (1980).
2. Fujinaga, K. *et al. Cold Spring Harb. Symp. quant. Biol.* **44,** 519–532 (1980).
3. Ortin, J., Scheidtmann, K. H., Greenberg, R., Westphal, M. & Doerfler, W. *J. Virol.* **20,** 355–372 (1976).
4. Wilson, M. C., Fraser, N. W. & Darnell, J. E. *Virology* **94,** 175–184 (1979).
5. Graham, F. L. *et al. Cold Spring Harb. Symp. quant. Biol.* **39,** 637–650 (1974).
6. Graham, F. L., Smiley, J., Russell, W. C. & Nairn, R. *J. gen. Virol.* **36,** 59–72 (1977).
7. Graham, F. L., Harrison, T. J. & Williams, J. *Virology* **86,** 10–21 (1978).
8. Shenk, T. E., Jones, N., Colby, W. & Fowlkes, D. *Cold Spring Harb. Symp. quant. Biol.* **44,** 367–375 (1980).
9. Byrd, P. J., Chia, W., Rigby, P. W. J. & Gallimore, P. H. *J. gen. Virol.* (in the press).
10. Mukai, N. *Prog. Neuropath.* **3,** 89–128 (1976).
11. Mukai, N. & Nishida, T. *Jap. J. Ophthal.* **22,** 326–330 (1978).
12. Mukai, N. *et al. Science* **210,** 1023–1025 (1980).
13. Southern, E. M. *J. molec. Biol.* **98,** 503–518 (1975).
14. Gallimore, P. H. & Paraskeva, C. *Cold Spring Harb. Symp. quant. Biol.* **44,** 703–713 (1980).
15. Paraskeva, C. & Gallimore, P. H. *Int. J. Cancer* **25,** 631–639 (1980).
16. Jochemsen, H., Daniels, G. S. G., Lupker, J. H. & van der Eb, A. J. *Virology* **105,** 551–563 (1980).
17. Bos, J. L. *et al. Cell* **27,** 121–131 (1981).
18. Ts'o, M. O. M. *Jap. J. Ophthal.* **22,** 351–357 (1978).
19. Ts'o, M. O. M., Fine, B. S. & Zimmermann, L. E. *Am. J. Ophthal.* **69,** 350–359 (1970).
20. Mackey, J. K., Rigden, P. M. & Green, M. *Proc. natn. Acad. Sci. U.S.A.* **73,** 4651–4661 (1976).
21. Wold, W. S. M., Mackey, J. K., Rigden, P. & Green, M. *Cancer Res.* **39,** 3479–3484 (1979).
22. Mackey, J. K., Green, M., Wold, W. S. M. & Rigden, P. *J. natn. Cancer Inst.* **62,** 23–26 (1979).
23. Green, M., Wold, W. S. M., Mackey, J. K. & Rigden, P. *Proc. natn. Acad. Sci. U.S.A.* **76,** 6606–6610 (1979).
24. Ibelgaufts, H., Jones, K. W., Maitland, N. & Shaw, J. F. *Acta neuropath. berl.* **56,** 113–117 (1982).
25. Graham, F. L. & van der Eb, A. J. *Virology* **52,** 456–467 (1973).
26. Frost, E. & Williams, J. *Virology* **91,** 39–50 (1978).
27. Paraskeva, C., Brown, K. W. & Gallimore, P. H. *J. gen Virol.* **58,** 73–81 (1982).
28. Laemmli, U. K. *Nature* **227,** 680–685 (1970).
29. Laskey, R. A. *Meth. Enzym.* **65,** 363–371 (1980).

Circulating immune complexes in infants fed on cow's milk

**R. D'Amelio*, R. Seminara*, E. Galli†,
G. Antoniazzi†, L. Businco† & F. Aiuti***

* Department of Clinical Immunology and † Pediatric Clinic I,
University of Rome, 00161 Rome, Italy

Delire *et al.*[1] have reported antigen–antibody (Ag–Ab) complexes in newborns, fed on cow's milk, 6 days after birth, whereas they were absent from breast-fed neonates. The method they used was the inhibition of latex-IgG agglutination by polyclonal rheumatoid factor (pRF), linked to the Ag–Ab complexes[2]. The presence of immune complexes was attributed to the passage through the placenta of maternal IgG with antibody activity against proteins in cow's milk. This interpretation was also based on the characterization of the Ag–Ab nature of the immune complex-like material. We have now used the same and a different method to study a similar population of newborns. Our results are very different from those of Delire *et al.* We conclude that the possible pathogenicity of immune complexes cannot be assessed on the basis of a single insensitive test and in the absence of symptoms of serum sickness.

We have studied a population of newborns similar to that examined by Delire *et al.*, 24 bottle-fed and 53 breast-fed, for the presence of immune complexes in cord sera and serum samples collected 6 days after birth. We have used the same method as Delire *et al.*[1] and, in addition, the Clq–SP assay of Hay *et al.*[3].

Our results obtained with the pFR-inhibition test were very different from those of Delire *et al.*; in fact we observed a very high incidence of immune complexes in umbilical cord sera, and no significant change 6 days after birth. Furthermore, there was no difference between breast-fed and bottle-fed neonates and the increase in the number of immune complexes was absolutely random (Table 1).

Table 1 Immune complexes detected by pRF-inhibition method in neonates

Subjects	*N*	Cord blood	Day 6
Breast-fed	53	20 (38%)	19 (36%)
Bottle-fed	24	5 (21%)	4 (17%)

In contrast, using the Clq–SP assay we found only three samples of cord sera positive for immune complexes and, 6 days after birth, only two sera were positive, both in the breast-fed group (Table 2).

These observations stress the fact that the same serum populations can give very different results with different methods for immune complex evaluation. In the Clq–SP assay, using *Staphylococcus aureus* protein A as detector, it is mainly IgG1 complexes that are identified, whereas the pRF-inhibition test has a wider spectrum of detection.

Table 2 Immune complexes detected by Clq–SP method in neonates

Subjects	*N*	Cord blood	Day 6
Breast-fed	53	3 (6%)	2 (4%)
Bottle-fed	24	0	0

The difference between our data and those of Delire could be due to the fact that the pFR-inhibition test used, although simple and easy to perform, has too subjective a reading, depends on the source of pFR used (which may affect agglutinating activity) and on the IgG levels on the surface of the latex particles. Furthermore, it is very important that the presence of immune complexes be linked with symptoms of serum sickness.

Thus, we believe that it is impossible to draw conclusions about the pathogenic role of Ag–Ab complexes on the basis of a single insensitive test and in the absence of characteristic symptoms.

Received 15 July 1981, accepted 6 April 1982.

1. Delire, M., Cambiaso, C. L. & Masson, P. L. *Nature* **272**, 632 (1978)
2. Lurhuma, A. Z. *et al. Clin. exp. Immun.* **25**, 212–226 (1976)
3. Hay, F. C., Nineham, L. J. & Roitt, I. M. *Clin. exp. Immun.* **24**, 396–400 (1976).

Binding of C3b proceeds by a transesterification reaction at the thiolester site

**Margaret K. Hostetter, Matthew L. Thomas,
Fred S. Rosen & Brian F. Tack†**

Department of Pediatrics, Harvard Medical School and the
Division of Immunology, Children's Hospital Medical Center,
300 Longwood Avenue, Boston, Massachusetts 02115, USA

The binding of C3b, the opsonic fragment of the third component of complement (C3), to bacterial surface structures mediates two events important in host defence: assembly of the $\overline{\mathrm{C5b\text{-}C9}}$ lytic complex and opsonic recognition by phagocytic cells (for reviews see refs 1, 2). These interactions proceed through a labile binding site[3] located on the α' chain of the C3b molecule, with the resultant formation of a covalent oxy-ester bond[4,5] in which the acyl group is contributed by the protein. By exposure of a titratable sulphydryl group[6,7] an internal thiolester of native C3 has also been localized to the α' chain. Studies with ^{14}C-methylamine, a nucleophile which is inherently reactive with a thiolester, have further indicated a stoichiometric (1:1) and covalent interaction, again within the α' chain[8–10]. After reaction of the native protein with ^{14}C-methylamine and radioalkylation of the exposed sulphydryl with ^{3}H-iodoacetic acid, a 35-residue tryptic peptide has been isolated that yields the sequence -Cys^{9}-Gly-Glu-Glu^{12}- on Edman degradation; tritium counts are released at step 9 (*S*[^{3}H]-(carboxymethyl)cysteine) and ^{14}C counts at step 12 (γ-glutamyl[^{14}C]methylamide)[8]. We now present data which directly demonstrate that the second glutamyl residue of the reactive thiolester can, on proteolytic cleavage of the protein, donate its carbonyl group in a transesterification reaction with appropriate acceptor molecules. These results provide a model for analysis of the interactions at the molecular level between surface constituents of microorganisms and C3b.

Small molecules such as oligosaccharides and amines have been shown to inhibit C3 uptake onto Sepharose–trypsin matrices[11,12], while other studies have shown direct incorporation of radiolabelled sugars and amino acids into nascent C3b and have localized the site of incorporation to the α' chain[13,14]. To define this site more precisely, purified human C3[15] was cleaved into fragments C3a and C3b in the fluid phase by limited tryptic digestion[16] in the presence of 100 mM ^{14}C-sucrose, ^{14}C-D-glucosamine or ^{14}C-glycerol (NEN; each diluted to a specific activity of 1.5 mCi mmol^{-1}). For all experiments, C3 was >80% native as assessed by sulphydryl group titration in the presence and absence of methylamine[8,16]. Controls for each reaction included native C3 without trypsin (C3) and pretrypsinized C3 (C3b), incubated in identical conditions of temperature

---

† Present address Department of Molecular Immunology, Research Institute of Scripps Clinic, La Jolla, California 92037, USA

Table 1 Incorporation (mol per mol) of radioactive ligand into total C3

	C3	C3b	C3 + trypsin
^{14}C-sucrose	0.42	0.45	0.72
^{14}C-glucosamine	0.19	0.13	0.20
^{14}C-glycerol	0.04	0.04	0.35
^{14}C-threonine	0.02	0.05	0.63

Incorporation was determined by measurements of radioactivity and absorbance at 280 nm ($E^{1\%}_{1\,\mathrm{cm}} = 9.3$)[24].

(37 °C) and time with each of the radiolabelled compounds. Results of SDS-polyacrylamide gel electrophoresis and autofluorography are presented in Fig. 1. For each sample, incorporation of ligand, expressed as mols of ligand per mol C3, is shown in Table 1. An identical study was performed with 100 mM ^{14}C-L-threonine (Amersham; uniformly labelled, diluted to a specific activity of 0.83 mCi mmol^{-1}), and the results are shown in Fig. 2 and Table 1.

These experiments demonstrate that generation of C3b (C3 + trypsin) in the presence of either ^{14}C-glycerol (Fig. 1) or ^{14}C-threonine (Fig. 2) results in covalent binding of the ligand specifically to the α′ chain. The negligible (≤0.05 mol per mol) incorporation of these two compounds into the control samples (C3, C3b) confirms that proteolytic cleavage of native C3 is a requirement for the covalent binding interaction and emphasizes the short lifetime of the labile binding site in C3b. In contrast, although ^{14}C-sucrose and ^{14}C-glucosamine are incorporated preferentially into the α′ chain (C3 + trypsin), a significant amount of label is associated with both chains of the control C3 and C3b samples (Fig. 1). These high levels of nonspecific incorporation for sucrose and glucosamine precluded their use in further studies (Table 1). By analogy, radiolabelled glucose preparations have frequently been shown to be contaminated with high specific activity components which react nonspecifically and covalently with proteins[17].

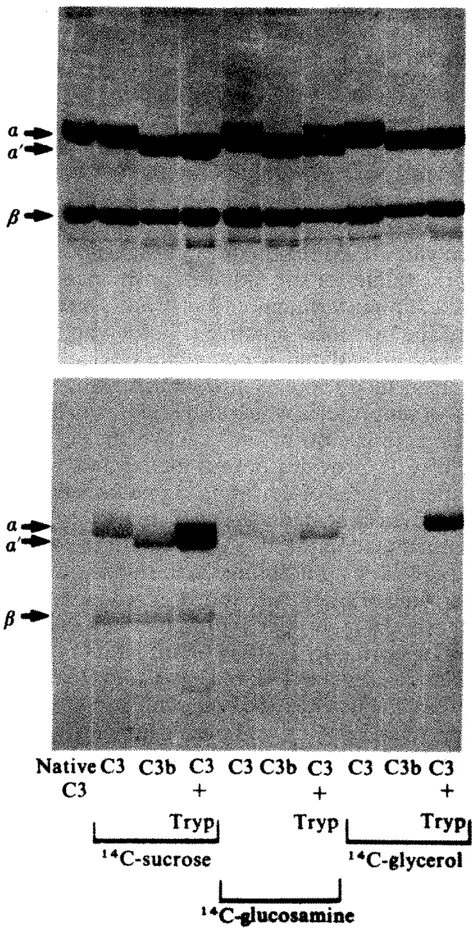

Fig. 1 SDS gel and autoradiogram of human C3 preparations reacted with ^{14}C-sucrose, ^{14}C-D-glucosamine and ^{14}C-glycerol. Each sugar derivative was reacted with the following C3 species: native (C3); pretrypsinized (C3b); trypsin-activated (C3 + trypsin). The far left lane represents untreated native C3. Purified C3 was dialysed overnight at 4 °C against 0.01 M Tris-HCl (*p*H 7.5), 0.15 M NaCl, 0.002 M Na$_2$EDTA. Trypsin digests (0.05%, w/w) were terminated at 16 min (37 °C) with the addition of a 10-fold molar excess of soybean trypsin inhibitor (Worthington). Samples were reduced in 1% SDS, 0.01 M dithiothreitol (2 h, 37 °C), alkylated with iodoacetamide (10% in excess of reducing thiol) and dialysed against 0.1 M Tris-HCl (*p*H 8.0), 0.01 M Na$_2$EDTA, 0.1% SDS. In the upper panel the chain structure of C3 (α, β) and C3b (α′, β) is visualized by staining the 7.5% polyacrylamide slab gel[25] with Coomassie blue R250. The lower panel shows the corresponding gel prepared for autofluorography[26].

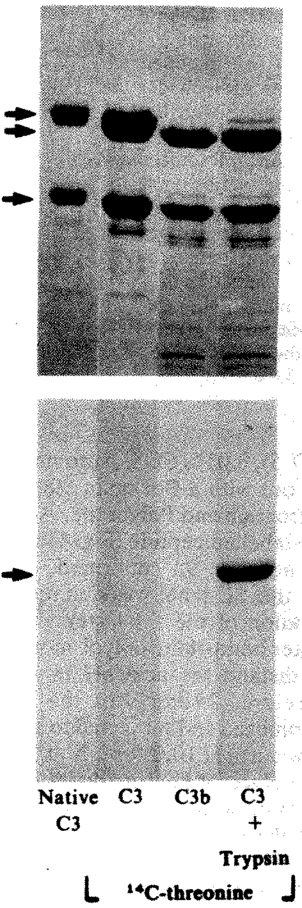

Fig. 2 SDS gel (upper panel) and autoradiogram (lower panel) of human C3 preparations reacted with ^{14}C-L-threonine. See Fig. 1 for description of method.

Accordingly, preparative experiments which would yield sufficient quantities of glycerol- or threonine-labelled protein for sequence analysis were performed. Purified human C3 (50 mg) was reacted with TPCK-trypsin in limited conditions in the presence of 100 mM ^{14}C-glycerol (0.25 mCi mmol^{-1}) or 100 mM ^{14}C-threonine (0.28 mCi mmol^{-1}). The mixture was treated with activated thiol–Sepharose and the bound C3b subjected to extensive trypsin digestion. Isolation of the tryptic peptide containing the labile binding site and radio-alkylation of the exposed sulphydryl group with ^{3}H-iodoacetic acid (54.6 mCi mmol^{-1}) were carried out as previously described[8]. On elution of the tryptic peptides from Sephadex G-75 (Superfine), ^{3}H and ^{14}C radioactivity (d.p.m.) coincided in a single peak (Fig. 3) which was subsequently subjected to Edman degradation. The mol fraction of C3 that incorporated ^{14}C-glycerol or ^{14}C-threonine was 0.35 and 0.38, respectively. For the threonine-labelled peptide, material in the excluded peak represented incompletely digested sample.

The threonine-bearing peptide was lyophilized, dissolved in 1.0 ml distilled water and dialysed against 0.001 M *N*-ethyl-

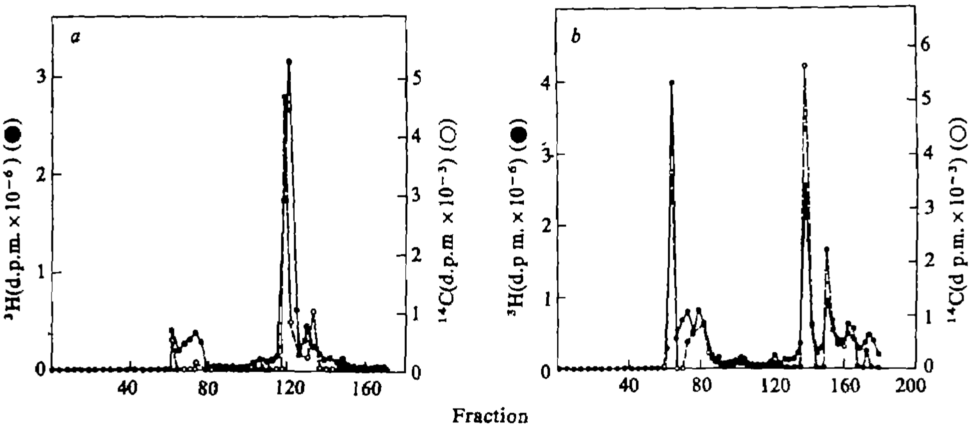

Fig. 3 Elution profile of the ^{14}C-glycerol-labelled (*a*) and ^{14}C-threonine-labelled (*b*) peptides. A 1.5×220 cm column of Sephadex G-75 SF was equilibrated with 0.01 M Tris-HCl (*p*H 8.0), 0.2% SDS, 0.001 M Na_2EDTA. Radioactivity coincided with the major peak of absorbance at 230 nm (not shown). The yield of glycerol-labelled peptide (35%) was calculated based on the known specific activity of ^{3}H-iodoacetic acid and nanomols of C3b bound to thiol-Sepharose. The yield of threonine-labelled peptide was 33%.

morpholine (*p*H 7.5), 0.01% SDS. Automated Edman degradation was carried out with a Beckman 890C sequencer using a 0.1 M Quadrol program and Polybrene. Analysis of 23.6 nmols of ^{14}C-threonine-labelled peptide (Fig. 4) showed the ^{3}H counts to be present at step 9, confirmed as *S*-[^{3}H]-(carboxymethyl)cysteine; the ^{14}C label was quantitatively recovered at step 12, the location of the thiolester glutamyl residue. The predicted oxy-ester bond of the polyol-modified peptide proved too labile to withstand the acid *p*H inherent in the Edman procedure. Therefore, 23 nmols of the ^{14}C-glycerol-bearing peptide were lyophilized and subjected to ammonolysis in 1.0 M ammonium acetate at *p*H 10.0 for 2 h at 37 °C. An additional 22.5 nmols of the glycerol-bearing peptide were left unreacted as a control, lyophilized and then dissolved in 1.0 ml distilled water. After dialysis against 0.001 M *N*-ethylmorpholine (*p*H 7.5), 0.01% SDS, the peptide treated with ammonium acetate released 66% of its ^{14}C counts, while all ^{14}C radioactivity remained bound in the control peptide. In neither peptide was release of ^{3}H counts detected. On Edman degradation of the amidated peptide, the ^{3}H label was recovered at step 9, identified as *S*-[^{3}H]-(carboxymethyl)cysteine, and >95% of the predicted glutamine was detected at step 12. For the experimental peptide, the recoveries of the phenylthiohydantoin derivatives were as follows for steps 9–13: (9) Cys, 2.3 nmols; (10) Gly, 1.6 nmols; (11) Glu, 1.1 nmols; (12) Glu, 0.7 nmols and Gln, 0.4 nmols; (13) Asn, 0.8 nmols. No glutamine was detected by HPLC at any of the first 14 steps in the non-amidated peptide.

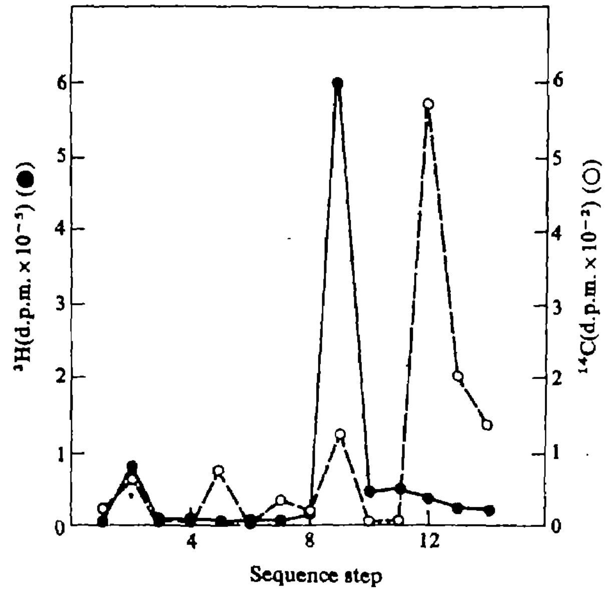

Fig. 4 Profile of the ^{3}H and ^{14}C counts observed on Edman degradation of the ^{14}C-threonine-labelled peptide. The recoveries of specific counts were 33% of the ^{3}H at step 9 and 16% of the ^{14}C at steps 12, 13 and 14.

The specific labelling data obtained in these studies clearly demonstrate that the second glutamyl residue, contained in the C3 sequence -Cys-Gly-Glu-Glu-, is the reactive species involved in covalent bonding with small molecules. In the native protein this residue participates in the formation of a thiolester bridge to the cysteinyl sulphydryl group. On proteolytic cleavage, this carbonyl group transesterifies with an acceptor molecule, releasing the cysteinyl sulphydryl. The reaction with glycerol is clearly one of *O*-acylation. For L-threonine, the resultant linkage with C3 is amide in nature (hydroxylamine insensitive[14], stable on Edman degradation). It is not possible, however, to distinguish between direct *N*-acylation of the α-amino group and/or *O*-acylation at the β-hydroxyl group with subsequent rearrangement through an *O–N* shift. *N*-acylation has been proposed to account for a stable linkage observed between C3b and the Fd region of rabbit IgG[18].

Recently, the thiolester site has been positioned by sequence analysis at the amino-terminal end of C3d[19], a subdomain of the α' chain. The presence in native C3 of a reactive thiolester is not, however, an isolated phenomenon: evidence has been presented for an identical site in α_2-macroglobulin[8,20] and in C4[21,22]—two other proteins which also function in host defence. Thus, the characterization of the reactive species involved in the binding of C3b provides both a model and a method for identifying specific sites of acylation on pathogenic organisms in which phagocytosis is mediated by C3b.

We thank Paul Gallop for his suggestion of the ammonolysis reaction and for discussion during these studies; we also thank Alex Law for suggesting the use of L-threonine. A preliminary report of these data has been presented elsewhere[23]. This research was supported by USPHS Grant AI 17146, American Heart Association grant 80-841 and by a Child Health Research Grant from the Charles H. Hood Foundation to M.K.H.; B.F.T. is the recipient of an Established Investigatorship (77-168) from the American Heart Association.

Received 8 February; accepted 16 April 1982.

1. Muller-Eberhard, H J & Schreiber, R D *Adv. Immun.* **29**, 1–53 (1980)
2 Reid, K. B. M. & Porter, R R. *A Rev Biochem* **50**, 433–464 (1981)
3 Muller-Eberhard, H. J , Dalmasso, A P. & Calcott, M A *J exp Med* **123**, 33–54 (1966)
4 Law, S. K & Levine, R P *Proc natn Acad. Sci. U S.A* **74**, 2701–2705 (1977)
5. Law, S K., Lichtenberg, N A & Levine, R. P *J. Immun.* **123**, 1388–1394 (1979).
6 Janatova, J , Lorenz, P , Schechter, A. M., Prahl, J W & Tack, B F *Biochemistry* **19**, 4471–4478 (1980).
7 Janatova, J., Tack, B. F & Prahl, J W *Biochemistry* **19**, 4479–4485 (1980).
8. Tack, B. F., Harrison, R A , Janatova, J., Thomas, M L & Prahl, J W *Proc natn Acad Sci. U.S.A.* **77**, 5764–5768 (1980)
9. Pangburn, M. K & Muller-Eberhard, H J *J. exp. Med* **152**, 1102–1114 (1980)
10. Howard, J B *J biol Chem.* **255**, 7082–7084 (1980)
11. Capel, P J A , Groeneboer, O., Grosveld, G. & Pondman, K H *J. Immun* **121**, 2566–2572 (1978).
12. Sim, R B , Twose, T M , Paterson, D. S & Sim, E. *Biochem. J.* **193**, 115–127 (1981)
13. Mann, J. *et al.*, *J Immun* **126**, 2370–2372 (1981)
14 Law, S. K , Minich, T. M & Levine, R P *Biochemistry* **20**, 7457–7463 (1981)
15 Hammer, C. H , Wirtz, G. H , Renfer, L , Gresham H D & Tack, B F *J biol Chem* **256**, 3995–4006 (1981)
16. Tack, B. F , Janatova, J., Thomas, M L , Harrison, R. A & Hammer, C H *Meth Enzym* **80** (in the press)
17. Trueb, B , Holenstein, C G., Fischer, R W. & Winterhalter, K. H. *J biol Chem.* **255**, 6717–6720 (1980).

18. Gadd, K J & Reid, K B. M. *Biochem J* **195**, 471–480 (1981)
19. Thomas, M L., Janatova, J, Gray, W R & Tack, B F *Proc natn Acad Sci U S.A.* **79**, 1054–1058 (1982)
20 Sottrup-Jensen, L, Peterson, T E & Magnusson, S *FEBS Lett* **121**, 275–279 (1980).
21. Campbell, R D., Gagnon, J & Porter, R R *Biosci Rep* **1**, 423–429 (1981)
22. Harrison, R A., Thomas, M L. & Tack, B F *Proc natn Acad. Sci U S A* **78**, 7388–7392 (1981)
23. Hostetter, M K, Thomas, M L & Tack, B F *IXth Int Complement Workshop*, Key Biscayne, Florida *Molec Immun* (in the press)
24. Tack, B F & Prahl, J. W *Biochemistry* **15**, 4513–4521 (1976)
25 Laemmli, U. K *Nature* **227**, 680–685 (1970)
26 Bonner, W. M & Laskey, R A *Eur J Biochem* **46**, 83–88 (1974).

Translation of mRNA for human granulocyte–macrophage colony stimulating factor

Aldons J. Lusis*†, David W. Golde*, Diana H. Quon* & Laurence A. Lasky‡

* Division of Hematology/Oncology, Department of Medicine,
UCLA School of Medicine, Los Angeles, California 90024, USA
† Department of Microbiology, University of California,
Los Angeles, California 90024, USA
‡ Genetics Institute, 225 Longwood Avenue, Boston,
Massachusetts 02115, USA

Granulocyte–macrophage colony stimulating factors (GM-CSFs) regulate the growth and differentiation of committed granulocyte and macrophage progenitor cells[1–3]. Operationally, the factors are recognized by their ability to stimulate the formation of granulocyte and macrophage colonies in semi-solid cultures of bone marrow cells. GM-CSFs are produced by a variety of tissues, and prominent cellular sources in man include T lymphocytes and mononuclear phagocytes[1,4–7]. The factors obtained from most sources are glycoproteins of molecular weight 20,000–70,000. At least two major GM-CSF subtypes have been distinguished in mice and humans on the basis of biological activity *in vitro*: one primarily stimulates the formation of macrophage colonies, while the other stimulates the fomation of both granulocyte and macrophage colonies[1,8]. We report here the translation and partial characterization of a messenger RNA for human GM-CSF that stimulates both granulocyte and macrophage colonies. The mRNA was isolated from a human T-lymphocyte cell line, and when injected into *Xenopus laevis* oocytes[9] it directed the synthesis of biologically active GM-CSF.

Human GM-CSFs have been partially purified and characterized from urine and from medium conditioned by placenta, leukocytes, lung and several tumour cell lines[1]. For our studies of GM-CSF mRNA we used a human cell line (Mo) containing predominantly helper T lymphocytes that constitutively produces and secretes into the medium a GM-CSF stimulating the formation of both granulocyte and macrophage colonies *in vitro*[10,11]. The Mo cell line is an exceptionally rich source of GM-CSF and unlike most other sources, appears to produce a single GM-CSF subtype. The production of GM-CSF is approximately doubled by the inclusion of phytohaemagglutinin in the culture medium[10]. Physically the Mo cell GM-CSF is an acidic glycoprotein of molecular weight ~30,000 (ref. 11).

Whole cell RNA was isolated from Mo cells using a guanidine thiocyanate extraction procedure[12], and poly (A)-containing RNA was enriched using oligo (dT)-cellulose chromatography[13]. The resultant poly(A) RNA was contaminated to ~50% with ribosomal RNA as judged by agarose gel electrophoresis and a tritiated poly(U) hybridization assay[14]. Oocytes were injected with 30–50 ng of the poly(A) RNA, and after 1–3 days' incubation the oocyte culture medium stimulated the formation of clusters and small colonies in agar cultures of human bone marrow. For example, when injected oocytes were incubated for 3 days in Barth's medium (20 µl medium per oocyte) containing 0.1% bovine serum albumin, 200 µl of the medium stimulated the formation of an average of ~40 small colonies containing 15 or more cells in the standard GM-CSF assay. The assay involves monitoring the formation of granulocyte and macrophage colonies in 1-ml cultures containing 10^5 light-density human bone marrow cells plated in 0.3% agar, α-medium and 10% fetal bovine serum[2,15,16]. In contrast, the medium from oocytes injected with water or poly(A)-containing RNA from rat liver did not stimulate colony formation.

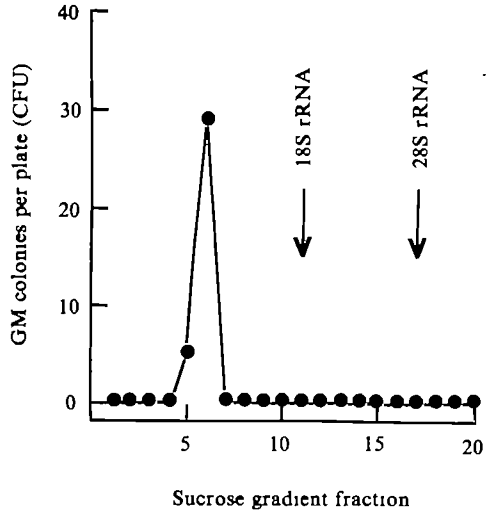

Fig. 1 Fractionation of Mo T-cell poly(A)-containing RNA using sucrose gradient centrifugation. Mo cells were grown and induced for 48 h with phytohaemagglutinin (Burroughs-Wellcome) as described previously[21] In these conditions GM-CSF production increased approximately two-fold over that of uninduced cells[10]. Total RNA was isolated by a procedure involving guanidine thiocyanate extraction followed by centrifugation through a caesium chloride cushion[12]. The poly(A) RNA was then isolated by chromatography on oligo(dT)-cellulose (Collaborative Research) Judging from electrophoretic analysis and a tritiated poly(U) hybridization assay, ~50% of the RNA at this stage was ribosomal[14]. The yield of total RNA from 10^9 cells averaged 3–4 mg, and of this ~3% was recovered following oligo(dT)-cellulose chromatography The RNA had a 260 nm/280 nm absorbance ratio of 2.1 or better, indicating low protein contamination. The poly(A) RNA was heated at 65 °C for 1 min and 100 µg was applied to a 10-ml 5–25% sucrose gradient containing 0.1 M sodium chloride, 10 mM Tris *p*H 7.4, and 1 mM EDTA. The gradient was centrifuged in a Beckman SW 41 rotor at 26,000 r.p.m. for 19 h at 4 °C and 0.5-ml fractions were collected and precipitated with two volumes of ethanol. The RNA precipitates were dissolved in 5 µl of water. An aliquot of the RNA was removed for analysis by electrophoresis on 1% agarose gels, the results indicated good separation of RNA on the basis of size, with 18S and 28S ribosomal RNA being present mainly in fractions 11 and 17. RNA from each fraction was injected into 20 oocytes (50 nl per oocyte) and the pooled oocytes from each fraction were incubated at room temperature in 200 µl of modified Barth's medium containing 1% bovine serum albumin (Sigma, crystallized) for 2 days. The medium from each fraction was then assayed for GM-CSF using cultures of human bone marrow as described in Fig. 2 legend Fraction 6, containing the bulk of the GM-CSF mRNA activity, contained ~4 µg of RNA. The arrows indicate the positions of 18S and 28S ribosomal RNA markers present in a gradient run in parallel CFU, colony-forming units.

For these experiments it was important to use non-adherent bone marrow cells in the assay because in some cases the presence of adherent cells in the cultures produced a background of clusters that made it difficult to detect the small amount of activity present in oocyte medium[15]. Also, the presence of protein (0.1% bovine serum albumin) in the oocyte medium appeared to stabilize the activity stimulating colony formation. Homogenates of oocytes injected with Mo poly(A) mRNA stimulated few colonies; this phenomenon may be attributed in part to an inhibitor of colony formation present in the oocytes (see below). The numbers of colonies produced in different experiments varied considerably, probably due to donor-specific differences in bone marrow and variability in frog oocytes. This variability made it difficult to ascertain whether treatment of the Mo cells with phytohaemagglutinin stimulated GM-CSF mRNA activity; nevertheless, for experi-

0028–0836/82/260075—03$01 00

ments described below, RNA was extracted from Mo cells treated with the lectin.

A control experiment in which mRNA preparations were added directly to bone marrow cultures indicated that contaminating GM-CSF in the RNA was not responsible for the stimulation of colony formation. The addition of 500 ng of sucrose gradient-purified GM-CSF mRNA (see below) to duplicate cultures of bone marrow cells did not result in the stimulation of colony formation, while medium derived from 10 oocytes injected with a comparable amount of the same mRNA stimulated the formation of up to 30 granulocyte–macrophage colonies containing ≥20 cells.

The CSF signal obtained when total poly(A) RNA was injected into oocytes was usually low, with few colonies containing relatively small numbers of cells. The poly(A) RNA was therefore fractionated according to size using sucrose gradient centrifugation, and the resultant fractions injected into oocytes. RNA in each fraction from the gradient was precipitated with ethanol and resuspended in 5 μl of H_2O. Agarose gel electrophoresis and *in vitro* translation using reticulocyte lysates[17] demonstrated the presence of translatable poly(A) mRNA in each fraction. An aliquot (50 nl) of each fraction was injected into each of 20 oocytes, and the oocytes from each fraction were incubated together in 20 μl of medium for 2 days. Assay of the medium in human bone marrow cultures indicated that the CSF activity was present in a single sharp peak of RNA from the sucrose gradient (Fig. 1). Using 18S and 28S ribosomal RNA markers, the size of the GM-CSF mRNA was estimated at about 1,200 nucleotides. A mRNA of this size could be translated into a protein having a maximum molecular weight of 44,000—this compares with a molecular weight of ~30,000 for GM-CSF produced by the Mo cells as estimated by gel filtration chromatography[11] or SDS-polyacrylamide gel electrophoresis (A.J.L., unpublished). As the Mo GM-CSF is glycosylated, the information content in the mRNA is more that sufficient to encode this protein. The sucrose gradient fractionation was performed three separate times with identical results.

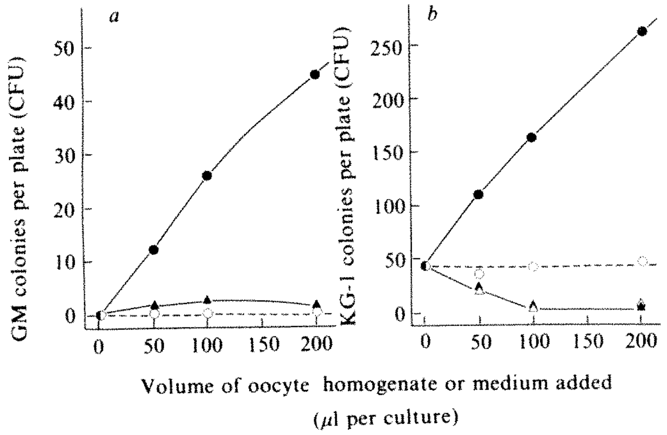

Fig. 2 Clonal assay of GM-CSF translated by oocytes using human bone marrow (*a*) and the KG-1 human myeloid leukaemia cell line (*b*). Oocytes were injected with 40 ng of RNA purified from the Mo T-cell line using oligo(dT)-cellulose chromatography and sucrose gradient centrifugation as described in Fig. 1 legend. The oocytes were incubated, in pools of 10, in 200 μl of modified Barth's medium containing 1% bovine serum albumin for 2 days at room temperature. The oocyte incubation medium was removed and the oocytes were homogenized in 0.02 M sodium phosphate, 0.15 M NaCl, *p*H 7.4 (20 μl per oocyte). The debris was removed by centrifugation at 12,000*g* for 10 min. The oocyte homogenates and media were then assayed in clonal assays using human bone marrow target cells as previously described[11,15,16]. Briefly, bone marrow cells were aspirated from healthy adult volunteers, and the light-density, non-adherent cells were isolated using sedimentation in Ficoll–Hypaque followed by Petri dish adherence. 10^5 fractionated cells were plated with varying amounts of oocyte homogenates or media in 1-ml cultures containing 0.3% agar, 10% fetal bovine serum, α-medium (Flow) and α-thioglycerol. The cultures were then incubated for 11 days at 37 °C in 7% carbon dioxide, when they were examined using a low power microscope and colonies of ≥30 cells counted. In tests on the KG-1 human myeloid leukaemia cell line, the cells were plated in agar and cultured at a density of 2×10^3 cells m^{-1} culture exactly as described for bone marrow cells. Colonies containing ≥20 cells were counted after 11 days. Each point represents the average of two determinations. Medium from oocytes injected with mRNA (●) or water (○); homogenates of oocytes injected with mRNA (▲) or water (△).

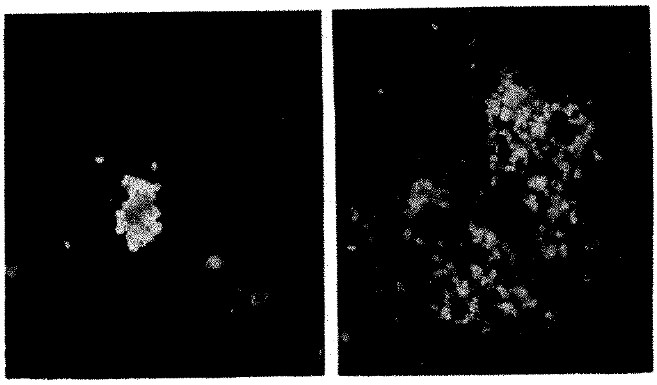

Fig. 3 Gross morphology of typical granulocyte–macrophage colonies stimulated by GM-CSF translated in frog oocytes. Both 'tight' (left) and 'loose' (right) colonies were also observed at low concentration of Mo T-cell conditioned medium (not shown). ×30

The enrichment of mRNA for GM-CSF by sucrose gradient fractionation resulted in a considerably stronger stimulation of colony formation by oocyte medium than was obtained using total poly(A)-containing RNA. In contrast to the relatively small colonies observed using unfractionated RNA, peak gradient fractions, when injected in quantities of 25–50 ng per oocyte, stimulated relatively large colonies containing up to ~300 cells. For example, in the experiment shown in Fig. 2, 200 μl of oocyte medium derived from 10 oocytes injected with fractionated mRNA and incubated for 2 days, stimulated more than 40 colonies containing ≥30 cells as well as numerous smaller clusters. In terms of colony number, size and morphology, the GM-CSF in 200 μl oocyte medium resulted in stimulation equivalent to ~4 μl of medium conditioned by the growth of Mo cells for 3 days at a final density of 5×10^6 cells ml^{-1} (Fig. 3). Because of its higher specific activity, sucrose gradient fractionated preparations of GM-CSF mRNA were used in the experiments described below.

The GM-CSF produced by frog oocytes stimulated colony formation dose dependently (Fig. 2). The curve resembles that found previously for the GM-CSF produced by Mo T cells[10,11]. Also, the activity in oocyte medium produced colonies that were similar morphologically to those observed using low levels of T-cell conditioned medium (Fig. 3). Microscopic examination of individual cells from the colonies indicated the presence of monocytic, granulocytic and mixed monocytic–granulocytic colonies (data not shown). For these experiments, single colonies were picked from agar cultures using a fine pipette, dissociated from the agar by a stream of air and stained with Wright's or Giemsa. Monocytic colonies were identified using a lipase stain specific for monocytes and macrophages[11]. Using this procedure, 50–100 μl of medium from injected oocytes stimulated an average of 56% monocytic colonies, 37% granulocytic colonies and 7% mixed colonies. A comparable concentration of T-cell-derived GM-CSF gave similar results, with 49% of the colonies being monocytic, 42% granulocytic and 9% mixed.

The bulk of the GM-CSF activity produced by the oocytes was apparently secreted into the medium (Fig. 2). However, the determination of GM-CSF activity in oocyte homogenates is complicated by the presence of a weak inhibitor of colony formation. For example, in mixing experiments, 200 μl of control oocyte homogenate from the experiment shown in Fig. 2 produced ~40% inhibition of the activity of added Mo T-cell GM-CSF. Taking this inhibition into account, ~90% of the GM-CSF produced by oocytes is present in the medium after 2 days. Because of the relatively small amount of activity produced by injected oocytes, a detailed physical characterization of the oocyte-derived GM-CSF has not been possible. However, preliminary experiments have shown that the activity produced by oocytes had a heat inactivation profile similar to that of the GM-CSF produced by Mo T cells. When incubated at neutral *p*H for 30 min both activities were stable at 60 °C but were almost completely inactivated at 80 °C.

The GM-CSF translated in oocytes also stimulated the growth in agar of a human myeloid leukaemia cell line, KG-1, that has previously been shown to be specifically responsive to GM-CSF[18,19] (Fig. 2). As in the case of bone marrow cells, medium from oocytes injected with water or control RNA had no effect on the growth of KG-1 cells. However, homogenates of both injected and uninjected oocytes significantly inhibited cell growth (Fig. 2).

The GM-CSF mRNA assay will undoubtedly be useful for the isolation of cloned cDNAs which contain GM-CSF nucleotide sequences. Similar oocyte translation systems have proved useful for studies of interferons[20]. Clearly, molecular genetic approaches should aid the examination of the structural and functional properties of these mediators of haematopoiesis. Our results also suggest that it should be feasible to use the oocyte system for the translation and characterization of mRNAs for other factors regulating the growth and differentiation of haematopoietic cells.

This work was supported by NIH grants AM 27008, CA 32737, CA 30388 and the Genetics Institute. We acknowledge the technical assistance of Kelly O'Donnell and Noelle Bersch, and thank Drs G. Watson, H. P. Koeffler and O. N. Witte for helpful advice. The Mo cell line supernatant is available on request.

Received 30 December 1981, accepted 14 April 1982

1. Burgess, A W & Metcalf, D *Blood* **56**, 947–958 (1980).
2. Metcalf, D. *Hemopoietic Colonies*: In Vitro *Cloning of Normal and Leukemic Cells* (Springer, New York, 1977)
3. Moore, M A S *Clin Hemat* **8**, 287–310 (1979)
4. Chervenick, P. A & LoBuglio, A F *Science* **178**, 164–166 (1977)
5. Golde, D W., Finley, T N & Cline, M J *Lancet* **ii**, 1397–1399 (1972)
6. Parker, J W & Metcalf, D *J Immun* **122**, 502–510 (1974)
7. Cline, M J & Golde, D W *Nature* **248**, 703–770 (1974)
8. Stanley, E R *Proc. natn Acad Sci U S A* **76**, 2969–2973 (1979)
9. Gurdon, J B *The Control of Gene Expression in Animal Development* (Harvard University Press, 1974)
10. Golde, D W, Quan, S G & Cline, M J *Blood* **52**, 1068–1072 (1978)
11. Lusis, A J, Quon, D H & Golde, D W. *Blood* **57**, 13–21 (1981).
12. Chirgwin, J M, Przybyla, A. E, MacDonald, R J & Rutter, W. I. *Biochemistry* **18**, 5294–5299 (1979)
13. Aviv, H & Leder, P. *Proc. natn. Acad Sci U S A* **69**, 1408–1412 (1972)
14. Bishop, J, Morton, J, Rosbash, M & Richardson, M *Nature* **250**, 199–204 (1974)
15. Golde, D W & Cline, M J *J. clin Invest* **51**, 2981–2983 (1972).
16. Messner, H. A, Till, J. E & McCulloch, E A *Blood* **52**, 701–710 (1973)
17. Pelham, H R B & Jackson, R. J *Eur. J. Biochem* **67**, 247–256 (1976).
18. Koeffler, H P & Golde, D W. *Science* **200**, 1153–1154 (1978)
19. Lusis, A J & Koeffler, H P *Proc natn Acad Sci U S A* **77**, 5346–5350 (1980)
20. Taniguchi, T, Pang, R H, Yip, Y K, Henriksen, D & Vilcek, J *Proc natn Acad. Sci U S A* **78**, 3469–3472 (1981)
21. Nathan, I, Groopman, J E., Quan, S G, Bersch, N & Golde, D. W *Nature* **292**, 842–844 (1981)

A common mechanism for the synthesis of membrane and secreted immunoglobulin α, γ and μ chains

W. Cushley*, B. E. H. Coupar, C. A. Mickelson* & A. R. Williamson†

Department of Biochemistry, University of Glasgow,
Glasgow G12 8QQ, UK

Immunoglobulins serve as both secreted effector antibodies and antigen receptors bound to the membrane of lymphocytes. Each newly generated B lymphocyte expresses membrane IgM and subsequently co-expresses membrane IgM and membrane IgD. Antigen-driven clonal proliferation is accompanied by further differentiation with the generation of B lymphocytes expressing, in membrane-bound form, other classes and subclasses of immunoglobulin[1]. Such memory cells are apparently capable of responding to antigen to generate further clones of cells secreting antibodies of particular classes and subclasses. The mechanism by which IgM functions as both a membrane-bound and a secreted immunoglobulin has been determined for both murine and human systems[2–4]. The difference between the two forms of IgM is entirely at the C-terminus. The μ_s (secreted) chain has a hydrophilic peptide additional to the Cμ4 domain and the μ_m (membrane-bound) chain has a hydrophobic peptide replacing the hydrophilic C-terminal peptide of the μ_s chain[2–4]. The μ_s and μ_m chains are translated from distinct mRNA molecules that are generated by alternative splicing and/or termination points of transcripts from a single rearranged μ gene[5,6]. Recent evidence supports the existence of a similar mechanism for the generation of δ_s and δ_m chains[7–9]. Structurally different γ_m and γ_s chains have been observed in human, mouse and chicken cells[10–12].The present study further distinguishes between γ_m and γ_s chains and characterizes the mRNA molecules encoding them in human cells. We have also characterized α_m and α_s chains in a human cell. The data reported here, together with other recent findings, suggest a common mechanism for the generation of membrane and secreted forms of α, γ and μ chains.

We have compared the biosynthesis of IgG in three different human B-cell lines (EB4, Bec-11 and Maja) with that of IgA in the human cell line Dakiki Arosros I and of IgM in the human line Bjab. The membrane and secretory heavy chains of Bec-11, Dakiki and Bjab immunoglobulins have been fully characterized previously[10,13]. Two forms of biosynthetically labelled, specifically immunoprecipitable γ chains of EB4 cells are clearly resolved by SDS-gel electrophoresis (Fig. 1), differing in apparent molecular weight by 12,000 whether glycosylated or not. The high molecular weight band can be identified as γ_m by iodination of intact cells (Fig. 1*e*), and the lower molecular weight γ chain as γ_s by demonstrating its secretion in either the glycosylated (Fig. 1*h*) or non-glycosylated (lane *i*) state. The cell line Maja synthesizes two γ polypeptide chains similar in size to the γ_m and γ_s chains of Bec-11 and EB4 cells. M. J. Owen (personal communication) has characterized the γ_m and γ_s chains of Maja cells. The three cell lines show three different patterns for glycosylation of γ chains: in EB4, both γ_m and γ_s seem to be singly glycosylated; in Bec-11 some γ_s chains have a second oligosaccharide unit added but γ_m chains are singly glycosylated; and in Maja cells a substantial proportion of both γ_m and γ_s chains have a second oligosaccharide unit added to the polypeptide chain.

When non-glycosylated, the γ chains of the three cell lines have different electrophoretic mobilities but in each line the apparent molecular weights of the γ_m and γ_s forms differ by ~12,000. This is in contrast to the difference in apparent

Table 1 C-terminal amino acid sequences of human immunoglobulin heavy chains

Protein*	H chain class	Residue no.	Sequence
Ou (16)	μ	609	G K P T L Y N V S L V M S D T A G T C Y
Bur (17)	α	477	G K P T H V N V S V V M A G V D G T C Y
Zuc (18)	γ	477	G (K)
ND (19)	ε	609	G K

The C-terminal amino acid sequences of human μ, α, γ and ε chains from the glycine residue located at the end of the last constant region domain to the end of the polypeptide are shown. The myeloma proteins given are representative of the equivalent sequences found in other myelomas. The C-terminal lysine of the γ-chain is shown in parentheses as it is not always found in the polypeptide although it is ubiquitous in the gene sequence[15].

* References given in parentheses.

---

* Present addresses Department of Microbiology, University of Texas Southwestern Medical School, Dallas, Texas 75235, USA (W.C), Department of Pathology, University of Melbourne, Parkville, Victoria 3052, Australia (C A M).

† To whom correspondence should be addressed at Glaxo Group Research Limited, Greenford Road, Greenford, Middlesex UB6 0HE, UK

0028–0836/82/260077—03$01.00

molecular weight between μ_m and μ_s (~3,000) and α_m and α_s (~2,000). Comparison of the C-terminal amino acid sequences of α_s, γ_s and μ_s chains reveals a conserved Gly-Lys sequence at the end of the terminal domain followed, in the case of α and μ chains, by highly homologous hydrophilic tail sequences (Table 1). Neither ε nor γ_s chains possess this tail sequence (Table 1). In the murine μ gene, the Gly-Lys sequence encodes a consensus splice site used in the generation of μ_m mRNA[3]. It is therefore proposed that this splice site is conserved in α and μ genes. The similarity between the hydrophilic tail sequences of α and μ genes would be consistent with a common evolutionary origin for the membrane exons for these two classes and this would explain the similar size difference between the membrane and secreted forms of the chains. In this model, the hydrophilic tailpiece of γ_s is a single lysine residue. We propose that the hydrophobic, immunoglobulin domain-sized tailpiece on γ_m chains had a separate evolutionary origin from the *M* exons of α and μ chains.

To test the hypothesis that the γ_m and γ_s polypeptides are translated from different mRNA molecules, the specific mRNAs coding for γ chains in cell lines EB4 and Bec-11 were identified. Total poly(A)-containing RNA was prepared from each cell line, resolved electrophoretically in denaturing conditions, transferred to diazobenzyloxymethyl paper and hybridized to a genomic γ2 DNA probe. This probe detects 3.3 and 1.4 kilobase (kb) γ mRNA in EB4 RNA (Fig. 2). The higher molecular weight mRNA is of lower intensity than the lower molecular weight RNA. This difference is consistent with our interpretation that the 3.3 kb mRNA encodes γ_m and the 1.4 kb species γ_s. In the highly stringent conditions used to obtain the data shown in Fig. 2, the γ2 probe only detects the 1.4 kb component in Bec-11 mRNA. In less stringent conditions, the γ2 probe gives a more intense hybridization signal in the 1.4 kb position and shows some hybridization to the 3.3 kb component (data not shown). The difference between the results obtained with EB4 and Bec-11 is consistent with the much lower ratio of γ_m to γ_s polypeptides in Bec-11 cells than in EB4 cells (Fig. 1) and might be related to a subclass difference between EB4 and Bec-11 γ chains.

To account for the molecular weight difference between γ_s and γ_m polypeptide chains the γ_m message would need to be only 0.3 kb larger than the γ_s mRNA. The observed size difference of 1.9 kb is in close agreement with the reported difference of 2 kb between murine γ^2a_s and γ^2a_m mRNAs[14]. The most likely explanation for the unexpected size difference between γ_m and γ_s mRNAs is the presence of an extended 3'-untranslated region in the γ_m message (we have found no evidence for any other coding region in the 3.3 kb mRNA as we can detect no γ chains larger than γ_m). For comparison, μ_m and μ_s mRNA molecules are 2.7 and 2.4 kb respectively. The predicted coding difference would account for 63 base pairs (bp) and gene sequencing shows that the 3'-untranslated region of μ_m is 142 bp longer than that of μ_s mRNA[3]. The close agreement between the human and murine γ chain data are consistent with an early evolutionary divergence or separate origin for the *M* exons of γ and μ chains.

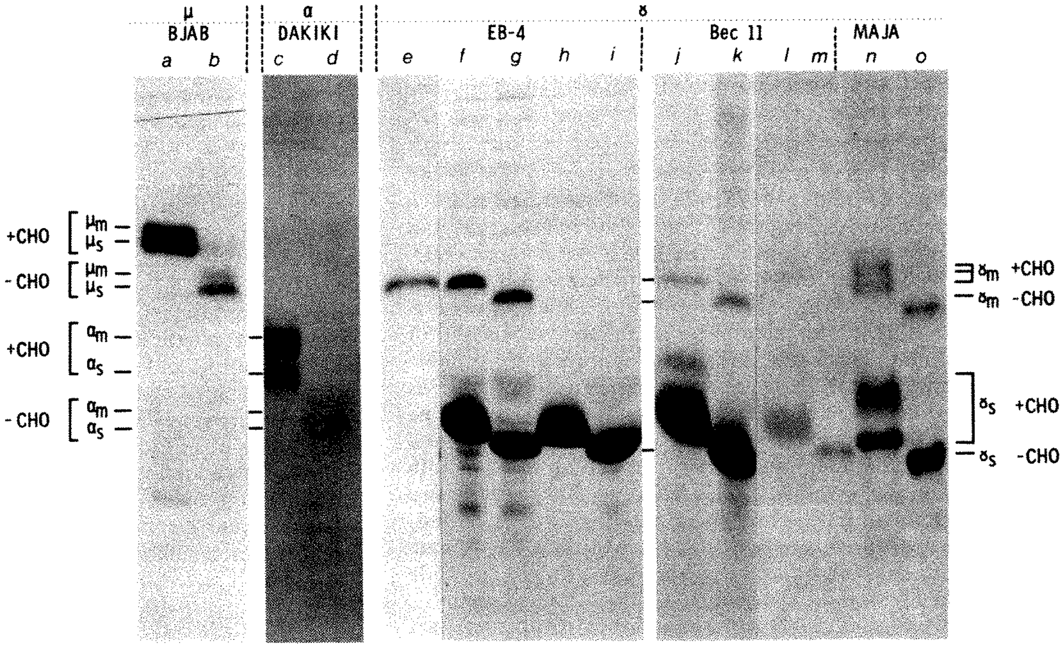

Fig. 1 Biosynthetic characterization of membrane and secretory forms of α, γ and μ polypeptide chains. The following human B-lymphoid cell lines were used: Bjab (IgM κ), Dakiki Arosros I (IgA λ), EB4 (IgG κ), Bec-11 (IgG κ), and Maja (IgG κ). An aliquot (2.5×10^6 cells) from log-phase cultures of each cell line was incubated in the presence or absence of tunicamycin (2 μg ml^{-1}) for 3 h at 37 °C in RPM1-1640 medium plus 10% (v/v) fetal calf serum (FCS). After preincubation, the cells were washed once in serum-free RPM1-1640 lacking methionine and then resuspended in 0.2 ml of the same medium containing 200 μCi ^{35}S-methionine and incubated at 38 °C for 90 min to effect metabolic labelling of cellular proteins. For pulse-chase experiments (lanes *h*, *i*), 50% of the culture was pelleted, resuspended in 0.5 ml of RPM1-1640 medium containing 10% (v/v) FCS and incubated at 37 °C for 4–6 h: the cells were pelleted and the supernate used for analysis of secreted proteins. Membrane proteins were radiolabelled by lactoperoxidase-catalysed iodoination. 10^7 cells were incubated for 3–4 min at 30°C in 70 μl of PBS-1 (50 mM sodium phosphate buffer *p*H 7.2; 150 mM NaCl) containing 10 μg lactoperoxidase and 1.25 mM H_2O_2: the reaction was terminated by addition of ice-cold 5 mM KI in PBS-I (1 ml). The cells were washed extensively before preparation of cell lysates. Cell lysates were prepared as follows[20]. Radiolabelled cells were washed once in ice-cold TKM buffer (0.1 M Tris-HCl *p*H 8.2, 0.1 M KCl and 5 mM $MgCl_2$) and resuspended in 235 μl of ice-cold 1% (w/v) Triton X-100 in TKM; the suspensions were placed on ice for 20–30 min to complete lysis. Nuclei were removed by centrifugation (5,000 *g* for 30 min) and deoxycholate and SDS were added to the supernatant to final concentrations of 1% (w/v) and 0.5% (w/v) respectively to yield lysates in 3D-TKM (1%(w/v) Triton X-100, 1% (w/v) deoxycholate and 0.5% (w/v) SDS in TKM buffer). Radiolabelled immunoglobulin was isolated by specific immunoprecipitation using 1 μl of rabbit antiserum to the appropriate light chain followed by addition of serological equivalence of goat anti-rabbit immunoglobulin antiserum. After overnight incubation at 4 °C, the immunoprecipitates were collected by centrifugation and washed by pelleting through a two-step discontinuous sucrose gradient in 3D-TKM. Aliquots of washed immunoprecipitates were dissolved in 25 μl of SDS polyacrylamide gel electrophoresis loading buffer [0.065 M Tris-HCl *p*H 6.8, 0.1% (w/v) SDS, 0.1 M dithiothreitol, 10% (w/v) glycerol and 0.001% (w/v) Bromophenol blue] and heated at 100 °C for 2 min. Reduced samples were electrophoresed on 10% (w/v) acrylamide slab gels using the discontinuous buffering system of Laemlli[21] [IgM samples derived from Bjab cells were analysed on a 12.5% (w/v) acrylamide slab gel]. Radioactive components were visualized by fluorography[22]. Lanes *a*, *b*, glycosylated and non-glycosylated μ chains respectively; *c*, *d*, equivalent samples derived from the α-chain-producing line Dakiki Arosros I. Radioiodinated membrane γ-chain of EB4 cells is shown in lane *e* and is compared with glycosylated and non-glycosylated γ-chains for EB-4 lysates (*f*, *g*) and supernatants (*h*, *i*); *j*, *k*, respectively glycosylated and non-glycosylated γ chains from Bec-11 cell lysates; *l*, *m*, similar results for Bec-11 cells (obtained in an independent experiment) compared with glycosylated (*n*) and non-glycosylated (*o*) γ chains of the cell line Maja to illustrate the ubiquity of the large size difference between γ_m and γ_s polypeptides.

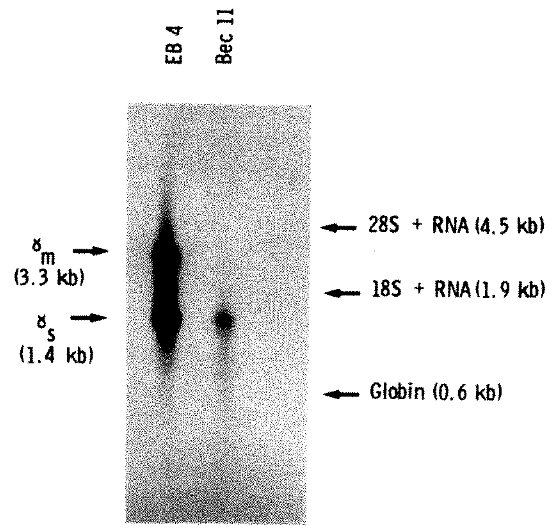

Fig. 2 Polyribosomes were prepared from 5×10^9 EB4 cells as previously described[20]. Poly(A)-containing RNA was extracted from polyribosomes by oligo(dT)-cellulose chromatography. Five μg of EB4 poly(A)-containing RNA was electrophoresed on a 1% (w/v) agarose gel containing 7.5 mM methyl mercury hydroxide. After electrophoresis, the separated RNA species were transferred to diazobenzyloxymethyl paper[23]. A DNA plasmid containing $\gamma2$ coding sequences of human genomic DNA was nick-translated to a specific activity of 1×10^8 d.p.m. μg^{-1} with [α-^{32}P]dATP and used as a probe for γ mRNA species contained in the EB4 poly(A)-containing RNA. Hybridization was done at 42 °C for 5 h in 50% formamide, $5\times$SSC, 0.1% bovine serum albumin, 0.1% polyvinylpyrrolidone, 0.1% Ficoll (molecular weight 400,000) 20 mM sodium phosphate *p*H 6.5, 10% sodium dextran sulphate 500 and 100 $\mu g\ ml^{-1}$ denatured sonicated salmon sperm DNA. Unhybridized label was removed by extensive washing in $0.3\times$SSC/0.1% SDS and hybridization visualized by autoradiography using an intensifier screen at −70 °C.

In cloned murine genomic DNA, two homologous regions, 270 and 250 bp long, are conserved at a position 1–2 kb 3′ to each of the γ subclass genes[15]. These regions are known to hybridize to the γ_m mRNA[14,15]. They are quite sufficient to encode the additional domain-size segment of γ_m chains but would not account for the size of the γ_m mRNA. The implication that the additional γ_m mRNA sequences are not conserved between γ subclasses further supports the argument that these additional sequences are non-coding.

We thank Irene Gall for assistance, George Klein for the Dakiki cell line, Mike Owen for the Maja cell line and Terry Rabbitts for the human $\gamma2$ DNA probe.

Received 10 February; accepted 16 April 1982.

1. Abney, E. R. *et al. J. Immun.* **120,** 2041–2049 (1978).
2. Alt, F. W. *et al. Cell* **20,** 293–301 (1980).
3. Rogers, J. *et al. Cell* **20,** 303–312 (1980).
4. Singer, P. A., Singer, H. H. & Williamson, A. R. *Nature* **285,** 294–300 (1980).
5. Early, P. W. *et al. Cell* **20,** 313–319 (1980).
6. Johnson, N., Douglas, R. & Hood, L. in *B Lymphocytes in the Immune Response* (eds Klinman, N., Mosier, D. E., Scher, I. & Vitetta, E. S.) 3 (Elsevier, New York, 1981).
7. Maki, R. *et al. Cell* **24,** 353–365 (1981).
8. Tucker, P. W., Liu, C.-P., Mushinski, J. F. & Blattner, F. R. *Science* **209,** 1353–1360 (1980).
9. Moore, K. W. *et al. Proc. natn. Acad. Sci. U.S.A.* **78,** 1800–1804 (1981).
10. Singer, P. A. & Williamson, A. R. *Eur. J. Immun.* **10,** 180–186 (1980).
11. Oi, V. T., Bryan, V. M., Herzenberg, L. A. & Herzenberg, L. A. *J. exp. Med.* **151,** 1260–1274 (1980).
12. Lifter, J., Higgins, G. & Choi, Y. S. *Molec. Immun.* **17,** 483–490 (1980).
13. Cushley, W. & Williamson, A. R. *Eur. J. Immun.* (submitted).
14. Tyler, B. M., Cowman, A. F., Adams, J. M. & Harris, A. W. *Nature* **293,** 406–408 (1981).
15. Honjo, T. *et al. Immun. Rev.* **59,** 33–67 (1981).
16. Putnam, F. W., Florent, G., Paul, C., Shinoda, T. & Shimizu, A. *Science* **182,** 287–291 (1973).
17. Low, T. L. K., Liu, Y. S. V. & Putnam, F. W. *Science* **191,** 390–392 (1976).
18. Wolfenstein-Todel, C., Frangione, B., Prelli, F. & Franklin, E. C. *Biochem. biophys. Res. Commun.* **71,** 907–914 (1976).
19. Bennich, H. & Von Bahr-Lindstrom, H. *Prog. Immun.* **1,** 49–58 (1974).
20. Mosmann, T. R. & Williamson, A. R. *Cell* **20,** 283–292 (1980).
21. Laemlli, U. K. *Nature* **227,** 680–685 (1970).
22. Bonner, W. M. & Laskey, R. A. *Eur. J. Biochem.* **46,** 83–88 (1974).
23. Alwine, J. C., Kemp, D. J. & Stark, G. R. *Proc. natn. Acad. Sci. U.S.A.* **74,** 5350–5354 (1977).

Production of colony-stimulating factors by murine T cells in limiting dilution and long-term cultures

Fritz G. Staber, Lothar Hültner, Fabrizio Marcucci* & Peter H. Krammer†

Abteilung für Experimentelle Hämatologie der Gesselschaft für
Strahlen- und Umweltforschung, Landwehrstr. 61,
D-8000 München 2, FRG

* Institut für Virologie, and † Institut für Immunologie und Genetik,
Deutsches Krebsforschungszentrum, Im Neuenheimer Feld 280,
D-6900 Heidelberg, FRG

Colony-stimulating factors (CSF) are glycoproteins essential for the formation of colonies of mature haematopoietic cells by single immature progenitor cells (colony-forming cells (CFC)). The number of colonies in semi-solid agar cultures can be used to determine the CSF concentration in biological fluids[1]. Various murine cells[2–6] are able to produce CSF *in vitro*. Supernatants of spleen cell cultures consisting of a mixture of T cells, B cells and macrophages are found to contain neutrophil-granulocyte–macrophage CSF (GM-CSF), CSF for megakaryocytes (Meg-CSF), eosinophilic granulocytes (Eo-CSF) and erythroid cells (E-CSF)[5]. The producer cells of these different CSF types, however, have not been defined[7]. We therefore determined here whether normal T cells produce CSF *in vitro* and whether GM-CSF, Meg-CSF, Eo-CSF and E-CSF are produced by different T-cell subsets or the progeny of single T-cell clones. Our results indicate that T cells at a high frequency (one out of three) produce CSF at variable amounts even in the absence of accessory cells following mitogen stimulation.

After stimulation of C57BL/6 (B6) spleen cells in bulk cultures with 5 $\mu g\ ml^{-1}$ concanavalin A (Con A) for 48 h, light density blasts were separated by centrifugation over Ficoll (1.077 $g\ cm^{-3}$). These cells (>95% Thy-1.2 positive) were subsequently grown in microcultures in limiting dilution conditions in the presence of allogeneic (AKR/J) irradiated (3300 r; ^{60}Co) peritoneal exudate filler cells (PEC) (10^4 per well) and 10% T-cell growth factor (TCGF) containing conditioned medium from 24 h Con A-stimulated rat (Sprague–Dawley) spleen cells (rat spleen cell conditioned medium (RSCM)). The T cells have a doubling time of ~15 h and clones derived from single or a few precursor cells grow to a clone size large enough to be tested in functional assays[8–12]. Following a growth period of 10 days during which the cells were fed twice with fresh RSCM, the cells were washed twice to remove CSF contained in RSCM and resuspended in fresh culture medium containing 10 $\mu g\ ml^{-1}$ Con A. After overnight incubation supernatants of all culture wells were assayed individually for CSF at a final concentration of 15% in 1 ml semi-solid agar cultures containing 7.5×10^4 CBA bone marrow cells. Seven days later the bone marrow cultures were scored for colony growth and the cellular composition of the colonies determined[13].

Table 1 % CSF-negative cultures of T cells plated in the presence of different numbers of filler cells

No. of PEC per well	T cells plated 1 per well	10 per well	20 per well
5×10^2	100	100	63
10^3	100	88	75
10^4	100	19	13
10^5	81	75	69

Limiting dilution analysis of B6 splenic T cells was performed as described in Fig. 1 legend.

0028-0836/82/260079—04$01.00

Table 2 Con A-induced CSF production by TCGF-dependent cells

Long-term cultured cells	Growth dependent on		Production of CSF				
			Total no. of colonies (±s.e.)	Colonies (%)			
	Antigen	TCGF		GM	Meg	Eo	E
PC-AKR-clone 29	−	+	78±9	97	3	0	0
AKR-anti-B6 line PK 7.1.1b	+	+	126±15	86	2	6	6
AKR-anti-B6 line PK 7.1.2	+	+	113±11	90	4	1	5

The establishment of PC AKR clone 29 in long-term culture from antigen (picryl chloride)-stimulated AKR/J T cells has been described previously[18,19], as has the establishment of the alloreactive AKR anti-B6 T-cell lines PK 7.1.1b and PK 7.1.2[9,20,21]. Antigen used was irradiated allogeneic B6 stimulator cells. The number of colonies (controls) with a standard CSF: 127±24, NaCl: 0±0.

A representative experiment (Fig. 1) shows that, analysed according to the Poisson distribution (least square fit as well as the method of Porter and Berry[14]), the growth frequency of Con A-activated T cells initially plated in limiting dilution was approximately one out of two to three cells ($f = 1/2.2$ (least square method), $f = 1/2.5$ ref. 14, 95% confidence limit $f = 1/2.1$ to $f = 1/2.9$ (ref. 14)). The frequency of CSF producer cells was close to $f = 1/6$ (Fig. 1). Lower frequencies found in other experiments (Table 1) were essentially due to lower plating efficiencies. The plot of our data (Fig. 1) gave a straight linear regression line ($\chi^2 \sim 1$ for fit[14]) with an intercept at the ordinate at or close to 1.0. This suggests single-hit kinetics, indicating that the only limiting component for CSF production was the number of T cells initially seeded in microculture. This is supported by our observation that no CSF production occurred in cultures devoid of proliferating T cells (data not shown). Moreover, CSF production was not constitutive but absolutely dependent on Con A stimulation (data not shown).

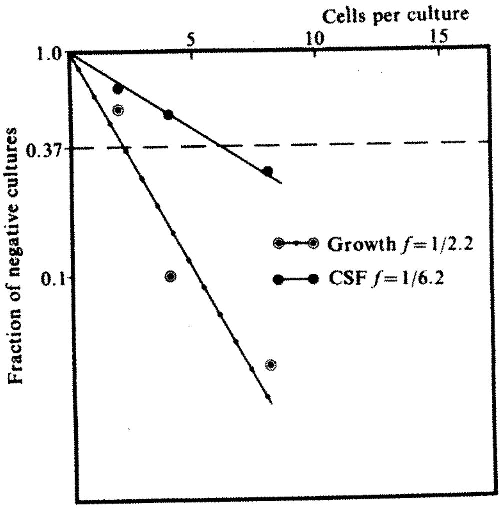

Fig. 1 Frequency of growing and CSF-producing Con A-activated splenic B6 T cells in limiting dilution. Two days after polyclonal activation by Con A and separation of the light density T-cell blasts over Ficoll, 2, 4 and 8 B6 cells were plated in microcultures (96 wells per group) and expanded on irradiated (3300 r) AKR/J PEC (10^4 per well) for 10 days in the presence of medium containing 10% RSCM from 24 h Con A-stimulated rat (Sprague–Dawley) spleen cells. After a growth period of 10 days the cells were washed twice to remove CSF contained in RSCM and resuspended in fresh culture medium containing 10 μg ml^{-1} Con A. After overnight incubation supernatants of all culture wells were assayed individually for CSF at a final concentration of 15% in 1 ml semi-solid agar cultures containing 75.000 CBA bone marrow cells. After 7 days the bone marrow cultures were scored for colony growth[13]. Cell growth in limiting dilution microwells was determined by microscopic inspection. Data were plotted according to Poisson's distribution and linear regression lines fitted to the least squares method. Frequencies were read from the number of responding cells corresponding to 37% negative cultures[8–12].

Note that the above procedure might favour selection of certain T-cell subpopulations. Con A activation (20–50% growth of Con A-activated murine spleen cells in bulk culture (data not shown)), Ficoll purification, growth in limiting dilution microcultures (growth frequency as high as $f = 1/2$) and induction of lymphokine release by Con A may have a selective effect. Nevertheless, we believe that this experimental system probably provides the most random evaluation available of the repertoire of functional T cells in non-immune mice[12].

Figure 2*a* shows the results of an analysis of CSF activity of supernatants from microcultures derived from the progeny of single or a few T-cell precursors. The quantity of CSF in such supernatants varied remarkably, and occasionally very high activities from low numbers of T cells could be observed. All active supernatants contained GM-CSF. Moreover, many supernatants with intermediate to high GM-CSF levels contained other types of CSF, for example, Meg-CSF, Eo-CSF and E-CSF. As the incidence of CFC for megakaryocytes, eosinophils and erythroid cells in the bone marrow is low, the semi-solid agar culture system only detects high concentrations of Meg-CSF, Eo-CSF and E-CSF. Therefore, some supernatants with only low GM-CSF levels may not be entirely negative for the other CSF types.

Table 3 Specificity of induction of proliferation and CSF release

Stimulator cells	*H-2* regions *K*	*A*	*J*	*E*	*C*	*S*	*G*	*D*	^{3}H-thymidine incorporation (±s.e.)	No. of colonies (±s.e.)
AKR	*k*	*k*	*k*	*k*	*k*	*k*	*k*	*k*	597±389	0
B6	*b*	*b*	*b*	*b*	*b*	*b*	*b*	*b*	25,089±3,545	18±5
B10.D2	*d*	*d*	*d*	*d*	*d*	*d*	*d*	*d*	734±474	0
B10.A(4R)	*k*	*k*	*b*	*b*	*b*	*b*	*b*	*b*	1,968±299	0
B10.A(5R)	*b*	*b*	*k*	*k*	*d*	*d*	*d*	*d*	31,263±2,596	17±2

10^4 Responder cells of the AKR anti-B6 T-cell line PK7.1.2 were used per well (triplicates, round-bottom microtitre plates, Greiner, Nürtingen, 96K). Irradiated (3300r) stimulator cells at a concentration of 10^5 per well were used after lysis of red blood cells. ^{3}H-thymidine incorporation (2.5 μCi per well) was determined after a 6-h pulse on day 5 of culture. CSF was induced by overnight stimulation with stimulator cells on days 4–5 of culture. The number of colonies (controls) with a standard CSF: 78±7, and NaCl: 0±0. Underlining indicates the presence of the *b* allele in the subregions of the *H-2* complex.

Figure 2 also shows that Meg-CSF and/or Eo-CSF and E-CSF were only found in supernatants which also contain GM-CSF. Possibly the colony-forming potential of CFC for megakaryocytes, eosinophils and erythroid cells is only expressed when stimulated by specific CSF and GM-CSF. This suggests that some supernatants might exist which only contain Meg-CSF and/or Eo-CSF and E-CSF but no GM-CSF and is compatible with data by Metcalf *et al.*[15]. Such supernatants would not be detectable in our standard assay. To investigate this we determined the CSF activity of one aliquot of a large number of supernatants from limiting dilution microcultures separately from another aliquot mixed with a standard CSF preparation from mouse lung conditioned medium (MLCM). This mixing experiment, however, gave no indication of the

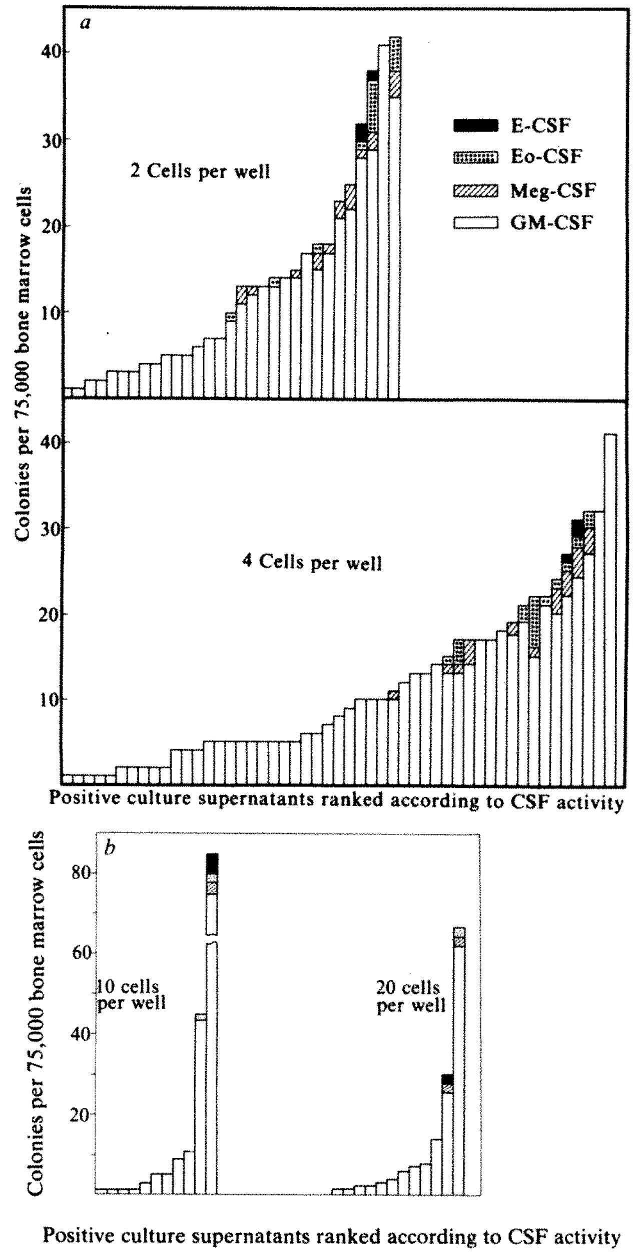

Fig. 2 *a*, Analysis of CSF types in CSF-positive culture supernatants. B6 splenic T cells were established in limiting dilution microcultures as described in Fig. 1 at an initial plating of two (upper) or four (lower) cells per well. The CSF-positive culture supernatants were ranked according to their activity. Number of colonies (controls) with a CSF standard: 84±5, and NaCl: 0±0. *b*, Analysis of CSF types in supernatants of T cells grown in limiting dilution microcultures in the presence of SRBC as filler cells. B6 splenic T cells were grown as described in Fig. 1 legend except that instead of irradiated allogeneic peritoneal exudate filler cells 10^6 SRBC from a selected batch particularly suitable for growth promotion were used as filler cells. Number of colonies (controls) with a CSF standard: 110±15, and NaCl: 0±0.

existence of supernatants containing only Meg-CSF and/or Eo-CSF and E-CSF, and the existence of potentiators or inhibitors of standard CSF in these supernatants could not be demonstrated (data not shown).

The above experiments suggest that different CSF types are produced by T cells. As T cells were plated in limiting dilution microcultures in the presence of allogeneic irradiated PEC it had to be excluded, however, that these PEC were involved in CSF production. Table 1 shows that no linear correlation could be found between the number of CSF-positive wells and the number of irradiated PEC used in the microculture system. In fact, at the highest number of PEC (10^5 per well) a decrease rather than an increase of CSF-positive culture supernatants occurred. In addition, when selected batches of sheep red blood cells (SRBC) instead of PEC were used as filler cells CSF production was still detectable. Although the growth frequency of T cells in these cultures was comparatively lower than with PEC as filler cells some supernatants contained very high levels of GM-CSF as well as the other CSF types (Fig. 2*b*).

CSF has recently been obtained from T-cell hybridomas[16]. That normal T cells produce CSF is supported by our experiments with TCGF-dependent cell lines in long-term cultures. Such lines and clones, however, might be aberrant with respect to karyotype, gene expression and regulation of their gene products but this may primarily be the case for T-cell clones growing in medium supplemented with TCGF[17]. Therefore, we have complemented our analysis of such clones with T-cell lines and clones growing in long-term culture in the presence of TCGF and antigen. Cells of this type were found to have a normal karyotype (M. Nabholz, personal communication). In addition, our T-cell lines in long-term culture have not shown TCGF-independent growth or tumorogenicity which may indicate a transformed phenotype. As these cells probably represent a highly selected population, results should be compared with those from analysis of T cells in limiting dilution. The following data are therefore in line with our limiting dilution analysis.

Three representatives of T-cell lines in long-term culture are shown in Table 2. PC-AKR clone 29, previously described to produce high amounts of immune interferon on Con A stimulation[18,19], has been passaged in permanent culture for over 18 months in the complete absence of antigen and adherent cells and in the presence of TCGF. The alloreactive AKR anti-B6 T-cell lines PK 7.1.1b and PK 7.1.2 grow in the presence of both TCGF and irradiated B6 stimulator cells[9,20,21]. PC-AKR clone 29 produced GM-CSF and Meg-CSF whereas both alloreactive T-cell lines and clones derived from them (data not shown) produced all four types of CSF after stimulation with Con A (Table 2). These results differed from previous reports where CSF production by continuous T-cell lines was found to be constitutive[22] or dependent on the presence of syngeneic accessory cells[23].

We further studied whether antigen-specific recognition is involved in triggering CSF release using the alloreactive AKR anti-B6 T-cell line PK 7.1.2. This line shows antigen-specific proliferation against stimulator cells from mice which carry the *b* allele in the *K* and *I–A* region of the *H–2* complex (Table 3). It can be seen from Table 3 that stimulator cells with the same *H–2* determinants as those that induce proliferation also induce CSF release.

In conclusion, our data indicate that a large proportion of T cells produce CSF on mitogen induction. CSF release is also triggered from T cells during specific antigen recognition. Accessory cells do not seem to be absolutely necessary for CSF production although they might have a potentiating physiological role. Furthermore, the supernatant of a single T-cell clone can contain different types of CSF. However, the production of Meg-CSF, Eo-CSF and E-CSF occurs only concomitantly with GM-CSF. This may indicate that the CSF genes belong to a gene family derived from a common precursor. Indeed, the different CSF types seem to have a striking biochemical similarity[24]. It is not yet clear whether in physiological conditions of induction of CSF release and of antigen-specific recognition all CSF types are always produced simultaneously or whether separate inductive signals trigger the release of different CSF types to assure a fine tuning of the formation of haematopoietic cells.

We thank Dr P. Dörmer for support, Drs U. Kees and P. Kisielow for critically reading the manuscript and A. Michnay, H. Broszeit and L. Wadeson for technical help.

Received 23 December 1981; accepted 17 May 1982.

1. Metcalf, D. in *Tissue Growth Factors*, (ed. Baserga, R.) (Springer, New York, 1980).
2. Stanley, E. R. & Heard, P. M. *J. biol. Chem.* **252**, 4305–4312 (1977).
3. Staber, F. G. *et al. Cell Immun.* **37**, 174–187 (1978).
4. Quesenberry, P. J., Gimbrone, M. A. & McDonald, M. J. *Expl Hemat.* **6**, Suppl. 3, 4 (1978).

5. Metcalf, D. & Johnson, G. R. *J. cell. Physiol.* **96,** 31–42 (1978).
6. Parker, J. W. & Metcalf, D. *Immunology* **26,** 1039–1049 (1974).
7. Metcalfe, D. in *Biology of the Lymphokines* (eds Cohen, S., Pick, E. & Oppenheim, J. J.) 515–525 (Academic, New York, 1973).
8. Krammer, P. H., Marcucci, F., Waller, M. & Kirchner, H. *Eur. J. Immun.* **12,** 200–204 (1982).
9. Krammer, P. H. *et al.* in *Isolation, Characterization, and Utilization of T Lymphocyte Clones* (eds Fathman, G. & Fitch, F.) 253–262 (Academic, New York, 1982).
10. Krammer, P. H. & Michnay, A. in *Mechanisms of Lymphocyte Activation,* 357–360 (Elsevier, Amsterdam, 1981).
11. Krammer, P. H. in *The Immune System,* 304–310 (Karger, Basel, 1981).
12. Eichmann, K., Falk, I., Melchers, I. & Simon, M. M. *J. exp. Med.* **152,** 477–492 (1980).
13. Staber, F. G. & Johnson, R. *J. cell. Physiol.* **105,** 143–152 (1980).
14. Porter, E. H. & Berry, R. J. *Br. J. Cancer* **17,** 583–595 (1963).
15. Metcalf, D., Johnson, G. R. & Burgess, A. W. *Blood* **55,** 138–147 (1980).
16. Schrader, J. W., Arnold, B. & Clark-Lewis, I. *Nature* **283,** 197–199 (1980).
17. Nabholz, M. *et al. Transplantn Rev.* **51,** 125–156 (1980).
18. Marcucci, F., Waller, M., Kirchner, H. & Krammer, P. H. *Nature* **291,** 79–81 (1981).
19. Waller, M., Marcucci, F., Kirchner, H., Michnay, A. & Krammer, P. H. *Immun. Lett.* **3,** 263–266 (1981).
20. Isakson, P., Puré, E., Vitetta, E. S. & Krammer, P. H. *J. exp. Med.* **155,** 734–749 (1982).
21. Krammer, P. H. *et al. UCLA Symp. molec. cell. Biol.* **24** (in the press).
22. Nabel, G., Greenberger, J. S., Sakekeeny, M. A. & Cantor, H. *Proc. natn. Acad. Sci. U.S.A.* **78,** 1157–1161 (1981).
23. Schreier, M. H. & Iscove, N. N., *Nature* **287,** 228–300 (1980).
24. Burgess, A. W., Metcalf, D., Russell, S. H. M. & Nicola, N. A. *Biochem. J.* **185,** 301–314 (1980).

Japanese wild mouse, *Mus musculus molossinus*, has duplicated immunoglobulin γ2a genes

Akira Shimizu, Yasushi Hamaguchi, Yoshio Yaoita, Kazuo Moriwaki*, Kyoji Kondo† & Tasuku Honjo

Department of Genetics, Osaka University, School of Medicine,
Osaka 530, Japan
* National Institute of Genetics, Mishima, Japan
† Faculty of Agriculture, Nagoya University, Nagoya, Japan

The immunoglobulin heavy chain loci of the mouse contain eight tightly linked genes that encode the constant region (C) of the immunoglobulin heavy chains (H). As no recombination occurred within the immunoglobulin C_H gene loci among more than 3,000 crosses of mice[1–3], the mouse C_H genes were believed to be inherited as a set, designated the *Igh* haplotype. Recent molecular cloning experiments[4–9] have demonstrated that the organization of the mouse *Igh* loci of BALB/c (*Igh*^{a} haplotype) is 5′-$C\mu$-(4.5 kilobases [kb])-C_δ-(55 kb)-$C_{\gamma3}$-(34 kb)-$C_{\gamma1}$-(21 kb)-$C_{\gamma2b}$-(15 kb)-$C_{\gamma2a}$-(14 kb)-C_ϵ-(12 kb)-C_α-3′. The structural analyses of four C_γ subclass genes have shown that they are essentially identical in terms of lengths and locations of each of the structural and intervening sequences[6,10–12]. Comparison of the nucleotide sequences of the $C_{\gamma1}$, $C_{\gamma2b}$ and $C_{\gamma2a}$ genes has shown that limited portions of the C_γ gene are conserved between compared pairs of the C_γ genes[12]. The results imply that the nucleotide sequences of the C_γ gene segments have been exchanged by recombination among related clustered genes. Similar studies on the $C_{\gamma2a}$ genes of different haplotypes, *Igh*^{a} and *Igh*^{b}, have also suggested that these two types of $C_{\gamma2a}$ gene have undergone recombinational exchange of a part of the gene sequence[13]. These results imply, in contrast to the previous belief, that frequent recombinational events have taken place within the *Igh* loci and that their nucleotide sequences have been rearranged during evolution. Here we present direct evidence that a Japanese wild mouse, *Mus musculus molossinus*, contains duplicated $C_{\gamma2a}$ genes while the copy numbers of the neighbouring C_H genes, that is, the $C_{\gamma1}$, $C_{\gamma2b}$ and C_ϵ genes, remain constant. The results indicate that the duplicated $C_{\gamma2a}$ genes of *M. m. molossinus* arose from unequal crossing-over between homologous chromosomes.

During our evolutionary study of immunoglobulin C_H genes (Y.Y. and T.H., in preparation) we found that DNAs of the Japanese wild mouse *M. m. molossinus* had several extra restriction DNA fragments which hybridized with a $C_{\gamma2b}$–$C_{\gamma2a}$ probe, whereas DNAs of many laboratory strain mice had a single fragment for each C_γ gene (ref. 6 and Y.Y. and H.T., in

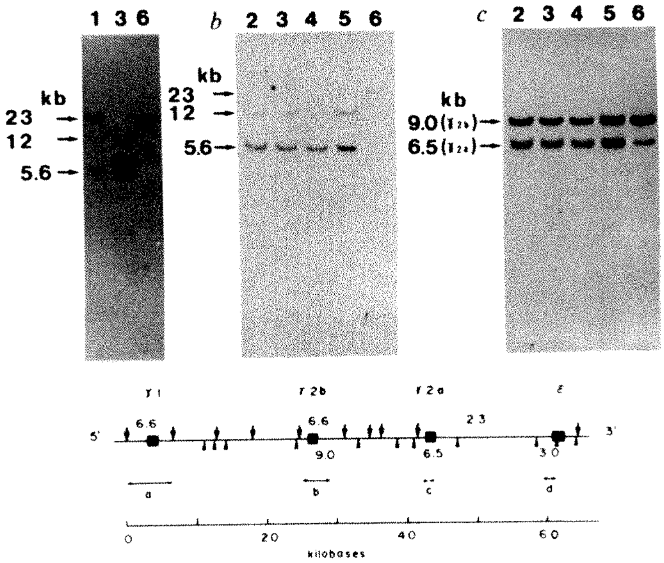

Fig. 1 Southern blot hybridization of *M. m. molossinus* liver DNA with $C_{\gamma2a}$ or $C_{\gamma2b}$–$C_{\gamma2a}$ gene probe. High molecular weight DNA was extracted from each individual liver of a wild heterozygous *M. m. molossinus* or inbred *M. m. molossinus* mice, or from livers of BALB/c mice as described previously[20]. We used three individual mice of inbred *M. m. molossinus* which are derived from wild mice trapped at Teine, Hokkaido Island. These mice are designated as Mol. Ten (individual numbers 101, 102 and 103). The other individual mouse of inbred *M. m. molossinus*, designated as MOL. A, is the progeny of wild mice trapped at Anjo, Aichi, Honshu Island. DNAs (1.5 μg each) were digested with *Eco*RI (*a*, *b*) or *Hin*dIII (*c*), electrophoresed in a 0.5% agarose gel and transferred to nitrocellulose filters as previously described[20,21]. Probes used are $C_{\gamma2a}$ (probe c) for *a* and *b* and $C_{\gamma2b}$–$C_{\gamma2a}$ (probe b) for *c*. Probes were labelled by nick-translation and hybridized as described elsewhere[20,22]. Origins of DNAs used are as follows: lane 1, a wild *M. m. molossinus*; lane 2, Mol. Ten 103; lane 3, Mol. Ten 102; lane 4, Mol. Ten 101; lane 5, MOL. A; lane 6, BALB/c. A restriction endonuclease cleavage map around the $C_{\gamma2a}$ gene of the BALB/c mouse and fragments used for probes are shown at the bottom. Data for the restriction map are taken from ref. 4. Structural genes are shown in closed boxes. Numbers above and below the top line indicate the sizes (kilobases) of *Eco*RI and *Hin*dIII fragments, respectively, which are described in the present study. Horizontal arrows under the top line indicate the fragments used as probes: a, 6.6-kb *Eco*RI fragment of γ1 gene[10]; b, 4-kb *Xba*I–*Hha*I fragment of $C_{\gamma2b}$ gene[11] which hybridizes to not only the $C_{\gamma2b}$ gene but also the $C_{\gamma2a}$ gene[4,20]; c, 217-base pair *Hae*III fragment of $C_{\gamma2a}$ gene which contains the 5′ 12 base pairs of the hinge region exon and the 3′ half of the intervening sequence between the C_H1 domain and the hinge region exons[12]; d, 2-kb *Bam*HI-*Hin*dIII fragment of C_ϵ gene[5]. ↓ and ▲ indicate *Eco*RI and *Hin*dIII sites, respectively.

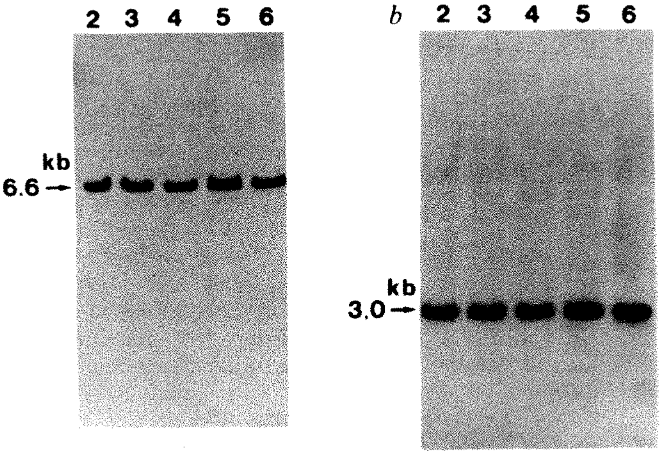

Fig. 2 Southern blot hybridization of *M. m. molossinus* liver DNA with $C_{\gamma1}$ or C_ϵ probe. DNAs (1.5 μg each) were digested with *Eco*RI (*a*) or *Hin*dIII (*b*) and electrophoresed, blotted and hybridized as described in Fig. 1 legend except that probes used are $C_{\gamma1}$ (probe a in Fig. 1) for *a* and C_ϵ (probe d in Fig. 1) for *b*. Origins of DNAs used in lanes indicated were the same as described in Fig. 1 legend.

0028-0836/82/260082—03$01.00

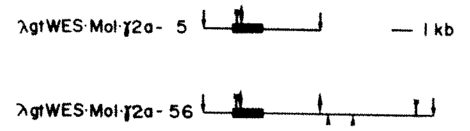

Fig. 3 Restriction map of two cloned $C_{\gamma 2a}$ genes of *M. m. molosssinus*. High molecular weight DNA of Mol. Ten 103 was digested with *Eco*RI to completion and the digests were fractionated by electrophoresis in a 0.5% agarose gel. Fragments of 5.6 and 12 kb were collected and ligated to λgtWES arms as described previously[9]. Ligated DNAs were packaged *in vitro* and screened with BALB/c $C_{\gamma 2b}$–$C_{\gamma 2a}$ probe (probe b in Fig. 1) as described elsewhere[4]. Two and three identical clones were isolated from 5.6- and 12-kb fragments, respectively. Inserts of λgtWES·Mol·γ2a-5 (5.6 kb) and λgtWES·Mol·γ2a–56 (12 kb) are shown by horizontal bars. Closed boxes indicate structure genes. Restriction enzyme cleavage sites are indicated as follows: ↓, *Eco*RI; ▲, *Hin*dIII; ◆, *Xho*I; ↑, *Bgl*I.

preparation). DNA of *M. m. molossinus* had four *Eco*RI fragments (12, 9.3, 5.6 and 1.85 kb) hybridizing with a $C_{\gamma 2b}$–$C_{\gamma 2a}$ probe in addition to the 23-kb $C_{\gamma 2a}$ and 6.6-kb $C_{\gamma 2b}$ fragments which are shared by BALB/c, C57BL and other inbred strain mice[6]. We used the $C_{\gamma 2b}$ gene fragment (probe b in Fig. 1) as a probe for both $C_{\gamma 2a}$ and $C_{\gamma 2b}$ genes. The $C_{\gamma 2a}$ gene fragments were usually less intense than the $C_{\gamma 2b}$ gene fragment because the $C_{\gamma 2a}$ gene sequence was detected by cross-hybridization to a part of the probe. As the 12- and 5.6-kb fragments were less intense than the 9.3- and 1.85-kb fragments, we presumed that the former fragments are the $C_{\gamma 2a}$ gene.

To determine unequivocally which of the above *Eco*RI fragments are the $C_{\gamma 2a}$ gene, we used as a probe the restriction DNA fragment that contains the 3′ half of the intervening sequence between the coding sequences for the C_H1 domain and the hinge region of the γ2a chain (probe c in Fig. 1). This probe has little cross-hybridization with the $C_{\gamma 2b}$ gene[12]. As shown in Fig. 1*a*, DNA of an individual *M. m. molossinus* mouse (which was trapped at Mishima, in Honshu Island) has three *Eco*RI fragments (23, 12 and 5.6 kb) that hybridize with the $C_{\gamma 2a}$ probe. The results seem to indicate that the $C_{\gamma 2a}$ gene is duplicated in this wild mouse, although the presence of heterozygous $C_{\gamma 2a}$ gene cannot be excluded.

We next examined DNAs of four individual mice of *M. m. molossinus* which have been maintained in laboratories by full-sibmating for 11 generations in the Mol. Ten strain and for 23 generations in the MOL. A strain. The Mol. Ten strain was derived from wild mice caught at Teine in Hokkaido Island and the MOL. A strain from those caught at Anjo in Honshu Island. *Eco*RI digestion of DNAs of these *M. m. molossinus* strains gave two DNA fragments (12 and 5.6 kb) which were identical for the two strains, whereas DNA of BALB/c mice had a single *Eco*RI fragment of 23 kb (Fig. 1*b*). The results strongly support the idea that *M. m. molossinus* has the duplicated $C_{\gamma 2a}$ genes, one of which is located in the 12-kb *Eco*RI fragment and the other in the 5.6-kb fragment. One can still argue the possibility, however, that *M. m. molossinus* has introduced point mutations which have created new *Eco*RI sites, thus converting the 23-kb fragment into the 12- and 5.6-kb fragments.

To exclude this possibility, we used another restriction enzyme, *Hin*dIII. *Hin*dIII digestion of *M. m. molossinus* produced the 9.0-kb $C_{\gamma 2b}$ fragment and the 6.5-kb $C_{\gamma 2a}$ fragment, both of which are identical in size to those of BALB/c DNA (Fig. 1*c*). However, 6.5-kb bands of the $C_{\gamma 2a}$ gene of *M. m. molossinus* DNAs are about twice as dark as that of the BALB/c DNA. In contrast, the intensity of the $C_{\gamma 2b}$ gene bands (9.0 kb) remains the same among DNAs of *M. m. molossinus* and BALB/c mice.

To examine whether neighbouring C_H genes are duplicated, we analysed the $C_{\gamma 1}$ and C_ϵ genes. As Fig. 2 clearly shows, the intensity and size of the $C_{\gamma 1}$ and C_ϵ genes in these wild mice are indistinguishable from those of BALB/c mice. We have also found that the $C_{\gamma 3}$ gene is not duplicated (data not shown). Previously we showed that the number of the C_μ and C_α gene fragments of *M. m. molossinus* are identical to those of many laboratory inbred strain mice although the sizes of the fragments vary slightly[6].

We have further cloned two DNA fragments, each containing a complete $C_{\gamma 2a}$ gene, from DNA of an individual *M. m. molossinus*. One $C_{\gamma 2a}$ gene is located in the 12-kb *Eco*RI fragment and other in the 5.6 kb *Eco*RI fragment (Fig. 3). The restriction sites in the cloned DNA fragments are consistent with those determined by Southern blot analyses.

These results demonstrate that *M. m. molossinus* has a new haplotype which contains the duplicated $C_{\gamma 2a}$ genes. In spite of the fact that these four mice are derived from two independent populations in different islands of Japan, the mice seem to have a similar haplotype, indicating that this haplotype is widely distributed among various local colonies of *M. m. molossinus*.

Lieberman and Potter[14] analysed allotype markers of serum immunoglobulins of homozygous *M. m. molossinus* (Kyushu) and found that this wild mouse had $IgG2a^a$ markers in addition to the $IgG1^b$, $IgG2b^b$, $IgG2a^b$ and IgA^b markers. They proposed that this haplotype is created by unequal crossing-over between the Igh^a and Igh^b haplotypes. Using monoclonal antibodies which can distinguish *a* and *b* allotypes, Herzenberg and his associates (personal communication) also found that two individual mice of inbred *M. m. molossinus* (Mol. Ten strain) have two allotypes of IgG2a, namely $IgG2a^a$ and $IgG2a^b$. Because the restriction sites around the coding regions of the $C_{\gamma 2b}$ and $C_{\gamma 2a}$ genes are well conserved between C57BL (Igh^b) and BALB/c (Igh^a)[6,9], we are unable to correlate the $C_{\gamma 2a}$ gene fragments with serological markers. The restriction map of the cloned $C_{\gamma 2b}$ gene of *M. m. molossinus* is different from those of BALB/c and C57BL (A.S. *et al.*, in preparation). As Fig. 4 shows, it is therefore likely that the duplicated $C_{\gamma 2a}$ genes of *M. m. molossinus* arose from unequal crossing-over between two different haplotypes which must be characterized and identified by nucleotide sequence determination.

Since immunoglobulin allotypes are distributed among various subspecies of *M. musculus*, the allotype seems to have evolved before the divergence of the subspecies of *M. musculus*.

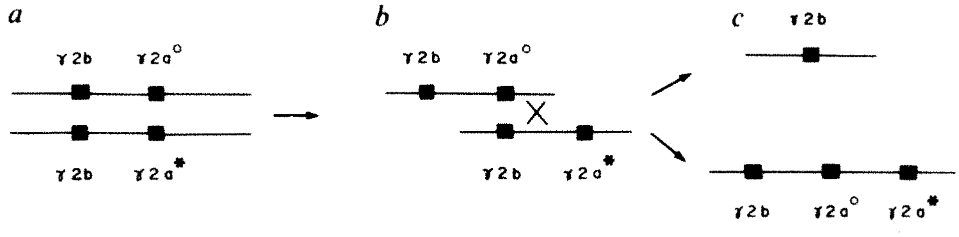

Fig. 4 A possible recombination that created duplicated $C_{\gamma 2a}$ genes with different allotypes. *a*, schematic representation of heterozygous mouse chromosomes containing two different $C_{\gamma 2a}$ genes. $\gamma_{2a}{}^*$ and $\gamma_{2a}{}^\circ$ indicate $C_{\gamma 2a}$ genes with different allotypes. *b*, Unequal pairing between homologues at meiosis and unequal crossing-over. As $C_{\gamma 2b}$ and $C_{\gamma 2a}$ genes have extensive homology[8,12], such a misalignment may occur at meiosis. *c*, Resultant chromosomes. In one chromosome (upper) the $C_{\gamma 2a}$ gene has been deleted, while the other chromosome contains the duplicated $C_{\gamma 2a}$ genes which have different allotypes. The latter chromosome may be an ancestor of the present chromosome in *M. m. molossinus*.

The duplication of the $C_{\gamma 2a}$ gene must have taken place after the divergence of *M. m. molossinus* and *M. m. domesticus*, an estimated one million years ago[15-17]. Duplication of immunoglobulin genes has also been suggested in humans by serological studies[18,19].

*Eco*RI digestion of DNA of the first heterozygous *M. m. molossinus* mouse produced three $C_{\gamma 2a}$ gene fragments (23, 12 and 5.6 kb) and three $C_{\gamma 2b}$ gene fragments (9.3, 6.6 and 1.85 kb). It is now clear that the 12- and 5.6-kb $C_{\gamma 2a}$ gene fragments are located on one chromosome and the 23-kb $C_{\gamma 2a}$ gene fragment on the other. We also know that the 6.6-kb $C_{\gamma 2b}$ gene fragment is derived from the chromosome containing the duplicated $C_{\gamma 2a}$ gene. Consequently, the other chromosome should contain two $C_{\gamma 2b}$ gene fragments (9.3 and 1.85 kb) and one $C_{\gamma 2a}$ gene (23 kb). It is not clear whether these two *Eco*RI fragments of the $C_{\gamma 2b}$ gene are due to the gene duplication or to the introduction of new *Eco*RI sites by point mutation.

The number of C_H genes has been thought to be invariant among inbred strains, although definitive proof is lacking. Previous studies (ref. 6 and Y.Y. and H.T., in preparation) using Southern blot analyses indicate the presence of a single gene for each of the C_μ . $C_{\gamma 1}$, $C_{\gamma 2b}$, $C_{\gamma 2a}$, C_ϵ and C_α genes in many inbred strains including BALB/c, C57BL, AKR, AJ, NZB and SJL. It may be safe to conclude that inbred strains mentioned above have similar sets of C_H genes although they have considerable divergence in the nucleotide sequence.

We thank Dr L. A. Herzenberg for providing us with unpublished data of allotype analyses and Miss F. Oguni for assistance in preparing the manuscript. This investigation was supported in part by grants from the Ministry of Education, Science and Culture of Japan, Torey Science Foundation, Mitsubishi Science Foundation and Naito Foundation.

Received 18 January; accepted 21 April 1982.

1. Herzenberg, L. A. *Cold Spring Harb. Symp. quant. Biol.* **29,** 455–462 (1964).
2. Lieberman, R. & Potter, M. *J. molec. Biol.* **18,** 516–528 (1966).
3. Potter, M. & Lieberman, R. *Adv. Immun.* **7,** 91–145 (1967).
4. Shimizu, A. *et al. Nature* **289,** 149–153 (1981).
5. Nishida, Y. *et al. Proc. natn. Acad. Sci. U.S.A.* **78,** 1581–1585 (1981).
6. Honjo, T. *et al. Immun. Rev.* **59,** 33–67 (1981).
7. Liu, C.-P., Tucker, P. W., Mushinski, G. F. & Blattner, F. R. *Science* **209,** 1348–1353 (1980).
8. Roeder, W.,Maki, R., Traunecker, A. & Tonegawa, S. *Proc. Natn. Acad. Sci. U.S.A.* **78,** 474–478 (1981).
9. Shimizu, A., Takahashi, N., Yaoita, Y. & Honjo, T. *Cell* **28,** 499–506 (1982).
10. Honjo, T. *et al. Cell* **18,** 559–568 (1979).
11. Yamawaki-Kataoka, Y., Kataoka, T., Takahashi, N., Obata, M. & Honjo, T. *Nature* **283,** 786–789 (1980).
12. Yamawaki-Kataoka, Y., Miyata, T. & Honjo, T. *Nucleic Acids Res.* **9,** 1365–1381 (1981).
13. Schreier, P. H., Bothwell, A. L. M., Mueller-Hill, B. & Baltimore, D. *Proc. natn. Acad. Sci. U.S.A.* **78,** 4495–4499 (1981).
14. Lieberman, R. & Potter, M. *J. exp. Med.* **130,** 519–541 (1969).
15. Yonekawa, H. *et al. Jap. J. Genet.* **55,** 289–296 (1980).
16. Moriwaki, K., Shiroishi, T., Minezawa, M., Aotsuka, T. & Kondo, K. *J. Immunogenet.* **6,** 99–113 (1979).
17. Minezawa, M., Moriwaki, K. & Kondo, K. *Jap. J. Genet.* **56,** 27–39 (1981).
18. Loghem, E. van. *et al. J. Immunogenet.* **7,** 285–299 (1980).
19. Matumoto, H. *et al. Jap. J. hum. Genet.* (in the press).
20. Yaoita, Y. & Honjo, T. *Nature* **286,** 850–853 (1980).
21. Southern, E. M. *J. molec. Biol.* **98,** 503–517 (1975).
22. Maniatis, T., Jeffrey, A. & Kleid, P. G. *Proc. natn. Acad. Sci. U.S.A.* **72,** 1184–1188 (1975).

Monoclonal antibodies show that neurofibrillary tangles and neurofilaments share antigenic determinants

Brian H. Anderton*, Deryck Breinburg*, Malcolm J. Downes*, Philip J. Green†, B. E. Tomlinson‡, J. Ulrich§, John N. Wood*‖ & Jacob Kahn†

* Department of Immunology, St George's Hospital Medical School, Cranmer Terrace, London SW17 ORE, UK.
† Department of Neuropathology, Institute of Psychiatry, De Crespigny Park, Denmark Hill, London SE5 8AF, UK
‡ Department of Pathology, Newcastle General Hospital, Westgate Road, Newcastle upon Tyne NE4 6BE, UK
§ Institut für Pathologie, University of Basle, 4003 Basle, Switzerland

Neurofibrillary tangles are a prominent feature in the pyramidal cells of the hippocampus and in neurones of the cerebral cortex of people suffering from senile dementia of the Alzheimer type (SDAT)[1]. Similar neuronal changes also occur in elderly Down's syndrome patients and to a lesser degree in intellectually normal old people[2]. The tangles are composed of bundles of paired helically twisted 10–13 nm filaments (PHF)[3,4], which may be either neurofilaments[3] or microtubules[5]. Attempts to isolate tangles from postmortem material have met with some success[6] but there is disagreement over the molecular weight (M_r) of presumptive PHF proteins enriched in these fractions, with conflicting claims of 50,000 (refs 6, 7) and 20,000 (ref. 8). Initially it seemed that the 50,000-M_r putative PHF protein and tubulin cross-react[9,10] but this result may have been a serological artefact, due to tangle-associated material in preparations of microtubule proteins used as immunogen and as test antigen[11]. We have used monoclonal antibodies to show here that neurofilament antigens are present in neurofibrillary tangles.

Monoclonal antibodies were produced as previously described using as immunogen either Triton X-100-insoluble rat brain protein[12] (monoclonal antibodies RT 97, RS 18, 147, 155) or a crude soluble protein fraction (1 h 150,000g_{av} supernatant) from two pooled hippocampi (SDAT cases U212 and U224, one of which was also studied immunohistochemically; see Table 2) (monoclonal antibody BF 10). Hybridomas secreting antibody to neurofilaments were screened as before[12] and to neurofibrillary tangles by the peroxidase–antiperoxidase (PAP) or by the indirect immunoperoxidase methods on paraffin sections of tangle-rich human brain[13]. Neuropathological samples were selected from postmortem brains of three

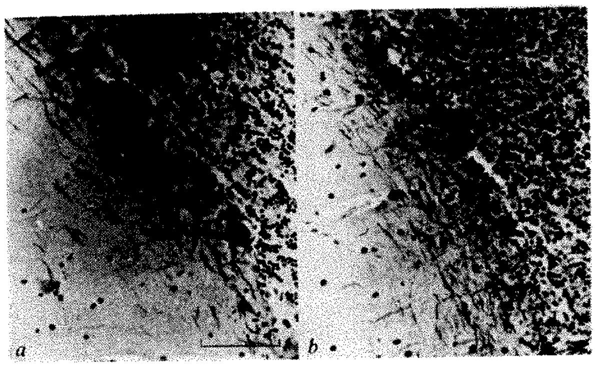

Fig. 1 Human cerebellum (paraffin sections) was stained by the PAP method[13]. *a*, Monoclonal antibody 147; *b*, monoclonal antibody BF 10 (counter-stained with Harris's haematoxylin). Baskets and neuronal fibres reacted strongly. Monoclonal antibodies were used both as tissue culture supernatants (undiluted) and as ascites fluid [diluted 1:1,000 with Tris-buffered saline, *p*H 7.6 (TBS)]. Normal horse serum (diluted 1:5 with TBS) was used instead of normal goat serum in the preincubation step to eliminate non-specific staining. After overnight incubation at ambient temperature with monoclonal antibodies, sections were washed in TBS (30 min), overlayed with rabbit anti-mouse IgG (H + L; Nordic) diluted 1:200 with TBS (30 min), washed in TBS (30 min), overlayed with goat anti-rabbit IgG (Fc fragment; Nordic) diluted 1:200 with TBS (30 min), washed in TBS (30 min), overlayed by PAP produced in rabbits (Miles) diluted 1:300 with TBS. The reaction was developed with diaminobenzidine (BDH). Scale bar, 100 μm.

‖ Present address: The Wellcome Research Laboratories, Beckenham, Kent BR3 3BS, UK

0028–0836/82/260084—03$01.00

cases of senile dementia of the Alzheimer type, one elderly Down's sydrome subject and one intellectually normal old subject. We found that five monoclonal antibodies (Table 1) resembled rabbit anti-bovine neurofilament 210,000-M_r polypeptide (anti-210K) sera previously described[13,14] in their reaction on human cerebellum, as they all reacted with basket cell axons around the Purkinje cells and neuronal fibres in the inner third of the molecular layer (Fig. 1). Monoclonal antibodies BF 10 and 147 and the rabbit anti-210K antiserum were found to react with some neuronal fibres in the cortex and subcortical white matter (Fig. 2*a*). BF 10 and RT 97 were the only antibodies to react with tangles, and did so in all cases studied (Tables 1, 2); the extent of reaction with tangles resembled that of similar slides after silver or Congo red staining. Initial studies of antibody RT 97 in tissue culture supernatants suggested that the antibody was not tangle reactive, but subsequent studies using ascites fluid showed that, like BF 10, it also stains tangles down to a dilution of ascites fluid of at least 1:2,000. Ascites fluid antibodies RS 18, 147 and 155 do not react with tangles even at 1:200 dilutions whereas all stain neurofilaments at 1:2,000 dilution. The ascites fluid was used at dilutions of at least 1:2,000, as, if more concentrated, background staining of sections becomes appreciable.

PHF can be associated with neuronal perikarya in the form of neurofibrillary tangles or with certain neurites in plaques. As well as staining tangles, BF 10 and RT 97 reacted strongly with numerous distended terminals or neurites which constitute the major part of the senile plaque (Fig. 2*c–e*). In case T/B, BF 10-positive material was found associated with plaques and only an occasional perikaryon (Fig. 2*f*); RT 97 was not studied in sufficient detail to know whether it reacted identically with BF 10 in this case. Only a minority of the neurites in plaques reacted with antibodies other than BF 10 and RT 97 (Fig. 2*b*; Table 1) and none of the antibodies stained amyloid. These results are consistent with our earlier observations of the lack of tangle-reactivity of rabbit anti-bovine neurofilament sera[13]. Absorption of BF 10 with purified bovine neurofilaments (polypeptide pattern shown in Fig. 3*a*) removed all staining with this antibody.

The monoclonal antibodies were analysed by immunoblotting[15] on purified bovine neurofilaments and on total protein from SDAT and control human hippocampi (Fig. 3). BF 10 and 155 react predominantly with the 155,000-M_r neurofilament protein of bovine neurofilaments and the corresponding polypeptide in human brain. RT 97, 147 and RS 18 bind most strongly to the 210,000-M_r bovine neurofilament protein and the equivalent human polypeptide. Several of the monoclonal antibodies seem to cross-react[14,16,17] with the 210,000- and 155,000-M_r neurofilament proteins. BF 10 reacts with both the 155,000- and 210,000-M_r polypeptides of bovine neurofilaments (Fig. 3*b*) but is specific for the 155,000-M_r polypeptide of human neurofilaments (Fig. 3*g*, *n*). RT 97 also seems to react with both polypeptides in bovine neurofilaments (Fig. 3*d*) but in human material may be specific for the 210,000-M_r protein (Fig. 3*i*, *p*). RS 18 (Fig. 3*e*, *j*, *q*) reacts similarly to RT 97 but 147 seems specific to the 210,000-M_r polypeptide of both bovine and human neurofilaments (Fig. 3*c*, *h*, *o*). Monoclonal antibody 155 is specific for the 155,000-M_r polypeptide in both species but reacts strongly with several lower molecular weight (50,000–60,000) bands (Fig. 3*f*, *k*, *r*). Antibody BF 10 also reacts strongly with two to four bands just below the 155,000-M_r polypeptide. We have tentatively attributed these extra bands to proteolytic degradation of the major neurofilament proteins; if this is the case, the corresponding antigenic determinants are probably well separated in the 155,000-M_r polypeptide. Other bands, which can be visualized on longer exposure of autoradiographs with all the antibodies (data not

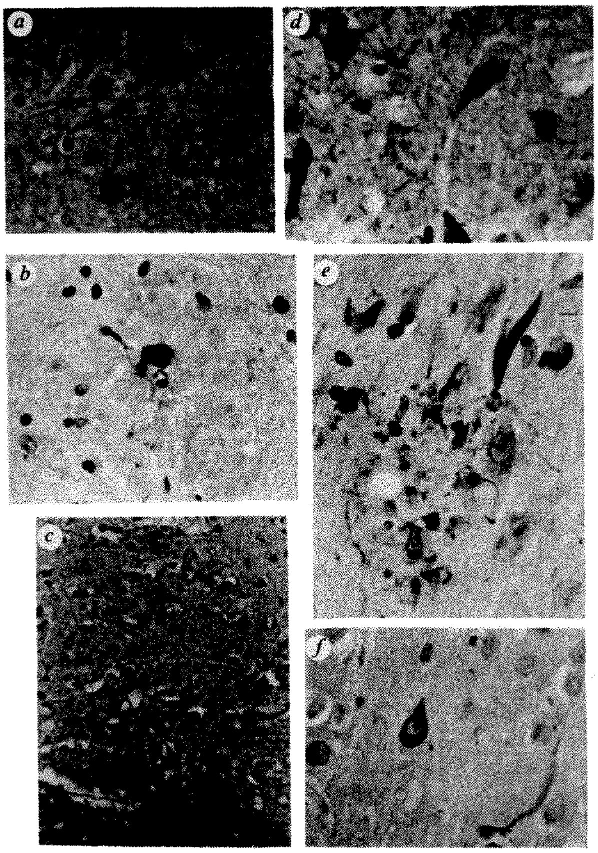

Fig. 2 Reaction of plaques and tangles with monoclonal antibodies 147 and BF 10. *a*, T/A fibres in cortex reacting with 147 (scale bar, 50 μm; applies to *a*, *b*, *d–f*); *b*, U/144 neurites in a plaque reacting with 147; *c*, T/A tangles in pyramidal cells in cortex reacting with BF 10 (scale bar, 100 μm); *d*, U/303 tangles in pyramidal cells of hippocampus reacting with BF 10; *e*, U/144 tangles and neurites in a plaque reacting with BF 10; *f*, T/B tangles in a pyramidal cell perikaryon reacting with BF 10.

Table 1 Immunohistochemical reaction pattern and antigenic specificities of antibodies

Clone	Immunoglobulin subclass	Reaction with neurofibrillary tangles	Reaction with human senile plaques	Reaction with human neurofilaments*	Neurofilament polypeptide with major antigenic determinant (M_r)
BF 10	IgG2a	+	N	+	155,000
RT 97	IgG1	+	N	+	210,000
RS 18	IgG1	–	n	+	210,000
147	IgG1	–	n	+	210,000
155	IgG1	–	n	+	155,000
BF 10-absorbed	–	–	–	–	ND
Rabbit anti-210K neurofilament sera	–	–	n	+	210,000, 155,000

N, most neurites; n, occasional neurites. ND, not determined.
*Determined by characteristic staining pattern on cerebellum.

Table 2 Comparison of immunohistochemical reaction pattern of two monoclonal antibodies on five different postmortem specimens

Case		Area examined	BF 10	Reaction pattern 147, rabbit anti-210K antiserum
U/224	(SDAT)	DG, H	T, N	n
U/303	(SDAT)	DG, H	T, N	n
T/A	(SDAT)	NC, SWM	T, N, A	n, A
U/144	(Down's syndrome)	DG, H	T, N	n
T/B	(old age)	NC, SWM	T, N, A	n, A

DG, dentate gyrus; H, hippocampus; NC, neocortex; SWM, subcortical white matter. T, neuronal perikaryal tangles; A, axons; N, most neurites in senile plaques; n, occasional neurites in senile plaques.

shown), are being investigated. Immunoblotting did not reveal any outstanding differences between normal and SDAT neurofilament antigens with any of the antibodies used, including BF 10 and RT 97. Differences such as the relative sharpness and intensities of individual bands are probably the result of postmortem degradation and variability in the efficiency of blotting and would only be significant if confirmed in analyses of many different postmortem specimens. The neurofilament proteins detected by the antibodies on the immunoblots are minor constituents of the total human hippocampal proteins present as neurofilament bands in the stained tracks (Fig. 3*l*, *m*) are not obviously visible; this attests to the sensitivity and specificity of the antibodies for immunochemical analysis of neurofilament antigens (neurofilaments are only a minor component of the total protein composition of grey matter even of fresh rat brain although white matter is relatively rich in neurofilaments).

Neurofibrillary tangles must share at least two antigenic determinants with neurofilaments as the immunoblots analysis has shown RT 97 and BF 10 to be clearly directed at different sites of the neurofilament structure and possibly different neurofilament polypeptides (Table 1). Some tangles contain a mixture of apparently normal neurofilaments and PHF[18,19] and are occasionally composed of bundles of straight filaments (B.E.T., unpublished) but the strength of the reaction with the BF 10 and RT 97 monoclonal antibodies with most of the tangles suggests that the reactive component is not simply due to inclusions of neurofilaments. Ultrastructural studies with this antibody are required to confirm this. As other monoclonal antibodies and rabbit antisera which react with normal human neurofilaments fail to stain tangles, any neurofilaments present in the PHF (or straight filaments) must be structurally different. The differential reactivity of RT 97 in tissue culture supernatants with tangles and normal neuronal fibres suggests that the corresponding antigenic determinant may be partially affected in tangles resulting in a failure of RT 97 to bind when the antibody concentration is low. The pattern of reactivity with the panel of antibodies is consistent for all tangles of a given case and for all five cases studied (three SDAT, one Down's syndrome, one normal old age), which implies that any change in neurofilament integrity is a precisely defined event and not a random breakdown of structure. Immunoblotting so far has failed to reveal any gross differences in molecular weight of neurofilament antigens from control and SDAT tissues and suggests that an altered antigenicity may be the result of either an intrinsic conformational change in the filament protein or a different packing and/or masking of antigenic determinants. BF 10 and RT 97 monoclonal antibodies should be useful new reagents for probing the chemical composition of neurofibrillary tangles.

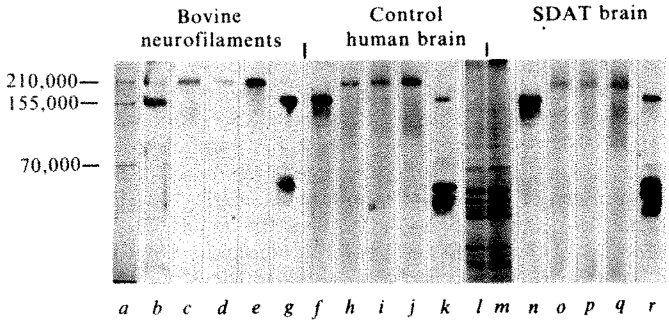

Fig. 3 Immunoblots showing the antigenic specificities of all five monoclonal antibodies on isolated bovine neurofilaments (*a–f*); total hippocampal proteins of control human brain (*g–l*); total hippocamal proteins of SDAT brain (*m–r*). *a*, *l*, *m* Are stained with Coomassie brilliant blue and are tracks cut from SDS slab gels[22]. The remainder of the tracks, with identical sample loadings, were blotted and processed essentially as according to Towbin *et al.*[15] on to nitrocellulose sheets which were then cut into strips and each strip incubated with a different antibody followed by ^{125}I-labelled rabbit anti-mouse immunoglobulins. The autoradiographs are aligned exactly with the stained gel strips to show the position of the labelled antigens present in the total sample proteins. BF 10 (*b*, *f*, *n*); 147 (*c*, *h*, *o*); RT 97 (*d*, *i*, *p*); RS 18 (*e*, *j*, *q*); 155 (*g*, *k*, *r*). Ascites fluid for the incubations with the nitrocellulose blots was diluted as follows: BF 10—$1:10^2$ (*b*), $1:5\times10^4$ (*f*, *n*); 147—$1:4\times10^3$ (*c*), $1:10^4$ (*h*, *o*); RT 97—$1:1.5\times10^3$ (d), $1:2\times10^4$ (i, p); RS 18—$1:2\times10^3$ (*e*), $1:5\times10^3$ (*j*, *q*); 155—$1:2\times10^3$ (*g*), $1:5\times10^3$ (*k*, *r*). The molecular weight of the individual bovine neurofilament triplet polypeptides are indicated at the left-hand side.

This work was supported by the Wellcome Trust and the MRC. We thank Dr L. H. Carrasco, Professor J. A. N. Corsellis, Dr B. Doshi, Dr I. Janota and Professor P. L. Lantos for advice and assistance in collecting specimens, and Dr R. Calvert for preparations of isolated bovine neurofilaments.

Note added in proof: Selkoe *et al.*[20] have claimed that PHF are insoluble in SDS which would therefore make it difficult to analyse these proteins by SDS-gel electrophoresis and immunoblotting. This same group[21] have also recently published evidence that the 20,000-M_r protein previously found to be enriched in the PHF fraction[8] is, in fact, myelin basic protein.

Received 5 October 1981; accepted 23 April 1982.

1. Wisniewski, H., Terry, R. D. & Hirano, A. *J. Neuropath. exp. Neurol.* **29,** 163–176 (1970).
2. Tomlinson, B. E. in *Dementia* 2nd edn (ed. Wells, C. E.) 113–153 (Davis, Philadelphia, 1977).
3. Kidd, M. *Nature* **197,** 192–193 (1963).
4. Wisniewski, H. M., Narang, H. K. & Terry, R. D. *J. neurol. Sci.* **27,** 173–181 (1976).
5. Terry, R. D. & Wisniewski, H. M. in *Alzheimer's Disease and Related Conditions* (eds Wolstenholme, G. E. W. & O'Connor, M.) 145–168 (Churchill, London, 1970).
6. Iqbal, K. *et al. Brain Res.* **77,** 337–343 (1974).
7. Iqbal, K., Wisniewski, H. M., Grundke-Iqbal, I., Korthals, J. K. & Terry, R. D. *J. Histochem. Cytochem.* **23,** 563–569 (1975).
8. Selkoe, D. J. *Ann. Neurol.* **8,** 468–478 (1980).
9. Grundke-Iqbal, I., Johnson, A. B., Terry, R. D., Wisniewski, H. M. & Iqbal, K. *Ann. Neurol.* **6,** 532–537 (1979).
10. Grundke-Iqbal, I., Johnson, A. B., Wisniewski, H. M., Terry, R. D. & Iqbal, K. *Lancet* **i,** 578–580 (1979).
11. Yen, S-H., Gaskin, F. & Terry, R. D. *Am. J. Path.* **104,** 77–89 (1981).
12. Wood, J. N. & Anderton, B. H. *Biosci. Rep.* **1,** 263–268 (1981).
13. Kahn, J., Green, P. J., Thorpe, R. & Anderton, B. H. *J. clin. exp. Gerontol.* **2,** 199–210 (1980).
14. Anderton, B. H., Thorpe, R., Cohen, J., Selvendran, S. & Woodhams, P. *J. Neurocytol.* **9,** 835–844 (1980).
15. Towbin, H., Staehelin, T. & Gordon, J. *Proc. natn. Acad. Sci. U.S.A.* **76,** 4350–4354 (1979).
16. Liem, R. K. H., Yen, S-H., Solomon, G. D. & Shelanski, M. L. *J. Cell Biol.* **79,** 637–645 (1978).
17. Yen, S-H. & Fields, K. L. *J. Cell Biol.* **88,** 115–126 (1981).
18. Yagashita, S., Itoh, Y., Wang, N. & Amano, N. *Acta neuropath.* **54,** 239–246 (1981).
19. Metuzals, J., Montpetit, V. & Clapin, D. F. *Cell Tissue Res.* **214,** 455–482 (1981).
20. Selkoe, D. J., Ihara, Y. & Salazar, F. J. *Science* **215,** 1243–1245 (1982).
21. Selkoe, D. J., Brown, B. A., Salazar, F. J. & Marotta, C. A. *Ann. Neurol.* **10,** 429–436 (1981).
22. Laemmli, U. K. & Favre, M. *J. molec. Biol.* **80,** 575–599 (1970).

A model for the molecular requirements of immunoglobulin heavy chain class switching

Kenneth B. Marcu, Rhonda B. Lang, Lawrence W. Stanton & Linda J. Harris

Biochemistry Department and Molecular Biology Graduate Program, State University of New York, Stony Brook, New York 11794, USA

Heavy chain immunoglobulin gene expression requires two independent DNA recombination systems[1-3]. The first DNA rearrangement event (V–D–J recombination) involves the formation of a complete variable region (V_H) gene in pre-B lymphocytes[3-6]. The second series of recombination events allows for a switch in heavy chain constant region class from μ to either $\gamma3$, $\gamma1$, $\gamma2b$, $\gamma2a$, ε or α[1-3]. These recombination events occur in intervening sequences but do not alter or generate new coding information which is a common feature of V–D–J unions[1-3]. Tandemly repeated DNA sequences, spanning ~2–5 kilobases (b), are localized ~1.5 kilobase pairs 5′ of each C_H gene and have been termed C_H switch (S) regions[2,7]. Two short, simple sequences that are shared by all switch region repeats (GAGCT and GGGGT) have been proposed to facilitate C_H switching by homologous DNA recombination[8]. Unlike other switch regions, a large portion of the S_μ region (3 kb) consists of essentially pure tandem repeats of GAGCT which are occasionally interrupted by a GGGGT[8]. However, the precise sites of switch-recombination in S_μ are generally located considerably 5′ of this genetically unstable stretch[9,10] of GAGCT repeats (Fig. 1). We now report the properties of a novel C_H S region sequence, YAGGTTG, which is 5′ of switch recombination sites and preferentially repeated in S regions.

The nucleotide sequences in the immediate vicinity of the switch-recombination sites used by 10 rearranged C_H genes are depicted in Fig. 2. Germ-line S_μ sequences are all referred to as 'donor sites' because all functional switch events must originate 5′ of the C_μ gene and then for simplicity all other germ-line S_H sites are termed 'acceptors'. Acceptors may also serve as donors when multiple recombination events result in a functional switch. Abortively rearranged C_H genes can either be generated by inter-switch region acceptor recombinations (that is, as with $S_{\gamma3}$ and $S_{\gamma2b}$ in MPC11)[11] or by the recombination of non-immunoglobulin-associated DNA sequences (that is, non-switch region DNA) with an S_H region[12,37,38]. The only common feature at or near all the recombination sites shown in Fig. 2 is the presence of a prevalent heptamer sequence, YAGGTTG. Several expressed C_H genes use an analogue of YAGGTTG in the identical sequence environment, suggesting that these may constitute preferred switch sites. Analogues of this prevalent heptamer are occasionally located 3′ of some of these recombination sites. However, GAGCT and GGGGT sequences are absent in 9 of these 21 DNA sequences. The poorest YAGGTTG analogues (4/7 matches) are utilized by the $S_{\gamma2b}$ acceptor in MOPC 141 and the S_μ donor of MC101 (a $\gamma1$ producer). However, the four matched nucleotides are contiguous in both cases. Therefore, we assume that the minimum criterion for a YAGGTTG sequence analogue is a 4/7 match with four contiguous matched nucleotides. As most of these putative recognition sequences are not perfect matches to a YAGGTTG heptamer, we analysed other properties of YAGGTTG-like sequences which might support the idea of their specific involvement in the C_H switching mechanism.

The majority of switch events appear to occur 8–16 nucleotides 3′ of this common sequence (Fig. 3). However, four of the rearrangement events shown in Fig. 2 occur within this prevalent sequence. Two of these examples are acceptor sites of abortively rearranged genes ($\gamma2b$ in MPC11, and α in MOPC 603)[11,12]. One of these events occurred within intervening sequence (IVS) I of the $C_{\gamma1}$ gene which resulted in a C_H1 domain deletion[13]. The fourth and last case ($\gamma2b$ in MOPC 141) occurred 1.0 kb beyond the 3′ boundary of the repetitive $S_{\gamma2b}$ acceptor region[3,14]. The expressed $\gamma2b$ gene in MOPC 141 is the only known example of a switch that occurs beyond the 3′ boundary of a repetitive switch region. We have failed to observe a reoccurrence of this rare event in any of 13 different $\gamma2b$-producing plasmacytomas (R.B.L. and K.B.M., in preparation). The significance of the preference for 8–16 nucleotides between a YAGGTTG analogue and the actual switch site will require further confirmation from analyses of other functionally switched C_H genes.

YAGGTTG analogues are repeated in switch regions. Twenty-eight YAGGTTG-like sequences are located in the

Table 1 YAGGTTG (Y = CorT) matches in five switch regions of heavy chain constant region genes

Switch region	Length (kb)	YAGGTTG matches $\frac{7}{7}$	$\frac{6}{7}$	$\frac{5}{7}$	$\frac{4}{7}$	Total	Prevalent matches to YAGGTTG						
S_μ	5.20	1	8	8	15	32	Y 71	A 53	G 82	G 100	T 82	T 88	G 82
$S_{\gamma3}$ 5′	0.56	0	5	3	8	16	Y 100	A 88	G 88	G 100	Y 75	T 63	G 63
$S_{\gamma3}$ 3′	0.85	3	9	21	7	40	Y 88	A 88	G 100	G 100	Y 70	T 58	G 67
$S_{\gamma1}$	0.59	1	4	5	12	22	C 90	A 100	G 100	G 100	Y 80	T 80	G 50
$S_{\gamma2b}$	1.60	0	14	5	21	40	Y 90	A 100	G 95	G 100	T 74	G 79	G 95
S_α	1.40	6	30	16	2	54	T 79	A 81	G 98	G 100	Y 88	T 94	G 81
Totals	10.2 $S_D = 5.2$ $S_A = 5.0$	11	70	58	65	204	Y 86	A 83	G 96	G 100	Y 80	T 71	G 76
C_H coding regions* (without IVS I)	6.8	0	3	40	72	115	Y 88	A 78	G 95	G 100	T 70	N	N

The minimum criteria for a match is 4/7 with all four nucleotides contiguous and all other matches (that is, 7/7, 6/7, 5/7) must also have four contiguous nucleotides. The switch region lengths only refer to sequenced DNA S_μ[3,8], $S_{\gamma3}$ 5′[11], $S_{\gamma3}$ 3′[27], $S_{\gamma1}$[11] $S_{\gamma2b}$[11] and S_α[7]. Prevalent matches to YAGGTTG were determined by only tabulating the 7/7, 6/7 and 5/7 matches. 4/7 matches only seem to be rarely used in functional C_H genes (Fig. 2) and the high probability to detect randomly such a non-specific match (a 1/51 chance) tends to randomize unnecessarily the resultant consensus sequences. The fit of a particular nucleotide is indicated as the percentage of its incidence in all 7/7, 6/7 and 5/7 matches combined. S_D refers to the entire S_μ region and S_A refers to all other S regions

* Data obtained from C_μ[28], $C_{\gamma1}$[29], $C_{\gamma2b}$[30 31], $C_{\gamma2a}$[32] and C_α[33] with IVS I contribution removed. N, any of the four nucleotides

0028–0836/82/260087—03$01 00

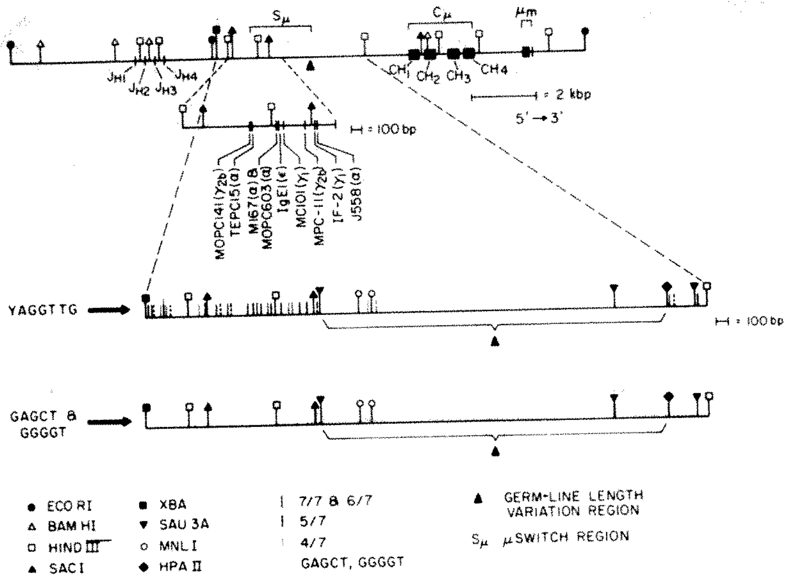

Fig. 1 The relative locations of C_H gene switch sites and two classes of hypothesized recognition sequences are indicated 5' of the mouse C_μ gene. Y represents a C or a T. The nucleotide sequence of the S_μ region were extracted from other publications[3,8]. The location of the unstable S_μ length variation region that consists of a relatively pure stretch of GAGCT and GGGGT sequences was determined from other published work[9,11] as well as our unpublished data. MOPC 141 (refs 3, 14), TEPC 15 (ref. 7), M167 (ref. 34), MOPC 603 (ref. 7), Ig E1 (ref. 8), MC101 (ref. 35), MPC 11 (ref. 36), IF-2 (ref. 14) and J558 (L.H. and K.B.M., in preparation).

immediate vicinity of all known S_μ sites used in C_H gene switches and S_H acceptor regions contain numerous repeats of YAGGTTG-like sequences (Table 1). Consensus sequences prepared for YAGGTTG analogues found in different switch regions closely resemble the YAGGTTG prototype sequence. Analogues of this recognition sequence are at least as prevalent as the common GAGCT sequences[8]. The S_α region is particularly rich in YAGGTTG-like sequences possessing 36 out of 54 examples that are either 7/7 or 6/7 matches in only 1,400 base pairs[7].

YAGGTTG sequences are not repeated in C_H coding regions. If similar amounts of C_H coding DNA (8.3 kb) and C_H switch region DNA (10.2 kb) are compared, the C_H coding regions are found to contain less than 10% of the total number of 7/7 and 6/7 YAGGTTG matches found within all switch regions (Tables 1, 2). The distribution of YAGGTTG analogues in C_H coding regions is below random expectations (Table 2). Indeed, these sequences are present in random amounts in three mouse globin genes[15,16] and in the entire J_K–C_K locus[17,18]. A lower frequency of YAGGTTG-like sequences in C_H coding regions may be selected for to avoid aberrant recombination events. More than 50% of the best YAGGTTG matches, that are found in C_H coding regions, occur in IVS I. If these are excluded from the C_H coding region analysis, the 3' end of the YAGGTTG-like heptamer appears random and gives a poor YAGGYNN composite (Table 1). These observations may be relevant to the phenomenon of rare C_H domain deletions in defective or mutant chains in mice[19] and humans[20]. Unlike the results observed for the entire C_H coding region, the presence of YAGGTTG analogues in IVS I agrees well with random expectations (Table 2).

Table 2 Observed frequencies of YAGGTTG sequences compared with their expected random frequencies

	No. YAGGTTG matches 7/7	6/7	5/7	4/7
C_H coding regions (8.3 kb)	0 (1)	6 (14)	58 (81)	105 (163)
C_H IVS I only (~1.5 kb)	0 (0)	3 (3)	18 (15)	33 (30)
C_H coding regions without IVS I (6.8 kb)	0 (0.8)	3 (12)	40 (67)	72 (133)
BALB/c α- and β-type globin genes (~5.0 kb)	3 (0.6)	18 (9)	51 (49)	87 (98)
Within 50 bp 5' of J_K and J_H (0.450 kb)	0 (0)	3 (0.8)	8 (4)	15 (9)
S_μ (without GAGCT repeat region; 2.2 kb)	1 (0)	9 (4)	17 (22)	30 (40)
All S regions (without S_μ GAGCT repeat region; 7.2 kb)	11 (1)	81 (12)	139 (70)	202 (140)

The total number of each of the four different categories for YAGGTTG matches are compared with their number derived from random expectations. The random probabilities used for 4/7, 5/7, 6/7 and 7/7 matches to YAGGTTG are 1/51, 1/102, 1/585 and 1/8192 respectively. Statistical probabilities were calculated with the assumption that the four matched nucleotides in the YAGGTTG sequence must be contiguous. Numbers in parentheses indicate the random expectation for the YAGGTTG analogue in a similar size sequence. YAGGTTG analogues were also observed to be random in the J_K–C_K and J_H loci and in the μ–δ intragenic region. C_H coding regions[28–33], BALB/c α- and β-type globin genes[15,16], J_K locus[17,18], J_K–C_K intragenic region and C_K[27], J_H locus[3], S_μ[3,8], other S regions[7,11,27].

We have compiled here considerable evidence for the involvement of a YAGGTTG-like sequence in the mechanism of C_H switch-recombination: (1) YAGGTTG-like sequences are predominant features of all functional switch sites so far identified. (2) YAGGTTG is 5' of the switch sites of both donor and acceptor sites for all C_H switches in a total of 21 examples. (3) Switch-recombination sites preferentially occur 8–16 nucleotides 3' of a YAGGTTG analogue. (4) YAGGTTG-like sequences are preferentially repeated in all S_H acceptor regions but appear unique to the S_μ donor region. (5) YAGGTTG analogues are present below random expectations in C_H domains and their IVSs except IVS Is.

As a model for C_H switch-recombination, we suggest that a YAGGTTG sequence or its close analogue acts with tandem repeats of a GAGCT sequence to mediate an efficient C_H gene switch. The S_μ donor region appears different and not only seems to require a YAGGTTG-like sequence close to the 5' side of the switch site but also to possess a very large region of GAGCT tandem repeats located considerably 3' of the actual switch site. The presence of 3 kb of GAGCT repeats in S_μ[8], the conservation of this repetitious region in mice and humans[21–23] and the existence of GAGCT and GGGGT in switch region consensus sequences[8] collectively argue that YAGGTTG analogues, as well as GAGCT repeats, are required for an efficient C_H switching process. The need for repeats of both YAGGTTG analogues as well as GAGCT and GGGGT sequences in switch acceptor regions may reflect the pairing process that allows for the proper alignment of C_H genes for an accurate switch event. After the initiation of this pairing event, a switch could perhaps occur close to any YAGGTTG analogue. However, this idea would not rule out that low-frequency switching events may not require the GAGCT epeats. This would be the case for the γ2b gene in MOPC 141 and the C_H1 domain deleted γ1 gene in IF-2 in which the switch acceptor sites have no GAGCT repeats. When considering recombination events associated with immunoglobulin genes, one must also be aware that rare V–J recombinations can occur with the participation of a conserved heptamer sequence in the absence of a nanomer sequence[18,24].

We consider this a working hypotheses which may stimulate further studies on C_H switch sites. The examination of other switch recombination events may confirm the role of the YAGGTTG-like sequences. One testable prediction of our model would be that C_H switches occurring in tissue culture variants of myeloma cell lines[25] utilize YAGGTTG analogues. A γ2b→γ2a switch in an MPC 11 switch variant has recently been shown to result from a DNA deletion event which encompasses the switch site of the γ2b-producing, parental MPC 11 cell and the entire γ2b-coding region[26]. We suggest that the endpoints of this deletion event may occur close to the 3′ side of YAGGTTG analogues. This type of secondary or variant cell switch would be an infrequent or rare event since the S_μ GAGCT repeat region is completely deleted on forming the original functional MPC 11 γ2b gene and is therefore unavailable for the secondary switch event. A direct functional test of the molecular requirements for C_H switching could use a gene transfer approach that would use B lymphocytes or switch variant myeloma cells as recipients of genetically modified, multi-C_H gene substrates whose germ-line switch regions have been deleted or specifically mutagenized.

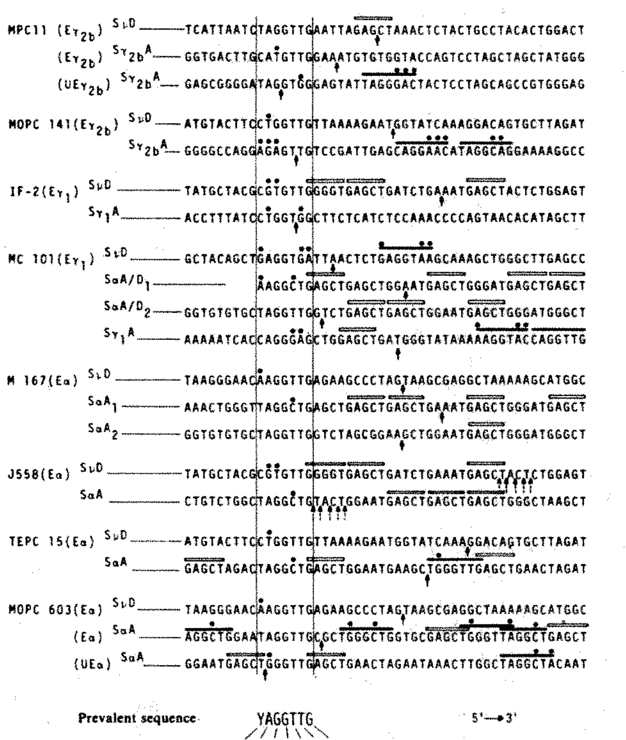
MPC11 (Eγ2b) SμD TCATTAATCTAGGTTGAATTAGAGCTAAACTCTACTGCCTACACTGGACT
(Eγ2b) Sγ2bA GGTGACTTGCATGTTGGAAATGTGTGGTACCAGTCCTAGCTAGCTATGGG
(UEγ2b) Sγ2bA GAGCGGGGATAGGTGGGAGTATTAGGGACTACTCCTAGCAGCCGTGGGAG
MOPC 141(Eγ2b) SμD ATGTACTTCCTGGTTGTTAAAAGAATGGTATCAAAGGACAGTGCTTAGAT
Sγ2bA GGGGCCAGGAGAGTTGTCCGATTGAGCAGGAACATAGGCAGGAAAAGGCC
IF-2(Eγ1) SμD TATGCTACGCGTGTTGGGGTGAGCTGATCTGAAATGAGCTACTCTGGAGT
Sγ1A ACCTTTATCCTGGTGGCTTCTCATCTCCAAACCCCAGTAACACATAGCTT
MC 101(Eγ1) SμD GCTACAGCTGAGGTGATTAACTCTGAGGTAAGCAAAGCTGGGCTTGAGCC
SαA/D1 AAGGCTGAGCTGAGCTGGAATGAGCTGGGATGAGCTGAGCT
SαA/D2 GGTGTGTGCTAGGTTGGTCTGAGCTGAGCTGGAATGAGCTGGGATGGGCT
Sγ1A AAAAATCACCAGGGAGCTGGAGCTGATGGGTATAAAAAGGTACCAGGTTG
M 167(Eα) SμD TAAGGGAACAAGGTTGAGAAGCCCTAGTAAGCGAGGCTAAAAAGCATGGC
SαA1 AAACTGGGTTAGGCTGAGCTGAGCTGAGCTGAAATGAGCTGGGATGAGCT
SαA2 GGTGTGTGCTAGGTTGGTCTAGCGGAAGCTGGAATGAGCTGGGATGGGCT
J558(Eα) SμD TATGCTACGCGTGTTGGGGTGAGCTGATCTGAAATGAGCTACTCTGGAGT
SαA CTGTCTGGCTAGGCTGTACTGGAATGAGCTGAGCTGAGCTGGGCTAAGCT
TEPC 15(Eα) SμD ATGTACTTCCTGGTTGTTAAAAGAATGGTATCAAAGGACAGTGCTTAGAT
SαA GAGCTAGACTAGGCTGAGCTGGAATGAAGCTGGGTTGAGCTGAACTAGAT
MOPC 603(Eα) SμD TAAGGGAACAAGGTTGAGAAGCCCTAGTAAGCGAGGCTAAAAAGCATGGC
(Eα) SαA AGGCTGGAATAGGTTGCGCTGGGCTGGTGCGAGCTGGGTTAGGCTGAGCT
(UEα) SαA GGAATGAGCTGGGTTGAGCTGAACTAGAATAAACTTGGCTAGGCTACAAT
Prevalent sequence YAGGTTG
16/21 14/21 17/21 21/21 16/21 17/21 20/21
5′→3′
E = Expressed $C_H$gene
UE = Unexpressed $C_H$gene
↑ = Switch-recombination sites

Fig. 2 Nucleotide sequences of the germ-line donor and acceptor environments of eight C_H gene switches and two aberrantly rearranged C_H genes. YAGGTTG sequences that are found in all switch-recombination events, and therefore hypothesized to be important recognition sites, lie between the two vertical lines. Arrows indicate the precise points of DNA breakage. Overhead solid bars indicate the locations of YAGGTTG analogues outside the hypothesized YAGGTTG recognition site. Overhead open bars indicate the locations of GAGCT and GGGGT sequences. Nucleotides in YAGGTTG analogues which do not match their counterparts in the prevalent sequence are marked with overhead dots. MPC11 $E_{\gamma 2b}$ (ref. 16), MPC11 $UE_{\gamma 2b}$ (ref. 11), MOPC 141 $E_{\gamma 2b}$ (refs 3, 14), IF-2 $E_{\gamma 1}$ (ref. 15), MC101 $E_{\gamma 1}$ (ref. 35), M167 E_α (ref. 34), J558 Eα (L.H. and K.B.M., in preparation), TEPC 15 Eα[7], MOPC 603 Eα[7] and MOPC 603 UEα[13].

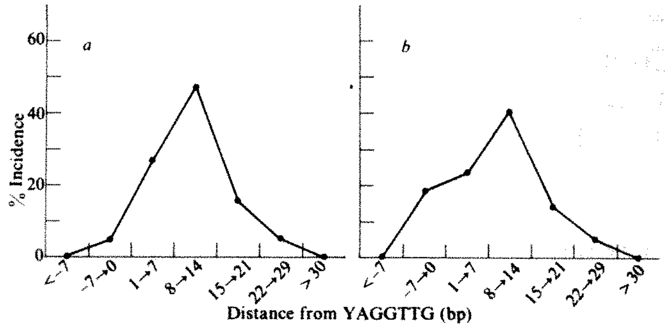

Fig. 3 C_H gene switch recombination sites are not randomly distributed around the YAGGTTG sequence. The percentage of examples of C_H switch events that occur at 7 bp intervals from the prevalent YAGGTTG recognition sequence are depicted as a function of this distance. The recognition sequence is in the −7→0 region of the graphs. *a*, Normally rearranged C_H genes. The abnormal C_H genes IF-$2_{\gamma 1}$, MPC11 $UE_{\gamma 2b}$ and MOPC 603 UEα) are not included in the analysis. *b*, All rearranged C_H genes. All 21 examples presented in Fig. 2 are used for the analysis.

We thank Robert P. Perry and Martin Weigert for helpful suggestions and critical evaluation of the manuscript, and T. Honjo and L. Hood for providing preprints of their manuscripts before publication. This work was supported by NIH grants GM26939 and AI00416 awarded to K.B.M. K.B.M. is a Research Career Development Awardee of the NIH and L.H. is a postdoctoral fellow of the Arthritis Foundation.

Received 26 January; accepted 16 April 1982.

1. Davis, M. M. *et al. Nature* **283**, 733–739 (1980).
2. Kataoka, T., Kawakami, T., Takahashi, N. & Honjo, T. *Proc. natn. Acad. Sci. U.S.A.* **77**, 919–923 (1980).
3. Sakano, H., Maki, R., Kurosawa, Y., Roeder, W. & Tonegawa, S. *Nature* **286**, 676–683 (1980).
4. Early, P., Huang, H., Davis, M., Calame, K. & Hood, L. *Cell* **19**, 981–992 (1980).
5. Matthyssens, G. & Rabbitts, T. H. *Proc. natn. Acad. Sci. U.S.A.* **77**, 6561–6565 (1980).
6. Siebenlist, U., Ravetch, J. U., Korsmeyer, S., Waldmann, T. & Leder, P. *Nature* **294**, 631–635 (1981).
7. Davis, M. M., Kim, S. K. & Hood, L. *Science* **209**, 1360–1365 (1980).
8. Nikaido, T., Nakai, S. & Honjo, T. *Nature* **292**, 845–848 (1981).
9. Marcu, K. B., Banerji, J., Penncavage, N. A., Lang, R. & Arnheim, N. *Cell* **22**, 187–196 (1980*a*).
10. Marcu, K. B. *et al. Cold Spring Harb. Symp. quant. Biol.* **45**, 899–911 (1980).
11. Kataoka, T., Miyata, T. & Honjo, T. *Cell* **23**, 357–368 (1981).
12. Hood, L. *et al. Cold Spring Harb. Symp. quant. Biol.* **45**, 887–898 (1980).
13. Dunnick, W., Rabbitts, T. H. & Milstein, C. *Nature* **286**, 669–675 (1980).
14. Takahashi, N., Kataoka, T. & Honjo, T. *Gene* **11**, 117–127 (1980).
15. Konkel, D. A., Maizel, J. V. & Leder, P. *Cell* **18**, 865–873 (1979).
16. Nishioka, Y. & Leder, P. *Cell* **18**, 875–882 (1979).
17. Sakano, H., Huppi, K., Heinrich, G. & Tonegawa, S. *Nature* **280**, 288–294 (1979).
18. Leder, P. *et al., Cold Spring Harb. Symp. quant. Biol.* **45**, 859–865 (1980).
19. Morrison, S. L. in *Cells of Immunoglobulin Synthesis* (eds Pernis, B. & Vogel, H. J.) 113–126 (Academic, New York, 1979).
20. Franklin, E. C., Frangione, B. & Buxbaum, J. in *Cells of Immunoglobulin Synthesis* (eds Pernis, B. & Vogel, H. J.) 89–95 (Academic, New York, 1979).
21. Takahashi, N., Nikai, S. & Honjo, T. *Nucleic Acids. Res.* **8**, 5983–5991 (1980).
22. Ravetch, J. V., Kirsch, I. R. & Leder, P. *Proc. natn. Acad. Sci. U.S.A.* **77**, 6734–6738 (1980).
23. Rabbitts, T. H., Forster, A. and Milstein, C. P. *Nucleic Acids Res.* **9**, 4509–4524 (1981).
24. Seidman, J. G. & Leder, P. *Nature* **286**, 779–783 (1980).
25. Kenter, A. L. Eckhardt, L. A., Tilley, S. A. Birshtein, B. K. in *Immunoglobulin Idiotypes and Their Expression*, ICN-UCLA Symp. molec. cell. Biol. (eds Janeway, C., Sercarz, E. E., Wigzell, H. & Fox, C. F.) (Academic, New York, in the press).
26. Eckhardt, L. A., Tilley, S. A., Lang, R. B., Marcu, K. B. & Birshtein, B. K. *Proc. natn. Acad. Sci. U.S.A.* **79**, 3006–3010 (1982).
27. Stanton, L. W. & Marcu, K. B. *Nucleic Acids Res.* (submitted).
28. Kawakami, T., Takahashi, N. & Honjo, T. *Nucleic Acids. Res.* **8**, 3933–3945 (1980).
29. Honjo, T. *et al. Cell* **18**, 559–568 (1979).
30. Tucker, P. W., Marcu, K. B., Newell, N., Richards, J. & Blattner, F. R. *Science* **206**, 1301–1306 (1979).
31. Yamawaki-Kataoka, Y., Kataoka, T., Takahashi, N., Obata, M. & Honjo, T. *Nature* **283**, 786–789 (1980).
32. Ollo, R., Auffray, C., Morchamps, C. & Rougeon, F. *Proc. natn. Acad. Sci. U.S.A.* **78**, 2442–2446 (1981).
33. Tucker, P. W., Slightom, J. L. & Blattner, F. R. *Proc. natn. Acad. Sci. U.S.A.* **78**, 7684–7688 (1981).
34. Kim, S., Davis, M. M., Sinn, E., Patten, P. & Hood. L. *Cell* **27**, 573–581 (1981).
35. Obata, M. *et al. Proc. natn. Acad. Sci. U.S.A.* **78**, 2437–2441 (1981).
36. Lang, R. B., Stanton, L. W. & Marcu, K. B. *Nucleic Acids Res.* **10**, 611–630 (1982).
37. Kirsch, I. R. *et al. Nature* **293**, 585–587 (1981).
38. Harris, L. J., Lang, R. B. & Marcu, K. B. *Proc. natn. Acad. Sci. U.S.A.* **79** (in the press).

Complete amino acid sequence and maturation of the mouse submaxillary gland renin precursor

Jean-Jacques Panthier*, Simon Foote†, Béatrice Chambraud*, A. Donny Strosberg‡, Pierre Corvol† & François Rougeon*

*Unité de Génétique et Biochimie du Développement, Institut Pasteur, ERA CNRS 851, 25 rue du Dr Roux, 75724 Paris Cedex 15, France
†Institut National de la Santé et de la Recherche Médicale U36, 17 rue du Fer à Moulin, 75005 Paris, France
‡Laboratoire d'Immunologie Moléculaire—Institut de Recherches en Biologie Moléculaire CNRS, Université Paris VII, 2 Place Jussieu, 75221 Paris Cedex 5, France

Renin, a protease which cleaves the prohormone angiotensinogen, releasing angiotensin I, has a major role in regulating blood pressure and electrolyte balance. However, the primary structure and the active structure of the enzyme remain unknown. The presence of an inactive form of the enzyme, activable by partial proteolysis, has led to the proposal that renin is synthesized as an inactive precursor[1]. Kidney juxtaglomerular cells constitute the principal source of renin, but its concentration in this tissue is too low to allow determination of its primary structure by conventional techniques. In some strains of mice, the male submaxillary glands synthesize and secrete very large amounts of an enzyme which appears indistinguishable from renal renin by immunological and physicochemical criteria[2,3], thereby representing a unique opportunity to delineate the detailed features of renin. We now present the analysis of bacterial DNA recombinant clones harbouring an essentially complete transcript of renin mRNA isolated from the mouse submaxillary gland. The deduced amino acid sequence shows that renin is synthesized as a 44,209 molecular weight (M_r) precursor. Comparison with other known acid proteases shows a good alignment of renin and acid protease sequences in the neighbourhood of residues involved in the active site. N-terminal sequence analysis of renin reveals that the precursor is converted by a protein cleavage into active renin consisting of two chains of M_r 35,000 and 3,000.

We have previously described the construction of cDNA clone pRn5.3 which contains ~1,100 nucleotides of a mouse renin mRNA sequence[4]. The presence of a poly(A) extension at one end of pRn5.3, as revealed by nucleotide sequence analysis, indicated that the cDNA sequence in this clone corresponds to the 3′ portion of renin mRNA. A clone, designated pRn4.7, containing a sequence 5′ upstream of pRn5.3 cDNA, has been isolated (see Fig. 1 legend), and contains ~1,250 nucleotides of renin mRNA sequence. As clones pRn5.3 and pRn4.7 share an identical segment of ~900 nucleotides in their central portion and as pRn5.3 codes for the 3′-terminal region of renin mRNA, together they harbour an essentially complete transcript of renin mRNA. The nucleotide sequence of cDNA inserts was determined using the partial chemical degradation method of Maxam and Gilbert[5] in conditions previously described[6]. The strategy for sequencing pRn5.3 and pRn4.7 plasmids is presented in Fig. 1*a*, while Fig. 1*b* shows the nucleotide sequence of cDNA in pRn5.3 and pRn4.7; the sequence is 1,424 nucleotides long.

The sequence bears one open reading frame of 1,203 nucleotides, the two other reading frames containing, respectively, 17 and 20 nonsense codons. A search for the ATG translation initiating codon in the open reading frame near the beginning of the 5′ region revealed two ATG codons located 41 and 56 nucleotides from the 5′-terminal region of pRn4.7 cDNA. If the first ATG codon is the starting codon, the amino-terminal sequence of renin precursor would contain 3 basic residues followed by 10 hydrophobic amino acids. Such a sequence is very similar to the signal sequences observed at the amino-terminal end of most precursors of secreted proteins[7], making it likely that the first ATG codon is the starting codon.

As the endoprotease responsible for the cleavage of signal segments splits the peptide bond on the carboxy-terminus side of small uncharged amino acids and as the residues located in the neighbourhood of the cleavage site exhibit a high potential for making β-turns or aperiodic conformations[8], we propose that the cleavage site for preprorenin probably lies after Cys 18. However, two other cleavage sites—after Ser 21 and Gly 25—cannot be ruled out.

The coding sequence of renin mRNA is 1,203 nucleotides long and ends with the translation stop codon UAA. The deduced amino acid sequence gives a molecular weight for the renin precursor of 44,209. The 3′-untranslated region, which is 180 nucleotides long, contains four more potential stop codons in the same reading frame. The consensus sequence proposed by Proudfoot *et al.*[9] AATAAA, occurred 12 nucleotides before the polyadenylation site.

Enzymatic studies have shown that renin shares certain catalytic features with acid proteases[10,11]. James *et al.*[12] have proposed a mechanism for the catalytic hydrolysis of peptide bonds by acid proteases involving the proton shared by Asp 32 and Asp 215 of penicillopepsin as the electrophilic component and Tyr 75 as a charge relay element. These authors have shown that, on substrate binding, Tyr 75, originally bound to Trp 39, is involved in a conformational change.

We aligned the primary amino acid sequences of some pepsin family proteins—bovine and porcine pepsinogens[13,14], bovine prochymosin[15] and pepcillopepsin from *Penicillium janthinellum*[16]—with the renin sequence so as to maximize the homology between proteins. As calculated from Fig. 2, a homology of 37–24% exists between these acid proteases and renin. In particular, the cysteine residues occur within the renin chain at almost identical positions to those in the pepsinogen chain, suggesting the same arrangement of the disulphide bridges, and similarities in tertiary structure for renin and acid protease molecules.

Figure 2 shows that the two regions of highest homology between renin and acid proteases are those surrounding the two renin aspartyl residues Asp 101 and Asp 286, corresponding to Asp 32 and Asp 215 of penicillopepsin. Furthermore, the two residues Tyr 75 and Trp 39 are conserved, occurrring, respectively, at positions 146 and 108 of the renin chain. As mechanistic features of proteases indicate that the ways in which residues of a protein attack peptide bonds are limited, this homology in the active site of renin suggests a detailed analogy in catalytic mechanism. Our results thus indicate that renin and acid proteases have arisen by a process of divergent evolution from a single ancestral prototype[17].

To establish the relationship between the renin precursor and the mature active enzyme, we have determined the N-terminal sequence of pure active renin[18]. Although renin appeared homogeneous on analytical HPLC and SDS-gel electrophoresis, a double sequence was obtained. After reduction by mercaptoethanol, the molecular weight shifted from 38,000 to 35,000 and a faint band appeared at the front of the gel. A similar observation was reported by Suzuki *et al.*[19]. The double sequence and the decrease in molecular weight following reduction suggested that renin exists as two chains linked by a disulphide bridge. Therefore, renin was reduced, carboxymethylated and the two chains separated by gel filtration and subjected to automated Edman degradation; their N-terminal sequences are shown in Fig. 3.

The N-terminal sequence of peptide A, corresponding to the main protein band, determined for 21 positions, coincides with the portion of renin starting at position 64, and the sequence of peptide B, corresponding to the minor band, determined for 21 positions, coincides with the portion of the enzyme starting at position 354. We propose the model of renin processing shown in Fig. 4. The peptide signal is first removed from the renin precursor by membrane processing enzymes, leading to

0028-0836/82/260090—03$01.00

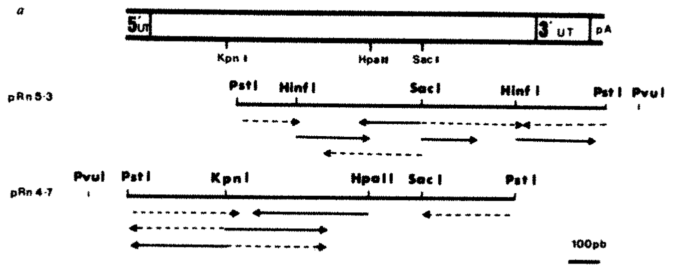

b

```
                                                          1                                10
                                                          MetAspArgArgArgMetProLeuTrpAlaLeuLeuLeuLeuTrpSer
 TCTGGGCTACACAGCTCTTAGAAAGCCTTGGCTGAACCAGATGGACAGGAGGAGGATGCCTCTCTGGGCACTCTTGTTGCTCTGGAGT   88

      20                               30                               40
ProCysThrPheSerLeuProThrGlyThrThrPheGluArgIleProLeuLysLysMetProSerValArgGluIleLeuGluGluArg
CCTTGCACCTTCAGTCTCCCAACGGGCACCACCTTTGAACGAATCCCACTCAAGAAAATGCCCTCTGTCCGGGAAATCCTGGAGGAGCGG  178

      50                               60                               70
GlyValAspMetThrArgLeuSerAlaGluTrpAspValPheThrLysArgSerSerLeuThrAspLeuIleSerProValValLeuThr
GGAGTGGACATGACCAGGCTCAGTGCTGAATGGGACGTATTCACAAAGAGGTCTTCCTTGACTGATCTTATCTCCCCCGTGGTCCTCACC  268

      80                               90                               100
AsnTyrLeuAsnSerGlnTyrTyrGlyGluIleGlyIleGlyThrProProGlnThrPheLysValIlePheAspThrGlySerAlaAsn
AACTACCTGAATAGCCAGTACTATGGCGAGATCGGCATTGGTACCCCACCCCAGACCTTCAAAGTCATGTTTGACACGGGCTCCGCCAAC  358

      110                              120                              130
LeuTrpValProSerThrLysCysSerArgLeuTyrLeuAlaCysGlyIleHisSerLeuTyrGluSerSerAspSerSerSerTyrMet
CTCTGGGTGCCCTCCACCAAGTGCAGCCGCCTCTACCTTGCTTGTGGGATTCACAGCCTCTATGAGTCCTCTGACTCCTCCAGCTACATG  448

      140                              150                              160
GluAsnGlyAspAspPheThrIleHisTyrGlySerGlyArgValLysGlyPheLeuSerGlnAspSerValThrValGlyGlyIleThr
GAGAATGGAGACGACTTCACCATCCACTACGGATCAGGGAGAGTCAAAGGTTTCCTCAGCCAGGACTCGGTGACTGTGGGTGGAATCACT  538

      170                              180                              190
ValThrGlnThrPheGlyGluValThrGluLeuProLeuIleProPheMetLeuAlaGlnPheAspGlyValLeuGlyMetGlyLeuSer
GTGACACAGACCTTTGGAGAGGTCACCGAGCTGCCCCTGATCCCTTTCATGCTGGCCCAGTTTGACGGGGTTCTAGGCATGGGCCTTTCC  628

      200                              210                              220
ArgSerAlaValGlyGlyValThrProValPheAspHisIleLeuSerGlnGlyValLeuLysGluLysValPheSerValTyrTyrAsn
CGCTCAGCCGTCGGCGGGGTCACCCCTGTCTTTGACCACATTCTCTCCCAGGGGGTGCTGAAGGAGAAAGTGTTCTCTGTCTACTACAAC  718

      230                              240                              250
ArgGlyProHisLeuLeuGlyGlyGluValValLeuGlyGlySerAspProGluHisTyrGlnGlyAspPheHisTyrValSerLeuSer
AGGGGTCCCCACCTGCTGGGGGGCGAGGTGGTGCTAGGAGGCAGCGACCCGGAGCATTACCAAGGCGATTTTCACTATGTGAGCCTCAGC  808

      260                              270                              280
LysThrAspSerTrpGlnIleThrMetLysGlyValSerValGlySerSerThrLeuLeuCysGluGluGlyCysGluValValValAsp
AAGACTGATTCCTGGCAGATCACAATGAAGGGGGTGTCTGTGGGGTCTTCCACCCTACTGTGTGAAGAAGGCTGTGAGGTAGTGGTGGAC  898

      290                              300                              310
ThrGlySerSerPheIleSerAlaProThrSerSerLeuLysLeuIleMetGlnAlaLeuGlyAlaLysGluLysArgLeuHisGluTyr
ACTGGTTCATCCTTTATCTCGGCTCCTACGAGCTCCCTGAAGTTGATCATGCAAGCCCTGGGAGCCAAGGAGAAGAGACTACATGAATAT  988

      320                              330                              340
ValValSerCysSerGlnValProThrLeuProAspIleSerPheAsnLeuGlyGlyArgAlaTyrThrLeuSerSerThrAspTyrVal
GTTGTGAGCTGTAGCCAGGTGCCCACCCTCCCCGACATCTCCTTCAACCTGGGAGGCAGGGCCTACACACTCAGCAGTACGGACTACGTG 1078

      350                              360                              370
LeuGlnTyrProAsnArgArgAspLysLeuCysThrValAlaLeuHisAlaMetAspIleProProProThrGlyProValTrpValLeu
CTACAGTATCCCAACAGGAGAGACAAGCTGTGCACAGTGGCTCTCCATGCCATGGACATCCCACCACCCACTGGGCCTGTCTGGGTCCTG 1168

      380                              390                              400
GlyAlaThrPheIleArgLysPheTyrThrGluPheAspArgHisAsnAsnArgValGlyPheAlaLeuAlaArg
GGTGCCACCTTCATCCGCAAGTTCTATACAGAGTTTGATCGGCATAACAATCGCGTTGGATTCGCCTTGGCCCGCTAAGGCCCTCTGCCA 1258


CCCAGTAACCCTAGGCCAAGCCAAGCTGGCACTCTTGGGGGCCATTTGTCTGGCTTTGTCCCAACATAGGGACACTGGACACAGAGACCC 1348


TAACGAGTGTTGCCCCTTCACCTGCACCTCACCCTTCCCTGCCTTTAAGGGAAAACCGAATAAAGATTTCATGTTT 1424
```

Fig. 1 *a*, Bacterial cloning and sequencing strategy of recombinant plasmids. Comparison of renin mRNA size, ~1,600 nucleotides as determined previously[4], and 1,100-nucleotide cDNA insert in pRn5.3 shows that ~400 nucleotides are required to complete the sequence of the renin message (if we assume that the poly(A) track is 100 nucleotides long). To clone the 5′ portion of renin mRNA, partially purified renin mRNA was used as a template for reverse transcription[23]. The cDNA obtained was converted into double-stranded S_1 nuclease-resistant DNA[23]. Double-stranded cDNA of 1.2–1.7 kilobases was eluted from a 3.5% acrylamide gel and inserted into the *Pst*I site of pBR322 by the oligo(d(CG)) tailing method[23]. Host bacteria were transformed and colonies were screened by hybridization with the nick-translated cDNA insert of pRn5.3 as a probe. The recombinant plasmid containing the largest 5′ portion of renin message was chosen for further analysis and designated pRn4.7. For sequencing experiments, sites of endonuclease cleavage are indicated at the top. As shown by the *Pvu*I site position of the pBR322 plasmid, the recombinant plasmids pRn5.3 and pRn4.7 are inserted in inverse orientation at the *Pst*I site of vector DNA. DNA fragments were labelled either at the 5′ end (———) or at the 3′ end (– – –). Arrows indicate the direction and extent of nucleotide reading. *b*, Nucleotide sequence of mouse submaxillary renin cDNA as deduced from the sequence of plasmids pRn5.3 and pRn4.7. The amino acid sequence is that predicted from the nucleotide sequence.

```
                       1                                                 50                                                100
Renin                  MDRRRMPLWALLLLWSPCTFSLPTGTTFERIPL( )KK( )MPSVREILEERGVDMTRLSAEWDVFTKRSSLTDLISPVVLTNYLNSQYYGEIGIGTPPQTFKVIF
Pepsinogen (bovine)                                           SVVK---VK--SLRQNLIENGKLKEF-RTHKYNLGSKYI-EAA-( )-V-EQP-Q---DTE-F-T------A-D-T---
Pepsinogen (pig)                                               LVKV--VR--SLRQNLIKDGKLKDFLKTHKHNPASKYFPEAAA( )--GDEP-E---DTE-F-T------A-D-T---
Prochymosin (bovine)                                         AEIT----YKG-SLRKALKEHGLLEDFLQKQQYGISSKY( )-( )GFGEVASVP-----D---F-K-YL-----E-T-L-
Penicillopepsin                                                                                   AASGVATNTP-AN-DEE-ITPVT--GT-( )-LNLN-

                       101                                               150                                               200
Renin                  DTGSANLWVPSTKCSRLYLACGIHSLYESSDSSSYMEN( )GDDFTIHYGSGRVKGFLSQ( )DSVTVGGITVT( )QTFGEVTELPLIPFMLAQ( )FDGVLGMGLSRSAV
Pepsinogen (bovine)    ----S------IY--( )SE--TN-NRFNPQ---( )TY-/
Pepsinogen (pig)       ----S------VY--( )SL--SD-NQFNPD---( )TF-ATSQELS-T--T-SMT-I-GY( )-T-Q----SD-N-I--LSETE-GS( )-LYYAP---I--LAYPSISA
Prochymosin (bovine)   ----SDF----IY-K( )SN--KN-QRFDPRK--( )TFQ-L-KPLS----T-SMQ-I-GY( )-T---SN-VDIQ--V-LS-QE-GD( )VFTTAE---I---AYPSL-S
Penicillopepsin        -----D---F--ELP( )ASQQSG--V-NP-ATG( )K--LS-YTWS-S--D-SSASGNVFT-------V-AHG-AVQAAQQISAQ( )-QQDTNN--I--LAF-SINT

                       201                                               250                                               300
Renin                  GGVT( )PVFDHILSQGVLKEKVFSVYYN( )RGPHLLGGEVVLGGSDPEHYQGDFHYVSLSKTDSWQITMKGVSVGSSTLLCEEGCEVVVDTGSSFISAPTSSLK
Pepsinogen (bovine)
Pepsinogen (pig)       S-A-( )----NLWD--LVSQDL----LSSNDDSGSVVLLGGID-SYYTGSLNWVP-( )SVE( )GY----LDSITMDGE-IA-SG--QAI----T-LLTG---AIA
Prochymosin (bovine)   EYSI( )----NMMNRHLVAQDL----M( )D-DGQESMLTLGAIDPSYYTGSLHWVP-( )TVQ( )QY--FYVDS-TISGVVVA--G--QAIL---T-KLVG-S-DIL
Penicillopepsin        VQPQSQTTFFDTVKSS-AQPL-A-AL( )KHQQPGVYDFGFID-SKYTGSLTYTG-DN-QGH( )-SFNVDSYTA--QSGDGFS-(   )IA---TTLLLLBD-VVS

                       301                                               350                                               400
Renin                  L( )MQALGAKEKRLH( )EYVVSCSQVPTLPDISFNLGGRAYTLSSTDYV( )LQYPNRRDKLCTVALHAMDIPPPTGPVWVLGATFIRKFYTEFDRHNNRVGFALAR
Pepsinogen (bovine)
Pepsinogen (pig)       ( )N-QSDI--S-NSD( )G-M-I---SIDS----V-TIN-VQ-P--PSA-I( )--D(    )DS--SGFEG--V-TSS-EL-I--DV---QY--V---A--K--I-PVA
Prochymosin (bovine)   ( )N-Q--I--TQNQY( )G-FDID-DNLSYM-TVV-EIN-KM-P-TPSA-T( )S-D(   )QGF--SGFQ(   )SENHSQK-I--DV---EY-SV---A--L--L-K-I
Penicillopepsin        QYYS-VS--QQDSNAGG--FB--SSVPBFSV-ISGYTATVPG-LIN-GPSGN(   )GST-LGGIQ(   )SNSGIGFLIF-DI-LKSQ-VV--SDGPQL---PQA
```

Fig. 2 Comparison of mouse submaxillary renin and acid proteases primary sequences. The upper line gives the predicted amino acid sequence of renin, the four lower lines give the amino acid sequences of bovine and porcine pepsinogens, bovine prochymosin and penicillopepsin from *P. janthinellum*. Data are from Dayhoff[24]. Only the amino acids which differ from the renin chain are shown. Homologous positions are indicated by dashes. Deletions are indicated by parentheses. The single code for amino acids is given in ref. 24.

10 20
A chain S S L T D L I S P V V L T N Y L N S Q Y Y

B chain D K L C T V A L H A M D I P P P T G P V W

Fig. 3 Amino-terminal sequence analysis of renin A and B chains; 30 nmol each of chain A and chain B were analysed by automated Edman degradation in a Beckman sequencer 890C exactly as described elsewhere[25].

the formation of prorenin. The prorenin is converted into active mature renin by two proteic cleavages, each occurring after two basic residues: Lys 62–Arg 63 and Arg 352–Arg 353. The exact length of the A and B chains is not known because the carboxyl terminus of the two chains has not been determined. However, the molecular weight of the A chain as determined by SDS-gel electrophoresis (35,000) is close to that calculated from the deduced amino acid sequence (31,347). The addition to A and B chain (5,379) M_r gives a M_r of 36,698, close to that found by SDS-gel electrophoresis and equilibrium sedimentation, making extensive processing of the C-terminus unlikely.

Our model is based on the presence of a disulphide bond between the A and B chains. Cys 4 present in the B chain (Cys 357) is probably linked to Cys 320 of the A chain, by analogy with pepsin. Similarly, because the position of the cysteines is conserved in the acid protease family, it is likely that there is a disulphide bond between Cys 114 and Cys 121, and between Cys 277 and Cys 281.

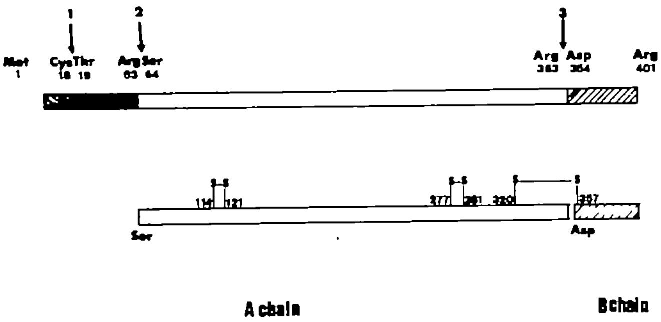

Fig. 4 A schematic representation of the possible maturation process of submaxillary gland renin. The model involves three cleavages: (1) removal of the peptide signal by membrane processing enzymes; (2), (3), conversion of the prorenin obtained into active mature renin by two cleavages occurring after a dibasic peptide and giving rise to the A and B renin chains linked by a disulphide bond.

Comparison of this model with the primary structures of carboxyl proteases and the mature form of these enzymes reveals interesting features: murine submaxillary renin and porcine cathepsin D[20] possess two chains; in the case of renin the processing of these two chains occurs after a dibasic peptide. This activation cleavage is distinctly different from the intramolecular activation mechanism of pepsinogen[21] but similar to that for proinsulin and other endocrine peptides[22]. It is not known whether submaxillary gland and kidney renins are identically processed from the same precursor molecule.

We thank J. L. Sikorav, P. Paraitaud and M. Cauvereys for help in DNA and protein sequence determinations, respectively, and H. Bedouelle for stimulating discussions. This work was supported by grants from the CNRS (ATP 4247), the Institut National de la Santé et de la Recherche Médicale (PRC 124024) and the Fondation pour la Recherche Médicale Française.

Received 4 March; accepted 21 May 1982.

1 Morris, B. J. & Lumbers, E. R *Biochim biophys Acta* **289**, 385–391 (1972).
2 Michelakis, A. M., Yoshida, H, Meume, J, Murakami, K. & Inagami, T *Endocrinology* **94**, 1101–1105 (1974).
3 Malling, C. & Poulsen, K. *Biochim biophys. Acta* **491**, 542–550 (1977).
4 Rougeon, F. *et al Proc natn Acad. Sci. U S A* **78**, 6367–6371 (1981).
5. Maxam, A. M & Gilbert, W *Proc natn Acad. Sci. U.S.A* **74**, 560–564 (1977).
6. Sikorav, J. L, Auffray, C. & Rougeon, F. *Nucleic Acids Res* **8**, 3143–3155 (1980).
7. Davis, B D. & Tai, P. C. *Nature* **283**, 433–438 (1980)
8. Garnier, J., Gaye, P, Mercier, J. C. & Robson, B. *Biochimie* **62**, 231–239 (1980).
9. Proudfoot, N J & Brownlee, G. G *Nature* **263**, 211–214 (1976).
10 Gross, F, Lazar, J. & Orth, H *Science* **175**, 656 (1972).
11 Misono, K. S. & Inagami, T *Biochemistry* **19**, 2619–2622 (1980).
12. James, M. N G, Hsu, I. N. & Delbaere, L T. J *Nature* **267**, 808–813 (1977).
13. Harboe, M. K. & Foltmann, B. *FEBS Lett* **60**, 133–135 (1975).
14. Sepulveda, P, Marciniszyn, J. Jr, Liu, D. & Tang, J *J. biol. Chem* **250**, 5082–5088 (1975)
15. Foltmann, B., Pedersen, V. B, Jacobsen, H, Kauffman, D & Wybrandt, G *Proc. natn Acad Sci. U S A.* **74**, 2321–2324 (1977).
16 Hsu, I N., Delbaere, L T. J., James, M. N. G. & Hofmann, T. *Nature* **266**, 140–145 (1977).
17. Tang, J. *Molec. cell. Biochem.* **26**, 93–109 (1979).
18 Soubrier, F. *et al. J. clin. Endocr. Metab.* **54**, 139–144 (1982).
19 Suzuki, F., Nakamura, Y., Nagata, Y, Ohsawa, T & Murakami, K *J Biochem* **89**, 1107–1112 (1981).
20 Huang, J. S, Huang, S. S & Tang, J *J. biol Chem* **254**, 11405–11417 (1979)
21 Marciniszyn, J Jr, Huang, J. S, Hartsuck, J A. & Tang, J. *J. biol. Chem* **251**, 7095–7102 (1976).
22. Steiner, D, Quinn, P., Chan, S, Marsh, J & Tager, H *Ann. N.Y. Acad Sci.* **343**, 1–16 (1980)
23. Rougeon, F. & Mach, B *J biol Chem* **252**, 2209–2217 (1977).
24. Dayhoff, M O. *Atlas of Protein Sequence and Structure*, 105–107 (National Biochemical Research Foundation, Silver Spring, 1978).
25. Hunkapiller, M. W. & Hood, L. E *Biochemistry* **17**, 2124–2133 (1978).

Prostatic steroid binding protein: gene duplication and steroid binding

Malcolm Parker, Maurice Needham & Roger White

Imperial Cancer Research Fund, PO Box 123, Lincoln's Inn Fields, London WC2A 3PX, UK

The principal secretory protein in rat prostatic fluid is a steroid binding protein[1–6] whose expression is stimulated by androgenic steroids[7,8]. This prostatic steroid binding protein is oligomeric, consisting of two subunits, one containing the polypeptides C1 and C3 and the other containing C2 and C3[9]. We have isolated cDNA clones specific for each of the mRNAs which code for prostatic binding protein and note here the considerable DNA sequence homology between C1 and C2. Therefore, it is likely that duplication of an ancestral gene occurred and the subsequent divergence results in the expression of two related polypeptides that form part of a single protein. Furthermore, in view of the structure of the protein it is possible that the divergence of one of the genes has resulted in the capacity of this prostatic protein to bind steroids.

Prostatic steroid binding protein is an oligomer consisting of two subunits[9]. In one subunit C3, a polypeptide of molecular weight (M_r) 12,000 is linked by disulphide bridges to C2, a polypeptide of M_r 10,000 and in the other subunit C3 is linked by disulphide bridges to C1, a polypeptide of M_r 8,000. These three polypeptides are encoded by discrete mRNAs and we have previously isolated cDNA clones for C1 and C3 mRNA[10] by using the ability of single-stranded cDNA to form a hairpin at its 3′ end in order to prime the synthesis of the second DNA strand[11]. As the cDNA inserts were much smaller than the estimated mRNA sizes, we have now used an alternative procedure which reduced the loss of DNA corresponding to the 5′ end of the mRNA[12,13]. Single-stranded cDNA was tailed with dCMP and synthesis of the second strand was primed with oligo(dG), thereby avoiding the use of S_1 nuclease which necessarily results in loss of DNA. After a second tailing reaction, dC-tailed double-stranded cDNA was inserted into the *Pst*I site of pAT153[14], which had been tailed with dGMP.

Transformants that contained the desired cDNA sequences were identified by *in situ* hybridization[15] using ^{32}P-labelled

Table 1 Relationships of prostatic binding proteins, mRNA and cDNA clones

Prostatic binding protein	Primary translation product	mRNA size (nucleotides)	cDNA plasmid	cDNA insert size (nucleotides)
8,000 (C1)	9,000	500–550	pA13	500
10,000 (C2)	11,000	550–600	pB44	500
12,000 (C3)	10,000	650–700	pA34	600

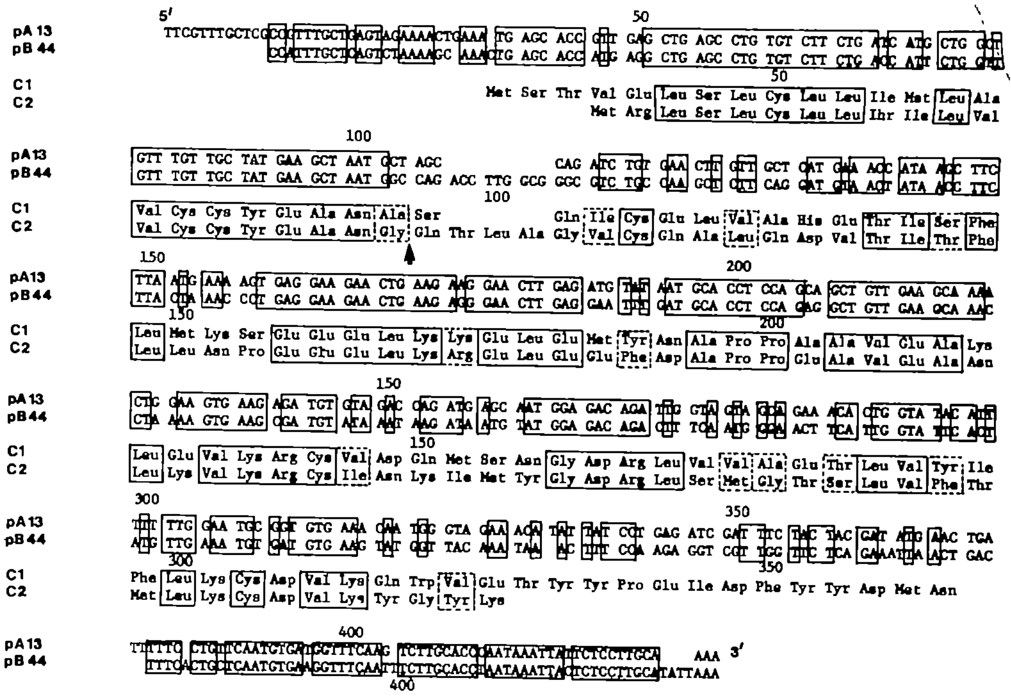

Fig. 1 Nucleotide sequence of prostatic binding protein mRNAs for C1 and C2 and deduced amino acid sequence The nucleotide numbers are shown above the sequence Gaps have been left to maximize homology; the solid boxes show perfect homologies and the dotted boxes show semi-conservative amino acid homologies The putative cleavage point of the signal peptide is represented by ↑. The cDNA clones pA13 and pB44 which were used to analyse the sequences of C1 and C2 were isolated as follows. Poly(A)-containing RNA was isolated from rat ventral prostate and used to synthesize prostate cDNA[8]. The cDNA was 'tailed' using terminal transferase with dCTP in the presence of 1 mM CoCl to yield molecules with ~20 dC at their 3′ ends[10]. After phenol extraction the tailed DNA was passed through a Sephadex G-150 column and annealed with oligo(dG) to prime the synthesis of the second DNA strand using reverse transcriptase[13] After phenol extraction and gel filtration the double-stranded cDNA was tailed again with dCTP using terminal transferase. pAT153[14] was digested with *Pst*I and tailed with ~20 dGMP molecules. Annealing of pAT153 and double-stranded DNA was carried out at a molar ratio of 1.1 by heating the mix at 60 °C for 2 h and cooling overnight. After transformation of *Escherichia coli* HB101 had been carried out, recombinant colonies were selected for tetracycline resistance. Further screening to distinguish colonies which contained the desired prostatic DNA sequences was carried out by *in situ* hybridization using ^{32}P-labelled cDNA[15] Plasmid DNA was isolated from transformed *E coli* by lysis with lysozyme and subsequent SDS treatment in alkaline conditions[34]. After purification on CsCl gradients the DNA was bound to diazobenzyloxymethyl paper as described previously[16] except that 25 μM sodium phosphate *p*H 6.5 was used in place of borate as buffer. The recombinant plasmid clones were then identified by mRNA purification. Total prostate poly(A)-containing RNA (6 μg) was hybridized to the filters, washed and the bound RNA eluted and translated in a cell-free system derived from wheat germ[35]. End-labelling of DNA with [γ-^{32}P]ATP and DNA sequence analysis were carried out using the methods of Maxam and Gilbert[19] The sequencing strategy was to 5′-end label pA13 that had been digested with *Bgl*II and *Hin*dIII and pB44 that had been digested with *Hin*f and *Hpa*II using [γ-^{32}P]ATP and T4 polynucleotide kinase.

cDNA. This was possible because the amount of hybridization with recombinant plasmids depends on the abundance of the individual cDNA species and the cDNAs that correspond to prostatic steroid binding protein mRNA represent by far the most abundant cDNA in the total mix. Individual recombinant plasmids were distinguished by mRNA purification[10,16]. Thus cDNA clones pA13, pB44 and pA34 (Table 1), which are specific for C1, C2 and C3, respectively, were selected for further studies. It was likely that they represented complete copies of the mRNAs because we and others[10,17,18] have estimated that the size of prostatic binding protein mRNAs, including the poly(A)-tail, was 450–700 nucleotides and the DNA insert sizes were consistent with the size of each corresponding mRNA (Table 1). Furthermore, preliminary mapping of mRNA transcripts synthesized *in vivo* indicates that the cDNA inserts extended to within 10 nucleotides of the 5′ ends of the mRNAs.

We sequenced the cDNA inserts[19] and found marked similarities between pA13 and pB44, resulting in extensive amino acid sequence homologies between C1 and C2 (Fig. 1). In contrast, the DNA sequence of pA34, which was consistent with the published protein sequence of C3[20], shows no significant homology with pA13 or pB44.

Both C1 and C2 mRNAs contain approximately 430 nucleotides. C1 mRNA contains: (i) A 5′ non-coding region of at least 36 nucleotides. (ii) A coding region of 333 nucleotides of which 264 correspond precisely to the secreted polypeptide of 88 amino acids[21]. In fact, there are two potential AUG initiation codons which could represent the NH$_2$ terminus of the protein. As these would result in signal peptides of 12 or 23 amino acids, we favour initiation of translation at nucleotide 37 because all signal peptides described so far contain 15–30 amino acids[22] and, in general, the first AUG initiation codon is utilized. (iii) A 3′ non-coding region of 60 nucleotides, including a UGA termination codon and a AAUAAA poly(A) addition signal 19 nucleotides preceding the poly(A)-tail. The C2 mRNA contains: (i) A 5′ non-coding region of 34 nucleotides. (ii) A postulated coding region of 294 nucleotides of which 60 probably comprise a signal peptides and 234 code for the secreted polypeptide, in agreement with the partial protein sequence which has been determined to date (B. Peeters and W. Rombauts, personal communication). This would be consistent with the sizes of the primary translation product synthesized *in vitro* and the processed polypeptide secreted *in vivo*[8]. In addition, we suggest that the signal peptide is cleaved at Asn-Gly-↑Gln which is used commonly by signal peptidases[22]. (iii) A 3′ noncoding region of 105 nucleotides which contains a UAA termination codon and a AAUAAA poly(A) addition signal 24 nucleotides preceding the poly(A)-tail.

The most remarkable feature of the two mRNAs, however, is the extent of sequence homology which occurs in both coding and non-coding regions and which results in a 50% amino acid sequence homology between the primary translation products and increases to 62% when semi-conservative amino acids are included (Fig. 1). The most striking homologies are shown in Fig. 2 and encompass: (i) the 5′ non-coding region of nucleotides 1–19 in pB44 and 13–31 in pA13 which share 79% homology, (ii) the signal peptide of nucleotides 22–99 in pB44 and 35–109 in pA13 which share 87% homology, (iii) the coding region of nucleotides 128–267 in pB44 and 131–269 in pA13 which share 76% homology and (iv) the 3′ non-coding region of

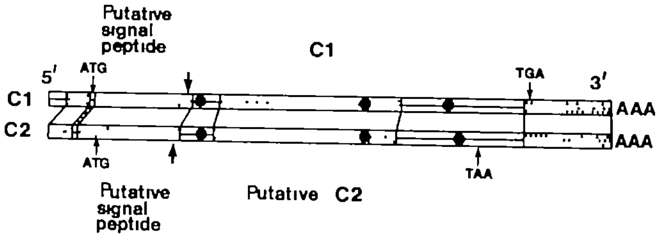

Fig. 2 Schematic representation of the major homologies between C1 and C2 mRNA. Hatched areas show regions of at least 75% DNA sequence homology. Possible homologous regions of less than 15 nucleotides have been omitted. The initiation codons ATG and termination codons TGA and TAA are shown by arrows and the putative signal peptides are shown preceding the arrows ↑ at which a signal peptidase may cleave. Cysteine residues (●) attach C1 and C2 to C3 by disulphide bridges.

nucleotides 362–432 in pB44 and 363–431 pA13 which share 81% homology. Several additional homologous regions of 15–20 nucleotides also exist but have been omitted for reasons of clarity.

The similarity in the DNA sequences in pA13 and pB44 suggest that the genes coding for C1 and C2 have probably arisen by duplication of an ancestral gene. There are now many examples of duplicated genes: some are pseudogenes[23–25], some are expressed at quite different levels with distinct control signals[26–28], and others are expressed in similar amounts[29,30]. C1 and C2 seem to fall into this last class, being similarly expressed and controlled by androgens in the rat ventral prostate and ultimately both forming part of a secreted steroid binding protein. It is also of interest that in blotting experiments[31] with rat and mouse DNA samples we find that pB44, but not pA13, hybridizes (at low as well as high stringency) with mouse DNA; therefore, we presume that gene duplication in the rat occurred after the evolutionary divergence of rat and mouse.

The divergence between the C1 and C2 genes may be of functional significance in view of the structure of prostate binding protein[9] and its steroid binding properties[2,6,32]. After dissociation of the protein into the two subunits, only C2–C3 continue to show steroid binding[9]. Although this experiment is open to several interpretations, the only apparent difference between the subunits is the composition of C1 and C2 and therefore one intriguing possibility is that a portion of C2 is crucial for steroid binding. In spite of this, it is extremely difficult to predict which regions of C2 are important because amino acid differences, which could markedly affect the conformation of the protein, occur throughout the two polypeptides. Moreover, it is conceivable that C2 does not bind steroids directly but may interact with C3 in such a way as to enable the C2–C3 subunit to bind steroids. Nevertheless, as estramustine, a nitrogen mustard derivative of oestradiol-17β, binds with a K_d of 2×10^{-8} M[32] and has been used as a therapeutic agent in the treatment of prostatic carcinoma[33], it will be of considerable interest to investigate whether similar genes can be detected in human DNA.

Received 18 March; accepted 10 May 1982.

1. Heyns, W., Peeters, B. & Mous, J. *Biochem. biophys. Res. Commun.* **77,** 1492–1499 (1977).
2. Heyns, W. & De Moor, P. *Eur. J. Biochem.* **78,** 221–230 (1977).
3. Parker, M. G., Scrace, G. T. & Mainwaring, W. I. P. *Biochem. J.* **170,** 115–121 (1978).
4. Forsgren, B. *et al. Proc. natn. Acad. Sci. U.S.A.* **76,** 3149–3153 (1979).
5. Lea, O. A., Petrusz, P. & French, F. S. *J. biol. Chem.* **254,** 6196–6202 (1979).
6. Chen, C., Hirpakha, R. A. & Liao, S. *J. Steroid Biochem.* **11,** 401–405 (1979).
7. Parker, M. G. & Mainwaring, W. I. P. *Cell* **12,** 401–407 (1977).
8. Parker, M. G. & Scrace, G. T. *Proc. natn. Acad. Sci. U.S.A.* **76,** 1580–1584 (1979).
9. Heyns, W., Peeters, B., Mous, J., Rombauts, W. & De Moor, P. *Eur. J. Biochem.* **89,** 181–186 (1978).
10. Parker, M. G., White, R. & Williams, J. G. *J. biol. Chem.* **255,** 6996–7001 (1980).
11. Maniatis, T., Kee, S. G., Efstratiadis, A. & Kafatos, F. C. *Cell* **8,** 163–182 (1976).
12. Rougeon, F., Kourilsky, P. & Mach, B. *Nucleic Acids Res.* **2,** 2365–2378 (1975).
13. Land, H., Grez, M., Hauser, H., Lindenmaier, W. & Schütz, G. *Nucleic Acids Res.* **9,** 2251–2266 (1981).
14. Twigg, A. J. & Sherratt, D. *Nature* **283,** 216–218 (1980).
15. Grunstein, M. & Hogness, D. S. *Proc. natn. Acad. Sci. U.S.A.* **72,** 3961–3965 (1975).
16. Alwine, J. C., Kemp, D. J. & Stark, G. R. *Proc. natn. Acad. Sci. U.S.A.* **74,** 5350–5354 (1977).
17. Peeters, B. L., Mous, J. M., Rombauts, W. A. & Heyns, W. J. *J. biol. Chem.* **255,** 7017–7023 (1980).
18. Mansson, P. E., Silverberg, A. B., Gipson, S. H. & Harris, S. E. *Molec. cell. Endocr.* **19,** 229–241 (1980).
19. Maxam, A. H. & Gilbert, W. *Proc. natn. Acad. Sci. U.S.A.* **74,** 560–564 (1977).
20. Peeters, B., Rombauts, W., Mous, J. & Heyns, W. *Eur. J. Biochem.* **115,** 115–121 (1981).
21. Peeters, B., Heyns, W., Mous, J. & Rombauts, W. *Eur. J. Biochem.* **123,** 55–62 (1982).
22. Austen, B. M. *FEBS Lett.* **103,** 308–313 (1979).
23. Jacq, C., Miller, J. R. & Brownlee, G. G. *Cell* **12,** 109–120 (1977).
24. Hardison, R. C. *et al. Cell* **18,** 1285–1297 (1979).
25. Fritsch, E. F., Lawn, R. M. & Maniatis, T. *Cell* **19,** 959–972 (1980).
26. Royal, A. *et al. Nature* **279,** 125–132 (1979).
27. Colbert, D. *et al. Biochemistry* **19,** 5586–5592 (1980).
28. Wood, W. G. *et al. Cell* **15,** 437–446 (1978).
29. Lomadico, P. *et al. Cell* **18,** 545–558 (1979).
30. Wahli, W. & Dawid, I. B. *Proc. natn. Acad. Sci. U.S.A.* **77,** 1437–1441 (1980).
31. Southern, E. M. *J. molec. Biol.* **98,** 503–517 (1975).
32. Forsgren, B., Gustafsson, J.-A., Pousette, A. & Hogberg, B. *Cancer Res.* **39,** 5155–5164 (1979).
33. Jönsson, G., Hogberg, B. & Nilsson, T. *Scand. J. Urol. Nephrol.* **11,** 231–238 (1977).
34. Birnboim, H. C. & Doly, J. *Nucleic Acids Res.* **7,** 1513–1523 (1979).
35. Paterson, B. M., Roberts, B. E. & Kuff, E. L. *Proc. natn. Acad. Sci. U.S.A.* **74,** 4370–4374 (1977).

Inverted repeats surround the ribitol–arabitol genes of *E. coli* C

Christopher D. Link* & Albey M. Reiner

Department of Microbiology, University of Massachusetts, Amherst, Massachusetts, 01003, USA

Only 10–20% of natural *Escherichia coli* strains can catabolize the pentitol sugars ribitol and D-arabitol[1]. This variability extends to common laboratory strains: *E. coli* C strains, but neither K12 nor B strains, can catabolize these sugars. In *E. coli* C, the genes responsible for these catabolic pathways are chromosomal and consist of two very closely linked, independent operons[2]. Genetic[1] and hybridization studies (C.D.L. and A.M.R., unpublished data) indicate that the genes are completely absent in K12. These observations led us to consider whether these genes had been acquired by horizontal, rather than vertical, genetic transmission, perhaps as an inserted transposable element. Here we report that the ribitol-arabitol genes of *E. coli* C are surrounded by 1.4 kilobase (kb) inverted repeats of imperfect homology. These genes may constitute an example of a vestigial transposable element recently acquired by the bacterial chromosome.

To examine the physical structure of the ribitol–arabitol chromosomal region, the ribitol–arabitol genes of *E. coli* C were cloned *in vivo* on a λ specialized-transducing phage (designated λdAR) and *in vitro* by recombinant DNA techniques. Preliminary electron microscopy with DNA from λdAR suggested that this phage contained inverted repeats, structures often associated with transposable elements[3,4]. To investigate this possibility further, single strands of λdAR and of two λ control phages were separated and purified by the poly(U, G)/CsCl equilibrium gradient method[5]. Renaturation of single-stranded phage DNA in the absence of its complementary strand yields duplex regions only by formation of intrastrand duplexes resulting from inverted repeat sequences in the original double-stranded molecule. These intrastrand duplex regions can be visualized and sized by degrading the unpaired single-stranded DNA with nuclease S_1 and displaying the remaining duplex DNA by gel electrophoresis[6].

The gel banding pattern produced when single-stranded DNA from λdAR and control phage λY199::*tn10* (which contains transposon Tn*10*) is treated with S_1 nuclease is shown in Fig. 1. Single-stranded λdAR DNA produces multiple bands with a major band having the mobility of an ~1.4 kb fragment, and minor bands running at ~0.7 and 0.6 kb (Fig. 1, lanes *f–i*). These bands are never observed with single-stranded DNA from Y199, the parent phage of λdAR. In contrast, DNA from phage λY199::Tn*10* produces a single sharp band (Fig. 1, lanes *b–e*) corresponding to 1.36 kb, which is the size of the Tn*10* inverted repeats as estimated by electron microscopy[7]. These results demonstrate that λdAR, like λY199::Tn*10*, contains inverted repeats. The multiple banding pattern of λdAR presumably reflects imperfect homology between two sequences of ~1.4 kb, resulting in single-strand 'bubbles' of non-homology in the intrastrand duplex which may be cleaved by S_1 nuclease. This view is supported by the observation that increasing the S_1 nuclease concentration shifts the banding pattern of λdAR towards smaller, more numerous fragments (Fig. 1), and by hybridization experiments described below.

To locate these imperfect repeats with respect to the ribitol–arabitol genes, and to exclude the possibility that the inverted repeats found on the λdAR genome are an artefact generated during *in vivo* formation of this phage, we also worked with the genes cloned by recombinant DNA techniques. Cloning was achieved by randomly ligating *Eco*RI fragments of *E. coli* C chromosomal DNA into the plasmid vector pBR322. (*Eco*RI was chosen after preliminary experiments demonstrated that an *Eco*RI fragment of λdAR includes both the ribitol–arabitol

---

* Present address: Department of Molecular, Cellular and Developmental Biology, University of Colorado, Boulder, Colorado 80309, USA.

0028-0836/82/260094—03$01.00

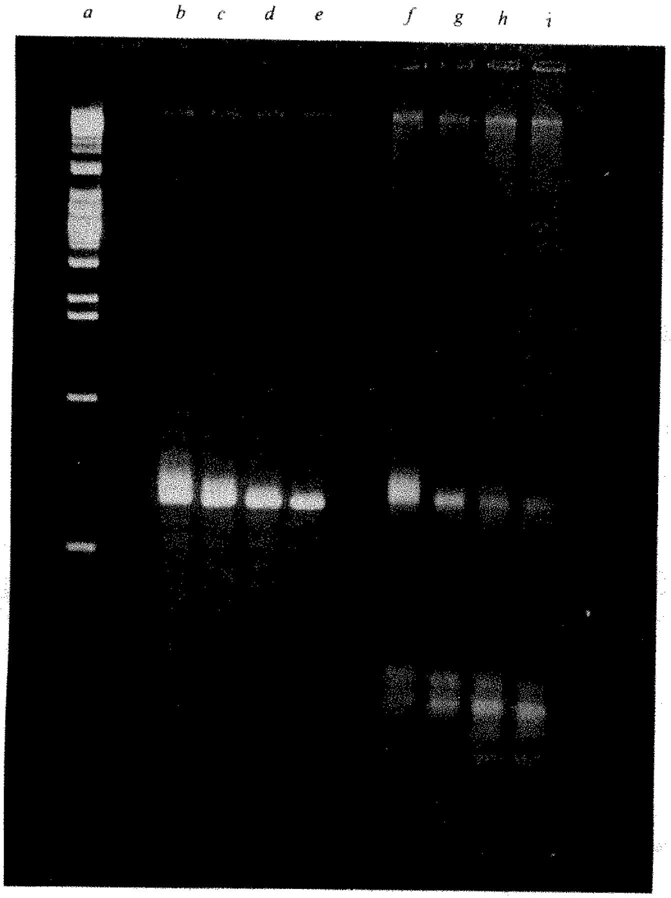

Fig. 1 Gel electrophoresis of intrastrand duplex fragments which survive S_1 nuclease digestion of renatured single-stranded DNA from λY199::Tn*10* (lanes *b–e*) and λdAR (*f–i*). Phage λY199::Tn*10*, used as a control, was constructed by selecting a recombinant between λY199 and the Tn*10*-containing phage λ561[18]. Preparations of separated strands of phage DNA were renatured by heating for 1 h in 0.3 M NaCl at 65 °C. S_1 nuclease digestions were done as described earlier[6] and the digested samples were run on a 1.4% agarose gel. Lane *a* contains an *Eco*RI-*Bam*HI double digest of λ^+ and pBR322 as a size standard. Lanes *b–e* contain 1.4 μg of λY199::Tn*10* DNA, *f–i* contain 3.2 μg of λdAR DNA. The digestions were done using 20 (*b, f*), 40 (*c, g*), 80 (*d, h*) or 120 (*e, i*) units of S_1.

genes and the inverted repeats.) All transformants selected for their ability to use ribitol or D-arabitol could utilize both sugars, and all examined further harboured a plasmid in which a large (16.5 kb) *Eco*RI fragment had been inserted into pBR322. One of these plasmids, designated pAR-2, was chosen for further restriction mapping.

The relative locations of the inverted repeat sequences were determined by preparing Southern transfers of restriction enzyme digests of pAR-2 and probing with ^{32}P-labelled inverted-repeat DNA. The probe was prepared by first extracting from an agarose gel the major intrastrand duplex fragment which survives S_1 nuclease treatment of λdAR (Fig. 1) and then labelling the fragment *in vitro* by nick translation[8]. Lane *a* of Fig. 2 is a positive control showing hybridization of the probe to the intrastrand duplex fragments produced by S_1 treatment of λdAR. (The hybridization of the probe to the minor bands demonstrates that the smaller fragments are derived from the major intrastrand duplex fragment.) The hybridization patterns of the pAR-2 digests (Fig. 2*b–e*) were used to locate the inverted repeats relative to previously mapped restriction fragments of this plasmid. The repeats were found to lie in two noncontiguous fragments separated by 7.2 kb (see Fig. 3).

Similar hybridization studies show that the inverted repeat probe does not hybridize to Tn*5*, Tn*10*, or *E. coli* K12 chromosomal DNA, even in conditions that would detect partially homologous sequences[9]. Hybridization of the probe to *E. coli* C chromosomal DNA was limited to fragments present in pAR-2, demonstrating that the only copies of the repeat unit in the *E. coli* C chromosome are those surrounding the ribitol–arabitol genes.

The location of the individual genes of the ribitol and D-arabitol operons relative to the inverted repeats was determined by experiments with pAR-2 plasmids into which the kanomycin-resistance transposon Tn*5* had been inserted[10]. Inserts which prevented either ribitol or D-arabitol use were mapped by restriction enzyme analysis, and the individual genes inactivated were determined by genetic complimentation. The gene order determined in this manner was in complete agreement with the order previously determined by standard genetic methods[2]. The repeats bound the ribitol–arabitol genes in a transposon-like arrangement (Fig. 3). Although these experiments do not exclude the possibility that distal portions of the ribitol or D-arabitol genes contribute to the repeated sequences, results with the ribitol–arabitol region of the related bacteria *Klebsiella* have shown that no detectable hybridization exists between these operons, although hybridizing fragments were detected outside the operons[11].

As the repeat sequences surrounding the ribitol–arabitol genes are not found elsewhere in the *E. coli* C chromosome, or anywhere in the *E. coli* K12 chromosome, it is unlikely that they represent insertion sequences which coincidentally surround the ribitol–arabitol genes. The inverted repeats could result from residual homology retained from an ancestral tandem inverted duplication[12]; this is improbable, however, in light of the non-homology of the ribitol and D-arabitol operons. We

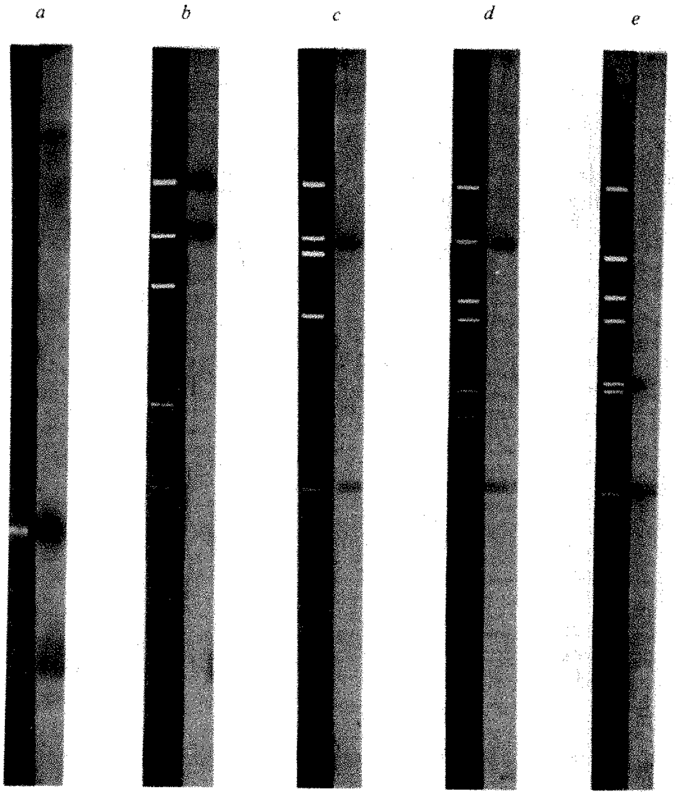

Fig. 2 Hybridization of the ribitol–arabitol inverted repeat probe to digests of pAR-2. The probe was created by electroeluting from an agarose gel the major intrastrand duplex fragment of λdAR (see Fig. 1) and then labelling this fragment with ^{32}P by nick translation[8]. Restriction fragments of pAR-2 and pAR-2 derivatives were fractionated on a 1% agarose gel and transferred to nitrocellulose by the method of Southern[19]. Pretreatment of nitrocellulose filters and hybridization incubations were done as described previously[20]. The probe was hybridized to: *a*, intrastrand duplex fragments generated by S_1 nuclease digestion of λdAR single-stranded DNA; *b*, *Eco*RI–*Bam*HI–*Hin*dIII triple digest of pAR-2; *c*, *Pst*I digest of pAR-2; *d*, *Pst*I digest of pAR-2 containing a Tn*5* insert in the gene for D-xylulose kinase; *e*, *Pst*I digest of pAR-2 containing a Tn*5* insert in the gene for D-ribulose kinase.

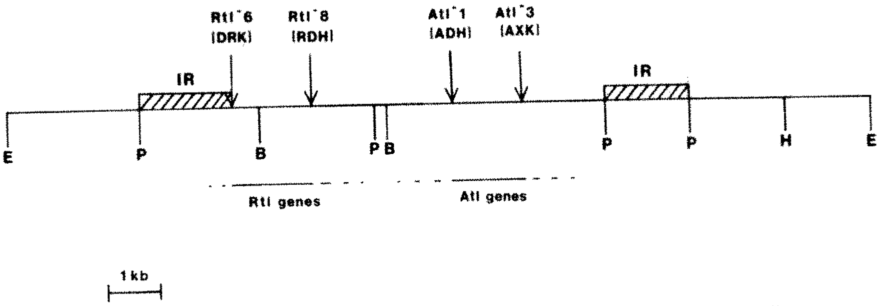

Fig. 3 Map of the 16.5 kb *Eco*RI fragment cloned in pAR-2. Hatched regions indicate fragments which hybridize to the inverted repeat (IR) probe. Arrows indicate location of representative TN*5* insertions which inactivate ribitol or D-arabitol genes. Tn*5* insertions were generated by delivering the Tn*5* element via defective λ phage[10] to strain AB1157 containing pAR-2. The subpopulation of pAR-2 plasmids which received Tn*5* inserts was enriched by preparing plasmid DNA from all transposon-receiving cells, then using this to transform another strain to kanamycin resistance. Those inserts in pAR-2 were identified by screening the kanamycin-resistant transformants for inability to use ribitol of D-arabitol. Complementation studies were done by transforming a strain containing active ribitol and D-arabitol dehydrogenases, but inactive D-ribulose and D-xylulose kinases, with insert-containing plasmids. Because of the polarity of Tn*5* insertions, this complementation test cannot distinguish between dehydrogenase and promoter insertions. Letters in parentheses indicate enzyme coded for by inactivated gene: DRK, D-ribulose kinase; RDH, ribitol dehydrogenase; ADH, D-arabitol dehydrogenase; AXK, arabitol-induced D-xylolose kinase. The maximum rightward extent of the left IR region was determined by experiments with pAR-2 containing Tn*5* insertion Rtl$^-$ 6, which show that only the left-hand plasmid–Tn*5* junction fragment hybridizes to the probe (see Fig. 2, lane *e*). Restriction sites for *Sal*I, *Hpa*I and *Bgl*II were omitted for clarity. B, *Bam*HI; E, *Eco*RI; H, *Hind*III: P, *Pst*I.

suggest that the inverted repeats are the structural remnants of an ancestral transposable element which carried the ribitol–arabitol genes into *E. coli*. This would account for the observation that only a subpopulation of *E. coli* strains can use ribitol and D-arabitol.

The imperfect homology of the inverted repeats suggests that they no longer function in transposition. Conjugation experiments (not shown) which demonstrate that the ribitol–arabitol genes do not seem to translocate from the chromosome ($<10^{-9}$ transpositions per gene copy) support this view. The hypothesis that the inverted repeats are derived from a transposable element could be further supported by demonstrating that the repeats themselves are flanked by short inverted repeats, or that the ends of the presumptive ribitol–arabitol transposon are flanked by a duplication of an oligonucleotide of target DNA. However, these transposon characteristics[4] may be difficult to detect in this case because of the genetic drift which has apparently occurred since the insertion of these genes.

If the *E. coli* ribitol–arabitol region did originate as a transposon, then these genes can be viewed as a rare example of genes for which there is a molecular record of their acquisition by a bacterial chromosome[13]. What other chromosomal genes might have been derived from transposable elements? As transposons seem to carry genes of potentially strong selective advantage, chromosomal genes conferring catabolic traits or resistance to toxic agents could be derived from transposable elements. For example, certain chromosomal genes which confer antibiotic resistance (such as *ampC* of *E. coli*[14]) might also be found to be surrounded by inverted repeats. The *E. coli* genes for restriction and modification (*hsd*), which are nonessential and can convey potentially strong selective advantage, may also be candidates for genes derived from transposons. (Restriction and modification genes have not yet been identified as part of transposable elements, although they can be phage or plasmid borne[15].) Some of the inverted repeat sequences detected in the *E. coli* chromosome by electron microscopy[16,17] may be evidence of past transposon insertions. The fraction of chromosomal genes derived from transposons may be significantly greater than the fraction of genes eventually found associated with inverted repeats, as one would expect the identifying structural features of genes derived from transposons to be lost with time.

We thank Tom Carbone, Anne Ferguson and Jeanne Bertonis for technical assistance. This work was supported by NSF grant PCM-7811161. C.D.L. was supported by NIH graduate traineeship grant 074 73-04.

Received 25 January; accepted 22 April 1982.

1. Reiner, A. M. *J. Bact.* **123,** 530–536 (1975).
2. Scangos, G. A. & Reiner, A. M. *J. Bact.* **134,** 492–500 (1978).
3. Kleckner, N. *Cell* **11,** 11–23 (1977).
4. Calos, M. P. & Miller, J. *Cell* **20,** 579–595 (1980).
5. Davis, R. W., Botstein, D. & Roth J. R. in *Advanced Bacterial Genetics*, 114–115 (Cold Spring Harbor Laboratory, New York, 1980).
6. Ohtsubo, H. & Ohtsubo, E. *Proc. natn. Acad. Sci. U.S.A.* **73,** 2316–2320 (1976).
7. Tye, B.-K., Chan. R. K. & Botstein, D. *J. molec. Biol.* **85,** 485–500 (1974).
8. Rigby, P. W. J., Dieckman, M., Rhodes, C. & Berg, P. *J. molec. Biol.* **113,** 237–251 (1977).
9. Hyman, R. W., Brunowski, I. & Summers, W. L. *J. molec. Biol.* **77,** 89–96 (1973).
10. Shaw, K. J. & Berg, C. M. *Genetics* **92,** 741–747 (1979).
11. Neuberger, M. S. & Hartley, B. S. *J. molec. Biol.* **132,** 435–470 (1979).
12. Inderlied, C. B. & Mortlock, R. P. *J. molec. Evol.* **9,** 181–190 (1977).
13. Cambell, A. *A. Rev. Microbiol.* **35,** 55–83 (1981).
14. Bobrowski, M. M. *et al. J. Bact.* **125,** 149–157 (1976).
15. Arber, W. & Linn, S. *A. Rev. Biochem.* **38,** 467–500 (1969).
16. Deonier, R. C. & Hadley, R. G. *Nature* **264,** 191–193 (1976).
17. Chow, L. T. in *DNA Insertion Elements, Plasmids and Episomes* (eds Bukhari, A. I., Shapiro, J. A. & Adhya, S. C.) 73–79, (Cold Spring Harbor Laboratory, New York, 1977).
18. Kleckner, N., Barker, D. F., Ross, D. G. & Botstein, D. *Genetics* **90,** 427–450 (1978).
19. Southern, E. M. *J. molec. Biol.* **98,** 503–517 (1975).
20. Botchan, M., Topp, W. & Sambrook, J. *Cell* **9,** 269–287 (1976).

LexA protein inhibits transcription of the *E. coli uvrA* gene *in vitro*

Aziz Sancar, Gwendolyn B. Sancar & W. Dean Rupp[*]

Departments of Therapeutic Radiology and of Molecular Biophysics
& Biochemistry, Yale University School of Medicine, 333 Cedar
Street, New Haven, Connecticut 06510, USA

John W. Little & David W. Mount

Departments of Therapeutic Radiology and of Molecular
Biophysics & Biochemistry, Yale University School of Medicine,
333 Cedar Street, New Haven, Connecticut 06510, USA

Treatment of *Escherichia coli* with radiation or chemical carcinogens induces a number of cellular functions to counteract the damage inflicted by such treatments (see ref. 1 for a review). One of these inducible functions is the SOS response, which is controlled by the *recA* and *lexA* genes: single-stranded DNA produced as a result of DNA damage binds to *recA* protein (RecA), activating its protease function; activated RecA cuts *lexA* protein (LexA), the repressor of the SOS genes, thereby inactivating it and turning on these genes[2–4]. The SOS genes include *recA* and *lexA* themselves, and recent work has shown that the two genes have similar operators where LexA binds *in vitro*, inhibiting their transcription[3,4]. It is anticipated that other genes under the control of *recA* and *lexA* will have similar operators. Recent genetic[5,6] and biochemical[7] data suggest that the excision repair genes *uvrA* and *uvrB* are part of the *recA–lexA* regulon and are at least partly responsible for *recA–lexA*-mediated inducible DNA repair. In support of these results we have reported that *uvrB* has a promoter that is repressed by LexA *in vitro*[8]. We now show that *uvrA* has an operator similar to those of other SOS genes and that LexA binds to this operator and inhibits the transcription of the *uvrA* gene *in vitro*.

---

[*] To whom correspondence should be addressed.

To study the regulation of *uvrA* we used the plasmid pDR1996 (see Fig. 1*a*) which carries both the *uvrA* and *ssb* genes[9]. The exact location of *ssb* on this plasmid was determined from DNA and protein sequencing[9]. The direction of transcription of *uvrA* and the approximate location of its promoter were determined by Tn*1000* mapping[10]. The exact location of the *uvrA* promoter was determined by subcloning and transcription experiments: removal of the *Bal*I–*Kpn*I fragment spanning 6.7–7.5 kilobases (kb) inactivated *uvrA* while transcriptional experiments indicated a single transcriptional start between the *Hae*III site at 6.73 kb and the *Hin*fI site at 7.03 kb (data not shown). This transcript was presumed to be that of *uvrA*, and this $(HaeIII\text{-}HinfI)_{325}$ fragment was sequenced to obtain the nucleotide sequence of the *uvrA* promoter shown in Fig. 1*b*. The transcriptional start point in this sequence was determined from RNA sequencing of the [γ-^{32}P]-labelled transcript made *in vitro* (data not shown) and is indicated as +1 in the figure.

To study the effect of LexA on *uvrA* transcription, LexA was included in the *in vitro* transcription reactions. As seen in Fig. 2, when present at concentrations similar to those used for *recA* and *lexA*[2], LexA markedly inhibits transcription of the *uvrA* gene. This inhibition is the result of specific binding of LexA to the promoter–operator region of *uvrA*, as is demonstrated by the DNase I protection experiments ('footprinting', see Fig. 3). As seen in Fig. 3, LexA protects from DNase I digestion a 25–30-base pair (bp) segment that overlaps the *uvrA* promoter.

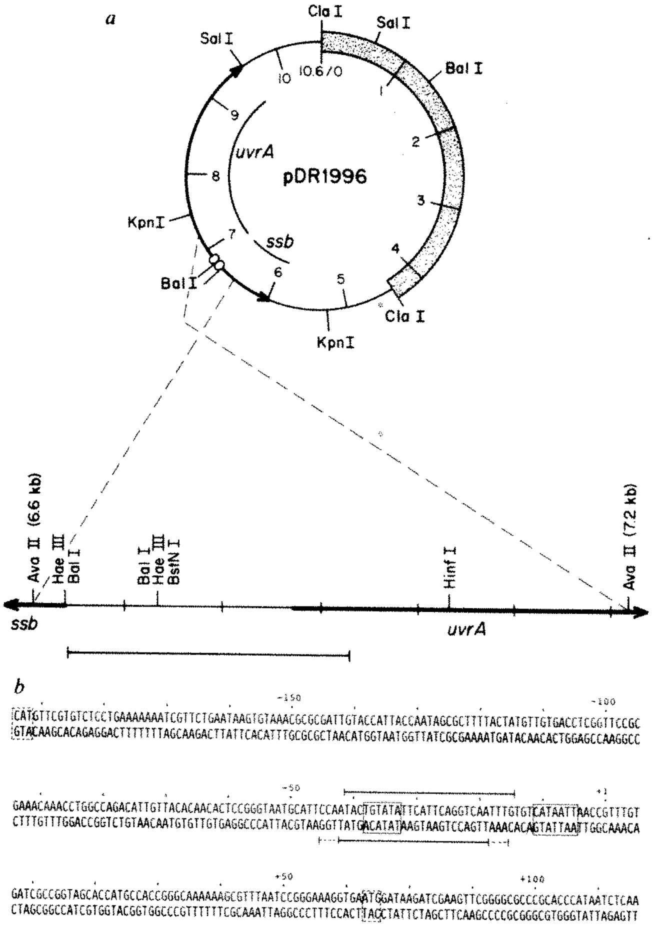
a
Sal I
Cla I
Sal I
Bal I
10.6/0
10
1
9
2
uvrA
pDR1996
8
3
KpnI
7
ssb
4
6
5
Bal I
Cla I
KpnI
Ava II (6.6 kb)
Hae III
Bal I
Bal I
Hae III
BstN I
Hinf I
Ava II (7.2 kb)
ssb
uvrA
b
-150
-100
CATGTTCGTGTCTCCTGAAAAAAATCGTTCTGAATAAGTGTAAACGCGCGATTGTACCATTACCAATAGCGCTTTTACTATGTTGTGACCTCGGTTCCGC
GTACAAGCACAGAGGACTTTTTTTAGCAAGACTTATTCACATTTGCGCGCTAACATGGTAATGGTTATCGCGAAAATGATACAACACTGGAGCCAAGGCC
-50
+1
GAAACAAACCTGGCCAGACATTGTTACACAACACTCCGGGTAATGCATTCCAATACTGTATATTCATTCAGGTCAATTTGTGTCATAATTAACCGTTTGT
CTTTGTTTGGACCGGTCTGTAACAATGTGTTGTGAGGCCCATTACGTAAGGTTATGACATATAAGTAAGTCCAGTTAAACACAGTATTAATTGGCAAACA
+50
+100
GATCGCCGGTAGCACCATGCCACCGGGCAAAAAAGCGTTTAATCCGGGAAAGGTGAATGGATAAGATCGAAGTTCGGGGCGCCCGCACCCATAATCTCAA
CTAGCGGCCATCGTGGTACGGTGGCCCGTTTTTTCGCAAATTAGGCCCTTTCCACTTACCTATTCTAGCTTCAAGCCCCGCGGGCGTGGGTATTAGAGTT

Fig. 1 *a*, Restriction map of the *uvrA* plasmid, pDR1996. The vector (pBR322) sequences are shaded. The locations and directions of transcription of *uvrA* and *ssb* are indicated by the heavy arrows on the map. The region whose sequence is shown in *b* is indicated by a bar beneath the detailed restriction map of the 0.6-kb *Ava*II fragment carrying the *uvrA* and *ssb* promoters. *b*, Sequence of the promoter–operator regions of *uvrA* and *ssb*. The −35 sequence and Pribnow box for *uvrA* are boxed. The previously determined[9] initiation codon of *ssb* and the initiation codon for *uvrA* (unpublished data) are indicated by dashed boxes. The region protected from DNase I by LexA is bracketed; dashed lines at the ends of the brackets indicate regions of uncertainty as to the extent of LexA protection. Numbering is from the transcription start site of *uvrA* determined by RNA sequence analysis as previously described[8].

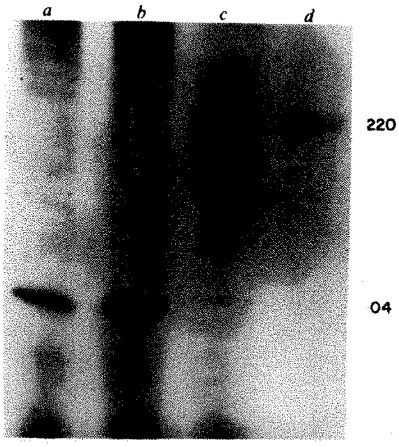

Fig. 2 Inhibition of *uvrA* transcription by LexA *in vitro*. pBR322 DNA and the $(HaeIII\text{-}HinfI)_{325}$ fragment of pDR1996 were transcribed *in vitro* in the presence and absence of LexA. Transcription reactions using 2.5 μg ml^{-1} of template and 14 μg ml^{-1} of LexA were performed as described previously[8] except that the transcription buffer contained 30 mM KCl. Transcripts were analysed on a 6% polyacrylamide gel containing 9 M urea and visualized by autoradiography. In lanes *a* and *b* 75% of the reaction mixture was loaded onto the gel while in lanes *c* and *d* 25% of the total reaction volume was loaded. The length of the transcript (shown in nucleotides at the right of the figure) was determined by comparison with ^{32}P-labelled ΦX174 DNA. The 104-nucleotide transcript from pBR322 (used here as a control) has been described previously by Levine and Rupp[13]. The 220 nucleotide-long transcript initiated from the *uvrA* promoter was found to consist of two discrete RNA species which differed in length by ~10 nucleotides but possessed the same sequence at their 5′ ends (data not shown). *a*, pBR322 minus LexA; *b*, pBR322 plus LexA; *c*, pDR1996 $(HaeIIIB\text{-}HinfI)_{325}$ minus LexA; *d*, pDR1996 $(HaeIIIB\text{-}HinfI)_{325}$ plus LexA.

Inspection of the protected region reveals that it has extensive sequence homology with the LexA binding sites found in the *recA*, *lexA* and *uvrB* genes[2,3,8] and the postulated LexA binding site in the colicin E1 gene, *cleI* (ref. 11). A comparison of these various operators is shown in Fig. 4, from which two conclusions can be reached. First, although all the operators have considerable sequence homology with the *recA* operator, which has a near-perfect dyad symmetry, the only conserved dyad symmetry is 5′CTG(N)$_{10}$CAG3′, suggesting that this structure might be an important feature of the LexA binding site. Second, the positioning of the LexA binding site relative to the two promoter defining sequences, the '−35 sequence' and the Pribnow box, varies in the different genes. Thus, the LexA binding site overlaps with the −35 sequence of *uvrA*, occupies the region extending from the −35 sequences to the Pribnow boxes of *recA* and *uvrB*, covers the Pribnow box and the transcriptional start site of *lexA* and occupies the region 3′ to the Pribnow box of *cleI*. These varied locations of the LexA binding site may provide flexibility for additional regulatory circuits for individual genes by leaving specific regions in the promoters accessible to regulatory factors other than LexA. In this regard, it is of interest that the *uvrA* and *uvrB* genes share a homologous sequence that is only partly included in the LexA binding site (see Fig. 4). This sequence may be the recognition site of a repressor specific for these genes. (Note that such a repressor would inhibit transcription from the first *uvrB* promoter, P1, which is not influenced by LexA *in vitro*[8].) Similarly, there is evidence that two other *recA*–*lexA*-controlled genes, *cleI* and *himA*, have second repressors in addition to LexA[11,12], and it is likely that the operators for these repressors do not or only partly overlap with the LexA binding site. The SOS response is a drastic reaction by the cell, causing a major perturbation in cell physiology and in some cases, even leading to cell death

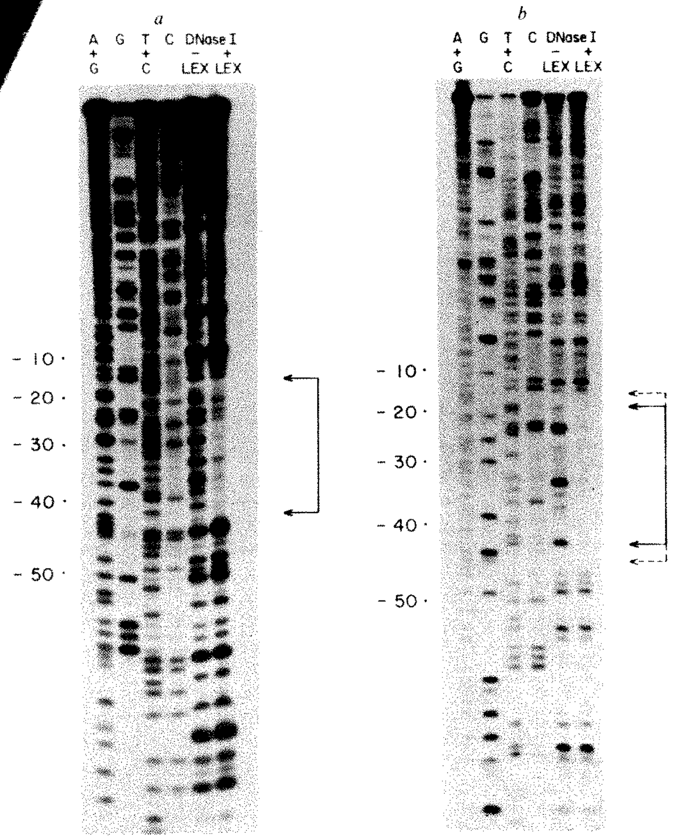

Fig. 3 Protection of the *uvrA* operator by LexA against digestion with DNase I (footprinting). The (*Hae*III–*Hin*fI)$_{325}$ fragment of pDR1996 was labelled with ^{32}P at the *Hae*III site at either the 5′ or 3′ end and then subjected to chemical sequencing[14] or DNase digestion[15] in the presence or absence of LexA. The conditions for footprinting were essentially as described before[4,8,15]. The bases are numbered relative to the start point of *uvrA* mRNA, which is designated +1. The protected regions are bracketed and the positions where the effect of LexA protection could not be determined due to lack of DNase I cleavage are indicated by broken lines. *a*, Top strand (5′ label); *b*, bottom strand (3′ label).

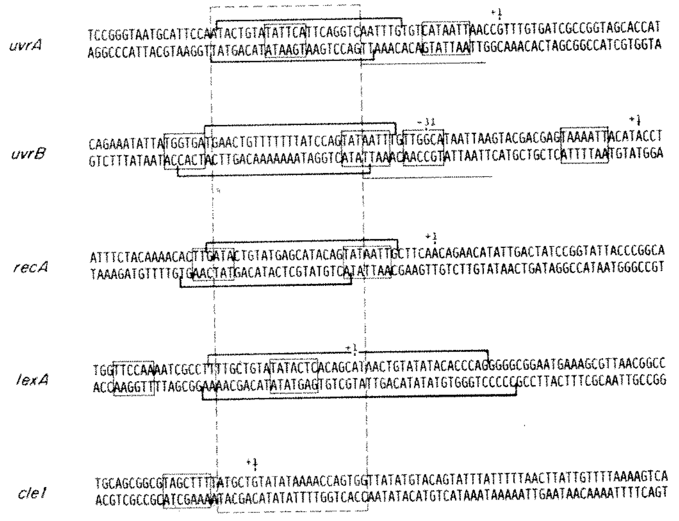
+1
uvrA
TCCGGGTAATGCATTCCAATACTGTATATTCATTCAGGTCAATTTGTGTCATAATTAACCGTTTGTGATCGCCGGTAGCACCAT
AGGCCCATTACGTAAGGTTATGACATATAAGTAAGTCCAGTTAAACACAGTATTAATTGGCAAACACTAGCGGCCATCGTGGTA
-31
+1
uvrB
CAGAAATATTATGGTGATGAACTGTTTTTTTATCCAGTATAATTTGTTGGCATAATTAAGTACGACGAGTAAAATTACATACCT
GTCTTTATAATACCACTACTTGACAAAAAAATAGGTCATATTAAACAACCGTATTAATTCATGCTGCTCATTTTAATGTATGGA
+1
recA
ATTTCTACAAAACACTTGATACTGTATGAGCATACAGTATAATTGCTTCAACAGAACATATTGACTATCCGGTATTACCCGGCA
TAAAGATGTTTTGTGAACTATGACATACTCGTATGTCATATTAACGAAGTTGTCTTGTATAACTGATAGGCCATAATGGGCCGT
+1
lexA
TGGTTCCAAAATCGCCTTTTGCTGTATATACTCACAGCATAACTGTATATACACCCAGGGGGCGGAATGAAAGCGTTAACGGCC
ACCAAGGTTTTAGCGGAAAACGACATATATGAGTGTCGTATTGACATATATGTGGGTCCCCCGCCTTACTTTCGCAATTGCCGG
+1
cle1
TGCAGCGGCGTAGCTTTTATGCTGTATATAAAACCAGTGGTTATATGTACAGTATTTATTTTTAACTTATTGTTTTAAAAGTCA
ACGTCGCCGCATCGAAAATACGACATATATTTTGGTCACCAATATACATGTCATAAATAAAAATTGAATAACAAAATTTTCAGT

Fig. 4 Location of LexA binding sites in the promoter–operator regions of various genes that are controlled by *recA* and *lexA*. The 22-base pair dyad symmetry in the *recA* gene and the sequences in the other genes corresponding to this palindrome are in the dashed box. The −35 sequence of *cle1* (colicin E1) is not included for simplicity. Note that there are two tandem operators in *lexA*[3] and that the potential LexA binding site of *cle1* is included in a larger dyad symmetry[11]. *uvrB* has at least two transcriptional start sites, one marked +1 and the second at −31. Transcription from −31 but not from +1 is inhibited by LexA[8]. The regions of sequence homology between *uvrA* and *uvrB* are underlined. Other symbols are as in Fig. 1.

(as in the case of lambda induction). Thus, it may be advantageous for genes repressed by LexA to have additional regulatory controls that can function to fine-tune the response of different genes to different inducing stimuli, and perhaps also to cause expression of some SOS genes in conditions that do not lead to a full-scale SOS response.

We thank Elizabeth Rapoport for technical assistance. This work was supported by NIH grants CA 06519, CA 09259, GM 24178 and American Cancer Society grant PDT-80.

Received 22 March; accepted 23 April 1982.

1. Howard-Flanders, P. *Scient. Am.* **245,** 72–80 (1981).
2. Little, J. W., Edmiston, S. H., Pacelli, L. Z. & Mount, D. W. *Proc. natn. Acad. Sci. U.S.A.* **77,** 3225–3229 (1980).
3. Little, J. W., Mount, D. W. & Yanisch-Perron, C. R. *Proc. natn. Acad. Sci. U.S.A.* **78,** 4199–4203 (1981).
4. Brent, R. & Ptashne, M. *Proc. natn. Acad. Sci. U.S.A.* **78,** 4204–4281 (1981).
5. Kenyon, C. J. & Walker, G. C. *Nature* **289,** 808–810 (1981).
6. Fogliano, M. & Schendel, P. *Nature* **289,** 196–198 (1981).
7. Kacinski, B. M., Sancar, A. & Rupp, W. D. *Nucleic Acids Res.* **9,** 4495–4508 (1981).
8. Sancar, G. B., Sancar, A., Little, J. W. & Rupp, W. D. *Cell* **28,** 523–530 (1982).
9. Sancar, A., Williams, K. R., Chase, J. W. & Rupp, W. D. *Proc. natn. Acad. Sci. U.S.A.* **78,** 4274–4278 (1981).
10. Sancar, A. *et al. J. molec. Biol.* **148,** 45–62 (1981).
11. Ebina, Y. *et al. Gene* **15,** 119–126 (1981).
12. Miller, H. I., Kirk, M. & Echols, H. *Proc. natn. Acad. Sci. U.S.A.* **78,** 6754–6758 (1980).
13. Levine, A. & Rupp, W. D. in *Microbiology-1978* (ed. Schlesinger, D.) 163–166 (American Society for Microbiology, Washington DC, 1978).
14. Maxam, A. & Gilbert, W. *Meth. Enzym.* **65,** 499–560 (1980).
15. Galas, D. & Schmitz, A. *Nucleic Acids Res.* **5,** 3157–3170 (1978).

The *uvrD* gene of *E. coli* encodes a DNA-dependent ATPase

Kenji Oeda, Takashi Horiuchi & Mutsuo Sekiguchi

Department of Biology, Faculty of Science, Kyushu University 33,
Fukuoka 812, Japan

Mutations in the *uvrD* gene of *Escherichia coli* K-12 result in multiple phenotypes, including increased sensitivity to UV light and ionizing radiation, decreased ability for host cell reactivation, increased spontaneous mutation frequency and decreased rate of genetic recombination[1–6]. It has been shown, moreover, that double mutants having mutations in both *uvrD* and *polA* genes are conditionally lethal[7–10]. The pleiotropic phenotypes of the *uvrD* mutants suggest that the *uvrD* gene product may have important roles in the processes of DNA repair, recombination and replication. To study the function of the *uvrD* gene, we have constructed hybrid phages and plasmids that carry the gene[11]. Here we have analysed the proteins synthesized by the hybrid phages and report that the *uvrD* gene product is a polypeptide of molecular weight (MW) 75,000. We present evidence that the *uvrD* protein possesses a DNA-dependent ATPase activity.

A hybrid phage, λ*uvrD*$^{+}$, which is able to complement *uvrD* mutations, was constructed using λgt·λc as cloning vector[11]. In addition to the *uvrD* gene, λ*uvrD*$^{+}$ carries the *corA* gene that controls transport of Mg^{2+}, Mn^{2+} and Co^{2+} through the cell membrane[12,13]. A hybrid phage, λ*corA*$^{+}$, which carries the *corA* gene alone, was also constructed[11]; this served as a control. We have isolated various deletion mutants from λ*uvrD*$^{+}$ using the method of Saito and Uchida[14]. Of these deletion mutants, Δ41 and Δ48 were able to complement *corA* but not *uvrD* mutations, while Δ49 was unable to complement either mutation.

λ*uvrD*$^{+}$ contains a 6.8-kilobase pair (kbp) DNA fragment derived from the *E. coli* chromosome and a part (4.0 kbp) of the γδ sequence (transposon Tn*1000*) derived from F plasmid[11]. DNA fragments generated from these phages using restriction endonucleases were analysed by agarose gel electrophoresis, and physical maps constructed (Fig. 1).

Proteins produced by the λ transducing phages were labelled with a ^{14}C-amino acid mixture and analysed by SDS-polyacrylamide gel electrophoresis (Fig. 2). Compared with cells infected with λgt·λc, two specific bands, corresponding to polypeptides

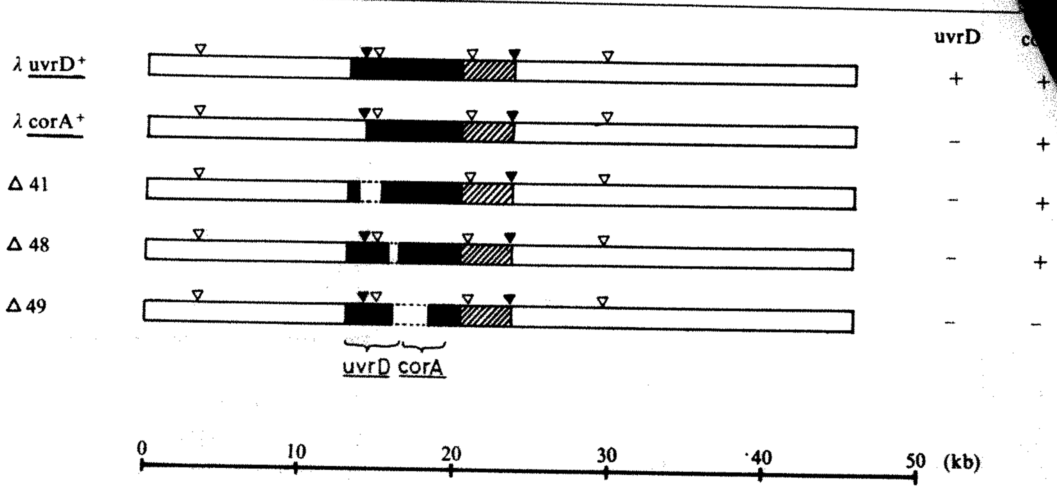

Fig. 1 Physical maps of transducing λ phages. Cleavage maps were constructed by digestion with restriction enzymes followed by agarose gel electrophoretic analysis as described previously[11]. Origins and restriction enzyme target sites are: ■, *E. coli* DNA; ▨, γδ sequence; □, λ phage DNA; [ ], deletion; ▽, *Bam*HI target sites; ▼, *Eco*RI target sites. Phenotypes of *uvrD3* or *corA5738* cells lysogenized with each transducing phage are shown on the right-hand side.

of molecular weight 75,000 and 37,000, were found in cells infected with λ*uvrD*⁺. The 75,000-MW polypeptide was identified as the *uvrD* gene product, because it was absent from cells infected with λ*corA*⁺, Δ41 or Δ48, which lack the intact *uvrD* gene. The 37,000-MW polypeptide seems to be the *corA* gene product; it is absent from Δ49.

Of the many proteins known to be involved in DNA metabolism, there are some whose molecular weight is ~75,000. These include DNA-dependent ATPase I[15,16] and DNA helicase II[17,18]. Recent studies suggested that they may be the same proteins[19]. Thus, we have examined DNA-dependent ATPase activity in cells infected with *uvrD*⁺ transducing phage. To overproduce the *uvrD* protein, the *susQ* mutation[20] was introduced into both λ*uvrD*⁺ and λ*corA*⁺ by recombination of each phage strain with λ*imm434 susQ21*. A culture of *E. coli* W3623 (*uvrD*⁺ *Su*⁻) infected with λ*uvrD*⁺ *susQ* was collected 195 min after infection, and an extract was subjected to DEAE-cellulose filtration, ammonium sulphate fractionation and phosphocellulose chromatography. As a control, an extract of λ*corA*⁺ *susQ*-infected cells was processed similarly.

Figure 3 shows elution profiles of DNA-dependent ATPase activity from phosphocellulose columns. Both samples showed activity eluting as a single peak at almost the same position as that reported for DNA-dependent ATPase I in these conditions[15]. The ATPase activity was totally dependent on denatured DNA and was sensitive to *N*-ethylmaleimide, as was observed with the enzyme from normal cells. We estimated that λ*uvrD*⁺-infected *uvrD*⁺ cells contain about 14 times more ATPase activity than λ*corA*⁺-infected *uvrD*⁺ cells. The small peaks in Fig. 3*b* may represent composites of ATPases, which were shown to be present in phosphocellulose eluates[21].

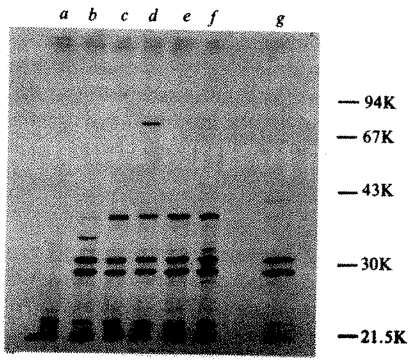

Fig. 2 Proteins produced by transducing λ phages. *E. coli* KY3304 lysogenic for λ*CI857* was grown in RM medium at 30 °C to a density of 2×10^8 cells ml^{-1} and infected with one of the transducing phages at a multiplicity of 10. The cells were labelled with ^{14}C-amino acid mixture at 30 °C for 50 min and extracts were prepared[28]. The polypeptides were analysed by electrophoresis on 10% SDS-polyacrylamide gels followed by fluorography, as described previously[29]. The positions of phosphorylase B [MW 94,000 (94K)], bovine serum albumin (67K), ovalbumin (43K), carbonic anhydrolase (30K) and soybean trypsin inhibitor (21.5K) are indicated. *a*, Uninfected; *b*, λgt·λc; *c*, λ*corA*⁺; *d*, λ*uvrD*⁺; *e*, Δ41; *f*, Δ48; g, Δ49.

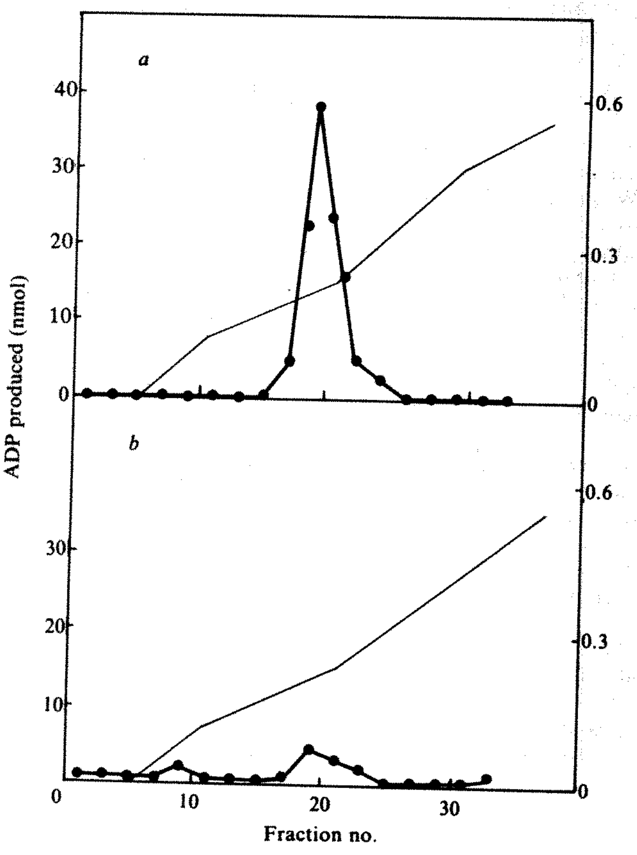

Fig. 3 Chromatographic resolution of DNA-dependent ATPase. *E. coli* strain W3623 (*uvrD*⁺ *Su*⁻) was infected with λ*uvrD*⁺ *susQ* (*a*) or λ*cor*⁺ *susQ* (*b*). The extracts were prepared from ~3 g of the infected cells and processed as described elsewhere[15]. Fraction II was applied to a phosphocellulose column (0.6×6 cm) and eluted with a linear gradient of 0.04–0.6 M NaCl in 0.02 M potassium phosphate buffer (*p*H 7.2). DNA-dependent ATPase activity was determined using 5 μl of each fraction. The reaction mixture (75 μl final volume) contained 50 mM Tris-HCl (*p*H 7.5), 20 mM 2-mercaptoethanol, 2 mM MgCl_2, 1 mM [γ-^{32}P]ATP (1×10^5 counts min^{-1}), 15 μg bovine serum albumin, and 7.5 nmol of heat-denatured calf thymus DNA. Incubation time, 20 min. A peak fraction (no. 19) of each sample was used for further analysis (see Fig. 4).

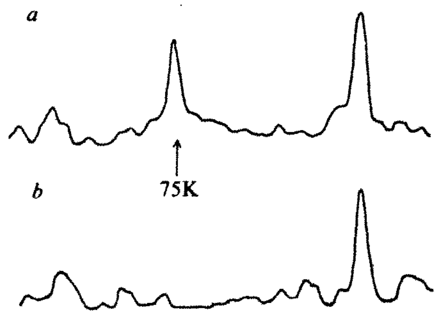

Fig. 4 Analysis of DNA-dependent ATPase fractions by SDS-polyacrylamide gel electrophoresis. Enzyme fractions (14 μl) from λ*uvrD*$^+$-infected (*a*) and λ*corA*$^+$-infected (*b*) cells were applied to 10% SDS-polyacrylamide gels and electrophoresed at 20 mA for 3 h. The gels were stained with Coomassie brilliant blue and scanned using a densitometer. Electrophoresis was from right to left. An arrow indicates the 75,000-MW polypeptide.

The enzyme fractions were further analysed by SDS-polyacrylamide gel electrophoresis. Figure 4 shows the patterns of proteins present in each of the peak fractions. In the λ*uvrD*$^+$ sample there was a large distinct band corresponding to the 75,000-MW protein whereas only a small band was observed at the corresponding position of the λ*corA*$^+$ sample, although the sizes of the other bands were almost the same for both samples. The ratio of the amounts of the 75,000-MW protein for the two samples was 12:1, very similar to that of the activities of the two samples.

These results suggest that the *uvrD* gene encodes a 75,000-MW protein which possesses a DNA-dependent ATPase activity. As this protein is similar in both size and chromatographic properties to DNA-dependent ATPase I[15,16], it is possible that the *uvrD* protein may be identical to DNA-dependent ATPase I. Recently, Richet *et al.*[19] isolated mutants that are defective in DNA-dependent ATPase I. Although they have correlated the mutations neither to certain phenotypes nor to a specific chromosomal locus, it is possible that the mutations might occur in the *uvrD* gene.

E. coli possesses several enzymes capable of unwinding DNA at the expense of ATP[17,18,21–27], and such enzymes may have vital roles in DNA replication, recombination and repair. Evidence has been presented that one of the enzymes, DNA helicase II, may be identical to DNA-dependent ATPase I[19]. Thus, it would be of interest to determine whether the *uvrD* protein possesses DNA unwinding activity. Studies on this are now in progress.

We thank Dr Yoshikazu Nakamura for sending us bacterial and bacteriophage strains and providing instruction in the method of protein labelling. This work was supported in part by Scientific and Cancer Research Grants from the Ministry of Education, Science and Culture of Japan.

Received 3 February; accepted 23 April 1982.

1. Ogawa, H., Shimada, K. & Tomizawa, J. *Molec. gen. Genet.* **101,** 227–244 (1968).
2. Smirnov, G. B. & Skavronskaya, A. G. *Molec. gen. Genet.* **113,** 217–221 (1971).
3. Siegel, E. G. *J. Bact.* **113,** 145–160 (1973).
4. Horii, Z. I. & Clark, A. J. *J. molec. Biol.* **80,** 327–344 (1973).
5. Kushner, S. R., Shaepherd, J., Edwards, G. & Maples, V. F. in *DNA Repair Mechanisms* (eds Hanawalt, P. C., Friedberg, E. C. & Fox, C. F.) 251–254 (Academic, New York, 1978).
6. Siegel, E. C. *Molec. gen. Genet.* **184,** 526–530 (1981).
7. Horiuchi, T. & Nagata, T. *Molec. gen. Genet.* **123,** 89–110 (1973).
8. Siegel, E. C. *J. Bact.* **113,** 161–166 (1973).
9. Smirnov, G. B., Filkova, E. V. & Skavronskaya, A. G. *Molec. gen. Genet.* **121,** 139–150 (1973).
10. Mattern, I. E. & Houtman, P. C. *Mutat. Res.* **25,** 281–287 (1974).
11. Oeda, K., Horiuchi, T. & Sekiguchi, M. *Molec. gen. Genet.* **184,** 191–199 (1981).
12. Nelson, D. L. & Kennedy, E. P. *Proc. natn. Acad. Sci. U.S.A.* **69,** 1091–1093 (1972).
13. Park, M. H., Wong, B. B. & Lusk, J. E. *J. Bact.* **126,** 1096–1103 (1976).
14. Saito, H. & Uchida, H. *Molec. gen. Genet.* **164,** 1–8 (1978).
15. Richet, E. & Kohiyama, M. *J. biol. Chem.* **251,** 808–812 (1976).
16. Richet, E. & Kohiyama, M. *J. biol. Chem.* **253,** 7490–7495 (1978).
17. Abdel-Monem, M. & Hoffmann-Berling, H. *Eur. J. Biochem.* **65,** 431–440 (1976).
18. Abdel-Monem, M., Chanal, M. C. & Hoffmann-Berling, H. *Eur. J. Biochem.* **79,** 33–38 (1977).
19. Richet, E., Kern, R., Kohiyama, M. & Hirota, Y. in *Mechanistic Studies of DNA Replication and Genetic Recombination* (ed. Alberts, B.) 606–608 (Academic, New York, 1980).
20. Moir, A. & Brammar, W. J. *Molec. gen. Genet.* **149,** 87–99 (1976).
21. Yarranton, G. T., Das, R. H. & Gefter, M. L. *J. biol. Chem.* **254,** 11997–12001 (1979).
22. Denhardt, D. T., Iwaya, M. & Larison, L. L. *Virology* **49,** 486–496 (1972).
23. Abdel-Monem, M., Dürwald, H. & Hoffmann-Berling, H. *Eur. J. Biochem.* **65,** 441–443 (1976).
24. Scott, J. F. & Kornberg, A. *J. biol. Chem.* **253,** 3292–3297 (1978).
25. Kornberg, A., Scott, J. F. & Bertsch, L. L. *J. biol. Chem.* **253,** 3298–3304 (1978).
26. Yarranton, G. T., Das, R. H. & Gefter, M. L. *J. biol. Chem.* **254,** 12002–12006 (1979).
27. Klinkert, M., Klein, A. & Abdel-Monem, M. *J. biol. Chem.* **255,** 9746–9752 (1980).
28. Saito, H., Nakamura, Y. & Uchida, H. *Molec. gen. Genet.* **165,** 247–256 (1978).
29. Laemmli, U. K. *Nature* **227,** 680–685 (1970).

A relationship between replicon size and supercoiled loop domains in the eukaryotic genome

Mario Buongiorno-Nardelli, Gioacchino Micheli, Maria Teresa Carrī & Monique Marilley*

Istituto di Istologia ed Embriologia, Facoltà di Scienze MFN,
Università di Roma, Rome, Italy

*Départment de Biologie Moleculaire et Cellulaire, Laboratoire de
Morphogénèse Animale, LA CNRS 179, UER Scientifique de
Luminy, F13288 Marseille Cedex 2, France

In interphase nuclei and metaphase chromosomes, eukaryotic chromosomal DNA is arranged in negatively supercoiled loops whose length averages several tens of kilobases (kb). Supercoiling indicates that the loops are tenaciously bound at both ends through the periodic attachment of DNA to a non-histone protein structural support, termed the nuclear matrix, skeleton or cage in interphase nuclei and the scaffold in metaphase chromosomes[1–16]. The looped organization has been envisaged to be important in DNA replication[2,11,15,17–25] and transcription[26–28]. We report here a close relationship between average loop length and replicon size in different animal and plant species. Autoradiographic experiments support the hypothesis that DNA synthesis occurs at fixed sites on the nuclear matrix[15,20]. We also describe a modification of the looped organization occurring during early embryonic development in *Xenopus laevis*.

We have investigated the supercoiled loop organization of erythrocytes (Fig. 1) and cultured cells (not shown) from *X. laevis* using the fluorescence halo technique[11]. Cells were treated with the non-ionic detergent NP40, dehistonized in 2 M NaCl containing various amounts of ethidium bromide or acridine orange and observed under the fluorescence microscope. The intercalation of either dye causes the dehistonized loops to form a DNase-sensitive and RNase-resistant fluorescence halo around the nuclear skeleton (Fig. 1*b*, *d*). The halo's radius (15 μm maximum) exhibits a characteristic 'breathing' in response to varying dye concentrations and prolonged UV irradiation (see Fig. 1 legend and refs 11, 23), thus supporting conclusions from different systems[11,23] that DNA is arranged in independent negatively supercoiled loops. Assuming that the largest fluorescence halo corresponds to completely unwound and extended DNA loops, then its radius gives a rough estimate of the average loop size (2 × 15 μm or ~90 kilobases in *X. laevis*).

We next investigated the relationship between the nuclear matrix, supercoiled loops and DNA replication in cultured *X. laevis* kidney cells using the fluorescence halo technique coupled with autoradiography. Asynchronous cells grown in monolayer on microscope slides were ^{3}H-thymidine-pulsed for 2 min. The cells were then treated *in situ* for maximal halo expansion and autoradiographed. After 2 min labelling, radioactivity covers almost exclusively the nuclear matrix (Fig. 2*a*).

0028–0836/82/260100–03$01.00

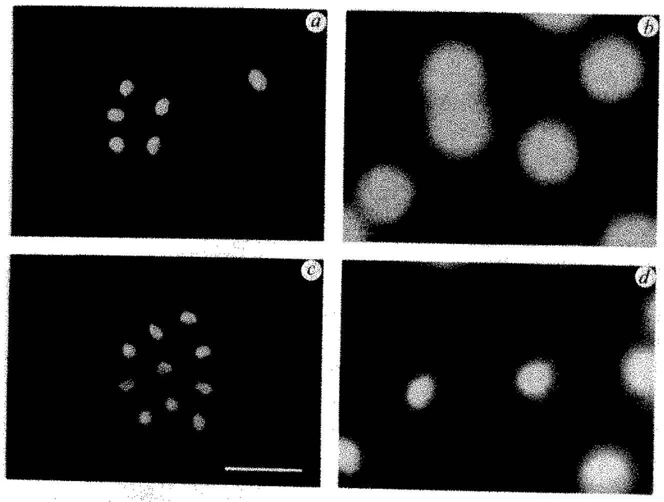

Fig. 1 Fluorescence micrograph of *X. laevis* erythrocyte nuclei. Freshly prepared blood smears were dipped for 30 s in ice-cold NP40 buffer (0.5% NP40, 10 mM MgCl, 0.5 mM $CaCl_2$, 1 mM phenylmethylsulphonyl fluoride, 50 mM Tris-HCl pH 7.5), stained with 5 μg ml^{-1} ethidium bromide (*a*) or 5 μg ml^{-1} acridine orange (*c*) and observed under the fluorescence microscope. When the dyes were dissolved in high-salt buffer (2 M NaCl, 0.2 mM MgCl, 10 mM Tris-HCl pH 7.5) at the same concentration a distinct fluorescence halo appeared (*b*, ethidium bromide; *d*, acridine orange). The halo radius (from the edge of the nuclear matrix to the edge of the halo) was measured using a micrometer eyepiece during the first few seconds following UV illumination. The radius reaches its maximum, ~15 μm, when the fluorochrome concentration is ~5 μg ml^{-1}; the lower or the higher the dye concentration, the smaller the halo (data not shown). However, at every dye concentration the maximal radius is attained following prolonged UV irradiation under the fluorescence microscope. These observations indicate that, with increasing dye concentrations, DNA loops are progressively unwound from a negatively supercoiled to a relaxed state and eventually forced into a positively supercoiled condition; whereas—independently from dye concentration—nicks introduced in the DNA by prolonged UV exposure remove the topological constraints thus lifting the maximal halo[11,23]. Scale bar, 45 μm.

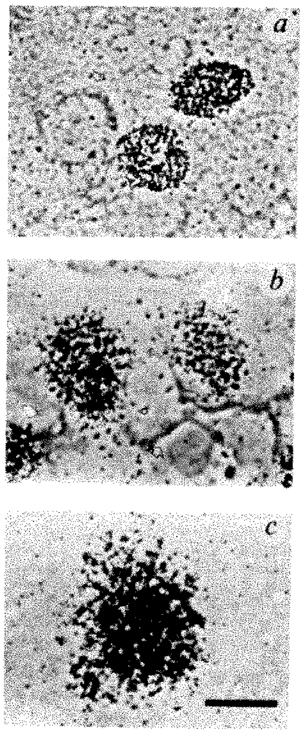

Fig. 2 Autoradioradiograms of *X. laevis* kidney culture cells pulsed with ^3H-thymidine and treated for maximal halo expansion. The fibroblast clone used stems from an established cell line (from Dr M. Cianfriglia, Siena). Cells were cultured in Eagle's minimal essential medium H_2O (100:40), supplemented with 10% fetal calf serum, at 26°C under 5% CO_2. Asynchronous cells growing in monolayer on microscope slides were pulsed with 20 μCi ml^{-1} ^3H-thymidine (42 Ci m-mol^{-1}; Amersham) for 2 (*a*), 10 (*b*), 30 (*c*) and 60 min or, in pulse-chase experiments (not shown), for 2 min followed by 0, 8, 28, 58 min chases with a 100-fold excess cold thymidine. The slides were then sequentially dipped in ice-cold distilled water for a few seconds, ice-cold NP40 buffer for ~30 s followed by 100 μg ml^{-1} ethidium bromide in high-salt buffer (see Fig. 1 legend) for ~1 min and exposed to a UV lamp (15 W, short wave) at a distance (~5 cm) and for a time sufficient for maximal halo expansion. After briefly rinsing with distilled water the slides were air dried and autoradiographed using Kodak NTB 2 undiluted autoradiographic emulsion. Exposure time was varied to obtain a roughly comparable grain density. Smoothed contours of several labelled areas, and of several unlabelled nuclear matrixes, were traced on enlarged prints of the autoradiograms, and assimilated to a circumference, using a Tektronix 4956 digitizer coupled to a 4051 desk top computer. Mean radius (in μm) of the labelled areas ±s.d. (number of measurements): 2 min pulse, 13.0 ± 0.85 (27); 10 min pulse, 17.2 ± 1.8 (30); 30 min pulse, 26.3 ± 1.9 (25); 60 min pulse, 27.6 ± 1.4 (29). Radius of the unlabelled nuclear matrix: 12.1 ± 0.9 μm (30). Average expansion rate of the labelled area: 0.47 μm min^{-1}. Arrows point to unlabelled nuclear matrixes. Scale bar, 25 μm.

Considering that the cells were in asynchronous growth active replicons were thus in all phases of replication, t observation suggests—in agreement with other investigation on different biological systems[2,11,18,20–23]—that in *X. laevis*, DNA synthesis occurs at fixed sites on the nuclear matrix. Nevertheless, the possibility that newly synthesized DNA binds nonspecifically to the nuclear matrix during extraction cannot be ruled out. Following 10 and 30 min pulses, the radioactivity distributes on a progressively wider area, which extends beyond the nuclear matrix (Fig. 2*b*, *c*). The radioactive area expands at a rate of ~0.47 μm min^{-1} (see Fig. 2 legend), in agreement with estimates of fork movement rate from DNA fibre autoradiography[29]. Almost identical results were obtained in pulse-chase experiments (data not shown) in which the expansion rate of the radioactive area was ~0.43 μm min^{-1}. Taking account of the bidirectionality of DNA replication and the average loop size in *X. laevis*, one loop would be predicted to be duplicated in ~30 min; hence pulses longer than 30 min should not result in a further increase of the labelled area. This was confirmed after 60 min labelling, since there was no substantial difference in the size of the labelled area compared with after 30 min.

The expansion of radioactivity on the halo with increasing pulse length suggests that replicating DNA loops are reeled through matrix-bound replication complexes, as proposed by Pardoll *et al.*[15,30]. On this interpretation, a relationship between the average loop size and the average replicon length would be predicted. We have chosen several animal and plant species

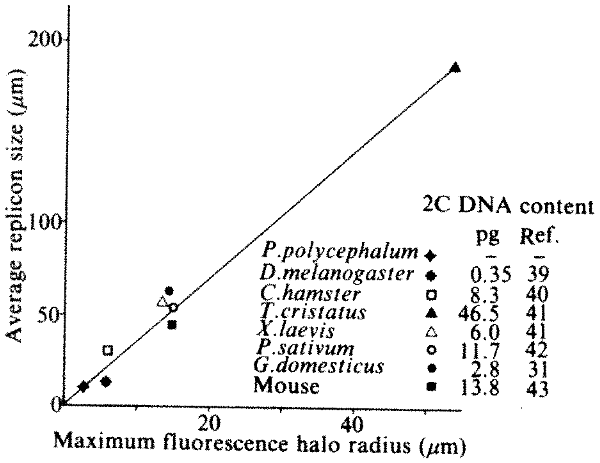

Fig. 3 Relationship between maximum fluorescence halo radius (MFHR) and average replicon size (av. RS). MFHR was determined by treating blood smears, cultured cells grown on microscope slides or isolated nuclei with ice-cold NP40 buffer and staining with 100 μg ml^{-1} ethidium bromide in high-salt buffer (see Fig. 1 legend). Maximal fluorescence halo expansion was induced by prolonged (⩾2 min) UV irradiation under the fluorescence microscope and measured using a micrometer eyepiece. Mean MFRH values (in μm) ± s.d. (number of measurements) are given below. MFHR data for *P. polycephalum* and mouse and all av. RS values (in μm determined by DNA fibre autoradiography) are taken from the literature. *P. polycephalum*: av. RS, 9[38]; MFHR 2.5–3[23]. *Drosophila melanogaster*: av. RS, on Schneider 2 cultured cells, 13.6[32]; MFHR, on GM 2 cultured cells (gift of Dr R. Caneva, Centro Acidi Nucleici, Rome) 6.0 ± 0.8 (25). Chinese hamster: av. RS, on B14FAF28 cultured cells, 30[33]; MFHR, on CHEF 125 cultured cells (grown in Eagle's minimal essential medium at 37 °C under 5% CO_2), 6.1 ± 0.7 (31). *X. laevis*: av. RS, on A6 cultured cells, 57.5[31]; MFHR, on kidney cultured cells (see Fig. 2 legend), 14.0 ± 3.2 (19). *Pisum sativum*: av. RS, on cells from root tip meristems, 54.7[34]; MFHR, on nuclei from root tips (isolation procedure as described in Fig. 4 legend) 14.8 ± 1.5 (25). *Gallus domesticus*: av. RS, on embryonic primary cell culture, 63[35]; MFHR, on freshly prepared blood smear, 14.1 ± 1.7 (15). Mouse: av. RS, on L929 cultured cells, 45.4[36]; MFHR, on 3T3 cultured cells, 15[11]. *Triturus cristatus*: av. RS, on liver primary cell culture, 188[31]; MFHR, on freshly prepared blood smear, 53.7 ± 4.2 (24). The 2C DNA contents in pg (ref. from which value is taken) for the various species examined are the following. *P. polycephalum* (◆), (—); *D. melanogaster* (★), 0.35[39]; Chinese hamster (□), 8.3[40]; *T. cristatus* (▲), 46.5[41]; *X. laevis* (△), 6.0[41]; *P. sativum* (○), 11.7[42]; *G. domesticus* (●) 2.8[31]; mouse (■) 13.8[43].

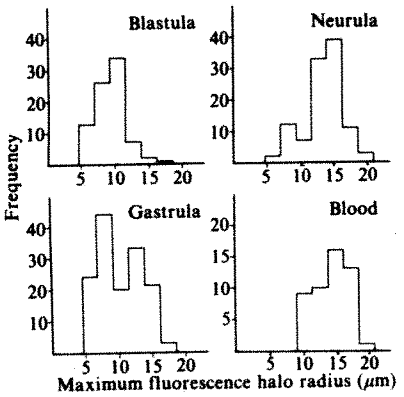

Fig. 4 Maximum fluorescence halo radius in different developmental stages of *X. laevis*. Ovulation and mating were stimulated by injection of gonadotropic hormone into the dorsal lymph sac a few hours before mating: females received 1,200 U of Pregnyl (Organon) and males 300 U. Mating and egg laying were allowed to occur overnight. The embryos were then collected, dejelled with 2.4% cysteine *p*H 7.5 and staged according to Nieuwkoop and Faber[37]. Nuclei were isolated by gently homogenizing the embryos in buffer A (60 mM KCl, 15 mM NaCl, 0.15 mM spermine, 0.5 mM spermidine, 15 mM 2-mercaptoethanol, 15 mM Tris-HCl *p*H 7.5) containing 0.34 M sucrose. One volume of ice-cold NP40 buffer (see Fig. 1 legend) was then added and the homogenate was centrifuged (~1,000*g* at 4 °C for 10 min) on a 1.37 M sucrose cushion in buffer A. the pellet was resuspended in a small volume of 20 mM EDTA, 10 mM Tris-HCl *p*H 7.5. A droplet of this suspension was diluted, directly on microscope slides, in an excess volume of 100 μg ml^{-1} ethidium bromide in high-salt buffer (see Fig. 1 legend) and covered with a coverslip. Maximum fluorescence halo radii were measured under the fluorescence microscope, using a micrometer eyepiece, after prolonged (≥2 min) UV illumination. Blood smears were treated for maximal fluorescence halo expansion as described in Fig. 3 legend. Mean values (in μm) ±s.d. (number of measurements): blastula (stage 8–9), 9.4 ± 2.4 (83); gastrula (stage 10–11), 10.3 ± 3.3 (145); neurula (stage 13–14) 13,5 ± 3.0 (107); (adult blood) 14.5 + 2.6 (49). The observation of fluorescent haloes on embryonic nuclei in suspension is quite difficult, as the DNA haloes, compared with those from blood smears or cells growing attached to glass surfaces (Fig. 3), can be easily distorted or destroyed by sudden currents or air bubbles in the liquid sheet between the microscope slide and the coverslip.

(Fig. 3) whose replicon sizes are known from DNA fibre autoradiography. The maximum halo radius seems to be species specific, varying from 2.5 μm (*Physarum polycephalum*) to 53.7 μm (*Triturus cristatus*), and is only roughly proportional to 2C DNA content (DNA content/diploid nucleus). On the other hand the halo radius (loop size) is directly proportional to the average replicon length, which strongly supports a general relationship between supercoiled loop structure and DNA replication.

It is of interest to speculate how DNA loops might be related to replication. A preliminary condition must be the existence of two adjacent matrix-bound replication complexes per replicon, in order to reconcile fixed replication sites with the bidirectionality of synthesis. As a further development of previous models[2,15,19,20,22,30] we propose that each replicon might actually correspond to two adjacent loops and be duplicated by the reeling of the DNA through a couple of matrix-bound replication complexes, alternate anchorage sites of the DNA to the nuclear matrix behaving as origins and termini of replication. Once a new nuclear matrix is assembled—whenever this happens with respect to the S phase—one of the two newly replicated origins, and one of the two termini, would remain bound to the old matrix while the other would bind to the newly assembled one. This, admittedly speculative, view was drawn from the data in Fig. 3. The average replicon length in all the species explored is roughly four times the maximum fluorescence halo radius, that is, twice the size of a DNA loop. Although the replicon lengths and halo radii are only approximations, our interpretation is appealing because it suggests how the whole chromosome structure can be faithfully reproduced at each cell cycle and how daughter DNA strands orderly segregate at mitosis.

An intriguing facet of DNA replication in multicellular organisms is the brevity of the S phase in early, compared with later, development. As the rate of fork movement is constant, the variation has been explained on the basis that during pregastrular stages, compared with later ones, the origins of replication are synchronously activated and the replicon size is smaller[31,32].

To check further the proposed correspondence between replicons and supercoiled loops we have determined the maximum halo radius in embryonic cells from *X. laevis* at pre- and post-gastrular stages. The maximum halo size in blastulae averages 9 μm (Fig. 4). A significant proportion of gastrula-stage nuclei are able to develop haloes of 10–15 μm, and at the tail bud stage, most of the dehistonized nuclei have 10–15 μm haloes. These results are consistent with the reduced replicon size in pregastrular stages[31,32] and further support a relationship between supercoiled loops and replication units[11]. They suggest that structural rearrangement of the chromosome occurs during gastrulation, when the embryonic genome enters a phase of active gene expression. However, the intrinsic limitations of the technique used here (see Fig. 4 legend) require that this structural transition be confirmed by different experimental approaches. It is nonetheless tempting to envisage such a transition in gastrula as of crucial importance in establishing novel patterns of supercoiled loop domains representing both replication and transcription units.

We thank Mrs M. T. Curtale and Miss T. Forte for carrying out some of the experiments on *X. laevis* fluorescence haloes, and Mr L. Lascari for technical assistance. This work was supported by grants CNR 78.01345.04 and 79.03191.04 to M.B.-N. M.M. was recipient of a NATO fellowship.

Received 10 November 1981; accepted 13 April 1982.

1. Piñon, R. & Salts, Y. *Proc. natn. Acad. Sci. U.S.A.* **74,** 2850–2854 (1977).
2. McCready, S. J. Godwin, J., Mason, D. W., Brazell, I. A. & Cook, P. R. *J. Cell Sci.* **46,** 365–386 (1980).
3. Benyajati, C. & Worcel, A. *Cell* **9,** 393–407 (1976).
4. Hartwig, M. *Acta biol. med. germ.* **37,** 421–432 (1978).
5. Marsden, M. P. F. & Laemmli, U. K. *Cell* **17,** 849–858 (1979).
6. Ide, T. Nakane, M., Anzai, K. & Andoh, T. *Nature* **258,** 445–447 (1975).
7. Igo-Kemenes, T. & Zachau, H. G. *Cold Spring Harb. Symp. quant. Biol.* **42,** 109–118 (1977).
8. Okada, T. A. & Comings, D. E. *Chromosoma* **72,** 1–14 (1979).
9. Mattern, M. R. & Painter, R. B. *Biochim. biophys. Acta* **563,** 293–305 (1979).
10. Mattern, M. R. & Painter, R. B. *Biochim. biophys. Acta* **563,** 306–312 (1979).
11. Vogelstein, B., Pardoll, D. M. & Coffey, D. S. *Cell* **22,** 79–85 (1980).
12. Laemmli, U. K. *et al. Cold Spring Harb. Symp. quant. Biol.* **42,** 351–360 (1977).
13. McCready, S. J. Cox, B. S. & McLaughlin, C. S. *Expl Cell Res.* **108,** 473–478 (1977).
14. Cook, P. R. & Brazell, I. A. *Nucleic Adids Res.* **8,** 2895–2906 (1980).
15. Shaper, J. H. *et al. Adv. Enzyme Regulation* **17,** 213–248 (1979).
16. Comings, D. E. in *The Cell Nucleus* Vol. 4 (ed. Bush, H.) 345–371 (Academic, New York, 1978).
17. Wilkins, A. S. *J. theor. Biol.* **89,** 715–717 (1981).
18. Berezney, R. *Expl Cell Res.* **123,** 411–414 (1979).
19. Berezney, R. & Buchholtz, L. A. *Expl Cell Res.* **132,** 1–13 (1981).
20. Pardoll, D. M., Vogelstein, B. & Coffey, D. S. *Cell* **19,** 527–536 (1980).
21. Berezney, R. & Coffey, D. S. *Science* **189,** 291–293 (1975).
22. Dijkwel, P. A., Mullenders, L. H. F. & Wanka, F. *Nucleic Acids Res.* **6,** 219–230 (1979).
23. Hunt, B. F. & Vogelstein, B. *Nucleic Acids Res.* **9,** 349–363 (1981).
24. Nelkin, B. D., Pardoll, D. M. & Vogelstein, B. *Nucleic Acids Res.* **8,** 5623–5633 (1980).
25. Buckler-White, A. J., Humphrey, G. W. & Pigiet, V. *Cell* **22,** 37–46 (1980).
26. Jackson, D. A., McCready, S. J. & Cook, P. R. *Nature* **292,** 552–555 (1981).
27. Smith, G. R. *Cell* **24,** 599–600 (1981).
28. Robinson, S. I., Nelkin, B. D. & Volgelstein, B. *Cell* **28,** 99–106 (1982).
29. Edenberg, H. J. & Huberman, J. A. *A. Rev. Genet.* **9,** 245–284 (1975).
30. Dingman, C. W. *J. theor. Biol.* **38,**187–195 (1974).
31. Callan, H. G. *Phil. Trans. R. Soc.* **B181,** 19–41 (1972).
32. Blumenthal, A. B., Kriegstein, H. J. & Hogness, D. S. *Cold Spring Harb. Symp. quant. Biol.* **38,** 205–224 (1974).
33. Huberman, J. A. & Riggs, J. D. *J. molec. Biol.* **39,** 327–341 (1968).
34. Van't Hof, J. *Expl Cell Res.* **93,** 95–104 (1975).
35. McFarlane, P. W. & Callan, H. G. *J. Cell Sci.* **13,** 821–839 (1973).
36. Hand, R. & Tamm, I. *J. molec. Biol.* **82,** 175–183 (1974).
37. Nieuwkoop, P. D. & Faber, J. *Normal Tables of Xenopus laevis* (North Holland, Amsterdam, 1967).
38. Funderud, S., Andreassen, R. & Haugli, F. *Nucleic Acids Res.* **6,** 1417–1431 (1979).
39. Rasch, E. M., Barr, H. J. & Rasch, R. W. *Chromosoma* **33,** 1–18 (1971).
40. Bachman, K. *Chromosoma* **37**, 85–93 (1972).
41. Buongiorno-Nardelli, M., Amaldi, F. & Lava-Sanchez, P. *Nature new Biol.* **238,** 134–137 (1972).
42. Van't Hof, J. & Sparrow, A. H. *Proc. natn. Acad. Sci. U.S.A.* **49,** 897–902 (1963).
43. Maul, G. G. & Deaven, L. *J. Cell Biol.* **73,** 748–760 (1977).

BOOK REVIEWS

Confronting the unanswerable

Marie Jahoda

The Mind's I: Fantasies and Reflections on Self and Soul. Composed and arranged by Douglas R. Hofstadter and Daniel C. Dennett. Pp.450. UK ISBN 0-7108-0352-4; US ISBN 0-465-04624-X. (Harvester/Basic Books: 1981.) £9.95, $16.95.

WHEN two nimble minds combine in the effort to produce a book designed, according to the preface, "to provoke, disturb and befuddle its readers" the chances of succeeding in this not obviously laudable enterprise must be high. Had Hofstadter and Dennett added to their aims amuse, disappoint and frustrate they would have encompassed the whole universe of possible readers' reactions to this particular book and their success, measured by their own standards, would have been total.

The themes addressed in the book concern eternal questions that have preoccupied great and not so great minds since the dawn of history: the nature of self, of consciousness, of reality, the body–mind problem, free will, the relation of mechanism to meaning. Every conceivable approach to these issues has in the past been adopted with conviction by some; none has withstood critical examination by others. All of them, however, whether based on religion, philosophy or science fulfil a major function: they enable their adherents to engage in a bootstrap operation, pulling themselves out of the inevitable ignorance about the ultimate why and wherefore. Once this operation is performed they can proceed to tackle answerable questions or develop consistent world views.

The debate about fundamental assumptions has in recent years gained new impetus through the development of computers and of artificial intelligence (AI); both play a dominant part in the book under review. The issues raised are, however, also tackled by other means without recourse to modern technology or to the spreading enthusiasm for AI. This variety of approaches is the result of the peculiar conception of this book. Hofstadter and Dennett have here reprinted pieces by 20 different authors, each of whom is known as a science fiction writer or a philosopher or a scientist or a literary figure. If one did not know their names it would be hard to classify them, for many write with remarkable ease in several of these idioms. Every contribution is followed by some reflections on it by one or both of the "composers" of this volume. These original contributions form less than a quarter of the text.

Many, though not all of the reprinted pieces are amusing and relevant to the major issues. My favourite science fiction writer, philosopher and scientist, Stanislav Lem, is represented by several pieces, outstanding among them *Non Serviam*, where his man-made creatures agonize about their origin and the qualities of their creator; agonize because the very essence of their being precludes the possibility of discovering answers.

The philosopher Dennett in his excursion into science fiction raises the fantasy of a disembodied brain kept functioning while connected to an empty cranium by radio links, thus directing a human body hundreds of miles away. In his reflections on his own story Dennett rightly says that the story "not only isn't true . . . but couldn't be true" (p.230) and is truly "outrageous" (p.231). On p.5, however, he commits himself differently by insisting that everything that is imaginable is hence possible in principle; befuddling with a vengeance and disturbing in raising the possibility of brain transplants.

Richard Dawkins in an excerpt from *The Selfish Gene* is at his well-known reductionist best, but he admits that the evolution of subjective consciousness is "the most profound mystery facing modern biology" (p.141). Thomas Nagel's question, "What is it like to be a Bat?", prompts an interesting discussion of the gap between subjective experience and objective fact and the not-unexpected answer that it is hard to know.

In his reflection on this contribution Hofstadter, who has so brilliantly demonstrated his ability to discuss profound problems playfully and with wit in his *Prelude . . . Ant Fugue* (reprinted in this volume), here lets himself down by raising some 50 rather silly questions, of which "What is is like to be Chopin's brother [he had none]?" is a typical example. Nagel's question posed the problem; 50 variations do not make it clearer. To be sure, he follows this with other reflections, some of them interesting, but less coherent than Nagel's argument.

Computer simulation and AI appear in many original and reprinted contributions; they are confronted head-on in John Searle's "Minds, Brains and Programs" and in the following reflections. This sharp and prolonged controversy forms the frustrating highlight of the book. Searle distinguishes the cautious claim of AI — that it is a powerful tool for the study of the mind — from the strong claim that computers given the right programs can be literally said to *understand* . . . the programs are not mere tools . . . to test psychological explanations; rather . . . themselves the explanations [p.353].

This claim provokes him to a sustained counter-argument, the gist of which is to insist on the difference between simulation and identity, based on the impossibility of separating mind from brain. Intentionality is a biological phenomenon . . . No one would suppose that we could produce milk and sugar by running a computer simulation of the formal sequences in lactation and photosynthesis, but where the mind is concerned many people are willing to believe in such a miracle . . . [p.372].

In their reflections on Searle, Hofstadter and Dennett say unequivocally "our position is quite opposed to Searle's" (p.373) but they do not proceed to face the issues straight on. By implication rather than direct statement they seem to support the strong claims of AI, though they admit that present technology has not yet established the identity of programmed intelligence and human intelligence. "Minds . . . may come to exist in programmed machines. . ." (p.382).

We shall all have to wait and see. Anybody who wishes to confront the unanswerable will enjoy this book; those who struggle with answerable questions will brush it aside.

Marie Jahoda is Professor Emeritus of Social Psychology and Consultant to the Science Policy Research Unit, University of Sussex.

Gentle violence

William H. Press

Violent Phenomena in the Universe. By Jayant V. Narlikar. Pp.218. ISBN 0-19-219160-8. (Oxford University Press: 1982.) £9.95, $19.95.

THE title of this book makes it seem like some tawdry imitation of Nigel Calder's *Violent Universe.* Perhaps some editor with an eye on sales can be blamed for such a blatancy, which does disservice to a excellent and uncompromising book on modern astrophysical theory and discovery. Not just inapt, the title seems quaintly *passé*: "violence" as a cosmic metaphor seems to have faded with the early 1970s. And who now remembers the "majestic" universe, before it became violent?

The universe through which Narlikar ads us is more rational than violent. Its phenomena can be discovered, explored and understood by careful analysis. Moreover, the facts and their analysis can be laid open to the scrutiny of the non-specialist reader.

Precision and economy of expression characterize the narrative as it takes the reader through prerequisite discussions of Newtonian gravitation (and its successful celestial mechanics) to Einstein's theory of gravitation, and then to quite a sophisticated discussion of the formation of black holes and the laws of black-hole physics. The emphasis then waxes astrophysical for a few chapters: stellar evolution, supernovae, neutron stars. By now the reader is ready for pulsars, binary X-ray sources, accretion disks, X-ray bursters, and then a chapter on active galaxies and quasars. The material is extremely up-to-date.

Finally, there are two chapters on cosmology. The first is a clear (if conventional) summary of the big bang, synthesis of the chemical elements, its observed echo in the cosmic microwave background. The second, unfortunately, is on the author's own alternative theory, one favoured by virtually no other practising cosmologist. The author is absolutely fair in introducing this chapter as a "non-standard" and "minority" view; but one is left wondering why he did not apply the same rigorous standard to this chapter as to the previous ones, and delete it *in toto* (an action which the reader should take on his own).

Several stylistic features set this book apart from the myriad other popular and semi-popular books on "black holes and all that stuff": its richness of factual detail; the implicit sophistication in its presentation of the scientific process, the interplay of observation with theoretical hypothesis; its uncompromisingly literate *and numerate* prose. Algebraic formulae are used freely; the reader is assumed to be comfortable with the use of symbols and numbers to represent physical quantities. Further, a sane, methodical organization pervades the whole book. A typical subchapter begins with a question, such as "Does the X-ray source Cygnus X-1 contain a black hole?". Observational facts are then concisely presented, before the author proceeds to discuss the bearing of each of the facts in turn on the question posed.

Probably too sophisticated for a lowest-common-denominator "popular" audience, this book can be recommended strongly to anyone with at least an undergraduate degree in any scientific subject who wants a precise narrative presentation of the excitement of modern astrophysical discovery — and no danger of being talked-down to! □

William H. Press is Professor of Astronomy and Physics at Harvard University.

Self-instruction in high energy physics

Maurice Jacob

Basics of Electron–Positron Collisons. By Fernand M. Renard. Pp.238. ISBN 2-86332-010-6. (Editions Frontières: 1981.) FF150, $30.

WITH the decision to build a Large Electron–Positron storage ring at CERN, the LEP project, a large part of future European activity in high energy physics became invested in the study of electron–positron interactions. Already, a tremendous wealth of results has been collected from the e^+e^- colliding ring machines at Stanford (SLAC) and Hamburg (DESY); the LEP project will further extend our ability to investigate the intriguing phenomena thus revealed.

Professor Renard's book on the basics of electron–positron collisions therefore comes at a particularly appropriate time. Many students and experimentalists wish to familiarize themselves with calculations which, over and over again, crop up in the analysis of such collisions. The book should be a good self-teaching guide for that purpose. The author surveys all the standard cases in great detail, giving both explicit formulae and enough of the intermediate steps for their derivation *ab initio*, while always being meticulous with notation. However, in his gallic approach he has a tendency to start with the most general case, discussing only later simpler particular cases, when the beginner might have found the reverse more helpful. The presentation is nevertheless clear enough to enable the reader to skip the general sections easily and go directly to the specific examples.

Reading this book, and making the effort to derive the many formulae given, should prove a very worthwhile investment of time for the dedicated student with some background in relativistic quantum mechanics. The numerous formulae which it contains will also make it useful to the experimentalist writing a Monte Carlo program to assess the response of a detector to expected reactions. To that extent, the book certainly meets a need.

This said, I should add that the newcomer to the field might feel frustrated at the paucity of figures, when the wealth of experimental results is such that calculated distributions and concepts such as jet structure could have been beautifully illustrated. The surprising absence of graphs or tables is also a serious drawback for the reader wishing to assess which kinematical configurations are the most appropriate for the observation of any particular process. For that reason it is difficult to recommend the book as a reference text; it is pitched, perhaps, too much at the computational level when one could have wished for a more global phenomenological approach. Also, while the scope is quite exhaustive, some sections should be considered merely as brief introductions to particular areas which have come into bloom only recently; this applies especially to the account of quarkonia and jets.

The book thus falls short of providing a balanced, critical survey of research on electron–positron collisions. It should, however, definitely be considered as a useful tool for the dedicated physicist entering this active and exciting field. □

Yale University Press have recently re-issued Richard Goldschmidt's *The Material Basis of Evolution*, first published in 1940. The reprint incorporates an introduction by Stephen Jay Gould and, in his words, "commemorates a strong reawakening of interest in Goldschmidt's views among evolutionary biologists". Prices are hbk $35, £25; pbk $12.95, £9.

Maurice Jacob is a Senior Scientist in the CERN Theory Division, Geneva. He was the organizer of the LEP Summer Study at Les Houches and CERN in 1978.

Dark reactions

M.C.W. Evans

Photosynthesis. Proceedings of the Fifth International Photosynthesis Congress. Edited by G. Akoyunoglou. Six volumes, pp.5,322 excluding indexes. ISBN 0-86689-012-2. (Balaban International Science Services: 1982.) $499. Single volumes also available. Distributors ISS, S. Pomerantz, 2242 Mt Carmel Ave., Glenside, PA 19038; ISS, Couwenhoven 62-49, 3703 HN Zeist, The Netherlands.

I MUST start this review with two admissions: first I am an author of a very small part of the books under consideration, and secondly I have not read very much of them. However, probably neither is a serious disability. Almost anyone who might review them is an author, and it is highly unlikely that anyone will ever read the entire work. It has 5,322 pages, plus 69 pages of index repeated in each volume, at least 10 million words, and weighs nearly 9 kg. It contains 650 papers written by 850 authors ranging from Abdourakhmanov, I.A., to Zurrer, H., who achieve authorship of between 1 and 13 papers each.

Enough statistics. The books contain the proceedings of a very successful conference held in Halkidiki, in Greece, late in 1980 (see *Nature* **289**, 122; 1981). They appear 18 months after the meeting and the question must be, was their publication necessary or worthwhile? The papers are unreviewed and cover a very wide range of subjects from the biophysical studies of light absorption in the picosecond time range, through biochemical work on CO_2 fixation, genetic analysis of chloroplast DNA, to physiological ecology. The wide range of subjects is of course a problem for the organizers of the triennial photosynthesis conference, but on balance it is probably a good thing for researchers at the extremes of photosynthesis research to have the chance to hear each other every so often. However they are unlikely, having listened to the talks, to read them again two years later. This is admitted by the editor, who has packaged the volumes into specialist areas for separate sale: the intention does not, then, seem to be to spread a wider view of the world.

Do the books contain much important information which is not available elsewhere? They certainly provide a total view of photosynthesis since so many people attended and dutifully handed in their manuscripts. Much of the work described is of course first class, but even for the best only an outline is provided in the space allocated. For major laboratories a few touches on the world randomizer overcame copyright problems, while for lesser mortals the opportunity to unload all that important work that the refereed journals didn't understand was not to be missed. It is really very unlikely that these volumes contain anything of major scientific importance which has not been published previously: indeed, the smart conferee knows better than to mention anything not already in press with a "good" journal.

Why then did the organizing committee publish the books, and why did the authors bother to submit their papers? The latter question is perhaps easier to explain. Invited speakers no doubt feel some duty to meet the organizers' requirements, while few of us can resist a "free" publication, although surely everyone who is supposed to be impressed by publication lists automatically discounts proceedings of this type. Why the organizers should want to record the proceedings in full is rather harder to understand. There is surely little money to be had from them and an enormous amount of work must have gone into their production. At the Fourth Congress in this series, held in England, no such book was produced, and I do not believe it was seriously missed. It is to be hoped that the organizers of the Sixth Conference next year will show similar restraint.

Who might buy one or all of these books? Libraries, for student use? — review volumes and textbooks are a far better buy. Research laboratories? — refereed journals offer virtually all the useful information. A souvenir of an excellent conference? — a case of ouzo and a set of pornographic coasters would be more fun. No! These volumes are really only for the man who has everything. □

M.C.W. Evans is Reader in Plant Chemistry at University College London.

Philosopher at the bedside

W.F. Bynum

Medical Thinking: A Historical Preface. By Lester S. King. Pp.336. ISBN 0-691-08297-9. (Princeton University Press: 1982.) $19.50, £14.50.

BRILLAT-Savarin's *Philosopher in the Kitchen* showed long ago that every human activity — even cooking and eating — is enhanced by due philosophical reflection. Lester King's philosopher has moved to the bedside where, *malgré lui,* he juggles philosophical concepts when examining his patient, making a diagnosis or prescribing a course of therapy. In using words such as *sign, symptom, syndrome, health, disease, normal, pathological, cause,* and *effect,* any doctor engages in language possessing a philosophical dimension. The quality of his medical thinking will be reflected in the precision and consistency with which he employs these and similar words. The purpose of King's book is to sharpen that thinking by the historical and philosophical glosses he provides on this central core of medical concepts. It is, King asserts, the kind of book he wishes he had had when he began medical school more than half a century ago.

King's credentials are impressive. After spending 30 years as a pathologist he became a senior editor of the *Journal of the American Medical Association,* a position which permitted him to devote a good deal of time to medical history. His historical researches have ranged widely, but he is a particular student of seventeenth- and eighteenth-century medicine. Those who have followed his earlier work will have noted its increasing philosophical preoccupation; they will also be familiar with many of the doctors — Daniel Sennert (1572-1637), Thomas Sydenham (1624-1689), Hermann Boerhaave (1668-1738), William Cullen (1710-1790) — who people the present volume. Throughout, there is a mixture of historical and contemporary material, as King seeks to identify certain constant features in the interactions between doctors and their suffering patients.

King's central theme may be baldly stated: there has always been good medical thinking, as well as bad, even though medicine's conceptual framework and the amount and quality of medical information available to a doctor have changed dramatically over time (and particularly in the past century or so). In one of the best chapters of the book, King illustrates this constancy in the midst of change by showing how the diagnosis of pulmonary phthisis evolved from the seventeenth to the late nineteenth century with the gradual abandonment of Greek humoralism, development of the tissue concept, invention of the stethoscope, increased use of microscopes and cell theory, and the emergence of bacteriology. The change in name from phthisis to tuberculosis was part of this process, but pulmonary phthisis was not simply the old name for tuberculosis. Rather, it was a separate disease, often of course including patients suffering from what we would call tuberculosis, but a disease which must be understood historically, within the intellectual frameworks of earlier times. Thus, Richard Morton (1635-1698) cannot be blamed for describing a different disease from the one which intrigued Robert Koch (1843-1910), nor does the fact that Koch worked with 'our' tuberculosis mean *a priori* that he was a better thinker than Morton. Good medical thinking is reflective, critical, and consistent, but is also historically contingent.

The other chapters of King's book are arranged primarily around those concepts intrinsic to medical diagnosis. He examines the historical relationships between signs and symptoms, between concepts of health and of disease, between the 'clinical entity' and the 'disease entity', between disease classification (nosology) and medical knowledge. He has useful things to say on all these and other topics, but some readers may find that three characteristics limit the book's scope. First, it is an extremely personal statement. Many of his references to the secondary literature are to his own earlier writings, and even when citing other work of direct relevance to his topic — for instance A.R. Feinstein's *Clinical Judgment* (Williams & Wilkins, 1967) or F. Kräupl Taylor's *The Concepts of Illness, Disease and Morbus* (Cambridge University Press, 1979) — he makes little attempt to place his own position within its contemporary context. While this gives King's book a greater internal coherence, it also unnecessarily isolates it.

More important, perhaps, is the relatively narrow perspective of disease which King espouses. He is aware of the cultural relativity of disease categories (Chinese women with bound feet are diseased by Western standards), and of the aesthetic judgements which enter definitions of health (straight teeth are 'healthier' than crooked ones). But King's own concept of disease is essentially lesion-orientated. Thus, there is nothing on the notion of mental disease, or of 'functional' illness, or psychosomatic medicine. These softer edges of contemporary medicine are important dimensions of current debate and deserve explicit treatment in a book which is designed to sharpen medical thinking.

Finally, King's philosophy of history has a surprisingly thin social base. Despite his wise injunctions to us to view historical characters historically, he fails to put Sydenham or Cullen in any concrete social milieu. Even epidemiology gets short shrift, an unfortunate omission in two otherwise perceptive chapters on historical contemporary concepts of disease usation. It would seem from King's nalysis that medicine has its own internal impetus for change, whereas most historians would place more emphasis on social and professional factors.

These lacunae in King's book by no means negate its value. It is a work which repays thoughtful reading, not least for the way it laments sloppy medical thinking in any age, our own included.

W.F. Bynum is at the Wellcome Institute for the History of Medicine, London, and a co-editor of the Dictionary of the History of Science *(Macmillan/Princeton University Press, 1981).*

Unity in diversity — or how to choose your animal

R.B. Moreton

Membrane Physiology of Invertebrates. Edited by Ronald B. Podesta. Pp.664. ISBN 0-8247-1503-9. (Dekker: 1982.) $87.50.

IN THE animal kingdom, invertebrates not only outnumber the vertebrates to an unimaginable extent, but also present a fascinating diversity of form and function, combined with a surprising unity of basic mechanisms. To those of us who study a specific tissue in depth this provides an opportunity to pick those animals where the particular tissue is especially large, simple or well-developed. Thus, as every physiologist knows, the squid has a giant axon, the sea-urchin lays eggs, the crayfish has a stretch-receptor, and so on. This theme is developed by the late P.C. Caldwell in the introduction to this book, and it runs through the entire volume despite efforts by some authors to collect more general information: invertebrate physiology is just like that.

Membrane Physiology of Invertebrates is a collection of essays by specialist authors, arranged roughly in order of complexity of the organisms covered. It begins with an outline of our disappointingly sketchy understanding of how *Amoeba* feeds, and a detailed analysis of the electrophysiology of the "slipper microbe" *Paramecium*, whose genetic variations have been exploited to study particular membrane functions in isolation.

A chapter on coelenterates (jellyfish and hydroids) provides interesting examples of specialized intercellular junctions, and of the way in which development, for example the growth of new "heads", is controlled by cellular secretions. Intercellular junctions are still more important in the helminths, dealt with in the next contribution, where whole sheets of cells can be fused to form the body-wall. Annelids are covered in chapters on epithelial transport (osmoregulation, digestion and excretion) and excitble cells. The former presents a mainly qualitative study of "what happens where"; the latter begins with a rather confusing attempt to compare the properties of nerve cells in leech and earthworm with those of other groups, but gets into its stride with quantitative modelling of the giant axon of *Myxicola.* Crustacea are treated similarly, with a detailed and well-illustrated chapter on the gastrointestinal tract, and a good summary of the diverse types of nerve cells and sensory organs that have been studied, including a brief section on barnacle photoreceptors. A chapter by G.A. Gerencser on molluscan digestion presents mainly the author's own work, but refers to other reviews on osmoregulation and transport across the body-wall. The much larger pool of knowledge on molluscan nerve cells is covered, inevitably rather selectively, by F.E. Dudek, who concentrates on gastropods — perhaps enough has been written about the squid axon for the time being! Dudek does include neuromodulators and neuropeptides, however, usefully integrating this relatively new topic with more conventional ideas on synaptic transmission.

Insects are represented by a contribution on gut physiology by W.R. Harvey, which includes an exposition of the thermodynamics of active transport systems, and by a neat summary of the properties of insect muscle, written by F.M. Ashcroft. There is no chapter on insect nerve cells, perhaps due to lack of space to treat this large subject properly. The book ends, unexpectedly, with a short chapter on the echinoderms, dealing mainly with the interesting electrical and chemical events accompanying fertilization of the egg.

This is not a book for the novice: most of the material is detailed and technical, with a fair amount of theory. Rather, it gives a comprehensive view "over the fence" for the specialist in transport or excitable tissue physiology, or for the researcher seeking to enter a new field. The title is misleading, in that much of the material relates to whole epithelia rather than membranes as such. But as a summary of our current knowledge of epithelial transport and excitable tissue physiology, right accross the invertebrate kingdom, the book is about as up-to-date as can be expected given the inevitable publication delays. Certainly, it should be in every library. ☐

R.B. Moreton is a Principal Scientific Officer with the ARC Unit of Invertebrate Chemistry and Physiology, Department of Zoology, University of Cambridge.

Molecular shapes

M.G.B. Drew

Inorganic Stereochemistry. By David L. Kepert. Pp.227. ISBN 3-540-10716-9; 0-387-10716-9. (Springer-Verlag: 1982.) DM154, $71.70.

CHEMISTS have always had a fundamental interest in the shapes of molecules and in evaluating the reasons for the adoption of a particular geometry. There are two theoretical approaches to such problems: the minimization of non-bonded repulsions and molecular orbital calculations. In this book, Professor Kepert uses simple repulsion theory to evaluate the various geometries of the metal coordination spheres of inorganic complexes in which one central metal atom is surrounded by 4–12 donor atoms.

The author takes each coordination number in turn and calculates the potential energy surface, allowing for possible combinations of unidentate and multidentate ligands. The theoretical results are then compared to the observed structural data provided by X-ray analysis. The enormous amount of structural information is thoroughly assimilated and well organized. There is excellent agreement between theory and experimental data, and in all the book amply demonstrates the validity of the repulsion approach to stereochemistry.

Kepert's work has undoubtedly been a major contribution to our understanding of molecular geometry. However it does not seem to have had much impact on the way in which chemists look at molecular geometry. There are probably two main reasons for this. First, the parameters used for the potential energy curves are often not simple to calculate; structural chemists prefer to analyse geometry on the basis of bond lengths, bond angles and δ angles and find Kepert's parameters unnecessarily complicated. Secondly, he does not compare his results with those obtained by other methods. To take just one example, many people find that δ angles are useful structural parameters but they are not mentioned here. Nor indeed are the results of molecular orbital calculations.

It is this single-mindedness that is both the strength and weakness of the Kepert approach: whilst the book is self-contained, it is not intended to provide a balanced view of current ideas on stereochemistry.

It is certainly useful to have Kepert's work brought together in one volume. However the book follows closely a series of reviews written for *Progress in Inorganic Chemistry* over the past few years, and those who have the previous articles may well find this present volume of limited additional value.

M.G.B. Drew is a Lecturer in Chemistry at the University of Reading.

nature

22 July 1982

24 NOV 1982

Who sells to the Soviet Union?

The Reagan Administration will probably decide to extend the grain agreement with the Soviet Union for a year. Can it then insist that West European governments should not buy gas from the East.

With the best will in the world, it will be hard for Europeans to be charitable about last week's special cabinet meeting called by President Reagan to help him decide whether United States farmers should continue to sell bulk cereals to the Soviet Union when present arrangements run out in September. Naturally, there will be much sympathy for Mr Reagan's dilemma. By denying it access to the Middle West, he could cause the Soviet Union a great deal of inconvenience (the need to shop around for other grain), physical discomfort (hunger) and even occasional starvation while establishing the powerful political point that United States farmers are more efficient than their Soviet counterparts. He would also provide the Soviet Union with a reminder that the *de facto* occupation of Afghanistan still rankles. These are great prizes, not lightly to be dismissed. But unfortunately for Mr Reagan, there is another millstone pressing on him — the unwillingness of farmers in the Middle West to sacrifice their occupations and their holdings by becoming bankrupt (more common already in the past twelve months than for several decades) in the cause of talking toughly to the Soviet Union. Politicians in most places will be full of fellow-feeling for the president. Especially because this is a mid-term election year (and because a decision must be made before polling day) they will weep with him as he sacrifices principles on the altar of prudence and renews the Soviet grain agreement for just one more year. But European politicians, no less given to calculations of how to square beliefs with the ballot box, will be asking why their acknowledgement of President Reagan's difficulty is not reciprocated in the matter of the natural gas pipeline between the Soviet Union and Western Europe.

That issue is more important than anybody in Washington seems to understand. (Mr George Shultz has made tactful noises, but is too new in his job as Secretary of State to be persuasive.) So far, three countries in Western Europe (France, Switzerland and West Germany) have committed themselves as customers for Soviet gas, and have agreed to make credits available for the construction cost of this gigantic project. (This in itself is not unusual; when did it most recently occur that Westinghouse, General Electric or Babcock-Wilcox built a nuclear power station n the hope of being able to sell the electricity production to some utility?) Sensibly enough, the countries concerned have done their best to ensure that they will not have to pay out too much (in the orm of convertible currency) in advance by securing Soviet agreement to buy in much of the advanced equipment that will be needed. Washington has for the past six months been doing verything it can to ensure that such agreements will not be ulfilled — and that the Soviet Union will have to look to other uppliers or even make the equipment for itself. Since the summit meeting a few weeks ago at the palace of Versailles, the governments of Western Europe have been bubbling with esentment at President Reagan's Administration's ruling on this question. How can one government tell commercial corporations egally registered under another's laws that they should renege on what is otherwise a binding contract?

Western Europe's sin, on President Reagan's view, goes even eeper — its willingness to pay out convertible currency year after ear in return for natural gas that may serve to keep its people warm and its industries in business but which will have the side-ffect of helping the Soviet Union to pay its bills and will make Western Europe strategically dependent on the East for a substantial part of its energy consumption. When Washington first woke up to the problems of the pipeline project eighteen months ago, it was principally alarmed at the prospect of strategic dependence, now mercifully seen in a less clear light. The present concern seems principally to deplore any arrangement that will make it less likely that the Soviet Union will cease to function overnight, and which may even offer it some assurance of an income-stream for thirty years or so. The long-term nature of the pipeline agreement is admittedly a more solemn undertaking than the one-year extension of the grain agreement that Washington now contemplates, but Western Europe could presumably repudiate its inital investment in the pipeline if the going became rough (or the price of gas too high). President Reagan is probably under-estimating the friendliness of his friends in Western Europe (one disservice) and is certainly bullying them too much by his complaints about the pipeline (another).

All this is especially disconcerting at a time when the Reagan Administration is in the box of having to talk to the Soviet Union, most days at Geneva, about the future of strategic arms. That contradiction is awkward and not easily avoided. Washington needs a Moscow willing to talk about strategic arms, but properly insists on its right to be huffy about Afghanistan and other transgressions. It wishes that it could also afford the luxury — all those farming votes — of standing firm on principle. Detente, the saying seems to be, is from time to time an expedient necessity. Western Europe, on the other hand, with no choice but that of being within a few minutes (by Intermediate Range Ballistic Missile) from the border, believes and behaves differently. Interdependence is a fact of life, but does not preclude the sudden breakdown of coexistence. The wisdom of the pipeline deal, in other words, is judged by relatively short-term criteria; for a half-continent whose separate existence could be quickly ended, long-term economic deals (lasting, say, thirty years) count for less than longer-term cultural connections — the sense of deprivation springing from people's inability to visit European cities such as Prague, Warsaw or even Leningrad when they choose.

Muddle about universities

The British government only seems to threaten university autonomy, but the precedent is bad.

Is the independence of the British university system, traditionally assured by the existence of the University Grants Committee as an intermediary between the government and the universities, now threatened? This is the obvious question provoked by last week's open letter to the committee from Sir Keith Joseph, the Secretary of State for Education and Science in the British government. For the letter, described as the first exchange in a "dialogue" between the government and the universities, finishes with the declaration that, in the development of British higher education and of the universities in particular, "there will be some strategic decisions for which it would be appropriate for ministers to take explicit responsibility and to answer in Parliament". After more than two years of abysmal relations between the government and the universities that it supports, beginning with the decision in the summer of 1979 that

028-0836/82/29031302$01.00

nceforth overseas students should pay arbitrarily defined economic fees", and with the later and equally arbitrary decision that direct support for the universities must be reduced by 8.5 per cent, it is natural that the universities should assume that the minister's intentions towards the University Grants Committee are malevolent.

Some consideration should therefore be given to the more or less moderate tone of the bulk of the Joseph letter, which among other things repeats the promise that direct support for the universities will level out when the academic year 1983–84 is over (at least if inflation does not run away again), pats the grants committee on the back for its selective distribution of reduced funds among British universities, applauds the more recent decision to allocate extra funds to biotechnology (see *Nature* 20 May, p.173) and sympathizes with the general concern that, as things are, the recruitment of "young able people" into the university system is virtually impossible. The letter even acknowledges that the grants committee has acted sensibly in revising some of the targets for student numbers at particular universities in the light of some special pleading, even though these decisions will marginally shade the government's insistence that student numbers should be fixed from on high. How, it may be asked, can such a reasonable minister have malign intentions towards the independence of the system?

On the evidence of the minister's letter, part of the trouble is simply that the British government remains in a muddle about higher education. Student numbers are a good illustration. The most illiberal feature of the present university contraction is that each British university has been given a ceiling for the number of students from the United Kingdom and European Community countries it can have on its books in 1983–84. The result, since most numbers are reductions, is that much educational plant will be less than fully used and that universities will not be able to work their way out of financial trouble by doing their jobs more efficiently. (The threat that if they take in more than their allotted quota of students they will be penalized financially has not been withdrawn even though the grants committee did not repeat it in the letters sent to individual universities in May.) Yet this offensive system, and the uncertainties that go with it, arises simply from the government's fear that if the universities exceed their quotas, the cost will be increased of maintenance awards to students, paid by local authorities but then laid off on the central government. Is it really beyond the wit of a government anxious to play a more active part in the planning of higher education to devise some different system of subsidizing students, one that would combine the legitimate objective of controlling the total cost with flexibility on numbers?

The Joseph letter is also muddled about the relationship between the universities and the higher education institutions formally supported (but with funds from the central government) by local authorities, chiefly the polytechnics. The coexistence of these two kinds of institutions in what is called the "binary system" is strictly a political matter, for the polytechnics were established (in the 1960s) because of the then government's conviction that there was a need for a more down to earth system of higher education than the universities chose to provide. The experiment has been only a patchy success but, to its credit, the present government has been trying since before Sir Keith Joseph's time at the Department of Education and Science to wrest full control of the polytechnics away from the local authorities. Indeed, there is now a National Advisory Body for the polytechnics in England, and there may soon be one for those in Wales. The Joseph letter now asks that the grants committee and its counterpart committee for the polytechnics should consult with each other and that, as well as working out schemes for collaboration between individual universities and polytechnics, they should also help to define the relationship between the two sectors of higher education. The objective is sensible and should have been sought a long time ago. But the issue, eminently political as it is, must in the long run be settled by the government.

What the Joseph letter says about the support of university research is more alarming. The letter applauds the grants committee's intention to play its part in the dual support system, welcomes the Merrison report on the subject and goes on to approve of the principle that there should be "selectivity of funding" not merely by the research councils that provide project grants for university research but also by the grants committee, which is responsible for supporting a "basic level of research activity". What, suspicious minds will ask, is the minister approving? A decision, not yet taken, that in future there will be two kinds of universities — those equipped for research and those which are not? The Merrison committee rightly argued that British universities are less deliberate than they should be in using the grants committee's general subvention for research, and acknowledged that even if the job were done intelligently, some university departments would be able to mount research programmes only in collaboration with others. But the Merrison committee also rejected the principle of a close correlation between research support provided by the grants committee and the research councils, for that would only undermine the dual support system as a whole.

The fear that the Department of Education and Science does not properly understand the system of higher education in whose management it now seeks a more decisive role is the worry underlying the declaration that in future ministers must take more responsibility for it. Higher education may be too important to be left to academics, but the British government hardly seems their natural successor. By all accounts, the present intention is merely that Sir Keith Joseph should from time to time give the grants committee general guidance about its sense of where priorities lie. The difficulty is that the government's sense of priorities is unlikely to make academic sense. The present concern is somehow to shape higher education so as to contribute to national prosperity, a question with which university systems elsewhere than in Britain have wrestled for decades, but without much success. The danger is that from frustration, ministers will slip into the habit of making their priorities particular, issuing edicts such as "Let there be more engineers!", "Let there be more computer engineers!" or even "Let there be more computer engineers training on British equipment!" Sir Keith Joseph himself may be aware of the dangers. But once the precedent of intervention has been established, his successors will be provided with countless opportunities for foolish interference.

Pity the luckless British

Great wars are said to bring out the best in people. Small wars appear to reveal the worst.

Who would have predicted that a mere month after a famous victory in the Falklands, the British government would be deeply embarrassed by a concatenation of domestic blunders — the false assumption that it would be able to comply with its bargain with its opponents when it won consent to send an amphibious force to the South Atlantic by mounting a Parliamentary enquiry on its own terms of reference? the discovery that an intruder could climb into Buckingham Palace and sit on the Queen's bed for ten minutes before being apprehended? and the growing likelihood that there has been another monumental breach of national security at one of the most technically advanced intelligence centres in the world? The British legend, especially common since the Second World War, is that the British are good at fighting (and even winning) wars but less endowed with flair in times of peace. The truth is different, as the events of the past few months have shown all too clearly. Most probably, the Parliamentary enquiry will show that the Falklands war was unnecessary, if not the consequence of a poor appraisal of intelligence then of indolence. Much the same is likely to be the case of the other conspicuous failures of public administration in the past few weeks. But who, or what, is to blame? The simple answer is the Civil Service, and its perennial pride in its technical innocence. The charge that this is so has been made repeatedly, and most governments have agreed that it is correct. When will one of them do something?

0028-0836/82/290314-01$01.00

JPL takes on classified research

General to be appointed as new director

Washington

General Lew Allen Jr, who recently retired as chief of staff of the US Air Force, is reported to be the leading candidate for the directorship of the Jet Propulsion Laboratory (JPL), managed on behalf of the National Aeronautics and Space Administration (NASA) by the California Institute of Technology (Caltech). An announcement of the appointment is expected in the next few weeks.

The selection of General Allen would intensify the concern of some scientists at Caltech and JPL over the growing military role of the laboratory. Last year, the Caltech faculty and NASA agreed that up to 30 per cent of the laboratory's operating funds might come from Department of Defense (DoD) research contracts. Before that, the laboratory had refused to do classified research, under a policy laid down by Dr Bruce Murray (who ceased to be director of JPL on 1 July). The decline in NASA funding prompted Dr Murray to seek a change in that policy.

Dr Marvin Goldberger, president of Caltech, maintains that neither that change nor the appointment of General Allen — who he says is a "serious candidate" — will affect JPL's fundamental character. "We have every intention that JPL shall have its primary objectives in the civilian space programme. I can assure you that General Allen's view is coincident with this view."

A JPL scientist involved in the selection process pointed out that Allen has a strong technical and management background. He holds a PhD in physics from the University of Illinois, and worked at Los Alamos from 1954 to 1957. Allen directed the Air Force space programme from 1965 to 1972.

Allen declined to comment on the report that he is the principal candidate for the JPL position, and would say only that any announcement would come from JPL. But JPL officials are clearly worried about reaction to the appointment of General Allen, both within the Caltech-JPL community and outside it. Similar worries prompted the laboratory to adopt a tacit policy of not carrying out weapons research and development even with the lifting of the prohibition on classified work. The laboratory also made clear that it would not do "secret work secretly" — that is, it would only accept such classified projects as it could at least announce its participation in.

Dr Goldberger stresses, too, that work for DoD is subject to scrutiny by a faculty committee which reviews its "propriety" and its effect on the "overall mission of the laboratory". He also insists "classified work will not jeopardize access to the laboratory by Caltech faculty and students".

Dr Arden Albee, JPL's chief scientist, agrees that these precautions are enough to ensure that JPL remains fundamentally a NASA laboratory. "Certainly it's something we have to worry about, but my own feeling is it's not going to cause a significant change in the character of the place", he said.

"I KNOW THE PAY'S GOOD—
IT'S THE NEW LAB-COATS
I DON'T LIKE."

JPL's principal function within NASA is to provide the engineering and scientific support for unmanned planetary exploration missions. Some of this responsibility is shared with NASA's Ames and Langley laboratories, although JPL is the "lead centre".

At present, "about 8 or 9 per cent" of JPL's support comes from military contracts, according to Dr Albee. These are mostly "small technology projects" involving simulation, sensing and surveillance. The only large project is the autonomous spacecraft project which arose from the Voyager spacecraft work and is of some interest to the Air Force.

Nor does Dr Albee see any new threats to the scientific mission of JPL from its increased involvement in DoD projects: "NASA has always been a development agency; science got done on its periphery. That's as dangerous to science as DoD projects." He also points out that more research is supported by DoD on the Caltech campus than at JPL.

We have to put it in perspective," he said. "DoD is a major part of the budget. NASA is a small part."

JPL's current budget is $321 million; the laboratory employs a full-time staff of 4,620. The proposed budget for 1983 is $330 million, which represents a cut in real terms. According to Dr Arden Albee the most telling indicator of falling NASA support is that the laboratory has not started on a new planetary mission for almost 10 years.

Stephen Budiansky

France ponders biotechnology

France has done no microbiology for 20 years, has few people who understand fermentation or fungi and has never developed food processing technology. This wild exaggeration is the opinion of a francophile British biotechnologist sketching the problems facing France in his field. Now, however, a fairy godmother has waved her wand: the ministry of research and industry in Paris has published a vast programme for biotechnology, to stretch over three years and cost the government FF 600 million (about £50 million). Will she get Cinderella to the ball?

It depends in part on what the report says in a large section marked "Secret and Confidential", which has not been published but which describes the actions to be taken by the ministry in concert with industry. And it depends on whether France can create enough microbiologists, whose star fell faster and further in France than elsewhere when molecular biology turned to the eukaryotic genome. The University of Strasbourg, for example, was granted a new professorship in microbiology last year, with emphasis on biotechnology; it has been unable to fill it, said a spokesman, with anyone with even a smattering of French.

The ministry's three-year programme promises to tackle the problem in partnership with the universities and the *grandes écoles*. And the Centre National de la Recherche Scientifique (CNRS), which supports much of the most advanced biology in France, plans to help double the number of French microbiologists.

Meanwhile, several important centres of biotechnology will now enjoy increased support. At Toulouse, for example, there are three laboratories grouped to form a kind of "transfer centre" between research and industry, directed by Professor Jean-Pierre Zaltar (a specialist in gene expression). At Marseilles, there is a laboratory for bacterial microbiology, which will be expanded next year with the help of Orsay biochemist Jean-Claude Patte. At Cadarache, there is a new laboratory for biomass studies run by CNRS in conjuction with the oil company Elf Aquitaine and the Commissariat à l'Energie Atomique. At Compiègne there is the University of Technology with Dr Daniel Thomas specializing in enzyme technology; in Paris, the Institut Pasteur is

0028-0836/82/290315-02$01.00

working hard to make up for past years; and at the University of Strasbourg, there are well-advanced plans for a laboratory of plant genetics (which is, incidentally, strongly supported by the new report).

This week's report surprisingly emphasises the plant sciences, with no fewer than ten recommendations for INRA, the agricultural research body. Even Professor Roger Monnier, director of life sciences at CNRS, believes plant science must receive the most attention.

Over biotechnology as a whole, the report considers France to be weakest in bioengineering — in the kinetics of growth and production, in techniques of culture of microorganisms and cells, in enzymology, in reactor design, in extraction and purification and in the provision of analytical control equipment. France also suffers because of an "excessive compartmentalization and specialization of disciplines, research organizations and industries" says the report. But it ends on a strong note: now more than ever, France must support fundamental research, which is "the unique source of the unpredictable".

Robert Walgate

British Telecom

Roll up!

The British government is embarking on the most significant phase in its plans to liberalize the telecommunications industry. Mr Patrick Jenkin, Secretary of State for Industry, said this week that he will be introducing legislation in November to sell off British Telecom (BT), the state-owned telecommunications monopoly. The subsequent sale of shares will be the "largest single issue on the London market and maybe the world".

The sale of British Telecom has been widely forecast. Earlier in the year it was suggested that the government was considering privatization to avoid acting as guarantor for the company's borrowings. This week, Mr Jenkin confirmed this. But the government clearly hopes that British Telecom will be able to keep down its customer charges, which have recently risen above the cost of services, simply to finance 90 per cent of the annual £2,200 million investment programme.

The proposal to sell British Telecom goes beyond measures earlier this year to liberalize British telecommunications. Last October, the government passed legislation allowing private companies to supply equipment for attachment to the network in competition with British Telecom. Equipment is still awaiting approval. Earlier this year, the Mercury Consortium, a group of three private companies, was licensed to operate a new telecommunications network in competition with British Telecom. And shortly, Mr Jenkin promises a general licence permitting the use of BT and Mercury networks by suppliers of value-added or third party services.

The new bill will transform British Telecom into a public limited company and allow the sale of up to 51 per cent of the shares to the public. As soon as half the shares have been sold, the government will relinquish its control, allowing the company to borrow from shareholders and private markets. British Telecom's present status as a licensing authority will be transferred to the industry secretary acting through a newly-created Office of Telecommunications. Regulations — balancing the interests of those involved in the supply and use of telecommunication services — will be controlled by the new office. Licences to operate services will be issued, according to Mr Jenkin, only to those companies willing to fulfil their public duties by, for example, supplying uneconomic services to rural areas.

No doubt still smarting from the embarrassment of under-estimating the share price of Amersham International, sold off earlier this year, Mr Jenkin is as yet unwilling to hazard a guess at the value of British Telecom or the shares that will be on sale. Neither does he seem in any hurry to push the sale through. The legislation can be expected to be enacted by the end of next year, he says. But the sale of shares is not scheduled before the next election, which must occur before May 1984. The present government is clearly confident that it will have another term to run.

Judy Redfearn

Britain's nuclear power

PWRs hit snag

Mr Ron Anthony, recently appointed Chief Inspector of Nuclear Installations in Britain, wants to be counted on the side of the angels. Last week his Nuclear Installations Inspectorate (NII) published a report critical of several aspects of the "preconstruction safety report" for a British version of the Westinghouse pressurized water reactor (PWR), thus confounding environmentalists' fears that NII is in the pocket of the nuclear industry.

"As far as we're concerned, no-one could go too far in the matter of safety" said Mr Anthony last week, stressing that assessment of the Central Electricity Generating Board (CEGB)'s design would be continuous right up to the moment of operation. Next January, there will be a planning inquiry on the PWR, but even if the inquiry favoured the reactor, NII would still have the right to refuse a licence.

Is this unexpected opponent causing shudders in the nuclear industry? Not yet. Mr Anthony's inspectoral bark is judged to be worse than his bite. The director of CEGB, Sir Walter Marshall — nuclear physicist and passionate advocate of the PWR — said he was delighted that NII had flexed its muscles, while at the same time giving CEGB a pass mark on all the difficult issues (such as containment vessel design). Moreover, the NII report says frequently that a satisfactory and safe PWR design is "achievable", and that CEGB has only to satisfy NII on certain points.

These are many, and include "human factors" now known to have played a great part in the Three Mile Island accident. "In the preconstruction safety report [for the British PWR] there is only brief mention of the role of the operator in testing and maintenance, operating procedures, operator training, the control room and operator response to faults" says the NII report. "The various sections give little indication of intent to design and operate on good ergonomic principles." NII is not unduly worried, however: CEGB is considering the problem, the inspectorate says, and NII will have evidence of the CEGB conclusion before a licence is granted.

More substantial, in NII eyes, are five concluding points gathered together as "not yet satisfactory". These are:

- Hazards presented by fire, earthquake and aircraft crash.
- "Ballooning" of the fuel cladding.
- Steam generator tube integrity.
- The automatic reactor protection system, which is a completely new design.
- CEGB's software models of fault development.

The report also says that the possible consequences of severe accidents will be the subject of a separate CEGB submission and NII report.

Of all these, Sir Walter Marshall is most worried about ballooning of the fuel cladding, a phenomenon discovered by UK Atomic Energy Authority researchers, Sir Walter's former colleagues. The problem is that uranium fuel rods necessarily contain a small amount of helium and that if the surrounding coolant pressure suddenly drops, this gas can balloon out of the cladding and close off coolant flow completely. For this to happen, the cladding ductility — and hence fuel-rod temperature — has to be just right, and the pressure must not fall too fast (otherwise the cladding simply bursts, allowing coolant past the ragged edges). The combination of conditions is unlikely, but it requires only a small loss-of-coolant accident, said Sir Walter. Experiments are under way in Canada to measure precisely the conditions in which ballooning occurs, but Sir Walter "stakes his reputation" in predicting that the phenomenon will prove to be no substantial obstacle to reactor safety.

The automatic reactor protection system is the other, more substantial, doubt. Relying on modern microelectronics and computer control, this system would handle major faults for 30 minutes before an operator was allowed to touch the controls. NII has no objection to the principle, but remains to be satisfied that it will work. That will require six years of software analysis and testing, said Sir Walter last week. He will set up a team of 10–20 specialists to do the job.

Robert Walgate

0028-0836/82/290316-01$01.00

Whales' Waterloo

Science, it seems, has once again failed the sperm whale. Among other issues, the annual meeting of the International Whaling Commission (IWC), which convenes this week in Brighton, must decide on sperm whale catch limits. Quite how it will do so is not at all clear. The Scientific Committee of IWC, which met two weeks before the main commission, has, as last year, failed to make a recommendation.

Indecision continues to cast a cloud over the sperm whale. At a special meeting in March (*Nature* 1 April, p.383) the Scientific Committee, using the computer model developed by the International Institute of Environment and Development (IIED) and supported by all but the Japanese scientists, estimated the number of exploitable whales at around 200,000. The analysis indicated that even with a zero catch, stocks would continue to decline. The Japanese presented their own computer model and pushed for a minimum quota of 890. A decision on catch limits was deferred to this week's annual meeting.

The recent meeting of the Scientific Committee produced a few surprises. A majority of the committee agreed that the IIED model estimate of population size had been too optimistic and that the population continues to decline. The Japanese did not re-present their earlier model but put forward a modification of the IIED model indicating that earlier population estimates were low.

In view of the Japanese dissent, the Scientific Committee was unable to recommend a catch limit or to classify the stock. Because of the disagreement on the state of the sperm whale stock it is difficult to assess whether a catch of 890 could be sustained without taking a serious toll on the population. The buck has now been firmly passed back to the IWC delegates. A political trade-off must now be made. The sperm whale is not the species in greatest danger of extinction. With the conservationist countries determined to stand firm and press for a total ban, some clever manoeuvring is now called for if IWC is to avoid even greater schism.

Jane Wynn

Badger gassing

Ferrets stand in

The study which earlier in the month precipitated the British government's abandonment of the policy of gassing badgers appears to have provided the most detailed information so far of the mortality of ferrets exposed to hydrogen cyanide. A total of 177 female ferrets were exposed to hydrogen cyanide in the course of the study, but only four badgers were thus used because of their scarcity.

The issue of gassing badgers with cyanide has been contentious since 1975, when the Ministry of Agriculture, Fisheries and Food began gassing badgers suspected of being carriers of bovine tuberculosis. The practice was suspended towards the end of 1979 after complaints from conservationists and wildlife organizations that it was unnecessary, inhumane and ineffectual, but resumed in October 1980 after a report from Lord Zuckerman that confirmed that badgers can be reservoirs for bovine tuberculosis, a conclusion disputed by some conservationists.

The Zuckerman report on badgers also pointed to the lack of experimental evidence of the effects of cyanide on badgers, when the study commissioned by the agriculture ministry from the Chemical Defence Establishment at Porton Down (not to be confused with the now-civil microbiology establishment at the same place). The report of that study, by anonymous officials at the establishment, was published last week.

The first objective of the study was to establish a kind of dose–response relationship for mortality among ferrets, chosen as experimental animals on the recommendation of Lord Zuckerman. One of the defects of the study is that the sample of ferrets (obtained from a commercial supplier) appeared to consist of two groups differing in body weight. The animals were exposed in groups of three to various concentrations for periods of 1, 5 and 25 minutes. Nothing is said in the report of the age of the animals, which had nevertheless been bred especially for the study.

Eric Hoskins

The exposure of ferrets is measured as the product of the concentration of cyanide in the air and the time in minutes for which the ferrets breathed it. The ferret part of the study was used so as to estimate the likely lethal doses for badgers, fourteen times heavier than ferrets on the average, by means of the rule that the exposure required to produce a specified mortality is proportional to (body-weight)$^{0.7}$.

On this basis, the estimated exposures to cyanide needed to kill 90 per cent of badgers after times of 1, 5 and 25 minutes are 2,000, 5,000 and 5,500 mg min m^{-3} respectively. The report says that these "crude" estimates are supported by the experiments in which four badgers were exposed to cyanide gas. The only badger that died was exposed to 6,560 mg min m^{-3} for 17 minutes; the other three have been returned to the wildlife park from which they came.

The government's decision to abandon the use of cyanide against badgers has been prompted by the knowledge that concentrations of cyanide in the tunnels of badger setts rarely approaches that needed to kill them within minutes, if at all. Its problem now is whether it can devise an alternative humane way of killing badgers — and do so quickly. Conservation interests will be able to exploit a prolonged hiatus in the control programme to reopen the question of its necessity. The use of carbon monoxide and nerve gases as alternative methods of control was ruled out in the Zuckerman report as being respectively ineffectual and "too dangerous".

British academic industry

Prize incentives

"We realize that we're just a football. We're here to be kicked by both sides." Thus a spokesman for the British Technology Group (BTG) on the group's present interest — the marriage of industry and academic science to put high technology on the market. In its latest venture, an academic enterprise competition, BTG hopes to encourage academics to don the entrepreneurial cap. Last week, Patrick Jenkin, Secretary of State for Industry, handed out cheques totalling £230,000 to twelve winning entries.

The academic enterprise competition, originally sponsored by the National Research Development Corporation (now part of BTG), was open to science researchers from British institutions of higher education who had set up, or planned to set up, a business based on their research work. At the award ceremony, enthusiasm ran high. Sir Alastair Pilkington, chairman of the panel of five judges, declared "We would like to see a large number of academics become millionaires every year". Patrick Jenkin described the occasion as one of "unique importance". The competition was all about the partnership between education and industry and aimed to dispel the feeling that "somehow for an academic to go into industry is disreputable". He issued a warning that the government's position was firmly on the sidelines. Public funds were but the seeds of support.

Professor W.A. Gambling of the University of Southampton, whose company York Technology Ltd took the top prize of £50,000, agreed that if Britain is to "seize the juicy plum" and commercialize high technology, higher education must play its part. But he added that the main occupation of the academic remains teaching and research.

Although legislation has yet to be passed, the National Research Develop-

0028-0836/82/290317-02$01.00

ment Corporation and the National Enterprise Board were merged to form BTG in September 1981. A Universities Coordination Unit was set up to go on the road and seek out entrepreneurs in the academic world. Last week's competition has at least provided a market survey. BTG now knows that there are at least 118 groups, the number of entries in the competition, keen to set up business ventures based on academic research.

Electronics and information technology dominated the entries but engineering, medical equipment and biotechnology were strongly represented. More than a third of the entries came from research institutions in the south of the United Kingdom. York Technology Ltd, the winner, was set up in 1980 to market products for the optical communications industry. Its first product, a "preform profiler" which measures the refractive-index distribution in glass preforms from which long lengths of optical fibre are drawn, was invented and patented at the University of Southampton. So far, £250,000 worth of equipment has been sold, 80 per cent as exports.

BTG may inject further cash, up to £250,000, in some of the prize-winning companies. It hopes, however, that private industry will become more interested and step in to bridge the investment gap. The competition seems to have established that while academics' sights may not yet be set on making a million, there is no shortage of people willing to give it a try. **Jane Wynn**

Synthetic fuels

Support wanes

Washington

The "synfuel fever" that led Congress in 1980 to launch a 12-year, $88,000 million development plan seems to have lapsed into a synfuel coma. The US Synthetic Fuels Corporation, established by Congress to distribute the funds, is off to a slow start — several large privately-supported projects have recently collapsed and the economic projections of the profitability of synfuels are becoming bleaker.

Last week, the board of directors of the synfuels corporation continued at its measured pace, eliminating about half of the 35 proposals received in the second round of applications. The corporation has taken a very cautious course, so far selecting only two projects out of the first round and pledging to be "tough negotiators" in settling on the details of the government support for those. Chairman Edward Noble has also made clear that once the corporation has spent the $14,600 million already appropriated to it, there will be no more funds available.

Yet even this is more than synfuel supporters had expected from the Reagan Administration. According to the Democratic staff of the House fossil and synthetic fuels subcommittee, the Administration now appears "to support at least the concept". But John Sawhill, who was Secretary of Energy and, briefly, chairman of the synfuels corporation under President Carter, says that the corporation is doing "the minimum possible that will keep Congress off its back".

But critics of synfuel development say the industry's real problems go deeper than the policies of the synfuels corporation. Technological uncertainty, high risks and a declining world price of oil are formidable obstacles. Earlier this year, two large private projects collapsed, apparently for these reasons. Exxon, the world's largest corporation, pulled out of the Colony oil shale project in Colorado after the estimated construction costs doubled — to $6,000 million.

The Alsands oil sands project in Alberta, Canada, suffered a similar fate, almost simultaneously, when both Shell Canada and Gulf Canada pulled out. And the two projects that the synfuels corporation has chosen to support — the Breckinridge oil-from-coal project in Kentucky and the Hampshire Energy gasoline-from-coal project in Wyoming — are reported to be having trouble finding equity backers.

An industry source said that Exxon's main trouble with the Colony project was that artificially high oil prices had made what are basically "neanderthal" technologies seem attractive.

Meanwhile, other projects are continuing. Union Oil is reported to be more than half-way to completion on its $2,000 million, 10,000 barrel per day shale project in Colorado, and work is also progressing on the $2,100 million Great Plains coal-gasification plant in North Dakota. Exxon, in spite of the setback on the Colony project, is going ahead with a small direct coal liquefaction plant in Texas and a coal gasification project in the Netherlands.

The industry is not dead; but neither is it just hibernating, as some of its supporters claim, waiting for the next rise in oil prices. The change of plan by Exxon was clearly a blow; as one observer put it, "it was a shock to everyone that Exxon couldn't do everything".

A reevaluation of the long-term economics of synfuels is at the heart of the industry's sickness. The draft of an Office of Technology Assessment study reports that even with the large loan guarantees available from the synfuels corporation, investment in particular projects seems attractive "only if current capital cost estimates for synfuels plants are correct and there are no cost overruns. Most industry experts, however, consider the chances of cost overruns to be high."

Some economists have also begun to question the rationale behind synfuel development. Arthur Wright of the University of Connecticut doubts that even a credible supply of synfuels at a credible price would insulate the American economy from the effects of oil price rises. "Synfuels might reduce imports, but not the source of the instability", he says.

Britain is odd-man-out on 2,4,5-T

The European Commission is urging the Community's member states to take greater precautions to ensure that herbicides containing 2,4,5-trichlorophenoxyacetic acid (2,4,5-T) do not contaminate food. In a surprising move, the Commission is recommending that the Council of Ministers adopt a directive forbidding the use of 2,4,5-T on cereals and woodlands when fruits and mushrooms are in season and in weedkillers for domestic use. The Commission is also recommending that the maximum permitted level of the toxic contaminant 2,3,7,8-tetrachlorodibenzo-*p*-dioxin (TCDD) be reduced immediately to 0.01 mg per kg of 2,4,5-T and later to 0.005 mg per kg when a method of control at such a low level is available.

The Commission's move may embarrass the British government, even though Britain, together with Belgium and West Germany, already operates the 0.01 mg per kg limit for TCDD in 2,4,5-T. The British Ministry of Agriculture has repeatedly given 2,4,5-T a clean bill of health provided that it is used as recommended. The ministry's view was challenged in 1980 by the National Union of Agricultural and Allied Workers (NUAAW) which claimed to have evidence of harm to individuals who had been in contact with 2,4,5-T. But the Advisory Committee on Pesticides, which the ministry asked to reply, saw little evidence to make it change its mind.

Thus, not surprisingly, NUAAW is greeting the Commission's move with enthusiasm while the agriculture ministry is more guarded, preferring to wait for the Council of Ministers' decision before responding to the Commission's recommendations.

The Commission's decision to move on the side of caution is the result of a review conducted in 1980 by its scientific committee for pesticides. Although that review found no evidence of direct harm from the proper use of herbicides containing 2,4,5-T, it nevertheless recommended lowering the level of TCDD in 2,4,5-T and greater precautions to minimize 2,4,5-T in food. Whether the Commission's recommendations become binding on EEC member states will depend on how they are greeted by the Council of Ministers. Whatever the outcome, however, Italy, the Netherlands, Denmark and West Germany will be unaffected. They have already banned use of the chemical as a herbicide.

Judy Redfearn

0028-0836/82/290318-02$01.00

The industry's sorry state is compounded by Congress's loss of enthusiasm in the past two years. The 1980 Energy Security Act, which set up the government synfuels projects, also authorized spending on solar energy and conservation. With the dropping of all but the synfuels portion of the act, the coalition of environmentalists and oil-industry supporters that passed the act has fallen apart. A new anti-synfuels coalition, now made up of environmentalists and the much larger body of fiscal conservatives, is trying to destroy government synfuels support. So far, this coalition has had little success, but the days of government support for synfuels are surely numbered.

Stephen Budiansky

High-energy physics

Labour intensive

They have been playing musical chairs at CERN, the European Centre for Nuclear Research near Geneva. Last week there were six proposed experiments for LEP, the large electron-positron collider due to start up at the end of 1987. Now there are four, after a preliminary examination of the proposals gave a cautious thumbs down to the other two*.

But the number of physicists remains the same, so that the 850 scientists involved in all six proposals will attempt to regroup to find jobs for all, in a process that CERN dubs "optimalization". Final approval of the arrangements will be given at a research board meeting in November.

The scale of the LEP collaborations is thus going to be vast, far bigger than foreseen only two years ago. Then, the European Committee for Future Accelerators (ECFA), in a report on the future employment of physicists in Europe, predicted collaborations averaging only 75 physicists on each of six LEP experiments. Now the figures seem likely to reach 200 on each of four experiments. Rutherford, where is you string and sealing wax now?

Dr Jack Mulvey of the University of Oxford, who produced the ECFA report, said this week that he thought the main problem was going to be project management. But particle physicists had shown a remarkable ability to adapt to new conditions. "We've realized that it takes an enormous effort to get these big experiments on the floor", he said, and that large collaborations are necessary.

The LEP collaborations will also need to be big to spread costs — for this time CERN is not following its usual policy of offering about half the capital cost of the equipment, but will restrict itself to one-fifth. Since the total sum for the four experiments is some £75 million, the matter is not negligible.

The other problem is whether there will be enough jobs for the 2,000 or so particle physicists in Europe when LEP is built. Mulvey thinks there will, as the ECFA report deemed the situation satisfactory with only 450 researchers at LEP. Although the intersecting storage rings at CERN will be closed down, and there will be less work at the Super-Proton Synchrotron, there will be enough to do at the proton-antiproton collider, at the low energy antiproton ring (LEAR) and at other European laboratories such as the Deutsches Elektronen-Synchrotron in Hamburg, the ECFA report concluded.

Although "four experiments" sounds rather modest, LEP should be an excellent physics factory, provided that the particle called the neutral intermediate vector boson (Z°) exists. LEP is designed to be tunable to this resonance, which is the predicted mediating particle of the electroweak interaction. If the resonance is not there, however, or if it proves difficult to tune to it, there will no doubt be 850 unhappy physicists.

Robert Walgate

Franco-Soviet space flight

Some hitches

The visit of "*spacionaute*" Jean-Loup Chrétien to the Salyut-7 space station last month has introduced an unprecedented degree of candour into the reporting of Soviet space flights. Usually, cosmonauts' post-flight press conferences gloss over technical hitches and report as "satisfactorily accomplished" even those missions that were quite obviously curtailed.

The Soviet planners clearly accepted that the presence of a Westerner would entail more candid reporting, and a few days before the launch even admitted that Salyut-7 suffered unexpected attitude changes that had had to be corrected before link-up. Attitude, however, continued to give trouble throughout the flight, both aboard the Soyuz-T transport craft and on Salyut-7 itself.

According to Chrétien, the on-board computer of Soyuz-T suddenly ceased its automatic plotting just as the craft was approaching the space station at speed. This left Soyuz-T in a rolling motion, from which the crew of three had to effect a manual docking. This, Chrétien later explained on French radio, was not a breakdown — but it came at a critical moment when the crew could not even see the space station.

Orientation problems continued on board Salyut. The French contribution to the programme included high-sensitivity photography of the Earth's atmosphere and the interplanetary environment in the visible and near-infrared range. Another experiment was to photograph very weak light sources, from noctilucent clouds to distant galaxies. Both experiments required both darkness and a high degree of stability.

According to the crew commander, Vladimir Dzhanibekov, both these factors caused difficulty. The cosmonauts repeatedly lost their equipment (cameras, cassettes and so on) in the dark. Worse, flare from the thruster rockets necessary to maintain stability interfered with the lengthy exposures necessary. Dzhabenov said that such a possibility had never occurred to them before the launch.

Similar problems seem also to have arisen with the various physiological experiments. The crew is said not to have been able to think them through before launch and therefore to have had to "carry out additional training" in space. This seems remarkable — the focus of the medical programme, the French "echography" project, a Doppler measurement of blood-flow in the arteries leading to the brain, was intended to compare cadiovascular function before, during and after the flight. The crew should therefore have been familiar with the apparatus long before take-off.

The apparent lack of preparation may perhaps be due to the international nature of the flight which, contrary to Soviet practice, tied the launch to a pre-announced date.

Vera Rich

Colonel Jean-Loup Chrétien (left) meets President Mitterrand at the Elysée Palace.

UPI

---

*The "indicated experiments are ALEPH (spokesman Jack Steinberger), OPAL (Aldo Michelini), L3 (Samuel Ting) and DELPHI (Ugo Amaldi). ELECTRA (Roger Cashmore) and LOGIC (Jim Kirkby) have been put on hold.

0028-0836/82/290319-01$01.00

CORRESPONDENCE

Nuclear dangers

SIR — Nils Ove Bielsten (*Nature* 25 March, p.284) claims on the basis of "fact" that nuclear power plants are safer than hydroelectric, causing far fewer fatal casualties (a rather dubious claim considering comparative risk analysis), "not a single one occurring to people outside the plants (except possibly in accidents due to construction work traffic)". Yet again the impeccable record of nuclear power is invoked and compared with other sources of energy.

Is it not time to recognize and admit to the dangers of the whole chain of supply of nuclear fuel from mining to its eventual and undecided disposal? Uranium mines where studies have been possible, including some in the United States, have recorded mortality rates between 50 and 100 per cent. Surrounding native American communities also suffer casualties with the additional destruction of their environment and traditional livelihoods, especially painful for people with a traditional respect for the health of the Earth. I believe that it is time for a wider perspective to be taken on large scale projects such as this. Debate over social cost-benefit analyses, environmental impact assessments and technology assessments, which are prone to value judgements, does not negate their usefulness.

The casualties of Britain's earlier plutonium/electricity plants are also becoming apparent and substantial sums have been paid in compensation for workers' deaths.

The economics of nuclear plants are not quite as simple as Mr Bielsten would have us believe either. Left to the electric utilities, as he approves, we find that in the United States no new plants have been ordered for years and several have been cancelled. Plant cost escalations have run up crippling debts for communities and have sent utilities to the federal government for help. In the United Kingdom, it is now suggested that Scottish electricity consumers are paying the price for an unnecessary plant at Torness whose claimed "robust economic case" rests on a possible four-year period when, if coal plants are closed early, it may be useful. Government and independent investigations cast some doubt on even this value to consumers now that costs, need and forecasts are at last being debated.

The writer claims that "nuclear power is the environmentally soundest way of producing the energy that we cannot do without". Yet the people of Sweden have voted not to build any further plants beyond those already started. Their closure is already decided and a transition has been embarked on for a programme of energy efficient development — ending waste to liberate extra available energy. Renewable energy technologies are increasingly the source of new space heating needs and other requirements.

This approach, and energy efficient developments in the United States, demonstrate the value of demand management as a crucial aspect of energy planning.

Finally, Mr Bielsten's reference to possible benefits of mutation in the population is worrying. If it is a serious point then further debate is necessary.

MARTIN S. FODOR

Milton Keynes, UK

Complicating SI

SIR — Like J.A. Nicoll (*Nature* 10 June, p.450) and probably many others I have considered a simplified notation for physical quantities in terms of SI units.

The appropriate unit is automatically implied by the quantity that must necessarily be specified. Thus the statement that a force is 12 should denote by the absence of units that the SI system is employed and that the force is thus 12 m kg s^{-2} or 12 N. Whenever SI is not utilized units must continue to be provided as in 0.237 lb ft min^{-2}. The convenience of omitting units might thus speed the general adoption of SI.

Prefixes (kilo etc.) are not merely clumsy but they conflict with a principal virtue of SI which is coherence. The nuisance of large or small numbers could of course be lessened by the method commonly practised in computer printouts where 67,000 is written as 6.7 E + 4. However, a simpler notation might be 4;6.7 which specifies the numbers as read from left to right in increasing detail. The semicolon indicates that the number to the left is the power of ten and the period between 6 and the 7 might in time be dropped by convention. Such numbers are subject to rather obvious and simple rules in algebraic procedures.

In this notation the speed of light is 10;2.99776 and the electron rest mass -31;9.109. For the rather unusual case where a physical quantity has a negative value some further symbolism would be required. Perhaps one might adopt the method used by accountants to indicate net loss rather than net profit. In this case the absolute zero temperature on the centigrade scale would be (-2;2.73) C.

Here the unit would have to be provided since the Kelvin scale can also be employed. Amongst other virtues the latter does not have negative values and one would have $-\infty$;0. Which seems a bit odd but could of course also be written conventionally as 0.

HARALD H. ROSSI

Department of Radiology,
College of Physicians and Surgeons
of Columbia University,
New York, USA

German universities

SIR — Thank you for the splendid review on "Science in West Germany", which was published in *Nature* on 27 May. There are, however, some additional points on the present situation of German universities which I would like to highlight.

The statement that government support of science will decrease by 2 per cent in real terms in 1982 is not quite true for the universities. For instance the universities in Nordrhein-Westfalen are facing severe budget cuts which give them only 55 per cent of the 1980 budget. For some institutes in the natural sciences this is less money than they had in 1975, and student numbers have risen by some 50 per cent since; readers of *Nature* will know themselves how much they had to spend on lab-ware and chemicals in the meantime.

Another point is that the measures taken to reform German universities are in fact cutting the numbers of teaching and research personnel at the universities. Only 50 per cent of the young scientists who pursued a university career and "habilitated" themselves in recent years are eligible for a university job in the new frame law-university structure. The Nordrhein-Westfalen measures to concentrate university studies especially in teacher training, which date from March 1982 and were covered in the *Nature* review, are said to last for at least 5 years in order to transform university jobs into jobs at the Aachen *Klinikum;* at the end of these 5 years the numbers of personnel in the physics and biology departments at Bonn University will have been reduced by 50 per cent.

Since nobody is talking about student number reductions, please add all this up: what you come out with is a catastrophe. Already experimental work for diploma and doctorate theses in biology often is not financed by the universities, but by money from Deutsche Forschungsgemeinschaft (DFG). Although nobody likes to talk about it aloud, DFG funds are also being spent for teaching jobs and so on. Teaching is severely affected: at Bonn the biology department will have to cut lab courses by one third, the chemistry department is seriously thinking about closing down its central chemicals store. All this makes orderly studies and research impossible. The outlook for Germany's universities is very, very grim.

THOMAS SIMON

Bonn, West Germany

Living in the past?

SIR — It would be unfortunate if the pungent style of S. Blinkhorn's review of *The Mismeasures of Man* by S. J. Gould, (*Nature* 8 April, p.506) should weaken the force of his criticism. Like Blinkhorn I think there is much to object to in this book and, for T. J. M. Schopf (*Nature* 13 May, p.98), I would like to document a few of its substantive faults.

Although he has references as recent as 1979, Gould ignores major studies and references of the 1970s relevant to the topics he is considering in depth. Consequently, the reader will not learn from Gould's book that most geneticists are *not* "biological determinists"[1,2] nor that modern studies of heredity of cognitive abilities do *not* rely on a single (mystical) measure of intelligence[3].

Gould devoted 83 pages to the demolition of nineteenth century claims for an association between cranial capacity and human intelligence and the casual reader undoubtedly will think that he has thoroughly covered this topic. But he omits a critical 1974 review of the subject by Van Valen[4] which concludes that there probably really is a small positive correlation. Interestingly, Van Valen's conclusion is also ignored by Lewontin (discussing the same subject) in his favourable review[5] of Gould's book although Van Valen thanks Lewontin for comments (as does Gould).

Gould documents in great detail some blatant errors of the past but, by not coming up to the present, misleadingly implies that it is no different from the past. One would like to know why.

T. EDWARD REED

Departments of Zoology and Anthropology,
University of Toronto, Canada

1. Russell, E. S. *Genetics* **83**,s99 (1976).
2. Dobzhansky, Th. *Persp. Biol. Med.* **19**, 156 (1976).
3. DeFries, J. C. *et al. Nature* **261**, 131 (1976).
4. Van Valen, L. *Am. J. phys. Anthropol.* **40**, 417 (1974).
5. Lewontin, R. C. *New York Rev. Books* (22 Oct. 1981).

NEWS AND VIEWS

New branches for old roots

from Barry Cox

THE battle seems now to have been joined in earnest. Waving their branching weapons of attack, some of the cladists are now assaulting even the most fundamental roots of the systems of relationship that the traditional evolutionary morphologists have developed. After the skirmish over the tetrapod-origin outpost, in which Rosen *et al.* (*Bull. Am. Mus. nat. Hist.* **167**, 159; 1981) suggested that lungfishes rather than rhipidistians were closest to tetrapod ancestry, Gardiner has now used cladistic techniques to transform the whole system of tetrapod classification (*Zool. J. Linn. Soc.* **74**, 207; 1982).

Gardiner's method is first to return to the criteria given by nineteenth century anatomists in their analyses of relationship of the major tetrapod groups. Thus he concludes that "the denial of any immediate relationship between the mammals and the other great homotherm (*sic*) group, the birds, was based on no more than three characters; the form of the heart, aortic arches and occipital condyle". These three characters he swiftly demolishes (in about a page of text), and immediately moves on to list a number of characteristics of homoiothermy and of the central nervous system that appear to link mammals and birds as sister-groups. He relates to these two, in order of increasing distance, the crocodiles, chelonians and lepidosaurs. In all these discussions, palaeontology is ignored and only the characteristics of living animals are used. Into the resulting classification, Gardiner then fits a few fossil groups, such as the pterosaurs (a sister-group of birds), dinosaurs in Owen's original sense (sisters to crocodiles), the cynodonts (far divorced from the mammals), the dicynodonts (sister-group to the chelonians) and the pelycosaurs (completely separated from the previous two groups). The results are so different from those that also incorporate palaeontological data that a headlong collision is inevitable, for there can be no minor shifting of viewpoints or emphasis that could lead to a reconciliation or synthesis.

Gardiner's methods can be illustrated particularly well in his treatment of the Synapsida, the splitting of which into three separate groups (pelycosaurs, dicynodonts and cynodonts) is, to a palaeontologist, one of the most revolutionary aspects of his work. Basically, he rejects previously established relationships if he can quote other workers to the contrary and can show that some members of any other group also share some of the features previously thought to support the accepted relationship. So "as long ago as 1926 Berg wrote that the mutual similarities between mammals and (advanced synapsids) were probably due to convergence" and "despite the fact that fenestrae might have arisen independently (as they have done within the Chelonia . . . and Amphibia . . .), today's unquestioned doctrine is that the Synapsida include the mammal's closest relatives".

Gardiner also underestimates the modern palaeontological evidence by restricting himself to out-dated authors; is it really true of the pelycosaurs that "Their claim to Synapsid relationship apparently rests on Cope's (1884) insistence on their closeness to mammals and the possession of a lateral temporal fenestra"? Reisz, himself a cladist, states that "The pelycosaurs, together with their descendants, form a natural group and possess such derived characters as broad anteriorly tilted occipital plate . . . reduced post-temporal fenestrae, single median post-parietal, and septomaxilla composed of a broad base and a dorsal process" (*Spec. Vol. Syst. Ass.* **15**, 553; 1980). The relationships of pelycosaurs to both dicynodonts and cynodonts (and also to other therapsid and theriodont groups) is also suggested by the fact that all these groups share with sphenacodontid pelycosaurs the synapomorphic feature of a reflected lamina on the angular bone of the lower jaw. All, except the turtle-beaked dicynodonts, also share in having a heterodont dentition.

The cynodonts, like some other advanced synapsids, show a progressive reduction of the post-canine dentition and of the post-dentary bones of the lower jaw, with the mammalian type of squamosal-dentary jaw articulation having evolved in a few forms, and various approaches to the mammalian condition in the secondary palate, dentition, limbs and girdles. Gardiner nevertheless dismisses any relationship between cynodonts and mammals because an examination of the British Museum (Natural History) specimens of the cynodont *Thrinaxodon* "failed to reveal a single mammalian synapomorphy" and, for example, showed that *Thrinaxodon* was not particularly mammalian in its tooth-replacement and braincase. But it is such later, mid-late Triassic cynodonts as ***Probainognathus*** and the trithelodonts that are thought to be close to the origin of mammals, and these do show far more mammalian conditions of the teeth and braincase.

It seems perverse to reject these complex similarities merely because our extensive knowledge of the osteology of both recent and fossil tetrapods reveals isolated instances where temporal fenestrae have evolved independently (and, in any case, the chelonian openings that Gardiner quotes are emarginations, not fenestrae). We have no such systematic knowledge of the soft-part anatomy, physiology or biochemistry that make up the 17 characters that Gardiner lists to support his contention that birds and mammals are closely related sister-groups. As Szalay (*Am. Zool.* **21**, 37; 1981) has commented: "I believe that at the very heart of the post-Hennigean cladistic approach to phylogeny reconstruction lies the implicit neglect for biological and functional scrutiny of the characters employed. As a result of this attitude the postulated homologies chosen (the units on which phylogenies are based) are not biologically investigated and therefore the chances of discovering whether these features are unique or parallel or convergent acquisitions, or whether they represent a pattern commonly attained by distant lineages because of epigenetic factors, or because they are rooted in a common heritage, weakens the very foundations of such analyses. In other words, character analysis commonly practised in cladistics is really a semantically masqued enumeration of characters without attempts to analyse and weight them".

Gardiner's suggestions are so completely at odds with the palaeontological record that some of Panchen's observations, in an incisive criticism of the cladistic method published in the same volume as Gardiner's work (*Zool. J. Linn. Soc.* **74**, 207; 1982), seem particularly relevant. "The first obvious fault of cladism in general is perhaps a temperamental and, one may hope, a temporary one. This is the temptation to produce new and revolutionary groupings of organisms, or to resurrect old and discredited ones, just to demonstrate that cladism is getting results." □

Barry Cox is a Professor in the Department of Zoology, King's College, University of London, London WC2.

0028-0836/82/290321-01$01.00

Chaos, randomness and dimension

from T. Geisel

CHAOS and randomness are ubiquitous. In many scientific disciplines, random time series are obtained from an experiment and analysed into their power spectra. Often enough, the irregular motion of a system will have been produced by an external noise source. On the other hand, irregular motion and irregular time series may also be self-generated by a purely deterministic system. In the latter situation the term 'chaos' is used and, in a state space description, its dynamics are often governed by strange-looking topological objects called 'strange attractors'. As the scientific community is becoming aware of this phenomenon, observations of irregular behaviour that previously might have been ignored are attracting attention. The following questions then arise: given only the irregular time series, is it possible to tell whether it is due to chaos in the above sense, that is, does it have intrinsic properties which allow such a decision? Is it even possible to reconstruct the strange attractor, the ID card of the system, from the time series? These questions have been addressed in several recent papers which are reviewed in this article.

When irregularity is due to thermal fluctuations in physical systems, a large number (10^{23}) of particles and degrees of freedom are involved, which make the measurements look noisy. In brownian motion, for example, the irregular motion of a heavy test particle only reflects the irregular dynamics of 10^{23} molecules in the surrounding liquid. The terms 'randomness' and 'noise' describe such situations. 'Chaos', in contrast, is reserved for an irregularity that is self-generated by a deterministic system with few degrees of freedom in the absence of external fluctuating forces. Simple examples are driven anharmonic oscillators[1], where the phase space is three dimensional, consisting of position x, velocity v and the phase ψ of the driving force. In an undriven damped harmonic oscillator, the motion would asymptotically settle down at $x=0$, $v=0$. This point is called an attractor because any initial condition x_0, v_0 in a given area of phase space would lead to this point. The dimension is thereby shrinking from two to zero. For chaotic systems which are dissipative, attractors called strange attractors[2,3] may occur. These are asymptotic limit sets in phase space which also have lower dimension than the phase space and which have an additional property: the motion on the attractor is characterized by an exponential divergence of neighbouring states in some direction. This sensitive dependence on initial conditions is the cause for their strange appearance. It also practically prevents long-term predictions since the initial conditions are usually not known exactly. The sensitive dependence and the degree of unpredictability are measured by a variable called a Lyapunov exponent.

Strange attractors may not only occur in systems with few degrees of freedom but also in systems where, *a priori*, the dimension of phase space is high or infinite. An example is provided by turbulence in fluids and other systems that can be described by partial differential equations. Due to the presence of dissipation (damping) the motion in multidimensional phase space may, with time, settle down on a strange attractor which acts like a low-dimensional trap. The motion can then be described by a few variables in phase space. If the topology of the strange attractor is known, the dynamics of the entire system is known. This explains the dominating role of low-dimensional strange attractors for the chaotic dynamics of systems that may have infinite dimensions. Due to the sensitive dependence on initial conditions, these attractors have a complex structure similar to a Cantor set. The fractal dimension[4,5] can be used to characterize their spatial organization. In contrast to the topological dimension, this number may be non-integral, reflecting the topological complexity.

When an irregular time series is observed in an experiment one may ask whether the irregularity is due to chaos or to randomness as distinguished above. When little is known about the system, one can only hope that the time series possesses intrinsic properties which make this distinction possible. Power spectral analysis, which is usually applied, is of little help but other techniques have recently been proposed. They can be used to determine the dimension of the underlying dynamics and the fractal dimension of strange attractors. It is even possible to reconstruct the strange attractors.

One procedure has been proposed by the Santa Cruz Dynamical Systems Collective (J.P. Crutchfield, J.D. Farmer, N.H. Packard and R.S. Shaw). They propose to use the observed signal $x(t)$ and its successive derivatives $\dot{x}(t)$, $\ddot{x}(t)$, . . . as variables spanning the subspace of phase space to be reconstructed[6]. The procedure has been applied successfully to a dynamical system due to O.E. Rössler. It cannot be applied when the time series is not detailed enough to determine the derivatives. Another procedure, suggested by D. Ruelle (personal communication), consists of using the signal $x(t)$ and delayed signals $x(t-\tau)$, $x(t-2\tau)$. . . . to span the phase space reconstruction. F. Takens[7] has given a formal justification of these procedures in terms of the Whitney embedding theorem.

Roughly speaking, the dimension is determined if, with increasing dimension, the objects produced by the motion start

T. Geisel is at the Institut für Theoretische Physik, Universität Regensburg, D-8400 Regensburg, FRG.

100 years ago

THE NEW AFRICAN EXPEDITION

It is now understood to be quite settled that a new African exploring expedition will start next year. The Royal Geographical Society have, as might have been expected, taken the opportunity of Mr. Joseph Thomson's return from the completion of his engagement to the Sultan of Zanzibar to obtain his services as leader, and it is certain that no better selection could have been made.

Mr. Thomson will leave England in the Spring of 1883, and proceed to Zanzibar to organise the expedition. From Mombas, a port on the East African coast, to the north of Zanzibar, he will direct his course straight to Kilimandjaro, and do his best to explore the snowy ranges of this celebrated mountain, which but one European has as yet ever reached. Passing across the waterparting he will then descend through an entirely unknown country to the eastern shore of Lake Victoria Nyanza, and return to the coast by a more northern route, in the course of which it is hoped he may be able to visit Lake Baringo and Mount Kenia — another peak known to run far above the snow-level, but concerning which further details would be very desirable.

As a mere geographical expedition it will be thus seen that the proposed route will be one of great interest, embracing, as it does, the transit through much utterly unknown country, and the exploration of two mysterious snow-crowned mountains, which, according to the usual view of the conformation of the African Continent, appear to be quite out of place in the districts in which they are situated. But still more interesting problems will be solved, if steps are taken to investigate the unknown fauna and flora of Kilimandjaro and Kenia.

GEOGRAPHICAL NOTES

Lieut. Giraud has sailed from Marseilles for Zanzibar, as leader of a French expedition which proposes to take up African exploration where Livingstone laid it down with his life on the south shore of Lake Bangweolo. Lieut. Giraud proposes to go either direct west to Lake Tanganyika, or, more probably, by the north shore of Lake Nyassa, to the Chambeze River. This he will follow to its outlet in Lake Bangweolo, which he proposes to circumnavigate he will then attempt, in canoes, to sail down the Luababa-Congo, to its mouth in the Atlantic Ocean. This is an ambitious programme; and every one interested in African exploration will wish the expedition complete success.

From *Nature* **26**, 304 & 309, 27 July, 1881.

0028-0836/82/290322-02$01.00

making sense. More systematic techniques, however, are now available. The Dynamical Systems Collective uses linear regression locally to fit the data to points, planes or higher-dimensional hyperplanes[5]. The goodness of the fit is determined by χ^2, the sum of the squared deviations divided by the dimension. When the dimension closest to the fractal dimension is reached, χ^2 drops sharply. In the example of the Rössler system, a drop by a factor of one million was found for the best fit. Once the strange attractor has been reconstructed, the fractal dimension may be determined according to its definition[5]. Techniques to determine the fractal dimension and another measure of chaos, the topological entropy, have been described by F. Takens[7]. The relationship between the fractal dimension and the Lyapunov exponents has been investigated by P. Frederickson *et al.*[8].

Procedures which are able to distinguish between chaos and randomness are also suggested in an article by J. Guckenheimer published in this issue of *Nature* (p.358). These procedures are based on the assumption that randomness means unpredictability of the short-term evolution of a system. Chaos, on the other hand, is characterized by an exponential divergence of neighbouring states in phase space. This brings about only a long-term unpredictability of the system. Consequently procedures are constructed that verify exponential divergence of neighbouring states in the reconstructed phase space. Exponential divergence has also been investigated in terms of the Lyapunov exponent by R.S. Shaw for a chemical reaction system[9].

The methods outlined here have been applied successfully in real experimental situations. Strange attractors have been reconstructed for chaotic chemical reactions by J.C. Roux *et al.*[10,11] by using the time series of the concentration of a single chemical species — the phase space may in principle consist of at least the concentrations of all chemical species involved (about 25). D. Farmer *et al.*[12] have recently used a phase space reconstruction for a baroclinic flow experiment. In addition, they have been able to determine quasi-one-dimensional Poincaré return maps. R.S. Shaw *et al.*[13] have studied the irregular dripping of a tap and derived one- and two-dimensional return maps and topological and metric entropies from their measurements. ☐

1. Huberman, B.A. & Crutchfield, J.P. *Phys. Rev. Lett.* **43**, 1743 (1979).
2. For an introductory article see, for example, Ruelle, D. *La Recherche* **11**, Feb. 1980, p.132; English translation in *Math. Intelligencer* **2**, 126 (1980).
3. Ruelle, D. & Takens, F. *Comm. Math. Phys.* **20**, 167 (1971); **23**, 343 (1971).
4. Mandelbrot, B.B. *Fractals: Form, Chance and Dimension* (Freeman, San Francisco, 1977).
5. Froehling, H., Crutchfield, J.P., Farmer, D., Packard, N.H. & Shaw, R. *Physica* **3D**, 605 (1981).
6. Packard, N.H., Crutchfield, J.P., Farmer, J.D. & Shaw, R.S. *Phys. Rev. Lett.* **45**, 712 (1980).
7. Takens, F. in *Dynamical Systems and Turbulence* (eds Rand, D.A. & Young, L.S.) *Lect. Notes Math.* **898**, 366 (1981).
8. Frederickson, P., Kaplan, J.L., Yorke, E.D. & Yorke, J.A. *J. different Equat.* (in the press).
9. Shaw, R.S. as quoted in Roux, J.C. & Swinney, H.L. in *Nonlinear Phenomena in Chemical Dynamics* (eds Vidal, C. & Pacault, A.) 38 (Springer, Berlin, 1981).
10. Roux, J.C., Rossi, A., Bachelart, S. & Vidal, C. *Phys. Lett.* **77A**, 391 (1980); *Physica* **2D**, 395 (1981).
11. Turner, J.S., Roux, J.C., McCormick, W.D. & Swinney, H.L. *Phys. Lett.* **85A**, 9 (1981).
12. Farmer, D., Hart, J. & Weidman, P. (in preparation).
13. Shaw, R.S. *et al.* (in preparation).

Do mitochondria share enzymes with the rest of the cell?

from Thomas Fox

In a rough way, the matrix of mitochondria can be thought of as a cell cytoplasm containing a chromosome, a transcription and translation apparatus, and a number of metabolically important soluble enzymes. The peculiar thing, of course, is that much of this — for reasons that are unknown — apparently duplicates functions present in the real cell cytoplasm and the nucleus. It has seemed, however, that in no case does the same protein species function both inside and outside the mitochondrial matrix. Even though virtually all of the proteins present in the matrix are coded by nuclear genes, the matrix proteins studied so far have been found to be biochemically distinguishable from their functional analogues outside the mitochondria. A new report from Hopper *et al.* (*Cell* **28**, 543; 1982) now provides evidence that this may not always be the case. Work on two yeast mutants that affect tRNA methylation suggests that these functions are indeed shared by mitochondria and their gracious hosts.

The nuclear mutations, *trm1* and *trm2*, cause the absence of tRNA (guanosine-N^2, N^2) dimethyltransferase and tRNA (uridine-5)methyltransferase activities respectively. This was clearly demonstrated by examining HPLC elution profiles of ribonucleosides derived from digests of whole-cell tRNA preparations: $\mathrm{m}^2_2\mathrm{G}$ is specifically absent from the tRNA of the *trm1* mutant, while $\mathrm{m}^5\mathrm{U}$ is specifically absent from the tRNA of the *trm2* mutant. The modification of those tRNAs encoded and transcribed within mitochondria was examined by preparing tRNA from well-washed, isolated organelles, digested and analysed by HPLC. What was striking was that the purified mitochondrial tRNAs from wild type contained both methylated nucleosides, but $\mathrm{m}^2_2\mathrm{G}$ and $\mathrm{m}^5\mathrm{U}$ were specifically lacking in the mitochondrial tRNA from the *trm1* and *trm2* mutants respectively. Thus, the phenotype of these mutants is the same at the level of whole-cell (primarily cytoplasmic) tRNA and mitochondrial tRNA. On the face of it, it appears that for both modifications, the same (or similarly regulated) enzyme activities function inside and outside the mitochondria. (One assumes that the tRNAs do not leave the matrix to be modified and then return.)

It is dangerous to jump from the fact that a mutation affects an enzyme activity inside and outside the mitochondria to the conclusion that the mutation is in a gene coding both enzymes, without examining the enzymes themselves. Studies by Gross and co-workers on the *LEU5* locus in *Neurospora crassa* have shown that a mutation there leads to the production of an altered cytoplasmic leucyl-tRNA synthetase and to the virtual lack of mitochondrial leucyl-tRNA synthetase. Both phenotypes co-revert, indicating that they are the result of a single mutation. Furthermore, the genetic determinant for a naturally occurring electrophoretic variant of the mitochondrial enzyme also maps to the LEU5 region, indicating that structural gene information for both enzymes is in the same place (Beauchamp *et al. Proc. natn. Acad. Sci. U.S.A.* **74**, 1172; 1977). However, they could find no immunological cross-reactivity between the cytoplasmic and mitochondrial enzymes leading them to propose two tightly linked or overlapping genes for these two enzymes. Since the lack of immunological cross-reactivity may not be the most reliable indication that two proteins are unrelated, one should not yet rule out the possibility that a single gene codes for two, perhaps differently modified, leucyl-tRNA synthetases in *N. crassa*. However, in the case of the *trm1* and *trm2* mutations of yeast, the possibility of distinct but tightly linked and co-regulated genes for tRNA methylases should probably not be dismissed either.

A single gene, with two possible modes of transcription and translation, could clearly code for two similar proteins that end up on opposite sides of a membrane, as has been shown by analysis of a yeast gene that codes for both intracellular and secreted invertase (Perlman and Halvorson *Cell* **25**, 525; 1981; Carlson and Botstein *Cell* **28**, 145; 1982). It seems quite possible that such a mechanism also plays a part in specifying some proteins inside and outside the mitochondrial matrix. Clearly, an examination of the *TRM1* and *TRM2* genes of yeast and the *LEU5* gene of *N. crassa*, as well as the proteins they encode, will prove very enlightening. ☐

Thomas Fox is Assistant Professor of Genetics, Division of Biological Sciences, Cornell University, New York 14853.

0028-0836/82/290323-01$01.00

Bone in the cartilaginous fishes

from Brian Hall

THE recent documentation by Peignoux-Deville *et al.*[1,2] of bone in the vertebrae of the backbone of the dogfish, *Scyliorhinous canicula*, a member of the cartilaginous fishes (Chondrichthyes), has important implications for biology because sharks and rays are grouped together as cartilaginous fishes on the basis of the presence of a cartilaginous skeleton in the adult and the absence of bone from any stage of the life cycle. In other vertebrates, such as man or the bony fishes, most of the cartilage of the embryo is replaced by bone in the adult.

Cartilage and bone are the two major skeletal tissues. The long debate in evolutionary circles over whether cartilage or bone arose first during vertebrate evolution resulted in classifications of the vertebrates that had cartilaginous fishes either on the main evolutionary line as the ancestors of all other fishes and amphibians, if you believed that bone arose late in vertebrate evolution, or as a side branch, if you believed that bone arose early[3].

Peignoux-Deville *et al.* examined vertebrae of the dogfish using X-ray analysis, labelling with tetracycline (a calcium-seeking fluorescent drug) and transmission electron microscopy. The upper halves (neural arches) of the vertebrae were found to consist of large-celled cartilage overlain by a layer of lamellar bone containing bone-forming cells (osteocytes). The bone was calcified, as confirmed by the uptake of tetracycline and by the presence of calcium phosphate (apatite) crystals. Average mineralization (1g mineral per cm^3 of bone) was the same in the cartilaginous and bony portions of the vertebrae. The association of the bone with the underlying large-celled cartilage suggests that the cartilage may have induced the bone to form in the same way as occurs in higher vertebrates[4]. Mutants are known in which cartilage fails to become large-celled (for example, *talpid* in the chick, *brachypod* in the mouse), with the consequence that bone fails to form around the cartilage. Cartilaginous fishes appear to use the same developmental mechanism to form bone. The cartilage of higher vertebrates also contains canals which both provide cells for centres of bone formation deep within cartilage and allow nutrients to reach the deeper recesses of cartilage, a tissue which lacks blood vessels. Hoenig and Walsh[5] examined vertebrae from 16 species of sharks and found that all had canals containing blood vessels and immature cartilage cells. They ruled out any bone-forming (osteogenic) function for these canals .... "the osteogenic function cannot apply to Elasmobranch vertebrae", following instead the traditional view that sharks lack bone. A closer examination of these vertebrae is clearly now required.

Previous studies had hinted at the presence of bone in the endoskeletons of sharks and definitely showed it to be present in the hard denticles which are embedded in the skin and at the base of the teeth[6-11]. The X-ray diffraction pattern of shark vertebrae is also identical to that obtained from bone[12], and this and the presence of the canals should encourage a closer examination of shark vertebrae. *Ornithoprion hertwigi*, a fossil shark from the Permian period, had a thick layer of bone around its lower jaw[13]. The presence of bone in both the jaw and the vertebrae is of especial interest as much of the head skeleton is derived from the neural crest[4,14], while vertebrae are mesodermal in origin. Sharks have retained bone-forming potential in cells with both of these embryological origins. Bone formation in cells on the surface of the vertebrae is presumably activated by association with underlying large-celled cartilage while cranial neural crest-derived cells are presumably activated by interaction with epithelia, as happens in other vertebrates[14].

The existence of bone in these sharks explains the previously paradoxical presence of the hormone calcitonin, which acts on bone to regulate calcium metabolism. The presence of bone also highlights the chanelling of thinking which follows the classification of a group of animal on the basis of the presence of one, albeit major, feature and the lack of another. Because the Chondrichthyes are classified as having a cartilaginous skeleton and lacking bone, we automatically think that they are incapable of forming bone. This lead to the spurious classifications of vertebrates mentioned earlier, to the conclusion that no feature (canals, calcitonin) could have anything to do with bone or bone formation, that the cartilaginous fishes have 'lost out' in evolution, not having the potential for growth, mineral metabolism and structural support possessed by their bony cousins, and that any suggestion of the presence of bone must be spurious for cartilaginous fishes lack bone. The simple observation of the presence of a tissue in one region of one species opens up many roads for future travel. □

---

1. Peignoux-Deville, J. *et al. C.R. hebd. Séanc. Acad. Sci., Paris* **292**, 73 (1981).
2. Peignoux-Deville, J. *et al. Cell Tissue Res.* **222**, 605 (1982).
3. Hall, B.K. *Am. Zool.* **15**, 329 (1975).
4. Hall, B.K. *Developmental and Cellular Skeletal Biology* (Academic, New York, 1978).
5. Hoenig, J.M. & Walsh, A.H. *Can. J. Zool.* **60**, 483 (1982).
6. Kemp, W.E. & Westrin, S.K. *J. Morph.* **160**, 75 (1979).
7. Moss, M.L. *Am. Zool.* **17**, 335 (1977).
8. Holmgren, N. *Acta zool.* **23**, 129 (1942).
9. Moss, M.L. *Acta anat.* **77**, 161 (1970).
10. Peyer, B. *Comparative Odontology* (University of Chicago Press, 1968).
11. Miles, R.S. & Moy-Thomas, J.A. *Palaeozoic Fishes* 2nd end (Chapman & Hall, London, 1971).
12. Gilbert, P.W. *et al. Sharks, Skates and Rays,* 37 (The Johns Hopkins Press, Baltimore, 1967).
13. Zangerl, R. *Fielddiana Geol.* **16**, 1 (1966).
14. Pratt, R.L. & Chirstiansen, R.L. *Current Research Trends in Prenatal Craniofacial Development* (Elsevier, New York, 1980).

Brian Hall is Professor and Chairman of Biology, Dalhousie University, Halifax, and a Nuffield Foundation Fellow and Visiting Fellow, University of Southampton.

Hipparcos: space-age astrometry

from A.M. Cruise

THE measurement and cataloguing of stellar positions is one of the oldest branches of science and the results, gathered over the centuries, have been crucial in the formulation of our present concept of the scale and structure of the Universe. But astrometry is hardwork. To achieve a precision very much better than the arc second resolution of ground-based optical telescopes in a homogeneous manner over the whole sky seems impossible, with present instruments at least. It is no wonder then that astrometry has fallen from the front ranks of astronomical science, and spectroscopy and theoretical astrophysics have gained favour. Nevertheless, astrometry has some simple but profound truths to tell that are fundamental to the development of all branches of astronomy. By choosing the space astrometry mission 'Hipparcos', scheduled for launch in late 1986, the European Space Agency will transform many branches of astronomy and astrophysics.

The astrometric observations made from Hipparcos are hoped to have a precision of one or two milliarc seconds — one hundred to a thousand times better than is currently available for most stars. Such accuracy will allow both radio VLBI measurements and optical results to be specified in a consistent coordinate system.

Increased precision is not the only attribute of the Hipparcos catalogue. The instruments scanning sequence will allow observation of the whole celestial sphere during the two and a half year mission. About 1000,000 stars will be measured, including all stars down to ninth magnitude, and careful selection will ensure that there are always two or three

A.M. Cruise is at the Mullard Space Science Laboratory, University College London, Holmbury St Mary, Dorking, Surrey RH5 6NT.

0028-0836/82/290324-02$01.00

Hipparcos stars in each square degree of sky. A convenient, homogeneous coordinate grid of high precision that covers the whole sky will thus be created. In addition, the Space Telescope will be able to determine the position of some extragalactic objects with respect to Hipparcos stars and so link the new coordinate system to an inertial frame.

The increase in precision gained from Hipparcos will allow the absolute determination, by trigonometric parallax, of distances 10–20 times greater than at present. It is the absolute nature of the method which is of overwhelming importance. All the overlapping cosmic distance scales which span the observable Universe ultimately depend on measurements of the distance to the Hyades cluster which is just close enough to show measurable angular motion in ground based telescopes. Calibration of the absolute luminosity of various stellar distance indicators in the Hyades provides the means by which apparent luminosities of very distant objects can be used to determine their distance.

Not only will Hipparcos improve on the absolute distance measurement for the Hyades and so reduce the statistical error on all cosmic distance scales but more important, the absolute distance of five clusters other than the Hyades will be measured. The calibration of distance indicators can then be scrutinized for dependences on metallicity and other factors that might vary from cluster to cluster. Hipparcos will also increase the number of stars accessible to direct distance measurement by a factor of about 1,000 and absolute luminosity measurements over a much wider range of stellar temperature will be made possible.

The accuracy of measurement will allow changes in stellar positions to be observed during the mission. This proper motion caused by the stars spatial velocity with respect to the Sun has been measured in the past for a relatively small number of stars by comparing positions measured at widely separated times. The high precision of Hipparcos will, however, be offset by the shortness of the two and a half year observation period so the accuracy of proper motion measurements will not be much increased — the really dramatic improvement will be in the large numbers of stars observed.

The performance of the Hipparcos instrument is closely coupled to the operation of the satellite and the design of both is being refined. The two main difficulties, which should be overcome by the concept first proposed by Lacroute, are the achievement of the necessary precision and the maintenance of the absolute calibration of the angular measurements. A modestly sized telescope will view a beam combiner so that two stars separated on the sky by about 70 degrees will be superimposed in the focal plane on a modulating grid that measures their relative separation. As the satellite rotates the two fields of view will scan along a great circle. By demanding that a closed chain of star separation measurements must sum to 360 degrees angular calibration can be accomplished with the desired frequency. When many intersecting great circle scans are combined the two coordinate stellar position can be found with an ultimate accuracy of one or two milliarc seconds.

There is already a great deal of scientific activity, including colloquia[1,2] and published papers[3-5], supporting the Hipparcos project. ESA has selected two separate consortia to perform the data analysis task and has issued a call for proposals to help define the list of stars to be observed. The deadline of 1 October 1982 gives some hint of how much work is required to put the observing list into the necessary form for the operation of the satellite.

Astrometry from space will still be hard work but at least the astrometric measurements from Hipparcos will stand more clearly above the noise and so attract the attention they deserve from astronomers in general. □

---

1. Barvieri, C. & Bernacca, P.L. *Colloq. European Satellite Astronomy*, University of Padova (1978).
2. ESA SP-177 *The Scientific Aspects of the Hipparcos Space Astrometry Mission* (ed. Perryman, M.A.C. & Guyenne, T.D.).
3. Hoyer, P. *et al. Astr. Astrophys.* **101**, 228 (1981).
4. Murray, C.A. *Mon. Not. R. astr. Soc.* **195**, 639 (1981).
5. Froeschle, M. & Mignard, F. *Appl. Optics* **20**, no. 18, 3521 (1981).

Monoclonal antibodies to human malignant melanoma

from Ralph A. Reisfeld

A RECENT international workshop on monoclonal antibodies to human melanoma-associated antigens* demonstrated rapid progress in the analysis of 30 monoclonal antibodies that had been produced and exchanged by 10 laboratories. There was general agreement that 24 antibodies defined 11 antigens that are expressed on melanoma cells to a considerably greater extent than on other normal or neoplastic cells and tissues. These antigens may be the products of amplified and/or altered normal genes and could provide a set of model targets for adjunct immunotherapy, as well as sensitive molecular probes for studies on the biology of malignant melanoma and the mechanism of neoplastic transformation.

Particularly striking were the consistency among reaction patterns of most antibodies, even though different target cells and techniques were used, and the variety of the antigens identified, even by using the same melanoma cell lines as immunogens. Although most monoclonal antibodies were elicited from melanoma lines in long-term tissue culture, they reacted in binding indirect immunofluorescence and immunoperoxidase assays with surgically removed, frozen tissue sections and, in some cases, with melanoma cell lines at early passage levels — suggesting few tissue culture artefacts and little antigenic drift. Only relatively few antibodies reacted with formalin-fixed, paraffin-embedded tissue sections, suggesting that most determinants recognized by the monoclonal antibodies are irreversibly denatured by this treatment.

Structural studies of the 11 selected antigens indicated 5 of them to be single-chain glycoproteins with molecular weights (M_r) of 70,000–100,000, one a single-chain glycoprotein with M_r 184,000 and two multiple-chain glycoprotein molecules with M_r of 116,000–130,000. One of the antigens is a sialoganglioside (G_{D3}) and two were identified as extracellular matrix proteins, that is, chondroitin sulphate proteoglycans consisting of a glycoprotein chain (M_r 250–280,000) and a series of components with $M_r > 780,000$. Antibodies to two of the antigens, p97 (gp95), a glycoprotein of M_r 97,000 which is structurally related to transferrin, and the proteoglycan molecules, have been identified which can react with distinct epitopes on the same or very similar molecules. Interestingly, all the 24 monoclonal antibodies selected react with cell membrane or matrix antigens. This may reflect a relatively low immunogenicity of cytoplasmic antigens and/or the choice of the procedures used in screening the hybridomas.

Several general conclusions were reached by the 10 participating laboratories. The antibodies analysed detect tumour-associated antigens but not tumour-specific antigens in the strict sense

---

*The workshop on 'Monoclonal Antibodies to Human Melanoma Antigens: II' held on 26–27 April 1982 at Bethesda, Maryland was organized by the Immunology Program, Cancer Biology Branch, Division of Cancer Biology and Diagnosis, National Cancer Institute. The participating laboratories were those of J.C. Bystryn, New York University School of Medicine; S. Ferrone, Columbia University, New York; K.E. and I. Hellstrom, Fred Hutchinson Cancer Center, Seattle; H. Koprowski, Wistar Institute, Philadelphia; J.P. Mach and S. Carrel, Ludwig Institute for Cancer Research, Lausanne; D.L. Morton, University of California, Los Angeles; R.A Reisfeld, Scripps Clinic and Research Foundation, La Jolla; G. Riethmuller, University of Munich; and H.F. Seigler, Duke University Medical Center, Durham. The proceedings of the workshop will be published in *Hybridoma* 2, No. 4, 1982.

Ralph A. Reisfeld is at Scripps Clinic and Research Foundation, La Jolla, California 92037.

0028-0836/82/290325-02$01.00

of the word; those selected are, however, sufficiently closely associated with melanomas that they should be further characterized and serious consideration given to their potential as *in vitro* and *in vivo* markers for diagnosis and as targets for immunotherapy. Simple screening of monoclonal antibodies by binding assays with cultured tumour cell lines is not sufficient to evaluate critically their specificity, and screening of a large variety of both normal and tumour tissues by indirect immunofluorescence or immunoperoxidase techniques appears necessary to make any meaningful comparisons. Quantification of antigen expression on normal and tumour cells is definitely necessary, either by saturation binding with Scatchard plot analyses or by quantitative binding assays with radiolabelled antibody or by analysis with the fluorescence-activated cell sorter. □

What limits photosynthesis?

from Christine Foyer, Richard Leegood and David Walker

ENHANCED plant productivity is one means by which world food and energy shortages may be alleviated. For this reason research into the photosynthetic process is increasingly favoured both in the UK and overseas. However, the crop physiologist is quick to remind us that the connection between photosynthesis and productivity is more apparent than real, in the sense that a correlation between short-term measurement of photosynthetic rate and crop yield is not easily demonstrated. Certainly the gulf between the plant scientist and the farmer is considerable. Even the highly valuable contributions of the plant breeder have been largely confined to factors such as disease resistance and the redistribution of assimilates within the plant. We have all lamented photorespiratory loss, worried over the inadequacies of ribulose bisphosphate carboxylase/oxygenase and wondered if we can turn, for solace, to C4. Perhaps, however, if we pause for thought, there is no reason to be unduly pessimistic about the future of photosynthesis in its relation to agriculture.

Plant growth is the best measure of net photosynthesis that we have and the limits to which the useful redistribution of assimilates can be achieved are fast being reached. To increase plant productivity by securing more vigorous growth through more effective photosynthesis we need to determine which existing limitation might be removed. A discussion meeting* was organized by the Agricultural Research Council to identify and characterize the reactions which limit the photosynthetic process in various environmental and developmental conditions, and to determine how basic research into photosynthesis may be directed towards increasing plant productivity. A workshop on the methodology and applications of the measurement of chlorophyll fluorescence preceded the meeting. This technique is now regarded as a valuable non-intrusive probe for photosynthesis *in vivo* providing, in the words of J. Barber (Imperial College, London), a 'stethoscope' for plants.

Many workers in photosynthesis disagree about the basis on which the rate of photosynthesis should be expressed, and doubt the validity of the present methods, especially since a single factor is unlikely to be constant. All quantitative means for expressing photosynthetic rate in current use (for example, ground area, fresh weight) carry inescapable disadvantages. In spite of this, chlorophyll is likely to remain the universal basis for expressing photosynthetic rate at the cellular level simply because it is easily measured (J. Ludwig, GCRI, Littlehampton). The use of the term 'photosynthetic efficacy', to relate capacity to performance (that is, an assessment of the actual performance of a given crop as a function of the potential performance), could help to determine the degree to which photosynthetic capacity is realized in a given circumstance (D. A. Walker, Sheffield University).

Although the basic climatic limitation to crop photosynthesis is the seasonal input of light energy, the degree to which this energy can be used by the plant is modified by local climatic factors, such as temperature, water and the requirements of particular farming systems (J. P. Cooper, WPBI, Aberystwyth). The rate of photosynthesis reaches a maximum at or just before full leaf expansion and declines thereafter. The length of the growing season before leaf senescence is, therefore, a limitation on crop yield (H. Thomas, WPBI, Aberystwyth). The efficiency of photosynthesis in relation to the balanced excitation of the photosystems is believed to be controlled by the phosphorylation of the light-harvesting chlorophyll *a/b* binding protein. Balanced excitation is necessary for efficient non-cyclic electron transport and also serves to poise cyclic electron flow by increasing excitation of photosystem I relative to photosystem II. Furthermore, the flexible distribution of available quanta between the two photosystems can be especially important under stress and allow a more efficient distribution of excitation in different cells of a leaf and different leaves in a canopy (P. Horton, Sheffield University).

The majority of temperature crops, particularly cereals, are exposed to suboptimal temperatures for most of their lives. Dramatic differences in temperature response occur between cold-tolerant and cold-intolerant plants. Even at the level of the chloroplast the partitioning of assimilate may be considerably influenced by temperature as transport generally outstrips production at low temperatures; the autocatalytic Benson–Calvin Cycle does not obey Arrhenius' law (Heber, Würzburg University). Low temperatures cause phase changes in the lipids of the thylakoid membranes and the resulting reduction of the fluidity of the thylakoids reduces the mobility of the electron carriers between photosystems I and II, for example by diminishing the diffusion rate of reduced plastoquinone (D. Chapman, Imperial College, London). This may well be the most temperature-dependent step of electron transport.

Ribulose bisphosphate carboxylase/oxygenase is the point of entry of carbon into the Benson–Calvin cycle and that of oxygen into the photorespiratory pathway. There is a broad correlation between ribulose bisphosphate carboxylase activity extractable from leaves and light-saturated rates of photosynthesis in plants taken from a wide range of growth conditions and genotypes. Ribulose bisphosphate carboxylase appears to limit photosynthesis only in the sense that the activity of the enzyme is close to that of the flux through the Benson–Calvin cycle. Plants synthesize only as much of this enzyme as they need (A. Keys, Rothamsted Experimental Station). This raises the question of whether a limitation imposed by this enzyme is a phenomenon perceived by the manipulator rather than the plant.

The purpose of photorespiration continues to be hotly debated. Selective inhibition of the oxygenase activity is improbable although some species have carboxylases with a significantly higher affinity for CO_2 than others (S. Gutteridge, Rothamsted Experimental Station). Other enzymes of the Benson–Calvin cycle, such as fructose bisphosphatase, show changes in activity in response to the redox state of ferredoxin, although the changes in fructose bisphosphatase activity do not have a role in regulation of the photosynthetic rate in leaves illuminated with saturating light.

No final answer as to 'What limits photosynthesis' arose from the meeting. The most popular candidate, proposed by O. Björkman (Carnegie Institute of Washington), was God. The question deserves future consideration and research if we are to secure increased plant productivity. □

Christine Foyer, Richard Leegood and David Walker are in the ARC Research Group on Photosynthesis, Department of Botany, Sheffied S10 2TN.

---

*The ARC discussion meeting on 'What limits photosynthesis' was held on 15–16 April 1982 and was hosted by the ARC Research Group on Photosynthesis at the University of Sheffield.

0028-0836/82/290326-01$01.00

New views of the immunoglobulin heavy-chain switch

from Kenneth B. Marcu and Max D. Cooper

DURING the differentiation of B lymphocytes, the immunoglobulin genes they express undergo a succession of rearrangements. The last of these determines the class of antibody expressed — whether it is IgM, IgG, IgA and so on. Just which of these classes or isotypes will predominate in an antibody response depends, among other things, on the nature of the antigen and in particular on the dependence of the B-cell response on T-cell help. Both the mechanism of the class switch and the nature of the T-cell influence were discussed at a meeting* in Sweden.

Antibody molecules (or immunoglobulins) consist of two identical heavy and light chains. In the mouse, these are encoded by linked families of V_H, D_H and J_H genes located 5′ to a cluster of eight heavy-chain constant-region (C_H) genes (μ, δ, $\gamma 3$, $\gamma 1$, $\gamma 2b$, $\gamma 2a$, ε and α) on chromosome 12 and V_L and J_L genes upstream from the κ and λ light-chain genes on chromosomes 6 and 16 respectively.

One of the first steps in differentiation of the B cell is the assembly by chromosomal rearrangement of one each of the V_H, D_H and J_H genes and the transcription of the V–D–J set along with the C_μ gene (see the figure). A cell expressing such μ mRNA is known as a pre-B cell, and at this stage few of the μ chains reach the cell surface. Thus the pre-B cell is not influenced by antigen until the next stage in differentiation, when one set of V_L and J_L genes is productively rearranged and a complete IgM molecule is expressed on the surface of the cell, which has now differentiated into an immature B lymphocyte.

Subsequent stages in B-cell differentiation entail changes in the expression of the C_H genes, and, in particular, isotype switching in which the same V_H–D_H–J_H set is expressed sequentially with different constant-region genes. Intermediate stages in B-lymphocyte differentiation are marked by the expression of a variety of cell-surface proteins involved in regulating B-cell migration, growth and differentiation. In its terminally differentiated state, the B cell, now a plasma cell, shifts from surface expression to secretion of its antibody.

All immature B lymphocytes at first express membrane-bound IgM, and later co-express surface IgD, sharing the same V_H–D_H–J_H and light chains. Some members of each B-cell clone make a further switch, from IgM (and IgD) to IgG, IgA or IgE — again with no change in the V–D–J genes. Heavy-chain isotype switching in B-cell clones was discovered more than a decade ago, when it was shown that treatment of immature B cells by infusions of anti-μ antibodies prevented subsequent development of plasma cells producing other immunoglobulin classes[1]. It is now known that in plasmacytomas secreting isotypes other than μ, the constant-region genes 5′ to the one that is expressed are deleted, the deletion occurring between switch (S) regions localized in the introns 5′ to the expressed C_γ, C_ε or C_α gene[2–6]. But many fundamental questions remain unanswered. What is the normal sequence of C_H gene expression — can cells switch directly from IgM to, say, IgE or must they express each successive isotype between? What are the precise switch mechanisms and when does a cell become committed? How is the switch regulated? The answers to these questions are beginning to emerge and were discussed at Umeå.

Mechanism of the switch

While it is generally accepted that deletion of the 5′ constant-region genes accompanies differentiation into an immunoglobulin-secreting plasma cell, it is still not known whether this occurs by intrachromosomal deletion[2] or by unequal exchange between sister chromatids[7]. In either case, there is now evidence that the C_H gene deletion may not occur until the switch from the surface to secreted immunoglobulin has taken place.

The existence of immature B lymphocytes exhibiting two cell-surface isotypes, for example IgM + IgG or IgM + IgA, has been known for some time. It was originally thought that this could be most simply explained by the stability of either the μ mRNA or the μ polypeptide, which would allow for the maintenance of cell-surface IgM for a B cell that has already genetically switched to either γ or α isotype. In the case of cells co-expressing μ and δ chains, however, it is now known that the two chains are produced by differential splicing of a single primary RNA transcript containing both the C_μ and the C_δ gene[8–10]. At the meeting it became clear that differential splicing of a long transcript may also underlie the expression of constant-region genes downstream of δ. T. Honjo (Osaka University) presented evidence that $\mu^+ \varepsilon^+$ B lymphocytes, purified from the spleens of parasite-infected SJA/9 mice (a congenic strain without detectable circulating IgE antibody), have no detectable C_H gene rearrangements and/or deletions. To explain this unexpected finding, Honjo proposes[23] that a transcription unit starting 5′ of V_H

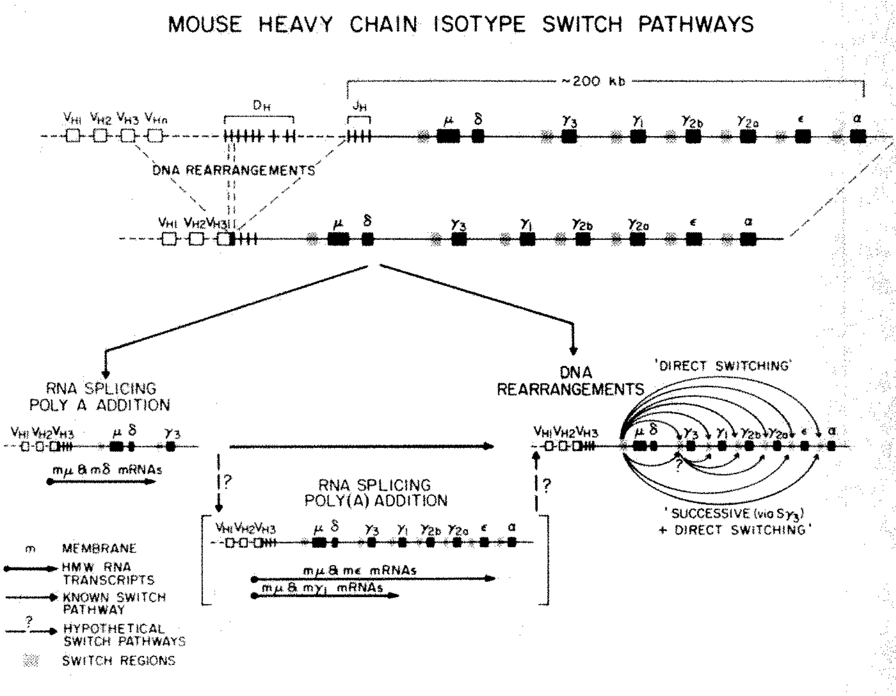
MOUSE HEAVY CHAIN ISOTYPE SWITCH PATHWAYS
~200 kb
V_{H1} V_{H2} V_{H3} V_{Hn}
D_H
J_H
μ δ γ_3 γ_1 γ_{2b} γ_{2a} ϵ α
DNA REARRANGEMENTS
RNA SPLICING
POLY A ADDITION
$m\mu$ & $m\delta$ mRNAs
?
RNA SPLICING
POLY(A) ADDITION
$m\mu$ & $m\epsilon$ mRNAs
$m\mu$ & $m\gamma_1$ mRNAs
DNA
REARRANGEMENTS
'DIRECT SWITCHING'
'SUCCESSIVE (via $S\gamma_3$)
+ DIRECT SWITCHING'
m MEMBRANE
HMW RNA TRANSCRIPTS
KNOWN SWITCH PATHWAY
HYPOTHETICAL SWITCH PATHWAYS
SWITCH REGIONS

In the course of B cell ontogeny, V_H, D_H and J_H DNA segments first become assembled to encode a complete heavy-chain variable region and later, the same assembly of V, D and J segments is associated sequentially with different C segments. The diagram shows the three possible ways in which this sequential switching may be achieved.

---

*A workshop on 'Immunoglobulin Heavy-Chain Class Switching' was organized by A. Coutinho and his colleagues at Umeå University, Sweden, on 16–19 February 1982.

Kenneth B. Marcu is at the Department of Biochemistry, State University of New York at Stony Brook, New York 11794, and Max D. Cooper is at the Cellular Immunobiology Unit, University of Alabama Medical Center, Birmingham, Alabama 35294.

0028-0836/82/290327-02$01.00

and terminating past ε is produced in $\mu^+ \varepsilon^+$ lymphocytes. This approximately 180 kilobase multi-C_H transcript could yield μ and ε membrane mRNAs by differential RNA splicing coupled with specific poly(A) addition (see the figure). Similar studies on a population of $\mu^+ \gamma 1^+$ B cells from normal mouse spleen have been interpreted in the same way[11]. However, cellular immunologists will want clear assurance that the immunoglobulin molecules on the surface of these cells are actually synthesized by them and not picked up from other cells, especially since the existence of a multi-C_H transcript in immature B lymphocytes may be very difficult to establish (none has yet been isolated for the μ–δ transcription unit). This hypothesis poses the intriguing problem of a mechanism for operating the switch first by RNA splicing and then by DNA rearrangement since γ^+ and α^+ B cells have been shown to give rise to plasma cells which produce the same heavy chain isotype.

Another hypothesis arises from observations on subclones of a pre-B cell line (18–81) transformed by Abelson virus. In these cells, switching from μ to γ2b (ref. 12) can apparently occur in the absence of μ-gene deletion, though not without some DNA rearrangement[13]. It is possible that at some point in the history of the 18–81 cell line, the δ, γ3 and γ1 genes were deleted and the γ2b gene was positioned immediately 3′ to the μ gene where it could give rise to a μ–γ2b transcript by the same mechanism that produces the μ–δ transcript. F. Blattner (University of Wisconsin) suggested that this might be a transitional step in isotype switching, the constant-region gene to be expressed in each case replacing the δ gene 3′ to μ. The next step would involve C_μ gene deletion before plasma cell differentiation.

Successive and direct switching

So far, there is evidence for both successive and direct isotype switching (see the figure). Both switching modes could operate on a purely stochastic basis[5], or under the influence of regulatory elements such as isotype-specific recombinases[14].

In addition to direct $\mu \rightarrow \gamma$ and $\mu \rightarrow \alpha$ switches, M. Wabl (University of Tübingen) reported evidence for a $\mu \rightarrow \varepsilon$ switch in lipopolysaccharide (LPS)-induced plasma blasts. Successive isotype switches are also suggested from studies using the splenic focus assay and limiting dilution as methods for examining these cell clones[15,16]. Using the limiting dilution of LPS-stimulated cells, A. Coutinho and co-workers (Umeå University) obtained results consistent with switches from μ to each of the other isotypes and for multiple patterns of successive 'downstream' switches. In the response to trinitrophenol-Ficoll, a T-independent antigen, the frequency of γ isotypes expressed follows the C_H gene order (that is, $\gamma3 > \gamma1 > \gamma2b > \gamma2a$), and results of splenic focus analysis suggested that γ3 cells may be pivotal for switches to other γ isotypes[16]. K. Marcu (SUNY, Stony Brook) showed that $S_{\gamma 3}$, S_α and S_ε possess extensive homology with S_μ, while $S_{\gamma 1}$, $S_{\gamma 2b}$ and $S_{\gamma 2a}$ have very limited S_μ homology, and suggested that this could provide a genetic basis for intermediate $S_{\gamma 3}$ switches to other γ isotypes (see the figure). Marcu also presented evidence for a new consensus DNA sequence, YAGGTTG, preferentially located 5′ of C_H switch sites and repeated in S regions[17,18], which, together with previously identified common S sequences (GAGCT and GGGGT)[19], may play a part in switch-site recognition[17–19].

Successive C_H gene switches have recently been explored at the molecular level in C_H switch-variant cell lines[20,21]. A switch from γ2b to γ2a in MPC-11 myeloma variants results in S region-mediated γ2b gene deletion[20]. F. Sablitzky (Genetics Institute, University of Cologne) presented some startling results from correlations of C_H gene rearrangements and deletions with isotype switching in clones of spontaneous class-switch variants derived from the X-63 hybridoma[15]. In X-63 hybridoma cells, 'backswitches' (for example $\gamma 2a \rightarrow \gamma 1$) occur at 100-fold higher frequency than forward switches (for example $\gamma 1 \rightarrow \gamma 2b \rightarrow \gamma 2a$), which arise at frequencies of 10^{-7}. The unprecedented finding of C_H backswitching could be most simply explained by either trans-homologous chromosome exchange or the presence of duplicated γ genes generated by unequal cross-over during sister chromatid exchange. Even though these findings may partly reflect peculiarities of the cell lines, they do clearly demonstrate that successive switching — for example, $\gamma 1 \rightarrow \gamma 2b \rightarrow \gamma 2a$ — can occur.

Role of T cells in isotype expression

It is well known that the nature of the antigen and responding T cells or their helper and suppressor factors can selectively influence the isotypes expressed by plasma cell progeny of responding B cells. J. Davies (Washington University, St Louis) reviewed evidence indicating that T-independent polysaccharide antigens elicit primarily μ and γ3 antibodies while the T-dependent protein antigens preferentially induce μ, γ1 and γ2 antibodies in the mouse. Coutinho showed that the same hapten can elicit different antibody isotypes when coupled to different carriers which determine the nature of the T-cell help. Y. Rosenberg (MRC, Mill Hill) showed that the isotype-specific influence of antigen-stimulated T cells may spill over to cause bystander B-cell clones to undergo plasma cell differentiation, the T-cell influence presumably being mediated by soluble factors.

Three groups of investigators represented at the Umeå meeting have analysed the immunoglobulin isotypes expressed by mouse B cells when cultured with established T-cell lines (A. Coutinho; and L. Forni, Basel) or soluble T-cell factors (P. Tucker, Dallas; & E. Severinsson, University of Stockholm). In each system, the polyclonal B-cell activator LPS by itself induced γ3 more than γ1 plasma cells. The addition of activated T cells, or soluble factors released from them favoured the reverse pattern, γ1 over γ3. L. Forni's data suggested that LPS induces both γ1 and γ3 B-cell blasts to proliferate, but only the γ3 blasts to differentiate into mature plasma cells; the subsequent addition of activated T cells, by contrast, reduces the frequency of γ3 cells and induces γ1 plasma cells. P. Tucker presented data on the state of the γ3 and γ1 mRNA species before and after the addition of a T-cell product (B-cell differentiation factor[22]) to LPS-stimulated B cells. LPS alone induced γ3 mRNAs, but very little γ1 mRNA. Following the addition of the T-cell factor, γ1 mRNAs were increased in quantity and γ3 mRNAs reduced. But all these results, while tantalizing, leave open the central question: do T cells instruct B cells to switch isotypes or do they select isotype-committed B cells for preferential induction of terminal differentiation?

Clearly, we still have important lessons to learn about the genetic basis for C_H isotype switching and its regulation. While solutions appear almost within reach, these genetic events remain elusive as they occur transiently and in minor subpopulations of cells. Clones of normal B cells undergoing isotype switches are unavailable. The C_H switching phenomenon may continue to challenge both cellular and molecular biologists for some time ☐

1. Kincade, P.W. *et al. Proc. natn. Acad. Sci. U.S.A.* **67**, 1918 (1970).
2. Honjo, T. & Kataoka, T. *Proc. natn. Acad. Sci. U.S.A.* **75**, 2140 (1978).
3. Cory, S. & Adams, J.M. *Cell* **19**, 37 (1980).
4. Rabbitts *et al. Nature* **283**, 351 (1980).
5. Coleclough, C., Cooper, D. & Perry, R.P. *Proc. natn. Acad. Sci. U.S.A.* **77**, 1422 (1980).
6. Shimizu, A. *et al. Cell* **28**, 499 (1982).
7. Obata *et al. Proc. natn. Acad. Sci. U.S.A.* **78**, 2437 (1981).
8. Liu, C.P. *et al. Science* **209**, 1348 (1980).
9. Maki, R. *et al. Cell* **24**, 353 (1981).
10. Moore, K.W. *et al. Proc. natn. Acad. Sci. U.S.A.* **78**, 1800 (1981).
11. Perlmutter, A.P. & Gilbert, W. *Proc. natn. Acad. Sci. U.S.A.* (in the press).
12. Burrows, P.D. *et al. Proc. natn. Acad. Sci. U.S.A.* **78**, 564 (1981).
13. Alt, F.W. *et al. Nature* **296** 325 (1982).
14. Davis, M.M., Kim, S.K. & Hood, L. *Science* **209**, 1360 (1980).
14 Gearhart, P.J. *et al. Proc. natn. Acad. Sci. U.S.A.* **77**, 5424 (1980).
16. Mongini, P., Metcalf, L. & Paul, W. *J. exp. Med.* **155**, 884 (1982).
17. Lang, R.B., Stanton, L.W. & Marcu, K.B. *Nucleic Acids Res.* **10**, 611 (1982).
18. Marcu, K.B. *et al. Nature* (in the press).
19. Nikaido, T., Kakai, S. & Honjo, T. *Nature* **292**, 845 (1981).
20. Eckhardt, L. *et al. Proc. natn. Acad. Sci. U.S.A.* **79**, 3006 (1982).
21. Beyreuther *et al. ICN-UCLA Symp. molec. cell. Biol.* **20**, 229 (1981).
22. Isakson, P.C. *et al. J. exp. Med.* **155**, 734 (1982).
23. Yaoita, Y. *et al. Nature* **297**, 697 (1982).

Corrigendum

In "Sons and daughters" from T.H. Clutton-Brock (*Nature* **298**, 11; 1982) the figures shown for *Papio cynocephalus* (Table 2) as "Per cent males" are actually totals; the percentage of males would be 35 (for high maternal rank) and 68 (for low maternal rank).

REVIEW ARTICLE

Structure and variation of human α_1–antitrypsin

Robin W. Carrell, Jan-Olof Jeppsson*, Carl-Bertil Laurell*,
Stephen O. Brennan, Maurice C. Owen, Lloyd Vaughan & D. Ross Boswell

Molecular Pathology Laboratory, Pathology Department (University of Otago), Christchurch Hospital, Christchurch, New Zealand, and *Department of Clinical Chemistry, University of Lund, Malmö General Hospital, S-214 01 Malmö, Sweden

The sequence of α_1–antitrypsin is in keeping with its role as a tissue scavenger of leukocyte elastase. Two abnormal variants commonly present in Europeans cause a deficiency that predisposes them to a progressive loss of lung elasticity. The nature of the reactive centre helps explain why cigarette smoking greatly accelerates the onset and severity of this degenerative process to give the disease emphysema.

As its name implies, α_1-antitrypsin (α_1–AT) is the major component of the α_1 electrophoretic band of the human plasma proteins and acts as an inhibitor of proteolytic enzymes. It inhibits serine proteinases and hence is also known as α_1-proteinase inhibitor. Interest in this protein stems largely from the observation that its genetic deficiency[1] is accompanied by the early onset of degenerative lung disease[2] and, in some instances, liver disease[3]. A puzzling feature of this genetic deficiency is its virtual confinement to Europeans, some 10% of whom are carriers of a pathological variant[4,5].

This association with disease has stimulated research into the structure and abnormalities of α_1–AT that is revealing new aspects of the molecular pathology of genetic disease. One example[6,7] is the way that genetic and environmental factors may interact to give disease. α_1–AT is a protective factor and its genetic deficiency renders the individual susceptible to cumulative lung damage from bouts of inflammation induced by outside stress such as pollutants. The proteolytic enzymes released during this inflammation can overwhelm the limited amounts of inhibitor present in the deficient individual, a situation that is aggravated by the additional ability of some pollutants to produce a direct inactivation of α_1–AT. The consequence is that whereas in a healthy environment α_1–AT deficiency may be compatible with a full lifespan, in a polluted environment or with heavy cigarette smoking it can result in crippling lung disease and early death[8].

This review discusses α_1–AT, its variants and their molecular pathology, with particular reference to the primary structure of the protein presented here in its completed form.

Structure

The structure of human α_1–AT shown in Fig. 1 is based on our amino acid sequence of the plasma protein and represents a consensus with that of the unpublished cDNA sequence of human α_1–AT (S. L. C. Woo and E. W. Davie, personal communication). Details of the sequence and its determination are given in Fig. 1 legend.

The structural features of α_1–AT are in keeping with its known functions. The molecule is relatively small and polar, allowing ready movement into the tissue fluids. It has a single polypeptide chain of 394 residues, with three carbohydrate side chains[9,10], giving an overall molecular weight of 51,000. The cDNA studies[11] confirm that α_1–AT does not have a propeptide but does have a 24-residue hydrophobic pre- or signal peptide[12]. The molecule has a single reactive site[13], centred on methionine[14] at position 358. For α_1–AT to act as a proteinase inhibitor, this reactive site must be held in a fixed conformation: the conformation of an ideal substrate[15]. Although the tertiary structure of α_1–AT is not known, physical measurements[16,17] and calculations[18] predict a highly ordered structure. The strength of this ordered structure is indicated by the fact that it is not buttressed by the disulphide bridges that are characteristic of most inhibitors, including the homologous antithrombin-III[19]. α_1–AT has only the one cysteine residue, located in a cavity on the surface of the molecule and available for SH–SS interchange reactions both *in vivo* and *in vitro*.[20]

A characteristic feature of α_1–AT is the multiple banding that it shows on acid electrophoresis (pH 4.9)[21] or on electrofocusing[22]. This banding is the result of a microheterogeneity that is primarily due to variations in its carbohydrate structure[23]. The three oligosaccharide groups of α_1–AT are N-linked to asparagine residues at positions 46, 83 and 247.[10] A physiologically controlled variation can occur in the structure of these side chains to give isoforms; physiological variants of α_1–AT in which the usual biantennary oligosaccharides may be replaced in position 83, and to a lesser extent 46, by triantennary oligosaccharides [9,23] (Fig. 2).

Reactive centre: Although it has been generally agreed that the reactive site of α_1–AT is centred on a methionine residue[14], its location in the sequence and the number of reactive sites has been controversial[13,14,24-26]. The overall sequence shows that the reactive centre methionine is Met 358, 37 residues from the C-terminus of the molecule[13,27,28].

Proteinase inhibition is accompanied by the formation of a 1:1 complex between α_1–AT and its target enzyme.[29] The reaction mimics that between the enzyme and its substrate, with the reactive centre of the inhibitor functioning as a bait for the active site of the proteinase. The mechanism of inhibition appears to involve a blockage of the reaction, probably at the stage of the tetrahedral adduct, and the evidence suggests that cleavage does not occur in physiological conditions[26]. Conversion of the adduct to an acyl-enzyme may be induced by gross changes in pH or by treatment with strong denaturing agents; only in these non-physiological conditions can the existence of the C-terminal, 36 residue, leaving group be demonstrated[28].

Homology: An interesting feature of the sequence of α_1–AT is its homology with those of antithrombin-III[19,30] and ovalbumin[31] (Fig. 1). It shares 29% common structure with antithrombin-III and 30% with ovalbumin, and ovalbumin and antithrombin-III share 32% common structure with each other. Together the three form a new superfamily[31] that probably diverged from a common ancestral proteinase inhibitor some 500 million years ago. However, this suggestion of a common origin has been questioned as a consequence of gene sequence studies[32] that indicate a complete difference in intron positions between α_1–AT, with three introns, and ovalbumin, with seven introns. This has raised the possibility that the similarity of the two proteins may be due to convergent evolution. However, comparison of aromatic amino acids (Fig. 1) confirms that the structural similarity of α_1–AT and ovalbumin extends

0028-0836/82/280329—06$01.00

Human α₁AT **- Glu Asp Pro**
Human AT-III His Gly Ser Pro Val Asp Ile Cys Thr Ala Lys Pro Arg Asp Ile Pro Met Asn Pro Met Cys Ile Tyr Arg Ser Pro Glu Lys
Ovalbumin -

10 20 30
Gln Gly Asp Ala Ala Gln Lys Thr Asp Thr Ser His His Asp Gln Asp His Pro Thr Phe Asn Lys Ile Thr Pro Asn Leu Ala Glu Phe Ala Phe
Lys Ala Thr Glu Asp Glu Gly Ser Glu Gln Lys Ile Pro Glu Ala Thr Asn Arg Arg Val Trp Glu Leu Ser Lys Ala Asn Ser Arg Phe Ala Thr
- Gly Ser Ile Gly Ala Ala Ser Met Glu Phe Cys Phe

40 50 60
Ser Leu Tyr Arg Gln Leu Ala His - Gln Ser Asn Ser Thr Asn Ile Phe Phe Ser Pro Val Ser Ile Ala Thr Ala Phe Ala Met Leu Ser Leu
Thr Phe Tyr Gln His Leu Ala Asp Ser Lys Asn Asp Asn Asp Asn Ile Phe Leu Ser Pro Leu Ser Ile Ser Thr Ala Phe Ala Met Thr Lys Leu
Asp Val Phe Lys Glu Leu - Lys Val His His Ala Asn Glu Asn Ile Phe Tyr Cys Pro Ile Ala Ile Met Ser Ala Leu Ala Met Val Tyr Leu

70 80 90
Gly Thr Lys Ala Asp Thr His Asp Glu Ile Leu Glu Gly Leu Asn Phe Asn - Leu Thr Glu Ile Pro Glu Ala - - - - - - - -
Gly Ala Cys Asn Asp Thr Leu Glx Glx Leu Met Glu Val Phe Lys Phe Asp Thr Ile Ser Glu - - - - - - - - - Lys Thr
Gly Ala Lys Asp Ser Thr Arg Thr Gln Ile Asn Lys Val Val Arg Phe Asp Lys Leu Pro Gly Phe Gly Asp Ser Ile Glu Ala Gln Cys Gly Thr

100 110
- - Gln Ile His Glu Gly Phe Gln Glu Leu Leu - Arg Thr Leu Asn Gln Pro Asp Ser Gln Leu Gln Leu Thr Thr Gly Asn Gly Leu Phe
Ser Asp Gln Ile His Phe Phe Phe Ala Lys Leu Asn Cys Arg Leu Tyr Arg Lys Ala Asn Lys Ser Ser Lys Leu Val Ser Ala Asn Arg Leu Phe
Ser Val Asn Val His Ser Ser Leu Arg Asp Ile Leu Asn Gln Ile - Thr Lys Pro Asn Asp Val Tyr Ser Phe Ser Leu Ala Ser Arg Leu Tyr

120 130 140 150
Leu Ser Glu Gly Leu Lys Leu Val Asp Lys Phe Leu Glu Asp Val Lys Lys Leu Tyr His Ser Glu Ala Phe Thr Val Asn Phe - Gly Asp Thr
Gly Asp Lys Ser Leu Thr Phe Asn Glu Thr Tyr Gln Asp Ile Ser Glu Leu Val Tyr Gly Ala Lys Leu Gln Pro Leu Asp Phe Lys Glu Asn Ala
Ala Glu Glu Arg Tyr Pro Ile Leu Pro Glu Tyr Leu Gln Cys Val Lys Glu Leu Tyr Arg Gly Gly Leu Glu Pro Ile Asn Phe Gln Thr Ala Ala

160 170 180
Glu Glu Ala Lys Lys Gln Ile Asn Asp Tyr Val Glu Lys Gly Thr Gln Gly Lys Ile Val Asp Leu Val Lys - - Glu Leu Asp Arg Asp Thr
Glu Gln Ser Arg Ala Ala Ile Asn Lys Trp Val Ser Asn Lys Thr Glu Gly Arg Ile Thr Asp Val Ile Pro Ser Glu Ala Ile Asn Glu Leu Thr
Asp Gln Ala Arg Glu Leu Ile Asn Ser Trp Val Glu Ser Gln Thr Asn Gly Ile Ile Arg Asn Val Leu Gln Pro Ser Ser Val Asp Ser Gln Thr

190 200 210
Val Phe Ala Leu Val Asn Tyr Ile Phe Phe Lys Gly Lys Trp Glu Arg Pro Phe Glu Val Lys Asp Thr Glu Glu Glu Asp Phe His Val Asp Gln
Val - - Leu Val Asn Thr xxx xxx xxx Lys Gly Leu Trp Lys Ser Lys Phe Ser Pro Glu Asn Thr Arg Lys Glu Leu Phe Tyr Lys Ala Asp
Ala Met Val Leu Val Asn Ala Ile Val Phe Lys Gly Leu Trp Glu Lys Ala Phe Lys Asp Glu Asp Thr Gln Ala Met Pro Phe Arg Val Thr Glu

220 230 240
Val Thr Thr Val Lys Val Pro Met Met Lys Arg Leu Gly Met Phe Asn Ile Gln His Cys Lys Lys Leu Ser Ser Trp Val Leu Leu Met Lys Tyr
Gly Glu Ser Cys Ser Ala Ser Met Met Tyr Gln Glu Gly Lys Phe Arg - Tyr Arg Arg Val Ala Glu Gly Thr Gln Val Leu Glu Leu Pro Phe
Gln Glu Ser Lys Pro Val Gln Met Met Tyr Gln Ile Gly Leu Phe Arg Val Ala Ser Met Ala Ser Glu Lys Met Lys Ile Leu Glu Leu Pro Phe

250 260 ▼ 270
Leu Gly Asn Ala - Thr Ala Ile Phe Phe Leu Pro Asp Glu Gly Lys - Leu Gln His Leu Glu Asn Glu Leu Thr His Asp Ile Ile Thr Lys
Lys Gly Asp Asp Ile Thr Met Val Leu Ile Leu Pro Lys Pro Glu Lys Ser Leu Ala Lys Val Glu Lys Glu Leu Thr Pro Glu Val Leu Gln Glu
Ala Ser Gly Thr Met Ser Met Leu Val Leu Leu Pro Asp Glu Val Ser Gly Leu Glu Gly Leu Glu Ser Ile Ile Asn Phe Glu Lys Leu Thr Glu

280 290 300
Phe Leu Glu Asn Glu - - Asp Arg Arg Ser Ala Ser Leu His Leu Pro Lys Leu Ser Ile Thr Gly Thr Tyr Asp Leu Lys Ser Val Leu Gly
Trp Leu Asp Glu Leu - - Glu Glu Met Met Leu Val Val His Met Pro Arg Phe Arg Ile Glu Asp Gly Phe Ser Leu Lys Glu Glx Leu Glx
Trp Thr Ser Ser Asn Val Met Glu Glu Arg Lys Ile Lys Val Tyr Leu Pro Arg Met Lys Met Glu Glu Lys Tyr Asn Leu Thr Ser Val Leu Met

310 320 330
Gln Leu Gly Ile Thr Lys Val Phe Ser - Asn Gly Ala Asp Leu Ser Gly Val Thr Glu Glu Ala Pro - - Leu Lys Leu Ser Lys Ala Val
Asx Met Gly Leu Val Asp Leu Phe Ser Pro Glu Lys Ser Lys Leu Pro Gly Ile Val Ala Glu Gly Arg Asp Asp Leu Tyr Val Ser Asp Ala Phe
Ala Met Gly Ile Thr Asp Val Phe Ser - Ser Ser Ala Asn Leu Ser Gly Ile Ser Ser Ala - - Glu Ser Leu Lys Ile Ser Gln Ala Val

340 ▼ 350 360
His Lys Ala Val Leu Thr Ile Asp Glu Lys Gly Thr Glu Ala Ala Gly Ala Met Phe Leu Glu Ala Ile Pro Met Ser Ile Pro Pro Glu - Val
His Lys Ala Phe Leu Glu Val Asn Glu Glu Gly Ser Glu Ala Ala Ala Ser Thr Ala Val Val Ile Ala Gly Arg Ser Leu Asn Pro Asn Arg Val
His Ala Ala His Ala Glu Ile Asn Glu Ala Gly Arg Glu Val Val Gly Ser Ala Glu Ala Gly Val Asp Ala Ala Ser Val Ser Glu Glu - -

370 380 390
Lys Phe - - Asn Lys Pro Phe Val Phe Leu Met Ile Glu Gln Asn Thr Lys Ser Pro Leu Phe Met Gly Lys Val Val Asn Pro Thr Gln Lys
Thr Phe Lys Ala Asn Arg Pro Phe Leu Val Phe Ile Arg Glu Val Pro Leu Asn Thr Ile Ile Phe Met Gly Arg Val Ala Asn Pro Cys Val Lys
- Phe Arg Ala Asp His Pro Phe Leu Phe Cys Ile Lys His Ile Ala Thr Asn Ala Val Leu Phe Phe Gly Arg Cys Val Ser Pro - - -

Fig. 1 The sequence of human α_1–AT aligned with that of human antithrombin-III[19] and chicken ovalbumin[68]. Sequence numbers refer to α_1–AT. The reactive centre Met-Ser 358–359 is boxed; the attachment points of the three oligosaccharide chains at Asn 46, Asn 83 and Asn 247 are encircled; ▼ shows the mutation sites of the *S* (264 Glu → Val) and *Z* (342 Glu → Lys) variants. Residues aligned with the bulky aromatic Phe and Trp of ovalbumin are shaded to indicate that structural homology is not confined to a single domain of the molecule; this confirms a relationship derived from divergent evolution. Homology of the reactive centre region 358–363 of α_1–AT and antithrombin-III is illustrated in Fig. 3; ovalbumin retains some homology at this site, although it apparently has no inhibitory function. There has also been some conservation in α^1–AT of the internal site (244–261) identified in ovalbumin as a hydrophobic signal sequence[71], but α_1–AT has an undoubted N-terminal signal sequence[11,12]. There are several striking differences as well as the difference in intron numbers and positions. There are three disulphide bonds in antithrombin-III, one in ovalbumin and none in α_1–AT; ovalbumin has a single oligosaccharide group, antithrombin-III has four and α_1–AT has three, none of the sites being homologously related. α_1–AT has a calculated molecular weight of 51,000 with a 13% carbohydrate content (isoform I). The sequence of human α_1–AT is based on our previously published peptide sequences[10,27,30] along with recent completion of overlap sequences. The sequence has been checked against that of the unpublished cDNA sequence for human α_1–AT (S. L. C. Woo and E. W. Davie, personal communication). Residue Leu 176, and amide assignments 158 and 159, have been made on the basis of the cDNA structure. The only sequence difference is at 213 where we obtain an unequivocal Val but the cDNA shows an Ala; this may represent a polymorphism. Our sequence gives a consistent Asp–Gly at 116–117 but post-synthetic deamidation is known to occur at Asn–Gly sequences[69,70] and residue 116 has therefore been assigned as an Asn, as found in the cDNA.

throughout the sequence. This would be highly improbable if the similarity were due to convergence.

The relationship of the two plasma proteins, α_1–AT and antithrombin-III, is not surprising. Both are serine proteinase inhibitors and both have become specialized to varying degrees as inhibitors of specific enzymes. This is most marked with antithrombin-III, which is a specific inhibitor of the coagulation proteinases. By comparison, α_1–AT is relatively unspecialized and will inhibit all serine proteinases including thrombin, its most effective target being leukocyte elastase[33,34]. An examination of the differences between the two inhibitors provides a clue as to the process involved in their specialization. Calculation of the evolutionary distance between α_1–AT and antithrombin-III gives a value of 160 accepted point mutations per 100 residues, which is similar to that between thrombin and elastase[13]. This similarity suggests that the specialization of the inhibitors has occurred in response to, and in concert with, the specialization of their target enzymes.

The alignment of the two sequences provides strong evidence for the positioning of their reactive centres, giving support[27] for a reactive centre in antithrombin-III at Arg 384. The similarity between these two proteins is an example of divergent evolution but, interestingly, the recognition of the sequence of the reactive centre of α_1–AT was greatly aided by a set of convergent homologies[14]. Figure 3 shows the remarkable similarity between the reactive centres of both proteins and those of the unrelated plant proteinase inhibitors.

Other features of the homology of the proteins are indicated in Fig. 1. One point of interest is that the 32-residue N-terminal portion of α_1–AT, which bears no resemblance to the other two proteins[10], is homologous to another plasma proteinase inhibitor, α_1-antichymotrypsin[35]. This has a similar function to that of α_1–AT as an inhibitor of a leukocyte enzyme, probably cathepsin G[33].

Function

There is good reason to believe that α_1–AT is primarily a defence protein whose function is to protect the tissues against attack from released proteolytic enzymes. It is synthesized in the liver and secreted into the plasma where it has a half life of 6 days[36]. As would be expected of a defence protein, it is an acute phase reactant and its normal plasma concentration[37] of 1.3 g l^{-1} can quadruple in response to the general stimulus of inflammation or oestrogens. This rise in plasma concentration is due to an increased synthesis of α_1–AT, particularly of its triantennary isoforms[38] (Fig. 2). The only other inhibitor present in blood in concentrations approaching that of α_1-AT is the much larger α_2-macroglobulin. Both inhibitors function as suicidal proteins that are taken up by the cells of the reticuloendothelial system once they have formed complexes with their target proteinases[39].

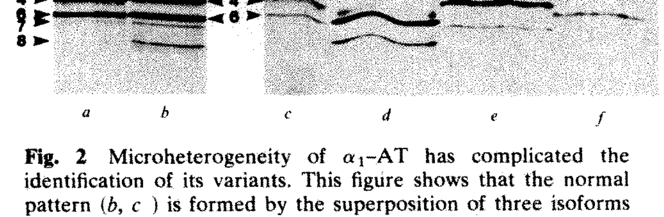

Fig. 2 Microheterogeneity of α_1–AT has complicated the identification of its variants. This figure shows that the normal pattern (*b*, *c*) is formed by the superposition of three isoforms (*d*, *e*, *f*). The isoforms differ in the degree of branching of their oligosaccharide groups and consequently in the number of their negatively charged sialic acids. Isoform I (*d*) has all biantennary chains and isoforms II (*e*) and III (*f*) have one and two, respectively, of these replaced by triantennary chains. The pattern is complicated by a subsidiary heterogeneity seen in each isoform that is explicable by known minor post-secretory changes in primary structure. A shift to increased production of isoforms II and III during inflammation results in an increased proportion of bands 2 and 4 (*a*). (Reproduced with permission from ref. 38.)

		P_1	P_1'	P_2'	P_3'	P_4'	P_5'	
Human α_1AT (Elastase)	**...**	**Met**	**Ser**	**Ile**	**Pro**	**Pro**	**Glu**	**...**
Human AT-III (Thrombin)	...	Arg	Ser	Leu	Asn	Pro	Asn	...
Soybean (Trypsin)	...	Lys	Ser	Asn	Pro	Pro	Gln	...
Garden Bean (Elastase)	...	Ala	Ser	Ile	Pro	Pro	Gln	...
Lima Bean (Trypsin)	...	Lys	Ser	Ile	Pro	Pro	Gln	...

Fig. 3 The reactive centres of α_1–AT and antithrombin-III bear a striking similarity to those of the much smaller and unrelated plant proteinase inhibitors[14]. The P_1 residue reflects the specificity of the target enzyme. Elastase preferentially cleaves at small hydrophobic residues such as alanine (as in the garden bean inhibitor) and valine. Methionine is found in some other inhibitors of elastase;[15] it probably confers a wider specificity but also its lability may be of advantage in allowing the deactivation of the inhibitor.

The evidence that the prime target of α_1–AT is leukocyte elastase is circumstantial but persuasive. The strongest evidence is the consequences of deficiency; the major effect is a progressive loss of elasticity in the lung, a loss that can be mimicked in model systems by the administration of elastase aerosols[40]. Secondary evidence is provided by the measurement of the association rate constants of α_1–AT with a range of proteinases[33]. These give a decreasing order with: leukocyte elastase > chymotrypsin > cathepsin G > anionic trypsin > cationic trypsin > plasmin > thrombin. These association rate constants together with clinical and *in vivo* experimental observations indicate that α_1–AT is a physiologically effective inhibitor of leukocyte elastase[39,41] but a relatively ineffective inhibitor of trypsin, plasmin and thrombin.

An initially puzzling aspect of the role of α_1–AT as a specific inhibitor of elastase is the occurrence of methionine at its reactive centre. Methionine in a Pro-Met sequence will provide a susceptible point for cleavage by elastase but valine[42] or alanine would seem to be a better and more specific choice. Furthermore, methionine has the apparent disadvantage of being readily oxidized to its sulphoxide which is polar and does not provide a favourable proteolytic cleavage site for elastase[43,44]. Consequently, α_1–AT is readily inactivated by oxidizing agents such as the oxygen radicals released by phagocytes[45,46]. However, a mechanism can be proposed in which this lability may provide a self-regulatory contribution to the process of inflammation.

Consider the formation of an abscess around a small foreign particle. An aggregation of leukocytes occurs to surround the particle and perform two separate functions—a discharge of bactericidal oxygen radicals and a release of granulocytic enzymes, including[47] elastase and cathepsin G. These enzymes facilitate the breakdown of adjacent connective tissue to give an area of liquefaction which isolates the foreign body in readiness for ejection. The spread of this liquefactive process by diffusion of the enzymes will be constrained by tissue proteinase inhibitors, predominantly α_1–AT. This will limit tissue breakdown at the periphery of the inflammation, but allow it to occur at the focus of activity where α_1–AT will itself be inhibited by released oxygen free radicals. In this way the lability of the methionine at the reactive centre of α_1–AT could be advantageous, if it allowed the inhibition to be switched off at the focus of inflammation but continued to provide protection for outlying tissue.

However, the lability of α_1–AT to oxidation will be distinctly disadvantageous in exposed situations such as occur in the fluids lining the respiratory tract. The elastic tissue of the lung is protected from surface attack primarily by two inhibitors: human bronchial inhibitor which predominates in the fluid lining the upper respiratory tract[34,41] and α_1–AT which predominates in the lower respiratory tract[7,34,41]. Normally there is ample inhibitory capacity but the defences of the lower respiratory tract, because they depend on α_1–AT, are vulnerable to combined oxidative and elastolytic attack, as is believed to occur as a consequence of heavy cigarette smoking[48].

Variation and disease

Genetic variation: There are several well established genetic polymorphisms of α_1-AT. The protein is encoded by two independent alleles at a single locus, resulting in autosomal codominant inheritance. The variants are classified alphabetically by the *Pi* (proteinase inhibitor) nomenclature[21], in terms of their electrophoretic mobility at *p*H 4.9. For example, *PiBB* is the homozygote for an anodal variant and *PiZZ* for a cathodal variant, with *PiMM* representing the homozygote for the normal *M* allele.

The variants of particular interest are the common *Z* and *S* mutants which are associated with plasma deficiency; the product of the *Z* allele gives concentrations equivalent to 15% of that of the normal *M* allele, whereas the product of the *S* allele gives concentrations of 60% of the normal allele[49]. Mixed heterozygotes, for example *MZ*, *MS* and *SZ*, will give proportionately altered plasma levels. The genotypes with a deficiency sufficient to pose a definite risk to health are: *PiZZ* (15% of normal concentration), *PiSZ* (35% of normal) and combinations with the unusual null (−) gene, for example, *PiZ*− (8% of normal).

The structural abnormalities of the *Z* and *S* variants have been characterized[50–52]. Both have single amino acid substitutions (Fig. 1) that have presumably arisen from single base mutations in the gene DNA. Otherwise the plasma forms of the two variants resemble the normal M protein; they have a similar half life in the circulation[37], normal inhibitory capacity and a similar carbohydrate composition. The Z protein, however, is something of an exception in that it is only partially secreted, and a considerable amount of the protein accumulates at the site of synthesis in the endoplasmic reticulum of the liver cells[3].

A summary of the findings of various populations surveys[5] shows that the *S* and *Z* variants are polymorphisms essentially confined to individuals of European descent. On average, some 3% of Europeans are carriers of the *Z* mutant (*PiMZ*) and some 7% are carriers of the *S* gene (*PiMS*). The frequency of the Z gene is somewhat higher in Northern Europeans and conversely that of the *S* gene is somewhat higher in Southern Europeans. About 1 in 1,000 Northern Europeans will have the *PiZZ* or *PiSZ* genotypes associated with severe deficiency of α_1-AT[53]. The relative confinement of these polymorphisms to the European is a puzzle. Both of the deficiency genes pose a real threat to health and there must be some balancing advantage to explain their survival at this frequency.

Deficiency and disease: Abnormal phenotypes of α_1-AT have been associated with a number of diseases[54] including renal disease, arthritis and malignancies. However, the two strongest associations are with lung and liver disease; 60% of those with severe deficiency will die of lung disease and 14% of those with the *ZZ* deficiency will die of liver disease[8]. Two separate features need to be considered regarding the pathology of these diseases in α_1-AT deficiency. These are the liver accumulation of the variant and the low plasma concentrations of inhibitor.

The accumulation of α_1-AT in the hepatocytes occurs only with those variants whose defect is assumed to be one of secretion, the *Z* variant being by far the most common example[55]. The *Z* protein that accumulates in the liver apparently has the same polypeptide structure[56] as the circulating Z protein, but its carbohydrate side chains are immature, with a high mannose content and no sialic acid[56,57]. This is compatible with the deficiency of the Z protein being due to a partial block in processing of the polypeptide, with some of the material proceeding to completion and subsequent secretion in the plasma whilst the remainder is stopped in its passage through the secretory pathway at the stage of partial glycosylation[5]. The accumulation takes the form of intracellular amorphous aggregations of α_1-AT that can be demonstrated microscopically as occasional deposits in the *PiMZ* liver and as massive deposits in the *PiZZ* liver (Fig. 4).

Liver disease is most apparent in the *PiZZ* newborn, where it occurs as a hepatitis with a wide variation in severity[58]. Some 50% of *PiZZ* infants have minor changes in liver function, some 7% develop a severe obstructive jaundice, and a smaller proportion go on to develop a fatal juvenile cirrhosis. The reason for this variation in severity is not known; there are probably a number of contributory factors, such as hormonal influences, since boys are more affected than girls, and genetic influences, since a familial predisposition seems to be involved[58]. Although the childhood cirrhosis is the most obvious and tragic form of the liver disease there is also an independent and substantial risk of developing cirrhosis in adult life. This increases with age to give cirrhosis levels near 20% in *PiZZ* individuals above the age[8] of 50. The pathophysiology of this liver disease is not understood. It is almost certainly related to the accumulation of α_1-AT in the hepatocyte rather than the associated plasma deficiency, because it only occurs in association with those variants that produce inclusions[5] and not with those, such as the *S* variant, that give an isolated plasma deficiency.

However, there is no doubt that the lung disease is a direct consequence of low plasma levels of α_1-AT. This conclusion is supported by a large body of evidence, both observational and experimental, that has been reviewed elsewhere[6,7]. It all indicates that the loss of lung elasticity that occurs in severe α_1-AT deficiency represents the summation of cumulative proteolytic damage. The end point of this loss of elasticity is the development of the irreversible lung disease, emphysema. This is a common disease and only some 1–2% of cases are due to a genetic deficiency of α_1-AT; however, the recognition of this relationship has opened up an understanding of the pathogenesis of emphysema in general as being due to a 'protease–antiprotease' imbalance[7,59].

The most common cause of emphysema is heavy cigarette smoking. Exposure of the lungs to tobacco smoke causes a considerable increase in the population of a phagocytic cell peculiar to the lung, the pulmonary alveolar macrophage[6,7]. The numbers of these in the lung increase up to 10-fold or more in proportion to the number of cigarettes smoked. The macrophages change in character and become activated to give increased proteolytic activity along with the secretion of a chemotactic factor that attracts leukocytes to the lungs[7]. This leads to a considerable change in the phagocytic population of the lung with a large increase in the elastolytic load. There is also an accompanying diminution of proteinase inhibitory capacity, due to an inactivation of inhibitor rather than a deficiency[44]. Normal amounts of α_1-AT are present in bronchial washings but its inhibitory capacity is almost halved[48]. Some of this loss may be due to direct oxidation of the reactive methionine of α_1-AT by cigarette smoke[60] but the main source of oxidation is almost certainly macrophage and leukocyte oxygen radicals[46,61]. The conclusion is that a combination of

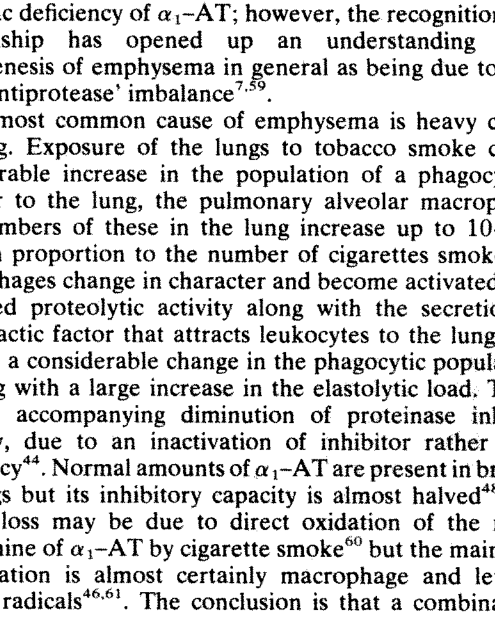

Fig. 4 Electron micrograph (×26,500) of a liver cell showing the accumulation of *Z* variant α_1-AT in the rough endoplasmic reticulum. The position of the inclusions and their composition are compatible with a blockage occurring at the stage of final processing of the oligosaccharide side-chains. These inclusions are clearly visible by light microscopy and can be specifically identified[3] with fluorescent antibody to α_1-AT.

the increased production of elastase along with the decrease in inhibitor activity results in an attack on the elastic tissue of the lower respiratory tract to give the development of emphysema[6,7,48].

The heavy cigarette smoker with homozygous α_1-AT deficiency is in double jeopardy and faces the likelihood of crippling emphysema before the age of 40 years[62] with a 20-year decrease in survival time as compared with the non-smoking homozygote[8]. This situation illustrates the interaction that occurs between environmental and genetic factors. On the one hand there is the risk posed by macrophage stimulation due to smoking and air pollution; on the other, there is a whole range of genetic deficiencies of the proteinase inhibitor. For example, an intermediate deficiency such as *PiSZ* may be compatible with a fully active life for the non-smoking office worker[58], whereas it can result in premature emphysema in a heavily-smoking industrial worker. Fortunately, the common heterozygous genotypes, *PiMS* and *PiMZ*, pose no real threat to respiratory health[63,64].

Molecular pathology: There is now no doubt that the common *Z* and *S* deficiencies of α_1-AT are due to single amino acid substitutions in its polypeptide chain. Independent analyses of plasma samples from several unrelated individuals have shown the change in structure in the *S* variant to be the replacement of glutamic acid by valine at position 264 and in the *Z* variant the replacement of glutamic acid by lysine at position 342[18,50-52,65].

In the absence of crystallographic data, the structural relationship of the two glutamic acids is unknown but an indication of their importance is their conservation in all the homologous proteins, including ovalbumin. The glutamic acid replaced in the S protein is in a predicted α-helical region[5] and in this way it resembles the mutation of the coincidentally named haemoglobin S. Both involve the introduction of a valine on the hydrophilic aspect of a helical region, the effect of which will be to favour intermolecular aggregation. Support for this is seen in the decreased stability of the *S* variant of α_1-AT[66]. This decrease in stability suggests that deficiency may be due to increased breakdown, although no gross difference has been detected between the half life of the S and that of the normal M protein[36]. The S protein does not accumulate in the liver and the problem is not apparently that of a failure of secretion, nor is it likely that a mutation of this type would affect translation rates. It is likely that the presence of the substituted valine results in incorrect folding of the nascent protein resulting in intracellular degradation and hence an apparent decrease in synthesis[5].

The *Z* mutation presumably acts in a different way to give a partial blockage in the processing of the protein. The sequence of the protein excludes some of the previously suggested mechanisms, that is, that the mutation might directly interfere with pre- or propeptide cleavage or with an oligosaccharide attachment site[3,37,67]. However, the sequence is of little help in suggesting alternative mechanisms. The mutation has occurred in a non-helical region but it must cause a perturbation in structure as the *Z* antitrypsin, like the *S*, has decreased *in vitro* heat stability[66]. The failure in processing of the polypeptide could be a consequence of this perturbation in structure; alternatively, it has been proposed[5] that it could be due to a misreading of the new Lys–Lys sequence 342–343 as a processing signal. No experimental evidence is available to support either proposal.

Conclusion

Knowledge of the structure of α_1-AT with other available information provides at least a partial outline of the pathophysiology of the function and dysfunction of the protein. In particular, it supports the previously proposed concept[6,7,59] that the emphysema associated with both α_1-AT deficiency and cigarette smoking is due to a protease–antiprotease imbalance. This understanding of the pathogenesis of the lung disease provides the basis for the design of therapy either by antiproteinase replacement or alternatively, by macrophage inhibition. One approach to replacement therapy is the development of low molecular weight analogues of the reactive centre of α_1-AT[42]. A more radical approach will be the use of recombinant DNA techniques to give a substitution of the reactive centre methionine to decrease lability and increase specificity for elastase. But the most useful therapy that follows from knowledge of the pathogenesis of the lung disease is the concise and effective counsel that can be given to the *PiZZ* individual: Don't smoke!

The detection of homozygous deficiency at birth is technically and logistically a simple task.[53] The problem is to devise a means of contacting affected individuals at adolescence, at a time when they can elect not to smoke and thus have a reasonable chance of a full and active life.

This work was supported by the MRC of New Zealand and the Swedish MRC (project no. B81-13X-581-14C). We thank Dr S. L. C. Woo, Professor E. W. Davie and colleagues for access to the unpublished sequence of the cDNA of human α_1-AT.

1. Laurell, C.-B. & Eriksson, S. *Scand. J. clin. Lab. Invest.* **15**, 132–140 (1963).
2. Eriksson, S. *Acta med. scand.* **175**, 197–205 (1964).
3. Sharp, H. L. *Hosp. Pract.* **6**, 83–96 (1971).
4. Fagerhol, M. K. *Postgrad. med. J.* **52** Suppl. 2, 73–83 (1976).
5. Carrell, R. W. & Owen, M. C. *Essays med. Biochem.* **4**, 83–119 (1979).
6. *Lancet* **i**, 743–745 (1980).
7. Gadek, J. E. *et al. Bull. Eur. Physiopath. Resp.* **16**, suppl., 27–40 (1980).
8. Larsson, C. *Acta med. scand.* **204**, 345–351 (1978).
9. Mega, T., Lujan, E. & Yoshida, A. *J. biol. Chem.* **255**, 4053–4056 (1980).
10. Carrell, R. W. *et al. FEBS Lett.* **135**, 301–303 (1981).
11. Kurachi, K. *et al. Proc. natn. Acad. Sci. U.S.A.* **78**, 6826–6830 (1981).
12. Carlson, J. & Stenflo, J. *FEBS Lett.* **130**, 297–300 (1981).
13. Boswell, D. R., Owen, M. C., Brennan, S. O., Carrell, R. W. & McLachlan, A. D. in *Protides of the Biological Fluids: 27th Colloqu.* **28**, 129–132 (1980).
14. Johnson, D. & Travis, J. *J. biol. Chem.* **253**, 7142–7144 (1978).
15. Kraut, J. *A. Rev. Biochem.* **46**, 331–358 (1977).
16. Jirgensons, B. *Biochim. biophys. Acta* **493**, 352–358 (1977).
17. Saklatvala, J., Wood, G. C. & White, D. D. *Biochem. J.* **157**, 339–351 (1976).
18. Owen, M. C. thesis, Univ. Otago, Dunedin (1979).
19. Peterson, T. E., Dudek-Wojciechowska, G., Sottrup-Jensen, L. & Magnusson, S. in *The Physiological Inhibitors of Blood Coagulation and Fibrinolysis* (eds Collen, D. *et al.*) 43–54 (Elsevier, Amsterdam, 1979).
20. Laurell, C.–B. in *The Chemistry and Physiology of the Human Plasma Proteins* (ed. Bing, D. H.) 329–338 (Pergamon, New York, 1979).
21. Fagerhol, M. K. *Ser. Haemat.* **1**, Suppl. 1, 153–161 (1968).
22. Allen, R. C., Harley, R. H. & Talamo, R. C. *Am. J. clin. Path.* **62**, 732–739 (1974).
23. Vaughan, L. & Carrell, R. W. *Biochem. Int.* **2**, 461–467 (1981).
24. Martodam, R. R. & Liener, I. E. *Biochim. biophys. Acta* **667**, 328–340 (1981).
25. Kress, L. F., Kurecki, T., Chan, S. K. & Laskowski, Srn. M. *J. biol. Chem.* **254**, 5317–5320 (1979).
26. James, H. L. & Cohen, A. B. *J. clin. Invest.* **62**, 1344–1353 (1978).
27. Carrell, R. W., Boswell, D. R. Brennan, S. O. & Owen, M. C. *Biochem. biophys. Res. Commun.* **93**, 399–402 (1980).
28. Morii, M., Odani, S. & Ikenaka, T. *J. Biochem.* **86**, 915–921 (1979).
29. Cohen, A. B. *J. biol. Chem.* **248**, 7055–7059 (1973).
30. Carrell, R. W., Owen, M. C., Brennan, S. O. & Vaughan, L. *Biochem. biophys. Res. Commun.* **91**, 1032–1037 (1979).
31. Hunt, L. T. & Dayhoff, M. O. *Biochem. biophys. Res. Commun.* **95**, 864–871 (1980).
32. Leicht, M. *et al. Nature* **297**, 655–659 (1982).
33. Beatty, K., Bieth, J. & Travis, J. *J. biol. Chem.* **255**, 3931–3934 (1980).
34. Gauthier, F., Fryksmark, U., Ohlsson, L. & Bieth, J. G. *Biochim. biophys. Acta* **700**, 178–183 (1982).
35. Travis, J., Garner, D. & Bowen, J. *Biochemistry* **17**, 5647–5651 (1978).
36. Jeppsson, J.-O., Laurell, C.-B., Nosslin, B. & Cox, D. W. *Clin. Sci. molec. Med.* **5**, 103–107 (1978).
37. Jeppsson, J.-O., Laurell, C.-B. & Fagerhol, M. K. *Eur. J. Biochem.* **83**, 143–153 (1978).
38. Vaughan, L., Lorier, M. A. & Carrell, R. W. *Biochim. biophys. Acta* **701**, 339–345 (1982).
39. Balldin, G., Laurell, C.-B. & Ohlsson, K. *Hoppe-Seylers Z. physiol. Chem.* **359**, 699–708 (1978).
40. Senior, R. *et al. Am. Rev. resp. Dis.* **116**, 469–475 (1977).
41. Gadek, J. E., Fells, G. A., Zimmerman, R. L., Rennard, S. I. & Crystal, R. G. *J. clin. Invest.* **68**, 889–898 (1981).
42. Nakajima, K., Powers, J. C. Ashe, B. M. & Zimmerman, M. *J. biol. Chem.* **254**, 4027–4032 (1979).
43. Shechter, Y., Burstein, Y. & Gertler, A. *Biochemistry* **16**, 992–997 (1977).
44. Beatty, K., Robertie, P., Senior, R. & Travis, J. *J. Lab. clin. Med.* (in the press).
45. Carp, H. & Janoff, A. *Am. Rev. resp. Dis.* **118**, 617–621 (1978).
46. Matheson, N. R., Wong, P. S. & Travis, J. *Biochem. biophys. Res. Commun.* **88**, 402–409 (1979).
47. Baglioni, M. in *The Cell Biology of Inflammation* (ed. Weissman, G.) 161–187 (Elsevier, Amsterdam, 1980).
48. Gadek, J. E., Fells, G. A. & Crystal, R. G. *Science* **206**, 1315–1316 (1979).
49. Laurell, C.-B. & Jeppsson, J.-O. in *The Plasma Proteins. Structure, Function and Genetic Control* Vol. 1, 2nd edn (ed. Putnam, F. W.) 229–264 (Academic, New York, 1975).
50. Owen, M. C. & Carrell, R. W. *Br. med. J.* **i**, 130–131 (1976).
51. Jeppsson, J.-O. *FEBS Lett.* **65**, 195–197 (1976).
52. Yoshida, A., Lieberman, J., Gaidulis, L. & Ewing, C. *Proc. natn. Acad. Sci. U.S.A.* **73**, 1324–1328 (1976).

53. Laurell, C.-B. & Sveger, T. *Am. J. hum. Genet.* **27,** 213–217 (1975).
54. Fagerhol, M. K. & Cox, D. W. *Adv. hum. Genet.* **11,** 1–62 (1981).
55. Blenkinsopp, W. K. & Haffenden, G. P. *J. clin. Path.* **30,** 132–137 (1977).
56. Jeppsson, J.-O., Larsson, C. & Eriksson, S. *New Engl. J. Med.* **293,** 576–579 (1975).
57. Hercz, A., Katona, E., Cutz, E., Wilson, J. R. & Barton, M. *Science* **201,** 1229–1232 (1978).
58. Sveger, T. *New Engl. J. Med.* **294,** 1316–1321 (1976).
59. Lieberman, J. *Chest* **70,** 62–67 (1976).
60. Janoff, A., Carp, H., Lee, D. K. & Drew, R. T. *Science* **206,** 1313–1316 (1979).
61. Carp, H. & Janoff, A. *J. clin. Invest.* **63,** 793–797 (1979).
62. Janus, E. D. & Carrell, R. W. *N. Z. med. J.* **81,** 461–467 (1975).
63. Larsson, C., Ericksson, S. & Dirkson, H. *Br. med. J.* **ii,** 922–925 (1977).
64. de Hamel, F. A. & Carrell, R. W. *N. Z. med. J.* **94,** 407–410 (1981).
65. Yoshida, A., Ewing, C., Wessels, M., Lieberman, J. & Gaidulis, L. *Am. J. hum. Genet.* **29,** 233–239 (1977).
66. Lieberman, J. *Chest.* **64,** 579–584 (1973).
67. Bell, O. F. & Carrell, R. W. *Nature* **243,** 410–411 (1973).
68. McReynolds, L. *et al. Nature* **273,** 723–728 (1978).
69. Moo-Penn, W. F. *et al. J. biol. Chem.* **251,** 7557–7562 (1976).
70. Perutz, M. F., Fogg, J. H. & Fox, J. A. *J. molec. Biol.* **138,** 669–670 (1980).
71. Lingappa, V. R., Lingappa, J. R. & Blobel, G. *Nature* **281,** 117–121 (1979).

ARTICLES

Internal rotation and gravitational quadrupole moment of the Sun

D. O. Gough

Institute of Astronomy, Madingley Road, Cambridge CB3 0HA, UK

The internal angular velocity of the Sun is estimated from observations of apparent rotational splitting of low-order low-degree global oscillations detected in fluctuations in the limb-darkening function. A sidereal rotation of 3 μHz is inferred for the deep interior; this is more than six times greater than the equatorial rotation frequency of the photosphere. The inferred angular velocity distribution does not vary strongly with latitude, and yields a gravitational quadrupole moment $J_2 \simeq 3.6 \times 10^{-6}$. When combined with the results of planetary radar observations to determine $(2-\beta+2\gamma)/3$, a combination of Eddington–Robertson post-newtonian parameters which in general relativity is unity, a value of about 0.994 ($\pm$0.012) is thus obtained.

ONE of the most important tests of theories of gravitation concerns the rates of precession of planetary orbits. In the fully conservative parameterized post-newtonian (PPN) formalism, for example, the predicted advance $\Delta\phi_0$ per orbital period of a planetary orbit with semi-major axis a and eccentricity e, after correcting for perturbations due to the other planets, is $6\pi GM\lambda_p/[a(1-e^2)c^2]$, where

$$\lambda_p = \tfrac{1}{3}(2-\beta+2\gamma) + \frac{R^2c^2}{2GMa(1-e^2)}J_2 \qquad (1)$$

Here M and R are the mass and radius of the Sun, G is the gravitational constant, c is the speed of light, and β and γ are Eddington–Robertson parameters of the PPN formalism[1,2]. In general relativity, for example, $\beta = 1$ and $\gamma = 1$, and hence $\frac{1}{3}(2-\beta+2\gamma) = 1$. The parameter J_2 measures the quadrupole moment of the Sun's gravitation field, normally presumed to arise from centrifugal distortion. It is defined such that the solar component of the gravitational potential outside the Sun, referred to spherical polar coordinates (r, θ, ϕ) with respect to the Sun's rotation axis, is

$$\Phi = \frac{GM}{r}\left[1 - J_2\left(\frac{R}{r}\right)^2 P_2(\cos\theta)\right] \qquad (2)$$

where P_2 is a Legendre function of second degree. Equation (1) was derived assuming the Sun's rotation axis to be perpendicular to the plane of the planetary orbit. The correction that should be made to account for the small tilt that exists is insignificant.

Since the contributions to $\Delta\phi_0$ from the quadrupole component of Φ and from the deviations from newtonian gravitation depend differently on $a(1-e^2)$, one should in principle be able to determine $\frac{1}{3}(2-\beta+2\gamma)$ and J_2 separately by combining observations of different planets. However, it has not been possible to do this, because the planetary precession rates are not yet known with adequate precision[3]. An independent measurement of J_2 is therefore required.

Attempts have been made to infer J_2 from the shape of the visible solar disk. The method relies on equating the oblateness E of the disk with that of the gravitational equipotentials, after accounting for the observed rotation of the photosphere and brightness inhomogeneities such as are produced by faculae. This yields $J_2 = \frac{2}{3}E$. It is interesting that modern observations have yielded quite different values: Dicke and Goldenberg[4] obtained

$$\tfrac{2}{3}E = (24.7 \pm 2.3) \times 10^{-6} \qquad (3)$$

whereas Hill and Stebbins[5] obtained

$$\tfrac{2}{3}E = (1.0 \pm 4.3) \times 10^{-6} \qquad (4)$$

The discrepancy has not been explained. Note, however, that the two measurements utilized different properties of the intensity distribution near the limb of the Sun, and that alone might prove to be the cause. Evidently one cannot infer J_2 until the discrepancy has been understood.

For the orbit of Mercury, equation (1) yields

$$\lambda_p = \tfrac{1}{3}(2-\beta+2\gamma) + 2.96 \times 10^3 J_2 \qquad (5)$$

Shapiro *et al.*[6], using radar measurements of the distance to Mercury, found

$$\lambda_p = 1.003 \pm 0.005 \qquad (6)$$

A similar analysis by Anderson *et al.*[3] gave

$$\lambda_p = 1.007 \pm 0.005 \qquad (7)$$

Shapiro *et al.* took J_2 to be equal to the value one calculates assuming the Sun to be rotating uniformly, which is 2×10^{-7} if the surface equatorial angular velocity is used, and thus arrived at a value for $\frac{1}{3}(2-\beta+2\gamma)$. It is evident from the uncertainty suggested by the difference between equations (3) and (4) that the passage from λ_p to the PPN parameters is premature.

The limitations imposed by the uncertainty in J_2 on the accuracy to which the precession data test theories of gravity has led to other proposals for probing the solar gravitational field. One method is to take advantage of the high eccentricity of Mercury's orbit to search for different periodic orbital variations. This would require tracking a spacecraft in orbit around Mercury. According to Anderson *et al.*[7] a precision of a few parts in 10^7 should be possible. Another suggestion is to track a spacecraft that passes by the Sun within a few solar radii[8]. Similar precision might be possible, though it could be affected by perturbations in Φ associated with long-period solar oscillations[9], especially if J_2 were as small as 2×10^{-7}. Preliminary calculations[7,10] suggest that J_2 could be measured to an accuracy

0028–0836/82/290334—06\$01.00

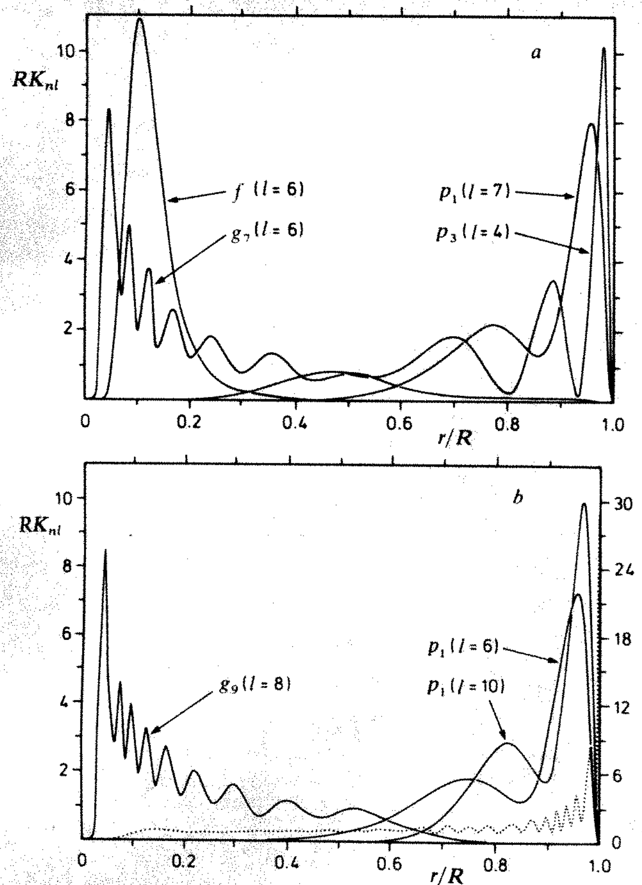

Fig. 1 Rotational splitting kernels RK_{nl} for the seven modes listed in Table 1. The dotted curve (to which the right-hand ordinate scale refers) is an average of the six kernels with $l=1$ and $l=2$ and frequencies closest to 2.5, 3.3 and 4.1 μHz. This is representative of the 5-min modes observed by Claverie *et al.*[25].

of a part in 10^8 if the spacecraft were in a bound orbit around the Sun.

The discovery of global solar oscillation by Hill and his collaborators[11], Severny *et al.*[12] and Brookes *et al.*[13] raised the possibility that the deep interior of the Sun could be measured more directly than had previously been possible[14]. In particular, rotational splitting of otherwise degenerate nonaxisymmetrical modes provides averages of the angular velocity Ω. Different modes weight Ω differently, and with a sufficient variety one can go some way towards determining the variation of Ω with position. I report here an attempt to estimate Ω from recent observations. This yields a preliminary rough estimate of the Sun's angular momentum, the rotational kinetic energy and J_2.

Properties of rotational splitting

Slow rotation causes nonaxisymmetrical standing wave patterns to precess about the rotation axis of the Sun. This is manifest as a splitting of the degeneracy in frequency with respect to the angular order m of the modes[15,16] (that is to say, the order m of the spherical harmonic that factors from the eigenfunctions). The splitting is an average of the angular velocity, weighted by a kernel that depends on the eigenfunction of oscillation of the nonrotating star. That kernel, which can be computed directly from the variational principle of Lynden-Bell and Ostriker[17], is discussed in refs 18–20. Here I assume that the solar angular velocity $\mathbf{\Omega}$ can be approximated by $\Omega\mathbf{k}$, where $\Omega(r,\theta)=\Omega_0(r)-\Omega_1(r)\cos^2\theta$ and $\mathbf{k}$ is a constant unit vector. In that case the cyclic frequency $\nu\equiv\nu_{nlm}$ of a mode of order n and degree l, with respect to an inertial frame of reference, is well approximated by $\nu_{nl}+\nu'_{nlm}$, where ν_{nl} is the corresponding frequency when $\Omega=0$, and

$$\nu'_{nlm}=\frac{m}{2\pi A}\int_0^R \rho\{\{(\xi-\eta)^2+[l(l+1)-2]\eta^2\}\Omega_0(r)$$

$$-[\![Q_{lm}\{(\xi-\eta)^2+[l(l+1)-7]\eta^2\}+\eta^2]\!]\Omega_1(r)\}r^2\,\mathrm{d}r \qquad (8)$$

$$\equiv\frac{m}{2\pi}\left\{\beta_{nl}\int_0^R K_{nl}(r)\Omega_0(r)\,\mathrm{d}r-\beta_{nlm}\int_0^R K_{nlm}(r)\Omega_1(r)\,\mathrm{d}r\right\} \qquad (9)$$

$$A=\int_0^R \rho[\xi^2+l(l+1)\eta^2]r^2\,\mathrm{d}r \qquad (10)$$

$$Q_{lm}\equiv\tfrac{1}{2}(2l+1)\frac{(l-|m|)!}{(l+|m|)!}\int_{-1}^{1}\mu^2[P_l^m(\mu)]^2\,\mathrm{d}\mu \qquad (11)$$

ξ and η, which depend on n and l but not on m, are measures of the radial and horizontal components of the adiabatic displacement eigenfunction $\delta\mathbf{r}$, defined in spherical polar coordinates by

$$\delta\mathbf{r}(\mathbf{r},t)=\mathrm{Re}\left\{\left[\xi(r)P_l^m(\cos\theta),\ \eta(r)\frac{\mathrm{d}}{\mathrm{d}\theta}P_l^m(\cos\theta)\right.\right.$$

$$\left.\left.im\eta(r)\,\mathrm{cosec}\,\theta\,P_l^m(\cos\theta)\right]\exp(im\phi-2\pi i\nu t)\right\} \qquad (12)$$

P_l^m is the associated Legendre function of the first kind, ρ is the equilibrium density of the Sun (which may be calculated ignoring the centrifugal distortion) and t is the time. The coefficients Q_{lm} can be expressed in terms of Gaunt integrals, which can be computed from the tables of Scott[21]. The factors β_{nl} and β_{nlm} are defined such that the kernels K_{nl} and K_{nlm} are unimodular (that is, their integrals are unity). Thus, if Ω_0 and Ω_1 were constant, the rotational perturbation ν'_{nlm} to the eigenfrequency would be $(m/2\pi)(\beta_{nl}\Omega_0-\beta_{nlm}\Omega_1)$.

If the latitudinal variation of Ω in the solar interior is no greater than the variation observed in the photosphere, then for p modes and low-order g modes of low degree, the second integral in equation (9) is considerably smaller than the first. Thus, since β_{nl} and K_{nl} are independent of m, the frequencies corresponding to the $2l+1$ possible values of m are approximately uniformly spaced.

Observations of apparent rotational splitting

Oscillations of the radial variation of intensity near the solar limb have been recorded by Bos and Hill[22]. Measurements were

Table 1 Rotationally split multiplets and the modes with which they have been identified

Multiplet	l_{min}	ν_c (μHz)	$\Delta\pm\sigma$ (μHz)	Mode	ν_{nl} (μHz)	$\beta_{nl}^{-1}(\Delta+\omega_e/2\pi)$ (μHz)
1	6	256.54	2.875±0.008	$g_7(l=6)$	258.8	2.945
2	8	260.38	2.902±0.006	$g_9(l=8)$	260.9	2.948
3	6	427.97	2.888±0.008	$f(l=6)$	425.6	2.958
4	6	471.10	0.96±0.02	$p_1(l=6)$	495.4	1.07
5	7	498.12	0.85±0.02	$p_1(l=7)$	518.7	0.94
6	10	592.65	0.74±0.01	$p_1(l=10)$	584.6	0.81
7	4	773.94	1.29±0.01	$p_3(l=4)$	759.2	1.39

The theoretical eigenfrequencies ν_{nl} are the frequencies ν_λ extrapolated from the frequencies ν_A, ν_B of models A and B of ref. 30 with $\lambda=1.26$. The corresponding frequencies of $f(l=32)$ and $p_2(l=10)$ are 588.5 and 780.1 μHz. Aside from possible errors in identification, the frequencies ν_c of the central components of the observed multiplets have standard error 0.07 μHz. The r.m.s. difference between ν_{nl} and ν_c is 13 μHz. Δ is the observed mean splitting, and σ is, according to Hill[24], a conservative estimate of the variation of the splitting with m. The last entry is numerically equal to the mean value of Ω_0, weighted by the appropriate kernel K_{nl} illustrated in Fig. 1.

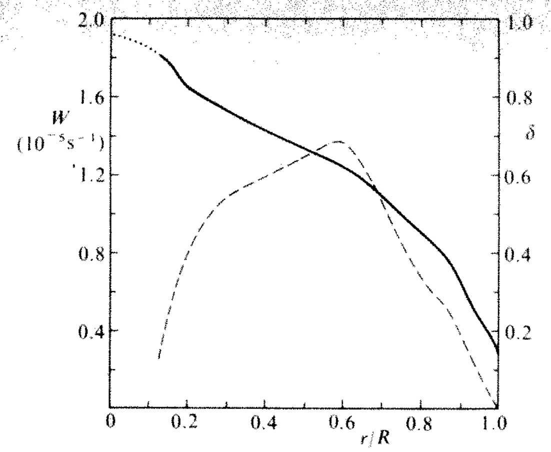

Fig. 2 Averages $W(r)$ of Ω_0 computed by the Backus–Gilbert optimal averaging procedure. Averaging kernels D with $\bar{r} < 0.12R$ cannot be constructed from the data kernels in Fig. 1, so W has been extrapolated to the origin with a cubic curve (dotted) that approximates W in the range $0.12 < r/R < 0.2$. Since $\mathscr{I}$ and $\mathscr{J}$ are both small near the origin (see Fig. 4), H, T, and J_2 are insensitive to the extrapolation procedure. The dashed line is the half-width δ of the averaging kernel D.

made simultaneously at three pairs of diametrically opposed locations, distributed symmetrically about the equator, and from them six functionals $\psi_i(t)$ of the limb-darkening function were constructed. For this discussion it does not matter how the functionals ψ_i are defined. It is necessary only to accept that their variation is produced by the ensemble of normal modes of oscillation of the Sun, whose frequencies are thus indicated by peaks in the power spectra of ψ_i. The solar origin of the signal is argued in refs 22, 23.

Observations of mean duration 9.3 h have been made on 18 days during a 41-day period[22]. Fourier transforms of $\psi_i(t)$ were computed, and from linear combinations of them power spectra of components of the oscillations satisfying certain symmetry relations could be isolated. For example, the power spectrum of $\sum_{i=1}^{6} \psi_i$ contains contributions from only those modes with even l and even m. Part of that spectrum is shown in ref. 22. Aliasing aside, the frequency resolution is 1/(41 day) = 0.28 μHz.

In the hope that the influence of the latitudinal variation of Ω on the splitting would be small, sequences of uniformly spaced peaks in the spectra were sought. Some care was taken to account for the side-bands imposed by the window function, but a systematic attempt to remove them was not made. To be acceptable, the spacing between the centres of the peaks was required to be uniform to 0.07 μHz. It is prudent to apply so stringent a condition, at least in a preliminary analysis, to guard against misinterpreting accidental sequences of peaks in the densely populated spectra. Seven sequences have been found. Their median frequencies ν_c, the mean frequency separations Δ and lower bounds $l_{\min}$ to l, inferred from the number of peaks in the sequences, were announced recently by Hill[24] and are reproduced in Table 1. For this investigation, I shall assume, with Hill, that these are sequences of rotationally split eigenfrequencies, and ask what that implies.

Before this analysis of the power spectrum, evidence of a mean rotational splitting of 0.75 μHz synodic in the low-degree 5-min oscillations was discovered by Claverie *et al.*[25]. The data are difficult to interpret because $2l+1$ components appear in the spectrum, whereas, owing to the symmetry of observing technique, only $l+1$ of the modes of degree l should be visible. Isaak[26] has suggested that the extra components are accounted for by an intense rotating magnetic field in the core of the Sun, as has been postulated by Dicke[27,28] to explain the 12.2-day variation in the Princeton oblateness data. However, it is not clear how that explains the 5-min oscillation data[29]. It is conceivable that a weak field could couple nearly resonant modes with different spatial symmetries, but in that case there is the danger that the coupling modifies the frequencies sufficiently to belie the apparent splitting that arises directly from rotation. Therefore a detailed account of the analysis that includes the 5-min modes will not be presented.

Identification of the modes

Tentative identifications were made by selecting those modes of the standard (nonrotating) solar model A of Christensen-Dalsgaard *et al.*[30] with l approximately equal to but not less than $l_{\min}$ whose frequencies are closest to the median frequencies of the groups of modes observed. It was borne in mind that if $l_{\min}$ underestimates l, as a result of failure to detect or recognize modes with $|m| = l$, the median frequency may differ from the frequency ν_{nl0} by an integral multiple of the frequency separation Δ. The identifications are listed in Table 1. In all cases $l = l_{\min}$.

It is important to realize that there is considerable uncertainty in the identification. This is true particularly of the multiplets 1–3 and multiplets 6 and 7. In the middle range there is less scope for error because the eigenfrequencies are more sparsely distributed.

Splitting kernels

Kernels $K_{nl}(r)$ are illustrated in Fig. 1 for the modes listed in Table 1. It is a property of all these modes that for given n and l the kernels K_{nlm} are nearly the same as K_{nl}. Therefore the kernels K_{nlm} are not displayed. This property also characterizes those other modes that might have been identified with the observed oscillations, and arises because the motion is nearly vertical wherever the amplitude of the mode is large.

It is immediately evident from Fig. 1 that the low-frequency modes sample mainly the rotation of the core, and the high-frequency modes the rotation near the surface. The greater values of Δ associated with the lower frequencies indicates immediately that the Sun's core is rotating more rapidly than the photosphere.

Latitudinal variation of Ω

Because, for the modes under consideration, $l(l+1)\eta^2$ is rather smaller than ξ^2, and $K_{nlm} \simeq K_{nl}$, the splitting formulae (8), (9) may be approximated by

$$\nu'_{nlm} \simeq \frac{m}{2\pi}\beta_{nl}(\bar{\Omega}_0 - Q_{lm}\bar{\Omega}_1) \qquad (13)$$

Table 2 Properties of estimates of Ω

Estimate	H	T	J_2	σ_Δ
1	5.0	25.7	3.6×10^{-6}	0.07
2	4.8	23.8	3.8×10^{-6}	0.01
3	5.3	31.5	4.3×10^{-6}	0
4	5.9	37.4	5.4×10^{-6}	0.04
5	5.4	31.3	4.1×10^{-6}	0.02
6	4.4	27.9	4.5×10^{-6}	0
7	1.0	3.8	1.4×10^{-6}	0

Estimate 1 is the result of the Backus–Gilbert inversion shown in Fig. 1. Estimates 2–5 are the curves 1–4 in Fig. 2. Estimate 6 is the seventh-degree polynomial in r with $\Omega(R) = \Omega_S$ that satisfies the splitting constraints (14) exactly. Estimate 7 is the function Ω_0 that minimizes J_2 and satisfies $\Omega_0(R) = \Omega_S$ and the splitting constraints (14). For any value J above the minimum J_2 there are infinitely many functions $\Omega(r)$ satisfying $J_2 = J$, the outer boundary condition and the splitting constraints (14). The entries σ_Δ are r.m.s. differences between Δ and the frequency splitting predicted by Ω_0, measured in units of the observed splitting Δ. The angular momentum H and the rotational kinetic energy T are measured in units of $I\Omega_S$ and $\frac{1}{2}I\Omega_S^2$ respectively, where $I \simeq 0.068MR^2$ is the moment of inertia of the extrapolated solar model about an axis through the centre. If the rotational splitting of low-degree 5-min modes claimed by Claverie *et al.*[25] is added to the data, the values of $10^6 J_2$ for the seven estimates of Ω listed above are 2.3, 2.1, 3.4, 2.9, 2.8, 14.4 and 1.4 respectively. In this case estimate 6 is the eighth-degree polynomial that satisfies the constraints. If the last two modes in Table 1 are replaced by $f(l=32)$ and $p_2(l=10)$, whose splitting kernels are somewhat more concentrated near the surface, the corresponding values of $10^6 J_2$ are 3.6, 2.1, 5.1, 5.9, 4.2, 438.4 and 1.2 when the 5-min datum is ignored, and 2.4, 1.7, 4.9, 2.9, 2.9, 790.3 and 1.2 when the 5-min datum is included.

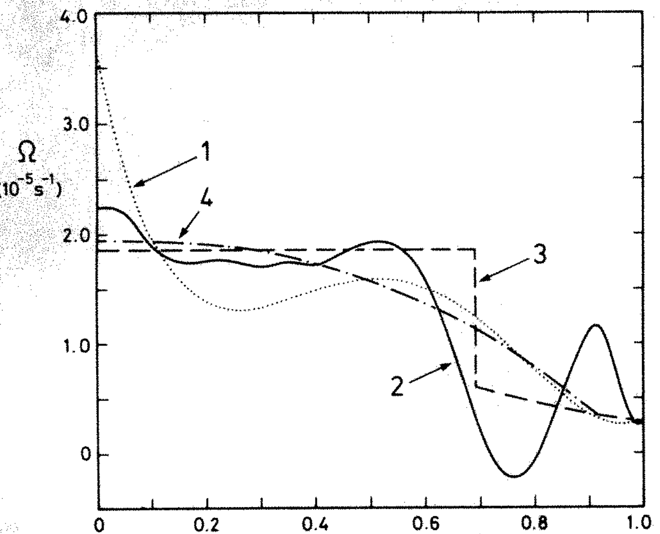

Fig. 3 Some possible rotation curves Ω_0 that are compatible with the data. Curve 1 is a fourth-degree polynomial and curve 2 minimizes the mean square gradient of Ω_0. Curves 3 and 4 vary inversely with r^2 for $r>r_c$; for $r<r_c$ curve 3 is constant whereas curve 4 is proportional to $1-\alpha(r/R)^b$. In each case the free parameters were chosen to fit to the constraints (14) by least squares, subject to curve 4 being continuous. Curve 2 satisfies (14) exactly. The data in Table 1 cannot distinguish between these curves.

where the overbar denotes the mean with weight K_{nl}. Thus from any observed nonuniformity in the splitting an estimate of $\bar{\Omega}_1/\bar{\Omega}_0$ may be obtained.

Nonuniformity in the splitting has several origins. Aside from observational error and differential rotation, the most likely source is a magnetic field. This can be distinguished from rotational splitting by a difference of symmetry. If, for example, $\nu^{\dagger}_{nlm}$ is the magnetic perturbation to frequency due to an axisymmetrical field, then $\nu^{\dagger}_{nl(-m)}=\nu^{\dagger}_{nlm}$, whereas $\nu'_{nl(-m)}=-\nu'_{nlm}$. This result holds even when the axis of symmetry does not coincide with the rotation axis, provided ν'_{nlm} is less than the width of the lines in the power spectrum. With sufficiently accurate data the two contributions could be separated.

It is a consequence of the different symmetries that ν'_{nlm} and $\nu^{\dagger}_{nlm}$ cannot cancel for all m. Therefore the deviations σ from uniform splitting listed in Table 1 can be used to estimate an upper bound to $\bar{\Omega}_1$. The standard deviation of the rotational contribution to the nonuniformity in the splitting can be computed easily from the approximation (13). If all detectable modes are present, the result, expressed in units of the mean splitting, varies monotonically from $0.32\bar{\Omega}_1/\bar{\Omega}_0$ to $0.40\bar{\Omega}_1/\bar{\Omega}_0$ as l varies from 4 to 10.

Consider first multiplets 4–7 in Table 1, whose kernels are concentrated near the surface of the Sun. The mean σ is about 0.015 of the mean splitting, which implies, if the modes have been identified correctly, that $\bar{\Omega}_1/\bar{\Omega}_0\leq 0.04$. This is to be compared with the differential rotation in the photosphere, which satisfies $\Omega_1(R)/\Omega_0(R)\simeq 0.2$. The result implies either that the θ-dependence of Ω is confined to a boundary layer about $0.05R$ deep, or that Ω_1 changes sign, so that at the base of the convection zone the rotation is faster at the poles than at the equator.

Note that among the surface modes, multiplets 6 and 7 are the more concentrated near the surface. Therefore one would expect their rotational splitting to be the less uniform, which is apparently not the case. Aside from the possibility that the data have been wrongly interpreted, this suggests either that the magnetic field increases with depth or that the modes have been incorrectly identified. According to equation (13), nonuniformity in the splitting increases as m increases, so it is quite conceivable that the components with the greatest values of m have not been recognized. The multiplet 6 could be a high-degree f mode, such as $f(l=32)$, and multiplet 7 could be $p_2(l=10)$. It is unlikely that multiplet 6 is a high-degree g mode, even though there are such modes with appropriate frequencies, because these modes are likely to be severely trapped beneath the convection zone and hence be unobservable[31,32].

Multiplets 1–3 in Table 1 are concentrated in the core. The high degree of uniformity observed in the splitting implies that the core's rotation is nearly uniform on spheres. The limits set by σ yield $\bar{\Omega}_1/\bar{\Omega}_0\leq 7\times 10^{-3}$. They also set limits on the magnetic field in the core. If a field of structure similar to that adopted by Dicke[27] is assumed, the mean field intensity is bounded above by about 3×10^4 G.

Radial variation of Ω

Because the contribution to ν'_{nlm} from Ω_1 is small, I shall neglect it. Then the mean observed splittings Δ listed in Table 1 yield seven differently weighted averages of Ω_0. These are

$$\int_0^R RK_{nl}(r)\Omega_0(r)\,\mathrm{d}(r/R)=\beta_{nl}^{-1}(2\pi\Delta+\omega_e) \qquad (14)$$

where ω_e is the orbital angular velocity of the Earth. The values of these averages are listed in Table 1.

Provided the data are not mutually inconsistent, inversion of equations (14) to obtain a plausible estimate of Ω_0 is possible, but not unique. Nonuniqueness arises partly because there are only a finite number of averages to constrain the function. Therefore one must adopt some criterion for preference. Here I follow an optimal averaging procedure of Backus and Gilbert[33]. For each value r_0 of r one attempts to construct a linear combination $D(r,r_0)=\sum\alpha_{nl}(r_0)K_{nl}(r)$ of the data kernels K_{nl} in such a way that D is concentrated near r_0. The α_{nl} are normalized to make D unimodular. The average $W(\bar{r})$ of Ω_0 weighted with the new kernel D is simply $\sum\alpha_{nl}\beta_{nl}^{-1}(2\pi\Delta+\omega_e)$. Here $\bar{r}$ is the median of D. If the attempt to concentrate D was successful, then D resembles a delta function, and one may safely set $\Omega_0(r)\simeq W(r)$. If D is not well concentrated, one may still adopt $W(r)$ as the least biased estimate of $\Omega_0(r)$, but one must bear in mind that structure on a scale smaller than the width of D cannot be resolved. Thus the function W is likely to be smoother than Ω_0. Moreover, it does not satisfy the constraints (14) precisely. Note, however, that W is an invariant property of data, in the sense that all functions $\Omega_0(r)$ that satisfy the constraints (14) have the same averages $W(\bar{r})$ when weighted with the averaging kernels D.

The Backus–Gilbert inversion procedure has been applied to the data listed in Table 1. In so doing, a further constraint of the form (14) was added, with a data kernel that is a delta function at $r=R$ and a right-hand side equal to $2\pi/(25.4\text{ days})=2.86\times 10^{-6}\,\mathrm{s}^{-1}\equiv\Omega_S$. This device ensures that $\Omega(R)=\Omega_S$. The function $W(r)$ is shown in Fig. 2.

To give an idea of the extent of the averaging, the half-width δ of D, defined as r_2-r_1 where

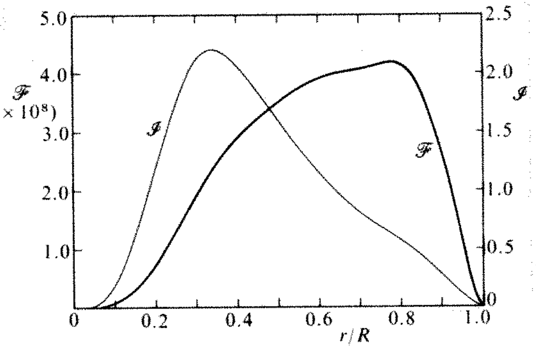

Fig. 4 The moment of inertia kernel $\mathcal{J}$ and the oblateness kernel $\mathcal{F}$, extrapolated linearly from the corresponding kernels of models A and B of ref. 30 as in equation (17) with $\lambda=1.26$. $\mathcal{J}$ is measured in units of the moment of inertia I, and $\mathcal{F}$ is measured in units of Ω_S^{-2}.

$$\int_{r_1}^{r} D\,\mathrm{d}r = \int_{r}^{r_2} D\,\mathrm{d}r = \tfrac{1}{4} \qquad (15)$$

is also displayed. The averages are quite well confined near the centre and the surface, but are very broad in the mid-range. This is not surprising, as none of the data kernels K_{nl} has a substantial amplitude where $0.2 \leqslant r/R \leqslant 0.8$. The failure of the Backus–Gilbert procedure to provide a kernel D that is well concentrated about any point in the mid-range results from a paucity of appropriate data, and does not reflect a deficiency in the procedure. Though $\Omega_0(r)$ is quite strongly constrained near the centre and the surface, there is a wide margin of uncertainty elsewhere.

An important goal of the inversion procedure is the attainment of a stable solution. If averaging kernels D are chosen so as to minimize δ, small changes to either the data or the kernels K_{nl} yield large changes in W when several different data, or linear combinations of them, provide nearly the same physical information. Thus errors are magnified and the solution is inaccurate. Backus and Gilbert[33] discuss how, at the expense of permitting somewhat broader averaging kernels D, a tradeoff between stability to errors in the data (or the mapping of those data on to Ω_0 via the data kernels K_{nl}) and formal mathematical accuracy can be achieved. That procedure has been adopted here. The rotation curve presented in Fig. 2 is stable to small changes in the data or the kernels, and is therefore more likely to be a good representation of the actual angular velocity of the Sun than is a curve constructed to fit the constraints (14) exactly.

As an indication of the uncertainty in $\Omega_0(r)$ I display four alternative possibilities in Fig. 3. The first is the fourth-degree polynomial in r satisfying $\Omega_0(R) = \Omega_S$ that best fits equations (14) by least squares. Its shape is quite sensitive to changes in the equilibrium solar model. (The corresponding seventh-degree polynomial, which is even more sensitive to the equilibrium model, satisfies equations (14) exactly. Some of its properties are listed in Table 2.) The second is in some sense the most slowly varying function that fits the data, for it minimizes the integral of $(\mathrm{d}\Omega_0/\mathrm{d}r)^2$ among all differentiable functions Ω_0 that satisfy the constraints (14) and $\Omega_0(R) = \Omega_S$. The third is of the form $\Omega_0 = \tilde{\Omega} =$ constant for $0 \leqslant r < r_c$ and $\Omega_0 = (R/r)^2\Omega_S$ for $r_c < r \leqslant R$. This function was chosen, somewhat arbitrarily, with the idea that the radiative interior might be rotating rigidly, aside from a thin boundary layer at the base of the convection zone. Because Ω_0 is very much smaller than the buoyancy frequency in the radiative zone, only a slight smoothing of the discontinuity would be necessary to satisfy the Solberg–Høiland dynamical stability criterion[34–36] in the equatorial plane, with negligible effect on the values of the angular momentum, rotational kinetic energy and J_2. Again the free parameters were chosen to give the closest fit to equation (14) by least squares, yielding $r_c = 0.69R$ and $\tilde{\Omega} = 1.86 \times 10^{-5}\,\mathrm{s}^{-1}$. The value of r_c is close to independent modern estimates[37–40] of the radius of the base of the convection zone. The fourth function is of the form $\Omega_0 = \tilde{\Omega}[1 - \alpha(r/R)^b]$ for $0 \leqslant r \leqslant r_c$ and $\Omega_0 = (R/r)^2\Omega_S$ for $r_c \leqslant r \leqslant R$, with $\tilde{\Omega}$, α, b, r_c chosen to give the least squares fit to equation (14) subject to Ω_0 being continuous.

Angular momentum, rotational kinetic energy and J_2

From each of the rotation curves displayed in Figs 2 and 3 it is straightforward to compute the angular momentum H, the rotational kinetic energy T and the measure J_2 of the gravitational quadrupole moment. These are given by

$$H \simeq \int_0^1 \mathscr{I}\Omega_0\,\mathrm{d}x, \qquad T \simeq \tfrac{1}{2}\int_0^1 \mathscr{I}\Omega_0^2\,\mathrm{d}x, \qquad J_2 \simeq \int_0^1 \mathscr{F}\Omega_0^2\,\mathrm{d}x \quad (16)$$

where $x = r/R$, $\mathscr{I}(x) = (8\pi/3)R^5\rho x^4$ and $\mathscr{F}$ is given in ref. 17. The results are listed in Table 2. The kernels $\mathscr{I}$ and $\mathscr{F}$ are displayed in Fig. 3. Notice that they are greatest where knowledge of Ω_0 is the least. This unfortunate property magnifies the undertainty in H, T and J_2.

On the solar helium abundance

A least squares fit of the frequencies

$$\nu_\lambda = \lambda\nu_A + (1-\lambda)\nu_B \qquad (17)$$

interpolated or extrapolated linearly from the eigenfrequencies ν_A and ν_B of models A and B of ref. 30 (which have initial helium abundances $Y = 0.25$, 0.19 respectively) to observed frequencies of low-degree 5-min modes[38] yields $\lambda = 1.36 \pm 0.12$. Thus it seems that Y is somewhat greater than 0.25. A similar fit to the frequencies in Table 1 yields $\lambda = 1.26 \pm 0.79$. The latter fit is hardly strong independent evidence that $Y > 0.25$, especially since the mode identifications are uncertain. Nevertheless, it does show that the data in Table 1 are apparently consistent with this result. All the computations listed in this paper used the extrapolated model with $\lambda = 1.26$. Using model A typically changes H^2, T and J_2 by no more than 10%.

Conclusion

If the sequence of peaks found in the spectra of Bos and Hill[22] really are a consequence of rotational splitting, then it may confidently be concluded that the central core of the Sun rotates on average some six times faster than the surface. Moreover, the angular velocity Ω in the core is almost independent of latitude. The distribution of angular velocity throughout the rest of the Sun is uncertain, but it is not unlikely to resemble the solid curve in Fig. 2. Of course, there may be variations about that curve on a scale less than δ (shown also in Fig. 2). Such structure cannot possibly be resolved by observations of only the modes listed in Table 1, however precise the measurements. What is needed is to observe modes with data kernels that have substantial amplitudes where $0.2 \leqslant r/R \leqslant 0.8$.

Aside from a smoothed version of curve 3 in Fig. 3, none of the estimates of Ω_0 is dynamically stable. All the estimates are unstable to the Rayleigh criterion $\mathrm{d}(\varpi^2\Omega_0)^2/\mathrm{d}\varpi > 0$, where ϖ is the distance from the rotation axis. This condition is relevant when thermal diffusion is taken into account[41–43]. Indeed, it is interesting that there exists no function Ω_0 satisfying $\Omega_0(R) = \Omega_S$ and the Rayleigh criterion that can reproduce the frequency splitting of multiplets 4–7 in Table 1. Therefore the data seem to imply either that the mean flow is stabilized by some agent, such as a magnetic field, or that the natural tendency of the instability to restore Ω_0 to a state satisfying the Rayleigh criterion is effectively countered by some other angular-momentum transporting process.

The splitting data alone cannot determine Ω_0. Thus, to arrive at an estimate it is necessary to impose at least one additional restriction. That chosen here is one of smoothness, and was applied by equating the solid curve in Fig. 2, which is a well-determined average of Ω_0 with a known kernel D, with Ω_0 itself. This procedure has been applied successfully in other inverse problems, particularly in geophysics. The result is likely to be smoother than the actual angular velocity.

The curve depicted in Fig. 2 implies that the measure J_2 of the gravitational quadrupole moment is 3.6×10^{-6}. It is difficult to judge how accurate this value is, partly because the identification of the modes is uncertain, and partly because even if the modes were known, the constraints imposed by the splitting alone do not restrain the possible functions Ω_0 within tight bounds. The smallest value of J_2 compatible with the data is about 1.2×10^{-6}; the data cannot bound J_2 above.

The implications the estimate has on the test of gravitation theories using the precession of the orbit of Mercury can be assessed from equations (5)–(7). Taking $J_2 = 3.6 \times 10^{-6}$ yields

$$\tfrac{1}{3}(2 - \beta + 2\gamma) = \begin{matrix} 0.992 \pm 0.005 & \text{(ref. 6)} \\ 0.996 \pm 0.005 & \text{(ref.3)} \end{matrix} \qquad (18)$$

The errors quoted are standard errors arising from the orbit analysis, and take no account of the uncertainty in J_2.

Finally, it should be remembered that a careful analysis of the power spectra has yet to be undertaken, and that the uniformly spaced sequences of peaks might have been interpreted wrongly.

I thank Professor H. A. Hill for collaboration in Cambridge last November when together we isolated some of the multiplets in the power spectrum, identified the modes of oscillation, constructed a crude rotation curve and made our first estimate of J_2. Since then our opinions about the implications of the data have diverged, and we have decided to publish our findings separately (see ref. 44). I thank J. Christensen-Dalsgaard for some computer programs and comments, and D. Gubbins, D. Lynden-Bell and K. Whaler for discussions, also J. E. Pringle for suggesting improvements on an early version of the paper.

Received 13 April; accepted 4 June 1982.

1. Misner, C., Thorne, K. S. & Wheeler, J. A. *Gravitation* (Freeman, San Francisco, 1973).
2. Will, C. M. *General Relativity: An Einstein Centenary Survey* (eds Hawkins, S. W. & Israel, W.) 24–89 (Cambridge University Press, 1979).
3. Anderson, J. D., Keesey, M. S. W., Lau, E. L., Standish, E. M. Jr & Newhall, xx *Astronautica* **5,** 43–61 (1978).
4. Dicke, R. H. & Goldenberg, H. M. *Astrophys. J. Suppl.* **27,** 131–182 (1974).
5. Hill, H. A. & Stebbins, R. T. *Astrophys. J.* **200,** 471–483 (1975).
6. Shapiro, I. I., Counselman, C. C. III & King, R. W. *Phys. Rev. Lett.* **36,** 555–558 (1976).
7. Anderson, J. D., Colombo, G., Friedman, L. D. & Lau, E. L. *Proc. Int. Meet. on Experimental Gravitation* (ed. Bertotti, B.) 393–422 (Academia Nazionale dei Lincei, Rome, 1977).
8. Esterbrook, F. B. *et al. Sources of Gravitational Radiation* (ed. Smarr, L. L.) 37–48 (Cambridge University Press).
9. Christensen-Dalsgaard, J. & Gough, D. O. *Nonradial and Nonlinear Stellar Pulsations* (eds Hill, H. A. & Dziembowski, W. A.) 369–380 (Springer, Heidelberg, 1980).
10. Nordtvedt, K. Jr *Proc. int. Meet. on Experimental Gravitation* (ed. Bertotti, B.) 247–256 (Academia Nazionale dei Lincei, Rome, 1977).
11. Hill, H. A. *The New Solar Physics* (ed. Eddy, J. A.) 135–214 (Westview, Boulder, 1978).
12. Severny, A. B., Kotov, V. A. & Tsap, T. T. *Nature* **259,** 87–89 (1976).
13. Brookes, J. R., Isaak, G. R. & van der Raay, H. B. *Nature* **259,** 92–95 (1976).
14. Christensen-Dalsgard, J. & Gough, D. O. *Nature* **259,** 89–92 (1976).
15. Cowling, T. G. & Newing, R. A. *Astrophys. J.* **109,** 149–158 (1949).
16. Ledoux, P. *Astrophys. J.* **144,** 373–384 (1951).
17. Lynden-Bell, D. & Ostriker, J. P. *Mon. Not. R. astr. Soc.* **136,** 293–310 (1967).
18. Hansen, C. J., Cox, J. P. & Van Horn, J. M. *Astrophys. J.* **217,** 151–159 (1977).
19. Cuypers, J. *Astr. Astrophys.* **89,** 207–208 (1980).
20. Gough, D. O. *Mon. Not. R. astr. Soc.* **196,** 731–745 (1981).
21. Scott, S. *The Application of Modern Physics to the Earth and Planetary Interiors* (ed. Runcorn, S. K.) 586–602 (Wiley–Interscience, London, 1969).
22. Bos, R. J. & Hill, H. A. *Solar Phys.* (in the press).
23. Hill, H. A., Bos, R. J. & Caudell, T. P. *Solar Phys.* (in the press).
24. Hill, H. A. *Proc. R. astr. Soc. Meet. in Dublin, Irish astr. J.* (in the press).
25. Claverie, A., Isaak, G. R., McLeod, C. P., van der Raay, H. B. & Roca Cortes, T. *Nature* **293,** 443–445 (1981).
26. Isaak, G. R. *Nature* **296,** 130–131 (1982).
27. Dicke, R. H. *Proc. Informal Conf. on Status and Future of Solar Neutrino Research* Vol. 2 (ed. Friedlander, G.) 109–143 (Brookhaven National Laboratory, Upton, 1978).
28. Dicke, R. H. *New Scient.* **83,** 12–14 (1979).
29. Gough, D. O. *Nature* **298,** 350–354 (1982).
30. Christensen-Dalsgaard, J., Gough, D. O. & Morgan, J. G. *Astr. Astrophys.* **73,** 121–128; **79,** 260 (1979).
31. Dziembowski, W. A. & Pamjatnykh, A. A. *Pleins Feux sur la Physique Solaire* (ed. Rösch, J.) 135–140 (CNRS, Paris, 1978).
32. Christensen-Dalsgaard, J., Dziembowski, W. A. & Gough, D. O. *Nonradial and Nonlinear Stellar Pulsation* (eds Hill, H. A. & Dziembowski, W. A.) 313–341 (Springer, Heidelberg, 1980).
33. Backus, G. & Gilbert, F. *Phil. Trans. R. Soc.* **A266,** 123–192 (1970).
34. Solberg, H. *Procès-verbaux de l'assn. de météor. UGGI 6^e Assemblée Générale (Edinburgh), Mém. et Disc.* **2,** 66–82 (1936).
35. Høiland, E. *Avhandl. Utgitt Norske Vidensk.—Akad. Oslo I. Mat.—naturv. Kl.* No. 11, 1–24 (1941).
36. Zahn, J.-P. *IAU Symp.* No. 59, 185–195 (1974).
37. Lubow, S. H., Rhodes, E. J. Jr & Ulrich, R. K. *Nonradial and Nonlinear Stellar Pulsation* (eds Hill, H. A. & Dziembowski, W. A.) 300–306 (Springer, Heidelberg, 1980).
38. Berthomieu, G. *et al. Nonradial and Nonlinear Stellar Pulsation* (eds Hill, H. A. & Dziembowski, W. A.) 307–312 (Springer, Heidelberg, 1980).
39. Christensen-Dalsgaard, J. & Gough, D. O. *Astr. Astrophys.* **104,** 173–176 (1981).
40. Scuflaire, R., Gabriel, M. & Noels, A. *Astr. Astrophys.* **99,** 39–42 (1981).
41. Yih, C.-S. *Phys. Fluids* **4,** 806–811 (1961).
42. Goldreich, P. & Schubert, G. *Astrophys. J.* **150,** 571–587 (1967).
43. Fricke, K. J. *Z. Astrophys.* **68,** 317–344 (1968).
44. Hill, H. A., Bos, R. & Goode, P. R. *Phys. Rev. Lett.* (submitted).

The thermal springs of Bath

J. N. Andrews*, W. G. Burgess†, W. M. Edmunds†, R. L. F. Kay‡ & D. J. Lee§

* School of Chemistry, University of Bath, Bath BA2 7AY, UK
† Institute of Geological Sciences, Hydrogeology Unit, Wallingford, Oxon OX10 8BB, UK
‡ Institute of Geological Sciences, Environmental Protection Unit, Harwell, Didcot, Oxon OX11 0RA, UK
§ United Kingdom Atomic Energy Authority, Winfrith, Dorset DT2 8DH, UK

Geochemical and hydrogeological evidence shows that the thermal springs at Bath originate from the Mendip Hills. A maximum subsurface temperature of 80 ± 16 °C is attained during circulation to between 2.7 and 4.3 km within the Carboniferous Limestone. The residence time of the bulk of the water is < 10,000 yr.

INTEREST in the evaluation of the geothermal resources of Britain has prompted a thorough geochemical investigation of the Bath thermal springs and their regional setting[1]. The King's Spring, the principal spring at Bath, emerges through Lower Lias shales within a reservoir of Roman construction. It has a flow of 13 l s^{-1} at a temperature of 46.5 °C which records show to have been constant within ±0.5 °C since 1754. Its thermal yield above a non-thermal groundwater temperature of 10 °C is 2.0 MW. Two smaller springs at Bath, the Cross Bath and Old Royal springs, have chemical compositions very similar to that of the King's Spring. Thermal water also occurs at Bristol where the Hotwells Spring discharges from Carboniferous Limestone into river muds just above low tide level in the Avon gorge. The flow is about 0.2 l s^{-1} at 24 °C and the thermal yield is only 7 kW.

The Bath/Bristol district is a complex synclinal structure formed between three intersecting fold axes[2]. The most important aquifers which might contribute to the flow of the thermal water, are in the Carboniferous Limestone and in Triassic deposits. The Old Red Sandstone (Devonian) and the Pennant Sandstones (Carboniferous) have only restricted hydraulic continuity.

The origin and composition of the Bath thermal waters have been the subject of much scientific curiosity. Notable associated discoveries include the extraction of helium from the exsolved gases by Sir James Dewar[3]; the identification of their radioactivity due to radium by Strutt[3] in 1904 and that due to radon by Munro[4] in 1928. However, no acceptable explanation of the heat source and circulation history of the waters has yet been proposed. The objective of the present study was to use a range of geochemical techniques to deduce the source, the circulation history, the temperature at depth and the age of groundwater[5].

Geochemical characteristics

(1) Inorganic chemistry: the King's Spring water has a total mineralization of 2,150 mg l^{-1} and Ca^{2+} and SO_4^{2-} are the dominant ions (Table 1). The chemical composition remained constant over the 2 yr period of investigation, and comparison with earlier work[6–9] suggests that the composition is stable over a long period. This stability is also reflected in the fact that the thermal water is in equilibrium with the minerals calcite, dolomite, gypsum, fluorite and barite as calculated using the WATEQF program[10].

Regional sampling of representative groundwaters from local aquifers was carried out and these results[5] show that no other groundwaters with a composition similar to that of Bath thermal water are found in the region, except locally in the Triassic aquifer, as discussed below. The Hotwells spring at Bristol has a composition equivalent to a mixture of Bath-type thermal water and shallow, Carboniferous Limestone water in the ratio 1 : 2.3.

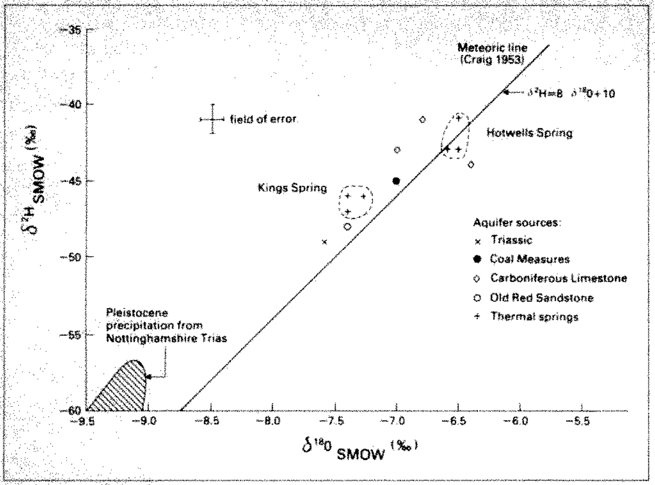

Fig. 1 Plot of hydrogen and oxygen stable isotope results for the thermal waters in relation to other groundwaters in the region.

(2) Dissolved radioelements: The isotope ^{234}U can be dissolved in preference to its precursor, ^{238}U, as a consequence of its genesis by decay processes and the $^{234}U/^{238}U$ activity ratio in groundwaters is frequently in excess of equilibrium[11]. The Bath thermal water is distinguished from other groundwaters in the region by a very low U-content and a high $^{234}U/^{238}U$ activity ratio (Table 1*c*). Only groundwaters from the Old Red Sandstone have similar activity ratios although they generally have higher U-contents than thermal water.

The high level of radioactivity in the King's Spring water is due to ^{222}Rn and during 1977 it gradually increased from 1,000 to 2,220 pCi kg^{-1}, the value determined[12] in 1972. This increase is attributed to a delayed piezometric recovery following the unusual drought conditions of 1976. Other radiochemical parameters and the radiogenic ^4He content similarly increased during 1977. ^{222}Rn contents similar to that of the King's Spring also occur locally in groundwaters from the Trias. Although the ^{226}Ra activity in the water is much lower than that of ^{222}Rn, it is the most significant radioelement present with regard to radiological hazard[13]. The short-lived β-emitting ^{222}Rn daughters, $^{214}Pb/^{214}Bi$ are present in equilibrium with ^{222}Rn. The isotope ^{210}Pb (half life 22 yr) requires about 100 yr to reach equilibrium with a constant ^{222}Rn source. Because the activity of ^{210}Pb in the thermal water is negligible although there is adequate natural Pb carrier present, this suggests either that the ^{222}Rn content has not been constant for a long period or that rapid wall-rock exchange of lead isotopes must be occurring.

The natural Th content of the King's Spring is below the detection limit of 0.002 µg per kg. The β-emitting ^{232}Th daughters, $^{212}Pb/^{212}Bi$, are present to the extent of 2.6 pCi kg^{-1}. These isotopes must be derived by ^{220}Rn release into the groundwater by mechanisms similar to those for ^{222}Rn release. The ratio of $^{222}Rn/^{220}Rn$ activities suggests that the U/Th ratio in the source rock could be as high as 250:1, though this may be an overestimate as the efficiency of ^{220}Rn release could be much less than that for ^{222}Rn. However, the uranium geochemistry also suggests that U deposition has occurred somewhere in the flow system.

(3) Dissolved gases: The gas composition (Table 1*d*) can be explained as the exsolution of atmospheric gases, which were dissolved at recharge, modified by the geochemical reaction of oxygen in the aquifer, by the addition of radiogenic ^4He due to radioelement decay and by the addition of hydrocarbon gases. At atmospheric pressure, the ratio of nitrogen solubility at 46.5 °C to that at 9.5 °C, the approximate recharge temperature, is 0.6, so that less than half of the dissolved gas should be exsolved as the thermal water re-equilibrates with the atmosphere. The total dissolved gas flow was calculated as 710 l h^{-1} in the present study and this may be compared with estimates[14] of the total exsolved gas flow of 208 l h^{-1}. Seasonal fluctuations

Table 1 The composition of thermal water from the King's Spring, Bath

a, **Major element composition** (mg kg^{-1})

Year source	1977–79 (this study) Range	Mean	1961 (ref. 6)	1936 (ref. 7)
Temperature (°C)	46.4–46.6	46.5	48	49
Flow (ls^{-1})	–	15.0	—	—
*p*H	6.39–6.94	6.68	7.1	—
Eh (mV)	+220–32	—	—	—
O_2(mg l^{-1})	0.5–6.0	1.8	—	—
Total solids	2,177–2,280	2,203	2,166	2,162
Na^+	169–190	183	174	177
K^+	16.2–20.3	17.4	15.7	15.4
Ca^{2+}	352–399	382	392	392
Mg^{2+}	52.0–55.4	53	54	51
HCO_3 –	184–206	192	216	193
SO_4 –	1.010–1,060	1,032	1,021	1,001
Cl^-	280–292	287	276	274

			1888 (ref. 8)	1874 (ref. 9)
Temperature (°C)	46.4–46.6	46.5	47	46
Flow (ls^{-1})	–	15.0	—	—
*p*H	6.39–6.94	6.68	—	—
Eh (mV)	+220–32	—	—	—
O_2(mg l^{-1})	0.5–6.0	1.8	—	—
Total solids	2,177–2,280	2,203	2,360	1,920
Na^+	169–190	183	135	129
K^+	16.2–20.3	17.4	31	39
Ca^{2+}	352–399	382	402	377
Mg^{2+}	52.0–55.4	53	52	47
HCO_3 –	184–206	192	88	86
SO_4 –	1.010–1,060	1,032	1,061	869
Cl^-	280–292	287	277	280

b, **Trace element composition** (mg kg^{-1})

			1961 (ref. 6)	1936 (ref. 7)
Li^+	0.240–0.255	0.242	0.050	0.22
Sr^{2+}	5.60–6.10	5.92	8.0	5.6
Ba^{2+}	—	0.024	0.8	0.1
Total Mn	0.065–0.085	0.068	0.059	0.027
Total Fe	0.950–1.320	0.879	0.009	1.45
Ni^{2+}	0.002–0.030	0.022	0.0005	—
Cu^{2+}	0.0005–0.0037	0.0021	0.0035	0.04
F^-	2.0–2.20	2.6	2.0	4.3
Br^-	1.00–1.50	1.32	6.9	1.3
NO_3^-	0.9–1.7	1.2	<0.0002	0.24
HPO_4^{2-}	—	0.020	0.0058	—
SiO_2	43.2–44.3	44.1	44.1	43.6

c, **Isotopic and radioelement composition** (this study)

$\delta^{18}O$	‰ rel. SMOW	−7.4
δ^2H	‰ rel. SMOW	−47.0
δ^3H	Tritium units	0–3.1
	pCi kg^{-1}	0–9.0
$\delta^{13}C$	‰ rel. PDB	−1.5
$\delta^{14}C$	% modern carbon	4.5

U-series isotopes		Mode	1977–79 Range
Natural U	µg kg^{-1}	0.05	0.025–0.094
^{238}U	pCi kg^{-1}	0.017	—
$^{234}U/^{238}U$	activity ratio	2.5	1.7–3.5
^{226}Ra	pCi kg^{-1}	11.0	5.9–11.7
^{222}Rn	pCi kg^{-1}	2,350	1,030–2,650
$^{214}Pb/^{214}Bi$	pCi kg^{-1}	2,367 ± 200	—
^{210}Pb	pCi kg^{-1}	<1.0	—

Th series isotopes		
Natural Th	µg kg^{-1}	<0.002
$^{212}Pb/^{212}Bi$	pCi kg^{-1}	2.61 ± 0.26
$^{224}Ra/^{220}Rn$	pCi kg^{-1}	2.61 ± 0.26

d, **Exsolved gas composition and dissolved noble gas content**

Exsolved gas composition	%
N_2	to 100%
O_2	<0.5
^4He	0.1
Ar	1.0
CO_2	3.5
CH_4	0.6
C_3H_8	0.8

Dissolved noble gases	cm^3 STP/cm^3 H_2O
^4He	$1,080 \times 10^{-8}$
Ne	2.10×10^{-7}
Ar	4.04×10^{-4}
Kr	0.91×10^{-7}
Xe	1.19×10^{-8}

in dissolved oxygen (<0.5–6.0 mg l^{-1}) and in *Eh* (redox potential) were also noted and may indicate some mixing of waters at intermediate depths.

Source of thermal groundwater and its recharge

The hydrogen and oxygen isotopic compositions of the thermal water demonstrate that it is of meteoric origin (Fig. 1). The isotopic compositions lie close to the worldwide meteoric line[15] and the ratios are similar to those of modern shallow groundwaters in the region. The Bath thermal water may be clearly distinguished from known occurrences[16] of late Pleistocene groundwater elsewhere in England where a recharge temperature some 5 °C cooler than postglacial climatic conditions has been indicated. The ratios of dissolved atmospheric inert gases in the thermal waters indicate recharge temperatures around 9 °C. The combined evidence shows that climatic conditions at recharge were similar to those of the present day.

The piezometric levels in the various aquifers in the Bath/Bristol region are shown in Fig. 2. The piezometric level of the King's Spring is known from the historical record for a well which encountered thermal water in Kingsmead Street[17] in 1836. It is 40 m above sea level (10 m above the elevation of the spring). The only location with sufficient head to cause flow at the King's Spring is the Mendip Hills, about 15 km to the south-west and on the margin of the basin.

Maximum temperature and circulation depth

Rock–water equilibration temperatures for groundwaters from geothermal areas have been estimated from the amounts of dissolved Na^+, K^+, Ca^{2+} and SiO_2 (refs 18, 19). It was found that the cation geothermometers were not valid for the sedimentary formations of the Bath/Bristol region. The application of the SiO_2 geothermometer depends on which silica polymorph controls its dissolution. The thermal groundwaters are closer to equilibrium with chalcedony ($SI = +0.18$) than with quartz ($SI = +0.60$) but because of the limited number of springs the control on SiO_2 solution is uncertain. Maximum rock equilibration temperatures of 64 °C (for chalcedony control) and 96 °C (for quartz control) have been calculated and the maximum temperature reached at depth probably lies within this range. The SiO_2 geothermometer indicates that the thermal component of the Hotwells source has been equilibrated in the range 49–72 °C before subsequent mixing with shallow groundwater from the Carboniferous Limestone.

The necessary circulation depth for meteoric water to reach these temperatures may be estimated from the geothermal gradient. The only geothermal gradient measurement[20] (11 °C km^{-1}) in the basin, however, is known to have been affected by cold water inflows in the borehole. On the assumption that the region is one of average heat flow (40 mW m^{-2}), a geothermal gradient close to 20 °C km^{-1} is more likely (J. R. Bloomer, personal communication). This would place the circulation depth of the Bath thermal water in the range 2,700–4,300 m to attain a temperature of 64–96 °C and this depth strongly implies that either the Carboniferous Limestone and/or the Old Red Sandstone must be the principal storage aquifer(s)

The slightly negative $\delta^{13}C$ (−1.5‰) of the dissolved bicarbonate is very strong evidence that the thermal water has equilibrated chemically with the marine Carboniferous Limestone rather than with the largely non-marine Old Red Sandstone. The value of $\delta^{13}C$ for the latter[21] is −10.7‰ and is too negative to permit the development of the observed $\delta^{13}C$ of the thermal water. It must be concluded that the most recent storage and chemical equilibration of the carbonate system takes place within the Carboniferous Limestone ($\delta^{13}C = -0.05$‰), although a proportion of the thermal water may previously have been transmitted in the Old Red Sandstone.

Thermal water age

Tritium, ^3H, produced by thermonuclear weapon testing, was used to identify any post-1950s recharge. The ^3H content of the King's Spring averaged 1 ± 2 TU over the monitoring period and the highest observed value was 3.1 ± 2 TU. This, together with the small amounts of nitrate present, variations in dissolved O_2, *Eh* and $^{234}U/^{238}U$ activity ratio, suggests that there could be some mixing of the thermal water with very small quantities of 'recent' waters from shallow aquifers.

The ^{14}C specific activity for the dissolved bicarbonate of the King's Spring averages 4.5% of that for modern carbon (Table 1*c*). The uncertain source and age of any 'young' mixing component leads to uncertainty in the interpretation of the carbon isotope data in terms of residence time for the thermal water. Assumptions about the extent of mixing, however, allow limiting conditions to be defined. If there is no mixing with recent groundwater, and the ^{14}C activity represents that remaining after decay of the original ^{14}C present, a corrected age for the thermal water of 20,000 yr may be derived on the basis of the stoichiometric reaction between biogenic CO_2 (100% modern carbon; $\delta^{13}C - 26.1$‰) and ^{14}C- dead carbonate in the recharge zone (no ^{14}C; $\delta^{13}C$ −0.05‰ for Carboniferous Limestone). Such a 1 : 1 reaction between carbonate and biogenic CO_2, however, would result in a $\delta^{13}C$ value of −13.0‰ for the dissolved bicarbonate.

The measured $\delta^{13}C$ of the thermal water bicarbonate (Table 1*c*) is −1.6‰, and this indicates that extensive bicarbonate/carbonate interphase exchange has occurred after the initial congruent solution of carbonate. It is not possible to estimate, or correct for, the concurrent loss of ^{14}C from the bicarbonate in solution to the aquifer carbonate in this process. The age estimate of 20,000 yr is therefore a maximum possible age, provided that no ^{14}C activity has been introduced by mixing with shallow groundwater of recent origin. Alternatively, if mixing with recent groundwater (which may be dead to ^3H, but contain appreciable ^{14}C) is sufficient to account for all the observed ^{14}C activity, then the thermal water itself is dead to ^{14}C and is older than 50,000 yr.

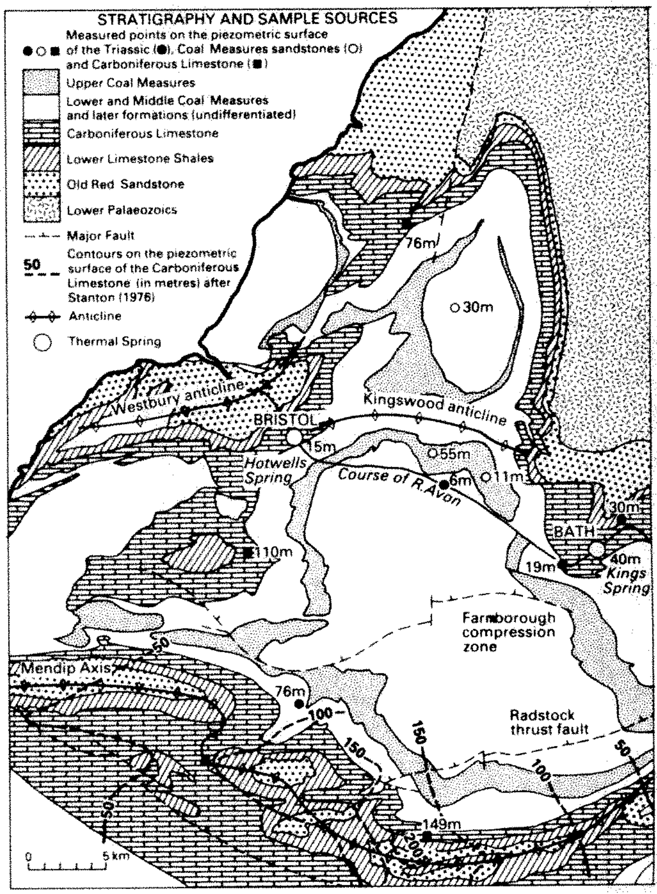
STRATIGRAPHY AND SAMPLE SOURCES
● ○ ■ Measured points on the piezometric surface of the Triassic (●), Coal Measures sandstones (O) and Carboniferous Limestone (■)
Upper Coal Measures
Lower and Middle Coal Measures and later formations (undifferentiated)
Carboniferous Limestone
Lower Limestone Shales
Old Red Sandstone
Lower Palaeozoics
Major Fault
50 Contours on the piezometric surface of the Carboniferous Limestone (in metres) after Stanton (1976)
Anticline
○ Thermal Spring
76m
o 30m
Westbury anticline
Kingswood anticline
BRISTOL
15m
Hotwells Spring
O55m
Course of R. Avon
6m
O11m
30m
BATH
110m
19m
40m
Kings Spring
Farmborough compression zone
50
Mendip Axis
76m
100
150
150
Radstock thrust fault
50
100
50
149m
200
0
5 km

Fig. 2 Outcrop and subcrop of Palaeozoic strata in the Bath–Bristol region, with major structural features (after G. A. Kellaway, unpublished data); the localities sampled during the study and the piezometric data are also shown.

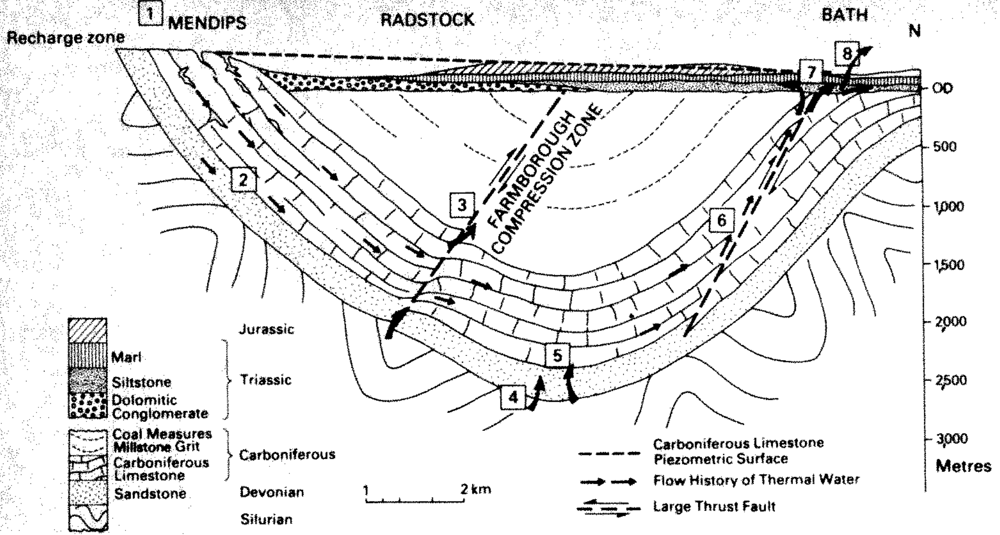

Fig. 3 Conceptual model of the flow path of thermal water in the Bath–Bristol Basin: 1, recharge (9–10 °C) at the Carboniferous Limestone/Old Red Sandstone outcrop; 2, down dip and down gradient flow, assisted by karstic development; 3, possible gain from Lower Palaeozoics and leakage to Upper Carboniferous via Farmborough compression zone; 4, some leakage of very old ^{4}He-bearing groundwater from Old Red Sandstone and possibly Lower Palaeozoics; 5, storage and chemical equilibration within the Carboniferous Limestone, at 64–96 °C; 6, relatively rapid ascent along thrust fault system; 7, some recharge of Triassic by thermal water at Bath; 8, discharge of the thermal springs at Bath (46.5 °C).

The temperature at which the thermal water was recharged (9–10 °C), estimated from its inert gas contents and its isotopic composition (δ^2H and δ^{18}O), shows that recharge took place in climatic conditions similar to those of the Holocene. This implies either that the water is younger than 10,000 yr (the beginning of the present climatic optimum), or older than 70,000 yr (the end of the last interglacial). It is therefore not possible to distinguish between the alternative explanations for the ^{14}C activity in the water, on the basis of its recharge temperature.

The ^{4}He content of a groundwater increases with its residence time in a formation of porosity, ϕ, and density, ρ, according to the equation[22]:

$$^4\text{He content, cm}^3/\text{cm}^3\ \text{H}_2\text{O} = \rho\,\phi^{-1}\,\{1.19\times10^{-13}\,[\text{U}]+2.88\times10^{-14}\,[\text{Th}]\}t \qquad (2)$$

where [U] and [Th] are the U and Th contents of the aquifer rock and t is the groundwater age in years if all the ^{4}He generated is dissolved in the pore fluids. This equation is not strictly applicable to the Carboniferous Limestone which is a fracture-flow system for which estimation of effective porosity is difficult. It is also unlikely that all the ^{4}He generated would be dissolved in the fracture fluids if the porosity is low. However, equation (2) yields a minimum age of 250,000 yr for a porosity of 1% and the radioelement contents of the Carboniferous Limestone. The Old Red Sandstone has radioelement contents about four times higher than those of the Carboniferous Limestone and for a similar porosity the minimum residence time to generate the ^{4}He in this formation is 60,000 yr. The generation of the observed ^{4}He content of the thermal water, within the Carboniferous Limestone, it is impossible for a residence time as short as 10,000 yr. At least a proportion of the thermal water must be much older and may be derived from the Old Red Sandstone.

Hydraulic controls and local conditions

The thermal water probably rises at Bath by way of a southerly-dipping east–west thrust fault in the vicinity. During the artesian flow of thermal water in Kingsmead Street[17], it was noted that an immediate and considerable decrease in flow occurred at the King's Spring and at the Cross Bath and Old Royal Springs. This indicates that the storage capacity of the Trias cannot be large. It was found that groundwaters which are chemically similar to Bath thermal water occur in the Trias at up to 2 km from the King's Spring. It therefore appears that the rising thermal water, under pressure, is recharging the Triassic sequence, probably by way of the Palaeozoic unconformity. This suggestion is supported by the available piezometric data (Fig. 1).

Limits on the likely hydraulic gradient between the Mendips and the Bath Spring are set by the level of the perennial discharge springs to the north of the pericline and the maximum level of the water table on Mendip. For a first approximation, a hydraulic gradient of 0.005 appears likely. Applying Darcy's law to the flow rate at Bath for an estimated cross-sectional area perpendicular to the direction of flow of 7×10^5 m^2 (the Carboniferous Limestone being ~700 m thick over a 1 km segment), the effective permeability controlling the flow of thermal water at depth is calculated as ~0.3 m day^{-1}. This is reasonably lower than the permeability to diffuse flow of 4 m day^{-1} in the Mendip Carboniferous Limestone outcrop[23]. For an effective porosity between 1 and 10%, volumetric considerations suggest the actual flow velocity would be between 0.1 and 0.01 m per day. Up to 4,000 yr would therefore be required to traverse the 15 km betweeen Mendip and Bath.

Discussion

The thermal water at Bath has very constant chemical and thermal characteristics. It is of meteoric origin, and was recharged in climatic conditions similar to those in the Holocene. Recharge probably takes place on the Mendips, where sufficient elevation provides the piezometric head controlling the flow across the basin. The Carboniferous Limestone acts as the last important storage aquifer for the thermal water where it equilibrates chemically and thermally at a depth of between 2,700 and 4,300 m at a temperature in the range of 64–96 °C, before relatively rapid ascent to the spring discharge points. At Bath, the thin Triassic aquifer which overlies the Palaeozoic unconformity is recharged by the rising thermal water but the major proportion discharges at the King's Spring through the Lower Lias. Although various techniques have been used to try to determine its residence time no unambiguous estimate can presently be made.

Although the hydraulic model is simplistic, it is in order of magnitude agreement with the conclusion that the bulk of the thermal water is <10,000 yr old and on balance we favour this interpretation. To account for the observed level of ^{4}He, this implies that a small proportion of the thermal water must have an extremely long residence history, probably in the Old Red Sandstone, before chemical re-equilibration in the Carboniferous Limestone.

Implications for geothermal development

At the King's Spring, Bath, a discharge of almost 50 m^{3}h^{-1} of water at 46 °C results from a natural head loss of 10 m. A pumped drawdown of 30 m in a borehole tapping the resource at depth might therefore provide a supply of 100–110 m^{3}h^{-1}. If the actual discharge were at 70 °C and the water were rejected from a heat exchanger at 25 °C, this would give a thermal yield of about 5 MW. The use of a heat pump would increase the thermal yield.

It is probable that the Carboniferous Limestone stores thermal water elsewhere along its 15-km strike between Bath and

Bristol. This is, however, only speculation and could only be proved by exploratory drilling.

It may be possible to exploit thermal groundwater stored in the Triassic aquifer at Bath without the need for wildcat drilling in the Carboniferous Limestone. The low effective bulk permeability of the Carboniferous Limestone at depth, however, is unlikely to support a flow of thermal water (across a 1 km wide section) much greater than the natural flow at the Bath springs. There could, therefore, be no exploitation of thermal water within a radius of several kilometres from Bath without risk of seriously affecting the spring discharge. The hydrogeological conditions at Bath must be thoroughly investigated before any such development, if the intrinsic historical and tourist value of the springs is to be protected.

We thank the City Councils of Bath and Bristol for permission to carry out work at the springs and for their assistance during sampling, the Wessex Water Authority for their collaboration in the regional groundwater sampling, and local landowners for providing access. We particularly thank colleagues at the IGS for analytical work and considerable help both during the sampling and in discussion of the results. We also acknowledge the help of SURRC, East Kilbride and AERE, Harwell for providing the radiocarbon and tritium analyses. We thank Dr G. A. Kellaway for valuable discussions concerning the geology of the region. The work was funded partly by the U.K. Department of Energy and the EEC under research contract 084–76–EG(UK) and partly by NERC research grand GR3/2622A. It is published with permisssion of the Director, Institute of Geological Sciences (NERC).

Received 19 January; accepted 19 May 1982.

1. *Final Rep. to EEC under contract* 084–76–*EG*(*UK*) (Institute of Geological Sciences, London, 1980).
2. Welch, F. B. A. & Crookall, R. *British Regional Geology: Bristol and Gloucester District* (HMSO, London 1948).
3. Dewar, J. & Strutt, R. J. *Reports to the Corporation of Bath* (1904).
4. Munro, J. M. H. *Report to the Corporation of Bath.* (1928).
5. Burgess, W. G., Edmunds, W. M., Andrews, J. N., Kay, R. L. F. & Lee D. J. *Inst. geol. Sci. Rep. to EEC under contract* 084–76–*EG*(*UK*) (1979).
6. Riley, J. P. *J. appl. Chem.* **11,** 190–192 (1961).
7. Judd-Lewis, S. in *Bath Official Handbook* (Mendip, Bath, 1938).
8. Heriot, M. *Proc. Bath Field Club* **3,** 171–177 (1877).
9. Ekin, C. in *The Thermal Baths of Bath* (ed Freeman, H. W.) (Hamilton, Adams and Co, London, 1888).
10. Plummer, L. N., Jones, B. F. & Truesdell, A. H. *U.S. geol. Surv. Wat. Res. Inv.* 76–13 (1976).
11. Osmond, J. K. & Cowart, J. B. *Atom. Energy Ref.* **14,** 621–679 (1976).
12. Andrews, J. N. & Wood, D. F. *Inst. Min. Metall. Trans.* **B81,** B197–210 (1972).
13. Andrews, J. N. & Wood, D. F. *Hlth Phys.* **27,** 307–310 (1974).
14. Masson, I. & Ramsey, Sir W. *Trans. J. chem. Soc.* **101,** 1370–1376 (1912).
15. Craig, H. *Science* **33,** 1702–1703 (1961).
16. Bath, A. H., Edmunds, W. M. & Andrews, J. N. in *Isotope Hydrology* Vol. 2, 545–568 (IAEA Vienna, 1979).
17. Armstrong, W. *An Account of the Tapping and Closing of a Hot Spring, Bath* (Privately published pamphlet, Bristol, 1838).
18. Fouriner, R. O. & Truesdell, A. H. *Geochim. cosmochim. Acta* **37,** 1255–1275 (1973).
19. Fournier, R. O. in *Proc. Symp. Hydrogeochemistry Biogeochemistry* Vol. 1, 122–139, (Clarke, Washington, 1973).
20. Kellaway, G. A. *Bull. geol. Surv. Gt Br.* No. 27, 49–153 (1967).
21. Evans, G. V., Otlet, R. L., Downing, R. A., Monkhouse, R. A. & Rae, G. in *Isotope Hydrology* Vol. 2, 679–708 (IAEA, Vienna, 1979).
22. Andrews, J. N. & Lee, D. J. *J. Hydrol.* **41,** 233–252 (1979).
23. Atkinson, T. C. *J. Hydrol.* **35,** 93–110 (1977).

T24 human bladder carcinoma oncogene is an activated form of the normal human homologue of BALB- and Harvey-MSV transforming genes

Eugenio Santos, Steven R. Tronick, Stuart A. Aaronson, Simonetta Pulciani & Mariano Barbacid

Laboratory of Cellular and Molecular Biology, National Cancer Institute, National Institutes of Health, Bethesda, Maryland 20205, USA

A transforming gene isolated from T24 human bladder carcinoma cells is closely related to the BALB murine sarcoma virus (MSV) onc *gene (v-*bas*). This transforming gene is localized to a 4.6 kilobase pair (kbp) region and is expressed as a 1.2-kbp polyadenylated transcript, which contains v-*bas *related sequences. Moreover, antisera known to detect the immunologically related* onc *gene products of BALB- and Harvey-MSVs recognized elevated levels of a related protein in T24 cells. The normal human homologue of v-*bas *was found to be indistinguishable from the T24 oncogene by heteroduplex and restriction enzyme analysis. These results imply that rather subtle genetic alterations have led to the activation of the normal human homologue of v-*bas *as a human transforming gene.*

THE genetic alterations that cause normal cells to become malignant in natural conditions are for the most part still obscure. A potentially important approach towards understanding such mechanisms has come from studies of acute transforming retroviruses. It is now well established that the majority of these viruses possess substituted viral genes necessary for replication with a discrete segment of host genetic information[1]. When incorporated within the retroviral genome, such transduced cellular (*onc*) sequences acquire the ability to induce neoplastic transformation. At least 24 independent acute transforming retrovirus isolates have been found to date, of which some contain the same or closely related *onc* genes[2–7]. These findings have suggested that vertebrates contain a limited number of cellular genes that can acquire transforming properties when recombined with retroviral sequences.

The development of DNA-mediated gene transfer techniques has recently made it possible to identify transforming genes in a variety of tumours, including some of human origin[8–19]. DNAs isolated from either naturally occurring human tumours or from human tumour cell lines, have been shown to induce morphological transformation when transfected into suitable assay cells[12–19]. In fact, a transforming gene has been isolated by molecular cloning techniques from the T24[20] and EJ[21] human bladder carcinoma cell lines[19,22,23]. Preliminary characterization of this bladder carcinoma oncogene has revealed it to be of human origin and small size (less than 6 kilobase pairs (kbp))[19,22,23]. We undertook the present studies to investigate whether this human bladder carcinoma oncogene was related to any of the cell-derived *onc* sequences that have acquired neoplastic properties on transduction into retroviruses.

A human bladder carcinoma transforming gene is related to v-*bas*

The availability of a molecularly cloned bladder carcinoma transforming gene, designated the T24 oncogene, enabled us to examine its relationship with the *onc* genes of a variety of

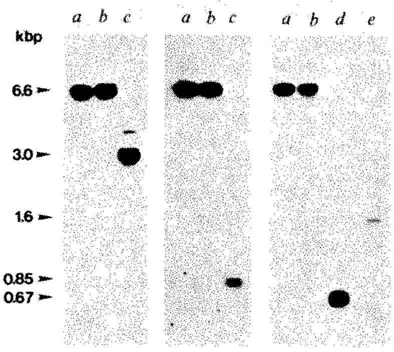

Fig. 1 Relationship between the T24 oncogene and the retroviral *onc* genes of BALB-MSV (v-*bas*) and of MC29 virus (v-*myc*). Molecularly cloned DNAs, including 100 ng of a 6.6-kbp *Bam*HI fragment containing the T24 oncogene, purified from λT24-15A DNA[19] (*a*), 100 ng of a 6.6-kbp *Bam*HI fragment containing the T24 oncogene purified from pT24-C3[32] (*b*), 200 ng of the above 6.6-kbp *Bam*HI fragment but digested with *Sac*I (*c*), 100 ng of 0.67-kbp *Hin*dIII to *Bam*HI fragment of v-*bas* (*d*), and 200 ng of 1.6-kbp *Sac*I to *Bam*HI fragment of v-*myc* (*e*), were electrophoresed in horizontal agarose (1% w/v) gels, blotted to nitrocellulose filters and hybridized in stringent conditions (50% formamide, 5×SSC and 42 °C) for 16 h to 5×10^6 c.p.m. of the following nick-translated probes: *A*, ^{32}P-labelled 0.67-kbp *Hind* III to *Bam*HI v-*bas* DNA; *B*, ^{32}P-labelled 1.6-kbp *Sac*I to *Bam*HI v-*myc* DNA; *C*, ^{32}P-labelled 6.6-kbp *Bam*HI T24 oncogene DNA, as described previously[42]. Hybridized blots were exposed to Kodak XR-5 film at −70 °C in the presence of intensifier screens for 4 h (*A*), 3 days (*B*) and 4 h (*C*). Arrows indicate the migration of each of the hybridized DNA fragments.

transforming retroviruses. We used probes obtained from DNA clones of transforming retroviruses capable of inducing a wide range of malignancies and known to contain different *onc* genes. These included avian isolates such as the MC29 virus[24], avian myeloblastosis virus (AMV)[25] and Rous sarcoma virus (RSV)[26], as well as mammalian viruses, including Abelson murine leukaemia virus (A-MuLV)[27], BALB[4] and Moloney[28,29] strains of murine sarcoma virus (MSV), the Snyder–Theilen strain of feline sarcoma virus (ST-FeSV)[30] and simian sarcoma virus (SSV)[31]. Each retroviral *onc* gene probe was prepared from a pBR322 subclone containing only *onc* sequences.

As shown in Fig. 1, the cloned 6.6-kbp *Bam*HI human DNA fragment harbouring the T24 oncogene was readily hybridized with a DNA probe containing 675 bp of v-*bas*, the *onc* gene of BALB-MSV. In the reciprocal experiment, v-*bas* DNA was detected with similar intensity with a probe composed of the T24 oncogene (Fig. 1). Cleavage of the cloned 6.6-kbp *Bam*HI human DNA with the restriction endonuclease *Sac*I is known to generate three fragments of 3.0, 2.7 and 0.85 kbp[32]. Only the 3.0-kbp *Sac*I fragment was detected using v-*bas* as a probe (Fig. 1). These findings firmly established a high degree of relationship between the T24 human bladder carcinoma oncogene and v-*bas*.

No homology was detected between the T24 oncogene and any other *onc* gene tested, with the exception of v-*myc*, the *onc* gene of MC29 virus. However, the degree of relationship between the T24 oncogene and v-*myc* was at least 20–50-fold lower than that detected with v-*bas*, as measured by the relative signal intensity observed (Fig. 1). The possibility that the v-*myc* probe was detecting the subset of T24 oncogene sequences related to v-*bas* was excluded by findings that v-*bas* and v-*myc* showed no homology in identical experimental conditions (data not shown). In fact, it was possible to localize the v-*myc*-related sequences within the 0.85-kbp *Sac*I fragment of the T24 oncogene rather than within the 3.0-kbp *Sac*I fragment containing v-*bas*-related sequences (Fig. 1). Recent studies have localized the transforming region of the T24 oncogene within a 4.6-kbp DNA fragment that contains both the 3.0- and 0.85-kbp *Sac*I fragments[32]. Therefore, these two sets of T24 oncogene sequences, those highly related to v-*bas* and those weakly related to v-*myc*, mapped within the region required for malignant transformation.

c-*bas* (human) is a nontransforming allele of T24 human bladder carcinoma oncogene

As normal human DNA is known to contain sequences related to a variety of retroviruses including v-*bas* and v-*myc*[33], we reasoned that characterization of normal human DNA sequences homologous to each of these transforming genes might shed light on the biological significance of their related sequences. Normal human DNA was digested with *Bam*HI and submitted to Southern blot analysis for detection of sequences related to the T24 oncogene as well as to v-*bas* and v-*myc*. The T24 oncogene and v-*bas* probes both hybridized with a 6.6-kbp *Bam*HI human DNA fragment, suggesting that the normal human v-*bas*-related sequences might represent a normal allele of the T24 oncogene (Fig. 2). In addition, v-*bas* recognized a 3.0-kbp *Bam*HI fragment known to contain another member of the c-*bas* family of genes (S.T. *et al.*, unpublished observations). We also detected hybridization of the T24 oncogene to this 3.0-kbp *Bam*HI human DNA fragment after prolonged exposure (data not shown). In contrast, the v-*myc* probe hybridized with a different subset of human DNA sequences (Fig. 2). These results established that the v-*myc*-related 0.85-kbp *Sac*I fragment of the T24 oncogene did not correspond to the human c-*myc* locus.

To compare the T24 oncogene with normal human sequences related to v-*bas* [designated c-*bas* (human)], we isolated c-*bas* (human) from a library of normal human fetal liver DNA[34]. A recombinant λ Charon 4A phage containing a 19-kbp *Eco*RI insert of human DNA exhibited a 6.4-kbp internal *Bam*HI segment that specifically hybridized with v-*bas*. This 6.4-kbp *Bam*HI fragment was subsequently subcloned in pBR322 and a representative plasmid, designated p344, used for restriction enzyme analysis. As shown in Fig. 3, the restriction map of this 6.4-kbp *Bam*HI fragment of normal human DNA closely

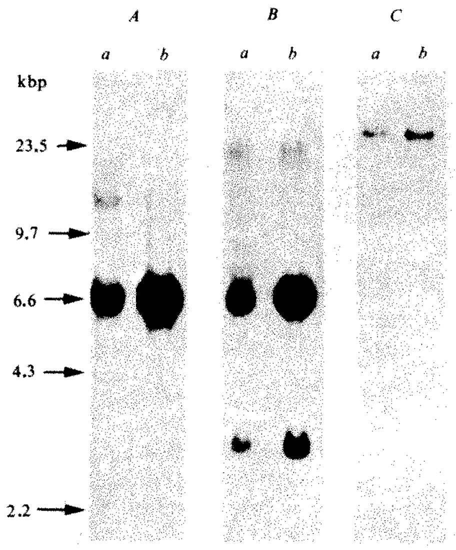

Fig. 2 Detection in human DNA of sequences related to T24 oncogene, v-*bas* and v-*myc*. Twenty microgrammes of high molecular weight DNA isolated from T24 bladder carcinoma (*a*) and M413 normal embryonic human cells (*b*) were digested with 20 U of *Bam*HI for 1 h at 37 °C, electrophoresed in horizontal agarose (0.6% w/v) gels (18 h at 30 V) and blotted to nitrocellulose filters as described previously[42]. Filters were then hybridized in stringent conditions (see Fig. 1 legend) for 44 h to 2×10^7 c.p.m. of the following nick-translated probes: *A*, ^{32}P-labelled 6.6-kbp *Bam*HI T24 oncogene; *B*, ^{32}P-labelled 0.67-kbp *Hin*dIII to *Bam*HI v-*bas*; *C*, ^{32}P-labelled 1.6-kbp *Sac*I to *Bam*HI v-*myc*. Hybridized blots were exposed to Kodak XR-5 film at −70 °C in the presence of intensifier screens for 2 days. Co-electrophoresed DNA fragments of *Hin*dIII-digested λ c1857 DNA served as size standards (labelled in kilobase pairs).

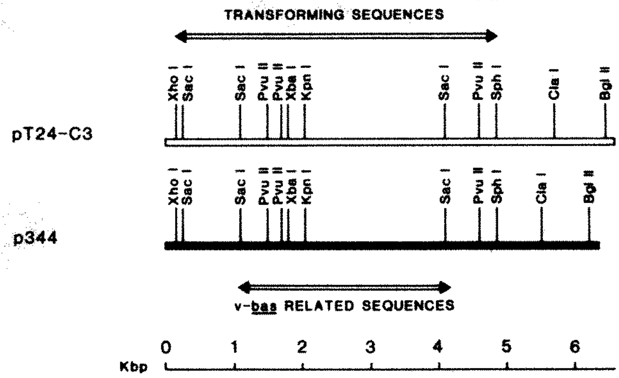

Fig. 3 Comparative restriction maps of the T24 oncogene and c-*bas* (human). The diagram depicts the location of the cleavage sites for *Xho*I, *Sac*I, *Pvu*II, *Xba*I, *Kpn*I, *Sph*I, *Cla*I and *Bgl*II restriction endonucleases within the subcloned *Bam*HI human DNA fragments containing the T24 oncogene (pT24-C3) and c-*bas* (human) (p344). The location of the transforming sequences of the T24 oncogene between the *Xho*I and *Sph*I cleavage sites has been determined elsewhere[32]. The location of the v-*bas*-related sequences within the 3.0-kbp *Sac*I internal fragment of both genes was determined in experiments depicted in Fig. 1.

matched that of the T24 oncogene. In fact, the only detectable difference between the two molecules was a 200-bp deletion that mapped between the *Sph*I and *Cla*I cleavage sites in c-*bas* (human) (Fig. 3). Note that this deletion maps outside the transforming sequences of the T24 oncogene[32], as well as outside the sequences related to v-*bas* (Fig. 3). These results established that c-*bas* (human) is an allele of the T24 bladder carcinoma oncogene.

The T24 oncogene has been shown to transform NIH/3T3 cells efficiently, with a specific activity of ~5×10^4 focus-forming units pmol^{-1} (refs 19, 22, 23). If was of obvious interest to determine whether molecularly cloned c-*bas* (human) sequences exhibited similar biological activity. As much as 1 μg of c-*bas* (human) DNA demonstrated no detectable focus-forming activity whereas in the same experiment, NIH/3T3 cells were readily transformed with as little as 1 ng of the T24 oncogene. The above results, taken together, strongly imply that the acquisition of transforming activity by the T24 oncogene must be the result of subtle genetic alterations.

Organization of v-*bas*-related sequences within the T24 oncogene

The structural relationship between the T24 oncogene and c-*bas* (human) and v-*bas* sequences was studied by heteroduplex analysis. As shown in Fig. 4*a*, c-*bas* (human) and the T24 oncogene were homologous along their entire length, with the exception of a 0.2–0.3 kbp 'loop' located ~1 kbp from one end. These results are consistent with the restriction enzyme maps of these two molecules depicted in Fig. 3. In contrast, heteroduplexes formed between the T24 oncogene and a 0.67-kbp subclone of v-*bas* revealed the presence of a region of homology of about 0.6 kbp in length interrupted by three single-stranded regions of 0.65, 0.14 and 0.27 kbp (Fig. 4*b*). Its v-*bas* homologous sequences were localized within the 3.0-kbp *Sac*I fragment of the T24 oncogene, in agreement with the results obtained by Southern blot analysis (Fig. 3). The coding sequences of v-*bas* are known to reside within the viral RNA strand of the DNA (P. R. Andersen and E. P. Reddy, unpublished observations). By heteroduplex analysis (Fig. 4*b*) it was thus possible to orientate the T24 oncogene as left to right with respect to v-*bas* coding sequences, as shown in Fig. 3.

T24 oncogene products are related to those of the BALB- and Harvey-MSV *onc* genes

Recently, Wigler *et al.* have reported that T24 bladder carcinoma cells exhibit elevated levels of a 1.1-kbp poly(A)-

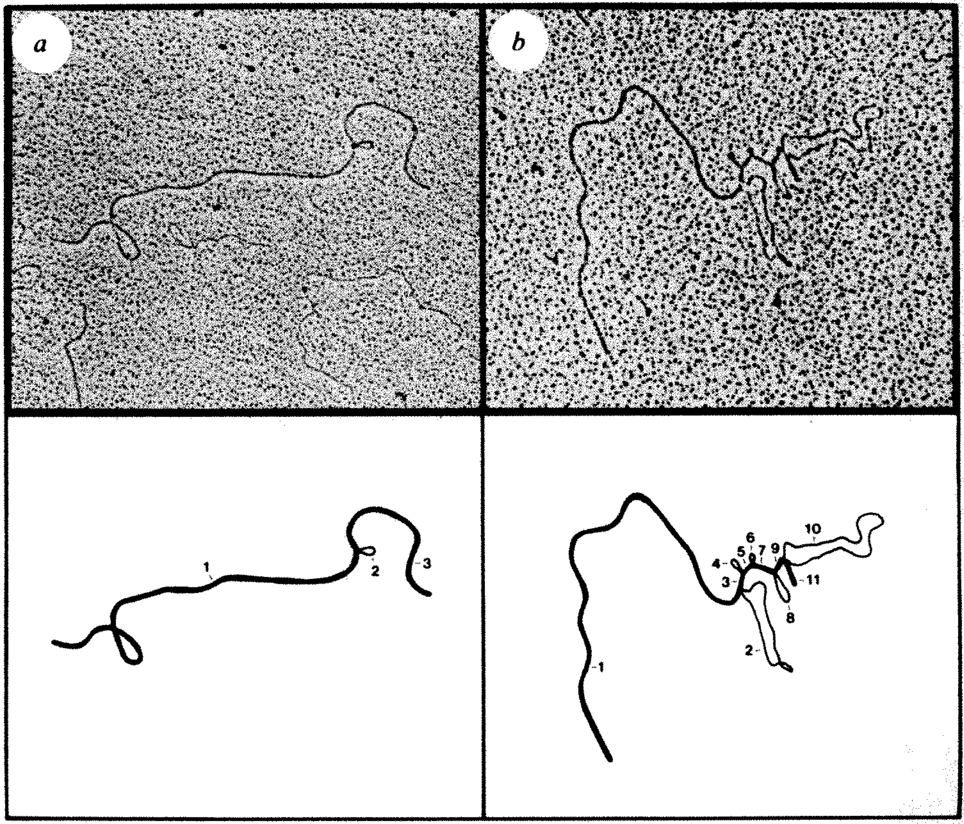

Fig. 4 Heteroduplex analysis of T24 oncogene, c-*bas* (human) and v-*bas*. Heteroduplexes were prepared as described previously[43]. Briefly, DNAs (2 μg ml^{-1}) were denatured with alkali, annealed in the presence of 50% formamide at room temperature for 16 h and spread on to a distilled water hypophase. When pBR322 subclones were used, the supercoiled DNAs were linearized by cleavage with *Sal*I, an enzyme which does not cut any of the inserts. *a*, Heteroduplex formed between T24 oncogene and c-*bas* (human). *Bam*HI inserts purified from pT24-C3 and p344 DNAs, respectively, were used. A representative heteroduplex and an interpretative sketch are represented. Contour lengths (in kbp) of features are as follows: $1=5.2\pm0.25$, $2=0.25\pm0.04$ and $3=1.15\pm0.1$. Fragments 1, 2 and 3 correspond to the 6.6-kbp *Bam*HI DNA fragment containing the T24 oncogene. Fragments 1 and 3 correspond to the 6.4-kbp *Bam*HI DNA fragment containing c-*bas* (human). *b*, Heteroduplex analysis of T24 oncogene and v-*bas*. A representative heteroduplex between pT24-C3 and pHB1 DNA, a plasmid that contains the 0.67-kbp *Hin*dIII to *Bam*HI fragment of v-*bas*, and an interpretative sketch are represented. Contour lengths (kbp) of relevant features are as follows: $1=3.9\pm0.2$, $2=1.8\pm0.2$, $3=0.10\pm0.02$, $4=0.27\pm0.03$, $5=0.10\pm0.02$, $6=0.14\pm0.02$, $7=0.2\pm0.02$, $8=0.65\pm0.05$, $9=0.25\pm0.03$, $10=3.0\pm0.2$, $11=0.25\pm0.03$. Fragments 1 and 11 correspond to pBR322 sequences. Fragments 3, 5, 7 and 9 correspond to v-*bas* sequences. Fragments 2, 4, 6, 8 and 10 correspond to the 6.6-kbp *Bam*HI DNA fragment containing the T24 oncogene.

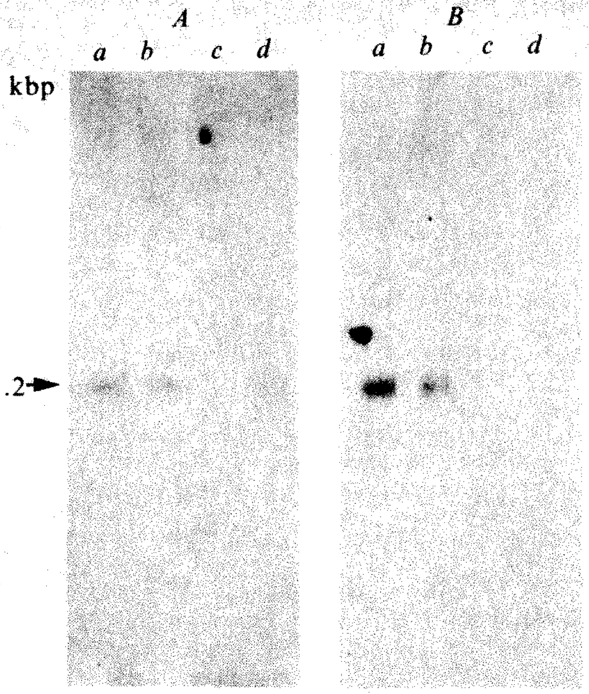

Fig. 5 T24 oncogene and v-*bas*-related transcripts in human cell lines. *a*, *b*, Poly(A)-containing RNA, isolated from T24 bladder carcinoma cells (two independent preparations); *c*, M413 normal embryo cells; *d*, HT-1080 fibrosarcoma cells were obtained as previously described[44,45]. RNA samples (5 μg) were denatured in 13 mM methylmercury hydroxide and size fractionated in horizontal agarose (1% w/v) gels containing 5 mM methyl mercury[46]. Electrophoresed gels were blotted to nitrocellulose filters which were subsequently hybridized with 10^7 c.p.m. of the following nick-translated probes: *A*, ^{32}P-labelled 6.6-kbp *Bam*HI T24 oncogene; *B*, ^{32}P-labelled 0.67-kbp *Hin*dIII to *Bam*HI v-*bas*. Hybridization was performed in 50% formamide, 5 × SSC at 37 °C for 44 h. Hybridized blots were exposed to Kodak XR-5 films at −70 °C in the presence of intensifier screens for 4 days. The arrow indicates the size of the detected transcript as deduced from its relative migration with respect to ribosomal RNA size standards.

containing RNA that specifically hybridized with the T24 oncogene[20]. This transcript was also detected in normal cells, although at much lower levels. As shown in Fig. 5*A*, similar results were obtained in our laboratory. To establish whether the v-*bas*-related sequences of the T24 oncogene were transcribed, poly(A)-containing RNA of T24 cells was submitted to Northern blot analysis. As shown in Fig. 5*B*, a 1.2-kbp RNA molecule hybridized with both the T24 oncogene and v-*bas* probes. These results indicated that v-*bas*-related sequences are an integral part of the T24 oncogene transcript.

The transforming gene product of v-*bas* has been identified as a polypeptide with an apparent molecular weight of 21,000, designated p21^{bas} (ref. 4). An antigenically related protein, p21^{ras}, has been identified as the gene product of Harvey-MSV[35], another murine sarcoma virus whose *onc* gene is closely related to that of BALB-MSV[4]. Antisera obtained from BALB- and Harvey-MSV tumour-bearing rats were used to search for the putative T24 oncogene translational product in a variety of human tumour cells including parental T24 bladder carcinoma cells. As shown in Fig. 6, low levels of a protein migrating with an apparent molecular weight of 21,000 were detected in M413 normal human embryo fibroblasts[36] as well as in HT-1080 human fibrosarcoma cells[37]. Similar results were observed with a variety of human tumour cell lines established from tumours other than bladder carcinomas (data not shown). This p21 protein was also detected in T24 cells but at somewhat elevated levels. In addition, T24 cells contained an antigenically related 23,000 molecular weight protein which was not detected in any of the other human cells analysed (Fig. 6).

To investigate further whether this protein was coded for by the T24 oncogene, we analysed NIH/3T3 cells transformed by this gene (Fig. 6*D*). Such transformants expressed levels of the p23 protein comparable with those detected in T24 cells. In addition, T24 oncogene-transformed NIH/3T3 cells expressed high levels of a p21 protein that co-migrated with the gene product of BALB-MSV (Fig. 6). Whether this protein represents a post-translationally modified human p23 molecule or the endogenous mouse p21 protein, remains to be determined. In either case, our findings support the concept that the T24 oncogene encodes a protein immunologically related to the transforming gene products of BALB- and Harvey-MSV.

Implications

Recent intensive investigation of acute transforming retroviruses has led to considerable knowledge concerning their genomes and translational products, as well as their interactions with the host[1]. Thus, our demonstration that the T24 oncogene represents an activated human cellular analogue of a retroviral *onc* gene should make it possible to apply this knowledge to understanding the mechanisms by which the T24 oncogene induces transformation. By use of high titred antisera directed against the BALB and Harvey MSV-coded p21 proteins[4,35], we were able to detect an antigenically related p23 protein specifically expressed in T24 cells. It should be possible to

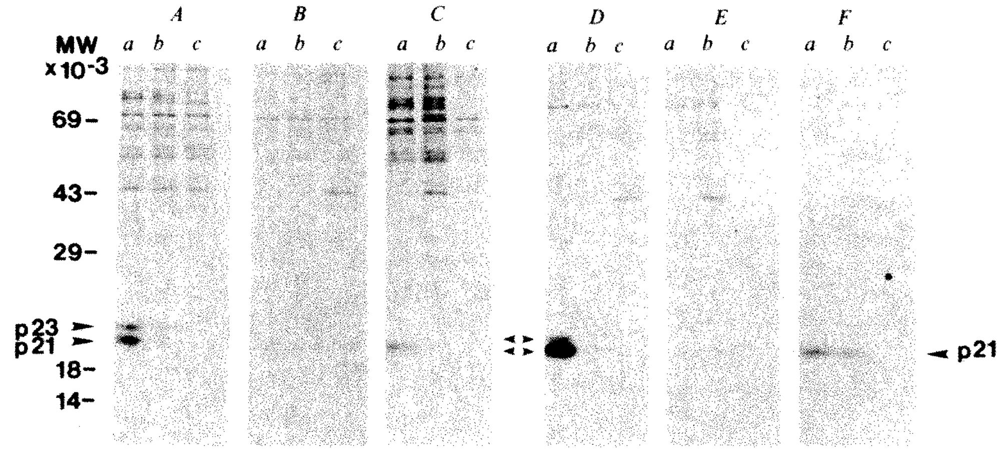

Fig. 6 Detection of proteins antigenically related to the *onc* gene products of BALB- and Harvey-MSV in human tumour cell lines and in NIH/3T3 cells transformed by the T24 oncogene. Exponentially growing cells (~2 × 10^6 cells per immunoprecipitation reaction) including: *A*, T24 human bladder carcinoma cells; *B*, M413 normal human embryonic fibroblasts; *C*, HT-1080 human fibrosarcoma cells; *D*, 44-91 NIH/3T3 cells transformed by the T24 oncogene; *E*, NIH/3T3 mouse cells; *F*, NIH/3T3 cells nonproductively transformed by BALB-MSV, were labelled with ^{35}S-methionine as previously described[47]. Radiolabelled cell extracts were incubated for 1 h at 4 °C with 0.005 ml of sera obtained from: *a*, Harvey-MSV-induced tumour-bearing rats; *b*, BALB-MSV-induced tumour-bearing rats; *c*, uninfected normal rats. Immunoprecipitates, collected with the aid of *Staphylococcus aureus* protein A bound to Sepharose 4B beads, were disrupted in the presence of 1% SDS and 2% 2-mercaptoethanol and analysed by electrophoresis in 8–16% linear gradient SDS-polyacrylamide gels. Electrophoresed gels were dried, fluorographed[48] and exposed to Kodak XR-5 films for 4 days at −70 °C. Molecular weight (MW) markers co-electrophoresed with the above samples included bovine serum albumin (69,000), ovalbumin, indicated by arrows.

establish whether this protein is present in other human bladder carcinoma cells or in other naturally occurring tumours. Such an approach may help in determining whether the T24 oncogene has an aetiological role in human neoplasia.

Detection of dominant human transforming genes by DNA-mediated gene transfer techniques has generally required the use of the NIH/3T3 cell line as the recipient assay cell[12-16,18,19]. As NIH/3T3 is a continuous, heteroploid cell line[38], it is possible that genes which transform this cell line might be unable to transform normal cells. It is known that both v-*bas* and v-*ras* are capable of inducing a variety of malignancies in animals[39-41]. Thus, it seems likely that when the human cellular homologue of these *onc* genes is activated, as in the case of the T24 oncogene, this gene would possess the capacity to transform normal cells as well.

The number of different genes that are activated as dominant transforming genes in human tumours is not known[12-19]. DNAs isolated from carcinomas of the colon and pancreas as well as from a fibrosarcoma and a rhabdomyosarcoma have been shown to transform NIH/3T3 cells in transfection assays (ref. 19 and M.B. *et al.*, unpublished). Although none of these putative human oncogenes has been found to correspond to the human homologues of retroviral *onc* genes used in the present studies, our findings that c-*bas* (human) is a nontransforming allele of the T24 oncogene suggest that additional relationships between human oncogenes and retroviral *onc* sequences may be uncovered.

It has been well established that the cellular sequences transduced by retroviruses require viral genetic information in order to induce malignancy. The present studies demonstrate that at least one of these cellular sequences, c-*bas* (human), can be activated by a mechanism not requiring recombination with retroviral sequences. Detailed restriction enzyme analysis of this gene and its transforming allele, the T24 oncogene, has not revealed detectable differences. Thus, we must conclude that subtle genetic changes have caused the activation of this gene. Comparative sequence analysis of the T24 oncogene and c-*bas* (human) will ultimately define, not only the nature, but the number of genetic changes that led to the acquisition of transforming activity by c-*bas* (human) in T24 bladder carcinoma cells.

We thank Anne V. Lauver, Carole K. Lengyel and Linda K. Long for technical assistance, Holly Fuhrer for photographic work, and the following investigators for providing *onc* gene probes: T. Papas (v-*myc*), M. Baluda (v-*myb*) and G. Cooper (v-*src*).

Received 7 May; accepted 8 June 1982.

1. *Cold Spring Harb. Symp. quant. Biol.* **44,** pt 2 (1980).
2. Frankel, A. E., Gilbert, J. H., Porzig, K. J., Scolnick, E. M. & Aaronson, S. A. *J. Virol.* **30,** 821–827 (1979).
3. Shibuya, M., Hanafusa, T., Hanafusa, H. & Stephenson, J. R. *Proc. natn. Acad. Sci. U.S.A.* **77,** 6536–6540 (1980).
4. Andersen, P. R. *et al. Cell* **26,** 129–134 (1981).
5. Barbacid, M., Breitman, M. L., Lauver, A. L., Long, L. K. & Vogt, P. K. *Virology* **110,** 411–419 (1981).
6. Beemon, K. *Cell* **24,** 145–153 (1981).
7. Wang, L. H. *et al. J. Virol.* **40,** 258–267 (1981).
8. Shih, C., Shilo, B. Z., Goldfarb, M. P., Dannenberg, A. & Weinberg, R. A. *Proc. natn. Acad. Sci. U.S.A.* **76,** 5714–5718 (1979).
9. Cooper, G. M., Okenquist, S. & Silverman, L. *Nature* **284,** 418–421 (1980).
10. Cooper, G. M. & Neiman, P. E. *Nature* **287,** 656–659 (1980).
11. Hopkins, N., Besmer, P., DeLeo, A. B. & Law, L. W. *Proc. natn. Acad. Sci. U.S.A.* **78,** 7555–7559 (1981).
12. Lane, M. A., Sainten, A. & Cooper, G. M. *Proc. natn. Acad. Sci. U.S.A.* **78,** 5185–5189 (1981).
13. Shih, C., Padhy, C., Murray, M. & Weinberg, R. A. *Nature* **290,** 261–264 (1981).
14. Krontikis, T. G. & Cooper, G. M. *Proc. natn. Acad. Sci. U.S.A.* **78,** 1181–1184 (1981).
15. Murray, M. J. *et al. Cell* **25,** 355–361 (1981).
16. Perucho, M. *et al. Cell* **27,** 467–476 (1981).
17. Smith, B. L., Anisowicz, A., Chodosh, L. A. & Sager, R. *Proc. natn. Acad. Sci. U.S.A.* **79,** 1964–1968 (1982).
18. Lane, M. A., Sainten, A. & Cooper, G. M. *Cell* **28,** 873–880 (1982).
19. Pulciani, S. *et al. Proc. natn. Acad. Sci. U.S.A.* **79,** 2845–2849 (1982).
20. Bubenik, J. *et al. Int. J. Cancer* **11,** 765–773 (1973).
21. Marshall, C. J., Franks, L. M. & Carbonell, A. W. *J. natn. Cancer Inst.* **58,** 1743–1747 (1977).
22. Goldfarb, M., Shimizu, K., Perucho, M. & Wigler, M. *Nature* **296,** 404–409 (1982).
23. Shih, C. & Weinberg, R. A. *Cell* **29,** 161–169 (1982).
24. Lautenberger, J. A., Schulz, R. A., Garon, C. F., Tsichlis, P. N. & Papas, T. S. *Proc. natn. Acad. Sci. U.S.A.* **78,** 1518–1522 (1981).
25. Souza, L. M., Komaromy, M. C. & Baluda, M. A. *Proc. natn. Acad. Sci. U.S.A.* **77,** 3004–3008 (1980).
26. Shalloway, D., Zelentz, A. D. & Cooper, G. M. *Cell* **24,** 531–541 (1981).
27. Srinivasan, A., Reddy, E. P. & Aaronson, S. A. *Proc. natn. Acad. Sci. U.S.A.* **78,** 2077–2081 (1981).
28. Vande Woude, G. F. *et al. Proc. natn. Acad. Sci. U.S.A.* **76,** 4464–4468 (1979).
29. Tronick, S. R. *et al. Proc. natn. Acad. Sci. U.S.A.* **76,** 6314–6318 (1979).
30. Sherr, C. J., Fedele, L. A., Oskarsson, M., Maizel, J. & Vande Woude, G. F. *J. Virol.* **34,** 200–212 (1980).
31. Robbins, K. C., Devare, S. G. & Aaronson, S. A. *Proc. natn. Acad. Sci. U.S.A.* **78,** 2918–2922 (1981).
32. Santos, E., Pulciani, S. & Barbacid, M. *Fedn Proc.* (in the press).
33. Eva, A. *et al., Nature* **295,** 116–119 (1982).
34. Lawn, R. M., Fritsch, E. F., Parker, R. C., Blake, G. & Maniatis, T. *Cell* **15,** 1157–1174 (1978).
35. Shih, T. Y., Weeks, M. O., Young, H. A. & Scolnick, E. M. *Virology* **96,** 64–79 (1979).
36. Aaronson, S. A. & Todaro, G. J. *Virology* **36,** 254–261 (1968).
37. Rasheed, S., Nelson-Rees, W. A., Toth, E. M., Arnstein, P. & Gardner, M. B. *Cancer* **33,** 1027–1033 (1974).
38. Jainchill, J. L., Aaronson, S. A. & Todaro, G. J. *J. Virol.* **4,** 549–553 (1969).
39. Peters, R. L., Rabstein, L. S., Van Vleck, R., Kelloff, G. J. & Huebner, R. J. *J. natn. Cancer Inst.* **53,** 1725–1731 (1974).
40. Harvey, J. J. *Nature* **204,** 1104–1107 (1964).
41. Scher, C. D., Scolnick, E. M. & Siegler, R. *Nature* **256,** 225–228 (1975).
42. Southern, E. M. *J. molec. Biol.* **98,** 503–517 (1975).
43. Davis, R. W., Simon, M. & Davidson, N. *Meth. Enzym.* **21,** 413–428 (1971).
44. Cox, R. A. *Meth. Enzym.* **12,** 120–129 (1967).
45. Aviv, H. & Leder, P. *Proc. natn. Acad. Sci. U.S.A.* **69,** 1408–1412 (1972).
46. Bailey, J. M. & Davidson, N. *Analyt. Biochem.* **70,** 75–85 (1976).
47. Barbacid, M., Lauver, A. L. & Devare, S. *J. Virol.* **33,** 196–207 (1980).
48. Bonner, W. M. & Laskey, R. A. *Eur. J. Biochem.* **46,** 83–88 (1974).

Synthesis and assembly of hepatitis B virus surface antigen particles in yeast

Pablo Valenzuela[*†], **Angelica Medina**[*] **& William J. Rutter**[*]

[*] Department of Biochemistry and Biophysics, University of California, San Francisco, California 94143, and [†] Chiron Corporation, 4560 Horton, Emeryville, California 94608, USA

Gustav Ammerer & Benjamin D. Hall

Department of Genetics, SK-50, University of Washington, Seattle, Washington 98195, USA

The surface antigen of hepatitis B virus (HBsAg) has been synthesized in the yeast Saccharomyces cerevisiae *by using an expression vector that employs the 5′-flanking region of yeast alcohol dehydrogenase I as a promoter to transcribe surface antigen coding sequences. The protein synthesized in yeast is assembled into particles having properties similar to the 22-nm particles secreted by human cells.*

HEPATITIS B virus[1-3] is a 42-nm particle (the Dane particle) consisting of a core containing the viral genome (~3,200 base pairs (bp) of partially single-stranded DNA[4]) bound to the core protein and its own DNA polymerase[5-9]; the virus core is surrounded by a phospholipid-containing envelope carrying the major surface antigenic determinants (HBsAg). These seem to

0028-0836/82/290347—04$01.00

reside mainly in a single protein, which occurs in both a glycosylated and non-glycosylated form (molecular weight (M_r) 27,000–29,000 and 23,000–25,000, respectively, as measured on SDS gels[10,11]). Infection with hepatitis B virus (HBV) leads not only to the production of Dane particles but also to a dramatic overproduction of 22-nm large particles and filaments (the HBsAg particle) that contain the elements of the surface envelope. These HBsAg particles are about 1,000-fold more immunogenic than the unassembled HBsAg protein[12]. Because of its narrow host range (humans and chimpanzees), and as it cannot be propagated in tissue culture, investigation of the structure and mechanism of infection of HBV has been severely restricted. The advent of molecular cloning has allowed the mplete virus genome to be cloned and sequenced[5–7,13–15], and the coding regions for the different antigens have been identified[5–7], raising the possibility of expressing HBV genes in alternative host systems. However, in previous attempts, high level production of HBsAg-related immunogenic material was not achieved in bacteria even in systems using powerful bacterial promoters[14,16,17]. We therefore examined yeast as an alternative host system; this organism has complex membrane systems and the ability to secrete and glycosylate proteins by processes resembling those observed in higher cells[18]. Recently, yeast has also been developed to give a system which allows the introduction, maintenance and expression of foreign genes[19–21]. Here we report the construction of an autonomously replicating plasmid containing HBsAg-coding sequences linked to the yeast alcohol dehydrogenase I promoter. Yeast transformed with these vectors synthesize and accumulate particulate material that specifically reacts with antibodies against HBsAg.

Construction of plasmids and expression of HBsAg in yeast

The HBsAg-coding sequence used in these studies was isolated on a 835-bp *Taq*I–*Hpa*I fragment[13,16]. This fragment contains 26 bp preceding the AUG which encodes the N-terminal methionine of mature HBsAg. It lacks the DNA sequence of 489 or 522 bp that encodes a presumptive precursor which can be deduced from the viral genomic sequence[7]. The HBsAg gene fragment was joined to the yeast alcohol dehydrogenase (ADHI) promoter as described in Fig. 1 legend. The plasmid

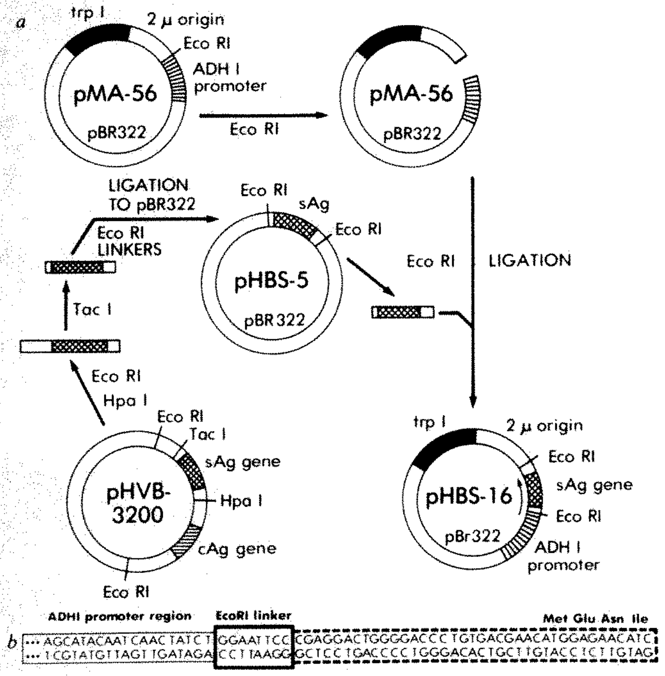

Fig. 1 *a*, Construction of plasmids for the expression of hepatitis B surface antigen in yeast. pMA-56 was constructed from YRp7 (ref. 27) by (1) removing one of its *Eco*RI sites (digestion with *Eco*RI, fill-in by DNA polymerase I Klenow fragment and blunt-end ligation); (2) replacing the yeast *ars*-1 replication origin by a *Pst*I–*Eco*RI fragment containing the replication origin of yeast 2 μ plasmid; and (3) replacing the smallest *Eco*RI–*Bam*HI of the resulting plasmids by a 1,500-bp *Eco*RI–*Bam*HI fragment containing the yeast ADHI promoter[21]. Sixty microgrammes of pHBV-3200[13] were digested with *Eco*RI and *Hpa*I, and the 1,000-bp fragment containing the surface antigen gene was isolated and digested with *Tac*I; 10 μg of the resulting 800-bp fragment were ligated to *Eco*RI linkers and cloned in the *Eco*RI site of pBR322 (pHBS-5). The *Eco*RI fragment containing the HBsAg was isolated from pHBS-5 by preparative gel electrophoresis after digestion with *Eco*RI, and ligated to pMA-56 (previously linearized by *Eco*RI and treated with bacterial alkaline phosphatase). After transformation of *E. coli* cells (RR1) and isolation of DNA by a small scale procedure[28], recombinant plasmids were analysed by cleavage with restriction endonucleases. Plasmids in which the HBsAg gene was in line with the ADHI promoter (pHBS-16), and those with these regions in the opposite orientation (pHBS-20) were amplified and used to transform strain XV610-8C *a ade2 ade6 leu2 lys1 trp1 can1* as described elsewhere[19]. *b*, DNA sequence of the ADHI–HBsAg gene junction present in pHBS-16. The sequence was obtained by the method of Maxam and Gilbert[29].

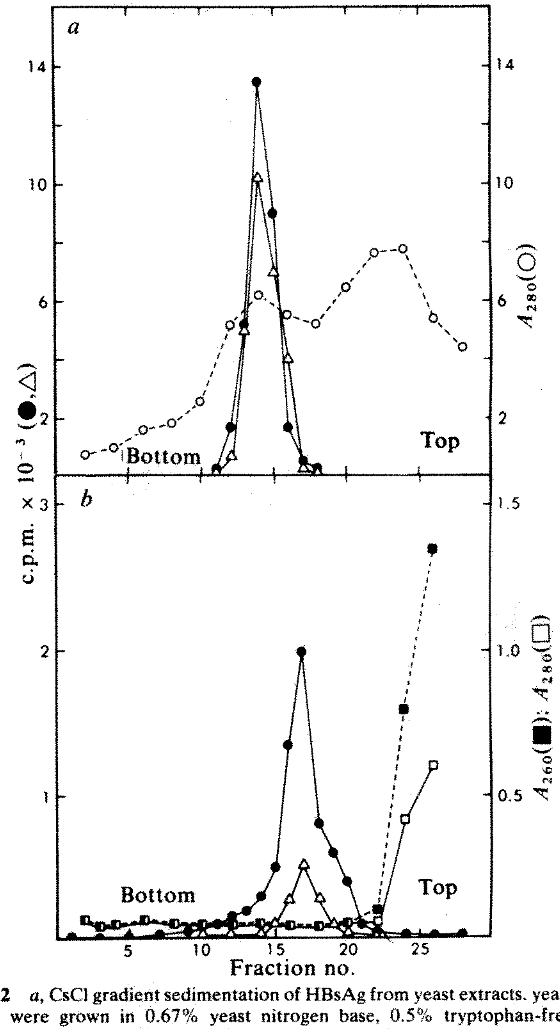

Fig. 2 *a*, CsCl gradient sedimentation of HBsAg from yeast extracts. yeast cells were grown in 0.67% yeast nitrogen base, 0.5% tryptophan-free casamino acids and 2% glucose. Cells from a 100 ml culture were pelleted, washed in 100 ml of buffer (10 mM phosphate *p*H 7.5, 0.1% Triton X-100), suspended in one volume of packed cells of the same buffer and broken by vortexing with glass beads (0.45–0.50 mm diameter). After centrifugation, a 0.5-ml aliquot of the extract was layered on to a 12 ml discontinuous 1.1–1.4 g cm^{-3} CsCl gradient in 10 mM phosphate buffer (*p*H 7.4) and run at 30,000 r.p.m. at 5 °C for 24 h in a beckman SW41 rotor. Fractions (0.5 ml) were collected from the bottom of the tube. The HBsAg activity was measured using the radioimmunoassay AUSRIA II (Abbott). The HBsAg used as standard was isolated from supernatants of PLC/PRF/5 cells[25,26]. *b*; Sucrose gradient sedimentation of HBsAg produced in yeast cells. Active fractions from the above CsCl gradient were pooled and dialysed against 10 mM phosphate buffer *p*H 7.5. A 0.5-ml aliquot was layered on to a 12 ml 5–30% sucrose gradient in 10 mM phosphate buffer containing 0.15 M NaCl and run at 33,000 r.p.m. at 5 °C for 6 h in a Beckman SW41 rotor. Fractions (0.5 ml) were collected and aliquots assayed as for *a*. A 0.5-ml sample of PCL/PRF/5 cell supernatant was used as standards in the same way. ●, Yeast; △, Alexander cells for *a* and *b*.

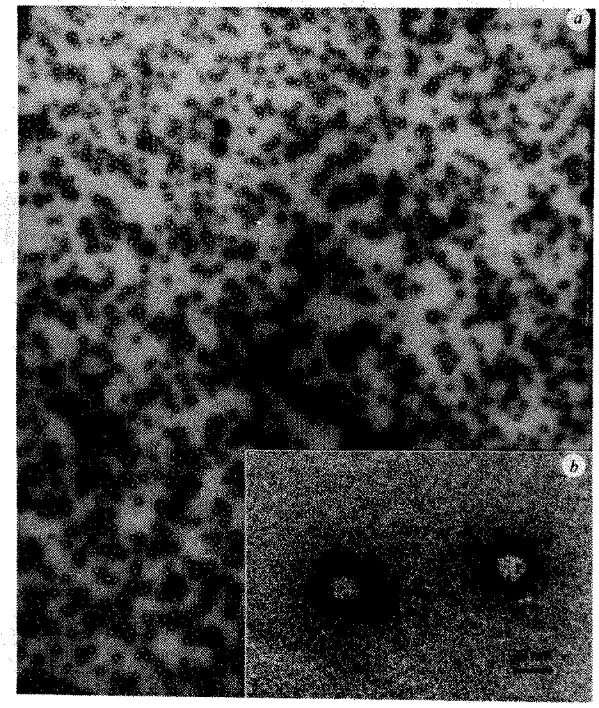

Fig. 3 Electron micrographs of HBsAg particles produced by yeast cells. *a*, Particles were purified by adsorption to a column of goat anti-HBsAg specific antibody covalently bound to Sepharose, eluted with 3 M potassium thiocyanate and visualized by negative staining with 2% phosphotungstic acid. ×25,000. *b*, Higher magnification of particles purified by a combination of CsCl and sucrose gradient sedimentation and visualized after negative staining with 2% uranyl acetate. ×250,000.

contains *Escherichia coli* vector pBR322, a replication origin derived from the yeast 2 μ plasmid, the *trp*1 gene for selection in yeast cells, and the ADHI promoter inserted into the *tet*^{r} region of pBR322. The efficacy of the ADHI promoter for expression of a linked coding sequence has recently been demonstrated by the production of interferon in this system[22]. Yeast cells (XV610-8C) were transformed by recombinant plasmids in which the HBsAg gene was placed either in the same 5′–3′ orientation as the ADHI promoter (pHBS-16) or in the opposite orientation (pHBS-20). Cell extracts from mid-log phase cultures of these strains were assayed for HBsAg by radioimmunoassay (AUSRIA II; Abbott). A substantial level of HBsAg was detected only in the cells transformed with pHBS-16; no surface antigen was observed in cells transformed with the plasmid in which the viral gene is incorrectly oriented. The amount of surface antigen protein made per 200 ml of yeast culture was ~2–5 μg, calculated from the radioimmunoassay data.

Nature of viral antigen produced in yeast

The predominant form of HBsAg produced by human cells is the so-called 22-nm particle. Its biophysical properties are well documented[23,24] and its immunological potency exceeds that of the pure protein[12]. To examine the form in which surface antigen is present in yeast, we subjected extracts to equilibrium sedimentation through a discontinuous CsCl gradient. A control tube containing HBsAg from a human hepatoma cell line (Alexander or PLC/PRF/5 cells[25,26]) was treated identically to provide a buoyant density marker. Surprisingly, HBsAg synthesized by yeast was found to band at the same density as that from the PLC/PRF/5 cell, that is, ~1.2 g cm^{-3} (Fig. 2*a*). Peak fractions of the CsCl gradient were analysed further by velocity sedimentation in sucrose gradients. Again the peak of HBsAg produced by yeast coincided exactly with HBsAg from human cells (Fig. 2*b*), which sediments at ~55S[24].

From the sedimentation data, it is apparent that HBsAg is synthesized in yeast in the form of particles or aggregates. The nature of these particles was further characterized by electron microscopy. HBsAg synthesized in yeast was purified again by a combination of sedimentation in CsCl and sucrose gradients. The immunoreactive material was adsorbed onto carbon film grids and negatively stained with uranyl acetate by Drs P. Bull and J. Garrido (Catholic University, Santiago, Chile). Alternatively, yeast HBsAg was purified by affinity chromatography and negatively stained with phosphotungstic acid by Drs G. Wampler, W. Ziegler, W. Miller and W. McAleer (Merck Sharp and Dohme Research Laboratories). When examined under the electron microscope, the yeast HBsAg preparation was found to contain particles (Fig. 3*a*,*b*) which appeared very similar to those secreted by Alexander cells. The particles purified and stained using the first method are ~20 nm in diameter. A more extensive analysis showed that the size of the purified particles eluting with 3 M ammonium thiocyanate from an affinity column is variable, the medium size being ~17 nm (W. Miller and W. McAleer, personal communication).

Preliminary tests have shown that these particles are antigenic, inducing antibodies in animal species (G. Buynak and W. McAleer, personal communication). It has been demonstrated previously[12] that integration of the HBsAg protein into a phospholipid structure to form the 22-nm particle dramatically increases its immunogenic properties. Thus the immunogenicity of the material synthesized in yeast is further evidence that its structure resembles that of the 22-nm particle.

The chemical composition of HBsAg molecules synthesized in yeast was determined by immunoprecipitation of ^{35}S-proteins labelled *in vivo* in a yeast strain transformed by the ADHI–HBsAg recombinant plasmid. SDS-gel electrophoresis of the anti-HBsAg immunoreactive material (Fig. 4) revealed a single band of apparent M_r 23,000, corresponding in size to the unglycosylated HBsAg component of PLC/PRF/5 cells[11]. No higher molecular weight bands could be detected, indicating that most of the molecules were not glycosylated in these conditions.

Conclusions

Expression of hepatitis B surface antigen coding sequences in yeast leads to the production of particles immunoreactive with anti-HBsAg antibodies. These particles are similar to those

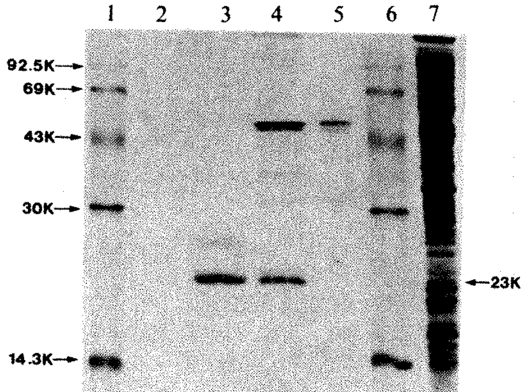

Fig. 4 Autoradiography of SDS-polyacrylamide gel of HBsAg proteins produced by yeast and PLC/PRF/5 cells. Yeast cultures and PLC/PRF/5 cells were grown in the presence of ^{35}S-methionine and ^{35}S-cysteine. Yeast cells were collected, broken by vortexing with glass beads and the resulting extracts clarified by centrifugation. Labelled HBsAg particles from PLC/PRF/5 cell supernants were concentrated by ultracentrifugation and used as a control. Proteins from yeast and PLC/PRF/5 cells were immunoprecipitated using the SAC technique[30]. Samples were run on 12.5% acrylamide gels according to Laemmli[31], subjected to fluorography[32], dried and exposed to X-ray film. Lanes 1 and 6, ^{14}C-methylated proteins as molecular weight standards: phosphorylase (92,500, 92.5K), bovine serum albumin (69K), ovalbumin (46K), carbonic anhydrase (30K) and lysozyme (14.3K); lane 2, PLC/PRF/5 cell supernatants plus normal human serum; lane 3, PLC/PRF/5 cell supernatant plus human anti-HBsAg serum; lane 4, yeast extracts from strain XV610-8C with pHBS-16 plus human anti-HBsAg serum; lane 5, yeast extracts from strain XV610-8C with pHBS-16 plus normal human serum; lane 7 aliquot of total yeast ^{35}S-labelled proteins. Numbers at the left refer to protein markers as above. The number at the right indicates the 23,000-M_r protein immunoprecipitated from yeast and PLC/PRF/5 cells.

made by human carrier patients or by a hepatoma cell line; they have identical sedimentation rates and buoyant density, suggesting a similar size and ratio of protein to lipid composition for yeast and for human particles. Electron microscopic observation established that the yeast particles are more variable in size and have a smaller mean diameter than the human particles. Furthermore, unlike the HBsAg from human cells, the yeast particle does not contain significant quantities of a higher molecular weight glycoprotein, indicating that glycosylation is required neither for the formation of the particulate structures nor for immunogenicity.

The construction we have used in the HBsAg-expressing plasmid eliminates that part of the gene encoding the leader peptide of putative pre-HBsAg[7]. Therefore, formation of particles in yeast implies that the polypeptide sequence of the surface antigen molecule contains the requisite instructions for assembly of apparently normal particles within the cytoplasmic milieu of the yeast cell. The leader region and other possible precursors formed by its translation are not required for the formation of this structure. Furthermore, no other hepatitis gene products or liver-specific cell products are necessary to form the particulate structure. It seems likely, therefore, that such particles can be formed in many other heterologous cell systems, perhaps even in bacteria. It remains to be determined where within the yeast cell the 22-nm particle is assembled, and what biochemical processes accompany it. An immediate advantage of the yeast system is that the physiological and genetic requirements for particle assembly may be systematically explored, making use of yeast mutants conditionally defective for the secretory pathway[18] and for other aspects of cellular metabolism.

The similarity in structure of the yeast particle to bona fide 22-nm particles and the high immunogenicity in animals emphasize the possible value of the HBsAg particle as a vaccine. The yeast HBsAg particles can in principle be produced in large quantities for this purpose. Further, the complete absence of intact HBV and/or human proteins in such preparations eliminates the possibility of secondary infections or autoimmunity problems as a result of the vaccine.

Finally, our findings illustrate the versatility of recombinant DNA methodology for the production of complex structures. Previously, recombinant DNA techniques as applied to microorganisms have only been used to produce simple proteins like insulin, growth hormone, interferon and enzymes. Our experiments suggest that more complicated structures can be formed in alternative hosts like yeast provided the genes for the requisite organizing proteins are introduced and efficiently expressed. This offers an effective approach for the analysis of organelles in higher organisms.

We thank P. Bull, J. Garrido and B. Wolanski, R. Ziegler, W. Miller and W. McAleer for the electron microscopic analysis; L. Rall for the preparation of ^{35}S-labelled HBsAg particles from PLC/PRF/5 cells; and M. Worthington and S. Bektech for the construction of pMA-56. This research was funded by grants from Merck Sharp and Dohme Research Laboratories. G.A. was supported by a grant from the Max Kade Foundation.

Note added in proof: Since the submission of this paper, particles containing a different HBV protein, the virus core antigen, have been reported in *E. coli* carrying a recombinant plasmid[33].

Received 2 March; accepted 25 May 1982.

1. Vyas, G. N., Cohen, S. N. & Schmid, R. (eds) *Viral Hepatitis. A Contemporary Assessment of Etiology, Epidemiology, Pathogenesis and Prevention* (Franklin Institute Press, Philadelphia, 1978).
2. Zuckerman, A. J. *J. Tox. envir. Hlth* **5,** 275–280 (1979).
3. Prince, A. M. *Hepatology* **1,** 73 (1981).
4. Summers, J., O'Connell, A. & Millman, I. *Proc. natn. Acad. Sci. U.S.A.* **72,** 4597–4601 (1975).
5. Pasek, M. *et al. Nature* **282,** 575–579 (1979).
6. Galibert, F., Mandart, E., Fitoussi, F., Tiollais, P. & Charnay, P. *Nature* **281,** 646–650 (1979).
7. Valenzuela, P., Quiroga, M., Zaldivar, J., Gray, P. & Rutter, W. J. in *Animal Virus Genetics* (eds Fields, B. N., Jaenisch, R. & Fox, C. F.) 55–77 (Academic, New York, 1980).
8. Robinson, W. S. & Greenman, R. C. *J. Virol.* **13,** 1231–1236 (1974).
9. Hruska, J. F. & Robinson, W. S. *J. med. Virol.* **1,** 119–124 (1977).
10. Shih, J. W. K. & Gerin, J. L. *J. Virol.* **21,** 1219–1222 (1977).
11. Peterson, D. L. *J. biol. Chem.* **256,** 6975–6983 (1981).
12. Cabral, G. A. *et al. J. gen. Virol.* **38,** 339–350 (1978).
13. Valenzuela, P. *et al. Nature* **280,** 815–819 (1979).
14. Burrell, C. J., Mackay, P., Greenway, P. J., Hofschneider, P. H. & Murray, K. *Nature* **279,** 43–47 (1979).
15. Sninsky, J. J., Siddiqui, A., Robinson, W. S. & Cohen, S. N. *Nature* **279,** 346–348 (1979).
16. Edman, J. C., Hallewell, R. A., Valenzuela, P., Goodman, H. M. & Rutter, W. J. *Nature* **291,** 503–506 (1981).
17. Mackay, P. *et al. Proc. natn. Acad. Sci. U.S.A.* **78,** 4510–4514 (1981).
18. Novick, P., Field, C. & Schekman, R. *Cell* **21,** 205–225 (1980).
19. Beggs, G. D. *Nature* **275,** 104–109 (1978).
20. Petes, P. D. *A. Rev. Biochem.* **49,** 845–876 (1980).
21. Ammerer, G., Hitzeman, R. A., Hagie, F. E., Barta, A. & Hall, B. D. *Recombinant DNA, Proc. 3rd Cleveland Symp. Macromolecules* (ed. Walton, A. G.) 185–197 (Elsevier, Amsterdam, 1981).
22. Hitzeman, R. A. *et al. Nature* **293,** 717–722 (1981).
23. Gerin, J. L., Purcell, R. H., Hoggan, M. D., Holland, P. V. & Chanock, R. M. *J. Virol.* **4,** 763–768 (1969).
24. Gerin, J. L., Holland, P. V. & Purcell, R. H. *J. Virol.* **7,** 569–576 (1971).
25. Macnab, G. M., Alexander, J. J., Letcasas, G., Bey, E. M. & Urbanowicz, J. M. *Br. J. Cancer* **34,** 509–515 (1976).
26. Alexander, J. J., Bey, E. M., Geddes, E. W. & Letcasas, G. *S. Afr. med. J.* **50,** 2124–2128 (1976).
27. Tschumper, G. & Carbon, J. *Gene* **10,** 157–166 (1980).
28. Birnboim, H. C. & Doly, J. J. *Nucleic Acids Res.* **7,** 1513–1523 (1979).
29. Maxam, A. M. & Gilbert, W. *Meth. Enzym.* **65,** 490–565 (1980).
30. Martial, J. A., Hallewell, R. A., Baxter, J. D. & Goodman, H. M. *Science* **205,** 602–607 (1979).
31. Laemmli, U. K. *Nature* **227,** 680–685 (1977).
32. Bonner, W. M. & Laskey, R. A. *Eur. J. Biochem.* **46,** 83–88 (1974).
33. Cohen, B. J. & Richmond, J. E. *Nature* **296,** 677–678 (1982).

LETTERS TO NATURE

Evidence for an oblique magnetic solar rotator

D. O. Gough

Institute of Astronomy, Madingley Road, Cambridge CB3 0HA, UK

The observation by Claverie *et al*[1]. of fine structure in the peaks in the power spectrum of low-degree 5-min solar oscillations has been interpreted as being a result of rotational splitting. Claverie *et al*.[1] claim that their measurements imply that an appropriately weighted average $\bar{\Omega}$ of the interior angular velocity $\Omega(r)$ of the Sun is about twice the value of Ω at the surface. At first sight their claim looks doubtful, because all $2l+1$ components of the set of modes of degree l appear in the spectrum, whereas only $l+1$ of them should be detectable. However, Isaak[2] has recently speculated that the additional components are produced by an intense rotating magnetic core, such as had been postulated by Dicke[3],[4] to account for the 12.2-day periodic component in the Princeton oblateness data[5-9]. Isaak[2] pointed out that the mean period $2\pi/\bar{\Omega} \simeq 15$ days of the solar interior that was inferred from the Birmingham data[1] is consistent with a central core rotating with the 12.2-day period and an outer envelope rotating with the photosphere. Moreover, his rough estimate of a few megagauss for the r.m.s. magnetic field that is required to support his conjecture is within about a factor 10 of that required by Dicke[3]. Thence he concluded that the Birmingham data[1] provide the first clear empirical evidence for an intense internal solar magnetic field. Here I examine this evidence in more detail, and show that the conclusion is premature. If the magnetic core does exist, the 5-min oscillations provide no clear evidence that it is rotating rapidly. Furthermore, unless one accepts a contrived magnetic-field configuration, an explanation for the $2l+1$ components of the multiplets is still lacking.

With respect to spherical polar coordinates (r, θ, ϕ) about any axis, the linear eigenfunctions of oscillation of a spherically symmetrical star of radius R are separable in radial and angular coordinates. For example, the radial component δr of the dis-

0028-0836/82/290350—05$01.00

placement eigenfunction can be written:

$$\delta r(\mathbf{r}, t) = Re[\xi(r) P_l^m(\cos\theta)\, e^{im\phi - i\omega t}], \qquad |m| \leq l \tag{1}$$

where P_l^m is the associated Legendre function. For any given value of the degree l, there is a discrete set of modes. Each mode in the set is labelled by an integer n, called the order of the mode, which is equal to the number of zeros of $\xi(r)$ for $0<r<R$, $(0\leq r<R$ when $l=0)$, except possibly when n is small. The frequencies of the p modes, which are the subject of this discussion, increase with n.

The degree l measures the total horizontal wavenumber. The angular order m measures its azimuthal component about the coordinate axis. Unlike m, l is independent of the orientation of the coordinate axis; indeed, any spherical harmonic of degree l transforms under coordinate rotations into a linear combination of the harmonics of that degree. Evidently the eigenfrequencies of a spherically symmetrical star cannot depend on the orientation of the axis. Therefore the frequencies ω and eigenfunctions $\xi(r)$ are independent of m.

Unless $m = 0$, the representation (1) is of a wave propagating about the axis with angular phase speed $m^{-1}\omega$. Since ξ and ω are independent of m, it is possible to combine two such waves with equal and opposite m to form a standing wave.

By comparing with theory the power spectra of the observed low-degree oscillations[1,10–17] it has been possible to identify the modes. In particular, the modes isolated by Claverie *et al.*[1] lie in the range: $0\leq l\leq 2$, $16\leq n\leq 27$. For this discussion, the values of n are sufficiently large for asymptotic theory[18,19] to be adequate. Furthermore, it is sufficient to assume the oscillations to be adiabatic, with ξ and ω real.

Any deviation of the equilibrium state of the star from spherical symmetry is liable to destroy the simple structure of the eigenfunctions exhibited in equation (1). In the Sun it is known that symmetry is broken by rotation. It is also broken by magnetic fields. The effect on the eigenfrequencies is to split the degeneracy with respect to m. The question under investigation here is whether the splitting that has been observed in the Sun compels us to conclude that strong magnetic fields are present.

Let us consider first the effect on the modes of rotation alone. Viewed from a coordinate frame rotating with angular velocity Ω_0 about the rotation axis of the Sun, and granted that the solar angular velocity Ω measured in an inertial frame is small, the principal modifications to the motion that arise are due to Coriolis forces and advection of the wave pattern by the relative angular velocity $\Omega-\Omega_0$. For high-order p modes the Coriolis effect is small; by substituting the appropriate asymptotic form[19] for the eigenfunction into equations (7), (8) of ref. 20 it can be shown that advection augments the frequency by approximately

$$\Delta\omega = mI^{-1}\int_0^R c^{-1}(\Omega-\Omega_0)\,\mathrm{d}r \equiv m(\bar{\Omega}-\Omega_0) \tag{2}$$

where

$$I=\int_0^R c^{-1}\,\mathrm{d}r \tag{3}$$

and c is the sound speed in the equilibrium state. Here it has been assumed that Ω is a function of r alone. Thus, with respect to an inertial spherical polar coordinate system about the rotation axis, the total frequency is

$$\omega = \omega_0 + m\Omega_0 + \Delta\omega = \omega_0 + m\bar{\Omega} \tag{4}$$

where ω_0 is the frequency of the corresponding mode of an equivalent nonrotating star[17]. Notice that $\bar{\Omega}$ is independent of m. Therefore the frequencies of the modes of given degree l and order n are uniformly spaced, with separation $\bar{\Omega}$. In particular, it follows from equation (4) that any standing wave pattern formed by a superposition of rotationally split modes precesses without dispersion about the rotation axis of the Sun with angular velocity $\bar{\Omega}$. In the frame of the standing wave, frequency is independent of m.

This behaviour is modified when one acknowledges that Ω is really a function of both r and θ. The splitting is no longer precisely uniform, because modes with different values of m sample the latitudinal variation of Ω differently. For example, if the angular velocity of the Sun is approximated by $\Omega(r)$ $(1-\alpha\cos^2\theta)$ with α constant and positive, the high-order p-mode eigenfrequencies can be shown to be

$$\begin{aligned}\omega &= \omega_0 + m\left\{1-\frac{\alpha}{2}(2l+1)\frac{(l-|m|)!}{(l+|m|)!}\int_{-1}^{1}[\mu P_l^m\mu)]^2 d\mu\right\}\bar{\Omega}\\ &\equiv \omega_0 + m\beta\bar{\Omega}\end{aligned} \tag{5}$$

Thus as $|m|$ increases at fixed l the splitting increases, because the eigenfunctions become more concentrated towards the more rapidly rotating equator. The concentration is accentuated as l increases, and the mean spacing, which is $[1-(2l+3)^{-1}\alpha]\bar{\Omega}$, approaches $\bar{\Omega}$ as $l\rightarrow\infty$. However, when l is small the variation is also small: taking $\alpha\simeq 0.2$ yields a splitting between quadrupole modes with $m=1$ and $m=2$ only 6% greater than the splitting between those with $m=0$ and $m=1$, and roughly equal to the splitting of the dipole modes.

According to Claverie *et al.*[1], the major peaks in the power spectrum of their data are either single, or split into approximately uniformly spaced triplets or quintuplets. The mean spacing of the triplets is ~0.67 μHz synodic, and that of the quintuplets, which are less clearly resolved, is ~25% greater. The overall mean spacing is 0.75 μHz.

The signal obtained by Claverie *et al.* is a measure of the time-varying shift in a solar spectrum line. The light is integrated over the entire solar disk[20]. Therefore, if the solar rotation axis were perpendicular to the line of sight, pure modes for which $l+m$ is odd could not contribute to the signal. This follows directly from the symmetry properties of tesseral harmonics. Thus, of all the modes of degree l, no more than $l+1$ of the $2l+1$ possible values of m should be detected. At the time of the observations the Sun's axis was tilted from the plane of the sky by about 6°. As pointed out by Isaak[2], this is insufficient to have produced a detectable signal from the otherwise invisible modes, unless of course, modes with odd $l+m$ systematically have 10 times the amplitude of the others.

If one were to assume with Claverie *et al.*[1] that the fine structure in the Birmingham power spectrum is rotational splitting, the most naive interpretation would be that the triplets correspond to $l=2$ and the quintuplets to $l=4$. Then the mean splitting between adjacent components of the multiplets would be $2\beta\bar{\Omega}\simeq 2\bar{\Omega}$, implying a mean interior rotation rate of ~0.38 μHz. This is similar to the rotation rate of the photosphere, which is 0.42 μHz synodic at the equator.

This interpretation faces several difficulties, such as the problem of explaining why doublets presumed to be associated with dipole modes (to which the observations are most sensitive[17]) are not prominent in the spectrum. But most important is that it is contradicted by the mode identification made previously[1,10,13–15], which depends on the qualitative structure of the patten apparent in the frequencies of the modes[13–18,21]. That pattern, which repeats as n increases, consists of approximately uniformly spaced groups of modes, of alternately odd and even degree. It is a basic signature of the eigenvalues of the wave equation that describes asymptotically high-order modes in any spherically symmetrical system. Though the absolute values of the theoretical eigenfrequencies are dependent on the solar model, the pattern in which they are distributed is a basic geometrical property. It is a consequence of the fact that the Sun is essentially a sphere (and not, for example,

Table 1 Frequencies of high-order dipole p modes in a rotating magnetic star

m'	$m=-1$	$m=0$	$m=+1$
0	$\omega_0+\delta_0\omega-\beta\bar{\Omega}$	$\omega_0+\delta_0\omega$	$\omega_0+\delta_0\omega+\beta\bar{\Omega}$
1	$\omega_0+\delta_1\omega-\beta\bar{\Omega}$	$\omega_0+\delta_1\omega$	$\omega_0+\delta_1\omega+\beta\bar{\Omega}$

a cube). Therefore, whilst one might suspect that n has been incorrectly assigned, the identification of l is robust: the triplets found by Claverie *et al.* have $l=1$, and the quintuplets $l=2$. So why is it that there are more components in the observed spectrum than should be expected?

Of course, all the components would be detectable if the solar interior were rotating about an axis that is inclined to that of the photosphere. In that case, because it would be quite unlikely that the axis of mean rotation would precess about the photospheric axis with the same angular velocity as the Earth's orbital rotation about the Sun, the relative heights of the rotationally split components in the power spectrum would be modulated on a time scale of a year. This could be checked by observation.

The presence of the central dipole component strongly suggests to Isaak[2] the existence of a perturbation which is inclined at a large angle from the axis of material rotation, and which precesses about it. Isaak contends that this perturbation is produced by an internal oblique magnetic rotator of a kind proposed previously by Dicke[3,4].

Both the magnetic effects and the rotational effects are small, producing frequency changes of $<0.1\%$. Therefore, as Isaak[2] acknowledged, it is quite adequate to linearize about the nonrotating nonmagnetic state, and treat the two perturbations separately. To this end it is conceptually convenient to work in a frame S' rotating with the magnetic field, say with angular velocity Ω_0, and transform to the inertial frame later. In S' the equilibrium state is steady, and the oscillations about that state can be described by eigenfunctions that are separable in space and time. I shall assume, with Dicke[3], that the field has an axis of symmetry, in a direction (Θ, Φ) with respect to an inertial coordinate system S whose axis coincides with the axis of rotation. The axis of magnetic symmetry is taken as the axis of spherical polar coordinates (r, θ', ϕ') in S'. With respect to these coordinates the angular order of a mode will be denoted by m'.

Perturbation theory for magnetic stars has been developed by Ledoux and Simon[22], and subsequently by Goossens[23]. Both the equilibrium state and the normal modes of oscillation are expanded in powers of a parameter λ, which characterizes the strength of the Lorentz force in relation to the pressure gradient; it measures both the deviation from spherical symmetry of the equilibrium configuration and the perturbation to the eigenfrequencies. In the Sun λ is small: if, for example, the magnetic field is confined to the core, and has intensity 5×10^7G, then $\lambda \simeq 10^{-3}$. Since the postulated magnetic field is buried in the solar interior, singular perturbations in the surface layers[24,25] are of no consequence.

Consider first the perturbation to the shape of the dipole wave pattern. Formally, the most striking effect of the magnetic field is to resolve the degeneracy in the eigenfunctions. The dipole oscillations are separated into three well-defined modes, however weak the field. But that does not change the number of peaks in the power spectrum. A new peak associated with the $m=0$ mode resulting from a modification to the geometry of the wave pattern can come about only by coupling to a mode of even degree l^*. If ω^* is the frequency of free oscillation of the coupled mode that is nearest to ω, the ratio of the amplitude of the coupled mode to that of the dipole mode is of order $\sigma = \min(1, \lambda\omega/|\omega-\omega^*|)$. If $l^*=0$ or $l^*=2$, $|\omega-\omega^*| \simeq 70$ μHz. Then $\sigma \simeq 40\lambda$, which is probably too small for the coupled mode to be detected. If $l>2$ it is conceivable that a chance resonance could make $\sigma = 0(1)$, but in that case the sensitivity of the observations is too low to account for the observed central peak[17]. Similar arguments apply to the quadrupole modes. Therefore the most significant influence the magnetic field is likely to exert is to change the speeds of propagation of the waves.

At this juncture it should be pointed out that any standing dipole mode has an axis of symmetry, and can be represented as a linear combination of the three modes with $l=1$. If somehow that pattern could be caused by the rotating magnetic field to rotate with angular velocity Ω_1 about the axis of the inertial frame S, the sole effect would be to augment the frequencies of the three components in S by $m\Omega_1$. After adding the effect of material rotation, the frequencies of the modes would become $\omega_0 + m(\Omega_1 + \bar{\Omega})$. This, of course, is completely analogous to, and observationally indistinguishable from, rotational splitting, and therefore could not introduce another component to the power spectrum.

The effect of the magnetic field $\mathbf{B}$, however, is not to induce a simple rotation of a standing mode. Because the Lorentz force is quadratic in the field, changing the sign of $\mathbf{B}$ has no effect. Hence there is no distinction between waves propagating positively and negatively about the axis of symmetry. Though frequency changes can depend on the magnitude of m', they cannot depend on its sign. In S', combinations of modes with like $|m'|$ yield standing waves that do not precess; but unlike rotationally split modes, the frequency splitting is sensitive to m', at least when l is small. It is an immediate corollary that to leading order in λ the frequencies observed are not influenced by the angular velocity of the buried magnetic field configuration: as is evident in equation (4), after adding the effect of rotation and transforming to the inertial frame (or, for that matter, to any other rotating frame that does not depend on Ω_0, such as the frame rotating with the Earth), Ω_0 cancels.

It is not inconceivable, however, that an observable dipole triplet could be induced by a magnetic field. Let us represent any mode of degree l by a superposition of the modes in S' of degree l and angular orders m'. Then the effect of the field is to augment the frequencies by $\delta_{m'}\omega$, say, where $\delta_{-m'}\omega = \delta_{m'}\omega$. After transforming the modes to S, and adding the effect of rotation, each component (l, m) is found to have multiple frequencies. These are listed in Table 1 for the dipole modes. Since in this case the $m=0$ modes cannot be detected, there are four frequencies that should appear in the spectrum. It is possible, however, to reduce these to a triplet, if the two inner components have identical frequencies. This occurs if

$$|\delta_1\omega - \delta_0\omega| = 2\beta\bar{\Omega} \qquad (6)$$

The frequency splitting is then $2\beta\bar{\Omega}$, which is again consistent with almost uniform rotation.

The hypothesis raises several issues. For example, condition (6) is a relationship between the magnetic field and the rotation, and was engineered to force agreement with observation. If it were satisfied in the Sun, it would be unlikely to be accidental. We know, of course, that there is a dynamical connection between Ω and $\mathbf{B}$. But why should it be such that particular oscillation frequencies coincide, especially since the energy in the oscillations is very much less than the field energy? Moreover, we must acknowledge that $\delta_{m'}\omega$ might vary with frequency, and question whether equation (6) can be satisfied sufficiently well by all the relevant modes. The observations would therefore set limits on how rapid the variation could be. There are also further conditions, analogous to equation (6), to be explained. They arise from demanding that quadrupole modes are split into only quintuplets. These would constrain Ω and $\mathbf{B}$ further.

It is also of interest to compare the amplitudes of the components of the multiplets. It can be shown that if the three dipole modes in S' have r.m.s. displacement amplitudes $A_{m'}$ in the atmosphere, the mean squared amplitudes in S, in ascending or descending order of frequency according to whether $\delta_1\omega$ is

Table 2 Frequency shifts (μHz) of those high-order solar quadrupole p modes that can be detected by whole-disk observations

m'	$m=-2$	$m=0$	$m=+2$
0	0.91	1.68	2.45
1	3.08	3.85	4.62
2	1.56	2.33	3.10

Observations are referred to a frame rotating with the Earth about the Sun and computed assuming the presence of a toroidal magnetic core chosen so as to reduce the dipole quadruplet to a triplet. Rotational splitting was computed from equation (5) with $\alpha = 0.2$.

greater or less than $\delta_0\omega$, should be in the ratios

$$A_0^2 \sin^2\theta :$$
$$A_0^2 \sin^2\theta + \tfrac{1}{2}(A_1^2 + A_{\bar{1}}^2)(1 - \tfrac{1}{2}\sin^2\theta) :$$
$$\tfrac{1}{2}(A_1^2 + A_{\bar{1}}^2)(1 - \tfrac{1}{2}\sin^2\theta) \tag{7}$$

Because the whole-disk observations are equally sensitive to modes with $m = -1$ and $m = +1$, these represent the ratios of the power in each peak of the triplet. Note that whatever the values of $A_{m'}$ and θ, the power in the central peak is the sum of the powers in its two neighbours. This appears not to be in accord with observation[1].

The magnetic core postulated by Dicke[3,4] is presumed to have been formed by field stretching produced by the differential rotation. This created an essentially toroidal field, about an axis which subsequently departed from the Sun's rotation axis, in a manner that has been discussed by Mestel *et al.*[26–28]. Now it lies almost in the equatorial plane, with $\theta = 86°$. I approximate the magnetic field by

$$\mathbf{B} = (0, 0, B(r)\sin\theta'\cos\theta') \tag{8}$$

without questioning its stability. This is the form originally adopted by Dicke[3], though a subsequent analysis of the oblateness data suggests a more complicated configuration[29].

The perturbations $\delta_{m'}\omega$ generated by $\mathbf{B}$ can be computed using Goossens's analysis[23]. In the limit of high-order p modes the result is

$$\delta_{m'}\omega \sim \frac{(2l+1)}{u(R)}\frac{(l-|m'|)!}{(l+|m'|)!}\left[\!\!\left[\int_0^R \left\{a\left[\frac{\mathrm{d}}{\mathrm{d}r}(r\xi B)\right]^2 + bm'^2\xi^2B^2\right\}\mathrm{d}r \right.\right.$$
$$\left.\left. - \frac{\omega}{4\pi}\int_0^R \mathrm{d}r\int_0^\pi c^{-1}(c_1^2 - \varepsilon)[P_l^{m'}(\cos\theta')]^2\sin\theta'\,\mathrm{d}\theta'\right]\!\!\right] \tag{9}$$

where

$$u = \int_0^r c^{-1}\,\mathrm{d}r \tag{10}$$

$$\xi = r^{-1}\rho^{-1}c^{-1}u^{1/2}J_{l+3/2}(\omega u) \tag{11}$$

$$a(l, m) = \int_{-1}^{1} [P_l^{m'}[(\mu)]^2\mu^2(1-\mu^2)\,\mathrm{d}\mu,$$

$$b(l, m') = \int_{-1}^{1} [P_l^{m'}(\mu)]^2\mu^2\,\mathrm{d}\mu \tag{12}$$

$\rho(r)$ is the density of the equilibrium model in the absence of $\mathbf{B}$, and J_ν is the Bessel function of the first kind. The variable c_1^2 is the small θ'-dependent part of the square of the adiabatic sound speed in the equilibrium configuration, measured in units of c^2, and $\varepsilon(\theta')$ is such that $r = (1+\varepsilon)R$ defines the equilibrium photosphere. The first integral in equation (9) represents the direct effect of the Lorentz force on the oscillations, and the second integral results from the axisymmetrical distortion to the equilibrium state.

It can now be argued that an intense large-scale magnetic field cannot pervade the entire radiative region of the Sun. If there were such a field, all the terms in the integrals in equation (9) would be of roughly the same magnitude. According to Dicke[3–9] ε is of order 3×10^{-5}, and according to Hill *et al.*[28] it must be even smaller. This sets an upper limit to the intensity of the magnetic field. It implies that the magnitude of $\delta_{m'}\omega$, to within a factor of order unity, can be no larger than $3\times10^{-5}\omega$, which is too small for equation (6) to be satisfied.

The distortion associated with a field confined to the core is relatively small at the photosphere. This permits the field to be stronger without it being ruled out by the oblateness measurements. Can it be strong enough to produce the frequency shift required? Note first that the contribution to $\delta_{m'}\omega$ from the distortion of the equilibrium structure is proportional to ω. Therefore, if that term dominated, it would not be possible to satisfy equation (6) over the entire frequency range. Admittedly, a variation of only 30% in ω is sufficient to encompass half the power in the spectrum of the 5-min modes, and such a variation in the splitting cannot convincingly be ruled out by the published data[1]. Nevertheless, in anticipation that cleaner results will be obtained in the future, I shall simplify the analysis by ignoring the second integral. Moreover, I shall choose a field amplitude $B(r)$ to render the first integral only weakly dependent on ω.

In the core, the major variation of ξ is produced by the Bessel function. Its argument is proportional to ω, and, in particular, the radius of the first node is roughly inversely proportional to ω. Since B is independent of ω, and ξ and B occur in the expression for $\delta_{m'}\omega$ only in the combination ξB, it follows that $\delta_{m'}\omega$ is stationary with respect to ω when ξ and B overlap maximally, in an appropriate sense. Therefore the variation of $\delta_{m'}\omega$ with ω can be made weak if B and ξ are similar functions at the median frequency $\bar{\omega}$. As an example, I choose

$$B(r) = \begin{cases} B_0 r\rho c u^{-1/2}J_{5/2}(\bar{\omega}u), & \bar{\omega}u \leqslant j_{5/2} \\ 0, & \bar{\omega}u \geqslant j_{5/2} \end{cases} \tag{13}$$

with $\bar{\omega}/2\pi = 3$ mHz and B_0 constant. Here j_ν is the first zero of J_ν. The factors in front of the Bessel function were chosen just for analytical convenience. The function $B(r)$ has a single maximum, near $r \simeq 0.14R$, and falls to zero at $r \simeq 0.22R$.

It is a straightforward matter to evaluate the frequency shifts $\delta_{m'}\omega$, and hence compute B_0 by insisting that the constraint (6) be satisfied at $\omega = \bar{\omega}$. The result is such that the maximum value of $B(r)$ is 1.1×10^8 G, which implies a total field energy of 3.5×10^{45} erg. This is to be compared with a similar field suggested by Dicke[3], which had been chosen to explain his oblateness data. That field extends to $r \simeq 0.33R$ and has a maximum value of 6.1×10^7 G at $r \simeq 0.16R$. Dicke does not exhibit the radial dependence of his field precisely, but if it were taken to be homologous to $B(r)$, the energy would be 3.6×10^{45} erg. Such a field is apparently incompatible with the oblateness data of Hill *et al.*[28].

The stationary value of the first integral in equation (9), with respect to variations in ω, is a minimum. Consequently, amongst function B generated from equation (13) by varying $\bar{\omega}$ and B_0 such as to preserve equation (6), 1.1×10^8 G is a maximum of the field strength.

Consider now the quadrupole modes. With respect to the coordinate system in S, only modes with $m = 0$ and $m = \pm2$ should be detectable in the whole-disk data. As with the dipole modes, the frequencies are split by rotation. Furthermore, the magnetic field splits the frequencies for each value of m in to three, corresponding to the three different values of $|m'|$. Consequently, there are nine, not five potentially observable components in the power spectrum. Table 2 lists the synodic deviations of those nine frequencies from ω_0, computed with that value of B_0 that reduces the dipole frequencies to a triplet. Note that there are three pairs of frequencies that are too close to have been resolved by Claverie *et al.* Thus there should be no more than six observable components, with median frequencies 0.91, 1.62, 2.39, 3.09, 3.85, 4.62 μHz above ω_0. These frequencies are nearly uniformly distributed, with a mean spacing of 0.74 μHz.

The coincidences of some of the quadrupole frequencies arise because the magnetic splittings $\delta_{m'}\omega - \delta_{m'-1}\omega$ of the modes are roughly integral multiples of the dipole splitting. The difference between the dipole and quadrupole eigenfunctions ξ is not very great in the core, so the integral of $[\mathrm{d}(r\xi B)/\mathrm{d}r]^2$ in particular is similar for the two values of l. That integral exceeds the integral of ξ^2B^2 by a factor of ~10. Therefore the near commensurability of the splittings is largely a product of the properties of the spherical harmonics, and is not dependent on the detailed structure of the function $B(r)$. Thus if the magnetic field in the solar core is intense enough to produce observable splitting, and is such as to reduce the expected dipole quadruplet to a triplet, then it is likely that the quadrupole frequencies constitute only a sextuplet, with a mean separation that is roughly the same as for the dipole triplet.

I have shown that some aspects of the Birmingham data might be rationalized if the Sun were to have an intense magnetic core; so might the Princeton oblateness data. However, that does not imply that the magnetic core exists. Aside from the contradiction by the oblateness measures of Hill *et al.*[30], there would be disturbing conflicts with certain properties of the oscillations. These may eventually be decisive. The incorrect ratios of the amplitudes of the dipole triplet, for example, would demand explanation, as would the absence of a component of the predicted quadrupole sextuplet. In superposed spectra such as those presented by Claverie *et al.*[1], it is hardly likely that some peaks are removed by interference. Nevertheless, there is the possibility that a magnetic field configuration rather different from that considered here could produce a quintuplet. Notice that in that case the splitting would still be $2\beta\Omega$, implying $\bar{\Omega} \simeq \Omega(R)$.

The high energy in the magnetic field would also need explaining. That energy is probably 50 or more times greater than the kinetic energy in the solar rotation today, though when the intense field was presumed to have been created the rotational energy may have been more than 1,000 times greater than its present value. Nevertheless, it would still be necessary to demonstrate that the regeneration of magnetic field by the differential rotation of the core, if it occurs, is sufficient to balance dissipation by instabilities.

And finally, what of the rotation itself? The potential explanation of the dipole triplet discussed here requires that the mean solar angular velocity, weighted by the reciprocal of the sound speed, is hardly different from the surface value. That is not easy to reconcile with the 12.2-day period of the core required by Dicke to explain the periodic component in his oblateness data. Moreover, it appears to be contradicted by the analyses of apparent rotational splitting inferred from oscillations in the limb-darkening function[31,32], which suggests that Ω is some six times greater at the centre of the Sun than it is at the surface. The condition $\bar{\Omega} \simeq 2\Omega(R)$ claimed by Claverie *et al.*[1] and Isaak[2] is not inconsistent with that result. Thus it seems likely that the solar magnetic field is not strong enough to have produced the splitting required to satisfy equation (6). Therefore the explanation for the fine structure in the whole-disk power spectrum needs still to be found and demonstrated, and until that is accomplished one cannot be confident that the separation of the multiplets results solely from rotational splitting.

Received 26 March; accepted 4 June 1982.

1. Claverie, A., Isaak, G. R., McLeod, C. P. & van der Raay, H. B. *Nature* **293,** 443–445 (1981).
2. Isaak, G. R. *Nature* **296,** 130–131 (1982).
3. Dicke, R. H. *Proc. Informal Conf. on Status and Future of Solar Neutrino Research* Vol. 2 (ed. Friedlander, G.) 109–143 (Brookhaven National Laboratory, Upton, 1978).
4. Dicke, R. H. *New Scient.* **83,** 12–14 (1979).
5. Dicke, R. H. & Goldenberg, H. M. *Astrophys. J. Suppl.* **27,** 131–182 (1974).
6. Dicke, R. H. *Phys. Rev. Lett.* **37,** 1240–1242 (1976).
7. Dicke, R. H. *Solar Phys.* **47,** 475–515 (1976).
8. Dicke, R. H. *Proc. natn. Acad. Sci. U.S.A.* **78,** 1309–1312 (1981).
9. Dicke, R. H. *Proc. natn. Acad. Sci. U.S.A.* **78,** 1989–1993 (1981).
10. Grec, G., Fossat, E. & Pomerantz, M. *Nature* **288,** 541–544 (1980).
11. Fossat, E., Grec, G. & Pomerantz, M. *Solar Phys.* **74,** 59–63 (1981).
12. Deubner, F.-L. *Nature* **290,** 682–683 (1981).
13. Christensen-Dalsgaard, J. & Gough, D. O. *Nature* **288,** 544–547 (1980).
14. Christensen-Dalsgaard, J. *Proc. 5th Eur. Meet. in Astronomy* (ed. Ledoux, P.) A.1.1–A.1.28 (Institut d'Astrophysique, Liège, 1980).
15. Scuflaire, R., Gabriel, M. & Noels, A. *Astr. Astrophys.* **99,** 39–42 (1981).
16. Christensen-Dalsgaard, J. & Gough, D. O. *Astr. Astrophys.* **104,** 173–176 (1981).
17. Christensen-Dalsgaard, J. & Gough, D. O. *Mon. Not. R. astr. Soc.* **198,** 141–171 (1982).
18. Vandakurov, Yu, V. *Astr. Zh.* **44,** 786–797 (1967).
19. Gough, D. O. *Mon. Not. R. Astr. Soc.* **196,** 731–745 (1981).
20. Brookes, J. R., Isaak, G. R. & van der Raay, H. B. *Mon. Not. R. astr. Soc.* **185,** 1–17 (1978).
21. Scherrer, P. H., Wilcox, J. M., Christensen-Dalsgaard, J. & Gough, D. O. *Solar Phys.* (in the press).
22. Ledoux, P. & Simon, R. *Ann. Astr.* **20,** 185–195 (1957).
23. Goossens, M. *Astrophys. Space Sci.* **16,** 386–404 (1972).
24. Goossens, M., Smeyers, P. & Denis, J. *Astrophys. Space Sci.* **39,** 257–272 (1976).
25. Biront, D., Goossens, M., Cousens, A. & Mestel, M. *Mon. Not. R. astr. Soc.* (in the press).
26. Mestel, L., *Q. Jl R. astr. Soc.* **12,** 402–416 (1971).
27. Mestel, L. & Takhar, H. S. *Mon. Not. R. astr. Soc.* **156,** 419–436 (1972).
28. Mestel, L., Nittman, J., Wood, W. P. & Wright, G. A. E. *Mon. Not. R. astr. Soc.* **195,** 979–1000 (1981).
29. Dicke, R. H. *Solar Phys.* **78,** 3–16 (1982).
30. Hill, H. A. *et al. Phys. Rev. Lett.* **33,** 1497–1500 (1974).
31. Bos, R., Goode, P. R. & Hill, H. A. *Phys. Rev. Lett.* (submitted).
32. Gough, D. O. *Nature* **298,** 334–339 (1982).

VHF Faraday polarization fluctuations and strong *L*-band amplitude scintillations near Appleton anomaly crests

A. DasGupta*, M. C. Lee† & J. A. Klobuchar*

* Air Force Geophysics Laboratory, Hanscom AFB,
Massachusetts 01731, USA
† Regis College Research Center, Weston,
Massachusetts 02139, USA

The Faraday rotation angle of a linearly polarized transionospheric very high frequency (VHF) signal near the crests of the Appleton anomaly, around the recent solar maximum period, often exhibits fast and intense fluctuations, when the amplitude of the signal shows saturated and very fast scintillations[1,2]. These fluctuations usually occur during the post-sunset hours and decay around midnight. The occurrence pattern has been found to be similar to that of microwave amplitude scintillations at *L*-band. We present here certain observed characteristics of the fast polarization fluctuations and report the results of an experiment, which shows that there is a loss of correlation between fadings on the two circularly polarized component modes of the signal during the periods of VHF polarization fluctuations. Hence, the usual concept of Faraday rotation is no longer valid during these times. The above features are discussed in terms of our present knowledge of small scale irregularity structures in the equatorial ionosphere.

Equatorial ionospheric irregularities have been extensively investigated during the past decade by techniques such as rocket and satellite *in situ* measurements, radar, airglow and propagation effects on transionospheric signals[3]. It has been shown that the plumes of equatorial irregularities associated with depletions in background electron content can be studied in a very simple and inexpensive manner from simultaneous measurements of amplitude scintillations and Faraday rotation of a VHF signal propagating through the ionosphere[4,5]. While the occurrence of depletions of the integrated electron content is commonly observed with Faraday rotation records obtained near the magnetic equator[6,7], a new feature, fast and intense fluctuations of the Faraday rotation angle, has recently been reported from stations situated near the crests of the Appleton anomaly[1,2], a region characterized by severe amplitude scintillations during solar maximum years[8,9]. Polarization fluctuations of 136-MHz signals have been observed at Ascension Island (31°S dip), which is situated close to the southern crest of the equatorial anomaly in the African zone, and at Calcutta (32°N dip) and Ahmedabad[10] (34°N dip) near the northern crest of the anomaly in the Indian sector. These have sometimes been observed even at Delhi (40°N dip) (Y. V. Somayajulu, personal communication) near the northern edge of the anomaly, but no such phenomenon has been observed at Arequipa (9°S dip), Peru or at Natal (10°S dip), Brazil which are close to the magnetic equator. Kaushika and deMendonca[11] possibly observed the same type of fluctuations in the polarization records of 137-MHz signals recorded at Sao Paulo (26° S dip) which is also situated near the crest of the anomaly, but they had no amplitude scintillation measurements. In their attempt to associate the fluctuations with atmospheric gravity waves, they were concerned with slower fluctuations of period 2 min and longer.

Figure 1 shows a typical polarimeter record obtained during post-sunset hours at Ascension Island (7.9° S, 14.4° W, 31° S dip). The channel at the top is the amplitude of the 136-MHz transmission from the geostationary satellite SIRIO (15° W) and the two bottom channels are the Faraday polarization angle of the signal with one shifted from the other by 90°. The polarization fluctuations are often too intense to render the Faraday data useful. The station also recorded signals from the

0028–0836/82/290354—04$01.00

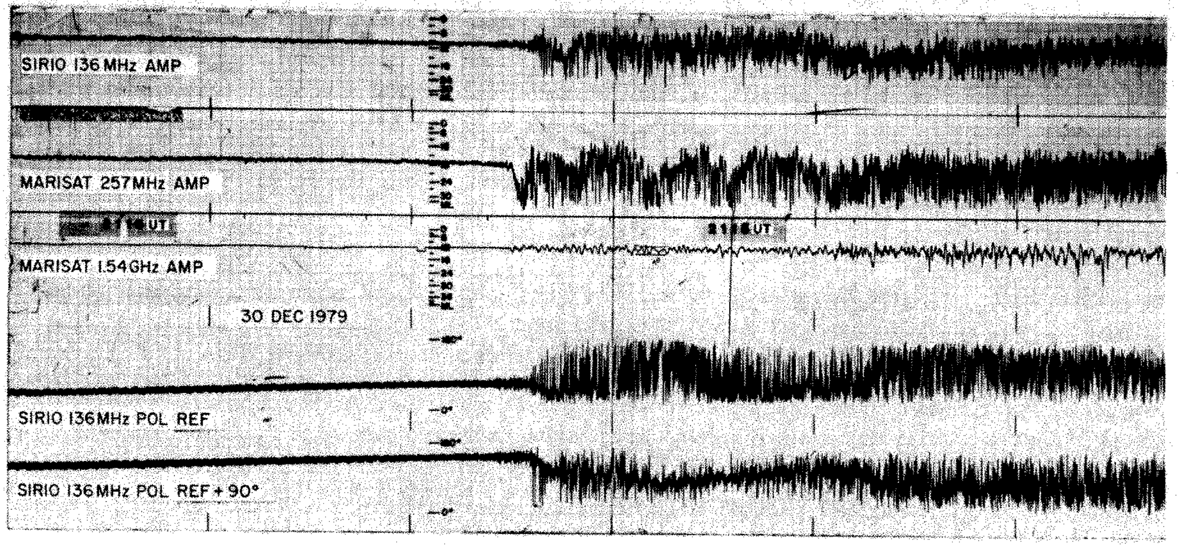

Fig. 1 Sample records of satellite signals obtained at Ascension Island. Time marks shown are in UT. Local time corresponds to UT − 1 h.

satellite Marisat (also at 15° W) at 257 MHz and 1.54 GHz for amplitude scintillation measurements. The sub-ionospheric points of the two satellites are essentially identical. The third channel from the top shows amplitude scintillations of the 1.54-GHz signal. Polarization fluctuations are found when the amplitude of the VHF signal shows saturated and very fast scintillations, which generally occur during the pre-midnight hours. We have found during more than 2 yr of observations around the recent solar maximum period that the polarization fluctuations coexist with intense *L*-band scintillations at 1.54 GHz. During the post-midnight period polarization fluctuations decay, even though VHF amplitude scintillation remains saturated, but with slower fading rates.

The change in fading rates of VHF amplitude scintillations, with and without polarization fluctuations, is clearly evident in the power spectra of 136-MHz scintillation measurements as presented in Fig. 2*a* and *b* respectively. The corresponding power spectra obtained at 257 MHz and 1.54 GHz are also shown. The approximate corner frequencies of the power spectra are indicated by arrows. The corner frequency of a power spectrum gives a measure of the fading rate, a higher corner frequency corresponding to a faster fading rate. In the present case, a lowering of the corner frequency is obvious in the late phase, as shown in Fig. 2*b*, when no polarization fluctuations are observed.

Power spectrum analysis of scintillation measurements is generally used to obtain information on the characteristics of the ionospheric irregularities responsible for scintillations. However, the interpretations of the power spectrum in conditions of weak and strong scintillations involve different scattering mechanisms by the ionospheric irregularities. According to the theory of radiowave propagation, for weak scintillation conditions, the amplitude fading rate of a transionospheric signal from a geostationary satellite is proportional to v/l_F, where v is the drift velocity of the irregularities and l_F the Fresnel dimension[6]. Because $l_F \propto \sqrt{\lambda}$ (where λ is the radiowave length), the fading rate should increase with observing frequency in weak scatter conditions. In contrast, in the case of severe scintillations, the wave propagation has to be considered in the framework of multiple scatter theory and the recorded scintillation data pertain to the ground diffraction pattern, which cannot be related to the irregularity pattern in the ionosphere in a simple manner[12]. The fading rate, in severe scintillation conditions, is inversely related to the autocorrelation distance of the ground pattern. The autocorrelation interval is determined by the drift velocity as well as by the strength of scattering. As the strength of scattering (in other words, scintillation index) increases, the autocorrelation distance decreases[13], and an increase in the fading rate is observed[14]. The scintillation index is usually inversely related to the observing frequency. Thus, in the case of severe scintillations, with an increase of the observing frequency the autocorrelation distance should increase and hence, a slowing down of the amplitude fading rate occurs.

In the equatorial region amplitude scintillations observed at 136 MHz and 250 MHz are usually severe (saturated or near saturated) for most of the time the phenomena are observed. Near the crests of the Appleton anomaly, severe scintillations in excess of 20 dB are quite frequent even at *L*-band (such as 1.54-GHz observations at Ascension Island) during the pre-midnight hours, particularly around the recent solar maximum[8]. The power spectra depicted in Fig. 2 are representative of scintillations observed at the corresponding frequencies in the developed and late phases of equatorial night-time ionospheric irregularities respectively.

During an intensive campaign of measurements in December 1979, in order to investigate the nature of fast polarization fluctuations, the left and right circular components of the 136-MHz signal were recorded separately in addition to the routine observations. The data were recorded on a magnetic tape in analog form, which was digitized at an 18 samples s^{-1} rate for later analysis. The cross-correlation between the amplitude fadings of the two component modes was computed over 3-min intervals. The scintillation index S_4 (refs 15, 16), which is a measure of the r.m.s. amplitude fluctuations about the mean level, is also computed for each 3 min interval at different observing frequencies. Figure 3 shows the variation of the cross-correlation coefficient between the amplitude fadings of the two circularly polarized component waves at 136 MHz with changes in the scintillation index S_4 observed at 1.54 GHz.

The correlation coefficient decreases as S_4 increases and attains low values (<0.2) when S_4 is 0.5 or more. The intervals with $S_4 > 0.5$ at 1.54 GHz generally exhibit fast polarization fluctuations at 136 MHz. In other words, the two circularly polarized components undergo quasi-independent fluctuations when strong *L*-band and polarization fluctuations are obtained. If the two modes become quasi-independent, the usual concept of Faraday rotation breaks down. The close correlation of occurrence of 136-MHz polarization fluctuations and the 1.54-GHz scintillation, clearly seen in Fig. 3, implies that either irregularities of nearly the same scale size are responsible for the two phenomena or that the irregularities causing the two phenomena coexist in the ionosphere.

Lee *et al.*[17] have shown that ionospheric power law density irregularities with an outer scale size in the range 50–200 m are responsible for the 136-MHz polarization fluctuations. Faraday polarization fluctuations result from differential phase shift and the differential change in the logarithmic amplitude of the two circularly polarized modes introduced by wave scattering from these short-scale density irregularities. The theory

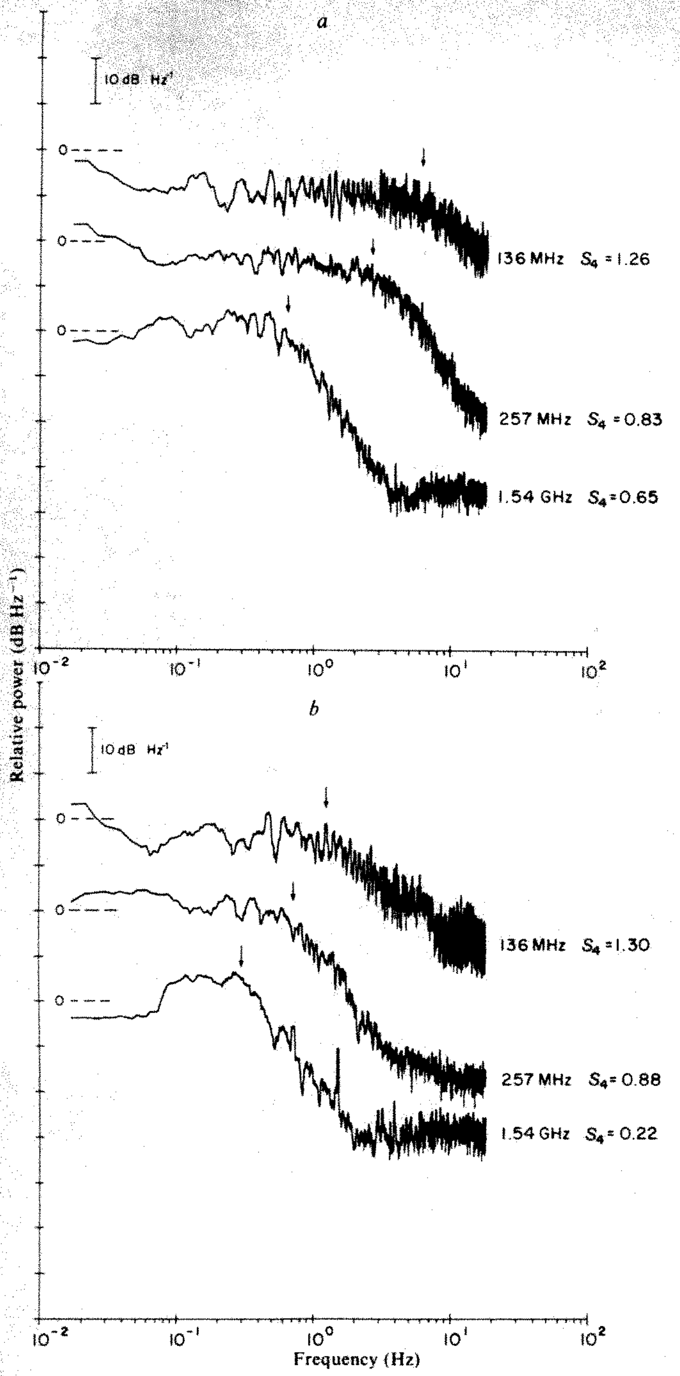

Fig. 2 Power spectra of amplitude scintillations at different frequencies for a 3-min sample centred on the time indicated. *a*, 21 h 46 min 30 s UT; Faraday polarization channels show intense and rapid fluctuations during this period. *b*, 22 h 34 min 30 s UT; no fast polarization fluctuation was observed during this period. The approximate corner frequencies are given by arrows.

shows that a deviation of ~1–2% in a high ambient ionization density, say, not less than $3.0\times10^{12}\,\mathrm{m}^{-3}$, corresponding to a plasma frequency of over 15 MHz, is required to provide a favourable environment for the 136-MHz fluctuations to occur. When the r.m.s. differential phase departure exceeds ~0.5 rad, the two circularly polarized modes are expected to become practically uncorrelated. Scintillations at 1.54 GHz are most effectively produced by irregularities with scale sizes of a few hundred metres (~300 m in the present case), which are of the same order as the Fresnel zone dimension. Both the 136-MHz polarization fluctuations and the 1.54-GHz scintillations involve density irregularities of a few hundred metres scale size. If the irregularity power spectrum follows a power law, with diminishing spectral density at shorter scale lengths, and if the overall strength of the irregularities is high enough to have spectral density in the 50–200 m scale size range sufficient to cause polarization fluctuations at 136 MHz, it is implied that irregularities at a ≳300 m scale size range will also have enough spectral power to produce appreciable amplitude scintillations at 1.54 GHz. Thus, the presence of fast polarization fluctuations at 136 MHz may be taken as an indication of the possible scintillations at *L*-band and lower frequencies. The reverse may not, however, always be true.

From multi-technique observations Basu *et al.*[18] have reported that, while during the pre-midnight period the power spectra of equatorial irregularities follow a power law, during post-midnight hours the overall strength of the irregularities is eroded and there is a transition to a quasi-gaussian type of spectrum indicating the decay of shorter-scale (typically <1 km) irregularities. As the 1.54-GHz scintillation became weak, with the decay of short-scale density irregularities, the two circularly polarized modes were seen to have high cross-correlation coefficients, reflecting no, or very small, polarization fluctuations.

Except in the HF band (for example, 20 MHz), the polarization fluctuations of satellite signals cannot be effectively caused by irregularities with quasi-gaussian spectra[19]. Near the Appleton anomaly crests, in solar maximum conditions, the ambient ionization density (n) is very high and the high level persists during the evening hours. As a result, the absolute value of the irregularity intensity (Δn) is also very high in the anomaly region[8]. In contrast, in regions near the magnetic equator, the relatively small n and Δn and the relatively large angles of propagation with respect to the geomagnetic field make it impossible to give rise to significant polarization fluctuations of 136-MHz signals[17].

We thank S. Basu, Sunanda Basu and C. L. Rino for discussions. The work at the Regis College Research Center was supported by AFGL contract F19628-80-C-0016. A.D.G is a NRC–NAS Senior Resident Research Associate on leave from the University of Calcutta, India.

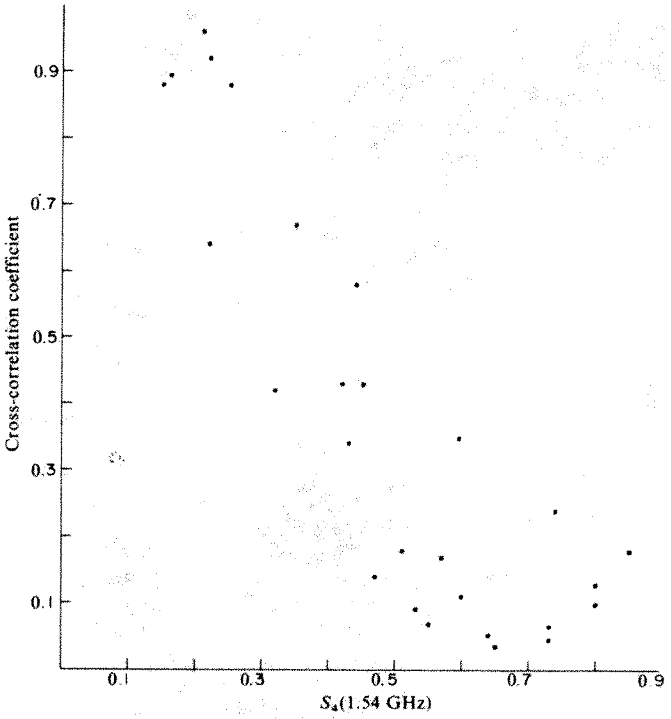

Fig. 3 Variation of cross-correlation coefficients of the fluctuations of the two opposite circularly polarized components of the 136-MHz signal with the amplitude scintillation index S_4 at 1.54 GHz. The intervals $S_4 > 0.5$ correspond to intense and fast Faraday polarization fluctuations.

Received 3 March; accepted 20 May 1982.

1. Klobuchar, J. A. & Aarons, J. *Alt. Frequenza* **49,** 345–349 (1980).
2. DasGupta, A. & Maitra, A. *Adv. Space Expl.* (COSPAR Ser.) **8,** 209–212 (1980).
3. Basu, S. & Basu, S. *J. atmos. terr. Phys.* **43,** 473–489 (1981).
4. Klobuchar, J. A., Aarons, J., Weber, E., Lucena, L. & Mendillo, M. *Paper* G.4 (Radio Science Meeting, US National URSI, Boulder, Colorado, 1978).
5. Yeh, K. C., Soicher, H., Liu, C. H. & Bonelli, E. *Geophys. Res. Lett.* **6,** 473–475 (1979).
6. Yeh, K. C., Soicher, H. & Liu, C. H. *J. geophys. Res.* **84,** 6589–6594 (1979).
7. DasGupta, A., Aarons, J., Klobuchar, J. A., Basu, S. & Bushby, A. *Geophys. Res. Lett.* **9,** 147–150 (1982).
8. Aarons, A., Whitney, H. E., MacKenzie, E. & Basu, S. *Radio Sci.* **16,** 939–945 (1981).
9. DasGupta, A., Maitra, A. & Basu, S. *Radio Sci.* **16,** 1455–1458 (1981).
10. Deshpande, M. R. *et al. Curr. Sci.* **50,** 221–222 (1981).
11. Kaushika, N. D. & de Mendonca, F. *Planet. Space Sci.* **22,** 1331–1334 (1974).
12. Yeh, K. C., Liu, C. H. & Youakim, M. Y. *Radio Sci.* **10,** 97–106 (1975).
13. Rino, C. L. & Owen, J. *Radio Sci.* **16,** 31–33 (1981).
14. Umeki, R., Liu, C. H. & Yeh, K. C. *J. geophys. Res.* **82,** 2752–2760 (1977).
15. Briggs, B. H. & Parkin, I. A. *J. atmos. terr. Phys.* **25,** 339–365 (1963).
16. Whitney, H. E., Aarons, J. & Malik, C. *Planet. Space Sci.* **17,** 1069–1073 (1969).
17. Lee, M. C., DasGupta, A., Klobuchar, J. A., Basu, S. & Basu, S. *Radio Sci.* **17,** 399–409 (1982).
18. Basu, S., McClure, J. P., Basu, S., Hanson, W. B. & Aarons, J. *J. geophys. Res.* **85,** 5119–5130 (1980).
19. Lee, M. C. *J. geophys. Res.* **87,** 751–755 (1982).

Is the olivine–spinel phase transformation martensitic?

P. J. Vaughan & H. W. Green II

Department of Geology, University of California, Davis,
California 95616, USA

R. S. Coe

Earth Sciences Board, University of California, Santa Cruz,
California 95060, USA

Olivine, the dominant mineral in the Earth's uppermost mantle, undergoes one, or possibly a series of phase transformations to adopt a spinel structure at pressures above ~13 GPa. The mechanism by which the transformation is accomplished could have important implications for understanding mantle dynamics and deep focus earthquakes. Recently, it has been proposed that the transformation may proceed by a martensitic mechanism[1–5]. We discuss here the characteristic properties of martensitic transformations and present evidence that the analogous transformation in Mg_2GeO_4 does not proceed by such a process.

Polymorphic transformations which occur by a martensitic mechanism involve a specific, coordinated movement of atoms. The interface which effects the transformation propagates by the movement of a series of partial dislocations resulting in the production of stacking faults. Such faults represent monolayers of the new phase[6]. This process contrasts with the nucleation and growth mechanism in which the interface propagates by a generally uncoordinated, thermally activated movement of atoms. Martensitic transformations involve a significant shear component in their transformation strain. This means that if the transformation is accomplished under nonhydrostatic stress, the process should be enhanced in favourably oriented parent crystals and retarded in unfavourably oriented parents. Higher stresses (and hence strain rates) will favour the transformation. The daughter phase generally grows as lamellae in the parent, whereas the nucleation and growth mechanism usually produces irregular interfaces due to more rapid migration in directions of greater stored strain energy in the deformed parent. Martensitic mechanisms always exhibit specific crystallographic relationships between parent and daughter crystals, whereas nucleation and growth (also proposed for olivine–spinel[7]) can, but normally does not, produce such relationships. The topotactic relation required by the martensitic mechanism proposed for the olivine–spinel transformation is $[100]_{ol}$ parallel to $\langle 111\rangle_{sp}$ and $[001]_{ol}$ parallel to $\langle 011\rangle_{sp}$ (refs 3,4). This crystallographic relationship has been reported in a few instances in Fe_2SiO_4 (ref. 3) and Ni_2SiO_4 (ref. 5); in the latter case only 3 out of 10 spinel crystals showed the exact relationship, and 5 showed large deviations. The occasional presence of topotaxy is compatible with any transformation mechanism, but it must be present in all instances to support the martensitic mechanism.

The olivine–spinel transformation for the chemical composition appropriate for the Earth's mantle, $(Mg_{0.9}, Fe_{0.1})_2SiO_4$, has been very difficult to study directly due to the very high transformation pressure[8,9]. Consequently, the transformation has been studied in other systems, principally Fe_2SiO_4, (ref. 3), Ni_2SiO_4 (ref. 5) and Mg_2GeO_4 (ref. 10), which undergo the transformation at lower pressures. Although systematic studies of these and other analogues have shown very great similarities between the various systems, one complication remains. Each of the analogue systems listed above undergoes the transition directly, whereas for the Mg-rich silicate olivine system there is another (β) phase with a distorted-spinel structure which is found at intermediate pressures[8,9]. Transmission electron microscopy (TEM) studies[1,2,11] indicate that in many cases the β-phase may be a quench product formed at the expense of the γ-phase. Considering these uncertainties, the simplest approach regards the direct transformation (olivine–spinel) as relevant to the mantle[12]. The martensitic mechanism was proposed on this basis and the topotactic relations found in Fe_2SiO_4 and Ni_2SiO_4 have been cited as support for the martensitic mechanism on the same basis. We continue this approach here while recognizing that the question of relevance to the mantle remains unresolved until the mineralogy is better known.

To test the martensitic hypothesis, we selected a deformed Mg_2GeO_4–olivine sample which had partially transformed to spinel. The run conditions of this creep experiment (no. 92) were: confining pressure, $P = 1.3$ GPa; average differential stress, $\sigma = 280$ MPa; total axial strain 5%; duration 55 h (ref. 11). The temperature along the 18.4-mm long sample varied from 950 °C at the lower end to 1,200 °C in the centre. Thus, the lower portion of the sample was well within the spinel field but the central portion was just inside the olivine field. Specimens were selected from a small region of 50–60% spinel near the lower end of the sample. TEM foils were prepared by

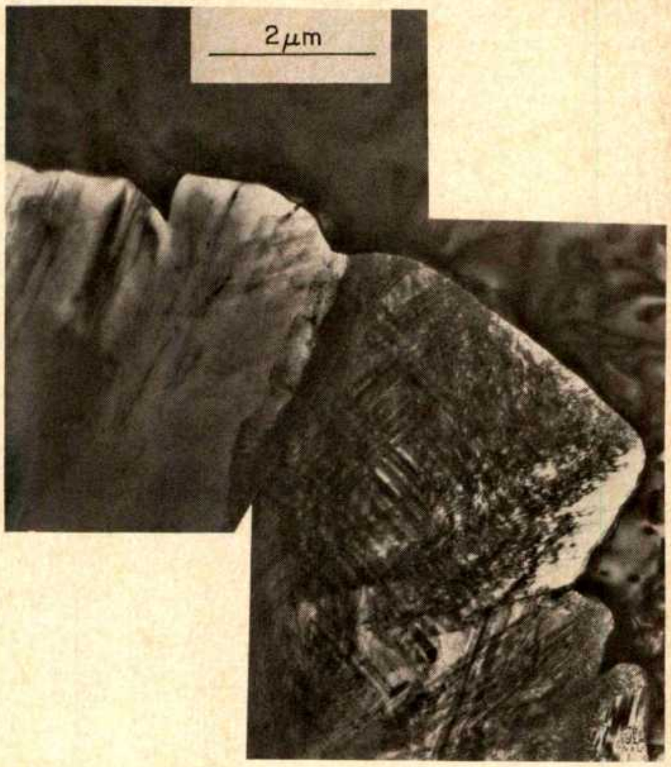

Fig. 1 High-voltage transmission electron micrograph of large spinel grains with a high density of stacking faults and parent olivine with moderate dislocation density (800 kV). The maximum compressive stress applied to the specimen lies NE–SW, parallel to the spinel–spinel grain boundaries.

0028–0836/82/290357—02$01.00

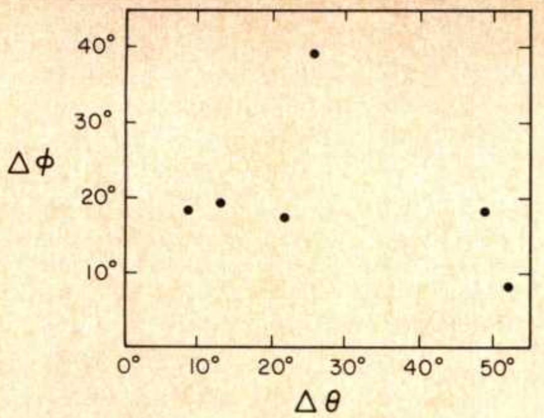

Fig. 2 Diagram showing the deviation from the orientations predicted for the martensitic transformation mechanism. $\Delta\theta$ measures the angle between $[100]_{ol}$ and the nearest $\langle 111\rangle_{sp}$; $\Delta\phi$ is the angle between $[001]_{ol}$ and the nearest $\langle 011\rangle_{sp}$. Data were obtained by selected area electron diffraction.

ion-thinning and examined in both optical and electron microscopes.

The following observations on this specimen suggest that the mechanism of the transformation was not martensitic:

(1) TEM images display no stacking faults in the olivine phase (Fig. 1); the substructure, both near to and far from olivine–spinel interfaces, is that normally produced during plastic deformation of germanate[13] and silicate[14] olivine. Thus, there is no direct evidence for operation of the martensitic mechanism. Stacking faults appear in the spinel phase (Fig. 1), but there is no indication that they are involved in the transformation process[15].

(2) Variations in the diffraction contrast images of the daughter spinel crystals growing into the same olivine parent grain indicate that the spinels have different orientations (Fig. 1). Moreover, selected-area electron diffraction of several parent–daughter clusters demonstrates that the topotactic relations required by the martensitic mechanism are not present (Fig. 2). Small deviations from topotaxy might be explained away as loss of coherency by accumulation of dislocations in the interface. However, the lack of evidence for the required dislocations and the extremely large deviations from coherency (Fig. 2) render such an argument untenable.

(3) The spinel crystals have an elongated growth habit, but the inequant shapes are independent of the crystal orientation of both olivine and spinel. The martensitic mechanism requires a crystallographic relationship and preferential growth of spinel in olivine crystals oriented with high shear stress on the hypothetical dislocations which effect the transformation.

(4) The spinel crystals have grown preferentially in the direction of the maximum compressive stress, resulting in subparallel fingers of spinel separated by residual spikes of olivine (Figs 1 and 3).

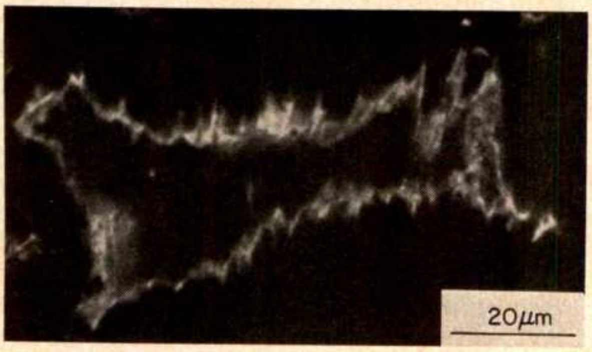

Fig. 3 Optical micrograph of a residual olivine grain surrounded by spinel. The prominent north–south spikes protruding from the olivine crystal are the remnants left between spinel grains which have grown preferentially parallel to the maximum compressive stress (crossed polarizers).

We have failed to find any evidence indicative of a martensitic transformation. On the other hand, the observation that the spinel displays a strong growth anisotropy reflecting the stress field is an interesting new discovery. This is consistent with a simple nucleation and growth mechanism in which the driving force for growth varies with the $P\Delta V$ term in the equation describing the difference in Gibbs free energy between the two phases (ref. 16, and work in preparation).

We thank J. P. Poirier and N. Hamaya for preprints and H.-R. Wenk for assistance with the electron microscopy. This work was supported by NSF EAR 74-21885A01.

Received 4 January; accepted 24 May 1982.

1. Putnis, A. & Price, G. D. *Nature* **280,** 217–218 (1979).
2. Price, G. D., Putnis, A. & Agrell, S. O. *Contr. Miner. Petrol.* **71,** 211–218 (1979).
3. Lacam, A., Madon, M. & Poirier, J. P. *Nature* **288,** 155–157 (1980).
4. Poirier, J. P. *Anelastic Properties and Related Processes in the Earth's Mantle* (AGU Monograph, in the press).
5. Hamaya, N. & Akimoto, S. in *High Pressure Research in Geophysics* (eds Akimoto, S. & Manghnani, M. H.) (Center Academic, Tokyo, in the press).
6. Brooks, J. W., Loretto, M. H. & Smallman, R. E. *Acta met.* **27,** 1839–1847 (1979).
7. Sung, C.-M. & Burns, R. G. *Tectonophysics* **31,** 1–32 (1976).
8. Ringwood, A. E. & Major, A. *Phys. Earth planet Inter.* **3,** 89–108 (1970).
9. Suito, K. *J. Phys. Earth* **20,** 225–243 (1972).
10. Dachille, F. & Roy, R. *Am. J. Sci.* **258,** 225–246 (1960).
11. Price, G. D., Putnis, A. & Smith, D. G. W. *Nature* **296,** 729–730 (1982).
12. Poirier, J. P. *Phys. Earth planet. Inter.* **26,** 179–186 (1981).
13. Vaughan, P. J. & Coe, R. S. *J. geophys. Res.* **86,** 389–404 (1981).
14. Green, H. W. in *Electron Microscopy in Mineralogy* (eds Wenk, H. R. *et al.*) 443–464 (Springer, Heidelberg, 1976).
15. Vaughan, P. J. & Kohlstedt, D. L. *Phys. Chem. Miner.* **7,** 241–245 (1981).
16. Green, H. W. & Vaughan, P. J. *EOS* **62,** 1030 (1981).

Noise in chaotic systems

John Guckenheimer

Division of Natural Sciences, University of California, Santa Cruz,
California 95064, USA

Procedures which estimate the noisiness of complicated, aperiodic data are outlined here and considered in the context of transitional fluid flow, although similar questions arise in many other fields[1,2]. Because this is the initial formulation of these ideas only qualitative results are presented; any attempt to develop quantitative measures of randomness will be postponed until more testing and refinement of the procedures have been completed.

Consider a fluid experiment such as Rayleigh–Bérnard convection or the flow between concentric cylinders in a regime which produces aperiodic flow[3]. Substantial theoretical and experimental attention has been given to the temporal characteristics of these flows as dynamical systems. The Landau–Hopf model of turbulence[4] portrays turbulent flow as quasiperiodic with many independent frequencies. This view was successfully challenged by Ruelle and Takens[5] with an argument based on the structural instability of quasiperiodic attractors for dynamical systems. Extensive high-precision experiments have demonstrated that the transition to aperiodic flow occurs directly from flows whose power spectra have few independent frequencies[6,7]. These measurements for small aspect ratio fluid experiments are evidence that fluid transitions in this regime are described reasonably well by the bifurcations of systems of differential equations with few degrees of freedom[8]. There is still disagreement, however, as to whether the aperiodicity of the post-transition flows has the characteristics which one finds in a trajectory of a system of ordinary differential equations with a state space of low dimension. In particular, it has been suggested that some aspects of the data are described much better by stochastic models. The methods proposed here may help resolve this matter.

Dynamical systems with few degrees of freedom can have 'strange attractors': bounded sets of aperiodic trajectories which are asymptotically stable[10,11]. Some features of a trajectory in

0028–0836/82/290358—04$01.00

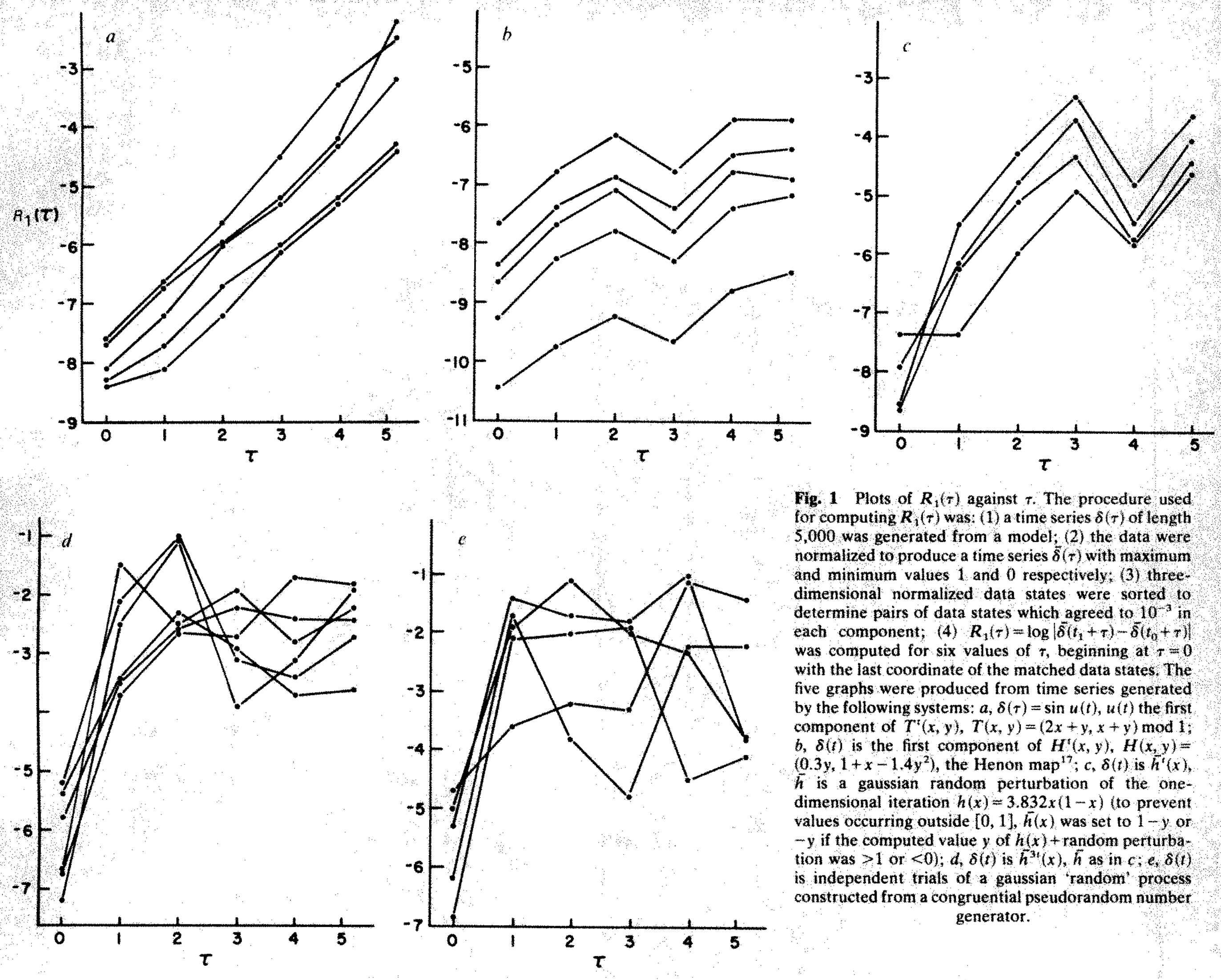

Fig. 1 Plots of $R_1(\tau)$ against τ. The procedure used for computing $R_1(\tau)$ was: (1) a time series $\delta(\tau)$ of length 5,000 was generated from a model; (2) the data were normalized to produce a time series $\bar{\delta}(\tau)$ with maximum and minimum values 1 and 0 respectively; (3) three-dimensional normalized data states were sorted to determine pairs of data states which agreed to 10^{-3} in each component; (4) $R_1(\tau) = \log|\bar{\delta}(t_1+\tau) - \bar{\delta}(t_0+\tau)|$ was computed for six values of τ, beginning at $\tau = 0$ with the last coordinate of the matched data states. The five graphs were produced from time series generated by the following systems: *a*, $\delta(\tau) = \sin u(t)$, $u(t)$ the first component of $T^t(x, y)$, $T(x, y) = (2x + y, x + y) \bmod 1$; *b*, $\delta(t)$ is the first component of $H^t(x, y)$, $H(x, y) = (0.3y, 1 + x - 1.4y^2)$, the Henon map[17]; *c*, $\delta(t)$ is $\bar{h}^t(x)$, $\bar{h}$ is a gaussian random perturbation of the one-dimensional iteration $h(x) = 3.832x(1-x)$ (to prevent values occurring outside [0, 1], $\bar{h}(x)$ was set to $1 - y$ or $-y$ if the computed value y of $h(x)$ + random perturbation was >1 or <0); *d*, $\delta(t)$ is $\bar{h}^{3t}(x)$, $\bar{h}$ as in *c*; *e*, $\delta(t)$ is independent trials of a gaussian 'random' process constructed from a congruential pseudorandom number generator.

a strange attractor appear chaotic even though its evolution is determined completely by initial conditions. There is a sensitive dependence to initial conditions which prevents long-term prediction of the location of a trajectory within the attractor due to the uncertainty in our measurements of initial conditions. I interpret the Ruelle–Takens theory as asserting that aperiodic fluid flow is described by a strange attractor. This behaviour contrasts with randomness in the flow. Here randomness is defined as unpredictability in the short term evolution of a system. The present aim is to estimate the extent of randomness or noise in a system from the data which it produces.

In analysing a time series, I begin with the hypothesis that it can be described by evaluating a function along a trajectory in a strange attractor of a system with few degrees of freedom. This hypothesis implies that the trajectory will visit some regions of the state space repeatedly, returning many times to positions that are close to ones that it occupied previously. When this happens, the corresponding observations in the time series approximate each other. Indeed, entire sections of the time series approximate each other over time intervals for which the trajectories remain close. A second assumption about the function defining the time series allows this observation to be reversed.

Packard *et al.*[12,13] and Takens[14] have developed a procedure for recovering the location of a point in the state space from a section of the time series based on the Whitney embedding theorem[15]. Specifically, the trajectory with initial condition x is denoted by $\phi(x, t)$ and a time interval Δt selected. We then assume that the functions f_i defined by $f_i(x) = f(\phi(x, i\Delta t))$ are in a general position. The embedding theorem then implies that the mapping F defined by $F(x) = (f_0, f_1, \ldots, f_k)$ is an embedding of the state space into R^{k+1} if K is at least twice the dimension of the state space. We need only observe here that if $\phi(x, t)$ is a trajectory, then the observations $f(\phi(x, t + i\Delta t))$, $0 \leq i \leq n$, determine uniquely the location of $\phi(x, t)$ when n is large enough.

Sections of a discrete time series $\delta(t)$ are now used which approximate each other to assess the extent to which the data $\delta(t)$ could have been generated by a dynamical system with a low dimensional state space. An integer k is selected and a $(k+1)$-dimensional data state $\Delta(t)$ defined to be a $(k+1)$ vector $(\delta(t), \delta(t+1), \ldots, \delta(t+k))$. If k is sufficiently large and the data can be generated by a strange attractor, then $\Delta(t+1)$ is determined by $\Delta(t)$ by means of an unknown $(k+1)$ order (nonlinear) difference equation.

The practical problems here are that (1) no physical process is entirely free of randomness, and (2) any experiment gives us limited quantities of data. Nonetheless, the data states defined above can be used to estimate the randomness in a system. In two procedures used as an initial test for these methods, the data states of a time series are sorted to locate efficiently the pairs and triples of data states which are close to each other. Longer sections of the data which include these data states can then be examined.

The first procedure is based on the observation that the divergence of trajectories from one another in a strange attractor is approximately exponential, at a rate determined by the

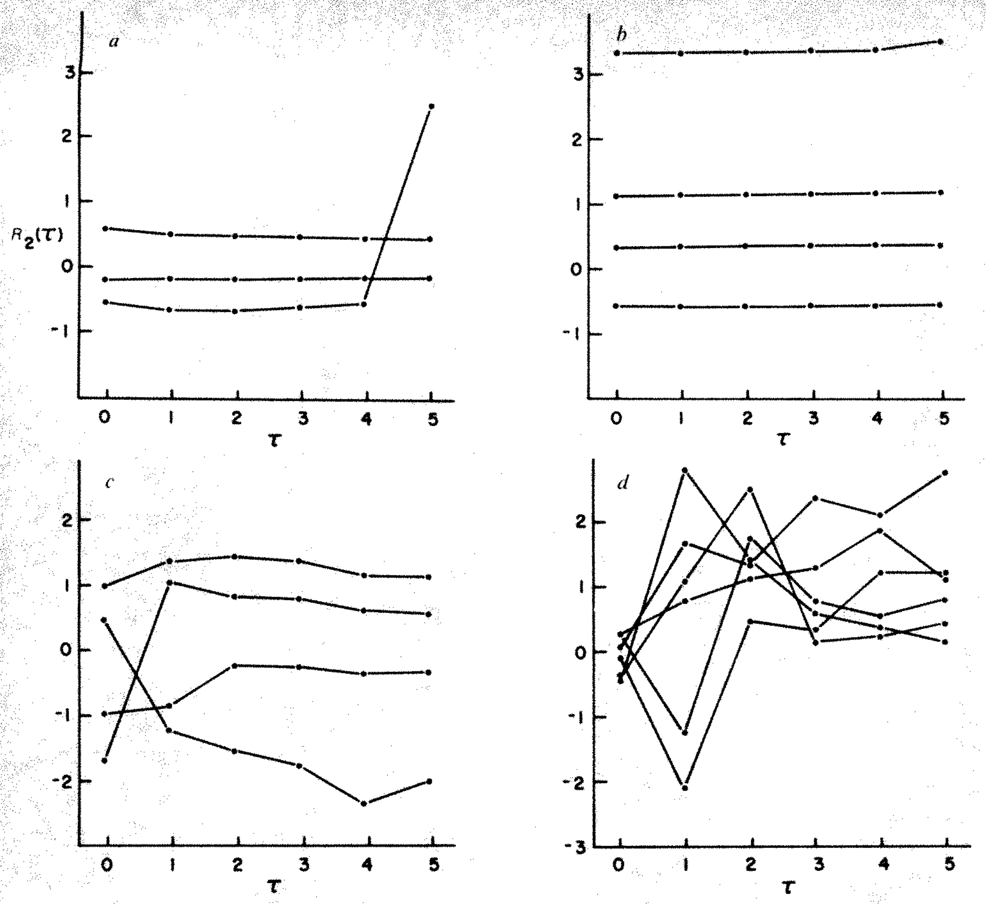

Fig. 2 Plots of $R_2(\tau)$ against τ for the same time series $\delta(t)$ used in Fig. 1*a–d*. To compute R_2 from $\delta(t)$, nearby triples of data states were located. With $\tau=0$ corresponding to the last component of the matched data states,

$$R_2(\tau)=\frac{\delta(t_2+\tau)-\delta(t_1+\tau)}{\delta(t_0+\tau)-\delta(t_1+\tau)}$$

was computed for $\tau=0,\ldots,5$.

largest Liapunov exponent of the trajectory. This suggests that the difference $R_1(\tau)=\log|\delta(t_1+\tau)-\delta(t_0+\tau)|$ of two sections of the time series $\delta(t)$ should be approximately linear in τ with slope which is generally independent of the sections of data chosen in a given region of the state space. Thus the first step is to measure $R_1(\tau)$ for sections of data which immediately follow pairs of nearby data states $\Delta(t_0)$ and $\Delta(t_1)$.

There is a limitation in using $R_1(\tau)$ due to the nonuniformity of the spreading of trajectories in different parts of a strange attractor and to the nonlinearity of the observing function f. The second procedure examined the statistics

$$R_2(\tau)=\frac{\delta(t_2+\tau)-\delta(t_1+\tau)}{\delta(t_0+\tau)-\delta(t_1+\tau)}$$

at times following the close approach of the corresponding triple of data states. In sections of a time series for which the strange attractor hypothesis indicates exponential divergence, $R_2(\tau)$ should be almost constant. In our present tests R_2 seems to be less susceptible to the nonlinearity of the observable and the nonuniformity of an attractor than R_1.

The statistics R_1 and R_2 are designed to examine more directly the extent of the randomness in a system than the procedures described by Takens[14] and Froehling *et al.*[12,13]. Takens partitions the space of k-dimensional data states into boxes of size ε. He uses the number $N(k,\varepsilon)$ of boxes populated for varying k and ε to estimate the topological entropy and capacity of a strange attractor. However, in a system with randomness, the noise can be expected to dominate the counts $N(k,\varepsilon)$ when ε is considerably smaller than the amplitude of the noise. This places limitations on the suitability of Takens' process for data with moderate amounts of noise. One might obtain an indication of the noise amplitude in a set of data if there is a pronounced plateau in $N(k,\varepsilon)$ with varying ε, but the issue of short term predictability is not addressed directly. Froehling *et al.*[12,13] use a method of local linear regression to fit the set of data states in a given region of the space of data states to a linear subspace. This procedure is complementary to the one described here and can be used to select an optimal value for the dimension of the data states which should be used when computing the statistics R_1 and R_2. The LLR method does not appear to be effective in assessing the issue of short term predictability.

The extreme examples which have been examined with these two procedures are a linear toral Anosov diffeomorphism[16] and independent trials of a gaussian random variable. The toral diffeomorphism is defined by $T(x,y)=(2x+y, x+y)$, where x and y are regarded as cyclic coordinates (mod 1). The whole two-dimensional torus is a strange attractor for T. The nonlinear function $f(x,y)=\sin x$ was used to generate time series $\delta(t)$ for this system. Examples have also been examined of the time series drawn from the x-coordinate of iterates of the Henon mapping[17] defined by $H(x,y)=(0.3y, 1+x-1.4y^2)$, and a random perturbation of a one-dimensional quadratic iteration $h(x)=3.832x(1-x)$. This perturbation was formed by adding to $h(x)$ a gaussian random variable constructed from a congruential pseudorandom number generator.

Figure 1 shows the results obtained from applying the first procedure to time series of 5,000 observations drawn from each of the examples. Nearby three-dimensional data states have been located, and then $R_1(\tau)$ has been plotted for the last components of the nearby data states and for the five observations immediately following these. The results clearly separate the deterministic systems from the pseudorandom gaussian process. The nonuniformity of the expansion in the Henon mapping is reflected in the smaller values of R_1 at the third observation following the matched data states compared to the second. For the one-dimensional iteration, the deterministic features dominate the randomness at this scale. To show the randomness more clearly, Fig. 1*d* shows the results of selecting every third data point (there is a stable period 3 cycle in the deterministic map) and then working on a finer scale of resolution. The randomness in the data shows clearly in Fig. 1*d*. Note also in Fig. 1*d* and *e* the large magnitude of the uncertainty in the knowledge of the next observation associated with our current knowledge of the data state.

Figure 2 shows R_2 statistics for the same time series. The gaussian process produced only one triple which was a close match, and this was very erratic. Only graphs with moderate values of the R_2 statistic are shown. The R_2 statistic works strikingly well for the Anosov and Henon mappings, while the one-dimensional iteration gives an indication of a small amount of randomness. Looking at the finer scale of resolution for the third iterate of this process, the randomness is once again dominant.

The results of these initial test on models of strange attractors and stochastic systems are promising. The differences between time series generated by strange attractors and those generated by systems with some randomness are apparent. There are three specific indications of determinism versus randomness in the tests we have performed with these model data:

(1) If $\tau = 0$ denotes the time of the last observations used in matching nearby data states, then a large value of $R_1(1) - R_1(0)$ shows that one state has exceeded the resolution at which one step prediction is possible.

(2) Approximately constant differences in the values of R_1 computed from different trajectories demonstrate a consistent pattern of separation of trajectories like that present in strange attractors.

(3) Approximately constant values of $R_2(\tau)$ compared with τ give an indication similar to (2) of the orderly separation of trajectories found in strange attractors.

I suggest that statistics such as R_1 and R_2 may help resolve questions about whether the irregularities of time series drawn from experimental observations are due to effects which can be described by deterministic systems with few degrees of freedom. The problems discussed above are related to questions about entropy and fractal dimension of data[14], but the methods reported here address the question of randomness as the cause of irregularity more directly.

Received 1 February; accepted 28 April 1982.

1. Guckenheimer, J. *Lect. Math. Life Sci.* **10,** 1–47 (1978).
2. Brillinger, D. R., Guckenheimer, J. Guttorp, P. & Oster, G. *Lect. Math. Life Sci.* **13,** 65–90 (1981).
3. Swinney, H. L. & Gollub, J. (eds) *Hydrodynamic Instabilities and the Transition to Turbulence* (Springer, New York, 1981).
4. Landau, L. & Lifshitz, E. M. *Fluid Mechanics* (Pergamon, Oxford, 1959).
5. Ruelle, D. & Takens, F. *Comm. Math. Phys.* **20,** 167–192 (1971).
6. Libchaber, A. & Maurer, J. *Nonlinear Phenomena and Phase Transitions* (ed. T. Riste) (Geilo Nato School, in the press).
7. Gollub, J. P. & Benson, S. V. *J. Fluid. Mech.* **100,** 449–470 (1980).
8. Eckmann, J.-P. *Rev. mod. Phys.* **53,** 643–654 (1981).
9. Greenside, H. S., Ahlers, G., Hohenberg, P. C. & Walden, R. W. *Physica* D (in the press).
10. Guckenheimer, J. Moser, J. & Newhouse, S. *Dynamical Systems* (Birkhäuser, Boston, 1980).
11. Ruelle, D. *Ann. N.Y. Acad. Sci.* **316,** 408–416 (1979).
12. Packard, N. H., Crutchfield, J. P., Farmer, J. D. & Shaw, R. S. *Phys. Rev. Lett.* **45,** 712–716 (1980).
13. Froehling, H., Crutchfield, J. P., Farmer, J. D., Packard, N. H. & Shaw, R. S. *Physica* **3D,** 605–617 (1981).
14. Takens, F. in *Dynamical Systems and Turbulence,* Warwick 366–381 (Springer, New York, 1981).
15. Hirsch, M. W. *Differential Topology* (Srpinger, New York, 1976).
16. Smale, S. *Bull. Am. math. Soc.* **73,** 747–817 (1967).
17. Henon, M. *Comm. Math. Phys.* **50,** 69–78 (1976).

Natural production of tritium in permeable rocks

J. N. Andrews

School of Chemistry, University of Bath, Claverton Down,
Bath BA2 7AY, UK

R. L. F. Kay

Institute of Geological Sciences, Environmental Protection Unit,
Building 151, Harwell Laboratory, Didcot, Oxon OX11 0RA, UK

Natural tritium production by the reaction, ${}^6_3\mathrm{Li}(n,\alpha){}^3_1\mathrm{H}$, may in some circumstances lead to ${}^3\mathrm{H}$ contents in the fracture fluids of a granite, which are significantly above the present natural ${}^3\mathrm{H}$ content (0.5 tritium units, TU) of pre-bomb precipitation. We show here that the principal factors which determine the ${}^3\mathrm{H}$ content of the fracture fluids are the U, Th, Li and B contents of the rock and its matrix porosity. Granites with high U, Th and Li contents; low B content and a low matrix porosity may have a naturally maintained ${}^3\mathrm{H}$ content of up to about 2.5 TU in water within the matrix. This has important implications for the interpretation of groundwater flow patterns from their ${}^3\mathrm{H}$ contents. Whereas it has generally been assumed that groundwaters with ${}^3\mathrm{H}$ contents greater than 0.5 TU have a proportion of post-1954 recharge present, this may not always be a valid conclusion.

Precipitation after 1954 contained ^{3}H which was produced by the thermonuclear weapon testing in the atmosphere. The ^{3}H content of rainfall in the UK has declined from a maximum of ~2,000 TU in 1963 to about 60 TU in 1975[1]. The pre-1954 ^{3}H content (due to cosmic ray production) of precipitation on the western coast of Europe was ~2.5 TU (ref. 2) and a groundwater which was recharged in 1953 with this ^{3}H content would at present (1982) contain only a residual 0.5 TU because of ^{3}H decay (half life, 12.3 yr). A groundwater with the natural ^{3}H input (2.5 TU) would need to be ~60-yr old to reduce its ^{3}H content to 0.1 TU by decay. This is about the analytical limit[3] for determining ^{3}H in water.

A groundwater with a ^{3}H content ≥ 0.1 TU is therefore generally considered to be younger than 60 yr and, especially if the ^{3}H content exceeds a few TU, to contain a proportion of post-1954 precipitation. Here, we consider whether or not it is possible that groundwaters older than 60 yr could contain levels of ${}^3\mathrm{H} > 0.1$ TU due to *in situ* production of ^{3}H. Such production is most likely for groundwaters from granites for which lithium and radioelement contents are comparatively high.

The only nuclear reaction which can produce significant ^{3}H natural activity by in-ground production is the neutron-induced reaction:

$$ {}^6_3\mathrm{Li}(n,\alpha){}^3_1\mathrm{H} \qquad (1)$$

The thermal neutron cross-section for this reaction[4] is large and neutrons are produced in rocks by both spontaneous fission of uranium and by (α, n) reactions on the major matrix elements; Si, O, Al, Mg. The activity of ^{3}H produced at a constant rate P by neutron irradiation of lithium for time t is given by:

$$\left(\frac{dN_r}{dt}\right)_t = \lambda (N_r)_t = P(1-e^{-\lambda t}) \qquad (2)$$

where $(N_r)_t$ is the number of ^{3}H atoms present after time t and λ is the decay constant for ^{3}H, from which

$$(N_r)_t = \frac{P}{\lambda}(1-e^{-\lambda t}) \qquad (3)$$

and

$$\lim_{t\to\infty} (N_r)_t = \frac{P}{\lambda} \qquad (4)$$

P may be estimated in a manner similar to that used by Zito *et al.*[5] to estimate in-ground ^{14}C production. The chance, F, of neutron absorption by Li relative to absorption by other neutron-absorbing elements is given by:

$$F = \sigma_{\mathrm{Li}} N_{\mathrm{Li}} \Big/ \sum_1^{92} \sigma_i N_i = \sigma_{\mathrm{Li}} N_{\mathrm{Li}} / C_t \qquad (5)$$

where σ_i, N_i are the total neutron absorption cross-sections and abundances for all elements in the matrix; σ_{Li} is the cross-section for reaction (1) and N_{Li} is the abundance of Li in the matrix. The $\sigma_i N_i$ summation, C_t, may be regarded as the total neutron capture probability for the rock matrix and the terms

0028–0836/82/29036 —03$01.00

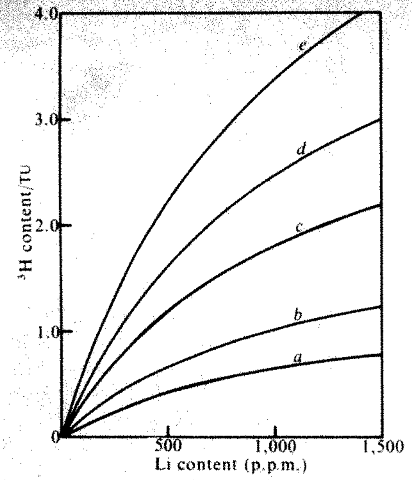

Fig. 1 Variation of the ^{3}H content of water in a granite with the Li, U and Th contents. A boron content of 15 μg per g (average granite, ref. 6) and an equivalent total porosity (see text) of 1% were assumed. *a*, 3.5 p.p.m. U+18 p.p.m. Th; *b*, 10 p.p.m. U+15 p.p.m. Th; *c*, 20 p.p.m. U+20 p.p.m. Th; *d*, 30 p.p.m. U+20 p.p.m. Th; *e*, 40 p.p.m. U+30 p.p.m. Th.

of this summation for various rocks are listed in Table 1. The Li-content of the rock matrix directly influences the ^{3}H production rate and B, because of its strong influence on the total capture probability, needs to be further considered. This may be facilitated by substituting for C_t in equation (5) as follows:

$$C_t = C + \sigma_{\text{Li}} N_{\text{Li}} + \sigma_{\text{B}} N_{\text{B}} \qquad (6)$$

where C is the total absorption probability excluding the contributions of Li and B. For a granite matrix, the fraction F, of thermal neutrons captured by Li may be shown to be:

$$F = [\text{Li}]/\{1.057\times10^{-7} + [\text{Li}] + 6.827[\text{B}]\} \qquad (7)$$

where [Li] and [B] are the Li and B contents of the rock in μg per g. This equation was derived for the elemental composition of average granite[6] using cross-sections for thermal neutron absorption. Only thermal neutron absorption has been considered as the cross-sections for fast neutron absorption reactions are generally very much smaller than those for thermal neutron reactions and the high abundance of light elements (O, Si) in the matrix ensures that neutrons are thermalized by scattering processes. The ^{3}H production rate, P, is given by:

$$P = Fn \quad \text{atoms s}^{-1}\,\text{cm}^{-3} \qquad (8)$$

where n = neutron production in the rock, neutrons $\text{s}^{-1}\,\text{cm}^{-3}$. The neutron production in granites has been estimated by Feige *et al.*[7] (Table 2).

Following neutron-induced fission of ^{6}Li, the ^{3}H nuclei formed capture electrons to form ^{3}H atoms which diffuse through the rock matrix much more readily than molecular hydrogen. Their ultimate fate is to combine to form $^3H_2$ or to exchange with the H atoms of water molecules to form ^{3}HHO. The latter is much more probable than direct combination in a matrix which contains aqueous fluids as the diffusing ^{3}H atoms are likely to encounter water molecules before they meet other ^{3}H atoms. Exchange of the diffusing ^{3}H atoms with structurally bound water or hydroxyl groups in the rock matrix is also likely to occur. The total water content of the matrix, that is, structurally bound water and pore- or fracture-contained water, may be combined to obtain an equivalent total porosity, ϕ, for the rock. The ^{3}H atoms are trapped on a random basis by the total water in the matrix and its specific activity in structurally bound and pore water is therefore identical with that in the fracture fluids from which samples are generally drawn.

The ^{3}H content of the fluid is given by the equation:

$$^3\text{H-content(TU)} = \frac{P}{\lambda\ \phi} \frac{18\times10^{18}}{\times 2\times6.02\times10^{23}} \qquad (9)$$

where λ (0.0559 yr^{-1}) is the decay constant of ^{3}H and P is the ^{3}H production rate (atoms yr^{-1}); as there are $2\times6.02\times10^{23}$ H atoms in 1 mole (18g) of water and 1 TU is defined as 1 ^{3}H atom in 10^{18} H atoms. The ^{3}H content is inversely proportional to the equivalent total porosity and will become most significant for rocks with both low porosity and only small amounts of structurally bound water. Recent measurements on various granites[8,9] suggest that the minimum porosity is in the range 0.3–0.5%. The amount of structurally bound water is also about 0.5% for unaltered granites[9]. The minimum equivalent total porosity for granite is therefore ~1% and *in situ* ^{3}H contents were calculated for this porosity. Figure 1 shows the variation of ^{3}H content with the Li and radioelement contents for a granite of average B content (15 μg per g). At high Li and radioelement contents, *in situ* ^{3}H production could lead to ^{3}H contents in the fracture fluids which exceed the maximum possible residual cosmogenic ^{3}H from recharge just before 1954

Table 1 Neutron capture probabilities (abundance × capture cross-section) in rock matrices

Element	Atomic No.	Cross-section (barns)	Neutron capture probability (mol barns) Ultramafic	Basalt	Granite	Sandstone	Limestone
Li	3	71	0.000005	0.00015	0.00040	0.00015	0.00034
B	5	755	0.00007	0.00035	0.00104	0.00244	0.00140
Na	11	0.534	0.00013	0.00045	0.00064	0.00007	0.00000
Mg	12	0.064	0.00068	0.00012	0.00000	0.00000	0.00012
Al	13	0.232	0.00004	0.00075	0.00066	0.00021	0.00004
Si	14	0.160	0.00108	0.00137	0.00184	0.00209	0.00014
Cl	17	33.6	0.00005	0.00005	0.00022	0.00014	0.00014
K	19	2.07	0.00002	0.00044	0.00176	0.00056	0.00014
Ca	20	0.44	0.00008	0.00074	0.00017	0.00042	0.00332
Ti	22	6.1	0.00004	0.00115	0.00029	0.00019	0.00005
Cr	24	3.1	0.00012	0.00001	0.00000	0.00000	0.00000
Mn	25	13.3	0.00036	0.00048	0.00014	0.00001	0.00027
Fe	26	2.56	0.00045	0.00039	0.00123	0.00044	0.00017
Co	27	37.5	0.00013	0.00003	0.00000	0.00000	0.00000
Ni	28	4.54	0.00015	0.00001	0.00000	0.00000	0.00000
Sm	62	5,820	0.00002	0.00019	0.00034	0.00038	0.00005
Gd	64	49,000	0.00016	0.00156	0.00280	0.00311	0.00040
Total capture probability			0.00358	0.00841	0.01177	0.01045	0.00668

Elements which do not contribute >1% of the total capture probability for at least one rock type, have not been tabulated. The average rock compositions of ref. 6 have been used.

Table 2 Neutron production in granites

a, Spontaneous fission (s.f.) neutrons

	s.f. half life (yr)	Neutrons per fission	Neutrons per year per μg of natural U
^{238}U	8.04×10^{15}	2.2	0.4762
^{235}U	1.87×10^{17}	2.5	0.0002
Total	—	—	0.4764

b, Neutrons produced by α-irradiation of light nuclei[7]

SiO_2 content (%)	Neutrons per year per g of rock for each p.p.m. U	Th
60	1.70	0.76
70	1.44	0.65

(0.5 TU). The effect of increased B contents is demonstrated by Table 3. In general, a 10-fold increase in B content results in a 3- to 5-fold reduction in the amount of *in situ* produced ^3H in the fracture fluids. Variation of the Gd content of the matrix would also significantly affect ^3H production.

The Carnmenellis granite, one of the major outcrops of the granite batholith of South West England[10], is known to have high radioelement and Li contents. High salinity groundwaters occur in tin mines at depths of up to 690 m, and these have been shown to result from alteration reactions of the granites with meteoric waters[11]. These waters had apparently constant ^3H contents of 6 ± 2 TU over a range of salinities and this could be a consequence of either *in situ* ^3H production or variations in the extent to which alteration reactions have proceeded.

Lithium is generally present in the biotite[12] and an average whole-rock Li content for the Carnmenellis granite is 278 μg per g, compared with an average Li content of 340 μg per g for the similar, poorly megacrystic, Dartmoor granite[13]. Higher average Li contents (~1,100 μg per g) are present in the St Austell granite[12].

The available data for the Carnmenellis granite suggest that its B content is of the order 250 μg per g, compared with 15 μg per g for average granite. Outcrop samples of the Bodmin granite have an average B content of 270 μg per g whilst the two available analyses (J. R. Hawkes personal communication) of the Carnmenellis granite are 85 and 230 μg per g respectively. Tourmaline is the principal B-bearing mineral and is present in both primary and secondary forms[10]. The variation of B content with depth in the granite is not known but it is likely that secondary tourmalinization is greater towards the granite margins. The B content at depth is therefore unlikely to be greater than that at outcrop. The Gd contents of the Cornish granites[14] are similar to those for average granite.

The dependence of ^3H production in the Carnmenellis granite on Li and B contents is indicated in Table 3. It is evident that for the probable geochemical conditions in this granite (250–500 μg per g of Li; 250 μg per g of B), the *in situ* ^3H production cannot supply more than 0.5 TU to the fracture fluids. Higher Li contents occur in the nearby St Austell granite for which the B content is lower (<50 μg per g), so that tritium in excess of 1 TU could be present in fracture fluids as a result of *in situ* production. It is, however, concluded that the 6 TU observed in the deep groundwaters from the Carnmenellis granite must be principally due to the presence of meteoric water of post-1954 origin. In the most favourable case for ^3H production, a granite with a high Li content and an average B content, the consequent fracture fluid ^3H content is unlikely to exceed 1 TU in most cases, or up to 2.5 TU for highly uraniferous granite.

Table 3 ^3H-content of fracture fluids resulting from *in situ* ^3H-production, for various Li and B contents in the Carnmenellis granite*

Li-content (μg per g)	^3H-content†, TU for B-contents (μg per g) 15	50	250	500	1,000
50	0.14	0.11	0.05	0.03	0.02
250	0.57	0.47	0.24	0.15	0.08
500	0.95	0.81	0.45	0.29	0.17
1,000	1.40	1.25	0.76	0.52	0.31
1,500	1.67	1.52	1.00	0.71	0.44

* U = 13.6 p.p.m.; Th = 16.9 p.p.m. (ref. 15).

† For an equivalent total porosity of 1.0% and a rock bulk-density of 2.6 g cm^{-3}.

We thank A. H. Bath, W. M. Edmunds, J. R. Hawkes and M. Stone for helpful discussions, J. R. Hawkes for access to unpublished analyses of the Cornish granites by the Laboratory of the Government Chemist. The support of the Natural Environment Research Council through research grant GR3/2622 is gratefully acknowledged. R.L.F.K. contributes to this paper with the permission of the director of the Institute of Geological Sciences.

Received 8 March; accepted 17 May 1982.

1. Foster, S. S. D. & Smith-Carrington, A. *J. Hydrol.* **46,** 343–364 (1980).
2. von Buttlar, H. & Libby, W. F. *J. Inorg. nucl. Chem.* **1,** 75–91 (1955).
3. Cameron, J. F. in *Radioactive Dating and Methods of Low-level Counting* 543–573 (IAEA, Vienna, 1967).
4. Hughes, D. J. & Schwarz, R. B., *Report BNL-325* (Brookhaven National Laboratory, New York, 1958).
5. Zito, R., Donahue, D. J., Davis, S. N., Bentley, H. W. & Fritz, P. *Geophys. Res. Lett.* **1,** 235–238 (1980).
6. Parker, R. L. *U.S. geol. Surv. Profess. Pap.* 440–D (1967).
7. Feige, Y., Oltman, B. G. & Kastner, J. *J. geophys. Res.* **73,** 3135–3142 (1968).
8. Hall, D. H., Black, J. H. & Storey, B. C. *Rep. ENPU 81–10,* (Institute of Geological Sciences, London, in the press).
9. Nelson, P. *et al., Rep. LBL-8280* (Lawrence Berkeley Laboratory, University of California 1979).
10. Edmonds, E. A., McKeown, M. C. & Williams, M. *British Regional Geology: South West England* (Institute of Geological Sciences, London, 1975).
11. Burgess, W. G., Edmunds, W. M., Andrews, J. N., Kay, R. L. F. & Lee, D. J. *The Origin and Circulation of Groundwater in the Carnmenellis Granite: the Hydrogeochemical Evidence* (Institute of Geological Sciences, London, 1982).
12. Beer, K. E., Edmunds, W. M. & Hawkes, J. R. *Energy* **3,** 281–292 (1978).
13. Hawkes, J. R. & Dangerfield, J., *Proc. Ussher Soc.* **4,** 158–171 (1978).
14. Alderton, D. H. M., Pearce, J. A. & Potts, J. A. *Earth planet. Sci. Lett.* **49,** 149–165 (1980).
15. Tammemagi, H. Y. & Wheildon, J. *Geophys. J. R. astr. Soc.* **38,** 83–94 (1974).

Role of Mn(IV) oxide in abiotic formation of humic substances in the environment

H. Shindo* & P. M. Huang

Saskatchewan Institute of Pedology, University of Saskatchewan,
Saskatoon, Saskatchewan, Canada S7N 0W0

The oxidative polymerization of polyphenols in soils is regarded as one of the main processes in the formation of humic substances[1–7]. The polymerization causes the darkening of the colour of polyphenols—the 'browning phenomenon'—which can be accelerated non-enzymatically as well as enzymatically[7–15]. However, the relative effectiveness of various inorganic components, especially noncrystalline to poorly crystalline Fe, Al, Mn and Si oxides commonly occurring in soils[16–19], in affecting the browning of polyphenols is still obscure. The elucidation of the relative effectiveness of these oxides is of importance in understanding their roles in the formation of humic substances in the environment. We report here that Mn(IV) oxide is a very effective oxidant with respect to the abiotic browning of hydroquinone solution over the *p*H range (4–8) common in soil. On the other hand, the accelerating effect of Fe oxide on the browning is extremely small. The promoting effects of Al and Si oxides were not observed in the conditions studied. The results obtained in the present study indicate that Mn(IV) oxides deserve close attention in the abiotic formation of humic substances in the environment.

---

* Permanent address: Faculty of Agriculture, University of Yamaguchi, Yamaguchi, Japan 753.

Table 1 Effects of Mn, Fe, Al and Si oxides on the browning of hydroquinone solution at different *p*H values at the end of the reaction period of 24 h

Oxide*	Initial *p*H of 4.0				Initial *p*H of 5.0				Initial *p*H of 6.0			
	Final		Absorbance		Final		Absorbance		Final		Absorbance	
	*p*H	*Eh*(V)	400 nm	600 nm	*p*H	*Eh*(V)	400 nm	600 nm	*p*H	*Eh*(V)	400 nm	600 nm
None	4.0	0·38	Colourless†		5.0	0.32	Colourless†		6.0	0.27	Colourless†	
Mn	4.1	0.44	1.64	0.46	5.3	0.38	0.88	0.20	7.5	0.32	7.44	1.84
Fe	4.0	0.40	0.06	0.02	5.0	0.33	0.01	Colourless†	6.1	0.27	Colourless†	
Al	4.0	0.38	Colourless†		5.0	0.32	Colourless†		6.0	0.27	Colourless†	
Si	4.0	0.38	Colourless†		5.0	0.32	Colourless†		6.0	0.27	Colourless†	

Oxide	Initial *p*H of 7.0				Initial *p*H of 7.8			
	Final		Absorbance		Final		Absorbance	
	*p*H	*Eh*(V)	400 nm	600 nm	*p*H	*Eh*(V)	400 nm	600 nm
None	6.9	0.24	0.30	0.09	6.9	0.24	0.70	0.17
Mn	7.7	0.29	8.62	2.06	7.7	0.32	8.86	2.12
Fe	6.9	0.25	0.10	0.02	7.0	0.25	0.37	0.10
Al	6.7	0.25	0.10	0.04	6.8	0.24	0.24	0.08
Si	6.8	0.24	0.20	0.06	6.9	0.24	0.49	0.12

* The experimental procedures were as stated in Fig. 1.

† The supernatant is visibly colourless and its absorbance is <0.01.

Noncrystalline or poorly crystalline oxides of manganese (birnessite, δ-MnO_2), iron, aluminium and silicon were prepared and used in this study as they commonly occur in soils[16–19]. Hydroquinone was used as the phenolic compound in this study, because benzoquinone derivatives are known to be parts of the chemical structure of humic acid[2,3,5,6], and the use of catechol derivatives which rapidly form coloured chelate complexes with iron[20] is inadequate for this study.

Figure 1 shows the absorption spectra of several browning solutions in the visible region at the end of the reaction period of 24 h. The colours of the solutions were light reddish brown to dark brown, and differed from the colour (yellow) of *p*-benzoquinone which is an oxidized monomeric product of hydroquinone. The shapes of their spectra varied with the reaction conditions, indicating that substances with varying degrees of polymerization were formed. Their absorbances in the visible region were distinct from each other. The degree of the browning of hydroquinone solution as influenced by the various oxides can be compared by using light absorption at given wavelengths. The degree of humification of humic acid is commonly determined using light absorbances at 400 and 600 nm (ref. 9). Therefore, in this study, the absorbances at 400 and 600 nm were used to determine the effects of the oxides on the browning.

Table 1 shows the effects of Mn, Fe, Al, and Si oxides on the browning of hydroquinone solution at different *p*H values at the end of the reaction period of 24 h. The control solution without the oxides became coloured only when the initial *p*H of the solution was 7.0 or higher. The degree of the browning at *p*H 7.8 was higher than that at *p*H 7.0, indicating that oxidative polymerization was promoted at the higher *p*H. The addition of Mn oxide greatly accelerated the browning over the *p*H range (4.0–7.8). The degree of the browning in the Mn oxide system was influenced by the *p*H values. In the case of *p*H 5.0, the degree of the browning was much lower than that at other *p*H values. In both solutions of *p*H 4.0 and 5.0, the

Table 2 Effects of antiseptic and inoculum on the browning of hydroquinone solution both in the absence and presence of birnessite at the end of the reaction period of 24 h

No.	Mn oxide*	Antiseptic	Inoculum†	Final *p*H	Growth of micro-organisms‡	Absorbance 400 nm	Absorbance 600 nm
1	–	–	–	6.0		Colourless‖	
2	–	$HgCl_2$	–	5.5		0·23	0·04
3	–	Toluene	–	6.0		Colourless‖	
4	–	–	+	6.0		Colourless‖	
5	+	–	–	7.4	ND§	6.70	1.66
6	+	$HgCl_2$	–	7.1	ND	5.00	1.42
7	+	Toluene	–	7.4	ND	6.70	1.66
8	+	–	+	7.4		6.70	1.66

* 20 mg of Mn oxide (birnessite)[21] was suspended in 20 ml of 0.1 M sodium acetate solution at *p*H 6.0 containing 10 μmol ml^{-1} hydroquinone; in certain cases, 2 ml of water, 2 ml of 1% $HgCl_2$, 1 ml of toluene or 2 ml of inoculum was added. The subsequent procedures are as stated in Fig. 1.

† Filtrate was obtained from the soil water suspension (soil:water ratio = 1:10). The fresh soil sample was taken from the Ap horizon of the Unity Orthic soil in Wilkie, Saskatchewan, Canada.

‡ The growth of microorganisms in the solution at the end of the reaction period of 24 h was examined using agar plates which contained nutrient broth and agar[24].

§ ND, no colonies were observed on the plates even after 4 days.

‖ The supernatant is visibly colourless and its absorbance is <0.01.

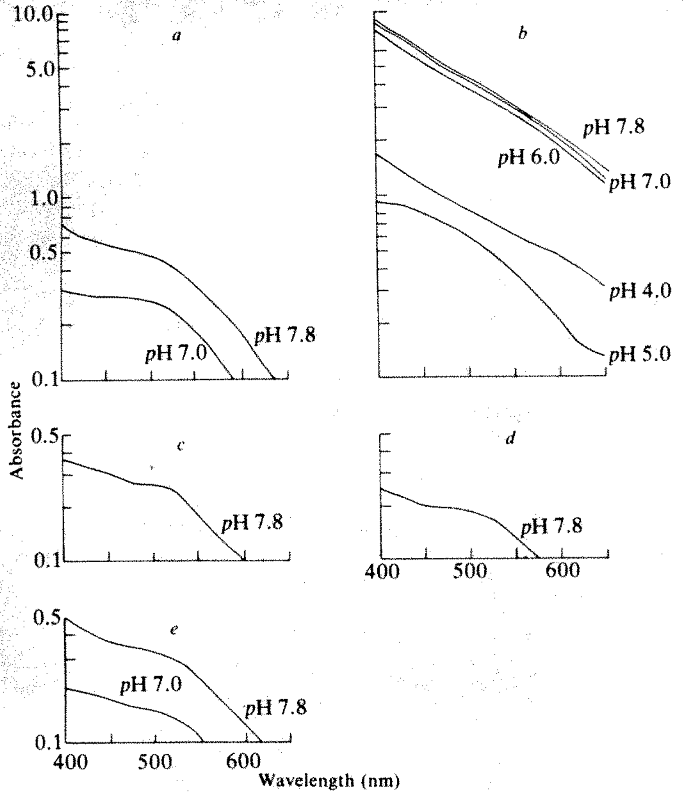

Fig. 1 The absorption spectra of several browning solutions in the visible region at the end of the reaction period of 24 h. *a*, Control (hydroquinone); *b*, Mn system; *c*, Fe system; *d*, Al system; *e*, Si system. pH means initial pH of the hydroquinone solution used. In systems *b* to *e* the Mn oxide (birnessite)[21], Fe (ref. 22), Al (ref. 22), and Si (ref. 23) oxides were prepared. Twenty mg of each oxide was suspended in 20 ml of 0.1 M sodium acetate solution at different pH values containing $10\ \mu mol\ ml^{-1}$ hydroquinone. The flasks (125 ml) containing the suspensions were placed in an oscillating shaker in a water bath at 25 °C for 24 h. After the reaction period, the suspension was centrifuged at 38,000*g* for 20 min. The absorbance of the supernatant was measured with a spectrophotometer directly or after dilution; the resulting absorbances were scaled by the dilution factor. The sodium acetate solution which did not contain hydroquinone was used as reference.

Mn oxide added was dissolved at the end of the reaction period of 24 h. In the solution of pH 5.0, a very broad absorption band ranging from 400 to 600 nm was observed; this is different from the other Mn systems (Fig. 1*b*). Therefore, the low degree of the browning at pH 5.0 may be attributed to the formation of a stable complex which does not polymerize further. In the cases of pH 6.0 or higher, the degree of the browning was much higher than that at pH 4.0 or 5.0. This result cannot be explained by the *Eh* values of the system, because *Eh* decreased with increasing pH. In the Mn oxide systems to which were added solutions of initial pH values of 6.0, 7.0 and 7.8, the final pH values ranged from 7.5 to 7.7. On the other hand, final pH values in the control systems ranged from 6.0 to 6.9. Therefore, the high degree of the browning in the Mn oxide systems at the initial pH values of 6.0 or higher is attributed to the following processes: (1) the Mn oxide acts as a Lewis acid which accepts electrons from hydroquinone leading to its oxidative polymerization and (2) the acceleration of oxidative polymerization which is driven by an increase of pH which is in turn caused by the reduction of Mn oxide.

The absorption spectra of the browning solutions in the Mn systems at pH 4.0, 6.0, 7.0 and 7.8 (Fig. 1*b*) were similar to those of humic acids[9]. Their $\Delta\log K$, namely, the logarithm of the ratio of the absorbance at 400 nm to that at 600 nm (ref. 9), ranged from 0.55 to 0.62. This indicates that Mn oxides are capable of accelerating the conversion of phenolic compounds such as hydroquinone to humic acid-like polymers with a relatively high degree of humification.

The promoting effect of Fe oxide on the browning was observed only in acidic conditions, and the effect was higher at pH 4.0 than at pH 5.0 (Table 1). The accelerating effects of Al and Si oxides on the browning were not observed at all the pH conditions studied.

The control solution became coloured when the solution was adjusted to pH 7.0 or 7.8. In the presence of Fe, Al and Si oxides, a decrease in the degree of the browning was observed. This decrease is attributed to the adsorption of the browning substances by the oxides.

To determine whether microorganisms influence the browning of hydroquinone solution in the conditions studied, antiseptic or inoculum was added to the system. The browning of hydroquinone solution was then studied. As shown in Table 2, the hydroquinone solution in the absence of Mn oxide was colourless both in the absence and presence of toluene or inoculum. The degree of the browning in the Mn oxide system was not influenced by the presence of either toluene or inoculum. $HgCl_2$ slightly accelerated the browning of hydroquinone solution without Mn oxide, indicating that $HgCl_2$ has a weak power in causing the browning. The presence of Hg(II) in the Mn oxide system slightly suppressed the browning. $HgCl_2$ is a considerably weaker oxidant than MnO_2 (Table 2). Therefore, the influence of $HgCl_2$ on the browning of hydroquinone solution by MnO_2 may be attributed to the blocking of a portion of Lewis acid sites on the surfaces of MnO_2 by Hg(II). Agar plates, inoculated with the browning solution, did not show any growth of microorganisms (Table 2). Therefore, the results clearly show that the browning of hydroquinone solution in the conditions studied occurs abiotically.

Our data reveal that Mn(IV) oxide is a very effective oxidant compared with Fe, Al and Si oxides in the abiotic browning of hydroquinone. This finding indicates that Mn(IV) oxide may have an important role in the formation of humic substances in the environment.

This study was supported by a grant from the Natural Sciences and Engineering Research Council of Canada. We thank Dr J. J. Germida in our Institute for help with the microbiological aspects of the experiment.

Received 18 March; accepted 10 May 1982.

1. Kononova, M. M. *Soil Organic Matter* 2nd edn, 544 (Pergamon, Oxford, 1966).
2. Flaig, W., Beutelspacher, H. & Rietz, E. in *Soil Components* Vol. 1 (ed. Gieseking, J. E.) 1-211 (Springer, Berlin, 1975).
3. Felbeck, G. T. Jr *Adv. Agron.* 17, 327-368 (1965).
4. Hurst, H. M. & Burges, N. A. in *Soil Biochemistry* Vol. 1 (eds McLaren, A. D. & Peterson, G. H.) 260-286 (Dekker, New York, 1967).
5. Martin, J. P. & Haider, K. *Soil Sci.* **111,** 54-63 (1971).
6. Schnitzer, M. & Khan, S. U. *Humic Substances in the Environment,* 327 (Dekker, New York, 1972).
7. Scheffer, F. & Ulrich, B. *Humus and Humusdüngung,* 260 (Ferdinand Enke, Stuttgart, 1960).
8. Kumada, K. & Kato, H. *Soil Sci. Pl. Nutr.* **16,** 195-200 (1970).
9. Kumada, K. *Chemistry of Soil Organic Matter* (in Japanese) 220 (University of Tokyo Press, 1977).
10. Kyuma, K. & Kawaguchi, K. *Proc. Soil Sci. Soc. Am.* **28,** 371-374 (1964).
11. Wang, T. S. C., Li, S. W. & Ferng, Y. L. *Soil Sci.* **126,** 15-21 (1978).
12. Wang, T. S. C., Kao, M. M. & Huang, P. M. *Soil Sci.* **129,** 333-338 (1980).
13. Haider, K., Frederick, L. R. & Flaig, W. *Plant and Soil* **22,** 49-64 (1965).
14. Scheffer, F., Meyer, B. & Niederbuddle, E. A. *Z. Pflanzenernähr. Düng., Bodenk.* **87,** 26-44 (1959).
15. Haider, K., Martin, J. P. & Filip, Z. in *Soil Biochemistry,* Vol. 4 (eds Paul, E. A. & McLaren, A. D.) 195-244 (Dekker, New York, 1975).
16. Hsu, P. H. in *Minerals in Soil Environments* (eds Dixon, J. B. & Weed, S. B.) 99-143 (Soil Science Society of America, Madison, 1977).
17. Schwertmann, U. & Taylor, R. M. in *Minerals in Soil Environments* (eds Dixon, J. B. & Weed, S. B.) 145-180 (Soil Science Society of America, Madison, 1977).
18. McKenzie, R. M. in *Minerals in Soil Environments* (eds Dixon, J. B. & Weed, S. B.) 181-193 (Soil Science Society of America, Madison, 1977).
19. Wilding, L. P., Smeck, N. E. & Dress, L. R. in *Minerals in Soil Environments* (eds Dixon, J. B. & Weed, S. B.) 471-552 (Soil Science Society of America, Madison, 1977).
20. Shindo, H. & Kuwatsuka, S. *Soil Sci. Plant Nutr.* **22,** 23-33 (1976).
21. McKenzie, R. M. *Miner. Mag.* **38,** 493-502 (1971).
22. Huang, P. M., Wang, T. S. C., Wang, M. K., Wu, M. H. & Hsu, N. W. *Soil Sci.* **123,** 213-219 (1977).
23. Mitchell, S. A. *Chemy Ind.* **23,** 924-933 (1966).
24. Germida, J. J. & Casida, L. E. Jr *J. Bact.* **144,** 1152-1158 (1980).

Is the CH_4, H_2 and CO venting from submarine hydrothermal systems produced by thermophilic bacteria?

John A. Baross, Marvin D. Lilley
& Louis I. Gordon

School of Oceanography, Oregon State University, Corvallis,
Oregon 97331, USA

Submarine hydrothermal vents are a major source of methane to the oceans[1,2]. The methane, as well as H_2 and CO, are generally believed to result from degassing of the mantle or from abiogenic water–rock reactions[1], a conclusion supported by direct correlations between ^3He and CH_4, and generally between CH_4, H_2 and CO and dissolved silicate in hydrothermal waters[2,3]. An alternative source for these gases might be microbiological. This would imply that active bacterial communities exist in deep-sea hot water environments, some of which have temperatures exceeding 100 °C; this inference is without precedent. We have now found that the super-heated waters emanating from sulphide chimneys at 21 °N along the East Pacific Rise and samples from the sulphide chimneys themselves harbour complex communities of bacteria capable of growing with generation times of 37–65 min, producing CH_4, CO, H_2 and traces of N_2O in media containing $S_2O_3^{2-}$, Mn^{2+} and Fe^{2+} as energy sources, and oxidizing CH_4, at 100±2 °C at 1 atm. These microbial communities consist of three to five morphologically distinct types and include both oxidative and anaerobic species. These mixed cultures will not grow at temperatures below 70–75 °C. Even though some of the communities originated from water of temperatures >300 °C, it is not known if they can grow and produce CH_4, CO and H_2 in super-heated waters kept liquid due to hydrostatic pressure. The discovery of these obligately thermophilic, gas-producing and consuming bacterial communities associated with submarine volcanic environments has interesting and important implications for prokaryotic evolution, marine geochemistry, industrial microbiology and exobiology.

Submarine hydrothermal systems located along tectonic rifts and ridges off the Galapagos Islands and along the East Pacific Rise[4–6] and the Gorda Ridge have been studied and sampled since 1977. Two groups of vents have been described: (1) cracks and small fissures which emit warm water (5–22 °C) at a flow rate of $\sim 2\,cm\,s^{-1}$ and (2) spectacular 3–10-m high conical sulphide mounds (chimneys) out of which spout super-heated waters with temperatures as high as 380±30 °C and flow rates of metres per second (ref. 5). At the depth of these hydrothermal systems (2,500–2,650 m) seawater can remain liquid at temperatures up to ~460 °C due to the effect of hydrostatic pressure[7]. Sulphide chimneys are found at 21° N along the East Pacific Rise, and the warm water vents are found at both the Galapagos Rift and at 21° N. Associated with each of these hydrothermal environments are extensive and diverse groups of animals which are now known to derive their energy from chemosynthetic bacteria[8,9]. These bacteria, which are found in large numbers in warm vent waters[4,9], on animal and rock surfaces[10,11], and as endosymbionts associated with specific vent animals[12], utilize S, metals and possibly organic gases and H_2 as energy sources. Bacteria had previously not been thought to exist in the super-heated waters associated with sulphide chimneys.

During October and November 1979, samples of hot vent water, sulphide chimney sections and associated fauna were obtained from the East Pacific Rise at 21° N using the manned submersible, *Alvin*. The present report is based on microbial cultures obtained from eight hot water samples from black and white smoking chimneys and one chimney wall sample. Initial chemical, physical and microbiological analyses of these waters were made on board the R/V *Gillis* shortly after the samples surfaced.

In general, the concentrations of the biologically important chemical constituents, H_2S, Mn and Fe, were high in all samples. The concentration of each chemical species was dependent on the degree of mixing with ambient seawater (Table 1). Degree of mixing is indicated by the difference in the water temperatures, both as measured with a temperature probe attached to the *Alvin* and as calculated from Mg numbers (see corrected temperature measurements, Table 1). Also, the presence of anaerobic and aerobic bacteria capable of growing at 25 °C in some of the samples indicate mixing of the sample with bacteria from ambient or warm vent water. This is particularly apparent

Table 1 Chemical and microbiological characteristics of hot water venting from sulphide chimneys at 21° N along the East Pacific Rise

Sample designation	Temperature (°C)		pH	Concentration of biologically important constituents (μM)				Total nos of bacteria			Presence of thermophiles
									Viable counts at 25 °C (ml^{-1})		
	Probe	Corrected		H_2S	Mn	Fe	Si	Direct counts (ml^{-1})	Aerobic	Anaerobic	
978 5/6	220	195	5.12	7.5	1,055	153	11,700	1.4×10^4	<1	80	+
978 7/8	120	22	6.04	600	120	20	1,300	7.4×10^5	<1	310	+
980 7/8	84	46	6.27	475	68	—	2,839	3.5×10^5	<1	<1	+
979 11/12	100	3	7.53	1.2	17	56	200	1.8×10^5	<1	25	+
979 1/2	120	6	6.96	3.4	46	14	390	3.6×10^5	5	40	+
980 3/4	170	160	4.91	1,300	286	206	9,600	2.5×10^5	<1	<1	+
980 5/6	30–60	34	6.46	5	96	137	2,100	No data	No data	No data	No data
982 7/8	290	306	4.24	4,300	800	—	18,320	4.7×10^5	<1	<1	+
978(Niskin)*	3	3	Sample not analysed chemically					8.6×10^5	5.3×10^3	<1	–

All water samples were obtained with 750 ml gold-plated stainless steel and brass (one valve) samplers (provided by Sandia Laboratories, New Mexico) using the submergence research vehicle *Alvin* in October 1979. Subsamples were taken into sterile 20–150-ml bottles. Corrected temperature measurements were calculated from the relationship: $T = 0.00667$ (°C μmol^{-1}) (Mg) where Mg = Mg ambient − Mg measured; T = sample temperature. Mg data were provided by J. Edmond. All chemical measurements and pH were from John Edmonds (unpublished). Total direct bacterial counts were measured by epifluorescent microscopy using the procedures of Zimmerman and Meyer-Reil[21]. Water samples were immediately fixed on shipboard with 2% glutaraldehyde (Tousimis, electron microscopy grade) and maintained at 1 °C until counted back in the laboratory; total aerobic viable bacteria were enumerated using a basal salt medium (MS) which contained: NaCl, 26 g; KCl, 0.8 g; $MgCl_2 \cdot 6H_2O$, 5.6 g; $MgSO_4 \cdot 7H_2O$, 7.6 g; $CaCl_2$, 0.1 g in 1 l twice distilled water; MS was supplemented with $Na_2S_2O_3 \cdot 5H_2O$, 0.5%; $FeSO_4 \cdot 7H_2O$, 0.02%; $MnSO_4 \cdot H_2O$, 0.08%; $Na_2MoO_4 \cdot 2H_2O$, 0.001%; Na_2HPO_4, 0.9%; KH_2PO_4, 0.15%; $NaNO_3$, 0.1% trace element mixture according to Rippka, *et al.*[22]; medium adjusted to pH 7.5. Total anaerobic viable bacteria were enumerated using MS supplemented with 0.25% sodium formate, 0.1% $NaNO_3$, trace element mixture and phosphate buffer (above) at pH 7.5 and incubated in anaerobic jars in an atmosphere of H_2 and CO_2 using BBL Gas Pax disposable gas generator envelopes. Bacto purified agar (Difco) was dialysed in twice distilled water to remove soluble organic compounds and $12\,g\,l^{-1}$ was used. Water samples were enumerated using the spread plate technique for dilutions of 0.1, 0.01 and 0.001 ml whereas 1-, 5- or 10-ml samples were concentrated using 0.22-μm Millipore type GS membrane filter. The filters were then placed on the surface of the agar plates. The presence of thermophiles was detected using enrichment medium containing MS supplemented as described above for aerobic plating medium. Duplicate enrichments were adjusted to pH 5 and 7.5. A dilute heterotrophic medium 1/10 strength Lib-X (ref. 23) was also used. Glass screw-cap culture tubes (1.8 × 12 cm) containing 10 ml of the enrichment media were inoculated with 1–2 ml of the water sample. The inoculated samples were then placed in a boiling water bath for 1 h to minimize contamination and then incubated at 86 °C on a generator in the engine room of the R/V *Gillis*. All of the inorganic media enrichments at both pH 5 and 7.5 showed positive growth within 4 days. No growth was detected in the heterotrophic medium after 10 days.

* Sterile Niskin bag sample used to collect water from sites located adjacent to vents.

0028-0836/82/290366—03$01.00

Table 2 Rate of H_2, CH_4 and CO production by 21° N hot water and sulphide-chimney associated bacterial communities at 100 ± 2 °C

				Gas production			
Sample	Inoculum size (per 30 ml)	Medium Type	pH	nmol per ml per h H_2	nmol per ml per h CH_4	nmol per ml^{-1} per 9 h CO	Presence of N_2O (nmol ml^{-1})
978 5/6 (water)	1.3×10^6	A(S–NH_4^+)	7	102	42	10	0.15 at 36 h
			5	71	39	9	ND
		C(formate)	7	31	27	11	0.12 at 36 h
		D(no energy source)	7	0.3	0.3	0.6	ND
		A(killed cells)*		ND	ND	ND	ND
982 7/8 (water)	3.0×10^5	A	7	54	22	14	Trace‡
		C	7	(110)†	(46)†	(22)†	Trace‡
		D	7	0.2	ND	ND	ND
		A(killed cells)		ND	ND	ND	ND
3140 (sulphide chimney rock)	6.1×10^5	B(S–NO_3^-)	7	24	24	7.5	Trace†
			5	23	22	10	ND
		C	7	26	25	10	1.3 at 36 h
		D	7	0.3	ND	ND	ND
		A(killed cells)		ND	ND	ND	ND

Inoculum size was determined using epifluorescent microscopy. All media were made with MS (see Table 1 legend) supplemented with trace element mix (Table 1) and buffered with 1.0 g l^{-1} HEPES (Sigma). Medium A contained 0.02% $FeSO_4\cdot7H_2O$; 0.06% $MnSO_4\cdot H_2O$; 0.002% $Na_2MoO_4\cdot2H_2O$; 0.02% $(NH_4)_2SO_4$; 0.2% $Na_2S_2O_3\cdot5H_2O$; 0.03% Na_2HPO_4; 0.05% $NaHCO_3$. Medium B is the same as medium A except 0.02% KNO_3 was used in place of $(NH_4)_2SO_4$ as a nitrogen source. Medium C contained 0.02% $FeSO_4\cdot7H_2O$; 0.06% $MnSO_4\cdot H_2O$; 0.002% $Na_2MoO_4\cdot2H_2O$; 0.02% $(NH_4)_2SO_4$; 0.02% sodium formate; 0.03% Na_2HPO_4. Medium D contained MS plus HEPES buffer and 0.03% Na_2HPO_4 and was used as a non-energy source medium. This medium was inoculated as described for other reactions. Cultures were inoculated into 60-ml serum bottles containing 30 ml medium. The serum bottles were capped with Teflon caps. All media were equilibrated at 98–100 °C before inoculation and capping. No gases were detected in any of the uninoculated medium controls. All gases were detected by gas chromatography using a modification of the procedure described by Swinnerton and Linnenbom[24] with a custom-built gas chromatograph equipped with helium ionization, flame ionization and electron capture detectors[25]. In all cases most of the H_2 and CH_4 was produced by these cultures within 3 h of inoculation. The levels of CO continued to increase over a period of 8–12 h. The rate of gas formation was calculated based on three measurements made at 45 min, 2 h and 3 h for H_2 and CH_4, and at 45 min, 3 h and 9 h for CO. ND, not detected.

* Inoculum was exposed to 5% neutralized formalin for 24 h at 15 °C. The cells were then centrifuged at 12,000g for 10 min in a Sorvall RC-2B, resuspended in medium A and diluted to 10^6 cells per ml after counting by epifluorescent microscopy.

† In these samples only one gas sample was measured after 30 h incubation. Based on other experimental results (see above) these concentrations of gases were probably reached within 3 h.

‡ Trace levels of N_2O were <0.1 nmol ml^{-1} but >0.025 nmol ml^{-1}.

in samples 979 11/12 and 979 1/2. These samples also showed the greatest degree of mixing based on the Mg temperature calculations. In all samples, except the ambient Niskin bag sample (978), bacteria capable of growing at 86 °C were detected by enrichment in media composed of inorganic energy sources at either pH 5 or 7, but not in a dilute heterotrophic medium. The hottest water sample (982 7/8), which came from a black smoker, had the highest concentration of H_2S, Mn and Si and the lowest pH. In contrast, the other hot sample (978 5/6), which originated from a white smoker, had considerably lower levels of H_2S. High concentrations of H_2, CH_4 and CO were detected in both these samples. Also, in samples 979 3/4 and 982 7/8 the concentrations of CH_4 and H_2 exceeded 20 and 200 μM, respectively (M.D.L. and L.I.G., unpublished). The mixed communities of thermophilic bacteria have been kept intact by incubating at 85 °C with the transfer of 50 ml of culture into 450 ml medium at 6–8-week intervals. The experimental results reported here used these cultured communities.

The mixed cultures of thermophilic bacteria from these hot waters grew slowly at 80–86 °C and there was no evidence of gas production. When the cultured bacterial communities were transferred to fresh medium and incubated at 100 ± 2 °C in a water bath using a high boiling commercial coolant, rapid growth and active gas ebullition were observed. Table 2 shows the specific gases synthesized by the cultures and their rate of formation at 100 ± 2 °C. The rapid production of CH_4 by these communities was unexpected because no precautions had been taken to maintain anaerobic conditions with the initial water samples or with subsequent cultures. The gases were formed at both pH 5 and 7 in inorganic media and in a formate medium. In contrast to the H_2 and CH_4, which were at detectable levels within minutes after the samples were prepared, CO and N_2O required 9–24 h of incubation to reach measurable concentrations. The sulphide chimney sample also harboured a thermophilic microflora capable of producing the same suite of gases as the hot water cultures. This suggests either that there is a resident population of these organisms associated with sulphide chimneys which could be washed off into the venting fluid, or that these sites are contaminated with hot water bacteria. The temperatures of the outer surfaces of the chimneys are not known, but observable schlieren indicate that they are considerably warmer than the ambient seawater (J.A.B. and L.I.G., unpublished observation).

The thermophilic communities investigated are composed of anaerobic and aerobic bacteria including methanogens and methylotrophs. Table 3 shows the rate of CH_4 oxidation by these cultures. Neither the proportion of methane oxidizers in the cultures nor the versatility of the organisms in oxidizing other gases and ammonia have been determined. Enrichments in CH_4 and methanol-containing media with the intent of isolating pure cultures have resulted in a predominance of bacteria having homogeneous morphological characteristics. However, due to the mixotrophic nature of the cultures (oxidize CH_4, Mn^{2+} and NH_4^+), we are not yet positive of their purity.

The generation times of the mixed cultures at 100 °C in a medium containing S, Mn, Fe and $NaHCO_3$ ranged from 37 to 65 min (Table 3). The bacteria associated with the hottest water sample (982 7/8 at 304 °C) also had the shortest generation time. The lack of any measurable lag phase in the growth of these cultures at 100 °C might help explain their rapid production of CH_4 and H_2 (Table 2). Within 12–15 h incubation, the total numbers of bacteria remained constant at $\sim10^9$ cells ml^{-1}, although morphologically distinct groups continued to replace other groups for up to 2 weeks. Rod-shaped bacteria (1–2 μm) and small cocci (0.5–0.7 μm) dominated young cultures (up to 7 h) whereas in older cultures, sheathed, budding and filamentous bacteria, and a coccus having spines, were observed.

Because very few microorganisms have been described which can grow above 90 °C and only one species has been shown[13–16] to grow above 100 °C, it is probable the vent thermophiles are new species. For example, the highest growth temperature previously reported for a methanogen and a methylotroph are ~70 and 55 °C, respectively[14,17]. Also, because of the uniqueness, of these marine thermophiles, nothing is known about the biochemical reactions involved in their formation of H_2, CH_4 and CO. The elucidation of these metabolic pathways awaits the isolation of pure cultures. Due to the growth temperature characteristics of these communities and their propensity to form clumps and sheaths, it has been difficult to obtain pure cultures.

Table 3 Growth rates and rates of methane oxidation by 21 °N thermophilic bacterial communities at 100±2 °C

	Growth rate			Methane oxidation rate	
Sample	Time (h)	No. of bacteria ($\text{ml}^{-1}\times10^4$)	Generation time (min)	^{14}C-CH$_4$ oxidized to CO$_2$ (nmol h^{-1})	Inoculum size (no. bacteria per 50 ml)
978 5/6 (water)	0	1.2	55	2.3	3.0×10^7
	2	4.0			
	3.5	34			
	7	98			
	11	3,900			
928 7/8 (water)	0	2.7	37	2.5–3.9	5.0×10^7
	2	15			
	3.5	150			
	7	2,800			
	11	11,000			
3140 (chimney rock)	0	2.4	65	3.1–3.9	1.5×10^7
	2	10			
	3.5	25			
	7	120			
	11	3,700			

Growth rates of bacterial communities at 100 °C were determined using epifluorescent microscopy. The growth medium was MS with 0.5% HEPES buffer supplemented with 0.2% $Na_2S_2O_3\cdot5H_2O$; 0.02% $MnSO_4\cdot H_2O$; 0.02% $FeSO_4\cdot7H_2O$; 0.05% $(NH_4)_2SO_4$; 0.01 $Ca(NO_3)_2$ 0.05% Na_2HPO_4; 0.05% $NaHCO_3$; trace element mix (see Table 1 legend); 0.001% Bacto-yeast extract (Difco) and adjusted to *p*H 7.0±0.2. Yeast extract to 0.001% was found to stimulate growth of the communities. Higher concentrations were inhibitory. The component(s) in yeast extract responsible for this growth response is not known. Growth rates were determined from duplicate 100-ml cultures in 150-ml screw-cap bottles. 10-ml subsamples from each culture were used in all the bacterial count measurements. Methane oxidation rates were measured using ^{14}C-CH$_4$ at a final concentration of 1 μCi ml^{-1} (50 mCi mmol^{-1}). The bacterial cultures were grown in MS supplemented with trace element mix, 0.02% $NaNO_3$; 0.03% Na_2HPO_4; 0.02% $MnSO_4$ H_2O; 0.5% HEPES buffer in 60-ml serum bottles containing 25 ml medium with a gas mixture consisting of 20% methane and 80% air. After 24 h incubation at 100 °C, the cultures were brought up to a volume of 50 ml with MS medium, flushed for 2 min with air, capped and 1 ml of ^{14}C-CH$_4$ was added. Three sets of triplicate samples were run for each culture and the rates of methane oxidation were measured after 1, 2 and 4 h. Oxidation of methane was terminated by adding 1 ml of 10 M NaOH. The samples were then transferred to 100-ml serum bottles fitted with rubber caps according to the procedures of Harrison *et al.*[26] and the ^{14}C-CO$_2$ was collected on β-phenylethylamine-impregnated filter paper. The level of ^{14}C-CH$_4$ incorporated into cells was determined as previously described[27]. All samples were counted using a Beckman LS 100-C scintillation counter in 10 ml toluene fluor (Omnifluor, NEN). All counts were corrected for counting efficiency by the channel-ratio method. In general, about 1–5% of the total ^{14}C-CH$_4$ taken up by these communities was incorporated into cellular material.

One of the important questions regarding the oxidative microbial activity in anaerobic submarine hydrothermal waters is the nature, source and concentrations of the electron acceptors. Oxygen and NO_3^-, the most abundant electron acceptors in ambient seawater, were either not detected or were present in low concentrations in waters from the Galapagos vents[4] or from 21° N chimneys (J. Edmond, personal communication). However, due either to the leaky nature of hydrothermal systems or to advection processes, it is possible that O_2 and NO_3^- are involved. As these electron acceptors would be the factors which most limit bacterial productivity, they would be rapidly utilized *in situ*. Many of the sulphur- and manganese-oxidizing bacteria isolated from the Galapagos and 21° N waters and animals are capable of coupling oxidation reactions with denitrification (J.A.B. unpublished data). An alternative hypothesis would be that other electron acceptors such as MnO_2 and N_2O could be abiogenically synthesized in hydrothermal waters.

Even though the temperatures of some water samples harbouring thermophiles were above 300 °C, we cannot conclude that these bacteria grow in those super-heated waters. As previously stated, seawater at the depths of these environments can remain liquid at temperatures up to 460 °C (ref. 7). Also, in some cases increased hydrostatic pressure can affect microorganisms in a manner analogous to a decrease in temperature[18]. Further experiments are needed to test the possibility that these thermophiles can grow in super-heated water at pressures equivalent to water depths of 2,500–3,000 m. Determining the maximum and optimum growth temperatures under such *in situ* pressures will help to characterize the distribution of actively growing thermophiles in submarine hydrothermal environments.

Although we do not know the extent to which microorganisms are contributing to the quantity of CH_4, H_2 and CO venting from hydrothermal systems, our preliminary findings indicate that these gases may not be produced entirely by abiogenic reactions. Particularly in the lower temperature vents, microbial formation of these gases may be very significant, but even in the high temperature vents at 21° N, this mechanism cannot be ruled out.

Finally, it has been suggested that the first group of microorganisms to evolve in the warm Archaean oceans were thermophiles and that submarine hydrothermal environments could be suitable sites for chemical and microbiological evolution to occur[19,20]. It is tempting, therefore, to suggest that some of these present day marine hydrothermal vent thermophiles may represent physiological analogues to Archaean ocean bacteria.

Support for this research was provided by Office of Naval Research grant N00014-79C-0004 and NSF grant 79-27283. We also thank the crews of the R/V *Lulu* and R/V *Gillis* for their assistance, John Edmond for his invitation to participate on the expedition and for use of unpublished data, R. Y. Morita for use of laboratory facilities, and Clifford Dahm and Sarah Hoffman for their helpful discussions and editorial comments.

Received 15 April; accepted 24 May 1982.

1. Welhan, J. A. & Craig, H. *Geophys. Res. Lett.* **6,** 829–831 (1979).
2. Lupton, J. E. & Craig, H. *Science* **214,** 13–18 (1981).
3. Lilley, M. D. & Gordon, L. I. *EOS* **60,** 863 (1979).
4. Corliss, J. B. *et al. Science* **203,** 1073–1083 (1979).
5. Spiess, F. N. *et al. Science* **207,** 1421–1432 (1980).
6. Hekinian, R., Fevrier, M., Bischoff, J. L., Picot, P. & Shanks, W. C. *Science* **207,** 1433–1444 (1980).
7. Chen, C-T.A. *Science* **211,** 298 (1981).
8. Williams, P. M., Smith, K. L., Druffel, E. M. & Linick, T. W. *Nature* **292,** 448–449 (1981).
9. Karl, D. M., Wirsen, C. O. & Jannasch, H. W. *Science* **207,** 1345–1347 (1980).
10. Jannasch, H. W. & Wirsen, C. O. *Appl. envir. Microbiol.* **41,** 528–538 (1981).
11. Hiatt, B. *Mosaic* **11,** 15–21 (1980).
12. Felbeck, H., Childress, J. J. & Somero, G. N. *Nature* **292,** 291–293 (1981).
13. Brock, T. D. *Thermophilic Microorganisms and Life at High Temperatures* (Springer, New York, 1978).
14. Tansey, M. R. & Brock, T. D. in *Microbial Life in Extreme Environments* (ed. Kushner, D. J.) 159–216 (Academic, London, 1978).
15. Zeikus, J. G. *Enzyme Microb. Technol.* **1,** 243–252 (1979).
16. Heinen, W. & Lauwers, A. M. *Archs Microbiol.* **129,** 127–128 (1981).
17. Zeikus, J. G., Ben-Bassat, A. & Hegg, P. *J. Bact.* **143,** 432–440 (1980).
18. Baross, J. A., Hanus, F. J. & Morita, R. Y. *Appl. Microbiol.* **30,** 309–318 (1975).
19. Fyfe, W. S. *Science* **213,** 105–110 (1981).
20. Corliss, J. B., Baross, J. A. & Hoffman, S. E. *Oceanologica Acta* No. SP, 56–69 (1981).
21. Zimmerman, R. & Meyer-Reil, L. A. *Kieler Meeresforschungen* **30,** 24–27 (1974).
22. Rippka, R., Deruelles, J., Waterbury, J. B., Herdman, M. & Stanier, R. Y. *J. gen. Microbiol.* **111,** 1–61 (1979).
23. Baross, J. A., Hanus, F. J. & Morita, R. Y. in *Effects of the Ocean Environment on Microbial Activities* (eds Colwell, R. R. & Morita, R. Y.) 180–202 (University Park Press, Baltimore, 1974).
24. Swinnerton, J. W. & Linnenbom, N. J. *J. chromat. Sci.* **5,** 570–573 (1967).
25. Lilley, M. D., Baross, J. A. & Gordon, L. I. *Deep-Sea Res.* (in the press).
26. Harrison, M. J., Wright, R. T. & Morita, R. Y. *Appl. Microbiol.* **21,** 698–702 (1971).
27. Baross, J. A., Hanus, F. J., Griffiths, R. P. & Morita, R. Y. *J. Fish. Res. Bd Can.* **32,** 1876–1879 (1975).

Evidence that patterning mechanisms in developing and regenerating limbs are the same

Ken Muneoka & Susan V. Bryant

Developmental Biology Center and Department of Developmental
and Cell Biology, University of California, Irvine,
California 92717, USA

Some amphibians have the ability to form new limbs throughout their lives. The essential similarity between limb regeneration and the original development of the limb is that both involve the elaboration of new patterns of structures. While some investigators believe that the two developing systems use similar mechanisms to generate the limb pattern[1-7], others have stressed the basic differences in developing and regenerating limbs, and have concluded that different mechanisms exist[8]. Both developing and regenerating urodele limbs can be caused to form supernumerary parts following tissue misalignment so that cells from normally disparate positions within the limb circumference confront each other (developing limbs[2,9,10]; regenerating limbs, see ref. 11 for review). If similar mechanisms are operating, the developing limb should respond to grafts of regenerating limb tissue, and vice versa, by forming supernumerary outgrowths. If different mechanisms are operating, either the grafts should fail or the response should be disorganized. Our results with the axolotl *Ambystoma mexicanum* suggest that the patterning mechanisms are the same.

Grafts between regenerating fore- and hindlimbs are as effective as grafts within the homologous limb in eliciting supernumerary limb formation[12,13]. Similar conclusions can be drawn from experiments performed on the developing leg and wing buds of birds[14-16]. We exploited this in our experiments on the axolotl where development of the hindlimb is retarded relative to that of the forelimb[17], thus enabling grafts to be made between animals of similar age in which the hindlimb is developing and the forelimb is regenerating. Forelimbs were amputated midway through the humerus at stage 46[17] and allowed to regenerate to the stage of palette[18]. Stage 46 hindlimb buds were amputated near the base and exchanged with palette stage blastemas removed from older sibling larvae. A section through a developing hindlimb bud at stage 46 is shown in Fig. 1. The limb bud is undifferentiated at this stage. In the experimental series, contralateral grafts were made between developing and regenerating limbs so as to confront anterior and posterior tissue. In the controls, ipsilateral grafts were made between developing and regenerating limbs so as to align all circumferential positions. In addition, developing hindlimb buds were grafted either contralaterally (experimentals) or ipsilaterally (controls) to other hindlimb bud stumps (Fig. 2).

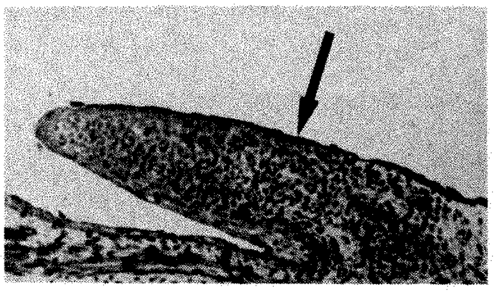

Fig. 1 A longitudinal section through a stage 46 hindlimb bud of the axolotl. No histological differentiation has yet occurred. The arrow indicates the level at which the limb bud was cut. Limbs were fixed in Bouin's and embedded in paraffin for serial sectioning. Sections were cut at 6 μm and stained with Mallory's triple stain. ×70.

The results are shown in Table 1. Control grafts, in which no positional disparity was created by grafting, mostly developed into normal limbs without supernumerary structures (Fig. 3*a*–*c*). In 3 out of 41 cases (one forelimb blastema to hindlimb bud stump and two hindlimb buds to forelimb blastema stumps), one extra digit formed at the anterior and/or posterior margin of the graft. The remaining 38 cases formed normal limbs according to the site of origin of the graft.

In the experimental series, where grafting created tissue disparities, supernumerary limbs formed in a high percentage of cases (Table 1). Contralateral exchange of developing hindlimb buds led to supernumerary limbs in 73% of the cases (Fig. 3*f*). Contralateral grafting of developing hindlimb buds to regenerating forelimb stumps led to supernumerary limbs in 70% of the cases (Fig. 3*d*), and the reciprocal experiment of contralateral grafting of regenerating forelimb blastema to developing hindlimb bud stump led to supernumerary limbs in 62% of the cases (Fig. 3*e*). In all the experimental series, extra structures formed either at the anterior, the posterior, or both borders of the graft junction (see Table 1), and in all cases the supernumerary limbs were of stump rather than graft handedness. Commonly, supernumerary limbs were not clearly separated from the grafted limb, and loss of digits along the line of symmetry between supernumerary and grafted limb was observed (see Fig. 3*e*). Similar types of limbs were observed by Iten and Bryant[19] after contralateral grafts of early stage forelimb blastemas of newts (*Notophthalmus viridescens*) to appose anterior and posterior tissues. How such fusions can occur is discussed in terms of the polar coordinate model by Bryant *et al.*[3].

The results of these experiments show that the interactions between developing and regenerating limbs of urodeles following confrontations between cells from disparate positions are similar to the interactions between similar limb bud and limb bud or blastema and blastema grafts. When developing axolotl forelimb buds were exchanged contralaterally to appose anterior and posterior tissues, Maden and Goodwin[9] found that 70% of the cases produced limbs with supernumerary structures. Our results on the developing hindlimb bud are very

Table 1 Grafts between developing and regenerating limbs

Operation	Total	Normal*	Uninterpretable	Supernumerary structures: Total	Anterior	Posterior	Both	Mean no. digits
Control series								
Hindlimb bud to hindlimb bud stump	12	12						
Hindlimb bud to forelimb blastema stump	17	15	2					
Forelimb blastema to hindlimb bud stump	12	11	1					
Experimental series								
Hindlimb bud to hindlimb bud stump	11	2†	1‡	8 (73%)	1	2	5	9.1
Hindlimb bud to forelimb blastema stump	20	2†	4	14 (70%)	4	3	7	7.8
Forelimb blastema to hindlimb bud stump	13	2†	3‡	8§ (62%)	2	2	3	7.8

* Developing according to the site of graft origin.
† Limbs were of stump handedness.
‡ Hypomorphic limbs.
§ One case formed a ventral supernumerary structure.

0028–0836/82/290369—03$01.00

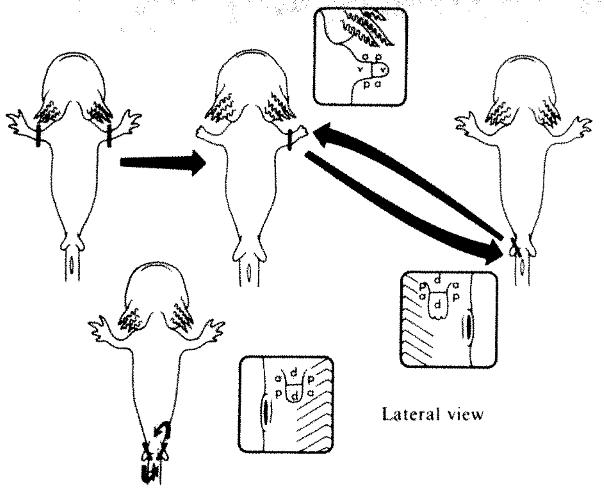

Fig. 2 Diagram of the grafting operations, shown here from the ventral aspect. *a*, The forelimbs of stage 46 (ref. 17) axolotls were amputated through the mid-humerus. Note that the forelimbs in the axolotl are fully differentiated when the hindlimbs are just beginning to grow out. After a period of 10–12 days the forelimb blastemas had regenerated to the stage of palette to early digits[18]. These animals were paired with more slowly developing stage 46 sibling axolotls. The regenerating forelimb blastema and the developing hindlimb bud were exchanged between the paired animals (usually between differently pigmented animals). Grafts were made either ipsilaterally (control series) matching anterior, posterior, dorsal and ventral limb tissues or contralaterally (experimental series) apposing anterior and posterior limb tissues. A contralateral graft is shown in the diagram. The insets show a closer ventral view of the limb bud to blastema stump graft and a lateral view of blastema to limb bud stump graft. *b*, The hindlimb buds of a stage 46 axolotl were exchanged either contralaterally (experimental series) as shown here, or simply amputated and replaced (control series). In the experimental series, the limb buds were oriented to appose anterior and posterior limb bud tissue while keeping dorsal and ventral limb bud tissue aligned. For all grafting operations animals were anaesthetized in MS222 (Eastman) diluted 1:3,000 in 50% Holtfreter solution. Operations were done in air with fine irridectomy scissors, forceps and microdissection scalpel. Operated animals were kept in individual dishes (100×25 mm plastic Petri dishes, Lab-tek), fed and changed daily, and checked (without anaesthetizing) every 2–3 days throughout the experiment. Camera lucida drawings were made every time the grafts were checked. In this way observations on the early stages of limb outgrowth were made and the positions of supernumerary outgrowths were recorded. a, Anterior; d, dorsal; p, posterior; v, ventral.

similar, with 73% of the cases producing supernumerary structures. Similar experiments by Thoms and Fallon[10] on the developing forelimb buds of three species of urodeles (*A. mexicanum*, *Ambystoma maculatum* and *N. viridescens*) resulted in supernumerary structures in 95% of the cases. Experiments by Tank[20] on the regeneration blastema of *A. mexicanum* grafted to oppose anterior and posterior tissues showed that supernumerary structures were produced in 57% of the cases. Iten and Bryant[19] showed in similar experiments in the newt that supernumerary structures were formed in 63% of the cases. In all these experiments on developing and regenerating limbs the position and handedness of the supernumerary structures which formed were similar, and are consistent with the polar coordinate model[3,5]. These results, taken with those reported here, suggest that the developing and regenerating limbs of urodeles use similar mechanisms for pattern regulation during limb outgrowth.

It also appears from grafting of developing limb bud tissues from evolutionarily diverse vertebrate species into the chick wing bud, that common pattern regulatory mechanisms are shared among many different vertebrates[14,21–23]. In these studies grafts of tissue from the posterior of the limb buds of mammals (man, hamster, mouse, pig and ferret), birds (Japanese quail, ringneck pheasant, chukar partridge and Peking duck) and reptiles (snapping turtle and painted turtle) into the anterior of chick wing buds resulted in the formation of supernumerary limb structures. Further, control grafts which were made so that no positional disparity was created resulted in the normal development of the host limb. The relationship between the developing amphibian limb bud and the developing chick limb bud is less clear because differences in the temperature tolerances of the two species make grafting experiments between them difficult to interpret[23]. However, grafting studies on the amphibian limb bud show that its behaviour after apposition of normally nonadjacent tissues is remarkably similar to that of the chick limb bud[2,9,10,24]. It seems therefore that the mechanisms of pattern formation in the development of vertebrate limbs are common to all vertebrates[22]. Our results here suggest that those patterning mechanisms common to vertebrate limb development are also the mechanisms that control patterning during limb regeneration in amphibians.

This conclusion may have important implications for the way we think about how the vertebrate limb pattern is formed as

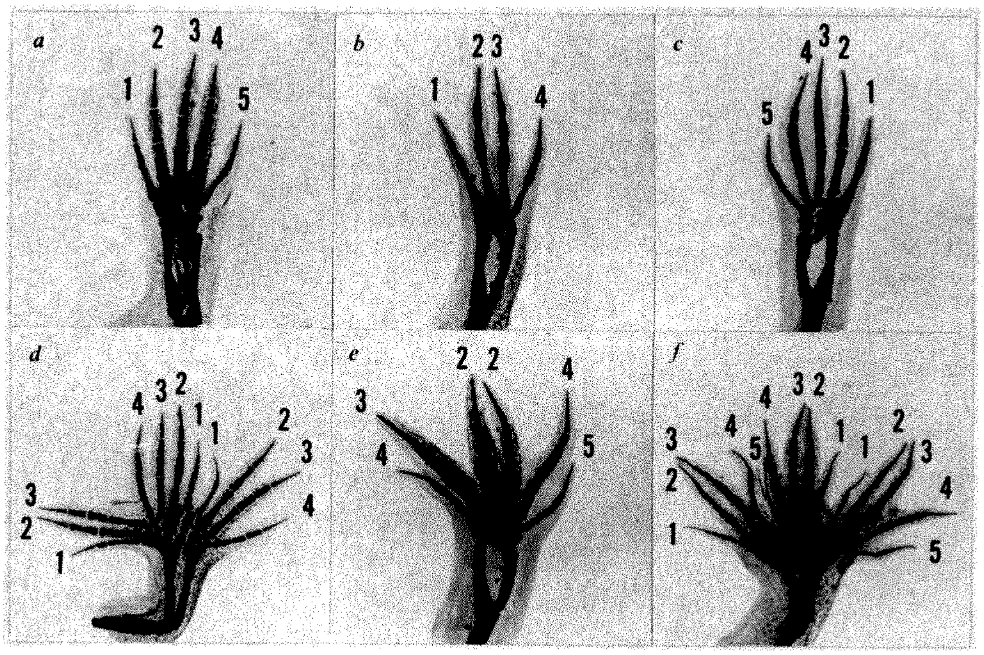

Fig. 3 Skeletal preparations of control and experimental limbs, prepared by the Victoria blue technique[25] 4 to 6 weeks after the grafting operation. *a*, A control ipsilateral graft of a developing right hindlimb bud put onto a regenerating right forelimb stump. A normal five-digit right hindlimb was formed on the forelimb stump. *b*, A control ipsilateral graft of a right regenerating forelimb blastema put onto a developing right hindlimb bud stump. The graft produced a normal four-digit right forelimb on the hindlimb stump. *c*, A control ipsilateral graft of a developing left hindlimb bud put onto a developing left hindlimb bud stump. The resulting limb is a normal five-digit left hindlimb. *d*, A limb which resulted from the contralateral graft of a left developing hindlimb bud to a right regenerating forelimb blastema stump. Supernumerary limb structures are present both anterior and posterior to the grafted hindlimb. *e*, A limb which resulted from the contralateral graft of a left regenerating forelimb blastema onto a right developing hindlimb bud stump. Digits derived from the graft are located on the left of the figure; supernumerary limb structures are present on the right. The two limbs have fused during outgrowth with loss of digits along the line of symmetry between them. *f*, A limb resulting from a contralateral graft of a left developing hindlimb bud to a right developing hindlimb bud stump. Supernumerary limb structures are present both anterior and posterior to the grafted hindlimb. *a–f*, ×5.

limb development and limb regeneration have mostly been regarded as two very different fields of study. Models of pattern formation during limb development have been drawn solely from data generated from work on limb development and the same is true for most models of pattern formation during limb regeneration. As there is now direct evidence that the mechanisms controlling pattern formation during limb development are the same as those for limb regeneration, we believe that the experimental data from both limb development and limb regeneration studies must be considered together to understand pattern formation. Why all vertebrates can develop limbs, but only a few can regenerate them remains puzzling. However, we propose that during evolution, the underlying patterning mechanisms have remained the same, but that the ability to call these mechanisms into use has been modified. In other words, the urodele limb can regenerate because it has maintained its ability to implement pattern mechanisms whereas the chick wing cannot regenerate because it loses this ability very early in its development.

These studies therefore show that it is possible to learn about limb development by studying limb regeneration. Conversely, studies of limb development may help us to understand the causes of failure of limb regeneration in higher vertebrates.

We thank Christine Rollman-Dinsmore, William P. Hayes, Laurie E. Iten, Nancy A. O'Rourke and L. David Wise for their comments and Warren F. Fox and Kate John-Alder for assistance. This research was supported by NIH grants HD 06082 and HD 07029.

Received 26 February; accepted 14 May 1982.

1. Bryant, S. V. & Iten, L. E. *Devl Biol.* **50,** 212–234 (1976).
2. Maden, M. *J. embryol. exp. Morph.* **63,** 243–265 (1981).
3. Bryant, S. V., French, V. & Bryant, P. J. *Science* **212,** 993–1002 (1981).
4. Carlson, B. M. in *XIX Morphological Congr. Symp.* 135–140 (Charles University, Prague, 1978).
5. French, V., Bryant, P. J. & Bryant, S. V. *Science* **193,** 969–981 (1976).
6. Faber, J. *Adv. Morph.* **9,** 127–147 (1971).
7. Stocum, D. L. *Differentiation* **3,** 167–182 (1975).
8. Tickle, C. *Am. Sci.* **69,** 639–646 (1981).
9. Maden, M. & Goodwin, B. C. *J. Embryol. exp. Morph.* **57,** 177–187 (1980).
10. Thoms, S. & Fallon, J. *J. Embryol. exp. Morph.* **60,** 33–55 (1980).
11. Tank, P. W. & Holder, N. *Q. Rev. Biol.* **56,** 113–142 (1981).
12. Rollman-Dinsmore, C. G. & Bryant, S. V. *J. exp. Zool.* (in the press).
13. Stocum, D. L. *Devl Biol.* **79,** 276–295 (1980).
14. Balcuns, A., Gasseling, M. T. & Saunders, J. W. Jr *Am. Zool.* **10,** 323 (1970).
15. Saunders, J. W. Jr *Ann. N.Y. Acad. Sci.* **193,** 29–42 (1972).
16. Saunders, J. W. Jr & Gasseling, M. T. in *Epithelial-Mesenchymal Interactions* (eds R. Fleischmajer & R. E. Billingham) 78–97 (Williams & Wilkins, Baltimore, 1968).
17. Schreckenberg, G. M. & Jacobson, A. G. *Devl Biol.* **42,** 391–400 (1975).
18. Tank, P. W., Carlson, B. M. & Connelly, T. G. *J. Morph.* **150,** 117–128 (1976).
19. Iten, L. E. & Bryant, S. V. *Devl Biol.* **44,** 119–147 (1975).
20. Tank, P. *Devl Biol.* **62,** 143–161 (1978).
21. MacCabe, J. A. & Parker, B. W. *J. exp. Zool.* **195,** 311–317 (1976).
22. Tickle, C., Shellswell, G., Crawley, A. & Wolpert, L. *Nature* **259,** 396–397 (1976).
23. Fallon, J. F. & Crosby, G. M. in *Vertebrate Limb and Somite Development* (eds D. A. Ede, J. R. Hinchliffe & M. Balls) 55–69 (Cambridge University Press, 1977).
24. Cameron, J. & Fallon, J. F. *Devl Biol.* **55,** 320–330 (1977).
25. Bryant, S. V. & Iten, L. E. *Wilhelm Roux Archiv.* **174,** 90–101 (1974).

Selective collateral elimination in early postnatal development restricts cortical distribution of rat pyramidal tract neurones

Brent B. Stanfield, Dennis D. M. O'Leary & Carl Fricks

The Salk Institute for Biological Studies and The Clayton Foundation for Research—California Division, PO Box 85800, San Diego, California 92138, USA

The pyramidal tract, comprising those axons which pass from the neocortex to the medulla and spinal cord, is among the most thoroughly studied projections of the mammalian cortex. Recent studies using anterograde axon tracing techniques have provided information concerning the time course of the growth of pyramidal tract fibres[1,2], yet much remains to be learned about its development. We have now begun to study the distribution of the neurones of origin of the pyramidal tract during the postnatal development of the rat neocortex using the recently introduced retrogradely transported fluorescent marker, True blue[3]. During the first postnatal week, injections of True blue into the pyramidal decussation result in the labelling of pyramidal tract neurones which are distributed virtually throughout the tangential extent of layer V of the neocortex, whereas after comparable injections during the fourth postnatal week the distribution of such cells is much more restricted and remains restricted into adult life. This developmental restriction is most dramatic in the occipital cortex: during the first postnatal week many pyramidal tract neurones are found throughout the visual cortex while none is seen in this area in the adult. When True blue is injected into the pyramidal decussation during the first postnatal week and the animals are allowed to survive until the fourth postnatal week, the distribution of pyramidal tract neurones is as widespread as in the immediate postnatal period and includes the entire visual cortex. This implies that many of the neurones in the occipital cortex initially send a collateral into the pyramidal tract which is later eliminated, although the neurones themselves persist. These findings, together with similar recent observations on the development of the callosal connections[4,5], indicate that the elimination of axon collaterals may be a general feature of the development of cortical projection systems, and that such transitory collaterals may traverse considerable distances.

The experimental procedure in all instances involved the injection of 0.3–1.0 μl of the fluorescent dye (a 2–5% solution of True blue) into the pyramidal tract at the level of its decussation at the spino-medullary junction. This injection site is convenient because: (1) of the ease with which consistent injections can be made; (2) of the considerable distance between this site and the targets of non-pyramidal tract cortical neurones; (3) it is known that in the rat the fibres of the pyramidal tract have reached the decussation at the time of birth[2,6]. The pyramidal decussation of the rat consists of corticospinal axons (which after crossing descend into the spinal cord) and crossed corticobulbar fibres which terminate in the dorsal column and other medullary nuclei[7,8]. Thus, we will refer to the retrogradely labelled cortical neurones in our experiments as pyramidal tract

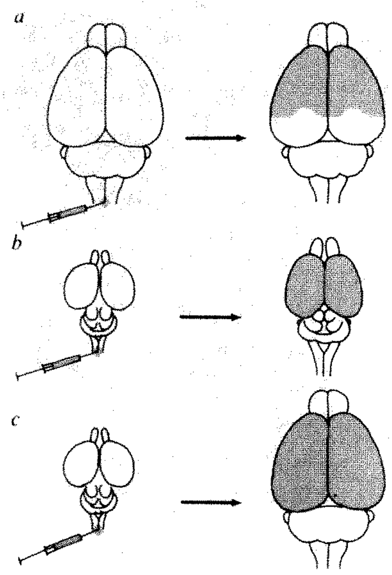

Fig. 1 Schematic illustrations of the three experimental paradigms used in this study, summarizing the results of each. *a*, When True blue is injected into the pyramidal decussation of adult rats, or rats at 20 days of age, the distribution of retrogradely labelled pyramidal tract neurones is widespread but limited to about the rostral two-thirds of the cerebral hemisphere. *b*, *c*, Following similar injections in 2-day-old rat pups, labelled cells are spread throughout the tangential extent of the cortex, whether the animals are killed on day 6 (*b*) or are allowed to survive until day 25 (*c*).

0028-0836/82/290371—03$01.00

neurones without distinguishing between the corticobulbar and corticospinal projections because both of these had access to the injected label. After a suitable survival period the animals were perfused with 10% buffered neutral formalin, the brains were removed and processed as described elsewhere[9] and the frozen sections were examined with a Leitz Dialux-20 fluorescence microscope.

Following injections of True blue (0.5–1.0 μl) into the pyramidal decussation of adult rats ($n = 7$), the distribution of labelled cells in the cortex after a 5–7 day survival period is similar to, but more extensive than, that of corticospinal cells, as recently shown through the use of similar techniques[10,11]. Although strictly limited in the radial dimension of the cortex to layer V (as identified in adjacent Nissl-stained sections), the labelled neurones occupy a large and continuous tangential sheet of cortex. This sheet of labelled cells spans virtually the entire frontal cortex and extends uninterruptedly into the parietal cortex (Fig. 1*a*). An essentially identical distribution of pyramidal tract neurones is seen in rats that are injected on postnatal day 20 and allowed to survive for 5 days ($n = 14$). We emphasize that although the extent of the cortex in which pyramidal tract neurones are found varies slightly from case to case (due no doubt to slight variations in the effective injection site), in none of these animals, nor in any of the adult cases, are retrogradely labelled neurones identifiable in the occipital cortex (Figs 2*a*, 3*a*).

In animals injected with True blue (0.3–0.5 μl) on postnatal day 2 and killed on postnatal day 6 ($n = 17$), a large number of retrogradely labelled cells can be seen in layer V of the cortex (Fig. 3*b*). In fact, the density of labelled cells in the early postnatal cortex is appreciably greater than that in the older animals. The band of labelled cells is spread across essentially the entire tangential extent of the cortex, from the frontal cortex to the caudal pole of the hemisphere (Fig. 1*b*). We emphasize that in none of the present experiments did the injected dye spread beyond the lower medulla and that we are confident that there was no involvement of the corticopontine projection.

Thus, during the first week of postnatal life pyramidal tract neurones seem to be confined to layer V, but are distributed throughout the tangential extent of the neocortex, whereas by the fourth week such cells are excluded from the posterior pole of the hemisphere, and in particular from the visual cortex[12,13]. This difference in the distribution of pyramidal tract neurones at these two ages is most clearly seen in sagittal sections as shown in Figs 2 and 3. To determine whether the developmental restriction in the distribution of pyramidal tract neurones is brought about by the selective elimination of axon collaterals or by cell death, in 15 animals we injected True blue (0.3–0.5 μl) into the pyramidal decussation on postnatal day 2 and allowed the rats to survive until postnatal day 25. As we have previously reported[5], True blue remains within labelled neurones for several weeks, without significant degradation or leakage. In these experiments the distribution of labelled cortical neurones is as widespread as that in animals which were injected on postnatal day 2 and allowed to survive for only a few days even though the adult distribution of pyramidal tract neurones is established by the time these animals were killed on day 25 (Fig. 1). Of course, the cortex in these animals had continued its normal course of maturation and was cytoarchitectonically indistinguishable from that of control animals of the same age. The band of retrogradely labelled neurones was again confined to layer V, but extended throughout the cortex, including the visual cortex, from which, as we have shown, pyramidal tract neurones are normally excluded by the fourth postnatal week (Figs 2, 3).

The most straightforward interpretation of these findings is that early in postnatal life there are neurones throughout the tangential extent of layer V which send axons into the pyramidal tract, and that during the next 3 weeks many of these cells (and especially those in the visual cortex) lose their pyramidal tract collaterals even though the neurones themselves survive. At present we cannot rule out the possibility that neuronal cell death also contributes to the exclusion of pyramidal tract neurones from the occipital cortex during postnatal development, but certainly this restriction is not due mainly to the death of these neurones, because when labelled by way of their pyramidal tract axon on postnatal day 2, many of these cells are still identifiable at 4 weeks of age. This result also excludes the possibility that the developmental change in the distribution of labelled neurones is due to a secondary, tangential migration of neurones. Although we cannot determine how many neurones lose pyramidal tract collaterals during postnatal development, within the occipital cortex collateral elimination is clearly a substantial event as it results in the disappearance of all pyramidal tract axons which initially arise from this part of the cortex.

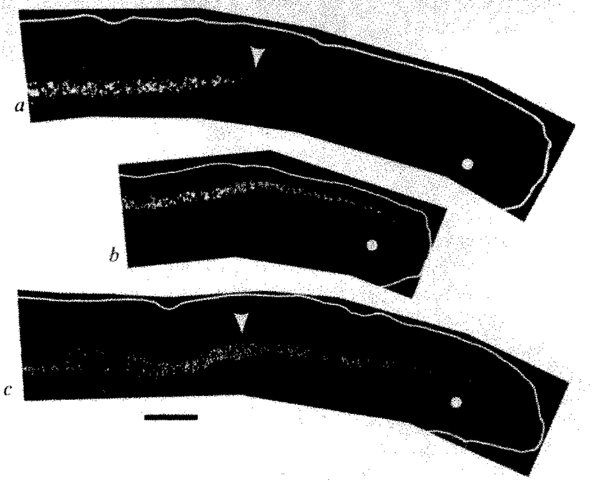

Fig. 3 These photomontages illustrate the distribution of True blue-labelled neurones in sagittal sections of the caudal part of the cortex from animals injected in the pyramidal decussation: *a*, at postnatal day 20 and surviving until postnatal day 25; *b*, at postnatal day 2 and surviving to postnatal day 6; *c*, at postnatal day 2 and surviving until postnatal day 25. The white line indicates the cortical surface; the splenium of the corpus callosum is marked with a large dot. The arrowhead in *a* marks the caudal limit of the band of labelled cells and that in *c* is at the same level. Scale bar, 1 mm.

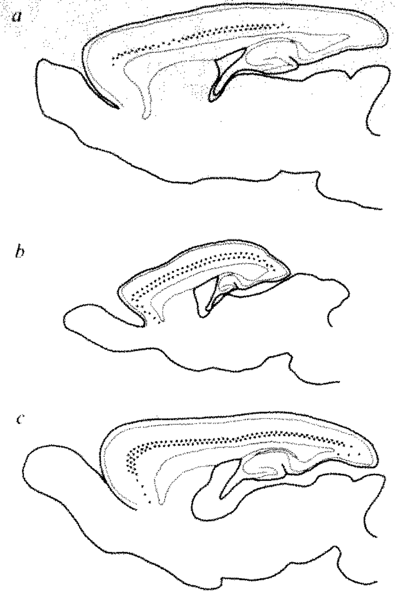

Fig. 2 Tracings of sagittal sections of rat brains at approximately the same medio-lateral position to show the distribution of retrogradely labelled neurones in the cortex of animals which: *a*, received an injection of True blue in the pyramidal decussation on postnatal day 20 and was killed on postnatal day 25; *b*, received a similar injection on postnatal day 2 and was killed on postnatal day 6; *c*, was injected on postnatal day 2 and killed on postnatal day 25. Each dot represents ~15 labelled neurones.

These observations on the development of pyramidal tract neurones are similar to those that we and others have recently made on the development of callosally projecting neurones[4,5]. In that instance, however, the developmental change results in a refinement of the distribution of callosal neurones within an area, whereas in the present study we have shown the complete elimination of a substantial projection from an entire region of cortex. However, together these studies suggest that a loss of collateral projections may be a rather general feature of the development of cortical efferent systems. We have not examined the time course of the restriction in the distribution of pyramidal tract neurones in detail, but the data available so far suggest that it is similar to that affecting the distribution of callosal neurones in the rat[14]. It would also be of interest to determine if some of early pyramidal tract collaterals reach and form synapses in the spinal cord before they are withdrawn. At present, it is not known whether collateral elimination of this type also involves synapse elimination—a phenomenon known to occur in several developing systems[15]. Interestingly in one of the systems in which synapse elimination has been shown to occur, there is apparently no change in the number of neurones which give rise to these synapses[16]. Finally, we emphasize that during the first postnatal week, when the tangential distribution of the pyramidal tract neurones is widespread, their radial distribution within layer V has already been determined.

We thank Madeline Farris and Kris Trulock for technical assistance, Pat Thomas for secretarial help, and Dr W. M. Cowan for support, advice and encouragement. This work was supported in part by NIH grants NS-16980, EY-03653 and GM-07198.

Received 1 March; accepted 14 May 1982.

1. Reh, T. & Kalil, K. *J. Comp. Neurol.* **200,** 55–67 (1981).
2. Schreyer, D. J. & Jones, E. G. *Neuroscience* (in the press).
3. Bentivoglio, M., Kuypers, H. G. J. M., Catsman-Berrevoets, C. E. & Dann, O. *Neurosci. Lett.* **12,** 235–240 (1979).
4. Innocenti, G. M. *Science* **212,** 824–827 (1981).
5. O'Leary, D. D. M., Stanfield, B. B. & Cowan, W. M. *Dev. Brain Res.* **1,** 607–617 (1981).
6. DeMyer, W. *Archs Neurol.* **16,** 203–211 (1967).
7. Valverde, F. *J. comp. Neurol.* **119,** 25–54 (1962).
8. Wise, S. P. & Jones, E. G. *J. comp. Neurol.* **175,** 129–158 (1977).
9. Sawchenko, P. E. & Swanson, L. W. *Brain Res.* **210,** 31–51 (1981).
10. Catsman-Berrevoets, C. E., Lemon, R. N., Verburgh, C. A., Bentivoglio, M. & Kuypers, H. G. J. M. *Expl Brain Res.* **39,** 433–440 (1980).
11. Catsman-Berrevoets, C. E. & Kuypers, H. G. J. M. *Brain Res.* **218,** 15–33 (1981).
12. Woolsey, C. N. in *Milbank Symp. on the Biology of Mental Health and Disease*, 193–206 (Hoeber, New York, 1952).
13. Montero, V. M. *Brain Res.* **53,** 192–196 (1973).
14. Ivy, G. O. & Killackey, H. P. *J. comp. Neurol.* **195,** 367–389 (1981).
15. Purves, D. & Lichtman, J. W. *Science* **210,** 153–157 (1980).
16. Johnson, D. A. & Purves, D. *J. Physiol., Lond.* **318,** 143–159 (1981).

Glycogenolysis induced by serotonin in brain: identification of a new class of receptor

T. T. Quach, C. Rose, A. M. Duchemin & J. C. Schwartz

Unité de Neurobiologie (U 109), Centre Paul Broca de l'INSERM, 2ter rue d'Alésia, 75014 Paris, France

Serotonin-containing neurones in brain have been proposed to have a role in the control of physiological mechanisms such as sleep, thermoregulation, pain perception and endocrine secretions as well as in the physiopathology of migraine or depressive illness[1–6]. One difficulty in testing these possibilities lies in the scarcity of pharmacological agents able to interact selectively with the probably multiple classes of serotonin receptors in the central nervous system. Development of such agents would be facilitated by simple *in vitro* models in which biological responses to serotonin in mammalian brain could be quantified. Thus a serotonin-sensitive adenylate cyclase has been characterized in rat brain, but the response to serotonin is weak in newborn and practically absent in adult animals[7–11]. In addition, two pharmacologically distinct classes of serotoninergic binding site have been identified using ^{3}H-serotonin and ^{3}H-spiperone as ligands[12–17], but their identification as receptors remains to be established. More recently, serotonin has been shown to stimulate phosphorylation of a neuronal protein in slices from the facial motor nucleus, although the receptors mediating this action were not characterized[18]. We now report that serotonin stimulates glycogen hydrolysis in slices of cerebral cortex, that this action is mediated by a novel class of receptors and that tricyclic antidepressants are among the best competitive antagonists of the indolamine.

The addition of serotonin to slices from mouse cerebral cortex preincubated with ^{3}H-glucose for 30 min, at a time when ^{3}H-glycogen level in tissue has reached a plateau[19], results in rapid hydrolysis of the ^{3}H-polymer. The serotonin-induced glycogenolysis is concentration dependent, occurs with a K_{act} of 20 ± 3 μM and reduces the ^{3}H-glycogen level by, at the most, $78 \pm 4\%$ (Fig. 1*a*). A similar effect is observed with other indolamine derivatives such as tryptamine or 5-methoxytryptamine, while tryptamine derivatives *N*-methylated on the side chain, such as *N*-methyltryptamine, bufotenine, psilocybin and psilocin, are only partially active and *N,N*-dimethyltryptamine is totally inactive (Fig. 1*a*, *b*). This latter observation prompted us to study *N,N*-dimethyltryptamine as antagonist: we found that increasing concentrations of this compound shift the concentration–response curve to serotonin rightwards, without modifying the maximal response (Fig. 2). This suggests that *N,N*-dimethyltryptamine acts as a competitive antagonist with

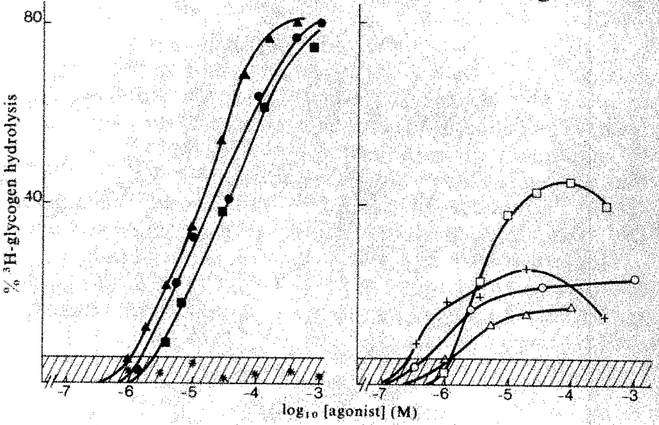

Fig. 1 ^{3}H-glycogen hydrolysis induced by serotonin and other tryptamine derivatives in slices from cerebral cortex. Male Swiss albino mice (18–20 g, Lessieux, France) were killed by decapitation, the cerebral cortex was quickly removed and slices (250 × 250 μm thick) were prepared in a cold room (4 °C) with a McIlwain tissue slicer. Pooled cortical slices from six animals were preincubated for 15 min at 37 °C in a slightly modified Krebs–Ringer bicarbonate medium (120 mM NaCl, 5 mM KCl, 2.6 mM $CaCl_2$, 0.67 mM $MgSO_4$, 1.2 mM KH_2PO_4, 3 mM glucose and 27.5 mM $NaHCO_3$) under a constant stream of O_2/CO_2 (95:5). The slices were then washed once with fresh medium, 300-μl aliquots of the tissue suspension corresponding to 0.5 mg protein were distributed in incubation tubes and 13.4 nmol of ^{3}H-glucose (500 mCi mmol^{-1}; Amersham) were added in a volume of 10 μl. Test agents were added when ^{3}H-glycogen level in tissue had reached a steady state, that is, after a 30 min incubation[19], and the slices were further incubated for 20 min. The incubations were stopped by rapid centrifugation. The supernatant was discarded and replaced by 300 μl of fresh medium in which the slices were sonicated. A fraction of the resulting homogenate was then immediately deproteinized by heating at 95 °C for 10 min and ^{3}H-glycogen assayed by the ethanol filter paper technique[19]. Results are expressed as per cent of the basal ^{3}H-glycogen level (26.3 ± 2.1 d.p.m. $\times 10^3$ per mg protein). The shaded area corresponds to the s.e.m. of basal ^{3}H-glycogen level. Values are the mean of 15–25 determinations performed in 3–5 independent experiments. ▲, Serotonin; *, *N,N*-dimethyltryptamine; ●, 5-methoxytryptamine; ■, tryptamine; △, *N*-methyltryptamine; +, bufotenine (5-hydroxy-*N,N*-dimethyltryptamine); ○, psilocybin (*O*-phosphoryl-4-hydroxy-*N,N*-dimethyltryptamine); and □, psilocin (4-hydroxy-*N,N*-dimethyltryptamine).

0028–0836/82/290373—03$01.00

an apparent K_i of 0.8 μM. The ergot derivative (+)LSD can elicit complete ^{3}H-glycogen hydrolysis but only at high concentrations; its action was also antagonized by *N,N*-dimethyltryptamine with an apparent K_i in the micromolar range. Typical serotoninergic antagonists such as methysergide, cyproheptadine and methiothepin fail to or weakly block the serotonin-induced response (Table 1).

Among neuroactive drugs, the antipsychotics chlorpromazine, spiperone, pipamperone and pimozide antagonize the serotonin-induced glycogenolysis with inhibition constants of between 4 and 20 μM; various tricyclic antidepressant compounds competitively block this response, all with inhibition constants of ~1 μM.

The glycogenolytic response elicited by serotonin in cortical slices suggests that this amine should be added to the list of neurotransmitters controlling carbohydrate metabolism in brain and which comprises the other glycogenolytic agents noradrenaline[19-21] (via β_1 receptors), histamine[22] (via H_1 receptors) and the neuropeptide vasoactive intestinal peptide (VIP)[23]. The serotonin-induced glycogenolysis requires higher concentrations of amine, however, particularly in comparison with VIP. Because the response to these agents occurs in the same cells (as shown by the almost total ^{3}H-glycogen hydrolysis in all cases), lower serotonin concentrations might be expected to be required in the presence of other glycogenolytic agents.

In a preparation such as brain slices, an effect observed with one neurotransmitter could be indirectly mediated by the release of another. The lack of antagonism by β-adrenergic and H_1-receptor blockers (Table 1) indicates that neither noradrenaline nor histamine is involved. Experiments with phosphodiesterase inhibitors or with various concentrations of calcium indicate that phosphorylase activation leading to glycogen hydrolysis seems to result in brain[20-22], as in other tissues[24-26], from one of two mechanisms: stimulation of an adenylate cyclase, as in the case of noradrenaline[19,20] and VIP[23], or translocation of calcium ions, as in the case of histamine[22]. The former mechanism is probably not involved in the response to serotonin as it is not modified in the presence of 0.7 μM isobutyl methylxanthine, a phosphodiesterase inhibitor, but is diminished when the calcium concentration is lowered (not shown). This suggests that VIP is probably not indirectly responsible for the serotonin effect, but this requires confirmation with antagonists of the neuropeptide, which are not available.

Serotonin induces phosphorylation of the 'protein I' in slices from facial motor nucleus at similar concentrations to those required for the glycogenolytic response, and both responses are blocked by 10 μM mianserin; however, only the former is potentiated by isobutyl methylxanthine[18]. Among the several other unidentified proteins which were phosphorylated in response to serotonin, one may correspond to phosphorylase.

Glycogen is the single largest energy reserve in the brain and the glycogenolytic effect of serotonin should result in an increased availability of glucose. The cellular location of this response remains to be identified, however, as the polymer is present both in neuronal and glial elements[27]. Nevertheless the observations that impairment of monoaminergic neurotransmission in mice subchronically treated with reserpine results in the development of hypersensitivity to the glycogenolytic actions of noradrenaline[20] as well as to those of serotonin (T.T.Q., C.R., A.M.D. and J.C.S., in preparation) suggest that the target cells are tonically controlled by the two monoaminergic systems. Interestingly, the three aminergic systems controlling glycogenolysis—the coeruleo-cortical noradrenergic[28], the raphe-cortical[29] and the histaminergic ascending[30] projections—are highly divergent neuronal circuits emanating from restricted areas of the brain stem and projecting throughout the telencephalon. This common anatomical feature probably facilitates a coordinated, quasi-hormonal control of energy supply in large areas of brain.

The strong influence of small changes in the structure of agonists on their activity (Fig. 1) and the apparently competitive nature of the antagonism exerted by substances such as *N,N*-dimethyltryptamine (Fig. 2) suggest that serotonin-induced glycogenolysis is a receptor-mediated response. The pharmacol-

Table 1 Comparison of drug potencies on the hydrolysis of ^{3}H-glycogen in cortical slices and other models

Drugs	K_{act} or K_i values (μM)			
	^{3}H-glycogen hydrolysis	^{3}H-serotonin binding sites	^{3}H-spiperone binding sites	Serotonin-sensitive adenylate cyclase
Agonists				
Serotonin	20	0.004 (14)	2.7 (14)	1 (9) 0.001 (10)
Tryptamine	26	>2 (12)		
5-methoxytryptamine	22	0.011 (14)	2.7 (14)	
N-methyltryptamine	9			
Bufotenine	5	0.037 (14)		
(+)LSD	60	0.010 (14)	0.013 (14)	
Antagonists				
a, Serotonergic				
Metergoline (7 μM)	6	0.009 (17)	0.002 (17)	1 (9)
Methysergide (7 μM)	NE	0.088 (14)	0.003 (14)	0.2 (10)
Cyproheptadine (30 μM)	NE	1.5 (14)	0.002 (14)	0.2 (9) 0.6 (10)
N,N-dimethyltryptamine (2 μM, 5 μM)	0.8	0.17 (12)		
Ketanserin (30 μM)	NE	NE (15)	0.002 (15)	
Methiothepin (20 μM)	20	0.3 (17)	0.004 (17)	0.3 (9)
b, Neuroleptics				
Spiperone* (50 μM)	20	0.73 (14)	0.001 (14)	0.3 (11)
Pimozide* (3 μM)	5	>4 (12)		
Pipamperone*	20	5 (15)	0.005 (15)	
Chlorpromazine* (3 μM)	4	6 (12)	0.02 (16)	0.4 (9)
c, Antidepressants				
Iprindole* (1 μM, 5 μM)	1	20 (17)	0.2 (17)	
Amitryptiline (0.5 μM)	1	5 (17)	0.01 (17)	
Mianserin (1 μM, 5 μM)	1.7	0.87 (14)	0.005 (14)	2.5 (11)
Doxepin (3 μM)	2.1			
Desimipramine (3 μM)	2.4	9 (17)	0.1 (17)	
Maprotiline* (3 μM)	1.6			
Inactive agents				
Alprenolol (100 μM), timolol (10 μM), mepyramine (30 μM), morphine (30 μM) and 5-hydroxyindoleacetic acid (100 μM), as either agonists or antagonists				

K_{act} values of compounds for ^{3}H-glycogen hydrolysis were obtained from the data of Fig. 1. K_i values were determined by one of two methods: (1) see Fig. 2. The rightward shift of the concentration–response curve to serotonin was determined in the presence of fixed concentration(s) of antagonists (concentrations indicated in parentheses) and the Cheng–Prussof equation[35] was then applied. (2) See Fig. 2 legend. The effect of 20 μM serotonin was antagonized by agents (indicated by *) in increasing concentrations and their K_i values were calculated from their IC_{50} values using the equation: $K_i = IC_{50}\,(1 + S/K_a)$. As shown for *N,N*-dimethyltryptamine in Fig. 2 legend, the two methods give K_i values which are always in good agreement, and the average is given. Concentration–response curves were established using six to eight concentrations of serotonin, agonists or antagonists (for each concentration 8–20 distinct determinations were performed in 2–5 separate experiments). Numbers in parentheses refer to references from which data were taken. NE, non-effective agents at the indicated concentration.

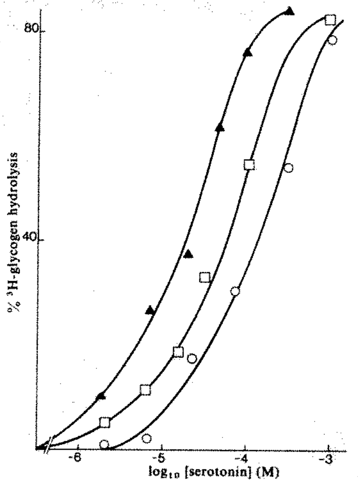

Fig. 2 Inhibition of the serotonin-induced glycogenolysis in slices from cerebral cortex by *N,N*-dimethyltryptamine. Following a 30 min preincubation in the presence of ^{3}H-glucose, serotonin was added at increasing concentrations and the incubation continued for a further 20 min. *N,N*-dimethyltryptamine was added 10 min before serotonin. Basal ^{3}H-glycogen level was 23.4 ± 1.2 d.p.m. $\times 10^3$ per mg protein. Values are the mean of 10–15 determinations performed in 2–5 independent experiments. The K_{act} values of serotonin alone or in the presence of *N,N*-dimethyltryptamine were determined by computer[36] and a K_i value of 0.8 µM was obtained from the equation. $K_i = I/[(K'_a/K_a) - 1]$, where K_a and K'_a are the K_{act} values of serotonin in the absence and presence of antagonist respectively, and I is the concentration of antagonist. In another experiment (not shown), using a fixed concentration of serotonin (100 µM) and increasing concentrations of *N,N*-dimethyltryptamine, the IC_{50} value of the latter compound was 10 µM, from which a K_i value of 1.7 µM was calculated from the equation[35]: $K_i = IC_{50}/(1 + S/K_a)$ where IC_{50} is the concentration of antagonist required to produce a 50% inhibition of the glycogenolytic effect of serotonin, S represents the concentration of serotonin and K_a is the K_{act} value of serotonin. ●, Serotonin; □, serotonin + 2×10^{-6} M *N,N*-dimethyltryptamine; ○, serotonin + 5×10^{-6} M *N,N*-dimethyltryptamine.

ogical specificity of the receptors mediating the serotonin-induced glycogenolysis does not correspond, however, to that of other serotoninergic receptors or putative receptors: for example, there are large differences in the apparent dissociation constants of the typical serotoninergic antagonists regarding inhibition of glycogenolysis, adenylate cyclase or binding of ^{3}H-spiperone or ^{3}H-serotonin respectively (Table 1). This suggests that a novel subclass of serotonin receptors mediates the glycogenolytic response.

It is unlikely that these receptors represent the common site of action of the potent hallucinogenic indole derivatives which display relatively low apparent affinity for the receptors and behave as either agonists (tryptamine) or antagonists (*N,N*-dimethyltryptamine). In view of the low apparent affinity of neuroleptics (compared with their affinity for dopamine receptors), it is also unlikely that significant occupation of serotonin receptors mediating glycogenolysis occurs during antipsychotic treatments which result in body fluid levels of these drugs in the nanomolar range[31]. On the other hand, micromolar concentrations of tricyclic antidepressants belonging to various chemical classes all antagonize competitively the serotonin-induced response. The antagonist effect of these compounds seems unrelated to their ability to block the serotonin uptake process as, for example, compounds such as iprindole or desimipramine are almost inactive on this process[32,33]. Because the effective concentrations of tricyclic compounds in the body fluids of patients undergoing antidepressant treatment seem to be in the micromolar range[34], it is likely that serotonin receptors mediating the glycogenolysis in brain are blocked during such treatments. It remains to be established whether this blockade participates in the antidepressant activity (or side effects) of these drugs.

Received 23 November 1981; accepted 21 May 1982.

1. Barchas, J. & Udsin, E. (eds) in *Serotonin and Behavior*, 1–316 (Academic, New York, 1973).
2. Fuxe, K., Schubert, J., Hokfelt T. & Jonsson, G. *Adv. biochem. Psychopharmac.* **10,** 67–74 (1974).
3. Green, A. R. & Grahame-Smith, *Nature* **260,** 487–491 (1976).
4. Aghajanian, G. K. & Wand, R. Y. in *Psychopharmacology: A Generation of Progress* (eds Lipton, M. A., Di Mascio, A. & Killam, K. F.) 171–193 (Raven, New York, 1978).
5. Besson, J. M. *Pain and Society* **17,** 161–182 (1980).
6. Garver, D. L. & Davis, J. M. *Life Sci.* **24,** 383–394 (1979).
7. Von Hungen, K., Roberts, S. & Hill, D. F. *Brain Res.* **84,** 257–267 (1975).
8. Enjalbert, A., Bourgoin, S., Hamon, M., Adrien, J. & Bockaert, J. *Molec. Pharmac.* **14,** 2–10 (1978).
9. Enjalbert, A., Hamon, M., Bourgoin, S. & Bockaert, J. *Molec. Pharmac.* **14,** 11–23 (1978).
10. Fillion, G. *et al. Life Sci.* **24,** 1813–1819 (1979).
11. Nelson, D., Herbet, A., Enjalbert, A., Bockaert, J. & Hamon, M. *Biochem. Pharmac.* **29,** 2445–2453 (1980).
12. Fillion G. M. B. *et al. Molec. Pharmac.* **14,** 50–59 (1978).
13. Nelson, D. L., Herbert, A., Bourgoin, S., Glowinski, J. & Hamon, M. *Molec. Pharmac.* **14,** 983–995 (1978).
14. Peroutka, S. J. & Snyder, S. H. *Molec. Pharmac.* **16,** 687–699 (1979).
15. Leysen, J. E. *et al. Life Sci.* **28,** 1015–1022 (1981).
16. Leysen, J. E. *J. Physiol., Paris* **77,** 351–362 (1981).
17. Peroutka, S. J., Lebovitz, R. M. & Snyder, S. H. *Science* **212,** 827–829 (1981).
18. Dolphin, A. C. & Greengard, P. *Nature* **289,** 76–79 (1981).
19. Quach, T. T., Rose, C. & Schwartz, J. C. *J. Neurochem.* **30,** 1335–1341 (1978).
20. Edwards, C., Nahorski, S. R. & Rogers, K. J. *J. Neurochem.* **22,** 564–572 (1974).
21. Schwartz, J. C., Martres, M. P., Rose, C., Quach, T. T. & Sokoloff, P. in *Chemical Neurotransmission, 75 Years* (eds Stjärne, L., Hedkvist, P., Lagercrantz, H. & Wennmalm, A.) 411–423 (Academic, New York, 1981).
22. Quach, T. T., Duchemin, A. M., Rose, C. & Schwartz, J. C. *Molec. Pharmac.* **17,** 301–308 (1980).
23. Magistretti, P., Morrisson, J. H., Shoemaker, W. J., Sapin, V. & Bloom, F. E. *Proc. natn. Acad. Sci. U.S.A.* **78,** 6535–6539 (1981).
24. Sutherland, E. W. & Robison, G. A. *Pharmac. Rev.* **18,** 145–164 (1966).
25. Haylett, D. G. & Jenkinson, D. H. *J. Physiol., Lond.* **225,** 751–772 (1972).
26. Assimacopoulos Jeannet, F. O., Blackmore, P. F. & Exton, J. *J. biol. Chem.* **252,** 2662–2669 (1977).
27. Koizumi, J. *Prog. Histochem. Cytochem.* **6,** 1–37 (1974).
28. Dahlstrom, A. & Fuxe, K. *Acta physiol. scand.* **62,** 1–35 (1964).
29. Dahlstrom, A., Haggendal, J. & Atack, C. in *Serotonin and Behavior* (eds Barchas, J. & Usdin, E.) 87–96 (Academic, New York, 1973).
30. Garbarg, M., Barbin, G., Feger, T. & Schwartz, J. C. *Science* **186,** 833–835 (1974).
31. Seeman, P. *Pharmac. Rev.* **32,** 229–313 (1980).
32. Ross, S. B., Renyi, A. L. & Ogren, S. O. *Life Sci.* **10,** 1267–1277 (1971).
33. Maas, J. W. *Archs gen. Psychiat.* **32,** 1357–1361 (1975).
34. Glassman, A. H. & Perel, J. M. in *Psychopharmacology: A Generation of Progress* (eds Lipton, M. A., Di Mascio, A. & Killam, K. F.) 917–922 (Raven, New York, 1979).
35. Cheng, C. & Prussoff, W. H. *Biochem. Pharmac.* **22,** 3099–3108 (1973).
36. Parker, R. B. & Waud, D. R. *J. Pharmac. exp. Ther.* **177,** 1–24 (1971).

Monoclonal antibodies against human T lymphocytes label Purkinje neurones of many species

J. A. Garson, P. C. L. Beverley,* H. B. Coakham & E. I. Harper

Brain Tumour Research Laboratory, Departments of Neuropathology and Neurosurgery, Frenchay Hospital, Bristol BS16 1LE, UK
*ICRF Human Tumour Immunology Group,
Faculty of Clinical Sciences, School of Medicine, University Street,
London WC1E 6JJ, UK

Conventional antibodies have long been used in an attempt to produce specific neural markers[1,2]. Such markers would be invaluable for studying the structural organization and development of the nervous system. Unfortunately, they have not generally been found to discriminate satisfactorily between neuronal subpopulations[3,4]. Recent developments of the hybridoma technique[5], however, promise to provide monoclonal antibodies of adequate specificity. Such antibodies have already been generated and shown to be capable of distinguishing between individual neurones of the leech nervous system[6]. We report here two monoclonal antibodies which, although generated against human T cells[7,8], react exclusively with Purkinje cells in the vertebrate central nervous system (CNS). This new specificity arose out of a fortuitous observation made during examination of the lymphocyte infiltration of human cerebellar tumours with the monoclonal antibody, UCHT1. Although widely used as a T-cell marker, its reaction with neural tissue has not hitherto been described. To our knowledge, this is the first description of a monoclonal antibody which recognises a functionally discrete neuronal population in the vertebrate brain.

0028–0836/82/290375—03$01.00

UCHT1 is an IgG1 mouse monoclonal antibody, derived from a fusion between P3/NS1/1-Ag4-1 myeloma cells and splenic lymphocytes from BALB/c mice immunized with human infant thymocytes and Sezary cells. The antibody had been previously characterized in detail[7] and was thought to bind exclusively to an antigen of 22,000 molecular weight (MW) present on the surface of human T lymphocytes. Therefore, we were surprised that it produced strong staining of Purkinje cells, by indirect immunofluorescence, when applied to frozen sections of human cerebellum.

Purkinje cells provide the only efferent pathway from the cerebellar cortex, their axons terminating chiefly in the deep cerebellar nuclei[9]. Their large flask-shaped cell bodies and extensive dendritic arborizations give them a unique appearance. Figure 1 shows intense cytoplasmic staining of Purkinje cells by UCHT1, extending throughout axons and dendrites. Note that cerebellar granule, stellate, basket and glial cells fail to stain. Human, mouse, rat, guinea pig and quail brains produced identical Purkinje cell staining. No other cells were stained in the cerebrum, cerebellum or spinal cord of any of the species tested. Extensive screening of other non-lymphoid tissues revealed no further cross-reactivity. The specificity of UCHT1 staining is summarized in Table 1. Absorption experiments (Table 2) confirmed restriction of the UCHT1 neural antigen to the cerebellum. The discovery of Purkinje cell labelling by UCHT1 led us to investigate other anti-haemopoietic cell monoclonal antibodies for similar cross-reactivity (see Table 3). Of 12 reagents tested, only one (Leu-4; Becton Dickson) had anti-Purkinje cell activity. It produced cytoplasmic staining which was indistinguishable from that of UCHT1. Cross blocking experiments on human T lymphocytes (unpublished data) indicate that UCHT1, Leu-4 and another pan T-cell marker, OKT3[10] (Ortho Pharmaceuticals), recognize closely related antigenic determinants. It is, therefore, of special interest to note that OKT3 does not react with Purkinje cells.

Table 1 UCHT1 reactivity

Positive	Negative Human	 Other species
Human T cells	Erythrocytes	Rat:
		Cerebellum†
Human Purkinje cells	Polymorphs	Olfactory bulb
Mouse Purkinje cells	Monocytes	Cerebrum
Guinea pig Purkinje cells	Platelets	Midbrain
Rat Purkinje cells*	Non T lymphocytes	Brain stem
Quail Purkinje cells	Cerebrum	Spinal cord
	Cerebellum†	Dorsal root ganglion
	Spinal cord	Spleen
	Pituitary	Kidney
	Muscle	Lung
	Liver	Bladder
	Kidney	Tongue
	Skin	Oesophagus
	Breast	Duodenum
	Thyroid	Aorta
	Adrenal	Mouse:
		Cerebellum†
	Colon	Cerebrum
	Oesophagus	Spinal cord
	Stomach	Kidney
	Tongue	Guinea pig:
		Cerebellum†
	Buccal mucosa	Spleen
	Connective tissue	Quail:
		Cerebellum†
	Primary cerebral tumours (25)	Cerebrum
	Secondary cerebral tumours (8)	Spinal cord

* Adult and 10-day-old neonates were tested.
† Cerebellum negative apart from Purkinje cells.

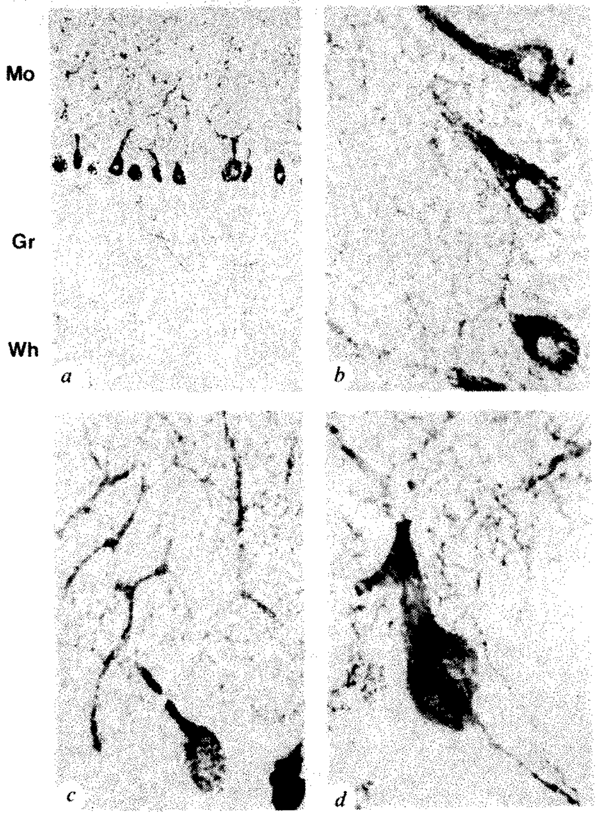

Fig. 1 Guinea pig Purkinje cells stained by UCHT1 using the indirect immunoperoxidase technique. Frozen sections (6 μm) of cerebellum were fixed briefly in acetone then incubated at 20 °C for 30 min with a purified IgG fraction of UCHT1 ascites, diluted 1:200. The slides were washed for 10 min in phosphate-buffered saline then incubated at 20 °C for 30 min with peroxidase-conjugated rabbit anti-mouse immunoglobulin (Dako), diluted 1:100. Diaminobenzidine (0.6 mg ml^{-1}) was used as the chromogenic substrate. *a* Shows Purkinje cell axons traversing the granule cell layer (Gr) to join other Purkinje axons of the cerebellar white matter (Wh). These axons were seen to terminate on neurones of the deep cerebellar nuclei. Such neurones showed no staining with UCHT1. Purkinje cell branching dendrites in the molecular layer (Mo) are clearly stained. *b*, The antigen is seen to be cytoplasmic, as the nuclei show no staining. *c* Shows the dendritic arborizations of the molecular layer; *d* shows an axon as it leaves the base of a Purkinje cell body.

The Purkinje cell antigen does not survive fixation in formaldehyde, paraformaldehyde, glutaraldehyde, osmium tetroxide, Carnoy's or Bouin's fixatives but is unaffected by fixation in acetone at room temperature for 5 min. The antigen is best demonstrated in fresh material but can be detected in sections stored for up to 3 days at −20 °C. Beyond this time, staining becomes unpredictable.

The relatively labile nature of the Purkinje antigen has so far prevented any determination of its molecular weight or biochemical characteristics. Without such data it is unsafe to assume that the UCHT1-defined Purkinje cell and T-cell antigens are identical[11,12]. Indeed, their differing species distributions and different locations within the cell (cytoplasm versus plasma membrane) suggest that they may be unrelated molecules which merely share a common antigenic determinant.

Although the nature of UCHT1-defined Purkinje specific antigen is unknown, it does not seem to match any of the other previously reported Purkinje cell-associated proteins such as P-400 (ref. 13). This 400,000 MW protein is not detectable in the Purkinje cell axon and is therefore unlikely to be the antigen recognized by UCHT1. Prostaglandin dehydrogenase[14] and the calcium binding protein parvalbumin[15] have also been reported to be Purkinje cell-related but lack the highly restricted localization of the UCHT1-defined antigen. The intestinal peptide hormone motilin has recently been detected in Purkinje cells[16]

Table 2 Absorption experiments with UCHT1

	T lymphocyte staining	Purkinje cell staining
UCHT1 unabsorbed	+ +	+ +
UCHT1 cerebrum absorbed	+ +	+ +
UCHT1 cerebellum absorbed	±*	−

UCHT1 was diluted to 1 : 1200 (one doubling dilution below end titre) and absorbed with homogenates of rat cerebrum and cerebellum. Absorption was carried out at 20 °C for 1 h with equal volumes of diluted antibody and homogenate. Following absorption, UCHT1 binding on human T cells and Purkinje cells in frozen section was visualized by indirect immunofluorescence using a fluorescein-conjugated goat anti-mouse immunoglobulin, diluted 1 : 80.

* Weak residual staining of T cells.

but, unlike the UCHT1-defined antigen, is only present in a proportion of Purkinje cells. Furthermore, UCHT1 fails to stain motilin-containing cells of the rat duodenum. Finally, cyclic GMP-dependent protein kinase has been shown, within the rodent nervous system, to be restricted almost exclusively to Purkinje cells[17]. However, in contrast to the UCHT1 antigen, the enzyme is also present in high concentration in the muscular wall of the aorta and in various other smooth muscle cells (see Table 1).

Purkinje-specific antigens have previously been demonstrated by immunological studies with two conventional polyclonal heteroantisera. The first[18], although operationally specific, was only effective at very low titre. The second[19], raised against a glycoprotein extracted from rat cerebellum, appeared Purkinje cell-specific, but specificity was demonstrated by absorption rather than by direct testing so that small populations of antigen-containing cells elsewhere in the nervous system might have been overlooked. In addition to these studies with polyclonal antisera, a monoclonal antibody, designated CE5, reactive with Purkinje cells, has also been described[20]. CE5, unlike UCHT1, however, is relatively nonspecific, reacting with many different types of neurone including dorsal root ganglion cells and pyramidal neurones; it also labels cardiac muscle and the protozoan *Trypanosoma cruzi*. The high titre, high specificity and unlimited supply of UCHT1 and Leu-4 make them ideal immunological markers for Purkinje cells.

The work described here, together with preliminary experiments on neonatal mouse cerebellum and cerebellar mutant strains, suggests that UCHT1 and Leu-4 will become invaluable tools for studying the organization and development of cerebellar architecture and connectivity.

This work was financed by the MRC, the Imperial Cancer Research Fund, Bristol Brain Tumour Research Fund and the Francis and Augustus Newman Foundation. We thank Dr D. B. Brownell, D. Rowe, T. Gradidge and J. Singh for their help and K. Caddy for providing the data on fixatives. Monoclonal antibody 308 was donated by J. Kemshead, RFB-1 by G. Janossy and CR3/43 by D. Y. Mason. OKT3, OKT4 and OKT8 were supplied by Ortho Pharmaceuticals and Leu-4 and Leu-2a donated by Becton Dickinson.

Table 3 Reactivity of anti-haematopoietic cell monoclonal antibodies with Purkinje cells

Monoclonal antibody	Haematopoietic cell reactivity	Purkinje cell staining
UCHT1	Pan T cell	+
Leu-4	Pan T cell	+
OKT3	Pan T cell	−
OKT4	Helper T cells	−
OKT8*	Suppressor/cytotoxic T cells	−
UCHT2	Pan T cell + B.CLL	−
UCHT3	Pan T cell + B.CLL	−
CR3/43	Anti HLA-Dr	−
Leu-2a	Suppressor/cytotoxic T cells	−
2D1	All leukocytes	−
TG1	Granulocytes	−
308	Granulocytes	−
RFB-1	Lymphoid stem cells	−

* OKT8 has recently been shown to exhibit anti-ovine oligodendrocyte cross-reactivity *in vitro*[21]. However, we have been unable to demonstrate OKT8 immunostaining of oligodendrocytes in frozen sections of human white matter, optic nerve, multiple sclerosis plaques or oligodendroglioma.

Received 22 March; accepted 18 May 1982.

1. Raff, M. C. *et al. Brain Res.* **174,** 283–308 (1979).
2. Schachner, M., Wortham, K. A. & Kincade, P. W. *Cell Immun.* **22,** 369–374 (1976).
3. Mirsky, R., Wendon, L. M. B., Black, P., Stolkin, C. & Bray, D. *Brain Res.* **148,** 251–259 (1978).
4. Rutishauser, U., Gall, W. E. & Edelman, G. M. *J. Cell Biol.* **79,** 382–393 (1978).
5. Kohler, G. & Milstein, C. *Nature* **256,** 495–497 (1975).
6. Zipser, B. & McKay, R. *Nature* **289,** 549–554 (1981).
7. Beverley, P. C. L. & Callard, R. E. *Eur. J. Immun.* **11,** 329–334 (1981).
8. Ledbetter, J. A., Frankel, A. E., Herzenberg, L. A. & Herzenberg, L. A. in *Monoclonal Antibodies and T Cell Hybridomas* (eds Hammerling, U., Kearney, J. & Hammerling, G.) (Elsevier, New York, in the press).
9. Eccles, J. C. in *Cerebro-Cerebellar Interaction* (eds Massion, J. & Sasaki, K.) (Elsevier, New York, 1979).
10. King, P. C., Goldstein, G., Reinhertz, E. L. & Schlossman, S. F. *Science* **206,** 347–349 (1979).
11. Dulbecco, R. *et al. Nature* **292,** 772–774 (1981).
12. Lane, D. & Koprowski, H. *Nature* **296,** 200–202 (1982).
13. Mikoshiba, K., Huchet, M. & Changeux, J. P. *Devl Neurosci.* **2,** 254–275 (1979).
14. Siggins, G., Hoffer, B. & Bloom, F. *Ann. N.Y. Acad. Sci.* **180,** 302–319 (1971).
15. Celio, M. R. & Heizmann, C. W. *Nature* **293,** 300–302 (1981).
16. Nilaver, G., Defendini, R., Zimmerman, E. A., Beinfeld, M. C. & O'Donohue, T. L. *Nature* **295,** 597–598 (1982).
17. Walter, U., DeCamilli, P., Lohmann, S. M., Miller, P. & Greengard, P. *Cold Spring Harb. Conf. Cell Proliferation* **8,** 141–157 (1981).
18. Woodhams, P., Mallet, J., Changeux, J. P. & Balazs, R. *Devl Biol.* **72,** 320–326 (1979).
19. Reeber, A., Vincendon, G. & Zanetta, J. P. *Brain Res.* **229,** 53–65 (1981).
20. Wood, J. N., Hudson, L., Jessell, T. M. & Yamamoto, M. *Nature* **296,** 34–38 (1982).
21. Oger, J., Szuchet, S., Antel, J. & Arnason, B. *Nature* **295,** 66–68 (1982).

Germinal centre B cells: antigen specificity and changes in heavy chain class expression

G. Kraal, I. L. Weissman & E. C. Butcher

Laboratory of Experimental Oncology, Department of Pathology,
Stanford University Medical Centre, Stanford,
California 94305, USA

Germinal centres are histologically defined aggregates of blast cells that occur in B-cell areas of lymphoid tissues after antigenic stimulation. They are believed to be associated with the development of B-cell memory and plasma cell (especially secondary, IgG and IgA) responses[1-3]. Recent studies of murine lymphoid tissues have defined cell-surface markers that distinguish germinal centre B cells from other mature B cells[4-7], permitting their identification and characterization in cell suspensions. Here we have used these markers to define and study germinal centre cells in lymph nodes, and have found that they constitute a unique population of B cells which (1) arises in response to antigenic stimulation, (2) contains nearly all of the demonstrably antigen-specific B cells in the stimulated organ, (3) bears surface IgM after primary stimulation and (4) as a population, demonstrates isotype switching to a predominant surface IgG phenotype after secondary stimulation with specific antigen. These findings demonstrate that germinal centres are a major site of proliferation and differentiation of antigen-specific B cells *in vivo*, and suggest that the germinal centre microenvironment may have an important role in heavy chain class switching during B-cell responses.

Germinal centre B cells possess unique cell-surface features. One of the most important of these is defined by peanut agglutinin (PNA)[4-7], a plant lectin with specificity for terminal galactosyl residues. In antigen-stimulated lymphoid organs, fluorescence-labelled PNA defines a discrete population of lymphocytes (termed PNA$^{\text{hi}}$) that bind 10–30 times as much PNA as the major population of lymphocytes[7] (PNA$^{\text{lo}}$). Immunohistological[4,5,7], electron microscopic[5] and cell suspension[4-7] studies of mouse Peyer's patches and stimulated lymph nodes have shown that the B cells in the PNA$^{\text{hi}}$ population are almost exclusively germinal centre lymphocytes. B cells

0028-0836/82/290377—03$01.00

outside germinal centres, as well as plasma cells and most T cells, bind only low levels of PNA[5,7]. A small proportion of T cells may also be PNA^{hi} (refs 7, 8). A secondary independent marker is IgD: immunohistological[9,10] and flow cytofluorometric[7] studies have shown that germinal centre lymphoid cells lack surface IgD, whereas essentially all other mature B cells are IgD$^+$ (ref. 7). Thus, germinal centre B cells can be identified confidently in cell suspensions of lymph nodes and Peyer's patches by virtue of their unique PNA^{hi}, IgD$^-$, Thy-1$^-$ phenotype.

BALB/c or BALB.B mice were immunized in the front foot pads with heterologous erythrocytes, and cell suspensions were made from brachial and axillary lymph nodes during or near the peak of germinal centre responses (6 days after primary or secondary immunization). Several studies were carried out to confirm the usefulness of PNA in identifying germinal centre lymphoid cells in these lymph nodes. Fluorescence activated cell sorter (FACS) analyses demonstrated the appearance of a discrete population of PNA^{hi} cells in the stimulated nodes, constituting up to 10–12% of the lymph node cells (and up to 20–30% of B cells) 6 days after primary immunization (see Fig. 1). Double fluorescence microscopy of frozen sections of stimulated nodes stained with tetramethylrhodamine isothiocyanate (TRITC)-conjugated PNA and counterstained with fluorescein-isothiocyanate (FITC)–rabbit anti-mouse Ig confirmed the remarkable specificity, within the B-cell lineage in this organ, of intense PNA staining for germinal centre cells (not shown, see Raedler *et al.*[5] for similar findings). Staining of FACS-separated PNA^{hi} and PNA^{lo} populations confirmed the observation, previously based on immunohistological studies[5,7], that plasma cells and plasmablasts are PNA^{lo} (see Fig. 1 legend).

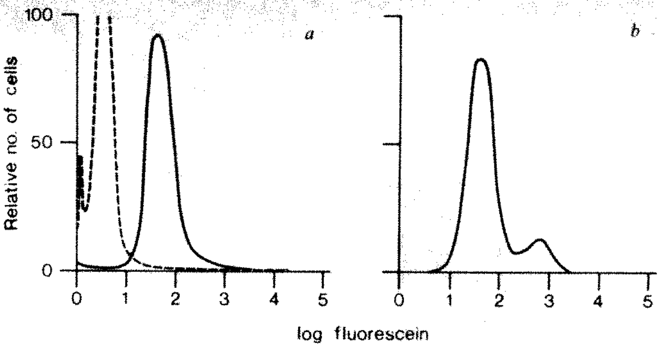

Fig. 1 Axillary and brachial lymph node cells from BALB/c mice were incubated for 5 min in an excess of FITC-conjugated PNA (EY Laboratories) at 100 μg ml^{-1} in phosphate-buffered saline, washed, and analysed on the FACS (Becton Dickinson). *a*, Unstimulated lymph node cells were stained with FITC–PNA in the presence (dotted line) or absence (solid line) of 0.2 M galactose. Most lymphocytes bind low levels of PNA to galactose-inhibitable sites, and are therefore referred to as PNA^{lo}. *b*, Six days after footpad immunizations with 1–2 × 10^7 SRBC, a discrete population of PNA^{hi} cells has arisen which binds about 20 times as much PNA as the PNA^{lo} lymphocytes. To determine if this PNA^{hi} population included significant numbers of plasma cells or plasmablasts, cytocentrifuge preparations of FACS-sorted PNA^{hi} and PNA^{lo} populations were air-dried, fixed 10 min in cold acetone, counterstained with rabbit anti-mouse immunoglobulin and examined by fluorescence microscopy. Cells containing cytoplasmic immunoglobulin segregated predominantly with the PNA^{lo} population. Of 400 sorted PNA^{lo} cells counted, 41 contained detectable internal immunoglobulin; 27 of these were mature plasma cells with eccentric nuclei, and the remaining 14 had the appearance of plasmablasts. Of 1,000 PNA^{hi} sorted cells examined, only one apparent plasma cell and seven plasmablasts were identified.

Table 1 The phenotype of PNA^{hi} sample cells in lymph nodes after immunization

	% Of cells stained	
Antibody directed against	Primary response	Secondary response
B cells (B220)	94	83
Total immunoglobulin	84	80
IgM	62	25
IgG	9	60
IgG + γ blockade	ND	1
IgG + α and μ blockade	ND	64
IgA	4	3
IgD	1	1
T cells (Thy-1 + Lyt-1)	9	10
Rabbit anti-KLH	0	1
RA3-2C1	0	0

BALB.B mice, 6–8 weeks of age, were injected with 1–2 × 10^7 SRBC in the front footpads. For analysis of the primary response, axillary and brachial lymph nodes were removed 6 days after immunization. For the secondary response lymph nodes were collected 6 days after a second injection of antigen with a 2-week interval between first and second injection. Cells were stained at a density of 10^6 cells per 10 μl of antiserum at saturating concentrations for 5–10 min and washed between first and second stages by centrifugation through serum. After incubating the cells in the second stage for 5 min, an equal volume of TRITC-conjugated PNA (EY Laboratories) at 100 μg ml^{-1} was added for another 3–4 min. The cells were then directly suspended in 1–2 ml of 2% formalin in phosphate-buffered saline washed through serum and examined microscopically. Affinity-purified anti-mouse total immunoglobulin, anti-keyhole limpet haemocyanin (KLH), and μ-chain-specific[16] and α-chain specific[7] antibodies (gifts from Drs C. Nottenburg and R. L. Coffman) and an Fab preparation of an anti-γ-serum[17] (a gift of Dr E. Vitetta) were produced in rabbits and used in combination with a fluoresceinated sheep anti-rabbit immunoglobulin second stage (Institut Pasteur, Paris). To detect δ chains a biotinylated monoclonal anti-Igh-5a, H10.4.22[18], was used in combination with fluoresceinated avidin (EY Laboratories). B cells were detected by a newly developed monoclonal rat antibody (RA3-6B2, a gift of Dr R. L. Coffman) specific for B220, the B-lineage-specific form of the T200 family of molecules[13]. A mixture of monoclonal anti-Lyt-1 (53-7.3) and anti-Thy-1 (30-H12)[19] was used to detect T cells with a highly specific fluoresceinated rabbit anti-rat immunoglobulin second stage. A monoclonal rat antibody (RA3-2Cl) with no known specificity was used as a control. The specificity of the rabbit anti-mouse γ chain reagent was tested by attempting to block staining either with a pool of IgG myeloma proteins or with a mixture of IgA and IgM myeloma proteins. Preincubation of the antiserum for 15 min with mouse IgGs totally inhibited staining but an excess of IgA (TEPC 15) and IgM myeloma proteins had no effect. 150–200 PNA^{hi} cells (with the characteristic large size and/or irregular outline of germinal centre cells) were scored, single-blind, using a Zeiss fluorescence microscope with exciter/barrier filter combinations for rhodamine and fluorescein. The data are pooled from two experiments with similar results and are expressed as the % of sample cells staining.

For studies of the surface phenotype of the PNA^{hi} population, cells were labelled with TRITC-conjugated PNA and counterstained with various (fluorescein-detected) monoclonal antibodies or heterologous antisera. Putative germinal centre cells were identified microscopically by their intense staining with PNA in combination with their characteristic larger size and frequently irregular cell outline. These criteria excluded most PNA^{hi} T cells, yet included nearly all B cells with the characteristic IgD$^-$ phenotype of germinal centre cells. Cells so identified were then examined under fluorescein filters for staining with immunological reagents.

Initial experiments describing the surface phenotype of germinal centre cells after primary and secondary immunizations are presented in Table 1. Only 10% of the sample PNA^{hi} population were contaminating T cells; the remainder were IgD$^-$ B cells. The results demonstrate that IgM is the predominant isotype of surface immunoglobulin during the primary response, but in a secondary response, germinal centre cells mainly express surface IgG. Although the present findings do not demonstrate that these B cells synthesize their surface immunoglobulin, we have previously presented evidence based on allelic exclusion that the comparable population of Peyer's patch germinal centre cells do synthesize their major class of surface immunoglobulin (IgA)[6,7]. (In striking contrast to the pattern of immunoglobulin expression by peripheral node germinal centre cells, 50–75% of germinal centre cells in Peyer's patches express surface IgA[7].) These findings suggest that germinal centres may have an important role in the process of isotype switching.

We wished therefore to determine if the B cells proliferating in germinal centres are specific for the immunizing antigen, as suggested by work of Sordat *et al.*[21], or if germinal centres merely represent sites of nonspecific expansion and perhaps isotype switching of all available B cells. Kanowith-Klein *et al.*[12] have shown that the proportion of antigen binding B cells bearing surface IgG increases during the immune response to heterologous erythrocytes. Thus the switch we observed from a predominance of IgM$^+$ to IgG$^+$ cells in germinal centres with restimulation with the same antigen suggested that these cells

Table 2 Heavy chain isotype switching of germinal centre cells is antigen specific

Antigen 1° Injection	 2° Injection	% Of PNA^{hi} cells with surface IgM	 IgG
SRBC	SRBC	31	48
SRBC	HuRBC	56	13
SRBC	None	46	14
HuRBC	SRBC	52	21
HuRBC	HuRBC	36	49

BALB.B mice were immunized in the front foot pads with either SRBC or HuRBC. After 3 weeks the animals were boosted with one of the two antigens. Five days later lymph node cells were prepared and stained as described in Table 1 legend. 150–200 PNA^{hi} cells were counted single-blind. The results are from a representative experiment, expressed as the percentage of PNA^{hi} sample cells staining with the antiserum.

might be antigen specific. This reasoning was greatly strengthened by the demonstration that this IgM to IgG switch was itself antigen specific. After priming with SRBC, secondary immunization with SRBC reproducibly caused a switch in the germinal centre cells to a predominance of IgG$^+$ cells, whereas secondary injection of human red cells (HuRBC) caused no shift (see Table 2). After HuRBC priming, secondary HuRBC but not SRBC injection caused the switch.

More direct evidence of antigen specificity has been obtained at the single cell level. By using rosetting techniques, we have found that almost all specific-antigen-binding B cells have the surface phenotype of germinal centre cells during the active immune response to SRBC. Suspensions of immunized lymph nodes were incubated with RBC briefly on ice, and subsequently stained with TRITC–PNA. Ten per cent of PNA^{hi}, IgD$^-$ cells in SRBC-immunized lymph nodes formed SRBC rosettes. As many SRBC antigens are probably either located on the erythrocyte surface, or not sufficiently represented to support rosette formation, this proportion of rosetting cells probably underestimates the percentage of germinal centre cells that are antigen specific. Furthermore, after removal of glass-adherent cells (presumably macrophages binding cytophilic antibody), 98% (104/106) or rosetting cells were PNA^{hi}, and 100% (100/100) stained with RA3-6B2, a monoclonal antibody against B220[13], the B-lineage specific form of the T200 family of molecules. Similar results were obtained after secondary injections.

Rosette formation was antigen-specific. Six days after foot pad injection of SRBC or HuRBC, immunized lymph node cells were incubated with a mixture of HuRBC, and FITC-labelled SRBC. As shown in Table 3, PNA^{hi} cells of SRBC recipients only rosetted with SRBC, whereas only HuRBC rosettes were formed after HuRBC immunization. To rule out the possibility that these results were simply due to cytophilic adsorption of anti-RBC antibodies, individual mice were immunized with a mixture of HuRBC and SRBC in the same footpad, and 6 days later the specificity of PNA^{hi} rosetting cells was determined. If cytophilic antibodies were involved, we could expect most rosettes to be mixed, containing both FITC–SRBC and unlabelled HuRBC. Instead, all rosettes were formed specifically with one or the other RBC type, providing strong evidence that PNA^{hi} cells form rosettes by synthesis and surface expression of specific antibody.

Table 3 Germinal centre cells form rosettes specifically with the immunizing antigen

Immunogen	HuRBC	No. of rosetting cells binding HuRBC and SRBC	SRBC
SRBC	0	0	100
HuRBC	113	0	0
SRBC and HuRBC	51	0	75

BALB.B mice were injected with SRBC, HuBRC or a 1:1 mixture of both erythrocyte types. After 6 days cell suspensions from axillary and brachial lymph nodes were prepared and incubated for 1 h at 37 °C in glass tubes to remove adherent cells. Nonadherent cells were then added to a 1:1 mixture of SRBC and HuRBC and allowed to form rosettes for 10 min at 4 °C. The cell mixtures were spun down and resuspended with rhodaminated PNA for 5 min after which they were diluted and directly examined in the fluorescence microscope. SRBC were labelled by incubation with FITC before rosette formation[20]. Rosettes were (1) first identified microscopically under dark-field illumination, (2) then examined under UV epi-illumination using the filter combination for rhodamine to determine if the rosetting cells were PNA^{hi}, and if so, (3) the type of erythrocyte in the rosette was determined using filters for fluorescein. Rosettes were scored when at least 10 erythrocytes surrounded one nucleated centre cell. Approximately 10–15% of the specific rosettes, thus defined, contained one or two heterologous contaminating erythrocytes, but the frequency was no greater in recipients of mixed erythrocytes than in animals immunized with only one type. All rosette-forming cells were B cells (100 RA3-6B2$^+$ per 100 rosettes counted); nearly all were PNA-binding (104 PNA^{hi} per 106 rosettes counted); and 10% (9.3; 10.1%) of PNA^{hi} cells formed rosettes. Similar results were obtained after secondary immunization. Truly mixed rosettes could be easily identified using this technique. In recipients immunized with both RBC types many mixed rosettes were observed before removal of adherent cells (presumably macrophages bearing cytophilically absorbed antibody).

The present findings support the concept that antigen-specific virgin B cells are recruited in the formation of germinal centres during a primary immune response, and subsequently undergo differentiation and selection in this site. Although many differentiation events may occur within the germinal centre population (for example, affinity maturation, suppression and/or reprogramming of normal lymphocyte migration mechanisms[6]), we have focused initially on changes in heavy chain class expression. If the precursors of germinal centre cells are IgD$^+$, IgM$^+$ lymphocytes (as seems likely, although other lineages cannot be ruled out[11,14]), the first such alteration in isotype expression, which may be necessary on entry into the germinal centre, is the loss of surface IgD. Occurrence and significance of IgD regulation however, remain speculative. More interesting is the direct demonstration of changes in the proportions of germinal centre cells expressing IgM and IgG during the immune response. The switch to a predominance of IgG bearing cells, and the observation that almost all antigen-specific B cells seem to be maintained in the PNA^{hi} pool, strongly argue that the genetic rearrangements leading to heavy chain class switching occur in the germinal centre. The specific lack of IgA expression in peripheral lymph node as opposed to Peyer's patch germinal centres suggests that the germinal centre microenvironment (perhaps in conjunction with T-cell influences[15]) may be capable of directing the heavy chain class switch, or perhaps of selecting cells that have randomly switched to the isotype appropriate to the site of the immune response. Although our findings support a role for germinal centres in the production of memory B cells and plasma cell precursors[1–3], a thorough understanding of the role of germinal centres in humoral immunity must await direct lineage analyses.

This work was supported by NIH grant AI 09072. G.K. is the recipient of a Research Fellowship award from the Fogarty International Center. E.C.B. is a Senior Fellow of the American Cancer Society.

Received 9 November 1981; accepted 5 May 1982.

1. Thorbecke, G. J., Romano, T. J. & Lerman, S. P. in *Prog. Immun. II* **3**, 25–34 (1974).
2. Nieuwenhuis, P., Gastkemper, N. A. & Opstelten, D. *Ciba Fdn Symp.* **84**, 246–264 (1981).
3. Klaus, G. G. B. & Kunkl, A. *Ciba Fdn Symp.* **84**, 264–280 (1981).
4. Rose, M. L., Birbeck, M. S. C., Wallis, V. J., Forrester, J. A. & Davies, A. J. S. *Nature* **284**, 364–366 (1980).
5. Raedler, A., Raedler, E., Arndt, R. & Thiele, H. G. *Immun. Lett.* **2**, 335–338 (1981).
6. Butcher, E. C., Reichert, R. A., Coffman, R. L., Nottenburg, C. & Weissman, I. L. *Adv. exp. Med. Biol.* (in the press).
7. Butcher, E. C. *et al. J. Immun.* (submitted).
8. London, J., Berrih, S. & Bach, J. F. *J. Immun.* **121**, 438–443 (1978).
9. Martin, L. N. & Leslie, G. A. *Immunology* **33**, 865–872 (1977).
10. Stein, H. *et al. J. Histochem. Cytochem.* **28**, 746–760 (1980).
11. Jacobson, E. B. *et al. J. exp. Med.* **154**, 318–322 (1981).
12. Kanowith-Klein, S., Vitetta, E. S., Korn, E. L. & Ashman, R. F. *J. Immun.* **122**, 2349–2355 (1979).
13. Coffman, R. L. & Weissman, I. L. *Nature* **289**, 681–683 (1981).
14. Opstelten, D., Stikker, R., Van der Heyden, D. & Nieuwenhuis, P. *Virchows Arch. path. Anat. Physiol.* **34**, 53–62 (1980).
15. Elson, C. O., Heck, J. A. & Strober, W. *J. exp. Med.* **149**, 632–643 (1979).
16. Coffman, R. L. & Cohn, M. *J. Immun.* **118**, 1806–1815 (1977).
17. Zan-bar, I., Strober, S. & Vietta, E. S. *J. Immun.* **123**, 925–930 (179).
18. Oi, V. T. P., Jones, P., Goding, S. W., Herzenberg, L. A. & Herzenberg, L. A. *Curr. Topics Microbiol. Immun.* **81**, 115–129 (1978).
19. Ledbetter, J. A. & Herzenberg, L. A. *Immun. Rev.* **47**, 63–90 (1979).
20. Butcher, E. C. & Weissman, I. L. *J. immun. Meth.* **37**, 97–108 (1980).
21. Sordat, B., Sordat, M., Hess, M. W., Stoner, R. D. & Cottier, H. *J. exp. Med.* **131**, 77–92 (1970).

Somatic variants of murine immunoglobulin λ light chains

Alfred L. M. Bothwell*†, Michael Paskind*†,
Michael Reth‡, Thereza Imanishi-Kari†,
Klaus Rajewsky‡ & David Baltimore*†

* Whitehead Institute for Biomedical Research, and
† Center for Cancer Research and Department of Biology,
Massachusetts Institute of Technology, Cambridge,
Massachusetts 02139, USA
‡ Institut für Genetik der Universitat zu Köln, 5000 Köln 41, FRG

Studies of the murine λ1 light chains produced by myeloma cells provided the first evidence for somatic point mutation of germ-line variable (V) region genes. An examination of the variable regions of 19 λ1 chains revealed seven which differed from a common sequence by one to three amino acid substitutions[1]. Subsequently, one of these presumed somatic variants of the single λ1 V gene was characterized by DNA sequence analysis of the rearranged functional gene[2]. The predicted DNA sequence alteration was observed and no silent mutation was evident. These studies of λ chain variants suggested that the hypervariable, complementarity-determining regions (CDRs) ht be a preferred site of somatic mutation because all seven characterized variants contained substitutions only in these regions. By contrast, comparisons of closely related κ chain variable region amino acid sequences, and more recently V_κ and V_H genes[8–12], have suggested that somatic mutation probably occurs in codons for both framework and CDR residues. To examine this apparent discrepancy between the sites of somatic mutation in λ and κ genes, we have determined the nucleotide sequence of two λ1 gene from hybridomas and a λ2 gene from a myeloma. These sequences demonstrate that somatic mutation in λ genes can occur in both the framework and CDR residues.

We have previously characterized the sequences of genes for the V_H regions of two antibodies which bear (4-hydroxy-3-nitrophenyl)acetyl (NP)[b] idiotypic determinants[8]. These antibodies were from hybridomas of C57BL/6 origin and possessed λ1 light chains: one was from hybridoma B1–8 which secretes an IgM antibody whose μ chain is specified by a germ-line nucleic acid sequence; another was from the S43 hybridoma which produces an IgG2a antibody in which 10 base pairs (bp) in the V_H region were altered from the germ-line configuration by somatic point mutations. We determined, therefore, whether somatic mutation in the λ1 light chains paralleled that observed in their associated V_H regions.

In addition, we have determined the nucleotide sequence of pλ2–1, the λ2 cDNA clone derived from MOPC-315[13]. A comparison of the amino acid sequence of this protein with the sequence predicted from the germ-line λ2 V gene indicated the presence of somatic mutation[14], which was further defined by determining the nucleotide sequence encoding this protein.

Molecular cDNA clones of the λ1 light chain mRNAs were constructed as previously described[8] using the DNA insert from pABλ1–1 as probe[13]. A preliminary characterization of several λ1-containing cDNA clones by restriction enzyme cleavage suggested the presence of somatic mutation in the S43-derived sequence. Restriction enzyme digests of three B1–8 clones were consistent with the sites predicted from the germ-line λ1 DNA sequence[2,13] but the S43-derived clone, pABλ1–15, had an additional *Kpn*I site in the J region (Fig. 1).

To precisely identify differences from the germ-line sequence, the longest cDNA clones pABλ1–9 (B1–8) and pABλ1–15 (S43), were sequenced. The sequence of the pABλ1–9 insert indicated that the clone began with codon 47 and extended in the 3′ direction through the poly(A) (Fig. 1). This nucleotide sequence was identical to that found in the BALB/c germ line. Peptide mapping of the B1–8 λ1 chain also suggested that this chain contained the germ line-encoded sequence (T.I., unpublished).

The DNA sequence of the longest S43-derived clone, pABλ1–15, encoding the leader, V, J and most of the C region (up to the *Pvu*II site at codon 195) is presented in Fig. 2. (The rest of the λ1 sequence in Fig. 2 was derived from pABλ1–9.) The S43 V-region sequence contained three somatic mutations when compared with the germ-line sequence; two in the $V_{\lambda 1}$ region at codons 80 and 87 and one in the J segment at codon 103. Otherwise the DNA sequence consisting of the leader, V, J and the available C region was exactly the same as that found in the B1–8-derived clone, pABλ1–9, or in the BALB/c λ germ-line DNA sequences[13]. The somatic mutations in the λ chain of S43 all occurred outside the CDRs—they are the first somatic mutations to be located outside these regions in a productive λ1 gene. The mutations in codons 80 and 87 result in fairly conservative amino acid replacements; the new methionine (Met) residue at codon 87 is also found at that position in the λ2 V region.

Comparison of the C57BL/6 and BALB/c λ1 germ-line cDNA sequences beginning with the initiator Met codon and extending 3′ to the poly(A) sequence showed complete identity. Given the polymorphisms evident in comparisons of heavy chain constant regions between these two strains[15], the complete absence of polymorphic differences in these λ1 sequences is notable.

To characterize somatic mutations present in the MOPC-315 λ2 chain, the DNA sequence of pλ – 1 was determined[13] (Fig. 2). Six somatic mutations in the V region were found, at codons 38, 50, 94, 95 and 96. This sequence corrects the published amino acid sequence at positions 55 (where MOPC-315 λ2 has the germ-line sequence), and at 145 and 146 and it removes the ambiguity at codons 147–148[16,17]. All of the observed somatic mutations occurred in CDRs except for those found in codon 38. The precise junction between the $V_{\lambda 2}$ and $J_{\lambda 2}$ segments can be defined because the $J_{\lambda 2}$ germ-line sequence has recently been determined[18,19]. The $J_{\lambda 2}$ sequence in pλ2–1 is identical to the germ-line sequence.

These analyses have shown that somatic mutations in λ chains need not be localized in the CDRs. The sequence of an aberrantly rearranged λ1 gene in MOPC-315 also showed somatic variation outside of the CDRs[20]. It therefore seems likely that for λ, as for κ[3–7] and V_H genes[8–12], somatic mutation occurs throughout the variable region sequence.

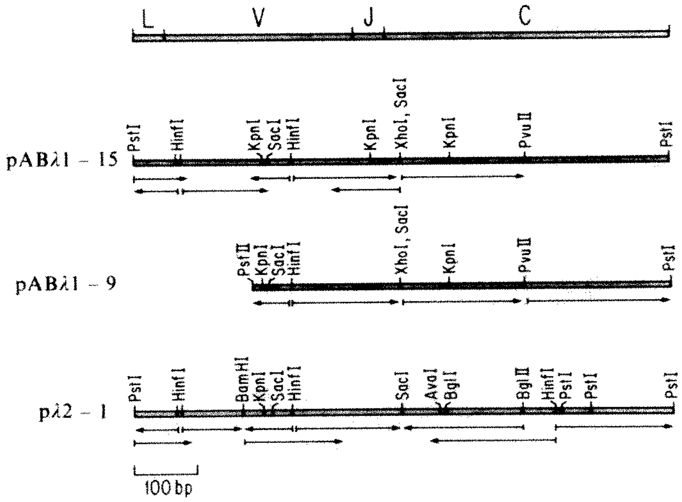

Fig. 1 Restriction map and DNA sequencing of λ cDNA clones. The clone pABλ1–15 was derived from the S43 hybridoma, pABλ1–9 from B1–8 and pλ2–1 from the MOPC–315 myeloma[13]. The DNA sequence was determined using the Maxam–Gilbert[25] procedure on 5′-kinased DNA. The arrows indicate the DNA sequences determined in the 5′ to 3′ direction.

0028–0836/82/290380—03$01.00

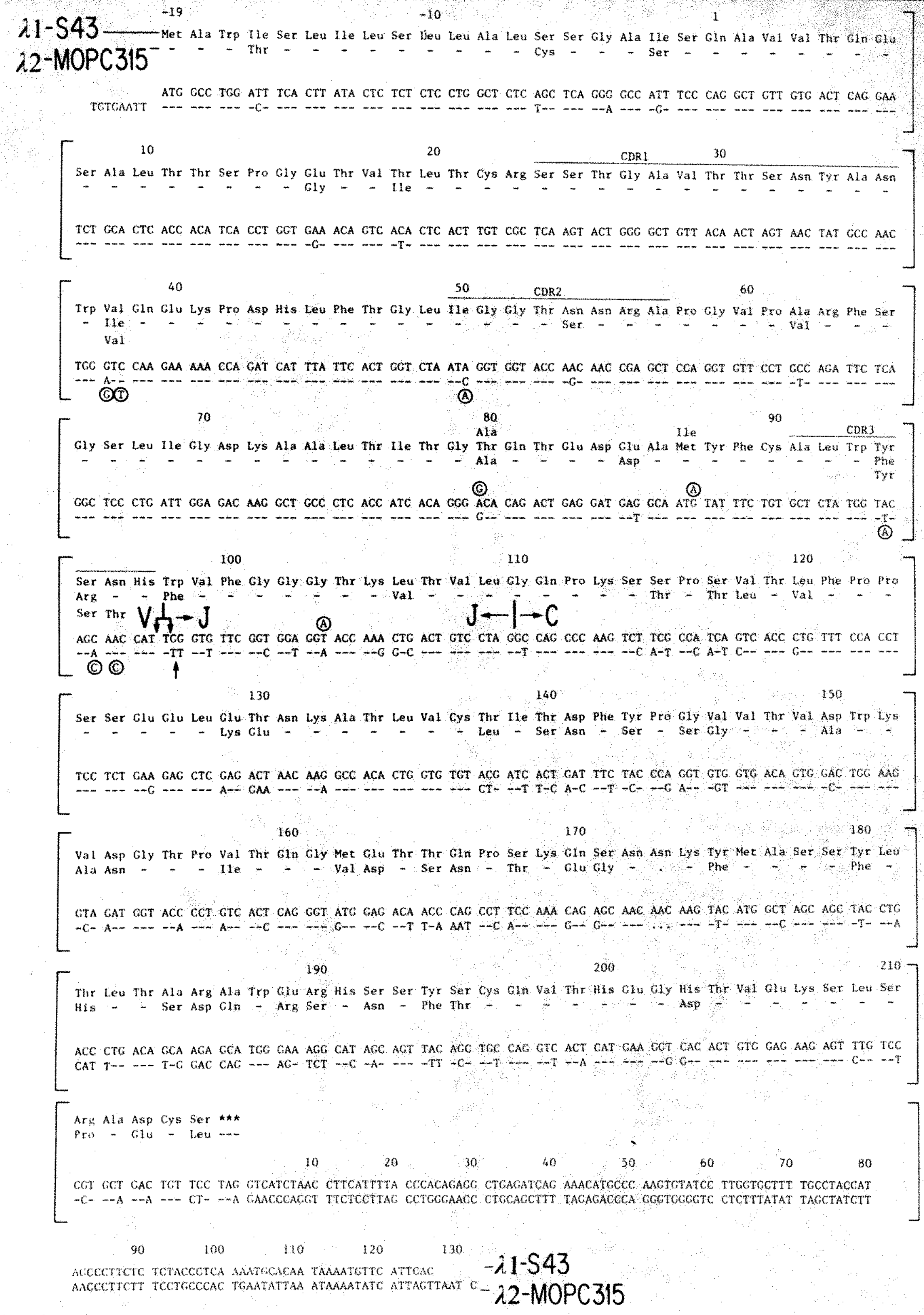

```
                    -19                                 -10                                      1
λ1-S43 ———————————— Met Ala Trp Ile Ser Leu Ile Leu Ser Leu Leu Ala Leu Ser Ser Gly Ala Ile Ser Gln Ala Val Val Thr Gln Glu
λ2-MOPC315           -   -   -  Thr  -   -   -   -   -   -   -   -   -  Cys  -   -   -  Ser  -   -   -   -   -   -   -   -

                    ATG GCC TGG ATT TCA CTT ATA CTC TCT CTC CTG GCT CTC AGC TCA GGG GCC ATT TCC CAG GCT GTT GTG ACT CAG GAA
           TCTGAATT --- --- --- -C- --- --- --- --- --- --- --- --- --- T-- --- --A --- -G- --- --- --- --- --- --- --- ---

        10                                      20                              CDR1    30
Ser Ala Leu Thr Thr Ser Pro Gly Glu Thr Val Thr Leu Thr Cys Arg Ser Ser Thr Gly Ala Val Thr Thr Ser Asn Tyr Ala Asn
 -   -   -   -   -   -   -   -  Gly  -   -  Ile  -   -   -   -   -   -   -   -   -   -   -   -   -   -   -   -   -

TCT GCA CTC ACC ACA TCA CCT GGT GAA ACA GTC ACA CTC ACT TGT CGC TCA AGT ACT GGG GCT GTT ACA ACT AGT AAC TAT GCC AAC
--- --- --- --- --- --- --- --- -G- --- --- -T- --- --- --- --- --- --- --- --- --- --- --- --- --- --- --- --- ---

            40                                      50          CDR2                        60
Trp Val Gln Glu Lys Pro Asp His Leu Phe Thr Gly Leu Ile Gly Gly Thr Asn Asn Arg Ala Pro Gly Val Pro Ala Arg Phe Ser
 -  Ile  -   -   -   -   -   -   -   -   -   -   -   -   -   -   -  Ser  -   -   -   -   -   -   -  Val  -   -   -
    Val

TGG GTC CAA GAA AAA CCA GAT CAT TTA TTC ACT GGT CTA ATA GGT GGT ACC AAC AAC CGA GCT CCA GGT GTT CCT GCC AGA TTC TCA
--- A-- --- --- --- --- --- --- --- --- --- --- --- --C --- --- --- -G- --- --- --- --- --- --- --- -T- --- --- ---
    ⒼⓉ                                               Ⓐ

                70                                      80                                      90          CDR3
                                                        Ala                         Ile
Gly Ser Leu Ile Gly Asp Lys Ala Ala Leu Thr Ile Thr Gly Thr Gln Thr Glu Asp Glu Ala Met Tyr Phe Cys Ala Leu Trp Tyr
 -   -   -   -   -   -   -   -   -   -   -   -   -   -  Ala  -   -   -   -  Asp  -   -   -   -   -   -   -   -  Phe
                                                                                                                Tyr
                                                         Ⓖ                           Ⓐ
GGC TCC CTG ATT GGA GAC AAG GCT GCC CTC ACC ATC ACA GGG ACA CAG ACT GAG GAT GAG GCA ATG TAT TTC TGT GCT CTA TGG TAC
--- --- --- --- --- --- --- --- --- --- --- --- --- --- G-- --- --- --- --- --T --- --- --- --- --- --- --- --- -T-
                                                                                                                 Ⓐ

                    100                                     110                                     120
Ser Asn His Trp Val Phe Gly Gly Gly Thr Lys Leu Thr Val Leu Gly Gln Pro Lys Ser Ser Pro Ser Val Thr Leu Phe Pro Pro
Arg  -   -  Phe  -   -   -   -   -   -   -  Val  -   -   -   -   -   -   -   -  Thr  -  Thr Leu  -  Val  -   -   -
Ser Thr  V↓↓→J                   Ⓐ                      J←|→C
AGC AAC CAT TCG GTG TTC GGT GGA GGT ACC AAA CTG ACT GTC CTA GGC CAG CCC AAG TCT TCG CCA TCA GTC ACC CTG TTT CCA CCT
--A --- --- -TT --T --- --C --T --A --- --G G-C --- --- --- --T --- --- --- --C A-T --C A-T C-- --- G-- --- --- ---
 Ⓒ   Ⓒ           ↑

                        130                                     140                                     150
Ser Ser Glu Glu Leu Glu Thr Asn Lys Ala Thr Leu Val Cys Thr Ile Thr Asp Phe Tyr Pro Gly Val Val Thr Val Asp Trp Lys
 -   -   -   -   -  Lys Glu  -   -   -   -   -   -   -  Leu  -  Ser Asn  -  Ser  -  Ser Gly  -   -   -  Ala  -   -

TCC TCT GAA GAG CTC GAG ACT AAC AAG GCC ACA CTG GTG TGT ACG ATC ACT GAT TTC TAC CCA GGT GTG GTG ACA GTG GAC TGG AAG
--- --- --G --- --- A-- GAA --- --A --- --- --- --- --- CT- --T T-C A-C --T -C- --G A-- -GT --- --- --- -C- --- ---

                            160                                     170                                     180
Val Asp Gly Thr Pro Val Thr Gln Gly Met Glu Thr Thr Gln Pro Ser Lys Gln Ser Asn Asn Lys Tyr Met Ala Ser Ser Tyr Leu
Ala Asn  -   -   -  Ile  -   -   -  Val Asp  -  Ser Asn  -  Thr  -  Glu Gly  -   .   -  Phe  -   -   -   -  Phe  -

GTA GAT GGT ACC CCT GTC ACT CAG GGT ATG GAG ACA ACC CAG CCT TCC AAA CAG AGC AAC AAC AAG TAC ATG GCT AGC AGC TAC CTG
-C- A-- --- --A --- A-- --C --- --- G-- --C --T T-A AAT --C A-- --- G-- G-- --- ... --- -T- --- --C --- --- -T- --A

                                190                                     200                                     210
Thr Leu Thr Ala Arg Ala Trp Glu Arg His Ser Ser Tyr Ser Cys Gln Val Thr His Glu Gly His Thr Val Glu Lys Ser Leu Ser
His  -   -  Ser Asp Gln  -  Arg Ser  -  Asn  -  Phe Thr  -   -   -   -   -   -   -  Asp  -   -   -   -   -   -   -

ACC CTG ACA GCA AGA GCA TGG GAA AGG CAT AGC AGT TAC AGC TGC CAG GTC ACT CAT GAA GGT CAC ACT GTG GAG AAG AGT TTG TCC
CAT T-- --- T-G GAC CAG --- AG- TCT --C -A- --- -TT -C- --T --- --T --A --- --- --G G-- --- --- --- --- --- C-- --T

Arg Ala Asp Cys Ser ***
Pro  -  Glu  -  Leu ---

                                10         20         30         40         50         60         70         80
CGT GCT GAC TGT TCC TAG GTCATCTAAC CTTCATTTTA CCCACAGACG CTGAGATCAG AAACATGCCC AAGTGTATCC TTGGTGCTTT TGCCTACCAT
-C- --A --A --- CT- --A GAACCCAGGT TTCTCCTTAG CCTGGGAACC CTGCAGCTTT TACAGACCCA GGGTGGGGTC CTCTTTATAT TAGCTATCTT

        90        100        110        120        130
ACCCCTTCTC TCTACCCTCA AAATGCACAA TAAAATGTTC ATTCAC        -λ1-S43
AACCCTTCTT TCCTGCCCAC TGAATATTAA ATAAAATATC ATTAGTTAAT C -λ2-MOPC315
```

Fig. 2 Nucleotide sequence of λ cDNA clones. The DNA sequence labelled λ1–S43 was derived from the pABλ1–15 (codons −19 to 195) and pABλ1–9 (codon 196 to the poly(A) sequence) plasmids and the λ2–MOPC-315 sequence was derived from the pλ2-1 plasmid[13] (Fig. 1). The predicted amino acid sequence is indicated above the nucleotide sequence and these residues are numbered. A dash (—) indicates a position where the λ2 sequence is identical to the λ1 sequence, and a period (.) indicates a gap used for sequence comparison at codon 173. The circled nucleotides immediately above the λ1 sequence at codons 80, 87 and 103 and immediately below the λ2 sequence at codons 38, 50, 94, 95 and 96 indicate the sequences of the corresponding germ-line genes: the λ1 and λ2 V and J germ-line sequences were determined by Tonegawa and co-workers[2,14,18]. The V, J and C region boundaries are indicated; arrows indicate the location of the V–J junction. The double arrow above the λ1 sequence indicates two possible sites for the actual junction. The arrow beneath the λ2 sequence indicates that there is no ambiguity in the assignment for the λ2 chain. The 3′ untranslated regions are numbered separately to facilitate reference to that region. One sequence error found in our previous sequence[13] is corrected here (the 3′-terminal λ1 sequence immediately preceding the poly(A) in BALB/c and C57BL/6 is AC and not ATC). All of these sequences were determined using the Maxam–Gilbert methods[25]. Restriction enzyme sites in the λ2 clone occur at the following codon positions: *Ava*I, 144; *Bam*HI, 38; *Bgl*I, 150; *Bgl*II, 189; *Hinf*I, 5, 7, 63 and 208; *Kpn*I, 52; *Pst*I, 212 (base pair position 31 in 3′ UT region); and *Sac*I, 57, 127. The inserted λ2 sequence at the *Pst*I site in the cloning vector is CTGCAG$_{20}$–insert–A$_{23}$–C$_{16}$ TGCAG. The corresponding sequence in pABλ1–15 is CTGCAG$_{13}$ CG$_6$–insert and in pABλ1–9, insert–A$_{26}$C$_{12}$ TGCAG.

In previous experiments, all of the observed somatic variation in myeloma $\lambda 1$ chains was restricted to the CDRs[1]. Furthermore, the existing data on V_κ and V_H shows a strong bias for somatic variation (as well as genetic variation) to occur in the CDRs (refs 8, 12 and A.B., M.P. & D.B., unpublished). There are two alternative possibilities for this clustering of somatic events: either there could be a predisposition for mutations in the CDRs, or selection could be operating. Preferential somatic mutation in the CDRs would require a remarkably specific mechanism but may occur. Selection could either act negatively, causing a loss of variants in the framework regions, or could act positively and favour proteins with variation in the CDRs. Negative selection seems unlikely because an excess of silent (synonymous) mutations in the framework compared to those from random mutational events would be expected. However the ratio between silent and replacement mutations in these λ sequences was approximately that expected from random mutation (25%): S43 and the MOPC-315 $\lambda 2$ had 1/3 and 1/6 silent mutations, respectively. Positive selection could be exerted either through better antigen binding due to variations in the CDRs or selective regulation by the immune system, but the expected bias in favour of replacement mutations might not be evident in the limited data available.

The constant regions of both the $\lambda 1$ light chain and $\gamma 2a$ heavy chain[15] of the S43 hybridoma are germ-line DNA sequences although both variable regions show mutation[8]. Studies of the spread of somatic mutation away from the coding sequence suggest that barriers must exist to the spread of mutational activity. For κ light chains, no spread outside of the coding regions was observed[5-7] although for $\lambda 1$, mutations just 3′ to the J segments have been observed[2,20]. Because the $V_{\lambda 1}$ gene is only 1,250 nucleotides from the $C_{\lambda 1}$ gene in the joined configuration[2], the lack of mutation in the S43$C_{\lambda 1}$ region suggests that the barrier to mutational spread in the $\lambda 1$ gene is within the 1,250 nucleotides 5′ to the $C_{\lambda 1}$ region. For heavy chains, extensive spread of mutation away from the rearranged V_H region has been observed[9,10].

There does not seem to be absolute specificity for mutations at particular nucleotides although similarities have been observed[21]. Interestingly, the three S43 $\lambda 1$ chain mutations occurred only at purine residues and we have noted a similar bias in the V_H region from the S43 hybridoma (9 out of 10)[8]. The six somatic mutations in the $\lambda 2$ cDNA, however, occurred at all four bases, three at purine and three at pyrimidine residues. The significance of a purine bias in some but not all data remains puzzling.

The MOPC-315 tumour expresses two λ mRNA species, one producing a normal $\lambda 2$ protein and the other producing a truncated $\lambda 1$ protein[13]. The V–J junction of the $\lambda 1$ sequence puts the reading of the rest of the mRNA out of frame[20]. Presumably in the progenitor MOPC-315 cell, the $\lambda 1$ gene rearranged first but because a functional polypeptide could not be synthesized, the $\lambda 2$ gene was later rearranged. Following the productive $\lambda 2$ rearrangement, a similar level of somatic mutation occurred in both rearranged λ genes, the $\lambda 1$ gene having seven somatic mutations in its coding sequence[20] and the $\lambda 2$ containing six mutated bases (Fig. 2). Pech *et al.*[5] found a related situation for κ genes where in one myeloma cell both an expressed and an unexpressed but rearranged κ gene showed similar levels of somatic variation.

Except for one report (HPC 16; ref. 22), data on somatic variation has revealed no variants appearing in association with the μ heavy chain isotype but many variants have occurred in association with other isotypes[8,23]. This again was seen in the λ data: B1-8 has a μ heavy chain and no somatic variation in its λ chain, S43 has a $\gamma 2a$ heavy chain and somatic variation in both its heavy and λ light chain, and MOPC-315, with an α heavy chain, has somatic variation in its $\lambda 2$ light chain. Somatic mutation is not, however, obligatory during isotype switching: protein sequencing has identified germ-line sequences in non-IgM antibodies[23] as has nucleotide sequencing (A.B., M.P. & D.B., in preparation). It seems that isotype switching may precede somatic mutation. Somatic mutation may be an inducible phenomenon (perhaps via T-cell help) in some stage of B-cell development after its encounter with antigen. More data will be needed to clarify these relationships.

Finally, these data allow a direct comparison of the nucleotide sequences of the $\lambda 1$ and $\lambda 2$ constant regions. The two genes are obviously related but differ at 30 out of 105 amino acids (Fig. 2). They are more different from one another than the three human λ sequences recently determined[24]. They differ so extensively in their 3′ flanking sequences that the homology is not very evident (and therefore in Fig. 2 the identities are not shown with dashes). The two genes probably diverged in a species ancestral to the present mouse species. By contrast, the human λ genes are closely related and therefore diverged quite recently, as did the mouse $\lambda 2$ and $\lambda 3$ genes as shown by protein sequence data[17].

This work was supported by grants from the American Cancer Society and the NCI and a contribution from the Whitehead Charitable Foundation. A.B. was a postdoctoral fellow of the Medical Foundation. D.B. is an American Cancer Society Research Professor.

Received 1 March, accepted 18 May 1982.

1. Weigert, M. & Riblet, R. *Cold Spring Harb Symp. quant. Biol.* **41,** 837–846 (1976).
2. Bernard, O., Hozumi, N. & Tonegawa, S. *Cell* **15,** 1133–1144 (1978).
3. Weigert, M., Gatmaitan, L., Loh, E., Schilling, J. & Hood, L. *Nature* **276,** 785–790 (1978).
4. Valbuena, O., Marcu, K. B., Weigert, M. & Perry, R. *Nature* **276,** 780–784 (1978).
5. Pech, M., Hochtl, J., Schnell, H. & Zachau, H. G. *Nature* **291,** 668–670 (1981).
6. Selsing, E. & Storb, U. *Cell* **25,** 47–58 (1981).
7. Gershenfeld, H. K., Tsukamoto, A., Weissman, I. L. & Joho, R. *Proc. natn. Acad. Sci. U.S.A.* **78,** 7674–7678 (1981).
8. Bothwell, A. L. M. *et al. Cell* **24,** 625–637 (1981).
9. Sakano, H., Maki, R., Kurosawa, Y., Roeder, W. & Tonegawa, S. *Nature* **286,** 676–683 (1980).
10. Kim, S., Davis, M., Sinn, E., Patten, P. & Hood, L. *Cell* **27,** 573–581 (1981).
11. Kataoka, T., Nikaido, T., Miyata, T., Moriwaki, K. & Honjo, T. *J. biol. Chem.* **257,** 277–285 (1982).
12. Crews, S., Griffen, J., Huang, H., Calame, K. & Hood, L. *Cell* **25,** 59–66 (1981).
13. Bothwell, A. L. M., *et al. Nature* **290,** 65–67 (1981).
14. Tonegawa, S., Maxam, A. M., Tizard, R., Bernard, O. & Gilbert, W. *Proc. natn. Acad. Sci. U.S.A.* **75,** 1485–1489 (1978).
15. Schreier, P. H., Bothwell, A. L. M., Mueller-Hill, B. & Baltimore, D. *Proc. natn. Acad. Sci. U.S.A.* **78,** 4495–4499 (1981).
16. Dugan, E. S., Bradshaw, R. A., Simms, E. S. & Eisen, H. N. *Biochemistry* **12,** 5400–5416 (1973).
17. Azuma, T., Steiner, L. A. & Eisen, H. N. *Proc. natn. Acad. Sci. U.S.A.* **78,** 569–573 (1981).
18. Blomberg, B. & Tonegawa, S. *Proc. natn. Acad. Sci. U.S.A.* **79,** 530–533 (1982).
19. Miller, J., Selsing, E. & Storb, U. *Nature* **295,** 428–430 (1982).
20. Hozumi, N. *et al. Proc. natn. Acad. Sci. U.S.A.* **78,** 7019–7023 (1981).
21. Baltimore, D. *Cell* **26,** 295–296 (1981).
22. Kocher, H. P., Berek, C., Schreier, M. H., Cosenza, H. & Jaton, J. C. *Eur. J. Immun.* **10,** 264–267 (1980).
23. Gearhart, P. J., Johnson, N. D., Douglas, R. & Hood, L. *Nature* **291,** 29–34 (1981).
24. Hieter, P. A., Hollis, G. F., Korsmeyer, S. J., Waldmann, T. A. & Leder, P. *Nature* **294,** 536–540 (1981).
25. Maxam, A. M. & Gilbert, W. *Proc. natn. Acad. Sci. U.S.A.* **74,** 560–564 (1977).

Mapping class I gene sequences in the major histocompatibility complex

Larry R. Pease, Stanley G. Nathenson & Leslie A. Leinwand

Department of Microbiology and Immunology and Department
of Cell Biology, Albert Einstein College of Medicine, Bronx,
New York 10461, USA

The class I glycoproteins of the major histocompatibility complex (MHC) are products of closely linked genes on the 17th chromosome of the mouse. Four highly homologous cell surface proteins, K, D, L, and Qa-2 (refs 1–4), belonging to this multigene family have been analysed. Several additional members[5–7], M, R, TL, are indicated by biochemical data and recent serological data suggest the family is larger[8]. Recent reports using recombinant DNA technology suggest that the class I system is an extensive multigene family[9–12]. In this report we describe results of experiments using restriction enzyme digestion of DNA from a group of standard, congeneic and MHC

0028-0836/82/290382—04$01.00

recombinant mouse strains followed by hybridization to H–2 cDNA probes. Particular bands of hybridization can be assigned to specific H–2 haplotypes and, therefore, to the MHC region of the 17th chromosome. A number of the MHC polymorphic bands have been assigned to genetic map positions in the K and D-L regions of the H–2 complex. Additional class I gene sequences map outside the boundaries of the traditional H–2 complex (K, I, S, D), into the Qa-T1a region. At least one sequence is centromeric to the K locus. Further, amino terminal and carboxy terminal probes show different restriction patterns, suggesting that the exons corresponding to the different domains of the class I glycoproteins may have different evolutionary histories.

We used two cDNA probes[9] to identify the DNA sequences bearing homology to the class I antigens. The first, pH-2.IIa, is homologous to the exons encoding from amino acid 167 through the carboxy terminus of the H–2K^{b} glycoprotein. The second probe, pH-2.III, is homologous to exons encoding from amino acid 63 to 160.

To determine whether the bands that hybridize to the cDNA probes are specific for any given haplotype and if these bands are located in the MHC, comparisons were made between hybridization patterns of class I cDNAS to genomic DNAs of standard mouse strains and those bearing (1) different MHC haplotypes but identical non-MHC backgrounds, and (2) identical MHC haplotypes but different non-MHC backgrounds. DNA from these standard and congeneic mouse strains was digested with *Bam*HI endonuclease and examined by hybridization to the carboxy terminal cDNA probe pH-IIa (Fig. 1*a*). The results show that approximately 50% of the bands in the DNA of each haplotype are polymorphic when compared with the other haplotypes (7/13 in the *b* haplotype, 9/16 in the *d* haplotype, 6/13 in the *k* haplotype). This polymorphism can be assigned to the MHC segment on the 17th chromosome because the congenic strains, BALB · B, BALB/c and BALB · K differ only at the MHC chromosomal segment. Schematic representation of the banding patterns and the distribution among three haplotypes is shown in Fig. 2. The degree of polymorphism observed by our analyses (approximately 50%) is probably an underestimate since dissimilar bands may be approximately equal in size and high molecular weight bands greater than 5 kilobases (kb) are not resolved as well as the smaller bands.

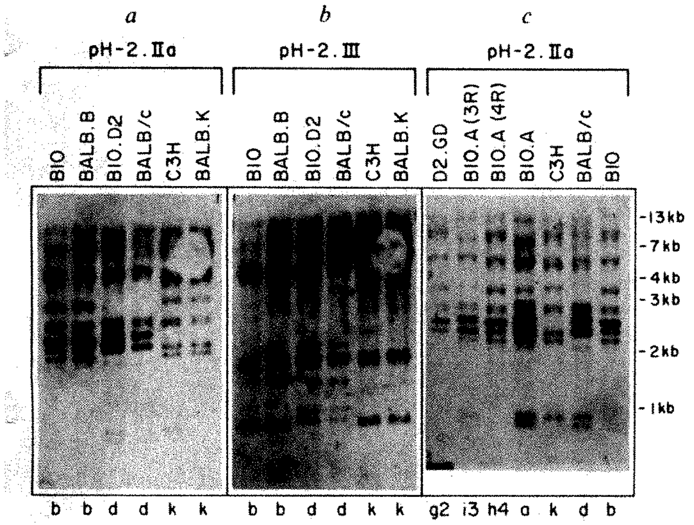

Fig. 1 Characterization of *Bam*HI genomic restriction fragments by hybridization to the cDNA probes, pH-2.IIa and pH-2.III. Splenic DNA was isolated from inbred strains maintained by Dr F. Lilly. Spleen cells were disrupted in 10 mM Tris (*p*H 7.4), 0.05 M EDTA, 0.5%SDS and 100 g ml^{-1} protinease K and incubated at 37 °C for 16 h. Protein contaminants were extracted from high molecular weight DNAs with phenol, chloroform, isoamyl alcohol, and the DNAs were recovered by ethanol precipitation. Samples of 12 μg of DNA from each strain were digested to completion with *Bam*HI and electrophoresed overnight on 0.8% Agarose gels in G-M buffer (0.18 M Tris, 0.18 M boric acid, 6 mM EDTA, *p*H 8.3) at 60 V. The DNA in the gels was transferred to nitrocellulose paper by the method of Southern[13]. Following transfer, the filters were prehybridized (5 × SSC, 50 mM PO$_4$, *p*H 7.4, 50 μg ml^{-1} salmon sperm DNA, 50 μg ml^{-1} poly(A), 1X Denhardts solution) at 65 °C for 6 h. Radioactively labelled cDNA clones (2×10^5 c.p.m. ml^{-1}) were added to prehybridization solution containing 20% dextran sulphate. After hybridizing for 6 h at 65 °C the filters were washed three times in 2 × SSC, 0.2% SDS at 65 °C and twice in 0.1 × SSC, 0.2% SDS at 55 °C for 20 min. The filters were exposed to X-ray film with an intensifying screen at −70 °C.

The distribution of *Bam*HI fragments homologous to the two probes was different (Fig 1*a*,*b*). Unlike the pattern of bands observed with the carboxy terminal probe H-2.IIa, the amino terminal probe, pH-2.III, distinguished between two groups of bands. One family consisted of four prominent bands which hybridized strongly to the probe while the remaining 7 to 9 bands hybridized weakly.

The availability of congeneic mouse strains as well as recombinant mouse strains, that were derived from previously defined arrays of class I alleles, provided the means to assign the class I hybridizing bands not only to the MHC of chromosome 17 but also to specific map positions within the MHC. The results of a series of experiments (as in Fig. 1*c*) utilizing *b*, *d*, and *k* haplotypes and recombinant haplotypes, *a*, *h4*, *i3*, *i5*, *g2* and *g* are shown in Fig. 3. The mapping patterns fall into several groups. Bands 1, 3, 4, 5, 6, 7 and 17 cannot be mapped to any specific region within the MHC since these segments of the genome do not contain detectably polymorphic *Bam*HI sites. Two *Bam*HI bands, 2 and 18, map to the K end of the H–2 complex. Band 2 is present in the *d* haplotype, also present in th *g2* and *g* haplotypes, but absent in the *b* haplotype. Since *g2* and *g* are haplotypes derived from recombination events that substituted a portion of the *b* haplotype at the D end of the H–2 complex, band 2 must map to the region containing the alleles derived from the *d* haplotype, namely the K end. Band 18 can also be mapped to the K end since it is present in the *b* haplotype but is absent in the *d*, *g2* and *g* haplotypes.

Another group of bands appears to map to the D end of the H–2 complex. Band 12, for example, is present in the *d* and *a* haplotypes but not in the *b* haplotype. Recombinants *i3* and *i5* contain band 12 and have *a* haplotype-specific genetic sequence from I–C through the T1a region. Thus the presence of band 12 in these strains indicates that the location of the DNA fragments contained in band 12 must be at the D end. The absence of band 12 from the recombinant *h4* which does not have either the *d* or *a* haplotype sequences in the D region further supports this mapping assignment. Similar analyses can be used for the mapping of the other bands, 10, 11, 13, 14, 16, 20 and 22 to the D end.

The remaining bands, 8, 9, 15, 19 and 21 cannot be directly mapped by the recombinants tested. The ambiguity about the location of these bands arises because the genetic regions homologous to class I cDNA probes may map to the centromeric as well as the distal side of the MHC because the boundaries defined by the congeneic and recombinant strains have not been established. However, it is possible to eliminate some regions of the MHC, where these bands cannot be located. For example, bands 15 and 19 which are present in the *a* haplotype but not the *k* haplotype must be absent from the K or I–A region of the H–2 complex. Similarly, bands 8 and 21, which are present in the *k* haplotype but in none of the other strains examined, should not be present in the K or Ia region. Band 9 is present in the *a* haplotype but absent from both *d* and *k* haplotypes and thus must map outside of the traditionally defined H–2 complex since the *a* haplotype contains both *d* and *k* alleles throughout the complex.

The genetic sequences mapping to the D-end of the H–2 complex have been analysed with additional restriction enzymes and a Qa-T1a congeneic mouse line, B6.T1a^{a} (data not shown). The recombinant MHC haplotype of this inbred strain includes the K, D and L alleles of the *b* haplotype and the Qa-T1a

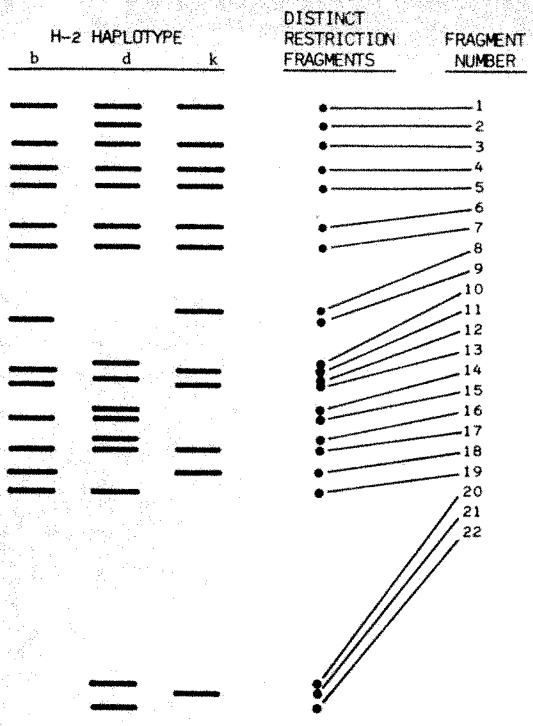

FRAGMENT NUMBER	SIZE (BASE PAIRS X 10^{-3})	PRESENCE OF FRAGMENT IN HAPLOTYPE		
1	13.5	b	d	k
2	9.5		d	
3	8.4	b	d	k
4	7.4	b	d	k
5	6.6	b*	d	k
6	5.1	b	d	k
7	4.5	b*	d	k
8	3.6			k
9	3.5			
10	3.1		d	
11	3.0	b		k
12	2.9		d	
13	2.9	b		k
14	2.7		d	
15	2.6	b	d	
16	2.4		d	
17	2.4	b	d	k
18	2.2	b		k
19	2.1	b	d	
20	1.0		d	
21	1.0			k
22	0.9		d	

* = FAINT BAND

Fig. 2 Schematic representation of *Bam*HI fragments hybridizing to the carboxy terminal probe pH-2.IIa. This summary is based on several analyses, including those shown in Fig. 1. Bands were assigned a number according to their relative migratory position on 0.8% agarose gels in G-M buffer (see Fig. 1). Bands not distinguishably different among haplotypes were assigned the same number. Size estimates are based on band mobility relative to *Hind*-III fragments of λ phage DNA.

alleles of the *a* haplotype. A comparison of the banding patterns of B6.T1a^a with those from the strains B10(H-2^b), B10.A (H-2^a), and B10.A(3R) (H-2^{i3}) (Fig. 3), subdivides the polymorphic D-end sequences into two groups, those mapping to the D-L region and those mapping to the Qa-T1a region. Similar mapping assignments of Class I genes to the Qa-T1a region have been reported by others[11,12].

A similar analysis has been carried out using the amino terminal probe pH-2.III (data not shown). Results are similar to the pattern seen with pH-2.IIa with the exceptions that two instead of one *d* haplotype specific fragment maps to the K end, and one fragment shared by the *d* and *a* haplotypes maps between H-2K and the centromere.

The different hybridization patterns observed with the amino terminal and carboxy terminal probes for the *Bam*HI fragments (Fig. 1), raise questions about the evolutionary relationships among the exons representing the protein domains of the class I antigens. For example, recent evidence suggests that the third protein domain of H-2K^b, (approximately amino acids 180 to 270), is critical for association with β_2-microglobulin (K. Yokoyama and S.G.N., unpublished data). This region is quite important for the function of the molecule. Since other class I glycoproteins are believed to associate with β_2-microglobulin[15], they may also retain a similarly conserved domain. This domain is homologous to the carboxy terminal probe (pH-2.IIa), but not to the amino terminal probe, a relationship which could be

Fig. 3 Summary of H-2 recombinant *Bam*HI banding patterns. As described in Fig. 1, DNAs from the inbred strains B10, BALB/c, and C3H were compared with the DNA from the presumed B10.A, the *a*×*b* haplotype recombinants B10.A(3R), B10.A(4R), B10.A(5R), and the *b*×*d* haplotype recombinants D2.GD and BALB.G. The approximate positions of recombinant sites, marked with a bar, in all recombinant strains have been established by classical mapping using serological markers[14]. The presence or absence of different pH-2.IIa homologous *Bam*HI bands, as defined in Fig. 2, are shown (blank versus filled space) next to each strain examined. Unique bands resulting from recombination were not observed. The relative position of bands on the 17th chromosome is presented schematically.

STRAINS	H-2	CTR	K	IA	IC	S	D	TLA
B10	b	b	b	b	b	b	b	b
BALB/C	d	d	d	d	d	d	d	c
C3H	k	k	k	k	k	k	k	b
B10.A	a	a	k	k	d	d	d	a
B10.A(4R)	h4	a	k	k ▌	b	b	b	b
B10.A(3R)	i3	b	b	b ▌	d	d	d	a
B10.A(5R)	i5	b	b	b ▌	d	d	d	a
D2.GD	g2	d	d	d ▌	b	b	b	b
BALB.G	g	d	d	d	d	d ▌	b	b

PH-211a (HOMOLOGOUS BAM HI BANDS)

STRAINS	1	2	3	4	5	6	7	8	9	10	11	12	13	14	15	16	17	18	19	20	21	22
B10	■	□	■	■	■	■	■	□	■	□	■	□	■	□	■	□	■				□	□
BALB/C	■	■	■	■	■	■	■	□	□	■	□	■	□	■	■	■	■			■	□	■
C3H	■	□	■	■	■	■	■	■	□	□	■	□	■	□	□	□	■			□	■	□
B10.A	■	□	■	■	■	■	■	□	■	■	□	■	□	■	■	■	■	■	■	■	□	■
B10.A(4R)	■	□	■	■	■	■	■	□	■	□	■	□	■	□	■	□	■		■	□	□	□
B10.A(3R)	■	□	■	■	■	■	■	□	■	■	□	■	□	■	■	■	■			■	□	■
B10.A(5R)	■	□	■	■	■	■	■	□	■	■	□	■	□	■	■	■	■			■	□	■
D2.GD	■	■	■	■	■	■	■	□	■	□	■	□	■	□	■	□	■		■	□	□	□
BALB.G	■	■	■	■	■	■	■	□	■	□	■	□	■	□	■	□	■			□	□	□

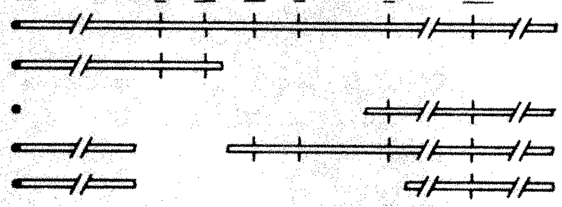

BAM HI BANDS

1,3,4,5,6,7,17

2,18

10,11,12,13,14,16,20,22

8,15,19,21

9

responsible for the extensive strong cross-hybridization of the probe with numerous class I sequences throughout the MHC. In contrast, the amino terminal probe hybridized to restriction fragments, with various intensities, suggesting that those sequences homologous to the amino terminal portion of the molecules have evolved more rapidly than those homologous to the C-terminal portion.

The findings reported in this study indicate that a multigene family, homologous to genes encoding class I H-2 antigens, extends from the centromeric side of the K region through the Qa-Tla region on chromosome 17. Most of the polymorphic bands map the gene sequences distal, with respect to the centromere, to the complement components (S region) of the H-2 complex. Many of these sequences clearly are associated with the Qa and Tla regions. These data suggest that the H-2 complex is only a small part of a larger set of genes comprising the major histocompatibility complex.

We thank Diane McGovern for technical assistance and Catherine Whelan and Angela Stockhausen for secretarial help. This work was supported by NIH grants AI-07289 and AI-10702 (S.G.N.), GM-29020 (L.A.L.), and ACS grants IM-236 (S.G.N.) and NP-348 (L.A.L.).

Received 12 February; accepted 6 May 1982.

1. Nathenson, S. G., Uehara, H., Ewenstein, B. M., Kindt, T. J. & Coligan, J. E. *A. Rev. Biochem.* **50,** 1025–1052 (1981).
2. Nairn, R., Nathenson, S. G. & Coligan, J. E. *Eur. J. Immun.* **7,** 495–503 (1980).
3. Coligan, J. E. *et al. Proc. natn. Acad. Sci. U.S.A.* **77,** 1134–1138 (1980).
4. Soloski, M. J., Uhr, J. W., Flaherty, L. & Vitetta, E. S. *J. exp. Med.* **153,** 1080–1093 (1981).
5. Ivanyi, D. & Demant, P. *Immunogenetics* **8,** 539–550 (1979).
6. Hansen, T. H. *et al. J. Immun.* **126,** 1713–1716 (1981).
7. Yokoyama, K., Stockert, E., Old, L. J. & Nathenson, S. G. *Proc. natn. Acad. Sci. U.S.A.* **78,** 7078–7082 (1981).
8. Ivanyi, D. & Demant, P. *Immunogenetics* **12,** 397–408 (1981).
9. Steinmetz, M. *et al. Cell* **24,** 125–134 (1981).
10. Cami, B., Bregegere, F., Ahastado, J. P. & Kourilsky, P. *Nature* **291,** 673–675 (1981).
11. Steinmetz, M. *et al. Cell* **25,** 683–692 (1981).
12. Margulies, D. H., Evans, G. A., Flaherty, L. & Seidman, J. G. *Nature,* **295,** 168–170 (1982).
13. Southern, E. M. *J. molec. Biol.* **98,** 503–517 (1975).
14. Altman, P. L. & Kutz, D. D. in *Inbred and Genetically Defined Strains of Laboratory Animals: Part 1,* 125–127 (Federation of American Societies for Experimental Biology, Bethesda, 1979).
15. Vitetta, E. S. & Capra, J. D. *Adv. Immun.* **26,** 147–193 (1979).

Reactivation of latent feline leukaemia virus infection

Jennifer L. Rojko*, Edward A. Hoover*†, Sandra L. Quackenbush* & Richard G. Olsen*†‡

* Department of Veterinary Pathobiology, † Comprehensive Cancer Center and ‡ Department of Microbiology, The Ohio State University, 484 W. 12th Avenue, Columbus, Ohio 43210, USA

In most cats exposed to the contagious[1] feline leukemia virus (FeLV), viral replication is contained in target haematopoietic tissues[2] and elicits humoral immunity to FeLV and to the feline oncornavirus-associated cell membrane antigen (FOCMA)[3–6]. Recently, we and others have considered that these ostensibly self-limiting infections might be persistent nonproductive (latent) infections in certain haematopoietic cells. This hypothesis could account for the relapsing viraemias[7], protracted incubation periods[8], persistently high titres of antiviral and anti-FOCMA antibodies[8], appearance of FeLV p27 antigen in serum of otherwise non-viraemic animals[9] and occurrence of FeLV-negative but FOCMA-positive leukaemias in naturally infected pet cats[10,11]. Here we describe the reactivation of latent FeLV from myelomonocytic and lymphoid cells of cats immune to FeLV, cats bearing FeLV-negative tumours, and kittens congenitally exposed to FeLV. Furthermore, the reappearance of FeLV infection is suppressed by the host's immune system but this can be altered by adrenal corticosteroid hormones *in vivo* and *in vitro*.

Self-limiting (regressive) FeLV infection was established in 10 adult specific pathogen-free cats by two oral-nasal exposures to 10^5 focus-forming units (FFU) of FeLV-R (Rickard) strain[12] and confirmed by demonstration of transient group specific antigen (GSA) in peripheral blood mononuclear leukocytes (PBML)[2,13], 1–3 weeks after exposure and persistent FOCMA-L[5,6,14] and FOCMA-S[14] antibody responses 2–4 weeks after exposure.

At 16–20 weeks after exposure, femoral bone marrow cells, mesenteric lymph node cells, peritoneal macrophages and PBML were collected. Freshly isolated cells were negative for GSA by fixed-cell immunofluorescence assay[13] and were negative for replicating FeLV by a viral infectivity assay[15] (Table 1). However, high titres of FeLV were reactivated following isolation and *in vitro* propagation of marrow from 8 of 10 FeLV-immune cats but not from any of 4 FeLV-naive cats (Table 1). Identification of the reactivated agent from four cats as FeLV was confirmed by neutralization[16] of its infectivity for clone 81 cells. This was achieved by preincubation with a 1:10 dilution of goat anti-FeLV serum or a 1:4 dilution of autochthonous cat anti-FeLV serum but not FeLV-naive goat or cat serum. Moreover, immunofluorescent examination of methanol-fixed, cytocentrifuged preparations of marrow cells demonstrated small clusters of GSA-positive proliferating myelomonocytic precursor cells (20% of total cells present). Neither the differentiated macrophage majority nor the mature granulocyte minority also present contained GSA. Refractoriness to retroviral replication, therefore, accompanies differentiation of feline myelomonocytic progenitor cells.

Stimulation of lymphocytes from lymph node but not bone arrow, by the feline T_γ cell mitogen staphylococcal Protein A (Protein A)[17] gave rise to low titres of recrudescent FeLV. Unstimulated nodal cells and PBML did not generate viral infectivity, nor was it found in cells activated by other T cell mitogens (phytohaemagglutinin, pokeweed mitogen, concanavalin A) or the B cell mitogen lipopolysaccharide[18]. Lymphocyte and macrophage growth factors and the tumour promotor, 12-*O*-tetradecanoyl-phorbol-acetate, also failed to reactivate GSA or viral infectivity in node cells or PBML. Thioglycollate-induced peritoneal macrophages did not reactivate GSA or viral infectivity (Table 1). Parallel cultures of marrow, lymphocytes and macrophages from FeLV-naive cats were negative (Table 1; ref. 19).

Bone marrow, tumour biopsies, PBML and serum were obtained from two pet cats referred to Ohio State University Veterinary Teaching Hospital for FeLV-negative lymphosarcoma of the mesenteric or popliteal lymph nodes (Table 1). In both cats, virus was reactivated from cultured marrow cells but not blood or tumour cells.

Finally, matings between two regressor females (cats 748B1, 1586) and two regressor males (cats 1604, 748B2) produced two litters of five kittens (kittens 1586-1, 2, 3; 748B1-1, 2) with evidence of congenital FeLV infections (Table 1). Both females were re-exposed by a single intraperitoneal dose of FeLV during the first week of gestation but remained negative for viraemia of marrow origin[2,13] throughout the 9-week gestation period. Freshly isolated fetal (1586-1, 45 days gestation) and neonatal (1586-2, 3; 748B1-1, 2) lymph node, thymus and maternal placenta (1586) were negative for GSA and viral infectivity. Infectious virus was expressed in cultured marrow from three kittens (1586-1, 2; 748B1-1), cultured thymus of two kittens (1586-1; 748B1-1) and freshly isolated, as well as cultured, liver haematopoietic cells of the fetal kitten (1586-1).

The presence of FeLV replication in fetal haematopoietic cells, but not maternal placenta, suggested that transplacental passage of FeLV was not prevented by maternal anti-FeLV responses. Other workers have shown that in cats the majority of maternal antibody was transferred in colostrum[20–22]. Passive (colostral) transfer of maternal FeLV-neutralizing antibody[23] to suckling neonates is perhaps responsible for maintenance of the neonatal infection in its non-productive, but reactivatable, form.

Therefore, latent FeLV infections are characterized by absence of infectious virus in freshly isolated marrow, node, macrophage and PBML, and reactivation of viral infectivity

0028–0836/82/290385—04$01.00

Table 1 Reactivation of latent FeLV infections

		Type of FeLV infection							
		FeLV-immune		FeLV-negative lymphosarcoma		Congenital		FeLV-naive	
Cell source	Days in culture	No. of cats positive for VI	VI	No. of cats positive for VI	VI	No. of cats positive for VI	VI	No. of cats positive for VI	VI
Marrow	0	0/10	<5	0/2	<5	0/5	<5	0/4	<5
Marrow	6	8/10	11,794 (580–74,500)	2/2	1,565 (975–2,060)	3/5	90 (40–120)	0/4	<5
PBML	0	0/10	<5	0/2	<5	0/2	<5	0/6	<5
PBML-PA	7	0/10	<5	0/2	<5	0/2	<5	0/6	<5
Lymph node	0	0/5	<5	ND	ND	0/4	<5	0/6	<5
Lymph node-PA	7	5/5	155 (10–675)	ND	ND	0/4	<5	0/6	<5
Peritoneal macrophages	0	0/3	<5	ND	ND	ND	ND	0/4	<5
Peritoneal macrophages	7	0/3	<5	ND	ND	ND	ND	0/4	<5
Tumour	0	ND	ND	0/2	<5	ND	ND	ND	ND
Tumour	7	ND	ND	0/2	<5	ND	ND	ND	ND
Tumour	28	ND	ND	0/2	<5	ND	ND	ND	ND
Thymus	0	ND	ND	ND	ND	0/4	<5	0/4	<5
Thymus	6	ND	ND	ND	ND	2/4	77 (44–110)	0/4	<5

Cells were collected by aspiration (marrow, peritoneal macrophages), surgical biopsy (node, tumour, thymus), or venipuncture (peripheral blood) from cats anaesthetized with ketamine. Peritoneal macrophages were collected 4 days after intraperitoneal inoculation of thioglycollate. Partial purification of mononuclear cells from marrow and blood was by density separation on Ficoll-metrizoate gradients (specific gravity 1,077). Marrow and peritoneal macrophages cultured in McCoys 5A with 20% (marrow) to 40% (macrophages) horse serum by modifications of the procedure of Dexter and Testa[34]. PBML, lymph node neoplastic lymph node, and thymus were cultured in RPMI 1640 and 20% fetal calf serum[19]. A minimum of 10^6 freshly isolated or cultured cells in 1 ml were disrupted by two freeze-thaw cycles prior to viral infectivity (VI) assay[23]; 0.2 ml of disrupted cell-associated inoculum and 0.2 ml of cell-free supernatant from each culture were each applied to 5×10^4 indicator clone 81 cells in 24 cluster dishes. VI data, expressed as FFU per 10^6 mononuclear cells, is the sum of cell-associated virus and cell-free virus for each cat positive for reactivated virus, averaged between the number of cats positive for reactivated virus from marrow versus node, etc. The ranges for the individual VI sums are indicated in brackets. ND, not determined.

from cultured marrow cells and a minor subset of nodal lymphocytes. These data suggest that self-limiting (regressive) FeLV infections are actually latent (nonproductive) infections of myelomonocytic precursor cells in the bone marrow and Protein A-reactive cells in the lymph nodes.

A similar coupling of virus latency *in vivo* with viral reactivation *in vitro* described for the putative human herpesviral oncogen, the Epstein–Barr Virus (EBV)[24,25] has been attributed to the presence versus absence of a host immune response against virally infected cells. By analogy, while those cells expressing FeLV antigens would be eliminated in regressor cats, nonproductively infected cells would survive. Therefore, we investigated the role of host antiviral defenses in the maintenance of FeLV infections in their dormant phases. Regressor cats mounted both cell-dependent and antibody-dependent killing of autochthonous marrow cells with reactivated virus (Table 2) but did not kill freshly isolated marrow cells. Cells from FeLV-naive cats had minimal cytotoxicity (<20%) against autochthonous freshly isolated or cultured marrow cells and peritoneal macrophages (data not shown). Regressor PBML (but not regressor sera) also were cytotoxic for autochthonous, non-transformed peritoneal macrophages (Table 2) negative for demonstrable FeLV production (Table 1); a finding that we do not understand, but is similar to the recognition of lymphocyte-defined membrane antigen on nonproductively infected B cells by killer cells in EBV-exposed people[26]. The biological relevance of the killing of FeLV-infected marrow cells by immune PBML and sera is suggested by the correlation of decreases in circulating neutrophil and lymphocyte numbers with curtailment of virus replication and appearance of FOCMA antibody in regressively infected cats[2,27].

The early containment in haemolymphatic tissues and establishment of regressive versus progressive infection *in vivo* is corticosteroid (CS)-sensitive[28]. *In vitro* studies have shown that minority populations of feline macrophages and lymphocytes are susceptible to productive FeLV infection[19,29] and that the permissiveness of macrophages but not lymphocytes to FeLV infection can be augmented by CS[19,29]. To examine this further we investigated the effect of CS on latent FeLV infections *in vivo* and *in vitro*. Cats with established regressive FeLV infection were treated with 10 mg per kg methylprednisolone acetate twice weekly for 4 successive weeks. They developed productive FeLV infection in marrow and diminished antibody to FOCMA-L 1–2 weeks after initiation of CS treatment (Table 3). While 3 of 5 cats were able to contain reactivated FeLV, 2 of 5 cats remained persistently viraemic 135 days after initiation of treatment. Comparable non-CS-treated untreated regressors maintained for 2–3 years in similar environments have never developed productive infection[4].

Reactivation of FeLV from latently infected marrow myelomonocytic precursor cells and from peritoneal macrophages but not from lymph node or PBML occurred *in vitro* following CS treatment (Table 4). Reactivation of FeLV was associated with induction of cytoplasmic GSA in 15–30% (mean 21%) of untreated regressor cat bone marrow cells and 20–32% (mean 25%) of CS-treated marrow cells. The CS-mediated 2–3-fold amplification of viral production, therefore, is perhaps due to increased viral replication in a fixed population (20–25%) of marrow cells that contain latent FeLV infection.

Both lymphocytes and macrophages are critical to the early restriction of reactivated FeLV infection. However, ultimately T cells of marrow origin which migrate to the thymus are transformed[2,30]. The relationships between the target cells for latent infection (myelomonocytic and T_γ cells), acute infection (B cells and myelomonocytic cells)[2,19] and transformation (T cells)[30] are as yet undetermined.

Our findings suggest that most cats infected by FeLV develop persistent viral infection of marrow cells. A minority of cats

Table 2 Cytotoxic immune responses of FeLV regressor cats with reactivated infections

	Microcytotoxicity (MCT) target					
	Marrow			Peritoneal macrophages		
		% Killing			% Killing	
Type of MCT	No. of cats positive	Mean	(Range)	No. of cats positive	Mean	(Range)
ADCC	6/6	89	(52–99)	2/5	46	(25–60)
CTL (PBML)	4/6	99	(84–99)	3/5	60	(59–61)
CML-regressor serum	5/6	91	(65–99)	0/5	<20	
CML-reference serum	5/6	72	(41–99)	0/5	<20	
CML-pre-exposure serum	0/3	<20		0/3	<20	
ΔH-regressor serum	4/6	88	(47–99)	ND	ND	
ΔH-reference serum	1/3	38	(38)	ND	ND	
ΔH-pre-exposure serum	0/3	<20		0/3	<20	
Media control	0/6	0		0/5	0	

500 marrow cells or peritoneal macrophages from regressor cats were seeded in triplicate in 96-well cluster dishes and cultured as described in Table 1 to permit *in vitro* FeLV reactivation. On day 6, nonadherent cells were aspirated and the adherent cells washed twice with fresh media before the addition of autochthonous cells, serum or reference serum. Serum were diluted 1:4 in media and added in 0.05-ml aliquots. For antibody-dependent cell-mediated cytotoxicity (ADCC), washed adherent cells were incubated with heat-inactivated (ΔH, 56 °C, 30 min) autochthonous serum for 30 min at 37 °C, washed twice and incubated with plastic nonadherent PBML at an effector:target (E:T) ratio of 50:1. For cytotoxic T lymphocytes (CTL), autochthonous plastic nonadherent BML only were added at an E:T ratio of 50:1. For complement-mediated lysis (CML), fresh or fresh-frozen autochthonous serum (regressor or pre-exposure serum) was added. Alternatively, ΔH reference goat anti-FeLV serum and 0.05 ml of fresh FeLV-naive cat complement[35] diluted 1:4 in media were added. To evaluate the complement-independent, cytostatic potential of regressor serum alone, ΔH regressor, reference, or pre-exposure serum was added. Cytotoxicity media was RPMI 1640–20% fetal calf serum. Plates were incubated for 20 h at 37 °C to allow lysis by cat complement[35] and nonadherent cells were removed by washing. Plates were stained with Wright Giemsa and examined for morphological evidence of target cell necrosis. % Killing is the arithmetic mean of triplicate wells for each of the no. of cats positive for MCT: (>30% killing of variable versus media control was significant at $P < 0.05$ by Student's paired *t*-test); and

$$\%\ \text{Killing} = 100 - \frac{\text{No. of viable adherent cells in variable well}}{\text{No. of viable adherent cells in media control well}}$$

Table 3 Effect of adrenal corticosteroids on latent FeLV infections *in vivo*

	No. of cats positive for GSA in:		Marrow VI			FOCMA-L	
				Titre		Antibody	
Days post treatment	Marrow	Blood	No. positive	Mean	(Range)	Mean	(Range)
0	0/5	0/5	0/5	<5		71	(32–256)
7–14	1/5	1/5	4/4	22	(15–30)	9	(<2–32)
28	2/5	2/5	2/5	30	(25–35)	4	(<2–8)
63–135	2/5	2/5	2/5	732	(200–1175)	32	(16–64)

Five adult regressors were treated with 10 mg per kg methylprednisolone acetate (Depo-Medrol, Upjohn) at days 0, 4, 7, 11, 14, 18, 21. Mononuclear and polymorphonuclear cells in blood and marrow smears were examined for FeLV GSA by fixed cell immunofluorescence[13]. A minimum of 10^6 freshly isolated marrow cells were disrupted by two freeze-thaw cycles and assayed for VI[15]. VI is expressed as mean FFU per 10^6 cells. Antibody to FOCMA was determined by indirect membrane immunofluorescence using FL-74 target cells[5,6] and is expressed as geometric mean titre.

Table 4 Effect of adrenal corticosteroids on reactivation of latent FeLV infections *in vitro*

				VI		% GSA-positive cells	
Cell source	Days in culture	CS treatment	No. of cats positive	Mean	(Range)	Mean	(Range)
Marrow	0	Absent	0/6	<5		0	
	6	Absent	8/10	11,794	(580–74,500)	21	(15–30)
	6	Present	9/10	30,500	(2,350–136,700)	25	(20–32)
Lymph node	0	Absent	0/10	<5		0	
	7	Absent	0/10	<5		0	
	7	Present	1/10	15		0	
PBML	0	Absent	0/10	<5		0	
	7	Absent	0/10	<5		0	
	7	Present	1/10	10		0	
Peritoneal macrophages	0	Absent	0/5	<5		0	
	7	Absent	0/5	<5		0	
	7	Present	3/5	517	(50–950)	ND	

Cells were obtained from adult regressors and cultured as described for Table 1. 10^{-6} M CS (hydrocorticosone hemisuccinate, Solucrotef, Abbot) was included as indicated. VI is expressed as FFU per 10^6 cells (freeze-thaw lysate); % GSA-positive cells is expressed as arithmetic mean.

experience highly expressed persistent infections of marrow haemolymphatic progenitor cells, lymphoid tissues and epithelia[2], with consequent virus excretion[31], immunosuppression[32,33] and subsequent FeLV-related proliferative or antiproliferative disease[4]. Most FeLV-exposed cats (>70%), however, develop transient productive infection of haemolymphatic cells which is curtailed by host immune responses[2,5]. Nevertheless, FeLV persists as an integrated latent infection in marrow myelomonocytic precursor cells and (certain nodal) T lymphocytes and can be reactivated by liberation from host immunological controls through culture *in vitro* or immunomodulation *in vivo*. Comparable degrees of viral recrudescence *in vivo* may occur in response to endogenous hormones, senescence, or other immunosuppressive or promoting influences. These observations provide both a progression and a link between host–retrovirus relationships in the cat and those species in which greater degrees of viral genomic latency predominate, such as the ecotropic retroviral infections of cattle, gibbon apes, wild mice and the oncogenic human, simian and avian herpesvirus infections.

Received 11 November 1981; accepted 5 May 1982.

1. Jarrett, W. F. H. *et al. J. natn. Cancer Inst.* **51,** 833–841 (1973).
2. Rojko, J. L., Hoover, E. A., Mathes, L. E., Olsen, R. G. & Schaller, J. P. *J. natn. Cancer Inst.* **63,** 759–768 (1979).
3. Sarma, P. S. & Log, T. *Virology* **54,** 160–169 (1973).
4. Hoover, E. A., Olsen, R. G., Hardy, W. D. Jr, Schaller, J. P. & Mathes, L. E. *J. natn. Cancer Inst.* **57,** 365–369 (1976).
5. Essex, M., Klein, G., Snyder, S. P. & Harrold, J. B. *Int. J. Cancer* **8,** 384–390 (1971).
6. Essex, M., Klein, G., Snyder, S. P. & Harrold, J. B. *Nature* **233,** 195–197 (1971).
7. Post, J. W. in *Feline Leukemia Virus* (eds Hardy, W. D., Essex, M. & McClelland, A. J.) 151–159 (Elsevier-North Holland, New York, 1980).
8. Essex, M., Hardy, W. D. Jr, Cotter, S. M., Jakowski, R. M. & Sliski, A. *Infect. Immunity* **11,** 470–475 (1975).
9. Lutz, H., Pedersen, N. C., Higgins, J., Harris, C. W. & Theilen, G. H. in *Feline Leukemia Virus* (eds Hardy, W. D., Essex, M. & McClelland, A. J.) 497–505 (Elsevier-North Holland, New York, 1980).
10. Hardy, W. D. Jr, Zuckerman, E. E., MacEwen, E. G., Hayes, A. A. & Essex, M. *Nature* **270,** 249–251 (1977).
11. Hardy, W. D. Jr. *et al. Cold Spring Harb. Conf. on Cell Proliferation* **7,** 677–699 (1980).
12. Rickard, C. G., Post, J. E., Noronha, F. & Barr, L. M. *J. natn. Cancer Inst.* **42,** 987–1014 (1969).
13. Hardy, W. D. Jr, Hirshaut, Y. & Hess, P. *Bibl. Haemat.* **39,** 778–799 (1973).
14. Sliski, A., Essex, M., Meyer, C. & Todaro, G. J. *Science* **196,** 1336–1339 (1977).
15. Fischinger, P. J., Blevins, C. S. & Nomura, S. *J. Virol.* **14,** 177–179 (1974).
16. Schaller, J. P. & Olsen, R. G. *Infect. Immunity* **12,** 1405–1410 (1975).
17. Rojko, J. L., Finn, B. L., Hoover, E. A. & Olsen, R. G. *Clin. exp. Immun.* (submitted).
18. Rojko, J. L., Hoover, E. A., Finn, B. L. & Olsen, R. G. *Int. Archs Allergy appl. Immun.* (in the press).
19. Rojko, J. L., Hoover, E. A., Finn, B. L. & Olsen, R. G. *J. natn. Cancer Inst.* **67,** 899–910 (1981).
20. Schultz, R. D., Scott, F. W., Duncan, J. R. & Gillespie, J. H. *Infect. Immunity* **9,** 391–393 (1974).
21. Causse-Vaills, C., Vérain, A. & Vérain, A. *C.r. hebd. Séanc. Acad. Sci., Paris* **252,** 2453–2455 (1961).
22. Tomada, I. *Jap. J. vet. Sci.* **24,** 337–348 (1962).
23. Hoover, E. A., Schaller, J. P., Mathes, L. E. & Olsen, R. G. *Infect. Immunity* **16,** 54–59 (1977).
24. Rickinson, A. B., Jarvis, J. E., Crawford, D. H. & Epstein, M. A. *Int. J. Cancer* **14,** 704–715 (1974).
25. Rickinson, A. B., Crawford, D. H. & Epstein, M. A. *Clin. exp. Immun.* **28,** 72–79 (1977).
26. Svedmyr, E. & Jondal, M. *Proc. natn. Acad. Sci. U.S.A.* **72,** 1622–1626 (1975).
27. Hoover, E. A., Rojko, J. L. & Olsen, R. G. *Cold Spring Harb. Conf. on Cell Proliferation* **7,** 635–651 (1980).
28. Rojko, J. L., Hoover, E. A., Mathes, L. E., Krakowka, S. & Olsen, R. G. *Cancer Res.* **39,** 3789–3791 (1979).
29. Hoover, E. A., Rojko, J. L., Wilson, P. L. & Olsen, R. G. *J. natn. Cancer Inst.* **67,** 889–898 (1981).
30. Cockerell, J. L., Krakowka, S., Hoover, E. A., Olsen, R. G. & Yohn, D. S. *J. natn. Cancer Inst.* **57,** 907–913 (1976).
31. Francis, D. P., Essex, M. & Hardy, W. D. Jr *Nature* **269,** 252–254 (1977).
32. Perryman, L. E., Hoover, E. A. & Yohn, D. S. *J. natn. Cancer Inst.* **49,** 1354–1362 (1972).
33. Mathes, L. E., Olsen, R. G., Hebebrand, L. C., Hoover, E. A. & Schaller, J. P. *Nature* **274,** 687–698 (1978).
34. Dexter, T. M. & Testa, N. G. *Meth. Cell Biol.* **14,** 387–405 (1976).
35. Grant, C. K., De Boer, D. J., Essex, M., Worley, M. B. & Higgins, J. *J. Immun.* **119,** 401–406 (1977).

Culture of macrophage cell lines from normal mouse bone marrow

Jaroslav Činátl, Eduard Paluska, Vladimír Chudomel, Věra Malasková & Milan Elleder*

Institute of Haematology and Blood Transfusion, 128 20 Prague 2, U nemocnice 1, Czechoslovakia
* 1st Department of Pathology, Faculty of Medicine, 128 00 Prague 2, Studničkova 2, Czechoslovakia

The use of semisolid medium for the culture and cloning of haematopoietic cells[1,2] has helped our understanding of their proliferation and differentiation. It has been shown that mixed colonies of granulocytes and macrophages developed, in the presence of colony-stimulating factor (CSF)[3,4], from their common precursor, granulocyte–macrophage colony-forming cells (GM–CFC)[5]. Attempts at recloning these colonies in semisolid medium suggested that granulocytes and macrophages were differentiated cells incapable of further proliferation[6,7]. However, our studies on cultures of larger numbers of cells[8] demonstrate that while this may be the case for granulocytes, macrophages seem to be capable of long-term proliferation.

The bone marrow for culture of GM-CFC was obtained from ICR SPF mice (Velaz). We used the technique of Metcalf[9] to establish the primary culture; MEM medium[10] was supplemented with 0.2% Bactotryptose (Difco)[11], 20% heat-inactivated pooled human serum (HS) or native fetal calf serum (FCS) (VŠV), 10% lung conditioned medium (LCM)[12], and 0.34% Bacto-Agar (Difco). For the culture we used Müller flasks (Cavalier). The primary culture was established from 5×10^5 nuclear bone marrow cells in 5 ml of medium. After 7 days at 37 °C in an ambient atmosphere plus 5% CO_2, the cells were counted and then transferred to fresh agar medium at a minimum concentration of 5×10^4 per 5 ml. Further passages were done in the same conditions approximately every 15 days. The cells in semisolid agar medium were stained with acetoorceine.

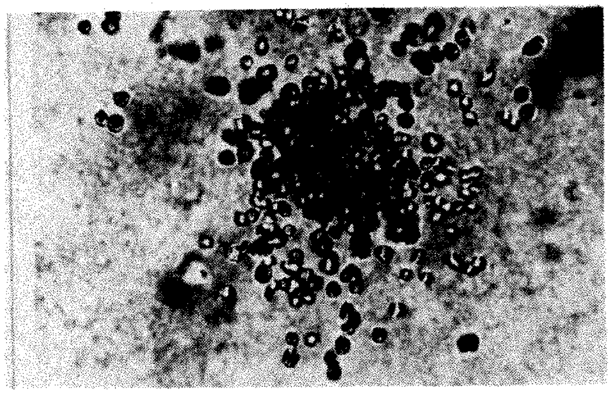

Fig. 1 A colony of macrophages from normal mouse bone marrow grown in semisolid medium; 15-day culture after the 22nd passage (330 days *in vitro*). Native preparation. ×63.

Cells of the 20th passage were transferred to liquid medium for examination and 1 ml aliquots were put into Leighton test tubes with a cover glass. After 3 weeks of culture, colonies of adhering cells suitable for processing were formed on the cover glass.

Pinocytosis was studied by means of dextran sulphate (molecular weight (MW) 5×10^5; Pharmacia); phagocytosis by means of latex particles (Imuna) and a suspension of autoclaved yeast. The receptors for IgG, complement, and IgM were determined by mouse antibodies to sheep erythrocytes. Lysozyme was demonstrated by anti-lysozymal serum using immunofluorescent techniques. The tests were performed according to Goud *et al.*[13] and the peroxidase reaction was carried out according to Graham and Karnovsky. For the determination of nonspecific esterase α-naphthyl acetate was used which could be blocked by E-600 (3×10^{-5} M). For the determination of chloroacetyl esterase, naphthol-ASD-chloroacetate and acid phosphatase naphthol-ASBI-phosphate were used. The coupler was hexazonium-*p*-rosaniline throughout. The procedures are described by Lojda *et al.*[14].

Ten macrophage cell lines have been obtained so far, the first of which is now in the 22nd passage (330 days *in vitro*) in

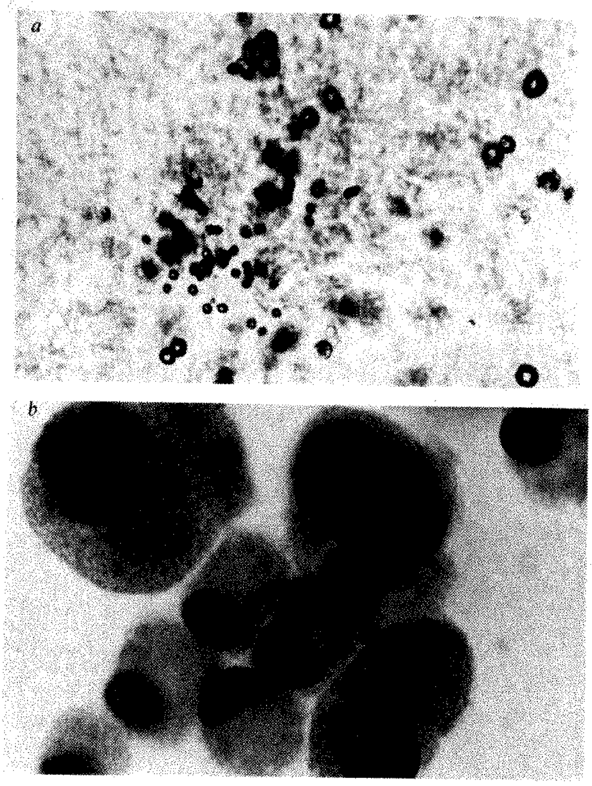

Fig. 2 *a*, A cluster of macrophages (starting colony) from a 7-day culture after the 15th passage in semisolid medium. The cluster consists of cells of various sizes. Small cells (10–14 μm in diameter) predominate in the culture. It is these cells which proliferate most readily are believed to maintain the continuous growth of the culture. Native preparation. ×30. *b*, Small and large macrophages; 15-day culture after the 15th passage in semisolid medium. Fixed and stained with acetoorceine. ×630.

medium with HS; the other three are in the 19th, 16th and 15th passage, and six lines are between the 5th and 10th passage. All of the latter nine lines were grown in FCS-containing medium. The number of seeded cells increased fivefold in ∼15 days after every passage. The macrophages grew in colonies (>40 cells) (Fig. 1), and clusters (3–40 cells), with cells varying in size from approximately 10 μm to 30 μm (Fig. 2). Larger colonies normally consist of smaller cells and large macrophages are frequently found singly or in clusters. When stained in agar medium, both large and small cells show excentrically located nuclei with relatively rich cytoplasm (Fig. 2*b*).

Pinocytosis was found in 97.2% of cells, 95.8% of cells phagocytosed latex particles, and 93.6% phagocytosed yeast (Fig. 3). Receptors for IgG and complement were present in 89.3% and 86.1%, respectively but IgM-receptors could not be demonstrated. The immunofluorescent test for lysozyme was positive.

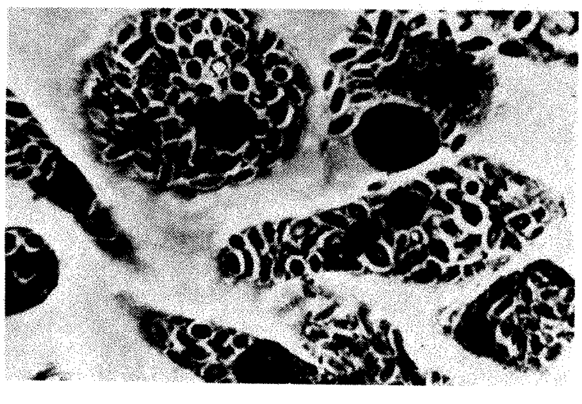

Fig. 3 Macrophage phagocytic activity after 20th passage. When transferred to liquid medium, phagocytes formed colonies of adhering cells on the surface of the cover glass. Oval forms within the cells are yeasts. Fixed with methanol. Phase contrast; ×360.

Peroxidase was negative in all cells. Nonspecific esterase was found in all cells, its activity being almost completely blocked by E600, and persisted only sporadically. Similarly, chloroacetyl esterase and acid phosphatase were positive in all cells. The activity of the hydrolases tested was high in most of the cells.

The assumption that the passaged cells are macrophages is supported by the demonstration of receptors for IgG and complement, and the absence of receptors for IgM[13], and by the cytochemical examination, despite remarkably high chloroacetyl esterase activity.

Macrophages can be preserved in liquid medium for many weeks[15,16], but are believed to be incapable of passaging[16]. However, the use of semisolid media, which minimizes the number of cells adhering to the culture surface, allows long-term growth of macrophage populations from the original mixed granulocyte–macrophage colonies. The medium for long-term culture and passaging of macrophages must be supplemented with a suitable serum and LCM. The establishment of long-term cultures and passaging of macrophages from normal mouse bone marrow *in vitro* will be a useful tool for the further characterization of these very important cells.

Received 16 October 1981; accepted 14 May 1982.

1. Pluznik, D. H. & Sachs, L. *J. cell. Physiol.* **66,** 319–324 (1965).
2. Bradley, T. R. & Metcalf, D. *Aust. J. exp. biol. Sci.* **44,** 287–300 (1966).
3. Pluznik, D. H. & Sachs, L. *Expl Cell Res.* **43,** 553–563 (1966).
4. Metcalf, D. *J. cell. Physiol.* **76,** 89–100 (1970).
5. Metcalf, D. in *Hemopoietic Colonies,* 5–11 (Springer, Berlin 1977).
6. Metcalf, D., Johnson, G. R. & Mandel, T. E. *J. cell. Physiol.* **98,** 401–420 (1978).
7. Dexter, T. M., Garland, J., Scott, D., Solnick, E. & Metcalf, D. *J. exp. Med.* **152,** 1036–1047 (1980).
8. Činátl, J., Paluska, E. & Chudomel, Vl. *Expl Hemat.* **9,** Suppl. 9,113–113 (1981).
9. Metcalf D. in *Hemopoietic Colonies,* 13–15(Springer, Berlin, 1977).
10. Eagle H. *Science* **130,** 432–437 (1959).
11. Činátl, J. *et al. Čs. fysiol.* **29,** 33–38 (1980).
12. Sheridan, J. W. & Metcalf, D. *J. cell. Physiol.* **81,** 11–32 (1973).
13. Goud, T. J. L. M., Schotte, C. & van Furth, R. *J. exp. Med.* **142,** 1180–1199 (1975).
14. Lojda, Z., Gossrau, R. & Schiebler, T. H. *Enzyme Histochemistry* (Springer, Berlin, 1979).
15. Bennet, B. *Am. J. Path.* **48,** 165–181 (1966).
16. Adams, D. O. *Meth. Enzym.* **58,** 494–506 (1979).

Biosynthesis of membrane factor B by mouse peritoneal macrophages

Yuet M Ooi & Boon S. Ooi

Division of Nephrology, Department of Internal Medicine,
University of Cincinnati Medical Center, Cincinnati,
Ohio 45267, USA

The biosynthesis of many of the complement proteins by cells of the monocyte-macrophage series has been established[1]. Studies on these cells using radiolabelled amino acids have demonstrated synthesis of precursor proteins (pro-complement)[2–5], and the native complement protein similar in size to that found in the plasma. However, synthesis of membrane complement proteins has not been demonstrated, although it has been suggested by previous studies using indirect techniques[6–10]. In particular, there is evidence for the membrane-associated factor B in human lymphocytes[11,12]. We report here that resident and thioglycollate-stimulated mouse peritoneal macrophages synthesized, in short-term primary cultures membrane factor B of molecular weight (MW) 95,000 and secreted factor B (MW 90,000) as single chain polypeptides. We also found a large single chain polypeptide with an approximate molecular weight of 195,000, which may be the putative factor B precursor.

Resident and thioglycollate-stimulated mouse (C57BL/6J) peritoneal macrophages were cultured at 37 °C for 18–48 h in Dulbecco's modified Eagle's medium (DMEM) in serum-free conditions in the presence of 60 mM 6-ε-amino caproic acid and radiolabelled with 35 S-methionine (150 μCi ml^{-1} of medium). At the end of the culture, the supernatants of the

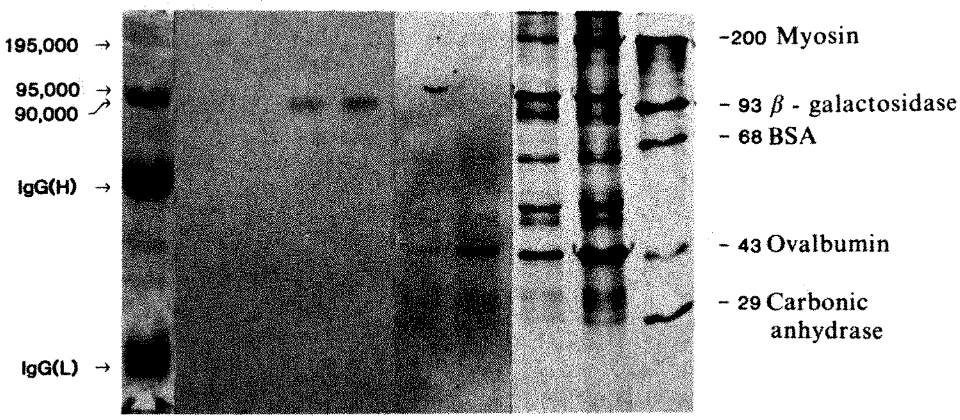

Fig. 1 SDS (1%)-polyacrylamide (9%) gel electrophoresis (Laemmli)[23] of reduced and alkylated ^{35}S-methionine labelled intracellular factor B antigen from resident and thioglycollate-stimulated mouse peritoneal macrophages (mouse strain C57BL/6J). Resident and thioglycollate-stimulated cells were collected and cultured as described previously[5]. Resident cells were plated at 13×10^6 and thioglycollate-stimulated cells at 10×10^6 cells on to 60×15 mm dishes in Dulbecco's modified Eagle's medium, 20% FCS (heated at 56 °C for 2 h). The cells were incubated in a humidified atmosphere of 95% air : 5% CO_2 at 37 °C for 45 min to allow adherence and then non-adherent cells were rinsed off by several washes with Hank's balanced salt solution (HBSS). The adherent cells were cultured for 18 h in DMEM lacking cold methionine (incomplete DMEM) and containing 60 mM 6-ε-amino caproic acid (EACA) and ^{35}S-methionine (150 μCi ml^{-1}) specific activity >50 Ci mmol^{-1}; NEN). At the end of the culture, the medium was collected and the adherent cells were lysed with cold lysate buffer consisting of Tris-HCl (50 mM), KCl (100 mM), Triton X-100 (0.5%), deoxycholate (0.5%), EDTA (10 mM), EACA (100 mM), and phenylmethylsulphonyl fluoride (PMSF; 2 mM). Radiolabelled culture material was centrifuged at 10,000 r.p.m. in a microfuge at 4 °C for 45 min. To the extracellular culture medium was added EDTA (10 mM), PMSF (2 mM), and EACA (100 mM) final concentration and the extracellular culture medium was centrifuged at 150*g* for 10 min. The radiolabelled supernatants were immunoprecipitated with cross-reactive goat IgG antibody to human factor B (Atlantic Antibodies), added at two-fold antibody excess to yield 30 μg of immunoprecipitate, in the presence of ovalbumin with normal mouse serum as cold carrier[5]. The control was mouse antiserum to ovalbumin reacted with ovalbumin in the presence of goat IgG; the antibody to ovalbumin was absorbed with mouse serum before use. After incubation for 3 h at room temperature, the immunoprecipitates were washed extensively. The precipitates were solubilized by boiling for 4 min in 80 μl of sample buffer *p*H 8.1 consisting of: SDS (1%), Tris-HCl (10 mM), Na_2-EDTA (1 mM) and β-mercaptoethanol (4%). After boiling, the sample was incubated with 120 mM iodacetamide for 1 h at 37 °C and centrifuged at 10,000 r.p.m. for 2 min. The fluorograph following SDS-PAGE was developed by standard techniques[24] after fixing the slab gel in 7% glacial acetic acid with 50% methanol, followed by 1 h in Enhance (NEN) and 1 h in distilled water. The gel was dried under vacuum and exposed to a Kodak X-Omat-RP film at −70 °C for 7–10 days, depending on the radioactivity of the immunoprecipitates. Lane *a* shows mouse factor B antigen precipitated from cold carrier mouse serum stained with Coomassie blue, migrating as a protein of MW 90,000. The goat antibody is also detected: H, heavy chain; L, light chain. Lanes *b* to *i* represent the fluorograph of the SDS-PAGE of immunoprecipitated ^{35}S-methionine-labelled protein. Lane *h* shows newly synthesized ^{35}S-methionine-labelled reduced and alkylated intracellular factor B antigen from lysates of cultures of resident mouse peritoneal macrophages. Note the presence of the 195,000-MW and 95,000-MW bands compared with the control immunoprecipitate (*f*). Lane *i* shows these bands but is from intracellular factor B antigen from thioglycollate-stimulated mouse macrophages, which is not found in the control immunoprecipitate from stimulated cells (*g*). In *d* (resident cells) and *e* (thioglycollate-stimulated cells), reduced and alkylated extracellular factor B antigen is shown as a protein band of 90,000 MW, not detected in the controls (*b*, resident cells; *c*, thioglycollate-stimulated cells). ^{14}C-labelled molecular weight markers are shown in *j*.

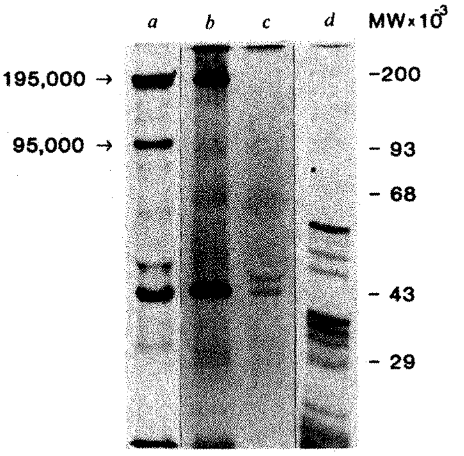

Fig. 2 For these experiments thioglycollate-stimulated and control cells cultured for 18 h in serum-free DMEM containing 60 mM ε-aminocaproic acid (EACA) and 150 μCi ml^{-1} ^{35}S-methionine. The cells were rinsed and incubated with trypsin (tosylphenylethylchloromethylketone, TPCK) added at 10 μg ml^{-1} of HBBS at 37 °C for 45 min. At the end of the incubation, the cells were rinsed and lysed with cold lysate buffer with added protease inhibitors (EDTA, EACA and PMSF). A similar lysate was prepared without protease inhibitors and then incubated at 37 °C for 45 min with 10 μg ml^{-1} of trypsin. At the end of the incubation a twofold excess of soybean trypsin inhibitior (SBTI) was added. Immunoprecipitation and SDS-PAGE was then performed. Lane *b* shows the factor B precipitate of the ^{35}S-labelled thioglycollate-stimulated macrophages trypsinized off the cell surface. Note the disappearance of the 95,000-MW protein band and the presence of the 195,000-MW polypeptide chain. In lane *a* is the non-trypsinized control. Lane *c* is the control immunoprecipitation with anti-ovalbumin of a culture following trypsinization showing absence of the corresponding bands. Lane *d* shows precipitate of the lysate not treated with protease inhibitors. Note the disappearance of the 195,000-MW and the 95,000-MW polypeptides and the generation of several small peptide fragments. ^{14}C-labelled molecular weight standards are shown on the right.

radiolabelled medium and of the cell lysates were immunoprecipitated with goat IgG antibody to human factor B, which is cross-reactive with mouse serum factor B. The antibody was shown by immunoelectrophoresis to be specific for factor B antigen of human and murine serum. Factor B antigen immunoprecipitated from mouse serum with the same antibody migrated as a single chain polypeptide of 90,000 MW (Fig. 1*a*) on SDS (1%) polyacrylamide gel (9%) electrophoresis (SDS-PAGE) of the immunoprecipitate. A similar SDS-PAGE of the immunoprecipitate obtained from ^{35}S-methionine labelled cell lysates of resident and thioglycollate-stimulated cells, detected several intracellular polypeptide chains and intermediate fragments: a large 195,000-MW polypeptide chain, a 95,000-MW chain, and several smaller MW polypeptide chains (88,000–64,000 and smaller) (Fig. 1*h* and *i*). The SDS-PAGE of the immunoprecipitate obtained from the extracellular culture yielded a single chain polypeptide of 90,000 MW (Fig. 1*d* and *e*) similar in size to that of mouse serum factor B.

^{35}S-methionine labelled thioglycollate-stimulated cells were incubated with trypsin (10 μg ml^{-1}) at 37 °C for 45 min, to remove membrane proteins, then rinsed and lysed. SDS-PAGE of the factor B immunoprecipitates of these cell lysates did not show the band representing the 95,000 MW polypeptide chain, suggesting its association with the membrane (Fig. 2*b*); control cells not incubated with trypsin retained their bands (Fig. 2*a*).

The intracellular 195,000-MW polypeptide was unaffected by trypsinization of the cell surface. Evidence for its intracellular location was obtained by experiments in which intracellular lysates were trypsinized; in these conditions the 195,000-MW protein and the 95,000-MW polypeptide were digested (Fig 2*d*). To establish whether the 95,000-MW polypeptide chain was a membrane component, macrophage plasma membrane proteins were labelled by lactoperoxidase-catalysed radioiodination. The immunoprecipitate showed the presence of the 95,000-MW polypeptide (Fig. 3*b*) identical in size to the newly synthesized 95,000-MW polypeptide chain obtained from ^{35}S-methionine labelled cells (Fig. 3*a*). Macrophages cultured in the presence of cycloheximide showed almost total abrogation of the expression of the 95,000-MW polypeptide chain (Fig. 3*c*) followed by its reappearance in cells radioiodinated after a 36 h culture in fresh medium following the removal of cycloheximide (Fig. 3*e*); these experiments therefore established *de novo* synthesis of this molecule and ruled out the possibility of absorption onto the cell membrane.

To further exclude absorption of membrane factor B studies were done using radiolabelled non-adherent peritoneal cells which did not show the presence of the 95,000-MW polypeptide chain (Fig. 3*f*). As a fourfold excess of radiolabelled non-adherent cells compared to the radioiodinated adherent cell population was examined, differential absorption of protein could not account for the different absorption patterns. Finally, it must be noted that on parallel SDS-PAGE analysis of intracellular, extracellular, and membrane labelled material, the extracellular (secreted) factor B has a different molecular size (MW 90,000) compared to the membrane and the cell lysate factor B (MW 95,000), which indicates that there are two distinct molecules one of which is a membrane component.

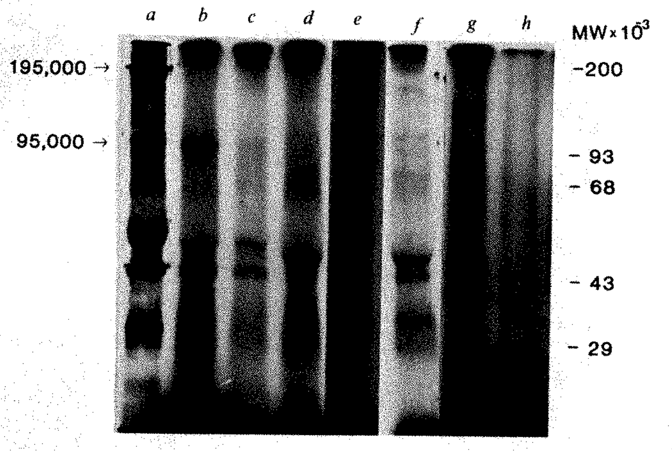

Fig. 3 SDS-PAGE of reduced and alkylated factor B antigen from ^{125}I-labelled mouse peritoneal macrophages radioiodinated for plasma membrane proteins radioiodinated by the Na^{125}I–lactoperoxidase-catalysed reaction[10] with slight modifications. For these experiments, resident and thioglycollate-stimulated peritoneal cells were cultured in serum-free complete DMEM, 60 mM EACA. After culture the cells were released by incubation at room temperature for 1 h with lidocaine (20 mM) in complete DMEM, 20% heated FCS, washed with PBS and then suspended at 1×10^7 cells ml^{-1} for lactoperoxidase radioiodination. The heated FCS contained no detectable factor B antigen. For the cycloheximide experiments, thioglycollate-stimulated cells were cultured for 4 h with cycloheximide added to a concentration of 7·5 μg ml^{-1} of complete DMEM. Cycloheximide was removed after 4 h, the cells were rinsed and the culture continued for 36 h in fresh medium containing 60 mM EACA; a control culture contained no cycloheximide. At the end of the culture, the adherent cells were released with lidocaine and radioiodinated for analysis of plasma membrane proteins. The cell suspension was reacted with 250 μCi of carrier-free Na ^{125}I, an equal volume of NaI (1 mM solution), lactoperoxidase (40 U; Sigma), glucose oxidase (1 U; Sigma), and the mixture was shaken intermittently at 4 °C for 25 min. After incubation, the cells were washed with PBS containing (mM): glucose 20, EDTA 10, PMSF 2, EACA 100 and NaI 75; and finally with complete DMEM, 20% heated FCS containing EDTA, PMSF, EACA and NaI as above. The cells were lysed with cold lysate buffer then centrifuged at 10,000 r.p.m. for 35 min; the supernatants were immunoprecipitated for factor B antigen. Parallel control precipitation was with control antiserum to ovalbumin. The immunoprecipitate was reduced and alkylated and subjected to SDS-PAGE; the autoradiograph is shown. Lane *a* shows ^{35}S-methionine-labelled factor B antigen from a 48 h culture of thioglycollate-stimulated mouse peritoneal macrophages for comparison with radioiodinated membrane factor B antigen. Note the smaller MW protein bands. Lanes *b–e* and *g, h* show lysates of peritoneal macrophages and *f* shows lysates from non-adherent peritoneal cells. Note (1) the presence of the 95,000-MW protein band in *b*, representing factor B antigen; (2) the almost total abrogation of the 95,000-MW band in cycloheximide-treated ^{125}I-labelled thioglycollate-stimulated macrophages (*c*); (3) the absence of the corresponding band from the control precipitate (*d*); (4) the presence of the corresponding 95,000-MW protein band in the stimulated cells after 36 h of culture in fresh medium following a 4 h exposure to cycloheximide (*e*); (5) the absence of this band from non-adherent stimulated cells from 48 h cultures (*f*); (6) the presence of 95,000-MW protein band in radioiodinated resident cells (*g*); and (7) the absence of the corresponding band in the control precipitate from macrophages (*h*). ^{14}C-labelled molecular weight markers are shown on the right.

These findings establish the 95,000-MW polypeptide chain detected in cell lysates of mouse macrophages as membrane factor B of molecular weight 95,000, synthesized in short-term primary culture. Secreted factor B of molecular weight 90,000 was also demonstrated. A larger 195,000-MW polypeptide, pro-factor B, has been identified. In studies[13] using pulse-chase and conversion experiments, the 195,000-MW molecule was shown to be precursor, giving rise to membrane and native factor B. Smaller fragments were also demonstrable and probably result from degradation by proteolytic digestion, as was evident in previous studies[4]. This was probably not due to the specificity of the antibody which was described earlier and is further supported by the presence of only a single band on analysis of immunoprecipitated extracellular material as well as of mouse serum. Another explanation, though less likely, is the presence of incompletely synthesized chains. The biosynthesis of native factor B by mouse macrophages and by human monocytes and the function of plasma factor B have been established previously[14–22]. The functionl activities of the three proteins reported here have yet to be determined. It may be that the macrophage assembles such complement proteins as a defence mechanism, either as a recognition or as an effector unit.

We thank Mrs V Henry for her help. This work was presented at the 9th International Complement Workshop in November 1981 and is supported in part by a grant AI 16729 from the N.I.A.I.D., NIH.

Received 5 January; accepted 5 May 1982.

1. Colten, H. R. *Adv. Immun.* **22,** 67–118 (1976).
2. Hall, R. E. & Colten, H. R. *Proc. natn. Acad. Sci. U.S.A.* **74,** 1705–1710 (1977).
3. Brade, V., Hall, R. E. & Colten, H. R. *J. exp. Med.* **146,** 759–768 (1977).
4. Roos, M. H., Atkinson, J. P. & Shreffler, D. C. *J. Immun.* **121,** 1106–1115 (1978).
5. Ooi, Y. M. & Colten, H. R. *J. Immun.* **123,** 2494–2498, (1979).
6. Saunders, D. & Edidin, M. *J. Immun.* **112,** 2210–2210, (1974).
7. Ferrone, S., Pellegrino, M. A. & Cooper, M. *Science* **193,** 53–55, (1976).
8. McConnell, I. & Lachmann, P. J. *Transplantn Rev.* **32,** 72–92 (1976).
9. McConnell, I. & Lachmann, P. J. *Immun. Commun.* **6,** 111–132 (1977).
10. Yin, H. L., Aley, S., Bianco, C. & Cohn, Z. A. *Proc. natn. Acad. Sci. U.S.A.* **77,** 2188–2191 (1980).
11. Halbwachs, L. & Lachmann, P. J. *Scan. J. Immun.* **5,** 697–704 (1976).
12. Woo, P. & Lachmann, P. J. *Immunology* **44,** 629–639 (1981).
13. Ooi *et al.* (submitted for publication).
14. Bentley, C., Bitterman, D., Hadding, U. & Brade, V. *Eur. J. Immun.* **6,** 393–398 (1976).
15. Whaley, K. *J. exp. Med.* **151,** 501–516 (1980).
16. Gotze, O. & Muller-Eberhard, H. J. *J. exp. Med.* **134,** 90S–108S (1971).
17. Muller-Eberhard, H. J. & Gotze, O. *J. exp. Med.* **135,** 1003–1008 (1972).
18. Gotze, O. *Proteases and Biological Control* (eds Reich, G., Rifkin, D. B. & Shaw, E.) 255–265 (Cold Spring Harbor Laboratory, 1975).
19. Lesavre, P. H., Hughli, T. E., Esser, A. F. & Muller-Eberhard, H. J. *J. Immun.* **123,** 529–534 (1979).
20. Gotze, O., Bianco, C. & Cohn, A. A. *J. exp. Med.* **149,** 372–386 (1979).
21. Sundsmo, J. S. & Gotze, O. *Cell. Immun.* **52,** 1–17 (1979).
22. Sundsmo, J. S. & Gotze, O. *J. exp. Med.* **154,** 768–777 (1981).
23. Laemmli, U. K. *Nature* **227,** 680–685 (1970).
24. Laskey, R. A. & Mills, A. D. *Eur. J. Biochem.* **56,** 335–341 (1975).

A bifunctional gene product involved in two phases of the yeast cell cycle

J. R. Piggott, R. Rai & B. L. A. Carter

Department of Genetics, University of Dublin, Trinity College,
Dublin 2, Ireland

The cell cycle in *Saccharomyces cerevisiae* is divided into two distinct phases. Unbudded, mononucleate cells in the G1 phase can react to relevant environmental changes by mating[1], sporulating[2], or by entering stationary phase[3]. DNA synthesis and bud initiation occur almost simultaneously and mark 'commitment' to the completion of mitosis. Temperature-sensitive mutations at the *cdc28* locus are known to cause arrest in the G1 phase of the cell cycle at the restrictive temperature[4,5]. Here we show that the *cdc28* gene product is also active in post-G1 cell cycle functions, and that a different property of the gene product may be required for each phase of the cycle in which it acts.

The *S. cerevisiae* strain RJB-1 was obtained during a search for nonsense mutations in the strain FM11 (ref. 6). At 37 °C, RJB-1 arrested with the budded, mononucleate morphology

0028–0836/82/290391—03$01.00

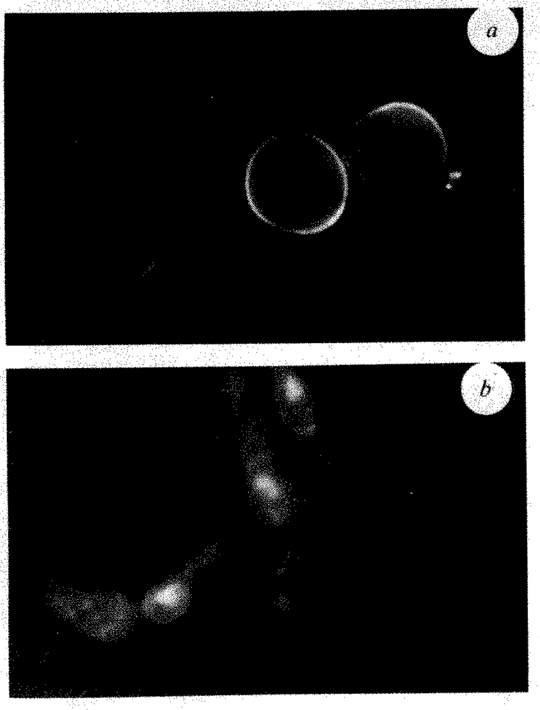

Fig. 1 *a*, The unbudded morphology characteristic of G_1 arrest seen in *cdc28-6* cells after 3.5 h at 37 °C, stained with calcofluor and photographed under UV light. *b*, The mononucleate, budded morphology of RJB-1 (*cdc28-1N*) cells after 3.5 h at 37 °C. The nuclei are stained with diamidinophenyl indole[18] and the cell outlines revealed by calcofluor under UV light.

illustrated in Fig. 1. When crossed with a wild-type strain, RJB-1 yielded a temperature-insensitive diploid, and 42 tetrads from this diploid showed four-spore survival and 2 : 2 segregation for temperature sensitivity. The homogeneity of its arrest phenotype suggested that RJB-1 carried a cell cycle mutation[7], and it was shown to complement the *cdc* mutants 1 to 40, except for *cdc28-1* and *cdc28-6*. Dissection of 32 tetrads from the RJB-1 × *cdc28-1* cross, and 59 tetrads from the RJB-1 × *cdc28-6* cross, yielded no wild-type spores. We therefore concluded that RJB-1 carried a new mutation at the *cdc28* locus. As the phenotype of the new mutant suggested a lesion in nuclear division, we provisionally named the new *cdc28* allele, *cdc28-1N*.

When yeast cells of *a* mating type are treated with *α*-factor, a hormone-like small polypeptide produced by cells of *α* mating type, they undergo reversible G_1 arrest[1]. The cells are sensitive to *α*-factor until ~15 min before the appearance of a visible bud[8]. Figure 2 shows the pattern of DNA synthesis in cells carrying the *cdc28-6* and *cdc28-1N* mutations at 37 °C after release from *α*-factor-induced arrest at 24 °C. The *cdc28-6* cells showed no significant DNA synthesis, remaining unbudded, while the *cdc28-1N* cells exhibited appreciable DNA synthesis. Microscopic examination revealed 100% bud initiation in the *cdc28-1N* culture, although there was no increase in cell number. In the reciprocal shift, that is, arrest at 37 °C followed by transfer to 24 °C in the presence of *α*-factor, *cdc28-6* cells remained arrested in G_1, as described by Hereford and Hartwell[9], while *cdc28-1N* cells divided once at 24 °C before undergoing *α*-factor arrest. Thus, the *cdc28-1N* mutation acts at a point in the cell cycle which is unambiguously later than the *α*-factor or 'start' step, while the *cdc28-1* and *cdc28-6* execution points cannot be separated from 'start' by the reciprocal shift technique[9].

Table 1 The behaviour of recently budded *cdc28-6* cells at 37 °C

Time after shift to 37 °C (min)	Unbudded, 1 nucleus (%)	Budded, 1 nucleus in mother (%)	Budded, 1 nucleus in bud (%)	Budded, nucleus dividing (%)	Budded, binucleate (%)
0	48	48	–	–	4
70	33	48	2	4	13
110	34	49	5	–	12
130	32	49	5	–	14

An exponentially growing culture of *cdc28-6* in YEPD (1.5×10^6 cells ml^{-1} in 2% glucose, 2% Bacto-peptone and 1% yeast extract solution) was arrested in G_1 by exposure to *α*-factor (10 U ml^{-1}) at 24 °C for 3h. The *α*-factor was removed by Millipore filtration of the cells, which were then washed with two volumes of fresh medium. The cells were resuspended in fresh YEPD and allowed to recover at 24 °C until 50% had initiated a bud, when a 25-ml sample was shifted to 37 °C. The control cells divided at 24 °C, 100 minutes after T_0 (zero time). Samples taken at the time indicated were stained with diamidinophenyl indole[18] to reveal nuclear morphology. The increase in per cent binucleate cells was due to cells which had already passed both cell cycle blocks at the time of the shift. At least 150 cells were scored for each sample.

The *cdc28-6* × *cdc28-1N* and *cdc28-1* × *cdc28-1N* diploids arrested at 37 °C with the budded morphology typical of *cdc28-1N*. As *cdc28-1N* is recessive, this suggested the presence of a nuclear division defect in the G_1 arrest alleles. To test this possibility, *α*-factor-arrested *cdc28-6* cells were allowed to recover from G_1 arrest at 24 °C, and at 20-min intervals, samples from the recovering culture were shifted to 37 °C. It was found that the cells were unable to divide at 37 °C until 35 min after bud initiation (that is, 'start'). The *cdc28-1N* mutant shows similar behaviour (data not shown). The results presented in Table 1 confirm that *cdc28-6* cells which have recently budded, and therefore passed the 'start' event, cannot complete cell division at the restrictive temperature. Thus *cdc28-6* harbours a lesion in the nuclear division process which has been masked previously by its temporal proximity to the 'start' lesion also present in this strain.

Evidently, mutation at the *cdc28* locus may confer a defect in nuclear division alone, or in both 'start' and nuclear division functions. So far, *cdc28-1N* is the only allele at this locus known to affect nuclear division exclusively. In contrast, a range of *cdc28* G_1 arrest mutants is already available. Whether or not all such mutants show the double cell cycle lesion reported here for *cdc28-6* is unknown. If 'start only' mutants of *cdc28* do exist, we might expect them to complement *cdc28-1N*, and test crosses with this allele should provide a useful preliminary screening procedure. An investigation of the mitotic behaviour of other G_1 arrest mutants (for example, *cdc37*)[5] is also required in view of these results.

The earliest cell cycle event known to be blocked by the *cdc28* mutation is spindle pole body duplication, which nor-

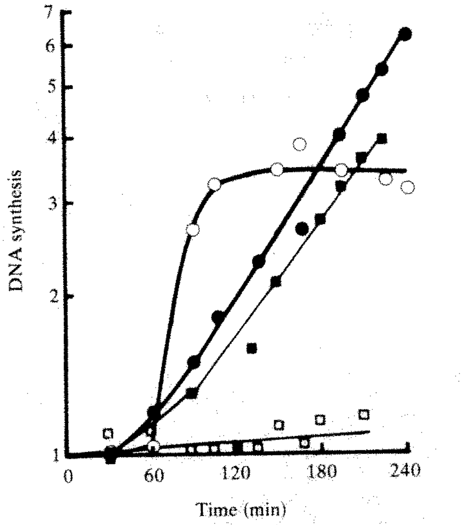

Fig. 2 DNA synthesis patterns following a shift from the *α*-factor block to 37 °C in RJB-1 (*cdc28-1N*) and ST10 (*cdc28-6*) cells. A log-phase culture (2×10^6 cells ml^{-1}) was arrested in G_1 by exposure for 3 h to *α*-factor (final concentration 10 U ml^{-1}). The *α*-factor was removed by Millipore filtration and washing with 100 ml of fresh nutrient medium. Cells were resuspended in fresh medium containing 1 μCi [2-C^{14}]uracil ml^{-1} and incubated at 24 °C or 37 °C. Samples were removed at intervals and the radioactivity incorporated into DNA was determined[19]. Results are expressed as c.p.m. relative to initial values in each experiment. ●, RJB-1 at 24 °C; ○, RJB-1 at 37 °C; ■, ST10 at 24 °C; □, ST10 at 37 °C.

mally precedes both initiation of DNA synthesis and budding[10]. As recently budded cells have already duplicated their spindle pole bodies, our results indicate that *cdc28* cannot be concerned exclusively with such duplication. Failure to complete this process does not suppress other 'start' activities in the cell cycle mutant *cdc31* (ref. 11), thus it is possible that such failure is a symptom of G_1 arrest, but not its primary cause. As bud formation can occur in the absence of DNA synthesis in *cdc7* (ref. 12), and DNA synthesis can occur in the absence of bud formation[13], it is likely that all three markers of the start event are normally subject to coordinate control by a process or structure which involves the *cdc28* gene product.

When recovering from α-factor arrest at 24 °C, *cdc28-6* and *cdc28-1N* cells showed nuclear migration into the bud before nuclear division, and this migration was inhibited at 37 °C (Table 1). As mid- and late-nuclear division require extensive nuclear mobility, and these events are apparently unaffected by *cdc28* mutations, it is unlikely that the early nuclear paralysis seen in both *cdc28-6* and *cdc28-1N* is due to a defect in microtubule formation. Nuclear division, however, requires that nuclear movements be spatially coordinated within the mother/bud junction of the dividing cell. Such coordination requires the presence of nuclear/cytoplasmic connections, and the mitotic spindle in yeast is known to connect with the cytoplasm via mictrotubules[14]. Inability to form such nuclear/cytoplasmic connections at 37 °C could well account for our results, and for the reported association of a *kar* phenotype (failure of nuclear fusion at zygote formation) with some *cdc28* mutants[15].

Nuclear division is prevented by the *cdc28-1N* mutation at the restrictive temperature, but start functions seem unaffected. This suggests that a different property of *cdc28* is required for each process in which it participates. The bifunctional nature of the *cdc28* protein may reflect functional segregation of the *cdc28* gene similar to that found at the *his4c* locus, where a single polypeptide has three enzymatic functions which can be independently eliminated by mutation[16]. On the other hand, the particular lesion present in *cdc28-1N* may be critical for nuclear division, but not start processes, at the restrictive temperature because of a different molecular environment for the gene product at both cell cycle stages. Extensive genetic and physical analysis will be required to elucidate this.

Whatever the physical basis of the bifunctionality of *cdc28*, it is interesting that the *cdc2* gene in *Schizosaccharomyces pombe* has a regulatory effect at start[17] and acts at two points in the cell cycle equivalent to those described here for *cdc28* in *S. cerevisiae*. Although no mutation has so far been reported in *S. pombe* which blocks one function in the cell cycle exclusively, it is possible that the *cdc28* gene of *S. cerevisiae* and the *cdc2* gene of *S. pombe* have equivalent roles, and that in both organisms a functional component of the nuclear division process has a role in regulation commitment to cell division.

This work was supported by grants from the MRC of Ireland and the National Board of Science and Technology.

Received 19 March; accepted 21 May 1982.

1. Bucking-Throm, E., Duntze, W., Hartwell, L. H. & Manney, T. R. *Expl Cell Res.* **76,** 99–110 (1973).
2. Hirschberg, J. & Simchen, G. *Expl Cell Res.* **105,** 245–252 (1977).
3. Johnston, G. C., Pringle, J. R. & Hartwell, L. H. *Expl Cell Res.* **105,** 79–98 (1977).
4. Hartwell, L. H., Mortimer, R. K., Culotti, J. & Culotti, M. *Genetics* **74,** 267–286 (1973).
5. Reed, S. I. *Genetics* **95,** 561–577 (1980).
6. Rai, R. & Carter, B. L. A. *Molec. gen. Genet.* **181,** 556–558 (1981).
7. Hartwell, L. H., Culotti, J. & Reid, B. *Proc. natn. Acad. Sci. U.S.A.* **66,** 352–359 (1970).
8. Carter, B. L. A. *The Cell Cycle* (ed. John, P. C. L.) (Cambridge University Press, 1981).
9. Hereford, L. M. & Hartwell, L. H. *J. molec. Biol.* **84,** 445–461 (1974).
10. Byers, B. & Goetsch, L. *Cold Spring Harb. Symp. quant. Biol.* **38,** 23–131 (1973).
11. Byers, B. *Molecular Genetics in Yeast. Alfred Benzon Symp.* **16** (Munksgaard, Copenhagen, 1981).
12. Hartwell, L. H. *J. Bact.* **115,** 966–974 (1973).
13. Sloat, B. F. & Pringle, J. R. *Science* **200,** 1171–1173 (1978).
14. Robinow, C. F. & Marak, J. *J. Cell Biol.* **29,** 129–151 (1966).
15. Pringle, J. R. & Hartwell, L. H. *Molecular Biology of the Yeast* Saccharomyces (eds Strathern, J. *et al.*). (Cold Spring Harbor Laboratory, New York, 1981).
16. Fink, G. R. *Genetics* **53,** 445–459 (1966).
17. Nurse, P. & Bissett, Y. *Nature* **292,** 558–560 (1981).
18. Williamson, D. H. & Fennell, D. J. *Methods in Cell Biology* (ed. Prescott, D. M.) 335–372 (Academic, 1975).
19. Hartwell, L. H. *J. Bact.* **104,** 1280–1285 (1975).

Ligation of oligonucleotides by pyrimidine dimers—a missing 'link' in the origin of life?

Roger J. Lewis & Philip C. Hanawalt

Department of Biological Sciences, Stanford University, Stanford, California 94305-2493, USA

One of the principal photochemical reactions of DNA on exposure to UV is the formation of intrastrand cyclobutane-type pyrimidine dimers[1,2]. The efficiency of this reaction depends on both the wavelength of the UV[2] and the specific nucleotide sequence in the DNA[3]. The formation of the pyrimidine dimer and its repair in living cells have been studied extensively[4]. We have examined the possibility that pyrimidines at the ends of DNA strands may be adequately juxtaposed for dimer formation by the presence of a complementary strand, even when no phosphodiester linkage joins their sugars. In these conditions the formation of a dimer will 'ligate' two DNA strands end-to-end. We report here that thymidine oligonucleotides annealed to polydeoxyadenylate can be ligated end-to-end by UV irradiation, via thymine dimerization of the terminal nucleotides in adjacent oligonucleotides. The linkages are susceptible to direct photoreversal by 254 nm UV, as expected for cyclobutane-type thymine dimers, but they are not cleaved by the bacteriophage T4 endonuclease V, a dimer-specific DNA repair enzyme. We demonstrate that the ligating dimers are also resistant to photolyase from *Escherichia coli*. Although the phosphodiester backbone is not required for dimer formation, it is required for recognition of dimers by these DNA repair enzymes. We discuss the possibility that high molecular weight polynucleotides in primordial seas might have been generated from oligonucleotides by pyrimidine dimerization under the intense solar UV flux unattenuated by an ozone layer.

Within a continuous DNA strand, pyrimidine dimer formation proceeds as follows. An absorbed photon excites a pyrimidine base from its singlet bonding ground state to a singlet antibonding excited state. The new electronic configuration of the base reduces its van der Waals' radius, allowing an adjacent pyrimidine to move closer than the usual 3.4 Å spacing and to share the excitation energy[5–7]. This 'excimer' state can then undergo inter-system crossing into the more stable triplet state from which a pyrimidine–pyrimidine cyclobutane dimer may arise.

Our model system consisted of oligodeoxythymidylate 10 residues long $[d(pT)_{10}]$ mixed with an equal weight of polydeoxyadenylate [poly(dA)] in solution. The resulting duplex[8] melts near 25°C (ref. 9). After labelling a small fraction of the 5′ ends with ^{32}P we irradiated the DNA with UV of wavelengths >290 nm, which we hereafter call long-wavelength UV. Electrophoretic analysis on denaturing polyacrylamide gels revealed the production of high molecular weight oligomers corresponding to integral multiples of the $d(pT)_{10}$ (Fig. 1). The presence of dimers, trimers and tetramers was apparent after 30 min of irradiation. This 'ligation' of oligonucleotides was caused presumably by the formation of dimers between the first and last thymines of oligonucleotides adjacent on the complementary poly(dA). Similar irradiation of single-strand $d(pT)_{10}$ produced no effect detectable by gel electrophoresis (data not shown). We concluded that hybridization to the poly(dA) is required to maintain the oligonucleotides in a photoligatable configuration.

To quantify the amount of material in each electrophoresis band, we excised the bands from the dried gel and assayed them for ^{32}P. This allowed us to measure the kinetics of the photoligation process (Fig. 2). To compare the photoligation process with the formation of thymine dimers at internal positions, we irradiated poly(dT)·poly(dA) in identical conditions and quantified the resulting thymine dimers by TLC[10]. During the initial phase (0–30 min) of irradiation, the production of

0028-0836/82/290393—04$01.00

dimers, trimers and tetramers of the oligomers occurred, with the expected loss of material from a 10-base band in the gels. The initial rate for internal dimer production in poly(dT) · poly(dA) was similar to or slightly less than the initial rate for the production of ligating thymine dimers in our substrate (Fig. 2).

During the next phase of the process (30–60 min of irradiation) the yield of material in each band reached a plateau. In contrast, the content of internal dimers in poly(dT) · poly(dA) continued to rise rapidly during this period. On continued irradiation (60–240 min) we observed no significant change in the relative quantity of material in the respective bands.

Why does formation of ligating dimers cease while internal dimer formation continues? One possible explanation involves denaturation of oligonucleotides by internal dimers. After 30 min irradiation each oligonucleotide contained an average of one internal dimer, assuming that the rate of internal dimer formation in $d(pT)_{10}$ is similar to that in poly(dT). A dimer in oligo $d(pT)_{10}$ · poly(dA) reduces the melting temperature below that of $d(pT)_6$ · poly(dA)[11]. As the melting temperature of $d(pT)_6$ · poly(dA) is less than 9 °C (ref. 9), it seems likely that after 45–60 min of irradiation at 5–10°C very little of the $d(pT)_{10}$ was still annealed to the poly(dA), thus eliminating the end-to-end juxtaposition required for the formation of ligating dimers. Another possible explanation is that the competing production of internal dimers between the first and second or ninth and tenth thymines within the oligonucleotides prevented the production of ligating dimers between the first and tenth thymines of adjacent oligonucleotides.

One distinctive characteristic of cyclobutane dimers is their reversibility by irradiation with UV of wavelengths shorter than ~260 nm (ref. 2). To confirm that the ligating dimers were reversible by UV, we exposed $d(pT)_{10}$ · poly(dA) to long-wavelength UV to produce 'ligated' oligonucleotides, then re-irradiated the DNA with UV of shorter wavelengths (mainly 254 nm). With doses of short-wavelength UV up to 1.6×10^4 J m^{-2}, the amount of material in the ligated oligomer bands clearly decreased (Fig. 3). Quantification of the material in the bands confirmed this (not shown). This observation demonstrates photoreversibility of the ligating dimers and, as discussed below, lends support to the hypothesis that dimer-induced denaturation limits formation of ligating dimers.

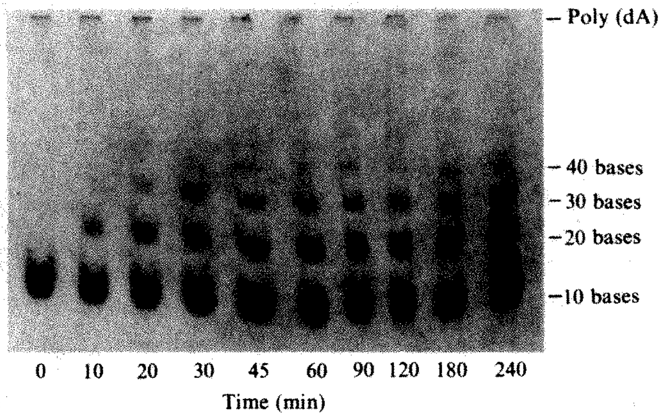

Fig. 1 Ligation of oligonucleotides by increasing irradiation with long-wavelength UV. This autoradiograph of a denaturing polyacrylamide gel shows the production of dimers (20 bases), trimers (30 bases), and tetramers (40 bases) of oligonucleotides (10 bases) by increasing irradiation with long-wavelength UV. Double-strand polymers of oligo ($d(pT)_{10}$) · poly(dA) (7850; P. L. Biochemicals) were dissolved in 0.5 ml phosphate buffer (50 mM sodium phosphate, 50 mM NaCl, *p*H 7.0) to an A_{260} of 6.0; 1 μg of this DNA was ^{32}P-labelled at the 5′ termini[20]. Mixing the unlabelled and labelled DNA yielded an activity of 10^3 c.p.m. μl^{-1} although less than 1% of the molecules were labelled. For irradiation, a fraction of the DNA solution was placed in a 1 cm glass cuvette, surrounded by water at 0 °C. The solution was stirred and nitrogen was bubbled through it before and during the irradiation. Light was provided by a focused 75 W low-pressure xenon lamp having an output of 2 J m^{-2} in the 250–260 nm band. The glass cuvette was opaque to wavelengths shorter than 290 nm and in these conditions a high equilibrium dimer yield was obtained[2]. At the times shown, 30-μl samples were removed, denatured with formaldehyde[21], and loaded onto the gel with 6 μl of 40% (w/v) sucrose. The 12.5% polyacrylamide gels were prepared and run in Peacock's buffer[22] to which formaldehyde had been added to a concentration of 2% (w/w). The buffer was recirculated during both the pre-run (> 8 h, 100 V) and the run (60 min, 250 V). The gel was dried and autoradiographed.

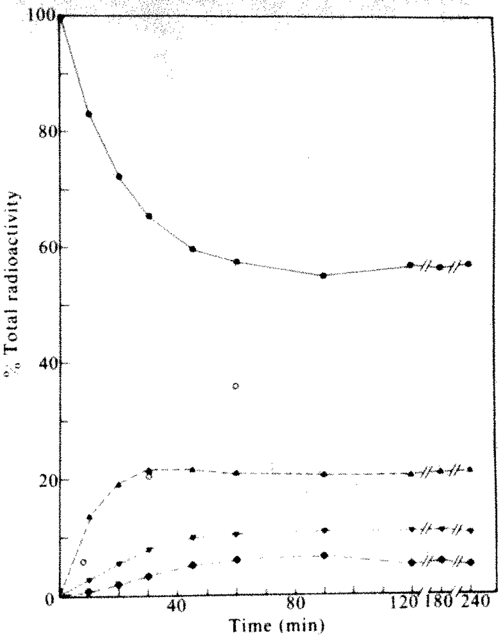

Fig. 2 Kinetics of photoligation. The radioactivity in each band (●, 10 bases; ▲, 20 bases; ▼, 30; ◆, 40) is expressed as a percentage of the total radioactivity entering each gel lane shown in Fig. 1. After the gel was autoradiographed, each band was excised and assayed for radioactivity by scintillation spectrometry in omnifluor/toluene (NEN). A separate experiment was set up to determine the kinetics of internal dimer formation in our irradiation conditions: a small amount of [2-^{14}C]poly(dT) · poly(dA) (10472; P. L. Biochemicals); was included in the cuvette during an identical irradiation of $d(pT)_{10}$ · poly(dA) and the fraction of thymines contained in dimers was measured by TLC[10]. The percentage of total ^{14}C contained in the dimer peak is shown (0). The initial rate of production for any of the products measured was determined by measuring the slope of the line joining the first two points (for example, 0 min and 10 min).

Short-wavelength UV (254 nm) can dimerize up to 39% of the thymines in poly(dT)[2], but only 20% of the thymines were dimerized after our initial long-wavelength UV irradiation of $d(pT)_{10}$ · poly(dA). Thus, the subsequent short-wavelength irradiation while apparently breaking the ligating dimers, should have actually increased the frequency of internal dimers within the oligomers. This dichotomy is understandable if one considers two effects of short-wavelength UV on a photoligated oligonucleotide. First, the internal dimers are both broken and formed, eventually resulting in a higher equilibrium frequency than originally present. This leads to denaturation of the oligonucleotide. Second, the ligating dimer is broken, but cannot be re-formed because the oligonucleotide is no longer hybridized to the poly(dA). Thus there is a loss of ligated oligonucleotides. Dimer-induced denaturation removes the oligonucleotides from a ligatable configuration after either extensive long-wavelength irradiation or after a shorter period of long-wavelength irradiation followed by short-wavelength irradiation. In the former case this simply stops the photoligation process, while in the latter case it allows us to observe photoreversibility of the ligating dimers.

It was of interest to determine whether enzymes specific for pyrimidine dimers in DNA would also recognize the ligating dimers, as this would elucidate both the nature of the ligating dimers and the mechanisms of action of these enzymes.

Photolyase from *E. coli* binds tightly to pyrimidine dimers and, on irradiation with visible light, catalyses the splitting of the dimers into the two original pyrimidines[12,13]. The splitting of a ligating dimer would result in the separation of the oligonucleotides as no phosphodiester bond connects them.

To determine whether the ligating dimers were sensitive to photolyase, we treated photoligated $d(pT)_{10} \cdot poly(dA)$ with the enzyme. We included in the reaction mixture a small amount of ^{14}C-labelled *E. coli*. DNA, the natural substrate, to confirm that the enzyme was active. After electrophoretic analysis we looked for a reduction in the amount of material in the 20-base band which would indicate splitting of the ligating dimers. We monitored splitting of pyrimidine dimers in *E. coli* DNA by TLC. In reaction conditions suggested by Betsy Sutherland (personal communication), 33% of the dimers in the *E. coli* DNA were split but we observed no significant reduction in the relative quantity of 20-base material. Although this suggested that the ligating dimers were insensitive to the enzyme, the possibility remained that the 20-base oligonucleotides were too small for efficient substrate recognition. Competition experiments have shown that photolyase from yeast will efficiently recognize dimers on oligonucleotides 20 base pairs (bp) long[14]. To interpret our negative result unambiguously we needed to demonstrate that the *E. coli* enzyme also recognized dimers on small oligomers. In a series of competition experiments analogous to those performed with the yeast photolyase, we demonstrated that irradiated $oligo(d(pT)_{10}) \cdot poly(dA)$, containing photoligated oligonucleotides 20 bp long, did in fact compete with irradiated *E. coli* DNA for the *E. coli* photolyase. Thus, photolyase was able to recognize the dimers in photoligated oligonucleotides 20 bp long and possibly in even smaller oligonucleotides. As photolyase did not break the linkages, we concluded that the lack of a phosphodiester bond at such sites reduces significantly the activity of the enzyme.

Another enzyme that is specific for the cyclobutane pyrimidine dimer is endonuclease V from *E. coli* infected with bacteriophage T4[15]. This enzyme (T4 endo V) incises DNA containing pyrimidine dimers by a two-step process. First, a dimer-specific DNA glycosylase cleaves the 5′ pyrimidine of the dimer from its sugar and then an apyrimidinic–apurinic endonuclease cuts the phosphodiester linkage between the dimerized bases, leaving an apyrimidinic site at the 3′ end at the nick[3,16]. As there is no phosphodiester linkage between the thymidines in the ligating dimer, the action of the glycosylase alone should break the linkage. We wished to compare the glycosylase activity of T4 endo V on ligating dimers with that on internal dimers. We irradiated $d(pT)_{10} \cdot poly(dA)$ with long-wavelength UV to produce both internal and ligating dimers.

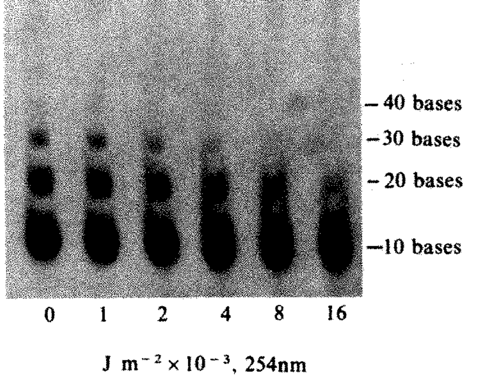

Fig. 3 Photoreversal of ligating dimers by 254 nm irradiation. $d(pT)_{10} \cdot poly(dA)$ was irradiated for 30 min with long-wavelength UV as described in Fig. 1 legend. The solution was then irradiated again at a distance of 10 cm from a 15 W mercury germicidal lamp whose principal output is 254 nm. At times corresponding to the doses shown, samples were removed and analysed by electrophoresis in the same conditions as before.

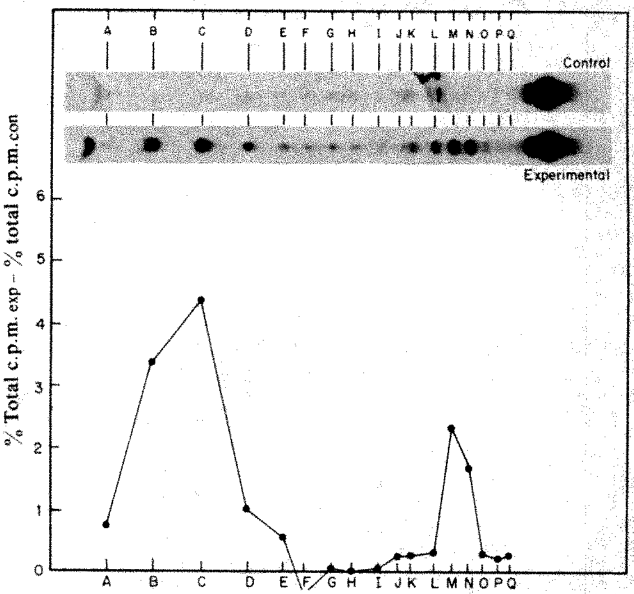

Fig. 4 Action of the glycosylase of T4 endo V on 20-base oligonucleotides containing a ligating dimer between the 10th and 11th positions. The top of the figure shows the electrophoresis patterns of photoligated oligonucleotides before and after treatment with T4 endo V and NaOH. The DNA moved from right to left. The very intense band at the origin represents the 20-base substrate and the bands to the left represent scission products of decreasing size. The top lane shows the pattern obtained for DNA treated with NaOH to hydrolyse the phosphodiester bond at apyrimidinic sites already present. The defect in the autoradiogram at the band labelled L was not the result of radioactivity in the gel. The bottom lane shows the pattern obtained for DNA that had been treated with T4 endo V followed by NaOH. Strand scissions occurred on both ends of the molecule (A–D and L–N). Although oligonucleotide markers were run in adjacent lanes (not shown), unambiguous assignment of lengths to each band was impossible, thus we have only lettered them. Action of the enzyme on the ligating dimer would have yielded a fragment migrating between I and K. Each band shown at the top of the figure was excised and assayed for radioactivity. After expressing the radioactivity of each band as a percentage of the total radioactivity in its lane, we subtrated the control values ($c.p.m._{con}$) from the experimental values ($c.p.m._{exp}$). No strand scissions occurred at the centre of the oligonucleotide although every molecule contained a ligating dimer at its centre. The substrate molecules for this experiment were isolated by electrophoresis (12% acrylamide, 7 M urea gel) of irradiated $d(pT)_{10} \cdot poly(dA)$ (20 min long-wavelength UV), followed by electroelution of the 20-base band. We 5′end-labelled these molecules with ^{32}P and precipitated them with ethanol. Enzyme reactions were carried out in 20 µl buffer (10 mM Tris, 10 mM EDTA, *p*H 8.0) at 37 °C for 30 min. NaOH was then added to 0.1 M and the samples were incubated at 90 °C for 30 min. After lyophilization the samples were resuspended in 5 µl formamide and run on a 20% acrylamide, 7 M urea gel[20].

After separation on a urea gel, we recovered the 20-base oligomers by electroelution and then ^{32}P-labelled their 5′ ends. Each 20-base oligonucleotide thus obtained contained a ligating thymine dimer between positions 10 and 11 and an average of one or two dimers randomly distributed over the other positions (except positions 9–10 and 11–12, which are prohibited in these molecules). The sample was then treated with excess T4 endo V, and heated in NaOH to ensure that strand scission would occur at all sites of glycosylase activity of the enzyme. A control sample was treated with NaOH after incubation without the enzyme. All enzyme reactions were performed on single-strand DNA to eliminate the possibility that denaturation differences between the locations of internal and ligating dimers might affect the results. The products of the reactions were analysed by electrophoresis on a 20% polyacrylamide DNA sequencing gel (Fig. 4); a band should appear for each dimer site sensitive to the enzyme plus NaOH. As there is a 100% probability of having a ligating dimer in the 10–11 position but a less than 10% chance of having an internal dimer at any other particular site, this experiment detects susceptibility of the linking dimer to the enzyme with a 10-fold greater sensitivity than that for internal dimers. Nevertheless, no breakage at the position of the linking dimers was detected (Fig. 4). In our laboratory it has been found that thymine dimers in $d(pT)_{17}$, treated in exactly the same manner, are sensitive to T4 endo V along the entire mid-section of the molecule (to be published), which excludes the possibility that the mid-section of an oligonucleotide is insensitive to the enzyme.

Thus, as was suggested with photolyase, the glycosylase activity of the T4 endo V seems to require a phosphodiester backbone. In this case, however, we demonstrated that internal dimers in our 20-base molecule were sensitive to the enzyme, while the ligating dimer was not. Proposed mechanisms for either enzyme must eventually take into account this feature of substrate recognition and action.

Could the pyrimidine dimer have served as a primordial 'ligase', linking short oligomers of nucleotides for the abiogenic assembly of high molecular weight duplex nucleic acids? In 1974 Tšo pointed out that in the laboratory "no satisfactory chemical synthesis of long-chain polynucleotides has succeeded under any conditions, prebiotic or otherwise"[17]. Since then, much progress has been made in template-directed non-enzymatic polymerization of nucleotide derivatives. For example, Zn^{2+} has been shown to serve as "an efficient catalyst for the oligomerization of guanosine 5'-phosphorimidazolide on a polycyticlylic acid template"[18].

Once high molecular weight polynucleotide templates existed, simple catalysts could make multiple complementary copies of them. But how did these templates originate and how did they increase in length? Small oligomers might have been created by a number of reactions: for example, condensation of 5' thymidine monophosphates by heating in the presence of histidine has been shown to yield oligomers up to 7 units long and containing predominantly the 3'–5' phosphodiester linkage[19]. The yields from such reactions fall off rapidly as the length of the oligomer increases, however, thus it is highly unlikely that the 'first' high molecular weight template formed exclusively by these reactions. Instead, we envisage the accumulation of overlapping oligomeric structures, followed by some ligation event(s) to generate much larger structures. This would occur simultaneously with template-directed polymerization reactions. The enhanced thermal stability of the larger duplex structures should help to drive the process forward.

The results presented here show that the ligation of short oligomers having thymidine nucleotides at their termini could have been accomplished by formation of cyclobutane pyrimidine dimers. In the primordial era there was no stratospheric ozone layer to attenuate the intense UV flux from the sun. Thus, it is fairly certain that pyrimidine-containing oligonucleotides accumulated dimers. We suggest that the cyclobutane pyrimidine dimer that poses a threat to DNA replication and survival in present day organisms, might have played a part in the prebiotic assembly of the first genetic material.

We thank Betsy Sutherland and Pat Seawell for supplying photolyase and T4 endo V, respectively; Ann Ganesan, Michel Philippe, Allen Smith and Mimi Zolan for support; and Evelyn Gates for repeatedly typing the text. This work was supported by a grant GM09901–20 from the National Institute of General Medical Sciences, USPHS.

Received 5 February; accepted 17 May 1982.

1. Smith, K. C. & Hanawalt, P. C. *Molecular Photobiology* (Academic, New York, 1969).
2. Deering, R. A. & Setlow, R. B. *Biochim. biophys. Acta* **68**, 526–531 (1963).
3. Haseltine, W. A. *et al. Nature* **285**, 634–641 (1980).
4. Hanawalt, P. C., Cooper, P. K., Ganesan, A. K. & Smith, C. A. *A. Rev. Biochem.* **48**, 783–836 (1979).
5. Wang, Shih Yi. *Photochemistry and Photobiology of Nucleic Acids* Vol. 2, 430 (Academic, New York, 1976).
6. Eisinger, J. *et al. Proc. natn. Acad. Sci. U.S.A.* **55**, 1015–1020 (1966).
7. Rahn, R. O. & Landry, L. C. *Photochem. Photobiol.* **18**, 29–38 (1973).
8. Spencer, J. H. *The Physics and Chemistry of DNA and RNA*, 92 (Saunders, Philadelphia, 1972).
9. Janik, B. *Physicochemical Characteristics of Oligonucleotides and Polynucleotides*, 108–109 (Plenum, New York, 1971).
10. Reynolds, R. J., Cook, K. H. & Friedberg, E. C. in *DNA Repair: A Laboratory Manual of Research Procedures* (eds Friedberg, E. C. & Hanawalt, P. C.) 11–22 (Dekker, New York, 1981).
11. Haynes, F. N., Wilkins, D. L., Ratliff, R. L., Varghese, A. J. & Rupert, C. S. *J. Am. chem. Soc.* **93**, 4940–4942 (1971).
12. Sutherland, J. C. *Photochem. Photobiol.* **25**, 435–440 (1977).
13. Snapka, R. M. & Sutherland, B. M. *Biochemistry* **19**, 4201–4208 (1980).
14. Setlow, J. K. & Bollem, F. J. *Biochim. biophys. Acta* **157**, 233–237 (1967).
15. Freidberg, E. C. *Mutat. Res.* **15**, 113–123 (1972).
16. Seawell, P. C., Smith, C. A. & Ganesan, A. K. *J. Virol*, **35**, 790–797 (1980).
17. Tšo, P. O. *Basic Principles in Nucleic Acid Chemistry* Vol. 1 (Academic, New York, 1974).
18. Bridson, P. K. & Orgel, L. E. *J. molec. Biol.* **144**, 567–577 (1980).
19. Ibanez, J. D., Kimball, A. P. & Oro, J. *Science* **173**, 444–446 (1971).
20. Maxam, A. & Gilbert, W. *Meth. Enzym.* **65**, 499–560 (1980).
21. Haselkorn, R. & Doty, P. *J. biol. Chem.* **236**(10), 2738–2745 (1961).
22. Peacock, A. C. & Dingman, C. W. *Biochemistry* **6**(b), 1818–1827 (1967).

Potential Z-DNA forming sequences are highly dispersed in the human genome

Hiroshi Hamada & Takeo Kakunaga

Cell Genetics Section, Laboratory of Molecular Carcinogenesis,
National Cancer Institute, NIH, Bethesda, Maryland 20205, USA

Recent analyses of the three-dimensional structure of synthetic DNA molecules has revealed the existence of a left-handed double-helical conformation of DNA, called Z-DNA[1–4]. The Z-DNA structure was first observed in molecules having alternating guanine and cytosine bases[1–3], but has now also been shown for molecules of sequence poly(dT-dG)·poly(dC-dA) (refs 4–7). If Z-DNA occurs naturally then it might have quite different reactivities with molecules such as proteins or carcinogens from right-handed B-DNA. The interconversion of sequences between B and Z forms, under the influence, for example, of DNA binding proteins or chemical modification, may be important in regulating DNA function[8,9]. So far, little data have been published on the occurrence of potential Z-DNA forming sequences in eukaryotic DNA. Here we report the presence of a sequence of 50 alternating dT and dG residues within one of the introns of a human cardiac muscle actin gene. Also, using a probe specific for poly(dT-dG) sequences, we have found that potential Z-DNA forming sequences are highly repeated in the human genome.

We have recently isolated a phage clone that contains a human cardiac muscle actin gene, λHa-25 (Fig. 1). This clone was obtained by screening of a human DNA library that had been constructed by partial *Eco*RI digestion of DNA from a β°-thalassaemia patient and ligation to Charon 4A phage vector[10]. The molecular structure (Fig. 1*a*) and nucleotide sequence of the entire coding region and some introns of the cloned cardiac muscle actin gene were determined[11]. In intron IV we found a sequence of 25 alternating dT and dG residues (abbreviated to $(dT\text{-}dG)_{25}$). Figure 1*b* shows the nucleotide sequence of the intron IV–exon 5 boundary region. The presence of $(dT\text{-}dG)_{25}$ near the intron–exon junction was confirmed by sequencing of both DNA strands by the Maxam–Gilbert method. The repeated sequences found are not an artefact of our cloning procedure because we used $RecA^-$ mutant *Escherichia coli* as a host, and we have further been able to isolate human cardiac muscle actin gene with exactly the same restriction map as that of λHa-25 by screening a second human DNA library constructed by partial *Eco*RI digestion of DNA from a chemically transformed human fibroblast cell line (our unpublished data). Our finding of a $(dT\text{-}dG)_{25}$ stretch is a direct demonstration of potential Z-DNA sequences in the eukaryote DNA. If poly(dT-dG) sequences are functionally important then it is to be expected that they should be found in other parts of the genome. To examine this possibility we carried out the following two Southern blotting analyses. In the first analysis we used ^{32}P-labelled total DNA from human HeLa cells on a probe to detect repeated sequences in the *Eco*RI–*Bam*HI 8-kilobase (kb) fragment of the λHa-25. In this method only

0028–0836/82/290396—03$01.00

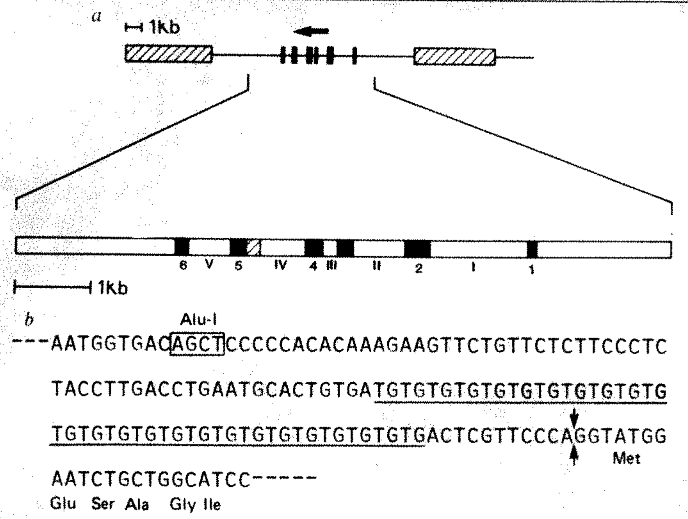
a
1Kb
6
V
5
IV
4
III
II
2
I
1
1Kb
b
Alu-I
---AATGGTGACAGCTCCCCCACACAAAGAAGTTCTGTTCTCTTCCCTC
TACCTTGACCTGAATGCACTGTGATGTGTGTGTGTGTGTGTGTGTG
TGTGTGTGTGTGTGTGTGTGTGTGTGTGACTCGTTCCCAGGTATGG
Met
AATCTGCTGGCATCC-----
Glu Ser Ala Gly Ile

Fig. 1 *a*, Molecular organization of the human cardiac muscle actin gene. The black blocks show the locations of six exons. The arrow above the map indicates the direction of transcription. Six exons and five introns are designated from 1 to 6 and from I to V, respectively, according to their locations. The hatched blocks show the presence of three different repeated elements. These locations were determined by hybridization to ^{32}P-labelled total human DNA or ^{32}P-labelled cloned human *Alu* family (provided by Dr Schmid) (data not shown). *b*, Nucleotide sequences of intron IV–exon 5 boundary region. DNA sequence was determined by the Maxam–Gilbert method[21]. The vertical arrow indicates the splicing site. *Alu*I site in intron IV is enclosed by a box. The sequence (dT-dG)$_{25}$ is underlined. The amino acid sequence corresponding to DNA sequence of exon 5 is shown under the nucleotide sequence.

highly repeated (>100 copies per cell) sequences are detected. When the 8-kb *Eco*RI–*Bam*HI fragment was digested with *Pst*I a 0.9-kb band hybridized to the probe (Fig. 2). A probe specific for the *Alu* family of repetitive sequences[12] did not hybridize to any region of the *Eco*RI–*Bam*HI fragment (data not shown). The 0.9-kb fragment contains all of exon 5 and a part of introns IV and V. In order to narrow further the location of the repeated element, we constructed a subclone of the 0.9-kb *Pst*I fragment in pBR322. By Southern blotting analysis of restriction digested 0.9-kb DNA fragment using ^{32}P-labelled total human DNA as a probe, the repeated element was mapped between the *Alu*I site in intron IV and *Sau*96I site in exon 5 (Fig. 2). As the actin-coding sequence is not highly repeated in the human genome, we conclude that a highly repeated element is located in the 110-base pair (bp) region between the *Alu*I site in intron IV and the 5′ splicing site—precisely the region where (dT-dG)$_{25}$ is located.

In the second analysis, the DNA used as a probe, and that probed were reversed. ^{32}P-labelled 0.9-kb *Pst*I fragment was used as a hybridization probe against *Eco*RI-digested human DNA. As shown in Fig. 3*a* a smear of hybridization was observed with the HeLa DNA, indicating again that the 0.9-kb *Pst*I fragment contains the highly repeated element. To demonstrate that the repeated element in the 110-bp region between *Alu*I site and splicing site is the sequence (dT-dG)$_{25}$, we prepared ^{32}P-labelled poly(dT-dG) · poly(dC-dA) as a probe to specifically recognize sequences. The specificity of the probe was confirmed by the exclusive hybridization of the probe to (dT-dG)$_{25}$-containing fragments when hybridized to restriction enzyme digested λHa-25 DNA (Fig. 3*b*). This probe also produced a smear of hybridization in gels containing *Eco*RI-digested total human DNA (Fig. 3*b*), thus indicating that (dT-dG)$_n$ is a repeated element. We also determined the copy number of (dT-dG)$_n$ sequences in the human genome by Dot analysis[13], using the (dT-dG)$_n$-specific probe (Fig. 4). The approximate number of (dT-dG)$_n$ copies was estimated as 10^5 per human genome, assuming that the average size of n is 25.

These results clearly indicate the widespread distribution in the human genome of sequences that cross-hybridize with the poly(dG-dT) · poly(dA-dC) probe. The following observations suggest that most of the hybridizing sequences are poly(dT-dG) stretches. First, the hybridization conditions used were so stringent that the sequences containing more than 15% of mismatched nucleotide sequence would not cross-hybridize with the probes. Second, large excess amounts of *E. coli* DNA did not compete at all with the probes for hybridization to human DNA. Third, sequence analysis of one of hybridizing clones containing *Eco*RI-digested human DNA proved to contain an exact (dT-dG)$_{15}$ sequence (unpublished data). Fourthly, a (dT-dG)$_{17}$ sequence has been found in human globin genes[14]. The observation that our probe did not hybridize to pBR322 DNA (data not shown), which contains a (dT-dG)$_3$ sequence indicates that the DNA fragments that cross-hybridized to the probe contain a significant stretch of alternating dT and dG residues.

It has been reported that the C(8) position of deoxyguanosine residues, which is the primary position of binding of mutagens and carcinogens such as *N*-acetoxy-*N*-2-acetylaminofluorene (*N*-AcO-AAF), is exposed on the outer surface of the DNA molecules in Z-DNA but not in B-DNA. *N*-AcO-AAF modification or methylation of cytidine in the 5-position in poly(dG-dC) · poly(dG-dC) has been found to favour the transition of the polymer from the B to Z conformation[15–17]. Mutational 'hot spots' have been shown to exist in the *hist D* gene of *Salmonella*, within which is a (dG-dC)$_4$ sequence[18]. Further, cloned segments of poly(dG-dC)$_{13}$ · poly(dG-dC)$_{13}$ in a plasmid undergo a B to Z transformation even though they are enclosed in plasmid segments containing B-DNA[19]. Nordheim *et al.* recently reported that antibodies specific to the Z-DNA conformation bind to interband regions of *Drosophila* polytene

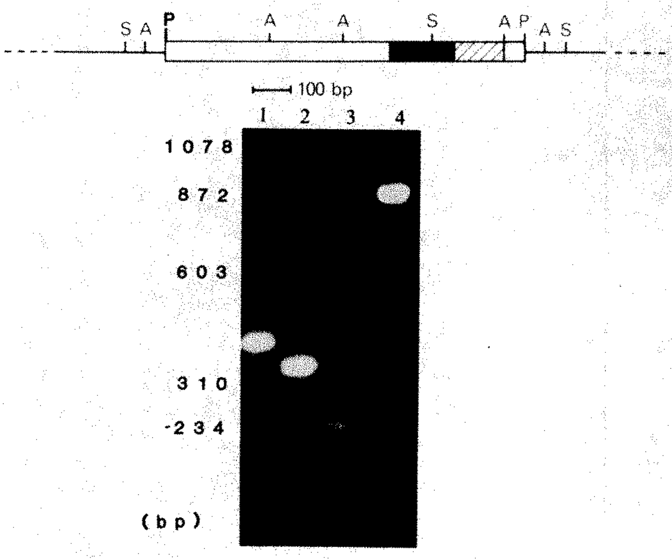

Fig. 2 Mapping of highly repeated sequences in human cardiac muscle actin gene. pEB 8.0 DNA, a subcloned DNA containing the *Eco*RI–*Bam*HI 8-kb fragment in pBR322, was digested with *Pst*I (lane 4). pPst 0.9-1 DNA, constructed by subcloning of the *Pst*I 0.9-kb fragment shown in Fig. 1 into pBR322, was digested with *Alu*I (lane 1), *Sau*96I (lane 2), or *Sau*96I and *Pst*I (lane 3). The resulting DNA fragments were separated on a 2% agarose gel, transferred to nitrocellulose filter, and hybridized to total HeLa cell DNA labelled with ^{32}P by nick-translation. Hybridization was carried out as described previously[22]. *E. coli* DNA was used as carrier DNA. The filter was washed in 1×SSC 0.1% SDS at 50 °C three times and in 0.1×SSC 0.1% SDS at 50 °C twice. The restriction map of pPst 0.9-1 DNA is shown above the autoradiogram. The solid and broken lines indicate pBR322 DNA. The box indicates the 0.9-kb *Pst*I fragment subcloned into pBR322. The black box and open boxes denote coding region and introns, respectively. The hatched region shows the location of the repeated sequence as determined by the results shown in this figure. The arrow above the map indicates the direction of transcription. The restriction enzyme sites are abbreviated as the following: A, *Alu*I; P, *Pst*I; S, *Sau*96I. *Hae*III digests of ΦX174 DNA served as a molecular size standard.

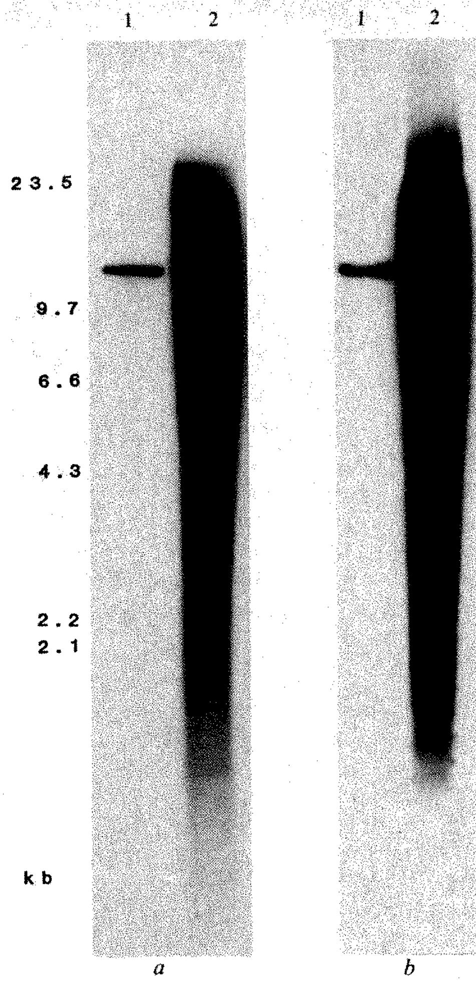

Fig. 3 Detection of poly(dT-dG) sequences in a human genome by Southern blot hybridization. 20 μg of HeLa cell DNA was completely digested with *Eco*RI (lane 2 in *a* and *b*). Fifty copies equivalent (lane 1 in *a* and *b*) amount of λHa-25 DNA was digested with *Eco*RI. These equivalent amounts were calculated based on the assumption that human genome size is 3×10^9 bp, and our data that $(dT\text{-}dG)_{25}$ exist only once in λHa-25 (data not shown). The resulting DNA digests were electrophoresed on 0.7% agarose gel, transferred to nitrocellulose filter and hybridized to ^{32}P-labelled probe. Hybridization was carried out as described above. The probes used here are nick-translated *Pst*I 0.9-kb fragment in *a* and nick-translated poly(dT-dG)·poly(dC-dA) in *b*. The latter probe was prepared by annealing of $(dT\text{-}dG)_{6-9}$ and $(dC\text{-}dA)_{6-9}$ (Collaborative Research) followed by nick-translation.

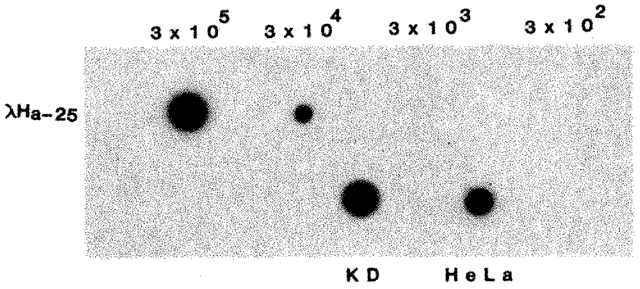

Fig. 4 Determination of copy number of poly(dT-dG) sequences in human genome. 0.25 μg of human DNA prepared from HeLa cell or KD cell (normal diploid human fibroblast) and 3×10^5, 3×10^4, 3×10^3 or 3×10^2 copies equivalent amount of λHa-25 DNA were denatured and spotted on nitrocellulose filter as described by Kafatos *et al.*[13]. These equivalent amounts were calculated as described above. The filter was hybridized to ^{32}P-labelled poly(dT-dG)·poly(dA-dC) as described above.

chromosomes[20]. It is plausible that a portion or all of the $(dT\text{-}dG)_n$ sequences that we have found to be highly dispersed in the human genome adopt a Z conformation depending on the circumstances and that these sequences may be important in mutagenesis, recombination and the control of gene expression.

We thank Dezider Grunberger and Che-Hung Lee for their valuable suggestions and Kenneth H. Kraemer for his help with and Linda Nischan for typing the manuscript.

Received 29 March; accepted 7 May 1982.

1. Wang, A. H. J. *et al. Nature* **282,** 680–686 (1979).
2. Arnott, S., Chandrasekaran, R., Birdsall, D. L., Leslie, A. G. W. & Ratliff, R. L. *Nature* **283,** 743–745 (1980).
3. Drew, H., Takano, T., Takano, S., Itakura, K. & Dickerson, R. E. *Nature* **286,** 567–573 (1980).
4. Crowford, J. L. *et al. Proc. natn. Acad. Sci. U.S.A.* **77,** 4016–4020 (1980).
5. Leslie, A. G. W., Arnott, S., Chandrasekaran, R. & Ratliff, R. L. *J. molec. Biol.* **143,** 49–72 (1980).
6. Vorlickova, M., Kypr, J., Stokrova, S. & Sponar, J. *Nucleic Acids Res.* **10,** 1071–1080 (1982).
7. Zimmer, C., Tymen, S., Marck, C. & Guschlbauer, W. *Nucleic Acids Res.* **10,** 1081–1091 (1982).
8. Pohl, F. M. & Jovin, T. M. *J. molec. Biol.* **67,** 375–396 (1972).
9. Thamann, T. J., Lord, R. C., Wang, A. H. J. & Rich, A. *Nucleic Acids Res.* **9,** 5443–5457 (1981).
10. Fritsch, E. F., Lawn, R. M. & Maniatis, T. *Cell* **19,** 959–972 (1980).
11. Hamada, H., Petrino, M. G. & Kakunaga, T. *Proc. natn. Acad. Sci. U.S.A.* (in the press).
12. Houck, C. M., Rinehart, F. P. & Schmit, C. W. J. *J. molec. Biol.* **132,** 289–306 (1979).
13. Kafatos, F. C., Jones, C. W. & Efstradiadis, A. *Nucleic Acids Res.* **7,** 1541–1552 (1979).
14. Misfeld, R., Krystal, M. & Arnheim, N. *Nucleic Acids Res.* **9,** 5931–5947 (1981).
15. Sage, E. & Leng, M. *Proc. natn. Acad. Sci. U.S.A.* **77,** 4597–4601 (1980).
16. Santella, R. M., Grunberger, D., Weinstein, I. B. & Rich, A. *Proc. natn. Acad. Sci. U.S.A.* **78,** 1451–1455 (1981).
17. Behe, M. & Felsenfeld, G. *Proc. natn. Acad. Sci. U.S.A.* **78,** 1619–1623 (1981).
18. Isono, K. & Yourno, J. *Proc. natn. Acad. Sci. U.S.A.* **71,** 1612–1617 (1974).
19. Klysik, J., Stirdivant, S. M., Larson, J. E., Hart, P. A. & Wells, R. D. *Nature* **290,** 672–677 (1981).
20. Nordheim, A. *et al. Nature* **294,** 417–422 (1981).
21. Maxam, A. M. & Gilbert, W. *Proc. natn. Acad. Sci. U.S.A.* **74,** 560–564 (1977).
22. Hamada, H., Leavitt, J. & Kakunaga, T. *Proc. natn. Acad. Sci. U.S.A.* **78,** 3634–3638 (1981).

Receptor-rich intracellular membrane vesicles transporting asialotransferrin and insulin in liver

M. T. Debanne, W. H. Evans*, N. Flint & E. Regoeczi

National Institute for Medical Research, Mill Hill,
London NW7 1AA, UK, and Department of Pathology,
McMaster University, Hamilton, Ontario, Canada L8N 3Z5

A wide range of receptors are located at the blood sinusoidal aspect of the hepatocyte plasma membrane[1,2]. Many circulating ligands that bind to receptors on the cell surfaces are interiorized along two pathways. Asialoglycoproteins[3] are transferred from the plasma membrane to lysosomes and degraded, whereas immunoglobulin A[4] and bile acids[5] are transported across the hepatocyte interior and released into bile. Asialotransferrin type 3 (ref. 6) follows a further pathway termed diacytosis[7]. After binding to the asialoglycoprotein receptor[8], asialotransferrin is endocytosed and then returned to blood with a proportion of its carbohydrate side chains resialylated[9]. We now describe in liver the properties of intracellular asialotransferrin-enclosing vesicles (diacytosomes) and show that they differ from Golgi, lysosome and plasma membrane fractions. Furthermore, we show that the asialoglycoprotein binding sites are located on the cytoplasmic (outer) surface of diacytosomes.

Asialotransferrin, after binding to the hepatic asialoglycoprotein receptor[3,10–13], is rapidly interiorized. Analytical centrifugation of liver homogenates in sucrose gradients shows that within 5 s of injecting asialotransferrin into the liver via the portal vein, the ligand equilibrates at a density corresponding to plasma membranes (1.16 g cm^{-3}) and then moves rapidly, through an intermediate density (1.13 g cm^{-3}) at 30 s, to a final density position of 1.10–1.11 g cm^{-3}, where it remains intact for long periods[14]. The components equilibrating at the latter

---

* To whom correspondence should be addressed at the National Institute for Medical Research.

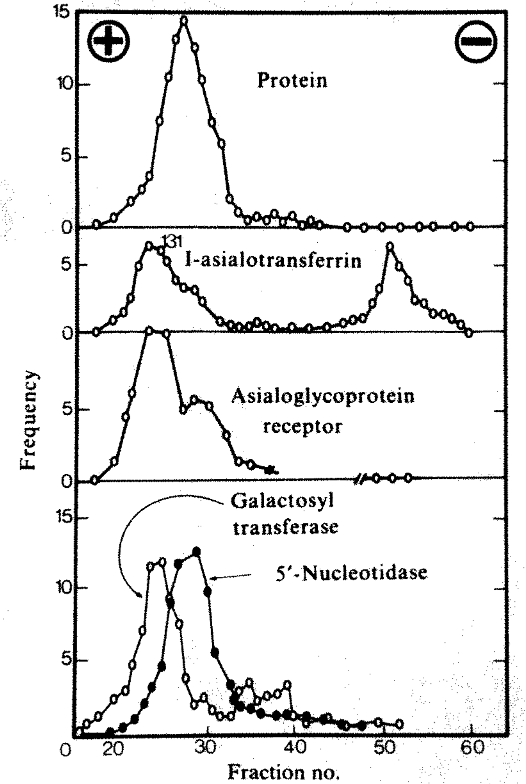

Fig. 1 Fractionation of the diacytosome fraction, prepared as described in Table 1 legend, by free-flow electrophoresis in an Elphor VaP5 apparatus (Bender and Hobein, Munich). The conditions used were essentially as reported by Menashi *et al.*[34]. Protein was determined by the microtannin turbidometric method[31], and asialoorosomucoid binding by the Pricer and Ashwell method[32]. Galactosyl transferase and 5'-nucleotidase activities were determined by standard methods[35]. The results are expressed as the frequency of distribution of components recovered from the apparatus from livers 15 min after administration of ^{125}I-asialotransferrin.

Table 1 Recovery and relative specific activities of radioiodinated ligands and marker enzymes in the diacytosome fraction

Component in diacytosome fraction	% Recovery from homogenate	Specific activity relative to homogenate
Protein	0.25 ± 0.04 (4)	—
Asialotransferrin type 3	19.4 ± 0.9 (4)	62.0
Asialoorosomucoid	2.7 (2)	6.5
Insulin	7.9 ± 1.1 (4)	25.0
Galactosyl transferase	21.0 (2)	65.0
Sialyl transferase	9.5 (2)	51.0
5'-Nucleotidase	6.7 ± 2.4 (4)	16.5
Alkaline phosphodiesterase	2.5 ± 0.4 (4)	6.5
Acid phosphatase	1.0 (2)	2.2
β-galactosidase	0.09 (2)	0.1

Diacytosomes were prepared from unstarved rat liver homogenates as described in detail elsewhere[22]. Briefly, nuclei, mitochondria and lysosomes, plasma membranes and Golgi components of livers homogenized in 0.25 M sucrose were removed by centrifugation sequentially at 1×10^4g min and 4×10^5g min. The final clear supernatant was centrifuged into a 10–40% w/v sucrose gradient at 97,000g_{av} for 4 h (Beckman SW27 rotor) and components equilibrating at densities of 1.097–1.117 g cm^{-3} were pooled and concentrated by vacuum dialysis. Radioactivity and enzymes (70–90%) and a protein peak (20–25%) were eluted in the void volume peak of a Sepharose 2B column equilibrated in 10 mM Tris-HCl *p*H 7.4, 1 mM EDTA and 0.15 M NaCl, and concentrated by centrifugation. The three ligands were iodinated using the iodogen method[36]. Asialotransferrin type 3 (5 μg), asialoorosomucoid (20 μg) or insulin (20 μg) were injected intraportally into rats (150 g body weight) and livers removed and homogenized 10–15 min later when most of the asialotransferrin and proportions of asialoorosomucoid and insulin equilibrated in the density range 1.095–1.12 g cm^{-3}. Enzyme activities and radioactivity were determined as previously described[14,15,24]. The complete distribution of all components in the fractions will be described elsewhere[22], and total recoveries were 89–103% of homogenate values. Standard errors of the mean and the number of experiments (in parentheses) are given.

density were isolated in a subcellular fraction now operationally defined as the diacytosome fraction, using a modified method for preparing blood sinusoidal plasma membranes[15]. The diacytosome fraction was obtained (Table 1) by centrifuging the homogenate supernatant in a continuous sucrose gradient after pelleting nuclei, plasma membranes, mitochondria, lysosomes and Golgi apparatus components. Soluble proteins associated with the diacytosome fraction were removed by permeation chromatography. The diacytosome fraction retained about 20% of the bound ^{125}I-labelled asialotransferrin and 10–20% of homogenate glycosyl transferase activities (Table 1); recovery of 5'-nucleotidase and alkaline phosphodiesterase was lower and more variable, and that of lysosomal enzymes very low.

On further resolution of the diacytosome fraction by free-flow electrophoresis[16] (Fig. 1), although a single protein peak emerged, the galactosyl transferase and residual 5'-nucleotidase activities separated into adjacent peaks. Importantly, however, the positions of the major asialotransferrin peak, the major peak representing asialoglycoprotein receptor-binding activity and the galactosyl transferase coincided. Although this result could have implied that asialotransferrin was interiorized to the Golgi apparatus, the morphological features and the ligand–receptor binding properties of diacytosomes showed that the recovered ligand resides in previously undocumented subcellular components.

Examination of the diacytosome fraction by electron microscopy showed a relatively homogeneous population of smooth-surfaced vesicular profiles, 600–1,200 Å in diameter. The cisternal tubular networks and vaculoles characteristic of Golgi apparatus fractions[17–19] were rarely seen. No coated vesicles[20] were detected, even when negatively stained preparations were examined. Fractions containing the ligands, receptors and galactosyl transferase (Fig. 1) contained a higher proportion of vesicles with single or compound intraluminal vesicular membrane components (Fig. 2). Similar vesicles were present as minor components in gross Golgi[17–19] and plasma membrane sinusoidal fractions[15] prepared from liver. Recently, similar multi-vesicular structures (termed 'receptosomes', although no receptors or receptor binding was measured) were described in cells that have interiorized ligands[21].

Table 2 shows that the diacytosome fraction has a much higher capacity for binding asialoglycoproteins than do the plasma membrane and Golgi subfractions. Examination of the orientation of the receptors on the vesicles by measuring the binding capacity of various fractions after treatment with Triton X-100 showed that the binding capacity of the Golgi subfractions increased two- to three-fold, indicating that most of the receptor sites were located inside the membrane-enclosed

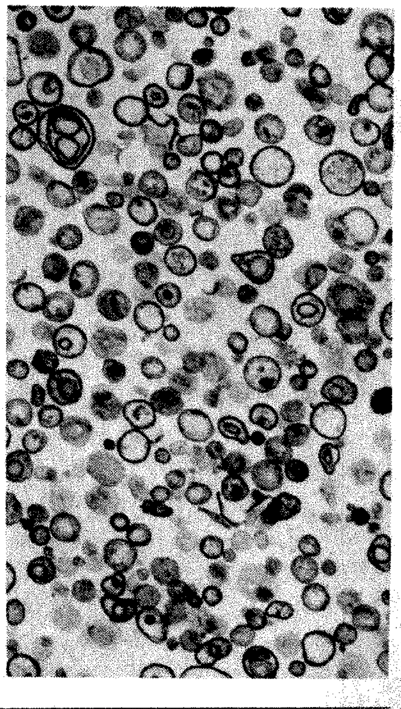

Fig. 2 Electron micrograph of fraction 23 from the free-flow electrophoresis separation (Fig. 1). Membranes were concentrated by centrifugation on to a 51% (w/v) sucrose cushion, and sections prepared for viewing by standard methods[15]. ×27,800.

Table 2 Effects of treatment with Triton X-100, trypsin and sonication on binding of asialoorosomucoid and insulin to diacytosome, Golgi and plasma membrane fractions

Fraction	Specific binding activity						
	Asialoorosomucoid (ng per μg protein)						Insulin (ng per mg protein)
	No treatment	0.1% Triton X-100	Sonication	Trypsin	Trypsin and sonication	Trypsin and 0.1% Triton X-100	
Diacytosome	6.1 ± 0.4	5.6 ± 0.6	6.2 ± 0.3	0.03 ± 0.01	0	0.05 ± 0.01	1.14 ± 0.11
Golgi—heavy	0.9 ± 0.2	2.7 ± 0.2	3.1 ± 0.1	0.17 ± 0.1	2.3 ± 0.6	3.3 ± 0.3	0.27 ± 0.02
Golgi—intermediate	0.8 ± 0.1	2.5 ± 0.6	—	—	—	—	0.57 ± 0.09
Plasma membrane (heavy)	1.4 ± 0.2	1.7 ± 0.3	—	—	—	—	0.71 ± 0.02
Plasma membrane (sinusoidal)	2.2 ± 0.3	2.7 ± 0.1	1.6	0.10	0.24	0.03	0.39 ± 0.02

The diacytosome fraction was prepared as described in Table 1 legend, and Golgi and plasma membrane fractions by standard procedures[15,18]. Asialoorosomucoid binding was carried out as described by Pricer and Ashwell[32], and insulin binding as described previously[33]. Sonication of membrane fractions was carried out in a Sonic Dismembrator (Fisher, Model 300) using 2 × 10 s bursts at setting '35'. Trypsin treatment was carried out before binding studies as follows. Membrane fractions (250 μg protein) were incubated for 15 min at 23 °C with trypsin (250 μg; P–L Biochemicals); control samples were incubated in the buffer 0.15 M NaCl, 0.005 M $CaCl_2$ 0.01 M Tris-HCl *p*H 8. Protease treatment was stopped by addition of a fivefold (w/w) excess of crystalline soybean trypsin inhibitor (Worthington). In separate studies, the trypsin inhibitor had no effect on ligand binding. Values are shown ± s.e.m. of three to five determinations.

compartments. In contrast, no increase in binding capacity was elicited by detergent treatment of the diacytosome fraction, thus indicating that the binding sites were located on the outer surface. Further evidence for an external location of the asialoglycoprotein receptor on diacytosomes was obtained by the finding that sonication had little effect on asialoorosomucoid binding by the diacytosome fraction, whereas a three-fold increase, similar to that elicited by treatment with Triton X-100, was obtained with a Golgi fraction. Trypsin treatment removed 96% of the asialoorosomucoid binding capacity of diacytosomes when carried out alone or in combination with sonication or exposure to Triton X-100, two treatments that should reveal any additional receptors located inside the vesicles. On the other hand, the diminution in binding capacity of the Golgi fraction occurring after trypsin treatment was low when compared with that measured after sonication or Triton X-100 treatment. These results provide strong evidence that the receptor-binding sites are located mainly on the outer (cytoplasmic) surface of the diacytosome.

A role for diacytosomes in the receptor-mediated uptake of insulin was also briefly investigated, for about 8% of the ^{125}I-labelled insulin associated with particulate components of the liver homogenate 10–15 min after injection was recovered in the diacytosome fraction (Table 1). Comparison of the insulin-binding capacity of the diacytosome with plasma membrane and Golgi fractions showed that diacytosomes possessed the highest activity (Table 2), and preliminary observations suggest that a proportion of the insulin receptors is cytoplasmically orientated.

The morphology, high concentration and external orientation of receptors, when taken with the simplified polypeptide composition relative to plasma membrane and Golgi fractions[22], indicate that diacytosomes cannot be categorized directly into the major hepatic classes of subcellular organelles and membrane systems described[23,24]. However, in view of the structural and functional complexity of the Golgi apparatus, especially in secretory tissues[25] the vesicles may originate from a region of the Golgi apparatus specialized for the processing of classes of ligands internalized by hepatocytes. A diacytotic pathway along which ligands move in and out of the hepatocyte can be divided into inward (endocytotic) and outward (exocytotic) sector legs. The association of glycosyl transferases with the diacytosome fraction indicates that the more electronegative vesicles separated by free-flow electrophoresis may arise from components comprising the intracellular terminus of the diacytotic pathway. The glycosyl transferases in the diacytosome fraction can also explain the glycosylation of internalized asialotransferrin demonstrated in *in vivo* experiments[9].

Finally, the cytoplasmic orientation of asialoglycoprotein receptors demonstrated on the diacytosomes indicates that the receptor–ligand complex formed at the plasma membrane has been rearranged during internalization. Either there is receptor reorganization in the membrane lipid bilayer[26], or engulfment of membrane components of the inward sector leg and multiple fusions have taken place, resulting in a dissociation of the complex with the receptors now becoming cytoplasmically orientated. Indeed, these results add to the increasing indirect evidence for discrete intracellular compartments bearing cytoplasmic receptors for lectins[27], phosphomannosyl enzyme[28], asialoglycoproteins[29] and human growth hormone[30]. External receptors on diacytosomes, while undoubtedly contributing to their high electronegativity exploited in the free-flow electrophoretic separation, may provide recognition potential ensuring specificity in the vesicular transport of ligands inside the cell. The high concentration of receptors on diacytosomes suggests a role in receptor recycling and therefore receptor turnover at the plasma membrane.

We thank Professor Neville Crawford and Dr Donald Stuart, Institute of Basic Medical Sciences, Royal College of Surgeons, London for their help and support in running the free-flow electrophoresis apparatus, and Miss Kate Sullivan for electron microscopy. Part of this study was supported by the MRC of Canada and the Ontario Heart Foundation.

Received 11 March; accepted 14 May 1982.

1. Evans, W. H. *Biochim. biophys. Acta* **604,** 27–64 (1980).
2. Evans, W. H. *Hepatology* **1,** 452–458 (1981).
3. Neufeld, E. F. & Ashwell, G. in *The Biochemistry of Glycoproteins and Proteoglycans* (ed. Lennarz, W. H.) 241–266 (Plenum, New York, 1980).
4. Renston, R. H., Jones, A. L., Christiansen, W. D., Hradek, G. T. & Underdown, B. J. *Science* **208,** 1276–1278 (1980).
5. Jones, A. L., Smuckler, D. L., Mooney, J. S., Ockner, R. K. & Alder, R. D. *Lab. Invest.* **40,** 512–517 (1979).
6. Regoeczi, E., Taylor, P., Debanne, M. T., März, L. & Hatton, M. W. C. *Biochem. J.* **184,** 399–407 (1979).
7. Tolleshaug, H., Chindemi, P. A. & Regoeczi, E. *J. biol. Chem.* **256,** 6526–6528 (1981).
8. Hudgin, R. L., Pricer, W. J., Ashwell, G., Stockert, R. I. & Morrel, A. G. *J. biol. Chem.* **249,** 5536–5543 (1974).
9. Regoeczi, E., Chindemi, P. A., Debanne, M. T. & Charlwood, P. A. *Proc. natn. Acad. Sci. U.S.A.* **79,** 2226–2230 (1982).
10. Regoeczi, E., Taylor, P., Hatton, M. W. C., Wong, K.-L. & Koj, A. *Biochem. J.* **174,** 171–178 (1978).
11. Hubbard, A. L., Wilson, G., Ashwell, G. & Stukenbrok, H. *J. Cell Biol.* **83,** 47–64 (1979).
12. Wall, D. A., Wilson, G. & Hubbard, A. L. *Cell* **21,** 79–93 (1980).
13. Steer, C. J. & Clarenberg, R. *J. biol. Chem.* **254,** 4457–4461 (1979).
14. Debanne, M.-T. & Regoeczi, E. *J. biol. Chem.* **256,** 11266–11272 (1981).
15. Wisher, M. H. & Evans, W. H. *Biochem. J.* **146,** 375–388 (1975).
16. Hannig, K. & Heidrich, H. G. *Meth. Enzym.* **31,** 746–761 (1974).
17. Ehrenreich, J. H., Bergeron, J. J. M., Siekevitz, P. & Palade, G. M. *J. Cell Biol.* **59,** 45–72 (1973).
18. Bergeron, J. J. M. *Biochim. biophys. Acta* **555,** 493–503 (1979).
19. Borgese, N. & Meldolesi, J. *J. Cell biol.* **90,** 687–696 (1981).
20. Pearse, B. M. F. & Bretscher, M. *A. rev. Biochem.* **50,** 85–101 (1981).
21. Pastan, I. & Willingham, M. C. *Science* **214,** 504–509 (1981).
22. Evans, W. H., Debanne, M. T., Flint, N. A. & Regoeczi, E. *J. biol. Chem.* (submitted).
23. De Duve, C. *Science* **189,** 186–194 (1975).
24. Evans, W. H. *Preparation and Characterisation of Mammalian Plasma Membranes* (North-Holland, Amsterdam, 1978).
25. Rothman, J. C. *Science* **213,** 1212–1219 (1981).
26. Blumenthal, R., Klausner, R. D. & Weinstein, J. N. *Nature* **288,** 333–338 (1980).
27. Pinto da Silva, P., Torrisi, M. R. & Kachar, B. *J. Cell Biol.* **91,** 361–372 (1981).
28. Fischer, H. D., Gonzalez-Noriega, A., Sly, W. S. & Morré, D. J. *J. biol. Chem.* **255,** 9608–9615 (1980).
29. Tanabe, T., Pricer, W. E. & Ashwell, G. *J. biol. Chem.* **254,** 1038–1043 (1979).
30. Bergeron, J. J. M., Rachubinski, R. A., Sikstrom, R. A., Posner, B. I. & Paiement, J. *J. Cell Biol.* **92,** 139–146 (1982).
31. Mejbaum-Katzenellenbogen, W. & Dobryszycha, W. M. *Clin. chim. Acta* **4,** 515–522 (1959).
32. Pricer, W. E. & Ashwell, G. *J. biol. Chem.* **251,** 7539–7544 (1976).
33. Evans, W. H., Bergeron, J. J. M. & Geshwind, I. I. *FEBS Lett.* **34,** 259–262 (1973).
34. Menashi, S., Weintraub, H. & Crawford, N. *J. biol. Chem.* **256,** 4095–4101 (1981).
35. Evans, W. H., Flint, N. A. & Vischer, P. *Biochem. J.* **192,** 903–910 (1980).
36. Fraker, P. J. & Speck, J. C. *Biochem. Biophys. Res. Commun.* **80,** 849–857 (1978).

MATTERS ARISING

Dielectric constant of ice

ADAMS has recently considered the dielectric constant of ice[1]. His Monte Carlo calculations fill a gap in the literature and complement previous calculations. However, his theoretical discussion, while displaying an important constraint on the Kirkwood–Frohlich (K–F) theory, falls short of the 'simple resolution' claimed.

Adams' primary equation[1] is

$$\langle \mu_1 \Sigma \mu_i \rangle_{\varepsilon'} N/9\varepsilon_0 kTV = (\varepsilon - 1)(2\varepsilon' + 1)/3(\varepsilon + 2\varepsilon') \qquad (1)$$

The right hand side (RHS) of equation (1) is obtained using macroscopic electrostatic theory for a spherical system of ice of dielectric constant ε surrounded by a much larger sphere of dielectric constant ε'. The left hand side (LHS) of equation (1) is obtained using microscopic statistical mechanics for a system of water dipoles in the central sphere which interact with each other as well as with the material in the outer sphere, whence the subscript ε'. The internal field E_{int} which acts on the dipoles in the calculation of the LHS of equation (1) is interpreted to be the cavity field which would have existed if the ice sphere were removed, whereas the polarization P is computed from the field actually present in the electrostatic calculation before the ice sphere is removed. The first problem is to determine specifically which intermolecular interactions are required in the calculation of the LHS to make it correspond to the RHS for which the cavity field is used. This has not been *a priori* obvious as evidenced by the fact that several researchers[1–7], including Adams, have performed calculations assuming only short range interactions which Adams correctly concludes is an inconsistent model in the context of equation (1).

For the ideal ice-rules model the numerical results for the correlation sums g_K and G for the LHS appear to agree with the RHS for the respective cases of $\varepsilon' = \varepsilon$ and $\varepsilon' = \infty$. However, as Adams acknowledges, for a finite concentration of Bjerrum defects, which is a necessary feature of real ice, equation (1) becomes inconsistent because statistical mechanics requires that the two correlations sums G and g_K are equal when the ideal ice rules are broken and only short range interactions are included. Adams tries to eliminate this dilemma by the proposal that dipolar interactions, previously left out of all but one primitive calculation[8], will restore the numerical values of G and g_K to those given by the ideal ice-rules. As Adams admits, this proposal cannot be exact because the ice rules determine G/g_K to be independent of the dipole moment and temperature which cannot be true for dipolar interactions. He also admits that dipolar interactions are likely to raise the numerical value of G which would reduce the calculated dipole moment below the value $\mu = 3.0$ D quoted in his paper. Therefore, Adams' simple resolution leaves us with a theory for which neither G nor g_K has been calculated and for which such calculations may be practically impossible due to the difficulty of doing statistical mechanical calculations on systems with long range dipolar interactions. Adams' real conclusion, also emphasized by Stillinger[10], is that G and g_K must satisfy a relation (Adams' equation (9)) if the proper interactions consistent with the internal cavity field are included in the calculation of the LHS of equation (1).

Adams' theory is essentially an extension of the K–F theory to include the cases $\varepsilon' \neq \varepsilon$ and this allows him to connect the K–F equation, given by equation (1) when $\varepsilon' = \varepsilon$ for which the LHS has a factor g_K, to an equation which is derived from equation (1) by setting $\varepsilon' = \infty$ for which the LHS has a factor which Adams identifies as G. If this last identification is made, then the Onsager–Slater (O–S) equation is recovered and must be equivalent to the K–F equation because they both come from the same unified derivation. However, this identification is incorrect because to calculate the G required by Adams' theory it is necessary to include dipolar interactions; in contrast dipolar interactions are completely absent in the calculation of G appropriate for the O–S theory. This astonishing feature has caused many to dismiss the O–S theory too lightly. However, elsewhere I have shown that the O–S theory consists of a renormalization of the electrostatic interactions in ice into a dipole-free effective Hamiltonian[9]. Therefore, the G required for the O–S theory cannot be the same as the quantity required for the LHS of equation (1) which should henceforth be called by a different name, $g_{\infty=\varepsilon'}$. It then follows that the use of equation (1) does not permit a derivation of the O–S theory which is fundamentally different from the K–F theory[2,3,9]; in particular, the internal field in the O–S theory is not the cavity field. A major advantage of the O–S theory to the K–F theory is that extant calculations of G, which do not include dipolar interactions, can be applied immediately and unambiguously to the O–S theory. However, it is to be hoped that the more difficult calculation of g_∞ necessary for the K–F theory may also be performed and that this might indeed result in complete resolution of the theory of the dielectric constant of ice.

J. F. NAGLE

Department of Physics,
Carnegie–Mellon University,
Pittsburgh,
Pennsylvania 15213, USA

1. Adams, D. J. *Nature* **293**, 447–449 (1981).
2. Hollins, G. T. *Proc. phys. Soc.* **84**, 1001–1016 (1964).
3. Nagle, J. F. *J. Glaciol.* **21**, 73–81 (1978).
4. Rahman, A. & Stillinger, F. H. *J. chem. Phys.* **57**, 4009–4017 (1972).
5. Gobush, W. & Hoeve, C. A. J. *J. chem. Phys.* **57**, 3416–3421 (1972).
6. Stillinger, F. H. & Cotter, M. A. *J. chem. Phys.* **58**, 2532–2541 (1973).
7. Yanagawa, A. & Nagle, J. F. *Chem. Phys.* **43**, 329–339 (1979).
8. Powles, J. G. *J. chem. Phys.* **20**, 1302–1309 (1952).
9. Nagle, J. F. *Chem. Phys.* **43**, 317–328 (1979).
10. Stillinger, F. H. in *Studies in Statistical Mechanics* (eds Lebowitz, J. L. & Montroll, E. W.) (North-Holland, Amsterdam, in the press).

ADAMS REPLIES—The 'simple resolution' which I claim is the observation that it is not necessary to choose between either the Onsager–Slater equation or the Kirkwood equation. The Onsager–Slater equation, $\varepsilon - 1 = 3yG$, becomes equivalent to the exact Kirkwood equation when G is identified with g_∞ which is obtained with $\varepsilon' = \infty$ (that is, the 'tin-foil' case) and when all the dipole–dipole and other interactions of the model hamiltonian are included in the calculation[1,2]. The approximation of the Onsager–Slater theory is that the dipole–dipole interactions are to be ignored in the calculation of G.

Perfect ice-rules ice is a very simple hamiltonian which despite having no dipole–dipole interactions produces long-range dipole–dipole correlations of the sort to be expected in real dielectrics. I have calculated unambiguous values of $G = g_\infty$ and g_K for this model. The identification of such a model with real ice must be done with caution and I have tried to make an informed guess as to the direction of the error. One major approximation of the model is that all configurations allowed under the ice rules have the same energy. This cannot be too drastic an approximation or the observed residual entropy of ice would not be predicted so well.[3]

The other major approximation I have made is to ignore the Bjerrum defects which undoubtedly occur in real ice. However, when non-interacting defects are introduced into the model then the long-range correlations are destroyed and $g_K = G = g_\infty$ which cannot be true for a real dielectric. I argue that to introduce defects without also including the long-range electrostatic interactions which occur in all real dielectrics is to make the model worse and not better. I agree with Nagle that complete resolution requires making difficult calculations with all electrostatic interactions included and using the formally exact expressions for the dielectric constant of the Kirkwood type.

0028-0836/82/290401—02$01.00

D. J. ADAMS
Department of Chemistry,
The University,
Southampton SO9 5NK, UK

1. De Leeuw, S. W., Perram, J. W. & Smith, E. R. *Proc. R. Soc.* **A373,** 27–56 (1980).
2. Pollock, E. L. & Alder, B. J. *Physica* **102A**, 1–21 (1980).
3. Nagle, J. F. *J. math. Phys.* **7,** 1484–1491 (1966).

Body temperature changes during the practice of g Tum-mo yoga

IN their recent letter[1], Benson *et al.* do not provide sufficient information to determine whether the temperature changes reported indeed resulted from the practice of yoga. The 'control' time shown on their graphs ranged from 5 to 10 min, and significant fluctuations in temperature appeared to occur within even that brief time. For example, if the 1 °C change in finger temperature recorded during this time for the first subject, V.G.J., were extrapolated for the 55-min meditation period, a temperature change of ~5 °C would result, which represents most of the reported effect of 5–9 °C. The change in the toe temperature was even greater than the finger temperature change during the 'control' period.

I would like to see results of tests on non-meditating individuals, and on those individuals studied, to determine how their temperatures vary over periods of 1–1.5 hours, corresponding to the duration of meditation. I would also want experiments to be performed in a temperature controlled environment, as I suggest that room temperature changes of 2 °C, such as occurred during the trial of the second subject, could lead to greater changes in the temperature of the extremities.

JAY M. PASACHOFF
Williams College,
Hopkins Observatory, Williamstown,
Massachusetts 01267, USA

1. Benson, H. *et al. Nature* **295,** 234–236 (1982).

BENSON *ET AL.*[1] present an interesting account of three persons who increase their finger and toe temperatures apparently by a Tibetan Buddhist meditational practice known as g Tum-mo (heat) yoga. To ensure that any observed changes in body temperature are directly attributable to this method of meditation, the use of a control group is desirable. As this study did not include a control group, it is possible that the observed effects were the result of some other factor, for example: (1) changes in the ambient air temperature (as was the case for two of the subjects, A and B, in this investigation); (2) the consumption of certain food known to increase metabolic activity; and (3) the placement of toe and fingers during the meditation and recovery period, for example, if toes or fingers were placed in an axillary cavity, this would effect a rapid rise in temperature. In addition, the location and method of attachment of the disk thermistors may be partly responsible for the changes in temperature. Further investigation should include the use of matched controls; possibly additional practitioners of g Tum-mo yoga could be used if they were willing to refrain from meditating during the testing period.

MARC A. STRASSBURG
County of Los Angeles
Department of Health Services,
313 North Figueroa Street,
Los Angeles, California 90012, USA

1. Benson, H. *et al. Nature* **295,** 234–236 (1982).

BENSON REPLIES—With regard to the comments of Strassburg and Pasachoff, the subjects in our experiment served as their own controls in an 'off–on–off' design. As the studies were performed in the isolated, mountain hermitages of the monks, it was not feasible to control the ambient temperature. The monks could not serve as their own matched controls at a later time because they would involuntarily lapse into g Tum-mo meditation while sitting quietly for prolonged periods, as we described for subject L.T. Closely-matched, simultaneously-studied controls would have been desirable, but this was not possible in a small Himalayan hut. Despite the changing ambient temperatures and lack of between-subject control, we believe the reported results are valid for the following reasons.

It is unlikely that the reported increases in skin temperature could have occurred spontaneously. Our study was performed in relatively cold to cool ambient temperatures[1]. There are two major modes of preserving body temperature in humans at cool ambient temperatures: heat conservation and increased heat production[2]. In the first adaptation, heat flow from the body centre to the skin is reduced through vasoconstriction of the arterioles in the skin. Thus, less heat is lost to the environment, but at the expense of decreased skin temperatures. When a comfortably warm individual enters an ambient temperature of 25 °C and does not change clothing or activity, his mean body skin temperature can decrease from ~33 °C to 31 °C, and heat loss to the environment is reduced by ~25%. Since the fingers and toes are thin cylinders with little mass in which to store heat, their temperatures usually decrease more, and much more rapidly, than those of the thorax and abdomen. Ordinarily, finger temperatures in environments such as those of our experiment are ~4 °C higher than ambient[3]. During the meditation period, however, the subjects' finger temperatures were 10–14 °C higher than ambient temperatures. The finger temperatures during the control period were already higher than expected. If the increases were spontaneous shifts, one would expect a return to normal, not a further deviation. In the second adaptation, the metabolic rate increases, and more heat is produced. Although it is possible that these men had learned to increase their metabolism to produce more body heat, this is also unlikely. Meditation practices generally have been associated with decreased metabolic rates[4]. Furthermore, the subjects' heart rates were within normal limits and relatively stable throughout. An increased heart rate would be expected in conditions of increased metabolism.

Pasachoff extrapolated several of the increasing, control-period temperatures of subject G.J; he disregarded those of the other subjects which were either stable or decreasing. Both Strassburg and Pasachoff mention the changing ambient temperatures as a possible confounding influence. There was, however, no consistent relationship between the temperature changes in the air and those of the skin of the subjects. For example, in G.J., the finger and toe temperature increases preceded the increases in air temperature; his finger temperature returned to baseline when ambient temperature was highest. In L.T., finger temperature increased during the meditative period at a time when ambient temperature was decreasing. As for the possibility that the location and method of attachment of the thermistors may have been partly responsible for the temperature changes, the thermistors were placed at representative skin sites of the thorax, abdomen and extremities and remained closely taped to the skin during each experiment. Both increases and decreases in skin temperature were recorded. Although there may have been some damping of the magnitude of the observed alterations in temperature, the method of application of the thermistors did not inhibit the decreases during the recovery period.

Finally, Strassburg mentions that placement of toes or fingers in an axillary cavity would bring about a rapid rise in temperature. This is true, but the subjects were under constant observation by four people throughout the experiments and assumed no such position. It is intriguing, however, to contemplate the resulting posture with one's toes in one's armpits or, perhaps, in someone else's armpits?

H. BENSON
Division of Behavioural Medicine,
Department of Medicine,
Beth Israel Hospital,
Harvard Medical School,
Boston, Massachusetts 02115, USA

1. Goldman, R. F. in *Energy Conservation Strategies in Buildings* (ed. Stolwijk, J. A. J.) (Pierce, Connecticut, 1978).
2. Berton, A. C. & Edholm, O. G. *Man in a Cold Environment* (Arnold, London, 1955).
3. VanDilla, M., Day, R. & Siple, P. A. in *Physiology of Heat Regulation and the Science of Clothing* (L. H. Newburgh, ed.) (Hafner, New York, 1968).
4. Wallace, R. K., Benson, H. & Wilson, A. F. *Am. J. Physiol.* **221,** 795–799 (1971).

BOOK REVIEWS

A kind of anthropology

R.D. Attenborough

Social Anthropology. By Edmund Leach. Pp.254. Hbk ISBN 0-19-520371-0; pbk ISBN 0-00-635533-1. (Oxford University Press/Fontana: 1982.) Hbk £9.50, $17.95; pbk £2.50.

FOR ALL his eminence, Professor Sir Edmund Leach apparently does not anticipate much critical acclaim for his contribution to Fontana's new *Masterguide* series. As he writes in the introduction, the book is not addressed to his anthropological colleagues,

> many of whom are likely to be contemptuous of the style of anthropology which it advocates, and which they may well denounce as old-fashioned, egocentric, unscientific, escapist, lacking in coherence, political commitment and so on.

So readers are forewarned of an unfavourable reaction among social anthropologists, which does indeed seem to be emerging, though not entirely on the grounds predicted (see the review by Maurice Bloch, *Times Literary Supplement*, April 16). As a biological anthropologist offering a view from just outside the subject, I differ in perspective but have arrived independently at partly similar conclusions.

Leach's intention in this book is quite expressly to write about "my kind of anthropology", and accordingly the unabashed pursuit of his own intellectual concerns is evident throughout. This strongly personal flavour has its drawbacks, in that the result is far from being a balanced portrait of social anthropology as a whole, and certainly it would not make a suitable textbook for undergraduates (nor is it intended to be one). It also appears to insulate the book from criticism, since some comments are simply irrelevant to the author's aims; the deficiencies cited above are, he says, mostly intentional. But the personal flavour has its rewards too: the book is more stimulating, even entertaining and certainly more readable than would have been likely had the author adopted a blandly balanced approach. Leach leads us through his vision of social anthropology, offering at best some subtle and ingenious ideas about the understanding of human society and culture that will challenge the reader (particularly the non-specialist) to real thought: and he does this in his usual admirable manner — clear and trenchant in expression, and direct and conversational in tone.

Roughly the first half of the book deals with general issues, mainly different views of humanity. Leach starts by distinguishing social anthropologists from cultural anthropologists, empiricists from rational idealists, and so on. As he gives his account of these and other cross-cutting distinctions, he naturally argues for his own position — British social anthropology as a kind of micro-sociology, blending Malinowskian empiricism and Levi-Straussian rationalism in the study of the day-to-day lives of small communities, with the aim of gaining insight, in a quasi-literary sense, into human behaviour. At the same time he denounces opposing positions, with polemical shots at conjectural historical reconstruction, cross-cultural comparison of isolated "traits", natural science thinking about human society, and other anthropological practices of which he disapproves. He then discusses criteria and concepts of humanity and animality, as a philosophical and anthropological problem rather than a purely taxonomic one. This first half concludes with what is perhaps a key declaration:

> I myself view the varieties of human society as alternative systems of moral order rather than as a sequence of specialized adaptations to different economic circumstances.

In the second half, the focus shifts to a closer look at what social anthropologists actually study. In Leach's view, the three main spheres of concern to social anthropology are economy, kinship and cosmology (or, roughly, religion). These are not treated equally. Kinship, traditionally a prime concern in social anthropology and one which extends well beyond what readers in modern industrial society might associate with the term, is discussed at some length: the conceptual complexities of the subject, and its connections with indebtedness, power, alliance and so forth are illustrated. The interlocking relationships between economy, kinship and cosmology are also explored, but economy in its own right is not dealt with at all, and cosmology only in a few pages, despite Leach's particular interest in the subject. The book ends defiantly. Leach grants that social anthropology is "the study of the statics of social systems", despite the dynamic nature of all actual social systems: but recalling that in his earlier career as an engineer he found all the basic theory in the statics, he rests his case for the genuine value of social anthropology as he has presented it.

What, then, should one make of all this? I find a good deal to respect in Leach's cogent exposition, and up to a point I also find it persuasive. But I have reservations too. For one thing, I cannot deny a certain disappointment at the proportions of the book: the first half seems too long for its material and the second too short, especially on subjects such as cosmology. For another, the vehemence of Leach's rhetoric certainly makes for lively reading, but I think he overdoes it. The attacks on opponents are apt to become overbearing, and are sometimes plain wrong. An example of the latter comes when he accuses ethologists of assuming, among other things, that "emotions and attitudes are just as much observable characteristics as colours or structures" — a remarkable misrepresentation that presumably reflects a lack of consultation with ethologists such as his Cambridge colleague and fellow "master", Robert Hinde (whose *Ethology* was reviewed in *Nature* **296**, 507; 1982).

Other attacks — for example on Geertz for an "unverifiable" statement about Balinese culture and society, on a sociobiological "just-so story", and on E.O. Wilson for the "startling incompetence" of his anthropology — may perhaps have more justice in them. The briskness with which such shortcomings are dismissed conveys the impression of commendably rigorous standards: but I think one may question whether everything Leach himself says has been scrutinized equally severely, or indeed whether it would have been reasonable to do so, given the nature of the subject matter. A possibly more straightforward issue of consistency arises within Leach's own arguments. On some points, including important ones such as the place of generalizing in social anthropology, he seems to argue in different directions as the book proceeds, creating a rather equivocal overall impression despite the clarity of particular passages.

It is conspicuous that Leach's most forceful points are frequently negative ones — not only criticizing opponents, but closing off avenues of enquiry and interdisciplinary contacts that he considers worthless. This no doubt reflects a sceptical habit of mind born of long experience, and in itself it seems defensible: indeed as an antidote to fashionable concerns it can be refreshing. Nonetheless, the cumulative effect seems to risk discouraging innovation. To my surprise, physical (biological) anthropology is one instance where Leach nods respectfully in the direction of interdisciplinary dialogue: yet this seems counter to the tenor of the argument, and the point is not pursued.

Finally, at a more mundane level, Leach is at times quite cavalier when it comes to matters of definition (e.g. species) and fact (e.g. confusing irrigation and drainage in New Guinea agriculture).

Like Aubrey Manning in his review of Hinde's *Ethology*, I am uncertain about the intended audience of the *Masterguide* series. Leach's imaginary reader is

> someone like myself at the age of twenty-five to whom learning about anthropology came as an unexpected intrusion into a deceptively well-organized existence.

Social Anthropology is lively and stimulating enough to be recommended to such a reader, with the important caution that is also personal in flavour and erratic in approach. It is, for once, a book that matches its description in the cover blurb — "fascinating and idiosyncratic". ☐

Robert Attenborough is a Lecturer in Biological Anthropology at the Australian National University, Canberra.

Not much that's new in cancer research

Peter Alexander

Cancer: A Comprehensive Treatise, 2nd Edn. Vol. 1, *Etiology: Chemical and Physical Carcinogenesis*. Edited by Frederick F. Becker. Pp.714. ISBN 0-306-40701-9. (Plenum: 1982.) $69.50, £43.79.

RESEARCH into cancer embraces an enormous range of disciplines, yet a broad understanding of the subject as a whole is necessary if the specialist investigator is to exploit the best opportunities available and is to evaluate the implications of his findings. A comprehensive treatment of cancer research, therefore, fills a very real need.

In 1975 such a treatise appeared. Edited by Professor F.F. Becker, the six-volume work was splendidly produced and most of the chapters were both readable and authoritative. Publication delays inherent in such a mammoth undertaking meant that the literature was only covered until 1973, and this most useful source is now only of value in some restricted areas. The pace of cancer research within the past decade has been rapid in most areas and some have changed out of all recognition. At the cellular and sub-cellular level the new techniques of gene cloning, production of monoclonal antibodies and the isolation and characterization of growth factors have provided a plethora of new facts and theories which supersede much of the earlier work.

A second edition of Becker's work was, therefore, keenly awaited and a revised version of Vol. 1 has now appeared. This, unfortunately, is a great disappointment because attempts to bring it up to date have been very patchy. The second edition contains 40 per cent more pages, but this increase is largely accounted for by the introduction of three new chapters and the extensive revision of three chapters dealing with the metabolism and biochemistry of chemical carcinogens. In all, there are 19 chapters of which six are direct reprints of the first edition with no alteration or additions; they contain no references beyond 1973 and cover the role in cancer induction of genetics, hormones, immunology and radiation. There is a further set of chapters which, while not identical reproductions of the first edition, have been changed only marginally and fail to reflect adequately the advances since 1973. Approximately half the book is, therefore, useless as a guide to the current state of knowledge. As a reference source to the older literature, these chapters have some worth, but why reprint them when copies of the first edition are readily accessible in so many libraries?

Much of the remainder is made up of some quite excellent contributions, however, which are of value both to those who wish to gain a general feel of the field as a whole and to researchers directly engaged in the area reviewed. In general, they do not suffer greatly from the fact that, even in the new chapters, the literature is only covered until 1979. Notable amongst these are the chapters on cytogenetics by P.C. Nowell, epidemiology (V.F. Guinee), the metabolism (J.H. Weisburger and S.M. Williams) and interaction with nucleic acids (S. Rajalakshimi *et al.*) of carcinogens, and two articles on the two-stage mechanism of carcinogens by, respectively, I. Berenblum and E. Farber. What a pity that these articles were not published by themselves, since it is difficult to recommend the purchase of an expensive book in which virtually half of the contents are available in an earlier edition. ☐

Peter Alexander is Professor and Head of the Division of Tumour Immunology at the Institute of Cancer Research, Sutton, Surrey.

Fusion forever

R.S. Pease

Fusion. Vol.1, *Magnetic Confinement*, 2 parts. Edited by Edward Teller. Part A, pp.491, ISBN 0-12-685201-4; Part B, pp.529, ISBN 0-12-685241-3. (Academic: 1982.) Part A $56, £37; Part B $59, £39.

IN 1930, the installed electricity generating capacity of the Soviet Union was 2. GWatts. According to Professor Teller' introduction to these books, the entir supply of Leningrad — perhaps a third o the 2.9 GWatts — was offered to Georg Gamow for experiments to create th fusion-energy-producing temperature the recently suggested as the source of th limitless solar energy. The offer (write Teller) was refused. Today, over 50 year later, we can anticipate such experiments a the Joint European Torus in Europe an the Tokamak Fusion Test Reactor i America coming into operation next year they indeed use power supplies of th magnitude offered to Gamow b Bukharin. The publication of these presen volumes, the first in a new series describin the state of fusion research and the hope and uncertainties of the researchers, is thu very timely.

The first eleven chapters of the tw companion volumes comprising Vol.1 ar devoted to accounts of research on th confinement of hydrogen isotopes b magnetic fields. A further two chapte describe the methods proposed to heat th plasma to the required 100M° temperatures; and the final three chapte describe the work on technology and engineering carried out to explore the possibility of practical extraction of power from the hoped-for large-scale fusion reactions.

Each chapter is largely self-contained, and is written by a leading authority at a level which, though demanding concentration, will be rewarding for many physicists and engineers outside this field of research. At the same time, for specialists in fusion research, the articles are comprehensive, accurate, up-to-date (to about 1980) and have excellent, though not exhaustive bibliographies. Each contribution is concerned with theory and experiment in one of the main configurations of magnetic field which might form the basis of a reactor: the Tokamak, the Stellarator, the Mirror Machine, the Reverse Field Pinch and so forth. This form of presentation has the advantage that it is relatively easy to comprehend the state of play in each of these approaches, even if the reader will sometimes have to take into account what is not said as well as what is. The disadvantages are that there is some duplication of material; that the overall presentation of confinement physics is somewhat haphazard; and that important investigations of magnetic-confinement using systems, such as the Levitron, not regarded as the basis of a reactor, are omitted.

The balance of the material reflects that of the current research programme in the United States, with major articles on the theory and experiment of Tokamaks and Mirror Machines, respectively; whilst the Stellarators, though a pioneering achievement of the early US programme, are here dealt with relatively briefly. Some of the contributions bring together important material hitherto unpublished or widely scattered throughout the literature, notably the short chapter on the so-called ELMO (after St Elmo's fire) Bumpy Torus, and the chapter on Advanced Fusion Reactors. Others — those on the Tokamak system and on Magnetic Fusion Reactors — achieve a mastery over a vast literature for which both specialists and non-specialists alike will be grateful. Professor Teller's own chapter and his assembly of authors and material has ensured that there is now available for graduate engineers and physicists in general — as well as for the specialists — an up-to-date account of the main features of the physics and engineering of magnetic confinement fusion.

On the wider issue of whether or not this research will finally come to fruition, the book offers a combination of long-term confidence and short-term caution appropriate when the main ideas are subject to the imminent test of major experimentation. □

R.S. Pease is the UKAEA's Programme Director for Fusion Research, and is currently Chairman of the International Fusion Research Council.

Between the laboratory and the patient

John P. Bunker & Jinnet Fowles

Biomedical Innovation. Edited by Edward B. Roberts *et al.* Pp.395. ISBN 0-262-18103-7. (MIT Press: 1982.) $30, £17.

Most of us would agree that an ideal model for biomedical innovation, the process by which new diagnostic and therapeutic technologies are conceived, developed and disseminated would look something like this: a strong, adequately funded, basic research capability; prompt evaluation of the new procedure by well-designed clinical trials; a favourable balance of benefits and risks; a well-informed public, able to appreciate the consequences of treatment; timely application of the medical technology to the relief of human suffering; translation of the results into appropriate standards for general clinical practice; and continued monitoring or surveillance for long-term effects. The authors of *Biomedical Innovation* make it clear how far we are from achieving such perfection.

We are encouraged at the outset by Julius Comroe, who recounts the landmark studies in which he and the late Robert Dripps documented the benefits of strong basic science. Comroe and Dripps conducted a six-year study of the top ten clinical advances in cardiovascular-pulmonary medicine between 1945 and 1975 to determine whether they were mainly the result of targeted or of untargeted research. Their study was, in fact, a response to a Department of Defense study of weapon development which had concluded that scientists were most effective when their effort was mission-oriented. The Comroe–Dripps study, based on an examination of 4,000 published articles, came to the opposite conclusion: that the great advances in the treatment of cardiovascular disease were based on a strong, undirected, basic research effort. Since this process is already established, the message is a simple one: don't meddle.

Prompt evaluation, or the process of "knowledge validation", is described in fascinating detail by Robert Levy and Edward Sondik of the National Heart, Lung, and Blood Institute (NHLBI) — the multiple steps by which the Institute decides which of a possible portfolio of clinical trials should be undertaken given that these trials draw funds away from the support of knowledge acquisition.

One could almost believe that the 15 per cent of its extramural budget devoted by NHLBI to clinical trials is a sufficient investment in evaluation. Unfortunately, NHLBI appears to be the exception, for ample evidence is presented elsewhere in *Biomedical Innovation* that current efforts at clinical evaluation are inadequate. Worse, we now know that the current federal administration, as a matter of policy, intends to reduce further its investment in clinical trials in favour of support for basic research.

However unsatisfactory the record of clinical evaluation may be, the goal of a well-informed public ("informed consent") appears to be even more distant. While providing no new insights, Laurence Tancredi calls attention to four of the major unsolved conceptual problems of informed consent: the ability of the patient to comprehend the information provided by physicians; the nature of the judgements made under this uncertainty; the placebo effect; and the accuracy of available data. He concludes that these conceptual issues "create serious questions about the validity and meaningfulness of informed consent as a protective device". In his pessimistic appraisal, Tancredi slights the evidence of randomized trials demonstrating improvements in patients' understanding of the implications of treatment and even in the medical outcomes. Nonetheless, although there are indeed many obstacles to an effective informed consent process, there have been undoubted gains in the effectiveness with which information can be made available to the patient. Emphasis on the timing of information, as well as appropriate levels of vocabulary and organization, have increased patient comprehension and thoughtful decision-making.

Timely application of new medical technology is barely mentioned as an issue, which seems odd in view of the recent discussions of the so-called "drug lag" in professional journals and the lay press. Acknowledging the past existence of "considerable lag time", the editors, in an introductory chapter, state that "whether lag time exists today is essentially unanswered . . . but . . . is a concern we must continually explore". Unfortunately the reader searching for enlightenment on this thorny and controversial issue will be disappointed.

We now come to the unresolved issue which Donald Young calls "deficiencies in the communication of research results". Dr Young examines the dissemination of findings from two large clinical trials, the Veterans' Administration Cooperative Study of Surgery for Coronary Artery Disease and the NHLBI Cooperative Study of Unstable Angina Pectoris. On the basis of these two studies, he concludes that the published medical research literature is largely irrelevant to the information needs of practitioners and that there is inadequate guidance for practising physicians attempting to resolve the frequent conflicts encountered in clinical trial results. The issue he raises, the lack of evaluation of medical technology that reflects users' needs, is a theme that recurs throughout the book — which is not surprising; in comparison with basic research, and despite their undoubted worth, evaluation studies have been woefully underfunded.

The final phase of our model, continued monitoring or surveillance, may be the most neglected. Herbert Klarman, in his chapter "Measuring Economic Effects of Biomedical Innovation", declares that monitoring the effects of technology is inherently superior to forecasting as a basis for planning. He even suggests that monitoring could serve as a basis for reimbursement of physicians and hospitals, and that this might be a better way to regulate biomedical innovation than certificate-of-need, which depends on forecasting. Great Britain has, of course, already opted for earlier introduction of drugs, relying more heavily on post-marketing surveillance. In the United States, unfortunately, and despite extensive professional debate and encouragement, no comprehensive programme of post-marketing surveillance is yet in sight.

The method used by Young and by Levy and Sondik, as well as by several of the other authors in *Biomedical Innovation*, is "research on research" — the study of the research process as revealed in the medical literature. Much of their material has been published in other forms previously, and sadly the opportunity to use this collection to develop a cohesive and comprehensive thesis has been largely missed. But it is too much to expect a multi-authored book emerging from a three-day conference to read as if it were the product of a single, all-knowing intelligence. Rather, it is a valuable collection of essays that contains much useful information and many insights. It will be a convenient sourcebook for those who wish to understand the current process of biomedical innovation or who choose to write about it in the future. □

John P. Bunker and Jinnet Fowles are in the Health Services Research Program at Stanford University.

Mulliken on molecular orbitals

W. G. Richards

Polyatomic Molecules: Results of ab Initio *Calculations.* By Robert S. Mulliken and Walter C. Ermler. Pp.431. ISBN 0-12-509860-X. (Academic: 1982.) $49, £32.40.

Charles Coulson once suggested that the acronym MO should stand for Mulliken Orbitals rather than for Molecular Orbitals. Robert Mulliken was one of the originators of the method of obtaining solutions of the Schrödinger equation for molecules in a manner paralleling that used for atoms, each electron having its own individual function or orbital. How heartening, then, that the great man should still be active and at the forefront of the discipline. Not for Mulliken the contempt for computers; he seizes on the power which can produce accurate functions and a precision in computed properties which may on occasion rival that available from experiment.

Together with Walter Ermler, in this book he presents a comprehensive survey of *ab initio* calculations on polyatomic molecules. The epithet *ab initio* may sometimes give a spurious impression of quality; merely performing all the integrations implied in a Roothaan–Hartree–Fock calculation does not cover over defects in the original theory. In an introduction the authors do go beyond the minimum required by their title, discussing matters such as configuration interaction, electron pair and many-body approaches to improvement of wavefunction, as well as pseudopotentials.

Subsequent chapters each treat general classes of molecules, for example AH$_2$; AB$_2$; ABC; molecules with specified symmetry; reaction surfaces and organic compounds. In every case general considerations are followed by specific results obtained for individual molecules. Copious references mean that this is a very comprehensive survey, invaluable to theoretical chemists, to spectroscopists and to the growing band of those who describe themselves as computational chemists.

The appetite for this type of work shows no sign of abating and indeed it is being stimulated by developments in computer hardware. Cheaper and more powerful minicomputers mean that experimental chemists can run *ab initio* calculations for themselves using freely available programs obtainable from the admirable Quantum Chemistry Program Exchange run from the University of Indiana. At the same time, the new breed of supercomputer with vector and array processors offers the chance of doing extremely accurate calculations on molecules which were until recently too complex to be contemplated.

Although there is no hint of a plateau in the output of quantum mechanical calculations the book is timely in that it surveys the field, describing what has been done before the new machines have a major impact. □

W. Graham Richards is a Lecturer in the Physical Chemistry Laboratory at Oxford University. The latest volume of his Bibliography of *Ab Initio* Molecular Wavefunctions *covering 1978–1980 was published by Oxford University Press last year.*

More for less

Peter W.J. Rigby

DNA Tumor Viruses, 2nd Edn revised. Edited by John Tooze. Pp.1,073. Hbk ISBN 0-87969-142-5; pbk ISBN 0-87969-141-7. (Cold Spring Harbor Laboratory: 1981.) US hbk $75, pbk $32.50; elsewhere hbk $90, pbk $39.

This revision of the bible of DNA tumour virology is to be warmly welcomed. That reprinting should be necessary within 18 months of publication of the original edition emphasizes the value of the book, and the editor is to be congratulated on having seized this opportunity to improve the text considerably.

The basic material is unaltered but the book has been updated by adding supplements to nine of the thirteen chapters. These supplements vary considerably in length and comprehensiveness, but they do describe the recent major advances in the field. The additional material deals effectively with such topics as polyoma middle T-antigen, the p53 protein associated with large T-antigen in SV40-transformed cells and the molecular biology of BKV, thus obviating criticisms expressed in my review of the original book (*Nature* **289**, 332; 1981). The appendices of DNA sequence data have been considerably enlarged. The SV40 sequence has been modified to take account of the extra nucleotides, and another welcome addition to this section is a tabulation of restriction fragments. The sections on human adenoviruses contain a large amount of fresh sequence data and there are new appendices dealing with simian and murine adenoviruses and adenovirus–SV40 hybrids.

The book now contains some 1,100 pages which, at a price of less than $40 for the paperback edition, represents extraordinary value. The appearance of a paperback version is the most pleasing aspect of the revision as the book is now within the economic reach of the many advanced undergraduate and graduate students who ought to own a copy. This excellent volume will be, for many years to come, compulsory reading for everyone with an interest in any aspect of DNA tumour virology. □

Peter W.J. Rigby is a member of the Cancer Research Campaign Eukaryotic Molecular Genetics Research Group and a Senior Lecturer in Biochemistry at Imperial College, University of London.

● The National Physical Laboratory has recently issued a second edition of their information poster, *Units of Measurement.* The chart summarizes the SI system and illustrates how the units are realized at the NPL. It may be obtained by writing to Information Services, NPL, Teddington Middlesex TW11 0LW, enclosing a stamped addressed C4 envelope.

nature

5 August 1982

James Watt and biotechnology

The British government is being deluged by advice about the proper exploitation of biotechnology, which is in itself a symptom of what is wrong. The government should think of cutting loose.

Just over two hundred years ago, when James Watt had developed his crucial improvement of Newcomen's steam engine, it seems not to have entered the heads of the British Parliament or of the Prime Minister of the day (the Marquis of Rockingham in the second half of 1765) to set up a committee to recommend how this important innovation could best be exploited. But, in the event, for the best part of the succeeding century, Britain profited enormously from James Watt's doings. So what is so different nowadays? That is what the present British government should ask itself before setting out to reply to the latest contribution to the stream of unsolicited advice it has been given in the past few years about the exploitation of biotechnology. Two years ago, a committee under the late Sir Alfred Spinks tried to persuade the government that it had an important role to play. A year later, the government issued a defensive and temporizing reply. Now, the Education, Science and Arts Committee of the House of Commons has predictably (see page 507) complained that the government has done too little about Spinks, and makes a string of suggestions of its own, some sensible and some not. The form now would be for the government to produce another defensive reply and for some other committee to protest that the reply is unsatisfactory. And so the cycle would continue. Because the process would do nothing (except perhaps harm) for biotechnology, the government should now bend its energies to asking how far it is prepared to go to create a climate in which innovation can flourish again.

Communication

To go back to James Watt would do no harm, as a consideration of the advice the government was offered last week will readily show. Thus the House of Commons asks that there should be a "formal channel of communication" between the Department of Industry (a huge department of state) and the University Grants Committee (a tiny and constitutionally ambiguous entity responsible for saying how what the government decides should be spent on universities should be divided among them) so that the former can tell the latter what it has already told the committee (and in public) — that it would like to see more of the universities' resources spent on science and technology. Can that channel of communication really be necessary? Simple-minded people might think that Mr Patrick Jenkin, the industry man, might simply write to Sir Keith Joseph, the education man (who also happens to be his predecessor), asking him to use his influence with the grants committee, to which he has in any case recently taken to writing open letters (see *Nature* 22 July, p.313). Or perhaps the two ministers might exchange a few civil words after some convenient meeting of the Cabinet to which they both belong? "What about a trenchant postscript, Keith, to your next letter to those . . . people?", Patrick might ask. By now, both participants know too well that such strategems will have no effect. For neither of them can speak freely to the other until what he thinks he might say has been solemnly considered by his own civil servants and then, perhaps, by an interdepartmental committee (which takes even longer to arrange). And the House of Commons committee, constitutionally the only defence against the executive, finds itself lending its name to a proposal that civil servants from yet another ministry should have a right to attend meetings of the grants committee. Is that how steam engines might have been exploited?

Of course not. The Marquis of Rockingham knew that by instinct. Why is the present British government, whose political inclinations are not very different, by comparison so diffident and unsure? Watt's steam engines made their way in the eighteenth century, and then made the nineteenth century for Britain, because there was an army of British manufacturers who fought their way to Watt's door (and later to that of Boulton and Watt) to place an order and to risk the money that went with it in the hope of being able to keep ahead (make a better profit or win a larger share of the market) of their competitors. To be sure, economic circumstances were different while direct taxes were negligible, so that capital expenditure (on, say, a steam engine) was a direct replacement for current expenditure and not, as it is at present, partly the purchase of a capital asset. The mechanisms of trade were also primitive, so that competition was less ferocious and, as a consequence, profit margins higher. But there were also people who thought the game worth the candle, who were prepared to take a risk — the risk that they might be wrong. What has happened to them? And if they have disappeared for good, what is being done to recreate them? So far, it seems, not very much.

Yet it is also plain the British government, three years after its election, is at a turning-point in its industrial affairs. Originally, the promise was that reducing income tax would create what were called incentives, persuading people to spend their tax rebates on industrial investment. That stratagem seems not to have worked as planned. But the government at the outset planned to pull back from the direct management of industry, selling off bits and pieces of previously nationalized industries wherever it could, on the grounds that governments are inherently bad managers but also because it had become impossible to finance the annual capital investment of major industries together with the increased social costs that modern states must pay out. The past few weeks have been a great disappointment. The state communications monopoly, British Telecom, is to be sold but not until after the next election. British Aerospace (which works primarily for the government) may have half-gone, but British Airways is destined to make such a huge loss in the present financial year that is unlikely to be saleable next year at more than the scrap value of its equipment. The hope that British Steel will be saleable has faded as the prospect has increased that its next reported loss will be getting on for two per cent of the GNP. Yet the Confederation of British Industry and the major clearing banks are at their wits' ends to know what should be done to keep quite substantial companies in business, while unemployment is well above three million. Who, in these circumstances, will suppose that the future for the British economy lies in the creation of a channel of communication between the Department of Industry and the University Grants Committee?

De-industrialization

The truth is that the de-industrialization of Britain is already well-advanced. After a decade of gloomy speculation on that theme, the prospect is now within sight of becoming a reality. The present government, a victim of circumstance its historians may claim, has to choose between the stark alternatives that lie ahead — gracefully to let the process continue (but nevertheless fighting for the channel of communication between the Department of

0028-0836/82/310501 02$01.00

Industry and the University Grants Committee) and recreating the circumstances that enabled Mr Watt to prosper. Even though the torrent of advice that the government is now given about the exploitation of biotechnology is largely empty of constructive content (because it supposes that all innovations will be conducted within the framework to which all have grown accustomed), the fact that there is so much of it must surely be a sign that something needs to be decided.

The case of biotechnology is marvellously illustrative of what lies ahead. Popular legend has it that laboratory discoveries in the immediate past could be made the foundation of a brave new industry, one so productive and profitable that, with a little luck, some entrepreneurial government might succeed as James Watt did. Modern biotechnology will indeed change the world in welcome ways, but not necessarily more profoundly than it has done so already. (Where would we be without bread, or cheese, or wine?) Equally, however, it is certain that in the long run the benefits will accrue to those commercial organizations that are so technically and financially strong, or so imaginative and fiscally free, that they can make the best bargains with their present customers and an uncertain future. Inevitably, of course, in the intervening years or decades, many small enterprises will spring into being (and some may even prosper in the long term), but those responsible for founding them will only rarely make their marks by becoming household words, names on some pharmaceutical package or other new commodity. Most will be content to sell out to larger partners, and some will be glad to do so. Those doubting that calculation should consider what happened to the manufacturers of automobiles who set out a century ago on their endeavour. The difference, now, is that the market, both for products and people, is international. The House of Commons committee at least knows that.

So why should not Britain follow in biotechnology where the government of France appears to be going in its attempt to make a new electronics industry (see page 507)? Because the British have been through that, most recently in the 1960s. Many of the projects mounted then in the belief that profligate public investment in new technology must be virtuous are only now being painfully abandoned — the aluminium smelter in the north of Scotland, for example. What has stuck in the British mind is merely that this is a recipe for an inflation rate that is insupportable. If the French avoid that painful trauma, it will be because their civil servants are more businessmen than bureaucrats.

The British government's concern, in the face of the conflicting advice being showered on it, must be to give British industry a sporting chance of survival. How should that be done? Most committees with an opinion on the subject say that British universities are even in penury remarkably productive of good fundamental research, but the research councils' own committee of officials acknowledges that the peer-review system may inhibit applied research in universities (see page 507). That is not, of course, a contradiction but a simple consequence. Who is to change it, and how? Certainly there is no room for change within the present system, although there might be if universities were genuinely autonomous and not as at present constrained by an invidious *numerus clausus* applied to their total size. The time has probably come when the British system for research support must follow the course being followed by universities in the United States, looking for closer links betwen universities and industry (with all the discomfort that must follow), in which case tax concessions are necessary — not merely matters to be studied. And while the research councils themselves are probably quite able managers of their own research and development, there is very little to be said for allowing them to continue as they are while the work they do might as well be done in the more flexible (and perhaps cheaper) environment of the universities. The House of Commons committee is right to say that change is overdue, but it underestimates the degree to which the necessary change must be radical. A formal channel of communication between the Department of Industry and the University Grants Committee is not a sufficient substitute.

Talk, guns and butter

President Reagan is more flexible about India than his predecessor, but still has much to learn.

President Reagan's diplomacy is better than that of his predecessor, Jimmy Carter, at least where relations with India are concerned. By working out an ingenious way round the impasse over the supply of nuclear fuel to India (see p.503), Reagan has extricated US diplomacy from the trap created by Carter, who campaigned against nuclear proliferation, supported the 1978 anti-proliferation act but then had to bend to Indian pressure and send nuclear fuels to a state that has consistently refused to forswear the development of nuclear weapons. The relief that greeted the Tarapur deal last week in Washington indicated that a thaw in US–Indian relations is overdue. But a thaw does not solve the problems of that part of the world nor signal a clear path for future US diplomacy. Indeed, the Tarapur deal may be a little too cynical. After all, why should the United States, with its long record of efforts to prevent proliferation, bow to a nation that was the chief opponent of the Nuclear Non-Proliferation Treaty, and which mightily inflamed the nuclear ambitions of other developing countries with its "peaceful" nuclear test in 1974?

Why should Mrs Gandhi, who otherwise seemed to be bearing olive branches to Washington last week, keep the nuclear weapons option open? "We do not have nuclear weapons", she told a gathering at the National Press Club, sounding faintly like those Israeli generals who always deny that Israel has "deliverable" nuclear bombs. Most people, especially the Pakistanis who seem to be bent on a nuclear weapons capability of thier own, assume that India could use a nuclear weapon if it so chose. Is it not, after all, an emblem of India's advanced science and technology? India says the reason for keeping the nuclear weapons option open is Pakistan, and has been highly critical of the new $3,200 million dollar arms package the Reagan Administration has put together for India's worst enemy. Ever since the Soviet invasion of Afghanistan in 1980, Washington has tried to treat the Pakistani government as some kind of Western bulwark. Yet the military aid, as usual, seems not to be going to fortify Pakistan defences along the Afghan border as intended. According to Mrs Gandhi, the arms keep massing on the Indian border, and attempts to sign a "no-war pact" seem always to end in failure.

This is one reason why Mrs Gandhi was in Washington last week: to rectify the long-standing impression that India "tilts" to the Soviet Union, and thus is forcing Washington to "tilt" to Pakistan. Asked point-blank which way India is tilting these days, Mrs Gandhi told a reporter "We stand upright" — and her American audience applauded. She also hinted that it might be possible for the Soviets to leave Afghanistan under some kind of negotiated agreement — a development that would also remove Washington's need to support Pakistan. But such global machinations could hardly be carried out in a single state visit. "Our main purpose is to put across the Indian point of view" she explained. She appeared to imply that she would be returning to Washington.

Mrs Gandhi also had a more specific purpose: to persuade the President that India needs substantial low-cost loans from other governments and international lending institutions if it is to become the kind of free-enterprise state the President would admire. On this point, however, she did not succeed. Although she stressed India's progressive Western-oriented view of development — hence India's interest in bilateral science cooperation with the United States — she failed to turn that impression into money. Apparently the President insisted that there could be no increase of the US contribution to the International Development Association (which mainly lends to India) and urged her to borrow in the commercial markets. So President Reagan has extended a handshake even while denying India a scrap of extra money to aid Indian development, science and technology. It is politic for the President to be that tough, but is it wise?

0028-0836/82/310502-01$01.00

Gandhi puts India's claim to USA

New science link agreed but no money

Washington

Indian Prime Minister Mrs Indira Gandhi made her first visit to Washington in 11 years last week, during which she and President Ronald Reagan announced not only a settlement of the long-standing dispute over nuclear fuels for the Indian nuclear reactors at Tarapur but also a new high-level agreement on cooperation in science and technology.

Like the agreements on science that Washington signed with Moscow and later with Peking in the early 1970s as a prelude to improved relations, the science accord could signal a new period of stable relations between Washington and New Delhi, which have been troubled for some years (see opposite).

In a day and a half of meetings with the President, members of Congress, the press and scientists, Mrs Gandhi made it clear that India does not consider itself a supplicant for US aid monies or hand-me-down technology from the United States. In a talk to the American Association for the Advancement of Science, she stressed India's strong indigenous high-science traditions, which have included world-class contributions in many basic fields.

"It is an inherent obligation of a great country such as India, with its traditions of scholarship and original thinking and its great cultural heritage, to participate fully in the march of science", said Mrs Gandhi, quoting from the latest resolution on national science policy.

On the other hand, India most needs science and technology to serve development down to the village level as with the "fitting of tyres on bullock carts and the use of biogas plants", she said.

The new accord establishes a committee to be chaired jointly by Dr George A. Keyworth, the President's science adviser, and Professor M.G.K. Menon, chairman of the Indian Science Advisory Council. Other members have still to be chosen. The committee should produce suggestions for collaborative work by early next year, according to the White House, But the new group, while enjoying prestige, has not had any money allocated to it and it is not clear how any programmes it suggests will be carried out or funded.

Nyle C. Brady, senior assistant administrator of the US Agency for International Development, who will help to select the members of the committee, says that some projects could be funded by reshuffling the existing $80 million in foreign aid that his agency gives to India each year. He estimated that 10–20 per cent of the money now goes on projects based on science and technology items. (Mrs Gandhi also tried to persuade the President of the importance of concessional financing to India for general development, but her arguments are said to have fallen on deaf ears.)

Likely areas of collaboration suggested by Mrs Gandhi and US officials include:

- Biomedical research to control leprosy, tuberculosis and waterborne diseases. India claims recently to have made advances in the control of leprosy, while US investigators are the source of its only natural host for experimental infection, the nine-banded armadillo.
- Nutritional blindness associated with severe vitamin A deficiency, a leading cause of blindness in many developing nations. Related work is already under way in the United States, and US–Indian collaboration is taking place at the National Institute of Nutrition in Hyderabad.
- Birth control, especially development of possible vaccines as anti-fertility measures.
- Agriculture and biomass. India has achieved self-sufficiency in grain production, a remarkable achievement for a nation of 700 million people. But, as Mrs Gandhi told reporters in Washington, most modern grain production increases consumption of energy. Energy conservation and cheap energy production are important priorities for the achivement of future increases in food production and overall standards of nutrition. The US Department of Agriculture and the land-grant colleges already contribute to this work.

India is especially interested in the possi-

France to supply Tarapur fuels

Washington

A major problem in US–Indian relations was removed last week when President Ronald Reagan and Prime Minister Indira Gandhi announced that they had resolved a long-standing dispute over whether the United States should continue to provide low-enriched uranium to Indian reactors at Tarapur, outside Bombay.

The two heads of state announced that the reactors would be able to keep operating because fuel would be provided by a third party, France. This circumvents a 1978 US law that appears to supersede the 1963 agreement and effectively bars US shipments to Tarapur. In return, India will continue to observe safeguards operated by the International Atomic Energy Agency.

Under the 1963 agreement, the United States became the exclusive supplier of low-enriched uranium to Tarapur. In return, India promised to observe bilateral safeguards.

But in 1978, Congress passed the nuclear anti-proliferation act which prohibited US export of nuclear fuels to any country that had not signed the 1968 Non-Proliferation Treaty. India has deliberately remained outside the treaty, so the act seemed to prevent continued shipments to Tarapur.

Under pressure from the Indian government, President Carter in 1980 used a provision in the 1978 act to authorize shipment of 38 tonnes of enriched uranium to Tarapur anyway. As recently as April 1981, the Reagan Administration was reported to be ready to cancel the 1963 agreement, and India was reported to be threatening to stop observing safeguards at Tarapur.

Under the new agreement, however, both the 1963 agreement and the 1978 act are upheld. The United States will not supply fuel to Tarapur — instead, the French will do so. But there are some sticking points, such as India's continued insistence that, under the 1963 agreement, it does not need US permission to reprocess spent fuel from Tarapur. It is estimated that there are 200 tonnes of fuel at Tarapur, 100 tonnes in the form of spent fuel and another 100 tonnes in the reactors. If all this were reprocessed into weapons grade material, it could be enough for 100 nuclear devices.

Two congressional watchdogs of nuclear proliferation, Representative Jonathan Bingham (Democrat, New York) and Senator John Glenn (Democrat, Ohio), say they are content with the Reagan–Gandhi deal. **Deborah Shapley**

France's decision

In France, the decision to supply the enriched uranium has been taken at the political level; commercial questions such as price have yet to be decided.

Moreover, some political problems may still remain. For the enriched fuel would be produced by the Eurodif plant at Tricastin in the Rhône valley and Eurodif is not French but an international consortium of France, Italy, Spain, Belgium and Iran. Through a surviving Franco-Iranian company, Sofidif, Iran still owns 10 per cent of in Eurodif.

In principle Cogema, the French nuclear fuel company which owns 51 per cent of Eurodif, could buy the enriched uranium from Eurodif and resell it to India; or Eurodif itself could make the deal. Both arrangements might be expected to require the agreement of the other Eurodif partners. No decision on either arrangement has yet been taken, say French sources. **Robert Walgate**

0028-0836/82/310503-02$01.00

Wide-World Photo

Secretary of State George Schultz follows Mrs Gandhi's lead.

bilities of genetic engineering for the improvement of crop yields and to produce quick-growing trees to provide fodder and firewood for rural populations. Biotechnology, some Indians say, is an area where high science and the needs of development meet. Last January, Mrs Gandhi announced the creation of a National Biotechnology Board, of which Dr M.S. Swaminathan will be chairman.

- Energy, minerals and materials. Indians are already being trained in the use of the Landsat satellite for mineral surveys, and collaboration exists in the field of earthquake engineering.

The White House explained that the new committee should overcome some of the problems afflicting the subcommission on science and technology formed under the Joint Commission on Economic, Commercial, Scientific, Technological, Educational and Cultural Cooperation. The commission was created in 1974 in an earlier effort at US–Indian detente, in spite of US unhappiness with India's nuclear test a few months earlier.

The science subcommission apparently did not include sufficiently high-ranking people and so was not influential enough with each country's bureaucracy to get major projects started. The new committee, under the joint chairmanship of Dr Keyworth and Dr Menon, should not have such difficulties.

In an oblique reference to the many meetings of developing countries, including one held in India last March, Mrs Gandhi noted that bilateral arrangements were the most effective path for development. "Global conferences end with inspiring and laudable statements. But their commitments are seldom honoured" she said.

Deborah Shapley

Electronics industries

French on march

The French government last week declared war on world electronics* markets with a FF140,000 million ($20,000 million) three to five-year investment programme in the French electronics industry. After nuclear power (France now has the largest and fastest-growing nuclear programme in the world) and space (where the Ariane launcher is now competing effectively with the space shuttle) comes electronics, now clearly marked out as *the* technological programme of the new socialist France.

The battle will begin in the United States. M. Abel Farnoux, principal architect of the French programme, is expected to move to an office in New York in September and one of his partners, M. Girard Compain, is to set up shop in California. Altogether, some ten French electronics policy-makers are to move to the United States this year.

Their objective will be, in part, to learn, but the real French goal is the American market. France would seek both to establish French companies in the United States and to set up cooperation agreements. But so far the French government has given no details of Farnoux's new role. The decision last week was to adopt the main lines of Farnoux's recent report on the industry (see *Nature* 27 May p.257) and to announce an investment figure.

The most difficult domestic question has been avoided — how to reorganize the French electronics industry at home. The problem is that some of the major companies — such as Thomson CSF, which produces military equipment, telephone exchanges, minicomputers, microchips, television sets and hi-fi equipment — have clear ideas of their own about their competence and company strategies, and have resented the government interference implied by their recent nationalization.

Thus Thomson was recently attempting to put its own foot in the American market through cooperation in the minicomputer market with an American company, but the French government stepped in and — despite Farnoux's attachment to the United States — insisted that Thomson link up instead with the mostly French computer company CII-Honeywell-Bull. This has riled the Thomson management, not least because the French company had earlier undermined Thomson's own minicomputer operation with the introduction of a Honeywell system (the "Level 6") despite an agreement not to do so.

Thus internal strife may make the French electronics adventure less of a threat than it might otherwise be. Meanwhile, money will certainly pour into the industry, and that alone may give it a competitive edge. It seems likely that the government will provide FF10,000 million in support of component manufacture (basically chips); FF7,000 million in consumer electronics; FF15,000 million in computers and office automation; FF15,000 million in the space industries; FF3,200 million in industrial automation; FF2,000 million in scientific instrument manufacture; FF3,000 million in medical electronics; and FF4,500 million in software production. On top of this, the industry itself is expected to invest some FF90,000 million over the planning period (to 1986), a rate not far from its present figure.

Robert Walgate

---

*The word "electronics" is used to include everything from materials production to television sets, communications and computers. The French see their 10 main competitors in the industry to be: AT&T, IBM, General Electric, ITT, Philips, Siemens, Matshushita, Hitachi, GTE and Toshiba.

Balancing the francs

The French Ministry of Research and Industry is doing its best to juggle with a tight budget for 1983 — and to make it seem not too different from the 4-year averages recently advertised in the research law passed by the National Assembly (17.8 per cent a year in real money, and 4.5 per cent a year in jobs). The budget will not be announced before September: it seems likely that the cash target will be achieved, but not the jobs.

This represents a political decision that in the short run it is more important to get on with research, and to re-equip laboratories, than to create new posts. The figures under discussion would give something like a 2–3 per cent increase in posts (up to 600 new positions) at the Centre National de la Recherche Scientifique, which is responsible for the bulk of basic science in France; 6 per cent (230 posts) at INSERM, which pursues medical research; and 3 per cent (200) at INRA (agriculture). The total civil research budget would rise the full 17.8 per cent to around FF32,000 million (£2,700 million).

All this takes place against a total government budget constrained to grow only 4.1 per cent in real terms next year, and a number of items written into the 1983 science budget that were not envisaged in the law, including FF1,000 million to help equip the science museum at La Villette, north of Paris, and FF500 million to support the computer firm CII-Honeywell-Bull.

Even so, the government is assuming only an 8 per cent inflation rate next year. Current inflation is in double figures. And in spite of the apparently large increases announced for 1982, the real increases in laboratory budgets have been eaten into by inflation and the weakness of the franc against the dollar. For example, despite a nominal 30 per cent increase, the budget of one director of a molecular biology laboratory in France this year was only 5 per cent up in buying power. But he was not complaining: "That's probably much better than my foreign colleagues".

Robert Walgate

0028-0836/82/310504-02$01.00

British biotechnology

Commons ask for action

The agreement that gives the British biotechnology company Celltech exclusive rights to research carried out by the Medical Research Council was condemned last week by the Education, Science and Arts Committee of the House of Commons. In an interim report on its continuing inquiry into British biotechnology, the committee said that it is opposed to exclusivity in patent rights arising from research council work, and urged that the government should review the issue before the Agricultural Research Council comes to a similar arrangement (see *Nature* 29 July, p.412).

The committee seems to have been influenced towards this conclusion by the arguments of one witness that Celltech, having been put in a "monopoly position", must be assumed to have "responsibilities commensurate with its privileged position". The fear seems to be that some good ideas might not be pursued effectively in these circumstances.

Consistently, the committee also advocates that the British Technology Group should be deprived of its monopoly right to the first refusal of patent rights developed in research council laboratories. This goes back to 1947, when the National Research Development Corporation (now merged in the British Technology Group) was given the right to exploit (if it chose) patent rights arising from publicly supported research.

On this point, the committee seems to be pushing at an open door: the Secretary of State for Industry, Mr Patrick Jenkin, told the committee that a consideration of this question was "long overdue". For the rest (and apart from a proposal that British universities should publish lists of their members of staff holding consultancy agreements with industry), the interim report is a complaint that the British government has responded too hesitantly to the advice it has been given in the past two years followed by a string of detailed recommendations for improving the machinery of government.

Thus, the committee says, the Department of Industry should have a formal channel of communication with the University Grants Committee (UGC) so as to be able to make its opinion felt that a greater share of the universities' budget should be spent on science and technology. UGC should conversely be represented on the department's biotechnology committee (which might raise constitutional difficulties) and should set up a "more specific decision-making structure" for "strategic decisions about biotechnology".

The essence of the committee's interim report is centralist — it pleads for a "more coherent science policy" and in particular for the restoration of support for research "within the dual support system". But the report also asks that there should be a study of tax incentives as a means of stimulating industrial links with the universities and more deliberate study by the British research councils of the earmarking of student training places for intending biotechnologists.

Entrepreneurship

Monsanto act

A new venture capital fund with ambitions in biotechnology has been set up in Britain on the initiative of Monsanto, the US chemical manufacturer. Other partners in the venture include the Universities of Oxford, Cambridge and St Andrews, Imperial College London and the Nuffield Foundation, to whom the project is primarily another kind of financial investment.

The new fund will have an initial capital of £10 million (of which Monsanto will be contributing a half). The fund will be called Advent Eurofund, and will be managed by a board whose chairman is Sir Kenneth Cork,a skilled accountant.

The prospectus of the new fund is wide, covering most fields of high technology — robotics as well as biotechnology. The immediate objective is to seek minority holdings in new and established companies, investing sums between £100,000 and five times as much in order to acquire them.

Advice on prospective investments will be provided by an advisory committee including Sir Peter Hirsch and Dr W. Graham Richards (both of the University of Oxford) and Sir Hans Kornberg (University of Cambridge). Dr G. Edward Paget, director of biomedical programmes at Monsanto, will also be a member.

One member of the advisory committee said this week that his chief interest was to find ways of helping academics in British universities and elsewhere to turn their bright ideas into commercial realities. In the past few months, the venture capital scene has unexpectedly come to life in Britain. The merchant bank N.M. Rothschild has a $50 million fund for investment in biotechnology (mostly overseas), while Technical Development Capital, a subsdiary of Finance for Industry (owned by the British clearing banks) has also been active in the field. In microelectronics, there has been ill-informed controversy about the activities of Mr Jack Melchor, the Californian entrepreneur, who has apparently been testing the nerves of potential British businessmen by using £2 million from the British Technology Group to back people with ideas only if they relinquish financial control.

Signs of hope

Biotechnology is alive and well and living in at least 22 British universities. This is the burden of the first report of a body of officials called the Inter-Research Council Coordinating Committee on Biotechnology, published before the House of Commons report. In effect, it is the research councils' reply to the report prepared two years ago by a group under the late Sir Alfred Spinks meeting under the auspices of the Advisory Board for the Research Councils, the Advisory Council on Applied Research and Development and the Royal Society.

The new document, emolliently out of tune with that of the House of Commons committee, says that even before the recommendation two years ago that research council spending on biotechnology should be at least £3 million a year, expenditure amounted to £4 million in 1979-80 (and was more than £7 million the following year).

The group says, however, that it cannot accept the suggestion that successful research grant applications should include some in which there is evidence of industrial interest, but reaffirms the commitment of the research councils to "support the best science".

The research council group also resists the proposal that a small number of the centres of excellence should be established in biotechnology on the grounds of "a lack of support from government", the breadth of biotechnology and the wide distribution of relevant studies in 22 British universities.

The group says that British institutions must reconcile themselves to the loss of a proportion of people trained in Britain to posts overseas, pours cold (or at least lukewarm) water on the European programme in biotechnology and raises two subversive questions for future decision. Should British scientists who have commercial links with companies overseas be denied research council grants to support "underpinning research"? And what should be done to equalize the rewards from commercial collaboration of full-time members of research council laboratories and their intellectual partners, who "stand to gain financially to a substantially greater degree"?

One of the Spinks recommendations is, however, accepted — the need for new mechanisms to bridge what is called the "predevelopment gap" between the bench and the manufacturing plant. The document acknowledges that under peer-review, proposals designed to produce useful products "may be regarded as scientifically interesting".

0028-0836/82/310505-02$01.00

US employment

Argonne's new ways with people

Washington

Argonne National Laboratory has repeatedly evaded limits on the numbers of staff employed by referring applicants to intermediary companies known as "body shops", which supplied Argonne with "resident consultants" in exchange for overhead payments as high as 184 per cent.

This practice was one of several management irregularities at Department of Energy (DoE) laboratories revealed last week by the Senate's permanent subcommittee on investigations. The laboratories, which are largely exempt from the normal federal contract procedures, have been the subject of a year-long investigation by the subcommittee and Congress's General Accounting Office (GAO).

The use of the "body shops" appears to be the most serious abuse unearthed by the subcommittee. In one typical case, an applicant was told that she could not be employed by Argonne because of a freeze on engaging new staff but that she would instead be offered a job by an intermediary company. Her salary was $10.34 per hour; the company was paid $25.54 per hour for her services. After working as a "residential consultant" at Argonne for a year, she was taken on by the laboratory directly. She continued to do exactly the same work, and received slightly less than the $10.34 per hour she had been making as a resident consultant.

GAO found that one division at Argonne had spent $7.2 million for resident consultants since 1977, of which overhead charges by the "body shops" accounted for $4 million.

The practice of hiring professional employees through intermediaries was also popular in Argonne's Washington office. In questioning GAO Comptroller General Charles Bowsher at the subcommittee hearings last week, Senator William Roth (Republican, Delaware) brought out the fact that the Washington office had hired a nuclear engineer through Kelly Girl, a temporary office-help agency. A similar arrangement was made through the Washington School for Secretaries, which runs a temporary service. A subcommittee staff member said that "five or six" professionals had been hired this way; according to GAO, Argonne could have saved $45,000 by hiring these employees directly and avoiding the agencies' commissions of up to 50 per cent.

Argonne appears to have used the body shops not only to avoid hiring limits but also to circumvent its own education requirements. Senate investigators found several resident consultants who did not meet the laboratory's graduate-degree requirements but who had been referred to body shops by the laboratory and hired by them, usually to continue work at Argonne that they had begun as undergraduates in Argonne's student programme.

The acting under-secretary of DoE, Jan Mares, offered a mild defence of the use of body shops before the subcommittee: "managers of these laboratories need the flexibility to hire temporary people", he said, especially in the face of annual budget uncertainties and fluctuations.

Argonne's official response to the GAO study points out that the resident consultants were needed particularly at a time when Argonne was being asked to shift quickly from a concentration on nuclear energy to a much broader coverage of energy research and development. Argonne says there are now fewer than 15 resident consultants — in 1980 there were 200.

The need for flexibility was also the issue in another area, the awarding of contracts without competitive bidding. The national laboratories are allowed considerable leeway here — with the result, as GAO reported earlier this year, that for example 72 per cent of Argonne's contracts were let without bidding. At Oak Ridge National Laboratory, GAO found several instances in which the company selected by the laboratory was informed of the laboratory's budget for the project. The company's proposed costs for the project tended to show a remarkable agreement with the amount budgeted.

The laboratories' exemption from the usual federal and DoE contracting procedures led to other abuses. DoE headquarters discovered that by going through the laboratories, it could avoid those regulations in awarding its own contracts. A contract official at Brookhaven National Laboratory, for instance, was directed by DoE to award $15,000 to a particular film-maker for production of an informational film unrelated to any work then going on at Brookhaven. The project collapsed six months later when the film-maker proved "incapable of performance", according to the Senate subcommittee staff. It also turned out, said the staff, that the film-maker's "only unique qualifications were that he was in the film business and has attended graduate school with a lab employee whose office was involved in the project".

The Senate investigators said that under these "directed procurements", the laboratory officials nominally in charge of awarding contracts and overseeing performance were in fact used simply as conduits for DoE, and often did not even see any of the work.

DoE last autumn issued an order for this practice to stop. But it is still permitted when the contract is directly related to the laboratory's technical mission. DoE officials told the Senate investigators that the procedure was sometimes necessary in order to cut through the red tape of the standard procurement channels.

Senator Roth emphasized that he appreciated the special mission of the laboratories and their need for flexibility. But he said there is "no assurance that money is well spent" without better safeguards. And he seemed less than satisfied by DoE assurances that the problem of directed procurements had been solved by last year's order. "The oldest game in town is to issue some instruction to satisfy some senator", he said. **Stephen Budiansky**

Anthrax island

Why worry?

How do you get rid of anthrax? The announcement last week in the House of Commons that the British Ministry of Defence intends to try and clean up Gruinard Island has left several people puzzled. The island, off the north-west coast of Scotland, is contaminated with *Bacillus anthracis* spores scattered during biological warfare tests carried out during the Second World War. The ministry will use laboratory-tested chemicals in the field trial which will begin next month. What these chemicals are and why such an operation is now called for are not at all clear.

Gruinard Island is in a popular tourist area, but has been out of bounds to man and animals for nearly 40 years. Scientists from the Chemical Defence Establishment at Porton Down have been testing soil samples and trying to find an effective decontaminant for many years. A survey in 1979 showed that viable spores of *Bacillus anthracis* lay in the top 6 cm of soil and were mainly concentrated in a small area in the southern end of the island.

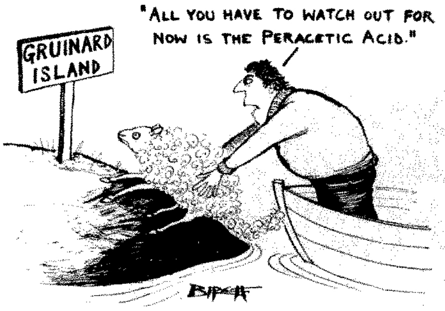
"ALL YOU HAVE TO WATCH OUT FOR NOW IS THE PERACETIC ACID."
GRUINARD ISLAND

The Ministry of Defence revealed its intention to carry out field trials in response to a question in the Commons by Mr Donald Stewart, MP for the Western Isles, who asked how much longer the island would be ruled unsafe for men and animals. The ministry plans to put a small party from the Chemical Defence Establishment onto the island to test the effectiveness of certain chemicals in destroying the anthrax spores. The ministry will not give any details of the chemicals in question. A representative of the Scottish Home and Health Department will accompany the scientists.

In spite of warning notices, tourists frequently stray onto Gruinard Island. In a recent incident a German and a Belgian on

0028-0836/82/310506-02$01.00

a fishing trip were apparently unable to understand the hazard warnings and wandered onto the island. *Bacillus anthracis* is particularly dangerous to humans when inhaled into the lungs — a low risk on Gruinard because the spores are buried in the soil. It can also enter the body through the gut or through cuts on the skin, when it causes spreading sores.

Officially *Bacillus anthracis* is described as a hypervirulent micro-organism which is difficult to destroy. In laboratory conditions it is susceptible to heat. Peracetic acid can also destroy anthrax spores but the acid must itself be carefully handled.

One knowledgeable person confessed himself perplexed as to why the Ministry of Defence is making such a fuss about the island. The strain of anthrax on Gruinard is not as virulent as some field strains and infection is easily treated with antibiotics. Animals can be vaccinated against the disease and in many areas, where the climate is less favourable, anthrax has been successfully eradicated through animal vaccination programmes. Gruinard Island, he said, poses no serious threat to humans. In the past anthrax has been found in animal bonemeal feed and its presence ignored. **Jane Wynn**

UK research councils

Sharing of spoils

One of the long-standing sources of jealousy among British scientists is likely to be stirred up by the decision announced last week to mount an inquiry into the ways in which research councils distribute their resources between in-house research and support for universities. The Advisory Board for the Research Councils has set up a committee under Mr J.R.S. Morris, chairman of the British subsidiary of the oil-drilling company Brown and Root, to make recommendations on the subject early in 1983.

The committee is a swift response to one of the more contentious recommendations of the Merrison report on university research, published last month (see *Nature* 10 June, p.445). The report said that when research councils are under pressure, "university support may be the only or chief area" in which they can economize. In a judicious but ominous phrase, the report went on to say "we are not satisfied" that the balance between in-house spending and university support "is always right".

The committee also pointed out that during the 1970s, when government support for the research councils increased by 8 per cent in real terms, the councils' collective support for university research increased by only 3 per cent. This comparison may, however, be misleading because of the importance of salary and equipment costs in in-house budgets and research grants respectively.

Even so, some research council employees see the setting up of the new committee as an attempt by the academic scientists who account for the majority of members of the advisory board to increase the funds available for university research. Others ruefully recall that in the 1960s, the Agricultural Research Council, relatively and absolutely the most modest supporter of university research, was, on account of its dependence on in-house research, the target of the complaints that led to the Rothschild reorganization of civil science.

In practice, the new committee will have to solve several awkward problems, not least that of deciding how to assess the present performance of the research councils. The accompanying chart, based on figures taken from the Merrison report, shows the use made of resources in 1978-79 by the four research councils supporting research in the natural sciences. The cost of commissioned research is that commissioned by government departments from the research councils under the Rothschild customer-contractor principle.

The pattern of spending by the Science and Engineering Research Council is anomalous in that, of the £144 million claimed as university support in 1978-79, only £51 million was spent directly in universities, with the remainder divided almost equally between service laboratories and subscriptions to international projects.

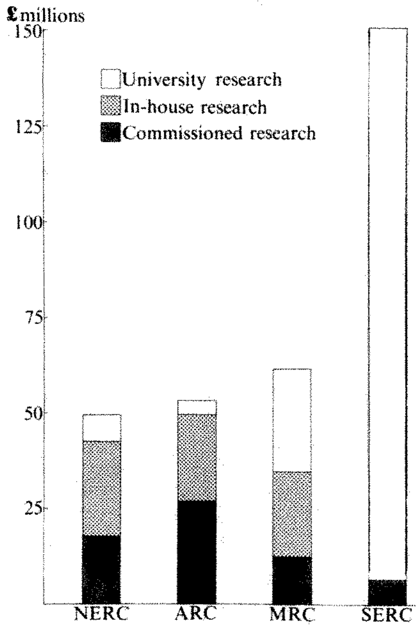

Research council spending, 1978-79. Spending by the Agricultural Research Council (ARC), Natural Environment Research Council (NERC), Medical Research Council (MRC) and Science and Engineering Research Council (SERC). Source: Cmnd 8567, HMSO.

For the committee (which will have met for the first time this Wednesday, 4 August), the most difficult task will be to establish criteria for deciding how the "right" balance between in-house research and university support should be struck. The chairman of the committee is thought to be impartial in the sense of being as impatient with the research councils as with academics.

Telecommunications

Battle hots up

Mercury, the private telecomminications network licensed last year in Britain to compete with British Telecom, the still-public network, is about to take off rather sooner than expected. Its founders (Cable and Wireless, British Petroleum and Barclays Bank) have brought foward to next spring the launch of a service in London, intended as the first element in a more extensive network.

Mercury says that demand from potential customers is the chief reason why its plans have been advanced, but there seems no doubt that the competitiveness of British Telecom is another. At the outset, Mercury hopes to gain some advantage because it will be offering high-speed digital transmission services, available from British Telecom only in the City of London. The plan is to do for Birmingham by next May what will have been done in London a little earlier, when the two cities will be linked by microwave. These two services are the first elements in what Mercury misleadingly calls a national network. The present goal (for 1984) is a figure-of-eight network linking only the major commercial cities in central England. Initially transmission within cities will be by microwave radio.

Initially, Mercury will be suitable only for customers wishing to send voice and data down leased lines at 64 kilobits or 2 megabits a second. Charges will be based on standard rates per channel, independent of distance. The basic network is expected to cost about £50 million, but the capital cost of providing a network to compete with British Telecom's will be far more. Investment of £1,000 million over 25 years has been mentioned to pay for, among other services, switching and possibly a link with British Telecom.

But plans for the future will depend on customer demand. Mercury is in touch with 25 potential customers for its London service, and government departments as well as large companies are said to be showing interest. Mercury believes that its chief attraction over British Telecom's digital service in London will be its transatlantic satellite-link. At one stage, plans for international links had seemed doomed to be obstructed by British Telecom which, as the signatory to Intelsat, is the recognized international carrier. But Mercury, which will be negotiating directly with Intelsat to carry traffic late next year from London, is unperturbed that British Telecom must sign the contract, seeing British Telecom's involvement as purely administrative.

How successful Mercury is in attracting its statutory allowance of 3 per cent of British Telecom's business by 1985 will also depend on the competition. The consensus is that the monopoly is putting the heat on. **Judy Redfearn**

0028-0836/82/310507-01$01.00

UK higher education

Call for change

A gang of lounge-suited revolutionaries issued last week a call to turn the British educational system on its head. Calling itself a study group of the Royal Society of Arts, and concealing its subversive message* in glossy covers decorated with an elegant engraving of the Adam building used as its accommodation address, the gang demanded nothing less than the reorganization of the Department of Education and Science (to include industrial training), tax deductibility for fees paid for technological education, the reform of the British school examinations system and a scheme for supporting institutions of higher education with public funds on a scale determined by "the funds which institutions succeed in raising for themselves".

The movement's front-man, and self-confessed chairman of the study group, is Sir Henry Chilver, vice-chancellor of Cranfield Insitute of Technology and chairman of the British government's Advisory Council on Applied Research and Development (ACARD). Sir Henry is widely tipped in Whitehall as the man most likely to succeed Sir Alec Merrison (vice-chancellor of the University of Bristol, chairman of the Advisory Board for the Research Councils, chairman of the council of CERN, etc.) as the chairman of most committees on British science policy during the 1980s.

Speaking last week to journalists (outnumbered two to one by members of the group), Sir Henry admitted that the manifesto called for a revolution in the British educational system. He said he would be infiltrating some of the proposals into ACARD's deliberations on the mechanisms for supporting British university research. The group hopes to accomplish its goals by putting pressure on politicians and civil servants, and by writing letters to influential people.

All-purpose chairman, Sir Henry Chilver

One objective is to change the education of young people aged 16–19, providing them with "flexibility of employment opportunities". The manifesto also demands a "shift in curriculum for 13–16 year olds", a new school examinations system "aimed at encouraging young people to be educated for their future capability in society" and the monitoring of "the effectiveness of education for wealth creation" by some method as yet undisclosed. To accomplish these objectives, the group admits, it would be necessary to rewrite both the Education Act (1944) and the more recent Training Act so as to give a new Department of Education and Training direct control of the education of the young.

There seems, however, to be an ideological split among the members of the group on central direction for higher education. One member, Dr Donald Moore (previously with Imperial Chemical Industries Limited), said that "a lot of money is wasted in universities" and called for strong central management of higher education. But Chilver seems to prefer a system of financial incentives to make universities more aware of industrial needs.

The most subversive proposal is that for replacing the present general subsidy of higher education with a system in which universities and other institutions would be supported on some scale related to the resources they had been able to recruit from industry and elsewhere. The manifesto says that "those most closely related to industry would attract continuing public support" but otherwise conceals its reasons for believing in a switch to "geared funding" and the means by which that would be accomplished, on the pretext of "keeping it short". **John Maddox**

Nuclear aftermath

Euthanasia plan

The Soviet media — not normally practitioners of sensation journalism — last week gave major coverage of alleged British plans for "selective treatment" and/or enforced euthanasia of victims of a nuclear disaster. According to the Soviets, plans prepared by the Royal College of Physicians for the British government insist that "anyone who is seriously injured must be destroyed" — preferably by the military or the police, since the doctors, allegedly, are unwilling to break the Hippocratic oath.

These remarkable reports are apparently based on an article in *The Guardian* of 22 July. Within three days it had been picked up by *Pravda* and then by Moscow Radio — remarkably fast for Soviet journalism.

The *Guardian* writer, Andrew Veitch, says that his story was based on "classified" government plans leaked to his newspaper and a "statement" prepared by the faculty of community medicine of the Royal College of Physicians. This statement, he says, was never published.

Acccording to the faculty members, however, the document to which Mr Veitch referred was never, in any sense, an official statement. It was, they say, simply a discussion paper written by a small "study group" which the faculty board felt itself, as a body, unable to accept.

The president of the faculty, Professor Alwyn Smith, who is also a signatory of the recent "Physicians against Nuclear War" declaration, describes the original paper as "somewhat forthright" and suggests that it would need "very extensive revision" before it would gain the support of the faculty's membership. It is presumably the latest version of this document, which was discussed last April at the faculty's meeting on medical planning in relation to nuclear war, that came into the hands of Andrew Veitch.

Since the speech of Mr Andrei Gromyko at the United Nations Disarmament Session in June, the Soviet media have repeatedly attacked the reluctance of Western governments to respond to Soviet "peace initiatives".

To that extent, their response is predictable. The curious error by which the study group's draft document, which called for a full public debate of the issues (including euthanasia) involved in disaster planning, becomes in the Russian version a secret government document prepared by "troglodytes from the world of medicine" and kept secret from the British people, must inevitably throw some doubt on the Soviet understanding of the Western-style nuclear debate. **Vera Rich**

Repression in Guatamala

Physician freed

A prominent Guatemalan physician and anthropologist, Dr Juan José Hurtado Vega, was released from government custody last Thursday after enquiries by a delegation from five US scientific societies.

Dr Hurtado had been held virtually incommunicado, and without charges, since 24 June, when he was abducted by armed men in civilian clothes outside his clinic in Guatemala City. Not until 4 July, in a speech by Guatemalan President Efrain Rios Montt, did the government admit that Dr Hurtado had been arrested.

According to the American Association for the Advancement of Science (AAAS) Clearinghouse on Science and Human Rights, Dr Hurtado was released to the custody of the International Red Cross Committee, which suggests that he was in need of medical treatment. The members of the US delegation that visited Guatemala to enquire after Dr Hurtado told reporters upon their return last week that they were seriously concerned that he had been physically mistreated and possibly tortured. Dr Hurtado's wife reported that during the five-minute visit she was allowed to her husband — a visit that was filmed and broadcast by the state-run television — she noticed that he was very weak, had lost a lot of weight and had a haematoma on his arm. The delegation was told by Guatemalan officials that Dr

---

**The Future of Technological Higher Education in Britain* (Report of a study group appointed by the Council of the Royal Society for the encouragement of Arts Manufactures and Commerce).

0028-0836/82/310508-02$01.00

Hurtado was in good health and was recovering from a gastro-intestinal illness. AAAS said that Dr Hurtado and his wife were going to leave Guatemala and were due in the United States within a few days.

The reasons for Dr Hurtado's arrest remain unclear. President Rios Montt, in his television address on 4 July, accused Dr Hurtado of being a communist; later, in an interview with a BBC correspondent, Rios Montt charged that "he is not merely a communist but a captain of many units, a member of the leadership group. His son, all his family have been killing people." The US delegates reported that many government officials they spoke to brought up the association of one of Dr Hurtado's daughters with the communist insurgents. She is now living in Nicaragua.

Dr Hurtado may also have come under suspicion for his work among the rural poor. Since 1976, he has run a private clinic offering free health care in San Juan Sacatepequea, an Indian village outside Guatemala City. The delegation doubted that this was the principal factor behind his arrest, especially since the government has made no effort to shut down the clinic.

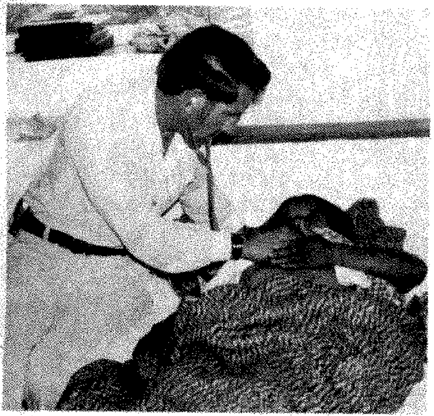

Dr Hurtado and patient

The most likely direct motive for his arrest may have been the kidnapping, the day before, of the Interior Minister's son by the Guatemalan communist party. The Interior Minister, or perhaps even a subordinate acting on his own, may have ordered the arrest of Dr Hurtado as a hostage. If so, it was apparently a miscalculation: when the communists issued a list of prisoners whose release they were demanding, Dr Hurtado's name was not on it.

The US delegation, which comprised AAAS, the American Public Health Association, the American Anthropological Association, the National Association of Social Workers and the Institute of Medicine of the National Academy of Sciences, expressed concern that this case may be a bellwether of a return to the repression of the previous regime in Guatemala. President Rios Montt, who came to power in March of this year, pledged to restore civil rights and constitutional law. On 1 July, however, the government declared a "state of siege", suspending all political activity and most civil liberties.

Stephen Budiansky

Plea from a Soviet refusnik

An open letter to Dr J.M. Legay, Secretary General of the World Federation of Scientific Workers.

SIR — Several times either alone or together with colleagues in the same position (having been refused permission to leave the Soviet Union), I have appealed to you and to the World Federation of Scientific Workers for help. But only recently have we received a reply — and that not directly, but in the pages of *Nature* (11 February, p.452). I regret to say that your answer was both surprising and disappointing. Being absolutely distressed by it I have to address you once again. Another, perhaps more important reason making me do it is that I am sincerely convinced of your honesty, humaneness and high moral standards — anything else would be incompatible with the high position you occupy. Besides, I believe that the contents of your answer suggest that you are not aware of the gravity of the situation of the scientists refused permission to leave the Soviet Union.

For more than 3 years I and my friends have been trying, through completely legal channels, to obtain permission to leave the country. All of us after many months of waiting have been refused permission and in most cases nobody took the trouble of explaining to us the reasons for this refusal. And none of us has ever dealt with military or state secrets. That is why I say that these refusals do not comply with the laws of the Soviet Union, with the International Human Rights Declaration and with the Helsinki Final Act. The only reason for these refusals is the fact that we have scientific degrees. And it has nothing to do with the problem of the notorious "brain-drain" since most of us are deprived of any professional work and have been deprived of it ever since we applied for permission to leave the USSR.

I have appealed more than 20 times to different Soviet bodies to cancel the illegal decision and to protect me from lawlessness but I have not received a single answer and the experience of many of my colleagues has been the same. Neither have I received any answer from the vice-president of the World Federation of Scientific Workers Mr N.N. Inozemtsev or from Mrs Janushevaskaya. But according to the federation's charter, it is their duty to defend the interests of scientists.

Addressing you, Mr Legay, I like many others expect sympathy and help. Maybe it is naive on my part but I consider it your moral duty and that of the federation to help us. It is not a question of me alone, a whole group of scientists is involved. It is not only our careers as scientists, but our whole lives that are threatened. We suffer material hardships and nervous stress beyond any normal limits. We are beginning to break down. Recently one of us, Dr Tsipkin, died after receiving a dismissal notice. Many of us have become seriously ill — and still we have to support aged parents or our children. We are in complete isolation, we are thrown out of society and in fact are not protected by law. And all this for one "fault", for one "crime" — our wish to leave the Soviet Union.

We are living in the world so strikingly depicted by Kafka, but the circumstances of our life are much harder than those of his characters. We have no possibility in our own country to protest openly, publicly. We can't defend our interests legally. We can hope only for help from our western colleagues. This is our only hope, the only thing that makes it possible for us to go on living.

Don't become a silent accomplice of the injustice, don't let evil take the upper hand, raise your voice for us. I want to believe, Mr Legay, that an appeal from you to the Soviet government, an appeal from the World Federation of Scientific Workers and from its journal *Scientific World* will change our position, will make it possible for us to leave the Soviet Union and to return to scientific work. Don't let our appeal get drowned in bureaucratic hold-ups and procrastinations.

Only an appeal to the Soviet government can change the situation. The more definite, the more public your stand, the sooner it will help the unfortunate. Take this stand, Mr Secretary General, and like any noble deed it will only add to your and the federation's authority.

You cannot but understand, Mr Secretary General, that our life and our fate have become part of an important problem — that of trust among scientists and their mutual understanding. You have to understand that the question of mutual trust and respect, the questions of scientific contacts will depend on the settlement of our problem. It cannot be right to let general and undoubtedly very important problems obscure the fates of individual people. It cannot be allowed that behind a torrent of beautiful words evil should be committed. Who but the World Federation of Scientific Workers and its head can realize and know it? Who but the federation and its Secretary General can and must stand on guard defending the members deprived of everything?

Moscow J.S. IRLIN, DSci

0028-0836/82/310509-01$01.00

CORRESPONDENCE

Imperial echoes

Sir — Your note on the establishment of Imperial College's Centre for Biotechnology (*Nature* 24 June, p.617) has caught the sentiment of the occasion, but lacks one or two points of detail.

Imperial Biotechnology Ltd (IBL) is jointly owned by Imperial College (35 per cent), TDC Developments Ltd (35 per cent) and its own staff, who hold the balance. The fermentation pilot plant will be managed by IBL, which will expand the business of development and pilot scale manufacture of specialized biological products. The company and the college are fully committed to maintain and expand the current college teaching programme. They have made a teaching agreement for the provision of adequate pilot plant and fermentation facilities for the college's programme of work. Like any other customer, the college may buy additional resources for research purposes from the company above the agreed level.

Resources that were absorbed by the non-commercial pilot plant operation may now be released for academic purposes; the college is applying part of them to the two lecturer posts shortly to be advertised (the Leverhulme chair is financially self-contained). The lecturers' positions will not therefore be so precarious as the comment ". . . salaries will be met by the fees earned from contracts with outside bodies" implies. They will be normally established posts.

The Centre for Biotechnology sees contract work as a major factor in the development of its research programmes — biotechnology is nothing if not an applied discipline. However, a substantial proportion of the investment in the centre must come from Imperial College's own efforts — unless the college clearly demonstrates its commitment to the subject, the centre will lack the credibility it needs amongst its potential customers.

Imperial College has found what it believes to be a workable combination of commercial risk and academic purposes that suits its own particular circumstances. It is firmly committed to producing the people and the products needed by the biotechnology industry by these means.

David Thomas

Centre for Biotechnology,
Imperial College of Science and Technology,
London SW7, UK

Meltdown risks

Sir — Robert J. Yaes has overstated the hazard of a major nuclear accident by two orders of magnitude in his letter of 24 June (*Nature*, p.622). Not even a meltdown in midtown Manhattan could produce the "several million" deaths he envisions. The number of fatalities from a "maximum credible" accident, which the US Nuclear Regulatory Commission has estimated would occur once in 100,000 meltdowns, is put at 45,000. This is comparable to the toll that might be expected from such "conventional" hazards as oil and gas explosions, and *one-fourth* the number of deaths that could occur if a certain major dam in the Southern California earthquake fault zone should break.

Dale H. Gieringer

Stanford, California, USA

Not by mirrors

Sir — In *News and Views* of 28 January (p.277), Jared Diamond discussed the occurrence of migratory birds in places outside their normal geographic range (vagrants)[1]. Such vagrancy has been noted in many parts of the world and a variety of hypotheses have been put forward to account for it. By discussing only the ingenious "mirror-image misorientation" hypothesis of DeSante[2], Diamond erroneously implied not only that it is the proven mechanism underlying the occurrence of vagrant warblers in California but also that it can account for vagrancy on a worldwide basis.

Based on the hypothesis that some individuals in a population of migrants make mirror-image orientational errors (such as heading SW instead of SE in autumn), DeSante predicted the relative frequency with which various species should occur. The pattern of records supported the hypothesis. The blackpoll warbler (*Dendroica striata*), which migrates towards the SE over North America in the fall, is the most numerous vagrant on the California coast. *A priori*, one would expect warblers captured off coastal California to show SW hopping in an orientation cage. DeSante tested blackpolls captured on the Farallon Islands off California. Unfortunately, almost none of the birds oriented toward SW; most mean directions were toward NE or NW. The results could be explained only by the *a posteriori* hypothesis that the birds have four preferred directions: the normal SE heading, the SW mirror-image, and the reverse of these two. The data, therefore, do not provide strong, clear support for the original hypothesis.

The mirror-image misorientation hypothesis is important and deserves further testing. It is premature, however, to regard it as proven or to extend it to other areas of the world. There are data to suggest that weather patterns, especially wind, may play a large role in bringing vagrants to California and other areas[3]. Recently, a strong association between the arrival of vagrants and particular wind patterns has been demonstrated in Great Britain. Interestingly, the blackpoll warbler is the most numerous warbler vagrant from North America, a fact very difficult to account for by mirror-image misorientation[4].

Kenneth P. Able
Scott B. Terrill
Jeffrey D. Cherry

Department of Biological Sciences,
State University of New York, USA

1. Diamond, J.M. *Nature* **295**, 277-278 (1982).
2. DeSante, D.F. thesis, Stanford Univ. (1973).
3. Able, K.P. in *Animal Migration, Orientation, and Navigation* (Academic, New York, 1980).
4. Elkins, N. *Br. Birds* **72**, 417 (1979).

Prions have feathers

Sir — In *News and Views* on 13 May[1], R.H. Kimberlin discusses S.B. Prusiner's recent suggestion in *Science* that scrapie is caused by some new sort of proteinaceous infective particle or "prion", to use the acronymic neologism suggested by Prusiner[2]. However, there can be no doubt that prions exist. They contain lots of nucleic acid, packaged in a wonderful variety of proteins. One of the more striking of the proteins is keratin, arranged in a complex structure, the feather, that enables the prions to maintain their temperatures well above ambient and to flutter above the southern oceans.

Today the prions are placed in the genus *Pachyptila*. Their vernacular name stems from the generic name given by Lacépède, after the serrated edge to the birds' mandibles (*πριων*, a saw). It was in use as an English name among ornithologists in the last century[3] and is given in the *Oxford English Dictionary*.

Perhaps in this case there is little chance of confusing the old and new meanings of the word. But precision and unambiguity are important in science — even if they are not in *Science*, whose editors do not wish to point out this unfortunate homonymy to their readers. I hope you will be more concerned and that *Pachyptila* will in future be the only prion to appear in *Nature*, whether or not "proteinaceous infective particles" occur in nature.

J.J.D. Greenwood

Department of Biochemistry,
University of Dundee, UK

1. Kimberlin, R.H. *Nature* **297**, 107-108 (1982).
2. Prusiner, S.B. *Science* **216**, 136 (1982).
3. Newton, A. *A Dictionary of Birds* (1896).

The parasitic balance

Sir — I am sure Professor Cox does not need me or anyone else to defend him, but Dr Palmieri's letter (*Nature* 15 July, p.220) does not seem to take account of the fact that Cox's original report (*Nature* 4 March, p.10) was an account of a symposium specifically devoted to *diseases* caused by parasites. Aside from this, of course, Palmieri's contention is true — most parasites are in balance, albeit maybe a delicate balance, with their hosts.

Notable examples are found amongst parasites of wild animals, in this country and elsewhere. Flagellates and sporozoans are almost ubiquitous amongst the wild vertebrates of this country, but direct pathogenic effects of their presence are rare. This does not necessarily mean, however, that such infections are not subtly harmful in conditions of unusual stress, or by virtue of immunodepressive effects. A deeper understanding of factors involved in maintaining the balance might help explain why it sometimes breaks down, with devastating effects among the host population, as exemplified by recent epidemic sleeping sickness (human trypanosomiasis) in parts of Africa.

J.R. Baker

The Institute of Terrestrial Ecology,
Cambridge, UK

Philosopher in gaol

Sir — I have received first-hand information concerning Professor Lessek Novak from the University in Poznan, a distinguished philosopher in Poland's strong tradition of logicians. He has been confined for seven months, held in a prison without daylight and infested with bugs. Professor Novak took part in the postgraduate courses at the Inter-University Centre in Dubrovnik and has been very active in international collaboration in science. His confinement is a grave violation of human rights, particularly that of freedom of thought. I appeal to the scientific community to do everything possible to bring about his liberation.

Ivan Supek

Institute for History and Philosophy of Science,
Zagreb, Yugoslavia

The NK cell: a phagocyte in lymphocyte's clothing?

from Bernard M. Babior and David W. Parkinson

ANIMALS under attack by invading microorganisms are able to kill their attackers by means of a group of exceedingly powerful oxidizing agents which are mobilized in response to the microorganisms' invasion. The earliest evidence for the existence of this oxygen-dependent killing system was reported some 20 years ago by Karnovsky[1] and by Quastel[2]. Since then, this system has been investigated in many laboratories (for reviews see refs 3,4), and it is now understood at least at an elementary level.

The critical step in the mobilization of the lethal oxidizing agents is the activation of a membrane-bound enzyme (or enzyme system) known as the 'NADPH oxidase'. This oxidase is dormant in an unstimulated cell, but comes to life when the cell encounters a microorganism. As its name suggests, the oxidase catalyses the transfer of electrons from NADPH to oxygen. What is unusual about this reaction is that the oxygen is reduced, not by two electrons to form H_2O_2, but by one electron to form the superoxide radical ($O_2^{\cdot-}$).

It is from this innocuous $O_2^{\cdot-}$ radical that all the system's lethal oxidants are formed. These oxidants include hypochlorite (OCl^-), known commercially as a powerful disinfectant, and a group of highly reactive oxidizing radicals, including the hydroxyl radical ($OH^\cdot$), one of the most reactive compounds known in chemistry. OCl^- arises through the peroxidase-catalysed oxidation of Cl^- by H_2O_2, which in turn is formed by the dismutation of superoxide ($O_2^{\cdot-} + O_2^{\cdot-} + 2H^+ \rightarrow H_2O_2 + O_2$), a very rapid reaction which consumes most of the $O_2^{\cdot-}$ manufactured by the cell. $OH^\cdot$ and the other reactive oxidizing radicals are made from the remaining $O_2^{\cdot-}$; the mechanism of their production is poorly understood apart from the fact that no peroxidase is required, though an iron-catalysed reaction between $O_2^{\cdot-}$ and H_2O_2 ($O_2^{\cdot-} + H_2O_2 \rightarrow OH^\cdot + OH^- + O_2$; the famous Haber–Weiss reaction) has been proposed as the source of the hydroxyl radical. It is a striking illustration of the versatility of biological systems that they are able to manufacture and put to use compounds as reactive and dangerous as OCl^- and $OH^\cdot$.

Until now, the oxygen-dependent killing system has been thought to be restricted to 'professional phagocytes' (granulocytes and mononuclear phagocytes), the front-line cells whose purpose in life is to engage and destroy invading pathogens. In this issue of *Nature* (p.569), however, Roder and his associates show for the first time that the same system is expressed by a lymphocyte. The lymphocyte that acts like a phagocyte is the natural killer (NK) cell.

The NK cell is a large lymphocyte whose most prominent morphological feature is a single large granule in its cytoplasm[5]. Many biological roles have been proposed for this enigmatic cell, both from experiments testing the effects of partially purified NK cell preparations on various targets[6] and from studies with intact NK-deficient animals and humans[7]. A function in host defense against infection has been postulated on the basis of the NK cell's ability to recognize and kill virus- and parasite-infected target cells. Its capacity to kill certain malignantly transformed cells has led to speculation about its participation in defense against cancer. Finally, it is able to kill certain types of cells in the normal bone marrow and thymus, suggesting that it may serve to control the function of these tissues on a day-to-day basis. The true physiological role of the NK cell, however, is still not fully understood. Even less well understood are the means by which it exerts its diverse effects. In particular, basic questions as to how target cells are recognized and destroyed are largely unanswered.

The work of Roder and his associates now appears to provide a partial answer to at least one of these questions. The ability of the NK cell when exposed to a susceptible target to produce $O_2^{\cdot-}$ (in staggering quantities too; the amount of $O_2^{\cdot-}$ manufactured by these cells can exceed by two orders of magnitude the amounts liberated by fully stimulated neutrophils or monocytes) and to use this $O_2^{\cdot-}$ to kill this target strongly implicates some form of the oxygen-dependent killing system in target cell destruction. This system must comprise more than just $O_2^{\cdot-}$ itself, because NK cells from patients with Chediak–Higashi disease exhibit greatly impaired killing ability despite a normal $O_2^{\cdot-}$-generating response to NK-susceptible targets[8]. The hallmark of Chediak–Higashi disease is the swollen, grotesquely misshapen lysosome that is found in the cells of affected subjects; perhaps the granule of the NK cell is another participant in its oxygen-dependent killing system, and it is the malfunction of this granule that accounts for the defect in NK cell activity in Chediak–Higashi disease. Supporting this notion are recent experiments with metabolic inhibitors which have been interpreted in terms of a 'stimulus–secretion' model of NK cell activity[9], consistent with the morphology of the cell as a large lymphocyte containing a granule which, after all, must be there for a reason.

Like all novel discoveries, the finding that NK cells can kill with oxygen raises more questions than it answers. Is NK cell function impaired in chronic granulomatous disease, the inherited disorder in which phagocytes are unable to manufacture their lethal oxidants[3]? What are the other components of the oxygen-dependent killing system of the NK cell? Does the NK cell possess oxygen-independent killing mechanisms like those described by Elsbach in the rabbit and human neutrophil[10]? What do these findings say about the relationship between the NK cell and other types of lymphocytes, some of which have killer activity of their own? Is the NK cell a true lymphocyte, or is it nothing but a phagocyte in lymphocyte's clothing? □

Bernard M. Babior and David W. Parkinson are at the Division of Hematology-Oncology, Tufts University School of Medicine, Boston, Massachusetts 02111.

---

1. Sbarra, A.J. & Karnovsky, M.L. *J. biol. Chem.* **234**, 1355 (1959).
2. Iyer, G.Y.N., Islam, M.F. & Quastel, J.H. *Nature* **192**, 583 (1961).
3. Babior, B.M. *New Engl. J. Med.* **289**, 659, 721 (1978).
4. Badway, J.A. & Karnovsky, M.L. *A. Rev. Biochem.* **49**, 695 (1980).
5. Timonen, T., Saksela, F., Ranki, A. & Hayry, P. *Cell. Immun.* **48**, 133 (1979).
6. Herberman, R.B. & Ortaldo, J.R. *Science* **214**, 24 (1981).
7. Heiberman, R.B. *Clin. Immun. Rev.* **1**, 1 (1981).
8. Roder, J.C. *et al. Nature* **284**, 553 (1980).
9. Quan, P.C., Ishizaka, T. & Bloom, B.R. *J. Immun.* **128**, 1786 (1982).
10. Weiss, J., Elsback, P., Olsson, I. & Odeberg, H. *J. biol. Chem.* **253**, 2664 (1978).

0028-0836/82/310511-01$01.00

The fifth major D/V *Challenger* operation in central equatorial waters

from the Scientific Staff, Leg 85, DSDP/IPOD

On 2 May 1982 the drilling vessel *Glomar Challenger* arrived back in Honolulu from Leg 85, the fifth major operation of the Deep Sea Drilling Project in the eastern and central equatorial Pacific. In her holds were well over 2 km of central equatorial sediments and 1.6 m of basalt, the products of 16 drill holes of which the deepest had reached to 525 m below the ocean bottom. From this material, some 21,000 samples have now been distributed to the scientific party aboard and to collaborators all around the world. Some preliminary conclusions, discussed below, have already been reached but ahead lies the main analysis of the core material. The ultimate aim is to understand the entire equatorial system, its behaviour through time, its reaction to stimulation from outside, its effect on and control of climate, and its feedback mechanisms.

The central equatorial Pacific has always been a primary target for DSDP drilling. Earlier legs (Fig. 1) had helped establish the global Tertiary tropical biostratigraphy and chronology that have shaped our understanding of past oceanographic events, and the development of tectonic models for the Pacific Plate. Tertiary equatorial sediments are very sensitive recorders of the interplay between tectonism, oceanic circulation patterns, fluctuations in biological productivity, dissolution and, ultimately, diagenesis.

In the past, drilling disturbances, particularly in the upper unconsolidated 100–300 m of sediments that often comprise much of the Neogene, have hampered really fine-scale reseach in sediments beyond the reach of conventional piston coring. Leg 85, with relatively new tool at its heart — the hydraulic piston corer — was designed to respond to the growing need to obtain environmental signals with frequencies measured in 10^3–10^4 yr.

The hydraulic piston corer (HPC) was developed by DSDP during the late 1970s and first successfully used during Leg 64 (1978); the HPC is a pressure-activated 9 m long piston coring device (with a 5 m option) which is lowered to the bottom of the drill string. It allows the recovery of successively deeper 9 (or 5) m sediment cores in sufficiently soft layers, without having to resort to rotary drilling. The disturbances that make rotary-drilled samples of softer sediments almost useless for high-frequency analyses are thus avoided.

The Joint Oceanographic Institutions for Deep Earth Sampling Ocean Palaeoenvironmental Panel designed Leg 85 to recover undisturbed, tropical Cenozoic sections for research on: (1) high-resolution bio-, magneto-, seismic-, carbonate and stable-isotope stratigraphy; (2) oceanographic and biological (evolutionary) changes associated with the Eocene–Oligocene boundary; (3) termination of Atlantic–Pacific circulation across the Central American isthmus and the evolution of modern Pacific circulation; (4) the origin of the fine-scale cyclicity seen in Pacific sediments of Oligocene to Quaternary age; and (5) carbonate and silica diagenesis in thick biogenic sections. In order to ensure the highest possible resolution and to avoid coring gaps, each hole was doubly piston-cored and then rotary-drilled to basement through the stiffer sediments below the reach of the HPC (generally 150–250 m sub-bottom).

Five sites, 571–575 (Table 1, Fig. 1), were drilled by Leg 85. With the exception of Sites 571 and 572 (Site 572 is a repeat of Site 81, of DSDP Leg 9), which were to terminate in the Miocene, latest Eocene was anticipated to be the basement age at all the sites. Thus, it was also hoped that complete, or near complete, records of the very 'elusive' Eocene–Oligocene (35–40 Myr) transition could be recovered.

Geologically, the dominant tectonic feature of the central–eastern Pacific region is the East Pacific Rise, which generates new oceanic crust at rates of 8–20 cm yr^{-1}, and which serves as a boundary to the Pacific (on which all the Leg 85 sites lie), North American, Cocos and Nazca Plates. In simple terms, during the past 50 Myr, new Pacific crust has been continuously spreading northwestwards, away from the East Pacific Rise. As it spreads it subsides from a depth of about 3,000 m. The motion has two crucial results: it continuously alters the relationship between the stationary equatorial high-productivity belt above and its depositional expression on the sea floor (Fig. 1), and the subsidence with age and cooling of the spreading crust brings about an increasing exposure of solution-susceptible calcium carbonate produced by plankton to deeper, more corrosive waters.

Biological processes are superimposed on this evolving tectonic framework. Upwelling associated with the equatorial current system creates, along the equator, a fertile planktonic belt of variable width (today 3–4° wide and having its maximum expression slightly offset to the north of the Equator) and dominated by carbonate and silica production.

Assuming that these present-day relationships between surface waters and productivity have remained roughly constant during the Cenozoic, a broadly lens-shaped body, with its apex offset to the north, of dominantly biogenous calcareous–siliceous sediments should have accumulated in this region. It should be dominated by calcareous sediments along its crest and be increasingly more siliceous towards its northern and southern flanks — as indeed has been confirmed by seismic profiling, piston coring and

Table 1 Summary of Leg 85 coring

Site	No. of holes	Water depth (corrected m)	Operations	No. of received cores	Maximum penetration (m)	Cored sub-bottom range (m)		Est. age of oldest seds (Myr)	Nature of basement
571	1	3,962	HPC Heat flow/ pore water	1	7.1	571	0–7.1	0.46	—
572	5	3,893	Double HPC Rotary core*	76	486.0	572 572A 572B 572C 572D*	0–19.0 0–154.0 154.0–172.1 0–169.5 151.0–486.0	14–15	Basalt
573	3	4,301	Double HPC Rotary core* Heat flow/ pore water	68	529.0	573 573A 573B*	0–158.6 0–53.2 138.5–529.0	38–39	Basalt
574	4	4,561	Double HPC Rotary core*	92	532.5	574 574A 574B* 574C*	0–206.5 0–180.2 185.0–204.0 194.5–532.5	38–39	Basalt
575	4	4,536	Double HPC	60	196.3	575 575A 575B 575C	0–98.6 93.8–196.8 0–99.8 0–15.8	22	—

Co-Chief Scientists Larry Mayer (University of Rhode Island, Kingston, Rhode Island 02881) and Fritz Theyer (Hawaii Institute of Geophysics, Honolulu, Hawaii 96822); John A. Barron (US Geological Survey, Menlo Park, California 94025), Dean A. Dunn (University of Rhode Island, Narragansett, Rhode Island), Tim Handyside (The University, Newcastle upon Tyne NE1 7RU), Scott Hills (Scripps Institution of Oceanography, La Jolla, California 92093), Ian Jarvis (City of London Polytechnic, London EC3A 7BU), Catherine A. Nigrini (Scripps Institution of Oceanography), Nicklas G. Pisias (Oregon State University, Corvallis, Oregon 97331), Annick Pujos (University of Bordeaux, 33405 Talence, France), Tsunemasa Saito (Yamagata University, Yamagata, Japan), Paul Stout (Scripps Institution of Oceanography), Ellen Thomas (Scripps Institution of Oceanography), Norbert Weinreich (Ruhr-Universitat Bochum, 4630 Bochum, FRG), Roy H. Wilkens (Massachusetts Institute of Technology, Cambridge, Massachusetts 02139).

0028-0836/82/310512-02$01.00

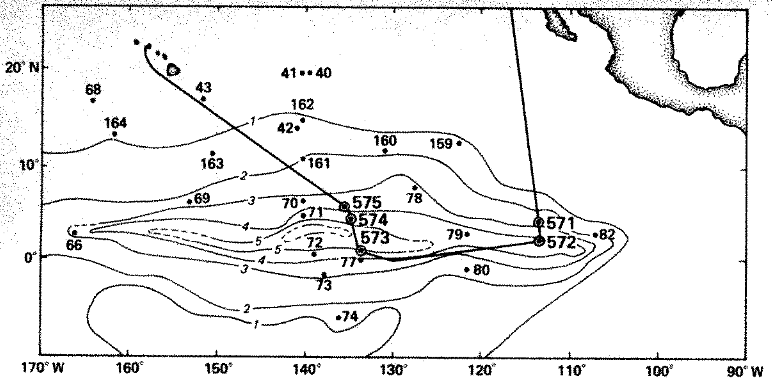

Fig. 1 Cruise track and site locations of Leg 85 of DSDP/IPOD in relation to acoustic sediment thickness (contours are in tenths of seconds of two-way travel time) and previous DSDP operations (Legs 5, 8, 9, 16, indicated by •).

previous DSDP drilling.

The product of this simple tectonic-productivity model of the equatorial region is further altered by changes in oceanographic conditions. The latter affect primarily solution of calcium carbonate or may, in the form of thermohaline bottom currents, physically remove and mix sections of the depositional record. Whereas solution of biogenous silica appears to be occurring throughout the water column, calcium carbonate is very responsive to changes in the corrosiveness of deeper waters. At the other end of the spectrum, numerous submarine outcrops of Tertiary sediments and the widespread hiatuses occurring in the equatorial Pacific testify to the effectiveness of bottom-water erosion throughout the Cenozoic.

Shipboard analyses made during Leg 85 obviously cannot do justice to the massive amount of data gathered but preliminary impressions indicate that of the factors affecting the Leg 85 drill sites, the most striking is the strong east–west productivity gradient. At Site 572, which is at 114°W, sedimentation and accumulation rates are extremely high (often 50 m Myr^{-1}). The sedimentation rate curve at Site 573, 2,100 km to the west, has the same shape as that at 572, but quite attenuated rates (except for the Plio-Pleistocene). Although depth and latitude also contribute to the differences between Sites 572 and 573, analyses of the carbonate and non-carbonate accumulation rates, foraminiferal dissolution index, and qualitative evaluation of diatom and benthic foraminiferal species distributions all support a strong east–west productivity gradient during the mid-Miocene to early Pliocene. This gradient is dominated by the production of siliceous microfossils (mostly diatoms) in the east and the observed lithological and stratigraphical variations appear to respond to this siliceous east–west gradient.

The increasing influence of silica productivity in the east is also indicated by a comparison of the carbonate and non-carbonate accumulation rates. (For all of the Leg 85 sites it is valid to assume that the non-carbonate fraction is mostly comprised of biogenous silica and that there is a consistent association of diatom species, indicative of upwelling, with times of increased non-carbonate accumulation.) At Site 572, a plot of carbonate rate increases positively and linearly with non-carbonate rates. At Site 573, 20° to the west, a comparison of the post-Oligocene carbonate and non-carbonate accumulation rates reveals a similar positive relationship but with a depressed slope,implying that the non-carbonate component decreases its dominance over deposition.

The influence of the east–west gradient of decreasing productivity is particularly noticeable when comparing accumulation rates, carbonate content and foraminiferal dissolution index curves between Sites 572 and 573. At Site 573, the carbonate and non-carbonate accumulation rate and carbonate contents follow one another nicely, high carbonate values being associated with high accumulation rates (productivity) and better preservation. In contrast, at Site 572, the more easterly site, the same relationships are found only during periods of relatively lower accumulation rates; times of high accumulation are associated with enhanced dissolution and decreased carbonate content. The explanation may lie in the magnitude of non-carbonate accumulation at each site: the highest non-carbonate rate at Site 573 is about 0.5 g per cm^2 per 1,000 yr, whereas the maximum value at Site 572 is almost three times higher. This suggests that, when a certain non-carbonate accumulation rate (productivity) threshold is reached, the abundant organic matter produces steep dissolution gradients and enhanced dissolution. We only see evidence for this phenomenon at Site 572, but the implications for palaeoceanographic modelling are intriguing. □

Protein folding by numbers

from Roger Pain

It has long been accepted that the folding of globular proteins from linear unstructured polypeptide chains must occur along closely defined pathways, so that the rate of folding can keep pace with the rate of biosynthesis. Proof of the existence of pathways has, however, been harder to come by. Experimental evidence is required of the identity of species intermediate between the fully unfolded and native states and, more precisely, of three of their properties. The structure of the intermediate, the rates of interconversion with other states and proof that the intermediate lies on the folding pathway and is not an artefact of the denaturation conditions must be obtained to characterize the part of the folding pathway associated with the intermediate under study.

In two recent papers (*J. molec. Biol.* **157**, 331 & 357; 1982), Labhardt has demonstrated the existence of four non-native states associated with ribonuclease, has studied the kinetics with which some of them are formed and has interpreted these results in terms of a sequential mechanism of folding in which a relatively stable β-sheet structural intermediate plays a rate-determining role.

Some may find it surprising that a fresh contribution about protein folding can be extracted from a study of the old biophysical workhorse, ribonuclease A (RNase A), using the relatively low-level information techniques of far-UV circular dichroism (CD) and tyrosine absorbance. Ribonuclease is classed as an $\alpha + \beta$ protein as its three-dimensional structure contains both α-helix and β-sheet secondary structures which are located in no regular orientation with respect to each other. It is peculiarly attractive as a model for folding studies because it can be cleaved specifically between residues 20 and 21 to give the S-peptide, which contains the elements termed α_1, and the S-protein, which contains elements β and the remaining α structure, α_2. The S-peptide and S-protein will combine spontaneously to give enzymatically active RNase S in which the two moieties undergo mutual stabilization of their secondary and tertiary structures.

There are thus three stable species, RNase A, RNase S and S-protein, whose structural relationship to each other is precisely known from X-ray crystallography. These have been partially denatured variously by heat, acid and guanidinium chloride, and the contents of α-helix and

---

Roger Pain is Professor of Physical Biochemistry in the Department of Biochemistry, The University of Newcastle upon Tyne, NE1 7RU.

β-pleated sheet in the products estimated with care from the far-UV CD spectra.

Labhardt correlated these results with the known structures of the three starting products so that he could identify four distinct products of unfolding. In terms of the three main regions of secondary structure, these are $\alpha_1\beta$, $\alpha_2\beta$, β and α_2^*. $\alpha_1\beta$ is not stable but may have a role as a folding intermediate, while α_2^*, which represents the occurrence of an α helix in the thermally unfolded state, cannot yet be assigned to a definitive structure and hence to a role on the folding pathway.

These experiments on the equilibria of the various unfolding reactions of ribonuclease and its derivatives, together with supporting data from the literature, lead to the conclusion that the three antiparallel strands of folded β-structure must be formed for the N-terminal helix (α_1) to be stabilized. However, the species $\alpha_1\beta$ requires the further independent folding and tertiary association of the α_2 group of helices to give it permanence as $\alpha_1\alpha_2\beta$ (RNase A or RNase S). Thus in the folding molecule, three different regions of secondary structure can form independently and associate with mutual stabilization to give the folded enzyme with its native structure and function.

Given some of the structural intermediates associated with the folding pathway, in what order do they form and associate and what are the rate-limiting stages? Labhardt goes on in a second paper in the same journal to monitor the kinetics of refolding of RNase S by the regain of 2′-CMP binding ability and, with identical results, by changes in tyrosine absorbance. The kinetics are, as we would now expect for a proline-containing protein (see *Nature* **290**, 187; 1981), complex. Three phases are resolved in refolding from initial conditions in which different proportions of the equilibrium species reported above have been shown to exist. Two interesting features emerge. The fastest phase is second order, reflecting the rate-limiting association of S-protein and S-peptide, and the amount of product, RNase S, formed from this phase is equal to the amount of S-protein with preformed structure existing in the initial conditions from which folding takes place. Thus, this particular part of the structure, and not, for example, the α_2 moiety, is essential and sufficient for the productive association with S-peptide to take place. It is a key intermediate on the folding pathway.

The two slower phases of refolding reflect the same folding pathway but starting a stage further back, that is from S-protein molecules whose β-structure is unfolded. These may collapse to a condensed species containing improper proline isomers which have to isomerize before the fully native structure is attained (species I in *Nature* **290**, 187; 1981). Labhardt's second key observation is that the rates of these two slower phases are linearly related to the thermal stability of RNase S in the final conditions of the folding experiments. Since the S-peptide has no direct effect on these kinetics, it is concluded that the species whose thermal stability dictates the rates of folding is the condensed structure with improper prolines. This is therefore identified as a transient precursor of the folded S-protein with its β-structure.

This work represents a significant clarification of intermediate species involved in the folding of ribonuclease. Structures which can be 'seen' by available techniques can be numbered and ordered into an overall sketch. However, just as painting by numbers does not result in a work of art, so folding by numbers does not give us the complete folding picture and there still remains much to be discovered. ☐

Measuring competition in plant communities

from Peter D. Moore

EXPLANATIONS of how similar species can coexist within a single area have, in general, been more satisfactory when dealing with animal species than with plants, and it is fairly evident why this should be. Animal species vary in their specific demands for food resources and may also vary in the manner in which they tap those resources, hence there is considerable opportunity for niche specialization and co-adaptation between species. In the case of autotrophic plants, there would appear to be far less room for diversification. All the various grass species in a meadow are basically doing the same things — gathering light energy, reducing carbon dioxide from the atmosphere, extracting water and required elements from the soil. Just how can so many morphologically similar species coexist? Is their coexistence accompanied by fierce competition for the habitat's resources, or has the process of niche specialization over evolutionary time scales resulted in competition interactions being minimized?

Such questions have great appeal to ecological theoreticians[1-3], particularly to animal ecologists who can base their models on the Lotka–Volterra population growth equations. Newman[4] has recently emphasized that this approach, which depends on the numerical assessment of populations, is not entirely satisfactory when applied to plants, in which vegetative proliferation of individuals can occur. He develops two alternative models more appropriate for plant studies, and concludes that the maximum number of plant species which could coexist with respect to a single habitat axis is two or three. But one is left with the problem of how many 'axes' are present within a habitat. Taking a proposed habitat with six niche axes, for example, and assuming a limitation of two species per axis, Newman's model permits the coexistence of $2^6 = 64$ species within the habitat, provided that all possible axis combinations are possible, that is, that the axes are non-related.

Theoretical models may be pleasing to the human mind, but their scientific value can only be ascertained by comparing them with observational or experimental data derived from nature. Here, however, it is usually necessary to confine one's attention to a single habitat axis and to a single pair or small group of species in order to document relationships with adequate precision. In this way one can isolate and study such aspects of competition as root interactions[5] and the effects of environmental modifications on the equilibrium attained by species pairs[6]. With static organisms like plants, initial access to the resource is obviously of great significance, with the result that much emphasis has been placed upon the dispersal propagule and its establishment as a critical phase in plant interactions[7-10].

An alternative approach to the field study of coexistence is the manipulation of a habitat, either by disturbance, fertilization or selective species removal, and then observing the outcome on the balance of remaining species. This approach has proved particularly valuable in studying species interactions in intertidal communities[11-13], but it has also proved useful in studying community dynamics in terrestrial ecosystems, for example the fertilization experiments of Hurd *et al.*[14], and the use of natural badger disturbance by Platt and Weig[15] in their studies of opportunistic plant species in prairies.

There has been little attempt to date to develop a disturbance experiment within a plant community which will permit the testing of theoretical concepts of coexistence. Such an experiment is now reported by Silander and Antonovics in this issue of *Nature* (see p.557). They have altered the community composition of maritime plant communities by the selective removal of certain plant species from sample plots and observed the consequences for the remaining species. The effects are quantified in terms of a single response coefficient, C_{ij}, which compares the change in abundance (point cover or tiller number) of species *j* (following the removal of species *i*) with the

---

Peter D. Moore is in the Department of Plant Sciences, King's College London, 68 Half Moon Lane, London SE24 9JF.

original abundance of species *i*. The response coefficient will approach unity if species *j* expands to fill the entire space that was occupied by species *i* before its removal. Such a result would be suggestive of considerable niche overlap and hence high levels of competition for available resources, though caution is necessary in interpreting artificial removal responses.

The graphic representation of the results in their Fig.2 (see p.559) illustrates the complexity of interactions seen. For example, in the high salt marsh (*d*), the removal of *Spartina patens* (Gramineae) results in a marked increase in one species in particular, that is, *Fimbristylis* (Cyperaceae), and the reciprocal effect is shown by the experiment in which *Fimbristylis* is removed — *S. patens* expands strongly ($C = 0.693$). It is tempting to believe that these two species must normally be in acute competition. In the high marsh, *Fimbristylis* is the most abundant subsidiary species, but this is not the most influential factor determining the course of replacement, for if *S. patens* is removed from the low salt-marsh system, where *S. alterniflora* is the most abundant species, then it is still *Fimbristylis* which shows the greatest expansion, though its C value is far lower (0.072). This suggests that the overlap of resource utilization in these conditions is considerably less. *S. alterniflora*, in fact, is not altered by the removal of *S. patens*, indicating a lack of niche overlap, perhaps an example of perfect coexistence.

The authors are also able to identify 'diffuse' interactions in which the removal of one species results in similar responses from several of those remaining. This can be expressed numerically simply by using an evenness (equitability) index based on the Shannon diversity index. Such an occurrence is clearly indicated in their Fig.2 where *Muhlenbergia* is removed from the swale habitat (*c*), resulting in an almost equal expansion of all the remaining six species.

The potentialities of both the experimental method and the means of data expression are considerable. What is displayed here is a representation of plant community interactions in a form reminiscent of Hutchinsonian niche theory, though to interpret the coefficients precisely in this way would be stepping beyond the limits inherent in an approach which involves severe disturbance to community structure. The removal of one species produces a situation that is essentially artificial. The empirical method does, however, provide a valuable new way of approaching the vexed question of how plant species coexist. □

---

1. May, R.M. *Stability and Complexity in Model Ecosystems* (Princeton University Press, 1973).
2. Slatkin, M. *Ecology* **55**, 128 (1974).
3. Schoener, T.W. *Science* **185**, 27 (1974).
4. Newman, E.I. in *The Plant Community as a Working Mechanism* (ed. Newman, E.I.) 61 (Blackwell Scientific, Oxford, 1982).
5. Litav, M. & Wolovitch, S. *Ann. Bot.* **35**, 1163 (1971).
6. Eagles, C.F. & Williams, D.H. *J. agric. Sci. Camb.* **77**, 187 (1971).
7. Horn, H.S. & MacArthur, R.H. *Ecology* **53**, 749 (1972).
8. Werner, P.A. & Platt, W.J. *Am. Nat.* **110**, 959 (1976).
9. Grubb, J.P. *Biol. Rev.* **52**, 107 (1977).
10. Hubbell, S.P. *Oikos* **35**, 2-4-229 (1980).
11. Paine, R.T. *Am. Nat.* **100**, 65 (1966).
12. Paine, R.T. & Vadas, R.L. *Limnol. Oceanogr.* **14**, 710 (1969).
13. Dayton, P.K. *Ecol. Monogr.* **41**, 351 (1971).
14. Hurd, L., Mellinger, M., Wolf, L. & McNaughton S. *Science* **173**, 1134 (1971).
15. Platt, W.J. & Weis, I.M. *Am. Nat.* **111**, 479 (1977).

Lysosome proton pump identified

from Michael Geisow

IN 1893 Metchnikoff[1] used what must have been the earliest spectroscopic probe in living cells. He observed that litmus particles ingested by amoeba turned red and was able to conclude that the vacuoles of free-living phagocytes were acid. Now, nearly a century later, the same approach (modestly updated) has revealed that acidification of digestive vacuoles — secondary lysosomes — is achieved by proton-translocating ATPases. The recent paper by Ohkuma and his colleagues[2], reporting the latter result, also ends a decade of minor biochemical controversy.

Continuous enzymatic disassembly of macromolecules in secondary lysosomes releases new acid–base equivalents. To maintain the *p*H within the operating range of the hydrolases responsible (4.5–5.0), transport of basic equivalents out, or acidic equivalents in, must occur. The nature of the transport mechanism provided the subject of the controversy. Chief among the contenders for lysosomal *p*H control were proton-pumping ATPases and variants of the Gibbs–Donnan effect.

The issue was partially resolved by measurements of the ionic permeability of the lysosomal membrane[3,4]. In a Gibbs–Donnan equilibrium, impermeant macromolecules — acid hydrolases — in the lysosomes could buffer the content at a low *p*H given two assumptions. First, the isoelectric points of these proteins must lie in the range 4–5. Second, the membrane must be relatively permeable to H^+. On the latter point the hypothesis fell down, since the membrane turned out to have a relatively low permeability to H^+ and cations Na^+ and K^+ at physiological temperatures. This made the classical Donnan equilibrium unlikely but a clear proof of the proton-pumping alternative was lacking.

Further advance came with the development of an effective lysosomal *p*H meter — the fluorescent *p*H indicator dye fluorescein that can be used as a conjugate with dextran. Pinocytic activity conveniently delivers the conjugate to secondary lysosomes wherein *p*H can be monitored by emission spectroscopy. The *p*H of macrophage lysosomes was found to be 4.5–4.7 (ref. 5).

The biochemical exploitation of this intralysosomal *p*H probe required the problem of the isolation of lysosomes to be solved. Usually liver lysosomes are prepared by injection of the compound Triton WR-1339 in rats, to produce abnormally buoyant 'tritosomes', the difficulty then being whether the resulting pure organelles are representative. In the new work reported by Ohkuma, the *p*H probe was uniquely within lysosomes[6] so the presence of contaminating organelles was acceptable.

Ohkuma and his colleagues found that the *p*H of isolated liver lysosomes gradually increased in K^+-containing medium from an initial *p*H 5.0. The indication was not one of lysis, but more probably of slow cation permeation. The mitochondrial proton uncoupler FCCP and the K^+ ionophore valinomycin separately induced minor increases in *p*H, in agreement with limited lysosomal permeability to H^+ or K^+. Together these agents produced the expected collapse of *p*H in the isolated lysosomes. Mg^{2+}-ATP reduced the upward drift of lysosomal *p*H and the supply of a permeant anion (SCN^- or Cl^-) facilitated acidification, indicating that the *p*H-maintaining mechanism is electrogenic.

These symptons are diagnostic of a proton-translocating ATPase (H^+-ATPase). A series of inhibitors designed to characterize this enzyme showed that the lysosomal ATPase was unlike mitochondrial H^+-ATPase in being sensitive to quercetin, but unaffected by oligomycin. Ca^{2+} could not support ATPase activity, nor could ouabain [an inhibitor of (K^+ + Na^+)ATPase] suppress it. The K_m for ATP of the lysosomal proton pump is 0.1–0.2 mM, indicating that it should be working flat out at normal intracellular levels.

The closest analogy with the action of the lysosomal H^+-ATPase is provided in the secretion granules (catecholamine-containing) of the adrenal chromaffin cells. A granule H^+-ATPase is widely recognized. This enzyme acidifies the interior of the granule to *p*H 5.5 (refs 6, 7) and is also quercetin sensitive but unaffected by oligomycin[8]. The granule membrane is equally impermeable to

---

Michael Geisow is at the National Institute for Medical Research, The Ridgeway, Mill Hill, London NW7 1AA.

0028-0836/82/310515-02$01.00

cations, but in this case, the high matrix concentration of weak acids (for example, nucleotides) more effectively buffers the *p*H than in the case of lysosomes. Hence the intragranular *p*H does not increase in the absence of ATP and is unaffected by external *p*H. Perhaps the two H^+-ATPases are identical since both derive from Golgi/endoplasmic reticulum.

The demonstration and partial characterization of the lysosomal H^+-ATPase will inevitably shift the focus of attention onto other cellular membranes where *p*H regulation may occur. Unfortunately, the present results cannot address the question of whether a *p*H-controlling mechanism is present in primary lysosomes or Golgi vesicles, since the delivery of the fluorescent conjugate is, by definition, to secondary lysosomes (endosome–lysosome fusion must have taken place). The method could, however, be used to measure the *p*H of endocytic vesicles which have not yet fused with lysosomes. The *p*H of phagocytic vacuoles has been considered to be reduced by a membrane NADPH oxidase; the *p*H of pinosomes is unclear. Do these organelles also possess proton pumps? ☐

1. Metchnikoff, E. in *Lectures on the Comparative Pathology of Inflammation* (Dover, London,).
2. Ohkuma, S., Moriyama, Y. & Takano, T. *Proc. natn. Acad. Sci. U.S.A.* **79**, 2758 (1982).
3. Dean, R. T. & Barrett, A. J. in *Essays in Biochemistry* Vol. 12 (eds Campbell, P. N. & Alridge, W. N.) 1 (Academic, New York, 1976).
4. Reijngoud, D. J. & Tager, J. M. *FEBS Lett.* **54**, 76 (1975).
5. Ohkuma, S. & Poole, B. *Proc. natn. Acad. Sci. U.S.A.* **75**, 3327 (1978).
6. Pollard, H. B., Shindo, H., Creutz, C. E., Pazoles, C. J. & Cohen, J. S. *J. biol. Chem.* **254**, 1170 (1979).
7. Johnson, R. G. & Scarpa, A. *J. biol. Chem.* **251**, 2189 (1976).
8. Apps, D. K. & Glover, L. A. *FEBS Lett.* **85**, 254 (1978).

The end of the message

from Nick Proudfoot

WITH the isolation and sequencing of eukaryotic genes now a standard, if sometimes tricky, procedure, attention is turning towards the question of how a eukaryotic gene works. Obviously, the first place to look at is the beginning of this process — transcriptional initiation and promoters — and much has already been achieved[1-3] with the discovery of CAT and TATA boxes. In the last year the focus on gene expression has shifted perceptibly '3'-wards'. Several studies have recently been reported on the transcriptional termination of eukaryotic RNA polymerase II (pol II) genes.

A picture now emerges of three different though related methods of mRNA 3'-end formation in eukaryotes. Histone genes generate their mRNA 3' ends by simply termination of transcription. This process involves the recognition of a specific termination sequence at the end of the mRNA. Yeast RNA polymerase II genes generate mRNA 3' ends by a coupled termination–polyadenylation process again apparently at a specific, although different, sequence. Finally, all other higher eukaryotic RNA polymerase II genes first terminate transcription, possibly at a specific sequence similar to the histone gene terminator. These mRNA precursors are then cut down close to an AAUAAA sequence and polyadenylated.

Early studies of mRNA sequence yielded the first clue to RNA polymerase II termination — several different mRNAs had the sequence AAUAAA about 15 base pairs from the 3'-terminal poly(A) sequence[4]. Since this was the only significant sequence homology close to the end of the mRNA, it was inferred that AAUAAA might constitute a recognition site for the enzymes involved in polyadenylation and/or pol II termination. Subsequently, this sequence was found at the 3' ends of all pol II genes (excluding histone genes and possibly all yeast genes) although in a few cases it varies by one base. In the case of histone genes, the mRNA produced is not polyadenylated, implying a link between the AAUAAA sequence and polyadenylation. However, the yeast genes that do not contain AAUAAA at their 3' ends do make polyadenylated mRNA.

The presence of AAUAAA at the end of viral mRNAs allowed the first direct tests of the sequence's function to be made. SV40 deletion mutants were constructed lacking the late gene AAUAAA sequence but containing the same sequence further downstream[5]. No wild-type 3' terminus was detected but rather polyadenylated 3' ends were formed 15 nucleotides away from the new AAUAAA sequence. These and similar experiments directly demonstrated the role of the sequence in positioning the poly(A) tail at the end of the mRNA[5]. Further complexities have followed for several different genes encode mRNAs with multiple 3' termini. First adenovirus[6], then dihydrofolate reductase[7] and immunoglobulin genes[8] were shown to have multiple 3' termini. In each mRNA, AAUAAA or a close homologue preceded the poly(A) tail by about 15 nucleotides. In some cases the selection of different 3' termini causes the expression of different gene products — secreted and membrane-bound forms of antibodies, for example[9].

An important advance in our understanding of these processes has recently come from Hofer and Darnell[10] at the Rockefeller University. They demonstrated the presence of RNA transcripts from the mouse β-globin gene that extended well beyond the 3' end of the mRNA sequence. Evidence that these 3'-extended transcripts were the precursors of mature mRNA was at first indirect but additional experiments that mapped the 3'-terminal position to a defined position 1,400 bases beyond the poly(A) addition site of the mouse β-globin gene have been described by Darnell at a recent conference*. Clearly the fact that these 3' extensions stop at a precise position suggests the transcripts are true globin mRNA precursors. In close agreement with these results, the primary transcripts of the DNA tumour viruses, adeno, SV40 and polyoma, have been unambiguously demonstrated to extend well beyond their poly(A) addition sites (see review, ref. 11). In polyoma, RNA transcripts have been found that are several times larger than the genome size, suggesting that RNA polymerase molecules transcribe in circles around the polyoma genome, never finding a terminator sequence that allows them to stop. These large transcripts must then be cut down to mRNA size by a specific endonuclease activity.

mRNA 3'-end formation thus appears to be a three-step process. First, RNA polymerase II terminates, at least in the case of mouse β-globin, at a defined sequence in the 3'-flanking region of the gene. Then an endonuclease cleaves this primary transcript down to 15 bases 3' to the AAUAAA sequence. Finally, this newly formed 3' end is polyadenylated. It seems plausible to suggest that both the RNA endonuclease and poly(A) polymerase activities recognize the same ubiquitous AAUAAA sequence.

A significantly different approach is revealed in the H2A histone gene of sea urchin[12]. Histone mRNA, although synthesized by RNA polymerase II, is not polyadenylated and does not possess the 3' AAUAAA sequence present in other mRNAs. However, a 23 base pair sequence, including an imperfect inverted repeat at the 3' end of the histone mRNA, is essential for 3'-end formation. When specific deletions of this sequence were constructed and the mutant genes injected into oocyte nuclei the resulting RNA transcripts were larger than histone mRNA and heterogeneous in size, due to multiple 3' termini in the 3'-flanking region or spacer sequence of the histone gene. It seems likely that the 23 base pair inverted repeat sequence is a termination signal for RNA polymerase II. Possibly the inverted repeat forms a secondary structure in the nascent RNA transcript that is recognized by pol II termination factors. Formally, it is still possible that extended 3' termini are

---

Nick Proudfoot is a University Lecturer and Fellow of Brasenose College, Oxford.

*The UCLA-CETUS meeting was held at Keystone, Colorado in April 1982.

0028-0836/82/310516-02$01.00

cleaved down to the mRNA 3′ terminus. However, no evidence for such extended 3′ termini in the normal gene has been obtained, unlike poly(A)-containing mRNAs. The histone genes may have a similar termination mechanism to other pol II genes, but simply miss out the additional endonucleolytic and polyadenylation steps — presumably due to the absence of a suitably positioned AAUAAA sequence. Such a theory seems more plausible given that the same RNA polymerase enzyme transcribes both types of gene. This model will soon be put to the test when the true termination sites of several different pol II genes (that encode poly(A) containing mRNAs) are mapped and sequenced. These genes may possess a sequence identical or similar to the histone termination signal. Unfortunately, most gene sequence studies extend only a few hundred base pairs beyond the poly(A) site. If termination occurs over 1 kb 3′ to the poly(A) site, as appears to be the case with mouse β-globin, then possible termination signals will not yet have been sequenced.

Yeast pol II genes provide yet another variation. Recent studies on a naturally occurring mutant of the yeast Iso-1-cytochrome *c* gene reveal transcripts that are much longer than in wild-type yeast, due to extended 3′ termini[13]. Detailed structural analysis reveals that the mutant gene contains a 38 base pair deletion at the 3′ end of the mRNA sequence. Sequence comparison of all characterized yeast pol II genes shows that the deleted region includes a sequence homology present in all the yeast genes but different from AAUAAA. Curiously, in this mutant all the 3′-extended RNA transcripts are polyadenylated as is the wild-type mRNA. This lack of specificity as to which 3′ end is adenylated is clearly different from the situation in higher eukaryotes. Presumably termination and polyadenylation are coupled events, so that only pol II transcripts end with poly(A) tails. It would appear that yeast pol II genes are intermediate between higher eukaryotic histone genes and other pol II genes encoding poly(A)-containing mRNAs. ☐

1. McKnight, S.L., Gavis, E.R., Kingsbury, R. & Axel, R. *Cell* **25**, 385 (1981).
2. Mellon, P., Parker, U., Gluzman, Y. & Maniatis, T. *Cell* **27**, 279 (1981).
3. Grosveld, G.C., de Boer, E., Shewmaker, C.K. & Flavell, R.A. *Nature* **295**, 120 (1981).
4. Proudfoot, N.J. & Brownlee, G.G. *Nature* **263**, 211 (1976).
5. Fitzgerald, M. & Shenk, T. *Cell* **24**, 251 (1981).
6. Flint, S.J. & Broker, T.R. in *DNA Tumour Viruses* Vol. 9 (ed. Tooze, J.) 433 (Cold Spring Harbor Laboratory, New York, 1981).
7. Setzer, D.R., McGrogan, M., Nunberg, J.H. & Schimke, R.T. *Cell* **22**, 361 (1980).
8. Early, P. *Cell* **20**, 313 (1980).
9. Rogers, J. *et al. Cell* **20**, 303 (1980).
10. Hofer, E. & Darnell, J.E. Jr *Cell* **23**, 585 (1981).
11. *DNA Tumour Viruses* (ed. Tooze, J.) (Cold Spring Harbor Laboratory, New York, 1981).
12. Birchmeier, C., Grosschedl, R. & Birnstiel, M. *Cell* **28**, 739-745 (1982).
13. Zaret, K.S & Sherman, F. *Cell* **28**, 563 (1982).

Two different viral transforming proteins bind the same host tumour antigen

from David Lane and Ed Harlow

A RECENT publication[1] by Sarnow and his colleagues shows that in adenovirus-transformed mouse cells, a host protein, p53, becomes tightly associated with a 58,000-molecular weight product of the adenovirus E1b region — one of the regions whose product is responsible for the transforming capability of adenovirus. What makes the finding of particular interest is that in SV40-transformed mouse cells, p53 also binds to the SV40-coded large T antigen[2,3], expression of which is thought sufficient to transform rodent cells. That proteins from unrelated DNA tumour viruses should both form a stable highly specific complex with p53 (ref. 4) immediately suggests the possibility of a common function in transformed cells for either the viral proteins or the complexes themselves.

Interest in p53 has not come solely from tumour virology, but also from the discovery of antibodies to p53 in sera from animals with a wide variety of tumours. Anti-p53 antibodies were first detected almost simultaneously in two separate fields. DeLeo and co-workers reported that a proportion of sera from mice with methylcholanthrene-induced tumours had anti-p53 antibodies[5] while workers with SV40 reported that p53 could be immunoprecipitated with sera from animals with tumours of SV40-transformed cells[2,3]. Subsequently, anti-p53 antibodies were found in mice with Abelson-induced leukaemia[6]. Why this host protein should become immunogenic in these animals is not clear but the presence of anti-p53 antibodies in tumour sera is not restricted to experimental animals. About 10 per cent of sera from human breast cancer patients also contain anti-p53 activity, while no activity against p53 can be detected in sera from normal patients[7].

It is commonly said that the level of p53 is higher in transformed cells than in normal cells[5,8,9]. Levels of p53 clearly increase following SV40 transformation, probably because of stabilization by binding to large T antigen: in mouse 3T3 cells, p53 has a half life of approximately 20 min which increases to more than 24 h in SV40-transformed 3T3 cells[10].

A similar set of observations might now be expected in adenovirus-transformed cells. Reports of metabolic labelling and immunoprecipitation experiments on a wide variety of non-SV40-transformed cells have suggested that they have higher levels of p53 than their non-transformed counterparts. Increased levels of p53 labelling have also been reported to follow lectin stimulation of lymphocytes[11] and to be associated with explants of early embryos[12].

These reports are consistent with the hypothesis that increased levels of p53 accompany transformation or rapid cell growth but it must be remembered that the incorporation of radiolabelled precursors into immunoprecipitated p53 may not be an accurate measure of the total protein levels of p53. For example, as judged by radiolabelled p53, SV40-transformed mouse cells have two to three times more p53 than mouse F9 teratocarcinoma cells, but when tested in a radioimmunoassay for total protein, F9 cells have approximately 50-fold less p53 than the SV40-transformed cells[13]. Until an accurate assay for total cold p53 is widely used, the claim that elevated levels of p53 frequently accompany transformation will have to be held in some doubt.

Although the ability to label p53 may be reduced in normal cells, careful examination has shown that p53 can be found in almost all cell cultures. The only known exceptions to this rule are the human tumour cell lines HeLa and EJ[9]. No detectable levels of p53 have been found in these cells, and if these negative data prove correct, p53 cannot be essential for cell viability. Likewise, p53 does not represent a universal marker for transformation as it is present in normal cells and absent from some transformed cells.

Although there are very few clues to understanding the role of p53 in normal or transformed cells, knowing what viral processes are dependent or altered on binding to p53 is probably one of the best avenues to determining its function. The fact that two DNA tumour viruses both produce proteins that complex p53 should greatly aid this search and may provide a clue to the immunogenicity of p53 in animals with cancer. ☐

David Lane is in the Eukaryotic Molecular Genetics Group, Imperial College of Science and Technology, London SW7 2AZ and Ed Harlow is in the Molecular Virology Laboratory, Imperial Cancer Research Fund Laboratories, London WC2A 3PX.

1. Sarnow, P. *et al. Cell* **28**, 38 (1982).
2. Lane, D. & Crawford, L. *Nature* **278**, 261 (1979).
3. Linzer, D. & Levine, A. *Cell* **17**, 43 (1979).
4. McCormick, F. & Harlow, E. *J. Virol.* **34**, 213 (1980).
5. DeLeo, A. *et al. Proc. natn. Acad. Sci. U.S.A.* **76**, 2420 (1979).
6. Rotter, V. *et al. J. Virol.* **36**, 547 (1980).
7. Crawford, L., Pim, D. & Bulbrook (in preparation).
8. Rotter, V., Boss, *et al. J. Virol.* **38**, 336 (1981).
9. Crawford, L. *et al. Proc. natn. Acad. Sci. U.S.A.* **78**, 41 (1981).
10. Oren, M. *et al. Molec. cell. Biol.* **1**, 101 (1981).
11. Milner, J. & Milner, S. *Virology* **112**, 785 (1981).
12. Chandrasekaran, K. *et al. Proc. natn. Acad. Sci. U.S.A.* **78**, 6953 (1981).
13. Benchinol, S. (in preparation).

0028-0836/82/310517-01$01.00

The beginnings of solar-terrestrial studies

from David W. Hughes

THE early years of the nineteenth century mark a watershed in astronomy. From that time astronomers ceased to concentrate on recording the positions and movement of celestial objects and astrophysics began its growth into the dominant force it is today. As documented in a recent review of the birth of the study of solar-terrestrial relations (*Vistas Astr.* **25**, 419; 1982), a factor that helped this transformation was the realization, as a result of geomagnetic, auroral and meteorological observations, that there was an obvious non-gravitational interaction between the Sun and the Earth.

Our knowledge of the existence of sunspots is centuries old but the periodicity of their occurrence, the so-called solar cycle, was only reported as recently as 1843. H. Schwabe, a one-time apothecary of Dessau, devoted himself to the observation and recording of sunspots (some say partly in the hope of discovering an intra-Mercurial planet). By 1838 he began to suspect that the 'spottiness' of the Sun changed with a period of about 10 years. He published his conclusions in *Astronomische Nachrichten* (**20**, no. 495) but his discovery did not become widely known until Baron von Humboldt publicized it in 1851 in the third volume of his popular work *Cosmos*. This popularization opened the flood gates.

Colonel Sabine of the British army had been analysing a series of magnetic field measurements taken from a group of observatories dotted throughout the British colonies. They showed that the Earth's field underwent small fluctuations, the amplitudes of which varied with time. As Sabine wrote: "It happens by a most curious coincidence" that the magnitude and frequency of magnetic disturbances, on a global scale, had a maximum in 1848 and a minimum in 1843, following the sunspots. Sabine published his findings in March 1852 and A. Gautier and Rudolf Wolf independently came to the same conclusions and published in the same year.

As far back as 1747, Hiorter queried

> "Who could have thought that the northern lights would have a connection and a sympathy with the magnet, and that these northern lights, when they draw southwards across our zenith or descend unequally towards the eastern and western horizons could, within a few minutes, cause considerable oscillations of the magnetic needle through whole degrees?"

Suggestions of a close link between solar cycle and the frequency of aurorae were quickly made in the 1850s but, unfortunately, the scarcity of records made the periodicity of the auroral occurrence frequency difficult to establish.

Speculation about a connection between spots and aurorae and spots and the weather had been made in the mid-eighteenth century. In 1801, William Herschel wen so far as to try and find a correlation between the number of spots and the price of corn, the latter obviously being influenced by the amount of fine weather. The 1850s was a time when all regularly observed meteorological variables were analysed for periodicities. The British with their colonial interests were especially involved and Indian weather reports were carefully perused with the hope of producing reliable long-range weather predictions.

The relationship between solar cycles and variations in magnetic activity was confirmed when scientists realized that predictions of magnetic disturbances made by using sunspot observation were reasonably good. Astrophysical mechanisms connecting changes on the Sun and the consequent particle and radiation flux to aurorae and magnetic disturbances on Earth were also speedily established. The importance of the solar cycle was recognized and John Herschel's question "What can there be to determine a periodicity of this kind in the Sun?" became, and still remains, an important stimulus to astrophysicists.

Sun–weather relationships were a different matter. *Post hoc* correlations might be detected but predictions from them lacked accuracy. There were also far too many weather parameters to choose from. Even today, though many causal relationships have been suggested between ground temperature, rainfall, pressure and storms and sunspot activity, none has been generally accepted. □

David W. Hughes is a lecturer in Astronomy and Physics at the University of Sheffield, Sheffield S3 7RH.

Air pollution in the Arctic

from B. Ottar

AN extensive study of pollutant transport and deposition in the Arctic has recently been begun by the Norwegian Institute for Air Research with the support of British Petroleum Ltd. Not only is the Arctic an important region climatologically, but the increasing interest in the exploitation of Arctic oil reserves makes it important to obtain baseline pollutant measurements as soon as possible.

Transport of air pollutants into the Arctic has received much attention recently, and it seems that the Arctic haze north of Barrow, first reported in 1956, is due to large-scale transport of polluted air masses. Aerosol samples from the Arctic show that the concentrations of trace elements associated with fossil fuel combustion reach a pronounced maximum in February–March (K.A. Rahn & R.J.M. Caffrey *Proc. WMO Symp. on Long-Range Transport of Pollutants,* Sofia, 25, WMO no.538; 1979). During summer, aerosol concentrations are very low (H. Lannefors, J. Herntzenberg & H.C. Hansson *Tellus* **34**A, no.1; in the press). This extreme variation is explained by the formation of a cold high-pressure centre over northern USSR and Siberia in winter, which forces the Atlantic westerlies northwards into the Barents Sea. This enhances the south to north advection associated with the low pressures in the Atlantic and the Norwegian Sea. In addition, pollutant transformation and deposition rates are very low in the cold and dark winter season. Polluted air masses from Europe and the USSR are transferred into the polar basin and across the North Pole towards northern Alaska and Canada. In summer, the circulation becomes more circumpolar, and dry deposition and precipitation prevent anthropogenic aerosols from reaching the high Arctic.

The new study includes an expansion of the present Norwegian measurement programme. Four ground stations in the high Arctic (Bear Island, Hopen, Spitsbergen, Jan Mayen) and two stations along the Norwegian coast will operate over a three year period, starting summer 1982, together with two inland stations. At all stations sulphur dioxide, sulphate aerosol and precipitation will be monitored throughout the year. More extensive supplementary measurements, including high-volume sampling and chemical analysis of aerosols and hydrocarbons, will be made during a few 1–2 month periods each year. In the same periods, intensive aerosol measurements will be carried out by aircraft and the vertical and horizontal extent of the polluted air masses mapped. Soil samples as well as biological samples will be collected to evaluate the deposition and accumulation of trace elements and organic components. In particular, the accumulation of chlorinated hydrocarbons, whose presence in the Arctic air has been demonstrated, will be examined in fish from isolated lakes.

Turbulent dispersion over ocean surfaces will also be studied in order to provide a better basis for calculation of hazard zones in connection with blow-outs and other accidents. Such studies and the background air pollution inventory will help the Norwegian Government evaluate possible damage from Arctic oil activities.

B. Ottar is Director of the Norwegian Institute for Air Research, PO Box 130, 2001 Lillestrom.

0028-0836/82/310518-01$01.00

ARTICLES

Nd, Sr and Pb isotopic systematics in a three-component mantle: a new perspective

Alan Zindler[*], **Emil Jagoutz**[†] **& Steven Goldstein**[*]

[*] Lamont-Doherty Geological Observatory and Department of Geological Sciences, Columbia University, Palisades, New York 10964, USA
[†] Max Planck Institut für Chemie, Saarstrasse 23, Mainz, FRG

Average Nd, Sr and Pb isotopic compositions for oceanic basalts indicate that the present day mantle consists of three chemically independent components. The recognition of a third mantle component obviates geochemical arguments which have been used to support chemical stratification and convective decoupling within the mantle, and the transport of lead to the core throughout geological time.

RECENT geochemical modelling of mantle differentiation and crustal growth[1-5] has suggested that Nd and Sr isotopic variations in young mantle-derived rocks may be explained by mixing of two mantle components, 'MORB-type' or 'depleted mantle' material and 'undifferentiated' or 'slightly enriched' mantle material. In this context, apparently enigmatic variations in Pb isotope ratios have been interpreted as indicating that the U–Th–Pb system has suffered a more complex evolution in the earth than either Sm–Nd or Rb–Sr. An alternative interpretation of the data has been proposed by Zindler and Jagoutz[6,7] who suggested that variations in Nd, Sr and Pb isotopic compositions of mantle-derived rocks indicate the existence of at least three chemically independent mantle components. The acquisition of Nd isotope data from St Helena (ref. 8 and Lamont unpublished data) was particularly important to the formulation of this hypothesis because it showed that St Helena, which is characterized by the highest $^{206}Pb/^{204}Pb$ ratios ever measured in young basalts (see Fig. 1*d*), falls below the 'mantle array' in a plot of $^{143}Nd/^{144}Nd$ against $^{87}Sr/^{86}Sr$ (see Fig. 1*a*).

The term 'component' is used so as not to imply the connotations of a word like 'reservoir', that a physical entity with these compositions actually exists in the mantle. We also do not mean to imply that only three isotopically distinct materials exist within the mantle (a brief look at the crust should dispel any such notion). However, the data indicate that, while any number of isotopically distinct materials may exist, they may all be described as linear combinations of three components.

The first-order difference between the two- and three-component models is not simply the number of mantle components invoked, for any subdivision of the mantle into two, three or *n* components is necessarily a simplification of the real situation. The basic difference lies in the nature of the mechanisms which must be called on to explain the differentiation of the mantle into its major observable components. Processes which involve the mobilization of silicate liquids or silica-rich fluids within the mantle are thought to fractionate parents from daughters in each of the isotope systems under consideration. Therefore, to propose that, in a gross sense, Nd and Sr isotopic variations may be explained by two mantle components while

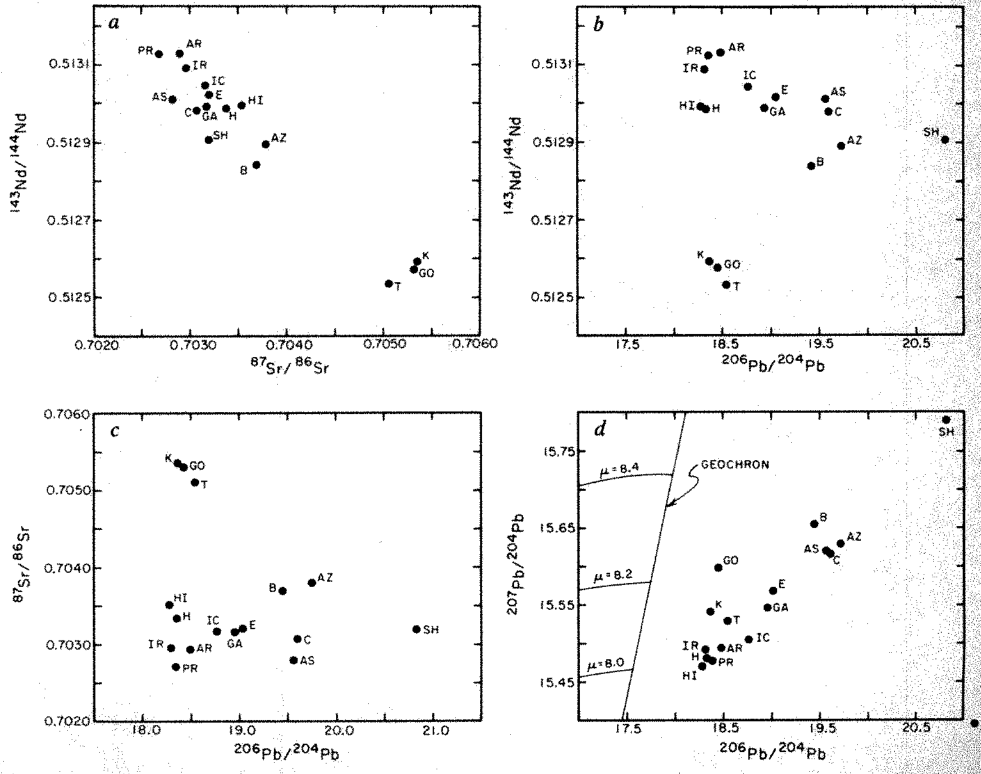

Fig. 1 Two-dimensional variation diagrams for average values of Pb, Nd and Sr isotopes in basalts from ocean islands and ridges. Localities are labelled as in Table 1. *a*, $^{143}Nd/^{144}Nd$ versus $^{87}Sr/^{86}Sr$; *b*, $^{143}Nd/^{144}Nd$ versus $^{206}Pb/^{204}Pb$; *c*, $^{87}Sr/^{86}Sr$ versus $^{206}Pb/^{204}Pb$, *d*, $^{207}Pb/^{204}Pb$ versus $^{206}Pb/^{204}Pb$.

0028–0836/82/310519—05$01.00

three or more components are required by Pb isotope variations is to imply that some geochemically active mantle process causes severe fractionations of U and Th from Pb without significantly affecting Rb/Sr and Sm/Nd ratios, and furthermore, that this process is not one governed solely by solid–liquid–fluid equilibria in a silicate system. Based on this kind of reasoning, several authors[9–11] have proposed that Pb has been transferred from the mantle to the core in a sulphide phase throughout geological time, causing a progressive increase in mantle U/Pb and Th/Pb ratios. Because the other elements under consideration are not chalcophile in nature, their relative abundances in the mantle will not have been affected by this process. In contrast, if Nd, Sr and Pb isotopic variations support the existence of more than two mantle components, then fractionations of all three parent–daughter systems may conceivably be in response to magmatic or metasomatic processes operating within the mantle without calling on a special process to fractionate U and Th from Pb.

We now examine mantle Nd, Sr and Pb isotopic variations in multi-dimensional space to investigate systematics which may be obscured in two-dimensional variation diagrams. In three, four or five dimensions, average isotopic compositions for individual ocean islands or island groups and mid-ocean ridges define a planar array with a high degree of precision and indicate that mantle isotopic variations are best described by mixing between three chemically independent mantle components. These results suggest that: (1) processes which involve the mobilization of silicate liquids or silica-rich fluids within the mantle, such as metasomatism of magma generation, can account for differentiation of the three isotope systems without calling on a special process to produce apparently complex Pb isotope variations; (2) mixing between mantle components must occur without significant fractionation of daughter element ratios (Sr/Nd, Sr/Pb and Nd/Pb); (3) mass-balance arguments which have been used to support convective isolation of the lower mantle[2–4] (and the resulting chemical stratification of the mantle) are not valid, due to the positive identification of an additional important mantle component; and (4) the 'bulk Earth' $^{87}Sr/^{86}Sr$ ratio is about 0.7052, significantly higher than the range of previous estimates (0.7045–0.7050)[12–14].

Recognition of these systematics in the mantle places strong constraints on the evolution of the continental crust. The continental crust is not constrained to lie on the 'mantle plane' of compositions. However, given that the continental crust has been derived from the mantle through time (albeit indirectly), the average continental crust must lie close to the plane, within a restricted range of compositions. Details of continental crust evolution, in the context of those mantle systematics, will be discussed elsewhere[15,16].

Results and discussion

Investigation of the large-scale chemical structure of the mantle is facilitated by averaging the small-scale isotopic heterogeneities known to exist in the mantle beneath specific volcanic centres (such as the Reykjanes Peninsula[17]). In other words, we would like to obtain representative isotope ratios for mantle segments which are large when compared with the scale of melting. In light of these considerations, we have calculated average Nd, Sr and Pb isotope ratios for individual islands, island groups and mid-ocean spreading centres. (This method was previously used[18] to examine Rb–Sr systematics in the sub-oceanic mantle.) Because we are attempting to evaluate mixing relationships between mantle components, the desired information will not be obscured by the enhanced or diminished representation of one or more components at a given locality.

The current data base is only marginally sufficient to accomplish this task with some statistical credibility, due to a lack of single samples for which there are Nd, Sr and Pb isotopic analyses. Hence, we included all available high-precision analyses of oceanic basalts for each isotope system. This typically results in average Pb isotope ratios which are based on analyses of different samples from those used to obtain the average Nd and Sr isotope ratios. Although the approach is not ideal, it is necessitated by the nature of available data. Had we been restricted to dealing only with those samples for which Nd, Sr and Pb isotopic analyses exist, the data base would simply not have been sufficient to perform the multidimensional analysis presented here.

Average Nd, Sr and Pb isotope ratios for various localities are reported in Table 1. Also shown are the number of samples used for computation and the sources for the data. The data set used to calculate these averages has been significantly augmented by the inclusion of unpublished analyses done at Lamont and by White. The average values are plotted using standard representations in Fig. 1. While the averaging tends to reduce noise, the patterns formed by the data in these diagrams are familiar from the literature. One should note that in Fig. 1*a*, the $^{143}Nd/^{144}Nd$ versus $^{87}Sr/^{86}Sr$ diagram, the data do form a convincingly linear array.

Planes have been fitted to the 10 possible combinations of 3 of the 5 isotope ratios using a standard multiple linear regression treatment. For 5 of the 10 combinations, the correlation coefficient, r, is >0.98; for other combinations, r can go as low as 0.72. Factor analysis techniques have been used to evaluate simultaneously the data in five dimensions ($^{143}Nd/^{144}Nd$, $^{87}Sr/^{86}Sr$, $^{206}Pb/^{204}Pb$, $^{207}Pb/^{204}Pb$, and $^{208}Pb/^{204}Pb$). Using an autoscaling technique[47], in which the data within each isotope system are normalized to the total variation within that system,

Table 1 Average Pb, Nd and Sr isotopic compositions for mid-ocean ridges and ocean islands

Locality		Data sources	$N_{Sr,Nd}$	N_{Pb}	N_C†	$^{87}Sr/^{86}Sr$	$^{143}Nd/^{144}Nd$	$^{206}Pb/^{204}Pb$	$^{207}Pb/^{204}Pb$	$^{208}Pb/^{204}Pb$
Mid-Atlantic Ridge	(AR)	8, 10, 12, 13, 19, 20, 35–38	47	52	23	0.70291	0.513129	18.490	15.491	38.019
Pacific Ocean Ridges	(PR)	8, 10, 19, 20, 36, 39, 40*	10	13	3	0.70269	0.513126	18.355	15.477	37.838
Indian Ocean	(IR)	20, 26, 39	4	6	2	0.70297	0.513093	18.304	15.490	38.048
Canary Islands‡	(C)	20*	5	17	0	0.70307	0.512980	19.600	15.613	39.419
Azores§	(AZ)	8, 20, 35	7	5	0	0.70379	0.512891	19.731	15.626	39.341
Ascension	(AS)	13, 20	4	4	0	0.70282	0.513010	19.568	15.618	39.112
St Helena	(SH)	8, 20*	8	12	1	0.70320	0.512907	20.804	15.789	40.091
Gough	(GO)	13, 20	1	8	1	0.70532	0.512574	18.435	15.599	38.917
Tristan da Cunha	(T)	8, 13, 20*	5	6	3	0.70507	0.512535	18.551	15.527	39.013
Bouvet	(B)	13, 20	4	3	0	0.70369	0.512840	19.445	15.652	39.065
Easter Island	(E)	8, 19	6	2	0	0.70320	0.513022	19.040	15.567	38.616
Hawaiian Islands	(HI)	8, 12, 13 19, 20, 41	32	31	0	0.70355	0.512993	18.282	15.472	37.953
Island of Hawaii	(H)	8, 13, 18, 41	20	20	0	0.70338	0.512985	18.338	15.479	38.016
Galapagos Islands	(GA)	42, 43	13	15	13	0.70317	0.512992	18.953	15.547	38.586
Kerguelen	(K)	8, 44, 45	25	25	25	0.70535	0.512592	18.374	15.538	38.910
Iceland	(IC)	13, 17, 35, 38, 46	17/19	12	0	0.70317	0.513045	18.752	15.502	38.382

All $^{143}Nd/^{144}Nd$ values are normalized to $^{146}Nd/^{144}Nd = 0.7219$, and where necessary, corrected to BCR – 1 = 0.51264. Symbols in parentheses are used to label figures.

* Plus Lamont-Doherty Geological Observatory, unpublished data.

† Number of samples for which Nd, Sr, and Pb isotope ratios have been measured.

‡ Gran Canaria, La Palma and Hierro only.

§ Does not include Sao Miguel.

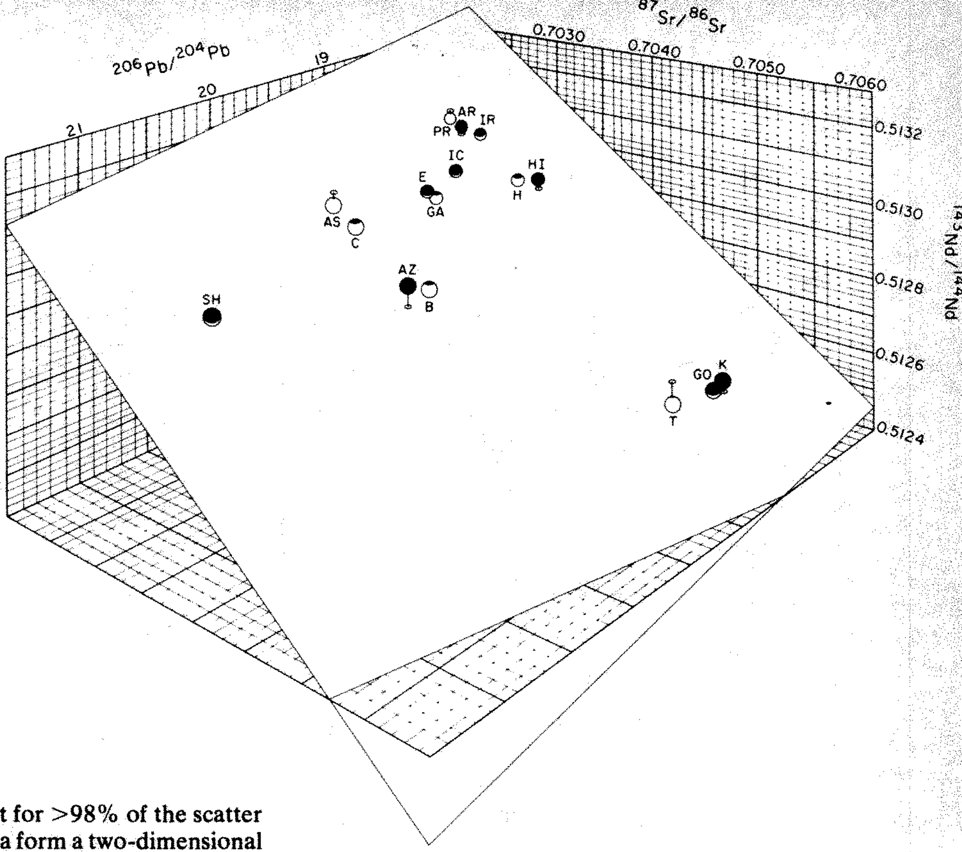

Fig. 2 Three-dimensional plot of average $^{206}Pb/^{204}Pb$, $^{143}Nd/^{144}Nd$ and $^{87}Sr/^{86}Sr$ for basalts from ocean islands and ridges. The best-fit plane is shown. Closed and open symbols lie above and below the 'mantle plane', respectively. Lines connecting data points to the plane are parallel to the $^{143}Nd/^{144}Nd$ axis and indicate those points which do not intersect the plane. Localities are labelled as in Table 1.

two vectors in five dimensions account for >98% of the scatter in the data, demonstrating that the data form a two-dimensional or planar array. The plane formed by these two vectors is not normal to the plane formed by the Nd and Sr axes. A complete treatment of results for the five isotope systems will be published elsewhere[15]. Only the results for $^{143}Nd/^{144}Nd$ versus $^{87}Sr/^{86}Sr$ versus $^{206}Pb/^{204}Pb$ will be discussed in detail here.

The plane fit to the data for $^{143}Nd/^{144}Nd$, $^{87}Sr/^{86}Sr$ and $^{206}Pb/^{204}Pb$ has a correlation coefficient of 0.984, is given by the equation

$$-0.334640(^{87}Sr/^{86}Sr)-1.48742(^{143}Nd/^{144}Nd)$$

$$-8.59379\times10^{-5}(^{206}Pb/^{204}Pb)+1=0$$

and is shown in Fig. 2. The small magnitude of the coefficient for $^{206}Pb/^{204}Pb$ results in part from the large magnitude of $^{206}Pb/^{204}Pb$ ratios compared with $^{87}Sr/^{86}Sr$ and $^{143}Nd/^{144}Nd$ ratios. The tie lines between the data points and the plane are drawn parallel to the $^{143}Nd/^{144}Nd$ direction and are meant to aid three-dimensional visualization. The fit of the data to the plane is extremely good. Deviations taken normal to the plane are smaller than experimental errors for $^{87}Sr/^{86}Sr$ and $^{206}Pb/^{204}Pb$ and average only slightly in excess of typical experimental errors for $^{143}Nd/^{144}Nd$.

While the fit of the data to the plane cannot be contested, one may wonder whether some special differentiation process has affected the U–Pb system, especially in light of the apparently linear correlation of $^{143}Nd/^{144}Nd$ and $^{87}Sr/^{86}Sr$ seen in Fig. 1*a*. In other words, it may be conceivable to have only two chemically independent components for $^{143}Nd/^{144}Nd$ and $^{87}Sr/^{86}Sr$, and three for $^{206}Pb/^{204}Pb$. If three components are appropriate for all three isotope systems, a two-dimensional projection taken parallel to the plane should yield an array which is significantly more linear than that seen in Fig. 1*a*. We have tested this by rotating the plane about the $^{87}Sr/^{86}Sr$ axis. The resulting diagram (Fig. 3) is a plot of $^{87}Sr/^{86}Sr$ versus a function of $^{143}Nd/^{144}Nd$ and $^{206}Pb/^{204}Pb$. Compared with Fig. 1*a*, many data points have been rotated into the trace of the plane in Fig. 3, resulting in a significantly improved linear correlation. Deviations from the trace of the plane in Fig. 3, parallel to the $^{87}Sr/^{86}Sr$ axis, average a factor of two smaller than those deviations from a best-fit line to the data in Fig. 1*a*. Thus, it becomes clear that, as suspected, there is important information contained in the scatter of data about the 'mantle array' in Fig. 1*a*. We consider that this critical test of the proposed three-component model has been passed.

Chemically independent mantle components are produced through differentiation of a mantle which is well-mixed subsequent to core formation. Differentiation of the mantle in response to magmatic processes, such as basalt generation or the extraction of continental crust, will cause fractionation of Sm/Nd, Rb/Sr and U/Pb ratios. Resulting mantle components will have distinct Nd, Sr and Pb isotope ratios. Models which have been proposed to explain Nd and Sr isotopic variations in oceanic basalts have generally called on two chemically distinct mantle components[1–5]. However, several authors[1,5,10–12,19,20] have noted that simple mixing of two components is not sufficient to explain Pb isotopic variations (see Fig. 1). To resolve this apparent dilemma, a process must be identified which fractionates U from Pb, but not Sm from Nd, nor Rb from Sr, thus affecting only Pb isotope systematics. The transport of Pb to the core throughout geological time has been proposed[1,9–11] as such a mechanism. Having recognized the coherence of Nd, Sr and Pb isotope systematics in the mantle, such *ad hoc* proposals may no longer be necessary. For the elements of interest then, we consider the mantle and crust to be a closed system. Subsequently, 'bulk Earth' shall refer only to the mantle–crust system and exclude the core. In this context, the 'bulk Earth' Pb isotopic composition must lie on the Pb–Pb geochron.

In the context of this three-component model for the mantle, we are able to make a new and more accurate estimate of $^{87}Sr/^{86}Sr$ in the 'bulk Earth'. Previous estimates average about 0.7047 (refs 12–14) and are made using only the $^{143}Nd/^{144}Nd$ versus $^{87}Sr/^{86}Sr$ correlation together with the chondritic value of $^{143}Nd/^{144}Nd$ (most recently and accurately determined by Jacobsen and Wasserburg[21]). By using the equation given for the 'mantle plane', a 'bulk-Earth' $^{206}Pb/^{204}Pb$ ratio of 17.767 (corresponding to a present-day μ equal to 8.2, an age for the Earth of 4,570 Myr and initial Pb isotopic compositions from

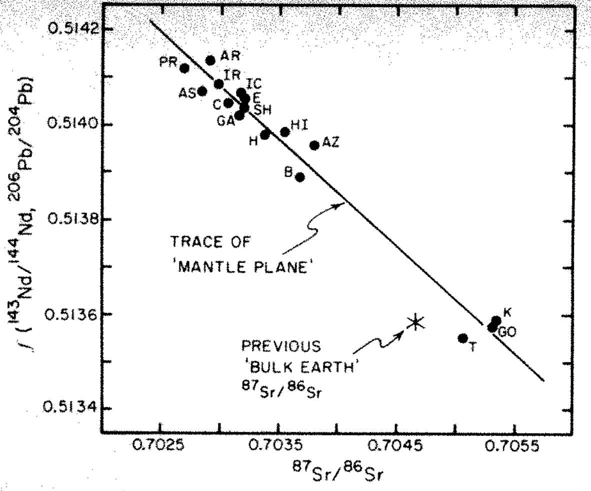

Fig. 3 Two-dimensional projection, taken parallel to the 'mantle plane', of average $^{206}Pb/^{204}Pb$, $^{143}Nd/^{144}Nd$ and $^{87}Sr/^{86}Sr$ values for basalts fron ocean islands and ridges. The coordinate system has been rotated about the $^{87}Sr/^{86}Sr$ axis so that the 'mantle plane' is normal to the page. The abcissa is $^{87}Sr/^{86}Sr$; the ordinate is a function of both $^{206}Pb/^{204}Pb$ and $^{143}Nd/^{144}Nd$ given by:

$$f(^{143}Nd/^{144}Nd,\ ^{206}Pb/^{204}Pb)$$
$$=[(^{143}Nd/^{144}Nd)^2+(^{206}Pb/^{204}Pb)^2]^{1/2}$$
$$\times[\sin[\arctan((^{143}Nd/^{144}Nd)/(^{206}Pb/^{204}Pb))+0.0031035]]$$

Localities are labelled as in Table 1. Note that this projection yields a significant decrease in scatter compared with Fig. 1*a*. The trace of the 'mantle plane' is shown for reference. The previous 'bulk Earth' estimate for $^{87}Sr/^{86}Sr$ of 0.7047 is shown to lie farther from the 'mantle plane' than any single data point, when plotted assuming 'bulk Earth' $^{143}Nd/^{144}Nd = 0.51262$ and $^{206}Pb/^{204}Pb = 17.767$ (corresponding to a present day $\mu = 8.2$, an age for the Earth of 4,570 Myr, and initial Pb isotopic compositions from Tatsumoto *et al.*[22]). A 'bulk Earth' estimate of $^{87}Sr/^{86}Sr = 0.7052$ is compatible with both the 'mantle plane' and reasonable values for 'bulk Earth' Nd and Pb isotope ratios.

ref. 22), and the chondritic $^{143}Nd/^{144}Nd$ value of 0.51262, we have estimated a 'bulk-Earth' $^{87}Sr/^{86}Sr$ ratio of 0.7052. (While a μ of 8.2 is considerably higher than μ values observed in Cl chondrites, it is less than μ values observed in some differentiated meteorites. If lead is treated as a volatile element, its depletion in the Earth, relative to Cl chondrites, is not inconsistent with depletions observed for other volatile elements.) An $^{87}Sr/^{86}Sr$ ratio of 0.7047 would imply a $^{206}Pb/^{204}Pb$ ratio of about 20 in the 'bulk Earth', clearly too high for any reasonable 'bulk Earth' μ value. The new value of 0.7052 for the 'bulk Earth' $^{87}Sr/^{86}Sr$ ratio implies a Rb/Sr ratio of 0.032. Also, when compared with the $^{230}Th/^{232}Th$ versus $^{87}Sr/^{86}Sr$ correlation of Condomines *et al.*[23], an $^{87}Sr/^{86}Sr$ ratio of 0.7052 yields a $^{232}Th/^{238}U$ ratio of about 3.9 in the 'bulk Earth'. This is compatible with Tatsumoto's[19] estimate that the 'bulk-Earth' κ value lies between 3.8 and 4.0.

The fit of the data points to a plane carries implications for the relative compositions of the three components, since mixing relationships are not planar in the general case. A planar mixing surface, rather than a curved surface or a cloud, will only result when the three components have Sr/Nd, Sr/Pb and Nd/Pb ratios which are not too dissimilar, and when the mixing process does not produce severe fractionations of these ratios. That such a planar array is observed offers some insight into mantle dynamics.

Examples from the literature document mantle metasomatism on a small scale[24,25] or call on mantle metasomatism as a precursor to melt generation in the mantle[17,24]. The present results suggest that metasomatic processes, which fractionate both parent/daughter ratios and daughter/daughter ratios, do not have an important role in determining the gross chemical characteristics of the mantle. The planar array is most easily understood if mixing between components in the mantle occurs in the solid state. However, the constancy of Sr/Nd in volcanic rocks[26] indicates that a planar array will result from mixing of magmas where Sr/Pb and Nd/Pb ratios are not fractionated by magma generation processes. At present, our knowledge of solid/liquid partitioning for Pb is not sufficient to resolve this point[19].

Source materials for magmas in the mantle may then be considered as composite mixtures of varying amounts of the three components without requiring chemical stratification within the mantle. This is a realistic scenario in which to produce the chemical and isotopic variations observed at individual volcanic centres[27]. In some areas, however, where metasomatism has affected the source mantle before basalt generation, isotopic compositions of basalts are expected to deviate from the 'mantle plane'.

Recent models[2–4] have proposed that the continental crust is the only geochemical complement to the depleted mantle observed at mid-ocean ridges. In such a context, material balance arguments have been used to show that only 20–50% of the mass of the mantle need be depleted to produce the continental crust. These arguments have been taken to support convective decoupling of the upper and lower mantle, and consequently, chemical stratification of the mantle. Having identified a third mantle component, we can no longer realistically consider that continental crust is the sole complement to the depleted mantle. (This was pointed out by Anderson[5] using arguments based on the presence of an enriched reservoir in the mantle). Therefore, the material balance arguments used previously are invalid, and from a geochemical standpoint the question of whole-mantle versus part-mantle convection remains open. This point has been made independently by Allegre *et al.*[28] who show that uncertainties in input parameters are sufficient to allow the possibility that the whole mantle has been depleted to produce the continental crust, even in the context of a two component mantle.

Nd, Sr and Pb isotope ratios have been shown to delineate three chemically distinct components within the Earth's mantle. Two of these components, undifferentiated or slightly enriched mantle material, and MORB-type or depleted mantle material, have received much attention recently[2,3,12,5,29]. On independent grounds, Hofmann and White[30–32], Chase[33], and Zindler and Jagoutz[6,7], have suggested that recycled oceanic crust may have a role in determining the chemical characteristics of volcanics at some ocean islands. Therefore, it is appropriate to consider whether subducted ocean crust will have the chemical characteristics required by the third component (high U/Pb and Th/Pb, low Th/U, and intermediate Sm/Nd and Rb/Sr ratios with respect to the other components). The chemical characteristics of subducted ocean crust are determined by magma generation processes at mid-ocean ridges and volcanic arcs, by sea-floor alteration processes, and by the presence of seamounts or ocean islands. The effects of these processes on Rb/Sr and Sm/Nd can be predicted on the basis of the geochemical behaviour of these elements. However, the behaviour of U and Pb during magma generation and ocean crust alteration is complex and poorly understood [19,34]. Further, a range of isotopic compositions will result from the subduction of ocean crust materials at different times during Earth history. An accurate assessment of the suitability of subducted ocean crust for the third component must await further work.

Summary and conclusions

Nd, Sr and Pb isotope ratios in mantle-derived rocks define a plane in three, four or five dimensions, and demonstrate that the interactive portion of the Earth's mantle is composed of three chemically distinct and independent components. The recognition of a third significant chemical component in the mantle obviates geochemical arguments which have been used to support chemical stratification and convective decoupling within the mantle, and the transport of Pb to the core throughout geological time.

We anticipate that the 'mantle plane' will be useful as an aid in understanding geochemical aspects of petrogenetic processes in different tectonic settings. As discussed above, specific conditions of mixing are required to generate magmas whose isotopic compositions lie on the plane. Where isotope ratios in volcanic products are observed to deviate significantly from the plane, constraints on the nature of magma generation processes and source materials can be inferred. For example, melting of metasomatically veined mantle may produce magmas with anomalous isotopic compositions. In addition, products of intracrustal differentiation are not constrained by mantle isotope systematics and may have isotopic compositions which lie far off the mantle plane. Where crustal materials are involved in igneous processes at volcanic arcs or sites of intra-continental volcanism, the isotopic compositions of resulting magmas are expected to lie off the plane.

We thank Stan Hart for encouragement and for a helpful review of an early version of this manuscript. Previously unpublished data supplied to us by Bill White were greatly appreciated. We thank Gerd Brey, Christa Goepel, Brendon Griffith and Bill White for a helpful evening of discussion, Claude Allegre, Don Anderson and Al Hofmann for constructive reviews and Dave Zindler and Patty Catanzaro for the graphics. Lamont–Doherty Geological Observatory contribution no. 3365.

Received 26 February; accepted 18 June 1982.

1. Allegre, C. J. *Tectonophysics* **81,** 109 (1982).
2. O'Nions, R. K., Evensen, N. M. & Hamilton, P. J. *J. geophys. Res.* **84,** 6091 (1979).
3. Jacobsen, S. B. & Wasserburg, G. J. *J. geophys. Res.* **84,** 7411 (1979).
4. DePaolo, D. J. *Geochim. cosmochim. Acta* **44,** 1185 (1980).
5. Anderson, D. L. *Earth planet. Sci. Lett.* **57,** 1 (1982).
6. Zindler, A. & Jagoutz, E. *Abstr. AGU Chapman Conf. on the Generation of the Oceanic Lithosphere*, 28 (1981).
7. Jagoutz, E. & Zindler, A. *Terra cognita* **1,** 40 (1981).
8. White, W. M. & Hofmann, A. W. *Nature* **296,** 821–825 (1981).
9. Vidal, P. & Dosso, L. *Geophys. Res. Lett.* **5,** 169 (1978).
10. Dupre, B. & Allegre, C. J. *Nature* **286,** 17 (1980).
11. Allegre, C. J., Brevart, O., Dupre, B. & Minster, J.-F. *Phil. Trans. R. Soc.* A**297,** 447 (1980).
12. DePaolo, D. J. & Wasserburg, G. J. *Geophys. Res. Lett* **3,** 249 (1976).
13. O'Nions, R. K., Hamilton, P. J. & Evensen, N. M. *Earth planet. Sci. Lett.* **34,** 13 (1977).
14. Allegre, C. J., Ben Othman, D., Polve, M. & Richard, P. *Phys. Earth planet. Inter.* **19,** 293 (1979).
15. Zindler, A., Jagoutz, E. & Goldstein, S. L. *Earth planet. Sci. Lett.* (submitted).
16. Goldstein, S. L. *et al. Earth planet. Sci. Lett.* (submitted)
17. Zindler, A., Hart, S. R., Frey, F. & Jakobsson, S. P. *Earth planet. Sci. Lett.* **45,** 249 (1979).
18. Brooks, C., Hart, S. R., Hofmann, A. W. & James, D. E. *Earth planet. Sci. Lett.* **32,** 51 (1976).
19. Tatsumoto, M. *Earth planet. Sci. Lett.* **38,** 63 (1978).
20. Sun, S.-S. *Phil. Trans. R. Soc.* A**297,** 273 (1980).
21. Jacobsen, S. B. & Wasserburg, G. J. *Earth planet. Sci. Lett.* **50,** 139 (1980).
22. Tatsumoto, M., Knight, R. J. & Allegre, C. J. *Science* **180,** 1279 (1973).
23. Condomines, M., Morand, P. & Allegre, C. J. *Earth planet. Sci. Lett.* **55,** 247 (1981).
24. Menzies, M. & Murthy, V. R. *Earth planet. Sci. Lett.* **46,** 323 (1980).
25. Zindler, A. & Jagoutz, E. *EOS* **61,** 374 (1980).
26. Zindler, A., Hart, S. R. & Brooks, C. *Earth planet. Sci. Lett.* **54,** 217 (1981).
27. Zindler, A. *et al. EOS* **62,** 424 (1981).
28. Allegre, C. J., Hart, S. R. & Minster, J. F. *Earth planet. Sci. Lett.* (in the press).
29. DePaolo, D. J. *Earth planet. Sci. Lett.* **43,** 201 (1979).
30. Hofmann, A. W. & White, W. M. *Earth planet. Sci. Lett.* **52,** 421 (1982).
31. Hofmann, A. & White, W. M. *26th int. Geol. Congr., Paris* Abstr. Vol. II, 777 (1980).
32. Hofmann, A. & White, W. M. *Yb Carnegie Instn. Wash.* **79,** 477 (1980).
33. Chase, C. G. *Earth planet. Sci. Lett.* **52,** 277 (1981).
34. Hart, S. R. & Staudigel, H. *Earth planet. Sci. Lett.* **58,** 202 (1982).
35. Richard, P., Shimizu, N. & Allegre, C. J. *Earth planet. Sci. Lett.* **34,** 269 (1977).
36. Cohen, R. S., Evensen, N. M., Hamilton, P. J. & O'Nions, R. K. *Nature* **283,** 149 (1980).
37. White, W. M. *Yb Carnegie Inst Wash.* **78,** 325 (1979).
38. Sun, S.-S., Tatsumoto, M. & Schilling, J.-G. *Science* **190,** 143 (1975).
39. Carlson, R. W. thesis, Univ. California (1980).
40. Church. S. & Tatsumoto, M. *Contr. Miner. Petrol.* **53,** 253 (1975).
41. Staudigel, H. *et al. EOS* **62,** 1083 (1981).
42. White, W. M. & Hofmann, A. W. *Yb Carnegie Instn Wash.* **77,** 596 (1978).
43. White, W. M. *Yb Carnegie Instn Wash.* **78,** 331 (1979).
44. Dosso, L. & Murthy, V. R. *Earth planet. Sci. Lett.* **48,** 268 (1980).
45. Dosso. L., Vidal, P., Cantagrel, J. M., Lameyre, J. & Marot, A. *Earth planet. Sci. Lett.* **43,** 46 (1979).
46. Sun, S.-S. & Jahn, B.-M. *Nature* **255,** 527 (1975).
47. Kowalski, B. R. in *Computers in Chemical and Geochemical Research* Vol. 2 (ed. Klopenstein, C. A.) (Academic, New York, 1974).

Palaeolimnology and archaeology of Holocene deposits north-east of Lake Turkana, Kenya

R. B. Owen*, J. W. Barthelme†, R. W. Renaut* & A. Vincens‡

* Department of Geological Sciences, Queen Mary College, University of London, Mile End Road, London E1 4NS, UK
† Department of Sociology and Anthropology, St Lawrence University, Canton, New York 13617, USA
‡ Laboratoire de Géologie du Quaternaire, CNRS-Case 907, Luminy, 13288 Marseille Cédex 2, France

Geological, diatom, pollen and archaeological studies, supported by 24 original radiocarbon dates, provide new evidence to illustrate the Holocene history of Lake Turkana, Kenya. High and intermediate lake levels are recorded between 10,000 and about 3,000 yr BP, *with a general regression during the later Holocene. Archaeological finds document the transition from a fishing-based economy to pastoralism.*

DURING the past 15 yr, considerable evidence has been presented to illustrate the Holocene limnological histories of many East African lakes[1-6]. Research has demonstrated several former periods when lake levels were higher than today, some of which were broadly synchronous in different basins, and which have generally been attributed to palaeoclimatic variations. We report here the principal results of a multidisciplinary study of the Holocene sediments of Lake Turkana, providing new evidence for lake level fluctuations, and for the palaeoclimatology, palaeoecology and archaeology of East Africa.

Lake Turkana, one of the oldest and largest African lakes (7,500 km^2, 125 m maximum depth), occupies a predominantly semi-arid basin of internal drainage at the northern end of the Kenya Rift (Fig. 1). Its waters, which are moderately saline and alkaline[7-10], are mostly derived from the Ethiopian Highlands, through the Omo River[11]. Like most non-outlet lakes, Turkana's waters have been subject to climatically-induced fluctuations in level and hydrochemistry of variable magnitude, frequency and duration[8,11,12].

Holocene lacustrine sediments lie around the margins of the lake, up to 80 m above the present (July 1976) lake surface (~375 m OD). Although sediments north of the lake have already been examined[13-16], Holocene deposits from the other shorelines have previously received little attention. North-east of the lake near Koobi Fora (Fig. 1), they are informally termed the 'Galana Boi beds'[17-21].

Geology and lithofacies of Galana Boi beds

The Galana Boi beds are a sequence of predominantly lacustrine and marginal lacustrine, poorly consolidated, diatomaceous silts and sands. They rest unconformably on Plio–Pleistocene sediments over an area of ~2,000 km^2. Where exposed, they are mostly <10 m thick, but attain an aggregate thickness of 32 m in Area 103 (Fig. 1). The deposits lie up to 80 m above the modern lake and are unaffected by tectonics, except locally near the Kokoi uplands (Fig. 1), where they have been uplifted.

Littoral sandy units crop out as discontinuous curvilinear

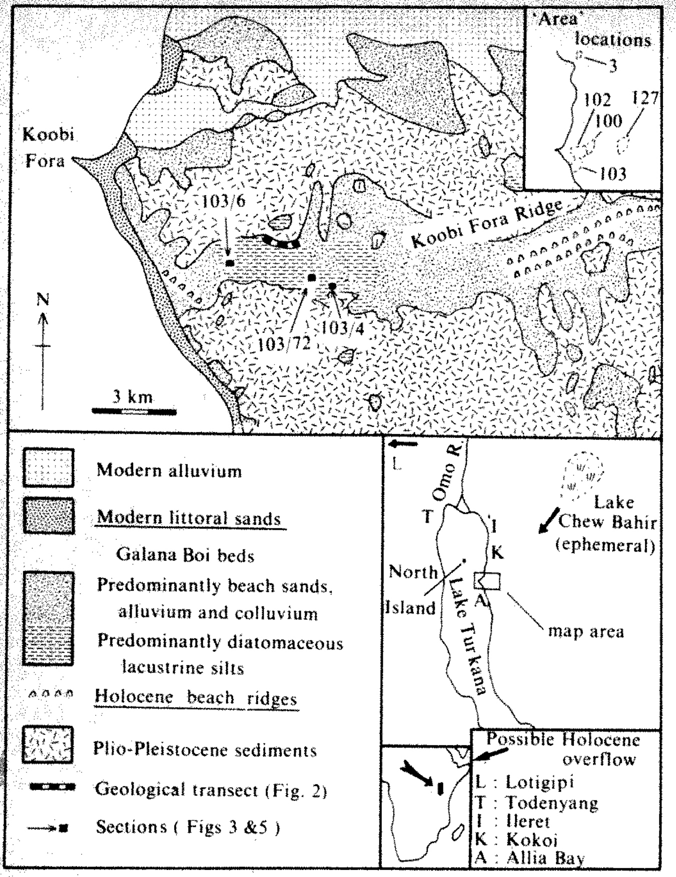

Fig. 1 Simplified geological map showing the distribution of the Galana Boi beds, east of Koobi Fora. Area numbers shown in the inset refer to fossil-collecting areas as designated by the Koobi Fora Research Project.

bodies parallel to former shorelines, while lacustrine silts have infilled palaeovalleys. Fluctuating lake levels during deposition have contributed to the development of lenticular and interdigitating sedimentary units, displaying vertical and lateral facies variations over short distances. Though commonly horizontal, primary depositional dips of up to 15° have developed where sediments drape over topographic highs.

Nearshore, moderate- to high-energy environments such as beach bars, barriers and sandy littoral shelves, are represented by a sublitharenite-quartz arenite lithofacies[10]. These heterogeneous sediments are typically well sorted (locally with distinct heavy mineral laminae) and although commonly massive due to bioturbation, many kinds of stratification are present. Typically they form linear bodies <2 m thick. Molluscs are common and include *Mutela emini*, *Etheria elliptica* and *Pila ovata*. Calcified root-tubules[22] and fish bones are locally numerous.

Distal alluvial and delta plain environments, and parts of shorelines adjacent to river mouths, are associated with a litharenite-arkosic arenite lithofacies[10]. This encompasses various sublithofacies that are moderately to poorly sorted. Stratification is generally poor and units are usually <2 m thick. $CaCO_3$ concretions, rhizoliths, root-marked palaeosols, molluscs, fish and other vertebrates are locally present.

Low energy lacustrine environments are represented by a diatomaceous silt, clay and fine sand lithofacies. The sediments are commonly well laminated (up to 1 cm), locally fissile and attain a maximum thickness of about 20 m. Diatom content ranges up to 10^8 individuals per g of sediment. Nitratine ($NaNO_3$) locally forms up to 8% of the deposits in Area 103. Molluscs are common and are dominated by *Melanoides tuberculata*, *Corbicula africana*, *Cleopatra pirothii* and *Bellamya unicolor*. Carbonaceous root-marks, calcite-cemented siltstone nodules, fish bones, pollen, sponge spicules and ostracods also occur.

There are three important biogenic lithofacies. In the first, *Etheria elliptica* forms reefs up to 4 m thick. Their relationship to other facies indicates a high-energy environment. In the second, *Melanoides tuberculata* and *Corbicula africana* variously dominate in silty sand units <10 cm thick. The degree of shell wear shows that both *in situ* and reworked assemblages are present. Third, a few outcrops of impure diatomite record former lagoons and areas of low clastic input.

Stratigraphy and chronology

Much of the data presented here originate in Areas 102 and 103 (Fig. 1). The stratigraphy of Area 102 is summarized by the transect in Fig. 2. The stratigraphies of Area 103 and other localities are shown in Fig. 3. Many new radiocarbon dates have been obtained[23] from the region and are listed in Table 1. The time-spans represented by the sections (Figs 2, 3) are shown in Fig. 4, together with a generalized plot of former lake levels against time. For descriptive purposes, three high level phases are recognized. These 'phases' do not represent continuously stable levels, but periods of varying duration in which the lake was high and fluctuating between +50 and +80 m.

Early Holocene sedimentation (phase 1): The diatomaceous silts of section C in Area 102 (Fig. 2) record a period of high lake levels (+75 to +80 m). They thicken to the east and south, and probably represent a large part of the early and middle Holocene. To the south-east, the basal units have been dated at 9,880 ± 670 yr BP (ref. 24) (section 103/4, Fig. 3).

South of the Kokoi uplands (Fig. 1), dates of 9,540 ± 260 and 9,260 ± 235 yr BP have been obtained from molluscs in high level spits (uplifted to +95 m). In the same area, mammal bones from littoral deposits have yielded ages of 8,395 ± 270 and 8,355 ± 235 yr BP.

Shells from littoral sands (+70 to +80 m) near Ileret (Fig. 1) have been dated at 9,360 ± 135 yr BP (ref. 17). Locally, these sands contain abundant stromatolites[10,25,26] (section 3/42, Fig. 3). In Area 127 (Fig. 1), subarkosic sands, silts, clays and impure diatomites represent former littoral and lagoonal environments. Shells from these deposits (+73 to +75 m) have yielded ages of 8,710 ± 130 and 8,520 ± 130 yr BP, while fish bone has given a date of 7,855 ± 160 yr BP. Locally, these sediments are overlain by reefs of *Etheria elliptica* (section 127/52, Fig. 3), which have given erroneous modern ^{14}C ages.

The dates reported above show that phase 1 (Fig. 4) accords with the high lake levels widely recorded in East Africa[1-6] for the early Holocene (~10,000–7,500 yr BP).

Middle Holocene sedimentation (phase 2): Following the early Holocene lake maxima, Butzer[16] found evidence in the Omo region (Fig. 1) for a fall to modern levels at 6,600 yr BP. Although the diaton record from section103/72 (Fig. 5) does suggest a regression that could relate to such an event, we lack evidence for a drop of such magnitude. This regression (Fig. 4) was followed by the higher, fluctuating levels of phase 2.

Phase 2 littoral deposits lie at ~+70 m in Area 103 (5,060 ± 245 yr BP) [24] and +67 m, 5 km north-east of Koobi Fora (4,540 ± 230 yr BP)[27]. Several dates (3,960 ± 60, 3,945 ± 135 and 4,100 ± 125 yr BP) have been recorded from littoral sands at +45 to +47 m (GaJi 4, Fig. 2). These units overlie diatomaceous clayey silts and silts (with *Stephanodiscus* and *Melosira* dominated diatom floras, Fig. 2) that formed under an expanded lake whose shoreline (~+55 m) may be marked by the planar cross-stratified sands of section B (Fig. 2).

Phase 2 represents a middle Holocene period of high (up to ~+75 m) fluctuating lake levels. However, the later stages were characterized by lower elevations of ~+50 to +55 m (Fig. 4).

Late Holocene sedimentation (phase 3): Phase 3 (Fig. 4) is recorded by 6 m of white, highly diatomaceous, laminated silts (section 103/6, Fig. 3), 5 km south-east of Koobi Fora. The base of this sequence lies at ~+35 to +40 m. Its stratigraphical relationship to sediments dated further east indicates a late Holocene age. An interbedded white vitric tuff (8 cm thick) probably represents a contemporary ashfall into the former

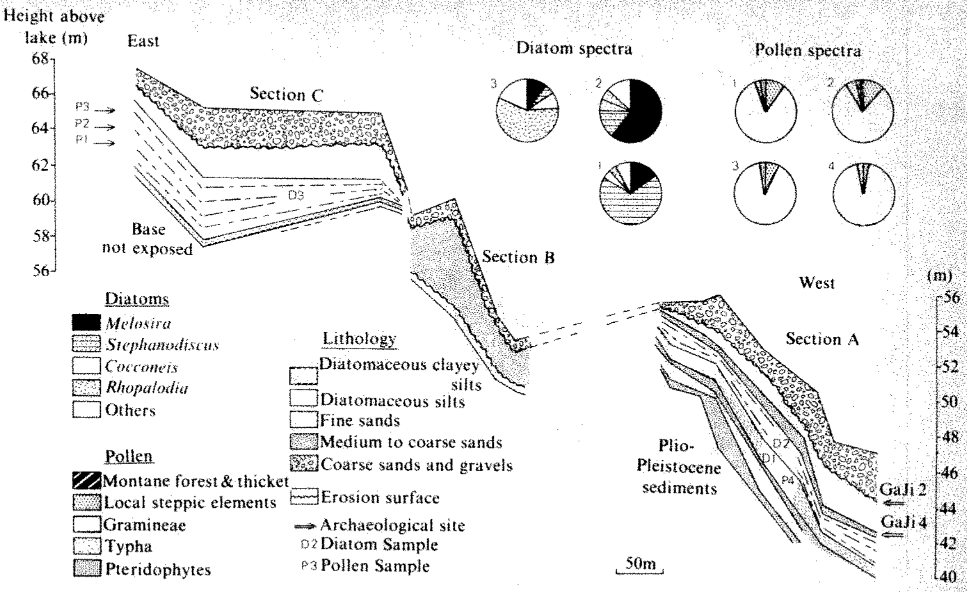

Fig. 2 Geological transect and representative microfossil spectra from Area 102. The location of the transect is shown in Fig. 1. The three sections were accurately levelled relative to one another and then related to the height of the lake surface (in July 1976) by using a barometric altimeter.

lake. One possible source may be the North Island volcano (Fig. 1), where trachytic lavas[28] overstep high-level, wave-cut platforms of probable early or middle Holocene age. An ill-defined series of beach ridges and regressive littoral sands record lower, fluctuating lake levels for the past two millennia.

Although the third phase remains to be dated radiometrically, it may be of broadly similar age to a late Holocene high stand recognized in the Omo region at 3,250 yr BP (ref. 14).

Other confirmed and probable Holocene lake sediments at +75 to +80 m have been reported from the southeastern[29], southwestern[30] and western[31–33] lake margins.

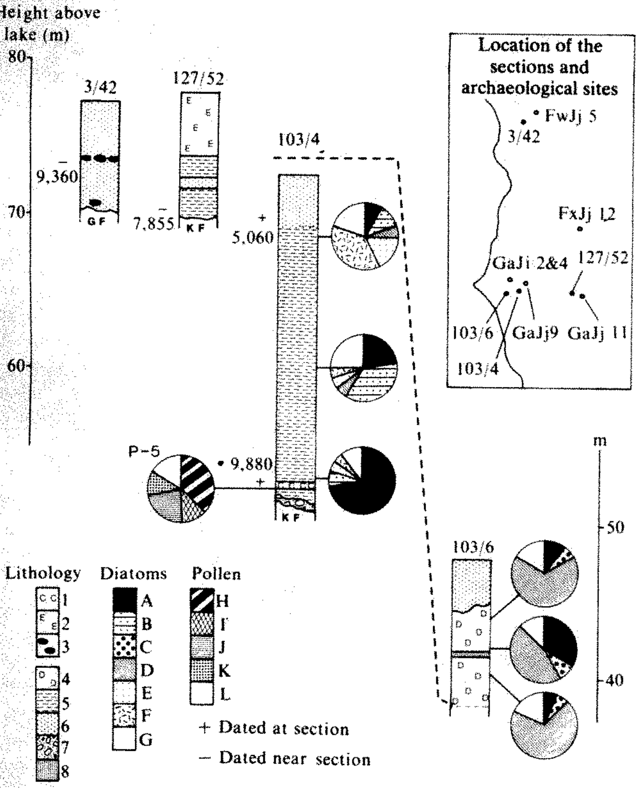

Fig. 3 Simplified litho- and microfossil stratigraphy of the Galana Boi beds. Lithologies: 1, coquina; 2, *Etheria* reef; 3, stromatolites; 4, impure diatomites; 5, diatomaceous silts; 6, sands; 7, orthoconglomerates; 8, tuff. The base of section 103/6 is not exposed. GF, Guomde Formation; KF, Koobi Fora Formation. Diatoms: *a*, *Melosira*; *b*, *Stephanodiscus*; *c*, *Cyclotella* and *Thalassiosira*; *d*, *Fragilaria*; *e*, *Cocconeis*; *f*, *Rhopalodia*; *g*, others. Pollen: *h*, montane forest and thicket; *i*, local steppic elements; *j*, *Gramineae*; *k*, *Typha*; *l*, *Pteridophytes*; *m*, others.

Diatom stratigraphy and lake palaeoecology

Figure 5 shows the diatom stratigraphy of section 103/72, which lies 9 km south-east of Koobi Fora (Fig. 1). Its base lies at ~+50 m and lateral tracing to locally dated units (section 103/4, Fig. 3) brackets it between ~9,880 and 5,060 yr BP (ref. 24).

Abundant planktonic diatoms in the lower 3.8 m of section 103/72, combined with a scarcity of benthic and epiphytic species, suggest a period of deep water and high lake level (phase 1). Lower levels are indicated by a dramatic decline in the planktonic species *Melosira agassizi* and *M. granulata-agassizi*, and by an increase in shallow water forms such as *Rhopalodia vermicularis* and *Cocconeis placentula*.

An increase in the planktonic component (dominated by *Stephanodiscus*) between 6 and 6.5 m reflects a second high level period, after which the lake was generally lower, but still covering the section site. Two, probably short-lived, transgressions can be inferred from increases in *Stephanodiscus minutula* (formerly *S. astraea v. minutula*) at 7.9 m and *Melosira nyassensis v. victoriae* at 7.2 m. At the top of the section, a decrease in diatom abundance, increasing grain size and littoral sands all indicate a fluctuating, regressing lake.

Although the basal silts of section 103/72 are certainly early Holocene, a lack of datable material at the top of the silts (10 m) has left the section open to two possible interpretations. First, the silts could be entirely of early Holocene age, the decline in *Melosira* at 3.8 m recording an early Holocene regression. This implies a very high average sedimentation rate of at least ~1 m 300 yr^{-1}, with even higher rates to the south and west where the silts thicken to ~20 m. Alternatively, the *Melosira* decline could reflect the fall in lake levels between phase 1 and phase 2 recorded elsewhere (Fig. 4). The subsequent transgression would then be of middle Holocene age, the record ending at ~5,000 yr BP. If the latter interpretation is correct, then the altimetric data, diatom stratigraphy and continuity of silt sedimentation would indicate that the lake did not fall below about +50 m for any extended period between ~10,000 and 5,000 yr BP.

The youngest diatomaceous units (phase 3 in Fig. 4; section 103/6 in Fig. 3) contain a flora dominated by *Fragilaria* spp. and *Melosira granulata*, but significantly include a few *Thalassiosira rudolfii* and *Cyclotella meneghiniana* for the first time. The latter diatoms occur in the modern saline, alkaline lake[10].

Ecological studies of modern East African diatoms[34–38] allow several inferences to be made concerning the former hydrochemistry. Today, Lake Turkana is saline (2.5 g l^{-1}) and alkaline (19–25 mequiv. l^{-1}) with a pH of ~9.2 and a SiO_2 concentration of ~18 mg l^{-1} (refs 7–9). The early and middle Holocene diatoms imply alkalinities ($HCO_3^- + CO_3^{2-}$) of ≤10 mequiv. l^{-1}, salinities below 2 g l^{-1}, a pH of ~7–8.5 and fluctuating SiO_2 concentrations of from ~1 to 10 mg l^{-1}.

Pollen of the Galana Boi beds

Figures 2 and 3 give the locations of five samples from which pollen was obtained. Sample P-5 is of early Holocene age, while the younger P-1 to P-4 material extends into the middle Holocene.

The oldest pollen spectrum was extracted from the base of a coquina dated at 9,880±670 yr BP (section 103/4, Fig. 3). It is characterized by abundant regional elements—montane forest and thicket taxa (36.8%), which do not occur in modern lake samples[39]. The pollen grains were probably transported to the lake by rivers originating in the Ethiopian Highlands. They suggest both increased runoff and an extension of the highland forests. This, together with a high percentage of *Pteridophytes* (14.7%), suggests increased rainfall over the catchment. Arboreal forms are uncommon (3.2%) among local elements, which are dominated by herbaceous types, notably *Gramineae* (21.2%) and *Compositae* (7.4%). The *Chenopodiaceae/Amaranthaceae*, which indicate saline soils, occur in low percentages (2.2%).

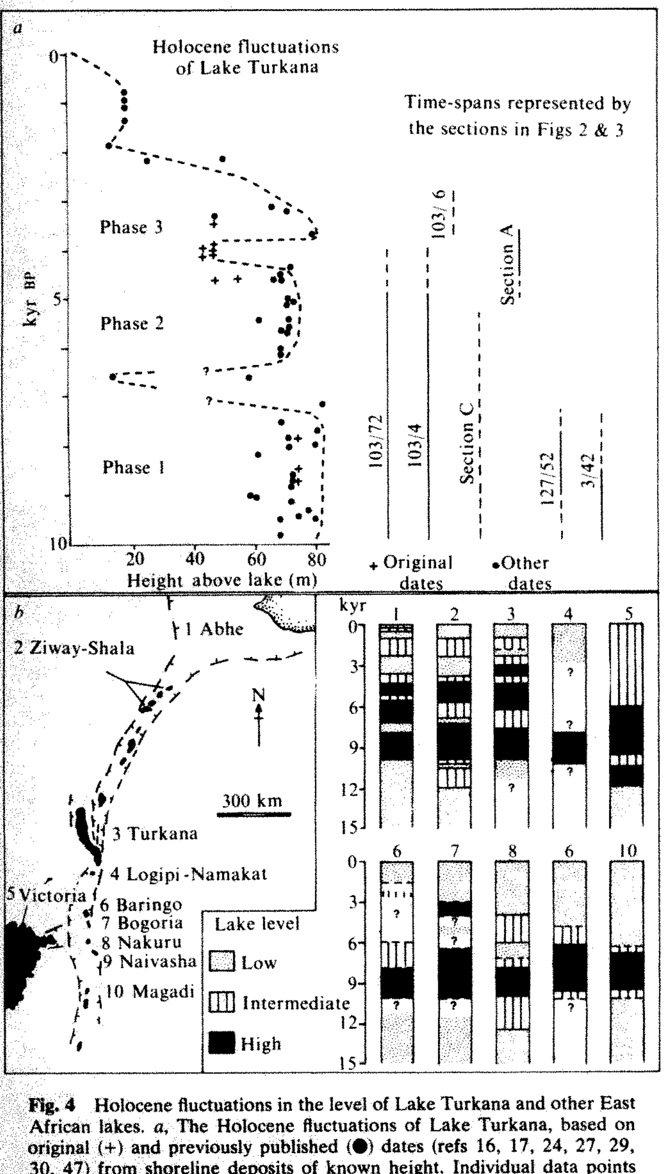

Fig. 4 Holocene fluctuations in the level of Lake Turkana and other East African lakes. *a*, The Holocene fluctuations of Lake Turkana, based on original (+) and previously published (●) dates (refs 16, 17, 24, 27, 29, 30, 47) from shoreline deposits of known height. Individual data points have not been joined together as this process can introduce a false sense of accuracy. The dates themselves commonly have error ranges of ±100–200 yr. Several dates from a single unit at the same level may give a wide variation. Dates from archaeological site GaJi 4 for example, range from 3,405 to 4,580 yr BP, with an exceptional date of 10,320 yr BP (probably from reworked material). As more dates become available so problems of scatter become apparent. For these reasons, we have traced only the general trends based on clusters of dates. *b*, Lake level trends for other East African lakes during the past 20,000 yr (includes original data for lakes Turkana, Baringo and Bogoria. Other sources: refs 1, 5, 49 and 56).

Samples P-1 to P-4 (sections A and C, Fig. 2) are younger and very different. They are dominated exclusively by taxa that typically inhabit lake margins in sub-desert zones[40]. Regional elements are absent or rare (0.4% in P-2) with only two taxa, *Juniperus* and *Myrica*, being represented. The occurrence of *Typha* and *Pteridophytes* in percentages >1% suggests the presence of rivers, although runoff was probably less than in the early Holocene. Local arboreal elements are rare (0.2–0.4%). Among local herbaceous forms, *Gramineae* are very abundant (77–99%). The *Chenopodiaceae/Amaranthaceae* again occur in low percentages (2.7% maximum). In two samples *Tribulus* constitutes 8.4–10.1% of the total pollen sum (P-2 and P-4, Fig. 2). This herbaceous taxon is today associated with refuse tips and is widely distributed in sub-desert zones[41]. Its occurrence may reflect the presence of local human encampments.

The early and middle Holocene lake margins were covered by a sub-desert steppe with well developed, herbaceous vegetation similar to that of today, although arboreal forms were more common at 9,880 yr BP. The poor representation of *Chenopodiaceae/Amaranthaceae* and the occurrence of *Typha* and *Pteridophytes* indicates the presence of freshwater rivers, supporting the other evidence for a lake less saline than today. The distribution of regional pollen suggests a more humid environment at 9,880 yr BP, but by the middle Holocene, climatic conditions had become more comparable with those of the present.

Archaeology

Two principal human economic adaptations are represented in the Holocene deposits. First, associated with early Holocene beaches, and continuing through into the middle Holocene deposits, are a distinctive set of lacustrine based occupations. Faunal refuse consists primarily of fish bones, while cultural materials include barbed bone harpoons and, at some sites, decorated and undecorated pottery. Seven large occupations are situated on the +75 to +80 m shoreline. Dates of 8,710±130 yr BP (GaJi 11, Fig. 3) and 8,395±270 yr BP (FxJj 12, Fig. 3) have been obtained from two of the sites. Importantly, ^{14}C ages of 9,540±260 and 9,260±235 yr BP were obtained from a basal *Melanoides* coquina at FxJj 12. This horizon contains a low density scatter of microlithic artefacts and fish-bone refuse. While the small excavation did not yield barbed bone harpoons, the lithic material indicates that by 9,500 yr BP, human groups with characteristic Later Stone Age lithic artefacts, were camping adjacent to the +75 to +80 m shoreline.

The lacustrine based sites exhibit broadly similar technological and economic features. The lithic assemblages are primarily composed of microlithic elements (especially crescents and curved backed blades), morphologically unstandardized scrapers, *outils écaillés* and core tools. Barbed bone harpoons, including uniserial, biserial and triserial examples, have been recovered. Two sites (FxJj 12 and GaJi 11) lack pottery remains suggesting a possible aceramic occupation phase. Decorated and undecorated pottery is represented at the remaining five shoreline sites. Numerous sherds similar to the well known 'wavy-line' pottery from the Sudan[42] are present at FxJj 12-North[43]. Fish remains, primarily several species of catfish and Nile Perch, constitute the major proportion of faunal refuse. Hippopotamus and crocodile, in addition to a wide variety of land mammals, are also represented. While freshwater molluscs, including such edible species as *Pila ovata* and *Etheria elliptica*, are commonly associated with the lacustrine sites, direct evidence for their consumption is lacking. Archaeological sites with similar lacus-

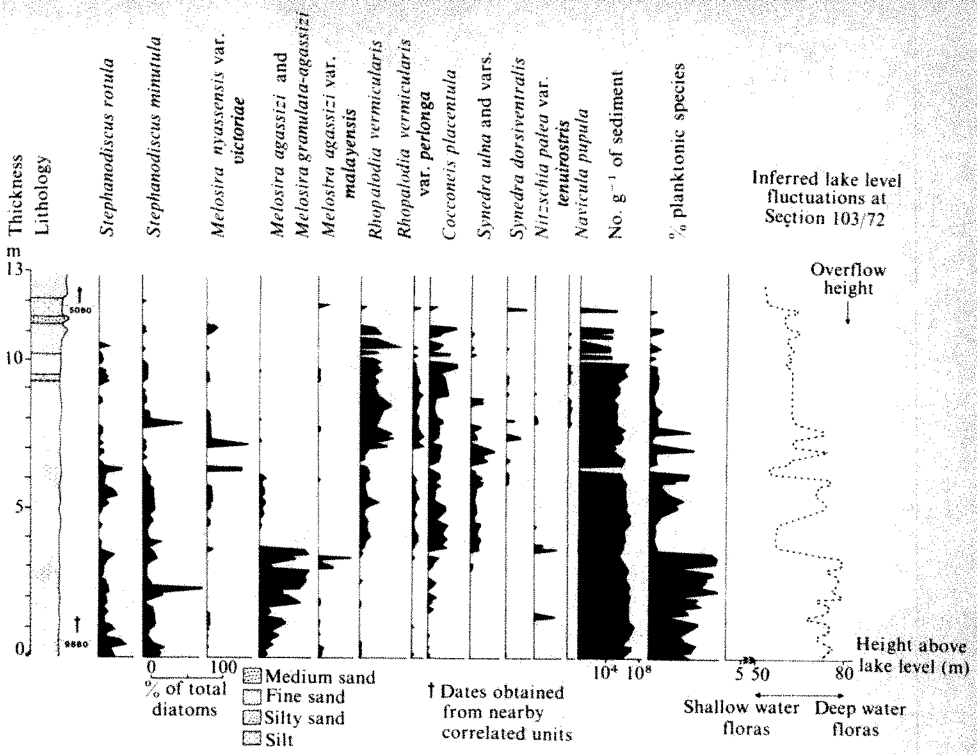

Fig. 5 Lithofacies, diatom stratigraphy and interpretation of section 103/72, north-east Turkana. The section site is shown in Fig. 1. Many species are present (96) but only the most important are included. The first five are planktonic types, whereas the remainder tend to be associated with shallow waters in East Africa. The lake level interpretation is relevant to the section site only, the base of which lies at about +50 m (barometric determination). The minimum and maximum levels of the fluctuation curve are provided by the known height of the section and the overflow level of Lake Turkana respectively. Within these limits the curve is generalized from the diatom data.

trine adaptation are known from the northern[16,44], south-western[30] and southeastern[29] margins of the basin.

The second principal economic tradition, the Pastoral Neolithic, is associated with the second phase of high lake levels. Domestic stock, including ovicaprids and probably cattle, are present at sites GaJi 2 and GaJi 4 (Fig. 3). A suite of ^{14}C determinations (Table 1) date the occupations to ~4,000 yr BP. These dates currently represent, along with preliminary dating results from North Horr[45], the earliest securely dated evidence for domestic animals in Eastern Africa[46]. At two sites, anomalously old shell dates of 8,915 ± 140 yr BP and 10,320 ± 150 yr BP have been recorded. These probably represent reworked debris and in both cases are associated with suites of younger dates from various materials.

Both pastoralist settlements lie within middle Holocene beach sands at +43 to +47 m. Stone artefact assemblages consist of typical Later Stone Age microliths and debitage. Several distinctive pottery types, including Nderit Ware, are represented. While fishing continued to play an important subsistence role, barbed bone harpoons are absent. The early pastoralists had apparently devised an alternative, as yet unidentified fishing strategy. Faunal remains of wild animals are noticeably scarce. A third pastoralist settlement, the Ileret Stone Bowl Site, yielded a single ^{14}C date of 4,000 ± 140 yr BP. Domestic cattle and ovicaprids are present in apparent association with stone bowls.

While little archaeological material is associated with the third phase, recent fieldwork to the south-west[47] suggests that human groups were pursuing a combination of aquatic and pastoral economic adaptations.

Discussion

Late Pleistocene high-stands are recorded for several East African lakes[1-5]. None has yet been recognized at Lake Turkana for the period 35,000–10,000 yr BP. This may reflect either a continuously low status or the erosion of any high-lake sediments that were deposited.

Lake Turkana expanded during the early Holocene, periodically reaching +80 m. Contemporary local hunter–gatherer groups camped adjacent to its fluctuating shorelines and increased their reliance on fishing.

Sandy silts at Todenyang (Fig. 1) that dip below the modern lake surface, have yielded a single mixed shell date of 6,600 ± 150 yr BP (ref. 14), which indicates a fall to modern levels during the middle Holocene. Although we do not reject this possibility, our experience of shells in the Turkana basin has shown that they may be reworked with little damage and should be interpreted with caution. If valid, the date implies major desiccation of a large lake at a time when the great majority of intertropical African lakes were at high or intermediate status[2,48]. No evidence has been found for significant contemporary erosion of the unconsolidated sediments in area 103 which span this period. Similarly, evidence is lacking for a fall of such magnitude to the south-east of the lake[29]. While accepting a possible drop to intermediate levels at this time, we lack evidence to confirm a fall to modern levels.

During the remainder of the middle Holocene the lake was fresh and fluctuated between high and intermediate levels. The local vegetation was dominated by *Gramineae* and by 4,500 yr BP, human groups with domestic animals were present.

Lake Turkana contracted during the late Holocene and became significantly more alkaline. While we have evidence for a lake standing at about +50 m, we lack data to confirm the rise to +75 m at 3,250 yr BP suggested by Butzer[16]. The lake level oscillated below about +50 m after 3,000 yr BP (refs 16, 30) (Fig. 4).

The lake demonstrates hydrological variability both in time and space. Hydrodynamic variations and consequent differences in the nature of the surface level record around the lake, partly reflect the influence of prevailing easterly winds. High energy shorelines predominate to the west, whereas more mixed energy environments occur to the east. The diatom record suggests that many minor oscillations were superimposed on the major fluctuations. In addition, alternating light and dark laminae in silts may reflect a cyclic input of flood waters, similar to those from the modern Omo River.

The lake level fluctuations can be mostly attributed to variations in the water balance caused by climatic change. The lake may have increased its catchment for periods during the early and middle Holocene by receiving overflows from Lake Chew Bahir[49] (Fig. 1) and a former lake in the Suguta Valley to the south[50,51]. At its maximum level (+80 m), Lake Turkana overflowed into the Lotigipi Plain (Fig. 1) and thence to the River Nile[16,52].

The archaeological data may provide a geographical and chronological link between the early food-producing traditions

Table 1 Radiocarbon dates from Lake Turkana

Site	Lithology/ environment of dated unit	Material dated	Laboratory	Laboratory date no.	Date (yr BP)	Elevation of dated unit above lake level (m)
Fishing settlements						
GaJi 3	Beach sands	Bone apatite (M)	Geochron	Gx-5475-A	4,560 ± 185	55–56
GaJi 11	*Etheria* reef	*Etheria* shell	Geochron	Gx-5477-A	Modern	75
GaJi 11	*Etheria* reef	*Etheria* shell	Helsinki	Hel-1275	Modern	75
GaJi 11	Sand bar	Shell	Helsinki	Hel-1276	8,520 ± 130	73–75
GaJi 11	Sand bar	*Etheria* shell	Helsinki	Hel-1277	8,710 ± 130	73–75
GaJi 11	Sand bar	Bone apatite (F)	Geochron	Gx-5476-A	7,855 ± 160	73–75
FxJj 12	Sand spits	Shell	Geochron	Gx-5479	9,260 ± 235	95 (uplifted)
FxJj 12	Sand spits	Shell	Radiocarbon Ltd.	R1-954	9,540 ± 260	95 (uplifted)
FxJj 12	Sand spits	Bone apatite (M)	Geochron	Gx-5481-A	8,395 ± 270	95 (uplifted)
FxJj 12	Sand spits	Bone apatite (M & F)	Geochron	Gx-5480-A	8,355 ± 235	95 (uplifted)
FxJj 12-N	Beach sands	Bone apatite (H)	Geochron	Gx-4733-A	3,215 ± 155	100 (uplifted)
Pastoral Neolithic						
GaJi 2	Beach sands	Charcoal	Un. Penn.	P-2609	3,970 ± 60	43–46
GaJi 2	Beach sands	Charcoal	Un. Sydney	SUA-634	4,160 ± 110	43–46
GaJi 2	Beach sands	Shell	Un. Sydney	SUA-635	8,915 ± 140	43–46
GaJi 4	Beach sands	Charcoal	Un. Sydney	SUA-637	3,945 ± 135	45–47
GaJi 4	Beach sands	Humic acid from SUA-637	Un. Sydney	SUA-637-B	4,100 ± 125	45–47
GaJi 4	Beach sands	Charcoal	Un. Penn.	P-2610	3,960 ± 60	45–47
GaJi 4	Beach sands	Bone apatite (M)	Geochron	Gx-4642-I-A	3,405 ± 130	45–47
GaJi 4	Beach sands	Bone apatite (F)	Geochron	Gx-4642-II-A	4,580 ± 170	45–47
GaJi 4	Beach sands	Shell	Un. Sydney	SUA-638	10,320 ± 150	45–47
FwJj 5	Fluvial sands	Bone apatite (M)	Geochron	Gx-4643-A	4,000 ± 140	–
Other sites						
Nderati	Sandy silts	Shell	Geochron	Gx-5478	13,040 ± 640	–
GaJj 9	Burial site 1	Bone apatite (H)	Geochron	Gx-4641-A	Modern	–
GaJj 9	Burial site 2	Bone apatite (H)	Geochron	Gx-6400-A	3,125 ± 210	–
Previously obtained dates						
Ileret[*17]	Sands	Shell	—	—	9,360 ± 135	70–75?
Area 103[*24]	Coquina	Shell	—	—	9,880 ± 670	52–55?
Area 103[*24]	Sandy silts	Shell	—	—	5,060 ± 245	70–73?
Area 103[*24]	Silts	Charcoal	—	—	4,390 ± 235	65–68?
Area 102[*27]	Beach sands	Shell	Un. Birm.	Birm-540	4,540 ± 230	67

M, Mammal bone; F, fish bone; H, human bone; Un., university. Heights quoted are based on barometric determinations. Site locations shown in Figs 1 and 3. For consistency with previous research, all shell dates are recalibrated to give an age 400 yr younger than that obtained by ^{14}C assay (for explanation, see ref. 14). The Ileret date of 9,360 yr BP is quoted as published as we have not been able to confirm any recalibration.

* Reference number.

in the Sudan and later pastoralist occupations in the central Kenya Rift. The appearance of early pastoralism in the Turkana basin may have been the result of small-scale population movements caused by middle Holocene climatic deterioration in the Sahel and Savannah zones, or the diffusion of pastoralist tradition[4]. Ehret[53] indicated that the linguistic evidence supports an ancestral Southern Cushitic identity for these early pastoralists. While this evidence is being evaluated[54], the archaeological data from the Turkana basin seem to support the Cushitic model[23,30].

An alternative model for the beginnings of pastoralism in East Africa has been proposed by Nelson (ref. 55 and unpublished data). He has uncovered evidence of domestic cattle some 40 km to the south of Nairobi, reported to date between 14,000 and 15,000 yr BP. This date would require rewriting of the history of animal domestication worldwide. However, it is based on a single ^{14}C determination on bone apatite (from our experience, a sometimes unreliable dating material) and faunal elements studied only in preliminary form. While a challenge to other models of early domestication in East Africa, including that presented here, more ^{14}C dates and extensive comparative examination of the fauna are needed before the far reaching implications of Nelson's work can be accepted.

We thank the late Professor W. W. Bishop, Professor G. L. Isaac, Dr R. Bonnefille, Mr A. T. Grove, Dr I. Findlater, Dr W. J. French, Mr P. Harvey and Mr R. E. F. Leakey for assistance. We acknowledge support from the NERC, Royal Society, NSF and CNRS.

Received 29 January; accepted 4 May 1982.

1. Butzer, K. W., Isaac, G. L., Richardson, R. L. & Washbourn-Kamau, C. K. *Science* **175,** 1069–1076 (1972).
2. Street, F. A. & Grove, A. T. *Quat. Res.* **12,** 83–118 (1979).
3. Gasse, F., Rognon, P. & Street, F. A. in *The Sahara and the Nile* (eds Williams, M. A. J. & Faure, H.) 361–400 (Balkema, Rotterdam, 1980).
4. Livingstone, D. A. *A. Rev. ecol. Syst.* **6,** 249–280 (1975).
5. Tiercelin, J. J., Renaut, R. W., Delibrias, G., Le Fournier, J. & Bieda, S. *Palaeoecol. Afr.* **13,** 105–120 (1981).
6. Renaut, R. W. & Owen, R. B. *Rech. Géol. Afr.* **5,** 130–133 (1980).
7. Yuretich, R. F. *Sedimentology* **26,** 313–331 (1979).
8. Cerling, T. E. *Palaeogeogr. Palaeoclimatol. Palaeoecol.* **27,** 247–285 (1979).
9. Talling, J. F. & Talling, I. B. *Int. Rev. Gesamt. Hydrobiol.* **50,** 421–463 (1965).
10. Owen, R. B. thesis, Univ. London (1981).
11. Butzer, K. W. *Res. Pap. Dept Geogr. Univ. Chicago* 136 (1971).
12. Cohen, A. *Palaeoecol. Afr.* **13,** 61–82 (1981).
13. Butzer, K. W. & Thurber, D. L. *Nature* **222,** 1138–1143 (1969).
14. Butzer, K. W., Brown, F. H. & Thurber, D. L. *Quaternaria* **11,** 15–30 (1969).
15. Butzer, K. W. in *Earliest Man and Environments in the Lake Rudolf Basin* (eds Coppens, Y., Howell, F. C., Isaac, G. L. & Leakey, R. E. F.) 12–33 (University of Chicago Press, 1976).
16. Butzer, K. W. *Phys. Geogr.* **1,** 42–58 (1980).
17. Vondra, C. F., Johnson, G. D., Behrensmeyer, A. K. & Bowen, B. E. *Nature* **231,** 245–248 (1971).
18. Bowen, B. E. & Vondra, C. F. *Nature* **242,** 391–393 (1973).
19. Vondra, C. F. & Bowen, B. E. in *Earliest Man and Environments in the Lake Rudolf Basin* (eds Coppens, Y., Howell, F. C., Isaac, G. L. & Leakey, R. E. F.) 79–93 (University of Chicago Press, 1976).
20. Vondra, C. F. & Bowen, B. E. in *Geological Background to Fossil Man* (ed. Bishop, W. W.) 395–414 (Scottish Academic, Edinburgh, 1978).
21. Findlater, I. in *Koobi Fora* Vol. 1 (eds Leakey, M. G. & Leakey R. E. F.) 14–31 (Oxford University Press, 1978).
22. Klappa, C. F. *Sedimentology* **27,** 613–629 (1980).
23. Barthelme, J. W. thesis, Univ. California (1981).
24. Raynolds, R. G. H. *Koobi Fora Res. Proj.* (1973).
25. Johnson, G. D. *Nature* **247,** 520–523 (1974).
26. Abell, P., Awramik, S. M. & Osborne, R. H. *Bull. Am. Soc. Petrol. Geol.* **63,** 478 (1978).
27. Bishop, W. W. *Radiocarbon* **18,** 248–267 (1976).
28. Brown, F. H. & Carmichael, I. S. E. *Lithos* **4,** 305–323 (1971).
29. Phillipson, D. W. *Azania* **12,** 1–32 (1977).
30. Robbins, L. H. *The Lothagam Site: A Late Stone Age Fishing Settlement in the Lake Rudolph Basin, Kenya* (Museum, Michigan State University, 1980).
31. Walsh, J. & Dodson, R. G. *Rep. geol. Surv. Kenya* 82 (1969).
32. Whitworth, T. *Durham Univ. J.* **5712,** 88–100 (1965).
33. Dodson, R. G. *Rep. geol. Surv. Kenya* 60 (1963).
34. Richardson, J. L. *Int. Rev. Gesamt. Hydrobiol.* **53,** 299–338 (1968).
35. Richardson, J. L., Harvey, T. J. & Holdship, S. A. *Pol. Arch. Hydrobiol.* **25,** 341–353 (1978).
36. Hecky, R. E. & Kilham, P. *Limnol. Oceanogr.* **18,** 53–71 (1973).
37. Kilham, P. *Limnol. Oceanogr.* **16,** 10–18 (1971).
38. Gasse, F. thesis, Univ. Paris (1975).
39. Vincens, A. *Bull. Ass. Sénégal. Etud. Quat. Afr.* **56–57,** 74–75 (1979).
40. Bonnefille, R. & Vincens, A. *Ass. Fr. Etud. Quat.* **50,** 235–247 (1977).
41. Agnew, A D. Q. *Upland Kenya Wild Flowers. A Flora of the Ferns and Herbaceous Flowering Plants of Upland Kenya* (Oxford University Press, 1974).
42. Arkell, A. J. *Early Khartoum* (Oxford University Press, 1949).
43. Barthelme, J. W. *Azania* **12,** 33–41 (1977).
44. Brown, F. H. *Azania* **10,** 144–175 (1975).

45. Phillipson, D. W. *The Later Prehistory of Eastern and Southern Africa* (Heinemann, London, 1977).
46. Barthelme, J. W. in *The Causes and Consequences of Food Production in Africa* (eds Clark, J. D. & Brandt, S. A.) (University of California Press, in the press).
47. Robbins, L. H. *Lopoy: a Late Stone Age Fishing and Pastoralist Settlement West of Lake Turkana, Kenya* (Museum, Michigan State University, 1980).
48. Street, F. A. & Grove, A. T. *Nature* **261**, 385–390 (1976).
49. Grove, A. T., Street, F. A. & Goudie, A. S. *Geogr. J.* **141**, 177–202 (1975).
50. Truckle, P. H. *Nature* **263**, 380–383 (1976).
51. Owen, R. B. & Renaut, R. W. *Rech. Géol. Afr.* **5**, 143–146 (1980).
52. Adamson, D. A., Gasse, F., Street, F. A. & Williams, M. A. J. *Nature* **287**, 50–55 (1980).
53. Ehret, C. *Ethiopians and East Africans: the Problem of Contacts* (East African Printing House, Nairobi, 1974).
54. Clark, J. D. & Brandt, S. A. (eds) *The Causes and Consequences of Food Production in Africa* (University of California Press, in the press).
55. Nelson, C. M. *Nyame Akuma* **14**, 28–30 (1979).
56. Gasse, F. *Nature* **265**, 42–45 (1977).

Expression of murine H–2K^{b} histocompatibility antigen in cells transformed with cloned *H–2* genes

A. L. Mellor[*], L. Golden[*], E. Weiss[*], H. Bullman[*], J. Hurst[*], E. Simpson[†], R. F. L. James[‡], A. R. M. Townsend[§], P. M. Taylor[§], W. Schmidt[¶], J. Ferluga[||], L. Leben[||], M. Santamaria[||], G. Atfield[||], H. Festenstein[||] & R. A. Flavell[*]

[*] Laboratory of Gene Structure and Expression, National Institute for Medical Research, The Ridgeway, Mill Hill, London NW7 1AA, UK
[†] Clinical Research Centre, Watford Road, Harrow, Middlesex HA1 3UJ, UK.
[‡] ICRF Tumour Immunology Unit, University College, Gower Street, London WC1E 6BT, UK
[§] Division of Immunology, National Institute for Medical Research, The Ridgeway, Mill Hill, London NW7 1AA, UK
[||] Department of Immunology, The London Hospital Medical School, University of London, Turner Street, London E1 2AD, UK

Cosmids containing H-2 *histocompatibility antigen genes of the* H-2^{b} *haplotype have been isolated. One of these genes expresses a 45,000 molecular weight protein, indistinguishable from* H-2K^{b} *when introduced into mouse L cells. These* H-2K^{b} *transformed L cells can be killed by allospecific anti-*H-2K^{b} *cytotoxic T cells. Moreover, when infected with influenza virus, they can be killed by an* H-2K^{b}*-restricted, influenza virus-specific cytotoxic T cell line. These results show that expression of the* H-2K^{b} *gene product on the L-cell surface is sufficient to make it a target for specific T-cell killing.*

CELL-surface glycoproteins encoded by the genes of the major histocompatibility complex (MHC), *H-2* in mouse, *HLA* in man, are important in regulating cell–cell interactions, especially those governing the functions of the immune system[1]. Class I molecules, of which the best characterized are encoded by genes on the H-2K, D and L regions (Fig. 1*a*) act as guides for presenting extrinsic antigen (for example viruses) to cytotoxic T cells, whilst class II molecules encoded by genes in the I–region perform a comparable function for T helper cells[1]. How extrinsic antigens are presented in association with self-MHC molecules is still very poorly understood, partly because the structure of the T-cell receptor is unknown. However the problem can be approached by study of MHC molecules themselves. Knowledge of the amino acid sequence and three-dimensional structure of these molecules has progressed very rapidly over the past few years (see, for example, ref. 2). The *H-2K* and *H-2D* gene products are highly polymorphic, which may reflect the importance of genetic variation of MHC molecules in overcoming virus infections. The mutation rate, particularly of class I H-2 molecules is extremely high[3] and of all of the *H-2* haplotypes studied, that of *H-2^{b}* is the highest. Within this haplotype it is the *H-2K^{b}* molecule which undergoes mutational change most frequently. Nathenson *et al.*[4] have determined the complete polypeptide sequence of the H-2K^{b} molecule of C57BL/10 mice and have also determined portions of the sequence of several mutants[5] which express an altered H-2K^{b} molecule. Information about the DNA coding for these molecules is thus of great interest, and may give insight into the mechanism of mutation and generation of new haplotypes.

Several groups have isolated cDNA[6,7] and genomic DNA clones[8-10] containing class I *H-2* or *H-2* related DNA sequences from BALB/c mice (*H-2^{d}* haplotype). We have isolated ~100 different cosmid clones, containing sequences mapping to the *H-2* and associated regions (Fig. 1*a*) of chromosome 17 from a cosmid library constructed using spleen DNA from C57BL/10 mice (*H-2^{b}* haplotype). A full description of the construction and screening of these libraries together with chromosomal mapping data for all the *H-2*-related cosmid clusters, will be given elsewhere. Here we describe a cluster of five overlapping cosmids (the H8 cluster) and show that one of the two *H-2* gene sequences cloned in this cluster encodes a cell-surface antigen which is recognised by *H-2K^{b}* restricted T cells. It therefore appears identical to the *H-2K^{b}* polypeptide found on cells derived from C57BL/10 mice.

Restriction map of the H8 cosmid cluster

The H8 cluster of cosmids consists of five overlapping cosmids containing two class I *H-2* related genes, approximately 15 kilobases (kb) apart, which hybridize to human genomic[11] and *H-2* cDNA class I gene probes[6] (Fig. 1*b*). The DNA cloned in this cluster spans about 65 (kb) of the C57BL/10 genome and the two *H-2* class I gene-related sequences are arranged in a head to tail configuration, as determined by hybridization to 5′ and 3′ probes obtained from the *HLA* or *H-2* probes. The left-hand gene (*H-2* genes are defined here as DNA sequences which hybridize to *HLA* and *H-2* class I probes) is present in cosmids H8, H25, H24 and H39 (A gene), whereas the right-hand gene sequence (B gene) is present only in H8 and H21. As polymorphic restriction site mapping of this cosmid cluster shows that the cloned region is derived from the *H-2K* (Fig. 1*a*) end of the *H-2* complex (manuscript in preparation), we investigated whether one (or both) of the two gene regions in the H8 cluster encoded an *H-2K^{b}* cell-surface antigen. Thus, we have introduced each cosmid into mouse Ltk^{-} (of *H-2^{k}* haplotype) cells using CaPO$_4$-mediated DNA transfer and tested the resulting tk^{+} clones for expression of new H-2^{b} cell-surface antigens using (1) direct monoclonal and allo-antibody binding (2) antibody-dependent complement-mediated lysis and (3) alloreactive anti-H-2K^{b} T-cell mediated lysis (CML) and (4) H-2K^{b}-restricted virus specific T-cell killing.

[¶] Present address: Institut für Virologie, Frankfurter Strasse, 107, 6300 Gissen, FRG.

0028–0836/82/310529—06$01.00

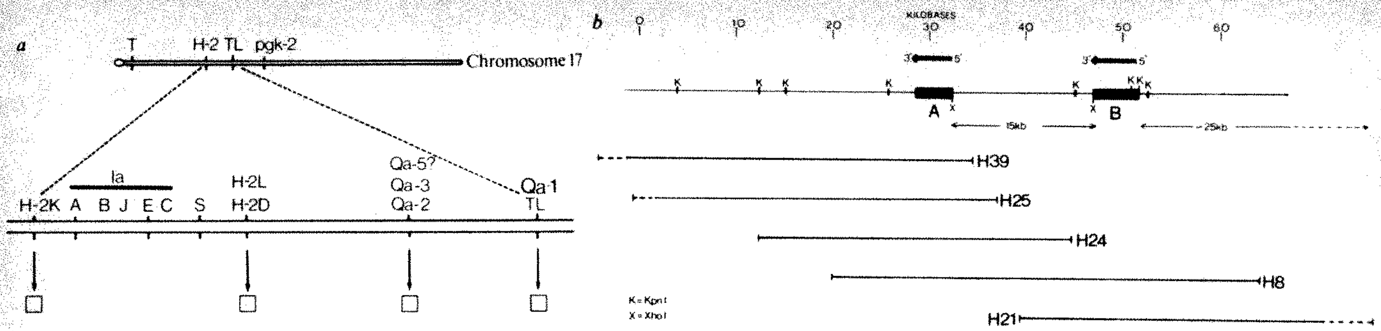

Fig. 1 *a*, Genetic map of the mouse *H-2* and associated genetic loci. The top line shows a diagram of chromosome 17 with the centromere on the left. The bottom line shows an expanded diagram of the regions between the *H-2K* locus on the left and the TL locus on the right. H-2 class 1 molecules (□) are expressed from at least four separate genetic loci as shown by the arrows below this line. *b*, A restriction enzyme map of the region cloned in the H8 cosmid cluster. The top line shows the extent of the cloned region and the approximate positions of *Xho*I(X) and *Kpn*I (K) restriction sites (see top scale calibrated in kilobase, kb). Class 1 gene regions (A and B) are shown as thick lines and their 5′ to 3′ orientation is indicated by the thick arrows over the line. The approximate extent of each cosmid is shown below the line beside the name assigned to each cosmid. Dotted lines at the end of cosmids indicate that the end of the cosmid has not been determined precisely.

Table 1 Antibody-dependent cytotoxicity assays

Antisera/antibodies		% Specific ^{51}Cr release (cell lines) Ltk$^-$	LH8	LH39
WS9/7B (αK^k)		73	71	61
D32(αD^k) NIH		63	71	61
D1 (αH–2^k) NIH		58	72	66
D8 (αH–2^k) NIH		21	70	44
100-5 (anti-H–2.11/αH–$2K^k$) monoclonal*		62	50	44
Anti-H–2.33 (αK^b)	NIH unabsorbed	2	72	6
(Ia–9–20)	B10 absorbed	0	0	0
	AKR absorbed	2	66	0
D28 (αH–2^b)	NIH unabsorbed	21	70	44
	B10 absorbed	1	1	0
	AKR absorbed	2	48	0
27–11–13 (αD^b)†		4	6	0

The chromium release assay was performed essentially as described by Sanderson[19]. Details of all antisera and monoclonal antibodies except 100–5[20] and 27–11–13[21] can be found in ref. 14. Absorptions of antisera were carried out before binding to cell lines using either C57BL/10 (B10) or AKR lymphocytes. Cell lines tested for lysis in this experiment were untransformed L cells (Ltk$^-$) and uncloned tk$^+$ cells transformed by cosmid H8 (LH8) or cosmid H39 (LH39). % Specific ^{51}Cr release was measured as (test c.p.m. − spontaneous c.p.m./maximum c.p.m.) × 100. Spontaneous release was 10–13%. Numbers shown in a box are significant results showing specific H-2K^b expression.

* Lemke *et al.*[20].

† Ozato and Sachs[21].

Introduction of cosmid DNA

The cosmid library used in this study was constructed using the cosmid vector pOPF1 (F. Grosveld *et al.*, in preparation). As this vector contains the herpes simplex virus thymidine kinase (*tk*) gene, cosmid DNA can be selected for its presence in transformed L cells by growing the cells in hypoxanthine/aminopterin/thymidine (HAT) medium. Thus, the five cosmids from the H8 cluster were used to generate tk$^+$ clones following CaPO$_4$-mediated DNA transfer and subsequent selection for tk$^+$ clones in HAT medium[12]. For each cosmid transformation, two subclones were isolated and the rest of the tk$^+$ clones were passaged as an uncloned tk$^+$ population. We experienced some difficulty with cosmid H21, due to its propensity to lose DNA sequences whilst replicating in host bacteria.

Analysis of transformed L-cells

Binding of antibodies: L cells transformed by individual cosmids and established as stable Ltk$^+$ transformed clones growing in HAT medium, were tested for their ability to bind anti-H-2K^b or anti-H-2D^b monoclonal antibodies in ^{125}I-radioimmunoassays. The results of a binding assay using Ltk$^+$ cell clones derived by transformations with H8, H24, H25, H39 and a control, H11 (a cosmid which maps to the H-2 related TL region; in preparation) are shown in Fig. 2. Both clones derived from H8 transformations (LH8.1 and LH8.2) bind anti-H-2K^b monoclonal antibody at a level higher than that of the positive control EL4 cell line (an H-2^b fibrosarcoma cell line). All other cell lines tested show only background levels of anti-H-2K^b monoclonal antibody binding. Anti-H-2D^b monoclonal antibody was not bound to any of the cell lines tested. Recently, Goodenow *et al.*[13] and Evans *et al.*[16], have both detected the expression of a cloned *H-2L^d* gene in transformed cells by using a monoclonal antibody binding assay.

In addition, a series of well characterized anti-H-2 alloantisera was used. In this case, binding of antibodies to L-cell lines was assessed using either complement-dependent chromium (^{51}Cr) release (Table 1) or complement-mediated growth inhibition assays (Table 2).

These assays both demonstrate that L cells transformed with cosmid H8 express a cell-surface polypeptide which is recog-

Table 2 Antibody-dependent growth inhibition

Antisera/antibodies		% Specific growth inhibition cell lines L cells	LH8.1	LH39
Anti-H–2.23 (αK^k) NIH		74.8	85.8	87.3
100–30 (anti-H–2.25/$\alpha K^k D^k$) monoclonal*		78.8	89.6	93.5
Anti-H–2.28 (αH–2^b)	NIH unabsorbed	4.2	66.2	7.1
	B10 absorbed	NT	6.3	3.9
	AKR absorbed	NT	40.5	0
Anti-H–2.33 (αK^b)	NIH unabsorbed	0	86.4	0
	B10 absorbed	NT	0	0
	AKR absorbed	NT	86.9	0

NT, not tested. For sera see Table 1. B10 = C57BL/10. The growth inhibition assays were performed as described previously[22]. L cells were cultured in Cooke flat-bottomed microculture plates at 10^4 per well in 4 μl for 45 min at 37 °C in RPMI with 10% fetal calf serum in CO$_2$ and air with 1 μl of antibody per well (final dilution 1/5). Rabbit complement (1/5 diluted) was then added and the incubation continued for another 30 min. ^{14}C-uridine was added and the incubation continued for 6 h. 0.025% Trypsin in phosphate-buffered saline was then added and incubated for 30 min. After three washes the wells containing adherent cells were punched out and counted in a scintillation counter. Cell lines tested in this assay were untransformed L cells (Ltk$^-$), a cloned L-cell line transformed by cosmid H8 (LH8.1) and uncloned tk$^+$ cells transformed by cosmid H39 (LH39). Numbers shown in a box are significant results showing specific H-2K^b expression.

* Lemke *et al.*[20].

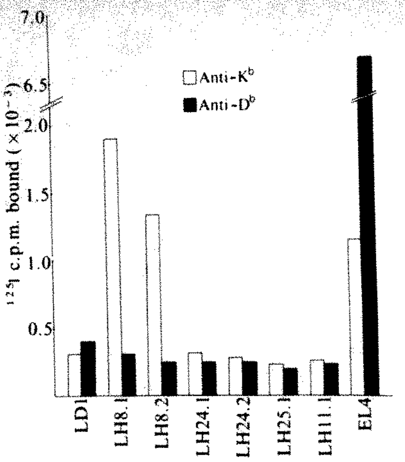

Fig. 2 Histogram showing the binding of monoclonal antibodies to transformed L cells. Binding studies were done in Titertek 96 well flexible plastic plates (Flow Laboratories). These were first blocked with radioimmunoassay RIA buffer (0.1 M phosphate-buffered saline, pH 7.2 plus 0.02% NaN_3 + 1% bovine serum albumin) and cells were assayed at 5×10^5 per well in triplicate. Cells were incubated with the first antibody in a volume of 100 µl of MEM-H (Eagle's minimal essential medium plus HEPES buffer + 0.1% NaN_3 + 5% calf serum) for 1 h at room temperature on a Titertek plate shaker (Flow), washed 3× with MEM-H and then incubated for 45 min with ^{125}I-labelled affinity purified sheep anti-mouse immunoglobulin (10–15 µCi per µg) in a volume of 100 µl containing ~10^5 c.p.m. per well. Cells were washed 3X and counted in a Nuclear Chicago γ scintillation counter. The monoclonal antibodies used were anti-H-2K^b(Y25, a gift of E. A. Lerner) used at a dilution of 1:2,000 or anti-H-2D^b (B22-249-R1, see ref. 23) used at a dilution of 1:100. LD1 cells are Ltk$^-$ control cells.

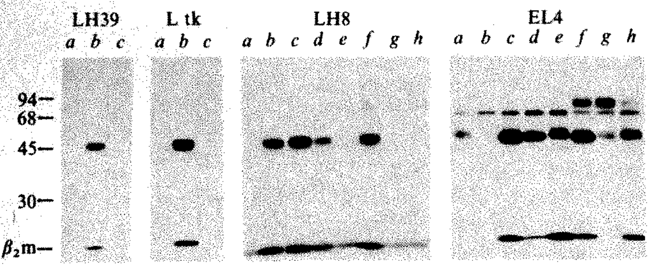

Fig. 3 Immunoprecipitation of radiolabelled cell-surface antigens from transformed L cells. Cell-surface proteins of cells indicated were radiolabelled with ^{125}I by the glucose oxidase–lactoperoxidase catalysed iodination technique[24] and lysed with nonionic detergent (0.5% NP40 in 0.01 M Tris-HCl buffer, pH 7.4, containing 0.15 M NaCl, 1.0 mM $MgCl_2$) in the presence of 1,000 KIE ml^{-1} Trasylol (soy bean trypsin inhibitor). Reaction of solubilized cell membrane proteins with monoclonal antibodies and alloantisera was determined by immunoprecipitation using *Staphylococcus aureus* and SDS-polyacrylamide gell electrophoresis of the resulting precipitates as previously described[25]. Precipitations were done with BALB/c-normal mouse serum (control) *a*, with monoclonal antibodies (refs. 19, 20) specific for H-2K^k (H100-5) *b*; H-2K^b (20-8-4s) *c*; H-2K^b, D^b (28-8-6s) *d*; H-2D^b, L^d(28-14-8s) *e*; and with alloantisera raised against the private specificities of H-2K^b *f*, *g*; and H-2D^b *h*. The anti-H-2K^b sera (A × B10.D2)F$_1$ anti-B10.A (5R)) were either preabsorbed with AKR (H-2^k) lymphocytes which remove antibody against murine leukaemia virus gp70 but not H-2 (*f*), or with B10 lymphocytes, which specifically remove anti-H-2K^b alloantibody (*g*). Note that both monoclonal antibodies and alloantiserum with specificity for the H-2K^b molecule precipitated a 46,000 molecular weight protein, which is identical in molecular weight to the H-2K^b expressed on EL4 (*H-2^b*) tumour cells. Co-precipitation of β_2-microglobulin (β_2m), incorporation of trititated mannose and glucosamine, and binding to *Lens culinaris* Sepharose (not shown) indicate that the cloned *H-2K^b* gene product is expressed on L cells in the same manner as in normal *H-2^b* lymphoid or tumour cells (ref. 4).

nized by public (anti-H-2.28) and private (anti-H-2.33) specificity alloantisera[14] reactive against the H-2K^b molecule. Antibody binding to these cell lines was shown to be specific for H-2^b antigens, because preabsorption of the antisera with spleen cells from B10, but not AKR (*H-2^k*) mice blocks binding. L cells transformed with cosmid H39, which contains the A gene, but not the B gene, do not express the public or private *H-2^b* determinants defined by the alloantisera we used. All cell lines, including untransformed Ltk$^-$ cells (which are derived from the C3H mouse of *H-2^k* haplotype) react with monoclonal antibodies and alloantisera directed against H-2^k cell-surface antigens. The data suggest that cell lines transformed with cosmid H8 express a cell-surface antigen which is indistinguishable from the H-K^b molecule using these antibodies. In addition, the lack of any significant anti-H-2K^b antibody binding to those cell lines transformed with cosmids H24, H25 and H39 suggests that the H-2K^b polypeptide detected in H8 transformed cells is expressed from the B gene in the cloned region.

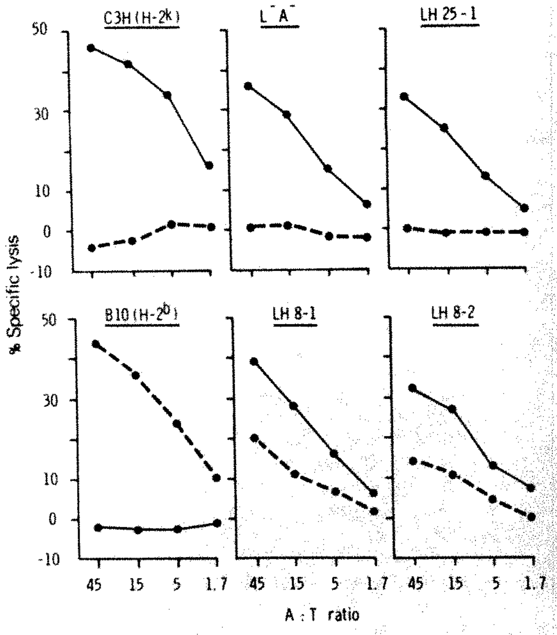

Fig. 4 1–2 × 10^6 target cells were labelled with 100 µCi ^{51}Cr-labelled sodium chromate for 1 h then washed twice. 1 × 10^4 Labelled target cells, in 100 µl volumes were placed in round-bottomed wells of microtitre plates. For the cytotoxic T-cell lysis (CML) killer cells, generated in 5-day mixed lymphocyte cultures (CBA anti-BALB.B = k anti-b, B10 anti-CBA = b anti-k) were added in 100 µl to give attacker: target (A:T) ratios of 45:1, 15:1, 5:1 and 1.7:1. Three triplicate wells of each A:T ratio were set up. After 5 h incubation at 37 °C in a 5% CO_2 humidified atmosphere the plates were spun and 100 µl of the supernatant from each well collected and counted for released γ counts. The per cent specific lysis was calculated according to the formula $(E - C/(M - C) \times 100\%$ where E = c.p.m. from target cells incubated with killer cells, C = c.p.m. from target cells incubated in medium alone and M = c.p.m. from target cells lysed with 5% Triton. L$^-$A$^-$ refers to control Ltk$^-$ cells.

Detection of H-2K^b in the L-cell membrane: Confirmation that L-cells transformed with cosmid H8 contain H-2K^b heavy chain polypeptides on the cell surface was obtained by labelling the cell surface proteins of transformed cells with ^{125}I and immunoprecipitating the cell extracts. This was done by using either alloantisera o monoclonal antibodies directed against the H-2K^b molecule. Immunoprecipitates were analysed by SDS–polyacrylamide gel electrophoresis and the results are shown in Fig. 3. The H-2K^d-specific alloantisera and two monoclonal antibodies (anti-H-2K^b and anti-H-2K^{b}D^b) precipitate cell-surface polypeptides of molecular weight 45,000 and 12,000 (H-2 heavy chain and β_2-microglobulin respectively) from extracts of L cells transformed with cosmid H8. No polypeptides were precipitated from the LH8 cells by the anti-H-2D^b/L^d-specific monoclonal antibody (Fig. 3, lane *e*).

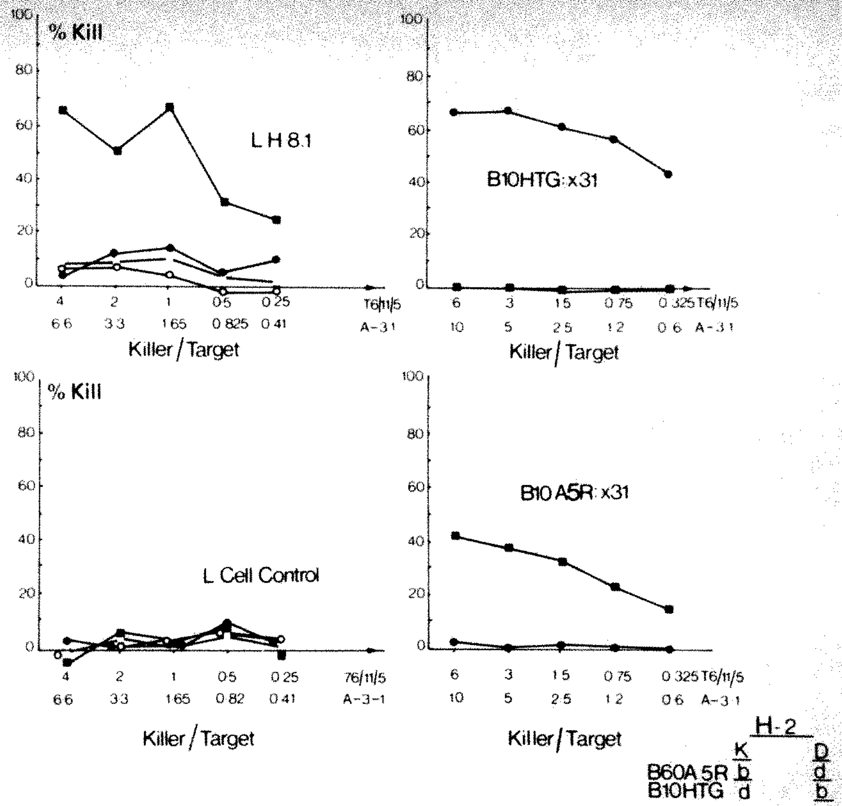

Fig. 5 T_c-cell mediated killing of transformed L cells infected with influenza virus. T_c-cell clones: The derivation of the two influenza-specific T_c clones T6/11/5 and A3.1 will be described in detail elsewhere (A.R.M.T. and P.M.T., manuscript in preparation). Clone A3.1 is restricted to H-2D^b and clone T6/11/5 to H-2K^b. In brief, C57BP6 mice were primed by ultranasal infection with A/X31 or A/JAP influenza virus. T_c-cell lines were established from spleen cell suspensions from these mice by repeated stimulation with 2,000R irradiated A/X31 infected syngeneic spleen cells, either in the presence (A3.1) or absence (T6/11/5) of a source of growth factors from concanavalin A-pulsed rat spleen. Cells from both sources were cloned at 0.5–10 cells per well onto 5×10^5 2,000R X31 infected syngeneic spleen in the presence of 10–20% concanavalin AS/N. 10–20 days later they were transferred to 2-ml wells and maintained by repeated antigenic stimulation with 2,000R X31 infected syngeneic spleen in the presence of 20% concanavalin AS/N every 5–10 days. Chromium release assay: Transformed and untransformed L cells were plated out at 3×10^4 per well in 100 μl α medium containing 10% fetal calf serum 18 h before assay into Nunc 96 well flat-bottomed wells plated in the presence of 2 μCi of sodium chromate (^{51}Cr). Before the assay the plates were spun at 1,000 r.p.m. for 5 min and the medium from wells containing cells to be infected removed by suction. To each of these wells was added 100 μl of serum free α medium containing 320 HA A/X31 and the plates incubated for a further 1.5 h. The plates were then washed four times with 200 μl per well balanced salt solution and the cells in all wells finally resuspended in 100 μl of RPMI medium plus 10% fetal calf serum. Control target cells were 3% thioglycollate-induced peritoneal exudate cells from B10A5R (*H-2K^b, D^d*) and B10 HTG (*H-2K^d, D^b*) mice. 10^7 cells were labelled with 100 μCi Na chromate (^{51}Cr) and infected with 3,200 HA A/X31 in 0.5 ml serum free RPMI for 1.5 h. Immediately before the assay they were washed four times in 10 ml phosphate-buffered saline and resuspended in RPMI 10% fetal calf serum. 2×10^4 targets were dispensed in 100 μl to wells of Nunc 96 well flat-bottomed microtitre plates. The cloned cytotoxic cells, at the ratio indicated in the figure, were added in 100 μl plus 10% fetal calf serum to experimental wells, 100 μl RPMI plus 10% fetal calf serum alone was added to control wells. The plates were spun at 1,000 r.p.m. for 1 min and then incubated for 6 h at 37 °C. The collection of ^{51}Cr-containing supernatants was done as previously described[26]. All samples were counted on a Wallac 80,000 γ counter for 2 min. Results were calculated as % specific ^{51}Cr release from target cells as follows:

$$\frac{\text{release in presence of cloned } T_c - \text{medium release}}{\text{Triton release} - \text{medium release}} \times 100\%.$$

All points are the mean from three identical wells. ○, Control target cells; A-3.1 H-2D^b (restricted) effectors. □, Control target cells; T6/11/5 (H-2K^b restricted) effectors. ●, Infected target cells; A-3.1 effectors. ■, Infected target cells; T6/11/5 effectors.

Anti-H-2K^b antibodies also fail to detect any polypeptides in untransformed Ltk$^-$ cells or in cells transformed with cosmid H39 which contains the A gene. Preabsorption of the anti-H-2K^b alloantisera using unlabelled B10, but not AKR lymphocytes prevents the precipitation of H-2K^b and β_2-microglobulin from extracts of cells transformed with cosmid H8 (Fig. 3, lanes *g* and *f* respectively).

Cytotoxic T-cell killing of L-cells: The presence of the H-2K^b molecule on a cell renders these cells as targets for allogeneic cytotoxic T-cell (T_c-cell)-mediated killing by T_c cells raised against H-2^b antigens[15]. A number of indirect arguments suggest that the presence on the cell membrane of a given H-2 polypeptide, such as the H-2K^b molecule is sufficient to generate a target for T_c-cells. For example, this process can be blocked by monoclonal antibodies directed against a single H-2 polypeptide[16]. To test this further, we generated T_c cells directed against H-2^b or H-2^k antigens and tested their ability to kill various target cells (Fig. 4, Table 3). Whereas anti-H-2^k T_c cells show specific killing of all L-cell lines tested, anti-H-2^b T_c-cells show specific killing of only control B10 target cells and two L-cell clones (LH8-1 and LH8-2) transformed by cosmid H8. Untransformed L cells (Ltk$^-$), a clone transformed by cosmid H25 (LH25-1) and other clones transformed by cosmids H24 and H39 (data not shown) were not killed by anti-H-2^b T_c cells. These data confirm that the H-2K^b molecule detected by serological assays in cosmid H8 transformed cells, can act as a target for anti-H-2^b T_c-cell killing.

We performed a similar experiment using B10.D2 (*H-2^d*) Tc cells generated by immunization with target spleen cells from the recombinant mouse B10.A (5R) *K^b, D^d*). Such T_c cells kill cells expressing the H-2K^b but not the H-2D^b molecule. These Tc cells also kill L cells transformed with cosmid H8, but not L cells transformed with cosmid H39 (Table 3).

Thus, these data suggest that the B gene present in cosmid H8, but not present in cosmids H24, H25 and H39, encodes a molecule carrying the determinant recognized by anti-H-2^b and anti-H-2K^b T_c cells.

T-cell killing of virus-infected L-cells: T_c cell mediated lysis of cells expressing viral antigens on their surface can only take place when the viral antigen is presented to T_c cells in association with an appropriate H-2 antigen; in this way H-2 antigens act as a restriction element for the T_c-cell response[15,17]. Thus, we tested the ability of the H-2K^b molecule expressed on the surface of L cells transformed by cosmid H8 to act as a restriction element for T_c-cell-mediated killing of influenza virus-infected cells.

Influenza-specific T_c clones restricted to one H-2 region can be selected and grown in the presence of T-cell growth factor[18]. L cells (*H-2^k*) and LH8-1 cells were infected with type A influenza virus (A/X31) and used as target cells for two influenza-specific H-2^b T_c clones, one restricted to H-2K^b (T6/11/5) and the other (A/3.1) to H-2D^b molecules (A. Townsend and P. M. Taylor, unpublished data). Figure 5 shows that X31 infected, untransformed L-cells (H-2^k) are unable to act as targets for killing by either the H-2K^b or H-2D^b restricted T_c-cell clones. LH8-1 cells infected with X31, however, act as targets for killing by the H-2K^b restricted T_c-cell clone, but not the H-2D^b restricted clone. This shows that the H-2K^b molecule expressed on the surface of LH8-1 cells is able to act as a restriction element for T_c-cell killing of X31 virus-infected cells.

Discussion

We have shown here that the H8 gene cluster contains two *H-2* genes, one of which (gene B) is an *H-2K^b* gene. The second gene (gene A) does not express a polypeptide that can be detected by any o the immunological criteria we have used

Table 3 Cell-mediated cytotoxicity

Responder strain (*H–2* haplotype)	Stimulator strain (*H–2* haplotype)		(Target cells)	% Specific lysis at effector: target ratio			
				100	50	10	1
B10.BR	C57BL/10		L cells	7.0		1.2	−0.6
($H–2^k$)	($H–2^b$)		LH8	52.7		28.9	3.6
		Expt 1	LH8.1	58.7		39.2	7.8
			LH39	6.0		4.5	1.4
			LH39.1	1.4		0.7	0.3
			LH8.1	45.0		19.1	2.6
			LH8.2	40.9		16.6	2.2
		Expt 2	LH39.1	7.1		1.9	1.8
			B10.blasts	59.5		48.6	18.0
			B10.BR blasts	8.0		8.1	3.2
B10.D2	B10A(5R)		L cells		11.0	12.7	0.7
($H–2^d$)	(*bbkkdddd*)		LH8		51.7	26.0	4.1
		Expt 1	LH8.1		53.3	32.0	3.9
			LH39		22.0	10.3	2.8
			LH39.1		18.8	8.0	1.6
			LH8.1	50.3		25.3	3.8
			LH8.2	50.8		21.6	2.4
			LH39.1	16.4		5.3	0.7
		Expt 2	B10 blasts	53.4		42.0	9.0
B10A(5R)							
			46.2				
			41.2				
			10.0				
			B10.D2	16.4		10.1	3.2

Cytotoxic T lymphocytes (CL) were generated *in vitro* from splenic lymphocytes of responder strain mice (B10.BR and B10.D2) which had been inoculated 1 week earlier with 4×10^7 stimulator strain (B10 and B10.A(5R) respectively) splenic lymphocytes. Responder lymphocytes were cultured in flasks at 2×10^7 per ml with an equal number of irradiated (2,000 rad) stimulator splenic lymphocytes in 10 ml culture medium (RPMI 1640 with 10% fetal calf serum, 100 U ml^{-1} penicillin, 10 μg ml^{-1} streptomycin, 5×10^{-5}M 2-mercaptoethanol). Cells were collected after 5 days' incubation at 37 °C in 8% CO_2 in air and assayed for cytotoxic activity against normal (L cells) or transfected (LH8, LH39) tumour cells labelled with ^{51}Cr-labelled sodium chromate. These cells were grown as monolayers and detached by treating for 5 min with 0.25% trypsin/versene in phosphate-buffered saline before being labelled with sodium chromate (100 μCi per 5×10^6 cells) for 2 h, washed four times to remove any free radioactivity, then suspended in assay medium (RPMI 1640 with 10% fetal calf serum) to 10^5 ml^{-1}. The CML assay was performed in round-bottomed microtitre plates. CL at 10^7, 5×10^6, 10^6 and 10^5 per ml were prepared and 0.1 ml samples added per well followed by 0.1 ml of transformed cell (TC) suspension. Plates were centrifuged at 100*g* for 45 s then incubated at 37 °C in 8% CO_2 in air. Each CL:TC ratio was performed in triplicate and controls for spontaneous release of radioactivity included (0.1 ml TC plus 0.1 ml assay medium). Maximum release of label was estimated by incubating 0.1 ml TC with 0.1 ml of 1% Triton X-100. After 4 h, plates were centrifuged again for 10 min to pellet cells and 0.1 ml supernatant collected from each well into small tubes for counting radioactivity released. The percent specific lysis or release was calculated as: (test c.p.m. − spontaneous c.p.m./maximum c.p.m.) × 100. Spontaneous release for all TC was ~12% and for all samples in the table the mean s.d. was 1.3, range 0.1–6.1. LH8 and LH39 are uncloned cell populations whereas LH8.1, 8.2 and 39.1 are cloned cell lines.

and may perhaps be a pseudogene. We have determined part of the DNA sequence which corresponds to the first and second domains of the A and B genes. While the sequence of the B gene is identical to that expected for an *H–2K^b* gene, the A gene shows only about 75% homology with this sequence (unpublished results). It is therefore clear that if the A gene does encode an H–2 protein, this protein is no more similar to the *H–2K^b* gene product than to any other H–2 molecule[4]. That the B gene is the *H–2K^b* gene is shown by a number of functional criteria. First, L cells transformed with the B gene from the H8 cluster express a 45,000 molecular weight polypeptide which carries determinants characteristic of the H–2K^b molecule and which reacts with a number of H–2K^b-specific monoclonals. This suggests that all the epitopes normally associated with the H–2K^b molecule are present on the surface of the transformed L cells. Second, L cells transformed with the B gene are recognized as targets for allogeneic (anti-H–2^b) T_c cell killing and for virus-specific, H–2 restricted T_c-cell killing of infected cells.

These results suggest that a detailed molecular analysis of the determinants recognized by antibodies and the T-cell receptor, using cells transformed with recombinant DNA will be possible. Specifically, L cells transformed with hybrid *H–2* genes, constructed *in vitro*, which contain DNA segments from, say, the *H–2K^b* and *H–2D^b* genes should help determine whether T_c-cell clones, either allospecific or H–2 restricted, can kill such target cells. In this way, we hope to map the determinants recognized by specific monoclonal antibodies and by the T-cell receptor.

We thank Professor N. A. Mitchison and Drs A. Fortunato (ICRF) and A. Alonzo for helpful discussions, B. Jordan, P. Kourilsky, M. Steinmetz and L. Hood for the probes, and Cora O'Carroll for preparing this manuscript. L.G. and E.W. were the recipients of postdoctoral fellowships from the Helen Hay Whitney Foundation and the Deutsche Forschungsgemeinschaft respectively. The work in the laboratories of R.A.F., E.S. and A.R.M.T. was supported by the MRC. Work in the laboratory of H.F. was supported by the Cancer Research Campaign and work in the laboratory of R.J. by the Imperial Cancer Research Fund.

Received 19 April; accepted 1 June 1982.

1. Mitchison, N. A. *Cell. Immun.* **62,** 258–263 (1981).
2. Ploegh, H. L., Orr, H. T. & Strominger, J. L. *Cell* **24,** 287–299 (1981).
3. Klein, J. in *Biology of the Mouse Histocompatibility-2 Complex*, 192–230 (Springer, New York).
4. Coligan, J. E., Kindt, T. J., Uehara, H., Martinko, J. & Nathenson, S. G. *Nature* **291,** 35–39 (1981).
5. Nairn, R., Yamaya, K. & Nathenson, S. G. *A. Rev. Genet.* **14,** 241–277 (1980).
6. Steinmetz, M. *et al. Cell* **24,** 125–134 (1981).
7. Kvist, S. *et al. Proc. natn. Acad. Sci. U.S.A.* **78,** 2772–2776 (1981).
8. Steinmetz, M. *et al. Cell* **25,** 683–692 (1981).
9. Steinmetz, M., Winoto, A., Minard, K. & Hood, L. *Cell* (in the press).
10. Evans, G. A., Margulies, D. H., Camerini-Obero, D., Ozato, K. & Seidman, J. G. *Proc. natn. Acad. Sci. U.S.A.* **79,** 1994–1998 (1982).
11. Malissen, M., Malissen, B. & Jordan, B. R. *Proc. natn. Acad. Sci. U.S.A.* **79,** 893–897 (1982).
12. Wigler, M. *et al. Proc. natn. Acad. Sci. U.S.A.* **76,** 1373–1376 (1979).

13. Goodenow, R. S. *et al. Science* **215,** 677–679 (1982).
14. Festenstein, H. & Demant, P. in *HLA and H-2. Basic Immunogenetics, Biology and Clinical Relevance* (ed. Turk, J.) 90–116 (Arnold, London, 1978).
15. Doherty, P. C. & Zinkernagel, R. M. *J. exp. Med.* **141,** 502–507 (1975).
16. Weyand, C., Hammerling, G. J. & Goronzy, J. *Nature* **292,** 627–629 (1981).
17. Zinkernagel, R. M. & Doherty, P. C. *Adv. Immun.* **27,** 51–177 (1979).
18. Lin, Y.-L. & Askonas, B. A. *J. exp. Med.* **154,** 225–234 (1981).
19. Sanderson, A. R. *Nature* **204,** 250–253 (1964).
20. Lemke, H., Hammerling, G. J., Hohmann, L. & Rajewsky, K. *Nature* **271,** 249–251 (1978).
21. Ozato, K. & Sachs, D. H. *J. Immun.* **126,** 317–321 (1981).
22. Schirrmacher, V. & Festenstein, H. *Tissue Antigens* **7,** 183–186 (1976).
23. Lemke, H., Hämmerling, G. J. & Hämmerling, U. *Immun. Rev.* **47,** 175–206 (1979).
24. Hubbard, A. L. & Colin, Z. A. J. *Cell. Biol.* **55,** 390–405 (1972).
25. Schmidt, W., Leben, L., Atfield, G. & Festenstein, H. *Immunogenetics* **14,** 323–339 (1981).
26. Zweerink, H. J., Courtneidge, S. A., Skehel, J. J., Crumpton, M. J. & Askonas, B. A. *Nature* **267,** 354–356 (1977).

Formation of transmembrane tubules by spontaneous polymerization of the hydrophilic complement protein C9

Jürg Tschopp, Hans J. Müller-Eberhard & Eckhard R. Podack

Department of Molecular Immunology, Research Institute of Scripps Clinic, La Jolla, California 92037, USA

The ninth component of complement C9 can undergo circular polymerization in the fluid phase and on lipid membranes. The concomitant hydrophilic–amphiphilic transition is the result of a conformational reorganization of C9 and allows insertion of poly C9 into membranes in the form of a transmembrane protein channel. The ultrastructure of poly C9 resembles that of membrane lesions caused by complement.

FIVE of the more than 20 complement proteins are directly involved in complement-dependent membrane damage and cytolysis[1,2]; these are C5, C6, C7, C8 and C9. Enzymatic cleavage of a single peptide bond in C5 initiates[3] self-assembly of the five proteins into a supramolecular organization termed the membrane attack complex (MAC) of complement[4]. Assembly proceeds from formation of the bimolecular complex C5b–6 to the reaction of C5b–6 with C7, which results in formation of the intermediate complex, C5b–7. After binding of C8 by C5b–7, the C5b–8 complex reacts with multiple C9 molecules, leading to the formation of the MAC. Assembly of the MAC results in the expression of hydrophobicity by the originally hydrophilic proteins. Hydrophobic protein domains seem to be responsible for the insertion of C5b–7 into target membranes[5] and for membrane damage caused by the binding to C5b–7 of C8 and C9 (refs 6, 7). Complement-induced membrane lesions can be visualized by electron microscopy as originally reported by Borsos, Dourmashkin and Humphrey[8]. By negative staining, an individual lesion appears as a circular stain-filled structure, which projects ~12 nm above the membrane surface and which has an inner and outer diameter of 10–11 nm and 21 nm, respectively[9]. As the isolated MAC extracted from complement-lysed cells[10,11] or assembled from the isolated precursor proteins[12–14], has an ultrastructure that resembles the image of an individual membrane lesion, it has been proposed that each membrane lesion actually constitutes one MAC[11,15].

Membrane damage and cytolysis caused by the MAC has been attributed to lipid bilayer perturbation[16,17] and to transmembrane channel formation[15,18,19]. A critical role for C9 in MAC function and structure is indicated by the following: (1) Although it is not an essential component of immune haemolysis, C9 markedly increases the rate of lysis of C5b–8-bearing erythrocytes[20]. (2) Up to six C9 molecules per C8 molecule were reported to be incorporated into the MAC[21] and subsequently, as many as 12–16 molecules per MAC have been estimated[22]. (3) C9 is essential for the formation of the MAC-induced ultrastructural membrane lesions[13,14]. (4) The size of the MAC-produced membrane pore was reported to be dependent on the concentration of C9[23]. (5) C9 within the membrane-bound MAC was found to be the MAC subunit that was predominantly labelled by membrane-restricted-photoactivatable probes[6,7]. (6) Isolated C9 underwent spontaneous polymerization at 37 °C to form circular polymers resembling the MAC in ultrastructure[24].

We report here that C9, a water-soluble plasma protein, can

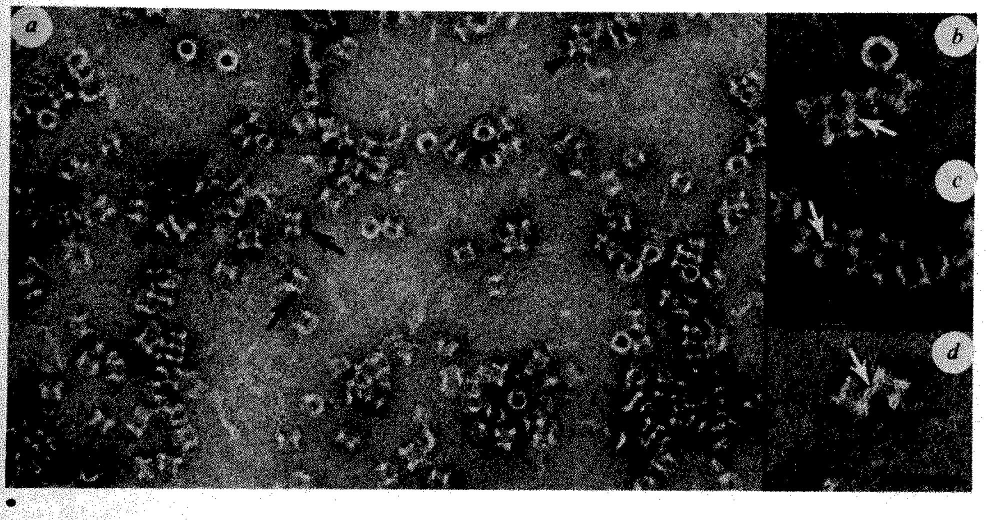

Fig. 1 Ultrastructure of poly C9. C9 was isolated according to Biesecker and Müller-Eberhard[25] and was incubated at a concentration of 5.3 μM in TBS at 37 °C for 64 h. Samples were negatively stained with 2% uranyl formate and examined in a Hitachi model 12A electron microscope at an initial magnification of ×19,550 (*a*). Poly C9 was visualized as a stain-filled tubule with an inner diameter of 11 nm (top views are imaged as rings) and a length of 16 nm (side view, black arrows). The thick-rimmed end comprises a ~3 nm-thick torus with 21 nm outer diameter (black arrowhead). The other end of the tubule terminates in a hydrophobic domain that forms side-by-side aggregates (*b–d*). The white arrows indicate the overlapping areas that presumably represent the hydrophobic segments with a length of 4 nm. Scale bars, 40 nm.

0028-0836/82/310534—05$01.00

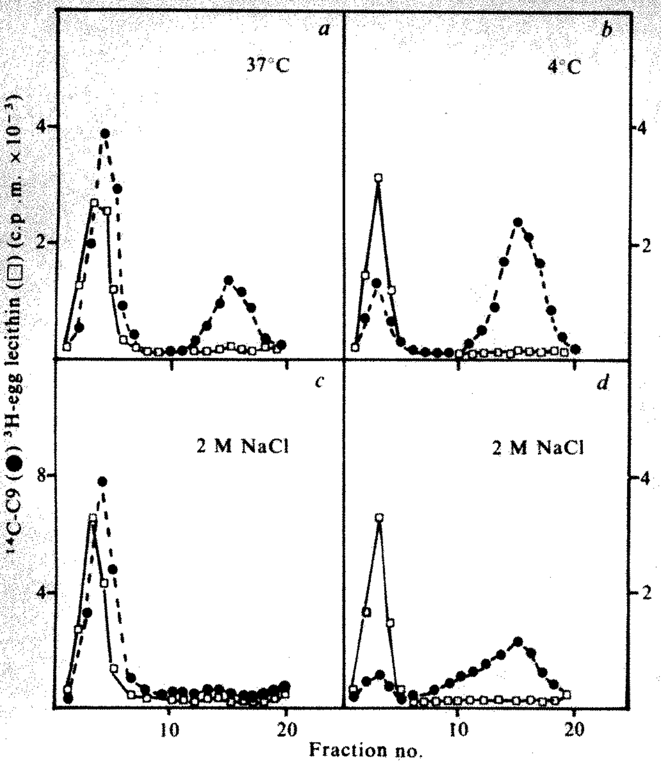

Fig. 2 Interaction of C9 with lipid membranes. Monomeric ^{14}C-labelled[31] C9 (2.6 μM) was incubated in TBS with ^{3}H-labelled egg lecithin vesicles (0.44 μM). Small unilamellar vesicles were prepared by sonication for 1 h as described elsewhere[32]. The samples were then floated through 35% (w/w) sucrose, dissolved in TBS; 1 ml of the sample was made 40% in sucrose, placed on top of a 0.75 ml cushion of 60% sucrose, overlayered with 3 ml of 35% sucrose and 1 ml TBS, then centrifuged to equilibrium at 120,000*g* for 20 h at 4 °C. Fractions (0.25 ml) were collected and analysed for ^{14}C and ^{3}H radioactivity. *a*, C9 was incubated with vesicles at 37 °C for 64 h and most of the C9 underwent flotation together with the vesicles. *b*, C9 was exposed to vesicles at 4 °C for 64 h; only a small fraction of C9 associated with the floating vesicles. *c*, When the vesicle-containing fraction of *a* was again ultracentrifuged in 35% sucrose containing 2 M NaCl, almost all the C9 remained bound to the lipid. *d*, When the corresponding fraction of *b* was treated similarly, most of the C9 dissociated and stayed behind the floating vesicles. The direction of flotation is towards the left.

polymerize and thereby become an integral membrane protein having membranolytic activity and the ultrastructural appearance characteristic of complement-induced membrane lesions.

C9 acquires hydrophobic domains on spontaneous polymerization

Isolated monomeric C9 is a water-soluble protein consisting of a single polypeptide chain with a molecular weight of ~71,000 (ref. 25). It is monodisperse on ultracentrifugal analysis and has a sedimentation coefficient of 4.5S. During incubation for 3 days at 37 °C, isolated monomeric C9 polymerized and assumed the ultrastructural appearance shown in Fig. 1. Views from the top and sides suggest that poly C9 is a 16 nm-long tubule with an internal channel of ~11 nm diameter. One end of the tubule is rimmed by a ~3 nm-thick torus of 11 nm inner and 21 nm outer diameter. Analytical ultracentrifugation of poly C9 showed a polydisperse sedimentation behaviour with sedimentation coefficients in the range 27–250S. Poly C9 aggregated to form arrays in which the tori of adjacent tubules pointed in opposite directions, and in which the smaller ends of the tubules combined side-by-side and overlapped by ~4 nm (Fig. 1*b*,*c*). These overlapping segments presumably constitute the hydrophobic domain of the poly C9 tubule. Poly C9 aggregates dissociated to a 27S species on treatment with detergents, that is, 1% sodium desoxycholate or 0.1 M octylglucoside, indicating hydrophobic interaction between individual poly C9 tubules. In these conditions, poly C9 itself did not dissociate into monomers. The ultrastructure of poly C9 suggests a dodecameric to hexadecameric composition. In view of the molecular weight of monomeric C9, the calculated molecular weight of poly C9 is $0.85–1.14 \times 10^6$, in agreement with preliminary molecular weight determinations.

The amphiphilic properties of poly C9 were tested by studying C9–phospholipid vesicle interaction. In a typical experiment, egg lecithin vesicles were incubated with monomeric C9 for 3 days at 37 °C to effect C9 polymerization. After ultracentrifugation of the protein–lipid mixture in 35% sucrose, most of the poly C9 (60–90%) underwent flotation together with the lipid vesicles (Fig. 2*a*). Incubation of C9 with vesicles at 4 °C did not promote C9 polymerization and resulted in only 10–30% binding of C9 to the vesicles (Fig. 2*b*). The latter protein–lipid interaction was ionic because C9 could be dissociated from the vesicles by 2 M NaCl (Fig. 2*d*). In contrast, the poly C9–lipid interaction at 37 °C was stable on exposure to 2 M NaCl (Fig. 2*c*), suggesting hydrophobic interactions between poly C9 and the hydrocarbon core of the lipid bilayer. The differential binding of C9 at 4 °C and 37 °C cannot be attributed to different physical properties of the egg lecithin vesicles because both temperatures are well above the phase transition. Therefore, the increased affinity of C9 for lipid at 37 °C must be due to C9 polymerization and concomitant acquisition of hydrophobic domains.

Membranolysis by poly C9

The acquisition of hydrophobic sites by polymerizing C9 correlated well with the expression of membranolytic activity (Fig. 3). The rate of appearance of hydrophobic sites on poly C9 was determined by the increase in 8-aminonaphthalene-1-sulphonic acid (ANS) binding. Figure 3*a* shows the increase in ANS fluorescence during incubation of C9 at 46 °C. At this temperature, the rate of C9 polymerization allows continuous monitoring of the reaction by fluorometry. At 20 °C, C9

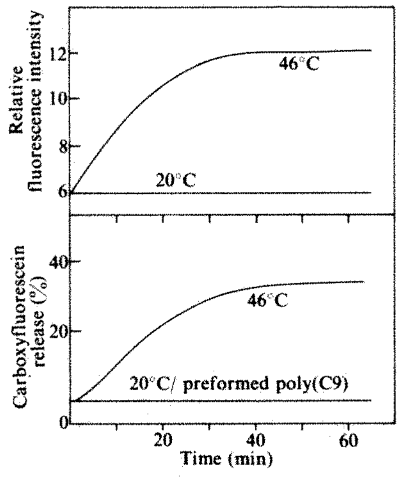

Fig. 3 Correlation of C9 polymerization and lipid vesicle lysis. Carboxyfluorescein (75 mM) was entrapped in large unilamellar egg lecithin vesicles prepared by the reversed-phase evaporation method[26]. C9 (2.6 μM) was incubated with the marker-containing vesicles (20 μM lipid concentration) in TBS in a microcuvette which was placed in a cell compartment with temperature regulation. Membranolysis was continuously monitored by means of the fluorescence increase observed on dilution of the originally self-quenched entrapped carboxyfluorescein[33]. Maximal release of marker was determined after the addition of 0.8% Triton X-100. The extent of lysis was corrected for a small amount of spontaneous marker release. *a*, Rate of acquisition of hydrophobic binding sites by C9, as assessed by ANS binding, which correlates with C9 polymerization[24]. *b*, Rate of marker release at 46 °C. The lines parallel to the abscissa represent controls: lack of C9 polymerization at 20 °C (*a*) and lack of marker release at 20 °C (*b*).

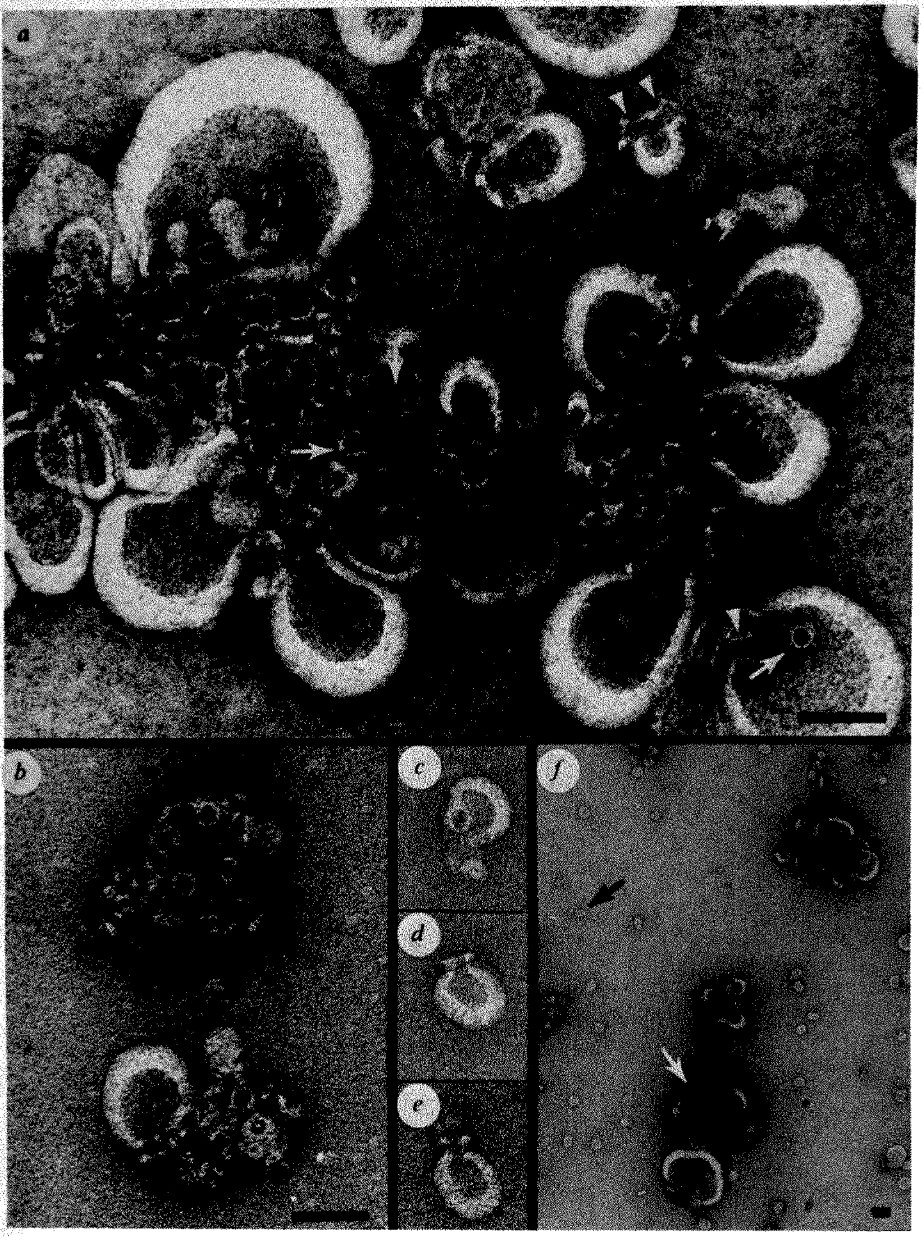

Fig. 4 Ultrastructure of poly C9–vesicle complexes. Poly C9–vesicle complexes were prepared by incubating sonicated and gel-filtered[32] egg lecithin vesicles of 21 nm diameter with monomeric C9 at 37 °C for 64 h. The ratios of C9 monomers per vesicle were: *a*, 6 : 1; *b*, 50 : 1; and *c*, *d*, *f*, 12 : 1. For comparison, a MAC–vesicle complex is shown in *e*. The field of view in *a* shows fused poly C9-vesicle complexes. White arrows indicate top views; white arrowheads, side views of poly C9 attached to bilayer membranes. The inner and outer diameters of the ring structure in top views are 11 nm and 21 nm, respectively; in side views poly C9 projects ~12 nm from the membrane surface. The dimensions of poly C9–vesicle complexes correspond closely to those of MAC–vesicle complexes shown for comparison in *e*. The effects of high C9 multiplicity per vesicle are shown in *b* (50 C9 monomers per vesicle). Multiple poly C9 complexes per vesicle caused bilayer disassembly. *c*, *d* Show single C9 tubules attached to single bilayer vesicles in comparison with a MAC–vesicle complex in *e*. *f*, The fusogenic effect of C9 on vesicles when incubated at a 12 : 1 or lower ratio. The originally small vesicles of ~21 nm (black arrow) fuse to form large vesicles (>100 nm) bearing poly C9 (white arrow). Note also the absence of stain penetration into vesicles lacking poly C9. Scale bars, 50 nm.

remained monomeric and no increase in fluorescence occurred. The membranolytic activity of poly C9 was measured by the release of entrapped carboxyfluorescein from large unilamellar vesicles[26]. C9 polymerization at 46 °C caused vesicle lysis, commencing after a lag period of 5 min, which proceeded at a rate which correlated with the rate of acquisition of ANS binding sites by the protein. After 40 min, 40% of the maximal dye release was observed. This value is only slightly lower than that observed for C9 in the presence of the C5b–8 complex (that is, 55%). C5b–8, however, increased the rate of C9-dependent dye release to the extent that only 2 min were required for maximal release compared with ~40 min for C9 alone. In control experiments, neither C5b–6, C7, C8 nor bovine serum albumin induced membranolysis. Preformed poly C9 added to vesicles expressed no membranolytic activity. Loss of activity may be due to aggregation of poly C9, which probably conceals the hydrophobic domains that are essential for contact with the lipid (Fig. 1). Alternatively, polymerization and insertion into the hydrophobic interior of lipid bilayers may have to occur simultaneously. It is probable that either dimeric or oligomeric C9 initiates the insertion process.

Ultrastructure of poly C9–vesicle complexes

Figure 4 shows electron micrographs of poly C9 attached to egg lecithin vesicles. Poly C9 is visualized as the thin-walled tubule described above for the fluid phase polymer. In profile, it projects ~12 nm from the outer surface of the vesicle membrane, indicating that a 4 nm-long domain is inserted into the lipid bilayer. This value correlates well with the length of the overlapping segments of poly C9 in aggregates of poly C9 (Fig. 1*b*–*d*). The ultrastructure of poly C9, and the presence of stain inside vesicles with bound poly C9, suggest that it forms a transmembrane channel. The fact that poly C9 bound to vesicles resembles the vesicle-bound MAC (Fig. 4*e*) suggests that poly C9 is an integral part of the fully assembled MAC and that it provides the transmembrane channel within the membrane-bound MAC. This interpretation is supported by the results of three-dimensional reconstruction of MAC-bearing vesicles[19], of freeze-fracture studies of MAC-bearing erythrocytes[27] and by studies showing membrane penetration of C9 (ref. 28). In addition to channel formation, poly C9 fuses small, single bilayer vesicles to large vesicles (Fig. 4*f*). Vesicle fusion was observed at an input of <12 C9 monomers per vesicle. An input of 50 C9 monomers per vesicle resulted in complete disruption of the vesicles (Fig. 4*b*), presumably due to the lipid-binding capacity of poly C9, which may be similar to that of the C5b–9 complex[16].

Conformational change on C9 polymerization

Conversion of monomeric C9 to membrane-inserted poly C9 was examined by circular dichroism (CD) spectroscopy. The weak interaction of monomeric C9 with small unilamellar vesicles at 4 °C was not accompanied by a conformational change. In contrast, C9 polymerization and membrane insertion resulted in a decrease in the ellipticity between 210 and 220 nm. Analysis of the spectra by the method of Provencher and Glöckner[29] yielded values of 24% α-helix and 32% β-sheet for monomeric C9 and 22% α-helix and 38% β-sheet for poly C9, indicating an increase in the amount of β-pleated sheet structure.

To determine whether the same conformational change of C9 occurs on MAC formation, C9 and C5b–8 bound to lipid vesicles were mixed at 4 °C and 37 °C at a molar ratio of 12:1. At 4 °C, C9 interacts reversibly with C5b–8 (refs 22, 30) without polymerizing. The circular dichroism (CD) spectrum recorded at 4 °C (Fig. 5*b*) therefore is the sum of the signals of monomeric C9 and C5b–8. When the same mixture was brought to 37 °C, C9 polymerization and MAC formation occurred, accompanied by a change in the CD spectrum similar to that observed during C9 polymerization on vesicles. The two CD difference spectra for poly C9 (poly C9 minus monomeric C9) and for MAC [MAC minus (C5b–8 plus C9)] (Fig. 5*a*,*b* insets) show the same conformational change. The occurrence of a structural change of the C9 monomer on polymerization was also indicated by electron microscopic analysis[24]. In contrast to the globular appearance of monomeric C9, the protomer dimensions of C9 in poly C9 indicated an extended conformation. In addition, comparative immunochemical analysis of poly C9 and MAC showed identical neo-antigenic (conformational) determinants that are specific for poly C9 but which are not detectable in monomeric C9 (ref. 22). These data further indicate that poly C9 constitutes the channel-like structure in the MAC.

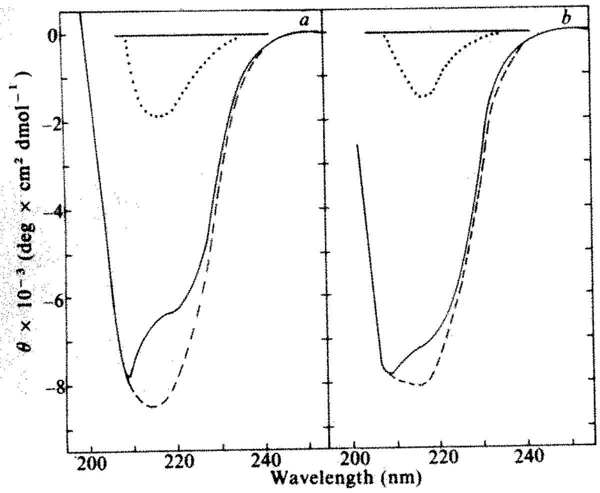

Fig. 5 Far-UV circular dichroism (CD) spectra of vesicle-bound poly C9 and MAC. CD measurements were performed in a Dichrograph III (Jobin Yvon Instruments). The absorbance value of the proteins in TBS at 280 nm was used to calculate their concentrations. The absorbance coefficients used were based on quantitative amino acid analysis and have been published elsewhere[22]. Using a Nicolet model 535 signal averager interfaced to the CD instrument, four individual CD scans were averaged and corrected for the baseline. Results are expressed as the mean residue ellipticity with a mean residue weight of 112. *a*, C9–vesicle complexes were prepared as described in Fig. 2 at a molar ratio of 1:2 poly C9 to vesicle, assuming 12 C9 monomers per poly C9. The solid line represents the CD spectrum of monomeric C9 mixed with vesicles. The broken line shows the spectrum of the same sample after C9 had been polymerized on the vesicle membrane by incubation at 37 °C. Protein concentration, 0.2 mg ml^{-1}. *b*, C5b–6, C7 and C8 (0.22 μM each) were mixed at 30 °C for 15 min with 0.45 μM small unilamellar vesicles, to form vesicle-bound C5b–8. The mixture was cooled on ice and 2.6 μM C9 added. The Cd spectrum was recorded at 4 °C (solid line). The same sample was then warmed to 37 °C for 30 min to allow MAC formation. After re-cooling to 4 °C, the CD spectrum was monitored (broken line). The dotted lines (insets) depict the CD difference spectra of poly C9 minus monomeric C9 (*a*) and of MAC minus (C5b–8 + C9) (*b*). The spectra were calculated by subtracting the solid line spectra from the broken line spectra using a Nicolet data processor. In the case of MAC formation (*b*), it was assumed that the observed change was due only to a secondary structure change in C9 without any contribution by C5b–8. The difference spectrum is therefore normalized and is expressed as mean residue ellipticity of C9.

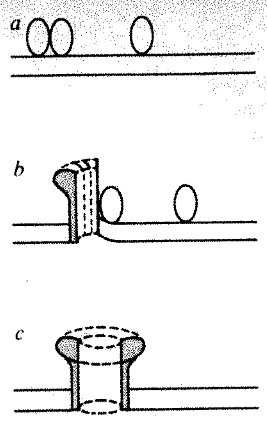

Fig. 6 Hypothetical model for circular polymerization of C9 on lipid membranes. *a*, Reversible binding of monomeric C9 to membranes by ionic interaction. *b*, Polymerization and conformational rearrangements of C9 lead to exposure of previously hidden hydrophobic domains which associate with the hydrophobic core of the lipid bilayer. *c*, Circular polymerization of C9 leads to the formation of a hydrophilic protein channel in the membrane.

Conclusions

The results reported here may be pertinent to the understanding of mechanisms of hydrophilic–amphiphilic transitions of proteins, and may therefore be of relevance to the mechanism of insertion of proteins into lipid bilayers during membrane biosynthesis. Specifically, poly C9 formation is closely related to the cytolytic function of complement and to the ultrastructure of the MAC.

Figure 6 shows a hypothetical model for C9 polymerization on lipid membranes. First, monomeric C9 binds reversibly to the membrane by ionic attraction. Then, multiple electrostatically bound C9 monomers associate and undergo a conformational change involving constrained unfolding of each molecule with exposure of hydrophobic regions that insert themselves into the hydrocarbon core of the lipid bilayer. Additional C9 monomers can then bind to C9 oligomers until the polymerization reaction is terminated by ring closure, one ring containing 12–16 molecules. Our model implies that polymerization of C9 occurs without chemical modification. However, cleavage of a small peptide from C9 by traces of contaminating proteases during the long incubation time has not been excluded.

Exposure of hydrophobic domains in an aqueous environment is thermodynamically unfavourable. The energy for the hydrophilic–amphiphilic transition of C9 is probably derived from the high-affinity C9–C9 interaction during poly C9 formation. Polymerization may cause conformational rearrangement of C9 monomers leading to exposure of hydrophobic domains. Hence, polymerization of C9 may be favoured within a hydrophobic environment, that is, in membranes. The rate of polymerization at 37 °C is highly accelerated by detergents[24]; this effect is of interest as the hydrocarbon core of detergent micelles provides an environment similar to the hydrocarbon core of membranes.

The membranolytic activity of poly C9 is demonstrable with artificial membrane vesicles (Fig. 3). Cytolytic activity of poly C9, however, is not readily apparent. Of the cells tested, only chicken erythrocytes showed a certain degree of susceptibility to lysis by polymerizing C9 (not shown). The inability of polymerizing C9 alone to perturb natural membranes protects host cells against the potential membranolytic activity of C9, and emphasizes the biological role of C5b-8 as C9 receptor and modulator in providing access to the lipid bilayer and promoting C9 polymerization.

There is strong evidence that poly C9 is an integral unit of the MAC: (1) Identical conformational changes occur on polymerization of isolated C9 and on binding of C9 to C5b-8 (Fig. 5). (2) The ultrastructural image of poly C9 and the MAC are very similar (Figs 1, 4). (3) C5b-8 can bind as many as 12-14 C9 molecules in forming the MAC[22]. (4) Identical C9-specific neo-antigens are expressed by poly C9 and the MAC[22]. Therefore, evidence suggests that poly C9 is part of the MAC and forms a transmembrane channel within the MAC assembly. The principle of circular polymerization accompanied by hydrophilic–amphiphilic transition of a soluble precursor may also be valid for cytotoxic effector systems other than complement.

We thank Dr Stephen Provencher for the computer program for secondary structure determination; Dr Klaus Preissner for contributing an electron micrograph; and K. Pangburn and S. Patthi for technical assistance. This work was supported by NIH grants AI 17354, CA 27489 and HL 16411. J.T. is supported by the Swiss National Science Foundation, H.M.-E. is the Cecil H. and Ida M. Green Investigator in Medical Research, Research Institute of Scripps Clinic, and E.R.P. is an Established Investigator of the American Heart Association (no. 79–149).

Received 24 February; accepted 6 May 1982.

1. Götze, O. & Müller-Eberhard, H. J. *J. exp. Med.* **132,** 898–915 (1970).
2. Lachmann, P. J. & Thompson, R. A. *J. exp. Med.* **131,** 643–657 (1970).
3. Fernandez, H. N. & Hugli, T. E. *J. Immun.* **117,** 1688–1694 (1976).
4. Kolb, W. P. & Müller-Eberhard, H. J. *J. exp. Med.* **138,** 438–451 (1973).
5. Podack, E. R. & Müller,-Eberhard, H. J. *J. Immun.* **121,** 1025–1030 (1978).
6. Podack, E. R., Stoffel, W., Esser, A. F. & Müller-Eberhard, H. J. *Proc. natn. Acad. Sci. U.S.A.* **78,** 4544–4548 (1981).
7. Hu, V. W., Esser, A. F., Podack, E. R. & Müller-Eberhard, H. H. *J. Immun.* **127,** 380–386 (1981).
8. Borsos, T., Dourmashkin, R. R. & Humphrey, J. H. *Nature* **202,** 251–252 (1964).
9. Humphrey, J. H. & Dourmashkin, R. R. *Adv. Immun.* **11,** 75–114 (1969).
10. Bhakdi, S., Bjerrum, O. J., Rother, U., Knufermann, H. & Wallach, D. F. H. *Biochim. biophys. Acta* **406,** 21–35 (1975).
11. Biesecker, G., Podack, E. R., Halverson, C. A. & Müller-Eberhard, H. J. *J. exp. Med.* **149,** 448–458 (1979).
12. Lachmann, P. J., Munn, E. A. & Weissmann, G. *Immunology* **19,** 983–986 (1970).
13. Dourmashkin, R. R. *Immunology* **35,** 205–212 (1978).
14. Podack, E. R., Esser, A. F., Biesecker, G. & Müller-Eberhard, H. J. *J. exp. Med.* **151,** 301–313 (1980).
15. Tranum-Jensen, J., Bhakdi, S., Bhakdi-Lehnen, B., Bjerrum, O. J. & Speth, V. *Scand. J. Immun.* **7,** 45–56 (1978).
16. Podack, E. R., Biesecker, G. & Müller-Eberhard, H. J. *Proc. natn. Acad. Sci. U.S.A.* **76,** 897–901 (1979).
17. Esser, A. F., Kolb, W. P., Podack, E. R. & Müller-Eberhard, H. J. *Proc. natn. Acad. Sci. U.S.A.* **76,** 1410–1414 (1979).
18. Mayer, M. M. *Proc. natn. Acad. Sci. U.S.A.* **69,** 2954–2958 (1972).
19. Podack, E. R., Müller-Eberhard, H. J., Horst, H. & Hoppe, H. *J. Immun.* (in the press).
20. Hadding, U. & Müller-Eberhard, H. J. *Immunology* **16,** 719–735 (1969).
21. Kolb, W. P., Haxby, J. A., Arroyave, C. M. & Müller-Eberhard, H. J. *J. exp. Med.* **135,** 549–566 (1972).
22. Podack, E. R., Tschopp, J. & Müller-Eberhard, H. J. *J. exp. Med.* (in the press).
23. Boyle, M. D. P. & Borsos, T. *J. Immun.* **123,** 71–76 (1979).
24. Podack, E. R. & Tschopp, J. *Proc. natn. Acad. Sci. U.S.A.* **79,** 574–578 (1982).
25. Biesecker, G. & Müller-Eberhard, H. J. *J. Immun.* **124,** 1291–1296 (1980).
26. Szoka, F. & Papahadjopoulos, D. *Proc. natn. Acad. Sci. U.S.A.* **75,** 4194–4198 (1978).
27. Tranum-Jensen, J. & Bhakdi, S. *Molec. Immun.* Abstr. (in the press).
28. Rautenberg, E. W. *Molec. Immun.* Abstr. (in the press).
29. Provencher, S. W. & Glöckner, J. *Biochemistry* **20,** 33–37 (1981).
30. Kolb, W. P. & Müller-Eberhard, H. J. *J. Immun.* **113,** 479–488 (1974).
31. Kreutzer, D. L., Kunkel, S., Ward, P. A., Showell, H. & McLean, R. H. *J. Immun.* **123,** 2278–2282 (1979).
32. Mason, J. T. & Huang, C. *Ann. N. Y. Acad. Sci.* **308,** 29–49 (1978).
33. Blumenthal, R., Weinstein, J. N., Sharrow, S. O. & Henkart, P. *Proc. natn. Acad. Sci. U.S.A.* **74,** 5603–5607 (1977).

LETTERS TO NATURE

Spontaneous generation of density perturbations in the early Universe

Matt Crawford & David N. Schramm

Astronomy and Astrophysics Center, The University of Chicago,
Chicago, Illinois 60637, USA

A long-standing problem in cosmology has been to understand the origins of density inhomogeneities in the Universe. Calculations involving inhomogeneities have for the most part required the assumption of some initial spectrum of perturbations, which is inserted 'by hand'. We present here a mechanism for the spontaneous creation of density perturbations during the transition in the early Universe from unconfined quark matter to hadronic matter. The subsequent evolution of these perturbations remains a problem for further study.

It is possible that some of these density perturbations, if sufficiently large, may become black holes with masses up to the horizon mass of 10^{30} g, smaller than a solar mass but greater than the mass of 10^{15} g which would evaporate by the Hawking mechanism in the age of the Universe. These black holes would survive to the present and could perhaps be an important component of the dark matter in clusters of galaxies and yet would not be constrained by the upper limit on baryonic mass density from big-bang nucleosynthesis. They would then satisfy the condition[1] that the dark matter in large clusters should be non-baryonic. These black holes would, however, be constrained by the limit on the total mass density derived from the deceleration parameter q_0. Therefore $<10^{-8}$ of all material going through the quark–hadron transition could become black holes.

At the time of transition[2] the age of the Universe is $\simeq 3\times 10^{-6}$ s and, as mentioned before, the horizon mass is far smaller than a solar mass, much less a galactic mass. Thus the existence by itself of the perturbations described here is not sufficient to explain the origin of galaxies. However, it may be that these perturbations can be 'seeds' which could grow through some other mechanisms to larger scales. Press and Vishniac[3] point out that for such growth to be possible, some correlated process is required, such as shocks which produce other shocks. Shock waves to start this process could come from explosions of objects created by these perturbations, or the baryons which form objects around black holes created at the transition. Such shocks could cause perturbation scales to grow as the horizon expands, in a manner similar to the idea proposed by Ostriker and Cowie[4].

We now consider quantitatively how the quark–hadron transition may lead to perturbation growth.[5] In particular, Olive[2] has mentioned that the transition may be a first-order phase transition with a duration comparable to the age of the Universe at the time when the transition occurs. Thus, there is enough time for the perturbations once formed to grow to scales that are some reasonable fraction of the horizon. (Recent unpublished work by Shenker supports the idea of a first-order phase transition for SU_3 with relativistic quarks.)

The physical principle that enables perturbations to form spontaneously and grow comes from the observation of quark–quark interactions in high-energy physics experiments. The experiments show that the Ψ/J- charmonium spectrum[6] and the Υ-bottomonium spectrum[7] are best fitted if the quark–quark interaction potential grows linearly in strength with distance of separation between quarks. Such a dependence is a natural consequence of the non-abelian SU_3 colour gauge theories. This idea of a potential increasing in strength at longer distance is fundamental to the concept of quark confinement and also will stimulate perturbation growth at the phase transition, where quarks combine to make hadrons. If we take, for example, a quark–anti-quark pair out of the quark soup or similarly a triplet of three quarks out of the quark soup to make a meson or baryon, the neighbouring quarks surrounding the site where the hadron has just formed will be able to see the colour charge of quarks further away across the gap where the hadron has formed, as opposed to other directions where colour screening results in a relatively short range interaction, thus there will be unstable growth of perturbations throughout the entire phase transition. However, some saturation in the growth occurs because the strength of the interaction at large distances is sufficiently high that quark–anti-quark pairs are spontaneously produced. The stimulation of the first hadron formation will just be the expansion of the Universe with normal thermal statistical fluctuations.

To investigate this effect, we have run a relativistic n-body stimulation of coloured quarks and antiquarks interacting classically with a two-body potential given by:

$$V(r, C^2) = \begin{cases} 0 & \text{if } C^2 > \frac{8}{3} \text{ and } r > 1.670 \text{ fm} \\ -\frac{1}{2}(C^2 - \frac{8}{3})\, f(r) & \text{otherwise} \end{cases} \tag{1}$$

where C^2 is the combined colour of two particles, assigned in accordance with the Clebsch–Gordon coefficients of SU(3) and

$$f(r) = \begin{cases} \dfrac{6\pi}{33 - 2n_f}\, \dfrac{\hbar c}{r} \left(\log \dfrac{\Lambda r}{\hbar c}\right)^{-1} & r \leqslant 0.132 \text{ fm} \\ (0.620 \text{ GeV fm}^{-1})\text{r} - 1.035 \text{ GeV} & r > 0.132 \text{ fm} \end{cases} \tag{2}$$

Here n_f is the number of quark flavours with mass $\leqslant \hbar c/r$. (Note that we have assumed the potential derived from Ψ and Υ mesons, it is not automatic that this should also apply identically to free quark interactions; however, our conclusions mainly depend on the functional forms.)

The effect of the cutoff in equation (1) is that repulsive forces have limited range while the range of attractive forces between quarks is limited only by the screening effects of nearer quarks.

A quark and an antiquark were deemed to have formed a meson if they were in a colour singlet state and if, in addition, their mutual interaction was at least 10 times greater in absolute value than the interaction of either of them with any other particle. The inclusion of baryon formation was regarded as not worth the added numerical difficulties as the excess of quarks over antiquarks at the time of the transition is approximately 1 part in 10^9 and the bulk of the hadronic matter in the Universe was in mesons rather than baryons at this time.

Taking $\Lambda = 500$ MeV, an initial temperature[2] of 400 MeV, and using the constituent quark masses $M_d = M_u = 300$ MeV, $M_s = 500$ MeV (all heavier quarks being scarce at this temperature), we find a generated perturbation spectrum $\phi(n) \equiv \delta\rho/\rho \approx n^{-\alpha}$ with $\alpha = 0.618 \pm 0.027$. (This is close to the Zeldovich $n^{-2/3}$ spectrum which is favourable[8] to black hole formation.) As we will show below, the amplitude of the fluctuation spectrum produced in our model is too low for very efficient immediate production of black holes. Efficient black hole production would require $\phi(n) \sim 1$ for $n = n_H$, where n_H is the number of particles inside the horizon. The uncertainty in the exponent includes statistical errors and the effects of varying the screening parameters. The screening was varied from run to run so that each quark in the initial state interacted with an average of from 5 to 12 of its nearest neighbours at each time step. If the average number of interactions per quark was more than ~16, the transition no longer took place in this model. The quark masses were not varied. However, it is expected that variations in assumptions about quark masses would have little effect on our conclusions, as their primary effect is to set the initial abundances of quarks due to the fact that the temperature is comparable to the masses.

The transition in our model proceeds by a nucleation process although it differs from vacuum phase transitions in that there is no apparent potential barrier. Our simulations do not show any characteristic 'bubble size' above which the fluctuation spectrum is damped from its power-law behaviour. This indicates that the induced correlations have either unlimited ranges (up to the horizon size) or that the range, if limited, is larger than the size which can be numerically simulated. In the latter case, subsequent rapid growth of perturbations is still a possibility due to the presumably unstable nature of the high-density meson aggregations formed by the transition.

It is reasonable to expect that the radiation participates in the density fluctuations along with the matter, as the clustering of the quarks takes place under the influence of the colour interaction which is stronger than the pressure of the electromagnetic radiation to which the quarks are also coupled. With this supposition we can estimate an upper limit to the direct formation of black holes of mass $\geqslant 10^{15}$ g. (As Carr[8] has emphasized smaller mass black holes lead to unacceptably large amounts of Hawking radiation.) Simply extrapolating the fluctuation spectrum $\phi(n)$ to a number of particles $n_c \approx 3 \times 10^{38}$ corresponding to a mass of 10^{15} g gives an upper limit $\phi(n_c) = 10^{-24\pm1}$ on the fraction of the total mass-energy at the time of the transition which could wind up in black holes of sufficient mass to survive to the present. After the annihilation of matter and anti-matter the mass density due to these black holes would amount to just $10^{-15\pm1}$ times the remaining baryon density. Forming even these black holes requires large compressions. (Note that the initial clustering is not due to traditional Jeans type instabilities but due to the long-range colour force.) Unless the behaviour of meson matter is very favourable to collapse, most black holes formed will be near the horizon mass of $\sim 10^{30}$ g, where the background density is already near the required density for collapse. In any case, we expect the black hole masses to be unaffected by accretion as the total mass gained by a black hole of initial mass M from the time of the quark–hadron transition to the present is $\leqslant 3 \times 10^{-4}\, M^2/10^{30}$ g.

We can show that even with the most generous possible rates of formation the evaporation of small ($< 10^{15}$ g) black holes would not produce γ rays in excess of observational limits. Let the black holes be produced on all scales up to the horizon with the same spectrum as the generated density fluctuations. Then the mass contained in black holes in the mass range $(M, M + \mathrm{d}m)$ is $M^{-\alpha+1}\,\mathrm{d}M$. If $M_{\text{big}}/M_{\text{small}} =$ the ratio of the total mass in black holes of mass 10^{15}–10^{30} g to the total mass in black holes smaller than 10^{15} g, $M_{\text{big}}/M_{\text{small}} = (10^{15})^{-\alpha+2} - 1 = 10^{20.7\pm0.4}$. Thus, if we leave aside problems of the normalization of the black hole spectrum, due to indirect subsequent balck hole formation, the higher mass black holes can contribute a density up to the critical density while the energy density of γ rays from the evaporation of smaller ones will be $\leqslant 10^{-28.5\pm0.4}$ erg cm^{-3}, below the observational value[8] of $\sim 10^{-15.8}$ erg cm^{-3}.

It is interesting to speculate on the subsequent evolution of a critical density ($\Omega \sim 1$) in planetary mass black holes. Because they have no charge they could begin to cluster gravitationally once they become the dominant mass of the Universe which could occur at an order of magnitude higher redshift than recombination. If there were primordial fluctuations, they would get trapped in them and make for example, excellent dark mass halo material. If there were no primordial fluctuations, one might expect a slow statistical cluster growth. These small clusters of black holes could then capture baryons once the baryon decoupled and had a low enough Jeans mass. The black hole cluster centred baryon objects might be the initial seeds for the Ostriker–Cowie scenario. However, if perturbations were built up in this latter manner they always fall within the horizon. Thus there would be no non-zero quadrupole moment to the 3° background. If the present measurements are real[9] then the planetary black holes are still allowable as dark matter but they do not produce galaxies.

We conclude that the quark–hadron transition in the early Universe can produce density fluctuations which might themselves propagate to large scales through some undetermined process, or which could produce black holes with a mass spectrum which allows them to provide the 'missing mass' on any scale. However, to discover whether these black holes can be produced in sufficient numbers to provide the required dark matter will require detailed study of the evolution of the density perturbations in the meson-rich material after the transition.

We thank Craig Hogan, Mike Turner and Keith Olive for valuable discussions. D.N.S. thanks P. B. Price and his colleagues at Berkeley and John Ellis and Alan Guth for stimulating discussions. This work was supported in part by the NSF and by the US Department of Energy at the University of Chicago.

Received 18 March; accepted 2 June 1982.

1. Schramm, D. N. & Steigman, G. *Gen. Rel. Grav.* **13,** 101–107 (1981).
2. Olive, K. A. *Nucl. Phys.* **B190,** 483–503 (1981).
3. Press, W. H. & Vishniac, E. T. *Astrophys. J.* **236,** 323–334 (1980).
4. Ostriker, J. P. & Cowie, L. *Astrophys. J. Lett.* **243,** L127–131 (1981).
5. Schramm, D. N., Crawford, M. & Olive, K. A. *Proc. Symp. on Ultra-High Energy Heavy Ion Collisions,* Berkeley (1979).
6. Eichten, E., Gottfried, K., Kinoshita, T., Lane, K. D. & Yan, T. M. *Phys. Rev.* D**17,** 3090–3117 (1978).
7. Celmaster, W., Georgi, H. & Machacek, M. *Phys. Rev.* D**17,** 879–885 (1978).
8. Carr, B. J. *Astrophys. J.* **201,** 1–19 (1975).
9. Wilkensen, D. *Proc. R. astr. Soc. Meet.*, London, (in the press).

The peculiar variable star R Aquarii and its jet

Minas Kafatos* & Andrew G. Michalitsianos

Laboratory for Astronomy and Solar Physics, NASA Goddard Space Flight Center, Code 685, Greenbelt, Maryland 20771, USA

Outward motion of the nebula associated with the symbiotic variable R Aquarii was suspected by Hubble[1] and confirmed by Baade[2], who estimated its ejection ~600 yr ago. A new feature of the nebulosity near the star appeared between 1970 and 1977 as found by Herbig from direct plates obtained with the 3-metre telescope at Lick Observatory. The 'spike' or 'jet' so-called by Wallerstein and Greenstein[3] appears as a protrusion from the central star. The observational properties of the jet in both the optical and radio are described by Sopka *et al.*[4]. The near UV image obtained in 1980 by Herbig and the VLA radio map[4] are shown combined in Fig. 1. Here we suggest that the jet is the result of supercritical accretion of mass transferred from the cool 387-day period Mira to the hot companion in a highly elliptical orbit. Ancient Japanese astronomical records suggest a nova outburst in AD 930 may be associated with R Aquarii which formed the outer extended nebulosity. The jet may help explain the outbursts of this object as well as the excitation of the R Aquarii nebula.

R. Aquarii undergoes erratic episodes in which the hot compact central ionizing source dominates the integrated visual light. In the 1928–35 outburst the optical spectrum was characterized by a blue continuum and hydrogen P-Cygni profile emission lines which dominated the normally strong absorption spectrum of the cool Mira[5]. Willson *et al*[6]. have studied the visual light curves of the Mira and found that maximum light associated with the 387-day light cycle undergoes unusually deep minima in 1934 and 1978. They suggest that an eclipse of the Mira occurred at these times in which a gas cloud or accretion disk in the system occulted the Mira for ~8.5 yr. Their interpretation suggests an orbital period of ~44 yr. In examining their work we find that the period may actually be ~22 yr, similar to that found by Merrill[7]. In what follows we adopt a 44 yr binary period. Our basic results are not sensitive to the exact value adopted in the 22- to 44-yr orbital period range.

Merrill[7,8] has discussed the spectroscopic properties of R Aquarii from 1920 to 1950, and from velocity measurements finds that the orbital eccentricity $e = 0.5$. Here, we suspect that the orbit is also highly elliptical, but disagree with the notion that the 'eclipse' or suppression of Mira light took place at apoastron as required by Willson *et al.*[6]. Examining the radial velocity curve of Merrill[7], we note that the 1934 eclipse may not have occurred near apoastron. It we take a binary period of 44 yr, apoastron would have occurred in 1920, and the eclipse of 1934 would more closely coincide with periastron. We believe that the appearance of the jet (sometime between 1970 and 1977) which coincided nearly with the eclipse or suppression of Mira light, provides a theoretical basis for believing that this event occurred at periastron.

If the Mira and secondary are in a highly elliptical orbit, near periastron the Mira envelope becomes extended due to the close proximity of the secondary at this particular orbital phase. Mass transfer to the companion occurs forming a spatially thick accretion disk ar supercritical accretion rates, which is accompanied by the formation of a jet, possibly driven by radiation pressure[9]. A few years later after the stars separate sufficiently the Mira relaxes to its previous undisturbed state. It is possible of course, for quasi-periodic outbursts to occur separated by the thermal time scale of the red giant envelope (see below) with no eccentricity in the binary model.

We have carried out theoretical analysis that supports this model Bath and Pringle[10] have made time-dependent accretion disk calculations in symbiotic binaries with separations of the primary and secondary $\sim 10^{13}$ cm. In their model the accretion disk forms around a main sequence star, or around a smaller star with effective photospheric radius $\sim 1R_\odot$. Even though the orbital separation of the stars is believed larger by one order of magnitude than that considered by Bath and Pringle[10], the high eccentricity[5,7], assumed here may allow accretion to occur at particular phases of the orbit, that is, at periastron. If the separation of the stars at periastron is ~1–2 times the radius of the Mira[11], supercritical mass transfer occurs through the critical Roche lobe, characterizing the system by episodic accretion events every 44 yr.

From the 387-day light cycle of the Mira (hereafter referred to with subscript '1', '2' denoting the companion) we find $R_1 \sim 250\text{–}300 R_\odot$ (refs 12, 13). For $M_1 \sim 1.5 M_\odot$ (ref. 12) and $M_2 \sim M_\odot$ and a binary period of 44 yr, we find that the semi-major axis of the ellipse $a \sim 2.5 \times 10^{14}$ cm. This value is in close agreement with that obtained by Merrill[7]. In a purely circular orbit the Mira would always fail to fill its Roche lobe by a factor of 5–7. In a highly elliptical orbit, however, episodic mass transfer could occur around periastron. Farther away from periastron the secondary would only accrete material expelled from the Mira in a stellar wind at much lower rates. Using the criterion for Roche lobe formation of Haynes *et al.*[11] we find that the eccentricity of the orbit is in the range $0.84 \lesssim e \lesssim 0.92$ if $R_1 \sim 2 \times 10^{13}$ cm and the semi-major axis is $a \sim 2.5 \times 10^{14}$ cm.

For a main sequence secondary the critical accretion rate is expressed as $M_C = 1.1 \times 10^{-3}\ (R_2/R_\odot)\ M_\odot\,\text{yr}^{-1}$, while for a white dwarf it is $M_C = 1.53 \times 10^{-5}\ (R_2/10^9\ \text{cm})\ M_\odot\,\text{yr}^{-1}$. Bath and Pringle[10] have shown that it is difficult for a white dwarf accreting at sub-critical rates to dominate the M giant optical continuum. It is possible, of course, that the secondary is a white dwarf or hot subdwarf with an effective photosphere ($\tau \sim 1$) at $r \sim 1R_\odot$. The accretion disk would have to be extended and cool in its outer regions if substantial eclipses of the Mira are to occur. If the eclipse occurs at or near apoastron as favoured by Willson *et al.*[6], then for $e = 0.85$, $M_1 + M_2 = 2.5\ M_\odot$ and for a 44 yr period, the minimum radius of the occulting disk R_d (for a line-of-sight to Earth along the semi-major axis of the ellipse) is $\sim 2R_1$. The value is essentially the same if different values of stellar masses are considered. We find that the visible light brightness of the disk should be not more than ~1/5 that of the Mira, and it should be spatially thick ($h/r \gtrsim \frac{1}{2}$). The disk temperature in the outer regions should then be appreciably less than the effective temperature of the Mira, say ~2,800 K (ref. 12). We find that $T_d \sim 2{,}300$ K in the outer regions of the disk, resulting in a disk that would be brighter than the Mira in the 1–3 μm wavelength region. In any case, if $R_d \gtrsim 2R_1$ at apoastron, it would indicate that the gravitational field of the secondary would have to be substantially stronger than that of the Mira to maintain such large disk dimensions

---

*Permanent address: George Mason University Department of Physics, Fairfax, Virginia 22030, USA.

0028-0836/82/310540—03$01.00

at maximum separation. Moreover, as the two stars approach each other the collision of such a substantial disk with the outer atmosphere of the Mira would likely cause a noticeable brightening in 1957-which was not seen-and which would occur again in the year 2000. Additionally, the large disk model does not explain the 1935 outburst which R Aquarii underwent.

Instead, we believe that the disk around the unseen companion is extended ($R_d \sim 1$–2×10^{13} cm), but not as large as $2R_1$ and achieves its largest extent at periastron. More moderate dimensions for the disk would be more consistent with a mass $\sim 1 M_\odot$ expected for a white dwarf, hot subdwarf or main sequence type companion. The outer regions of the disk in this case would have temperatures $\sim$3,000 K, and would be moderately thick, $h/r \sim v_s/v_K \sim 0.25$ (refs. 14–16), where v_K is the keplerian velocity, v_s the sound speed and h the semi-thickness of the disk[14]. The drift time scale of the disk is $t_r = r/v_r$, where the drift velocity $v_r = \alpha[v_s^2/v_K]$, and α is the usual viscosity parameter[14]. We assume following Bath and Pringle[10] that the α-viscosity model holds. For values of $\alpha \sim 0.1$–1.0 expected for symbiotics[10], we find that $t_r \sim 1.7$–17 yr. At periastron the two stars remain close, say within a few R_1, for ~ 1 yr. The jet forms and persists for a comparable period of time. As the two stars recede from each other the disk dissipates over time scales of the order ot t_r. We estimate that material with a total mass $\gtrsim 10^{-3} M_\odot$ is ejected in the form of a jet if the companion is a quasi-main sequence type star, and $\gtrsim 10^{-5} M_\odot$ if the companion is a white dwarf. The orbit will decay over time scales $t_e \equiv |e/\langle\dot{e}\rangle|$, $t_a \equiv |a/\langle\dot{a}\rangle|$, where $\langle\dot{e}\rangle$ and $\langle\dot{a}\rangle$ are the orbit average rates which can be computed from Alexander, Chau and Henriksen[17]. During quiescent phases away from periastron, and assuming an orbit average lass loss rate for the Mira $\langle\dot{M}\rangle \sim 2\times10^{-5} M_\odot\,\mathrm{yr}^{-1}$ (main sequence type companion), or $\sim 10^{-6} M_\odot\,\mathrm{yr}^{-1}$ (white dwarf companion), we find that the semi-major axis of the ellipse diminishes over time scales $t_a \sim 1.7\times10^5$ yr to 3.4×10^6 yr, respectively. The quantity $\langle\dot{M}\rangle$ is defined as $[\dot{M}_C \times 1\,\mathrm{yr} + \dot{M}_W \times 43\,\mathrm{yr}]/44$, where $\dot{M}_W \sim 10^{-6} M_\odot\,\mathrm{yr}^{-1}$ is the quiescent Mira mass loss rate that occurs well away from periastron. The orbit actually becomes more eccentric over timescales longer than t_a. In any case, if we impose the requirement that during successive episodic mass transfer events between primary and secondary the Mira retains essentially most of its envelope[18] ($M_{env} \sim 0.8\,\dot{M}_\odot$), then the system cannot be older than $M_{env}/\langle\dot{M}\rangle$, or 4×10^4 yr for a main sequence type companion, and 8×10^5 yr for a white dwarf.

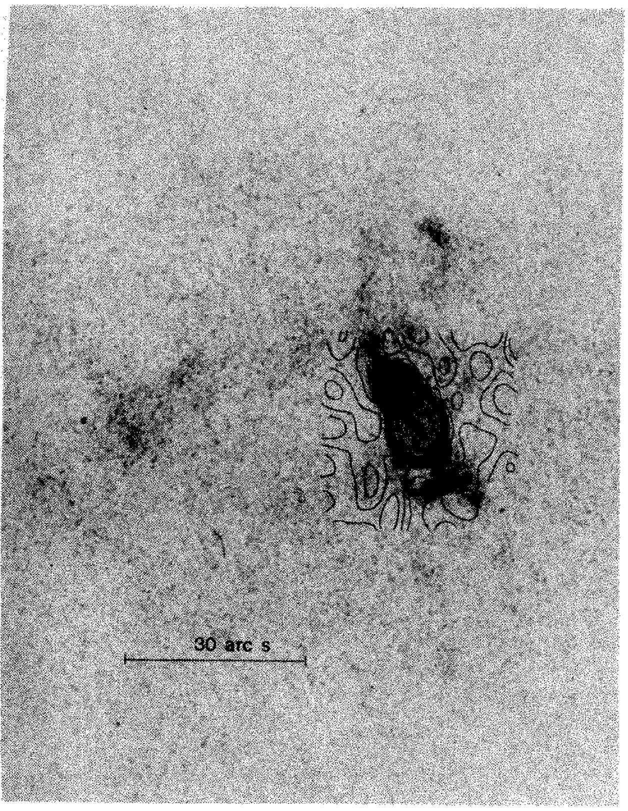

Fig. 1 Optical image of R Aquarii obtained in the near-UV with the 3-m telescope at Lick Observatory (courtesy George Herbig) in October 1980, shown combined with a Very Large Array radio map at 6-cm obtained by Sopka *et al.* on 5 November 1981. The protruding jet features extending from the central star was first noticed by Wallerstein and Greenstein[3] in 1977, and appears to have grown in brilliance over the past several years.

The Mira envelope will relax over thermal (Kelvin–Helmholtz) time scales. We find for typical Mira parameters $L_1 \sim 4\times10^3 L_\odot$, $M_1 \sim 1.5 M_\odot$ and $R_1 \sim 2\times10^{13}$ cm, that $t_{th} \sim 20$ yr. This rough estimate is in agreement with the thermal time scales in the envelopes of the Mira models of Wood[19], which are $\sim$1–10 yr. We also note that some material outside the disk will eventually rain back on the Mira over the free-fall time scale $t_{ff} \sim 0.3$–30 yr, for densities in the outer regions of the disk that are in the range 10^{15}–10^{13} cm^{-3} (main sequence or white dwarf companions, respectively). It is curious that all these time scales are in the range comparable with the 8.5-yr eclipse[6] duration. As such, this phase may not represent an eclipse at periastron (it would last only $\sim$1 yr), but would in fact be the characteristic dynamical time scale required by the Mira to recover to its pre-periastron, quiescent state. Although no detailed calculations of such a complicated system as R Aquarii exist at present to check this hypothesis of disk and jet formation, we believe the overall properties of the system support this model, namely: (1) the brightening of the secondary and the appearance of P-Cygni profiles in 1928 through 1935, indicating mass loss and mass accretion forming a disk; (2) the appearance of the jet between 1970 and 1977 occurred close to the time of periastron predicted in our model. A test of our model can be provided by radial velocity measurements of R Aquarii in the next 10–20 yr to determine the orbital characeristics, and check whether the eclipse of 1978 took place near periastron.

The question whether the secondary is a main sequence star, hot subdwarf or white dwarf has not been conclusively resolved. Important clues concerning its exact nature can be obtained from UV and optical observations of the nebula. We find that the inner nebula responsible for the UV emission lines and UV continuum observed has a radius $\sim 2.5\times10^{14}$ cm, and electron density $n_e \sim 5\times10^6$ cm^{-3} (ref. 21). If the hot subdwarf photoionizes this nebula, thus accounting for the line emission observed in the UV and in the optical, the temperature of the secondary would have to be less than $T_{eff} = 65{,}000$ K in order to explain the weakness or absence of the He II λ1640A line[20]. Accordingly, such a star would be located in the lower part of the *H–R* diagram, generally occupied by central stars of planetary nebulae[21]. Temperatures near 60,000 K are also favoured by Kaler[22]. Such a star would photoionize the inner, higher density nebula, but lacks a sufficient flux to photoionize the entire extended nebulosity.

The extended nebula is still expanding with an average velocity 50–100 km s^{-1} (ref. 1). From the electron densities derived by Wallerstein and Greenstein[3] for the nebula, and using a filling factor value of 0.1, we find an average electron density $\langle n_e\rangle \sim 10^4$ cm^{-3}. The mass of the nebula is $\sim 0.2 M_\odot$ and its kinetic energy $> 2\times10^{46}$ erg. We note that typical nova light output is in the range 10^{44}–10^{45} erg (ref. 24), while for slow-novae such as RR Tel and RT Ser, that resemble more R Aquarii, the output is of the order of 10^{45} erg. The R Aquarii nebula radiates more than 5×10^{44} erg yr^{-1} in the Balmer and Lyman continua and emission lines. The corresponding cooling time scale of the nebula is estimated to be $\sim$2 yr. The question arises naturally, what has been powering this extended nebulosity for the past 600 yr (ref. 1). Photoionization is unlikely because it would require a secondary much brighter than the Mira, which would have to radiate in excess of the Eddington limit for a $1 M_\odot$ star. The luminosity of the secondary was found to be $\gtrsim 3\times10^{38}$ erg s^{-1} using the Stromgren relation with a root-mean-square electron density $\langle n_e^2\rangle^{1/2}\sim3\times10^4$ cm^{-3}.

Alternatively, from purely energetic arguments, the jet could be the source of excitation. Taking a minimum size for the jet feature of 7 arc s (ref. 4), that corresponds to a linear size of $\sim2\times10^{16}$ cm (at a distance 200 pc)[4], and assuming it travelled since 1970, we find an average jet velocity of 700 km s^{-1}. If the mass of the jet is $\sim10^{-3}M_\odot$, then its kinetic energy would be $\sim5\times10^{45}$ erg, in reasonable agreement with estimates for radiation cooling given above. However, most of the material in the extended nebula that surrounds R Aquarii is confined to rings, generally perpendicular to the axis of the jet. Morphologically, this structure argues for the nebula being formed in a single explosive event hundreds of years ago. If formed in an explosion, the ejection which created the present nebula is possibly reflected in the composition of the nebular dust grains, which appear chemically distinct from the material in the interstellar medium[24]. Moreover, the richness of the R Aquarii nebula in He and particularly N (ref. 3) is in agreement with models of recurrent novae[25] and further argues in favour of the nebula having been formed in a single nova-type event.

The present expansion rate of the nebula of 50–100 km s^{-1} and angular extent of ~1 arc min argues for an outburst ~1,100–550 yr ago. We find that only one recorded nova outburst during historical times in the general vicinity (within 10° × 10° box, the uncertainty of ancient records) of R Aquarius is found in ancient oriental astronomical records[26,27]. Specifically, the outburst of AD930 is described as a "guest star entering Yülin" in Japanese astronomical records, for which Yülin is a faint ancient Chinese asterism in Aquarius. The term 'entering' can mean at the edge or periphery (D. H. Clark, personal communication). The approximate coordinates of the guest star of AD 930 are RA ~ 23 h, Dec. ~ −20°, within 10° of R Aquarii, and near the edge of Yülin[27]. A nova outburst would have been discovered and recorded in the Oriental chronicles if its magnitude at maximum was ~2 mag. (ref. 28). In our Galaxy, the frequency of nova outbursts brighter than 2 mag. recorded in the past 100 yr is at a rate ~9 novae per century[23]. The galactic distribution of novae is also known for recent novae[23] and for ancient sightings[26–28]. The probability, therefore, of finding a random nova (different from R Aquarii) within 10° × 10° of this object (with $b = 70.32°$) is small, only ~0.02 for the past 1,000 yr.

From the duration of the outburst of AD930 of a couple of months, adopting a maximum light $m_V\sim2$ mag., we find that if the effective temperature of the hot component during the outburst was in the range 10^4 to 5×10^4 K, then the total light output of the nova is estimated to be $\sim10^{45}$–10^{47} erg. Based on these rough estimates the total energy could account for the kinetic energy presently estimated for the nebula. If correct, R Aquarii would be the first object related to slow-novae and recurrent novae whose outburst was recorded in ancient astronomical records.

The very interesting star R Aquarii has provided us with a number of recent surprises: a jet in the only star besides SS433, the existence of a plausible accretion disk that likely forms at supercritical accretion rates, and a possible ancient Japanese sighting of the initial outburst that produced the nebula. It is obvious this star should be followed carefully in the next 10–20 yr, particularly the radial velocity displacements of emission lines which can provide an indication of the orbit characteristics. Moreover, because of its relatively close proximity of ~200 pc, it may just be possible to spatially resolve an accretion disk around the hot component in the system with Space Telescope.

Other galactic objects associated with jet activity such as SS 433 for example[29] are much further than R Aquarii. Similarly, extragalactic objects[30] are far too distant. R Aquarii offers a much better opportunity to study the formation of jets in suspected accreting systems, and affords us a means of possibly checking directly the physics of accretion disk formation and jet activity.

It is curious that jets tend to form in such widely disparate astrophysical sites as the nuclei of active galaxies[30], in a neutron star or black hole in objects such as SS 433 (ref. 29), and here in hot subdwarfs or main sequence-like companions that accrete. Surely this implies that jet formation is quite a general phenomenon occurring in a variety of astronomical objects.

Received 10 May; accepted 11 June 1982.

1. Hubble, E. P. *A. Rep. Dir. Mt. Wilson Obs.* 1942–43, 17 (1943).
2. Baade, W. *A. Rep. Dir. Mt. Wilson Obs.* 1943–44, 12 (1944).
3. Wallerstein, G. & Greenstein, J. L. *Publs. astr. Soc. Pacific* **92,** 275–283 (1980).
4. Sopka, R. J., Herbig, G., Kafatos, M. & Michalitsianos, A. G. *Astrophys. J. Lett.* **258,** (in the press).
5. Mattei, J. A. & Allen, J. *J. R. astr. soc. Canada* **73,** 173–175 (1979).
6. Willson, L. A., Garnavich, P. & Mattei, J. A. *Int. Bull. of Variable Stars* 1961–1963 (1981).
7. Merrill, P. W. *Astrophys. J.* **112,** 514–519 (1950).
8. Merrill, P. W. *Astrophys. J.* **81,** 312–333 (1935).
9. Bath, G. T. *Mon. Not. R. astr. Soc.* **178,** 203–217 (1977).
10. Bath, G. T. & Pringle, J. E. *Mon. Not. R. astr. Soc.* in press (1982).
11. Haynes, R. F., Lerche, I. & Wright, A. E. *Astron. Astrophys.* **81,** 83–87 (1980).
12. Willson, L. A. in *Physical Processes in Red Giants* (eds Iben, I. & Renzini, A.) (Reidel, Dordrecht, 1981).
13. Robertson, B. S. C. & Feast, M. W. *S. Afr. Astrophys. Obs. Rep.* 227 (1980).
14. Shakura, N. J. & Sunyaev, R. A. *Astron. Astrophys.* **24,** 337–355 (1973).
15. Bath, G. T., Evans, W. D., Papaloizou, J. & Pringle, J. E. *Mon. Not. R. astr. Soc.* **169,** 447–470 (1974).
16. Bath, G. T. & Pringle, J. E. *Mon. Not. R. astr. Soc.* **194,** 967–986 (1981).
17. Alexander, M. E., Chau, W. Y. & Henriksen, R. N. *Astrophys. J.* **204,** 879–888 (1976).
18. Wood, P. R. & Cahn, J. H. *Astrophys. J.* **211,** 499–508 (1977).
19. Wood, P. R. *Astrophys. J.* **190,** 609–630 (1974).
20. Michalitsianos, A. G., Kafatos, M. & Hobbs, R. W. *Astrophys. J.* **237,** 506–512 (1980).
21. Kafatos, M., Michalitsianos, A. G. & Hobbs, R. W. *Astrophys. J.* **240,** 114–124 (1980).
22. Kaler, J. B. *Astrophys. J.* **245,** 568–573 (1981).
23. Payne-Gaposchkin, C. *The Galactic Novae* (Dover, New York, 1964).
24. Johnson, H. M. *Astrophys. J.* **235,** 66–75 (1980).
25. Starrfield, S. G., Sparks, W. M. & Williams, R. E. in *Advances in Ultraviolet Astronomy-Four Years of IUE Research* (eds Kondo, Y. & Kalinowski, K.) (in the press).
26. Hsi Tse-tsung *Smithsonian Contr. Astrophys.* **2,** 109–130 (1958).
27. Pskovskii, Y. P. *Soviet Astr.* **16,** 23–31 (1972).
28. Clark, D. H. & Stephenson, F. R. *The Historical Supernovae* (Pergamon, Oxford, 1977).
29. Margon, B. *Science* **215,** 247–252 (1982).
30. Rees, M. J., Bergelman, M. C., Blandford, R. D. & Phinney, E. S. *Nature* **295,** 17–21 (1982).

Magnetostrictive control of coercive force in multidomain magnetite

J. P. Hodych

Department of Earth Sciences, Memorial University of
Newfoundland, St John's, Newfoundland, Canada A1B 3X7

Although the natural remanent magnetization of terrestrial igneous rock is often due to multidomain grains of magnetite or titanomagnetite, it is not certain what controls the coercivity of the multidomain grains and hence the stability of their remanence[1]. Even the related but simpler problem of what controls the bulk coercive force H_c of multidomain magnetite is still not solved. I consider this simpler problem here by noting[2,3] that the coercive force of multidomain magnetite powders[4] varies with low temperature approximately in proportion to the magnetostriction[5] coefficient λ. I find the same approximate proportionality between H_c and λ on cooling six igneous rocks bearing multidomain magnetite. Hence, the coercive force of these powders and rocks seems mainly to be magnetostrictively controlled–presumably through internal stresses. This is even true of the three rocks with high enough H_c (~150 Oe) to be classed as pseudo-single-domain, including two with the fine magnetite–ilmenite intergrowths often observed in terrestrial igneous rocks with stable remanence[6].

There have been several suggestions as to what controls the coercive force of multidomain magnetite. If internal stresses mainly control H_c as suggested for titanomagnetite by Syono[7], the temperature variation of H_c should be given[8] by $H_c \propto G\lambda/J_s$ where G is the shear modulus and J_s is the saturation magnetization. If dislocations impeding domain wall motion mainly control H_c as favoured by Stacey and Wise[9], the temperature variation of H_c should lie[8] between $H_c \propto G\lambda/J_s(K_1)^{1/2}$ and $H_c \propto G\lambda/J_s(K_1)^{1/4}$ where K_1 is the magnetocrystalline anisotropy

0028-0836/82/310542—03$01.00

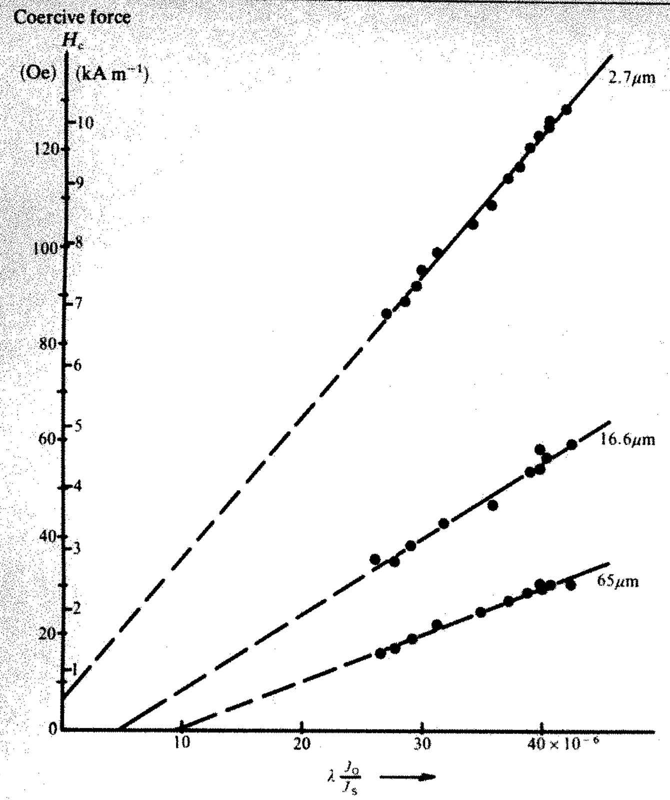

Fig. 1 Coercive force H_c of three grain sizes of crushed natural magnetite measured between ~300 and ~130 K by Morrish and Watt[4] plotted against the corresponding $\lambda(J_o/J_s)$. The polycrystalline magnetostriction coefficient[5] is used for λ. The ratio J_o/J_s of saturation magnetization at 0 K to saturation magnetization at the measurement temperature varies little[14] compared with λ.

coefficient. The possible importance of internal stresses or dislocations to H_c is supported by the observation[10,11] that annealing can substantially reduce H_c of multidomain magnetite. If inclusions mainly control H_c as favoured by Day *et al.*[12] to explain why H_c of their coarse synthetic titanomagnetites does not vary greatly with titanium content, then the temperature variation of H_c should be given[13] approximately by $H_c \propto K_1/J_s$.

It may be possible to decide which of the suggested controls on H_c dominates in a given sample by observing how H_c varies with low temperature. The variation of J_s, K_1, and λ with low temperature is known[5,7,14]. Although the variation of G with low temperature is unknown, it can probably be neglected since G only changes by ~8% between 20 and 255 °C for magnetite[15].

Morrish and Watt[4] measured H_c as a function of low temperature for three grain sizes of multidomain magnetite powder. They concluded that most of the thermal variation of H_c is controlled by K_1 because H_c is a minimum when $K_1 = 0$ (at 130 K). However, H_c is only reduced by 45% or less of its room temperature value when $K_1 = 0$. Furthermore, I find[2,3] that their values of H_c vary approximately in proportion to λ not K_1 from ~300 to ~130 K. Hence, λ rather than K_1 seems mainly to control H_c.

Figure 1 shows the measurements of Morrish and Watt[4] for H_c from ~300 to ~130 K plotted against the corresponding $\lambda(J_o/J_s)$ where J_o is J_s at 0 K. The thermal variation of the polycrystalline $\lambda = 0.4\lambda_{100} + 0.6\lambda_{111}$ was calculated from the smoothed curves of Bickford *et al.*[5] for λ_{100} and λ_{111} versus low temperature. The thermal variation of J_s is comparatively small[14]. For all three grain sizes of crushed unannealed natural magnetite, H_c seems to vary as a linear function of $\lambda(J_o/J_s)$ as expected if H_c is mainly controlled by λ through internal stresses. The line for 2.7-μm grains passes above the origin perhaps because a small fraction of H_c is magnetostatically controlled. The lines for 16.6- and 65-μm grains pass below the origin perhaps because a small fraction of H_c is controlled by K_1 through inclusions. Dislocations impeding domain wall motion do not appear to be the main control on H_c as there is no linear relation between H_c and $\lambda/J_s(K_1)^{1/2}$ or $\lambda/J_s(K_1)^{1/4}$ using K_1 versus low temperature reported by Syono[7].

To test whether magnetostrictive control of H_c is common in rocks bearing multidomain magnetite, the six rocks of Table 1 were studied. Most of the magnetite in each rock is likely multidomain since the ratio j_R/j_s of saturation remanence to saturation magnetization (estimated from 1,200 Oe hysteresis loops) decreases roughly in proportion to H_c on cooling[3].

Figure 2 shows H_c of the six rocks as a function of low temperature. Most of the samples show a minimum in H_c near 130 K followed by an increase in H_c at lower temperatures as expected from the large increase in magnetocrystalline anisotropy accompanying magnetite's cubic to orthorhombic transition below ~120 K. For the two diabases, the minimum in H_c is shifted to lower temperature perhaps due to a little titanium in the magnetite.

Figure 3 shows that for all six rocks, H_c seems to be a linear function of $\lambda(J_o/J_s)$ from near room temperature to ~130 K as expected if H_c is mainly magnetostrictively controlled through internal stresses. The lines for the Shelburne diabase, the peridotite and the basalt pass above the origin perhaps

Table 1 Properties of six igneous rocks containing multidomain magnetite

Rock type	Locality	H_c* (Oe)	j_R/j_s†	Curie point ±7 (°C)
Diabase	Palisades Sill, New York	165	0.23	573
Diabase	Shelburne dyke, Nova Scotia	149	0.22	590
Serpentinized peridotite	Table Mountain, Newfoundland	149	0.30	599
Basalt	India	52	0.08	597
Diorite	Lake Superior	23	0.04	591
Metabasalt	Tweed, Ontario	8	0.02	591

* Coercive force in 1,200 Oe cycles near room temperature.

† Ratio of saturation remanence to saturation magnetization in 1,200 Oe cycles near room temperature.

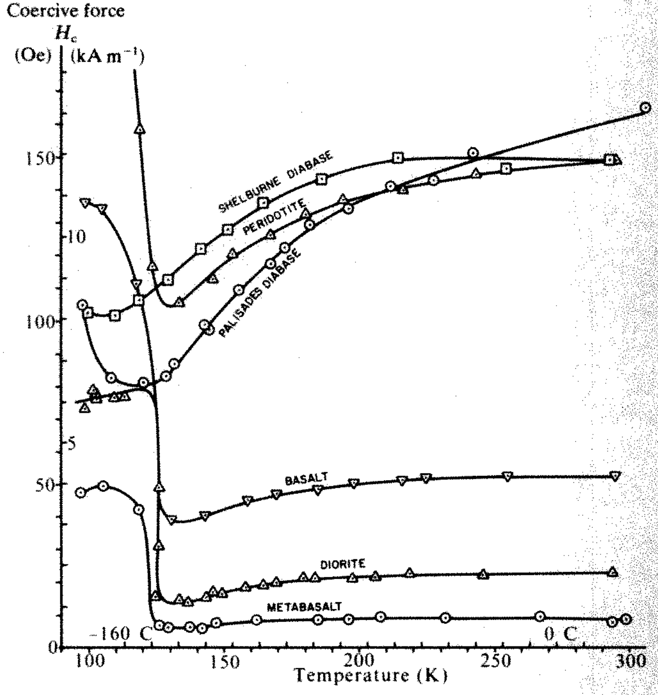

Fig. 2 Coercive force H_c of the six magnetite-bearing rocks of Table 1 measured as a function of low temperature. See ref. 3 for experimental details. For a given sample, the relative error in H_c should be ~±2 Oe but may be greater near room temperature and below 130 K.

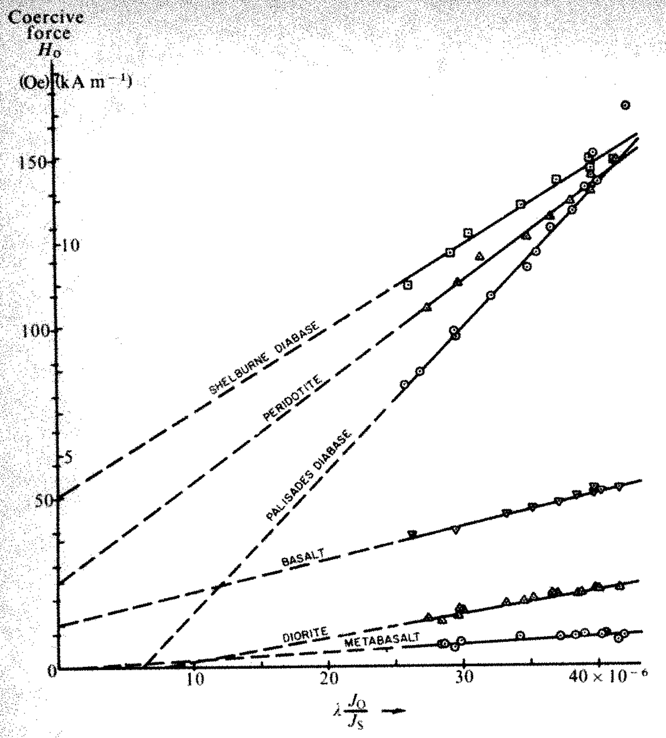

Fig. 3 Coercive force H_c of the six magnetite-bearing rocks of Table 1 measured between ~300 and ~130 K plotted against the corresponding $\lambda\,(J_o/J_s)$ as in Fig. 1.

because a fraction of H_c is magnetostatically controlled. The lines for the Palisades diabase and the diorite pass below the origin perhaps because a fraction of H_c is controlled by K_1 through inclusions. (In the case of the Palisades diabase, the measurements at 300 and 243 K were not included in calculating the least-squares fit line.)

Thus, magnetostrictive control of H_c, probably through internal stresses, does seem common in multidomain magnetite and in rocks bearing it. This even seems true of the upper part of the pseudo-single-domain grain size range judging from the 2.7-μm magnetite and from the peridotite and two diabases with $H_c \sim 150$ Oe and $j_R/j_s \sim 0.2$. Note that the two diabases contain magnetite finely intergrown with ilmenite lamellae in what were originally titanomagnetite grains—a common feature of terrestrial igneous rocks with stable remanence[6].

Magnetostrictive control of H_c may also be common in natural multidomain titanomagnetite with a mole fraction $x = 0.6$ of ulvospinel. I find that H_c increases in proportion to λ on cooling deep-sea basalts containing such grains[3,16]. The same could be true for x between 0 (pure magnetite) and 0.6 since the ratio λ/K_1 for these compositions does not fall much below that of pure magnetite[7].

This research was aided by a grant from the Natural Sciences and Engineering Research Council of Canada and was reported at the International Association of Geomagnetism and Aeronomy assembly in Edinburgh in August 1981[2].

Received 6 April; accepted 26 May 1982.

1. Dunlop, D. J. *Phys. Earth planet. Inter.* **26,** 1–26 (1981).
2. Hodych, J. P. *Bull. int. Ass. Geomagn. Aeron.* **45,** 255 (1981).
3. Hodych, J. P. *Can. J. Earth Sci.* **19,** 144–152 (1982).
4. Morrish, A. H. & Watt, L. A. K. *J. appl. Phys.* **29,** 1029–1033 (1958).
5. Bickford, L. R. Jr, Pappis, J. & Stull, J. L. *Phys. Rev.* **99,** 1210–1214 (1955).
6. Larson, E. E., Ozima, M., Ozima, M., Nagata, T. & Strangway, D. W. *Geophys. J. R. astr. Soc.* **17,** 263–292 (1964).
7. Syono, Y. *Jap. J. Geophys.* **4,** 71–143 (1965).
8. Träuble, H. in *Magnetism and Metallurgy* (eds Berkowitz, A. E. & Kneller, E.) 621–687 (Academic, New York, 1969).
9. Stacey, F. D. & Wise, K. N. *Aust. J. Phys.* **20,** 507–513 (1967).
10. Parry, L. G. *Phil. Mag.* **11,** 303–312 (1965).
11. Lowrie, W. & Fuller, M. *J. geophys. Res.* **74,** 2698–2710 (1969).
12. Day, R., Fuller, M. D. & Schmidt, V. A. *J. geophys. Res.* **81,** 873–880 (1976).
13. Néel, L. *Annls Univ. Grenoble* **22,** 299–343 (1946).
14. Pauthenet, R. *C.R. hebd. Séanc. Acad. Sci., Paris.* **230,** 1842–1843 (1950).
15. Bhagavantam, S. *Proc. Ind. Acad. Sci.* **A41,** 72–90 (1955).
16. Hodych, J. P. *Bull. int. Ass. Geomagn. Aeron.* **45,** 223 (1981).

Langmuir–Blodgett films of long-chain amines

George L. Gaines Jr

General Electric Corporate Research and Development,
Schenectady, New York 12301, USA

Widespread interest has developed in the potentialities of molecular films built up on solids by the Langmuir–Blodgett (L–B) technique of sequential transfer of monomolecular layers from a water surface[1,2]. For certain purposes, the fatty acid soaps which are the classical, and most extensively studied, constituents of L–B films, may be unusable. For example, it may be desired to incorporate acid-sensitive molecules, or the presence of heavy-metal ions such as barium or cadmium, which are required to produce the most stable soap layers, may be undesirable. These problems may be overcome in some instances by the use of fatty alcohols or esters, but multilayers of these substances are generally less stable (especially with respect to thermal disruption or vaporization) than those of the heavy-metal soaps. I now report methods for the facile formation of L–B layers of long-chain amine salts which offer comparable, as well as complementary, advantages compared with soap films.

Early studies of long-chain amine monolayers have been reviewed elsewhere[3], while more recent studies[4,5] have provided further information on counter-ion selectivities at low *p*H. *n*-Alkyl amines with chains of 18 or fewer carbon atoms form expanded monolayers, and dissolve relatively rapidly, when they are spread on acidic subphases at room temperature. The addition of strongly bound multivalent counter-ions, such as sulphate[3] or hydrogen phosphate[6], can reduce this tendency. Over a relatively narrow *p*H range, it has been found that facile L–B film deposition of octadecylamine can be carried out in the presence of such anions[6].

With *n*-docosylamine, however, condensed monolayers are formed in a wide range of conditions (Fig. 1). After a few minutes for equilibration with the atmosphere (*vide infra*), the surface pressure–area isotherms are reversible without hysteresis, and the films are stable, showing negligible changes of area when maintained at pressures up to at least 30 dyn cm^{-1}. Especially at *p*H < 7 and room temperature, their monolayers are readily and quickly built into multilayers of excellent optical uniformity by the usual L–B technique. At high *p*H (10^{-3} M NaOH) in air, the layers emerge with an entrapped solution layer and this must be allowed to drain and dry before reimmersion. If this is done, good multilayers can also be obtained although the process is slow. (The same is true for octadecylamine spread on alkaline solutions where a condensed monolayer is formed[6].)

Amines in contact with alkaline solutions form carbamates very readily by reaction with atmospheric carbon dioxide[7]. The facility with which this reaction occurs had not been generally appreciated, and it undoubtedly accounts for many of the peculiarities noted in early studies of amine monolayers[3]. Direct evidence of carbamate formation in spread monolayers can be easily obtained. A monolayer of octadecylamine (melting point 53–54 °C) was spread on 10^{-3} M NaOH and exposed to room air for 10 min, then collapsed and skimmed from the surface. The skim was rinsed with water and dried in vacuum; its melting point was found to be 75–78 °C, identical to that observed for a sample of the carbamate obtained by passing dry CO_2 into an ethanol solution of octadecylamine. IR spectra (Fig. 2) also demonstrate the presence of carbamate in multilayers built from amine monolayers on alkaline subphases in air, as well as incorporated sulphate counter-ions in L–B films formed at low *p*H. Carbamates are not stable in neutral or only slightly basic solutions[7], and the spectrum of a film built up in this *p*H range (Fig. 2, curve *b*) shows reduced levels of both sulphate and carbamate; further study is required, however, to decide

0028–0836/82/310544—02$01.00

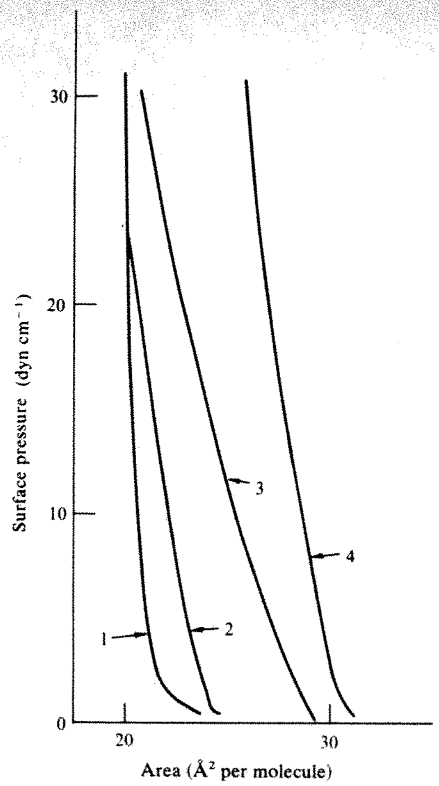

Fig. 1 Surface pressure–area isotherms for *n*-docosylamine in air at 25 °C. Subphase 10^{-3} M NaOH (curve 1) or 0.05 M $(NH_4)_2SO_4$, *p*H 8.3 (curve 2), *p*H 7.5 (curve 3), *p*H $<$ 6.0 (curve 4).

whether these in fact contain free amine. It has also been found that treatment of the carbamate-containing films with sulphate solutions, or sulphate-containing films with NaOH, after they have been built up, can lead to at least partial interconversion of these species as judged by IR spectra, with no significant effect on their visual optical properties (clarity or interference colours).

Multilayers built from 10^{-3} M NaOH exhibit substantial optical changes when heated above 60 °C, while the films formed from sulphate solutions at *p*H $<$ 6 show no detectable changes to at least 100 °C. A 40-layer film deposited on chromium from 0.05 M $(NH_4)_2SO_4$, *p*H 5.6, was baked at 130 °C for 1 h; after cooling, it was found to have developed a hazy appearance, although the interference colours in reflected white light (at either normal or grazing incidence) were unchanged.

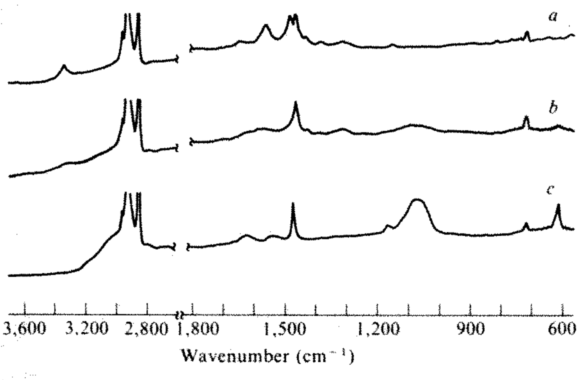

Fig. 2 Transmission IR spectra of 60-layer L–B films of *n*-docosylamine (on Ge plates) built in air from: *a*, 10^{-3} M NaOH; *b*, 0.05 M $(NH_4)_2SO_4$, *p*H 8.7; and *c*, 0.05 M $(NH_4)_2SO_4$, *p*H 5.5. Bands at 617 and 1,080 cm^{-1} are characteristic of sulphate ion; those at 1,570 and 3,340 cm^{-1} are associated with carbamate[11]. The relative intensities of the CH_2 bands at 2,855 and 2,920 cm^{-1} are consistent with the relative molecular packing inferred from the pressure–area curves of Fig. 1.

Multilayers of amines and their salts clearly possess several characteristics analogous to those of fatty acids and their soaps. The degree of counter-ion incorporation (which can affect deposition conditions as well as the properties of the built-up layers) will depend on the composition (especially *p*H) of the subphase from which they are built. Although no extensive results are yet available, I have found that some films built at *p*H 7–8, where only partial salt formation may occur, exhibit interference colour changes after being immersed in solvents which are reminiscent of the 'skeletonization' of acid–soap layers[8].

Treatment of the multilayers with aqueous solutions containing polymeric anions, such as soluble silicates, alginate or tannic acid, renders them hydrophilic (in some cases with interference colour changes indicating increments of thickness); that is the analogue of the 'conditioning' of soap films with solutions of thorium and aluminum complex cations[9].

In addition to the chemical reactions already considered, it would appear that several other well-known reactions of amines offer potential for interesting modification of these L–B layers. Condensation with aldehydes has already been considered in the context of spread monolayers[10]. The formation of carbamate esters by reaction with chloroformates, or diazotization with nitrous acid, may also be possible. The amines, therefore, would seem to provide a highly useful addition to the materials suitable for L–B film fabrication.

I thank Dr R. S. McDonald for assistance with IR spectroscopy.

Received 31 March; accepted 18 May 1982.

1. Vincett, P. S. & Roberts, G. G. *Thin Solid Films* **68**, 135–171 (1980).
2. Barlow, W. A. (ed.) *Langmuir-Blodgett Films* (Elsevier, Amsterdam, 1980).
3. Gaines, G. L. Jr *Insoluble Monolayers at Liquid-Gas Interfaces*, 226–233 (Wiley-Interscience, New York, 1966).
4. Goddard, E. D., Kao, O. & Kung, H. C. *J. Colloid Interface Sci.* **27**, 616–624 (1968).
5. Patil, G. S., Matthews, R. H. & Cornwell, D. G. *J. Lipid Res.* **17**, 197–202 (1976).
6. Petrov, J. G., Kuhn, H. & Möbius, D. *J. Colloid Interface Sci.* **73**, 66–75 (1980).
7. Frahn, J. L. & Mills, J. A. *Aust. J. Chem.* **17**, 256–273 (1964).
8. Blodgett, K. B. & Langmuir, I. *Phys. Rev.* **51**, 964–982 (1937).
9. Langmuir, I. & Schaefer, V. J. *J. Am. chem. Soc.* **59**, 1762–1763 (1937).
10. Valenty, S. J. *Macromolecules* **11**, 1221–1228 1978).
11. Bellamy, L. J. *The Infra-red Spectra of Complex Molecules* 2nd edn, 222 (Methuen, London, 1958).

Photoreduction of methyl viologen in aqueous neutral solution without additives

Thomas W. Ebbesen, Gerrit Levey & Larry K. Patterson

Radiation Laboratory, University of Notre Dame, Notre Dame,
Indiana 46556, USA

Methyl viologen (paraquat; 1,1′-dimethyl-4,4′-dipyridinium dichloride; $MV^{2+}(Cl^-)_2$) has been of great interest not only for its herbicidal activity[1], but also for its use as an electron relay in photochemical systems designed for solar energy conversion[2–12]. In both cases principal attention has been directed towards the reduced species, that is the radical cation $MV^{+\cdot}Cl^-$ which can be generated through the photosensitized reduction of $MV^{2+}(Cl^-)_2$. Such reduction can be achieved *in vivo* by the photosynthetic system[1] or *in vitro* by Ru (II) tris-bipyridine derivatives[2–6], porphyrins[7–9], proflavine[10] and other aromatic compounds[12–14]. Direct photoreduction of $MV^{2+}(Cl^-)_2$ has been widely investigated in the presence of alcohols[15–18] and has also been noted in alkaline[19] and acid[20] solutions. Solid phase photoreduction of $MV^{2+}(Cl^-)_2$ on cellulose involving the oxidation of the substrate has recently been reported[21]. We describe here the direct photoreduction of methyl viologen in neutral aqueous solution to give the complex $MV^{+\cdot}Cl_3^-$. This is potentially important for the understanding of the herbicidal activity of methyl viologen. It also suggests an explanation for the photoreduction process of methyl viologen in alcohols and a possible extension of the role of methyl viologen in the photochemical conversion of solar energy.

Commercial $\mathrm{MV^{2+}(Cl^-)_2}$ (Aldrich) was recrystallized in pure ethanol and dried for 5 h at 70 °C. All solutions were prepared in 0.1 M phosphate buffer at $p\mathrm{H}=7$ and deoxygenated with $\mathrm{N_2}$. Using a Cary 219 spectrophotometer the absorption spectrum of $\mathrm{MV^{2+}(Cl^-)_2}$ was found not to obey Beer's law and may be shown to vary with added $\mathrm{Cl^-}$ concentration. This suggests formation of a complex between methyl viologen and the chloride ions. Indeed an association constant ($0.9\ \mathrm{M^{-1}}$) may be determined from the variation in the absorption spectrum. We believe this results from the complexation of the second $\mathrm{Cl^-}$ on the methyl viologen as has been suggested by others; conductance measurements have given an estimate of this association constant of the order of $10\ \mathrm{M^{-1}}$ (ref. 22). The behaviour of this complex is of great importance to the yield of photoproducts as will be discussed below.

On excitation of $\mathrm{MV^{2+}(Cl^-)_2}$ (0.1 M in 1 M NaCl) at 337 nm with a nitrogen laser (Molectron UV 400, pulse width 8–10 ns), transient spectra were observed (Fig. 1) which exhibit peaks at 395 and 605 nm characteristic of $\mathrm{MV^{\dot{+}}Cl^-}$ (ref. 23). The overall absorption by the initial transient (Fig. 1*a*) below 400 nm is, however, significantly higher than may be predicted from the known spectrum of $\mathrm{MV^{\dot{+}}Cl^-}$ (ref. 23) and the absorption measured at 605 nm. The presence of another transient species absorbing in the region below 400 nm is indicated. It may be seen from Fig. 2*a* that the transient formation occurs at a rate $>10^8\ \mathrm{s^{-1}}$, that is beyond the limits of our time resolution, and that decay occurs in a two step process (Fig. 2*b*, *c*). The initial transient spectrum (Fig. 1*a*) disappears with an overall experimental first-order rate constant, $k_\mathrm{D}=6\times10^4\ \mathrm{s^{-1}}$ (Fig. 2*b*), to a second transient spectrum (Fig. 1*b*). The latter spectrum is long lived, $>10^{-3}$ s (Fig. 2*c*).

While the long-lived transient may be assigned to $\mathrm{MV^{\dot{+}}Cl^-}$ alone (ref. 23), the initial spectrum, as indicated above, may not. However, it may be synthesized by summing the absorbances of equimola quantities of $\mathrm{MV^{\dot{+}}}$ (ref. 23) and $\mathrm{Cl_2^{\dot{-}}}$ (ref. 24). This is illustrated in Fig. 3 and is seen to give a good fit of the synthetic curve to the experimental points.

Such observation would suggest the oxidation of $\mathrm{Cl^-}$ by the excited state of $\mathrm{MV^{2+}}$ generated by photolysis:

$$\mathrm{MV^{2+}(Cl^-)_2} \xrightarrow{h\nu} \mathrm{MV^{\dot{+}}Cl_2^{\dot{-}}} \quad k_\mathrm{f}>10^8\ \mathrm{s^{-1}} \qquad (1)$$

This reaction is analogous to the photoreduction of the alkyl pyridinium ion in 1-alkyl pyridinium iodide[25] and of methyl viologen in the presence of carboxylate ions[22]. An equivalent reaction was previously[20] suggested to explain the simultaneous appearance of $\mathrm{Cl_2^{\dot{-}}}$ and $\mathrm{MV^{\dot{+}}}$ in acid solutions when irradiated in the UV with conventional flash photolysis. However, the transient spectrum given show that considerably more $\mathrm{Cl_2^{\dot{-}}}$ than $\mathrm{MV^{\dot{+}}}$ is formed. Furthermore, $\mathrm{Cl_2^{\dot{-}}}$ was formed in similar conditions in the absence of methyl viologen. Irradiation of chloride solutions in the far UV is known to produce $\mathrm{Cl_2^{\dot{-}}}$ as well as the hydrated electron, e^-_aq (ref. 26) and e^-_aq will reduce methyl viologen with a diffusion controlled rate constant ($8.4\times10^{10}\ \mathrm{M^{-1}\,s^{-1}}$) (ref. 23). The participation of such processes significantly complicates the mechanism for $\mathrm{Cl_2^{\dot{-}}}$ and $\mathrm{MV^{\dot{+}}}$ generation previously reported. In the present study, however, direct electron transfer occurs on excitation of the complex with light well into the visible part of the spectrum (see below) at biological pH.

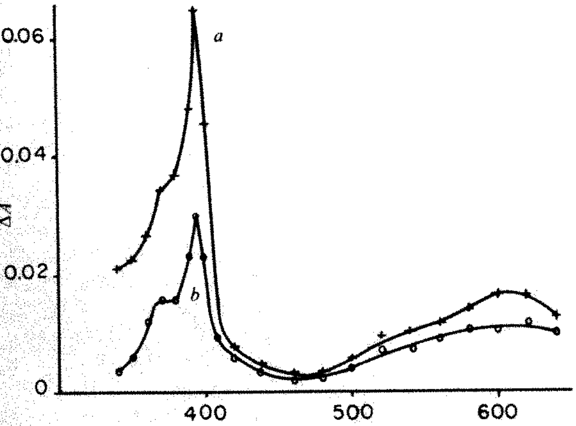

Fig. 1 Differential absorption (*A*) spectra of 0.1 M $\mathrm{MV^{2+}(Cl^-)_2}$ (1 M NaCl) after excitation at 337 nm with $\mathrm{N_2}$ laser (*a*, 1 μs; *b*, 35 μs after flash).

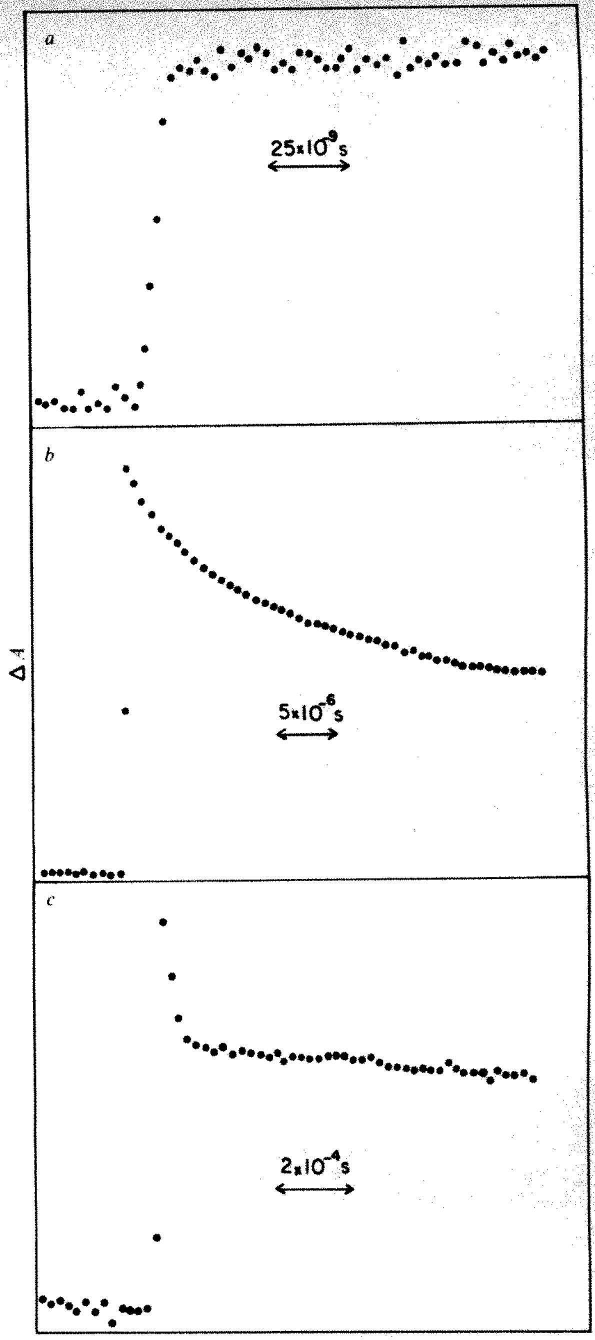

Fig. 2 Experimental kinetic traces of methyl viologen radical generation (*a*), its initial decay (*b*) and its long time disappearance (*c*) as observed at 395 nm after excitation at 337 nm of a 0.1 M $\mathrm{MV^{2+}(Cl^-)_2}$ (1 M NaCl) solution.

The quantum yield of reaction (1) strongly depends on the amount of ground state complex present. Using anthracene as reference[27,28] the quantum yield for reaction (1) with an excitation at 337 nm was estimated to be 0.2, in the experimental conditions described above.

The experimental first-order rate constant, k_D, is independent of wavelength, that is identical for $\mathrm{Cl_2^{\dot{-}}}$ at 340 nm and for $\mathrm{MV^{\dot{+}}}$

at 395 nm (absorption maxima for these species). k_D was also found to remain constant when the flash intensity was varied by a factor of 3. As a significant proportion of the radical cation $MV^{+\cdot}$ (spectrum Fig. 1*b*) remains after $Cl_2^{-\cdot}$ has disappeared, $MV^{+\cdot}Cl_2^{-\cdot}$ must decay by two different reactions. One of the reactions is the obvious back electron transfer:

$$MV^{+\cdot}Cl_2^{-\cdot} \rightarrow MV^{2+}(Cl^-)_2 \quad k_2\,(s^{-1}) \qquad (2)$$

The other reaction was found to involve $MV^{2+}(Cl^-)_2$ which was in excess in the solution:

$$MV^{+\cdot}Cl_2^{-\cdot} + MV^{2+}(Cl^-)_2 \rightarrow MV^{+\cdot}Cl^- + \ldots X \quad k_3\,(M^{-1}\,s^{-1}) \quad (3)$$

A simple kinetic analysis shows that the observed rate constant k_D is equal to the sum of k_2 and $k_3\,[MV^{2+}(Cl^-)_2]$. Values of k_2 and k_3 were determined to be $1.5(\pm1)\times10^4\,s^{-1}$ and $4.5(\pm1)\times10^5\,M^{-1}\,s^{-1}$ respectively. The rather large error limits arise from the limited concentration range over which the experiment can be performed. $MV^{+\cdot}Cl^-$ decays with a rate $<10^3\,s^{-1}$ (slow component in Fig. 2*c*) and no accumulation of the radical is observed under steady-state irradiation.

It is commonly believed that the toxicity of $MV^{2+}(Cl^-)_2$ in plants proceeds initially through its reduction by the photosynthetic system[1] and that the cation radical $MV^{+\cdot}(Cl^-)$ thus produced reacts with O_2 to give several toxic products[23,29–32]. While this is unquestionably the major toxic pathway, our results indicate, however, a potential parallel pathway: $MV^{2+}(Cl^-)_2$ absorbs light well into the solar spectrum (Fig. 4) and will thus directly generate not only $MV^{+\cdot}$ but also $Cl_2^{-\cdot}$. The presence of the radical $Cl_2^{-\cdot}$ adds another dimension to the toxicity of methyl viologen because $Cl_2^{-\cdot}$ is known to react at rates between 10^9 and $10^7\,M^{-1}\,s^{-1}$ with molecules such as: thymine, uracil, guanine, histidine, thyrosine, tryptophan, cysteine, ascorbic acid and other important biological molecules[33,34]. The redox potentials of $MV^{2+}/MV^{+\cdot}$ and $Cl_2^{-\cdot}/(Cl^-)_2$ are −0.44 V (ref. 35) and 2.3 V (ref. 36) respectively. Thus the energy necessary to drive reaction (1) can be estimated to be ~2.7 eV or a photon of 460 nm wavelength. However, the actual energy required might be less as the reaction proceeds with the complexed forms of methyl viologen. Using a dye laser with an excitation wavelength of 460 nm we were able to observe reaction (1), confirming, in accord with the theoretical estimate, that this phenomena is not limited to the near UV spectrum.

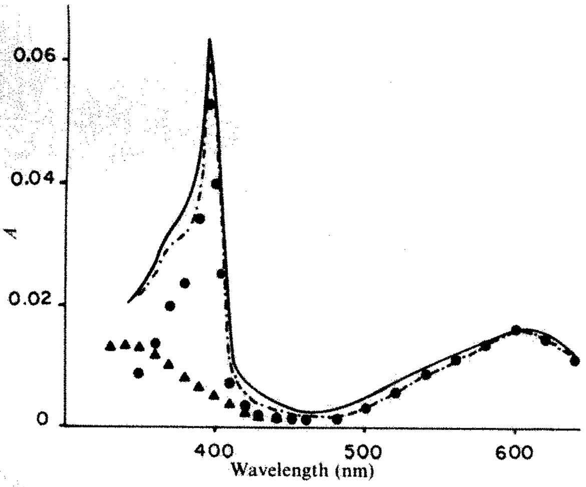

Fig. 3 Comparison between the experimental initial transient spectrum (———) of Fig. 1*a* and the theoretical spectrum (–·–·–) calculated assuming it to be the sum of the spectra of $MV^{+\cdot}$ ($\varepsilon_{605} = 11{,}000\,M^{-1}\,cm^{-1}$)(●) and of $Cl_2^{-\cdot}$ ($\varepsilon_{340} = 8{,}800\,M^{-1}\,cm^{-1}$) (▲) at an equimolar concentration of 1.5×10^{-6} M.

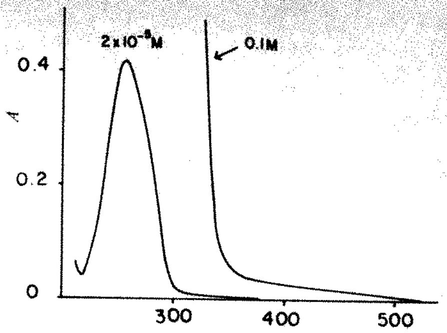

Fig. 4 Absorption spectra of $MV^{2+}(Cl^-)_2$ at 2×10^{-5} M and 0.1 M concentrations.

It is obvious that direct photoreduction of $MV^{2+}(Cl^-)_2$ in aqueous solution can compete with other indirect photosensitization pathways in solar energy conversion systems especially when near UV light is used. In fact, care must be taken to distinguish between the direct photoreduction and the photosensitized contribution in such situations. The methyl viologen radical is known to reduce H^+ in the presence of a catalyst, conversely $Cl_2^{-\cdot}$ can oxidize OH^- ($7.3\times10^6\,M^{-1}\,s^{-1}$) (ref. 34), H_2O_2 ($1.4\times10^5\,M^{-1}\,s^{-1}$) (ref. 34) and HO_2 ($4.5\times10^9\,M^{-1}\,s^{-1}$) (ref. 34). It is therefore not inconceivable that $MV^{+\cdot}Cl_2^{-\cdot}$ could have an important role in both reduction and oxidation of water.

The well known photoreduction of methyl viologen and its derivatives in alcohols has been shown to occur through two processes[37,38] (in certain cases quantum yields >1 have been reported[39]). The initial process may well resemble that observed here. $Cl^{\cdot}$ and $Cl_2^{-\cdot}$ are known to react with alcohols[26,40] and might generate the alcohol radical which in turn reduces another $MV^{2+}(Cl^-)_2$, thus accounting for the second process. While the presence of $Cl_2^{-\cdot}$ has not been previously suggested, a methyl viologen–alcohol–counter-anion complex has already been evoked to explain steady-state irradiation results of methyl viologen and aqueous alcoholic solutions[41]. Further study is in progress to elucidate this mechanism and other questions pertaining to the photoreduction of methyl viologen such as *p*H and temperature effects.

This research was supported by the Office of Basic Energy Sciences of the Department of Energy. This is document no. NDRL-2310 from the Notre Dame Radiation Laboratory.

Received 8 April; accepted 26 May 1982.

1. Dodge, A. D. *Endeavour* **30,** 130–135 (1971).
2. Borgarello, E., Kiwi, J., Pelizetti, E., Visia, M. & Gratzel, M. *Nature* **289,** 158–160 (1981).
3. Kirch, M., Lehn, J. M. & Sauvage, J. P. *Helv. chim. Acta* **62,** 1345–1384 (1979).
4. Matsuo, T., Sakamoto, T., Takuma, K., Sakura, K. & Ohsako, T. *J. phys. Chem.* **85,** 1277–1279 (1981).
5. Chan, S. F., Chou, M., Creutz, C., Matsubara, T. & Sutin, N. *J. Am. chem. Soc.* **103,** 369–379 (1981).
6. Amouyal, E., Keller, P. & Moradpour, A. *JCS Chem. Commun.* 1019–1020 (1980).
7. Harriman, A., Porter, G. & Richoux, M. C. *JCS Faraday Trans.* **2,** 77, 833–844 (1981).
8. Kalyanasundaram, K. & Gratzel, M. *Helv. chim. Acta* **63,** 478–485 (1980).
9. McLendon, G. & Miller, D. S. *JCS Chem. Commun.* 533–534 (1980).
10. Sweetser, P. B. *Analyt. Chem.* **39,** 979–982 (1967).
11. Bellin, J. S., Alexander, R. & Mahoney, R. D. *Photochem. Photobiol.* **17,** 17–24 (1973).
12. Das, P. K. *Tetrahedron Lett.* **22,** 1307–1310 (1981).
13. Davidson, R. S., Bonneau, R., Fornier de Violet, Ph. & Joussot-Dubien, F. *Chem. phys. Lett.* **78,** 475–478 (1981).
14. Hyde, P. & Ledwith, A. *JCS Perkin Trans.* **2,** 1768–1772 (1974).
15. Ledwith, A. *Acct. chem. Res.* **5,** 133–139 (1972).
16. Evans, A. G., Dodson, N. K. & Raes, N. H. *JCS Perkin Trans.* **2,** 859–863 (1976).
17. Brown, N. M. D., Cowley, D. J. & Hashmi, M. *JCS Perkin Trans.* **2,** 462–468 (1978).
18. Furue, M. & Nozakura, S. *Chem. Lett.* **7,** 821–824 (1980).
19. Shchegoleva, I. S. *Khim. Vys. Energii* **10,** 398–400 (1976).
20. McKellar, J. F. & Turner, P. H. *Photochem. Photobiol.* **13,** 437–440 (1971).
21. Kaneko, M., Motoyoshi, J. & Yamada, A. *Nature* **285,** 468–470 (1980).
22. Barnett, J. R., Hopkins, A. S. & Ledwith, A. *JCS Perkin Trans.* **2,** 80–84 (1973).
23. Farrington, J. A., Ebert, M., Land, E. J. & Fletcher, K. *Biochim. biophys. Acta* **314,** 372–381 (1973).
24. Hug, G. L. *NSRDS–NBS 69* (NBS, Washington DC 1981).
25. Kosower, E. M., Skorcz, J. A., Schwarz, W. M. & Patton, J. W. *J. Am. chem. Soc.* **82,** 2188–2191 (1960).
26. Matheson, M. A., Mulac, W. A. & Rabani, J. *J. phys. Chem.* **67,** 2613–2617 (1963).
27. Amand, B. & Bensasson, R. *Chem. phys. Lett.* **34,** 44–48 (1975).
28. Bensasson, R. & Land, E. J. *Photochemical and Photobiological Rev.* Vol. 3 (ed. Smith, K. C.) 163–191 (Plenum, New York, 1978).
29. Patterson, L. K., Small, R. D. & Scaiano, J. C. *Radiat. Res.* **72,** 218–225 (1977).
30. Levey, G., Rieger, A. L. & Edwards, J. O. *J. org. Chem.* **46,** 1255–1260 (1981).
31. Nanni, E. J., Angelis, Ch. T., Dickson, J. & Sawyer, D. T. *J. Am. chem. Soc.* **103,** 4268–4270 (1981).

32. Winterbourn, C. *FEBS Lett.* **128**, 339–342 (1981).
33. Patterson, L. K. *et al. J. Am. chem. Soc.* **94**, 9028–9032 (1972).
34. Ross, A. B. & Neta, P. *NSRDS-NBS 65* (NBS, Washington DC 1979).
35. Homer, R. F., Mees, G. C. & Tomlinson, T. E. *J. Sci. Fd. Agr.* **11**, 309 (1960).
36. Endicott, J. F. *Concepts of Inorganic Photochemistry* Ch. 3 (eds Adamson, A. W. & Fleischauer, P. D.) (Wiley-Interscience, New York, 1975).
37. Rodgers, M. A. J. *Photochem. Photobiol.* **29**, 1031–1033 (1979).
38. Hopkins, A. S., Ledwith, A. & Stam, M. F. *Chem. Commun.* 494–495 (1970).
39. Brown, N. M. D., Cowley, D. J. & Hashmi, M. *JCS Perkin Trans.* **2**, 462–468 (1978).
40. Hasegawa, K. & Neta, P. *J. phys. Chem.* **82**, 854–857 (1978).
41. Brown, N. M. D., Cowley, D. J. & Murphy, W. J. *Chem. Commun.* 592–593 (1973).

Air hydrate inclusions in fresh ice core

Hitoshi Shoji & Chester C. Langway Jr

Ice Core Laboratory, Department of Geological Sciences,
State University of New York at Buffalo, 4240 Ridge Lea Road,
Amherst, New York 14226, USA

One of the characteristic features of polar glacier ice is the abundance of air bubbles[1–3]. With increasing depth from the surface of the ice sheet, the size of the bubbles generally decreases in response to the change of overburden pressure. Below a certain depth, the bubbles start to shrink faster than expected and finally become invisible. Although not visible to the naked eye, unit mass of the bubble-free (clear) ice includes almost the same volume of air as unit mass of bubbly ice[4,5]. It is hypothesized that the air exists in the ice structure probably in the form of clathrate hydrates as suggested by Miller[6,7] but until now the location of the air has been unknown. Direct observations of air hydrate inclusions were carried out for the first time in fresh ice cores from Dye-3, Greenland. When the ice structure surrounding air hydrate was melted, an explosive transition occurred releasing a gas bubble into the melt cavity.

Optical microscope observations were carried out immediately after ice core recovery, as part of the mechanical property study project, during the 1980 and 1981 field seasons of the Greenland Ice Sheet Program (GISP) at Dye-3 (65°12′ N, 43°47′ W). The core was examined to locate the sites of the entrapped air in both bubbly and 'clear' looking ice samples. The work was conducted in a snow trench at −10 °C. Samples (2 × 2 × 1 cm) were cut from fresh ice cores using a band saw and then the surface was planed using a microtome. Silicone oil was applied between the ice sample and a glass plate and the upper surface was allowed to sublimate to diminish the light scattering. A tinker-dam made of shaved ice and supercooled water was applied around the sample to secure it to the glass plate. Thirteen samples were selected over the core profile as follows: 235, 504, 708 and 896 m depths from the 1980 ice core, and 939, 994, 1,280, 1,293, 1,537, 1,642, 1,711, 1,814 and 1,992 m depths from the 1981 ice core. Below 600 m, the ice became brittle with increasing depth and badly fractured between 800 and 1,200 m. The physical property of the core progressively improved and below ~1,400 m was of excellent quality. Total gas content measurements made on core samples at approximately the same depth levels showed a nearby constant gas volume concentration whether the samples were cut from bubbly or 'clear' ice. (S. Herron and C.C.L., in preparation).

To investigate the air sites, a device was constructed consisting of a variable transformer and a heated rod which permitted controlled melting. Microscopic observations were made at least 2 mm below the sample surface to avoid the strained layer near the surface.

Microscopic observations revealed that air bubbles disappeared completely at 1,642 m. However, transparent air hydrate inclusions appeared in the samples starting at a depth of 1,280 m. As is shown in Fig. 1, various shapes were observed for the air hydrate inclusions. They include platelet forms—triangular (*a*), hexagonal (*b*) and polygonal (*c*)—as well as forms classified as tetrahedron (*d*), polyhedron (*e*), graupel-like (*f*) and spheroid (*g*). These inclusions are easily distinguished from air bubbles by their low image contrast under the microscope. These transparent inclusions are not to be confused with Tyndall figures[8] (which consist of water vapour and liquid water), vapour figures[8] (only water vapour) or pressure cracks[1] (water vapour and air formed during the core relaxation process). The optical Becke test on the air hydrate inclusions revealed that the index of refraction of the inclusions is slightly higher than that of ice matrix surrounding them. This indicates that the transparent inclusions in Fig. 1 are not in a gas phase.

Figure 2 shows a typical response of an air hydrate inclusion when the temperature surrounding the inclusion is raised close to the melting point by the heated rod. An ice–water interface is located ~100 μm fron the inclusion and appears in the upper right-hand corner in Fig. 2*a–d*. A protuberance appears (a dark spot) at a position on the inclusion edge nearest to the ice–water interface as shown in Fig. 2*a*. The protuberance (a highly pressurized mixture of melt water and air from the inclusion) is further elongated as a column towards the ice–water interface (towards the high temperature side due to pressure melting) in Fig. 2*b* and finally the elongated column separates (Fig. 2*c*) and quickly migrates to the ice–water interface with a speed of 50 μm^{-1} s^{-1} merging in the melt water. This indicates that the

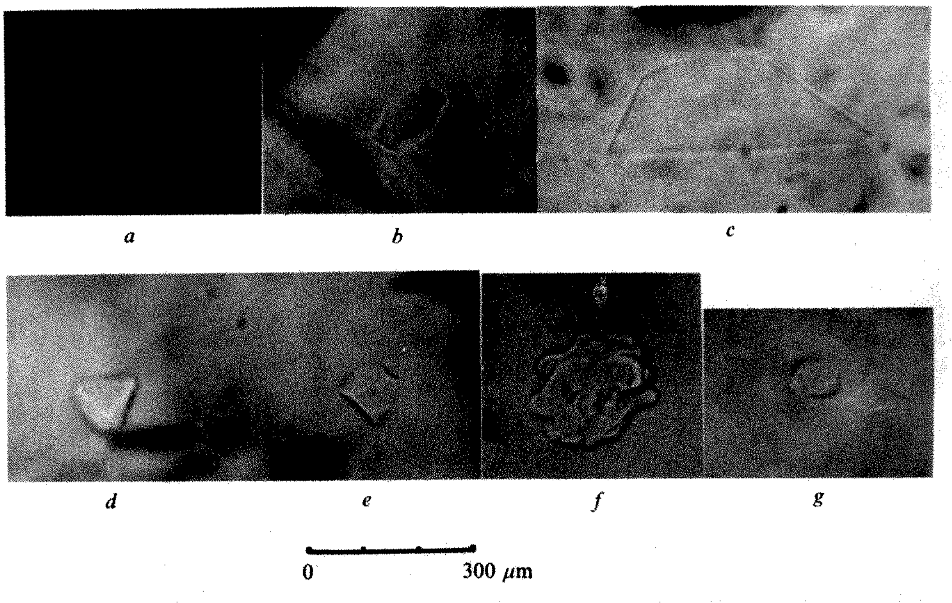

Fig. 1 Shape of air hydrate inclusion: *a*, triangular platelet; *b*, hexagonal platelet; *c*, polygonal platelet; *d*, tetrahedron; *e*, polyhedron; *f*, graupel-like; *g*, spheroid.

0028-0836/82/310548—03$01.00

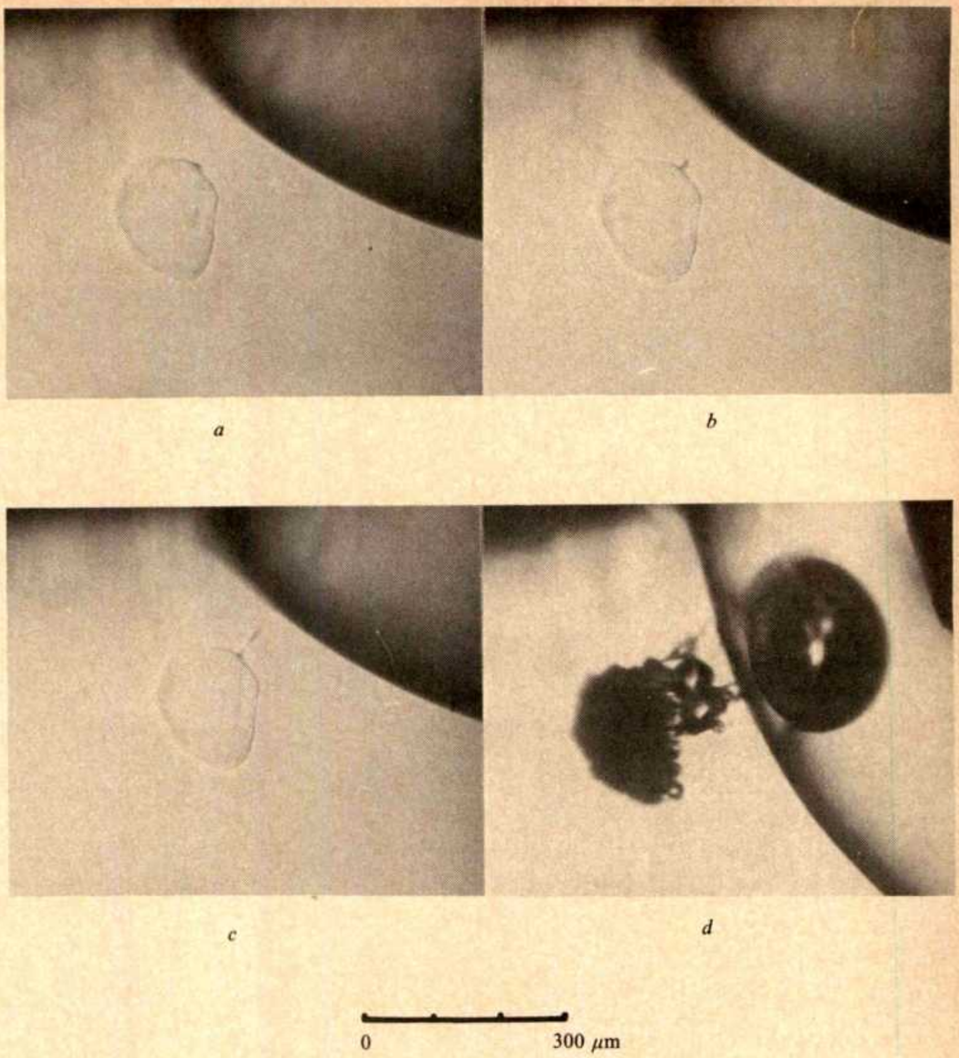

Fig. 2 The melting procedure of an air hydrate inclusion without air bubbles: *a*, embryo protuberance; *b*, elongated column; *c*, column separation (a jet); *d*, the transition of an air hydrate inclusion into air bubbles. Tip of heated rod is to be seen in the outermost upper right-hand corner of *d*; *d* also shows the explosive nature of the transformation of the air hydrate inclusion into a group of smaller air bubbles and the emergence of a huge amount of air into the melt water in the form of a large bubble.

inclusion is not in a gas or liquid phase under pressure. If it were, we would expect a migration or an expansion of the inclusion. In the examples shown in Fig. 2*b*, *c*, additional jets emerged every 20 s, but this frequency changed with each experiment. The rate of jet release is a function of distance between the inclusion and ice–water interface. The experimental procedure used created the end point shown in Fig. 2*d*. When the ice–water interface was moved forward by advancing the heated rod and made contact with the elongated column, an explosive transition of the inclusion into small bubbles occurred and a huge amount of air streamed out through the connecting channel to form a large bubble in the melt water as can be seen in Fig. 2*d*. When air bubbles exist in contact around the air hydrate inclusion before the heat treatment experiment as shown in Fig. 3, the response is different from that of air hydrate inclusions without air bubbles (Fig. 2*a*). A long channel (several hundred micrometres) formed perpendicular to the ice–water interface and air streamed out along this conduit into the melt water. A generation and expansion of multiple bubbles also occur inside the air hydrate inclusion. These observations under the heat treatment indicate that the transparent inclusion is a localized position for the air in clear bubble-free ice. Figure 4 shows a gradual transition of air hydrate inclusions into elongated air bubbles at −10 °C. Photographs shown in Fig. 4*a*, *b*, *c* were taken of the same transparent air hydrate inclusions at 12.5, 71 and 180 h. after core recovery from the bore hole. The two inclusions on the right side of Fig. 4 show air bubble appearance and growth. The size of the air bubble becomes greater than that of the transparent air hydrate inclusion in both cases (Fig. 4*c*), while the transparent inclusion remains the same size and shape. This clearly indicates that the transparent inclusion is in solid phase, otherwise appreciable change in the size or shape of the transparent inclusion would be affected by the hydrostatic pressure difference creating the growing air bubbles. On the other hand, the air hydrate inclusion on the left-hand side of Fig. 4 is still without air

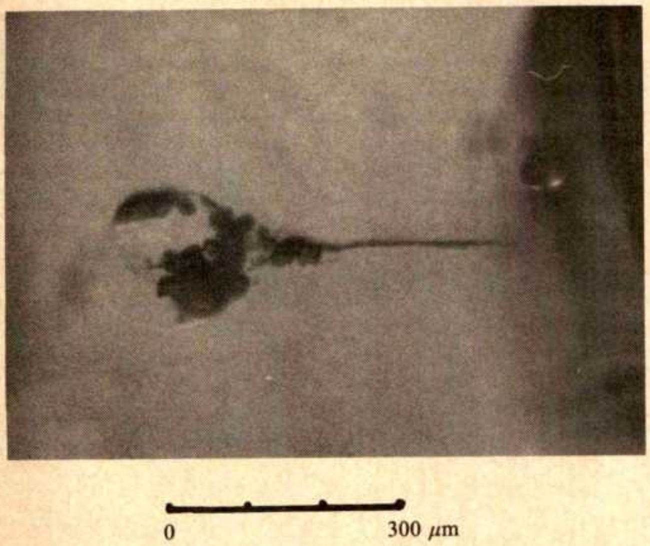

Fig. 3 A long channel formation from an air hydrate inclusion with existing air bubbles under heat treatment.

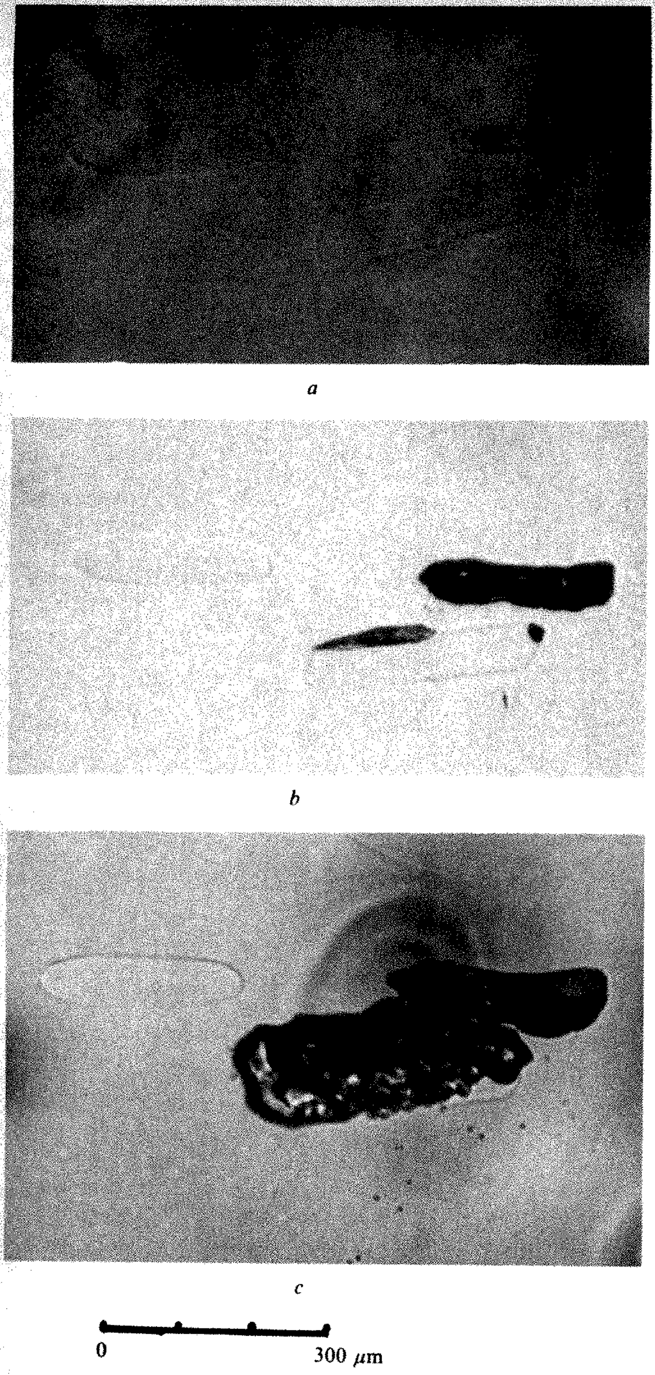

Fig. 4 Air bubble formation and growth process from air hydrate inclusions. *a*, *b* and *c* were taken at 12.5, 71 and 180 h respectively after core recovery.

bubbles even at the end of the 180-h experiment (Fig. 4*c*). This suggests that the nucleation for the phase transition of air hydrate inclusions fron solid to gas determines the rate of relaxation process of bubble-free ice.

The observations and results of this study indicate that the transparent inclusions are in solid phase and mainly composed of water and air molecules, that is, air hydrate inclusions. General information about the clathrate hydrate in ice cores have been given earlier by Miller[6,7] who has proposed calling it craigite. The amount of clathrate hydrate was calculated by Miller on the assumption that 10% of the volume of polar glacier ice consists of air bubbles. These bubbles originated at the surface as air voids and subsequently, through natural compaction processes, became entrapped in the ice. This is the situation at Dye-3. On the basis of the formula used by Miller, $(N_2,O_2)\cdot 6H_2O$, he calculated that 0.06% of the ice in volume would be clathrate hydrate of structure I. Our measurements show that 0.02% of the ice is occupied by air hydrate inclusions which are >10 μm in diameter and represents one-third the amount of the earlier calculation. This suggests that additional locations or smaller sized inclusions (<10 μm diameter) exist; for example, at interstitial positions[9] or grain boundaries. The depth for the first appearance of the air hydrate inclusions is somewhere between 994 and 1,280 m (a zone of highly fractured ice core) which nearly agrees but is slightly deeper than the 950 m value given by Miller for the clathrate hydrate at an *in situ* ice sheet temperature of about −20 °C. Supplemental observations on wedge-shaped thin section between crossed polaroids showed that the colour at the air hydrate inclusion is always shifted from that around the inclusion to that in the thinner part of the sample, which would be expected as the clathrate hydrate structure I is optically isotropic. These findings strongly support the possibility of the inclusion being a clathrate hydrate. A complete X-ray analysis for the crystallographic structure of the air hydrate is planned.

We thank Dr K. Itagaki and Dr B. Kamb for useful discussions. This work was supported by the NSF, Division of Polar Programs.

Received 2 February; accepted 16 April 1982.

1. Langway, C. C. Jr in *Physics of the Movement of the Ice*, 336–349 (IAHS Publ. 47, 1958).
2. Langway, C. C. Jr in *Variation of the Regime of Existing Glaciers*, 101–118 (IASH Publ. 58, 1962).
3. Langway, C. C. Jr *USACRREL Res. Rep.* No. 77 (1967).
4. Gow, A. J. in *Int. Symp. on Antarctic Glaciological Exploration*, 78–90 (IAHS Publ. 86, 1970).
5. Gow, A. J. *J. geophys. Res.* **76**, 2533–2541 (1971).
6. Miller, S. L. *Science* **165**, 489–490 (1969).
7. Miller, S. L. in *Physics and Chemistry of Ice* (eds Whalley, E. *et al.*) 42–50 (Royal Society of Canada, 1973).
8. Nakaya, U. *USASIPRE Res. Rep.* No. 13 (1956).
9. Jones, S. J. & Johari, G. P. in *Isotopes and Impurities in Snow and Ice*, 23–28 (IAHS Publ. 118, 1977).

Major ion chemistry of some large Chinese rivers

Hu Ming-hui[*], R. F. Stallard[†] & J. M. Edmond

Department of Earth and Planetary Sciences E34-201, Massachusetts
Institute of Technology, Cambridge, Massachusetts 02139, USA

There is very little information available in the western literature on the chemical compositions of the major rivers of the People's Republic of China[1,2]. Since these include the largest in terms of sediment transport[3] (Huang He or Yellow), the third largest in terms of flow[4] (Chiang Jiang or Yangtze) and major streams draining the Tibetan plateau, this lack of data represents a significant gap in our knowledge of the chemical denudation rates of the continents as a whole and of south, central and eastern Asia in particular. To begin to rectify this situation, advantage has been taken of recent visits by US scientists to the People's Republic of China to collect suitable samples for analysis. It was found that the chemistry of such rivers is dominated by the weathering of carbonates and evaporites, with no pronounced effects of the degradation of aluminosilicates.

Given the *ad hoc* nature of the project samples were collected and processed in various ways. Those obtained by one of us (J.M.E.) were filtered and acidified soon after sampling. Those provided by our colleagues were either stored intact until

---

[*] Permanent address: Department of Oceanography, Amoy University, Xiamen, Fujian Province, People's Republic of China.

[†] Present address: Department of Geological and Geophysical Sciences, Princeton University, Princeton, New Jersey 08544, USA.

0028-0836/82/310550—04$01.00

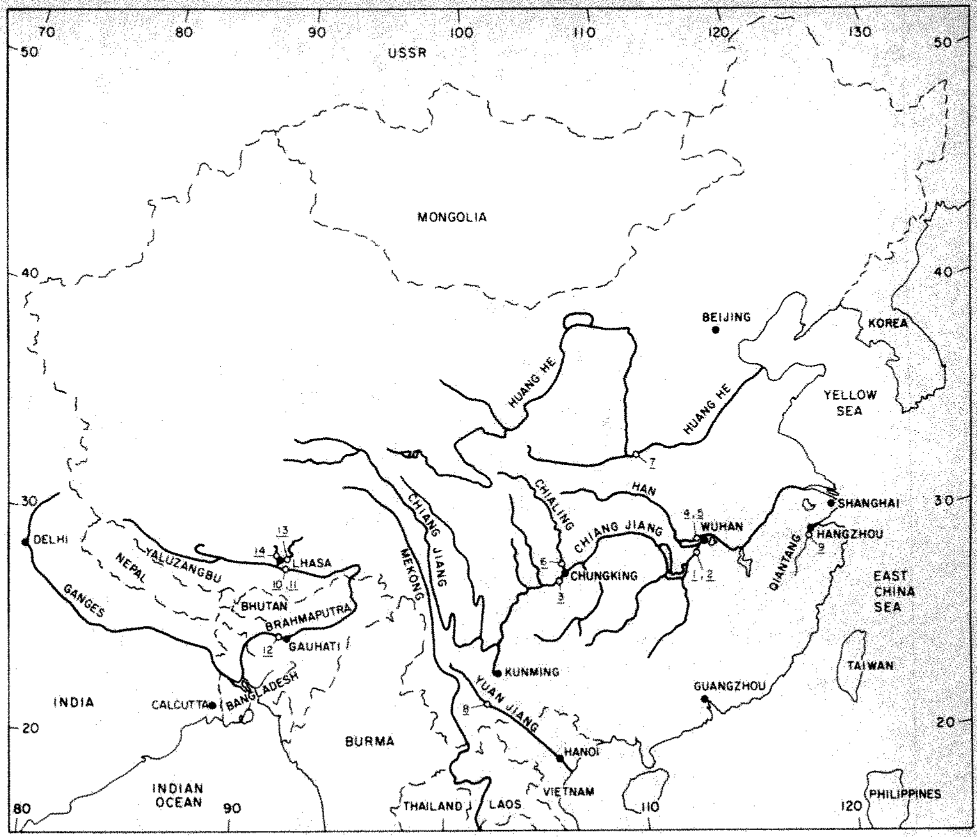

Fig. 1 Location map of the samples.

returned to the Massachusetts Institute of Technology laboratory, a period of several months, or were decanted after the bulk of the suspended material had settled out (within 24 h). The sampling locations are shown in Fig. 1 and these and the details of the processing are summarized in Table 1. The analytical procedures followed were as described previously[5]. The data are presented in Table 2.

Samples were obtained from the main channel of the Chiang Jiang at Chungking, above the Gorges, and at Wuhan in the central part of the flood plain (Table 1, Fig. 1). Two important southwards draining tributaries were also sampled at their confluence with the Chiang Jiang, the Chialing (at Chungking) and the Han (at Wuhan).

The tributaries are typical carbonate rivers with alkalinity accounting for over half the anion balance (including silica) (Fig. 2*a*). Calcium and magnesium are the major cations (Fig. H2*b*): (Ca+Mg)/(Na+K) is around 10 equiv. for the Han and 19 equiv. for the Chialing. In both rivers sulphate is substantially higher than chloride indicating a major contribution from the dissolution of gypsum and minor halite. The low silica and Na:Cl ratios confirm this and demonstrate the lesser relative importance of aluminosilicate weathering inputs in these basins. The main channel above Wuhan is rather similar in its properties, the chemistry being dominated by carbonate weathering (Fig. 2). At Chungking ($Cl+SO_4$) are more significant in the anion balance (Fig. 2*a*) with sulphate being particularly enhanced. This is a reflection of evaporite dissolution in the upper reaches of the river. There is a long established trade in salt in Szechwan and Yunan Provinces exploiting both salt springs and rock salt and supplying halite and gypsum to much of western China[6]. Aluminosilicate weathering is of minor importance consistent with the predominantly sedimentary geology of the drainage.

The Quiantang, sampled at Hangzhou, is an extreme example of carbonate weathering. Calcium and alkalinity account for over 85% of the cation and anion balances.

The Huang He is characterized by a very high content of dissolved solids ($0.46\ g\ l^{-1}$), over double that of the Chiang Jiang (Table 2). Chloride plus sulphate account for over 40% of the anions (Fig. 2*a*) and identify a major contribution from evaporites and soil salts[6,7]. It is estimated that the river loses ~50% of its flow to evaporation during transit around the Great Bend in a region of high aridity[8]. The Mg:Ca ratio of 0.72 and the high alkalinity suggest that carbonate is precipitated in this region also. The sodium excess over chloride (Na:Cl = 1.9) requires significant input from aluminosilicate

Table 1 Sample collection and processing

Sample no.	River	Date	Location	Processing
1	Chiang Jiang	October 1978	Mid-channel above Wuhan	Filtered within a few hours of collection
2	Chiang Jiang	June 1980	Mid-channel above Wuhan	Decanted after settling of suspended load
3	Chiang Jiang	June 1980	Jetty at Chungking	Decanted after settling suspended load
4	Han	October 1978	Mid-channel above confluence	Filtered
5	Han	June 1980	Mid-channel above confluence	Decanted
6	Chialing	June 1980	Mid-channel above confluence	Decanted
7	Huang He	October 1978	From river bank below dam	Stored untreated for 3 months
8	Yuan Jiang	July 1979	From river bank at bridge south of Kunming	Decanted
9	Qiantang	October 1978	Mid-channel above Hangzhou	Filtered
10	Yaluzangbu	July 1979	From river bank at bridge south of Lhasa	Decanted
11	Yaluzangbu	June 1980	From river bank at bridge south of Lhasa	Decanted
12	Brahmaputra	July 1979	From river bank at Gauhati	Decanted
13	Zangbo	June 1980	From river bank above Lhasa	Decanted
14	Doilung	June 1980	From river bank above Lhasa	Decanted

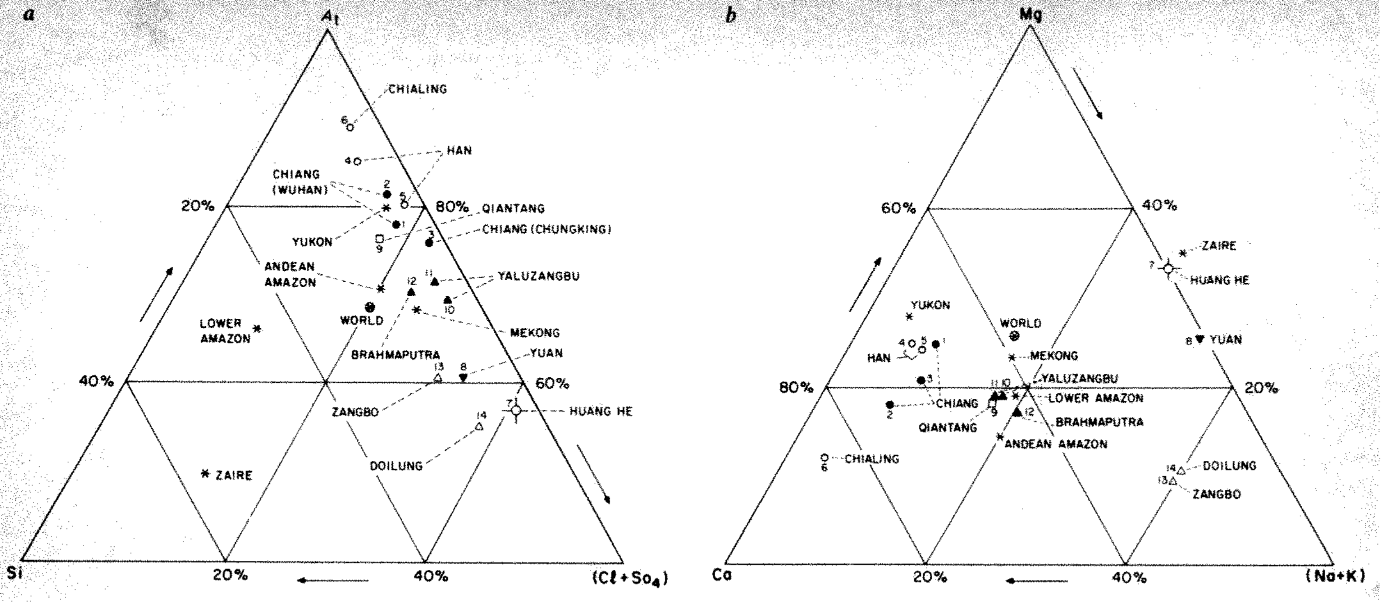

Fig. 2 *a*, Portion of the ternary diagram for the anions (including silica). The data are in equiv l^{-1}. Rivers draining siliceous terranes plot in the left-hand region (Si-A_t dominated). Those draining young orogenic belts rich in uplifted platform carbonates plot in the upper region (A_t dominated). The influence of evaporites is seen in the spread in the right-hand portion ($A_t - [Cl + SO_4]$ dominated). Rivers draining black shales plot in the lower central region owing to sulphuric acid weathering. *b*, Portion of the ternary diagram for the cations. While not as diagnostic as that for the anions parallel relationships are well developed.

weathering. The low silica value may be an artefact of removal by diatoms in the reservoirs upstream from the sampling site[8].

The Yuan Jiang has a chemistry rather similar to the Huang He although the concentration levels are much lower (Table 2, Fig. 2). Salt is mined extensively in the region of the drainage[9] and can account for the pronounced evaporite input. A similar effect is seen in the Mekong[10]. The sodium excess over chloride, the relatively high Mg:Ca ratio and the elevated silica require also a significant input from aluminosilicate weathering.

The chemistry of the Yaluzangbu–Brahmaputra in Tibet is offset from that of the Chiang Jiang in the direction of relatively higher evaporite inputs with sulphate substantially greater than chloride (Fig. 2). Published stratigraphical columns show evaporites in the Tertiary as well as reduced and perhaps pyritic sediments throughout[11]. The Tibetan samples are in marked contrast to that from the flood plain in the sub-Himalayan lowlands especially as regards the K:Na ratio. In rivers draining the Amazonian Andes, which like the Himalayas have an extremely moist 'front range' and dry interior[5,12], the chemistry is controlled by inputs from the well-watered tributaries[5]. While poorly described, the dominant lithologies of the moist slopes of the Himalayas appear to be reduced shales, gneisses, carbonates and perhaps volcanic rocks. Reduced shales are notably potassic[13] as are the gneisses and granites reported from the Himalayas[12]. Intense chemical weathering of these lithologies is consistent with the evolution of the river chemistry.

The two tributaries sampled drain portions of the Tibetan Plateau north of the main channel. They are carbonate–evaporite streams strongly enriched in sodium and chloride (Table 2).

The chemistry of the major rivers of China is dominated by the weathering of carbonates and evaporites (gypsum, halite) in varying proportions. The effects of the degradation of aluminosilicates are nowhere pronounced. In this, these rivers are typical of streams draining young orogenic belts. Thus the Chiang Jiang is very similar to the Yukon at the US–Canadian border (R.F.S and J.M.E. unpublished data) (Fig. 2) and the Yaluzangbu–Brahmaputra to the Andean Amazon in Peru[5]. In the latter case large-scale inputs of evaporite material from salt springs and exposed salt domes have been well documented[5].

The effects of aluminosilicate weathering have most influence on the anion diagram as they are uniquely characterized by high concentrations of dissolved silica. For illustrative purposes the Zaire (Congo) (R.F.S. and J.M.E. unpublished data) and lower Amazon[5] are plotted in Fig. 2. Both rivers receive a substantial component of their dissolved load from streams draining shield areas or, in the case of the Amazon, from basins whose surficial geology is dominated by shales or alluvial detritus. They are distinctively separated from the Chinese rivers on the anion diagram (Fig. 2*a*).

The Yaluzangbu–Brahmaputra, like the Mekong and the Andean Amazon, is close to the world average river water[1,2] in composition (Fig. 2). The Chiang Jiang and the Yukon are more calcareous, less siliceous and have lower relative abundances of alkalies, chloride and sulphate. The Huang He and Yuan Jiang are separate from the other rivers reflecting their

Table 2 Analytical data

Sample no.	River	Location	Date	Na	K	Mg	Ca (μmol l^{-1})	Cl	SO_4	Si	A_t (μequiv l^{-1})
1	Chiang Jiang	Wuhan	October 1978	227	34.8	318	794	159	147	115	2,011
2	Chiang Jiang	Wuhan	June 1980	179	31.8	269	1,120	116	186	95.5	2,420
3	Chiang Jiang	Chungking	June 1980	300	39.0	343	1,089	183	310	104	2,550
4	Han	Wuhan	October 1978	186	36.4	294	824	68.7	114	94.0	2,156
5	Han	Wuhan	June 1980	234	33.0	322	916	124	182	71.5	2,280
6	Chialing	Chungking	June 1980	159	35.8	230	1,160	116	130	124	3,550
7	Huang He	Gorges Dam	October 1978	2,120	61.9	903	1,249	1,134	760	95.0	3,700
8	Yuan Jiang	South Kumming	July 1979	482	38.5	335	413	234	238	164	1,340
9	Qiantang	Hongzhou	October 1978	204	38.7	122	451	127	54	76.0	1,110
10	Yaluzangbu	South Lhasa	July 1979	396	31.8	209	752	156	255	127	1,670
11	Yaluzangbu	South Lhasa	June 1980	446	37.4	191	717	198	223	125	1,740
12	Brahmaputra	Gauhati	July 1979	159	78.5	119	425	107	100	123	884
13	Zangbo	Lhasa	June 1980	380	35.5	38.6	270	200	75	134	751
14	Doilung	Lhasa	June 1980	300	48.4	35.0	224	262	60	88.0	558

Table 3 Chemical transports and denudation rates

Sample no.	River	Discharge (10^{12} l yr^{-1})	Area (10^3 km^2)	Na	K	Mg	Ca	Cl	SO$_4$	Si	A_t	A*	Si* (10^6 mol km^{-2} yr^{-1})	Salt discharge (M tonnes yr^{-1})	Salt discharge (tonnes km^{-2} yr^{-1})
							(10^8 mol yr^{-1})								
1	Chiang	1,063	1,950	241	37.0	338	844	169	156	122	2,140	1.10	0.063	226	116
2	Chiang	1,063	1,960	190	33.8	286	1,190	123	198	102	2,570	1.32	0.052		
7	Huang He	48	745	102	3.0	43	60	54	37	4.5	178	0.24	0.006	22.4	30
12	Brahmaputra	603	580	96	47.3	72	256	65	60	74	533	0.92	0.13	61.0	105
—	Mekong	666	795	89	27.5	73	200	168	22	83	538	0.68	0.10	58.7	74
—	Zaire	1,230	4,104	74	32.8	58	64	34	15	177	242	0.06	0.043	35.6	8.7
—	Amazon	5,500	6,300	440	140	230	750	200	120	83	1,870	0.30	0.13	223	35
—	World (10^{12} mol yr^{-1})	31,400	101,000	6.0	1.2	5.2	12.5	3.3	3.0	6.5	32	0.31	0.064	3,600	35

large evaporite inputs and, in the case of the Huang He, probable artefacts of carbonate and silica removal during evaporative loss or in reservoirs.

A rough estimate can be obtained of the transport of dissolved material by these streams by combining the compositional data reported here with the existing discharge measurements[4] (Table 3). Note that such calculations are uncertain by as much as 50% because of the variations in the discharge-composition relationship over the range of the discharge and because of the lack of information on the actual flow rates at the time of sampling. These effects can be seen by comparison of values of the chemical transport from rivers resampled on different dates (Tables 1.3). Estimates for the Amazon[5], Zaire (R.E.S. and J.M.E., unpublished data) and Mekong[10] are shown for comparison as are the global estimates[1,2].

Although its discharge is less than one-fifth that of the Amazon, the Chiang Jiang carries substantially more calcium, magnesium, sulphate and alkalinity to the ocean. It supplies lesser but still relatively large amounts of sodium and chloride. Its transport of potassium and silica is similar to that of Zaire; the latter is a relatively minor supplier of the other major ions reflecting the low weathering yields from siliceous terranes.

The Huang He, although its discharge is small (1% of that of the Amazon) is a significant source of sodium, chloride and sulphate. It contributes only a small amount of potassium.

The Yaluzanbgu–Brahmaputra, with a discharge of ~60% of that of the Chiang Jiang, supplies considerably more potassium and appreciable amounts of sodium, chloride and sulphate. It is much more potassic than the Mekong, with similar discharge, but comparable for the other elements.

In the global context, the Chiang Jiang accounts for over 5% of the flux of magnesium, calcium, chloride, sulphate and alkalinity to the oceans. Neither the Yaluzangbu–Brahmaputra nor the Huang He make contributions of similar magnitudes. The total salt discharge of the Chiang Jiang is $\sim 220 \times 10^6$ tonnes yr^{-1} or 226 including silica. This places it equal to the Amazon at 223×10^6 tonnes yr^{-1}.

Estimates of the average chemical denudation rates for the basins can also be derived from the data (Table 3). As compared with the world average[1,2] these are high for rivers with well-watered, topographically elevated drainages composed of young orogenic belts—Chiang Jiang, Yaluzangbu–Brahmaputra, Mekong. They are close to the average for streams draining arid mountainous regions—Huang He—or extensive lowland areas—Amazon. They are very low for rivers such as the Zaire which drain predominantly shield terranes.

The inferences as to carbonate–evaporite versus aluminosilicate weathering are substantiated by the variations in the ratio of the areal yields of alkalinity and silica. These range from 20 for the Chiang Jiang (40 for the Huang He, probably an artefact), 7 for the Yaluzangbu–Brahmaputra and Mekong to 1.4 for the Zaire. The world average is 4.8 again emphasizing the extreme chemistry for the Chiang Jiang.

With the exception of the Huang He the major rivers of the People's Republic of China are free from large-scale hydrological development. Outside of their lowermost reaches agriculture is the only anthropogenic modification that can be expected to have a significant influence on the water chemistry. It is to be hoped that systematic geochemical studies will be initiated before and pursued in parallel with the planned industrial development of the basins.

We thank the US Committee for Scholarly Communications with the People's Republic of China and especially Mr Halsey Beemer for their generosity and support. We also thank the parallel organizations in the People's Republic of China. We are grateful to H. and V. Craig, B. Lyons, P. Molnar and C. Nordin for contributing samples. R.F.S. acknowledges the receipt of an NSF graduate fellowship.

Received 24 February; accepted 18 May 1982.

1. Livingston, D. A. *U.S. geol. Surv. Prof. Pap.* **400-G,** G1–G64 (1963).
2. Meybeck, M. *Rev. Geol. Dyn. Geogr. Phys.* **21,** 215–246 (1979).
3. Holeman, J. N. *Water Resour. Res.* **4,** 737–747 (1968).
4. van der Leeden F. *Water Resources of the World* (Water Info Center, New York, 1975).
5. Stallard, R. F. & Edmond J. M. *J. geophys. Res.* **86,** 9844–9858 (1981).
6. Spencer, J. E. *Geogr. Rev.* **25,** 353–366 (1935).
7. Tregear, T. R. *China, A geographical Survey* (Halstead, New York, 1980).
8. Greer, C. *Water Management in the Yellow River Basin of China* (University of Texas Press, Austin, 1979).
9. Lefond, S. J. *Handbook of World Salt Resources* (Plenum, New York, 1963).
10. Meybeck, M. & Carbonnel, J. P. *Nature* **255,** 134–136 (1975).
11. Bally A. W. *et al. U.S. geol. Surv. Open File Rep.* **80-501,** 100 pp (1980).
12. Gansser, A. *Geology of the Himalayas* (Wiley, New York, 1964).
13. Pettijohn, F. J. *Sedimentary Rocks* (Harper and Row, New York, 1975).

Dynamic uplift of the Himalaya

Chi-yuen Wang & Yao-lin Shi

Department of Geology and Geophysics, University of California, Berkeley, California 94720, USA

Wen-hu Zhou

Institute of Geophysics, Academia Sinica, China

It has become widely accepted that the Himalaya is the product of collision between the Indian landmass and the Eurasian continent. Holmes[1] conjectured that the Indian Shield was carried northwards by sub-lithospheric mantle flow to cause a double thickening of crust beneath the Himalayas and the Tibetan Plateau. Wager[2] hypothesized that the extra height of the great peaks of the Himalaya over Tibet was due to isostatic readjustment following the removal of load by intense erosion. Molnar *et al.*[3], relate the uplift to the shear stress on the boundary faults beneath the Himalayas. Relevant data have recently become available from the northern flank of the Himalaya and the Tibet Plateau, of which especially important are: (1) a gravity profile across central Tibet; (2) seismic crustal structures of the region from explosion seismology; (3) seismicity; (4) geothermal activities; (5) geodetic, palaeogeographical, and radiometric data bearing on the uplift rate of the region; and (6) field observation of the surface fault patterns. The combined data-set has imposed strong constraints on theories of the dynamic processes in this region. We summarize here the relevant observations and discuss the results and implications of our model analysis; details of the modelling procedure are given elsewhere[4].

Gravity surveys along a 1,200 km highway across central and eastern Tibet, from Yadong (27.88° N, 88.56° E) to Golmud

0028-0836/82/310553—04$01.00

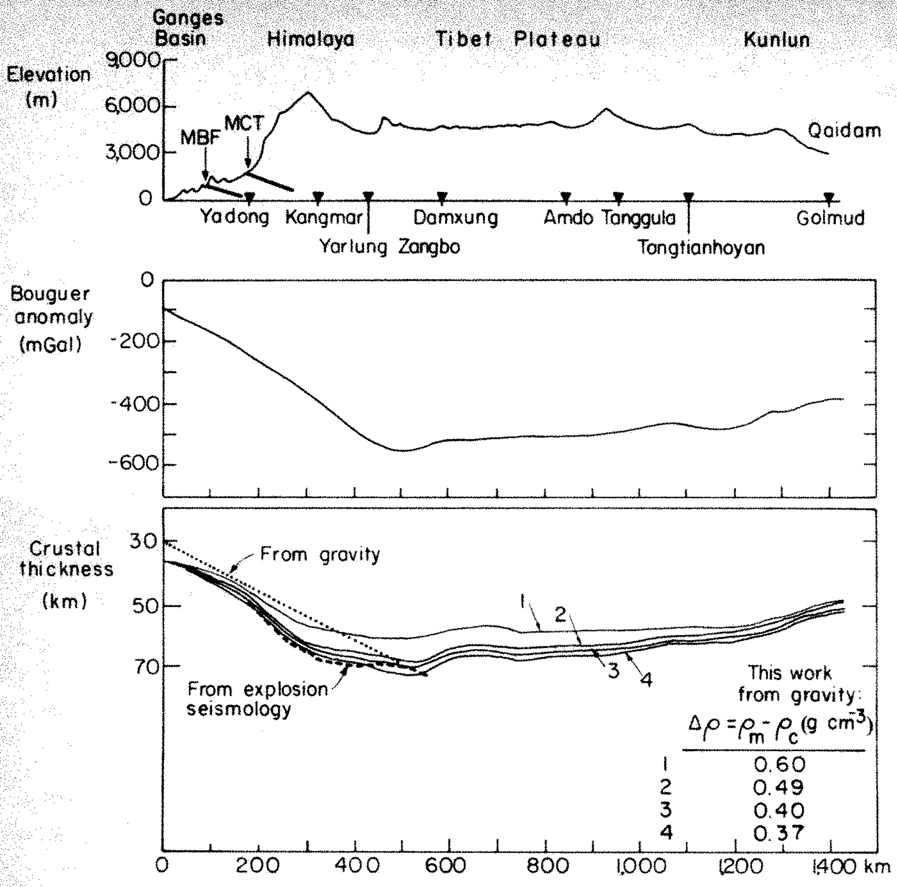

Fig. 1 Topography and Bouguer gravity anomaly along the cross-section from Yadong (27.88° N, 88.56° E) to Golmud (36.22° N, 94.55° E). The corresponding boundaries for an Airy crust are also plotted, based on a normal crustal thickness of 30 km and several values for the density contrast between the crust and the upper mantle. The dotted line shows the boundary given by Kono[35]. The dashed curve shows the Moho boundary obtained from the explosion seismology[5].

(36.22° N, 94.55° E), were carried out in 1975–77. Figure 1 shows the topography and the Bouguer gravity anomaly along this route. North of the Zangbo River, Tibet is characterized by a large negative Bouguer anomaly of about −500 mGal. Southward from the Zangbo River, Bouguer anomaly increases from about −500 to −300 mGal over the High Himalaya and to about −50 mGal over the Ganges Basin. The Airy crust constructed from this gravity profile is also shown, which is about 70 km thick beneath the Tibet Plateau, but thins southward to about 50 km beneath the High Himalaya. This model is supported by its general agreement with the latest information on the seismic velocity structures of this region.

Seismic profiling in central Tibet along the 90° E meridian[5] has provided the most detailed information for the crustal structures. The crusts on the two sides of the Zangbo River are significantly different. North of the river the crust is 70–73 km in thickness; south of the river the crust thins from 65 to 45 km near Yadung (27.5° N). Deep seismic sounding in the Kashmir Himalaya shows northward dipping of the Moho at an average angle of 15°–20° (ref. 6). Thus, the Moho boundary has the same general features as the lower boundary of the Airy crust.

Most of the seismic activity is confined to the southern slope of the Himalaya. Along most of the Himalaya the seismic activity appears to be associated with the Main Boundary Fault (MBF)[3]. On the other hand, Chandra[7] located earthquakes in a broad zone of 200-km width along the Main Central Thrust (MCT), and considered both the MBF and MCT to be active. Most earthquakes are generated by thrust faulting, with one plane dipping gently beneath the Himalaya[3]. This is consistent with the theory that the Indian subcontinent underthrusts at shallow angles, and implies that the processes that formed the Himalaya are still at work.

Within the Tibet Plateau, seismic activities are less vigorous, and the fault plane solutions generally show strike-slip faulting, with the P-axis oriented approximately north–south[8], or normal faulting, with the T-axis oriented approximately east–west[9–11]. Studies of Landsat imageries[10] and recent field observations[12,13] also revealed abundant evidences for active strike-slip and normal faulting inside Tibet.

Geothermal activities in Tibet (Fig. 2) are extremely energetic with numerous boiling springs, geysers, and hot springs scattered across the highland. Cenozoic volcanism is extensive over much of Tibet. Youthful geology also points towards a high regional heat flow.

Also important is the uplift rate of the Himalaya. Geodetic surveys[14] in northern India during the past 75 yr revealed that the block north of the MBF is uplifting with respect to the southern block at an average rate of 0.8 mm yr^{-1}. Fossil fauna, including *Hipparion*, were recently found in the horizontally bedded lake deposits of Jilong Basin (20°30′ N, 85°10′ E), now at an elevation of about 5,000 m (refs 15, 16). Widely distributed peneplains in the High Himalaya at similar elevations are thought to be the remains of an originally continuous peneplains formed in the Pliocene at about 1,000 m above sea level[17]. Evidences from abundant pollen, plant fossils, and traces of ancient snowlines have made possible the separation of the influences of the climatic factor from the tectonic one[18–20]. These palaeogeographical investigations have yielded a consistent estimate that an average uplift rate of ~1 mm yr^{-1} has occurred in the High Himalaya since the late Pliocene. A third type of estimate of the Himalayan uplift rate came from modelling fission-track dates of minerals from this region; a consistent estimate of uplift rate from 0.7 to 1.5 mm yr^{-1} also emerges from these studies[21,22]. Clearly, there is much uncertainty in each of these estimates, and more extensive work is needed to gain a more precise knowledge of the Himalayan uplift rate; but when all the evidence is taken together, the close agreement in the different estimates is not likely to be coincidental, and the estimate of an average rate of uplift of 1 mm yr^{-1} seems to be reasonable.

Based on these observations, we have attempted to model the present tectonic process in this region by using a two-dimensional, finite element technique[4]. Deformation was approximated by plane-strain in a vertical plane perpendicular to the major structural lines, with the north–south width of the model extending northward from the Ganges Basin, through the Himalaya and the Tibet Plateau, to the Kunlun Mountains. Such an approach is common for problems where the vertical motion is of main concern[23]. As mentioned above, however, most earthquakes inside Tibet are either due to strike-slip faulting, with the P-axis nearly in the north–south direction[8], or due to normal faulting, with the T-axis in the east–west direction[9–11]. Thus, the problem of modelling the tectonics in the Himalayan–Tibet region is intrinsically three-dimensional. Nevertheless, a two-dimensional approximation of the problem may be worthwhile, not only because it is far less expensive but because it may provide insight to the complex problem at hand.

The detailed modelling procedure is given elsewhere[4]. We assumed that at shallow depth the crust is permeated with fractures so that deformation is controlled by frictional sliding. At deeper levels ($\geq \sim 25$ km) ductile flow becomes more important; the controlling mode of deformation is assumed to be the one that requires less shear stress to activate. For frictional sliding, the shear stress (τ) and the normal stress (σ_n) across the sliding surface are related by $\tau = \mu\sigma_n$ where μ is the frictional coefficient and is ~ 0.6–0.8 for rock-on-rock sliding[24,25] and may decrease to 0.2 for faults filled with saturated clayey gouge[26]; the latter value is used for friction on the boundary faults beneath the Himalaya. For steady-state flow of rocks at high temperature, the general relation between strain rate ($\dot{\varepsilon}$) and the deviatoric stress ($\delta\sigma$) may be expressed at $\dot{\varepsilon} = A(\delta\sigma)^n \exp(-Q/RT)$, where T is the absolute temperature, R is the gas constant, and A and n are material constants. From the steady state flow laws for several crustal rocks recently reported by Shelton and Tullis[27] we chose for the lower crust the following parameters: $Q = 60$ kcal mol^{-1} (251 kJ mol^{-1}), $n = 3$, and $A = 1.33 \times 10^3$ kbar^{-3} s^{-1}. For the upper mantle we assume that the steady state flow is controlled by the mechanical properties of olivine. The experimental results are summarized by Tullis[28]. For our numerical work, we chose the following parameters: $Q = 100$ kcal mol^{-1}, $n = 3$, and $A = 3 \times 10^8$ kbar^{-3} s^{-1}.

Because the mechanical properties of rocks depend strongly on temperature, its value beneath the Himalaya and its vicinity is a most important factor. Unfortunately, relevant data for the construction of geotherms in this region are tenuous. Beneath the Ganges Basin, we adopted the thermal model of Bird[29] for the Indian platform. Chen and Molnar[30] recently interpreted the upper mantle seismic velocities beneath Tibet, using laboratory data for olivine at high temperature and pressure, they concluded that the upper mantle temperature beneath Tibet is about 250 °C higher than that beneath the Indian Shield at the same depth. This conclusion is consistent with the high geothermal activities in this area (Fig. 2), and confirms a geotherm we constructed from an assumed high conductive heat flow (2 HFU) and some broad geophysical constraints[4].

With these assumptions of rheology and geotherms, the mechanical property of our model is defined. The depth where ductile flow becomes dominant depends on the local strain rate and the geotherm. In general terms, the upper 25 km or so is stiff, below which ductile deformation becomes more important and the 'strength' of the lithosphere decreases rapidly with depth.

Assuming that the observed gravity anomalies and uplift in this region is the product of a tectonic process still in operation, we looked for a set of boundary conditions which led to predictions compatible with observations. The successful boundary conditions were then used to constrain the mechanism which may now be operating for the Himalayan uplift.

From the many models we tested[4], the best one was acquired by imposing the following boundary conditions (Fig. 3): the south boundary moves northwards with a velocity of 50 mm yr^{-1}. On the bottom boundary, vertical movement is $\sim$2 mm yr^{-1} under the thrust zone and 1 mm yr^{-1} under the Tibet Plateau, horizontal displacement is not constrained, except under Tibet, where a basal shear of a few bars is applied in the direction opposing the plate motion. The northern boundary is fixed in position at its lower end, but the upper 25 km is constrained to move northward at a rate of 10 mm yr^{-1}. This causes the lower crust and the upper mantle to experience a horizontal shear.

Results of calculation for this model (Fig. 3) show that the Ganges Basin sinks and the Himalaya rises, with a calculated uplift rate for the Himalaya of $\sim$0.6 mm yr^{-1}, relative to the Ganges Basin. Considering the substantial uncertainty usually present in such data, and considering the crudity of our model, we think the agreement between the calculated and the observed values are satisfactory. The Tibet Plateau also uplifts; at the same time it remains in isostatic balance. But the Himalaya and the Ganges Basin do not; the Himalaya develops a positive isostatic anomaly, and the Ganges Basin a negative anomaly. The thickening of the crust in Tibet is accompanied by shortening of the entire region, with $\sim$15% in the Ganges Basin, $\sim$30% in the Himalaya, and $\sim$55% in Tibet. When the stability of this model was examined with respect to changes in material properties and boundary conditions, it was found that it was stable to minor changes of material properties and boundary conditions.

An interesting result is the differential uplift rates between the Tibet Plateau and the Himalaya—the annual rate of uplift of the Himalaya is $\sim$0.2 mm yr^{-1} greater than that of Tibet. This difference in uplift rates implies that the Himalaya was lower than Tibet some 2 Myr ago. Spectacular evidence for this speculation is provided by the many antecedent rivers flowing southward across the main ridges of the Himalaya[1,2]. Following Wager[2], we suggest that the rivers established their courses on a slope which formed the descent from a northern highland (which was later elevated to become the Tibet Plateau) to the Ganges plain, and since then the Himalaya has risen faster than

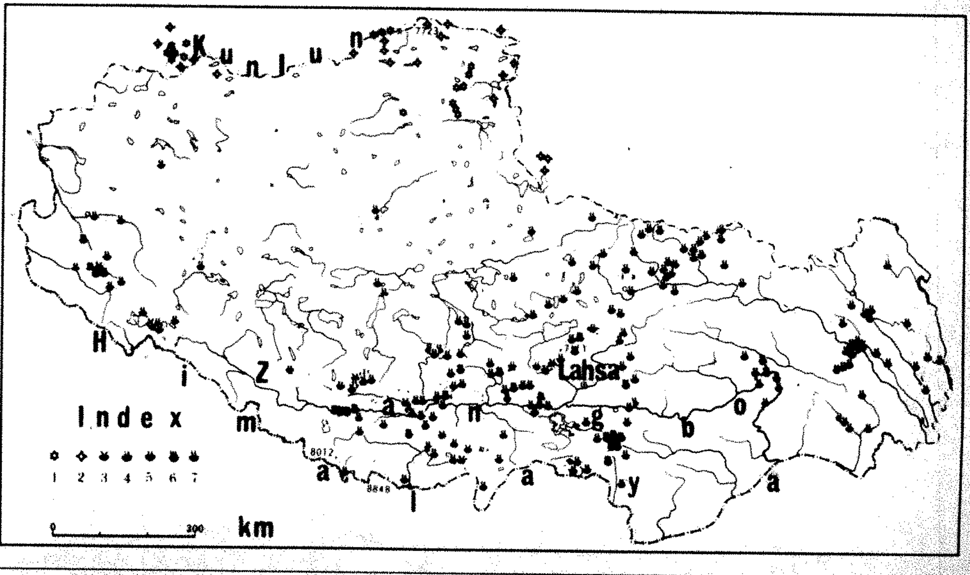

Fig. 2 Geothermal activities in Tibet[36]. 1, Quaternary volcanic cones; 2, eroded volcanic cones; 3, steam blasts; 4, intermittent hot springs; 5, geysers and fumaroles; 6, boiling springs; 7, hot springs.

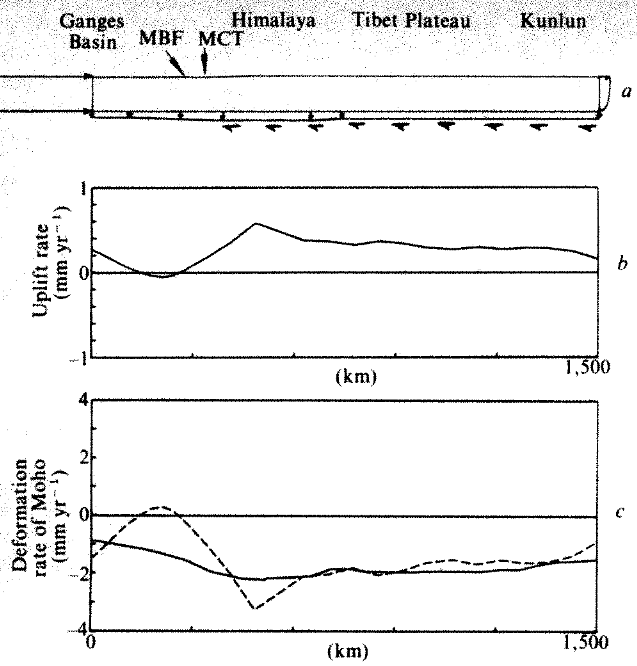

Fig. 3 *a*, Boundary conditions used in obtaining our 'best-fitting' model. The displacement boundary condition is indicated by arrows. The traction at the bottom boundary of the model is indicated by the 'half' arrows. *b*, Calculated annual rate of deformation at the surface. *c*, Calculated annual rate of deformation at the Moho boundary. The solid curve gives the deformation rate for the model; the dashed curve shows the hypothetical position of the boundary if local isostasy is achieved. Thus, if the dashed boundary lies above the solid boundary, the region is overcompensated and will show a negative isostatic gravity anomaly; on the other hand, if the dashed boundary lies below the solid boundary, the local region is undercompensated and will show a positive isostatic gravity anomaly.

Tibet to cross the rivers' courses. More evidence is provided by the studies of the palaeoclimate on the northern flank of the Himalaya[19,20]. These studies show that up until the middle Pleistocene the Himalaya did not significantly block the moisture from the south. Since the late Pleistocene, however, the mountain range has become a barrier effective enough to cause a dramatic change to a dry and cold continental climate on the northern flank of the mountain range and inside Tibet.

The calculated maximum principal stress in the model is compression in the horizontal plane and along the north–south direction. Under the Himalaya, the stresses along the thrust faults are also compressive, in conformity to the seismic focal mechanism. The magnitude of the predicted stresses depends critically on the assumed rheology and, in the lower crust and the upper mantle, on the assumed geothermal profiles. Our predicted stresses, however, are compatible with the current thinking on the formation of the Himalaya. On the average, our calculated maximum shear stress increases from about 1 kbar at a depth of 5 km to a maximum of 3 kbar, and then decreases to about 1 kbar at 45 km, 100 bar at 60 km, and about 1 bar at 100 km. The maximum stress difference beneath Tibet required to support the static loading due to the anomalous mass associated with the topography was estimated to be 0.5–1.5 kbar. Our calculation shows, however, that the tectonic stresses in this region may be significantly greater than the static stresses induced by surface loading. This tectonic stress has caused India to underthrust the Himalaya and is resisted by buoyant forces and friction. The push from the south and the resistance from below may have forced the Himalaya to uplift quickly to reach its great heights within recent geological time.

The highest values of the maximum shear stress, as predicted by our models, occur near the southern boundary and the lowest values under Tibet. The differences between these values remain within a factor of 2–5. This lateral variation of shear stress may be partially responsible for the southward migration of faulting in the Himalaya. Molnar *et al.*[3] relate this southward migration of faulting to increasing friction on the active fault beneath the rising Himalaya. The mechanism we suggested above is complementary to that suggested by Molnar *et al.*

Because of the two-dimensional nature of our model, we cannot predict the observed patterns of normal faulting or strike-slip faulting in Tibet. Surface deformation patterns, however, are not clearly related to the state of stress at depth. To demonstrate this point, we have carried out a preliminary, three-dimensional finite element calculation of the deformation of a model consisting of a upper, stiff, layer overlying a lower ductile substratum under uniform north–south compression. Our results show that east–west tensile stress may be induced in the upper layer to cause extensional features. A similar conclusion was reached qualitatively by Molnar and Tapponnier[31,32]. Other mechanisms, such as doming and stress concentration near the tips of pre-existing faults may also produce east–west extension under north–south compression. Thus, the observed tensional features on the surface in Tibet do not necessarily contradict our suggestion that the entire region is under a north–south compression. Studies of the focal mechanism of intermediate depth earthquakes beneath Tibet would provide crucial evidence for further modelling. Hong *et al.*[33] studied the focal mechanisms of seven earthquakes of intermediate depths in this region and showed a consistent picture of slightly inclined *P*-axes perpendicular to the main structural lines. Chen *et al.*[34] did a more detailed study of one intermediate depth earthquake in Tibet; their results, however, shows the *P*-axis to be vertical. Clearly, more work needs to be done towards a better understanding of the tectonics of this region.

We thank Peter Bird, and John Verhoogen for helpful comments. C-y. W. thanks the University of California for financial support, the Academia Sinica for making possible his trip to the studied area, and Zhang Zhi-fei for permission to include his geothermal data.

Received 10 November 1981; accepted 6 April 1982.

1. Holmes, A. *Principles of Physical Geology* (Ronald, New York, 1965).
2. Wager, L. R. *Geogr. J.* **89,** 239 (1937).
3. Molnar, P. *et al. Collques int. Cent. natn. Rech. scient.* No. 268, 463 (1977).
4. Wang, C. Y., Shi, Y. & Zhou, W. *J. geophys. Res.* **87,** 2949 (1982).
5. Teng, J. *et al. Proc. Sym. Qinghai-Xizang (Tibet) Plateau, Abstr.* 81 (Academia Sinica, Beijing, 1980).
6. Kaila, K. L. & Narain, H. *Himalaya Geology Seminar,* Dehli (1976).
7. Chandra, U. *Phys. Earth planet. Inter.* **16,** 109 (1978).
8. Huan, W., Wang, S., Shi, Z. & Yan, J. *Acta geophys. sin.* **23,** 269 (1980).
9. Fitch, T. J. *J. geophys. Res.* **75,** 2699 (1970).
10. Molnar, P. & Tapponnier, P. *J. geophys. Res.* **83,** 5361 (1978).
11. Ni, J. & York, J. E. *J. geophys. Res.* **83,** 5377 (1978).
12. Tapponnier, P. *et al. Nature* **294,** 405 (1981).
13. Tapponnier, P., Mercier, J. L., A mijo, R., Han, T. & Zhou, J. *Nature* **294,** 410, (1981).
14. Survey of India, *National Report of Geodetic and Gravimetric Work Done in India by Various Organizations and Institutions During 1971–74, 6th Gen. Assem.* Meet. (IUGG, Grenoble, 1974).
15. Cheng, W. *Proc. Sym. Qinghai-Xizang (Tibet) Plateau, Abstr.* 23 (Academia Sinica, Beijing, 1980).
16. Cheng, T., Feng, Z., Zhang, Y. & Hu, S. *Proc. Sym. Qinghai-Xizang (Tibet) Plateau, Abstr.* 111 (Academia Sinica, Beijing, 1980).
17. Yang, Y., Li, B., Yin, Z., Zhang, Q. & Wang, F. *Proc. Sym. Qinghai-Xizang (Tibet) Plateau, Abstr.* 256 (Academia Sinica, Beijing, 1980).
18. Song, Z. & Liu, G. *Proc. Sym. Qinghai-Xizang (Tibet) Plateau, Abstr.* 14 (Academia Sinica, Beijing, 1980).
19. Zhao, X. *Sci Geol. Sinica* **3,** 243 (1975).
20. Guo, X. *Sci. Geol. Sinica* **1,** 59 (1974).
21. Krummenacher, D. *Région de la Takkhola* (eds Bordet, P. *et al.*) 187 (CNRS, Paris, 1971).
22. Mehta, P. K. *Tectonophysics* **62,** 205 (1980).
23. Bird, P. *Tectonophysics* **50,** 307 (1978a).
24. Byerlee, J. *Pure appl. Geophys.* **116,** 615 (1978).
25. Stesky, R. M., Brace, W. F. & Robin, P.-Y. *Tectonophysics* **23,** 117 (1974).
26. Chu, C. L., Wang, C.-Y. & Lin, W. *Geophys. Res. Lett.* **8,** 565 (1981).
27. Shelton, G. L. thesis, Brown Univ. (1981).
28. Tullis, J. A. *Rev. Geophys. Space Phys.* **17,** 1137 (1979).
29. Bird, P. *J. geophys. Res.* **83,** 4875 (1978).
30. Chen, W. P. & Molnar, P. *J. geophys. Res.* **86,** 5937 (1981).
31. Molnar, P. & Tapponnier, P. *Science* **189,** 419 (1975).
32. Molnar, P. & Tapponnier, P. *J. geophys. Res.* **83,** 5361 (1978).
33. Hong, Y., Zhang, W., Yu, Z. & Xiu, Q. *Seismol. Geol.* **3,** 9 (1981).
34. Chen, W. P., Nábělek, J. L., Fitch, T. J. & Molnar, P. *J. geophys. Res.* **86,** 2836 (1981).
35. Kono, M. *Geophys. J.R. astro. Soc.* **39,** 283 (1974).
36. Zhang, Z. *et al. Acta geophys. sin.* **25,** 34 (1982).

Analysis of interspecific interactions in a coastal plant community—a perturbation approach

J. A. Silander & J. Antonovics

Ecology Section, Biological Sciences Group,
University of Connecticut, Storrs, Connecticut 06268, USA
and Department of Botany, Duke University, Durham,
North Carolina 27706, USA

Most studies of plant communities attempt to correlate species distributions with environmental variables[1-5]. Such studies provide some insight into the contribution of density-independent variables to plant community structure[1-6] but contribute little to our understanding of niche relationships and levels of competitive interactions among coexisting species. In contrast, experimental perturbation studies where species are added or removed, have the advantage of testing specific biotic interactions among community components in natural conditions. Such approaches, for example, have proved valuable in elucidating the role of competition and predation in structuring sessile marine invertebrate communities[7-9]. Despite an empirical approach championed by Clemments[10], few terrestrial plant ecologists have conducted analogous perturbation–response studies[11-14]. We have performed perturbation experiments on a set of closely adjacent coastal plant communities. Our observations indicate that species interactions are important in structuring these plant communities, and that these interactions may be specific or diffuse, reciprocal or non-reciprocal and may vary in different environments. We suggest a general approach to quantifying species interactions, derived from perturbation experiments, as a framework for generalizations and comparisons of biotic interactions in natural communities.

A series of adjacent coastal plant communities was examined along a gradient across Core Banks, a barrier island on the coast of North Carolina. The vegetation was surveyed by measuring optical point cover in 448 0.25 m^2 contiguous quadrats located along two main transects across the island and several smaller transects chosen to include the total range of communities encountered in the area. A single environmental scalar was developed from two measured environmental variables (distance from beach berm crest and depth to water table), using direct gradient ordination[1,15]. From relative cover values, we obtained running average curves for each species along the scalar (Fig. 1). Detailed analyses of these ordinations will be presented elsewhere. Several workers have attempted to make interpretations regarding niche relationships among coincident species from such descriptive data[16-20], but these purely observational data beg the question of whether species both coexist and compete, or coexist because they do not compete.

Experimental perturbations were carried out at five sites approximately 50 m apart along one of the main transects in the primary dune, rear dune, swale-grassland, high salt marsh, and low salt marsh. Dominant and subdominant species were removed singly or in groups within 1 m^2 plots by weeding, combined with selective herbicides. At each site there were two or four selective removal treatments (see Fig. 2 and Table 1), complete vegetation removal, plus a control. Grasses and sedges were spot- or broadcast-treated with Dalapon (2,2-dichloropropionic acid) and dicotyledons with (2,4-dichlorophenoxyacetic acid (2,4-D). Treatments were repeated as necessary to ensure that vegetative regrowth did not occur during the first 3 months of the study (June–August). At each site, treatments were assigned randomly to cells in each of three replicate blocks. Four samples were taken per cell for a total of 12 replicates per treatment per site. Species responses were analysed by optical point cover (0–81 counts per replicate) and, for grasses, by change in the number of tillers per year. The results of both methods were very similar[21], and only values based on optical point cover are presented (Fig. 2 and Table 1).

Removal effects were tested by analysis of variance (after square root transformation) in which treatments were contrasted with controls in paired comparisons. Using block × treatment mean square as the error mean square, significant removal treatment effects were found in 8 of 48 comparisons [$\alpha = 0.05\ (1,2)$] (Fig. 2 and Table 1) whereas <3 would have been expected by chance at this level. We use this result to show that significant species interactions can potentially be resolved by such perturbation–removal experiments.

It is possible that the within-block replication differs from that between blocks; in this case it would be invalid to combine error variation. A subjective assessment of the experimental area indicated that the two levels of variation were similar for most of the cells. In addition, the mean square errors associated with the within-cell replicates were approximately equivalent to the block × treatment mean square errors for 40 of 48 comparisons. We therefore pooled the error variation for each comparison[22] and have given the appropriate standard errors in Table 1.

We now introduce a general approach to analysing these biotic interactions: the response of species j to the removal of species i can be quantified in terms of a removal response coefficient defined as $C_{ij} = N_{ij}/N_i$, where, N_{ij} is the change in importance of species j following the removal of a coincident species i, and N_i is the importance value of species i coexisting with species j before the imposed perturbation. Here importance values are based on per cent cover, but abundance, biomass, reproductive output and so on, might be used. N_i is equivalent to the relative area of the central, darker circle in

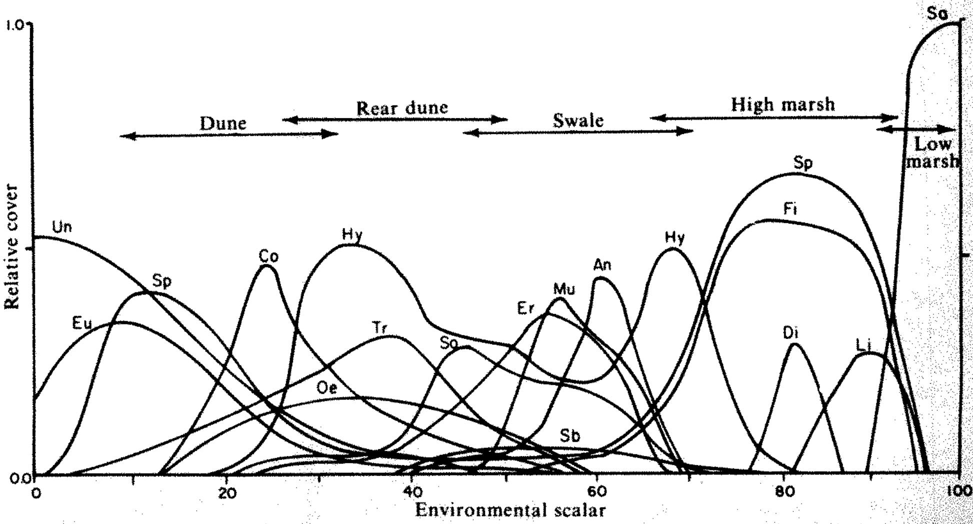

Fig. 1 Direct gradient ordination for 16 herbaceous species occurring along the Core Banks, North Carolina transects. The environmental scalar is based on a weighted distance from the beach and the inverse of depth to the water table. Species curves were plotted from running averages. Abbreviations for species are as follows: Un, *Uniola paniculata*; Eu, *Euphorbia polygonifolia*; Sp, *Spartina patens*; Co, *Conyza canadensis*; Oe, *Oenothera humifusa*; Hy, *Hydrocotyle bonariensis*; Tr, *Triplasis purpurea*; So, *Solidago sempervirens*; Er, *Eragrostis pilosa*; Mu, *Muhlenbergia capillaris*; Sb, *Sabatia stellaris*; An, *Andropogon scoparius*; Fi, *Fimbristylis spadiceae*; Di, *Distichlis spicata*; Li, *Limonium carolinianum*; Sa, *Spartina alterniflora*.

0028–0836/82/310557—04$01.00

each diagram of Fig. 2; N_{ij} is equivalent to the relative area of the jth inner, tangential circle associated with each N_i.

In most cases, coexisting species increased in importance after the removals. However, in one case, *Eragrostis* showed a large decrease in importance (negative C_{ij} value) following the removal of *Spartina patens* from the swale. This effect has been confirmed recently in controlled competition experiments (data not shown). These observations are not necessarily consistent with any predictions that could be made from purely descriptive data (Fig. 1). For example, significant and apparently strong competitive interactions occur between *Fimbristylis* (i) and *S. patens* (j) ($C_{ij} = 0.498$, $C_{ji} = 0.693$; see Fig. 2*d* and Table 1), species which have almost complete distributional overlap in the high marsh (compare with Fig. 1). However, little interaction is indicated between *S. patens* and *Uniola* ($C_{ij} = -0.028$, $C_{ji} = -0.078$; see Fig. 2*a* and Table 1) which have a similar distribution in the dune (Fig. 1). Again, from Fig. 1, the pattern of distributional overlap in the swale between *Muhlenbergia* and *S. patens*, *Hydrocotyle*, *Solidago*, *Andropogon*, *Paspalum* and *Eragrostis*, varies continuously from inverse to broadly overlapping, yet significant interactions are revealed between *Muhlenbergia* and at least two of the six associated species ($C_{ij} = 0.055$, 0.085, 0.130, 0.085, 0.065 and 0.100, respectively; see Fig. 2*c* and Table 1). Species interactions are abundant, but the way in which they structure these plant communities and lead to the zonation patterns observed in Fig. 1 is complex.

The interactions found were both specific and diffuse. We can quantify these based on the equitability of responses among j species to the removal of a particular species i. A high equitability would indicate diffuse interactions whereas a low equitability would indicate species-specific effects. Using the standard Shannon information measure[23], equitability $E_i = H_i/H_{\max}$, where

$$H_i = -\sum_{i=1}^{s}\left(N_{ij}/\sum_{i=1}^{s}N_{ij}\right)\ln\left(N_{ij}/\sum_{i=1}^{s}N_{ij}\right),$$

s = number of j species coexisting with i, and $H_{\max}$ is equal to H_i calculated assuming that all N_{ij} values are equal. In the high

Table 1 Species removal response coefficients

Community type	Species or guild: Removed (i)	Retained (j)	Response*: Control	Removal	SE	C_{ij}
Dune						
	Uniola	*S. patens*	1.96	1.86	0.23	−0.028
	Uniola	*Hydrocotyle*	2.34	1.80	0.20	−0.166
	Uniola	*Conyza*	2.22	1.29	0.32	−0.241
	Uniola	*Oenothera*	0.74	1.07	0.20	0.044
	S. patens	*Uniola*	3.68	3.72	0.30	0.078
	S. patens	*Hydrocotyle*	2.34	2.96	0.26	0.857
	S. patens	*Conyza*	2.22	2.25	0.33	0.034
	S. patens	*Oenothera*	0.74	1.03	0.13	0.156
Rear dune						
	Hydrocotyle	*S. patens*	0.66	2.39	0.24	0.344
	Hydrocotyle	*Conyza*	1.48	2.27	0.23	0.193
	S. patens	*Hydrocotyle*	3.92	3.60	0.15	−5.409
	S. patens	*Conyza*	1.48	1.53	0.20	0.341
Swale						
	Muhlenbergia	*S. patens*	1.55	2.23	0.26	0.055
	Muhlenbergia	*Hydrocotyle*	2.28	3.03	0.21	0.085
	Muhlenbergia	*Solidago*	2.00	3.18	0.26	0.130
	Muhlenbergia	*Andropogon*	2.19	2.96	0.31	0.085
	Muhlenbergia	*Eragrostis*	1.77	2.80	0.30	0.100
	Muhlenbergia	*Paspalum*	0.21	1.59	0.29	0.065
	S. patens	*Muhlenbergia*	6.85	5.87	0.35	−5.218
	S. patens	*Hydrocotyle*	2.28	2.60	0.18	0.653
	S. patens	*Solidago*	2.00	3.39	0.35	3.134
	S. patens	*Andropogon*	2.19	2.00	0.31	−0.335
	S. patens	*Eragrostis*	1.77	0.90	0.30	0.971
	S. patens	*Paspalum*	0.21	0.30	0.11	0.019
	Hydrocotyle and *Solidago*	*Muhlenbergia*	6.85	6.43	0.22	−0.608
	Hydrocotyle and *Solidago*	*S. patens*	1.55	1.54	0.23	−0.003
	Hydrocotyle and *Solidago*	*Andropogon*	2.19	1.72	0.35	−0.200
	Hydrocotyle and *Solidago*	*Eragrostis*	1.77	2.12	0.29	0.148
	Andropogon and *Eragrostis*	*Muhlenbergia*	6.85	6.19	0.25	−1.084
	Andropogon and *Eragrostis*	*S. patens*	1.55	2.51	0.20	0.491
	Andropogon and *Eragrostis*	*Hydrocotyle*	2.28	2.94	0.18	0.435
	Andropogon and *Eragrostis*	*Solidago*	2.00	3.01	0.23	0.637
High marsh						
	Fimbristylis	*S. patens*	5.54	7.57	0.20	0.693
	Fimbristylis	*Aster*	1.10	1.54	0.25	0.030
	Fimbristylis	*Limonium*	0.18	0.99	0.15	0.025
	Fimbristylis	*Satabia*	0.48	0.48	0.20	0
	S. patens	*Fimbristylis*	6.20	7.33	0.24	0.498
	S. patens	*Aster*	1.10	0.35	0.21	−0.036
	S. patens	*Limonium*	0.18	0.24	0.12	0.001
	S. patens	*Sabatia*	0.48	0.63	0.19	0.006
Low marsh						
	S. alterniflora	*S. patens*	4.73	5.24	0.32	0.143
	S. alterniflora	*Fimbristylis*	2.05	1.86	0.28	−0.021
	S. alterniflora	*Aster*	0.91	1.71	0.30	0.059
	S. alterniflora	*Limonium*	1.07	1.59	0.26	0.039
	S. patens	*S. alterniflora*	5.97	5.63	0.25	−0.176
	S. patens	*Fimbristylis*	2.05	2.41	0.34	0.072
	S. patens	*Aster*	0.91	0.83	0.15	−0.006
	S. patens	*Limonium*	1.07	1.09	0.19	0.002

SE, standard error of responses are based on combined error variation: within block mean square and block × treatment mean square. C_{ij} values were determined from back-transformed N_i and N_{ij} values.

* Mean cover values (after square root $(x+0.1)$ transformation) for control and removal treatment.

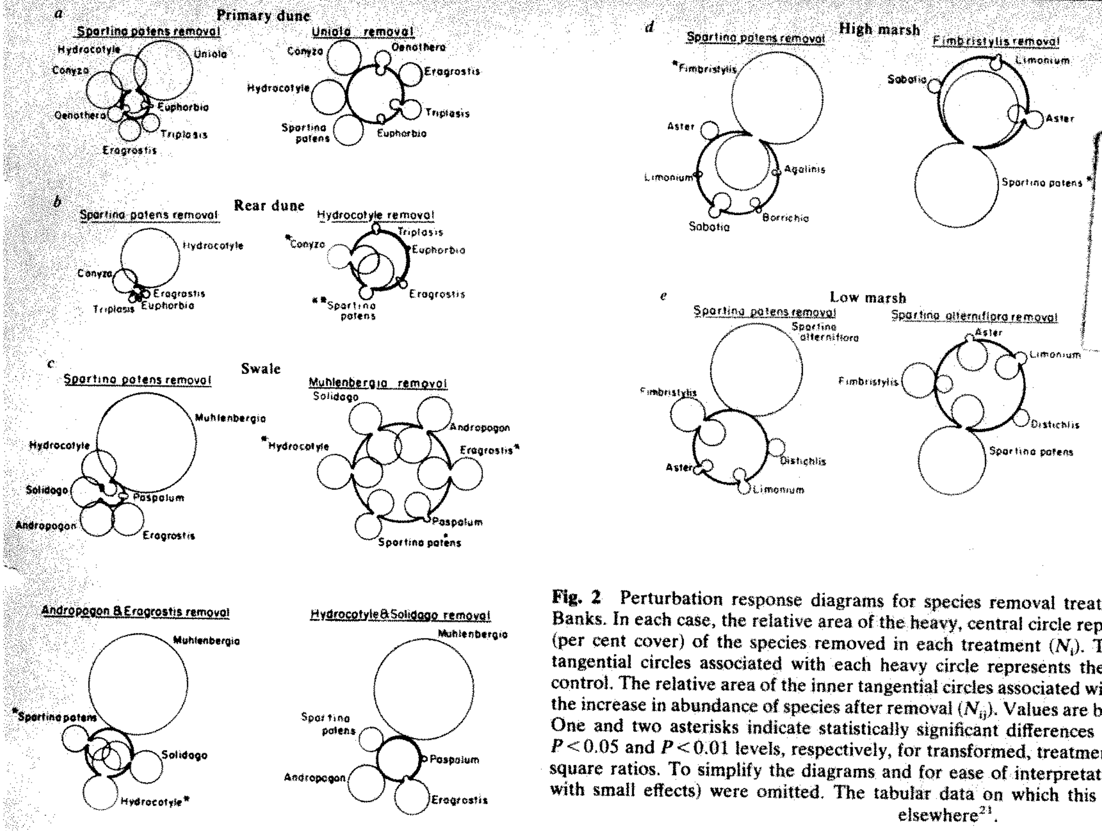

Fig. 2 Perturbation response diagrams for species removal treatments at five sites from Core Banks. In each case, the relative area of the heavy, central circle represents the relative abundance (per cent cover) of the species removed in each treatment (N_i). The relative area of the outer, tangential circles associated with each heavy circle represents the abundance of species in the control. The relative area of the inner tangential circles associated with each heavy circle represents the increase in abundance of species after removal (N_{ij}). Values are based on untransformed means. One and two asterisks indicate statistically significant differences compared with the control at $P<0.05$ and $P<0.01$ levels, respectively, for transformed, treatment and block × treatment mean square ratios. To simplify the diagrams and for ease of interpretation, negative N_{ij} values (most with small effects) were omitted. The tabular data on which this figure is based are presented elsewhere[21].

University College of Science & Technology
LIBRARY COMPLEX
4 NOV [illegible]

marsh, removal of *S. patens* produced a large and significant response from *Fimbristylis* alone among six competitors ($E_i = 0.225$, for 4 of 6 competitors as listed in Table 1, Fig. 2*d*; absolute N_{ij} values were used). This contrasts with the swale where there were more nearly equal interactions among the six subdominant species after removal of *Muhlenbergia* ($E_i = 0.978$; Fig. 2*c*).

Non-reciprocal responses seem common across these sites. We can define reciprocity of species i with j as $R_{ij} = C_{ij}/C_{ji}$, where $\|C_{ij}\| < \|C_{ji}\|$. In four of the five sites the interactions between the dominant and subdominant species were largely non-reciprocal. In the rear dune and low marsh, $R_{ij} = -0.064$ and -0.813, respectively, for *Hydrocotyle* with *S. patens* and *Spartina alterniflora* with *S. patens* (Fig. 2). Negative values would result from non-reciprocal contraction of species j in response to the removal of species i. In the swale the dominant *Muhlenbergia* was consistently involved in non-reciprocal responses with the three subdominant components: *S. patens*, *Andropogon* plus *Eragrostis*, and *Hydrocotyle* plus *Solidago* ($R_{ij} = -0.010$, -0.171 and -0.354, respectively; Fig. 2*c*). In the primary dune, *S. patens* and *Uniola* both showed little interaction but $R_{ij} = -0.359$ (Fig. 2*a*). Only in the high marsh were the responses relatively reciprocal between *S. patens* and *Fimbristylis*, $R_{ij} = 0.719$ (Fig. 2*d*).

Site-specific effects were also prevalent. The nature, degree and reciprocity of significant species interaction between *Hydrocotyle* and *S. patens* changed depending on the habitat considered: C_{ji} for the primary dune $= 0.857$; C_{ij} and C_{ji} for the rear dune were 0.344 and -5.409, respectively; and C_{ij} and C_{ji} for the swale (*Solidago* included with *Hydrocotyle* in i) were -0.003 and 3.787 (Fig. 2a–c). Similarly the interactions of *S. patens* with *Fimbristylis* changed for high compared with low marsh ($C_{ij} = 0.498$ and 0.072; Fig. 2*d*, *e*). We cannot distinguish whether these site-specific effects are a direct effect of the environment on the species interaction, or the result of changes in background species composition, or both.

One major problem in assessing species interactions by perturbation–response studies is that the results may be time-specific and biased towards fugitive species. However, we do not believe this is applicable to the present study. The complete removal treatments allowed us to identify *Sabatia*, *Salicornia*, *Triglochin* and *Setaria* as fugitive species because they were either absent or persisted at low frequency in the community and expanded following complete removal[21]; only one of these species was found in one of the partial removal treatments. These results show that while our observations were time specific, they were not necessarily biased towards fugitive species. Clearly one could quantify fugitivity of a species by observing the change in its C_{ij} with time; however this was not done in the present study.

This experimental approach, with the associated parameters, could be extended to the level of the entire community if all species were reciprocally removed. We could then examine interference among coexisting species across the community by considering a C_{ij} matrix[24], where the elements are removal response coefficients indicating covariation in abundance of species i and j. Sets of covarying species can then be identified, and may be considered to constitute guilds[25]. Moreover, the parameters relating to diffuseness and reciprocity of the interactions can be extended, by simple weighting, to the entire community, and can then be used for comparisons between different communities, or among different classes of species (based on, for example, abundance, life form or breeding system) within particular communities. By performing single species and multi-species removals, the existence of higher order community interactions can also be tested. We have deliberately avoided interpreting C_{ij} in explicit biological terms: for example, C_{ij} could be thought of as representing the degree of overlap in resource utilization of species j on species i, but this is a presumption not warranted by either the nature of this study or any other perturbation experiment *per se*. Even if we excluded interaction effects due to predators or pathogens, deriving competition coefficients from such perturbation responses would require an *a priori* assumption as to the appropriateness of the competition model used to make such calculations.

Clearly, the information about community structuring gained from such perturbation experiments is far greater and more accurate than any inferences that might be made from purely descriptive studies. Such experiments provide a definitive test of interference among community components; the nature of this interference can then be tested either by constructing synthetic communities in controlled conditions, or by further field experimentation. Above all, when perturbation responses are quantified using the indices suggested here, they can be used in a comparative way, to generate and test hypotheses regarding the manner in which different communities are organized.

We thank R. Whitlatch, J. Hartman, F. Bazzaz, R. Mead and U. Koehn for helpful comments.

Received 19 January 1981; accepted 17 May 1982.

1. Whittaker, R. H. (ed.) *Ordination of Plant Communities* (Junk, The Hague, 1978).
2. Austin, M. P. in *Mathematical Models in Ecology* (ed. Jeffers, J. N. R.) (Blackwell, Oxford, 1971).
3. Grieg-Smith, P. *Quantitative Plant Ecology* (Butterworth, London, 1964).
4. Strain, B. R. & Billings, W. D. (eds) *Vegetation and Environment* (Junk, The Hague, 1974).
5. Mueller-Dombois, D. & Ellenberg, H. *Aims and Methods of Vegetation Ecology* (Wiley, New York, 1974).
6. Pamadasa, M. A., Grieg-Smith, P. & Lovell, P. H. *J. Ecol.* **67**, 246–268 (1974).
7. Paine, R. T. *Oecologia* **15**, 93–120 (1974).
8. Sutherland, J. P. *Am. Nat.* **108**, 859–873 (1974).
9. Dayton, P. K. *Ecol. Monogr.* **41**, 351–389 (1971).
10. Clemments, F. E. & Goldsmith, G. W. *The Phytometer Method in Ecology* (Carnegie Inst. Wash. Publ. 356, 1924).
Clemments, F. E., Weaver, J. E. & Hanson, H. C. *Plant Competition: An Analysis of Community Functions* (Carnegie Inst. Wash. Publ. 398, 1929).
11. Harper, J. L. *Population Biology of Plants*, 721–727 (Academic, New York, 1977).
12. Abul-Fatih, H. A. & Bazzaz, F. A. *New Phytol.* **83**, 813–816 (1979).
13. Fonteyn, P. J. & Mahall, B. E. *Nature* **275**, 244–245 (1978).
14. Colwell, R. K. & Fuentes, E. R. *A. Rev. Ecol. Syst.* **6**, 281–310 (1975).
15. Loucks, O. L. *Ecol. Monogr.* **32**, 137–166 (1962).
16. May, R. M. *Stability and Complexity in Model Ecosystems* (Princeton University Press, 1973).
17. Whittaker, R. H., Levin, S. A. & Root, R. B. *Am. Nat.* **107**, 321–338 (1973).
18. Platt, W. J. & Weis, I. M. *Am. Nat.* **111**, 479–513.
19. Colwell, R. K. & Futuyma, D. J. *Ecology* **52**, 567–576 (1971).
20. Werner, P. A. *Syst. Bot.* **1**, 246–268 (1976).
21. Silander, J. A. thesis, Duke Univ. (1976).
22. Bozivich, A., Bancroft, T. A. & Hartley, H. V. *Ann. math. Statist.* **27**, 1017–1043 (1956).
23. Peet, R. K. *A. Rev. Ecol. Syst.* **5**, 285–307 (1974).
24. Vandermeer, J. *Am. Nat.* **104**, 73–83 (1970).
25. Root, R. B. *Ecol. Monogr.* **37**, 317–350 (1967).

Inhibition of experimental ascending urinary tract infection by an epithelial cell-surface receptor analogue

**C. Svanborg Edén*, R. Freter†, L. Hagberg*,
R. Hull‡, S. Hull‡, H. Leffler§ & G. Schoolnik||**

* Department of Clinical Immunology, University of Göteborg, Göteborg, Sweden
† Department of Microbiology and Immunology, University of Michigan, Ann Arbor, Michigan 48109, USA
‡ Department of Microbiology and Immunology, Baylor College of Medicine, Texas Medical Center, Houston, Texas 77025, USA
§ Department of Medical Biochemistry, University of Göteborg, Göteborg, Sweden
|| The Rockefeller University, 1230 York Avenue, New York, New York 10021, USA

It has been shown that the establishment of urinary tract infection by *Escherichia coli* is dependent on attachment of the bacteria to epithelial cells[1–4]. The attachment involves specific epithelial cell receptors, which have been characterized as glycolipids[5–10]. Reversible binding to cell-surface mannosides may also be important[4,11–13]. This suggests an approach to the treatment of infections—that of blocking bacterial attachment with cell membrane receptor analogues. Using *E. coli* mutants lacking one or other of the two binding specificities (glycolipid and mannose), we show here that glycolipid analogues can block *in vitro* adhesion and *in vivo* urinary tract infection.

Table 1 lists the properties of the *E. coli* strains used. *E. coli* HU 824 and HU 742 were selected after a two-step chemical mutagenesis of *E. coli* GR 12, isolated from a patient with acute pyelonephritis, as having either surface ligands attaching to epithelial cells through globoseries glycolipid receptors or mannose-reversible binding properties. The mutants HU 742 and HU 824 were obtained after *N*-methyl-*N*-nitro-*N*-nitrosoguanidine treatment of a lactose-negative mutant of GR 12. Further details on the construction and stability of the mutants will be reported elsewhere[14]. The mutants and the parent were identical by the following genotypic and phenotypic characteristics available for testing: electrophoretic mobility of 13 chromosomally determined enzymes[15], three plasmid bands of the same size[16], serotype[17], resistance to the bactericidal effect of serum[18], inability to haemolyse horse erythrocytes[17] and api 20 E pattern. Clearly, these tests or other techniques are insufficient to demonstrate genetic identity between the mutants. The only discernible difference between these strains was, however, the receptor specificity of their adhesins. Initially,

Table 1 Properties of the *E. coli* strains HU 824 Str^R and HU 742 Nal^R, used for experimental ascending urinary tract infection

Property	*E. coli* strain HU 824 Str^R	 HU 742 Nal^R
Serotype	075 Knt	075 Knt
Antibiotic resistance		
Streptomycin	R	S
Nalidixic acid	S	R
Trimethoprim	S	S
Sulphadiazine	R	R
Tetracycline	S	S
Cephalothin	S	S
Mecillinam	S	S
Ampicillin	R	R
Nitrofurantoin	S	S
Bactericidal effect of human serum	R	R
Haemolysin production	0	0
Adhesion to uroepithelial cells (bacteria per cell)		
Human	65	0
Mouse	51	12
Receptor sugar inhibiting adhesion		
Globotetraos	9 μg ml^{-1}	NI
α-Mn	NI	~92 μg ml^{-1}
Agglutination of guinea pig erythrocytes		
Uncoated in PBS	−	+
in α-Mn	−	−
Coated with globotetraosylceramide		
in PBS	+	+
in α-Mn	+	−

E. coli HU 824 and HU 742, mutants of a wild-type pyelonephritogenic *E. coli* strain, were identical for the genotypic and phenotypic traits listed, but differed in specificity of their adhesins. R, resistant; S, sensitive; Knt, nontypable for Kantigens[17]. To permit separate detection out of a mixture, mutants resistant to 1 mg ml^{-1} of streptomycin (HU 824 Str^R) or to 50 μg ml^{-1} of nalidixic acid (HU 742 Nal^R) were selected by the gradient plate technique (without mutagenesis). The resistant mutants grew equally well on TSA with or without antibiotic after passage on antibiotic-free medium, retained the adhesive and haemagglutinating properties and showed no difference in *in vivo* infectivity compared with the respective parent. Adhesion to uroepithelial cells from the urinary sediment of a healthy female donor (blood group P_1) and the bladder of BALB/c mice was assessed as described elsewhere[1–3]. Adhesion = mean no. of bacteria attached to 40 epithelial cells. For adhesion inhibition, bacteria were preincubated with decreasing concentrations of globotetraose or αMn, epithelial cells were added and adhesion testing was performed[5,7]. The concentration required for 50% inhibition of the adherence of 10^9 bacteria is shown. NI, no inhibition. Induction of binding of *E. coli* HU 824 Str^R was studied by agglutination of guinea pig erythrocytes coated with globotetraosylceramide[5,6]. Agglutination after but not before coating, and in the presence of αMn, was credited to the receptor. The oligosaccharide globotetraose, released from globoside by ozonolysis, and purified by Folch partitioning and alkaline fragmentation, was analysed by gas-liquid chromatography and NMR (ref. 23). The NMR spectroscopy in D_2O spectrum showed signals from three anomeric protons with chemical shifts, as expected for globotetraose: β-hexoseamine, β-hexose and α-hexose. The fourth anomeric signal from the reducing glucose residue was split into two, corresponding to the α and β form in the proportions 1:2.

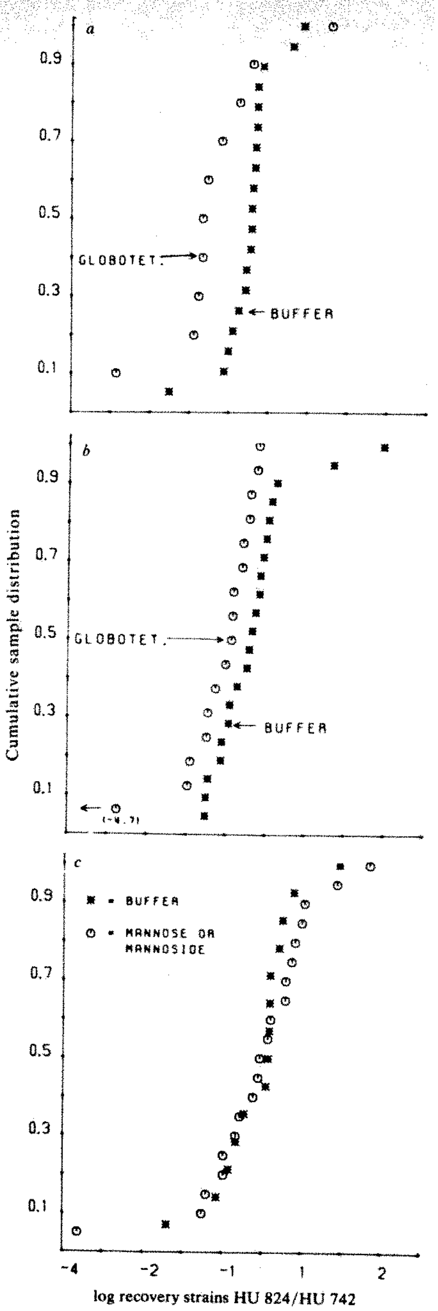

Fig. 1 Recovery of *E. coli* HU 824 Str$^{\rm R}$ and HU 742 Nal$^{\rm R}$ in the presence and absence of receptor sugar. The strains were grown on antibiotic-free media, collected into PBS with globotetraose (50 μg ml^{-1}) for expt 1 and 30 μg ml^{-1} for expt 2, which were, respectively, four and three times the *in vitro* IC$_{50}$ for *E. coli* HU 824) or into PBS with αMn (5 mg ml^{-1} for both experiments which was 50 times the IC$_{50}$ of HU 742 *in vitro* adhesion), and incubated for 60 min at 37 °C. Viable counts on the inoculum before and after incubation excluded changes in bacterial numbers due to the presence of the sugars. The inocula (per animal) for expt 1 were: PBS, $3.9\times10^8+8.3\times10^7$; globotetraose, $9.7\times10^7+8.3\times10^7$. For experiment 2: PBS, $3.0\times10^8+3.9\times10^7$; globotetraose, $2.9\times10^8+3.3\times10^7$ of HU 824 Str$^{\rm R}$ and HU 742 Nal$^{\rm R}$ respectively. The inocula per animal for the αMn experiments were for expt 1: PBS, $2.3\times10^9+1.4\times10^8$; αMn, $3.7\times10^9+1.1\times10^8$. For expt 2: PBS, $6.4\times10^8+8.3\times10^7$; αMn, $4.4\times10^8+1.0\times10^8$ of HU 824 Str$^{\rm R}$ and HU 742 Nal$^{\rm R}$ respectively. The mixed inocula with or without receptor sugar were injected into the bladder of mice which were killed 2 or 16 h later. Serial dilutions of the homogenized kidneys and bladders were cultured on TSA (BBL, Cockeysville, Maryland), TSA streptomycin (1 mg ml^{-1}) or ISA nalidixic acid (50 μg ml^{-1}). The relative recovery from each animal and tissue of the two strains is given as log (RHU 824/RHU 742). The cumulative sample distribution[24] of the recovery ratio is presented, starting from the animal with the lowest recovery and adding up to all animals (=100%). Both in kidneys (a) and bladders (b) a significant shift towards lower recovery of HU 824 Str$^{\rm R}$ was observed after globotetraose treatment. No significant effect of αMn treatment was observed (c). The differences obtained with globotetraose were significant both at 2 and at 16 h, and the results from these animals have been pooled.

the two strains had identical antibiotic resistance patterns. To allow separate detection from a mixed inoculum, mutants resistant to 1 mg ml^{-1} of streptomycin (HU 824 Str$^{\rm R}$) or to 50 μg ml^{-1} of nalidixic acid (HU 742 Nal$^{\rm R}$) were selected (see Table 1 legend).

The difference in receptor specificity between the adhesins of *E. coli* HU 824 Str$^{\rm R}$ and HU 742 Nal$^{\rm R}$ was characterized by adhesion inhibition by soluble receptor sugars or induction of binding to previously unreactive cells by receptor coating[5–7] (Table 1 legend). The adhesion to human uroepithelial cells of 10^9 *E. coli* HU 824 Str$^{\rm R}$ was reduced to 50% by 9 μg ml^{-1} of globotetraose, the oligosaccharide obtained from globoside (a receptor glycolipid) by ozonolysis[19] (Table 1 legend). *E. coli* HU 742 carried mannose-binding adhesins defined by mannose-reversible agglutination of guinea pig erythrocytes[21]. The adhesion of *E. coli* HU 742 Nal$^{\rm R}$ to human or mouse epithelial cells was inhibited by α-methylmannoside (αMn), although inhibition was too low to allow exact determination of the 50% inhibitory αMn concentration (IC$_{50}$). Association with urinary slime[13] could not be assayed quantitatively. The agglutination by *E. coli* HU 742 of guinea pig erythrocytes was inhibited by αMn both before and after coating with globoside. *E. coli* HU 824 Str$^{\rm R}$ agglutinated guinea pig erythrocytes after, but not before globoside coating. This reaction was unaffected by αMn.

Female BALB/c mice, aged 6–8 weeks, were infected by catheterization of the urethra and injection of 0.05 ml of a bacterial suspension (L.H. *et al.*, in preparation). The animals were killed at various times later, kidneys and bladders homogenized and viable counts performed. It was soon recognized that the high degree of variation among animals in the recovery of *E. coli* from kidney or bladder would tend to mask moderate differences between experimental and control groups. For this reason, each mouse was infected with a mixture of *E. coli* HU 824 Str$^{\rm R}$ and HU 742 Nal$^{\rm R}$, separable from the mixture by their different antibiotic resistance. At the end of an experiment, kidneys and bladders of each animal were homogenized separately, and quantitative cultures of each strain prepared on agar plates containing the appropriate antimicrobial agent. The recovery, R, of a given strain was then determined as R = no. of bacteria in the organ cultured/no. of bacteria in the inoculum.

To evaluate the *in vivo* effectiveness of a given treatment (for example, the addition of globotetraose or αMn to the inoculum), the two *E. coli* strains were chosen such that one was susceptible and the other resistant to the *in vitro* effects of the treatment under test. The *in vivo* effectiveness of the treatment was then evaluated by comparing the recoveries of the two strains as the recovery ratio, R (susceptible)/R (resistant). Consequently, if the recovery ratio in the experimental group was significantly lower than in the control group, it could be concluded that the treatment had been effective *in vivo*. In this manner, the randomizing effects of individual differences among animals were overcome by having one *E. coli* strain serve as an intrinsic control in each animal.

Inocula consisting of *E. coli* HU 824 Str$^{\rm R}$ and HU 742 Nal$^{\rm R}$ were prepared as detailed in Fig. 1 legend. After incubation with globotetraose or αMn, respectively, the *in vitro* attachment to mouse epithelial cells and agglutination of human or guinea pig erythrocytes was abolished. The inocula in phosphate-buffered (saline PBS) retained these properties. After intravesicular injection of the inocula, the animals were killed and viable counts of the homogenized kidneys and bladders on trypticase soy agar (TSA), TSA-streptomycin or TSA-nalidixic acid were performed. The result of globotetraose treatment is shown in Fig. 1a for kidney cultures and in 1b for bladder cultures, while Fig. 1c shows the result of αMn treatment. The recovery of *E. coli* HU 824 Str$^{\rm R}$ was significantly reduced, both in kidneys and bladders after globotetraose treatment, as seen by the shift of the cumulative sample distribution curve towards the left ($P=0.019$, Mann–Whitney U-test). After αMn treatment the opposite effect, a decrease of HU 742 Nal$^{\rm R}$ recovery with a shift of the cumulative sample distribution to the right, might have been expected. No significant difference from the PBS control was observed.

We propose the following interpretation of the results. Capacity to attach to the mucosal lining of the mouse urinary tract was an important survival mechanism for *E. coli* HU 824, as seen by its efficient adherence to mouse bladder cells *in vitro* and the decrease of *in vivo* infectivity after pretreatment with globotetraose. *E. coli* HU 742 attached in low numbers *in vitro* to the mouse bladder cells, but might bind to urinary slime. An inhibitory effect of αMn *in vivo*, as reported in other systems[20], may be masked by a dual effect of αMn. Blocking of binding to mucus may facilitate the ascent of bacteria to the kidney, as well as increase the elimination of bacteria from the urinary tract. The inhibition of experimental infection by globotetraose, on the other hand, illustrates a new approach to prophylaxis and treatment of infections occurring via mucous membranes. Compounds mimicking the host receptors may competitively bind to bacterial surface ligands[20,22]. This might decrease the number of bacteria attaching to the mucosa sufficiently to alter the delicate balance of host-parasite interaction in favour of the host.

This study was supported by grants from the Swedish MRC (projects 215 and 3967, 6034), the University of Göteborg, the Ellen, Walter and Lennart Hesselman Foundation for Scientific Research, the Swedish Board for Technical Development and the Volkswagen Foundation. C.S.E. was supported by a Fogarty Fellowship (018497). The BALB/c mice were purchased from Dr B. Murphy. Mutant construction and the cloning of the pilus genes were performed in the laboratory of S. Falkow, University of Washington, under NSF grant PCM 8015722 and NIH grant AI 10885-07. S.H. was a trainee under NIH grant 07149-02. R.H. was a fellow of NKF and the NIH.

Received 18 January; accepted 2 June 1982.

1. Svanborg-Edén, C. *et al. Ciba Fdn Symp.* **80,** 161–187 (1981).
2. Svanborg-Edén, C. *et al.* in *Bacterial Vaccines* (eds Robbins, J. B., Hill, J. C. & Sadoff, C.) 113–131 (Thieme-Stratton, New York, 1982).
3. Svanborg-Edén, C., Eriksson, B. & Hanson, L. A. *Infect. Immun.* **18,** 767–774 (1977).
4. Hughes, R. C. & Sharon, N. *Trends biochem. Sci.* **3,** 275–278 (1978).
5. Leffler, H. & Svanborg Edén, C. *FEMS microbiol. Lett.* **8,** 127–134 (1980).
6. Leffler, H. & Svanborg-Edén, C. *Infect. Immun.* **34,** 920–929 (1982).
7. Leffler, H. *et al. Scand. J. infect. Dis.* (in the press).
8. Källenius, G. *et al. Lancet* **ii,** 604–606 (1981).
9. Källenius, G. *et al. Lancet* **ii,** 1369–1372 (1981).
10. Väisänen, V. *et al. Lancet* **ii,** 1366–1369 (1981).
11. Salit, I. E. & Gotschlich, E. C. *J. exp. Med.* **146,** 1169–1181 (1977).
12. Beachey, E. H. *J. infect. Dis.* **143,** 325–345 (1981).
13. Ørskov, I., Ørskov, F. & Birch-Andersen, A. *Infect. Immun.* **27,** 657–666 (1980).
14. Hull, R., Falkow, S., Leffler, H., Svanborg-Edén, C. (in preparation).
15. Selander, R. K. & Levin, B. R. *Science* **210,** 545–547 (1980).
16. Caugant, D. A., Levin B. R. & Selander, R. K. *Genetics* **98,** 467–490 (1981).
17. Lidin-Janson, G., Falsen, E., Jodal, U., Kaijser, B. & Lincoln, K. *J. med. Microbiol.* **10,** 299–308 (1977).
18. Olling, S. *et al. Infection* **1,** 23–28 (1973).
19. Wiegandt, H. & Baschang, G. *Z. Naturforsch.* **206,** 164–166 (1965).
20. Aronson, M. *et al. J. infect. Dis.* **139,** 329–332 (1979).
21. Duguid, J. P. & Old, D. C. in *Bacterial Adherence* (ed. Beachey, E. H.) 185–217 (Chapman & Hall, London, 1980).
22. Holmgren, J. *Nature* **292,** 413–417 (1981).
23. Falk, K.-E., Jovall, P.-Å., Winyard, P. *Acta chem. scand.* (in the press).
24. Colton, T. *Statistics in Medicine*, 35 (Little, Brown, Boston, 1974).

A stem cell for stem cells in murine haematopoiesis

D. I. Burton, J. D. Ansell, R. A. Gray & H. S. Micklem

Department of Zoology, University of Edinburgh,
Edinburgh EH9 3JT, UK

Mature erythrocytes and granulocytes have limited lifespans, do not replicate and must therefore be replenished constantly. They are derived from pluripotent stem cells (PSCs) which are capable of self-renewal[1]. The numbers and properties of PSCs can be inferred in part from studies of their progeny. Such studies have depended largely on highly artificial experimental systems, involving such procedures as X-ray irradiation, bone marrow transplantation and parabiosis[2]. We now describe a method for studying the behaviour of haematopoietic cell populations in normal mice, and show that erythropoiesis is maintained by the products of a very small number of clones which, as predicted by Kay[3], arise and decline in succession. These results suggest that spleen colony-forming cells (CFC), usually regarded as stem cells, are themselves members of substantial clones which differentiate in sequence.

In female mammals, one of the two X chromosomes becomes irreversibly inactivated early in embryogenesis; subsequently any somatic cell and its descendants fail to express genes carried on the inactivated chromosome[4,5]. X-linked genetic variants can therefore provide markers for cell population studies, and have been used to estimate embryonic founder cell numbers for the haematopoietic system[6,7]. Recently, the discovery of an electrophoretic variant of the X chromosome-encoded enzyme phosphoglycerate kinase (PGK-1)[8], and the development of improved methods for measuring PGK activity in electrophoresis strips[9], have provided a convenient marker system in the mouse.

Female mice heterozygous at the PGK-1 locus were bled at 14-day intervals for 16 weeks and then at 28-day intervals for a further 40 weeks. The enzyme phenotypes were determined electrophoretically from haemolysates using a modification of the technique of Bücher *et al.*[9].

The percentages of PGK-1A alloenzyme in serial blood samples from 10 normal heterozygous mice are shown in Fig. 1. Large, and frequently sudden, variations in the relative amounts of A and B alloenzymes are evident in every individual,

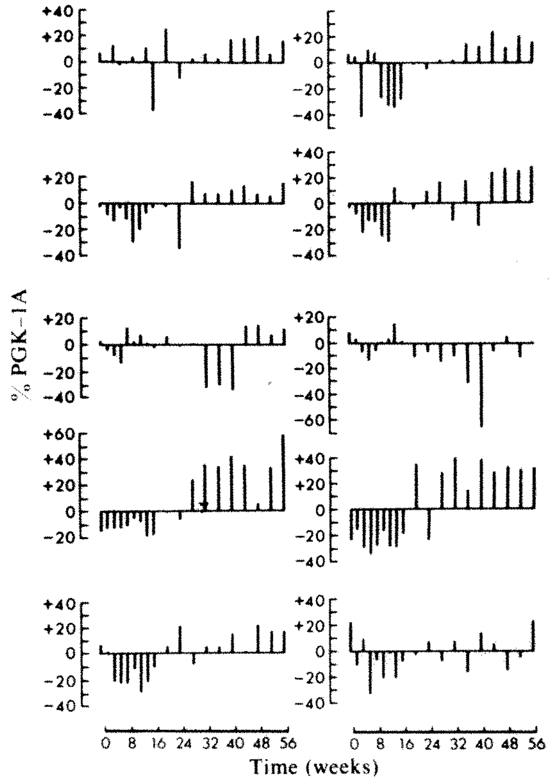

Fig. 1 Percentages of PGK activity attributable to the A alloenzyme in serial blood samples from 10 PGK-1A/B heterozygous female mice. The data for each mouse are plotted as the deviation of individual samples from the overall percentage of A alloenzyme in the mouse; this was estimated as the mean of the readings obtained on day 0 and at 56-day intervals thereafter (see text). The percentages of A and B alloenzymes were determined electrophoretically from haemolysates as described by Bücher *et al.*[9], with the following modification. After electrophoresis, the Cellogel electrophoresis strips were applied to a polyethylene imine (PEI) TLC sheet on which had been spread a solution of the enzymes, substrates and co-factors necessary for the visualization of PGK activity[9], with added ^{14}C-labelled D-glucose. The radioactive final products of the linked enzyme reactions (glucose-6-phosphate and 6-phosphogluconolactone) were adsorbed onto the PEI sheet[14], which was then autoradiographed on Kodak XS X-ray film. The autoradiographs were scanned with a double-beam recording densitometer and the area under each peak integrated. The figures obtained were corrected to compensate for the log-linear response of the X-ray film to exposure, as determined by calibration with a series of known alloenzyme mixtures, and the proportions of the A and B alloenzymes were calculated. In most animals the overall A:B ratio was $\sim$7:3, a value consistent with the expected linkage of *xce* alleles (controlling the probability of a given X chromosome excaping inactivation) to the PGK-1A and 1B alleles[15]. The mice used were from the eighth generation back-cross of PGK-1A onto the CBA/Ca (PGK-1B) strain.

0028-0836/82/310562—02$01.00

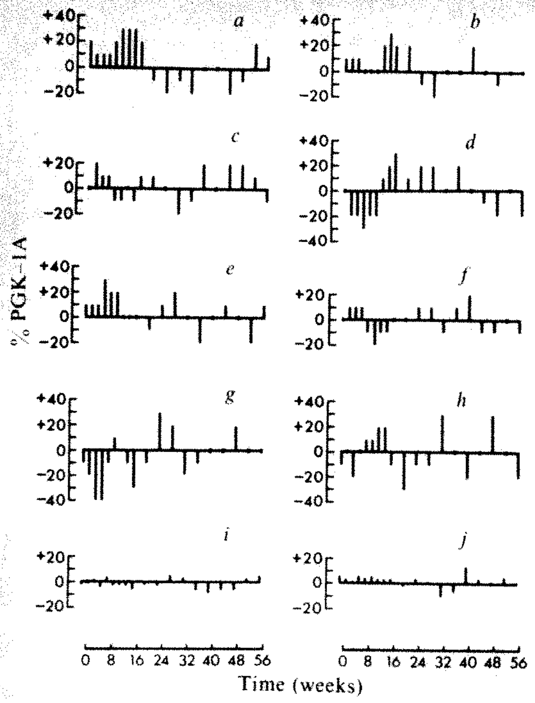

Fig. 2 Computer simulations of PGK phenotypes in serial blood samples, generated on the assumptions that (1) erythrocyte lifespan = 45 days; (2) PGK-1A and 1B-expressing clonogenic cells are selected at random; and (3) each clone produces erythrocytes for only a limited period before becoming extinct or quiescent. Three (*a–h*) or 15 (*i*, *j*) clones productive over any 14-day period. The simulations shown are unselected, i.e. first series generated.

suggesting that only a few clones of cells are represented in each blood sample and that the identity of these can change rapidly. On the simplifying assumption that all erythropoietic clones are of equal size, the number of clones (n) can be estimated by the binomial equation $n = p(1-p)/s^2$ (refs 10, 11) where p is the best estimate of the overall proportion of A alloenzyme in the haematopoietic system, calculated as the mean from several blood samples; $1-p$ is the proportion of B alloenzyme; and s^2 is the variance of individual and independent samples around p. As the lifespan of erythrocytes in the mouse is ~40–45 days[12], blood samples taken at 14- and 28-day intervals are not independent and therefore cannot all be used to estimate p and s^2. Accordingly, n was calculated from the samples taken at day 0 and at 56-day intervals thereafter. The mean value of n was 10 and the range 2–30. This wide estimated range is largely due to statistical error, as only eight independent blood samples were obtainable over the 56-week period of the study. Using the value 10, and assuming 10^{10} erythrocytes per ml of blood with a blood volume of 2 ml, each clone must average 2×10^9 erythrocytes and is therefore large enough alone to provide the total steady-state erythrocyte requirements for 4.5 days; three clones could provide for 14 days. The large changes that can occur in A : B ratios within 14 days suggest that clones do indeed arise and decline in quite rapid succession. Computer simulations of our data, assuming that three clones maintain the whole burden of erythropoiesis for 14 days and then cease production, are shown in Fig. 2(*a–h*). These simulations correspond quite closely to the actual data, while simulations using any substantially larger number of clones—for example 50 in a blood sample, corresponding to 15 over a 14-day period—do not generate sufficient variability (Fig. 2*i–j*).

To make a clone of 2×10^9 cells requires a production line of 31 doublings, which is far longer than has been estimated for the production of erythrocytes from CFC—about 12–14 doublings[13]. CFC have long been regarded as haematopoietic stem cells and some of them at least have the stem cell properties of self-renewal and pluripotency. Our data show that those CFC which undergo erythroid differentiation are themselves substantial clones, separated by 17–19 doublings from the clonogenic cell, and that these clones are used sequentially to maintain erythropoiesis.

This work was supported by the Melville Trust and by the MRC, of which D.I.B. is a research student. We thank Dr J. D. West for the gift of our initial breeding stock of PGK-1A mice

Received 23 April; accepted 2 June 1982.

1. Lajtha, L. G. *Differentiation* **14,** 23–34 (1979).
2. Schofield, R. *Blood Cells* **4,** 7–25 (1978).
3. Kay, H. E. M. *Lancet* **ii,** 418–419 (1965).
4. Lyon, M. F. *Proc. R. Soc.* B **187,** 243–268 (1974).
5. Monk, M. & Harper, M. I. *Nature* **281,** 311–313 (1979).
6. Fialkow, P. J. *Ann. hum. Genet.* **37,** 39–48 (1973).
7. Gandini, E., Gartler, S. M., Agioni, G., Argiolas, N. & Dell Acqua, G. *Proc. natn. Acad. Sci. U.S.A.* **61,** 945–948 (1968).
8. Nielsen, J. T. & Chapman, V. M. *Genetics* **87,** 319–326 (1977).
9. Bücher, T., Bender, W., Fundele, R., Hofner, H. & Linke, I. *FEBS Lett.* **115,** 319–324 (1980).
10. Wallis, V. J., Leuchars, E., Chwalinski, S. & Davies, A. J. S. *Transplantation* **19,** 2–11 (1975).
11. Micklem, H. S. & Ross, E. in *Human Lymphocyte Differentiation: Its Application to Cancer* (eds Serrou, B. & Rosenfeld, C.) 15–22 (Elsevier, Amsterdam, 1978).
12. Russell, E. S. & Bernstein, S. E. in *Biology of the Laboratory Mouse,* 2nd edn (ed. Green, E. L.) 352 (McGraw-Hill, New York, 1966).
13. Testa, N. *Clinics Haemat.* 8, 311–333 (1979).
14. Chasin, L. A. & Urlaub, G. *Somatic Cell Genet.* **2,** 453–467 (1976).
15. Johnston, P. & Cattanach, B. M. *Genet. Res.* **37,** 151–160 (1981).

Analysis of fibroblast proteins from patients with Duchenne muscular dystrophy by two-dimensional gel electrophoresis

E. Rosenmann, C. Kreis, R. G. Thompson, M. Dobbs, J. L. Hamerton & K. Wrogemann

Departments of Biochemistry and Pediatrics (Genetics),
University of Manitoba, Winnipeg, Canada R3E OW3

Duchenne muscular dystrophy (DMD), the most common and severe form of the muscular dystrophies, is an X-linked inborn error of metabolism with multiple tissue involvement. Although the major pathological changes are observed in skeletal muscle, abnormalities have also been detected in the heart[1], nervous system[2], red blood cells[3], lymphocytes[4] and cultured skin fibroblasts[5–7]. For many reasons, such as readily available tissue material, fewer secondary changes and the potential for prenatal diagnosis, cultured skin fibroblasts should be the tissue of choice to search for the primary defect. Several abnormalities have been reported in DMD fibroblasts, suggesting that the genetic abnormality is expressed in these cells[5–7]. To search for potentially mutant protein(s) we have compared the protein composition of normal and DMD fibroblasts by two-dimensional gel electrophoresis and have now found one protein spot consistently missing in DMD cells. The nature of this protein and its relation to the DMD gene are unknown.

Genetic alterations responsible for a disease are generally reflected in specific proteins which could be structurally altered, synthesized in abnormal quantities or not made at all. We have searched previously for mutant proteins in DMD fibroblasts using one-dimensional polyacrylamide gel electrophoresis in combination with a dual labelling technique and found no consistent abnormality[8]. This indicated that the most abundant proteins in fibroblasts are not affected by the DMD gene. With the development of two-dimensional polyacrylamide gel electrophoresis[9], the power of resolution for protein composition was greatly improved. However, using the O'Farrell technique[9] we encountered problems in obtaining absolute consistency between the protein maps of separate experiments. We therefore used a dual labelling approach, in which normal and DMD cells are labelled with two different isotopes (^{14}C- and ^{3}H-leucine), mixed and then co-electrophoresed on the same gel.

0028-0836/82/310563—03$01.00

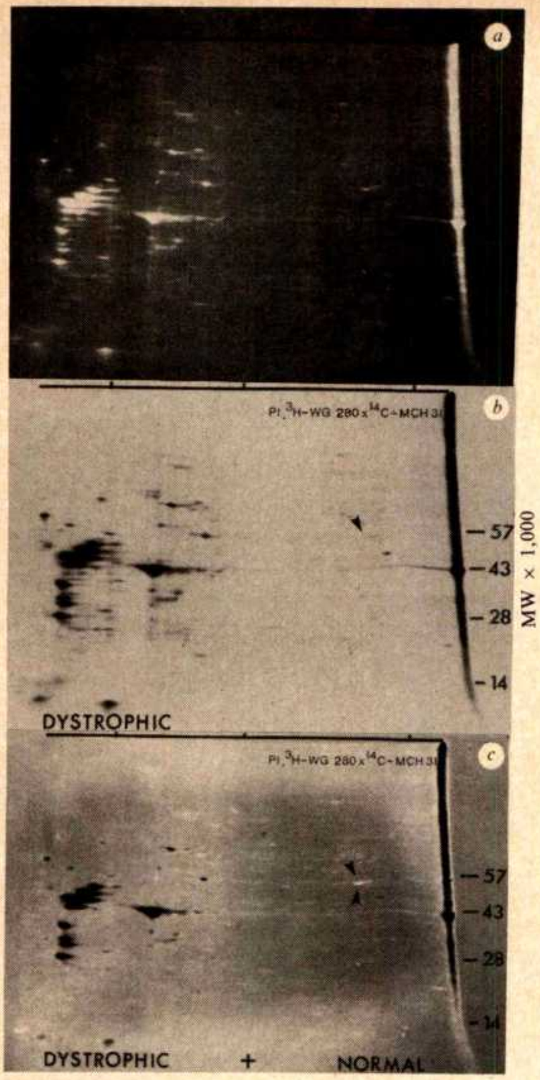

Fig. 1 Analysis of protein composition of normal and dystrophic human fibroblasts by two-dimensional gel electrophoresis in combination with double-label autoradiography[10]. *a*, The negative of an autoradiogram (to give white spots) showing protein spots from normal cells; *b*, a fluorogram showing the protein map of dystrophic cells. The arrows indicate a protein spot of M_r 56,000 and a pI of ~6.7 present in normal cells (*a*) but not in dystrophic cells (*b*). *c*, A superimposition of *a* and *b*. White spots (normal) identical to black spots (dystrophic) are covered by this procedure. The 56 K spot indicated by arrows is not covered. Cells were seeded in 60-mm Petri plates at a concentration of 1×10^5 cells per plate in McCoy's medium (10% in fetal calf serum, FCS) and grown at 37 °C for 14 days, at which time they were always confluent. Media were changed twice weekly. For labelling, the medium was replaced with 1.5 ml of a similar medium containing 36.3% FCS and either 1 mCi of [4, 5-^{3}H]leucine or 25 μCi of [U-^{14}C]leucine (Amersham) and the cells were labelled for 48 h at 37 °C. In some experiments, cells were seeded in 100-mm plates and conditions were adjusted accordingly. Cell lysates were prepared according to O'Farrell[9]. For isoelectric focusing (IEF) the lysates from normal and dystrophic fibroblasts were combined in a ratio of 400:1 ^{3}H d.p.m. to ^{14}C d.p.m. Two-dimensional electrophoresis was performed according to O'Farrell[9] with minor modifications. IEF gels were prepared using 0.4% pH 3.5–10 and 1.6% pH 5–7 ampholines (LKB) and polymerized in glass rods 12.5 cm long and 3 mm in diameter. A sample consisting of ~200 μl of radioactive cell lysate containing ^{3}H-labelled and ^{14}C-labelled protein and ~100 μg of total protein was applied to each gel. With every double-labelled gel, a control gel was run which only contained ^{14}C-labelled proteins. IEF was carried out for 16 h at 400 V followed by 45 min at 800 V for a total of 7,000 V h. Electrophoresis in the second dimension was done in slab gels 0.75 mm thick with an 8–14% exponential gradient of acrylamide. The IEF gel was applied to the second dimension with or without prior freezing and was not equilibrated. After completion of electrophoresis, gels were fixed and prepared for fluorography by standard procedures. For double-label autoradiography, the procedure of Walton *et al.*[10] was followed. Gels containing double-labelled material and gels containing ^{14}C-labelled material, in the same amount as that of the double-labelled gels, were prepared for fluorography. Exposure of the fluorograms to X-ray film showed that there was no spillover of ^{14}C-labelled material during ^{3}H exposure except for the most prominent spots. To determine the pH of the gradient formed in the first dimension, a parallel IEF gel containing unlabelled protein from normal fibroblasts was extruded and rapidly sliced into 10-mm sections. Each section was then equilibrated in capped tubes containing 0.5 ml of water per tube. Molecular weights were determined on the second dimension by the use of appropriate markers. The photographs show the protein pattern of homogenates of normal and dystrophic fibroblasts which were mixed and electrophoresed on the same IEF gel. In this experiment (pair 1 of Table 1) the dystrophic fibroblasts were labelled with ^{3}H-leucine. The normal fibroblasts were labelled with ^{14}C-leucine.

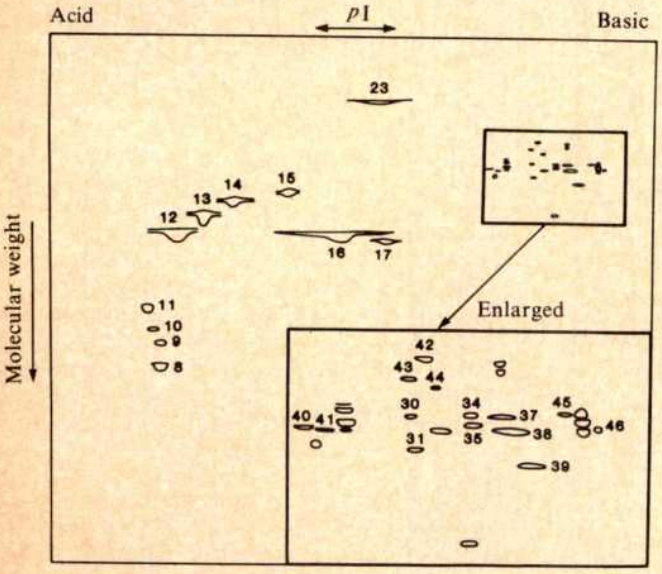

Fig. 2 Diagram of spots cut out from a two-dimensional gel for analysis by liquid scintillation counting. Cells from the normal strain MCH 40 labelled with [4, 5-^{3}H]leucine were combined with cells from the DMD strain DC (male, 13 yr, Department of Pediatrics, Winnipeg) labelled with [U-^{14}C]leucine and co-electrophoresed essentially as in Fig. 1, except that the acrylamide concentration of the second dimension was 10%. The gel was silver stained[11] and the spots indicated were cut out for dual label liquid scintillation counting[13]. Spot no. 35 corresponds to the 56 K/6.7 protein of Fig. 1. Additional spots were cut out to provide a reliable mean ratio of ^{3}H/^{14}C for reference (see Fig. 3).

Whether protein spots come from normal and/or dystrophic cells is determined by dual label autoradiography[10] which produces two superimposable X-ray films: one shows only ^{3}H-labelled spots, the other only ^{14}C-labelled spots.

With this technique we detected numerous differences between normal and DMD fibroblast proteins (Table 1) but only one difference was seen consistently: the absence in DMD of a protein spot of molecular weight (M_r) ~56,000 (56 K) with an approximate isoelectric point of 6.7 (Fig. 1). This abnormality was seen in fibroblasts from six different patients with DMD, which were compared with six control strains in eight different combinations. The protein spot was missing irrespective of whether the dystrophic cells were labelled with ^{3}H-leucine or ^{14}C-leucine (Table 1). In two pairs, overexposure of the fluorography for tritium (dystrophic cells) did not reveal a spot, although extreme overexposure will always reveal a spot due to ^{14}C-leucine from the normal cells.

A problem was encountered with pair 6 (Table 1): based on the constellation of spots in the 56 K/6.7 area it appears that both normal and dystrophic cells do not have the 56 K/6.7 protein. However, an extra spot of the same apparent molecular weight was seen at an approximate pI of 6.5 in normal cells. We are now exploring the hypothesis that this spot represents a variant of the normal 56 K/6.7 protein.

Some of the autoradiograms of the dual-label study had to be exposed for over 6 months. However, three more rapid techniques were successfully used to confirm our original findings (to be published elsewhere in detail). The absence of the 56 K/6.7 protein spot in DMD cells was also detected when the cell strains were labelled with ^{35}S-methionine or when unlabelled proteins were visualized by a sensitive silver staining method[11]. Furthermore, when silver-stained spots from gels containing dual-labelled samples of an additional pair of normal

Table 1 Polypeptide map comparison of normal and DMD fibroblast strains by two-dimensional polyacrylamide gel electrophoresis in combination with dual-label autoradiography

Pair	Normal (age) Label	Dystrophic (age) Label	No. of spots compared	Extra spots in Normal	Extra spots in Dystrophic
1	MCH 31(8 yr)	WG 280(7 yr)	193	56/6.7	—
	^{14}C	^{3}H		21/5.3	
				42/5.4	
				65/5.7	>65/5.8
2	MCH 40(6 yr)	WG 348(5 yr)	129	56/6.7	—
	^{3}H	^{14}C		43/5.5	
3	MCH 7(3 yr)	WG 448(6 yr)	130	56/6.7	—
	^{3}H	^{14}C		25/5.3	42/5.4
4	MCH 35(3 yr)	WG 466(6 yr)	178	56/6.7	—
	^{14}C	^{3}H		40/5.4	42/4.5
				29/5.5	40/4.8
5	MCH 48(5 yr)	WG 502(6 yr)	253	56/6.7	—
	^{3}H	^{14}C		45/5.5	28/6.4
6	MW (9 yr)	JB (11 yr)	577	56/6.5	—
	^{14}C	^{3}H		>80/4.5	29/6.6
				43/5.8	61/6.7
				15/6.2	
				16/6.2	
				28/6.2	
				75/6.8	
7	MCH 40(6 yr)	WG 448(6 yr)	970	56/6.7	—
	^{14}C	^{3}H		27/5.8	28/5.9
				43/6.6	65/6.1
				42/6.6	50/6.1
				20/6.8	42/6.1
					20/6.4
8	MCH 48(5 yr)	WG 348(5 yr)	490	56/6.7	—
	^{14}C	^{3}H		57/7.1	29/6.9
					38/7.0
					57/7.1

MCH and WG cell strains were obtained from the Repository for Mutant Human Cell Strains, Montreal, Canada; MW and JB from the Department of Pediatrics (Genetics), University of Manitoba, Winnipeg, Canada. All cell strains were from male individuals, matched closely for passage number and were used at passage 18 or less. The position of protein spots is given in approximate coordinates of $M_r \times 1{,}000/pI$. These coordinates have to be considered gross approximations, as no internal markers for M_r and pI were included in the experiments.

and dystrophic cells were excised (Fig. 2) and their radioactivity determined by liquid scintillation counting, the 56 K/6.7 protein spot showed <20% of radioactivity of the isotope of DMD cells (^{14}C) as documented by the highly abnormal ratio of ^{3}H/^{14}C of spot number 35 (Fig. 3).

If the 'missing' protein described here is responsible for DMD, it should be missing in all fibroblast strains from DMD patients, unless there is genetic heterogeneity in this disease. The protein should be coded for by the X chromosome, and one should be able to show evidence for lyonization[12] in fibroblasts cloned from carriers of DMD. Experiments to test these points are in progress. At present, the nature and significance of this missing protein are not known. Whether a direct or a secondary result of the DMD gene, these findings provide further support to the hypothesis that DMD is indeed expressed in cultured skin fibroblasts and can be studied in these cells.

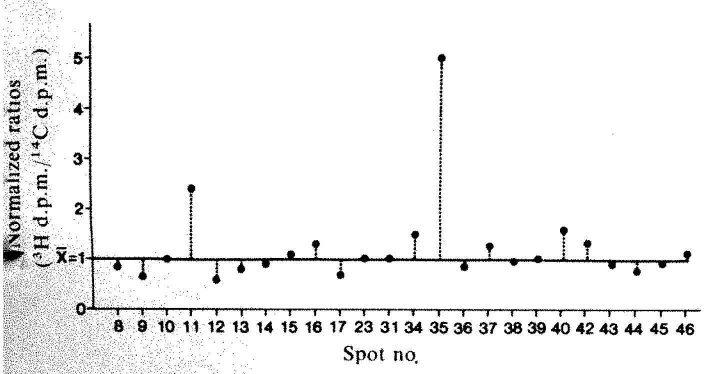

Fig. 3 Normalized ratios of ^{3}H/^{14}C d.p.m. of the protein spots designated in Fig. 2. Scintillation counting and analysis were done as described elsewhere[13,14]. The mean of the normalized ratio of all spots equals one and the dotted lines indicate the deviation from the mean.

We thank A.-M. Adachi, A. Vust, T. Trottershaw and M. LaFleur for technical assistance. This work was supported by the Muscular Dystrophy Association of Canada, the Manitoba Heart Foundation and the MRC of Canada.

Received 21 January; accepted 21 May 1982.

1. Hunter, S. *Br. med. Bull.* **36,** 133–134 (1980).
2. Emery, A. E. H. & Gosden, C. *J. med. Genet.* **11,** 76–79 (1974).
3. Plishker, G. A. & Appel, S. H. *Muscle Nerve* **3,** 70–81 (1980).
4. Hornstein, A. L. & Emery, A. E. H. *Neurology* **30,** 1330–1332 (1980).
5. Jones, G. E. & Witkowski, J. A. *J. neurol. Sci.* **43,** 465–470 (1979).
6. Gelman, B. B. *et al. J. clin. Invest.* **65,** 1398–1406 (1980).
7. Rounds, P. S. *et al. Biochem. biophys. Res. Commun.* **97,** 1384–1390 (1980).
8. Pena, S. D. J. *et al. Clin. Genet.* **14,** 50–54 (1978).
9. O'Farrell, P. H. *J. biol. Chem.* **250,** 4007–4021 (1975).
10. Walton, K. E., Styer, D. & Gruenstein, E. *J. biol. Chem.* **254,** 7951–7960 (1980).
11. Oakley, B. R., Kirsch, D. R. & Morris, N. R. *Analyt. Biochem.* **105,** 361–363 (1980).
12. Lyon, M. F. *A. Rev. Genet.* **2,** 31–52 (1968).
13. Pena, S. D. J. & Wrogemann, K. *Pediat. Res.* **12,** 887–893 (1978).
14. Wrogemann, K. *et al. Analyt. Biochem.* **81,** 472–477 (1977).

Recognition of a polymorphic monocyte antigen in HLA

A. van Leeuwen, A. Termijtelen, S. Shaw*
& J. J. van Rood

Department of Immunohaematology and Blood Bank,
University Hospital, 2333 Leiden, The Netherlands
* Department of Health & Human Services, National Institutes of Health, Bethesda, Maryland 20205, USA

The serological recognition of 'new' gene products of the *HLA* system can be accomplished by selecting sera with strong leucocyte antibodies and testing these against a panel of cells obtained from donors which are compatible for the known HLA antigens with the antibody producer. This approach, which we termed the HLA-CAP approach (compatible with antibody producer), was essential in the recognition of what is now called the *HLA-DR* locus[1] and of non HLA-linked T-cell subgroups[2]. Using the same technique, we have defined here several sera recognizing a structure on monocytes similar to one of the alleles of the HLA-linked PL3[3,4] or secondary B-cell (SB)[5,6] system, so far only recognized by cellular techniques.

Over 100 sera obtained from HLA-A1-B8-DR3 positive women which produced strong leukocyte antibodies, were tested against lymphocyte suspensions obtained from HLA-A1-B8-DR3 homozygous individuals. The two colour fluorescence (TCF) technique[7] was used, which allows the recognition of antibodies against B cells, T cells and monocytes independently, without the need to separate these cells. In this technique, which is a complement dependent cytotoxicity test, ethidium bromide was used as a dye for dead cells, which is a more sensitive reagent to test for viability than the eosine stain normally used.

Using these techniques, antibodies that reacted with T cell subsets were identified[2] and also a cluster of antibodies that reacted primarily with monocytes. The reaction pattern of 22 of these sera is given in Table 1. When the homozygous panel cells were tested by means of the primed lymphocyte test (PLT) for the five alleles of the recently described SB system[5], four of the sera showed an almost perfect fit with SB4 and one with SB1+4.

Because the sera also contained strong anti-HLA class I and class II antibodies they were absorbed with buffycoat cells obtained from donors which were SB4 negative so that they could be used to type a random panel of cells. After absorption the sera were tested against 25 unrelated SB typed individuals (Table 2). There is a highly significant and clearcut correlation between the SB4 determinant as recognized in PLT testing, and the antisera 37270, 35572 and 34155. However, one of the panel donors was positive with these sera, but negative for SB4 when tested with the PLT-SB4 reagents. This discrepancy may be an artefact as the SB4 is the most poorly defined allele of the SB system but it may be that SB4 as recognized in PLT is distinct from the determinant recognized by our sera. In other

0028-0836/82/310565—03$01.00

Table 1 Anti-monocyte antibodies in sera from parous women

Donor	SB	Serum no. 30422	35242	34135	42062	38731	1950	30147	35572	37270	34155	24777	32361	19505	1941	40862	13373	38736	12681	21859	41845	22878	25031
BER	1, 4	+	+	+	+	+	+	+	+	+	+	+	+	+	−	−	−	−	−	−	−	−	−
EYS	1, 4	−	−	−	+	+	+	+	+	+	+	+	+	+	+	+	+	+	−	−	−	−	−
HOV	4	−	−	−	−	−	+	+	+	+	+	−	−	−	+	+	−	−	+	+	+	−	−
HAR	4	−	−	−	−	−	+	+	+	+	+	+	+	−	+	−	+	+	−	−	−	−	+
POU	1	−	−	−	−	−	−	−	−	−	+	−	−	−	−	−	−	−	−	−	−	+	+
HAG	1, 2	−	−	−	+	−	−	−	−	−	+	+	+	+	−	−	−	−	−	−	−	+	+
OVE	ND	−	−	−	−	−	−	−	−	−	−	−	−	−	−	−	−	−	−	−	−	−	−
JAN	2	−	−	−	−	−	−	−	−	−	−	+	+	+	−	−	+	+	−	−	−	−	+
GYS	1, 3	−	−	−	−	−	−	−	−	−	+	−	−	−	−	−	−	−	−	−	−	+	+

ND, not determined.

Sera were obtained from women that had HLA–A1, –B8 and DR3 determinants. These sera were tested on mononuclear cells from donors which were homozygous for HLA–A1–B8 and –DR3 in the two colour fluorescence (TCF) technique, described previously[7]. In brief, B lymphocytes and monocytes from a lymphocyte suspension obtained after Ficoll-Hypaque density gradient separation, were labelled with a goat anti-human immunoglobulin FITC conjugate. This cell suspension was used in a micro lymphocytotoxicity assay with antisera and complement. Dead cells were stained with ethidium bromide. The reading of the test was carried out with an inverted microscope containing a Ploemopak filter combination. Excitation filters: LP 455- SP 490, barrier filter: LP 520, Zeiss filter combination no. 487709). If 20–50% of the monocytes were lysed, the reaction was considered to be positive (indicated by +).

Table 2 Two-by-two comparison of SB4 with 5 different sera

SB4 serum no.	+ +	− +	+ −	− −	P*
37270	15	1	0	9	<0.0001
35572	15	1	0	9	<0.0001
34155	15	1	0	9	<0.0001
30147	15	8	0	2	0.15
1950	11	1	4	9	0.003

The relevant sera were absorbed with selected buffycoat lymphocytes which carried the HLA–A, –B, –C and /or –DR antigens corresponding to the antibodies in the sera, but lacking the SB4 determinant. The reactivity of serum 34155 with SB1 positive donors was eliminated due to absorption with SB1 positive buffycoat lymphocytes.

* Fisher's exact P value.

words, the relationship of SB and the presently described serologically defined determinant may be as confusing as the relationship between HLA–D and HLA–DR.

The husbands of the women whose sera had shown positive SB4 reactivity were tested with all the SB4 associated antisera (Table 3). These results showed that the monocytes of the women were negative with the 'anti SB4' sera, but the husbands' monocytes reacted positively. Preliminary data indicate that in this way also antibodies can be identified which react with SB1 or SB5 positive cells.

The data presented here show that it is possible to recognize a product, by serotyping on monocytes, which shows a very significant association with a product recognized by cellular (that is PLT) typing. It appears that this structure is encoded in the *HLA* region but it is not clear why this structure is detected only on monocytes. CML studies[5] suggested the presence of SB determinants on B cell lines. Moreover a monoclonal antibody, I-LR1, first described by Nadler *et al.*[8], recently has been shown to react with an epitope present on lymphocytes of SB2, 3 and a low number of SB4 positive individuals. This monoclonal antibody was reactive (as shown in an immunofluorescence technique) with a class II molecule, present on B cells, monocytes and activated T cells[8]. This observation is in contradiction to our present findings which indicate that the SB-like determinants, as recognized by serology, are primarily expressed on monocytes. There are at least two explanations for this discrepancy.[1] The determinant recognized by our sera is present on B cells as well, but for technical reasons (for example the distance of antigenic sites) the complement dependent cytotoxicity test could be negative[2]. Alternatively it could be that the determinant recognized by our sera is not expressed on B cells. Paul and coworkers[9] found a polymorphic determinant expressed on monocytes and some endothelial cells but not on B cells. Absorption studies are under way to determine whether this possibly more sensitive technique may show that the structures recognized by our sera are present on B cells.

Recent studies suggest that there may be many more loci[10,11] in the *HLA* region than those presently recognized and our results show the importance of using antibodies which react with only subsets of mononuclear cells and more sensitive techniques than those commonly used in tissue typing should be used.

We conclude that the antibodies described here recognize an epitope on a gene product which is highly associated with or identical to SB. These antibodies will enable biochemical analysis of this gene product, but will not answer the question of identity or non-identity of SB and the determinant recognized by the antibodies. As long as uncertainty exists about the identity of SB determinants recognized by cellular techniques and the determinants identified by means of serology, we suggest an independent nomenclature. Following HLA–A, –B, –C, and –D we recently described the serologically defined DR linked determinant LB–E[12] (similar to or identical with MB[13]). The presently described determinant will be referred to as LB–F. For convenience, the number indicating the allele of the LB–F system should be identical to the number of the corresponding SB allele, i.e. in our case LB–F4.

Table 3 Reactivity of the SB4 associated antisera tested against monocytes from the antibody producers and their husbands

Monocytes from the producers of serum no.	Serum no. 37270	35572	34155
37270	−	−	−
35572	−	−	−
34155	−	−	−
Monocytes from husbands of the producers of serum no.			
37270	+	+	+
35572	+	+	+
34155	+	+	+

The experiment was performed with the TCF method as indicated in Table 1.

We thank Ms J. S. G. Niterink, Ms S. van den Berge, Ms L. Thung, Ms M. Jager and Mrs G. de Groot-Swings for technical assistance and Ms C. S. L. Mackenzie for preparing the manuscript.

Received 23 March; accepted 7 June 1982.

1. Leeuwen, A. van, Schuit, H. R. E. & van Rood, J. J. *Transplantn Proc.* **5**, 1539–1542 (1973).
2. Leeuwen, A. van, Festenstein, H. & van Rood, J. J. *J. exp. Med.* **152**, 235s–242s (1980).
3. Termijtelen, A., Bradley, B. A. & van Rood, J. J. *Tissue Antigens* **15**, 267–274 (1980).
4. Termijtelen, A. & van Rood, J. J. *Tissue Antigens* **17**, 57–63 (1981).
5. Shaw, S., Johnson, A. H. & Shearer, G. M. *J. exp. Med.* **152**, 565–580 (1980).
6. Shaw, S., Kavathas, P., Pollack, M. S., Charmot, D. & Mawas, C. *Nature* **293**, 745–747 (1981).
7. Rood, J. J. van, van Leeuwen, A. & Ploem, J. S. *Nature* **262**, 795–797 (1976).
8. Nadler, L. M. *et al. Nature* **290**, 591–593 (1981).
9. Paul, L. C., Claas, F. H. J., van Es, L. A., Kalff, M. W. & de Graeff, J. *New Engl. J. Med.* **300**, 1258–1260 (1979).
10. Cami, B., Brégégère, F., Abastado, J. P. & Kourilsky, P. *Nature* **291**, 673–675 (1981).
11. Kratzin, H. *et al. Hoppe-Seyler's Z. physiol. Chem.* **362**, 1665–1669 (1981).
12. Schreuder, G. M. Th. *et al. Hum. Immun.* (in the press).
13. Duquesnoy, R. J., Marrari, M. & Annen, K. *Transplantn Proc.* **11**, 1757–1760 (1979).

Immunotherapy in nude mice of human hepatoma using monoclonal antibodies against hepatitis B virus

Daniel Shouval, David A. Shafritz,
Vincent R. Zurawski Jr*, Kurt J. Isselbacher†
& Jack R. Wands†

Liver Research Center, Department of Medicine and Cell Biology,
Albert Einstein College of Medicine, Bronx, New York 10461, USA
* Centocor, Malvern, Pennsylvania 19355, USA
† Gastrointestinal Unit, Massachusetts General Hospital, Boston,
Massachusetts 02114, USA

The human hepatoma cell line PLC/PRF/5, which contains integrated hepatitis B virus DNA, synthesises and secretes hepatitis B virus surface antigen (HBsAg)[1,2]. When injected into BALB/c nude mice, these cells produce well-vascularized, encapsulated tumours in almost 100% of animals[1]. HBsAg has been demonstrated on the surface and in the cytoplasm of PLC/PRF/5 cells using immunofluorescence techniques[1,3–5]. Recently, we reported that monoclonal antibodies to HBsAg (IgG1, IgG2a and IgM isotypes) bind to HBsAg-associated viral determinants of PLC/PRF/5 cells in culture and immunoprecipitate HBsAg secreted into the growth medium[6]. Also IgG2a and IgM antibodies to HBsAg (anti-HBs) produce specific lysis of PLC/PRF/5 cells in culture in the presence of complement, but have no lytic effect on human hepatoma cells which do not express HBsAg[6]. In the present study, we demonstrate that IgM and IgG2a, but not IgG1, monoclonal anti-HBs specifically prevent or suppress tumour formation in a substantial number of athymic nude mice injected with PLC/PRF/5 cells.

For immunotherapy, we used three anti-HBs producing hybridoma clones developed by Wands *et al.* which bind with high affinity and specificity to distinct viral determinants on HBsAg[7,8]. In preliminary experiments, we determined the dose required to maintain detectable levels of monoclonal anti-HBs in nude mouse serum. When 1×10^6 c.p.m. of ^{125}I-labelled monoclonal anti-HBs IgM (specific activity 7–10 μCi μg^{-1}) was injected intravenously (i.v.), 10,000–20,000 c.p.m. of ^{125}I anti-HBs per ml was present in nude mouse serum 3 days later. Following i.v. injection of 1×10^6 c.p.m. of ^{125}I anti-HBs IgM every 48 hours for 8 days, ^{125}I anti-HBs was detected in nude mouse serum 5 days after the last injection. Intraperitoneal (i.p.) injection of ^{125}I anti-HBs IgG1 or IgG2a produced similar levels of anti-HBs in nude mouse serum.

The effect of ascitic fluid containing anti-HBs hydridoma antibodies on production and growth of PLC/PRF/5 tumours was then determined. Treated BALB/c male nude mice received IgM anti-HBs (i.v.), IgG2a anti-HBs (i.p.), or IgG1 anti-HBs (i.p.), and control mice received 100 μl of phosphate-buffered saline (PBS) i.v. or i.p. Subcutaneous injection of PLC/PRF/5 cells produced tumours in 37/39 control nude mice (Table 1). Treatment of tumour-injected mice with anti-HBs IgM prevented tumour formation in 15/23 animals, and suppressed tumour growth in 4 others ($P<0.001$). Anti-HBs IgG2a showed a protective response in 18/26 animals, with prevention of tumour formation in 8 mice and suppression of tumour growth in 10 mice ($P<0.01$). Monoclonal IgG1 anti-HBs, which bound effectively to PLC/PRF/5 cells in culture[6], had no effect on tumour growth (Table 1). These results correlated well with our previous *in vitro* studies[6].

Two additional groups of animals were treated with monoclonal antibodies to non-HBV determinants. Ascitic fluid containing monoclonal IgM antibodies against influenza HA antigen[9] (i.v.) or IgG1–IgG2b monoclonal antibodies to tetanus toxin[10] (i.p.) showed an effect in that some treated mice did not develop PLC/PRF/5 tumours. However, no response was observed in 11/16 of these animals and once tumours became established during treatment with monoclonal anti-influenza HA protein or anti-tetanus toxin, there was no suppression of

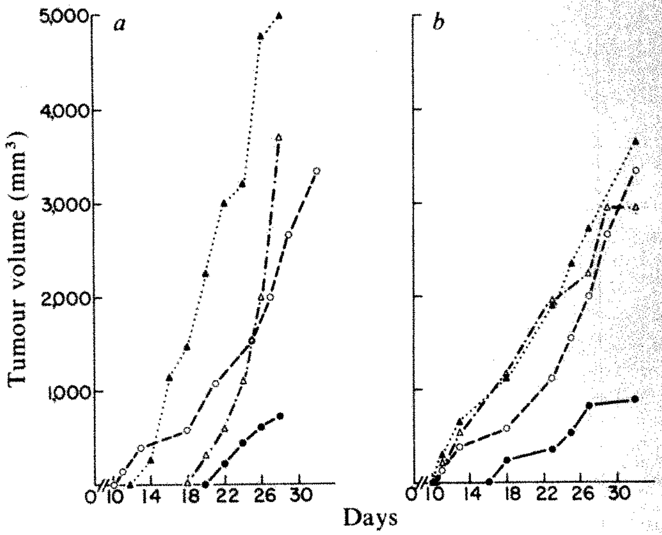

Fig. 1 Passive immunotherapy of PLC/PRF/5 human hepatoma with monoclonal antibodies to hepatitis B surface antigen. Four-to six-weeks-old male BALB/c *nu/nu* mice were injected subcutaneously with 10^7 PLC/PRF/5 cells on day 0. Mice were injected with 100 μl monoclonal antibodies to HBsAg IgM (i.v.) or with 100 μl anti-HBs IgG2a or IgG1 (i.p.). Control mice were injected either with 100 μl of monoclonal antibody to influenza HA antigen (i.v.) or with PBS (i.v. or i.p.). These data represent the results of one experiment in which all animals were injected with the same preparation of PLC/PRF/5 cells on the same day. Monoclonal antibody treatment was started within 1 h after tumour cell injection and was repeated every 48 h for 28–32 days. Mice were examined daily for tumour formation and the volume of palpable tumours was determined by a standard protocol with a calipers. The tumour volume is the mean of the maximal longitudinal diameter multiplied by the square of the maximal horizontal diameter. Numbers in parenthesis refer to the number of animals in each group. At the termination of experiments, tumours were excised and weighed, and mean weights of tumours in each group are expressed as mg per g mouse body weight. *a*, Treatment with monoclonal anti-HBs, IgM: ●, 'suppressed' tumours ($n=4$; tumour weight 6.2 ± 2.3 mg per g); ○, control tumours in untreated mice ($n=6$; 60 ± 25 mg); △, tumours in anti-influenza HA antigen treated mice ($n=4$; 60 ± 17 mg); and ▲, 'non-responder' tumour ($n=1$, 131 mg). *b*, Treatment with monoclonal anti-HBs, IgG2a or IgG1: ●, 'suppressed' tumours in mice treated with anti-HBs IgG2a ($n=9$; 10 ± 2.5 mg); △, 'non-responder' tumours in anti-HBs IgG1 treated mice ($n=9$; 56 ± 17 mg); ○, control tumours in untreated mice ($n=8$; 60 ± 25 mg); and ▲, 'non-responder' tumours in mice treated with anti-HBs IgG2a ($n=5$; 78 ± 33 mg).

0028–0836/82/310567—03$01.00

Table 1 Effect of monoclonal antibodies on tumorigenicity

Monoclonal antibody treatment	Effect on tumour growth Protective response	No response	*P*
None	2/39	37/39	—
Anti-HBs IgM (i.v.)	19/23	4/23	$P<0.001$
Anti-HBs IgG2a (i.p.)	18/26	8/26	$P<0.01$
Anti-HBs IgG1 (i.p.)	1/10	9/10	NS
Anti-influenza HA IgM (i.v.)	2/6	4/6	NS
Anti-tetanus toxin IgG1–IgG2b (i.p.)	3/10	7/10	NS

All mice were injected into the flank region with 1×10^7 PLC/PRF/5 cells on day 0, followed in one hour by injection of ascitic fluid containing monoclonal antibodies i.p. or i.v. as indicated, or PBS in animals not receiving monoclonal antibodies. The concentrations of anti-HBs in ascitic fluid were as follows: IgM clone 5D3, 5.6 mg ml^{-1}; IgG2a clone 5C3, 22.6 mg ml^{-1}; and IgG1 clone 2C6, 25.0 mg ml^{-1}. For anti-influenza HA antigen IgM and anti-tetanus toxin IgG1–IgG2b, the concentrations were 3.8 mg ml^{-1} and 10 mg ml^{-1}, respectively. 100 μl of ascites fluid containing IgM or IgG was administered every 48 hours i.v. or i.p., respectively. Nude mice tolerated repeated injection of ascitic fluid for up to 4 weeks (3% mortality compared to 2% in noninjected controls). Mice were killed within 28–33 days after tumour cell injection. Significance *P* was determined by comparing experimental mice to PBS treated controls, using the χ^2 test.

the tumour growth rate (see below). Thus, in animals receiving ascites fluid containing monoclonal anti-HBs IgM or IgG2a, there was a response in 27/49 animals, whereas in the combined groups treated with monoclonal anti-HBs IgG1, anti-influenza HA protein IgM or anti-tetanus toxin IgG1–IgG2b, there was a response in only 6/26 animals ($P<0.001$) which was not significantly different to control animals (2/39) with $0.05<P<0.1$.

Further evidence for suppression of tumour growth by monoclonal anti-HBs IgM or IgG2a was shown by an increased tumour latency (defined as the time from PLC/PRF/5 cell injection until the onset of gross tumour development), a slower tumour growth rate (determined by measurement of tumour volume) and a decreased tumour weight at necropsy compared to control animals. Figure 1 shows the latency and tumour growth rate in 46 nude mice injected with the same batch of PLC/PRF/5 cells and treated with various monoclonal antibodies. Most animals receiving monoclonal anti-HBs IgM did not develop tumours. In the four anti-HBs IgM-treated mice with suppressed tumour growth (Fig. 1*a*), latency was prolonged to 20–22 days as compared to 10 days in control animals. For reasons which are unclear, tumour latency was also prolonged to 16–18 days in anti-influenza HA IgM-treated mice. However, once tumours became established in anti-influenza HA protein-treated animals, their growth rate was most rapid (Fig. 1*a*). Tumour latency was also prolonged in IgG2a anti-HBs-treated mice (Fig. 1*b*). Mean tumour volume was decreased in IgM and IgG2a anti-HBs-treated mice with suppressed tumours (Fig. 1*a*, *b*) but was unchanged in mice treated with IgM monoclonal antibodies to anti-influenza HA protein (Fig. 1*a*). There was also no change in latency or tumour growth rate in IgG1 anti-HBs-treated mice (Fig. 1*b*). In animals with suppressed tumours, the mean tumour weight at termination of the experiment was reduced six- to tenfold (Fig. 1*a*, *b*). Tumour weight was unaffected in monoclonal anti-tetanus toxin-treated animals (data not shown). With one exception, when gross tumours did not develop following anti-HBs treatment, tumour cells were not identified histologically at the injection site.

In one anti-HBs IgM-treated mouse and five anti-HBs IgG2a-treated mice very large tumours developed (Fig. 1*a*, *b*). This 'escape' phenomenon, which has also been observed in other systems[11], was not due to inadequate monoclonal antibody treatment. HBsAg was completely neutralized in the serum of all anti-HBs-treated mice (Table 2), and HBs antigen was also identified in the medium cultured sublines established from three 'escape' tumours. Therefore, selection of non-HBsAg producing variants did not explain this phenomenon (our unpublished results).

The gross appearance of PLC/PRF/5 tumours in nude mice treated with IgM anti-HBs monoclonal antibody is shown in Fig. 2. An example of a mouse with a PLC/PRF/5 tumour in each category is illustrated; *a*, 'prevented', *b*, 'suppressed', *c*, control (untreated) and *d*, 'nonresponder' or 'escape'.

In the present study, the difference in effectiveness of IgG2a and IgM anti-HBs on PLC/PRF/5 tumour growth is not clear but may merely reflect the relatively small number of animals in each group. Although IgG2a anti-HBs can lyse PLC/PRF/5 cells *in vitro*[6] and was injected in a fivefold excess over IgM anti-HBs to reach comparable serum levels, it had primarily a suppressive rather than a preventive effect. This may be due to differences in the affinity or avidity of IgG2a and IgM monoclonal anti-HBs for HBsAg on the surface of PLC/PRF/5 cells or that these monoclonal antibodies recognize different HBsAg viral determinants[6–8]. Alternatively, mechanisms other than complement-mediated lysis may be involved in inhibition of tumour formation and growth in nude mice. To test this a panel of monoclonal antibodies of the same affinity and/or directed against the same or different viral epitopes of various isotopes would be useful. It is also possible that a combination of monoclonal antibodies directed against different viral epitopes might enhance effectiveness in suppressing or preventing PLC/PRF/5 tumour development.

Despite previous failures of polyspecific antisera in tumour immunotherapy[11], suppression of tumour growth in mice by monoclonal antibodies has been reported in mouse lymphoma[12] or leukaemia[13] and in solid tumours of human origin, such as malignant melanoma[14] and colorectal carcinoma[15]. A limited effect has also been observed recently in several patients with non-Hodgkins and T-cell lymphomas[16,17]. However, in some studies, monoclonal antibodies to tumour cell determinants have been shown to recognize more than one specific cell type[18–20], thereby limiting their potential effectiveness. The present experiments suggest that immunotherapy with monoclonal antibodies directed toward viral epitopes on HBsAg may alter the growth of a human hepatocellular carcinoma, when

Table 2 Detection of anti-HBs in the serum of PLC/PRF/5 tumour-bearing mice

Monoclonal antibody	No. of mice	Effect on tumour growth	Serum HBsAg and anti-HBs levels (c.p.m. ± s.e.) HBsAg	anti-HBs
None	8	None	9,910 ± 1,792	1,692 ± 439
Anti-HBs IgM	4	Suppressed	219 ± 25	29,239 ± 414
Anti-HBs IgM	7	Prevented	207 ± 15	28,816 ± 907
Anti-HBs IgM	1	Non-suppressed	179	28,144
Anti-HBs IgG2a	5	Suppressed	580 ± 243	19,178 ± 1,375
Anti-HBs IgG2a	5	Non-Suppressed	360 ± 46	19,893 ± 980
Anti-HBs IgG1	9	None	232 ± 17	21,368 ± 833
Anti-influenza HA antigen IgM	4	None	2,794* ± 656	639 ± 62

Mice were killed 28–32 days after tumour cell injection. HBsAg and anti-HBs were determined on the day of killing, using commercially available radioimmunoassay kits as previously described[1]. HBsAg in normal nude mouse serum was 252 ± 15 c.p.m. by RIA.

* IgM monoclonal antibodies to influenza HA antigen partially interfered with the RIA for detection of HBsAg.

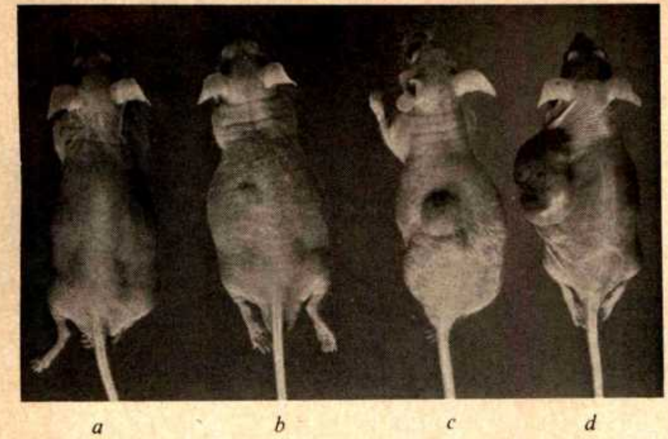

Fig. 2 Gross appearance of PLC/PRF/5 tumours in BALB/c nude mice receiving monoclonal IgM anti-HBs antibody treatment. BALB/c *nu/nu* mice were injected with 1× 10^7 PLC/PRF/5 cells and were treated with monoclonal anti-HBs IgM antibodies (i.v.) every other day, beginning 1 hour after tumour cell injection. This photograph was taken on the 28th day after PLC/PRF/5 cell injection. *a*, Tumour 'prevented'; *b*, tumour growth 'suppressed'; *c*, control tumour in untreated mouse; *d*, 'non-suppressed' or 'escape' tumour.

such viral determinants are expressed on the tumour cell surface. This study shows that a high affinity monoclonal antibody to a viral determinant can inhibit tumour growth and thereby overcome the problem of cross-reactivity with normal cell membrane constituents. While this approach might be applicable only in situations where specific viral proteins are expressed on the host cell surface, its potential use in heptatitis B virus carriers, especially in those patients with chronic liver disease, would seem possible.

We thank Drs B. R. Bloom, D. Rager Zisman and P. C. Quan for advice, Mrs E. Hurston for technical assistance and Dr W. Gerhard for the gift of H28-A2-1 cell line. This study was supported in part by NIH grants AM-17609, AM-17702, AA-20309, AG-04145, the Chait Memorial Foundation and the Gail I. Zuckerman Foundation. Daniel Shouval is the recipient of an NIH Fogarty International Research Fellowship Award 3F05 TW02764 on leave from the Department of Medicine A, Hadassah University Hospital, Jerusalem, Israel (also his present address). Jack R. Wands is the recipient of an NIH Research Scientist Development Award 1-K02-AA-00048.

Received 11 February; accepted 8 June 1982.

1. Shouval D. *et al. Cancer Res.* **41,** 1342–1350 (1980).
2. Chakraborty, P. R., Ruiz-Opazo, N., Shouval D. & Shafritz, D. A. *Nature* **286,** 531–533 (1980).
3. Gerber, M. A., Garfinkel, E., Hirschman, S. Z., Thung, S. N. & Panagiotatos, T. *J. Immun.*, **126,** 1085–1089 (1981).
4. Daemer, R. J., Feinstone, S. M. & Purcell, R. H. in *Viral Hepatitis* (eds Vyas, G. N., Cohen, S. N. & Schmid, R.) 724 (Franklin Institute Press, Philadelphia, 1978).
5. Chisari, F. V., Bieber, M. S., Josephe, C. A., Xavier, C. & Anderson, D. S., *J. Immun.* **126,** 45–49 (1981).
6. Shouval, D., Wands, J. R., Zurawski, V. R. Jr, Isselbacher, K. J. & Shafritz, D. A., *Proc. natn. Acad. Sci. U.S.A.*, **79,** 625–629 (1982).
7. Wands, J. R. & Zurawski, V. R. Jr *Gastroenterology* **80,** 225–232 (1981).
8. Wands, J. R., Carlson, R. I., Schoemaker, H., Isselbacher K. J. & Zurawski, V. R. Jr *Proc. natn. Acad. Sci. U.S.A.* **78,** 1214–1218 (1981).
9. Gerhard, W., Croce, C. M., Lopes, D. & Koprowski, H. *Proc. natn. Acad. Sci. U.S.A.* **75,** 1510–1514 (1978).
10. Zurawski, V. R., Hurrell, J. G. R., Latham, W. C., Black, P. H. & Haber, E. *Fedn Proc.* **39,** 1204 (1980).
11. Rosenberg, S. A. & Terry, W. O. *Adv. Cancer Res.* **25,** 323–388 (1977).
12. Young, W. W. Jr, & Hakomori, S. *Science* **211,** 487–489 (1981).
14. Bernstein, I. D., Tam, M. R. & Nowinski, R. C. *Science* **207,** 68–71 (1980).
14. Koprowski, H., Steplewski, Z., Herlyn, D. & Herlyn, M. *Proc. natn. Acad. Sci. U.S.A.* **75,** 3405–3409 (1978).
15. Herlyn, D. M., Steplewski, Z., Herlyn, M. F. & Koprowski, H. *Cancer Res.* **40,** 717–721 (1980).
16. Nadler, L. M. *et al. Cancer Res.* **40,** 3147–3154 (1980).
17. Miller, R. A. & Levy, R. *Lancet* **ii,** 226–230 (1981).
18. Yeh, M. Y., Hellstrom, I., Brown, J. P., Warner, G. A., Hansen, J. A. & Hellstrom, K. E. *Proc. natn. Acad. Sci. U.S.A.* **76,** 2927–2931 (1979).
19. Herlyn, M. *et al. Cancer Res.* **40,** 3602–3609 (1980).
20. Seeger, R. C., Rosenblatt, H. M., Imai, K. & Ferrone, S. Cancer *Res.* **41,** 2714–2717 (1981).

Oxygen intermediates are triggered early in the cytolytic pathway of human NK cells

John C. Roder, Stephen L. Helfand*, Jerome Werkmeister, Ronald McGarry, Timothy J. Beaumont & Axel Duwe†

Department of Microbiology and Immunology, Queen's University, Kingston, Ontario, Canada K7L 3N6
* Department of Neurology, Massachusetts General Hospital, Harvard Medical School, Harvard University, Boston, Massachusetts 03128, USA
† Department of Medical Microbiology, University of Toronto, Banting Institute, 100 College Street, Toronto, Ontario, Canada M5G 1L5

The mechanism of tumour cell destruction by natural killer (NK) cells or other lymphocytes is not understood. NK cells appear to represent a primitive anti-tumour surveillance system more analogous to macrophages than lymphocytes[1]. Free oxygen radicals (O_2^-, OH) and H_2O_2 are thought to be involved in cell destruction by macrophages[2] and therefore we looked for similar cytocidal intermediates of oxygen in NK cells. These highly reactive molecular species can easily be detected in the presence of luminol by the emission of light[3]. We show here that highly enriched human NK cells respond to NK-sensitive but not NK-insensitive tumour cells with a rapid burst of oxygen metabolites as detected both by chemiluminescence and cytochrome *c* reduction. Agents which can prevent chemiluminescence and cytochrome *c* reduction, such as superoxide dismutase (SOD), reduced NK-mediated cytolysis and agents which increased chemiluminescence, such as interferon, also increased NK-mediated cytolysis. These results suggest that the production of oxygen species may be the earliest event to occur in the NK cell following tumour cell contact, and these products are involved in NK-mediated cytolysis.

Peripheral blood lymphocytes were depleted of monocytes and separated on a discontinuous Percoll density gradient[4]. Lymphocytes from the NK-enriched fraction were dark-adapted in the presence of luminol, to achieve a stable background, and then stimulated by the addition of tumour cells at a 10:1 tumour cell/lymphocyte ratio. As shown in Fig. 1, the addition of K562 cells (a human erythroleukaemia) caused a rapid increase in chemiluminescence, reaching a peak of 167×10^3 c.p.m. within 30 s followed by a rapid decline and a second peak of 120×10^3 c.p.m. at 3 min followed by a more gradual decline to low levels at 8 min. Parallel experiments using a cytochrome *c* reduction assay revealed rather slower kinetics with a reaction velocity of 200 pmol cytochrome *c* reduced per min per 10^6 Percoll fractionated cells. No further cytochrome *c* reduction occurred after 8 min, by which time the chemiluminescence response had returned almost to the background level. Addition of P815-2 cells (a murine mastocytoma) to Percoll fraction 2 cells caused a low chemiluminescence response (35×10^3 c.p.m.) and little cytochrome *c* reduction (<200 pmol) (Fig. 1). The area under the anti-P815-2 chemiluminescence curve was 36% of that under the anti-K562 curve. Addition of 100 μg (280 U) of SOD caused an 80–90% inhibition of both chemiluminescence and cytochrome *c* reduction. Even concentrations as low as 10 $\mu g\ ml^{-1}$ had a small but significant effect (data not shown).

To investigate the cells generating chemiluminescence, NK cells were enriched on a Percoll density gradient[4]. As shown in Fig. 2, there was a striking parallel between those fractions enriched in NK cytolytic activity and those fractions yielding the highest levels of chemiluminescence. In addition, Percoll fraction 2 cells reduced 210 pmol cytochrome *c* per min per

0028-0836/82/310569—04$01.00

Table 1 Production of oxygen species after target-cell binding

		% Control			
Expt	Condition	Chemiluminescence	Cytochrome *c* reduction	Cytolysis	Conjugates
a	R anti-mIgM(1/10) + C′	100	100	100	100
	Anti-HNK-1 (100 μg ml^{-1}) + R anti-mIgM + C′	44	38	25	30
b	HEF	164	NT	210	120
	K562	100	NT	100	100
	K562-induced clone B	48	NT	33	25
	Chang	29	NT	20	26
	L5178Y	15	NT	5	5
c	Control	100	NT	100	100
	Fixed target (K562)	97	NT	NT	90
	Fixed effector (NK)	0	NT	0	88
	K562 p.m. vesicles	80	NT	NT	NT
	P815 p.m. vesicles	0	NT	NT	NT
d	Normal NK responder ($n = 10$)	100	100	100	100
	Low NK responder ($n = 4$)	47	50	20	98
	CH patients ($n = 3$)	100	NT	2	105
e	Control	100	100	100	100
	SOD (100 μg ml^{-1}; 280 U)	11	8	25	105
	SOD-boiled	100	100	100	99
	Catalase (100 μg ml^{-1}; 1,150 U)	100	100	100	100
f	Control	100	NT	100	100
	β-Interferon (200 U ml^{-1})	150		200	95
	α-Interferon (500 U ml^{-1}	120	NT	150	110
	α-Interferon + anti-interferon (1/50)	100	NT	110	105

Macrophage-depleted, peripheral blood lymphocytes were prepared and separated on Percoll density gradients as described in Fig. 2 legend. Each fraction was tested in a 2-h ^{51}Cr-release assay against K562 and the most active fraction (usually fraction 2) was treated as shown, and tested in parallel for (1) K562-stimulated chemiluminescence, calculated as the area under a 10-min curve (control values were 4–9 × 10^5 total counts); (2) cytochrome *c* reduction calculated as pmol cytochrome *c* reduced per min per 10^6 cells during the first 6 min of reaction (control values = 175–225); (3) cytolysis of K562 in a 4-h ^{51}Cr-release assay, calculated as lytic units at 20% lysis (control values were 8–16 × 10^2 lytic units per 10^7 cells); (4) the per cent fraction 2 cells binding to K562 cells in a single cell assay[19] (control values were 40–60%). All values are expressed as per cent control for ease of comparison. *a*, 2 × 10^6 fraction 2 cells were treated for 1 h at 0 °C with medium as control or 100 μg ml^{-1} (1/1,000 ascites fluid) of monoclonal, mouse anti-human NK antibody (HNK-1) (provided by T. Abo and C. Balch), washed and then treated for 1 h at 0 °C with 1/10 rabbit anti-mouse IgM (Cappel) (R anti-mIgM) followed by a 1-h treatment at 37 °C with 1/2 rabbit complement (C′) previously absorbed with human lymphocytes. *b*, 10^7 cells from various cell lines were added to fraction 2 cells. HEF, human embryonic fibroblasts; K562, human erythroleukaemia; clone B from K562 cultures induced to differentiate with sodium butyrate[13]; Chang, human hepatocarcinoma; and L5178Y, a lymphoma induced in DBA/2 mice with methylcholanthrene. *c*, K562 cells or Percoll fraction 2 cells were treated for 1 h at 37 °C with 0.2% glutaraldehyde and then mixed with unfixed effectors or targets respectively. K562 or P815 cells were also disrupted in a nitrogen bomb and plasma membrane vesicles were isolated on sucrose density gradients. The equivalent of 10^7 intact tumour cells (28 μg protein) were added to the effectors. *d*, Ten normal and four stably low NK responders were selected from a pool of 600 multiply tested, healthy donors, previously identified by Dr H. Pross. Cells from three Chediak-Higashi (CH) patients were provided by Drs L. Boxer and A. S. Fauci. *e*, Superoxide dismutase (Sigma, 2,800 U per mg protein), catalase (11,500 units per mg) and boiled (30 min) SOD as control was added to fraction 2 cells approximately 1 min before addition of K562. Cytotoxicity was measured in a 2-h assay. SOD activity was confirmed in a xanthine oxidase system[20]. *f*, Fraction 2 cells were preincubated for 30 min at 20 °C with 200 or 500 U human β-interferon (10^8 units per mg protein, provided by C. Tan) and α-interferon respectively. α-Interferon was incubated for 2 h at 4 °C with 1/50 monoclonal anti-human leukocyte interferon[21] (clone NK2; provided by Dr D. S. Secher) followed by 1/10 goat anti-mouse immunoglobulin. Precipitates were removed by centrifugation. Each experiment was repeated three times with similar results. NT, not tested.

10^6 cells in response to K562 compared with zero in Percoll fraction 5, the only fraction tested. Immunofluorescence assays with monoclonal antibodies revealed that fraction 2 cells were enriched fivefold in the following NK markers compared with unfractionated lymphocytes: 60% HNK−1$^+$ (NK specific[5]), 52% OKM1$^+$ (ref. 6), 38% mac−1$^+$ (ref. 7) and depleted severalfold in the following non-NK markers: 15% OKT3$^+$ (T cells)[8] and 3% Ia$^+$ (B cells + monocytes + activated T cells)[9]. In addition, fraction 2 cells were >50% large granular lymphocytes (LGL), a morphological marker of human NK cells[4], and <0.1% granulocytes as judged by morphology in Giemsa-stained cytocentrifuge preparations or by immunofluorescent staining with a monoclonal antibody specific for human polymorphonuclear leukocytes (PMN). Over 50% of fraction 2 cells bound to ox erythrocytes coated with rabbit IgG anti-ox erythrocytes antibody (EA$^+$) which is another NK characteristic, whereas <0.1% phagocytosed the erythrocytes to which they were attached. In addition, <0.1% of the cells expressed the Mo2 marker[10] specific for human monocytes and <0.1% stained cytochemically for acid esterase. Therefore Percoll fraction 2 cells were contaminated with few (<0.1%) granulocytes or phagocytic macrophages and over half expressed NK markers and morphology. The few T cells in the preparation were probably not important since Percoll fractions 5 and 6 consisted of 90% T3$^+$ cells and did not generate significant chemiluminescence. When monocytes (purified by plastic adherence) or granulocytes (isolated on Ficoll–Hypaque followed by hypotonic shock of the cell pellets) were incubated together with Percoll fraction 2 cells at a cell dose approaching 1% contamination (10^4 cells ml^{-1}), the chemiluminescence response to K562 was not altered. In addition, 10^4–10^5 monocytes or PMN alone gave an insignificant response (< 10 × 10^3 c.p.m. above background) to K562 over the 10-min period of the chemiluminescence assay. Furthermore, 10^{-8}M phorbol-12-myristate-13-acetate-4-*O*-methyl ether (PMA) caused no chemiluminescence in Percoll fraction 2 cells although Percoll fraction 1 cells and purified monocytes or granulocytes generated >4 × 10^6 c.p.m. within seconds after addition. It is unlikely, therefore, that monocyte or PMN contamination can account for the response of the NK-enriched populations. Furthermore, we[11] as well as others[12] have shown that PMN- and macrophage-mediated cytoxicity of certain tumour cells is inhibited by catalase but not SOD, whereas NK-mediated cytotoxicity can be inhibited by SOD but not catalase as shown below. Finally, pretreatment of fraction 2 cells with monoclonal anti-HNK-1 antibody and complement, a procedure known to selectively remove NK cells[5], reduced the chemiluminescence, cytochrome *c* reduction, conjugate formation and cytolytic response against K562 by 56–75% (Table 1, expt *a*). It is likely, therefore, that most of the these responses are mediated by NK cells.

We then asked if the generation of chemiluminescence was

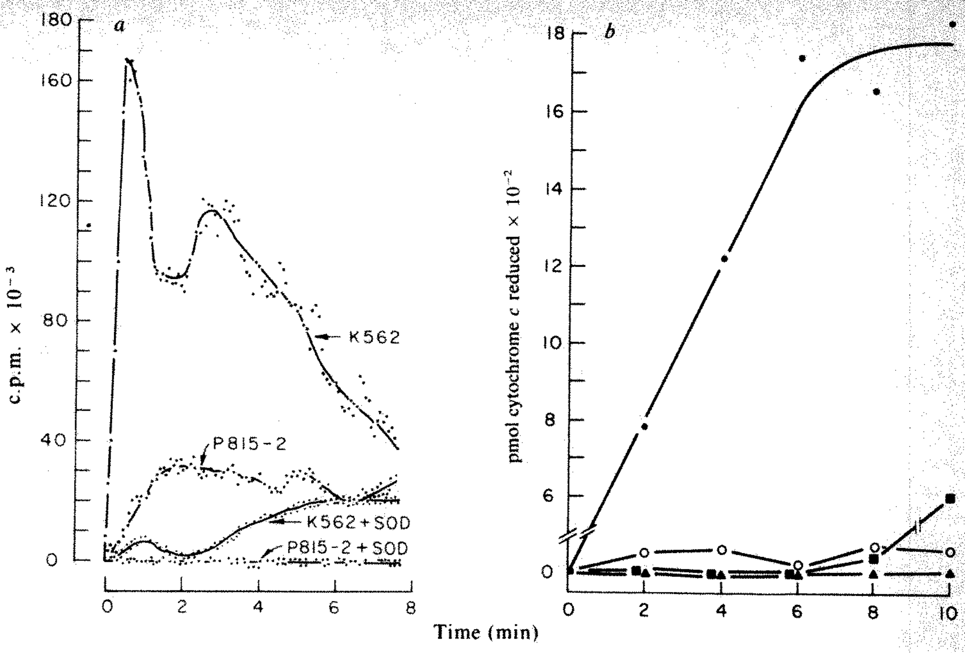

Fig. 1 Chemiluminescence and cytochrome *c* reduction in large granular lymphocytes (LGL) induced by NK-sensitive tumour cells. Peripheral blood was treated for 30 min at 37 °C with carbonyl-iron and a magnet to remove monocytes. Mononuclear cells were isolated by centrifugation on Ficoll-Hypaque (1.077 g cm^{-3}) and were further depleted by adherence on autologous serum-coated plastic dishes for 1 h at 37 °C. The non-adherent lymphocytes were layered on a five-step, discontinuous, Percoll density gradient and centrifuged for 30 min at 20 °C as described by Timonen and Saksela[4] and elaborated in Fig. 2 legend. Fraction 2 cells were enriched fivefold in cytolytic activity against K562; 60% of fraction 2 cells were LGL as detected morphologically in Giemsa smears, whereas <0.1% phagocytosed antibody-coated erythrocytes. *a*, 10^6 Percoll fraction 2 cells were dark-adapted for 30 min in 1.0 ml of 10% luminol-saturated, fetal calf serum in plastic scintillation vials. 10^7 tumour cells, medium alone, or tumour cells + 100 μg superoxide dismutase (280 U) was added in 0.1 ml volumes and mixed. Chemiluminescence was measured at ambient temperature (20 °C) in an LKB liquid scintillation counter in the out of coincidence mode. Values represent c.p.m. above background, measured in successive 5-s intervals. Luminol alone gave 35×10^3 c.p.m. and fraction 2 cells + luminol gave a stable background of 50×10^3 c.p.m. throughout the 8 min of the assay. This experiment was repeated 10 times with similar results and in replicate samples within each experiment the area under the curves varied <3%. *b*, 10^6 fraction 2 cells were combined with 10^7 K562 cells (●), 10^7 P815-2 cells (○), 10^7 K562 cells + 100 μg per ml SOD (280 U) (■), 10^7 P815-2 cells + 100 μg per ml SOD (280 U) (▲) in 1 ml of balanced salt solution (BSS) containing 0.2% bovine serum albumin in 10 μM KCN, 200 U catalase (Sigma; thymol-free) and 0.01 mM cytochrome *c* (Sigma, type III). After varying periods of incubation at 20 °C the reaction was stopped at 0 °C. Supernatants were measured spectrophotometrically at A_{550}. Maximum, reducible cytochrome *c* was determined with an excess of sodium dithionite. Absorbance readings were converted to pmol cytochrome *c* reduced after subtracting a small background response (<500 pmol) by tumour cells alone. Fraction 2 cells gave zero background over the 10-min period of assay. This experiment was repeated five times with similar results and values for replicate samples at each point varied <10%.

triggered in NK cells by a selective membrane binding event. As shown in Table 1, expt *b*, the degree of chemiluminescence correlated well ($r = 0.96$) with the degree of target cell binding in a survey of five different cell lines. One of the lines was a clone from K562 cultures which had been induced to differentiate in the presence of haemin[13]. Cell-free culture supernatants of K562 were inactive but plasma membrane vesicles also triggered chemiluminescence (Table 1*c*). Vesicles from a NK-insensitive target (P815) were not effective. The directionality of the response was indicated by the fact that mild glutaraldehyde fixation of NK cells abolished the chemiluminescence response to untreated K562 cells although conjugate formation was not markedly altered. Glutaraldehyde-fixed targets, on the other hand, stimulated a normal response in unfixed NK cells. It is likely therefore that target–effector binding stimulates the effector, rather than target, to generate chemiluminescence.

We emphasize that target-cell binding may not be a sufficient stimulus for release of oxygen species. Hence, stably low NK responders, selected from 600 screened normals, exhibited normal frequencies of HNK-1$^+$ NK cells and normal target cell binding but failed to generate normal levels of chemiluminescence, cytochrome *c* reduction or cytolysis (Table 1*d*). Furthermore, genetically NK-defective, Chediak-Higashi (CH) patients[14] also had normal frequencies of HNK-1$^+$ NK cells, normal target-cell binding and normal levels of chemiluminescence but markedly deficient cytolysis. Therefore, the generation of chemiluminescence may be necessary but not sufficient for cytolysis.

The generation of oxygen intermediates, particularly the superoxide anion, O_2^-, may be necessary for cytolysis because SOD (100 μg ml^{-1}, 280 U) inhibited 90% of chemiluminescence and cytochrome *c* reduction and consequently reduced cytolysis by 75% in a short-term (<2 h) ^{51}Cr-release assay (Table 1, expt *e*). Target-cell binding was not effected by SOD and denatured SOD did not inhibit chemiluminescence, cytochrome *c* reduction or cytolysis. Catalase was also non-inhibitory, as shown, although similar concentrations prevented monocytes from generating chemiluminescence and mediating cytotoxicity against L5178Y in parallel experiments (data not shown). In contrast to the inhibitory effects of SOD, both human α- and β-interferon were shown to augment chemiluminescence in parallel with cytotoxicity (Table 1*f*). Target binding was not effected.

Other cell subpopulations have also been shown to generate oxygen intermediates. Thymocytes stimulated with phytohaemagglutinin generated a peak chemiluminescence response of 15×10^3 c.p.m. per 10^8 cells[15] which compares with a peak NK response of 170×10^3 c.p.m. from only 10^6 Percoll fraction 2 cells in the present study (Fig. 1). Neutrophils (10^7) and mononuclear cells (5×10^7) generated up to 30×10^3 c.p.m. and 10×10^3 c.p.m. respectively, in response to opsonized bacteria[16]. Neutrophils stimulated with PHA generated 800 pmol cytochrome *c* reduced per min per 10^6 cells[17] compared with 200 pmol cytochrome *c* per min per 10^6 NK-enriched cells stimulated with K562 (Fig. 1). Therefore the NK cell response to K562 targets is similar to the response of other cell types to various stimuli.

In comparison with our findings with NK cells, alloimmune killer T cells in mice were not inhibited in function by any concentration of SOD tested (100–1,500 μg ml^{-1})[18]. Therefore killer T cells may function by a SOD-resistant mechanism[18] and monocyte-mediated cytolysis is catalase-sensitive and SOD-resistant[12]. The SOD-sensitive triggering of cytolysis in NK cells may be a unique phenomenon.

In conclusion, these results suggest that human NK cells are triggered to release oxygen intermediates including O_2^-, by contact with NK-sensitive targets. Although these oxygen species appear to be involved in cytolysis, their function may be to activate a subsequent step in the cascade of events leading to target cell destruction.

We thank I. Louwman and A. Wade for assistance and Drs Toru Abo and Charles Balch for the HNK-1 antibody. This

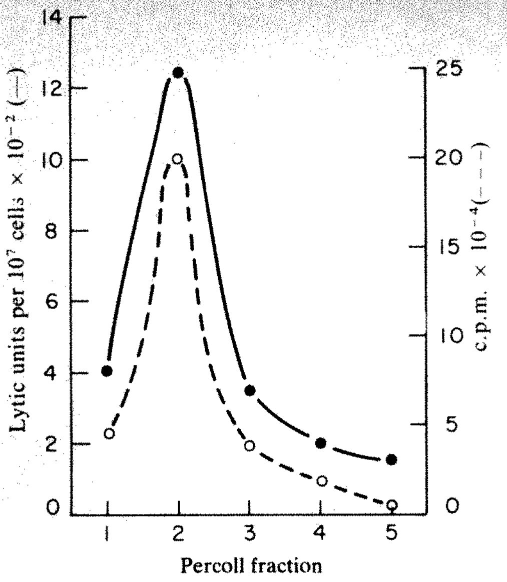

Fig. 2 Correlation between NK enrichment or depletion and chemiluminescence. Peripheral blood lymphocytes were prepared as outlined in Fig. 1 legend and layered on a five-step discontinuous Percoll (Pharmacia) density gradient[4]. The top layer consisted of 40% Percoll (v/v) diluted in medium and adjusted to 285 mosmol with a refractive index of 1.3432. Each 2-ml layer varied by 2.5% Percoll. The gradient was loaded with 10^8 lymphocytes and centrifuged at 550 g for 30 min at 20 °C. Cell yields were as follows ($\times 10^{-6}$): fraction 1, 13.3; fraction 2, 7.5; fraction 3, 48.4; fraction 4, 24.4; fraction 5, 8.3. Cytolysis was measured in a 4-h ^{51}Cr-release against K562. Values are expressed in lytic units per 10^7 lymphocytes where one lytic unit is the number of lymphocytes required for 20% lysis. To measure chemiluminescence, 10^6 lymphocytes in luminol were stimulated with 10^7 K562 cells as described in Fig. 1 legend. Values represent the c.p.m. above background in the first peak. A similar curve was generated using a calculation based on the area under the entire curve for cells from each Percoll fraction. Unfractionated lymphocytes yielded 240 lytic units per 10^7 cells and 3×10^4 c.p.m. This experiment was repeated five times with similar results.

work was supported by grants to J.C.R. from the MRC and NCI of Canada. J.W. and R.M. are recipients of a NCI Senior Research Fellowship and a Multiple Sclerosis Society Fellowship, respectively. S.L.H. was supported by a Principal's Development grant from Queen's University.

Note added in proof: Recent experiments reveal partially depressed NK-mediated cytolysis in strictly anaerobic conditions, which confirms an oxygen-dependent component in the cytolytic pathway.

Received 2 October 1981; accepted 13 May 1982.

1. Babior, B. M. *New Engl. J. Med.* **298,** 659–668 (1978).
2. Roder, J. C., Karre, K. & Kiessling, R. *Prog. Allergy*, **28,** 66–159 (1981).
3. Allen, R. C., Stjernholm, R. L. & Steele, R. H. *Biochem. biophys. Res. Commun.* **47,** 679–684.
4. Timonen, T. & Saksela, E. *J. immun. Meth.* **36,** 285–291 (1980).
5. Abo, T. & Balch, C. M. *J. Immun.* **127,** 1024–1029 (1981).
6. Zarling, J. M. & Kung, P. C. *Nature* **288,** 394–396 (1980).
7. Ault, K. & Springer, T. *J. Immun.* **126,** 359–364 (1981).
8. Kung, P. C., Goldstein, G., Reinherz, E. & Schlossman, S. *Science* **206,** 347–349 (1979).
9. Reinherz, E. *et al. J. exp. Med.* **150,** 1472–1482 (1979).
10. Todd, R. F., Nadlér, L. M. & Schlossman, S. *J. Immun.* **126,** 1435–1442 (1981).
11. Helfand, S, Werkmeister, J. & Roder, J. C. *J. exp. Med.* **156** (in the press).
12. Nathan, C. F., Silverstein, S. C., Brukner, L. H. & Cohn, Z. A. *J. exp. Med.* **149,** 100–113 (1979).
13. Werkmeister, J. *et al. Cell. Immun.* **68** (in the press).
14. Roder, J. C. *et al. Nature* **284,** 553–555 (1980).
15. Wrogemann, K., Weidemann, M. J., Ketelson, U. P., Wekerle, H. & Fisher, H. *Eur. J. Immun.* **10,** 36–40 (1980).
16. Nelson, R. D., Mills, E. L., Simmons, R. L. & Quil, P. G. *Infect. Immunity* **14,** 129–134 (1976).
17. Simchowitz, L. & Spilberg, I. *Immunology* **37,** 301–309 (1979).
18. Devlin, R. G., Lin, C. S., Peper, R. J. & Dougherty, H. *Immunopharmacology* **3,** 147–159 (1981).
19. Timonen, T., Ortaldo, J. R. & Herberman, R. B. *J. exp. Med.* **153,** 569–582 (1981).
20. McCord, J. M. & Fridovich, I. *J. biol. Chem.* **244,** 6049–6055 (1969).
21. Secher, D. S. & Burke, D. C. *Nature* **285,** 446–450 (1980).

Adenosine-induced slow ionic currents in the *Xenopus* oocyte

Ilana Lotan, Nathan Dascal, Sasson Cohen & Yoram Lass

Department of Physiology and Pharmacology, Sackler School of Medicine, Tel-Aviv University, Ramat-Aviv 69 978, Israel

Adenosine and its 5′-phosphorylated congeners evoke specific membrane-mediated responses in excitable tissues[1,2]. Available data suggest that inhibition of the target cell occurs due to hyperpolarization[3,4], and in some preparations a compound effect of ATP (excitation and inhibition) has been found[5,6]. However, the ionic mechanism of the purinergic-mediated response has not been studied by standard intracellular voltage-clamping techniques. Recently, we have discovered purinergic receptors in the *Xenopus* oocyte, a well defined giant cell amenable to rigorous electrophysiological[7] and biochemical[8] studies. We report here that in these cells, adenosine-induced slow membrane responses consisted of an early depolarizing (D) transient current carried by Cl^- ions, followed by a steady hyperpolarizing (H) current involving K^+ ions. The relative potency sequence for the D current was ATP ≃ ADP > AMP ≃ adenosine; this order was reversed for the H current.

Fully grown oocytes (stages 5 and 6)[9] were dissected from an ovary of *Xenopus laevis*, mounted in a 1-ml Perspex bath and continuously perfused at room temperature with Ringer's solution (mM): Na^+, 116; K^+, 2; Ca^{2+}, 1.8; Cl^-, 128.6; Mg^{2+}, 1; Tris, 5. In a standard experiment the oocyte was impaled with two microelectrodes and the cell was clamped at −50 mV. The cell was then exposed to one of the active compounds and the induced membrane current recorded on a paper chart (YEW 3022).

Typical responses to 4×10^{-5} M adenosine and 4×10^{-5} M ATP are shown in Fig. 1. The basic response consists of an initial 'fast' inward current of 10–30 s duration (D), followed by a long-lasting outward current (H). The relative potency sequence for the H-response was: adenosine ≃ AMP > ADP ≃ ATP, whereas that for the D response was: ATP ≃ ADP > AMP ≃ adenosine. In some preparations, adenosine failed to evoke the D response and the H response was the only current recorded. In these cells, the latency of the H response was 25–40 s, well beyond the 'dead time' of the perfusion system (5–10 s). The latency of the D response was the same as the perfusion 'dead time'.

Voltage–current curves were obtained using a ramp command voltage. The reversal potentials of the D and H responses, measured as described in Fig. 2 legend, were [mean (mV) ± s.e.m. (number of cells)] −21.86 ± 2.34(7) for the D current and −102.7 ± 3.6(7) for the H current. A plot of the D reversal potential as a function of the log external Cl^- concentration showed a strict Nernst relationship (Fig. 3*a*), which suggests

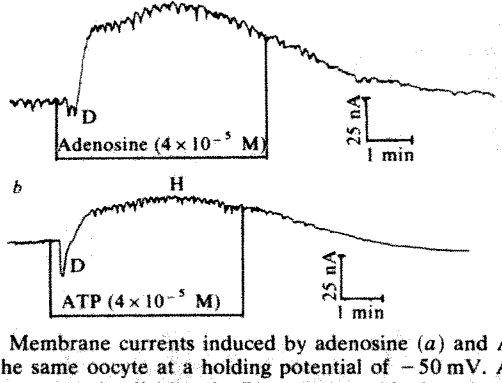

Fig. 1 Membrane currents induced by adenosine (*a*) and ATP (*b*) in the same oocyte at a holding potential of −50 mV. ATP was more potent in eliciting the D response, and adenosine was more potent in eliciting the H response.

0028–0836/82/310572—03$01.00

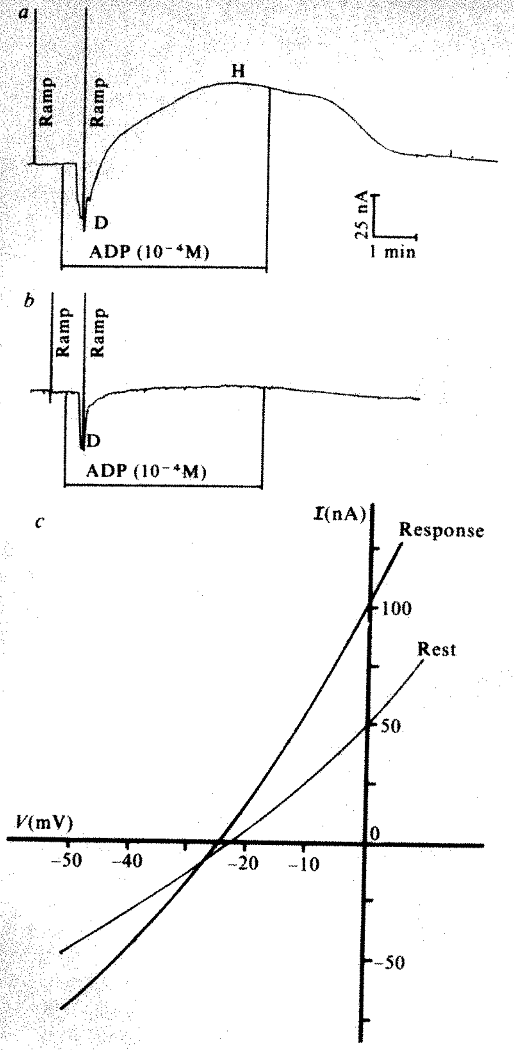

Fig. 2 *a*, Oocyte response to 10^{-4} M ADP at a holding potential of −50 mV. *b*, Blocking of the H current by tetraethylammonium (3×10^{-2} M) in the same cell. Two ramp-like changes of the holding potential (duration 0.8 s) were applied, one just before application of ADP and a second at the plateau of the D current. The voltage electrode was connected to the *x* axis of the *x–y* plotter, the current electrode to the *y* axis, and the voltage–current relationships were plotted automatically (*c*). The reversal potential of the D current was obtained from the cross-over point.

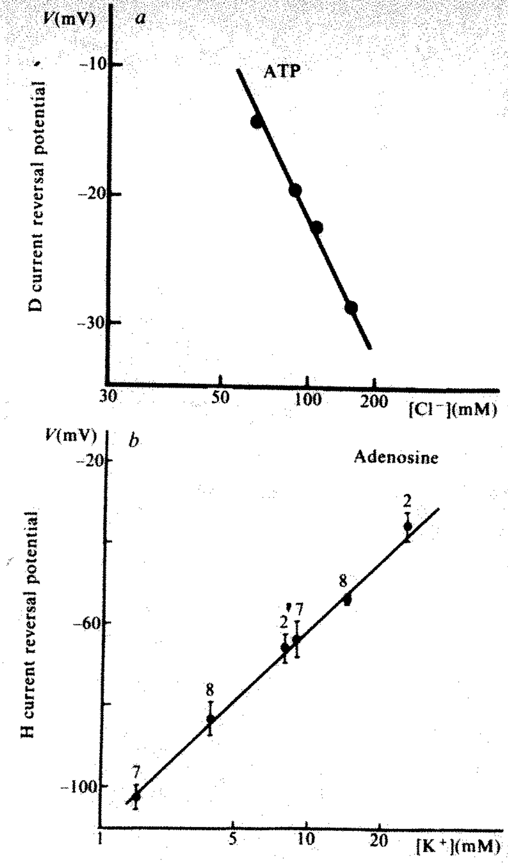

Fig. 3 *a*, Relationship between the D current reversal potential and bath Cl⁻ concentration in the same oocyte. SO_4^{2-} was substituted for Cl⁻ and tonicity was kept constant with sucrose. A strict Nernst relationship was obtained with a slope of 58 mV for a 10-fold change in Cl⁻ concentration. *b*, Reversal potential of the H current plotted against bath K⁺ concentration in several oocytes. KCl was replaced by $MgCl_2$, with the Cl⁻ concentration kept constant, and tonicity balanced by sucrose. In control experiments, increased Mg^{2+} had no effect on the H current reversal potential: again a strict Nernst relationship was obtained.

that the D current is carried by Cl⁻ ions. The involvement of Cl⁻ in mediating the oocyte membrane depolarization has already been postulated[7]. A similar Nernst plot showed that the H current is carried by K⁺ ions (Fig. 3*b*). Moreover, tetraethylammonium (3×10^{-2} M) almost completely abolished the H current (Fig. 2*b*), with no effect on the D current. Based on the measured reversal potential and the Nernst equation, the intracellular concentrations of K⁺ and Cl⁻ were calculated to be (mM) 117.0 and 54.0, respectively. The value for K⁺ correlates well with intracellular [K⁺] measurements (102 ± 2 mM) for *Rana pipiens* oocytes[10].

The spontaneous membrane current fluctuations shown in Fig. 1*a* were observed in ~20% of the cells. The reversal potential of the fluctuations was the same as the D current reversal potential. Thus Cl⁻ may be involved in generating these currents. In most cases, ATP increased the amplitude of the fluctuations (Fig. 1*b*).

The purinergic response was preserved after complete removal of the follicular cells, which normally envelop the oocyte. The follicular cells were removed by shaking for 2.5 h in collagenase (2 mg ml^{-1}, dissolved in Steinberg solution (mM): 58 = Na⁺, 1 = K⁺, 1.8 = Ca²⁺, 69.6 = Cl⁻). The oocyte was then returned to normal Ringer's for 1 h and tested for the presence of purinergic responses. The same cell was fixed, embedded in paraffin, sectioned and stained with haematoxylin-eosin. In eight oocytes examined morphologically, the follicular cells were completely removed but the purinergic response was preserved; the H current, however, was rather reduced.

These results demonstrate a compound membrane response to adenosine, generated by two distinct ionic mechanisms having different relative potency sequences for the purinergic agonists. Further pharmacological characterization of the oocyte purinergic response was achieved using theophylline. Figure 4 shows selective and reversible blocking of the H current by 5×10^{-5} M theophylline. This blocking action was tested in the range 10^{-6} M–10^{-4} M theophylline, and was found to be dose dependent. The D current was augmented, probably due to the removal of the H current, and remained unaffected even at 10^{-4} M theophylline. The reported heterogeneity among

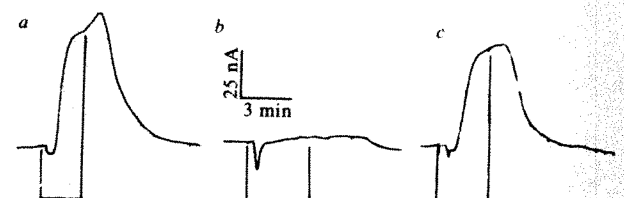

Fig. 4 Selective blocking of the H current by theophylline. *a*, Control response; *b*, a response of the same oocyte after 20 min incubation in 5×10^{-5} M theophylline; *c*, a response of the same oocyte after a 20 min wash period in normal Ringer's.

purinergic receptors[11-14] might represent the biochemical and pharmacological basis of this diversity in electrophysiological response. More specifically, the H current is probably mediated by the P1-receptor type[15].

The oocyte response to adenosine is qualitatively similar to muscarinic cholinergic responses described previously[7,16]. However, the adenosine response was not blocked by atropine (10^{-5} M), which suggests that the various membrane receptors may have the same biochemical mechanism, possibly mediated by cyclic nucleotides[17], for opening 'slow' ionic channels in the oocyte membrane.

We thank the Recanti Fund for Medical Research for support.

Received 10 December 1981; accepted 11 May 1982.

1. Burnstock, G. *Circulation Res.* **46,** 1175–1182 (1980).
2. Urthaler, F., Woods, W. T., James, T. N. & Walker, A. A. *J. Pharmac. exp. Ther.* **216,** 254–260 (1981).
3. Hartzell, H. C. *J. Physiol., Lond.* **293,** 23–50 (1979).
4. Tomita, T. & Watanabe, H. *J. Physiol., Lond.* **231,** 167–178 (1973).
5. Flitney, F. W. & Singh, I. *J. Physiol., Lond.* **304,** 21–42 (1980).
6. Yatani, A., Goto, M. & Tsuda, Y. *Jap. J. Physiol.* **28,** 47–61 (1978).
7. Kusano, K., Miledi, R. & Stinnakre, J. *Nature* **270,** 739–741 (1977).
8. Maller, J. L., Butcher, F. R. & Krebs, E. G. *J. biol. Chem.* **254,** 579–582 (1979).
9. Dumont, J. N. *J. Morph.* **136,** 153–180 (1972).
10. Morrill, G. A. & Ziegler, D. *Devl Biol.* **14,** 216–223 (1980).
11. Burnstock, G. *J. Physiol., Lond.* **313,** 1–34 (1981).
12. Van Calker, D., Muller, M. & Hamprecht, B. *Nature* **276,** 839–841 (1978).
13. Londos, C. & Wolff, J. *Proc. natn. Acad. Sci. U.S.A.* **74,** 5482–5486 (1977).
14. Londos, C., Cooper, D. M. F. & Wolff, J. *Proc. natn. Acad. Sci. U.S.A.* **77,** 2551–2554 (1980).
15. Brown, C. M. & Burnstock, G. *Br. J. Pharmac.* **73,** 617–624 (1981).
16. Dascal, N. & Landau, E. M. *Life Sci.* **27,** 1423–1428 (1980).
17. Rodbell, M. *Nature* **284,** 17–22 (1980).

Presence of cyclic nucleotide–Ca^{2+} independent protein kinase in bovine brain coated vesicles

A. Pauloin, I. Bernier & P. Jollès

Laboratory of Proteins, University of Paris V, CNRS ER 102 and
INSERM Unité U-116, 45 rue des Saints-Pères,
F75270 Paris Cedex 06, France

Coated vesicles, which are membrane vesicles enclosed by a polyhedral protein lattice, are involved in many cellular events[1-6], including intracellular membrane transport and protein secretion, in which they must be able to undergo repeated membrane fusion and fission. The icosahedral lattice of protein surrounding the core of coated vesicles is composed predominantly of clathrin, a 180,000 (180 K) molecular weight protein, and other 30 K and 36 K polypeptides[7,8]. In native conditions, the basic subunit of the coat consists of a trimer of clathrin with probably three polypeptides of 30K and/or 36K (refs 9–11). Additional minor proteins of 100K and 55K have been reported in purified coated vesicles[12]. We describe here the presence of cyclic nucleotide- and Ca^{2+}-independent protein kinase activity in coated vesicles. This protein kinase phosphorylates specifically a unique 50K protein which can be co-purified with clathrin and seems to be an integral protein of coated vesicles.

Coated vesicles were isolated from fresh bovine brain according to a slightly modified procedure of Keen *et al.*[13] The highly enriched upper 5% sucrose solution of the second gradient was used for the final purification using a self-generated density gradient centrifugation of Percoll (Pharmacia). We verified the homogeneity of this material by submitting samples from the upper and lower opalescent Percoll zones to agarose gel electrophoresis. The lower Percoll fraction corresponds to the more slowly migrating agarose zone which contains smooth vesicles and membrane fragments while the upper Percoll fraction corresponds to the faster migrating agarose zone which contains only coated vesicles and empty coats (see Fig. 1 and ref. 12). Aliquots of coated vesicles obtained after the different purification steps were incubated in presence of [γ-^{32}P]ATP. Figure 2 shows an analysis by SDS-polyacrylamide gel electrophoresis of the radiolabelled and stained proteins.

Many proteins are phosphorylated in the grey matter homogenate but only one 50K phosphoprotein, which is poorly stained by Coomassie blue, can be co-purified with clathrin. The pattern of radioactive proteins indicates that neither clathrin nor the 30–36K polypeptides are phosphorylated. We verified the presence of both the 50K protein substrate and its specific kinase in coated vesicles after agarose gel electrophoresis[12]. Following the electrophoresis, the different supernatants from the centrifuged broken agarose gel fractions (see Fig. 3 legend) were incubated with [γ-^{32}P]ATP. The 50K radiolabelled protein co-purified with clathrin (Fig. 3). Using radiolabelled ATP, a slight phosphorylation of a 100K band could be observed in our experimental conditions, but not after the incubation of coated vesicles just purified by Percoll centrifugation: this unexpected observation is now being investigated. Fig. 3 shows not only the association of the 50K protein substrate with coated vesicles but also that the kinase activity is a constitutive part of the vesicles. Phosphorylation of the 50K protein occurred without cyclic AMP or cyclic GMP in the reaction mixture, and addition of 40 μM cyclic AMP or cyclic GMP did not modify the phosphorylation (Fig. 4, lanes 6, 7).

The presence of calmodulin in coated vesicles[14] and the dependence of the phosphorylation of many proteins on calmodulin and Ca^{2+} have been described. We therefore investigated whether Ca^{2+} and calmodulin had any effect on the *in vitro* phosphorylation of the 50K protein. The addition of 1 mM EGTA or 10 μg exogenous calmodulin or calmodulin inhibitors, such as 1 mM dibucaine[15] or 50 μM trifluoperazine[16], to the reaction mixture had no effect on the 50K polypeptide labelling (Fig. 4, lanes 1–4). Furthermore, the isolation of coated vesicles in Ca^{2+}-depleted MES buffer (see Fig. 2 legend) did not modify the purification of either clathrin or 50K protein, or the phosphorylation of the latter (data not shown). Note that a high concentration of trifluoperazine (400 μM) blocks the phosphorylation of the 50K protein but allows that of the 100K coated vesicles protein (Fig. 4, lane 5). Dibucaine (10 mM) induced the same effect (data not shown).

The 50K phosphoprotein and its kinase are not membrane contaminants or traces of smooth vesicles, as they cannot be eliminated even by agarose gel electrophoresis, which is considered to be the most powerful purification technique. Recently, Pfeffer and Kelly[17] reported further data on minor components of coated vesicles. Using permeation

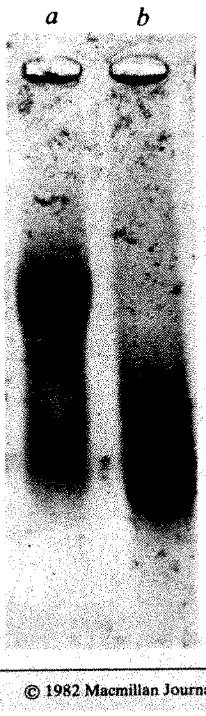

Fig. 1 Coomassie blue-stained 0.15% agarose gel of lower (*a*) and upper (*b*) fractions from Percoll gradient centrifugation.

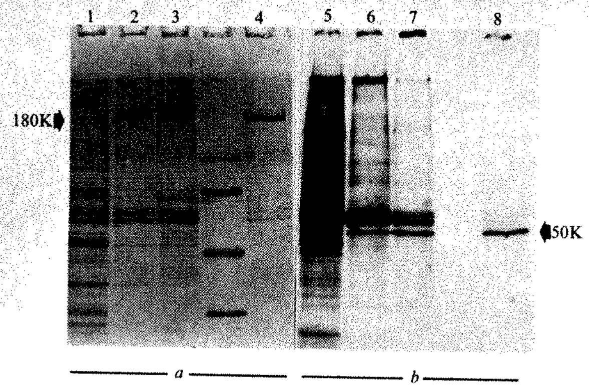

Fig. 2 Comparison of the protein gel patterns after Coomassie blue staining (*a*) and autoradiography (*b*) of the coated vesicles purification steps. The purification procedure was carried out at 4 °C. Bovine brains were cleansed of meninges and the white matter removed by dissection. The grey matter was homogenized in 1 vol of a 2-(*N*-morpholino)ethanesulphonic acid (MES)–Ca^{2+} buffer: 0.1 M MES, *p*H 6.5, 0.1 mM EGTA, 2 mM $MgCl_2$, 1.1 mM $CaCl_2$, 0.2% NaN_3, 50 µg ml^{-1} phenylmethlsulphonyl fluoride (PMSF). The homogenate was centrifuged at 20,000*g* for 30 min in a Sorvall GSA rotor. The resulting pellet was subjected twice to the same procedure. All the supernatants were pooled and centrifuged at 100,000*g* for 1 h in a Beckman 60 Ti rotor. The soluble fraction was removed and the pellet was resuspended in the MES–Ca^{2+} buffer. Coated vesicles were purified by two successive sucrose gradients[13]. The highly enriched upper 5% sucrose solution of the second gradient was used for the final purification using a self-generated density gradient centrifugation of Percoll (Pharmacia). A 2-ml aliquot of the coated vesicle preparation in 5% sucrose was mixed with 3.96 ml Percoll, 0.44 ml 2.5 M sucrose and 15.6 ml 0.25 M sucrose in the MES–Ca^{2+} buffer. After centrifugation at 100,000*g* for 15 min, the upper opalescent zone contained the highly purified coated vesicles. The reaction mixture (15 µl) for phosphorylation tests was made in ice and contained 12 mM Tris-HCl, *p*H 7.5, 32 mM KCl, 2 mM $MgCl_2$, 2.3 mM 2-mercaptoethanol, 0.2 A_{280} aliquots of coated vesicles obtained after various purification steps, 0.1 mM ATP and 10 µCi [γ-^{32}P]ATP. It was incubated for 12 min at 30 °C as previously described[21]. The reaction was stopped by addition of 30 µl SDS-gel electrophoresis sample buffer and the polypeptide composition was analysed by SDS-polyacrylamide gel (5–10%) electrophoresis according to Laemmli[22]. The electrophoresis was carried out at 20 mA for 6 h at constant current until the Bromophenol blue as tracking dye was eluted. Autoradiography was done by exposing the stained gel to Royal X-Omat Kodak film. Lanes 1, 5, grey matter homogenate; 2, 6, middle zone of first sucrose gradient; 3, 7, upper 5% zone of second sucrose gradient; 4, 8, upper opalescent zone of self-generated density gradient of Percoll. The following proteins were run in parallel as molecular weight markers: phosphorylase *b* (94K), bovine serum albumin (67K), ovalbumin (43K) and carbonic anhydrase (30K).

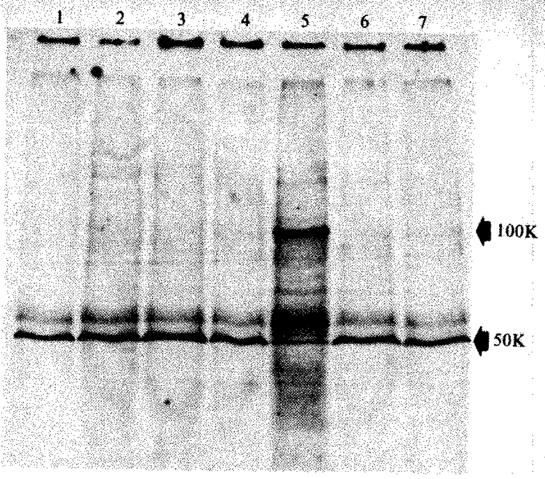

Fig. 4 Effect of cyclic nucleotides and Ca^{2+} inhibitors on the coated vesicle protein ^{32}P-labelling. The following substances were added to the phosphorylation reaction mixture: lane 1, 1 mM EGTA; lane 2, 10 µg calmodulin; 3, 1 mM dibucaine; 4, 50 µM trifluoperazine; 5, 400 µM trifluoperazine; 6, 40 µM cyclic AMP; 7, 40 µM cyclic GMP. Following the incubation, the phosphoproteins were analysed on a 10% SDS-polyacrylamide gel and visualized by autoradiography.

chromatography, they also identified a thin 50K protein band in their highly purified preparations.

Dissociation and reassembly of coat structures seem to be reversible, and both energy[13,18,19] and phosphorylation independent. In comparison, membrane transport, secretion and internalization generally require more complex control. Thus, before internalization, the coated pits act as a molecular filter, selecting some proteins and excluding others. Although the molecular mechanisms remain uncertain, proteins selected to enter the cell are supposed to interact directly or indirectly with clathrin[20]. Such a selection might depend on a phosphorylation step. If the 50K protein is involved in regulation, one or a few molecules per coated vesicle would be sufficient. This would explain its presence in trace amounts in coated vesicles preparations.

This work was supported by INSERM (Unité U-116) and CNRS (ER 102). We thank Dr G. Petrissand and Dr Feure for providing the bovine brains, Professor C. Chany for the use of his laboratory and Dr M. F. Dubois for supplying the [γ-^{32}P]ATP.

Received 5 October 1981; accepted 9 June 1982.

1. Friend, D. S. & Farquhar, M. G. *J. Cell Biol.* **35**, 357-376 (1967).
2. Heuser, J. E. & Reese, T. S. *J. Cell Biol.* **57**, 315–344 (1973).
3. Rothman, J. E. & Fine, R. E. *Proc. natn. Acad. Sci. U.S.A.* **77**, 780–784 (1980).
4. Franke, W. W., Luder, M. R., Kartenbeck, J., Zerban, H. & Keenan, T. W. *J. Cell Biol.* **69**, 173–195 (1976).
5. Goldstein, J. O., Anderson, R. G. & Brown, M. S. *Nature* **279**, 679–685 (1979).

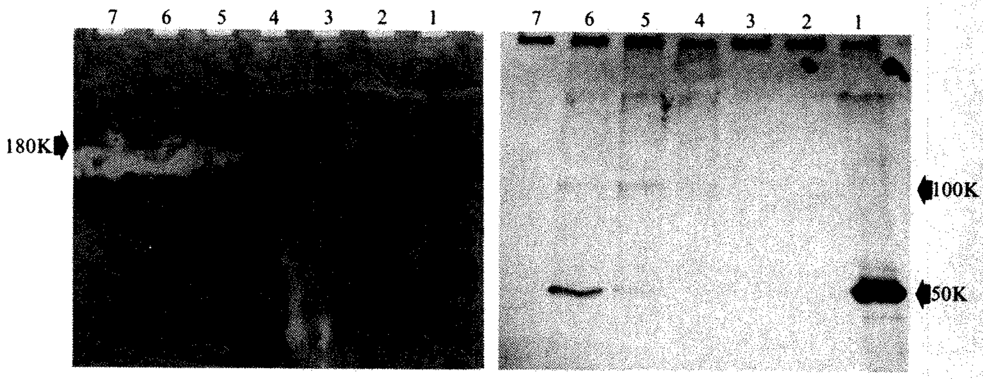

Fig. 3 Analysis of the agarose gel fraction by SDS-polyacrylamide gel electrophoresis and autoradiography. Percoll-purified coated vesicles were electrophoresed in a 0.15% agarose gel as described in ref. 12. At the end of the migration the gel was cut into 1-cm slices and each fraction was homogenized in 5 ml MES–Ca^{2+} buffer. Broken agarose was removed by centrifugation at 15,000*g* for 5 min. Supernatants were concentrated by polyethylene glycol, labelled with [γ-^{32}P]ATP as described in Fig. 2 legend and analysed on a 10% SDS-polyacrylamide gel. The protein patterns are after *a*, Coomassie blue staining and *b*, autoradiography. Lane 1, Percoll-purified coated vesicles; lanes 2–7, agarose gel fractions. The direction of the agarose gel electrophoresis was from lane 2 to lane 7.

6. Baldwin D. Jr, Prince, M., Marshall, S., Davies, P. & Olefsky, J. M. *Proc. natn. Acad. Sci. U.S.A.* **77,** 5975–5978 (1980).
7. Pearse, B. M. F. *J. molec. Biol.* **97,** 93–98 (1975).
8. Pearse, B. M. F. *J. molec. Biol.* **103,** 785–798 (1976).
9. Ungewickell, E. & Branton, D. *Nature* **289,** 420–422 (1981).
10. Pretorius, H. T. *et al. Biochemistry* **20,** 2777–2782 (1981).
11. Kirchhausen, T. & Harrison, S. C. *Cell* **23,** 755–761 (1981).
12. Rubenstein, J. L. R., Fine, R. E., Luskey, B. O. & Rothman, J. E. *J. Cell Biol.* **89,** 357–361 (1981).
13. Keen, J. H., Willingham, M. C. & Pastan, I. H. *Cell* **16,** 303–312 (1979).
14. Linden, C. D., Dedman, J. R., Chafouleas, J. G., Means, A. R. & Roth, T. F. *Proc. natn. Acad. Sci. U.S.A.* **78,** 308–312 (1981).
15. Tanaka, T. & Hidaka, H. *Biochem. biophys. Res. Commun.* **101,** 447–453 (1981).
16. Levin, R. M. & Weiss, B. *Biochim. biophys. Acta* **540,** 197–204 (1978).
17. Pfeffer, S. R. & Kelly, R. B. *J. Cell Biol.* **91,** 385–391 (1981).
18. Woodward, M. P. & Roth, T. F. *Proc. natn. Acad. Sci. U.S.A.* **75,** 4394–4398 (1978).
19. Bloom, W. S., Schook, W., Feageson, E., Ores, C. & Puszkin, S. *Biochim. biophys. Acta* **598,** 447–455 (1980).
20. Bretscher, M. S., Thomson, N. & Pearse, B. M. F. *Proc. natn. Acad. Sci. U.S.A.* **77,** 4156–4159 (1980).
21. Lebleu, B., Sen, G. C., Shaila, S., Cabrer, B. & Lengyel, P. *Proc. natn. Acad. Sci. U.S.A.* **73,** 3107–3111 (1976).
22. Laemmli, U. K. *Nature* **227,** 680–685 (1970).

Injection of subunits of cyclic AMP-dependent protein kinase into cardiac myocytes modulates Ca^{2+} current

W. Osterrieder, G. Brum, J. Hescheler & W. Trautwein

II. Physiologisches Institut der Universität des Saarlandes,
D-6650 Homburg/Saar, FRG

V. Flockerzi & F. Hofmann

Pharmakologisches Institut der Universität Heidelberg,
Im Neuenheimer Feld 366, D-6900 Heidelberg, FRG

β-Adrenergic stimulation of the heart is thought to increase cardiac muscle contractility by activation of cyclic AMP-dependent protein kinase and concomitant increase in the phosphorylation of certain proteins (for refs see refs 1–6). Electrophysiological studies have shown that the stimulation of cardiac β-adrenoreceptors[7], the external application of cyclic AMP or its analogues to Purkinje fibres[8], or the injection of cyclic AMP into single myocytes[9] can increase the slow inward current (I_{si}) during the plateau phase of the action potential (AP). In heart muscle this current is mainly carried by Ca^{2+} (refs 10, 11) and it has been suggested that cyclic AMP-dependent phosphorylation of some component of the calcium channel increases the amount of Ca^{2+} which enters the cell during depolarization[10]. We have investigated this hypothesis by examining the electrical responses of isolated guinea pig ventricular myocytes to pressure injections of subunits of the cyclic AMP-dependent protein kinase. We report here that injection of the catalytic subunit (C) resulted in a lengthening of the action potential duration (APD) and an increase in the height of the plateau as well as the amplitude of I_{si}. By contrast, the injection of regulatory subunit (R) shortened the APD of fast and slow response APs, an effect which was reversed by adrenaline.

Isolated ventricular cells[12] stimulated at 0.33 Hz through the injection electrode had a resting potential of approximately −80 mV and stable action potentials of 150–300 ms duration. Injection of C prolonged the APD measured at 80% repolarization (APD_{80}) from 130 to 315 ms and increased AP amplitude by about 20 mV without affecting the resting potential (Fig. 1*A*). These changes occurred during the 60 s injection period and were still present 20 min after the cessation of injection pressure (Fig. 1*B*). Visual inspection of the cells revealed that the injection of C also produced a dramatic increase in the force of contraction. After the injection of C the addition of adrenaline (0.5 μM) to the bathing solution had no effect on the AP or force of contraction. The injection of buffer A (see Fig. 1 legend) or of C inactivated by incubation at 60 °C for 30 min had little or no effect on the configuration of the AP. These controls confirm an earlier conclusion that injection-related increases in intracellular volume and pressure have minimal effects on the AP[9]. Thus, it is highly likely that the molecular basis of the changes observed after C injection is quite similar or identical to that found after stimulation of the β-adrenoreceptor by adrenaline[7] or after the intracellular application of cyclic AMP[8,9]. Similar changes of the AP have been observed after C injection into bag cell neurones obtained from the abdominal ganglion of *Aplysia*[13].

The experiments suggested that C altered the AP configuration by increasing the Ca^{2+}-dependent I_{si}. Therefore, I_{si} was determined in cells in which the membrane potential was clamped by current being supplied through a second microelectrode. In five experiments, changes in I_{si} in response to depolarizing clamp pulses were recorded before and after the pressure injection of C through the voltage-sensing electrode. Figure 2*A* shows that the injection of C increased the inward current from 2.2 to 6.0 nA. This increase in current was not reversed when the pressure was terminated but was completely abolished by the addition of the Ca^{2+} channel blocker, D-600 (Fig. 2*B*). The time constant for inactivation of I_{si} was 17 ms before the injection of C, and 15 ms after C injection. The similarity of these time constants suggests that C does not alter the time during which the voltage-dependent Ca^{2+} channel is open. The recording of Fig. 2*A* suggests that injected catalytic subunit slightly increased the outward current.

The present experiments indicate that elevation of the intracellular concentration of free C increases I_{si} during the plateau phase of the AP. As free C is an active phosphotransferase, its injection probably results in enhanced phosphorylation of cytosolic and membrane proteins. Therefore, phosphorylation of certain membrane proteins may be intimately involved in the hormonal regulation of I_{si}. However, the results do not eliminate the possibility that in physiological conditions in the absence of hormones either the phosphorylation of certain membrane proteins is not important for the opening of the Ca^{2+} channel, or these proteins are phosphorylated by a protein kinase other than C. The latter point arises because the injected subunit might phosphorylate proteins usually not accessible to C.

To establish whether C is involved in physiological conditions, we examined the effects of the regulatorys subunit, R. The rationale for this experiment was that, as far as is known, the only function of R is to bind C and thereby inhibit its phosphotransferase activity[6]. The pressure injection of R into isolated ventricular cells decreased the APD_{80} from 240 to 130 ms and the AP amplitude by about 15 mV (Fig. 3*A*). Both decreases were slowly reversed after the termination of injection, suggesting the occurrence of some compensatory regulation, presumably cyclic AMP production. However, a compensation of the inhibitory effects of R on the AP was no longer observed after multiple injections of R. On the other hand, the AP depression produced by R was reversed by the addition of adrenaline (0.1 μM) to the bathing solution. Finally, the injection of heat-inactivated R had no significant effect on the configuration of the AP. It is therefore quite likely that the R-induced depression in the AP was brought about by inhibition of the phosphotransferase activity of free C. To substantiate an effect of R on I_{si}, the resting membrane potential of some cells was decreased to −50 mV by increasing the extracellular K^+ concentration, $[K^+]_O$, to 22 mM (Fig. 3*B*). The fast sodium channel is inactivated in this condition and the upstroke of the AP is mainly carried by I_{si} (slow response AP). In this condition, R injection had the same effect as discussed above.

The data strongly support the hypothesis that injection of catalytic or regulatory subunit of cyclic AMP-dependent protein kinase affects the phosphorylation of one or several proteins and thereby alters Ca^{2+} influx. Changes in the AP and I_{si} caused by the injection of free C are indistinguishable from those produced in ventricular myocytes by extracellular adrenaline[14]

0028-0836/82/310576—03$01.00

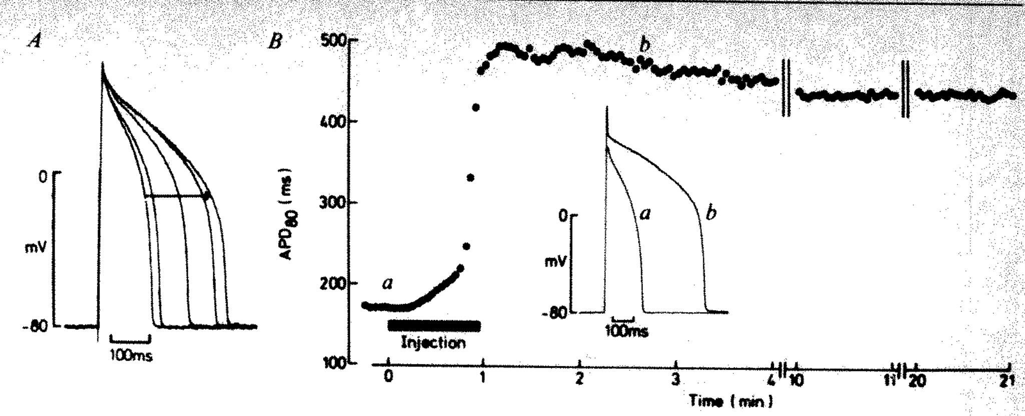

Fig. 1 Injection of the catalytic subunit (C) prolongs the action potential and increases the amplitude. *A*, a microelectrode containing C (9.6 mg ml^{-1}) was impaled into a myocyte and C was injected by pressure (4 bar, for 60s). The injection prolonged the AP from 130 to 315 ms. The arrow indicates the direction of change. *B*, the same procedure as in *A* was used. The injection pressure was gradually increased from 2 to 5 bar during 60 s. Injection of C prolonged the AP from 170 to 490 ms. The inset shows an AP before (*a*) and 1.5 min after (*b*) the injection of C. A different cell from that used in *A* is shown. Cells were isolated from the ventricle of adult guinea pig hearts as described previously[12] and were incubated in Tyrode solution containing 150 mM NaCl, 5.4 mM KCl, 1.8 mM $CaCl_2$, 1 mM $MgCl_2$, 10 mM glucose and 5 mM HEPES, *p*H 7.4. Injection experiments were carried out at 37 °C in a Perspex chamber perfused with the same Tyrode solution. Cells were visualized on a TV screen after 1,000-fold magnification. Glass microelectrodes containing 2 mM HEPES *p*H 7.2, and 150 mM KCl (buffer A) and having a resistance of 100–150 MΩ were used for pacing the cells at 0.33 Hz, recording the membrane potential and pressure injection of proteins or buffer. The volume injected was of the order of 1 pl and that of the cells 30 pl (the injected volume was estimated by measuring the size of the drop released by pressure into oil (×250 magnification)). APD was taken as the time between the beginning of the stimulating current pulse and 80% repolarization, and AP amplitude was measured 30 ms after the stimulating current pulse. Homogeneous preparations of catalytic subunit (C) and cyclic AMP-free regulatory subunits (R) of cyclic AMP-dependent protein kinase II were prepared from fresh bovine heart muscle as described earlier[17,18]. Proteins used for injection were chromatographed on a Biogel-P6 column (2.5 × 9 cm) equilibrated in buffer A. Fractions containing protein were pooled and concentrated by vacuum dialysis against buffer A at 4 °C. Dialysis was continued after the concentration step for at least 18 h with several changes of buffer. Thereafter, denatured protein was removed by centrifugation and the clear supernatant containing active subunits at a concentration of 5–10 mg ml^{-1} was stored in aliquots at 4 °C. For control experiments aliquots of the dialysis buffer were always used. The purity of all proteins used was better than 95%. During this investigation, we used five and three different preparations of C and R (free of cyclic AMP), respectively. No apparent differences between these preparations were observed.

or intracellular cyclic AMP[9], suggesting that all three agents affect the AP by the same basic mechanism. This is not surprising because each agent increases the intracellular concentration of the active species of cyclic AMP-dependent protein kinase. A previously proposed mechanism for the enhancement of I_{si} is that adrenaline and cyclic AMP increase the number of Ca^{2+} channels which are opened by depolarization[10]. Some evidence has been obtained (see Fig. 3) that in the absence of hormone, C is involved in the regulation of I_{si}, although a complete suppression of the plateau phase of the AP by injection of free R has not been observed. This might suggest that cyclic AMP-dependent phosphorylation of membrane proteins is not an absolute requirement for the ability of Ca^{2+} channels to open on depolarization. However, the data do not rule out the possibility that in the absence of hormone, cyclic AMP-dependent phosphorylation of some membrane protein(s) occurs and that this covalent modification is a necessary condition for depolarization-activated Ca^{2+} channels. The data are also compatible with the existence of two types of Ca^{2+} channel or with two states of one Ca^{2+} channel. One type or state would allow voltage-dependent Ca^{2+} influx in the absence of protein phosphorylation, while the other would allow this only after phosphorylation of a specific membrane protein.

The positive inotropic effect of adrenaline, injected cyclic AMP or C on the heart is at least partially mediated through

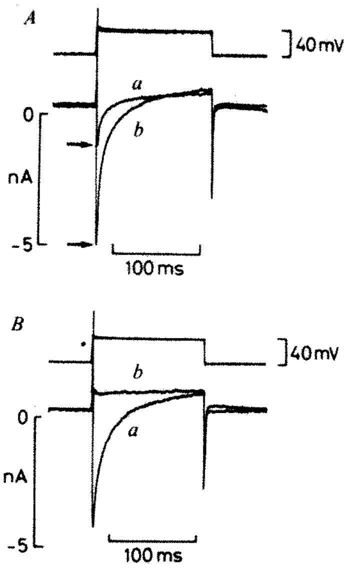

Fig. 2 *A*, injection of C increases I_{si}. Two microelectrodes, one containing C (16 mg ml^{-1}) and a second containing 2 M KCl (20–30 MΩ resistance), were impaled in a single cell for voltage clamp. Depolarizing clamp pulses from −50 mV (holding potential) to −10 mV were applied continuously at a rate of 0.33 Hz throughout the experiment. Superimposed potential (top) and current (bottom) traces before (*a*) and after (*b*) the injection of C (3 bar; 30 s) are shown. Arrows indicate peak I_{si} which was increased from 2.2 to 6.0 nA. The peak amplitude of I_{si} was measured as the difference between peak inward current and the current amplitude 100 ms after the pulse. *B*, the calcium channel blocker D-600 (10 μM) abolishes the effect of injected C on I_{si}. The same procedure as in *A* was applied to a different cell. The injection of C (9.6 mg ml^{-1}) into the cell resulted in a large I_{si} (*a*) which was blocked within 60 s by the addition of D-600 to the bathing solution (*b*). For further details see Fig. 1 legend.

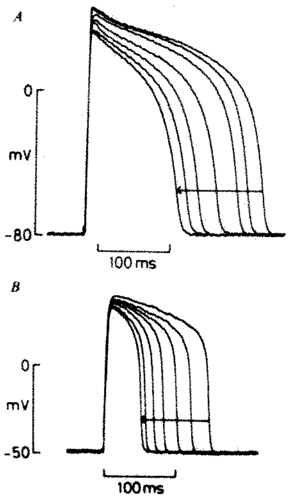

Fig. 3 Injection of the regulatory subunit (R) shortens the action potential. *A*, injection of cyclic AMP-free R (0.1 mg ml^{-1}) at 3 bar for 30 s shortened the AP_{80} within 30 s from 240 to 130 ms. The arrow indicates the direction of change. *B*, in a different cell slow response APs were recorded after increasing extracellular KCl to 22 mM. Injection of R (0.1 mg ml^{-1}) at 5 bar for 15 s shortened the AP from 150 to 50 ms. The control AP and successive APs during the injection are shown. The arrow indicates the direction of change. The upstrokes of APs are blurred by the stimulation artefact. For further details see Fig. 1 legend.

their effect on the slow Ca^{2+} channel. It can be estimated from the data of Fig. 2 that I_{si} measured after C injection amounts maximally to 1.3×10^{-16} mol of Ca^{2+} entering the cell during each depolarization. Taking into account an average total cell volume of 30 pl and a cytosolic space of ~50% of the total cell volume, this indicates that the intracellular Ca^{2+} concentration was elevated by 1.3 μM during depolarization. This crude estimation could indicate that more than just the trigger calcium enters isolated cells through maximally phosphorylated Ca^{2+} channels.

The nature and localization of the proteins phosphorylated by injected C have not been determined. Studies in intact hearts stimulated by adrenaline indicate a rapid phosphorylation of a sarcolemmal protein of molecular weight 27,000 (ref. 15). Several groups have shown that a 22,000 or 11,000 molecular weight peptide is phosphorylated by an endogenous cyclic AMP-dependent protein kinase in purified sarcolemmal membranes[1,3,4]. In addition, some evidence has been obtained that *in vitro* phosphorylation of this peptide is associated with an increased Ca^{2+} uptake by sarcolemmal vesicles[16]. Thus, there is a growing body of evidence supporting the concept that cyclic AMP-dependent protein kinase and phosphorylation of distinct membrane proteins are intimately involved in the regulation of I_{si} of myocardial cells.

This work was supported by grants from Deutsche Forschungsgemeinschaft to W.T. (SFB 38, Membranforschung, Projekt G1) and to F.H. (Ho 579/5 and 579/6-1) and by Fonds der Chemischen Industrie.

Received 29 March; accepted 16 May 1982.

1. England, P. J. in *Recently Discovered System of Enzymes; Regulation by Reversible Phosphorylation* (ed. Cohen, P.) 153–173 (Elsevier, Amsterdam, 1980).
2. Tsien, R. W. *Adv. Cyclic Nucleotide Res.* **8,** 369–421 (1977).
3. Mewes, R. & Hofmann, F. in *Catecholamines and the Heart* (eds Delius, W., Gerlach, E., Grobecker, H. & Kübler, W.) 118–127 (Springer, Berlin, 1981).
4. Wollenberger, A. & Will, H. *Life Sci.* **22,** 1159–1178 (1978).
5. Katz, A. M. *Adv. Cyclic Nucleotide Res.* **11,** 303–343 (1979).
6. Krebs, E. G., Beavo, J. A. *A. Rev. Biochem.* **48,** 923–959 (1979).
7. Reuter, H. *J. Physiol., Lond.* **242,** 429–451 (1974).
8. Tsien, R. W. *Nature new Biol.* **245,** 120–122 (1973).
9. Trautwein, W., Taniguchi, J. & Noma, A. *Pflügers Arch. Ges. Physiol.* **392,** 307–314 (1982).
10. Reuter, H. *A. Rev. Physiol.* **41,** 415–424 (1979).
11. McDonald, T. F. *A. Rev. Physiol.* **44,** 425–434 (1982).
12. Isenberg, G. & Klöckner, U. *Nature* **284,** 358–360 (1980).
13. Kaczmarek, L. K. *et al. Proc. natn. Acad. Sci. U.S.A.* **77,** 7487–7491 (1980).
14. Taniguchi, J., Kokubun, S., Noma, A. & Irisawa, H. *Japan J. Physiol.* **31,** 547–558 (1981).
15. Walsh, D. A., Clippinger, M. S., Sivaramakrishan, S. & McCullough, T. E. *Biochemistry* **18,** 871–877 (1979).
16. Rinaldi, M. L., Le Peuch, L. J. & Demaille, J. G. *FEBS Lett.* **129,** 277–281 (1981).
17. Beavo, J. A., Bechtel, P. J. & Krebs, E. G. *Meth. Enzym.* **38,** 299–308 (1974).
18. Hofmann, F. *J. biol. Chem.* **255,** 1559–1564 (1980).

The DNase I sensitivity of *Xenopus laevis* genes transcribed by RNA polymerase III

J. Coveney & H. R. Woodland

Department of Biological Sciences, University of Warwick,
Coventry CV4 7AL, UK

Since the initial discovery that the DNase I sensitivity of the globin genes in different cell types correlates with globin gene expression[1], this relationship has been shown to hold true for a variety of genes, including the genes for ovalbumin[2], conalbumin[3], α- and β-globin in chicken[4,5], several heat-shock proteins in *Drosophila*[6,7], the r-chromatin of *Tetrahymena*[8] and the viral polyoma minichromosome[9]. Although genes transcribed by RNA polymerases I and II have been studied extensively, the genes transcribed by RNA polymerase III have not. We have therefore investigated the DNase I sensitivity of transfer RNA (tRNA) and oogenetic 5S RNA genes in the liver and erythocyte nuclei of *Xenopus laevis*. The oogenetic 5S genes are not transcribed in any known somatic cell[10,11], and tRNA genes are transcribed in the hepatocyte but are inactive in the erythrocyte. We show here that, although in these two cell types the correspondence between DNase I sensitivity and gene transcription holds good for globin and the ribosomal genes, the tRNA and oogenetic 5S genes are DNase I sensitive in both liver and erythrocyte nuclei. Thus for the genes transcribed by polymerase III the correspondence of sensitivity and expression breaks down.

There are two types of 5S ribosomal gene in *X. laevis*: oocyte specific ($5S_{ooc}$) and somatic ($5S_{som}$)[10,11]. The $5S_{ooc}$ genes are a family of about 20,000 genes per haploid genome[12], interspersed with an equal number of 5S pseudogenes, representing residues 1–101 of the normal 120 bp gene[13]. Transcripts of the pseudogene *in vivo* have never been detected, but their occurrence remains a possibility[14]. The $5S_{ooc}$ genes are transcribed exclusively during oogenesis, whilst in other cells it is the $5S_{som}$ genes (of which there are fewer, about 400)[15] which are used[10,11]. This number is far too small for the somatic genes to be detected by the straightforward hybridization experiments described here. A rough calculation of gene number from Fig. 1*a* (11,000–21,000 copies of the gene per pseudogene repeat per haploid genome, depending on the amount of vector sequences involved in the hybridization) confirms that, in effect, we measure only $5S_{ooc}$ genes in these hybridizations. Figure 1*a* and Table 1 show that the $5S_{ooc}$ genes are sensitive to DNase I in both liver and erythrocyte nuclei. No 5S genes are transcribed in erythrocytes, which have lost all RNA polymerase III molecules during maturation[16], nor are the $5S_{ooc}$ genes believed to be transcribed in hepatocytes[17]. In the latter cells, the $5S_{som}$ genes should provide all the 5S RNA. These genes are hidden by the 50 times more numerous $5S_{ooc}$ genes.

Equally surprising is the finding (Fig. 1*b*) that certain of the tRNA genes, which are transcribed in the hepatocyte but not in the erythrocyte, are equally sensitive in both types of nucleus. The probe used contains two $tRNA^{Met}$ genes and one each of the tRNAs accepting phenylalanine, tryosine, asparagine, alanine, leucine and lysine[18]. The complete 3.18 kilobase (kb) unit is repeated about 100 times per haploid genome[19]. The probe probably reveals all of these tRNA species present in the genome, but some of them may be pseudogenes and never expressed. Even if this were the case, it would not alter the conclusion that these tRNA genes are hypersensitive to DNase I, even when they are not expressed.

Thus in blood and liver cells, many, and perhaps all, genes transcribed by polymerase III seem to be DNase I sensitive, regardless of their transcriptional activity. Maternal $5S_{ooc}$ genes have not been active since oogenesis, a period of at least 2 yr. In the case of the paternal $5S_{ooc}$ genes, it is not known whether they were even active during gametogenesis, but this seems unlikely as the accumulation of vast numbers of ribosomes, transcribed in part from the $5S_{ooc}$ genes, which is a feature of oogenesis, does not occur during spermatogenesis. Thus this half of the $5S_{ooc}$ gene complement may have been inactive for as much as 4 yr (two life cycles).

Table 1 Degree of hybridization of various probes to DNase I-digested erythrocyte and liver nuclei as a percentage of binding to undigested DNA

	% Probe binding			
		Ribosomal		
DNA	$5S_{ooc}$	tRNA	DNA	Globin
Total, undigested	100	100	100	100
Erthrocyte nuclei;				
5% DNase I digestion	34.9	51.0	100	42.5
Liver;				
5% DNase I digestion	39.5	47.8	54.5	100

The data are calculated from the experiments shown in Figs 1 and 2. The saturation values were calculated by fitting straight lines to double reciprocal plots using linear regression by least squares.

0028-0836/82/310578—03$01.00

It might be suspected that these results reflect an artefact in the preparation and digestion of the nuclei, and therefore that many other genes would also show unexpectedly high nuclease sensitivity. However, measurement of the concentrations of several other genes in the same DNA samples yielded the predicted results. For example, ribosomal genes are not transcribed in erythrocytes[16], nor is RNA polymerase I present in their nuclei, but the opposite is true of liver. As expected the ribosomal DNA from liver was more sensitive to DNase I digestion than bulk DNA, but equally resistant in erythrocytes (Fig. 2*a*). Globin genes are active in the immature erythrocyte of *Xenopus*, but not in the adult cell. The latter, however, contains RNA polymerase II molecules tightly bound to the chromatin[16] and in avian erthrocytes the frozen polymerases are to be found on the globin genes[20]. In this sense the globin genes could be regarded as 'active genes', which correlates with the observation that in avian erthrocytes, globin sequences are preferentially digested by DNase I[1,4,5]. The same is the case in human erythrocytes (Fig. 2*b*), but not hepatocytes, which do not synthesize globin. Our results confirm those of others[1-7], and show that the crude approach of DNase I solubilization is capable of detecting different DNase I sensitivity in genes active in one cell type and inactive in another.

The results of Figs 1 and 2 show a single time point of digestion and leave open the posibility that the inactive tRNA or 5S genes show different kinetics of digestion from active genes. Figure 3 shows that this is not the case; in fact, $5S_{ooc}$ genes demonstrate even greater sensitivity to DNase I than do the active ribosomal genes of liver.

It has been argued[1,21] that any gene that has been transcribed at a given stage of the life cycle of an organism remains DNase I sensitive, even if the gene becomes inactive later. This argument could be used to explain the sensitivity of the tRNA genes in the erythrocyte nuclei. It is harder, however, to sustain this argument in the case of the $5S_{ooc}$ genes, which show a similar DNase I sensitivity. It would mean that any gene active in oocytes (and this would probably amount to ~15% of the DNA[22]) would always be in the sensitive state, even when it passed through the male for one or more generations (as 50% of the $5S_{ooc}$ genes have done). The insensitivity of ribosomal genes in the erythrocyte nuclei is also inconsistent with this idea, since these genes must have been active in erythroblasts. It seems more likely that the genes transcribed by RNA polymerase III have a different structure from other genes, at least in their inactive state, with the result that they are always DNase I sensitive. The difference might simply relate to their very small size and tandem repetition. Several RNA polymerase

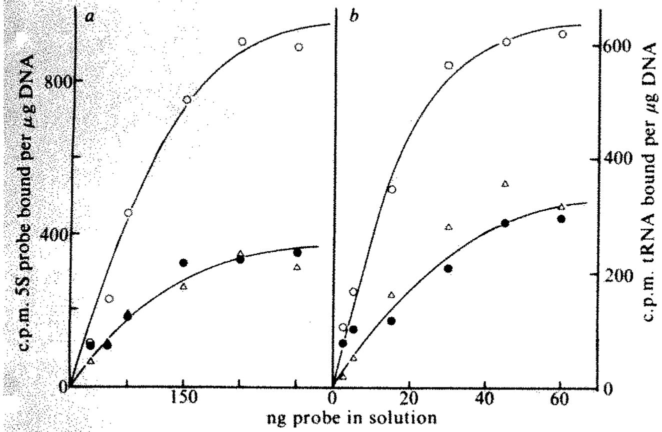

Fig. 1 DNase I sensitivity of 5S (*a*) and tRNA (*b*) genes in erythrocyte and liver nuclei. Erythrocyte nuclei were prepared according to the method of ref. 26 and the liver nuclei by the method of Scribler and Weber[27]. Nuclei from the two tissues were digested with pancreatic DNase I (20 μg ml^{-1}) for 5 min, which is sufficient to release 5–10% of the DNA from the nuclei. The nuclei were pelleted by centrifugation for a few seconds in an Eppendorf microfuge and their DNA extracted according to the method of Weintraub and Groudine[1]. The alkali-denatured DNA was loaded onto nitrocellulose filters[28] and hybridized with nick-translated recombinant DNA[29] containing the relevant gene sequences. This procedure will not detect a hypersensitive site[30] in the way that a blot-transfer hybridization of electrophoresed DNA would, but it gives a more quantitative assay of the DNase I sensitivity of the genes as a whole[5]. The $5S_{ooc}$ probe used was pXlo31 which contains a single repeat of the 5S gene plus a pseudogene[31]. It was labelled with ^{3}H-dCTP to a specific activity of 5.5×10^5 c.p.m. μg^{-1}. The tRNA probe used was λt210, which contains two copies of tRNA$_1^{Met}$ and one copy each of tRNA^{Phe}, tRNA^{Leu}, tRNA^{Lys}, tRNA^{Asp}, tRNA^{Ala} and tRNA^{Tyr} (refs 18, 19) it was labelled with ^{3}H-dCTP to a specific activity of 3.9×10^6 c.p.m. μg^{-1}. Undigested liver DNA gave a result identical to that for erythrocyte, so the data are not shown. ○, Undigested erythrocyte DNA; △, digested erythrocyte DNA; ●, digested liver DNA.

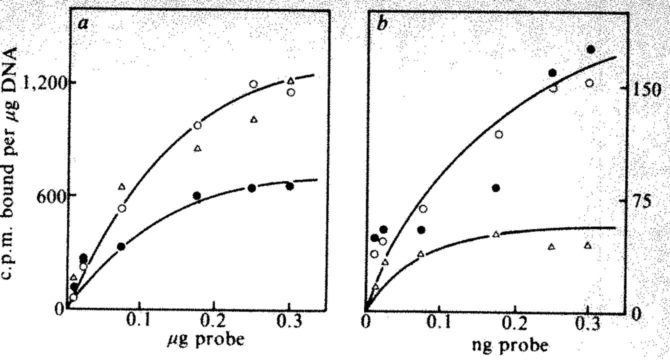

Fig. 2 DNase I sensitivity of ribosomal RNA (*a*) and globin (*b*) genes in erythrocyte and liver nuclei. The DNA samples and procedures were as for Fig. 1. The ribosomal probe used was pXlr101, constructed by Dr R. Reeder; it contains a complete repeat of the 40S precursor plus non-transcribed spacer. It was nick-translated with ^{3}H-dCTP to 2.2×10^5 c.p.m. μg^{-1}. The globin probe was labelled with ^{32}P-dGTP to 1.1×10^7 c.p.m. μg^{-1}. It was a gift from Dr R. W. Old, and contains an~300 bp sequence complementary to a globin mRNA. ○, Undigested erythrocyte DNA (liver gave identical results); △, DNase I-digested erythrocyte DNA; ●, DNase I-digested liver DNA.

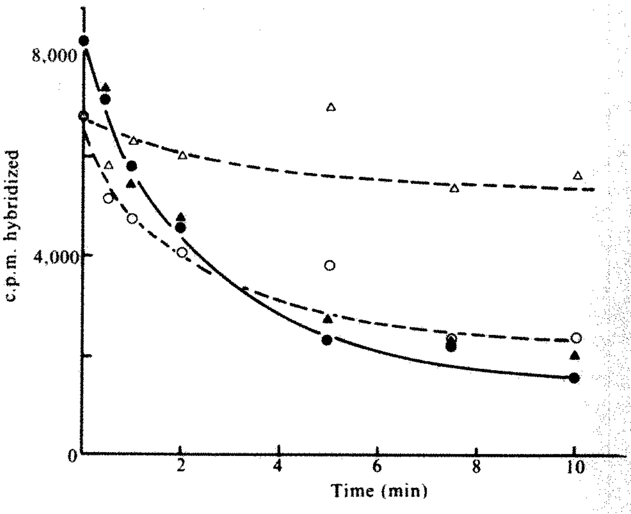

Fig. 3 Time course of DNase I digestion. Erythrocyte and liver nuclei were digested with 20 μg ml^{-1} DNase I for increasing periods of time, the reaction was stopped by the addition of SDS and EDTA to a final concentration of 0.5% SDS, 12.5 mM EDTA, and the DNA extracted as previously described. One μg DNA from each time point was loaded onto duplicate nitrocellulose filters, which were hybridized in a final volume of 200 μl with either 250 ng ^{32}P-pXlr101 or 200 ng ^{32}P-pXlo8 for 24 h before washing and counting. pXlr101 and pXlo8 were labelled with ^{32}P-dCTP to a specific activity of 5.6×10^7 and 3.6×10^7 c.p.m. μg^{-1} respectively; pXlo8 contains three copies of the gene–pseudogene 5S repeat[32]. Further details are given in Fig. 1 legend. Erythrocyte ribosomal genes; ○, liver ribosomal genes; ▲, erythrocyte 5S genes; ●, liver 5S genes.

II-transcribed genes have been shown to be associated with sites hypersensitive to DNase I[3,6,7,23] and for some genes these sites are always sensitive, regardless of the activity of the genes[6]. For genes in which small units are tandemly repeated this might be a serious problem. We have therefore examined the $5S_{ooc}$ repeat unit by digesting the DNA samples of Fig. 3 with the restriction enzyme *Hin*dIII, running the digested DNAs on agarose gels, transferring them to nitrocellulose and probing with pXlo31. *Hin*dIII cuts once within the $5S_{ooc}$ gene/pseudogene repeat, yielding a 700 bp fragment. If a hypersensitive site were present it would act like another restriction site, giving a defined fragment or fragments smaller than 700 bp. The 700 bp repeat disappeared with the expected kinetics and without revealing discrete smaller fragments (data not shown). Thus it does not seem that our results can be explained by the presence of specific hypersensitive sites. Another possible explanation of the $5S_{ooc}$ sensitivity is that the location of these genes at the telomeres of several chromosomes[24] confers special nuclease sensitivity on them. This possibility could be tested by studying a species, such as *Rana temporaria*, in which the 5S genes are not telomeric[25]. In any case, the tRNA repeat studied here does not have a telomeric location. (See G. Fostel, M. L. Pardue and S. G. Clarkson, quoted in ref. 18.) Whatever the reason for the phenomenon, it appears that ready DNase I solubilization cannot be used as an indication of activity in genes transcribed by polymerase III.

Received 22 December 1981; accepted 10 June 1982.

1. Weintraub, H. & Groudine, M. *Science* **193**, 848–856 (1976).
2. Garel, A. & Axel, R. *Proc. natn. Acad. Sci. U.S.A.* **73**, 3966–3970 (1976).
3. Kuo, M. T., Mandel, J. L. & Chambon, P. *Nucleic Acids Res.* **7**, 2105–2113 (1979).
4. Stadler, J. *et al. Cell* **20**, 451–460 (1980).
5. Bellard, M., Kuo, M. I., Dretzen, G. & Chambon, P. *Nucleic Acids Res.* **8**, 2737–2757 (1980).
6. Wu, C. *Nature* **286**, 854–860 (1980).
7. Keene, M. A., Corces, V., Lowenhaupt, K. & Elgin, S. C. R. *Proc. natn. Acad. Sci. U.S.A.* **78**, 143–146 (1981).
8. Borchsensius, S., Bonven, B., Leer, J. C. & Westergaard, O. *Eur. J. Biochem.* **117**, 245–250 (1981).
9. Herbomel, P., Saragosti, S., Blangy, D. & Yaniv, M. *Cell* **25**, 651–658 (1981).
10. Wegnez, M., Monier, R. & Denis, H. *FEBS Lett.* **25**, 13–20 (1972).
11. Ford, P. J. & Southern, E. M. *Nature new Biol.* **241**, 7–12 (1973).
12. Brown, D. D., Wensink, P. C. & Jordan, E. *Proc. natn. Acad. Sci. U.S.A.* **68**, 3175–3179 (1971).
13. Jacq, C., Miller, J. R. & Brownlee, G. G. *Cell* **12**, 109–120 (1977).
14. Miller, J. R. & Melton, D. A. *Cell* **24**, 829–835 (1981).
15. Peterson, R. C., Doering, J. L. & Brown, D. D. *Cell* **20**, 131–141 (1980).
16. Hentschell, C. C. & Tata, J. R. *Devl Biol.* **65**, 496–507 (1978).
17. Korn, K. J. & Gurdon, J. B. *Nature* **289**, 461–465 (1981).
18. Bryan, P. N., Hofstetter, H. & Birnstiel, M. L. *Cell* **27**, 459–466 (1981).
19. Clarkson, S. G., Kurer, V. & Smith, H. O. *Cell* **14**, 713–724 (1978).
20. Gariglio, P., Bellard, M. & Chambon, P. *Nucleic Acids Res.* **9**, 2589–2598 (1981).
21. Young, N. S., Benz, E. J., Kantor, J. A., Kretschmer, P. & Weinhuis, A. W. *Proc. natn. Acad. Sci. U.S.A.* **75**, 5884–5888 (1978).
22. Davidson, E. H. *Gene Activity in Early Development* 2nd edn (Academic, New York, 1976).
23. Samal, B., Worcel, A., Louis, C. & Schedl, P. *Cell* **23**, 401–409 (1981).
24. Pardue, M. L., Brown, D. D. & Birnstiel, M. L. *Chromosoma Berl.* **42**, 191–203 (1973).
25. Vitelli, L., Batistoni, R., Andronico, F., Nardi, I. & Barsacchi-Pilone, G. *Chromosoma Berl.* **84**, 475–491 (1982).
26. Marzluff, W. F., Murphy, E. C. & Huang, R. C. C. *Biochemistry* **12**, 3440–3446 (1973).
27. Schribler, U. & Weber, R. *Analyt. Biochem.* **58**, 225–230 (1974).
28. Gillespie, D. *Meth. Enzym.* **12B**, 641–668 (1968).
29. Maniatis, T., Jeffrey, A. & Kleid, D. G. *Proc. natn. Acad. Sci. U.S.A.* **72**, 1184–1188 (1975).
30. Wu, C., Bingham, P. M., Livak, K. J., Holmgren, R. & Elgin, S. C. R. *Cell* **16**, 797–806 (1979).
31. Federoff, N. V. & Brown, D. D. *Cell* **13**, 701–716 (1978).
32. Brown, D. D. & Gurdon, J. B. *Proc. natn. Acad. Sci. U.S.A.* **75**, 2849–2853 (1978).

Is avian adeno-associated virus an endogenous virus of chicken cells?

G. J. Dawson*, V. J. Yates, P. W. Chang & J. J. Oprandy

Department of Animal and Veterinary Science,
University of Rhode Island, Kingston, Rhode Island 02881, USA

The adeno-associated viruses (AAV) are defective parvoviruses which produce infective progeny only in cells co-infected with a 'helper' adenovirus (Ad)[1]. Both human and simian AAV have been recovered from human and simian primary cell cultures following their inoculation with 'AAV-free' Ad. Whereas some studies have suggested that AAV exists in a latent state in these cells[2,3], others have indicated that the AAV genome is capable of establishing and maintaining a latent state in defined laboratory conditions[4–7] which mimic the situation proposed for the 'latent' AAV recovered from human and simian tissues. Here, avian adeno-associated virus (AAAV) was consistently recovered from limiting dilutions of purified and unpurified avian Ad stocks propagated in embryonating chicken eggs derived from two independently raised flocks of White Leghorn (WL) chickens but not when these Ad stocks were propagated in duck cells. These observations suggest that AAAV is a latent endogenous virus of at least some flocks of WL chickens.

Infectious AAV has been vertically transmitted *in utero* in both naturally occurring and experimentally induced infections of hens[8,9] and in experimentally infected mice[10]. An advantage of using chickens for virological studies is the availability of specific -pathogen-free (SPF) embryonating eggs derived from WL chickens which had not been exposed to avian Ad or to AAAV. By using SPF embryos, the possibility of an *in utero* infection with either infectious Ad or AAAV was eliminated. Antibodies to avian Ad or AAAV were not detected either in the SPF chickens during serological surveys conducted by the producer or in the yolks of SPF embryos we tested using the virus neutralization test and the enzyme-linked immunosorbent assay[8,11]. (We had previously demonstrated that yolk antibody levels to avian Ad and AAAV were similiar or identical to those present in hens experimentally infected with these viruses[11].)

Two avian Ad strains, CELO virus (serotype 1) and Irish strain 506 (serotype 4), were treated with antiserum to AAAV and inoculated in chicken embryo kidney (CEK) cells prepared from SPF embryos. Various dilutions of the cell lysate were inoculated into sets of 10-day-old embryonating eggs. The allantoamniotic fluids were collected and tested for AAAV as described in Table 1. legend. AAAV was detected in all inoculated eggs by the second passage, even though these Ad stocks were pretreated with AAAV antiserum of high titre. Because our antiserum may not have neutralized all of the AAAV, the CELO virus stock was purified as indicated (Table 1, experiment 2). Three successive isopycnic centrifugations were performed[12,13] to separate possible contaminating AAAV (buoyant density 1.38 and 1.42 g cm^{-3}) from CELO virus (buoyant density 1.34 g cm^{-3}). AAAV was not detected when this purifed stock was examined by electron microscopy. Two thousand CELO virus particles were counted without detecting a single AAAV particle. However, AAAV was detected in all embryos infected with purified CELO virus (Table 1, experiment 2). In some cases, the allantoamniotic fluids of eggs inoculated with higher dilutions of CELO virus (for example, eggs inoculated with a 10^{-9} dilution of CELO virus) had Ad antigens but not AAAV antigens until the second passage. These results suggested that several cycles of viral replication are needed to produce enough AAAV to be detected by the agar gel precipitation test. Similar results were obtained when the above experiment was repeated using embryonating eggs from a second flock of WL hens housed in isolation at the University of Rhode Island Experimental Farm.

Our findings were of great concern because the usual means of assaying AAAV involved inoculating embryonating eggs with CELO virus and various dilutions of AAAV. In previous studies the incubation period was limited to 96 h when the CELO virus inoculum was 10^4 plaque-forming units (PFU) per ml. AAAV was only detected when added to this system; eggs inoculated with CELO virus alone did not produce detectable AAAV antigens. In the present study, AAAV was invariably produced in embryonating eggs when either the incubation time

---

* Present address: Laboratory of Neurovirology, Department of Neurology, Mount Sinai School of Medicine, New York 10029, USA.

0028–0836/82/310580—03$01.00

Table 1 The detection of AAAV in Ad stock virus

Avian Ad	Virus dilution	Detection of AAAV (no. positive/total eggs tested)		Detection of avian Ad (no. of positive/ total eggs tested)	
		First passage	Second passage	First passage	Second passage
Expt 1					
Irish strain 506 (serotype 4)	10^{-6}	2/3	3/3	3/3	3/3
	10^{-7}	1/2	2/2	2/2	2/2
	10^{-8}	0/3	3/3	2/3	3/3
	10^{-9}	1/4	2/4	2/4	2/4
	10^{-10}	0/4	0/4	0/4	0/4
CELO virus (serotype 1)	10^{-6}	3/4	4/4	4/4	4/4
	10^{-7}	2/3	3/3	2/3	3/3
	10^{-8}	1/3	3/3	1/3	3/3
	10^{-9}	0/3	1/3	0/3	1/3
	10^{-10}	0/4	0/4	0/4	0/4
Expt 2					
Purified CELO virus (serotype 1)	10^{-6}	4/6	6/6	6/6	6/6
	10^{-7}	2/4	4/4	4/4	4/4
	10^{-8}	1/3	3/3	3/3	3/3
	10^{-9}	0/4	4/4	4/4	4/4
	10^{-10}	0/3	3/3	2/3	3/3
	10^{-11}	0/4	2/4	1/4	2/4
	10^{-12}	0/4	0/4	0/4	0/4

In experiment 1, Ad stocks were mixed with an equal volume of 1:10 dilution of hyperimmune rabbit antiserum to avian AAV for 30 min before inoculating monolayers of CEK cells made from SPF embryos. (Rabbit hyperimmune serum to AAAV, prepared as described elsewhere[13], had a neutralizing titre of 1:2,560 when 250 ID_{50} AAAV was used as the challenge virus.) After an adsorption period of 1 h, the supernatant fluid was decanted and the cell sheet was rinsed three times with sterile phosphate-buffered saline (PBS). At 72 h post-infection, the tissue culture fluid was clarified, diluted in sterile PBS and inoculated into the chorioallantoic sac of 10-day-old SPF embryonating eggs. At 120–144 h post-infection the allantoamniotic fluids were collected, concentrated with polyethylene glycol and tested for AAAV and Ad antigens using the agar gel precipitation test performed as previously described[8]. Second passages were performed by inoculating SPF 10-day-old embryonating eggs with 0.1 ml allantoamniotic fluids from the first passage and testing for viral antigens by the agar gel precipitation test at 96 h post-infection. In experiment 2, the CELO viral stock was purified by performing three successive isopycnic density gradient centrifugations; in each case viral suspensions were centrifuged at 45,000 r.p.m. (210,000*g*) for 22 h. Discrete CELO viral bands of buoyant density 1.34 g cm^{-3} were collected after each centrifugation and tested for avian Ad and AAAV as described above.

Table 2 Detection of AAAV in chicken and duck embryos

Inoculum	Virus propagation system	Presence of AAAV (no. positive/total no. tested)
Ad*	Duck eggs	0/6
Ad + AAAV*	Duck eggs	5/5
AV	Chicken eggs	5/5
Ad + AAAV	Chicken eggs	5/5

Viruses were propagated in DEK cells for two passages and inoculated into either duck or chicken 10–11-day old embryonating eggs. The AAF from these inoculated eggs were collected at 120 h post-infection and tested for AAAV using the agar gel precipitation test[8].

* Ad = 10^5 ID_{50} units of purified CELO virus were used as inoculant. AAAV = 10^5 ID_{50} units of purified avian adeno-associated virus were used as inoculant.

was extended to 120–168 h or when collected material was passaged in a second set of eggs.

To provide further evidence that AAAV was not present as discrete virions in the purified CELO virus stock, 10^5 50% infectious doses (ID_{50}) CELO virus were grown in duck embryo kidney (DEK) cells and then passaged twice in embryonating duck eggs before being tested for AAAV. If AAAV were present as discrete virions in limiting dilutions of the purified CELO virus stock, a dose of 10^5 CELO virus would also contain at least 10^5 ID_{50} AAAV. AAAV was not detected in duck eggs inoculated with purified CELO virus stock before being propagated in DEK cells (Table 2). Therefore, duck cells can support the growth of both viruses, but AAAV was only detected when added to the inoculum.

We tentatively conclude that AAAV did not have its source in the CELO virus stock but rather may be present in these chicken cells as an endogenous virus.

If AAAV is latent in chicken embryos, it is likely that all Ad propagated in chicken cells would eventually become contaminated with AAAV. It was previously reported that AAAV was detected in 6 of the 11 Ad strains which had been propagated in CEK cells[14]. (The origin of these viral stocks has been described in this report.) The Ad strains had been purified by isopycnic density gradient centrifugation and fractions with a buoyant density of 1.34 g cm^{-3} were examined by electron microscopy. Recently, this experiment was repeated, and fractions with densities of 1.38 and 1.42 g cm^{-3} were examined. AAAV was found in four of the five Ad strains (CELO, 506, 685 and AP-1) previously reported negative. The other Ad strain was not available.

We have previously reported that individual plaques (clones) of CELO virus propagated in SPF CEK cells produced AAAV when inoculated into embryonating eggs (Table 3)[15]. As the CELO virus stock was diluted to contain 100 PFU ml^{-1} and then treated with a 1:10 dilution of rabbit anti-AAAV antiserum, our results provide additional evidence that AAAV may be endogenous to chicken cells.

The concept of vertically transmitted latent AAAV is further supported, though indirectly, by field studies, Avian Ad infections in the field are commonly accompanied by AAAV[16]. In fact, antibodies to AAAV so commonly precede detectable antibody to Ad during field infections that we have suggested rapid screening for precipitating antibodies to AAAV as a reliable means of detecting avian Ad infections[16].

A second possible explanation of our findings is that the information for AAAV is contained in the Ad virion either as separate DNA strands or as a hybrid with Ad DNA. There are no available data to support this hypothesis but it is an interesting possibility especially when one considers that the CELO virus genome is several million daltons larger than Ads of man or ducks[17].

Several studies have shown that AAV can enhance or inhibit Ad replication *in vitro* and modify Ad pathogenicity *in vivo*[18–23]. Our present study raises questions as to the role of

Table 3 The detection of endogenous AAAV in the embryonating eggs of a specific-pathogen flock of hens following the inoculation of eggs with single clones of CELO virus.

Clone no. (plaque no.)	Detection of AAAV* (no. positive/total tested)		Detection of avian adenoviral antigen* (no. positive/total tested)	
	First passage	Second passage†	First passage	Second passage
1	1/4	4/4	4/4	4/4
2	2/4	4/4	4/4	4/4
3	0/3	3/3	2/3	3/3
4	1/3	3/3	3/3	3/3

Individual plaques were picked from a monolayer of CEK cells prepared from SPF chicken embryos infected with 100 PFU CELO virus. The inoculum was reacted with rabbit antiserum to AAAV for 30 min before infecting the cells. After an absorption period of 1 h at 37 °C, the cell sheet was washed with PBS before adding nutritive agar.

* Individual plaques were crushed and dissolved in 2 ml PBS; then 0.2 ml of this virus suspension was inoculated into 10-day-old embryonating eggs from SPF chickens. The allantoamniotic fluid was collected at 120 h post-infection and tested for avian adenoviral antigen using the agar gel precipitation test.

† 0.1 ml concentrated amnioallantoic fluid from the first passage was inoculated into 10-day-old embryonating eggs; the fluid was collected at 96 h postinfection and tested for viral antigens using the agar gel precipitation test.

a possible endogenous virus in modifying the pathogenicity of a second virus.

Our preliminary results suggest that AAAV may be transmitted in the germ line of chicken cells, This is the first report indicating that a DNA virus can be transmitted in this fashion. Further studies should provide interesting data as to whether AAAV is endogenous in WL and other strains of chickens. It would also be valuable to determine if the AAV of other animals are carried as endogenous viruses.

Received 20 December 1981; accepted 16 April 1982.

1. Atchison, R. W., Casto, B. C. & Hammon, W. McD. *Science* **149,** 754–756 (1965).
2. Rapoza, N. P. & Atchison, R. W. *Nature* **215,** 1186–1187 (1967).
3. Hoggan, M. D. *Prog. med. Virol.* **12,** 211–239 (1970).
4. Hoggan, M. D., Thomas, G. F. & Johnson, F. B. *Possible Episomes in Eukaryotes* (ed. Silvestri, L. G.) 243 (North-Holland, Amsterdam, 1973).
5. Berns, K. I., Pinkerton, T. C., Thomas, G. F. & Hoggan, M. D. *Virology* **68,** 556–560 (1975).
6. Handa, H., Shiroki, K. & Shijmojo, H. *Virology* **82,** 84–92 (1977).
7. Cheung, A. K. M., Hoggan, M. D., Hauswirth, W. M. & Berns, K. I. *J. Virol.* **33,** 739–748 (1980).
8. Dawson, G. J., Yates V. J., Chang, P. W., Orsi, L. N. & Pronovost, A. D. *Am. J. vet. Res.* **40,** 1624–1627 (1979).
9. Dawson, G. J., Yates, V. J., Chang, P. W. & Wattanavijarin, W. *Am. J. vet. Res.* **42,** 1833–1837 (1981).
10. Lipps, B. V. & Mayor, H. D. *Intervirology* **14,** 118–123 (1980).
11. Dawson, G. J., Chang, P. W., Yates, V. J. & Fry, D. E. *Avian Dis.* **24,** 890–895 (1980).
12. Hoggan, M. D., Blacklow, N. R. & Rowe, W. P. *Proc. natn. Acad. Sci. U.S.A.* **55,** 1467–1474 (1966).
13. Yates, V. J., El Mishad, A. M., McCormick, K. J. & Trentin, J. J. *Infect. Immun.* **7,** 973–980 (1973).
14. El Mishad, A. M., McCormick, K. J., Yates, V. J. & Trentin, J. J. *Infect. Immun.* **11,** 287–289 (1975).
15. Yates, V. J., Dawson, G. J. & Pronovost, A. D. *Am. Vet. med Ass. Mtg*, Washington, DC (1980).
16. Yates, V. J., Pronovost, A. D., Rhee, Y. O. & Fry, D. E. *Am. J. vet. Res.* **40,** 277–279 (1979).
17. Zsak, L. & Kisary, J. *J. gen. Virol.* **56,** 87–95 (1981).
18. Parks, W. P., Casazza, A. M., Alcott, J. & Melnick, J. L. *J. exp. Med.* **127,** 91–108 (1968).
19. Casto, B. C. & Goodheart, C. R. *Proc. Soc. exp. Biol. Med.* **140,** 72 (1972).
20. Mayor, H. D., Houlditch, G. S. & Mumford, D. M. *Nature new Biol.* **241,** 44–46 (1973).
21. Pronovost, A. D., Yates, V. J. & Fry, D. E. *Avian Dis.* **22,** 354–357 (1978).
22. Pronovost, A. D., Yates, V. J. & Fry, D. E. *Am. J. vet. Res.* **40,** 549–551 (1979).
23. Bagshaw, C. Yates, V. J., Provovost, A. D. & Chang, P. W. *J. Wildl. Dis.* **16,** 287–291 (1980).

Evolutionary selection for perfect hairpin structures in viral DNAs

Uwe R. Müller* & Walter M. Fitch†

* Department of Microbiology, School of Medicine,
East Carolina University, Greenville, North Carolina 27834, USA
† Department of Physiological Chemistry, University of Wisconsin,
Madison, Wisconsin 53706, USA

Several recent discoveries[1] have pointed to nucleic acid secondary structure as an additional dimension in gene expression[2]. Further evidence for the formation of hairpins in RNA is the fact that cruciforms exist in negatively supercoiled DNAs[3–5]. As potential binding sites for proteins, these structures have been proposed to play a part in the regulation of various crucial reactions, such as replication[6,7], transcription[8], or RNA processing[9]. As any random nucleotide sequence can self-anneal with an approximately 50% chance of forming some Watson–Crick-type base pairs[10], it is difficult to assess which, if any, of all possible hairpin-like secondary structures may be biologically relevant. We have computed the expected distribution of perfectly base-paired structures as a function of loop size and stem length and compared it with the distribution observed in the complete genome of eight DNA viruses from animals, plants and bacteria. We report here that hairpins having six or more consecutive base pairs in the stem are not distributed randomly along the genome, occur much more often than chance would predict, and are particularly over-represented in regions that appear to have regulatory significance. The average loop size was found to decrease with an increase in stem length. These results support our previous hypothesis that these structures are biologically relevant[11].

The sequenced genomes of bacteriophages ΦX174 (ref. 12), G4 (ref. 13) and fd (ref. 14) and of the eukaryotic viruses simian virus 40 (SV40)[15] and polyoma[16] were searched by computer for invert repeat DNA sequences, which can form hairpin (or cruciform)[2]-like secondary structures. The search was restricted to those hairpins with perfectly base-paired stems (no G–T pairing, no interruptions) and loop sizes of at least 3 but not more than 20 nucleotides. Occurring naturally in a circular form, these genomes were aligned for comparison according to functional similarities among their genetic maps. The start codon of the first gene following the structural gene block was used as a cleavage point for the icosahedral viruses (SV40, polyoma, ΦX174 and G4) and the linearized genomes were plotted on a per cent scale (Fig. 1). In this alignment the leftward 40–45% of each genome contains all the non-structural genes, while the remainder carries all the structural genes and intercistronic regions[2]. The genome of filamentous phage fd was linearized beginning with the start codon of gene II, the product of which (an endonuclease)[17] is functionally homologous to the G4 and ΦX174 gene A products[18]. In this arrangement the largest intercistronic region containing the origin of replication[19] occupies the right end of the genome and aligns with the largest intercistronic regions of SV40 and polyoma, which also contain the replication origins[15,16].

The positions of potential hairpins plotted on these genetic maps, revealed a remarkable similarity in their distribution. As shown in Fig. 1, the major hairpins are not randomly distributed, but consistently more concentrated in the right half of each genome, that is, the portion encoding the intercistronic regions and structural genes. Despite considerable variation in the total number of major hairpins between these genomes, there are always more in the right half than in the left (Table 1). In the case of SV40 and fd, the discrepancy between the left and right halves is even more pronounced when only hairpins with ≥7 base pairs in the stem are considered (Table 1).

Although intercistronic regions occupy only 4% (ΦX174) to 13.7% (SV40) of the total genome, they contain 20–40% of all major hairpins and, when corrected for differences in length, between 2 and 8 times as much secondary structure as translated regions (Table 1). Furthermore, the largest (or at least one of the largest) hairpins can always be found in an intercistronic region (Fig. 1). It appears that most of the hairpins occur in the two largest intercistronic regions of each genome, and the structural gene block between them.

The genomes of hepatitis B virus (HBV)[20] and cauliflower mosaic virus (CaMV)[21] have been cloned and sequenced and only two genes and their products have been described for each agent. For HBV, one of the surface antigens (S antigen) has been identified as the major envelope protein(s)[22], and its gene has been localized in open reading frame 7 (ref. 20; Fig. 2). The core antigen (gene 8) was found to be a DNA-binding protein[23]. The identified gene products of CaMV are capsid protein (gene 4)[21] and the inclusion body protein (gene 6)[24]. Both circular genomes were linearized such that the major capsid (or envelope) protein gene (gene S and gene 4, respectively) would align with the major capsid protein genes of the other icosahedral viruses (VPI and F). For CaMV it was also possible to place the start codon of gene 6 (a non-structural protein)[24] to the extreme left and an intercistronic region at the right end. In the case of HBV, the stop codon of gene 8 was localized at the extreme left, thereby aligning this gene with the DNA-binding protein genes of the other viruses. In this arrangement, the gap on the L-strand is in approximately the same position as the gap in the CaMV α-strand (Fig. 2). As shown in Fig. 2, the similarities in gene arrangements among all virus genomes analysed are congruent with similarities in the distribution of DNA secondary structure. Both the hepatitis and CaMV DNAs have the potential for these structures concentrated in the right half of the genome, although for CaMV this is only true for hairpins with seven or more base pairs in the stem (Table 1). Furthermore, the largest (CaMV) or one of the two largest hairpins (HVB) are localized at the right end,

0028-0836/82/310582—04$01.00

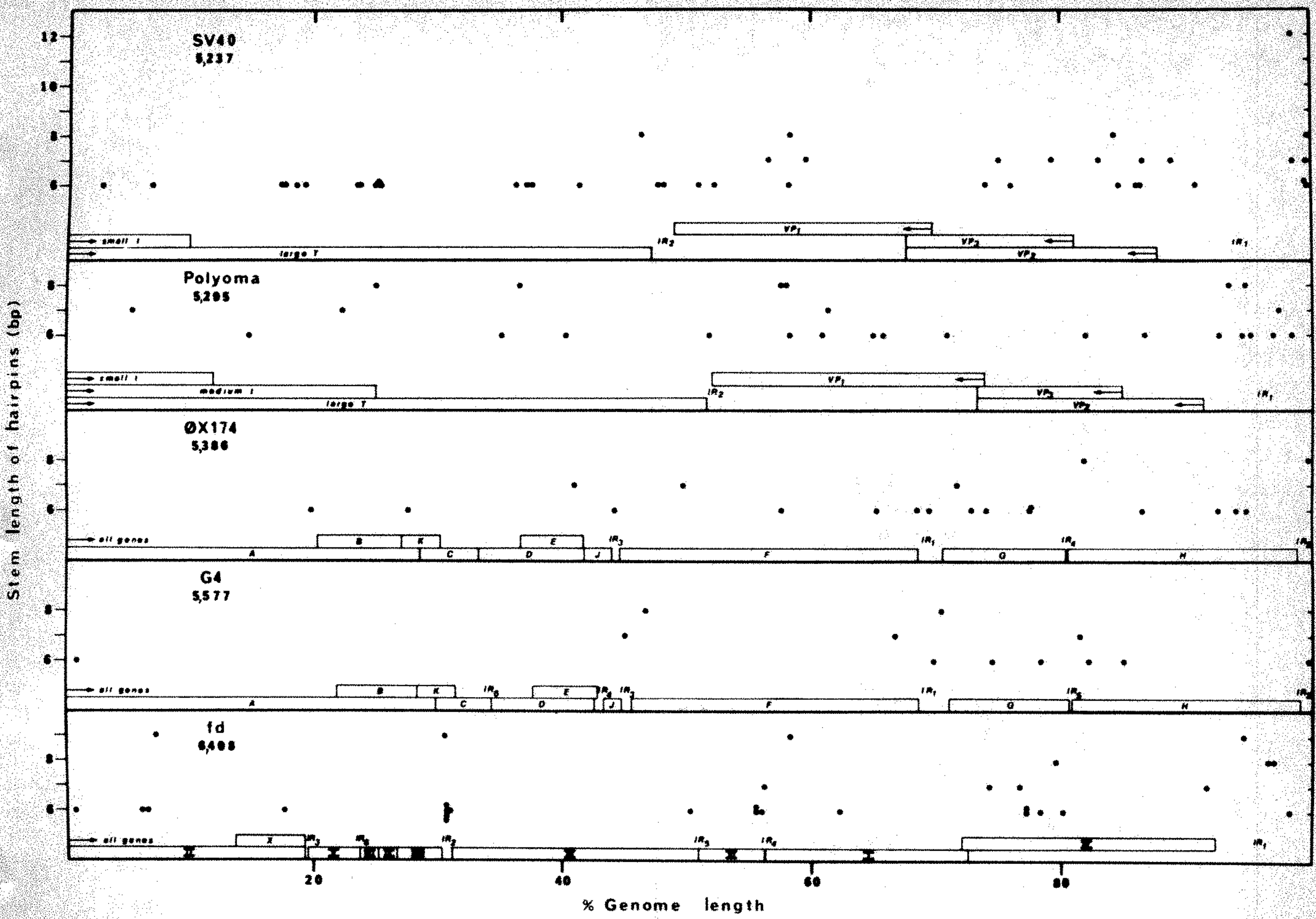

Fig. 1 Distribution of hairpins in the genomes of SV40, polyoma, ΦX174, G4 and fd. The genomes were linearized as described in the text and plotted on a per cent scale. The length in base pairs and name of each genome are indicated. The positions of perfect hairpins (as defined in the text) with ⩾6 base pairs in the stems are indicated by dots. Genes have been labelled according to the original literature and the arrows indicate the direction of transcription. Intercistronic regions (IR) have been labelled sequentially according to size.

which is also characteristic of most of the other genomes. Despite these similarities, the relatively small size and number of hairpins in the intercistronic regions of CaMV make this genome rather unusual compared with the others (Fig. 2 and Table 1).

For comparison, the sequence of the *Escherichia coli* plasmid pBR322 (ref. 26) was analysed and then linearized such that the intercistronic region containing the largest hairpins was placed to the right side (Fig. 2). In this arrangement the observations made for the viral genomes hold true also for this DNA (Table 1), supporting the generality of our findings.

The possibility of a non-uniform distribution of the four nucleotides and consequently an artefactual concentration of hairpins in one region of the genome makes a statistical evaluation of our findings necessary. The detailed mathematical approach and the computer program will be published elsewhere. Briefly, a program was written to compute E_n, the expected number of perfect hairpin structures with stem length n and loop sizes of 3–20 nucleotides, as a function of the total length and composition of the sequence; F_n is the number actually observed in a specific genome of that length and composition. The ratio of observed to expected numbers, Q_n, for a

Table 1 Relative distribution of hairpins in the genomes analysed

Genome type	Genome length (bp)	No. of hairpins in genome with stem length $n \geqslant 6$ bp	$n \geqslant 7$ bp	Ratio of number of hairpins in RH/LH* for $n \geqslant 6$ bp	$n \geqslant 7$ bp	% Of all hairpins in intercistronic regions for $n \geqslant 6$ bp	$n \geqslant 7$ bp	Ratio of number of hairpins in IR/TR† $n \geqslant 6$ bp	$n \geqslant 7$ bp
SV40	5,337	42	14	1.3	13.0	24	36	1.9	3.5
Polyoma	5,295	26	10	2.7	1.5	35	30	5.3	4.3
ΦX174	5,386	20	5	3.0	1.5	20	20	5.6	5.6
G4	5,577	13	5	3.3	1.5	31	40	7.9	11.9
fd	6,408	30	11	1.7	4.5	40	46	6.7	8.3
Hepatitis	3,182	19	7	2.8	1.3				
CaMV	8,024	77	25	0.9	1.8	13	0	0.9	0
pBR322	4,362	27	9	1.7	3.5	59	67	3.8	5.3
Mean	5,446	31.8	10.8	2.2	3.6	31.7	34	4.5	5.6

References for the DNA sequences are given in the text. The SV40 sequence[15] was updated according to ref. 28.

* RH and LH refer to right and left half of the genome, respectively.

† IR and TR refer to intercistronic regions and translated regions, respectively. The values were corrected for the length of the regions.

stem length $\geq n$, is the ratio of the two sums

$$Q_n = \sum_{i=n}^{15} F_i \Big/ \sum_{i=n}^{15} E_i$$

Thus, values for $Q_n > 1$ show more structures of stem length $\geq n$ than expected by chance alone.

Using this approach we analysed the known intercistronic and translated regions separately. The results indicate an intrinsic difference between them (Fig. 3). While short hairpins are found in both regions with the expected frequency ($Q_n \simeq 1$), larger hairpins are definitely over-represented in intercistronic regions with an excess ranging from approximately 4-fold ($n \geq 6$ bp) to 2,000-fold ($n \geq 12$ bp). For translated regions the curve is shifted by about 2 bp, and hairpins with 8 or 9 base pairs in the stem are over-represented. Note also that the uneven distribution of hairpins between structural (late) and non-structural (early) genes in icosahedral viruses (Table 1) is matched by a difference between these regions with regard to Q_n values (Fig. 3). Of particular interest here are the non-structural genes of ΦX174 and G4. Hairpins with 5 or more base pairs in the stem are under-represented in these regions with a Q_n for $n = 6$ as low as 0.38 (ΦX174) or 0.16 (G4) (data not shown). The situation is reversed, however, in the filamentous phage fd, which has an over-representation of hairpins in the non-structural genes, but an expected frequency in the structural genes[25] (data not shown).

As thermodynamic considerations favour the formation of secondary structures having small loops[27], we determined the average loop size for the hairpins of all eight genomes with stem length $n \geq 4$ bp. For $n \leq 5$, the loop sizes average ~11.5 nucleotides, indicating a random distribution between the minimum and maximum values allowed in this study. For stem length $n > 6$ bp a preference for smaller loop sizes was discernible. Compared to the average loop size of 11.18 for hairpins with $n = 4$, the 12 hairpins with $n > 8$ averaged 7.9 bases in the loop, and the 2 with $n > 10$ both have a loop size of 3.

We have demonstrated that the potential to form perfectly base-paired hairpin structures with six or more base pairs in the stem is non-randomly distributed and generally larger than expected in viral DNA genomes. This, together with the preference for small loop sizes, implies an evolutionary selection and therefore a function. Their predominance in intercistronic regions strongly supports the speculations[2,11] that they have evolved as regulatory loci expressing their functions via DNA (or RNA) secondary, rather than primary, structure. Furthermore, it may be argued that secondary structure may also be needed in translated regions and can evolve whenever compatible with the coding requirements. The difference between structural and non-structural genes in this regard cannot be easily explained, but is probably not an intrinsic feature of the genes themselves, as the fd genome shows, but rather a function of their location in the genome, for example, their proximity to the origin of replication.

Though we do not claim that a given loop size or the absence of G–T (or G–U) pairing is fundamental to the biological significance of a hairpin, we are certain that the type of secondary structure on which we have focused here either has some biological role or is at least part of a more complex structure which may be universal to all genomes, as is the genetic code itself.

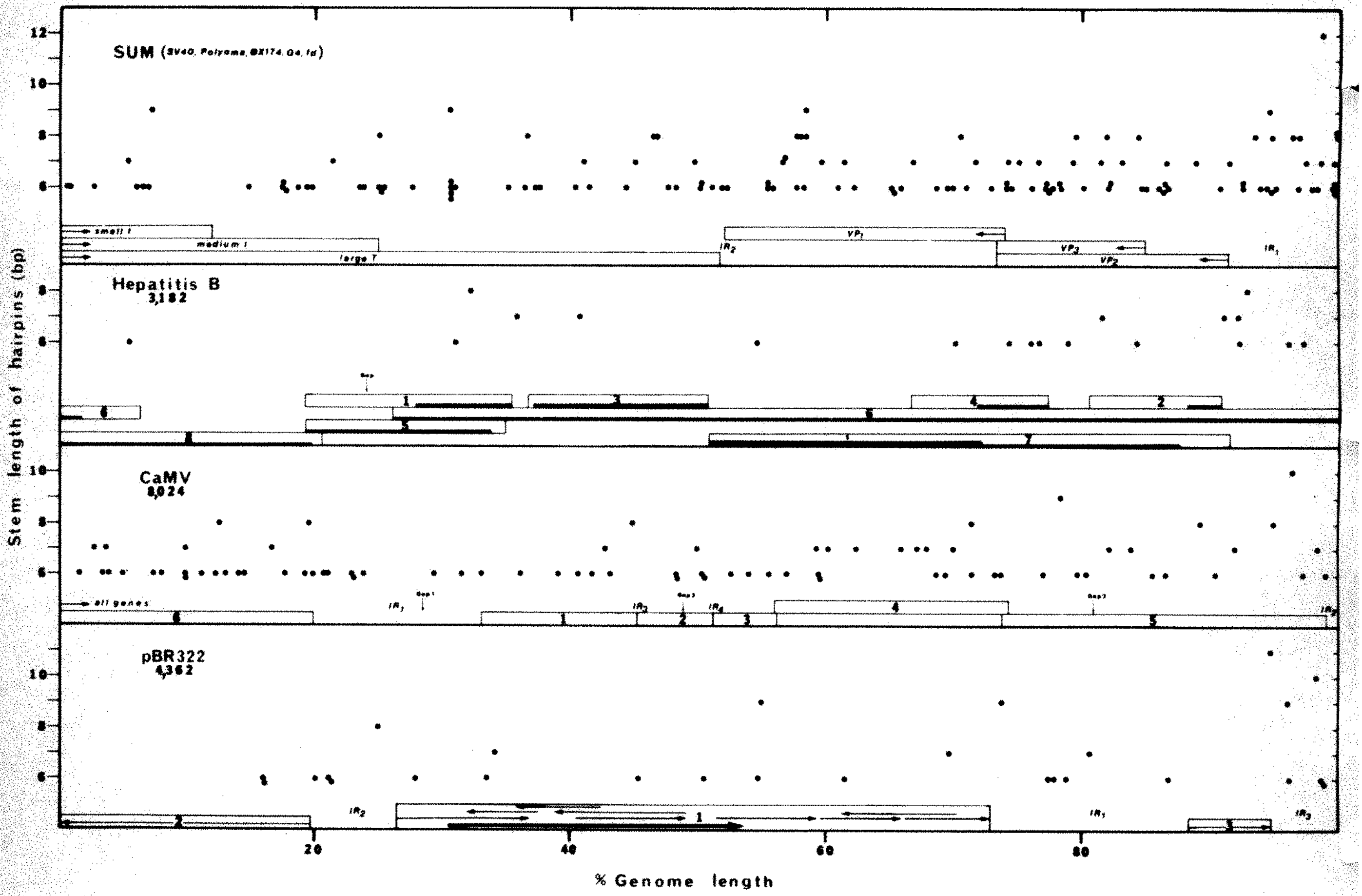

Fig. 2 Distribution of hairpins in the genomes of hepatitis B, CaMV and the plasmid pBR322. The position of hairpins was plotted against % genome length as described in Fig. 1 legend. The top panel represents a summary of Fig. 1 with respect to type and position of hairpins; the genetic map of polyoma virus has been included for comparison. The open reading frames of hepatitis B are indicated by boxes and labelled as in ref. 20. The heavier line at the base of each box has been drawn from the first start codon to the first stop codon within that reading frame and therefore indicates the direction of their transcription and the potentially translated segment. The identified gene product (S) is identified by an additional heavier line in reading frame 7. For pBR322, the boxes indicate possible genes or gene blocks. The arrows indicate the direction of transcription and the length of the putative genes[26].

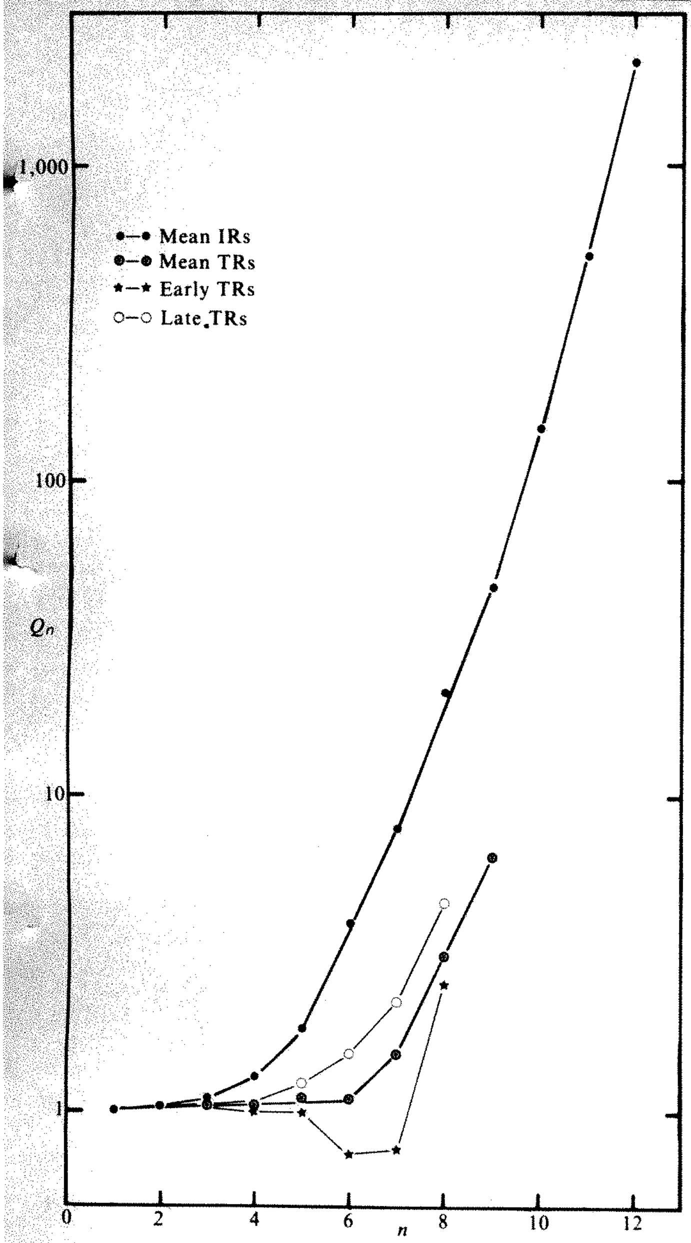

Fig. 3 The distribution of hairpins in intercistronic and translated regions. The intercistronic regions (IRs) and the genes or gene blocks (TRs) between them of the SV40, polyoma, ΦX174, G4, fd and pBR322 genomes were analysed individually and the Q_n values determined as described in the text. After weighting these values according to the length of each region, they were arranged and plotted on a log scale versus the stem length, n. The translated regions of SV40, polyoma, ΦX174 and G4 were separated into early (non-structural) and late (structural) genes and the weighted Q_n values were averaged.

This work was partially supported by NSF grant DEB 78-14197 to W.M.F. We thank Drs P. Deininger, R. Staden and H. Schaller for their computer sequence files.

Received 25 November 1981; accepted 19 May 1982.

1. Cantor, C. R. *Cell* **25**, 293–295 (1981).
2. Wells, R. D. *et al. Prog. Nucleic Acid Res. molec. Biol.* **24**, 167–267 (1980).
3. Panayotatos, N. & Wells, R. D. *Nature* **289**, 466–470 (1981).
4. Hassanoot, C. A. G. *et al. Nucleic Acids Res.* **8**, 169–181 (1980).
5. Lilley, D. M. J. *Nucleic Acids Res.* **9**, 1271–1289 (1981).
6. Sims, J. *et al. J. biol. Chem.* **254**, 12615–12628 (1979).
7. Suggs, S. V. & Ray, D. S. *Cold Spring Harb. Symp. quant. Biol.* **43**, 379–388 (1978).
8. Rosenberg, M. *et al. Nature* **272**, 414–423 (1978).
9. Guaneros, G. *et al. 7th Int. Biophys. Congr. 3rd Pan-Am. Biochem. Congr.*, Mexico City (Abstr. TH-0-42, 1981).
10. Fitch, W. M. *J. molec. Evolut.* **3**, 279–291 (1974).
11. Müller, U. R. & Fitch, W. M. in *Bacteriophage Assembly* (ed. DuBow, M. S.) 285–297 (Liss, New York, 1981).
12. Sanger, F. *et al. J. molec. Biol.* **125**, 225–246 (1978).
13. Godson, G. N. *et al. Nature* **276**, 236–247 (1978).
14. Beck, E. *et al. Nucleic Acids Res.* **5**, 4495–4503 (1978).
15. Reddy, V. B. *et al. Science* **200**, 494–502 (1978).
16. Deininger, P. L. *et al. Nucleic Acids Res.* **8**, 855–860 (1980).
17. Meyer, T. F. & Geider, K. *J. biol. Chem.* **254**, 12642–12646 (1979).
18. Weisbeek, P. *et al. Eur. J. Biochem.* **114**, 501–507 (1981).
19. Schaller, H. *et al.* in *The Single-Stranded DNA Phages* (eds Denhardt, D. T., Dressler, D. & Ray, D. S.) 139–163 (Cold Spring Harbor Laboratory, New York, 1978).
20. Galibert, F. *et al. Nature* **281**, 646–650 (1979).
21. Franck, A. *et al. Cell* **21**, 285–294 (1980).
22. Charnay, P. *et al. Nucleic Acids Res.* **7**, 335–346 (1979).
23. Pasek, M. *et al. Nature* **282**, 575–579 (1979).
24. Covey, S. N. & Hull, R. *Virology* **111**, 463–474 (1981).
25. Simons, G. F. M. *et al.* in *Bacteriophage Assembly* (ed. DuBow, M. S.) 401–411 (Liss, New York, 1981).
26. Sutcliffe, J. G. *Cold Spring Harb. Symp. quant. Biol.* **43**, 77–90 (1978).
27. Tinoco, J. *et al. Nature new Biol.* **246**, 40–41 (1973).
28. Van Heuverswyn, H. & Fiers, W. *Eur. J. Biochem.* **100**, 51–60 (1979).

Evolution of early mechanisms of translation of genetic information into polypeptides

Hans Kuhn* & Jürg Waser†

* Max-Planck Institut für biophysikalische Chemie,
D3400 Göttingen-Nikolausberg, FRG
† Terryhill Drive, San Diego, La Jolla, California 92093, USA

In devising models of the origin of life it is necessary to tackle the problems that the processes of genetic information transfer that are central to life depend on molecules that are themselves the products of such processes—enzymes. A proposed model must eventually yield a detailed chain of processes that can be checked experimentally. We have developed a model in which interactions between the helices of hairpin-loop 'adaptor' RNA molecules (amino acid carrying), lined up side-by-side by sequence complementarity to another 'messenger' RNA, promotes polypeptide synthesis.

Our model involves a picket-fence like linear array of hairpin molecules $B_1, B_2, \ldots, B_i, \ldots$ (Fig. 1), each of which consists of an RNA strand of some 40 monomers. The three nucleotides in the middle of such a strand form the loop of the hairpin, while its ends, twisted into a base-paired double helix, form the hairpin legs. The nucleotides in the hairpin loop hydrogen bond to complementary nucleotides contained in an extended RNA filament C, which is attached to another hairpin that forms the endpost of the picket-fence and is rotated 180° relative to the units B_i. The open ends of hairpin B_i possess affinity towards activated amino acids, and facilitate the formation of polypeptide bonds between amino acids attached to them. The hairpin RNAs are envisaged as the precursors of tRNAs, the nucleotides in the hairpin loop serving as anticodons to the codons along filament C, the precursor of mRNA. The endpost hairpin A would evolve into the messenger end used in the recognition of the start of the genetic message.

In many details, including the hairpin conformation of adapter molecules, this model is similar to one described several years ago[1]. Hairpin conformation of ancestral adapters is supported by tRNA sequence analysis[2,3]. We also suggest that another double-helical RNA-strand facilitates polypeptide synthesis, moving along the ribbon-like aggregate of hairpins, functioning as an early ribosome[4]. In the present model DNA became involved much later[1,3,4].

The assumptions underlying our approach are: (1) the presence of activated nucleotides and amino acids; (2) the existence of periodic temperature changes, as caused by sunlight and shadow-casting objects; and (3) a structurally diversified environment, such as pores of different sizes in rocks. Conditions (1) and (2) favour the creation, and later drive the replication and evolution of short nucleotide strands, with (+) strands acting as templates for (−) strands and vice versa; (3) provides confinement as well as all-important evolutionary pressure, because of the existence of a large variety of 'niches' available for 'colonization' by emerging life forms of increasing sophistication. For example, pores above a certain size cannot be colonized by strands that are too short, because they diffuse too quickly from the favorable sites. Calculations[3-5] show that

0028-0836/82/310585—02$01.00

strands of about 10 monomers may form directly. Longer strands may arise by fusion of shorter strands, but there is a limit to the length of a replicable strand of some 40 nucleotides, because of copying errors.

This impasse is broken by convolution of the strands into a conformation allowing aggregate formation. This permits the invasion of larger pores and, of the utmost importance, it eliminates erroneous copies because aggregate formation is crucially governed by RNA conformation and thus nucleotide sequence. The simplest conformation that permits such interlocking is that of the twisted hairpin B_i described earlier. A huge selective premium is associated with machinery that facilitates such aggregation, and the units described earlier provide such machinery (Fig. 2). C acts as collector strand, guiding the hairpins B_1, B_2, ... to the growth region of the aggregate, while A (to which C has become fused accidentally) acts as nucleation site that facilitates the onset of aggregation.

Our molecular model exhibits an astonishingly good fit between neighbouring hairpins, and between codons and anticodons, permitting stacking of bases. The model is based on left-handed GC RNA helices analogous to the Rich–Arnott–Dickerson Z conformation of DNA,[6-8], which has recently been shown to be possible for RNA as well (J. H. Van DeSande and T. M. Jovin, personal communication). All these steric fits require that the 3′5′ direction of strands connected by codon-anticodon interactions be opposite. In a model in which the hairpins have the conformation of a right-handed A helix the fits are not as good, but probably still adequate. The aggregates might be stabilized by polyvalent cations (Mg^{2+}, Ca^{2+}) that form links between negatively charged phosphatidyl groups on the outside of neighbouring hairpin strands. C would remain unconvoluted because convolution into a hairpin requires specific nucleotide sequences.

The presence of pores too large to curb strand diffusion favors the evolution of polypeptide-producing devices because polypeptides would block pore channels and at a later stage would coalesce into confining 'cellular' envelopes. The aggregates described develop catalytic properties toward polypeptide formation as follows.

Complementary (+) and (−) base-paired hairpins are identical (Fig. 2) except for the nucleotides in the mid-position and at the open ends. Ancestral tRNA contained largely, and perhaps exclusively, G and C[2], with C in the first and G in the third anti-codon position, and we assume the same for our (+) and (−) hairpins, leaving the midposition for purposes of an ancestral code, while the open ends possess or develop affinity towards activated amino acids. This view is also supported by a DNA sequence analysis[9] that suggests an ancestral reading frame PuNPy (Pu purine, Py pyrimidine, N either). If the midpositions and ends of (+) strands are occupied by C residues and those of (−) strands by G residues, and amino acids a_1 and a_2 activated by linkage with C and G respectively existed prebiotically[3,5] the two types of hairpins would serve as adapters.

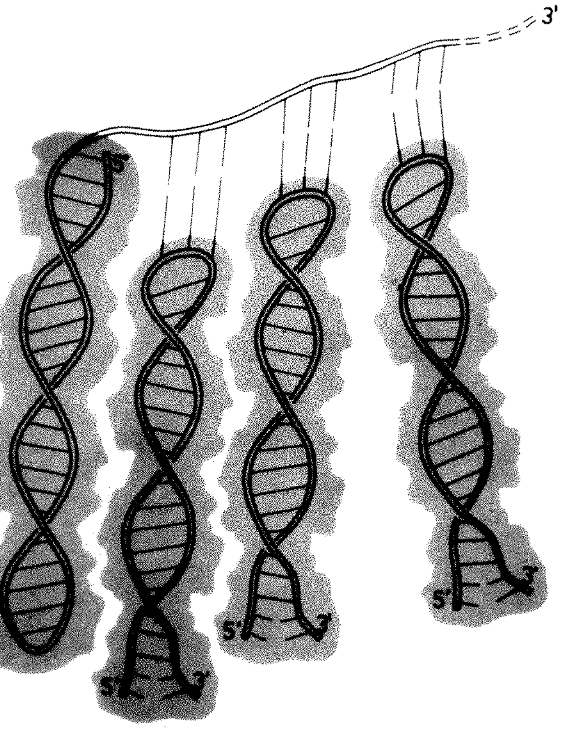

Fig. 1 Hairpin strands forming the beginnings of an aggregate. Legs of hairpins are twisted into double helices and outlines are as expected for van der Waals contacts.

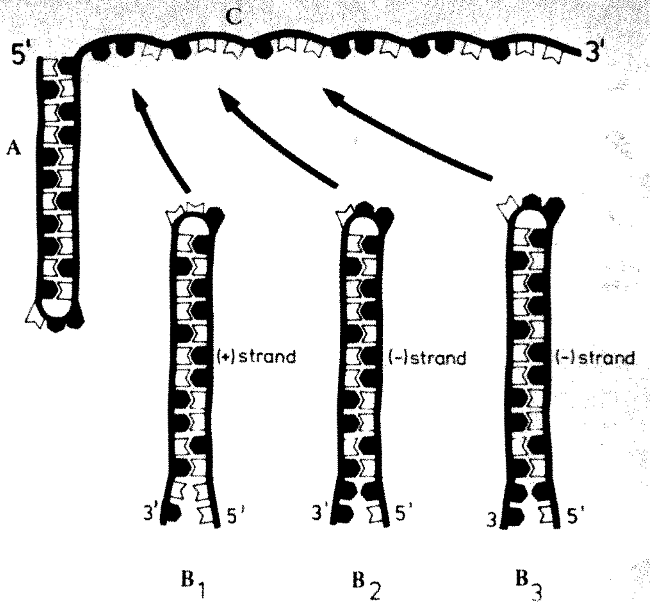

Fig. 2 Schematic view of strand C attached to hairpin A and hairpins B_1, B_2, B_3 in the act of forming a picket-fence like aggregate.

Eventually a sequence along C arises encoding a polypeptide acting as a primitive RNA replicase that decreases replication errors sufficiently so the information coding for it is not lost. (An increase of the survival rate by 10% by a replicase of 10 amino acids would only require a reduction of the error rate by a factor 3 for it to be fixed by selection. Such a 'replicase' might be a short polypeptide that fits into a notch of the double helix that exists during strand replication, slipping along in the notch as the new strand is lengthened (see ref. 10 for a discussion of the plausibility of this assumption).

The rate of evolution can be increased enormously once a 'replicase' has been produced. More diversified 'enzymes' evolve, the base pairs A and U become part of the code, the first and third anticodon positions gradually become used for coding purposes, and the number of amino acids being integrated into polypeptides increases during each of these steps[11]. Details of the proposed molecular model do not affect the potency of our methodology and we encourage others to think of improved scenarios.

We thank Drs Dietmar Möbius, Mary Price and Nickolas Waser for valuable discussions.

Received 23 February; accepted 2 June 1982.

1. Kuhn, H. *Angew. Chem. Ausg. B* **11,** 798 (1972).
2. Eigen, M. & Winkler, R. *Naturwiss enschafter* **68,** 217, 282 (1981).
3. Kuhn, H. & Waser, J., *Angew. Chem. Ausg. B* **20,** 500 (1981).
4. Kuhn, H. & Waser, J. in *Biophysics* (eds Hoppe, W., Lohmann, W., Markl, H. & Ziegler, H.) (Springer, Berlin, 1982).
5. Kuhn, H. *Naturwissenschaften* **63,** 68 (1976).
6. Wang, E. H.-J. *et al. Nature* **282,** 680 (1979).
7. Drew, H., Takano, T., Takano, S., Itakura, K. & Dickerson, R. E. *Nature* **286,** 567 (1980).
8. Arnott, S., Chadrasekaran, R., Birdsall, D. L., Leslie, A. G. W. & Ratliff, R. L. *Nature* **283,** 743 (1980).
9. Shepherd, J. C. W., *J. molec. Evol.* **17,** 94 (1981); *Proc. natn. Acad. Sci. U.S.A.* **78,** 1596 (1981).
10. Anderson, W. F., Ohlendorf, D. H., Takeda, Y. & Mattheus, B. W. *Nature* **290,** 754 (1981).
11. Kuhn, H. & Kuhn, Ch. *Origins of Life* **9,** 137 (1978).

BOOK REVIEWS

Colleges of Science & Technology
92, A.P.C. Rd., Cal. 9
LIBRARY COMPLEX
Departments of :
...mical Engineering
...mical Technology
...stics & Rubber Technology

Koestler glimpsed

Nicholas Wade

Koestler: A Biography. By Iain Hamilton. Pp.398. UK ISBN 0-436-19101-6; US ISBN 0-02-547660-2. (Secker & Warburg, London/Macmillan, New York:1982.) £10, $19.95.

ARTHUR Koestler must have led one of the most varied and interesting lives of the twentieth century. For a life so filled with thought and action, and which reflects so accurately the major political and intellectual preoccupations of the time, parallels are hard to find. André Malraux and George Orwell are perhaps the closest, yet even they didn't venture into science, the realm of the century's most distinctive achievements.

The range of Koestler's interests is as formidable as his skill in pursuing them. Most of us find it difficult enough to write well in one language: Koestler, whose native tongue is Hungarian, wrote his famous novel *Darkness at Noon* in German, and his later work in English. As a novelist, political activist and historian of science, he has fitted at least three careers, each performed with unusual distinction, into one lifetime. There could be few greater challenges to a biographer.

Iain Hamilton, the poet and former editor of *The Spectator,* has made a creditable attempt to capture the protean nature of his subject. He dexterously follows Koestler through the changing milieus of his life, from student president of a Zionist duelling fraternity at the University of Vienna, to correspondent and science adviser for the Ullstein chain of newspapers, to his establishment in the English-speaking literary world. Yet the biography has several serious faults which spring, I think, from a severe lack of empathy that has somehow developed between the writer and his subject.

Mr Hamilton is too good a reporter to be anyone's Boswell. He has read everything and interviewed everyone relevant to his subject. He has unearthed many details of Koestler's private life, some of which Koestler might prefer not to have seen in print. Yet despite the close-up view, the nature of the subject remains blurred. Hamilton had access to Koestler's papers and diaries, yet does not quote from his interviews with Koestler himself. His desire to be totally independent seems to have led in places beyond detachment, to the point of rivalry with his subject. Too many of his own views obtrude into the portrait, while at the same time he frankly refuses to discuss Koestler's interests from 1970 onward, which have been focused on extrasensory perception. It may well be, as Hamilton implies, that Koestler's writings in this intractable field are worthless: all the more reason for a biographer to try to explain what led him into it.

Admirers of Koestler will be disappointed at the way Hamilton all but ignores the substance of his *oeuvre.* Since Koestler has written four volumes of autobiography covering his early life, perhaps there is little point in going over the same ground. But Hamilton does not have much to say about the subject matter even of *Darkness at Noon,* which along with *Animal Farm* surely ranks as one of the most important and influential political novels of the century. The French edition of *Darkness at Noon* sold by the thousands of copies just before the first post-War election in France, which the Communist Party was expected to win, and the book's impact has been held responsible for the party's narrow defeat. But Hamilton does not evaluate this claim, or discuss the book's influence on the many Western intellectuals who even in the late 1940s could not believe the Soviet experiment had so grossly betrayed its ideals.

Koestler's writings on the nature of scientific discovery are also given rather short shrift. *The Sleepwalkers,* a brilliantly fresh and stimulating account of the early history of astronomy, receives eleven pages of discussion in this 364-page book; *The Act of Creation,* an inquiry into the modes of scientific creativity, is dismissed in eight, and the treatment is thin. Yet these are two of Koestler's major post-War works.

A minor book produced during this period was *The Case of the Midwife Toad,* a passionate defence of the Austrian biologist Paul Kammerer who, like Koestler, was interested in psychic phenomena. Kammerer committed suicide in 1926 after the discovery by the American biologist G. K. Noble that nuptial pads on Kammerer's specimens of midwife toads, interpreted as evidence for Lamarckian inheritance, had been faked. Koestler argued that Kammerer was innocent, and that the pads, which really existed at one time, were perhaps touched up by an overzealous lab assistant. But a brilliant review by Lester Aronson (*Behavior Genetics* **5**, 115–125; 1975), a former assistant to Noble, persuades me that Koestler, in this instance, carried defence to the point of whitewash.

The Case of the Midwife Toad, like most of Koestler's other works, receives little substantive attention in Hamilton's biography, presumably on the assumption that they speak for themselves. The trouble with this approach is that the matters which Hamilton discusses at length, such as Koestler's relationships with his wives, or his problems in getting an American visa, are of little interest except in as far as they throw light on Koestler's public achievements. Hamilton does not use them to this end. Indeed the reader is occasionally led to wonder whether the purpose of some of the more trivial episodes isn't to belittle Koestler.

This cannot be the main purpose because, as Hamilton explains in the preface, he for many years "had admired Koestler's work (the greater part of it, at any rate)". Yet the reasons for that admiration are not clearly explained. There are few sustained themes or insights to unify the mass of chronological material presented here. Hamilton also remarks in the preface that:

> My reading of Koestler's works has convinced me that he is *au fond* a deeply religious man. He has never admitted this, confessing only to several experiences of the quasi-mystical Freudian 'oceanic' feeling . . . .

This is an interesting observation, yet one that is not further explored in the text.

Koestler's life can perhaps be seen as a search for faith. As a young man he embraced Zionism but quickly grew disenchanted. The next faith was Communism, but that was the god that failed. Pursuit of the divine spark led Koestler into the study of Kepler and scientific creativity. More recently came the interest in the paranormal. Like Sisyphus with his stone, Koestler has laboured mightily to ascend the peak, and when the effort fails, he has picked up the pieces and started again. It is this relentless search that has created work after work of intellectual inquiry, each exploring a new area with Koestler's own combination of intensity and clarity. Hamilton's biography portrays the private man behind these public explorations. It is well written and thoroughly researched, yet despite these substantial merits the portrait does not fully capture the essence of its subject.

Nicholas Wade is a Member of the Editorial Board of the New York Times, and author of The Nobel Duel *(Anchor Press/Doubleday, 1981).*

Stars, listed and mapped for a new epoch

David W. Hughes

Sky Atlas 2000.0. By Wil Tirion. ISBN 0-521-24467-6. (Cambridge University Press/Sky Publishing: 1982.) £15, $29.95.
Sky Catalogue 2000.0. Volume 1, *Stars to Magnitude 8.0.* Edited by Alan Hirshfeld and Roger W. Sinnott. Pp.604. Hbk ISBN 0-521-24710-1; pbk ISBN 0-521-28913-0. (Cambridge University Press/Sky Publishing: 1982.) Hbk £32.50, $45; pbk £14.95, $29.95.

ATLASES and catalogues of the sky have one important characteristic for the publisher, and that is they get out of date quickly. The poles of the sky move, thus slowly changing the stellar co-ordinates. This is indicated by the epoch figure 2000.0 in the titles of the two books under review. The star positions given in the atlas and catalogue are only correct for that date. The last epoch was 1950.0 and these two books are the first comprehensive works for the new co-ordinate epoch. The pole does not move very quickly, the precession about the vertical to the Earth's orbital plane taking about 25,750 years, but still astonomers like being up to date and like to have the latest atlas and catalogue to hand.

The second thing to say about Tirion's atlas is that it is a joy to the eye. The sky is divided into 26 areas each represented by a chart measuring 12¼ by 17¾ inches. Stars are represented by black dots which decrease in size as the stars get fainter. Galaxies are red, nebulae green, clusters yellow and the Milky Way is represented by two shades of blue, following Pannekoek's isophotes. Secant conic and secant cylindrical projections are used which reproduce the constellation figures with minimum distortion. The labelling is clear. Simply to see this book is to want it.

The charts contain some 43,000 stars down to visual magnitude 8 and about 2,500 deep-sky objects. Brighter stars are labelled with both their name and their Bayer letter and Flamsteed number. Deep sky objects have their NGC or IC number as well as their Messier number. The Andromeda galaxy is, for example, shown as 224.M31.

Volume 1 of the *Sky Catalogue 2000.0* starts with an extremely useful ten-page introduction which is followed by 600 pages of tables. Each line in the table refers to one star, and 45,269 are tabulated. The brightest, Canopus, is 40 million times more luminous than the faintest, HD 153336. Thirty-seven thousand of them are visible with the naked eye from Earth. Following normal practice the stars are listed in order of increasing right ascension. Henry Draper and Smithsonian Astrophysical Observatory numbers are given, as are the name (where applicable), right ascension, declination, proper motion, visual magnitude, colour index, absolute visual magnitude, spectral type, MK type, radial velocity and distance. An example of the care taken by the authors is indicated by the way in which the distances are labelled according to whether they originate from trigonometric or spectroscopic parallax techniques or are just maximum or minimum values. Ninety-one per cent of the stars in the catalogue have their distances given.

Still to come, to complete the set, is Vol.2 of the *Sky Catalogue* which will describe in full the multiple and variable stars as well as the clusters, nebulae and galaxies. This is due to appear early next year.

Both the *Sky Atlas* and the *Sky Catalogue* are beautifully produced, good value for money and in my opinion essential acquisitions for all active astronomical observers.

David W. Hughes is a Lecturer in Astronomy and Physics at the University of Sheffield.

The great chain of non-being

A. Rupert Hall

Plurality of Worlds: The Origins of the Extraterrestrial Life Debate from Democritus to Kant. By Steven J. Dick. Pp.246. ISBN 0-521-24308-4. (Cambridge University Press: 1982.) £19, $34.50.

WHY should fairies be intrinsically any more absurd than Astrans? Partly, it is obvious, because the bottom of the garden is easier to inspect than even the planets of our own Solar System, and partly because the non-human qualities of pixy or fairy make this kind of being fantastic while we may imagine Astrans to be just as human-like as we wish. Indeed, the very principle of universal similitude which encourages us to contemplate the existence of Astrans — or in earlier days Lunatics and Martians — requires us, in starting from the assumption that these creatures are living, sentient and intelligent beings, to suppose them in some recognizable measure of behaviour to be like ourselves, however morphologically unfamiliar. The same argument applies to the imagination of extra-terrestrial animals and plants: a Venusian tree that runs, or an Astran flying elephant, are just as absurd as if we placed the same creatures in some unexplored Amazonian backwoods.

Nonetheless, for living things of all kinds the principle of universal similitude remains to this day an unsupported speculation. It is a principle, common to Epicuros and Hoyle, resting on a metaphysical belief that nothing in the cosmos can be unique, which many (including presumably most if not all religious believers) regard as unacceptable. In its original form, as adopted by the Greek atomists, it embraced the idea that no substance and no type of being can be unique, since everything is subject to probability and the occurrence of an event in one place does not reduce the likelihood of its repetition there or elsewhere. Hence time's arrow pointed in all directions at once as on a three-dimensional compass-card or, more exactly, must be interpreted as having but a local and reversible effect. Accordingly, the metaphysical rejection of singularity — and indeed the principle of universal similitude itself — are inconsistent with such an attribution of time-direction to the cosmos as the prevailing scientific view of its evolution seems to require; but as Dr Dick's consideration stops with Kant in the late eighteenth century, the relation of the Perfect Cosmological Principle and of the Primordial Bang to universal similitude falls outside his scope.

Throughout late antiquity and the Middle Ages Aristotle's rational arguments for a finite universe and a unique Earth held sway, though latterly mitigated by the contention, founded on God's omnipotence, that the creation of more universes than one was within his power. However, since it seems that mediaeval philosophers regarded such alien universes as in principle unobservable — surely a logical position to adopt — the assertion or denial of their existence was meaningless except perhaps in a theological sense. Then, as Dr Dick emphasizes, the Copernican revolution opened the door to a more effective version of universal similitude in that the Earth was now seen as a member of a class of bodies, planets, and later the Sun was placed in another class, stars. Since then, and with renewed emphasis from Newton, universal similitude has become a firm principle in thought about the physical structure of the cosmos though, paradoxically enough, the progress of scientific investigation has always increased rather than diminished our sense of the diversity within the classes of stars and satellites. Whereas the seventeenth century could (with some little violence to observation and plausibility) imagine the Moon as not at all unsuited to the existence of intelligent living beings, and the nineteenth century could similarly view Mars, we now recognize that the chances of finding another Earth-like planet, if finite, are quite small. The fact is that our search for analogues in the cosmos has had to be pushed ever further and further from home as our knowledge of the cosmos has become more positive. Even the bottom of the galaxy is now perhaps too close.

Dr Dick's interest is very much more in the philosophical rather than in the scientific stage of the debate about the plurality of worlds. Newton, to whom worlds of anti-matter — or at any rate "Worlds of several sorts in several parts of the Universe" — were by no means inconceivable, appears only 50 pages before the end of the 190-page text. I think this is a pity. The principle of universal similitude is much less interesting in the period where it was justified only by the experientially dubious argument that things are more probably like than unlike, than in the age of modern science when it has been justified by observational and theoretical successes. We have built up a fair body of knowledge of how this principle can be applied, and where it fails to work. Moreover, since Kant's time we have learnt a great deal about similitude in living things on Earth and have related this knowledge to a theory of their evolution in such a way as to transform the discussion of the possibility of living phenomena elsewhere. True, none of this has come near answering the question: "Are there other inhabited worlds?" but it has taught us at least where such worlds are not, and hardened the distinction between scientific imagination and scientific romance. The question: "Was Jesus Christ to be seen as the planet-hopping Savior in the new cosmology?" (Dr Dick's phrase), once so poignant to theologians, would not disturb a modern astrophysicist but scientist and theologian might agree that the most profitable working hypothesis for the present is to assume the Earth's singularity. Earths outside our galaxy seem likely to remain as unknowable to us as God's alternative universes in mediaeval thought.

Dr Dick's painstaking account contains few surprises. No one has made assertion or denial of the plurality of worlds the pole of a philosophical or scientific system; rather, the idea has been exploited or refuted as an exemplary consequence of more fundamental ideas about space, time and being. Very often, as in that most famous book of all on the subject, Fontenelle's *Entretiens* (1686), plurality has been defended in a fanciful or fictional manner. Belief in the plurality of worlds has also long been an intellectual symbol, like the expropriation of the expropriators or free love, a sign that he who holds this belief is fettered by no conventional dogmas of religion or science. It never seems to have done anyone much harm to assert this belief, not even Giordano Bruno (and Galileo rejected it). Whether it has ever done anyone any good I shall not attempt to say. ☐

A. Rupert Hall is Emeritus Professor of the History of Science, Imperial College, University of London.

There is a tide in the affairs of men . . .

Arthur T. Winfree

The Clocks That Time Us: Physiology of the Circadian Timing System. By Martin C. Moore-Ede, Frank M. Sulzman and Charles A. Fuller. Pp.448. ISBN 0-674-13580-6. (Harvard University Press: 1982.) $25, £17.50.

If you have cancer, don't accept another dose of cytotoxins or X-rays at a time scheduled for clinical convenience: the damage to your healthy tissue can be devastating at one time of day, yet go relatively unnoticed at another. If you read this en route across time zones, don't sleep off your jet-lag behind drawn curtains: exposure to people and sunlight will markedly shorten the time of discomfort. If you want a stimulating book to read, try this one.

Why this one? Wide-ranging books on circadian rhythms have appeared before: Bunning's classic *The Physiological Clock*, updated in 1973; Luce's popular *Biological Rhythms in Psychiatry and Medicine* in 1970; Ward's still-more-popular *Living Clocks* in 1971; Wever's 1979 classic-to-be *The Circadian System of Man*; my own *Geometry of Biological Time* in 1980; plus abundant, more specialized monographs and symposium proceedings. So who needs another?

You do if you found Winfree too mathematical, Wever too preoccupied with data and statistics, the journalists too excited for scientific reliability, and Bunning too preoccupied with invertebrates and plants. We mammals have clocks too, and clock physiology has immediate medical pertinence. A lot has been discovered by mammalian physiologists and medical doctors in the past decade, especially about sleep timing in human beings and the origin of sleep rhythms in the lower brain. *The Clocks That Time Us* is absolutely up-to-date in these respects, and does a superb job of presenting the major results in jargon-free English.

As with most scientists cum writers, the authors are liveliest on topics more distant from their scholarly speciality. The chapters on neuroanatomy and monkey physiology may become tiresome unless you are professionally involved. But if you are, you will appreciate the 150 or so figures, mostly depicting data, and some 900 reference citations, most of them less than a decade old. Regardless, you cannot help but appreciate the rich variety of illustrations drawn from *human* physiology, psychology and medicine.

Every author must compromise accuracy somewhat for a lively presentation and I might have chosen a different balance in some of the more theoretical sections. For example, the 30-page section about phase-resetting and entrainment, though well done, is drawn from outdated theory of the 1950s, and in any case is never referred to again. And a "mathematical model", vintage 1981, for the human temperature rhythm and sleep/wake alternations occupies most of a short chapter, but to my mind gives the misleading impression that we know a lot more than we do.

Though sceptically alert, even to the point of peppering pages with "howevers" in the physiology chapters, Moore-Ede *et al.* seem to me to accept many other, oftimes rather sensational, data too nearly at face value. For example, were I assigned to edit the next edition, I would urge less emphasis on the likelihood that we harbour two or more separate sources of circadian timekeeping in our various organs, unless more persuasive experiments appear. Nonetheless, every suggestive observation in this book deserves the emphasis given if it provokes immediate testing: for example, that the only four successful "test-tube baby" implantations carried out at the time of writing were performed between 10pm and midnight, and the 75 failures were attempted at other times.

The long last chapter was the most exciting to me: "Medical Implications of Circadian Rhythmicity". The effectiveness (and toxicity) of drugs and anaesthetics show marked rhythms which should be charted to improve the safety of medical procedures; this has already been done and reduced to clinical practice in the case of cortisone therapy. We also learn about jet lag and the inconveniences of disparity between external time and internal body time. Unfortunately, no evidence is presented that internal desynchronization is, in itself, part of the problem. The prospect of a "jet-lag pill" is discussed, but no drug more reliable than caffeine is suggested. Whoever invents this one seems sure to get rich. Note is made that shift-workers suffer from desynchronization while responsible for critical decisions in hospitals, nuclear power plants and submarines; the Three Mile Island incident occurred at 4am. Psychiatric disorders, too, may sometimes stem from derangement of circadian coordination: success has been reported in some attempts to cure insomnia and recurrent depression by phase-resetting.

So do not buy this book lightly — you may end by habitually charting your body temperature and hours of sleep. ☐

Arthur T. Winfree is a Professor of Biological Science at Purdue University, Indiana.

Richard D. Alexander's *Darwinism and Human Affairs*, first published in 1980 and reviewed in *Nature* **287**, 173 (1980), has now appeared in paperback. The book is published by the University of Washington Press and costs $9.95.

Bewitched by a computer

Simon Lavington

The Soul of a New Machine. By Tracy Kidder. Pp.254. US ISBN 0-316-49170-5; UK ISBN 0-7139-1482-3. (Little, Brown/Allen Lane: 1982.) $12.95, £7.50.

COMPUTERS are created by teams — for the simple reason that even the smallest of them is too complicated to be designed in a reasonable time by one person alone. This team approach is common to many other complex engineering projects, and yet a hint of sorcery does surround the birth of a new computer. In *The Soul of a New Machine*, Tracy Kidder examines this mystique through the eyes of a computer design team operating in the United States in the late 1970s.

The book is somewhat retrospective, for few computers are today things of mystery. Market forces and the increased use of design automation are producing a convergence of approaches amongst manufacturers. Standard computers are off-the-shelf items and it is only in the areas of very high performance or special-purpose computers that there is much scope for engineering innovation. It has not always been thus. Not too many years ago every computer was special. They were special not only in the engineering sense but also because of the unexpected avenues they opened up for human endeavour. Man could comprehend machines which enhanced his physical strength, mobility or range of communication, but here was a new type of machine which cooperated with and enhanced his very thoughts.

Of course the difficulty was — and is — that computers do not speak the same language or share the same preconceptions as human beings. The computer is simpler, faster, more rigorous, less forgiving than its designer and nowhere is this mis-match felt so keenly as during the testing of new hardware or software. Getting a computer to work properly — especially under commercial pressures — demands a particular kind of mental and physical stamina for which there are few parallels. There is all the difference in the world between thinking about a new computer and actually building one, though a result of modern design methodology has been to reduce the areas of uncertainty. A computer design team has thus to operate in an unusual environment and, until quite recently, the team morale was strengthened by the unspoken feeling that the members were in some way pioneers of a new age.

The Soul of a New Machine is something of a misnomer, for the book is really about the soul of the design team. Brought together and sustained by the god-like personality of their leader, the team is given the challenge of designing a relatively high performance machine within severe political constraints imposed by the company's top management. In describing this political background, Mr Kidder provides an interesting analysis of the minicomputer market at a time which saw the progression from 16-bit to 32-bit machines. In particular, the development of the Data General Company is charted with the financial precision of a business journal, and students of modern industrial development will find this very revealing. The machine itself remains in the wings for most of the story. It is in any case somewhat of a hybrid — an attempt to achieve large computer performance whilst maintaining compatibility with a small computer marketing base. Although by no means a technical landmark, the project does involve the solution of some unusual design problems and the emphasis on processing speed makes fault-finding the more difficult. Few hints are given about the precise tricks played by the engineers to obtain the performance they required, but this omission is perhaps just as well. Mr Kidder is not at home with computer terminology; his attempts to interpret the jargon for a lay readership are at times ungainly, and *cognoscente* will recognize instances where his simplifications are based on misconceptions.

Luckily, however, a precise technical understanding is not necessary for an appreciation of the book's underlying theme: the response of young engineers to stress. Mr Kidder's unease in some ways emphasizes the gulf between computer terminology and everyday language, a gulf which tends to place computer engineers apart from other mortals. The jargon, the project deadlines, the group pressure to work long and unsociable hours, the mental effort of pinning down faults from the most sketchy of clues — it is no wonder the engineers become totally absorbed by their machine.

There is also a subtle yet pervasive managerial influence applied to the team. To most of the engineers this is their first chance to make a personal contribution to the design of a new computer and the team leader appears to exploit this. The ephemeral glory of "having your name on the machine" is offered only to those who are willing to devote their total waking hours to the project. As the project progresses, any lesser commitment becomes unthinkable by the young engineers themselves; peer pressure ensures finally that they are not so much enslaved as bewitched. Wives and families receive scant mention in the book, but they probably felt that the machine was being weaned on men's souls.

The story will ring true for anyone who has been involved in the design of a new computer, and yet these same readers will find Mr Kidder at times frustrating. This is because the tantalizing glimpses of engineering problems leave unassuaged a thirst for more detail. But if the book is — thankfully — not a technical report, it is also not a novel. It fails to do justice to the dramatis personae; the character sketches dwell excessively on the scientific career of the team members and few of them emerge from the pages as flesh and blood. In a sense this criticism is unfair, since the book should be judged as a documentary which makes a successful attempt to bridge the gap between high technology and everyday experience. With computers, for better or worse, pervading every corner of society, such bridge-building books are badly needed. ☐

Simon Lavington is a Senior Lecturer in Computer Science at the University of Manchester, and author of Early British Computers *(Manchester University Press, 1980).*

Harvested thoughts

Wolfgang Pauli: I don't mind your thinking slowly: I mind your publishing faster than you think.

[Sir] Francis Galton: [Statistics are] the only tools by which an opening can be cut through the formidable thicket of difficulties that bars the path of those who pursue the Science of Man.

[Lord] Ernest Rutherford: If your experiment needs statistics, you ought to have done a better experiment.

Michael Flanders: One of the great problems of the world today is undoubtedly this problem of not being able to talk to scientists, because we don't understand science; they can't talk to us because they don't understand anything else, poor dears.

Francis [Lord] Jeffery: 'Damn the Solar System. Bad light; planets too distant; pestered with comets; feeble contrivance; could make a better myself.'

Samuel Butler: We shall never get people whose time is money to take much interest in atoms.

[Lord] John [of Selmeston] Wilmot [Minister of Supply 1945–1947]: What I like about scientists is that they are a team, so that one need not know their names.

Victor Frederick Weisskopf: Science has become adult: I am not sure whether scientists have.

Leo Szilard: Don't lie if you don't have to.

Eric Temple Bell: The cowboys have a way of trussing up a steer or a pugnacious bronco which fixes the brute so that it can neither move nor think. This is the hog-tie, and it is what Euclid did to geometry.

These quotations are taken from Alan L. Mackay's delightful collection, *Harvest of a Quiet Eye*, first published in 1977 by The Institute of Physics. The book contains well over a thousand such aphorisms and quotations, and has just appeared in paperback, price £3.95, $9.95. Hardback is £8.50, $22.50.

BOOKS RECEIVED

Astronomy

FICHTEL, C.E. and TROMBKA, J.I. Gamma Ray Astrophysics. New Insight into the Universe. Pp.401. No ISBN. (National Aeronautics and Space Administration, Washington: 1981.) Np.

FRICKE, K.J. and SHAHAM, J. (eds). Proceedings of the 5th Gottingen–Jerusalem Symposium on Astrophysics held October 6-9, 1980, Gottingen. Pp.298. ISBN 3-525-82107-7. (Vandenhoeck & Ruprecht, Germany: 1981.) Kart DM 44.

HEESCHEN, D.S. and WADE, C.M. (eds). Extragalactic Radio Sources. Proceedings of IAU Symposium No.97. in cooperation with URSI held August 3–7 1981, Albuquerque, USA. Pp.490. Hbk ISBN 90-277-1384-7; pbk ISBN 90-277-1385-5. (Reidel: 1982.) Hbk Dfl.125, $54.50; pbk Dfl.60, $26.

SPITZER, L. Jr. Searching Between the Stars. Pp.180. ISBN 0-300-02709-5. (Yale University Press, London: 1982.) £17.50.

SZEBEHELEY, V. (ed.). Applications of Modern Dynamics to Celestial Mechanics and Astrodynamics. Proceedings of the NATO Advanced Study Institute held August 2–14, 1981, Italy. Pp.400. ISBN 90-277-1390-1. (Reidel: 1982.) Dfl.100, $43.50.

Physics

CLARK, H. A First Course in Quantum Mechanics, Revised Edn. Pp.368. ISBN 0-442-30173-1. (Van Nostrand Reinhold: 1982.) £4.95.

DORNER, B. Coherent Inelastic Neutron Scattering in Lattice Dynamics. Pp.96. ISBN 3-540-11049-6/0-387-11049-6. (Springer-Verlag: 1982.) DM 44, $20.50.

GEORGI, H. Lie Algebras in Particle Physics: From Isospin to Unified Theories. Frontiers in Physics, Vol.54. Pp.255. ISBN 0-8053-3153-0. (Benjamin/Cummings: 1982.) $14.50.

HUDSON, A. and NELSON, R. University Physics. IE. Pp.975. No Hbk ISBN; pbk ISBN 0-15-592963-1. (Harcourt Brace Jovanovich, London: 1982.) Hbk £22; pbk £14.75.

MILLER, F. Jr. College Physics, 5th Edn. Pp.876. Hbk ISBN 0-15-511737-8; no pbk ISBN. (Harcourt Brace Jovanovich, London: 1982.) Hbk £15.60; pbk £12.20.

MUGHABGHAB, S.F., DIVADEENAM, M. and HOLDEN, N.E. Neutron Cross Sections. Vol.1: Neutron Resonance Parameters and Thermal Cross Sections, Part A. ISBN 0-12-509701-8. (Academic: 1981.) $58.

ORTON, C.G. (ed.). Progress in Medical Radiation Physics, Vol.1. Pp.388. ISBN 0-306-40713-2. (Plenum: 1982.) $45.

RISTE, T. (ed.). Nonlinear Phenomena at Phase Transitions and Instabilities, Vol.77. Pp.481. ISBN 0-306-40896-1. (Plenum: 1982.) Np.

Chemistry

ANTELMAN, M.S. and HARRIS, F.J. Jr. The Encyclopedia of Chemical Electrode Potentials. Pp.288. ISBN 0-306-40903-8. (Plenum: 1982.) Np.

BENNINGHOVEN, A., GIVER, J. *et al.* (eds). Secondary Ion Mass Spectrometry SIMS III. Proceedings of the 3rd International Conference held August 30--September 5, 1981, Budapest. Springer Series in Chemical Physics, Vol.19. Pp.444. ISBN 3-540-11372-X/0-387-11372-X. (Springer-Verlag: 1982.) DM 80, $37.30.

BERGER, R. and MARSHALL LIBBY, L. Radiocarbon & Tritium. Collected Papers of Willard Frank Libby. Vol.1. ISBN 0-941054-01-2. (Geo Science Analytical, Santa Monica: 1981.) Np.

Biological Sciences

BRADFIELD, A. E. and LLEWELLYN, M. J. Animal Energetics. Pp.168. UK Hbk ISBN 0-216-91255-5; pbk ISBN 0-216-91254-7: US Hbk ISBN 0-412-00021-0; pbk ISBN 0-412-00031-8. (Blackie/Chapman & Hall: 1982.) UK Hbk £16.95; pbk £7.95. US np.

BROWN, I. R. (ed.). Molecular Approaches to Neurobiology. Pp.420. ISBN 0-12-137020-8. (Academic: 1982.) $49.50.

BURGDORFER, W. and ANACKER, R. L. (eds). Rickettsiae and Rickettsial Diseases. Pp.650. ISBN 0-12-143150-9. (Academic: 1981.) $47.50.

CAPLAN, D. (ed.). Biological Studies of Mental Processes. Pp.335. Hbk ISBN 0-262-03061-6; pbk ISBN 0-262-53041-4. (MIT Press: 1982.) Hbk np; pbk $8.95.

CARAFOLI, E. (ed.). Membrane Transport of Calcium. Pp.266. ISBN 0-12-159320-7. (Academic: 1982.) £21.80, $45.

CASE, R. M., GARNER, A. *et al.* (eds). Electrolyte and Water Transport Across Gastrointestinal Epithelia. Pp.334. ISBN 0-89004-765-0. (Raven: 1982.) $37.

CASPARI, E. W. (ed.). Advances in Genetics, Vol. 21. Pp.373. ISBN 0-12-017621-1. (Academic: 1982.) $36.

CATLING, D. and GRAYSON, J. Idenitification of Vegetable Fibres. Pp.89 + plates. ISBN 0-412-22300-7. (Chapman & Hall, London: 1982.) £12.50.

CHANTLER, E. N., ELDER, J. B. and ELSTEIN, M. (eds). Misus in Health and Disease–II, Vol. 144. Pp.441. ISBN 0-306-40906-2. (Plenum: 1982.) Np.

CHAPMAN, D. (ed.). Biological Membranes, Vol. 4. Pp.526. ISBN 0-12-168545-4. (Academic: 1982.) £36.20, $74.50.

CHIARELLI, A. B. and CORRUCCINI, R. S. (eds). Primate Evolutionary Biology. Selected Papers (Part A) of the 8th Congress of the International Primatological Society, held July 7-12 1980, Florence. Pp.119. ISBN 3-540-11023-2/0-387-11023-2. (Springer-Verlag: 1981.) Np.

COCKRUM, E. L. Mammals of the Southwest. Pp.176. Hbk ISBN 0-8165-0760-0; pbk ISBN 0-8165-0759-7. (University of Arizona Press: 1982.) Hbk $11.95; pbk $5.95.

CROFT, L. R. The Last Dinosaurs: A New Look at the Extinction of the Dinosaurs. Pp.80. Hbk ISBN 0-946019-00-2; pbk ISBN 0-946019-01-0. (Elmwood, London: 1982.) Hbk £4.95; pbk £2.25.

CUNNINGHAM, L. W. and FREDERIKSEN, D. W. (eds). Structural and Contractile Proteins. Part A: Extracellular Matrix. Methods in Enzymology, Vol. 82. Pp.913. ISBN 0-12-181982-5. (Academic: 1982.) $69.50.

DENNO, R. F. and DINGLE, H. (eds). Insect Life History Patterns: Habitat and Geographic Variation. Pp.225. ISBN 0-387-90591-X/3-540-90591-X. (Springer-Verlag: 1981.) Np.

DRIESSENS, F. C. M. Mineral Aspects of Dentistry. Monographs in Oral Science, Vol. 10. Pp.216. ISBN 3-8055-3469-8. (Karger: 1982.) SwFr.148, DM177, $88.75.

DUBROV, A. P. and PUSHKIN, V. N. Parapsychology and Contemporary Science. Pp.221. ISBN 0-306-10973-5. (Plenum: 1982.) $39.50.

FRIEDMAN, H., KLEIN, T. W. and SZENTIVANYI, A. (eds). Immunomodulation by Bacteria and their Products. Pp.308. ISBN 0-306-40885-6. (Plenum: 1981.) $42.50.

GANONG, W. F. and MARTINI, L. (eds). Frontiers in Neuroendocrinology, Vol. 7. Pp.400. ISBN 0-89004-694-8. (Raven: 1982.) $61.20.

GILLING, D and BRIGHTWELL, R. The Human Brain. Pp.192. ISBN 0-85613-424-4. (Orbis, London: 1982.) £8.95.

HALL, D. A. and JACKSON, D. S. (eds). International Review of Connective Tissue Research, Vol. 9. Pp.338. ISBN 0-12-363709-0. (Academic: 1981.) $49.

HAND, A. R. and OLIVER, C. (eds). Methods in Cell Biology, Vol. 23. Basic Mechanisms of Cellular Secretion. Pp.588. ISBN 0-12-564123-0. (Academic: 1981.) $64.50.

HARRIS, J. T. The Peregrine Falcon in Greenland. Observing an Endangered Species. Pp.254. ISBN 0-8262-0343-4. (University of Missouri Press: 1981.) $8.95.

HARRISON, R.J. and NAVARATNAM, V. (eds). Progress in Anatomy, Vol.2. Pp.220. ISBN 0-521-24420-X. (Cambridge University Press: 1982.) £30.

HEINZ, E. Electrical Potentials in Biological Membrane Transport. Molecular Biology, Biochemistry and Biophysics, Vol.33. Pp.85. ISBN 3-540-10928-5/0-387-10928-5. (Springer-Verlag: 1981.) Np.

HUSKISSON, E.C. and KATONA, G. (eds). New Trends in Osteoarthritis, Vol.7. International Symposium held October 9, 1981, Monte Carlo. Pp.200. ISBN 3-8055-3487-6. (Karger: 1982.) SwFr. 80, DM 96, $48.

JAHN, G. (ed.). Application of Vegetation Science to Forestry. Handbook of Vegetation Science, 12. Pp.405. ISBN 90-6193-193-2. (Junk, The Netherlands: 1982.) Dfl.185, $79.50.

JANEWAY, C., SERCARZ, E.E. *et al.* (eds). Immunoglobulin Idiotypes. ICN–UCLA Symposia on Molecular and Cellular Biology, Vol. 20, 1981. Pp.902. ISBN 0-12-380380-2. (Academic: 1981.) $54.

JOHNS, E.W. (ed.). The HMG Chromosomal Proteins. Pp.251. ISBN 0-12-386050-4. (Academic: 1982.) £19.20, $39.50.

JONES, D. Garden Wildlife. The Living World of your Garden. Pp.152. ISBN 0-85223-213-6. (Ebury Press, London: 1982.) £7.95.

JONES, G. (ed.).Quinolines, Part II. Pp.685. ISBN 0-471-28055-0. (Wiley: 1982.) £70.

KENNER, T., BUSSE, R. and HINGHOFER-SZALKAY, H. (eds). Cardiovascular System Dynamics. Models and Measurements. Pp.668. ISBN 0-306-40727-2. (Plenum: 1982.) Np.

KING, J.C. The Biology of Race. Pp.180. ISBN 0-520-04223-9. (University of California Press: 1982.) £11.25.

KLAUBER, L.M. Rattlesnakes. Their Habits, Life Histories, and Influence on Mankind. Pp.350. ISBN 0-520-04038-4. (University of California Press: 1982.) £14, $24.95.

KOHN, L.D. (ed.). Hormone Receptors. Horizons in Biochemistry and Biophysics, Vol.6. Pp.392. ISBN 0-471-10049-8. (Wiley: 1982.) £28.50.

LANGE, O.L., NOBEL, P.S. *et al.* (eds). Physiological Plant Ecology I. Responses to the Physical Environment. Encyclopedia of Plant Physiology, Vol.12, Part A (in 4 parts). Pp.625. ISBN 3-540-10763-0/0-387-10763-0. (Springer-Verlag: 1981.) DM 239, $111.30.

LEHNINGER, A.L. Principles of Biochemistry. Pp.1011. ISBN 0-87901-136-X. (Worth, New York: 1982.) £13.

LEVY, C.K. Elements of Biology, 3rd Edn. Pp.550. ISBN 0-201-04564-8. (Addision-Wesley: 1982.) $23.95.

LORAND, L. (ed.). Proteolytic Enzymes, Part C: Methods in Enzymology, Vol.80. Pp.919. ISBN 0-12-181980-9. (Academic: 1982.) $74.

LOWENSTEIN, J.M. (ed.). Lipids, Part D. Methods in Enzymology, Vol.72. Pp.842. ISBN 0-12-181972-8. (Academic: 1981.) $65.

LYON, J. and SLOAN, P.R. (eds). From Natural History to the History of Nature: Readings from Buffon and His Critics. Pp.406. ISBN 0-268-00955-4. (University of Notre Dame Press, London: 1981.) £11.95.

MACFADYEN, A. and FORD, E.D. (eds). Advances in Ecological Research, Vol.12. Pp.252. ISBN 0-12-013912-X. (Academic: 1982.) £19, $39.

MANNUCCI, P.M. and D'ANGELO, A. (eds). Urokinase: Basic and Clinical Aspects.. Proceedings of the Serono Symposia, Vol.48. Pp.265. ISBN 0-12-469280-X. (Academic: 1982.) £19.20, $39.50.

MANSKE, R.H.F. and RODRIGO, R.G.A. (eds). The Alkaloids. Chemistry and Physiology, Vol.20. Pp.341. ISBN 0-12-469520-5. (Academic: 1982.) $59.50.

MARGULIS, L. and SCHWARTZ, K.V. Five Kingdoms. An Illustrated Guide to the Phyla of Life on Earth. Pp.338. ISBN 0-7167-1212-1. (Freeman: 1982.) £17.30.

MARSAN, C.A. and MATTHIES, H. (eds). Neuronal Plasticity and Memory Formation, Vol.9. Pp.682. ISBN 0-89004-681-6. (Raven: 1982.) $88.40.

PESTKA, S. (ed.). Interferons, Part A. Methods in Enzymology, Vol. 78. Pp.632. ISBN 0-12-181978-7. (Academic: 1981.) $59.

PETTIGREW, W. (ed.). Conservation. Pp.179. ISBN 0-340-26821-2. (Hodder & Stoughton: 1982.) £2.50.

PFALLER, W. Structure Function Correlation on Rat Kidney: Quantitative Correlation of Structure and Function in the Normal and Injured Rat Kidney. Advances in Anatomy, Embryology and Cell Biology, Vol. 70. Pp.106. ISBN 3-540-11074-7/0-387-11074-7. (Springer-Verlag: 1982.) DM 59, $27.50.

PICKLES, J.O. An Introduction to the Physiology of Hearing. Pp.341. Hbk ISBN 0-12-554750-1; pbk ISBN 0-12-554752-8. (Academic: 1982.) Hbk £16, $33; pbk £6.95, $14.50.

PITCHER, T.J. and HART, P.J.B. Fisheries Ecology. Pp.414. ISBN 0-85664-894-9. (Croom Helm, London: 1982.) £16.95.

PLATT, T. (ed.). Physiological Bases of Phytoplankton Ecology: Canadian Bulletin of Fisheries and Aquatic Sciences No. 210. Pp.346. (Dept. of Fisheries & Ocean, Ontario: 1981.) $17.95 (Canada), $21.95 (elsewhere).

RADZIALOWSKI, F.M. (ed.). Hypertension Research. Methods and Models. Pp.472. ISBN 0-8247-1344-3. (Marcel Dekker: 1982.) SwFr. 188.

RENTZ, D.C.F. and WEISSMAN, D.B. Faunal Affinities, Systematics, and Bionomics of the Orthoptera of the California Channel Islands. Entomology, Vol. 94. Pp.240. ISBN 0-520-09640-1. (University of California Press: 1982.) $22.

REVOLTELLA, R.P. *et al.* (eds). Expression of Differentiated Functions in Cancer Cells. Pp.542. ISBN 0-89004-693-X. (Raven: 1982.) $78.20.

RICHES, H.R.C. Hypersensitivity to Bee Venom. IBRA Reprint M109. Pp.42. No ISBN. (International Bee Research Assoc., Bucks: 1982.) 95p, $2.30.

ROCHE, A.F., SIERVOGEL, R.M. *et al.* Serial Changes in Subcutaneous Fat Thicknesses of Children and Adults. Monographs in Paediatrics, Vol. 17. Pp.110. ISBN 3-8055-3496-5. (Karger: 1982.) SwFr. 79, DM 95, $47.50.

RODGERS, M.A.J. and POWERS, E.L. (eds). Oxygen and Oxy-radicals in Chemistry and Biology. Pp.808. ISBN 0-12-592050-4. (Academic: 1981.) $54.

ROSE, A.H. and MORRIS, J.G. (eds). Advances in Microbial Physiology, Vol.23. ISBN 0-12-027723-9. (Academic: 1982.) £23.40, $48.

ROSSI, F. and PATRIARCA, P. (eds). Biochemistry and Function of Phagocytes. Advances in Experimental Medicine and Biology, Vol. 141. Pp.699. ISBN 0-306-40887-2. (Plenum: 1982.) Np.

ROTHSCHILD, H. (ed.). Biocultural Aspects of Disease. Pp.653. ISBN 0-12-598720-X. (Academic: 1981.) $65.

SALZMAN. E.W. (ed.). Interaction of the Blood with Natural and Artificial Surfaces. Pp.240. ISBN 0-8247-1582-9. (Marcel Dekker: 1981.) SwFr. 105.

SANADI, D.R. (ed.). Current Topics in Bioenergetics, Vol. 12. Pp.261. ISBN 0-12-152512-0. (Academic: 1981.) $37.

SANDS, H. (ed.). Epilepsy: A Handbook for the Mental Health Professional. Pp.296. ISBN 0-87630-272-X. (Brunner/Mazel, New York: 1982.) $30.

SCHIMKE, R.T. (ed.). Biological Mechanisms in Aging. Proceedings of a Conference held June 1980, Maryland. (US Department of Health & Human Services: 1981.) Np.

SCHLEIF, R.F. and WENSINK, P.C. Practical Methods in Molecular Biology. Pp.220. ISBN 0-387-90603-7/0-540-90603-7. (Springer-Verlag: 1981.) DM 69, $32.20.

SCHLESINGER, D.H. (ed.). Neurohypophyseal Peptide Hormones and other Biologically Active Peptides. Proceedings of the International Symposium held September 1980, Chicago, in memory of Dr. Roderick Walter. Developments in Endocrinology, Vol. 13. Pp.293. ISBN 0-444-00605-2. (Elsevier/North Holland: 1981.) $55, Dfl. 143 (outside N. America).

SCHMIDT, W. Natural and Experimental Succession of Fallow Land, Vol. 15. Pp.199. ISBN 3-88452-514-X. (Erich Goltze, Gottingen: 1981.) DM 40.

SCHUH, J., HECHT, K. and ROMANOW, A. (eds). Chronobiologie–Chronomedizin. Pp.883. No ISBN. (Akademie-Verlag, Berlin: 1981.) Np.

SELA, M. (ed.). The Antigens, Vol. 6. Pp.453. ISBN 0-12-635506-1. (Academic: 1982.) $56.

SEMENZA, G. (ed.). Of Oxygen, Fuels, and Living Matter, Part 2. Evolving Life Sciences, Vol. 1. Pp.508. ISBN 0-471-27924-2. (Wiley: 1982.) £27.50, $59.95.

SHEPHERD, S.A. And THOMAS, I.M. (eds). Marine Invertebrates of Southern Australia, Part 1. Pp.491. No ISBN. (South Australian Government: 1982.) Np.

SIMPSON, T.L. and VOLCANI, B.E. (eds). Silicon and Siliceous Structures in Biological Systems. Pp.587. ISBN 3-540-90592-8/0-387-90592-8. (Springer-Verlag: 1981.) DM 240, $111.80.

SOPER, J.H. and HEIMBURGER, M.L. Shrubs of Ontario. Pp.495. ISBN 0-88854-283-6. (Royal Ontario Museum: 1982.) $20.

SPAIN, J.D. Basic Microcomputer Models in Biology. Pp.354. ISBN 0-201-10678-7. (Addison-Wesley: 1981.) $23.50.

SZEJTLI, J. Cyclodextrins and Their Inclusion Complexes. Pp.296. ISBN 963-05-2850-9. (Akademiai Kiado, Budapest: 1982.) $30.

TANNER, W. and LOEWUS, F.A. (eds). Plant Carbohydrates II: Extracellular Carbohydrates. Encyclopedia of Plant Physiology, New Series, Vol. 13, Part B. Pp.769. ISBN 3-540-11007-0/0-387-11007-0. (Springer-Verlag: 1981.) DM 268, $124.80.

TENORIO, J.M. and GOFF, M.L. Ectoparasites of Hawaiian Rodents. Pp.32. No ISBN. (Bishop Museum Press: 1980.) $4.

VANDERPLANK, J.E. Host–Pathogen Interactions in Plant Disease. Pp.207. ISBN 0-12-711420-3. (Academic: 1982.) $26.

WACHTEL, P.L. (ed.). Resistance: Psychodynamic and Behavioral Approaches. Pp.267. ISBN 0-306-40769-8. (Plenum: 1982.) $22.50.

WEATHERALL, D.J., FIORELLI, G. and GORINI, S. (eds). Advances in Red Blood Cell Biology. Pp.444. ISBN 0-89004-647-6. (Raven: 1982.) $65.28.

WECKER, E. and HORAK, I. (eds). Retrovirus Genes in Lymphocyte Function and Growth. Topics in Microbiology and Immunology, Vol.98. Pp.142. ISBN 3-540-11225-1/0-387-11225-1. (Springer-Verlag: 1982.) DM 66, $30.80.

WILLIAMS, J.I. and SHAW, M. Micro–organisms, 2nd Edn. Pp.176. ISBN 0-7135-1321-7. (Bell & Hyman, London: 1982.) £4.95.

ZIMMERMAN, A.M. and FORER, A. (eds). Mitosis/Cytokinesis. Pp.481. ISBN 0-12-781240-7. (Academic: 1981.) $55.

Applied Biological Sciences

ADOLPH, L. and LORENZ, R. Enzyme Diagnosis in Diseases of the Heart, Liver and Pancreas. Pp.128. ISBN 3-8055-3079-X. (Karger: 1982.) DM 34, $20.50.

AMERICAN SOCIETY OF PEDIATRIC NEUROSURGERY. Concepts in Pediatric Neurosurgery, 1. Pp.238. ISBN 3-8055-2904-X. (Karger: 1982.) SwFr. 190, DM 228, $114.

AOKI, T., URUSHIZAKI, I. and TSUBURA, E. (eds). Manipulation of Host Defence Mechanisms. Pp.281. ISBN 90-219-0516-7/0-444-90245-7. (Excerpta Medica/Elsevier: 1981.) $51.25, Dfl. 110.

ATKINSON, P. and WOODCOCK, J.P. Doppler Ultrasound and Its Use in Clinical Measurement. Pp.288. ISBN 0-12-066260-4. (Academic: 1982.) £24, $49.50.

BROWN, D.D. (ed.). Developmental Biology using Purified Genes. ICN–UCLA Symposia on Molecular and Cellular Biology, Vol. 23, 1981. Pp.702. ISBN 0-12-137420-3. (Academic: 1981.) $58.

BRUNNER, H.R. and GAVRAS, H. (eds). Clinical Hypertension and Hypotension. Pp.522. ISBN 0-8247-1279-X. (Marcel Dekker: 1982.) SwFr. 188.

COLNAGHI, M.I., BURAGGI, G.L. and GHIONE, M. (eds). Markers for Diagnosis and Monitoring of Human Cancer. Proceedings of the Serono Symposium, Vol.46. Pp.280. ISBN 0-12-181520-X. (Academic: 1982.) £21.60, $44.50.

COSTA, E. and RACAGNI, G. (eds). Typical and Atypical Antidepressants: Clinical Practice. Advances in Biochemical Psychopharmacology, Vol. 32. Pp.422. ISBN 0-89004-830-4. (Raven: 1982.) $53.72.

DOLEYS, D.M., MEREDITH, R.L. and CIMINERO, A.R. Behavioral Medicine: Assessment and Treatment Strategies. Pp.628. ISBN 0-306-40841-4. (Plenum: 1982.) Np.

DUKES, M.N.G. (ed.). Side Effects of Drugs Annual 6. Pp.478. ISBN 90-219-3060-9/0-444-90211-2. (Excerpta Medica/Elsevier-North Holland: 1982.) $69.75, Dfl. 150.

ELLIS, G.P. and WEST, G.B. (eds). Progress in Medicinal Chemistry, Vol. 18. Pp.236. ISBN 0-444-80345-9. (Elsevier-North Holland: 1981.) $63.75, Dfl. 150.

FRANK, R.M. and LEACH, S.A. (eds). Surface and Cilloid Phenomena in the Oral Cavity: Methodological Aspects. Proceedings of a Workshop on Saliva–Dental Plaque and Enamel Surface Interactions held October 15–17 1981, Strasbourg. Pp.274. ISBN 0-904147-36-3. (IRL Press, Oxford: 1982.) £12, $24.

GELBOIN, H.V. and TS'O, P.O.P. (eds). Polycyclic Hydrocarbons and Cancer, Vol. 3. Pp.351. ISBN 0-12-279203-3. (Academic: 1981.) $49.50.

HARPER, A.E. and DAVIS, G.K. (eds). Nutrition in Health and Disease and International Development. Symposia from the 12th International Congress of Nutrition: Clinical and Biological Research, Vol. 77. Pp.1060. ISBN 0-8451-0077-7. (Alan R. Liss: 1982.) $85.

HUSBAND, J.E. and KELSEY FRY, I. Computed Tomography of the Body: A Radiological and Clinical Approach. Pp.222. Hbk ISBN 0-333-25584-4; pbk ISBN 0-333-25585-2. (Macmillan Press: 1981.) Np.

LEHMANN, H.E. (ed.). Non–Tricyclic and Non–Monoamine Oxidase Inhibitors. Modern Problems of Pharmacopsychiatry, Vol.18. Pp.216. ISBN 3-8055-3428-0. (Karger: 1982.) SwFr. 115, DM 138, $69.

MCBRIEN, D.C.H. and SLATER, T.F. (eds). Free Radicals, Lipid Peroxidation and Cancer. Pp.448. ISBN 0-12-481780-7. (Academic: 1982.) £24, $49.50.

MELNICK, J.L. (ed.). Progress in Medical Virology, Vol.28. Pp.234. ISBN 3-8055-2983-X. (Karger: 1982.) SwFr. 148, DM 177, $88.75.

OADES, R.D. Attention and Schizophrenia: Neurobiological Bases. Pp.343. ISBN 0-273-08490-9. (Pitman, London: 1982.) £22.

PARRAT, D., MCKENZIE, H. *et al.* Radioimmunoassay of Antibody and its Clinical Applications. Pp.156. ISBN 0-471-10061-7. (Wiley: 1982.) £15, $35.

PICKLEMAN, J. Problems in General Surgery. Pp.363. ISBN 0-306-40765-5. (Plenum: 1982.) $39.50.

POWANDA, M.C. and CANONICO, P.G. (eds). Infection: The Physiologic and Metabolic Responses of the Host. Pp.435. ISBN 0-444-80336-X. (Elsevier/North Holland: 1981.) $111, Dfl. 261.

REYNIAK, J.V. and LAUERSEN, N.H. (eds). Principles of Microsurgical Techniques in Infertility. Pp.294. ISBN 0-306-40781-7. (Plenum: 1982.) Np.

RICHTER, G.W. and EPSTEIN, M.A. (eds). International Review of Experimental Pathology, Vol. 23. Pp.274. ISBN 0-12-364923-4. (Academic: 1982.) $34.50.

ROPER-HALL, M.J. (ed.). Microsurgery of the Anterior and Posterior Segments of the Eye. Developments in Ophthalmology, Vol. 5. Meeting of the International Micro-surgical Group, Mallorca, 1980. Pp.134. ISBN 3-8055-2711-X. (Karger: 1981.) SwFr. 90, DM 108, $54.

TERRY, R.D., BOLIS, C.L. and TOFFANO, G. (eds). Neural Aging and Its Implications in Human Neurological Pathology. Aging, Vol. 18. Pp.270. ISBN 0-89004-677-8. (Raven: 1982.) $38.08.

VARGHA, GY. Pharmacoangiography in the Diagnosis of Tumours. Pp.253. ISBN 963-05-2912-2. (Akadémiai Kiadó, Budapest: 1981.) $32.

WARNER, N.L. and METCALF, D. (eds). Leukaemia. UICC Technical Reports Series, Vol.61. Workshops on the Biology of Human Cancer Report No.14. Pp.232. ISBN 92-9018-061-7. (International Union Against Cancer, Geneva: 1981.) SwFr.44, $22.

WEILL, H. and TURNER-WARWICK, M. (eds). Occupational Lung Diseases: Research Approaches and Methods. Lung Biology in Health and Disease, Vol.18. Pp.528. ISBN 0-8247-1362-1. (Marcel Dekker: 1981.) SwFr.178.

WILLIAMSON, R. (ed.). Genetic Engineering 3. Pp.173. ISBN 0-12-270303-0. (Academic: 1982.) £11.80, $24.50.

WINGARD, L.B. Jr. *et al.* (eds). Applied Biochemistry and Bioengineering, Vol.3: Analytical Applications of Immobilized Enzymes and Cells. Pp.314. ISBN 0-12-041103-2. (Academic: 1981.) $42.50.

WORLD HEALTH ORGANIZATION. International Histological Classification of Tumours, No.1. Histological Typing of Lung Tumours, 2nd Edn. Pp.36 + Figs. ISBN 92-4-176101-6. (WHO: 1981.) SwFr. 22.

nature

12 August 1982

Disunited nations in outer space

The UN conference on space technology opened in Vienna earlier this week is certain not to ask the questions that need answering. So should conferences like these take place at all?

The United Nations conference on the peaceful uses of outer space, which opened this week in Vienna, seems to have set off on a familiar track (see page 595). It is right and proper, but also predictable, that the Austrian Foreign Minister, Dr Willibald Pahr, should have opened the proceedings with a declaration that the most urgent need is somehow to rid what the United Nations calls outer space of all military connotations. Better this, it may be thought, than that the keynote address should be yet another plea that the benefits of remote sensing satellites (whatever they may be) should be made freely accessible to all sovereign states that think they have a need of them, or which are just curious to know what they look like from aloft. Certainly it is far better than that the members of the group of seventy-seven, the developing countries whose interests in development are a part but only a small part (witness present anxieties about the Lebanon) of the proper objectives of the United Nations, should set up a howl that they do not have the direct-broadcasting satellites to put into the geosynchronous orbits with which the United Nations (through the International Telecommunications Union) endowed them in 1979. Even so, it is a serious question for the United Nations to consider whether conferences like these should continue to be held.

None of this is to suggest that the military use of space technology is not a serious problem. The past few years have shown all too well that the contrary is the truth. The major powers, principally the United States and the Soviet Union, are already dependent on satellites for much of their military intelligence. Quite soon there may be systems for putting other systems out of action (see *Nature* 15 July, p.211). And the process seems destined to catch on. Other states (France, for example) will soon be up there too. Other systems, perhaps laser weapons, will be added to the orbital ironmongery. Moreover, there seems no doubt that once these systems have multiplied the danger that they will be used provocatively if not in anger will be substantial. The trouble, unfortunately, is that no amount of speech-making at United Nations conferences will bring the perpetrators of these new devices to an agreement on restraint. Only hard-headed negotiations between parties willing that negotiations should take place could arrive at such a conclusion. Some international organization could, it is true, help to bring those who now use orbits for military (but not destructive) purposes to heel by keeping a close watch on what they are about, and then publishing the results. This is what governments such as that of Sweden have been urging. Unfortunately, for the United Nations to act in such a sense, either the political backing of the major powers or the financial backing of the others would be necessary. Neither is likely to be forthcoming.

So what, in these circumstances, can the latest conference hope to accomplish? By the end of next week, the delegations will no doubt be hard at work on the draft of a declaration so stuffed with anodyne pieties that even hard-headed governments will be shamed into endorsement. One certain ingredient in the communique — would that this prediction were proved wrong — will be that the benefits of telecommunications by satellite, the only commercially proven benefit of these devices, should be more freely available and more widely shared. Ever since the disastrous United Nations Conference on Science, Technology and Development (also at Vienna) in 1979, the notion has become entrenched that it is somehow inequitable that high technology should be exploited first by highly developed industrialized states. But this clamour is entirely mistaken. If industrialized states are to be persuaded not to win some commercial benefit from their high technology, how can they be asked (as they should be asked) to throw open their domestic markets more freely to imports from the developing countries?

This contradiction lies at the heart of much of what the United Nations seeks to accomplish in these periodic and increasingly gigantic conferences. Their form ensures that all parties go away frustrated — the high-technology states because they have been shamed into promises whose only saving grace is that they are empty, the others because they believe (or pretend) that the promises mean what the words say. The outcome, mutual despair, may be as dangerous as the militarization of space over which Dr Pahr wrung his hands this week. Has the time come when somebody should say no to the next conference (on nuclear energy next year) or at least to the one after that?

Gamekeeper turned poacher

The British need a new university boss; herewith some nominations and a job description.

Dr Edward Parkes seems a glutton for punishment. Most of his spell as chairman of the University Grants Committee has been spent in forcing arbitrary government economies on British universities. His decision now to quit is understandable, and would have been forgiven at any time in the past few years. His decision to be instead the next vice-chancellor of the University of Leeds is more surprising. Is it self-sacrificing heroism, a wish to be seen lying on the bed of nails that universities accuse him of having fashioned for them? Or bravado, an ambition to show that the economies are not so bad after all? Either way, the University of Leeds, already distinguished among British universities not merely for its academic strength but, these days even more important, for the strong regional loyalty that sustains it, must count itself lucky. For a university to have as its chief officer someone who knows how the grants committee functions must be an advantage of some kind. Parkes is unlikely to use his position to win extra leverage for Leeds with the grants committee, although many of his new colleagues are hoping that he is not that straight. But at the worst, he will be able to help his new university to understand more readily than others what may lie behind the inscrutable instructions that issue from time to time from the committee he is now leaving.

For the British government, Parkes's departure now is probably more of an embarrassment than an opportunity to fill the empty office with a kind of stool-pigeon or Uncle Tom. Not that there is a shortage of potential successors to Parkes. Sir Alec Merrison, vice-chancellor at Bristol, would suit quite well, even if Sir Peter Swinnerton-Dyer from Cambridge would be more interesting. Lord Flowers, rector of Imperial College London, would be a strong appointment, but would the government welcome a grants committee chairman free to speak his mind in the House of Lords? Lord Swann, under-employed since quitting as head of Oriel College, Oxford, a year ago, is similarly

0028-0836/82/320593 02$01.00

encumbered by a peerage. But then Sir Ronald Mason will be leaving his post as scientific adviser to the Ministry of Defence later in the year, while Mr Geoffrey Caston, who has administered the vice-chancellors' own lobby (the Committee of Vice-Chancellors and Principals) for the past five years, probably knows as intimately as anybody how the British university system functions. Any one of these, and no doubt a host of others, could embark on a stint as chairman of the grants committee without having first to win the confidence of British universities. The government would even find that most of them accept its own view that even when direct support for the universities has levelled off in 1984-85, continuing reorganization will be necessary within the British system. But none of them would take Parkes's job without certain assurances, the most important of which is that there should be an understanding between the government and the universities on what the grants committee is for.

What should they ask for? The natural temptation is to ask for more independence, but that will not be as simple as it seems. Although the grants committee was established to be an independent buffer between the universities and the government, it has never been autonomous. In principle, in the old days, the government would say what subsidy it could afford, the committee would recommend how that should be divided and the government would send out cheques to individual universities accordingly. In practice, of course, the grants committee was very much a spokesman for the university system, arguing the case for new developments in some field or other (more medicine, more science perhaps), whose credibility with the government stemmed from its periodic invigilation of how universities individually conducted their affairs. So even in the halcyon days when the committee dealt with the Treasury rather than with the Department of Education and Science, and when the scale of spending on the universities was settled five years ahead, the government was inevitably drawn into decisions about the character as well as the scale of British higher education. Most of the changes that have come about in the past few years are changes only of degree. After the government decreed at the end of 1980 that its subsidies for the universities should be reduced by 8.5 per cent in real terms, it seems genuinely to have been left to the grants committee to decide how the misery should be distributed. The declaration a few weeks ago by the Secretary of State for Education and Science that ministers might in future shoulder more responsibility for issues of university policy is therefore not an innovation of principle. The danger is merely that they will choose to intervene too often and too trivially.

Candidates for Parkes's job will therefore ask for an assurance that they will have a job to do, and not be mere office-boys (or girls?) for ministers. More important, they should also ask for a restoration of the old civilities by which the grants committee was consulted in advance on important issues of public policy on higher education. Parkes appears to have been told in advance of the two decisions that have most affected British universities in the past few years, the increase of fees for students from overseas and the reduction of the general subsidy (coupled with limits on student numbers). The government may now regret that on enither occasion was the grants committee given a chance to suggest how its objectives might be more sensibly, and more equitably, attained. Yet even these examples of the present government's disrespect for the grants committee (to some extent made good by Sir Keith Joseph's offer of a "dialogue") are not unprecedented. The creation in the 1960s of what is called the "binary" system of higher education, with parallel systems of universities and polytechnics, was presented to the universities by the late Mr Anthony Crosland as a bolt from the blue. Yet that has become the most serious unsolved problem in British higher education. In the government's interest as well as his own, Parkes's successor should make it clear in advance that if he first learns of radical changes in his working environment from the morning newspapers, he will be up and off before the day is out.

Given suitable assurances, Parkes's successor could have a rewarding job. In the promised period of stability after the present contraction is over, it should be possible to make a start on the restoration of the spirits of academics and of their universities. The new grants committee chairman will have the advantage of dealing with universities that, by definition, will have survived, sometimes to their own surprise. Many of them will by then be enlivened by innovations forced out of them in these hard times, from science parks and essays in continuing education to the discovery that research of high quality does not necessarily require an entail on the output of a gold mine. Administratively, so far as the universities are concerned, the trick must be to find a way of giving all universities a sense that they are more fully than at present in control of their own destinies, from which would follow the beneficent consequence that they have an incentive to be different from each other, not an incentive to ape each other — or Oxbridge. (The criteria of academic standards and the conventions of "peer review" might have to be subordinated to others, the interests of students perhaps.) Politically, the objective would be to provide the government with a solution to the problem of the binary system, showing how it might be made unitary. Philosophically the need is for a chairman who could help to redefine the functions of higher education in countries such as Britain now that the participation rate is high enough to falsify the traditional academic assumption that the purpose of being a student is to become an academic. Such a chairman might even be able to find a way of creating some tangible linkage between higher education and national prosperity — everybody's ambition and nobody's boast. Then, so the daydream goes, British universities might have friends again in the House of Commons . . . Is that too much to hope for?

Jumpiness of bankers

Science and technology, usually respectful of banking, will suffer if bankers lose their nerve.

Why are the world's bankers so much on edge? In the past few weeks, these ordinarily imperturbable figures have taken to whispering behind their hands as if they were selling not credit (a respected commodity) but something disreputable. The change of demeanour is in the short term easily explicable. The bankers worry that they may not be permitted by their governments to roll over their credits to Poland when that question has to be decided next month, or that some unsophisticated member of their community may not agree to forgo payment on its Polish loan even if the governments concerned suggest that bankers should be compliant. But that is very much a short-term calculation. The sum of what the Polish government owes the Western banks, estimated at $15,000 million or thereabouts, is perhaps only 5 per cent of what the commercial banks of the industrialized West have lent overseas in the past few years. Obviously, a default by Poland would be an inconvenience, but arithmetically it should not spell the end of the Western way of life. Western bankers will not be readily forgiven if they let the Polish credits jeopardize their survival — and that of their depositors.

So what really makes them jumpy? A sense of guilt, the certain knowledge that they are no longer as much in charge of their own affairs as they pretend they are. Once upon a time, when bankers earned their reputation for probity, banks undertook to look after the money entrusted to them by depositors, lent that to borrowers who had a need of it, and made their living on the turn. For at least half a century, however, the banks have been partly the prisoners of their governments — or suckers for their governments' propaganda. In the 1960s, the banks helped pay for the Vietnam war by exporting the US government's excess expenditure through the Eurodollar market, exporting inflation at the same time. More recently, in countries such as Britain and the United States, the banks have helped their governments both fiscally (with high interest rates that cause deflation) and politically (by lending to unknown clients overseas). Their profit margins have been assured, but their assets have been just as much at risk as are other people's. Discrimination, the banker's stock in trade, has gone by the board. Who, except the rest of us, will cry if they go bust?

0028-0836/82/320594-01$01.00

More trouble for Stanford's patent

US patent office gives reasons for refusal

Washington

Further doubt has been cast on the validity of the key Cohen–Boyer patent covering basic processes in genetic manipulation by a decision on a second patent application taken last week by the US Patent and Trademark Office. On 30 June, the office announced that the granting of the second patent, originally planned for 13 July, would be postponed (see *Nature* 29 July, p.409). Last week, the office took a further step in the minuet-like US patent process and notified Stanford University (acting on its own behalf and that of the University of California, San Francisco) that the second patent application was to be rejected.

The decision of the patent office seems to turn on the status and origin of the plasmid called pSC101, that first used by Cohen and Boyer as a means of cloning foreign genes in *Escherichia coli* plasmids. Originally, Cohen and Boyer considered that this plasmid had been derived from a naturally occurring plasmid called R6-5 by recircularization of some fragment itself produced by hydrodynamic shear.

Last week, the US patent office cited an article published by co-inventor Stanley Cohen and a collaborator in 1977 (Cohen, S.N. and Chang, A.C.Y. *J. Bact.* **132,** 734; 1977) in which other possible origins of pSC101 were canvassed. The possibility of a relationship with the *Salmonella* plasmid SP219 was mentioned.

The patent office now says that the 1977 article "sets forth a revised view of the origin of the pSC101 plasmid. That view conflicts with the origin of pSC101 as set forth in this application".

The first patent, which was issued to Stanford and the University of California at San Francisco in December 1980, presumably suffers from the same potential defect. The patent office has the authority to reexamine an already-issued patent, but has only exercised this option once since it was given the authority in 1980. Alternatively, a third party could file a challenge to the first patent.

A possible counter to the patent office's objection would be to show that the plasmid was publicly available at the time of application, and thus the claims in the patent for how the plasmid is used as a starting point in the creation of recombinant plasmids does not depend on the accuracy of the recipe for making pSC101. This matter is open to question; Cohen and his co-worker Herbert Boyer did make the plasmid available to qualified scientists who requested it, but with some restrictions. The patent office asked Stanford to provide data on how many scientists were supplied the plasmid and whether any were refused.

Cohen said last week that the 1977 *Journal of Bacteriology* article "did not admit an error in the original procedure" but rather only in the "interpretation" of where the pSC101 plasmid came from. He said that procedure was totally reproducible.

Stanford has already sold one-year licences to the first patent to 73 companies. Stanford has three months to respond to the patent office's action; a Stanford official said he did not see any "insurmountable obstacles" in successfully asserting its claim.

Stephen Budiansky

Space wars at UN conference

Vienna

Austrian Foreign Minister Willibald Pahr has called on the world scientific community to "oppose vigorously" the increased militarization of space. He was addressing the opening session of Unispace 82, the second United Nations conference on the exploitation and peaceful uses of outer space, now meeting here. Dr Pahr had just been elected president of the conference, an honour shared with Dr Kurt Waldheim, who, in 1968, had been Austrian Foreign Secretary when the first Unispace conference was held in Vienna.

Unispace-1 had been mainly concerned with the potential of the new space technologies. Unispace-2, fifteen years later, is interested primarily in what can be done with those technologies to improve the quality of life of mankind. An exhibition, staged parallel to the conference, shows an impressive range of space technologies.

In one respect, Unispace-2 might be considered as a showcase for the space techniques of the more developed nations, in their hopes that these benefits could be extended to the less fortunate.

UK Minister of State Kenneth Baker observed that, "Unispace is particularly significant for those countries which do not have their own space industry, but who seek quite rightly the assurance that the way that space applications are developing is of value to all".

The prestige element was, of course, present. The Soviet exhibit was under the direction of Dr A. P. Kapitsa, son of the Nobel prizewinner. The Americans brought to their stand not only their shuttle astronaut Henry Hartsfield but also a female trainee astronaut. The American impact, however, was somewhat lessened by the recent Soviet media campaign which stressed the military aspects of the shuttle and by fears of what President Reagan's 4 July speech about a "more permanent" US presence in space might mean — a subject on which US delegates to Unispace 82 were remarkably non-communicative.

The idea that the "demilitarization" of space was a prime prerequisite for its peaceful exploitation was taken up by many of the delegates, including the representatives of non-governmental organizations, who have a special session on this theme scheduled for Saturday. If, unlike its predecessor, Unispace-2 produces some concrete recommendations, the peace issue is almost certain to be among them. So far, however, no concrete proposals for the "demilitarization" of space have emerged.

Vera Rich

India's space hopes

Bangalore

India's ambitions in space remain high despite a number of setbacks. Next month, the indigenous rocket, SLV-3, will carry a 42-kg satellite during its first operational flight and next year the first Indian astronaut will fly aboard the Soviet spacecraft Salyut-7. But the country's most ambitious space project yet, the multi-purpose operational domestic satellite INSAT-1A, has been crippled by the failure of its solar sail to deploy.

INSAT-1A, the world's first civilian telecommunications, weather and direct broadcasting satellite rolled into one, was built by the Ford Aerospace Corporation under contract from the Indian Space Department and launched by the US National Aeronautics and Space Administration aboard a Thor Delta rocket. The Indian government had planned to use the satellite for meteorology, long distance communications and for broadcasting direct to remote villages, but the failure of the solar sail will reduce the satellite's lifespan to two and a half years and limit its usefulness. The Indian Space Department is hoping for better luck with INSAT-2, due for launch aboard the space shuttle in July 1983.

High hopes are also pinned on the operational launch of SLV-3, India's own solid-fuelled, four-stage rocket. After a disastrous first test flight in 1979, SLV-3 had a successful test flight in July 1980 and was partially successful in May 1981 when it placed a small satellite into an unexpectedly low orbit, thereby condemning the satellite to 9 rather than 90 days of life.

B. Radhakrishna Rao

0028-0836/82/320595-02$01.00

US astronomy

Arrays in, dishes out

Washington

The US radioastronomy community, after much agonizing, has decided to give first priority to the construction of the Very Long Baseline Array (VLBA) radio telescope — a decision that effectively means that the 25 metre telescope — which it has sought for several years without obtaining funds — will not now be built.

Associated Universities Inc., the management group that runs most major US radioastronomy facilities, recently submitted a formal proposal to the government asking for $51 million in 1982 dollars to build the network, which would extend from Alaska to Hawaii and across the continental United States to New England.

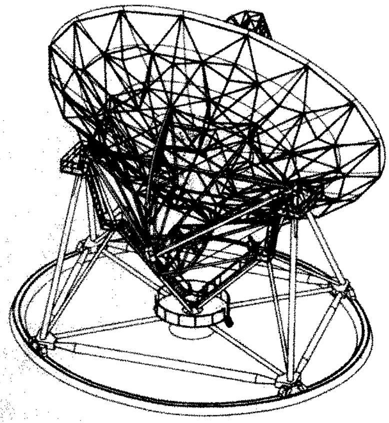

The 25-m millimetre wavelength telescope

Using interferometric techniques, VLBA will have a baseline on the order of the radius of the Earth, and so will be able to achieve extraordinary resolutions of 0.3 milliarcsecond. Thus it will be able to study many aspects of the so-called "violent universe", such as explosive events in quasars and in the nucleii of galaxies. It may also permit precise distance determinations to maser sources in our own galactic system."

The 25-metre telescope, on the other hand, would have used very short, millimetre wavelengths to investigate interstellar molecular chemistry. It was first recommended in 1972 by a committee of the National Academy of Sciences (NAS) headed by Jesse L. Greenstein of the California Institute of Technology. The National Radio Astronomy Observatory in Charlottesville, Virginia, has sought funds for the 25-metre telescope since 1977; in some of those years, the National Science Foundation forwarded the request to the White House, where, for unrelated budgetary reasons, it stopped. Meanwhile, related work has continued at smaller dishes at Caltech, the University of California at Berkeley, Bell Laboratories and the University of Massachusetts.

Other countries, too, entered the promising field: the United Kingdom has a 15-metre dish at Mauna Kea, in Hawaii, while the Franco-German telescope institute IRAM (Institut de la Radioastronomie Millimetique), based at Grenoble in France, plan two telescopes — one almost ready at Pico Veleta in the Sierra Nevada near Granada in Spain, the other under construction at the Plateau de Bure in the southern French Alps (near Grenoble). The Japanese, too, plan to build one, and a copy of the dish destined for Granada has even been ordered by the government of Iraq.

But in spite of its once-widespread support in the United States, "time has passed the 25-meter by", as one astronomer said last week. The most recent review of astronomical priorities, a report by another NAS committee headed by Harvard astronomer George Field (see *Nature* 8 April, p.482), included a subcommittee to set priorities in radio astronomy hardware, headed by Pat Thaddeus of Columbia University's Institute for Space Studies. At that time, the 25-metre telescope seemed likely to be funded, so the final Field report gave top priority to the need for VLBA. Only afterwards, was it clear that even in fiscal year 1983, the 25-metre telescope would not be funded. So its virtual omission from the Field report meant it was doomed.

US radioastronomers hold mixed views about this gap in the field, in which the United States was a pioneer.

On the other hand, nobody disputes that VLBA, if it is built, will be a major advance, as nothing like it is planned elsewhere in the world.

Deborah Shapley

Fields Medal awards

Two Americans and a Frenchman are the 1982 winners of the Fields Medal, the "Nobel Prize" of mathematics, it was announced in Warsaw on Sunday.

The International Congress of Mathematicians (ICM), meeting this year in Poland, awarded the medal to William Thurston of Princeton University, S. T. Yau of the Princeton Institute of Advanced Studies, and Alain Connes, who is at present a director of research at the headquarters of the Centre National de la Recherche Scientifique in Paris. As a mathematician, Connes is attached to the Ecole Normale Superieure and the University of Paris VI.

The Fields Medal, an inspiration of an early president of ICM, is awarded every four years. These are the ninth and tenth awards for Americans, and the sixth for a Frenchman — a remarkable record for France, bearing in mind that the United States has four times the population of France.

Robert Walgate

British academic pay

Five per cent

Last Wednesday a council meeting of the Association of University Teachers (AUT) approved a 5 per cent pay increase for university lecturers. It had little choice. When talks between AUT and the Universities Authorities Panel (the body nominated by the Committee of Vice-Chancellors and Principals to negotiate salaries) reached an impasse, the matter went to arbitration and 5 per cent was recommended. The award, which has been approved by Sir Keith Joseph, Secretary of State for Education, means that the universities will be faced with yet another book-balancing feat. The outcome may be further job losses.

Negotiations between AUT and the vice-chancellors were mainly over how much the universities could afford to set aside for salaries. Initially the vice-chancellors said they could afford nothing. The body both sides most wanted to negotiate with was the government. Each made representations to the government for more money to meet a pay increase. But the government remained adamant that any award must be met from the grants given to the universities by the University Grants Committee. The government did decide, however, to provide £770,000 to meet two-thirds of the cost of the 6 per cent award made to clinical academics to maintain their parity with National Health Service workers. "That is in some way understandable", commented Mr Laurie Sapper, general secretary of AUT, "After all, most government ministers are over 50 and don't want to upset the medics".

AUT was hoping for a much higher award to keep in line with other public sector settlements and to compensate for inflation. The vice-chancellors were in agreement with AUT that it was unfair for members of university staff to have their pay further depressed in relation to other employees in public institutions. But they insisted that an award over 4 per cent, the amount allowed for in the government-set cash limits, could not be met without outside help.

Dr Albert Sloman, chairman of the Committee of Vice-Chancellors, pressed the case for more money in a meeting with Sir Keith Joseph on 25 June. In a further letter on 23 July, after the settlement of the award, Dr Sloman pointed out that the rising salary costs would mean a further running down of the university system. In his written reply Sir Keith Joseph made it clear that additional money would not be forthcoming.

Given the universities' stringent cash limits, the negotiations between AUT and the vice-chancellors left little room for manoeuvre. In giving a 5 per cent award the government's attitude seems to be, if the unions want more money, they know it may mean fewer staff.

Jane Wynn

0028-0836/82/320596-01$01.00

US drug regulation

Congress finds FDA wanting

Washington

Eli Lilly and Company has repeatedly failed to report adverse findings about drugs it was testing or marketing, according to Food and Drug Administration (FDA) documents made public last week. Sales of one of the drugs mentioned in the documents, Oraflex (benoxaprofen), were suspended last week in both Britain and the United States after a review of British data revealed 61 deaths associated with its use (see box).

The allegations against Lilly are spelled out in a series of internal FDA memoranda released by the House intergovernmental relations subcommittee, which was holding hearings on FDA's proposed streamlining of the new drug evaluation process.

One of the most serious charges is that "data for benoxaprofen appear to have been deliberately withheld, thus biasing the NDA (new drug application) in favour of approval". The investigator who reached that conclusion, Dr Michael Hensley, recommended last September that FDA "consider prosecution of appropriate Lilly employees".

Dr Hensley's investigation revealed in particular that 65 adverse effects that occurred during the clinical trials of Oraflex were not reported to FDA, even though they were apparently related to the drug, and were in Lilly's files when the application was made in December 1979. These effects were principally photosensitivity and onycholysis (loosening of the fingernails), and all occurred after the "cut-off date" of November 1978 that Lilly had set on data that were to go into their application. The cut-off is apparently a usual procedure.

But the Lilly employee in charge of the application, Dr H.A. Bartlett, did review the adverse effect reports from trials that continued after the "cut-off date", and included "serious" reactions in the application, according to a memorandum written by Dr Hensley on 16 September 1981. This memorandum then states that Dr Bartlett instructed an employee "not to report others (such as onycholysis and photosensitivity) which he allegedly felt were, because of their frequent occurrence, no longer alarming" (*sic*). In fact, the new data showed a sharp increase in the incidence of these side effects. A letter from Dr Marion Finkel, then associate director for new drug evaluation, to R.D. Wood, chairman of the board of Lilly, on 12 March this year charges that "the consequence was a biased presentation clearly more favourable to the drug than was warranted by the data".

Lilly's answer is that FDA regulations simply do not require applications to include data on all adverse reactions observed after the cut-off date. At the subcommittee hearings, Dr Robert Temple, acting director of the office of new drug evaluation, agreed. He called it a "defect in the regulations".

A similar mix-up occurred over the reporting of four deaths from jaundice associated with the drug. Attention was focused on this matter by reports (Goudie, E.M. *et al. Lancet* **i**, 959; 1982/Halsey, J.P. & Cardoe, N. *Br. med. J.* **284**, 1365; 1982.) of several jaundice deaths in Britain associated with Oraflex. On 23 June, FDA officials met Lilly officials to discuss the matter, and "expressed surprise that (American) cases of jaundice had not been submitted prominently to the NDA (new drug application) prior to its approval".

"I'M AFRAID YOU HAVE DOW JONES SYNDROME!"
LILLY
CLINICAL TRIALS
BIRCH

Lilly officials claimed that they had in fact submitted two reports to the IND file before approval. At the subcommittee hearings, FDA officials said they had had no way of checking that, since there was a six-month backlog in processing the IND files. They said they have since found that all four cases were reported to FDA by Lilly — but that FDA reviewers apparently approved the application without seeing the reports. FDA Commissioner Arthur Hayes Jr says that it "wouldn't have made any difference" in the approval, since the reviewers knew about the problem.

Dr Hensley's memorandum of 29 September 1981, in which he recommended possible prosecution of Lilly employees, referred to three other drugs about which he said "allegations . . . . that Lilly has repeatedly failed to make required reports of important adverse findings" had been "confirmed" by FDA investigators. About aprindine, an anti-arrhythmia drug, Dr Hensley found that "Lilly employees may have engaged in highly objectionable, perhaps ethically questionable practices in their handling of the aprindine clinical programme". Furthermore, Lilly apparently ignored findings from its own experiments with dogs of a possibly lethal side effect of the drug, fibrillation. It was not until January 1974, after four patients in the aprindine clinical trials had died, that the dog studies were reviewed and finally reported to FDA on 4 February 1974. An FDA memorandum dated 4 February 1982 recommends that Lilly be issued a "Notification of Adverse Findings" for failing to incorporate the data from the

Arthritis drug proscribed in Britain

A voluntary decision by Eli Lilly to withdraw the anti-arthritis drug benoxaprofen from sale in all countries came soon after the imposition of a 90-day ban on UK sale by the Committee on Safety of Medicines (CMS). The Department of Health withdrew the product licence for the drug (sold under the trade name Opren in the United Kingdom) to allow time to assess the alarming total of 3,500 reports of serious side effects, especially in the elderly.

Benoxaprofen had rapidly become one of the most prescribed of anti-rheumatic drugs since the UK product licence was issued in 1980, and the CMS review cites 61 deaths associated with its use. In the United States the drug (sold as Oraflex) was given FDA approval only in April of this year, but already at least 11 deaths have been linked with benoxaprofen, again mostly in elderly patients and mostly involving liver or kidney damage.

In withdrawing the drug, Eli Lilly was at pains to explain that it still believed benoxaprofen to be safe and effective if used as directed. But after seven years of development before being allowed on the market, the question of why possible contraindications seem to be emerging only at this stage will be taxing regulatory authorities and Lilly's medical teams on both sides of the Atlantic.

Benoxaprofen is undoubtedly effective in many cases of rheumatoid arthritis and osteoarthritis but it is probably not irreplaceable — other non-steroid anti-inflammatory agents with similar activity include aspirin, naproxen, ibuprofen and fenoprofen. For Eli Lilly, though, the whole episode is a major setback. Even if benoxaprofen is allowed back onto the market, the damage will have been done and doctors will be reluctant to prescribe it and patients to take it.

The latest events surrounding benoxaprofen provide another reminder of the high risks involved for companies attempting to reap the high rewards that accompany a successful new drug launch. Only two weeks ago the London Stock Market witnessed extraordinary fluctuations in the price of shares in the pharmaceuticals company Glaxo. High hopes of massive profits from sales of the new anti-ulcer drug Zantac (ranitidine) were dampened when a few reports of possible side effects were publicized with little analysis in the financial press. Share prices recovered when Glaxo and others pointed out the relatively minor nature of the reported effects, but predictably the price has not matched the high levels seen before the fracas.

Charles Wenz

0028-0836/82/320597-02$01.00

animal studies into the clinical protocols and failing to report properly to FDA.

Dr Hensley's memorandum of 29 September 1981 concludes that for a third drug, drobuline, proper case report records were not maintained, and protocols were not followed. In the case of the fourth drug, monensin, the FDA documents charge that Lilly failed to report adverse effects in animals and humans exposed to the drug, or delayed reporting these effects by as much as 23 months. Lilly was issued a notice of adverse findings on monensin on 6 July 1981.

At the subcommittee hearings, Lilly issued a statement to reporters denying the charges. "Eli Lilly and Company takes vigorous exception to any implication that it withheld data, maintained inadequate records, or failed to comply with the requirements of the FDA".

Stephen Budiansky

FDA regulations

Saving time, but carefully

Washington

The Food and Drug Administration (FDA)'s plans to relax some of its requirements for new drug applications came under congressional scrutiny last week during two days of hearings that also raised serious questions about Eli Lilly and Company's reporting of adverse effects of its drugs (see p.597).

FDA Commissioner Arthur Hull Hayes Jr, testified that the proposed changes in FDA procedures should shorten the approval process for the average application by six months. It now takes nearly two years. An FDA spokesman said, however, that the new procedures would probably have little effect on applications for drugs deemed important, since they are already given expedited treatment.

Representative L. H. Fountain (Democrat, North Carolina), chairman of the House subcommittee that conducted the hearings, focused strongly on two of FDA's proposed changes. One would drop the requirement that drug companies submit the detailed "case report forms" from clinical trials of the drug; the other would allow FDA to approve a new drug application on the basis of foreign studies.

At present, applicants are required to turn over to FDA all case report forms. These are the reports made by the clinical investigators on each patient; according to FDA, they make up 70 per cent of the applications now, often running into hundreds of volumes. FDA is proposing that, instead, the drug companies should be allowed to submit tabulations of the raw data, and only submit the case reports for cases that raise significant safety questions, such as patients who died, or dropped out of the study because of an adverse effect. The companies would still have to supply the case reports if requested by FDA.

Dr Robert Temple, acting director of the office of new drug evaluation, assured the subcommittee that FDA would not lose anything in the change. But detailed reports "will still be asked for as they're needed", he said; and Commissioner Hayes argued that tabulation of the raw data is "more consistent with current scientific practices".

Subcommittee staff members, however, noted that two in-house reviews at FDA found tabulations which did not agree with the case reports they were supposedly drawn for. They were also concerned that FDA reviewers might be intimidated by the prospect of having to make a special request for the case reports, if for no other reason than the time it would take.

On the issue of foreign data, FDA officials similarly tried to be reassuring that the proposed changes would not undermine FDA's ability to make a thorough evaluation. FDA rules now allow foreign studies to be accepted if the investigators are "well-qualified" and if they make background data available to FDA. But in almost all cases, at least one domestic study is also required.

That would change under the new rules. A drug could be approved solely on the basis of foreign data; Hayes suggested that this would be especially important when requiring domestic trials would "cause an unjustifiable delay in the drug's availability to the public", would result in "unnecessary or duplicative testing", or would present an "unnecessary burden on the drug sponsor".

Foreign data would still have to meet US standards and be the product of "investigators of recognized competence". Critics worry that standards will nonetheless be lowered. Dr Sidney Wolfe of Ralph Nader's Health Research Group, said, "The main problem with the use of foreign data is that the drug laws and the protection of human subjects are weaker everywhere in the world" than they are in the United States. And according to Dr John Nestor, a retired FDA employee who worked for many years reviewing drug applications in the agency's cardio-renal drug division, the main effect of the change will be that "the drug companies will be getting their studies done in Mexico and Canada and everywhere else because it's easier to escape surveillance by FDA". At the subcommittee hearing, Representative Fountain released evidence that FDA had encountered just such problems when it attempted to investigate studies done in Mexico and Canada.

The changes FDA is planning appear to enjoy support in Congress. But there are some reservations. Representative Elliot Levitas (Democrat, Georgia) enthused about the benefits of deregulation, and then implied that the only weapon against the drug companies is vigilance.

Stephen Budiansky

Venture capital investment

Now Monsanto

Britain now has one of the best environments in Europe for innovation, a director of the US chemicals company Monsanto said last week. And Mr Richard A. Onians has put Monsanto's money where its mouth is, investing £4.75 million in a new £9.7 million venture capital fund launched last week in London (see *Nature* 5 August, p.505).

Onians describes Monsanto's investment as a window on European technology, but what the company will see through it is mostly British work. The fund is to be managed by Advent Management, which already controls another £10 million fund, Advent Technology, now 15 months old and with ten British investments already under its belt. Monsanto will have no control over the new fund, but Advent Management will use Monsanto for technology assessment.

Monsanto itself seems to have been tempted to Britain for its "window" because of government willingness to allow foreign investment (France would not let Monsanto invest there, in spite of a desperate need to rebuild the French chemical industry), low capital gains taxes and because of what Onians called British inventiveness. There are probably plenty of potential British entrepreneurs as well, he thinks, if only the money is made available.

Sir Kenneth Cork, the accountant and ex-Lord Mayor of London who is chairman of the new fund, believes Britain could make good use of £500 million of venture capital, ten times the total probably now on offer. "But the Trades Union Council plan of £1,000 million from government and £1,000 million from industry just wouldn't work", he said; venture money needs to be hard to get.

Advent Management has certainly found it harder to raise the money for Advent Eurofund than it was two years ago to raise it for Advent Technology, an essentially similar fund. The fashion among finance houses and insurance companies for investing in such funds seems to have been short-lived, says Advent director David Cooksey.

University investment in high technology venture funds seems, however, to be new — new certainly for Cambridge (£500,000) and Oxford (£100,000). St Andrews, Imperial College London, the Nuffield Foundation and Boston University (Massachusetts) have also invested, reaching a total academic interest of £1.5 million. Some 20 other British universities were interested, said Cooksey, but they had not got the cash.

From the universities' point of view, these investments are dealt with like any other but offer a chance of protecting assets against inflation. Cooksey, however, clearly sees them as a window on potential invention, and this is bound to be

0028-0836/82/320598-02$01.00

the case even though no formal arrangements have been made. There is no need for formal committees, Mr W. Hyde, Secretary of the Chest (finance officer) at the University of Oxford, says the "old boy network" will suffice. **Robert Walgate**

Polish students abroad

A helping hand

Polish University students stranded in Britain by the declaration of martial law last December should be able to continue their education in Britain under a scheme launched by a group of academics at the London School of Economics (LSE). Following a personal appeal to university principals by Lord James of Rusholme, thirty universities and colleges have offered free places to Polish students unable to continue their studies in Poland.

A preliminary count of students last spring suggested that between forty and fifty places would be needed. Since 22 July, however, when General Jaruzelski made it clear that there would be no early end to martial law, some fifty more students have applied for assistance.

Most of the students had come to Britain on temporary leave of absence from their universities in order to learn English. Many of them, at the same time, had been appointed as roving delegates of the Independent Students' Association (NZS), which hoped to build up strong ties with students unions abroad. NZS was outlawed last January (unlike Solidarity, which technically is only "suspended"), a factor which has undoubtedly influenced the students' decision to remain abroad.

Incorporating the Polish students into the British university structure involves a number of difficulties, even with science students where the curriculum differences are least. Poland has no bachelor's degree; university courses normally last five years, ending with a master's degree.

A compromise has been worked out, whereby students who should be beginning fourth or fifth year work in Poland will enter the second year in British universities, while their juniors will begin again from the beginning. The students themselves seem fairly happy with this plan, since a few terms of what is essentially revision will offset the difficulties of studying in English.

The LSE team, which is acting as an unofficial placement board, feels confident that places will be found for all Polish students who genuinely wish to continue their studies in Britain. The main problem is now that of maintenance; the team estimates that, to take advantage of the places so far offered, it will have to raise some £200,000 for the students' maintenance over three years. A charitable trust — the Polish Students' Appeal Fund — has been launched, and possibilities such as local authority rent rebates are being explored. **Vera Rich**

Nature guide to bio-riches

As a service to readers working in biotechnology, to those who may have invested in this new technology or who may regard its commercial fortunes as an indicator of the success with which bright ideas can be turned into commercial reality, *Nature* will in future publish a monthly listing of the stock performance of 15 representative biotechnology companies in the United States.

This scoreboard of performance will appear in the second issue each month, and will record the price of each of the stocks as traded on the last Friday of the month immediately preceding, the traded price at the end of the preceding month, and the high and low prices during the calendar year.

Where the stocks concerned are traded on the New York Stock Exchange or the American Exchange, the prices listed are those traded. For stocks traded over-the-counter, the prices listed are the bid prices.

***Nature* will also publish once a month a weighted index of the listed stocks, taking an initial value of 100 as of 25 June 1982. In the calculation of this index, the contributions of the 15 listed stocks to the index are weighted according to the total value of the issued stock.**

Between the Fridays of 25 June and 30 July, the *Nature* Biotechnology Index increased from 100 to 102.7.

The data (as of 25 June 1982) on which these calculations will be based are shown in the following table.

Market value of biotechnology stocks, 25 June 1982

	Outstanding shares (millions)	Closing price 25/6/82 ($)	Total market value ($ million)	% of all total market values
A.B. Fortia	19	23.375	444.1	21
Bio-Response	5.5	4.25	23.4	01
Cetus	22	8.0	176.0	08
Collaborative Research	8	8.0	64.0	03
Collagen	5.1	17.875	91.2	04
Damon	6.6	6.5	42.9	02
Enzo-Biochem	5.0	14.75	73.8	04
Flow General	8.0	8.5	68.0	03
Genentech	8.1	32.75	265.3	13
Hybritech	8.8	12.5	110.0	05
Molecular Genetics	4.0	8.5	34.0	02
Novo Industri A/S	16.6	38.25	635	30
Monoclonal Antibodies	2.0	9.5	19	01
Genetic Systems	13.7	2.75	37.7	02
Bio Logicals	5.9	2.75	16.2	01
Total			2,100.6	100

From time to time, *Nature* will also publish graphical analyses of the performance of stocks of particular interest, perhaps because the corporation is going through an eventful period or because the industry as a whole is at some turning point.

The stocks listed have been selected from among the much larger number for which data are available on somewhat arbitrary criteria — because of the volume of transactions, for example. It is intended to review the listing from time to time.

***Nature* is grateful to E.F. Hutton and Co., Inc., for advice on the design of this service and for assistance with the compilation of the data. Suggestions from readers will be welcome.**

Performance of biotechnology stocks, 30 July 1982

1982 high	1982 low		Close previous month	Close July 30	Change
28	16$^1/_8$	**A. B. Fortia**	23$^3/_8$	25¾	+2$^3/_8$
7	3$^5/_8$	**Bio-Response**	4¼	4$^7/_8$	+ $^5/_8$
14$^1/_8$	8	**Cetus**	8	9	+1
11	6$^1/_8$	**Collaborative Research**	8	8$^3/_8$	+ $^3/_8$
21$^7/_8$	14¾	**Collagen**	17$^7/_8$	17¾	- $^1/_8$
8$^7/_8$	5¾	**Damon**	6½	6¼	- ¼
17¼	11¼	**Enzo-Biochem**	14¾	11¼*	-3½
28	6$^5/_8$	**Flow General**	8½	7$^5/_8$	- $^7/_8$
37¾	26	**Genentech**	32¾	30¾	-2
17$^7/_8$	9$^5/_8$	**Hybritech**	12½	13¾	+1¼
9	6¼	**Molecular Genetics**	8½	6$^3/_8$	-2$^1/_8$
44$^5/_8$	34$^7/_8$	**Novo Industri A/S**	38¼	39$^8/_8$	+1$^5/_8$
12$^3/_8$	8	**Monoclonal Antibodies**	9½	9¼	- ¼
3$^3/_8$	2¼	**Genetic Systems**	2¾	2¾	0
8	2	**Bio Logicals**	2¾	3	+ ¼

Close of month prices at the close of business on the last Friday of the month. Where stocks are traded over the counter, the price quoted is the bid price. For stocks listed on the American and New York Stock Exchanges the price quoted is the actual transaction price.
*High or low for the calendar year.

0028-0836/82/320599-01$01.00

CORRESPONDENCE

Celltech and MRC

Sir — The House of Commons Select Committee's remarks (*Nature* 5 August, p.505) on Celltech's links with the Medical Research Council (MRC) raise some important issues:

(i) The cost of developing a discovery and bringing it to the market often makes a degree of monopoly essential if it is to be worthwhile for anyone to take on the development risk. On the other hand, giving one body monopoly rights for all inventions for all time may lead to stultification. So a good balance between exclusivity and competition needs to be struck.

(ii) Industry and academia quite rightly differ in their aims and ways of doing things, so collaboration between them will not be productive unless mutual understanding about aims and methods reaches a high enough level. This probably requires individuals and organizations to work together quite closely over a period of time.

The agreement between Celltech and MRC gives Celltech only a first option — MRC must always be satisfied with the commercial plans. It has other features novel in the United Kingdom which bring MRC and Celltech scientists closer together. Experimentation with a variety of frameworks for industrial/academic collaboration is highly desirable and that between MRC and Celltech may turn out to be worth copying. It has been operating for less than two years but has already led to commercial success, for example, in anti-interferon. The time is perhaps too short to have tested the ideas fully but if a review at this stage could be helpful to others, I would be happy to see it.

G.H. Fairtlough

Chief Executive,
Celltech Limited,
Slough, Bucks, UK

The numbers game

Sir — Dr H. H. Rossi (*Nature* 22 July, p.320) makes a plea for a modification of our way of writing quantities in the SI system.

This raises various issues. The numbers we write in English speaking countries as 1.234 and 1,234 tend to be written the other way round in continental Europe (with a "decimal comma" instead of a decimal point, and a dot for thousands). This is a dangerous confusion, and one has to be thankful that so far it hasn't resulted in catastrophe. What makes it worse is that especially in handwriting (and sometimes also in print) not only may dots and commas be difficult to distinguish reliably, but also they may be so faint as to escape notice altogether.

What is wanted is a good clear symbol for the decimal point, which ideally should be already present on all ordinary typewriters, and not already used as a symbol for a unit of measurement or easily confused in handwriting with such a symbol.

About the only symbols satisfying all these conditions are "&" and the letter "u". If we wrote "2&34" or "2u34" for "2.34" there would be little danger of confusion. There is also a lot to be said for the admirable brevity of the occasional continental habit of writing, say, 2.34 m as "2m34". It is quicker to write and to say, and is unambiguous. Brevity is a great help to clarity. Although "0.700" means exactly the same as ".7", it is ".7" which makes the quickest and strongest impression on the mind.

For representing numbers in so-called scientific notation, I would suggest that we write, for example, 2(6)34 for 2.34×10^6. This notation is brief and more flexible than the traditional one. There is no objection to writing 1(3)234(0)567(-3)g if one wishes, showing simultaneously that this is 1.234567 kg, or 1234.567 g, or 1234567 mg, according to which units are most convenient. In addition, 2(3), meaning 2000, could be written unambiguously as 2(3 with the second bracket understood, again encouraging brevity, and similarly (6)14 (= .14 million) could be written 6)14.

Of course some problems remain; for example most computers already use brackets in at least two other senses already. Perhaps a convention should be made of using square brackets in computer programs, writing 2[68]34 for what is now more clumsily written 2.34E06 or 2.34×10^6. But these problems should resolve themselves in due course.

Cedric A.B. Smith

Department of Genetics and Biometry,
University College London, UK

Drugs as carcinogens

Sir — The main impression given by Dr M. Weatherall (*Nature* 1 April, p.387) is that the maintenance and improvement of the health of humans should be based principally on the development of new drugs, and that any delay, such as compliance with government regulations, in the introduction of a new drug would result in an increased loss of human health.

Fortunately the approach of regulatory agencies differs from that of the pharmaceutical industries. The agencies attempt to reduce the occurrence in the population of side effects of drugs and to assess the benefits of drug therapy. The causes of the major diseases are only partly known, and an incomplete rationale behind the therapy for such diseases results in what L. Thomas has called "halfway technology"[1], involving very high costs and relatively unsatisfactory results. An additional problem is that the effectiveness of medicines is oversold[2].

Improvement of human health in the future will depend on greater knowledge of the aetiopathogenesis of diseases, on improvements in social conditions and on more specific treatments[1-7]. Priority should be given to maintaining a proper balance among these different approaches.

There are certainly limitations in the capacity of *in vitro* assays and *in vivo* carcinogenicity tests for the detection of possible carcinogenicity in humans. However, the intelligent use of such tools has proven valid in predicting carcinogenic effects in man[8]. Of the drugs mentioned by Dr Weatherall, phenacetin induces tumours of the urinary system of rats, and epidemiological studies[9] show the same organ system to be the target for its carcinogenic effect in humans; there is also evidence that phenacetin is a mutagen in bacteria and mammalian cells[9]. Azathioprine, chlorambucil and cyclophosphamide, known to be responsible for an increased risk of developing tumours among patients undergoing kidney transplantation, are carcinogenic in experimental animals and mutagenic in various systems[9]. Metronidazole is carcinogenic in mice and rats and mutagenic in bacteria and fungi, while the available epidemiological data are inadequate for a proper assessment of its carcinogenicity in humans. The following drugs or treatments, proven to be carcinogenic in humans, were also found to be carcinogenic in experimental animals: chlornaphazine, myleran, melphalan, methoxsalen (in combination with ultraviolet A irradiation, PUVA), and diethylstilboestrol. Chlornaphazine, myleran, melphalan and PUVA are also mutagens[9].

Thus evidence of an adverse effect observed in experimental systems should not be underestimated, and in some cases, it can have value as a predictor for a similar effect in humans. This value should increase as more is known of the mechanisms of carcinogenesis.

A summary by Dollery[10] of a recent meeting concludes that there is still a tendency to underestimate risks and to overestimate benefits when evaluating drugs. It seems reasonable that the experimental tests to detect possible side effects of drugs should remain a part of the process of the development of a drug, one of the main aims being the provision of reliable information on which a risk-benefit evaluation can be made. The argument that this process is expensive is tenuous, when one considers that approximately 10 per cent of the budget of the pharmaceutical industry is devoted to research and development and 20 per cent to the marketing of drugs. It is worth mentioning that recently, WHO has listed a total of approximately 200 essential drugs to help in the maintenance of health[11], a very small number compared with the number of drugs now on the market.

R. Montesano

International Agency for Research on Cancer,
Lyon, France

1. Thomas, L. *J. med. Educ.* **51**, 23-29 (1976).
2. Ingelfinger, F.J. *Science* **200**, 942-946 (1978).
3. Knowles, J. (ed.) *Doing Better and Feeling Worse: Health in the United States* (Norton, New York, 1977).
4. Mechanic, D. *New Engl. J. Med.* **298**, 249-254 (1978).
5. McKeown, T. *The Role of Medicine: Dream, Mirage and Nemesis* (Nuffield Provincial Hospitals Trust, London, 1976).
6. Saward, E. & Sorensen, A. *Science* **200**, 889-894 (1978).
7. Lalonde, M. *A New Perspective on the Health of Canadians* (Ministry of National Health and Welfare, Ottawa, 1974).
8. Tomatis, L., Breslow, N.E. & Bartsch, H. in *Cancer Epidemiology and Prevention* (eds Schottenfeld, D. & Fraumeni, J.F. Jr) 44-73 (Saunders, Philadelphia, 1982).
9. *IARC Monographs on the Evaluation of the Carcinogenic Risk of Chemicals to Humans* Suppl.4. (International Agency for Research on Cancer, Lyon, 1982).
10. Dollery, C.T. in *Risk-Benefit Analysis in Drug Research* (ed. Cavalla,J.F.) (MTP Press, Lancaster, 1981).
11. *WHO Tech. Rep. Ser.* 635, (1979.

Correction

The letter from J. A. Nicoll in *Nature* of 10 June (p.450) on "Logarithmic SI" contained the following errors. In line 10 $\bar{p}2.3$ should read $p\bar{2}.3$; in line 25 pDO stands for density, 1 kg m^{-3} not m^{-2}; in line 29 $\bar{p}$L*8.5 should read pL*8.5; and in line 30 pL*9 should read $\bar{p}$L*9.

NEWS AND VIEWS

College of Science & Technology
LIBRARY COMPLEX
Engineering
Technology
& Rubber Technology
NOV 1982

What are quarks made of?

from Louis Lyons

In 1964, the properties of the hundreds of 'elementary' particles then known were explained in terms of just three quarks. But, since then, the number of quark types has grown. Added to the original up, down and strange quarks are the charmed and bottom quarks and a sixth, the top quark, is presumed to exist. Furthermore, each quark is now known to exist in three different 'colours' and a further eight particles, the gluons, are required to mediate the binding forces between them.

History thus seems to be repeating itself for in each past attempt to explain the ultimate structure of matter, an initial reduction in the number of entities required — be they atoms, nuclei or elementary particles — has been followed by further discoveries of similar objects until, finally, the cycle has repeated itself and another level of substructure has been proposed at which the number of basic particles has again become small. Are we to believe then that quarks are not, after all, elementary?

In addition to quarks, which are the constituents of the strongly interacting particles mentioned above, the world also contains leptons. The best known are the electron and its neutrino, but nature has twice replicated them with the muon and the tau leptons, which both appear to be simply heavier versions of the electron and both of which have their own neutrino. Some of the properties of leptons and quarks are listed in the table.

The repetitive similarities of both the quarks and leptons suggest that they be grouped in families or generations with increasing mass, in a manner somewhat reminiscent of the chemical periodic table. This in itself is suggestive of another level of substructure for quarks and leptons. Again, further generations may also exist, still waiting to be discovered.

A wide variety of suggestions concerning substructure has been made in the past couple of years[1]. Any prospective model must address a number of issues: (1) How many preons (the name given to the substructure elements) make a quark or lepton? (2) Should quarks and leptons be constructed entirely from the same preons or should at least one preon in a quark and in a lepton differ? (3) Are the preons bound together by gravity, electromagnetism or some new extra strong force? (4) What is the energy scale Λ or distance scale r on which quarks and leptons are composite? Popular values congregate around about 10^3 GeV or 10^{15}–10^{19} GeV (equivalent to $r \sim 10^{-17}$ cm or 10^{-39}–10^{-33} cm [the mass of the proton is ~ 1 GeV]). (5) What makes the different generations, and how many are there? Are the higher ones simply some form of excitation of the first, do they contain extra combinations of preons, does one preon exist in a few different forms, do they correspond to a fine structure type splitting, or something entirely different? (6) What is a plausible scenario for making the composite systems so light on the scale of Λ, and yet still have an interesting mass spectrum (see Table 1)? (7) What other dynamical predictions can be made?

Louis Lyons is in the Department of Nuclear Physics, University of Oxford, Keble Road, Oxford OX1 3RH.

One model[2] has preons T and V of charge 1/3 and zero respectively. The first generation quarks are TTV and $\bar{T}\bar{V}\bar{V}$ composites while the electron and its neutrino are $\bar{T}\bar{T}\bar{T}$ and VVV (the bar above a preon denotes its antiparticle). In another model[3] the preons are labelled h_i, w_j and c_k, where h_1, h_2 and h_3 determine the generation, w_1 and w_2 are two different charged preons, and c_1, c_2 and c_3 give the three colours to the quarks while c_0 is the charged colourless lepton's preon. Here the blue up and down quarks are $h_1 w_1 c_3$ and $h_1 w_2 c_3$, while the μ^- is $h_2 w_2 c_0$.

Most models nowadays try to do more than simply obtain the quantum numbers (that is spin, charge, colour, generation number, etc.) of the observed quarks and leptons. However, there are not many testable predictions and those that exist are often not very specific to substructure models. Thus many composite models suggest that neutrinos should not be exactly massless and that the proton should decay at a very slow rate; but other non-composite models make these predictions as well. A significant advance would be if a mass formula were deduced, which enables as yet undiscovered quarks and/or leptons to be predicted.

The obvious question is whether there is any experimental evidence in favour of quarks or leptons being composite. The answer to date is 'No'. The relevant experiments can then be used to set lower limits on Λ.

For example, the magnetic moments of truly elementary particles can be predicted from quantum electrodynamics. Substructure effects are likely to produce deviations; the composite nature of atoms, nuclei and even 'elementary' particles results in their magnetic moments differing from the predictions for point-like objects. The fact that the magnetic moment of the electron and muon agree with point-like values, to accuracies of 1 in 10^9 and 1 in 10^8 respectively, results in stringent constraints on their composite structure.

Other sources of information on Λ include reactions such as $e^+e^- \rightarrow \mu^+\mu^-$, e^+e^- annihilations producing strongly interacting particles, and the scattering of muons or neutrinos off nuclei. In all cases

Table 1 Properties of quarks and leptons

Generation 1	Up(u)	Down(d)	Electron(e^-)	Neutrino(ν_e)
Mass (GeV c^{-2})	0.3	0.3	5×10^{-4}	$<5 \times 10^{-8}$
Generation 2	Charm(c)	Strange(s)	Muon(μ^-)	Neutrino(ν_μ)
Mass (GeV c^{-2})	1.5	0.5	0.1	$<6 \times 10^{-4}$
Generation 3	[Top(t)]	Bottom(b)	Tau(τ^-)	Neutrino(ν_τ)
Mass (GeV c^{-2})	?	5	1.8	<0.3
Quark or lepton	Quark	Quark	Lepton	Lepton
Electric charge	+2/3	−1/3	−1	0
Colour	Red, green, blue		Colourless	Colourless
Directly observed?	No		Yes	Yes
Forces	Strong Electromagnetic Weak		Electromagnetic Weak	Weak

0028-0836/82/320601-02$01.00

to date, the predictions based on a point-like nature of quarks and leptons agree with experiment.

The above data can be used to deduce that Λ is greater than 600 GeV. Thus quarks and leptons, if they are composite, must be very tightly bound systems, since their masses are so much smaller than Λ.

There are other reactions and decays which are expected in some models of substructure. Thus if the muon is an excited state of an electron, the decay $\mu \rightarrow e\gamma$ should occur. Similarly, if the quarks in a proton share a common substructure with leptons, proton decay becomes possible. Again none of these types of processes has been seen, but because of the model dependence of the predictions, no firm limit on Λ can be deduced.

Theoretical speculation to date has thus been unhampered by any positive experimental evidence. Models have thus become exercises in self-consistency with the main constraints coming from the need to produce almost massless composite states and the necessity of not violating any experimental bounds which have been set in attempts to observe substructure effects.

The main hope for the future is that experiments at the new accelerators becoming available during this decade may reveal direct evidence for quarks and/or leptons possessing substructure. This would then change the motivation for the subject from the realms of aesthetics, history, psychology and sociology to that of physics. □

---

1. Lyons, L. *Progress in Particle and Nuclear Physics* (in the press).
2. Harari, H. *Phys. Lett.* **86B**, 83 (1979); Shupe, M.A. *Phys. Lett.* **86B**, 87 (1979).
3. Terazawa, H. *Phys. Rev.* **D15**, 480 (1977); Pati, J.C., Salam, A. & Strathdee, J. *Phys. Lett.* **59B**, 265 (1975).

Proteins containing nickel

from Andrew J. Thomson

NICKEL long stood out among the six metallic elements of the latter half of the first transition series, namely, Mn, Fe, Co, Ni, Cu and Zn, as being apparently without biological function apart from its toxicity. The situation has changed rapidly in the last few years[1]. Nickel is now known to be a nutritional requirement for many eukaryotic and prokaryotic organisms.

The element has been shown to be a component of urease in plant cells growing on urea as sole nitrogen source[2], to be present in the hydrogenases from several types of bacteria including those which can perform the Knallgas reaction ($2H_2 + O_2 \rightarrow 2H_2O$)[3] and the sulphate-reducing bacterium *Desulphovibrio gigas* [4,5], to be in the enzyme carbon monoxide dehydrogenase in acetogenic bacteria[6] and, lastly so far, in a low molecular weight tetrapyrrole present in methanogenic bacteria[7,8]. Other roles for nickel are also apparent in, for example, a plant such as *Alyssum* which accumulates large amounts of nickel[9] and in a strain of *Bacillus cereus* which forms a nickel-containing intracellular pigment that is probably a protein[1]. It has also been suggested that nickel is involved in endosphere formation of these bacteria[1].

Urease catalyses the hydrolysis of urea in the reaction

$$(NH_2)_2CO + H_2O \rightarrow CO_2 + 2NH_3$$

The enzyme from jack bean contains about 6–8 mol of nickel per mol of protein (molecular weight 480,000). The metal appears to be in the oxidation state +II (ref. 2). This contrasts with the nickel centres recently discovered in some hydrogenases from *Methanobacterium thermoautotrophicum*[3] and from *D. gigas* which have been ascribed to nickel in the trivalent or +III state since electron paramagnetic resonance (EPR) signals are readily detectable[4,5]. These discoveries stemmed from earlier observations that nickel is required for the biosynthesis of hydrogenase in 'Knallgas' bacteria[10] and that there is an EPR signal in both soluble and membrane-bound fractions from the methanogen *M. bryantii* [11]. The assignment of the EPR signals in this latter case to Ni III, by Lancaster [11], was a bold one. The Ni III/Ni II potential of inorganic complexes of peptides was known to be above 0.7V, making Ni III an unlikely species in a hydrogenase[12].

However, Lancaster was persuaded of this assignment for the following reasons[11]. The signals occurred at $g_1 = 2.30$, 2.23 and 2.02, all above the free-electron value and therefore unlikely to arise from haem. They were observable up to 80K and were quite unlike those of any known iron-sulphur centres. The *g*-factors pointed to a metal ion with the electronic structure low-spin d^7. The lack of nuclear hyperfine structure eliminated cobalt(II). This left Ni III as the only candidate, however unlikely on chemical grounds.

It has since been shown that the hydrogenase from *M. thermoautotrophicum*[3] also gives the characteristic nickel EPR signals at *g*-factors of 2.3, 2.2 and 2.0. Studies of the hydrogenase purified from cells grown on a medium enriched in ^{61}Ni, an isotope with a nuclear spin of 3/2, showed nuclear hyperfine structure on the lines at 2.23 and 2.01, which proved beyond doubt that these signals arise from nickel. A spin quantification of the nickel EPR signals gives a value in close correspondence with the chemically determined nickel content, being about 0.6 mol Ni per mol enzyme.

The assignment of the nickel ion to the trivalent state has now been confirmed by a study of the EPR spectrum of the periplasmic hydrogenase from *D. gigas* [4,5]. A redox titration of the $g = 2.24$ signal from nickel in this enzyme shows that it is lost on reduction with a mid-point potential (E_m) of −145 mV at *p*H 7.2 (ref. 5). Moreover the E_m value is *p*H dependent, showing that one proton is picked up during reduction[5]. These potentials are higher than those of the $2H^+/H_2$ couple by about 280 mV, raising obvious mechanistic difficulties for the involvement of the nickel centre directly.

The low redox potential for the Ni III/Ni II couple also raises interesting questions about the likely coordination site of the metal ion in the protein. Several nickel–peptide complexes have been prepared which involve a rather narrow range of amino acids, including leucine, phenylalanine, histidine and aspartic acid[12]. The complexes can be electrochemically oxidized to the trivalent state at E_m values of between +0.79 and +0.96 V. The oxidized state appears to involve the deprotonated peptide linkage. The EPR properties of the Ni III peptides are not dissimilar from those of the protein-bound Ni III ion. However, the remarkably different redox properties argue for a very different site of ligation in the protein possibly involving sulphur ligands.

The periplasmic hydrogenase from *D. gigas* also contains about 12 Fe atoms per mol, undoubtedly arranged into several separate iron-sulphur centres[4]. EPR signals are also observed from these centres both in the oxidized and reduced states of the enzyme. Curiously, however, Albracht *et al.* could detect no iron-sulphur EPR signals in the hydrogenase purified from *M. thermoautotrophicum*[3]. All hydrogenases purified before this report contain iron-sulphur centres. The authors do not yet discount the possibility that the iron-sulphur centres could have been lost during aerobic purification of the enzyme. If not, this will be an intriguing case of a hydrogenase containing only nickel as its metal component.

Pre-dating much of this work on the EPR detection of Ni III in hydrogenases were the observations that nickel is necessary for the biosynthesis of carbon monoxide dehydrogenase in acetogenic bacteria such as *Clostridium thermoaceticum*, *C. aceticum* and *Acetobacter Woodii*[13] and also for the growth of methanogenic bacteria with H_2 plus CO_2 as sole energy source[10]. The two classes of reaction being catalysed are respectively

$$8[H] + 2O_2 \rightarrow CH_3COOH + 2H_2O$$
$$4H_2 + CO_2 \rightarrow CH_4 + 2H_2O$$

Andrew J. Thomson is in the School of Chemical Sciences, University of East Anglia, Norwich NR4 7TJ.

0028-0836/82/320602-02$01.00

From the methanogenic bacterium *M. thermoautotrophicum* it is possible to isolate a yellow, low molecular weight nickel-containing compound with an absorption maximum at 430 nm, hence named factor F$_{430}$ (ref. 7). This factor has been found in every methanogenic bacterium so far examined[8]. The extinction coefficient at 430 nm is high, $\sim 23 \times 10^3$ per cm per mol Ni. The exact structure of this pigment has not yet been elucidated but there is evidence from the biosynthetic incorporation of δ-amino laevulinic acid that F$_{430}$ is a nickel tetrapyrrole[14]. Chemical degradation products of F$_{430}$ have appreciable absorption in the region 500–600 nm and react with cyanide. It has been suggested that the spectrum resembles that of vitamin B$_{12}$ with, presumably, the implication that the nickel species is related to nirrin, the nickel analogue of corrin[1]. There is evidence of a mechanistic kind that the carbon monoxide oxidation in acetogenic bacteria may also involve a prosthetic group similar in structure in vitamin B$_{12}$ but with nickel in place of cobalt[15]. There is a very recent report that the co-enzyme of the purified methyl reductase of *M. thermoautotrophicum* is F$_{430}$, with a stochiometry of 1 mol of nickel per mol of F$_{430}$ and 2 mol of F$_{430}$ per mol of methyl reductase[16].

Thus it is now clear that there are at least two new classes of nickel-containing enzymes: the nickel-containing hydrogenases and those with a nickel tetrapyrrole-related co-factor. Much work on their structural elucidation needs to be carried through. □

---

1. Thauer, R.K., Diekert, G. & Schonheit, P. *Trends biochem. Sci.* **11**, 304 (1980).
2. Dixon, N.E., Gazzola, C., Blakeley, R.L. & Zerner, B. *J. Am. chem. Soc.* **97**, 413 (1975).
3. Albracht, S.P.J., Graf, E.G. & Thauer, R.K. *FEBS Lett.* **140**, 311 (1982).
4. Legall, J. *et al. Biochim. biophys. Res. Commun.* **106**, 610 (1982).
5. Cammack, R., Patil, D., Afluire, R. & Htchikian, E.C. *FEBS Lett.* **142**, 289 (1982).
6. Drake, H.L., Hu, S.L. & Wood, H.G. *J. biol. Chem.* **255**, 7174 (1980).
7. Diekert, G., Klee, B. & Thauer, R.K. *Arch. Microbiol.* **124**, 103 (1980).
8. Whitman, W.B. & Wolfe, R.S. *Biochem. biophys. Res. Commun.* **92**, 1196 (1980).
9. Brooks, R.R., Morrison, R.S., Reeves, R.D., Dudley, T.R. & Akman, Y. *Proc. R. Soc.* **203**, 387 (1979).
10. Bartha, R. & Ordal, E.J. *J. Bact.* **89**, 1015 (1975).
11. Lancaster, J.R. Jr *FEBS Lett.* **115**, 285 (1980).
12. Bossu, F.P. & Margerum, D.W. *Inorg. Chem.* **16**, 1210 (1977).
13. Diekert, G.B. & Thauer, R.K. *FEMS Microbiol. Lett.* **7**, 187 (1980).
14. Diekert, G., Jaenchen, R. & Thauer, R.K. *FEBS Lett.* **199**, 118 (1980).
15. Diekert, G.B. & Thauer, R.K. *J. Bact.* **134**, 597 (1978).
16. Ellefson, W.L., Whitman, W.B. & Wolfe, K.S. *Proc. natn. Acad. Sci. U.S.A.* **79**, 3707 (1982).

Remote operation of telescopes

from Michael Penston

BRITISH astronomers have recently moved to the fore in several branches of optical astronomy, thanks largely to the building of new telescopes in favourable sites abroad — in particular the Anglo-Australian Telescope at Coonabarabran, New South Wales, and the UK Infrared Telescope (UKIRT) on Mauna Kea in Hawaii. Access to the telescopes has, not surprisingly, so far depended on the opportunities provided by air travel. Now, astronomers have begun discussing whether modern communications technology offers an alternative way of working. Early in June experts in communcations and computer technology came together with astronomers and builders of astronomical instruments at the Royal Greenwich Observatory (RGO) to discuss the feasibility of remote operation of telescopes*.

Remote operations of telescopes is possible and, indeed, has already been carried out in an experimental way by Kitt Peak National Observatory and UKIRT. The Kitt Peak 4 m and 2.1 m telescopes have been used by observers at the end of telephone lines both from nearby downtown Tucson and at distant sites in Michigan and the East Coast of the United States. Three lines were used — one for voice, one for TV pictures needed by the astronomer to identify his target star and one to run a remote terminal linked to the computer in the telescope dome. UKIRT is running a similar system which offers the major advantage of being able to diagnose and solve instrumental problems from sea level without suffering the problems of lack of oxygen at the Mauna Kea telescope site 14,000 feet higher up.

There is little difficulty in sending the acquisition images of star fields. Images with 10,000–20,000 pixels with 3–4 grey levels transmitted each 10–20 seconds are perfectly adequate as this update rate is used by current integrating TV systems on telescopes. These could pass down a standard 9.6 kbit line even without data compression. In fact, the Kitt Peak experiment had found a 30 second update rate to be satisfactory. On the other hand, present astronomical practises regarding weather monitoring and protection of the instruments from damage were not so easily compatible with remote operation. A better ways of determining whether the humidity is high enough to hazard the telescope mirror than the traditional test of 'whether the dome rail is wet' needs to be developed. A more professional approach would even benefit conventional observing with the observer present.

The financial benefits of remote observing are obvious, given rising air fares and falling communications costs. Advantages in flexibility might also be provided — the difficulties of scheduling simultaneous observations on different telescope and/or satellites might, for example, be eased. When some particularly demanding meteorological requirement is expected to be met for only a short time (for example, conditions dry enough to use an IR telescope in the 350 μm 'window') it would be easier to put a different observer on the telescope if he did not have to travel so far to exploit this short period. Efficiency would also be improved as astronomers would spend less time travelling and recovering from jet-lag.

There are individual problems in communicating from different sites as reports by Paul Bryant (Rutherford and Appleton Laboratories) and Peter Kirstein (University College London) showed a somewhat anarchic situation in the communications field. There are differences in computer-to-computer communication protocols, in line tariffs and in regulations from country to country so that the best solution at one observatory might not apply at another. Obviously, however, common requirements exist and common solutions and standards are highly desirable as participants, looking ahead, foresaw a network for remote operation of telescopes linking Australia, Hawaii, Chile, continental United States, the Canary Islands and Europe. One solution to the present problem was to separate the difficulties of communication and control, defining interfaces between these segments only. Thus cheap entry to the field could be obtained with use of dial-up telephone lines, as at present, and when wide band lines or public packet switching networks become cheaper it would be possible to change to them with minimum distruption. The eventual use of wide-band 50 kbit lines was foreseen since that would allow near-real-time transmission of astronomical data from the telescope to the site of remote operations. In the meantime it seems most practical to progress using two to three dedicated telephone lines.

At the end of the meeting Alec Boksenberg, Director of the RGO, undertook to have remote operation from Herstmonceux of the 2.5 m Isaac Newton and 1.0 m telescopes on La Palma working by the end of next year. Obviously at this pace, the sky is the limit in the remote operations field. □

Michael Penston is at the Royal Greenwich Observatory, Herstmonceux Castle, Hailsham, East Sussex BN27 1RP.

---

*The two-day workshop on 'Remote operation of telescopes' was held at Herstmonceux Castle, home of the Royal Greenwich Observatory. Participants included representatives from UKIRT, Kitt Peak National Observatory, the European Southern Observatory and the European Space Agency as well as British astronomers and experts in computer networking.

0028-0836/82/320603-01$01.00

The biogeography of the Pacific Basin

from Jared M. Diamond

THE Pacific Basin includes the world's largest and deepest ocean as well as most of the world's islands. It constitutes the eastern half of the richest province of marine biogeography, and is bordered by five of the six provinces of terrestrial biogeography. Its biota includes textbook examples of adaptive radiation, such as the Galapagos finches, the honey-creepers and *Drosophila* of Hawaii, and the marsupials of Australia and New Guinea. Little wonder then, that it has long held a fascination for biogeographers.

The last major symposium on Pacific Basin biogeography was convened 21 years ago in Honolulu at the 10th Pacific Science Congress, by J.L. Gressitt[1]. For the recent 10th annual meeting of the Association of Systematics Collections* Gressitt again organized a symposium on Pacific Basin biogeography at Honolulu's Bishop Museum. Sadly, the symposium took place without him — a month before the conference he died in an aeroplane crash in China.

The 1961 symposium was marked by polemical discussions about the relative contributions of long-distance overwater dispersal, former land bridges and continental drift to the founding of Pacific biotas. Proponents of one factor often dismissed the possibility of any significant role of the other factors in scathing terms. In retrospect, we can now see that the polemics arose because convincing evidence to settle the dispute was unavailable in 1961. At that time it equally strained one's credulity to accept that continental drift had occurred, or to accept that long-distance dispersal could explain everything in the absence of drift. In the following 21 years new types of evidence have made continental drift an accepted fact. Participants at the 1982 symposium took it for granted that drift and dispersal were both significant, and they proceeded without polemics to seek explanations for distributional patterns in terms of both.

Carson's studies on Hawaiian *Drosophila* provide a good example. In Hawaii, this genus is represented by hundreds of endemic species, whose interrelationships can be determined from the banding patterns of giant chromosomes[2]. For all of the 26 large picture-winged species of Big Island, the nearest relative among the species on the older islands of Maui, Oahu and Kauai (respectively 1.8, 3.3 and 5.6 Myr old) has been identified. As Big Island is only 700,000 years old, these 26 populations (25 of them endemic to Big Island at the species level) must have arisen within that time by overwater colonizations from known sources, followed by reorganization of the gene pool (see J.S. Jones *News & Views* **289** 743; 1981). One infers similarly rapid speciation in the Hawaiian honey-creepers (Drepanididae) and other Hawaiian taxa, and in the tree sunflowers of the Juan Fernandez islands (about 1–4 Myr old).

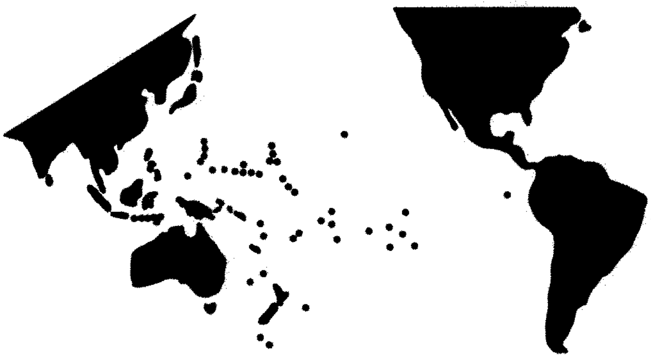

Above, Pacific distribution of herons of genus *Egretta,* resulting from overwater dispersal that continues today. These birds are strong fliers and reach almost every scrap of land in the Pacific, no matter how remote. Herons have landed on ships in mid-ocean thousands of miles from land. Below, Pacific distribution of araucarias, resulting from continental drift. The huge cones and large seeds of these trees are unsuitable for overwater dispersal. Today, native araucarias are confined to South America (1), New Caledonia (2), Norfolk Island (3), Queensland (4) and New Guinea (5). After the breakup of the supercontinent Gondwanaland 50–100 Myr ago, araucarias survived on some of its fragments and were rafted by continental drift to their present locations. On other fragments, such as Antarctica, New Zealand, India and South Africa, araucarias became extinct and are known only as fossils.

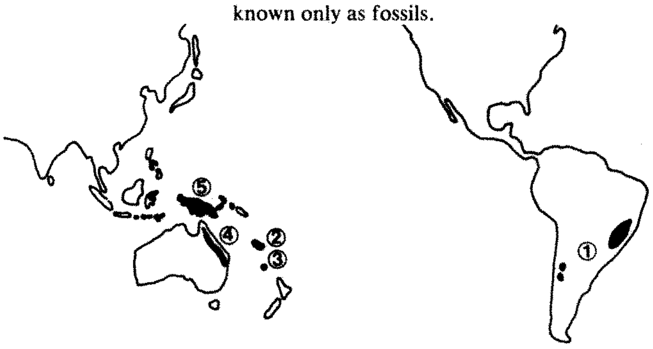

Yet biochemical dating indicates that the Hawaiian *Drosophila*[3] and honey-creepers[4] diverged from their mainland relatives at a date estimated at 15–42 Myr ago, considerably before the oldest of the existing Hawaiian high islands rose above the sea! The explanation is that the existing Hawaiian high islands are merely the youngest in a chain of volcanoes formed by relative motion of the Pacific Plate and a volcanic hot spot, and subject to gradual erosion and submergence after formation. The Hawaiian low islands (11–27 Myr old) and the submerged Emperor Seamounts (37–70 Myr old) are the modern remains of older high islands on which the ancestors of the Hawaiian *Drosophila* and honey-creepers presumably made their initial colonization and then diverged.

In contrast to this explosive radiation of *Drosophila*, some other taxa, such as ferns, bats, inshore marine fishes and molluscs, and plants of coral atolls, exhibit little or no local adaptive radiation and little local endemism beyond the species level on Pacific islands east of New Guinea. At the opposite extreme, achatinellid land snails have evolved numerous endemic genera on Hawaii, Juan Fernandez and the Australs, including nine endemic genera and one nearly endemic subfamily on the small (16 mi²) island of Rapa alone[5]! Numerous groups of insects and flowering plants are also prone to local endemism and adaptive radiation, while Pacific land birds have radiated only on Hawaii, the Galapagos and New Zealand and belong elsewhere mainly to New Guinea genera or closely related genera. Why such differences among taxa? A large part of the explanation is intertaxon differences in dispersal ability. Differentiation and radiation proceed rapidly when a rare colonist of a sedentary group, such as land snails, reaches an island. However, differentiation and radiation are inhibited by the rain of colonists in mobile species such as ferns, with their wind-borne spores, or marine fish and molluscs, with their planktonic larvae. Another relevant factor is inter-taxon differences in propensity for evolutionary losses of dispersal ability[6,7]: colonizing birds and insects often evolve to become literally flightless, and plants figuratively so, but there is no case of a flightless bat (how could one forage?).

A major contribution of continental drift has been to clarify how certain taxa of poor overwater crossing ability came to

---

*The participants in the symposium were P. Raven (Missouri Botanical Garden, St Louis), E. Kay and H. Carson (University of Hawaii, Honolulu), J. Diamond (UCLA), T. Stuessy (Ohio State University), E. Bousfield (National Museum of Natural Sciences, Ottawa), J. Holloway (Commonwealth Institute of Entomology, London), P. Morat (ORSTOM, Noumea) and F. Fosberg (US National Museum of Natural History, Washington DC).

Jared M. Diamond is Professor of Physiology at the University of California Medical Center, Los Angeles, California 90024.

0028-0836/82/320604-02$01.00

have far-flung representatives on New Caledonia, New Zealand, Australia, New Guinea and South America. The numerous examples include southern beech (*Nothofagus*), hoop pines (*Araucaria*), marsupials, leptodactylid frogs, migadopine carabid beetles and peloridiid bugs. It was tacitly assumed without argument at the 1982 symposium, and hotly debated at the 1961 symposium, that these land masses were formerly joined in Gondwanaland and that these taxa were rafted to their present locations by the motion of Gondwanaland's fragments. Yet a mystery remains why the rafted survivors constitute such a selective fraction of Gondwanaland's former biota. With the doubtful exception of a flightless bird (the Kagu), New Caledonia has no Gondwanan relict vertebrates: in fact its only other flightless vertebrates are some lizards and one other flightless bird, endemic but recently derived. The sole candidates for Gondwanan relict vertebrates on New Zealand are its flightless birds, its two frogs and a primitive reptile (the Tuatara). How did New Caledonia and New Zealand come to lack marsupials and other Gondwanan vertebrates that survived in Australia and South America? Could New Caledonia and New Zealand somehow have acquired Gondwanan trees without the vertebrates living in them, and Gondwanan insects without the vertebrates eating them[8]? Or, did most of the old vertebrates become extinct in the confined areas of New Caledonia and New Zealand, because vertebrates require larger areas for long-term survival than do many insects and plants? Could some of the flying birds of Australia be Gondwanan relicts, like the marsupials[9,10]? □

1. Gressitt *Pacific Basin Biogeography* (Bishop Museum Press, Honolulu, 1963).
2. Carson *Science* **168**, 1414 (1970).
3. Beverley *2nd int. Congr. Syst. Evol. Biol. Abstr.* 112 (1980).
4. Sibley & Ahlquist *Auk* **99**, 130 (1982).
5. Cooke & Kondo *Bishop Mus. Bull.* **221** (1960).
6. Carlquist *Island Biology* (Columbia University Press, New York, 1974).
7. Diamond *Nature* **293**, 507 (1982).
8. Raven & Axelrod *Ann. Missouri Bot. Gard.* **61**, 539 (1974).
9. Cracraft *J. Zool. Lond.* **169**, 455 (1973).
10. Rich *Emu* **75**, 97 (1975).

Warts and all

from M. Saveria Campo

THE last few years have seen a remarkable progress in our knowledge of papillomaviruses, as was very evident at a recent workshop* involving clinicians, pathologists and virologists and held in Freiburg. Papillomaviruses are the aetiological agents of papillomas or warts in their natural hosts, and are widespread and heterogeneous: so far twelve different types of human papillomavirus (HPV1-12) and six types of bovine papillomavirus (BPV1-6) have been characterized (Orth, Institut Pasteur; Jarrett, University of Glasgow).

Although originally benign, some papillomas can become malignant under the influence of environmental and genetic factors, as in the case of epidermodysplasia verruciformis lesions in humans[1], papillomas of the upper alimentary tract in cattle[2] and papillomas of the cottontail rabbit[3].

In addition to these well documented cases, ample evidence was presented at the workshop of the possible pathogenic role of papillomaviruses in some anogenital malignancies in humans. Thus, HPV6 DNA has been found in several types of genital warts (Gissmann, University of Freiburg; Mounts, Johns Hopkins Medical School; Grussendorf, University of Aachen; De Villiers, Onderstepoort, Pretoria) and HPV particles and antigens have been detected in anal warts (Oriel, University College London) and in several lesions of the uterine cervix (Pixley, University of Western Australia; Rilke, Istituto dei Tumori, Milan; Meisel; Morin, University of Quebec; Braun, Johns Hopkins Medical School). Both anal and genital warts have occasionally been found associated with malignant tumours.

In a particularly extensive survey of 250,000 unselected individuals, Meisel found that about two-thirds of the cases of mild and moderate atypia of the cervix are in fact papillomavirus-induced flat warts. In a more selected sample of cone biopsies, flat warts were frequently found associated with cervical displasia, *in situ* carcinoma and microinvasive carcinoma. These findings confirmed the view held by the clinicians and the pathologists present at the workshop that, although it is commonly accepted that severe atypia of the cervix is the result of direct progression from mild and moderate atypia, most cases of the latter are in fact papillomavirus lesions, and thus different entities from severe atypia. However, the question of whether or not there is a direct transformation from flat warts to frankly malignant structures is still open.

Perhaps the most striking and best known example of the malignant conversion of virus-induced tumours is provided by epidermodysplasia verruciformis (Orth; Jablonska, Warsaw Medical School). Several types of HPVs with different degrees of oncogenicity have been found in EV lesions, but despite this multiplicity, only HPV5 DNA is found in the squamous carcinomas, as multiple non-integrated episomes (Orth; Jablonska; Pfister, University of Freiburg; Faras, University of Minnesota).

Malignant transformation of papillomas is observed also in animals, where the synergism between the virus and other co-carcinogens can be studied experimentally.

Injection of bovine papillomavirus in the urinary bladder of cattle causes lesions which usually regress with time, but can occasionally progress to malignancy, particularly in animals eating bracken fern (Olson, University of Wisconsin), which contains both immunosuppressant and co-carcinogenic substances[4].

Papillomatosis of the upper alimentary canal, adenocarcinomas of the large intestine, and transitional carcinomas and haemangiosarcomas of the urinary bladder have been experimentally reproduced in cattle injected with virus and either fed with bracken or immunosuppressed with azothioprene. Non-integrated multiple copies of viral DNA have been found in both the experimentally induced bladder cancers and in naturally occurring ones (Jarrett).

Multiple copies of non-integrated non-methylated BPV DNA have been found also in *in vitro* transformed cells (Moar, University of Edinburgh; Pfister). Non-integration and non-methylation of papillomavirus genomes in tumours and transformed cells seems to be the general rule. One exception, however, is provided by papillomas and carcinomas induced by the cottontail rabbit papillomavirus in the domestic rabbit, where the viral DNA is partially methylated and some of it is integrated as long tandem repeats (Wettstein, University of California, Los Angeles).

The complete DNA sequences of BPV1 (7,945 base pairs; obtained by Chen, Levison and Seeburg of Genentech, and presented by Howley, National Cancer Institute, Bethesda) and of HPV1 (7,811 base pairs; Danos, Institut Pasteur) and the almost complete sequence of HPV6 (6,860 base pairs; Schwarz, University of Freiburg) were presented. In all cases, the viral genetic information is probably contained in only one strand, where four overlapping coding regions have been identified, as the other strand is blocked by stop codons in all three frames. The presumptive genes for both structural and non-structural proteins have been identified, and several putative splicing signals have been found in the non-structural region, strongly suggesting that appropriate splicing may generate a variety of transcripts.

The interpretation of the sequence data is coroborated by the mapping of the BPV1 transcripts. In productive warts (Howley; Amtmann, Cancer Research Center, Heidelberg), RNA species are found which

M. Saveria Campo is at The Beatson Institute for Cancer Research, Garscube Estate, Switchback Road, Glasgow G61 1BD.

---

*The workshop on 'Papillomaviruses and Cancer' was held in Freiburg, 7-8 April 1982, and was sponsored by the Deutsche Forschungsgemeinshaft.

0028-0836/82/320605-02$01.00

are absent in non-productive transformed cells and which only hybridize to the 30 per cent DNA fragment that is not necessary for cell transformation and contains the putative structural genes. These RNAs can be translated *in vitro*, and their polypeptide products appear to be genuine capsid proteins (Howley).

Four viral RNA species have been identified in BPV1-transformed cells, which, not surprisingly, hybridize to the 70 per cent DNA fragment capable of cellular transformation and thought to encode the non-structural viral antigens (Amtmann; Freese, University of Freiburg). More surprisingly, they are all co-terminal at their 3′ end, but extend for different lengths to the 5′ end where a 5′-leader sequence has been found (Amtmann). Thus, during the genesis of the non-structural BPV RNAs, the same 5′-leader sequence would be spliced onto different bodies, to give rise to a family of several distinct transcripts, as predicted from the sequence data.

By the end of the workshop it had become clear that, if the progress of our knowledge of papillomaviruses continues at the same break-neck speed of the past few years, we can soon expect to learn about their mechanisms for interaction with, and transformation of, the host cell. □

---

1. Orth, G. *et al.* in *Viruses in Naturally Occurring Cancers* (eds Essex, Todaro & zur Hansen) 259 (7th Cold Spring Harb. Conf. on Cell Proliferation, 1980).
2. Jarrett, W. *et al. Nature* **274**, 215 (1978).
3. Kreider, W. in *Viruses in Naturally Occurring Cancers* (eds Essex, Todaro & zur Hansen) 283 (7th Cold Spring Harb. Conf. on Cell proliferation, 1980).
4. Evans, I.A. in *Naturally Occurring Chemical Carcinogens*, 10th int. Cancer Congress (1970).

Antigenic variation in the trypanosome

from Mervyn Turner

PARASITES have evolved many methods of evading the immune system of their host[1], but perhaps none is so spectacular as the mechanism of antigenic variation adopted by the salivarian trypanosomes. These tsetse fly-transmitted parasites inhabit the bloodstream and tissue spaces of their mammalian hosts, where they rapidly stimulate the production of trypanocidal antibody. Before all the trypanosomes can be eliminated, however, antigenically distinct variants appear in the bloodstream which perpetuate the infection until they in turn are removed by antibody. Usually, the trypanosome can outstrip the immune system in this cycle, which leads eventually to the death of the host. How can such a simple eukaryotic organism produce sufficient antigenically distinct forms to subvert the sophisticated mechanisms possessed by the host for the generation of antibody diversity?

The antigenic profile of the trypanosome is governed by the structure of its surface coat, which in turn is made up of a densely packed layer of glycoprotein molecules, the variant surface glycoproteins (VSGs), whose composition is unique for each variant antigen type. The trypanosome genome contains in excess of 100 variant antigen genes probably generated by gene duplication and mutation[2], and by controlling the expression of these genes, the trypanosome is able to parade a sequence of different variants past the immune system of the host. Naturally, the mechanism by which expression is controlled has attracted much attention and a recent edition of *Nature* contains a contribution (Majiwa *et al.* **297**, 514; 1982) which is sure to add fuel to the controversy surrounding the subject. Furthermore, a second contribution this week (Rice-Ficht *et al.*, p. 676) shows how the trypanosome may have developed a mechanism to extend its repertoire of antigens, perhaps indefinitely.

It has been clear for some time that VSG genes are capable of undergoing rearrangements. These rearrangements do not generate new variants in a fashion analogous to that used by immunoglobulins, but they are detected as alterations in the sequences flanking the VSG gene. Thus, Hoeijmakers *et al.*[3] showed that expression of some VSG genes is accompanied by the generation of an additional copy of that gene, the expression-linked copy (ELC), in a different chromosomal location. Similar findings have been reported from other laboratories[4], and Pays *et al.*[5], by comparing the sensitivity to DNase I of both the basic copy and ELC of a VSG gene, concluded that the ELC was in transcriptionally active chromatin. To date, it has not proved possible to clone the ELC, but on the basis of R-looping, S_1 nuclease protection experiments and comparison of restriction enzyme sites in cDNA and in the ELC it has become apparent that VSG gene activation involves a duplication–transposition mechanism in which the 3′ end of the gene is replaced in the formation of the ELC[6].

Sequencing of cDNA clones has revealed that the 3′ region of VSG mRNA encodes a 17–23 amino acid C-terminal extension[7,8]. It is presumed that this largely hydrophobic sequence serves to anchor the VSG to the membrane at some stage during its biosynthesis, although it is certainly absent from mature VSGs. One possibility is that VSG gene activation involves the generation of a functional end, but DNA sequencing has shown that the codons specifying the hydrophobic tail are present in the basic copy genes[9]. The recombination event at the 3′ end of the gene that leads to the generation of an ELC probably takes place just outside the coding region. In contrast, comparison of restriction enzyme sites around basic copy and ELC genes shows that a 1–2 kilobase (kb) 5′ sequence is transposed with the gene in the generation of the ELC[10]. It is not known whether this sequence contains the promoter sequences allowing VSG expression when placed in transcriptionally active chromatin, or whether such promoters are present only at the expression locus. Nor is it known at what stage in the cell cycle of the bloodstream trypomastigote this duplication/transposition occurs.

So much is clear. What is in dispute is whether activation of VSG genes can occur only by the generation of an ELC. In particular, a group working at the International Laboratory for Research on Animal Diseases (ILRAD), Kenya, has consistently claimed that expression need not be linked to a specific duplication–transposition event. Thus an early analysis of one VSG gene was consistent with the presence of two gene copies, irrespective of whether that gene was being expressed or not[11,12]. Sequence rearrangements around the two copies were observed in all trypanosome clones, even in different clones expressing the same antigen, and restriction enzyme mapping was compatible with the insertion and deletion of lengths of DNA between the 3′ end of the cloned cDNA sequence and a group of restriction enzyme sites some 5–15 kb downstream from the end of the gene. No alterations in sequence were observed within at least 1–5 kb upstream from the 5′ end of the cDNA sequence used as a probe. These results have now been extended to an analysis of VSG gene rearrangements in three different variants, A, B and C, all related by descent from a common, single trypanosome (see Majiwa *et al. Nature* **297**, 514; 1982), and surprisingly, each of the three variant antigen genes behaves differently. Probes specific for variant A recognize the same single fragment in Southern blots of total genome digests from variants A, B and C when using restriction enzymes which do not cut the cDNA, but also recognize an additional, larger fragment in DNA from the clone expressing VSG A. Such results are fully consistent with the ELC model. In contrast, as in the earlier studies, probes specific for VSG B recognize two fragments in the DNA from cells expressing VSGs A, B or C, but the size of

---

Mervyn Turner is at the University of Cambridge Molteno Institute, Downing Street, Cambridge CB2 3EE.

0028-0836/82/320606-02$01.00

both fragments differs in each variant. Has B lost its basic copy gene? This seems unlikely, because B was generated from A, which should therefore contain the basic copy of gene B. Is one of the B genes in an environment such that it is susceptible to the action of DNase I? Are both copies truly in chromosomal DNA? Answers to both questions are unknown. There appear to be four copies of gene C, in clones A, B and C. Two copies are invariant, whereas the sizes of the fragments carrying the other two genes alters in a way similar to that observed for variant antigen B.

Such results imply that different mechanisms may exist to control expression of VSG genes. The ELC model is attractive because it offers a ready explanation for control of antigenic variation, but as the principal proponents of the model themselves admit[2,3], not all the data are consistent with generation of an ELC. Another problem relates to the ploidy of trypanosomes. It has been estimated that ELC genes and basic copy genes exist in a ratio of 1:1 (ref. 4). If this estimate is correct, and if trypanosomes are diploid as generally assumed[13], this implies coordinate expression of the products of two alleles. If the estimate is incorrect, some mechanism of allelic exclusion must operate. Such problems are not resolved by incorporating the results of the ILRAD group for their findings suggest no obvious mechanism for the control of antigenic variation. The two B-specific genes identified could, for example, be allelic forms of the same antigen, but it is not apparent how expression of each is controlled. Is one copy silent, and can the other be activated? Hence the importance of the DNase I protection experiment. Perhaps a very large fragment of DNA (>50 kb) is transposed into a site allowing expression. Such a phenomenon could be identified only by using restriction enzymes which cut outside the transposed unit and a detection system which allowed resolution of very large fragments. All groups agree that the sequence on the 3′ side of the active gene is unusual[2,12] in that it is apparently devoid of restriction enzyme sites for up to 15 kb, and is therefore presumably a simple repetitive sequence. The apparent clustering of many restriction enzyme sites at the end of this sequence could represent the end of the DNA molecule. Resolution of these paradoxes is awaited with interest.

As a further sophistication, VSG genes appear to be capable of localized 'somatic' hypermutation which may extend the antigenic diversity yet further. Sequence analyses of VSGs have shown that the N-terminal 350–400 amino acids are highly variable. The next 100 or so amino acids form a homology region which can be used to divide VSGs into two subsets, followed by the hydrophobic tail of about 20 amino acids which is absent from mature VSGs[7,8,14-16]. Rice-Ficht *et al.* (see p.676) have now compared the DNA sequence of the basic copy gene with cDNA sequences corresponding to the mRNA transcribed from the ELC of variant antigen gene A described by Majiwa *et al.* Surprisingly, considerable differences were observed in the variable region and in the C-terminal hydrophobic tail, amounting to nucleotide changes at four per cent of all codon positions. The homology region is identical in the two sequences. As previously recorded, the 3′-non-translated sequences are quite different in the two clones, consistent with generation of the ELC through recombination in this region. What could be the significance of such findings?

One possibility, which cannot be rigorously excluded, is that the 'wrong' basic copy gene has been cloned and sequenced. A second is that cDNA cloning artefacts are responsible. However, sequences from different cDNA clones were compared and found to be identical, and cloning artefacts are unlikely to respect homology regions. The assumption must therefore be that such sequence alterations are generated in the formation of the ELC, with the possibilities for 'somatic' diversity that that implies. Changes at nine per cent of codon positions in the influenza haemagglutinin are sufficient to produce new variants, corresponding to alterations at four antigenic determinants[17], hence the trypanosome may be using this mechanism to extend enormously its repertoire of VSGs.

Two difficulties remain. First, only half the VSG variable region has so far been analysed in this way. Does the N-terminal region show similar hypermutation? Second, how much of this variable region is exposed on the trypanosome? It has been known for some time that immunizations with either living trypanosomes, or pure VSG can lead to the production of a high proportion of variant-specific monoclonal antibodies which will react with soluble VSG, but not with the surface of the trypanosome[18,19].

Trypanosomes readily shed their VSG during infection, so much of the immune response must be against soluble VSG, but why have variant-specific determinants on soluble VSGs which are not exposed on the surface of the trypanosome, and which are therefore not under selective pressure? Of the several potential antigenic determinants on the VSG molecule only a small number may be exposed on the closely packed surface coat, and such sites may be 'hot spots' for the 'somatic' hypermutation described by Rice-Ficht *et al.* For the trypanosome to then induce the host to make variant-specific antibody which cannot recognize the trypanosome surface could be a diversionary form of antigenic competition which surely would be the ultimate caprice of this virtuoso parasite? ☐

---

1. Bloom, B.R. *Nature* **279**, 21 (1979).
2. Borst, P. *et al. Cold Spring Harb. Symp. quant. Biol.* **45**, 935 (1980).
3. Hoeijmakers, J.H.J., Frach, A.C.C., Bernards, A., Borst, P. & Cross, G.A.M. *Nature* **284**, 78 (1980).
4. Pays, E., Van Meirvenne, N., Le Ray, D. & Steinert, M. *Proc. natn. Acad. Sci. U.S.A.* **78**, 2673 (1981).
5. Pays, E., Lheureux, M. & Steinert, M. *Nature* **292**, 265 (1981).
6. Bernards, A. *et al. Cell* **27**, 497 (1981).
7. Rice-Ficht, A.C., Chen, K.K. & Donelson, J.E. *Nature* **294**, 53 (1981).
8. Boothroyd, J.C., Cross, G.A.M., Hoeijmakers, J.H.J. & Borst, P. *Nature* **288**, 624 (1980).
9. Boothroyd, J.C., Paynter, C.A., Cross, G.A.M., Bernards, A. & Borst, P. *Nucleic Acids Res.* **9**, 4735 (1981).
10. Van der Ploeg, L.H.T., Bernards, A., Rijsewijk & Borst, P. *Nucleix Acids Res.* **10**, 593 (1982).
11. Williams, R.O., Young, J.R. & Majiwa, P.A.O. *Nature* **282**, 847 (1979).
12. Williams, R.O., Young, J.R., Majiwa, P.A.O., Doyle, J.J. & Shapiro, S.Z. *Cold Spring Harb. Symp. quant. Biol.* **45**, 945 (1980).
13. Tait, A. *Nature* **287**, 536 (1980).
14. Bridgen, P.J., Cross, G.A.M. & Bridgen, J. *Nature* **263**, 613 (1976).
15. Holder, A.A. & Cross, G.A.M. *Molec. biochem. Parasit.* **2**, 135 (1981).
16. Matthyseens, G., Michiels, F., Hammers, R., Pays, E. & Steinert, M. *Nature* **293**, 230 (1981).
17. Webster, R.G., Laver, W.G., Air, G.M. & Schild, G.C. *Nature* **296**, 115 (1982).
18. Pearson, T.W. *et al. J. immun. Meth.* **34**, 141 (1980).
19. Lyon, J.A., Pratt, J.M., Travis, R.W., Doctor, B.P. & Olenick, J.G. *J. Immun.* **126**, 134 (1981).

---

100 years ago

We observe that a correspondent of a daily paper proposes that men addicted to the pursuits of science should be called *scientiates*, after the Italian *scienziati;* and in like manner the studies of science, *sciential* studies (*studj scienziali*). The substitution of the American *scientist* for our unsatisfactory phrase *men of science* is of course much to be deprecated; perhaps we shall come to accept Sir William Thomson's proposed use of *naturalist* for the designation in question, if its sense may be extended. *Scientific studies* is a phrase which cannot be commended for accuracy.

A curious and little-known experiment, showing the resistance of the air in guns, is described by Prof. Daniel Colladon, of Geneva. It resembles a feat that was sometimes performed by soldiers with the old Swiss carbines. M. Colladon fully charged with compressed air the hollow iron breech of an air-gun, serving as reservoir. Having screwed up the gun, he introduced a round lead ball, running freely, but nearly filling the bore; then, placing the gun vertical, he seized the upper end and pressed his thumb vigorously on the mouth. The gun was then "fired" by an assistant; the thumb remained in position, and the ball was heard to fall back in the bore. Thereupon, after recharging the breech and with the same ball, he shot the latter at a pine board about 4in. thick and it passed through. The experiment, M. Colladon says, is without danger, if the operator is sure of the strength of his thumb, if the gun is more than 32in. long, and if the ball is spherical and nearly fills the gun (in which it must act like a piston). While M. Colladon has repeated the experiment twenty or thirty times, without the least inconvenience a trial of it is perhaps hardly to be recommended.

From *Nature* **26**, 353; August 10, 1882.

0028-0836/82/320607-01$01.00

Anilides and the Spanish toxic oil syndrome

from A. Pestaña and E. Muñoz

During May and June, 1981, an epidemic outbreak of interstitial pneumonitis occurred in Spain. Over 20,000 people were affected, and nearly five per cent subsequently developed persistent neurodistrophic- and schlerodermia-like conditions. More than 300 people have died. The disease, at first attributed to a never isolated mycoplasm, is now thought to be due to the consumption of adulterated cooking oil containing the processed products of crude rapeseed oil denatured with 2 per cent aniline. The oil was enriched in fatty acid anilides (up to 2,000 p.p.m.) and almost freed from aniline (less than 30 p.p.m.), as a result of thermal processing (220°C) under vacuum.

Comprehensive research into the causes of the toxic oil syndrome was slow to start but tremendous efforts are now being made by many clinical and research institutes — although lack of effective coordination still remains a problem. Progress made so far was reviewed at a National Symposium[1] organized by the Ministry of Health and held in Madrid on 11–12 June.

Initial doubts about the toxicity of anilides and uncertainties in the cause–effect relationships between the disease and the available samples of suspicious oils led the Consejo Superior Investigaciones Cientificas (CSIC) to a research programme based on two priorities. First, a series of screening tests of a wide sample of oils was to be carried out in HeLa cells to uncover toxic factors. Second, a comparative study of synthetic anilides and suspicious oils would be made in several animal models, such as chick embryo, mouse, rat and rabbits. After 9 months of intensive research, a working hypothesis of the toxic oil syndrome can be put forward in light of the clinical findings reported at the meeting.

Toxicological screening of more than 100 samples of oil led the CSIC researchers to conclude that the *in vitro* test is probably not directly relevant to human and animal pathology. No correlation was found between cell toxicity and anilide content of the oils, and the synthetic anilides were found to be almost devoid of *in vitro* toxicity. The direct toxicity of the oils seems to depend on their content of free linoleic acid and/or its oxidation products, such as hydroxy and epoxy derivatives.

Most of the suspicious oils were found to be a mixture of vegetable oils (rapeseed, olive seeds and grapeseeds) and liquid fats, extracted from lard. Their average linoleic acid content was high (42 per cent of the total fatty acid) and their content of lipid peroxides was also very high (four times higher than the legal limits, on average). Furthermore, all the oil samples were very susceptible to oxidative damage, indicating a low content of natural antioxidants, the tocopherols.

As it is generally thought that the tocopherols (vitamin E compounds) mainly function as antioxidants for unsaturated lipids and so protect lipid membranes from attack by free radicals, it is possible that consumers of the oil mixtures may have developed vitamin E deficiency. They would have been subjected both to a higher requirement for vitamin E (because of the oil's high linoleic and peroxide contents) and to a decreased dietary supply (because of the oil's lack of tocopherols).

We do not, however,believe that this would suffice to explain the epidemic outbreak of the toxic oil syndrome as suggested by McMurray[2], since it is generally accepted that similar mixtures (devoid of anilides) have been fraudulently marketed for years. But we think that it must be considered an important pathogenic factor, in association with fatty acid anilides or their presumed imino-quinone derivatives, as has been shown with *p*-hydroxy acetanilides[3].

There are no clinical data in support of free radical pathology. A systematic study of the vitamin E content in humans affected by the toxic oil syndrome is also lacking. However, an increase in the product of peroxidative damage of membrane lipids (assayable with thiobarbituric acid) has been reported in human necropsies and experimental animals after anilide treatment. A marked decrease in T-cell immunosupressive functions in toxic oil syndrome patients, which is an expected result of free-radical pathology[4] and vitamin E deficiency[5], was also reported.

Working with chicken embryo, Garcia-Gancedo *et al.* have shown that the toxic effects of synthetic anilides can be prevented by the simultaneous administration of tocopherol. The result indicates that the anilides are acting, at least in this experimental model, through a toxic route susceptible to free radical scavengers. Clinical trials with vitamin E were ineffective, but it should be remembered that the disease was at an advanced stage when the treatment was applied.

The experiments employing chicken embryo, carried out by the CSIC, deserve a few comments. First, the toxicity of anilides is dose related. Second, toxicity appears only 2–3 days after hatching and does not affect embryonic development, suggesting the involvement of inhaled oxygen on the toxicity of anilides. Last, but not least, the toxic syndrome in chicken evolves rapidly towards respiratory distress and paralysis. Histopathological study of the affected animals reveals a perivascular infiltrate with eosinophils, interstitial pneumonitis with abundant eosinophils in the alveolar lumen and widespread lesions in the cerebellum, with pycnotic degeneration of the Purkinje cells and vacuolar degeneration of the white matter. These same pathological signs were found in rabbits treated with low doses of synthetic anilides.

Work with rabbits was aimed at elucidating the involvement of immunological mechanism in the toxicity of anilides — a possibility that arises from the clinical signs (fever, rash with marked eosinophilia and large titres of IgE) and the structural relationships between anilides and pentadecil cathecol, the agent of the delayed hypersensitivity to poison ivy[6]. Rabbits treated for 15 days with oral anilides (10 μg per kg) showed a typical delayed response in a skin test with anilides and titratable antibodies against the same synthetic anilides. Moreover, anilide-treated animals developed a syndrome of progressive paralysis and the cerebellar lesions (Purkinje cells and white matter) described above, in close resemblance to the Gordon phenomenon[7]. In addition, eosinophilic infiltrates were seen in the skin lesions after challenge with anilides and in the pia madre around the cerebellar cortex.

Some results from human necropsies indicate the occurrence of similar lesions in human brains. There is also histochemical and electron microscopic evidence (Rycoll, personal communication) of peroxidase-positive granula in the vicinity of the neural lesions observed in muscle biopsies from toxic oil patients.

On the basis of these clinical and experimental observations, we think that the pathogenesis of the toxic oil syndrome could be explained by an eosinophil-mediated cytotoxicity, probably directed by specific antibodies towards anilides, that could be incorporated in the cellular plasma membranes[8]. These inmunopathological causative effects (relatively well documented in toxic oil syndrome humans with depression in T-cell supressor functions, eosinophilia, high IgE levels and autoantibodies) could have arisen through the synergistic effects of anilides and the peroxidative status, resulting from the poor nutritional quality of the oil mixtures. Although we do not exclude other pathogenic possibilities, we think that these ideas may provide a conceptual framework and working hypothesis by which the Spanish toxic oil syndrome could be experimentally approached. □

A. Pestaña, Instituto de Enzimologia, CSIC, is responsible for the coordination of the CSIC programme on toxic oil syndrome and E. Muñoz, Unidad de Biomembranas, Centro de Investigaciones Biológicas, is Vicepresident for Scientific Affairs at the CSIC.

---

1. *Simposium Nacional "Síndrome Tóxico"* (Spanish Ministry of Health, Madrid, 1982).
2. McMurray, C.H. & Rice, D.A. *Nature* **293**, 332 (1981).
3. Nelson, S.D., Dahlin, D.C., Rauchman, E.J. & Rosen, G.M. *Molec. Pharmac.* **20**, 195 (1981).
4. Anderson, R.E. & Lefkovits, I. *Am. J. Path.* **97**, 456 (1979).
5. Sheffy, B.E. & Schult, R.D. *Fedn Proc.* **38**, 2139 (1979).
6. Godfrey, H.P., Harold, B. & Watkins, R.C. *J. Immun.* **106**, 91 (1971).
7. Durack, D.T., Mark Sumi, S. & Klebanoff, S.J. *Proc. natn. Acad. Sci. U.S.A.* **76**, 1443 (1979).
8. Murphy, R.B. & Vodyanoy, V. *Lancet* i, 98 (1982).

ARTICLES

Aspherical Earth structure from fundamental spheroidal-mode data

Guy Masters, Thomas H. Jordan, Paul G. Silver & Freeman Gilbert

Institute of Geophysics and Planetary Physics, University of California, San Diego, La Jolla, California 92093, USA

Free-oscillation data reveal heterogeneity in the Earth's mantle whose geographical pattern is dominated by spherical harmonics of angular degree two and correlates well with the hydrostatically referenced geoid. The heterogeneity can be modelled as localized in the transition zone (420–670 km depth) and may be related to a large-scale component of mantle convection.

THE study of the Earth's lateral, or aspherical, heterogeneity using long-period seismic observations has since 1966[1] been based on the 'pure-path' approximation; variations in the phase velocities of travelling waves are represented as a sum of their fractional dispersion across several types of tectonic structures. Recently, this sort of analysis has been extended to normal-mode frequency shifts[2]. We investigate here a new data set of nearly 4,000 fundamental-mode frequencies measured from over 500 records of the International Deployment of Accelerometers (IDA) network. The extensive coverage provided by these measurements shows that the present schemes of tectonic regionalization are inappropriate at periods longer than ~200 s; the lateral heterogeneity revealed by the low-order fundamental modes is more suitably represented by a spherical-harmonic expansion with the dominant power in the degree-two terms. A drawback of this representation is that the data do not constrain the odd-order harmonics[3,4], a fact which must be kept in mind when interpreting the observed patterns. The source of the observed signal cannot be determined unambiguously, but our analysis suggests that the transition zone of the Earth's mantle (between about 400 and 700 km depth) is the most plausible location of the dominant heterogeneity.

Observations of fundamental-mode frequencies

In a recent study of fundamental-mode attenuation the complex frequencies of the modes ${}_0S_8$ to ${}_0S_{46}$ from 557 IDA recordings were measured[5]. Because the primary goal was to obtain reliable Q determinations, only large-amplitude peaks showing little signs of overtone interference or beating due to splitting were retained. A by-product of this analysis was 3,934 reliable measurements of fundamental-mode frequencies, forming the data base for the present study. Below $l = 39$ each mode has an average of 118 independent observations, but the number of measurements decreases rapidly at higher angular orders. The modes above $l = 43$ had <20 observations and were dropped from the data set. A complete account of the data analysis techniques can be found in ref. 5.

A convenient way of displaying the data is to plot the observed frequency shifts at the location of the pole of the great circle joining the source and receiver. In the geometrical optics limit, when the horizontal wavelength of the heterogeneity is much greater than that of the mode, the frequency shift is solely a function of the pole position[6]. If this condition is not met in the Earth, then effects not described by this asymptotic theory become important, and a more complete interpretation may be required[6,7]. In particular, the exact first-order expressions for the frequency shifts depend on the details of the source mechanisms, so that if non-asymptotic effects were to dominate the signal, the apparent frequencies would not be a smooth function of pole position. Figure 1 shows the frequency shifts for several sets of angular orders. The patterns revealed by these diagrams have a large-scale simplicity and are consistent from angular order to angular order; this suggests that the geometrical optics limit is a valid approximation and that the asymptotic theory can provide an adequate framework for the interpretation of the data.

Theoretical developments[6,8] define the peak location in terms of the ratio of the first polynomial moment of the multiplet spectrum to its zeroth moment, an estimator employed in the first systematic observational study[2]. The values used here were derived by least-squares fitting of a singlet shape to the observed spectrum[5]. However, for the large-amplitude, singlet-like peaks considered in the present study, these different estimators give almost identical results, a behaviour consistent with the asymptotic theory[8]. The least-squares estimation technique is less sensitive to contamination by nearby higher modes and has the additional benefit of a comprehensive error analysis[9]. The errors in the frequency estimates are typically 0.05%, roughly a factor of 10 less than the frequency variations ascribed to aspherical heterogeneity.

One well determined feature of the Earth's asphericity is its ellipticity of figure, which causes a positive frequency shift for poles at low latitudes and a negative shift at high latitudes. The expected variation with latitude—amounting to 2.2 μHz for ${}_0S_8$ and 9.3 μHz for ${}_0S_{43}$—is evident at low angular orders, but above $l = 16$ or so it disappears almost completely. This behaviour has been attributed by Silver and Jordan[2] to the existence of some sort of lateral heterogeneity which, in terms of its effects on the fundamental spheroidal modes, is anti-correlated with the ellipticity of figure. The present study confirms this conclusion. Because we believe the hydrostatic component of ellipticity is well modelled by the Clairaut theory, we have adopted an elliptical Earth as a reference model and have corrected the raw peak frequencies for this signal using the asymptotic formula derived by Dahlen[10].

Table 1 Localized models of degree-two aspherical heterogeneity

		Normalized coefficients					Total variance reduction
Zone	Amplitude*	δm_2^0	Re δm_2^1	Im δm_2^1	Re δm_2^2	Im δm_2^2	(%)
1	1.84	−0.70	0.27	−0.17	0.12	0.62	52
2	1.76	−0.72	0.26	−0.15	0.20	0.59	61
3	2.10	−0.69	0.25	−0.13	0.27	0.60	49
4	7.74	−0.67	0.26	−0.13	0.26	0.63	46
5	10.62	−0.70	0.26	−0.16	0.19	0.61	59

* Amplitude of the heterogeneity as a percentage of shear velocity; perturbations in density and compressional velocity are constrained to have relative amplitudes of 0.4 and 0.8 of the shear-velocity perturbation (see text).

0028–0836/82/320609—05$01.00

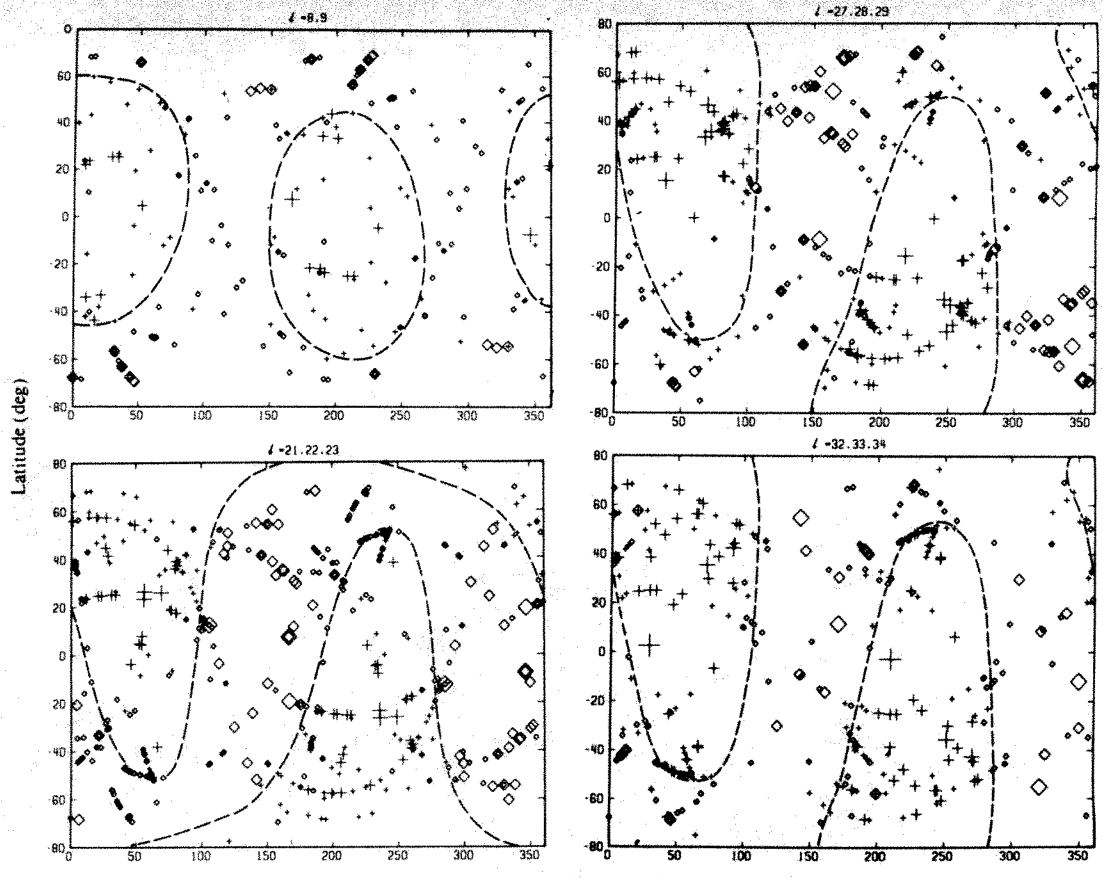

Fig. 1 Multiplet-location data from selected fundamental spheroidal modes plotted at the poles of the great circles connecting the sources and receivers. Frequency shifts are relative to the estimated degenerate eigenfrequencies of Fig. 2*c*. Symbol type indicates sign of the frequency shift (+, positive; ◇, negative); symbol size indicates its magnitude (smallest symbols correspond to shifts of 0.0–0.1%; the largest to 0.3–0.4%). Dashed lines are the nodes of the best-fitting degree-two patterns for $\delta\omega_{\text{local}}$ uncorrected for ellipticity of figure; the patterns are very similar except for the P_2^0 components, which are large for $l = 8, 9$ but small for the other modes shown.

Models of the heterogeneity

The elastic part of the terrestrial monopole is specified by $\bar{\mathbf{m}}(r)=[\bar\rho(r),\bar v_p(r),\bar v_s(r)]$, where r is radius ($0\leq r\leq a=6{,}371$ km) and $\bar\rho$, $\bar v_p$ and $\bar v_s$ are the spherically averaged mass density, compressional velocity and shear velocity, respectively. The degenerate eigenfrequency of the kth mode of this spherically symmetric model is denoted $\bar\omega_k$. Aspherical heterogeneity is represented by the perturbation

$$\delta\mathbf{m}(r,\theta,\phi)=\sum_{s=1}^{\infty}\sum_{t=-s}^{s}\delta\mathbf{m}_s^t(r)Y_s^t(\theta,\phi) \qquad (1)$$

where Y_s^t is the complex surface spherical harmonic of degree s and order t; the conventions of Edmonds[11] are adopted, so that $Y_s^{-t}=(-1)^tY_s^{t*}$. Because the perturbation is real, $\delta\mathbf{m}_s^{-t}=(-1)^t\delta\mathbf{m}_s^{t*}$.

The asymptotic first-order theory relating the multiplet locations to the aspherical model (1) is well developed[6,8]; for a source and receiver connected by a great circle with pole at colatitude Θ and longitude Φ, the peak frequency of a mode of radial order n and angular order $l\gg n$ is

$$\omega_k=\bar\omega_k+\sum_{\substack{s=2\\ s\ \text{even}}}^{\infty}P_s(0)\sum_{t=-s}^{s}(\delta\omega_{\text{local}}^{(k)})_s^tY_s^t(\Theta,\Phi) \qquad (2)$$

The coefficients in this expansion are given by

$$(\delta\omega_{\text{local}}^{(k)})_s^t=\int_0^a\mathbf{M}_0^{(k)}(r)\cdot\delta\mathbf{m}_s^t(r)r^2\,\mathrm{d}r \qquad (3)$$

where $\mathbf{M}_0^{(k)}$ is a triplet of functional derivatives computable from the eigenfunctions of the terrestrial monopole[12]. The apparent eigenfrequency (2) can be shown to equal the great-circular average of the 'local eigenfrequency' $\bar\omega_k+\delta\omega_{\text{local}}^{(k)}(\theta,\phi)$, whose harmonic coefficients are defined by equation (3). Such averages place no constraints whatsoever on the odd-parity (s-odd) part of the aspherical perturbation, a point first noted by Backus[3] in his analysis of great-circle dispersion. Equations (2) and (3) can be combined to give a linear inverse problem for the even part of $\delta\mathbf{m}$.

Alternatively, equation (2) can be solved directly for $\delta\omega_{\text{local}}^{(k)}$, permitting an investigation of the even part of the spherical harmonic patterns underlying individual modes without introducing the additional questions of nonuniqueness associated with the complete inverse problem. Figure 2 shows the results of this analysis assuming $\delta\omega_{\text{local}}^{(k)}$ is representable by harmonics of degree two. To reduce the variance and ensure a good sampling of the sphere, the data from three consecutive angular orders were combined in each calculation. The inversion determined estimates of the degenerate eigenfrequencies and the complex coefficients of $s=2$, for a total of eight independent parameters per mode triplet. The coefficients in Fig. 2*a* have been normalized to unit power to facilitate comparisons among the modes; their normalization scalars are shown in Fig. 2*b*.

The estimated degenerate eigenfrequencies are plotted relative to the PEM-A model[13] in Fig. 2*c*, together with the weighted means of the apparent frequencies and the estimates given in ref. 2. (Figure 2*c* was constructed using the PEM-A eigenfrequencies published by Dziewonski *et al.*[13]; these differ from the values calculated from the PEM-A model by up to 2 μHz.) The offset in the eigenfrequencies between ${}_0S_{11}$ and ${}_0S_{18}$, is prominent. Present Earth models predict significant quasi-degenerate Coriolis coupling between the ${}_0S_l$ and ${}_0T_{l+1}$ modes at the ends of this band[14], which could explain the shifts of ${}_0S_{11}$ and ${}_0S_{18}$, but the reason for a nearly constant offset of the

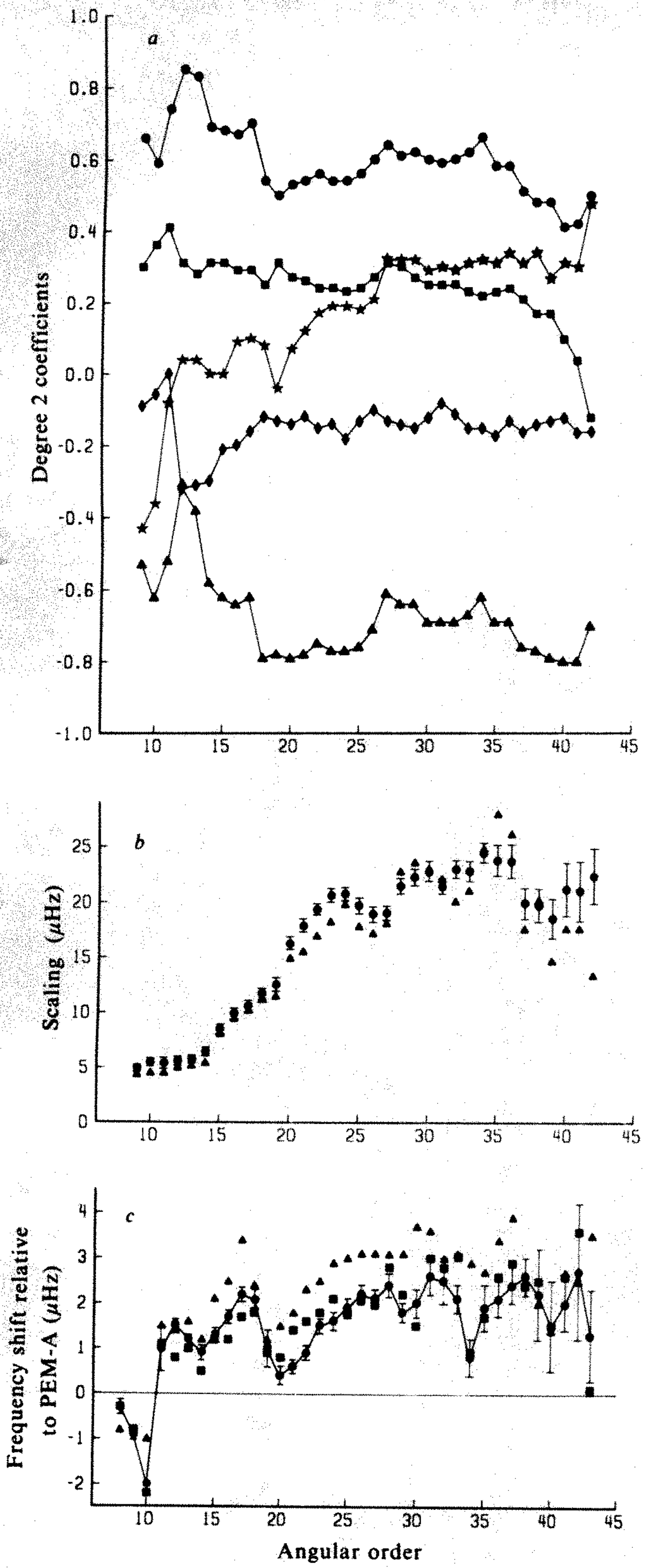

Fig. 2 *a*, Normalized degree-two coefficients of $\delta\omega_{\text{local}}$ from a least-squares fit to the ellipticity-corrected multiplet locations assuming $s_{\max}=2$(▲, P_2^0;■, Re P_2^1; ◆, Im P_2^1; ★, Re P_2^2; ●, Im P_2^2). Three consecutive angular orders were combined in each calculation (eight-parameter inversion). *b*, Scale factors for these coefficients, with 1σ error bars. ▲, Degree-two scale factors for 30-parameter ($s_{\max}=6$) inversions. *c*, Estimates of the degenerate eigenfrequencies $\bar{\omega}_k$ plotted as residuals with respect to published eigenfrequencies of the PEM-A model[13]. Values from eight-parameter inversions are connected by a solid line; error bars are 1σ. Simple weighted means of our data (■) and those from ref. 2 (▲) are shown. The latter two estimates are more sensitive to bias caused by incomplete sampling of the aspherical heterogeneity.

intermediate modes remains obscure. This important observation, previously noted in ref. 2, may provide strong constraints on the spherically averaged Earth structure.

Note that the average eigenfrequencies estimated by the degree-two inversion form a generally smoother function of angular order than the simple weighted means, particularly at the higher angular orders. This is because the pole positions for our data set are biased to temperate latitudes and there consequently exists a significant tradeoff between $\bar{\omega}_k$ and any P_2^0 component of $\delta\omega_{\text{local}}^{(k)}$. At the higher angular orders the acceptable data are fewer, the sampling is more variable, and the P_2^0 component is large; hence, a simple averaging of the data can introduce spurious variations in estimates of $\bar{\omega}_k$. The small positive shift of the Silver–Jordan means relative to our estimates appears to be ascribable to a bias in the way their pole positions sample the patterns shown in Fig. 1.

Several conclusions can be immediately drawn from Fig. 2*a*, *b*. The normalized spherical harmonic pattern of $\delta\omega_{\text{local}}^{(k)}$ is quite stable, especially for the modes ${}_0S_{20}$–${}_0S_{38}$, where only the real part of the P_2^2 term appears to exhibit a significant trend. The pattern consists of a large P_2^2 component and a large negative P_2^0 component. It is this latter term which at the higher angular orders almost cancels the signal due to the ellipticity of figure. The P_2^1 component is comparatively small, accounting for only ~10% of the total power. The scale factors multiplying this nearly constant pattern increase with angular order to $l\sim35$, but level off at higher angular orders.

The variance reduction provided by this simple model is remarkable (Fig. 3). Except for ${}_0S_{11}$ whose scatter is probably dominated by the vagaries of quasi-degenerate coupling, the median variance reduction is 60% and, in the centre of our mode band where the data are most numerous, it exceeds 70%.

This variance reduction is far superior to that achievable by tectonic regionalizations with comparable numbers of parameters. We have, for example, inverted these data using a six-parameter regionalization[2,15]. The median variance reduction is only 24% and for only nine of the 35 modes does it exceed 30% (Fig. 3). Furthermore, the patterns in $\delta\omega_{\text{local}}^{(k)}$ derived from the tectonic regionalization are much less stable with respect to variations in angular order number.

The possibility that power is aliased into the degree-two coefficients from higher-degree heterogeneity by inadequate sampling of the sphere can be checked by comparing these results with inversions allowing higher harmonics in $\delta\omega_{\text{local}}^{(k)}$. The scale factors for the degree-two coefficients from inversions with $s_{\max}=6$ (30 parameters per mode triplet) are plotted with those from the eight-parameter inversions in Fig. 2*b*. Throughout most of the band the agreement is quite good. In fact, below $l=36$ the power in the higher harmonics is down by a factor of four or more. Above $l=36$ the scale factors for the 30-parameter inversion are generally lower, the power in the higher harmonics increases, and the possibility of appreciable aliasing cannot be discounted. As shown in Fig. 2*b*, ignoring higher harmonics tends to increase the degree-two scale factors for $l>36$. Because this bias appears to be small and the variance reduction at the lower angular-order numbers is not significantly improved by the addition of the higher-degree terms, we shall restrict further attention to the degree-two components.

The uniformity of the $\delta\omega_{\text{local}}^{(k)}$ patterns suggests that the dominant signal arises from anomalies localized in radius. If this is true, the variation of the pattern's amplitude with angular order constrains the position of the heterogeneity inside the Earth. We consider five zones based on the major seismological divisions of the mantle as defined by the PEM-A model:

Zone 1:	5,350–5,701 km (top of the lower mantle)
Zone 2:	5,701–5,951 km(transition zone)
Zone 3:	5,951–6,151 km
Zone 4:	6,151–6,291 km (low-velocity zone)
Zone 5:	6,291–6,352 km (lid)

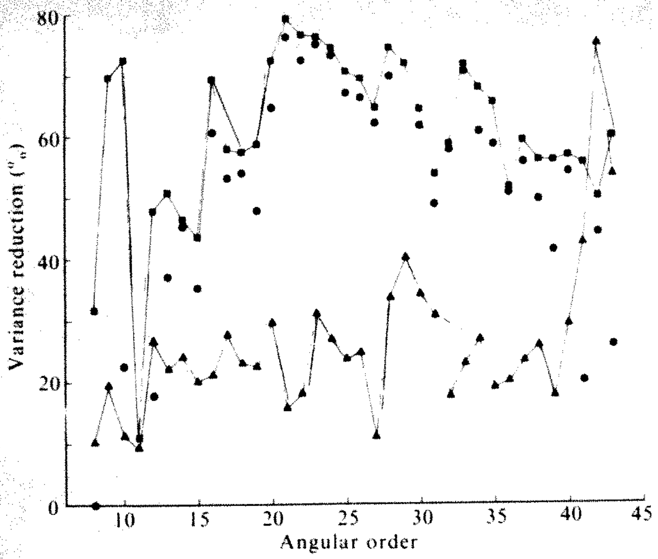

Fig. 3 Percentage variance reductions achieved by the degree-two representation of $\delta\omega_{\text{local}}$ given by Fig. 2 (–■–), the tectonic regionalization of Jordan[15] (–▲–), and the degree-two transition-zone (zone 2) model of Table 1 (●).

Five models of degree-two heterogeneity have been constructed by least-squares inversion of the entire data set (excluding ${}_0S_{11}$) assuming the perturbations to ρ, v_p and v_s are constant functions of radius localized in one of these zones. Of course, the radii of the discontinuities separating zones could be (and probably are) laterally variable, but their effects on the data have been shown by numerical experiments to be similar to constant perturbations in adjacent zones; for these preliminary experiments we have therefore fixed these radii.

If ρ, v_p and v_s are allowed to be independently variable in the inversion, then the results depend strongly on the integrals of the functional derivatives across each layer. In zones 4 and 5, for example, the differential kernels for ρ and v_p are of the same magnitude but opposite sign, and the inversion yields models with large positive ρ perturbations correlated with large negative v_p perturbations, and vice versa. From what we know about mantle properties this behaviour is unphysical. To eliminate such models we have scaled *a priori* the perturbations in density and compressional velocity to those in shear velocity by assuming $d\ln\rho/d\ln v_s = 0.4$ and $d\ln v_p/d\ln v_s = 0.8$. These scalings were derived from the temperature derivatives of possible mantle constituents given by Anderson *et al.*[16], but they are equally appropriate for the chemical variations observed in naturally occurring periodotites[17,18]. If the heterogeneity is confined to zones 1, 2 or 3, then the scaling is unimportant, as the modes are primarily sensitive to only the v_s perturbations in these regions. This is not true for zones 4 and 5, where the ρ and v_p perturbations predominate, although it is unlikely that any reasonable scaling will alter our conclusions.

The results of the inversions for the five zones are listed in Table 1. The spherical-harmonic pattern is essentially the same for each zone, but the magnitude of the requisite perturbation increases rapidly for the shallower zones. The localized perturbation giving the best overall fit to the data is the zone-2 (transition-zone) model with a total normalized variance reduction of 61%. Except at the very low and high ends of the mode band, the variance reduction provided by this simple model is almost as great as the optimal values for a degree-two parameterization attained by the $\delta\omega_{\text{local}}^{(k)}$ inversions (Fig. 3). Zones 1, 3 and 4 have much less satisfactory residuals. Although the zone-5 (lid) model is better, it systematically under-predicts the magnitude of the frequency shifts in the band ${}_0S_{20}$–${}_0S_{30}$ and overpredicts the shifts above ${}_0S_{35}$.

These aspects of the data fit are illustrated in Fig. 4, which compares the scaling of the degree-two pattern derived from the $\delta\omega_{\text{local}}^{(k)}$ inversions with the scalings predicted by the various models. The dependence of the scaling on angular-order number is clearly best matched by the transition-zone model. The zone-1 solution predicts too rapid a roll-off, whereas the models for zones above the 420-km discontinuity do not roll off fast enough.

Correlation with the geoid

The geographical pattern of aspherical heterogeneity synthesized from the transition-zone model of Table 1 is mapped in Fig. 5 (the contours for the other models are very similar). High-velocity anomalies are centred near the Equator in the western Pacific and central Atlantic, whereas lows occur at high latitudes in the southeastern Pacific and northern Eurasia. These features are remarkably similar to the dominant large-scale undulations of the geoid when the latter is referenced to the hydrostatic ellipsoid. The correlation coefficient between the degree-two harmonics of the transition-zone model and the GEM 9 geoid[19] corrected for Jeffreys' hydrostatic value of J_2 (ref. 20) is +0.79, which is significant at the 94% confidence level. We hypothesize, therefore, that the heterogeneity detected by the multiplet-location data is responsible, at least in part, for the degree-two geoid anomalies.

None of the localized perturbations in Table 1 can by itself adequately account for these anomalies, however; the predicted amplitudes are too large. For example, the root-mean-square (r.m.s.) geoid amplitude calculated for the transition-zone

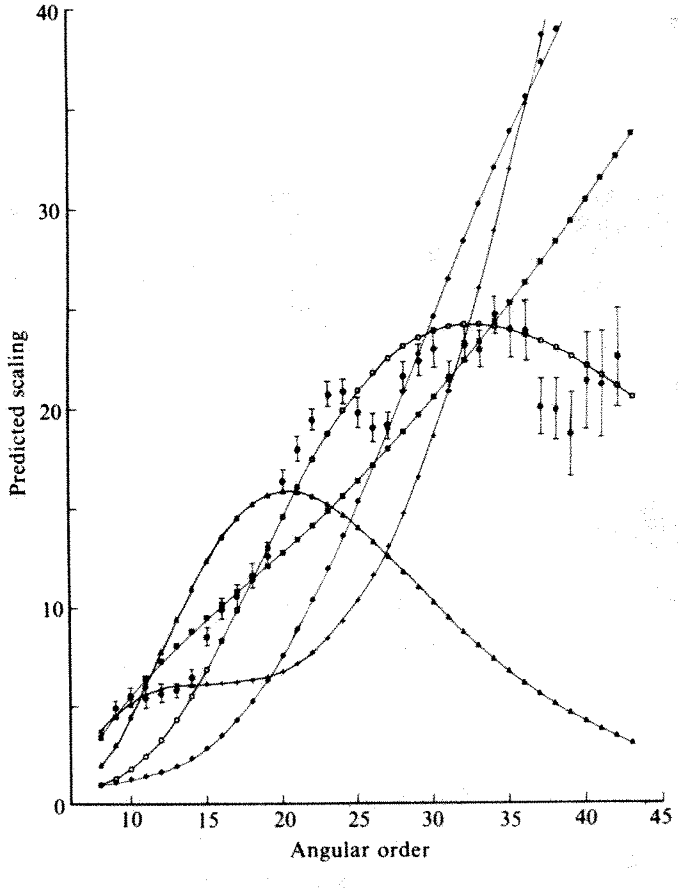

Fig. 4 Variation of degree-two scale factors with angular order predicted by localized models of aspherical heterogeneity (△, zone 1; □, zone 2; ◇, zone 3; +, zone 4; *, zone 5). Solid circles with 1σ error bars are the degree-two scalings from the eight-parameter inversions shown in Fig. 2*b*.

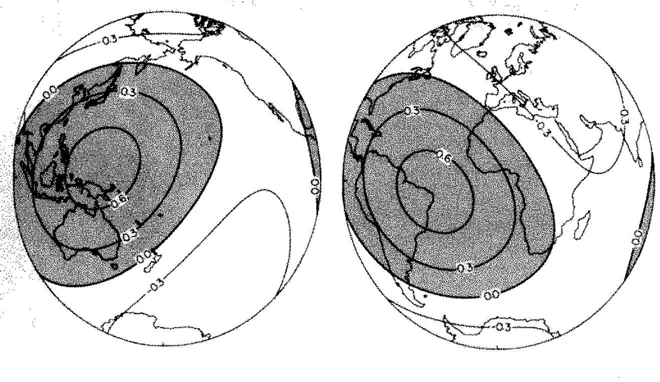

Fig. 5 Lambert equal-area projections of the Earth showing the degree-two heterogeneity of the transition-zone model, normalized such that its square integrates to unity on the unit sphere. Regions of positive anomaly are shaded; contour interval is 0.3 units.

models exceeds the observed degree-two value by about a factor of five. The discrepancy for the zone-5 model is even larger, nearly a factor of nine. Either the velocity-density scaling adopted in the inversions is grossly incorrect or the heterogeneity sensed by the multiplet-location data is compensated at other levels within the Earth. We prefer the latter hypothesis, as the former would imply substantial lateral variations in mean atomic weight[17] which would be difficult to maintain in a convecting mantle.

The compensation is not likely to be confined to the upper mantle. If our scaling parameters are roughly correct, then only models with large and nearly cancelling radial excursions in upper-mantle properties can satisfy both the multiplet-location data and the geoid. It seems improbable that any mechanism responsible for such excursions would yield multiplet-location patterns so similar at different angular orders. A lower-mantle compensation is more plausible. The changes in the $\delta\omega_{\rm local}^{(k)}$ patterns at low angular orders are suggestive of a deeper-seated heterogeneity, as are the observations of splitting of high-Q, low-angular-order modes[21]. In fact, heterogeneities anti-correlated with the geoid have already been proposed for depths greater than 1,100 km by Dziewonski *et al.*[22] to explain certain large-scale variations in P-wave travel times.

Discussion

Aspherical heterogeneity of the sort implied by the transition-zone model could be produced by lateral temperature differences of the order of 200–300 °C associated with a large-scale component of mantle convection. Such variations could occur in a thermal boundary layer between the upper and lower mantle, or alternatively, in a mantle-wide system of convective flow. To differentiate between these possibilities will require better resolution of the heterogeneity distribution as a function of depth. Although the simple scaling of the $\delta\omega_{\rm local}^{(k)}$ patterns with angular order suggests some localization in depth and motivates the modelling experiments of Table 1, the data now in hand certainly do not exclude models wherein the aspherical variations are distributed throughout the Earth. Indeed, we have argued that the geoid requires the heterogeneity constrained by the multiplet-location data to be largely compensated elsewhere in the mantle, most likely near its base.

There are at least four additional sources of seismic data which should help to increase our vertical resolution of structure. The first is the measurement of phase-velocity dispersion at periods shorter than 200s. We have attempted to extend our data set using published phase-velocity observations, but these have proved inadequate in both quantity and quality to improve our spherical-harmonic models of lateral heterogeneity. The second is the study of fundamental toroidal modes whose energy is more strongly concentrated near the surface than spheroidal modes, and the third is the measurement of resolvably split high-Q modes of low angular order. Finally, the inversion of large sets of teleseismic travel times[22] can be used to constrain the odd-order harmonics of deep-seated heterogeneity to which the free-oscillation data are insensitive. With the addition of these data detailed models of the Earth's large-scale lateral heterogeneity should be within our reach in the near future.

Conclusions

A data set comprising 3,886 apparent centre frequencies of the modes ${}_0S_8$–${}_0S_{43}$ measured from over 500 IDA records has been analysed for aspherical Earth structure. When plotted as a function of the pole position of the great circle connecting the source and receiver the frequency shifts show a remarkably coherent geographical pattern clearly dominated by surface spherical harmonics of degree two. Although the degree-two pattern is well constrained by the data, the depth distribution of the aspherical heterogeneity cannot be determined unambiguously. Models of degree-two heterogeneity localized in various mantle layers have been constructed using the asymptotic theory of multiplet locations by scaling the density and compressional-velocity perturbations to those in shear velocity. The best fit to the data is obtained by localizing the degree-two perturbations in the mantle transition zone (420–670 km depth). This transition-zone model is characterized by shear-velocity variations of 1.7% (r.m.s. amplitude). The overall variance reduction provided by the model is 61%, more than a factor of two better than that achievable by tectonic regionalization. The degree-two pattern has high-velocity anomalies centred near the Equator in the western Pacific and central Atlantic and lows at high latitudes in the southeastern Pacific and northern Eurasia; these features correlate well with the hydrostatically referenced geoid. The transition-zone model predicts geoidal undulations too large by about a factor of five, however, suggesting a compensation mechanism which we infer to be heterogeneity in the lower mantle. Aspherical heterogeneity of the sort implied by our data could be produced by lateral temperature differences of the order of 200–300 °C associated with a large-scale component of mantle convection.

We thank Jon Berger, Duncan Agnew and the other members of the Project IDA team for providing data which made this study possible, and Loren Shure for assistance in constructing Fig. 5. This research has been supported by NSF grants EAR-80-07823 and EAR-80-25261.

Received 22 March; accepted 14 May 1982.

1. Toksöz, M. N. & Anderson, D. L. *J. geophys. Res.* **71,** 1649 (1966).
2. Silver, P. G. & Jordan, T. H. *Geophys. J. R. astr. Soc.* **64,** 605 (1981).
3. Backus, G. E. *Bull. seism. Soc. Am.* **54,** 571 (1964).
4. Zharkov, B. N. & Lyubimov, V. M. *Bull. Izv. Akad. Sci. USSR, Earth Phys.* **10,** 613 (1970).
5. Masters, G. & Gilbert, F. *Phil. Trans. R. Soc.* (in the press).
6. Jordan T. H. *Geophys. J. R. astr. Soc.* **52,** 441 (1978).
7. Woodhouse, J. H. & Girnius, T. P. *Geophys. J.R. astr. Soc.* **68,** 653 (1982).
8. Dahlen, F. A. *Geophys. J. R. astr. Soc.* **58,** 1 (1979).
9. Dahlen, F. A. *Geophys. J. R. astr. Soc.* **69,** 537 (1982).
10. Dahlen, F. A. *J. geophys. Res.* **80,** 4895 (1975).
11. Edmonds, A. R. *Angular Momentum in Quantum Mechanics* (Princeton University Press, 1960).
12. Woodhouse, J. H. & Dahlen, F. A. *Geophys. J. R. astr. Soc.* **53,** 335 (1978).
13. Dziewonski, A. M., Hales, A. & Lapwood, E. *Phys. Earth planet. Inter.* **10,** 12 (1975).
14. Woodhouse, J. H. *Geophys. J. R. astr. Soc.* **61,** 261 (1980).
15. Jordan, T. H. *Bull. seism. Soc. Am.* **69,** 271 (1981).
16. Anderson, O. L., Schreiber, E., Liebermann, R. C. & Soga, N. *Rev. geophys. Space Phys.* **6,** 491 (1968).
17. Birch, F. *J. geophys. Res.* **66,** 2199 (1961).
18. Christensen, N. I. *J. geophys. Res.* **71,** 5921 (1966).
19. Lerch, F. J., Klosko, S. M., Laubscher, R. E. & Wagner, C. A. *J. geophys. Res.* **84,** 3897 (1979).
20. Jeffreys, H. *The Earth* 5th edn (Cambridge University Press, 1970).
21. Masters, G. & Gilbert, F. *Geophys. Res. Lett.* **8,** 569 (1981).
22. Dziewonski, A. M., Hager, B. H. & O'Connell, R. J. *J. geophys. Res.* **82,** 239 (1977).

Sm–Nd, Rb–Sr and U–Th–Pb systematics of granulite facies rocks from Fyfe Hills, Enderby Land, Antarctica

D. J. DePaolo*, W. I. Manton†, E. S. Grew* & Martin Halpern†‡

* Department of Earth and Space Sciences, University of California, Los Angeles, California 90024, USA
† Geosciences Programs, University of Texas at Dallas, Richardson, Texas 75080, USA
‡ Present address: Enserch Exploration, Inc., Dallas, Texas 75221, USA

New Sm–Nd isotopic measurements made on granulite-facies metamorphic rocks from East Antarctica provide firm evidence that crust of ~3,500-Myr age exists in the Fyfe Hills. Zircon U–Pb data provide further documentation for a granulite-facies event 2,500 Myr ago, during which Rb, U, Sm and Nd were highly mobile. The U–Pb and Rb–Sr isotopic systems were seriously disrupted and in most samples give meaningless model ages. In contrast, Sm–Nd model ages were offset only slightly. A large time interval of 1,000 Myr between the times of crust formation and granulite-facies metamorphism has not previously been reported for Archaean rocks, and suggests that 2,500 Myr ago the Fyfe Hills may have been located in an Andean- or Himalayan-type continental margin where crust already 1,000-Myr old was involved in an orogenic event.

THE Napier complex of coastal Enderby Land, East Antarctica (46°–57°E) (Fig. 1) is an Archaean granulite-facies terrane[1–3] that was cut by pegmatites 2,500 Myr ago at about the time of metamorphism[3,4]. Sobotovich *et al.*[5,6] reported a 4,000-Myr Pb isochron age for six whole rock samples of enderbite and granulite of the Napier complex at Fyfe Hills (67°22′S, 49°12′E). This age was calculated assuming a two-stage development of the U–Pb system, an assumption that has been invalidated by the evidence for a 2,500 Myr metamorphism[4]. Nonetheless, recalculation of Sobotovich *et al.*'s data, assuming a three-stage development, yields a minimum age of 3,500 Myr (ref. 4).

If this age is correct, the Napier complex would represent the first documented example of an Archaean granulite-facies metamorphic event that significantly post-dated crust formation. This in turn places a new perspective on the mode of formation of the early crust and the causes of granulite-facies metamorphism. In view of these implications, we have reanalysed Sobotovich *et al.*'s Fyfe Hills samples for U–Pb isotopes, and also analysed them for Rb–Sr and Sm–Nd isotopes. U–Pb isotopic systematics are often ambiguous in granulite terranes[7]. However, Sm–Nd isotopes can place more stringent constraints on the age of the complex[8]. Furthermore, the concurrent study of the entire suite of chemically diverse elements provides a much better understanding of the geological processes which affected this part of the Antarctic crust during the Archaean. We have also analysed zircons in one of the Fyfe Hills granulites for U–Pb isotopes to document further the ~2,500-Myr age of metamorphism inferred from previous measurements on pegmatite minerals[4].

Samples

Grikurov provided seven samples (28-I to 28-VII) collected by Kamenev and co-workers in 1970–71, and Kamenev provided a sample 28-VIII, collected in 1978. The samples include garnet-two pyroxene granulite (28-I, IV), magnesian pyroxene granulite (28-II, III), quartzofeldspathic granulite (28-VI, VII and VIII) and magnetite–garnet–orthopyroxene ironstone (28-V) (Table 1). The granulites are medium grained (0.1–3.5 mm) and lack a marked foliation while the ironstone has a cataclastic fabric. The mineral identified as perrierite or chevkinite in 28-VII forms rare brown isotropic (metamict) grains containing major Si, Ti and Ce, and subordinate Ca, Al and Th (energy dispersive scan). Minor biotite, chlorite, hornblende, or a low Ca-amphibole appear to result from post-metamorphic alteration.

Table 1 Modes* of the Fyfe Hills rocks and calculated distribution coefficients

Rock type	Garnet-two pyroxene granulite		Magnesian pyroxene granulite		Quartzofeldspathic granulites			Ironstone
Sample no.	28-I	28-IV	28-II	28-III	28-VIII	28-VI	28-VII	28-V
Quartz	2	3	—	—	48	72	12	50
K-feldspar	—	—	—	—	—	—	15	—
Plagioclase	66	59	71	77	30	25	66	—
Orthopyroxene	5	10	28	20	9	3	5	20
Clinopyroxene	17	12	—	1	T	T	—	—
Colourless amphibole	—	—	T	T	—	—	—	—
Hornblende	—	T	—	—	—	T	T	—
Garnet	7	12	—	—	12	—	—	15
Biotite	T	T	1	2	T	T	T	T
Chlorite	—	—	—	—	T	—	T	—
Opaque	3	4	T	—	1	T	1	15
Apatite	T	T	—	—	—	—	1	T
Zircon	T	—	—	—	T	—	T	—
Monazite	—	—	—	—	—	—	T	—
Perrierite or chevkinite	—	—	—	—	—	—	T	—
D^{Rb}	0.05	0.05	0.08	0.11	0.03	0.02	0.27	<0.01
D^{Sr}	1.2	1.1	1.3	1.4	0.6	0.5	1.5	<0.1
D^{Nd}	0.185	0.120	0.024	0.029	0.115	0.032	0.279	0.109

* Visual estimates (volume %). T, trace amounts.

0028–0836/82/320614—05$01.00

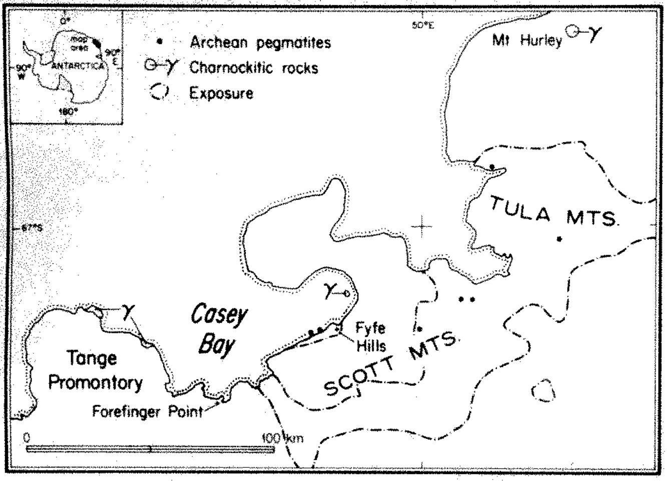

Fig. 1 Map of a portion of the Napier complex in Enderby Land showing Archaean pegmatites of possible plutonic origin[31] and intrusive charnockitic rocks (γ) on Tange Promontory (ref. 1, p. 494; ref. 3), east end of Casey Bay (J. W. Sheraton, personal communication), and Mt Hurley (ref. 1, p. 494). Specific localities of Soviet samples provided by Ye. N. Kamenev (personal communication).

The rocks vary considerably in major and trace element composition, especially in their SiO_2 content and in the relative proportions of Fe and Mg (Tables 1 and 2). Samples I and IV have igneous compositions corresponding to Fe-rich tholeiitic basalt. The other rocks, with the exception of the ironstone (sample V) have compositions that are broadly igneous except for a notable deficiency in Na_2O and K_2O. In general, the rocks are especially poor in K_2O, Rb and U, have low values of Rb/Sr and U/Pb, and high values of Th/U and K/Rb. All of these features are characteristic of granulite facies rocks[9,10]. An additional feature is the low Sr abundances of all the rocks, some three or more times lower than typical crustal abundances[11]. Sample VII, the only sample containing significant K-feldspar, is unique in that it contains much higher concentrations of K, Rb, Th and Nd than the other rocks, and has a high Rb/Sr ratio. Only sample VII has high U/Pb and low Th/U values. From the chemical compositions, we infer the protoliths for the samples to be volcanic rocks or immature detritus shed from an igneous terrane. The ironstone is clearly of sedimentary origin. The protolith for the magnesian pyroxene granulites is enigmatic. Their chemical compositions are not similar to igneous rock compositions, as both granulites have relatively high Mg/Fe ratios and Al_2O_3 contents, and low alkali contents.

Analytical techniques and data representation

The isotopic data were obtained using techniques described previously[12-14]. The U–Th–Pb and Rb–Sr data were obtained at the University of Texas; the X-ray fluorescence and Sm–Nd data were obtained at the University of California at Los Angeles. The Nd isotopic data were monitored for internal consistency by measuring all seven isotopes in all runs. Tracers for Sm and Nd concentration determinations were calibrated against gravimetric standard solutions using ultrapure metals from the Ames Laboratory[15,16]. All Sm–Nd analyses were by the total spike method. The measured $^{143}Nd/^{144}Nd$ ratios are expressed here in the ε-notation:

$$\varepsilon_{\mathrm{Nd}}(0) = 10^4\left[\frac{(^{143}\mathrm{Nd}/^{144}\mathrm{Nd})_{\mathrm{sample}}}{0.511836} - 1\right]$$

We also use the Sm–Nd enrichment factor, defined:

$$f_{\mathrm{Sm/Nd}} = \left[\frac{(^{147}\mathrm{Sm}/^{144}\mathrm{Nd})_{\mathrm{sample}}}{0.1967} - 1\right]$$

The values in the denominators are the isotopic ratios determined for average chondritic meteorites[17]. Our $\varepsilon_{\mathrm{Nd}}$ values as defined here are comparable with those of ref. 16 to within ±0.1 units.

Results

Sample 28-VIII contained abundant rounded, unzoned zircon for which U–Pb data have been obtained (Table 3). Two fractions were dated. The 100–200 mesh fraction is nearly concordant at 2,500 Myr (Fig. 2). The >100 mesh fraction is discordant and indicated an age of 2,550 Myr on the basis of a discordia line passing through 500 Myr (by analogy with the pegmatite minerals of Grew and Manton[4]). A 2,500-Myr age for the granulite-facies metamorphism, which Grew and Manton[4] inferred to be nearly coeval with the 2,500-Myr-old hypersthene-bearing pegmatites found throughout the Napier complex, is supported by the ages obtained from the zircons in this study. These zircons appear to have been reset at about the same time the pegmatites were emplaced. We have taken the 2,550-Myr value as the time of metamorphism for the purpose of discussion of the other isotopic data. It has been proposed that the Napier complex was also affected by a granulite-facies metamorphism about 3,000 Myr ago[18,32], but a second metamorphic event antedating 2,550 Myr would not affect the following arguments significantly.

Figure 3 shows the isotopic evolution of the samples as a function of time. We represented the data for each of the three isotopic systems in an analogous fashion. In all three plots, the trajectory labelled 'Mantle' represents an approximation to the isotopic evolution of the parental reservoir from which continental crust is derived by magmatic processes. It is assumed that any segment of continental crust must have had isotope ratios that lay on the mantle lines at the time it was originally derived from the mantle.

The Sm–Nd isotopic data (Fig. 3*a*) give the most direct indication of an ancient age of crust formation. The measured values of $\varepsilon_{\mathrm{Nd}}(0)$ (Table 2), shown at $T = 0$, are extrapolated back in time using the measured values of $^{147}Sm/^{144}Nd$. The points at which these lines intersect the mantle curve correspond to the Sm–Nd model crust-formation ages (T_{DM}) (ref. 8). We have used T_{DM}, rather than T_{CHUR} (ref. 19), because there is an increasing amount of evidence that continental crust is derived mainly from depleted mantle (DM), even as far back as the Archaean[8,17,20]. The model ages clearly show that crust formation predated 3,100-Myr ago. Probably much of the crust represented by these samples formed before 3,300 Myr. The spread of model ages does not allow precise definition of crust-formation ages for these rocks. Nonetheless, the data clearly confirm the existence of early Archaean crust at Fyfe Hills. The interpretation of the T_{DM} ages is discussed further below.

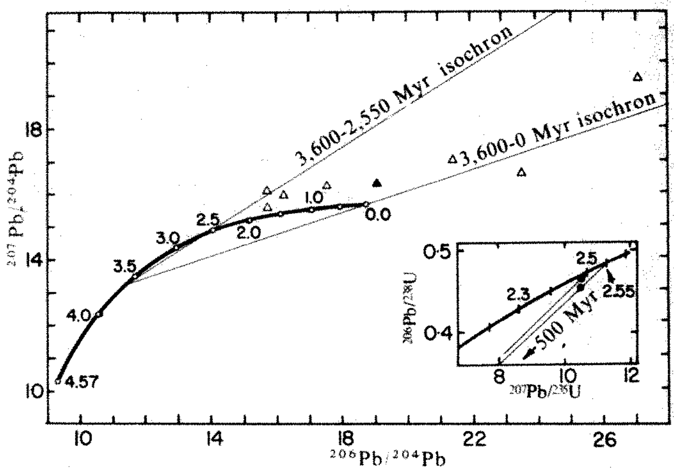

Fig. 2 $^{207}Pb/^{204}Pb$ versus $^{206}Pb/^{204}Pb$ diagram showing assumed mantle growth curve[19] and data from the Enderby Land rocks. △, Fyfe Hills: ▲, K-feldspar from pegmatite at Forefinger Point (67°37′S, 48°04′E) (see ref. 4). Inset, portion of the concordia plot showing zircon data from sample 28-VIII.

Table 2 Chemical composition and isotope ratios of Fyfe Hills rocks

Rock type	Garnet-two pyroxene granulite		Magnesian pyroxene granulite		Quartzofeldspathic granulite			Ironstone
Sample no.	28-I	28-IV	28-II	28-III	28-VIII	28-VI	28-VII	28-V
Field no.	28	28e	28g	28d	—	28a	28v	—
SiO_2(%)	51.02	50.00	48.30	47.83	70.00	73.94	63.61	50.29
Al_2O_3	14.32	13.34	19.50	22.38	12.86	13.58	14.67	3.40
CaO	10.11	9.01	8.95	12.29	5.59	3.93	4.81	0.89
Na_2O	2.77	2.20	1.39	1.02	1.85	2.47	2.32	ND
K_2O	0.42	0.40	0.23	0.40	0.38	0.38	3.02	0.15
Fe_2O_3	14.00	17.80	9.90	4.43	5.70	3.51	6.41	40.78
MgO	5.64	5.43	11.34	11.25	2.35	1.48	3.25	3.24
TiO_2	1.11	1.05	0.15	0.07	0.70	0.37	0.93	0.64
MnO	0.193	0.351	0.199	0.095	0.099	0.055	0.087	0.208
P_2O_5	0.19	0.10	ND	ND	0.17	0.04	0.45	0.17
Cr (p.p.m.)	132	103	329	222	60	50	60	286
Ni	138	94	188	110	69	55	31	46
Zr	164	60	27	2	490	38	450	ND
U (p.p.m.)	0.15	0.16	0.02	0.07	2.44	0.09	3.52	0.23
Th	2.90	1.64	0.24	1.92	4.06	1.04	107	2.38
Pb	3.72	8.91	7.47	5.08	5.73	5.72	29.7	2.76
κ	20.2	10.9	13.5	26.5	1.73	11.5	31.4	10.5
$^{206}Pb/^{204}Pb$*	16.17	15.68	15.73	17.57	21.32	17.50	27.05	23.46
$^{207}Pb/^{204}Pb$	15.91	15.61	16.04	16.24	17.04	16.26	19.52	16.65
$^{208}Pb/^{204}Pb$	40.60	36.09	35.50	36.92	42.46	38.20	126.6	64.91
Rb(p.p.m.)	2.63	1.09	3.66	13.4	2.25	2.03	76.2	0.31
Sr	105	124	128	44.8	110	116	103.6	6.77
$^{87}Sr/^{86}Sr$*	0.7120	0.7078	0.7164	0.7372	0.7134	0.7157	0.8160	0.7189
Nd (p.p.m.)	—	15.57	8.41	1.46	21.41	4.70	187.65	16.52
$^{147}Sm/^{144}Nd$	—	0.1566	0.0909	0.1112	0.1169	0.0782	0.0889	0.0864
$\varepsilon_{Nd}(0)$*	—	−19.2	−43.4	−36.6	−32.1	−46.9	−47.0	−41.9
T_{DM}(Myr)†	—	3,870	3,310	3,450	3,280	3,200	3,490	3,090

Sample numbers refer to the numbers as supplied to us. The Soviet field numbers were deduced from Table 5 of ref. 6 in which the same Rb–Sr data are presented.

All Fe as Fe_2O_3. ND, none detected. U, Th, Pb, Rb, Sr, Sm, Nd measured by isotope dilution; all other by X-ray fluorescence.

* Analytical precision is ±0.0003 for $^{87}Sr/^{86}Sr$, ±0.5 for $\varepsilon_{Nd}(0)$, and ±0.1% for Pb isotopic ratios.

† Uncertainty in model ages is typically 1–2%.

Our U–Pb and Rb–Sr data (Fig. 3*b, c*) also require that crust formation substantially predates the granulite-facies metamorphism. For U–Pb, the extremely low measured μ values ($\mu = {}^{238}U/{}^{204}Pb$) give calculated $^{206}Pb/^{204}Pb$ ratios that lie above the mantle evolution curve at 2,550 Myr ago[21]. Consequently, the rocks must have had much higher μ values during all or part of the time interval between crust formation and 2,550 Myr ago. The broken lines on Fig. 3*b* show the Pb isotopic evolution before 2,550 Myr for an arbitrarily assumed crust formation age of 3,600 Myr. The measured μ values, compared with those calculated for the time interval between crust formation and metamorphism, suggest that μ decreased by factors of 2–100 during the metamorphism as a result of severe U loss. This conclusion is independent of the value assumed for the crust-formation age. If instead of using the measured μ values, we use the measured $^{206}Pb/^{204}Pb$ and $^{207}Pb/^{204}Pb$ ratios to calculate a self-consistent set of values for μ_1 (3,600–2,550 Myr ago) and μ_2 (2,550 Myr ago to the present, see ref. 7), the calculated values of μ_2 agree with the measured values to within a factor of two. This agreement indicates that the low measured μs are a real feature that cannot be explained by loss of U in the outcrop by recent weathering. Sample 28-VIII differs in that it apparently has recently acquired a high μ value, possibly because of a gain in U, for Pb loss is ruled out by the Th–Pb data.

The Rb–Sr data (Fig. 3*c*) are analogous to the U–Pb data because the calculated $^{87}Sr/^{86}Sr$ ratios at the time of granulite metamorphism lie well above the mantle curve. This requires the rocks to have had high values of $^{87}Rb/^{86}Sr$ over an extended time interval before 2,550 Myr ago. $^{87}Rb/^{86}Sr$ apparently decreased during the granulite facies event by factors of 10–20 in most of the rocks. The marked loss of U and Rb observed in the Napier complex is characteristic of granulite grade terranes but is more extreme than examples from younger terranes. The resultant changes in μ and $^{87}Rb/^{86}Sr$ cause the model ages, as determined by the point of intersection of the sample evolution line with the mantle evolution line (Fig. 2), to be either unreasonably young (U–Pb) or undefined (Rb–Sr and some U–Pb data). In contrast, the Sm/Nd model ages are not shifted by more than ~10%.

The U–Pb isotopic data are displayed in Fig. 2. Our analyses confirm the high ^{207}Pb contents reported by Sobotovich *et al.*[6] but do not reproduce the linear array which was the basis of their 4,000 Myr age. The Th and Pb concentrations reported here are similar to those reported by Sobotovich *et al.*[6], but our U concentrations are lower by nearly an order of magnitude (except for sample 28-VII). The data (Fig. 3*c*) would be reasonably consistent with a model of crust formation at ~3,600 Myr ago and metamorphism at 2,500 Myr (3,600–2,500 Myr isochron), but this evidence is not sufficient to fix the crust-formation age.

Discussion

There is little evidence from other areas for metamorphic disturbance of Sm–Nd ages[8,17,19]. Our Sm–Nd data could be interpreted, therefore, to indicate that the protoliths of the Fyfe Hills granulites represent crust formed in multiple events over a large interval of time (3,090–3,870 Myr). However, geochronological data from other areas indicate that crust formation in a given continent or province within a continent is distinctly episodic, typically lasting ~100 Myr (see refs 7, 8 and 22). Thus, we wish to consider the evidence that some of the scatter of T_{DM} ages observed at Fyfe Hills is a result of Sm–Nd redistribution during the granulite-facies metamorphism.

The metamorphic effects can be modelled for a rock sequence having a uniform crust-formation age, τ, for Sm–Nd and subsequently subjected to redistribution of Sm and Nd isotopes at some age $\tau_m < \tau$. We will assume that in the affected volume of rock, V, which has an overall value of the Sm/Nd enrichment

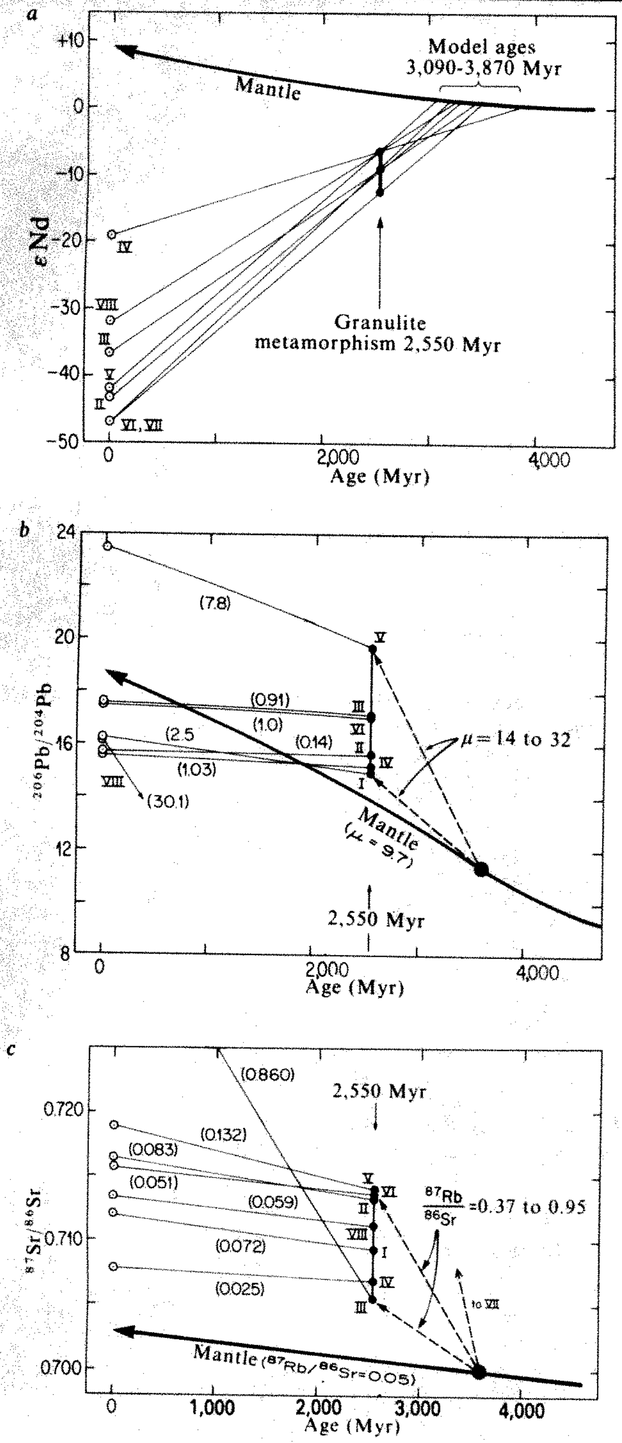

Fig. 3 *a*, Nd isotopic evolution of Fyfe Hills samples, showing model ages. *b*, Evolution of ^{206}Pb/^{204}Pb in Fyfe Hills samples. For illustration, the crustal evolution is shown to commence at 3,600 Myr ago (large ●). The μ ($= ^{238}$U/^{204}Pb) values required during the time interval 3,600–2,550 Myr ago are much higher than the measured μ values, shown in parentheses. Sample VIII shows evidence for recent gain of U. *c*, Evolution of ^{87}Sr/^{86}Sr in Fyfe Hills samples. The range of ^{87}Rb/^{86}Sr ratios required during the interval 3,600–2,550 Myr are given at the right; the measured values are shown in parentheses. Large ●, crust-formation age (see *b*).

factor equal to $f^{V}_{\rm Sm/Nd}$, Nd isotopic redistribution is complete, so that $\varepsilon_{\rm Nd}$ is uniform in V at time τ_m. If the volume of a particular analysed rock specimen is $\nu < V$, then $f^{\nu}_{\rm Sm/Nd}$ may differ from $f^{V}_{\rm Sm/Nd}$ by a factor, β, depending on the mineralogy in the volume, ν. The model age, $T^{\nu}_{\rm DM}$, is related to τ, the crust-formation age, by:

$$\tau \approx \tau_m + (T^{\nu}_{\rm DM} - \tau_m)\beta \qquad (1)$$

If an arbitrary τ value of 3,500 Myr and $\tau_m = 2{,}550$ Myr are used for the Fyfe Hills samples, β is calculated to be 0.72–1.46 for six of the samples, and 1.76 for sample V, the ironstone. With the exception of sample V, the calculated β values are not unreasonable, considering the relatively small sample size (10^{-4} m^3) and the variable mineralogy (Table 1). The β values depend on the assumed age, τ, but are plausible for any τ in the range 3,200–3,800 Myr.

The Fyfe Hills rocks show clear evidence for bulk removal of U and Rb, and thus the volume, V, for redistribution may have been large (km^3). Large-scale transport probably requires either magma or a volatile-rich fluid which can move through the rocks and selectively leach out certain elements. In this situation, which is analogous to ion-exchange chromatography[23], the average transport distance for any element will vary roughly as D^{-1} where D is the solid–fluid distribution coefficient. For a given volume of rock undergoing this metamorphic leaching, the amount of change in the elemental ratios Rb/Sr, U/Pb and Sm/Nd will depend on the absolute value of D for each element and the integrated fluid/rock ratio. For any volume of rock, ν, a bulk rock value of D^{α}_{ν} for element α could theoretically be calculated from the mineralogy:

$$D^{\alpha}_{\nu} = \sum_{p} D^{\alpha}_{p}\omega^{\nu}_{p} \qquad (2)$$

where: ω^{ν}_{p} is the weight fraction of mineral p in volume ν, and where D^{α}_{p} is the mineral–fluid distribution coefficient for element α in mineral p. Assuming local equilibrium, if $D^{\alpha} \ll 1$, even a small amount of fluid would quickly shift the concentration of α, C^{α}_{ν}, to a value of:

$$C^{\alpha}_{\nu} = D^{\alpha}_{\nu} C^{\alpha}_{\rm fluid} \qquad (3)$$

whereas if $D^{\alpha} \gg 1$, C^{α} could be essentially unaffected by the fluid interaction.

For our hand-sized samples from a single large outcrop in the Fyfe Hills, a gauge of mobility for an element would be the extent to which $C^{\alpha} \propto D^{\alpha}$ for all the samples. In practice, this test is difficult because D^{α}_{p} values are poorly constrained, and depend on fluid composition. Nevertheless, an estimate is possible because of the relatively simple mineralogy of the Fyfe Hills samples (Table 1). D^{α}_{p} values are available for mineral/magma partitioning for Rb, Sr, Sm and Nd (refs 24, 25). The absolute values are likely to be very different for an intergranular fluid in rock undergoing granulite-facies metamorphism, but the relative values for different minerals would be similar, except for possible temperature effects ($\log D^{\alpha}_{1}/D^{\alpha}_{2}$ would be approximately proportional to inverse absolute temperature).

Computed values for $D^{\rm Rb}$, $D^{\rm Sr}$ and $D^{\rm Nd}$ based on the modes are given in Table 1. For $D^{\rm Nd}$, modal apatite was calculated from the measured P$_2$O$_5$ (Table 2). For Rb, where the isotopic data clearly indicate mobility, there is a significant correlation between $D^{\rm Rb}$ and $C^{\rm Rb}$ (Table 2); $C^{\rm Rb}$ versus modal K-feldspar + biotite also yields a good correlation. A correlation is also found between $D^{\rm Nd}$ (or P$_2$O$_5$) and $C^{\rm Nd}$. No correlation is evident between $D^{\rm Sr}$ and $C^{\rm Sr}$ for the samples with large values of $D^{\rm Sr}$, but the sample with low $D^{\rm Sr}$ (28-V) has low $C^{\rm Sr}$, as would be predicted. These observations suggest that Nd and Sm, in addition to Rb, were mobile during the metamorphism because they were partitioned into the fluid. On the other hand, Sr was much less mobile because most of the rocks have large $D^{\rm Sr}$ values reflecting abundant plagioclase.

This analysis indicates that disturbance of the Sm–Nd system may have been sufficient to explain the range of observed $T_{\rm DM}$ ages. The Sm–Nd ages are less disturbed than those of Rb–Sr (and U–Pb) presumably because $D^{\rm Nd}$ and $D^{\rm Sm}$ are similar. In

Table 3 U–Pb Concentrations and Isotope ratios of two zircon fractions from sample 28-VIII

Fraction	U (p.p.m.)	Pb (p.p.m.)	$^{206}Pb/^{204}Pb$	$^{206}Pb/^{207}Pb$	$^{206}Pb/^{208}Pb$	$^{206}Pb^*/^{238}U$	$^{207}Pb^*/^{235}U$
>100 mesh	630.8	326.6	1.11×10^4	5.979	6.519	0.4556	10.51
100–200 mesh	590.5	316.5	3.44×10^4	6.096	5.838	0.4662	10.55

general, the least disturbed samples should be those with large values of D for both the parent and daughter element. One of our samples (28-VII) has the requisite large values of D^{Rb}, D^{Nd} and C^{Rb}, C^{Sm} and C^{Nd}. This sample is also the only one with roughly concordant model ages for Sm–Nd (3,490 Myr) and Rb–Sr (3,740 Myr).

The T_{DM} age and the low $^{147}Sm/^{144}Nd$ ratio of sample VII provide independent evidence for some crust ~3,500 Myr old in the Fyfe Hills. An age of crust formation younger than the T_{DM} for this sample requires that $^{147}Sm/^{144}Nd$ increased during the granulite-facies metamorphism. Such an increase is unlikely given the low $^{147}Sm/^{144}Nd$ in this sample. For example, if the crust-formation age were assumed to be 100 Myr younger than T_{DM}, the protolith would have to have had $f_{Sm/Nd} = -0.63$ [equation (1)]. Rocks with such low values of $f_{Sm/Nd}$ are extremely rare; the lowest value reported is −0.61 (ref. 26) and the mean for crustal rocks is about −0.35 (ref. 11).

Conclusions

The evidence for Nd mobility during granulite-facies metamorphism demonstrates that Sm–Nd model ages cannot be taken at face value in high-grade terranes. However, because of the relatively small net shifts in the model ages, Sm–Nd still provides a much better means of determining crust-formation ages than does either Rb–Sr or U–Pb. We have too few data from the Fyfe Hills to fix precisely the crust-formation age or determine the number of crust-forming events. Based on our analysis, the best indication of the crust-formation age is probably provided by T_{DM} of 3,500 Myr for sample VII. It is not clear whether this age, if correct, would apply to all of the rocks sampled. Reported isotopic evidence for an additional event at ~3,000 Myr ago[18,32] allows the possibility that crust formation occurred at that time also.

We conclude that the geological history of the Fyfe Hills commenced with the differentiation of magmatic rocks from the mantle at a time tentatively estimated to be ~3,500 Myr ago. The igneous crust must have become chemically layered at or about the time of formation with enrichment of Rb, U and K, and high Rb/Sr and U/Pb in the upper crust. During granulite-facies metamorphism ~2,500 Myr ago, the rocks lost most of their Rb and U, profoundly disturbing the isotopic systematics of Sr and Pb.

Our data show that a granulite-facies metamorphism post-dated crust formation by ~1,000 Myr in these rocks. Comparable time separation between crust formation and granulite-facies metamorphism has been demonstrated previously for Proterozoic granulite events[7,27], but not for an Archaean (>2,500 Myr) event. In the Archaean granulite terranes for which sufficient geochronological data are available[22,28], crust formation and granulite-facies metamorphism appear to have been contemporaneous within the resolution of the dating techniques (~100 Myr). Hamilton *et al.*[28] have attributed this to rapid heating after crust formation caused by *in situ* radioactive decay of U, Th and ^{40}K. Such a heat source is a possible cause for granulite-facies metamorphism that does not require plate tectonics. However, the conclusion was based on an erroneous heat flow calculation. Hamilton *et al.*[28] modelled the crust as a semi-infinite solid, whereas it should be modelled as a finite-thickness slab. In either case, *in situ* radioactive decay is not a satisfactory heat source for a granulite-facies metamorphic event post-dating crust formation by 1,000 Myr.

In general, the continental crust cannot reach granulite-facies conditions at depths corresponding to pressures of 7–10 kbar unless there is heat supplied from deeper levels. One possible heat source is magma, which in orogenic zones rises from the mantle into the crust on a regional scale over an extended period of time[29]. Another mechanism for generating granulite-facies conditions is large-scale underthrusting in a Himalayan-type continental collision zone[30]. Either of these mechanisms can account for a long time delay before metamorphism, and both require plate tectonics. In orogenic zones associated with subduction (magmatic arcs), granulite-facies metamorphism would be closely associated with crust formation, and at Andean-type continental margins old rocks comprising the continent may also be metamorphosed at a time much later than the time they were differentiated from the mantle. The Napier complex may represent the site of a former continental margin magmatic arc, or a continental collision zone that was active ~2,500 Myr ago, and resulted in metamorphism of ~3,500-Myr-old continental crust. If it were a magmatic arc, we would expect to find evidence in the Napier complex for the production of new crust in the form of magma ~2,500 Myr ago. Rocks of possible plutonic origin in the Napier complex, such as intrusive charnockite (Fig. 1 and ref. 3) should be investigated. Further isotopic studies of the Napier complex and other Archaean granulite terranes presently exposed in crystalline shields could provide important evidence that a plate tectonic regime similar to the Wilson cycle was operative in Archaean time.

We thank G. E. Grikurov and Ye. N. Kamenev for the samples from Fyfe Hills, G. Stummer for the X-ray fluorescence analyses, and B. Nelson for comments. NSF grants DDP76-80957, DPP80-19527 and EAR78-12966 are gratefully acknowledged.

Received 23 October 1981; accepted 3 June 1982.

1. Ravich, M. G. & Kamenev, E. N. *Crystalline Basement of the Antarctic Platform* (Wiley, New York, 1975).
2. Kamenev, Ye. N. *Antark. Doklady Komissii* **18,** 11 (1979).
3. Sheraton, J. W., Offe, L. A., Tingey, R. J. & Ellis, D. J. *J. geol. Soc. Aust.* **27,** 1 (1980).
4. Grew, E. S. & Manton, W. I. *Science* **206,** 443 (1979).
5. Sobotovich, E. V., Kamenev, Ye. N., Komaristyy, A. A. & Rudnik, V. A. *Int. geol. Rev.* **18,** 371 (1976).
6. Sobotovich, E. V. *et al.* in *Opredeleniye Absolyutnogo Vozrasta Rudnykh Mestorozhdeniy I Molodykh Magmaticheskikh Porod*, 59–70 (XVIII sessiya, Nauka, Moscow, 1976).
7. Jacobsen, S. B. & Wasserburg, G. J. *Earth planet. Sci. Lett.* **41,** 245 (1978).
8. DePaolo, D. J. *Nature* **291,** 193 (1981).
9. Heier, K. S. & Adams, J. A. X. *Geochim. cosmochim. Acta* **29,** 53 (1965).
10. Moorbath, S., Welke, H. & Gale, N. H. *Earth planet. Sci. Lett.* **6,** 245 (1969).
11. Taylor, S. R. in *Island Arcs, Deep Sea Trenches and Back-Arc Basins* (American Geophysics Union, Washington DC, 1977).
12. DePaolo, D. J. *J. geophys. Res.* **86,** 10470–10488 (1981).
13. Manton, W. I. *J. Petrol.* **9,** 23–29 (1968).
14. Manton, W. I. *Earth planet. Sci. Lett.* **19,** 83–89 (1973).
15. Papanastassiou, D. A., DePaolo, D. J. & Wasserburg, G. J. *Proc. 8th Lunar planet. Sci. Conf.*, 1639–1672 (1977).
16. Wasserburg, G. J., Jacobsen, S. B., DePaolo, D. J., McCulloch, M. T. & Wen, T. *Geochim. cosmochim. Acta* **45,** 2311–2323 (1981).
17. Jacobsen, S. B. & Wasserburg, G. J. *Earth planet. Sci. Lett.* **50,** 139–155 (1980).
18. Black, L. P. & James, P. R. *J. geol. Soc. Aust.* **26,** 266 (1979).
19. McCulloch, M. T. & Wasserburg, G. J. *Science* **200,** 1003 (1978).
20. McCulloch, M. T. & Compston, W. *Nature* **294,** 322–327 (1981).
21. Stacey, J. S. & Kramers, J. D. *Earth planet. Sci. Lett.* **26,** 207 (1975).
22. Moorbath, S. *Scient. Am.* **236,** 92–104 (1977).
23. Helferrich, R. *Ion Exchange* (McGraw Hill, New York, 1962).
24. Arth, J. G. *J. Res. U.S. geol. Surv.* **4,** 41–47 (1976).
25. Hanson. G. N. *Earth planet. Sci. Lett.* **38,** 26–43 (1978).
26. McCulloch, M. T. & Wasserburg, G. J. *Geol. Soc. Am. Spec. Pap.* **182,** 135–138 (1980).
27. Montgomery, C. W. & Hurley, P. M. *Earth planet. Sci. Lett.* **38,** 281 (1978).
28. Hamilton, P. J., Evensen, N. M., O'Nions, R. K. & Tarney, J. *Nature* **277,** 25 (1979).
29. Newton, R. C., Smith, J. V. & Windley, B. F. *Nature* **288,** 45–50 (1980).
30. Newton, R. C. & Perkins, D. *EOS* **62,** 420 (1981).
31. Grew, E. S. *Am. Miner.* **66,** 1022 (1981).
32. James, P. R. & Black, L. P. *Spec. Publ. geol. Soc. Aust.* **7,** 71 (1981).

An inter-laboratory comparison of radiocarbon measurements in tree rings

International Study Group[*]

Results from a collaborative study designed by the Glasgow ^{14}C laboratory to assess experimental variability in radiocarbon dating are presented. A series of eight replicate samples from one tree were dated independently by 20 ^{14}C laboratories. While the results are in general agreement they reveal the existence of systematic bias and unexplained variability. Thus as a general guideline for users of ^{14}C dates, quoted errors, particularly those derived solely on the basis of the counting procedure, should be multiplied by a factor of between 2 and 3.

THE method of radiocarbon dating, since its practical inception ~30 yr ago, has seen considerable development in methods of ^{14}C assay and in archaeological and geological applications requiring ever-more precise measurement[1-3]. The corresponding increase in the number of laboratories performing such work has not, however, produced an equivalent emphasis on a necessary programme of inter-laboratory checks on analytical methods. Thus the normal procedure for assessing errors in laboratory procedures using replicate sample analysis has been long neglected in the radiocarbon dating field. This project represents the first collaborative attempt to rationalize and quantify by experiment the uncertainty involved in ^{14}C dating of a typical sample and thus its major aims have been to collect quantitative information on the variability of ^{14}C dates and to estimate the extent of inter-laboratory variability.

Organization and design of the study

Although there are at present over 100 laboratories[4] providing a ^{14}C dating service using various analytical techniques, the logistics of the study required initial selection, at a fairly arbitrary level, of an, at least approximately, representative subgroup of laboratories, covering most, if not all, of the common experimental procedures. To this end, 30 laboratories were invited to participate in the study, with ultimately, results from 20 laboratories being submitted. The participants are listed in Table 1. It was agreed, as a prerequisite of participation, that because the aims of the study were not directed towards assessing errors in individual laboratories but rather towards monitoring group performance, anonymity would be preserved and laboratories would be assigned code letters A–T. Included in the original group of 30 was a smaller subgroup of 'high precision' laboratories, three of which agreed to take part.

The design of the study envisaged that each laboratory would date eight samples, hereafter referred to as time points 1–8, selected from a wood section spanning ~200 yr growth. Each sample, of 10 rings width, would be identified on a tree ring width plot to ensure that the same samples would be assayed by each laboratory. The sections of oak were themselves taken from one tree trunk from a submerged forest exposure at Stolford, UK (51°12′ N, 3°06′ W). The wood was well preserved, available in considerable quantity and sensitive ring patterns enabled accurate cross-matching of subsections. Each European laboratory received a complete section, while for reasons of postal economy non-European laboratories received the samples already extracted from their sections.

To reduce possible sources of variability in the results, each laboratory was asked to extract and date the cellulose fraction of the samples, and to this end, a standard recipe[5] involving KOH digestion followed by $NaClO_2/HCl$ bleaching, was circulated. A few laboratories chose not to extract cellulose preferring to adopt alternative procedures. However, subsequent additional work by both the La Jolla and Uppsala laboratories indicated that the method of pretreatment was, in this case, not important. Apart from pretreatment, each laboratory was asked to treat the replicate samples routinely and, in addition, to spread the measurements over as long a time period as possible to model more precisely the normal mode of operation.

The information requested from each laboratory included $\delta^{13}C$, which is the per mil deviation of the $^{13}C/^{12}C$ ratio from the PDB (belemnite) standard ratio, d ^{14}C, the per mil depletion or enrichment in ^{14}C with regard to the NBS oxalic acid standard, D ^{14}C which is d ^{14}C normalized for isotopic fractionation, conventional radiocarbon age (using the 5,568 yr Libby half life) and its error (based solely on the counting statistics), the overall error on the result, if different, and details of the counting method. One area in which it was considered necessary to provide clear instructions to participants concerned the age and error calculations themselves. The method of age calculation was constrained to the convention recommended by Stuiver and Polach[6]. However, no similar series of instructions exists for error calculations, some laboratories commonly quoting errors based solely on theoretical estimates of the uncertainty resulting from the radioactivity measurement process alone and others including additional error terms. Thus to ensure that results would be directly comparable a method of calculating a common error term was described, the final error being arrived at through propagation of the counting uncertainties on the sample, standard and background activities alone.

Table 1 Members of the study group

	Name	Laboratory
1.	**V. Alexeev, A. Lavrukhina, I. Smirnov, Z. Milnikova, L. Sulerzhitsky**	Academy of Sciences, Moscow, USSR
2.	**M. Baxter**[†], **M. Scott, T. C. Aitchison**	University of Glasgow, UK
3.	**R. Burleigh, J. Ambers, K. Matthews**	British Museum, London, UK
4.	**J. Evin, J. Marechal, G. Marien**	University of Claude Bernard, Lyon, France
5.	**A. Fairhall**	University of Washington, Seattle, USA
6.	**M. Geyh**	Niedersach. Land., Hanover, FRG
7.	**D. Harkness**	Scottish Universities Research & Reactor Centre, UK
8.	**T. Kankainen**	Geological Survey of Finland
9.	**W. Mook**	State University, Groningen, Netherlands
10.	**R. Nydal, S. Gulliksen**	Norwegian Institute of Technology, Norway
11.	**M. Stenhouse**	University of Glasgow UK
12.	**H. Oeschger**	University of Bern, Switzerland
13.	**I. Olsson, M. Söderman, T. Kronberg**	University of Uppsala, Sweden
14.	**G. Pearson**	Queen's University, Northern Ireland, UK
15.	**H. Polach**	Australian National University, Australia
16.	**A. Rafter, H. Jansen**	Institute of Nuclear Science, New Zealand
17.	**M. Stuiver**	University of Washington, Seattle, USA
18.	**H. Suess, T. Linnick**	University of California, USA
19.	**R. Switsur**	University of Cambridge, UK
20.	**R. Williams**	University of Birmingham, UK
Dendrochronology and sample distribution		
	A. Heyworth	University College of Wales, Aberystwyth, UK

[†] To whom correspondence should be addressed at the Department of Chemistry.

---

[*] See Table 1.

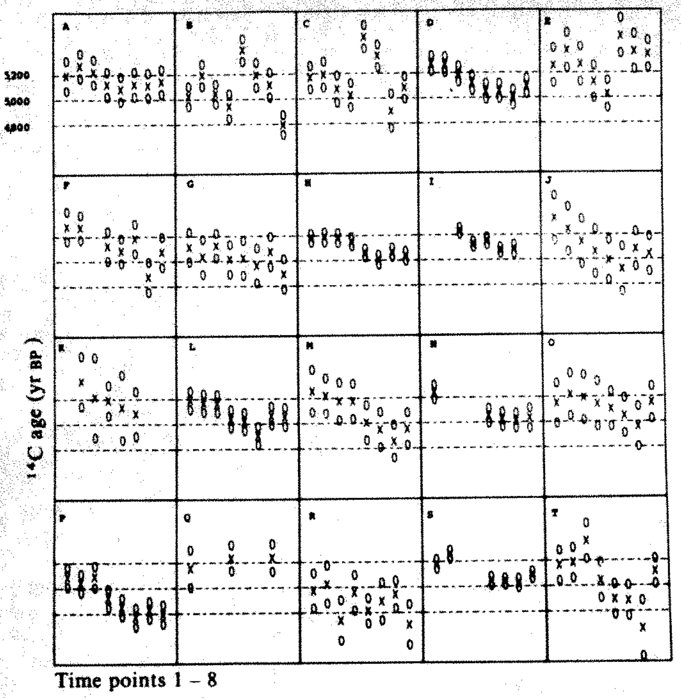

Fig. 1 Radiocarbon age (yr BP), along with 2σ error estimates versus time point for each laboratory. – – –, Reference lines at 5,200, 5,000 and 4,800 yr BP.

Before discussing the results it is important to mention their limitations, these being due primarily to the small sample numbers per laboratory—eight—and to the short study period—6–9 months. Conclusions concerning individual laboratory performance can therefore only be tentative and the more general conclusions can be drawn only for this one type of material and for this specific age. In addition, only short-term variability could contribute to the observed errors. Further results, however, reported by Stenhouse and Baxter[7] point to the relevance of the study results to routine archaeological dating over a wider range of sample types, artefact ages and laboratory time.

Results and preliminary comments

Of the results received from 20 laboratories six sets were for various reasons incomplete and thus a total of 143 measurements was obtained for this single tree. The results for each laboratory are shown in Fig. 1, the ^{14}C data across the eight time points being graphed for each laboratory, along with ± twice the quoted errors on each date. Horizontal reference lines at 5,200, 5,000 and 4,800 yr BP are shown to aid comparison. Figure 1 shows that the laboratory results all overlap in the age-range 5,000–5,200 yr BP and are thus in broad agreement. However, inspection of the results indicates the existence of considerable variability; for individual time points, results differ by between 316 and 724 yr, while, for individual laboratories, age differences of between 190 and 690 yr are observed.

The first stage of data analysis involved a preliminary estimation of the time trend through the results by calculating their weighted average at each time point, the weights in the averaging process being inversely proportional to the quoted error. The results are presented below, the trend showing the effect of ^{14}C decay during wood growth and implying the existence of a small fluctuation in mid-section.

Time point	1	2	3	4
Mean	5,168.5	5,196.1	5,173.1	5,094.4
s.e.m.	8.9	9.5	8.9	7.9
Time point	5	6	7	8
Mean	5,070.0	5,031.4	5,025.2	5,030.7
s.e.m.	7.6	7.0	8.1	8.5

Of primary interest, however, was an assessment of the variability observed about this trend relative to the claimed variability as measured by quoted errors. This analysis was performed by estimating the 'standardized residuals'—the differences between the observed and estimated time trend divided by the quoted errors. By normalizing results in this way it is reasonable to postulate that if the quoted error does measure the true error then most, if not all, of such residuals should be within the range −2 and +2. Figure 2 shows the series of standardized residual plots, with horizontal reference lines at −2, 0 and 2. Such plots visually confirm the impressions of the existence of bias for some laboratories and of the more variable nature of others.

The relative wealth of data available, however, offers the opportunity to provide (1) a more rigorous assessment of bias and additional variability for individual laboratories (of particular interest to the ^{14}C analyst), and more importantly (2) an estimate of the variability in a typical ^{14}C date for the benefit of an archaeologist or other user.

Evaluation of results

Throughout the interpretation of the results we have chosen to model the true variability using a multiplicative factor θ, such that $\theta \times$ quoted error gives a more realistic measure of reproducibility. There are two main reasons for the choice of a multiplicative factor rather than an additive term: (1) that a multiplicative factor gives a more immediate and simple understanding of the relative magnitude of the true error involved; and (2) the estimation of such a factor θ is mathematically slightly more straightforward, particularly for interval estimates. (The intervals are a range of plausible values for θ, a property of the method being that 95% of the time they will contain the true θ value.)

Nevertheless we concede that in reality any extra variability is almost certainly additive in nature. Use of a θ factor, however, effectively produces the same results as an additive term since each laboratory has more or less constant quoted error over these samples.

The significance of θ is such that $\theta = 1$ implies that the quoted error adequately represents the true error, while $\theta < 1$ and $\theta > 1$ imply over- and under-estimation respectively by the quoted error. Point and interval estimates for θ are produced throughout by use of likelihood methods[8].

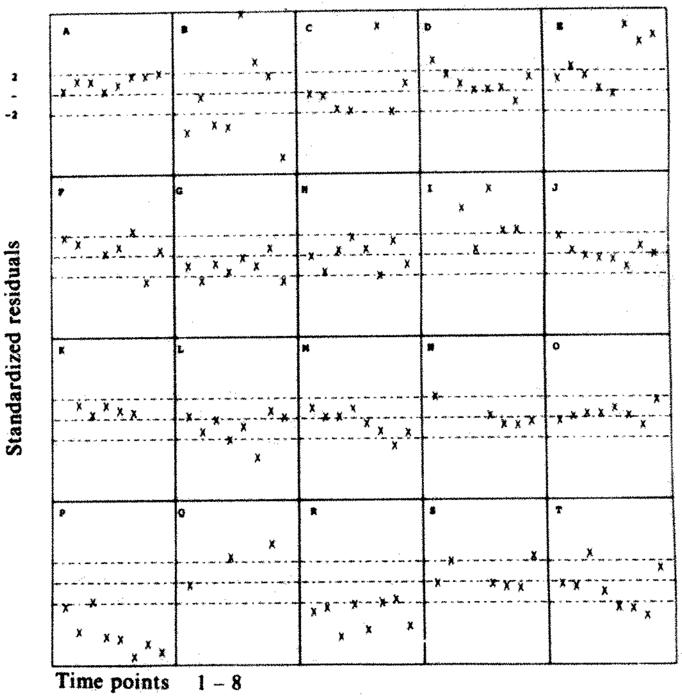

Fig. 2 Standardized residuals plotted against time point for each laboratory. – – –, Reference lines at −2, 0 and 2.

Table 2 Point and interval estimates for bias relative to baselines (1), (2) and (3)

	Baseline (1)		(2)		(3)	
Lab.	Bias	Interval estimate	Bias	Interval estimate	Bias	Interval estimate
A	53.02	(15.90)	56.28	(35.5, 85)	52.5	(13,87)
B	−37.46	(−185,110)	−43.34	(−192,107)	−40.24	(−185,93)
C	77.38	(−90,236)	70.75	(−90,230)	74.46	(78,214)
D	24.17	(−20,65)	19.78	(−15,55)	22.63	(−12,56)
E	168.51	(36,300)	163.16	(40,302)	166.86	(36,290)
F	37.67	(−57,120)	32.85	(−60,120)	31.27	(−53,110)
G	−76.85	(−120,35)	−78.89	(−125,−35)	−77.97	(−125,−41.5)
H	–		−4.08	(−21,15)	–	
I	33.62	(−10,85)	39.68	(22.5,57)	42.83	(−2,87)
J	−3.35	(−65,50)	−6.85	(−70,50)	–	
K	72.36	(25,115)	73.71	(40,110)	72.65	(28,113)
L	−33.70	(−70,0)	−38.65	(−80,0)	−35.19	(−72,0)
M	−43.85	(−112,20)	−48.44	(−115,20)	−45.09	(−106,14)
N	6.17	(−50,60)	−4.91	(−45,30)	–	
O	21.51	(−25,70)	14.82	(−30,55)	–	
P	−189.63	(−240,−145)	−194.11	(−245,−150)	−191.2	(−237,−150)
Q	94.37	(−25,205)	123.19	(−10,250)	98.86	(−37,225)
R	−216.35	(−295,−145)	−219.57	(−300,−45)	−215.97	(−295,−144)
S	25.12	(−20,65)	7.40	(−25,35)	17.56	(−12,50)
T	−37.09	(−135,63)	−46.26	(−150,55)	−41.14	(−137,54)

The analysis falls into two main sections, relevant to individual laboratory and group performances. First, individual laboratories were assessed for possible bias and θ factors.

Two obvious choices of baseline and one other justifiable choice were: (1) results from high precision laboratories; (2) the weighted average of all the results, that is as before; and (3) the new weighted average of results from laboratories with identifying letters H, J, N and O giving the following results at each time point:

Weighted average	5,186	5,176	5,165	5,134
Standard error	15	19	19	18

Weighted average	5,044	4,997	5,035	5,029
Standard error	15	16	15	17

(In all cases the error on the estimates of true age were assumed to be adequately measured by the quoted errors, that is either counting errors for baseline (1) or standard errors for baselines (2) and (3).) With respect to baseline (1) only one high precision laboratory's results were used, that is H, since it had provided a complete set of eight results, while laboratory S was not quite in statistical agreement with H and I appeared systematically biased with respect to H and S). For baseline (2) no results were rejected from the study, the main reason for this being the assumption that the laboratories in the study form a representative cross-section of ^{14}C laboratories as a whole. However, laboratories showing a great deal of variability and/or bias may influence age results excessively and the baseline for the data may then best be defined by considering only laboratories whose quoted errors measure their true error and which are unbiased relative to each other. Any criterion used for rejection of results is necessarily subjective (partly due to lack of absolute knowledge about the chronology and the inadequacy of additional information concerning each laboratory's replicate error). Our approach has been to consider the two groups of laboratories which were consistent with the baselines described in (1) and (2) (the definition of consistent being that there is inconclusive evidence that bias and θ factor are different from 0 and 1 respectively). The laboratories contained in both groups were used to provide a basis for calculation of the new weighted average for baseline (3).

Results for each laboratory relative to these baselines are shown in Tables 2 and 3, the major conclusions being that:

(1) Many laboratories show bias estimates ranging up to 200 yr. Only six, however, have statistically significant biases at the 5% level while three have point estimates of <20 yr. It is, of course, conceivable that, for any laboratory, bias itself may be variable with time when factors such as different standardizations and laboratory procedures are employed. The results imply that for most laboratories greater intercalibration efforts are necessary. (2) Individual θ factor estimates range from 0.35 to 4.3, with a median value of 1.4, and thus, in general, quoted errors do not adequately express true variability. This seems to be the case even if detailed intercalibration could remove bias factors for a given laboratory. Increased emphasis on assessment of θ factors by routine replicate assays seems necessary for each laboratory.

(3) Variability in laboratories quoting errors ⩾80 yr (that is, laboratories J, K and O) is considerably less than expected. High precision laboratories (H, I and S) are not in agreement, either through existence of a bias or through their true errors being in excess of their quoted errors. (Relative to baselines (1) and (3), $\hat{\theta}$ factors for I and S are 2.6 (I), 2.0 (S) and 2.57, 1.70 respectively; relative to baseline (2), $\hat{\theta}$ factors for H, I and S are 1.27, 1.08 and 1.72.)

Reasons for the differing levels of performance were investigated by considering results for each laboratory relative to baseline (1) (since results relative to other baselines do not differ significantly). The factors evaluated included type of pretreatment and method of counting. As mentioned previously, differences due to pretreatment were small. However, the method of counting did appear to be relevant, most gas laboratories having a positive bias, the liquid scintillation laboratories having a tendency to be negatively biased and most interestingly gas laboratories having smaller $\hat{\theta}$ factors than liquid scintillation laboratories.

Summary statistics on the $\delta^{13}C$ measurements from each laboratory were also prepared. The average laboratory measurements ranged between −23‰ and −26‰, with most clustered around −24‰. Correlations between $\delta\ ^{13}C$ and quoted ^{14}C ages were also calculated, several being significantly different from zero. Due to the small nature of these deviations and the both natural- and laboratory-induced sources of fractionation, no further analysis of these measurements was performed.

Analysis of the group results is, however, of greater significance to a user of ^{14}C dates because he is often required to interpret results from several laboratories and must do so with a realistic awareness of analytical errors. The subsequent analysis was therefore aimed at assessing the variability of results in small subgroups formed on the basis of level of median quoted error (m.q.e.) or method of counting. The subgroups considered were (1) m.q.e. ⩽20; (2) 20<m.q.e. ⩽45; (3) 45< m.q.e. ⩽75; (4) m.q.e. ⩾80; (5) gas counting laboratories; and (6) liquid scintillation laboratories (the latter two groups excluding high precision results).

The first analysis of the group results involved treating each subgroup separately, producing an estimate of bias for each individual laboratory and culminating in a common θ factor estimate for all members of the group. The results are shown

Table 3 Point and interval estimates for multiplicative factor θ relative to baselines (1), (2) and (3)

		Baseline (1)			(2)			(3)	
Lab.	$\hat{\theta}$	Interval estimate	$\hat{\theta}\times$m.q.e.	$\hat{\theta}$	Interval estimate	$\hat{\theta}\times$m.q.e.	$\hat{\theta}$	Interval estimate	$\hat{\theta}\times$m.q.e.
A	0.84	(0.48,1.6)	48	0.57	(0.36,1.1)	29	0.83	(0.5,1.5)	42
B	4.23	(2,8,7.7)	190.3	4.02	(2.9,7.8)	180.9	4.32	(2.6,7.2)	194.4
C	4.10	(2.6,7.4)	233.7	3.75	(2.6,7.3)	213.75	4.09	(2.3,6.8)	233.1
D	1.56	(0.9,2.96)	48	1.30	(0.83,2.35)	40	1.30	(0.8,2.45)	40
E	2.64	(1.7,4.7)	184.8	2.55	(1.7,4.7)	178.5	2.63	(1.5,4.6)	184.1
F	1.70	(1.13,3.66)	102	1.61	(1.0,3.2)	97	1.67	(1.05,3.2)	100
G	0.81	(0.46,1.53)	48	0.94	(0.6,1.7)	56	0.91	(0.5,1.7)	54
H	–			1.27	(0.8,2.4)	25	–	–	
I	2.61	(1.14,6.57)	37	1.08	(0.6,2.6)	15	2.57	(1.1,6.2)	36
J	0.84	(0.53,1.54)	76	0.92	(0.6,1.6)	83	–		
K	0.40	(0.18,0.99)	40	0.34	(0.2,0.8)	34	0.37	(0.14,0.94)	37
L	1.12	(0.62,2.16)	41	1.36	(0.9,2.5)	50	1.12	(0.7,2.1)	41
M	1.15	(0.72,2.11)	80	1.17	(0.8,2.1)	82	1.07	(0.7,1.97)	75
N	1.23	(0.53,3.3)	37	1.08	(0.6,2.4)	32	–	–	
O	0.77	(0.45,1.43)	62	0.68	(0.5,1.2)	54	–	–	
P	1.50	(1.21,2.81)	57	1.59	(1.05,2.8)	60	1.40	(0.84,2.6)	53
Q	1.22	(0.63,3.81)	67	1.40	(0.7,4.3)	77	1.45	(0.74,4.7)	80
R	1.37	(0.85,2.51)	96	1.51	(1.0,2.7)	105	1.43	(0.9,2.6)	100
S	2.08	(0.88,4.88)	37	1.72	(1.0,3.5)	31	1.70	(0.9,3.8)	31
T	2.03	(1.31,3.66)	122	2.03	(1.3,4.0)	122	1.97	(1.3,3.7)	118

in Table 4*a*. Time trends through the eight samples for each group were also estimated and found, in some cases, to differ significantly. The explanation of such differences, however, is related to the presence, in some groups, of laboratories with large biases which thus affect the overall group trend.

More importantly the major implications of the Table 4*a* results are as follows:

(1) For the study group as a whole, the best estimate of θ is 1.85 (1.65–2.1) so that, if the laboratories in the study are representative of all ^{14}C laboratories the true error on a typical ^{14}C date may be approximately double the quoted error for a sample of ~5,000 yr age.

(2) Excluding the high precision laboratories, the value of θ decreases as quoted error (m.q.e.) increases. The value for laboratories of high m.q.e. ($\geq$80) is surprisingly low, the interval estimate being completely <1 and the true error in years being actually less than that for laboratories quoting m.q.e.s of 30–75 yr. It seems likely therefore that, for these high m.q.e. laboratories, quoted errors are being calculated on a highly conservative basis and indeed do represent overestimates. In fact, much of the importance of this inter-calibration exercise centres on the significance of quoted errors and on the lack of a universal method of error calculation. It is therefore to be desired that, some time in the future, ^{14}C laboratories should adopt a universal method of error estimation.

(3) For high precision (low m.q.e.) laboratories, while we cannot reject the possibility that the quoted error does quantify the observed variability, it is likely that, with a $\hat{\theta}$ of 1.30 and an interval estimate of 0.98–1.88, it does underestimate the true error slightly. Nevertheless, from the value for $\hat{\theta}\times$m.q.e. of 23.4 it is evident that the procedures inherent in high precision analysis are highly significant in reducing errors; the value of 23.4 is considerably lower than the corresponding value for other groups.

(4) The estimate of θ for gas proportional laboratories is approximately half that for liquid scintillation laboratories, the implications being that, in general, the latter are more variable and that perhaps in the future some attention might be paid to identifying the apparently uncorrected sources of variability in liquid scintillation methodology.

From (3) above, it seems likely that many of the answers may be found in the high precision procedures already adopted in the Belfast liquid scintillation laboratory.

For a user, however, information concerning relative laboratory bias is generally unknown and thus a more realistic analysis would discount possible laboratory bias and would attempt to assess the scatter of results purely in terms of θ. This is also particularly relevant since bias for any particular laboratory may well be variable through time. Using the same grouping as in the previous analysis the estimated θ values are presented in Table 4*b*. The values for θ have all increased as would be expected, the difference in θ estimates reflecting the effective reduction in unexplained variability when information about bias is available. The conclusions can be summarized as follows:

(1) Quoted errors are inadequate for the study group as a whole, with an interval estimate for θ of 2.3–3.0, and for all subgroups other than the high m.q.e. group. The latter in fact seems to be more accurate than all but the high precision laboratories. It is clear from the range of values for θ that its value is highly dependent on the size of the quoted error and thus it is difficult to give a single 'best' value for it; use of the factor θ for the entire group supposes no information about the dating laboratory.

(2) For the high precision laboratories, a θ multiple of 1.8 is suggested and, because the interval estimate excludes 1, the quoted error represents an inadequate measure of true error.

(3) The value of θ for gas laboratories is approximately half the value for liquid scintillation laboratories so that values of 1.7 and 3.5 respectively might be recommended for users of each (for normal precision laboratories only, that is m.q.e. > 20).

Conclusions

The results from the study group provide clear indications for some laboratories at least of the existence of systematic labora-

Table 4 Group estimates of θ

	a After bias removal				*b* No bias removal		
Groups	No. of labs in group	$\hat{\theta}$	Interval estimate for $\hat{\theta}$	$\hat{\theta}\times$m.q.e.	θ	Interval estimate	$\theta\times$m.q.e.
1 m.q.e. $\leq$ 20	3	1.30	0.98–1.88	23.4	1.73	1.35–2.2	31.1
2. 20 $\leq$ m.q.e. $\leq$ 45	5	2.14	1.87–2.63	81.3	3.01	2.42–3.87	114
3. 45 < m.q.e. $\leq$ 75	9	1.90	1.62–2.30	114	2.57	2.21–3.1	154
4. m.q.e. $\geq$ 80	3	0.60	0.46–0.85	54	0.71	0.54–1.01	64
5. All gas laboratories (non-high precision)	9	1.23	1.04–1.48	74	1.65	1.4–2.0	99
6. All liquid scintillation (non-high precision)	8	2.29	1.93–2.78	126	2.97	2.5–3.62	169.3
7. Entire study group	20	1.85	1.65–2.1	92	2.60	2.33–2.95	143

tory bias (both gas and liquid scintillation laboratories being equally susceptible) and of a level of variability not entirely explained by the quoted errors. One possible indicator of level of true error compared to quoted error is provided by the factor θ. The appropriate value for θ is found to be dependent on the information available; first, concerning the dating laboratory itself (knowledge of bias, counting method, size and derivation of quoted error) and, second, concerning the sample context. For the study group as a whole, the interval estimates for θ are (1) 1.65–2.1 with a point estimate of 1.85 and (2) 2.30–3.0 with a point estimator of 2.6 for situations in which (1) laboratory bias is known and has been removed and (2) no bias has been removed. In both these situations differences in performance (as measured by θ) have been observed between normal precision gas and liquid scintillation laboratories: in situation (1) above, for gas and liquid scintillation laboratories, point and interval estimates for θ are 1.23 (1.04–1.48) and 2.3 (1.93–2.78) respectively and in (2) 1.65 (1.4–2.0) and 3.0 (2.5–3.6) respectively. Thus for gas and liquid scintillation laboratories we would propose quoted error multiples of 1.2 and 2.3 for situation (1) and 1.65 and 3.0 for situation (2), the latter condition being presumably more commonly relevant.

With respect to the three high precision laboratories, there seems to be some indication that their results are more variable than claimed, but, nevertheless, their procedures do produce significant improvements in levels of precision.

Note that this study is only a first step towards rationalization of $^{14}\mathrm{C}$ dating variability. No conclusions should be overstated as each laboratory performed at most eight analyses on only one wood sample and because a great many variables remain unknown. There is, however, considerable need for further research of an intercalibrative nature involving different sample types and ages. There is apparent need also for investigation of internal replicate errors and of additional error sources (in liquid scintillation methods particularly) and for adoption of a universally acceptable method of error calculation. One should also bear in mind that in many ways the sample and laboratory procedures in this short study were close to ideal, with well preserved and sufficient sample assayed over a short period of laboratory time. Most laboratories extracted cellulose before assay, thereby presumably removing any minor cross-contamination effects. It might seem therefore that the error estimates discussed here represent minimum values which would possibly require enlargement for: degraded/small/contaminated materials; different sample types; and replicate samples counted over a longer time period. The results urge increased caution in attempting to resolve $^{14}\mathrm{C}$ differences of <200 yr.

We thank Dr A. Heyworth for supplying the samples of dendrochronologically dated wood. E. M. Scott acknowledges financial support of the NERC.

Received 30 November 1981; accepted 8 April 1982.

1. Pearson, G. W., Pilcher, J. R., Baillie, M. G. L. & Hillam, J. *Nature* **270**, 25–28 (1977).
2. Stuiver, M. *Nature* **273**, 271–274 (1978).
3. De Jong, A. F. & Mook, W. G. *Radiocarbon* **22**, 267–272 (1980).
4. Radiocarbon Laboratory List, *Radiocarbon* **22**, 1130–1140 (1980).
5. Campbell, J. A. & Baxter, M. S. *Nature* **278**, 409–413 (1979).
6. Stuiver, M. & Polach, H. A. *Radiocarbon* **19**, 355–363 (1977).
7. Stenhouse, M. J. & Baxter, M. S. *Proc.* ^{14}*C and Archaeology*, Groningen (1981).
8. Kalbfleisch, J. G. *Probability and Statistical Inference* Vol. II (Springer, New York, 1979).

De novo methylation and expression of retroviral genomes during mouse embryogenesis

Detlev Jähner, Heidi Stuhlmann, Colin L. Stewart, Klaus Harbers, Jürgen Löhler, Iva Simon & Rudolf Jaenisch

Heinrich-Pette-Institut für Experimentelle Virologie und Immunologie an der Universität Hamburg, Martinistrasse 52, 2000 Hamburg 20, FRG

Retrovirus genomes introduced into mouse zygotes by microinjection of cloned DNA, or into morula stage pre-implantation mouse embryos by infection with Moloney murine leukaemia virus (M-MuLV), became de novo *methylated and were blocked in expression. No restriction of virus expression and no* de novo *methylation were observed when post-implantation mouse embryos were infected with virus. Efficient* de novo *methylation activity may be an important characteristic of gene regulation in early mouse embryos.*

THE introduction of foreign cellular and retroviral genomes into early mouse embryos has been used to investigate the regulation of gene expression in mammalian development[1-10]. Early mouse embryos and embryonal carcinoma cells have been shown to be non-permissive for DNA virus as well as retrovirus gene expression[11-16]. Recently, we correlated the lack of expression of genetically transmitted Moloney murine leukaemia (M-MuLV) proviral genomes with their high degree of methylation[17,18]. As the retroviral genomes introduced into the germ line of these mice were unmethylated, *de novo* methylation of the proviral genomes must have occurred at some point, either during the development of the infected embryo and/or as a consequence of their transmission through the germ line. To investigate this, we have introduced M-MuLV genomes into pre- and post-implantation embryos. Here we show that efficient *de novo* methylation occurred after the introduction of virus into pre-implantation but not into post-implantation embryos. The resulting *de novo* methylated genomes were not active in a DNA transfection assay and were apparently not expressed in early embryos.

Integration of M-MuLV genomes into mouse embryo

M-MuLV genomes were introduced into mouse embryos at different stages of embryogenesis (see Table 1). Pre-implantation embryos were infected at the zygote stage by injecting the cloned M-MuLV-containing *Eco*RI fragment from Mov-3 mice either into the male pronucleus (animal 69) or into the cytoplasm (animal 158)[6] and, at the 4–16-cell stage, by exposure to M-MuLV virus[4]. Post-implantation embryos were injected at day 8 of gestation with purified M-MuLV virus as described previously[19].

The number of M-MuLV genomes present in mouse DNA extracted from 2–4-month-old animals was determined by digestion with *Sst*I (see Fig. 1). The intensities of the M-MuLV-

0028–0836/82/320623—06$01.00

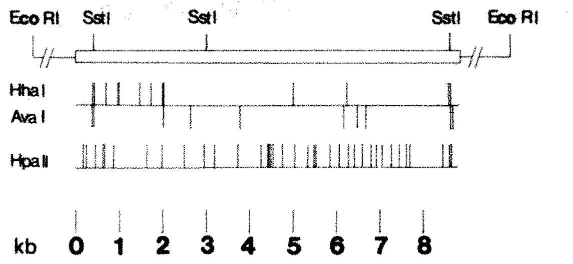

Fig. 1 Restriction enzyme map of a M-MuLV provirus. The open bar represents a M-MuLV provirus within flanking mouse DNA. Restriction sites of M-MuLV were taken from published maps[44] and sequences[45].

specific *Sst*I fragments of 5.6 and 2.6 kilobases (kb) from DNA of the experimental mice were compared with those from DNA of Mov-1 mice, thus permitting estimation of the total number of M-MuLV copies present per cell, as described elsewhere[6]. Figure 2 shows the presence of approximately 10 M-MuLV copies per cell in the DNA from mouse 69 and one copy in the DNA from mouse 158. Animals infected at day 3 of development carried between one and three copies and animals infected at day 8 of development carried between one and eight M-MuLV copies per cell in different tissues (Fig. 2, Table 1; compare ref. 19).

M-MuLV proviruses become integrated at multiple sites into pre-implantation embryos[4,5], mouse lymphocytes[20] and fibroblasts[21]. Because *Eco*RI does not cut within the M-MuLV genome, different integration sites of individual proviruses are characterized by different sizes of M-MuLV-containing *Eco*RI fragments. The number and intensities of such *Eco*RI fragments were used here to determine the time at which provirus integration took place in embryonal development. A single proviral copy inserted into the genome of the zygote will subsequently be present in every cell in all tissues of the mouse, resulting in an *Eco*RI fragment with the same intensity as the fragment which represents the single-copy M-MuLV genome in Mov mice. This has, indeed, been demonstrated for mouse 158 (Fig. 3, lane *b*, and ref. 6). DNA from mouse 69, which was derived from a zygote microinjected with cloned Mov-3 DNA into the male pronucleus, contained a strong band of 17 kb representing approximately 10 M-MuLV copies and a single copy fragment of higher molecular weight (Fig. 3, lane *a*). Further restriction enzyme analysis indicated tandem head-to-tail integration of the injected Mov-3 DNA, the single copy band representing Mov-3 DNA together with flanking mouse DNA (data not shown).

Table 1 Organization of M-MuLV copies introduced into mice at different stages of embryogenesis

Time of infection	Animal	Organ	No. of copies	No. of integration sites
Pre-implantation stage				
Day 1	69	Li	10–15	1
	158	Li	1	1
Day 3	58–1, 58–2 61, 62 100–19, 100–21	Li, Ki, Br	1–3	1–3
Post-implantation stage				
Day 8	B58, B59	Li	0.5–1	Multiple
		Ki	2–4	
		Br	4–8	
Control	Mov-13	Li	1	1

M-MuLV genomes were introduced into pre-implantation mouse embryos by DNA injection at day 1 or virus infection at day 3 of gestation. Microinjection of the cloned 16.8-kb *Eco*RI fragment from Mov-3 mice into the male pronucleus (animal 69) or into the cytoplasm (animal 158) of mouse zygotes at the day of fertilization was performed as described for mouse 158 (ref. 6). Four- to eight-cell embryos (that is, day 3 embryos) were infected *in vitro* as described for animal 62 (ref. 4). Post-implantation embryos were injected with virus *in utero* at day 8 of gestation as described elsewhere[19]. The data from mice B58 and B59 were representative of several similarly infected mice. The number of M-MuLV copies per cell was obtained by *Sst*I digestion with DNAs from liver (Li), kidney (Ki) or brain (Br) by comparison with the Mov-13 DNA (see Fig. 2). This DNA contained one M-MuLV genome per diploid genome. *Eco*RI digestion of DNA was used to determine the number of integration sites of M-MuLV in a given organ (see Fig. 3). All embryos were of strain C57BL/6 except animals 62, 100–19 and 100–21, which were ICR and 129 mice, respectively.

When exposure to virus takes place at a later stage (the 4–16-cell stage), integration can occur at different chromosomal sites as well as in different blastomeres. This will lead to less intense *Eco*RI fragments, depending on the segregation of the descendants of the infected blastomere during later development and their contribution to a given organ. Several *Eco*RI fragments of varying intensity were, indeed, observed in the DNA of such animals (Fig. 3, lanes *c*, *g*), indicating that these animals were mosaics with respect to the integrated M-MuLV copies (compare ref. 4). Germ-line mosaicism of such mice had been demonstrated previously[3–5]. The results shown in Fig. 3 revealed that the M-MuLV genomes present in the DNA of mice that were infected as pre-implantation embryos integrated in only a few chromosomal sites in a given animal. This indicated that the integration of M-MuLV genomes in these embryos occurred soon after the time of infection. Little or no reintegration of viral genomes had occurred during later stages of development (see below).

A different pattern of M-MuLV-specific *Eco*RI fragments was observed after infection with M-MuLV at a later stage, for example, day 8 of development, when the embryo consists of 10^4–10^5 cells. A broad smear of hybridization was seen and no discrete *Eco*RI fragments were detectable in any organ of such animals (Fig. 3, lanes *i*, *k*). This suggested that integration of virus took place at multiple sites in a heterogeneous population of cells. Each infected cell divided to form only a small fraction of the total number of cells in the respective tissue. We have shown previously that after postnatal infection of mice with M-MuLV, significant amounts of proviruses were not found in cells other than those of lymphopoietic origin[19]. The copies of M-MuLV in the non-lymphatic organs liver, kidney and brain of day-8 infected mice (Fig. 2*b*) therefore indicated prenatal virus spread. This conclusion was supported by *in situ* hybridization experiments (Fig. 4). At 4 days after injection of virus, multiple foci of cells expressing viral RNA were detected in liver and brain cells as well as in cells of other tissues. Viral proteins were detected similarly in multiple cells by immunofluorescence (not shown). Thus, efficient virus replication and infection took place at mid-gestation. These results, summarized in Table 1, suggested that the M-MuLV DNA detected in the adult integrated into the mouse genome at or soon after the time of the introduction of viral genomes.

De novo methylation of M-MuLV proviruses

The methylation of CpG dinucleotides in M-MuLV genomes present in the DNA of animals infected during different stages of embryogenesis (see Table 1) was analysed with methylation-sensitive enzymes[22–24]. Because newly synthesized retroviral DNA, the precursor of the provirus, is not methylated, the presence of 5-methylcytosine will reveal that *de novo* methylation has occurred between the time of integration and the time of DNA preparation. A given site can either be methylated or unmethylated. However, when studying the DNA from a population of cells, the same restriction site can be methylated in some molecules and unmethylated in the rest. Due to this heterogeneity, intermediate levels of methylation have been found in several analyses[25–28]. The presence of methyl groups in M-MuLV genomes was analysed by the resistance of the M-MuLV-specific *Sst*I or *Eco*RI fragments to digestion with the methylation-sensitive enzymes *Hha*I, *Ava*I or *Hpa*II (see Fig. 1). In all the DNAs from animals infected as pre-implantation embryos, the 2.6-kb *Sst*I fragment was highly resistant to digestion with all three enzymes (see Fig. 5). The 5.6-kb *Sst*I

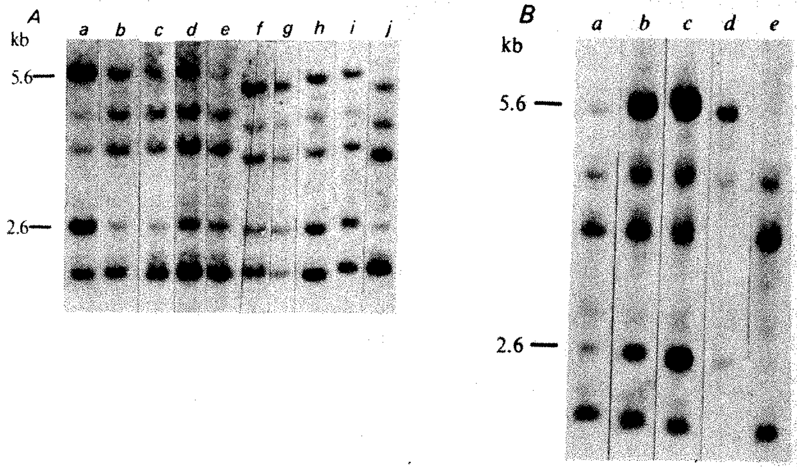

Fig. 2 Estimation of M-MuLV copies in DNAs from mice infected during embryogenesis. High molecular weight DNA was prepared, samples of 5–10 μg were cleaved with *Sst*I, separated on a 0.7% agarose gel and transferred to a nitrocellulose filter as described previously[17]. The filters were hybridized with a cDNA enriched for sequences specific for M-MuLV and washed after hybridization at 50 °C as described elsewhere[20]. *A*, DNAs from animals infected as pre-implantation embryos. Lanes *a*, *b*, liver DNA from animals 69 and 158, respectively; lanes *c*–*e*, DNA from liver, kidney and brain, respectively, of animal 58–1; lanes *f*, *g*, DNA from liver and brain, respectively, of animal 58–2; lanes *h*, *i*, liver DNA from animals 100–19 and 100–21, respectively; lane *j*, embryo DNA from Mov-13 mice[5], containing one copy of M-MuLV per cell. *B*, DNAs derived after infection of post-implantation embryos. Lanes *a*–*c*, DNAs from liver, kidney and brain, respectively, of animal B58; lane *d*, embryo DNA from Mov-1 mice, containing two copies of M-MuLV per cell; lane *e*, DNA from C57BL/6 mice. The bands present in all DNAs are due to cross-hybridization of the probe to DNA of endogenous retroviral genomes of the mouse[20]. These bands served as an internal standard for the amount of DNA present in each lane. The intensities of the 5.6- and 2.6-kb M-MuLV-specific *Sst*I fragments in DNAs from Mov mice, *A*, lane *j* and *B*, lane *d*, were used to estimate the number of M-MuLV copies in the other DNAs (see Table 1). As Mov-1 is of BALB/c background, bands derived from endogenous viruses are weaker with this probe than in C57BL/6 (compare lane *d* with lane *j*, *A*).

fragment was similarly resistant to cleavage with *Hha*I and *Ava*I and to some extent with *Hpa*II.

From the results shown in Fig. 5*A* we calculated that 70–95% of each of the sites had become *de novo* methylated in these DNAs (see Table 2). Our calculation was based on the assumption that every site was methylated to the same extent. This is supported by the following observations: (1) The resistance of both *Sst*I fragments did correspond to the number of cleavage sites present. Such a cumulative effect of multiple sites argued against the presence of certain sites with low levels of methylation. (2) No digestion products were found in the digests with the methylation-sensitive enzymes. Therefore, no detectable fraction of the total M-MuLV genomes had remained completely unmethylated, nor was there evidence for a number of sites methylated to a low degree. The latter conclusion was valid only for the *Hha*I and *Ava*I digestions, as *Hpa*II digestions could result in many undetectable digestion products (see Fig. 1). The above results suggested that the observed digestion of *Sst*I fragments of M-MuLV with *Hpa*II was only due to the presence of multiple sites, all of them methylated at a high level (see Table 2 for calculation) rather than to a lower level of methylation at such sites in a fraction of genomes. *Eco*RI/*Hha*I digestions of these DNAs revealed that some of the *Eco*RI fragments containing a M-MuLV provirus and several kilobases of flanking mouse DNA were highly methylated in all *Hha*I sites present (see Fig. 3, lanes *d*, *f*, *h*).

Table 2 *De novo* methylation of M-MuLV genomes at *Hha*I, *Ava*I and *Hpa*II sites in organs of animals infected during embryogenesis

Time of infection	DNA	Level of methylation at individual sites (%)	No. of sites
Pre-implantation stage	69 Li	70–95	44
	158 Li	70–90	44
	58–1 Li	70–95	22
	58–1 Ki	70–95	22
	58–1 Br	70–95	22
	58–2 Li	80–95	44
	58–2 Ki	70–90	22
	58–2 Br	70–90	22
	61 Li	70–95	44
	62 Li	70–95	22
	100–19 Li	70–95	44
	100–21 Li	70–95	44
Post-implantation stage	B58 B59 Li	<20	11
	Ki	<20	11
	Br	<20	11

See Table 1 legend fo details of infection and organ description. The level of *de novo* methylation in M-MuLV genomes present after infection of pre-implantation embryos was determined by the resistance of the M-MuLV-specific 5.6- and 2.6-kb *Sst*I fragments to digestion with *Hha*I, *Ava*I or *Hpa*II (see Fig. 5). Only sites sufficiently distant from the *Sst*I sites to reduce the size of the *Sst* fragments are included in the results. The 5.6-kb fragment has 25 *Hpa*II sites, the 2.6-kb fragment 7 *Hpa*II and 7 *Hha*I sites (see further in Fig. 1). With the exception of some *Ava*I sites in liver DNA of animal 69 (Fig. 5*A*, lane 1*c*), no preferential sensitivity of any site was seen. Therefore, assuming similar levels L of methylation in all n sites of a given enzyme present in an *Sst*I fragment, $L = \sqrt[n]{I}$, where I is the resistant fraction of the fragment obtained from the autoradiogram by visual inspection. If a fragment containing two sites for, for example, *Hha*I, is 70% resistant to cleavage with *Hha*I, then the level of methylation in both sites is 84%. The range in the percentage of methylation is due to differences observed with several enzymes and to the inaccuracy of determination of intensities. The level of *de novo* methylation in DNAs from animals infected at the post-implantation stage was estimated from the intensity of fragments appearing after digestion with *Hha*I or *Ava*I. The intensity of each fragment appearing is dependent on the presence of two unmethylated sites, thus $L = 1 - \sqrt[2]{I}$. I was >70% for all the M-MuLV fragments, compared with fragments of similar size derived by methylation-insensitive enzymes from the same DNA (see Fig. 6). In some cases no results for the *Hpa*II digestion of the 5.6-kb fragment are given, because a low number of M-MuLV copies per cell does not allow determination due to the multiple sites (see above). Four *Hha*I and seven *Ava*I sites resulting in fragments >0.6 kb were included in the analysis of appearing fragments (see Figs 1, 6).

In contrast to the above results, the M-MuLV genomes that integrated in post-implantation embryos showed a low degree of *de novo* methylation. The *Sst*I and *Eco*I fragments (see Fig. 5*B* and Fig. 3, lanes *j*, *l*) were almost completely digested with methylation-sensitive enzymes. No digestion products due to partial methylation of sites were visible. The levels of methylation in these DNAs were determined by digestions with *Hha*I or *Ava*I (see Table 2 for calculation). The intensities of the fragments appearing were compared with those of fragments of similar length derived from digestion of the same DNAs with the methylation-insensitive enzyme *Sst*I (see Fig. 6). Methylation of some of the sites would reveal fragments

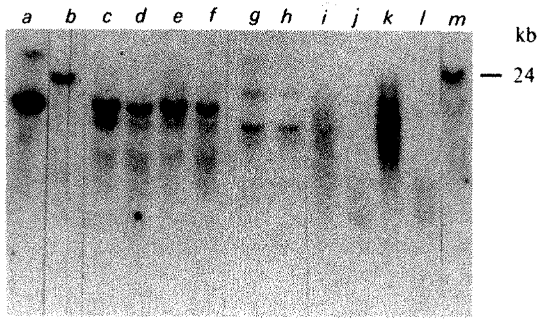

Fig. 3 Integration sites of M-MuLV genomes introduced into mouse embryos. The DNA samples were digested with *Eco*RI (lanes *a*, *b*, *c*, *e*, *g*, *i*, *k*, *m*) or *Eco*RI plus *Hha*I (lanes *d*, *f*, *h*, *j*, *l*). The completeness of the digestions was tested by addition of cloned M-MuLV DNA to a part of each digestion mix. The DNAs were separated on 0.5% agarose gels, a M-MuLV-specific cDNA being used for hybridization. Lane *a*, 5 μg of liver DNA from mouse 69; lane *b*, 10 μg of liver DNA from animal 158; lanes *c*–*f*, 20 μg DNA from animal 58–2, from kidney (*c*, *d*) and brain (*e*, *f*). Lanes *g*, *h*, 10 μg of DNA from kidney of mouse 100–21; lanes *i*–*l*: 10 μg DNA from animal B58, from kidney (*i*, *j*) and brain (*k*, *l*); lane *m*, 10 μg of embryo DNA from Mov-13 mice, containing one copy of M-MuLV per cell.

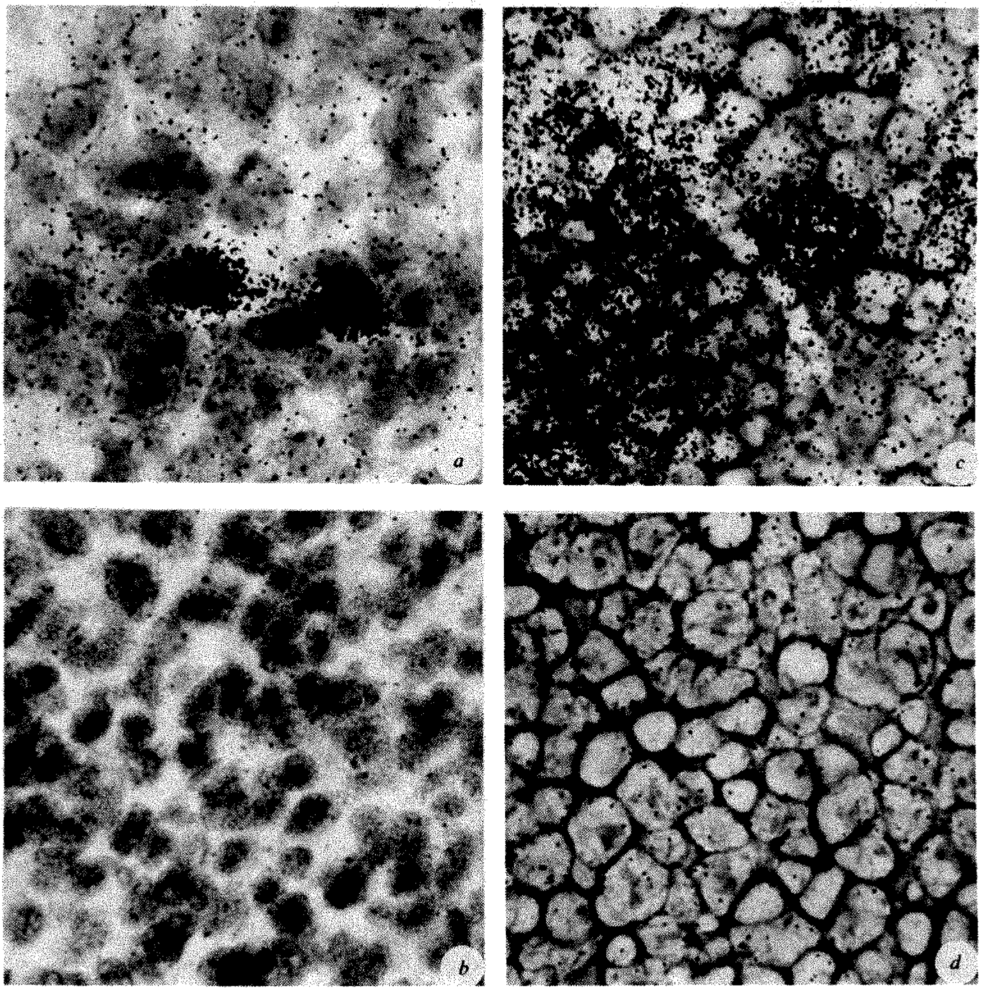

Fig. 4 Detection of M-MuLV RNA in post-implantation mouse embryos by *in situ* hybridization. Mouse embryos were infected *in utero* at day 8.5 of gestation with M-MuLV (see Table 1). Four to five days after infection, frozen sections of whole embryos were prepared, hybridized *in situ* with ^{3}H-labelled M-MuLV cDNA, and finally counter-stained with Giemsa stain as described previously[46]. *a*, Mantle layer of cerebral cortex showing focal expression of M-MuLV RNA; *b*, cerebral cortex of control embryo; *c*, foci of viral RNA in liver tissue; *d*, liver of control embryo. ×486.

differing in length and intensity from those derived from a completely unmethylated (that is, cloned) genome. Our analysis showed that at least 80% of the genomes introduced into post-implantation embryos remained completely unmethylated in 11 sites analysed. Because no partial digestion products or completely methylated genomes were visible (see also Fig. 5), we conclude that all 11 sites were methylated to less than 20% (see Table 2). Thus, these experiments demonstrated a striking difference in *de novo* methylation of M-MuLV genomes: a highly efficient *de novo* methylating activity is present only in pre-implantation embryos but not in post-implantation embryos or after birth. Furthermore, the methylation of M-MuLV genomes introduced into pre-implantation embryos was maintained over many cell generations.

Table 3 Infectivity of DNA from organs of mice infected with M-MuLV during embryogenesis

Time of infection	DNA	No. of XC PFU	Specific infectivity $\times 10^6$
Pre-implantation stage	69 Li	0	<0.01
	58–1 Li	0	<0.1
	58–1 Ki	0	
	61 Li	0	
	100–19 Li	0	
Post-implantation stage	B58 Li	8	1.4
	B58 Ki	24	0.7
	B58 Br	46	1.0
Controls	Mov-1 Sp	10–20	1.8
	C57BL Li	0	0
	1 ng pMov-3	500	8

The number of XC plaque-forming units (PFU) is given as a mean value from 30 μg DNA tested in two independent transfection assays as previously described[17]. Specific infectivity of DNA, defined as the number of XC PFU per viral genome, was calculated from the number of M-MuLV copies present in the respective DNA (compare Table 1). Infectivity of DNA from preleukaemic Mov-1 spleen is due to one to two M-MuLV copies acquired postnatally[17]. DNA from the highly infectious pMov-3 clone (specific infectivity 8×10^{-6} PFU per viral genome)[18], which was used for injection into zygotes (animal 69), was included as a control.

Expression of M-MuLV in infected embryos correlates with the infectivity of proviral DNA in the adult

Previous results have shown that pre-implantation mouse embryos are not permissive for virus replication[2,6,16]. The *Eco*RI pattern of M-MuLV-specific fragments indicated that infection with M-MuLV and integration of viral DNA did occur; however, virus spread, that is, virus expression, was not detectable in early mouse embryos, but did occur later in development in an unknown population of cells, leading to viraemia in the adult (compare ref. 5). In contrast, virus integration into cells of mid-gestation embryos led to expression and efficient spread throughout cells of all tissues of the infected embryo (Fig. 4). Therefore, those viral copies found in adult animals derived from infections of post-implantation embryos have been actively expressed after integration in most of the cells.

DNA transfection was used to study the biological activity of the same M-MuLV genomes as were analysed in previous sections. Table 3 shows that DNA containing M-MuLV genomes integrated in pre-implantation embryos was not infectious. The DNA from animal 69 carried 10–15 copies of pMov-3 DNA per cell. Thus, the injected DNA was several hundredfold less infectious after passage in the mouse than before injection. In contrast, the copies that were introduced

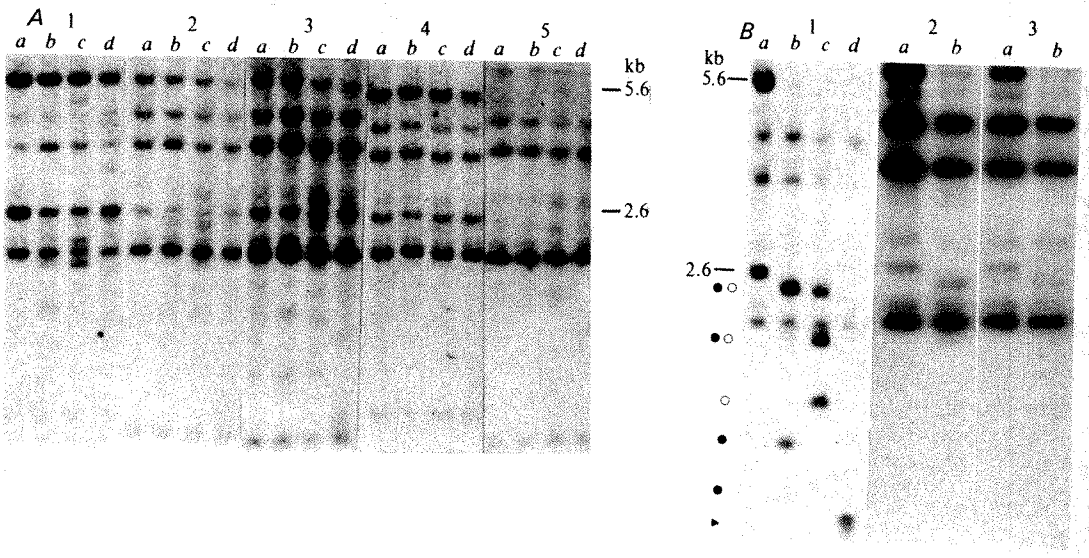

Fig. 5 Methylation of M-MuLV genomes. DNAs were analysed from mice infected as pre-implantation (*A*) or as post-implantation (*B*) embryos. All samples were digested with *Sst*I and also with: *b*, *Hha*I; *c*, *Ava*I; *d*, *Hpa*II. *A*, DNA from liver of mouse 69 (1*a*–*d*), liver of mouse 158 (2*a*–*d*), kidney of mouse 58-1 (3*a*–*d*), liver of mouse 58-2 (4*a*–*d*), C57BL/6 mice (5*a*–*d*). *B*, DNA from kidney of mouse B58 (1*a*–*d*), kidney of mouse Bv11 (2*a*, *b*), brain of mouse Bv12 (3*a*, *b*). The positions of DNA fragments of M-MuLV derived after double digestion with: ●, *Hha*I; ○, *Ava*I; ►, *Hpa*II are indicated. The cDNA was not representative of all sequences of M-MuLV; therefore, the intensities of the fragments did not correspond to their sizes (compare ref. 4).

into post-implantation embryos were as infectious as those integrated after birth. Previous results from this laboratory have correlated DNA methylation and expression of M-MuLV genomes with infectivity in a transfection assay[17,18,29]. The results described in Table 3 indicate that viral genomes which were *de novo* methylated after integration into pre-implantation embryos are non-infectious in the adult animal. Thus, both persistence of viral genome methylation and non-infectivity may be sustained by a maintenance methylase activity[24,30,31] for as long as 5 months after birth. In contrast, viral genomes inserted in cells of mid-gestation embryos are expressed, remain unmethylated and are infectious in a transfection assay when isolated from the adult.

Discussion

We have shown previously that pre-implantation mouse embryos are not permissive for replication of M-MuLV[2,6]. Viral DNA, however, can integrate efficiently into the embryo DNA and mouse substrains designated as Mov-1 to Mov-13 that carry M-MuLV in their germ line have been derived from infected embryos[3–5]. Virus is activated in some of these substrains and the available evidence suggested that the developmental stage at which virus activation occurs depends on the chromosomal position of the provirus[5]. Further analysis showed that the genetically transmitted proviral genomes in several organs of Mov substrains were highly methylated and non-infectious in a transfection assay[17,18].

We have shown here that retroviral DNAs become *de novo* methylated on integration into the genome of pre-implantation embryos as assayed in organs of the adult derived from the infected embryo. This was observed after exposure of the embryos to infectious virus as well as after microinjection of cloned viral DNA with flanking mouse sequences. In contrast, virus introduced into post-implantation embryos replicated efficiently in most or all embryonal cells and the integrated proviral genomes remained largely unmethylated when assayed in the adult animal. The difference in *de novo* methylation was also reflected in the transfection assay: DNA from animals exposed to virus at the pre-implantation stage was not infectious, in contrast to DNA from animals exposed to virus at mid-gestation. Thus, our results suggest that an efficient *de novo* methylation activity may be characteristic of cells of the pre-implantation stage and may be absent or less effective in cells of later embryos. This activity correlates with non-permissivity to virus expression. Furthermore, our results show that the maintenance methylation activity is faithful in preserving the respective methylation pattern of the proviral genomes throughout the life of the animal. The *de novo* methylation activity in embryonal cells may be of general significance, as not only viral but also globin DNA (F. Costantini and E. Lacy, personal communication) and a metallothionein–thymidine kinase fusion plasmid[32] became *de novo* methylated after microinjection into mouse zygotes..

Recent experiments obtained in tissue culture systems have demonstrated that embryonal carcinoma cells have an efficient *de novo* methylation activity, in contrast to differentiated cells[33], and that methylation correlated with gene expression. In these experiments we analysed the fate of the infecting DNA: the viral DNA remained unmethylated as long as it was unintegrated and became *de novo* methylated soon after genomic integration. This is relevant for the observation that DNA microinjected into mouse zygotes[6,34] or into *Xenopus* eggs[35] is

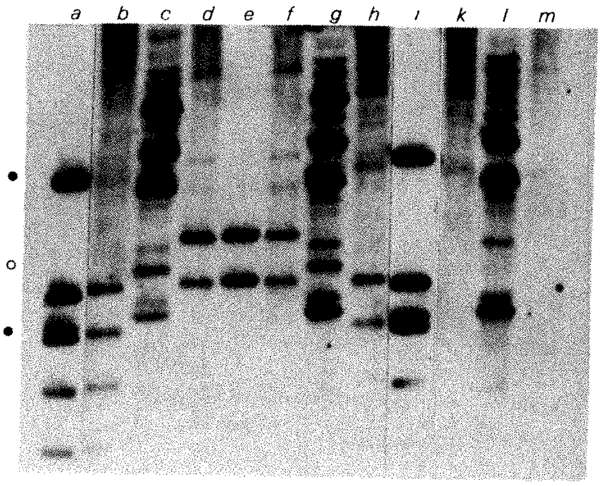

Fig. 6 M-MuLV genomes are not methylated in DNA from mice infected at the post-implantation stage. Lack of methylation was demonstrated by (1) appearance of equimolar M-MuLV-specific fragments after digestion of DNAs from mouse B59 and cloned M-MuLV DNA with *Ava*I and *Hha*I and (2) by comparing the intensity of the 2.6-kb fragment derived from digestion of DNAs from B59 with the methylation-insensitive enzyme *Sst*I to the intensity of fragments of similar size derived from digestion of the same DNAs with the methylation-sensitive enzymes *Hha*I and *Ava*I. DNA (10 μg) from brain and kidney of animal B59 were separated on a 0.8% agarose gel. The hybridization was performed with a nick-translated M-MuLV DNA. Lane *a*, *Ava*I- digest of plasmid p9-2, containing M-MuLV DNA[29]; lanes *b*–*d*, *Ava*I-, *Sst*I- and *Hha*I- digested brain DNA, respectively; lane *e*, *Hha*I digest of 9-2; lanes *f*–*h*, *Hha*I-, *Sst*I- and *Ava*I- digested kidney DNA, respectively; lane *i*, *Ava*I digest of p9-2; lanes *k*–*m*: *Ava*I-, *Sst*I- and *Hha*I- digested C57BL/6 DNA, respectively. The positions of the M-MuLV-specific 2.6-kb *Sst* fragment (○) and of the two plasmid sequences containing *Ava*I fragments of p9-2 (●), which are therefore not found in DNA from B59, are indicated.

expressed as long as it remains in an episomal state. Unintegrated DNA injected into *Xenopus* eggs was shown to remain unmethylated[36]. So far, *de novo* methylation activity has only been observed as a rare event in differentiated cell lines after long-term cultivation to select cell clones[37–40].

If the *de novo* methylation activity in embryonal and efficient maintenance methylation in later cells are involved in repression of proviral genomes, what is the origin of infectious virus in mice derived from pre-implantation embryos exposed to virus? Because virus, once activated, will infect all susceptible cells and spread throughout the animal, demethylation and activation of virus at a given stage of development and in a specific, as yet unidentified, population of cells would be sufficient to lead to viraemia. Demethylation of a given provirus in specific cells may depend on the chromosomal position where integration took place, and proviral genome activation may thus be regulated by similar mechanisms to those proposed for the tissue-specific activation of developmentally regulated genes[41,42]. Gene activation of the proviral genome in Mov-1 mice seems to be compatible with such a hypothesis[43].

Our results suggest that embryonal cells may possess an efficient *de novo* methylation activity that inactivates any DNA which is introduced into the early embryo. This may have evolved as a mechanism to protect the developing embryo against the deleterious consequences of virus infections. Finally, our results pose intriguing questions concerning the control of gene expression during early development, and it will be of great interest to study the methylation of genes that are active in pre-implantation embryos and embryonal carcinoma cells.

We thank Drs M. Breindl and W. Ostertag for helpful discussions, and D. Grotkopp, K. Haase and I. Humburg for technical assistance. This work was supported by grants from the Deutsche Forschungsgemeinschaft and the Stiftung Volkswagenwerk. The Heinrich-Pette-Institut is financially supported by Freie und Hansestadt Hamburg and Bundesministerium für Jugend, Familie und Gesundheit.

Received 13 April; accepted 7 June 1982.

1. Jaenisch, R. & Mintz, B. *Proc. natn. Acad. Sci. U.S.A.* **71,** 1250–1254 (1974).
2. Jaenisch, R., Fan, H. & Croker, B. *Proc. natn. Acad. Sci. U.S.A.* **72,** 4008–4012 (1975).
3. Jaenisch, R. *Proc. natn. Acad. Sci. U.S.A.* **73,** 1260–1264 (1976).
4. Jähner, D. & Jaenisch, R. *Nature* **287,** 456–458 (1980).
5. Jaenisch, R. *et al. Cell* **24,** 519–529 (1981).
6. Harbers, K., Jähner, D. & Jaenisch, R. *Nature* **293,** 540–542 (1981).
7. Costantini, F. & Lacy, E. *Nature* **294,** 92–94 (1981).
8. Wagner, E. F., Stewart, T. & Mintz, B. *Proc. natn. Acad. Sci. U.S.A.* **78,** 5016–5020 (1981).
9. Gordon, J. W. & Ruddle, F. H. *Science* **214,** 1244–1246 (1981).
10. Brinster, R. L. *et al. Cell* **27,** 223–231 (1981).
11. Lehman, J. M., Klein, I. B. & Hackenberg, R. M. in *Teratomas and Differentiation* (eds Sherman, M. I. & Solter, D.) 289–301 (Academic, New York, 1975).
12. Sekikawa, K. & Levine, A. J. *Proc. natn. Acad. Sci. U.S.A.* **78,** 1100–1104 (1981).
13. Vasseur, M., Kress, C., Montreau, N. & Blangy, D. *Proc. natn. Acad. Sci. U.S.A.* **77,** 1068–1072 (1980).
14. Teich, N. M., Weiss, R. A., Martin, G. R. & Lowy, D. R. *Cell* **12,** 973–982 (1977).
15. Speers, W. C., Gautsch, J. W. & Dixon, F. J. *Virology* **105,** 241–244 (1980).
16. Jaenisch, R. & Berns, A. in *Concepts in Mammalian Embryogenesis* (ed. Sherman, M. I.) 267–314 (MIT Press, 1977).
17. Stuhlmann, H., Jähner, D. & Jaenisch, R. *Cell* **26,** 221–232 (1981).
18. Harbers, K., Schnieke, A., Stuhlmann, H., Jähner, D. & Jaenisch, R. *Proc. natn. Acad. Sci. U.S.A.* **78,** 7609–7613 (1981).
19. Jaenisch, R. *Cell* **19,** 181–188 (1980).
20. Jähner, D., Stuhlmann, H. & Jaenisch, R. *Virology* **101,** 111–123 (1980).
21. Steffen, D. & Weinberg, R. A. *Cell* **15,** 1003–1010 (1978).
22. Gautier, F., Bünemann, H. & Grotjahn, L. *Eur. J. Biochem.* **80,** 175–183 (1977).
23. Waalwijk, C. & Flavell, R. A. *Nucleic Acids Res.* **5,** 4631–4641 (1978).
24. Bird, A. P. & Southern, E. M. *J. molec. Biol.* **118,** 27–47 (1978).
25. Mandel, J. L. & Chambon, P. *Nucleic Acids Res.* **7,** 2081–2103 (1979).
26. van der Ploeg, L. H. T. & Flavell, R. A. *Cell* **19,** 947–958 (1980).
27. Shen, C.-K. J. & Maniatis, T. *Proc. natn. Acad. Sci. U.S.A.* **77,** 6634–6638 (1980).
28. Bird, A., Taggart, M. & Macleod, D. *Cell* **26,** 381–390 (1981).
29. Chumakov, I., Stuhlmann, H., Harbers, K. & Jaenisch, R. *J. Virol.* **42,** 1088–1098 (1982).
30. Wigler, M., Levy, D. & Perucho, M. *Cell* **24,** 33–40 (1981).
31. Stein, R., Gruenbaum, Y., Pollack, Y., Razin, A. & Cedar, H. *Proc. natn. Acad. Sci. U.S.A.* **79,** 61–65 (1982).
32. Palmiter, R. D., Chen, H. Y. & Brinster, R. L. Cell **29,** 701–710 (1982).
33. Stewart, C. L., Stuhlmann, H., Jähner, D. & Jaenisch, R. *Proc. natn. Acad. Sci. U.S.A.* **79,** 4098–4102 (1982).
34. Brinster, R. L., Chen, H. Y., Warren, R., Sarthy, A. & Palmiter, R. D. *Nature* **296,** 39–42 (1982).
35. Kressmann, A., Clarkson, S., Telford, J. & Birnstiel, M. *Cold Spring Harb. Symp. quant. Biol.* **42,** 1077–1082 (1977).
36. Harland, R. *Proc. natn. Acad. Sci. U.S.A.* **79,** 2323–2327 (1982).
37. Desrosiers, R., Mulder, C. & Fleckenstein, B. *Proc. natn. Acad. Sci. U.S.A.* **76,** 3839–3843 (1979).
38. Sutter, D. & Doerfler, W. *Proc. natn. Acad. Sci. U.S.A.* **77,** 253–256 (1980).
39. Pollack, Y., Stein, R., Razin, A. & Cedar, H. *Proc. natn. Acad. Sci. U.S.A.* **77,** 6463–6467 (1980).
40. Guntaka, R. V., Rao, P. Y., Mitsialis, S. A. & Katz, R. *J. Virol.* **34,** 569–572 (1980).
41. Razin, A. & Riggs, A. *Science* **210,** 604–610 (1980).
42. Stalder, J., Groudine, M., Dodgson, J. B., Engel, J. D. & Weintraub, H. *Cell* **19,** 973–980 (1980).
43. Fiedler, W., Nobis, P., Jähner, D. & Jaenisch, R. *Proc. natn. Acad. Sci. U.S.A.* **79,** 1874–1878 (1982).
44. Gilboa, E. *et al. Cell* **16,** 863–874 (1979).
45. Shinnick, T. M., Lerner, R. A. & Sutcliffe, J. G. *Nature* **293,** 543–548 (1981).
46. Simon, I., Löhler, J. & Jaenisch, R. *Virology* (in the press).

Single base substitution in an intron of oxidase gene compensates splicing defects of the cytochrome *b* gene

Geneviève Dujardin, Claude Jacq & Piotr P. Slonimski

Centre de Génétique Moléculaire, Laboratoire propre du CNRS, associé à l'Université Pierre et Marie Curie, Paris VI,
F-91190 Gif-sur-Yvette, France

An extragenic suppressor mutation, mim2-1, *which compensates yeast mitochondrial mutants deficient in splicing of the cytochrome* b *gene, has been mapped and sequenced. The mutation is due to a single G → A transition in the long open reading frame of the fourth intron of the oxidase subunit one gene. It causes the replacement of a glutamic codon by a lysine codon and the expression of a novel mRNA maturase active in splicing. Evolution and regulatory connections between homologous introns of nonhomologous genes are discussed.*

THE mitochondrial gene *cob-box* of *Saccharomyces cerevisiae*, which specifies the apocytochrome *b*, exhibits a mosaic organization of exons and introns[1–6]. Respiration-deficient mutants have been mapped in both the exons and introns of this gene. Exon mutants belong to a single complementation group while intron mutants belong to separate complementation groups[7]. Intron mutations have been shown to block the processing of mRNA[8,9]. DNA sequence analyses of *trans*-recessive intron mutations and characterization of the mitochondrial translation products suggest that *trans*-acting proteins, 'mRNA maturases', involved in splicing are encoded by the two long open reading frames present in the two main introns of the *cob-box* gene,

0028-0836/82/320628—05$01.00

bI2 and *bI4* (refs 6, 10). The mRNA maturase model of splicing homeostasis can be used as a paradigm of the regulation of split genes in yeast mitochondria[6,10,11].

Numerous intron mutations of the *cob-box* gene result in a pleiotropic phenotype: they prevent not only the synthesis of cytochrome *b* but also that of subunit I of cytochrome oxidase. This protein is itself encoded by another mosaic mitochondrial gene, *oxi3*. The lack of expression is due to a block in the correct processing of the oxidase pre-mRNA[8]. More precisely, the fourth intron *bI4* of the *cob-box* gene has been shown to control the expression of *oxi3*[12,13]. The fourth intron *aI4* of the *oxi3* gene displays a very striking sequence homology to the intron *bI4* but no sequence homology is found between the exons of the two genes[14]. There is evidence that the mRNA maturase encoded by the intron *bI4* is involved in excising the two introns *bI4* and *aI4* of the two distant genes[10].

To investigate the function of introns and various components of the mitochondrial splicing machinery, we have developed a general method of selecting and genetically characterizing extragenic suppressors of splicing-deficient mutations located in introns[15]. The suppressor *mim2-1* is particularly interesting as (1) it is localized in mitochondrial (mt) DNA; (2) it compensates all the *trans*-recessive *box7*$^{-}$ mutations in intron *bI4*, but does not compensate any of some 450 mutations located elsewhere in the mitochondrial genome; (3) when *mim2-1* is associated with a complete deletion of the *cob-box* gene (leading to a total deficiency of cytochrome *b* and oxidase) oxidase synthesis is partially restored while cytochrome *b* is still absent[16]. These observations suggest that in the presence of *mim2-1*, the *cob-box* gene and the mRNA maturase encoded by it are no longer required for splicing and expression of the oxidase gene.

We have now localized the suppressor *mim2-1* in the intron *aI4* of the *oxi3* gene, determined its nucleotide sequence and compared it with that of the wild type. We show here that the suppressor mutation is due to a single base substitution in the intron open reading frame and we suggest that it brings about the synthesis of an active compensating mRNA maturase encoded by intron *aI4*.

Suppressor mutation is on mitochondrial DNA in the oxidase gene

The suppressor mutation *mim2-1* was localized on the mitochondrial genome by using *rho*$^{-}$ deletion mapping according to the first procedure described in ref 15. Three *rho*$^{-}$ (respiratory-deficient mutants that have large deletions of the mitochondrial genome) clones which retained the *mim2-1* mutation were obtained (see Fig. 1) and genetically characterized for the retention or loss of various markers that had previously been mapped in different mitochondrial genes. The *rho*$^{-}$ clones were able to restore, in crosses, the respiratory sufficiency of two classes of mitochondrial mutations from two distinct regions. (1) They successfully restored all *box7*$^{-}$ mutations of the cytochrome *b* gene at 28 °C and poorly or not all at 18 °C. This is consistent with the observation that the *mim2-1* suppressor, which they carry, is cryosensitive[15]. (2) The clones restored equally well at both 28 °C and 18 °C several *oxi3* mutations of the oxidase gene, showing that they have always retained the suppressor *mim2-1* and several *oxi3* markers which can be introduced by recombination. We conclude that the *mim2-1* mutation is located in or near the *oxi3* gene.

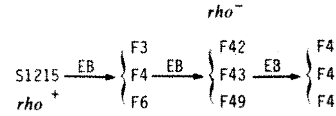

Fig. 1 Genealogy of *rho*$^{-}$ derivatives carrying the suppressor mutation. *rho*$^{-}$ were selected after ethidium bromide (EB) mutagenesis of the revertant *rho*$^{+}$ S1215 and subcloned as described in ref. 15.

Additional *rho*$^{-}$ subclones with smaller mitochondrial genomes, but still carrying the suppressor, were generated (see Fig. 1). Table 1 represents a simplified genetic map of the *oxi3* gene and the segments of mitochondrial genome retained by the nine *rho*$^{-}$ clones studied. The clones display distinctive genotypes but have retained a coherent region of mtDNA with no internal rearrangements. The retained segments of the *rho*$^{-}$ clones overlap a precise region, located approximately in the middle of the genetic map of the *oxi3* gene, where the *oxi3*$^{-}$ mutations *oxi3-G192* and *oxi3-G2190* are also located[17].

Thus the suppressor *mim2-1* can be localized in the *oxi3* gene near the *oxi3* mutations *G192* and *G2190*.

Suppressor mutation is in the fourth intron of oxidase gene

To determine which segment of the *oxi3* gene contains *mim2-1* we prepared mtDNAs of the two overlapping and genetically simple *rho*$^{-}$ clones carrying *mim2-1*, F431 and F439. We performed restriction analyses of the two genomes and compared the results with detailed restriction maps of the wild-type *oxi3* gene[14,18–20]. The genomes of these two *rho*$^{-}$ clones exist as tandem repeats with unit lengths of 2.2 (F439) and 5 (F431) kilobases (kb). The restriction maps of the two clones are completely consistent with the *rho*$^{+}$ maps already reported. They have retained contiguous segments of mtDNAs with no internal deletions or inversions. The absence of a *Hae*III site in F439 and any *Hin*dIII site in F431 shows that the overlap between the two genomes spans the segment between the *Hae*III and the *Hin*dIII sites (Fig. 2). This 865-base pair (bp) fragment contains an internal *Hph*I site present both in F439 and F431. The *mim2-1* mutation can thus be assigned to this

Table 1 Genetic mapping of the suppressor mutation in the oxidase gene

	oxi3 mutants														
rho^{-}	G20	G789	G2342	G656	G2133	G2027	G2508	G2190	G192	G3015	G1979	G421	G433	G1683	G922
F3	+	+	+	+	+	+	+	+	+	+	+	+	+	+	+
F4	−	+	+	+	+	+	+	+	+	+	+	+	+	+	−
F6	−	−	−	+	+	+	+	+	+	+	+	−	−	−	−
F42	−	+	+	+	+	+	+	+	+	+	+	+	−	−	−
F49	−	−	+	+	+	+	+	+	+	+	+	+	+	+	−
F43	−	−	−	−	+	+	+	+	+	+	+	+	+	+	−
F431	−	−	−	−	−	+	+	+	+	−	−	−	−	−	−
F434	−	−	−	−	−	−	−	+	+	+	+	+	+	−	−
F439	−	−	−	−	−	−	−	+	+	+	+	−	−	−	−

rho^{-} clones which have retained the *mim2-1* mutation have been crossed with different *rho*$^{+}$*oxi3*$^{-}$ mutants; +/− denotes presence/absence of wild-type *rho*$^{+}$ *oxi3*$^{+}$ recombinants in the diploid progeny. As expected from their lineage (Fig. 1), the genomes F42, F43 and F49 are included within the larger genome F4 and the genomes F434, F439 and F431 within the genome of F43. The *oxi3* map is consistent with previous results[17]. Strains and genetic methods have been described previously[15,16].

Fig. 2 *a*, Physical mapping of the suppressor mutation in intron *aI4* of the oxidase gene and strategy for sequencing. The two upper bars represent the segments of mitochondrial genome retained in *rho*⁻ clones F431 and F439 both carrying the *mim2-1* mutation. The uncertainties due to junction fragments are represented by slanted edges. The middle bar represents the general organization of intron *aI4* and flanking exons *A4* and *A5* (solid area). The restriction sites used for physical mapping, cloning and sequencing are shown. The bottom panel represents the DNA sequencing strategy: arrows indicate the direction and approximate length of the fragments sequenced, the restriction sites used for 5′-end-labelling are denoted by a short vertical bar. Nucleotide distances are given from the *Hae*III site (0) located at the beginning of intron *aI4*. The mutation *mim2-1* is at position +354. Mitochondrial DNAs were prepared according to ref. 10. A 1,440-bp fragment between the cleavage sites of *Bam*HI and *Hin*dIII was isolated from the *rho*⁻ genome F43 (Fig. 1, Table 1) and inserted into the plasmid vector pBR322 by *in vitro* recombination following the method described in ref. 24. Plasmid DNAs were prepared according to ref. 25. The recombinant DNA was digested with *Hae*III and *Hin*dIII and an 865-bp fragment was isolated by agarose gel electrophoresis. This fragment was entirely sequenced by the method of Maxam and Gilbert[26]. The *Hae*III–*Hin*dIII fragment was then further digested by *Sau*3A (= *Mbo*I), or by *Hph*I and labelled at the 5′ ends with [γ-^{32}P]ATP. Three of the four resulting fragments were then denatured and separated by gel electrophoresis. The fourth one (the largest 347-bp *Mbo*I fragment) was recut by either *Alu*I or *Mnl*I, allowing a good sequencing across the central part of the fragment. *b*, Nucleotide sequence of the intron fragment carrying the suppressor mutation *mim2-1*. Upper-case letters represent the nucleotide sequence established in the present work of the 865-bp fragment carrying the suppressor *mim2-1* between the *Hae*III and *Hin*dIII sites in intron *aI4* (see *a*). The sequence of the sense strand is displayed in the 5′→3′ orientation. The amino acid sequence of the intron open reading frame is indicated in lower case. The two lines represent the corresponding wild-type sequence established by Netter *et al.*[20]. The first rectangle shows that the suppressor mutation is due to a G→A substitution; the second shows the polymorphic variation between different wild types (see refs 14 and 20).

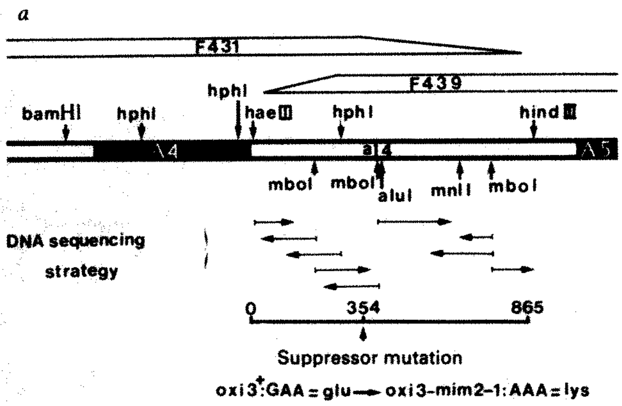

b

CC CTT ATT ATT ATA TTA ATA ATA TAT AAT GAT ATG CAT TTT TCT AAA TGC TGG AAA TTA TTA AAA AAA TGA ATT ACA AAT ATT ATA AGT CTA TTA TTT AAA
thr ile ile ile leu ile ile tyr asn asp met his phe ser lys cys trp lys leu leu lys lys trp ile thr asn ile ile ser thr leu phe lys

GCC TTA TTT GTA AAA ATA TTC ATA TCT TAT AAT AAT CAG CAG GAT AAG ATA ATA AAT AAT CTT ATA TTA AAA AAA GAT AAT ATT AAA AGA TCC TCA GAG ACT
ala leu phe val lys ile phe ile ser tyr asn asn gln gln asp lys ile ile asn asn thr ile leu lys lys asp asn ile lys arg ser ser glu thr

ACA AGA AAA ATA TTA AAT AAT TCA ATA AAT AAA AAA TTT AAT CAA TGA TTA GCT GGA TTA ATT GAT GGT GAT GGA TAT TTT GGT ATT GTA AGT AAG AAA TAT
thr arg lys ile leu asn asn ser ile asn lys lys phe asn gln trp leu ala gly leu ile asp gly asp gly tyr phe gly ile val ser lys lys tyr

GTA TCA TTA GAA ATT CTA GTA GCA TTA GAA GAT GAA ATA GCT TTA AAA AAA ATT CAA AAT AAA TTT GGT GGT TCT ATT AAA TTA AGA TCA GGT GTA AAA GCT
val ser leu glu ile thr val ala leu glu asp glu ile ala leu lys lys ile gln asn lys phe gly gly ser ile lys leu arg ser gly val lys ala
G
glu

ATT AGA TAT AGA TTA CTT AAT AAA ACT GGT ATA ATT AAA TTA ATT AAT GCA GTT AAT GGT AAT ATT AGA AAT ACT AAA AGA TTA GTA CAA TTT AAT AAA GTT
ile arg tyr arg leu thr asn lys thr gly ile ile lys leu ile asn ala val asn gly asn ile arg asn thr lys arg leu val gln phe asn lys val

TGT ATT TTA TTA GGT ATT GAT TTT ATT TAT CCA ATT AAA TTA ACT AAA GAT AAT AGT TGA TTT GTT GGA TTT TTT GAT GCT GAT GGT ACA ATT AAT TAT TCA
cys ile leu leu gly ile asp phe ile tyr pro ile lys leu thr lys asp asn ser trp phe val gly phe phe asp ala asp gly thr ile asn tyr ser

TTT AAA AAT AAT CAT CCT CAA TTA ACA ATT TCT GTA ACT AAT AAA TAT TTA CAA GAT GTA CAA GAA TAT AAA AAT ATT TTA GGT GGT AAT ATT TAT TTT GAT
phe lys asn asn his pro gln leu thr ile ser val thr asn lys tyr leu gln asp val gln glu tyr lys asn ile leu gly gly asn ile tyr phe asp

AAA TCA CAA AAT GGT TAT TAT AAA TGA TCC ATT CAA TCA AAA GAT ATA GTA TTA AAT TTT ATT AAT GAT TAT ATT AAA ATA AAT CCA TCA AGA ACA CTA AAA
lys ser gln asn gly tyr tyr lys trp ser ile gln ser lys asp ile val leu asn phe ile asn asp tyr ile lys ile asn pro ser arg thr thr lys

ATA AAT AAA TTA TAT TTA AGT AAA GAA TTT TAT AAT TTA AAA GAA TTA AA
ile asn lys leu tyr leu ser lys glu phe tyr asn leu lys glu leu

*Hin*dIII–*Hae*III segment in the *oxi3* gene. According to Bonitz *et al.*[14], this fragment is part of the fourth intron *aI4* of the *oxi3* gene: the *Hae*III site is located 9 bp downstream from the beginning of the intron and the *Hin*dIII site is located well inside the intron. The 865-bp fragment carrying the *mim2-1* mutation is therefore entirely within intron *aI4*. This physical location is in good agreement with the genetic one, as Netter *et al.*[20] have shown by sequence analysis that the mutations *oxi3-G-192* and *oxi3-G2190* are placed inside the intron *aI4* and, as discussed above, the *mim2-1* is linked to *G192* and *G2190*. We conclude that the suppressor *mim2-1* is located completely inside intron *aI4* of oxidase gene.

Suppressor mutation results from single base substitution in intron open reading frame

We have sequenced the *Hae*III–*Hin*dIII fragment containing the *mim2-1* mutation according to the strategy described in Fig. 2. This sequence was compared with the corresponding wild-type sequence of the isomitochondrial strain 777-3A (ref. 20). The suppression is due to a single G→A transition (Fig. 3) in the intron open reading frame at position +354 (Fig. 2). This substitution replaces a glutamic acid codon in the wild type by a lysine codon in the suppressor. No other changes occur in the entire sequence.

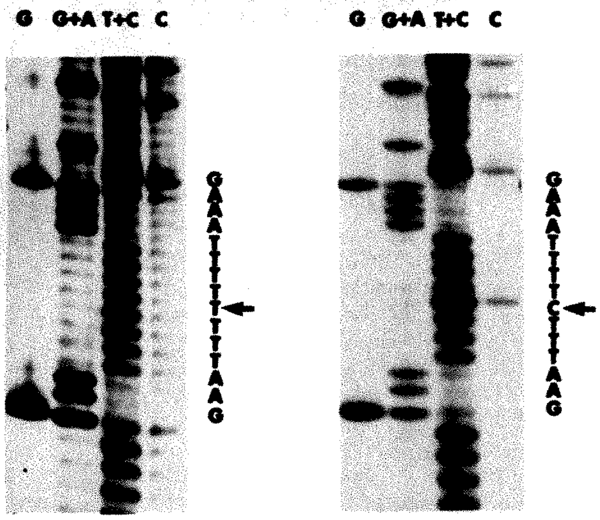

oxi3-mim2-1 oxi3⁺

Fig. 3 Sequencing gel demonstrating the base substitution of the suppressor mutation. The mutated *mim2-1* and corresponding wild-type sequences are shown on 8% acrylamide sequencing gels. Both strands of *Mbo*I fragment were sequenced. The base change corresponding to the *mim2-1* mutation that is 36 bp distant from the *Mbo*I site is more visible on the sequence of the nonsense strand. The mutation corresponds to a substitution on the nonsense strand of a C in the wild type by a T in the mutant. On the sense strand this gives a G→A substitution at position +354 (Fig. 2).

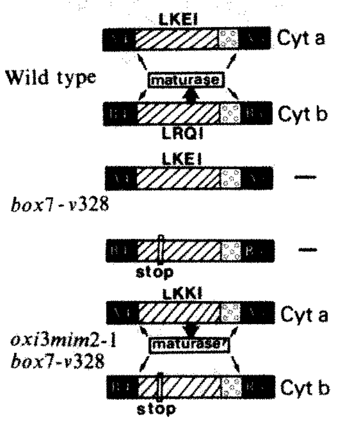

Fig. 5 A model for the normal, deficient and compensatory regulations between the introns of two genes. The drawing represents pre-mRNA molecules transcribed from two genes. The oxidase subunit I (Cyt a) and cytochrome *b* (Cyt b) exons are shown in solid and intron open reading frames in hatched areas. The reading frames are 966 and 1,158 bp long respectively. In the wild type (top), intron *bI4* encodes (thick arrow) a *trans*-acting mRNA maturase which is involved in splicing of both introns, *bI4* and *aI4* (thin arrows). A *box7* mutation (middle) that creates a stop codon at position 405 (AAA→TAA) in *bI4* prevents the synthesis of the maturase and the two introns are no longer excised[10]. The unspliced pre-mRNA of *aI4* accumulates and could be translated into a p56 protein devoid of maturase activity (see text). In a double mutant carrying the *oxi3–mim2-1* mutation (bottom), the protein translated from *aI4* has acquired the maturase activity due to the replacement of the glutamic (E) by the lysine residue (K). This novel protein permits splicing and expression of both genes.

Novel mRNA maturase translated from oxidase intron replaced normal maturase translated from cytochrome *b* intron

There is recent evidence that, in the wild type, the splicing of both introns *aI4* of the oxidase gene and *bI4* of the cytochrome *b* gene is controlled by a pleiotropic mRNA maturase translated from *bI4* (refs 10, 20). The activity of this maturase, designated *bI4* maturase, involves the same set of *cis*-acting signals present in both introns, in particular *box9*⁺ and *box2*⁺ nucleotide sequences in *bI4* and their equivalents in *aI4* (see Fig. 4 and refs 10, 20). We propose that the *mim2-1* mutation induces the synthesis of an active *aI4* maturase that would not occur in the wild type and that it is translated from the oxidase intron. This novel maturase would act as a substitute for a deficient *bI4* maturase, using the same set of critical sequences present in both pre-mRNAs. Such a hypothesis (summarized in Fig. 5) explains all the known facts: the suppression by *mim2-1* of *bI4* maturase-deficient mutants and the absence of suppression of *box9*⁻ or *box2*⁻ mutants; the synthesis of oxidase in the presence of a complete deletion of the cytochrome *b* gene[16]; and sequence homology between *aI4* and *bI4* (refs 10, 14, 20).

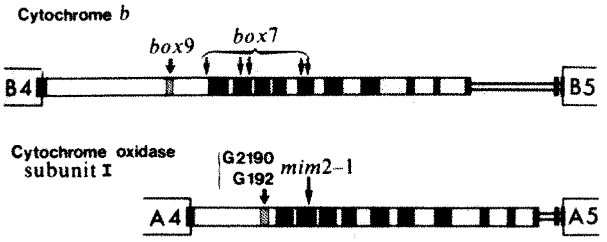

Fig. 4 General organization of the two homologous introns, *bI4* and *aI4*, of cytochrome *b* and cytochrome oxidase genes. *B4, B5* and *A4, A5* represent respectively the exons of cytochrome *b* and cytochrome oxidase genes. The regions of extensive sequence homology betweem the introns *bI4* and *aI4* are depicted by solid and hatched segments. Both introns are physically composed of two distinct regions: a long open reading frame (large rectangle) followed by a blocked frame (narrow rectangle)[10,14,20]. In intron *bI4*, two clusters of *box*⁻ mutational sites, which prevent splicing[8,9,27], have been mapped: (1) *box7* cluster composed of *trans*-recessive mutations[7] which generate nonsense codons in the intron's open reading frame[10]; (2) *box9* cluster composed of *cis*-dominant mutations[7] which are all localized in a dodecanucleotide signal sequence[10]. In intron *aI4*, two *cis*-dominant mutations have been localized in the homologous signal sequence (hatched area)[20]; no *oxi3*⁻ *trans*-recessive mutations have been found until now. The *oxi3–mim2-1* mutation occurs 150 bp downstream from the *cis*-acting signal sequence.

How is a new maturase formed from an inactive intron?

One could imagine, for example, that, in the wild type, intron *aI4* is not translated at all because an internal splice destroys the continuity of its open reading frame; the *mim2-1* mutation would remove the internal splice point and modify the splicing pathway such that the continuity of the reading frame would be restored. It might also be possible that, in the wild type, intron *aI4* is translated but the protein is destroyed by proteolysis; the *mim2-1* mutation could have removed a specific proteolytic site. Alternatively, the wild-type protein could be inactive and the *mim2-1* mutation, by creating a proteolytic site, would permit the formation of an active fragment involved in splicing. We find these conjectures unattractive, however, because they do not explain why an open reading frame is preserved in the wild-type oxidase intron *aI4*. We therefore favour the hypothesis that *aI4* is normally translated into a protein. If this is the case, what is its function in the wild type, why is it not *trans*-active in splicing (while *bI4* is) and how does *mim2-1* restore the splicing activity?

We believe that the ability of *mim2-1* to restore splicing activity is due to a local increase of positive charges in a part of a protein that is essential for its catalytic activity. Arguments favouring this idea are: (1) *mim2-1* causes a replacement of a glutamic codon by a lysine codon and thus increases the charge by +2. Interestingly, this change occurs in an α-helical region as shown by our calculation of the secondary structure carried out according to ref. 21 (data not shown). This α-helix is the longest (15–18 amino acids) that can be traced in the translation products of introns *bI4* and *aI4*, and occupies homologous positions in both proteins. The α-helix of the wild-type *bI4* translation product (active) is more basic than that of the wild-type *aI4* product (inactive) by two or four charges (depending on the local polymorphism between the strains D273-10B and 777-3A)[10,20]. The *mim2-1* mutation, by increasing the charge by +2, renders the *aI4* translation product more similar to its normal *bI4* counterpart and we believe that this change is sufficient to explain the acquisition of splicing activity. That a protein which interacts with nucleic acids should be positively charged is plausible, and other active mRNA maturases, such as that of *bI2*, are overall highly basic[6,13].

(2) A second line of evidence favouring the idea that *aI4* can be translated even in the absence of *mim2-1* mutation comes from the analysis of mitochondrially synthesized proteins in splicing-deficient mutants resulting from *bI4* maturase-deficient mutation or $oxi3^{-}$-*G192* and -*G2190* mutations in *aI4* (O. Groudinsky, personal communication). These mutants accumulate a protein of apparent molecular weight 56,000 (referred to as p56). We conjecture that p56 results from translation of the previously fused oxidase exons *A1–A4* with the *aI4* open reading frame. The size of p56 is consistent with this idea and fingerprint comparisons show that p56 displays some peptide homologies with the subunit I of cytochrome oxidase[22]. Analyses of double mutants indicate that the N-terminal sequences of the *oxi3* exons control the synthesis of p56 (O. Groudinsky, unpublished results) and this protein disappears in an *oxi3* deletion mutant[23]. All these data are easily explained by the model shown in Fig. 5: in the wild type, splicing of *oxi3* mRNA is efficient and no p56 accumulates because the *oxi3* pre-mRNA does not accumulate. In mutants deficient for the *bI4* maturase ($box7^{-}$ mutants[10]) or *cis*-dominant *aI4* mutants, such as $oxi3^{-}$-*G192* (ref. 20), the pre-mRNA containing the non-excised intron *aI4* would accumulate and its translation would lead to an accumulation of p56. In a double mutant carrying simultaneously a $box7^{-}$ mutation and a *mim2-1* mutation, a p56 protein should still be detectable because the suppression is only partial, probably because the *aI4* maturase is less efficient than its normal *bI4* counterpart; this has indeed been observed[16]. Our model predicts that p56 from an *oxi3 mim2-1* strain should differ slightly from the $oxi3^{+}$ in its fingerprint pattern, and preliminary experiments (O. Groudinsky *et al.*, unpublished results) suggest that this is indeed the case.

Evolution of two homologous introns in two non-homologous genes

Sequence homologies between *bI4* and *aI4* (refs 10, 14, 20) and functional compensations between their translation products (this work) strongly suggest that the two introns are derived from a common ancestral sequence. We do not know when this duplication, transposition or insertion took place, but depending on whether it is recent or ancient even, two evolutionary histories can be proposed. If it is a recent event, then the fact that *aI4* still has an open reading frame could be purely accidental. The *bI4* descendant of the common ancestor would have kept the splicing function and the *aI4* descendant would have lost it by accumulating missense mutations. The divergence would not have been large enough to prevent a single base substitution, such as in *mim2-1*, still being able to restore or readjust the function. In other words, *aI4* may have just become (or be in the process of becoming) a pseudogene and we have caught it during the very early part of its evolutionary drift! Although this hypothesis cannot be formally excluded, we do not find it plausible and prefer to think that the duplication, transposition or insertion event took place a long time ago. We propose the following evolutionary scheme.

An identical ancestral base sequence, encoding a protein, was originally present or has been inserted, in two non-identical genes. This sequence has diverged during evolution in two directions: the first one has led to a diffusible protein endowed with a pleiotropic splicing activity (the *bI4* sequence) and the second to a protein with no catalytic splicing activity (the *aI4* sequence). Numerous missense mutations have been fixed during this period: for the region of strongest homology between *aI4* and *bI4*, which is 170 residues long, some 38–40 amino acid replacements have taken place[10,14,20]. With such an amount of evolutionary divergence there must be a selective pressure that has prevented the accumulation of nonsense mutations in *aI4*. What is the role of *aI4*? One hypothesis is that the normal translation product of *aI4* has a different and unknown function. It could, for example, be a structural part of the mitochondrial splicing and/or translation apparatus, it could be used as a handle to position correctly, by quaternary interactions, the *bI4* maturase on its second substrate, that is, on the pre-mRNA of oxidase. Alternatively, the travelling of a ribosome through *aI4*'s open reading frame could be a necessary but insufficient condition for the processive splicing (see refs 10, 20). In both hypotheses, the splicing of the two genes will be catalysed by a single maturase and not by two independent ones. This could confer a selective advantage because a coordinate expression of both genes would be facilitated.

Evolutionary conjectures are not easy to test. The finding of a converse situation to the normal one and the demonstration that it results from a single base change in an intron do, however, provide a striking example of intergeneic communications through intron-encoded proteins. It is thus of interest for the evolutionary history of mosaic genes.

We thank P. Netter and O. Groudinsky for helpful discussions and personal communications, B. Poirier and M. Even for help in preparing the manuscript. This work was supported by grants from CNRS, DGRST, INSERM and Ligue Nationale Française contre le Cancer.

Received 24 March; accepted 2 June 1982.

1. Slonimski, *et al.* in *Biochemistry and Genetics of Yeast* (eds Bacila, M., Horecker, B. L. & Stoppani, A. M.) 339–368 (Academic, Sao Paulo, 1978).
2. Grivell, L. A. *et al. ICN–UCLA Symp. molec. cell. Biol.* **15,** 305–324 (1979).
3. Haid, A. *et al. Eur. J. Biochem.* **94,** 451–465 (1979).
4. Alexander, N. J., Perlman, P. S., Hanson, D. L. & Mahler, H. R. *Cell* **20,** 199–206 (1980).
5. Nobrega, F. G. & Tzagoloff, A. *J. biol. Chem.* **255,** 9828–9837 (1980).
6. Lazowska, J., Jacq. C. & Slonimski, P. P. *Cell* **22,** 333–348 (1980).
7. Lamouroux, A., Pajot, P., Kochko, A., Halbreich, A. & Slonimski, P. P. in *The Organization and Expression of the Mitochondrial Genome* (eds Kroon, A. M. & Saccone, C.) 153–156 (North-Holland, Amsterdam, 1980).
8. Church, G. M., Slonimski, P. P. & Gilbert, W. *Cell* **18,** 1209–1215 (1979).
9. Halbreich, A., Pajot, P., Foucher, M., Grandchamp, C. & Slonimski, P. P. *Cell* **19,** 321–329 (1980).
10. De La Salle, H., Jacq, C. & Slonimski, P. P. *Cell* **28,** 721–732 (1982).
11. Borst, P. & Grivell, L. A. *Nature* **285,** 439–440 (1981).
12. Dhawale, S., Hanson, D. L., Alexander, N. J., Perlman, P. S. & Mahler, H. R. *Proc. natn. Acad. Sci. U.S.A.* **78,** 1778–1782 (1981).
13. Jacq, C. *et al.* in *Mitochondrial Genes*, Monogr. 12, 155–183 (Cold Spring Harbor Laboratory, New York, 1982).
14. Bonitz, S., Coruzzi, G., Thalenfeld, B., Tzagoloff, A. & Macino, G. *J. biol. Chem.* **255,** 11927–11941 (1980).
15. Dujardin, G., Pajot, P., Groudinsky, O. & Slonimski, P. P. *Molec. gen. Genet.* **179,** 469–482 (1980).
16. Groudinsky, O., Dujardin, G. & Slonimski, P. P. *Molec. gen. Genet.* **184,** 493–503 (1981).
17. Carignani, G., Dujardin, G. & Slonimski, P. P. *Molec. gen. Genet.* **167,** 301–308, (1979).
18. Grivell, L. A. & Moorman, A. F. M. in *Mitochondria 1977* (eds Bandlow *et al.*) 371–384 (de Gruyter, Berlin, 1977).
19. Morimoto, R., Lewin, A. & Rabinowitz, M. *Molec. gen. Genet.* **170,** 1–9 (1979).
20. Netter, P., Jacq, C., Carignani, G. & Slonimski, P. P. *Cell* **28,** 733–738 (1982).
21. Garnier, J., Osguthorpe, D. J. & Robson, B. *J. molec. Biol.* **120,** 97–120 (1978).
22. Claisse, M. L., Slonimski, P. P., Johnson, J. & Mahler, H. R. *Molec. gen. Genet.* **177,** 375–387 (1980).
23. Hanson, D. K., Lamb, M. R., Mahler, H. R. & Perlman, P. S. *J. biol. Chem.* **257,** 3218–3224 (1982).
24. Bolivar, F. & Beckman, K. *Meth. Enzym.* **68,** 245–267 (1979).
25. Clewell, D. B. & Helinski, D. R. *Proc. natn. Acad. Sci. U.S.A.* **62,** 1159–116 6 (1969).
26. Maxam, A. & Gilbert, W. *Meth. Enzym.* **65,** 499–560 (1980).
27. Schmelzer, C., Haid, A., Gorsch, G., Schweyen, R. J. & Kaudewitz, F. *J. biol. Chem* **256,** 7610–7619 (1981).

LETTERS TO NATURE

Is our vacuum metastable?

Michael S. Turner

Astronomy and Astrophysics Center, The University of Chicago,
Chicago, Illinois 60637, USA

Frank Wilczek

Institute for Theoretical Physics, University of California,
Santa Barbara, California 93106, USA

In spontaneously broken gauge theories of particle interactions there are sometimes several local minima of the effective potential. Any of these minima can serve as a vacuum in the sense that we can expand the fields around their values at the minimum, interpret the quantized fluctuations around the minimum as particles, and compare the properties of these particles with experiment. One might think that only the state with absolutely minimum energy could be what we ordinarily call our vacuum, as the other local minima will inevitably decay into this lowest one. However, this is not necessarily the case, because it is possible for the lifetime of a metastable vacuum to be very long, even when compared with the age of the Universe. Furthermore, the energy densities available in present laboratory or astrophysical environments are much less than the barriers which exist in field space between the different local minima, and so we have no direct sensitivity to the presence of a possibly lower vacuum state. (A possible exception to this are magnetic monopoles which do probe the large field region.) If it is not the absolute minimization of the effective potential, what does determine the present vacuum state of the Universe? We argue here that it is determined cosmologically by the dynamical evolution of the Universe from the hot, dense phase which existed shortly after the big bang to the present[1,2].

At finite temperature, the free energy tends to be minimized in phases which contain light particles. Therefore, we expect that in general, at extremely high temperatures the thermodynamically favoured phase is the symmetric one which contains the most massless particles. Assuming that very near the big bang this phase is realized[3-5], one can follow the subsequent dynamical evolution to determine the present state. The present vacuum is properly determined by evolutionary, not merely energetic, considerations. This point is relevant for all proposed models of elementary particle interactions.

In what conditions might we convince ourselves that we live in a metastable vacuum (or, not finding these conditions, assure ourselves that we do not)? Of course, we must demand that the putative vacuum has an extremely long lifetime, and that small fluctuations around it describe known physics. In addition, it should have been realized in the dynamical evolution of the Universe, starting from the symmetric phase at extremely high temperatures.

First, consider the question of metastability. For a ϕ^4 scalar field theory in which the energy difference between the two minima is not too large, the decay rate of the 'false vacuum' (per unit volume per unit time) at zero temperature is[6]

$$\Gamma \simeq A \exp[-(32\pi^2/(3\varepsilon^3\lambda)] \qquad (1)$$

where λ is the quartic self-coupling, ε is the ratio of the energy difference between the two minima to the barrier height between them, and A has dimensions of mass^6 and should be $0(\mu^4)$. Here μ^2 is the bare mass of the scalar field. Taking μ to be of the order of the grand scale ($\sim 10^{14}$ GeV), and the spatial volume to be that of the present observable Universe ($V \sim 10^{84}$ cm^3), the probability that an energetically less favourable minimum has decayed during the age of the Universe is exponentially <1 so long as

$$\varepsilon \ll 0.6\,\lambda^{-1/3} \qquad (2)$$

a condition which is easily satisfied.

We now examine the second and third issues in the context of the simplest unified model of particle interactions, the minimal SU(5) theory[7].

At zero temperature the effective potential can be written as[8,9]:

$$\begin{aligned} V(h,A) = {} & \frac{-\mu^2}{2}\operatorname{tr} A^2 + \frac{a}{4}(\operatorname{tr} A^2)^2 + \frac{b}{2}\operatorname{tr} A^4 \\ & - \frac{\nu^2}{2} h^\dagger h + \frac{\lambda}{4}(h^\dagger h)^2 + \alpha (h^\dagger h)\operatorname{tr} A^2 + \beta h^\dagger A^2 h \end{aligned} \qquad (3)$$

where the discrete symmetry $A \rightarrow -A$ has been imposed, h is an SU(5) vector **5** Higgs field, and A is an SU(5) adjoint **24** Higgs field (traceless hermitian matrix). To reproduce the standard (and thus far very successful) SU(5) phenomenology, there must be a local minimum where A acquires a large vacuum expectation value of the form,

$$\langle A \rangle = \begin{pmatrix} 1 & & & & 0 \\ & 1 & & & \\ & & 1 & & \\ & & & -3/2 & \\ 0 & & & & -3/2 \end{pmatrix} \delta \qquad (4)$$

This vacuum expectation value breaks SU(5) down to SU(3) × SU(2) × U(1).

The second stage of symmetry breaking involves the fifth component of h acquiring a vacuum expectation value much less than δ (the small vacuum expectation value $\langle h \rangle$ will slightly perturb $\langle A \rangle$ from the form given in equation (4); see refs 8–10). In addition, we must also ensure that the colour triplet component of h has a large mass $\simeq 0(\delta)$ as it can mediate proton decay. Both of these requirements are fulfilled if:

$$\beta < 0 \qquad (5a)$$

$$-m_{\text{eff}}^2 \equiv \nu^2 - 3\mu^2(10\alpha + 3\beta)/a' \approx 0 \qquad (5b)$$

$$(\alpha + \beta/2) > -[\lambda(a+b)]^{1/2}/2 \qquad (5c)$$

$$\mu^2, a', b > 0 \qquad (5d)$$

$$\lambda > 9\beta^2/10b \qquad (5e)$$

where $a' \equiv 15a + 7b$. Condition (5*b*) specifies that the SU(2) doublet component of h (the ordinary Weinberg–Salam doublet) has a small, negative bare mass. Quantitatively, m_{eff} must be about 13 orders of magnitude smaller than $\delta = (2\mu^2/a')^{1/2}$.

For our purpose, the crucial observation is that condition (5*b*), along with the others, can be satisfied with ν^2 large and positive. Looking back at equation (3), it is perhaps not surprising that in this case another very different type of vacuum might be energetically favourable: one in which $\langle h \rangle$ is large. Indeed, if

$$2\alpha\nu^2/\lambda > \mu^2 \qquad (6a)$$

$$2(\alpha + 4\beta/5)\nu^2/\lambda > \mu^2 \qquad (6b)$$

then the potential also has a local minimum at $\langle h_5 \rangle^2 = \nu^2/\lambda$ and $\langle A \rangle = 0$. In this vacuum SU(5) has broken down to SU(4). When we compare the value of the effective potential at this local minimum with the usual one (when both exist), we find that for the following range of parameters:

0028–0836/82/320633—02$01.00

$$\mu^2, \lambda, a', b, -\beta > 0 \quad (7a)$$

$$\lambda > 9\beta^2/10b \quad (7b)$$

$$(\alpha + \beta/2) > -[\lambda(a+b)]^{1/2}/2 \quad (7c)$$

$$(5\alpha + 4\beta)(10\alpha + 3\beta) > 5\lambda a'/6 \quad (7d)$$

$$\nu^2 \approx 3\mu^2(10\alpha + 3\beta)/a' \quad (7e)$$

the usual vacuum corresponds to a local, but not a global, minimum.

From the point of view of microphysics, then, it is quite conceivable that our vacuum is metastable. We must now investigate the dynamical question, whether it is reasonable that during the course of its temperature evolution, the Universe could get 'hung up' in our vacuum in spite of its only being metastable. Basically, we must determine which of the two asymmetric vacua becomes lower than the fully symmetric vacuum first as the Universe cools down from very high temperatures. Although we have not investigated this question in quantitative detail, it seems that a 'hang up' can occur. Finite-temperature modifications to the zero-temperature potential tend to increase the free energy, and those due to the most strongly coupled fields are most important[3-5]. Suppose that the usual vacuum and the SU(4) vacuum discussed above have roughly the same energy at zero temperature. The high temperature state continuously related to the SU(4) vacuum will then be disfavoured if it feels stronger finite-temperature corrections. This will occur, for instance, if all the Higgs self-couplings are small and h, but not A, couples strongly to some fermion field.

It seems distinctly possible in simple unified models, that our present vacuum is only metastable, and that nevertheless, the Universe would have chosen to get 'hung up' in it. If this is the case, then without warning, a bubble of true vacuum could nucleate somewhere in the Universe and move outwards at the speed of light, and before we realized what swept by us our protons would decay away. There is no immediate cause for concern, however, because the lifetime of our metastable vacuum could easily be 10^{30} yr (or only 10^{10} yr for that matter).

This work was supported in part by the NSF through grant PHY 77-27084 (at Santa Barbara) and by the DOE through grant AC02-80ER-10773 (at Chicago).

Received 24 May; accepted 30 June 1982.

1. Linde, A. D. *Phys. Lett.* **70B**, 306 (1977).
2. Srednicki, M. Preprint (Princeton University, 1982).
3. Kirzhnits, D. A. & Linde, A. D. *Phys. Lett.* **42B**, 471 (1972).
4. Dolan, L. & Jackiw, R. *Phys. Rev.* **D9**, 3320 (1974).
5. Weinberg, S. *Phys. Rev.* **D9**, 3357 (1974).
6. Coleman, S. *Phys. Rev.* **D15**, 2929 (1977).
7. Georgi, H. & Glashow, S. L. *Phys. Rev. Lett.* **32**, 438 (1974).
8. Buras, A. J., Ellis, J., Gaillard, M. K., & Nanopoulos, D. V., *Nucl. Phys.* **B135**, 66 (1978).
9. Magg, M. & Shafi, Q. *Z. Phys.* **C4**, 63 (1980).
10. Sherry, T. N. *J. Phys.* **A13**, 2205 (1980).

A search for evidence of superheavy-element fission in chondritic metal

R. K. Bull*‡ & P. Mold*†

* Department of Physics, University of Birmingham B15 2TT, UK
† West Midlands College of Higher Education, Walsall,
West Midlands, UK

There is evidence for the early melting of the Moon[1,2], and Runcorn[2-4] has concluded from palaeomagnetic data that a fluid core dynamo must have been present for ~10^9 yr and that the decay of a siderophile superheavy element (SHE) with a half life of ~10^8 yr may have been responsible for these phenomena[3-5] Libby and co-workers[6] have suggested that SHE-decay could have produced certain trace-element abundance patterns in iron meteorites. Several searches[7-9] have failed to detect evidence for SHE decay in iron meteorites. We describe here a search for SHE in metal fragments within ordinary chondrites. The absence of excesses of tracks along the boundaries between olivines and metal grains allows upper limits to the SHE content of the metal of ~2.5×10^{-13} to ~2.5×10^{-15} kg per kg to be set at a time ~4×10^9 yr ago, determined from the ^{244}Pu fission track densities in chondritic phosphates.

Our experimental methods are essentially similar to those described previously[7]. Slices and coarse fragments from three chondrites, Estacado (type H6), Wold Cottage (L6) and Alta'ameem (LL5), were ground and polished. They were then etched in WN solution at pH 8 and 50% of the usual concentration to reveal tracks in olivine crystals[10]. The etched samples were then examined under an optical microscope at a magnification of approximately ×630 and under a scanning electron microscope at about ×5,000 magnification. Abundant cosmic ray tracks (identification as cosmic ray tracks was based on the anisotropic angular distribution of the tracks and a length distribution peaking at short track lengths) were observed throughout the olivine grains from Alta'ameem but track densities were observed to be much lower in Wold Cottage and Estacado (see Table 1). The boundaries between the olivine crystals and metal grains were carefully examined using both scanning electron microscopy and optical microscopy, and no significant excesses of tracks were detected in these regions in any of the three meteorites. For the purposes of calculation it is assumed that the contribution of fission tracks from the metal is, in each case, equal to the cosmic ray track density. These track densities (column 4 of Table 1) allow upper limits to the SHE content of the metal to be calculated and these are displayed in column 5 of Table 1. In obtaining these estimates it is assumed that the SHE have decayed to extinction during the time since tracks began to be retained by the olivine. These limits apply to the times at which track retention in the olivine began for each of the three meteorites and for any conclusions to be drawn from these data it is necessary to establish a time scale for track retention by the olivine.

An estimate of the track retention time for these meteorites can be made by examining the fission track densities in apatite and merrillite crystals from each meteorite. These phosphate crystals are usually found to contain tracks produced by the fission of ^{238}U and ^{244}Pu. Since the latter has a half life of ~10^8 yr, the identification of ^{244}Pu tracks in these phases would provide strong evidence that track retention in the olivine occurred relatively close to the time of formation of the meteorites, because olivine is believed to retain tracks at higher temperatures than apatite and merrillite[11].

Phosphates were concentrated in non-magnetic fractions of density between 2.8 and 3.3 g cm^{-3} and grain size between 63 and 106 μm. These were then etched in aqueous HNO_3 solutions at room temperature. The precise etching conditions used in each case are shown in Table 2. The track densities were obtained from scanning electron microscopy photographs at a magnification of about ×5,000. The uranium concentrations in the phosphates were determined by irradiating them with thermal neutrons (fluences of about 10^{18} neutrons cm^{-2}) in the Herald reactor at Aldermaston. Induced-fission fragments were detected in adjacent sheets of uranium-poor mica. The neutron fluence was monitored by irradiating standard reference glasses along with the meteorite samples.

Fission track density and uranium content data are shown in Table 2. The track density figures for Alta'ameem have been

---

‡ Present address: Atomic Weapons Research Establishment, Aldermaston, Reading, Berks RG7 4PR, UK.

0028-0836/82/320634—02$01.00

Table 1 Track densities in olivines

Meteorite (class)	Central track density in olivines* (cm^{-2})	Track density along boundary with metal† (cm^{-2})	Upper limit to contribution from fission in metal (cm^{-2})	Upper limit to SHE concentration at time of track retention by olivine (kg per kg)
Wold Cottage (L6)	$<10^4$	$<10^4$	10^4	2.5×10^{-15}
Alta'ameem (LL5)	$(0.9\text{–}1.3)\times10^6$	$\sim10^6$	10^6	2.5×10^{-13}
Estacado (H6)	$<10^4$	$<10^4$	10^4	2.5×10^{-15}

* Mainly due to heavy cosmic ray primaries.
† Measured within a strip of olivine 10 μm wide immediately adjacent to metal grains.

Table 2 Summary of track data for phosphates

Meteorite	Mineral	Etching conditions	Track density† (10^6 cm^{-2})	U content (10^{-6} kg per kg)	Approximate average ratio of ^{244}Pu fission tracks to ^{238}U fission tracks
Wold Cottage	Merrillite*	75s, 0.25% HNO_3, 20 °C	67–82 (6)	0.08–0.19	165
	Apatite		16–25 (2)	1.8–3.7	2
Alta'ameem	Merrillite	20s, 1% HNO_3, 20 °C	34 (1)	0.1	100
	Apatite		7–16 (20)	0.3–1.7	4
Estacado (This work)	Merrillite	50s, 1% HNO_3, 20 °C	33 (18)	0.1	120
(Pellas and Storzer[15])	Merrillite		37.5 (15)	0.19	75
	Apatite		8.2 (15)	3.26	<1

* In many earlier papers on meteoritic phosphates, this mineral is referred to as whitlookite.
† Number of crystals shown in parentheses.

corrected for a cosmic ray track background of $\sim10^6$ cm^{-2}. The contribution to the total track density from the spontaneous fission of ^{238}U can be calculated from the measured uranium content of each phase. The excess fission tracks are assumed to be due to the spontaneous fission of ^{244}Pu and the last column of Table 2 gives the ratio of ^{244}Pu to ^{238}U fission tracks. The assumption of a ^{244}Pu source for these tracks rests on numerous determinations of ^{244}Pu fission Xe in merrillites[12–14] (formerly known as whitlockites) and in apatites[13] from chondritic meteorites. In particular, Kirsten and co-workers[13] have measured the fissiogenic Xe content of Estacado. The fission track data for Estacado obtained by Pellas and Storzer[15] is included in Table 2.

Merrillites from all three of the meteorites that we studied show large excesses of ^{244}Pu fission tracks and notwithstanding uncertainties in the initial Pu content of these crystals, it seems unlikely that these three meteorites could have cooled to the track retention temperature of merrillite (and therefore of olivine) much later than $\sim4\times10^9$ yr ago. The upper limits to SHE concentrations given in Table 1 therefore apply to approxomately this time. Runcorn[4] requires a SHE concentration in the lunar core of $\sim10^{-7}$ kg per kg at $\sim4.1\times10^9$ yr ago. The concentration would have fallen to $\sim6\times10^{-9}$ kg per kg at $\sim3.7\times10^9$ yr ago, assuming a SHE half life of $\sim10^8$ yr. Our results indicate that the SHE content of chondritic metal was lower by at least 4–6 orders of magnitude at that time.

These results, taken together with the failure to find evidence for SHE in the metal from iron meteorites[7–9], indicate that the abundance of SHE in meteoritic metal was very low $\sim4\times10^9$ yr ago and unless the metal of the lunar core was very much enriched in siderophiles relative to meteorites, SHE could not have played an important role in the early heating of the Moon.

We thank Drs P. F. Green and S. A. Durrani for useful comments and the staff of the Herald reactor at the Atomic Weapons Research Establishment, Aldermaston, for carrying out the neutron irradiations. Meteorite samples were provided by Dr R. Hutchison (British Museum) and by Dr Y. Al-Rawi (College of Science, Baghdad, Iraq). The financial support of the SERC is gratefully acknowledged.

Received 13 April; accepted 30 June 1982.

1. Taylor, S. R. *Lunar Science: A Post Apollo View* (Pergamon, New York, 1975).
2. Runcorn, S. K. *Proc. 8th lunar Sci. Conf.*, 463–469 (1977).
3. Runcorn, S. K. *Science* **199,** 771–773 (1978).
4. Runcorn, S. K. *Earth planet. Sci. Lett.* **39,** 193–198 (1978).
5. Runcorn, S. K., Libby, L. M. & Libby, W. F. *Nature* **270,** 678–681 (1977).
6. Libby, W. L., Libby, W. F. & Runcorn, S. K. *Nature* **278,** 613–617 (1979).
7. Bull, R. K. *Nature* **282,** 393–394 (1979).
8. Nozette, S. & Boynton, W. V. *Meteoritics* **15,** 501 (1979).
9. Kaiser, T., Piepgras, D. & Wasserburg, G. J. *Earth planet. Sci. Lett.* **52,** 239–250 (1981).
10. Krishnaswami, S., Lal, D., Prabhu, N. & Tamhane, A. S. *Science* **174,** 287–291 (1971).
11. Fleischer, R. L., Price, P. B. & Walker, R. M. *Nuclear Tracks in Solids* (University of California Press, Berkeley, 1975).
12. Wasserburg, G. J., Huneke, J. C. & Burnett, D. S. *J. geophys. Res.* **74,** 4221–4322 (1969).
13. Kirsten, T., Jordan, J., Richter, H., Pellas, P. & Storzer, D. *Meteoritics* **12,** 279–281 (1977).
14. Lewis, R. S. *Geochim. cosmochim. Acta* **39,** 417–432 (1975).
15. Pellas, P. & Storzer, D. *Proc. R. Soc.* **A374,** 253–270 (1981).

Detection of nitrogen at {100} platelets in diamond

S. D. Berger & S. J. Pennycook

Cavendish Laboratory, Madingley Road, Cambridge CB3 0HE, UK

Platelets in type Ia diamond were first directly observed with transmission electron microscopy by Evans and Phaal[1] in 1962. Considerable controversy still exists over their structure and chemical composition. One of the earliest models of the platelet structure was that proposed by Lang[2] in which nitrogen, the major impurity in type Ia diamonds, is segregated into plate-like structures, only two atoms thick, lying on the cube planes. Later evidence seemed to favour interstitial carbon as the major component of the platelets[3–5], although more recent evidence from the production of platelets in synthetic diamond[6] again points to nitrogen as forming an important constituent. High resolution electron microscopy also supports this view[7,8]. Here we report for the first time the direct observation of nitrogen at platelets using the technique of electron energy loss spectroscopy (EELS).

A type Ia diamond was cut and thinned parallel to an (001) plane. The platelets were studied using a VG Microscopes' HB5 scanning transmission electron microscope (STEM). In the STEM transmitted electron images showing diffraction or phase contrast can be obtained similar in all respects to those obtained in a conventional TEM, but in addition elemental analysis and diffraction patterns can be obtained at very high

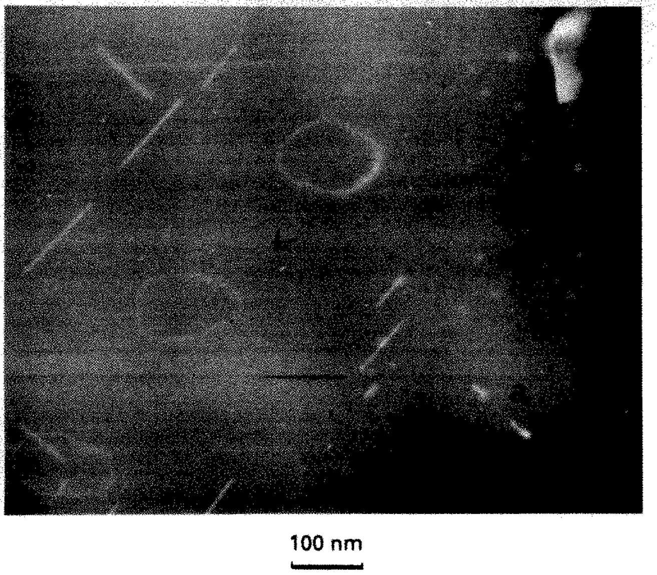

Fig. 1 Weak beam image of platelets in type Ia diamond. The dark marks are burns in the phosphor of the display tube.

spatial resolution (see ref. 9 for a full discussion of the techniques). Figure 1 shows an edge of the diamond flake containing several platelets. The image is obtained using an annular dark field detector, which detects electrons scattered out of the main beam. The diamond is orientated with the electron beam incident exactly along the [001] direction, so that the image is formed mainly from the four 220 Bragg reflections, weakly excited. Three sets of platelets are visible. Those lying on the (100) and (010) planes are seen as two sets of straight lines perpendicular to each other, while those lying on the (001) plane within the foil have a roughly circular shape, made visible by the partial dislocation around the circumference of the platelet. In thinner regions of the diamond, platelets lying parallel to the beam may extend through the thickness of the specimen (platelet a in Fig. 1 for example). In such regions the diffraction contrast along the length of the platelet is lost but it is still visible at the ends where the defect terminates inside the crystal. The central region of such platelets can be imaged by phase contrast microscopy giving images similar to those shown by Bursill *et al.*[8], although the resolution is limited to about 0.7 nm, in our case, due to stray magnetic fields around the field emission gun.

A previous attempt[10] to find nitrogen by EELS failed due to insufficient sensitivity to nitrogen in the experimental conditions used. Several factors must be optimized to achieve the highest sensitivity when analysing a platelet with a fine electron probe. First, steps must be taken to prevent the build-up of carbon contamination on the area analysed. This can be a severe limitation to microanalysis at the highest spatial resolution, but was completely eliminated by baking both the microscope and specimen at 120 °C for 10 h before analysis. Second, the specimen geometry was optimized by choosing platelets parallel to the beam running right through the thickness of the diamond. The highest sensitivity to the elemental composition is then achieved by passing the smallest electron probe down the centre of the platelet. The third factor is the correction for electron beam or specimen drift. As type Ia diamond is an insulating material, drift tends to occur as the specimen charges up and it is important to keep the electron probe over the platelet throughout the analysis. By scanning the smallest possible area (~1 nm^2) an image is available on the annular dark field detector while the electrons in the bright field beam are analysed by the spectrometer. In this way drift can be continuously compensated for using electrical beam shift controls. To facilitate this correction, improved contrast in the annular detector image was obtained by tilting the diamond slightly off the [001] direction into a two-beam condition, typical images being shown in Fig. 2.

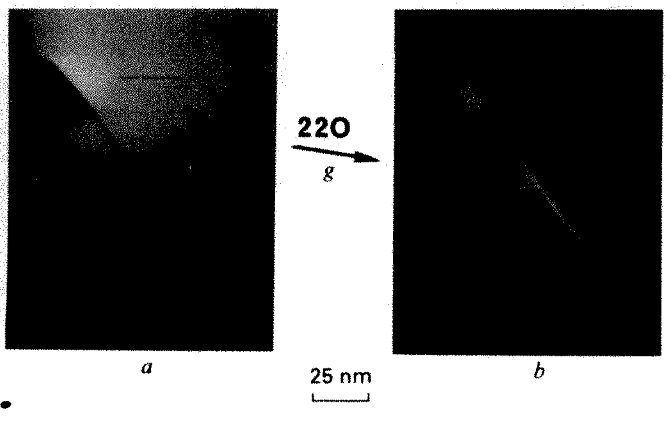

Fig. 2 Typical two-beam bright field (*a*) and annular dark field (*b*) images of platelets suitable for microanalysis.

The fourth and possibly most important factor is to achieve the most accurate background subtraction under the nitrogen edge in the energy loss spectrum. This would normally be done by extrapolation from the region of the spectrum just before the edge. However, due to strong intensity modulations following the carbon K-edge this technique would be inaccurate in this case. The spectrum from the normal diamond lattice shows the same modulations and hence provides a much more accurate background for subtraction.

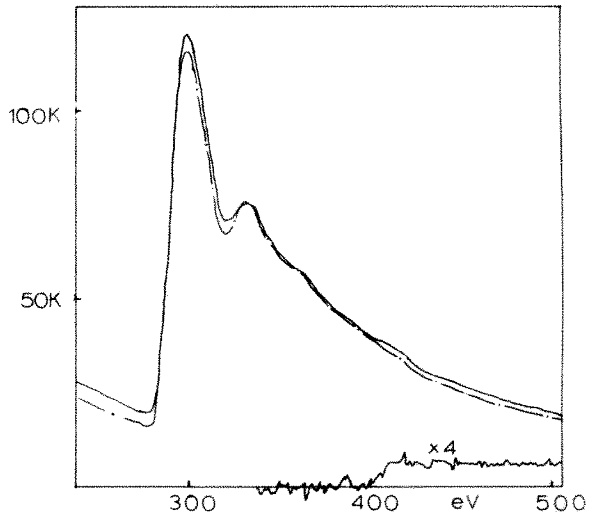

Fig. 3 Electron energy loss spectra from the centre of a platelet (solid line) and from just off the platelet (broken line). Also shown is the difference (×4) which shows the nitrogen-*K* edge at ≈406 eV from the platelet.

The spectra were obtained by scanning an isolated drift tube to give an absolute energy calibration[11] with digital data acquisition using a Link Systems 860 analyser. The incident beam semi-angle $\alpha = 8.3$ mrad and spectrometer acceptance semi-angle $\beta = 3$ mrad were chosen to give good spatial resolution together with a high count rate in the spectrometer with an energy resolution of about 12 eV.

The spectrum from the platelet acquired in this way is shown in Fig. 3 and is compared with the spectrum taken from the diamond just adjacent to the platelet. As well as the carbon *K*-edge at ≈290 eV an edge is clearly visible at ≈406 eV from the platelet which corresponds to the nitrogen K loss (both edges are shifted by ~7 eV from their expected positions[12] due to band structure effects[13]). The mismatch between the spectra in the region of the carbon edge is due to a slight change in specimen thickness between the two areas analysed. The area of normal lattice analysed was slightly thicker due, possibly, to preferential etching of the platelet during preparation. Generally, the effect of taking a matrix spectrum from a thicker region would be to decrease the slope of the decaying carbon edge as a result of multiple scattering. This would manifest

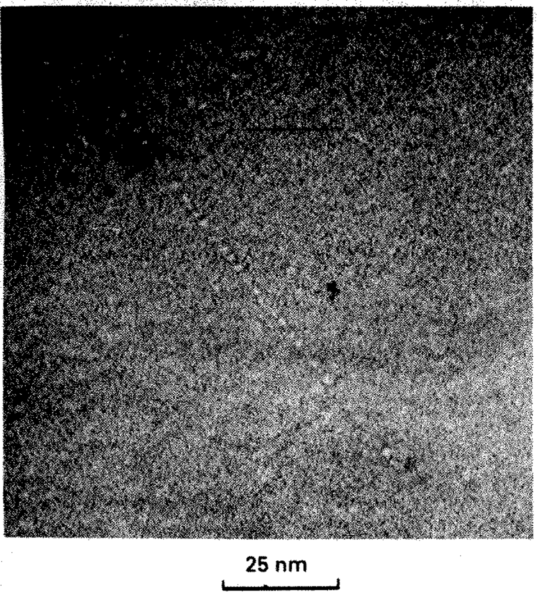

Fig. 4 Bright field image of an inhomogeneous platelet, or 'voidite' (noisy image is due to a shorter exposure time than in Figs 1 and 2).

itself, after subtraction from the platelet spectrum, in a slow modulation on the difference curve. In our case the change in thickness is ~3% and, as can be seen, produces negligible modulation of the difference between the spectra. The feature at ~406 eV rises over ~12 eV, corresponding to the spectrometer resolution, continues for the rest of the spectrum and can only be due to a nitrogen *K*-absorption edge. It has been shown[14] that most of the nitrogen in type Ia diamonds is in a dispersed form. Any signal due to this nitrogen will appear in both the background spectrum and the spectrum from the platelet. Thus when the two spectra are subtracted, only the nitrogen signal associated with the platelet will remain. However, the concent ations of the dispersed forms of nitrogen are so low that it is unlikely that they will be detected at all by this technique. The result of subtracting the two spectra is shown on an increased vertical scale and the nitrogen edge is very clearly visible.

So far, five platelets have been analysed, of which four contained nitrogen to a significant extent, while one contained no detectable nitrogen (<10% of the amounts found in the other platelets). By scanning an accurately known area and integrating the counts under the carbon and nitrogen edges in the spectrum, it is possible to obtain the percentage of nitrogen present in the volume analysed, and this can be compared with the expected percentage of nitrogen present if the platelet followed the Lang model. We found that the percentage of nitrogen detected varied significantly and no platelet contained as much nitrogen as the model predicts. Sequential spectra were then taken from the same platelet and it was found that nitrogen was being gradually lost from the defects. Although this would appear to account for the variation in nitrogen content already seen, early results indicate that some platelets are more susceptible to damage than others and further experiments are being carried out to clarify this point.

One platelet was found which showed a particularly interesting form of inhomogeneous contrast and is shown in Fig. 4. Analysis showed the bright regions of Fig. 4 contained at least three times as much nitrogen as the dark regions. The contrast seen from this platelet is very similar to that seen from 'voidites' (T. Evans and J. Macguire, and J. L. Hutchinson, personal communications) which appear to be a form of collapsed or semi-collapsed platelet. If the bright regions of Fig. 4 do not extend through a significant fraction of the thickness then they must contain a very high concentration of nitrogen.

The results from this work show directly that nitrogen is associated with platelet defects in type 1a diamond. The fact that some platelets are susceptible to beam damage at an energy of 80 keV indicates perhaps that the nitrogen is not bonded into the lattice in the covalent manner that the Lang model suggests. Also, if beam damage is unable to account for the variable nitrogen content seen, then again a modification to the simple models is called for.

We thank Professor T. Evans and Miss J. Maguire for providing the thinned specimen and for many useful discussions, together with Drs L. M. Brown and A. Howie. We are grateful to the SERC for financial support.

Received 11 March; accepted 10 June 1982.

1. Evans, T. & Phaal, C. *Proc. R. Soc.* **A270,** 535–552 (1962).
2. Lang, A. R. *Proc. phys. Soc. Lond.* **84,** 871–876 (1964).
3. Evans, T. *Diamond Research,* 2–5 (Industrial Diamond Information Bureau, London, 1973).
4. Evans, T. & Rainey, P. *Proc. R. Soc.* **A344,** 111–130 (1975).
5. Evans, T. *Contemp. Phys.* **17,** 45–70 (1976).
6. Evans, T., Qi, Z. & Maguire, J. *J. Phys.* **C14,** L379–L384 (1981).
7. Hutchison, J. L., Bursill, L. A. & Barry, J. C. *Electron Microscopy and Analysis 1981,* 369–372 (*Inst. Phys. Conf. Ser.* No. 61, London, 1982).
8. Bursill, L. A., Barry, J. C. & Hudson, P. R. *Phil. Mag.* **A37,** 789–812 (1978).
9. Brown, L. M. *J. Phys.* **F11,** 1–26 (1981).
10. Bursill, L. A. Egerton, R. F., Thomas, J. M. & Pennycook, S. J. *J.C.S. Faraday Trans. 2* **77,** 1367–1373 (1981).
11. Batson, P. E., Pennycook, S. J. & Jones, L. G. P. *Ultramicroscopy* **6,** 287–290 (1981).
12. Siegbahn, K. *et al. Nova Acta Reg. Soc. Scient. Uppsala,* Ser. IV **20,** 224–229 (1967).
13. Egerton, R. F., Whelan, M. J. *J. Electron Spectrosc.* **3,** 232–236 (1974).
14. Sobolev, E. V., Lisoivan, V. I. & Lenskaya, S. V. *Sov. Phys.-Doklady* **12,** 665–668 (1968).

Reconstruction of past ice conditions in a Hudson Bay estuary using tree rings

Gordon C. Jacoby & Linda D. Ulan

Lamont-Doherty Geological Observatory, Columbia University,
Palisades, New York 10964, USA

Descriptions of ice conditions, ranging from lake and sea ice to glacial advances and retreats, form an important portion of the climatic record. Ice formation, deterioration and changing areal extent are of increasing interest in climatology, sea transportation, petroleum exploration and the fishing industry. With few exceptions, quantitative information on ice conditions is generally brief, with many records in the US and Canada beginning only in the 1950s[1]. Tree-ring data from long-lived trees can be used as quantitative proxy data for past climatically related parameters. The record of first complete freezing of the Churchill River estuary on Hudson Bay is reconstructed here for 298 yr (1680–1977) by means of tree-ring analysis.

Both high-latitude tree growth and ice are influenced by many factors but can be significantly related to temperature[2–5]. In areas where ice conditions are influenced by a complex set of factors, a simple or direct relationship with climate may be difficult to establish. However, ice conditions in some areas show a more direct relationship to particular climate parameters (P. M. Kelly, personal communication). It is in these latter areas that we are investigating the possibility of using selected tree-ring data as a proxy series for past ice conditions.

A promising location to test the feasibility of reconstruction is near Churchill, Manitoba, Canada (see Fig. 1). Both a recent record of ice conditions and an independent, historical record are available, and we have developed a tree-ring chronology from the same location. The historical record of ice conditions is now used to calibrate the tree-ring time series which is in turn used to reconstruct the ice conditions for almost three centuries. The reconstruction is verified by modern data.

The tree-ring chronology is based on annual ring-width measurements of 15 increment cores from 7 white spruce (*Picea glauca* [Moench] Voss) from flat, poorly drained muskeg overlying permafrost. Ten of the 15 cores extend back to 1686 or

0028–0836/82/320637—03$01.00

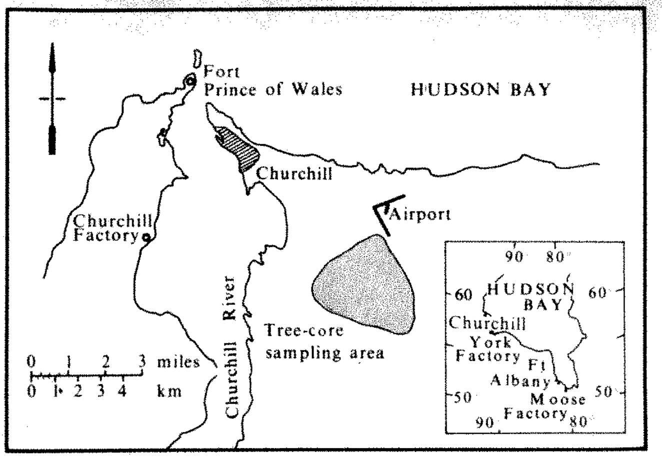

Fig. 1 Map of the Churchill area showing tree-core sampling site, Fort Prince of Wales, airport (meteorological station) and modern Churchill. Although total collection at this site was 39 cores from 15 trees, we feel that objective screening out of cores with abnormal anatomy (mainly reaction wood—eccentric growth due to leaning) and use of principal component analysis (PCA) to determine the most homogeneous subgroup produces a chronology with a better climatic signal-to-noise ratio. The PCA procedures are used before and independently of comparisons between the tree-ring data and meteorological information. The purpose is to determine a subgroup of tree cores with maximum common variance, which presumably is dominated by climate. The PCA results in ref. 20 show that, even from one site, smaller, homogeneous subgroups of cores can produce equally good or better climatically sensitive time series than larger numbers of cores. Cross-spectral analysis has also been used in selecting coherent subsets of cores from sites in Switzerland to maximize the signal-to-noise ratio of the resulting chronologies (J. Guiot, personal communication). Because we calibrated with historical data from 1741 to 1764, we also deleted cores younger than 1741 so that the sample size would not change between the calibration and verification periods. The deletions proceeded as follows: 17 cores due to abnormal growth or extreme youth of tree, 3 cores (all from one tree) shown by PCA to be heterogeneous with respect to the common variance of the rest of the cores, and 4 cores younger than 1740. Due to heterogeneous low-frequency variations in ring widths, conventional standardization methods did not produce a usable time series of ring-width indices for these tree cores. The s.d. of mean indices for individual years were above acceptable levels. The cubic-spline technique has been very useful in some of our analyses of trees from the subarctic and from the closed-canopy forests of the eastern US[6]. This group of trees does not exhibit the coherent, common, low-frequency trends that have been observed in some other subarctic trees[2–4]. This could be attributed in part to the standardization method but, additionally, inspection of the cores and the raw data do not show such trends to be as evident as they are in cores from other subarctic sites sampled.

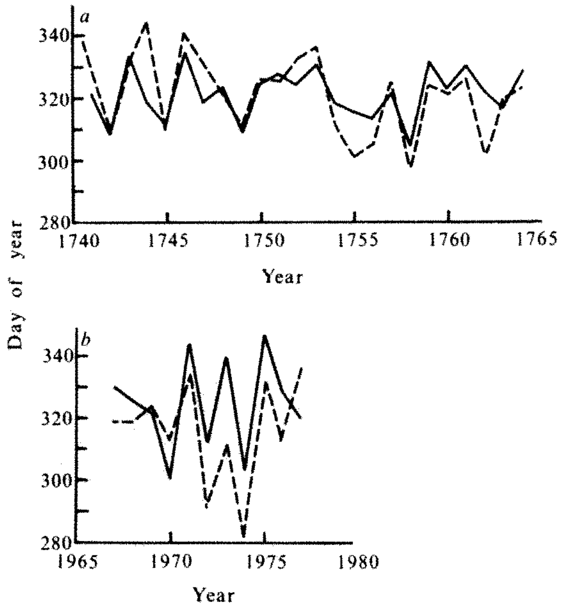

Fig. 2 *a*, Calibration data (dashed line) and reconstructed data (solid line) for first complete freeze of the Churchill Estuary. *b*, Verification data (dashed line) and reconstructed data (solid line) for first complete freeze.

earlier (see Fig. 1 legend). In an attempt to remove much of the nonclimatic variation, the raw ring-width data were standardized using cubic smoothing splines[6] which removed much of the variance with periods of 100 yr or more in length. The mean sensitivity of the standardized ring-width indices[7] for this chronology is 0.15, standard deviation (s.d.) is 0.17 and serial correlation is 0.44. Average values for these parameters for subarctic chronologies are 0.16, 0.25 and 0.62 respectively[4]. Based on a common period of 182 yr (1718–1899), the first principal component of the normalized ring-width indices for the cores accounts for 34% of the total variance.

One of the serious problems in reconstructing climate-related phenomena in the subarctic is the shortness of records and the lack of data for verification. The ice record for Churchill is unusual in that there are both recent and historical data. The older records result from an exhaustive analysis of old Hudson Bay Company records by Moodie and Catchpole[8] who were able to construct time series of quantitative data on ice conditions for several sites near old Hudson Bay Company factories along the south and south-west coast of Hudson Bay.

The historical ice data contain the following parameters for the nearby estuaries: days of first breaking, first partial freezing and first complete freezing. Not all the ice parameters have a clear relationship with climate nor are they equally reliable. The Churchill record is considered most reliable with respect to the records at York Factory, Fort Albany and Moose Factory[8] (see Fig. 1). The ice parameters at Churchill are, in order of increasing reliability: first partial freezing, first complete freezing and first breaking[8]. A fourth parameter, first ice free, shows very low reliability.

Table 1 Mean and standard deviation of first-full-freeze time series used or reconstructed

	Mean	s.d.
Prince of Wales—all data	321	11.96
Prince of Wales—calibration period (1751–64)	322	11.95
Modern Churchill—all data	317	15.10
Modern Churchill—verification period (1967–77)	317	15.08
Reconstruction (1680–1977)	323	10.31

The first-breaking data are judged to be most reliable from the standpoint of observational accuracy but for the following reasons may be less reliable as a simple climatic parameter. Ice breakup in many north-flowing, high-latitude rivers results from a combination of climatic and hydrological factors. In relatively low-relief regions such as Manitoba, the southern, headwater areas thaw sooner than the northern, outflow areas. The flow of water from the south causes hydraulic pressure and can either overflow or rupture the ice in the more northerly portions of rivers. These hydrodynamic effects of spring meltwater on breakup produce a more complex response to climate than the freeze response.

Modern Churchill River ice data are recorded by the Canadian Meteorological Service and extend from 1957 to 1980[9]. Precise definitions of specific ice events and observer judgement are crucial to the quality of ice record[1]. Due to changes in freeze-up definition[8], an 'approximate only' value for 1965 and a missing value for 1966, we used only the past 14 yr of reliable record for our analyses.

The meteorological data used are from the Churchill A station at the Churchill airport, ~7 km east of the estuary and 1 km north of the tree-core sampling area. This record of mean monthly temperatures and total monthly precipitation starts in January 1943. First subfreezing temperatures occur in September and, in the historical and modern ice records, complete freezing of ice takes place during October or November, usually the latter. Temperature data for these 3 months successfully passed tests for homogeneity[10,11].

We concluded that, for this study, any proxy time series should be based on tree-ring samples from the same locality

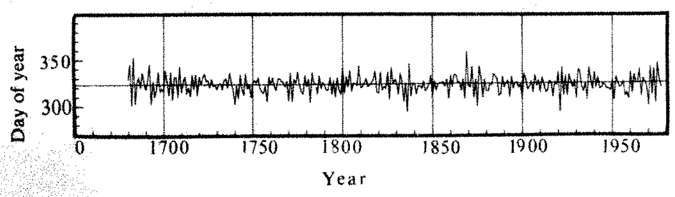

Fig. 3 Day of first complete freeze of the Churchill Estuary, Manitoba, Canada, reconstructed using rree rings, 1680–1978.

as the particular set of ice data because (1) plots of ice-condition time series and tree-ring series from distant locations showed little correspondence; and (2) similarly, the graphical relationships and correlations between the historical ice records at different stations were generally low.

Comparison of graphical plots of tree-ring and ice-condition data from Churchill indicated a correspondence between complete-freeze day and tree growth the next year. Response-function analysis[12] indicated a significant positive relationship between July temperature and ring-width indices as is common in most high-latitude forest–ecotone chronologies[4]. More importantly, a significantly positive ring-width response to warm October and November of the earlier year was shown. Although increased tree growth after a warm autumn the previous year has shown up in other dendroclimatic analyses of subarctic chronologies, generally only one autumn month, November, shows a significant positive relation to radial growth of the next year[2,3].

The freezing of the estuary at Churchill may be influenced by river flow and wind effects but, based on correlations with monthly meterological data, the major apparent influence is autumn temperature. The simple correlation coefficients between complete freeze day and monthly mean air temperatures for September, October and November are 0.67, 0.73 and −0.02, respectively, for the period of reliable modern ice data 1967–79. The first two coefficients are significant at the 95% level, the third obviously not. One can infer that most of the heat loss from the estuarine waters takes place in September and October, although the mean modern full-freeze day is 12 November for this same period.

Two sets of historical ice data comprise the Churchill record, one for Churchill Factory and the other for Fort Prince of Wales (see Fig. 1)[8]. Although the first-complete-freeze subset of data includes more values for Churchill Factory, more of these values have been inferred during the continuous period used for calibration[8]. Therefore, we based our calibration and reconstruction on the Fort Prince of Wales record.

Based on the graphical comparisons, response–function results and the correlations between fall temperatures and freeze-up, we performed multiple linear regression (MLR) using tree growth of the next year and current year as predictors of complete freeze day for the longest continuous freeze-up record, 1741–64. The multiple correlation coefficient (R) is 0.69, variance explained (R^2) is 0.47 and R^2 adjusted for loss of degrees of freedon due to the regression is 0.42 (ref. 13). The standard error of estimate is 9.00 and the F-ratio after the second step is 9.44. The latter is significant beyond the 99% level. The first variable entered is the ring-width index for the following year. This relationship concurs with the response–function result showing a positive relationship between tree growth and a warm autumn the previous year. The negative relationship with current year's growth is due to the difference between autoregressive properties of the tree-ring series and the ice data. The calibration equation resulting from the MLR is

$$\text{Full freeze day} \hat{=} 301.7 + 68.5 I_{t+1} - 46.6 I_t$$

where I_{t+1} = ring width index, following year, and I_t = ring width index, current year.

A regression between Churchill Factory first-complete-freeze data and the tree-ring data is not significantly different from the regression between Fort Prince of Wales record and the tree-ring data for the calibration period (1741–64). MLRs between the other ice parameters from Fort Prince of Wales and Churchill Factory and tree-ring data are not as strong as the first-complete-freeze data results.

Figure 2 compares the reconstructed first-complete-freeze record to the calibration period and the verification period. The entire reconstruction record from 1680 to 1978 is shown in Fig. 3. The reliable portion of the modern record from 1967 onwards, verifies the reconstruction with a correlation coefficient for the common period of 0.62 and a coefficient of determination of 0.38; both are significant at the 95% level. The more rigorous reduction of error statistic (*Re*) (ref. 14) is +0.14, also verifying some skill at estimating first-full-freeze day. The *Re* statistic should be viewed with caution in this case as it is unstable for small ($N \leq 20$) data sets[14].

Although 38% explanation of variance is not too impressive, the reconstruction passes the two verification tests. This reconstruction is calibrated by data developed from 200-yr-old descriptive accounts, is based on trees that respond to other factors besides those affecting the full-freeze conditions, and is verified by modern observation. Both the historical and modern ice data involve subjective observer decisions[1] and thus can be sources of error. In view of these difficulties, the graphical comparisons in Fig. 2 and the verification tests are good indications of the validity of the reconstruction.

Temporal and spatial ice variations in the Arctic have an important interactive role with climate[15]. Increase and decrease in areal extent of ice responds to climate[16] and also causes feedback into climatic change[17]. Very few long-term quantitative records of ice are available. This reconstruction of almost 300 yr demonstrates the feasibility of reconstructing ice data in one location. For this first effort we deliberately chose a favourable estuarine area. Other studies have related tree rings to atmospheric pressure variations[18] and pressure to ice variations[5,19]. From these earlier studies and the significant relationships indicated by this study, we are confident that additional reconstructions of ice conditions over wider areas can be achieved using tree-ring information.

We thank E. R. Cook and J. M. Duncanson for advice and assistance and P. M. Kelly, K. R. Briffa and P. D. Jones for helpful comments. A. J. W. Catchpole of the University of Manitoba and the Canadian Atmospheric Environment Service in Downsview, Ontario and Winnipeg, Manitoba provided essential information and data. This material is based on work supported by the NSF under grants ATM79-19223 and ATM81-16184.

Received 21 April; accepted 3 June 1982.

1. Singh, B. *Break-up and Freeze-up Dates: A Case Study of Inconsistencies in Climatological Data* (University of Manitoba, Winnipeg, 1973).
2. Jacoby, G. C. & Cook, E. R. *Arctic Alpine Res.* **13,** 409–418 (1981).
3. Garfinkel, H. L. & Brubaker, L. B. *Nature* **286,** 872–874 (1980).
4. Cropper, J. P. & Fritts, H. C. *Arctic Alpine Res.* **13,** 245–260 (1981).
5. Rogers, J. C. *Mon. Weath. Rev.* **106,** 890–897 (1978).
6. Cook, E. R. & Peters, K. *Tree-Ring Bull.* **41,** 45–53 (1981).
7. Fritts, H. C. *Tree Rings and Climate* (Academic, New York, 1976).
8. Moodie, D. W. & Catchpole, A. J. W. *Environmental Data from Historical Documents by Content Analysis* (University of Manitoba, Winnipeg, 1975).
9. Allen, W. T. R. *Freeze-up, Break-up and Ice Thickness in Canada* (Atmospheric Environment (AE)/Canada, Downsview, Ontario, 1977).
10. Siegel, S. *Nonparametric Statistics for the Behavioral Sciences* (McGraw-Hill, New York, 1956).
11. Mitchell, J. M. Jr *et al. Climatic Change* (World Meterological Organisation, Geneva, 1966).
12. Fritts, H. C. *Reconstruction of Past Climatic Variability* (University of Arizona, Tucson, 1976).
13. Neter, J. & Wasserman, W. *Applied Linear Statistical Models* (Irvin, Homewood, 1974).
14. Gordon, G. A. & LeDuc, S. K. *Proc. Conf. on Probability and Statistics in Atmospheric Science*, Monterey (1981).
15. Lamb, H. H. & Mörth, H. T. *Geogr. J.* **144,** 1–22 (1978).
16. Kukla, G. & Gavin, J. *Science* **214,** 497–503 (1981).
17. Hansen, *et al. Science* **213,** 957–967 (1981).
18. Blasing, T. J. & Fritts, H. C. *Climate of the Arctic/Proceedings Univ. Alaska 24th Alaska Science Conf.* (1975).
19. Barnett, T. P. *Mon. Weath. Rev.* **106,** 1353–1367 (1978).
20. Peters, K., Jacoby, G. C. & Cook, E. R. *Tree-Ring Bull.* **41,** 1–19 (1981).

Isotope evidence for Pleistocene climatic changes in Kashmir, India

R. V. Krishnamurthy* **& Michael J. DeNiro**

Department of Earth and Space Sciences, University of California,
Los Angeles, California 90024, USA

R. K. Pant

Physical Research Laboratory, Ahmedabad 380 009, India

Stable carbon isotope ratios of organic carbon from palaeosols in loess, and oxygen isotope ratios of pedogenic and lacustrine carbonates reveal significant Pleistocene climatic changes in the Kashmir basin. The extreme $\delta^{13}C$ values of −16 and −25‰ reported here indicate a shift from arid to sub-humid conditions. The $\delta^{18}O$ values of pedogenic carbonates is ~2‰ higher than that of the underlying lacustrine carbonates, suggesting that they were deposited in different climatic conditions.

The Plio-Pleistocene infillings in the intermontane Kashmir basin preserve a sequence of climatic events in the form of the Karewa sediments which have an estimated thickness of ~1,000 m and have been identified as glacio-fluvio-lacustrine, capped by a mantle of loess. At various localities in the valley, these sediments have been exposed by tectonic events[1,2]. Preliminary palaeomagnetic measurements suggest that the upper part of the Karewas are within the Brunhes normal epoch and therefore should preserve a large segment of the Pleistocene climatic record[3]. Figure 1 shows a schematic section at Burzahom (34°10′ N, 74°53′ E), ~25 km north-east of Srinagar. Member 1 represents a lacustrine regime with $CaCO_3$-rich marl layer said to represent periodic drying of the lake. Member 2 is a structureless mud facies representing swampy conditions after the draining out of this lake. Member 3 is a loess deposit of 15 m with three palaeosols and member 4 is the top archaeological deposit. Dilpur (33°56′ N, 74°57′ E) section follows the same sequence of events except that member 2 here is a gravelly deposit. Member 3 is ~22m thick while member 4 is absent.

Loess constitutes the top of the Karewas[4]. Loess, a silt-sized sediment, is generally wind-deposited in periglacial environments and represents cold, arid conditions. Palaeosols, or buried soils, in the loess are indicative of warmer/wetter phases. Extensive studies on loess and palaeosols have revealed their value as continental palaeoclimatic indicators[5–7].

We have studied the carbon and oxygen isotope variations in the palaeosols and pedogenic carbonates respectively from Burzahom (member 3, Fig. 1). The palaeosols are relatively rich in organic carbon and the pedogenic carbonates occur in dense, nodular forms, deposited through secondary dissolution—reprecipitation cycles. Oxygen isotope ratios of the lacustrine carbonates from Burzahom (member 1, Fig. 1) pedogenic and lacustrine carbonates from Dilpur have also been studied.

Buried soils in the loess indicate phases of vegetation growth due to climatic amelioration. The organic fraction of the buried soils is derived largely from the terrestrial plant community which fall into two major categories, C3 and C4, characterized by distinct $\delta^{13}C$ values and ecological preferences[8]. The C3 plants have an average $\delta^{13}C$ value of −27‰ and the C4 plants −14‰ on the PDB scale. The C4 plants are mostly distributed in deserts and salt marshes. Carbon isotope measurements indicate that while there are differences in isotope ratios among individual metabolates, the total organic matter in a sediment is a reliable indicator of the source ratio[9]. "Most studies of carbon isotopic composition in plants have made use of unfractionated organic matter. Gross differences in metabolism (C3 compared with C4) can be readily distinguished from such experiments"[10]. The $\delta^{13}C$ values of the organic fraction of a buried soil should therefore document the type of vegetation it supported and hence the ambient climate.

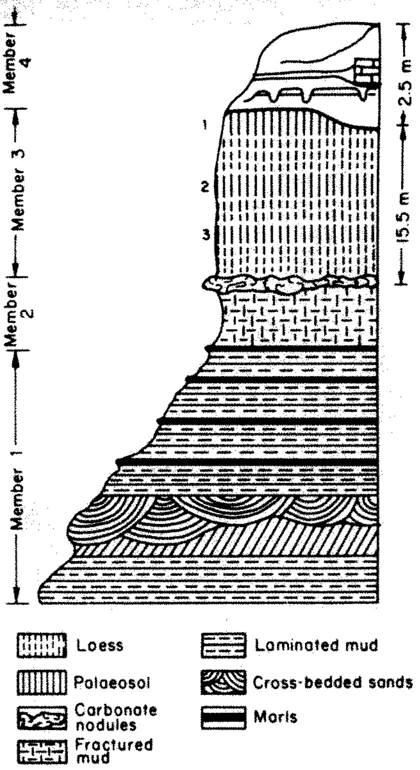

Fig. 1 Schematic section at Burzahom, near Srinagar. Member 1 comprises laminated muds, cross-bedded sands and marls, representing lacustrine and fluvial conditions. Member 2 represents swampy conditions when the lake drained out. Member 3 is the loessic deposit intercalated with three palaeosols (1, 2, 3); the top (member 4) 2.5 m is an archaeological deposit (~4,500 yr BP) (not to scale).

The results of the stable isotope measurements on the organic fraction are shown in Table 1. For organic carbon, samples were first demineralized by 20% HCl, freeze-dried and combusted to give CO_2 using a method described by Stump and Frazer[11]. Carbonate samples were treated with 'Chlorox' to remove any organics present and reacted with 100% H_3PO_4 at 25 °C. (All the measurements were carried out at the University of California, Los Angeles.)

The $\delta^{13}C$ values of the organic fractions range from −16.2 to −25‰ and indicate a clear dominance of the C4 type of plants in palaeosol 2. A gradual increase in the contribution of the C4 type vegetation towards the top of palaeosol 2 indicates an increasing aridity, which merges with the arid, unweathered loessic phase. In this the bottommost layer marks a transition from the laminated member to loess. If the loess deposition there commenced at the termination of a lacustrine regime, therefore, marking the onset of glacial aridity, our isotope measurements point to episodic soil formations through climatic

Table 1 Stable carbon isotope ratios of organic fraction of palaeosols

Site	Depth (cm)	Material	$\delta^{13}C$* (‰)	^{14}C date ($t_{\frac{1}{2}} = 5{,}568$yr) (yr BP)
Burzahom	250–300	Palaeosol 1	−25.3	$18{,}890^{+830}_{-750}$†
	300–350	Palaeosol 2	−16.2	>31,000
	350–400	Palaeosol 2	−18.3	>31,000
	400–450	Palaeosol 2	−20.3	
	1,400–1,550	Palaeosol 3	−21.9	>31,000

* Reproducibility on a single sample is 0.2‰.
† Quoted with 2σ error. The error is one of counting statistics only.

---

* Permanent address: Physical Research Laboratory, Ahmedabad 380009, India.

0028–0836/82/320640—02$01.00

Table 2 Stable oxygen isotope ratios of pedogenic and lacustrine carbonates

Site	Material	$\delta^{18}O$(‰)	No. of samples analysed
Burzahom	Pedogenic carbonates	−7 ± 0.3	12
	Lacustrine carbonates	−8.8 ± 0.2	15
Dilpur	Pedogenic carbonates	−7 ± 0.3	10
	Lacustrine carbonates	−8.4 ± 0.2	8

* Reproducibility on a single sample is 0.2‰.

amelioration, but not so dramatic as represented by palaeosol 1 when the region had a less arid climate, and a C3 type of vegetation reflected in the $\delta^{13}C$ value of −25‰. Note that palaeosol 1 is dated to ~18 kyr BP (ref. 12), which represents a relatively more humid climate. The relatively wetter-warmer conditions seem to have continued up to 15 kyr BP at higher altitudes of ~3,000 m as reflected by the pollen profile at Toshmaidan in Kashmir[13].

In many areas the period 18 kyr BP coincides with the last glacial maximum[14–17]. Peninsular Rajasthan also shows an intense sand dune building at this period[18]. This anti-correlation between Kashmir and Rajasthan could be explained either by an early deglaciation in certain parts of the world[19], or better still, by the strengthening of the northeastern monsoon and heavier winter precipitations during this period of weaker southwestern monsoon as indicated by Duplessey[20]. During the past 3 Myr the rise of the Pir Panjal range (≃5,000m) has effectively shielded off the Kashmir valley from the Indian southwestern monsoon (D. P. Agrawal, personal communication). Present-day rainfall pattern in the region is dominated by heavier winter rains as opposed to the southwestern monsoon in most of Peninsular India.

Oxygen isotope ratios of carbonates, precipitated in equilibrium conditions, are determined by the oxygen isotope composition of the water from which they form (ice-volume effect) and the temperature of precipitation (temperature effect)[21]. For lacustrine and pedogenic carbonates, conditions of isotopic equilibrium are generally assumed but not proved. Interpretation of the isotopic record of continental carbonates require also that the 'meteoric effect'[22] and possible changes in the local hydrological conditions be taken into account. The meteoric effect makes the carbonates heavier with increasing temperature as opposed to the temperature and ice volume effects, which make the carbonates lighter with increasing temperature. The role played by changing local hydrological conditions are often of an unknown magnitude but could be indirectly climate-controlled. Studies on speleothems have indicated that the meteoric effect may be insignificant thus carbonate isotope record interpretation can be made less complicated[23].

The carbonates that we studied are massive and laminated or large-sized nodules, sandwiched between impervious clay members, and therefore represent sealed environments. Moreover, we have analysed a population of carbonates from various layers to check on possible post-depositional exchanges. The rather negligible scatter within a population suggests minimal such exchanges as any secondary exchange is more likely to produce a wide scatter.

The lacustrine carbonates and the pedogenic carbonates from the loess fall into two oxygen isotope groups, the latter being heavier by 2‰ (Table 2). This depletion in the lacustrine carbonates could point to a warmer period during the lake phase. Sedimentologically, the carbonates are associated with finer particles typical of melt water load, therefore snow melt contribution to the lake, making carbonates lighter, is a distinct possibility. Such an effect also points indirectly to a warmer phase. Therefore, despite the 2‰ variation being small and following the observations by Cerling *et al.*[24] and Magaritz *et al.*[25], it appears from our preliminary measurements that these sedimentary carbonates may provide useful palaeoclimatic evidence. Analysis of many more carbonates from the basin, together with present day meteoric and lake waters should provide a firmer interpretation of the carbonate isotopic data.

These, the first isotope measurements from the continental sediments of Kashmir, have proved to be useful markers of climatic change. For detailed and definitive palaeoclimatic inferences, much wider data are needed—these are being obtained as part of a 5-yr project.

This work was carried out as part of the Kashmir Palaeoclimate Project funded by the Department of Science and Technology, Government of India. We thank Drs D. P. Agrawal, Ravi Korisettar and S. K. Tandon for discussions and Dr D. Winter for technical assistance. Partial financial assistance from Dr R. Berger of the Institute of Geophysics and Planetary Physics at UCLA, the Academic Senate Committee on Research at UCLA and NSF grants BNS 79-24756 and ATM-79-24581 are acknowledged.

Received 9 February; accepted 8 June 1982.

1. De Terra & Paterson, T. T. *Studies on the Ice Age in India and Associated Human Cultures* (Carnegie Institute, Washington, 1939).
2. Bhatt, D. K. *Himalayan Geol.* **6,** 197–208 (1976).
3. Agrawal, D. P. *et al. Acta geol hung.* **22,** 185–196 (1979).
4. Pant, R. K., Agrawal, D. P. & Krishnamurthy, R. V. in *Scanning Electron Microscopy in the Study of Sediments* (ed. Whalley, W. B.) (Geo Abstracts, Norwich, 1978).
5. Kukla, G. *Trans. Nebraska Acad. Sci.* **6,** 57–93 (1978).
6. Lazarenko, A. A. *The Neogene Quaternary Boundary* (Geological Institute of Academy of Sciences, Moscow, 1980).
7. Lomov, S. P. *The Neogene Quaternary Boundary* (Geological Institute of Academy of Sciences, Moscow, 1980).
8. Smith, B. N., & Epstein, S. *Pl. Physiol.* **47**, 380–384 (1971).
9. Deines, P. in *Handbk of Environmental Isotope Geochemistry: The Terrestrial Environment A* (eds Fritz, P. & Fontes, J. Ch.) (Elsevier, Amsterdam, 1980).
10. O'Leary, M. H. *Phytochemistry* **20,** 553–567 (1981).
11. Stump, R. K. & Frazer, J. W. *Nucl. Sci. Abstr.* **28,** 746 (1973).
12. Kusumgar, S., Agrawal, D. P. & Krishnamurthy, R. V. *Radiocarbon* **22,** 757–762 (1980).
13. Singh, G. & Agrawal, D. P. *Nature* **260,** 232 (1976).
14. McClure, H. A. *Nature* **263,** 755 (1976).
15. Sarntheim, M. & Diester-Hass, L. *J. sedim. Petrol.* **47,** 868–889 (1977).
16. Bryson, R. A. & Swain, A. M. *Quat. Res.* **16,** 135–145 (1981).
17. Zeist, W. Van. *Palaeobot. Palynol.* **2,** 301–311 (1967).
18. Misra, V. N., Rajaguru, S. N., Raju, D. R., Raghavan, H. & Gaillard, C. *Man Envir.* **6,** 72–86 (1982).
19. *Report of a Committee on Climatic Change* No. 21 (Australian Academy of Sciences, Canberra, 1976).
20. Duplessy, J. C. *Nature* **295,** 494–498 (1982).
21. Epstein, S., Buchsbaum, R., Lowenstam, H. A. & Urey, H. C. *Bull. Am. geol. Soc.* **64,** 1315–1324 (1953).
22. Dansgaard, W. *Tellus* **16,** 436–468 (1964).
23. Schwarez, P. H., Harmon, S. R., Thompson, P. Ford, C. D. *Geochim. cosmochim. Acta* **40,** 657–665 (1976).
24. Cerling, T. R., Hay, R. L. & O'Neil, J. R. *Nature* **267,** 137–138 (1977).
25. Magaritz, M., Kaufman, A. & Yallon, D. H. *Geoderma* **25,** 157–172 (1981).

An anomalous Suess effect above Europe

A. F. M. de Jong

Vening Meinesz Laboratory, Department of Geochemistry,
University of Utrecht, 80.021, 3508 TA Utrecht, The Netherlands

W. G. Mook

Isotope Physics Laboratory, University of Groningen,
Westersingel 34, 9718 CM Groningen, The Netherlands

The major impact that man is likely to have on climate comes from the artificial increase of the atmospheric CO_2 level, caused by the combustion of fossil fuels[1,2]. To predict its magnitude, the future rise of the global atmospheric CO_2 level must be calculated using carbon reservoir models. Because fossil fuel CO_2 lacks ^{14}C and has a $^{13}C/^{12}C$ ratio which is 18‰ lower than the present average atmospheric $^{13}C/^{12}C$ ratio, the validity of such geochemical models can be tested using past temporal variations in the atmospheric concentration of these isotopes. However, the past variation of the $^{13}C/^{12}C$ ratio in global

reservoirs is very difficult to infer[3]. Using $\Delta^{14}C$ data of tree rings Suess measured a depletion in the atmospheric ^{14}C concentration over the past century of <10‰ (ref. 4). Some years later more accurate data gave a value for this 'Suess effect' of 15–25‰ (ref. 5). As the models have been improved considerably over the past few years[6–8] the availability of $\Delta^{14}C$ data with an accuracy of better than 1.5‰ was thought to be essential to test these[9,10]. The present results indicate a good correlation with model predictions taking into account natural ^{14}C variations. However, deviations between American and European tree ring data after AD 1920 suggest a European continental CO_2 effect.

As the Netherlands are bordered by the most industrialized regions in Europe, it was suspected that the ^{14}C level of the local air masses was depressed below the average ^{14}C level[9]. We therefore selected two oaks grown in southern Germany near Unterfahlheim (48°24′ N, 10°10′ E) and Sindelfingen (48°43′ N, 9°0′ E). Comparison with the absolute master chronology showed that no rings were missing. To avoid the influence of radial transport of material with nuclear-bomb produced ^{14}C, cellulose was extracted from those tree rings which were part of the estimated sap–wood section when the nuclear bomb tests began[10–12]. All other tree rings were pretreated according to the AAA method[13]. In several cases a combination of material from several tree rings was required to obtain the 100–200 g of wood necessary for a ^{14}C analysis with a standard deviation of 1.2‰. The system stability and counting corrections for the set of seven proportional counters used have been described elsewhere[12,14].

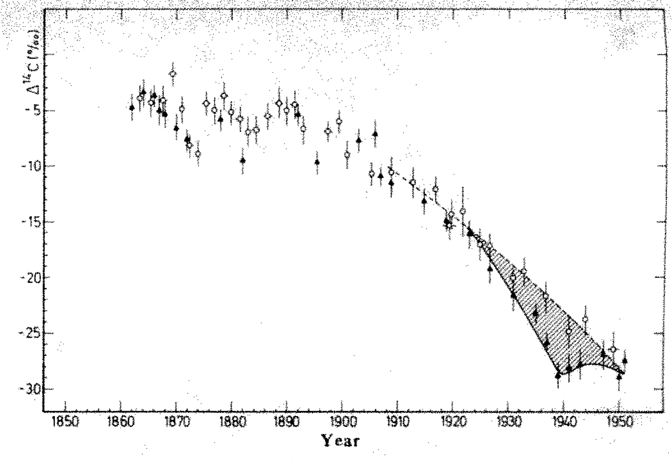

Fig. 1 A compilation of the $\Delta^{14}C$ results for both the Dutch (▲) and German (○) material. The dashed area indicates the local fuel contamination at the Dutch sampling site.

Table 1 Radiocarbon content in tree rings of south German oaks calculated with the half life of 5,730 yr and corrected for isotopic fractionation

Year of growth	Laboratory no. GrN-	$\delta^{13}C_{PDB}$ (‰)	$\Delta^{14}C$ (‰)
Unterfahlheim (48°24′ N, 10°10′ E)			
1948–50	9620*	−25.19	−26.5 ± 1.7
1943–45	9439*	−25.76	−23.8 ± 1.4
1941	9253	−26.70	−24.9 ± 1.6
1937	9290	−26.46	−21.8 ± 1.5
1933	9291	−26.68	−19.6 ± 1.3
1927	9365	−26.99	−17.2 ± 1.1
1925	9386	−26.79	−17.1 ± 1.5
1922	9366	−26.49	−14.1 ± 2.3
1918–21	9440*	−25.37	−15.4 ± 1.4
1917	9367	−26.93	−12.1 ± 1.2
Sindelfingen (48°43′ N, 9°0′ E)			
1931	9387	−25.94	−20.1 ± 0.8
1920	9388	−25.52	−14.4 ± 1.5
1913	9441	−25.52	−11.5 ± 1.4
1909	9442	−25.89	−10.6 ± 1.5
1905–06	9619	−25.30	−10.7 ± 1.1
1901	9477	−25.37	−9.0 ± 1.4
1899–1900	9806	−25.11	−6.0 ± 1.1
1897–98	9621	−25.40	−6.9 ± 1.0
1893	9478	−24.17	−6.7 ± 1.4
1891–92	9805	−25.44	−4.5 ± 1.4
1890	9642	−25.46	−5.0 ± 1.3
1888–89	9773	−25.80	−4.4 ± 1.3
1886–87	9774	−25.15	−5.5 ± 1.3
1884–85	9775	−25.10	−6.8 ± 1.3
1883	9690	−25.57	−6.9 ± 1.4
1881–82	9691	−25.65	−5.8 ± 1.1
1880	9692	−25.61	−5.2 ± 1.0
1878–79	9776	−25.70	−3.7 ± 1.3
1877	9777	−25.00	−5.0 ± 1.3
1875–76	9778	−25.43	−4.4 ± 1.1
1874	9779	−25.65	−8.9 ± 1.1
1872–73	9780	−25.19	−8.2 ± 1.1
1871	9781	−25.30	−4.9 ± 1.2
1869–70	9782	−25.01	−1.8 ± 1.0
1867–68	9783	−25.16	−4.1 ± 1.4
1865–66	9882	−25.09	−4.3 ± 1.2
1863–64	9919	−24.93	−3.9 ± 1.3

* Cellulose pretreatment; the other samples were pretreated according to the standard AAA extraction procedure[13].

The results obtained for the south German oaks are presented in Fig. 1 and are listed in Table 1 as the age ($t_{\frac{1}{2}}$ = 5,730 yr) and fractionation corrected deviation from A_{ox}, the standard 0.95× NBS oxalic acid activity:

$$\Delta^{14}C = \left(\frac{A - A_{ox}}{A_{ox}}\right) \times 1,000 \quad (‰)$$

where A_{ox} is corrected to 1950 and −19‰, and A to the year of growth and −25‰, respectively.

For the period before AD 1900, when the dilution of the atmospheric ^{14}C level was still negligible, our results are in good agreement with the results previously obtained for the Dutch oaks[9]. We suggest that the fine structure superimposed on the rather constant ^{14}C level during the nineteenth century is caused by solar-cycle induced changes in the natural ^{14}C production.

For the period AD 1920–40, however, there is an increasing divergence between the two data sets (Fig. 2). This effect is confirmed by the results obtained for three additional tree ring samples from the Dutch tree (*Quercus rubra*, Sleen) (Fig. 2 and Table 2). The maximum local depression of the atmospheric ^{14}C level at the Dutch sampling site appears to be 26%, with an average of slightly less. This must be caused by a regional contamination. However, after AD 1940 the divergence decreases and disappears around AD 1950. An explanation for this can be found in either a decreased regional effect at the Dutch site or an increased local effect at the German sampling site. To investigate this, our results are compared with ^{14}C data from the US West Coast with a comparable accuracy, covering

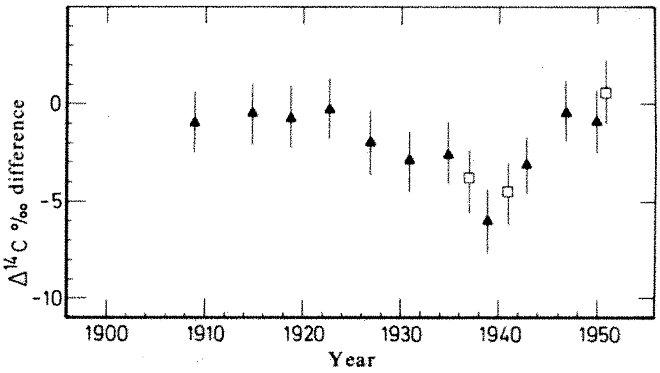

Fig. 2 The calculated difference between the $\Delta^{14}C$ results for the Dutch oak (*Quercus rubra*, Sleen[9]) and a curve calculated through the ^{14}C results for the German trees. Additional samples (□) confirm the existence of a local fossil fuel effect.

the same time interval. These data were obtained from material from two American Douglass firs[10]. These trees grew in oceanic air at the Olympic Peninsula (47°46′ N, 124°06′ W). Due to a lack of reliable data between AD 1895 and 1915, a comparison could not be made for the entire period (Fig. 3) but three points of interest can be noticed:

(1) During the nineteenth century the average $\Delta^{14}C$ level between both European and American data sets is almost identical. However, the correlation in fine structure as observed to exist between the Dutch and south German $\Delta^{14}C$ data sets is absent.

(2) The south German $\Delta^{14}C$ data also seem to be 2–3‰ lower than the American data during the period AD 1920–40. This would reflect a 10% local depression at the German sampling site.

(3) Also for the German material the divergence seems to decrease after AD 1940. The observation that the Dutch, south German as well as the American data indicate an almost identical ^{14}C level in 1950 must mean than this change can hardly be attributed to a natural variation in the ^{14}C production. This effect would be identical for all three sites and the divergence would be maintained.

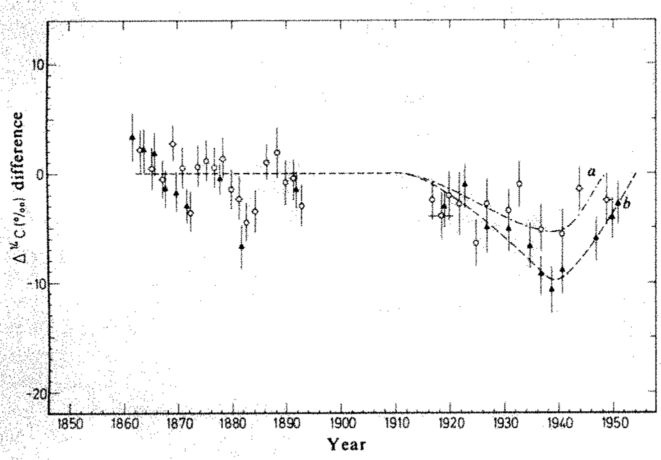

Fig. 3 The calculated difference between the $\Delta^{14}C$ results for the American Douglass firs and: *a*, the south German oaks (○); *b*, the Dutch oak (▲) allowed some curves to be drawn by hand. During the nineteenth century the correlation between $\Delta^{14}C$ results for the Dutch and German oaks does not exist for the American Douglass fir.

We suggest that this has been caused by changes in the relative rates of local influence. As the American data are believed to be a true representation of the atmospheric ^{14}C concentration above the ocean and therefore more widely representative, the effect most probably indicates that the decrease in fossil fuel consumption during the Second World War was more dramatic in the industrialized part of Western Europe than in the rest of the world.

We conclude that until AD 1920 the time variation in the dilution of the atmospheric ^{14}C level for northwestern and central Europe on the average seems to be identical with the ^{14}C level above the ocean. The results for the period after AD 1920, however, suggest a variable European continental ^{14}C effect. Large air masses may have a ^{14}C level which differs by 10–30% from the ^{14}C level of the oceanic air masses. If this is confirmed by more measurements for material from both the European and American continent, the true global time variation of the atmospheric ^{14}C concentration during the past 150 yr cannot easily be established. If the $\Delta^{14}C$ data of the Suess effect are obtained from a single tree, this will reduce its use for testing the accuracy of global carbon reservoir models. Only a global sample network, including the Southern Hemisphere, can thus give more information about the size and distribution of the diluted continental air masses in the past.

Although these ^{14}C results are probably only representative of the variations in ^{14}C concentrations of the European air masses, we have made a comparison with a recent global reservoir model calculation (Fig. 4)[10] carried out using a box diffusion model[7,15]. Values of the annual production during the period AD 1860–1950 were taken from ref. 16. In this calculation the varying background ^{14}C level has also been taken into account. Both the long-term geomagnetically- and medium-term solar-induced ^{14}C variations were calculated, respectively, using the relation derived by Houtermans[17] and an empirical relation between the average 11-yr solar cycle sunspot number and the ^{14}C production rate as determined for the pre-industrial interval AD 1723–1885 [18]. A short-term annual variation has been introduced superimposed on the medium-term contribution, as established from neutron flux observations[18,19].

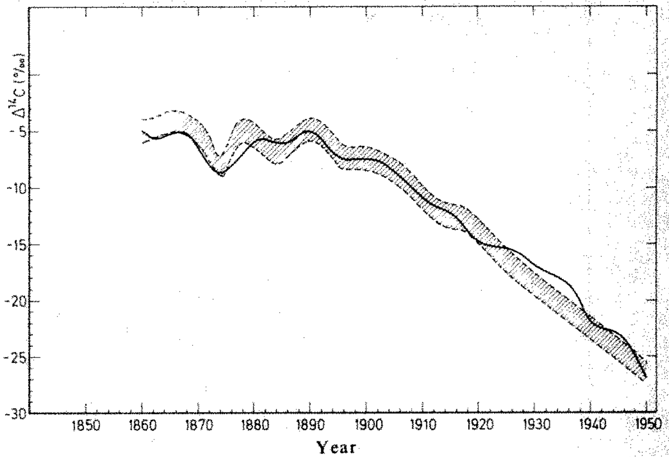

Fig. 4 A comparison of the changes in the atmospheric ^{14}C concentration calculated by model C in ref. 10 (solid curve) with a smoothed spline function with its standard deviation, calculated using the tree ring measurements (dashed area)[20]. The data from both Dutch and German oaks were used. For the period after AD 1920 the Dutch results were neglected.

Table 2 Radiocarbon content in tree rings of a Dutch oak (*Quercus rubra*, Sleen, 52°45′ N, 6°45′ E)

Year of growth	Laboratory no. GrN-	$\delta^{13}C_{PDB}$ (‰)	$\Delta^{14}C$ (‰)
1951	9293	−25.45	−27.6 ± 1.2
1941	9480*	−23.90	−28.1 ± 1.3
1937	9479*	−24.65	−25.9 ± 0.9

Radiocarbon content is calculated with the half life 5,730 yr and corrected for isotopic fractionation. More results from this tree have been published previously[9].

* Cellulose pretreatment; the other sample was pretreated according to the standard AAA extraction procedure[13].

If we now compare our ^{14}C results with these model calculations then apart from the local dilution effect after AD 1920, the fine structure during the nineteenth century is in rather good agreement. Because during that period there was only a minor effect of fossil fuel combustion, the influence on the variation in the model-calculated ^{14}C level is minimal. Therefore, the influence of changes in the solar activity on the ^{14}C production within an 11-yr solar cycle, as given in the model, seems to explain quite acceptably our measured short-term ^{14}C variations. However, especially for this fine structure, which can hardly be influenced by regional effects during this period, a better correlation between trees grown at different sites in the Northern Hemisphere is thought to be essential to establish a ^{14}C variation modulated by the 11-yr solar cycle.

We thank Dr B. Becker for providing samples of oaks grown in southern Germany.

Received 13 April; accepted 15 June 1982.

1. Manabe, S. & Wetherald, S. T. *J. atmos. Sci.* **32**, 3–15 (1975).
2. Marland, G. & Rotty, R. M. *Rev. Geophys. Space Phys.* **17**, 1813–1824 (1979).
3. Tans, P. P. & Mook, W. G. *Tellus* **32**, 268–283 (1980).
4. Suess, H. E. *Science* **122**, 415 (1955).

5. Lerman, J. C., Mook, W. G. & Vogel, J. C. in *Radiocarbon Variations and Absolute Chronology* (ed. Olsson, I. U.) 275–301 (Wiley, New York, 1970).
6. Bacastow, R. & Keeling, C. D. in *Carbon and the Biosphere* (eds Woodweel, G. M. & Pecan, E. V.) 86–135 (US Atomic Energy Commission, 1973).
7. Oescher, H., Siegenthaler, U., Schotterer, U. & Gugelmann, A. *Tellus* **27**, 168–192 (1975).
8. Broecker, W. S., Takahashi, T., Simpson, H. J. & Peng, T. H. *Science* **206**, 409–418 (1979).
9. Tans, P. P., de Jong, A. F. M. & Mook, W. G. *Nature* **280**, 826–828 (1979).
10. Stuiver, M. & Quay, P. D. *Earth planet. Sci. Lett.* **53**, 349–362 (1981).
11. Cain, W. F. & Suess, H. E. *J. geophys. Res.* **81**, 3688–3694 (1976).
12. de Jong, A. F. M. thesis, Univ. Groningen (1981).
13. Tans, P. P., de Jong, A. F. M. & Mook, W. G. *Nature* **271**, 234–235 (1978).
14. Tans, P. P. & Mook, W. G. *Radiocarbon* **21**, 22–40 (1978).
15. Siegenthaler, U. & Oeschger, H. *Science* **199**, 388–395 (1978).
16. Keeling, C. D. *Tellus* **25**, 174–197 (1973).
17. Houtermans, J. C. thesis, Bern Univ. (1971).
18. Stuiver, M. & Quay, P. D. *Science* **207**, 11–19 (1980).
19. O'Brien, K. *J. geophys. Res.* **84**, 423 (1979).
20. Reinsch, C. H. *Num. Math.* **10**, 177–183 (1967).

Triassic bedded cherts in central Japan are not pelagic

Ryuichi Sugisaki, Koshi Yamamoto & Mamoru Adachi

Department of Earth Sciences, Nagoya University, Nagoya, Japan

Although the origin of bedded radiolarian cherts in orogenic belts has been widely debated[1-15], their geochemistry is still poorly understood. Triassic bedded radiolarian cherts occur extensively in the Japanese Islands and are generally not associated with ophiolitic rocks but rather with clastic rocks. We present here chemical data on the Triassic bedded cherts of Kamiaso in central Japan. The relationship of SiO_2 with Al_2O_3, TiO_2 and Zr shows that the bedded cherts have been formed by a simple mixing of biogenic silica derived from radiolarians and sponge spicules with lithogenic materials. The ratios of several elements relative to TiO_2 strongly suggest that the shale partings and lithogenic portions of the cherts are consanguineous. Sedimentary structures as well as the geochemical evidence suggest that most Kamiaso cherts are turbidity current deposits. Our geochemical and geological data compared with those of recent marine sediments from various environments, demonstrate that the Triassic cherts and associated shale partings are not deep pelagic in origin but formed in an offshore or marginal sea environment.

Samples were collected from an extensive continuous outcrop of a Triassic chert formation[16-18] along the Hida river, Kamiaso, Gifu Prefecture, central Japan (Fig. 1). The chert formation, ~100 m thick, is conformably overlain by a series of Lower(?)–Middle Jurassic strata[19] of chert, siliceous shale and turbidite and is underlain by Triassic siliceous shale with chert layers. No ophiolitic rocks occur spatially associated with the cherts. The bedded chert consists of rhythmically interbedded chert and thinner shale (Fig. 1*a*); chert layers are from 1 to 30 cm thick, mostly 2–7 cm, and shale layers from paper-thin to 1.5 cm thick. The chert has a wide colour range: green, grey, dark red-brown, red, white and black. Some dark red-brown chert has a less vitreous appearance and yields best-preserved Triassic radiolarians. Bedding surfaces are generally smooth, but where shale partings become thicker they tend to be knobby and pinch-and-swell structures and load casts are common. The chert layers occasionally show parallel lamination, whereas graded bedding is rare and inconspicuous because detrital grains of quartz, feldspar or lithic fragments are not present in the cherts. Locally, graded bedding is displayed either by the upwards increase of clay content or by the upwards size grading of siliceous remains within one lamina. The chert is made up largely of cryptocrystalline quartz with a small amount of illite, chlorite and opaques; radiolarian tests and sponge spicules filled with cryptocrystalline quartz or length-fast chalcedony are ubiquitous (Fig. 1*b*). Some radiolarians are cut by vertical microstylolites. Secondary minerals such as quartz, chlorite, carbonate and opaques are generally present in trace amounts except for white chert which is invariably veined by microcrystalline quartz and chalcedony.

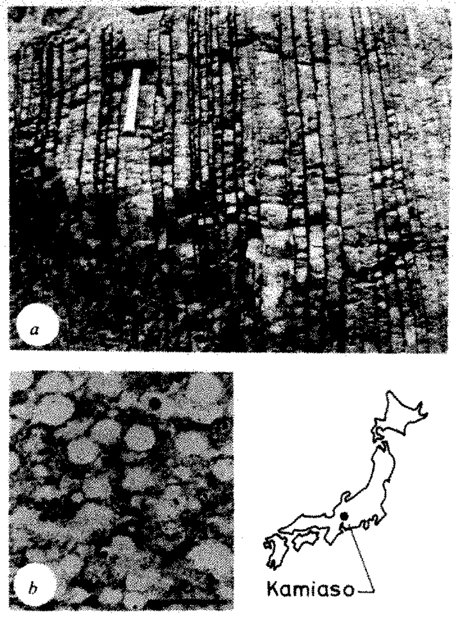

Fig. 1 Triassic bedded radiolarian chert at Kamiaso, Gifu Prefecture, central Japan. *a*, Rhythmically interbedded chert and thinner shale (hammer head, 20 cm); *b*, photomicrograph of black chert containing abundant silica-filled tests of radiolaria (scale bar, 0.2 mm).

The shale partings are very fissile and soft compared with cherts, have the same colour as associated cherts, and are composed essentially of a fine aggregate of illite, quartz, chlorite and opaques with or without radiolarian remains. Some partings have a conspicuous fracture cleavage with flattened radiolarians and well-oriented clay minerals.

Sixty-nine chert samples and 37 shale partings collected from the outcrop were analysed with an automatic X-ray fluorescence spectrometer (Table 1). Figure 2 shows the SiO_2 content in cherts and shale partings plotted against Al_2O_3, TiO_2 and Zr. That the composition of the chert samples trends to $SiO_2 = 100\%$ indicates that pure silica from a separate source is diluting other components during sedimentation. We thus conclude that the SiO_2 of the bedded cherts can be regarded as biogenic; the biogenic silica in each sample experienced different degrees of mixing with other elements which are considered mostly as lithogenic.

To examine the depositional environment of the Triassic cherts, the analytical data were compared with those of about 750 marine argillaceous sediments, which were collected during

Table 1 Chemical composition of cherts and shale partings in averages and their standard deviations (water, carbonate free basis)

	Cherts	Shale partings
No. of analyses	69	37
(%)		
SiO_2	96.22 ± 2.23	63.60 ± 6.48
TiO_2	0.077 ± 0.04	0.77 ± 0.16
Al_2O_3	1.74 ± 0.86	16.98 ± 3.11
Total Fe_2O_3	0.77 ± 0.38	6.37 ± 1.16
MnO	0.018 ± 0.012	0.13 ± 0.15
MgO	0.44 ± 0.30	2.48 ± 0.51
CaO	0.35 ± 0.02	0.19 ± 0.22
Na_2O	0.082 ± 0.023	0.17 ± 0.24
K_2O	0.40 ± 0.23	4.81 ± 0.95
P_2O_5	0.035 ± 0.015	0.24 ± 0.16
(p.p.m.)		
Co	3.3 ± 2.2	17 ± 11
Ni	14 ± 5.4	66 ± 22
Cu	60 ± 26	126 ± 101
Zr	23 ± 23	164 ± 47
Pb	8.2 ± 6.0	29 ± 34

0028-0836/82/320644—04$01.00

Table 2 TiO_2 normalized values of marine sediments[*] in various regions and Triassic cherts and shale partings in central Japan

Sediment type	Area	Environment	Cruise (ref.)	Distance from land (km)	Water depth (m)	No. of samples analysed	Al_2O_3/TiO_2	Total Fe_2O_3/TiO_2	MnO/TiO_2
Marine argillaceous sediments	Nishitsugaru (140° E, 41° N)	Continental shelf and slope	GH77-3II (25)	30	1,400	87	24.11±1.98	8.73±0.75	0.109±0.112
Marine argillaceous sediments	Pacific Coast, South-west Japan	Continental shelf and slope, Nankai Trough	GH75-4 (20)	110	2,900	29	23.11±1.99	8.35±0.51	0.121±0.078
Marine argillaceous sediments	Pacific Coast, North-east Japan	Continental shelf and slope, Japan Trench	GH76-2 (26)	150	3,800	67	22.16±1.20	9.23±1.14	0.112±0.044
Marine argillaceous sediments	Central Sea of Japan	Marginal sea	GH78-2 (21)	260	2,300	61	22.72±1.59	9.30±1.64	0.298±0.596
Marine argillaceous sediments	Shikoku Basin	Marginal sea	Site 443 (22)	480	4,400	114	23.54±1.51	9.08±0.72	0.488±0.221
Marine argillaceous sediments	Shikoku Basin	Marginal sea	Site 444 (22)	560	4,800	74	22.82±0.56	9.16±0.45	0.455±0.296
Marine argillaceous sediments[†]	Around Ogasawara Ridge	Around basaltic islands	GH79-2, 3, 4 (23)	930	2,600	32	18.52±1.76	11.09±0.95	0.295±0.117
Marine argillaceous sediments[‡]	Ogasawara Trench	Trench	GH79-2, 3, 4 (23)	600	7,400	40	21.90±0.86	10.40±0.50	0.569±0.508
Pelagic sediments	Pacific Ocean floor on the east of the Ogasawara Trench	Deep ocean floor	GH79-2, 3, 4 (23)	820	5,600	22	21.98±1.04	10.28±0.40	0.971±0.720
Pelagic sediments	Northern Central Pacific Basin	Deep ocean floor	GH79-1 (24)	1,000<	5,200	34	19.63±3.41	9.82±0.80	0.497±0.289
Pelagic sediments	Northern Central Pacific Basin, Wake to Tahiti	Deep ocean floor	GH80-1 (27)	1,000<	5,500	72	23.28±2.05	11.83±0.91	2.11±0.60
Pelagic sediments[§]	Northern Central Pacific Basin, Wake to Tahiti	On the basaltic plateau	GH80-1 (27)	1,000<	4,700	15	12.36±2.30	8.40±1.25	1.33±0.40
Pelagic sediments	Northern Central Pacific Basin (174° W, 10° N)	Deep ocean floor	GH80-4 (28)	1,000<	6,000	76	22.97±1.66	10.95±1.21	2.19±0.80
Marine argillaceous sediments[‖]	Northern Central Pacific Basin (174° W, 10° N)	Deep ocean floor	GH80-4 (28)	1,000<	6,000	31	27.82±2.73	13.09±0.96	3.52±0.85
Radiolarian cherts	Kamiaso, central Japan	'Chichibu geo-syncline'				69	22.08±2.32	10.21±2.44	0.254±0.196
Shale partings	Kamiaso, central Japan	'Chichibu geo-syncline'				37	21.97±1.07	8.89±2.03	0.168±0.191

[*] Samples of marine sediments are mostly collected from piston cores and deep sea drilling cores. 'Distance from land' and 'water depth' are expressed as values in averaged locations of a core group.

[†] The low Al_2O_3/TiO_2 ratio can be attributed to basalts of the Ogasawara Islands.

[‡] Some samples of this group show high ratios of Al_2O_3/TiO_2 and high content of SiO_2 (ref. 23); these contain much acidic tuff.

[§] The low Al_2O_3/TiO_2 ratio can be attributed to basalts from the Manihiki Plateau.

[‖] The high Al_2O_3/TiO_2 ratio is due to zeolites which are derived from acidic tuff.

cruises of the Geological Survey of Japan and Deep Sea Drilling Project (DSDP) and analysed in our laboratory with the same method used for cherts[20–28]. Si, Al, Ti and Zr tend to remain in the resistates and hydrozates during the sedimentation process: accordingly, the mutual abundances of these elements generally remain stationary during weathering and transportation. We examined the relative abundances of these 'conservative' elements by using TiO_2 concentration as a standard. For example, the Al_2O_3/TiO_2 ratio of sediment hardly changes, even if the sediment is diluted by biogenic silica. Thus, several oxides were normalized to TiO_2 for the marine argillaceous sediments in several regions (Table 2, Fig. 3). We noticed that the ratios of Al_2O_3/TiO_2 and total Fe_2O_3/TiO_2 fall in a narrow range in each region with a few exceptions; the ratios are from 22 to 24 and from 8 to 11, respectively. It is particularly interesting that the ratios are similar to mean values of those of granites and basalts (Fig. 3) because this suggests that the lithogenic part of the marine argillaceous sediments is derived mostly from the continental crust. The exceptions can be attributed to the contribution from oceanic island basalt, acidic tuff and others as noted in Table 2.

The chemical features of the shale partings in the bedded cherts can be compared with those of marine argillaceous sediments to examine the environment of formation for the cherts. The average ratios of Al_2O_3/TiO_2 and total Fe_2O_3/TiO_2 fall into the general range for the marine argillaceous sediments (Table 2, Fig. 3). The partings, however, are especially lacking in CaO and Na_2O (Table 1). This feature is usually observed in fault clay and gouge[29], suggesting that elements other than the 'conservative' elements would be soluble through weathering. As the shale partings are very fissile compared with cherts, meteoric waters will selectively soak into the partings and wash out mobile elements, as is the case with shear zones of faults. Accordingly, the elements other than the 'conservative' elements in the shale are of no use for comparison.

On the other hand, the average ratio of Al_2O_3/TiO_2 in the cherts (22.1) is remarkably close to that of the shale partings (22.0) in spite of errors in sampling and analysis. The ratios of total Fe_2O_3/TiO_2 in the chert and in the shale are also similar to each other, although Fe cannot be regarded as conservative. This similarity strongly suggests that the shale partings and lithogenic portions of the cherts are consanguineous. This is

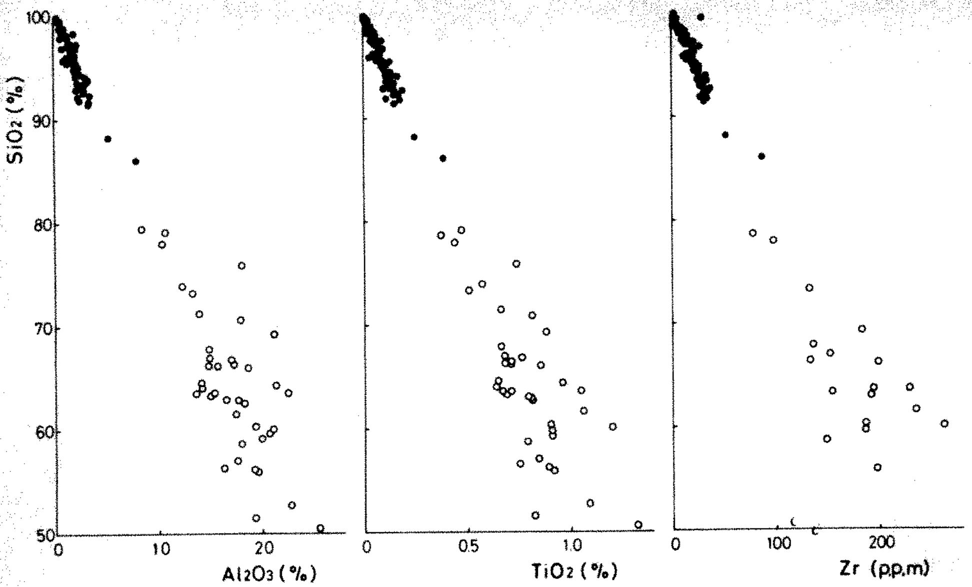

Fig. 2 Relation between SiO_2 and Al_2O_3, TiO_2 and Zr. ●, Cherts; ○, shale partings.

also implicitly shown in Fig. 2 where points for cherts and those for partings are approximately aligned. Cherts, which resist weathering, are expected to have kept their original composition: most TiO_2 normalized compositions, except for SiO_2/TiO_2 in the cherts, therefore, show the chemical feature of the lithogenic portion deposited with biogenic silica. From this, we can deduce the sedimentation environment of the lithogenic portion and ultimately that of the whole chert.

Most cherts are the same colour as associated shales; some cherts display parallel lamination and/or graded bedding, and some appear to grade upwards into overlying shales. These data strongly suggest that the Triassic bedded cherts of Kamiaso are turbidites[2,6,7,9,14], derived mostly from a previously gathered accumulation of biogenic silica, shale partings being deposited as the tail of the currents. This conclusion is compatible with the chemical inference that the shale partings are consanguineous to the lithogenic portions of cherts.

Support for a turbidite origin of Kamiaso cherts also comes from microfossil evidence: both late Triassic conodonts and early Jurassic radiolarians occur together in some green cherts of the uppermost part of the chert formation[18]. A similar reworking of conodonts is also known in the bedded cherts of Inuyama[30], ~20 km south of Kamiaso, which are stratigraphically almost in the same horizon as of Kamiaso. Presumably the conodonts would have been reworked at times when the original silica-rich material was transported from shallow sites to deeper depositional basins by turbidity currents. Because detrital grains other than fine clayey materials are not contained in both the cherts and shales, the depositional sites must have been sea basins where little or no coarser terrigenous sediments reached. Where did such basins occur during Triassic time, and where can we find such basins in the modern ocean?

A useful criterion for discriminating depositional environments of marine sediments is the MnO/TiO_2 ratio. This ratio in nearshore sediments remains generally low and does not fluctuate much because granites and basalts regarded as a main source of the sediments have a uniform and low ratio (Fig. 3). As the distance from land and the water depth increase, terrigenous materials decrease while Mn precipitates nearly uniformly from ocean water (Table 2, Fig. 3). The ratio shows almost two orders of magnitude of variation from the nearshore area to the abyssal area. The MnO/TiO_2 ratio of the Triassic cherts under consideration is 0.254 ± 0.196 and is close to those of the argillaceous sediments from the Central Sea of Japan and the continental shelf and slope off South-west Japan. The distance from land to both areas is at most 300 km. The fact that the ratio of the Triassic bedded cherts is quite different from that of deep ocean sediments implies that the cherts are not deep pelagic but would have formed in an offshore or shallow marginal sea within ~300 km from land. Furthermore, our preliminary analyses of 37 cherts from DSDP Leg 32 give 6.28 for the average MnO/TiO_2 ratio, which is much larger than that of the Triassic cherts. The study of rare-earth elements on DSDP and on-land cherts suggests that some Triassic radiolarian cherts of Kamiaso formed in coastal areas, marginal seas or land-enclosed seas[11]. All these facts confirm our view that the Triassic bedded cherts in central Japan are not pelagic in origin.

Another factor enhancing the MnO/TiO_2 ratio is the contribution of hydrothermal components resulting from submarine volcanism[31]. For example, Jurassic cherts overlying ophiolites

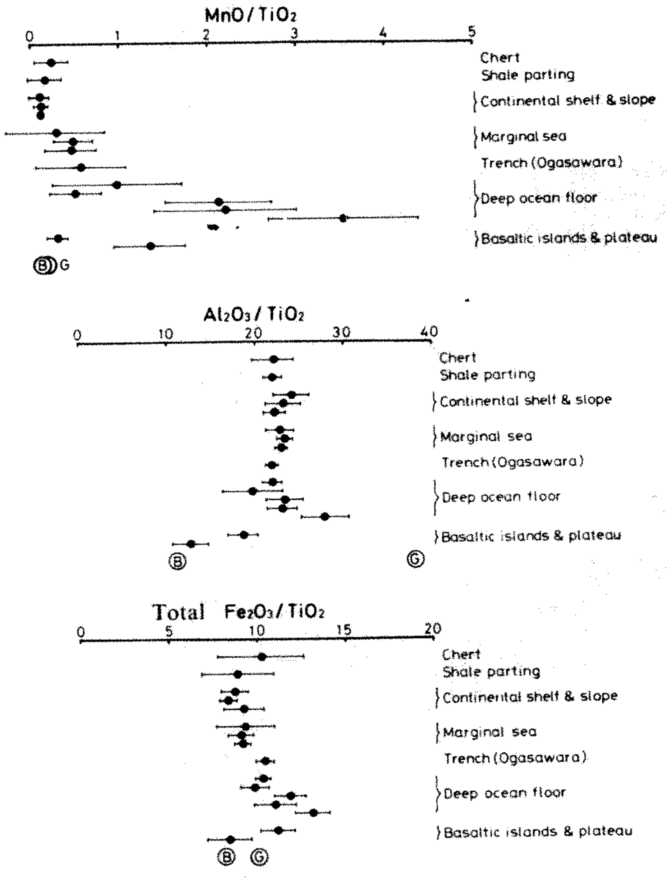

Fig. 3 Comparison of TiO_2 normalized values of marine argillaceous sediments in various environments and Triassic cherts and shale partings. The detailed description is listed in Table 2. The horizontal line indicates $\pm 1\sigma$. G and B represent the averaged values of granites and basalts, respectively[34].

in Italy show a higher range of the ratio (0.53–1.40) (refs 4, 32) and they contain much Ni, Co and Cu. The features of these elemental abundance and Pb isotopic compositions[33] have been ascribed to hydrothermal activity during submarine volcanism which gave rise to ophiolites. The MnO/TiO_2 ratio and the concentration of Co, Ni and Cu in the Japanese Triassic bedded cherts (Tables 1, 2) are significantly lower than those in the Italian cherts. This suggests that bedded cherts in close association with ophiolites as in Steinmann Trinity[1] are different in genesis from those intercalated within sedimentary sequences treated here. Clearly the study of bedded cherts from geochemical aspects in various orogenic belts will provide an important key to understanding the environment of ancient geosynclines.

We thank Setsuo Yogo and Miss Yumiko Isobe for technical assistance.

Received 2 February; accepted 26 May 1982.

1. Steinmann, G. 14*th int. Geol. Congr.* **2,** 637–668 (1927).
2. Fagan, J. J. *Bull. geol. Soc. Am.* **73,** 595–612 (1962).
3. Bailey, E. H., Irwin, W. P. & Jones, D. L. *Bull. Calif. Div. Mines Geol.* 183 (1964).
4. Thurston, D. R. *Contr. Miner. Petrol.* **36,** 329–334 (1972).
5. Kanmera, K. *Spec. Publ. Soc. Econ. Paleontol. Miner.* **19,** 161–173 (1974).
6. Nisbet, E. G. & Price, I. *Spec. Publ. Int. Ass. Sedim.* **1,** 351–366 (1974).
7. Garrison, R. E. *Spec. Publ. Int. Ass. Sedim.* **1,** 367–399 (1974).
8. Kimura, T., Yoshida, S. & Toyohara, F. *J. Fac. Sci. Univ. Tokyo*, Sec. II **19,** 149–177 (1975).
9. Imoto, N. & Fukutomi, M. *Monog. Ass. Geol. Collab. Jap.* **19,** 35–42 (1975).
10. Adachi, M. *J. Earth Sci., Nagoya Univ.* **23/24,** 13–55 (1976).
11. Shimizu, H. & Masuda, A. *Nature* **266,** 346–348 (1977).
12. McBride, E. F. & Folk, R. L. *J. sedim. Petrol.* **47,** 1261–1276 (1977).
13. Steinberg, M. *et al. Sedimentology* **24,** 547–563 (1977).
14. Folk, R. L. & McBride, E. F. *J. sedim. Petrol.* **48,** 1069–1102 (1978).
15. Iijima, A., Kakuwa, Y., Yamazaki, K. & Yanagimoto, Y. *J. Fac. Sci. Univ. Tokyo*, Sec. II **19,** 369–400 (1978).
16. Igo, H. & Koike, T. *J. geol. Soc. Japan* **81,** 197–198 (1975).
17. Nakaseko, K. & Nishimura, A. *Sci. Rep. Col. Gen. Educ. Osaka Univ.* **28,** 61–85 (1979).
18. Kido, S. *Spec. Vol. News Osaka Micropaleontol.* (in the press).
19. Mizutani, S. *et al. Proc. Japan Acad.* **57**B, 194–199 (1980).
20. Sugisaki, R. *Geol. Surv. Japan, Cruise Rep.* **9,** 65–73 (1978).
21. Sugisaki, R. *Geol. Surv. Japan, Cruise Rep.* **13,** 75–88 (1979).
22. Sugisaki, R. *Init. Rep. DSDP* Leg **58,** 719–735 (1980).
23. Sugisaki, R. & Kinoshita, T. *Geol. Surv. Japan, Cruise Rep.* **14,** 146–158 (1981).
24. Sugisaki, R. *Geol. Surv. Japan, Cruise Rep.* **15,** 236–244 (1981).
25. Sugisaki, R. *Geol. Surv. Japan, Cruise Rep.* (in the press).
26. Sugisaki, R. & Honza, E. *Bull. geol. Surv. Jap.* (in the press).
27. Sugisaki, R. & Kinoshita, T. *Geol. Surv. Japan, Cruise Rep.* (in the press).
28. Sugisaki, R. & Yamamoto, K. *Geol. Surv. Japan, Cruise Rep.* (in the press).
29. Sugisaki, R., Anno, M., Adachi, M. & Ui, H. *Geochem. J.* **14,** 101–112 (1980).
30. Kondo, N. & Adachi, M. *J. geol. Soc. Japan* **81,** 373–386 (1975).
31. Boström, K. & Peterson, M. N. A. *Mar. Geol.* **7,** 427–447 (1969).
32. Barrett, T. J. *Chem. Geol.* **34,** 289–317 (1981).
33. Barrett, T. J. *Earth planet. Sci. Lett.* **49,** 193–204 (1980).
34. Taylor, S. R. *Geochim. cosmochim. Acta* **28,** 1273–1285 (1964).

Mid-Palaeozoic travels of Arctic–Alaska

J. F. Sweeney*

Earth Physics Branch, Department of Energy, Mines and Resources, Ottawa, Canada K1A 0Y3

One of the most persistent proposals[1] for the origin of the Arctic sea floor is that Alaska, or parts thereof, broke away from polar Canada and rotated as much as 70° anticlockwise relative to the North American craton. Subsequent modifications[2–8] reduced the size of the rotated block (Fig. 1) and put the date of rotation at latest Jurassic–early Cretaceous (refs 4, 6, 7, 9, 10, and A. Grantz and S. May in preparation). Although restoration of the block provides a good geological fit between northern Alaska and the Arctic islands for late Palaeozoic and younger pre-rift age rocks,[8] the character of Devonian and older Palaeozoic rocks across the restored boundary is anomalous, with deformed and thermally altered rocks of northern Alaska lying against unaltered sediments on Banks Island (Fig. 2*b*). Here I compare the known geology of mid-and early Palaeozoic rocks along the margins of the restored rift and explain the anomalous Arctic–Alaska terrane as a block that was displaced southwestwards in mid-Palaeozoic time by as much as 2,000 km from its initial orogenic site to the north and east of Ellesmere Island.

Devonian and older rocks outcrop in northern Greenland[11], northern Axel Heiberg and Ellesmere islands[12] and northern Alaska[13] and are found in the subsurface along the modern polar margin on Ellef Ringnes and Brock islands[14], Banks Island[15], beneath the Mackenzie Delta[16], in northernmost Alaska, Chukotsk Peninsula and the adjacent continental shelf[17]. Across northern Greenland and adjacent parts of Canada, shallow-dipping Cambrian platform rocks pass northward from the craton into dominantly carbonate shelf facies which in turn grade northward into a dominantly clastic filled ensialic trough that on Ellesmere Island was two-sided and bounded on the north by a volcanic arc[11,12,18]. Trough sediments on Ellesmere Island were derived from both margins although the source to the north declined steadily during the Cambrian interval[18]. At this time in northern Greenland, detritus was derived from cratonic sources to the south[19].

In early and middle Ordovician time, felsic to intermediate volcanism prevailed on northernmost Ellesmere Island and was followed by local deformation and rapid deposition of flysch derived, at least in part, from Cambrian or older low-grade metamorphic rocks[12,18] within a major new or rejuvenated source terrane to the north (Fig. 2*c*). This terrane also delivered clastic debris to northern Greenland beginning in Ordovician time[19]. Clastic deposition advanced southward in both regions during the Silurian and early Devonian periods[12,18,19] and on Ellesmere Island both the volume and grade of deposited material increased to the north-east[18].

To the west of Mackenzie Delta across northeastern Alaska outcrop and borehole data indicate that in Cambrian and Ordovician time shallow-water carbonate arches graded northward into shale–chert basinal sequences that contained substantial volcanic deposits[13,16,17,20]. In later Ordovician and Silurian time this setting was interrupted by major uplift (Fig. 2*c*) within the shale–chert zone and was accompanied by deformation, emplacement of a felsic pluton at 431 ± 13 Myr (K/Ar hornblende date)[20,21] and erosion that exposed Cambrian and older low-grade metamorphic assemblages along the uplift axis[13]. The grain size of early and (?) middle Devonian clastic debris in northernmost Alaska increased towards what is now the west along the present coast[13].

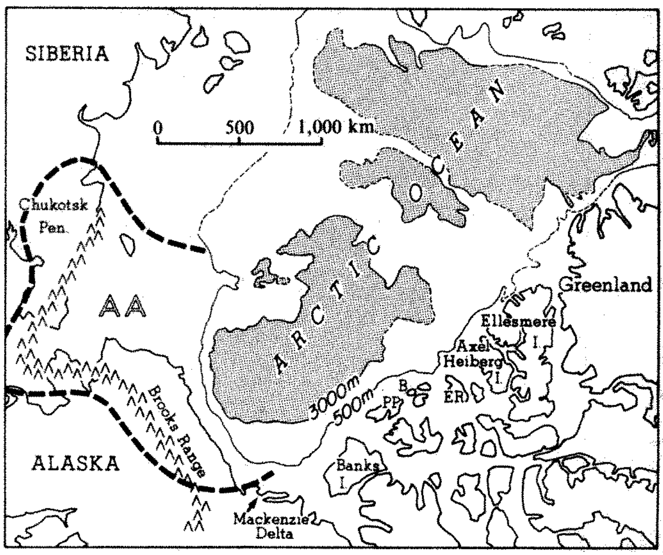

Fig. 1 Boundaries of the terrane[26,31], designated Arctic–Alaska[6] (AA), presumed to have rotated. B, Brock Island; ER, Ellef Ringnes Island; PP, Prince Patrick Island.

---

* Present address: Pacific Geoscience Centre, PO Box 6000, Sidney, British Columbia, Canada V8L 4B2.

0028-0836/82/320647—03$01.00

Plutonic rocks occur mainly along the southern Brooks Range in a relatively narrow belt (Fig. 2*a*) that extends northeastwards into the Mackenzie Delta region[21]. A second belt of small intrusions is found along northernmost Axel Heiberg and Ellesmere islands[12]. Intrusive rocks in each belt are dominantly felsic and most were emplaced during middle and late Devonian time[12,21]. Several small ultramafic to felsic bodies of late Silurian or early Devonian age are present within the Axel Heiberg–Ellesmere belt[12,18]. In both regions, shallow marine conditions at the time of emplacement suggest that the plutonic rocks may represent an ensialic island arc or a continental margin magmatic belt[18,21].

Metamorphic grade declines westward from amphibolite facies in northeastern Greenland[11] to greenschist–subgreenschist facies with local amphibolites on northernmost Ellesmere Island[18,22] to virtually unmetamorphosed rocks at Ellef Ringnes Island and beyond[14] (Fig. 2*a*). West from the Mackenzie Delta thermal effects are variable and reach greenschist grade along the coast but amphibolite grade rocks are associated with the magmatic arc in the southern Brooks Range[17,21,23].

Except for the Banks Island area, these regions experienced one or more early Palaeozoic periods of thermal and structural alteration that generally increased in intensity towards the north and culminated during middle Devonian to early Mississippian time with the deposition of thick southward-tapering clastic sediments that palaeocurrent studies suggest were transported mainly from north-east to south-west in both northern Alaska and the Canadian Arctic Islands[12,13,24,25]. Uplift and clastic wedge formation that began on northern Ellesmere and Axel Heiberg islands in early Middle Devonian time expanded southwestwards at an average rate close to 3 cm yr^{-1} to include Prince Patrick Island by the outset of the Mississippian[24]. A similar orogenic progression is not documented in northern Alaska where, as in Arctic Canada, the mid-Palaeozoic zone of uplift and related clastic deposition extends hundreds of kilometres south of the present continental margin[13,25] (Fig. 2*b*).

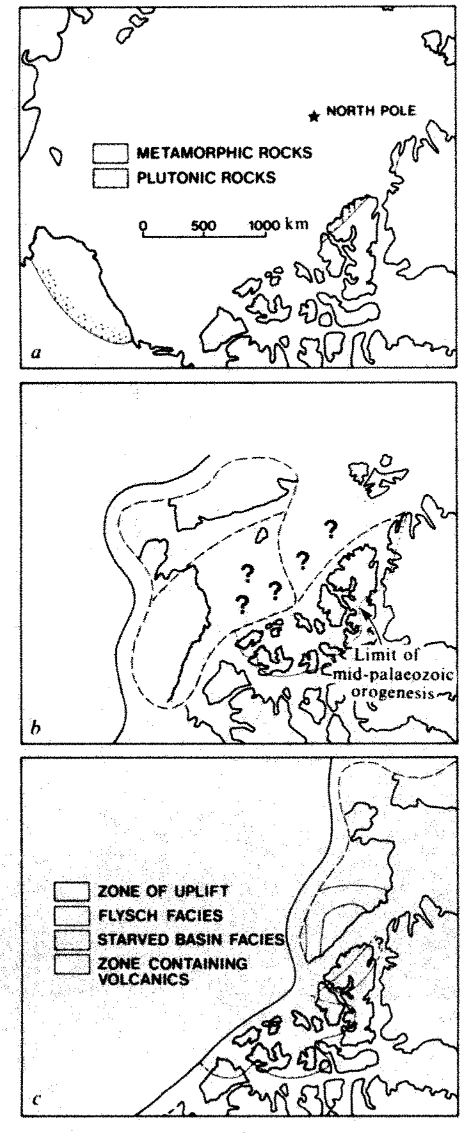

Fig. 2 Early and mid-Palaeozoic orogenic features[12,13,17,18,21] with continental blocks arranged: *a*, as at present; *b*, as they may have appeared before presumed rotation of Arctic–Alaska; *c*, before onset of mid-Palaeozoic tectonism.

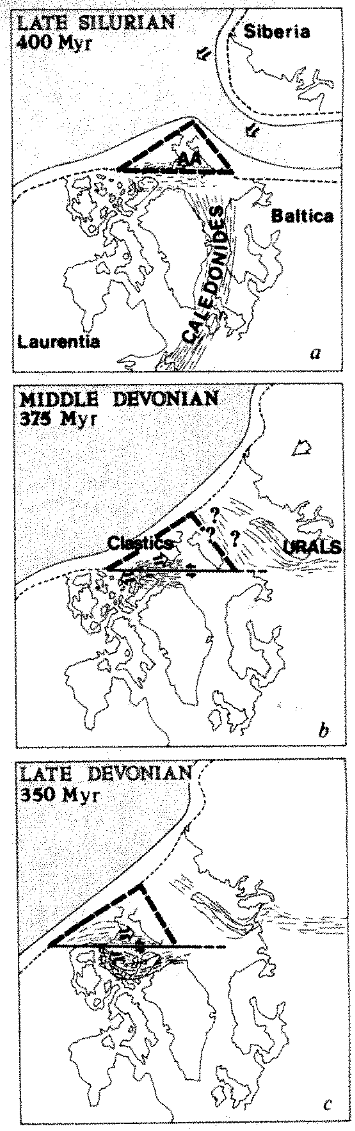

Fig. 3 Possible Devonian tectonic development of the Arctic region. Large arrows in *b* and *c* indicate expected directions of sediment and tectonic transport on opposite sides of the fault zone. *a*, Late Silurian 400 Myr; *b*, middle Devonian 375 Myr; *c*, late Devonian 350 Myr.

In the early 1970s it was proposed that from Greenland to Alaska, the major source of early and mid-Palaeozoic sediments may have been offshore orogenic welts produced by subduction of sea floor beneath the Laurentian continental mass, followed in mid-Palaeozoic time by closure of an ancestral Arctic Ocean and suturing of the opposing cratonic blocks[2,11,12]. The Banks Island area in this view lay opposite an embayment in the approaching landmass and was therefore spared the orogenic effects of continent–continent collision[15]. In a restored rotation, however, no appropriate embayment is evident in palaeogeographical reconstructions of northern Alaska[16]. More recent studies indicate that, in Canada, early and mid-Palaeozoic clastic sources to the north did not extend further south-west than Axel Heiberg Island[18,24] and also that significant left-lateral movements may have been associated with development of the orogen.

The gross similarity in mid- and early Palaeozoic stratigraphy, tectonism and metamorphic grade between Arctic–Alaska and northeastern Laurentia has long been noted[12,17]. Several of these comparative features may be explained if the two terranes were once joined, polar margin to polar margin (Figs 2*c*, 3*a*). The ensialic trough and associated volcanism noted for the Cambrian in the northern part of each region may indicate the presence of an adjacent consuming margin that ceased activity when the opposing Arctic–Alaska block collided with northeastern Laurentia in middle Ordovician time[18,19]. Uplift, metamorphism, deformation and plutonism in northern Alaska at about this time is matched by contemporary metamorphism, deformation and volcanism on northernmost Ellesmere Island. Uplift in Arctic–Alaska may thereby have become the source region for Ordovician through early Devonian clastics derived from the north in the Greenland–Ellesmere region (Fig. 2*c*). The crystalline fraction of detritus delivered to the latter region and rocks within the core of the eroded zone in Alaska are similar in age and metamorphic grade. Further, with Arctic–Alaska so oriented, the present westerly coarsening of early Devonian sediments in coastal Alaska becomes, in mid-Palaeozoic time, a northeasterly coarsening in agreement with the textural trend noted in contemporary clastics on what was then the adjacent landmass of Ellesmere Island. For middle Devonian to early Mississippian syntectonic deposits, however, the proposed reconstruction places major sediment transport directions within adjacent terranes in opposition, northeasterly in Arctic–Alaska, southwesterly in Arctic Canada[26].

Preliminary palaeomagnetic reconstructions[27,28] show that the Siberian Shield may have approached the ancestral polar margin of Laurentia from what is now the east during the early Palaeozoic and that intervening sea floor was probably eliminated during Devonian time (Fig. 3*a*, *b*). The approach of the Siberian block may have ruptured the weld between Arctic–Alaska and northeastern Laurentia and caused the former to move with compression accompanied by significant left-lateral motion against the Laurentian front to produce a broad zone of uplift and erosion within each block. In Laurentia, the affected zone expanded to the south-west as the Arctic–Alaska block proceeded (Fig. 3*b*, *c*). Significant but undated south-west -directed thrusting is also documented on northernmost Ellesmere Island[18]. By early Mississippian time, the migrating Arctic–Alaska terrane presumably came to rest against a zone that included the Banks Island area although, as earlier noted, the deformed belt did not extend beyond Prince Patrick Island. Final late- to post-orogenic movements in the region may not have been attended by significant disruption along the zone of contact between the two plates.

This reconstruction implies that Arctic–Alaska also moved against oceanic lithosphere as it advanced to the south-west (Fig. 3). Underthrusting or subduction of the latter beneath the encroaching continental block in middle and late Devonian time may be indicated by the belt of plutonic rocks along the southern Brooks Range (Fig. 2*a*), which would have been close to the leading edge of the Arctic–Alaska block during this interval (Fig. 3*b*, *c*). Contemporary magmatism in northernmost Ellesmere Island may be related to the initial stages of this event. Late Silurian–early Devonian intrusions within the Ellesmere belt may mark the line of separation between Laurentia and Arctic–Alaska or they could be the intrusive equivalents of nearby Ordovician volcanics[18] (Fig. 2*c*).

A key feature of this concept is that compression combined with left-lateral translation between adjacent continental blocks produces a region of uplift and clastic deposition that advances in each terrane as the zone of contact between them progresses. In Laurentia, the contact zone is seen to move to the south-west as does the region of middle and late Devonian uplift and clastic deposition[24] (Fig. 3*b*, *c*). In Arctic–Alaska, the opposing Laurentian block will appear to move to the north-east. Mid-Palaeozoic uplift and sediment transport in Arctic–Alaska should therefore proceed also towards the north-east. That is, the relative motions should produce overall directions of orogenic expansion and sediment transport in each block that, when compared, will be diametrically opposed. As indicated earlier, this is the case for mid-Palaeozoic palaeocurrent directions when Arctic–Alaska is placed in its pre-rotated position against polar Canada[25,26]. However, there is little evidence of corresponding northeastward orogenic expansion at this time in northern Alaska, perhaps because the entire facing side of the smaller Arctic–Alaska block was already in contact with the larger Laurentian block at the start of the tectonic episode (Fig. 3*a*).

This scheme was anticipated as early as 1965 by Harland[29] who proposed left-lateral shearing north of Greenland and Ellesmere Island as an extension of major sinistral faulting in late Devonian time within the Caledonian foldbelt. Recent palaeomagnetic evidence[30] assigns a Carboniferous age to the latter displacement which implies that Devonian shearing along the polar margin was an earlier and therefore separate event as suggested here.

The present scenario is attractive in that it explains early Palaeozoic and Devonian geological and tectonic similarities between what are now widely separated regions and, in a restored rotation, it accounts for dissimilarities between pre-Carboniferous sequences in the Banks Island area and in northern Alaska. The location as well as the linearity of the present polar margin from Greenland to the Mackenzie Delta are also explained as having been the site of a major mid-Palaeozoic shear.

At the end of Jurassic time, some 200 Myr after its Palaeozoic travels came to an end, Arctic–Alaska moved again, this time in anticlockwise rotation to begin the process of opening the modern Arctic Ocean basin.

I thank W. P. Brosgé, M. Churkin Jr, R. L. Coles, M. R. Dence, A. K. Goodacre, A. Grantz, B. W. Harland, C. G. Mull, N. J. Soper and H. P. Trettin for helpful comments and suggestions. Earth Physics Branch contribution 1005.

Received 8 April; accepted 2 June 1982.

1. Carey, S. W. *R. Soc. Tasm. Pap. Proc.* **89,** 255–288 (1955).
2. Tailleur, I. L. *Oil Gas J.* 128–130 (1969); *Am. Ass. petrol. Geol. Mem.* **19,** 526–535 (1973).
3. Tailleur, I. L. & Brosgé, W. P. in *Proc. Geological Seminar on the North Slope of Alaska* (eds Adkison, W. L. & Brosgé, M. M.) EL-E20 (Pacific Section American Association of Petroleum Geologists, Los Angeles, 1970).
4. Rickwood, F. K. in *Proc. Geological Seminar on the North Slope of Alaska* (eds Adkison, W. L. & Brosgé, M. M.) L1–L11 (Pacific Section American Association of Petroleum Geologists, Los Angeles, 1970).
5. Freeland, G. L. & Dietz, R. S. *Tectonophysics* **18,** 379–389 (1973).
6. Newman, G. W., Mull, C. G. & Watkins, N. D. *Proc. Alaska geol. Soc. Symp.*, Anchorage C1–C7 (1979).
7. Sweeney, J. F., Irving, E. & Geuer, J. W. *Publ. Earth Phys. Br.* **45,** 91–100 (1978).
8. Grantz, A., Ettreim, S. & Dinter, D. A. *Tectonophysics* **59,** 263–291 (1979).
9. Sweeney, J. F. in *Geodynamics Ser.* Vol. 6, 17–29 (American Geophysical Union, Washington DC, 1982).
10. Taylor, P. T., Kovacs, L. C., Vogt, P. R. & Johnson, G. L. *J. geophys. Res.* **86,** 6323–6333 (1981).
11. Dawes, P. R. & Soper, N. J. *Am. Assoc. petrol. Geol. Mem.* **19,** 117–134 (1973); *Gronlands Geol. Under. Rep.* **93,** 1–40 (1979).
12. Trettin, H. P. *et al. Geol. Ass. Can. Spec. Pap.* **11,** 83–179 (1972).
13. Brosgé, W. P. & Dutro, J. T. *Am. Ass. petrol. Geol. Mem.* **19,** 361–375 (1973).
14. Meneley, R. A., Henao, D. & Merritt, R. K. *Can. Soc. petrol. Geol. Mem.* **4,** 531–544 (1975).
15. Miall, A. D. *Bull. geol. Soc. Am.* **87,** 1599–1608 (1976).
16. Lerand, M. *Can. Soc. petrol. Geol. Mem.* **1,** 315–386 (1973).
17. Churkin, M. *Science* **165,** 549–555 (1969); *U.S. geol. Surv. Prof. Pap.* **740,** 1–64 (1973).
18. Trettin, H. P. & Balkwill, H. R. *Can. J. Earth Sci.* **16,** 748–769 (1979).
19. Dawes, P. R. in *Geology of Greenland* (eds Escher, A. & Watt, W. S.) 248–303 (Geological Survey Greenland, Copenhagen, 1976).
20. Reiser, H. N. in *Proc. Geological Seminar on the North Slope of Alaska* (eds Adkison, W. L. & Brosgé, M. M.) K1–K14 (Pacific Section American Association of Petroleum Geologists, Los Angeles, 1970).
21. Dillon, J. T., Pessel, G. H., Chem, J. H. & Veach, N. C. *Geology* **8,** 338–343 (1980).
22. Frisch, T. *Bull. geol. Surv. Can.* **229,** 1–87 (1974).
23. Dutro, J. T., Brosgé, W. P. & Reiser, H. N. *Bull. Am. Ass. petrol. Geol.* **56,** 808–814 (1972).
24. Embry, A. F. & Klovan, J. E. *Bull. Can. petrol. Geol.* **24,** 485–639 (1976).
25. Nilsen, T. H., Moore, T. E., Brosgé, W. P. & Dutro, J. T. *U.S. geol. Surv. Open-file Rep.* **81–506,** 1–39 (1981).
26. Churkin, M. & Trexler, J. H. *Earth planet. Sci. Lett.* **48,** 356–362 (1980).
27. Morel, P. & Irving, E. *J. Geol.* **86,** 535–561 (1978).
28. Scotese, C., Bambach, R. K., Barton, C., Van der Voo, R. & Ziegler, A. M. *J. Geol.* **87,** 217–277 (1979).
29. Harland, W. B. *Phil. Soc. Trans. R. Soc.* **258,** 59–75 (1965); *Am. Ass. petrol. Geol. Mem.* **19,** 599–608 (1973).
30. Van der Voo, R. & Scotese, C. *Geology* **9,** 583–589 (1981).
31. Fujita, K. *J. Geol.* **86,** 159–172 (1978).

A mutation in *Drosophila* alters normal connectivity between two identified neurones

John B. Thomas & Robert J. Wyman

Department of Biology, Yale University, Box 6666, New Haven, Connecticut 06511, USA

The mechanisms involved in producing the vast number of specific connections in the nervous system are unknown. As nerve cells grow during development and seek out their targets there must be some sort of molecular cues for axonal guidance and final target recognition. One strategy for identifying such factors is to locate the genes which code for or control the expression of the molecules. To identify these genes, we have chosen a simple network of eight neurones in *Drosophila melanogaster*, comprising the giant fibre (GF) system[1-3], in which we can detect the effect of mutations on connectivity. We report here the isolation of an X-linked, recessive mutation, *bendless* (*ben*), which deletes one process of the GF while leaving other portions functionally unaltered.

The GF network is activated by a light-off visual stimulus and mediates the early events of an escape response consisting of a jump and subsequent flight[4]. To isolate potential connectivity mutants we used standard mutagenesis techniques and a behavioural screen to select flies failing to jump to the light-off stimulus. Males 1 or 2 days old were fed the mutagen ethyl methane sulphonate (EMS)[5] and mated to $C(1)M3/Y$ females[6]; the F_1 male progeny from this cross inherit the mutagenized paternal X chromosome. We screened 50,000 F_1 males. The screening device consists of a flask inverted in a beaker. Flies are placed inside the flask and are free to walk along its inner surface. A light-off stimulus causes them to jump, but because activation of the flight muscle does not always result in maintained flight, the flies fall a small distance. After several stimuli, jumpers fall into the beaker where they are unable to re-enter the testing area; non-jumpers remain in the flask. White-eyed flies, which lack the visual screening pigments, show greater reliability than wild type in jumping to the light-off stimulus. Therefore, white-eyed flies of the *brown*; *scarlet* (*bw*; *st*) genotype were used. Both the morphology of the GF and its motor output in *bw*; *st* flies are indistinguishable from wild type.

Non-jumping lines were established from individuals selected in the screen. Males from these mutant lines were then tested physiologically for defects in the GF system by stimulating the GFs extracellularly in the brain and recording from thoracic muscles known to be driven by them[3]. Underlying structural abnormalities in the GF were revealed by intracellularly injecting the GF with the fluorescent dye Lucifer yellow. From these experiments several X-linked mutations have been isolated which disrupt the normal physiology and morphology of GF system neurones. The *bendless* mutation is one of these and maps between *vermilion* and *forked*.

The GFs themselves are a pair of large interneurones having cell bodies located ipsilaterally in the brain[2]. Each sends an axon along the dorsal midline of the cervical connective to the thoracic ganglion where it courses ventrally. Within the mesothoracic neuromere the GF axon makes a lateral bend and ends abruptly[1,2] (Fig. 1*a*, *b*). Just before this lateral bend, the GF makes an electrical synapse with the peripherally synapsing interneurone (PSI)[1], which crosses the ganglion and chemically synapses onto the five motoneurones of the contralateral dorsal longitudinal flight muscle (DLM). At the terminus of its bend, the GF makes another electrical synapse with a large motoneurone innervating the tergotrochanteral muscle (TTM, or jump muscle)[1].

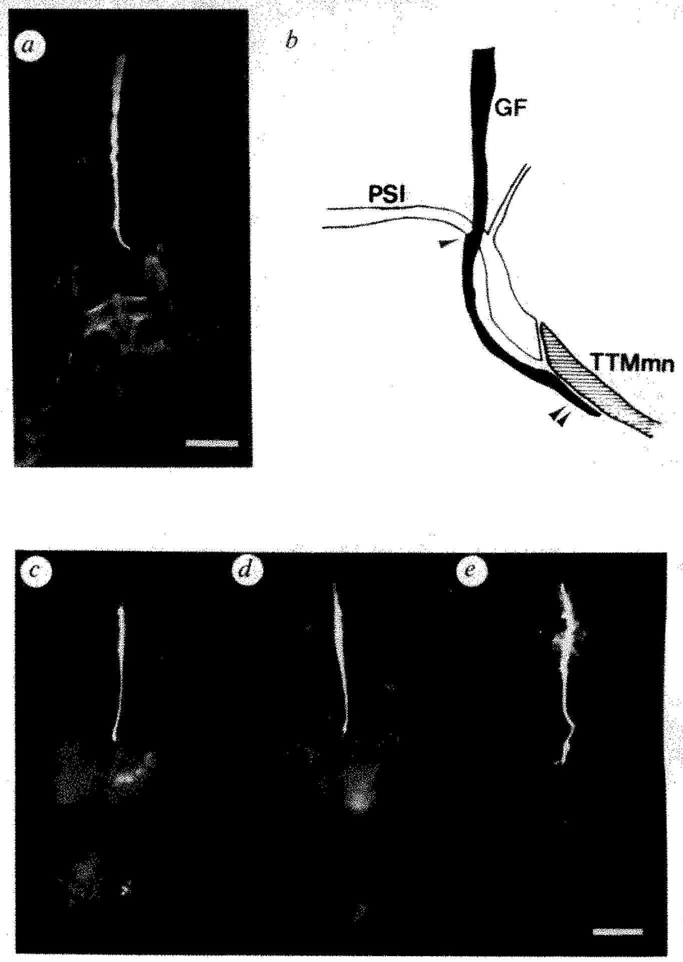

Fig. 1 *a*, *c*–*e*, Whole mounted thoracic ganglia, viewed with fluorescence optics, from a wild-type (*a*) and three *bendless* (*c*–*e*) individuals. In each the GF has been injected with Lucifer yellow. Techniques of dye injection are as described by Koto *et al.*[2]. *a*, *c*, *d*, Dorsal views; *e*, a dorso-lateral view in which the normal ventral bend and abnormal branches are visible. Anterior is up; scale bar, 100 μm. *b*, Schematic diagram of the GF bend region from an electron micrograph reconstruction[1] showing the location of synapses between the GF and PSI (single arrowhead) and between the GF and TTM motoneurone (double arrowhead).

In mutant flies ($n = 10$) the GF cell body position and dendritic morphology are indistinguishable from wild type (data not shown) and the GF axon descends unbranched to the thoracic ganglion. However, within the ganglion the GF fails to make the lateral bend characteristic of wild type and terminates before making the bend (Fig. 1*c*, *d*). Extending from the tip are numerous fine processes ~3–5 μm long. Occasionally, this branching is more extensive ($n = 2$), consisting of processes up to 30 μm long (Fig. 1*e*). In neither case does the GF extend to the region where it normally makes synaptic contact with the TTM motoneurone. The TTM motoneurone itself is present and drives the TTM normally. Preliminary experiments using retrograde labelling with horseradish peroxidase indicate that the TTM motoneurone morphology is normal in *ben* flies (M. Koto, personal communication).

Physiological experiments show that in the mutant the GF drives the DLM normally, but the TTM is driven abnormally. In wild type a spike in the GF drives the TTM and DLM with short and constant latencies. Figure 2*a* shows the response recorded in the TTM and DLM to intracellular stimulation of the GF in a wild-type individual. The TTM, whose motoneurone is driven monosynaptically by the GF, has a response latency

0028-0836/82/320650—02$01.00

of 0.8 ms; the DLM, whose motoneurones are driven disynaptically via the PSI, has a response latency of 1.2 ms. Figure 2*b* shows the GF output to the TTM and DLM of a *ben* individual. It can be seen that the DLM response latency of the mutant is indistinguishable from that of wild type. However, the TTM latency is abnormally long at 2.2 ms. All *ben* flies examined physiologically ($n = 40$) had abnormal TTM response latencies of 2.2–3.0 ms. Whether the giant fibre in the mutant actually does make synaptic contact with the TTM motoneurone, albeit in an abnormal region, is not known. However, as the TTM latency is 1.4–2.2 ms greater than wild type, and a normal synaptic delay is of the order of 0.5 ms, it is unlikely that there is direct functional contact between the GF and the TTM motoneurone. Instead, it is likely that the GF is driving the TTM via an as yet unidentified polysynaptic pathway.

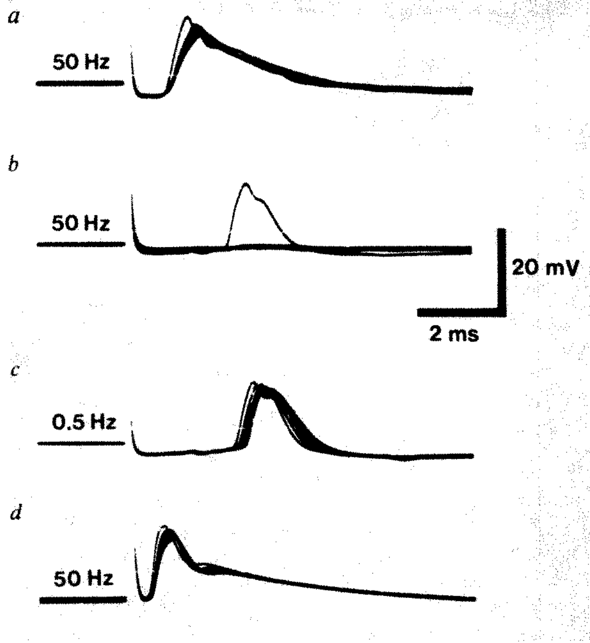

Fig. 3 *a*, GF stimulation at 50 Hz while recording the response in the TTM of a wild-type individual. *b*, Same as *a* but in the mutant *ben*. *c*, GF stimulation at 0.5 Hz while recording the response in the TTM of a *ben* individual. *d*, TTM motoneurone stimulation at 50 Hz in *ben*. In each trace 10 effective stimuli were delivered. Insulated tungsten electrodes were used for stimulating and recording in all experiments.

Evidence from following frequency experiments supports the conclusion that the normal GF–TTM motoneurone synapse is absent. The TTM of wild-type flies can be driven by GF stimulation at frequencies >100 Hz (ref. 3), but in the mutant, the TTM can be driven 1 : 1 only at frequencies <1 Hz. In contrast, the normal DLM following frequency to GF stimulation is unaffected in the mutant. Figure 3*a* shows the response in the TTM of wild type to extracellular stimulation of the GF at 50 Hz. The pathway can respond to each of the stimuli with its characteristically short and constant latency. Figure 3*b* shows the response in the TTM of a *ben* individual to GF stimulation at 50 Hz. The pathway can only follow the first stimulus. As the DLM responded normally to all stimuli in the train, each stimulus was effective in eliciting a spike in the GF. Figure 3*c* shows that the TTM pathway of *ben* flies is capable of following low frequencies of GF stimulation without failure. In this experiment the GF was stimulated at a frequency of 0.5 Hz; the TTM followed 1 : 1. To exclude the possibility of a defect in motoneurone spike conduction, neuromuscular transmission or the muscle membrane, the TTM motoneurone was stimulated extracellularly in the ganglion while recording from the TTM itself. Figure 3*d* shows the TTM response to stimulation of its motoneurone at 50 Hz; the muscle follows the train of stimuli without a failure. This indicates that the site of lability in the pathway mediating the abnormal TTM response lies centrally, between the GF and TTM motoneurone.

One of the more interesting possibilities for the mutation's mechanism of action is that some molecule necessary for the recognition between the GF and the TTM motoneurone is either missing or defective in the mutant. During normal development, insect neurones often send out many branches and retract them at approximately the time synaptic contact is made with their targets[7]. In this case, the presence of abnormal branches in *ben* may be the result of the GF failing to make normal synaptic contact with the TTM motoneurone. Further genetic analysis of mutations such as *ben* may lead to the identification of genes encoding developmentally important molecules involved in connectivity. Ultimately, the molecules themselves may be identified using the techniques of molecular biology.

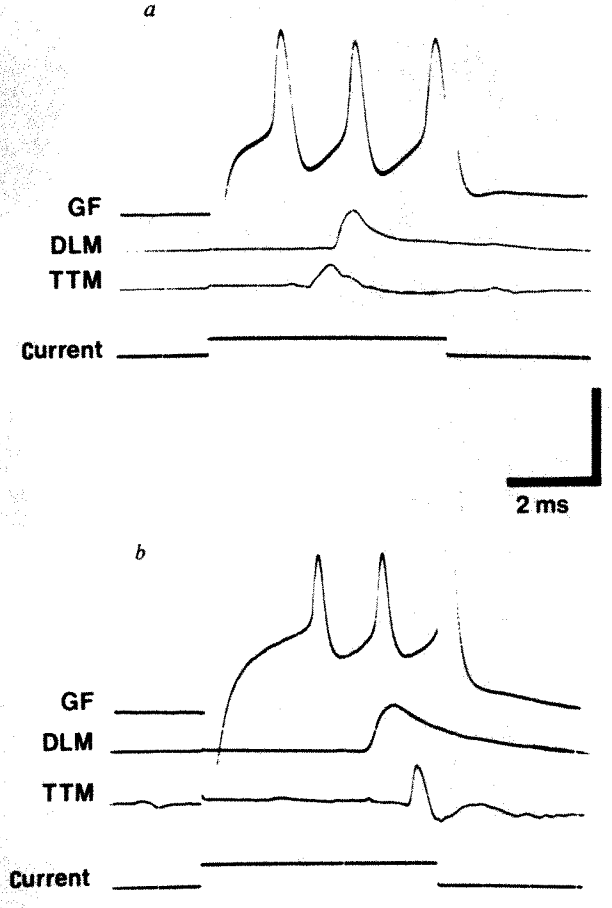

Fig. 2 Response in TTM and DLM to intracellular stimulation of the GF in wild-type (*a*) and *ben* (*b*). Top traces are the intracellular records of the GF. Current is shown in the lower traces. Muscle responses shown in the middle trace are driven by the first GF spike. Vertical calibration is 40 mV for the GF and DLM, 20 mV for the TTM; 10 nA for the current.

We thank Dr Lawrence Salkoff for helpful comments on the manuscript. This work was supported by USPHS grant NS-07314 to R.J.W. and an NIH predoctoral training grant to J.B.T.

Received 11 March; accepted 2 June 1982.

1. King, D. G. & Wyman, R. J. *J. Neurocytol.* **9,** 753–770 (1980).
2. Koto, M., Tanouye, M. A., Ferrus, A., Thomas, J. B. & Wyman, R. J. *Brain Res.* **221,** 213–217 (1981).
3. Tanouye, M. A. & Wyman, R. J. *J. Neurophysiol.* **44,** 405–421 (1980).
4. Thomas, J. B. *Soc. Neurosci.* **6,** 742 (1980).
5. Lewis, E. B. & Bacher, F. *Drosoph. Inform. Serv.* **43,** 193 (1968).
6. Lindsley, D. L. & Grell, E. H. *Genetic Variations of* Drosophila melanogaster (Carnegie Inst. Publ. 627, 1968).
7. Goodman, C. S. & Spitzer, N. C. *Nature* **280,** 208–214 (1979).

Cross-species neural grafting in a rat model of Parkinson's disease

Anders Björklund, Ulf Stenevi, Stephen B. Dunnett & Fred H. Gage

Department of Histology, University of Lund, Lund, Sweden

Previous studies[1-7] have shown that intracerebral implants of embryonic mesencephalic dopamine (DA) neurones, grafted between individuals of the same inbred rat strain, can reverse some of the functional deficits caused by damage to the nigrostriatal DA pathway. These observations have raised the possibility that the intracerebral neural grafting technique may eventually find a clinical application in the treatment of neurodegenerative disorders, particularly Parkinson's disease. One obvious obstacle to any such attempts is the immunological rejection mechanisms associated with allogeneic or xenogeneic grafting. Thus, neural tissue (sensory and sympathetic ganglia), transplanted across immunological barriers to sites outside the central nervous system (CNS), are known to be rejected[8,9]. The brain has, however, been described as an immunologically 'privileged' site, partly perhaps because of its protective blood–brain barrier[10-12]. This may be the case for grafts of embryonic tissue, in particular. Thus, Zalewski *et al.*[13] have reported rejection of allografts of adult ganglionic neurones transplanted o the spinal cord, while Low *et al.*[14] found prolonged survival of embryonic brain tissue in the hippocampal region, grafted between rats of different strains. We report here long-lasting functional cross-species transplantation of mesencephalic DA neurones, taken from mouse embryos, to the dopaminergically denervated neostriatum of adult recipient rats.

Grafts were taken from the ventral mesencephalon (containing the developing substantia nigra–ventral tegmental area DA cell group) of 16–17-day-old mouse embryos (NMRI-strain, Anticimex, Stockholm). The recipients were 18 young adult female rats (Sprague–Dawley strain, Anticimex AB) subjected to a unilateral 6-hydroxydopamine (6-OHDA) lesion of the right nigrostriatal DA pathway 1 month before transplantation. The lesion was performed by local injection of 8 μg 6-OHDA-HCl (Hässle) into the nigrostriatal pathway[15]. The lesion of the nigrostriatal DA pathway was complete in all recipients as assessed by the intensity of the amphetamine-induced turning response. The criterion rate >6 full ipsilateral turns per min over 90 min in response to 5 mg per kg metamphetamine (intraperitoneally) has previously been shown to correspond to a permanent reduction of neostriatal DA of more than 97% (refs 3, 16). The rotation tests were made in automated rotometer bowls according to Ungerstedt and Arbuthnott[17]. The grafts were placed on the dorsal surface of the denervated neostriatum, within a cavity made by aspiration through the anterior parietal cortex and the corpus callosum, as described elsewhere[1,3]. Further rotation tests were conducted $1\frac{1}{2}$, $3\frac{1}{2}$ and $5\frac{1}{2}$ months after transplantation. Turning in response to a low dose of apomorphine (0.05 mg per kg, subcutaneously) was tested twice, at 4 and 5 months after transplantation. All animals were killed at 6 months after transplantation and the brains processed for catecholamine fluorescence histochemistry according to the ALFA method[18]. Alternate sections were stained with cresyl violet.

In 10 of the 18 rats the fluorescence histochemistry revealed surviving DA neurones and reinnervation of the denervated neostriatum. In the remaining 8 animals the transplantation cavities were empty (except for some connective tissue and residual Gelfoam remnants) and there was no trace of surviving DA neurones, suggesting that the grafts in these cases had been totally resorbed (Fig. 1*b*). In the 10 positive cases the actual transplant piece, within the cavity, had also been largely resorbed. The surviving DA-containing neurones occurred either in small, apparently non-vascularized cell clusters at the surface of the caudate-putamen, or scattered within the dorsal part of the caudate-putamen (Fig. 1*a*). These DA neurones were mostly small and rounded, and exhibited a DA fluorescence of widely varying intensity. The cresyl violet stain suggested the presence also of some non-DA neurones in the cell clusters, but there were no obvious signs of lymphocytic infiltration within these clusters, or within the caudate-putamen of the host.

The most striking microscopic finding was the newly formed DA-fluorescent terminal network within the caudate-putamen of the positive cases. In 8 of the 10 specimens this reinnervation was rich and covered large areas of the head of the host caudate-putamen (Fig. 1*a*). In several cases the DA fibres occurred in patches which were seemingly derived from single DA-containing cell bodies in their vicinity. In two of the positive cases the ingrowth of DA fibres was poor and confined to a few small patches close to the transplantation cavity.

For behavioural analysis the rats were allocated in a blind manner to one of three groups: rich ingrowth, poor ingrowth or no ingrowth. The amphetamine and apomorphine rotation tests revealed a striking relationship between graft ingrowth and compensation of the turning response in the lesioned rats (Fig. 2). Thus, whereas the rats with no DA neurone survival (open circles in Fig. 2*a*) increased their amphetamine-induced turning response, from an average of 8.1 turns per min before grafting, to an average of 15 turns per min by $5\frac{1}{2}$ months, the rats with DA neurone survival and rich ingrowth into the caudate-putamen (filled circles in Fig. 2*a*) reduced their turning response from 9.6 turns per min to 1.0 turns per min. The compensation of the turning response developed over the first $3\frac{1}{2}$ months and remained stable between $3\frac{1}{2}$ and $5\frac{1}{2}$ months after transplantation. Both the magnitude and the time course of compensation of the turning response in the xenografted animals are very similar to those previously observed in rats with homologous nigral grafts[3]. In the rats with poor DA ingrowth into the caudate-putamen, the compensation of the amphetamine-induced turning followed a different time course and became evident only between $3\frac{1}{2}$ and $5\frac{1}{2}$ months after transplantation (open triangles in Fig. 2*a*). The differences between the groups are statistically significant (Fig. 2).

The contralateral turning response to a low dose of the DA receptor agonist, apomorphine (0.05 mg per kg), which can be taken as a measure of the degree of DA receptor supersensitivity in the denervated neostriatum[19], was on the average reduced by 65–75% in the richly reinnervated rats compared with the rats with no or poor DA ingrowth (Fig. 2*b*). This reduction is statistically significant and similar to that previously recorded from rats with homologous grafts[5].

The present results demonstrate that long-term survival of cross-species grafts of embryonic DA neurones can be achieved in the adult rat CNS in the absence of any immunosuppressive treatment. It is interesting that the surviving DA neurones were found on the surface and in the depth of the host caudate-putamen, whereas the bulk of the discrete transplant had been almost totally resorbed. This suggests that the migratory capacity of the embryonic neurones or neuroblasts in the graft is of critical importance for their ability to escape rejection. Although a blood–brain barrier is known to develop within grafts of embryonic CNS tissue, it is likely that it is established by vessels derived from the graft itself rather than from the host[20,21]. Thus, if the blood–brain barrier is important for long-term survival of immunologically imcompatible grafts in the CNS, our results would support the idea that grafted neurones can escape rejection by migration into the protected environment behind the barrier of the host. This would also explain the ability of the xenogeneic DA neurones to reinnervate and establish a new, long-lasting terminal network within the host caudate-putamen.

0028–0836/82/320652—03$01.00

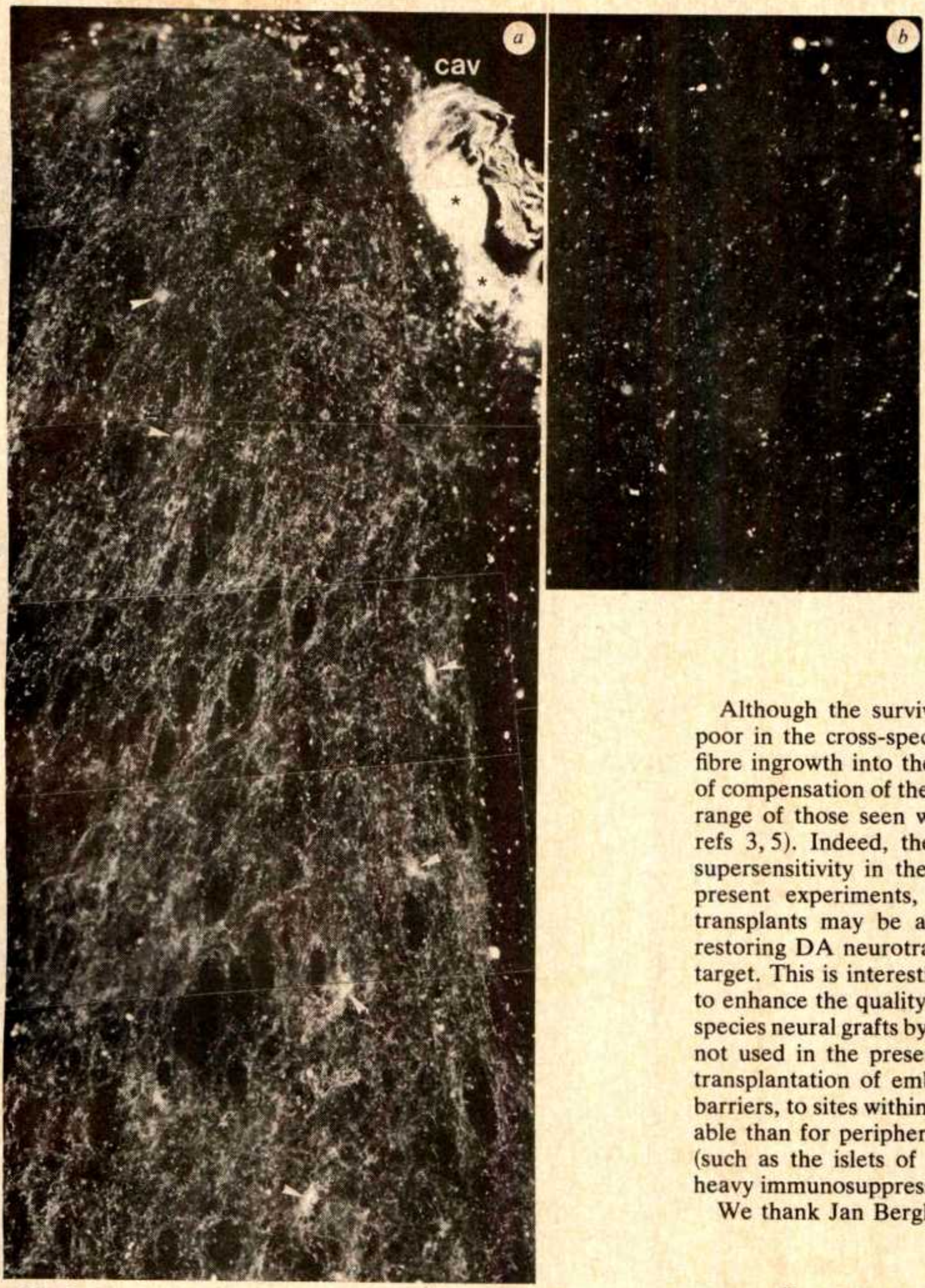

Fig. 1 The dorsal part of the caudate-putamen: *a*, in a case with surviving grafted DA neurones and a rich dopaminergic reinnervation of the dorsal caudate-putamen, and *b*, in a case with no surviving graft and a persisting total dopaminergic denervation of the caudate-putamen. Both rats were killed 6 months after transplantation. Asterisks in *a* denote clusters of intensely fluorescent DA-containing neurones at the bottom of the transplantation cavity (cav). Some fluorescent DA-containing cells within the caudate-putamen of the host are marked with arrow heads. (×160.)

Although the survival of the discrete grafts was generally poor in the cross-species experiments, the magnitude of DA fibre ingrowth into the host caudate-putamen and the degree of compensation of the turning asymmetry were well within the range of those seen with homologous nigral grafts (compare refs 3, 5). Indeed, the degree of reduction in DA receptor supersensitivity in the reinnervated neostriatum, seen in the present experiments, suggests that the cross-species nigral transplants may be as effective as the homotypic grafts in restoring DA neurotransmission in the previously denervated target. This is interesting not least because it may be possible to enhance the quality and magnitude of survival of the cross-species neural grafts by applying immunosuppressive treatment, not used in the present study. The conditions for functional transplantation of embryonic neurones across immunological barriers, to sites within the brain, thus seem to be more favourable than for peripheral grafts of neurones or endocrine cells (such as the islets of Langerhans) which are rejected unless heavy immunosuppressive treatments are applied[8,9,22–24].

We thank Jan Berglund, Ulla Jarl and Gertrude Stridsberg

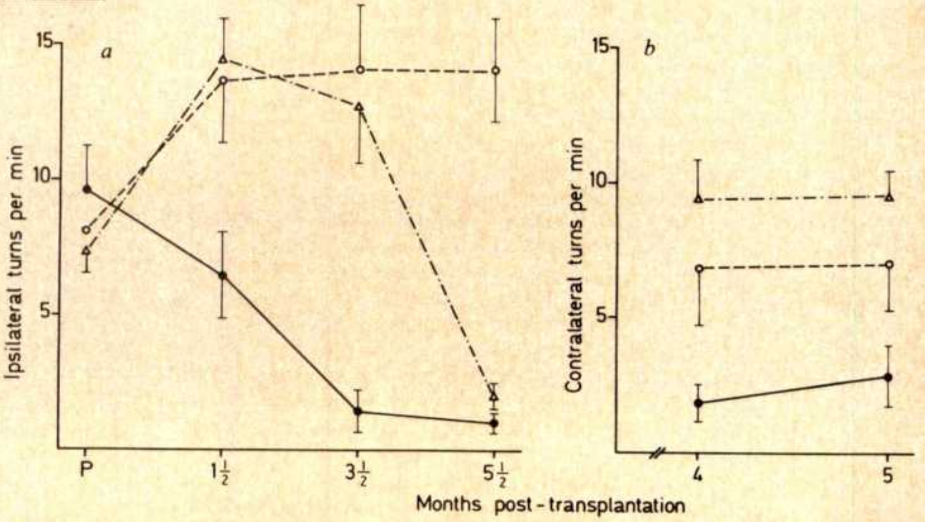

Fig. 2 Drug-induced rotation in rats with unilateral 6-OHDA lesions of the nigrostriatal pathway, followed 1 month later by grafts of DA-rich embryonic mouse mesencephalon to the neostriatum on the same side as the initial lesion. Rats were allocated to three groups on the basis of subsequent blind histological analysis: ∘- - -∘, no detectable surviving fluorescent DA cells or fibre ingrowth ($n = 8$); △- · -· △, poor fibre ingrowth in small patches in the host rat caudate-putamen ($n = 2$); •—•, rich surviving fluorescent fibre ingrowth in dorsal portions of the host caudate-putamen ($n = 8$). Values plotted are means ±s.e.m. *a*, Ipsilateral rotation over 90 min following intraperitoneal injection of 5.0 mg per kg metamphetamine, before (*P*) and at regular intervals following transplantation. Difference between groups: $F(2, 15) = 10.59$, $P < 0.01$; group × time interaction: $F(6, 45) = 9.41$, $P < 0.01$. *b*, Contralateral rotation over 40 min following subcutaneous (s.c.) injection of 0.05 mg per kg apomorphine, 4 and 5 months following transplantation. Difference between groups: $F(2, 15) = 3.97$, $P < 0.05$; group × time interaction: $F(6, 45) = 0.23$, not significant.

for technical assistance. The work was supported by grants from the Swedish MFR (04X-3874), the Syskonen Svensson and Kock Foundations and the NSF Division of International Programs.

Received 23 March; accepted 10 June 1982.

1. Björklund, A. & Stenevi, U. *Brain Res.* **177,** 555–560 (1979).
2. Perlow, M. J. *et al. Science* **204,** 643–647 (1979).
3. Björklund, A., Dunnett, S. B., Stenevi, U., Lewis, M. E. & Iversen, S. D. *Brain Res.* **199,** 307–333 (1980).
4. Freed, W. J. *et al. Ann. Neurol.* **8,** 510–519 (1980).
5. Dunnett, S. B., Björklund, A., Stenevi, U. & Iversen, S. D. *Brain Res.* **215,** 147–161 (1981).
6. Dunnett, S. B., Björklund, A., Stenevi, U. & Iversen, S. D. *Brain Res.* **229,** 457–470 (1981).
7. Björklund, A., Stenevi, U., Dunnett, S. B. & Iversen, S. D. *Nature* **289,** 497–499 (1981).
8. Zalewski, A. A. *Expl Neurol.* **32,** 218–229 (1971).
9. Zalewski, A. A. & Silvers, W. K. *Expl Neurol.* **52,** 507–514 (1976).
10. Greene, H. S. N. *Cancer Res.* **11,** 529–534 (1951).
11. Scheinberg, L. C., Edelman, F. L. & Levy, W. A. *Archs Neurol.* **11,** 248–264 (1964).
12. Barker, C. F. & Billingham, R. E. *Adv. Immun.* **25,** 1–54 (1977).
13. Zalewski, A. A., Goshgarian, H. G. & Silvers, W. K. *Expl Neurol.* **59,** 322–330 (1978).
14. Low, W. C., Lewis, P. R. & Bunch, S. T. *Brain Res.* (submitted).
15. Marshall, J. F. & Ungerstedt, U. *Science* **198,** 62–64 (1977).
16. Schmidt, R. H., Ingvar, M., Lindvall, O., Stenevi, U. & Björklund, A. *J. Neurochem.* **38,** 737–748 (1982).
17. Ungerstedt, U. & Arbuthnott, G. W. *Brain Res.* **24,** 485–493 (1970).
18. Lorén, I., Björklund, A., Falck, B. & Lindvall, O. *J. neurosci. Meth.* **2,** 277–300 (1980).
19. Ungerstedt, U. *Acta physiol. scand.* Suppl. **367,** 69–93 (1971).
20. Svendgaard, N. A., Björklund, A., Hardebo, J. E. & Stenevi, U. *Nature* **255,** 334–337 (1975).
21. Møllgard, K., Lundberg, J. J., Beebe, B. K., Björklund, A. & Stenevi, U. *Neurosci. Lett.* **8,** 295–301 (1978).
22. Marquet, R. L. & Heystek, G. A. *Transplantation* **20,** 428–431 (1975).
23. Finch, D. R. A., Wise, P. H. & Morris, P. J. *Diabetologia* **13,** 195–199 (1977).
24. Bowen, K. M., Andrus, L. & Lafferty, K. J. *Diabetes* **29,** Suppl. 1, 98–104 (1980).

Association amacrine cells could mediate directional selectivity in pigeon retina

Andrew P. Mariani

Laboratory of Vision Research, National Eye Institute,
National Institutes of Health, Bethesda, Maryland 20205, USA

Ganglion cell receptive fields in the vertebrate retina are classified as 'simple' if they display mutually antagonistic, concentric on and off responses to stimulation by light[1], or 'complex' if they respond maximally to a stimulus which moves in a certain direction or has a particular orientation[2]. One complex unit frequently reported is directionally selective[3–6]. It is excited by stimuli moving through its receptive field in only one direction, the preferred direction, and is inhibited by motion in the reverse or null direction. In species such as cats and monkeys which have a predominantly simple centre-surround organization of ganglion cell receptive fields, there is a low ratio of conventional (amacrine cell) to ribbon (bipolar cell) synapses in the inner plexiform layer, while in species such as pigeons and frogs which have a large percentage of complex ganglion cell receptive fields, there is a high ratio of conventional to ribbon synapses. It is therefore thought that amacrine cells, which are laterally interconnecting neurones in the inner plexiform layer, form the complex ganglion cell receptive field[7,8]. Although quantitative electron microscopy of the inner plexiform layer has indicated that amacrine cells may form the complex receptive field properties of ganglion cells, it offers no clues to the particular morphology of amacrine cells involved. I have therefore now studied amacrine cells in pigeon retina using Golgi impregnation in both whole-mounted and radially sectioned material to see whether there is a correlation between the morphology of amacrine cells and the receptive fields of ganglion cells. In 30 Golgi-impregnated retinas, I have found many different morphological types of amacrine cell. One of these is so clearly different from all other amacrine cells that it requires the separation of pigeon amacrine cells into two distinct classes, those which lack axons (class I cells) and those which have axons (class II cells).

Class I amacrine cells have dendrites radially organized with respect to their cell bodies when viewed in flat preparations (Fig. 1*b–e*). The cells have diverse morphology, and may include cells with dendritic trees which are multiply stratified, but which nevertheless display a radial symmetry when viewed in flat preparations. In comparison class II amacrine cells of the pigeon retina are not radially organized. In addition to their dendritic processes, they have a short axon with a terminal arborization in the same stratum of the inner plexiform layer as their dendrites. These cells were first described by Cajal[9] in another avian species, and he termed them 'association' amacrines, but their presence has not been reported since that time[10]. They differ from 'ordinary' amacrines (class I cells) as they clearly have an axon.

In the 30 Golgi preparations of the pigeon retina, the association amacrine cells are frequently stained: over a 100 may be found in a single retina, but only 5 have been stained completely through their axon terminal arborization.

Association amacrine cells (Fig. 1*a*) have 13 μm diameter cell bodies, which makes them larger than all other amacrines (6–10 μm), and are situated in the innermost part of the inner nuclear layer where they are exceeded in size only by the Dogiel (displaced ganglion) cells. Four or five dendrites about 2 μm thick arise from the vitreal part of the cell body and branch once or twice. Large 3–4 μm spiny varicosities occur on the dendrites near branch points, and the dendrites then taper to very fine processes and terminate in the outermost stratum of the inner plexiform layer, with a total length of no more than 35 μm. An axon of 1.5 μm diameter arises directly from the cell body or one of the dendrites and courses just beneath the inner nuclear layer for 200–700 μm. Collaterals may arise from the axon, but two axons are rarely observed; if the two axons do exist, both follow the same course. At its terminal arborization in the outermost stratum of the inner plexiform layer the axon thins to 0.5 μm, bears many 1–2 μm terminal and preterminal boutons and spans up to 200 μm. The axons of different cells appear to be non-preferentially oriented: those arising from nearby cells may cross each other at various angles. The association amacrine cells, due to their morphological polarization, might be involved in the organization of directionally selective receptive fields of ganglion cells in pigeon retina.

Directionally selective units in the pigeon retina respond to movement through their receptive fields in the preferred direction with a vigorous discharge of spikes[4,5]. There is virtually no response to a moving stimulus in the opposite or null direction[3] and a small response to a stationary stimulus over the receptive field[4]. The null directional movements, which are inhibitory and determine the null-preferred axes, are oriented in many directions so that different directionally selective units may have different null-preferred axes[6]. Other evidence[3] indicates that there is an inhibitory patch offset from the receptive field centre which determines the null direction, and when examined at this offset patch, the receptive field is non-directional as it is inhibited by moving stimuli in both the null-preferred and orthogonal axes. Similarly, the field centre is non-directional when examined at the preferred side since it may be activated by preferred, null and orthogonal movements[3].

Association amacrine cells could be the anatomical basis for the directionally selective responses recorded in the pigeon retina. Their having an axon which separates morphologically distinct parts of the cell is clearly consistent with a physiological

0028-0836/82/320654-03$01.00

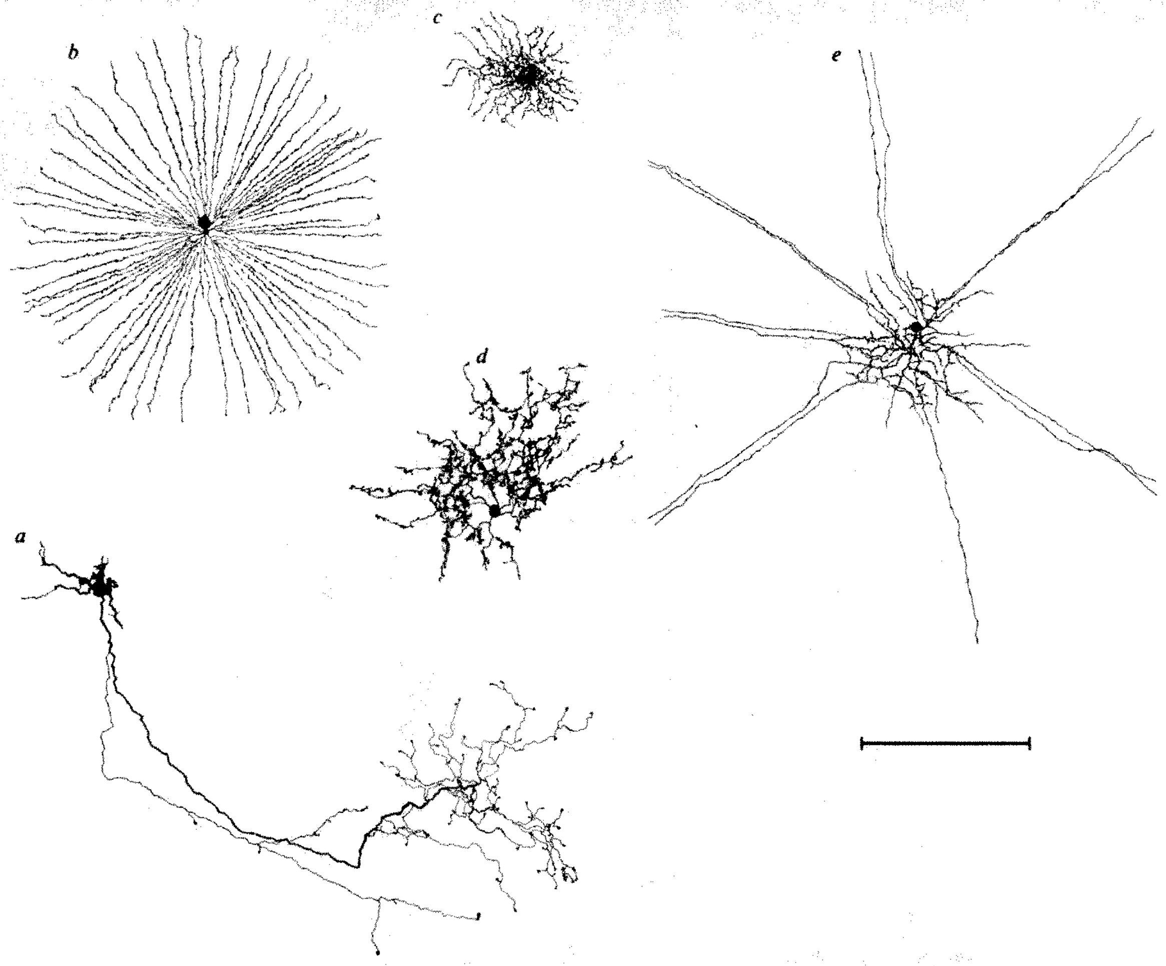

Fig. 1 Camera lucida drawings of Golgi-impregnated amacrine cells in whole, flat-mounted pigeon retina. 'Ordinary' amacrine cells (*b-e*) lack an axon and their dendrites display radial symmetry. 'Association' amacrine cells (*a*) clearly have an intraretinal axon which separates the dendritic end and the axon terminal arborization, and thus are morphologically polarized. This morphological polarization could mediate directional selectivity in pigeon retina. Bar, 100 μm.

concept of asymmetric lateral inhibition extending in only one direction which determines the null-preferred axis[11]. Like different directionally selective units, the axons of association amacrines have different orientations. The axon terminal arborization could be located over the receptive field centre of the ganglion cell. The soma and dendrites of the cell are then offset from the field centre, and activation of the association amacrine by motion in the null direction as a patch offset from the field centre could inhibit the ganglion cell. Thus motion in the preferred direction could excite the ganglion cell. This model can account for the non-directionality of responses at the receptive field centre and the non-directionality of inhibition which appears to be offset from the receptive field centre and determines the null direction[3].

Received 16 February; accepted 2 June 1982.

1. Kuffler, S. W. *J. Neurophysiol.* **16,** 37–68 (1953).
2. Lettvin, J. Y., Maturana, H. R., McCulloch, W. S. & Pitts, W. H. *Proc. Instn Radio Engrs Aust.* **47,** 1940–1951 (1959).
3. Holden, A. L. *J. Physiol., Lond.* **270,** 253–269 (1977).
4. Maturana, H. R. *22nd int. Cong. physiol. Sci.*, Leyden, 170–178 (Excerpta Medica, Amsterdam, 1962).
5. Maturana, H. R. & Frenk, S. *Science* **142,** 977–979 (1963).
6. Pearlman, A. L. & Hughes, C. P. *J. comp. Neurol.* **166,** 111–122 (1976).
7. Dowling, J. E. *Proc. R. Soc.* **B170,** 205–228 (1968).
8. Dubin, M. W. *J. comp. Neurol.* **140,** 479–506 (1970).
9. Cajal, S. R. (1933) as trans. in *The Structure of the Retina* (eds Thorpe, S. A. & Glickstein, M.) 76–92 (Thomas, Springfield, Illinois, 1972).
10. Stell, W. K. in *Handbook of Sensory Physiology* Vol. VII/2 (Springer, Berlin, 1972).
11. Wyatt, H. J. & Daw, N. W. *J. Neurophysiol.* **38,** 613–626 (1975).

Glycine receptor alteration in the mutant mouse *spastic*

W. F. White* & A. H. Heller†

Department of Neuroscience, Children's Hospital Medical Center
and Departments of *Neuropathology and †Neurology,
Harvard Medical School, Boston, Massachusetts 02115, USA

The mutant mouse *spastic*, which carries a single-locus, recessive mutation[1] on chromosome 3 (refs 2, 3), is characterized by hyperexcitability, rapid tremor, rigidity and prolonged righting reflexes[1]. No anatomical abnormalities have been found in preliminary histological studies of muscle or the central nervous system (CNS)[1]. Electromyographic studies in *spastic* mice demonstrate abnormal electrical bursts during activity and abnormal stereotyped reflexes[4]. Drugs which increase γ-aminobutyric acid (GABA)[5] or enhance GABA synaptic action[6] reduce *spastic* symptoms, suggesting that they result from an imbalance in excitatory and inhibitory influences in the *spastic* CNS. Strychnine antagonizes the synaptic action of glycine[7], and binds to a membrane site with the characteristics of the postsynaptic glycine receptor[8–11]. The behavioural and electrophysiological abnormalities of *spastic* mice are reproduced in normal mice given subconvulsive doses of strychnine[4], suggesting that *spastic* symptoms might result from a deficiency in glycine-mediated inhibition[4]. We describe here evidence that supports this hypothesis: a decrease in ^{3}H-strychnine binding in membrane fractions prepared from *spastic* compared with littermate control mice. We also demonstrate an involvement of the benzodiazepine, and possibly the GABA, binding site in the *spastic* phenotype.

0028-0836/82/320655—03$01.00

Adult mice of both sexes were produced on site from matings between B6C3-a/a-*spa*/+ hybrids (Jackson Laboratory) and homozygous *spa* mice (*spa*/*spa*) were identified by tremor and difficulty in regaining upright posture when turned on their backs. Unaffected littermates (+/?) of the same sex were used as controls in all studies. *Spastic* mutants are significantly smaller than control animals: a sample of adult *spastic* animals ($n = 7$) weighed 81.7±4.4% (mean±s.e.m.) of their littermate controls and the *spa*/*spa* brain regions (spinal cord, brain stem, midbrain and cortex) weighed an average of 88.4±8.4% of comparable +/? regions. There were no significant differences among the *spastic* to control weight ratios for the individual regions.

The binding of ^{3}H-strychnine in *spa*/*spa* and +/? animals is presented in Table 1. In all regions tested, specific ^{3}H-strychnine binding is reduced in *spa*/*spa* compared with +/?. The low level of binding seen in the *spastic* CNS makes accurate quantification difficult.

Because only a small amount of ^{3}H-strychnine binding in *spastic* animals is specific, we used several methods for determining nonspecific binding: excess glycine (10 mM) (Table 1), excess strychnine (100 μM), or heat inactivation (80 °C for 30 min) (data not shown). We find that ^{3}H-strychnine binding is <20% of control in the *spastic* spinal cord, brain stem and midbrain, using any of the measures of nonspecific binding, and <35% of control in cortex using excess glycine to determine nonspecific binding; neither the excess strychnine nor the heat inactivation methods for determining nonspecific binding yielded any specific binding in cortex.

Very different results are obtained in binding studies of the GABA, benzodiazepine and muscarinic acetylcholine receptors (Table 2). Generally, there is more specific ^{3}H-GABA binding in the spinal cord and brain stem of *spastic* compared with control animals. However, because of the low level of specific ^{3}H-GABA binding (10–20%) in these two brain regions, the results were relatively more variable, and the observed difference was not statistically significant ($P > 0.05$). Specific binding of ^{3}H-flunitrazepam is 40% greater in the spinal cord, and 17% greater in the brain stem of *spastic* compared with control animals ($P < 0.05$, both regions); again there are no differences in the midbrain and cortex. These increases in binding to the benzodiazepine binding site and potentially to the GABA binding site are consistent with preliminary studies using ^{3}H-flunitrazepam and ^{3}H-muscimol as ligands for the benzodiazepine and GABA binding sites[12]. In contrast, there are no significant differences in the binding of ^{3}H-QNB (quinuclidinyl benzilate) in any of the regions investigated. The magnitude and regional distribution of the binding of all four ligands in control animals are similar to published values for rodent brain[8,13–15].

Table 1 Specific binding of ^{3}H-strychnine to the CNS of *spastic* and littermate control mice

Region	Genotype	% Specific binding	pmol per mg protein	% Of paired littermate control
Spinal cord	+/?	68	1.26±0.08	
	spa/*spa*	29	0.22±0.06*	16±4*
Brain stem	+/?	87	1.79±0.11	
	spa/*spa*	45	0.34±0.04*	19±2*
Midbrain	+/?	60	0.60±0.04	
	spa/*spa*	28	0.086±0.031*	14±5*
Cortex	+/?	23	0.14±0.02	
	spa/*spa*	5	0.047±0.009*	34±6*

Mice were decapitated and the brains and spinal cords rapidly dissected, weighed, homogenized in a glass–glass homogenizer in ice-cold 200 mM KCl, 50 mM NaKHPO$_4$, pH 7.1, and centrifuged at 100,000*g* for 20 min. The pellet was then washed four times by replacing the supernatant with fresh buffer, sonicating to disperse the pellet and recentrifuging. The final pellet was resuspended at a concentration of 5 mg (original wet wt) per ml for use in the binding assays. In ^{3}H-strychnine binding studies, 500 μl of tissue were added to microcentrifuge tubes (Biorad) containing 500 μl of buffer and 12 nM ^{3}H-strychnine. Nonspecific binding was determined in parallel incubations containing excess glycine (10 mM). Following a 20 min incubation at 4 °C the samples were centrifuged for 10 min in an Eppendorf microcentrifuge. The supernatant was carefully removed and the pellet washed twice with 1 ml of buffer. The pellet was solubilized overnight in 1 ml 1% SDS, 20 mM EDTA, adjusted to pH 8.5 with NaOH, and counted in a Triton X-100, toluene, Omnifluor liquid scintillation cocktail. Parallel studies of ^{3}H-strychnine binding using excess strychnine (100 μM) and heat inactivation (80 °C for 30 min) to determine nonspecific binding values were also performed (data not shown). A small amount of ^{3}H-strychnine was displaced from the assay tube by 100 μM strychnine. Thus, when excess strychnine was used to determine nonspecific binding, nonspecific binding equalled the binding in the presence of excess strychnine plus the binding displaced from the tube. The ^{3}H-strychnine (19.3 Ci mmol^{-1}) was purchased from Amersham. All experiments on a given sample were performed at least in triplicate and samples were obtained from at least four pairs of animals. Specific binding equals total binding minus nonspecific binding. Per cent specific binding equals specific binding divided by total binding times 100. Proteins were assayed by the method of Bradford[25]. Values are the mean±s.e.m. and all values reported are significantly different from 0. Percentage values are the mean±s.e.m. of the percentages derived from comparisons between littermate pairs.

* *Spastic* animals differ from paired littermate control (+/?) at $P \leq 0.05$; Student's *t*-test for paired observations; two-tailed.

Table 2 Specific binding of ^{3}H-GABA, ^{3}H-flunitrazepam and ^{3}H-QNB to the CNS of *spastic* and littermate control mice

Region	Genotype	% Specific binding	pmol per mg protein	% Of paired littermate control
^{3}H-GABA binding ($n = 6$)				
Spinal cord	+/?	10	0.068±0.014	
	spa/*spa*	10	0.089±0.028	132±27
Brain stem	+/?	15	0.12±0.03	
	spa/*spa*	20	0.16±0.02	165±34
Midbrain	+/?	39	0.37±0.03	
	spa/*spa*	43	0.35±0.04	96±10
Cortex	+/?	61	0.92±0.04	
	spa/*spa*	61	0.93±0.08	101±7
^{3}H-flunitrazepam binding ($n = 4$)				
Spinal cord	+/?	74	0.45±0.03	
	spa/*spa*	84	0.62±0.03*	140±8*
Brain stem	+/?	87	0.85±0.02	
	spa/*spa*	90	0.99±0.02*	117±5*
Midbrain	+/?	94	2.17±0.06	
	spa/*spa*	95	2.20±0.01	102±3
Cortex	+/?	95	2.87±0.04	
	spa/*spa*	94	2.77±0.12	96±4
^{3}H-QNB binding ($n = 4$)				
Spinal cord	+/?	71	0.92±0.06	
	spa/*spa*	72	0.93±0.05	102±8
Cortex	+/?	91	5.14±0.28	
	spa/*spa*	90	5.22±0.33	102±4

A centrifugation assay similar to that used for the strychnine binding assays was used for the GABA binding studies. The tissues used in the GABA binding assay were prepared in Tris-citrate buffer (4 °C, pH 7.1) by washing four times followed by three freeze–thaw–wash cycles. The equivalent of 10 mg of tissue (original wet weight) in 1 ml was used in each tube. The ^{3}H-GABA concentration was 30 nM, and 1 mM GABA was used to determine nonspecific binding. A 10 min centrifugation followed the 10 min incubation. Pellets were washed twice with 1 ml ice-cold Tris-citrate (pH 7.1), solubilized and counted. The binding of both ^{3}H-flunitrazepam and ^{3}H-QNB was investigated using a filtration assay. Briefly, 500 μl of the same tissue suspension used for the strychnine binding studies were added to 500 μl of buffer containing either ^{3}H-flunitrazepam (1 nM) or ^{3}H-QNB (1 nM). Clonazepam (1 μM) or atropine (1 μM) were added to parallel incubations to determine nonspecific binding. Following a 1 h incubation (4 °C flunitrazepam, 24 °C QNB) the bound radioactivity was collected on a 24 mm glass fibre filter (Whatman GF-B) and washed three times with 5 ml of ice-cold 200 mM KCl buffered to pH 7.1 with 50 mM NaKHPO$_4$. The filters were air-dried and counted in liquid scintillation cocktail. The ^{3}H-GABA (34.3 Ci mmol^{-1}), ^{3}H-flunitrazepam (86.4 Ci mmol^{-1}) and ^{3}H-QNB (29.1 Ci mmol^{-1}) were from NEN. See Table 1 legend for further details.

The alterations in the binding of ligands for several neurotransmitters in *spa*/*spa* mice is very provocative. The very low binding of ^{3}H-strychnine in the *spa*/*spa* CNS demonstrates an alteration in the receptor for glycine, the major inhibitory neurotransmitter in spinal cord and brain stem, and a significant inhibitory neurotransmitter in midbrain[7]. This alteration might be expected to decrease the efficacy of glycine-mediated inhibition in these brain areas. On the other hand, the trend towards greater binding of ^{3}H-GABA to the GABA receptor and the greater binding of ^{3}H-flunitrazepam to the benzodiazepine binding site (which is believed to modulate the GABA receptor[16]) in the spinal cord and brain stem would potentially increase the efficacy of inhibition mediated by GABA, the other major inhibitory neurotransmitter in these brain areas[7]. It is tempting to speculate that this alteration in the GABA-benzodiazepine system represents a compensatory response to the decrease in glycine-mediated inhibition. The ability of drugs that enhance GABA-mediated inhibition to reduce the severity of the behavioural[5] and electromyographic[6] symptoms of the *spastic* mutant mouse is consistent with this hypothesis. The localization of the increase in GABA and benzodiazepine binding to the spinal cord and brain stem may result from an inability of the normal GABAergic tone to regulate neuronal excitability in these regions when their normal preponderance of glycine-mediated inhibition is reduced. The absence of this effect in the midbrain and cortex may result from the secondary role of glycine-mediated inhibition in these brain areas and thus the availability of sufficient GABAergic tone to control neuronal excitability. The lack of any difference in the binding of ^{3}H-QNB to the muscarinic acetylcholine receptor in any of the brain regions tested indicates specificity in the alterations produced by the spastic mutation.

Alterations in neurotransmitter receptors have been reported for other murine mutants, and have been attributed to morphological changes in the mutant animal. Both *nervous* and *staggerer* mice, mutants which have a reduced number of Purkinje cells and lack synaptic spines on Purkinje cells respectively, have fewer benzodiazepine binding sites in cerebellum than controls[17-20]. The opposite situation—a greater number of cerebellar benzodiazepine binding sites—has been reported for *weaver* and *reeler* mice, mutants having a reduced number of cerebellar granule cells[17,20]. Fewer GABA receptors have also been reported for all these cerebellar mutants[20,21].

Unlike the cerebellar mutants, the *spastic* mutant shows no obvious anatomical abnormalities in either nervous system or musculature in preliminary histological studies[1]. In addition, the widespread distribution of binding sites for GABA, benzodiazepines and strychnine in the spinal cord, brain stem and midbrain[22-24] makes it seem improbable that the alterations could result from an anatomical abnormality. These preliminary anatomical studies must, however, be confirmed by further, more detailed investigations on the morphological organization of the *spastic* CNS, and in particular of proposed glycinergic and GABAergic inhibitory systems in the affected areas.

These results, together with those from electromyographic studies[4], indicate an alteration in the glycine system in the *spa/spa* mouse which is the probable explanation of the behavioural and electromyographic abnormalities in these mice. They also demonstrate an involvement of the benzodiazepine binding site, and possibly the GABA binding site, in the expression of the *spastic* mutation. The molecular basis of the mutation in the *spastic* mouse which produces these observed alterations in the receptors for neurotransmitters mediating CNS inhibition is unknown. The mutation may result in a direct alteration in one of the receptors, in a component directly associated with one of the receptors, or in some other aspect of one of the affected neurotransmitter systems. On the other hand, the observed effects may be only a few of many widespread secondary effects produced by the mutation. A more complete characterization of both the glycine and GABA-benzodiazepine inhibitory systems in *spa/spa*, proven heterozygous and +/+ animals will further clarify the relationship between these systems and the mutation, and may elucidate the nature of the mutation. The *spastic* mutant mouse should be a valuable system for future investigations on the characteristics of CNS inhibition.

We thank Drs Marc Dichter and Tom Fox for criticism of the manuscript. These studies were supported by NIH grants NS06274, NS00623, NS11237, and the Children's Hospital Mental Retardation Center core grant HD 06276.

Received 3 February; accepted 2 June 1982.

1. Chai, C. K. *J. Hered.* **52,** 241–243 (1961).
2. Lane, P. W. *J. Hered.* **63,** 135–140 (1972).
3. Lane, P. W. & Eicher, E. M. *J. Hered.* **70,** 239–244 (1979); **71,** 315–318 (1980).
4. Heller, A. H. & Hallett, M. *Brain Res.* **234,** 299–308 (1982).
5. Chai, C. K., Roberts, E. & Sidman, R. L. *Proc. Soc. exp. Biol. Med.* **109,** 491–495 (1962).
6. Biscoe, T. J. & Fry, J. P. *Br. J. Pharmac.* **75,** 23–35 (1982).
7. Curtis, D. R. & Johnston, G. A. R. *Ergebn. Physiol.* **69,** 97–188 (1974).
8. Young, A. B. & Snyder, S. H. *Proc. natn. Acad. Sci. U.S.A.* **70,** 2832–2836 (1973).
9. Mackerer, C. R., Kochman, R. L., Shen, T. F. & Hershensen, F. M. *J. Pharmac. exp. Ther.* **201,** 326–331 (1977).
10. Young, A. B. & Snyder, S. H. *Proc. natn. Acad. Sci. U.S.A.* **71,** 4002–4005 (1974).
11. Muller, W. E. & Snyder, S. H. *Brain Res.* **147,** 107–116 (1978).
12. Biscoe, T. J., Fry, J. P., Martin, I. L. & Rickets, C. *J. Physiol., Lond.* **317,** 32p–33p (1981).
13. Enna, S. J. & Snyder, S. H. *Brain Res.* **100,** 81–97 (1975).
14. Speth, R. C. *et al. Fedn Proc.* **39,** 3032–3038 (1980).
15. Yamamura, H. I. & Snyder, S. H. *Proc. natn. Acad. Sci. U.S.A.* **71,** 1725–1729 (1974).
16. Tallman, J. F., Thomas, J. W. & Gallager, D. W. *Nature* **274,** 383–385 (1978).
17. Speth, R. C. & Yamamura, H. I. *Eur. J. Pharmac.* **54,** 397–399 (1979).
18. Skolnick, P., Syapin, P. J., Paugh, B. & Paul, S. M. *Nature* **277,** 397–398 (1979).
19. Lippa, A. S., Sano, M. C., Coupet, J., Klepner, C. A. & Beer, B. *Life Sci.* **23,** 2213–2218 (1978).
20. Chang, R. S. L., Tran, V. T. & Snyder, S. H. *Brain Res.* **190,** 95–110 (1980).
21. Olsen, R. W. & Mikoshiba, K. *J. Neurochem.* **30,** 1633–1636 (1978).
22. Palacios, J. M., Wamsley, J. K. & Kuhar, M. J. *Brain Res.* **222,** 285–307 (1981).
23. Zarbin, M. A., Wamsley, J. K. & Kuhar, M. J. *J. Neurosci.* **1,** 532–547 (1981).
24. Young, W. S. III & Kuhar, M. J. *J. Pharmac. exp. Ther.* **212,** 337–346 (1980).
25. Bradford, M. M. *Analyt. Biochem.* **72,** 248–254 (1976).

Aspartate aminotransferase-like immunoreactivity as a marker for aspartate/glutamate in guinea pig photoreceptors

Richard A. Altschuler*, Judith L. Mosinger†*, George G. Harmison,* Marianne H. Parakkal* & Robert J. Wenthold*

* Laboratory of Neuro-otolaryngology, National Institute of
Neurological and Communicative Disorders and Stroke,
National Institutes of Health, Bethesda, Maryland 20205, USA
† Department of Cellular and Developmental Biology,
Harvard University, Cambridge, Massachusetts 02138, USA

Immunocytochemical techniques have increased our ability to identify neurones containing a specific neurotransmitter. These techniques could not, however, be applied to two major neurotransmitter candidates, aspartate and glutamate, until our recent study in which aspartate aminotransferase (L-aspartate:2-oxoglutarate aminotransferase, EC 2.6.1.1, AATase) was proposed as a marker[1]. This enzyme catalyses the reversible reactions of aspartate to oxaloacetate and α-ketoglutarate to glutamate. In the auditory nerve, which is considered to be aspartergic/glutamergic[2-4], AATase was immunocytochemically localized in primary afferent terminals in the cochlear nucleus[1]. These results suggest a presynaptic enrichment of AATase is associated with aspartergic/glutamergic neurotransmitter function. We have now investigated the distribution of AAT-ase-like immunoreactivity in the retina where previous work suggests that glutamate or aspartate is the neurotransmitter of photoreceptors[5-14]. Our results, reported here, show AATase-like immunoreactivity localized in cones and their terminals in the guinea pig retina.

We used 12 female NIH strain guinea pigs, 150–250 g, in this study. Six guinea pigs were pretreated with colchicine: 10 μg in 5 μl were injected into the vitreous of the left eye 24–48 h before perfusion in guinea pigs under ether anaesthesia. Guinea pigs were anaesthetized with chloral hydrate (0.3 g per kg body weight) and perfused through the heart with 25 ml 0.1 M sodium cacodylate buffer followed by 500 ml of fixative containing 4% paraformaldehyde (w/v) in 0.1 M sodium cacodylate buffer, *p*H 7.2 at 4 °C. In some animals, 50 μl of the fixative were injected intravitreally immediately before vascular perfusion. Retinae from both eyes were placed in the same fixative for 1 h on ice and then rinsed in phosphate-buffered saline (PBS) *p*H 7.2, with 6% (w/v) sucrose at 4 °C for 16–48 h. Ten-μm cryostat sections were cut through the central and peripheral retina and the indirect immunofluorescence technique of Coons[15], modified as described previously[1], was applied using antiserum, raised in rabbits, to cytoplasmic AATase[1]. Sections were incubated for 18 h at 4 °C with antiserum diluted 1:400 in PBS with 0.3% Triton X-100. Absorption controls were prepared by adding 20 μg of AATase (Boehringer Mannheim) to 10 μl of antiserum and were used at a 1:400 dilution on adjacent sections as a control for specificity of staining. The second incubation was carried out with fluorescein-labelled swine antiserum to rabbit immunoglobulin (Bio-Rad) diluted 1:10, for 30 min at 37 °C. Sections were viewed with a Zeiss photomicroscope under epifluorescent illumination.

In the retinae of animals without colchicine pretreatment, a band of AATase-like immunofluorescence was seen in the outer plexiform layer (OPL; Fig. 1*a*). In absorption controls, as in the AATase-immunostained preparations, the inner segments of photoreceptors fluoresced non specifically. This was the only fluorescence seen in the retina on absorption control sections (Fig. 1*b*). Colchicine has often been used to concentrate particular antigens in cell bodies[16] and we therefore used colchicine to determine the source of the band of immunoflourescence in the OPL. In retinae pertreated with colchicine, this band could more easily be resolved into individual swellings (Fig. 2*c*). AATase-like immunofluorescence also was seen in cell bodies, in the outer portion of the outer nuclear layer (ONL), giving rise to thin processes ending in large swellings in the OPL (Fig. 2*c*,*d*). This is consistent with the morphological critera of cones and cone pedicles[17].

In retinae with and without colchicine pretreatment, AATase-like immunoreactivity was often seen in a subpopulation of cells along the innermost margin of the inner nuclear layer (INL; Fig. 2*a*–*c*) and in a laminar pattern in the inner plexiform layer (IPL; Figs 1*a*, 2*a*–*d*). These are likely to be a subpopulation of amacrine cells and their fibres.

Immunoreactive cells were also seen in the ganglion cell layer (GCL; Fig. 2*a*), though much less frequently than cells in the IPL. These were easiest to identify in retina prefixed intravitreally due to the better preservation of the ganglion layers. The immunoreactive cells in the GCL might be displaced amacrine cells or may correspond to the class of ganglion cells in which selective uptake of tritiated D-aspartate has been described[11,18].

Several lines of evidence have suggested that aspartate and/or glutamate is a vertebrate photoreceptor transmitter. Physiological studies have shown that glutamate and aspartate mimic the effects of the natural photoreceptor on horizontal and bipolar cells[5-9] and these effects can be eliminated by excitatory amino acid inhibitors[9,10]. Recently Ehinger[11] has demonstrated uptake of D-aspartate into photoreceptors, probably cones, in guinea pig, rabbit and pigeon. Uptake of aspartate and glutamate has also been shown in goldfish photoreceptors[12] where both amino acids were found to be concentrated in red and green cones while only glutamate was concentrated in rods. In rabbit retina, aspartate release has been found to decrease in response to light as would be expected of the natural photoreceptor[13]. Our findings of AATase-like immunoreactivity in cones and cone pedicles provide further evidence that aspartate or glutamate is the neurotransmitter of cones. A recent study showing L-aspartate enhanced excitation of sustained ganglion cells in the cat[19,20] is consistent with our finding of AATase-like immunoreactivity in amacrine cels and suggests aspartate or glutamate as a transmitter for a class of amacrine cells. Ultrastructural immunocytochemical studies are in progress to determine whether AATase is enriched in rod terminals as well as cones and to characterize the immunoreactive cells and fibres in the INL and IPL.

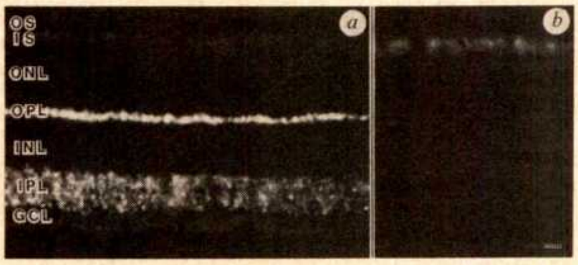

Fig. 1 Fluorescence micrographs of 10 μm cryostat sections of guinea pig retina incubated with antiserum to AATase (*a*) or to AATase preabsorbed with AATase (*b*). *a*, Section showing a band of AATase-like immunofluorescence in the outer plexiform layer and immunofluorescent fibres in the inner plexiform layer. *b*, Absorption control section showing nonspecific fluorescence in inner segments of photoreceptors. OS, outer segments; IS, inner segments; ONL, outer nuclear layer; OPL, outer plexiform layer; INL; inner nuclear layer; IPL, inner plexiform layer; GCL, ganglion cell layer. Scale bar, 20 μm.

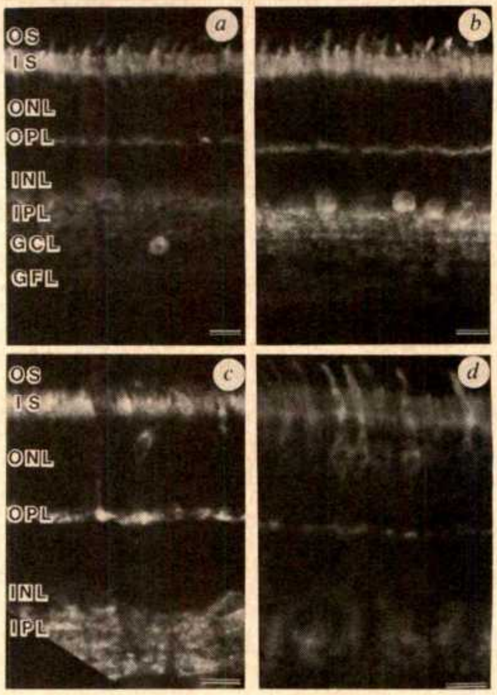

Fig. 2 Fluorescence micrographs of 10 μm cryostat sections of guinea pig retina incubated with antiserum to AATase. *a*, Section through central retina showing AATase-like immunoreactivity in the outer plexiform layer and immunofluorescent cells in the inner nuclear layer and ganglion cell layer. *b*, Section through central retina showing a band of AATase-like immunoreactivity in the outer plexiform layer, immunofluorescent cells in the inner nuclear layer and immunofluorescent fibres in the inner plexiform layer. *c*, Section through retina pretreated with colchicine as described in the text. AATase-like immunoreactivity can be seen in a cone cell body and a cone process and terminal, and immunofluorescent cell bodies and fibres in the inner nuclear and inner plexiform layers. *d*, Section through non-colchicine pretreated retina showing immunofluorescent cones and cone processes. OS, outer segments; IS, inner segments; ONL, outer nuclear layer; OPL, outer plexiform layer; INL, inner nuclear layer; IPL, inner plexiform layer; GCL, ganglion cell layer; GFL, ganglion fibre layer. Scale bars, 20 μm.

The present results support our hypotheses that aspartate aminotransferase can serve as a marker for synapses using aspartate or glutamate as a neurotransmitter. While it is a ubiquitous enzyme, aspartate aminotransferase is enriched in terminals of cones where it may be involved in the specialized role of neurotransmitter synthesis.

We thank Drs John E. Dowling, Berndt Ehinger and Jörgen Fex for helpful comments and suggestions and Mary Lou Adams for secretarial assistance.

Received 18 Februray; accepted 1 July 1982.

1. Altschuler, R. A., Neises, G. R., Harmison, G. G., Wenthold, R. J. & Fex, J. *Proc. natn. Acad. Sci. U.S.A.* **78**, 1255–1259 (1981).
2. Wenthold, R. J. in *Glutamate as a Neurotransmitter* (eds DiChiara, G. & Gessa, G. L.) 69–78 (Raven, New York, 1981).

3. Guth, P. S., Sewell, W. F. & Tachibana, M. in *Pharmacology of Hearing* (eds Brown, R. D. & Diagneault, E. A.) 99–136 (Wiley, New York, 1981).
4. Klinke, R. *Acta otolar* **91**, 541–554 (1981).
5. Cervetto, L. & MacNichol, E. F. *Science* **178**, 767–768 (1972).
6. Murakami, M., Ohtsu, K. & Ohtuska, T. *J. Physiol. Lond.* **227**, 899–913 (1972).
7. Sugawara, K. & Negishi, K. *Vision Res.* **13**, 977–981 (1973).
8. Murakami, M., Ohtsuki, T. & Shimazaki, H. *Vision Res.* **15**, 456–458 (1975).
9. Wu, S. M. & Dowling, J. E. *Proc. natn. Acad. Sci. U.S.A.* **75**, 5205–5209 (1978).
10. Slaughter, M. D. & Miller, R. F. *Science* **211**, 182–185 (1981).
11. Ehinger, B. *Expl Eye Res.* **33**, 381–392 (1981).
12. Marc, R. E. & Lam, D. M. K. *Proc. natn. Acad. Sci. U.S.A.* **78**, 7185–7189 (1981).
13. Neal, M. J. & Massey, S. C. *Neurochemistry* **1**, 191–208 (1980).
14. Yazulla, S. & Kleinschmidt, J. *Brain Res.* **182**, 287–301 (1980).
15. Coons, A. H. in *General Cytochemical Methods* (ed. Danielli, J. F.) 399–422 (Academic, New York, 1958).
16. Hökfelt, T., Elde, R., Johanson, O., Terenius, L. & Stein, L. *Neurosci. Lett.* **5**, 23–32 (1977).
17. Cajal, S. R. *La Cellule* **9**, 17–257 (1982).
18. Beaudet, A., Burkhalter, A., Reubi, J. C. & Cuenod, M. *Neuroscience* **6**, 2021–2034 (1981).
19. Ikeda, H. & Sheardown, M. J. *J. Physiol. Lond.* **319**, 77P (1981).
20. Ikeda, H. & Sheardown, M. J. *Neuroscience* **7**, 25–37 (1982).

Origin of lignans in mammals and identification of a precursor from plants

M. Axelson*, J. Sjövall*, B. E. Gustafsson† & K. D. R. Setchell‡

* Department of Physiological Chemistry and † Department of Germfree Research, Karolinska Institutet, S-104 01 Stockholm, Sweden
‡ Division of Clinical Chemistry, Clinical Research Centre, Harrow, Middlesex HA1 3UJ, UK

Lignans are a class of compounds with a dibenzylbutane skeleton[1] which until recently had only been found in higher plants[2,3]. The first lignans to be identified in humans and animals were *trans*-2,3-*bis*(3-hydroxybenzyl)-γ-butyrolactone (enterolactone)[4–6] and 2,3-*bis*(3-hydroxybenzyl)butane-1,4-diol (enterodiol)[4,5]. These structures differ from those of plant lignans by having aromatic rings substituted only in the *meta* position. Enterolactone and enterodiol are excreted in the urine and bile, predominantly as glucuronide conjugates[7,8], and intestinal microflora is required for their formation[8,9]. It is not known, however, whether they are synthesized *de novo* by microorganisms or are formed from dietary precursors. We report here evidence that these mammalian lignans are formed by microbial action on precursor lignans which are present as dietary constituents of plant origin. Precursors are found in seeds of different species, being particularly abundant in linseed. From this source, 2,3-bis(3-methoxy-4-hydroxybenzyl)butane-1,4-diol (secoisolariciresinol) has been identified as a glycoside.

Evidence for dietary precursor(s) was first obtained by changing the diet given to adult rats from commercial pellets to a semisynthetic diet, D7 (ref. 10), which resulted in a marked and rapid decrease in the excretion of mammlian lignans in urine (Fig. 1). When the diet was reverted to commercial pellets, lignans reappeared in the urine.

The minimum concentration of lignan precursors in different food constituents was determined by adding the latter to the semisynthetic diet and measuring the total excretion of lignans in urine. In decreasing order, rye, buckwheat, millet, soya, oat and barley gave from 6 to 2 μg of lignans in urine per g of meal added. Wheat bran gave about 8 μg per g, wheat and corn meal gave less than 1 μg per g, while linseed was by far the richest source of precursor(s), giving about 800 μg per g of meal. The corresponding value for linseed oil was only 17 μg per g.

Preliminary experiments to isolate the precursor(s) from barley, rye, wheat bran and linseed revealed that the compound(s) were polar and could be extracted with 80% aqueous methanol and separated from fibre. After removal of salts and lipids and fractionation on a column of TEAP-LH-20 $[\mathrm{OH}^-]$[7], about 70% of the precursor(s) in linseed was found in the phenolic fraction. Further separation on DEAE-Sephadex[11] yielded more than 80% of the precursor(s) in the diphenolic fraction. Analytical TLC showed a major highly polar component. Mass spectra of the trimethylsilyl (TMS) ether derivative were recorded using a direct probe. Peaks at m/z 451, 361 (base peak), 319, 271, 243, 217 and 204 were indicative of a TMS ether of a hexoside[12]. An intense peak at m/z 209 suggested a benzyl group substituted with a methoxy and a trimethylsiloxy group[13]. This interpretation was supported by the mass spectrum of the perdeuterated TMS ether derivative. Hydrolysis with β-glucosidase (Emulsin, Sigma) yielded a compound the TMS ether of which had the same retention time on SE–30 (1.54 relative to 5α-cholestane) and OV–17 and the same mass spectrum as the TMS ether of a reference sample of secoisolariciresinol. The fragmentation of the latter compound has been discussed previously[13]. The TLC mobilities of the non-derivatized compounds were also identical. When the reference compound (300 μg) was added to the semisynthetic diet for 1 day, approximately 85 μg of lignans of the mammalian type, predominantly enterolactone, were excreted in the urine, confirming that secoisolariciresinol is the major precursor of enterolactone in rats given linseeds.

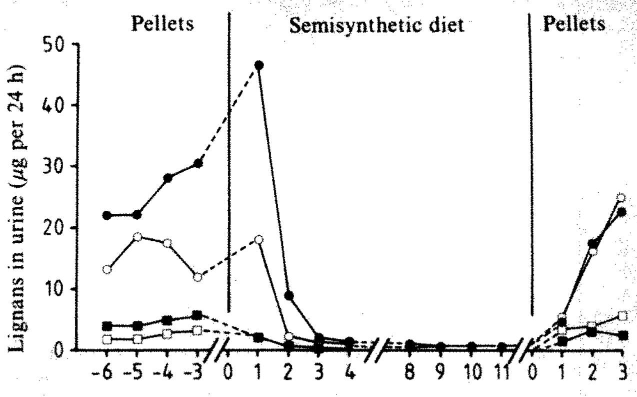

Fig. 1 Daily urinary excretion of enterolactone (circles) and enterodiol (squares) by two adult Long Evans rats (female, body weight 200 g) fed commercial pellets (Astra Ewos, Sweden) or a semisynthetic diet, D7 (ref. 10), composed of wheat starch, casein, arachis oil, salts and vitamins. Lignans were purified and measured by gas chromatography[7,8,11].

Extending these studies to man, the 'normal' diet of adults was supplemented with linseeds and the urinary excretion of enterolactone and enterodiol measured. The response to this diet was analogous to that observed in rats, indicating that the precursor–product relationships are similar in man and rats (Fig. 2).

Our results show that the precursor present in linseeds is a hexoside of 2,3-*bis*(2-methoxy-4-hydroxybenzyl)butane-1,4-diol. The tentative structure proposed in Fig. 3 is based on the previous finding of a diglucoside of a lignan in linseeds[14].

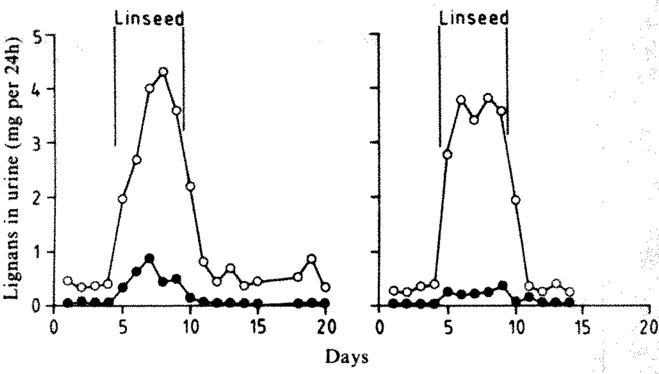

Fig. 2 Daily urinary excretion of enterolactone (○) and enterodiol (●) by two healthy adults before and after the addition of linseeds (10 g per day) to the normal diet over a period of 5 days.

0028–0836/82/320659—02$01.00

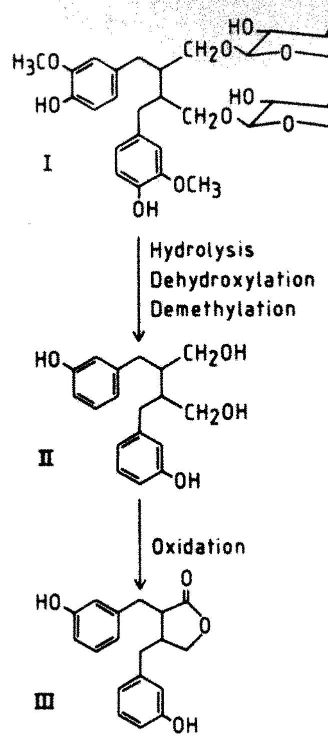

Fig. 3 A simplified scheme for the formation of enterodiol (II) and enterolactone (III) from the dietary precursor secoisolariciresinol glycoside (I). The structure of the sugar moiety is tentative and the exact sequence of reactions is not fully understood.

However, further studies are required to determine the number and position of hexose residues and the stereochemistry of the compound. Other precursors may also exist in plants. Thus, when rats were fed the more abundant plant lignan, matairesinol, enterolactone was excreted in the urine.

Conversion of secoisolariciresinol glycoside to enterodiol requires reactions depicted in Fig. 3. This type of reaction can be carried out by microbial enzymes[15,16]. Extensive formation of enterolactone from enterodiol was demonstrated by feeding 50 μg of the latter[17] to rats in a semisynthetic diet. Enterolactone was not detected when enterodiol was administered orally to germ-free rats, or injected intraperitoneally to bile fistula rats. This indicates that enterolactone can be formed from enterodiol by microbial action.

Lignans have been extensively investigated for their potential anticancer activity, and several have been used as chemotherapeutic agents[3,18]. It is therefore of interest that several common foodstuffs contain lignans. The compounds usually exist in optically pure form; however, enterolactone in human urine is racemic[4-6]. Whether this is due to its formation from precursors of different origin or to isomerization by exchange of a hydrogen vicinal to the carbonyl group of the lactone is unknown. The rate of formation of enterolactone and enterodiol is conceivably influenced by the composition of the microflora, the intestinal transit time and the redox level in the large intestine. Progesterone decreases intestinal motility[19], and this might explain the finding that the excretion of lignans in urine varies during the menstrual cycle[4,6,20,21].

We thank Ms B. Mörk, Mr M. Corrie and Ms E. Conway for technical assistance. Professors T. Norin and D. N. Kirk provided samples of matairesinol, which was reduced to secoisolariciresinol and synthetic enterolactone. Dr R. Ryhage provided mass spectrometric facilities. The work was supported by grants from the Swedish MRC (grants 03X-219 and 16X-206) and Karolinska Institutet.

Received 10 February; accepted 2 June 1982.

1. Haworth, R. D. & Slinger, F. H. *JCS chem. Commun.*, 1098 (1940).
2. Rao, C. B. S. *The Chemistry of Lignans* (Andhra University Press, Waltair, 1978).
3. Hartwell, J. L. *Cancer Treat. Rep.* **60,** 1031 (1976).
4. Setchell, K. D. R. *et al. Nature* **287,** 740 (1980).
5. Setchell, K. D. R. *et al. Biochem. J.* **197,** 447 (1981).
6. Stitch, S. R. *et al. Nature* **287,** 738 (1980).
7. Exelson, M. & Setchell, K. D. R. *FEBS Lett.* **122,** 49 (1980).
8. Axelson, M. & Setchell, K. D. R. *FEBS Lett.* **123,** 337 (1981).
9. Setchell, K. D. R. *et al. Lancet* **ii,** 4 (1981).
10. Midtvedt, T. & Gustafsson, B. E. *Curr. Microbiol.* **6,** 13 (1981).
11. Axelson, M. *et al. Biochem. J.* **201,** 353 (1982).
12. Laine, R. A. & Elbein, A. D. *Biochemistry* **10,** 2547 (1971).
13. Ekman, R. *Holzforschung* **30,** 79 (1976).
14. Bakke, J. E. & Klosterman, H. J. *Proc. N. Dakota Acad. Sci.* **10,** 18 (1956).
15. Drasar, B. S. & Hill, M. J. *Human Intestinal Flora.* (Academic, London, 1974).
16. Nilsson, A., Hill, J. L. & Davies, H. L. *Biochim. biophys. Acta* **148,** 92 (1967).
17. Cooley, G., Farrant, R. D., Kirk, D. N. & Wynn, S. *Tetrahedron Lett.* **22,** 349 (1981).
18. Barclay, A. S. & Perdue, R. E. Jr *Cancer Treat. Rep.* **60,** 1081 (1976).
19. Kumar, D. A,. *J. Obstet. Gynec.* **84,** 1300 (1962).
20. Setchell, K. D. R., Bull, R. & Adlercreutz, H. *J. Steroid Biochem.* **12,** 375 (1980).
21. Setchell, K. D. R., Lawson, A. M., Axelson, M. & Adlercreutz, H. *Int. Congr. Ser. Excerpta Medica Fdn* **515,** 207 (1980).

Fibronectin in adhesion, spreading and cytoskeletal organization of cultured fibroblasts

I. Virtanen*, T. Vartio*†, R. A. Badley‡ & V.-P. Lehto*

Departments of Pathology* and Virology†, University of Helsinki,
Haartmaninkatu 3, SF-00290 Helsinki 29, Finland
‡ Unilever Research, Colworth Laboratory, Sharnbrook,
Bedford MK44 1LQ, UK

The pericellular glycoprotein fibronectin, which has been localized in the pericellular matrix and at the adhesion sites of cells[1-5], has been considered to be important in cell attachment to other cells and to surfaces[1-8]. Using the ionophore monensin, which blocks the secretion of endogenous fibronectin[9,10], we have now shown that human fibroblasts do not require endogenous or exogenous fibronectin for adhesion and spreading, although its absence does prevent formation of the microfilament–vinculin system and the focal adhesion sites.

The indirect immunofluorescence (IIF) technique was used to stain for the presence of fibronectin. Figure 1 shows that trypsinized human embryonal fibroblasts, which adhere to and spread on plastic Petri dishes after plating, develop a typically fuzzy fibronectin-containing plaque after 5 h (Fig. 1*a, b*) and a fibrillar extracellular network of fibronectin after 24 h in culture (Fig. 1*c, d*). No cell-surface-associated fibronectin could be detected on monensin-treated cells (Fig. 1*e, g*) which did, however, adhere and spread in the same way as control cells (Fig. 1*f, h*). Monensin-treated cells do stain for fibronectin in their cytoplasm (Fig. 1*j*), and treatment with the protein synthesis inhibitor puromycin, which causes the cytoplasmic staining of control cells to disappear (Fig. 2*e*), results in an accumulation of fibronectin in the Golgi apparatus (Fig. 2*f*).

The blockage of fibronectin secretion by monensin is further illustrated in Fig. 3, which shows the lack of a polypeptide of molecular weight (M_r) 220,000 (220 K) which corresponds to fibronectin[11], and is the major product in ^{35}S-methionine-labelled control cells, in monensin-treated cells. As shown in Fig. 3*b*, surface labelling of control cells, using the galactose oxidase/sodium borohydride technique[12], also shows up a 220 K polypeptide as a major glycoprotein, lacking in monensin-exposed cells. After 24 h in normal medium, monensin-treated cells recovered the characteristics of normal cells. The surface labelling results also draw attention to the role of cell membrane proteins in cell adhesion and spreading. Interestingly, recent studies have suggested distinct cell-surface glycoproteins[13-16] to be important in cell adhesion. A cell-surface glycoprotein of M_r 140 K could also be shown in this study to be a major cell-surface glycoprotein in cells plated and allowed to spread in the presence of monensin (Fig. 3*b*, asterisk). We have previously shown[14] that the 140 K glycoprotein is the

0028-0836/82/320660—04$01.00

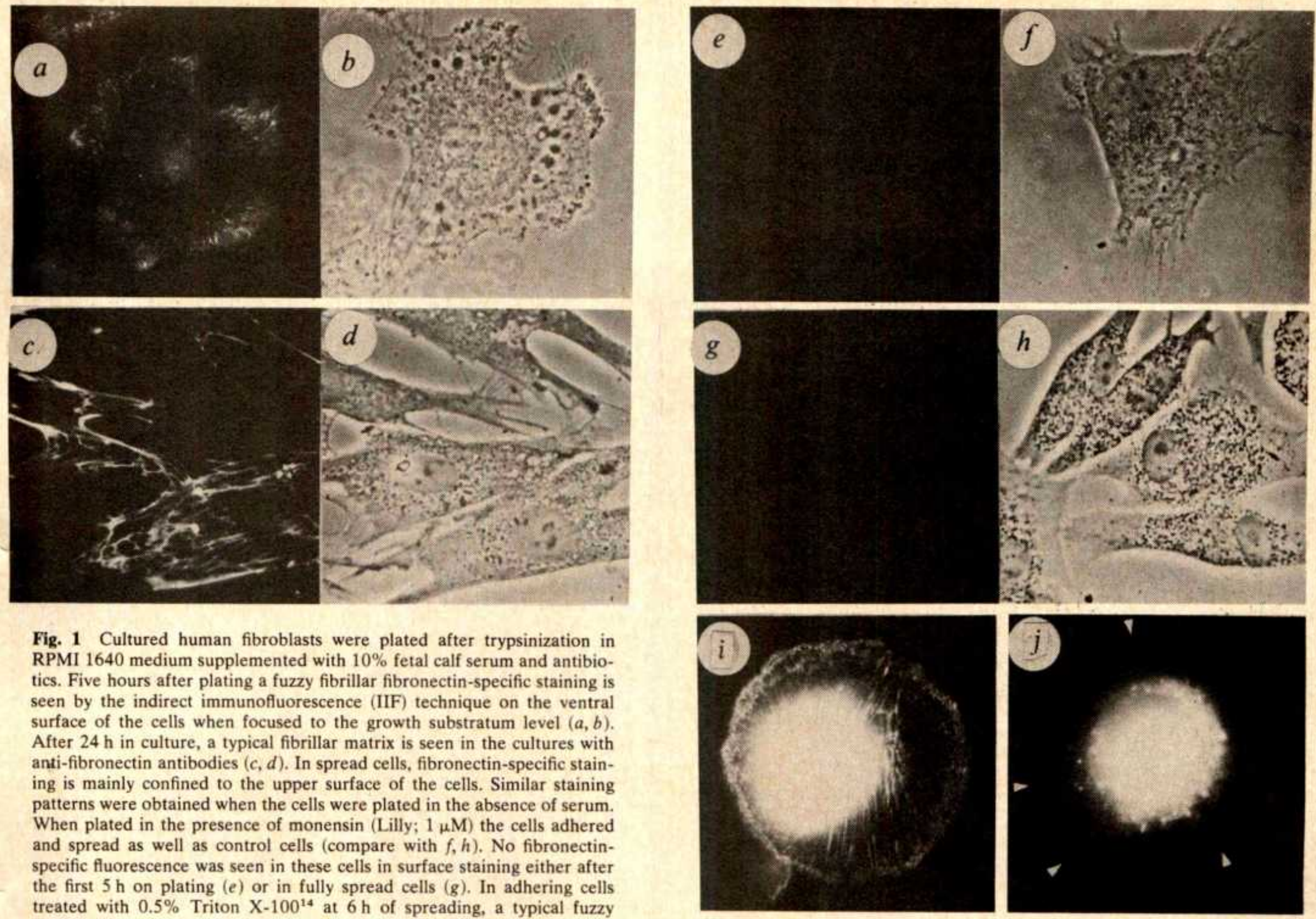

Fig. 1 Cultured human fibroblasts were plated after trypsinization in RPMI 1640 medium supplemented with 10% fetal calf serum and antibiotics. Five hours after plating a fuzzy fibrillar fibronectin-specific staining is seen by the indirect immunofluorescence (IIF) technique on the ventral surface of the cells when focused to the growth substratum level (*a*, *b*). After 24 h in culture, a typical fibrillar matrix is seen in the cultures with anti-fibronectin antibodies (*c*, *d*). In spread cells, fibronectin-specific staining is mainly confined to the upper surface of the cells. Similar staining patterns were obtained when the cells were plated in the absence of serum. When plated in the presence of monensin (Lilly; 1 μM) the cells adhered and spread as well as control cells (compare with *f*, *h*). No fibronectin-specific fluorescence was seen in these cells in surface staining either after the first 5 h on plating (*e*) or in fully spread cells (*g*). In adhering cells treated with 0.5% Triton X-100[14] at 6 h of spreading, a typical fuzzy fibrillar fibronectin-specific fluorescence is seen beneath the control cells, with some diffuse staining in the cytoplasmic domain (*i*) whereas the cells allowed to spread in the presence of monensin only show the remnant cytoplasmic staining following Triton treatment (*j*). In *j* the cell margins are indicated by arrowheads. For surface staining, unfixed cells were exposed to the first antibody washed in phosphate-buffered saline, fixed in 3.5% paraformaldehyde and then exposed to the second antibody, fluorescein isothiocyanate (FITC)-coupled goat anti-rabbit IgG (Cappel). Rabbit antifibronectin antibodies were obtained from Cappel. *a*, *b*, *e*, *f*, *i*, *j*: ×800; *c*, *d*, *g*, *h*: ×400.

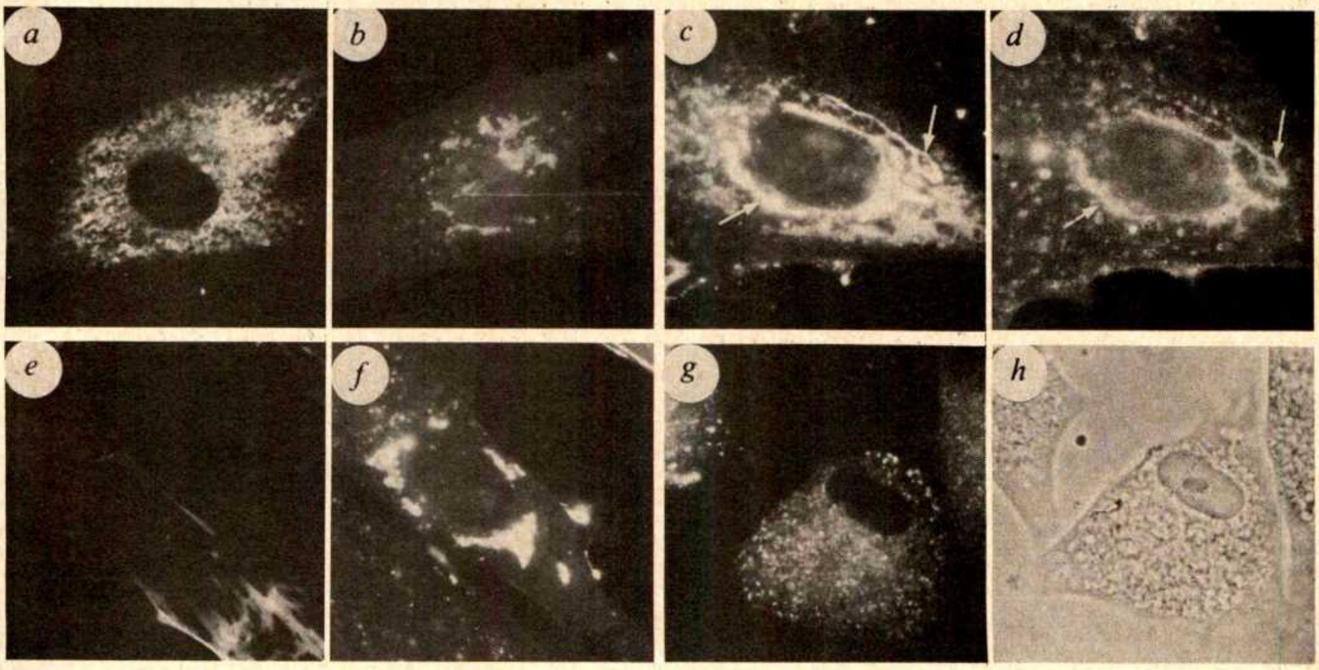

Fig. 2 In control cells fixed in 3.5% paraformaldehyde and permeabilized with 0.1% NP40, a cytoplasmic granular perinuclear staining is seen (*a*). In double-staining with TRITC-wheat germ agglutinin (WGA, Vector Laboratories), used here as a marker for the Golgi apparatus[40], a distinctly different reticular juxtanuclear staining was seen (*b*). Note that no apparent labelling of the Golgi region is seen in *a*. When the cells were exposed to monensin (1 μM) for 1 h, a diffuse cytoplasmic but also a pronounced reticular juxtanuclear fibronectin-specific staining was seen (*c*). The reticular staining (arrows in *c*, *d*) coincided with that obtained with TRITC-WGA (*d*), marking the Golgi apparatus. After exposure to puromycin (2 $\mu g\ ml^{-1}$) for 2 h, no cytoplasmic fluorescence could be detected in control cells (*e*) whereas cells first exposed to monensin (1 μM, 1 h) still showed a bright juxtanuclear fibronectin-specific fluorescence after puromycin treatment (*f*). Cells cultured in the presence of monensin for 24 h, on the other hand, showed a granular cytoplasmic accumulation of fibronectin in IIF but no fibrillar matrix-type fibronectin (*g*, *h*, cells plated in the presence of monensin). ×800.

only surface membrane glycoprotein present in detergent-resistant cytoskeletons of human fibroblasts still anchored to the culture substratum.

With the IIF technique using anti-actin (Fig. 4*a*) and anti-vinculin (Fig. 4*b*) antibodies control cells showed the typical organization of stress fibres and vinculin plaques. Interference reflection microscopy revealed 'black' arrays of focal adhesions in control cells (Fig. 5*a*). In contrast to control cells, IIF of cells plated in the presence of monensin showed only a diffuse actin- and vinculin-specific staining (Fig. 4*c*, *d*). They displayed, however, typical fibrillar arrays of both vimentin-type intermediate filaments and microtubules (Fig. 4*e*, *f*). Monensin-exposed cells did not exhibit focal adhesion sites in interference reflection microscopy but instead showed large grey-coloured areas representing sites of close adhesion (Fig. 5*d*). However, cells first spread in normal medium and then exposed to monensin showed normal arrays of both microfilament bundles (Fig. 4*g*, *h*) and vinculin plaques. A mouse fibroblastoid cell line (3T3), which is known to require exogenous fibronectin for both adhesion and spreading[1], spread on exposure to monensin only if serum was present, but did not develop stress fibres or vinculin plaques (data not shown).

Focal adhesions are specialized cell-surface areas of cell-to-substratum adhesion of cultured cells[17-20] and emerge concomitantly with the formation of bundles of microfilaments[18,19] during cell spreading. Both the vinculin plaques[21,22] and the focal contacts[17,22,23] have been reported to be in close apposition to pericellular fibronectin, and isolated focal adhesions have been reported to contain both actin and fibronectin[17]. During cell spreading, fibronectin seeks to co-align closely with microfilaments[23-25]. Transformed cells, lacking cell-surface-associated fibronectin[4,5], also lack bundles of microfilaments[26,27], but normal arrays of microfilaments are restored on addition of cell-derived fibronectin[28]. However, recent results[29-31] have indicated that fibronectin might be absent or even actively removed from focal adhesions. Based on such an observation, Chen and Singer[29] recently proposed two different molecular mechanisms for microfilament–cell membrane interaction in cultured cells, involving fibronectin differently in cytoskeletal organization and adhesive functions of cultured cells.

Our results with monensin-exposed cells suggest that fibronectin is not needed for fibroblast adhesion to and spreading on culture substrata. On the other hand, endogenous fibronectin seems to be required for the development of focal

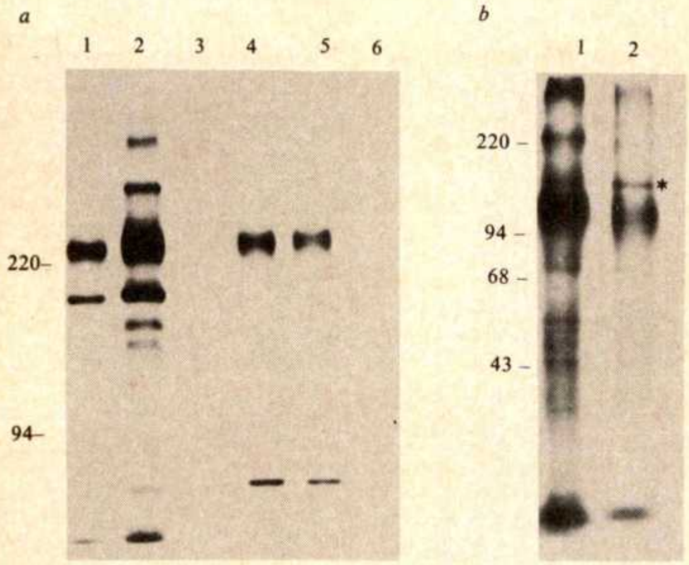

Fig. 3 *a*, Electrophoretic analysis of secreted polypeptides in the culture medium of control cells labelled with L-^{35}S-methionine for 24 h (1,000 Ci mmol^{-1}; 10 μCi ml^{-1}; Radiochemical Centre) showed several polypeptides both after 5 h and 24 h of plating (lanes 1, 2) whereas cultures plated in the presence of monensin and cultured for 24 h did not contain any secreted proteins (lane 3). A prominent 220 K gelatin-binding polypeptide, corresponding to fibronectin[11], was seen in the medium of both spreading (5 h, lane 4) and wholly spread control cultures (24 h, lane 5), but not in cultures plated in the presence of monensin (24 h, lane 6). *b*, Surface labelling experiments using the neuraminidase/galactose oxidase/sodium borohydride method[12] showed a distinct polypeptide with M_r 220 K and several polypeptides of lower molecular weight in control cultures (lane 1). Instead, cells exposed to monensin during plating lacked the 220 K glycoprotein but showed a prominent 140 K glycoprotein (asterisk in lane 2) together with some other polypeptides (lane 2).

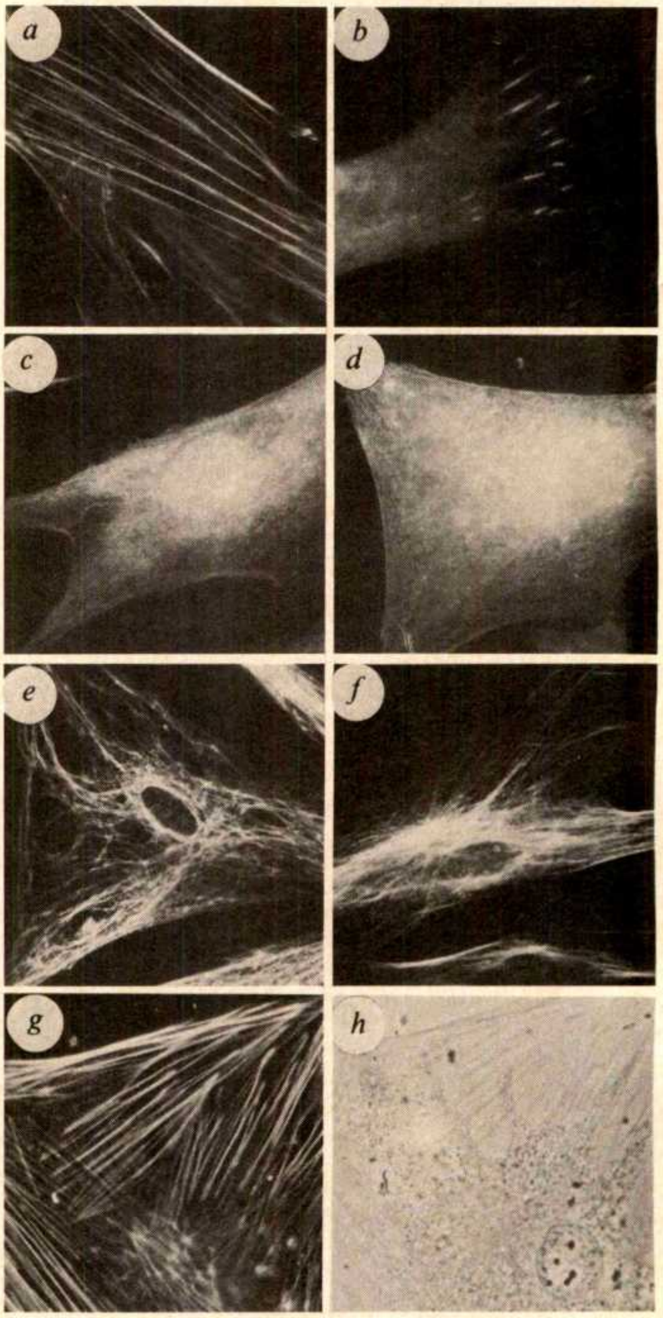

Fig. 4 Control human embryonal fibroblasts showed a stress fibre-type of actin organization in IIF with anti-actin antibodies[17] both when plated with (*a*) or without serum. Typical plaques of vinculin were also seen in these cells in IIF (*b*). Vinculin was isolated from chicken gizzard according to Feramisco and Burridge[41]. Antibodies were raised in rabbits and purified on antigen coupled to Sepharose 4B. Cells exposed to monensin on subcultivation showed only a diffuse actin-specific (*c*) or vinculin-specific (*d*) fluorescene in IIF. Such cells showed, however, typical arrays of both intermediate filaments (*e*), as shown with anti-vimentin antibodies[42], and microtubules (*f*), as revealed with anti-tubulin antibodies[17]. When spread cells were exposed to monensin (1 μM, 24 h), normal arrays of both microfilaments (*g*), phase-dense stress fibres (*h*) and vinculin plaques were still seen. For cytoskeletal antibodies the cells were fixed in −20 °C methanol for 5 min and stained for IIF as in Fig. 1. ×500.

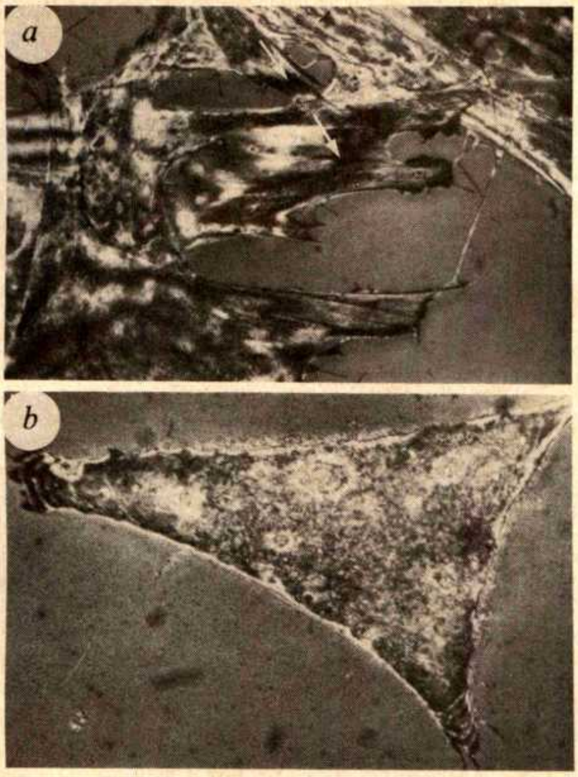

Fig. 5 Interference reflection microscopy[17] of control human fibroblasts (*a*) and of cells exposed to monensin on subcultivation (*b*). Note the black areas of focal adhesion (arrows in *a*) and extensive grey areas of close adhesion in monensin exposed cells (*b*). ×900.

adhesion sites, bundles of microfilaments and plaques of vinculin. This sequence of events corresponds to recent observations distinguishing a cell-independent and a cell-dependent phase in cell-to-substratum adhesion[13,32–35]. We suggest that a prerequisite for cells to enter into the cell-dependent phase of spreading is the deposition of endogenous pericellular fibronectin and subsequent formation of focal adhesion sites and the microfilament–vinculin system which, in turn, are needed to maintain an isometric contraction in cells[36].

Interestingly, human embryonal fibroblasts which were allowed to spread in the presence of monensin, could not acquire the matrix-type of fibronectin even from the culture medium[37]. This might be due to the lack of receptors for exogenous fibronectin in monensin-treated cells, as trypsinized cells are also apparently unable to retain exogenously added fibronectin[38]. A recent study by Atherton and Hynes[39] using monoclonal antibodies has revealed differences in plasma and cellular fibronectins which may be of importance in their apparently different roles in cell adhesion, as suggested by our results.

We thank Ms Raili Taavela, Ms Pipsa Kaipainen and Ms Hannele Laaksonen for technical assistance. This study was supported by grants from the Finnish MRC, the Sigrid Jusélius Foundation, the Finnish Cancer Research Fund and by a grant from the Finnish Life Insurance Companies.

Received 18 January; accepted 25 May 1982.

1. Grinnell, F. *Int. Rev. Cytol* **53**, 65–144 (1978).
2. Kleinman, H. K., Klebe, R. J. & Martin, G. R. *J. Cell Biol.* **88**, 473–485 (1981).
3. Hughes, R. C. & Pena, S. D. J. *Carbohydrate Metab. Disorders* **3**, 363–423 (1981).
4. Vaheri, A. & Mosher, D. F. *Biochim. biophys. Acta* **516**, 4–25 (1978).
5. Yamada, K. M. & Olden, K. *Nature* **275**, 179–184 (1978).
6. Hughes, R. C., Pena, S. D. J., Clark, J. & Dourmashkin, R. R. *Expl Cell Res.* **121**, 307–314 (1979).
7. Grinnell, F., Feld, M. & Minter, D. *Cell* **19**, 517–525 (1980).
8. Grinnell, F. & Feld, M. K. *Cell* **17**, 117–129 (1979).
9. Ledger, P. W., Uchida, N. & Tanzer, M. L. *J. Cell Biol.* **87**, 663–671 (1981).
10. Tartakoff, A. M. *Int. Rev. exp. Path.* **22**, 227–251 (1980).
11. Engvall, E. & Ruoslahti, E. *Int. J. Cancer* **20**, 1–5 (1977).
12. Gahmberg, C. G. & Hakomori, S.-I. *J. biol. Chem.* **248**, 4311–4317 (1973).
13. Rauvala, H. & Hakomori, S.-I. *J. Cell Biol.* **88**, 149–159 (1981).
14. Lehto, V.-P., Vartio, T. & Virtanen, I. *Biochem. biophys. Res. Commun.* **95**, 909–916 (1980).
15. Knudsen, K. A., Rao, P. E., Damsky, C. H. & Buck, C. A. *Proc. natn. Acad. Sci. U.S.A.* **78**, 6071–6075 (1981).
16. Hughes, R. C., Butters, T. C. & Aplin, J. D. *Eur. J. Cell Biol.* **26**, 198–207 (1981).
17. Badley, R. A. *et al. Expl Cell Res.* **117**, 231–244 (1978).
18. Heath, J. P. & Dunn, G. A. *J. Cell Sci.* **29**, 197–212 (1978).
19. Izzard, C. S. & Lochner, L. R. *J. Cell Sci.* **41**, 81–116 (1980).
20. Geiger, B. *Cell* **18**, 193–205 (1979).
21. Burridge, K. & Feramisco, J. R. *Cell* **19**, 587–595 (1980).
22. Singer, I. I. & Paradiso, P. R. *Cell* **24**, 481–492 (1981).
23. Birchmeier, C., Kreis, T. E., Eppenberger, H. M., Winterhalter, K. H. & Birchmeier, W. *Proc. natn. Acad. Sci. U.S.A.* **77**, 4108–4112 (1980).
24. Mautner, V. & Hynes, R. O. *J. Cell Biol.* **75**, 743–768 (1977).
25. Singer, I. I. *Cell* **16**, 675–685 (1979).
26. Weber, K., Lazarides, E., Goldman, R. D., Vogel, A. & Pollack, R. *Cold Spring Harb. Symp. quant. Biol.* **39**, 363–369 (1975).
27. Tucker, R. W., Sanford, K. K. & Frankel, F. R. *Cell* **13**, 629–642 (1978).
28. Ali, I. U., Mautner, V., Lanza, R. & Hynes, R. O. *Cell* **11**, 115–126 (1977).
29. Chen, W.-T. & Singer, S. J. *Proc. natn. Acad. Sci. U.S.A.* **77**, 7318–7322 (1980).
30. Fox, C. H., Cottler-Fox, M. H. & Yamada, K. M. *Expl Cell Res.* **130**, 477–481 (1980).
31. Avnur, Z. & Geiger, R. *Cell* **25**, 121–132 (1981).
32. Rees, D. A., Lloyd, C. S. & Thom, D. *Nature* **267**, 124–238 (1977).
33. Rauvala, H., Carter, W. G. & Hakomori, S.-I. *J. Cell Biol.* **88**, 127–137 (1981).
34. Butlers, T. D., Devalia, D., Aplin, J. D. & Hughes, R. C. *J. Cell Sci.* **44**, 33–58 (1981).
35. Aplin, J. D. & Hughes, R. C. *J. Cell Sci.* **50**, 89–103 (1981).
36. Burridge, K. *Nature* **294**, 691–692 (1981).
37. Hayman, E. G. & Ruoslahti, E. *J. Cell Biol.* **83**, 255–259 (1979).
38. Rennard, S. I., Wrud, M. I., Hewitt, A. T. & Kleinman, H. K. *Archs Biochem. Biophys.* **206**, 205–212 (1981).
39. Atherton, B. T. & Hynes, R. O. *Cell* **25**, 133–141 (1981).
40. Virtanen, I., Ekblom, P. & Laurila, P. *J. Cell Biol.* **85**, 429–434 (1980).
41. Feramisco, J. R. & Burridge, K. *J. biol. Chem.* **255**, 1194 (1980).
42. Virtanen, I. *et al. J. Cell Sci.* **50**, 45–63 (1981).

Evidence for contractile flexing of the gliding bacterium *Flexibacter* FS-1

Robert P. Burchard

Department of Biological Sciences, University of Maryland,
Baltimore County, Catonsville, Maryland 21228, USA

Flexing movements have been described in a variety of gliding bacteria and cyanobacteria (blue-green algae)[1–7]. Flexing of trichomes (chains of cells) of the genera *Oscillatoria* and *Beggiatoa* was attributed[8] to a "certain degree of elasticity"; it was concluded that there is no spontaneous flexibility. In contrast, observations of active flexing of free ends of otherwise immobilized *Oscillatoria* trichomes suggested[9] that active contractions are involved. It has been proposed that flexing and gliding motility are powered by the same mechanism[10]. No organelles have been demonstrated irrefutably to be responsible for these movements, although several mechanistic hypotheses have been proposed[11]. I demonstrate here that flexing movements by the bacterium *Flexibacter* FS-1 require no more than one point of attachment by the cell to its substratum, which suggests that flexing may result from a unilateral, longitudinal contraction. As the same motility mechanism is thought to operate for both flexing and gliding, the latter may be powered by a contractile apparatus, at least in this species.

I and others[6] have observed that flexing, like gliding, requires contact with a surface, such as another cell, a glass slide or an agar gel; in suspension such cells do not move actively. Gliding motility itself could account for flexing: for example, if the two polar regions of a cell or chain of cells were attached to a surface and were gliding in an uncoordinated fashion so as to be moving towards one another, the central portion of the cell(s) would, if not firmly attached to the surface, bow outwards and thus appear to flex. Reversal of the flexion could be explained by reversal of the direction of gliding at both ends. Uncoordinated gliding has been described in trichomes of the cyanobacterium *Oscillatoria*[12,13].

I have investigated this phenomenon by using a simple experimental design. *Flexibacter* FS-1, which grows as long filaments with widely spaced septa[6,14], was cultured in YE/2 medium[10] at ambient temperature or at 30 °C with little or no agitation. Cultures at absorbance (A_{540}) = 0.1, containing filaments ≤200 μm long (capable of active flexing in a wet mount

0028-0836/82/320663—03$01.00

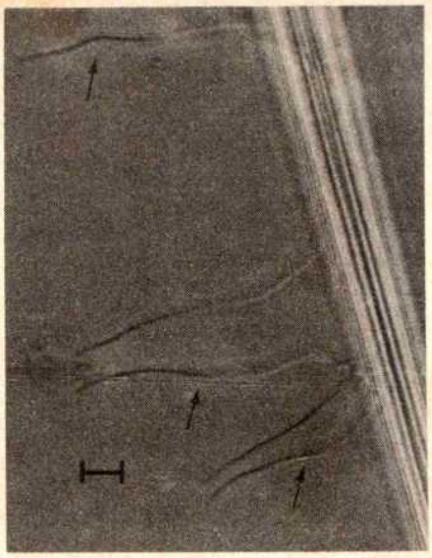

Fig. 1 Flexing *Flexibacter* FS-1 filaments attached to a glass wool fibre. Flexion points are indicated by arrows. Scale bar, 10 μm.

preparation), were diluted in YE/2 to ~10^4 filaments ml^{-1} and loaded into a 1 cm deep chamber mounted on a glass slide. A small tuft of glass wool fibres was submerged in the suspension. The chamber was then covered with a coverslip, and vacuum grease used to prevent leakage. The chamber was inverted and mounted on the stage of an inverted, phase-contrast microscope equipped with a ×10 Zeiss achromat objective (5 mm working distance). It was thus possible to observe individual filaments which readily but reversibly attached at or near one pole (or by their lateral surfaces) to a glass wool fibre and made no contact with any other surface.

Some of these multicellular filaments were observed to flex and relax repeatedly (Figs 1, 2). Flexing assumed various forms, including localized bending and undulating of the filaments. Flexions could be observed to move along a filament towards the unattached end. This end sometimes abruptly flexed so as to form a distinct hook and then very rapidly straightened out, as though the hook were spring-loaded or under some tension. As soon as the filaments detached from the glass wool, flexing ceased. The movements observed were active, as addition of dinitrophenol (5×10^{-4} M final concentration) inhibited flexing, although attachment appeared to have been unaffected. This agent also inhibited flexing in wet mounts and is known to inhibit gliding motility of *Flexibacter* and other gliding bacteria[11].

To ensure further that the observed flexing is an active process rather than one resulting from turbulence in the chamber, I examined the behaviour of strain Ng 7, a UV induced, non-gliding mutant of FS-1. The filaments (≤40 μm long) of this mutant also attached to the glass wool fibres but did not flex in the conditions used nor in wet mounts.

This active flexing by multicellular filaments attached via one pole can most readily be explained by a contractile mechanism which is longitudinally arrayed and unilateral. Similarly, flexional and swinging movements by the free ends of aggregated *Oscillatoria* trichomes[9,15] may also result from contractions. If gliding motility and flexing are indeed powered by the same mechanism, then gliding presumably also involves a contractile mechanism in *Flexibacter* FS-1.

Other theories to account for gliding motility have been proposed. The rotary assembly model[16] is attractive as it provides a unified theory of prokaryotic motility; both flagellated[17,18] and gliding bacteria would be driven by rotary motors. However, it is not clear how the spinning of rotary assemblies could explain the flexing movements described here, especially as flexing was observed in filaments with one end wrapped around a glass wool fibril and in those attached by one point on their lateral surface (Fig. 3). Similarly, 'make and break' interactions within the envelope[19], the elaboration of surfactant gradients[20,21], directed production of extracellular slime[22], and an electrokinetic mechanism[23] cannot account for the observed flexing.

Contractions have been described in a mycoplasma which also demonstrates a form of surface translocation called gliding[24]. However, I am unaware of any previous definitive reports of contractile phenomena among enveloped prokaryotes.

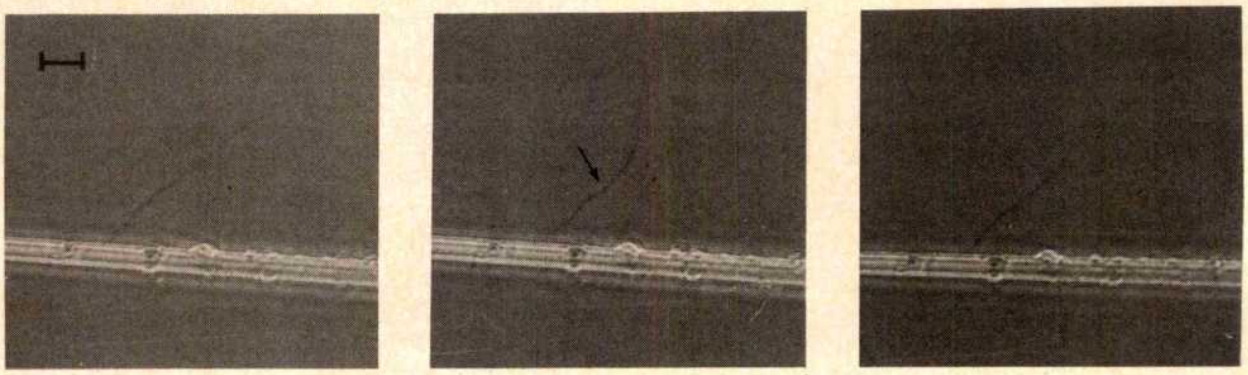

Fig. 2 A *Flexibacter* filament before and during a flexion (arrow). Scale bar, 10 μm.

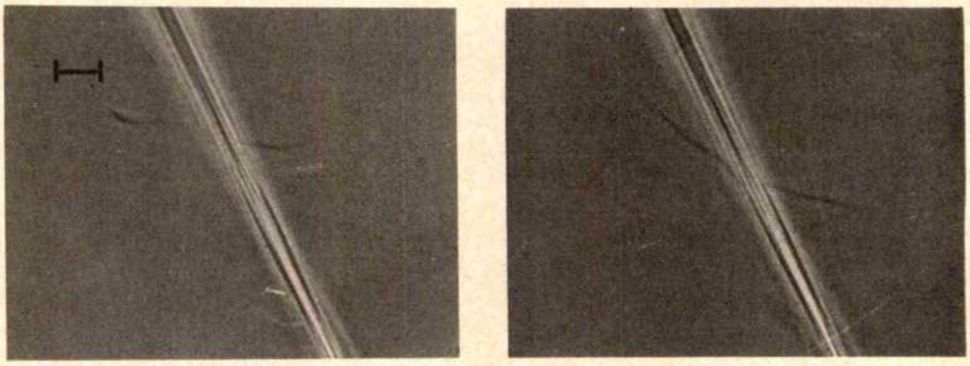

Fig. 3 A flexing *Flexibacter* filament attached to a glass wool fibril along its lateral surface, Scale bar, 10 μm.

There is no known structural basis for contractility in *Flexibacter*. Attempts to isolate eukaryotic-like actin from this bacterium have been unsuccessful (R.P.B. and S. Mockrin, unpublished results). Organelles proposed to have contractile or bending properties and to be mechanistically involved in gliding have been described in *Myxococcus*[25] and in *Oscillatoria*[26]. A contractile mechanism may, in fact, account for all of the forms of movement demonstrated by gliding bacteria[27].

A puzzling question which arises from these observations is why any point of attachment to a substratum should be required for flexing if this movement results from a contractile event. It may be that contact of the cell envelope with a surface is required to initiate such contractions.

I thank Sandra Rollins and James Dicke for technical assistance. This work was supported by NSF grant PCM-801150.

Received 3 April; accepted 7 June 1982

1. Correns, C. *Ber. dt. bot. Ges.* **15,** 139–148 (1897).
2. Kolkwitz, R. *Ber. dt. bot. Ges.* **15,** 460–467 (1897).
3. Stapp, C. & Bortels, H. *Zentbl. Bakt. ParasitKde* **90,** (11) 28–66 (1934).
4. Stanier, R. Y. *J. Bact.* **40,** 619–635 (1940).
5. Garnjobst, I., *J. Bact.* **49,** 113–128 (1945).
6. Simon, G. D. & White, D. *Arch. Mikrobiol.* **78,** 1–16 (1971).
7. Reichenbach, H., Kleinig, K. & Achenbach, H. *Arch. Mikrobiol.* **101,** 131–144 (1974).
8. Pringsheim, E. G. *Bact. Rev.* **13,** 47–98 (1949).
9. Castenholz, R. W. *Nature* **215,** 1285–1286 (1967).
10. Dayrell-Hart, B. & Burchard, R. P. *J. Bact.* **137,** 1417–1420 (1979).
11. Burchard, R. P. *A. Rev. Microbiol.* **35,** 497–529 (1981).
12. Drews, G. & Nultsch, W. in *Encyclopedia of Plant Physiology* Vol. 17, Pt 2 (ed. Ruhland, W.) 876–919 (Springer, Berlin, 1962).
13. Walsby, A. E. *Protoplasma* **65,** 223–238 (1968).
14. Poos, J. C. *et al. J. Bact.* **112,** 1387–1395 (1972).
15. Burkholder, P. R. *Q. Rev. Biol.* **9,** 438–459 (1934).
16. Pate, J. L. & Chang, L.-Y. E. *Curr. Microbiol.* **2,** 59–64 (1979).
17. Silverman, M. & Simon, M. I. *A. Rev. Microbiol.* **31,** 397–419 (1977).
18. Doetsch, R. N. & Sjoblad, R. D. *A. Rev. Microbiol.* **34,** 69–108 (1980).
19. Humphrey, B. A., Dickson, M. R. & Marshall, K. C. *Arch. Microbiol.* **120,** 231–238 (1979).
20. Coupin, H. *C. r. hebd. Séanc. Acad. Sci., Paris* **176,** 1491–1493 (1923).
21. Dworkin, M., Keller, K. H., Grady, M. & Weisberg, D. *8th int. Conf. Biology of the Myxobacteria,* Bloomington, Indiana (1981).
22. Schulz, G. *Arch. Mikrobiol.* **21,** 335–370 (1955).
23. Mitchell, P. *Proc. R. phys. Soc. Edinb.* **25,** 32–34 (1956).
24. Bredt, W., Heunert, H. H., Hofling, K. H. & Milthaler, B. *J. Bact.* **113,** 1223–1227 (1973).
25. Burchard, A. C., Burchard, R. P. & Kloetzel, J. A. *J. Bact.* **132,** 666–672 (1977).
26. Halfen, L. N. & Castenholz, R. W. *J. Phycol.* **7,** 133–145 (1971).
27. Hughes, B. L. & Burchard, R. P. *J. theor. Biol.* (submitted).

X-ray scattering by myosin S-1: implications for the steric blocking model of muscle control

Robert Mendelson

Department of Biochemistry and Biophysics, and Cardiovascular
Research Institute, University of California, San Francisco,
California 94143, USA

Steric blocking and unblocking[1–3] of the myosin interaction sites in muscle thin filaments by tropomyosin provides a simple yet elegant method of regulating contraction in skeletal muscle. Recently, this model was challenged[4] by the finding that tropomyosin is located on the opposite side of the thin filament helix axis from where Moore *et al.* reported that the myosin cross-bridge, S-1, bound[5]. However, new three-dimensional image reconstructions of electron micrographs of thin filaments decorated with S-1 were obtained by Taylor and Amos[6], who proposed that the prior assignment of the S-1 binding site of Moore *et al.*[5] was incorrect, and that consequently tropomyosin and S-1 are located on the same side of the actin helix. These past difficulties and the current lack of agreement[7] on the location of the S-1 binding site suggested that another technique would be useful. We report here that the shape of S-1, derived from reconstructions using the Taylor and Amos actomyosin interpretation, gives a better fit to the X-ray scattering pattern observed from S-1 in solution than alternative interpretations.

The two assignments of S-1 position in the three-dimensional reconstructions are illustrated in Fig. 1. The original assignment by Moore *et al.* was based on the supposition that a radial expansion of the acto-S-1 helix had occurred, as had been found in some isolated F-actin reconstructions. Using minimal dose electron microscopy with improved specimen preparation, Taylor and Amos found additional mass near the helix axis which they assigned to actin. They argued that the filaments of Moore *et al.* had not expanded radially and the mass previously assigned to actin was actually part of S-1. Although their assignment agrees well with the known mean radius of actin, the Moore *et al.* interpretation is difficult to refute with certainty because of the inherent ambiguity in defining a boundary between two complexed molecules whose individual structures are not highly determined. As the S-1 derived from the two proposed locations of the S-1 binding sites have very different shapes, we tested these contrasting models by X-ray scattering from isolated S-1 in solution.

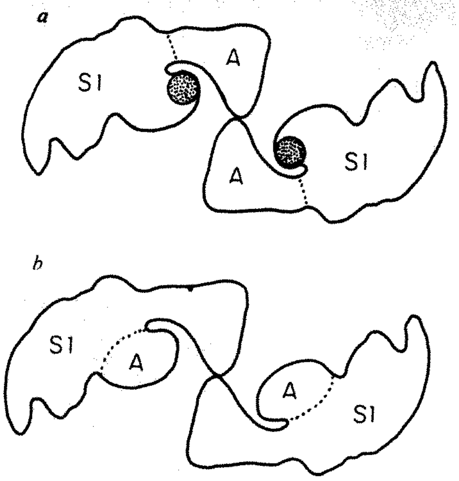

Fig. 1 A projected view (from the three-dimensional reconstructions of ref. 5) looking down the thin filament axis towards the Z-line with the S-1 position drawn according to the interpretation of: *a*, Taylor and Amos, and *b*, Moore *et al.* In the steric blocking model the tropomyosin (shaded in *a*) is thought to unblock the S-1 attachment site as the amount of Ca^{2+} binding to troponin (located at every seventh actin monomer) increases. The position of tropomyosin shown is approximately that given by ref. 4 for the rigor or activated state. If the interpretation of Taylor and Amos is correct, the S-1 binding site is nearer tropomyosin, and the shape of S-1 is more compact than in the Moore *et al.* interpretation. The structure of Moore *et al.* is similar to that shown, except that a significant amount of the mass labelled A is missing at low radii.

Previous X-ray scattering results[8] showed that S-1 shapes derived from three-dimensional helical electron micrograph reconstructions were capable of giving a better fit to scattering data than many simple models that might resemble S-1. Recent high resolution reconstructions, in addition to raising the question of S-1 position, suggest that the shape of S-1 is significantly altered by the presence of the 18,000 molecular weight (M_r) light chain[9]. Previously reported scattering data were from S-1 that contained only a fraction of the 18,000-M_r light chain. Thus, scattering data were accumulated on S-1 both with and without this light chain. The fractional change in the radius of gyration (R_g) was 0.01 ± 0.005 for S-1 with and without the light chain (five double preparations[10,11], seven trials), and the scattering patterns (Fig. 2) and chord distributions were almost identical, indicating that the 18,000-M_r light chain is not a significant determinant of S-1 shape. Thus, the present results validate the results of previous modelling studies[8] for S-1s that have varying amounts of light chain.

If the addition of light chain causes an isotropic increase in size, it would be expected that $\Delta R_g/R_g = 1/3\ (\Delta M_r/M_r) = 0.05$, when using the molecular weights of Margossian *et al.*[12]. Thus, S-1 with 18,000-M_r light chain is slightly more symmetrical than S-1 without it. The disagreement of the present result with those computed from reconstructions of decoration of actin by scallop S-1 ($\Delta R_g/R_g = 0.15$)[9] may be only apparent; our studies

0028-0836/82/320665—03$01.00

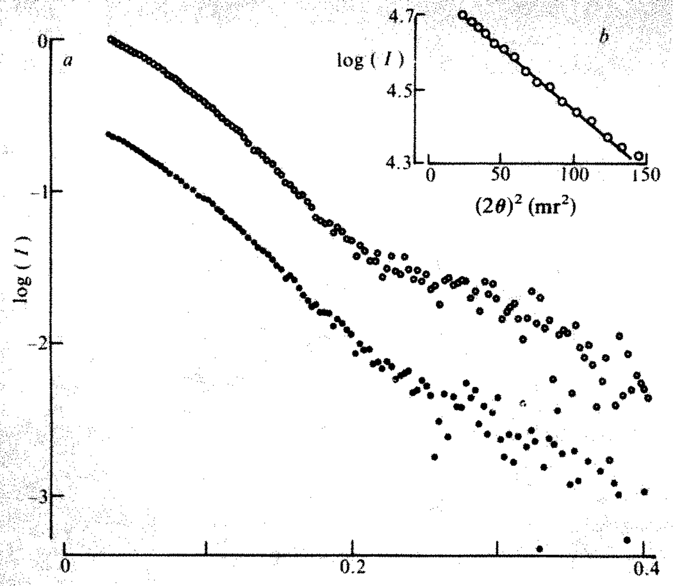

Fig. 2 *a*, Typical scattering patterns from S-1 with (●) and without (○) the 18,000-M_r light chain. Rabbit S-1 with this light chain was prepared and purified as described in ref. 10 except that the S-1 yield was kept below 20% so as to minimize heavy chain degradation. S-1 without the light chain was prepared as in ref. 11 except that purification was by S-200 gel filtration, which did not separate S-1 isoenzymes. The buffer contained 150 mM KCl; 20 mM tri[hydroxymethyl]methylaminoethane sulphonic acid; 0.1 mM NaN_3; 1 mM dithiothreitol, *p*H 7 at $T = 4°C$; [S-1] = 7 mg ml^{-1}. *b*, A Guinier plot from the lowest angle portion of the scattering curve, where *I* is the scattering intensity, and 2θ is the scattering angle. Guinier plots and chord distributions appeared virtually identical with and without light chain. Data were accumulated from $s = 1/38$ nm^{-1} to about $s = 1/2.5$ nm^{-1} (where $s = 2\sin\theta/\lambda$) using a Kratky camera with a position-sensitive proportional counter. The sample-to-registration-plane distance was 214 mm. The range of S-1 concentrations was 7–32 mg ml^{-1}. mr = milliradians.

were performed on rabbit skeletal S-1, which shows a less barbed structure than scallop S-1 in acto–S-1 micrographs[13]. In addition, the R_g and chord distribution (not shown) of scallop S-1 without 18,000-M_r light chain were in good agreement with the data; thus, an intact, flexible, light chain could be oriented most frequently along the surface of the S-1 heavy chain to give on average a compact S-1 structure in solution, while the electron microscopy stain could cause it to be visualized only in an extended orientation which would make the overall structure appear more elongate.

Comparison of the S-1 shapes derived from the two different interpretations is shown in Table 1 and Fig. 3. The radius of gyration (R_g), which is derived from the lowest resolution portion (smallest angle) of the scattering curve, most directly reflects the overall shape of the protein. As shown in Table 1, the R_g's showed a consistent preference for the Taylor and Amos interpretation in the micrographs of both Moore *et al.* and Taylor and Amos. The interpretations of the Wakabayashi and Toyoshima[7] reconstruction in terms of the two aforementioned S-1 positions are not fully consistent with the findings of other workers; their assignment of the Moore *et al.* actin position has a lower radius than that of their Taylor and Amos actin position. Further, their proposed actin structure, in both interpretations, has a smaller volume, relative to S-1, than actin in the reconstruction of Taylor and Amos. However, even this study favours a Taylor and Amos type of S-1 binding position. The mean and the maximum chord can be extracted from the chord distributions[14] and directly compared with these parameters from the reconstructions. As the mean chord (and R_g) is an average that depends on the entire structure of the molecule, it is a better parameter for experimental comparison than the maximum chord. The mean chord and relative goodness of fit factors to the chord distributions obtained in this study also favour the Taylor and Amos interpretation, although the maximum chord was inconclusive.

The choice of different micrograph contour levels had little effect on the overall shape of S-1; the difference in R_g using two plausible extreme contours of the model in ref. 5 (provided by K. Taylor) was only 0.05 nm when the contours were scaled to give the correct S-1 volume. In the previous X-ray scattering study[8], a good fit was obtained using a different reconstruction (J. Seymour and E. J. O'Brien, unpublished). Although the actin and tropomyosin were not fully resolved from S-1 in this reconstruction, their subtraction was consistent with that of Taylor and Amos (J. Seymour, personal communication). Indeed, alignment of this reconstruction with that of Taylor and Amos indicated that the shape and location of S-1 were very similar to those of Taylor and Amos. The results of X-ray scattering by S-1 in solution substantiate the shape of S-1 derived when it is attached to actin in the manner proposed by Taylor and Amos rather than in the position of Moore *et al.* Although we cannot formally exclude the possibility that the

Table 1 Structural parameters of S-1 from electron microscopy and X-ray scattering

Author and S-1 position	R_g (nm)	Mean chord (nm)	Max chord (nm)	*R*(Moore)/*R*(Taylor)*
Moore *et al.* (*x, y, z*)				
Moore *et al.* S-1	3.83	4.80	15.1	11
Taylor & Amos S-1	3.38	4.35	12.8	
Taylor & Amos (*x, y*)				
Moore *et al.* S-1	3.93	4.97	13.5	7
Taylor & Amos S-1	3.18	4.06	12.8	
Wakabayashi & Toyoshima (*x, y*)				
Moore *et al.* S-1	3.51	4.46	12.8	
Taylor & Amos S-1	3.14	4.07	11.5	1.3
Wakabayashi & Toyoshima (*x, y, z*)				
Moore *et al.* S-1	3.49	4.43	12.5	
Taylor & Amos S-1	3.21	4.14	11.0	1.5
Experimental†				
No LC2 (M_r = 110 K)	3.27 (0.1)	4.25 (0.15)	12 (1)	
Part LC2 (M_r = 122 K)	3.28 (0.06)	4.25 (0.15)	12 (1)	
Full LC2 (M_r = 130 K)	3.3 (0.1)	4.25 (0.15)	12 (1)	

Letters in parentheses denote the method of scaling suggested by each author. Wakabayashi and Toyoshima's maps were also scaled on *x, y, z* to illustrate the effect of a different scaling method on the parameters. K, molecular weight 1,000.

$$* \; R \equiv \frac{\{\Sigma_i[p_0(r_i) - p_c(r_i)]\}^2}{\{\Sigma_i\, p_0(r_i)\}^2}$$

where $p_0(r)$ is the observed and $p_c(r)$ is the calculated chord distribution function.

† All maps are to be compared with 'no LC2' except those of Moore *et al.*, which is to be compared with 'part LC2'. Any error in the findings that true molecular weight scales with LC2 content will improve the agreement with the Taylor and Amos interpretation.

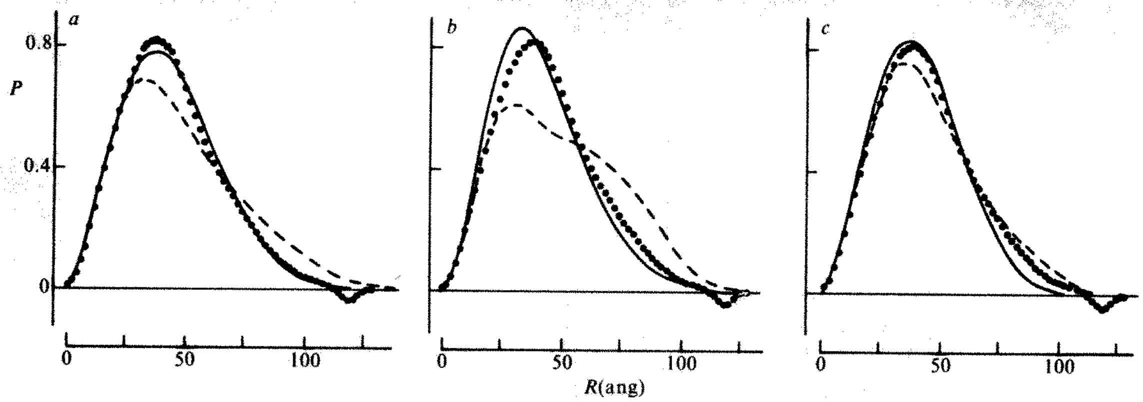

Fig. 3 A comparison of the S-1 experimental (●) chord distribution with the predictions from electron microscopy using the Taylor and Amos interpretation (solid lines) and the Moore *et al.* interpretation (dashed lines). The electron density maps were from: *a*, Moore *et al.*; *b*, Taylor and Amos; *c*, Wakabayashi and Toyoshima. The maps were furnished with the actin–S-1 interfaces delimited by their authors except in the case of the Moore *et al.* map, where the interface was delimited by L. Amos. The maps were scaled to the correct volume. This was done by scaling each *x* and *y* coordinate or each *x*, *y* and *z* (helix axis) coordinate as recommended by the author. Typically, the scaling changed these dimensions by only 10–20%. Tests showed that the method of scaling had only a small effect on the predicted chord distributions and on the overall molecular shape (see Table 1). Chord distributions were obtained by Fourier transforming the experimental and model scattering curves using the method of Glatter[14].

S-1 solution could have a shape similar to that found by Taylor and Amos and yet makes a conformational change to the shape described by Moore on binding to actin[7], such a large change seems improbable because the accompanying R_g change would be of an unprecendented magnitude. Thus, the present results are consistent with the notion that regulation of muscle contraction occurs by the steric blocking of the actin–S-1 interaction.

Received 10 March; accepted 4 June 1982.

I thank Drs L. Amos, P. Moore, M. Morales, E. O'Brien, J. Seymour, K. Taylor, P. Vibert, P. Wagner and T. Wakabayashi for many helpful communications, and Mr E. Giniger for technical assistance. This work was supported by NIH grant HL-16683 and NSF grant PCM 75-22698. I acknowledge use of the UCSF Pharmaceutical Chemistry Graphics Facility which is supported by NIH grant RR-1081.

1. Haselgrove, J. C. *Cold Spring Harb. Symp. quant. Biol.* **37,** 341–352 (1972).
2. Huxley, H. E. *Cold Spring Harb. Symp. quant. Biol.* **37,** 361–376 (1972).
3. Parry, D. A. D. & Squire, J. *J. molec. Biol.* **75,** 33–55 (1973).
4. Seymour, J. & O'Brien, E. J. *Nature* **283,** 680–682 (1980).
5. Moore, P. B., Huxley, H. E. & De Roosier, D. J. *J. molec. Biol.* **50,** 279–295 (1970).
6. Taylor, K. A. & Amos, L. *J. molec. Biol.* **147,** 297–324 (1981).
7. Wakabayashi, T. & Toyoshima, C. *J. Biochem.* **90,** 683–701 (1981).
8. Mendelson, R. A. & Kretzschmar, K. M. *Biochemistry* **19,** 4103–4108 (1980).
9. Vibert, P. & Craig, R. *J. molec. Biol.* **157,** 299–319 (1982).
10. Margossian, S. S., Lowey, S. & Barshop, B. *Nature* **258,** 163–165 (1975).
11. Weeds, A. G. & Taylor, R. S. *Nature* **257,** 54–56 (1975).
12. Margossian, S. S., Stafford, W. III & Lowey, S. *Biochemistry* **20,** 2151–2155 (1981).
13. Craig, R. *et al. J. molec. Biol.* **140,** 35–55 (1980).
14. Glatter, O. *J. appl. Crystallogr.* **10,** 415–421 (1977).

Insulin stimulates tyrosine phosphorylation of the insulin receptor in a cell-free system

Masato Kasuga*, Yehiel Zick†, Diana L. Blithe‡, Marco Crettaz* & C. Ronald Kahn*

* Elliott P. Joslin Research Laboratory, Joslin Diabetes Center and
Department of Medicine, Brigham and Women's Hospital,
Harvard Medical School, Boston, Massachusetts 02215, USA
† Diabetes Branch, National Institutes of Arthritis, Diabetes and
Digestive and Kidney Diseases, and ‡ Developmental Endocrinology
Branch, National Institutes of Child Health and Human
Development, Bethesda, Maryland 20205, USA

Insulin forms a complex with its receptors on the plasma membrane of cells and initiates a series of biochemical events which lead to the hormone's recognized effects[1,2]. The exact mechanism that initiates these events is unknown. We previously reported that insulin stimulates the phosphorylation of the 95,000 molecular weight (M_r) (β) subunit of its own receptor in intact cells and proposed that this phosphorylation reaction could be a very early step in insulin action[3]. To clarify the molecular basis of this reaction, we have now investigated the phosphorylation of insulin receptor in a cell-free system. Using [γ-^{32}P]ATP in solubilized and partially purified receptor preparations from rat liver plasma membrane, we find that both the α and β subunits of the insulin receptor are phosphorylated. Furthermore, insulin stimulates the incorporation of ^{32}P into both receptor subunits in a specific and dose-dependent manner. Phosphoamino acid determination of the β subunit after insulin stimulation reveals only phosphotyrosine. These findings suggest that the elements required for phosphorylation are associated with the plasma membrane of the cell and that specific phosphorylation of the insulin receptor on tyrosine residues can be activated in a solubilized preparation.

Rat liver plasma membranes were prepared by the procedure of Neville[4] and phosphorylation studied using [γ-^{32}P]ATP as described in Fig. 1 legend. Insulin receptors in this rat liver membrane fraction and solubilized insulin receptors prepared from these membranes have been well characterized[5,6]. Further, as previously shown lectin chromatography allows a 20-fold purification with nearly 100% recovery of insulin receptors as determined by ^{125}I-insulin binding[7]. The insulin receptor subunits were identified by immunoprecipitation with antibodies against insulin receptor followed by SDS-polyacrylamide gel electrophoresis (SDS-PAGE) and autoradiography[3,8].

When the immunoprecipitates were analysed in SDS-PAGE in reducing conditions (100 mM dithiothreitol; DTT), one major band of M_r 95,000 and a minor band of M_r 135,000 were specifically phosphorylated in basal state (Fig. 1*A*, lane *b*). These 135,000- and 95,000-M_r phosphoproteins have been tentatively identified as the α and β subunits of insulin receptor, respectively, by their immunoprecipitation by anti-receptor antibody and by the fact that they migrate in the same position in SDS-PAGE as α and β subunits of insulin receptor labelled either biosynthetically or externally[3,8]. After incubation of the solubilized fraction with insulin (10^{-6} M), the incorporation of ^{32}P into these two proteins was increased approximately fivefold as determined by scanning densitometry (Fig. 1*A*, lane *d*). A phosphoprotein band corresponding to M_r ~50,000 is also observed; this may represent phosphorylation of the heavy chain of IgG.

In the native insulin receptor, the receptor subunits are thought to be linked by disulphide bonds to form high molecular weight oligomers[9,10]. When the same samples were analysed without reduction of disulphide bonds, five bands were observed (Fig. 1*B*, lane *b*). Two bands had molecular weights higher than 300,000. In addition, there were phosphoproteins of M_rs 240,000, 130,000 and 90,000 in basal state (Fig. 1*B*, lane *b*); these bands are identical to those found when the receptor

0028–0836/82/320667—03$01.00

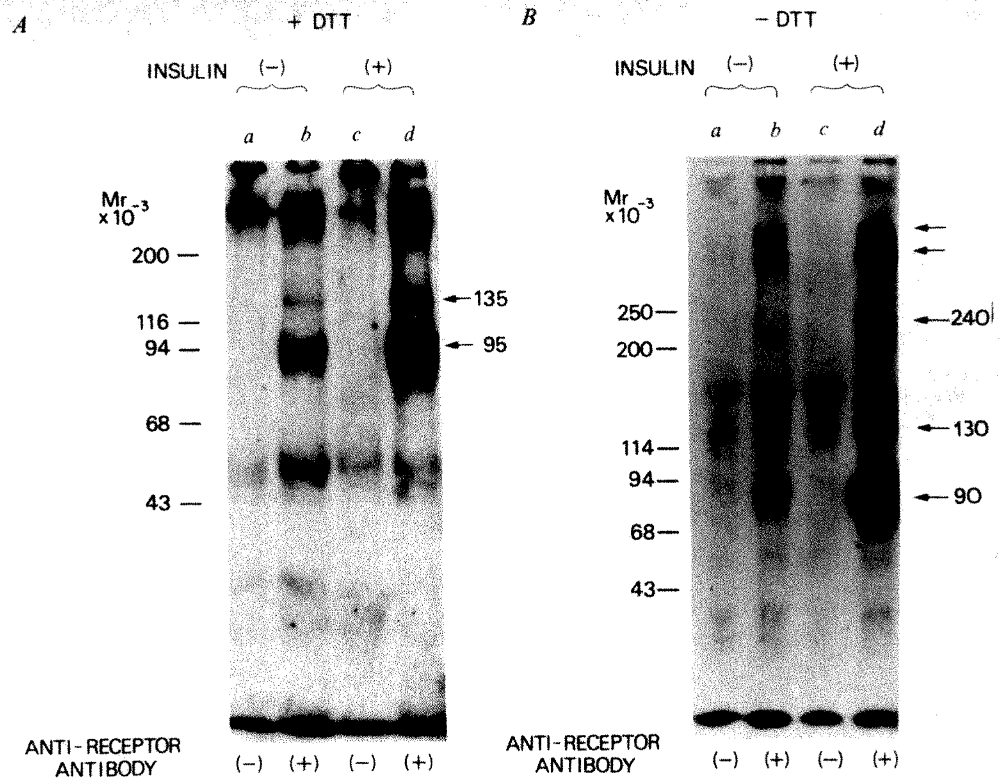

Fig. 1 Autoradiogram showing the incorporation of the ^{32}P from [γ-^{32}P]ATP into solubilized insulin receptor from rat liver plasma membrane. Rat liver plasma membranes were prepared by the procedure of Neville[4]. Protease inhibitors (2 mM phenylmethylsulphonyl fluoride; 1,000 trypsin inhibitor units per ml aprotinin) were added throughout the purification beginning with the first step of homogenization. The plasma membrane fraction was solubilized by 1% (v/v) Triton X-100 in 50 mM HEPES buffer, *p*H 7.6, containing protease inhibitors. The insulin receptors were further enriched by chromatography on a wheat germ agglutinin–agarose column[7] after elution by 0.3 N *M*-acetyl glucosamine in 50 mM HEPES buffer, *p*H 7.6, containing 0.1% (v/v) Triton X-100. Aliquots of these eluted fractions (150–300 μg per tube) were incubated with or without insulin (10^{-6} M) overnight at 4 °C. A 1-h incubation with insulin at room temperature was also used. Essentially the same result was obtained in the two different incubation conditions. The aliquots were then assayed for the incorporation of ^{32}P from [γ-^{32}P]ATP at 4 °C in a final volume of 1,350 μl. For the experiment shown, the reaction mixture contained 6 mM $MgCl_2$, 2 mM $Mn(CH_3COO)_2$, 5 μM [γ-^{32}P]ATP (~30 μCi $nmol^{-1}$) in 30 mM HEPES buffer, *p*H 7.6. Similar results were obtained with 20 mM $MgCl_2$ and 1 mM $MnCl_2$ in a 100 mM HEPES buffer, *p*H 7.4. Assays were initiated by the addition of ATP. After 10 min incubation, NaF, sodium pyrophosphate, EDTA, ATP and Triton were added to get final concentration of 50, 10, 5 and 5 mM and 0.1% (v/v) respectively. The insulin receptor was quantitatively immunoprecipitated by serum containing antibody against insulin receptor (serum B-2, 1:200 dilution) or normal control serum[8]. After 2.5 h at 4 °C, 200 μl of Protein A (Pansorbin; 10% w/v) were added and the incubation continued for 1 h at 4 °C. The precipitates were then collected by centrifugation at 10,000*g* for 5 min at 4 °C and washed twice with 1% Triton and 0.1% SDS[8]. Immunoprecipitates were solubilized by boiling for 3 min in 2% SDS in 10 mM sodium phosphate, *p*H 7.0, with (*A*) or without (*B*) dithiothreitol (DTT). The labelled components were separated electrophoretically in 5 or 7.5% polyacrylamide slab gels in the presence of 0.1% SDS as described by Laemmli[32]. After electrophoresis, the slab gels were stained, destained, dried and autoradiographed for 3–7 days as previously described[8]. Subunit molecular weights were calculated by using as standards (M_r): filamin (250,000), myosin (200,000), β-galactosidase (116,000), phosphorylase *b* (94,000), bovine serum albumin (68,000) and ovalbumin (43,000).

is labelled by ^{35}S-methionine or ^{3}H-sugars and analysed without reduction[11]. Using two-dimensional (non-reducing/reducing) gel electrophoresis, we have previously shown that the two highest molecular weight bands are composed of α and β subunits, and three other bands are an α–α dimer and 'free' α and β subunits respectively[11]. After incubating with insulin (10^{-6} M), the phosphorylation of all five bands was increased approximately five- to six-fold.

To evaluate further the mechanism of phosphorylation of insulin receptors, the solubilized fractions were incubated with several concentrations of insulin (10^{-10} to ~10^{-6} M), desoctapeptide (DOP) insulin and multiplication-stimulating activity (MSA), one of the insulin-like growth factors, and the phosphorylation was carried out as described above. Physiological concentrations of insulin (3×10^{-10} M) increased the phosphorylation of both subunits approximately threefold (Table 1). Stimulation was maximal with insulin concentrations of 10^{-8} to ~10^{-6} M (Table 1; Fig. 1). DOP insulin, which has ≤1% of the potency of porcine insulin in displacing bound ^{125}I-insulin from rat liver membrane insulin receptor and stimulating glucose metabolism[6], stimulated phosphorylation only minimally. MSA (10^{-7} M) was also far less potent than the same concentration of porcine insulin (Table 1), as expected from previous studies of the affinity of MSA for the insulin receptor in rat liver plasma membrane[12,13]. Thus, the 135,000- and 95,000-M_r bands were phosphorylated in dose-dependent fashion and specificity consistent with the affinity of the insulin receptor for insulin analogues.

To determine the phosphoamino acids of the β subunit of the insulin receptor, this ^{32}P-labelled phosphoprotein was cut from the gel and partially hydrolysed in 6 M HCl for 2 h at 110 °C. The resulting hydrolysates were separated by two-dimensional electrophoresis (*p*H 2.0 and *p*H 3.5) in the presence of unlabelled phosphoserine, phosphothreonine and phosphotyrosine, and the autoradiograms of the separated phosphoamino acids were compared with the ninhydrin-stained standards. Only trace amounts of phosphotyrosine could be detected in the basal state (data not shown). After insulin stimulation (10^{-7} M), there was a dramatic increase in the amount of phosphotyrosine (Fig. 2). Because of the low radioactivity, phosphoamino acid in α subunit could not be identified.

There is considerable evidence that phosphorylation and dephosphorylation may have various roles in insulin action[14–20]. Recently, we found that insulin stimulates the phosphorylation

Table 1 Effects of insulin and insulin analogues on ^{32}P incorporation into solubilized insulin receptor subunits from rat liver plasma membrane

Addition	Concentration (M)	^{32}P incorporated into insulin receptor subunits (arbitrary units)	
		M_r 135,000	M_r 95,000
Expt 1			
None	—	3.7	20.2
Porcine insulin	3×10^{-10}	12.9	64.0
Porcine insulin	1×10^{-7}	21.5	116.0
Desoctapeptide insulin	1×10^{-7}	4.1	27.2
Expt 2			
None	—	<0.5	5.2
Porcine insulin	1×10^{-7}	4.0	38.2
Multiplication-stimulating activity	1×10^{-7}	<0.5	6.6

Experiments 1 and 2 were performed with solubilized fractions derived from different membrane preparations. The studies were carried out as described in Fig. 1 legend. The autoradiograms were scanned in a Joyce-Loebl microdensitometer and the peak areas corresponding to the 135,000- and 95,000-M_r bands were calculated and expressed in arbitrary units.

of the β subunit of the insulin receptor in intact cells, indicating that this may be an early step in insulin action. This study demonstrates that the same phenomenon can be reproduced in cell-free systems and suggests several interesting points. First, although we are unable to determine the source of the phosphate used to phosphorylate the 95,000-M_r protein in an intact cell, in the broken cell system this protein clearly accepts the phosphate from γ-labelled ATP. Second, the results suggest that an endogenous protein kinase(s) is(are) involved in this reaction and that this endogenous protein kinase activity exists in the plasma membrane fraction and after affinity chromatography on wheat germ agglutinin–agarose. Furthermore, insulin stimulates the incorporation of ^{32}P into the β subunit of insulin receptor at tyrosine residues only. Phosphorylation of tyrosine is rare in normal cells[21], but specific tyrosine phosphorylation of other proteins has been observed after cellular transformation by RNA tumour viruses[21–25] or stimulation of cell growth by epidermal growth factor (EGF)[26,27], platelet-derived growth factor[28] and a human transforming growth factor[29]. Insulin is also a strong growth promoter.

Although phosphorylation has been demonstrated in both the intact and broken cell, there are some differences between them. First, the dose–response curve of phosphorylation is shifted to the left, that is, it is more sensitive, in a cell-free system than in the intact cell. This may depend on several factors, including the conditions of assay and the source of membranes. Second, in the intact cell only the β subunit is phosphorylated, whereas in the cell-free system, both subunits of the insulin receptor are phosphorylated. This suggests the α subunit can also be a substrate for endogenous protein kinases, although the amount of phosphorylation of the α subunit is usually 15% or less than that of the β subunit. The reason we cannot detect the phosphorylation of α subunit in intact cells may be related to the low level of phosphorylation, to the topography of insulin receptor subunits in intact cells, to differences in the level of endogenous phosphorylation, or to differences between these liver membranes derived from normal rats and cultured tumour cells. Third, we have found that in the intact cell, the content of both phosphoserine and phosphotyrosine in the β subunit of the insulin receptor is increased after insulin stimulation[30], although in the intact cell the absolute amount of phosphotyrosine is very small compared with phosphoserine. In the broken cell system, however, only phosphotyrosine is found. These results suggest that the tyrosine phosphorylation of the β subunit may be the initial reaction which occurs on insulin binding and that phosphorylation of serine requires other components absent in cell-free systems. Similar differences of phosphoamino acid composition between intact cells and cell-free systems have been observed in the phosphorylation of RNA tumour virus oncogene products[21,23–25], and the receptor for EGF[26,27].

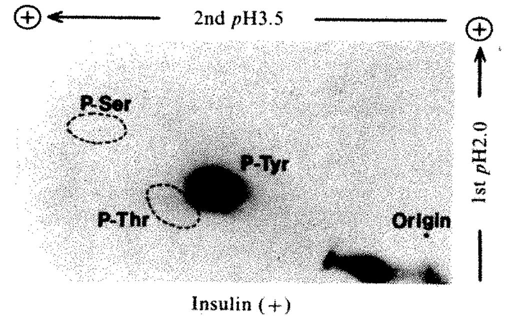

Fig. 2 Identification of phosphoamino acids in the 95,000-M_r phosphoprotein. The phosphoamino acids were analysed by a modification of the method of Hunter and Sefton[21]. The phosphorylation of the 95,000-M_r protein (β subunit of insulin receptor) was stimulated by insulin (10^{-7} M) as shown in Fig. 1. The 95,000-M_r bands, localized by autoradiography, were excised from the gel and the proteins eluted by electrophoresis at 150 V for 20 h into a dialysis bag containing 10 mM sodium phosphate buffer (*p*H 7.0) and 0.05% SDS. The samples were dialysed against 10 mM NH_4HCO_3, lyophilized, extracted by ethanol/ether (1 : 1 v/v) and then subjected to acid hydrolysis in 6 M HCl for 2 h at 110 °C. After lyophilization, the hydrolysates were spotted on Whatman 3MM paper. Electrophoresis was performed at *p*H 2.0 (formic acid/acetic acid/H_2O, 81 : 25 : 879) and 550 V for 60 min at 12 °C in the first dimension, and at *p*H 3.5 (pyridine/acetic acid/H_2O, 1 : 10 : 189) and 1,000 V for 105 min in the second dimension. Samples of authentic phosphoserine (Sigma), phosphothreonine (Sigma) and phosphotyrosine (a gift from Dr T. Hunter, Salk Institute) were added to all radioactive samples analysed. The standards were located by ninhydrin and are delineated by the broken lines. The radioactive material was located by autoradiography.

Our results provide the first demonstration, in a cell-free system of a covalent modification of the solubilized insulin receptor as a consequence of insulin–receptor complex formation. The mechanism by which insulin stimulates the incorporation of ^{32}P from [γ-^{32}P]ATP into its own receptor at tyrosine residue is not known. This system does, however, provide the opportunity to investigate whether the insulin receptor is a tyrosine protein kinase, as suggested for the EGF receptor[31], or a regulator of phosphoprotein phosphatase.

We thank Dr K. Yamada, J. Rath and M. Rechler for critical reading of the manuscript and for the gift of multiplication-stimulating activity. M.K. is a Capps Diabetes Scholar. This work was supported in part by a grant from the Juvenile Diabetes Foundation.

Received 8 February; accepted 4 June 1982.

1. Kahn, C. R. *et al. Recent Prog. Horm. Res.* **37,** 477–538 (1981).
2. Czech, M. P. *A. Rev. Biochem.* **46,** 359–384 (1977).
3. Kasuga, M., Karlsson, F. A. & Kahn, C. R. *Science* **215,** 185–187 (1982).
4. Neville, D. M. Jr *Biochim. biophys. Acta* **154,** 540–552 (1968).
5. Freychet, P., Roth, J. & Neville, D. M. Jr *Proc. natn. Acad. Sci. U.S.A.* **68,** 1833–1837 (1971).
6. Cuatrecasas, P. *Proc. natn. Acad. Sci. U.S.A.* **69,** 318–322 (1972).
7. Hedo, J., Harrison, L. C. & Roth, J. *Biochemistry* **20,** 3385–3393 (1981).
8. Kasuga, M., Kahn, C. R., Hedo, J., Van Obberghen, E. & Yamada, K. M. *Proc. natn. Acad. Sci. U.S.A.* **78,** 6917–6921 (1981).
9. Jacobs, S., Hazum, E., Schechter, Y. & Cuatrecasas, P. *Proc. natn. Acad. Sci. U.S.A.* **76,** 4918–4921 (1979).
10. Pilch, P. F. & Czech, M. P. *J. biol. Chem.* **255,** 1722–1731 (1980).
11. Kasuga, M., Hedo, J., Yamada, K. M. & Kahn, C. R. *J. biol. Chem.* (in the press).
12. Rechler, M. M., Podskalny, J. M. & Nissley, S. P. *Nature* **259,** 134–136 (1976).
13. Kasuga, M., Van Obberghen, E., Nissley, S. P. & Rechler, P. *J. biol. Chem.* **256,** 5305–5308 (1981).
14. Avruch, J., Leone, G. R. & Martin, D. B. *J. biol. Chem.* **251,** 1511–1515 (1976).
15. Benjamin, G. J. & Clayton, N. C. *J. biol. Chem.* **253,** 1700–1709 (1978).
16. Seals, J. R., McDonald, J. M. & Jarrett, L. *J. biol. Chem.* **254,** 6991–6996 (1979).
17. Smith, C. J., Wejksnora, P. J., Warner, J. R., Rubin, S. & Rosen, O. M. *Proc. natn. Acad. Sci. U.S.A.* **76,** 2725–2729 (1979).
18. Larner, J. *et al. Science* **206,** 1407–1408 (1979).
19. Marchmont, R. J. & Houslay, M. D. *Nature* **286,** 904–906 (1980).
20. Brownsey, R. W., Belsham, G. J. & Denton, R. M. *FEBS Lett.* **124,** 145–150 (1981).
21. Hunter, T. & Sefton, B. M. *Proc. natn. Acad. Sci. U.S.A.* **77,** 1311–1315 (1980).
22. Witte, O. N., Dasgupta, A. & Baltimore, D. *Nature* **283,** 826–831 (1980).
23. Collet, M. S., Purchio, A. F. & Erikson, R. L. *Nature* **285,** 167–169 (1980).
24. Feldman, R., Hanafusa, T. & Hanafusa, H. *Cell* **22,** 757–765 (1980).
25. Kawai, S. *et al. Proc. natn. Acad. Sci. U.S.A.* **77,** 6199–6203 (1980).
26. Ushiro, H. & Cohen, S. J. *J. biol. Chem.* **255,** 8363–8365 (1980).
27. Hunter, T. & Cooper, J. A. *Cell* **24,** 741–752 (1981).
28. Ek, B., Westermark, B., Wasteson, A. & Heldin, C-H. *Nature* **295,** 419–420 (1982).
29. Reynolds, F. H. Jr, Todaro, G. J., Fryling, C. & Stephenson, J. R. *Nature* **292,** 259–262 (1981).
30. Kasuga, M. *et al. J. biol. Chem.* (in the press).
31. Cohen, S., Carpenter, G. & King, L. Jr *J. biol. Chem.* **255,** 4834–4842 (1980).
32. Laemmli, U. K. *Nature* **227,** 680–685 (1970).

Insertion of diphtheria toxin into and across membranes: role of phosphoinositide asymmetry

James J. Donovan*†, Melvin I. Simon* & Mauricio Montal*†

Departments of *Biology and †Physics, University of California, San Diego, La Jolla, California 92093, USA

Diphtheria toxin (DT), a 63,000-molecular weight soluble protein, is toxic to most mammalian cells. The mechanism of intoxication involves a step in which one part of the molecule inserts into a membrane, facilitating the transport of the enzymatic fragment of the protein into the cytoplasm[1,2]. This event requires an acidic environment and seems to occur at the membrane of an endocytic vesicle[3,4]. Different cell lines and species differ in their sensitivities to DT—this is due at least in part to differences in the number of DT surface receptors on the cells[5], but may also arise from differences in the membrane transport step. It is generally recognized that protein–lipid

0028–0836/82/320669—04$01.00

interactions are of critical importance in membrane transport phenomena (see ref. 6). Thus, it is of interest to determine whether the interaction of DT with membranes is modulated by their composition. We have shown previously that DT interacts with planar lipid bilayers at acidic *p*H to produce voltage-dependent channels[7]. We report here that this interaction of DT with bilayers depends on membrane phospholipid composition; the interaction is optimal when inositides are present within the membrane, and the inositides are required on the side of the membrane opposite to that in which DT is introduced.

We investigated the effect of membrane composition on the interaction of DT with lipid bilayer membranes. Figure 1*a* illustrates the time course of the membrane current at a constant applied voltage of −40 mV recorded from two different membranes. The upper trace corresponds to a phosphatidylethanolamine (PE) membrane and the lower to an asolectin (AL, soybean phospholipids) membrane. AL is a mixture of phospholipids, the major components of which are PE, phosphatidylcholine (PC), phosphatidylinositol (PI), and phosphatidylserine (PS), and contains a small amount of α-tocopherol. The conductance of each unmodified membrane was low, as indicated by the small current in response to a voltage step. On addition of DT to the aqueous compartment, the conductance of the asolectin membrane increased due to the formation of ionic channels, whereas the current through the PE membrane remained almost unchanged. Channels do form in PE membranes if sufficient time is allowed, and if higher DT concentrations are used, but PE membranes are consistently much less sensitive to DT.

Alving *et al.*[8] have shown that the binding of DT to phospholipid vesicles at acidic *p*H is correlated with the membrane surface charge. This suggests that the difference between asolectin (~20% negative lipids) and PE membranes might be due to differential binding resulting from differences in surface charge or lipid composition. To evaluate this hypothesis, we tested a variety of lipids in our bilayer system. The data are summarized in Table 1, where the average rate of conductance increase for several lipids is shown normalized to the rate of increase for asolectin at a DT concentration of 100 ng ml^{-1}. Membranes consisting of the neutral lipids PC and PE are relatively insensitive to DT, but the same is true for the negative phospholipid, PS and the negative lipid oleoyl phosphate (OP) at surface charge concentrations comparable to asolectin. Similarly, glycolipids or gangliosides do not sensitize the membrane to DT. Diphosphatidylglycerol (DPG, cardiolipin) seems to confer some slight sensitivity to DT, but greater effects result from the presence of inositides in the membrane. As phosphatidylinositol is a major component of asolectin (~14%)[9,10], we believe that the PI in asolectin membranes is responsible for their sensitivity to DT. The fact that the PI–PC mixture is less DT-sensitive than asolectin could be due to the phytanoic acid chains on the PC because the acyl chain composition of the lipids affects DT binding[8]. Indeed, membranes formed with purified soybean PC, PE and PI exhibited DT-induced conductances comparable to asolectin, whereas substitution of PS for PI in this mixture rendered the membranes insensitive to DT (see Table 1). Channels do form in inositide-free membranes, but at a slower rate.

The rate of channel formation induced by DT is enhanced by the presence of a *p*H gradient. Similar results have been reported by Kagan *et al.*[11] who showed that a mutant form of DT, CRM 45, forms channels, and that the rate of conductance increase is greater in the presence of a *p*H gradient. For DT, we observed that in the presence of a 2-unit *p*H gradient (4.9–6.9, acid on the DT-containing side), the rate of channel formation was enhanced ~50-fold, regardless of the composition of the membrane. Thus, the relative conductances are unchanged by the *p*H gradient. To separate clearly the effects of *p*H and membrane composition, all the experiments reported here were performed with both sides of the membrane at *p*H 4.85.

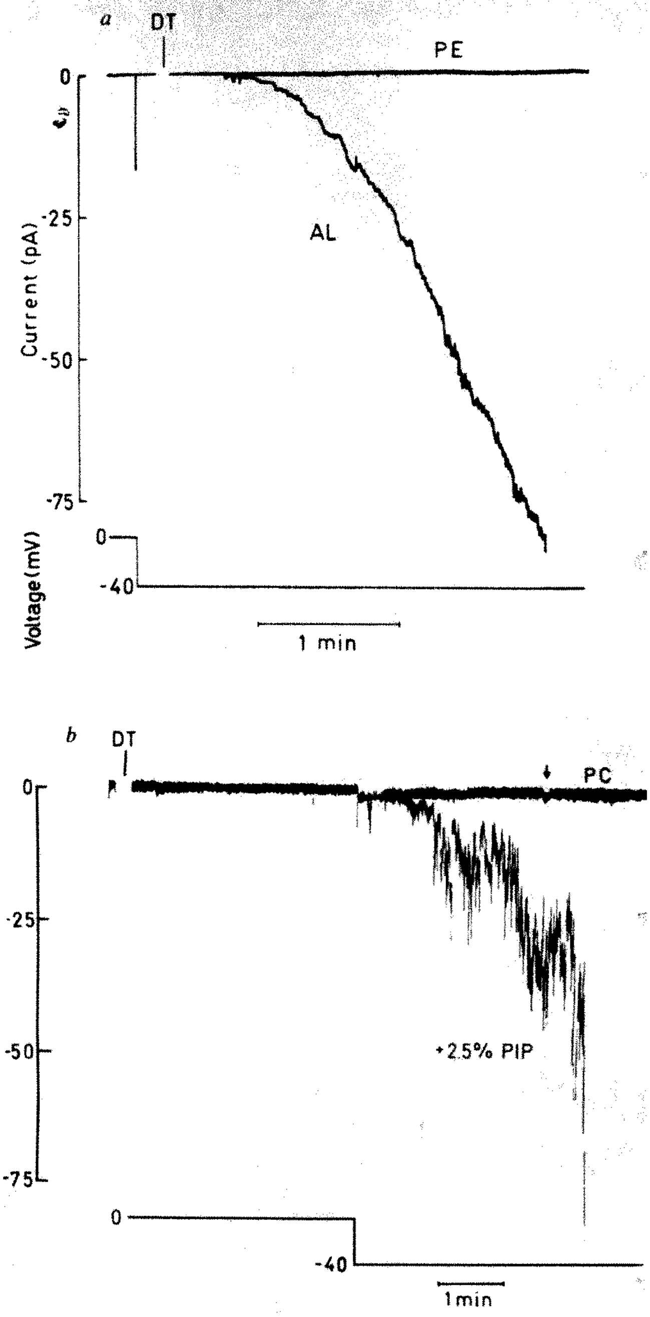

Fig. 1 Membrane currents at a constant applied voltage through symmetrical membranes treated with DT. Planar lipid bilayers were formed from monolayers as described elsewhere[23] across a 200-μm hole in a 12 μm-thick Teflon partition separating two 4-ml capacity Teflon compartments. The hole was treated with a 1% solution of squalene in pentane. Voltage was applied, and current measured using Ag/AgCl electrodes with an Analog Devices AD515 amplifier having a 1-GΩ feedback resistor. The DT-containing compartment is defined as being at zero potential, and positive current is the flow of positive ions into this compartment. *a*. Shows the current through two membranes before and after the addition of DT. The upper trace corresponds to a PE membrane, and the lower trace to an AL (soybean lipids purified by the method of Labarca *et al.*[24]) membrane. *b* Shows two current traces: the upper trace is from a membrane consisting of 100% PC (diphytanoyl phosphatidylcholine, DPPC) and exhibits a low conductance during which a single channel of DT opens and closes (arrow). The lower trace is from a membrane containing 97.5% PC and 2.5% PIP. Because of the low solubility of PIP in alkane solvents, the lipid solution was sonicated briefly before spreading the monolayers. All experiments shown were done at room temperature using 0.2 M NaCl/20 mM citrate buffer, *p*H 4.85. The DT concentration was 100 ng ml^{-1}. DT (Connaught) was purified by DE52 chromatography[25].

Another parameter which affects the potency of DT is nicking of the toxin. DT was nicked according to Drazin *et al.*[12]. The conductance induced by nicked toxin was increased relative to un-nicked toxin by an order of magnitude, and showed less variability.

Most interesting among the lipids studied here is phosphatidylinositol-4-monophosphate (PIP)[8]. This lipid (PI with an extra phosphate on the inositol ring) has a double negative charge at the *p*H of these experiments. It is most effective at sensitizing the membrane to DT, which seems to be due to the inositol or phosphoinositol moiety and not the charge, as diphosphoglycerate is also doubly charged, but is much less effective. Figure 1*b* illustrates the ability of PIP to sensitize a membrane to DT. The two superimposed current traces are for two different membranes, one of 100% PC and another of 97.5% PC with only 2.5% PIP. The addition of this small amount of PIP caused the current to increase dramatically in the presence of DT, even though the surface charge density was about one-quarter that for an asolectin membrane. Such current increases were not seen in the absence of DT.

The simplest explanation for these data is that DT binds to inositides, especially PIP, on the bilayer surface[8,13]. To test this notion, we prepared asymmetric lipid bilayers containing PIP exclusively in one monolayer. These membranes were made with lipid mixtures designed to have the same surface charge density in both monolayers. All other conditions, including DT concentration and *p*H, were also symmetric. Two superimposed traces of the current through asymmetric bilayers after the addition of DT are shown in Fig. 2*a*. When DT was added to the chamber in contact with the PIP face of the membrane, the membrane current was unaffected, except for some incidental current drift. In contrast, when DT was added to the PS side, the current increased dramatically after a significant lag time. Thus, although PIP does bind DT[8], it does not mediate channel formation primarily through DT binding, but has a more subtle role. We have shown previously[7] that the DT insertion and channel formation steps are distinct from the binding step. Our results indicate that phosphoinositides exert their effect not so much on the binding of DT but rather on either the insertion or channel formation step, and that they mediate this effect from the side opposite to that on which the DT is bound.

Table 1 Relative conductances induced by DT in symmetrical lipid bilayers of different composition

Membrane composition	Relative conductance*	
Asolectin	1.0±0.2	(10)
PE	≤0.001	(2)
DPPC	0.015±0.006	(3)
20% PS/80% DPPC	0.02±0.006	(3)
33% OP/67% DPPC	≤0.001	(2)
10% Glucocerebroside/90% DPPC	0.01±0.007	(2)
25% DPG/75% DPPC	0.058±0.022	(4)
10% Ganglioside/90% DPPC	0.02±0.015	(5)
25% PI/75% DPPC	0.16±0.07	(4)
5% PIP/95% DPPC	0.31±0.023	(3)
40% Soybean PC/40% PE/20% PI	0.82±0.022	(3)
40% Soybean PC/40% PE/20% PS	0.08±0.06	(3)

Values shown are mean conductance ±s.e.m. divided by the mean conductance for asolectin (number of experiments in parentheses). All conductances were obtained by incubating the membrane in the presence of DT for 4 min at 0 mV applied potential. Then, the potential was switched to −30 mV, and the conductance measured 1 min later. Asolectin membranes were generally treated with 100 ng ml^{-1} of DT; other membranes often needed higher DT concentrations. In these cases, the rate of conductance increase was taken as proportional to the square of the DT concentration[7,11]. Other conditions were as indicated in Fig. 1 legend. PE, PS, PI, PIP and soybean PC were obtained from Sigma, diphytanoyl phosphatidylcholine (DPPC) from Avanti, glucocerebroside and DPG from Supelco; OP was from Hooker Chemical. Gangliosides (mixed bovine brain) were the gift of E. Yavin; HPLC-purified soybean PC was given by M. Conrad. Lipids were dissolved in $CHCl_3$ (PIP in water-saturated $CHCl_3$) or $CHCl_3$/MeOH (2:1), and stored at −80 °C until use.

The effect of phosphoinositides seems to be due to an interaction of the inositol phosphate moiety with DT which is satisfied even if the inositol is added to the solution in contact with the membrane. Figure 2*b* shows the effect of adding inositol hexaphosphate (IHP, phytic acid) to the compartment on the toxin-free side of a PS-containing membrane. A current increase was apparent after DT addition only after IHP was added to a concentration of 0.5 mM; further addition of IHP further increased the conductance. In membranes untreated with DT, IHP had no effect on membrane conductance, and addition of IHP to the DT-containing side also had no effect (Fig. 3). The effect of IHP was the same in the presence of 1 mM EGTA or 1 mM Ca^{2+}, indicating that this effect is not due to any Ca^{2+} bound to the phosphate groups of the IHP. Rather, the inositol phosphate moiety seems to be essential for channel formation.

It is known that DT in solution binds IHP together with nucleotides and other polyphosphates[14,15]. Thus, the inositol phosphate effect could conceivably be due to its binding to the DT phosphate binding site, thereby anchoring the DT in a transmembrane conformation. If this were the case, presumably any polyphosphate should have the same effect. However, ATP, when added to the *trans* side of the membrane, does not affect DT channel formation (data not shown). Thus, the effect is specific: only phosphoinositide (or inositol phosphate) on the opposite side of the membrane induces DT channel formation.

We suggest a mechanism in which the DT first binds to the membrane surface, and then extends a process across the

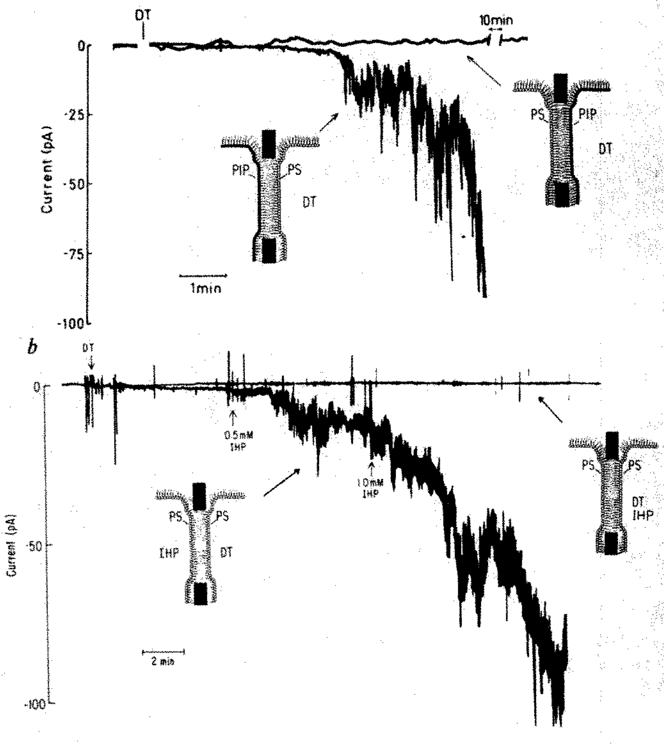

Fig. 2 *a*, Membrane currents through two asymmetric membranes treated with DT. The membranes were formed from two monolayers of different composition: one monolayer contained 10% PS and 90% PC, the other contained 5% PIP and 95% PC. The upper and lower traces show the current through the membrane when DT was added to the solution on the PIP-containing and PS-containing side, respectively. The applied potential was −30 mV throughout. DT concentration, 100 ng ml^{-1}. *b*, Membrane current through two symmetrical membranes in the presence of IHP. The membrane composition was 20% PS, 80% PC. The addition of DT to a concentration of 100 ng ml^{-1} caused no significant increase in conductance in either membrane. The lower trace shows the current after IHP (Sigma) was added to the side of the membrane opposite to that to which DT was added, and the upper trace shows the current obtained when IHP was added to the same side of the membrane as DT. The voltage was kept constant at −30 mV for both traces.

membrane core which probes the other side. If the DT finds phosphoinositide, and binds to it, anchoring it in place and allowing channel formation to occur. Thus, the critical steps in intoxication may be as follows. DT binds to a cell-surface receptor and is internalized. Once in the endosome, the acidic environment induces a conformational change in DT that, in concert with the membrane potential, promotes the binding and insertion of DT into the endosomal bilayer. The consequent binding to phosphoinositides anchors DT, allowing channel formation and, concomitantly, the translocation of the enzymatic moiety of DT into the cytoplasm. The notion that translocation of proteins across membranes involves conformational changes in the protein and the insertion of portions of the polypeptide chain has been suggested in a variety of contexts[16–19]. The requirements for insertion of the 'signal sequence' of some polypeptides are very similar to the requirements for DT channel formation[20–22]. The remarkable observation that channel formation is facilitated by the presence of inositides in the transmembrane monolayer suggests that specific polypeptide–lipid interactions can play a part in protein translocation.

This work was supported by NIH grants EY-02084, GM-07199-07; NSF grant PCM7726862; and ONR grant N00014-79-C-0798. During this work, M.M. was a John Simon Guggenheim Foundation Fellow.

Received 22 March; accepted 3 June 1982.

1. Collier, R. J. *Bact. Rev.* **39,** 54–85 (1975).
2. Pappenheimer, A. M. *A. Rev. Biochem.* **46,** 69–94 (1977).
3. Draper, R. K. & Simon, M. I. *J. Cell Biol.* **87,** 849–854 (1980).
4. Sandvig, K. & Olsnes, S. *J. Cell Biol.* **87,** 828–832 (1980).
5. Middlebrook, J. L., Dorland, R. B. & Leppla, S. H. *J. biol. Chem.* **254,** 7325–7330 (1979).
6. Parsegian, A. (ed.) *Proc. 3rd Biophys. Discussions* (1982); *Biophys. J.* **37,** 1–401 (1982).
7. Donovan, J. J., Simon, M. I., Draper, R. K. & Montal, M. *Proc. natn. Acad. Sci. U.S.A.* **78,** 172–176 (1981).
8. Alving, C. R. *et al. Proc. natn. Acad. Sci. U.S.A.* **77,** 1986–1990 (1980).
9. Miller, C. & Racker, E. *J. Membrane Biol.* **26,** 319–333 (1976).
10. O'Brien, D., Costa, L. F. & Ott, R. A. *Biochemistry* **16,** 1295–1303 (1977).
11. Kagan, B. L., Finkelstein, A. & Colombini, M. *Proc. natn. Acad. Sci. U.S.A.* **78,** 4950–4954 (1981).
12. Drazin, R., Kandel, J. & Collier, R. J. *J. biol. Chem.* **246,** 1504–1510 (1971).
13. Friedman, R. L., Iglewski, B. H., Roerdink, F. & Alving, C. R. *Biophys. J.* **37,** 23–24 (1982).
14. Middlebrook, J. L. & Dorland, R. B. *Can. J. Microbiol.* **25,** 285–290 (1979).
15. Lory, S. & Collier, R. J. *Proc. natn. Acad. Sci. U.S.A.* **77,** 267–271 (1980).
16. Inouye, M. & Halegoua, S. *CRC crit. Rev. Biochem.*, 339–371 (1980).
17. Ito, K., Mandel, G. & Wickner, W. *Proc. natn. Acad. Sci. U.S.A.* **76,** 1199–1203 (1979).
18. Ito, K., Date, T. & Wickner, W. *J. biol. Chem.* **225,** 2123–2130 (1980).
19. Blobel, G. *Proc. natn. Acad. Sci. U.S.A.* **77,** 1496–1500 (1980).
20. Date, T., Goodman, J. M. & Wickner, W. *Proc. natn. Acad. Sci. U.S.A.* **77,** 4669–4673 (1980).
21. Engelman, D. M. & Steitz, T. A. *Cell* **23,** 411–422 (1981).
22. Skehel, J. J. *et al. Proc. natn. Acad. Sci. U.S.A.* **79,** 968–972 (1982).
23. Montal, M. *Meth. Enzym.* **32B,** 545–554 (1974).
24. Labarca, P., Coronado, R. & Miller, C. *J. gen. Physiol.* **76,** 397–424 (1980).
25. Collier, R. J. & Kandel, J. *J. biol. Chem.* **246,** 1496–1503 (1971).

Genetic recombination and directional selection for DDT resistance in *Drosophila melanogaster*

Phillip B. Flexon

School or Medicine, Case Western Reserve University, Cleveland, Ohio 44106, USA

Charles F. Rodell*

Department of Biology, College of St Benedict–St John's University, Collegeville, Minnesota 56321, USA

It is generally agreed that recombination offers a long-term evolutionary advantage[1,2]. It is argued, however, that because genetic variability exists for recombination rates in natural populations, response to immediate demands for adaptation should result in reduced recombination regardless of the long-term consequences. Nevertheless, genetic recombination persists. Numerous models have been developed to examine this fact[1,2]. There exists, however, a notable lack of empiricism on the recombination question. Here we demonstrate in *Drosophila* that the response of a polygenic character (DDT resistance) to directional selection is sufficiently correlated with the genetic variability generated by recombination to bring about a corresponding increase in recombination rate. We draw attention to the relationship of these results to existing models, notably the 'hitch-hiking' model[3].

Twenty-eight single female lines of *Drosophila melanogaster*, free from chromosomal inversions, were cultured from individuals collected in central Tennessee. On 8 August 1978, five inseminated females from each line were combined to establish two control populations (C1 and C2) and three selected populations (R1, R2 and R3). Populations were maintained in population units consisting of two 1/2-pint bottles united by a 7.6-cm piece of hose[4]. The cultures were maintained at 25 ± 1 °C and the bottles replaced alternatively every 2 weeks throughout the study. On 20 August 1978, selection for DDT (1,1,1-trichloro-2,2-bis(*p*-chlorophenyl)ethane) resistance was initiated on populations R1, R2 and R3 by placing a 2.5 × 7.5 cm strip of filter paper impregnated with DDT on the medium surface in each fresh bottle. Selection was carried out by gradually increasing the amount of DDT from 0.1 mg to 190.0 mg over the next 555 days.

Three kinds of data were gathered from these populations. Population levels of DDT resistance were measured to demonstrate that directional selection had occurred; cross-over frequencies for portions of chromosomes I, II and III were determined to detect differences in recombination rates between initial, control and selected populations; and individual chromosomes from the selected populations were tested for resistance. The level of chromosomal resistance attained was then related to changes in chromosomal recombination rates.

DDT resistance was measured by subjecting the daughters of sampled females to a knockdown test[4]. After 330 days of selection, populations R1, R2 and R3 achieved resistance levels 10–40 times greater than those of the control populations, demonstrating that selection was effective. The median effective dose (ED_{50}) for DDT was 5.3 and 6.4 mg for populations C1 and C2, respectively, and 207.5, 160.4 and 54.1 mg for R1, R2 and R3, respectively[5]. Population levels of DDT resistance were not tested again even though selection continued for another 165 days.

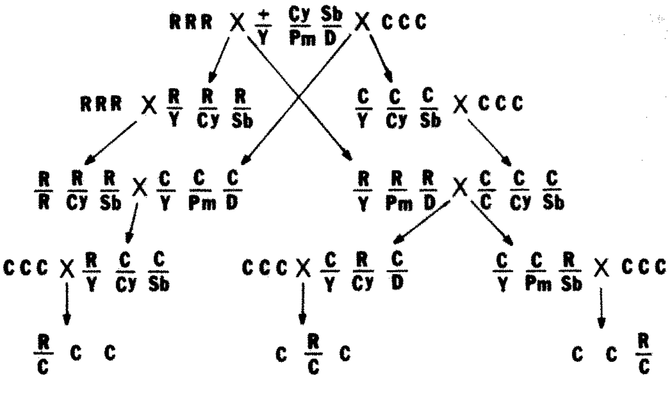

Fig. 1 Mating scheme that allows for the isolation of females possessing individual I, II or III chromosomes from the selected population. R, chromosome from the selected population; C, chromosome from the control population; +, wild-type I chromosome; Cy, curly; Sb, stubble; Y, Y chromosome; Pm, plum; and D, dichaete.

---

* To whom correspondence should be addressed.

0028-0836/82/320672—03$01.00

Table 1 Recombination rates for portions of chromosomes I, II and III in control and selected populations of *Drosophila melanogaster*

Population	Chromosome	Mean recombination index ±95% confidence interval	No. of females sampled from each population	No. of individuals counted	Months of DDT selection before recombination tests
Wild type	I†	0.286±0.041	10	1,500	0
C1		0.277±0.027	25	991	19*
C2		0.290±0.026	25	962	18*
R1		0.276±0.020	25	986	19
R2		0.283±0.021	24	958	19
R3		0.288±0.026	24	1,119	18
C1	II‡	0.330±0.020	36	1,910	12*
C2		0.309±0.035	26	1,313	12*
R1		0.369±0.023	23	1,675	11
R2		0.373±0.031	20	1,063	12
R3		0.398±0.021	37	1,899	12
Wild type	III§	0.056±0.013	12	1,153	0
C1		0.059±0.014	20	976	13*
C2		0.057±0.014	30	1,575	13*
R1		0.096±0.020	33	1,914	13
R2		0.098±0.022	24	1,323	14
R3		0.094±0.018	25	1,359	14

The 'recombination index' represents the number of recombination events observed divided by the total number of possible recombination events.

* Populations C1 and C2 were not exposed to DDT but in all other aspects were treated identically for the period of time shown.

† Recombination index determined for markers *w,m,f*.

‡ Recombination index determined for markers *dp, cn, bw*.

† Recombination index determined for markers *wmf*.

§ Recombination index determined for markers *Gl, Sb*.

The recombination data are summarized in Table 1. Following selection, recombination rates between loosely linked markers were determined for the major chromosomes in all populations. Initial rates were also determined for chromosomes I and III. It became necessary to change the markers for chromosome II after the experiment began; because of this change there are no initial data for that chromosome. These rates were obtained by crossing daughters of sampled females to marker stock males. F_1 daughters were again crossed to marker males and F_2 individuals scored for recombinant phenotypes. The data are expressed as a recombination index, representing the number of recombination events observed divided by the total number of possible recombination events. For chromosomes I and II with three markers per chromosome, the recombination index is computed by dividing the number of recombination events among F_2 individuals by twice the total number of F_2 individuals, as it is possible to observe a maximum of two recombination events in each individual. Chromosome III data are based on two markers; thus, the recombination index is the number of recombination events observed divided by the total number of F_2 individuals. One-way analysis of variance of the recombination index values for each chromosome indicated significant differences between populations for chromosomes II ($F_{4,137} = 8.64$; $P < 0.001$) and III ($F_{5,138} = 3.34$; $P < 0.01$) but no significant differences for chromosome I ($F_{5,127} = 0.45$; $P > 0.10$). Least-squares difference tests for the chromosome II values indicated no significant difference between the mean recombination index values for populations C1 and C2 and no significant differences between the means of the selected populations. However, each of the selected populations has a recombination rate ratio index significantly greater than each control population ($P < 0.05$ for all comparisons). The same results were obtained for the chromosome III data, that is $P < 0.05$ for each R population compared with each C population. These results indicate that a change in the level of DDT resistance brought about by directional selection was accompanied by a significant increase in the intrachromosomal recombination rate for portions of two of the three major chromosomes in this species.

The final step consisted of testing the level of DDT resistance for each chromosome separately. The rationale behind this step is as follows. If genes affecting recombination rates are maintained to any significant extent in populations as a result of producing new favourable recombinants, then the recombination genes must be sufficiently linked to these recombinants in order to 'hitch-hike' their way to a higher frequency. As significant increases in recombination frequency were found on chromosomes II and III, the hitch-hiking hypothesis predicts that these same chromosomes would possess the major genetic component for DDT resistance.

Individuals with the desired combination of unselected (C) and selected (R) chromosomes were obtained from a series of crosses by using inversion-containing marker chromosomes (Fig. 1). Again, females alone were evaluated for resistance by knockdown tests[4]. The results are striking when the chromosomal level of resistance, as indicated by the ED_{50} values[5], is compared with the ratio of selected chromosome recombination rate to that of the control chromosomes (Fig. 2), that is, chromosomal response for DDT resistance compared with chromosomal response in recombination rate. The greater the chromosomal response in recombination rate, the greater was the chromosomal response for DDT resistance; this significant positive correlation supports the hitch-hiking hypothesis.

It is necessary to consider whether the increases in recombination rate observed in the selected populations might be due to some factor other than selection. It seems unlikely that mutation could have caused this change. Studies on the

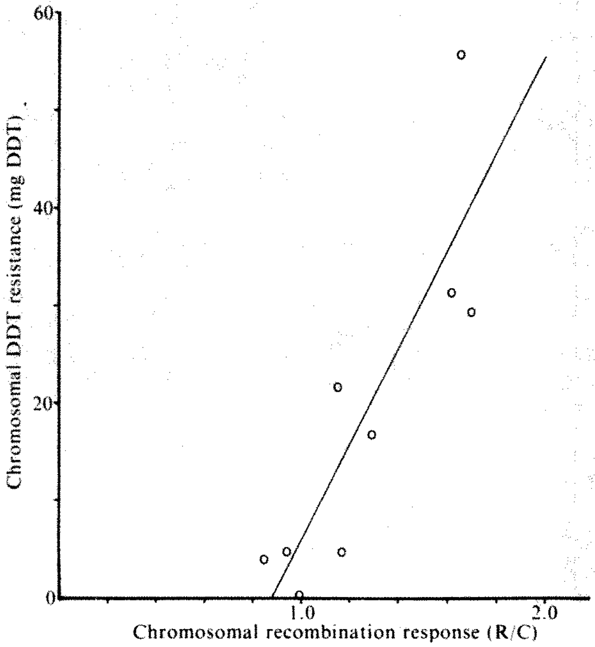

Fig. 2 The relationship between the level of chromosomal DDT resistance and chromosomal recombination response. The latter is taken as the ratio of the R population recombination index to the mean recombination index of the two C populations for a given chromosome: $y = 49.7x - 43.7$; $r_{yx} = 0.86$, $P < 0.01$ for H_0: $r_{yx} = 0$.)

mutagenic ability of DDT indicate that it is either nonmutagenic[6-9] or is only a weak mutagen[10,11]. It is possible that the increases were brought about by genetic drift. Because the selected populations were smaller in number than the control populations, the high rate alleles may have drifted to high frequencies. However, the fact that all populations responded in the same way favours directional selection as the major determinant of recombination rate increases.

These results are of interest in two respects: they provide the first demonstration of increased recombination correlated with the response to directional selection by a different quantitative character, and confirm the proposal that recombinant genes generating genotypes favoured by selection can 'hitch-hike' to increased allele frequencies[3]. For hitch-hiking to be a major factor in maintaining recombination in natural populations, these populations must experience either continuing directional selection or normalizing selection with a moving optimum[12]. Whenever a balancing selection model is analysed , selection for decreased recombination results[1,2,13]. The question becomes one of the relative importance of normalizing selection with a stable optimum as opposed to selection where the optimum is changing with time. The stabilizing selective mode might be favoured by those who prefer to think of adaptation as a response primarily to abiotic stresses such as temperature and humidity, or intraspecific interactions such as courtship, which present a more or less fixed range in which the species must adapt. It can be argued that adaptations to interspecific biotic stresses may be more important and more prevalent than those to abiotic stress[14-16]. Such co-evolutionary relationships are more likely to involve selection of the kind favouring recombination.

We thank Lisa D. Brooks, David J. Merrell and Michael J. Simmons for their critical comments on an earlier version of the manuscript. The marker stocks were supplied by the Mid-America Drosophila Stock Center, Bowling Green, Ohio.

Received 26 April; accepted 11 June 1982.

1. Felsenstein, J. *Genetics* **78,** 737–756 (1974).
2. Maynard Smith, J. *Nature* **268,** 693–696 (1977).
3. Strobeck, C., Maynard Smith, J. & Charlesworth, B. *Genetics* **82,** 547–558 (1976).
4. Merrell, D. J. & Underhill, J. C. *J. econ. Ent.* **49,** 300–306 (1956).
5. Finney, D. J. *Probit Analysis* 4th edn (Cambridge University Press, Cambridge, 1971).
6. Epstein, S. S. & Shafner, H. *Nature* **219,** 385–386 (1968).
7. Hart, M. M., Whang-Peng, J., Sieber, S. M., Fabro, S. & Adamson, R. H. *Xenobiotica* **2,** 567–574 (1972).
8. Luers, H. *Naturwissenschaften* **40,** 293–294 (1953).
9. Pielow, D. P. *Can. J. Zool.* **30,** 375–377 (1952).
10. Rabello, M. N. *et al. Mutat. Res.* **28,** 449–454 (1975).
11. Vogel, E. *Mutat. Res.* **16,** 157–164 (1972).
12. Maynard Smith, J. *Genet. Res.* **35,** 269–277 (1980).
13. Feldman, M. W., Christianson, F. B. & Brooks, L. D. *Proc. natn. Acad. Sci. U.S.A.* **77,** 4838–4841 (1980).
14. Whittaker, R. H. *Brookhaven Symp. Biol.* **22,** 178–185 (1969).
15. Levin, D. *Am. Nat.* **109,** 437–451 (1975).
16. Gilbert, L. E. in *Coevolution of Animals and Plants* (eds Gilbert, L. E. & Raven, P. H.) 210–240 (University of Texas Press, Austin, 1975).

Maintenance of broad host range plasmid RK2 replicons in *Pseudomonas aeruginosa*

Christopher M. Thomas, Atta A. K. Hussain & Christopher A. Smith

Department of Genetics, University of Birmingham, PO Box 363,
Birmingham B15 2TT, UK

Certain members of the *Escherichia coli* plasmid incompatibility group P are capable of efficient transfer between and maintenance in most Gram-negative bacterial species[1-4]. Of fundamental interest is whether this broad host range results from differences between the mechanisms of replication and partitioning during cell division used by IncP plasmids and by narrow host range plasmids. The genetic regions of IncP plasmid RK2 (similar or identical to RP4 and RP1) required for plasmid maintenance in *E. coli* have previously been defined as a vegetative replication origin (ori_{RK2}) and a gene specifying a positively required *trans*-acting product (*trfA*)[5-8]. Here we have tested various mini RK2 replicons for their ability to become established after transformation into *Pseudomonas aeruginosa* PAO as a model non-*E. coli* host. We chose *P. aeruginosa* for this purpose as it is a Gram-negative species relatively phylogenetically distant from *E. coli*. Our studies have defined a plasmid segment that contains a region which must be linked in *cis* to the ori_{RK2} replicon to allow mini RK2 plasmid maintenance in *P. aeruginosa* PAO and suggest that RK2 may carry genes which adapt the basic replicon to allow autonomous maintenance in specific groups of hosts.

A simplified physical and genetic map of plasmid RK2 is shown in Fig. 1. A segment of the plasmid genome (from coordinates 54.0 to 56.0 kilobases (kb)) has been designated the *trfB* region because experiments carried out in *E. coli* indicate that it contains a gene, *trfB*, that specifies a *trans*-acting product acting in plasmid replication or maintenance when the *trfB* region is part of the RK2 replicon[7,8]. The requirement for at least part of this region for establishment in *P. aeruginosa* has been suggested by the inability of unstable RP4 mutants with transposon Tn*7* inserted in the *trfB* region to transfer from *E. coli* to *P. aeruginosa*[9]. Also, a mutation has been described[10] that renders RP4 temperature-sensitive for maintenance in *P. aeruginosa* but not in *E. coli* and which physically maps in a plasmid segment that contains *trfB* but not *trfA* or ori_{RK2}.

We have analysed the *trfB* region requirement by testing the ability of mini replicons derived from RK2 by *in vitro* recombination and isolated from *E. coli* to be introduced by transformation into the restriction-deficient *P. aeruginosa* PAO1161. The structures of the plasmids we have used are shown in Fig. 2 and the results of transformation in Table 1. If a plasmid seemed to become established in PAO1161, plasmid DNA was isolated by the alkaline extraction method of Birnboim and Doly[11] and its structure verified by restriction endonuclease digestion pattern analysis. Our initial observation was that whereas mini RK2 replicons carrying all three regions, ori_{RK2}, *trfA* and *trfB* (pRK248), were capable of establishment in PAO1161,

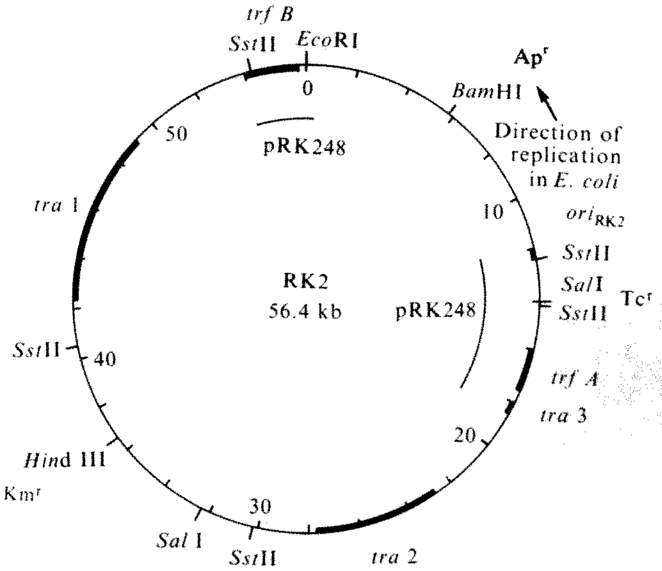

Fig. 1 Simplified physical and genetic map of broad host range plasmid RK2 (RP4 and RP1). Only a few restriction sites are shown as reference points. The single *Eco*RI site is used as the origin of kilobase pair (kb) coordinates. The regions specifying resistance to ampicillin (Ap^r), tetracycline (Tc^r) and kanamycin (Km^r) are shown together with regions (indicated by heavy lines) specifying genes required for conjugal transfer (*tra*), the vegetative replication origin (ori_{RK2}) and regions containing genes specifying *trans*-acting replication or maintenance functions (*trf*). The segments of RK2 present in the mini replicon pRK248 are shown.

Table 1 Results of transforming *P. aeruginosa* PAO1161 (Leu$^-$Res$^-$Mod$^+$) with DNA of mini RK2 replicons isolated from *E. coli* K12 C600 ΔtrpE5

	Average no. of transformants per plate*		
Plasmid	PAO1161	PAO1161 (pCT407)	PAO1161 (pCT408)
pRK248	2,000	89	2,000
pCT201	0	0	0 (6)†
pCT398	1,500	104	1,500
pCT427	200	14	1,000
pCT428	600	20	1,200

PAO1161 was made competent for transformation by pelleting 10 ml of late exponential phase culture ($A_{1\text{cm},625} \approx 1.0$) grown in L broth (10 g tryptone, 5 g yeast extract, 5 g l^{-1} NaCl) at 30 °C, washing with 4 ml ice-cold 100 mM $MgSO_4$, incubating in 4 ml ice-cold 100 mM $CaCl_2$ for 20 min and finally resuspending in 1 ml ice-cold 100 mM $CaCl_2$. Approximately 1 μg of DNA was mixed with 100 μl of competent bacteria and incubated at 0 °C for 60 min. After 2 min at 42 °C, 1.0 ml of L broth was added and after 120 min at 30 °C, 9 ml of L broth with tetracycline to 10 μg ml^{-1} was added. After overnight incubation at 30 °C, 0.2-ml samples were plated on L agar (L broth with 15 g l^{-1} agar) with 100 μg ml^{-1} tetracycline and incubated at 30 °C. pCT407 is an IncQ plasmid, R300B[9] (conferring resistance to streptomycin and sulphonamide) linked to *trfB*. pCT408 is R300B linked to *trfA* and *trfB*.

* If Tc$^{\text{r}}$ transformants were obtained the presence of independent plasmid DNA was verified by extraction and examination of plasmid DNA[11].

† On one occasion Tc$^{\text{r}}$ transformants were obtained but examination of plasmid DNA indicated that the tetracycline resistance was conferred by a recombinant between pCT201 and pCT408.

pCT201, which lacks all but 150 base pairs of the *trfB* region, was not. The *trfB* region was reinserted into pCT201 by *in vitro* recombination and the resultant plasmid (pCT398) was found to be capable of transforming and being maintained in PAO1161 (pCT398 is lost from PAO1161 at ~4–5% per generation in the absence of selection for plasmid markers). Therefore, the inability of pCT201 to transform PAO1161 is due to the lack of the *trfB* region rather than to a secondary defect located elsewhere on the plasmid.

To determine whether the requirement for all or part of the *trfB* region is solely to provide a *trans*-acting product necessary for *ori*$_{\text{RK2}}$ or *trfA* function in PAO1161, we cloned both *trfB* alone (pCT407) and *trfA* together with *trfB* (pCT408) into IncQ broad host range plasmid R300B by *in vitro* recombination and introduced these plasmids into PAO1161. The presence of *trfA* and *trfB* in the PAO1161 host did not significantly increase its ability to be transformed by pCT201. In one experiment, transformants were obtained but the restriction pattern of the plasmid DNA isolated from these transformants suggested that they contained a hybrid plasmid resulting from recombination between pCT201 and pCT408 after entry rather than pCT201 and pCT408 existing as separate plasmids. These results were interpreted to mean that part or all of the *trfB* region is needed linked in *cis* to pCT201 to allow establishment and maintenance in PAO1161 rather than simply for DNA entry into competent bacteria. Insertion of only part of the *trfB* region into pCT201 also restores the plasmid's ability to transform PAO1161, although the stability of these plasmids (pCT427 and pCT428) without selection for plasmid markers in PAO1161 is less than for pCT398 (pCT427 is lost at 5–10% per generation and pCT428 at 8–12% per generation). The limits of the essential segment of the *trfB* region are not known. The orientation of the inserted *trfB* segment relative to *ori*$_{\text{RK2}}$ and *trfA* (pCT427 and pCT428) does not matter so it seems unlikely that the *trfB* region is providing a transcription promoter active in *P. aeruginosa* that is necessary for *ori*$_{\text{RK2}}$ or *trfA* function.

As these results indicate that *ori*$_{\text{RK2}}$ and *trfA* as defined in *E. coli* are not sufficient for establishment and maintenance in *P. aeruginosa*, it could be that one or both of these regions is not needed in *P. aeruginosa*. However, we were unable to transform a plasmid containing *trfA* and *trfB* but lacking *ori*$_{\text{RK2}}$ (pCT141) into PAO1161. Also RP4.ColE1 hybrids with transposon Tn*7* inserted either into *ori*$_{\text{RK2}}$ or *trfA* (obtained from A. Stepanov) are incapable of conjugal transfer from *E. coli* to *P. aeruginosa* and *trfA* temperature-sensitive mutants are unstable at the non-permissive temperature in *P. aeruginosa*.

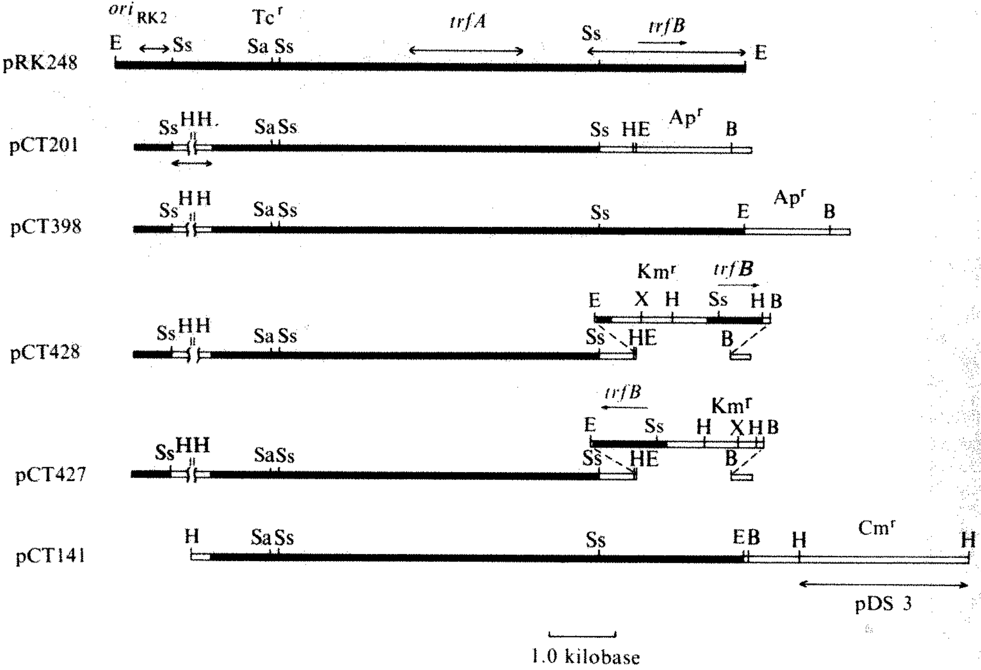

Fig. 2 Structure of mini RK2 replicons used to investigate the requirement for segments of the *trfB* region in *P. aeruginosa*. Sites for restriction endonuclease cleavage are labelled as follows: *Bam*HI, B; *Eco*RI, E; *Hin*dIII, H; *Sal*I, Sa; *Sst*II, Ss; *Xho*I, X. The segments of DNA derived from RK2 are shown as solid lines, non-RK2-derived DNA as open lines. The circular plasmids are represented as linear molecules with the break point defined by the *Eco*RI site for pRK248 and the other plasmids aligned with respect to the RK2 maintenance functions. pRK248 (9.6 kb) was produced indirectly from RK2 by partial digestion with restriction endonuclease *Hae*II and ligation[7] (Fig. 1). pCT201 (10.5 kb) was constructed by ligating two *Hin*dIII fragments, one containing Tc$^{\text{r}}$, *trfA* and ~150 base pairs of the *trfB* region and the other Ap$^{\text{r}}$ and *ori*$_{\text{RK2}}$. pCT398 (12.0 kb) was constructed by linking pCT201 to a hybrid plasmid carrying *trfB* and then carrying out *Sst*II partial digestion to delete the intervening DNA segment and join the partial *trfB* segment already present in pCT201 to the rest of the region containing *trfB*. pCT427 and pCT428 were constructed by replacing the Ap$^{\text{r}}$ *Bam*HI to *Eco*RI segment of pCT201 by a Km$^{\text{r}}$ *Bam*HI to *Eco*RI segment from hybrid plasmids containing segments of a mini RK2–Km$^{\text{r}}$ plasmid inserted into the *Cla*I site of pBR322. The two derivatives used have Km$^{\text{r}}$ and part of the *trfB* segment as shown inserted in opposite orientations relative to the *Bam*HI and *Eco*RI sites. pCT141 (11.8 kb) is a hybrid with a Tc$^{\text{r}}$ *Hin*dIII fragment carrying *trfA* and *trfB* inserted into a chloramphenicol resistance-conferring (Cm$^{\text{r}}$)Tc$^{\text{s}}$ derivative, pDS3, of pACYC184.

We therefore concluded that both ori_{RK2} and *trfA* are required in *P. aeruginosa* as well as part of the *trfB* region.

In *E. coli*, RK2 is known to code for several host lethal functions (*kil*) whose effects are normally suppressed in *trans* by other RK2 genes (*kor* functions)[12]. However, it seems unlikely that the phenomenon described here is solely due to the action of such a *kil* function that is active in *P. aeruginosa* but not in *E. coli*, because these might be expected to be suppressed by *trfB* in *trans* as well as in *cis*, which is not observed. Although we have demonstrated a *cis* requirement for part of the *trfB* region the results do not rule out the possibility that the *trfB* region also provides a necessary *trans*-acting product. The requirement for this extra DNA in *P. aeruginosa* may be at any or all of the stages of establishment (between DNA entry by transformation or conjugation and steady-state maintenance), replication or segregation. A defect in segregation, however, might be expected to lead only to unstable maintenance rather than to an absolute defect in maintenance[13–15]. Possible *cis* functions for the *trfB* region in establishment or replication in *P. aeruginosa* but not *E. coli* include: the provision of a replication origin used in *P. aeruginosa* (the mode of replication of RK2 in *P. aeruginosa* might require two functionally distinct replication origins, as in animal mitochondrial DNA replication[16]); the provision of a binding site for a protein that may subsequently migrate to a site of action elsewhere in the replicon—for example, at ori_{RK2}; the provision of a recombination site functional in *P. aeruginosa*, to allow the resolution of plasmid multimers, as these are thought to interfere with plasmid maintenance in other systems[17,18].

It is clear in the case of the mini RK2 derivatives used in the present study that whereas ori_{RK2} and *trfA* are sufficient to form a functional replicon in *E. coli*, they are not sufficient in *P. aeruginosa*. Linkage of the *trfB* region in *cis* to ori_{RK2} and *trfA* can overcome this defect, forming a replicon functional in *P. aeruginosa*. However, it is not known whether the *trfB* region is essential in any other bacterial host. One interpretation of our results is that RK2 may possess a basic replicon similar to that of other plasmids (ori_{RK2} and *trfA*) plus additional genetic information which enables this replicon to function in diverse Gram-negative bacterial species, for example, the *trfB* region in *P. aeruginosa*. We do not know whether other broad host range plasmids contain regions functionally analogous to the *trfB* region of RK2. If they do, analysis of the role of the *trfB* region in RK2 maintenance may shed light on the reason that certain groups of plasmids have a broader host range than many others.

C.A.S. is supported by a MRC project grant awarded to C.M.T. and this research was partly financed by this project grant.

Received 8 January; accepted 11 June 1982.

1. Datta, N. & Hedges, R. W. *J. gen. Microbiol.* **70,** 453–360 (1972).
2. Olsen, R. H. & Shipley, P. *J. Bact.* **113,** 772–780 (1973).
3. Beringer, J. E. *J. gen. Microbiol.* **84,** 188–198 (1974).
4. Cho, J. J., Panopoulos, N. J. & Schroth, M. N. *J. Bact.* **122,** 192–198 (1975).
5. Meyer, R. & Helinski, D. R. *Biochim. biophys. Acta* **478,** 109–113 (1977).
6. Figurski, D. & Helinski, D. R. *Proc. natn. Acad. Sci. U.S.A.* **76,** 1648–1652 (1979).
7. Thomas, C. M., Meyer, R. & Helinski, D. R. *J. Bact.* **141,** 213–222 (1980).
8. Thomas, C. M. *Plasmid* **5,** 277–291 (1981).
9. Barth, P. T. in *Plasmids of Medical, Environmental and Commercial Importance* (eds Timmis, K. N. & Pühler, A.) 399–410 (Elsevier, Amsterdam, 1979).
10. Haas, D. & Watson, J. *Soc. gen. Microbiol. Q.* **8,** 88–89 (1981).
11. Birnboim, H. C. & Doly, J. *Nucleic Acids Res.* **7,** 1513–1523 (1979).
12. Figurski, D. H., Pohlman, R. F., Bechhofer, D. H., Prince, A. S. & Kelton, C. A. *Proc. natn. Acad. Sci. U.S.A.* **79,** 1935–1939 (1982).
13. Meacock, P. A. & Cohen, S. N. *Cell* **20,** 529–542 (1980).
14. Miki, T., Easton, A. M. & Rownd, R. H. *J. Bact.* **141,** 87–99 (1980).
15. Nordstrom, K., Molin, S. & Aagaard-Hansen, A. *Plasmid* **4,** 215–227 (1980).
16. Robberson, D. L., Kasamatsu, H. & Vinograd, J. *Proc. natn. Acad. Sci. U.S.A.* **69,** 737–741 (1972).
17. Thomas, C. M. *Plasmid* **5,** 10–19 (1981).
18. Sternberg, N. & Austin, S. *Plasmid* **5,** 20–31 (1981).

Point mutations during generation of expression-linked extra copy of trypanosome surface glycoprotein gene

Allison C. Rice-Ficht, Kenneth K. Chen & John E. Donelson

Department of Biochemistry, University of Iowa, Iowa City,
Iowa 52242, USA

Trypanosomes exhibit antigenic variation by the sequential expression of a series of antigenically distinct variable surface glycoproteins (VSGs). On the basis of cDNA sequencing and/or terminal amino acid analyses of 10 *Trypanosoma brucei* VSGs[1–6], the approximately 500 amino acids of a nascent VSG can be divided into (N-terminus to C-terminus) a hydrophobic signal peptide (~20 amino acids), a variable region (~360 amino acids), a homology region (~100 amino acids) which can be used to classify the VSGs into one of two homology subsets and a hydrophobic tail (~20 amino acids) that is not present in the mature VSG[4,5]. Expression of some VSGs is accompanied by the production of an expression-linked extra copy (ELC) of a basic copy (BC) VSG gene[7–9]. We have now compared the sequence of a cDNA representing an ELC gene with its corresponding BC gene sequence. We find that the codons specifying the variable region contain nucleotide changes at 4% of the positions, while those specifying the homology region of the VSG are identical and the 17 codons specifying the C-terminal hydrophobic tail contain 11 nucleotide changes. The 3′-nontranslated region between the termination codon and the poly(A) (in the cDNA) is quite different in the two sequences. As the trypanosome serodeme contains only one BC gene coding for this VSG, point mutations seem to be actively introduced into specific areas of the coding sequence during the generation of the ELC gene. These point changes potentially increase the repertoire of immunologically distinct VSGs available to the trypanosome, similar to the way in which somatic mutations contribute to the diversity of the variable regions of immunoglobulins[10]. An alternative interpretation that cannot be completely eliminated is that a second BC gene is lost during the generation of the ELC.

One hundred or more different VSG genes exist in the trypanosome genome, and only one of them appears to be expressed at a given time (see refs 11–13 for reviews). The evidence suggests that this differential expression is controlled at the level of DNA transposition/recombination. On the basis of Southern hybridization data, these transpositions involve either the production of a transcriptionally active ELC from a transcriptionally silent BC gene[7,9,14] or a rearrangement of sequences flanking the 3′ end of a transcribed VSG gene[7,8,15]. For example, we have recently reported[4] the cDNA sequences of four VSGs from well-characterized *T. brucei* clones[9,15,16] that are serially related as follows:

$$\begin{tikzcd}[row sep=tiny] & & \text{ILTAT 1.3} \\ \text{ILTAT 1.1} \arrow[r] & \text{ILTAT 1.2} \arrow[ur] \arrow[dr] & \\ & & \text{ILTAT 1.4} \end{tikzcd}$$

Southern hybridization data described previously[9] indicated that a single BC gene for the ILTAT 1.1 (clone A in ref. 9) VSG is expressed via the ELC mechanism. In contrast, the VSGs expressed in ILTATs 1.2, 1.3 and 1.4 (clones B, C, D in ref. 9) are each specified by a pre-existing gene (one of two to four closely related genes) in which rearrangements on the 3′ side of the termination codon are detected in the different trypanosome clones[9,15,16].

The BC gene for the ILTAT 1.1 VSG occurs on a 2.8 kilobase (kb) *Eco*RI fragment in the genomic DNAs of all four ILTATs while its corresponding ELC occurs in the genomic DNA of only ILTAT 1.1 on an *Eco*RI fragment of ~20 kb (ref. 9, Fig. 3). Attempts to identify the ELC in a partial *Sau*3A

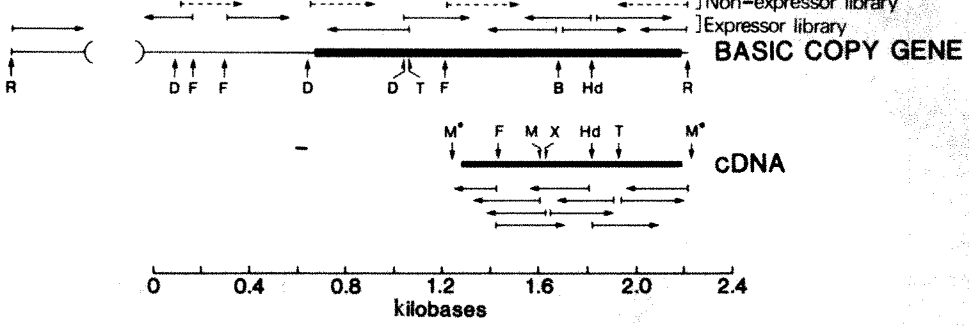

Fig. 1 The regions sequenced (indicated by horizontal arrows) in the BC gene and the cDNA for the VSG of ILTAT 1.1. The BC gene (thick line of upper diagram) is on a 2.8 kb *Eco*RI fragment that was initially identified in bacteriophage λ Charon 4A libraries of ILTAT 1.1 (expressor library) and ILTAT 1.3 (non-expressor library) genomic DNA. The 2.8 kb *Eco*RI fragment isolated from a phage clone of each library was subcloned into the *Eco*RI site of pBR322 for sequence determination using the Maxam–Gilbert technique[18]. The dashed arrows show the locations of sequences determined in the 2.8 kb fragment isolated from the ILTAT 1.3 (non-expressor) library and the solid arrows sequences determined in the same fragment isolated from the ILTAT 1.1 (expressor) library. Parentheses show a region of about 250 bp where the sequence was not obtained. The bottom diagram shows the restriction sites used to determine the sequence of the cDNA. In both diagrams, arrows pointing to the left and right are sequences obtained on the upper and lower strands respectively. Restriction sites labelled by the DNA polymerase I repair reaction[33] for Maxam and Gilbert sequencing were *Eco*RI (R), *Dde*I (D), *Hin*fI (F), *Taq*I (T), *Bam*HI (B), *Hin*dIII (Hd), *Xba*I (X), *Msp*I (M) and *Msp*I sites in pBR322 (M*).

library of ILTAT 1.1 DNA cloned in bacteriophage λ Charon 28 have not been successful (J. R. Young, P. A. O. Majiwa, P. T. Englund, R. O. Williams and J.E.D., unpublished) for unknown reasons that may be related to flanking repetitive sequences and/or the chromosomal location of the ELC[17]. However, the 2.8 kb *Eco*RI fragment containing the BC gene was found in bacteriophage libraries of all four ILTAT DNAs. This fragment was isolated from a phage clone of the ILTAT 1.1 DNA (expressor) library and an ILTAT 1.3 DNA (non-expressor) library and both fragments were subcloned into the *Eco*RI site of plasmid pBR322 for sequence determination via the Maxam and Gilbert technique[18]. Figure 1 shows the strategies used to determine these two genomic DNA sequences and the sequence of an ILTAT 1.1 VSG cDNA. More than 95% of the BC gene sequence was determined in the 2.8 kb fragment from the non-expressor library (dashed arrows) and about 90% in the fragment from the expressor library (solid arrows), so that taken together the complete sequence of the BC gene could be deduced. No differences were detected in the 2,100 nucleotides of each of the two genomic fragments that were determined separately, but many differences with the ILTAT 1.1 VSG cDNA were found.

Figure 2 compares the BC gene and cDNA sequences. Boxes indicate the non-homologous nucleotides. Also shown is the VSG amino acid sequence predicted by the BC gene sequence and those amino acids affected by the cDNA differences. The 696 nucleotides preceding the BC gene contain many termination codons in all three reading frames. A potential initiator methionine codon at position 697 is followed by an open translation reading frame of 471 codons which would code for a protein in the size range reported for different VSGs[12]; this suggests that the gene is not split by an intervening sequence. The first 15 codons specify a rather hydrophobic N-terminus which may be a signal peptide, although this cannot be confirmed on the basis of nucleotide sequence alone. The comparison with the cDNA sequence starts at nucleotide position 1,287 and in the next 450 nucleotides, there are 18 nucleotide differences (4% of the nucleotides) which affect 13 of the amino acids specified (9% of the amino acids). There is no obvious pattern to these changes with respect to either relative position or purine versus pyrimidine replacements. No differences occur in the next 324 nucleotides but then 11 changes occur in the last 46 nucleotides before the termination codon. The two sequences are very different in the 3′-non-translated region.

To ensure that these nucleotide differences were not the result of copying mistakes by enzymes used *in vitro* to construct the cDNA, portions of the sequences of two additional cDNAs containing the ILTAT 1.1 VSG coding sequence were determined (not shown). The same point changes were also present in the other two cDNAs, reducing substantially the possibility that they were the result of copying or cloning mistakes. Interestingly, one of the cDNAs did contain only four adenosines at positions 1,689–1,693 (and four thymidines in the complementary strand) in comparison with the five adenosines at this location in the other two cDNAs and the two genomic fragments. Since other cloned cDNAs with sequence errors have been reported previously[19,20], it seems likely that this single base pair deletion is the result of an enzymatic mistake during the synthesis of that cloned cDNA molecule *in vitro* or during its replication after transformation into *Escherichia coli*. Another less likely possibility is the occurrence of incorrect VSG mRNA transcription *in vivo*. At the very least, this observation demonstrates the hazard of relying on a single cloned cDNA molecule to determine a coding sequence.

Further confirmation that the point changes occur during the generation of the ELC *in vivo* was derived from previous Southern hybridization data which predicted that the ILTAT 1.1 BC gene contains a *Bam*HI site while the ELC gene does not[9]. And indeed, the sequence of the BC gene has a *Bam*HI site at positions 1,697–1,702 while the cDNA sequence does not because of a single nucleotide difference at position 1,700. Similarly, Southern hybridizations demonstrate that if there are two copies of the BC gene because the parasite is diploid[21], then both copies contain a *Bam*HI site while the ELC does not. Thus it appears that these nucleotide changes occur during the duplication and translocation events that generate the ELC from the pre-existing BC.

Figure 3 shows the locations of the nucleotide changes with respect to the different VSG regions specified. Eighteen changes occur in the variable region, none in the homology region, eleven in the hydrophobic tail and many in the 3′-non-translated region which possesses no more homology than would be expected of two random 80% (dA + T) sequences (49 differences in 84 nucleotides = 58%).

An alternative explanation of the results is the loss of a second BC gene concomitant with the appearance of the ELC but this seems unlikely for at least two reasons. Unfortunately this possibility cannot be formally eliminated, however, because ILTAT 1.1 is the first clone in the ILTAT series to be maintained (R. O. Williams, personal communication) so that genomic DNA from a trypanosome clone preceding ILTAT 1.1 is unavailable. However, when ILTAT 1.1 cDNA is used as a radioactive probe in Southern hybridizations with genomic DNA from *T. brucei* clones unrelated to the ILTAT series, only one BC gene is detected (not shown). In addition there is no evidence that the appearance of ELCs of other VSG genes being studied by other research groups is accompanied by the loss of a BC gene[5–8,14]. Thus if a second BC gene existed, the simultaneous loss of one BC gene and appearance of an ELC would represent a third type of DNA rearrangement associated with VSG expression. Furthermore, a hypothetical second BC gene still would not account for the confinement of random

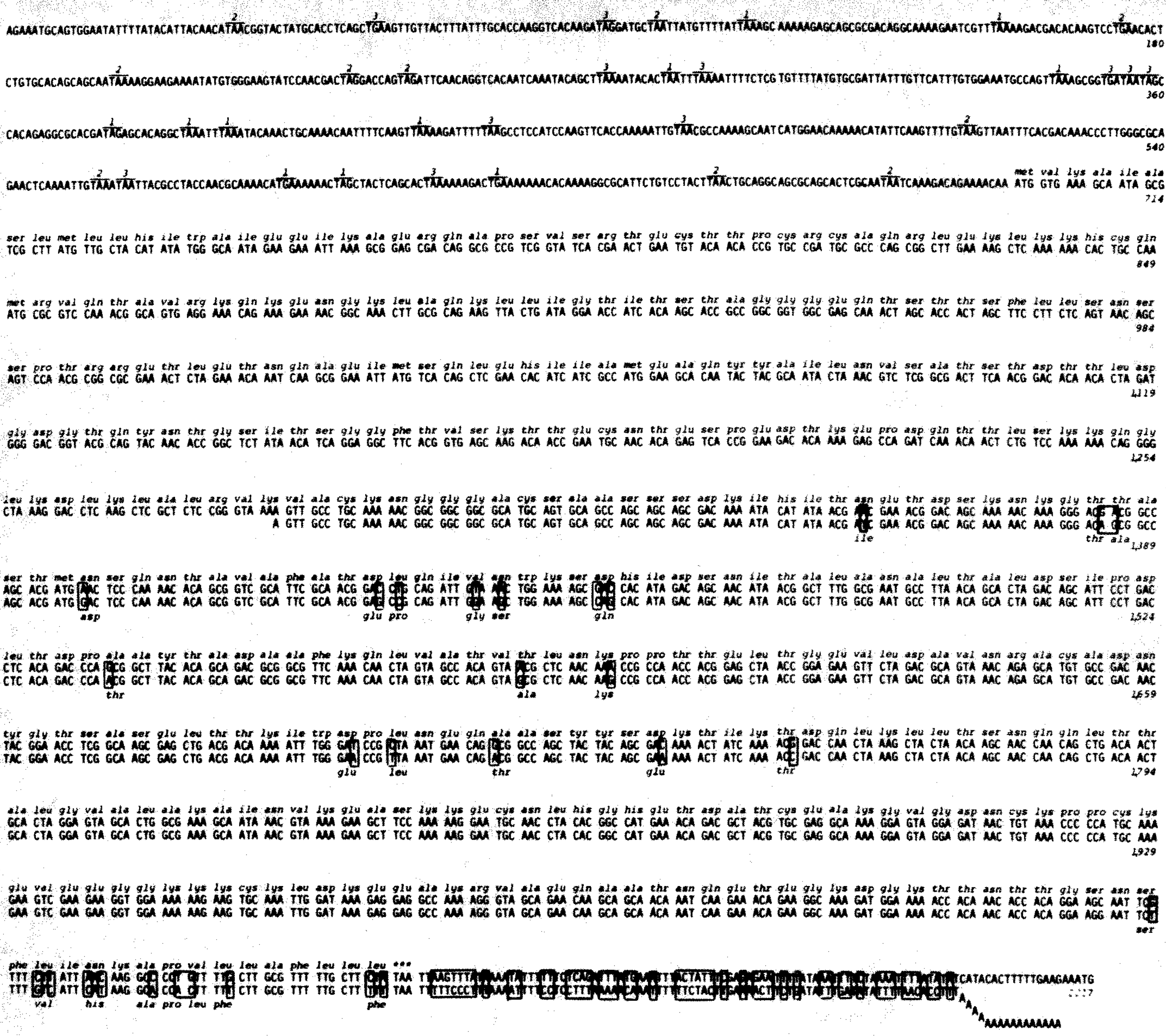

Fig. 2 Comparison of the coding strands of the BC gene (upper sequence) and the cDNA (lower sequence beginning at nucleotide 1,287) and the corresponding amino acid sequences predicted by the two nucleotide sequences. Boxes indicate nucleotides that differ in the two sequences. The amino acids below the cDNA are predicted from the cDNA sequence at locations where the cDNA and BC gene sequences differ. At all other locations the predicted amino acids are the same. ***, The termination codon at the end of the basic copy gene. The numbers above the first 696 nucleotides before the start of the BC gene indicate in which of the three reading frames the termination codons occur. The BC gene itself is in reading frame 1.

point changes to only the sequence coding for the variable and hydrophobic tail regions (see next paragraph).

Therefore the simplest interpretation of the data is that the generation of the ELC involves (1) a homologous recombinational event at a site just before or including the region coding for the hydrophobic tail and (2) a DNA polymerase system that replicates with low fidelity during the duplication event. Unexplained is the absence of point mutations in the homology region. If nucleotide changes were introduced with the same frequency here as in the variable region (4%) one would expect about 13 differences instead of none. Thus it seems unlikely that this region has escaped mutation just by chance although this possibility cannot be eliminated on the basis of this one example. Other possibilities are that a localized mutagenesis mechanism exists which does not act on this area or that mutations in this area are lethal because they result in a VSG that is non-functional. The latter possibility also seems unlikely because we have shown previously[4] that, although the homology region is highly conserved in VSG subsets, many amino acid changes and even deletions are tolerated. Although localized mutagenesis seems the most feasible explanation for this one example, sequence comparisons of other BC genes with their ELCs or cDNAs are needed to confirm its occurrence.

Although the mechanism(s) that generate(s) these mutations may be obscure, their biological significance is not. In influenza virus, a difference in less than 5% of the amino acids of the surface antigen is sufficient to change the antigenic specificity[22]. Therefore the trypanosome mutations could potentially increase the repertoire of immunologically distinct VSGs that are coded for by a limited number of different genes. They may in fact generate virtually an infinite number of potential VSGs for the trypanosome in the same way that somatic mutations are responsible, in part, for the immense diversity of antibodies generated by lymphocytes in the immune response (for a recent review, see ref. 10). These somatic mutations in the V segments of antibody genes occur in both the hypervariable regions and the framework residues and sometimes occur during the isotype switch from one constant region gene to another[23], so they may be introduced by a different and less localized mutation than the changes described here in the generation of the ELC. The

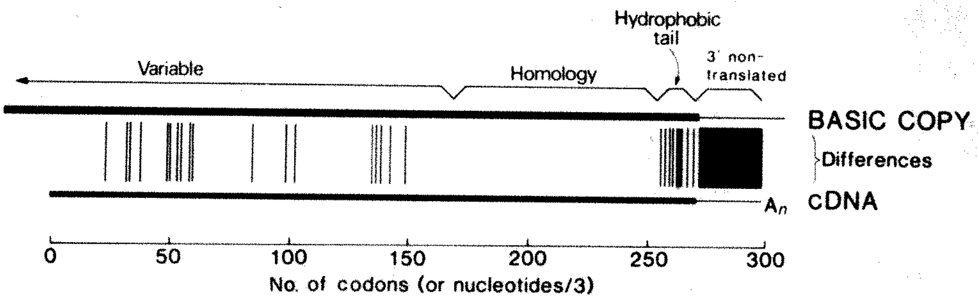

Fig. 3 Schematic comparison of the sequences of the BC gene and cDNA showing the 3'-non-translated region and poly(A)$_n$, the locations of coding portions that specify the various regions in the VSG (variable, homology and C-terminal hydrophobic tail regions) and the locations of nucleotide differences between the basic copy gene and the cDNA (vertical lines and solid rectangle).

two mutational processes are similar, however, in that there is no simple preference for purines or pyrimidines and some mutations are silent. Both processes are clearly important for generating the diversity of amino acid sequences found in the two types of protein.

Van der Ploeg *et al.*[17] have recently reported from Southern hybridization data (see below) that the DNA segment duplicated and translocated to generate the ELC of another VSG gene, VSG 117, begins 1–2 kb before the start of the BC gene. If the ILTAT 1.1 system is similar, then the 696 nucleotides reported here that precede the initiator methionine codon probably do not contain the 5'-recombination site. Indeed, by inspection or computer searches, we have been unable to identify a sequence that resembles switch sites of immunoglobulin genes or the yeast mating-type locus[24–27], sequences common to other eukaryotic transposable elements[28,29] or bacteriophage 'Chi' site sequences[30]. The sequence of another 300 nucleotides upstream has been determined (from the left-hand *Eco*RI site shown in Fig. 1) but is not shown in Fig. 2 because it is not contiguous with the sequence presented. This 300 nucleotide sequence, which is within 1–2 kb in front of the BC gene, also does not contain an obvious potential recombination site.

Bernards *et al.*[31] have reported a partial sequence comparison of the BC gene of VSG 117 and its corresponding cDNA which includes the hydrophobic tail and 3'-non-translated regions, but not the homology region or variable region. The VSG 117 system, like ILTAT 1.1, exhibits nucleotide changes in the hydrophobic tail region. Some of these changes, however, are nucleotide additions in the cDNA relative to the BC gene, a feature not present in the ILTAT 1.1 system. Another difference is that the VSG 117 system exhibits substantially more homology in the 3'-non-translated regions of the cDNA and BC gene than does the ILTAT 1.1 system. The significance, if any, of these differences is not known. Recently, Frasch *et al.*[32] reported Southern hybridization studies that suggested the occurrence of 'local hypermutagenesis' in subsets of closely related (cross-hybridizing) VSG genes which may correspond to the localized mutagenesis observed in the variable region of the ILTAT 1.1 BC gene (Fig. 3). Thus the occurrence of mutations during the generation of ELCs may be part of a general property of the entire VSG gene family, further demonstrating the intricate mechanisms that evolved in trypanosomes, permitting them to evade their hosts' immune defences.

This research was supported by USPHS grant AI16950. A.C.R.-F. is supported by USPHS postdoctoral grant AM07018. We thank John Young, Phelix Majiwa and Richard Williams in whose laboratory J.E.D. spent a sabbatical leave and where the ILTAT 1.1 cDNA clones and genomic library were constructed and identified.

Received 18 January; accepted 10 June 1982.

1. Bridgen, P. J., Cross, G. A. M. & Bridgen, J. *Nature* **263,** 613–614 (1976).
2. Johnson, J. G. & Cross, G. A. M. *Biochem. J.* **178,** 689–697 (1979).
3. Holder, A. A. & Cross, G. A. M. *Molec. biochem. Parasit.* **2,** 135–150 (1981).
4. Rice-Ficht, A. C., Chen, K. K. & Donelson, J. E. *Nature* **294,** 53–57 (1981).
5. Boothroyd, J. C., Cross, G. A. M., Hoeijmakers, J. H. J. & Borst, P. *Nature* **288,** 624–626 (1980).
6. Matthyssens, G., Michiels, F., Hamers, R., Pays, E. & Steinert, M. *Nature* **293,** 230–233 (1981).
7. Hoeijmakers, J. H. J., Frasch, A. C. C., Bernards, A., Borst, P. & Cross, G. A. M. *Nature* **284,** 78–80 (1980).
8. Pays, E., Van Meirvenne, N., LeRay, D. & Steinert, M. *Proc. natn. Acad. Sci. U.S.A.* **78,** 2673–2677 (1981).
9. Majiwa, P. A. O., Young, J. R., Englund, P. T., Shapiro, S. Z. & Williams, R. O. *Nature* **297,** 514–516 (1982).
10. Baltimore, D. *Cell* **26,** 295–296 (1981).
11. Vickerman, K. *Nature* **273,** 613–617 (1978).
12. Cross, G. A. M. *Proc. R. Soc.* **B202,** 55–72 (1978).
13. Marcu, K. B. & Williams, R. O. *Genetic Engineering* Vol. 3 (eds Setlow, J. K. & Hollaender, A.) 129–155 (Plenum, New York, 1981).
14. Pays, E., Lheureux, M. & Steinert, M. *Nature* **292,** 265–267 (1981).
15. Williams, R. O., Young, J. R. & Majiwa, P. A. O. *Nature* **282,** 847–849 (1979).
16. Williams, R. O., Young, J. R., Majiwa, P. A. O., Doyle, J. J. & Shapiro, S. Z. *Cold Spring Harb. Symp. quant. Biol.* **45,** 945–949 (1980).
17. van der Ploeg, L. H. T., Bernards, A., Rijsewijk, F. A. M. & Borst, P. *Nucleic Acids Res.* **10,** 593–609 (1982).
18. Maxam, A. M. & Gilbert, W. *Proc. natn. Acad. Sci. U.S.A.* **74,** 560–564 (1977).
19. Fagan, J. B., Pastan, I. & deCrombrugghe, B. *Nucleic Acids Res.* **8,** 3055–3064 (1980).
20. Gopinathen, K. P., Weymouth, L. A., Kunkel, T. A. & Loeb, L. *Nature* **278,** 857–859 (1979).
21. Tait, A. *Nature* **287,** 536–538 (1980).
22. Wiley, D. C., Wilson, I. A. & Skehel, J. J. *Nature* **289,** 373–378 (1981).
23. Pech, M., Höchtl, J., Schnell, H. & Zachau, H. G. *Nature* **291,** 668–670 (1981).
24. Astell, C. R. *et al. Cell* **27,** 15–23 (1981).
25. Klar, A. J. S., McIndoo, J., Strathern, J. N. & Hicks, J. B. *Cell* **22,** 291–298 (1980).
26. Tonegawa, S. *et al. Cold Spring Harb. Symp. quant. Biol.* **45,** 839–858 (1980).
27. Rabbitts, T. H. *et al. Cold Spring Harb. Symp. quant. Biol.* **45,** 867–878 (1981).
28. Rubin, G. M. *et al. Cold Spring Harb. Symp. quant. Biol.* **45,** 619–628 (1980).
29. Skalka, A., Ju, G., Hishinuma, F., DeBona, P. J. & Astrin, S. *Cold Spring Harb. Symp. quant. Biol.* **45,** 739–746 (1980).
30. Kenter, A. L. & Birshtein, B. K. *Nature* **293,** 402–404 (1981).
31. Bernards, A. *et al. Cell* **27,** 497–505 (1981).
32. Frasch, A. C. C., Borst, P. & Van den Burg, J. *Gene* **17,** 197–211.
33. Hartley, J. L. & Donelson, J. E. *Nature* **286,** 860–865 (1980).

Amplification of endogenous *myc*-related DNA sequences in a human myeloid leukaemia cell line

Steven Collins

Veterans Administration Hospital, 4435 Beacon Avenue South,
Seattle, Washington 98108, USA

Mark Groudine

Fred Hutchinson Cancer Research Center, 1124 Columbia Street,
Seattle, Washington 98104; Department of Radiation Oncology,
University of Washington Hospital, Seattle, Washington 98195,
USA

Malignant transformation of cells by acute transforming RNA tumour viruses is mediated by the expression of certain specific proviral DNA sequences ('oncogenes'). These sequences have been well characterized and, in many cases, molecularly cloned[1–8]. These viral oncogenes are related to similar genes found in normal uninfected cells[9,10]. Moreover, these particular sequences are highly conserved in evolution[4,11], suggesting that these genes have an important, albeit unknown, role in normal cell function. It has been suggested that an increased dosage of products of such endogenous oncogenes may be responsible for malignant transformation[10,12,13]. For example, increased expression of the endogenous chick c-*myc* oncogene has been observed in avian leukosis virus-induced transformation of chick bursal lymphocytes[12]. Here we demonstrate that sequences in normal human DNA homologous to the avian *myc* oncogene are present in multiple copies in the chromosomal DNA of the human leukaemia cell line HL-60. Other transformation-specific genes derived from the Abelson leukaemia virus[4] and feline sarcoma virus[6] are not amplified in HL-60. This *myc*-related gene amplification is not present in other cultured human myeloid leukaemia cells, including K-562[14] and KG-1[15].

The HL-60 cell line is a culture of malignant promyelocytes derived from the peripheral blood leukocytes of a patient with

0028–0836/82/320679—03$01.00

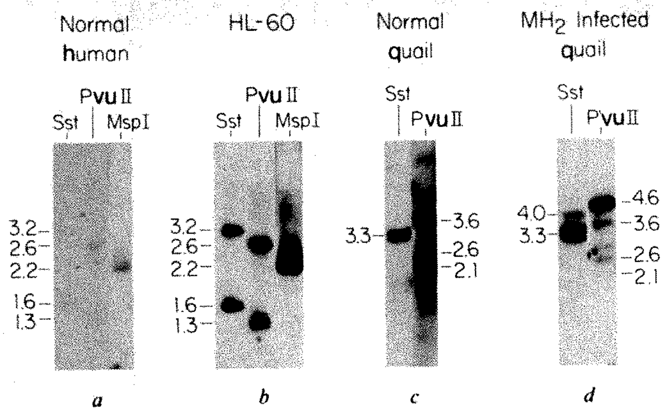

Fig. 1 *myc*-related sequences in DNA of HL-60, normal human and avian cells. Cells analysed included: *a*, normal human cells obtained by PHA stimulation of peripheral blood mononuclear cells from a normal human donor; *b*, HL-60 cells, passage 40, cultured as previously described[16]; *c*, normal quail embryo fibroblasts; *d* a cloned subline of quail embryo fibroblasts non-productively transformed with the MH$_2$ virus (a member of the MC-29 family of avian retroviruses) and obtained from M. Linial. DNA from these cells were restricted with the designated enzymes, subjected to agarose gel electrophoresis (1.2%) (10 μg of DNA per lane) followed by Southern blot hybridization[26] using a ^{32}P-labelled probe prepared by nick translation[27] of the c-*myc* probe. c-*myc* is a 3.3-kb *Sst* fragment obtained from a bacteriophage clone of c-*myc* that was isolated from a library of random chicken DNA fragments. This fragment encompasses almost the entire c-*myc* locus as detailed elsewhere[28]. The c-*myc Sst* fragment was subcloned in a derivative of pBr322 containing a single *Sst* site. Hybridizations were carried out in 50% formamide, 10% dextran sulphate 3 × SSC at 42 °C. Following hybridization, the filters were washed in 0.1% SDS, 0.1 × SSC at 50 °C and then exposed to Kodak XAR-5 film with intensifying screens. All blots were exposed for 72 h. Molecular weights of fragments are given in kilobases.

acute promyelocytic leukaemia[16]. DNA samples extracted from cells of this line and from phytohaemagglutinin (PHA) stimulated peripheral blood lymphocytes from a normal donor were digested with restriction endonucleases, separated by electrophoresis on agarose gels and transferred to nitrocellulose. The resultant blots were hybridized to a ^{32}P-labelled DNA probe specific for the chick c-*myc* gene, the cellular homologue of the transforming sequences of acute transforming retroviruses within the MC-29 family[17,18]. This c-*myc* probe gave faint but distinct bands when hybridized to various endonuclease digests of normal human DNA (Fig. 1*a*), indicating homology between certain sequences within the human genome and the chick c-*myc* probe, as reported by others[19]. From the same blot, bands of identical size were noted in endonuclease digests of HL-60 DNA, but the intensity of hybridization was much greater (Fig. 1*b*). The total amount of normal human and HL-60 DNA loaded in each lane was the same for all DNA preparations (10 μg). Moreover, when the same normal and HL-60 samples were hybridized with other ^{32}P-labelled probes, bands of similar intensity were noted in both normal and HL-60 DNA (Fig. 2). This indicates that the enhanced hydridization of the c-*myc* probe to HL-60 DNA is not a result of differences in the amount of DNA loaded on the gels.

The intensity of hybridization of the c-*myc* probe to HL-60 DNA is comparable with that noted in DNA extracted from normal avian cells and from avian cells infected with the acute transforming MH$_2$ virus (Fig. 1*b*–*d*). However, the similarity in restriction patterns of HL-60 and normal human DNA using the c-*myc* probe (Fig. 1*a*, *b*) makes it unlikely that the intense hybridization seen with HL-60 DNA is a result of inadvertent infection of HL-60 cells with a retrovirus such as MH$_2$ containing *myc* sequences or of contamination of HL-60 DNA with avian DNA.

The increased hybridization of the c-*myc* probe to HL-60 DNA compared with normal human DNA could be the result of either multiple copies (amplification) in HL-60 cells of the endogenous human sequences homologous to c-*myc* or to increased homology of these endogenous HL-60 c-*myc*-related sequences to the chick c-*myc* probe. The similarity in restriction enzyme patterns of HL-60 and normal human DNA hybridized to c-*myc* (Fig. 1) indicates that HL-60 and normal human *myc*-related DNA sequences are similar. Therefore, this increased HL-60 hybridization to c-*myc* most probably results from amplification in HL-60 DNA of c-*myc*-related sequences. To confirm this, we 'dot-blotted' serial dilutions of HL-60, normal human and avian DNA onto nitrocellulose as previously described[20], hybridized the filter with ^{32}P-labelled c-*myc* probe, and then estimated the melting point of the resultant hybrids by washing the filters at progressively higher temperatures (Fig. 3). If the enhanced hybridization of HL-60 DNA to the c-*myc* probe results from increased homology of *myc*-related HL-60 sequences to this probe, the melting points of avian and HL-60 c-*myc* hybrids should be similar. Alternatively, if endogenous *myc*-related genes are amplified in HL-60, then the melting points of HL-60 and normal human DNA-*myc* hybrids should be similar and should be lower than that seen with avian DNA. As demonstrated in Fig. 3, the intensity of hybridization of the *myc* probe to equal quantities of HL-60 and avian DNA is similar, but both HL-60 and normal human DNA c-*myc* hybrids are denatured at lower temperatures than avian DNA c-*myc* hybrids. The relative denaturation of both HL-60 and normal human DNA hybrids at a given temperature appears similar (Fig. 3). These results indicate that the enhanced hybridization of the c-*myc* probe to HL-60 DNA is a result of HL-60 amplification of the endogenous human *myc*-related sequences rather than to increased homology of these sequences to the c-*myc* probe. Moreover, one can estimate by comparing the intensity of hybridization of the c-*myc* probe to serial dilutions of HL-60 and normal human DNA (Fig. 3) that c-*myc* related sequences are amplified some 8–16-fold in HL-60 DNA compared with normal human DNA.

Identical restriction fragments are noted when the c-*myc* probe is hybridized to normal human and HL-60 DNA digested

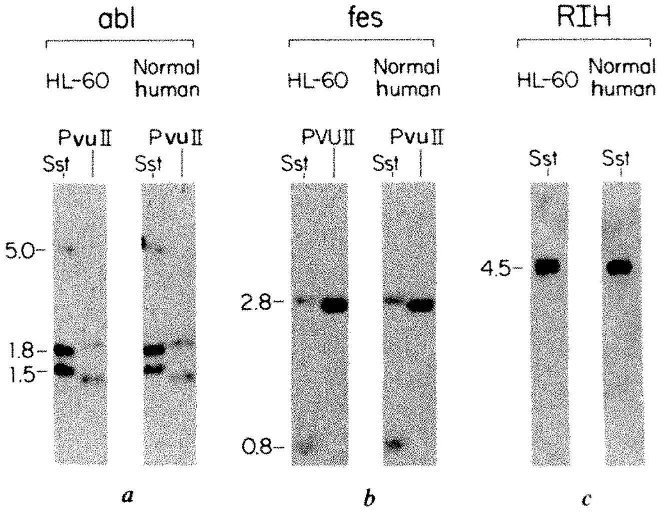

Fig. 2 Absence of amplification of non-*myc* sequences in HL-60 DNA. DNA samples from HL-60 cells and from PHA-stimulated normal human lymphocytes were digested with the designated enzymes, electrophoresed in 1.2% agarose (10 μg DNA per lane), and Southern blot hybridized to the indicated ^{32}P-labelled probes in conditions described in Fig. 1 legend. The *abl* probe contains the transforming sequences of Abelson leukaemia virus[4]. The *fes* probe contains the transforming sequences of the feline sarcoma virus[6]. The RIH probe is a 0.5-kb clone containing flanking sequences between the human γ and ∂ globin genes[29].

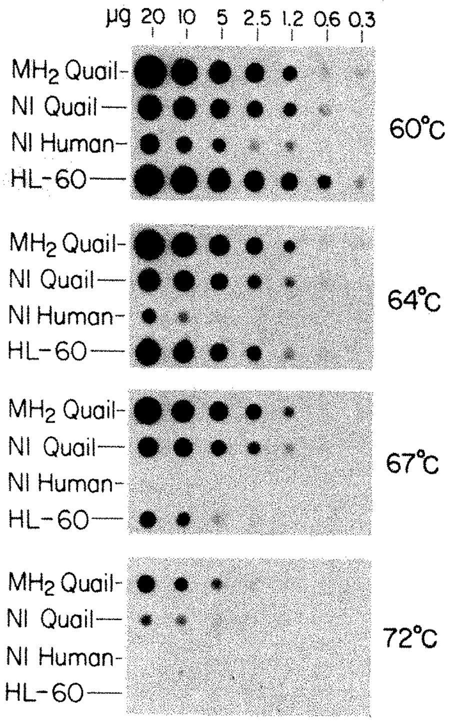

Fig. 3 Melting points of HL-60, normal human and avian DNA c-*myc* hybrids utilizing 'dot-blot' analysis. DNA samples obtained from HL-60 cells, PHA-stimulated human lymphocytes, quail embryo fibroblasts and quail embryo fibroblasts non-productively transformed with the MH_2 virus were treated with RNase A (Sigma) at 50 µg ml^{-1} for 20 min at 37 °C and then serially two fold diluted followed by denaturation in 1 M ammonium acetate and 0.2 NaOH as previously described[20]. The indicated quantities of DNA were then applied to a nitrocellulose filter, previously soaked in 1 M ammonium acetate, using a 'Hybri-Dot' manifold (Bethesda Research Laboratories). The filter was then hybridized to the c-*myc* probe, in conditions described in Fig. 1 legend. Following hybridization, the filter was washed in 0.1% SDS, 0.1 × SSC at 50 °C for 20 min, and then exposed for 24 h to XAR-5 film (Kodak) at −70 °C. Following this initial exposure, the filter on consecutive days was washed for 20 min in 0.1% SDS, 0.1 × SSC at progressively higher temperatures as indicated. After each wash, the filter was reexposed for 24 h to XAR-5 film.

with other enzymes, including *Kpn*, *Eco*RI and *Hin*dIII, although in every case the intensity of hybridization to the HL-60 DNA is much greater (blots not shown). As some of these enzymes presumably cut in sequences flanking, as well as within the human *myc* gene, the identical restriction patterns suggest that the *myc*-containing chromosomal unit amplified in HL-60 may be relatively large. This has been previously noted with amplified CAD[21] and DHFR[22] genes, where the amplified unit seems to be ~500–1,000 kilobases (kb). Thus, as in the examples of CAD and DHFR, it may be difficult to determine by restriction enzyme analysis of HL-60 cellular DNA whether *myc* amplification in HL-60 is tandem or non-tandem.

The *myc* amplification in HL-60 is not a result of hyperdiploidy of the *myc*-containing chromosome because this cell line is hypodiploid (modal chromosome number of 45) and exhibits no hyperdiploidy of individual chromosomes[23]. However, we have noted that some HL-60 metaphases contain double minutes and we are now attempting to determine whether these chromosome structures contain amplified *myc*-related sequences.

Hybridization of HL-60 DNA to other 'oncogene' probes derived from the Abelson leukaemia virus[4] and the feline sarcoma virus[6] gives a pattern and intensity of hybridization similar to those of normal human DNA (Fig. 2*a*, *b*). Moreover, the c-*myc* probe, when hybridized to endonuclease digests of DNA from the human myeloid leukaemia cell lines K-562[14] and KG-1[15] as well as to digests from several fresh leukaemia cells, exhibits a pattern and intensity of hybridization similar to those of normal human DNA (blots not shown). This preliminary screen suggests that amplification of endogenous human c-*myc*-related sequences may be an unusual phenomenon in both cultured and fresh human leukaemia cells.

Current speculations on the origin of cancer suggest that malignant transformation may result from the enhanced expression of certain normal cellular genes[10,12,13]. Indeed, in the case of avian retrovirus-induced bursal lymphomas, increased amounts of c-*myc* RNA as well as amplification of *myc*-related chromosomal DNA sequences have been reported[12,24]. While the levels of *myc*-related RNA in HL-60 cells and other normal or leukaemic human cells have not been rigorously defined, our own unpublished observations (in collaboration with Paul Neiman) and the results of others[30] have revealed relatively high levels of *myc*-related RNA sequences in HL-60. In addition, high levels of *myc*-related RNA have been observed in other leukaemic cells in which the *myc* gene is not amplified (S. Astrin and P. Neiman, personal communications). Thus, these observations may indicate that increased expression of this gene may follow at least two pathways, one involving amplification of c-*myc* DNA (under no obvious selective pressure), and another resulting from increased transcription or stabilization of transcription products from one copy of this gene. It is also possible that the amplification of c-*myc* observed in HL-60 is a normal developmental process in granulocytic differentiation, and that HL-60 represents a specific maturational compartment of these cells, arrested in this state[25].

We thank Mary Peretz and Carol Paschl for help in isolating the c-*myc* clone from the chick library, and Paul Neiman and Hal Weintraub for many helpful discussions. This work was supported by the Veterans Administration and by grants from the NIH and NSF. S.C. is a Special Fellow of the Leukaemia Society of America. M.G. is a Scholar of the Leukaemia Society of America.

Received 9 February; accepted 3 June 1982.

1. Czermlofsky, A. P. *et al.*, *Nature* **287**, 198–203 (1980).
2. Lautenberger, J. A., Schulz, R. A., Garon, C. F., Tsichlio, P. N. & Papas, T. S. *Proc. natn. Acad. Sci. U.S.A.* **78**, 1518–1522 (1981).
3. Vennstrom, B., Moscovici, C., Goodman, H. M. & Bishop, J. M. *J. Virol.* **39**, 625–631 (1981).
4. Goff, S. P., Gilboa, E., Witte, O. N. & Baltimore, D. *Cell* **22**, 777–785 (1980).
5. Vande Woude, G. F. *et al. Proc. natn. Acad. Sci. U.S.A.* **76**, 4464–4468 (1979).
6. Sherr, C. J., Fedele, L. A., Oskarsson, M., Maizel, J. & Vande Woude, G. F. *J. Virol.* **34**, 200–212 (1980).
7. Gelmann, E. P., Wong-Staal, F., Kramer, R. & Gallo, R. C. *Proc. natn. Acad. Sci. U.S.A.* **78**, 3373–3377 (1981).
8. Robbins, K. C., Devare, S. G. & Aaronson, S. A. *Proc. natn. Acad. Sci. U.S.A.* **78**, 2918–2922 (1981).
9. Stehelin, D., Varmus, H. E., Bishop, J. M. & Vogt, P. K. *Nature* **260**, 170–173 (1976).
10. Bishop, J. M. *Cell* **23**, 5–6 (1981).
11. Wong-Staal, F., Dalla-Favera, R., Franchini, G., Gelmann, E. & Gallo, R. C. *Science* **213**, 226–228 (1981).
12. Hayward, W. S., Neel, B. G. & Astrin, S. M. *Nature* **290**, 475–479 (1981).
13. Klein, G. *Nature* **294**, 313–318 (1981).
14. Lozzio, C. B. & Lozzio, B. B. *Blood* **45**, 321–334 (1975).
15. Koeffler, H. P. & Golde, D. W. *Science* **200**, 1153–1154 (1978).
16. Collins, S. J., Gallo, R. C. & Gallagher, R. E. *Nature* **270**, 347–349 (1977).
17. Graf, T. & Beug, H. *Biochim. Biophys. Acta* **516**, 269–299 (1978).
18. Roussel, M. *et al. Nature* **281**, 452–455 (1979).
19. Eva, A. *et al. Nature* **295**, 116–119 (1982).
20. Kafatos, F. C., Jones, C. W. & Efstratiadis, A. *Nucleic Acids Res.* **7**, 1541–1552 (1979).
21. de Saint Vincent, B. *et al. Cell* **27**, 267–277 (1981).
22. Nunberg, J. H., Kaufman, R. J., Chang, A. C. Y., Cohen, S. N. & Schimke, R. T. *Cell* **19**, 355–364 (1980).
23. Gallagher, R. *et al. Blood* **54**, 713–733 (1979).
24. Noori-Daloii, M. R., Swift, R. A., Kung, H. J., Crittenden, L. B. & Witter, R. L. *Nature* **294**, 574–576 (1981).
25. Collins, S. J., Ruscetti, F. W., Gallagher, R. E. & Gallo, R. C. *Proc. natn. Acad. Sci. U.S.A.* **75**, 2458–2462 (1978).
26. Southern, E. M. *J. molec. Biol.* **98**, 503–517 (1975).
27. Rigby, P. W., Dieckmann, M., Rhodes, C. & Berg, P. *J. molec. Biol.* **113**, 237–258 (1977).
28. Robins, T., Bister, K., Garon, C., Papas, T. & Duesberg, P. *J. Virol.* **41**, 635–642 (1982).
29. Fritsch, E. F., Lawn, R. M. & Maniatis, T. *Nature* **279**, 598–603 (1979).
30. Westin, E. H. *et al. Proc. natn. Acad. Sci. U.S.A.* **79**, 2490–2494 (1982).

Sequences on the human Y chromosome homologous to the autosomal gene for argininosuccinate synthetase

S. P. Daiger*, R. S. Wildin & T.-S. Su

Department of Pediatrics, Baylor College of Medicine, Houston, Texas 77030, USA

We have used a probe (pAS-1) to the human urea cycle enzyme argininosuccinate synthetase (AS) to detect individual variation in restriction enzyme digests of human DNA from lymphocytes, fibroblasts and transformed cell lines (including HeLa). pAS-1 is a 1.55 kilobase (kb) sequence of cDNA from poly(A)$^+$ RNA cloned in pBR322; it represents more than 90% of the AS message[1]. At least 15 genomic fragments are detected with pAS-1 in DNA digested with restriction enzymes recognizing 6-base sequences[2]. This multiplicity of fragments is explained in part by the observation that AS-like sequences are found on more than seven human chromosomes[3]. We report here population data and gene dosage experiments demonstrating an AS-like sequence on the human Y chromosome and confirming an AS-like sequence on the human X chromosome.

The pAS-1 probe was isolated by plasmid-selected mRNA translation and immunoprecipitation from a bank of cloned human cDNA. The cDNA recombinants were prepared in pBR322 plasmid using sucrose gradient-enriched mRNA from a canavine-resistant colony of the human cell line RPMI 2650. The translation product of mRNA selected by pAS-1 has the immunological properties, molecular weight and substrate specificity of human AS[1].

Human genomic DNA produces more than 15 AS-like fragments when digested with restriction endonucleases recognizing 6-base sequences and more than 25 fragments when digested with 4-base enzymes (Figs 1, 2; Table 1). Restriction analysis with pAS-1 of human–hamster cell lines containing one or two human chromosomes demonstrates that AS-like sequences are found on several human chromosomes including chromosomes 6, 9 and X (ref. 3). (The human AS structural gene is tentatively assigned [4,5] to 9q34.) The multiplicity of separable DNA fragments and the wide chromosomal dispersion of AS-like sequences makes pAS-1 an excellent probe for restriction site variation in human populations.

In a population survey of restriction site variation, we isolated DNA from more than 50 individuals, digested the DNAs with a panel of six restriction enzymes and probed with pAS-1 following agarose gel electrophoresis and Southern transfer (see Fig. 1 legend for details). DNA was from peripheral blood lymphocytes ($n = 37$), fibroblasts (12), lymphoblasts (4) and transformed cell lines (RPMI 2650 and HeLa). Considerable population variation was detected but this was independent of the type of cell from which the DNA was isolated. Four enzymes, *Bam*HI, *Hin*dII, *Hin*dIII and *Msp*I, revealed independent, high-frequency polymorphic variation in restriction fragments from more than one human autosome. This variation is described elsewhere (S.P.D., R.S.W., N. Hoffman and T-S.S., in preparation).

A more striking type of variation is apparent in digests with *Bam*HI, *Eco*RI, *Kpn*I and *Msp*I: one or two fragments are always present in males and always absent from females (Table 1, Fig. 1). *Bam*HI, *Eco*RI and *Kpn*I (6-base enzymes) produce one male-specific fragment and *Msp*I (a 4-base enzyme) produces two such fragments. We have observed male-only transmission of these fragments in several three-generation families. Male-specific fragments were also observed in chimpanzees, comparing two male and two female DNAs hybridized with pAS-1.

The most probable explanation for this sexual dimorphism is the presence of an AS-like sequence on the Y chromosome. To confirm this possibility we compared restriction digests of DNA from normal males and from an adult male with an XYY karyotype. (Peripheral blood lymphocytes were used for both DNA and karyotype determination. All of ten cells typed were XYY [Cytogenetics Laboratory, Baylor College of Medicine].) Table 2 shows mean-normal microdensitometry values of the autoradiographs produced in this and related experiments. For the *Bam*HI digest the only significant difference between the normal and XYY male is that the putative Y band (2.45 kb) is nearly twice as dense in the latter, suggesting that roughly twice the normal amount of DNA is present. The male-specific fragments produced by other enzymes (Table 3) are also significantly denser in the XYY DNA. One XX male fibroblast line tested (GM 2626, Human Genetic Mutant Cell Repository, Camden, New Jersey) did not produce a male-specific fragment.

There is one difficulty with this hypothesis: two enzymes, *Hin*dIII and *Pst*I, produce no apparent male-specific fragment. Double digests with *Hin*dIII plus *Pst*I also show no difference. We have since tested a few DNAs with four additional enzymes. Two of these enzymes, *Bgl*II and *Sst*I, do produce male-specific fragments and two, *Bcl*I and *Hin*dII, apparently do not. The most likely explanation for this discrepancy is that male-specific fragments are present in these digests but are obscured by the multiplicity of other fragments. In the typical X ray picture, 20% of the region from 1.0 to 50 kb contains bands that would obscure additional nearby bands unless they are unusually dense. In general, the putative Y bands are relatively less dense

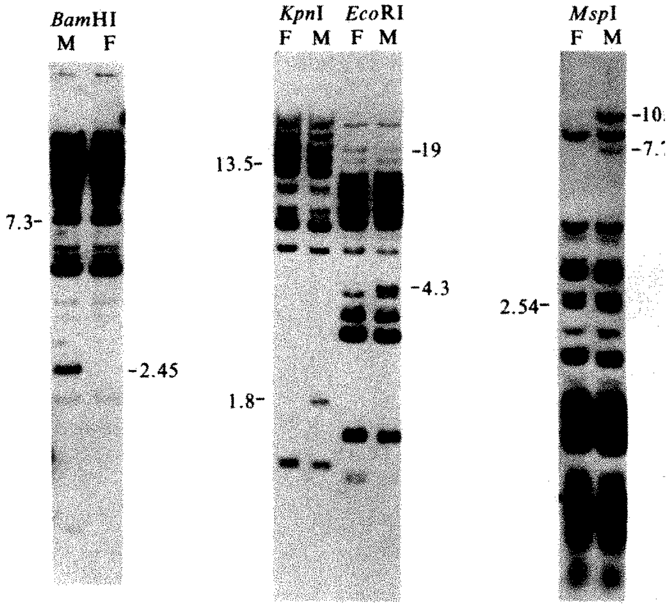

Fig. 1 Human genomic DNA digests probed with ^{32}P-pAS-1: enzymes producing male-specific fragments. DNA was prepared from 30 cm^3 of EDTA–whole blood by recovery of white blood cells from ammonium chloride/ammonium bicarbonate and digestion at 37 °C for 18 h with proteinase K and 0.1% SDS in 50 mM Tris buffer, *p*H 7.8. DNA was extracted twice with buffer-saturated phenol and precipitated in ethanol, resuspended and digested 1.5 h at 37 °C with RNase A, re-extracted with phenol and dialysed extensively against 10 mM Tris, 0.1 mM EDTA, *p*H 7.6 (ref. 17). Digestions were 5 μg DNA with 10–40 U restriction enzyme at 37 °C for 6 h. DNA was separated in 0.8% agarose gels, blotted onto nitrocellulose by Southern transfer and hybridized at 65 °C for 36 h with 8×10^5 d.p.m. per lane of pAS-1 (plasmid insert only) labelled with ^{32}P by nick-translation[18,19]. Hybridized nitrocellulose was washed at 65 °C with 0.1% SDS and decreasing amounts of sodium chloride/sodium citrate (2 × SSC to 0.5 × SSC). Autoradiography was for 4 days at −70 °C on Kodak SB-5 X-ray film using a DuPont Cronex enhancing screen. Higher-stringency conditions (70 °C, 0.1 × SSC) also produce a faint Y-chromosome fragment. F, female; M, male. Labelled bands are X- and Y-chromosome fragments (in kb); see Table 3.

---

* Present address: Center for Demographic and Population Genetics, University of Texas Health Science Center, PO Box 20334, Houston, Texas 77025, USA.

0028-0836/82/320682—03$01.00

Table 1 Number of individuals with male-specific fragments detected with pAS-1

Enzyme	*Bam*HI	*Eco*RI	*Kpn*I	*Msp*I	*Hin*dIII	*Pst*I
Total no. fragments observed	17	18	16	25	19	16
Male-specific fragments	+ −	+ −	+ −	+ −	None	None
Females	0 20	0 17	0 14	0 17	20	15
Males	30 0	23 0	16 0	18 0	31	22

+, Fragment present; −, fragment absent; none, no male-specific variation observed.

than other bands in the same lane so it is unlikely that microdensitometry alone would detect a male-specific band (Fig. 1; Table 2). (Such density differences may reflect differences in the extent of homology between particular fragments and pAS-1 or differences in the length of homologous sequences.) As no other known biological mechanism would account for these male-specific fragments and since it is certain that some fragments will occasionally obscure other fragments, we believe that all enzymes produce a Y-chromosome fragment containing an AS-like sequence but that these fragments are not always detectable by our methods.

Microdensitometry reveals another type of sexual dimorphism in genomic digests probed with pAS-1: one or two fragments are always denser in females than in males (Table 2). This is consistent with the assignment of an AS-like sequence to the human X chromosome using somatic cell hybridization[3]. Confirmation by microdensitometry is provided by DNA from a human XO (Turner's syndrome) fibroblast line (GM 857) and an XXXX fibroblast line (GM 1415). The putative X fragments are of equal density in males and in the XO DNA, significantly denser in normal females and most dense in XXXX DNA (Table 2).

Note that although the density ratio of the *Bam*HI Y fragment (2.45 kb), comparing normal male with XYY male DNA, is ~1:2 as expected, the ratio of the X fragment (7.3 kb), comparing normal male with normal female with XXXX female DNA, is 1:1.6:1.8, not the expected 1:2:4. (The XXXX karyotype was confirmed by Barr body determination on cells of the same passage as those used for DNA preparation.) The X-fragment differences, though, are statistically significant and in the correct direction. Conversely, the density of autosomal fragments do not differ between males and females. With such complex patterns it is possible that an autosomal fragment underlies the X fragment in *Bam*HI digests; this is the most likely explanation for the discrepancy in X-fragment ratios. Because DNA transfer, hybridization and autoradiography are generally non-linear processes, determination of absolute DNA concentration by microdensitometry is not reliable. In this application, though, with identical internal standards (autosomal fragments) and a sufficient number of controls, microdensitometry is very effective at detecting relative differences in fragment copy number.

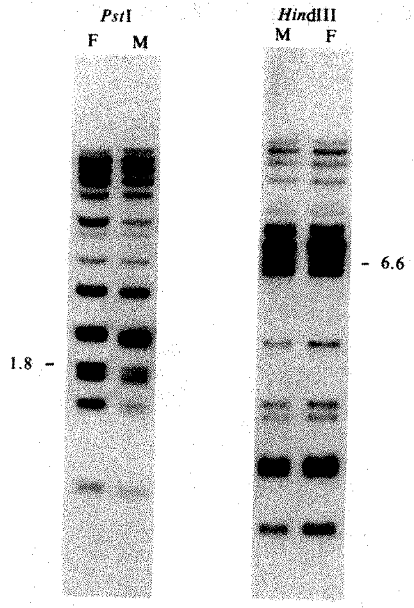

Fig. 2 Human genomic DNA digests probed with ^{32}P-pAS-1; enzymes failing to produce male-specific fragments. Methods as for Fig. 1. Labelled bands are X-chromosome fragments (in kb); see Table 3. M, male; F, female.

Table 3 lists the molecular weights (in kb) of the Y-chromosome and X-chromosome fragments detected in genomic digests and by microdensitometry.

Although Y-chromosome DNA represents ~1% of the total human genome, very few single gene traits have been mapped to this chromosome. 'Hairy ears' has been ascribed to the Y but this assignment is controversial[6,7]. A 'testis-determining factor' is most certainly on the Y and is associated with the Y histocompatibility antigen (H–Y)[8]. The structural locus for the

Table 2 Mean-normal microdensitometry data

	*Bam*HI					*Eco*RI			*Hin*dIII		
kb	Female $n = 7$	Male $n = 13$	XYY 3*	XO 1	XXXX 1	kb	Female $n = 3$	Male $n = 4$	kb	Female $n = 4$	Male $n = 10$
50	4.9±1.2	4.8±0.8	4.7±0.2	4.7	3.8	31	4.3±1.0	5.0±0.3	32	3.8±0.5	3.8±1.0
30	8.6±1.2	8.7±0.8	6.5±0.7	7.7	6.6	19	6.2±0.8	3.4±0.5	27	5.7±0.4	5.7±0.5
18	11.2±1.2	10.6±0.9	10.7±0.7	10.2	11.8	15	5.1±0.8	4.6±0.4	20	4.5±0.8	4.6±0.6
15	11.5±1.3	11.4±1.5	12.4±0.7	11.0	12.7	11	8.7±0.1	8.0±0.3	16	3.9±0.6	3.9±0.7
13	9.1±0.8	9.7±1.1	10.7±0.1	9.9	10.8	10.5	9.8±0.1	9.4±0.8	11	2.5±0.3	2.2±0.4
11	9.4±1.1	9.8±0.9	10.2±0.5	9.9	9.4	9.5	10.5±0.2	10.2±0.8	9.5	3.2±0.3	2.9±0.8
10.8	9.9±1.2	10.6±1.2	11.1±0.3	10.5	9.9	9.0	9.1±0.9	9.0±1.0	8.6	5.8±0.8	6.1±1.0
10.1	6.1±0.9	5.7±0.7	6.4±0.9	7.5	6.6	7.7	12.0±0.6	12.0±1.2	8.2	5.8±0.6	6.0±1.0
8.9	6.1±1.3	7.3±1.4	7.8±0.3	7.7	6.1	6.9	7.7±0.3	7.6±0.2	7.3	10.2±0.3	10.9±1.1
8.1	4.5±2.1	4.3±2.2	3.3±0.2	5.0	4.7	6.2	1.1±0.2	1.5±0.4	7.2	10.1±0.4	10.3±1.4
7.3	9.9±1.4	6.3±0.7	6.5±0.6	6.4	11.3	5.6	1.7±0.0	1.9±0.6	6.6	9.0±0.5	7.3±0.7
5.9	3.2±0.7	2.7±0.7	2.0±0.3	3.9	2.8	4.3	0.0	3.7±0.9	6.1	7.5±0.2	7.2±0.5
5.5	3.1±0.6	2.8±0.7	1.7±0.2	3.6	3.3	4.0	1.6±0.1	2.9±0.3	3.9	3.9±1.2	4.0±3.0
3.8	1.6±0.5	1.3±0.8	0.6±0.2	1.9	0.5	3.7	2.0±0.1	2.3±0.5	2.7	2.1±1.6	2.3±2.3
2.45	0.0	2.9±1.2	5.0±1.0	0.0	0.0	3.4	5.2±0.2	5.1±0.7	2.5	2.0±0.5	2.1±0.5
						3.0	9.9±0.2	9.0±0.2	2.1	7.1±0.3	7.2±0.5
						1.6	4.0±0.2	4.0±0.6	1.9	7.0±0.2	7.3±0.6
									1.4	4.9±0.3	5.2±0.9

Autoradiographs were scanned with a Helena Laboratories Microdensitometer. Values were normalized by dividing each peak height by the sum of all peaks in a given lane. Data storage and analysis were done on an Apple II microcomputer. Values are arithmetic mean ± 1 s.d. Putative X and Y fragments are underlined. There is an autosomal polymorphism of the *Bam*HI 8.1 kb fragment and of the *Hin*dIII 2.7 and 3.9 kb fragments. All *Bam*HI individuals in this table are 8.1^{+}; all *Hin*dIII individuals are 3.9^{+}/2.7^{+}. Some very faint fragments are not included.

* Replicates.

Table 3 Summary of molecular weights (in kb) of sex-specific DNA fragments detected with pAS-1

	*Bam*HI	*Eco*RI	*Hin*dIII	*Kpn*I	*Msp*I	*Pst*I
Y chromosome	2.45	4.3	—	1.8	10.9, 7.7	—
X chromosome	7.3	19	6.6	13.5	2.54	1.8

Assignment of Y-chromosome fragments is based on male-specific bands detected in genomic digests; –, none detected. Assignment of X-chromosome fragments is based on microdensitometry and human-hamster hybrid cell lines.

H-Y antigen itself, though, may be on another chromosome with regulatory loci on the X and Y[9]. Genes controlling embryonic gonadal differentiation, spermatogenesis and height have also been assigned to the Y[10]; these may or may not be independent of the other factors. At best it is reasonable to ascribe only four or five mendelian traits to the Y chromosome.

An explanation for the disparity between the amount of DNA present on the Y and the paucity of convincing gene assignments is that at least 50% of the Y is non-functional heterochromatin. There is considerable cytological variation in human heterochromatin, usually resulting in heritable differences in the size of the Y[11]. At the DNA level at least two male-specific mid-repeat sequences are detectable with *Hae*III (or BSu) digestion[12,13]. The heterochromatin and mid-repeat sequences are present on the 'inactive' long arm of the Y, whereas genes involved in sexual differentiation map to the short arm apparently. With the exception of heterochromatin differences (and hairy ears possibly), no polymorphic variation in either Y-chromosome DNA or genes has been reported in humans.

Our observation of a Y-chromosome restriction fragment containing an AS-like sequence in humans may provide a unique tool for probing Y-chromosome organization and function. It is highly probable that polymorphic restriction site variation will be detected with at least one of the dozens of restriction enzymes currently in use. These considerations also apply to the AS-like sequence on the X chromosome, though in this case excellent polymorphic markers are already known and many DNA probes are available[14].

The relationship between the AS structural locus and AS-like sequences on the X and Y chromosomes is not yet known in detail. The sequences are short relative to the structural locus but they contain sequences homologous to both 3′ and 5′ portions of pAS-1 (ref. 3). This arrangement is compatible with pseudogenes that lack introns[15,16]. The extraordinary dispersion of the AS-like sequence to both X and Y chromosomes and to several autosomes is unprecedented and intriguing.

We thank Nancy Hoffman for technical assistance. This work was supported by NIH grant GM 27593, NIH fellowship GM 08199 and grants from the Faculty Research and Fellowship Support Committee, Baylor College of Medicine and the O'Brien family of Houston, Texas.

Received 22 March; accepted 4 June 1982.

1. Su, T.-S., Bock, H.-G., O'Brien, W. E. & Beaudet, A. L. *J. biol. Chem.* **256,** 11826–11831 (1981).
2. Daiger, S. P., Wildin, R. S. & Su, T.-S. *Am. J. hum. Genet.* **33,** 136*a* (1981).
3. Beaudet, A. L. *et al. Cell* (in the press).
4. Carritt, B. & Povey, S. *Cytogenet. Cell Genet.* **23,** 171–181 (1979).
5. Meera Khan, P. & Robson, E. B. *Cytogenet. Cell Genet.* **25,** 39–46 (1979).
6. Rao, D. C. *Hum. Hered.* **20,** 486–492 (1970).
7. Stern, C., Centerwall, W. R. & Sarkar, S. S. *Am. J. hum. Genet.* **16,** 455–471 (1964).
8. Wachtel, S. S., Ohno, S., Koo, G. C. & Boyse, E. A. *Nature* **257,** 235–236 (1975).
9. Wolf, U. *Hum. Genet.* **58,** 25 (1981).
10. McKusick, V. M. *Mendelian Inheritance in Man*, 5th edn, 1xxiv, (Johns Hopkins Press, Boston, 1978).
11. Bobrow, M., Pearson, P. L., Pike, M. C. & El-Alfo, O. *Cytogenetics* **10,** 190–198 (1971).
12. Kunkel, L. M., Smith, K. D. & Boyer, S. H. *Science* **191,** 1189–1190 (1976).
13. Cooke, H. *Nature* **262,** 182–186 (1976).
14. Davies, K. E., Young, B. D., Elles, R. G., Hill, M. E. & Williamson, R. *Nature* **293,** 374–376 (1981).
15. Nishioka, Y., Leder, A. & Leder, P. *Proc. natn. Acad. Sci. U.S.A.* **77,** 2806–2809 (1980).
16. Vanin, E. F., Goldberg, G. I., Tucker, P. W. & Smithies, O. *Nature* **286,** 222–226 (1980).
17. Kan, Y. W., Dozey, A. M., Trecartin, R. & Todd, D. *New Engl. J. Med.* **297,** 1081–1084 (1977).
18. Southern, E. M. *J. molec. Biol.* **98,** 503–517 (1975).
19. Rigby, P. W. J., Dieckmann, M., Rhodes, C. & Berg, P. *J. molec. Biol.* **113,** 237–251 (1977).

Initiator tRNAs from archaebacteria show common unique sequence characteristics

Yoshiyuki Kuchino, Makoto Ihara, Yuko Yabusaki & Susumu Nishimura

Biology Division, National Cancer Center Research Institute,
Tsukiji 5-1-1, Chuo-ku, Tokyo 104, Japan

Archaebacteria have recently become of interest in studies on the phylogeny of organisms, for they are quite different from true bacteria as well as from eukaryotes and are thought to be derived from a separate primary line of descents from true bacteria[1]. This conclusion is based mainly on nucleotide sequence analysis of 16S ribosomal RNA by Woese and his co-workers, and other genotypic and phenotypic analysis of archaebacteria. To obtain more information on the phylogeny of archaebacteria, we examined the nucleotide sequences of their initiator tRNAs, because much information is available on initiator tRNAs of various organisms, and distinct differences have been found between the sequences of initiator tRNAs of prokaryotes and eukaryotes[2]. We have now determined the nucleotide sequences of initiator tRNAs from *Sulfolobus acidocaldarius*, *Halococcus morrhuae* and *Thermoplasma acidophilum*, and have found that they have a common unique structural feature that differs from both true bacterial initiator tRNAs and eukaryotic initiator tRNAs.

Initiator tRNAs from *S. acidocaldarius*, *H. morrhuae* and *T. acidophilum* were purified from unfractionated tRNA by successive column chromatographies of DEAE–Sephadex A-50, BD-cellulose and RPC-5 (refs. 3,4). Final purification of these tRNAs was achieved by two-dimensional polyacrylamide gel electrophoresis[5,6]. Heterologous charging of methionine by *Escherichia coli* aminoacyl-tRNA synthetase was adapted to pick up initiator tRNA species during purification[7]. In the case of *T. acidophilum*, two methionine tRNAs were detected when fractionated by BD-cellulose column chromatography (*p*H 7.5). The formylation reaction with *E. coli* enzyme was used to determine which species was initiator; only one species was formylated, and the other was found to be methionine tRNA for elongation[8].

The total primary sequences of the three initiator tRNAs were obtained by post-labelling procedures as described previously[5,6], and the sequences, arranged in cloverleaf form, are shown in Fig. 1. Eukaryotic initiator tRNAs are distinct from prokaryotic initiator tRNAs in having A_1, t^6A_{37}, A_{54}, G_{57}, A_{60} and U_{72} in place of C_1, A_{37}, T_{54} (U or uridine derivatives), A_{57}, U_{60} and A_{72} (ref. 2). These characteristics have been found in all prokaryotic and eukaryotic (cytoplasmic unicellular and multicellular) initiator tRNAs so far sequenced. By contrast, the three archaebacteria initiator tRNAs all contained A_1, A_{37}, uridine derivative$_{54}$, $(N_4)_{57}$ (adenine derivative), U_{60} and U_{72}. In other words, these particular residues in archaebacteria initiator tRNAs are not the same as those of either prokaryotic initiator tRNAs or eukaryotic initiator tRNAs. These data of archaebacteria initiator tRNAs clearly indicate that archaebacteria are unique prokaryotes distinct from true bacteria. This is further supported by the recent sequence data on 5S RNA[9] and ribosomal A protein[10].

It is also noteworthy that among archaebacteria initiator tRNAs, *S. acidocaldarius* initiator tRNA shows remarkable resemblance to yeast initiator tRNA; the two tRNAs have almost identical sequences in the CCA-stem, anticodon-stem

0028-0836/82/320684—02$01.00

Table 1 Sequence homology of initiator tRNAs from archaebacteria, *E. coli*, yeast, vertebrate and wheat germ

	E. coli	Yeast	Vertebrate	Wheat germ	*Thermoplasma*	*Halococcus*	*Sulfolobus*
E. coli	—	72	71	67	78	71	72
Yeast	—	—	76	73	70	62	82
Vertebrate	—	—	—	87	76	64	74
Wheat germ	—	—	—	—	66	62	71
Thermoplasma	—	—	—	—	—	82	79
Halococcus	—	—	—	—	—	—	72
Sulfolobus	—	—	—	—	—	—	—

D-loops of different chain lengths were arranged to have maximal homology. Unknown modified nucleosides were counted as not having homology. Values are percentage homologies of sequences of initiator tRNAs.

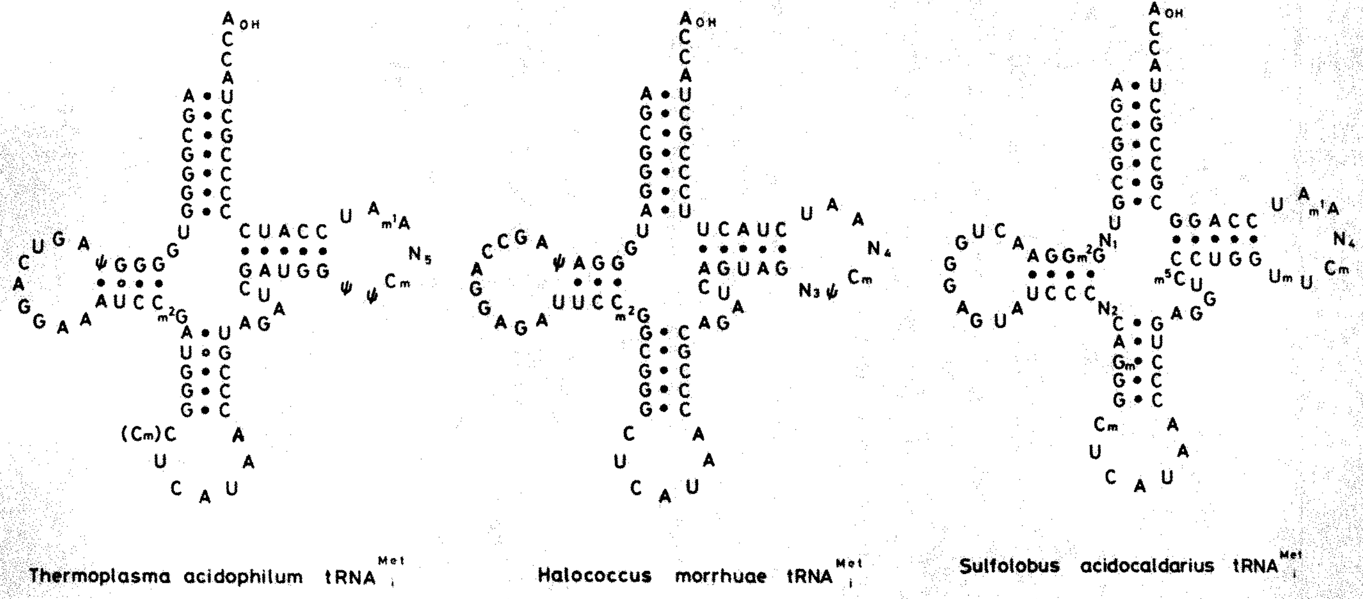
Thermoplasma acidophilum $tRNA_i^{Met}$ Halococcus morrhuae $tRNA_i^{Met}$ Sulfolobus acidocaldarius $tRNA_i^{Met}$

Fig. 1 Nucleotide sequence of initiator tRNAs from *S. acidocaldarius*, *H. morrhuae* and *T. acidophilum* in cloverleaf form. N_3 was recently characterized as 1-methylpseudouridine[11]. N_2, N_4 and N_5 are presumably m_2^2Gm, m^1I and I, respectively (Z. Yamaizumi, Y.K., M.I., W. Zillig and S.N., unpublished results). N_1 is an unidentified modified nucleoside. R. Gupta and C. R. Woese reported (personal communication) that *H. volcani* initiator tRNA contains triphosphate at the 5′ end. As we determined the sequences of the tRNAs by the post-labelling technique, we do not know whether they have triphosphate or monophosphate groups at the 5′ end.

and anticodon-loop[2], and the overall homology of *S. acidocaldarius* initiator tRNA to yeast initiator tRNA is 82% while its homology to *E. coli* initiator tRNA is only 72% (Table 1)[2]. By contrast, *H. morrhuae* and *T. acidophilum* initiator tRNAs do not resemble yeast initiator tRNA, or any other eukaryotic initiator tRNAs (Table 1).

All three archaebacteria initiator tRNAs contain two to four methylated nucleosides in the TψC-loop. In addition, *S. acidocaldarius* initiator tRNA contains three more 2′-O-methylated nucleosides in other regions. This characteristic is probably related to the tolerance of these tRNAs to extreme growth conditions.

A marked similarity among the three archaebacterial initiator tRNAs is the identical sequence of five stretches of base pairs in the CCA-stem, although the overall homology between them is not substantially high (Table 1). Fox and his co-workers reported that archaebacteria can be classified into several major subclusters[1]. Judging the phylogeny from 16S rRNA data, *S. acidocaldarius* seems to have separated first from *H. morrhuae* and *T. acidophilum*. The sequence data on initiator tRNAs reported have also suggested that *S. acidocaldarius* is distinct from *H. morrhuae* and *T. acidophilum*. It will obviously be interesting to compare sequences of initiator tRNAs from other archaebacteria with 16S rRNA data, and work on this line is in progress. The nucleotide sequences of initiator tRNAs from *Halobacterium cutirubrum* and *Halobacterium volcani* have recently been determined by U. L. RajBhandary and S. T. Bayley and by R. Gupta and C. R. Woese (personal communication), respectively. These sequences are almost the same as that of *H. morrhuae* except for a few base alterations in stem regions and thus are consistent with the above conclusion.

We thank Dr W. Zillig of Max-Plank-Institut für Biochemie for gifts of cells of *S. acidocaldarius*, *H. morrhuae* and *T. acidophilum*. This work was partly supported by a Grant-in-Aid for Scientific Research from the Ministry of Education, Science and Culture of Japan.

Received 1 March; accepted 26 May 1982.

1. Fox, G. E. *et al. Science* **209**, 457–463 (1980).
2. Gauss, D. H. & Sprinzl, M. *Nucleic Acids Res.* **10**, r1–r55 (1982).
3. Nishimura, S. in *Procedures in Nucleic Acids Research* Vol. 2 (eds Cantoni, G. L. & Davies, D. R.) 542–564 (Harper & Row, New York, 1971).
4. Taya, Y. & Nishimura, S. *Biochem. biophys. Res. Commun.* **51**, 1062–1068 (1973).
5. Kuchino, Y., Kato, M., Sugisaki, H. & Nishimura, S. *Nucleic Acids Res.* **6**, 3459–3469 (1979).
6. Kuchino, Y., Watanabe, S., Harada, F. & Nichimura, S. *Biochemistry* **19**, 2085–2089 (1980).
7. Takeishi, K., Ukita, T. & Nishimura, S. *J. biol. Chem.* **243**, 5761–5769 (1968).
8. Kilpatrick, M. W. & Walker, R. T. *Nucleic Acids Res.* **9**, 4387–4390 (1981).
9. Luehrsen, K. R., Nicholson, D. E., Eubanks, D. C. & Fox, G. E. *Nature* **293**, 755–756 (1981).
10. Matheson, A. T. & Yaguchi, M. in *International Cell Biology, 1980–1981* (ed. Schweizer, H. G.) 104–110 (Springer, Berlin, 1981).
11. Pang, H. *et al. J. biol. Chem.* **257**, 3589–3592 (1982).

Mechanism of C-terminal amide formation by pituitary enzymes

A. F. Bradbury, M. D. A. Finnie* & D. G. Smyth

National Institute for Medical Research, The Ridgeway, Mill Hill, London NW7 1AA, UK
* Department of Mass Spectrometry, St Bartholomew's Hospital, London EC1A 7BE, UK

The amino acid sequences of peptide hormones that terminate in an α-amide group seem usually to be followed by glycine in the sequence of their precursor molecules. Thus it has long been known that the sequence of α-melanotropin, which terminates in Lys-Pro-Val-$CONH_2$ (ref. 1), occurs adjacent to glycine in the sequence of corticotropin[2] and more recently it has been shown that the peptide hormone mellitin, which terminates in glutamine amide[3], is synthesized as a prohormone that terminates in glutaminyl-glycine[4]. A similar relationship is suggested by comparison of the primary structures of adipokinetic hormone[5] and red pigment-concentrating hormone[6]. These observations indicate that biosynthesis of the C-terminal amide may involve the action of a specific enzyme which has a requirement for C-terminal glycine. We present here direct evidence that porcine pituitary contains an enzyme with the ability to convert peptides that terminate in glycine to the corresponding des-glycine peptide amide. We have investigated the substrate specificity of the enzyme and with the aid of isotopic labelling have demonstrated that its mechanism of action involves dehydrogenation and hydrolysis of the glycine-containing substrate.

An assay system for detecting and estimating amidating activity in pituitary was obtained by examining the ability of enzyme preparations to convert the synthetic tripeptide D-tyrosylvalylglycine to the corresponding dipeptide amide D-tyrosylvaline amide. The sequence Val-Gly was selected because it seemed likely to contain the minimum structural elements of corticotropin necessary for formation of the valine amide group present at the C-terminus of α-melanotropin. The D-tyrosine residue conferred stability against degradation by aminopeptidases present in tissue homogenates and provided a site for radioiodination. The ^{125}I-labelled tripeptide D-tyrosylvalylglycine was incubated with pituitary homogenates (0.5 g porcine pituitary in 1 ml of phosphate-buffered saline, *p*H 7.4) or with chromatographed preparations of amidating enzyme obtained from porcine pituitary, and the degree of conversion of the D-Tyr-Val-Gly to D-Tyr-Val-$CONH_2$ was determined by column chromatography of the radiolabelled peptides on sulphopropyl Sephadex C25. The elution positions of the iodinated tripeptide and dipeptide amide were established with the use of synthetic peptides.

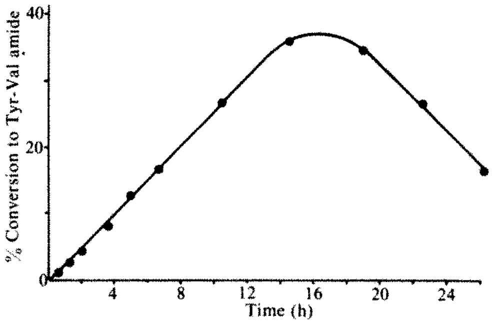

Fig. 1 Formation of D-Tyr-Val amide from D-Tyr-Val-Gly catalysed by an amidating enzyme from porcine pituitary. D-Tyrosylvalylglycine (100 pmol, 10^6 c.p.m. of ^{125}I) was incubated at 37 °C with an enzyme preparation obtained by gel filtration on Sephadex G100, as described in Fig. 3 legend. The incubation was performed with 0.25 ml of the peak fraction in 200 mM sodium chloride, 50 mM sodium phosphate at *p*H 7. At intervals, 20-μl aliquots of the reaction mixture were removed, acidified with 10 μl of 1 M hydrochloric acid and chromatographed on a column (15 × 1 cm) of SP Sephadex C25 eluted in 200 mM sodium chloride and 50 mM sodium phosphate at *p*H 5.5. The yield of D-Tyr-Val amide was calculated from the proportion of the total radioactivity that emerged in a peak corresponding to the position of an ^{131}I-labelled marker peptide. The iodinated tripeptide emerged at 20 ml and the iodinated dipeptide amide at 51 ml.

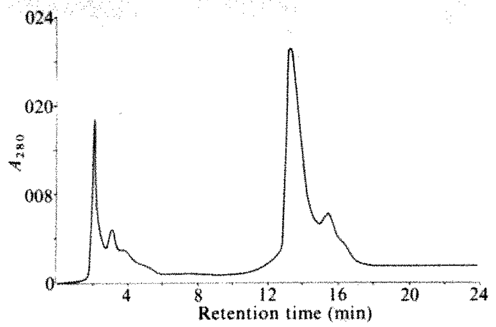

Fig. 2 Isolation of D-Tyr-Val amide produced by incubation of D-Tyr-Val-Gly with amidating enzyme extracted from porcine pituitary. The fraction containing the tritium-labelled dipeptide amide, obtained by ion-exchange chromatography as described in Fig. 1 legend, was concentrated *in vacuo* and submitted to HPLC on a C18 Microbondapak column (25 × 0.4 cm) eluted in 2 mM hydrochloric acid with a linear gradient (20 min) from 5–15% methanol. Fraction size was 0.5 ml. The D-Tyr-Val amide emerged at 27 ml.

Incubation of D-tyrosylvalylglycine with a preparation of the amidating enzyme obtained by gel fitration on Sephadex G100 led to the progressive formation of D-tyrosylvaline amide (Fig. 1). In the conditions used, the yield of the dipeptide amide reached a maximum value of 38% in 17 h, then slowly declined. Control experiments showed that when synthetic ^{125}I-labelled D-tyrosylvaline amide was incubated in the same conditions it was slowly degraded. Thus the formation of the dipeptide amide by the pituitary enzyme is followed by its descruction by other enzymes present in the pituitary extract. The reaction product, D-tyrosylvaline amide, was identified by co-elution with ^{131}I-labelled synthetic D-Tyr-Val amide; and in further experiments co-chromatography was demonstrated with D-Tyr-^{3}H-valine amide formed from D-Tyr-^{3}H-valylglycine with the corresponding synthetic dipeptide amide. The identity of the D-Tyr-Val-$CONH_2$ generated by the pituitary enzyme was further confirmed by its isolation in sufficient quantity for amino acid analysis. The incubation was performed using chemical amounts

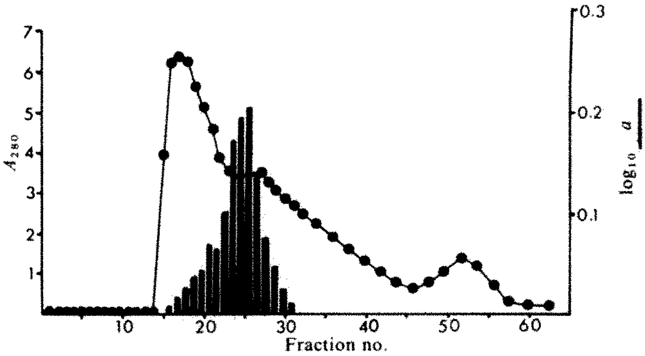

Fig. 3 Purification of amidating enzyme from porcine pituitary by gel filtration on Sephadex G100. The soluble enzyme obtained from the secretory granule fraction of porcine pituitary (50 g) was concentrated by vacuum dialysis and chromatographed on a column (60 × 1.5 cm) of Sephadex G100 eluted in 200 mM sodium chloride and 50 mM sodium phosphate at *p*H 7; fraction size was 2.5 ml. The enzyme was assayed by incubating 50-μl portions of each fraction with ^{125}I-D-Tyr-Val-Gly (20 pmol, 2 × 10^5 c.p.m.) at *p*H 7 for 5 h at 37 °C. The yields of dipeptide amide formed were determined as described in Fig. 1 legend.

0028–0836/82/320686—03$01.00

of D-Tyr-Val-Gly (100 nmol containing 2 μCi of ^{3}H-labelled peptide) in 10 ml of 200 mM sodium chloride, 50 mM sodium phosphate, *p*H 7.0, at 37°C for 10 h in the presence of enzyme purified on Sephadex G100. The resulting dipeptide amide was isolated in homogeneous form by gel filtration on Sephadex G25 to remove higher molecular weight material, by ion exchange chromatography as in Fig. 1 and by reverse-phase HPLC (Fig. 2). The reaction product (6 nmol) gave an amino acid composition of Tyr, 1.0; Val, 0.9; Gly, <0.1; NH_3, 1.1 residue.

The amidating enzyme was shown to be present in the secretory granule fraction of porcine pituitary. The granules, prepared from 50 g porcine pituitary by differential centrifugation[7], were solubilized by repeated sonication in 10 mM sodium phosphate at *p*H 7.0. The extracted enzyme was concentrated by dialysis under reduced pressure and purified by chromatography on Sephadex G100 (Fig. 3). The amidating activity emerged in a broad fraction, indicating that the minimum apparent molecular weight of the enzyme was ~60,000. Significant amidating activity could also be demonstrated, however, in the fractions corresponding to a molecular weight greater than 100,000 but further gel filtration of the higher molecular weight material gave a similar elution pattern to the initial granule extract, suggesting that the enzyme can undergo reversible aggregation. The yields of dipeptide amide obtained with the purified enzyme were ~40%, which is an order of magnitude greater than could be obtained with unfractionated pituitary homogenates.

To investigate the mechanism of amidation, the reaction was carried out with isotopically labelled tripeptides. D-Tyrosylvalylglycine was synthesized using both ^{14}N-glycine and ^{15}N-glycine and the corresponding D-tyrosylvaline amides were isolated after incubation with the purified pituitary enzyme. The molecular structures of the products were confirmed by high- and low-resolution mass spectrometric analysis of the trifluoracetyl derivatives (Fig. 4) prepared by reaction of the peptide amides with trifluoracetic anhydride in anhydrous conditions[8]. The low resolution mass spectra obtained from the enzymatically derived dipeptide amides were compared with those obtained from the corresponding synthetic dipeptide amides (Fig. 5). Three of the ions obtained showed the single mass unit increment expected from the incorporation of the ^{15}N isotope. High-resolution mass measurements of the molecular ions at 549 and 550 AMU (atomic mass units) and the base peaks of the spectra at 346 and 347 AMU gave unequivocal evidence for the empirical formulae of these compounds (Table 1), proving that the ^{15}N isotope from the glycine residue was retained in the peptide amide. This finding rules

Table 1 Mass measurements of the ions in the spectra of products formed enzymatically from D-Tyr-Val-^{14}N-Gly (a) and D-Tyr-Val-^{15}N-Gly (b)

Nominal mass	Empirical formula	Calculated mass	Measured mass	Error
346(a)	$C_{11}H_{10}O_3N_3F_6$	346.0624	346.0612	−0.0012
549(a)	$C_{20}H_{16}O_5N_3F_9$	549.0942	549.0954	+0.0012
347(b)	$C_{11}H_{10}O_3{}^{15}N \cdot N_2F_6$	347.0594	347.0596	+0.0002
550(b)	$C_{20}H_{16}O_5{}^{15}N \cdot N_2F_9$	550.0912	550.0928	+0.0016

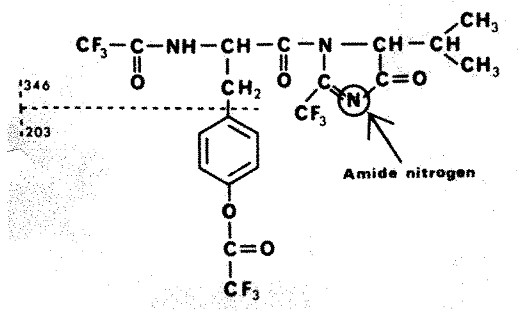

Fig. 4 Structural formula of the trifluoracetyl derivative tyrosylvaline amide.

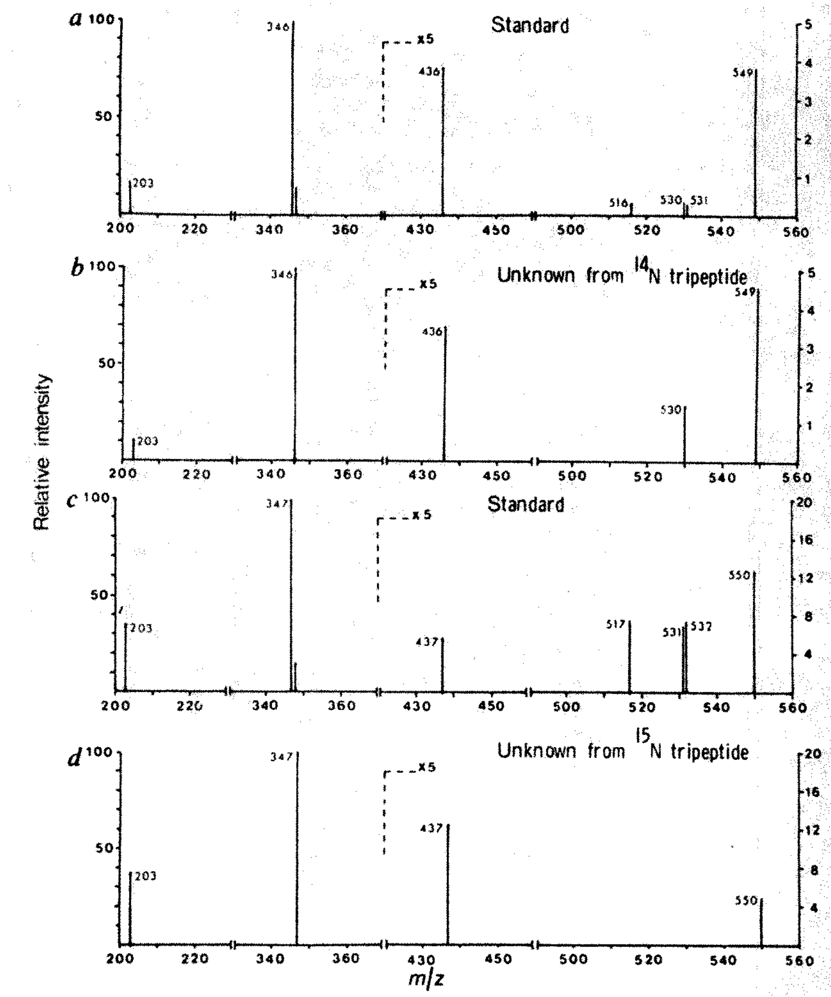

Fig. 5 Normalized partial mass spectra of the trifluoracetyl derivative of Tyr-Val amide. *a*, Synthetic D-Tyr-Val ^{14}N-amide. *b*, D-Tyr-Val amide formed enzymatically from Tyr-Val-^{14}N-Gly. *c*, Synthetic D-Tyr-Val ^{15}N-amide. *d*, D-Tyr-Val amide formed enzymatically from Tyr-Val-^{15}Gly.

out the possibility that the amide group might arise from ammonia, either by direct amidation of the valine carboxyl group[9] or by transamidation of the valylglycine peptide bond[10]. The data obtained support a mechanism involving removal of hydrogen from the C-terminal glycine and spontaneous hydrolysis of the resulting imino linkage:

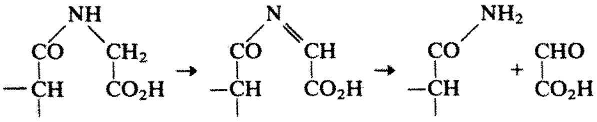

Consistent with this oxidative mechanism, it was found that when the incubation was performed with D-Tyr-Val-Gly synthesized with ^{14}C-glycine, the isotope was incorporated into glyoxylate. Furthermore, the amidation reaction was not affected by the presence of 1 mM ammonium ion, glutamine or asparagine at similar concentrations. The proposed mechanism is also consistent with previous suggestions that unsaturated peptides may be formed transiently during the biosynthesis of C-terminal amides[11,12].

The substrate specificity of the amidating enzyme was examined with a range of synthetic tripeptides. It was found that glycine was a mandatory amino acid in the C-terminal position of the tripeptide D-Tyr-Val-Gly; substrates containing leucine, alanine, sarcosine, lysine or glutamic acid in place of the glycine did not give rise to a detectable amount of dipeptide amide. Thus no amidation would be expected to take place with D-Tyr-Val-COOH as substrate, and none was observed. It can be concluded that the dipeptide carboxylate is not an intermediate in the formation of D-Tyr-Val amide from D-Tyr-Val-Gly. That C-terminal glycine should act as a signal for amidation is consistent with recent reports that the sequence of vasopressin is followed by glycine in the prohormone of vasopressin[13] and that glycine is present immediately after the C-termainal residue of calcitonin in the sequence of its biosynthetic precursor[14].

Amidation of the tripeptide D-Tyr-Val-Gly was found to take place when the valine in position 2 was replaced by phenylalanine or glycine but not when it was replaced by D-alanine, lysine or aspartic acid. This suggests that the pituitary enzyme can catalyse the formation of the amide group from the precursors of gastrin, choleocystokinin, oxytocin or vasopressin, hormones that terminate in phenylalanine or glycine amide. Furthermore, as the pituitary enzyme can form amides only with neutral amino acids in position 2 of the tripeptide substrates, and all known hormone amides appear to contain a neutral amino acid in the C-terminal position, it is clear that the pituitary enzyme has similar properties to the enzymes involved in the amidation of hormones in other tissues. The amidating enzyme in porcine pituitary may prove to be common to all tissues that biosynthesize the C-terminal carboxamide group.

We thank D. M. Carter for performing high-resolution mass measurements and product spectra. The Mass Spectrometry Unit is supported by grants from the Wellcome Trust.

Received 1 April; accepted 25 May 1982.

1. Harris, G. I. & Lerner, A. B. *Nature* **179**, 1346–1347 (1957).
2. Shepherd, R. G. *et al. J. Am. chem. Soc.* **78**, 5067–5076 (1956).
3. Habermann, E. & Jentsch, J. *J. Physiol. Chemie.* **348**, 37–50 (1967).
4. Suchanek, G. & Kreil, G. *Proc. natn. Acad. Sci. U.S.A.* **74**, 975–978 (1977).
5. Stone, J. V., Mordue, W., Batley, K. E. & Morris, H. R. *Nature* **263**, 207–211 (1976).
6. Fernhurd, P. *Biochim. biophys. Acta* **371**, 304–311 (1974).
7. Jacobs, L. S., McKeel, D. W., Jarett, L. & Daughaday, W. H. *Endocrinology* **92**, 477–486 (1973).
8. Engelfried, C., Koenig, W. A. & Voelter, W. *Biomed. Mass Spectrom.* **3**, 241–244 (1976).
9. Scott, A. P. *et al. Nature* **244**, 65 (1973).
10. Fruton, J. S., Johnson, R. B. & Fried, M. *J. biol. Chem.* **190**, 39–53 (1951).
11. Gross, E. in *Peptides, Chemistry, Structure and Biology* (eds Walter, R. & Meienhofer, J.) 31–42 (Ann Arbor Science, Michigan, 1975).
12. Barrett, G. C., Chowdhury, L. A. & Usmani, A. A. *Tetrahedron Lett.* **2063** (1978).
13. Land, H., Schütz, G., Schmale, H. & Richter, D. *Nature* **295**, 299–303 (1982).
14. Amara, S. G., David, D. N., Rosenfeld, M. G., Roos, B. A. & Evans, R. M. *Proc. natn. Acad. Sci. U.S.A.* **77**, 4444–4448 (1980).

Effect of an allozyme polymorphism on regulation of cell volume

Thomas J. Hilbish, Lewis E. Deaton & Richard K. Koehn

Department of Ecology and Evolution, State University of
New York, Stony Brook, New York 11794, USA

Biochemical differences have been described among allozymes[1–4], but the physiological consequences (that is, physiological phenotypes) of such differences have only rarely been demonstrated[5–7]. Such a relationship is necessary both to the argument that natural selection maintains allozymic diversity in natural populations and for understanding biochemical mechanisms of adaptation[8]. We report here a genotype-dependent difference in the rate of cellular free amino acid accumulation during adjustment to hyperosmotic conditions in the mussel *Mytilus edulis*. The product of the *Lap* locus in *M. edulis* is the lysosomal enzyme aminopeptidase-I (AM-I; E.C.3.4.11.-) which hydrolyses oligopeptides to their constituent amino acids[9]. Total AM-I activity is positively correlated with salinity; a 120% increase in salinity increases AM-I activity twofold[10–13]. Adjustment to hyperosmotic stress in osmoconforming marine bivalves, including *M. edulis*, involves rapid accumulation of cellular free amino acids[14,15]. The biochemical properties of AM-I, and its activation by salinity changes, suggest that it is important for providing cellular free amino acid pools during adjustment to hyperosmotic stress[11]. We show that individuals carrying the allele for high catalytic efficiency (k_{cat}) accumulated cellular amino acids more rapidly than other genotypes. The difference in accumulation rate was also demonstrated by an interruption of hyperosmotic adjustment, which resulted in genotype-dependent rates of amino acid excretion. These results demonstrate the role of AM-I in the physiological processes that regulate cell volume. Thus, differing catalytic properties of allozymes are manifested as phenotypic differences at the physiological level and provide a mechanism for the known selective mortality of mussels in natural populations[7].

Allozymes of AM-I have different catalytic properties; genotypes with the Lap^{94} allele (in either the homozygous or heterozygous condition) exhibit about 20% greater activity per unit enzyme protein, due to the higher k_{cat} of this allele[2]. This difference in specific activity, together with the proposed function of the enzyme in cell volume regulation, dictates that: first, on exposure to hyperosmotic stress, individuals with the Lap^{94} allele should accumulate cellular free amino acids at a greater rate. As the cellular response to hypo-osmotic stress consists of the release of amino acids to the haemolymph, some of which

Table 1 Tissue-specific levels of amino acids (ninhydrin-positive substances) as a function of AM-I genotype

	Adductor	Mantle	Digestive gland
Control	539 ± 15.0 (10)	566 ± 27.8 (10)	439 ± 7.3 (9)
Lap^{94}	681 ± 12.7 (29)	680 ± 21.8 (28)	617 ± 6.4 (29)
Non-Lap^{94}	664 ± 15.8 (11)*	655 ± 25.2 (15)*	570 ± 14.7 (16)†

All measurements were made 70 h after transfer of individuals from 15 p.p.t. to 30 p.p.t. salinity. Lap^{94} indicates those genotypes with the allele and non-Lap^{94} refers to all other genotypes. All values are mean ± s.e. in nmol per mg dry weight. Sample size is in parentheses.

* Difference between the two non-control groups not significant at $P < 0.05$; one-tailed t-test.

† Significant difference ($P < 0.005$).

are ultimately excreted[16], differences among animals in the size of the amino acid pool should result from different rates of amino acid excretion. Therefore, a second prediction is that during adjustment to hyperosmotic stress, transfer to hypo-osmotic conditions will produce a greater rate of excretion of amino acids by Lap^{94} individuals.

To test these predictions, animals were acclimated in 15 parts per trillion (p.p.t.) salinity for 2 weeks, then transferred to 30 p.p.t. and the concentration of cellular free amino acids observed during hyperosmotic adjustment. In the digestive gland, there was an increase in ninhydrin-positive substances (NPS; that is, principally free amino acids) of ~160 nmol per mg dry weight. Ten individuals maintained at 15 p.p.t. were taken at each sample period as controls, to demonstrate significant NPS accumulation in high salinity treatments. While the controls were heterogeneous ($P<0.025$; analysis of variance), the variance was due to an elevated mean of the 48-h sample; variation among controls will not affect the tests for relative differences among genotypes. All control variates were combined to give an overall mean and standard error (Fig. 1). The increase in NPS was clearly genotype-dependent (Fig. 1; Table 1); after 48 h at 30 p.p.t. the differences between Lap^{94} and other genotypes approached significance ($P<0.1$; one-tailed *t*-test) and after 70 h at 30 p.p.t., Lap^{94} genotypes had a 24% greater net increase in NPS ($P<0.005$) than other genotypes. One-tailed comparisons were dictated by the *a priori* prediction of greater NPS accumulation in Lap^{94} genotypes because of the higher catalytic efficiency of individuals carrying this allele.

The digestive gland has the greatest AM-I activity of any tissue; mantle and adductor tissues have maximally 50% and 5%, respectively, of the activity found in the digestive gland[13,17]. There were no significant contributions of genotype to the rates of accumulation of NPS in either mantle or adductor tissues, even after 70 h of hyperosmotic adjustment, although the results suggested greater rates of NPS accumulation for genotypes containing Lap^{94} (Table 1). We interpret the lack of genotype-dependent differences in mantle and adductor tissues as being due to the low AM-I activity in these tissues.

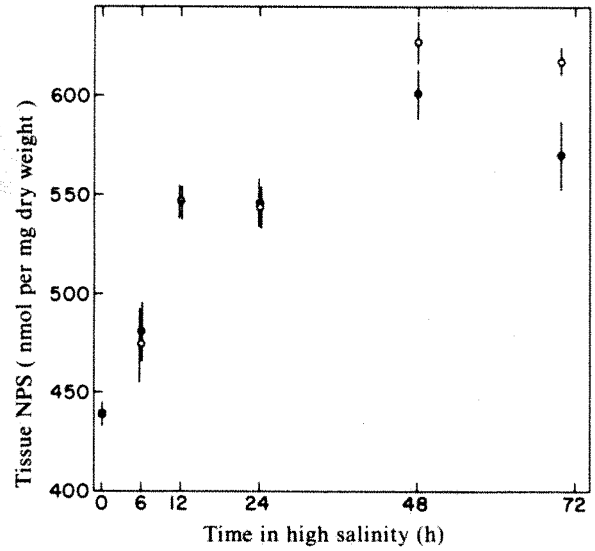

Fig. 1 Accumulation of ninhydrin-positive substances (NPS, nmol per mg dry tissue weight) in digestive gland of *Mytilus edulis* after transfer from 15 p.p.t. to 30 p.p.t. salinity. ○, Genotypes containing Lap^{94}; ●, genotypes without Lap^{94}; ■, overall mean for controls. The determination of NPS was modified for small samples[19]. *Lap* genotypes were determined by starch gel electrophoresis[20].

Table 2 Genotype-specific rates of amino acid excretion during hypo-osmotic stress

	24 h	48 h	70 h
Lap^{94}	304 ± 103 (17)	150 ± 38 (25)	497 ± 75.0 (31)
Non-Lap^{94}	296 ± 78.1 (9)*	183 ± 49.3 (16)*	271 ± 55.5 (15)†

Animals were acclimated to 15 p.p.t. salinity, 15 °C for 2 weeks before transfer to 30 p.p.t. After 24–70 h, animals were returned to 15 p.p.t. for 2 h. They were then placed in 150 ml of 15 p.p.t. filtered (0.45 μm pores) artificial seawater for 2.5 h. The amino acid concentration of duplicate 1-ml samples was determined using the fluorimetric method[18]. Results are expressed as nmol of glycine equivalents per g dry weight per h.

* Difference between genotypic groups not significant at $P<0.05$.

† Significant difference ($P<0.01$; one-tailed *t*-test) assuming inequality of variances.

In animals returned to 15 p.p.t. salinity after 70 h at 30 p.p.t., amino acid excretion reflected the genotype-dependent accumulation differences (Table 2). Genotypes with the Lap^{94} allele showed almost twice the excretion rate of genotypes without the allele. There was a notable concordance between genotype-dependent differences in accumulation during hyperosmotic adjustment and genotype-dependent excretion during hypo-osmotic stress; there were no significant differences in excretion rates until sufficient time had elapsed for significant differences in NPS accumulation to occur (Table 2).

Thus we have demonstrated that known catalytic differences among allozymes have predictable and measurable physiological consequences. In natural situations of diminished or fluctuating salinity, there is a direct ecological 'cost' to possessing the Lap^{94} allele. Our results provide a possible mechanism for the demonstrated selective mortality of Lap^{94} genotypes among natural populations experiencing differing salinities[7]. In a situation of natural environmental variation, an imbalance between accumulation and excretion of amino acids may lead to differential and excessive loss of nitrogenous resources by Lap^{94} genotypes. Specific studies of nitrogen balance in field populations are presently underway.

This is contribution 421 from Ecology and Evolution, State University of New York. The work was supported by NSF grant DEB 7908802 and USPHS grant GM 21133.

Received 12 March; accepted 17 June 1982.

1. Place, A. R. & Powers, D. A. *Proc. natn. Acad. Sci. U.S.A.* **76,** 2354–2358 (1979).
2. Koehn, R. K. & Siebenaller, J. F. *Biochem. Genet.* **19,** 1143–1162 (1981).
3. McDonald, J. F., Anderson, S. M. & Santos, M. *Genetics* **95,** 1013–1022 (1980).
4. Hoffmann, R. J. *Biochem. Genet.* **19,** 129–144 (1981).
5. Powers, D. A., Greaney, G. S. & Place, A. R. *Nature* **277,** 240–241 (1979).
6. Cavener, D. R. & Clegg, M. T. *Proc. natn. Acad. Sci. U.S.A.* **78,** 4444–4447 (1981).
7. Koehn, R. K., Newell, R. I. E. & Immermann, F. W. *Proc. natn. Acad. Sci. U.S.A.* **77,** 5385–5389 (1980).
8. Koehn, R. K. in *Ecological Genetics: The Interface* (ed. Brussard, P.) 51–72 (Springer, New York, 1978).
9. Young, J. P. W., Koehn, R. K. & Arnheim, N. *Biochem. Genet.* **17,** 305–323 (1979).
10. Moore, M. N., Koehn, R. K. & Bayne, B. L. *J. exp. Zool.* **214,** 239–249 (1980).
11. Koehn, R. K., Bayne, B. L., Moore, M. N. & Siebenaller, J. S. *Biol. J. Linn. Soc. Lond.* **14,** 319–334 (1980).
12. Bayne, B. L., Moore, M. N. & Koehn, R. K. *Mar. Biol. Lett.* **2,** 193–204 (1981).
13. Koehn, R. K. & Immermann, F. W. *Biochem. Genet.* **19,** 1115–1142 (1981).
14. Bishop, S. H. in *Estuarine Processes* (ed. Wiley, M.) 414–431 (Academic, New York, 1976).
15. Baginski, R. M. & Pierce, S. K. *J. exp. Zool.* **203,** 419–428 (1978).
16. Pierce, S. K. & Greenberg, M. J. *J. exp. Zool.* **57,** 681–692 (1972).
17. Graff, G. L. A., Brouet-Yager, M. & Kleiner, H. *Comp. Biochem. Physiol.* **49,** 381–386 (1964).
18. North, B. B. *Limnol. Oceanogr.* **20,** 20–27 (1975).
19. Matheson, A. T. & Tattrie, B. L. *Can. J. Biochem.* **42,** 95–103 (1964).
20. Koehn, R. K., Milkman, R. & Mitton, J. B. *Evolution* **30,** 2–32 (1976).

ANNOUNCEMENTS

Awards

The eighth Marconi Fellowship for Communications, Science and Technology has been awarded to **Arthur C. Clarke** for his contributions to the invention of the communications satellite. Most of the $35,000 grant will be used at the proposed Centre for Third World Communication, Energy and Space Technologies, at the University of Moratuwa, near Columbo, Sri Lanka, of which he is chancellor.

The World Academy of Art and Science has awarded the II Stuart Mudd Award to **Professor Leonardo J. Mata** (Institute of Research in Health, University of Costa Rica) for his pioneer work on intestinal microecology of poor and traditional populations of Central America living in different ecosystems.

The trustees of the Lady Tata Memorial Trust have made international awards for research in leukaemia to **H. Abrams** (USA), **H.J. Allen** (UK), **D.W. Anderson** (USA) (renewed awards); **R.J. Baer** (USA), **A.P. Gee** (USA), and **A.R. Venkitaraman** (India) (new awards).

Sir Alastair Pilkington has been awarded the Messel Medal of the Society of Chemical Industry for 1982. The Medal is the premier award of the Society and is awarded every second year.

The Royal Society of Chemistry presented its annual film prize on 8 June to the producers of the German film *Juncture* which describes work at the BASF chemical plant at Ludwigshafen.

The Royal Society of Chemistry has awarded the Meldola Medal and Prize jointly to **Dr D.C. Clary** (UMIST), for contributions to the theory of molecular energy transfer and chemical reactions, and to **Dr A. Dilks** (Xerox Corporation in Rochester, New York), for work on the characterization and plasma modifications of polymer surfaces.

The Meldola Medal, now accompanied by a prize of £100, will next be awarded in 1983 to the chemist who, being a British subject and under 30 years of age at 31 December 1982, shows the most promise as indicated by published chemical work. Applications, by 31 December 1982, to The President, The Royal Society of Chemistry, Burlington House, London W1, UK, the envelope being marked Meldola Medal.

An award of SF5,000 and a silver medal is available every three years, for the best paper or report devoted to significant work pertaining to coal tar products, plant or processes. Full details and conditions from BTIA, 132/135 Sloane Street, London SW1, UK.

The Beilby Awards, which consists of a medal and a prize of £250, are made to British investigators in science in recognition of original work of exceptional merit which has led to advances of practical significance. This work should have involved the development and application of scientific principles in chemical engineering, fuel technology or metallurgy. The awards are intended as an encouragement to younger men and women, normally under the age of 40. Applications, by 31 December 1982, to The Convener of the Administrators, Sir George Beilby Memorial Fund, The Royal Society of Chemistry, Burlington House, London W1, UK.

The W.K. Kellogg Foundation of America is providing $3 million to enable Oxford University to develop a major centre for continuing education. The Rewley House site in Wellington Square, part of which was acquired and converted into a residential centre for adult students with considerable financial help from the Foundation in 1963, will be redeveloped. Its new conference facilities will include a large lecture theatre, eight fully-equipped seminar rooms, a library and an administrative block. Existing residential accommodation will be upgraded, and catering facilities enlarged.

Appointments

Dr Lewis M. Branscomb has been re-elected chairman and **Dr Mary L. Good** vice chairman of the National Science Board, the governing body of the National Science Foundation.

Dr George Bugliarello (President of the Polytechnic Institute of New York) is the new Council Secretary of the Marconi International Fellowship Council following the retirement of Dr Walter Orr Roberts.

Prof. Alvin M. Kaye, has been named as the first incumbent of the Joseph Moss Chair in Molecular Endocrinology, established at the Weizmann Institute of Science.

Prof. R.J. Berry (University College, London) has been elected president of the Linnean Society for the next three years, succeeding Prof. W.T. Stearn. **Dr Colin Patterson** was elected as editorial secretary and the other officers were re-elected.

The Zoological Society of London has elected **Professor John Phillips** (Director of the Wolfson Institute in the University of Hull) as its next Secretary.

Prof. Janet V. Watson (Geology, Imperial College of Science and Technology) has been elected president of the Geological Society.

Prof. David G. Harnden (Department of Cancer Studies, University of Birmingham) has been appointed Director Designate of the Paterson Laboratories, Christie Hospital and Holt Radium Institute at the University of Manchester, to succeed the present Director, Professor L.G. Lajtha on his retirement in June 1983.

Meetings

1-3 September, **International Hepatitis Workshop,** Stirling (Miss E.K.S. Grant, Nuclear Enterprises Ltd, Sighthill, Edinburgh, UK).

1-3 September, **Annual Symposium Uranium Institute,** London (Mrs C. Scott Barrett, Conference Associates UIS, 34 Stanford Rd, London W8, UK).

1-3 September, **Fast Reactions in Solution,** Leuven (Dr A. Persoons, Dept of Chemistry, University of Leuven, Leuven, Belgium).

1-3 September, **The International Environment and Safety Exhibition and Conference,** Wembley (Labmate Ltd, Sandpit Lane, St Albans, Herts, UK).

3-9 September, **Science and Technology in the Service of Conservation,** Washington DC (IIC American Meeting, 1511 K Street NW, Suite 725, Washington DC 20005, USA).

5-9 September, **Protein Metabolism and Nutrition**, Clermont-Ferrand (4ème SIMNA, INRA-Theix, Laboratoire d'Etude de Metabolisme Azoté, 63110 Beaumont, France).

5-11 September, **World Congress on Medical Physics and Biomedical Engineering,** Hamburg (Hamburg Messr, Congress Organisation, D-2000 Hamburg 36, PO Box 30 23 60, FRG).

5-15 September, **Charles Coulson Summer School in Theoretical Chemistry,** Oxford (Dr P.J. Grout, Theoretical Chemistry Dept, 1 South Parks Rd, Oxford, UK).

6-8 September, **Charged Particles Management of Electrostatic Hazards and Problems,** Southampton (Miss L. Claff, Scientific and Technical Studies, Oyez IBC Ltd, 11-13 Norwich St, London EC4, UK).

6-8 September, **Modern Aspects of Heterocyclic Chemistry,** Sussex (Miss L. Hart, Royal Society of Chemistry, 30 Russell Square, London WC1, UK).

6-9 September, **Distillation,** Geneva (The Center for Professional Advancement, Postbus 19865, 1000 GW Amsterdam, The Netherlands).

6-10 September, **Annual Meeting, British Association for the Advancement of Science,** Liverpool (Ms U. Laver, BAAS, Fortress House, 23 Savile Row, London W1, UK).

6-10 September, **Linear Programming and Operational Planning in the Petroleum Chemical and Process Industries,** Edinburgh (Education Secretary, Institution of Chemical Engineers, 12 Gayfere St, London SW1, UK).

BOOK REVIEWS

The vision of David Marr

Stuart Sutherland

IN 1973 David Marr, then 28 years old, moved from Cambridge, England, to Cambridge, Massachusetts; seven years later he died of leukaemia. During this period he formulated a new approach to the theory of vision and published his results in a series of papers of great depth. Much of Marr's originality lay in his insistence that one must have a rigorous theory of how a particular task is performed before proceeding to construct a computer model of how the brain carries it out. *Vision,* posthumously published, presents a survey of his own work and that of the group of exceptionally clever young scientists whom he inspired with his ideas.

Despite his originality, Marr's papers were often flawed. Many were poorly written and unnecessarily opaque. Moreover, each paper tackled a particular aspect of vision and it was sometimes hard to see the connections. Marr's book overcomes both problems. It is written in a lively style and is for the most part lucid and free from technicalities. In addition, it has a clear structure that integrates the different aspects of his research.

Marr believed that there are three main levels of visual processing, at each of which a separate representation of the world is formed. At the lowest level is "the primal sketch", a representation of the retinal image that makes explicit the size and disposition of the intensity changes present. The primal sketch itself contains several levels of representation. At its highest levels it represents boundaries formed by grouping lower level elements. Such a boundary may be formed, for example, by a change in the density or size of a set of circles present in the retinal image. The purpose of the primal sketch is to deliver to higher level processes an explicit description of the boundaries that exist in the image and to enable these processes to determine whether the boundaries found are caused by a change in reflectance, a change in light intensity, an occluding contour or an edge at which two visible surfaces of a body meet.

Much the longest section of Marr's book is devoted to the processes that operate on the primal sketch in order to recover a 3-dimensional representation of the world. Amongst these processes are stereopsis, and those that use shading, texture, occluding contours and various aspects of motion. From these cues the second level of representation, the "2½-D sketch", is constructed: this is a representation of the scene based on viewer-centred coordinates, which makes explicit the slope relative to the viewer at each point on all visible surfaces. For the purpose of recognizing objects, a 3-D model, the highest level of representation, is formed from the 2½-D sketch. This model represents objects in object-centred coordinates (based either on the direction of elongation of the object or on its symmetry) and it makes explicit the volumetric structure of the object by representing its parts as generalized cones (the volume swept out by moving a cross section of a particular shape along an axis).

Vision: A Computational Investigation into the Human Representation and Processing of Visual Information. By David Marr. Pp.397. ISBN 0-7167-1284-9. (W.H. Freeman: 1982.) £22.50, $39.95.

Not only does *Vision* have a clear structure, it also gives an integrated treatment of each stage of processing, based on Marr's philosophy of the nature of explanation in psychology. He distinguishes three levels of explanation. At the highest level is a *computational theory,* that is a theory of how a task can be performed. At the next level is a *representation* and an *algorithm* to achieve that representation. At the lowest level lies the question of how the algorithm is actually implemented in the *hardware* of the system.

Marr's originality and much of the depth of his own thinking stems from his emphasis on the top level type of explanation, which few had previously even considered. The computational theory for a given stage in processing should, according to Marr, specify what is being computed, and why this is a useful thing to compute. It should in addition specify the ways in which the image is related to the world, that is to say, the constraints on how the image can be interpreted. It is only the existence of these constraints that makes it possible to recover from the image the properties of the scene. Thus, in recovering the shape of a rotating body from successive views of it, it is necessary to assume that the body is rigid, since otherwise there is an infinite number of possible interpretations. The assumption will normally hold true; where it does not, no solution to recovering a body's 3-D shape from its motion will emerge. Again, stereopsis depends on the constraints that in general one and only one point on one retina receives light from the same source as a single point on the other, and that local changes in disparity will be small. Both constraints have exceptions — in parts of the visual field there will be objects or parts of objects that are seen by one eye but not the other, and where one object occludes another there will be sudden changes in disparity. But for the most part the constraints hold, because the world is largely made up of surfaces that are comparatively smooth. Only by using these constraints is it possible to decide which point in the image on one retina corresponds to a given point in the image on the other.

The computational theory of a given task not only constrains the nature of the algorithm, it also constrains the nature of the representation of the results of a given stage of processing. Thus, Marr justifies the primitives used in the primal sketch (for example, segments of lines and edges formed by brightness changes, and higher level boundaries) by noting that it is just this sort of information that is needed to recover at the level of the 2½-D sketch the

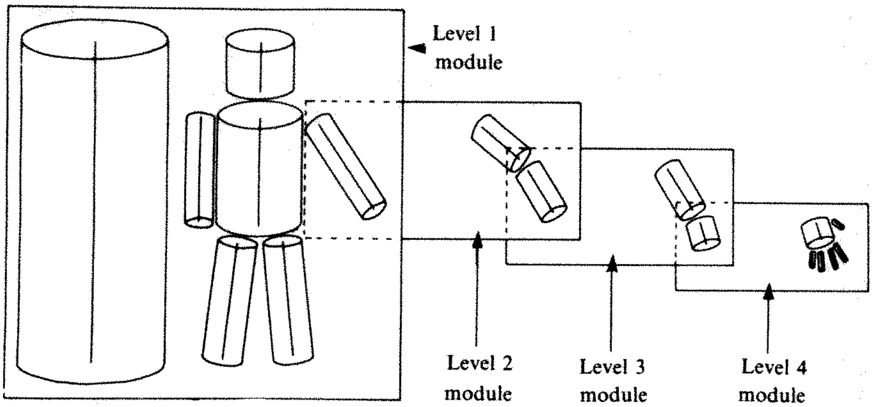

Hierarchical organization of a 3-D model: the visual object (here a person) is decomposed into parts, and each part is decomposed into successively finer and finer detail — in this case whole body, arm, forearm and hand. Each part is represented by its central axis and a generalized cone that corresponds to the volumetric shape of its surface. This method of representation preserves gross similarities between objects whilst making explicit variations in detail.

local orientation of surfaces and their reflectance. Again, in deciding how to represent the 3-D model of an object, Marr is guided by a computational theory of the process of recognition. First, the representation has to be accessible, that is, it must be possible to compute it economically from the image. Second, it should have a wide scope in that it must be possible to represent any object that can be recognized. Third, it must provide a unique description of a given object, otherwise different descriptions would be formed on different occasions and hence recognition would fail. Fourth, the representation should reflect the similarity between similar objects, but should also make explicit small differences: we can both see the similarity between different people and can also recognize individuals. Marr's method of representing 3-D objects meets all these constraints. Thus, the last constraint is satisfied by organizing the representation hierarchically so that the coarse shape of an object is represented in one module with other modules representing successively finer and finer detail (see diagram p.693).

There is a further way in which Marr's work is superior to that of most of his contemporaries. Other vision programs have usually taken no account of psychological or neurophysiological findings. In deciding what algorithm to employ, Marr makes use of both kinds of evidence where relevant results exist. For example, having proposed a simple and elegant model of stereopsis, he abandoned it because it did not fit the psychophysical findings. He put forward a second model, which although considerably more complex is consistent with the psychophysical results. In essence it begins by matching large features in the two images and allows for the use of eye-movements to reduce disparities in matching finer detail. Again, in his account of motion perception, he suggests that Y-cells may subtract a measure of the brightness at time $t+60$ msec from the same measure at time t: hence a cell will fire only if an edge is moving with the lighter part leading. He makes out a case that this idea is consistent with the known physiological properties of Y-cells. This is an ingenious idea for motion detection, but there is so much confusion amongst neurophysiologists about the role of X- and Y-cells that it may be premature.

"It is science and technology which has made other countries wealthy and prosperous, and it is only through the growth of technology that India shall become a wealthy and prosperous nation."
Jawaharlal Nehru

Science and
technology in
INDIA
the past, present, and future.

As appeared in the August 1982 issue of
SCIENTIFIC
AMERICAN

A SPECIAL ADVERTISING
REPORT IN THE AUGUST
SCIENTIFIC
AMERICAN

Circle No.10 on Reader Service Card.

Vision has two faults. First, despite Marr's emphasis on the importance of implementing algorithms as computer programs to make sure they work, it is often unclear whether he has actually written and tested a computer program to perform a particular task. Moreover, even when he claims to have implemented an algorithm, he rarely discusses how successful the program is and he gives no clear indication of the range of scenes on which it succeeds and those on which it fails. This nonchalant approach to computer modelling is unfortunately typical of the Artificial Intelligence community. Second, he is sometimes unduly dismissive of the research of others. For example, he scorns the work of Waltz and Mackworth, who wrote programs to recover depth from polyhedra, on the grounds that they were dealing with "mini-worlds". His allegation is correct, but it remains true that people can readily see depth in line-drawings of such objects and Marr provides no alternative account of how this task is performed. Both Waltz and Mackworth in fact succeeded (at different levels) in working out the constraints that enable this task to be carried out and to that extent they were amongst the few of Marr's predecessors who had a computational theory of the task they simulated.

Marr begins his preface by writing "This book is meant to be enjoyed": his intention will be fulfilled. The book is not only enjoyable, it is exciting and contains many stimulating ideas. For example, he gives good reasons for supposing that the brain cannot use iterative processes unless they converge very fast. *Vision* is perhaps the most important book on the subject to appear since Helmholtz's *Physiological Optics* was published over a hundred years ago. Marr's untimely death was a grievous loss to psychology. □

Stuart Sutherland is Director of the Centre for Research on Perception and Cognition at the University of Sussex.

NMR of biopolymers

Alfred G. Redfield

NMR in Molecular Biology. By Oleg Jardetzky and G. C. K. Roberts. Pp.681. ISBN 0-12-380580-5. (Academic: 1982.) $59, £39.

ALTHOUGH nuclear magnetic resonance does not occupy the central role in the biological sciences that it has in analytical organic chemistry, there is hardly a branch of biochemistry or biology to which it has not been applied in recent years. The physical basis for these biological applications is the same as for organic chemistry, but the goals and general methodology differ significantly. While no unusually subtle new ideas are used, biologically relevant NMR is often complicated and controversial in its interpretation, owing to the complexity of the systems involved, and it forms a new and flourishing sub-discipline. Most current research is directed toward fine-grained local structural studies, and the determination of dynamic behaviour which only NMR can provide.

The authors of this treatise were among the innovators, and continue to be active, in this field. Their book is a thorough treatment of the most mature application of NMR to biological problems, namely the study of small molecules and macromolecules in solution, alone and in interaction with each other. Topics such as *in vivo* metabolism and NMR imaging are omitted, as is a comprehensive treatment of NMR of partly immobilized or frozen structures (commonly called "solid state NMR") except for a brief description of its application to membranes and related problems. The emphasis is therefore on proteins, especially enzymes, reflecting both the majority of current applications and the experience of the authors. Restricting the content of the book in this way was wise, since the areas not covered were in early stages of development at the time (early 1981) when the book was completed, and because the treatment of solution-state NMR could then be comprehensive in a book of reasonable length.

There are short introductory sections on fundamentals and instrumentation, and also descriptions of theories of relaxation, both paramagnetic and diamagnetic. Most

Climate and history

Nineteen eighty two seems to be the year for books on climate and history. In addition to the two volumes reviewed by Stephen Schneider (*Nature* **298**, 499) are *Climatic Change in Later Prehistory*, edited by Anthony Harding and published by Edinburgh University Press, and *Food-Climate Interactions* with Wilfrid Bach *et al.* as editors and Reidel as publisher. Both books are the records of meetings. Prices are (EUP) pbk £9.75, (Reidel) hbk Dfl. 135, $58; pbk Dfl. 65, $28.50.

of the book is devoted to a descriptive, often case-history, treatment of individual problems and their attempted solution. Nearly half the text covers applications to enzymes and proteins, and it concludes with chapters on nucleic acids and on membranes. There are approximately 1,500 references (out of, we are told, a possible 6,000 on the subject) and a significant number of them are discussed at least briefly.

The style is refreshingly critical, with the inevitable result that every experienced reader will find points of disagreement with certain statements or with the emphasis. For example, I felt that the treatment of nuclear spin relaxation as a tool for studies of protein dynamics overemphasizes the methods used by Professor Jardetzky and his colleagues. The novice should be warned that nearly every topic in this field is subject to dispute but for the most part the authors do present both sides of complex issues, in references if not in their discussions. Unavoidably, certain areas are developing so rapidly that the text can provide only a useful indication of very recent advances: examples of such areas are studies of nucleic acids and of the conformation of small proteins by two-dimensional NMR.

Jardetzky and Roberts have written the most thorough treatment of the subject now available, and the first such treatise to appear in some time. Their book will be extremely useful to both experienced NMR research workers and novices alike. □

Alfred G. Redfield is Professor of Biochemistry and Physics at Brandeis University.

Tackling the bugaboos of solar flares

Robert Rosner

Solar Flare Magnetohydrodynamics. Edited by E.R. Priest. Pp.563. ISBN 0-677-05530-7. (Gordon & Breach: 1982.) $89.50.

SOLAR flares have long been an enigma. Along with such problems as how the solar corona is heated, and where the "missing" solar neutrinos are, the solar flare puzzle has been a persistent reminder to astrophysicists that the gap between observation and theory is still uncomfortably large whenever the data are of sufficient quality to rigorously test the details of theoretical models.

In the case of solar flares, the difficulties may be attributed both to the classic bugaboo of theoreticians, namely phenomena in which nonlinear effects dominate (in the present case, derived from the non-linear equations of magnetohydrodynamics); and to the virtual certainty that much of the crucial physics takes place on spatial scales which are not likely to be observable in the forseeable future (hence theory in this respect remains unconstrained by data). Given the complexity of the subject, it is welcome news that *Solar Flare Magnetohydrodynamics* does a commendable job of reviewing much of the theory relevant to present-day solar flare research.

The book is largely complementary to the recent NASA monograph on solar flares, *Proceedings of the Skylab Workshop on Solar Flares* edited by P.A. Sturrock (Colorado Associated University Press, 1980) and, if read in conjunction with this second tome, the student of solar flares will have in hand a full account of research prior to the recent flight of the Solar Maximum Mission (SMM) satellite. As such, the book should be of interest to all concerned with time-dependent (magneto-)hydrodynamics and plasma physics in astrophysics. The material is written at a fairly advanced level, but is not so esoteric as to be inaccessible to students.

With the exception of Z. Svestka's brief chapter which reviews observations (a topic covered far better in the NASA/Skylab monograph), the book is true to its title and gives a systematic exposition of the physics of flaring plasmas, from equilibrium to possible instability, and along the way treats the associated microphysics leading to explosive heating and particle acceleration. Chapters are written by active, prominent researchers in the field, and generally convey a good sense of the current status of work in this area. Particularly noteworthy and complete are the discussions of current sheet dynamics by E. Priest, time-dependent hydrodynamics (I. Craig), evolution of post-flare plasma (G. Pneuman) and flare particle acceleration processes (J. Heyvaerts).

With the exception of J. Birn and K. Schindler's discussion of magnetic field equilibria, the chapters are well-integrated; this exceptional case, though competent in content, has a rather formal style, with virtually no attempt to mesh theory with observation.

A pleasant surprise is Priest's superb overview in the introduction, in which a précis of the entire book is given; this chapter not only ties the various contributions together, but also gives a nice perspective of the solar flare problem as a whole. The overall result is a monograph of great value; it is a must for solar physicists, and for all interested in sudden magnetic energy release and its consequences in astrophysics. □

Robert Rosner is an Assistant Professor of Astronomy at Harvard University.

Energy and life

Robert M. Macnab

Biological Energy Transduction: The Uroboros. By Ronald F. Fox. Pp.279. ISBN 0-471-09026-3. (Wiley: 1982.) £24.50, $43.80.

THE dual purpose of this book is given in its preface: first, it is intended to be an introduction, for physical scientists, to advances that have taken place in molecular biology in the past few decades; second, a description of biology from the viewpoint of energetics, suitable for senior undergraduates or graduates. These would seem to be rather distinct aims, and it is unclear why they should be pursued in a single volume — or, for that matter, why physical scientists require a special exposition of molecular biology.

An emphasis on energetic considerations in biology and their use as a unifying concept is what the title of the book leads one to expect, and, in general, the author has been successful in presenting this point of view. His style is clear and entertaining, and the major topics of interest in bioenergetics (e.g. control of metabolic pathways, storage of energy across membranes, chemi-osmosis, energetics of macromolecular synthesis) are treated well, provided one does not examine too closely the factual details presented.

In this latter regard, the book is flawed. Sometimes the error (e.g. that the bacterial flagellum is a triple helix) is incidental to the argument, but it is irritating nonetheless and one wonders how it came about. In other instances, the errors are more serious. I will cite two examples. First, on p.203, an erroneously high value for the cytoplasmic *p*H of bacteria is given, and then used in subsequent bioenergetic calculations. The author comments that

> Many microbiologists and biochemists will be surprised to read that for bacteria grown in a medium of *p*H 7 the internal *p*H is as high as 9.

Indeed they will — did he ever ask them? (Typical experimental values are around 7.5.) Second, the choice of standard state for H_2O in conventional tabulations of free energy changes, redox potentials and so on, is incorrectly believed by the author (p.62) to be 1 M; based on this belief, he proceeds to make adjustments to 55.6 M, which of course was the standard state chosen in the original tabulations. A variety of conclusions regarding the energetics of electron transport and oxidative phosphorylation are then based on these adjusted values, and the rest of the scientific community is taken to task (p.211) for failing to make these "corrections". It is unfortunate that the author apparently did not discuss these questions with physical chemists or biochemists before codifying his viewpoint in a textbook.

The final part of the book is devoted to a

Similarities in Physics

John N Shive and Robert L Weber

A new educational text stressing the similarities between apparently quite different areas of physics. The authors' unusual mission is best summarised by these extracts from their preface, addressed to the student reader:
The edifice of physics is not nearly as complicated as it often appears. The purpose of this book is to tie similar phenomena together, wherever they may appear, in mechanics, acoustics, optics, electricity, heat, or theoretical physics, and to call your attention to the similarities between them. Physics may be simpler than you think; nature is marvellously regular in its behaviour; analogies helpfully link what is being studied with what is already understood . . . Sharpen your ability by being alert to similarities. That's the keynote of this book!

September 1982 xv + 277pp illus
0-85274-540-0 flexicover £9.95

A Handbook of Public Speaking for Scientists and Engineers

Peter Kenny

The only handbook offering guidance to scientists and engineers called upon to speak in public on technical matters. Peter Kenny aims to give every person in a technical or specialist field the opportunity of becoming a competent speaker. In his own words:
This book will show you how best to prepare your paper for presentation at a technical conference, how to put your case at your next committee meeting, and how to make a good impression on those visitors you will be talking to tomorrow. Not only does the book deal with specific events, but it also provides you with the techniques that will make you a more effective speaker whether presenting papers, answering questions, or speaking 'off-the-cuff'.
The book is intended for quick and easy reference, and also for more detailed study.

September 1982 viii + 192pp illus
0-85274-553-2 flexicover £6.50

Adam Hilger Ltd

Techno House
Redcliffe Way
Bristol BS1 6NX
England

Adam Hilger

Circle No.06 on Reader Service Card.

consideration of the evolution of the "uroboros", defined as an interlocking and at least partially self-sustaining macromolecular assembly of considerable complexity. It is suggested that, after several pre-biotic steps, an RNA polymer (generated under hygroscopic conditions) placed some selectivity on self amino-acylations; these eventually resulted, via "ur-" (= primitive) t-RNAs and ur-ribosomes, in a selectivity of linkage of the amino acids to each other. How closely the description approaches the actual process by which cells evolved is of course difficult to ascertain, but earnest attempts such as this to construct models, which are at least plausible in terms of the properties of biomolecules, help to take the question of the origin of life out of the realm of the utterly mysterious.

Overall, I found this to be an interesting and instructive book but, in light of the factual errors it contains, it cannot be recommended as a textbook. ☐

Robert M. Macnab is an Associate Professor of Molecular Biophysics and Biochemistry at Yale University.

From terrestrial processes to martian features

Lionel Wilson

The Channels of Mars. By Victor R. Baker. Pp.198. US ISBN 0-292-71068-2; UK ISBN 0-85274-467-6 (University of Texas Press/Adam Hilger: 1982.) £22.50, $39.95.

AMONG all the bodies of the Solar System yet explored in detail, Mars appears to be the only one which has had an evolutionary history sufficiently like that of the Earth to make extensive comparisons readily possible, and, at the same time, sufficiently different to make the comparisons profitable in the study of both planets.

The least-readily understood surface features of the planet are the several varieties of channel and valley showing many of the characteristics which would be associated on Earth with fluvial, glacial or permafrost processes. Present-day surface temperature and atmospheric pressure conditions on Mars preclude the existence of liquid water for other than very short periods unless large volumes of water are involved. Thus, any model of the channel-forming process which requires protracted periods of gentle water action has profound implications for the environmental conditions prevailing at the time the channels were formed. It is clearly vital to establish the duration of the channel-forming events and the times in martian history at which they occurred.

Victor Baker has been associated with the study of the martian channels since their discovery. In this welcome survey, he succeeds in presenting a generally well-balanced review of the classification systems and morphological features of the channels and of ideas on their origins, appealing widely to Earth analogues. The overall picture which emerges is one of very slow, periglacial activity alternating with brief periods of catastrophic water release. The morphological evidence for the proposed ice-related mechanisms is strong and the physical models for the processes involving ground ice migration seem well founded.

Much of the book is devoted to those aspects of the larger channels which appear to demand catastrophic flooding by large and rapidly-released volumes of water. An extensive comparison is made between the martian features and the landforms developed in the Channeled Scabland of the north-western United States as a result of abrupt and massive water release from glacial lakes after failure of their ice dams. The morphological comparison is supported by calculation of a number of the fluid dynamic parameters associated with both martian and terrestrial floods. While the evidence for the formation of the martian channel forms by water flooding is compelling, the author is at pains to point out that we are not yet sure of the mechanisms whereby huge quantities of water are released abruptly from within the martian crust — though he does review a number of the suggestions which have appeared in print.

The style of Baker's presentation is such that it is hard to read individual chapters of this book in isolation: appreciation of the complete story requires reading the entire book. The work seems to be pitched at the undergraduate/postgraduate level, though the lay reader will have little difficulty in following the arguments and the large collection of references will be of value to the planetary science specialist. A notable feature of the book is the high quality of the many black-and-white photographs. The few typographical errors are almost all associated with numbers and equations and will be readily detected by the attentive reader. As much as anything else, the book whets one's appetite for further advances in this field. ☐

Lionel Wilson is a Lecturer in Planetary Sciences with the Department of Environmental Sciences, University of Lancaster.

nature

19 August 1982

LIBRARY COMPLEX
Department of :
14 NOV 1983

Nuclear LUAnacy or sensible choice?

The policy of launch under nuclear attack seems to be finding increasing favour in unexpected quarters. But can we rely on machines to push the button?

Long derided as highly dangerous, the policy of launch under attack (LUA), in which one superpower would launch its land-based nuclear missiles on certification of a nuclear attack by the other, is enjoying new respectability in Washington and Moscow. This heightened interest is important because LUA has been regarded as so crazy for so long by so many and because it may well be the way in which President Reagan and Mr Caspar Weinberger, the US Secretary of Defense, end up solving the problem of how to protect the US land-based missile force. Indeed, in the future, LUA may be a more reasonable strategic option than it is now or has been — but the Department of Defense and the arms control community should study it carefully before deciding to proceed down that path.

At present the United States does not tell the Soviet Union outright whether it would launch upon warning of attack or not. And in light of the number of errors which the warning and command system could produce, and the consequent difficulty the President would have in making rapid decisions, a US policy of LUA hardly seems practical. On the other hand, the annual defence posture statements setting out US military policy, during the term of former Secretary of Defense Harold Brown, contained explicit references to the possibility that the Soviet Union must consider the likelihood of LUA before deciding to attack the United States. These hints were doubtless read with interest in Moscow.

Now, however, the issue is shifting away from official verbal hints and the obvious problems of the present system towards a discussion of future US goals. The new issue is whether, in future, the United States could build a warning and command system it could rely on to execute LUA policy, not merely preserving LUA as an option.

The interest is coming from some surprising quarters. In early July, Soviet defence minister Dmitri F. Ustinov suggested — without using those exact words — that the Soviet Union might move to an LUA policy. Ustinov was echoing what another Soviet analyst had told a group of visiting Americans. Last year, the Office of Technology Assessment of the US Congress offered a surprisingly bright view of LUA as a possible alternative to mobile basing of the MX missile. Finally, Dr Richard L. Garwin, a well known defence expert for IBM, advocates LUA. Among other LUA advocates is Harold Agnew, former director of Los Alamos National Laboratory, who is now president of the General Atomic Company. But Mr Weinberger, although continuing to mention the possibility of LUA in his posture statements, has not shown any real interest in such a policy.

Ustinov and the other Soviet official who hinted at a possible Soviet LUA policy were apparently intending to counter US nuclear weapons modernization. If you get a hair-trigger ability against us with your MX and other programmes, they seemed to say, we will be forced to respond rapidly, with LUA. Another interpretation, offered recently by Paul Bracken of the Yale School of Organization and Management, is that the Soviet Union feels it was backed in a corner by President Jimmy Carter's Presidential Decision Memorandum 59, which in 1980 shifted US policy towards fighting out a nuclear war through the macabre idea of "limited nuclear war". If the United States makes a target of Soviet command authorities rather than Soviet cities, the Soviet Union has to consider launching its missiles early while it can still command them before the US missiles could reach the target.

There is, in fact, a debate about whether the Soviets could execute a LUA policy, no matter what they say. Soviet rockets are liquid fuelled, and cannot be kept ready to be fired at a moment's notice, unlike US rockets which are solid-fuelled. Nor is Soviet command and control on a high state of alert, normally, (partly, it is said, to prevent Soviet generals from commandeering their nuclear weapons as part of some coup). On the other hand, since any nuclear attack is likely to start during a period of general high tension, these drawbacks may not obtain, and the Soviet Union may have some chance, it is argued, of bringing off an LUA. Clearly a Soviet LUA policy, if only a declaratory one, should worry US leaders: among other things it would make Western Europe even more impressed by the Soviet bear.

The possibility of a US policy of LUA is more interesting, because a practical LUA capability is for the United States only several years and billions of dollars away (while the MX with its basing system would cost tens of billions of dollars). This was the conclusion, at least, of the OTA panel under Harry Woolf, director of the Institute for Advanced Study in Princeton. In a remarkable chapter on LUA, it said, in effect, that technology is not an obstacle to achieving some sort of meaningful LUA capability. "Doctrine and procedures — issues of national policy, not technology — more than anything else . . . determine the architecture of an LUA system," it said. The overall report, of course, did not favour any particular MX basing mode, or LUA. It merely presented several of the options to Congress.

This view contradicts the conventional view, based on past and present capabilities, that there are too many ways in which warning and communications could be disrupted or go wrong or simply be ambiguous. The President cannot, it has been said, have enough reliable information to make the cosmic decision in the 30 minutes afforded by an intercontinental ballistic missile (ICBM) attack or the 5–15 minutes in the case of a submarine-launched ballistic missile (SLBM) attack. Early warning satellites could be blinded by preemptive nuclear explosions in space, or mistake the signature of the missiles, or be so delicate as to trigger a false alert internally: and the government has revealed that the existing system triggers many such errors each year. Futhermore, SLBM's computer accessory equipment can set off false alarms: the DEW line radars have "seen" an attack when they were only looking at a flight of geese or the rising Moon.

The OTA report suggested that future systems could overcome many of these defects — although it made no claim that a system could be invulnerable. Early warning satellites could be moved out of crowded, geosynchronous orbit where a Soviet "space mine" could attack them. Instead they could be placed by themselves, further out, in unique deep orbits chosen at random, so there would be reason to suspect the innocence of any unidentified object that approached them. Since non-synchronous orbits would be used, there would have to be many warning satellites to assure that at any given time, one would be "watching" Soviet territory. If the satellites were high enough it would take a long

0028-0836/82/330695 02$01.00

time — as much as 18 hours — for a ground-launched missile to reach them and knock them out.

The peculiar and varying orbits, and the use of "dormant" satellites as reserves, could make it very difficult for a Soviet anti-satellite system to knock them all out. In short, the warning system itself would contribute to security, by buying leaders more time.

The report also suggested that communications links could be maintained in a variety of ways: satellite communications could use millimetre wavelengths to avoid ionospheric disturbances due to high-altitude nuclear explosions. Rocket-launched reconstitution satellites could be on ready alert; existing communications satellites could be prepared to serve as back-ups. An LUA communications net would have an advantage over the alternative communications nets for other MX options, in that its most crucial period of use would be before the atmosphere was disrupted by nuclear attack.

In sum, the OTA report foresaw a future LUA system resilient enough to warn of a major attack — such as the lightning bolt-from-the-blue that the MX is meant to counter. The report implies that the President would not be faced with only a few minutes to think, panicked generals and blinking machines, but a relatively well ordered set of options: knowledge through early-warning of anti-satellite efforts, time to use the "hot line", and sure information about the attack itself. The report went so far as to suggest a series of automatic LUA programmes for response, that might not need the President's decision, in case he was incapacitated or unavailable.

Garwin takes this one step farther. If the United States had an announced, self-evident and reliable capability for LUA, the Soviet Union should be deterred from ever attempting to attack, he says. In attacking, the Soviet Union would have to launch its missiles all at once to minimize US foreknowledge. Thus, submarine-launched missiles would start hitting US bomber bases and US submarines in port 5 to 15 minutes after the launch, when the long-range ICBMs still had 15 minutes or more to go before reaching their targets.

All the President needs to be able to do, Garwin argues, is to certify that this attack is under way, based on information his machines can surely provide. He would then authorize a pre-planned launch of the US land-based ICBMs, his only surviving force. If the Soviet Union realized how automatic and surely this retaliation would come, Garwin says, it would be deterred from attacking in the first place, even against the vulnerable force of US land-based ICBMs. Thus for Garwin, LUA is the solution to the problem of Minuteman vulnerability.

Garwin's proposed LUA policy, with its elements of automatic response and certainty of destruction of the attacking side thus has much in common with MAD — the 1960s doctrine of "mutual assured destruction" under which the United States (which then had less accurate weapons than it does now) pledged to destroy Soviet industry and society if it were ever attacked. One way to look at a possible LUA policy, therefore, is as a high-precision version of MAD.

Is all this technological hubris of the first order? What sane president, or sane society, would entrust the decision about its likely end almost entirely to machines? If the warning could not be made reliable, LUA could make a mockery of human judgement and morality.

But if technology has evolved to the point where the machinery could be made reliable we must think again. Should we decline to upgrade strategic warning, and decide not to give leaders the best information they can get? What sane president, faced with a possible nuclear attack, would want to turn the calculations over to rows of men with abacuses to make sure the "human element" was not lost in the final decision? Every day, jetliners carry innocent passengers across oceans and continents on automatic pilot systems, yet this is not morally outrageous, so long as the pilot is there to back up the machines.

A society that has already delegated so much to technology, ought, when it comes to make a final choice, to consider technology an ally, too.

An almighty crash

AEG brought about its own collapse, but there are lessons for all to learn

The collapse last week of the West German corporation AEG-Telefunken has been on the cards for more than a decade, but is none the less to be mourned on that account. The seventh largest corporation in West Germany, AEG-Telefunken is a monument to the optimism of the 1950s and 1960s, so that its decision to appeal to the courts for relief from three-fifths of its still unspecified debts marks the passing of an era. For much of the past twenty years, AEG-Telefunken had around its neck the albatross of its 40 per cent share in Kraftwerk-Union, the nuclear construction consortium — until Siemens obligingly bought it out in 1978. During the same period, but especially at the beginning of it, AEG seems accurately to have appreciated that high technology was waiting around every corner and to have determined to be strongly represented in them all. So was it just bad luck that it was not then possible to guess how high would be the cost of development in most of these new fields; or that technological conglomerates would become unfashionable; and that they would prove to be so hard to manage?

Hardly. Compared with Siemens, the obvious analogue, AEG has been run by accountants rather than by technologists. They have been skilled at raising extra capital — no less than DM1,000 million in 1979 from the West German banks, for example — but apparently less skilled at matching their technical ambitions to reality. Even so, the efforts they have made in the past three years to sell off parts of the business, and to form joint ventures with other corporations (as with Bosch over telecommunications) have been insufficient. The most obvious difficulty has been that AEG has not been technically outstanding in any of the fields in which it has taken an interest. The moral, for other corporations, should be familiar. A technically based conglomerate, however large, can survive in the long run only by technical excellence.

To many outside West Germany, it has been a surprise that one of the impediments to the reconstruction of AEG has been the resistance of the labour unions to the threat of redundancy, one of the reasons why the British General Electric Company last week pulled out of negotiations about a partnership with AEG in the manufacture of heavy electrical machinery. Despite the record of harmonious industrial relations in West Germany since the Second World War, it should be no surprise that unions are less compliant with their employers' needs on the downturn than they were during the economic miracle. But the prospect now is that AEG will have to shed at least 40,000 of the 100,000 people it employs in West Germany and perhaps an even larger proportion of its 20,000 employees elsewhere. It is almost too much to ask that flesh and blood should stomach redundancies on such a scale. Represented as they are by law on the supervisory board of AEG, the unions have behaved predictability. Elsewhere governments have stepped in to avoid trouble of this kind (as at Chrysler and British Leyland).

So what will be the consequences of the decline of AEG? Those who will lose their jobs, like those who have lost a large part of their investment in the company, will be more than merely inconvenienced. So too in the short run will be the host of smaller companies working as suppliers for AEG. Its competitors will now find the market for their goods more buoyant and more easily attacked. The business that AEG is forced to shed will in due course be picked up by others, with the result that some of those now destined to lose their jobs will be re-employed. In the long run, there will be two conspicuous losers. First, the legend of West German industrial cleverness will be permanently tarnished. Second, Chancellor Helmut Schmidt's coalition government, which has steadfastly declined to intervene on AEG's behalf (and which was politically and economically powerless to intervene) will be unfairly blamed by its opponents for not having lifted a finger and for having created the economic climate that brought AEG to its knees.

0028-0836/82/330696-02$01.00

Japan reaches for the stars

Radio-dish looks set to excel

Japan is now poised to take a world lead in millimetre-wave radioastronomy — the study of molecular clouds and star-formation regions — thanks to a far-sighted decision by the Japanese Ministry of Education more than a decade ago to support the plans of Tokyo Observatory.

For while American molecular astronomers smart under the effective abandonment of their own country's plans for a large (25-metre) dish to operate in this wavelength range (see *Nature* 12 August, p.596), Professor Kenji Akabane of the Tokyo Obervatory will announce this week at the International Astronomical Union meeting at Patras, Greece, his first observations with a 45-metre dish and a 5 × 10-metre-dish interferometer — a combination which is likely to outclass the millimetre-wave equipment of other nations for a number of years.

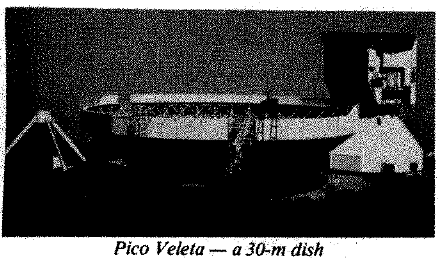

Pico Veleta — a 30-m dish

This telescope complex, which took 13 years to construct and cost £20 million, is now in operation at Nobeyama, 200 km north of Tokyo.

There is only one doubt about the telescopes — that they are sited in Japan. There they are limited by a relatively humid atmosphere, which absorbs low wavelengths. Thus, said a British millimetre-wave radioastronomer this week, Japan may be restricted to measurements at wavelengths not much shorter than 1 cm, which in molecular terms means a limitation to the observations of relatively rare long molecules. Studies of isotopic abundances in the Universe — an important project for millimetre-wave astronomy — need shorter wavelengths. The Tokyo observatory, however, reckons that Nobeyama will reach down to 2 mm.

If the Nobeyama telescope fails to reach down that far there is a chance that it will be suspassed within a few years by other millimetre-wave telescopes, planned or under construction.

France, Germany, and Spain will be next, with the £15-million Institut de Radioastronomie Millimetrique (IRAM). IRAM has an administrative headquarters in Grenoble and two telescope sites: one in southern Spain, on Pico Veleta near Granada, and one in the southern French Alps at the Plateau de Bure.

Pico Veleta is to have a 30-metre dish, whose steel-work is nearly complete — but the telescope is unlikely to be taking data before early 1984. According to Dr Dennis Downes, one of the IRAM team, this telescope should reach down to 1-mm wavelengths. But doubts have been expressed about that objective: the IRAM telescopes are to be open to the air and Sun, and so they will be distorted by wind and differential solar heating.

The exact shape of the dish must be maintained to within a wavelength of the radiation being studied — in other words 1 mm. To achieve this, the steelwork of the Pico Veleta telescope is to be heated to a uniform temperature; and the Plateau de Bure 15-metre dishes (of which there will be three making a T-shaped interferometer) will be stiffened with carbon fibre, cost allowing. Whether these untried methods will achieve the necessary accuracy is yet to be seen. Moreover the interferometer, will take some time to construct.

Besides IRAM, Britain, together with The Netherlands, plan to build a £7-million, 15-metre dish in Hawaii. These plans require environmental approval by the Hawaii State legislature, expected towards the end of this year. The British–Dutch dish, protected by a dome transparent to the radiation, should reach down almost to the edge of the millimetre-wave atmospheric "window" at 0.35 mm. But observations are not expected there before 1986.

Thus Japan is likely to enjoy a substantial lead in this branch of astronomy, possibly the first basic science in which it might take a world lead, at least until 1984.

Robert Walgate and Alun Anderson

Remote sensing for all at UN

Vienna

Remote sensing capabilities are emerging as a keynote of Unispace-82, the Second United Nations Conference on the Peaceful Exploration and Utilization of Outer Space, now taking place in Vienna. Virtually every national delegation expressed its committment to, and hopes for, remote sensing, and although some delegates privately expressed the views that remote sensing was still a solution in search of a problem, such sentiments were kept strictly outside of the official proceedings.

Remote sensing, for example, is to be the mainstay of the United States "global habitability" programme which is expected, during the 1980s, to develop into an umbrella for the research scheduled for the US space platform. "Global habitability" is intended to open up the entire land mass of the Earth to human habitation.

Yet the use of such techniques to survey another country contains the seeds of international tension. One of the problems to which remote sensing is repeatedly urged as a solution is the more rational use of land resources. But such techniques inevitably cut across traditional concepts of national and even personal privacy. The Soviet Union is a strong supporter of new international legislation to outlaw the improper use of data gained by satellite. As Dr Andrei P. Kapitsa, director of the Soviet stand at the exhibition associated with Unispace-82 pointed out, the publication in the Western press of predicted shortfalls in the Soviet harvest (based on satellite data) immediately raised world wheat prices, causing an extra drain on Soviet hard currency reserves.

Significantly, one of the most fervent pleas for the establishment of international principles on the use of satellite data came from Brazil, a country frequently quoted as a classic case where only remote sensing can provide adequate survey facilities. President Joao Baptista de Oliveira Figueiredo spoke of remote sensing as an "instrument both valuable and dangerous" since it "impinges on the sovereignty of states over their natural resources".

The problem becomes even more complex with marine resources. One of the greatest advantages which Cuba derived from participation in the manned "Interkosmos" programme, according the Cuban cosmonaut Arnaldo Tamayo Mendez, was the discovery of new fishing grounds. However, although one of the purposes of Unispace-82 was to show third world countries what space techniques are available, and although the European Space Agency has recently offered African states experimental facilities aboard Spacelab some 25 per cent of the nations represented in the United Nations have not yet reached a level of development where participation of any kind in a remote sensing survey is an economic possibility. The use of satellites to determine fishshoals in international waters could mean that those shoals fail to reach the traditional fishing grounds of the disadvantaged nations.

To obviate such inequities, some speakers at the forum of non-governmental organizations (NGOs), which took place in parallel to the main sessions, urged that the third world should strive for its own launch capability, but without clearly suggesting how this might be achieved. More practical would be the creation of an international pool of land-resource data as part of the United Nations committment to space. The two space superpowers already have a data-pooling

0028-0836/82/330697-02$01.00

programme, which is apparently continuing, although, as the administrator of the National Aeronautics and Space Administration, James M. Beggs, made it clear there can be no resumption of joint US–USSR experiments or missions until the international political climate improves considerably.

Several countries including India, France and the host country, Austria, have already established their own cooperation programmes with both the capitalist and the socialist worlds. Yet it was occasionally difficult to pin down the delegates from these countries on the advantages their countries have derived from such cooperation. And the Polish cosmonaut, Miroslat Hermaszewski, expertly fielded the question of what benefits Poland had derived from participating in the Comecon space programme — although, only a few metres away, the Polish Institute of Cartography had on display an excellent series of maps, which synthesized data from both the Interkosmos and the Landsat programmes.

Vera Rich

Remote sensing satellites

French plans for spot satellites

The French national space agency, the Centre National d'Etudes Spatiales (CNES), believes there is money to be made by remote sensing from space. Sales of data recorded by the two Spot satellites, France's first national remote sensing satellites due for launch in 1984 and 1986, are expected to offset the capital cost of the satellites' development and running costs in about ten years. Responsibility for earning the revenue will rest with Spot-Image, the independent company created early last month to market Spot data worldwide.

CNES's approach to the commercialization of remote sensing data differs markedly from that in the United States. The US National Aeronautics and Space Administration (NASA), like CNES chiefly a research and development agency, has been an unwilling operator of the service forced upon it when data from the early Landsat satellites proved commercially attractive. Potential users have complained that NASA was sometimes insensitive to their needs.

NASA will indeed be administering the distribution of data from Landsat-D, the latest satellite in the series launched last month, and from Landsat-D′, its successor, but beyond 1987 the Reagan Administration has insisted that NASA will have to get out of commerce so that the operational service will have to be taken up by private industry. Thus the fortunes of Spot-Image will be keenly watched in the United States as well as by the European Space Agency, now debating how to make available data from its planned remote sensing satellite ERS1, and the British government, which is contemplating a major effort in remote sensing.

Spot-Image's main shareholders are CNES with a 34 per cent holding, three French government agencies each with 10 per cent — the Institut Cartographique Nationale, the Institut Français du Petrole and the Bureau de Recherche Géologique des Minières — and two companies, Matra and Societé Européen de Propulsion, with 7.5 per cent each. Organizations from Sweden and Belgium which have collaborated to some extent on Spot, will also have small sharehodings. Spot-Image will buy data from CNES and sell them.

NASA's early experience in selling remote sensing data, however, seems not to augur well for Spot-Image. Although there has been great interest in Landsat data, there has been no prospect that fees would match development costs. But, according to Gérard Brachet, director-general of Spot-Image, the market for data from the second generation of remote sensing satellites should grow by leaps and bounds — he reckons that Spot should earn about $900 million, to cover development and running costs, within ten years.

The chief advantages of Spot and Landsat-D over earlier generations of remote sensing satellites is their increased resolution and number of spectral bands. Spot, for example, whose chief instrument is a multilinear array, will observe in three bands in the infrared and visible regions of the spectrum with a ground resolution of 20 m and in a broad band with 10 m resolution. Stereoscopic images are also available.

Spot data will be received and interpreted in Europe at ground stations in Toulouse (France) and Kiruna (Sweden). Spot-Image plans to turn round data within 48 hours for dispatch to users. The charge for one scene in digital form is expected to be about $1,000, but the fee for a photographic image has yet to be worked out, although it will be less. Brachet is confident that prices will compare favourably with those for images generated by the multi-spectra scanner aboard Landsat-D although comparisons with the thematic mapper, Landsat-D's most innovative instrument, are more uncertain.

Spot-Image is negotiating with some countries to receive Spot data direct via their own Earth stations, in which case there will be a copyright fee of only about FF220 ($40) per scene, less than the cost of images bought from Toulouse or Kiruna. The apparent discrepancy is explained, according to Brachet, by the prospective loss of about 70 per cent of potential images due to cloud as well as the cost of processing images.

Judy Redfearn

South African funds

The UK Science and Engineering Research Council (SERC), is reviewing its future commitment to the South African Observatory (SAO), because of financial pressures. South African astronomers currently take up 65 per cent of the viewing time of SAO, and SERC "buys" the rest for UK astronomers; has been suggested that this proportion be decreased. A recent questionnaire, however, revealed a strong desire within the UK astronomical community for this level of involvement to continue.

In terms of technical sophistication and size, the telescopes of the SAO (near Capetown) are outranked by others available to British astronomers in the Southern Hemisphere, particularly the Anglo-Australian and UK Schmidt telescopes in Australia. Paradoxically, SAO's usefulness is increased because its telescopes are not so advanced as to be oversubscribed in demand and yet are sufficiently powerful to do valuable work. In particular, SAO is heavily used for optical and infrared photometry with such objects as the brighter active galaxies and also cataclysmic variable and Cepheid-variable stars.

Earlier this year, while reviewing its plans for the financial year 1983–84 and the following three years, the Astronomy, Space and Radio Board of SERC set up a working group to ascertain the need for continuing use of SAO. The group circulated a questionnaire, to which it received replies from 60 or so groups in the United Kingdom. SERC says the working group reported to the board in July that there was a strong user demand for SAO.

The position of the board is that the decision will depend on scientific and financial considerations and that political issues are not relevant. According to SERC, however, a handful of the questionnaires raised political reasons for discontinuing the use of SAO. One astronomer, Dr Michael Rowan-Robinson, who has just completed a period of service on the SERC committee responsible for SAO, feels particularly strongly: "I seem to be in a minority in feeling that SERC should not maintain an official link of this kind with the South African government. Use of the telescope should be left more to the consciences of individual astronomers."

SERC is due soon to start negotiating its next contract with SAO, to which it now pays about £240,000 a year (about 25 per cent of the annual budget of the observatory) for 35 per cent of the total observing time. The British astronomical community will have a chance to review its use of all observatories in the Southern Hemisphere at the Anglo-Australian Telescope symposium to be held next month.

Philip Campbell

0028-0836/82/330698-01$01.00

French Comité National

Democracy, confusion abounds

One of the major and unique institutions of French scientific democracy, the Comité National, a king of scientific parliament with effective power over the work and careers of thousands of French researchers, is to be transformed.

That fact alone would lead to a great deal of heat, given the generally polemical French nature. But the fire has been stoked even higher by the decree, just published, which describes the transformation. It leaves so many loose ends that many French scientists remain unclear whether they can vote for candidates to the new parliament or not.

This is important, because of the potential power invested in the Comité National: if a scientist can vote for a candidate, at least he or she is assured of some kind of representation.

The Comité is the 1,200-strong board of assessment of the Centre National de la Recherche Scientifique (CNRS). CNRS is only one of the principal French research organizations, but it is the biggest and arguably the most important — at least for basic science; this year CNRS controls a budget of more than FF 6,000 million (over £500 million), and supports 9,322 scientists and 14,514 engineers, technicians and administrators. In general, the best of the university laboratories are at least "associated" with (or partly supported by) CNRS. And within this organization the Comité National plays a role by giving its advice (which is usually accepted) to the CNRS research directors on such matters as the hiring and firing of staff, opening and closing laboratories, and the awarding of grants.

The Comité National may appear to be no more than a collection of peer review committees — and it certainly does function in that way, divided into 45 sections each of 25 people according to subject or research. But the Comité is unique because it is an *elected* body, with a French electorate now totalling perhaps 20,000 people; and the key to the squabbles over the Comité is the question of what groups will be represented and to what extent?

Jean-Pierre Chevènement, minister for science and industry, was unhappy with the Comité that he inherited (the last election to the Comité National was in 1980; President Mitterrand came to power in mid-1981) for two main reasons — its subject structure was out of date, and it lacked representation from the technicians and administrators.

The new decree for the Comité sorts out these matters, and others besides. Chevènement has slightly increased the number of Comité seats that he can name himself, on advice from the CNRS directorate. He can now name eight rather than nine of the 25 members of each Comité (the rest being elected); and four seats per section are now reserved for election by engineers, technicians and administrators. The remaining 12 seats per section (just under half) are to be determined by election by scientists. But how is a scientist to be defined in that context? It is here that the new decree is unclear, and it is here that there will be plenty of discussion and acrimony before the next elections to the Comité National, planned for early 1983.

For the new decree actually decreases the right of certain university researchers to an automatic vote. Previously any researcher could vote; now only researchers with a "link" (the word is deliberately ambiguous) to CNRS may vote. This may be quite reasonable — after all, the Comité directly affects only CNRS employees — but CNRS is so important that researchers were pleased to have their little right to "meddle" in CNRS affairs.

Now that right seems to have gone. Or has it? According to the decree, scientific institutions that are not part of the CNRS may still appoint certain of their staff to vote for the Comité. Among those institutions could be universities. So there may yet be a back door to a voting right. And certain other categories of people do not have an automatic vote, but may receive one if they themselves apply to CNRS for the right.

What this means in effect is that almost every scientist and technician in France will have some way of getting a vote for the Comité; but for some a vote will come more easily than for others. It seems the ministry hopes that this solution will reduce political argument about rights to vote, but at the same time it will be a hard winter for the CNRS elector committee which, between now and January, will have to decide exactly who can vote and why. This process alone will take fully six months, CNRS estimates.

Robert Walgate

US computer industry

Paying the price

Washington

Federal Judge Harold H. Greene has raised the price that American Telephone and Telegraph Company (AT&T) will have to pay for the privilege of entering the data processing and computer game.

Ruling on 11 August on the proposed anti-trust settlement between AT&T and the Justice Department, Judge Greene said he would accept the basic deal, under which AT&T gives up its local telephone companies in exchange for the right to enter the unregulated computer market. But he insisted on certain modifications. The local telephone companies should be allowed to keep publishing the Yellow Pages directories, which are a big money-maker; they should also be permitted to market, but not manufacture, telephone equipment, he said. Under the original settlement, both of these options would be reserved for the parent AT&T company.

The judge also insisted that AT&T be barred from entering the "electronic publishing" field for at least seven years. This excludes AT&T for the time being from a variety of electronic information and news services; newspaper publishers have been especially worried that AT&T's grip on the country's communication system would give it an unfair advantage in this fledgling industry. Under Judge Greene's proposal, AT&T apparently could still supply transmission lines and terminal equipment for such ventures, but could not do the actual collection and compilation of information.

The anti-trust law limits the judge to making suggestions; he cannot order changes in the settlement. He can, however, reject it, and Judge Greene did not mince words: if the parties do not agree to his "suggestions", he will throw out the settlement and reopen the anti-trust case — which has already dragged on for eight years.

AT&T's vice-president and general counsel, William Keefauver, said "AT&T has a strong incentive to accept a decree and free ourselves from the business restrictions of the 1956 decree". (The 1956 settlement barred AT&T from entering the unregulated computer market. It resulted from earlier charges that AT&T was using revenues from its monopoly telephone business to subsidize its competitive ventures.) Failure to accept Judge Greene's terms means that those barriers remain. Keefauver said that the judge's suggested modifications "don't dramatically impact the thrust of the decree".

The Justice Department is less certain to go along with the changes. It had demanded that local companies should not market telephone equipment — a competitive business — while operating as regulated monopolies. The judge ruled that this was merely "theoretical consistency", when in fact allowing the companies to market equipment would increase competition — and at the same time keep rates down.

AT&T and the Justice Department have 15 days to respond to the judge. Earlier this year, Representative Timothy Wirth (Democrat, Colorado) introduced legislation to stiffen the terms of the anti-trust settlement; he later withdrew it in the face of heavy lobbying by AT&T.

The judge's suggested changes appear to incorporate a substantial portion of the Wirth plan, in particular letting the local companies keep the Yellow Pages and the right to market equipment. But, significantly, the judge did not recommend the other major point in Wirth's package: breaking off Long Lines (AT&T's long-distance network, which holds a virtual monopoly on interstate communications) from the more competitive divisions of the company. AT&T would thus retain Long Lines, Western Electric (which manufactures communications equipment), American Bell (the new subsidiary entering the computer market), and Bell Labs without restrictions on how research and development funds are allocated.

Stephen Budiansky

US biotechnology

Re-entry plans

Washington

E.F. Hutton, the large US financial company, is making its second entry into the potentially lucrative field of founding and backing fledgling biotechnology companies. In September, Hutton will begin offering investors limited partnerships in California Biotechnology Inc., a new company organized around the talents of three prominent university researchers. Hutton has already grossed $5.4 million in startup capital for the firm, which is now building a laboratory in Mountain View, in the San Francisco area.

Cal Biotech, as the firm is called, will have as director of research Professor Brian J. McCarthy on leave of absence from his position at the University of California, at Irvine. John Baxter of the University of California at San Francisco, has agreed to consult exclusively for Cal Biotech, although he will retain his professorship at the university. The third star is to be John Shine of Australia National University at Canberra. Shine will also consult exclusively for Cal Biotech, and work for the company under contract at his lab in Canberra, according to Hutton official Zsolt Harsanyi.

The company plans to use DNA techniques to develop pharmaceutical drugs, which could be tested and marketed by major pharmaceutical firms. Cal Biotech's role will be limited to development and ownership of the drugs themselves. Initially, the group plans to pursue development of human pharmaceuticals including those useful for cardiovascular diseases and anti-inflammatory purposes. However, Baxter and Shine have developed a way to produce beta-endorphin, the patent for which is held by the University of California. Baxter's laboratory has also cloned human and bovine growth hormone gene, so the company's work could proceed in those areas as well.

"What makes our company different from other biotechnology companies" says the firm's president Alfred G. Scheid, a long term consultant and former Hutton employee who makes rather a speciality of founding new companies, "is the combination of top scientists and access to a continuing flow of capital." Besides sponsoring the company financially, Hutton has also lent one of its executive vice presidents, William G. Baker, to be chairman of the board. Hutton itself invested an undisclosed amount as part of the $5.4 million fundraising.

Harsanyi says that come September, investors can put up a minimum of $5,000 to become limited partners in Cal Biotech. Using a little-noted provision in the tax law (that has been available for research and developments partnerships since the mid-1970s), they will be able to deduct perhaps as much as 99 per cent of the money they invest if the company spends the money in that year. Thus, the attractiveness of the investment depends on Cal Biotech's financial planning, which may explain why Hutton is taking such a deep interest in its management. Besides the tax writeoff, investors will receive a share of any instant royalties and profits the company earns from drugs that are sold, which could start as early as 1988, Harsanyi says. The company itself will be the general partner, splitting profits and royalties with the group of limited partners.

The approach of forming a company around a group of researchers and limiting its scope to their research is a major switch for E.F. Hutton following its failure with an alternative approach. In February 1981 Hutton raised $40 million to start DNA Science, a company planned to sponsor biotechnology research in many institutions around the world. Most of the initial investment was to go to the Weizmann Institute in Rehovot, Israel, to support work directed by Christian B. Anfinsen who had moved there after retiring from his post at the US National Institutes of Health. Baxter's laboratory in California was also due for support.

Research funding by DNA Science was mixed up with possible marketing rights granted to two major firms, and the whole cabbodle was to be managed by a businessman, E. Russell Eggers, with two Hutton officials, Harsanyi and Nelson Schneider, as vice presidents. But the structure of the company was too unwieldy and the 1981 tax law cancelled out some of the expected tax benefits from investment. So on 4 August 1981, the investors got their money back.

The lesson of DNA Science, Harsanyi says, is that investors in biotechnology are attracted by key people, such as Anfinsen and Baxter. The most promising approach, therefore, is to structure a company around these people, not expecting them to do management and marketing but assuring their access to capital for research and development. Whether Cal Biotech can develop a group of important products, to see them through the hurdles of trials and testing, and bring its investors golden returns, remains to be seen.

Deborah Shapley

Biotechnology centre

Links between industry and biotechnology research are thriving at the University of Leicester. Four companies are putting up approximately £1 million between them to establish a new biotechnology centre at the university. And the Science and Engineering Research Council (SERC) has promised the new centre £180,000 for capital equipment.

Industry's interest in Leicester is particularly timely. The University Grants Committee (UGC) recently awarded the university £50,000 of its grant earmarked for biotechnology to create three new lectureships. The university is now hoping to persuade the grants committee that one of those posts, for a yeast specialist, should be created within the new biocentre. The others are reserved for a plant biotechnologist and a mammalian geneticist within the university proper.

The companies prepared to put their money into research at Leicester are Whitbread, the brewers, Gallaher, the tobacco company, Dalgety-Spillers, the food manufactures and John Brown Engineers and Constructors whose main claim to biotechnical fame is the construction of the Pruteen plant for ICI. They have guaranteed support to the new centre for five years and have already agreed a programme of research. The centre will be concerned primarily with recombinant DNA technology, although questions of scale-up may be considered later. The research programme will consider plasmid DNA regulation and protein secretion in yeasts and the analysis and structure of genes in higher plants.

Money from the four companies should be sufficient to keep about eight researchers employed for five years, but the centre will also be trying to build up a sound contract research business. Patents resulting from work carried out under the core programme will be shared between the four companies and the university. The share of revenue will depend on how the patent is licensed. Ultimately, the centre hopes to build up a contract research business, the profits from which will be ploughed back into the centre. Precisely how much the university will earn from its association with the centre remains uncertain.

Even if the university has little to gain financially, it is intended to benefit from the small teaching commitment that the centre will take on. Training is also to be provided for employees seconded from industry. Initially, the centre will be housed in a suite of laboratories in the university's pre-clinical medical sciences building (for which it may pay no rent), but it may later build its own accommodation if cash can be raised.

Judy Redfearn

0028-0836/82/330700-01$01.00

New sights for Land

Washington

Dr Edwin H. Land, a legendary figure in US industrial history for his invention of the instant camera and for founding the Polaroid Corporation, announced on 27 July that he would resign as a director and chairman of the board of the company. When a remaining role as a consultant expires at the end of the year, Land will have relinquished all direct responsibility for the company identified with his name. Since 1975, he has been gradually breaking his links with the corporation in order to devote himself to research on colour vision and related fields. He is now 73.

Freedom ideal

As an inventor, however, Land has surprised no one in inventing an entirely new setting for his new career as a full-time scientist. Earlier this month, he gave me an exclusive tour of the Rowland Institute, a luxurious new building of brick, slate and oak that he has built and endowed on the banks of the Charles River in Cambridge, Massachusetts, only a few blocks from his old centre of operations at Polaroid.

At present, only 25 of the 80 people expected to work at the institute have been engaged, but Land is in no hurry to fill it up quickly, he explained, as he mounted, two steps at a time, a circular stairway carved in poplar wood leading to a large two-storey atrium housing a Japanese style garden and off which lay two storeys of eight double-laboratories.

Land's favourite word to describe the idea of the institute is freedom. Here, he and colleagues will be free from the pressures of writing government funding proposals or the demands of industry — or, perhaps, the burden of running Polaroid, which has had its troubles in recent years. To ensure this freedom, Land has endowed the institute with $20 million. "This is an experiment to see what will happen if a group of competent, intelligent and bright people were pursuing the substance of science itself for its own sake, without thought of product or profit", he says.

Some of the basic work to be undertaken, such as the study of light-induced heat transfer across molecular surfaces, is not far from work done at Polaroid, which was famous for exploring the frontiers of the science that underlay its projects. "We were very proud of the basic work we did at Polaroid. But while we were doing it we carried a very different and very proud burden.

"It was a joy to make new films, new dyes and new cameras" said the holder of 533 patents, who is a member of the US Inventors Hall of Fame, along with Thomas Alva Edison and others. "It is a different kind of joy if the product is deep insight into natural phenomena from which there may be by-products internally". The institute, like any other non-profit group, will be eligible to apply for patents and to accept royalties. But, Land stresses, basic science will be the product, with any inventions that transpire the by-product — not the other way around. Perhaps the Rowland Institute is Polaroid in reverse.

The institute aims to be collegial in style, explains James Foley, an organic chemist from Polaroid whom Land hired nine months ago. "Each of us is a sun on our own project, with the others as satellites, and I will be a satellite on Jim's project" says Land. Projects at present contemplated range from Land's own work on the physics of colour vision to an examination of the structure of biologically important molecules.

Edwin Land, new perspectives

For all its newness, its large, quiet library, Mexican grey pebbles and whisper-perfect auditorium, the institute is avoiding stocking up on fancy equipment (although each scientist may have a computer terminal in his office). Nor is Land hiring "teams" of people to work on a single project. He is opposed to both as too likely to drag researchers away from pursuing a clear, logical line of enquiry. Once you have a big machine, he says, you tend to work on problems the machine can do, rather than those that are most important or interesting.

The enormous darkroom in the basement, for example, has only a few items in it. There, Land happily shows off a phenomenon he discovered only the day before, in which the eye, after exposure to a certain kind of light, sees the fan-shaped spokes on a wheel become narrower. "We're going to look at one thing, then the next, and the next, without trying to explain too much at first. In a sense, we're returning to an older style of doing science. This was how Faraday worked."

Base of success

Back at Polaroid, the reins of power are now firmly in the hands of William J. McCune Jr who has been with the company since 1939, and whom Land made president in 1975, chief executive officer in 1980, and who now becomes chairman of the board too. McCune, who is 67, is an independent Polaroid power in his own right. One story has it that he recently rebuffed two would-be kidnappers in a local parking lot. Most discussions of Polaroid's health and future tend to show McCune and the board of directors seeing things differently from Land, although there is no indication of an outright break being the cause of Land's present departure.

Indeed, Polaroid, while highly successful with sales of $1,400 million, has had several things to disagree about internally. The film manufacturers have been hard hit by the rising price of silver in the late 1970s. In addition, the amateur camera market, which accounts for 80 per cent of Polaroid's business, levelled in those years in response to the recession, at a time when Polaroid had doubled its camera and film-making capacity in what proved to be a mistaken expectation of continued growth. Both US sales and sales in Europe, which had grown spectacularly, tailed off. The company workforce, which numbered 20,000 in 1979, now stands at approximately 15,000, and a number of high executives have been offered generous terms to leave to reduce management too.

Finally, the company has gone on introducing the kind of spectacular, unique inventions for which Land was famous — such as Time Zero film, an improvement on the SX-70 film first introduced in 1972. But it has also recently experienced its first real failure: Polavision, an instant movie camera and film system introduced in 1977 and withdrawn in 1979. The system came just when video products were coming along, and cost more than a comparable video system; the company had to write off an estimated $68 million and opinions vary over the extent to which Land bears the blame. McCune is seen as strongly favouring the company's decision, in recent years, to expand out of the volatile amateur camera market and into commerical, industrial and scientific products. Polaroid now offers cameras for computer graphics to industry and cameras for medical purposes, including nuclear medicine for example.

Will Polaroid go on being inventive after Land? He says "One of my functions was — innocently — to insulate the company from many of the conventional criteria by which companies are judged on a monthly or quarterly basis.

"If with my insulation removed, the company becomes susceptible to these judgements . . . this will lead to a basic conflict between two different approaches: first, the long-term, imaginative approach of sensing an unmet human need and bringing it, by way of science, to fulfillment; and second, responding to a chorus of external contemporary voices." What will be Polaroid's next big invention? Land laughs, but won't say. "I hope they guess what I hope it will be", he replies.

Deborah Shapley

0028-0836/82/330701-01$01.00

CORRESPONDENCE

Coal in reserve

Sir — Robert Olby's article "Britain's resources of coal and spent uranium fuel" (*Nature* 29 April; **296** 797-801) puts into sharp perspective the opposing arguments about fossil fuels versus nuclear fuels.

For the first time, the previously murky distinctions between the different classes of coal reserves have been made fairly clear. Previous attempts to do this have usually been obscured by the question of the future of coal versus other forms of energy. For example, those who believe that limited government resources should not be invested in the coal industry have tended to use the most restricting definitions of coal reserves, coupled with the lowest figures of percentage extraction, in order to suggest that coal has no future. As Olby points out, referring to A.M. Clarke, the future of coal is hardly unaffected by government policy. However, Olby himself is impartial in the matter of policy; he is simply clarifying the distinctions between different classes of coal reserves.

His brief account of Jevons's much misunderstood work of 1865 is also impressive. Jevons's point is just as valid today and, apparently, just as misunderstood. The finite extent of our recoverable fuel reserves does not define the period of time for which we can exist as we are before we run out of fuel. It defines the *much shorter period* for which we can continue to expand for the same production-to-fuel consumption ratio. A statement such as "At present rates of consumption, we have enough coal for 300 years" is thus meaningless.

Mr A.M. Clarke, ex-Chief Geologist of the National Coal Board, has probably done more than anyone else in Britain to stir up thought on these issues. It is good to see that his work is acknowledged in your pages, despite the continuing efforts both inside and outside the National Coal Board to denigrate his achievements.

Anton Ziolkowski

Department of Mining Engineering,
Delft University of Technology,
Delft, The Netherlands

Ball of fire?

Sir — On Tuesday, 3 August, shortly after 4.00 p.m., the Cavendish Laboratory and the surroundings were struck by lightning several times during an exceptionally intense storm. No structural damage ensued, but immediately after one of the discharges a ball of light was seen by a number of observers. Their descriptions are not entirely consistent but certain features are agreed upon well enough to enable a broad description to be given. The discharge apparently responsible struck near the centre of the Bragg Building, which runs east-west. An observer on the ground floor of the Mott Building, whose back was to the window, saw his room momentarily lit as if by a very bright object moving past rapidly towards the west, between the Bragg and Mott buildings. Another observer on the first floor saw the space between the buildings filled with a luminous haze at least to the first floor level, and on looking to the west noticed a blue-white light that he thought at first was a warning light on a distant tower. He apparently noticed no motion, but his companion in the same room must have seen it an instant earlier for she had the impression that it was moving past and away, and possibly expanding as it went, being about the size of a grapefruit when first seen. Three people who saw it after that, as it moved over the ground to the west, agreed it looked about the size of the moon, was blue-white in colour, very bright, and was visible for some 4-5 seconds before suddenly vanishing.

To this reasonably well attested observation must be added that while an assistant in the duplicating room, on the ground floor, was closing a small window she was startled by a noise that made her think the window had been knocked in; a bright sparkling object, resembling the lights thrown out by expensive rockets, entered by her head, rebounded from a machine and left as it came. The window was in fact undamaged, and when examined next morning entirely unmarked. Both assistants who were there at the time are convinced something came into the room.

Brian Pippard

Department of Physics,
University of Cambridge, UK

Badgers still snared

Sir — I understand that the Royal Society for Nature Conservation, while welcoming the ending of the gassing of badgers by the Ministry of Agriculture (*Nature* 22 July, p.317) because of its inhumanity, is adamant that only badgers that are positively found to be infected with tuberculosis should be destroyed. We learn, however, that snaring of badgers is to continue (which is surely as inhumane if not more so than their gassing) which makes it impossible to test for infection before killing.

Gwendolen Barter

Margate, Kent, UK

Nuclear risks

Sir — I find the claims of Martin Fodor concerning the dangers of nuclear power (*Nature* 22 July, p.320) both confusing and inconsistent with the available evidence. Studies in a number of countries have compared the number of fatalities from the routine operations of the complete fuel cycle for nuclear, coal-fired and oil-fired generation. They all show that nuclear generation is at least as safe, and probably a good deal safer, per unit output than using coal or oil. Martin Fodor is quite wrong to imply otherwise.

These evaluations include the contribution from uranium mining to the hazards of nuclear generation. I am not aware of any studies showing 50-100 per cent occupational mortality among uranium miners, but it has been known since the fifteenth century that underground metalliferous mines give rise to enhanced mortality from lung disease among the workforce. Modern radiation safety standards based on the recommendations of the International Commission for Radiological Protection (ICRP) are designed to ensure that working with radiation safety ensures that the main occupational hazard in uranium mining is the physical risk.

Comparative estimates of the routine risks from the alternative energy sources are not so reliably established as for nuclear and fossil fuels. However, such information as is available suggests that the risk per unit generation is within the range of the other fuels. Professor Fremlin has pointed out that the idyllic village millpond has only to account for one drowning every 200 years to be classified as the most hazardous energy source, and generating electricity from wavepower, the renewable resource with which the United Kingdom is most generously endowed, is likely to involve substantial risks.

Rare major accidents invariably give rise to a much smaller death rate than the routine operational risks for all technologies. Despite this, they are of particular concern because of society's abhorrence of multiple fatality accidents. Nuclear electricity generation is particularly well protected against such events: not a single death from radiation has been recorded from any accident during the 25 years such plants have been operating. Whilst the probability of nuclear power accidents is certainly not zero, all the evidence indicates that the risk is much smaller than for many other accepted activities. Anyone concerned about accidents which may kill large numbers of people should worry about technologies other than nuclear power which are over 100 times more likely to cause such accidents.

The overall conclusion can only be that no practicable method of electricity generation is particularly hazardous, nor is any so safe as to merit particular preference. Nuclear electricity generation is certainly not the most hazardous of the technologies we use, and may be one of the safer options.

Safety is only one aspect of the environmental impact of electricity generation. In other respects nuclear power has an inherent advantage because it is the most compact energy resource available. Consideration of land use, visual intrusion, water supply, transport requirements and biological effects, together with the safety aspects, gives good grounds for the view that on balance nuclear power is the least environmentally damaging of the available options for providing the electricity we need.

Brian Wade

AERE Harwell,
Oxfordshire, UK

Oxygen treatment

Sir — In view of the recent press publicity, which we understand has embarrassed many neurologists and general practitioners, on the use of hyperbaric oxygen in the treatment of multiple sclerosis, the Multiple Sclerosis Society wishes to state that at no time has it recommended its members to seek treatment with hyperbaric oxygen.

We are awaiting with interest the results of a carefully monitored double-blind controlled study recently undertaken in America with the support of the American National Multiple Sclerosis Society. Upon receipt of the results of this trial the society's medical advisers will immediately review this matter.

John Walford

Multiple Sclerosis Society,
London, UK

Mitochondrial mosaics — maturases on the move

from Leslie A. Grivell and Piet Borst

To the initiated, the idea that mitochondria have opted for unusual modes of gene expression must surely be becoming a familiar one. A paper just published in *Nature* (**298**, 628; 1982) by Dujardin *et al.* shows, however, that additional surprises may still be in store regarding the proteins that mtDNA encodes. The paper illustrates that mutations are not necessarily changes for the worse: a single amino acid substitution in an intron-encoded protein is responsible for generating a new enzymatic function, leading to the expression of a novel mRNA maturase active in splicing.

Two years ago, Lazowska *et al.*[1] showed that a protein encoded in part by the second intron in the yeast mitochondrial gene for cytochrome *b* (*cob*) is required for the splicing out of that same intron sequence from its own mRNA, one of the precursors to the mRNA for cytochrome *b*. The protein, *box3* (or bI$_2$) RNA maturase, is a chimaera, consisting of the amino-terminal half of cytochrome *b*, fused to an intron-specific sequence. Since it controls its own synthesis by destroying the mRNA which encoded it, Lazowska *et al.*[1] coined the term 'splicing homeostasis' to describe the self-regulation of RNA processing that results.

Other mitochondrial introns, both in yeast and other fungi, also contain long unassigned reading frames (URFs)[2-5] and many, if not all of them, may encode proteins with maturase action. Two series of observations support this view. First, the URFs display varying degrees of sequence conservation, suggestive of constraints on protein structure and indicating that their products have similar functions[3,6,7]. Second, *trans*-recessive mutants defective in splicing have been identified in the URFs of the other two main introns of the cytochrome *b* gene (bI$_3$ and bI$_4$)[3-10].

An unexpected complication was the finding that numerous intron mutations of the cytochrome *b* gene are pleiotropic. They prevent the synthesis not only of cytochrome *b*, but also of subunit I of cytochrome *c* oxidase[11]. This protein is also specified by a mosaic gene (*oxi3*) and the lack of expression is known to be due to a defect in the processing of the oxidase pre-mRNA[12,13]. The effect on expression works in only one direction as mutations in *oxi3*, including large deletions, have no effect on the expression of the cytochrome *b* gene[12,13]. The link is positive as deletion of all or part of the cytochrome *b* gene similarly blocks oxidase synthesis[14]. The key factor has been traced by genetic experiments to the fourth intron of the long form of the cytochrome *b* gene (bI$_4$)[15]. Several lines of evidence[9,16] now strongly suggest that the RNA maturase encoded by bI$_4$ is also involved in excision of aI$_4$, the fourth intron of the *oxi3* gene and one which is highly homologous to bI$_4$ (ref.3).

To learn more about the requirements for mitochondrial splicing and about the components involved, Slonimski and his associates have developed a general method for the selection and characterization of extragenetic suppressors of splicing-deficient mutations located in introns[17].

One of these mutations has been fully described in the recent report by Dujardin *et al.* The mutation (*mim* [*mi*tochondrial–*m*itochondrial interaction] *2-1*) is a single G→A transition in the open reading frame of aI$_4$, where it produces a glutamate to lysine substitution. In its presence, the cytochrome *b* gene and the mRNA maturase encoded by bI$_4$ are no longer required for the splicing and expression of the oxidase gene and, just as remarkable, expression of the cytochrome *b* gene in mutants with a defective bI$_4$ maturase is once again possible. Evidently, the *mim 2-1* mutation induces the synthesis of an aI$_4$ maturase with an activity different from that present in wild type. This novel maturase can presumably act as a substitute for a defective bI$_4$ maturase, using the same set of recognition sequences present in both pre-mRNAs[16]. This explanation is appealingly simple; nevertheless it raises a number of intriguing questions about the origin, evolution and function of the URFs in yeast mtDNA, some of which are addressed by Dujardin and his colleagues.

First, how is a new maturase formed from an 'inactive' one and what is the normal function of the aI$_4$ URF? Dujardin *et al.* propose that the replacement of a glutamate by lysine, which changes the overall charge of the protein by +2, may bring about a local increase in positive charge in a region of the protein that is essential for catalytic activity. The *mim2-1* change occurs in a α-helical region of 15–18 amino acids, which occupies homologous positions in the bI$_4$ and aI$_4$ URFs. The α-helix of wild-type bI$_4$ is more basic than that of wild-type aI$_4$ by two or four charges, dependent on strain polymorphism. The *mim2-1* mutation would make the aI$_4$ translation product more similar to its bI$_4$ counterpart.

What is the normal function of the aI$_4$ translation product? The aI$_4$ and bI$_4$ URFs display a high (>70 per cent) homology at the protein level and are presumably derived from a common ancestor. On this basis Dujardin *et al.* consider two scenarios. First, the aI$_4$ protein may simply be a pseudogene. A single substitution might (somewhat implausibly) still be capable of resurrecting the gene and restoring its function. Second, evolutionary divergence of aI$_4$ and bI$_4$ could have led to a diffusible protein, endowed with a pleiotropic splicing activity (bI$_4$) and to a protein with no catalytic splicing activity at all (aI$_4$). A selective pressure against the accumulation of chain-termination mutations in aI$_4$ would be provided if it had retained, or acquired, other functions, for example as a structural component of the mitochondrial splicing and/or translation apparatus. However, because of the extent and nature of sequence conservation between the two URFs, we prefer the idea that the wild-type aI$_4$ translation product fulfils a maturase function, that has so far escaped detection by mutagenesis. The main effect of the *mim 2-1* mutation may then be to alter substrate specificity.

What do maturases do and how do they do it? These are somewhat embarrassing questions, since not a single maturase has been isolated. They appear to be present in such low concentrations in wild-type yeast cells that they even escape detection by pulse-labelling. Conclusions about their structure and mode of action can, therefore, only be drawn from their DNA sequences and other indirect evidence. All URFs code for proteins which are rich in basic and hydrophobic residues and whose overall characters are suggestive of globular, non-membrane-associated proteins. Characteristics seen in similar distributions of charged residues, or residues

---

Leslie A. Grivell and Piet Borst are in the section for Medical Enzymology and Molecular Biology of the Laboratory of Biochemistry, University of Amsterdam.

0028-0836/82/330703-02$01.00

disrupting helical structure[6,7], are conserved within a central 115 amino acid stretch of each URF. This region, which is bounded by characteristic decapeptide motifs, is thus likely to play a key part in determining both protein structure and enzymatic function, as does a region immediately downstream, in which numerous *trans*-recessive mutations affecting splicing have been identified[9,10].

Two indirect observations concerning maturase function are important. First, intron mutants, with defective mitochondrial maturases, generally accumulate only high molecular weight, intron-containing pre-mRNAs[12,13]. Second, nuclear mutants defective in mitochondrial splicing reactions have been isolated and partially characterized. The defects are surprisingly specific, often involving an inability to cut or ligate the ends of a single intron in the gene for cytochrome *b* or subunit I of cytochrome *c* oxidase. In one group of cytochrome *b*-deficient mutants recently studied by Diekmann *et al.*[18], transcripts consisting of bI_4 linked to downstream exon sequences accumulated, indicating first that a nuclear gene product is required for scission of the bI_4–exon boundary and second, by implication, that the bI_4 maturase may itself be involved in the initial scission at the upstream exon-bI_4 border.

With such an intricate systems for RNA processing, it is remarkable that many individual introns and their maturases are dispensable, in that various yeast strains, either found in nature[19] or constructed in the laboratory[8,15], can lack them entirely and suffer no ill-effect. So, why have introns?

One view is that they are evolutionary relics, left over from a primitive, genes-in-pieces type of genome organization. Indeed, the high homology observed between introns in mtDNA of yeast and *Aspergillus nidulans*[4,5] indicates that at least some introns pre-date the common ancestor of these fungi. On the other hand, whatever role introns may have had in the evolution of mitochondrial genes, their continued retention in fungal mtDNAs cannot be an accident. The distribution of introns is highly non-random: two of the seven major protein-coding genes, one of the two rRNA genes and none of the tRNA genes contain introns. The maintenance of the introns requires a large number of genes involved in splicing; this complex system must be vulnerable to disruption by mutation. Nature is not without means to eliminate this costly genetic investment, because it can produce mtDNAs with fewer or no introns. The introns in the fungal mtDNAs must therefore confer a selective advantage now.

Among possible advantages, the most plausible is that additional splicing steps allow a more precise control over mitochondrial gene expression. This could permit, for example, the selective suppression of the synthesis of mitochondrial components during growth in the presence of fermentable sugars. Such an explanation may not, however, hold for all introns and all fungi. The gene for the mitochondrial large rRNA contains an intron plus URF, yet accurate splicing is possible in the absence of the URF product[20] (albeit somewhat inefficiently) and rRNA synthesis does not seem to be selectively repressible. Again, *Aspergillus* has also retained introns and their reading frames in the genes for cytochrome *b* and subunit I of cytochrome *c* oxidase, yet does not repress mitochondrial synthesis. There is obviously room for further speculation about the selective advantage of having mitochondrial introns and maturases.

Finally, where do the introns and their maturases come from? We suggested previously[21] that they might have arisen from insertion elements which lost their mobility in the course of evolution and this idea remains plausible. First, the sequence homologies found between the URFs of yeast mtDNA argue for a common origin with subsequent dispersal around the genome[7]. Second, the hypothesis correctly predicts that sequences homologous to intronic reading frames may also be found outside genes[22]. Third, all yeast URFs display codon usage which deviates markedly from the characteristic pattern observed in genes for known, major translation products[3,23]. Such usage could be the last visible trace of a separate genetic orgin of URF sequences. □

1. Lazowska, J., Jacq, C. & Slonimski, P.P. *Cell* **22**, 333 (1980).
2. Nobrega, F.G. & Tzagoloff, A. *J. biol. Chem.* **255**, 9828 (1980).
3. Bonitz, S.G., Coruzzi, G., Thalenfeld, B.E., Tzagoloff, A. & Macino, G. *J. biol. Chem.* **255**, 11927 (1980).
4. Waring, R.B. *et al. Cell* **27**, 4 (1981).
5. Netzker, R., Köchel, H.G., Basak, N. & Küntzel, H. *Nucleic Acids Res.* (in the press).
6. Michel, F., Jacquire, A. & Dujon, B. *Biochemie* (in the press).
7. Hensgens, L.A.M., Bonen, L., de Haan, M., Van der Horst, G. & Grivell, L.A. *Cell* (submitted).
8. Jacq, C. *et al.* in *Mitochondrial Genes* (eds Slonimski, P.P., Borst, P. & Attardi, G.) 155 (Cold Spring Harbour Laboratory, New York, 1982).
9. De la Salle, H., Jacq, C. & Slonimski, P.P. *Cell* **28**, 721 (1982).
10. Weiss-Brummer, B., Rödel, G., Schweyen, R.J. & Kaudewitz, F. *Cell* **29**, 527 (1982).
11. Pajot, P., Wambier-Kluppel, M.L., Kotylak, Z. & Slonimski, P.P. in *Genetics and Biogenesis of Chloroplasts and Mitochondria* (eds Bücher *et al.*) 443 (Elsevier, Amsterdam, 1976).
12. Church, G.M., Slonimski, P.P. & Gilbert, W. *Cell* **18**, 1209 (1979).
13. Van Ommen, G.J.B. *et al. Cell* **20**, 173 (1980).
14. Alexander, N.J., Perlmann, P.S., Hansen, D.K. & Mahler, H.R. *Cell* **20**, 199 (1980).
15. Dhawale, S., Hansen, D.K., Alexander, N.J., Perlman, P.S. & Mahler, H.R. *Proc. natn. Acad. Sci. U.S.A* **78**, 1778 (1981).
16. Netter, P., Jacq, C., Carignani, G. & Slonimski, P.P. *Cell* **28**, 733 (1982).
17. Dujardin, G., Pajot, P., Groudinsky, O. & Slonimski, P.P. *Molec. gen. Genet.* **179**, 469 (1980).
18. Dieckmann, C.L., Pape, L.K. & Tzagoloff, A. *Proc. natn. Acad. Sci. U.S.A.* **79**, 1805 (1982).
19. Borst, P. in *31. Colloquium-Mosbach 1980: Biological Chemistry of Organelle Formation* (eds Bücher, T., Sebald, W. & Weiss, H.) 27 (Springer, Berlin, 1980).
20. Tabak, H.F. *et al. Nucleic Acids Res.* **9**, 4475 (1981).
21. Borst, P. & Grivell, L.A. *Nature* **289**, 439 (1981).
22. Coruzzi, G., Bonitz, S.G., Thalenfeld, B.E. & Tzagoloff, A. *J. biol. Chem.* **256**, 12780 (1981).
23. Dujon, B. in *Molecular Biology of the Yeast Saccharomyces: Life Cycle and Inheritance* (Cold Spring Harbour Laboratory, New York, 1981).
24. Hudspeth, M.E.S., Ainley, W.M., Shumard, D.S., Butow, R.A. & Grossman, L.I. *Cell* (in the press).

Where has that Moon been?

from Kurt Lambeck

THAT tidal forces play a most significant part in the dynamical evolution of the Earth–Moon system is beyond dispute. What is in dispute is the time scale of this evolution. One more attempt at resolving this vexing question has recently been discussed by Webb in the *Geophysical Journal of the Royal Astronomical Society* (**70**, 261; 1982).

That this ancient subject continues to draw the attention of scientists in diverse disciplines may seem curious but is a reflection of the important ramifications of tidal evolution models as well as their intellectually satisfying nature. Few other subjects require one to delve into the rigours of celestial mechanics or into the ambiguity of an observational record that includes eighteenth century telescope observations, ancient records of eclipses and the life styles of Palaeozoic corals. It requires investigations into the solid Earth's structure, into ocean tides, speculations on the evolution of the Earth and an initiation into the mysteries of lunar chemistry.

A central difficulty in modelling the past orbital and spin configurations of the Moon and Earth is to extrapolate from present-day tide models and tidal accelerations. It is inescapable that most of the tidal energy is dissipated in the oceans[1] and that this must have been so for much of the Earth's past history. Any extrapolation backwards into geological time is, therefore, only as good as the assumption that past and present tides are identical or that past tides can be characterized by some mathematically convenient law. Such extrapolations lead to the conclusion that the Moon must have been very close to the Earth some 1.5–2 billion years ago. This conclusion is unsavoury to most lunar scientists[2].

Can this close approach, so late in the Earth's history, be avoided without invalidating the orbital evolution calculations?. Is it possible to push it back into the Earth's remote past? This is the problem that Webb sets out to solve; how to compute representative tidal dissipation estimates for past epochs when the requisite detailed oceanic data are

Kurt Lambeck is Visiting Professor at the University of Paris-Sud, on leave from the Australian National University, Canberra.

0028-0836/82/330704-02$01.00

unavailable. His approach is not to consider detailed models at specific geological epochs as others have attempted[3]. Instead Webb adopts an 'average' ocean model and then investigates how dissipation may vary in response to the evolving Earth–Moon system. In particular, he investigates the dependence of dissipation on the frequency of the tide-raising force. His important result is that the rate of tidal energy dissipation has been less in the past than it is now and that the calamitous consequences of a close approach of the Moon can be readily averted.

Present rates of energy dissipation are now quite well established as about 4.0 × 10^{12} Watts (ref. 4). It is also clear that at least 90 per cent of this energy is dissipated in the oceans. What remains less obvious is the mechanism by which this dissipation takes place. Is it by bottom friction in a few shallow seas, or by a more global mechanism such as the breaking of tidal waves along shorelines or the scattering of tidal waves into internal modes? Advocates of all mechanisms can be found but it seems that the actual assumptions made have little influence on the numerical solutions or interpolations of the Laplace tidal equations. Compare, for example, the recent tidal models for the dominant lunar tide[5-8]. All solutions require that dissipation is fairly uniformly distributed through the world's oceans, and all give very comparable results once corrections for the solid tide are made where appropriate[4]. That this is so is at least partly because all solutions are either explicitly or implicitly constrained by observations of the tides. But it makes Webb's approach of considerable interest for he does not have to make assumptions about the detailed ocean geometry. Instead, he considers tides on a hemispherical ocean[9] whose orientation with respect to the Earth's rotation axis is allowed to vary through all possible values. Dissipation is introduced by requiring that the decay time of tidal energy equals the average observed value. For a given frequency of the tide — defined by the Earth–Moon distance and the Earth's spin rate — Webb averages the power estimates over all orientation angles with the acceptable rationale that the time constant for plate tectonics is much less than the age of the oceans. The variation in the ocean geometry with time is therefore accounted for in this statistical manner. At any one frequency, strong resonances are encountered as a function of the orientation but Webb finds that, when averaged, these isolated resonances are smoothed out and that any resonances in the averaged power curve occur at frequencies that are lower than present and past values: the further one goes into the past the greater becomes the separation between the forcing and resonance frequencies.

Consequentially, past rates of orbital evolution will be less than if the Q or dissipation function of the ocean had been held constant, and Webb concludes that the close approach may never have occurred at all. Quantitatively his results may not be very significant but the general trend that emerges is. Evidence for reduced dissipation in the geological past has also been found in palaeontological records of the Earth's rotation where growth rhythms in corals and bivalves point to less dissipation over the past 400 million years than occurs at present[4]. A similar conclusion was also reached from explicit model studies of past ocean tides[3].

A word of caution seems appropriate however. The resonance frequencies of the ocean basins depend on the ocean scale as well as on the ocean depth. Thus by fixing the decay time, Webb also assumes that these factors have not changed much. The approximate period of the free oscillation is given by $2L/(gh)^{1/2}$ where L is the characteristic length scale, h the average depth and g is gravity. If, on the average, L is greater than today, as when the oceans were clustered into the Pangea continent, then the driving force will have been further away from resonance than it is now. If the ocean depths were less in the past, if the present basins evolved only relatively late in the Earth's history, then the difference between the forcing and resonance frequencies also increases. Thus some cancellation of Webb's result may occur. I rather doubt that this will be significant and those who argue that the Moon formed close to the Earth can sleep in peace. ☐

---

1. Lambeck, K. *Phil. Trans. R. Soc.* **A287**, 545 (1977).
2. Ringwood, A.E. *The Origin of the Earth and Moon* (Springer, Berlin, 1979).
3. Sundermann, J. & Brosche, P. *Tidal Friction and the Earth's Rotation*, 125 (Springer, Berlin, 1978).
4. Lambeck, K. *The Earth's Variable Rotation* (Cambridge University Press, 1980).
5. Zahel, W. *Ann. Geophys.* **33**, 31 (1977).
6. Accad, Y. & Pekeris, C.L. *Phil. Trans. R. Soc.* **A290**, 235 (1978).
7. Parke, M.E. & Hendershott, M.C. *J. mar. Geod.* (1980).
8. Schwiderski, E.W. *Rev. Geophys. Space Phys.* **18**, 243 (1980).
9. Webb, D.J. *Geophys. J. R. astr. Soc.* **61**, 573 (1980); **68**, 689 (1982).

From CoA to complement: thioesters as the spring in the molecular mouse trap

from John Fothergill

To most biochemists, thioesters mean coenzyme A and fatty acid metabolism. They are remarkable for their high free energy of hydrolysis and their participation as metabolic intermediates. With this background, the discovery of thioesters in proteins came as something of a surprise.

There is now good evidence that two of the complement proteins, C3 and C4, and the plasma proteinase inhibitor α_2-macroglobulin contain an internal thioester formed from the side chains of a cysteinyl and a glutamyl residue four positions apart on the polypeptide chain. In the native protein, the thioester is apparently buried, but on activation of the protein by proteolytic cleavage the thioester is exposed to the surroundings, readily generating a free thiol and an active acyl group that can react with nucleophilic amino or hydroxyl groups. This leads to covalent attachment of the thioester protein to adjacent protein or carbohydrate. Thus a single proteolytic cleavage of the protein containing the thioester leads to covalent linking of the activated protein to a nucleophilic group in its immediate environment. What are we to make of this 'molecular mouse trap'?

It has been known for a long time that complement components, once activated, adhere strongly to cell surfaces. This was explained as an interaction between a hydrophobic region on the complement component, revealed during proteolytic activation, and the cell membrane. The relatively short half life of the activated complement components was explained in terms of conformational rearrangement of this hydrophobic binding region. The first evidence[1] that the reaction could be a covalent one came from the detection of proteins in SDS-polyacrylamide gel electrophoresis that had higher molecular weights than the C3 polypeptide chains they were known to contain. Similar evidence has been obtained for the covalent binding of C4 (ref. 2) and C3 (ref. 3) to antigen–antibody aggregates. During the last two years evidence for this internal thioester has been accumulating rapidly. Publications have been overwhelmingly confirmatory, if somewhat repetitious.

Much of the evidence for the thioester in C3 has come from the work of Janatova

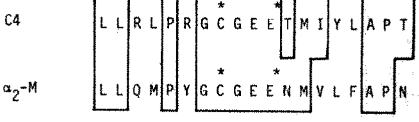
C3
L I V T P S G C G E E N M I G M T P T
C4
L L R L P R G C G E E T M I Y L A P T
α2-M
L L Q M P Y G C G E E N M V L F A P N
*
*

Fig. 1. Amino acid sequences around the thioester site of C3 (ref. 4), C4 (ref. 5) and α_2-macroglobulin (ref. 6). The cysteinyl and glutamyl residues contributing to the thioester are marked by an asterisk.

John Fothergill is in the Department of Biochemistry, University of Aberdeen, Aberdeen AB9 1AS.

0028-0836/82/330705-02$01.00

and Tack, and a recent paper[4] summarizes the present position. The glutamyl residue of the thioester can be labelled with radioactive methylamine producing the corresponding γ-glutamylmethylamide; the thiol group reacts with the usual reagents. Labelling studies have shown clearly that the reactive residues are in the C3d part of the C3b molecule which is known to contain the membrane-binding site. The amino acid sequence of this part of the polypeptide chain has been determined and it is obviously homologous not only to the corresponding region in C4 (ref. 5) but also to the thioester sequence in α_2-macroglobulin[6] (Fig. 1). Model-building studies have shown that the thioester cannot form if the polypeptide adopts an α-helix, β-sheet or β-turn conformation, but it is possible to arrange the atoms without undue strain in an unusually sharp bend that allows the glutamyl carboxyl and cysteinyl thiol groups to approach close enough to form the thioester.

The whole thioester story is intimately bound up with the question of conformational rearrangement during activation. Intact C3 is known to show circular dichroism spectra that are significantly different from those of a mixture of its activation products C3a and C3b (ref. 7). Treatment of C3 with methylamine or by freezing and thawing also produces evidence of conformational changes[8] and renders the C3 haemolytically inactive. Interestingly, evidence for an increase in exposed hydrophobic surface occurring concomitantly with this conformational change was also obtained[9]. Whether the biological activity of C3 and C4 depends on both covalent attachment by virtue of the thioester cleavage and hydrophobic interactions resulting from conformational rearrangement remains to be unequivocally demonstrated. It is noteworthy that the structurally homologous complement protein C5 has similar properties but no thioester.

The discovery of these thioesters has opened up many new possibilities in mechanisms of complement activation and in more general aspects of protein chemistry. The suggestion has been made that spontaneous hydrolysis of the thioester in C3 may generate C3b-like activity that could form the nucleus of a C3 convertase for the alternative pathway[10]. The implications for biosynthesis are particularly fascinating. At what stage of maturation is the thioester formed? Is there a thiokinase, with requirements for a nucleoside triphosphate, or does the folding of the nascent polypeptide chain contribute all that is necessary? Is the Lippman 'squiggle' the spring of this molecular mouse trap? ☐

---

1. Law, S. K. & Levine, R. P. *Proc. natn. Acad. Sci. U.S.A.* **74,** 2701 (1977).
2. Campbell, R. D., Dodds, A. W. & Porter, R. R. *Biochem. J.* **189,** 67 (1980).
3. Gadd, K. J. & Reid, K. B. M. *Biochem. J.* **195,** 471 (1981).
4. Thomas, M. L., Janatova, J., Gray, W. R. & Tack, B. F. *Proc. natn. Acad. Sci. U.S.A.* **79,** 1054, (1982).
5. Campbell, R. D., Gagnon, J. & Porter, R. R. *Biochem. J.* **199,** 359 (1981).
6. Swenson, R. P. & Howard, J. B. *J. biol. Chem.* **255,** 8087 (1980).
7. Hugli, T. E., Morgan, W. T. & Müller-Eberhard, H. J. *J. biol. Chem.* **250,** 1479 (1975).
8. Isenman, D. E., Kells, D. I. C., Cooper, N. R., Müller-Eberhard, H. J. & Pangburn, M. K. *Biochemistry* **20,** 4458 (1981).
9. Isenman, D. E. & Cooper, N. R. *Molec. Immun.* **18,** 331 (1981).
10. Pangburn, M. K., Schreiber, R. D. & Müller-Eberhard, H.J. *J. exp.Med.* **154,** 856 (1981).

Focus on filaments: embryology to pathology

from Birgitte Lane and Brian Anderton

A RECENT workshop* provided a useful summary of current research on intermediate filaments. With actin and tubulin, these filaments constitute the third fibre system of the cytoskeleton. They are morphologically well defined (as 10 nm filaments) and stable *in vitro,* and show a biochemical heterogeneity which is developmentally regulated. Each class of intermediate filament is restricted *in vivo* by tissue differentiation: vimentin to mesenchymal cells, desmin to muscle tissues, keratins to epithelia, glial fibrillary acidic protein (GFAP) to astroglia and neurofilament proteins to neurones. Given this apparently ideal experimental system, it is frustrating that so little is yet known about intermediate filament function.

However, progress is being made. Some synthesis is becoming possible regarding molecular structure, as Geisler (Max Planck Institute, Goettingen) showed in proposing a model for vimentin-like proteins, based on primary sequence data. The model molecule has three domains separated by enzyme-sensitive hinge regions: (1) a short, basic, folded head piece (about 7.5K) sensitive to proteolysis; (2) a long (38K) middle piece, helical and very acidic; and (3) a short tail piece, about 5.5 K and probably globular. The mid-piece helix has a hydrophobic edge which may stabilize the intertwining of molecules into protofilaments, while charged patches on other parts of the helix may aid association into 10 nm filaments. Mid-pieces can aggregate into filamentous and sheet-like structures, but the head and tail pieces seem to be necessary for correct assembly of filaments.

Quax (University of Nijmegen) reported the DNA sequence of a cloned hamster vimentin gene: there may only be a single gene for vimentin in mammals, in contrast to the multiple genes for keratins described by Green (Harvard Medical School). Surprisingly, keratin, and not vimentin, is the first type of intermediate filament to appear in ontogeny. The first keratins appear in the morula (Jackson, University of Geneva) as a pair of polypeptides of 53K (basic group) and 44K (acidic group). Franke (German Cancer Research Centre, Heidelberg) declared this to be the simplest keratin profile, therefore presumably the minimum required for filament formation. It was clear from many two-dimensional gels shown at the meeting that keratins can be classified as either acidic (smaller) or basic (generally larger). Presumably it is this complementarity of charge and size that restricts the major epidermal keratins to obligate heteropolymerization, as described by Steinert and colleagues some years ago.

Although some adult epithelia retain an almost embryonic simplicity of keratins, most differentiating epithelia acquire a more eleborate keratin profile, culminating in epidermal keratinocytes. Franke reported that 19 separate human keratins have now been identified. Sun (Johns Hopkins Medical Institute) suggested an ontogenic 'tree' model to help visualize the developmental complexity of the epidermis, which he demonstrated using three complementary monoclonal antibodies. Monoclonal antibodies to keratins can be used to detect non-keratinocytes in complex epithelial tissues (Lane, ICRF), and an elegant presentation by Moll (German Cancer Reserch Centre) showed how keratin microheterogeneity within a tissue or tumour could be scrutinized by two-dimensional gel electrophoresis of laser-dissected frozen sections.

Co-expression *in situ* of different types of intermediate filaments in one cell has only been reported in restricted situations, usually involving an overlap early in development between vimentin and the later-appearing tissue-specific class. Two cases of filament co-expression in adult cells were described at the meeting: astroglia, which by consensus of opinion usually contain vimentin as well as GFAP, and aortic smooth muscle, where cells may contain desmin or vimentin or both (Frank, Wistar Institute). Otherwise, the tissue specificity *in situ* of the non-vimentin filament classes remains clear-cut.

Do tumours express the filament type characteristic of the normal cell from

---

*The EMBO-sponsored workshop 'Intermediate filaments in differentiation and pathology' was held at the end of April in Gunzburg, FRG.

Birgitte Lane is at the Imperial Cancer Research Fund Laboratories, Lincoln's Inn Fields, London WC2A 2PX, and Brian Anderton is at St George's Hospital Medical School, Cranmer Terrace, London SW17 0RE.

0028-0836/82/330706-02$01.00

which they arise? The answer to this question is clearly yes — tissue specificity of intermediate filaments is retained in the tumour, and vimentin does not appear inappropriately. This was demonstrated by Osborn (Max Planck Institute, Goettingen) in the keratin-positive, vimentin-negative phenotype of intestinal cancers, and the desmin-positive, vimentin-negative phenotype of rhabdomyosarcomas.

On the other hand, tissue culture can modify filament expression, in that vimentin appears in most cultured cells. The meeting heard the first report of vimentin in epithelial cells in the body, however. Ramaekers (Catholic University of Nijmegen) observed vimentin in carcinoma cells growing as ascites, that is, in suspension, but when growing as a solid tumour these cells only expressed keratin. This may be a clue to the significance of vimentin induction.

Pathologists at the meeting agreed that intermediate filament antibodies are useful for identifying the origin of tumour metastases when standard histological methods are inconclusive. Improvements were suggested to avoid the need for frozen sections, since most intermediate filament antibodies react poorly with aldehyde-fixed material. Osborn showed high-quality immunofluorescence preparations of methanol-fixed, paraffin wax-embedded material; Coggi (University of Milan) used formalin-fixed material, but amplified sensitivity with multiple biotin-avidin complexes.

It is sometimes of immense medical value to be able to identify the origin of displaced cells. Virtanen (University of Helsinki) reported the presence of GFAP-positive (that is, astroglial) cells in amniotic fluid from anencephalic fetuses, and in many cases of spina bifida; normals were negative, since unless nervous tissue is exposed the glial cells cannot get into the aminiotic cavity.

Two examples of a pathological expression of intermediate filaments were discussed: Mallory bodies (containing keratin) of liver cells in alcoholic cirrhosis (Denk, University of Vienna) and neurofibrillary tangles of Alzheimer's senile dementia (Anderton, London, and Bignami, Havard Medical School). Anderton reported that the neurofibrillary tangles could only be stained by some of a group of neurofilament-staining monoclonal antibodies, and similar partial cross-reactivity with conventional antisera was reported by Bignami, implying that neurofibrillary tangles contain structurally altered neurofilaments.

Perhaps the most unexpected reports came from studies of mitosis. Franke and Lane independently described how keratin filaments break up into balls during mitosis in epithelial cell lines. This fact is not widely known, probably because of the preference for fibroblast models in cytoskeleton studies. Lane described how the balls, which form in prophase, may be associated with the plasma membrane, and Franke described associated 2 nm filaments, and said there was no evidence for the involvement of proteolysis. This disruption during mitosis is apparently not a tissue culture artefact, since Franke showed the effect in a human carcinoma. It was agreed that not all cell lines show the phenomenon, and Lane suggested a link with the speed of the cell cycle, such that more slowly dividing cells maintain intact filaments. Since keratins are difficult to depolymerize in non-denaturing conditions, this may be an interesting experimental system.

Thus, with some useful data on molecular structure, and the availability of systems in which the cell reorganizes its filaments *in situ*, we may soon understand how, and why, these molecules interact in the cell. Meanwhile the usefulness of filament antibodies in medical diagnosis should attract a greater commitment to this field of cell biology. □

Do steroid receptors recognize DNA sequences?

from J.R. Tata

On the twentieth anniversary of the Jensen two-step model of steroid hormonal regulation of gene expression[1] there is, at last, good evidence for one of its chief predictions. According to the model, steroid hormones interact in their target tissues with a high-affinity cytoplasmic receptor protein, and the interaction leads to a conformational change in the receptor such that the hormone–receptor complex is rapidly translocated into the nucleus. The receptor or receptor–hormone complex is then thought to interact with a variety of nuclear components in order to induce or modulate transcription of a few well specified genes. A prime nuclear target is DNA itself, but only recently has there emerged the first strong evidence to suggest sequence specificity of the interaction, at least *in vitro*.

In a recent study from Strasbourg, Mulvihill *et al.*[1] have most effectively exploited recombinant DNA technology and affinity chromatography to investigate the possible sequence specificity of interaction between the progesterone receptor and the genes of the egg-white protein that are induced by progesterone in the chicken oviduct. By adaptation of the oestrogen receptor DNA competition assay of Kallos and Hollander[2], Mulvihill *et al.* identified several cloned fragments from five chicken egg-white protein genes regulated by oestrogen and progesterone which could compete with calf thymus DNA for the progesterone receptor.

By testing deletion mutants, produced *in vitro*, of a fragment of the ovalbumin gene, Mulvihill *et al.* were able to narrow down the receptor recognition site to a region 250–300 base pairs (bp) 5′-upstream from the transcription initiation site, although recombinant fragments from other regions of all five genes (including exons and introns) were also found to be efficient competitors for the receptor. They then derived a consensus sequence of 19 nucleotides

$$\mathrm{ATC}\genfrac{}{}{0pt}{}{\mathrm{CC}}{\mathrm{TT}}\mathrm{ATT}\genfrac{}{}{0pt}{}{\mathrm{A}}{\mathrm{T}}\mathrm{TCTG}\genfrac{}{}{0pt}{}{\mathrm{G}}{\mathrm{T}}\mathrm{TTGTA}$$

not detected in a similar region of the globin gene, which is thought to be recognized by the progesterone–receptor complex.

It is interesting to compare the results of the Strasbourg group with findings from Schrader and his co-workers in Houston who have used a direct nitrocellulose DNA-binding assay[3-5]. Schrader also recently reported an A+T-rich region 135–250 bp upstream from the mRNA start site which is recognized by the progesterone receptor[6]. Photoaffinity labelling of the receptor with a synthetic analogue of progesterone (R5020) enabled this group to confirm their earlier suggestion that only one of the two subunits (A subunit) of the receptor recognizes DNA, while the other binds to chromatin (presumably to a protein component). However, the results of the two groups differ in some important respects. Whereas Mulvihill *et al.* find that the progesterone receptor specifically recognizes and binds to double-stranded DNA, the Houston group reported that the progesterone receptor acts as an unwinding or helix-destabilizing protein and has a preference for single-stranded DNA. The Strasbourg group ascribes this major inconsistency to several differences in methodology. They stress that they have used a crude cytoplasmic extract, in contrast to the highly purified preparation used in Schrader's laboratory, and that over-purification may have removed another component essential for the sequence-specific recognition of double-stranded DNA. They also point out that their assay measures the extent of competition by soluble DNA of progesterone–receptor complex to DNA already bound to cellulose, whereas the DNA filter-binding assay only gives the rate of association between the receptor and DNA.

J. R. Tata is Head of the Laboratory of Developmental Biochemistry at the National Institute for Medical Research, Mill Hill, London NW7 1AA.

0028-0836/82/330707-02$01.00

The sequence specificity of DNA binding by another steroid hormone receptor has also been reported recently. In a collaborative study between the University of California, San Francisco, and the Karolinska Institute in Stockholm, Payvar *et al.*[7] have suggested that the receptor for glucocorticoid hormones recognizes specific DNA sequences of murine mammary tumour virus (MMTV) within or neighbouring the gene, although the precise location of all possible sequences has not yet been determined. Their receptor preparation was purified 10,000-fold (that is, to about 50 per cent homogeneity) and tagged with the synthetic glucocorticoid ^{3}H-triamcinolone acetonide as the radioactive ligand. In a separate report, the San Francisco group has described how a 4.5 kilobase pair (kbp) *Eco*RI fragment of MMTV DNA cloned in plasmid pMTV2, which contains the long terminal repeats encoding the transcription start site but lacks 4.4 kbp of the rest of MMTV DNA, induced glucocorticoid-responsive transcription when introduced into cellular DNA[8]. Payvar *et al.* showed by ^{32}P end-labelling that the MMTV DNA fragment was specifically retained on nitrocellulose filters when bound to the glucocorticoid receptor preparation. Three different types of competition binding experiments demonstrated that the receptor selectively binds to at least four widely separated regions of MMTV proviral DNA. One of these binding sites was located 110–449 bp upstream of the promoter for MMTV transcription. Preliminary observations (for which experimental data have not yet been provided) revealed that at least one receptor binding site is located several kilobase pairs downstream from the start site of MMTV transcription.

How relevant are these *in vitro* receptor DNA binding studies to the physiological action of steroid hormones? Pongs and his colleagues in Bochum have provided the first direct evidence for the *in vivo* localization of a steroid hormone–receptor complex at the site of hormone-activated genes[9]. In the first of two papers, they showed that the insect metamorphic hormone β-ecdysterone can be covalently fixed by photolabelling to specific hormone-induced puffs of the polytenic chromosomes in the salivary glands of the third instar larvae of *Drosophila*. By using the 'Western' blotting technique of localization of ecdysterone antibody on cellulose nitrate filters, and two-dimensional gel electrophoresis, the second paper convincingly demonstrates that UV irradiation cross-links ecdysterone to a single protein of molecular weight 130,000 in both *Drosophila* larval salivary glands and K_c *Drosophila* tissue culture cells. This single protein exhibits all the characteristics of a steroid hormone receptor, including translocation from the cytoplasm to the nucleus.

The technical innovations in these recent studies represent a major step forwards in unravelling the role of steroid hormones in regulating gene expression, but they leave unanswered some important questions and raise a few new ones. First of all, discrepancies resulting from different techniques must be resolved. Then, there is the unresolved question of the high number of nuclear receptor molecules associated with full hormonal response. Although 42 sequences homologous to the 19 bp consensus segment were detected in the 14 kbp of known egg-white protein gene sequences, this number, even after generous extrapolation, does not explain the several thousand receptor binding sites normally found per cell nucleus. In this context, it is worth pointing out that the relative intensity of interaction between the progesterone receptor and specific 5′-upstream DNA sequence is only 10–40 times that observed with non-specific sequences such as calf thymus DNA or cloned globin genes[1,5]. Does this fact suggest that numerous other binding sites, not on DNA but on chromosomal proteins (also known as 'acceptor' sites), ribonucleoproteins, nuclear matrix and even non-nuclear sites, are required to induce alterations in overall structural conformation in order fully to maintain transcriptional activity? Will the results with progesterone receptor apply equally well to oestradiol, the major physiological regulator of egg-white gene expression?

In vivo functional tests, such as the introduction of viral sequences in a cell containing the rat glucocorticoid receptor, or the photoaffinity bonding of ecdysterone to its receptors in *Drosophila* cells, represent important approaches to be explored further. The next major advance will be the successful introduction of receptors in cells lacking these regulatory molecules and the manipulation of genes coding for the receptors. There is still some way to go before we can derive a unified concept of how hormones regulate gene activity, but what we learn along the way will be most valuable for our understanding of the multiple mechanisms of eukaryotic gene expression. □

---

1. Mulvihill *et al. Cell* **24**, 621 (1982).
2. Kallos & Hollander *Nature* **272**, 177 (1978).
3. Coty *et al. J. Steroid Biochem.* **10**, 1 (1979).
4. Hughes *et al. Biochemistry* **20**, 2481 (1981).
5. Compton *et al. Biochem. biophys. Res. Commun.* **105**, 96 (1982).
6. Schrader *UCLA Symp. on Gene Regulation*, Keystone, 28 March–3 April (1982).
7. Payvar *et al. Proc. natn. Acad. Sci. U.S.A.* **78**, 6628 (1981); *UCLA Symp. molec. cell. Biol.*, Squaw Valley (March 1982).
8. Yamamoto *et al. Cold Spring Harb. Symp. quant. Biol.* **45**, 681 (1981).
9. Gronemeyer & Pongs *Proc. natn. Acad. Sci. U.S.A.* **77**, 2108 (1980); Schaltmann & Pongs *Proc. natn. Acad. Sci. U.S.A.* **79**, 6 (1982).

Molecular heterogeneity and the nervous system

from Colin J. Barnstable

THE nervous system has an anatomical and physiological complexity that is considerably greater than that of other tissues and is seemingly part of a generally increased level of molecular complexity. The complexity arises both because the nervous system consists of more cell types and subtypes than other tissues and because a given neural cell seems to have a greater molecular complexity. Monoclonal antibodies are now providing an important new means of tackling this heterogeneity and of recognizing similarities and differences in neural cell types. Indeed, the use of monoclonal antibodies has grown so rapidly that two major review volumes on the fledgling subject of 'neuroimmunology' have already been published[1,2]. Two recent papers[3,4] provide good examples of the approach currently being taken by a number of laboratories.

In one paper, Hawkes *et al.*[3] used a synaptic plasma membrane fraction from rat cerebellum to immunize mice for monoclonal antibody production. In the other, Sternberger *et al.*[4] used a crude homogenate of rat hypothalamus as the immunogen.

Both papers describe antibodies that stain sections of rat brain in a manner characteristic of neurofibrillar staining. This makes it likely, though not certain, that these antibodies are staining neurofilaments, the class of intermediate filaments unique to neurones. Unlike intermediate filament types of other tissues, which consist of similarly sized polypeptide chains, neurofilaments have been isolated as a triplet of distinct polypeptides of molecular weights 200,000, 140,000 and 68,000 (ref. 5). Hawkes *et al.* found one such antibody that stained the cerebellum and reacted with a polypeptide of molecular weight 30,000. It is not yet clear whether this represents a new neurofilament polypeptide or whether it is some neurofilament-associated molecule. The staining patterns given by the other neurofibrillar antibodies were not identical, which suggests that either the neurofilament polypeptides are distributed differently between various neuronal cell types or that one or more of the neurofilament polypeptides exists in a

---

Colin J. Barnstable is in the Department of Neurobiology, Harvard Medical School, Boston, Massachusetts 02115.

variety of isotypic forms. Biochemical analysis of the antigens recognized by these monoclonal antibodies should resolve this question.

An important point to emerge from these papers is that an antibody can label different subpopulations of neurones in different brain regions. An example given by Sternberger *et al.* is the antibody 02-135 which labels pyramidal cells in area CA2 but not CA1 of the hippocampus, Purkinje cells but not granule cells of the cerebellum, and stellate cells but not pyramidal cells of the cerebral cortex.

The interpretation of such results is complex. Similar results using antibodies raised against the leech nervous system were interpreted as suggesting a possible functional interaction or neural subnetwork between the labelled cells[6]. While this is indeed possible, mammalian studies suggest a different interpretation. It seems as if each antigen can be used for one class of cells in an area of the nervous system that is physiologically and anatomically separated from other regions in which the same antigen appears. Clearly further characterization of the respective antigens is required since any interpretation will depend on whether or not the same molecule is being detected in the various cells. Hawkes *et al.* have shown that some antibodies that give very distinct immunocytochemical staining can react with a number of polypeptides of different molecular weights and the general problems of cross-reaction of monoclonal antibodies have been discussed in these pages recently[7]. If we view the nervous system as having evolved by duplication and divergence of cell types or even whole neuronal networks, then the problem of cross-reactions between related molecules is going to be particularly acute.

One antibody produced by Hawkes *et al.* has been characterized more fully[8] and shown to recognize a 23,000 molecular weight polypeptide that is present in all neurones. Both anatomical studies and subcellular fractionation experiments suggest that this antigen, named MIT-23, is restricted to neuronal mitochondria. During cerebellar development this antigen appears after the final cell division or migration of the neurones. It is at present unknown whether this molecule carries out a function that only appears in postmitotic neurones or whether it is a neurone-specific isozyme of a common mitochondrial component, another isozyme of which is present in the dividing neuroblast. This latter possibility would be reminiscent of one of the first immunologically identified 'brain-specific antigens', the 14-3-2 protein, that turned out to be a brain-specific subunit of the enzyme enolase that is only expressed in postmitotic neurones[9].

Because of the different methods being used to characterize antibodies by different laboratories, and the different extents of characterization, it is often difficult to compare results in different papers. A particularly acute problem arises when some of the results are based on reactions of uncloned antibodies, as in the case above. One thing that is clear, however, is that we do not yet know the full extent of the molecular complexity of the nervous system. The challenge facing those who would like to find molecules carrying out a particular function is to identify them against what is clearly a high background of molecular complexity that may be completely incidental to those functions.

---

1. McKay, R., Raff, M. C. & Reichert, L.F. (eds) *Monoclonal Antibodies to Neural Antigens* (Cold Spring Harbor Laboratory, New York, 1981).
2. Brockes, J. (ed.) *Neuroimmunology* (Plenum, New York, 1982).
3. Hawkes, R., Niday, E. & Matus, A. *Proc. natn. Acad. Sci. U.S.A.* **79**, 2410 (1982).
4. Sternberger, L.A., Harwell, L.W. & Sternberger, N.H. *Proc. natn. Acad. Sci. U.S.A.* **79**, 1326 (1982).
5. Lazarides, E. *Nature* **283**, 249 (1980).
6. Zipser, B. & McKay, R. *Nature* **289**, 549 (1981).
7. Lane, D. & Koprowski, H. *Nature* **296**, 200 (1982).
8. Hawkes, R., Niday, E. & Matus, A. *Cell* **28**, 253, (1982).
9. Bock, E. *J. Neurochem.* **30**, 7 (1978).

BIRPS: deep seismic reflection profiling around the British Isles

from D.H. Matthews

BIRPS* is investigating the geological structure of the lower part of the continental crust and of the underlying uppermost part of the Earth's mantle in and around the British Isles, using seismic reflection profiling techniques developed by the oil industry. The technique can be used at sea or on land and is similar to echo sounding: sound from an explosion at the surface passes down through the rock layers and is reflected back to a detector at the surface from inter-layer boundaries, across which there is a change in acoustic impedance (the product of sound velocity and density).

Two lines (MOIST and WINCH) have been shot so far — both offshore, as shown on the map (Fig. 1). The sound source was an array of air-guns which released compressed air into the sea every 50 m along the ship's track. Reflected sound was detected by a towed streamer, 3 km long, containing hydrophones arranged in 60 sections each 50 m long. By adding the returns from 30 consecutive shots recorded from sections 2, 4, 6 . . . 58, 60 and correcting for the increasing length of the raypath it was possible to add 30 reflections from a common point on the reflector (30-fold coverage). The recording equipment was run for 15 s; sufficient for the sound to travel to about 45 km beneath the surface and back again if the mean crustal sound velocity is 6 km s^{-1}.

MOIST obtained what are arguably the best deep seismic reflection data in the world[1,2] (Fig. 2). The crust–mantle boundary, the Moho, can be traced as a strong reflector along the greater part of the profile westwards from the Pentland Firth until it apparently terminates against a second strong reflector (the Flannan Thrust?) which can be followed down to 40 km depth. The Moho depth of 27 km agrees with that obtained on the LISPB refraction line where the two lines intersect[3]. Further velocity information was obtained from two-ship multichannel experiments[4]. The Outer Isles Thrust, which was reactivated as a normal fault in Mesozoic time, can be traced down as a planar reflector dipping at about 30°

Fig. 1 Outline of the British Isles with the positions of deep reflection lines: MOIST (Moine and Outer Isles Seismic Traverse, 180 km, shot 1981 by Western Geophysical), WINCH (Western Isles and North Channel Traverse, 1,000 km, shot 1982 by GECO International), SWAT (South West Approaches Traverse, planned for 1983). Meridians 0° and 10°W and parallels 50° and 60°N (the top border) are shown.

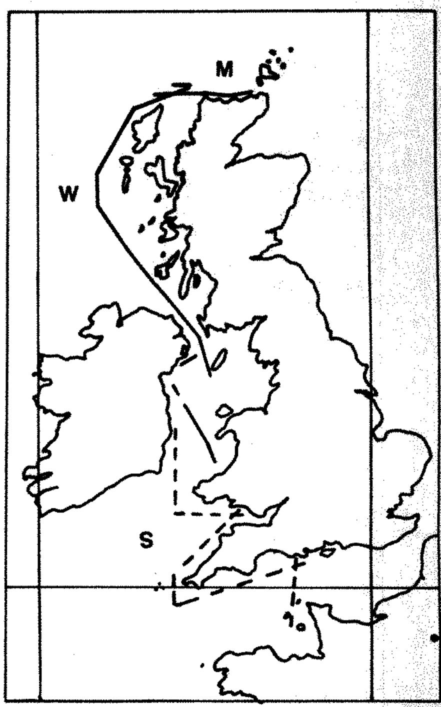

---

*BIRPS (The British Institutions Reflection Profiling Syndicate) is made up of members of university earth science departments and the Institute of Geological Sciences. The core group receives an annual grant from the Natural Environment Research Council and Shell (UK) supports a visiting scientist. Data from the first seismic reflection line shot (MOIST) are on open file at the Institute of Geological Sciences, Edinburgh, and are available for the cost of reproduction. The data from the second line (WINCH) will be available in July 1983.

From 1 October 1982 D.H. Matthews will be a senior research associate in the University of Cambridge, Director of the BIRPS core group.

0028-0836/82/330709-02$01.00

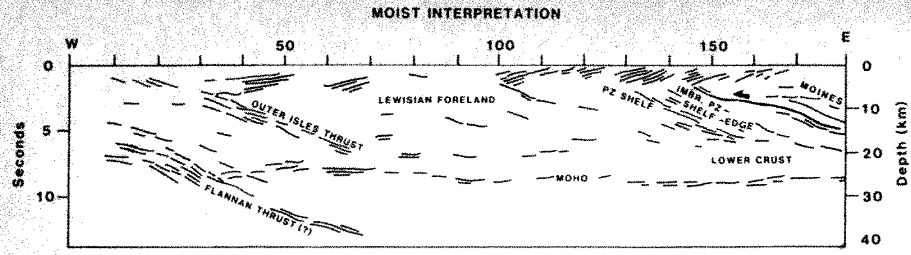

Fig. 2 Line drawing of reflection line-ups identified on MOIST (migrated data). The arrows indicate one plausible position of the Mone Thrust and the lettering in the border indicates one plausible geological interpretation[2]. Migration was done for BIRPS by Shell UK.

almost to the Moho, but the Moine Thrust is less easy to identify. At the eastern end of the profile there are easterly dipping reflectors which appear to pass up into the boundary faults of rotated blocks of Devonian sediments and are interpreted as imbricate thrusts reactivated as normal faults during a later period of stretching. There is a close parallel here with easterly dipping reflectors seen at the seaward end of COCORP profiles across the Appalachians[2,5].

WINCH was intended to elucidate the Flannan Thrust and to cross the principal faults of the Caledonides. Processing of the data has begun, as has planning for profiling in financial year 1983–84 around Cornwall and probably across the English Channel towards Guernsey to investigate Hercynian structures, the Cornubian batholith and the Brioverian basement. It is intended to work with the French ECORS group which is forming to carry out deep seismic profiling in France.

A start has thus been made on investigating the deep geological structure under the British Isles using the only technique that promises to have sufficient resolution. Also, two short deep profiles have been shot by the deep-geology unit of the Institute of Geological Sciences on land and one by the University of Leicester. The oil industry has also begun to obtain some deep profiles at sea and on land. Resolution is limited by the low frequencies of the returns from deep reflectors: a frequency of 20 Hz in rock with sound velocity $V_p = 6$ km s^{-1} implies a wavelength of 300 m and the possibility, at a depth of 30 km, of resolving two reflecting points 75 km apart vertically and 2,100 m apart horizontally. The recording parameters are chosen to look at deep features so that the resolution of shallow events is less good than that of standard industry reflection profiling which is usually run for about 5 s two-way time. For resolving details of relatively shallow sedimentary strata a wealth of data obtained by the oil industry is held by the Department of Energy.

The main objectives of BIRPS are threefold. First, structural geology, particularly to trace the attitude of major faults which are known at outcrop or subcrop to deep within the crust. Do the normal faults curve, to 'sole out' at relatively shallow depths? Are many thrust faults splays off sub-horizontal *decollement* surfaces like the Brevard zone[5] in the southern Appalachians? What is the shape of the Moho under sedimentary basins? Are all granites floored at about 6 s two-way time?

Second, continental rheology. A glance at a map of earthquake distribution is sufficient to convince that plate tectonics does not work in Eurasia: it is impossible to define aseismic plates delineated by lines of epicentres at their edges, as one can in the deep oceans, anywhere between Spain and Singapore. Is this because the hot continental lithosphere responds to stress by flowing, generating earthquakes only at shallow depths, or is it because the continents have such a long history of faulting that they can always respond to stress by reactivating some older fault surface, producing the widespread belt of earthquakes with random mechanism solutions that we observe in Eurasia. In the latter case, we should commonly find faults extending right through the crust into the upper mantle. In this context, it is likely that depth or penetration could be extended deeper than the 15 s that we have so far tried. Attenuation is low in crystalline rocks ($Q \sim 400$) and signal-to-noise ratios are still workable at the bottom of the record if reflectors are there.

Third, imaging. There is a perceived need, both in industry and in academic deep seismics, for better techniques of imaging steeply dipping reflectors. Groups of theoretical seismologists are working on this problem both in industry and at Cambridge, Princeton and Stanford. We also need to compute the reflection profiles that we would expect from model structures, for comparison with observed profiles, if we are to understand how we get apparently flat-lying reflections, albeit discontinuous, from the foliation surfaces of the high-grade metamorphic rocks that we expect to occur deep in the continental crust and which we observe exposed at outcrop on the continental shields.

BIRPS will try to contribute to all three objectives, and perhaps in the future we may be able to profile abroad in areas of active mountain building. Working deep within the crust sounds esoteric, of interest only to academic structural geologists. But, like COCORP in the USA, to whom we are deeply indebted[6], we are investigating the skeleton of the continent which supports and delimits the soft sediments of the oil basins. ☐

1. Smythe, D.K. *et al. Nature* (in the press).
2. Brewer, J.A. & Smythe, D.K. (in preparation).
3. Bamford, D., Nunn, K., Prodehl, C. & Jacob, B. *Geophys. J. R. astr. Soc.* **54** (1), 43 (1978).
4. White, R.S., Jones, E.J.W., Hughes, V.J. & Matthews, D.H. *Tectonophysics* (in the press).
5. Cook, F.A., Brown, L.D. & Oliver, J.E. *Scient. Am.* **243** (4), 156 (1980).
6. Oliver, J.E. *Nature* **275**, 485 (1978).

---

100 years ago

SCIENTIFIC EXPLORATION IN EGYPT

Now that we have embarked in a war in Egypt, it is to be hoped that steps will be taken to have a proper staff of scientific explorers attached to the army with facilities for conducting their investigations. There are periods of rest in a campaign during which soldiers and others may be usefully employed in conducting excavations at comparatively slight cost; and difficulties in the way of investigation, arising from the requirements of trade and industry, disappear in time of war. The deposits of the Delta require to be examined. The gravels of the Nile Valley have to be connected with their animal remains. Much has to be done for the earliest and best period of Egyptian art, and the Stone Age of Egypt has to be fixed with certainty.

I trust also that we shall not rob Egypt of her antiquities to any great extent. It may be useful to complete our typical series to a limited extent, but if Boulak should be happily preserved, I hope it will be preserved for Egypt and not brought home. Nothing would serve more to prove that we go there to civilise and not to rob. The means of communications are now so easy that all who are interested in Egyptology can see it there. Steam and railways have materially altered the requirements of education in this respect. Humanity, and British humanity in particular, now pours through all the great arteries of the world, and people observe and study more abroad than at home. The time has passed when antiquities should be regarded as trophies of war. It is no longer necessary for instruction to hoard up valuable specimens of foreign antiquities in European museums. So long as science has access to the materials of knowledge, that is all that it is necessary to bring away. Besides which, it should be remembered that the atmosphere of Egypt preserves antiquities in a way that no other climate can do; and when this fact hereafter becomes fully impressed upon the public mind, the time may come when subscriptions will be raised to take back obelisks and put them up again in their proper places; at any rate we have enough of them weathering and withering in smoke and damp. But the opportunity for exploration should not be lost. The French savants did their work thoroughly during their military operations in that country, and it would be shameful if, with the knowledge now at our disposal, the British expedition did not achieve more for the promotion of science than was effected by Napoleon half a century ago.

From *Nature* **26**, 364, 17 August 1882.

0028-0836/82/330710-01$01.00

ARTICLES

A pregalactic Population III: primordial helium and heavy elements and the microwave background

P. W. Tarbet & M. Rowan-Robinson

Department of Applied Mathematics, Queen Mary College, Mile End Road, London E1 4NS, UK

The helium, heavy elements and dark remnants produced by a pregalactic generation of stars, Population III, are discussed quantitatively for three scenarios: (1) Population III is responsible for the distortion of the microwave background spectrum measured by Woody and Richards; (2) Population III objects generate the whole of the microwave background; (3) Population III provides the oldest metals found in our Galaxy today.

A NATURAL consequence of the isothermal density fluctuation picture is the possibility of a pregalactic generation of stars, Population III, where 'stars' includes objects up to 10^6 or 10^7 solar masses. Consequences of such a population have been considered elsewhere (see ref. 1 and refs therein). Here we investigate three different roles for Population III. First, to generate the distortion of the microwave background measured by Woody and Richards[2,3], as proposed in ref. 4. Second, to produce the entire microwave background, and the observed 'primordial' helium abundance. Third, to manufacture the first metals in galaxies.

These three possibilities are explored quantitively with assumptions about the mass spectrum of the stars, the helium and heavy element yields of stars of different masses and the remnants.

Helium and metal yields of Population III

The mean mass density parameter of the Universe at the present epoch, $\Omega_0 (= 8\pi G\rho_0/3H_0^2 = (\rho_0/2\times10^{-29}\ \text{g cm}^{-3})\ (H_0/100)^{-2})$, can be considered to have three components; Ω_g, the contribution from visible matter, Ω_r, that due to dark matter, such as black holes and neutron stars, which we will assume are the remnants of Population III, and Ω_ν, from non-baryonic matter, such as neutrinos with mass $\Omega_0 = \Omega_g + \Omega_r + \Omega_\nu = \Omega_b + \Omega_\nu$, where Ω_b is the total baryonic contribution.

We assume that at some epoch in the early Universe a population of stars was born and subsequently died at a later epoch z_f (z_f is the redshift at which the objects cease to produce radiation, so in the case of black holes it is the epoch when they stop accreting at an appreciable rate).

If $Y(M)$ and $Z(M)$ are the fraction of a star's mass returned as helium and heavy elements respectively, then the fraction of visible matter in the form of helium and heavy elements is

$$Y = (1 - \Omega_{ej}/\Omega_g)Y_P + (8\pi G/3H_0^2\Omega_g)(1+z_f)^{-3}A\int_{M_1}^{M_2} Y(M)MN(M)\,dM$$

$$Z = (8\pi G/3H_0^2\Omega_g)(1+z_f)^{-3}A\int_{M_1}^{M_2} Z(M)MN(M)\,dM$$

where Y_P is the cosmic (pre-Population III) helium abundance, Ω_{ej} is the contribution to Ω_g that was cycled in pregalactic stars, H_0 is the Hubble constant and $AN(M)\,dM$ is the number-density of stars with masses in the range M to $M+dM$ at epoch z_f, having upper and lower limits of M_2 and M_1 respectively. We shall take $N(M) = M^{-\alpha}$. Similarly if $R(M)$ denotes the fraction of a star's mass left behind as dark matter, then

$$\Omega_r = (8\pi G/3H_0^2)\cdot(1+z_f)^{-3} \times A\left(\int_{M_1}^{M_b} R(M)MN(M)\,dM + (1+\mu_B)\cdot\int_{M_b}^{M_2} R(M)MN(M)\,dM\right)$$

where it is assumed that the remnant is a black hole for $M > M_b$, and μ_B is the ratio of the mass accreted by a black hole to the mass of an initial black hole.

The coefficient A of the mass function is related to the radiation output of these objects. If they enhance the background by a factor β and $\varepsilon(M)$ is the fraction of a star's mass converted into radiation, then

$$\beta a T_0^4(1+z_f)^4 = A\int_{M_1}^{M_2} \varepsilon(M)MN(M)c^2\,dM$$

$T_0(1+z_f)$ being the temperature of the primordial cosmic background at epoch z_f. If the efficiency of producing radiation in the conversion of H to He is $\varepsilon_Y(\sim 0.007)$ and from He to metals is $\varepsilon_Z(\sim 0.003)$, then

$$\varepsilon(M) = \varepsilon_Y(Y(M) + Z(M) - Y_P) + \varepsilon_Z Z(M)$$

for the nucleosynthetic contribution; and for those stars which produce black holes at their deaths, which then accrete a fraction μ_B of their initial mass with efficiency ε_B

$$\varepsilon(M) = \varepsilon_B\mu_B R(M)$$

The value of $\varepsilon_B\mu_B$ is difficult to determine as the accretion rate depends on the temperature of the material being accreted

Table 1 The effect of varying the parameters M_2, α, μ_B and H_0 on models producing the distortion of the microwave background

M_2	α	μ_B	H_0	Ω_g	Ω_b	Y_{min}	Y_P	Z
10^6	1.0	5.0	50	0.043	0.100	0.259	0.256	2.85×10^{-5}
10^6	1.25	5.0	100	0.016	0.030	0.262	0.258	1.32×10^{-4}
10^5	0.75	5.0	50	0.375	0.432	0.275	0.268	1.63×10^{-5}
10^7	1.25	5.0	50	0.021	0.078	0.256	0.254	6.63×10^{-5}
10^6	1.0	1.0	50	0.147	0.243	0.268	0.263	4.16×10^{-5}
10^6	0.75	0.5	50	0.173	0.316	0.270	0.266	1.02×10^{-5}
10^6	0.75	0.1	50	0.769	1.294	0.282	0.277	1.15×10^{-5}

Y_{min} is the minimum net helium yield given by the parameters M_2, α, μ_B, H_0 and Ω_g; the corresponding Ω_b, Y_P and Z are also shown.

0028-0836/82/330711—05$01.00

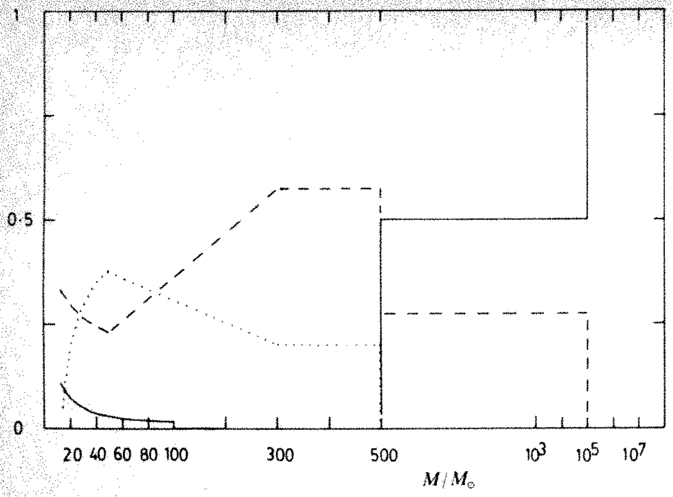

Fig. 1 The fraction of a star's mass ejected as helium ($Y(M)$, dashed curve) and heavy elements ($Z(M)$, dotted curve), and left as a remnant ($R(M)$, solid curve), as a function of the star's mass. Note that the mass scale changes at 100, 500 and $1{,}000M_\odot$.

which in turn is determined by the accretion, and the efficiency depends on the details of the flow and cooling processes[5]. The efficiency, ε_B, is of the order of 0.1 and if we consider $\varepsilon_B\mu_B = L_{ED}t/Mc^2$, where the Eddington luminosity $L_{ED} = 10^{38}(M/M_\odot)$, and $t = 10^{17.5}\Omega^{-1/2}z_f^{-3/2}$, then $\varepsilon_B\mu_B = 0.02$ for $\Omega = 0.15$ and $z_f = 200$. But it was found that in the models having $z_f = 200$, $\varepsilon_B\mu_B$ could not be much less than 0.1, (see ref. 6), to avoid excessive amounts of matter or high yields from Population III.

Schramm and Steigman[7] give $(0.9\text{–}3.5)\times10^{-3}h_0^{-1}$, where $h_0 = H_0/100$, as a firm lower limit to the nucleon density parameter, based on observations of the light producing stars in the solar neighbourhood. This is taken as the lower limit for Ω_g.

The functions $N(M)$, $Y(M)$, $Z(M)$, $R(M)$

The function $N(M)$ is assumed to have the form $M^{-\alpha}$. For the solar neighbourhood $\alpha = 2.35$, the Salpeter value[8], $M_1 = 0.01\text{–}0.1M_\odot$ and $M_2 = 60\text{–}100M_\odot$. In a zero metal abundance medium, cooling will be less efficient and fragmentation inhibited[9]. We may therefore expect M_1 to be increased (Silk[9] argues that $M_1 \sim 20M_\odot$) and α reduced. For $\alpha < 2$, M_1 is not a very important parameter; $M_1 = 13M_\odot$ was adopted. The cocoon star mechanism that limits M_2 in the solar neighbourhood[10] also does not apply in the metal-free primordial environment, and we assume that M_2 can extend up to the scale of the Jeans mass at decoupling.

In the range $12 < M/M_\odot < 100$ stars are believed to be able to burn all of their nuclear fuels through to iron without mishap[11]. The core then undergoes hydrodynamic collapse but the implosion is reversed when nuclear densities are reached and a large amplitude bounce reflects the incoming kinetic energy, blowing off all layers external to the core in a supernova explosion[12,13]. The exact details of core bounce are not yet known and the complex reaction networks of static and dynamic burning make yield determinations uncertain. Here, the helium yields of Arnett[14] (scaled for an initial helium content of Y_P) are used, the formula of Weaver and Woosley[15] is used for the metals, and the neutron star core remnants are taken to be $1.4M_\odot$.

Stars with initial mass greater than about $100M_\odot$ do not burn fuels all the way through to iron but encounter the e^+e^- pair instability and undergo core collapse[16]. The question is, can subsequent fast nuclear burning reverse this collapse or is the ultimate fate a black hole? Woosley and Weaver[17] and Bond *et al.*[18] calculate that stars having an initial mass much exceeding $300M_\odot$ (the uncertainty coming from the uncertainty in mass loss) will be unable to reverse this collapse, whilst those in the range $100\text{–}300M_\odot$ suffer complete disruption.

It has often been pointed out that massive stars ($M \gtrsim 60M_\odot$) are unstable to nuclear energized pulsations[19–21]. But studies by, for example, Appenzeller[22,23], Talbot[24,25] and Papaloizou[26] imply that these pulsations do not completely disrupt the stars. For those of initial mass $>300M_\odot$ a substantial fraction of the star may be lost on a time scale much shorter than the hydrogen burning phase, whilst those below $100M_\odot$ suffer little from this instability[23].

Talbot and Arnett[27] looked at helium production from massive stars, with no initial helium, suffering mass loss due to nuclear pulsations and concluded that 17% of the star could be shed in the form of helium with a net helium yield of about 0.5 for stars $>300M_\odot$. However, other mechanisms (radiatively driven winds) may be important and the observations of Humphreys and Davidson[28] seem to point to the possibility that mass loss severely restricts the evolution of stars with initial masses $50\text{–}60M_\odot$ to cooler regions of the H-R diagram. It has been suggested[29] that OH-IRII sources with deep silicate absorption may be the remnants of massive stars which have suffered substantial mass loss.

Considering the uncertainties in mass loss and the upper limit of complete disruption the following simple approach was taken. Stars of mass $>M_a = 300M_\odot$ are assumed to lose half their mass due to winds and so (scaling for $Y_P = 0.25$) shed 0.275 of their mass as helium. The remnant then contributes to the yield after disruption to give a total fraction of 0.575 as helium and 0.2 as metals. Those above $M_b = 500M_\odot$ (up to $10^5M_\odot$) return the 0.275 wind component but the remnants collapse to black holes. For stars in the range $50\text{–}300M_\odot$, $Y(M)$ and $Z(M)$ were interpolated linearly between the values adopted at 50 and $300M_\odot$.

Objects exceeding $10^5M_\odot$ encounter a general relativistic instability during quasi-static collapse[30] and if they contain no heavy elements, nuclear burning cannot proceed rapidly enough to prevent catastrophic collapse[31]. Thus virtually the whole star collapses to a black hole on a short time scale.

The adopted forms for $Y(M)$, $Z(M)$ and $R(M)$ are summarized in Fig. 1.

Viable scenarios of Population III

(1) The distortion of the microwave background: To produce the spectrum observed by Woody and Richards[2], Negroponte *et al.*[32] found it necessary to have z_f in the range 150–225, β in the range 0.2–0.4, and a metal abundance relative to the total mass of $2.5\text{–}7.5\times10^{-6}$ for $\Omega_0 = 1$ and $1\text{–}3\times10^{-5}$ for $\Omega_0 = 0.1$ ($H_0 = 100$), depending on the grain material. To test this type of model we take $z_f = 200$, $\beta = 0.25$ and look for values of the parameters Ω_g, H_0, M_2, α, μ_B, which give a heavy element abundance in the right range. Allowing for the uncertainties in the type of grain material and the observed distortion, we take this to be $\Omega_g Z = 5\text{–}50\times10^{-7}$ for $H_0 = 100$, and $10^{-6}\text{–}10^{-5}$ for $H_0 = 50$.

We have taken $H_0 = 50$ or 100; $\log_{10} M_2/M_\odot = 2(1)7$; $\alpha = 0.5(0.25)2.5$; $\mu_B = 1, 5$; and in each case varied Ω_g from 0.001 to 1.

Table 2 Models in which Population III stars produce all the microwave background

a	M_2	α	μ_B	H_0	Ω_g	Ω_b	Y	Z
	10^5	0.5	5.0	50	0.091	0.394	0.223	9.26×10^{-5}
	10^5	0.5	5.0	100	0.023	0.099	0.223	9.26×10^{-5}
	10^6	0.75	1.0	50	0.013	0.522	0.220	3.51×10^{-4}
	10^6	0.75	1.0	100	0.003	0.130	0.220	3.51×10^{-4}
b	10^5	0.25	5.0	50	0.091	0.394	0.223	4.56×10^{-5}
	10^5	0.25	5.0	100	0.023	0.099	0.223	4.56×10^{-5}
	10^5	0.5	5.0	100	0.023	0.099	0.223	1.69×10^{-4}
	10^6	0.5	1.0	50	0.007	0.516	0.231	1.74×10^{-4}

a, The only models producing all of the microwave background and providing enough helium without overproducing heavy elements; *b*, as *a* but with $Z(M)$ increased at the expense of $Y(M)$ in the stellar mass range $300\text{–}500M_\odot$. Y is the net helium yield given by the parameters M_2, α, μ_B, H_0 and Ω_g; Z is the corresponding net heavy element yield.

Table 3 The effect of varying the parameters α, M_1 and M_2 on initial enrichment models

α	M_1	M_2	Ω_{III}	Ω_{ej}	Ω_{r}	Y_{III}	β
2.35	20	100	3.18×10^{-5}	3.06×10^{-5}	1.19×10^{-6}	8.37×10^{-5}	3.93×10^{-4}
1.0	20	100	2.96×10^{-5}	2.87×10^{-5}	8.33×10^{-7}	7.74×10^{-5}	3.91×10^{-4}
2.35	13	100	3.90×10^{-5}	3.70×10^{-5}	1.99×10^{-6}	1.08×10^{-4}	4.11×10^{-4}
2.35	30	100	2.88×10^{-5}	2.80×10^{-5}	8.13×10^{-7}	7.30×10^{-5}	3.85×10^{-4}
2.35	20	300	3.27×10^{-5}	3.18×10^{-5}	8.58×10^{-7}	9.95×10^{-5}	4.30×10^{-4}
2.35	20	500	3.38×10^{-5}	3.30×10^{-5}	8.04×10^{-7}	1.11×10^{-4}	4.54×10^{-4}

See text for definitions of the parameters and their functional dependence on Z, Ω_g and z_f.

Because the Jeans mass at decoupling is $\sim10^6M_\odot$ it is natural to look first for models with $M_2=10^6M_\odot$ which produce the required Ω_gZ. $M_2=10^6M_\odot$, $H_0=50$, $\alpha=1.0$ and $\mu_B=5.0$ fits the required Ω_gZ and has a minimum helium yield of $Y=0.259$ at $\Omega_g=0.043$, $\Omega_b=0.100$, $Z=2.85\times10^{-5}$ and $Y_P=0.256$. The dependence of Y (and Y_P) on Z and Ω_g for this model is shown in Fig. 2. For low values of Ω_g the net metal and helium yields from Population III are high but decrease as Ω_g increases. At higher Ω_g, and hence Ω_b, the primordial helium yield increases so Y starts to increase again. The model cited above is seen to have a net helium yield slightly higher than some recently deduced primordial values; $Y=0.216\pm0.015$ (ref. 33), $Y=0.228\pm0.014$ (ref. 34). As most of the helium comes from primordial nucleosynthesis this problem is shared by the standard model unless $\Omega_b<0.03$ (ref. 7). However, these low values are disputed by Kunth[35], who deduces $Y=0.243\pm0.010$.

We have used the work of Yang *et al.*[36] to determine Y_P, which in turn adopts the nucleosynthesis code of Wagoner[37]. As discussed by Olive *et al.*[38], Y_P (and consequently Y) could be reduced by taking a lower value for the free neutron half life, $\tau_{1/2}$. Bondarenko *et al.*[39] have determined $\tau_{1/2}=10.13\pm0.09$ min, compared with $\tau_{1/2}=10.7$ used by Wagoner and $\tau_{1/2}=10.56\pm0.09$ recommended in ref. 40. This could reduce Y_P by ~0.01. If the τ-neutrino has a mass >1 MeV/c^2, then the two-neutrino case rather than the three-neutrino case should be used in the helium nucleosynthesis calculation (see the dotted curve in Fig. 2). However, this case leads to implausibly high values of Ω_ν unless the mass of the τ-neutrino is greater than 2 GeV/c^2 and this is inconsistent with the experimental upper limit of 250 MeV/c^2 (ref. 41).

The deuterium in these models is given by

$$D=(1-\Omega_{\mathrm{ej}}/\Omega_g)D_P$$

and since, for the case cited, $\Omega_{\mathrm{ej}}=5.06\times10^{-4}$, $D=0.988D_P$, (almost identical to the standard model).

We consider the effect of varying the other parameters of our model. Changing H_0 to 100 decreases Ω_gZ by a factor of 4 whilst the required range in Ω_gZ is reduced by a factor of 2. The net effect of changing H_0 is therefore small. To recover a model giving Ω_gZ in the required range we need to increase α from 1 to 1.25 when H_0 is changed from 50 to 100. The dependence of Ω_gZ on α is more significant. Increasing α to 1.25 with other parameters unchanged still leaves Ω_gZ in the required range, but $\alpha=1.5$ gives $\Omega_gZ=5.70\times10^{-5}$ and $\alpha=0.5$ gives $\Omega_gZ=2.55\times10^{-8}$. Since the radiation is mainly from accreting black holes, the upper end of the mass spectrum, the effect of reducing M_2 is to require a lower value of α to maintain Ω_gZ in the required range. The yields are also increased as M_2 is reduced because the contribution to the radiation from objects returning processed material is higher. It was found that M_2 must exceed $10^4M_\odot$ unless $\alpha<0.5$. Lowering μ_B increases the yields from Population III and such models also require more matter (higher Ω_r to provide the required radiation), hence Y_P is increased. Table 1 illustrates the effects of varying the parameters M_2, α, μ_B and H_0.

Thus a pregalactic stellar population can provide a distortion of the microwave background as in the scheme outlined in ref. 4, but to give acceptable values of Y and Z the mass function must be flat and extend to super-massive objects, so that most of the light is generated by accreting black holes.

(2) Generation of the whole of the microwave background: As pointed out by Carr[6], if a pregalactic generation of stars could have generated 25% of the microwave background, could it not be possible for them to have generated all of it? In this case $\beta=1.0$ and we take $T_0=2.9$ K so as to give a total energy density equal to that observed by Woody and Richards[2,3]. The primordial helium yield now has to be generated entirely by Population III stars (nucleosynthesis needs to be suppressed in a cold Universe by taking the lepton-to-baryon ratio >1.3 to prevent most of the Universe being synthesized into helium and heavy elements)[42]. If we are still trying to fit the claimed distorted spectrum then the required Ω_gZ is as in the previous case, and we take $z_f=200$. We have also looked at $z_f=1{,}000$ because, in the Carr model, the extra 75% of the background radiation produced in these models has to be generated at this earlier epoch for thermalization by free–free processes to be effective. (The Rowan-Robinson *et al.*[4] scheme requires only that the radiation be produced by $z_f\sim200$. The constraints on Ω_gZ are due to the optical depth in dust back to $z_f\sim200$ required in this scheme, so are unchanged.)

The only models giving the required Ω_gZ and enough helium are given in Table 2*a*. All other models (with $\mu_B=1.0$ or 5.0) satisfying the constraints on Ω_gZ and Z, from old Population II, produced too little helium.

Models with lower μ_B were found. With $M_2=10^6M_\odot$, $\alpha=0.75$ and $\mu_B=0.5$, we found $Y=0.220$ and $Z=3.51\times10^{-4}$ with $\Omega_g=0.007h_0^{-2}$, $\Omega_b=0.197h_0^{-2}$ ($\Omega_r=0.190h_0^{-2}$), but the only two cases with acceptable yields for $\mu_B=0.1$ were $M_2=10^6M_\odot$, $\alpha=0.5$ and $M_2=10^7M_\odot$, $\alpha=0.75$ which had $\Omega_r=0.697h_0^{-2}$ and $\Omega_r=0.670h_0^{-2}$, respectively, which are rather high. We also found acceptable models with $z_f=1{,}000$ but these also required high densities ($\Omega_r>0.6h_0^{-2}$) or had <1% of the total baryonic matter in visible form today, so are rather implausible.

Note that none of these models produce any deuterium and it is therefore necessary to appeal to some *ad hoc* astrophysical mechanism for this (see ref. 43). However, as there are models that imply that the Carr scenario can simultaneously produce all of the microwave background, explain the Woody and Richards distortion with the mechanism proposed in ref. 4, and give the correct helium yield and Population II metals, it would perhaps be worthwhile to investigate the predicted background spectrum of these models in more detail, taking into account the staggered way in which the radiation from different stellar masses is generated. The capacity of free–free processes to thermalize the bulk of the radiation has been disputed by Wright[44]. He argues that for adequate thermalization at long wavelengths, needle-shaped conducting grains are required, with a length-to-width ratio of at least 210; a similar mechanism is proposed in ref. 45.

(3) Initial enrichment: The need for a non-zero initial metal content for the Galaxy has been argued by many authors (see refs 46–48) and most recently by Bond[49] who deduces a mean metal abundance of $0.0181Z_\odot$ for Population II and an initial metal content of $2.51\times10^{-3}Z_\odot$.

It has been seen that models (1) and (2) can provide this initial enrichment, but here we suppose the radiation requirement on Population III to be minimal and try to produce the required metal abundance without adding significantly to the primordial helium.

Individual galaxies are believed to condense out at about

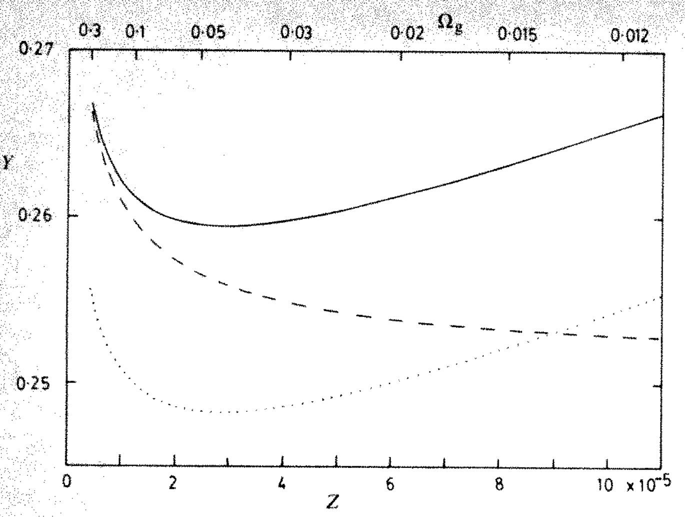

Fig. 2 The total helium abundance, Y (solid curve) and the primordial helium abundance, Y_P (broken curve), plotted as a function of the heavy element abundance, Z (lower scale). The contribution to Ω_b due to visible matter, Ω_g, is labelled on the upper scale. The dotted curve shows the two-neutrino case. Model parameters are given in the text.

redshifts 10, so z_f is relaxed to this value. However, β is not a relevant parameter in these models as we are not concerned with the effect of the stars on the microwave background. Instead we consider the fraction of the Universe that needs to go into a pregalactic stellar generation to provide the initial metals. We define Ω_{III}, the density parameter today for these objects if they had not ejected any of their mass (or accreted any).

$$\Omega_{III} = (8\pi G/3H_0^2)\cdot(1+z_t)^{-3}\mathrm{A}\int_{M_1}^{M_2} MN(M)\,\mathrm{d}M$$

First let us consider $M_1 = 20M_\odot$ (ref. 9), $\alpha = 2.35$ (the Salpeter[8] value), and $M_2 = 100M_\odot$. For this set of parameters we find $\Omega_{III} = 3.18\times10^{-5}\,(Z/10^{-4})\,(\Omega_g/0.1)$, $\Omega_{ej} = 3.06\times10^{-5}\,(Z/10^{-4})\,(\Omega_g/0.1)$, $\Omega_r = 1.19\times10^{-6}\,(Z/10^{-4})\,(\Omega_g/0.1)$, $Y_{III} = 8.37\times10^{-5}\,(Z/10^{-4})$, (where Y_{III} is the net helium yield from Population III) and $\beta = 3.93\times10^{-4}h_0^2\,(Z/10^{-4})\,(\Omega_g/0.1)\,(11/1+z_f)$.

It is therefore possible to provide the initial metal content of galaxies without resorting to a flat mass function extending to SMOs, and with only a very small amount of the Universe being cycled in pregalactic stars. Such models have a negligible effect on primordial helium and deuterium abundances and on the microwave background.

The effect on these values of variation of the parameters α, M_1 and M_2 is illustrated in Table 3.

Only for high values of M_2 and low values of α, comparable with those required in cases (1) and (2), does β, and hence the distortion of the microwave background, become significant.

Discussion

Because of uncertainties in Fig. 1 we now discuss the effects on our results of varying some of the values adopted for the yield functions.

(1) We have redone the calculations for scenarios (1) and (2) ($\mu_B = 1.0$ and 5.0, $z_f = 200$) varying the limit M_a, where a star loses half its mass due to pulsations, between 300 and $500M_\odot$, and the limit M_b, where black hole formation occurs, between 300 and $1{,}000M_\odot$. Varying these limits was found to have no qualitative effect on our previous conclusions and a negligible effect on the quantitative results.

(2) Klapp[50] has performed numerical calculations of the evolution of very massive stars and obtained yields which differ from those we have adopted (Fig. 1). We therefore consider the effects of changing $Y(M)$ and $Z(M)$ in two different ways: (i) increasing $Z(M)$ from 0.2 to 0.45 in the mass range 300–$500M_\odot$ at the expense of $Y(M)$, so more helium is cycled through to metals than assumed previously (we still linearly interpolate $Y(M)$ and $Z(M)$ between the values adopted at 50 and $300M_\odot$), and (ii) increasing $Z(M)$ from 0.0 to 0.02 in the mass range 500–$10^5M_\odot$, so a small amount of the material processed into metals is able to diffuse up to the surface of the star and is shed before the collapse to a black hole occurs (see ref. 50).

(i) The effect of increasing $Z(M)$ at the expense of $Y(M)$ over a small section of the mass spectrum is, generally, that α has to be reduced fractionally for a given model to keep Ω_gZ in the required range. However, in our case (1) above (producing the distortion of the microwave background) it was found that our best model ($M_2 = 10^6M_\odot$, $H_0 = 50$, $\alpha = 1.0$ and $\mu_B = 5.0$) is still viable and gave $Y = 0.259$ at $\Omega_g = 0.041$, $\Omega_b = 0.098$, $Z = 4.99\times10^{-5}$ and $Y_P = 0.256$. For models producing all of the microwave background (case (2)) the only cases giving Ω_gZ in the required range and enough helium, without violating the constraints on Z are given in Table 2*b*.

(ii) In this case $Z(M)$ has been increased over a large range of the mass spectrum and it is therefore necessary to reduce α more substantially than in case (i) to recover viable models. Our best model now has $\Omega_gZ = 2.13\times10^{-5}$ and is therefore invalid. Reducing α from 1.0 to 0.5, with all other parameters held constant, brings Ω_gZ back into the required range and gives $Y = 0.256$ at $\Omega_g = 0.021$, $\Omega_b = 0.078$, $Z = 2.94\times10^{-4}$ and $Y_P = 0.254$. The effect of varying the parameters of this model are again as previously discussed, but it was found that M_2 must exceed $10^5M_\odot$ unless $\alpha < 0.25$. No models were found that produced all of the microwave background and enough helium without overproducing metals. These models are much more dependent on the helium to metal production ratio of Population III than those producing only the distortion of the microwave background, because for the latter most of the helium is provided by nucleosynthesis in the fireball phase of the Universe.

We conclude that small changes in our adopted yield functions (case (1)) only affect the details of our results, not the general conclusions. But if Klapp's conclusion that even very massive stars which collapse to black holes return some of their mass in the form of heavy elements is correct, then models trying to produce all of the microwave background and the initial helium from Population III are untenable.

There are several viable and interesting roles for Population III and the best hope of testing these ideas observationally is improved measurements of the spectrum of the microwave background near the peak.

P.W.T. is supported by an SERC research studentship. We thank B. Carr, S. Woosley and J. Klapp for providing results before publication.

Received 22 March; accepted 2 June 1982.

1. Rowan-Robinson, M. & Tarbet, P. in *Progress in Cosmology* (ed. Wolfendale, A.) (Reidel, Dordrecht, 1982).
2. Woody, D. P. & Richards, P. L. *Phys. Rev. Lett.* **42,** 925–929 (1979).
3. Woody, D. P. & Richards, P. L. *Astrophys. J.* **248,** 18–37 (1981).
4. Rowan-Robinson, M., Negroponte, J. & Silk, J. *Nature* **281,** 635–638 (1979).
5. Carr, B. J. *Mon. Not. R. astr. Soc.* **189,** 123–136 (1979).
6. Carr, B. J. *Mon. Not. R. astr. Soc.* **195,** 639–668 (1981).
7. Schramm, D. N. & Steigman, G. *Astrophys. J.* **243,** 1–7 (1981).
8. Salpeter, E. E. *Astrophys. J.* **121,** 161–167 (1955).
9. Silk, J. *Astrophys. J.* **211,** 638–648 (1977).
10. Kahn, F. D. *Astr. Astrophys.* **37,** 149–162 (1974).
11. Weaver, T. A., Zimmerman, G. B. & Woosley, S. E. *Astrophys. J.* **225,** 1021–1029 (1978).
12. Arnett, W. D. *Ann. N.Y. Acad. Sci.* **336,** 366–379 (1980).
13. Van Riper, K. A. *Astrophys. J.* **232,** 558–571 (1979).
14. Arnett, W. D. *Astrophys. J.* **219,** 1008–1016 (1978).
15. Weaver, T. A. & Woosley, S. E. *Ann. N.Y. Acad. Sci.* **336,** 335–357 (1980).
16. Barkat, Z., Rakavy, G. & Sack, N. *Phys. Rev. Lett.* **18,** 379–381 (1967).
17. Woosley, S. E. & Weaver, T. A. *Supernovae* (eds Rees, M. & Stoneham, R. J.) (Reidel, Dordrecht, 1982).
18. Bond, J. R., Arnett, W. D. & Carr, B. J. *Supernovae* (eds Rees, M. & Stoneham, R. J.) (Reidel, Dordrecht, 1982).
19. Stothers, R. in *Stellar Evolution* (eds Hong-Yee Chiu & Muriel, A.) (Massachusetts Institute of Technology Press, 1972).
20. Schwarzschild, M. & Harm, R. *Astrophys. J.* **129,** 637–646 (1959).
21. Stothers, R. & Simon, N. R. *Astrophys. J.* **160,** 1019–1029 (1970).
22. Appenzeller, I. *Astr. Astrophys.* **5,** 355–371 (1970).
23. Appenzeller, I. *Astr. Astrophys.* **9,** 216–220 (1970).
24. Talbot, R. J. *Astrophys. J.* **163,** 17–27 (1971).
25. Talbot, R. J. *Astrophys. J.* **165,** 121–138 (1971).
26. Papalpoisou, J. C. B. *Mon. Not. R. astr. Soc.* **162,** 169–187 (1973).
27. Talbot, R. J. & Arnett, W. D. *Nature Phys. Sci.* **229,** 150–151 (1971).
28. Humphreys, R. M. & Davidson, K. *Astrophys. J.* **232,** 409–420 (1979).

29. Rowan-Robinson, M. *Mon. Not. R. astr. Soc.* (in the press).
30. Zeldovich, Ya. B. & Novikov, I. D. *Relativistic Astrophysics* Vol. 1 (University of Chicago Press, 1971).
31. Fricke, K. J. *Astrophys. J.* **183,** 941–958 (1973).
32. Negroponte, J., Rowan-Robinson, M. & Silk, J. *Astrophys. J.* **248,** 38–46 (1981).
33. French, H. B. *Bull. Lick Obs.* No. 863 (1979).
34. Lequeux, J., Peimbert, M., Rayo, J. F., Serrano, A. & Torres-Peimbert, S. *Astr. Astrophys.* **80,** 155–166 (1979).
35. Kunth, D. in *Cosmology and Particles* (eds Audouze, J. *et al.*) 241 (Frontières, Paris 1981).
36. Yang, J., Schramm, D. N., Steigman, G. & Rood, R. T. *Astrophys. J.* **227,** 697–704 (1979).
37. Wagoner, R. V. *Astrophys. J.* **179,** 343–360 (1973).
38. Olive, K. A., Schramm, D. N., Steigman, G., Turner, M. S. & Yang, J. *Astrophys. J.* **246,** 557–568 (1981).
39. Bondarenko, L. N., Kurguzov, V. V., Prokof'ev, Yu. A., Rogov, E. V. & Spivak, P. E. *JEPT Lett.* **28,** 303–306 (1978).
40. Wilkinson, D. H. in *Proc. of the Erice School on Nuclear Astrophys* (1980).
41. Cowsik, R. in *Cosmology and Particles* (ed. Adouze *et al.*) 157 (Frontiéres, Paris, 1981).
42. Carr, B. J. *Astr. Astrophys.* **60,** 13–26 (1977).
43. Epstein, R. I. *Astrophys. J.* **212,** 595–601 (1977).
44. Wright, E. L. *Astrophys. J.* **255,** 401–407 (1982).
45. Rana, N. C. *Mon. Not. R. astr. Soc.* **197,** 1125–1138 (1981).
46. Adouze, J. & Tinsley, B. M., *Ann. Rev. Astr. Astrophys.* **14,** 43–79 (1976).
47. Truran, J. W. & Cameron, A. G. W. *Astr. Space Sci.* **14,** 179–222 (1971).
48. Hartquist, T. W. & Cameron, A. G. W. *Astr. Space Sci.* **48,** 145–158 (1977).
49. Bond, H. E. *Astrophys. J.* **248,** 606–611 (1981).
50. Klapp, J. thesis, Univ. Oxford (1982).

Vitrification of pure liquid water by high pressure jet freezing

Erwin Mayer & Peter Brüggeller

Institut für Anorganische und Analytische Chemie, Universität Innsbruck, A 6020 Innsbruck, Austria

The vitrification of pure liquid water by projecting a thin jet of liquid water at high speed into a liquid cryomedium is reported. The influence of the experimental parameters on the cooling rate and the devitrification of the jet-frozen vitrified material have been investigated. A structural difference between vitrified liquid water and amorphous solid water prepared from the vapour phase is inferred from a comparison of the X-ray diffraction patterns.

FINDING a method for vitrifying pure liquid water is important for several reasons. The investigation of vitrified liquid water will help to elucidate the structure of liquid water because the effects of thermal and static disorder can be largely separated[1–4]. It might help in interpreting the anomalous properties of supercooled water[5–8]. Vitrification of biological systems without cryoprotectants is another application that could enable studies to be made of morphology without freezing artefacts and of the mechanism of freezing damage[9,10]. When applied to dilute aqueous solutions complete vitrification means the simultaneous matrix isolation of dissolved species. This extends the well known matrix isolation from the gas phase[11] to nonvolatile solutes such as ionic systems or biomolecules and allows, among others, spectroscopic investigations at low temperatures in the dissolved state. Attempts to form vitreous ice by rapid cooling of liquid water have invariably led to formation of ice I_h (ref. 12). (Pryde and Jones[13] did report a heat capacity change of rapidly cooled water at 126 K which they attributed to a glass transition, but could not reproduce this result in subsequent experiments.) We have recently described the complete vitrification of liquid water and dilute aqueous solutions by jet-freezing of aqueous droplets distributed in *n*-heptane as an emulsion, where the combination of emulsification and high cooling rate was essential for vitrification[14]. We have since increased the cooling rate by orders of magnitude and report here the vitrification of pure liquid water without emulsification by injecting a thin fluid jet of liquid water at high pressures *in vacuo* into a liquid cryomedium. This is an extension of the jet-freezing method developed by Bachmann and Schmitt for freeze etching[15]. Our technique differs from that of splat-cooling on a cold metal surface by using a liquid cryomedium, and gives for liquid water and dilute aqueous solutions much higher cooling rates[14]. [It has been reported that D. R. Uhlmann has vitrified liquid water by splat-quenching (ref. 16 in our ref. 6). However, to our knowledge no report has appeared since then.]

Conditions for vitrification

We have investigated the following parameters, considered to be important for a high cooling rate, with the ESR method described previously[14]: aperture diameter from 5 to 100 μm, working pressures between 10 and 400 atm, effect of the liquid cryomedium and of stirring. Small aperture diameter together with high working pressure were found to be most important for high cooling rates. With increasing working pressures the liquid jet is broken up by air resistance closer and closer to the exit hole of the aperture and dispersed into a fine mist. Therefore vacuum is essential for working at pressures above 100 atm. Liquid ethane, propane and butene-1 were investigated as cryomedia and gave for small apertures very similar cooling rates. Figure 1*a* shows the X-ray diffraction pattern of a jet-frozen sample of liquid water using the best conditions for vitrification emerging from hundreds of experiments: jetting through a 10-μm aperture with 400 atm working pressure (the

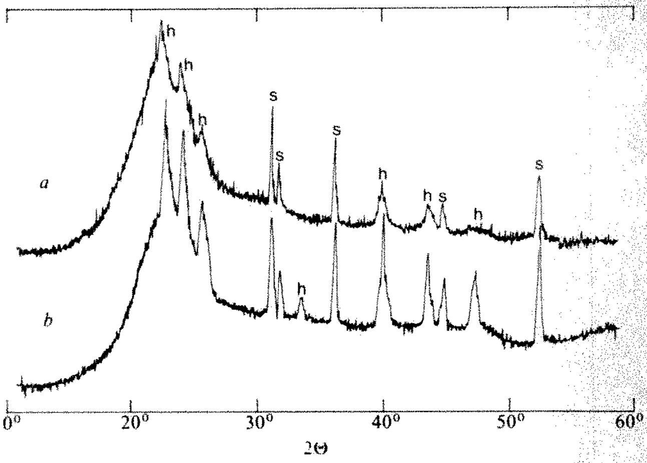

Fig. 1 X-ray diffraction patterns (CuKα, 90 K) of jet-frozen pure liquid water with: *a*, 400 atm; *b*, 100 atm working pressure (s, substrate reflexes; h, reflexes from crystalline ice). Samples were jet-frozen as follows: between 2 and 5 ml of pure liquid water were jetted through an aperture with a 10-μm opening (Balzers Union no. 16001), using working pressures of at most 400 atm, into 120 ml of vigorously stirred liquid propane cooled to 80 K. Liquid consumption at 100 atm: 0.4 ml min^{-1}, at 400 atm: 1.1 ml min^{-1}. The working pressures were generated with a hydraulic pump (type Maximator MSF 72), plugging of the 10-μm aperture was prevented by two filters (a Nupro 2-μm metal filter and a Millipore high pressure filter unit with a 0.2 μm filter). The experiment was started at normal pressure and vacuum applied as quickly as possible. Starting and stopping the jet already *in vacuo* gave identical X-ray diffraction patterns, but seemed to give apertures that clogged more easily. The suspension was filtered at liquid nitrogen temperature and the remaining mixture of frozen water and liquid cryomedium was transferred quickly with a liquid-nitrogen cooled spoon into the precooled apparatus. All operations at normal pressure were carried out under a cover of dry nitrogen gas. At liquid-nitrogen temperatures special care has to be taken to prevent accumulation of liquid oxygen in the cryomedium. The X-ray data were recorded on a Kristalloflex 4 (Siemens), using a vertical flat sample holder and samples between 0.5 and 1 mm thick.

0028-0836/82/330715-04$01.00

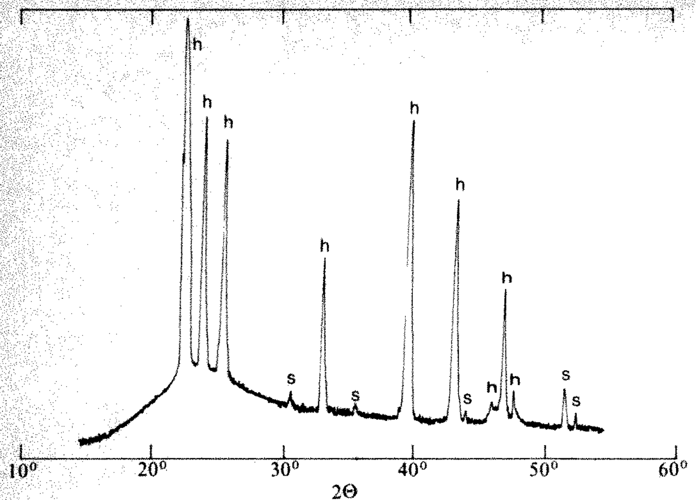

Fig. 2 X-ray diffraction pattern (CuKα, 90 K) of jet-frozen pure liquid water with 10 atm working pressure, showing the contribution of the liquid cryomedium at $2\theta = 23°$ (s, substrate reflexes; h, reflexes from ice I_h). The experimental conditions and the instrument gain were the same as conditions for Fig. 1 except for the working pressure and an aperture with a 20-μm opening. A 20-μm aperture was used because we could not start the jet through a 10-μm aperture with only 10 atm working pressure. However, from jet-freezing experiments with 50 atm we know that apertures with 10 and 20 μm openings give comparable cooling rates in this range of working pressures. With 10 atm working pressure the comparatively slow jet is not broken up by air over a long distance and thus the cooling rate is not increased by jetting *in vacuo*. The sharp reflexes are due to ice I_h, the intensity changes at small angles being caused by texture.

highest pressure used) into vigorously stirred propane at 80 K *in vacuo*. The X-ray diffraction pattern contains only a small amount of crystalline—mainly hexagonal—ice and is dominated by the broad feature characteristic of vitreous or microcrystalline substances. The effect of high working pressures is clearly seen by comparison with Fig. 1*b* where the pressure was reduced to 100 atm, using otherwise jet-freezing conditions identical with the experiment of Fig. 1*a*, and where the amount of hexagonal ice increases strongly. In several experiments we obtained nearly identical X-ray diffraction patterns with the same set of jet-freezing conditions which means that this method of vitrification is highly reproducible.

The vitrified liquid water inevitably contains some liquid cryomedium which cannot be removed without partial devitrification. The effect of the liquid cryomedium on the X-ray diffraction pattern of vitrified liquid water is demonstrated by Fig. 2, where the pattern of jet-frozen water using 10 atm working pressure only is shown with approximately the same intensity as in Fig. 1*a*, *b*: by differential thermal analysis (DTA) and by the ESR method reported previously[14] we confirmed that jet-freezing with 10 atm working pressure gives only crystalline ice. The X-ray diffraction pattern contains a broad peak centred at $2\theta = 23°$ in addition to the strong reflexes of ice I_h and is very similar to the pattern of a mixture of the liquid cryomedium with crystalline ice. The broad peak in Fig. 2 is therefore caused by the liquid cryomedium[16] and not by vitrified liquid water. The comparatively strong X-ray intensity of the liquid hydrocarbon might at first seem surprising. The small absorption coefficient for X rays of the solid water and the resulting transparency of the sample provide a simple explanation. In addition a matrix effect of the liquid cryomedium leading to strongly enhanced Compton scattering[17] and a particle size effect[18] might have a role. In any case the jet-freezing conditions for Fig. 2 are useful as a 'null-experiment', showing clearly in comparison with Fig. 1 the effect of high working pressures on the relative X-ray intensities of crystalline and amorphous material. We do not consider it useful to correct the X-ray diffraction pattern of vitrified liquid water for the effect of the cryomedium quantitatively because the amount of liquid and thus the size of the broad peak in Fig. 2 varied somewhat, and the possible additional effects considered above cannot be evaluated.

The vitrified material is definitely liquid water and not water vapour because: (1) the liquid enters the cryomedium as a continuous fluid jet of ~10 μm diameter. Typically between 2 and 5 ml of liquid water were jetted using a vacuum of 1 torr total pressure. The jetting time depends on the working pressure and the diameter of the aperture and was varied between 1 and 5 min. Therefore the amount of water vapour present during the experiment is negligible in comparison to the total amount of liquid water jetted. (2) We had tried to vitrify liquid water in the form of a very fine mist of small water droplets using working pressures of 1 to 2 atm only. The water droplets were generated by an ultrasonically vibrating 10-μm orifice similar to the aerosol generator of Berglund and Liu[19]. These experiments were carried out with a very small flow rate over considerable periods of time and therefore represent conditions where the amount of water entering the liquid cryomedium from the vapour phase becomes increasingly important. However, we have found no indication that material was vitrified using this arrangement. (3) The ESR spectra of jet-frozen 0.10 M aqueous $CuCl_2$ solutions depend strongly on the working pressures and were used as a good indicator for relative cooling rates[14]. We found that with a 200-atm working pressure the jet-frozen ESR spectrum is already nearly identical to the ESR spectrum of a perfectly vitrified 0.10 M $CuCl_2$ solution containing 50% glycerol for vitrification. While this does not prove that the jet-frozen solid has been vitrified completely, it still proves that the solute $CuCl_2$ has been matrix isolated and hence, that the liquid has experienced very high cooling rates.

Our jet-freezing conditions give a clear improvement, in terms of the amount of the vitrified material, over the previously reported vitrification of emulsified liquid water droplets[14] where we had obtained yields of ~13 and 16% for pure water and a 0.10 M $CuCl_2$ solution by DTA. These yields had been only barely noticeable in the X-ray diffraction pattern as a broadening underneath the sharp reflexes of the crystalline material between $2\theta = 20°$ and 28° (see Fig. 1*a* in ref. 14), whereas in Fig. 1*a* we have only a small amount of crystalline material on top of the broad feature. The determination of the relative amount of vitrified liquid water by DTA does not have any meaning for samples prepared as described in Fig. 1*a*, because the DTA method is not accurate enough, and the crystalline material comes mainly from condensation of water vapour during the preparation and transfer of the sample to the X-ray camera.

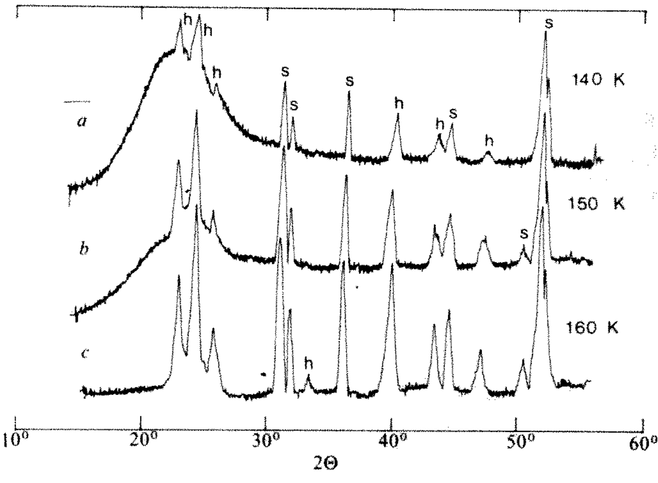

Fig. 3 X-ray diffraction patterns (CuKα) of jet-frozen pure liquid water warmed consecutively for 30 min to *a*, 140 K; *b*, 150 K; *c*, 160 K. The sampe was prepared as described in Fig. 1 with 400 atm working pressure except that liquid butene-1 was used as cryomedium at 100 K instead of propane. From 90 to 140 K the relative intensities of amorphous to crystalline reflexes were approximately constant, only the overall intensity decreased, probably due to movement of the viscous paste on the vertical sample holder with increasing temperature.

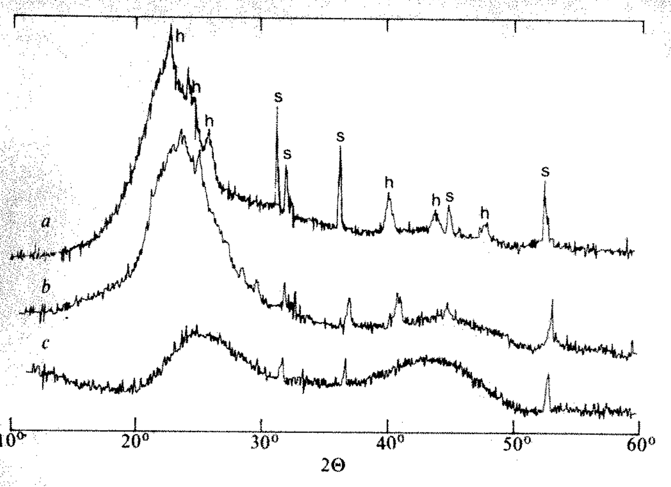

Fig. 4 X-ray diffraction patterns (CuKα, 90 K) of: *a*, jet-frozen pure liquid water prepared as described for Fig. 1*a* and thus containing some liquid propane; *b*, $(H_2O)_{as}$ mulled with liquid propane; *c*, $(H_2O)_{as}$ without propane. $(H_2O)_{as}$ was prepared as described in ref. 22 by vapour condensation at 77 K on a Cu-plate from a bath for the reservoir of water held at 210 K, using high vacuum conditions. For comparison with the pattern in Fig. 4*a* $(H_2O)_{as}$ was mixed thoroughly at 80 K with 20 ml of liquid propane, filtered and the remaining paste transferred to the precooled apparatus, using the same technique as for jet-frozen liquid water samples. As the pattern of $(H_2O)_{as}$ in Fig. 4*c* contains no reflexes of crystalline impurities, the amount of crystalline material in Fig. 4*b* represents the contamination of vitrified samples by crystalline ice due to condensation of water vapour during the experimental procedure.

We have investigated the devitrification and found that within the time scale of our X-ray measurements (30 min at every consecutive 10 K, starting at 90 K) the formation of ice I_c starts at 150 K (Fig. 3). This agrees very well with the devitrification of a vitrified 0.10 M $CuCl_2$ solution investigated previously within a similar time scale using ESR where a devitrification temperature of 153 K was deduced from signal broadening[14]. We found that the cryomedium used for vitrification affects the devitrification temperature. The sample giving the X-ray diffraction patterns in Fig. 3 had been prepared by jetting liquid water into butene-1 and therefore contained some butene-1. Vitrified liquid water containing some propane had started to devitrify already at 130 K. We think that this difference comes from the higher vapour pressure of liquid propane (1 torr at 144 K) and that devitrification is possibly induced by evaporating propane. At low temperatures the X-ray diffraction patterns of vitrified samples prepared with butene-1 or propane as cryomedia, using otherwise identical jet-freezing conditions, are very similar. The X-ray diffraction patterns of jet-frozen samples stored at 77 K for 3 months did not show any change.

Comparison with $(H_2O)_{as}$

In Fig. 4 the X-ray diffraction pattern of vitrified liquid water containing some liquid propane (Fig. 4*a*) is compared with the pattern of amorphous solid water prepared by condensation from the vapour phase (called $(H_2O)_{as}$ in accordance with Rice[1], Fig. 4*b*, *c*). Figure 4*c* shows the published X-ray diffraction pattern of $(H_2O)_{as}$ (refs 3, 20). Figure 4*b* the pattern of $(H_2O)_{as}$ mulled with liquid propane. A comparison has meaning only between the patterns of samples treated both with liquid cryomedium and has to be made between the patterns shown in Fig. 4*a*, *b*. A difference might possibly be found at high angles where the broad feature in the pattern of $(H_2O)_{as}$ centred around $2\theta = 44°$ appears to be less intense or absent in the pattern of vitrified liquid water. For further comparison we have tried to remove the cryomedium by washing the sample with liquid methane. However, this procedure leads to partial devitrification of the sample. In Fig. 5 the X-ray diffraction pattern of vitrified liquid water washed with liquid methane (Fig. 5*b*) is compared with the pattern of $(H_2O)_{as}$ treated identically (Fig. 5*a*), showing again for vitrified liquid water no clear amorphous peak at $2\theta = 44°$ underneath the sharp reflexes of crystalline ice in contrast to the pattern of $(H_2O)_{as}$. The X-ray diffraction pattern of the devitrified sample in Fig. 5*c* can be used as background of Fig. 5*b*. However, only a presentation of the X-ray data in the form of the structurally sensitive part of the scattered X-ray intensity will make a clear differentiation possible, and we cannot do this because we have not been able to compensate for the effect of the liquid cryomedium.

Discussion

The influence of high working pressures on the amount of vitrified material and thus on the cooling rate is certainly connected with the speed of the liquid jet. For 10, 100 and 400 atm working pressures approximate jet speeds of 20, 100 and 250 m s^{-1} can be calculated from the diameter of the 10-μm aperture and consumption of liquid. The effect of jet speed can be easily demonstrated by jetting at room temperature into paraffin oil with a viscosity similar to liquid propane at 80 K. With 10 atm working pressure the liquid jet hardly penetrates the surface, whereas with 100 atm working pressure penetration goes up to 20–30 mm. Therefore the liquid jet passes within a given time with increasing jet speed a larger volume of cryomedium, causing more efficient heat transfer from water to the cryomedium and giving higher cooling rates. In addition, vigorous stirring of the cryomedium enforces a circular movement onto the liquid jet, probably breaking up the jet into small droplets.

It is impossible to measure the cooling rates obtainable with high pressure jet-freezing. Fletcher[12] estimated the cooling rate necessary for vitrifying a micrometre-sized droplet of water to be $>10^{10}$ K s^{-1} from the theory of the homogeneous nucleation of freezing, whereas Uhlmann[21] calculated a cooling rate of $>10^7$ K s^{-1}. We do not know how the liquid jet breaks up in the cryomedium at high pressures, but we consider it likely that the jet breaks up into droplets of approximately the size of the jet diameter. Therefore a minimum cooling rate of 10^{10} K s^{-1} is obtained from Fletcher's value and of 10^7 K s^{-1} from Uhlmann's. As the minimum cooling rate depends strongly on droplet diameter and was calculated for 1-μm droplets[12,21] much higher cooling rates would result for larger droplet diameters. For a 10-μm droplet minimum cooling rates of 10^{13} and 10^{10} K s^{-1} follow from Fletcher's and Uhlmann's calculations. An idea about the distribution of cooling rates can be obtained from an inspection of the frozen products. We had

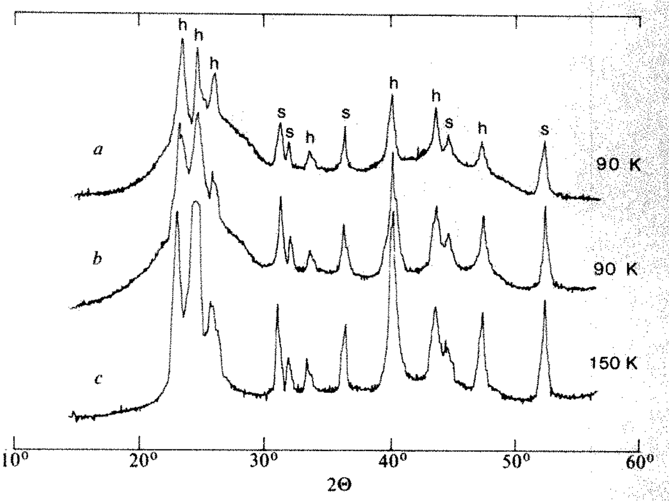

Fig. 5 X-ray diffraction patterns (CuKα) of: *a*, $(H_2O)_{as}$ from Fig. 4*b* washed with liquid methane; *b*, jet-frozen liquid water from Fig. 4*a* washed with liquid methane; *c*, the sample in *b* devitrified by warming up to 150 K. To remove liquid propane or butene-1 the samples were washed with liquid methane, filtered at ~90 K as described in Fig. 1 for propane, and the remaining methane pumped off at 77 K from the sample. This procedure leads inevitably to strong contamination and/or partial devitrification of the samples as shown by a comparison of Fig. 5*a* with Fig. 4*b* and *c*. The reflex at $2\theta = 24.3°$ in Fig. 5*c* was truncated.

expected that with increasing working pressure, increasing amounts of ice I_c and then of vitrified liquid water would be formed. This was frequently observed for the preparation of $(H_2O)_{as}$ from the vapour phase[20,22]. However, Fig. 1*b* shows that the crystalline fraction consists mainly of ice I_h in addition to the vitrified material. Thus the liquid jet apparently experiences either low cooling rates, giving ice I_h, or very high cooling rates leading to vitrified water. We believe that this is due to the vortex of the vigorously stirred cryomedium.

The thermodynamic conditions necessary for vitrifying liquid water have been discussed recently by Angell and Tucker[8]. The argument is based on the incompatibility of an extrapolated value of the glass transition temperature of vitrified liquid water with Kauzmann's entropy paradox[23] which states that a liquid can be supercooled only by a limited number of degrees before it loses all its excess entropy over the crystal, that is before its total entropy becomes equal to that of the crystal. This presents a problem, especially for liquid water, because in supercooled water a drastic increase of C_p occurs with decreasing temperature[5] among other anomalies. To resolve the entropy paradox Angell and co-workers postulated the existence of a λ-type heat capacity anomaly at 228 K associated either with some liquid state mechanical instability or with the cooperative formation of a long-range hydrogen-bonded network with decreasing temperature[6–8]. Angell and Tucker speculate that liquid water departs during cooling (assuming a rate of 10^8 K s^{-1}) from the metastable heat capacity already below the maximum observed value (which has been recorded at 235 K (refs 6, 24)) due to the 'freezing out' of the 'anomalous fluctuations' (see Fig. 5 in ref. 8). From the C_p versus temperature curve we wonder whether liquid water does not diverge at much higher temperatures—thereby avoiding the anomalous C_p increase altogether—and lose its internal equilibrium than that suggested by Angell and Tucker, considering the extreme cooling rates discussed above. In analogy to SiO_2 the vitrified solid is supposed to have different densities depending on the temperature at which internal equilibrium was established before quenching[25,26]. However, a determination of the density of vitrified liquid water is not possible at present due to the presence of the liquid cryomedium.

The similarity of structure between vitrified liquid water and $(H_2O)_{as}$ has been disputed recently. Rice[1,3,27] and Angell[8] believe that there is a continuity of state between liquid water and $(H_2O)_{as}$, that $(H_2O)_{as}$ is essentially liquid water, especially because the observed glass transition temperature of $(H_2O)_{as}$ is identical with the extrapolated value for vitrified liquid water. This hypothesis is the basis of the random network model of water recently proposed by Rice *et al.*[4,28]. In contrast Johari[29] argues on thermodynamic grounds mentioned above that a discontinuity of states exists, and that therefore "the structure of $(H_2O)_{as}$ is different from the one towards which supercooled water would tend". We have tried without success to observe a glass transition temperature in our vitrified water samples. A structural difference between vitrified liquid water and $(H_2O)_{as}$ could possibly emerge from a comparison of the X-ray diffraction patterns (see Figs 4 and 5). We do not know yet if the absence of the broad peak at $2\theta = 44°$ in vitrified liquid water is real or is only an artefact caused by the presence of the liquid cryomedium. According to Narten and Levy[30] a change of the double maximum in the structure functions of liquid water around 2.5 $Å^{-1}$ into a single peak corresponds to a disappearance of the maxima and minima between 3.5 and 8 Å in the correlation functions.

We thank Professor E. Schnell for help with the X-ray work.

Received 10 December 1981; accepted 10 May 1982.

1. Olander, D. S. & Rice, S. A. *Proc. natn. Acad. Sci. U.S.A.* **69,** 98–100 (1972).
2. Rice, S. A. & Sceats, M. G. *J. phys. Chem.* **85,** 1108–1119 (1981).
3. Narten, A. H., Venkatesh, C. G. & Rice, S. A. *J. chem. Phys.* **64,** 1106–1121 (1976).
4. Rice, S. A. *Topics curr. Chem.* **60,** 109–200 (1975).
5. Angell, C. A. in *Treatise on Water* Vol. 7 (ed. Franks F.) (in the press).
6. Angell, C. A., Shuppert, J. & Tucker, J. C. *J. phys. Chem.* **77,** 3092–3099 (1973).
7. Speedy, R. J. & Angell, C. A. *J. chem. Phys.* **65,** 851–858 (1976).
8. Angell, C. A. & Tucker, J. C. *J. phys. Chem.* **84,** 268–272 (1980).
9. Mazur, P. *Science* **168,** 939–949 (1970).
10. Wolstenholme, G. E. W. & O'Connor, M. *The Frozen Cell* (Churchill, London, 1970).
11. Becker, E. D. & Pimentel, G. C. *J. chem. Phys.* **25,** 224–228 (1956).
12. Fletcher, N. H. *Rep. Prog. Phys.* **34,** 913–994 (1971).
13. Pryde, J. A. & Jones, G. O. *Nature* **170,** 685–688 (1952).
14. Brüggeller, P. & Mayer, E. *Nature* **288,** 569–571 (1980).
15. Bachmann, L. & Schmitt, W. W. *Proc. natn. Acad. Sci. U.S.A.* **68,** 2149–2152 (1971); in *Freeze Etching* (eds Benedetti, E. L. & Favard, P.) 73–79 (Soc. Frac. Microsc. Electron, Paris 1973).
16. Stewart, G. W. & Mannheimer, M. *Z. anorg. allg. Chem.* **171,** 61–72 (1928).
17. Sahores, J. J. *Adv. X-ray Analysis* **16,** 186–197 (1973).
18. Berry, P. F., Furuta, T. & Rhodes, J. R. *Adv. X-ray Analysis* **12,** 612–632 (1969).
19. Berglund, R. N. & Lui, B. Y. H. *Envir. Sci. Technol.* **7,** 147–153 (1973).
20. Dowell, L. G. & Rinfret, A. P. *Nature* **188,** 1144–1148 (1960).
21. Uhlmann, D. R. *J. Non-Cryst. Solids* **7,** 337–348 (1972).
22. Hobbs, P. *Ice Physics* (Clarendon, Oxford, 1974).
23. Kauzmann, W. *Chem. Rev.* **43,** 219–256 (1948).
24. Rasmussen, D. H., MacKenzie, A. P., Tucker, J. C. & Angell, C. A. *Science* **181,** 342–344 (1973).
25. Kanno, H. & Angell, C. A. *J. chem. Phys.* **73,** 1940–1947 (1980).
26. Bruckner, R. *J. Non-Cryst. Solids* **5,** 281 (1971).
27. Rice, S. A., Bergren, M. S. & Swingle, L. *Chem. Phys. Lett.* **59,** 14–16 (1978).
28. Rice, S. A. & Sceats, M. G. *J. phys. Chem.* **85,** 1108–1119 (1981).
29. Johari, G. P. *Phil. Mag.* **35,** 1077–1090 (1977).
30. Narten, A. H. & Levy H. A. *J. chem. Phys.* **55,** 2263–2269 (1971).

The molecular basis of DNA–protein recognition inferred from the structure of cro repressor

D. H. Ohlendorf[*], W. F. Anderson[†], R. G. Fisher[*], Y. Takeda[‡] & B. W. Matthews[*]

*Institute of Molecular Biology and Department of Physics, University of Oregon, Eugene, Oregon 97403, USA
†MRC Group on Protein Structure and Function, Department of Biochemistry, University of Alberta, Edmonton, Alberta, Canada T6G 2H7
‡Chemistry Department, University of Maryland, Baltimore County, Catonsville, Maryland 21228, USA

Recognition by cro repressor protein of its specific DNA binding sites appears to occur via multidentate hydrogen bonds between amino acid side chains of the protein and base-pair atoms in the major groove of right-handed B-form DNA. Most of the sequence-specific interactions between cro and DNA, as well as a number of sequence-independent ones, are mediated by a two-α-helical unit which appears to be common to many proteins that regulate gene expression.

THE structures of three proteins that specifically bind to DNA have recently been determined, namely, the cro repressor protein (hereafter called 'cro') from bacteriophage λ[1], the catabolite gene activator protein (CAP) from *Escherichia coli*[2] and the amino-terminal fragment of the *c*I repressor protein (cI) from bacteriophage λ[3]. It has been proposed that these proteins bind to DNA with protruding α-helices penetrating[1,2] or partly penetrating[3] the major grooves of the DNA (in the case of CAP, the DNA has been postulated to be left-handed[2]).

In this article we propose a detailed model for the complex between cro and DNA. The model is consistent with the relative binding affinities of cro for the six operator sites within bacteriophage λ at which it binds specifically, and can also be used to rationalize known changes in binding affinity caused by mutations within these sites.

Cro is one of a number of proteins that participate in the

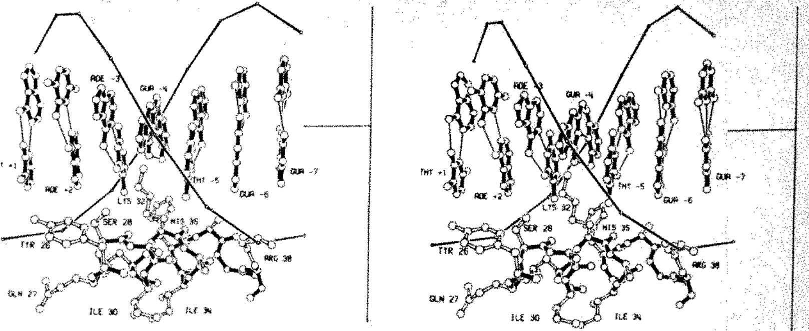

Fig. 1 Stereo drawing illustrating the initial alignment of residues 26–38 of cro repressor within the major groove of the DNA. Only the left half of the 17-base-pair binding site is shown. The vertical line at the right of the figure is the common protein and DNA twofold-symmetry axis which relates the other half of the binding site to that shown here. The horizontal line at the right coincides with the long axis of the DNA. The conformations of the individual protein side chains are those determined from the crystal structre of cro repressor protein. The base sequence is that for O_R3, with numbering as defined in the text. For clarity the details of the DNA backbone have been omitted and replaced by lines connecting the phosphates.

commitment to either the lytic or lysogenic pathway during the development of bacteriophage λ (for review see refs 4–6). Cro recognizes six binding sites on the bacteriophage genome, three within the left operator region (O_L1, O_L2 and O_L3) and three within the right operator region (O_R1, O_R2 and O_R3). Each binding site consists of 17 base pairs with approximate twofold symmetry. The base sequences of all six sites are similar but not identical[7].

Starting parameters

Coordinates for the DNA were derived from the fibre diffraction analysis of B-DNA by Arnott and colleagues (refs 8, 9 and S. Arnott, personal communication). Initially, the rise per base-pair, z, was set at 3.4 Å and the twist per base-pair, θ, was set at 34.6° (10.4 base-pairs per turn). These parameters are representative of values obtained by others[10–12].

The coordinates for cro were based on the previously reported structure determination[1]. The quality of the electron density map has been improved by a process of electron density averaging and phase extension[13] in which the final agreement between observed and electron-density-averaged structure factors was 22.3% at 2.8 Å resolution (R.G.F., D.H.O. and B.W.M., unpublished results). Also the cro structure has been partially refined, the coordinates used here being taken from the present stage of refinement, for which the crystallographic residual is 27% at 2.2 Å resolution (23% at 2.8 Å resolution) (D.H.O. and B.W.M., unpublished). The estimated error in the protein coordinates is about 0.4 Å.

The protein dimer was placed so that its twofold axis of symmetry coincided with that of the DNA[1], leaving two adjustable parameters, one the separation, d, between the protein and the DNA, and the other the rotation, τ, of the protein dimer relative to the DNA about the common protein-DNA symmetry axis. In addition to the above four parameters, z, θ, d and τ, adjustments were allowed in the radius of curvature, r, of the DNA. Because of the twofold symmetry of the protein–DNA complex, bending was constrained to occur only about points on the dyad axis.

Model building

Our general approach was to carry out model building on an MMS-X computer graphics facility[14] and to supplement this with energy minimization using the program EREF of Jack and Levitt[15]. Use of computer graphics permitted the screening of a large number of potential interactions between the protein and the DNA while energy minimization ensured that the stereochemistry of a proposed DNA–protein complex was reasonable.

The energy minimization procedure gives the calculated energy for the system under consideration, and, as such, provides an indication of the relative strength of a postulated cro:DNA complex. However, the energy minimization algorithm does not take account of solvent, and has other limitations which prevent its use for the reliable estimation of absolute interaction energies. Therefore, in attempting to optimize a given cro:DNA complex, we used energy minimization as a guide, but supplemented this with additional criteria such as the adherence of postulated hydrogen bonds to acceptable stereochemistry.

There has been considerable speculation that the free energy of stabilization of DNA:protein complexes comes primarily from relatively nonspecific interactions[16] while specificity derives largely from hydrogen bonds between protein side chains and the parts of the base pairs exposed in the grooves of the DNA[16–19]. Therefore, in model building we attempted to maximize the number of hydrogen bonds and other interactions between cro and the DNA, and assumed that each 'mispositioned' (that is, unsatisfied) hydrogen bond decreased the affinity of the DNA–protein complex, although it is understood that other factors such as shape complementary, hydrophobic and dipolar interactions and the role of solvent are also important. Since the binding constant, K, for the cro:DNA interaction is related to the free energy of the interaction, ΔG, by the formula $K = \exp(-\Delta G/RT)$, it follows that each improperly positioned hydrogen bond donor or acceptor, which reduces the free energy by about 1 kcal mol^{-1} (refs 16, 20), results in a reduction of the binding constant by a factor of approximately seven.

The presumed complexes between cro and DNA were initially subjected to energy minimization in which the protein backbone was kept rigid and only those side chains which appeared to interact with the DNA were allowed to move. A specialized version of EREF was used which allowed the explicit specification of hydrogen bonds. The five interaction parameters z, θ, d, τ and r (see above) were then systematically varied in small increments to determine which values gave the best value for the calculated energy of interaction. (This stepwise approach was necessary because EREF tends to make changes in local geometry, but not in the global interaction parameters.) In the final stages of the energy minimization, the local geometry of the DNA was allowed to vary, and, in addition, small adjustments were permitted in the protein backbone.

Interaction of cro with DNA

The initial structure determination of cro suggested that it bound to the DNA with a pair of dyad-related helices penetrating the major groove of the DNA[1]. This overall complementarity between the surface of the protein and the DNA not only suggests the approximate alignment of the protein relative to the DNA, but (short of making major conformational changes in the protein which we shall consider below), makes it sterically difficult to devise alternative interaction schemes which seem plausible.

Since both cro and the DNA binding site have approximate twofold symmetry it is, in the first instance, sufficient to consider the interaction between one monomer of cro and half of the binding site. We have numbered the base pairs within each half-site from 1 to 9 starting at the distal base pair. Bases +1 and −1 constitute a base pair, and so on. The '+' base is the one for which the inward direction of numbering is from 5′ to 3′.

The initial alignment of cro (Fig. 1) suggested that the amino acid side chains most likely to participate in interactions within the major groove of the DNA were Tyr 26, Gln 27, Ser 28, Asn 31, Lys 32, His 35 and Arg 38. Based on the framework of the potential hydrogen bonds and the cro:DNA geometry suggested by the energy calculations, it is possible to construct a set of rules which can be used to predict the hydrogen bonds

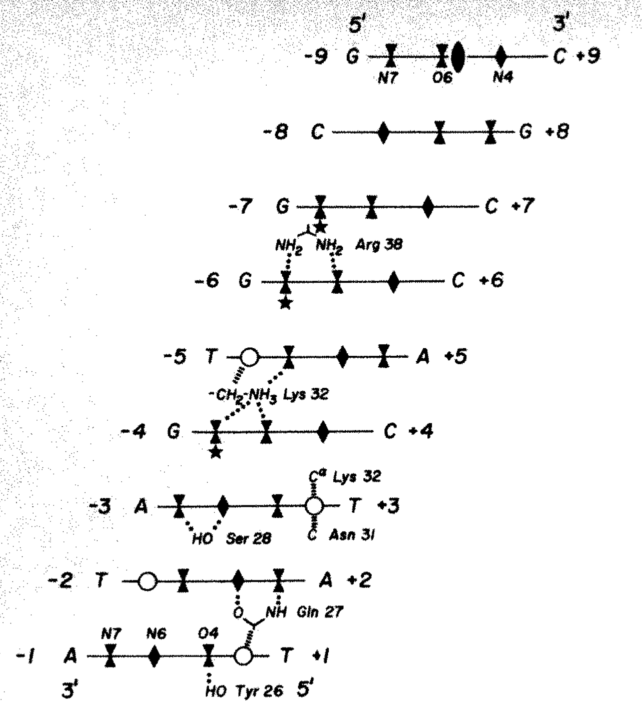

Fig. 2 Schematic representation, following Woodbury *et al.*[20], of the presumed sequence-specific interactions between cro and the parts of the base pairs exposed within the major groove of the DNA. The direction of view is imagined to be directly into the major groove of the DNA with the base-pairs seen edge-on. The dyad symbol within the topmost base pair indicates the center of the overall 17-base-pair binding region. The symbols are as follows: ⧗, hydrogen bond acceptor; ◆, hydrogen bond donor; ○, methyl group of thymine; ★, guanine N7 which is protected from methylation when cro is bound[22,23]. Presumed hydrogen bonds between cro side chains and the bases are indicated (. . . .). Apparent van der Waals contacts between cro and the thymine methyl groups are shown (||||||). Other van der Waals contacts are not shown.

expected when cro interacts with a given sequence of DNA. The proposed rules for hydrogen bonding are as follows:

(1) Arg 38 forms two hydrogen bonds to O6 and N7 of guanine −6. If base −6 is an adenine then Arg 38 makes a hydrogen bond with either the N7 of this adenine or the N7 of a purine at −7. If base −6 is a thymine then Arg 38 can make no hydrogen bonds to this base because of the blocking methyl group on C6 but can form one hydrogen bond to N7 of a purine at −7 (that is, a net loss of one hydrogen bond).

(2) Lys 32 N^{ζ} forms one hydrogen bond with either a purine N7 or an O4 of thymine at position −5. In addition, it forms a second hydrogen bond with O6 of guanine −4 and possibly a third hydrogen bond with N7 of guanine −4.

(3) Ser 28 O^{γ} forms two hydrogen bonds with N6 and N7 of adenine −3 or, alternatively, one hydrogen bond to N7 of guanine, N4 of cytosine, or O4 of thymine at −3. In the case of a thymine at position −3 there is a second hydrogen bond from the N6 of the adenine at +3 to the carbonyl oxygen of the serine.

(4) Gln 27 forms two hydrogen bonds to N6 and N7 of an adenine at +2. In all other cases it forms a single hydrogen bond.

(5) Tyr 26 O^{η} forms a hydrogen bond with either O4 of thymine +1 or N7 of a purine at +1, but cannot be placed in a stereochemically acceptable position to accept a hydrogen bond from N6 of adenine or N4 of cytosine.

As shown in Table 1, this model for the interaction between cro and DNA is consistent with the known relative affinities of cro for its six binding sites and for mutant sites as well.

The presumed sequence-specific hydrogen-bonding between cro and O_R3 is shown in Fig. 2 using a schematic representation based on that proposed by Woodbury *et al.*[20] and is shown in stereo in Fig. 3. The apparent interactions between the protein and the DNA backbone, which are not sequence-specific, and, presumbly, provide much of the overall energy of interaction, are summarized in Fig. 4. The overall conformation of cro repressor when bound to its specific binding site is illustrated in Fig. 5.

In the proposed cro:O_R3 complex, there are about 20 sequence-specific hydrogen bonds (Fig. 2) as well as many sequence-independent interactions (Fig. 4). These interactions could easily account for the observed dissociation constant of about 10^{-10} M (refs 21, 22).

Because cro is known to bind most tightly to O_R3 (refs 23–25) we used this for the initial model building and for most of the energy calculations. After refinement of the cro:O_R3 complex, the DNA had a mean z of 3.48 ± 0.09 Å with a range of 3.30 Å to 3.56 Å and a mean twist θ of $34.7 \pm 3.2°$ with a range of 26.9° to 39.8°. These values compare well with previously reported values for these parameters[10,26,27].

The optimization procedure suggests that the DNA is bent to a radius of about 75 Å. This degree of curvature is not excessive, as might at first be supposed. In the crystallized B-DNA dodecamer CGCGAATTCGCG, the DNA bends to a radius of 110 Å (ref. 28). Also, when associated with proteins in the nucleosome, DNA adopts a radius of about 45 Å (ref. 29). It can be estimated that the energy required to bend a 17 base-pair segment of DNA to a radius of 75 Å is between 0.85 and 1.7 kcal mol^{-1} (refs 30, 31), an amount of energy approximately equivalent to the formation of one hydrogen bond per monomer. As an alternative to the bending of the DNA, an essentially equivalent result could be obtained by a 'hinge-bending' motion of the two cro monomers in the vicinity of the antiparallel β-sheet strands, Glu 54–Lys 56. These residues form part of the C-terminal 'arms' (residues 52–60) which appear to be the major determinant in stabilizing the cro dimer. Other than the contacts mediated by these two arms there are only very tenuous interactions between the respective monomers, suggesting that a 'hinge-bending' motion could easily occur (Fig. 5; see also Figs 3, 4 and 6 of ref. 1).

Specific and nonspecific cro:DNA interactions

The proposed model for the complex between cro and DNA suggests that interactions occur predominantly within two regions of the protein, namely residues 15–38, that is, essentially the α_2 and α_3 helices, and residues 54–66 which include part of the third β-sheet strand and the carboxyl terminus of the molecule.

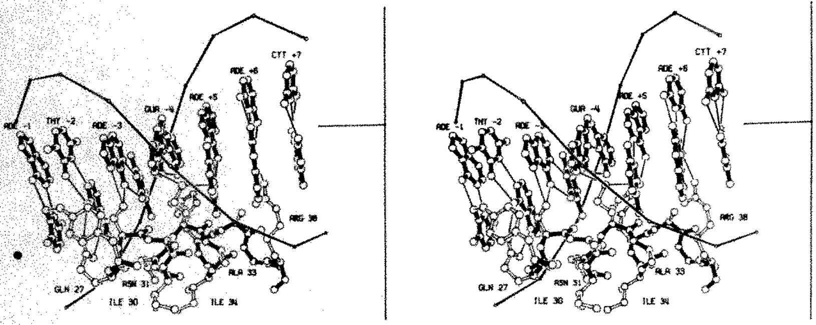

Fig. 3 Stereo drawing (Compare Fig. 1) showing the presumed hydrogen bonding of cro to base pairs in the major groove of O_R3, following model building and energy refinement.

Table 1 Cro binding to different DNA sites

Site	Sequence	Mutant	Affinity relative to O_R3	Predicted H-bonds relative to O_R3
O_R3	1 5 9 13 17 TATCACCGCAAGGGATA ATAGTGGCGTTCCCTAT		1	0
	G C	v3C	1/10	−1
	T A	r1	1/3	0
	T A	r2	<1	0
	A T	r3	<1	0
	G C	c12		−1
	C G	c10	1/10	−1
O_R2	TAACACCGTGCGTGTTG ATTGTGGCACGCACAAC		1/8	−1
	G C	v3C	1/80	−2
	A T	vi or vH		−2
	AA TT	virC23	1/400	−3
	T A	vN or vC34	<1/8	−3
O_R1	TACCTCTGGCGGTGATA ATGGAGACCGCCACTAT		1/8	−1
	G C	vR18		−2
	A T	vs326	1/40	−2
	A T	v3		−1
	C G	vs387	<1/8	−2
	T A	vC1	1/40	−2
O_L1	TACCACTGGCGGTGATA ATGGTGACCGCCACTAT		~1/2	−1
	G C	v101		−2
	T A	v2		−2
	A T	v003		−2
O_L2	TATCTCTGGCGGTGTTG ATAGAGACCGCCACAAC		~1/2	−1
	A T	v305		−1
O_L3	AACCATCTGCGGTGATA TTGGTAGACGCCACTAT 1 5 9 13 17		~1/10	−2
Amino acid	26 Lys Arg Arg Lys 26 −28 32 38 38 32 −28			

DNA sequences and relative affinities are shown for the six 17-base pair sites to which cro binds specifically in phage λ. Mutations in these sites with known relative affinities for cro binding are also shown. (Data taken from refs 23, 24.) The relative binding affinities are to be compared with the change in the number of sequence-specific hydrogen bonds between cro and the DNA site as predicted from the model for cro binding proposed in the text. If the model is correct, and if hydrogen bonding is a major determinant in the specificity of cro: DNA recognition, then the loss of successive hydrogen bonds ought to correspond to successive reductions in the affinity of binding by about a factor of seven.

The α_3 helix (residues 27–36) penetrates the major groove of the DNA and appears to contribute most of the sequence-specific interactions (Figs 2, 3). Interactions of Lys 32 and Arg 38 with bases in positions −4, −5 and −6 account for the observed protection from methylation of guanine N7 at these positions[4,23,24]. In the presumed complex between cro and O_R3 (Figs 2, 3) there is no hydrogen bonding at the N7 of guanine −7. This is, perhaps, surprising in view of the observed protection of this nitrogen from methylation. However, the close proximity of the guanidinium group of Arg 38 to guanine −7 (Fig. 3) might sterically inhibit the access of dimethyl sulphate to this base.

The α_2 helix (residues 15–23) appears to make a number of sequence-independent interactions with the outermost part of the DNA binding site (Fig. 4). Altogether, residues in the α_2 and α_3 helices may contribute as many as five hydrogen bonds to the phosphate backbone. In the model, there are no sequence-specific interactions between cro and the central three

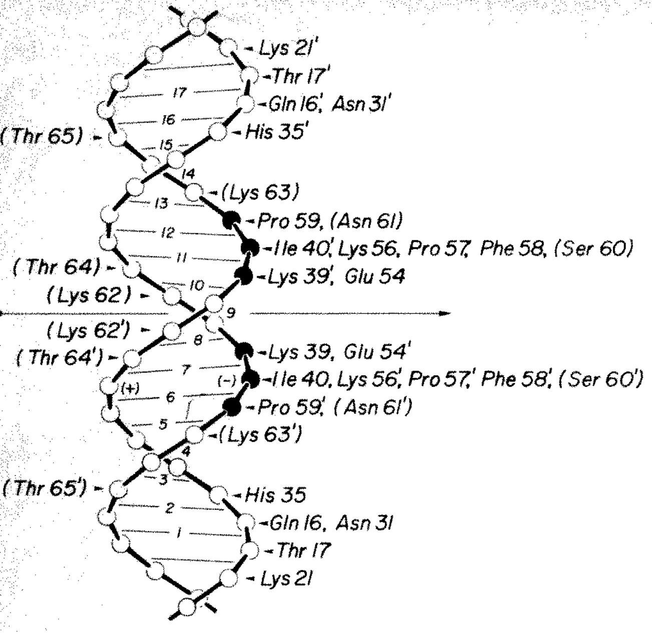

Fig. 4 Schematic representation of the contacts and interactions which are presumed to occur between cro and the phosphates in the DNA backbone. In the presumed cro: DNA complex, at least one close approach occurs between a given phosphate group and the named amino acids. Those phosphates for which ethylation interferes with cro binding[23] are drawn solid. Numbering of the base pairs and the signs (+) and (−) correspond to the identification used in the text. Amino acids belonging to 'lower' and 'upper' cro monomers related by the horizontal dyad axis are non-primed and primed, respectively. Amino acids in parentheses are those at the C-terminus of the molecule which are disordered in the crystal (residues 62–66) or for which the backbone conformation has been adjusted (residues 60, 61) to improve the contact with the DNA.

base pairs of the binding site, consistent with the observation that, for these three base-pairs, nitrogens N3 of the adenines exposed in the minor groove and N7 of the guanines exposed in the major groove are susceptible to methylation by dimethyl sulphate[4,23,24].

Residues Glu 54–Lys 56 of the third β-strand, together with the twofold-related strand in the adjacent cro monomer, are located close to the centre of the binding site and lie parallel to the minor groove, but, in part because of the bending of the DNA, do not lie within the minor groove (compare refs 1, 32). Rather, their contact with the DNA appears to be limited to interactions between the side chains and the phosphate backbone (Fig. 4). In the model for the presumed cro:DNA complex, the phosphate at position −6 (between base pairs 6 and 7 in Fig. 4) and possibly one or two solvent atoms or cations are surrounded by protein. The two neighbouring phosphates also appear to be partly 'covered' by protein (see Fig. 4), consistent with the observation that ethylation of these three phosphates interferes with the formation of the cro:DNA complex[4,23]. In the presumed cro:DNA complex, it appears that the seven C-terminal residues, including Lys 62 and Lys 63, could lie along the minor groove of the DNA with the side chains interacting with the phosphate backbone (Figs 4, 5). Since the five C-terminal residues are disordered in the crystals of the native protein[1] it has to be emphasized that the details of such interactions remain very speculative.

Inferences for protein–DNA recognition

The proposed complex between cro and DNA has a numnber of features which may be of general significance for recognition by proteins of specific sites on DNA.

The initial determination of the cro structure[1] revealed a pair of twofold-related α-helices arranged in such a way that they could be placed within successive major grooves of right-handed Watson–Crick B-form DNA. This result gave credence to previous suggestions that α-helices of proteins might bind within the major groove of B-DNA[33–36].

The present study strongly suggests that sequence-specific recognition of DNA is mediated by hydrogen bonds between protein side chains and the parts of the base pairs exposed within the grooves of the DNA as has been advocated by a number of authors[16,19,35–38]. In particular, it is of interest to note that the specificity of recognition appears to be enhanced by multiple interactions between a given side chain and appropriate hydrogen bond donors and acceptors on the base pairs. The apparent bidentate interaction of Gln 27 with nitrogens N6 and N7 of adenine +2 as well as the interaction of Arg 38 with O6 and N7 of guanine −6 (Figs 2, 3) are as anticipated[18,39]. Ser 28 and Lys 32 are also presumed to participate in multiple interactions. Such interactions had not been postulated previously, although von Hippel and colleagues[16,19] have suggested that bridging interactions could occur between atoms on successive base pairs, as seems to be the case with cro, in some instances. Also Drew and Dickerson[40] have observed a solvent molecule (molecule 66 in their numbering scheme) which forms hydrogen bonds with both the N6 and N7 nitrogens of an adenine, precisely as is proposed to occur between O^{γ} of Ser 28 and adenine −3.

In addition to the above hydrogen bonding within the major groove of the DNA, there are a number of apparent van der Waals contacts which are presumably also important in sequence-specific recognition. In particular, the C7 methyl groups of thymines +1, +3 and −5 appear to interact, respectively, with C^{δ} of Gln 27, with the carbonyl carbon of Asn 31 and the α-carbon of Lys 32 and with C^{γ} and C^{ϵ} of Lys 32 (Fig. 2). The importance of such hydrophobic interactions in the recognition of *lac* operator by lac repressor has been shown by Caruthers[41].

Another feature of the model which may be of general relevance is the combination of sequence-specific interactions, mediated by the more rigid parts of the protein structure, together with non-specific interactions that are assumed to derive, in part, from flexibility in the cro structure. Two distinct types of flexible motion seem likely. First, the C-terminal residues (62–66) are not ordered in the crystals of the native protein, and are presumably free to move in solution. Because of this freedom of motion, and also because the C-terminal residues do not seem to be involved in sequence-specific interactions, we suggest that these residues are involved in the initial binding of the protein to the DNA. The second type of flexible

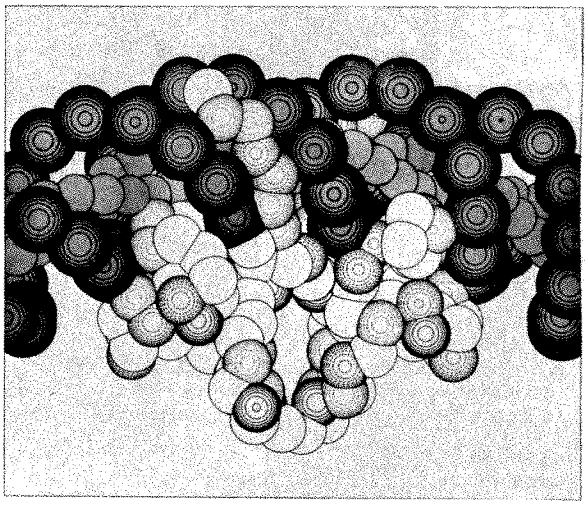

Fig. 5 Schematic drawing of the proposed sequence-specific complex of cro with DNA. For the stylized DNA (shaded) the large concentric circles indicate the positions of the phosphate groups and the smaller circles follow the bottom of the major and minor grooves. For the cro dimer, one circle is drawn for each amino acid; continuous concentric circles indicate acidic residues, broken circles indicate basic residues, dotted circles indicate non-charged hydrophilic residues and open circles show hydrophobic residues.

motion suggested by the cro structure is the 'hinge bending' motion described above. We suggest that such flexibility may be of general importance in facilitating 'sliding' along the DNA as has been proposed to occur for lac repressor[42–47]. Inspection of the structures of CAP[2] and *c*I repressor[3] indicates that 'hinge' motion seems possible for these structures as well, suggesting that this type of flexibility may be of general significance. One could imagine that a hinge motion of the protein, as well as flexibility in the DNA, would give each of the cro monomers some freedom to 'sample' adjacent base pair atoms in the major groove of the DNA. Only at the correct twofold-symmetric binding site would the full DNA-binding specificity be satisfied for both cro subunits simultaneously. Because a dimer rather than a monomer of cro binds to DNA, the overall recognition site extends over 17 base pairs (~60 Å). However, the cro:DNA complex is presumably optimized for control rather than tightness of binding so that not all of the 17 base pairs need contact the protein and, in addition, departures from exact twofold symmetry of the base sequence could be used to 'fine tune' the strength of the cro:DNA complex.

Finally, we note that in the proposed cro:DNA complex, most of the sequence-specific interactions, as well as a number of the sequence-independent ones, come from the α_2–α_3 helical unit. It has been striking to find, on the basis of recent sequence and structure comparisons, that a similar two-helical fold appears to occur in a number of other DNA-binding proteins[48–54] indicating that the principles of specific protein–DNA recognition suggested by the proposed model may be of general significance.

We thank Alan Bender for help with model-building and Dr. P. H. von Hippel for discussions. This work was supported in part by an NIH postdoctoral fellowship to D.H.O. (GM08403), a Damon Runyon-Walter Winchell Cancer Fund postdoctoral fellowship to R.G.F. (DRG-388-FT), by the MRC of Canada through the Group on Protein Structure and Function (to W.F.A.), by NIH grants to B.W.M. (GM20066) and Y.T. (GM28138) and by grants to B.W.M. from the NSF (PCM-8014311) and the M. J. Murdock Charitable Trust.

Received 27 April; accepted 2 July 1982.

1. Anderson, W. F., Ohlendorf, D. H., Takeda, Y. & Matthews, B. W. *Nature* **290,** 754–758 (1981).
2. McKay, D. B. & Steitz, T. A. *Nature* **290,** 744–749 (1981).
3. Pabo, C. O. & Lewis, M. *Nature* **298,** 443–447 (1982).
4. Ptashne, M. *et al. Cell* **19,** 1–11 (1980).
5. Echols, H. in *The Molecular Genetics of Development* (eds Loomis, W. & Leighton, T.) 1–16 (Academic, New York, 1980).
6. Herskowitz, I. & Hagen, D. A. *Rev. Genet.* **14,** 399–445 (1980).
7. Maniatis, T. *et al. Cell* **5,** 109–113 (1975).
8. Watson, J. D. & Crick, F. H. C. *Nature* **171,** 737–738 (1953).
9. Arnott, S. & Hukins, D. W. L. *Biochem. biophys. Res. Commun.* **47,** 1504–1509 (1972).
10. Drew, H. R. *et al. Proc. natn. Acad. Sci. U.S.A.* **78,** 2179–2183 (1981).
11. Peck, L. J. & Wang, J. C. *Nature* **292,** 375–378 (1981).
12. Rhodes, D. & Klug, A. *Nature* **292,** 378–390 (1981).
13. Bricogne, G. *Acta crystallogr.* **A30,** 395–405 (1974).
14. Molnar, C. E., Barry, C. D. & Rosenberger, F. U. *Tech. Memo.* No. **229** (Computer Systems Laboratory, Washington University, St Louis, 1976).
15. Jack, A. & Levitt, M. *Acta crystallogr.* **A34,** 931–935 (1971).
16. von Hippel, P. H. in *Biological Regulation and Development* Vol. 1 (ed. Goldberger, R. F.) 279–347 (Plenum, New York, 1979).
17. Yarus, M. A. *Rev. Biochem.* **38,** 841–880 (1969).
18. Seeman, N. C., Rosenberg, J. M. & Rich, A. *Proc. natn. Acad. Sci. U.S.A.* **73,** 804–808 (1976).
19. Woodbury, C. P., Hagenbuchle & von Hippel, P. H. *J. biol. Chem.* **255,** 11534–11546 (1980).
20. Levitt, M. *J. molec. Biol.* **82,** 393–420 (1974).
21. Takeda, Y., Folkmanis, A. & Echols, H. *J. biol. Chem.* **252,** 6177–6183 (1977).
22. Johnson, A. D., Pabo, C. O. & Sauer, R. T. *Meth. Enzym.* **65,** 839–856 (1980).
23. Johnson, A. thesis, Harvard Univ. (1980).
24. Johnson, A., Meyer, B. J. & Ptashne, M. *Proc. natn. Acad. Sci. U.S.A.* **76,** 5061–5065 (1979).
25. Takeda, Y. *J. molec. Biol.* **127,** 177–191 (1979).
26. Wang, J. C. *Proc. natn. Acad. Sci. U.S.A.* **76,** 200–203 (1979).
27. Mandelkern, M., Elias, J. G., Eden, F. & Crothers, D. M. *J. molec. Biol.* **152,** 153–161 (1981).
28. Dickerson, R. E. & Drew, H. R. *J. molec. Biol.* **149,** 761–786 (1981).
29. Finch, J. T. *et al. Nature* **269,** 29–36 (1977).
30. Schellman, J. A. *Biopolymers* **13,** 217–226 (1974).
31. Hats, J. B., Magar, M. E. & Zimm, B. H. *Biopolymers,* **8,** 531–536 (1969).
32. Church, G. M., Sussman, J. L. & Kim, S.-H. *Proc. natn. Acad. Sci. U.S.A.* **74,** 1458–1462,
33. Zubay, G. & Doty, P. *J. molec. Biol.* **1,** 1–2 (1959).
34. Sung, M. T. & Dixon, G. H. *Proc. natn. Acad. Sci. U.S.A.* **67,** 1616–1623 (1970).
35. Adler, K. *et al. Nature* **237**, 322–327 (1972).
36. Warrant, R. W. & Kim, S. H. *Nature* **271,** 130–135 (1978).
37. von Hippel, P. H., Bear, D. G., Winter, R. B. & Berg. O. G. *Promoters: Structure and Function* (Eds Rodriguez, R. & Chamberlin, M.) (Praeger Scientific, New York, in the press).
38. Woodbury, C. P. & von Hippel, P. H. in *Gene Amplification and Analysis* Vol. 1 (ed. Chirikjian, J. C.) (Elsevier, New York, 1981).
39. Helene, C. *FEBS Lett.* **74,** 10–13 (1977).
40. Drew, H. R. & Dickerson, R. E. *J. molec. Biol.* **151,** 535–556 (1981).
41. Caruthers, M. H. *Accts Chem. Res.* **13,** 155–160 (1980).
42. Richter, R. H. & Eigen, M. *Biophys. Chem.* **2,** 255–263 (1974).
43. Berg, O. G. & Blomberg, C. *Biophys. Chem.* **4,** 367–381 (1976).
44. Berg, O. G., Winter, R. B. & von Hippel, P. H. *Biochemistry* **20,** 6929–6948 (1981).
45. Winter, R. B. & von Hippel, P. H. *Biochemistry* **20,** 6948–6960 (1981).
46. Winter, R. B., Berg, O. G. & von Hippel, P. H. *Biochemistry* **20,** 6961–6977 (1981).
47. Berg, O. G., Winter, R. B. & von Hippel, P. H. *Trends biochem. Sci.* **7,** 52–55 (1982).
48. Anderson, W. F., Takeda, Y., Ohlendorf, D. H. & Matthews, B. W. *J. molec. Biol.* (in the press).
49. Matthews, B. W., Ohlendorf, D. H., Anderson, W. F. & Takeda, Y. *Proc. natn. Acad. Sci. U.S.A.* **79,** 1428–1432 (1982).
50. Steitz, T. A., Ohlendorf, D. H., McKay, D. B., Anderson, W. F. & Matthews, B. W. *Proc. natn. Acad. Sci. U.S.A.* **79,** 3097–3100 (1982).
51. Ohlendorf, D. H., Anderson, W. F. & Matthews, B. W. *J. molec. Evol.* (submitted).
52. Sauer, R. T., Yocum, R. R., Doolittle, R. F., Lewis, M. & Pabo, C. O. *Nature* **298,** 447–451 (1982).
53. Weber, I. T., McKay, D. B. & Steitz, T. A. *Nucleic Acids Res.* (submitted).
54. Matthews, B. W., Ohlendorf, D. H., Anderson, W. F., Fisher, R. G. & Takeda, Y. *Cold Spring Harbor Symp. quant. Biol.* **47** (in the press).

Complete nucleotide sequence and identification of membrane components of the histidine transport operon of *S. typhimurium*

C. F. Higgins*, P. D. Haag, K. Nikaido, F. Ardeshir*, G. Garcia & G. Ferro-Luzzi Ames

Department of Biochemistry, University of California, Berkeley, California 94720, USA

The nucleotide sequence of the entire histidine transport operon from Salmonella typhimurium *has been determined and is shown to consist of four genes,* hisJ, hisQ, hisM *and* hisP. *This operon provides the only example of a binding protein-dependent transport system for which the total number of protein components is known. Determination of the amino acid compositions and sequences of these four transport proteins, together with analysis of various transport mutants, allows us to propose a molecular model for binding protein-dependent transport.*

AT least five separate transport systems are involved in the uptake of histidine by *Salmonella typhimurium*[1]. One of these, the high-affinity histidine permease, has been extensively characterized and is among the best understood of all bacterial transport systems. This permease belongs to a broad group of 'shock-sensitive' transport systems that require for function specific substrate-binding proteins that are located in the periplasmic space and released by osmotic shock[2]. Such periplasmic binding proteins are also involved in chemotaxis. Shock-sensi-

---

* Present addresses: Department of Biochemistry, University of Dundee, Dundee DD1 4HN, UK (C.F.H.); Department of Biochemistry, Stanford University, California 94305, USA (F.A.).

0028–0836/82/330723—05$01.00

tive transport systems usually involve multiple components, in contrast to shock-resistant systems which require only a single, membrane-bound component (such as the lactose permease[3]). Previous studies of the high-affinity histidine permease have identified three essential genes, *hisJ*, *hisQ* and *hisP*, which together with a regulatory locus, *dhuA*, form a single operon located at 48.5 minutes on the *S. typhimurium* chromosomal map[4] (Fig. 1). The *hisJ* gene encodes the periplasmic histidine-binding protein, J, which has been purified and characterized[5]. The *hisP* gene encodes a basic protein, P, which is located in the inner cytoplasmic membrane[6]. The previously defined *hisQ* gene is here shown to consist of two separate cistrons, *hisQ* and *hisM*. Thus, four protein components are required for high-affinity histidine transport.

The periplasmic protein J and the membrane-bound protein P interact with each other during histidine transport[7]. Complementation studies suggest that Q, M and P also interact with each other[6], possibly existing as a multicomponent complex located in the cytoplasmic membrane. The Q, M and P proteins, but not the J protein, are also essential for an arginine transport system that requires an alternative periplasmic component, the lysine–arginine–ornithine-binding protein, LAO[8,9]. The amino acid sequences of LAO and J are 70% homologous and the two proteins are believed to interact with the same site on the membrane-bound P protein during arginine or histidine transport, respectively[10]. Thus, the P protein provides a common membrane-bound receptor for two independent binding proteins. LAO is encoded by the *argT* gene which is located immediately upstream (Fig. 1) and is transcribed independently of the histidine transport operon[11].

Nucleotide sequence

The entire histidine transport operon has been cloned as a 12.4-kilobase (kb) *Eco*RI fragment in the phage vector λgt4 (ref. 12). The precise locations of the transport genes on this fragment were determined by correlating accurately a restriction map with the genetic map of the histidine transport operon[13]. The various genes of the operon were sequenced by subcloning appropriate restriction fragments into the plasmid vectors pBR322 and pBR322-SVa[13]. Figure 1 shows schematically the histidine transport operon and the restriction fragments used in our study, while the complete nucleotide sequence of the histidine transport operon, a total of 3,700 base pairs (bp), is presented in Fig. 2.

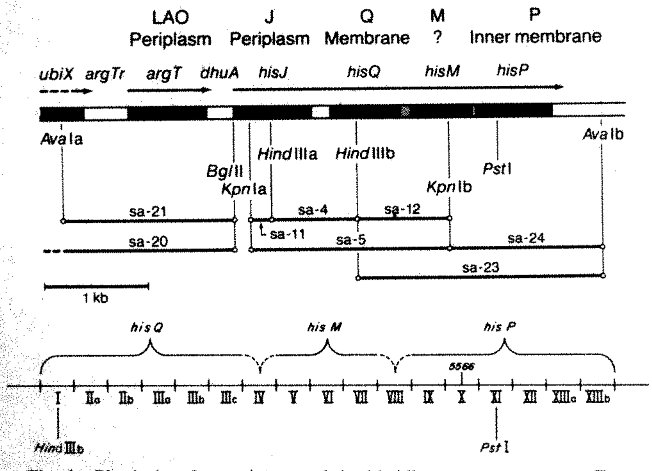

Fig. 1 Physical and genetic map of the histidine transport operon. Top: the structural genes (solid bars) and the intercistronic and regulatory regions (open bars) are all drawn to scale and include the *argTr*/*argT* operon. The dashed bar indicates uncertainty about the initiation site for *hisM* (see text). Arrows above the genes indicate length and direction of transcripts, as deduced from the sequences. The transcription terminator sequence for the histidine transport operon is located 0.11 kb 3′ to the end of *hisP*. The horizontal lines below the chromosome indicate specific restriction fragments subcloned for sequencing purposes. All are derived from the original clone of the entire region sa-1 (a 12.4-kb *Eco*RI fragment[13]). Bottom: genetic regions within the *hisQ*, *hisM* and *hisP* genes. These regions (in roman numerals) were defined by deletion mapping and biochemical analysis of mutants (refs 4, 6 and unpublished data).

Identification of the coding sequences

hisJ. The reading frame between bases 1 and 780 has previously been shown[10] to be the coding sequence for *hisJ*. The amino acid sequence deduced from this nucleotide sequence corresponds with the known amino acid sequence of the J protein[14]. Salient features of the amino acid sequence of J and its relation to the LAO protein have been discussed elsewhere[10].

hisP. All *hisP* mutations are located within eight genetic regions (IX–XIIIb; see Fig. 1)[4,6] (unpublished results). The structural gene encoding the P protein (as opposed to a possible regulatory region) must begin in or before region X because two-dimensional gel electrophoresis[6] shows that one mutant mapping in this region (*hisP5566*, Fig. 1) results in a P protein with an altered mobility. As the *Pst*I site is located in region XI[13], the coding sequence for the P protein must include this site. The only open reading frame of any length spanning the *Pst*I site is from position 2,367 to 3,140. This reading frame encodes a basic protein with a calculated molecular weight (M_r) of 28,738. The P protein has been confirmed experimentally to be basic and of ~24,000 M_r on SDS gels[6]: a discrepancy between the calculated molecular weight and the molecular weight determined on SDS gel is not unusual (see, for example, ref. 15). We confirmed that this reading frame encodes the P protein by purifying P protein, double-labelled with ^{35}S-methionine and ^{3}H-leucine, from several two-dimensional gels and analysing the first 12 amino acids on a sequenator. ^{3}H-leucine appeared in steps 5 and 10 (data not presented), and a very small amount of ^{35}S-methionine appeared in steps 1 and 2. These results are consistent with the predicted P sequence at the NH_2-terminus if we assume that most of the molecules have both N-terminal methionines removed post-translationally, but a few have only one or none of them removed.

hisQ. The region between *hisJ* and *hisP* has previously been defined genetically as *hisQ* and divided into regions (I–VIII)[6]. The sequence (1,586 bp) between the termination codon of the J protein (position 781) and the initiation codon of the P protein (position 2,367) could potentially encode a single polypeptide of M_r 53,000. However, examination of the nucleotide sequence does not reveal a reading frame covering this entire region. We have identified a protein, which we call Q, by non-equilibrium two-dimensional gel electrophoresis[16] either of whole cells or UV-irradiated cells[17] following infection with λ phages carrying the cloned transport operon[12] (data not shown). It is a basic protein, of apparent M_r 21,000, located in the membrane, and present in extremely small amounts (10–100 times less than J; we have been unable to determine its NH_2-terminal amino acids). The Q protein is absent from mutants in regions I–IV, but present in mutants in regions V–VIII. Thus, the *hisQ* gene proper does not extend beyond region IV. Region I of *hisQ* contains the *Hind*III site b (Fig. 1)[13]: therefore, the *hisQ* coding sequence must start 5′ to this restriction site. Of all the potential initiation codons (ATG, GTG and TTG[18]) between the end of *hisJ* and *Hind*III site b, only one, at position 966, could initiate a peptide of more than a few amino acids. This initiation codon is preceded by a strong ribosome-binding site and would initiate a basic protein of 24,573 M_r. Both the molecular weight and basicity of this protein are consistent with those of the Q protein. Therefore, we conclude that base pairs 966–1,649 are indeed the coding sequence for the Q protein and we re-define the *hisQ* gene as comprising this coding sequence only. Regions V–VIII (and part of IV) must code for one or more additional structural genes, or may comprise an extensive intercistronic region.

hisM. Between the termination codon for *hisQ* (position 1,650) and the beginning of *hisP* (position 2,367) is a sequence of position 717 which must correspond to regions V–VIII of the previously defined *hisQ* gene[6]. Mutants mapping in these regions are indistinguishable phenotypically from *hisP* and *hisQ*

```
                     -200 →  ←                    -150                             -100
GGGAAGGGGATAACGCGCCGCGCTGGGGAACTATCACGGTGCAAAATAGATGTTTTGCACCTTTTTGGTGCATAAGCCGTTGCGGAACAGGCGCATAAATGCATACTTAATCGATTTTTATGCAAAATAAACCGGCTGACAAGGTAGAAT

                     -50                    J protein →  1                          50
GCTTTGCCTTGTCGGCCTGATTAATGGCACGATAGTCGCATCGGATCTGTAAAGATCTCTTGGAAAGACAGTCTGTTGAGGATAGTTATGAAAAAACTGGCGTTATCCCTTTCTCTGGTGCTGGCATTTTCCAGCGCTACCGCAGCATTT
                                                                                          MetLysLysLeuAlaLeuSerLeuSerLeuValLeuAlaPheSerSerAlaThrAlaAlaPhe
↓
                     100                           150                             200
GCCGCTATTCCACAAAAGATTCGCATCGGTACCGATCCTACATACGCACCGTTTGAATCCAAAAATGCACAAGGTGAATTGGTCGGCTTTGATATCGATCTGGCCAAAGAGCTGTGCAAACGTATCAACACACAGTGTACGTTCGTGGAA
AlaAlaIleProGlnLysIleArgIleGlyThrAspProThrTyrAlaProPheGluSerLysAsnAlaGlnGlyGluLeuValGlyPheAspIleAspLeuAlaLysGluLeuCysLysArgIleAsnThrGlnCysThrPheValGlu
 1                                                          25

                     250                           300                             350
AACCCGCTGGATGCGCTGATTCCGTCTTTAAAAGCGAAGAAAATTGATGCCATCATGTCCTCGCTGTCCATCACTGAAAAGCGCCAGCAGGAAATCGCGTTTACCGACAAGCTTTACGCCGCTGATTCCCGTCTGGTGGTGGCGAAGAAC
AsnProLeuAspAlaLeuIleProSerLeuLysAlaLysLysIleAspAlaIleMetSerSerLeuSerIleThrGluLysArgGlnGlnGluIleAlaPheThrAspLysLeuTyrAlaAlaAspSerArgLeuValValAlaLysAsn
50                                                          75

                     400                           450                             500
TCTGATATTCAGCCGACCGTCGCGTCGCTGAAAGGCAAGCGCGTCGGCGTGCTACAGGGGACGACGCAGGAGACCTTCGGCAATGAGCACTGGGCGCCGAAAGGGATTGAGATCGTCTCTTACCAGGGGCAGGACAACATTTATTCCGAC
SerAspIleGlnProThrValAlaSerLeuLysGlyLysArgValGlyValLeuGlnGlyThrThrGlnGluThrPheGlyAsnGluHisTrpAlaProLysGlyIleGluIleValSerTyrGlnGlyGlnAspAsnIleTyrSerAsp
100                                                         125

                     550                           600                             650
CTGACGGCTGGCCGTATTGATGCGGCGTTCCAGGACGAGGTCGCGGCCAGCGAAGGTTTCCTTAAACAGCCCGTCGGAAAAGACTATAAATTCGGCGGCCCGGCGGTGAAAGATGAGAAGTTATTCGGCGTAGGAACCGGTATGGGGCTG
LeuThrAlaGlyArgIleAspAlaAlaPheGlnAspGluValAlaAlaSerGluGlyPheLeuLysGlnProValGlyLysAspTyrLysPheGlyGlyProAlaValLysAspGluLysLeuPheGlyValGlyThrGlyMetGlyLeu
150                                                         175

                     700                           750                             800
CGCAAAGAGGATAACGAGCTGCGCGAAGCGCTGAACAAAGCCTTTGCTGAAATGCGTGCTGACGGTACTTACGAAAAGCTGGCGAAAAAGTACTTTGATTTTGATGTTTATGGCGGTTAATCACCGTCGGTGCAGATAAAGCCCAAAGAA
ArgLysGluAspAsnGluLeuArgGluAlaLeuAsnLysAlaPheAlaGluMetArgAlaAspGlyThrTyrGluLysLeuAlaLysLysTyrPheAspPheAspValTyrGlyGlyEND
200                                                         225
         ⟶                                       ⟵
                     850                           900                             950
TGTTGACTGTCTGCATTGCCTGATGGCGCTGTGCGTGTCAGGCCTACGGGGAGCATCGTAGGCCGGGCAAGGCACAGCCGCCATCCGGCGTGATGTGAGGCAAAAATGCAAAAGAGGCTTATTACTTCACCACACACAACAGGACAGGCT

Q protein →
                     1000                          1050                            1100
GCATGTTGTACGGGTTTTCAGGCGTAATTTTACAGGGCGCGATCGTCACGCTGGAACTGGCGCTCAGTTCCGTGGTGCTGGCCGTGCTTATCGGTCTCGTCGGCGCGGGGGCGAAGCTTTCGCAAAACCGGGTAACGGGGCTTATTTTTG
 MetLeuTyrGlyPheSerGlyValIleLeuGlnGlyAlaIleValThrLeuGluLeuAlaLeuSerSerValValLeuAlaValLeuIleGlyLeuValGlyAlaGlyAlaLysLeuSerGlnAsnArgValThrGlyLeuIlePheG
  1                                                         25

                     1150                          1200                            1250
AAGGGTACACCACCCTGATTCGCGGGGTGCCGGATCTGGTCTTAATGCTGCTGATATTTTACGGATTGCAAATCGCGCTTAACGTGGTGACCGATTCGCTGGGTATCGACCAGATAGATATTGATCCGATGGTGGCCGGTATTATCACCC
luGlyTyrThrThrLeuIleArgGlyValProAspLeuValLeuMetLeuLeuIlePheTyrGlyLeuGlnIleAlaLeuAsnValValThrAspSerLeuGlyIleAspGlnIleAspIleAspProMetValAlaGlyIleIleThrL
50                                                          75                                                                                          1

                     1300                          1350                            1400
TTGGTTTCATCTACGGCGCCTATTTTACCGAAACCTTTCGCGGCGCGTTTATGGCGGTGCCGAAAGGCCATATCGAGGCGGCGACGGCCTTTGGTTTTACCCACGGGCAAACCTTCCGGCGGATTATGTTCCCGGCGATGATGCGTTACG
euGlyPheIleTyrGlyAlaTyrPheThrGluThrPheArgGlyAlaPheMetAlaValProLysGlyHisIleGluAlaAlaThrAlaPheGlyPheThrHisGlyGlnThrPheArgArgIleMetPheProAlaMetMetArgTyrA
00                                                          125                                                                                         1

                     1450                          1500                            1550
CCCTGCCGGGGATCGGCAATAACTGGCAGGTGATACTCAAAGCGACGGCGCTGGTGTCGCTGCTGGGCCTGGAAGATGTCGTCAAAGCCACGCAGCTTGCCGGTAAAAGTACCTGGGAGCCTTTCTATTTTGCCGTGGTCTGTGGACTTA
laLeuProGlyIleGlyAsnAsnTrpGlnValIleLeuLysAlaThrAlaLeuValSerLeuLeuGlyLeuGluAspValValLysAlaThrGlnLeuAlaGlyLysSerThrTrpGluProPheTyrPheAlaValValCysGlyLeuI
50                                                          175       M protein →                                                                       2
                     1600                          1650                            1700
TCTACCTGGTATTTACCACCGTTTCCAATGGTGTGCTGCTCTTACTTGAGCGTCGCTATTCCGTGGGCGTGAAGAGGGCCGATTTGTGATTGAGATCATTCAGGAGTACTGGAAATCCCTGCTTTGGACGGATGGCTATCGTTTTACCGG
leTyrLeuValPheThrThrValSerAsnGlyValLeuLeuLeuLeuGluArgArgTyrSerValGlyValLysArgAlaAspLeuEND  GluIleIleGlnGluTyrTrpLysSerLeuLeuTrpThrAspGlyTyrArgPheThrGl
00                                                          225       MetIle

                     1750                          1800                            1850
CGTGGCGATTACGCTGTGGCTGTTAATTTCATCGGTGGTGATGGGCGGTCTTCTGGCGGTGATTCTGGCGGTAGGCCGCGTTTCCAGTAATAAATTCATCCGTTTTCCCATCTGGCTGTTTACGTATATTTTTCGCGGCACGCCGCTGTA
yValAlaIleThrLeuTrpLeuLeuIleSerSerValValMetGlyGlyLeuLeuAlaValIleLeuAlaValGlyArgValSerSerAsnLysPheIleArgPheProIleTrpLeuPheThrTyrIlePheArgGlyThrProLeuTy
    25                                                                 50

                     1900                          1950                            2000
CGTACAGCTACTGGTGTTCTATTCGGGGATGTATACGCTGGAGATAGTCAAAGGCACCGATCTTCTTAACGCGTTTTTCCGCAGCGGACTAAACTGTACCGTACTGGCGCTGACGCTGAATACCTGCGCGTACACCACGGAAATTTTCGC
rValGlnLeuLeuValPheTyrSerGlyMetTyrThrLeuGluIleValLysGlyThrAspLeuLeuAsnAlaPhePheArgSerGlyLeuAsnCysThrValLeuAlaLeuThrLeuAsnThrCysAlaTyrThrThrGluIlePheAl
    75                                                                 100

                     2050                          2100                            2150
CGGGGCGATTCGCTCGGTACCGCACGGTGAAATTGAAGCGGCACGGGCCTATGGCTTCTCGTCATTTAAAATGTATCGCTGCATTATTTTGCCGTCGGCATTACGCATCGCCTTGCCTGCCTACAGCAACGAAGTGATTTTAATGCTGCA
aGlyAlaIleArgSerValProHisGlyGluIleGluAlaAlaArgAlaTyrGlyPheSerSerPheLysMetTyrArgCysIleIleLeuProSerAlaLeuArgIleAlaLeuProAlaTyrSerAsnGluValIleLeuMetLeuHi
    125                                                                150

                     2200                          2250                            2300
CTCTACGGCGCTGGCGTTTACCGCGACGGTGCCGGATTTGTTGAAAATCGCCCGCGATATTAACTCAGCGACTTACCAGCCGTTTACCGCGTTTGGCATTGCCGCCGTGTTGTATTTACTCATTTCGTATGTCCTGATAAGCCTGTTCCG
sSerThrAlaLeuAlaPheThrAlaThrValProAspLeuLeuLysIleAlaArgAspIleAsnSerAlaThrTyrGlnProPheThrAlaPheGlyIleAlaAlaValLeuTyrLeuLeuIleSerTyrValLeuIleSerLeuPheAr
    175                                      P protein →               200
                     2350                          2400                            2450
TCGGGCGGAAAGACGCTGGTTGCAGCACGTGTCCTCTAAATAATTCGAGTAACATGATGTCAGAAAATAAATTACACGTTATCGATTTGCACAAACGCTACGGCGGTCATGAAGTGCTGAAAGGGGTATCGCTGCAGGCCCGCGCCGGAG
gArgAlaGluArgArgTrpLeuGlnHisValSerSerLysEND          MetMetSerGluAsnLysLeuHisValIleAspLeuHisLysArgTyrGlyGlyHisGluValLeuLysGlyValSerLeuGlnAlaArgAlaGlyA
    225                                                1                                                                     25

                     2500                          2550                            2600
ATGTGATTAGCATCATCGGCTCGTCCGGCTCCGGTAAAAGCACTTTTTTGCGCTGTATTAACTTCCTCGAAAAACCGAGCGAAGGCGCGATTATCGTGAACGGTCAGAACATTAATCTGGTGCGCGACAAAGATGGCCAGCTCAAAGTGG
spValIleSerIleIleGlySerSerGlySerGlyLysSerThrPheLeuArgCysIleAsnPheLeuGluLysProSerGluGlyAlaIleIleValAsnGlyGlnAsnIleAsnLeuValArgAspLysAspGlyGlnLeuLysValA
                                                   50                                                                        75

                     2650                          2700                            2750
CGGATAAAAATCAGCTACGCTTGTTGCGTACCCGCCTGACGATGGTGTTTCAGCACTTCAACCTCTGGAGCCACATGACGGTGCTGGAAAATGTGATGGAAGCGCCGATTCAGGTACTGGGATTAAGCAAGCACGACGCGCGCGAGCGG
laAspLysAsnGlnLeuArgLeuLeuArgThrArgLeuThrMetValPheGlnHisPheAsnLeuTrpSerHisMetThrValLeuGluAsnValMetGluAlaProIleGlnValLeuGlyLeuSerLysHisAspAlaArgGluArgA
                                                   100                                                                       125

                     2800                          2850                            2900
CGTTGAAATATCTGGCGAAGGTGGGGATTGATGAGCGCGCTCAGGGCAAATATCCCGTCCATCTCTCCGGCGGCCAACAGCAGCGCGTTTCTATTGCGCGCGCGCTGGCGATGGAACCTGACGTTTTACTGTTCGATGAACCCACATCGG
laLeuLysTyrLeuAlaLysValGlyIleAspGluArgAlaGlnGlyLysTyrProValHisLeuSerGlyGlyGlnGlnGlnArgValSerIleAlaArgAlaLeuAlaMetGluProAspValLeuLeuPheAspGluProThrSerA
                                                   150                                                                       175

                     2950                          3000                            3050
CGCTCGATCCTGAACTGGTCGGCGAAGTGTTGCGCATCATGCAACAACTGGCGGAAGAAGGCAAAACGATGGTGGTGGTCACGCATGAAATGGGCTTCGCTCGCCATGTCTCTTCGCACGTTATTTTTCTGCATCAGGGGAAAATTGAAG
laLeuAspProGluLeuValGlyGluValLeuArgIleMetGlnGlnLeuAlaGluGluGlyLysThrMetValValValThrHisGluMetGlyPheAlaArgHisValSerSerHisValIlePheLeuHisGlnGlyLysIleGluG
                                                   200                                                                       225

                     3100                          3150                            3200
AAGAGGGTGATCCGGAGCAGGTATTCGGCAATCCGCAAAGCCCGCGTTTACAGCAATTCCTGAAAGGCTCGCTGAAATAAAAGAAGCCCGGCGGCGCATCGCTCACCGGGCAGGATACGGCGCTTTGGGAACTAGCGAATCACATCCGCC
luGluGlyAspProGluGlnValPheGlyAsnProGlnSerProArgLeuGlnGlnPheLeuLysGlySerLeuLysEND

                     3250  →  ← 250                3300                            3350
AGCGCCTCTTCTAAATCATACCAGCGAAATGCGAATCCGGCGGCTTCAAGCCGTTTTGGCAGCGCCCCGCTGTCCGCCCAACACCAGCACTGACGACTCTCCCATCAATAAGCGAATTGCCGTCGCCGGAATGCGAATAATCGCCGGACGC

                     3400                          3450
GCAGCGCGCGACCCAGCGCATGAGCAAAATGCTCATTATGGACGGGATACGGCGAGACCATATTGAAGGGACCGCGAAGATCGTTATCCAGCAGCCACAG
```

Fig. 2 Nucleotide sequence of the histidine transport operon and amino acid sequence of the gene products. The sequence presented (nonsense strand) begins immediately after the termination codon of the *argT* gene (see Fig. 1) and is numbered with base 1 being the first base of the *hisJ* gene; bases 5′ to this initiation codon are numbered negatively. The amino acid sequences have been determined (J protein[14]) or predicted (all others); the P protein amino terminus has been confirmed by sequencing (see text). The promoter region in *dhuA* is marked by two solid bars above the −10 and −35 regions, joined by a line. The vertical arrow at position 66 indicates the site of processing of the J protein precursor. Horizontal arrows at bases 3,254–3,266 indicate the region of dyad symmetry which is the presumed transription terminator signal for the transport operon. The horizontal arrows at −200 to −177 indicate a presumed transcription terminator signal for the *argT* gene which is immediately upstream from *dhuA*. Horizontal arrows at bases 831–902 indicate a region of dyad symmetry which is believed to serve a regulatory function[20]. The *hisM* gene is assumed to start with the GTG at position 1,649, although initiation may be at the in-phase ATG at position 1,754 (see text). The entire nucleotide sequence was obtained by the method of Maxam and Gilbert[44], both strands being sequenced at least once in their entirety. All restriction sites were sequenced over. The sequences of *dhuA* and *hisJ* have been published previously[10,11], but are presented here for completeness.

mutants and produce normal levels of unaltered P protein, indicating that this region is not regulatory and encodes at least one additional polypeptide. The nucleotide sequence of this region contains only one open reading frame of any length, beginning with either the GTG at position 1,649 or the ATG at 1,754. Each of these initiation codons is preceded by a ribosome-binding site. We call this sequence, between the GTG at 1,649 and the TAA translation termination codon at 2,353, *hisM*. This sequence encodes a basic protein of M_r 26,404, which we refer to as the M protein. This protein has not been identified, probably because of its hydrophobicity, strongly basic character and probable low level.

Noncoding regions

The region 240 bp 5' to the *hisJ* structural gene comprises the regulatory region for the histidine transport operon, *dhuA*. This region has previously been defined as the noncoding region between the termination codon of *argT* (position -240), the structural gene immediately upstream from the histidine transport operon, and the initiation codon (+1) of *hisJ*[10]. The promoter for the histidine transport operon occurs within the region -55 to -84 as indicated in Fig. 2. Features of the nucleotide sequence of *dhuA* important in regulating expression of the histidine transport operon have been discussed elsewhere[11].

Between *hisJ* and *hisQ* there is an intergenic region of 183 bp which contains an exceptionally long inverted repeat that, when transcribed, could form a very stable stem-loop structure ($\Delta G = -54$ kcal mol^{-1})[19]. As *hisJ* is expressed at a level at least 10 times that of *hisQ*, *hisM* and *hisP*, it seems probable that this intergenic element has a regulatory role in reducing the expression of the distal genes of the operon. The function of this element is discussed in the accompanying article[20].

There is no untranslated intergenic region between *hisQ* and *hisM* if the M protein starts with the GTG codon at position 1,649, as the first codon of *hisM* overlaps the termination codon of *hisQ*. However, if the initiation codon is the ATG at 1,754, the *hisQ–hisM* intergenic region consists of 101 bp: no inverted repeats or other features of potential regulatory interest have been found in this region. The third intergenic region, *hisM–hisP*, is only a few base pairs long. Such short intergenic regions, as seen for *hisQ–hisM* and *hisM–hisP*, are typical of multicistronic operons where the flanking genes are expressed to approximately the same extent[21,22].

Preceding each of the four genes of the histidine transport operon are presumed ribosome-binding sites, sequences homologous to the 3' end of 16S rRNA[23].

We have shown that the 5.4-kb *Ava*I fragment (Fig. 1) contains all the genes required for normal high-affinity histidine transport (data not presented). Every transport mutation we have isolated maps within this fragment[13]. Thus, if any histidine transport genes are located downstream from the *hisP* gene, they cannot be any larger than ~400 bp, this value being determined by *Ava*I site b (Fig. 1). However, no open reading frame of any length is found between the end of *hisP* and *Ava*I site b. A typical transcription termination signal (a G+C-rich dyad symmetry followed by several Ts; ref. 24) is found following *hisP* at positions 3,254–3,270. Thus, it is clear that we have identified all the genes required for high-affinity histidine transport.

Amino acid compositions of the histidine transport proteins

Figure 2 gives the predicted amino acid sequences of the four histidine transport proteins. The sequence of the J protein matches the determined amino acid sequence[10,14].

Of the four genes of the operon, only that for *hisJ*, the periplasmic histidine-binding protein, encodes a typical signal peptide (see examples in ref. 25), consisting of 22 mostly hydrophobic residues with two lysines located close to the NH_2-terminus. We have shown that the J protein is synthesized as a precursor, which is processed by removal of the signal peptide, presumably during secretion into the periplasm (G.F.-L.A. and K.N., unpublished data). All other known periplasmic and outer-membrane proteins (including the *tra* proteins; E. G. Minkley, personal communication) are synthesized as precursors with a signal peptide.

The other three proteins of the operon do not have a typical NH_2-terminal signal peptide and indeed, for P we have shown that the NH_2-terminal sequence of the mature protein is the same as that predicted by the nucleotide sequence. We have previously shown P to be located in the inner (cytoplasmic) membrane; as it interacts with the J protein[7], it is presumably exposed on the outside of the membrane. The Q protein is also located in either the inner or outer membrane (see above). It seems likely that the M protein also is located in the inner membrane because it is hydrophobic and the complementation pattern for mutants in these genes[6] implies that all three proteins, P, Q and M, interact with each other. Thus, although an NH_2-terminal signal peptide seems to be essential for a protein to pass through the inner membrane, it is not required for insertion of proteins into the membrane. This is consistent with results obtained for several other inner membrane proteins whose genes have been sequenced and which also lack a typical NH_2-terminal signal peptide[18,26]. However, there do seem to be certain exceptions to this general difference between inner membrane and outer membrane/periplasmic proteins. For example, the integral membrane protein bacteriohodopsin from *Halobacterium halobium* is apparently synthesized as a precursor which is processed, although its structural gene does not code for a typical signal peptide[27,28]; penicillin-binding proteins from *Escherichia coli* are also synthesized as precursors, though in this case it is not known whether their genes encode a typical signal peptide or whether processing occurs at the amino terminus[29]. The lactose permease gene codes for what might possibly be a signal peptide, although no processing occurs[3,30]. It is possible that in cases such as *hisM*, *hisQ* and *hisP* where no processing occurs, an internal hydrophobic region functions as a signal sequence, such as is found for the eukaryotic ovalbumin gene[31].

Consideration of the amino acid composition of the four transport proteins shows that the Q, M and P proteins are basic, in contrast to the J protein and the bulk (~90%) of the bacterial cell proteins, which have pI values of about 7 or less (as estimated by two-dimensional gel electrophoresis of total cell protein[32]). Two other inner membrane proteins, the lactose permease[3] and NADH dehydrogenase[18], are also basic, their basic character possibly being related to their need to interact with the negatively charged phospholipids of the membrane. Calculation of the hydrophobicity index[33] shows that proteins

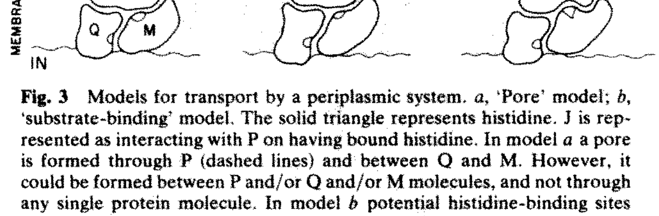

Fig. 3 Models for transport by a periplasmic system. *a*, 'Pore' model; *b*, 'substrate-binding' model. The solid triangle represents histidine. J is represented as interacting with P on having bound histidine. In model *a* a pore is formed through P (dashed lines) and between Q and M. However, it could be formed between P and/or Q and/or M molecules, and not through any single protein molecule. In model *b* potential histidine-binding sites on the membrane components are represented by hemispherical identations which are sequentially 'activated' to functional sites (indicated by triangles). Only the initial transfer of histidine from J to P, with the concomitant conformational changes, is illustrated. The transfer of histidine from P to M and from M to Q can be imagined to occur by a similar series of events. See text for discussion of these models.

Q and M have several uncharged stretches of 10 or more amino acids (residues 62–80, 92–109 and 190–215 in Q; 20–47, 57–66, 68–85, 192–221 in M) which are more hydrophobic than water-soluble proteins[33]. However, the P protein has no significantly hydrophobic stretches and in this respect is comparable with the water-soluble hydrophilic J protein. The percentage of charged amino acids in each of these proteins parallels the hydrophobicity calculations. The unusually low hydrophobicity of the membrane-bound P protein presumably reflects the fact that this protein interacts with the J protein[7] and may therefore protrude extensively into the periplasm. Notably, histidine is found in all four transport proteins and is particularly abundant in the P protein (11 histidines). The predicted sequences of two histidine biosynthetic proteins, HisG and HisD, show that they also contain histidine (W. Barnes, personal communication). Thus, despite the fact that all these proteins serve to supply histidine to the cell, they also require histidine for their own synthesis. An analysis of codon usage in the four histidine transport genes shows clearly that codon usage is non-random, condons recognized by the major iso-accepting species of tRNA being most frequently used.

Mechanisms of transport

We have shown that the high-affinity histidine transport system requires the function of four separate proteins. One of these, the histidine-binding protein, J, is located in the periplasmic space. Of the other proteins, at least two (Q and P), and probably all three, are associated with the membrane. This provides the only example of a shock-sensitive, binding protein-dependent transport system for which the total number of essential components is known. However, all other binding protein-dependent systems which have been studied in detail also seem to require other components in addition to a binding protein[34–41]. This multiplicity of components is in marked contrast to the lower-affinity, shock-resistant, binding protein-independent systems, such as the lactose permease (*lacY*), where only a single, membrane-bound component seems to be required.

The present determination of the number and location of the proteins required for transport, together with studies of transport mutants described previously and below, now allow us to begin to understand the molecular events involved in transport by a binding protein-dependent system (Fig. 3). The periplasmic protein J binds histidine[5], inducing a conformational change (such a change has been shown to occur; ref. 42 and S. Zukin, personal communication), which then allows the J–histidine complex to interact with the membrane-bound protein P[7]. Proteins P, Q and M form a cytoplasmic membrane-bound complex[6], with P exposed at the periplasmic face of the membrane. The membrane-bound complex of P, Q and M could promote the passage of histidine through the membrane either by forming a simple diffusion pore through the membrane, or they might possess specific binding sites for the transported substrate. These two possibilities are shown schematically in Fig. 3*a* and *b*, respectively. As P, Q and M do not mediate transport to any significant extent in the absence of J, the interaction of the J–histidine complex with P must induce a conformational change in the membrane complex. In Fig. 3*a* the 'pore' model (modified from ref. 43) indicates that the J–histidine complex, on interaction with P, induces a conformational change allowing P, Q and M to form an open pore through which histidine can diffuse into the cell interior. In Fig. 3*b*, the 'binding site' model indicates that one or more of the three membrane-bound proteins has a histidine-binding site[6,7]. These sites are 'activated' in a cascade-like manner, with histidine passing from one protein to the next, thus being carried across the membrane. It is also possible to envisage models which combine features from each of the two models described. In both models an energy-coupling step is presumably involved, although the mechanism by which this is achieved remains unknown.

The existence of certain classes of histidine transport mutant could help us distinguish between the two models. The wild-type histidine permease transports L-histidine efficiently; it also transports D-histidine and the histidine analogue HIPA with lower affinity. The isolation of mutants in *hisQ*, *hisM* or *hisP*, which differentially transport these substrates, suggests that the corresponding proteins have a substrate-binding site rather than being strictly part of a diffusion pore. We have found two types of such mutants: (1) *hisQ6699* transports L-histidine normally (K_m within 10% of normal) but does not transport D-histidine or HIPA at all within the limits of our measurements; (2) some *hisM* mutants (the 'odd group'[4]) result in the loss of transport of L- and D-histidine, and of HIPA, but also in an improved ability to transport L-histidinol. Both types of mutant can best be explained by an alteration in a substrate-binding site in a membrane-bound protein. This evidence supports the 'substrate-binding' model: isolation and characterization of additional mutants is required for confirmation. It has also been suggested that a membrane-bound component of the maltose permease may have a substrate-binding site (H. Shuman, personal communication).

The membrane-bound components of the histidine transport system are only present in very small amounts in the cell, and hence are extremely difficult to purify. The cloning and characterization of the genes encoding transport proteins thus provide the most powerful technique available for studying such systems. Given the many similarities between the histidine and other binding protein-dependent permeases, it seems likely that the model presented here can be generalized to most, if not all, such transport systems.

This work was supported by NIH grant AM12121 to G.F.-L.A., C.F.H. was supported by a NATO/SRC fellowship. P.D.H. was partially supported by a NSF predoctoral fellowship. We thank Dr R. Tjian and members of his laboratory for advice and for supplying us with ^{32}P-ATP, D. Cole and J. Sample for help with the sequenator experiment and W. Barnes for showing us DNA sequences of the histidine biosynthetic operon before their publication.

Received 9 February; accepted 16 June 1982.

1. Ames, G. F.-L. in *1st ICN–UCLA Symp. molec. Biol.* (ed. Fox, C. F.) 409–426 (Academic, New York, 1972).
2. Oxender, D. L. & Quay, S. C. in *Methods of Membrane Biology* Vol. 6 (ed. Korn, E. D.) 183–242 (Plenum, New York, 1976).
3. Buchel, D. E., Gronenborn, B. & Muller-Hill, B. *Nature* **283,** 541–545 (1980).
4. Ames, G. F.–L. *et al. J. Bact.* **129,** 1289–1297 (1977).
5. Ames, G. F.–L. & Lever, J. E. *J. biol. Chem.* **247,** 4309–4316 (1972).
6. Ames, G. F.–L. & Nikaido, K. *Proc. natn. Acad. Sci. U.S.A.* **75,** 5447–5451 (1978).
7. Ames, G. F.–L. & Spudich, E. N. *Proc. natn. Acad. Sci. U.S.A.* **73,** 1887–1881 (1976).
8. Kustu, S. G. & Ames, G. F.-L. *J. Bact.* **166,** 107–113 (1973).
9. Kustu, S. G., McFarland, N. C., Hui, S. P., Esmond, B. & Ames, G. F.-L. *J. Bact.* **138,** 218–234 (1979).
10. Higgins, C. F. & Ames, G. F.–L. *Proc. natn. Acad. Sci. U.S.A.* **78,** 6038–6042 (1981).
11. Higgins, C. F. & Ames, G. F.–L. *Proc. natn. Acad. Sci. U.S.A.* **79,** 1083–1087 (1982).
12. Ardeshir, F. & Ames, G. F.–L. *J. supramolec. Struct.* **13,** 117–130 (1980).
13. Ardeshir, F., Higgins, C. F. & Ames, G. F.–L. *J. Bact.* **147,** 401–409 (1981).
14. Hogg, R. W. *J. biol. Chem.* **256,** 1935–1939 (1981).
15. Noel, D., Nikaido, K. & Ames, G. F.–L. *Biochemistry* **18,** 4159–4165 (1979).
16. O'Farrell, P. Z., Goodman, H. M. & O'Farrell, P. H. *Cell* **12,** 1133–1142 (1977).
17. Jaskunas, S. R., Lindahl, L. & Nomura, M. *Proc. natn. Acad. Sci. U.S.A.* **72,** 6–10 (1975).
18. Young, I. G., Rogers, B. L., Campbell, H. D., Jaworowski, A. & Shaw, D. C. *Eur. J. Biochem.* **116,** 165–170 (1981).
19. Borer, P. N., Dengler, B. & Tinoco, I. *J. molec. Biol.* **86,** 845–853 (1974).
20. Higgins, C. F., Ames, G. F.-L., Barnes, W., Clement, J.-M. & Hofnung, M. *Nature* **298,** 760–762 (1982).
21. Selker, E. & Yanofsky, C. *J. molec. Biol.* **130,** 135–143 (1979).
22. Christie, G. E. & Platt, T. *J. molec. Biol.* **142,** 519–530 (1980).
23. Shine, J. & Dalgarno, L. *Proc. natn. Acad. Sci. U.S.A.* **71,** 1342–1346 (1974).
24. Rosenberg, M. & Court, D. *A. Rev. Genet.* **13,** 319–353 (1979).
25. Emr, S. D., Hall, M. N. & Silhavy, T. J. *J. Cell Biol.* **86,** 701–711 (1980).
26. Gay, N. J. & Walker, J. E. *Nucleic Acids Res.* **9,** 2187–2194, 3919-3926 (1981).
27. Chang, S. M. *et al. Proc. natn. Acad. Sci. U.S.A.* **78,** 3398–3402 (1981).
28. Dellwag, H. G. & Sumper, M. *FEBS Lett.* **116,** 303–309 (1980).
29. Pratt, J. M., Holland, I. B. & Spratt, B. G. *Nature* **293,** 307–309 (1981).
30. Ehring, R., Beyreuther, K., Wright, J. K. & Overath, P. *Nature* **283,** 537–540 (1980).
31. Palmiter, R. D., Gagnon, J. & Walsh, K. A. *Proc. natn. Acad. Sci. U.S.A.* **75,** 94–98 (1978).
32. O'Farrell, P. H. *J. biol. Chem.* **250,** 4007–4021 (1975).
33. Segrest, J. P. & Feldman, R. J. *J. molec. Biol.* **87,** 853–858 (1974).
34. Randall, L. & Schwartz, M. *J. Bact.* **116,** 1436–1446 (1973).
35. Shuman, H. A., Silhavy, T. J. & Beckwith, J. R. *J. biol. Chem.* **255,** 168–174 (1981).
36. Bavoil, P., Hofnung, M. & Nikaido, H. *J. biol. Chem.* **255,** 8366–8369 (1980).
37. Shuman, H. A. & Silhavy, T. J. *J. biol. Chem.* **256,** 560–562 (1981).
38. Silhavy, T. J. *et al. Molec. gen. Genet.* **174,** 249–259 (1979).
39. Anderson, J. J. & Oxender, D. L. *J. Bact.* **130,** 384–392 (1977).
40. Lo, T. C. Y. *J. supramolec. Struct.* **7,** 463–480 (1977).
41. Ordal, G. W. & Adler, J. *J. Bact.* **117,** 517–526 (1974).
42. Robertson, D. E., Kroon, P. A. & Ho, C. *Biochemistry* **16,** 1443–1451 (1977).
43. Singer, S. J. *A. Rev. Biochem.* **43,** 805–833 (1974).
44. Maxam, A. & Gilbert, W. *Meth. Enzym.* **65,** 499–560 (1980).

Character of 'prolate' galaxies

Douglas O. Richstone & Michael D. Potter

Department of Astronomy, University of Michigan, Ann Arbor, Michigan 48109, USA

It is still not known whether elliptical galaxies are oblate, prolate or triaxial. The prototype 'prolate' galaxy NGC2685 has a rapid observed stellar rotation rate around the projected minor axis. We show here that a steady figure, exactly prolate model can have no such rotation, and that a nearly prolate model fails by a factor of 7. We suggest that the galaxy is oblate and that the gas disk is the wreck of a dwarf companion.

There has recently been much interest over the determination of the three-dimensional figure of elliptical galaxies. This interest can be classified into four areas—statistical studies of surface brightness[1-3], theoretical models[4,5], detailed surface photometry[6-8] and the study of the distribution of embedded gas[9]. The last approach is distinguished by its potential ability to make statements about individual galaxies.

In the absence of figure rotation (for example, the tumbling of a bar) a gaseous disk is thought to settle into the fundamental plane of a biaxial galaxy in a time scale given by

$$\tau \approx T\left(6J_2\cos\theta\left|\frac{\mathrm{d}\ln T}{\mathrm{d}\ln r}\right|\frac{\Delta r}{r}\right)^{-1} \qquad (1)$$

where τ is the settling time, T is the orbital time, J_2 is the quadrupole moment of the gravitational potential, θ is the angle between the disk plane and the fundamental plane of the galaxy, r is the disk radius and Δr is the characteristic excursion in radius of gas clouds in the disk[10]. That excursion can be related to the peculiar velocity Δv of the gas clouds through $\Delta r = \Delta v/K$ where K is the epicycle frequency. Specializing now to a logarithmic potential (flat rotation curve), we can use $K = \sqrt{2}v_c/r$ (where v_c is the circular velocity) to write

$$\tau \approx T\left(3\sqrt{2}J_2\cos\theta\frac{\Delta v}{v_c}\right)^{-1} \qquad (2)$$

Noting that J_2 is <0.5 even for very flat galaxies and that $\Delta v/v_c \approx 0.1$ (a reasonable assumption), we see that the settling time from an inclination of 60° or more is always $>\tau_0 \sim 9T$.

The fact that the characteristic settling time is less than the age of the Universe has been used to argue that NGC2685[11] is, in fact, a prolate object with a small pattern speed[12].

The next step is to construct a prolate stellar dynamical model for NGC2685 which is consistent with the observed stellar rotation. We attempted such a construction as part of a systematic study of prolate stellar systems using Schwarzschild's[4] self-consistent field method. That method chooses a specific potential, follows stellar orbits in that potential and finally adds up the time averaged stellar orbits to produce a density distribution corresponding to the original potential. We used a logarithmic potential with a flattening corresponding to an E5 galaxy[5].

Such a model must reproduce the large observed rotation rate about the projected minor axis. The observed rotation parameter v/σ is ~ 1 (ref. 13), while σ is $\sim 100\ \mathrm{km\ s^{-1}}$. (This dimensionless rotation rate is 3–10 times the normal observed value for an elliptical, and is much more consistent with an S0 disk). There is some evidence also for minor axis notation. If this is true, it would suggest that the galaxy is triaxial.

Because the figure is fixed, the observed rotation must be derived from orbits which stream through the figure. Such an orbit is shown in Fig. 1*a*. Maximizing the polar streaming velocity (using linear programming techniques) permits a maximum streaming velocity—corresponding to an observed v/σ of only 0.075 on the projected major axis. Moreover, this large streaming velocity can only be obtained if the y component l_y of the total angular momentum of each orbit is >0 for all $l_z = 0$ orbits (no orbit circulates in the opposite sense). Because these orbits are only neutrally stable against perturbations which cause rapid precession about the z axis, this configuration is implausible. Even if the orbits were stable, the model's v/σ completely fails to reproduce the observed one of unity.

A model more consistent with the observations can be constructed with a slightly triaxial figure. The orbit of Fig. 1*a* can easily be followed in a gravitational potential of the form

$$\Phi = \frac{1}{2}\ln\left(x^2+\frac{y^2}{p^2}+\frac{z^2}{q^2}\right) \qquad (3)$$

If $p < 1$ the orbit is stable but l_z is no longer conserved and the orbit is no longer required to reach $z = 0$ frequently (see Fig. 1*b*). Therefore a larger number of these orbits can be incorporated into the model. A nearly prolate model was constructed maximizing the influence of these streaming orbits with $p = 0.9$. Viewed from the x axis (edge on) its $v/\sigma = 0.1$. The maximum v/σ was achieved from $\sim 30°$ from the x axis in the x–z plane. From that vantage point $v/\sigma = 0.14$. Thus we cannot construct a nearly prolate model with no figure motion and large v/σ. We emphasize that this method maximizes v/σ within the set of all self-similar solutions of this general form.

The failure to construct a figure fixed prolate model with large v/σ indicates that the galaxy is not prolate. An alternative explanation for the gas ring is that it is the wreck of a dwarf

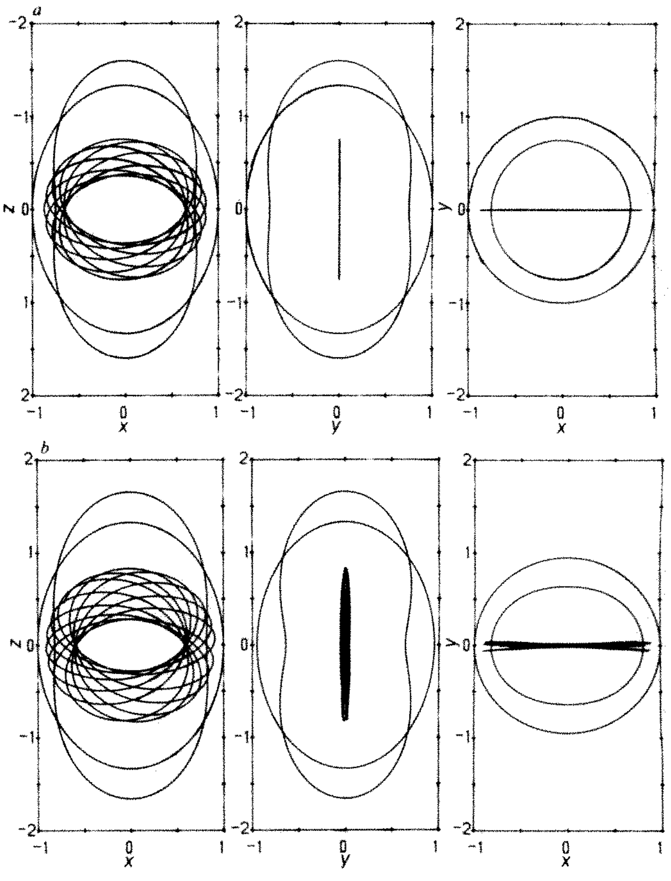

Fig. 1 *a*, Three orthogonal views of an orbit in a fixed biaxial prolate potential (with $p = 1$, $q = 1.333$, see equation (3)). The envelopes are cuts through the equipotential and equal-density surfaces. Note that the orbit streams through the galaxy maintaining a well defined circulation in the x–z plane. This orbit has no z angular momentum and is only neutrally stable. *b*, As *a* but with a triaxial potential with $p = 0.95$ and $q = 1.333$. This orbit also streams. It is a stable orbit with fluctuating z angular momentum.

0028–0836/82/330728—02$01.00

companion, which has not yet decayed to the fundamental plane of the galaxy.

Such a scenario does not, by itself, constrain the age of this gas disk. The disk is very inclined, and equation (2) suggests that for exact polar alignment ($\theta = 90°$), the disk lifetime is infinite.

In fact, equation (2) for the settling time also provides the means to calculate the time independent (or ensemble average) distribution of ring angles. From equation (2), $d\mu/dt \propto \mu^2$ where $\mu = \cos\theta$ is the cosine of the tilt angle ($\mu = 0$ for a polar ring). Because rings are inserted at some angle and then decay to the plane, they obey a continuity equation of the form

$$\frac{\partial n}{\partial t} + \frac{\partial}{\partial \mu}\left(\frac{d\mu}{dt} n\right) = \left(\frac{\partial n}{\partial t}\right)_i \tag{4}$$

where $n = n(\mu, t)$ is the chance of finding a disk at inclination μ at time t, and $(\partial n/\partial t)_i$ is the insertion rate. In steady state, $\partial n/\partial t = 0$. For insertion in strictly polar orbits it is easy to show that $n \propto \mu^{-2}$, while for an insertion rate independent of μ, $n \propto \mu^{-1}$ (to verify these results it is necessary to apply the appropriate boundary conditions at $\mu = 0$).

Note that the above results indicate a preference for disks in non-steady state but relatively long-lived nearly polar configurations regardless of the injection rate. The number of inclined disks will, however, be set by the ratio of the injection rate to the decay rate. Since the latter is $\approx \tau_0 \approx 10T$ ($\approx 10^9$ yr), a frequent incidence of tilted disks is required to demand an insertion time scale much shorter than the age of galaxies. However, these objects may be more common than we realize judging from a flurry of recent discoveries (ref. 14 and P. Schechter, unpublished data). Note that our Galaxy may be about to acquire such rings as the Magellanic clouds come apart[15].

Although we have presented a strong case for the view that this particular galaxy is axisymmetric with two long axes, we have not explicitly ruled out a slowly tumbling bar.

There is, however, an argument which suggests that slow figure motion does not alter the small values of v/σ derived above. Schwarzschild[16] and Miller and Smith[17] have constructed models of tumbling triaxial and biaxial prolate galaxies of very different rotation rates. In both studies the observable rotational velocity is never more than 1.5 times the pattern speed at any radius. Because the pattern speed must be small to avoid disrupting the polar rings in the galaxy under consideration if it is a tumbling bar[12], these models also indicate a small value of v/σ.

We conclude that it is easy to model NGC2685 as an oblate galaxy with polar rings of gas which are the wreck of a dwarf companion. It is impossible to construct a fixed figure prolate model which reproduces the observed stellar rotation rate. It is doubtful that a tumbling prolate model would resolve the discrepancy. It may be that a number of galaxies which have been identified as prolate objects because of embedded disks are in fact oblate objects.

We thank G. Lake, S. Tremaine, M. Schwarzschild and P. Schechter for advice and encouragement. This research was partially supported by NSF grant AST 82-02930 and by NASA grant NGR 23-005464.

Received 24 May; accepted 24 June 1982.

1. Marchant, A. B. & Olson, D. W. *Astrophys. J. Lett.* **230,** L157–L159 (1979).
2. Richstone, D. O. *Astrophys. J.* **234,** 825–828 (1979).
3. Olson, D. W. & de Vaucouleurs, G. *Astrophys. J.* **249,** 68–75 (1981).
4. Schwarzschild M. *Astrophys. J.* **232,** 236–247 (1979).
5. Richstone, D. O. *Astrophys. J.* **238,** 103–110 (1980).
6. Williams, T. B. & Schwarzschild, M. *Astrophys. J.* **227,** 56–63 (1979).
7. Williams, T. B. & Schwarschild, M. *Astrophys. J. Suppl.* **41,** 209–213 (1979).
8. Bertola, F. & Galleta, G. *Astr. Astrophys.* **77,** 363–365 (1979).
9. Bertola, F. & Galleta, G. *Astrophys. J. Lett.* **226**, L115–L118 (1978).
10. Tohline, J. E., Simonson, G. F. & Caldwell, N. *Astrophys. J.* **252,** 92–101 (1981).
11. Sandage, A. *The Hubble Atlas of Galaxies*, 7 (Carnegie Institution, Washington DC, 1961).
12. Tohline, J. E. & Durisen, R. H. *Astrophys. J.* **257,** 94–102 (1982).
13. Schechter, P. L. & Gunn, J. E. *Astr. J.* **83,** 1360–1362 (1978).
14. Hawarden, T. G., Elson, R. A. W. Longmore, A. J., Tritton, S. B. & Corwin, H. G. *Mon. Not. R. astr. Soc.* **196,** 747–750 (1981).
15. Tremaine, S. D. *Astrophys. J.* **203,** 72–74 (1976).
16. Schwarzchild, M. Preprint (Princeton University, 1982).
17. Miller, R. H. & Smith, B. F. *Astrophys. J.* **227,** 785–797 (1979).

Composition-dependent glass-transition temperatures and copolymers

P. R. Couchman

Department of Mechanics and Materials Science, Rutgers University,
PO Box 909, Piscataway, New Jersey 08854, USA

The glass transition is of primary relevance to the forming conditions and end-use properties of polymeric materials. Several polymers of industrial importance, most notably polyvinyl chloride (PVC), contain small molecules as processing lubricants (plasticizers) and are, therefore, solutions. Separately, economic and materials advantages have spurred the use of one-phase mixtures (miscible blends) of high polymers. The general theme of the compositional variation of glass-transition temperatures (T_g) includes, in addition, the variation of T_g with degree of polymerization, with cross-link density (network formation) and with copolymer composition. An attempt is made here to find a unified basis for the prediction of these several aspects of an identifiably single topic.

For solutions which are largely random and for phenomena which can be modelled in terms of such solutions, a recent thermodynamic theory for the compositional variation of glass-transition temperatures[1] has provided a method for calculating solution glass-transition temperatures, T_g, from pure-component glass-transition temperatures, T_{gi}, their corresponding glass-transition increments of heat capacity, ΔC_{pi}, and the mole or mass fractions, X_i, of these components. The equation for the glass-transition temperature of a c-component blend is, in the temperature-independent approximation for the ΔC_{pi},

$$\ln T_g = \frac{\sum_{i=1}^{c} X_i\,\Delta C_{pi} \ln T_{gi}}{\sum_{i=1}^{c} X_i\,\Delta C_{pi}} \tag{1}$$

Systems to which this entropic expression has been applied successfully include miscible blends of polymers[1-3] and plasticized straight-chain[4] and network[5] polymers. Additionally, the effect of degree of polymerization[6] and of cross-link density[7] on T_g have been accounted for by the theory.

For binary solutions, the derivative

$$\frac{d \ln T_g}{dX_2} = \frac{\Delta C_{p1} \Delta C_{p2} \ln T_{g2}/T_{g1}}{(X_1 \Delta C_{p1} + X_2 \Delta C_{p2})^2} \tag{2}$$

does not vanish (except in the trivial case) and, therefore, equation (1) predicts a monotonic dependence of T_g on overall composition. For near-random (and other) copolymers T_g can, however, manifest a compositional absolute extreme value. Thus, any model of copolymers as binary solutions cannot be generally acceptable. Nevertheless, as outlined below, it is possible to include copolymers of arbitrary ordering within the theory by recognizing formally that when differences between primary bonds must be considered in connection with the glass-transition properties of entities comprising a solution, the microscopic rather than overall composition determines the solution behaviour.

Sequence-distribution effects on T_g can be accounted for in the nearest-neighbour approximation by formal treatment of the general copolymer as a random solution of mer pairs, fractions f_{ii}, f_{jj}, f_{ij}. The particular version of equation (1) which then arises is

$$\ln T_g = \frac{f_{ii}\,\Delta C_{pii} \ln T_{gii} + f_{ij}\,\Delta C_{pij} \ln T_{gij} + f_{jj}\,\Delta C_{pjj} \ln T_{gjj}}{f_{ii}\,\Delta C_{pii} + f_{ij}\,\Delta C_{pij} + f_{jj}\,\Delta C_{pjj}} \tag{3}$$

The denominator of this relation is, as for equation (1), the solution transition increment of heat capacity, ΔC_p (ref. 1). For copolymers formed by continuous reaction of i and j monomers

0028-0836/82/330729—02$01.00

at constant feed composition, the dyad fractions of equation (3) can be rewritten as a function of the fraction, f_i, of i monomers in the feed and of the monomer reactivity ratios[8]. r_i, r_j (these are a measure of the relative rates at which a chain end grows by the addition of like and unlike mers). The consequent relation,

$$\ln T_g = \frac{r_i f_i^2 \Delta C_{p_{ii}} \ln T_{g_{ii}} + 2f_i(1-f_i)\,\Delta C_{p_{ij}} \ln T_{g_{ij}} + r_j(1-f_i)^2\,\Delta C_{p_{jj}} \ln T_{g_{jj}}}{r_i f_i^2\,\Delta C_{p_{ii}} + 2f_i(1-f_i)\,\Delta C_{p_{ij}} + r_j(1-f_i)^2\,\Delta C_{p_{jj}}} \qquad (4)$$

provides a formal method for the calculation of glass-transition temperatures of the quasi-binary solution from glass-transition properties of the corresponding homopolymers, the fully alternating copolymer, and the monomer reactivity ratios. For values of these properties which admit a physically acceptable value of f_i as a solution of the quadratic equation obtained from the condition $\mathrm{d}\ln T_g/\mathrm{d}f_i = 0$, the copolymer glass-transition temperature will pass through an absolute extremum. The sign of the second derivative $\mathrm{d}^2 \ln T_g/\mathrm{d}f_i^2$ at this value of f_i determines the nature of the extremum. If the quadratic equation gives no admissible value of f_i, the copolymer glass-transition temperature is a monotonic function of feed composition. The compositional variation of the copolymer glass-transition increment of heat capacity can be analysed in a similar manner. Generally, extreme values of T_g and ΔC_p occur at different compositions.

A considerable simplification of the theory occurs for an ideal azeotropic copolymerization ($r_i = r_j = 1$) of monomers for which $T_{g_{ii}} = T_{g_{jj}}$ and $\Delta C_{p_{ii}} = \Delta C_{p_{jj}}$. In these circumstances, the extreme value of the copolymer glass-transition temperature, T_g^*, occurs at $f_i = \frac{1}{2}$ and is given by

$$\ln T_g^* = \frac{\Delta C_{p_{ii}} \ln T_{g_{ii}} + \Delta C_{p_{ij}} \ln T_{g_{ij}}}{\Delta C_{p_{ii}} + \Delta C_{p_{ij}}} \qquad (5)$$

If, further, the difference between $\Delta C_{p_{ii}}$ and $\Delta C_{p_{ij}}$ can be neglected,

$$T_g^* = (T_{g_{ii}} T_{g_{ij}})^{1/2} \qquad (6)$$

Comparison of theory and experiment for ethylacrylate–vinylidene chloride copolymers affords a critical test of the theory, as a well-defined extreme value of T_g occurs. For this system[9], $r_i \simeq r_j \simeq 1$, $T_{g_{ii}} \simeq T_{g_{jj}} \simeq 250$ K and $T_{g_{ij}} = 408$ K. In the absence of information on the dyad transition increments of heat capacity, the approximation $\Delta C_{p_{ii}} = \Delta C_{p_{jj}} = \Delta C_{p_{ij}}$ allows equation (6) to be used, predicting a maximum value of the copolymer glass-transition temperature of 319 K, at $f_i = \frac{1}{2}$. The observed maximum value of T_g is 308 K and occurs at $f_i \simeq \frac{1}{2}$ (ref. 9).

Previous applications of the theory[16] have placed in a more general context a variety of empirical and semi-empirical expressions for specific aspects of the compositional variation of T_g. Similarly, the formal treatment outlined here gives as first or second-order approximations current relations for the variation of copolymer glass-transition temperatures with composition. Finally, note that equations (1) and (3) are in effect integrated, predictive forms of an entropic formal tautology for composition-dependent transitions of the second-order kind[10,11].

This work was supported by the NSF, Polymers Program.

Received 15 April; accepted 24 June 1982.

1. Couchman, P. R. *Macromolecules* **13,** 1272–1276 (1980).
2. Leisz, D. M., Kleiner, L. W. & Gertenbach, P. G. *Thermochim. Acta* **35,** 51–58 (1980).
3. Ryan, C. L. thesis, Univ. Massachusetts (1981).
4. Bair, H. E. & Warren, P. C. *J. macromolec. Sci.-Phys.* **B20,** 381–402 (1981).
5. Ellis, T., Karasz, F. E. & Moy, P. *Polym. Preprints* **22,** 121–122 (1981).
6. Couchman, P. R. *J. mater. Sci.* **15,** 1680–1683 (1980).
7. Martin, C. G., Mehta, R. K. & Lott, S. E. *Polym. Preprints* **22,** 319–320 (1981).
8. Wall, F. T. *J. Am. chem. Soc.* **66,** 2050–2057 (1944).
9. Comyn, J. & Fernandez, R. A. *Eur. Polym. J.* **11,** 149–151 (1975).
10. Landau, L. & Lifschitz, E. M. *Statistical Physics* 2nd edn (Pergamon, Oxford, 1969).
11. Angell, C. A., Sare, J. M. & Sare, E. J. *J. phys. Chem.* **82,** 2622–2629 (1978).

Gold deposition at low temperature on sulphide minerals

G. Michael Bancroft & Gilles Jean

Department of Chemistry, University of Western Ontario, London, Ontario, Canada N6A 5B7

Gold deposits are commonly associated with quartz veins containing variable amounts of pyrite and other sulphides. Gold is thought to be transported as $AuCl_2^-$ or $AuCl_4^-$ in strongly acidic and saline solutions and as AuS^- or $Au(S_2O_3)_2^{3-}$ in weakly acidic and alkaline solutions by hydrothermal solutions coming from great depth and rising in rock formations through faults[1,2]. In some cases gold occurs as finely divided particles, intimately intergrown with pyrite, suggesting that gold, quartz and pyrite were probably precipitated in response to a change in temperature. Fyfe and Henley[3] showed that the solubility of gold increases from 10 p.p.m. at 300 °C to 1,000 p.p.m. at 510 °C. In other cases gold may be aggregated in one spot in abundance while the remainder of the ore is barren, indicating preferential precipitation in one site. Using ESCA (electron spectroscopy for chemical analysis), we have studied the reaction between $KAuCl_4$ in solution and various sulphide minerals. Gold(III) was rapidly reduced to metallic gold on the surface of these minerals, suggesting a new mechanism for the deposition of gold at low solution concentration and temperature.

Various sulphide minerals [pyrite (FeS_2), pyrrhotite (FeS), sphalerite (ZnS), galena (PbS)] were cut into plates of 1 × 1 × 1 cm and were reacted with $KAuCl_4$ solutions of 1, 10 and 100 p.p.m. at different pH for various periods of time. Figure 1*a* shows the ESCA spectrum of the gold 4f lines of the original $KAuCl_4$ solution evaporated on Teflon. The binding energy of the gold $4f_{7/2}$ line at ≃87.4 eV (relative to carbon 1s line at 284.5 eV) is representative of Au(III) compounds[4]. Figure 1*d* is the spectrum of pure metallic gold and shows a binding energy for the gold $4f_{7/2}$ line of ≃83.5 eV which is 3.9 eV lower than Au(III). Figure 1*b* shows the ESCA spectrum of sphalerite (ZnS) reacted with a solution of $KAuCl_4$ (10 p.p.m.) at room temperature. This spectrum clearly shows that both Au(III) and Au(0) are present on the surface. Figure 1*c* shows the ESCA spectrum of pyrite (FeS_2) reacted with

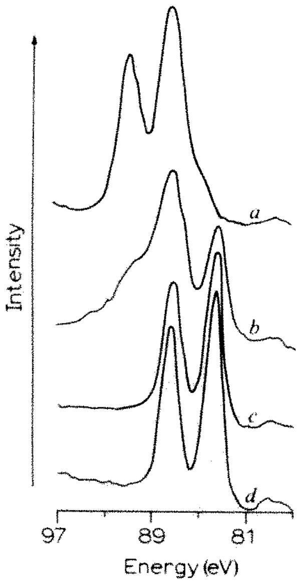

Fig. 1 Gold 4f ESCA spectra for: *a*, $KAuCl_4$ solution (10 p.p.m.) evaporated onto Teflon; *b*, sphalerite (ZnS) plate reacted with this $KAuCl_4$ solution; *c*, pyrite (FeS_2) plate reacted with this $KAuCl_4$ solution; *d*, metallic Au.

0028–0836/82/330730—02$01.00

$KAuCl_4$ in solution. The binding energy of $\approx$83.5 eV indicates that Au(0) only is present on the surface.

The reduction of Au(III) was found to be independent of either the pH or the initial concentration of gold and was found to occur even in saturated KCl solution. Gold was reduced from Au(III) to Au(0) within a minute by every mineral studied except sphalerite. In this latter case, the reduction was slower since both species, Au(III) and Au(0), were observed. This suggests that the nature of metal ion in the sulphide may have an important role in the deposition of gold. Further work is being done to clarify this point.

The mechanism that is thought to occur is: adsorption of Au(III) as the hydrated or the hydrolysed species (chloride is not seen on the surface), followed by reduction of the gold by the sulphide.

$$8\mathrm{Au(III)} + 3S^{2-} + 12H_2O \rightarrow 8\mathrm{Au(0)} + 3SO_4^{2-} + 24H^+$$

The deposition of gold goes on even after the surface is entirely covered, and can actually be seen with the naked eye. After the first layer of Au(0) is deposited, electrons for the reduction are probably coming from the interior of the crystal. This phenomenon is similar to the observed reduction of gold on activated carbon[5]. These results suggest that adsorption of Au(III) by sulphide minerals followed by reduction could have an important role in the deposition of gold in natural systems, especially at low temperature and low solution concentrations of gold.

We thank the NSERC (Canada) for research funds, Professor R. J. Puddephatt for the $KAuCl_4$, and Professor W. S. Fyfe for helpful discussions.

Received 29 March; accepted 28 June 1982.

1. Wedepohl, K. H. in *Handbook of Geochemistry* Vol. II-S, 79.F.1 (Springer, Berlin, 1978).
2. Goleva, G. A., Krivenkov, V. A. & Gutz, Z. G. *Geochem. Int.* **7,** 518–529 (1970).
3. Fyfe, W. S. & Henley, R. W. *Miner. Sci. Engng* **5,** 295–303 (1973).
4. Carlson T. A. *Photoelectron and Auger Spectroscopy* (Plenum, New York, 1975).
5. McDougall, G. J. & Hancock, D. *Gold Bull.* **14,** 138–153 (1981).

Layered convection and crystal layers in multicomponent systems

R. C. Kerr[*] & J. S. Turner

Research School of Earth Sciences, The Australian National University, Box 4, Canberra 2600, Australia

Laboratory experiments[1–5] in aqueous solutions have been used to model some of the physical and dynamical processes occurring during crystallization in magma chambers. In particular, it has been demonstrated[2,3,5] that crystallization at the side walls can lead to density stratification and layering in an initially homogeneous container, and also to the formation of vertical compositional gradients (that is, to 'differentiation') when more than one solute is present. Density gradients and compositional layers can alternatively be set up by replenishing a container from below with fluid of different temperature and composition[4,6,7]. Underlying all this work has been the concept that some aspects of the regularity and large horizontal extent of layering in well-documented igneous intrusions[8,9] might be explained in terms of 'double-diffusive' effects in the fluid state, with the growth of crystals subsequently being affected by these pre-existing layers. In the latest experiments reported here, we have explicitly addressed the problems of horizontal layering produced in the crystals themselves, when a compositionally-stratified tank of fluid containing several solutes has been cooled from either below or above. The relationship between the scales of the layers in the fluid and in the crystals has also been examined.

Earlier experiments[1,4] in which crystals of a constant composition were grown at the top or bottom of an experimental tank were of two kinds, in both of which layered structures were produced. When an aqueous solution of a single solute (usually Na_2CO_3) was cooled from the top[1], crystals of $Na_2CO_3 \cdot 10H_2O$ formed in horizontal layers, whether the initial fluid was homogeneous, was smoothly stratified, or was set up with several distinct layers of different densities. The dominant effect in all cases was the formation of a cold but less dense fluid layer against the cooled upper boundary as the denser crystals grew (because the density of the saturated solution decreased as the temperature fell). When the top boundary was held below the eutectic temperature, bands were observed in the eutectic layer at levels corresponding to pre-existing fluid interfaces; the advancing front of the crystals growing below this also remained nearly horizontal, and the growth rate was clearly influenced by the positions of the fluid layers. Cooling a compositional gradient from below produced a compact layer of dense crystals of nearly uniform thickness, above which was a fluid layer which increased in depth with time. In this layer convection was driven by the compositional change in the residual fluid generated by the removal of the solid phase at the lower boundary, and the changing depth was a measure of the total volume of less dense fluid produced.

The second type of experiment involving bottom crystallization was conducted[4] to model the evolution of a magma chamber following the sudden influx of a new layer of hot but heavy magma at the base. This lower layer remained chemically isolated from the rest of the chamber, while it cooled rapidly through the interface and crystallization proceeded[6]. In the laboratory model of this process, the lower layer was hot KNO_3 solution and the upper layer was a colder, less dense $NaNO_3$ or K_2CO_3 solution. Crystallization of KNO_3 took place on the bottom, often extending upwards to the interface, which produced a sharp horizontal top to the crystal layer. At the same time the density of the residual liquid in the lower layer decreased due to the compositional change. When this density became equal to that of the upper layer, the interface broke down, so that the two layers mixed thoroughly together leaving a layer of KNO_3 crystals at the base. Related experiments[7] have been conducted with a compositional gradient above the lower layer, and these show that the overturned lower-layer fluid is then confined by the gradient to the lower part of the upper region.

The present experiments represent extensions of each of these cases, with the additional feature that more than one component crystallized out during the course of an experiment, in a sequence and manner which were determined by the evolution of the layered fluid system. Examples have been chosen to illustrate different ways in which crystallization can be controlled by the compositional stratification.

The experimental tank used was a Perspex cube of 20 cm internal dimensions, fitted with a metal base through which coolant could be circulated at a controlled temperature. The procedure was to fill the tank with one or more layers of solution of known composition and temperature (and hence density), to insulate all the side boundaries, and to monitor at intervals the development of the fluid and crystal layers, and in some cases the properties of the residual fluid. Usually the bottom was cooled slowly, by lowering the temperature of the coolant in small steps, but in several experiments the bottom crystallization was produced by cooling from the top, followed by internal heat transfer (through the interfaces between the layers).

Consider first an experiment in which the whole tank was filled with a homogeneously mixed aqueous solution of $CuSO_4$ and Na_2SO_4. The initial compositions were ~19 wt% $CuSO_4$ and 9 wt% Na_2SO_4, well in the range where the copper salt will crystallize first. (The conditions used in this and later experiments are summarized in Fig. 1, where the four cases *a–d* correspond to the photographs in Fig. 3.) When this solution was cooled slowly through the bottom of the tank, a layer of $CuSO_4 \cdot 5H_2O$ crystals did indeed grow, to a thickness of ~1 cm.

---

[*] Present address: Department of Applied Mathematics and Theoretical Physics, University of Cambridge, Silver Street, Cambridge CB3 9EW, UK.

0028-0836/82/330731—03$01.00

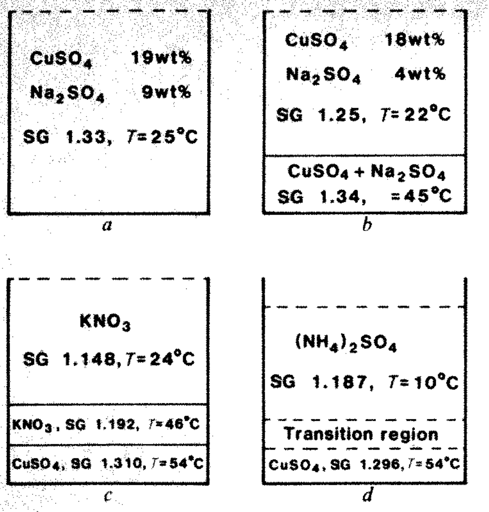

Fig. 1 Summary of the initial conditions in the four experiments for which the final crystal products are shown in Fig. 3*a–d*. The tank was cooled through the base in each case, and insulated at the sides and the top.

At the same time the composition of the residual fluid, well-mixed by 'compositional convection', moved towards the cotectic line as shown on Fig. 2, which is part of a phase diagram prepared for a more detailed study[5] of crystallization of these two components in a different geometry. Before the cotectic line was reached, however, $Na_2SO_4 \cdot 10H_2O$ crystals started growing on top of the previous layer (with just a few crystals of $CuSO_4 \cdot 5H_2O$ visible between them), and built up to a nearly uniform depth of 2 cm, as shown in Fig. 3*a*, while the composition evolved further back into the copper field. This behaviour has been attributed[5] to disequilibrium effects, and the different kinetics of crystallization of the two components, which made it possible for the growth of the copper salt to be suppressed when it was covered by the faster-growing $Na_2SO_4 \cdot 10H_2O$. Similar kinetic effects are also likely in crystallizing magmas, but even if these remained much closer to the equilibrium conditions, the evolution towards, and then along, a cotectic line would nevertheless produce an abrupt change in composition of the crystallizing phases.

The next experiment to be discussed (Fig. 1*b*) started with a 6-cm deep layer of similar composition to that used in the preceding experiment, with specific gravity 1.34 and temperature 45 °C, underlying a layer of depth 14 cm which was relatively rich in $CuSO_4$ and less concentrated in Na_2SO_4 (specific gravity, SG = 1.25 at T = 22 °C). Cooling from below produced the same sequence of crystal layers, first the copper, then the sodium salt, but with the changeover occurring sooner because the composition changes were confined to a shallower fluid layer. During this process, however, the density of the lower layer was decreasing, until eventually it overturned and mixed with the upper layer. This suddenly brought the top of the crystals into contact with a Cu-rich solution, and another layer of $CuSO_4 \cdot 5H_2O$ built up on top of the previous layers, as shown in Fig. 3*b*. Note that though the fluid layers undoubtedly controlled the growth and sequence of the crystal layers, the thicknesses in the two states were not identical, and only indirectly related.

When a layer of mixed solution of copper and sodium sulphates, with a depth of 6 cm and composition similar to that used in the experiments already described, was cooled from above through an interface (using a metal chamber containing coolant in contact with a less dense (SG = 1.055) upper layer of cold Na_2SO_4 solution), the same sequence of crystallization was observed as in the first experiment. A compact layer of $CuSO_4 \cdot 5H_2O$ formed right across the (insulated) bottom and grew to a thickness of 4 mm. On top of this, there was a sudden change to $Na_2SO_4 \cdot 10H_2O$ crystals, which began to grow after about 18 h in a long, spikey form (rather than as a compact mass as they did with bottom cooling) and built up to a nearly uniform thickness of 4.0 cm after about 4 days. There was no overturning in this case, because of the large density difference across the interface between the two layers.

There is no doubt that more complicated crystal sequences can be produced when more fluid layers are present initially, when there are more components which can crystallize over the temperature and composition ranges attainable in an experiment, or when the cooling conditions (for example the temperature of the base of the tank) are changed. The next case to be discussed is a three-layer system in which two solutes were present initially. The top, 12-cm deep, layer was KNO_3 solution at 24 °C, SG = 1.148; the middle layer was also KNO_3 at 46°C, SG = 1.192, 4 cm deep; and the bottom layer (put in last) was $CuSO_4$ solution at 54 °C, SG = 1.310, 4 cm deep (Fig. 1*c*). Cooling from the bottom (with the coolant at 8 °C) produced a 5 mm thick layer of $CuSO_4 \cdot 5H_2O$ crystals in 5.5 h, during which time the three fluid layers remained distinct. Overnight, after a total of 19.5 h, the bottom interface had broken down; some of the $CuSO_4 \cdot 5H_2O$ crystals had redissolved, but a thinner layer survived, above which was an 8-mm layer of paler blue crystals, identified (by X-ray diffraction) as the double sulphate $K_2SO_4 \cdot CuSO_4 \cdot 6H_2O$. The coolant temperature was dropped to 0 °C, and after a further day (a total of 45.5 h) the second interface had broken down, and convection extended over the whole depth of the fluid. On top of the two previously observed crystal layers was a thicker layer of KNO_3 crystals, compact at the bottom but with needles on top (see Fig. 3*c*). Thus each time an interface broke down, the composition of the fluid in contact with the cooled bottom changed abruptly, allowing one or more new solid phases to crystallize.

An example will now be given in which the thickness of the crystal layers was more directly controlled by the depth of the compositional layers in the fluid. A 12-cm deep layer of $(NH_4)_2SO_4$ solution at 10 °C, SG = 1.187, was set up above a 5-cm deep layer of $CuSO_4$ solution at 54 °C, SG = 1.296 (Fig. 1*d*). The interface was initially sharp, but it was stirred gently to produce a transition region 4 cm thick. The coolant circulating through the base was brought down from room temperature to 5 °C; on this occasion the thin insulating layer (usually built into the base of the tank to maintain a uniform temperature over the whole area) was left out, and the coldest temperature were therefore close to the back face. After 1.5 h, a layer of

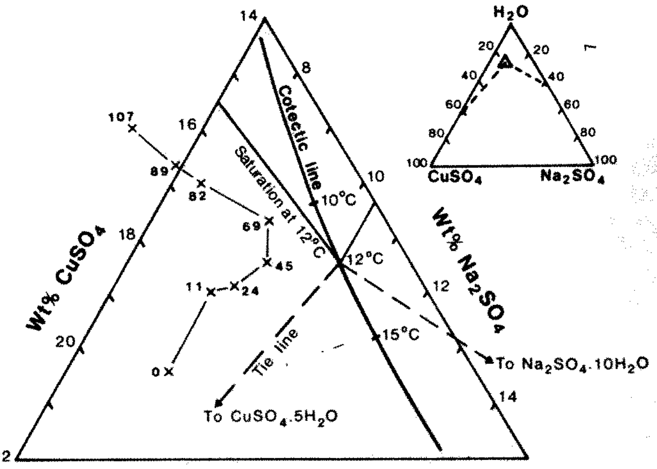

Fig. 2 Part of the phase diagram of the $CuSO_4$–Na_2SO_4–H_2O system, showing the cotectic line (representing solutions in equilibrium with both $CuSO_4 \cdot 5H_2O$ and $Na_2SO_4 \cdot 10H_2O$), and the saturation lines for the two components separately. The region detailed is contained in the small triangle on the full phase diagram sketched at the upper right. The evolution of the bulk composition of the fluid, during the experiment corresponding to Figs 1*a* and 3*a*, is also plotted. Times (in hours since the start of cooling) are marked against the measured points.

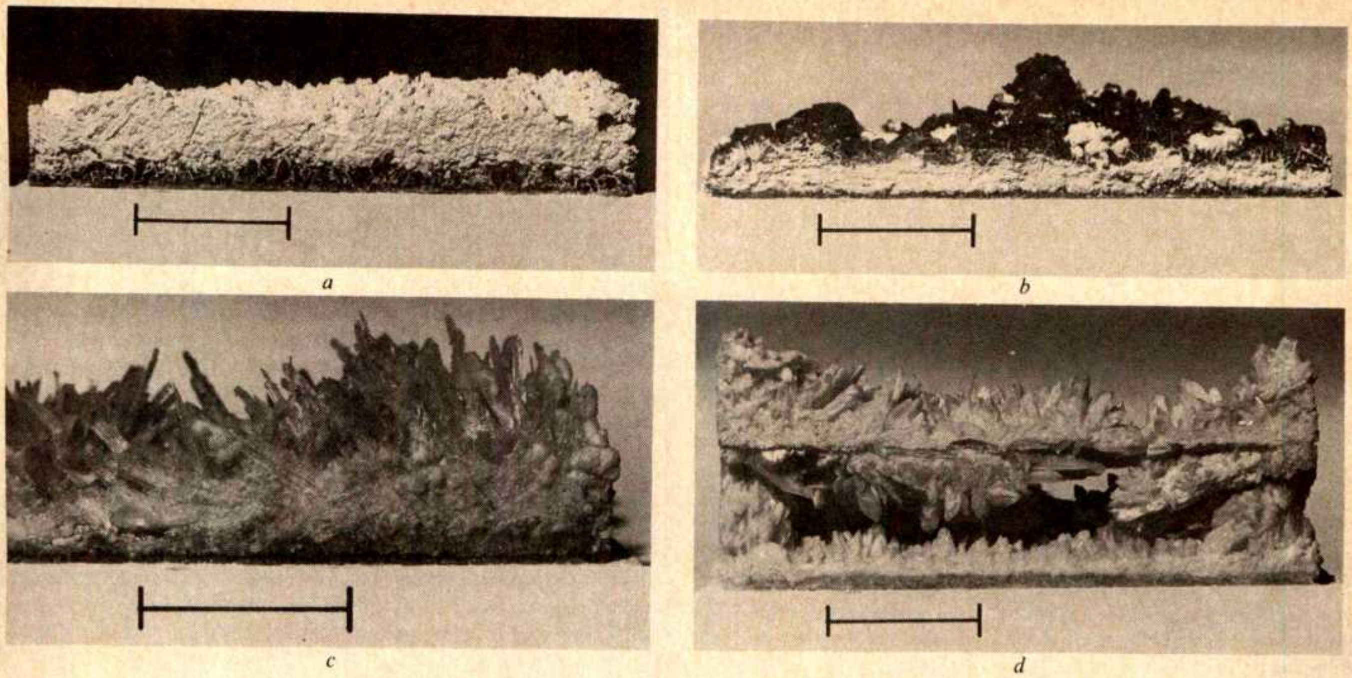

Fig. 3 *a*, Horizontal layers of first $CuSO_4 \cdot 5H_2O$, then $Na_2SO_4 \cdot 10H_2O$ crystals, produced by cooling from below, as the composition of a layer of mixed solution of Cu and Na sulphates evolved with time (see Figs 1*a* and 2). The photograph was taken after the sodium sulphate crystals had dehydrated. (All scale bars, 5 cm.) *b*, The crystal structure produced by cooling a two-layer fluid system from below. The lower layer consisted of a mixture of Cu and Na sulphates similar to that recorded in Fig. 1*a*, and the first two crystal layers grew as described in *a*. The density of the lower layer decreased until overturning occurred, and another layer of $CuSO_4 \cdot 5H_2O$ then grew on top from the Cu-rich solution newly in contact with the crystals. The first indication of a second layer of sodium sulphate is also seen above this. *c*, The crystal structure produced by cooling a three-layer fluid system from below. The upper two layers were KNO_3 (with different concentrations and temperatures, as detailed in Fig. 1*c*), and the lowest was hot $CuSO_4$ solution. The crystal layer which first formed over the bottom was $CuSO_4 \cdot 5H_2O$. As the two interfaces broke down successively, and the composition of the fluid in contact with the top of the crystals changed abruptly, layers of the double sulphate crystals ($K_2SO_4 \cdot CuSO_4 \cdot 6H_2O$) and then KNO_3 crystals formed on top. *d*, Crystal layers which correspond directly to the pre-existing compositional layering in the fluid from which they grew (Fig. 1*d*). A 5-cm deep layer of hot $CuSO_4$ solution was placed below a 12-cm deep layer of less dense cool $(NH_4)_2SO_4$ solution, and the interface thickened by stirring. Cooling from below produced a uniform layer of $CuSO_4 \cdot 5H_2O$ on the bottom and a horizontal band of the double sulphate $(NH_4)_2SO_4 \cdot CuSO_4 \cdot 6H_2O$, with a small fraction of $(NH_4)_2SO_4$, in the interfacial region. When overturning occurred, to produce a single convecting fluid layer, further growth of the double salt took place, extending away from the previous deposit.

$CuSO_4 \cdot 5H_2O$ crystals had begun to grow over the whole floor, and a few paler blue crystals (probably the double sulphate $(NH_4)_2SO_4$. $CuSO_2 \cdot 6H_2O$) were observed on the walls and corners at the centre of the transition layer. No observations were made overnight, but by 19 h the fluid in the tank had overturned, and the structures shown in Fig. 3*d* were observed (looking from the back—above the most strongly cooled region). There is a layer of copper sulphate on the base, with above it a uniform layer of the double sulphate crystals, mixed with a small fraction of $(NH_4)_2SO_4$ crystals. A horizontal layer of the double sulphate plus some ammonium sulphate is also visible at the level of the original interface, and it can be deduced that this is where the composition of the mixed solution initially favoured the formation of these two phases; further crystallization has occurred upwards and downwards from this level following the overturn and complete mixing.

Thus at least three mechanisms have been identified whereby a series of horizontal crystal layers of nearly constant thickness and abruptly changing composition can be produced in a layered multicomponent fluid system cooled from below. First, the composition of a single isolated layer may evolve (more rapidly than would otherwise be the case in a very deep well-mixed container), so that crystallization of a new phase with different kinetics becomes possible above the crystals originally formed on the bottom. Second, the decrease in density of the residual fluid which accompanies crystallization can lead to a sudden overturning and mixing, which rapidly changes the composition of the deeper combined layer in contact with the top of the crystals previously formed. Third, the interfacial region between fluid layers of different composition can provide an environment in which some species will crystallize preferentially, at higher temperatures than any crystals can form in either layer separately. In general the thickness of the various crystal layers is determined only indirectly by the depth of the fluid layers, but in the third case there is a direct relationship between the two scales.

The dynamical principles sketched here should be directly applicable to crystallizing magmas. The justification for transferring results from one fluid system to another, and the associated scaling problems, have been discussed elsewhere[1,5] and the need for this type of study has already been recognized in the recent literature[9,10] on layered intrusions. Further work in progress is aimed at providing a more quantitative understanding of the evolution of crystal layers and the solutions in which they are growing, so that the laboratory results can be generalized and used predictively for more complex magmatic systems.

We thank D. L. Corrigan and R. Wylde-Browne for assistance at all stages of these experiments, and P. W. Berrie for help with the X-ray diffraction analyses.

Received 11 March; accepted 15 June 1982.

1. Chen, C. F. & Turner, J. S. *J. geophys. Res.* **85**, 2573–2593 (1980).
2. Turner, J. S. *Nature* **285**, 213–215 (1980).
3. McBirney, A. R. *J. Volcanol. geotherm. Res.* **7**, 357–371 (1980).
4. Huppert, H. E. & Turner, J. S. *Earth planet. Sci. Lett.* **54**, 144–152 (1981).
5. Turner, J. S. & Gustafson, L. B. *J. Volcan. geotherm. Res.* **11**, 93–125 (1981).
6. Huppert, H. E. & Sparks, R. S. J. *Contr. Miner. Petrol.* **75**, 279–289 (1980).
7. Huppert, H. E., Turner, J. S. & Sparks, R. S. J. *Earth planet. Sci. Lett.* **57**, 345–357 (1982).
8. Wager, L. R. & Brown, G. M. *Layered Igneous Rocks* (Oliver and Boyd, Edinburgh, 196[illegible]).
9. McBirney, A. R. & Noyes, R. M. *J. Petrol.* **20**, 487–554 (1979).
10. Irvine, T. N. in *Physics of Magmatic Processes* (ed. Hargreaves, R. B.) Ch. 8 (Princeton University Press, 1980).

Lithospheric thinning associated with rifting in East Africa

Richard F. Wendlandt & Paul Morgan

Lunar and Planetary Institute, 3303 NASA Road One, Houston, Texas 77058, USA

A fundamental mechanism of some continental rifting processes appears to be the transmission of thermal energy into the lithosphere by asthenospheric upwelling (the 'active' mechanism of Sengör and Burke[1]), for which the East African rift system is a classic example. The abundance and variety of magma types of predominantly alkaline affinities in the East Rift which derive from the thermal perturbation suggest that studies of igneous petrogenesis may offer a method of investigating the physical as well as the chemical conditions of the upwelling. Systematic variations in the temporal–spatial–compositional relations of igneous rocks associated with rifts are becoming well documented for several different rifts[2–13], and it is generally observed that the degree of silica-saturation of lavas within these rifts increases with time, while incompatible element contents decrease. Furthermore, at any given instant, lavas erupted within the rifts are less silica-undersaturated than lavas erupted outside the rift. These observations are consistent with decreasing depths of origin of magmas with time as would be predicted for magmagenesis associated with an upwelling source region. Here, by deducing the physical conditions of origin of various magmatic products associated with a thermotectonic event in East Africa, the rate of upwelling is calculated and compared with the results of a simple thermal model of lithospheric thinning.

The diversity of eruptive rock types in the Kenya Dome region of the East African rift, corresponding to depths of origin ranging from >170 km to the lower crust (25–30 km), combined with an abundance of dated occurrences permits calculation of the rate of ascent of the thermal perturbation (Fig. 1). As a first approximation it is assumed that the magmas being considered in the analysis were generated and/or segregated from the lithosphere–asthenosphere boundary. The points in Fig. 1 were selected so as to minimize the depth of origin of magmas for a given age. The physical and chemical conditions of origin of the more primitive alkalic varieties of magmas and the flood volcanism in the East Rift are emphasized inasmuch as it is believed that the compositions of these rocks can be related to the depth from which they erupted. The deepest and oldest point in Fig. 1 is defined by the most recent diamond-bearing kimberlite eruption in northern Tanzania, 41 Myr (ref. 14); the depth of origin is based on the intersection of the theoretical and experimentally derived conditions for kimberlite genesis with the diamond–graphite equilibria[15–18], and represents a minimum estimate. The next younger point in Fig. 1, 31 Myr, is based on the oldest known carbonatite associated with rifting, Tororo in eastern Uganda[19]; the range of depths of origin is based on partial melting experiments on carbonated, and carbonated and hydrated peridotite[16,20–27]. The point at ~22 Myr represents the initiation of eruption of ~50,000 km^3 of Miocene flood basalts in northwestern and western Kenya[5]; the depth of origin is estimated from experimental results[28–30]. The two youngest points represent the onset of eruption of flood phonolites and trachytes, respectively, in the East Rift in southwestern Kenya and northern Tanzania[31]; the depths of origin are constrained by experiments in model peridotite systems[16,32] and thermobarometric estimates[33]. Approximately 65,000 km^3 of flood phonolite and trachyte were erupted[5,34]. The depth of origin estimates for the flood trachytes are probably realistic, being situated in the lower crust, although any model assumed in deriving the depth estimate will be, at best, contentious: of greater importance to the analysis is the observation that significant ascent of mantle isotherms must have occurred to enable the accumulation of 10^4–10^5 km^3 of melts of trachytic composition.

The magmatic events forming the basis of the analysis comprise >10^5 km^3 of eruptive rock, an amount approaching estimates of the total volume associated with the Kenya Dome. The data in Fig. 1 are represented by points with respect to time; however, it is important to emphasize, at least with regard to the flood eruptives, that it is the initiation of magmatic events, perhaps comprising many tens of flows and lasting up to several million years, which forms the basis for the analysis. While the general trend of melt composition variation with time is well documented[4–9], the volcanic stratigraphy is complex with intermingling of eruptives of different compositions, and, thus, of different depths of origin, particularly for younger magmas erupted from shallower depths; that is, the progression of deep sourced eruptives to those from shallower depths is not without exceptions, perhaps attesting to complex convective processes in the asthenosphere (textural and structural evidence of episodic deformation and melting that is believed to have originated in an diapirically rising mass has been reported for ultramafic nodules from Lashaine Volcano, Tanzania)[35]. If all the available ages versus depth of origin for volcanics were plotted, however, they would cluster on the concave side of the envelope (Fig. 1), without affecting the exponential trend of the minimum depth of origin for a given age. A systematic decrease in the rate of ascent of asthenosphere is evident (Fig. 1). Complete thinning of the lithospheric upper mantle by asthenospheric upwelling is accomplished over a time interval of ~30–40 Myr.

To understand better the lithospheric attenuation predicted by the analysis of eruptives in East Africa, a simple thermal model of lithospheric thinning has been developed. The lithosphere–asthenosphere boundary (LAB) is assumed to lie at or above the top of the upper thermal boundary layer of mantle convection, with its temperature at the mantle solidus. Heat

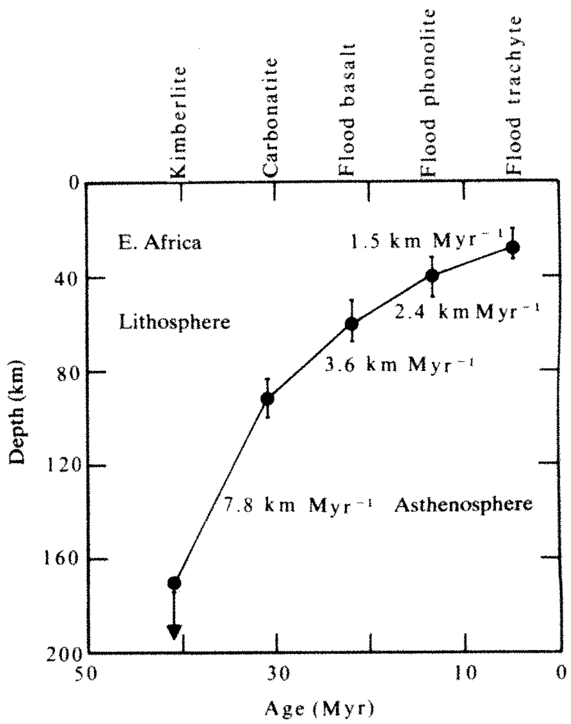

Fig. 1 Asthenosphere ascent rate associated with active type rifting in the Kenya Dome portion of the East African rift system as estimated by changes in the depth of origin of magmatic products with time. Data points are discussed in the text. The ranges of experimentally determined depths of origin are shown by brackets; the selected points are considered to be the best estimates except for the depth of origin of kimberlite which is a minimum estimate.

0028-0836/82/330734–03$01.00

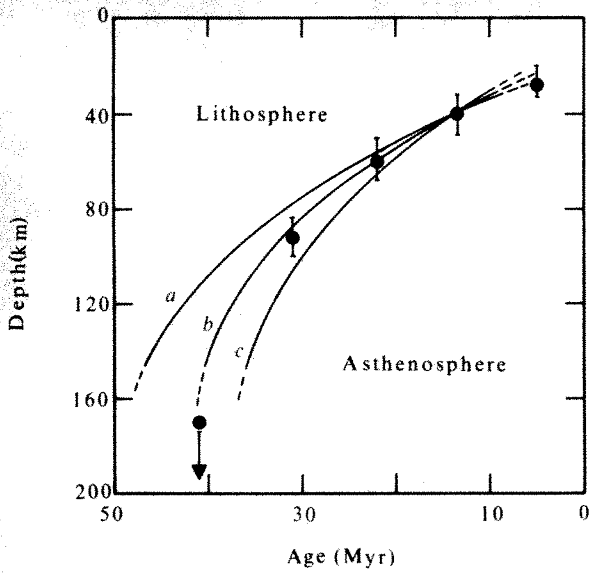

Fig. 2 Asthenosphere ascent, constrained to pass through the phonolite (40 km, 13.5 Myr) data point, calculated from thermal thinning model for 50 km radius lithosphere–asthenosphere boundary perturbation and different temperature gradient increases across the lithosphere–asthenosphere boundary: *a*, 70 °C km^{-1}; *b*, 60 °C km^{-1}; *c*, 50 °C km^{-1}. Curves for 100 km radius perturbation are similar for 65, 55 and 45 °C km^{-1} gradient increases respectively. Data points from Fig. 1 are shown for comparison.

transfer in the lithosphere is assumed to be by conduction only. In stable conditions, heat is conducted through the lithosphere at the same rate that it is input through the boundary layer. If locally the heat supply is increased (mantle 'hotspot'), however, temperatures will increase in the lithosphere, and a perturbation in the LAB will ascend to maintain its position on the mantle solidus. It is this ascent rate, as a function of the undisturbed lithosphere geotherm, the mantle solidus, and the increased heat supply, that we seek to determine.

By simplifying the geometry of the LAB perturbation to be spherical over the heat source, the following equation has been derived for the relationship between the increased heat supply (increased gradient dT'/dr), the temperature increase (T') at the LAB, and the ascent rate (W) of the LAB perturbation, from the solution for the temperature from a stationary constant-strength point-source in a medium moving at constant velocity[36]:

$$\frac{dT'/dr}{T'} = \left[\frac{(1+Wr/k)\exp(-Wr/k)}{r^2} + \frac{(1+W(r+2z)/k)\exp(-W(r+2z)/k)}{(r+2z)^2}\right] \Bigg/ \left[\frac{\exp(-Wr/k)}{r} - \frac{\exp(-W(r+2z)/k)}{r+2z}\right] \tag{1}$$

where r is the radius of the LAB perturbation, z is the depth of its shallowest point and k is the thermal diffusivity of the lithosphere. Although this equation is derived for a constant velocity ascent, a parameter study has shown that it can be used to determine instantaneous velocities at various depths, even if the ascent rate is variable, for radii $\geq$40 km and ascent velocities $\geq$1 km Myr^{-1} (3.17×10^{-11} m s^{-1}), for a typical mantle diffusivity of 1 mm^2 s^{-1}. This approximation is satisfactory because at velocities >1 km Myr^{-1} the ascent rate is effectively faster than the thermal conduction rate above the LAB.

The temperature increase in equation (1) is the temperature required to raise the lithosphere geotherm to the solidus. This has been calculated from a shield geotherm, considered to be appropriate for East Africa before rifting, given by model C1 of Sclater *et al.*[37], and a mantle solidus derived from published experimental data[16]. This mantle solidus was selected because it is internally consistent over a large pressure range, and is a model for the genesis of alkalic magmas, carbonatites and kimberlites, assuming the presence of small amounts of H_2O and CO_2 in the mantle. A thermal diffusivity of 1 mm^2 s^{-1} was assumed, and equation (1) was solved iteratively for ascent velocity at 10-km depth intervals from 150 to 30 km, assuming different radii for the LAB perturbation and different temperature gradient increases across the LAB.

Excellent fits to the experimentally derived LAB ascent rates were obtained for radii of 50 and 100 km and constant gradient increases within the range 55–60 °C km^{-1} over the LAB ascent depth range, as shown in Fig. 2. These radii can reconcile the lateral extent of the eruptives in East Africa[38], as the ascent rate is not sensitive to the radius if the latter is >100 km. The range of gradient increase is more difficult to evaluate, but is not unrealistic, being of the same order in a fixed heat source–lithosphere reference frame as that required in a moving reference frame to reheat the Pacific plate to a bathymetric age of 25 Myr over hotspots, as reported by Detrick and Crough[39]. The ascent rate is sensitive to changes in dT'/dr; a 1 °C km^{-1} change in gradient approximately results in a 0.55 Myr change (~1.5%) in the total ascent time from 150 to 30 km. The apparent 'exponential' decrease in ascent rate with time is predicted even with a constant heat supply (constant dT'/dr). This decrease is due to the increasing differential (T') between the geotherm and the solidus as the depth decreases, and the increasing rate of heat loss to the surface as the thermal wave in front of the LAB perturbation impinges on the surface.

Two direct predictions result from the thermal model. The rapid ascent rate of the thermal perturbation indicates little thermal disturbance above the LAB. The experimental data indicate that the perturbation reached a depth of 30 km 4.8 Myr ago, hence only a small surface heat flow anomaly is predicted outside the areas of Quaternary volcanism and plutonism. This prediction is consistent with surface heat flow data across the Kenya rift[40]. The thermal perturbation should cause thermal expansion in the lithosphere–asthenosphere column as it rises, however, resulting in uplift contemporaneous with lithospheric thinning. Using a volume thermal expansion coefficient of 3×10^{-5} °C^{-1} the model predicts a mean decrease in density of 0.035 g cm^{-3} from 160 to 20 km depth during thinning, which, assuming the lithosphere to be supported buoyantly by the asthenosphere[41], results in an uplift of a little over 1.5 km. This uplift is in good agreement with the uplift determined from geological criteria in Kenya[5].

The temporal–spatial–compositional relations of eruptives in the Kenya Dome region of the East African rift system suggest a shallowing of magma source regions with time, an observation implying encroachment of a thermal anomaly as might be expected from asthenospheric upwelling. Thermal modelling indicates that the rate of this upwelling, and the experimentally determined decrease in this rate at shallower depths can be explained by a constant supply of heat from the asthenosphere, with a magnitude similar to that deduced for other inferred mantle hotspots. The experimentally determined and theoretically modelled lithospheric thinning gives results consistent with observed surface heat flow and uplift across the Kenya rift, and supports the concept of a convective upwelling of the asthenosphere driving rifting in East Africa.

We thank R. J. Phillips, W. Harrison and G. Wadge for helpful discussions and constructive criticism. This work was carried out at the Lunar and Planetary Institute, operated by the Universities Space Research Association under contract NASW 3389 from NASA. Lunar and Planetary Contribution No. 478.

Received 22 February; accepted 8 June 1982.

1. Şengör, A. M. C. & Burke, K. *Geophys. Res. Lett.* **5**, 419–421 (1978).
2. Gass, I. G. *Phil. Trans. R. Soc.* **A267**, 369–381 (1970).
3. Mohr, P. A. *Bull. Volcanol.* **34**, 141–157 (1970).

4. Baker, B. H. *et al. Tectonophysics* **11,** 191–215 (1971).
5. Baker, B. H. *et al. Geol. Soc. Am. Spec. Pap.* **136,** (1972).
6. King, B. C. & Chapman, G. R. *Phil. Trans. R. Soc.* **A271,** 185–208 (1972).
7. Williams, L. A. J. *Tectonophysics* **15,** 83–96 (1972).
8. Lippard, S. J. & Truckle, P. H. in *Petrology and Geochemistry of Continental Rifts* (eds Neumann, E.-R. & Ramberg, I. B.) 123–131 (Reidel, Dordrecht, 1978).
9. Norry, M. J. *et al. Phil. Trans. R. Soc.* **A297,** 259–271 (1980).
10. Lipman, P. W. *Bull. geol. Soc. Am.* **80,** 1343–1354 (1969).
11. Dungen, M. A. *et al.* in *Pap. Conf. on the Processes of Planetary Rifting,* 137–140 (Lunar and Planetary Institute, Houston, 1981).
12. Duncan, R. A. *et al. Nature* **239,** 82–86 (1972).
13. Brooks, C. K. & Rucklidge, J. C. *Lithos* **7,** 239–248 (1974).
14. Davis, G. L. *Yb. Carnegie Instn Wash.* **77,** 895–897 (1978).
15. Eggler, D. H. & Wendlandt, R. F. in *Kimberlites, Diatremes, and Diamonds: Their Geology, Petrology, and Geochemistry* (eds Boyd, F. R. & Meyer, H. O. A.) 330–338 (American Geophysical Union, Washington DC, 1979).
16. Wendlandt, R. F. & Eggler, D. H. *Am. J. Sci.* **280,** 421–458 (1980).
17. Wyllie, P. J. *J. geophys. Res.* **85,** 6902–6910 (1980).
18. Kennedy, C. S. & Kennedy, G. C. *J. geophys. Res.* **81**, 2467–2470 (1976).
19. King, B. C. *et al. J. geol. Soc.* **128,** 173–205 (1972).
20. Wyllie, P. J. & Huang, W. L. *Nature* **257,** 297–299 (1975).
21. Wyllie, P. J. & Huang, W. L. *Geology* **3,** 621–624 (1975).
22. Wyllie, P. J. & Huang, W. L. *Contr. Miner. Petrol.* **54,** 79–107 (1976).
23. Eggler, D. H. *Yb. Carnegie Instn. Wash.* **74,** 468–474 (1975).
24. Eggler, D. H. *Geology* **4,** 69–72 (1976).
25. Eggler, D. H. *Am. J. Sci.* **278,** 305–343 (1978).
26. Wendlandt, R. F. & Mysen, B. O. *Am. Miner.* **65,** 37–44 (1980).
27. Wendlandt, R. F. & Eggler, D. H. *Am. J. Sci.* **280,** 385–420 (1980).
28. Green, D. H. *Phys. Earth planet. Inter.* **3,** 221–235 (1970).
29. Thompson, R. N. *Contr. Miner. Petrol.* **45,** 317–341 (1974).
30. Jaques, A. L. & Green, D. H. *Contr. Miner. Petrol.* **73,** 287–310 (1980).
31. King, B. C. & Chapman, G. R. *Phil. Trans. R. Soc.* **A271,** 185–208 (1972).
32. Kushiro, I. *J. geophys. Res.* **73,** 619–634 (1968).
33. Irving, A. J. & Price, R. C. *Geochim. cosmochim. Acta* **45,** 1309–1320 (1981).
34. Lippard, S. J. *Lithos* **6,** 217–234 (1973).
35. Pike, J. E. N. *et al. J. Geol.* **88,** 343–352 (1980).
36. Carslaw, H. S. & Jaeger, J. C. *Heat Conduction in Solids,* 266–267 (Oxford University Press, London, 1959).
37. Sclater, J. G. *et al. Rev. Geophys. Space Phys.* **18,** 269–311 (1980).
38. Wendlandt, R. F. in *Pap. Conf. on the Processes of Planetary Rifting,* 126–133 (Lunar and Planetary Institute, Houston, 1981).
39. Detrick, R. S. & Crough, S. T. *J. geophys. Res.* **83,** 1236–1244 (1978).
40. Morgan, P. & Wheildon, J. *J. geophys. Res.* (submitted).
41. Crough, S. T. & Thompson, G. A. *J. geophys. Res.* **81,** 4857–4862 (1976).

Oligo-Miocene rift of Sardinia and the early history of the Western Mediterranean Basin

A. Cherchi

Istituto di Geologia, Paleontologia e Geografia Fisica,
Università di Cagliari, via Trentino 51, 09100 Cagliari, Italy

L. Montadert

Istituto di Geologia, Paleontologia e Geografia Fisica,
Università di Cagliari, via Trentino 51, 09100 Cagliari, Italy

The geodynamic evolution of the Western Mediterranean Basin, in spite of many studies, is still uncertain. There is some consensus for interpreting this basin as a kind of small oceanic marginal basin. Its opening has generally been related to a subduction process which was active during the Oligocene–Miocene somewhere east of Sardinia–Corsica[1–7]. As the margins of the basin are deeply buried below Miocene-to-present sediments, direct lithological and stratigraphical data which could explain the events responsible for its formation are rare[8–10] or missing altogether. To obtain such data, detailed field studies have been undertaken in Sardinia (Fig. 1), and the first results are presented here. This approach is justified by the fact that in that island, Oligocene and Miocene sediments were deposited in a rift (*fossa tettonica sarda* of Verdabasso[11]), which is the easternmost arm of the complex rift system that affected the European plate during Oligocene and Miocene times. One of these arms evolved towards a small oceanic basin—the Western Mediterranean or Algero–Provençal Basin—while others such as the Gulf of Valencia and the Sardinia rift aborted and remained at the rift stage. Its exceptional exposures make it possible to examine the Sardinia rift to clarify the sequence of events which created it, and to establish a sedimentological model which we believe is directly applicable to the Western Mediterranean Basin.

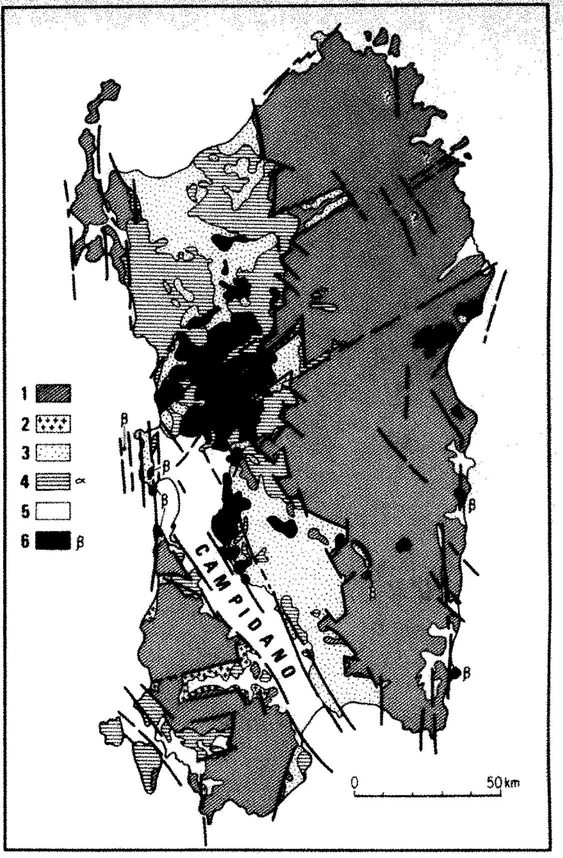

Fig. 1 Geological map of Sardinia. 1, Basement with its Mesozoic and Eocene cover; 2, Cixerri Formation; 3, Oligocene–Miocene rifted basin; 4, Oligocene–Miocene calc-alkaline volcanics; 5, continental Pliocene–Quaternary basin; 6, alkaline Pliocene–Quaternary volcanics.

The Sardinian Oligocene–Miocene rift, which crosses all of Sardinia's 220 km on a N–S trend, must be distinguished from the Pliocene–Quaternary graben of Campidano; the two are often confused. Figures 1, 2*a* and 3 show that the Campidano graben is superimposed on the southwestern part of the Oligocene–Miocene graben, but in an oblique NW–SE direction. It corresponds to an entirely different event, which affected the Central and Western Mediterranean[12]. Detailed structural and sedimentological observations, supported by a good biostratigraphy, can therefore be made of the eastern part of the Oligocene–Miocene rift which appears as a typical rift edge. The Palaeozoic basement of Sardinia, sometimes including its Mesozoic and Eocene cover, is downfaulted by a succession of tilted blocks. The vertical lowering of the pre-rift basement is estimated at at least 1,200 m, and probably much more. The complicated fault pattern can be explained by the complex structure and lithology of the basement. While the general trend of the rift is N–S, local faults vary from N–S to NNW–SSE, and are interrupted by transverse accidents. Among the succession of faults which downfaulted the basement, a master fault is generally observed whose throw can be as wide as 500 m (Fig. 2*b*). It is clearly evident in the morphology of the Sardinian rift, and explains the wall aspect on the eastern edge. Tilted blocks with shorter throw are observed westward and eastward of this master fault. The tectonic style is identical to those described in various intracontinental rifts and on some rifted passive continental margins[13]. This complex pattern controlled the palaeogeography of the basin and the nature and deposition of the sediments along the rift. The width between the two master faults delineating the main trough is 40–50 km.

The Sardinian rift has been infilled by Oligocene–Miocene continental-to-marine sediments ~1 km thick. Volcanics occurring from the late Oligocene, 29.9 ± 1.5 Myr to the middle

0028–0836/82/330736—04$01.00

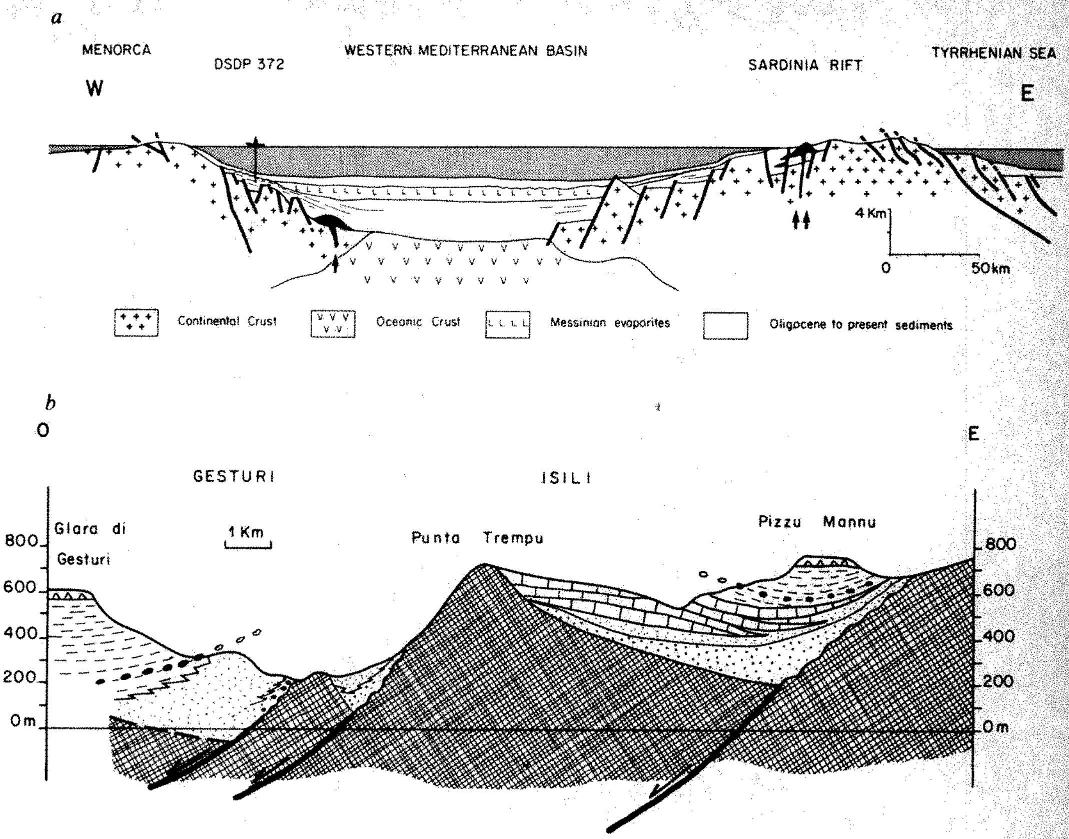

Fig. 2 *a*, Schematic geological cross-section from Menorca to Sardinia through the Western Mediterranean basin. Modified from Biju-Duval *et al.*[5]. The section crosses western Sardinia near Oristano. *b*, Geological cross-section on the eastern edge of the Oligocene–Miocene rift showing the tilted block of Isili bounded westward by a master fault. Conglomerates, sandstones and limestones are Oligocene–Aquitanian continental and marine synrift deposits. The black dotted line corresponds to the early Burdigalian post-rift marls.

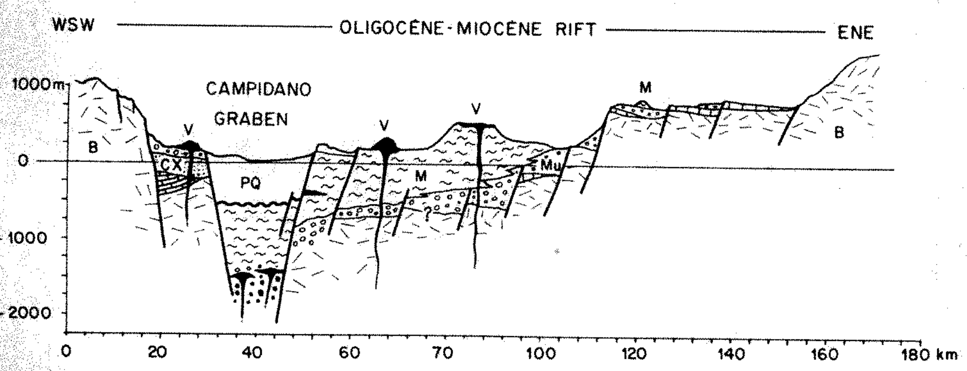

Fig. 3 Schematic geological cross-section through the Oligocene–Miocene rift of Sardinia, with the superimposed Pliocene–Quaternary Campidano graben. B, Palaeozoic basement with sometimes its Mesozoic and Eocene cover. Cx, Cixerri Formation; Mu, Oligocene–Miocene synrift Ussana Formation; M, late Oligocene–Miocene marls; PQ, Pliocene–Quaternary; V, volcanics.

Miocene, 13–14 Myr (refs 6–14) can be up to 1 km thick. They are believed to be the products of the volcanic arc linked with the subduction process which was active east of Sardinia. The sediments can be studied in their structural context to determine the timing of the formation, the evolution of the Sardinian rift and the age and nature of the prerift, synrift and postrift deposits.

Before the formation of the Western Mediterranean Basin, the Corsica Sardinia block joined the European plate. Lithological and biostratigraphical data demonstrate this proximity until the early to middle Oligocene. Indeed the continental Cixerri Formation (~300 m thick) outcrops in southwestern Sardinia where it is unconformable to various strata: Palaeozoic, Mesozoic and mainly Lower-base–Middle Eocene. This unconformity corresponds to the Eocene Pyrenean compressional phase recognized and recorded in Sardinia[15,16] with a NW–SE shortening direction[17]. The microfaunal composition and the direction of currents measured on these clastics[18], demonstrate a provenance from northeastern Iberia[19–21] for the material constituting the Cixerri Formation. These observations, and the absence of pebbles of local origin, suggest that the clastics were deposited after the Pyrenean phase and before the initiation of the rift system of the Western Mediterranean. The Cixerri Formation is dated Lutetian at its base by Charophyta and pollen assemblage[22]. It is cut by andesites, the older ones being dated 29.9 ± 1.5 Myr. It can be compared with conglomerates in Provence and in Menorca[19].

The fundamental structural change corresponding to the formation of the rift is recorded by the onset of deposition of the thick clastic Ussana Formation[23]. Its age is post 29.9 ± 1.5 Myr, early Middle Oligocene, in accordance with a Stampian age

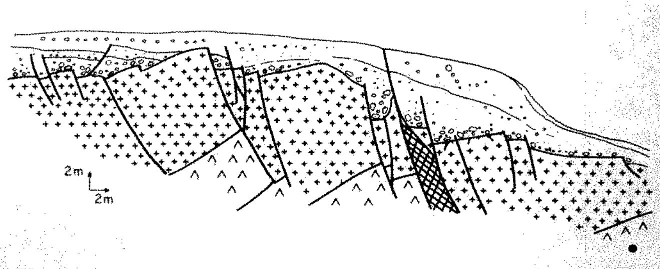

Fig. 4 Detail of the rift tectonics with faulting synchronous of continental conglomerates deposition (north of Cagliari).

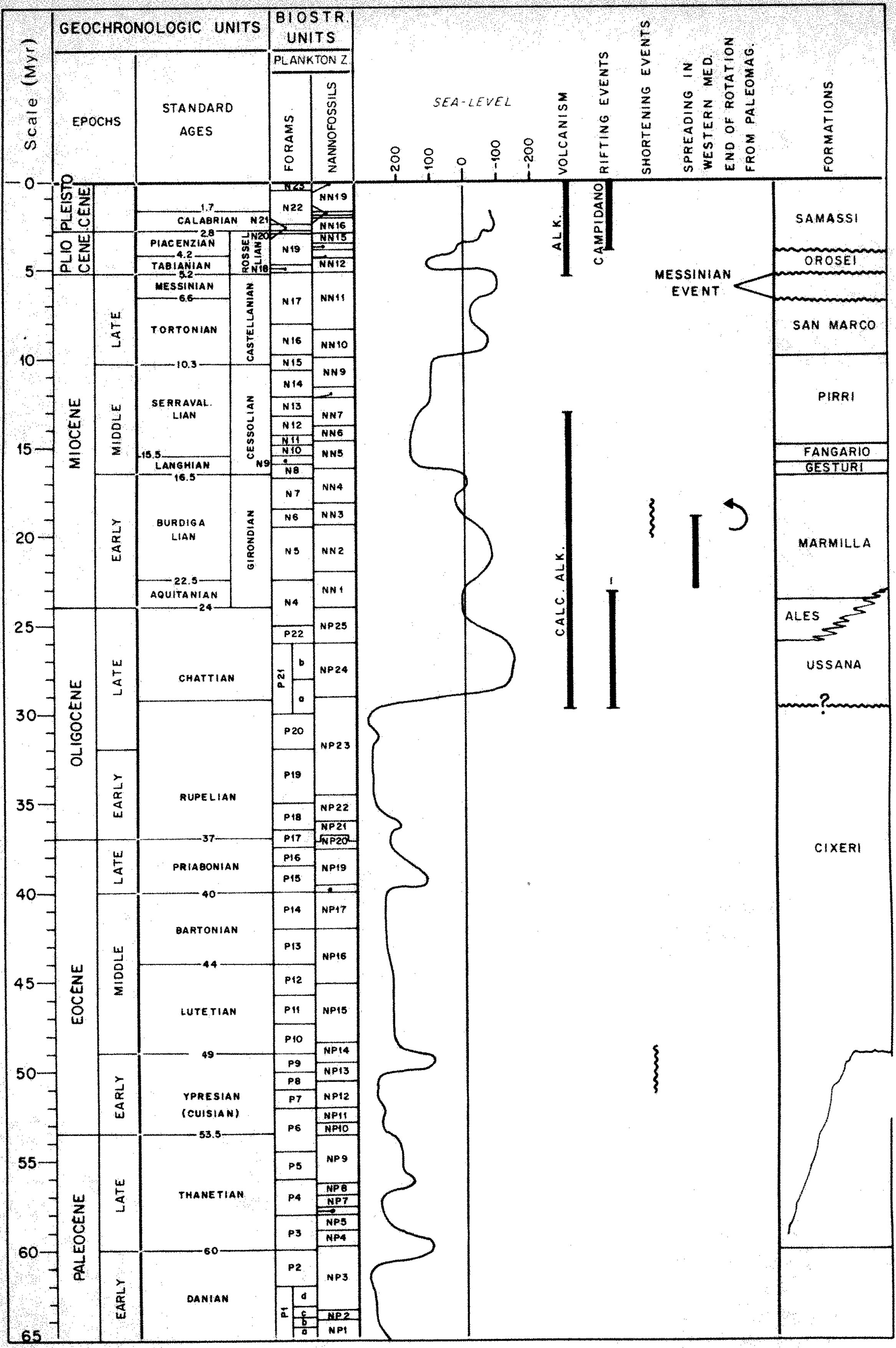

Fig. 5 Main geological events in Sardinia. Time scale and eustatic changes of sea level from ref. 38.

established for grabens in Languedoc (Southern France)[24]. The creation of new reliefs and fault escarpments caused intensive erosion.

First, continental breccias and heterometric conglomerates (from a few centimetres to several metres) embedded in a red-violine sandy-clayey matrix were deposited on and along these escarpments. Their structure is typical of slope deposits, alluvial fans or torrential deposits and they are clearly contemporaneous with faulting (Fig. 4). These observations demonstrate that in its early phase, rifting occurred in a continental environment. Then, fluviatile conglomerates with sandy matrices sometimes including breccias and intercalations of marine limestones with corals, oysters, bryozoans, red algae and pectinids, indicate progressive invasion of the rift by the sea. Thick sandstones are also present. This Ussana Formation, as much as 500 m thick, developed along the edge of the rift, its complex distribution of deposits controlled by the nature and topography of the basement. Locally, along the crest of some tilted blocks, shallow water carbonates made of red algae and >200 m thick were deposited (Fig. 2*b*). As it approaches the axis of the rift the upper Ussana Formation rapidly changes to open marine marls rich in pelagic microfossils (Ales and Marmilla Formations)[25], while on the flank, shallow-water limestones are present. The change from the continental, fluviatile or shallow marine environment to the deeper basin is indicated by intercalations of sands, conglomerates and breccias, with blocks up to several metres, deposited as turbidites and debris flows.

Rifting originated in a continental environment during the early Middle Oligocene. But these data, the pelagic microfossils present in the oldest open marine marls (which are Chattian—P22–NP25—in age), and the shallow-water limestones on the flanks (dated with *Lepidocyclina* and *Miogypsina* gr. *bantamensis*) indicate that the sea invaded the rapidly subsiding axis of the rift during the late Oligocene. The deposition of the Ussana Formation continued until the Aquitanian (N4). Quantitative study[26] of benthic and planktonic foraminifera has resulted in some estimates of the bathymetry at that time. For the Aquitanian deposited at the foot of the master fault, palaeodepths of ~1–1.3 km have been determined, while palaeodepths of 200–300 m were found in Aquitanian deposited higher up. Thus the sea bottom at that time was characterized by high relief.

Deposits equivalent to the Ussana, Ales and Marmilla Formations have been found around the Western Mediterranean. For example, conglomerates and late marine Oligocene have been found in exploration wells in the Camargue trough[27] and in the Gulf of Lions[10] and by submarine sampling on the continental slope of Provence[28–30]. In the Balearic Islands synrift deposits of early Miocene age have also been described[31,32]. Since the Aquitanian, Miocene deposits are essentially marine marls throughout the basin, with the exception of a sandy and carbonate episode in the Upper Serravallian–Lower Tortonian. Calc-alkaline volcanics[33–35] are interbedded throughout the Oligocene–Miocene deposits, and are dated from 29.9± 1.5 Myr to 13–14 Myr (refs 6, 14). They were emplaced either in the air (ignimbrites) or under the sea (pillow-lavas). Associated with them, thick and frequent series of tuffites were deposited. Major events are shown in Fig. 5. Late Miocene-to-present deposits are not considered here.

Thus there is a good set of evidence to support the thesis that rifting in Sardinia, and elsewhere in the European plate, began in the middle Oligocene around 30 Myr ago in a continental environment. At the end of the Oligocene, the trough was deep enough to allow invasion by the sea. The precise estimate of the end of rifting in the Aquitanian 23–24 Myr ago, is based on the following evidence: (1) the typical arrangement of Aquitanian sediments in half grabens, demonstrating that they are synrift deposits; (2) the vertical offset of several hundred metres of shallow marine lower Aquitanian limestones along the master fault; (3) the sealing of faulted blocks by Aquitanian sediments. Further extension with accretion of new oceanic crust was confined to the Western Mediterranean basin. There is no sedimentological evidence in the Miocene marine marls of Sardinia to indicate the end of oceanic accretion in the Western Mediterranean marginal basin, that is the end of rotation of the Corsica–Sardinia microplate. But an intra-Burdigalian compressional phase was recently determined in Sardinia. The shortening direction trends NE–SW[17], as in adjacent areas of Italy and Tunisia. We interpret this as a change in the stress field in the area at that time. The tensional regime in the Western Mediterranean ceased with the end of spreading and rotation of Corsica–Sardinia, because collision occurred east of Sardinia. This timing is in good accordance: (1) with the reinterpretation of the K/Ar ages and palaeomagnetic data of the volcanics of Sardinia[36], as a 19-Myr age (intra-Burdigalian) is proposed for the end of rotation; and (2) with the 19-Myr age of the Tristanite dredged from the axis of the Ligurian sea[37].

We thank Drs De Graciansky, Chenet, Lemoine, Heydman and Grosjean for useful discussions.

Received 24 March; accepted 23 June 1982.

1. Boccaletti, M. & Guazzone, G. *Mem. Soc. Geol. It.* **11,** 201–216 (1972).
2. Boccaletti, M. & Guazzone, G. in *Paleogeografia del Terziario sardo nell'ambito del Mediterraneo occidentale* (ed. Cherchi, A.) 57–68 (1974).
3. Auzende, J. M., Bonnin, J. & Olivet, J. L. *J. geol. soc. Lond.* **129,** 607–620 (1973).
4. Biju-Duval, B. *et al.* in *The Geology of Continental Margins* (eds Burk, C. A. & Drake, C. L.) 695–721 (1974).
5. Biju-Duval, B., Letouzey, J. & Montadert, L. *Init. Rep. DSDP* Leg **42A,** 951–984 (1978).
6. Bellon, H., Coulon, C. & Edel, J. B. *Bull. Soc. géol. Fr.* **19,** 825–831 (1977).
7. Tapponnier, P. *Bull. Soc. géol. Fr.* **19,** 437–460 (1977).
8. Ryan, W. B. F. *et al. Init. Rep. DSDP* Leg **13,** 1–1448 (1973).
9. Hsü, K. J. *et al. Init. Rep. DSDP* Leg. **42A,** 1 (1978).
10. Cravatte, J. *et al. Not. Mém. Compagnie Fr. Pétrole* **11,** 209–274 (1974).
11. Vardabasso, S. *Geol. Rdsch.* **53,** 613–630 (1963).
12. Mauffret, A. *et al. Bull. Am. Ass. petrol. Geol.* **57,** 2245–2262 (1973).
13. Montadert, L. *et al. Maurice Ewing Symp.* Ser. 3, 154 (1979).
14. Savelli, C. *et al. J. Volcan. Geotherm. Res.* **5,** 257 (1979).
15. Vardabasso, S. *56° Congr. Soc. Geol. It., Guida alle escursioni,* 1–75 (1952); *Soc. Geol. It.* **21,** 159–179 (1955).
16. Chabrier, G. *C.r. hebd. Séanc. Acad. Sci., Paris* **271,** 1251–1255 (1970).
17. Letouzey, J., Wannesson, J. & Cherchi, A. *C.r. hebd. Séanc. Acad. Sci., Paris* **294,** 596–602 (1982).
18. Barca, S. & Palmerini, V. *Boll. Soc. Sarda Sc. Nat.* **12,** 13–50 (1973).
19. Cherchi, A. & Schroeder, R. *Bull. Soc. géol. Fr.* **18,** 1217–1219 (1976).
20. Cherchi, A. *Riv. Ital. Paleont. Strat.* **35,** 353–410 (1979).
21. Cherchi, A. & Schroeder, R. *Boll. Soc. Sarda Sc. Nat.* **20,** 27–36 (1981).
22. Pittau, P. *Boll. Soc. Paleont. It.* **18,** 303–314 (1979).
23. Pecorini, G. & Cherchi, A. *Mem. Soc. geol. It.* **8**, 421–451 (1969).
24. Mattauer, M. *C.r. Som. Soc. géol. Fr.* No. 10, 316–317 (1962).
25. Cherchi, A. *V Congr. Néogène Méditerr. Lyon 1971, BRGM* **78,** 433–445 (1974).
26. Wright, R. *Init. Rep. DSDP* Leg **42A,** 837–844 (1978).
27. Arthaud, F., Ogier, M. & Seguret, M. *Bull. BRGM* 1.3., 175–193 (1980–1981).
28. Bellaiche, G. *et al. Mar. Geol.* **16,** 47–56 (1974).
29. Bellaiche, G. *et al.* (Groupe Cyaligure) *Bull. Soc. géol. Fr.* **21,** 533–543 (1979).
30. Bourrouilh, R. thesis, Univ. Paris VI (1974).
31. Colom, G. *Rev. R. Acad. Cienc. Ex. Fis. nat. Madrid* **70,** 353–408 (1976).
32. Pomar, L. & Colom, G. *Bol. Soc. Hist. Nat. Baleares* **22,** 119–136 (1977).
33. Deriu, M. *Mem. Soc. Geol. It.* **3,** 675–706 (1962).
34. Maccioni, L. in *Paleogeografia del Terziario sardo nell'ambito dell Mediterraneo occidentale* (ed. Cherchi, A.) 277–282 (1974).
35. Coulon, C. thesis, Univ. Marseille III (1977).
36. Montigny, R., Edel, J. B. & Thuizat, R. *Earth planet. Sci. Lett.* **54,** 261–271 (1981).
37. Rehaut, J. P. thesis, Univ. Paris VI (1981).
38. Vail, P. R. & Hardenbohl, J. *Oceanus* **22,** 71–79 (1979).

High rock stresses as a consequence of glaciation

Anders Carlsson

Swedish State Power Board, S-162 87 Vällingby, Sweden

Tommy Olsson

K-Konsult, S-117 80 Stockholm, Sweden

Knowledge of the stress field in the Earth's crust is crucial for the understanding of processes such as faulting and fracturing. It is also of fundamental importance for the design and construction of underground structures. The two most common methods used for *in situ* stress determinations for engineering geology purposes are (1) the stress relief method, in which the differences in strain resulting from induced stress relaxation are studied, and (2) the hydraulic fracturing method, in which one of the presumed principal stresses is replaced by a hydraulic pressure. Of these, the stress relief method is more applicable to design and construction problems as it enables the three-dimensional stress tensor to be measured. The *in situ* rock stress measurements reported here were carried out in a 500-m deep borehole in Precambrian bedrocks in Sweden and show high stress levels throughout the rock mass. A comparison between the actual recorded stresses and the theoretical stress field from a 2,000 m-thick land ice may provide a possible explanation for the measured stress situation.

0028-0836/82/330739—04$01.00

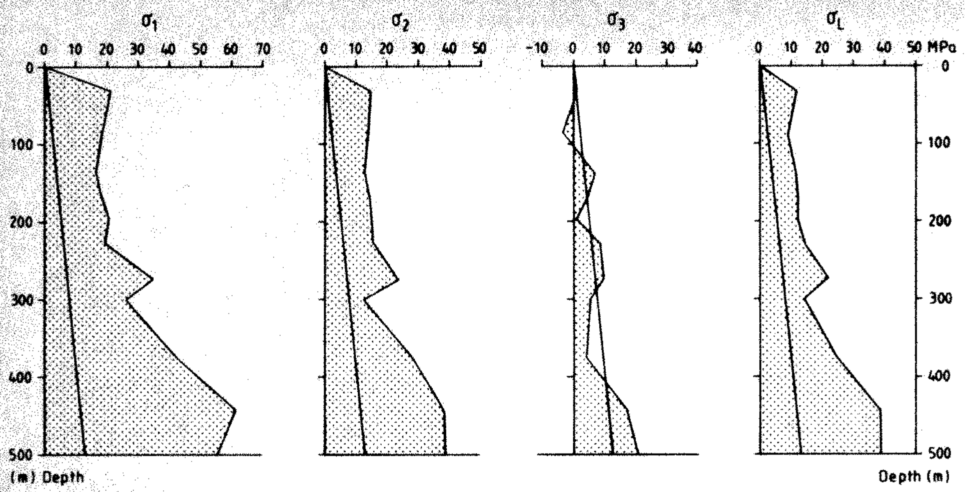

Fig. 1 Principal stresses (σ_1, σ_2 and σ_3) versus depth obtained in borehole DBT1. σ_1 and σ_2 are both nearly horizontal and σ_3 is nearly vertical. The stress level (σ_L), defined as the mean value of the principal stresses, is also shown. The straight lines represent the lithostatic stresses given by the weight of the overburden.

The only one stress relief device that we know of that is suitable for measurements in deep, water-filled boreholes has been developed at the Swedish State Power Board[1]. It is based on Leeman's three-dimensional theories and has been used in Sweden during the past 5 years where recordings have been taken at different locations in virgin parts of the Swedish bedrock.

Measurements have been made in several boreholes drilled from the ground surface, with readings taken at certain intervals down the hole. In the Forsmark area in southern, central Sweden, 30 successful measurements, concentrated to 11 levels, were taken during drilling of a 503 m-deep borehole (borehole DBT1). Another five boreholes have been studied in this area, but with fewer measurements and at shallower depths.

The magnitudes of the principal stresses at each of the 11 levels are shown in Fig. 1 as well as the stress level, defined as the mean value of the principal stresses. Figure 2 indicates the distribution of the orientation of the principal stresses. As may be seen, the stresses are generally high, compared with the weight of the overburden given by the straight line in Fig. 1. The maximum principal stress is ~70 MPa and acts in a plane near the horizontal. The dominating direction of the maximum principal stress (σ_1) is roughly WNW–ESE in the uppermost 300 m, below which level it shifts to a more NW–SE direction. This is indicated by the clockwise arrow in Fig. 2. The dip is approximately horizontal. The smallest of the principal stresses (σ_3) is approximately vertical, acting in a direction that dips steeply to the south. Note that there is a marked increase in the magnitude of stresses below 300 m, which coincides with the observed shift in direction.

The geology of Sweden is characterized by a basement of crystalline rocks of Svecocarelian age (1,500 Myr), which is covered by a thin layer of Quaternary deposits, mainly till. Sweden is located on the western edge of the Eurasian Precambrian shield, bounded to the west by the Caledonian Mountain Range, which forms the border between Norway and Sweden. In large areas, such as Forsmark, the crystalline basement has been eroded down to a peneplain of Precambrian age.

The bedrock at Forsmark is composed chiefly of gneiss granites, mica gneiss and mica schists. The rock stress measurements were performed in the gneiss granitic part of the area.

As shown in Fig. 1, the principal stresses found are of a higher magnitude than would be expected if the stress field were governed by the weight of the overburden alone. This is

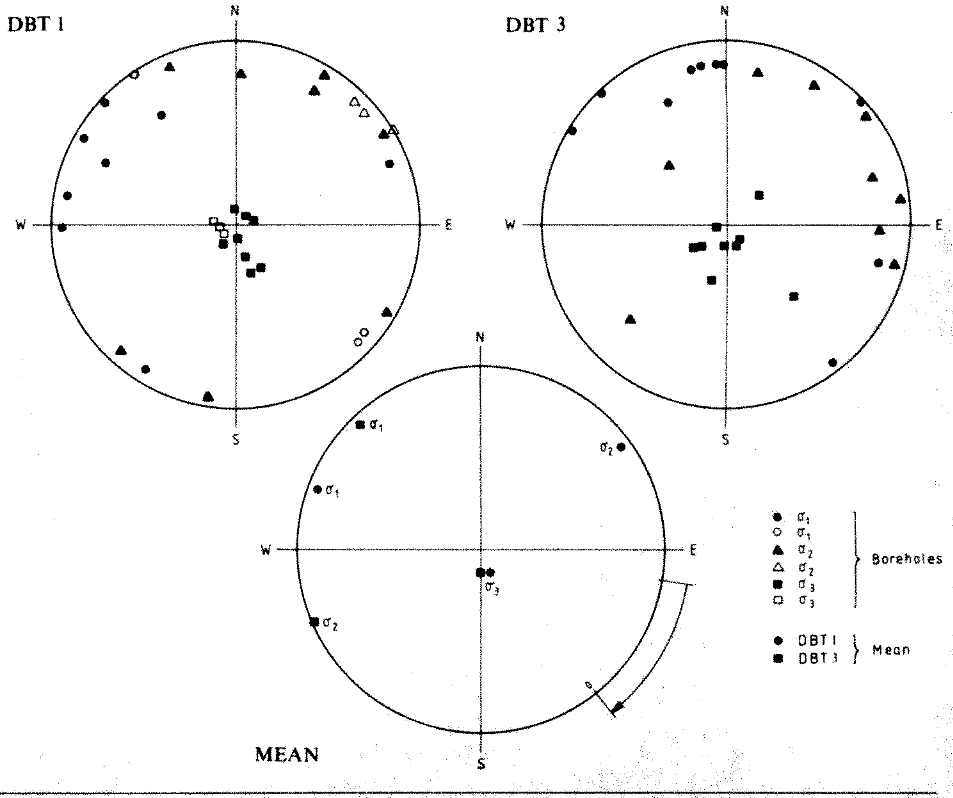

Fig. 2 Orientation of the individual principal stresses and mean values for the boreholes DBT1 and DBT3. The orientations are given as equal-area plots of the intersection of the principal axes with the lower hemisphere. The clockwise shift indicated by the arrow in the lower figure denotes a shift in direction at the passage of the fracture zone at 320 m. Filled and open symbols in DBT1 represent recordings taken above and below the 320-m depth, respectively.

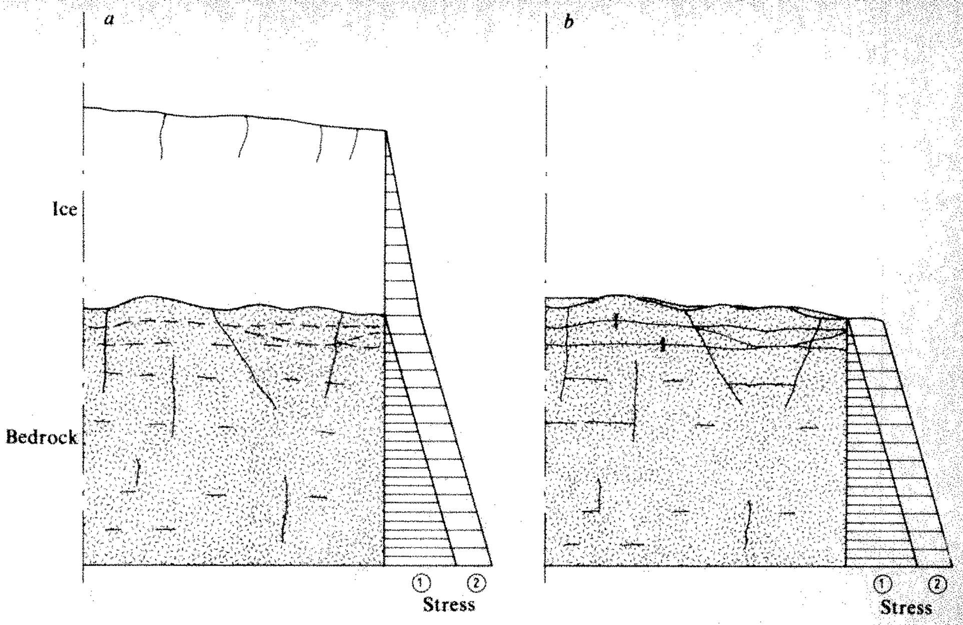

Fig. 3 Hypothetical influence of glaciation. The stress level: *a*, during glaciation; *b*, after deglaciation. Stresses 1 and 2 denote the gravitional stresses due to bedrock and ice respectively.

the case for all principal stresses including the nearly vertical one (σ_3). For the vertical component, the correspondence between the measured stress and the lithostatic is fairly good in the uppermost 300 m, but below this depth, the vertical component is much higher than the theoretically expected value. It is therefore not possible to explain the high stresses which actually exist as gravitional stresses; they must be of some other origin.

A high stress level in the bedrock may be due to many factors. An explanation frequently proposed is that denudation of the rock surface has occurred and this has decreased the weight of the overburden significantly. The lateral stress field created by the earlier formation should then remain, as long as the strength of the rock is not exceeded (allowing for an elastic adjustment of lateral stresses due to vertical stress decrease).

Voight[2] and others have chosen this theory to explain anomalous stress situations. This theory may be applicable to many areas, but not to Forsmark. Here the major denudation occurred in the Precambrian and it is not reasonable to believe that the present stress situation should have its origin back in this age.

Jamison and Cook[3] have analysed many rock stress measurements, and concluded that stresses may be influenced by the frictional resistance to sliding between individual blocks. This explanation is suitable for the stress situation obtained, but it does not provide any information on the origin of the stresses in the Forsmark area, sited as it is on the Precambrian peneplain, on a stable shield of old, crystalline rocks. Other explanations must be sought for the measured magnitude of the stress field at Forsmark. Comparing the results observed with theoretical stresses that could be expected to prevail during a glaciation, it is possible to give a theory for the state of stress in the Forsmark area. Deglaciation is a very rapid process (in the geological time scale) which may be compared with a very rapid denudation, and thus accords with the Voight hypothesis.

At the glaciation maximum the surface of the underlying bedrock is exposed to a vertical stress determined by the weight of the ice cap. By adopting Voight's theories, it is seen that the ice also creates lateral horizontal stresses initially of the magnitude of one-quarter of the vertical stress. This is based on a Poisson's ratio of 0.2 for the rock mass at Forsmark (33 determinations in the range 0.17–0.23). The lateral stress will increase in time due to creep to a value higher than a quarter of, but lower than, the vertical stress. During deglaciation, the vertical stress falls elastically down to zero, while the horizontal stress only falls by one-quarter. Thus it is possible to assume

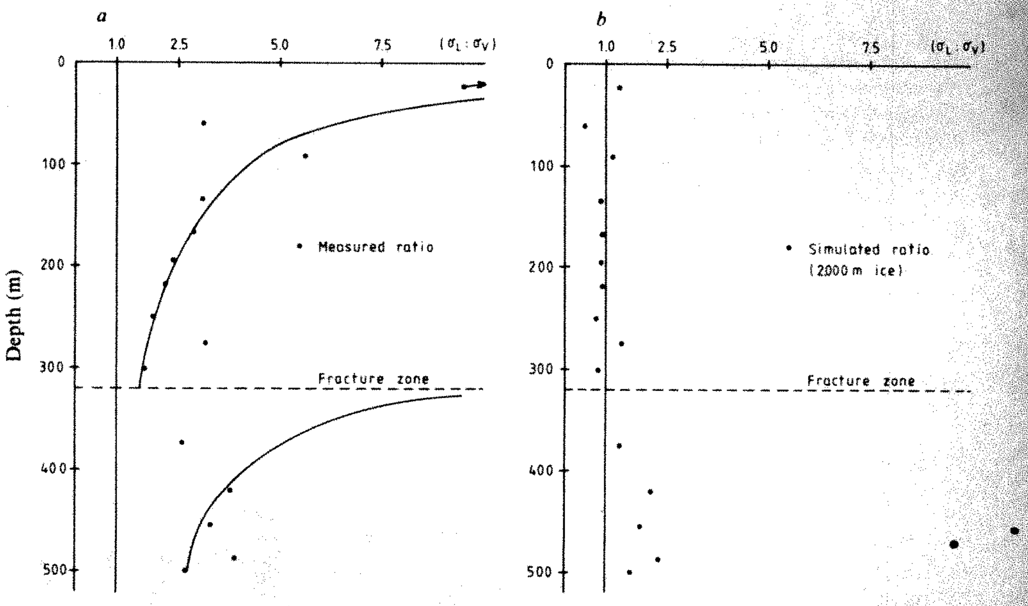

Fig. 4 The ratio between measured (σ_L) and theoretical (σ_V) stress level plotted against depth. *a*, The ratio between the recorded values and the theoretical as it is today. *b*, The ratio between the recorded values and a theoretical value given by the weight of a 2,000 m-thick ice and the weight of the rock mass.

that the glaciation could have created a stress situation as shown in Fig. 3.

To test this theory, the present results of stress measurements have been compared with theoretical effects of an assumed ice cap, 2,000 m thick. The result of the comparison is shown in Fig. 4, where Fig. 4*a* plots the ratio between the actual measured stress level (mean stress) and the theoretical lithostatic stress field (σ_L:σ_V ratio) against depth. This curve indicates that the discrepancy between the measured stress level and the theoretical level decreases with increasing depth. Simulating the pressure from a 2,000 m-thick ice cap gives a stress level of 20 MPa at the bedrock surface, in lithostatical conditions.

Using the sum of this ice-induced stress and a lithostatic stress level in the rock due to the weight of the overlying rock mass to give a new value for σ_V, it is possible to recalculate the σ_L: σ_V ratio, which includes the effects of a glaciation. Figure 4*b* shows that the theoretical, lithostatic stress level equals the measured one. Hence the present stress level, as measured at Forsmark, may be an effect of Quaternary glaciations, where the deglaciation resembles a rapid denudation.

However, the glaciation cannot be the sole cause of the high stresses recorded below a fracture zone at 320 m indicated in Fig. 4. Below this level readings of about 70 MPa for the maximum principal stress were taken. These high stresses could be explained as being stresses of palaeotectonic origin.

The effect of a glaciation on the stress field is discussed more completely in ref. 4.

Received 22 December 1981; accepted 9 June 1982.

1. Hiltscher, R., Martna, J. & Strindell, L. *Proc. 4th int. Congr. Rock Mech.* **2,** 227–234 (1979).
2. Voight, B. *Proc. 1st int. Congr. Rock Mech.* **2,** 45–50 (1966).
3. Jamison, O. B. & Cook, N. G. W. *J. geophys. Res.* **85,** B4, 1833–1838 (1980).
4. Carlsson, A. & Olsson, T. *Swedish State Power Board, Research and Development* Rep. 5:1 (1982).

Evidence for ^{13}C/^{12}C fractionation between tree leaves and wood

Steven W. Leavitt & Austin Long

Laboratory of Isotope Geochemistry, Department of Geosciences, University of Arizona, Tucson, Arizona 85721, USA

An isotopic fractionation step between carbon fixed in the leaves and that assimilated into wood cellulose has not previously been included in atmosphere–plant fractionation models. Data presented here, however, show that the magnitude of such a fractionation step may be significant. In an experiment which involved 10 juniper trees from around Arizona, cellulose of leaves was found to be isotopically lighter than that of the corresponding tree rings in all trees by an average of 2‰. In a second experiment, the δ^{13}C of leaf material from a juniper tree sampled at monthly intervals was compared with the δ^{13}C of the corresponding ring. For cellulose, δ^{13}C of the wood varied with changes in δ^{13}C of the leaves and was persistently isotopically heavier by 3–4‰. Furthermore, the observed change in δ^{13}C through the growing season suggests a temperature coefficient of about −0.27‰ °C^{-1}. The direction of this leaf–wood fractionation precludes diffusion processes as the primary cause.

For the most part, the carbon assimilated into woody tissue of trees is initially fixed from atmospheric carbon dioxide by chlorenchyma of the leaves. This process serves as the basis for using tree rings to decipher past changes in atmospheric radiocarbon production or dilution[1], and more recently to determine the role of the biosphere as a CO_2 source or sink from tree-ring δ^{13}C measurements[2]. The δ^{13}C fractionation between atmospheric CO_2 and C_3 plants, including most trees, is typically about −18‰, the greatest portion of which takes place at the enzyme fixation step. However, models which attempt to account for the atmosphere–plant fractionation either do not consider isotopic fractionation after glucose formation[3,4], or consider any fractionation during the formation of other compounds (including cellulose in tree rings) from photosynthesized sugars to be relatively slight or negligible[5,6,20].

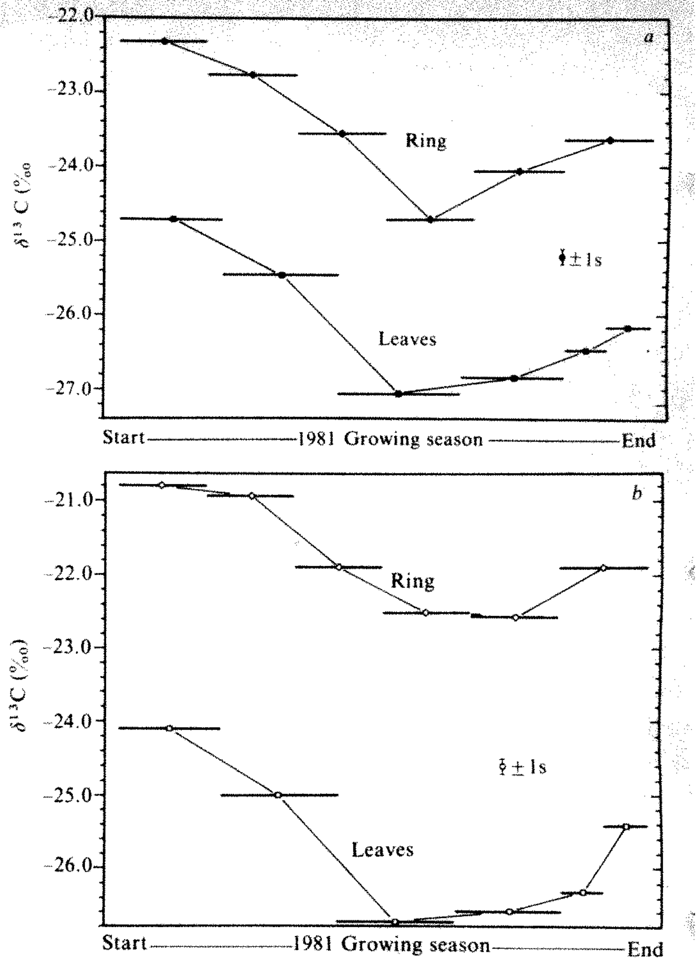

Fig. 1 *a*, Whole-tissue δ^{13}C analyses; *b*, cellulose δ^{13}C analyses of *J. monosperma* ring subdivisions and leaves from the 1981 growing season. Positions of leaf analyses in time have been scaled to their proportion of the total seasonal growth (Table 1).

Evidence, however, suggests isotopic selection during formation of individual organic compounds within plants. For example, a range of several per mil δ^{13}C among different organic constituents is well documented[7,8]. Analysis of whole tissue indicates that leaves are lighter than wood by 1–2‰[6,9,11], which implies isotopic differences between tissues also. Unfortunately, this evidence of leaf–wood δ^{13}C fractionation is inconclusive because of the possibility that such whole-tissue differences may simply reflect varied proportions of organic compounds, each of which has a different isotopic composition. Therefore, analyses of individual compounds such as cellulose are necessary to test more conclusively for this fractionation. So far, such information is scarce. One study (A. L. and J. C. Lerman, unpublished data) examined δ^{13}C of cellulose from leaves and wood of several bristlecone pine individuals and found in most cases that the leaf cellulose was isotopically lighter. Unfortunately, although the leaves were compared with wood of the same sites and of the same age, the leaves and wood were not from the same individual trees.

We conducted two experiments which provide insight into the nature of fractionation between leaves and wood. At the end of the 1979 growing season we sampled juniper trees in Arizona growing at elevations ranging from 1,200 to 2,300 m. Leaf samples were pooled from the four cardinal directions and

0028–0836/82/330742—03$01.00

Table 1 $\delta^{13}C$ values of cellulose from leaves and wood of Arizona juniper trees harvested after 1979 growing season

Site	Species	Elevation (m)	$\bar{\delta}^{\text{wood}}$ (1970–79) (‰)	$\bar{\delta}^{\text{leaves}}$ (‰)	$\Delta\delta^{\text{wood-leaves}}$ (‰)
Globe	*Juniperus monosperma*	1,195	−19.3	−21.6	+2.3
Jerome	*J. monosperma*	1,845	−21.6	−22.8	+1.2
Oracle	*J. deppeana*	1,450	−18.9	−22.4	+3.5
Prescott	*J. deppeana*	1,705	−20.8	−22.2	+1.4
St Johns	*J. monosperma*	1,790	−20.4	−21.7	+1.3
Santa Rita	*J. deppeana*	1,370	−20.8	−22.3	+1.5
Seligman	*J. osteosperma*	1,605	−21.0	−23.0	+2.0
Snowflake	*J. monosperma*	1,735	−20.0	−22.8	+2.8
Springerville	*J. monosperma*	2,315	−20.9	−22.9	+2.0
Williams	*J. osteosperma*	2,055	−20.3	−22.8	+2.5

$\bar{x} = +2.0$; $s = 0.7$.

Table 2 Leaf sampling schedule for the *J. monosperma* individual

Harvest date	No. of leaves sampled	Mean net growth (mm)	s.d. (mm)
6 May 1981	28	5.1	1.8
7 June 1981	34	5.6	2.2
9 July 1981	43	6.1	3.1
6 August 1981	37	5.1	2.0
7 September 1981	43	2.1	1.1
4 October 1981	35	2.0	1.2

a section of wood was taken from the base of the tree. Because junipers retain ~10 yr of leaves at any time[12], the rings representing 1970–79, taken about their full circumference, were collected for comparison. Cellulose from the leaf and wood samples was isolated using an acidified sodium chlorite solution in a procedure modified after Green[13]. After combustion of the samples to CO_2, carbon isotopic analyses were performed with a Micromass 602C mass spectrometer. The results reported in Table 1 are expressed in the standard δ notation with respect to the PDB standard[14], with the reproducibility of combustion and analysis estimated to be ±0.1‰. The $\delta^{13}C$ of cellulose in leaves in all cases was lower than the corresponding wood by an average of 2.0±0.7‰.

In the second experiment, we harvested leaf material at approximately monthly intervals over the 1981 growing season from a juniper tree (*Juniperus monosperma*) in the grounds of the University of Arizona. Marking of leaf tips along one major branch at the beginning of the intervals ensured that only the growth for that particular interval would be harvested. Furthermore, marking a large number of tips allowed some to be harvested while others could be remarked for harvesting later. Additional leaf tips, not previously marked, were also marked at the beginning of new intervals. These precautions minimized the effects that the cutting may have had on growth and provided a large pool of leaf tips for cutting at the end of each interval.

Table 2 summarizes the harvesting schedule and average amount of growth for only those tips which were harvested. The average growth values for the 6 August–7 September and the 7 September–4 October periods are higher than the actual growth of all tips during those two intervals because ~20% and 50%, respectively, of the tips marked at the beginning of each of these intervals did not grow at all and were not included in the averages. Finally, on 4 October, several tree-ring cores were taken from the trunk and branch. The 1981 ring from one core was divided into six approximately equal sections and cellulose was isolated from splits of these ring subdivisions and from the leaf samples.

Results of carbon isotopic analysis of the whole-tissue and the cellulose component of these samples are shown in Fig. 1. Strictly speaking, direct comparison of the wood and leaves is difficult because the time period represented by each of the wood subdivisions is unknown. However, as a first approximation we have plotted the wood analysis as equal lengths in time and then scaled the position of each leaf analysis to its proportion of the overall seasonal leaf growth. The major result is that leaves are persistently lighter than wood for both whole-tissue and cellulose by ~2.5 and 3.5‰, respectively, although leaf whole-tissue and cellulose values are quite similar. A pattern of decreasing $\delta^{13}C$ is evident in the spring and early summer followed by increasing values for the remainder of the sampling periods. The magnitude of the $\delta^{13}C$ decrease cannot be explained by the seasonal variation of $\delta^{13}C$ of atmospheric CO_2 which only changes ~0.4‰ in this region[15]. Moisture may be considered non-limiting because this tree is well irrigated, however, allowing us to calculate a significant temperature response of −0.27‰ $\delta^{13}C$ °C^{-1} ($r^2 = 0.86$). This coefficient results from regression of the April to September mean monthly temperatures for 1981 (9.7, 13.6, 18.9, 22.7, 20.2 and 20.4 °C, respectively) with their associated leaf cellulose $\delta^{13}C$ results (−24.1, −25.0, −26.7, −26.6, −26.2 and −25.4‰, respectively). This coefficient is opposite in sign to that calculated in an intra-annual study of *Pinus radiata* tree rings from New Zealand[16]. However, it is similar in sign and magnitude to temperature coefficients from several *in vitro* studies with the carbon-fixing enzyme RuBP-C[17,18].

If we infer similar leaf–wood isotopic differences for other species and locations, these results indicate that detailed models for atmosphere-to-plant carbon isotopic fractionation will need to include an additional fractionation step of +2‰ or more between the leaves and wood. This fractionation probably cannot be explained by diffusive processes because of the large molecular weight of glucose and because diffusion away from the leaves would tend to enrich them in ^{13}C, just the opposite of these results. If some type of ^{12}C preference operates during assimilation, similar to the preference for ^{12}C in carbon fixation, then this may be manifested in a $\delta^{13}C$ change in cellulose away from the photosynthate source. We had hoped to test this explanation of an isotopic gradient from leaves to wood with the other cores, but unfortunately they did not display a clear ring pattern with which to distinguish the 1981 growth-ring boundaries. One previous study[19] of longitudinal variation of $\delta^{13}C$ in *Quercus rubra* found a fairly constant $\delta^{13}C$ in a ring when measured over the relatively short distance of 40 cm.

Received 5 March; accepted 17 May 1982.

1. Damon, P. E., Lerman, J. C. & Long, A. *A. Rev. Earth planet. Sci.* **6,** 457–494 (1978).
2. Stuiver, M. *Science* **199,** 253–258 (1978).
3. Troughton, J. H. in *Proc. 8th int. Conf. Radiocarbon Dating*, E39–E57 (Royal Society of New Zealand, Wellington, 1972).
4. Grinsted, M. J. thesis, Univ. Waikato (1977).
5. Park, R. & Epstein, S. *Geochim. cosmochim. Acta* **21,** 110–126 (1960).
6. Francey, R. J. in *Carbon Dioxide and Climate: Australian Research* (ed. Pearman, G. I.) 95–104 (Australian Academy of Science, Canberra, 1980).
7. Park, R. & Epstein, S. *Pl. Physiol.* **36,** 133–138 (1961).
8. Degens, E. T., Guillard, R. R. L., Sackett, W. M. & Helleburst, J. A. *Deep-Sea Res.* **15,** 1–9 (1968).
9. Craig, H. *Geochim. cosmochim. Acta* **3,** 53–92 (1953).
10. Lerman, J. C. in *Proc. 8th int. Conf. Radiocarbon Dating*, H16–H28 (Royal Society of New Zealand, Wellington, 1972).
11. Stout, J. D. & Rafter, T. A. *DSIR Bull.* **220,** 75–83 (1978).
12. Arnold, L. D. thesis, Univ. Arizona (1979).
13. Green, J. W. in *Methods of Carbohydrate Chemistry III* (ed. Whistler, R. L.) 9–21 (Academic, New York, 1963).

14. Craig, H. *Geochim. cosmochim. Acta* **12,** 133–149 (1957).
15. Keeling, C. D. *Geochim. cosmochim. Acta* **24,** 277–298 (1961).
16. Wilson, A. T. & Grinsted, M. J. *Nature* **265,** 133–135 (1977).
17. Christeller, J. T., Laing, W. A. & Troughton, J. H. *Pl. Physiol.* **52,** 580–582 (1976).
18. Estep, M. F., Tabita, F. R., Parker, P. L. & Van Baalen, C. *Pl. Physiol.* **61,** 680–687 (1978).
19. Tans, P. P. & Mook, W. G. *Tellus* **32,** 268–283 (1980).
20. Francey, R. J. & Farquhar, G. D. *Nature* **297,** 28–31 (1982).

Oxic diagenetic products as indicators of past oceanic algal populations and diversity

F. T. Gillan* & R. B. Johns

Department of Organic Chemistry, University of Melbourne,
Parkville, Victoria 3052, Australia

Marine sediments contain a great diversity of organic molecules which have originated *in situ* and from planktonic organisms. The establishment of a direct relationship between possible 'chemical markers' and source organisms would enable studies of biomass-turnover time to be undertaken, using dated sediment cores as temporal records. Studies of the influence of long-term environmental variations on the abundance of planktonic flora and fauna are potentially amenable to this approach. Chemical compounds biosynthesized by organisms in the water column are, however, subjected to microbial attack, oxidation and other degradative processes before, and indeed after, sedimentary incorporation[1]. We show here that changes in the sedimentary abundances and distribution of selected chemical moieties produced by oxidative degradation of fatty acids of planktonic origin, can provide evidence for a change in algal abundance and distribution in the overlying oceanic waters.

As part of a continuing study[2] of the geochemistry of Patton escarpment sediments (32°34′.4 N, 120°28′.0 W; depth: 3,800 m), a sediment core has been analysed in detail. Four samples (1), 0–5 cm; (2), 12.5–17.5 cm; (3), 27.5–32.5 cm; (4), 42.5–47.5 cm) from the core were solvent-extracted and the residues from the extraction were saponified. Selected lipid classes from the bound acidic fraction were examined (after derivatization as the methyl esters, trimethylsilyl ethers) by capillary GC on a SCOT SE30 column, and by GC/MS (HP 5995A GC/MS with fused silica SE30 WCOT capillary column). α,ω-Dicarboxylic acids ('diacids') were readily identifiable by their characteristic mass spectra[3]. A group of compounds with a strong m/z 175 in their mass spectra, which did not co-elute with β-hydroxy acids was also observed. These compounds were not observed unless the methyl esters were trimethylsilylated. The mass spectrum of the major component was m/z (I):73(100); 75(62); 89(77); 133(54); 159(31); 175(45); 261(96) and 292(58). The ions: m/z 73, 75, 89, 133, 159 and 175 are indicative of a β-trimethylsilyl ether-methyl ester, while the intense M-31 fragmentation suggests an α,ω-dimethoxyl function in the molecule. The m/z 75 : m/z 73 ratio is higher than we have observed with typical β-hydroxy acid derivatives and probably indicates some contribution to m/z 75 from the characteristic m/z 75 fragmentation of a dimethyl acetal[4]. The most probable structure for this compound is the dimethyl acetal, trimethylsilyl ether, methyl ester derivative of β-hydroxy-ω-oxo-heptanoic acid: such compounds have not previously been reported in sediments. No authentic sample of a compound of this type was available for mass spectral comparison.

Table 1 lists the abundances of bound diacids in the four sediment samples examined. Note that the bound diacid abundance is much greater than that of any other lipid fraction we have determined (for example, solvent-extractable monocarboxylic acids: 6.5 p.p.m., hydrocarbons (aliphatic): 1.3 p.p.m.)[2]. The main component in each sample is the C_9 diacid (9:0), which constitutes ~70% of the total observed diacids; 7:0, 8:0, 10:0 and 11:0 diacids are also major components. The longer chain-length ($>C_{11}$) diacids constitute only a small percentage of the total diacid abundance (~3%). In contrast, in an anaerobic deep-sea sediment from the Santa Catalina Basin, bound 9:0 diacid is a minor constituent (<2% of the diacids) (our unpublished results). This indicates that the short-chain diacids probably originate by oxidation of lipids input to the oxic sediment. The high abundance of the C_9 diacid precludes a major contribution from, for example, higher plant sources. The production of similar diacid distributions to those observed here, in oxidations of algal kerogens[5], supports the probable origin of the short-chain diacids by oxidative degradation of suitable organic substrates present in the lipid mixture deposited in these sediments. $\Delta 9$ monoenoic, monocarboxylic acids are major components of the lipids of marine sediments, 16:1$\Delta 9$ being the most abundant monoenoic acid in many sediments we have studied[6]. Oxidation of this acid could lead to a variety of products (see Table 2). Direct cleavage at the double bond would produce only the C_9 diacid, while hydration followed by oxidative cleavage either side of the hydroxyl would lead to a mixture of C_8, C_9 and C_{10} diacids. ω-Oxidation (to Di-16:1$\Delta 7$)

Table 1 Depth profiles of bound dicarboxylic acids in the Patton escarpment sediments

Diacid	Abundance (p.p.m. wet wt)†			
	(1)	(2)	(3)	(4)
7:0*	0.73	1.86	3.3	2.4
8:0	1.40	1.28	2.5	1.60
9:0	10.9	11.4	13.5	10.9
10:0	0.45	0.42	0.75	0.65
11:0	0.42	0.55	1.19	0.94
12:0	0.043	0.058	0.128	0.099
13:0	0.015	0.041	0.066	0.032
14:0	0.014	0.027	0.052	0.017
15:0	0.033	0.035	0.059	0.020
16:0	0.025	0.031	0.049	0.017
16:1	0.016	0.010	0.007	0.001
17:0	0.014	0.023	0.037	0.018
18:0	0.016	0.023	0.050	0.027
18:1	0.017	0.002	0.001	0.001
19:0	0.023	0.022	0.052	0.029
20:0	0.025	0.021	0.064	0.031
21:0	0.019	0.017	0.050	0.026
22:0	0.013	0.016	0.035	0.022
23:0	0.017	0.016	0.034	0.024
24:0	0.014	0.018	0.038	0.027
25:0	0.012	0.013	0.029	0.025
26:0	0.005	0.013	0.024	0.022
27:0	0.001	0.011	0.014	0.016
Σ	14.2	15.9	22.1	16.9

* Diacids are denoted by $M:N$, where M is the number of carbon atoms and N the number of double bonds.

† All sediments 68 ± 2% moisture.

Table 2 Expected diacid products from oxic diagenesis of palmitoleic acid (16:1 $\Delta 9$)

Process	Diacid products*				
	6:0	7:0	8:0	9:0	10:0
Direct cleavage	0	0	0	1	0
Hydration then cleavage*	0	0	1	2	1
ω-Oxidation then cleavage	0	1	0	1	0
ω-Oxidation, hydration then cleavage	1	1	2	1	1

* These product ratios assume that hydration will produce equal amounts of the 9-OH and 10-OH products and cleavage of a hydroxy-acid will occur equally on either side of the hydroxyl-carbon atom (for example, for 9-OH 16:0 FA, C_9/C_{10} and C_8/C_9 cleavages are equally probable).

---

* Present address: Australian Institute of Marine Science, Townsville MSO, 4810, Queensland, Australia.

0028–0836/82/330744—03$01.00

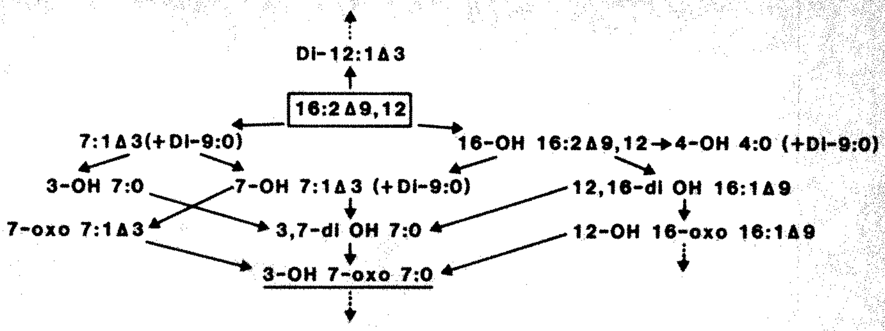

Fig. 1 Oxic diagenesis of a common, diatom-derived dienoic acid.

before oxidative cleavage is also possible. The observed diacid distribution indicates that direct cleavage is the predominant process, and the much higher abundance of C_8 diacid relative to the C_{10} diacid supports some contribution from the ω-oxidation, hydroxylation and then cleavage pathway (the alternate pathway:hydration then cleavage would result in a ~1:1 C_8:C_{10} ratio). The other major diacid, Di-11:0, will probably result from oxidation of $\Delta11$ monoenoic acids. These acids are the second most abundant group of monoenoic acids in marine sediments[6]. Oxidation of the $\Delta11$ acids would result in the production of a small quantity of Di-12:0. This proposed interrelationship of C_{11} and C_{12} diacids is supported by the high correlation of these data ($R^2 = 0.9996$). Whilst ω-oxidation is a known microbial process, microbial degradation of fatty acids generally proceeds through a series of both β-oxidations and ω-oxidations[7]. Reactions such as this would not lead to the observed diacid distribution. No evidence for a microbially-mediated direct cleavage or hydration/cleavage process has been reported: the major degradative pathway is probably abiological. The observed diacid distribution is thus consistent with an input to the sediment of $\Delta9$ (probably $16:1\Delta9$ and $18:1\Delta9$) and $\Delta11$ (probably $18:1\Delta11$) monocarboxylic acids, and subsequent oxidation.

As indicated above, the monoenoic acid distributions of intertidal marine sediments are dominated by $16:1\Delta9$, $18:1\Delta9$ and $18:1\Delta11$ (ref. 6). These acids are believed to originate from *in situ* algae. In the Patton escarpment sediment there is no chemical evidence for the presence of *in situ* algae (algal carotenoids are not detectable[2]), however, particulates derived from planktonic algae are expected to contribute to the lipids of the sediments. The presence of typical algal sterols in these sediments[2], in particular, supports the proposed contribution to the sedimenta y organic matter from algal debris.

The long-chain diacids detected in these sediments exhibit fairly smooth distribution envelopes with Carbon Preference Indices (CPI) near unity. If these acids were derived from a higher plant input the CPI would be expected to be large (>3) (ref. 8). Rather, these acids are probably diagenetic products possibly produced by microbial di-terminal oxidation of alkanes or ω-oxidation of long-chain fatty acids, and subsequent α- and β-oxidations. The traces of monounsaturated diacids detected could originate by ω-oxidation of the corresponding monocarboxylic acid, or may indicate a contribution to the sedimentary lipids from higher plant suberins[8].

The abundances of the β-hydroxy ω-oxo acids are listed in Table 3. By analogy with the mode of formation of the major diacids (Table 2), one can envisage a series of double bond cleavages, terminal oxidations and hydrations that would lead to such acids from a dienoic acid starting material (see Fig. 1). Note that these polyfunctional acids would be intermediates in the overall degradative pathway: it is expected that they would not be very abundant, as observed. The major acid of this class, C_7, could originate from $16:2$ $\Delta9$, 12 monocarboxylic acid, whilst the second most abundant component, C_9, would be derived from dienoic acids such as $18:2$ $\Delta9,12$ or $16:2$ $\Delta7$, 10. The major monoenoic and dienoic acids present in planktonic algae are algal class dependent. A change in the abundances of the different algal classes contributing to a sediment would result in a concomitant change in the input of unsaturated fatty acids, and thus in the abundances in the sediments of their diagenetic products.

Diatoms biosynthesize large amounts of $16:1$ $\Delta9$ and $16:2$ $\Delta9$, 12 compared with most other algae[9], and would thus be expected to be major contributors to the abundances of the C_9

Table 3 β-Hydroxy ω-oxo acids in the Patton escarpment sediments

Acid	Abundance (parts per 10^9 wet wt) (1)	(2)	(3)	(4)
6:0	3	4	9	6
7:0	60	59	114	110
8:0	12	9	18	11
9:0	19	23	54	38
10:0	10	10	31	17
11:0	5	8	27	14
12:0	4	8	29	16
13:0	3	4	10	5
14:0	2	2	6	4
15:0	1	2	4	3
16:0	1	2	6	3
17:0	3	3	18	5
18:0	4	5	21	10
19:0	3	6	31	15
20:0	2	3	18	8
21:0	1	1	7	4
22:0	—	1	4	3
23:0	—	1	4	3
Σ	133	151	411	275

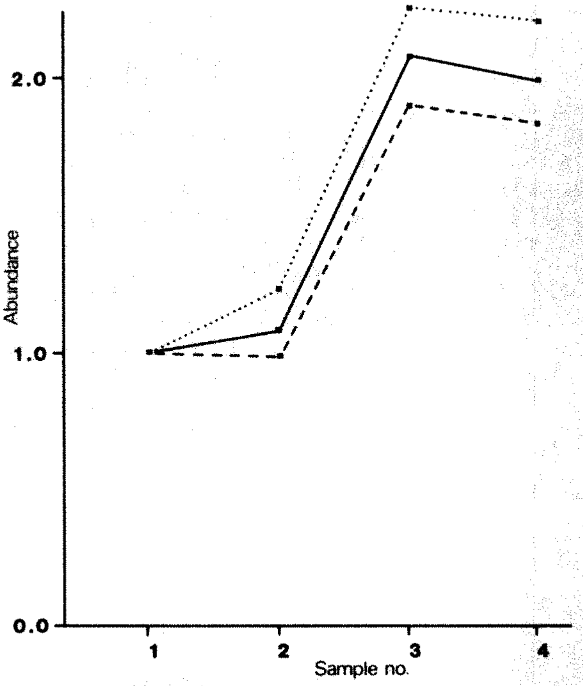

Fig. 2 Diacid ratios (C_{11}/C_9) and abundances of C_7 β-hydroxy-ω-oxo acid and 24-methylcholesta-5,22-dien-3β-ol (all data normalized to 1.00 for sample (1)). · · ·, Diacid; – – –, hydroxy acid; ——, sterol.

diacid and the C_7 β-hydroxy ω-oxo acid found in these sediments. In contrast, coccolithophores produce virtually no dienoic acids that would lead to the formation of the C_7 polyfunctional compound[10]: only C_9 precursors are present in these algae. The $\Delta 11:\Delta 9$ monoenoic acid ratios for the few algae of this class that have been analysed in detail also differ from those of diatoms. Similarly, certain green algae have been observed[11] to biosynthesize some $18:1\ \Delta 11$. Changes in the chain-length distributions of the diagenetically-derived acids could thus be indicative of changes in the algal populations contributing to the sedimentary lipids. 24-Methylcholesta-5,22-dien-3β-ol is a common major sterol in coccolithoptores[10] although it also is found in diatoms[13]. A change in the diatom and/or coccolithophore abundance or distribution should result in a change in the abundance of this sterol.

The dicarboxylic acids (Table 1) exhibit a marked change in the $C_{11}:C_9$ ratio between samples (2) and (3) (ratios: (1):(2):(3):(4):0.039:0.048:0.088:0.086) due mainly to a large increase in the C_{11} diacid abundance. The abundance of β-hydroxy ω-oxo 7:0 similarly changes abruptly between samples (2) and (3). Figure 2 shows a plot of these data together with the abundance of 'bound' 24-methylcholesta-5,22-dien-3β-ol. The high correlation of the data (diacid:hydroxy-oxo-acid $R^2=0.973$; diacid:sterol $R^2=0.996$; hydroxy-oxo-acid:sterol $R^2=0.991$) supports the proposed algal origin for the acids and indicates a probable change in the algal abundance and/or distribution between deposition of samples (3) and (2). The sedimentation rate for these sediments has not been determined, though a rate in the range 0.5–2.0 cm kyr^{-1} could be expected for this near-shore environment[12]. It is tempting to speculate that it may be of the order of 1.5 cm kyr^{-1}: samples (3) and (4) would then have been deposited during the last ice age, at a time when the algal abundance and distribution would surely have differed from that at present.

We thank Dr A. Yayanos for the sediment core and Dr R. Esdaile and CSIRO Division of Materials Science for access to the HP 5995A GC/MS. F.T.G. acknowledges financial assistance from a CPG Research Award. We thank the secretarial staff at the Australian Institute of Marine Science for their assistance.

Received 8 April; accepted 29 June 1982.

1. Didyk, B. M., Simoneit, B. R. T., Brassell, S. C. & Eglinton, G. *Nature* **272,** 216–222 (1978).
2. Gillan, F. T., Johns, R. B. & Volkman, J. K. *Geochim. cosmochim. Acta* (submitted).
3. Ryhage, R. & Stenhagen, E. *Arkiv. Kemi* **14,** 483–496 (1959).
4. Beynon, J. K., Saunders, R. A. & Williams, A. E. *The Mass Spectra of Organic Molecules* (Elsevier, Amsterdam, 1968).
5. Philp, R. P. *Nature* **262,** 134–136 (1976).
6. Gillan, F. T. *et al.* in *Advances in Organic Geochemistry 1981* (in the press).
7. Doelle, H. W. *Bacterial Metabolism* 2nd edn (Academic, New York, 1975).
8. Kolattukudy, P. E., Croteau, R. & Buckner, J. S. in *Chemistry and Biochemistry of Natural Waxes* (ed. Kolattukudy, P. E.) 289–347 (Elsevier, Amsterdam, 1976).
9. Chuecas, L. & Riley, J. P. *J. mar. biol. Ass. U.K.* **49,** 97–116 (1969).
10. Volkman, J. K., Smith, D. J., Eglinton, G., Forsberg, T. E. V. & Corner, E. D. S. *J. mar. biol. Ass. U.K.* **61,** 509–527 (1981).
11. Johns, R. B., Nichols, P. D. & Perry, G. J. *Phytochemistry* **18,** 799–802 (1979).
12. Bostrom, K., Kraemer, T. & Gartner, S. *Chem. Geol.* **11,** 123–148 (1973).
13. Volkman, J. K., Gillan, F. T., Johns, R. B. & Eglinton, G. *Geochim. cosmochim. Acta* **45,** 1817–1828 (1981).

Age of the Lufeng, China, hominoid locality

Lawrence J. Flynn

Department of Geosciences, University of Arizona, Tucson,
Arizona 85721, USA

Qi Guo-qin

Institute of Vertebrate Paleontology and Paleoanthropology,
Academia Sinica, PO Box 643, Beijing (27),
People's Republic of China

Recently discovered hominoids from a locality near Lufeng, China, are crucial to the understanding of the biogeographical distribution and the pattern of evolution of all later Miocene hominoids. However, the significance of these finds is difficult to assess fully without knowing their age accurately. The Lufeng fauna is diverse and includes several species of the rodent family Rhizomyidae. Rhizomyid evolution is well documented in the Siwalik deposits of Pakistan and provides the most precise method available at present for dating the Lufeng fauna. Based on co-occurrence of *Brachyrhizomys nagrii*, *Brachyrhizomys tetracharax* and cf. *Brachyrhizomys pilgrimi*, we conclude that hominoids inhabited southern China and Pakistan at about the same time, 8 Myr ago.

The success of expeditions in Pakistan[1] and Europe[2] in recovering late Miocene hominoids has stimulated fossil hunting in terrestrial deposits throughout southern Asia. Chinese scientists have recovered remarkably complete fossils from a site near Lufeng, Yunnan. Diverse rodents are frequently associated with hominoid remains and contribute to chronological correlation because evolution in some lineages was relatively rapid and is well documented. Fossil rhizomyids (bamboo rats of Asia and mole rats of Africa) are especially well represented in Pakistan[3] and occur at Lufeng.

The Lufeng fossil locality is near Shihuiba, a small village ~9 km north of Lufeng city (102°4′ E, 25°3′ N). Within a Cenozoic sequence of fluvial-lacustrine deposits, fossils are concentrated in ~3 m of lignite in a small area[4]. This fauna is diverse and includes abundant hominoid primates, numerous ungulates, and several carnivores and large rodents[4]. Unlike Siwalik faunas which span >10 Myr (Miocene–Pleistocene), the Lufeng fauna probably accumulated over a geologically short period of time. The Lufeng fauna resembles late Miocene faunal assemblages almost 3,300 km to the west in Pakistan, but differs from more northerly Chinese faunas[5]. Lufeng and the Pakistan sites apparently occupied the same general biogeographical province distinct from that of northern China in the late Miocene.

The Siwalik deposits of Pakistan are thousands of metres thick and vertebrates are widely distributed throughout the sequence. Palaeontological expeditions have recovered large collections of vertebrates, with documented stratigraphical provenance. Temporal calibration of Siwalik fossil horizons is based on palaeomagnetic reversal sequences and on several radiometric dates. Strata in the temporal interval from ~9 to 6.5 Myr are particularly well documented because the magnetic sequence includes many distinctive reversals, sedimentation was relatively continuous at this time, and magnetic properties of the sediment preserved the polarity sequence without ambiguity. Many palaeomagnetic sections through the 8-Myr

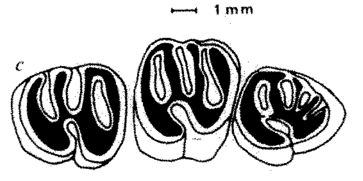

Fig. 1 Rhizomyid dentitions from Lufeng. *a*, *Brachyrhizomys nagrii*; *b* and *c*, *B. tetracharax*.

0028-0836/82/330746—02$01.00

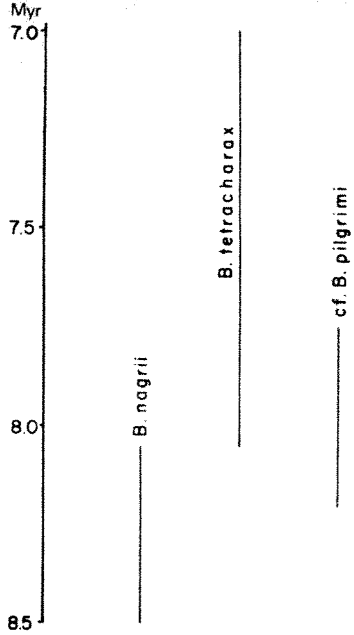

Fig. 2 Temporal ranges in Pakistan of three species of *Brachyrhizomys*.

hominoid level[6] offer exceptionally precise temporal control on Siwalik fossils in this interval.

Temporal ranges of rhizomyid species of the Siwaliks are well documented and evolutionary patterns of the family are clear[3]. The primitive genus *Kanisamys* appeared by 13 Myr and represents a long lineage of small rhizomyids that is not presently known from Lufeng. By 9.5 Myr *Brachyrhizomys* evolved, radiating after 8.5 Myr with as many as four large, burrowing contemporaneous species. After 7 Myr both genera became extinct locally, while three new genera appeared. By the Pleistocene, Rhizomyidae disappeared from Pakistan, but they persist in south-east Asia and in Africa. Today Asian rhizomyids occur throughout southern China, south to Sumatra. Most species have wide geographical ranges, for example *Rhizomys pruinosus* (south-east China, west to Assam), which certainly spans >3,000 km of territory.

The presence of at least three advanced species of *Brachyrhizomys* in the Lufeng fauna demonstrates that Lufeng vertebrates cannot be older than 8.5 Myr on the basis of Siwalik rhizomyid phylogeny. Lufeng *Brachyrhizomys* represent species that occur in the Siwaliks and are described below from casts of four specimens, each with three molars. The original material, collected by one of us (Q.G.) is in Beijing.

The smallest specimen (Fig. 1*a*) is a dentary referable to *B. nagrii*. Size (M_{1-3} length = 11.75 mm) agrees well with Siwalik specimens and M_3 is short (width = 90% of length), a derived character known only in *B. nagrii*. Furthermore, M_2 bears an elongated mesolophid, a primitive trait retained in this species.

Lower and upper dentitions (Fig. 1*b*, *c*) are referable to *B. tetracharax*. Although M_2 is moderately worn, the hypoconid has a weak anterior arm. Suppression of this connection is a derived trait of *B. tetracharax* and later rhizomyids. In addition, M_3 is elongated (width = 70% of length) and M_2 bears a rather long mesolophid, which are primitive characters retained in this species. Tooth row length is comparable to Siwalik *B. tetracharax* for both lower ($M_{1-3} = 14.88$) and upper ($M^{1-3} = 12.56$) dentitions. The upper row in Rhizomyidae is usually shorter than the lower. Aside from this, identification of this upper dentition is preliminary.

A fourth specimen is bigger than the others ($M_{1-3} = 15.6$) but smaller than the holotype of *B. pilgrimi*, the largest known species of *Brachyrhizomys*. Although the cast does not reveal diagnostic details of occlusal surfaces, this individual is closest to a population from Pakistan that has been provisionally named[3] *Brachyrhizomys* cf. *B. pilgrimi*.

Brachyrhizomys nagrii, *B. tetracharax*, and cf. *B. pilgrimi* have well known temporal ranges in Pakistan and coexisted for a short time at ~8 Myr (Fig. 2). Assuming that rhizomyid species ranged geographically about as far as they do now and had similar temporal ranges in southern China and Pakistan, this places the Lufeng hominoid fauna at ~8 Myr also. Further collecting at Lufeng will improve samples of fossil species and screenwashing will probably add smaller taxa to the faunal list that will help to refine this correlation.

It is probable that hominoids in Pakistan and southern China coexisted in the same broad biogeographical province at 8 Myr. Knowledge of temporal relations of samples of fossil hominoids is essential to reconstructing their pattern of evolution and palaeobiogeography and analysis of other faunal elements can elucidate the palaeoecological setting in which hominoids evolved. Continued synthesis of all available data will offer the fullest understanding attainable of human evolution in southern Asia.

We thank Drs E. H. Lindsay, D. R. Pilbeam and L. L. Jacobs for reviewing the manuscript, and Dr Li Chuan-Kuei for many valuable discussions. We are grateful for the cooperation of S. M. Ibrahim Shah (Geological Survey of Pakistan) and the Institute of Vertebrate Paleontology and Paleoanthropology. The work was partially supported by NSF grants BNS 772-5984 and DEB 7809539 and by SFCP grant FC80254100.

Received 29 March; accepted 28 June 1982.

1. Pilbeam, D. R., Rose, M. D., Badgley, C. & Lipschutz, B. *Postilla* **181**, 1–94 (1980).
2. Kretzoi, M. *Nature* **257**, 578–581 (1975).
3. Flynn, L. J. *Geobios* **15** (in the press).
4. Qi, G. *Vert. PalAsiatica* **14**, 14–22 (1979).
5. Chiu, C.-S., Li, C.-K. & Chiu, C.-T. *Ann. Géol. Pays Hellén.* **1**, 263–272 (1979).
6. Tauxe, L. & Opdyke, N. D. *Paleogeogr. Paleoclimatol. Paleoecol.* **37**, 43–61 (1982).

Natural selection on body size and proportions in house sparrows

Robert C. Fleischer & Richard F. Johnston

Museum of Natural History and Department of Systematics and Ecology, University of Kansas, Lawrence, Kansas 66045, USA

Variation in morphology across a species range is largely a function of climatic conditions. Evidence for this comes primarily from correlations of latitudinal trends of climate with those of body size or shape (the classic ecogeographic rules of Bergmann and Allen[1]). Few studies have documented a temporal sequence of natural selection on size variables within a single population[2–7], and no study precisely documents selection on shape variables. For birds in temperate regions, winter climate can be a major source of mortality[8], and is likely to be an important agent of selection on overall size[2–6]. We reported previously[6] that severe winter weather produced significant changes in the distribution of size classes of a population of house sparrows (*Passer domesticus*). In that study, post-winter males were on average significantly larger than pre-winter males and post-winter females averaged significantly smaller than pre-winter females. We report here further analyses indicating that sparrows also undergo selection for refinement of bodily proportions, consistent with predictions from Allen's ecogeographic rule. Such selection for increased core-to-limb proportions probably results in greater thermoregulatory efficiency. The changes in proportions accompany the changes in overall size[6] and there are major inter-sexual differences in how such proportions are achieved.

The study is based on 14 skeletal measurements[9] from 240 autumn (November 1978) and 196 Spring (March 1979) specimens of house sparrows from Lawrence, Kansas. The 1978–79 winter in Lawrence was one of the most severe on record[11]. Monthly mean temperatures for December–February averaged 4.8 °C below normal, and snow cover lasted for 55 days of the

Table 1 Selection intensities for skeletal elements of autumn and spring groups

	First-year autumn versus all spring					
	Male (n = 81 vs. 115)			Female (n = 60 vs. 81)		
	Mean (s.d.)		P*	Mean (s.d.)		P*
Skull elements (5)	0.040	+	<0.05	0.008	+	NS
Core elements (3)	0.125	+	<0.01, <0.05	0.042	−	NS
Limb elements (6)	0.059	+	<0.05, <0.05	0.135	−	<0.01, <0.05, <0.05
PC1	0.154	+	<0.01	0.056	−	NS
PC3	0.021	+	NS	0.046	+	NS
	First-year autumn versus first-year spring					
	Male (n = 81 vs. 15)			Female (n = 60 vs. 10)		
Skull elements (5)	0.003	±	NS	0.030	−	NS
Core elements (3)	0.106	+	<0.05	0.006	±	NS
Limb elements (6)	0.010	±	NS	0.105	−	NS
PC1	0.045	+	NS	0.119	−	NS
PC3	0.037	+	NS	0.135	+	NS

Values given are mean selection intensities for element groups (number of elements per group in parentheses), selection intensities for PC scores, and a summary of the significant overwinter differences (by t-test) among elements within their respective groupings. + Indicates an increase in the value(s) of the element or PC overwriter, − means a decrease, and ± indicates ambiguity in the direction of selection.

* Significance levels for those elements were significantly different by t-test between autumn and spring samples. No variances differed between autumn and spring samples. Univariate analysis presented elsewhere[6,14]. NS, not significant.

3-month period, compared with about 15 days in an average year.

Within each sex, different comparisons of autumn and spring groups were possible, but only autumn specimens could be satisfactorily identified as first-year birds by the incomplete ossification of their skulls[12]. However, a large number of banded specimens was included in the sample, from a previous study at the site[13]. From these birds of known age, samples of first-year spring specimens were identified and compared with first-year autumn birds. These provide the most useful comparison, in terms of measuring levels of wintertime selection, but a comparison is also made of first-year autumn versus all spring specimens. This mixes a number of separate age classes in the spring specimens, but all members of the group are similar in having had at least one wintertime selective experience. First-year autumn birds had completed skeletal growth[6].

Univariate analyses of the 14 variables over these specimen sets are provided elsewhere[6,14]. Spring means differed significantly by t-test from autumn means for several variables. Variances did not differ among the samples by Levene tests. To analyse the major trends of variation in the skeletal variables, the variance–covariance matrix of the entire log-transformed data set was subjected to principal component analysis[15] (PCA) and PC scores were computed for each specimen. Three principal axes contained significant proportions of variance and were easily interpretable. PC1 contained 42% of the variance and, because of its large, positive loadings for all variables, represents overall size. PC2 (13%) seems to represent a skull to body proportion, and is not included in the present analysis. PC3 contained 10% of the variance, had positive loadings on core variables, negative loadings on limb variables and insignificant loadings on skull variables. Thus, PC3 represents a core-to-limb ratio. Scores on PC1 and PC3 were averaged over each group as defined above.

- Here we compare morphology of autumn and spring groups using calculations of selection intensity[16] (measured as the proportional change in mean fitness, $\Delta\bar{w}/\bar{w}$). Selection intensities estimate the relative amount of morphological change from a pre-selection (autumn) to a post-selection (spring) sample. They are advantageous in that they are standardized and comparable over characters. Because selection acted primarily on the character means in the comparisons, we assume a linear fitness function[7,16–18].

Selection intensities were calculated for each of the 14 skeletal elements, grouped according to their respective bodily component (skull, core or limb) and averaged. These mean values, and the selection intensities for the PC scores, are presented in Table 1, which also includes a summary of significant differences. Selection intensities were large for certain characters. For example, $\Delta\bar{w}/\bar{w}$ was 0.237 for decrease in humerus length in females. By comparison, $\Delta\bar{w}/\bar{w}$ for change in humerus length from O'Donald's[17] re-analysis of Bumpus' data on storm-generated selection in *P. domesticus* was only 0.103. Drought-mediated selection on *Geospiza fortis*[7] produced the largest intensities ever noted: for example, $\Delta\bar{w}/\bar{w}$ on wing chord over a 2-yr period was 0.39.

The pattern of selection intensities differs to some extent between the sexes. On PC1, males show strong selection for increased body size, but females show strong selection for decreased body size. Selection intensities on PC3 are weak to moderate; mean changes are not significant, but all indicate an increased core-to-limb ratio. Selection intensities averaged over body components indicate more clearly a reproportioning of body parts. In males, selection intensities over skull and limb elements are weak, although generally showing a trend towards increased size. In comparison, average selection intensities for core elements are considerably larger for both the first-year autumn versus all spring comparison and for the first-year autumn versus first-year spring comparison. Male core elements, therefore, show a disproportionate increase relative to their limb or skull elements.

For females, the basic pattern of selection is opposite to that of males. Females exhibit low selection intensities in variable directions for skull and core characters, but extremely strong selection for decreased limb size. Females limb elements thus show a disproportionately greater decrease relative to their core or skull elements. In summary, Table 1 reveals that while spring males are larger overall and spring females are smaller overall, each sex has also experienced a differing mode of selection on body components that results for both sexes, in an increased core-to-limb ratio.

Individuals with a high core-to-limb ratio clearly have a selective advantage in severe winter weather. A decreased surface-to-mass ratio results from such a core-to-limb trend, which in turn may result in lower rates of metabolism and heat loss[19,20]. Such trends in the proportioning of body parts are evident in geographical comparisons within a number of species[1], and within house sparrows such a cline also exists[9]. However, we believe this report to be the first to indicate selection for proportioning of body parts on a temporal basis. As there are constraints on body size in each sex, for males to be larger and females smaller post-selection, there must also be constraints on the way each sex accommodates selection for optimal proportioning of body parts. Spring males must have greatly increased cores in relation to their also larger limb elements, and spring females must have considerably smaller limbs in relation to their also smaller core elements.

In house sparrows, therefore, males and females are selectively distinct morphometric entities: sexual selection results in larger-sized males[21]; and females perhaps undergo selection for small size because of reproductive constraints[22]. As shown here, given intense selection pressures, overwinter mortality can support or augment these trends[6]. Even so, males and females, although probably allowed to differ in size because of sex-limited loci, cannot be totally distinct in an evolutionary sense because of the effects of syngamy and recombination. Sexual reproduction annually generates cohorts of offspring of interparental size or shape that cannot wholly anticipate wintertime climate. Selection sometimes then acts on this new cohort to generate post-winter phenotypic distributions better approximating optimal distributions.

Support of the NSF (DBS-7912412) and the General Research Fund of the University of Kansas is hereby acknowledged.

Received 3 November 1981; accepted 27 May 1982.

1. Mayr, E. *Evolution* **10**, 105–108 (1956).
2. Bumpus, H. C. *Biol. Lect., Marine Biol. Lab. Woods Hole*, 1–15 (1898).
3. Johnston, R. F., Niles, D. M. & Rowher, S. A. *Evolution* **26**, 20–31 (1972).
4. Rising, J. D. in *Productivity, Population Dynamics and Systematics of Granivorous Birds* (eds Kendeigh, S. C. & Pinowski, J.) (Polish Scientific Publishers, Polish Academy of Sciences, Warszawa, 1972).
5. Baker, M. C. & Fox, S. F. *Am. Nat.* **112**, 675–682 (1978).
6. Johnston, R. F. & Fleischer, R. C. *Auk* **98**, 503–511 (1981).
7. Boag, P. T. & Grant, P. R. *Science* **214**, 82–85 (1981).
8. Fretwell, S. D. *Populations in a Seasonal Environment* (Princeton University Press, 1972).
9. Johnston, R. F. & Selander, R. K. *Evolution* **21**, 1–28 (1971).
10. Johnston, R. F. *Systematic Zool.* **22**, 219–226 (1973).
11. Matson, M. & Weisnet, D. R. *Nature* **289**, 451–453 (1981).
12. Niles, D. M. *Condor* **75**, 354–356 (1973).
13. Lowther, P. E. thesis, Kansas Univ. (1979).
14. Fleischer, R. C. thesis, Kansas Univ. (1982).
15. Harris, R. J. *A Primer of Multivariate Statistics* (Academic, New York, 1975).
16. O'Donald, P. *Theor. Population Biol.* **1**, 219–232 (1970).
17. O'Donald, P. *Evolution* **27**, 398–404 (1973).
18. Lowther, P. E. *Evolution* **31**, 649–656 (1977).
19. Kendeigh, S. C. *Auk* **86**, 13–25 (1969).
20. Blem, C. R. *Comp. Biochem. Physiol.* **47A**, 101–108 (1974).
21. Selander, R. K. in *Sexual Selection and the Descent of Man* (ed. Campbell, B.) Ch. 8 (Aldine, Chicago, 1972).
22. Downhower, J. F. *Nature* **263**, 558–563 (1976).

Genetic differences in individual behaviour associated with shell polymorphism in the snail *Cepaea nemoralis*

J. S. Jones

Department of Genetics and Biometry, University College London, Wolfson House, 4 Stephenson Way, London NW1 2HE, UK

It is often supposed that genetic polymorphism in a population will be favoured if individuals of different genotype occupy an ecological niche in which they are relatively fit[1]. There are great practical difficulties in establishing whether such genetic differences in behaviour influence the niches chosen by polymorphic animals in nature. I report here a new technique for investigating habitat selection in the land snail *Cepaea nemoralis*. This species is polymorphic for shell colour and banding and hence for shell reflectivity. Differences in the efficiency of absorption of solar energy by the various phenotypes lead to geographical changes in allele frequency[2]. In this study snails of different phenotype in the same population were marked with a paint which fades at a measurable rate when exposed to daylight. This detects individual differences in daytime activity too slight to be identified by direct observation and shows that within a population there are differences in the behaviour of individuals of contrasting shell phenotype when exposed to sunlight. Habitat selection may therefore be partially responsible for the extensive genetic polymorphism of *C. nemoralis*.

There are great differences in gene frequency among geographically separated populations of *C. nemoralis*. Some of these differences result from climatic selection; dark-coloured snails absorb more solar energy than do light-coloured, and hence may be at an advantage in cold and shady microclimates but liable to death through overheating in warm sunny places[2–4]. Much less is known of the forces which maintain genetic variation within a population than of those which lead to genetic change among populations. Individual differences in thermal relations in sunshine might influence the habitat chosen by snails of different genotype, so that the shell polymorphism may be associated with behavioural differences which help to maintain the various alleles in the population.

Observation of differences in behaviour in natural populations is difficult as the snails are often buried or hidden by vegetation. What is needed is to measure the activity of single snails over a period long enough to detect slight individual differences. Most techniques of measuring exposure to daylight are unsuitable as they involve complex instruments or undue physical interference[5]. There are, however, several chemical or electronic methods of integrating solar energy falling on a surface. Chemicals which degrade at a known rate when exposed to the Sun[6–8] are not usually practical for field use as they involve the spectrophotometry of degradation products. I have modified a technique used to measure the stability of textile dyes to give a convenient method of assessing the behaviour of individual animals in daylight.

The Blue Scale is a series of pigments of differing resistance to fading which are dyed onto cloth[9]. The technique can be improved for field use by dissolving the pigments in a stable yellow paint to give a green paint which fades to yellow. The extent of fading is assessed by comparison with a scale produced by mixing this paint with increasing proportions of the yellow base. The paint is primarily sensitive to UV light (which represents only a small part of the Sun's thermal energy[10]) so that paint fading integrates exposure to daylight over time rather than directly assessing thermal stress. Paint fading gives an indication of the activity of individuals over an extended period.

A saturated solution of benzyl blue in monoethyleneglycolmonoethylether was added to yellow polyurethane paint (International Paint Co., Series 101) to produce a dark green compound. Experimental snails were collected in the valley of the Garonne in the Spanish Pyrenees, where *C. nemoralis* is highly polymorphic[11]. Behavioural responses were tested in seminatural conditions in cages in the field at Nettlecombe Court Field Centre, Somerset, UK. These cages have been used by Bantock[12] to study mortality in *C. nemoralis*. His results seem to reflect the fitness differences between shell morphs which exist in natural populations. The cages have the great practical advantage that all surviving marked snails can be recaptured.

Twenty adult yellow unbanded and the same number of yellow five-banded snails were collected from each of 10 natural populations of *C. nemoralis* during the period 19–23 June 1981. In every case snails were collected from an area smaller than that of a panmictic population[13]. Each snail was marked with a small spot of paint placed 5 mm behind the lip at the equator of the shell, and the populations were placed in 10 field cages planted with nettles and grass on 3 July 1981. The extent of paint fading was measured 60 days later (Table 1).

There are significant differences between banded and unbanded snails in mean exposure to daylight. In every cage,

Table 1 Degree of paint fading on banded and unbanded snails

		Faded to point							
Cage		1	2	3	4	5	6	7	8
1	U		3	6	7	3			
	B			1	3	10	4		
2	U		3	3	5	3			
	B				6	9	1		
3	U		2	10	3	3			
	B			6	8	1			
4	U			4	7	4	3		
	B			1	3	12	3		
5	U		1	6	7	3			
	B			1	11	6	1		
6	U			4	9	7			
	B			4	3	10	3		
7	U		2	10	5	1			2
	B			2	7	9	1		
8	U			8	10				
	B				14	4			
9	U			1	9	8	2		
	B				4	12	2		1
10	U			7	9	2	1		
	B				11	6			

Paint fading on green to yellow scale of marked *C. nemoralis* in field population cages. U, unbanded snails; B, banded.

0028–0836/82/330749–02$01.00

unbanded shells show a lower mean paint fading than do banded. This is in itself significant (sign test: $P = 0.002$), and in five cages the effect is shown by a Mann–Whitney U-test to be individually significant at the 5% level. The overall difference between the mean fading of unbanded (3.85 points) and banded (4.55 points) is highly significant ($t = 7.54$; $P < 0.001$). In addition, in 9 of the 10 cages there is a greater variance of fading among unbanded shells (sign test: $P = 0.022$). There are therefore considerable behavioural differences associated with the shell polymorphism of *C. nemoralis*.

Partitioning of the environment by snails of different genotype may result either from temporal or from spatial differences in activity. There is a general tendency for related coexisting species of small poikilotherm to differ in their times of activity[14]. *C. nemoralis* and *Cepaea hortensis* differ in their period of maximum activity in a way which is related to their preferred microclimate[15]. Australian *Theba pisana* show differences in the seasonal activity of dark and light-coloured snails which depend on their thermal relations in sunshine[16]. This effect might also be important in *C. nemoralis*, so that the dark-coloured banded shells are active for a higher proportion of the day in the cool English climate.

Banded and unbanded snails might also choose to live at a different height above the surface. Behaviour in sunlight is the prime mode of thermoregulation in invertebrates[17]. Temperature stresses are often greater near the ground because of the development of a layer of heated air on sunny days[10] and many organisms exposed to solar stress choose to live at some distance above the surface. Mediterranean *Helicella virgata*, for example, reach a lethal temperature much more often when resting at 3 cm above the ground than when at 70 cm (ref. 18). In *C. nemoralis*, also, snails climb most actively in hot dry weather[19]. Behavioural thermoregulation of this kind is likely to be particularly important in banded *C. nemoralis*, which are more liable than are unbandeds to die of heat shock when exposed on the ground surface on sunny days[20]. Banded snails will therefore climb higher than do unbanded, so that their paint spots will fade to a greater extent. The greater variance of fading scores among unbanded snails suggests that they have a wider range of behaviours and hence a broader niche with respect to general activity, perhaps because they can penetrate both into the layer of heated air near the ground and the direct rays of the Sun at the top of the vegetation. Experiments with *Drosophila* show that temporal fluctuations in habitat are as effective in maintaining polymorphism as are spatial changes[21], so that differences in either time or location of activity by snails of different shell phenotype might favour the evolution of shell polymorphism.

In laboratory populations of various organisms, genetic differences in habitat selection increase the fitness of particular alleles[22–24], and allow a *Drosophila* mutant to be maintained in a heterogeneous environment although it is otherwise harmful to its carriers[25]. Very few examples of genetic polymorphism for habitat selection have been established in natural or semi-natural conditions[16,26]. The experiments described here show that different shell genotypes of *C. nemoralis* have differences in patterns of activity which may influence their fitness and hence promote shell polymorphism. This technique of integrating activity over time may be generally useful in exploring the behavioural ecology of the individual differences thought to exist in various animals as they search for food, for mates or for territory.

This work was supported by the NERC and the Royal Society. I thank the Field Studies Council and Dr S. M. Tilling for help at Nettlecombe Court; Dr C. R. Bantock for the use of his field cages; Professor C. A. B. Smith for statistical advice; Messrs S. Borfield, P. Slepokura and D. Young for help in the field; and Dr M. Tordoff of the Society of Dyers and Colourists, Dr A. Davis of the Propellants, Explosives and Rocket Motors Establishment and Dr K. L. Rabone of Unilever Research for advice on measuring solar radiation.

Received 1 April; accepted 24 May 1982.

1. Taylor, C. E. *Genetics* **83,** 887–894 (1976).
2. Jones, J. S., Leith, B. H. & Rawlings, P. A. *Rev. ecol. Systematics* **8,** 109–143 (1977).
3. Cain, A. J. *Phil. Trans. R. Soc.* B**253,** 499–517 (1968).
4. Jones, J. S. *Science* **182,** 546–552 (1973).
5. Monteith, J. L. *Int. biol. Progm. Hbk* **22,** 1–263 (1972).
6. Davis, A., Deane, G. H. W., Gordon, D., Howell, J. V. & Ledbury, K. J. *J. appl. Polym. Sci.* **20,** 1165–1174 (1976).
7. Davies, R. E. in *The Biological Effects of Ultraviolet Radiation* (ed. Urbach, F.) 437–443 (Pergamon, Oxford, 1969).
8. Diffey, B. L. & Davis, A. *Phys. Med. Biol.* **23,** 318–323 (1978).
9. *British Standard* No. 1006 (British Standards Institution, London, 1961).
10. Monteith, J. L. *Principles of Environmental Physics* (Arnold, London, 1973).
11. Arnold, R. W. *Phil. Trans. R. Soc.* B**253,** 549–593 (1968).
12. Bantock, C. R. *J. Linn. Soc. Biol.* **13,** 47–64 (1980).
13. Lamotte, M. *Bull. biol. Fr. Belg.* Suppl. **35,** 1–239 (1951).
14. Schoener, T. W. *Science* **185,** 27–39 (1974).
15. Cameron, R. A. D. *J. Zool.* **162,** 303–315 (1970).
16. Johnson, M. S. *Heredity* **47,** 121–134 (1981).
17. Henwood, K. *Ecology* **56,** 1329–1342 (1975).
18. Pomeroy, D. E. *Aust. J. Zool.* **16,** 857–869 (1968).
19. Jaremovic, R. & Rollo, C. D. *Can. J. Zool.* **57,** 1010–1014 (1979).
20. Richardson, A. M. M. *Nature* **247,** 572–573 (1974).
21. Mackay, T. F. C. *Genet. Res.* **37,** 79–94 (1981).
22. Christensen, B. *Hereditas* **87,** 21–26 (1977).
23. Cavener, D. *Behav. Genet.* **9,** 359–365 (1979).
24. Steward, R. C. *J. Zool.* **178,** 107–115 (1976).
25. Jones, J. S. & Probert, R. F. *Nature* **287,** 632–633 (1980).
26. Schoener, T. W. & Schoener, A. *Evolution* **30,** 650–658 (1976).

Pluripotent embryonic stem cell lines can be derived from t^{w5}/t^{w5} blastocysts

Terry Magnuson*, Charles J. Epstein*†,
Lee M. Silver‡ & Gail R. Martin§

Departments of * Pediatrics, † Biochemistry and Biophysics and
§ Anatomy, University of California, San Francisco,
California 94143, USA
‡ Cold Spring Harbor Laboratory, Cold Spring Harbor,
New York 11724, USA

Mouse embryos homozygous for t^{w5}, a recessive lethal mutation in the t complex located on chromosome 17, develop normally until the elongated egg cylinder stage, approximately 6.5 days after fertilization. At this time, the endoderm is morphologically abnormal and the embryonic ectoderm begins to show signs of pyknosis. Death of the embryo usually occurs within the next 2 days (ref. 1). A serious difficulty in the study of lethal t-mutant gene expression during embryogenesis has been to obtain appropriate experimental material, particularly during the period immediately following implantation. Recently, a method involving the use of teratocarcinoma-conditioned medium was devised for establishing pluripotent stem cell cultures directly from the inner cell mass (ICM) of a normal mouse blastocyst[2]. Using this method, we have established three embryonic stem cell lines derived from embryos carrying t^{w5}. We report here that one of the cell lines is homozygous for the mutation (t^{w5}/t^{w5}), whereas the other two are heterozygous ($+/t^{w5}$). When injected into athymic mice, each cell line is capable of forming tumours that contain differentiated derivatives of all three primary germ layers.

The three embryonic stem cell lines were obtained from cultures of 10 ICMs isolated from t^{w5}-bearing blastocysts. Mass cultures of the cell lines are indistinguishable from other established embryonic stem cell and teratocarcinoma stem cell lines in both morphological and growth characteristics. When tested for expression of the SSEA-1 cell-surface antigen[3], which is common to teratocarcinoma stem cells and early embryos but not to most differentiated cell types, all three cell lines derived from t^{w5}-bearing embryos were found to be positive by indirect immunofluorescence.

It would be desirable, of course, to identify the genotypes of these embryonic stem cell lines by determining whether they produce the wild-type or mutant t^{w5} gene products. However, as these products are unknown, we have used other genetic markers which identify three different regions of the t^{w5}-bearing chromosome. The validity of the markers depends on the fact that the t^{w5} lethal mutation is carried in the context of a

0028–0836/82/330750—04$01.00

complete t^{w5} haplotype. This t^{w5} haplotype, like all other complete *t* haplotypes, represents a variant form of a large region of chromosome 17 extending from the *T* locus near the centromere to beyond the *H-2* complex (reviewed in ref. 4). In addition to the mutation affecting embryonic development, which for t^{w5} has been mapped near the centre of the complete t^{w5} haplotype[5], all *t* haplotypes carry variant alleles of several other genes, including factors that affect sperm differentiation and function. The integrity of a *t* haplotype is maintained by an extreme suppression of meiotic recombination between *t*-haplotype and wild-type chromatin (for reviews see refs 4,6–8).

The first marker we used identifies the presence or absence of a t^{w5}-bearing chromosome. The embryos from which the stem cell lines were derived were obtained by crossing t^{w5}/Rb(16.17)7Bnr mice. In these embryos, the t^{w5} mutation is carried on an acrocentric chromosome 17, whereas the wild-type allele is carried on the Rb(16.17)7Bnr translocation chromosome (comprising chromosomes 16 and 17 fused at the centromere) which thus serves as a marker for its presence. Consequently, in the absence of recombination, chromosome spreads from embryonic stem cells homozygous for t^{w5} will not have a translocation chromosome, heterozygous cells will have one and wild-type cells will have two. When the karyotype of embryonic stem cell line 1 was examined, none of the spreads contained a translocation chromosome (Fig. 1*a*). In contrast, embryonic stem cell lines 2 and 3 both had a translocation chromosome (Fig. 1*c*).

Because there is a 4–6% chance of meiotic recombination occurring between the centromere and the start of the *t*-

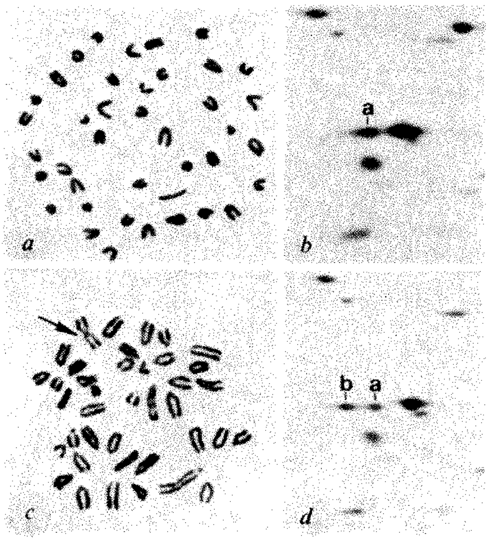

Fig. 1 Identification of embryonic stem cell genotype. Ten ICMs were isolated from blastocysts obtained by mating t^{w5}/Rb(16.17)7Bnr mice. (As the transmission ratio of the t^{w5} haplotype on our background is 87%, we would expect four to five of the ICMs to be t^{w5} homozygotes.) They were seeded on confluent monolayers of mitomycin C-treated fibroblasts in Dulbecco's modified Eagle's medium supplemented with 10% calf serum, 10^{-4} M 2-mercaptoethanol and concentrated conditioned medium[2]. Within 1 week, three of the ICMs had proliferated to form undifferentiated stem cell colonies. These colonies were disaggregated by treatment with trypsin and, with the use of a micropipette, were subcultured to new feeder layers. The cell populations were then expanded according to the procedures outlined by Martin[2], except that the addition of concentrated conditioned medium was discontinued after three passages. When the karyotype of embryonic stem cell line 1 was examined (*a*), 38% of the cells had 40 chromosomes, 30% had 41 and 10% had 42. A translocation chromosome was not observed in any spread. In addition, only the p63a protein was found marked a in (*b*). These data identify line 1 as homozygous for t^{w5}. 39% of the cells of embryo-derived cell line 2 were found to have 42 chromosomes and 22% had 41. 84% of the cells of line 3 had 40 chromosomes. The presence of a translocation chromosome (arrowed in (*c*) and p63a and p63b (a and b respectively in *d*) identifies lines 2 and 3 as heterozygous for t^{w5}. For karyotyping, 10^7 stem cells were seeded in 60 mm^2 tissue culture dishes and cultured overnight. They were then incubated for 30 min in medium containing 10 μg ml^{-1} colcemid (Gibco), washed with phosphate-buffered saline (PBS) and collected after exposure to trypsin. The cells were centrifuged, and the pellet resuspended in 10 ml of 0.56% KCl. After 25 min, the cells were again centrifuged and the resulting pellet resuspended in 10 ml of 3:1 methanol/acetic acid fixative. The fixative solution was changed three times and then refrigerated overnight. The following day, the pellet was resuspended in 1 ml of a freshly made fixative solution, and chromosome spreads were prepared by placing a drop of the cell suspension on cleaned, wetted microscope slides. The chromosomes were stained with 3% Giemsa (GURR) for 5 min. For two-dimensional gel electrophoresis, embryonic stem cells were separated from feeder layer cells by a double preplating technique[2]. The stem cells were then seeded in 16 mm^2 multi-well tissue culture plates (Flow Labs) at a density of 10^6 and cultured overnight. After washing with PBS, the stem cells were incubated in methionine-free medium for 30 min and then for 5 h in methionine-free medium containing 250 μCi ml^{-1} of ^{35}S-methionine (specific activity of 900–1,100 Ci mmol^{-1}; Amersham). The labelled cells were washed with PBS and lysed with 100 μl of isoelectric focusing sample buffer[18]). Two-dimensional gel electrophoresis was performed as outlined by O'Farrell[18] with a 4.5% stacking gel and a 10% separating gel being used in the second dimension. Kodak NS-2T film was used for autoradiography of the dried gels. Only the area of the gel pattern containing p63 is shown.

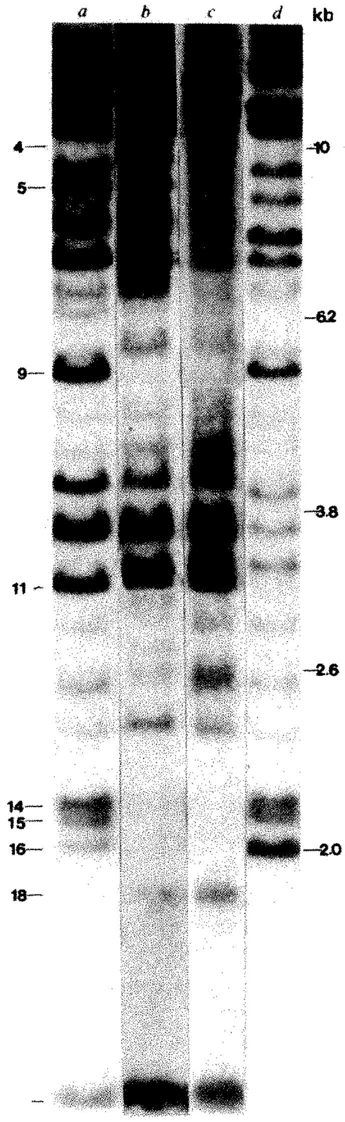

Fig. 2 Blot hybridization analysis of *H-2*-like genes from embryonic stem cell line 1. *Eco*RI restriction patterns of *a*, 129(t^{0}/t^{w5}); *b*, 129(+/t^{w5}); *c*, embryonic stem cell line 1; and *d*, Rb(16.17)7Bnr/Rb(16.17)7Bnr. High molecular weight DNA was prepared from adult livers or embryonic stem cells as described previously[13]. DNA was digested to completion with *Eco*RI and 5-μg aliquots of each sample were electrophoresed through a 1% agarose gel at 0.7 V cm^{-1} for 36 h. Southern blot hybridization was performed with clone pHIIa DNA[19] nick-translated to a specific activity of 2×10^8 c.p.m. μg^{-1}, and used at 8.2×10^4 c.p.m. cm^{-2} of filter. Hybridization and washing conditions were as described previously. Particular *t*-specific *Eco*RI fragments are numbered at the left according to Silver[13]. The numbers at the right denote the size and positions of the DNA length standards, in kilobases (kb). Lanes *b* and *c* are composites of different exposures of the same gel.

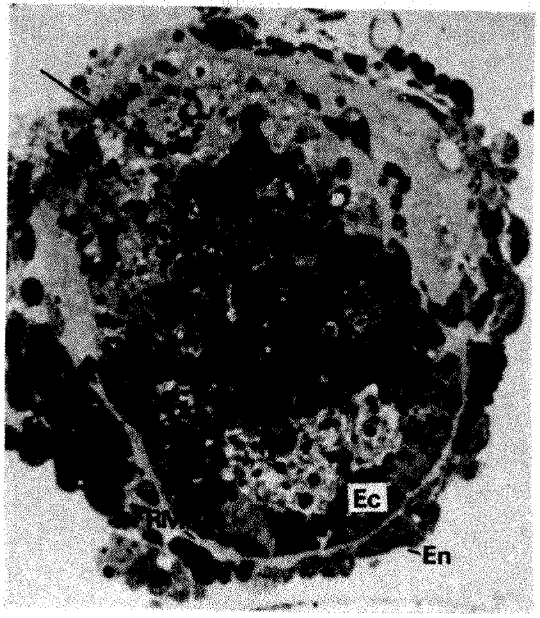

Fig. 3 Section of an embryoid body formed by t^{w5}/t^{w5} embryonic stem cells. Aggregates of cells were cultured in Petri dishes for 16 days. The embryoid bodies which formed were fixed in 2.5% glutaraldehyde, dehydrated and embedded in Epon, and 1.5-μm sections were prepared. Part of a cavitating embryoid body, consisting of columnar ectoderm (Ec) surrounded by a layer of endoderm-like cells (En) with underlying Reichert's membrane-like material (RM), is shown. There are numerous pyknotic cells (arrow) in this embryoid body. ×240.

haplotype region[9], the second marker we used was the *Tcp-1* gene located in the region of the t^{w5} haplotype proximal to the lethal gene[10]. All complete *t* haplotypes, including t^{w5}, carry a variant *Tcp-1* allele (*Tcp-1*^{a}) which encodes a polypeptide p63/6.9a (abbreviated p63a) that is readily distinguishable from the wild-type gene (*Tcp-1*^{b}) product (p63/6.9b or p63b) by two-dimensional gel electrophoresis[11]. Thus, t^{w5} homozygous cells express only the p63a form of the polypeptide, heterozygous cells express both p63a and p63b in equal amounts and wild-type cells express only the p63b form. When the protein gel pattern of embryonic stem cell line 1 was examined, only the p63a form of the polypeptide was observed (Fig. 1*b*). In contrast, both p63a and p63b were expressed in roughly equal amounts by embryonic cell lines 2 and 3 (Fig. 1*d*).

As meiotic recombination within the *t* complex is highly suppressed (recombination frequency between 0.001 and 0.002)[6], the probability that *Tcp-1* has been separated from the t^{w5} lethal mutation and that cell line 1 is not homozygous for t^{w5} is extremely low (≤0.004). Nevertheless, we used the family of genes comprising the *H-2* complex as a third marker to demonstrate that cell line 1 carries only the t^{w5} haplotype. The *H-2* complex is located in the region of the t^{w5} haplotype distal to the lethal factor[5]. *t*-haplotype-specific restriction fragments carrying DNA sequences homologous to the *H-2* class I genes have recently been described[12,13]. With the use of the restriction enzyme *Eco*RI, multiple *t*-haplotype-specific fragments can be observed in the context of the 129/SvJ background pattern (Fig. 2, lane *a*). Although fragments 5, 11 and 17 are shared by all complete *t* haplotypes, fragments 4 and 18 are unique to the t^{w5} haplotype (Fig. 2, lane *b*) and are not present in genomic DNA from other lethal and semilethal haplotypes such as t^{0}, t^{w2}, t^{w12} or t^{12}. All the other well characterized *t* haplotypes display fragments 9, 14, 15 and 16 whereas t^{w5} does not[13]. The *H-2* haplotype associated with the Rb(16.17)7Bnr chromosome also displays *Eco*RI fragments which migrate in the same regions as *t* fragments 9, 14–16 (Fig. 2, lane *d*).

*Eco*RI-digested DNA from embryonic cell line 1 displays *t*-specific *H-2* fragments 5, 11 and 17, and t^{w5}-specific fragments 4 and 18 (Fig. 2, lane *c*). This pattern of *Eco*RI fragments is characteristic of the t^{w5} haplotype. The absence of fragments 9, 14–16 rules out the unlikely possibility that a lethal or semi-lethal haplotype other than t^{w5} is present in this cell line, and also verifies the absence of the *H-2* genomic region of the Rb(16.17)7Bnr chromosome.

Taken together, the analyses of the three markers demonstrates conclusively that line 1 is homozygous for regions of the t^{w5} haplotype both proximal and distal to the t^{w5} lethal gene. As suppression of recombination along the t^{w5} haplotype reduces the probability of a double recombination event to $\sim 10^{-6}$, we can definitely conclude that this cell line is homozygous for the t^{w5} lethal gene.

To determine whether the embryonic stem cells can mimic early embryogenesis, the homozygous and one of the hetero-

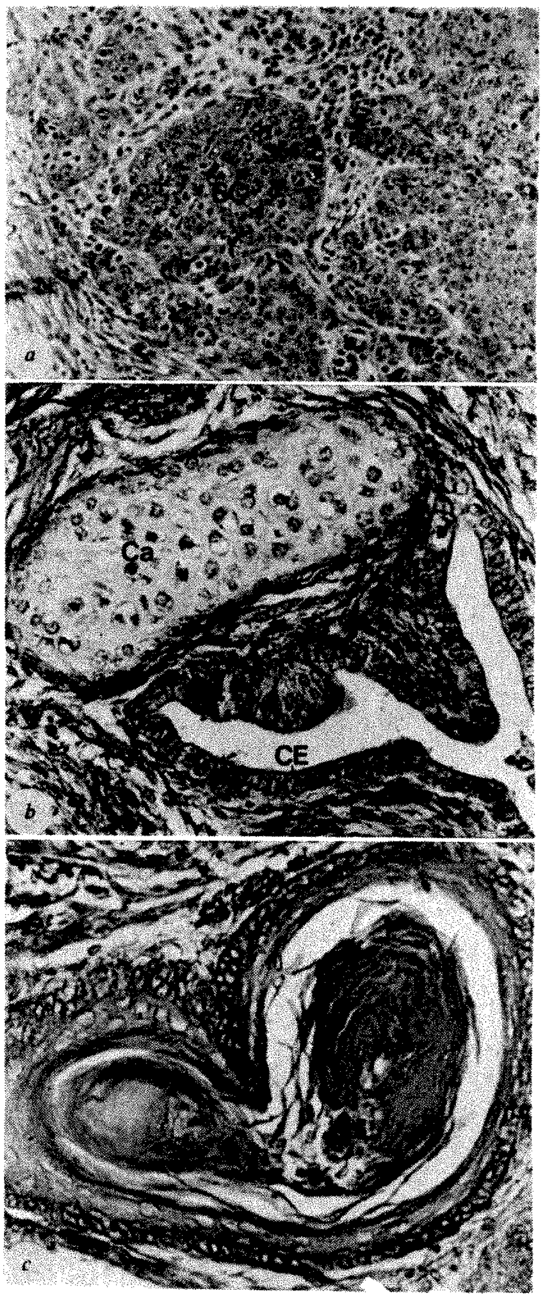

Fig. 4 Sections of tumours formed after subcutaneous injection of 5×10^{6} t^{w5}/t^{w5} embryonic stem cells into an athymic nude mouse. After 2–6 weeks the tumours that had formed were removed, fixed in Bouin's solution, embedded in paraffin and sectioned. The cell types observed in the tumours included *a*, groups of undifferentiated stem cells (SC); *b*, cartilage (Ca) and columnar epithelium (CE); and *c*, keratinizing epithelium. *a*, ×80; *b*, ×104; *c*, ×112.

zygous cell lines were cultured in appropriate conditions[14]. Both cell lines were able to form embryoid bodies. Under the light microscope, the t^{w5}/t^{w5} embryoid bodies were observed to consist of a core of ectoderm-like cells surrounded by a layer of endoderm-like cells. Typical Reichert's membrane-like material, presumably secreted by the endodermal cells, was observed in almost all the t^{w5}-homozygous embryoid bodies, and the beginning of pro-amniotic cavity formation was observed in the core of some (Fig. 3). Extensive death of core cells was observed in some of the t^{w5}/t^{w5} embryoid bodies. However, although ectoderm degeneration is characteristic of t^{w5}/t^{w5} embryos *in utero*, the cell death observed in the t^{w5}/t^{w5} embryoid bodies cannot necessarily be attributed to the effects of the t^{w5} lethal mutation as numerous pyknotic cells have also been observed in the core of embryoid bodies formed by some wild-type teratocarcinoma stem cell lines (G.R.M., unpublished data).

As the variety of cell types formed during the development of embryoid bodies is always limited, each of the t^{w5}-bearing embryonic stem cell lines was injected into several athymic mice (*nu*/*nu*) to determine the extent of their differentiative capacities. Within 2–6 weeks, all the cell lines produced tumours containing undifferentiated stem cells as well as differentiated derivatives of all three primary germ layers. The differentiated cell types included neural, keratinizing, pigmented and columnar epithelium, yolk sac endoderm, cartilage, muscle and connective tissue (Fig. 4*a*–*c*). Similar results were obtained with a subclone of the t^{w5}/t^{w5} embryonic stem cell line. We thus conclude that the t^{w5}-homozygous embryonic stem cell line is pluripotent and capable of differentiating into a large number of differentiated cell types. Many of these cell types are not formed by t^{w5}/t^{w5} embryos *in utero* because the embryo dies before all three primary germ layers are established[1].

The mechanisms of *t*-mutant lethality are not yet understood. One hypothesis is that at least the earlier-acting lethal *t* mutations, such as t^{12}, t^{0} and t^{w5}, are generalized cell lethals that cause embryonic death by perturbing processes such as intermediary metabolism, which are essential for the survival of all cells in the embryo[15]. Wudl and Sherman[16] interpreted their observation that all cells in cultured presumptive t^{w5}/t^{w5} blastocysts die at earlier times than do cells of control embryos as evidence that t^{w5} is a generalized cell lethal. Hogan *et al.*[17] also showed that presumptive t^{w5}/t^{w5} ICMs are smaller, abnormally organized and apparently moribund when compared with ICMs from normal embryos. Our results, however, demonstrate that t^{w5}/t^{w5} ICM cells are sufficiently viable to give rise to an embryonic stem cell line which, in the appropriate environment, can differentiate into a wide variety of cell types. The simplest explanation of these results is that the t^{w5} mutation does not result in generalized cell lethality. Death of t^{w5}/t^{w5} embryos must therefore be due to other causes. The availability of the t^{w5}-homozygous embryonic stem cell line described here should make possible new approaches to the study of how such lethal *t* mutations affect normal development.

We thank Estrella Lamella, Theodosia Zamora, Marianne Gallup and Jane Uman for technical assistance and Dave Akers for assistance in preparing the figures. This work was supported by NIH grants HD-03132, HD-16091, CA-25966 and basic research grant 1-770 from the March of Dimes Birth Defects Foundation. T.M. is a recipient of a NIH National Research Service Award and G.R.M. of an American Cancer Society Faculty Research Award.

Received 6 May; accepted 15 June 1982.

1. Bennett, D. & Dunn, L. C. *J. Morph.* **103,** 135–157 (1958).
2. Martin, G. R. *Proc. natn. Acad. Sci. U.S.A.* **78,** 7634–7638 (1981).
3. Solter, D. & Knowles, B. B. *Proc. natn. Acad. Sci. U.S.A.* **75,** 5565–5569 (1978).
4. Silver, L. M. *Cell* **27,** 239–240 (1981).
5. Artzt, K., Shin, H-.S. & Bennett, D. *Cell* **28,** 471–476 (1982).
6. Bennett, D. *Cell* **6,** 441–454 (1975).
7. Sherman, M. I. & Wudl, L. R. in *Concepts in Mammalian Embryogenesis* (ed. Sherman, M. I.) 136–234 (MIT Press, 1977).
8. Lyon, M. F. *Symp. zool. Soc. Lond.* **47,** 455–477 (1981).
9. Magnuson, T. & Epstein, C. J. *Biol. Rev.* **56,** 369–408 (1981).
10. Silver, L. M., White, M. & Artzt, K. *Proc. natn. Acad. Sci. U.S.A.* **77,** 6077–6080 (1980).
11. Silver, L. M., Artzt, K. & Bennett, D. *Cell* **17,** 275–284 (1979).
12. Shin, H-.S., Stavenezer, J., Artzt, K. & Bennett, D. *Cell* (in the press).
13. Silver, L. M. *Cell* (in the press).
14. Martin, G. R., Wiley, L. M. & Damjanov, I. *Devl Biol.* **61,** 230–244 (1977).
15. Wudl, L. R., Sherman, M. I. & Hillman, N. *Nature* **270,** 137–140 (1977).
16. Wudl, L. R. & Sherman, M. I. *Cell* **9,** 523–531 (1976).
17. Hogan, B., Spiegelman, M. & Bennett, D. *J. Embryol. exp. Morph.* **60,** 419–428 (1980).
18. O'Farrell, P. H. *J. biol. Chem.* **250,** 4007–4021 (1975).
19. Steinmetz, M. *et al. Cell* **24,** 125–134 (1981).

Plasminogen activator–plasmin system and neuronal migration

G. Moonen*, M. P. Grau-Wagemans† & I. Selak*

* Departement de Clinique et de Pathologie médicales,
Secteur de Neurologie and † Service de Cytologie et d'Histologie,
Université de Liège, 20 rue de Pitteurs, 4020 Liège, Belgium

Neuroontogenesis results from a synchronized series of elementary events including cellular proliferation, migration, differentiation, recognition and death. Neuronal migration is a key step in neural morphogenesis since inadequately located neurones may not establish the appropriate connections and this may lead to neuronal death or to functional deficit of synaptic circuits. Impairment of neuronal migration has been implicated in human pathology[1] and well documented in animal pathology, such as the *weaver* mutation in mice[2]. The cerebellum of small rodents is particularly well suited for the study of neuronal migration because a subpial neuronogenesis occurs postnatally. The subsequent inward migration of postmitotic neurones (mostly granule cells) has been studied using classical neuroanatomical methods, such as the Golgi stain[3], and autoradiography after systemic injection of ^{3}H-thymidine[4]. Systematic ultrastructural investigation of neuronal migration at different levels of the central nervous system and in different species led Rakic to propose the radial glia hypothesis—that neurones migrate along radial glia cells which serve as guides during migration[5]. The observation that neurones migrate inside a densely packed neuropile has prompted us to consider the possible role of extracellular neutral proteolysis during neuronal migration. We have focused on the plasminogen activator (PA) serine proteases because these enzymes are known to be involved in several phenomena that involve cell migration or tissue remodelling[6]. The usual substrate for PA is plasminogen, which is converted to plasmin, although other substrates may exist[7]. We report here that both PA and plasmin are released by cultived 7-day-old rat paraflocculus, but not by 1-month-old or adult rat paraflocculus (that is, after granule cell migration), and that inward migration of cerebellar granule neurones, which account for 95% of the cells in adult cerebellum, can be inhibited by inhibitors of the PA–plasmin system.

We have studied PA and plasmin activity with the use of the classical fibrin plate assay[8,9]. When standard plates are used, it is possible to demonstrate both endogenous PA and plasmin activity; with heated plates only endogenous plasmin activity can be detected (see Fig. 1 legend). When a 7-day rat cerebellum paraflocculus (the most lateral part of the cerebellum) was explanted for 24 h at 37 °C on a standard fibrin plate, a fibrinolytic zone formed around it; the fibrinolysis could be inhibited by 6-aminocaproic acid. In the same conditions, but using heated fibrin plates, a smaller but definite fibrinolytic zone could be seen, demonstrating that not only PA but also plasmin are released by the 7-day rat paraflocculus. If these enzymes were to have a role in neuronal migration, we reasoned that 1- or 3-month (adult) rat paraflocculus should not release PA and plasmin. We found that, indeed, provided the meninges were carefully dissected, in neither case could a release of PA or plasmin be demonstrated (see Fig. 1 for example). We also conclude from this experiment that the fibrinolysis observed with the 7-day rat paraflocculus is not due to damage (such as anoxia or nonspecific release of proteolytic enzymes). Extracellular release of PA and plasmin activity is even more obvious

0028-0836/82/330753—03$01.00

if the conditioned medium from 7-day rat paraflocculus suspension culture is assayed using standard or heated fibrin plates. 6-Aminocaproic acid again inhibits the fibrinolytic activity and in these conditions neither PA nor plasmin activity could be demonstrated in medium conditioned by 1-month or adult rat paraflocculus.

We next investigated whether inhibition of PA or plasmin affected cell migration, using organotypic suspension cultures of the 7-day paraflocculus. In these cultures, the external granular layer (EGL) disappears within 2 days. Further experiments, including sequential autoradiography after intraperitoneal injection of ^{3}H-thymidine 60 min before dissecting the paraflocculus, showed that the disappearance of the EGL was due to inward migration of EGL cells such as occurs *in vivo* (in preparation). The persistence of the EGL beyond 2 days could thus be considered as a criterion for migration blockade. The following inhibitors were used: 6-aminocaproic acid, which binds to plasminogen and inhibits the transformation of plasminogen to plasmin; diisopropylfluorophosphate, a general inhibitor of serine proteases; trasylol and soybean trypsin inhibitors which are antiplasmin agents; and D-Phe-Pro-Arg-CH_2Cl and D-Val-Phe-Lys-CH_2Cl which are specific and potent inhibitors of tissue PA and plasmin respectively (ref. 10 and D. Collen, personal communication). All the inhibitors inhibited inward migration of EGL cells (Fig. 2), and, judging from phase-contrast examination of dissociated 7-day rat cerebellum cultures, at the concentration used they had no toxic effect. The data show that (1) not only PA but also plasmin activity are released into the extracellular space of the cerebellum during migration and (2) neuronal migration is inhibited by agents which act on PA and plasmin activity.

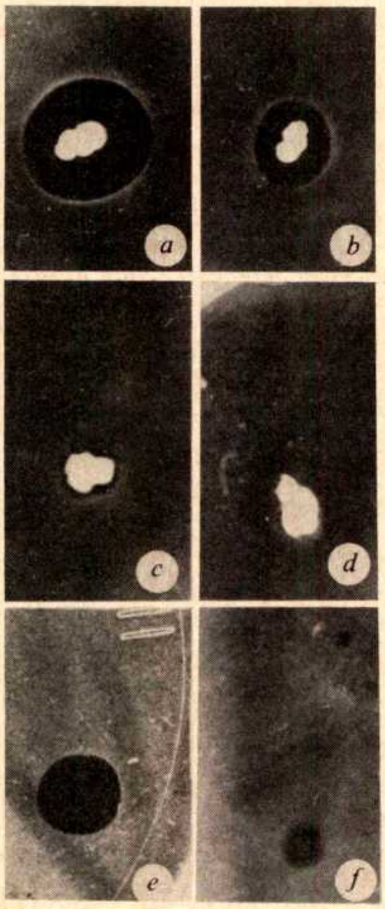

Fig. 1 Demonstration of plasminogen activator and plasmin release by 7-day-old rat paraflocculus. Fibrin plates were prepared as described in ref. 8; 200 mg of crude bovine fibrinogen (containing plasminogen) were dissolved in 100 ml of veronal buffer (*p*H 7.3) with 0.5 ml of 1% merthiolate solution added. To 3 ml of fresh fibrinogen solution (kept at 37 °C), 0.7 ml of thrombin (100 NIH units per ml of Veronal buffer) was added and the mixture layered in the compartments of Petri dishes (Falcon 1004 Y). If the plates are kept at 37 °C, both PA and plasmin activities can be detected. If the plates are heated to 80 °C for 20 minutes, the plasminogen is inactivated and the tissue must generate not only endogenous PA but also endogenous plasmin in order to induce fibrinolysis[9]. The diminished lytic zone, as compared with standard plates, indicates that plasminogen in the tissue sample is the limiting factor. Paraflocculi were dissected from 7-day (*a*–*c*) or 1 month (*d*) rat cerebella. Meninges were carefully removed under the dissecting microscope. The whole (7-day-old) or part (1-month-old) paraflocculus was then explanted in 0.5 ml of N_1MEM medium serum-free culture medium[15] on the fibrin plates which were incubated at 37 °C for 24 h, and then photographed. Serum-free conditioned medium was obtained from suspension cultures of cerebellar paraflocculus in some experiments or of slices of the whole cerebellum in other experiments (see Fig. 2 legend for details on the tissue culture). The medium was collected, centrifuged (100,000*g*, 60 min) and filtered through a 0.22 μm Millipore filter. The conditioned medium was used immediately although activity was not modified by freezing at −20 °C for 1 week. Forty μl of the conditioned medium were then seeded on either 37 °C or 80 °C fibrin plates, which were photographed after 24 h. *a*, 7-day-old rat paraflocculus, 37 °C plate; *b*, 7-day-old rat paraflocculus, 37 °C plate. 5×10^{-4} M 6-aminocaproic acid was added to the medium. At that concentration partial inhibition of the fibrinolysis is observed. Complete inhibition was obtained at 5×10^{-3} M; *c*, 7-day-old rat paraflocculus, 80 °C plate; *d*, 1-month-old rat paraflocculus, 37 °C plate; *e*, conditioned medium from 7-day-old rat paraflocculus suspension culture, 37 °C plate; *f*, conditioned medium from 7-day-old rat paraflocculus suspension culture, 80 °C plate. ×1.7.

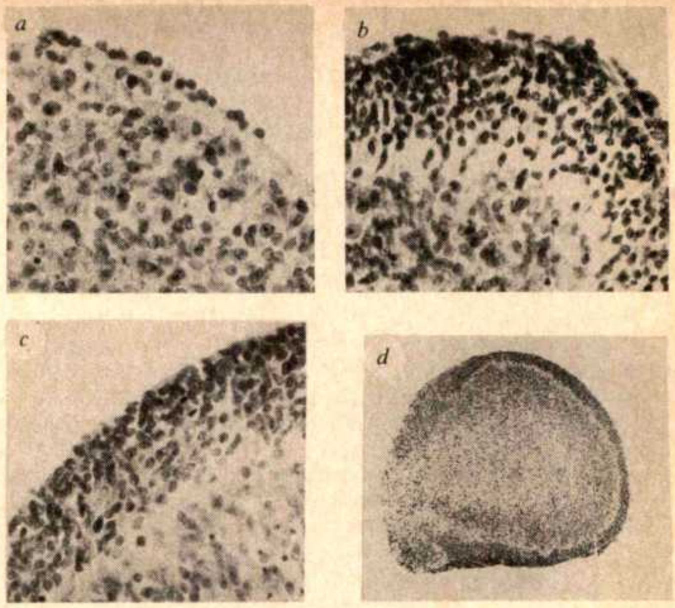

Fig. 2 Effects of inhibitors on neuronal migration. Cerebellar paraflocculi were dissected from 7-day-old rats and cultured in suspension (gyrotory shaker New Brunswick G2, 100 r.p.m.) for 48 h in high-glucose (600 mg%) minimal essential medium supplemented with either 10% heat-inactivated horse serum or with the N_1 component[15] (the same results were obtained with both media). Different inhibitors of the PA–plasminogen–plasmin system were added (see text). *a*, Control culture showing the disappearance of the external granule cell layer after 2 days. *b*–*d* Illustrate the effect of some of the inhibitors used: *b*, 10^{-3} M EACA; *c*, 10^{-4} M D-Val-Phe-Lys-CH_2Cl; *d*, 10^{-4} M D-Phe-Pro-Arg-CH_2Cl. In the presence of inhibitor, the EGL does not disappear, showing that the inward neuronal migration is blocked. At least five samples were examined in each condition. Paraffin sectioning. Gallocyanin stain. *a*–*c*, ×240; *d*, ×42.

The present study is not concerned with cellular location of PA or plasminogen. Recent reports[11–14] suggest, however, that PA is released by neurones and, in the case of the 7–9-day postnatal mouse cerebellum, by granule neurones. The tissue localization of plasminogen is unknown, although there are several possibilities. For example, it could be present on the outer surface of the radial glia or released by the radial glia in the neighbouring extracellular space. Plasmin would be locally generated and the modification of cell surfaces or spaces on or near the glial process would generate an area permissive for inward migration of granule cells. This mechanism is consistent with the radial glia hypothesis. Alternatively, plasminogen could be distributed throughout the extracellular fluid and not restricted to the Golgi epithelial cell. Finally, it should be noted that the molecular nature of the substrate(s) for plasmin in the brain is at present unknown.

G.M. and I.S. acknowledge support from Fonds National de la Recherche Scientifique, Belgium.

Received 2 March; accepted 2 June 1982.

1. Swaiman, K. F. & Wright, F. S. in *Clinical Neurology* (eds Baker, A. B. & Baker, L. H.) 1–186 (Harper and Row, New York, 1977).
2. Sidman, R. L., Green, M. G. & Appel, S. M. *Catalog of the Neurological Mutants of the Mouse* (Harvard University Press, 1965).
3. Cajal, Ramon y S. *Histologie du Système Nerveux de l'Homme et des Vertebres* Vols 1, 2 (Maloine, Paris, 1909–1911).
4. Miale, I. L. & Sidman, R. L. *Expl Neurol.* **4,** 277–296 (1966).
5. Rakic, P. *Trends Neurosci.* **4,** 240–244 (1981).
6. Reich, E. in *Biological Markers of Neoplasia: Basic and Applied Aspects* (ed. Ruddon, R. W.) 491–500 (Elsevier, Amsterdam, 1978).
7. Quickley, J. P. *Cell* **17,** 131–141 (1979).
8. Astrup, T. & Mullertz, S. *Archs Biochem. Biophys.* **40,** 346–351 (1952).
9. Lassen, M. *Acta physiol. scand.* **27,** 371–376 (1952).
10. Collen, D., Lijnen, H. R., De Cock, F., Durieux, J. P. & Loffet, A. *Biochim. biophys. Acta* **165,** 158–166 (1980).
11. Sorecq, H. & Miskin, R. *Brain Res.* **216,** 361–374 (1981).
12. Seeds, N. W., Haffke, S. C. & Krystocek, A. in *Tissue Culture in Neurobiology* (eds Giacobini, E., Vernadakis, A. & Shahar, A.) 145–154 (Raven, New York, 1980).
13. Krystocek, A. & Seeds, N. W. *Science* **213,** 1532–1534 (1981).
14. Krystocek, A. & Seeds, N. W. *Proc. natn. Acad. Sci. U.S.A.* **78,** 7810–7814 (1981).
15. Bottenstein, J. E. & Sato, G. H. *Proc. natn. Acad. Sci. U.S.A.* **76,** 514–517 (1979).

Transformation of fast fibres to slow prevented by lack of activity in developing lobster muscle

C. K. Govind* & Karla S. Kent†‡

* Scarborough College, University of Toronto, West Hill, Ontario, Canada M1C 1A4
† Boston University Marine Program, Marine Biological Laboratory, Woods Hole, Massachusetts 02543, USA

Adult mammalian twitch muscle fibres are extremely plastic, being able to transform from one type to another under the direction of their motoneurones[1–3]. The most unequivocal type of fibre transformation is that of fast-twitch to slow-twitch type, either with cross-reinnervation of the fast muscle with a slow nerve[4–6], or with chronic low frequency stimulation of the intact nerve to a fast muscle[7,8]. Moreover, direct electrical stimulation of the muscle itself with a tonic pattern is just as effective in converting fast fibres to slow[9]. All these experiments suggest that activity of the muscle itself, imposed by whatever means, is crucial in the transformation of fast to slow fibres[8,10]. A similar transformation during development may be responsible for producing the adult diversity of fibre types, as fibres begin by synthesizing myosin of an embryonic type which is replaced by a neonatal type and finally the adult type of fast[11] and slow[12], which occurs concurrently with innervation. We report here that during development of the paired claw closer muscle in lobsters, reducing or eliminating activity in one of the muscles by tenotomy or denervation prevents its fast fibres from becoming transformed into slow. Our results therefore suggest a regulatory role for activity in the differentiation of lobster slow fibres.

The adult lobster *Homarus americanus* has dimorphic claws consisting of a slender fast-acting cutter claw and a stout, slow-acting crusher claw[13,14]. The claw closer muscles are similarly differentiated, the cutter having a majority (60–80%) of fast fibres and the crusher having all slow fibres[15,16]. However, in the three larval[17] and first juvenile[18] stage the paired claws and closer muscles are symmetrical. Each muscle has ~30% fast fibres in a central band, with the remaining slow fibres distributed above and below the fast band[19]. During subsequent development, one of the muscles differentiates into a cutter with a majority of fast fibres and the other into a crusher with all slow fibres[18]. Claw and closer muscle type becomes determined some time during the 4th and early 5th stage and remains fixed thereafter[20]. As claw laterality (whether the crusher appears on the right or left side) is not genetically prespecified, extrinsic factors may influence the determination of claw type and muscle fibre type during the critical 4th and early 5th stage. Indeed, rearing juvenile lobsters without a substrate suppresses development of a crusher claw (and slow fibres) and instead produces paired cutter claws[21]. Because juvenile lobsters normally manipulate the substrate with their claws, it was proposed that the lack of exercise in the absence of a substrate suppressed the differentiation of a crusher claw. To test this hypothesis, we have examined the effects on claw dimorphism of rearing lobsters with or without substrates that they could manipulate and while restricting the use of one of the paired claws.

Larval lobsters were obtained from a hatchery and reared communally until the moult to the 4th stage, when they were placed individually in plastic trays[22]. Following experimental manipulation in the 4th and 5th stages, claw laterality was assessed in the 9th stage or beyond. At this stage the cutter claw is distinctly slender, covered with sensory bristles and has a major incisor-like tooth on its pollex. In contrast, the crusher is stout, has few sensory bristles and has a major molar-like tooth. The fibre composition of the claw closer muscles was based on histochemical demonstration of myofibrillar ATPase in frozen serial sections of the entire claw using the method of Padykula and Hermann[23], modified for lobster muscle[24]. As the specific activity of myofibrillar ATPase is two to three times higher in fast crustacean muscle than in slow[25,26], the former fibres stained more intensely than the latter (Fig. 1). Usually,

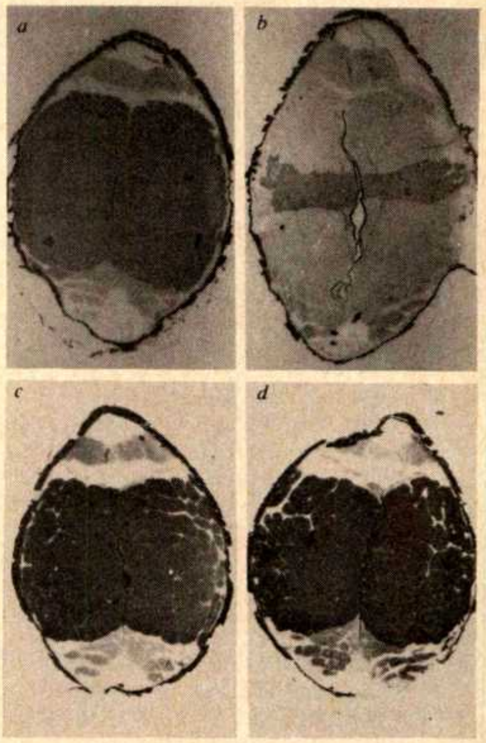

Fig. 1 Representative cross-sections midway through a serial series treated histochemically for myofibrillar ATPase in a pair of dimorphic cutter (*a*) and crusher (*b*) claws and a pair of cutter (*c, d*) claws from 9th stage juvenile lobsters reared with and without oyster chips, respectively. At this stage the closer muscle in the cutter claw (*a*) has almost completely differentiated, consisting mostly of intensely staining fast fibres with a small ventral band of less intensely staining slow fibres. Staining intensity of these ventral fibres is similar to that of the opener muscle which is known to be composed of all slow fibres. The closer muscle in the crusher claw (*b*) has a majority of fibres staining with the same intensity as the opener muscle thus denoting slow fibres except for a narrow central band of intensely staining fast fibres which are transformed into slow fibres in subsequent stages. In a juvenile lobster reared without a substrate, however, the closer muscles in the paired claws (*c, d*) are identical, having the fibre composition of a typical cutter muscle; a crusher muscle is completely suppressed. A detailed description of fibre types based on enzyme histochemistry in the lobster claw closer muscles has been published elsewhere[19]. ×18.

---

‡ Present address: Department of Biological Sciences, Columbia University, New York, New York 10027, USA.

Table 1 Configurations of paired claws in juvenile lobsters reared with a variety of substrates and without any substrate

	Configurations of paired claws					
	Right cutter and left crusher	Right crusher and left cutter	Double cutter	Total no. reared	No. tested histochemically	*P*
Oyster chips	15	14	3	32	8	
Mud	7	12	3	22	5	NS
Gravel	13	7	2	22	5	NS
Plastic chips	13	9	1	23	8	NS
All substrate	48	42	9	99	26	
No substrate	1	0	33	34	9	<0.001

For each condition the lobsters were reared individually from the 4th stage until the 9th stage or beyond, when the configuration of the paired claws was assessed visually in all lobsters and histochemically in a few lobsters to determine the fibre composition of their closer muscles. The table lists the number of lobsters with each claw configuration, the total number reared and the number examined histochemically. With the oyster chips as the control condition, significance was assessed for each of the other substrate and no substrate conditions using the contingency χ^2 test. A cumulative tally of the different substrate-reared lobsters is given under the 'all substrate' condition. NS, not significant.

for each experimental condition 25% of the animals were tested histochemically (Tables 1, 2) and in each case the external claw type accurately reflected the fibre composition of its closer muscle. In other words, the cutter muscle consisted entirely of fast fibres except for some ventral slow fibres while the crusher possessed all slow fibres except for a central band of fast fibres (Fig. 1*a*, *b*). As the juvenile closer muscles were separated into these two distinct types, the external claw type served as a reliable indicator of the type of closer muscle within it.

We began by repeating the original experiment[21] in which lack of a substrate suppressed development of a crusher claw and hence of slow fibres in 30% of the lobsters. In the original experiment juvenile lobsters were seen pinching the rubber stoppers over the drain hole with their claws. To prevent this, we covered the rubber stopper with a plastic tube and now found that 97% of the lobsters failed to develop a crusher claw (Fig. 1, Table 1). This was significantly different from the control condition of raising lobsters with oyster chips as substrate, which produced 91% with dimorphic claws and only 9% with both cutter claws. The two dimorphic configurations appeared in approximately equal proportions. Clearly, the lack of oyster chips as a substrate prevented transformation of fast fibres to slow and differentiation of a crusher muscle.

To test that it was not any special properties of the oyster chips which was the determining factor but rather their physical presence, we reared lobsters with mud, gravel and even plastic chips as substrate (Table 1). In each case, the majority (78.5%) of lobsters grew dimorphic claws; a minority failed to grow a crusher claw. For each of the different substrate conditions, the claw configurations were not significantly different from the control condition. Consequently, the presence of a substrate, of any kind, as long as it could be manipulated, is necessary for the differentiation of a crusher closer muscle. Furthermore, in the dimorphic condition, the crusher claw appears with almost equal probability on the right or left side, as shown when a tally is made of all substrate conditions (Table 1). This suggests that before the 4th and early 5th stage, each claw of a pair has the potential for developing into a crusher but greater use of one claw in the critical period is the determining factor.

We therefore reared lobsters with oyster chips, but restricted the use of one of the claws to varying degrees. We arbitrarily chose to restrict use of the right claw while leaving the left one intact (Table 2). Keeping the claw immobilized in the closed position with a rubber band or cutting of most of its dactyl did not prevent differentiation of a crusher claw; the right, or restricted claw became a crusher as often as the left, or unrestricted claw. This suggests that use of the claw *per se* was not critical in the differentiation of the crusher claw but that possibly some other minimal condition such as muscle activity was responsible. With neither immobilization nor dactylotomy is activity of the closer muscle prevented.

Consequently, we attempted to reduce muscle activity using more drastic procedures such as deafferentation. This was done by painting either the entire claw or just the pollex and dactyl with a fast-drying lacquer. In the former case the dactyl usually remained in the closed position simply because the entire claw was painted whereas in the latter case it was free to open and close and was seen to do so. Both forms of deafferentation appeared at first glance to suppress differentiation of a crusher claw (Table 2) because the majority of the right claws were cutters. However, when tested statistically the number of right cutter claws in these two experimental groups was not significantly different from those in the control group. These forms of deafferentation with their consequent reduction in motor output were not sufficient to suppress development of a crusher claw and of slow fibres in the closer muscle.

We therefore eliminated activity of the closer muscle by cutting its tendon where it attaches to the movable dactyl, thereby disconnecting the muscle. Tenotomy of the right closer muscle effectively inhibited the treated claw from becoming a crusher compared with its untreated counterpart in the control group (Table 2). As tenotomy has several effects on the closer muscle, it is difficult to determine which particular effect suppressed transformation of fast to slow fibres. For instance,

Table 2 Form of the right claw—whether cutter or crusher, when untreated or treated in various ways

	Right claw				
	Cutter	Crusher	Total no. reared	No. treated histochemically	*P*
Control	18	14	32	8	
Immobilization	9	11	20	5	NS
Dactylotomy	8	7	15	5	NS
Paint claw	15	4	19	5	NS
Paint pollex and dactyl	15	3	18	5	NS
Closer tenotomy	34	3	37	9	<0.001
Opener tenotomy	19	3	22	5	<0.02
Denervation	27	5	32	10	<0.02

* For each experimental group the right claw was manipulated in the 4th and again in the 5th stage and reared to the 9th stage, when its form was assessed visually in all lobsters and histochemically in a few lobsters for determining muscle fibre composition. Significance was determined between the control and each of the experimental conditions using the contingency χ^2 test.

tenotomy not only eliminates activity of the closer muscle but also eliminates its passive stretch and reduces the motor output to the claw muscles by disrupting the proprioceptive feedback.

On the other hand, tenotomy of the opener muscle which is an antagonist to the closer and is a small muscle occupying less than 10% of the claw muscle mass, also inhibited the treated claw from differentiating into a crusher (Table 2). Because this procedure allows the closer muscle to maintain its passive stretch, it rules out the possibility that loss of this stretch when the closer muscle was tenotomized suppressed the transformation of fast to slow fibres. Also, the relatively small size of the opener muscle would not seriously hinder contraction of the massive closer muscle when the opener is tenotomized. It is far more likely that tenotomy of the opener decreased motor output to the claw muscles because of reduction in proprioceptive feedback and sensory input from other sources. For example, some sensory nerve fibres from the dactyl run close to the insertion of the opener tendon and are presumably severed during tenotomy. Therefore, the failure to achieve some critical level of activity in fibres of the closer muscle prevents their transformation from fast to slow type.

As activity of the closer muscle is under the control of its nerve supply, we attempted denervation as a means of eliminating it without interfering with the muscle itself. This was done by destroying the anterior part of one side (right side) of the ganglion in intact animals. The cell bodies of the excitor motoneurones to the claw closer and opener muscles are located in this region of the ganglion in adult lobsters[27]. It was possible to destroy a relatively small anterior region of the ganglion with a finely sharpened pin. The efficacy of this surgery was confirmed by noting the loss of reflex activity in the claws and the destruction of the anterior part of the ganglion in post-mortem dissections of a few test lobsters. This form of denervation had a dramatic effect in that most lobsters failed to develop a crusher on the treated side (Table 2). Eliminating motor activity to the closer muscle prevents its fast fibres from transforming to slow.

Although denervation completely eliminates motor activity to the claw muscles, a reduction in activity such as with tenotomy of the opener muscle is just as effective in inhibiting formation of a crusher claw. Other, less acute treatments such as painting the claw, immobilization or dactylotomy, however, did not suppress development of a crusher claw, suggesting that a minimal level of muscle activity is required for the formation of a crusher claw. Our results therefore show that the reduction or elimination of muscle activity prevents the transformation of fast fibres to slow during development of the claw closer muscles in juvenile lobsters. Furthermore, the denervation experiments demonstrate the regulatory role of motoneurones in the differentiation of fibre types in lobster muscle. Such a crucial role for motoneurones in maintaining and determining fibre properties is well established for adult vertebrate muscle but has not previously been demonstrated in invertebrates and during development.

This work was inspired by the late Fred Lang. We thank H. L. Atwood for criticizing the manuscript, I. M. Campbell for help with statistical analysis, Joanne Pearce and Lena Hill for technical assistance and John Hughes of the Massachusetts State Lobster Hatchery on Martha's Vineyard for supplying us with larval lobsters. The work was supported by grants from the Natural Sciences and Engineering Research Council and the Muscular Dystrophy Association of Canada to C.K.G. and from the NIH (NINCDS) and the Graff Foundation to the late Fred Lang and A. G. Humes, Director, Boston University Marine Program.

Received 24 February; accepted 4 June 1982.

1. Guth, L. *Physiol. Rev.* **48,** 645–687 (1968).
2. Harris A. J. *A. Rev. Physiol.* **36,** 251–305 (1974).
3. Gutmann, E. *A. Rev. Physiol.* **38,** 177–216 (1976).
4. Buller, A. J. & Pope, R. *Phil. Trans. R. Soc.* **278,** 295–305 (1977).
5. Close, R. *J. Physiol., Lond.* **204,** 331–346 (1969).
6. Sreter, F. A., Luff, A. R. & Gergely, J. *J. gen. Physiol.* **66,** 811–821 (1975).
7. Salmons, S. & Sreter, F. A. *Nature* **263,** 30–34 (1976).
8. Salmons, S. & Henrikson, J. *Muscle Nerve* **4,** 94–105 (1981).
9. Pette, D., Smith, M. F., Staudte, H. W. & Vrbova, G. *Pflügers Arch. ges. Physiol.* **338,** 257–272 (1973).
10. Jolesz, F. & Sreter, F. A. *A. Rev. Physiol.* **43,** 531–552 (1981).
11. Whalen, R. G. *et al. Nature* **292,** 805–809 (1981).
12. Gauthier, G. F., Lowey, S. & Hobbs, A. *Nature* **274,** 25–29 (1978).
13. Herrick, F. H. *Bull. U.S. Fish. Commn.* **15,** 1–252 (1895).
14. Govind, C. K. & Lang, F. *J. exp. Zool.* **190,** 281–288 (1974).
15. Jahromi, S. S. & Atwood, H. L. *J. exp. Zool.* **176,** 475–486 (1971).
16. Lang, F., Costello, W. J. & Govind, C. K. *Biol. Bull.* **152,** 75–83 (1977).
17. Lang, F., Govind, C. K. & She, J. *Biol. Bull.* **152,** 382–391 (1977).
18. Govind, C. K. & Lang, F. *Biol. Bull.* **154,** 55–67 (1978).
19. Ogonowski, M. M., Lang, F. & Govind, C. K. *J. exp. Zool.* **213,** 359–367 (1980).
20. Emmel, V. E. *J. exp. Zool.* **5,** 471–484 (1908).
21. Lang, F., Govind, C. K. & Costello, W. J. *Science* **201,** 1037–1039 (1978).
22. Lang, F. *Aquaculture* **6,** 389–393 (1975).
23. Padykula, H. A. & Hermann, E. *J. Histochem. Cytochem.* **4,** 161–169 (1955).
24. Ogonowski, M. M. & Lang, F. *J. exp. Zool.* **207,** 143–151 (1979).
25. Hajek, I., Chari, N., Bass, A. & Gutmann, E. *Physiol. Bohemslov.* **22,** 603–612 (1973).
26. Lehman, W. & Szent-Gyorgi, A. G. *J. gen. Physiol.* **66,** 1–30 (1975).
27. Govind, C. K. & Lang, F. *J. exp. Biol.* **94,** 329–339 (1981).

Kainic acid stimulates excitatory amino acid neurotransmitter release at presynaptic receptors

John W. Ferkany, Robert Zaczek & Joseph T. Coyle*

Departments of Neuroscience, Pharmacology and Experimental
Therapeutics, and Psychiatry and the Behavioral Sciences,
Johns Hopkins University, School of Medicine, Baltimore,
Maryland 21205, USA

Kainic acid (KA), a conformationally restricted analogue of glutamic acid, exhibits potent neuroexcitatory[1] and neurotoxic properties[2]. The mechanism of the neurotoxicity of KA, however, seems to be complex and indirect because in many brain areas neuronal vulnerability requires the integrity of excitatory afferents[3–6]. Nevertheless, neurophysiological studies indicate that the neuroexcitatory effects of KA in the mammalian brain are direct[7]. We have now examined the effects of KA and other excitatory amino acids on the stimulation of cyclic GMP formation in brain slices incubated *in vitro* as a method for monitoring their depolarizing effects[8]. We show in the adult mouse cerebellum that the excitatory amino acid antagonist, D-α-aminoadipate (DAA)[9], blocks the stimulation of cyclic GMP produced by *N*-methyl-D,L-aspartate (NMDLA) but potentiates the effects of KA. Whereas KA causes a significant release of both aspartic (Asp) and glutamic (Glu) acids by a calcium-dependent process, NMDLA is without effect; furthermore, the effects of KA on Glu release are markedly reduced in cerebellum deficient in granule cells. KA also releases Glu and Asp from hippocampal and striatal slices, indicating that this response is not unique to the cerebellum. The results are consistent with evidence that KA has direct excitatory effects on neurones[7] but suggest that its potent neurotoxic action involves the activation of presynaptic receptors on glutamatergic and aspartergic terminals, thereby releasing Asp and Glu.

Male albino mice weighing 25–35 g (Blue Spruce Farms) were used in all experiments. Some mice had been treated with methylazoxymethanol acetate (25 mg per kg) by intraperitoneal injection on the day of birth; this causes a selective deletion of granule cells[10]. Immediately after decapitation the brain was removed, and the cerebellum was rapidly isolated and sliced mechanically at 275 μm at 2 °C before being placed in oxygenated Krebs–bicarbonate buffer. Histological analysis of the slices indicated preservation of the neuronal components in the conditions of slice preparation and incubation used. The cerebellar slices were preincubated for 60 min at 37 °C in Krebs–bicarbonate buffer constantly bubbled with O_2–CO_2 (95:5), with three changes of buffer. Portions of the tissue were

---

* To whom correspondence should be addressed at the Department of Neuroscience.

0028–0836/82/330757—03$01.00

Table 1 Effects of excitatory amino acids on cerebellar cyclic GMP

Condition	Cyclic GMP formed (% of control)
L-glutamate (10 mM)	198 ± 15 (9)*
N-methyl-D, L-aspartate (0.5 mM)	159 ± 10 (9)*
N-methyl-D, L-aspartate (10 mM)	234 ± 22 (4)*
α-Kainic acid (0.1 mM)	156 + 15 (4)*
α-Kainic acid (0.5 mM)	163 ± 9 (11)*
D-α-aminoadipate (0.25 mM)	116 ± 10 (22)
N-methyl-D, L-aspartate (0.5 mM) and D-α-aminoadipate (0.25 mM)	122 ± 14 (9)
α-Kainic acid (0.5 mM) and D-α-aminoadipate (0.25 mM)	251 ± 23 (11)*†

Cerebellar slices prepared from adult mice were incubated in conditions described in the text with the concentrations of amino acids indicated in parentheses and the amount of cyclic GMP formed was measured. The results are expressed in terms of per cent (±s.e.m.) of the cyclic GMP levels in control slices incubated in parallel; basal cyclic GMP levels were 5.4 ± 0.5 pmol per mg protein ($n = 33$). Statistical comparisons were made on the basis of absolute levels of cyclic GMP by ANOVA.

* $P < 0.001$ versus control; † $P < 0.02$ versus kainate alone.

then transferred to vials with 2 ml of fresh buffer containing the compounds of interest, and incubation was continued for an additional 15 min. The reaction was terminated by brief centrifugation, the supernatant was removed, 1 ml of 0.05 M Tris-HCl buffer containing 0.5 mM EGTA was added, and the tissue was immediately boiled for 10 min at 100 °C and then dispersed by sonication. The tissue extract was assayed for cyclic GMP content by the method of Steiner *et al.*[11]. In some experiments, slices were perfused with oxygenated buffer and the fractions were collected as previously described[12]. Amino acids in the medium were measured by HPLC fluorescent detection by the pre-column derivatization method of Hill *et al.*[13].

Incubation of the cerebellar slices with 10 mM Glu or 10 mM NMDLA caused a doubling of cyclic GMP levels (Table 1). Co-incubation of the slices with DAA (0.25 mM) blocked the cyclic GMP formation induced by NMDLA (0.5 mM). Dose–response curves with KA indicated that maximal stimulation of cyclic GMP formation occurred at 0.1 mM, but this concentration caused only a 60% increase in the cyclic GMP levels. However, the addition of DAA, which antagonizes the effects of the granule cell excitatory neurotransmitter[14], markedly potentiated the effects of KA on cyclic GMP formation. This observation raised the question of whether release of endogenous excitatory amino acids in the presence of KA might be attenuating the cyclic GMP response by promoting the neurotoxic effects of KA.

The possible influence of KA on excitatory neurotransmitter release was evaluated by measuring the amount of endogenous amino acids released in the medium during drug exposure (Table 2). With KA (0.5 mM), the concentration of Asp in the medium increased to 233 ± 33% (±s.e.m.; $P < 0.001$; $n = 6$) of control and that of Glu increased to 304 ± 33% ($P < 0.001$) of control whereas the concentrations of glutamine, alanine, tyrosine and taurine did not differ significantly from control. Notably, γ-aminobutyric acid (GABA) was not detected in the medium in the presence or absence of KA. The net release of Glu and Asp stimulated by KA was comparable with that found with a depolarizing concentration of potassium (40 mM). In contrast, neither NMDLA nor dihydro-KA (an analogue with low affinity for KA receptors[1,15]) significantly altered the concentration of the Glu or glutamine in the medium. As dihydro-KA is a more potent inhibitor of the sodium-dependent, high-affinity uptake process for Glu[5,16] than is KA, this result indicates that the KA-induced accumulation of Glu and Asp in the medium did not result simply from inhibition of the uptake process. Tetrodotoxin blocked the depolarization-induced release of Glu and Asp caused by the 40 mM KCl medium whereas tetrodotoxin did not antagonize the effects of KA. Thus, the effect of KA did not depend on the generation of action potentials nor did it result simply from an increased extracellular concentration of potassium, a reported effect of KA[17]. Nevertheless, incubation of the slices in calcium-free medium containing EGTA (1 mM) markedly inhibited the amount of Glu and Asp released by KA although basal release was increased somewhat in this condition; thus, the KA-induced release probably involved stimulus–secretion coupling.

To establish that KA was acting on a neuronal pool of Glu, we examined the effect of KA on Glu release from cerebellar slices deficient in granule cells. Treatment of newborn mice with methylazoxymethanol acetate, a potent alkylating agent, causes a marked and selective depletion of the cerebellar granule cells which are undergoing mitosis at the time[10]. In slices prepared from the granule cell-deficient adult mice, KA (0.5 mM) did not cause a significant release of Glu ($P > 0.10$); rather, the net release of Glu in the presence of KA was only 38 ± 14% of that observed in unlesioned cerebella from littermate controls ($n = 9$). Thus, the granule cells, a reputed glutamatergic system[18,19], seem to be the primary source of Glu released by KA. However, KA did cause a significant release of Asp ($P < 0.01$; $n = 9$) in the granulo-prival slices which was 91% of the amount observed in controls; this is noteworthy because Asp seems to be a neurotransmitter of one of the climbing fibre systems[20], which are spared by the granule cell lesion[21].

The presynaptic effects of KA on excitatory amino acid terminals were not limited to the cerebellum. In perfused slices prepared from cerebellum, hippocampus and striatum, 1 mM KA significantly increased the efflux of Asp and Glu (Table 3). Notably, the ratio of Asp to Glu differed among the three regions, with a greater increase in the Asp than Glu efflux stimulated by KA in the hippocampus. As observed in cerebellum, KA did not cause a release of GABA nor did it affect the efflux of glutamine or alanine. Perfusion with Ca^{2+}-free medium containing EGTA (1 mM) inhibited the KA efflux of Asp and Glu by >80% ($n = 4$; $P < 0.01$) in the hippocampus.

Results of these experiments suggest a resolution to the conundrum that KA has direct excitatory effects[7] although its neurotoxic effects seem to be primarily indirect and require the functional integrity of excitatory inputs[3–6]. The cerebellum offers a particularly favourable region for examining these interactions *in vitro* because the glutamatergic granule cell–parallel fibre system is intrinsic to the region. The present results

Table 2 Release of endogenous glutamate and aspartate from cerebellar slices

Condition	Net release (nmol per mg protein) Glutamate	Aspartate
α-Kainic acid (0.5 mM)	2.04 ± 0.33*	0.61 ± 0.15*
Potassium (40 mM)	2.48 ± 0.02*	0.54 ± 0.14*
N-methyl-D, L-aspartate (0.5 mM)	1.02 ± 0.50	NM
α-Dihydrokainic acid (0.5 mM)	(−)0.03 ± 0.09	0.01 ± 0.14
Tetrodotoxin (5 μM)	0.06 ± 0.12	(−)0.19 ± 0.07
Potassium (40 μM) and tetrodotoxin (5 μM)	0.13 ± 0.14	0.01 ± 0.09
α-Kainic acid (0.5 mM) and tetrodotoxin (5 μM)	2.61 ± 0.70*	1.49 ± 0.28*
α-Kainic acid (0.5 mM) and no Ca^{2+} and EGTA (1 mM)	0.59 ± 0.32	0.36 ± 0.19

Cerebellar slices prepared from adult mice were incubated in the conditions described in the text with the concentrations of drugs indicated in parentheses. The results are expressed in terms of the net amount of amino acids released into the medium in the presence of drug compared with control slices incubated in parallel. Values are the mean ± s.e.m. of five or more preparations. In no condition did the levels of Gln differ significantly from control. NM, not measurable due to interference of *N*-methyl-D, L-aspartate in medium.

* $P < 0.01$ versus control by Student's *t*-test.

Table 3 Effects of kainic acid on the efflux of aspartate and glutamate from perfused slices of mouse brain regions

Region	Aspartate	Glutamate
	(% of baseline)	
Cerebellum	440 ± 79*	963 ± 205*
Hippocampus	1,000 ± 280*	724 ± 57*
Corpus striatum	177 ± 44†	355 ± 66*

Immediately after decapitation, the relevant brain regions of the mice were isolated by dissection at 4 °C and placed in ice-cold oxygenated Krebs–bicarbonate buffer. The tissue blocks were then sectioned at 275 μm. After rinsing in Krebs buffer, the slices were transferred to syringe holders and supported on a bed of Sephadex G-10 (~15 mg wet weight tissue per chamber). The chambers were individually perfused at a rate of 0.5 ml min^{-1} with oxygenated Krebs buffer maintained at 37 °C in a Haake constant temperature circulator. After 60 min of perfusion, spontaneous release of endogenous amino acids stabilized at a constant low rate. Three 3-min samples were collected for baseline values, then buffer containing 1 mM KA was substituted and three 3-min samples were collected for measurement of endogenous amino acid in the buffer by the HPLC method. The results are the mean ± s.e.m. of 4–8 separate preparations.

* $P < 0.01$ versus baseline; † $P < 0.05$ versus baseline.

demonstrate that the activation of guanylate cyclase in cerebellar slices by KA is significantly enhanced by DAA, which antagonizes the effects of NMDLA. The potentiating effect of DAA on KA is compatible with the interpretation that the stimulation of KA receptors combined with the release of endogenous excitatory amino acids has direct neurotoxic effects in the cerebella Purkinje cells, thereby attenuating the cyclic GMP response. This interpretation is consistent with the conclusions of Foster and Roberts[22], who described cooperative interactions between exogenous excitatory amino acids and kainate on cyclic GMP stimulation in cerebellar slices prepared from 8-day-old rats. However, our study demonstrates, for the first time, the existence of presynaptic receptors for KA on the excitatory terminals.

In support of this hypothesis, Nicklas *et al.*[23] have previously demonstrated that KA alone profoundly depresses ATP levels in cerebellar slices, indicative of neurotoxicity[24]. Furthermore, KA stimulates the release of both Glu and Asp in a calcium-dependent, tetrodotoxin-insensitive manner consistent with its action at a presynaptic receptor on parallel fibre and climbing fibre terminals. Ligand binding studies have demonstrated a partial, presynaptic localization of the specific binding sites for ^{3}H-KA on the granule cells as these sites are reduced by 40% in the granule cell-deficient cerebellum[10]. Axonal receptors for KA on dorsal root fibres have also been described by neurophysiological methods[25]. In conclusion, KA seems to act at two sites, one postsynaptic, which accounts for its direct excitatory effects, and the other presynaptic on glutamatergic and aspartergic terminals, which causes release of these excitatory amino acids and may enhance its neurotoxic effects.

This research was supported by USPHS grants NS-13584, MH-26654, DA-00266, USPHS postdoctoral fellowship NS-06798 to J.W.F. and RSDA II MH-00125 to J.T.C.

Received 2 November 1981; accepted 8 June 1982.

1. Biscoe, T. J., Evans, R. H., Headley, P. M., Martin, M. R. & Watkins, J. C. *Br. J. Pharmac.* **58,** 373–382 (1976).
2. Olney, J. W., Rhee, V. & Ho, O. L. *Brain Res.* **77,** 507–512 (1974).
3. Coyle, J. T. & Schwarcz, R. *Nature* **263,** 244–246 (1976).
4. McGeer, E. G., McGeer, P. L. & Singh, K. *Brain Res.* **139,** 381–383 (1978).
5. Biziere, K. & Coyle, J. T. *Neurosci. Lett.* **8,** 303–310 (1978).
6. Kohler, C., Schwarcz, R. & Fuze, K. *Neurosci. Lett.* **10,** 241–24 (1978).
7. McLennan, H. *Neurosci. Lett.* **18,** 313–316 (1980).
8. Foster, G. A. & Roberts, P. J. *Life Sci.* **27,** 215–221 (1980).
9. Watkins, J. C. & Evans, K. H. *A. Rev. Pharmac.* **21,** 165–203 (1981).
10. Slevin, J., Johnston, M. V., Biziere, K. & Coyle, J. T. *Dev. Neurosci.* **5,** 3–12 (1982).
11. Steiner, A. L., Ferrendelli, J. A. & Kipnis, R. M. *J. biol. Chem.* **247,** 1121–1124 (1972).
12. Nelson, M. F., Zaczek, R. & Coyle, J. T. *J. Pharmac. exp. Ther.* **214,** 694–702 (1980).
13. Hill, P. W., Walters, F. H., Wilson, T. D. & Stuart, J. D. *Analyt. Chem.* **51,** 1338–1341 (1979).
14. Stone, T. W. *Br. J. Pharmac.* **66,** 291–296 (1979).
15. London, E. D. & Coyle, J. T. *Molec. Pharmac.* **15,** 492–505 (1979).
16. Johnston, G. A. R., Kennedy, S. M. E. & Twitchin, B. *J. Neurochem.* **32,** 121–127 (1979).
17. Evans, R. H. *J. Physiol., Lond.* **298,** 25–35 (1980).
18. Young, A., Oster-Granite, M., Herndon, R. & Snyder, S. H. *Brain Res.* **73,** 1–13 (1974).
19. Sandoval, M. & Cotman, C. *Neurosciences* **3,** 199–206 (1978).
20. Wiklund, L., Toggenburger, G. & Cuenod, M. *Science* **216,** 78–80 (1982).
21. Nadi, N. S., Kanter, D., McBride, W. J. & Aprison, M. H. *J. Neurochem.* **28,** 661–662 (1977).
22. Foster, G. A. & Roberts, P. J. *Neurosci. Lett.* **23,** 67–70 (1981).
23. Nicklas, W., Krespan, B. & Berl, S. B. *Eur. J. Pharmac.* **62,** 209–213 (1980).
24. Retz, K. C. & Coyle, J. T. *J. Neurochem.* **38,** 196–203 (1982).
25. Davies, J., Evans, R. H., Francis, A. A. & Watkins, J. C. *J. physiol., Paris* **75,** 641–654 (1979).

An opioid benzodiazepine

D. Römer, H. H. Büscher, R. C. Hill, R. Maurer & T. J. Petcher

Sandoz Ltd, Pharmaceutical Division, Preclinical Research,
CH-4002 Basle, Switzerland

H. Zeugner, W. Benson, E. Finner, W. Milkowski & P. W. Thies

Kali-Chemie Pharma Ltd, D-3000 Hannover, FRG

Although the benzodiazepines have been extensively investigated since their discovery about 20 years ago[1], only recently have antagonists of the classical actions of benzodiazepines been described[2]. We have now discovered a class of benzodiazepines which have lost all affinity for benzodiazepine binding sites but which have moderate to high affinity for opiate receptors. Depending on the substituents introduced, it is possible to obtain compounds with selective actions on μ, δ and κ subpopulations of opiate receptors. The compounds are effective analgesics in various animal models of pain, exhibit an opioid activity spectrum in various test systems, and show none of the typical effects of minor tranquillizers. Here we report that 1-methyl-2(3-thienylcarbonyl)-aminomethyl-5-(2-fluorophenyl)-*H*-2,3-dihydro-1,4-benzodiazepine (KC5103; tifluadom), acts selectively on opiate κ-receptors.

It has been believed previously that 1,4-benzodiazepines are a unique class of anxiolytic, anticonvulsant and sedative drugs belonging to the group of minor tranquillizers[1] and indeed the recently described antagonist Ro 15-1788 (ref. 2) is specific for these actions on the central nervous system (CNS). It is well established that most of these clinically active substances bind with high affinity to specific benzodiazepine binding sites in the brain and probably exert their specific effects by modulation of neuronal transmission of γ-aminobutyric acid (GABA).

We have studied benzodiazepines having an alkyl group at position 2, in particular the effect that various changes to this alkyl group[3] have on the affinities of these compounds for CNS receptors[4]. We synthesized the 2-methoxymethyl derivative metaclazepam (patent DE-PS 250937; ref. 5), which is a clinically effective anxiolytic[6] although having only low affinity for benzodiazepine receptors. As an extension of this work we developed 2-acylaminomethyl-1,4-benzodiazepines with a variety of substituents on the phenyl rings and in the side chain (patent DE-OS 2952279; ref. 7). Such compounds are effective in the hot-plate test in mice but this analgesia is not typical of the muscle-relaxant pseudoanalgesia shown by diazepam[8], rather the compounds exhibit affinity for opiate receptors and have lost their affinity for benzodiazepine binding sites.

In comparative binding studies on rat brain homogenates, tifluadom (Fig. 1) displaces ^{3}H-naloxone from its binding sites

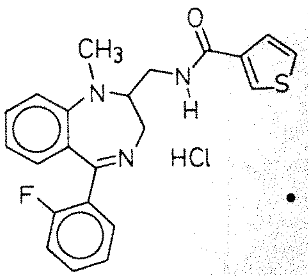

Fig. 1 Structural formula of tifluadom.

Table 1 Displacement of ^{3}H-(−)bremazocine from guinea pig brain homogenates

Substance	IC_{50} (nM)
Tifluadom	14 ± 6 (0.87)
Morphine	350 ± 170 (0.55)
Ketazocine	22 ± 12 (0.85)
Bremazocine	0.75 ± 0.5 (0.95)

Crude guinea pig membrane homogenates (minus cerebellum) were prepared essentially as described elsewhere[16]. ^{3}H-(−)bremazocine (0.5 nM) was incubated with membrane homogenates (17 mg per g wet weight per assay tube) for 40 min at ambient temperature in Tris-HCl buffer (50 mM, pH 7.4), filtered through Whatman GF/B glass fibre filters and washed twice with ice-cold assay buffer. All incubations were done in triplicate, and nonspecific binding was determined in the presence of 0.1 μM bremazocine. IC_{50} values were calculated by appropriately weighted regression analysis (at least four concentrations per decade); Hill coefficients are given in parentheses.

with an IC_{50} (50% inhibitory concentration) of 12 nM and has no effect on ^{3}H-flunitrazepam binding in concentrations up to 1 μM. In contrast, diazepam has no affinity for naloxone sites and displaces ^{3}H-flunitrazepam with an IC_{50} of 15 nM. In the arthritis pain test in the rat[9], a model of chronic pain processes in which classical benzodiazepines are known to give false positive reactions, tifluadom is effective with a 50% effective dose (ED_{50}) of 11 mg per kg orally (p.o.) and this action is partially reversed by pretreatment with 10 mg per kg naloxone subcutaneously (s.c.) but not by doses of up to 32 mg per kg intraperitoneally (i.p.) of the benzodiazepine antagonist Ro 15–1788. In the same test, diazepam is effective at a dose of 6 mg per kg p.o. and its action is readily abolished by Ro 15–1788 at 32 mg per kg i.p. but not by 10 mg per kg s.c. of naloxone. We conclude that tifluadom is an opiate analgesic with none of the actions typical of benzodiazepines.

Receptor binding studies with the universal opiate ligand ^{3}H-(−)bremazocine on guinea pig brain homogenates, a tissue preparation particularly rich in κ- and δ-opiate receptors[10], suggested no particular preference for κ sites compared with μ and δ binding sites. Pharmacological evidence, however, suggested a preference for κ-receptors, therefore we performed comparative studies with the classical μ-agonist morphine, the prototypic κ-agonist ketazocine, tifluadom, and the highly potent κ-agonist bremazocine[11] (see Table 1). Table 2 summarizes the results obtained in electrically-stimulated isolated organs. The rabbit vas deferens (RVD) is unusually specific in its sensitivity to κ-agonists[12,13]. Table 3 shows the effects of the four compounds in the mouse tail flick test[14] and the reversal of these effects by the μ-antagonist naloxone and the putative κ-agonist Mr 2266 (ref. 15).

It is clear from these results that tifluadom is an effective opioid analgesic with a preference for opiate κ-receptors. In keeping with these findings, the compound produces no respiratory depression in rats, is not self-applied by rhesus monkeys, and after programmed administration in the same species does not give rise to opiate withdrawal symptoms on cessation of treatment or after naloxone challenge. The existence of this new class of opioids suggests exciting possibilities for the study of opiate receptor subpopulations.

Table 2 Effects on electrically-stimulated guinea pig myenteric plexus–longitudinal muscle preparation, and mouse and rabbit vasa deferentia

Substance	IC_{50} (nM)			Potency ratio (normorphine = 1)	
	GPI	MVD	RVD	GPI	MVD
Tifluadom	1.7	2.6	4.9	234	43
Morphine	238	159	>10,000	0.9	0.8
Ketazocine	4.7	19.3	54	62	10.1
Bremazocine	0.25	0.5	6.4	1403	453

GPI, guinea pig myenteric plexus–longitudinal muscle preparation; MVD, mouse vasa deferentia[18]; RVD, rabbit vasa deferentia[12]. The IC_{50} is defined as the concentration required to produce 50% inhibition of the supramaximally electrically induced twitch response in each isolated tissue. Results are the means of several experiments: GPI n = 6–12, MVD n = 6–10, RVD n = 5. The absolute potency of normorphine varies strongly from tissue to tissue but is typically 150–400 nM (GPI) and 50–150 nM (MVD).

Table 3 Actions of test substances in the mouse tail flick test and their antagonism by naloxone and Mr 2266

Test substance	ED_{50} (mg per kg s.c., 30 min)	AD_{50} naloxone (mg per kg i.v.)	AD_{50} Mr 2266 (mg per kg i.v.)
Tifluadom	1.1 (0.5–2.4)	0.56 (0.31–1.02)	0.19 (0.08–0.45)
Morphine	3.0 (2.7–4.5)	0.005 (0.002–0.009)	0.08 (0.039–0.16)
Ketazocine	0.3* (0.1–0.5)	0.07 (0.03–0.1)	0.04 (0.02–0.08)
Bremazocine	0.7 (0.3–1.4)	~3.2	0.46 (0.24–0.87)

The ED_{50}(P = 0.05) is defined as the dose that prolonged the reaction time in seconds by >75% in half of the mice. The AD_{50} (P = 0.05) is defined as the dose (intravenous, i.v.) of the antagonist needed to reduce by 50% the analgesic effect of equi-active doses (ED_{90}) of the agonists. The antagonist was injected 15 min after the agonists (ketazocine, 7 min); readings were made 15 min later (ketazocine, 8 min): 5–10 animals were used per dose. Figures in parentheses indicate 95% confidence limits.

* 15 min.

Received 7 June; accepted 29 June 1982.

1. Sternbach, L. H. *J. med. Chem.* **22,** 1–7 (1979); *Arzneimittel-Forsch.* **30,** 851–916 (1980).
2. Hunkler, W. *et al. Nature* **290,** 514–516 (1981).
3. Liepmann, H., Milkowski , W. & Zeugner, H. *Eur. J. med. Chem.* **11,** 501 (1976).
4. Li, P.-L. in *Proc. Workshop on Cell Surface Receptors—Basic and Clinical Aspects* Cambridge, 1982 (Horwood, London, in the press).
5. Milkowski, W. *et al. Chem. Abstr.* **86,** 89913W (1977).
6. Laakman G. & Hippius, H. *Adv. Biosci.* **31,** 125–134 (1981).
7. Zeugner, H. *et al. Chem. Abstr.* **95,** 169234*b* (1981).
8. Garattini, S., Mussini, E. & Randall, L. O. in *The Benzodiazepines* 36ff (Raven, New York, 1973).
9. Pircio, A. W., Fedele, C. T. & Bierwagen, M. E. *Eur. J. Pharmac.* **31,** 207–215 (1975).
10. Kosterlitz, H. W., Paterson, S. J. & Robson, L. E. *Br. J. Pharmac.* **73,** 939–949 (1981).
11. Römer, D. *et al. Life Sci.* **27,** 971–978 (1980).
12. Oka, T. *et al. Eur. J. Pharmac.* **73,** 235–236 (1981).
13. Römer, D., Hill, R. C. & Maurer, R. in *Proc. 3rd World Cong. on Pain*, Edinburgh, 1981 (Raven, New York, in the press).
14. D'Amour D. E. & Smith, D. L. *J. Pharmac. exp. Theor.* **72,** 74–78 (1941).
15. Lord, J. A. H., Waterfield, A. A., Hughes, J. & Kosterlitz, H. W. *Nature* **267,** 495–499 (1977).
16. Pert, C. B. & Snyder, S. H. *Proc. natn. Acad. Sci. U.S.A.* **70,** 2243–2247 (1973).
17. Kosterlitz, H. W. & Watt, A. J. *Br. J. Pharmac.* **33,** 266–276 (1968).
18. Henderson, G., Hughes, J. & Kosterlitz, H. W. *Br. J. Pharmac.* **46,** 764–766 (1972).

A novel intercistronic regulatory element of prokaryotic operons

Christopher F. Higgins*§, Giovanna Ferro-Luzzi Ames*, Wayne M. Barnes†, Jean Marie Clement‡ & Maurice Hofnung‡

* Department of Biochemistry, University of California, Berkeley, California 94720, USA
† Department of Biological Chemistry, Washington University School of Medicine, St Louis, Missouri 63110, USA
‡ Unité de Programmation Moléculaire et Toxicologie Génétique, CNRS LA271 INSERM U-163, Institut Pasteur, 75015 Paris, France
§ Present address: Molecular Genetics Laboratory, Department of Biochemistry, University of Dundee, Dundee DD1 4HN, UK

The nucleotide sequences of the intercistronic regions from several multicistronic operons have recently been determined. In many cases such intercistronic regions consist of only a few base pairs (bp); in certain extreme cases, where the initiation codon of one gene overlaps the termination codon of the previous gene, intercistronic regions are essentially absent[1,2]. However, in other cases intercistronic regions can be up to several hundred base pairs long; it seems reasonable to suppose that, at least in these cases, such regions have a role in regulating expression of the operon. Indeed, a regulatory function for the large intercistronic region of the *rplJL–rpoBC* operon has been demonstrated[3]. We have now identified a genetic element, common to intercistronic regions from three independent

0028-0836/82/330760—03$01.00

bacterial operons (the histidine transport and the histidine biosynthetic operons of *Salmonella typhimurium* and the *malK–lamB* operon of the malB region of *Escherichia coli*), which we believe to be important in regulating the differential expression of individual genes in these multicistronic operons. A similar element is also found immediately following the *trpR* gene of *E. coli* although in this case it is not known whether or not a distal gene exists. Each of these elements consists of a long dyad symmetry which, once transcribed, could form an exceptionally stable stem–loop structure with a stem of up to 35 bp. In each case smaller palindromic units are also found, some of which overlap the main symmetry. The stem–loop structures show remarkable homology (~90%) and probably have a common evolutionary origin, possibly an insertion element. It seems that the function of these structures is to effect a decrease in expression of distal genes in an operon.

The histidine transport operon of *S. typhimurium* consists of four cistrons, coordinately transcribed from a single promoter (see accompanying letter[4]). Between the first two genes of this operon, *hisJ* (encoding the periplasmic histidine-binding protein) and *hisQ* (encoding a membrane-bound protein), there is an intercistronic region of 183 bp. An exceptionally long dyad symmetry (32 bases in each arm of the repeat) is evident within this region which, once transcribed, could form a very stable stem–loop structure ($\Delta G = -54.4\ \text{kcal mol}^{-1}$)[5] (Fig. 1*a*). The *hisG–hisD* intercistronic region of the histidine biosynthetic operon of *S. typhimurium* also contains a long dyad symmetry (Fig. 1*c*) which shows remarkable sequence homology with the dyad symmetry in the *hisJ–hisQ* intergenic region. A third example of this long intercistronic dyad symmetry is found in the *malK–lamB* operon of *E. coli*[6] (Fig. 1*e*) and again, it is almost identical in sequence to the two examples described above. This third example lies between *lamB* (encoding the λ receptor) and *molA*, a gene whose function is unknown[6]. As no obvious promoter or terminator is found between *lamB* and *molA* it is reasonable to assume that these two genes form part of the same operon. A further example of this long dyad symmetry is found immediately following the *trpR* gene of *E. coli*[7,8]. However, in this case it is not known whether the region is intercistronic (that is, whether a distally located gene exists and is co-transcribed with *trpR*) or whether it marks the end of a transcription unit.

The remarkable homology between these dyad symmetries is shown in Fig. 2. For example, the long dyad symmetries in *hisJ–hisQ* and *hisG–hisD* show 90% homology (42/47 bases); a comparably high level of homology is evident whichever combination of regions is compared. Interestingly, the loops of these potential stem–loop structures show no significant homology.

Detailed analysis of sequences in and around these long dyad symmetries shows the presence of several copies of a smaller palindromic unit (Figs 2, 3). A computer search of sequence data banks did not reveal further copies of this unit at any other locus. These smaller palindromic units are not completely symmetrical (Fig. 3) and consecutive copies are always in opposite orientations. Thus, once transcribed, stem–loop structures could not only be formed within each unit (Fig. 1*b*, *d*, *f*), but could also form between units, giving rise to a variety of larger, secondary structures. Indeed, the intercistronic elements (long dyad symmetries) described above are the result of just such base-pairing between two of these smaller palindromic units. Thus, stem–loop structures, some of which are mutually exclusive with the intercistronic element, can be formed; such structures may or may not be functionally significant. Interestingly, the attenuator of the *rplJL–rpoBC* operon[3] also shows considerable homology with this smaller palindromic unit.

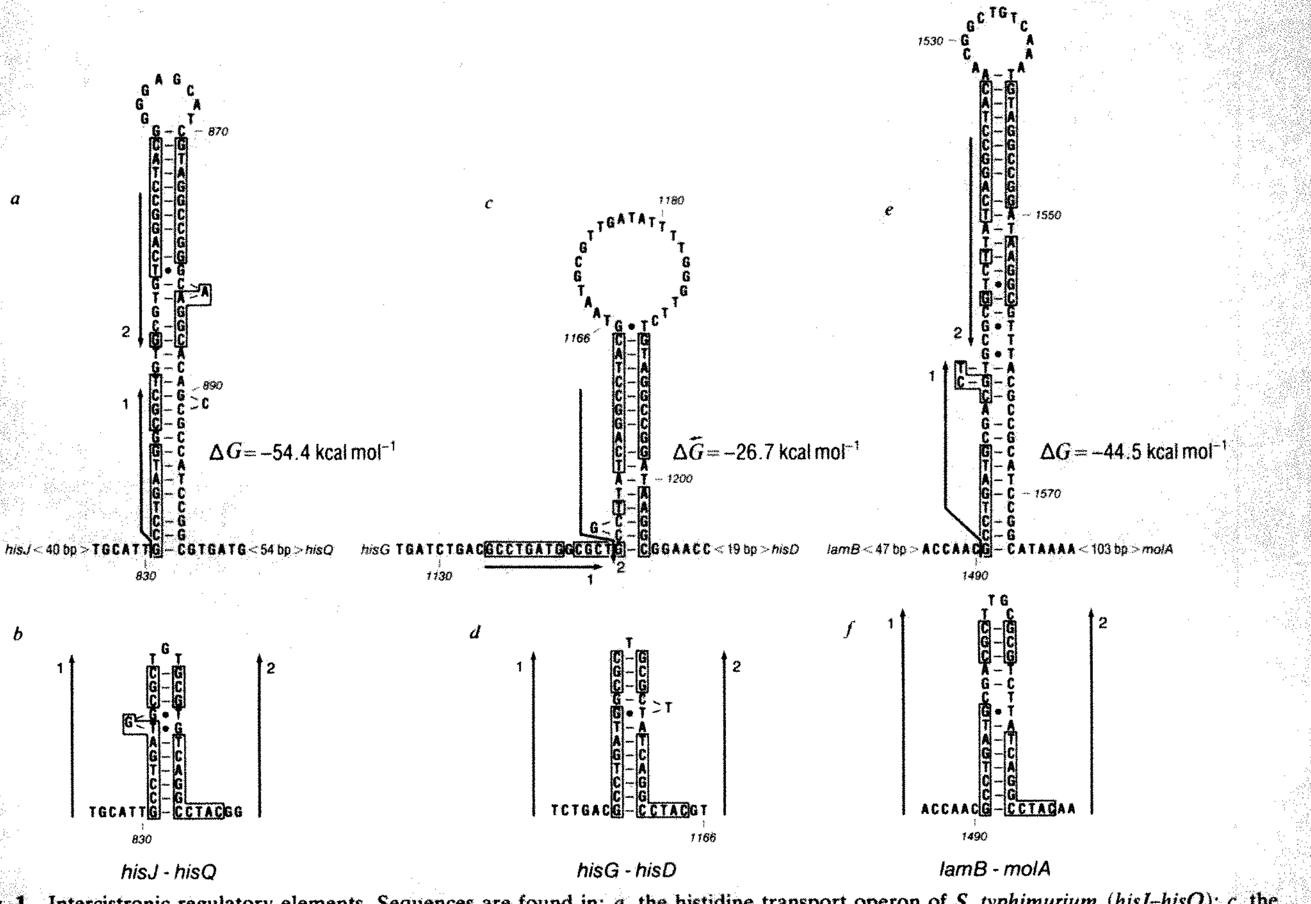
a
c
e
b
d
f
870
890
830
1180
1166
1200
1130
1530
1550
1570
1490
ΔG = −54.4 kcal mol⁻¹
ΔG = −26.7 kcal mol⁻¹
ΔG = −44.5 kcal mol⁻¹
hisJ < 40 bp > TGCATTG – CGTGATG < 54 bp > hisQ
hisG TGATCTGACGCCTGATGGCGCTG – CGGAACC < 19 bp > hisD
lamB < 47 bp > ACCAACG – CATAAAA < 103 bp > molA
1
2
hisJ - hisQ
hisG - hisD
lamB - molA

Fig. 1 Intercistronic regulatory elements. Sequences are found in: *a*, the histidine transport operon of *S. typhimurium* (*hisJ–hisQ*); *c*, the histidine biosynthetic operon of *S. typhimurium* (*hisG–hisD*); *e*, the *malK–lamB* operon of *E. coli* (*lamB–molA*). For each region alternative stem–loop structures are shown (*b*, *d* and *f*, respectively). The overlapping nature of these alternative structures is shown by the arrows (labelled 1 and 2) alongside the major structure which indicate the position of the alternative symmetry. Bases identical in all three sets of structures are boxed. Nucleotide sequences and base numberings are from ref. 4 (*hisJ–hisQ*), ref. 6 (*lamB–molA*) or unpublished data of W.B. (*hisG–hisD*).

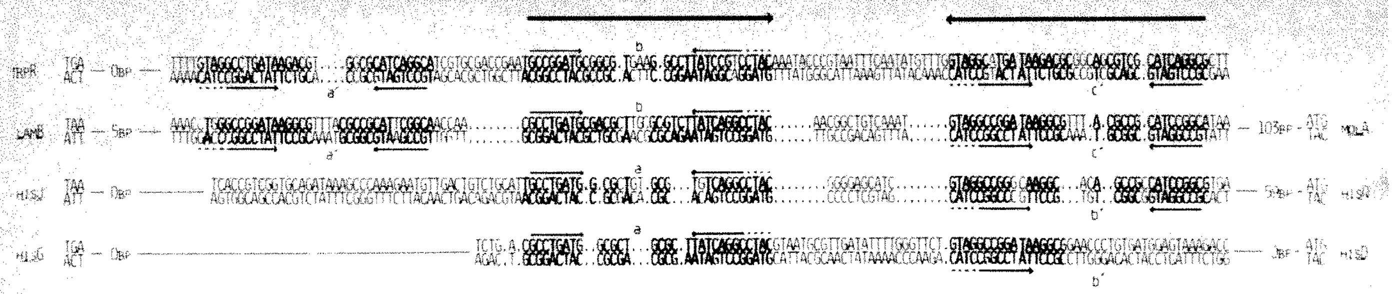

Fig. 2 Alignment of intercistronic regions. The *hisJ–hisQ*, *hisG–hisD* and *lamB–molA* intercistronic regions together with sequences immediately following the *trpR* gene are aligned for homology. Shaded bases indicate significant homologies between the sequences, corresponding to the consensus sequence for the smaller palindromic unit (Fig. 3). A dot in the sequences indicates the absence of a base. Arrows above the sequences indicate the position of the long dyad symmetry (intercistronic element) discussed in the text. The shorter arrows above and below each sequence indicate the position of the smaller palindromic units. The homologous sequence 5′ to each of these smaller palindromic units (see Fig. 3) is indicated by a series of dots following the arrows. Nucleotide sequences were obtained and are numbered as described in Fig. 1 legend or were taken from refs 7 and 8 (*trpR*).

What is the function of the intercistronic elements? Because of their location, we postulate that they are responsible for the lowered expression of distally located genes in a multicistronic operon. In the histidine transport operon, *hisJ* is expressed about 10 times more efficiently than *hisQ*[4]. Similarly, in the histidine biosynthetic operon, the dyad symmetry is found between two genes expressed to different extents: *hisG* is expressed at about three times the level of the distal *hisD* gene[9]. Unfortunately, in the *malK–lamB* operon the relative levels of expression of *lamB* and *molA* are unknown, although the *lamB* protein is known to be expressed at very high levels. It seems unlikely that regulation by these elements operates at a translational level: they are clearly separated from the ribosome-binding sites of the genes immediately downstream and bear no constant spatial relationship to the translation initiation codon. Indeed, evidence that regulation is transcriptional, rather than translational, has been obtained in studies of β-galactosidase production in strains carrying fusions of *lacZ* to *hisJ* and *hisQ* (M. Stern, C. F. H. and G. F.-L. A., in preparation). The elements might either cause premature termination of transcription, or they might serve as a processing site in the message after transcription. It is known that RNase III can cleave certain large stem–loop structures in mRNA[10–12] and it has been postulated that in doing so it regulates gene expression[3]. Perhaps, after RNase III cleavage, the distal portion of the message is rapidly degraded. It is also possible that these elements serve to protect long untranslated intercistronic regions from degradation, thus affecting the expression of distally located genes.

What is the origin of these elements? It seems unlikely that these homologous sequences have arisen independently to allow specific interactions with a common nucleic acid sequence or protein: sufficient specificity could be imparted by very much shorter sequences. More probably, the extensive homology reflects a common evolutionary origin. It is interesting to speculate that these intergenic regulatory elements may have arisen from insertion sequence-like elements, that is, 'regulatory building blocks', becoming fixed at locations in which they provide a selective advantage. The lack of a short direct repeat on either side of the regulatory elements, typical of insertion sequences[13], may be a result of mutational fixation of the element at these specific locations. Note, however, that these intergenic regulatory elements show no homology with known insertion elements of *E. coli*[13].

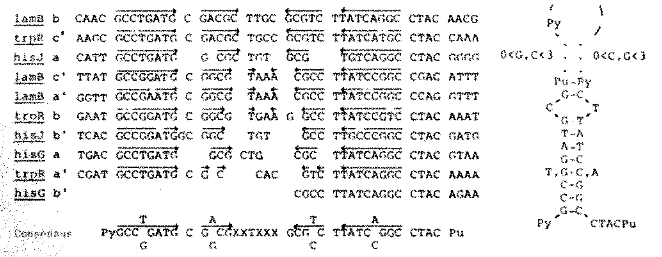
lamB b CAAC GCCTGATG C GACGC TTGC GCGTC TTATCAGGC CTAC AACG
trpR c' AAGC GCCTGATG C GACGC TGCC GCGTC TTATCATGC CTAC CAAA
hisJ a CATT GCCTGATG G CGC TGT GCG TGTCAGGC CTAC GGGG
lamB c' TTAT GCCGGATG C GGCG TAAA CGCC TTATCCGGC CGAC ATTT
lamB a' GGTT GCCGAATG C GGCG TAAA CGCC TTATCCGGC CCAG GTTT
trpR b GAAT GCCGGATG C GGCG TGAA G GCC TTATCCGTC CTAC AAAT
hisJ b' TCAC GCCGGATGGC GGC TGT GCC TTGCCCGGC CTAC GATG
hisG a TGAC GCCTGATG GCG CTG CGC TTATCAGGC CTAC GTAA
trpR a' CGAT GCCTGATG C G C CAC GTC TTATCAGGC CTAC AAAA
hisG b' CGCC TTATCAGGC CTAC AGAA
Consensus
T A T A
PyGCC GATG C G CGXXTXXX GCG C TTATC GGC CTAC Pu
G G C C
Py
0<G,C<3
0<C,G<3
Pu-Py
G-C
C
T
G·T
T-A
A-T
G-C
T,G-C,A
C-G
C-G
G-C
Py
CTACPu

Fig. 3 Consensus sequence of palindromic units. The several copies of the smaller palindromic units identified in and around the intercistronic elements are aligned for maximum homology. Arrows above the sequence indicate regions of dyad symmetry. The location of these sequences with respect to each other is indicated in Fig. 2. A consensus sequence for these palindromic units is given: Py indicates a pyrimidine base, Pu a purine. Note that the units are not completely symmetrical; a conserved sequence, CTAC, is found 3′ to each of the dyad symmetries, giving directionality to each unit. The potential stem–loop structure which might be formed by these units is shown schematically. Sequences were obtained as described in Figs 1 and 2.

Although we have identified three of these stem–loop structures in operons whose nucleotide sequences have been partially or completely determined, two lines of evidence indicate that very similar, if not identical, structures also occur at several other locations on the chromosome, presumably in other intercistronic regions where a step-down in expression of distal genes occurs. First, chromosomal rearrangements involving the histidine biosynthetic operon frequently have one end point within the *hisG–hisD* intergenic region[14]. It has previously been suggested that such *recA*-dependent rearrangements involve recombination with homologous sequences elsewhere on the chromosome[14]. Second, we have observed[15] that a clone of the histidine transport operon of *S. typhimurium* hybridizes with a number of fragments from a total chromosomal digest, in addition to those fragments which cover the transport operon itself. This may be due to hybridization with homologous sequences dispersed throughout the chromosome. The precise number and location of these additional elements remain to be determined.

We thank Bruce Ames and D. Brutlag for many helpful discussions. This work was supported by NIH grants AM12121 and GM24956 to G.F.-L.A. and W.M.B., respectively, by a NATO/SRC fellowship to C.F.H., and by grants from the DDRST and the Fondation pour la Recherche Medicale to M.H.

Received 9 February; accepted 15 June 1982.

1. Christie, G. E. & Platt, T. *J. molec. Biol.* **142**, 519–530 (1980).
2. Selker, E. & Yanofsky, C. *J. molec. Biol.* **130**, 135–143 (1979).
3. Barry, G., Squires, C. & Squires, C. L. *Proc. natn. Acad. Sci. U.S.A.* **77**, 3331–3335 (1980).
4. Higgins, C. F. *et al. Nature* **298**, 723–727 (1982).
5. Borer, P. N., Dengler, B. & Tinoco, I. *J. molec. Biol.* **86**, 845–853 (1974).
6. Clement, J. M. & Hofnung, M. *Cell* **27**, 507–514 (1981).
7. Gunsalus, R. P. & Yanofsky, C. *Proc. natn. Acad. Sci. U.S.A.* **77**, 7117–7121 (1980).
8. Singleton, C. K., Roeder, W. D., Bogosian, G., Somerville, R. L. & Weith, H. L. *Nucleic Acids Res.* **8**, 1551–1560 (1980).
9. Whitfield, H. J. *et al. J. molec. Biol.* **49**, 245–249 (1970).
10. Gegenheimer, P., Watson, N. & Apirion, D. *J. biol. Chem.* **252**, 3064–3073 (1977).
11. Robertson, H. D., Dickson, E. & Dunn, J. J. *Proc. natn. Acad. Sci. U.S.A.* **74**, 822–826 (1977).
12. Bram, R. J., Young, R. A. & Steitz, J. A. *Cell* **19**, 393–401 (1980).
13. Calos, M. P. & Miller, J. H. *Cell* **20**, 579–595 (1980).
14. Anderson, R. P. & Roth, J. R. *J. molec. Biol.* **119**, 147–166 (1978).
15. Ardeshir, F., Higgins, C. F. & Ames, G. F.-L. *J. Bact.* **147**, 401–409 (1981).

Identification of a centriole-associated protein by antibodies present in normal rabbit sera

K. Turksen*, J. E. Aubin† & V. I. Kalnins*

* Division of Histology, Department of Anatomy and
† MRC Group in Periodontal Physiology, Medical Sciences Building,
University of Toronto, Toronto, Ontario, Canada M5S 1A8

The centriolar region is a complex structural entity comprising not only centrioles, but also an abundance of associated electron-dense material identified at present only at the ultrastructural level[1,2]. It is known to contain initiation sites necessary for the assembly of both cytoplasmic and spindle microtubules. Basal bodies, which are structurally related to centrioles, contain the template and serve as initiation sites for the assembly of other microtubule-containing structures, such as the axonemes of cilia and flagella. Immunoglobulins in the sera of some apparently normal rabbits have the ability to bind specifically to centrioles and basal bodies, and have allowed the distribution of these structures to be localized at the light microscope level by immunofluorescence[3–5]. The identity of the molecule(s) detected by these sera in the centriolar region is unknown, although it is not tubulin, the major identified protein of centrioles[4]. We describe here the identification of a protein recognized by the immunoglobulins in some normal rabbit sera, of approximate molecular weight (MW) 50,000 in both basal bodies isolated from *Tetrahymena pyriformis* and in extracts of chicken tracheal epithelial cells.

When a monolayer of mammalian cells is stained with one of these sera the centrioles are strongly labelled and their position in cells can be readily identified[4]. The staining of centrioles is not species-specific and can be seen in basal bodies and centrioles in a wide variety of species including protozoans such as *Tetrahymena* (Fig. 1*a*). When cells are treated with 0.5% Triton X-100 before fixation, the immunofluorescence staining of centrioles and basal bodies by these normal sera is abolished, suggesting that the centriolar antigen(s) is loosely bound to the centriole. Because it would be advantageous to use Triton X-100 to disrupt membranes and thus isolate the basal bodies from the pellicles of *Tetrahymena*, the basal body staining was stabilized by using EDTA (see Fig. 1*b*), a method previously used to stabilize the basal bodies in *Chlamydomonas*[6].

A preparation enriched in basal bodies and retaining the centriolar antigen was made by breaking deciliated cells by vortex agitation in Triton X-100 containing 10 mM EDTA, *p*H 6.8, and separating the basal bodies from the cells and cellular debris by differential centrifugation (Fig. 2). Basal bodies were further purified by centrifugation on a discontinuous sucrose gradient. When basal bodies prepared in this way were stained for immunofluorescence with centriole-specific sera, the presence of the reacting antigen was clear. The protein components of the isolated basal bodies were then examined by SDS-polyacrylamide gel electrophoresis (SDS-PAGE). Numerous bands could be seen, including prominent ones at positions corresponding to molecular weights of 30–35,000, 45–47,000 and 55,000 and numerous less abundant ones at higher molecular weight (Fig. 2*a*). The band at about 55,000 apparently corresponded to tubulin, as it had the same electrophoretic mobility as the phosphocellulose-purified pig brain tubulin that was co-electrophoresed in a companion slot. This identity was confirmed by immunoautoradiography of nitrocellulose[7] sheets with antibody against pig brain tubulin.

To identify conclusively the antigen in the basal bodies which is responsible for the staining of the centrioles, we used the same electrophoretic blotting procedure. The basal body proteins were separated by SDS-PAGE (Fig. 2*a*) and electrophoretically transferred onto a nitrocellulose sheet (Fig. 2*b*). The sheets were then treated with several different centriole-positive normal rabbit sera and autoradiographed. With all the sera, one band could be readily detected in the autoradiographs (Fig. 2*c*) which, by comparison with marker molecules, corresponded to a molecular weight of 50,000 (Fig. 2). The band was not labelled with antisera to tubulin or with normal sera lacking specificity for centrioles (Fig. 2*c*), indicating that these sera did not contain any immunoglobulin against the 50,000-MW basal body protein. Treatment of the nitrocellulose sheets with ^{125}I-labelled protein A alone showed no binding between the

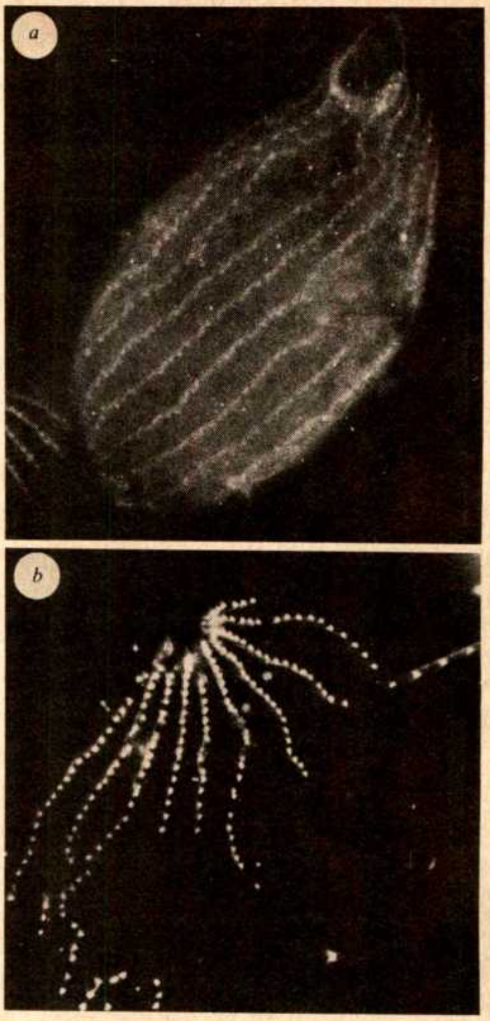

Fig. 1 Immunofluorescence micrograph showing typical basal body staining of isolated *Tetrahymena* pellicles by normal rabbit sera before (*a*) and after treatment with Triton X-100 + EDTA (*b*) stained with the same serum. Mass cultures of *T. pyriformis* strain GL cells were grown at 28 °C for 18–21 h in 6-l Erlenmeyer flasks, each with 1 l of culture medium containing 2% w/v protease peptone (Difco), 0.1% w/v liver extract L (US Biochemical). Cells were collected by centrifugation, and deciliated according to the procedure of Bird and Zimmerman[10]. Pellicles were isolated according to ref. 11. For immunofluorescence, purified pellicles were allowed to settle onto poly-L-lysine (Sigma, 0.1% w/v)-coated coverslips; they were fixed in methanol at −20 °C for 4 min, washed in phosphate-buffered saline (PBS) and then processed for indirect immunofluorescence (see below). For extraction, pellicles on poly-L-lysine-coated coverslips were fixed in freshly prepared 3% paraformaldehyde (Fisher) in PBS. The coverslips were then extracted in 1% Triton X-100 (Sigma)-containing 10 mM EDTA (Fisher) *p*H 6.8, for 5 min at room temperature and washed in PBS. They were then processed for indirect immunofluorescence. Standard indirect immunofluorescence: the coverslips after fixation were washed briefly in PBS, then incubated with normal rabbit serum (1:20 dilution in PBS) for 30 min at room temperature in a humidified chamber. The coverslips were then washed three times with PBS for 10 min and incubated for 30 min with fluorescein-labelled goat IgG against rabbit IgG (FITC-GAR, Hyland, diluted 1:5 in PBS) which was preabsorbed with *T. pyriformis* acetone powder. Finally, coverslips were washed three further times with PBS for 10 min. Coverslips were mounted in 50% glycerol in PBS, *p*H 7.8. The preparations were viewed with a Zeiss Photomicroscope-II equipped with epifluorescent illumination. Pictures were taken using Ilford FP-4 film. *a*, *b*, ×1,080.

0028–0836/82/330763—03$01.00

^{125}I-protein A and *Tetrahymena* basal body proteins (data not shown). Although the antisera to tubulin did stain the tubulin bands, this staining was clearly not due to the centriole-associated protein, as in companion gel slots the bands recognized by tubulin antisera and centriole sera were different. This was demonstrated further by labelling a nitrocellulose sheet containing basal body proteins simultaneously with both centriole-specific normal serum and tubulin-specific immune serum. This procedure clearly distinguished the tubulin band from the lower molecular weight (50,000) protein recognized by the centriole-specific serum (Fig. 2). Non-centriole-staining normal rabbit sera did not label any bands in these basal body extracts (not shown).

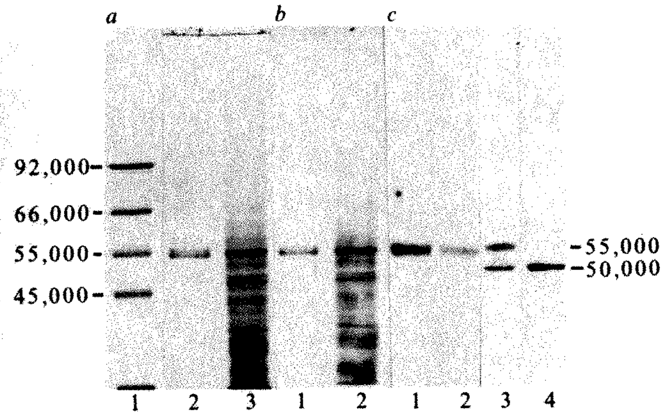

Fig. 2 Immunoelectrophoretic detection of the centriole-associated protein. *a*, SDS-PAGE stained with Coomassie blue. Lane 1, molecular weight standards phosphorylase *b* (92,000), bovine serum albumin (66,000), ovalbumin (45,000; Bio-Rad) and pig brain tubulin (57,000 and 55,000); 2, pig brain tubulin; 3, basal body-enriched fraction from *T. pyriformis*. *b*, Nitrocellulose sheet corresponding to gel in *a* after electrophoretic protein transfer and amido black staining. *c*, Immunoautoradiogram from nitrocellulose sheets labelled with antibodies and ^{125}I-protein A. Lane 1, pig brain tubulin labelled with rabbit antiserum (1:750) to pig brain tubulin; 2, basal body-enriched fraction labelled with rabbit antiserum (1:500) to pig brain tubulin; 3, basal body-enriched fraction labelled simultaneously with rabbit antiserum (1:500) to pig brain tubulin and with centriole-staining rabbit serum CT-2 (1:500); 4, basal body-enriched faction labelled with centriole-staining rabbit serum HMW-3 (1:200). To isolate fractions enriched in basal bodies, deciliated cells were washed twice with fresh medium and broken in 1% Triton X-100 containing 10 mM EDTA, *p*H 6.8, by vortex agitation for 30 s. Unbroken cells and large debris were removed by centrifugation at 4,000*g* (Sorvall HB-4 rotor) at 4 °C, for 10 min. The supernatant was further centrifuged at 8,000*g* for 10 min at 4 °C. Finally, basal bodies were pelleted by centrifugation at 12,000*g* for 30 min at 4 °C. This pellet is called the basal body-enriched fraction. In some experiments, the above pellet was run on a discontinuous sucrose gradient for further purification of basal bodies. For sucrose gradients, the basal body-enriched pellet was suspended in 1 ml of a 5% sucrose solution and was layered on a 0.7:1.2:1.7 M sucrose gradient (10 ml each) and centrifuged at 4,000*g* for 1.5 h using a Sorvall HB-4 swinging bucket rotor at 4 °C. The band containing the basal bodies was at the 1.2:1.7 M interface. This band was removed carefully and diluted with distilled water. The basal bodies were pelleted by centrifugation at 12,000*g* for 30 min at 4 °C. Basal body proteins were separated by SDS-PAGE using the buffer system of Laemmli[12]. The samples were electrophoresed at a constant current of 30 mA, using a Bio-Rad slab gel apparatus model 220. A 3% stacking gel and 8% resolving gel were used. Basal body proteins were transferred to nitrocellulose sheets as described in ref. 7, and antigens were detected using ^{125}I-protein A. Briefly, the nitrocellulose sheets were saturated with 3% bovine serum albumin (BSA, Fraction V, Sigma) in 10 mM Tris-buffered saline (TBS), *p*H 7.4 by incubating for 1 h at 37 °C. Sheets were then washed with TBS at room temperature and incubated for 24 h with rabbit sera in TBS buffer containing 3% BSA. The nirocellulose sheets were washed for 1 h with TBS and incubated for 3 h with ^{125}I-protein A in TBS buffer containing 3% BSA. The nitrocellulose sheets were then washed in TBS containing 0.1% Tween 20 (Sigma) and dried in air. The blots were exposed to Kodak X-Omat XAR-5 film with an intensifying screen (Dupont) at −70 °C. Protein A was iodinated at room temperature for 15 min in a reaction mixture (50 µl) containing 100 µg protein A (Pharmacia), 0.5 mCi carrier-free Na^{125}I (Amersham), 2.5 µg chloramine-T (Kodak), 5 µl dimethyl sulphoxide (Fisher). The reaction was stopped by addition of 5 µg of sodium metabisulphite (Sigma). The labelled protein and unreacted ^{125}I were separated on Sephadex G-25. The radioactively labelled protein A was rechromatographed on Sephadex G-25. Pig brain tubulin was purified as described[13]. The tubulin antiserum used in these studies was prepared against electrophoretically purified tubulin isolated from pig brain as previously described[14].

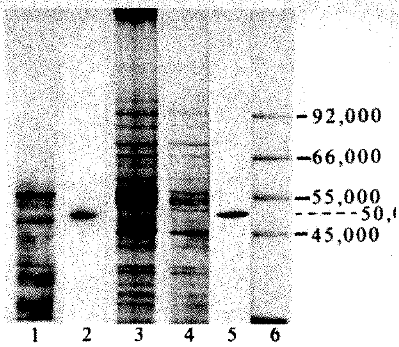

Fig. 3 Immunoelectrophoretic detection of the centriole-associated protein in ciliated chicken trachea cell extracts. Lane 1, nitrocellulose sheet with basal body-enriched fraction as in Fig. 2*b*, lane 2. Lane 2, immunoautoradiogram corresponding to lane 1 but labelled with a centriole-staining serum CT-2 (1:200) and ^{125}I-protein A. Lane 3, SDS-PAGE of Triton X-100 extract of ciliated cells from chicken trachea. Lane 4, nitrocellulose sheet corresponding to gel in lane 3 after electrophoretic protein transfer and amido black staining. Lane 5, immunoautoradiogram corresponding to lane 4 with nitrocellulose sheet labelled with centriole-staining rabbit serum CT-2 (1:200). Lane 6, molecular weight standards (see Fig. 2 legend). Ciliated cells were isolated from adult chicken trachea, obtained from a local abbatoir, as described previously[3]. Briefly, the tracheae were rinsed with PBS and cut open at the midline. The tracheal epithelium was removed by gently scraping with a glass coverslip. Cells were collected by centrifugation at 4,000*g* (Sorvall HB-4 rotor) at 4 °C for 10 min and extracted with Triton X-100 (Sigma) for 10 min. Cellular debris was removed by centrifugation at 12,000*g* for 10 min at 4 °C. The supernatant was used in identification of the centriole-associated protein. The samples were electrophoresed and incubated as for Fig. 2.

Since the centriole-specific sera were known to label cells from diverse species of higher organisms, it was of interest to determine whether or not the same or a similar 50,000-MW protein could be detected in the centriolar structures in any of these organisms. Thus ciliated cells from chicken trachea were treated with Triton X-100, as the centriole staining of these cells was known to be lost by Triton X-100 extraction. When the detergent extracts of the ciliated cells were used for immunoautoradiography, the centriole serum specifically labelled a band corresponding to MW 50,000 which co-migrated with the antigenicity detected in basal body preparations (Fig. 3).

These results show that certain centriole-staining normal rabbit sera have IgG molecules directed against a protein with a mobility on SDS-PAGE corresponding to a MW of ~50,000. Similar IgGs are absent from sera which do not stain centrioles, or stain only the tubulin-containing component of centrioles.

The function—whether enzymatic or structural—of the 50,000-MW protein is unknown. However, it, or a very similar protein, seems to be present in centrioles and basal bodies of diverse cell types and organisms ranging from protozoa to mammals, suggesting that it has been conserved and may be functionally important. Recently, two other polypeptides (of MW 14,000 and 17,000) have been localized at the centriolar region using other preimmune or immune sera[8]. The use of these, and perhaps other, sera, as well as precise biochemical analyses (for example, ref. 9), may help to decipher important constituents of these complex structures which have not previously been defined. Finally, it would also be of interest to determine whether the ability to make these antibodies to centriolar proteins is genetically inherited or whether they are produced by the rabbits as a result of infection by basal body-containing microorganisms, or as a result of an immune response to centrioles, basal bodies or their constituents released by dying cells into the circulation.

We thank Dr A. Zimmerman for providing *T. pyriformis* strain GL. This work was supported by grant MT-3302 from the MRC of Canada to V.I.K.

Received 15 February; accepted 23 June 1982.

1. Roberts, K. & Hyams, J. S. (eds) *Microtubules* (Academic, New York, 1980).
2. Peterson, S. P. & Berns, M. W. *Int. Rev. Cytol.* **64,** 81–106 (1980).
3. Connolly, J. A., Kalnins, V. I., Cleveland, D. W. & Kirschner, M. W. *Proc. natn. Acad. Sci. U.S.A.* **74,** 2437–2440 (1977).
4. Connolly, J. A. & Kalnins, V. I. *J. Cell Biol.* **79,** 526–532 (1978).

5. Wang, E., Connolly, J. A., Kalnins, V. I. & Choppin, P. W. *Proc. natn. Acad. Sci. U.S.A.* **76**, 5719–5723 (1979).
6. Gould, R. R. *J. Cell Biol.* **65**, 65–74 (1975).
7. Towbin, H., Staehelin, T. & Gordon, J. *Proc. natn. Acad. Sci. U.S.A.* **76**, 4350–4354 (1979).
8. Lin, W., Fung, B., Shyamala, M. & Kasamatsu, H. *Proc. natn. Acad. Sci. U.S.A.* **78**, 2373–2377 (1981).
9. Anderson, R. G. W. & Floyd, A. K. *Biochemistry* **19**, 5625–5631 (1980).
10. Bird, C. & Zimmerman, A. *Expl Cell Res.* **128**, 199–204 (1980).
11. Nozawa, Y. & Thompson, G. A. in *Biochemistry and Physiology of Protozoa* Vol. 2 (eds Levan Dowsk, M. & Hunter, S. H.) 275–338 (Academic, New York, 1979).
12. Laemmli, U. K. *Nature* **227**, 680–685 (1970).
13. Weingarten, M. D., Suter, M. M., Littman, D. R. & Kirschner, M. W. *Biochemistry* **13**, 5529–5537 (1974).
14. Connolly, J. A., Kalnins, V. I., Cleveland, D. W. & Kirschner, M. W. *J. Cell Biol.* **76**, 781–786 (1978).

Mycoplasma pneumoniae adhesin localized to tip structure by monoclonal antibody

J. Feldner, U. Göbel & W. Bredt

Institute for General Hygiene and Bacteriology, Center for Hygiene, University of Freiburg, D-7800 Freiburg, FRG

The human respiratory pathogen *Mycoplasma pneumoniae* has several peculiar properties: despite its diminutive size[1] it possesses a specialized tip structure[2–4]; it is motile and glides with considerable speed along inert surfaces[5,6], and it exhibits strong attachment to animal cells[7] and to inert surfaces[8]. The latter property is a prerequisite for the survival of this obligate parasite in the host organism. Experimental evidence[9–12] suggested that the binding site(s) mediating attachment of the pathogen is a protein, but so far this substance has not been characterized, nor has it been localized in the cell. By using a monoclonal antibody we have been able to localize the adhesin at the surface of the tip structure; it was identified by autoradiography as a protein of molecular weight (M_r) 160,000–190,000. We report that the monoclonal antibody inhibited erythrocyte adherence, attachment to glass and gliding motility of *M. pneumoniae*.

A hybridoma cell line was isolated according to the hybridization protocol described elsewhere[13]. Briefly, 6-week-old BALB/c mice were injected intraperitoneally with 0.5 ml of a *M. pneumoniae* (strain FH) cell suspension (1 mg ml^{-1}) in phosphate-buffered saline (PBS) *p*H 7.2. The injections were repeated four times at 2-week intervals. Mice were killed 3 days after the final injection, and their spleens removed. Lymphocytes were fused with Sp 2/0 myeloma cells[14] and macrophages were used as feeder cells. The hybridoma clones were screened after 10 days for adherence-inhibiting properties by a haemadsorption method[11] and positive wells were cloned by limiting dilution. The supernatants were also tested by indirect immunofluorescence on *M. pneumoniae* cells grown on glass[15]. Of the 120 hybridomas examined, one clone was found to have adherence-inhibiting antibody, designated M43. On immunofluorescence, this antibody stained only one pole of the cell (Fig. 1*a*). The association of antibody with the tip structure of the *M. pneumoniae* cell was confirmed by electron microscopy using ferritin-labelled antibodies to mouse immunoglobulins (Fig. 1*c*). Controls treated with an unrelated mouse monoclonal antibody were negative (Fig. 1*d*). The immunofluorescence was reduced by pretreatment of the *M. pneumoniae* cells with trypsin (10–20 µg ml^{-1}) at 37 °C for 30 min).

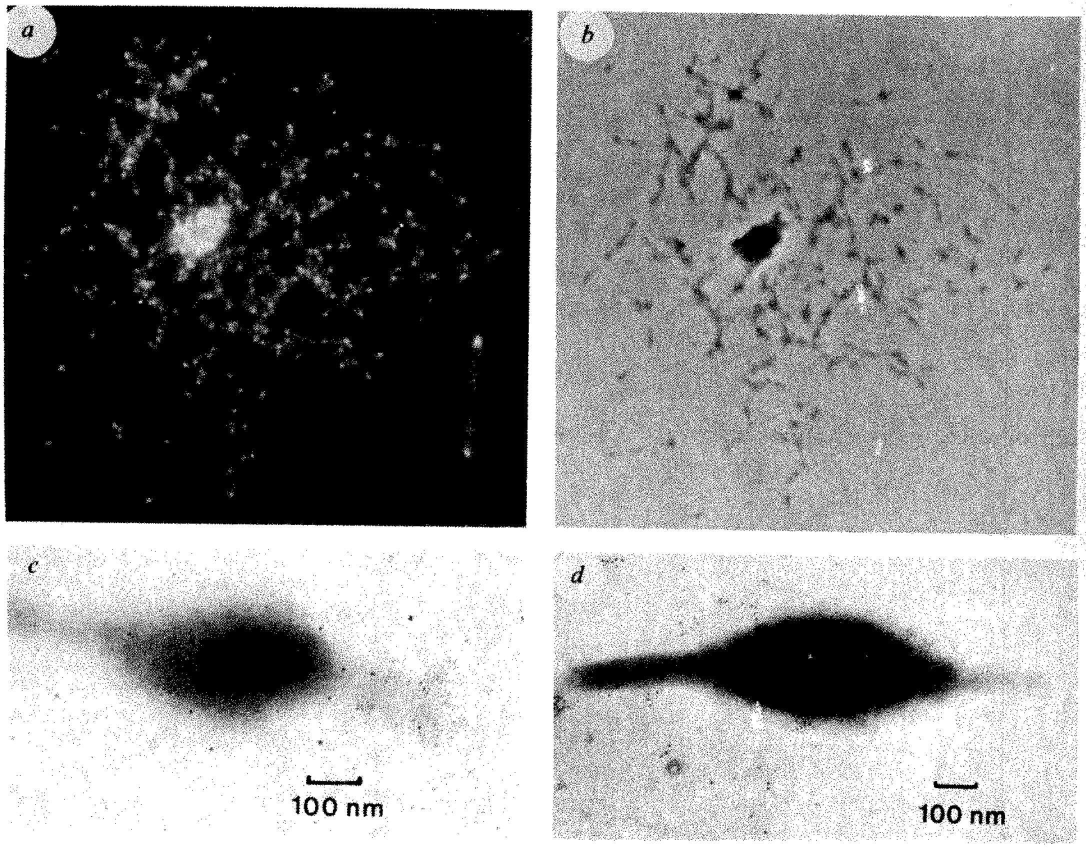

Fig. 1 Immunofluorescent and immunoferritin labelling of *M. pneumoniae* cells by monoclonal antibody M43. *a*, For indirect immunofluorescence the glass-attached mycoplasmas were fixed either in 0.1% glutaraldehyde or in 5% formaldehyde in PBS for 15 min at room temperature and rinsed twice with PBS. The cells were then treated with M43 hybridoma supernatant at 37 °C for 15 min, rinsed with PBS, and fluorescein isothiocyanate-conjugated goat anti-mouse antiserum (1:40) was added as second antibody. Incubation at 37 °C for 15 min was followed by two rinses with PBS. Finally, the cells were covered with a buffered glycerol–phenylenediamine solution to reduce the fading of the fluorescence[21]. The preparations were examined in a Zeiss photomicroscope equipped with epifluorescence illumination. The photographs (3-min exposures) were taken using 400 ASA film (Ilford) and show a microcolony consisting of single cells (×2,200). The insert shows dividing cells (×4,400). *b*, Phase contrast of *a* without the insert. *c*, *M. pneumoniae* cells grown on parlodion–carbon-coated platinum grids were pre-fixed with 0.1% glutaraldehyde in PBS at room temperature for 15 min. After washing they were incubated with anti-adherence antibody (1:100) at room temperature for 15 min, then washed and incubated with ferritin-labelled goat anti-mouse immunoglobulin at room temperature for 15 min. The grids were then rinsed six times with PBS, fixed with 2.5% glutaraldehyde at room temperature for 15 min and examined in a Siemens Elmiskop 102 at 80 kV. Ferritin molecules are seen predominantly at the tip structure. *d*, As a specificity control, *M. pneumoniae* preparations were incubated with mouse monoclonal anti-human immunoglobulin instead of the M43 antibody. Further controls used bovine serum albumin, fetal calf serum or the ferritin-labelled antibody alone (not shown).

0028–0836/82/330765—03$01.00

The antibody was identified as belonging to the IgM class by immunodiffusion and gel filtration on Sephacryl S-300. Pretreatment of *M. pneumoniae* sheets with antibody M43 caused strong inhibition of adherence of sheep erythrocytes (Table 1). Similar results were obtained with human, rabbit and guinea pig erythrocytes. The adherence inhibition titre of hybridoma supernatant was 1:16; this increased to 1:256 when the antibody was precipitated with 40% ammonium sulphate and resuspended in PBS to 30 mg ml^{-1}. Similar titres (1:10 and 1:128, respectively) were found also for the inhibition of attachment to glass surfaces (Table 1).

Table 1 Monoclonal antibody M43 inhibits erythrocyte adherence and attachment to glass

	Adherence of sheep erythrocytes to mycoplasma sheet	Attachment of mycoplasmas to glass
Control	100	100
M43		
1: 32	3	1
1: 64	5	3
1:128	17	23
1:256	21	57
1:512	77	Not tested

Attachment of sheep erythrocytes was assessed by a haemadsorption technique[11] which allows photometric measurement of lysates of sheep erythrocytes attached to sheets of *M. pneumoniae*. Attachment of glucose-energized mycoplasmas to glass was quantitated in an experimental system[12,20] which measures the settling of ^{3}H-palmitic acid-labelled cells on to glass coverslips. After incubation and rinsing of the coverslips, the radioactivity attached to the glass was determined.

The monoclonal antibody caused no growth inhibition and was ineffective in the metabolic inhibition test[16]. Furthermore, no complement-mediated lysis of antibody-coated cells was observed. These negative results suggest a localization of the corresponding antigen at a non-vital site.

To identify the binding substance, the monoclonal antibody was labelled by adding ^{35}S-methionine to the hybridoma culture medium[13]. *M. pneumoniae* cells were solubilized by SDS and the proteins separated on a SDS-polyacrylamide gel[17]. The gel was then treated with the labelled antibody. Autoradiography revealed that the activity bound to a protein at a position corresponding to a molecular weight of 160–190K (Fig. 2*a*). The same protein band was reactive when a similar gel was overlaid with sheep erythrocytes (Fig. 2*b*), suggesting that this polypeptide was not only antigenically but also functionally identical to the binding site material.

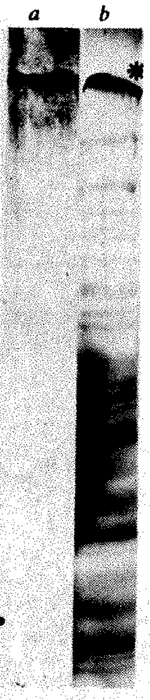

Fig. 2 Localization of the proteins stained by monoclonal antibody or by sheep erythrocytes after polyacrylamide gel electrophoresis[17] of whole *M. pneumoniae* cells. After electrophoresis, the SDS was eluted from the gel by washing with PBS at room temperature for 45 min. *a*, The gel was then covered with ^{35}S-methionine-labelled antibody, incubated at 4 °C for 20 h, then washed with PBS. The fixed gel was impregnated with Enhance (NEN), then dried and exposed at −70 °C for 2 days to Kodak X-Omat X-ray film. *b*, Instead of antibody, sheep erythrocytes were used to overlay the gel (room temperature for 45 min). After several washes with PBS the gel was stained with Coomassie blue. The asterisk indicates the position of the erythrocyte-labelled protein.

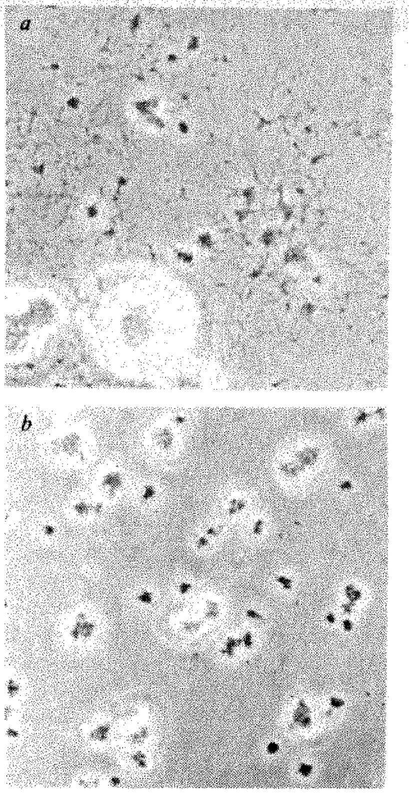

Fig. 3 Effect of antibody M43 on migration of *M. pneumoniae* cells. Mycoplasmas were grown on glass in coverslip chambers[15] in the absence (*a*) or presence (*b*) of antibody M43 (1:3,200). In *b*, normal growth of microcolonies can be seen but no individual cells migrated out of the colonies.

The gliding movements of *M. pneumoniae* were completely abolished when antibody (up to 1:1,000) purified by ammonium sulphate precipitation was added to the medium. This inhibition occurred within 5 min; the shape of the cells was not affected nor did they lose contact with the glass surface. When the antibody was added to growing cultures, the single cells remained aggregated in clusters and did not migrate out of the microcolonies to spread over the coverslip (Fig. 3). The immobilization of the cells suggests that some mobility of the binding site within the membrane that is required for gliding, is inhibited by the bound antibody.

Attempts to isolate the adhesin protein of *M. pneumoniae* have so far had only limited success[18]. Using the specific monoclonal antibody described here it should be possible to purify and characterize the binding site protein, which may further elucidate the mechanisms of motility and adherence. Furthermore it could be used to study parasite–host interactions, and may have potential value in diagnosis and immunoprophylaxis.

After submission of this letter, an article describing a similar antibody[19] was published. We thank A. Vogt for stimulating discussions, and D. Preusse and U. Burger for technical assistance.

Received 29 April; accepted 23 June 1982.

1. Razin, S. *Microbiol. Rev.* **42,** 414–470 (1978).
2. Biberfeld, G. & Biberfeld, P. *J. Bact.* **102,** 855–861 (1970).
3. Collier, A. M. in *Pathogenic Mycoplasmas* (eds Elliott, K. & Birch, K.) 307–327 (Associated Scientific, Amsterdam, 1972).
4. Göbel, U., Speth, V. & Bredt, W. *J. Cell Biol.* **91,** 537–543 (1981).
5. Radestock, U. & Bredt, W. *J. Bact.* **129,** 1495–1501 (1977).
6. Bredt, W. in *The Mycoplasmas* Vol. 1 (eds Barile, M. F. & Razin, S.) 141–155 (Academic, New York, 1979).
7. Razin, S., Kehane, I., Banai, M. & Bredt, W. *Ciba Fdn Symp.* **80,** 98–118 (1981).
8. Bredt, W., Feldner, J. & Kahane, I. *Ciba Fedn Symp.* **80,** 3–16 (1981).

9. Gorsky, F. & Bredt, W. *FEMS Microbiol. Lett.* **1**, 265–268 (1977).
10. Hu, P. C., Collier, A. M. & Baseman, J. B. *J. exp. Med.* **145**, 1328–1343 (1977).
11. Feldner, J., Bredt, W. & Kahane, I. *Infect. Immunity* **25**, 60–67 (1979).
12. Feldner, J., Bredt, W. & Razin, S. *Infect. Immunity* **31**, 107–113 (1981).
13. Fazekas de St Groth, S. & Scheidegger, D. *J. immun. Meth.* **35**, 1–21 (1980).
14. Shulman, M., Wilde, C. D. & Köhler, G. *Nature* **276**, 269–70 (1978).
15. Bredt, W. *Proc. Soc. exp. Biol. Med.* **128**, 338–340 (1968).
16. Senterfit, L. B. & Jensen, K. E. *Proc. Soc. exp. Biol. Med.* **122**, 786–790 (1966).
17. Laemmli, U. K. *Nature* **227**, 680–685 (1970).
18. Banai, M., Razin, S., Bredt, W. & Kahane, I. *Infect. Immunity* **30**, 628–634 (1980).
19. Hu, P. C. *et al. Science* **216**, 313–315 (1982).
20. Feldner, J., Bredt, W. & Razin, S. *Infect. Immunity* **26**, 70–75 (1979).
21. Johnson, G. D. & de C. Nogueira Araujo, G. M. *J. immun. Meth.* **43**, 349–350 (1981).

A multicopy insertion sequence in the bovine genome with structural homology to the long terminal repeats of retroviruses

R. E. Streeck

Institut Pasteur, 28 rue du Docteur Roux, 75724 Paris Cedex 15, France

Many of the transposable elements characterized so far in eukaryotes are a few thousand base pairs (bp) long and there are usually 20–50 copies per genome[1]. In addition, families of short interspersed repeated sequences have been discovered, some of which may also be transposable[2]. During analysis of the bovine satellite DNAs, I have found two types of sequence which have structural features in common with insertion elements[3]. They are only 0.6 and 1.2 kilobases (kb) long and are present in two different satellites at frequencies of 3.5×10^4 and 5×10^4 per genome, respectively. Sequence analysis of the 1.2-kb insertion and of satellite repeats carrying or lacking this sequence has now shown that a 6-bp duplication is generated at the site of insertion. I report here that the organization of this sequence is very similar to a retrovirus long terminal repeat (LTR). The 1.2-kb insertion and the related 0.6-kb sequence are highly homologous near their ends but unrelated in their internal sequences. These two elements may constitute precursors or descendants of an unknown retrovirus.

The bovine genome contains at least seven satellite DNAs, two of which have a density of 1.711 g cm^{-3} in CsCl (1.711A, 1.711B)[4]. Restriction and hybridization analysis of the 1.711B satellite (7.1% of the genome) has previously shown that it consists of two types of repeat unit: 1.4-kb units homologous to the 1.4-kb repeat units of another bovine satellite (1.715 g cm^{-3})[5,6] and 2.6-kb units which correspond to 1.4-kb units carrying in addition a 1.2-kb insertion[3]. About 50% of the repeat units carry this insert, each at the same position. Thus, digestion of the satellite with *Sst*I, which cleaves once in the 1.4-kb sequence but not in the insert (Fig. 1*a*), yields mainly fragments of 1.4 and 2.6 kb. *Hin*dIII digestion, which cleaves once in the insert but not in the 1.4-kb sequence (Fig. 1*a*), gives mainly 2.6- and 4.0-fragments, while fragments ≥5.4 kb are less frequently found. This indicates that the 1.2-kb insertions occur most often in repeat units that are neighbouring or separated by one additional 1.4-kb unit, and with less probability in more distant ones.

I have determined the nucleotide sequence of the entire 2.6-kb repeat unit and have compared it to the 1.4-kb sequence derived from the 1.715 satellite DNA[7]. Uncloned restriction fragments were used for both sequences. They were therefore 'prototype sequences' corresponding to the most frequent nucleotides at each position of the repeat units. The sequence analysis confirmed that the 2.6-kb repeat unit consists of a 1.4-kb sequence highly homologous to the 1.4-kb repeat units, and an unrelated 1.2-kb sequence interrupting the 1.4-kb sequence. The homology between the 1.4-kb sequences in the repeat units carrying or lacking the 1.2-kb insertion is of the order of 95% (to be published). The nucleotide sequence of the 1.2-kb insertion (which is termed INS-1.711B) has several remarkable features:

(1) It is flanked by a 6-bp direct repeat (CCCTAC) which occurs only once at the corresponding position in the 1.4-kb unit (Fig. 1*b*–*d*). Such a duplication is highly characteristic for the insertion of transposable elements[1].

(2) The insertion is bounded by a 3-bp terminal inverted repeat TGC ... GCA (Fig. 2). If some mismatches are taken into account, the repeat could be extended to 13 bp.

(3) Following the terminal repeat, at the 5′ end there is a repetitious sequence of ~100 bp consisting of several tri- to heptanucleotides repeated two to five times and interspersed with each other and some non-repeated DNA: for example, there are five copies of GCATATT. (These oligonucleotides are underlined in Fig. 2*a*.)

(4) An open reading frame of ~200 bp is found in the 5′ half of the sequence. It is terminated by two successive TAA codons that are boxed in Fig. 2*a*.

(5) Several sequences thought to be important for the regulation of transcription are found in the 3′ half of INS-1.711B (Fig. 2). These are a Goldberg–Hogness box, TATAAAAA, at positions 947–954 and a polyadenylation signal, AATAAA, at 966–971 which is followed 15 bp later by a polyadenylation site, Ca. The sequence GCAAG (900–904) precedes the Goldberg–Hogness box in a position where the related sequence CCAAT is frequently found. Finally, TTGGT (995–999) is found in a region where TTGT or related sequences are thought to have a role in the termination of RNA synthesis[8] (Fig. 2).

The arrangement of these sequences in INS-1.711B is remarkably similar to that in a LTR of retroviruses. A comparison between INS-1.711B and the prototype of a retrovirus LTR is shown in Fig. 2*b*. A LTR contains sequences derived from both the 3′ and 5′ ends of the viral RNA (U3, U5) as well as one copy of the terminal redundancy (R), thus signals for the initiation and termination of transcription and for polyadenylation occur characteristically close to each other at fairly constant positions (Fig. 2*b*). In INS-1.711B the same or closely related sequences (see above) occur in these positions. Furthermore, the TG, CA-termini and the terminal inverted repeat present in all LTRs are also found in INS-1.711B. By analogy to retroviruses, the sequence 1–977 would then be U3-like, 978–987 would be R-like, and 988–1198 U5-like. It is not known, however, whether INS-1.711B is transcribed in bovine cells.

There are two structural features in INS-1.711B which have not been found in any of the sequenced LTRs: one is the repetitious region at the 5′ end (Fig. 2*a*); the other is a 13 bp sequence (position 116–128), at the end of the repetitious

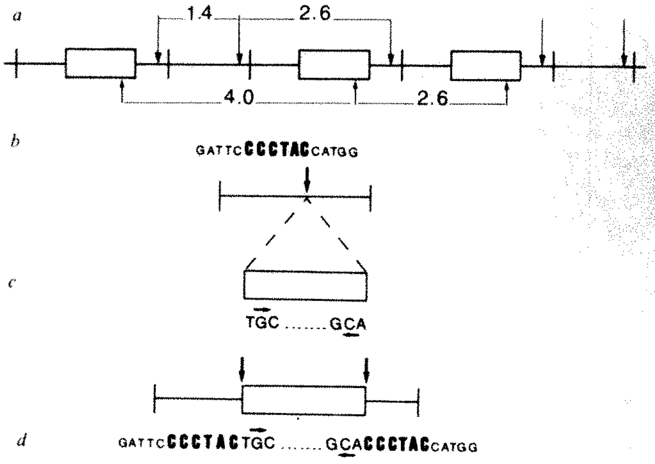

Fig. 1 Organization and partial sequences of repeat units in the 1.711B satellite DNA. *a*, Possible arrangement of 1.4-kb units lacking and 2.6-kb units carrying the 1.2-kb insertion. The sizes of fragments obtained by digestion with *Sst*I(↓) or *Hin*dIII(↑) are given in kb. *b*, 1.4-kb repeat unit. The arrow indicates the site of insertion. The nucleotide sequence at this site is given[7]. *c*, 1.2-kb inserted sequence (INS-1.711B). The 3-bp terminal inverted repeat is indicated. *d*, 2.6-kb repeat unit carrying INS-1.711B. The sequences flanking the insertion and its 3-bp terminal inverted repeats are given, the duplicated hexanucleotide in bold letters.

0028–0836/82/330767—03$01.00

region, that is related to the terminal repeats. In fact, this sequence forms a closer inverted repeat with the 3′-terminal sequence than does the 5′-terminal sequence (Fig. 2*a*).

No major differences were found when DNAs from thymus, liver and brain of different animals were digested by restriction nucleases and compared by Southern blot analysis[9] using cloned INS-1.711B as a probe. Therefore, major rearrangements of INS-1.711B in the satellite DNA during ontogenesis can be excluded. Some background smears observed in the hybridization experiment suggest that INS-1.711B-like sequences are dispersed throughout the genome.

I have shown previously that a 0.6-kb sequence related to INS-1.711B occurs in the repeat unit of the bovine 1.711A satellite (termed INS-1.711A)[3]. It was therefore interesting to compare INS-711B with INS-1.711A, which also exhibits some features of an insertion element[3]. The homologous regions of the two sequences are the first 250 bp of INS-1.711A, which correspond to the sequence 116–358 in INS-1.711B, and the last 140 bp of both elements; their internal sequences are completely unrelated (Fig. 3). The homology is greatest near the ends, for example, two transitions being the only base changes in the last 35 bp at their 3′ ends. The homology then gradually decreases to ~80% before ending abruptly. The 100-bp repetitious sequence found in INS-1.711B is absent from INS-1.711A. The region of homology near the 5′ end which contains the largest open reading frame in INS-1.711B (Fig. 2*a*) is also conserved in INS-1.711A. The region of homology at the 3′ end contains sequences characteristic of a polymerase II promoter in INS-1.711A[3]. In INS-1.711B this region is interrupted by a 19-bp sequence that is non-homologous. In summary, the homology found strongly suggests a common origin of the two sequences.

a

```
TGCGTGAGCC GGCATATTGC ATATTGAGTG CATATTGCAT ATTGCATATT GAGTGCAGCA CTTTCCACAG CATCATCTTT   80
CAGGATCTGG AATAGCTCCA CTGGAATTCT ATCACTGCTG GGAGCCAGTG AGGAACTCCG CCTATGATAA AGGTTATGAG  160
GAAGGAGGCT CGGCATACGC AAAGGCGGGA TCGAGCTTCA GGAGTCCCCC TGGAAATTCT CGAGCATATA CCCCCAAAAC  240
CAGAGTCTGC CTACTTTCTG CTTGTGCTTT CACCTAAACC TCTGACTTTA CGGGGGGCTC TCCCCCACTA CCTCTCTCTG  320
AAAAAAGAGT TAGCTTACAG TTCCAGTTAA TAATTCCTGG GTGTGACAGT GTTTAACCTA CAAACTCCTT TGGAAATCCT  400
CTAGCCTGCC TGAATAGGTT TTTTCGGCCA CATGGGATTG TTCAGAGCCT CCCAACTGTG AGAGGCAGGA GATGTTCTAA  480
ACTGTCTAAA CACAGATTCT TTTGAGTAGT TACAAGATTG ATTAGAAATT GTATTGGTGA ATGGTTTTTC ACTTGTTGGG  560
CCATTGTTTG CTGCTAAGTT TCCATATCCC TTACCTGCTG TGTCCCTGGC AGTGTATTGA TTAATATAAT TGGTGTAAGT  640
AGTAGCTTTA ATGTTTGTAA CCTGGGACCC TTGAGTTAAT TCTTTTTCTT GTTATAGCCC ACCACACCTT TGCTCTGTAG  720
GAATGCAACT TTATCTAATG CTTTTTTGGA GGGTGGCTCC TGACCAACCA CCTTTAGAGA AAAATAAGTT TTCTGAAGAA  800
AAGGTCTTAA AATGTTAACA GGCCTCCGGG CCAGAAGATG ATGCAAATCA CCTAAGCTTT TGCATATGAT AAGTTTGCAG  880
GAAGAAAGCC TGGTTTGCTG CAAGACTCGA CCCCTTCCCC CATTATCCTC TATGCATAAC TTAAGGTATA AAAACTACTT  960
TGAAAAATAA AGTGCGGGCC TTGTTCACCG AAACTTGGTC TCACCATGTC GTTCTTTCTC TTACCTTCTG GCTGAATTAT 1040
TCAGCCTCTT TTCTCCACTG AATTTCCTCA CTGAGCTATC CTCATTCTAT TACTCTTTAT ATCCTTAATT AACATTTAAT 1120
TAAGCAGTGG TTTCCTGATC TTCGCCTACG CCGTCTCTCC TTCGAATACC CTGGATCAGC CGGGGCTGGT CCCCGGCA   1198
```

b

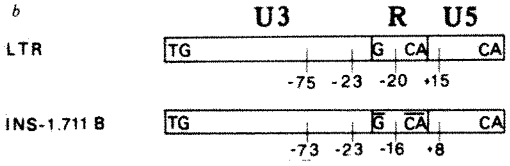

Fig. 2 Nucleotide sequence of INS-1.711B. Bovine 1.711B satellite DNA was purified from calf thymus DNA (Boehringer Mannheim) by isopycnic centrifugation[4] analogous to that described for bovine 1.706 satellite DNA [illegible]. Sequence analysis of restriction fragments from the purified satellite was carried out according to Maxam and Gilbert[13], using the *Alu*I, *Dde*I, *Hin*dIII, *Hin*fI, *Sau*3A and *Sau*96 sites in the insertion sequence for terminal labelling; 96% of the sequence was determined from at least two different overlapping restriction fragments, 40% being determined from both strands. *a*, Location of sequences mentioned in the text: the 3-bp terminal inverted repeats are indicated by arrows; the repeated oligonucleotide sequences near the 5′ end are underlined; and the largest open reading frame is marked by the boxed ATG and the two successive TAA codons. the other boxes indicate regulatory signals and related sequences thought to be important in transcription and polyadenylation. They are, in succession, a CCAAT-like sequence, a Goldberg–Hogness box, a polyadenylation signal and a transcription termination signal. A possible adenylation site, CA, and a presumptive cap site, G, are overlined. *b*, Diagrammatic representation of a LTR[8] and INS-1.711B. U3 and U5 correspond to sequences derived from the 3′ and 5′ ends, respectively, of the viral RNA; R indicates the terminal redundancy. The location of the regulatory signals mentioned above is marked. Their distances from the U3–R boundary (−75, −23) and R–U5 boundary (−20, +15)[8] are given in bp. The locations of the homologous signals in INS-1.711B (boxed in *a*) are analogously indicated assuming that the sequence 978–987 (Fig. 2*a*) corresponds to R. The overlined G and CA in the R-like region correspond to those of *a*.

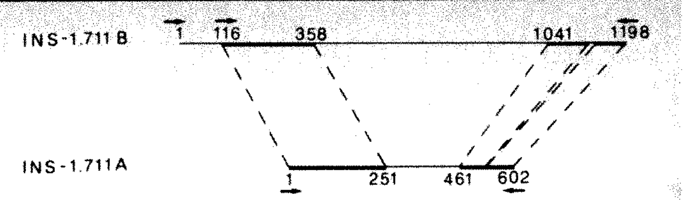

Fig. 3 Homologous regions of INS-1.711A and INS-1.711B. The nucleotide sequence of INS-1.711A is from ref. 3. INS-1.711A has been re-defined as the sequence bracketed by the inverted repeats, that is, the sequence 550–1,151 of the 1,413-bp repeat unit of bovine 1.711A satellite DNA[3]. The homologous sequences are indicated by bold lines, and their limits are represented by the corresponding nucleotide numbers. The arrows indicate the terminal inverted repeats and their internal repetition in INS-1.711B, respectively.

It is not known whether the high copy number of INS-1.711B is due to multiple insertion events or, more likely, to a passive amplification in the satellite DNA. In addition, it is not known whether INS-1.711B itself is transposable. Although the duplicated target sequence flanking the insertion is a strong indication of integration by transposition[1], it is also possible that INS-1.711B was a LTR of a larger movable element, for example, a retrovirus, which was first integrated and then excised by homologous recombination between the two LTRs (before being amplified in the satellite DNA). An analogous situation can be found for the solo δ-sequences of the Ty*1* elements in yeast[10]. Bovine leukaemia virus, the only bovine retrovirus for which partial sequences are known (A. Burny, personal communication), is unrelated to INS-1.711B.

Alternatively, INS-1.711A and INS-1.711B may be different stages in the evolution of a cellular insertion sequence, which were conserved by (or possibly evolved through) their integration into repetitive sequences. According to Temin's hypothesis on the genesis of retroviruses[11], INS-1.711B might then be an immediate precursor of a retroviral LTR.

This work was carried out at the Institut für Physiologische Chemie, Physikalische Biochemie und Zellbiologie der Universität München, D-8000 München 2, FRG, and was supported by Deutsche Forchungsgemeinschaft. I thank A. Burny for the communication of unpublished results, D. Brutlag for help in using the computer facilities at Stanford University, and K. Beer for technical assistance.

Received 29 March; accepted 24 June 1982.

1. Calos, M. P. & Miller, J. J. *Cell* **20**, 579–595 (1980).
2. Singer, M. F. *Int. Rev. Cytol.* (in the press).
3. Streeck, R. E. *Science* **213**, 443–445 (1981).
4. Macaya, G., Cortadas, J. & Bernardi, G. *Eur. J. Biochem.* **84**, 179–188 (1978).
5. Botchan, M. R. *Nature* **251**, 288–292 (1974).
6. Philippsen, P., Streeck, R. E., Zachau, H. G. & Müller, W. *Eur. J. Biochem.* **57**, 55–68 (1975).
7. Plucienniczak, A., Skowronski, J. & Jaworski, J. *J. molec. Biol.* **158**, 293–304 (1982).
8. Temin, H. M. *Cell* **27**, 1–3 (1982).

9. Southern, E. M. *J. molec. Biol.* **98,** 503–517 (1975).
10. Farabaugh, P. J. & Fink, G. R. *Nature* **286,** 352–356 (1980).
11. Temin, H. M. *Cell* **21,** 599–600 (1980).
12. Streeck, R. E. & Zachau, H. G. *Eur. J. Biochem.* **89,** 267–279 (1978).
13. Maxam, A. M. & Gilbert, W. *Meth. Enzym.* **65,** 499–560 (1980).

DNA synthesis in purified DNA–membrane complexes extracted from a *Bacillus subtilis* pol A mutant

Patricia Benjamin, Paul Strumph, Mark Kenny & William Firshein

Department of Biology, Wesleyan University, Middletown, Connecticut 06457, USA

The cell membrane of prokaryotes has been implicated as the site of DNA replication in the replicon model first proposed by Jacob, Brenner and Cuzin[1]. Ultrastructural, genetic and biochemical data have since been compiled suggesting an association between the cell membrane and replicating DNA (for review, see ref. 2). However, few studies have attempted to test this aspect of the replicon model directly by investigating the ability of DNA–membrane complexes to synthesize DNA *in vitro*. Such studies have been performed mainly with *Pneumococcus* and it has been shown that DNA–membrane complexes extracted by the M-band technique[3] retain their capacity to synthesize DNA even after extensive purification[4]. However, mutants defective in various aspects of DNA replication are unavailable in *Pneumococcus*, and this is an important requirement for elucidating the physiological significance of the complex. Fortunately, they are available in *Escherichia coli* and *Bacillus subtilis*, and of the two organisms, much of the important work with the complex has been accomplished with *B. subtilis*[5-12]. These studies have indicated that the origin and terminus of replication are permanently associated with the cell membrane. Nonetheless, there have been no previous studies of the synthetic capacity of *B. subtilis* DNA–membrane complexes. We now offer evidence that two DNA–membrane subcomplexes extracted and purified from a pol A mutant of *B. subtilis* are capable of synthesizing DNA *in vitro* and that these activities are inhibited by hydroxyphenyl azouracil, a specific inhibitor of DNA polymerase III activity in *B. subtilis*.

Many studies involving the DNA–membrane complex have been performed with only crude material, basically one step removed from whole cells. Because such complexes probably contain a variety of nonspecifically adsorbed components, it was considered essential to 'purify' the complex before analysing DNA synthesis. The purification procedure followed that developed for pneumococci[4] because it fulfilled three important criteria. First, a large amount of excess macromolecules was dissociated during the purification procedure. Second, the complex retained its ability to synthesize DNA *in vitro* without added template or enzymes. Third, the specific activity of DNA polymerase(s) increased throughout the purification procedure (except in one step, see below). Table 1 shows the percentages of macromolecules remaining in the complex after the various purification steps. CsCl centrifugation separated membrane-bound DNA from the crude M-band[3] into two peaks, one (corresponding to 94% of the total DNA in the crude complex) which sedimented at the buoyant density of free *B. subtilis* DNA, the other (corresponding to only 0.9% of the total DNA) floating at the top of the gradient as a pellicle together with 90% of the total lipid and 35% of the total protein.

These results indicate that DNA firmly bound to membrane represents a small fraction of the total DNA in the crude complex. One problem in this procedure is the possible contamination of the complex with 'free' protein which also floats at the top of the CsCl gradient. However, ~22% of the total protein of the crude complex was still associated with the subcomplexes after the final purification step described below. This suggests that at least this portion of the protein was firmly bound. The pellicle was dialysed to remove CsCl and centrifuged in a 5–20% (w/v) neutral sucrose gradient. Two peaks of DNA were observed (Fig. 1), one sedimenting near the bottom of the gradient and the other sedimenting near (but not at) the top. Both peaks contained varying amounts of co-sedimenting lipids (Fig. 1) and proteins (Table 1), suggesting that two DNA–membrane subcomplexes were resolved in the neutral sucrose gradient. Note that 'free' DNA and protein did

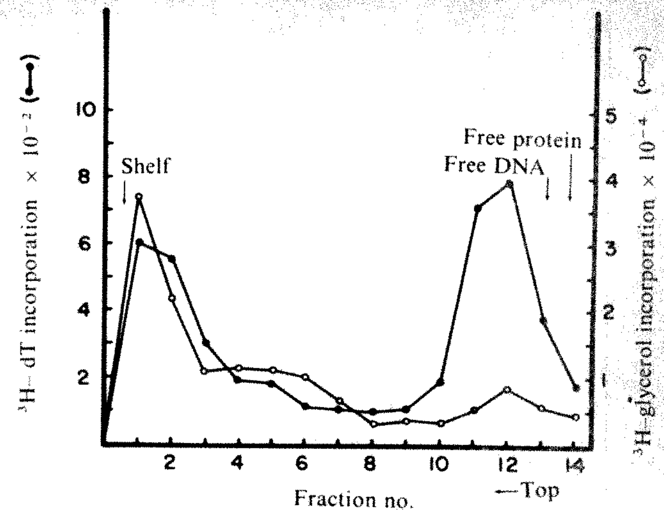

Fig. 1 Distribution of two DNA–phospholipid subcomplexes in a sucrose gradient. Methods are described in Table 1 legend. The experiment was repeated twice, once with a single label for DNA synthesis (^{3}H-thymidine) and once with a single label for phospholipid synthesis (^{3}H-glycerol).

Table 1 Purification of the DNA–membrane complex

Treatment of complex	% DNA	Macromolecule protein	Remaining lipid
1 DNA–membrane dialysis	100	100	100
2 CsCl centrifugation, dialysis	0.86	35.6	90.0
3 Sucrose gradient centrifugation (total)	0.64	22.3	49.0
(*a*) More slowly sedimenting complex	0.28	18.9	9.1
(*b*) Faster-sedimenting complex	0.36	3.4	39.9

Cultures (500 ml) of *B. subtilis* strain 841 (thy, tryp, pol A) were labelled with 100 μCi of ^{3}H-thymidine or 100 μCi of ^{3}H-glycerol and grown to the mid-logarithmic phase in Penassay broth. Cells were washed twice with TMK buffer, *p*H 7.0 (0.01 M Tris, 0.01 magnesium acetate, 0.1 M KCl) and incubated in the same buffer containing 25% sucrose (w/v) and lysozyme (20 μg ml^{-1}) at 4 °C for 10 min. Protoplasts were collected, resuspended in TMK buffer containing 0.3% sarkosyl and 1 mM phenylmethylsulphonyl fluoride (PMSF), and incubated for 10 min at 4 °C. The cell lysate was layered onto a biphasic 25/60% (w/v) sucrose gradient and centrifuged at 18,000 r.p.m. for 20 min at 4 °C in an Sw 41 rotor and Beckman L2 65B ultracentrifuge. The M-band was collected from the 25/60% interphase and dialysed overnight in TK buffer (0.01 M Tris, *p*H 7.0; 0.1 M KCl) containing 1 mM PMSF at 4 °C. Solid CsCl was added to the dialysate to obtain a mean density of 1.7001 at 30,000 r.p.m. for 48 h at 25 °C in an Sw 50.1 rotor. The pellicle was removed from the top of each gradient, pooled and dialysed in TK buffer overnight at 4 °C. The dialysate was layered onto 5–20% (w/v) neutral linear sucrose gradients containing an 80% sucrose shelf and centrifuged at 35,000 r.p.m. for 90 min at 4 °C in an Sw 50.1 rotor. The gradients were fractionated by puncturing the bottom of the tube, each fraction precipitated with trichloroacetic acid (5%, final concentration) and assayed for radioactivity in a Mark III liquid scintillation counter. Samples were also taken from the pellicle fraction and other areas of the CsCl gradient for assay of radioactivity as well as from the M-band fraction. Protein content was determined by the Bio-Rad reagent.

0028-0836/82/330769—03$01.00

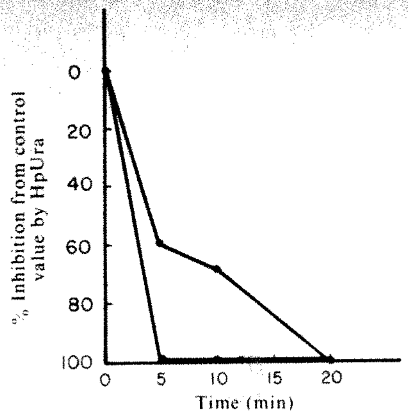

Fig. 2 Inhibitory effects of 6-(p-hydroxyphenyl azouracil) on DNA synthesis by the two subcomplexes. Methods are described in Table 2 legend. The concentration of reduced Hpura (with sodium dithionate) was 400 μM. The greater inhibitory activity (sharper slope) is observed in the fast-sedimenting subcomplex which is totally inhibited after 5 min, whereas the activity of the slowly sedimenting complex is totally inhibited only after 20 min. After 5 min the activity of the latter subcomplex is inhibited 60% from control values.

not sediment in the areas of the two subcomplexes but remained at or near the top of the gradient away from the slowly sedimenting subcomplex.

To determine whether the various complexes could synthesize DNA *in vitro* and whether purification of this activity was achieved, DNA polymerase assays were performed with the crude M-band, the CsCl pellicle fraction and the two subcomplexes detected in the sucrose gradient. Table 2 shows that both the total activity and the specific activity decreased after CsCl centrifugation and dialysis but increased significantly after sucrose gradient centrifugation. The reasons for this inhibition are unknown, but it has been observed consistently in our experiments. One possible explanation is that inhibiting factors are activated after this step but are removed after the subsequent sucrose gradient procedure. The more slowly sedimenting subcomplex showed a slight increase in specific activity while that of the faster-sedimenting complex was markedly enhanced. It is interesting that the more active complex contained a higher concentration of lipids. Firshein and co-workers[13] have shown that membrane glycolipids which are present only in Gram-positive bacteria stimulate DNA polymerase III activity in *Pneumococcus*. A similar phenomenon may be operating in *B. subtilis* if, in fact, the activity observed in both complexes is related to DNA polymerase III. Although it is probable that such is the case because of the pol A mutation (which virtually eliminates pol I activity), it was important to confirm this possibility by other means. Fortunately, 6-(p-hydroxyphenyl azouracil)(HpUra) specifically inhibits the activity of DNA pol III in *B. subtilis*[14]. Tests on the effects of this drug on the activity of the two subcomplexes show (Fig. 2) that with the addition of HpUra DNA synthesis is almost totally inhibited within 5–20 min, depending on the subcomplex, relative to controls.

Considerable evidence regarding the nature of membrane-associated DNA in *B. subtilis* has been provided by Sueoka and co-workers[8,11,12] and Yoshikawa and co-workers[7,9]. Their experiments have revealed several facts, which include (1) that the origin and terminus of replication are attached to the cell membrane throughout the cell cycle and (2) that the DNA–membrane complex can also be separated into two subcomplexes, both of which contain markers close to the origin. Although their subcomplexes were extracted and separated by different methods[9,11,12] from those used in the present experiments, it was of interest to determine whether there was any similarity in the composition of the complexes, at least with respect to some of the genetic markers present. Accordingly, the ability of the DNA in each of the complexes to transform markers near the origin, terminus and middle of the *B. subtilis* genome was compared.

Table 3 shows that both the slow- and fast-sedimenting subcomplexes (as well as CsCl-derived complex) were enriched for a genetic marker (gua Al) which is located less than 1° from the origin of replication on the *B. subtilis* genetic map[16]. The commonly used origin marker (pur A), which has been mapped to ~10° from the replication origin[16] and a genetic marker (met B5) which has been frequently used to detect enrichment for the terminus of replication, were not enriched in any of the DNA–membrane complexes isolated. In addition, no enrichment was detected for a marker (leu 8) located in the middle of the chromosome.

These results suggest that an unusually small area of the origin region may be represented in the subcomplexes. Although no enrichment for the terminus marker (met B5) was detected in the DNA–membrane complexes, it is possible that a smaller portion of the terminus region (including the actual terminus) is present in at least one of the subcomplexes. This suggestion is based on the possibility that the terminus marker (met B5) is positioned ~20° from the actual terminus of replication[16], whereas only 0.64% of the DNA in the M-band complex

Table 2 DNA synthesis *in vitro* in various fractions during purification of the DNA–membrane complex

Fraction	Total activity (counts per min)	Specific activity (counts per min per mg protein)
1 DNA–membrane, dialysis	725,940	2,902
2 CsCl centrifugation, dialysis	52,425	526
3*a* Sucrose gradient centrifugation, more slowly sedimenting complex	119,040	3,737
3*b* Sucrose gradient centrifugation, faster-sedimenting complex	150,240	19,603

Cultures (4 l) of *B. subtilis* strain 841 were grown to the mid-logarithmic phase in Penassay broth in the same conditions as for Table 1 except that radioactively labelled precursors were omitted. The DNA–membrane complex was extracted and purified according to the conditions described in Table 1 legend. The fractions were assayed for DNA polymerase activity in a reaction mixture containing 1.7 mM triethanolamine phosphate buffer, pH 7.5; 0.5 mM EDTA; 0.025% Triton X-100; 2.0 mM β-mercaptoethanol; 0.01 M $MgCl_2$; dATP, dCTP, dGTP (25 μg ml^{-1}); and ^{3}H-dTTP (73 Ci mmol^{-1}), 1 μCi per assay tube. Each assay tube was incubated at 37 °C for 30 min and the reaction terminated with the addition of ice-cold 5% trichloroacetic acid containing 1% (w/v) sodium pyrophosphate. Acid-insoluble radioactivity was determined by liquid scintillation techniques.

Table 3 Transformation for genetic markers in the DNA–membrane complex

Transforming *B. subtilis* DNA	Transformants per ml cells gua Al$^+$/leu 8$^+$	pur A$^+$/leu 8$^+$	met B5$^+$/leu 8$^+$
M-band-derived complex	20,000/445	413,000/104,000	40,000/5,500
CsCl-derived complex	600,000/10	90/40	38,240/610
Slowly sedimenting subcomplex	100,000/25	150/50	500/420
Fast-sedimenting subcomplex	120,000/20	60/30	660/80

Bulk *B. subtilis* DNA was extracted according to the method of Anagnostopoulos and Spizizen[17]. Although not shown, the ratios of the various transformations for bulk DNA were similar to those of the M-band because the M-band contains ~80% of the total cellular DNA. The DNA membrane complexes were prepared as described in the legend (Table 1). These fractions were used at concentrations of 2.5 μg ml^{-1} to transform recipient *B. subtilis* 1A177 (gua Al, ery-1), BUL717 (pur A, leu 8, met C), Mu8u5716 (pur A, met B5, leu 8) and a derivative of Mu8u5716 (gua Al, leu 8, pur A).

remains firmly bound in the subcomplexes (Table 1), a percentage corresponding to less than 2° of the *B. subtilis* chromosome. That this relatively small percentage does not represent a random area of the chromosome is indicated by the enrichment for the gua marker in most of the DNA–membrane complexes, but not for the pur A marker.

Finally, concerning the nature of the DNA synthesized, we can only surmise that since the assay solution does not contain components required for initiation of DNA replication (such as ribonucleoside triphosphates and high concentrations of ATP), an extension of strands from the replication fork is occurring with DNA pol III, rather than initiation of new strands. This possibility as well as attempts to determine whether initiation can be detected *in vitro* will be investigated. Nevertheless, this is the first report of a 'purified' DNA–membrane complex that can synthesize *B. subtilis* DNA *in vitro* using DNA pol III as the native enzyme.

This study was supported in part by NSF grant PCM 8110082 and by biomedical funds from Wesleyan University.

Received 29 March; accepted 14 June 1982.

1. Jacob, F., Brenner, S. & Cuzin, F. *Cold Spring Harb. Symp. quant. Biol.* **28,** 329–348 (1963).
2. Leibowitz, P. J. & Schaechter, M. *Int. Rev. Cytol.* **41,** 1–28 (1975).
3. Tremblay, G. Y., Daniels, M. J. & Schaechter, M. *J. molec. Biol.* **40,** 65–76 (1969).
4. Firshein, W. *J. molec. Biol.* **70,** 383–397 (1972).
5. O'Sullivan, A. & Sueoka, N. *J. molec. Biol.* **69,** 237–248 (1972).
6. Horowitz, S., Doyle, R. J., Young, F. E. & Streips, U. N. *J. Bact.* **138,** 915–922 (1979).
7. Yamaguchi, Y. & Yoshikawa, H. *Nature new Biol.* **224,** 204–206 (1973).
8. Beeson, J. & Sueoka, N. *J. Bact.* **139,** 911–916 (1979).
9. Yamaguchi, Y. & Yoshikawa, H. *J. molec. Biol.* **110,** 219–253 (1977).
10. Sueoka, N. & Quinn, W. G. *Cold Spring Harb. Symp. quant. Biol.* **33,** 695–705 (1968).
11. Sueoka, N. & Hammers, J. *Proc. natn. Acad. Sci. U.S.A.* **71,** 4787–4791 (1974).
12. Imada, S., Carroll, L. E. & Sueoka, N. *ICN-UCLA Symp. molec. Cell Biol.* **3,** 187–200 (1975).
13. Zerial, A., Gelman, I. & Firshein, W. *J. Bact.* **135,** 78–89 (1978).
14. Mackenzie, J. M., Neville, M. M., Wright, G. E. & Brown, N. C. *Proc. natn. Acad. Sci. U.S.A.* **70,** 512–516 (1973).
15. Kornberg, A. *DNA Replication*, 347–412 (Freeman, San Francisco, 1980).
16. Henner, D. J. & Hoch, J. A. *Microbiol. Rev.* **44,** 57–92 (1980).
17. Anagnostopoulos, C. & Spizizen, J. *J. Bact.* **81,** 741–746 (1961).

In vivo aminoacylation of brome mosaic and barley stripe mosaic virus RNAs

L. Sue Loesch-Fries* & Timothy C. Hall

Department of Horticulture, University of Wisconsin, Madison,
Wisconsin 53706, USA

The genomic RNAs of several plant viruses are now known to be able to bind a specific amino acid at their 3′ ends in a tRNA-like manner. Where the nucleotide sequence of the 3′-terminal region is known, it can be folded into an extensively base-paired secondary structure having the essential features of tRNAs[1,2]. The high degree of nucleotide sequence conservation of the 3′-terminal regions of the four RNAs of the three known bromoviruses[3], and the loss of infectivity of brome mosaic virus (BMV) RNA after chemical modification of its 3′ end[4], strongly suggest that the tRNA-like structure has a biological function in infection[2]. To elucidate this it has been important to determine whether viral RNAs are aminoacylated within infected host cells. We studied BMV and barley stripe mosaic virus (BSMV), which belong to very different groups but which have genomic RNAs that are capable of both accepting tyrosine and infecting barley protoplasts. We report here that single-stranded RNAs of both viruses are aminoacylated *in vivo*, but that the encapsidated RNAs of BMV are not.

Both BMV and BSMV have segmented genomes. The molecular weights (MWs) of the genomic RNAs of BMV are 1.1×10^6 (RNA1), 0.99×10^6 (RNA2), and 0.75×10^6 (RNA3). RNA 4, a subgenomic RNA coding for coat protein, is encapsidated with RNA3 and has a MW of 0.28×10^6 (ref. 7). The RNA of the Type strain of BSMV (ATTC strain 43) used in this investigation can be resolved by gel electrophoresis into two RNAs of MW 1.4×10^6 (RNA1) and 1.25×10^6 (RNA2)[8,9]. BMV and BSMV differ widely in their physical properties and transmissibility and thus have been assigned to separate virus groups; however, RNAs of both specifically accept tyrosine in an *in vitro* reaction catalysed by aminoacyl tRNA synthetase[5,6] *In vitro* studies have shown that aminoacylation of BMV RNA does not have a direct role in translation events[10,11]; however, it may be necessary for RNA transcription or encapsidation[12,13].

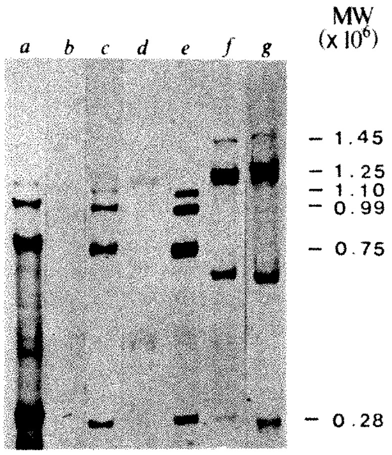

Fig. 1 Electrophoretic analysis of ^{3}H-labelled RNAs from: *a*, BMV Tyr-RNA charged *in vitro*[3]; *b*, mock-inoculated protoplasts cultured in ^{3}H-Tyr; *c*, BMV-infected protoplasts cultured in ^{3}H-Tyr; *d*, mock-inoculated protoplasts cultured in ^{3}H-uridine; *e*, BMV-infected protoplasts cultured in ^{3}H-uridine; *f*, BSMV-infected protoplasts cultured in ^{3}H-uridine; g, BSMV-infected protoplasts cultured in ^{3}H-Tyr. BMV and BSMV were extracted from infected *Hordeum vulgare* L. cv. 'Dickson' or 'black hulless', respectively[8,17]. Viral RNA was isolated by phenol extraction[8,18]. Protoplasts from primary leaves of 'black hulless' barley (20 ml, 1×10^5 ml^{-1}) were mock-inoculated or inoculated with BMV or BSMV RNA at 5 μg ml^{-1} and cultured in the presence of ^{3}H-Tyr (30–60 Ci mmol^{-1}) at 30 μCi ml^{-1} for 18–20 h, or ^{3}H-uridine (40–60 Ci mmol^{-1}) at 40 μCi ml^{-1} and actinomycin D at 10 μg ml^{-1} for 24 h. RNA was phenol-extracted from the protoplasts using buffer containing 100 mM sodium acetate, 10 mM EDTA *p*H 4.5, 1% SDS and 1 mg ml^{-1} bentonite for the samples labelled with ^{3}H-Tyr, or buffer containing 10 mM glycine, 10 mM EDTA, 100 mM NaCl *p*H 9.5, 1% SDS and 1 mg ml^{-1} bentonite for samples labelled with ^{3}H-uridine. After ethanol precipitation, the RNA samples were suspended in water and stored at −80 °C. Samples containing 2,000–3,000 c.p.m. were analysed by electrophoresis in 12.5 cm × 15.5 cm × 1.5 mm slab polyacrylamide gels containing 2.4% acrylamide, 0.1% methylene bisacrylamide and 0.45% agarose, using 90 mM Tris-borate *p*H 8.3, 2.5 mM EDTA (TBE buffer). Electrophoresis was at 25 mA for 2 h at 4 °C. The radioactive bands were detected by fluorography using EN^{3}HANCE (NEN). Exposures of 30–50 days were required to detect radioactive bands. The MWs of the viral RNA bands are indicated.

Primary leaf protoplasts of barley were inoculated with BMV or BSMV RNA[14]; for mock-inoculation RNA was omitted. Protoplasts were cultured either in the presence of ^{3}H-uridine and actinomycin D to label virus RNAs synthesized during infection, or in the presence of ^{3}H-tyrosine (^{3}H-Tyr) to label aminoacylated RNAs. Samples of RNA from inoculated protoplasts labelled with ^{3}H-Tyr had approximately the same number of trichloroacetic acid (TCA)-precipitable counts as did a comparable sample from mock-inoculated protoplasts. However, striking differences in the patterns of aminoacylation became evident when the samples were analysed by gel electrophoresis (Fig. 1). Protoplasts inoculated with either BMV or BSMV RNA and cultured in ^{3}H-Tyr (Fig. 1*c*,*g*) contained radioactive RNA species that co-migrated with the ^{3}H-uridine-labelled viral species from infected protoplasts (Fig. 1*e*,*f*). The four radioactive bands of BMV RNA also co-migrated with BMV Tyr-RNA prepared by aminoacylation *in vitro* (Fig. 1*a*). RNA preparations from mock-inoculated (uninfected) protoplasts did not contain these labelled RNA bands. In addition to the genomic RNAs of BSMV, two smaller RNA bands were present in samples labelled with either ^{3}H-Tyr or ^{3}H-uridine. Low levels of these RNAs (MWs ~0.65×10^6 and 0.30×10^6) are present in virion preparations; considerable amounts of them occur in infected protoplasts and they may represent subgenomic

---

*Present address: Agrigenetics Research Park, 5649 East Buckeye Road, Madison, Wisconsin 53716, USA.

0028-0836/82/330771—03$01.00

messengers that are infrequently encapsidated[15]. They are also present in polysome preparations from infected barley; however, their translation products have not yet been identified (J. E. McFarland and A. O. Jackson, personal communication).

The ester bond between the amino acid and the viral RNA is readily hydrolysed. Therefore, although the viral RNAs from protoplasts cultured in ^{3}H-Tyr were labelled, it was possible that the radioactivity did not represent an aminoacylated tyrosine. When BMV Tyr-RNA was heated in Tris-borate, *p*H 8.3 at 60 °C for 30 min, only 4% of the original radioactivity remained TCA-precipitable; if ^{3}H-uridine labelled BMV RNA was similarly treated, 96% of the radioactivity remained TCA-precipitable. Electrophoretic analysis of these samples is shown in Fig. 2*a*–*d*. BMV Tyr-RNA (Fig. 2, lane *c*) contained an RNA that migrated as a broad band ahead of RNA4—this probably resulted from slight degradation during *in vitro* aminoacylation. This band is present in Fig. 2*m*, which also contains BMV Tyr-RNA. The RNA samples from BSMV- and BMV-infected protoplasts cultured in ^{3}H-Tyr (Fig. 2*e*,*f*,*i*,*j*) behaved as expected for aminoacylated RNAs in that all radioactive viral bands lost most of their radioactivity during heating. Gels containing RNA samples from protoplasts cultured in ^{3}H-Tyr subjected to electrophoresis for a shorter time (Fig. 2*h*–*j*) contained a rapidly migrating radioactive RNA band that appeared to be tyrosylated tRNA. This was confirmed by comparison of its electrophoretic migration with wheat germ tRNA aminoacylated *in vitro* (Fig. 2*k*,*l*).

RNA isolated from infected protoplasts includes viral molecules involved in translation and transcription as well as those encapsidated into virions. To determine whether encapsidated RNA was tyrosylated, virus was purified from infected protoplasts cultured in ^{3}H-Tyr by a modified extraction procedure using differential centrifugation with unlabelled carrier virus[14]. RNA was isolated from the virus and analysed by polyacrylamide gel electrophoresis; RNA collected 18 h after inoculation contained only trace levels of radioactivity, but RNA from virus collected 24 h after inoculation contained detectable levels of radioactivity. Figure 3 shows that all four encapsidated RNAs were radioactive—this was surprising as comparisons of the acceptor capacity for batches of RNA isolated in acidic or alkaline conditions from virions suggested that encapsidated BMV RNA was not tyrosylated[2]. Therefore, the RNA was tested for the ability to lose radioactivity by deacylation in alkaline conditions. Figure 3*c*,*d* shows that most of the radioactivity remained after heating, suggesting that the radioactivity associated with the encapsidated RNA was not due to an aminoacylated tyrosine. It is likely that turnover of the ^{3}H-Tyr during the 24 h incubation period resulted in the formation of ^{3}H-labelled nucleotides that were subsequently incorporated into viral RNA, and thus the radioactivity was relatively stable to hydrolysis.

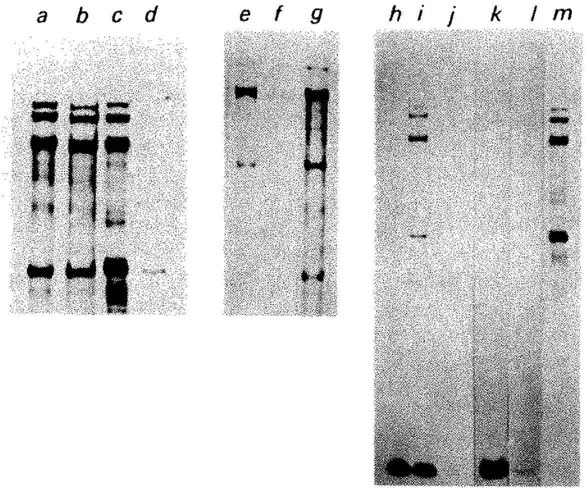

Fig. 2 Electrophoretic analysis of deacylated RNAs. Aliquots of RNA were prepared in either TBE buffer (see Fig. 1 legend) or in water as a control. The RNA samples suspended in TBE buffer were heated to 60 °C for 30 min and cooled on ice; samples suspended in water were brought to 50 °C for 5 min. All samples were made dense with urea. Electrophoresis was as described in Fig. 1 legend, except that RNAs in lanes *h*–*m* were subjected to electrophoresis for only 1.5 h. RNAs added to the gel lanes were: *a* and *b*, ^{3}H-uridine-labelled BMV RNA from infected protoplasts; *c* and *d*, BMV Tyr-RNA aminoacylated *in vitro*; *e* and *f*, RNA from BSMV-infected protoplasts cultured in ^{3}H-Tyr; *g*, RNA from BSMV-infected protoplasts cultured in ^{3}H-uridine; *h*, RNA from mock-inoculated protoplasts cultured in ^{3}H-Tyr; *i* and *j*, RNA from BMV-infected protoplasts cultured in ^{3}H-Tyr; *k* and *l*, wheat germ Tyr-tRNA aminoacylated *in vitro*; *m*, BMV Tyr-RNA aminoacylated *in vitro*. RNAs in lanes *b*, *d*, *f*, *j* and *l* were heated in TBE buffer; the other lanes contain control RNA.

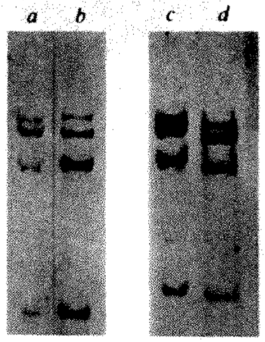

Fig. 3 Analysis of encapsidated RNA. Infected protoplasts (~1×10^6) collected 24 h after inoculation were homogenized in 500 mM sodium acetate, 80 mM magnesium acetate *p*H 4.5, using a ground-glass tissue homogenizer. Unlabelled BMV (200 μg) was added as a carrier and the sample was subjected to differential centrifugation to isolate virions[14]. The virus pellet was resuspended in 400 μl of a 1:10 dilution of the above buffer. RNA extraction and electrophoresis were as described in Fig. 1 legend except that 1M sodium salicylate was used as the autoradiographic enhancer for lanes *c* and *d*. Mock-inoculated protoplasts contained no radioactivity. *a*, *c*, *d*, RNA isolated from virus extracted from BMV-infected protoplasts cultured in ^{3}H-Tyr; *b*, BMV Tyr-RNA charged *in vitro*. RNA contained in lane *a* was from a separate experiment than that contained in *c* and *d*. RNA in *d* was heated in TBE buffer (as in Fig. 2).

These results demonstrate that non-encapsidated viral RNA is aminoacylated within a natural host cell. The tyrosylated viral RNA appeared to be full-length as it co-migrated in polyacrylamide gels with full-length BMV RNA. This differs from the situation described by Joshi *et al.*[16] for aminoacylation of turnip yellow mosaic virus RNA with valine in *Xenopus laevis* oocytes, in which the aminoacylated RNA appeared to have been cleaved into a fragment similar in size to tRNA; no full-length charged viral RNA could be detected. This discrepancy may reflect differences between plant and animal cells or possibly differences in methods of detecting charged RNAs.

Subgenomic RNA4 of BMV and two putative subgenomic messengers of BSMV were found to be aminoacylated. If aminoacylation is involved in RNA replication, such as the mechanism postulated by Hall and Wepprich[12] wherein aminoacylated viral RNA binds elongation factor and subsequently replicase, these results suggest replication of the subgenomic RNAs via their own templates.

We thank Dr A. O. Jackson for 'black hulless' barley seed and BSMV Type culture and for useful discussions. We also thank P. A. Kiberstis for the gift of *in vitro* aminoacylated BMV Tyr-RNA. This work was supported by NIH grant AI 11572 and NSF grant PCM 78-22526.

Received 26 January; accepted 8 June 1982.

1. Ahlquist, P., Dasgupta, R. & Kaesberg, P. *Cell* **23,** 183–189 (1981).
2. Hall, T. C. *Int. Rev. Cytol.* **60,** 1–26 (1979).
3. Dasgupta, R. & Kaesberg, P. *Proc. natn. Acad. Sci. U.S.A.* **74,** 4900–4904 (1977).
4. Kohl, R. & Hall, T. C. *Proc. natn. Acad. Sci. U.S.A.* **74,** 2682–2686 (1977).
5. Hall, T. C., Shih, D. S. & Kaesberg, P. *Biochem. J.* **129,** 969–976 (1972).
6. Agranovsky, A. A., Dolja, V. V., Gorbulev, V. G., Kozlov, Yu. V. & Atabekov, J. G. *Virology* **113,** 174–187 (1981).
7. Lane, L. C. & Kaesberg, P. *Nature new Biol.* **232,** 40–43 (1971).

8. Jackson, A. O. & Brakke, M. K. *Virology* **55**, 483–494 (1973).
9. Lane, L. C. *Virology* **58**, 323–333 (1974).
10. Shih, D. S., Kaesberg, P. & Hall, T. C. *Nature* **249**, 353–355 (1974).
11. Chen, J. & Hall, T. C. *Biochemistry* **12**, 4570–4574 (1973).
12. Hall, T. C. & Wepprich, R. K. *Ann. Microbiol*, **127A**, 143–152 (1976).
13. Dasgupta, R., Ahlquist, P. & Kaesberg, P. *Virology* **104**, 339–346 (1980).
14. Loesch-Fries, L. S. & Hall, T. C. *J. gen. Virol.* **47**, 323–332 (1980).
15. Gustafson, G. D. *et al. Virology* (in the press).
16. Joshi, S., Haenni, A. L., Hubert, E., Huez, G. & Marbaix, G. *Nature* **275**, 339–341 (1978).
17. Shih, D. S., Lane, L. C. & Kaesberg, P. *J. molec. Biol.* **64**, 353–362 (1972).
18. Bockstahler, L. E. & Kaesberg, P. *J. molec. Biol.* **13**, 127–137 (1965).

Differential scattering of circularly polarized light by the helical sperm head from the octopus *Eledone cirrhosa*

Marcos F. Maestre*, Carlos Bustamante†,
Thomas L. Hayes*, Juan A. Subirana‡
& Ignacio Tinoco Jr†

* Donner Laboratory, Lawrence Berkeley Laboratory, University of California, Berkeley, California 94720, USA
† Chemistry Department, Laboratory of Chemical Biodynamics, University of California, Berkeley, California 94720, USA
‡ Departamento de Quimica Macromolecular, Escuela Tecnica Superior de Ingenieros Industriales, Barcelona (28), Spain

Helices are expected to scatter circularly polarized light preferentially. According to theory, the scattering depends on the pitch, radius and sense of helix[1–4]; however, experimental data have been lacking. We now report quantitative measurements of the differential scattering of left and right circularly polarized light from the sperm head of the octopus *Eledone cirrhosa*. This sperm head is a left-handed helix with pitch and diameter of about 1 μm. It preferentially scatters left circularly polarized light versus right circularly polarized light in the forward direction, with a maximum differential scattering of 2% at 35° to the incident beam (wavelength = 0.442 μm). The preferential forward scattering of left circularly polarized light is consistent with theory[1–4]. As a differential scattering of 0.1% is easily measured, this can be a useful new method to characterize helical biological objects.

Circular dichroism (CD) studies of complex biological macrostructures sometimes produce anomalies in the measured spectra. CD signals are observed outside the absorption bands of the chromophores, thus making the interpretation of the spectra difficult[5–7]. These artefacts have been shown to arise from a difference in scattered intensities when left and right circularly polarized light is incident on the sample[8–11]. This differential scattering produces a differential extinction, which is recorded by the CD spectrophotometer as if it were differential absorption. Experimental techniques exist to characterize these spurious scattering effects and to eliminate them[9,12]. However, recent theoretical work[1–4] has shown that the differential scattering contains detailed structural information. The theory shows that the angular dependence of the circular intensity differential scattering, CIDS $= (I_L - I_R)/(I_L + I_R)$, reflects the structure of the chiral macromolecule. Here I_L and I_R are the intensities of the scattered light at a given angle when left and right circularly polarized light is incident. Application of the general theory to helices shows that polar plots of CIDS versus scattering angle give lobes whose sign, number and position are characteristic of the sense, pitch and radius of the helix.

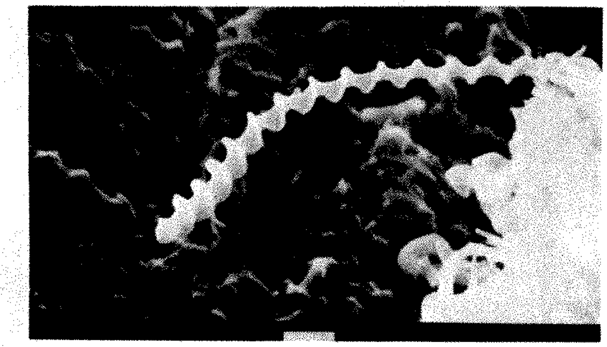

Fig. 1 Scanning electron micrograph of a freeze-dried sperm head from the octopus *Eledone cirrhosa*. The sperm head is a left-handed helix with a pitch of about 0.65 μm. Scale bar, 1 μm.

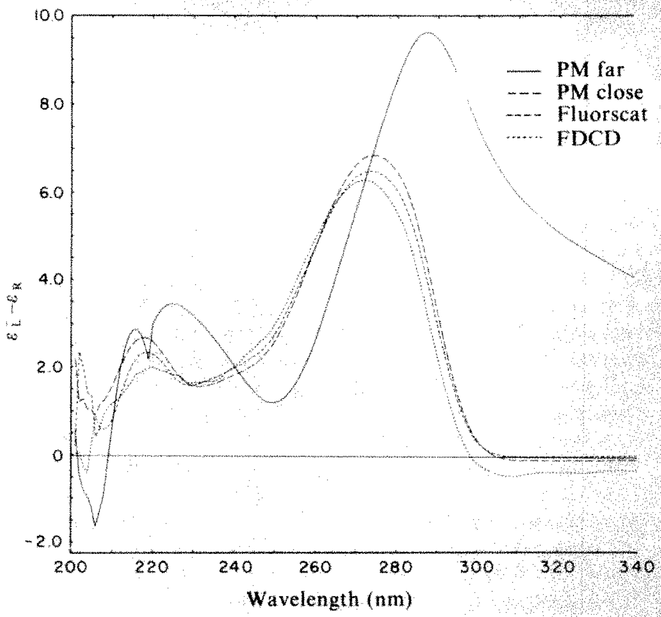

Fig. 2 Circular dichroism spectra in arbitrary units of *E. cirrhosa* sperm heads, measured by techniques having different solid angles of detection of scattered light. ——'PM far' is the conventional configuration; — —, 'PM close' has the photomultiplier detector close to the sample to detect most of the forward scattered light; - - -, fluorscat method; · · · · ·, fluorescence detected circular dichroism, FDCD, method. Sample contained 1 mg lyophilized heads in 10 ml of a 0.1 M NaCl, 10 mM Tris, *p*H 7.5 buffer.

We have built an instrument to measure the angular dependence of differential scattering of circularly polarized light (CIDS), and report some preliminary results that indicate the usefulness of such measurements. The nuclei of sperm cells from the octopus *E. cirrhosa* were chosen for initial study, because their large helical structure ensures large CIDS values, and their chirality and dimensions could be measured independently. Figure 1 illustrates the remarkable size and complexity of the helical head of the mature sperm from *E. cirrhosa*. These rigid nuclei have been measured by light microscopy to be 43 μm long, and to form a left-handed helix with a pitch of 1 μm and radius of 0.5 μm (ref. 13) Our measurements in the scanning electron microscope gave values for the pitch of 0.65 μm, with an outside diameter of 0.60–0.65 μm and an inner diameter of 0.25 μm. The difference in the two sets of values probably reflects the difference in techniques. On suspending purified nuclei in a buffer solution, intense light scattering is observed. Figure 2 shows the CD spectrum of the suspended nuclei. The curve labelled 'PM far' is the usual experimental arrangement, in which the photomultiplier mainly detects the transmitted beam; only light scattered very close to this beam is also detected. Note that the CD signal is very strong at long wavelengths, where the components of the nuclei (DNA and protein) do not absorb light, suggesting a large contribution from differential scattering of circularly polarized light. Of particular interest is the fact that this differential scattering effect is essentially eliminated by bringing the photomultiplier close to the sample and thus increasing the angle of acceptance of the scattered light (Fig. 2, curve labelled 'PM close').

Further small corrections were achieved by use of fluorscat cuvettes[8] and fluorescent detected circular dichroism (FDCD) techniques[9]. Fluorscat is a double-chambered cuvette with the outer chamber filled with a fluorescent solution that captures all light not absorbed by the sample, except for a small sector

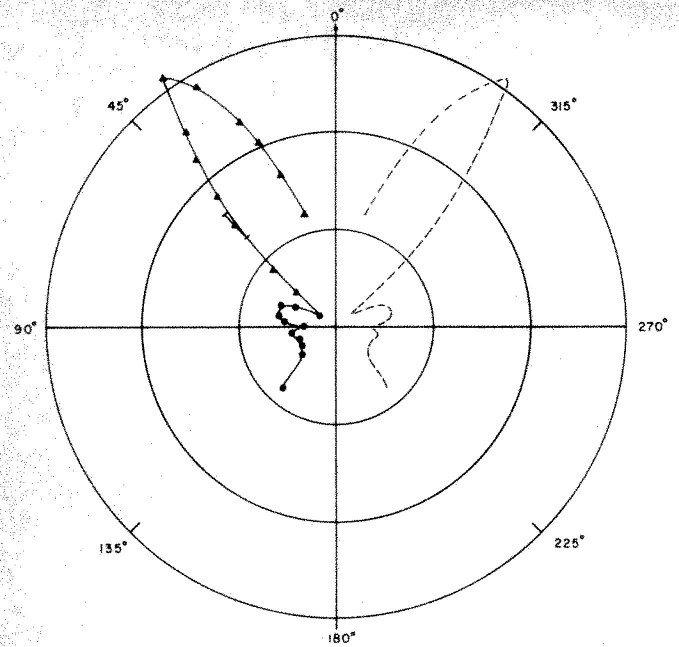

Fig. 3 Plot of CIDS $[(I_L - I_R)/(I_L + I_R)]$ versus scattering angle for *E. cirrhosa* sperm heads at a concentration of 0.25 mg ml^{-1} in the buffer of Fig. 2; the arrow illustrates the direction of incident beam (wavelength = 442 mm). ▲, Positive values; ●, negative values; ——, measured data; – – –, constructed by symmetry. The plot has a maximum positive value of 1.4×10^{-2} at about 35°; the positive value means left circularly polarized light is preferentially scattered.

in the back direction of the scattering envelope. The FDCD technique involves the use of a fluorescer molecule that is not optically active and that does not bind to the particle being measured. Each scattering particle is now surrounded by a cloud of fluorescent molecules which measure all the light that is not absorbed, including light scattered backwards along the incoming light beam. Considering the minor corrections to the measured CD by the fluorscat and FDCD techniques (Fig. 2), we conclude that the sperm heads mainly scatter light differentially in the forward direction.

The apparatus used to measure CIDS directs linearly polarized light from a He–Cd laser (442 nm) through a Pockels' cell (an electro-optical quarter wave plate) with an applied square voltage pulse which produces alternately pure left and right circularly polarized light. The circularly polarized light is incident on the sample cuvette, and the scattered radiation is measured by a detector mounted on a goniometer. The signal from the detector is processed by a modified Cary 60 spectrophotometer and analysed in terms of CIDS.

Figure 3 shows the resulting polar plots of CIDS versus scattering angle for the sperm heads; a reference sample of polystyrene beads shows no differential scattering in the same conditions. This plot shows that the CIDS does occur mostly in the forward scattering direction (with a maximum at 35° from the incident beam), and also that left circularly polarized light is scattered more intensely than right circularly polarized light, that is, the forward lobe is positive. There is evidence of small negative differential scattering to the sides (90°) as is predicted from the minor correction of the fluorscat method (Fig. 2). The results presented here are preliminary and have been obtained with a maximum angular resolution of 5°; however they are very reproducible. We are now working to improve the resolution of the apparatus to obtain more detailed information about the angular dependence of the differential scattering intensities.

The data shown in Fig. 3 are of the type expected from theory for a helix whose pitch or radius is larger than, but similar to the wavelength of incident light. The preferential forward scattering of left circularly polarized light indicates a left-handed helix. We have measured differential scattering from T4 and T7 bacteriophage[14] which are very different from each other and from the octopus sperm. We think that differential scattering of circularly polarized light can be very useful in determining the packing of DNA in bacteriophages[15,16], and the higher order structures of DNA in chromosomes[17].

We thank Dr Phillip Burns for help with some of these measurements. This work was supported by NIH grants AI08247(M.F.M) and GM 10840(I.T.) and by the Office of Health and Environmental Research of the US Department of Energy under contract 98, DE-AC03-76SF00098.

Received 22 April; accepted 11 June 1982.

1. Bustamante, C., Maestre, M. F. & Tinoco, I. Jr *J. chem. Phys.* **73,** 4273–4281 (1980).
2. Bustamante, C., Maestre, M. F. & Tinoco, I. Jr *J. chem. Phys.* **73,** 6046–6055 (1980).
3. Bustamante, C., Tinoco, I. Jr & Maestre, M. F. *J. chem. Phys.* **74,** 4839–4850 (1981).
4. Bustamante, C., Tinoco, I. Jr & Maestre, M. F. *J. chem. Phys.* **76,** 3440–3446 (1982).
5. Urry, D. W., Massoti, L. & Krivacic, J. *Biochem. biophys. Res. Commun.* **41,** 521–524 (1970).
6. Schneider, A. S., Schneider, M. J. & Rosenheck, K. *Proc. natn. Acad. Sci. U.S.A.* **66,** 793–798 (1970).
7. Maestre, M. F., Gray, D. M. & Cook, R. B. *Biopolymers* **10,** 2537–2553 (1971).
8. Dorman, B. P. & Maestre, M. F. *Proc. natn. Acad. Sci. U.S.A.* **70,** 255–259 (1973).
9. Reich, C., Maestre, M. F., Edmonson, S. & Gray, D. M. *Biochemistry* **19,** 5208–5213 (1980).
10. Tinoco, Jr., I., Bustamante, C. & Maestre, M. F. *A. Rev. Biophys. Bioengng* **9,** 107–141 (1980).
11. Maestre, M. F. & Reich, C. *Biochemistry* **19,** 5214–5223 (1980).
12. Dorman, B. P., Hearst, J. E. & Maestre, M. F. *Meth. Enzym.* **27,** 767–796 (1973).
13. Maxwell, W. L. *Proc. R. Soc.* **B186,** 181–190 (1974).
14. Tinoco, I. Jr, Bustamante, C. & Maestre, M. F. in *Structural Molecular Biology: Methods and Applications* (eds Davies, D. B., Saenger, W. & Danyluk, S. S.) (Plenum, New York, 1982).
15. Tikchonenko, T. I. *Comprehensive Virol.* **5,** 1–117 (1975).
16. Black, L. W. & Silverman, D. J. *J. Virol.* **28,** 643–655 (1978).
17. Sedat, J. & Manuelidis, L. *Cold Spring Harb. Symp. quant. Biol.* **42,** 331–350 (1977).

Erratum

In the letter 'Atmospheric angular momentum and the length of day: a common fluctuation with a period near 50 days' by R. B. Langley *et al. Nature* **294,** 730–732 (1982), the curves in a panel of Fig. 1 were rotated through 180°. The figure is shown correctly in reprints and (reduced in size) below.

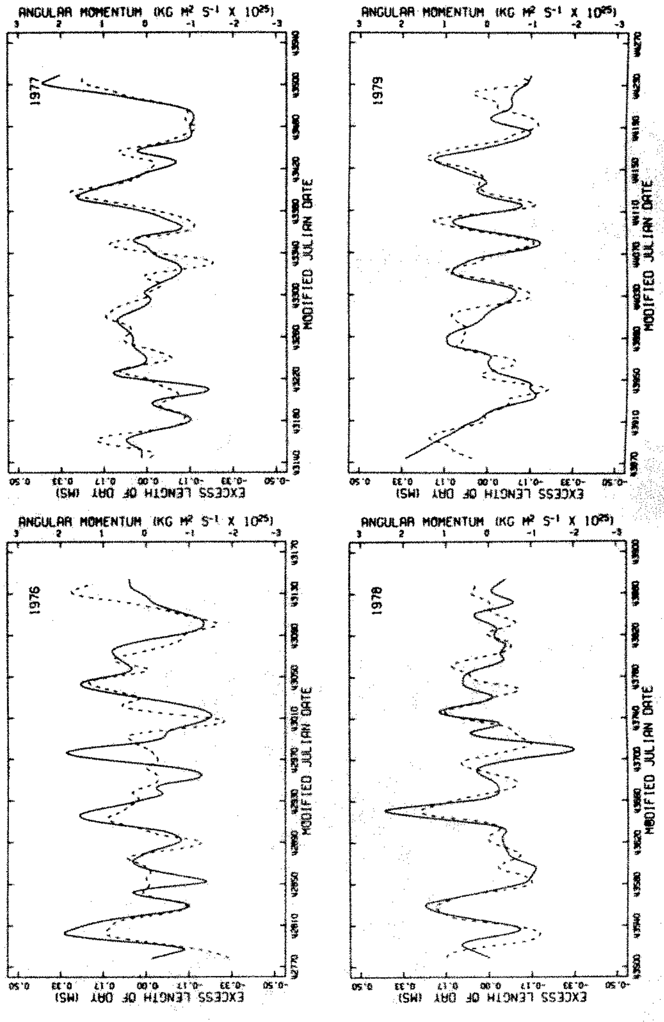

BOOK REVIEWS

Blunders in the business of risk

Dorothy Nelkin

IN 1885 a British tourist in the United States was travelling on a train when it began to shake violently. Panicked, he asked the conductor to stop the train, but to no avail. The train jumped its tracks and most of the cars were smashed. Yet to his amazement, his fellow passengers applauded the conductor's efforts to arrive on time. So consumed were they by the idea of progress, they failed to recognize a near fatal disaster.

Clearly, attitudes have changed. Today, the United States has been described as a "risk-aversive" society, and some feel that our preoccupation with risks is threatening our commitment to technological progress and economic growth. In this environment the field of risk assessment has become a veritable industry. The assessment, management and adjustment to risk is estimated to cost between $200 and $300 billion per year, that is, from 10 to 15 per cent of the gross national product. The fear of risk is reflected in legislation and regulation. A programme within the National Science Foundation supports research on risk, hoping to provide a rational and reasonable basis for technical decisions. The availability of funds has encouraged a proliferation of consulting firms and academic research programmes. Indeed, the field of risk assessment, engaging geographers and engineers, economists and systems analysts, psychologists and anthropologists, has replaced technology assessment as the fashion of the day.

Risk analysts are preoccupied with two central questions: "How safe is safe enough?" and "What factors influence perception of risk?". Systematic efforts to estimate and evaluate the risks inherent in different technologies and then to quantify the acceptability of risk began to burgeon in response to environmental controversies, in particular over nuclear power. Hoping to develop a "rational" means to make decisions about hazardous technologies, a number of scholars from the field of engineering safety analysis sought to establish a quantitative basis to compare risks from different technological choices and to calculate their relative costs and benefits. They were encouraged by legislation requiring the risks of technological choices to be systematically weighed against social benefits. Their analytical approaches to risk, based on engineering and economic models, included a variety of forecasting and systems analysis techniques. They confronted serious methodological dilemmas. Indeed, the uncertainty about the nature and extent of the risks inherent in many technological choices seems to defy systematic and objective analysis. In any case, the various efforts to calculate the risks and benefits of technology proved to be poor indicators of the political and social acceptability of risk.

Risk and Culture: An Essay on the Selection of Technological and Environmental Dangers. By Mary Douglas and Aaron Wildavsky. Pp.224. ISBN 0-520-04491-6. (University of California Press: 1982.) $14.95, £11.25.

Difficulties in predicting public attitudes focused attention on the psychological and attitudinal factors that enter subjective perceptions of risk. Psychologists began to study risk perception through laboratory experiments, gaming situations and survey techniques in order to identify the subjective values that guide individual choices. Their work on the characteristics of risk that influence judgements about acceptability suggests that risks that are involuntary, uncertain, unfamiliar and potentially catastrophic are most difficult for people to accept. In their studies, psychologists try to arrive at a quantitative determination of risk acceptance. However, limited by their focus on the individual, they often fail to account for variations in the perception of risk in different social and cultural contexts. Why indeed did the British tourist perceive risks so differently from his fellow travellers?

These social dimensions of risk perception are the focus of *Risk and Culture*. Seeking to explain the preoccupation with risk in American society, the authors start with a provocative and promising premise — that it is inappropriate to define simply the problem of risk either in terms of objectively calculated physical risks or subjectively biased individual perceptions. Between subjective perceptions and physical science, they argue, lies a culture; and perceptions of risk are necessarily embodied in the complex system of beliefs, values and ideals which constitute this culture. This premise carries the debate about risk beyond the narrow technical questions of safety and into the domain of values and social choices.

This view of risk as a socially constructed phenomenon is a creative and refreshing addition to the risk analysis literature. It could lead to research into a variety of questions, shedding light on the social and political dimensions of risk perception. However, instead, the authors carry their argument in a direction that reflects their personal concerns with challenges to the *status quo*.

Their argument is as follows. Risk is a kind of euphemism for social and moral issues. Both modern and primitive societies select dangers to buttress their view of the social system. Risk becomes an explanation of failure, a way of attributing blame, a moral judgement about conduct inspired by a vision of the social and moral order. People predisposed to prefer different forms of social organization will perceive different dangers. Douglas and Wildavsky thus shift the critical question in risk analysis from "What are the real risks?" to "Why do different people perceive risks in different ways?" — "What issues of accountability or values are at stake?".

They build their argument by rejecting the conventional assumptions of most risk analyses. They dispose of explanations based on scientific evidence, pointing to the disputes among scientists and the real uncertainties surrounding many questions of risk. They observe how scientific judgements themselves are rooted in social expectations. Similarly, they account for the rigid categories of voluntary and involuntary risk underlying "objective" analyses by observing how the choices of risk assessment methods are themselves biased by underlying cultural assumptions. Then they turn to their own analysis, suggesting how different cultures with shared values and social institutions will select or highlight certain risks and minimize others.

The argument is built on Douglas's superb work on "pollution" — the idea that "pollution beliefs" are used by all societies to define boundaries that will preserve social categories and political relationships. It is a convincing thesis. The very language of those concerned with risks vividly reveals their social and political orientation. Why else would critics of nuclear technology talk of "electro-fascism" or "nucleocracy"? However, my enthusiasm for this approach to risk begins to wane when Douglas and Wildavsky develop a three-part typology of "risk portfolios" in American society. They assert that the evaluation of risk is based on (i) hierarchical assumptions, (ii) market or individualistic rationality, or (iii) sectarian values. The first two comprise a "centre" in which maintenance of the existing system is the primary goal. "Sectarian" rationality comprises a border, remote from the centre of power. The perspectives of sectarian groups on risks reflect their rebellion against the centre and their own needs to maintain group allegiance. Their views are marked by "disdain of the world, fear of pollution, of cancerous contamination" and are propelled by "moral fervor". The sectarian "wins adherence if he can threaten bigger dangers and associate them with the corruption of the system".

The authors develop their model of the sectarian society less from evidence than from their own opinion of the radical wing of the environmental movement. They quickly lapse into pejorative language that hardly masks their disdain. They portray such groups as self-indulgent and living in permanent and nagging opposition to the centre with no intention of assuming responsibility or power. And they denigrate the strengths of sectarian ideals suggesting that, when not allowed to enjoy government subsidy, such groups simply become part of the very system they reject.

The authors feel that such sectarian values are increasingly important in American society and have won "extraordinary success". They do, indeed, account for our preoccupation with risk. There are, however, many problems with their argument. After all, the "sustained assault" by public interest and environmental groups lasted but a decade. In the context of today's politics the "extraordinary success" of environmental groups as compared to business interests is hardly convincing. Moral fervour in the United States today comes from other directions, indeed from the centre itself. Concerned about challenges to the hierarchical and market values that constitute the centre, the authors ignore the usefulness of sectarian groups as a source of constructive criticism and countervailing power. They neglect, for example, the positive contributions of "border groups" such as the alternative technology movement who have put forward specific proposals for minimizing risk. And to suggest that such sectarian — i.e. powerless — groups could gain power if they really wanted it, is to totally ignore political and economic constraints. In their criticism of such groups, the authors describe "lobbying, litigation and non-violent obstruction" as "border strategies", forgetting that these are also conventional political actions exploited by bureaucracies and businesses.

The authors also dismiss the possibility that the reality of risk has changed in any significant way, essentially ignoring the increased scale and changing character of technology-induced risk. Associating the fear of risk with radical groups, their theory has no place for those who work in genuinely dangerous jobs, or the residents of Love Canal, or the 700,000 middle-class people who converged in New York City to protest against the risk of nuclear war.

A cultural theory of risk could be developed in a different direction with greater emphasis on the social position and the special vulnerability of certain groups with limited economic or political choice. It could call attention to the experience and perspectives of people who deal with risks as a fact of everyday life. Clearly judgements of risk reflect cultural values. But after all there is a social reality. If indeed the issue of risk has become an arena for disputes over power, why not take off from this approach to examine critically corporate perceptions and behaviour with respect to risk? Why not ask how factors at work and in daily life influence people's risk perceptions?

Douglas and Wildavsky end their book by frankly stating their own bias towards the centre. Basing their analysis on the acceptance of given institutional arrangements, they, along with other risk analysts, have masked many problems by avoiding critical questions about the very political and social relationships that they themselves admit are fundamental to the selection and perception of risks. ☐

Dorothy Nelkin is a Professor in the Cornell University Program on Science, Technology and Society and the Department of Sociology.

An enlarged Universe

Owen Gingerich

The Expanding Universe: Astronomy's 'Great Debate' 1900–1931. By Robert W. Smith. Pp.220. ISBN 0-521-23212-0. (Cambridge University Press: 1982.) £19, $29.50.

ONE of the extraordinary developments of twentieth-century science has been the recognition and measurement of the great size of the Universe. The most dramatic moments in this revolutionary understanding took place from 1918 to 1924, primarily at the great mountain observatories in the American West, and a focal event was the debate on the scale of the Universe between Harlow Shapley and H.D. Curtis in Washington, in June 1920.

The Shapley–Curtis debate has achieved something of near mythological status among astronomers. Robert Smith capitalizes on the mystique of the specific debate in his subtitle to extend the argumentation over a broader time span; and well he might, for, as he informs us, the actual encounter before the National Academy of Sciences left a great deal to be desired as far as scientific depth was concerned. The main title is likewise stretched beyond its specific technical connotation, and in an almost punning fashion refers more to a Universe ever larger in man's conception than in physical expansion.

The Shapley–Curtis–Hubble era has attracted a variety of historical treatments in the past decade. Smith's in-depth research fills in the contemporary details too often blurred by our 20–20 hindsight. For example, the status of the globular clusters as possible external galaxies has been almost entirely neglected in modern historical accounts of the 1915–1925 period. Similarly, he fills in the story of the first faltering attempts in the 1920s to derive a relation between the velocities and distances of the spirals, without which certain aspects of Edwin Hubble's approach to the problem can scarcely be comprehended.

In giving us a near-definitive account of the fascinating and turbulent growth in astronomical knowledge, Smith has assiduously avoided the historian's sin of evaluating the past with today's standards. Yet it would have been illuminating, I think, for him to have allowed that Shapley's joining of the period–luminosity relations for cluster-type variables and the Cepheids, for which he was criticized at the time, was in fact incorrect. Equally, Shapley's own criticism of Hubble's assumptions about the similarity of certain galaxies and their components has today proved valid. In the event both Shapley and Hubble pushed on with their faulty programmes, to the considerable advance of science in their day. This may well be telling us something interesting about the nature of scientific progress, but Smith's strictly historical approach prevents any such speculation. ☐

Owen Gingerich is a Professor of Astronomy and History of Science at the Harvard–Smithsonian Center for Astrophysics, Cambridge, Massachusetts.

An experiment of Otto von Guericke (1602–1686), a predecessor of Robert Boyle, attempting to produce a vacuum by exhausting a sealed cask filled with water. The illustration is taken from a corrected reprint of A. Rupert Hall's *From Galileo to Newton*, first published in 1963. The new edition is published by Dover in the United States and Constable in Britain, prices $6, £4.50 respectively (pbk).

Polymeric molecules in motion

Warner L. Peticolas

The Theory of Vibrational Spectroscopy and Its Application to Polymeric Materials. By Paul C. Painter, Michael M. Coleman and Jack L. Koenig. Pp.530. ISBN 0-471-09346-7. (Wiley: 1982.) £44.50, $80.

A DISTINGUISHED figure in the field of vibrational spectroscopy, Professor Jack Koenig of Case Western Reserve University has collaborated with two of his younger colleagues to produce a book which should be, for some time to come, the definitive work on the application of the theory of molecular vibrations to polymeric materials. Starting with a clear treatment of the classical mechanics of the vibrations of small molecules using both Cartesian and internal coordinates, the book takes the reader in a logical way to calculations of the normal modes of vibrations of polymer chains.

Due to the exigencies of space, some short cuts have been taken. For example, although the book starts with a discussion of small molecules, there is no mention of the formulae for calculating molecular internal coordinates from molecular Cartesian coordinates. Instead, the general concept of internal coordinates and their relationship to Cartesian coordinates is worked out in detail using matrix techniques. If the reader would like to work out the G matrix for small molecules with a desk calculator, he will have to turn to one of the listed references.

However, one gets the feeling that this book is really for readers who wish to do their calculations using computers. With a good computer program, it is possible to carry out normal mode calculations without actually going into a detailed derivation of the precise mathematical formulae for calculating each type of internal coordinate. Computer programs are available which define the internal coordinates and then immediately give instructions for calculating them from the coordinates of the atoms, which must be supplied as data. This approach is stressed in Chapter 7, entitled "Solving the Vibrational Problem Using Computer Methods". The authors note that it is difficult to use a desk calculator to solve secular matrices whose dimensions are greater than 3 by 3 and that it is much easier to go directly to a computer. They conclude their discussion of simple molecules with a detailed analysis of the benzene molecule. This is an area to which they themselves have made an important contribution in elucidating the vibrational spectra of benzene and its two important carbon-13 isotopic derivatives, as well as those of numerous deuterium substitutive derivatives.

After giving a brief account of the quantum mechanical description of infrared and Raman intensities, the authors discuss the lattice dynamics of chain molecules. This is the strongest feature of the book. Starting with the simple linear diatomic chain, and going to a detailed mathematical discussion of the Wilson–GF method, they present a clear method for calculating the normal modes of helical polymeric chains. The theory is followed by consideration of the normal modes calculations of many common polymeric materials. The book closes with an introduction to biological polymers which includes a discussion of the normal modes of polyglycine I.

Anyone wishing to do research in the field of vibrational spectroscopy of polymeric materials, including biological polymers, or anyone interested in the force fields of macromolecules, will find this book a time-saving, helpful introduction to a very complex but fascinating subject. ☐

Warner L. Peticolas is a Professor of Biophysical Chemistry at the University of Oregon, Eugene.

Alternative hosts for genetic engineers

Noreen Murray

Gene Cloning in Organisms Other than E. coli. Vol.96 *Current Topics in Microbiology and Immunology.* Edited by P. H. Hofschneider and W. Goebel. Pp.259. ISBN 0-387-11117-4/3-540-11117-4. (Springer–Verlag: 1982.) DM92, $42.90.

BIOCHEMICAL approaches to the molecular cloning of DNA became simple when, in 1972, it was shown that DNA digested with certain endonucleases yielded discrete fragments with cohesive ends. In the intervening decade, molecular cloning techniques using *E. coli* K12 as host have led to a detailed understanding of the mechanism of action of several prokaryotic genes and have revolutionized our concept of the organization of the eukaryotic genome. The full impact of this technology cannot, however, be realized just by cloning, sequencing and changing genes. A complete understanding of gene expression requires the cloned genes to be studied within the environment of their provenance, whilst commercial production of polypeptides may demand hosts free of endotoxins from which products can be exported across the cell membrane.

Volume 96 of *Current Topics in Microbiology and Immunology* surveys the current and potential use of *Bacillus subtilis,* pseudomonads, streptomycetes, fungi, animal and plant cells as hosts for molecular cloning. In many instances a more complete view of any one genetic system is achieved by including two chapters covering one system. For each system the following topics are documented: vectors; uptake of DNA into cells; the recognition of cells carrying recombinant DNA molecules; and the fate of the donor DNA following its uptake.

The development of alternative prokaryotic systems inevitably draws heavily upon experience with *E. coli* where the concepts of vector construction are well established. Consequently, novel information is often relatively specialized and likely to be of most interest to those readers who wish to use bacteria other than *E. coli* as hosts for cloning experiments. For *Streptomyces* much useful technical information, including laboratory methods and recipes, is provided. Of more general concern are the justifications for studying different bacterial species and the accounts of experiments relevant to the barriers preventing expression of heterologous genes.

The fungi are represented by a brief article documenting the beginnings of molecular cloning in *Neurospora crassa* and two chapters conveying some of the dramatic advances achieved in the molecular biology of *Saccharomyces.* The second of these two articles is in no way redundant, but the first (by Hinnen and Meyhack) is so clearly presented that it should be enjoyed by students of both genetics and molecular biology.

I approached the contributions on higher cells as an interested outsider, anxious to be informed of some of the more exciting developments in molecular biology. In the event I found them somewhat disappointing. The chapter on selectable markers for gene transfer was indeed useful, covering the systems and their use in transformation with some critical evaluation of the resulting studies of gene expression. However, a detailed diagram summarizing the relevant features of the Herpes TK gene and a chart indicating those aspects of nucleotide metabolism of relevance to the selective systems in use would have been welcome. In contrast, the short chapter on animal viral vectors, principally SV40, presents only a limited account of the field. Perhaps the authors anticipated the inclusion of a second and complementary article; certainly the space devoted to animal viral vectors is only a half or a third that for either *Bacillus subtilis* or pseudomonads. Unfortunately the volume was conceived too early to take account of recent success in the transformation of *Drosophila* cells.

A detailed survey of liposomes as a

NEW

FORAMINIFERA

J. R. HAYNES
Reader in Geology
University College of Wales

December 1981; £50.00;
480pp; 34pp plates; ISBN 0
333 28681 2

CONTENTS
Preface; The Scope of Foraminiferal Studies; Collection, Preparation and Examination (including Annotated Literature on Technical Methods); The Living Foraminifer; Test Morphology and Composition; Classification of the Foraminifera; The Agglutinating Foraminifera; The Fusulinida – The Miliolida; The Nodosariida; The Buliminida; The Robertinida; The Rotaliida (Smaller); The Rotaliida (Larger); The Globigerinida; References; Index.

This work is an advanced text covering the biology, morphology and classification of the Foraminifera and their use in stratigraphy and palaeoecology.

Superbly illustrated, the text draws on the author's experience in oil exploration and twenty years' teaching at both undergraduate and postgraduate level.

The main features of this work are:
- A new classification, illustrated by hand-drawn figures of the main genera, selected scanning electron micrographs and photomicrographs of thin sections.
- New theories linking the morphology of the foraminiferal shell with its adaptive function.
- The integration of the study of each of the orders which tend to succeed each other in time to illustrate their use in biostratigraphy and palaeoecology from the Cambrian to the Recent.
- It brings the student up against current problems and the dangers of an over- simplified approach to palaeoecology, evolutionary studies and biostratigraphy, and synthesises the result of recent research which is at present widely scattered in the literature.

For further information write to
FRANCES ROACH, Product Manager,
Scientific & Medical Division,
Macmillan Press Ltd., Houndmills,
Basingstoke, Hampshire RG21 2XS,
U.K.

SCIENTIFIC & MEDICAL M MACMILLAN PRESS LTD

carrier system is included but there is no chapter devoted either to microinjection, or protoplast fusion, as a means of DNA or RNA transfer. Plant systems are represented by comprehensive accounts of cauliflower mosiac virus and Ti plasmids of *Agrobacterium*. The former includes as appendices a computer print-out of the viral DNA sequence and derivative information.

The broad topic of genetic engineering in hosts other than *E.coli* should appeal to a wide audience, and I would hope to find a copy of this useful reference material in all university libraries. □

Noreen Murray, currently on leave of absence in the European Molecular Biology Laboratory, Heidelberg, is Reader in the Department of Molecular Biology at the University of Edinburgh.

Pollution in context

Eirene White

Principles of Pollution Control. By Francis Sandbach. Pp.174. Pbk ISBN 0-582-30042-8. (Longman: 1982.) £5.95, $11.95.

THIS is not a book addressed to the serious natural scientist. To be fair, it does not pretend to be. It is the first study in a series entitled "Themes in Resource Management".

The manifold objectives of the series, as stated by the editor-in-chief, Professor Bruce Mitchell, are, first

> to identify and examine enduring resource management and development problems [and thence] to assess responses to these problems in a variety of world regions.

Of particular concern are research and action programmes. The former are to be evaluated in terms of the nature and adequacy of data, the theoretical and practical understanding displayed and the identification of special problem areas. Action programmes are to be reviewed in terms of their effectiveness in promoting "economic efficiency, social equity and environmental harmony".

> This orientation [writes Professor Mitchell] should provide a departure point for considering the transferability of experience from one jurisdiction to another.

A final objective is

> to explore the way in which resource analysis, management and development might be made more complementary to one another.

Set against these fairly demanding requirements, one may ask how far in his study of the principles of pollution control Francis Sandbach can be said to have complied with them, and in any case to what readership his book is directed. It would not satisfy a reader looking for a scientifically-based account of pollution control over the past few decades or the scientific outlook for the future. But that is not what Mr Sandbach envisages. As a lecturer in interdisciplinary studies at the University of Kent, it is natural that he should seek to paint with a broad brush. One needs to go no further than the introduction to realize that although he has indeed read widely and assiduously about pollution in its various manifestations and provides a great deal of helpful factual information about how it is handled in Britain and elsewhere, he is really turned on by social and political theory rather than by science or technology.

Anyone who wants a schematic view of pollution control would do better to turn to Martin Holdgate's *A Perspective of Environment Pollution*, published by Cambridge University Press in 1979. Nevertheless, there is some validity in Francis Sandbach's thesis, as he forcefully illustrates in his case study of asbestos, the classic example of the clash of interests between health and profits. He devotes another chapter to a not very satisfactory attempt to discredit what he describes as the pluralist/behavioural perspective of those such as Eric Ashby and Mary Anderson who in their historical account of air pollution control in Britain (*The Politics of Clean Air*; for review see *Nature* **298**, 207; 1982) pay less attention than he thinks fit to economic determinants.

The six preceding chapters comprise a rapid and necessarily superficial survey of risk/dose/response relationships; cost effectiveness; the alternatives of recycling or of using a less polluting technology; "the polluter pays" principle and the possible use of pollution taxes; the setting of standards or threshold limit values; the choice of strategies; and the administrative and legal framework for pollution control in the United Kingdom, the EEC and the United States, with glimpses of China, Japan and Scandinavia.

There is much of interest in the book, but it is all rather breathless, plucking a fact here and picking up a figure there. An extensive bibliography includes many useful references to periodical literature (including some that may be more emotive than scientific). The index, by contrast, is exceedingly thin and anyone wishing to look up Seveso or Minamata, for example, has to scan the text.

As a means of introducing students to the general problems of pollution control set in a comprehensive context, this study, in the hands of a well-informed lecturer, could be very helpful. For the more general reader, such as an elected member of a local authority, who might well be in need of guidance, it is likely to be too allusive and, at times, bewildering in its range of detail. □

Baroness White is a Member of the House of Lords Select Committee on Science and Technology (Water Sub-Committee), and was a Member of the Royal Commission on Environmental Pollution from 1974 to 1981.

nature

26 August 1982

Life as a wonderful one-hoss shay

In the next 20 years at normal fertility rates, the US population will age dramatically. Are science and medicine prepared for the challenge and will they respond in the best possible way?

It is a general human failing, or a failing of our culture, to turn a blind eye to the fact that one day we will be old and infirm. The search for eternal youth brings with it avoidance of the inevitability of old age. But a few researchers in the United States have been asking in recent years whether old age must entail senility, illness and loneliness or whether through research, people who are now in their 30s, 40s and 50s stand a chance of living out their lives in relative good health until the very end. Unfortunately, most biomedical researchers and doctors are merely human, they share the human preference to not think about old age — let alone about how to cure it.

Two who have held out this new goal, Lewis Thomas, chancellor of the Memorial Sloan-Kettering Cancer Center in New York, and James Fries of Stanford University Medical Center, invoke a poem by Oliver Wendell Holmes, called the "wonderful one-hoss shay". The one-hoss shay — American slang for a small carriage — worked without a hitch until one day it gave out all at once and died. Holmes wished that death would be so kind to us and spare us the gradual loss of our hubs, tyres, springs and thills.

Thomas argues that basic biomedical research at the cellular level — the breakthroughs in Alzheimer's disease (presenile dementia) and work on the fundamental processes of memory, the ageing of cells, the possible switches that are key to vascular abnormalities and even cancer — may be found through a steady assault at the fundamental level in coming years. In 1978 he made a prediction: "I believe that the major diseases of human beings have become approachable biological puzzles, ultimately solvable. It follows from this that it is now possible to begin thinking about a human society relatively free from disease . . . What can we die of, if not disease?"

Fries has advanced the concept of the "compression of morbidity". Reduction in the acute illnesses from which people used to die continues to add to life expectancy in the United States. It is well known that a person celebrating their 65th birthday in 1953 could expect to live another 14 years; the person celebrating their 65th birthday in 1978 could expect to live another 16.3 years. On the other hand, Fries says that the life *span* of human beings will remain at 85. Medical science will enable more people to avoid premature death from an acute illness only to have them suffer from the familiar array of chronic diseases: cancer, emphysema and chronic bronchitis, vascular diseases, osteoarthritis and Alzheimer' disease.

The challenge of both arguments is the same: given the extraordinary increase in the numbers of old relative to the numbers of young in the future (see figure), can science make the lives of the old healthier, and relieve their dependence on younger family members, institutions, and the state? Although the challenge of the demographics is widely accepted, there are many arguments about how science and medicine should organize itself for this challenge.

One debate particularly among doctors is whether to establish geriatrics as a separate, licensed specialty, equivalent, for example, to pediatrics, cardiology and other medical fields. The debate going on in teaching hospitals and medical schools currently centres on whether a separate set of skills is required for dealing with the elderly and if so, what they are. In the United States, the problem is aggravated by the fact that a rather small proportion of doctors is family practitioners, and most are specialists. In the United Kingdom, which has a large proportion of old people, the problem is less serious, because most doctors are general practitioners, and treat the elderly as a matter of course.

Another debate is over whether or not to create new institutes within the US National Institutes of Health to focus attention on particular diseases of the elderly in order to attract money and political attention. There is already a National Institute of Aging, founded in 1976 and now consuming $82 million a year. And some diseases of the elderly are already encompassed within other institutes; arthritis, for example, is covered by the National Institute on Arthritis, Metabolism and Digestive Diseases. But with the prospect of a new National Arthritis Institute being foisted upon him by Congress, Dr James B. Wyngaarde, director

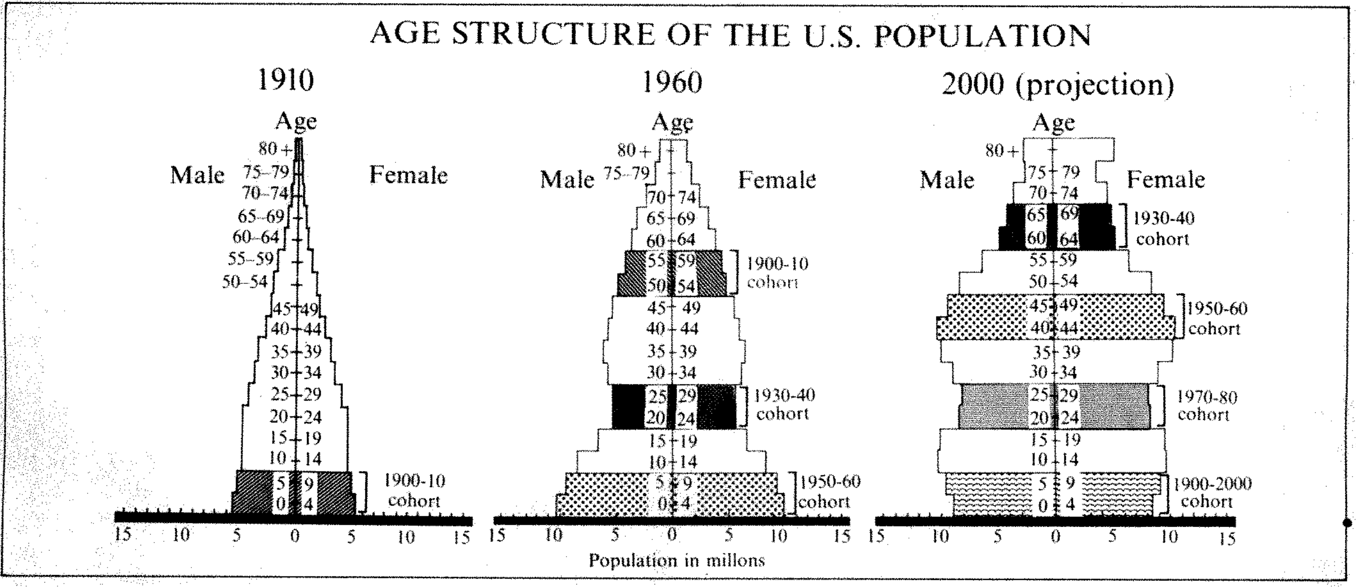

AGE STRUCTURE OF THE U.S. POPULATION

0028-0836/82/340779 02$01.00

of the National Institutes of Health, has been raising the kind of objection to focused institutes that is held by many serious biomedical researchers. Why fragment research, he argues, sensibly, just when the extraordinary interconnectedness of different diseases — for instance of the arthritis family with osteoporosis and systemic lupus erythematosus — is just becoming evident?

Typical short cycles for funding pose another obstacle to attacking the long-term, chronic diseases of the elderly. Most researchers (and doctors) prefer to work on problems that show quick, discernible results. But whether senile dementia is linked to nutrition or to early health, obviously cannot be answered in time for the next one- or three-year grant application.

Fortunately, more private benefactors are realizing that they can offer alternatives to traditional, government inspired approaches. Last week, Philippe Villiers, a Boston businessman, gave $40 million to endow a new foundation dedicated to research and study of the elderly. Robert N. Butler, who is leaving the directorship of NIA after six years, will take a privately endowed chair as head of the country's first department of geriatrics, also privately endowed, at the Mount Sinai School of Medicine. But the profession would be better off, obviously, with some overall plan for how to address these new problems, rather than letting the whims of benefactors or the political process shape the future.

A start will be made soon by the National Academy of Sciences, which has just designated a chairman (Robert I. Berliner, dean of the Medical School at Yale) for its Committee on the Aging, now being formed under the auspices of the Institute of Medicine. It should be no surprise that the government did not see the need to fund an overall study (hence much of it will be paid for with academy funds) and that assembling the committee and subgroups has taken time. Ageing is not exactly the status-ridden scientific bandwagon that cancer was 10 years ago. But the scope of the study is very broad, ranging from the impact of the demographics on society to the needs of science and medicine, so the study will be a step in the right direction.

In his diary in exile, in 1935, Leon Trotsky wrote: "old age is the most unexpected of all things that can happen to a man". But there is nothing unexpected about the ageing of US population, and the future, greyer constituency for the results of research and for health care. If Thomas is right, biomedical scientists may have it within their power to make life more comfortable for these people — indeed for themselves in their old age. But to do this they must look the problems in the eye and face up to certain organisational and philosophical choices. One choice is for the US biomedical science community to follow the path of least resistance and set up new 'advocacy' specialities and institutes that would focus political attention on the problems of the elderly. The alternative, harder, but probably sounder, choice is to inject knowledge of, and concern for, the diseases of the elderly into all biomedical research to maximize the chances of the unexpected discovery that would lead, ultimately, to improved treatment or even cure of the diseases. Similarly, for the medical profession it would be better to make the needs of the elderly part of all medical training than to establish yet more specialities.

Language of love

French scientists are under pressure to communicate in French. But can they afford to?

The English edition of *Scientific American* used to sell only 5,000 copies a month in France. But the new French edition, *Pour la Science*, sells 50,000, its editor, M. Philippe Boulanger has claimed. So a mere change from one language to another increased communication tenfold.

This is what preys on the minds of those in France who wish to re-establish "French as a language of science". While French scientists rush to the microphone at conferences to address their American colleagues in English (see this issue p.784), and while more and more French scientists publish in English rather than French (82 per cent of French papers were published in French in 1976, but only 67 per cent in 1980), a hunger — and a need — for knowledge among the rest of the French nation may go forgotten. Moreover, it is from this forgotten part of the nation that the next generation of scientists, technologists and technicians will emerge. What is more, it is imperative, from the point of view of a socialist government, that the same sector of the nation should, at the very least, be equipped to play an educated role in the democratic management of science and technology in the country. Meanwhile, many French primary scientific journals are declining — the best work being published in English — while few good textbooks are now published in French, and science is almost absent from radio and television. Is this the nation destined to become the technological leader of Europe?

One can therefore sympathize with M. Jean-Pierre Chevènement, Minister of State for Science and Industry, when he insists that French scientific culture must be based on the French language. His version of the French nation requires it. He does not decry international communications. There, he is the first to acknowledge, the universalism of English is a distinct advantage. Chevènement is determined to improve national communication and in pursuit of that goal Chevènement's scientist must look not only outwards, but inwards, towards his own countrymen and his own media.

But in practice, what can the minister do? He starts with the knowledge that most French scientists are against him. Professor Alfred Kastler, France's sole Nobel physicist, is a passionate Francophone, but he puts the Anglophone argument succinctly: "If we publish in French," the argument goes "the international scientific community doesn't read us. And if we speak in French at an international conference, most of the audience leaves the room". Briefly: to make contact with Americans, to keep in touch with his field, the French scientist must speak English. There is no simple solution to the dilemma that is posed for the French scientist sympathetic towards Chevènement's proposals but having to survive in a world dominated by the English language.

Professor Kastler has recommended "taking the offensive". But there is only one real offensive: to establish French science as a world force — just as the establishment of American science in the world (for whatever historical and economic reasons) led to the dominance of English. France can still dominate in one or two subjects — certain branches of mathematics, for example, and of social anthropology — but for the rest the battle will be arduous and the outcome must be gloomy.

Therefore, in most areas of science, French policy seems to grasp at straws. The provision of simultaneous translations at conferences has already been rejected as too expensive. The alternatives of partial translation by pre-print, transparencies or by a colleague (as now being suggested) seem artificial. In the matter of publication, to publish a paper in French as well as English is expensive and time-consuming; and will the editors of *Comptes Rendues* agree to become mere echoes of their counterparts on some English or American journal? Some have suggested more rigorous editing and selectivity in the French journals, and "vigorous marketing". This is a worthy proposal and can do no harm to the journals but if French scientists will not submit their best work to these journals anyhow, rigour and vigour are of little avail.

So is all lost for the French plan? Not entirely, insofar as early enthusiasms are now being tempered by reality. Certain small, but practical things are being done. Data banks and other forms of electronically stored information are being developed in French, for example, to make France independent of American data sources (there is a strategic imperative here also). And there are exercises to establish new, firmly edited journals in fields in which France does excel. Small things, perhaps, but the only practical ones. It is impossible to stage a complete revolution against English now. And as for French scientists: the measure of the success of the programme, in the end, will not be how many papers are published in French — but how many foreigners are forced to read them.

0028-0836/82/340780-01$01.00

Vienna accord on remote sensing

Conference calls for bigger UN role

Vienna

New and expanded space-related activities, recommended to the United Nations by the Unispace-82 conference which ended last Saturday, should cost the United Nations $3.2 million annually — almost four times the 1980–81 budget of the existing Outer Space Affairs Division of the UN Secretariat. These activities, the conference proposed, should be funded voluntarily by the member nations, and the UN General Assembly should rearrange its budget so that the increase in personnel costs may be absorbed within the available resources.

The proposed activities are largely information related, including consultancy services to assist developing countries in selecting space technology systems, study tours, seminars, and training fellowships, the creation of an international space information service, expansion of the existing space library and the establishment of a regular newsletter on space.

The need for such services became abundantly clear during the two weeks of Unispace-82; remote sensing has been constantly hailed as the answer to environmental and resource problems, and a bewilderingly large range of systems was on display for developing countries shopping for hardware or know-how. Yet the suppliers of these products were often first to admit that their data are simply not reaching those who most need the information. One representative of the UK Natural Environmental Research Council quoted the case of a remote sensing programme which identified icebergs heading directly for a Canadian off-shore oil-rig — with no organizational framework through which a warning could be transmitted to the rig at risk.

The conference report called for the formulation of international principles on satellite remote sensing which would allow the "sensed" state "timely and non-discriminatory access under reasonable conditions" to primary data relating to its territory.

The conference also expressed "real concern" over the approaching saturation of the geostationary orbit with communications satellites in certain frequency bands. Research into ways of facilitating the closer siting of satellites is "imperative", and the feasibility of using highly elliptical orbits for communications satellites should be re-examined. The International Telecommunications Union was recommended to consider introducing into its future regulations a clause stating that a satellite owner was responsible for removing its hardware from orbit when it became inoperable.

Similarly, although the conference urged member countries to examine the feasibility of direct television broadcasting satellites for education in remote rural areas, it also urged them to consider the possibility of international or regional satellite space segments, shared by neighbouring countries.

In general, the conference confined itself to the specifics of space technology and its applications but there was also a full discussion of the problem of preserving peace in space. After the three main committees of the conference had failed to reach consensus on this issue, Dr Willibald Pahr, the Austrian foreign secretary and president of the conference, convened a 15-member drafting group, called the "Friends of the president" which represented all regional groups and which finally, and with the conference in extra time, found an acceptable consensus wording calling on all nations, "in particular those with major space capabilities" to "contribute actively to preventing an arms race in outer space".

Vera Rich

Few winners in Australian budget

Sydney

The Australian government's latest budget, framed amid growing speculation about an early election, once again cuts back on funding for most areas of scientific research. The budget, released last week, was built around tax cuts and other handouts for the middle income earners. The government proved once again that they see very few votes in research funding.

Australia spends less than 1 per cent of gross domestic product on research, considerably less than most Western countries. The government provides about 70 per cent of this funding, which is an unusually large proportion by world standards. This year over half this money will go to the Commonwealth Scientific and Industrial Research Organization (CSIRO) and the rest to the other government agencies and the universities.

One of the few bright spots in the budget is the re-allocation of A$49 million (£27 million) to a scheme that favours research projects with product-oriented goals. This re-allocation came as a surprise because the scheme, funded under the Industrial Research and Incentives Act, was left up in the air last year when its budget was frozen after only A$24 million was spent.

In the budget, basic research in universities has been given A$19 million, around 4 per cent less in real terms than in 1981. This continues the steady decline which has gone on since 1975. The funds are channelled through the Australian Research Grants Scheme (ARGS) which now contributes only 15 per cent of the total national research spending compared with 24 per cent in 1975. If ARGS uses its reduced budget to maintain the top research groups, it will be unable to support about 100 projects that would otherwise have been accepted, according to Professor Max Brennan, chairman of the committee administering the scheme.

But there were some winners in the area of basic research. In astronomy, prior to the budget, two proposals were vying for patronage. One was the radioastronomers'

Canada's array poised

While Australian radioastronomers have just received the go ahead for their long baseline array of telescopes (see above) the fate of a Canadian counterpart is still in the balance.

The Canadian Long Baseline Array (CLBA) has already been approved in principle by the National Research Council (NRC) which has selected it over several competing big-science projects, such as the Canadian high energy electron ring and Starlab. A final proposal for the CLBA will probably be approved by NRC in September. The economic development committee of the Canadian cabinet will then have to decide whether it can afford the Canadian $70 million needed to construct CLBA — with $6.5 million per year running costs — in the midst of a recession.

The current proposal for CLBA calls for eight 32-metre dishes spread from British Colombia across to Newfoundland and one smaller dish in the North West Territories. Thomas H. Legg, the originator of the project, says the CLBA could be operating within four to five years of approval. The schedule is important, for the United States is planning its own very long baseline array that would stretch across the continent and include sites in Hawaii and Alaska. A proposal for building the system has been submitted to the US National Science Foundation (*Nature* 12 August, p.596) but whether it will be included in the US budget for fiscal 1984 is anybody's guess. There is a debate about the need for two separate systems of this size and both the Canadian and the US sides have thought about a possible link but nothing concrete has yet been proposed.

0028-0836/82/340781-02$01.00

"Australia Telescope", the other the optical astronomers' "Starlab" project.

With the news that the Australian Telescope has been funded to the tune of A$25 million, CSIRO can now proceed to develop a continental-scale, radio-linked interferometer network. When completed in 6 years' time, this should provide a Southern Hemisphere radio facility comparable to the most sophisticated interferometers in the north, complementing the activities in the optical and infrared bands of the Anglo-Australian Telescope.

The Australian Telescope will consist of a linear array of five 22-metre dishes at Culgoora in New South Wales, a 22-metre dish at Siding Spring (the site of the Anglo-Australian Telescope) and a 64-metre dish at Parkes. The total array will be equivalent to a dish 300 km across with a revolution of 0.1 seconds of arc — comparable to the US/European space telescope. It is also proposed that five other sites, covering much of the continent, can be radio-linked to the network, improving the resolution to one-thousandth of a second of arc.

The Starlab project has not been so fortunate. This joint Canadian, US, Australian scheme aims to place a 1-metre telescope in Earth-orbit by 1989. Australia's contribution was to have been the instrument package for the telescope. At this stage the government is not prepared to commit the full A$28 million that would be necessary if Australia is to participate. But it is keeping the project alive by providing A$3.3 million to local industry for some preliminary work.

Australian postgraduate research scholars were another notable group to gain in the budget. About one third of all full-time research students enrolled for higher degrees are supported on these scholarships. They have just been awarded a 50 per cent salary increase, presumably in recognition of the importance of their work as integral members of university research teams, and as Australia's future research scientists. Although this increase sounds impressive, the salary of a scholar has now only climbed from below the official poverty line to a generous A$40 a week above (A$6,850 a year). This is still less than half the average wage and no doubt a measure of the high esteem in which many Australian politicians hold Australian science.

Peter Hunt

US plant patent disputed

A fierce protest against the validity of a US patent dealing with plant breeding has been made public by Professor N.L. Innes, chairman of the British Association of Plant Breeders and a member of the staff of the British National Vegetable Research Station. The patent complained of was awarded in April this year to the Colorado based corporation Agrigenetics Research Associates, a seed firm with annual revenues of $100 million.

The invention for which the patent has been awarded is described in the published version (US patent number 4,326,358) as a technique for accelerated production of new hybrid strains of plants and rapid commercial production of seeds from such hybrids. The patent claims that seeds of desirable new hybrids can be readied for marketing in as little as three years rather than the present eight to twelve years.

In conventional hybrid production, the plant breeder first has to breed two different homozygous plant lines from which a hybrid is produced and tested. Not only can it take many years to breed the homozygous lines but homozygous plants often produce low numbers of seeds.

In its essentials the invention covered by the patent starts with the crossing of any heterozygous plant — of which there is a great variety of good seed producers — with a heterozygous or homozygous partner. The hybrid offspring of such a cross will not be genetically identical but, on occasion, the plants will still be sufficiently similar to be worth testing as a potential crop.

If they have desirable crop qualities, the breeder then returns to the parent plants and propagates them, asexually, as clones. The large numbers of each parent so generated are then crossed to produce large numbers of hybrids, equivalent to those of the original cross of the individual parents.

The protest from the British Association of Plant Breeders (published in full on page 786) boils down to the assertion that the use and advantages of heterozygous parental plants as breeding stock are well known and that clonal propagation of individual plants is now a standard technique in plant breeding, so that the particular combination of the two principles for which a US patent has been awarded must be obvious and thus not qualified for protection.

Even the combination of techniques described in the patent is very similar to that used in practice by, for example, British sugar beet breeders, says Dr Richard Macer, secretary of the British Association of Plant Breeders.

According to Rene Tegtmeyer, of the US Patent Office, to which Professor Innes has sent a copy of the letter, a formal request for reexamination can be filed after a patent is issued, but only on the grounds of a prior patent or publication that was overlooked by the patent office in its original examination. Prior public use or sale is not sufficient grounds for reopening an already-issued patent. Even in the original examination of an application, Tegtmeyer says, a foreign use would not bar patenting in the United States, although a foreign publication could.

"Any given detail or sequence may seem obvious, but the way they're put together may be original", so far as the patent law is concerned, says Dr David Padwa, chairman of Agrigenetics, who will shortly announce licensing terms that will be "fair and reasonable".

A second Agrigenetics patent, applying the techniques to a specific species, was recently allowed by the patent office and should soon be issued. Meanwhile Agrigenetics awaits the outcome of its application last January to the European Patent Office for a patent similar to the one issued in the United States.

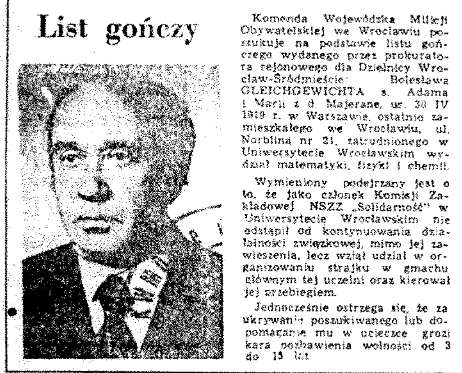

List gończy

Komenda Wojewódzka Milicji Obywatelskiej we Wrocławiu poszukuje na podstawie listu gończego wydanego przez prokuratora rejonowego dla Dzielnicy Wrocław-Śródmieście Bolesława GLEICHGEWICHTA s. Adama i Marii z d. Majerane, ur. 30 IV 1919 r. w Warszawie, ostatnio zamieszkałego we Wrocławiu, ul. Norblina nr 21, zatrudnionego w Uniwersytecie Wrocławskim wydział matematyki, fizyki i chemii.

Wymieniony podejrzany jest o to, że jako członek Komisji Zakładowej NSZZ „Solidarność" w Uniwersytecie Wrocławskim nie odstąpił od kontynuowania działalności związkowej, mimo jej zawieszenia, lecz wziął udział w organizowaniu strajku w gmachu głównym tej uczelni oraz kierował jej przebiegiem.

Jednocześnie ostrzega się, że za ukrywanie poszukiwanego lub dopomaganie mu w ucieczce grozi kara pozbawienia wolności od 3 do 15 lat

"WANTED for continuing trade union activities under martial law, and for organizing a strike in Wroclaw University" says this notice from a recent issue of the Wroclaw daily *Gazeta Robontnicza*. Professor Boleslaw Gleichgewicht, the subject of this notice, is a leading Polish mathematician, a former organizer of the clandestine "Flying University" and one of the founder-members of the Wroclaw University chapter of Solidarity. He is now in hiding.

The notice includes a warning that the penalty for hiding or assisting the "fugitive" is from three to fifteen years loss of liberty.

Australian patents bill

Seeds of doubt

Canberra

The Australian government's first attempt to legislate for the protection of new plant varieties has blown up in its face. The Plant Variety Rights Bill, introduced a year ago and passed by the House of Representatives in April, is now the focus of a political storm. And the Senate has referred the bill to its Standing Commission on Natural Resources, a procedural device for postponing a decision.

The objective of the bill, of crucial importance in a country with a large agriculture industry, is to enable plant breeders to acquire the same kind of proprietary rights in new plant varieties as have long been available in some European countries. The present Patents Act, dependent as it is on the criterion of reproducibility, does not protect most plant varieties.

Five years ago, the Australian Agricultural Council (a political body representing federal and state ministers) recommended legislation on plant varieties protection with the objectives of stimulating the commercial plant breeding

0028-0836/82/340782-02$01.00

industry, giving Australian farmers access to varieties developed overseas under the proposed bill's protection and enabling Australia to join L'Union Internationale pour la Protection des Obtentions Vegetales (UPOV).

As amended during the past year, the bill offers protection to Australian plant breeders producing plant varieties, including hybrids, that are novel, distinctive, stable and uniform. Existing varieties will not be entitled to protection.

Both government and opposition have been surprised at the controversy the bill has aroused. Its opponents include farmers, scientists, church groups, environmentalists, alternative life-stylers and consumer organizations. Many people employed by the federal and state governments on plant breeding fear that the bill, by making commercial plant-breeding more profitable, will give the governments an excuse to reduce support for plant breeding and also increase competition from the private sector, perhaps by the production of "cosmetic" varieties.

Even the claim that protecting plant varieties will stimulate the Australian private sector is disputed on the grounds that Australian farmers are at present only buying in one per cent of the seeds they sow each year — too little to generate much revenue. Some critics say that the most probable result will be to flood the market with seeds imported from overseas.

The fate of the bill is at this stage unclear. Hitherto, it had been thought that the fate of the bill would depend on the votes of the Australian Democrats, the minority party that holds the balance of power in the Senate and which sees its role as a watchdog over the machinations of the major parties. ("Keep the bastards honest" is its motto.) But several government senators now have cold feet about the bill.

One possibility is that nothing is decided until after the next election, particularly if that is called as early as the beginning of 1983. If there is an early election, everything will depend on which party is returned to Canberra. The present government might simply reintroduce the bill. The Labour Party, if elected, would probably let it die a natural death — and then find that it had to devise an alternative of its own.

Vimala Sarma

German nuclear power

Modest advance

Heidelberg

Four new nuclear power plants at a go may seem like a boom but appearances are deceptive. The Federal German atomic power industry has problems. Although work began recently on the sites at Isar II (Bavaria) and Emsland, Lingen (Lower Saxony) and approval for Biblis C (Hesse) and Neckar-Westheim (Baden-Würtemburg) seems little more than a formality, all four reactors are of the same conventional high pressure light water, type — defensive planning that aims to expedite technical approval and confine local enquiries to siting and radioecology.

The electricity industry in West Germany is private, with a legal monopoly position based on laws dating from the 1930s. Most new power stations are financed by consortia, usually combinations of power companies and local government. The two-stage Federal–Land vetting procedure which keeps nuclear issues in political focus, stringent safety regulations, lengthy planning processes, and battles with environmentalist groups have turned the construction of atomic power plants in the West Germany into an obstacle race. Costs are now double those in France. Electricity prices are disappointingly high and industries now renegotiating 20-year contracts signed in the optimistic 1960s may consider importing from France. It is suggested that heavy industries may eventually emigrate to sites close to the French power plants. While West Germany has only 11 functioning nuclear power plants and 14 awaiting approval or under construction, *Electricité de France* has 24 functioning units and 26 in various stages of planning and construction.

Atomic power is controversial in West Germany: The CDU/CSU accuse the government of damaging the industry by ambivalence, imposing unnecessary controls, and dragging its feet on the reprocessing facility. The SPD is divided on the issue and the Greens (*Nature* 17 June) oppose use of atomic power categorically. Not only is the Bonn SPD/FDP coalition shakey and the SPD losing votes on the right to the CDU and on the left to the Greens, but the CDU itself is on the brink of a leadership conflict. With the Greens set to gain 10 per cent in the House election on 26 September and over 5 per cent in the Bavarian elections on 10 October, the major parties want to play down the nuclear power issue. For the time being there will be no decision on Biblis C which will add 1,300 megawatts to what at 2,500 megawatts is already the biggest atomic power complex in the country.

The Federal government participates financially only in prototype reactors. The fate of the fast breeder at Kalkar on the lower Rhine and the high temperature reactor at Schmehausen in the Ruhr await a meeting of the *Nuklearkabinett* on 31 October. In June this year, escalating costs led research and technology minister Andreas von Bulow to advocate halting both these projects. They were reprieved by Helmut Schmidt, chairman of the *Nuklearkabinett*, who insisted that for reasons of national prestige the projects should be retained.

Meanwhile the future of the Federal German nuclear industry looks as unclear as that of the Bonn government.

Sarah Tooze

Belgian nuclear fuel

Plant to restart

Waalre, The Netherlands

Eurochemic, a nuclear fuel reprocessing plant in Mol (Belgium) which was closed in 1974, is likely to begin work again. The international project shut down when Britain, France and Germany decided to go their own way, but on 2 July one of the two chambers of the Belgian Parliament voted to reopen the plant and it is expected that the Senate will do the same, at the earliest in October.

If the Senate agrees, a new fuel cycle company will be formed covering the whole nuclear cycle, with the Belgian government and the utilities taking equal shares. One or two subsidiary companies will take care of reprocessing and fuel fabrication. A new fuel will be produced: a mixture of uranium and plutonium.

The capacity of the reprocessing plant, which is now 60 tonnes per year, will probably be doubled. Without the plant, Belgian nuclear power stations would have had no place for spent fuel after 1985. A 120-tonne capacity at Mol also provides an opportunity to reprocess spent fuel from other countries.

The Belgian plant at Mol is now — after decontamination — cleaner than many experts thought possible, according to Dr Jacques van Gell. Radiation levels in the cells are only slightly higher than natural background levels, after 200 million curies have passed through them. "This is a world achievement", says Detilleux.

The reprocessing process will be changed at Mol, from the dissolving method to the mechanical chop and leach process. The existing fuel fabrication company Belgonucleaire, on the same site at Mol, will become part of the second subsidiary company and will produce plutonium for fast breeders but also for thermal reactors. Although Dr Detilleux considers that breeder reactors will not be needed for the next 15 years, using plutonium in conventional thermal reactors should give Belgium a more secure supply of fuel.

There has been considerable criticism of the Belgian vote in the Netherlands. The plant is only 15 km from the border, and after a number of ex-employees had told of incidents at the plant between 1966 and 1974, Dutch public interest groups protested against reopening and regional authorities asked for more information and for early warning systems in case of accidents. The Dutch under-minister for the environment, Mrs Ineke Lambers, was disappointed about the Belgian decision. Only the previous day, she had recommended in the EEC Council of Ministers that arrangements should be made for the European Parliament to settle such trans-border pollution issues. "This is a proof that such settlements are far away", she said.

Casper Schuuring

0028-0836/82/340783-01$01.00

Language of science

French plans

The French government's campaign to re-establish French as a language of science is under severe stress — as thousands of foreign scientists descend on France for the 1982 conference season, attracted by the climate, the food and wine and, of course, the science. But these scientists mostly wish to speak English, not French, and there are not enough technical translaters to go round (nor money to pay them.)

Breaking point came a couple of weeks ago at the 21st international conference on high energy physics in Paris, where even the French spoke English.

Government determination to push on with the language programme is unbowed. But there has been a shift of emphasis from the tone of the circular sent out to researchers last September, which spoke of the need for French scientists to make presentations "in our language". For at the high energy conference participants were faced with a questionnaire in four languages (French, German, English and Spanish) asking them what they thought of simultaneous translation, multilingual posters and other means of dealing with the language barrier. The point is that the government is now supporting not just French as a language of science, but also Italian, Russian, Japanese, Spanish, Arabic, Chinese and the rest. "We will do all we can to demolish the monopoly of English", said the programme director.

The objection to English is that — outside Anglophone countries — it leads to the creation of an artificial barrier between those scientists who can cope easily with the language and those who cannot, so that English is used as a matter of status and hence of isolation of one group from another. English thus militates against "democracy" in French science. Moreover, in France the government has taken an overriding interest in all means of increasing communication between scientists and industry, and this "snobbish" division is seen as a real barrier to industrial development.

Government determination, however, is not enough. Money is also required. To provide simultaneous translation for a number of languages at a major conference is expensive — about FF350,000 (£30,000) for a conference of 1,500–3,000 participants for three or four days, estimates MIDIST, the Mission Interministerielle de l'Information Scientifique et Technique in which the "French as a language of science" programme is based. Short of the necessary wherewithal, and of technically-trained translators who can deal with immunology on the one hand or high-energy physics on the other, MIDIST this year is resorting to experiments on means cheaper than simultaneous translation.

For a total cost of FF600,000 at 20 conferences over the next couple of months, MIDIST will therefore try out:

- Simultaneous translation at plenary sessions, but not at working groups, which would be divided by subject and language.
- Distribution of a typed resumé of presentations in various languages.
- Bilingual transparencies, to be prepared before each talk.
- Paragraphy-by-paragraph translation of a talk by a bilingual colleague.
- The résumé on request, by a participant, of the essential points of a talk in the language requested.

The results of these experiments will be tested in part by questionnaire, and may result in more positive action during the conference season of 1983. **Robert Walgate**

Astronomer on fast

Patras, Greece

Professor Leonid Ozernoi of the P.N. Lebedev Physical Institute in Moscow began a hunger strike on 17 August in the face of the refusal of the Soviet authorities to grant him and his family visas for emigration to the United States. His case was being widely publicized at the General Assembly of the International Astronomical Union at Patras, Greece which finishes on 26 August.

Professor Ozernoi is well-known for his work in high-energy astrophysics including theoretical studies of processes in quasars and the nuclei of active galaxies. He applied for emigration in June 1979. Following the application, his wife lost her job as a sociologist and has since been unable to obtain another postion; he was barred from attending international conferences, removed from the board of *Letters to the Astronomical Journal of the USSR* and prevented from teaching. A paper of his was omitted from a book for which it was scheduled. Nearly 2½ years after applying to leave the country he was refused, his departure being "considered inexpedient at this time".

The Harvard-Smithsonian Centre for Astrophysics has invited Professor Ozernoi to work there, while the executive committee of the International Astronomical Union (IAU) will be considering whether or not to become involved officially at its next meeting in September.

A petition on behalf of Professor Ozernoi was cirulated at the IAU Assembly. Addressed to E.R. Mustel, Chairman of the Astronomical Council of the USSR Academy of Sciences, it also concerned Dr Alpert of the Institute of Terrestrial Magnetism Radio Research and the Ionosphere of the USSR Academy of Sciences, who has experienced demotion and restrictions on his work since his application for exit in 1975.

Philip Campbell

Drug promotion

FDA steps in

Washington

"A new choice for freedom from arthritis pain. . . Coming soon from Geigy."

This advertisement, accompanied by a colour illustration of a dove flying from a pair of outstretched hands, appeared in medical journals last autumn. At first glance, it seemed much like the many other eye-catching advertising pieces that the drug companies invest in so heavily to promote their wares in their highly competitive business. The strange thing about this advertisement, though, is that nowhere is the name of the drug mentioned. In fact, the drug had not yet received approval from the Food and Drug Administration (FDA).

Over the past year or so, this tactic and others for the pre-approval promotion of drugs have become increasingly common. Recently, FDA has been trying to do something about it.

FDA has broad powers under the federal drug laws to regulate the labelling of prescription drugs it has approved. By extension, this has been applied to advertising and other promotional literature. Any advertisement for a prescription drug must, for instance, include complete information on side effects, precautions and proper dosage. FDA also scrutinizes headlines and claims made in promotional material for accuracy and proper balance. A false or misleading promotion can render a drug "misbranded" and liable for seizure — a remedy FDA has occasionally used.

FDA regulations also prohibit the promotion of a drug's safety or usefulness before approval, since it is the safety and usefulness that FDA is attempting to determine in its review of a new drug application. But what if the drug's name is not mentioned in pre-approval advertising? That was apparently what the drug companies asked themselves; and thus a loophole was opened.

Possibly the most effective of these pre-approval advertisements are of the variety shown opposite. A graphic motif is introduced in the pre-approval advertisement, which is carried over to the post-approval — and, the advertiser hopes, the favourable first impression is carried over as well.

No warnings, precautions or contraindications encumber the pre-approval advertisements. But neither does the drug's name, and that puts FDA in an awkward position. "Without the mention of a drug product, it becomes difficult for us to say that is an advertisement" under FDA regulations, says Kenneth Feather, acting chief of FDA's drug advertising regulation branch.

Now the agency hopes to set limits on pre-approval advertisments. Last month, FDA issued a list of "recommendations" aimed to stop what it sees as infringements of the spirit of the law.

0028-0836/82/340784-02$01.00

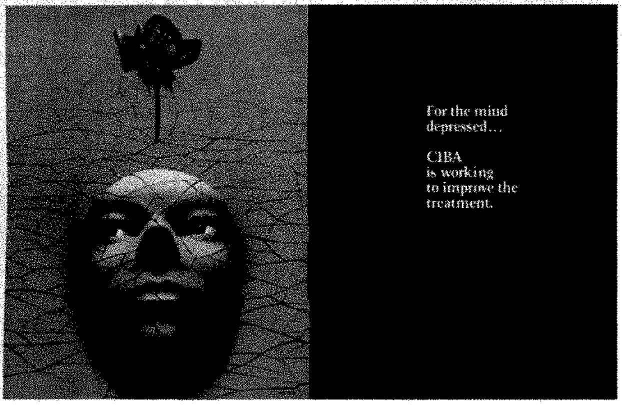

For the mind
depressed…

CIBA
is working
to improve the
treatment.

An impressionistic pre-launch . . .

In particular, the agency said, it will object to any advertisements that "make claims of safety and efficacy even if the new drug is not specified". On the other hand, if the name is specified, FDA says, advertising copy may not suggest the drug's indications, uses, safety or effectiveness, nor may any other advertisements or even the graphics that appear. In other words, the advertisement can say only "Fribulate, coming soon from Wonder Drugs, Inc.".

Pre-approval advertisements such as that shown here for Ciba's Ludiomil fall in a middle ground. The FDA says they are in general acceptable, but the dividing line is fine.

A case that came nearer to that line was Marion Laboratories' pre-approval campaign for Carafate, an antiulcer drug. The advertisements proclaimed the new, unnamed drug "a new era in ulcer therapy", a claim that FDA might well take exception to if it appeared in post-approval advertisements naming the drug.

Another loophole that concerns FDA is pre-approval promotion of drugs at scientific meetings. The FDA regulations specifically exempt seminars and scientific publications from its ban on representing a drug as "safe or useful" prior to approval; this is to allow a full exchange of scientific information concerning the drug. But according to Kenneth Feather of FDA, some firms have been stretching their interpretation of this exemption. He says he has seen several "scientific exhibits" at meetings that had all the hallmarks of promotional exhibits of the "flashing lights variety".

At the recent Pan-American Congress of Rheumatology, for example, Lederle Laboratories, had an exhibit which offered to visitors who stopped by free computer photographs along with a flyer with the headline "Fenbufen: a highly effective non-steroidal anti-infammatory drug with an unusually low incidence of serious GI complications". According to a letter that Feather sent Lederle, the exhibit was promoting Fenbufen, which the FDA has not yet approved for sale in the United States, although it is sold elsewhere.

After FDA objected, Lederle issued a statement that it "regarded the congress as an international meeting" and that "since requirements and practices differ from country to country . . . it does not appear equitable to adhere to those of any single country". FDA officials say, however, that it is nothing new for US laws to apply within the United States to US companies.

A similar incident occurred last year at the American Rheumatism Association meeting in Boston, where Pfizer Pharmaceuticals showed a film promoting Piroxicam, an anti-arthritis drug not yet approved. FDA said that the film hardly qualified as a "scientific exchange" since it was shown at a cocktail and buffet reception sponsored by Pfizer and that there was virtually no scientific discussion. According to FDA, the only question from the audience following the screening was, "When will the drug be available?"

FDA's recourse in these cases is unclear. They may order the companies to stop an advertisement or not to show a film again, but this, says Feather, is "shutting the barn door after the horse has bolted", since most of these pre-approval promotions are designed to be one-shot campaigns. And the remedies available after a drug is on the market, such as seizure, do not apply beforehand.

The recent Oraflex case, though, may cast a chill over the industry's own eagerness to pursue aggressive promotional campaigns. In late July, shortly before sales of Oraflex were suspended following reports of 61 deaths among users in Britain, FDA notified Lilly that a press kit prepared for Oraflex contained false or misleading statements. FDA said it seriously understated the drug's side effects and implied that Oraflex had a unique ability to fight the underlying disease in arthritis patients. In fact, FDA says, Oraflex is just another non-steroidal anti-inflammatory agent, and any claims about its disease-fighting ability are based solely on speculative inferences from animal studies.

After such a hard sell, the backlash that came when the reports of adverse effects started accumulating was all the greater. If the drug is ever cleared for sale again, FDA will probably require stiffer labelling designed to counter the false impression that Lilly's press campaign created.

FDA officials have raised the spectre of stiffer labelling requirements to counter pre-approval claims as well, a threat that will probably weigh heavily in the industry's decisions on future promotions.

Stephen Budiansky

. . . . succeeded by the complete story — and a name

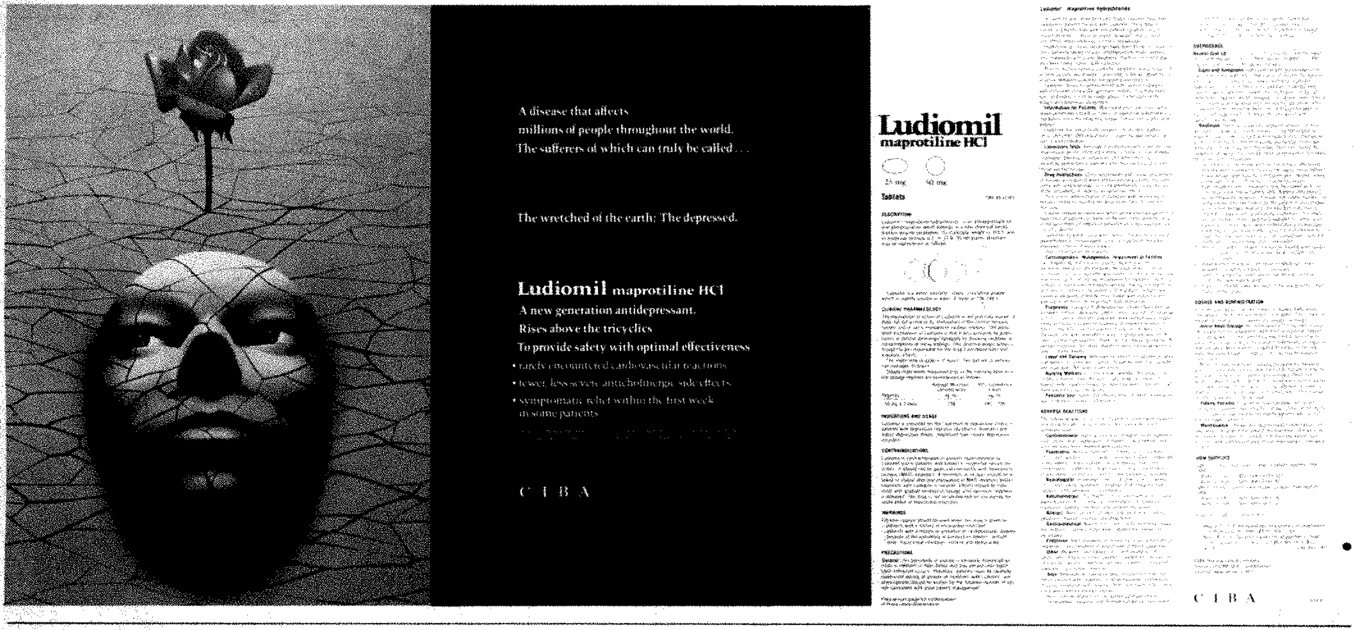

A disease that affects
millions of people throughout the world.
The sufferers of which can truly be called . . .

The wretched of the earth: The depressed.

Ludiomil maprotiline HCl
A new generation antidepressant.
Rises above the tricyclics
To provide safety with optimal effectiveness
- rarely encountered cardiovascular reactions
- fewer, less severe anticholinergic side effects
- symptomatic relief within the first week in some patients

C I B A

Ludiomil
maprotiline HCl

CORRESPONDENCE

Patents and plant breeding

SIR — In the United States a patent (No. 4,326,358 of 27 April 1982) has recently been granted to Agrigenetics Research Associates Ltd of Denver, Colorado for the use of tissue culture (micropropagation *in vitro*) for the multiplication of parental plants to produce hybrid seed of crop varieties. The patented procedure is intended for the rapid development, evaluation and commercial production of hybrid seed from pairs of parental plants chosen for their specific combining ability and uniformity of the hybrid between them irrespective of their degree of homozygosity. The specific example describes the application of the technique to tomatoes. It is understood that equivalent patents in other countries have also been sought.

Both public and private plant breeders must feel concern that this patent purports to give rights over the use of techniques that have been part of the stock-in-trade of plant breeders for some considerable time and have already been used commercially. We would therefore like to draw attention to the conditions governing the validity of patents on plant tissue culture in the United States, as well as to evidence in the scientific literature on the widespread use of tissue culture techniques by plant breeders before the US patent application was made.

Bagwill[1] has summarized the validity of patents on plant tissue culture techniques in the United States. Among the key points made by Bagwill are:

- A person shall be entitled to a patent unless — (a) The invention was known or used by others in this country, or patented or described in a printed publication in this or a foreign country, before the invention thereof by the applicant for patent.
  (b) The invention was patented or described in a printed publication in this or a foreign country or in public use or on sale in this country, more than one year prior to the date of the application for patent in the United States.
- A patent may not be obtained . . . if the differences between the subject matter sought to be patented and the prior art are such that the subject matter as a whole would have been obvious at the time the invention was made to a person having ordinary skill in the art to which said subject matter pertains.

In the light of Bagwill's remarks it is pertinent to observe that: (1) The essential principles and techniques in the patent were known and practised by others well before the patent application was filed. (2) The practical value of the particular combination of pre-existing principles and techniques outlined in the application had been recognized previously by others. (3) The value of the approaches outlined in the application to variety development and production were already obvious to any person having ordinary skills in the relevant disciplines.

The case for patentability is based on a number of premises which merit comment:

Utilization of hybrid vigour in developing crop varieties: The value of hybrid vigour in developing superior crop varieties has been recognized and exploited by plant breeders for more than 100 years. Beal was the first to recommend the use of hybrid varieties of maize; recognition of their commercial worth in other crops followed later. This principle is now universally acknowledged by biologists and is discussed in most textbooks on plant breeding[2].

Phenotype uniformity obtained from specific combination of heterozygous parents: The concept that first generation hybrids of acceptable phenotype can be obtained by crossing two heterozygous stocks has been known and used for a very long time. For example, varietal hybrids of maize were exploited commercially at least 150 years ago[3]. Controlled experiments on varietal hybrids of maize were reported in the 1870s[3] and interest in them was revived in the 1960s[4]. The difference between a varietal hybrid and the type of hybrid described in the patent is one of degree rather than of kind.

In the description of the patented procedure it is noted that some, but not all, hybrids of pair-crossed heterozygous plants are sufficiently uniform in phenotype to be acceptable as commercial varieties. This is not a new idea. Differences in uniformity for important traits were noted among double-cross hybrids of maize more than 40 years ago[5]. To any person with a knowledge of genetics it is obvious that if there are differences in phenotypic uniformity among double-cross hybrids, they would also occur among hybrids produced by crossing heterozygous single plants because the same genetical principles apply in both cases.

Progeny testing and specific combing ability: In the patented procedure, selection among potential parents of hybrids is based on the field performance of their hybrid progeny. It acknowledges that the best way to exploit specific combining ability is to make and test the hybrid that will eventually be released as a new variety. The concept of exploiting specific combining ability in this manner is not new. It was the basis of Hull's[6] recommendation that an inbred tester be used in developing new single-cross hybrids and is also an important feature of the full-sib selection systems developed by Hallauer[7], Lonnquist and Williams[8] and Hallauer and Eberhart[9] for maize. The only significant difference between these methods and the patented method is the manner in which selected heterozygous plants are propagated.

Seed yields from heterozygous parents: The principle that greater yields of good quality hybrid seed are obtained if the parents of a hybrid are themselves heterozygous has long been known to breeders of cross-pollinated crops. It was embodied in Jones'[10] proposal of 1918 that double-cross hybrids of maize should be used as commercial varieties. The same principle was later exploited in three-way cross hybrids and again in modified single crosses and sister line crosses[2]. It has also been used in the production of kale hybrids[11] and is a concept used in the breeding of hybrid Brussels sprouts[12] and onions[13].

Vegetative propagation: The vegetative propagation of heterozygous plants to provide adequate stocks of genetically identical plants for hybrid seed production is crucial to the procedure patented. However, the idea that cloning can be used to perpetuate and increase unique genotypes that cannot be maintained without genetic change by sexual methods of reproduction is common knowledge[2,14–17]. Its particular use in the production of hybrid seed has also been repeatedly recommended[2,11,14,18–25]. The special value of micropropagation *in vitro* as a potentially more efficient substitute for vegetative propagation *in vivo* is also generally acknowledged[14,15].

On the basis of our interpretation of Bagwill's paper[1] and the evidence presented here, we find it difficult as scientists to see how the conditions recited by Bagwill can have been satisfied in the process of obtaining this patent. We strongly urge the United States Patent and Trademark Office to re-examine this particular patent and if similar applications are made elsewhere to consult specialist opinion more widely before granting other plant patents that may similarly restrict the use of techniques and combinations of techniques that are common currency among plant breeders worldwide.

N. L. INNES

British Association of Plant Breeders,
The Plant Royalty Bureau Ltd,
Woolpack Chambers,
Market Street,
Ely, Cambs. CB7 4ND, UK

1. Bagwill, R.E. *Envir. exp. Bot.* **21**, 383-387 (1981).
2. Allard, R.W. *Principles of Plant Breeding* (Wiley, New York, 1960).
3. Sprague, G.F. & Eberhart, S.A. in *Corn and Corn Improvement* (ed. Sprague, G.F.) 305-362 (American Society of Agronomy, Madison, 1977).
4. Eberhart, S.A., Harrison, M.N. & Ogada, F. *Der Zuchter* **37**, 169-173 (1967).
5. Jugenheimer, R.W. *Agricultural Development Paper* No. 62 (FAO, Rome, 1958).
6. Hull, F.H. *J. Am. Soc. Agron.* **37**, 134-145 (1945).
7. Hallauer, A.R. *Crop Sci.* **7**, 192-195 (1967).
8. Lonnquist, J.H. & Williams, N.E. *Crop Sci.* **7**, 369-370 (1967).
9. Hallauer, A.R. & Eberhart, S.A. *Crop Sci.* **10**, 315-316 (1970).
10. Jones, D.F. *Connecticut Agricultural Experimental Station Bulletin* **207**, 1-100 (1918).
11. Thompson, K.F. *Agriculture, Lond.* **65**, 487-491 (1959).
12. Johnson, A.G. *Commercial Grower* **4014**, 831-832 (1972).
13. Erickson, H.T. & Gabelman, W.H. *Proc. Am. Soc. hortic. Sci.* **64**, 393-398 (1954).
14. Hussey, G. *Scient. Prog., Oxford* **65**, 185-208 (1978).
15. Hussey, G. & Hepher, A. *Annls Bot.* **42**, 477-479 (1978).
16. Fosberg, R.A. & Smith, R.R. in *Hybridization of Crop Plants* (eds Fehr, W.R. & Hadley, H.H.) 65-81 (American Society of Agronomy and Crop Science Society of America, Madison, 1980).
17. Smith, G.A. in *Hybridization of Crop Plants* (eds Fehr, W.R. & Hadley, H.H.) 601-616 (American Society of Agronomy and Crop Science Society of America, Madison, 1980).
18. Rogers, H.H. *New Varieties of Cocoa in West Africa*, 76-79 (Report of the Cocoa Conference held at Grosvenor House, London 13th to 15th September 1955).
19. Burton, G.W. *7th International Grassland Congress Proceedings*, 439-448 (Palmerston North, New Zealand, 1956).
20. Glendinning, D.R. & Edwards, D.F. *Report of the 1961 Cocoa Conference*, 137-140 (1962).
21. McWilliam, J.R. *J. agric. Res.* **13**, 1-9 (1962).
22. Toxopeus, H. *Cocoa Growers' Bull.* **12**, 14-16 (1969).
23. Edwards, D.F. *Cocoa Growers' Bull.* **13**, 14-19 (1969).
24. Wood, G.A.R. *Cocoa* 3rd edn (Longmans, London, 1975).
25. Watts, L.E. *Flower and Vegetable Plant Breeding* (Grower Books, London, 1980).

University Colleges of Science & Technology
92, A.P.C. Rd., Cal.-9
LIBRARY COMPLEX
Departments of:
Chemical Engineering
Chemical Technology
Plastics & Rubber Technology
NOV

Man the exterminator

from Jared M. Diamond

THE spread of European populations over the globe that followed the discovery of America soon led to the extinction of many species and local populations, including populations of man himself. Among the best known cases are those of the Dodo, Passenger Pigeon, Steller's Sea Cow, Tasmanian Wolf and Tasmanian humans. The colonizing Europeans often encountered local hunting groups who obeyed taboos that effectively promoted conservation of the wild life on which they depended. So arose the legend that man the hunter-gatherer is prudent, and only civilized man is an exterminator. Accumulating evidence, much of it recent or controversial, suggests that the truth may be very different.

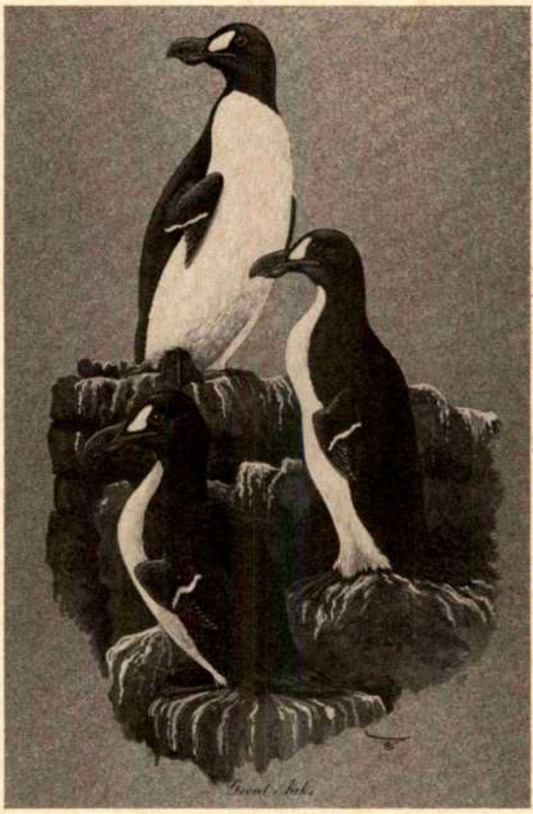

From Tim Halliday *Vanishing Birds* (Sidgwick & Jackson, 1978).

Hunter-gatherers and neolithic agriculturalists seem now to have played the part of exterminator whenever they occupied new areas of the globe. That the areas occupied by man in the past 50 millennia have suffered extinctions, especially of large animals, is undisputed. What remains controversial is which extinctions preceded and which followed man's arrival and how the latter extinctions took place.

Many other waves of human migration preceded that of the Europeans. Only in Africa and Eurasia is man's antiquity measured in millions or hundreds of thousands of years. Present estimates suggest humans reached Australia and New Guinea 50,000 yr BP, North and South America 20,000 yr BP, the West Indies 5,000 yr BP, outer Melanesia (New Caledonia and Fiji) 3–4,000 yr BP, and Madagascar, New Zealand and Hawaii 1–1,500 yr BP.

The best understood of the early extinction waves occurred on New Zealand. In the 200 years since Europeans arrived, eight bird species are known to have become extinct. The discovery of moa bones, however, testifies to earlier extinctions. Until about 25 years ago, it was generally thought that moas had been dying out naturally[1,2], and that few remained when Polynesian colonists arrived around AD 1000. Excavations and radiocarbon dating have now shown that these colonists encountered at least 30 bird species, including the 13 moas and 9 other flightless species, that had vanished by the time Europeans began surveying the avifauna in the 1800s[3–8]. The moas disappeared in a north-to-south wave ending at the south of New Zealand's South Island in the 1600s[9]. In the same period, breeding fur seals became extinct on North Island (now confined to South Island), and large lizards, frogs and flightless insects became extinct on the New Zealand mainland (now confined to offshore islands).

Graphic witness to a role of overhunting in at least some of these extinctions are archaeological sites with stone ovens and hundreds of butchered moa skeletons[5]. But overhunting could hardly explain the extinctions of frogs and flightless insects. Even for the moas, it is hard to accept overhunting as the sole explanation on South Island, where human population densities were very low. Other causes, including the clearing of forest, predation by introduced Polynesian rats and introduced diseases, must also have contributed to the Polynesian-linked extinctions[5–7,10–12].

In New Zealand, both the arrival of man and the extinctions are very recent and well documented. Yet it was long uncertain whether the New Zealand extinctions were even contemporary with human settlement, and it is not clear exactly how they took place, as is indeed often the case even for extinctions occurring under biologist's eyes today. No wonder then that the facts are disputed for earlier extinctions that are less accessible archaeologically, elsewhere in the world.

Around the time that Polynesians reached New Zealand, two other isolated islands with rich biotas were also first settled by man: Hawaii and Madagascar. When Europeans surveyed the Hawaiian avifauna in the nineteenth century, they found 49 land and freshwater bird species (two of them flightless), of which at least 15 are now extinct. This European-linked extinction wave is well known, but studies of subfossil bird bones reported in the current issue of *Science* show that it was preceded by an even larger Polynesian-linked extinction wave[13,14]. At least 39 recent fossil species have been discovered that had disappeared before European arrival. Bones of most of these species have been found either in Polynesian archaeological sites or in deposits contemporary with these sites, proving that the extinctions followed the arrival of man. The lost prehistoric avifauna includes at least 7 species of goose, many of them flightless, plus two flightless ibis, seven flightless rails and at least fifteen subfossil species of the Hawaiian endemic tribe Drepanidini (the Hawaiian finches or 'honeycreepers'). The radiation of Hawaii's geese, as of New Zealand moas, presumably filled grazer niches in the absence of mammals other than bats.

Madagascar also had a remarkable subfossil fauna that disappeared before the Europeans arrived[15–18]. It included about 14 large or giant lemurs, which together with about 19 surviving species constituted the richest sympatric primate community on Earth; 6–12 species of the giant flightless elephant birds (Aepyornthidae); 2 giant tortoises; and a hippopotamus, aardvark and large viverrid. The elephant birds and tortoises would have been the dominant terrestrial herbivores, equivalent to the moas and Hawaiian geese. Humans

Jared M. Diamond is Professor of Physiology at the University of California Medical School.

0028-0836/82/340787-03$01.00

arrived around AD 500, and extinction of most of the megafauna apparently followed in the next six centuries.

For New Zealand, Hawaii and Madagascar the arrival of man was so recent, and (at least for New Zealand and Hawaii) the occurrence of extinct species in archaeological sites or levels so well documented, that the extinctions are obviously due to man rather than to late-Pleistocene climate changes. In the West Indies[19,20], the story becomes more complicated, because humans arrived earlier (about 5,000 yr ago) and fossil extinctions have yet to be dated. Fossil mammals included about nine ground sloths, numerous rodents up to the size of a bear, insectivores and a distinctive but enigmatic monkey. Carnivorous birds radiated in the absence of carnivorous mammals: a condor, giant eagle, barn owls of three different sizes (normal, giant and enormous), and an enormous and possibly flightless strigid owl. Other extinct species include lizards and giant tortoises, as well as other birds. When each species went extinct is largely unknown, but there seems to have been at least three stages: late-Pleistocene extinctions due to moister climate and rising sea level and especially affecting species of dry habitats; a wave of extinctions when Amerindians arrived five millennia ago; and another, continuing wave that began with the arrival of Europeans in 1492.

On the North and South American continents a wave of extinctions peaking around 10,000–12,000 yr ago eliminated about three-quarters of the genera of large mammals (weight > 100 lb)[15,21-26]. Although there is now no dispute that the extinctions occurred after man arrived, the question of whether the extinctions were due to man or to the late-Pleistocene climate changes remains controversial for several reasons. First, the New World differs from the previously discussed cases in that the arrival of a wave of human hunters around 12,000 yr BP (the Clovis hunters)[26] coincided with the rapid climate changes at the end of the Pleistocene. Second, most archaeologists believe that other humans had already reached the New World well before 12,000 yr BP, so that those who maintain the extinctions to be man-related have to postulate that the earlier colonists were either inefficient or indifferent big-game hunters. Third, clear associations of human artefacts with extinct fauna are very few, a fact which Mosimann and Martin[23] explained by a 'blitzkreig model' of extinction — that is, hunters encountering native large animals decimate them so quickly that the period of coexistence between animals and man is brief, leaving few remains for archaeologists to distinguish from carcasses of animals that died naturally. This reconstruction seemed daring when first proposed, but it now appears to describe exactly the speed of extinction in New Zealand, Hawaii and Madagascar.

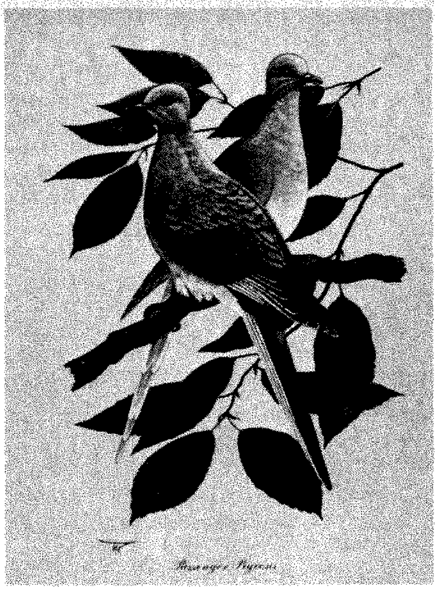

From Tim Halliday *Vanishing Birds* (Sidgwick & Jackson, 1978).

The alternative, climate-based interpretation of New World extinctions also faces difficulties. For instance, the Shasta ground sloth disappeared abruptly when Clovis hunters reached its range around 11,000 yr BP, yet radiocarbon-dated dung samples show it to have been common during the five centuries immediately preceding its extinction, and the plants on which the sloth fed still occur today at its fossil sites[24].

The other continent colonized by Pleistocene man, Australia, lost a bigger fraction of its megafauna than any other continent[27-29]. Along with a giant snake (*Wonambi*), giant lizard (*Megalania*), giant tortoise (*Meiolania*) and giant flightless birds (*Genyornis*), Australia lost all its large mammals (>100 lb) except 4 kangaroos: 17 extinct genera and 46 extinct species of marsupials up to the size of the rhinoceros-sized herbivore *Diprotodon* and the lion-sized carnivore *Thylacoleo*, plus several species of giant kangaroos. As in the New World, the relative roles of climate and man in the extinctions are controversial. Evidence for association of megafaunal remains with human artefacts has yet to be found in Australia. Unlike the New World, Australia gained humans and lost megafauna long before the end of the Pleistocene. Humans arrived at least by 30,000 yr BP, and evidence for survival of megafauna much after that time is inconclusive.

These changes on land produced secondary effects at sea. It is likely that the populations of pelagic turtles[30] and birds[31] that we see today are a tiny fraction of those existing before breeding colonies on oceanic islands were decimated by the first human colonists. Evidence includes abundant remains of subfossil petrels on Hawaii[14] and in Polynesian middens on the Chathams[32], and the recent discovery of breeding petrels in the remote interior of the Solomon island of Bougainville[33].

Evidence of man-linked faunal extinctions remains to be sought on many islands that have been little explored by palaeontologists but that were reached by man before the European expansion of the past 500 yr. Such islands include New Caledonia, New Britain, Fiji, the Solomons, Canaries, Comoros and Mediterranean islands. Of equal interest will be islands such as Lord Howe, the Galapagos and the remote islands of the Indian and Atlantic Oceans, that were not reached by man until the recent European expansion. Such islands will be controls that show the 'pure' effect of climate changes in the absence of man.

Man's hand fell especially on species that were large, flightless, or both. Large animals fared badly as the preferred prey of hunters, and because they tend to occur with low population densities and low reproductive potentials. Flightless birds fared badly as the easiest prey, whether to man or to his accompanying mammalian pests. For example, New Zealand lost its 19 largest birds; Madagascar, 14 of its 15 largest lemurs; Australia, 37 of its 41 largest marsupials; the New World, two-thirds of its largest mammals. An exception is Hawaii, whch lost 15 small drepanidine finches along with large geese, crows and an eagle (see below). The Chathams lost all 6 of their flightless birds; Hawaii lost all but 2 of its 14–18 flightless birds to the Polynesians, and the remaining 2 to Europeans; and New Zealand lost 22 of its

---

1. Oliver *Dominion Mus. Bull.* **15**, 1 (1949).
2. Duff *Canterbury Mus. Bull.* **1** (1956).
3. Kinsky *Annotated Checklist of the Birds of New Zealand* (Reed, Wellington, 1970).
4. Kuschel *Biogeography and Ecology in New Zealand* (Junk, Hague, 1975).
5. Cassels *Wildl. mon. Mag.* **21**, 31 (1979).
6. Cassels in *Quaternary Extinctions* (eds Martin & Klein) (University of Arizona Press, Tucson, in the press).
7. Mills & Williams in *The Status of Endangered Australian Wildlife* (ed. Tyler) (Royal Zoological Society of South Australia, Adelaide, 1979).
8. Anderson *Birds of a Feather* (British Archaeological Reports, Oxford, 1979).
9. McCulloch & Trotter *N.Z. archaeol. Ass. Newsletter* **18**, 2 (1975).
10. Fleming *Notornis* **10**, 113 (1962).
11. Williams *Nortonis* **10**, 15 (1962).
12. Bell *N.Z. Dept Internal Affairs Wildl. Publ.* No.181 (1975).
13. Olson & Wetmore *Proc. biol. Soc. Wash.* **89**, 247 (1976).
14. Olson & James *Science* **217**, 633 (1982).
15. Martin & Wright *Pleistocene Extinctions* (Yale University Press, 1967).
16. Battistini & Richard-Vindard *Biogeography and Ecology in Madagascar* (Junk, Hague, 1972).
17. Tattersall *Primates of Madagascar* (Columbia University Press, New York, 1982).
18. Dewar in *Quaternary Extinctions* (eds Martin & Klein) (University of Arizona Press, Tucson, in the press).
19. Olson *Philadelphia Acad. nat. Sci. spec. Publ.* **13**, 99 (1978).
20. Pregill & Olson *A. Rev. Ecol. Syst.* **12**, 75 (1981).
21. Martin *Science* **179**, 969 (1973).
22. Long & Martin *Science* **186**, 638 (1974).
23. Mosimann & Martin *Am. Sci.* **68**, 304 (1975).
24. Thomson *et al. Quat. Res.* **14**, 360 (1980).
25. Martin & Neuner *Trans. Nebraska Acad. Sci.* **6**, 117 (1978).
26. Haynes *Can. J. Anthrop.* **1**, 115 (1980).
27. Jones *Archaeol. phys. anthrop. Oceania* **3**, 186 (1968).
28. Gillespie *et al. Science* **200**, 1044 (1978).
29. Martin & Murray *Abstr. 52nd ANZAAS Congr.* **25**A, 5 (1982).
30. Green in *The Prehistory of Polynesia* (ed. Jennings) (Harvard University Press, 1975).
31. Olson *Smithsonian Contr. Paleobiol.* No.23 (1975).
32. Bourne *Ibis* **109**, 1 (1967).
33. Hadden *Birds of the North Solomons* (Wau Ecology Institute, 1981).
34. Greenway *Extinct and Vanishing Birds of the World* (Dover, New York, 1967).
35. Atkinson *Pac. Sci.* **31**, 109 (1977).
36. Kepler *Auk* **84**, 426 (1967).
37. Myers *Conversion of the Tropical Moist Forest* (National Academy of Sciences, Washington, 1980).

29 flightless birds to Polynesians, and has lost or nearly lost 4 of the remaining 7 to Europeans. Dozens of other remote islands lost flightless birds to Europeans.

While the fact of human-related extinction waves is clearly established for some areas, at least six different mechanisms have been proposed, and their relative importance is debated. The most obvious is overhunting, the mechanism by which modern European hunters exterminated the Greak Auk and Steller's Sea Cow under the eyes of other Europeans. For example, the last two Great Auk were clubbed to death at Eldey Rock off Iceland on 3 June 1844. Animal populations that had never experienced man did not fear him, and this helps explain why extinction waves proceeded so quickly when man first reached remote islands and continents. Today one can still glimpse a surviving fragment of the world of 50,000 yr ago in New Guinea's isolated, completely uninhabited Foja Mountains. Here large marsupials are abundant and tame, in contrast to their rareness and shyness even in areas of New Guinea with only sparse populations of nomadic hunter-gatherers.

A second, related mechanism of man-linked extinction is the impact of predators introduced by man, such as rats, cats, dogs, weasels and mongooses, especially on nesting birds and ground-dwelling animals. Notorious examples include the extinctions of four birds, a bat and numerous invertebrates on Big South Cape Island off New Zealand within three years of the arrival of rats[3]; and a similar extinction wave after rats reached Lord Howe Island[34]. The correlation between the spread of rats and the post-European extinctions of Hawaiian birds also suggests such an explanation[35]. Even large animals can fall victim to man's pests: rats have been seen to kill adult albatross on the nest[36], and young of Galapagos Giant Tortoises are destroyed by feral pigs unless reared in captivity to a pig-proof size. Numerous species of New Zealand birds, reptiles, frogs and insects have disappeared from the mainland and now survive only on rat-free offshore islands.

A third mechanism attested by innumerable examples is destruction of habitat, whether by fire, by clearing or draining for agriculture, or by introduced browsing animals. Clearing of Hawaii's lowland forest probably explains why the Polynesian-linked extinction wave carried off at least 15 small songbirds not worth hunting, as well as 'game' birds such as geese[14]. Deforestation by fire and introduced animals eliminated much of the habitat on which Madagascar's megafauna depended[18]. By the time that the first European biologists arrived, Easter Island had no land birds at all, and St Helena only one species: their original complement disappeared with the cutting of the forests by Polynesians and Europeans respectively, before the biologists came.

Three other suggested mechanisms of extinction involve introduced competitors, disease and social disruption. While man has exterminated native species, he has also introduced exotics that may compete with surviving natives. Disease is the primary mechanism by which colonizing Europeans have exterminated or reduced many non-European human groups they encountered in the last 500 yr. (Disease in the form of avian malaria may also have eliminated native Hawaiian forest birds from surviving forest below the malaria ceiling of 3,000 ft.) Finally, breeding in colonial species depends on social stimulation, so that a remnant population with its social structure disrupted may be incapable of recovery. This is probably why surviving Passenger Pigeons[34], and surviving human Tasmanians, dwindled to extinction after the hunting that had decimated their numbers ended.

What can past history teach us about future risks? We risk more of the same, in different places: overharvesting of the cichlid fish fauna of East African lakes; arrival of rats at still rat-free Rennell Island, which has 5 endemic bird species and 17 endemic subspecies; and continuing destruction of Himalayan hill forest. But the major extinction wave of the near future will surely be through the swiftly advancing destruction of the continental tropical rainforests, the most species-rich habitats on Earth. While extinction waves cost New Zealand, Hawaii and Madagascar a considerable fraction of their biotas, these biotas were tiny compared with the biotas of Amazonia and tropical south-east Asia. The rainforests are already gone in much of the mountains of Colombia, and in coastal south-east Brazil. At present rates of destruction they will be virtually gone in lowland Malaysia, west Africa, Cambodia, Sri Lanka, Guatemala and Chiapas by the year 2000. Man the exterminator risks eliminating more species in the next few decades than in all his previous history. □

Twinkle, twinkle quasi star . . .

from Marek Abramowicz

WAS our Galaxy a quasar? Could it become a quasar in the future? In a recent issue of *Monthly Notes of the Royal Astronomical Society* (**200**, 247; 1982), Bailey argues that the Galaxy has indeed undergone at least one event of quasar-like activity in the recent past and may do so again.

Short, active periods recur in most galaxies. In Bailey's picture of galactic evolution, the mass lost by stars slowly settles in a central rotating disk. This continues quietly until the disk density exceeds M/r^3, where M is the mass of the galactic nucleus and r is the disk radius. At this point the self-gravity of the disk becomes important and local instabilities, similar to the Jeans instability, develop. According to Paczyński[1], if the optical depth is so large that the cooling time scale is much longer than the rotational period, the instabilities will not produce condensations but will increase the velocity dispersion in the gas. Without condensations no star formation is possible. Velocity dispersion produces turbulence, thereby enhancing viscous stresses, which drive accretion by transporting angular momentum outwards and producing heat.

Bailey modifies this idea: he assumes that condensations will form and a sequential star formation occur. He suggests that this will produce turbulent motions in the gas which in turn increase viscosity. As in Paczyński's model, the rapid viscous evolution of the disk fuels the activity of the nucleus by accretion of gas onto a supermassive central black hole. Alternatively, in the absence of such a hole, a massive central cloud may form which eventually collapses to form a black hole or spinar.

The evolution goes through the sequence of long, quiet phases interrupted by short periods of high activity; the quasars twinkle, very much like cataclysmic variables in our Galaxy. But does this idea agree with what we know about quasars?

Despite the substantial progress in our understanding of the nature of active galactic nuclei, a few fundamental problems have not yet been solved: (1) The supply problem — how can a galaxy supply enough matter to fuel the activity of its nucleus? (2) The efficiency problem — what physical mechanism provides a high enough efficiency of accretion? (Efficiency is the number of ergs of energy radiated per gramme of matter swallowed by the nucleus.) (3) The verification problem — how can observations confirm or rule out the different theoretical models (black hole/spinar)?

The supply problem

The galaxy supplies fuel to its nucleus either through mass loss from stars, or by more exotic processes of star captures and disruptions which can be very effective near the central black hole. Some questions remain open — among them, how to compute the stellar capture and disruption rates, and how to determine the fate of the resulting debris. As pointed out by Rees[2] and others, the classical estimations of

---

Marek Abramowicz is in the Department of Astrophysics, University of Oxford, South Parks Road, Oxford OX1 3RQ.

0028-0836/82/340789-02$01.00

Hills are over-optimistic because they do not allow for the fact that once all the stars whose orbits pass close to the central hole have been destroyed, further capture can occur only when dynamical interaction between the stars repopulates the orbits, that is, on a time scale longer than 10^{10} yr. This means that the rate of supply from the galaxy may be insufficient to fuel continuously the activity of the nucleus. Obviously, Bailey's scenario gives an opportunity to solve this problem: the disk deposits a large mass by accumulating a low income over a very long time — it can therefore afford short time losses at a rate much higher than the income.

The efficiency problem

Black holes, once formed, cannot be destroyed. Soltan[3] uses this fundamental fact to discuss the masses of quasars and the efficiency of accretion. If quasar-like events are common and if they involve black holes, then there should be black holes in most galaxies. The mass of the hole must be smaller than that of its host galaxy. Since we know the masses of galaxies from observation, we can set an upper limit to the black hole masses, which is also the upper limit for the mass of the fuel swallowed by the hole during the active phases. Soltan also estimates (from quasar counts and bolometric luminosities) an absolute lower limit for the total energy produced by the quasars per unit volume. His estimate is independent of cosmological model and agrees with a similar estimate of Schmidt. The upper limit for mass, together with the lower limit for energy, give the lower limit for efficiency, which is close to 0.1. Such a high efficiency cannot be consistent with very thick, stationary accretion disks. However, there are strong arguments in favour of very thick disks as models of active galactic nuclei. Thick disks can generate huge, super-Eddington luminosities observed in some BL Lac objects and produce long, jet-like structures in which matter moves with apparently superluminal velocities. It was suggested (by myself, Paczyński, Blandford and probably by others) that non-stationary disks can radiate away most of their energy while being geometrically thick from time to time. Between these flare-ups most of the matter is accreted onto a black hole from $r = 3\,r_G$. Such disks may be both efficient and thick. Their behaviour resembles the short, active, recurrent events advocated by Bailey.

The verification problem

Bailey shows that the observations of several nearby galaxies are consistent with his theory. However, in the case of our Galactic Centre, his theory agrees with both the black hole and the spinar models, thus leaving unanswered the question, raised by Lynden-Bell, is there a black hole in the centre of our Galaxy? Previously Bailey has argued[4] that the Galactic Centre may contain a compact object (black hole?) with a mass greater than $10^6\,M_\odot$. Other authors, particularly Ozernol[2], maintain that in this case the Galactic Centre would have a much higher luminosity than is observed. This controversy will probably last for some time to come, because its source lies mainly in genuine difficulties of theoretical interpretation and cannot be resolved by progress in technology.

Bailey discussed some indirect observational tests of his theory. A direct test is also possible. Preliminary, unpublished results of Sikora and Soltan, who have analysed statistically the observed ratio of the radio luminosity of extended sources to the bolometric luminosity of their central nuclei as a function of redshift, seem to indicate that the galactic nuclei do indeed twinkle. The intensity and frequency of twinkling falls off with time.

Some of Bailey's calculations employ astrophysical theories that are still likely to experience new developments and substantial revisions. In addition, a few of his results are in conflict with those of other investigators. This may indicate that some details of Bailey's theory will need reconsideration. However, the main idea, that active galactic nuclei switch on and off, or that 'quasars twinkle', is, in my opinion, both very important and correct. Some elements of this idea have been discussed by other authors before Bailey. However, he presented it for the first time in a wide context of galactic evolution and endowed it with astrophysically realistic scenarios. The richness and complexity of Bailey's theory will guide many theoreticians and observers in their work on active galactic nuclei in years to come.

1. Paczyński, B. *Acta astr.* **28**, 91 (1978).
2. Rees, M.J. Preprint *The Compact Source at the Galactic Center* (1982).
3. Soltan, A. *Mon. Not. R. astr. Soc.* **200**, 115 (1982).
4. Bailey, M.E. *Mon. Not. R. astr. Soc.* **190**, 217 (1980).

Opioids at Cape Cod

from Brian M. Cox

A DECADE ago the presence of a specific receptor activated by opiate drugs was accepted, but those who sought direct measures of drug binding to the receptor were still struggling to reduce background binding to acceptable levels. Only a few visionaries had begun the search for the endogenous ligand, and it was always referred to in the singular, if mentioned at all. Now the occurrence of at least three sets of endogenous opioids derived from three different genes is clearly established and, as emerged at the recent International Narcotics Conference*, evidence of an extraordinary degree of complexity in endogenous opioid systems is rapidly accumulating.

Conference sessions on the endogenous opioids were dominated by rumours that Numa's group in Kyoto had characterized a common precursor for dynorphin and the neo-endorphins. Now these rumours have been confirmed and the precursor sequence recently published in *Nature* (**298**, 245). Much evidence presented at the conference was consistent with Numa's findings. Measurements of tissue levels of dynorphin and α-neo-endorphin revealed closely similar anatomic and subcellular distributions (B. Seizinger, Max-Planck-Institut, Munich; C. Molineaux, Uniformed Services University, Bethesda). Immunocytochemical studies by E. Weber (Stanford University), recently discussed in these pages (*News & Views* **298**, 221), were strongly suggestive of co-localization of these peptides in the same neurones. However, processing of the dynorphin precursor appeared to be differentially regulated in different tissues; both Seizinger and Weber provided evidence for the presence of substantial amounts of the dynorphin fragment dynorphin$_{1-8}$ in hypothalamus. The distribution of dynorphin in brain differs from that of the enkephalins and β-endorphin, although there are several areas where dynorphin and enkephalin precursors are both present (S. Watson, University of Michigan). Several studies emphasized that in the magnocellular neurones of the hypothalamo-hypophyseal tract, dynorphin and vasopressin are localized in the same cells, while K. Voight (University of Ulm) reported that enkephalins are present in the oxytocin-containing cells.

But what of the roles of the products of the three opioid peptide genes? There is now general agreement that opioid receptors can be classified into at least three types, designated μ, κ and δ. The enkephalins have long been known to have preferential affinity for δ receptors. Over the past year it has become apparent that dynorphin has selective affinity for κ receptors; at the meeting, evidence was presented that the other products of the dynorphin gene, α-neo-endorphin, dynorphin B and dynorphin$_{1-8}$, also show marked κ-receptor selectivity (W. Fischli, Addiction Research Foundation; A. McKnight, Unit for Research on Addictive Drugs, Aberdeen). Thus the dynorphin gene generates opioids with preferential κ

Brian M. Cox is Professor of Pharmacology at the Uniformed Services University of the Health Sciences, 4301 Jones Bridge Road, Bethesda, Maryland 20014.

---

*The International Narcotics Research Conference held its 13th meeting in North Falmouth, Cape Cod, Massachusetts on 13–18 June. The proceedings will be published later this year by *Life Sciences*.

0028-0836/82/340790-02$01.00

activity and the enkephalin gene agonists with preferential δ activity. β-Endorphin is, however, more promiscuous, interacting with comparable affinity at μ, κ and δ sites. There is no known endogenous opioid with selective affinity for the μ sites, although both β-endorphin and the enkephalins have good affinity and could well function as physiological ligands at μ receptors.

Whether these various receptor forms represent different molecular entities or result from conformational changes of a single receptor species is still unclear. C. Pert (NIMH) argued that μ- and δ-binding sites in the striatum were interconvertible, the conversion being regulated by local Na^+ and GTP concentrations. However, I. James (Addiction Research Foundation) was unable to demonstrate any re-equilibration of receptor types in isolated brain membranes after the selective inactivation of one or more classes by the alkylating opioid antagonist β-chlornaltrexamine. Autoradiographic studies suggest that the distributions of the μ- and κ-receptor forms in brain are different. S. Snyder (Johns Hopkins University) reported the presence of a particularly prominent band of κ receptors in the deep layers of the rat cerebral cortex, which he postulated might be linked to the sedative properties of κ receptor agonists. F. Leslie (University of California, Irvine) found the neonatal rat brain contained predominantly μ and κ receptors, with few δ receptors demonstrable. In the adult rat, the proportion of κ receptors falls substantially, while the proportion of δ receptors increases to levels comparable with μ-receptor densities. The rat, however, is apparently atypical in the low proportion of κ receptors observed in the adult animal. Higher levels have been observed in other species, and Y. Itzhak (New York University) reported that relatively high levels of κ receptors were observed in most regions of human brain.

The analysis of the functions of the different receptor classes has been facilitated by the development of several new drugs and reagents. The alkylating agents with opioid receptor affinity, such as β-chlornaltrexamine, initially developed by P. Portoghese (University of Minnesota), have been found useful by several groups. G. Pasternak (Memorial Sloan-Kettering Cancer Center) reported the use of another irreversible receptor ligand, naloxazone, in the discrimination of opioid receptor subtypes. However, all these irreversible ligands have proved to have lower affinity for δ receptors than other receptor forms. The development, therefore, of a peptide analogue with selective competitive antagonist activity at δ receptors, reported by J. Shaw and M. Turnbull (ICI), promises to be very useful in identifying functions mediated by this receptor class. An approach to the identification of the roles of specific opioids in physiological processes is the use of selective inhibitors of degradation. R. Greenberg (Squibb) and R.E. Chipkin (Schering) reported that thiorphan, an inhibitor of enkephalinase, potentiated analgesia induced by restraint or foot-shock stress. Interpretation of these results was complicated, however, by the observation that thiorphan also potentiated the analgesic effects of peptides not subject to degradation by enkephalinase.

Some progress has been made in identifying functions regulated by specific receptor subtypes. P. Wood (Douglas Hospital, Quebec) demonstrated that analgesia induced by opiate injection into the periaqueductal gray region of the midbrain is mediated by activation of μ receptors, while κ receptor-selective opioids are relatively inactive. However, M. Piercey (Upjohn) reported that injection of either dynorphin or a κ receptor-specific drug, U50488H, into the spinal cord in mice produced pronounced analgesia. The analgesic action of dynorphin in spinal cord was also confirmed by J. Han (Beijing Medical College). A possible role for dynorphin in the physiological regulation at the spinal cord level of the perception of noxious stimuli is suggested by Han's demonstration that electroacupuncture analgesia was suppressed by the localized administration to the spinal cord of dynorphin antiserum. The presence of relatively high concentrations of dynorphin in the dorsal horn of spinal cord has previously been reported.

The role of opioids in the nigrostriatal system has been much studied because it is known that there is a very close relationship between dopaminergic and opioid systems in this part of the brain. Wood reported that μ- and δ-receptor agonists increased the levels of dopamine metabolites in the striatum, while κ-selective agonists, such as ethylketocyclazocine, had little direct effect, but antagonized morphine action. M-F. Chesselet (College de France) showed that the selective δ ligand D-Ser^2-Thr^6-Leu-enkephalin, injected into the fluid perfusing the caudate nucleus, induced a localized release of dopamine. Selective μ agonists such as morphine produced a weaker effect which was followed by inhibition of release. Since the enkephalin analogue, but not morphine, enhanced the release of dopamine from striatal slices *in vitro*, it was suggested that δ agonists act directly, while μ agonists act indirectly, to promote the release of dopamine in the caudate. The induction of muscular rigidity by morphine in the rat, probably by an inhibitory action of γ-aminobutyric acid neurones in the zona reticulata of the substantia nigra, was discussed by U. Havemann (Max-Planck-Institut, Gottingen). Thus in this, as in so many systems, several component structures seem to be influenced by one or other form of opioid. □

Do antigen-presenting cells distinguish self from non-self?

from Martin C. Raff

THERE is substantial evidence suggesting that helper T cells recognize a foreign antigen only after it has been taken up by specialized antigen-presenting cells (APCs) and that the antigen is recognized on the surface of the APC in association with class II (Ia) MHC glycoproteins[1]. But this view of antigen presentation is fundamentally incomplete in that it does not provide answers to two central questions: how do APCs recognize antigens, and do they distinguish foreign molecules from self molecules?

If APCs do not discriminate between self and non-self, why are their recognition and processing pathways not saturated by the high concentration of self macromolecules in the extracellular fluid? If they do distinguish self from non-self, how do they do so? How can they pick out a molecule of tetanus toxin from a sea of self proteins? One possibility is that they use a non-immunological recognition mechanism akin to those used by certain invertebrate cells for distinguishing self from non-self: although the molecular mechanisms involved are still poorly understood, it is clear that such discrimination operates when, for example, yeast cells mate[2], or a mixture of cells dissociated from two different species of sponges reaggregates in a species-specific way[3], or invertebrate haematocytes react against foreign particles, cells or organisms[4]. However, the discrimination required of APCs, were they to distinguish the many thousands of different self molecules from the many millions of different foreign antigens that are capable of stimulating an immune response, would be far more demanding than that required of invertebrate cells. Teleologically, therefore, it seems more likely that APCs would take advantage of the sophisticated antigen recognition mechanisms evolved by the vertebrate immune system. For example, APCs might only efficiently bind and/or process molecules that are complexed to antibodies secreted by T cell-independent B cells. However, some APCs, such as splenic dendritic cells, apparently do not have Fc receptors with which to bind antigen–

Martin C. Raff is in the Department of Zoology, University College London, Gower Street, London WC1E 6BT.

0028-0836/82/340791-02$01.00

antibody complexes[5], and B cell-deficient animals seem to be able to make helper T cell-dependent immune responses[6]. Therefore, if APCs require lymphocyte help to recognize foreign antigens, this help might be in the form of antigen-specific T cell products (which must themselves be made without the aid of APCs). The recent report that suppressor T cells can inhibit the function of APCs[7] is consistent with the view that communication between T cells and APCs is bidirectional.

The idea that antigen binding and/or processing by APCs is lymphocyte-dependent would be untenable if pure APCs (especially antigen-presenting cell lines) were found to be as efficiently 'loaded' with antigen in the absence of lymphocytes as in their presence. It would also be unlikely if the recent evidence (cited but not documented in ref. 8; and G. Sunshine, M. Cyrus and G. Winchester, unpublished results) that APCs do not discriminate between self and non-self forms of the F serum glycoprotein is confirmed for other molecules. In either case, an important question in antigen presentation, which has so far been ignored, would remain unanswered: why are APCs not saturated by self molecules?

---

1. Rosenthal, A. S. *Immun. Rev.* **40**, 136 (1978).
2. Manney, T. R. & Meade, J. H. in *Microbial Interactions, Vol. 3. Receptors and Recognition* Series B (ed. Reissig, J. L.) 281 (Chapman & Hall, London, 1977).
3. Wilsnon, H. V. *J. exp. Zool.* **5**, 245 (1907).
4. Salt, G. *Parasitology* **53**, 527 (1963).
5. Nussenzweig, M. C. & Steinmann, R. M. *Immun. Today* **3**, 65 (1982).
6. Maguire, H. C., Fanis, L. & Weidanz, W. *Immunology* **37**, 367 (1979).
7. Ptak, W. & Gershon, R. K. *Proc. natn. Acad. Sci. U.S.A.* **79**, 2645 (1982).
8. Czitrom, A., Mitchison, N. A. & Sunshine, G. H. *Immunobiology of the Major Histocompatibility Complex*, 7th int. Convoc. Immun., Niagara Falls, 243 (Karger, Basel, 1981).

Iron-sulphur cluster interconversions and the activation of aconitase

from Richard Cammack

IRON-SULPHUR clusters in proteins may not always be such static entities as has been supposed. Recent experiments have shown that some of the newly discovered [3Fe-3S] clusters can be converted reversibly into [4Fe-4S] clusters. H. Beinert's group, working in Madison, Wisconsin, has proposed that an interconversion of this type is the key to the activation of the mitochondrial enzyme aconitase. It has long been known that aconitase, when isolated, is in an inactive form and can be activated by incubation with iron salts. Some authors have suggested that this iron atom is involved in the catalytic centre of the enzyme. Now it is recognized that aconitase contains an iron-sulphur cluster, of the recently discovered three-iron type (see *News and Views* **286**, 442; 1980). The additional iron appears to convert this to a [4Fe-4S] cluster which somehow is required for the activity of the enzyme.

Recent advances in the use of spectroscopic techniques, including ESR, magnetic circular dichroism (MCD), ^{57}Fe-Mössbauer and resonance Raman (RR) spectroscopy, have made it possible to observe the individual clusters in the iron-sulphur proteins. Though each technique provides different information about the type of cluster in a protein (paramagnetism, vibrational modes, and so on), they all provide ways of comparing an unknown iron-sulphur protein with the 'benchmark' proteins whose structures have been determined by X-ray crystallography. A series of ferredoxins is now known which contain [4Fe-4S] and [3Fe-3S] clusters in various combinations. The advantage of studying these instead of proteins such as aconitase is that their relatively low molecular weights means that there is relatively more iron to observe.

The [4Fe-4S] cluster can be visualized as a cube, with iron and sulphide atoms at alternate corners. The [3Fe-3S] cluster is more like a flat hexagon of alternate iron and sulphur atoms[1]. In each cluster, the iron atoms are also bound to ligands from the protein; in the [4Fe-4S] cluster, they are four sulphur atoms of the amino acid cysteine; the [3Fe-3S] cluster requires six ligands, which in ferredoxin of *Azotobacter vinelandii* are provided by five cysteine sulphurs and possibly a water or glutamate oxygen atom[1]. Cluster interconversion therefore requires a considerable rearrangement of the protein structure.

Atomic arrangements in the four-iron and three-iron clusters. Iron atoms are the solid circles.

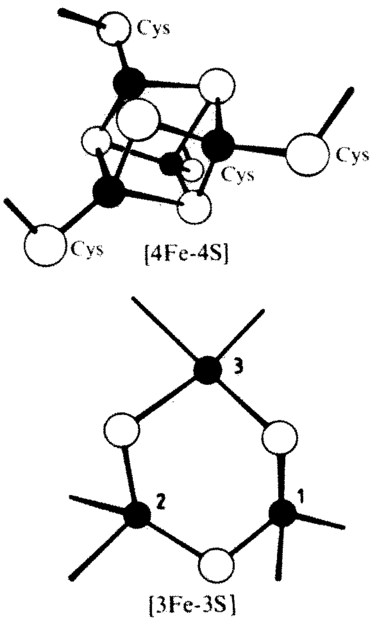

The function of the clusters in most iron-sulphur proteins is to transfer electrons. (This cannot, however, be the case in aconitase, which is not an oxidoreductase.) A major class of iron-sulphur proteins has clusters that undergo oxidation–reduction between the [Fe-4S]$^{2+}$ and [4Fe-4S]$^{1+}$ oxidation levels. When such proteins are isolated, they often contain small and variable amounts of material which gives an ESR signal in the oxidized state of $g = 2.01$. The amount of this material can be increased by treatment with the artifical oxidizing agent ferricyanide. At first this was thought to be due to conversion to the [4Fe-4S]$^{3+}$ oxidation level; however, if this occurs, the cluster is probably unstable and undergoes further modification, because the process cannot be reversed by simple reducing agents. The material which results from this modification, and which gives the $g = 2.01$ signal, has recently been shown by MCD[2], RR[3] and Mössbauer[4] spectroscopy to contain [3Fe-3S] clusters. Evidently oxidative treatment results in the loss of an iron atom from the [4Fe-4S] cluster, and rearrangement.

The change was referred to as 'oxidative damage'[3], implying that the [3Fe-3S] clusters found are artefacts caused by the exposure of [4Fe-4S] proteins to oxygen during isolation. The question then arises as to whether any of the [3Fe-3S] clusters observed in isolated proteins are of physiological significance.

A test case is provided by the ferredoxins isolated from *Desulfovibrio gigas* by J. Le Gall (University of Marseille), J. J. G. Moura, I. Moura and A.V. Xavier (University of Lisbon). Although designated ferredoxins I and II, these are in fact two different assemblages of the same polypeptide of molecular weight 6,000. Fd I is a trimeric unit in which each protein subunit contain a [4Fe-4S] cluster; Fd II is a tetrameric unit in which most of the subunits contains [3Fe-3S] clusters. Both ferredoxins are obtained in substantial quantities when the bacteria are extracted. They have different redox potentials and different activities with the enzymatic systems of *Desulfovibrio*. Fd I is active in the phosphoroclastic cleavage of pyruvate while Fd II is more active in sulphite reduction[5]. Various treatments have been found to interconvert the ferredoxins. Incubation of Fd II with cell extracts and pyruvate (reducing conditions) causes the appearance of Fd I, as seen by ESR. Oxidation of Fd I with ferricyanide

---

Richard Cammack is a lecturer in the Department of Plant Sciences, King's College London, 68 Half Moon Lane, London SE24 9JF.

converts it into something resembling Fd II. The protein has six cysteines and thus can readily accommodate a [3Fe-3S] cluster. The finely tuned balance between the cluster types was shown by reconstitution experiments in which the iron and sulphide were removed entirely and then replaced[6]. With an excess of iron present (5 per protein molecule), only [4Fe-4S] clusters were produced. With limiting iron (3 per protein molecule), up to 50 per cent of the clusters formed were of the [3Fe-3S] type.

Moura *et al.*[6] have developed a procedure to add the extra iron atom to Fd II and produce [4Fe-4S] clusters. This provides a unique opportunity to examine a specific iron atom in a [4Fe-4S] cluster. Using Mössbauer spectroscopy one can observe the isotope ^{57}Fe (which has an abundance of only 2.2 per cent in natural iron), so that by adding either enriched ^{57}Fe or ^{56}Fe to Fd II it is possible to obtain spectra from either the added iron atom, or the average of the other three. The studies were carried out by E. Münck and coworkers in Minnesota.

The spectra show that the added iron atom probably goes into a specific site in the [4Fe-4S] cluster, though the possibility of two equivalent subsites cannot be excluded[7].

The inequivalence between the iron atoms in this type of cluster is not understood at present. For example, in the reduced cluster, when the valence state corresponds to one Fe III and three Fe II atoms, the iron atoms as seen by Mössbauer spectroscopy appear to be present in two equivalent pairs[8]. A theoretical understanding of these clusters can now be assisted by the determination of the electron distribution and hyperfine field at the individual iron atoms.

Similar experiments have been carried out on the iron-sulphur cluster in aconitase[9]. The enzyme is activated by reductive treatments in which an iron atom is introduced into a particular site in the [4Fe-4S] cluster. The incorporated iron atom is relatively loosely bound, since added ^{56}Fe will exchange in a few minutes with ^{57}Fe-activated enzyme. By contrast, in *D. gigas* Fd I, the incorporated Fe will not readily exchange. Oxidative treatments, which reconvert the cluster to the [3Fe-3S] form, inactivate the protein, but it is still not clear why.

It has not yet been demonstrated that this interconversion occurs *in vivo*, apart from an early report[10] that the ESR signal at $g = 2.01$ resembling that of the aconitase [3Fe-3S] cluster can be observed in mitochondria. If it does, it would represent a totally new form of covalent modification of enzyme activity. It may not be unique; other enzymes, notably some hydrogenases, exist in inactive forms and show $g = 2.01$ ESR signals. □

---

1. Ghosh, D., Furey, W. Jr, O'Donnell, S. & Stout, C.D. *J. biol. Chem.* **256**, 4185 (1981).
2. Thomson, A.J. *et al. Biochim. biophys. Acta* **637**, 423 (1981).
3. Johnson, M.K., Spiro, T.G. & Mortenson, L.E. *J. biol. Chem.* **257**, 2447 (1982).
4. Bell, S.H. *et al. FEBS Lett.* **142**, 142 (1982).
5. Moura, J.J.G., Xavier, A.V., Hatchikian, E.C. & Le Gall, J. *FEBS Lett.* **89**, 177 (1978).
6. Moura, J.J.G. *et al. J. biol. Chem.* (in the press).
7. Kent, T.A. *et al. FEBS Lett.* **138** (1982).
8. Middleton, P., Dickson, D.P.E., Jonson, C.E. & Rush, J.D. *Eur. J. Biochem.* **88**, 135 (1978).
9. Kent, T.A. *et al. Proc. natn. Acad. Sci. U.S.A.* **79**, 1096 (1982).
10. Ohnishi, T., Ingledew, W.J. & Shiraishi, S. *Biochem. biophys. Res. Commun.* **63**, 694 (1975).

Evolution and molecular biology

from Andrew Leigh Brown

DESPITE the flush of publications commemorating the centenary of Darwin's death, those outside the field could be forgiven for believing that evolutionary biology has lost its way. While the horizons of the rest of biology are being dramatically extended by new technologies, evolutionary biology seems to be becoming more and more introspective. A recurrent discussion of 'tempo and mode' in evolution has reached such prominence that 'punctuated equilibria' appear to constitute the only issue of importance. In fact, this is far from being the case.

A more fundamental problem raised by developments in molecular biology has so far passed almost unnoticed: the concepts and language of population genetics, in which the behaviour of genes in populations is described in the terms of classical genetics, are no longer adequate. The very words 'locus' and 'allele' have become almost meaningless. A new phraseology is required which can accommodate data on both restriction site polymorphisms and nucleotide substitutions, as well as more radical types of genetic variation: insertion polymorphism, 'concerted evolution' and transposition of repeated elements. Some of the first steps in erecting this new framework could be seen at two recent meetings* intended to foster understanding of the relationship between molecular and evolutionary biology.

The mitochondrial genome was used for the first essays in the molecular study of evolution because of its small size and ease of isolation. Population structure was analysed by restriction site variation and detailed phylogenetic trees were constructed. Now the first results of DNA sequence analysis of mitochondrial (mt) DNA are becoming available. In 900 base pairs (bp) of DNA sequence around the D-loop region of human mtDNA from seven individuals, nucleotide substitutions were found at 45 sites and DNA insertions at three positions (C. Aquadro, National Institute of Environmental Health Sciences, North Carolina).

Nucleotide substitutions were almost always transitions (that is, A→G or T→C changes), transversions accounted for only four per cent of the total. A phylogenetic tree, constructed by a maximum parsimony procedure that minimizes the number of changes between each sequence in the finished tree, reveals that convergent or parallel substitutions have occurred in at least five positions. In addition, the distribution of substitutions along the sequence was highly non-random because multiple substitutions occur at certain sites. These results raise doubts about the estimation of genetic variability from DNA sequence data that depend on pairwise comparisons, for these would greatly underestimate the sequence change inferred by the phylogenetic approach. Perhaps more worrying is that a restriction enzyme analysis would produce quite incorrect trees, because of the localized occurrence of base substitution.

Turning to nuclear genes, more is known of the evolution of the mammalian β-globin gene family than any other system. In man, these genes are arranged in the order:

$$5'\ \psi\beta_2,\ \varepsilon,\ {}^{G}\gamma,\ {}^{A}\gamma,\ \psi\beta_1,\ \delta,\ \beta\ 3'$$

Sequence homology between the δ- and β-globin genes in man suggested that they arose by duplication about 40 million years ago. However, DNA sequence analysis shows that the 3′ portion of the mouse βH2 gene has nearly 80 per cent homology to the human δ gene but only 58 per cent to the human β gene (M. Edgell, University of North Carolina). In addition, part of the single pseudogene in the lemur β-globin cluster appears to be a δ-globin sequence that has undergone gene conversion with an embryonic gene (A. Jeffreys, University of Leicester). These results strongly suggest that the β/δ-globin duplication predates the mammalian radiation of 80 million years ago. Where gene conversion can occur, overall sequence homology cannot be used to estimate the times of gene duplication events.

A large body of data collected on variants in the human β-globin gene cluster has revealed some remarkable aspects of the relationship between linkage disequilibrium and recombination distance (H.K. Kazazian, Johns Hopkins University). Thirteen polymorphic restriction site markers have been studied in several hundred individuals. Seven are located in a

---

*The Annual Meeting of the Society for the Study of Evolution and the American Society of Naturalists was held at Stony Brook, New York from 21 to 24 June 1982. The London Darwin Meeting was held on 5 July 1982 at University College London.

Andrew Leigh Brown is at the Imperial Cancer Research Fund Mill Hill Laboratories, Burtonhole Lane, London NW7 1AD.

0028-0836/82/340793-02$01.00

32-kilobase (kb) region on the 5′ side of the δ-globin gene which includes the γ, ε and ψβ$_1$ genes. Six sites are found in a separate 20kb block across and to the 3′ side of the β gene. Theoretically, the variants at the seven restriction sites might be found in over one hundred different combinations in the 5′ region. Remarkably, only three combinations are common, all of which are distinguished from each other at at least two sites. Similarly, in the 3′ block, only three more combinations are found. This high degree of linkage association would be unsurprising in view of the short distance separating the markers, but for the observation that across an 11 kb region spanning the δ gene, random association between 5′ and 3′ haplotypes is found. However, this recombination hot spot is unlikely to be a function of the δ-globin gene itself, as the flanking blocks include all the other genes in this cluster.

In surveys of the β-globin region, few DNA insertion variants have been found. In contrast, studies of restriction site polymorphism at two genes in *Drosophila* indicate that insertion/deletion events are an important source of variation. In a 12 kb region around the alcohol dehydrogenase (*Adh*) gene in *D. melanogaster*, five insertion/deletion variants were discovered in 18 lines from natural populations (C.H. Langley, NIEHS, North Carolina). However, the commonest restriction map in *D. melanogaster* showed little divergence that could be ascribed to DNA insertion from those obtained for two other species, *D. simulans* and *D. mauritiana*. Similar results are seen for the *87A* heat-shock locus in *Drosophila* (A. Leigh Brown, Imperial Cancer Research Fund). It is not yet known whether these other *Drosophila* species also show insertional variation but it could be that 'the spaces between the genes' are important in as yet undefined ways such that insertions or deletions are generally screened out by natural selection. The strong conservation of the distances between genes in the β-globin cluster of higher primates has prompted similar speculations (Jeffreys).

The *Adh* gene in *D. melanogaster* is also the first nuclear gene to be used for a systematic survey of variation in natural populations using DNA sequencing (M. Kreitman, Harvard University). Of 1,750 bp which have been sequenced in 11 isogenic strains, 36 nucleotide positions are variable. Unlike mtDNA, transitions and transversions are equally frequent. No amino acid substitutions were detected apart from the Thr-Lys substitution which causes the well known 'fast-slow' electrophoretic polymorphism. If it is assumed that the only substitutions permitted are silent ones whch do not result in an amino acid change, the frequency of polymorphic nucleotide sites relative to the number of silent sites in exons is very similar to the total frequency found in the introns. A much lower frequency was found in the 5′-non-coding regions of the transcripts, suggesting that some constraints on nucleotide substitution may be acting upstream of the protein-coding region. However, these apparently do not extend to the transcription start point, around which substitutions were quite frequent.

Finally, population genetics theory is now being applied to the behaviour of transposable elements in eukaryotic populations. A simple mathematical model has been developed that gives the expected frequencies of occupation of a particular chromosomal site by a mobile element in a natural population under the action of random genetic drift (J. Brookfield and C.H. Langley, NIEHS). Testing this model with data on the sites of hybridization to *Drosophila* polytene chromosomes of three mobile elements, *copia*, *412* and *297*, Brookfield and Langley showed that the data give a good fit for a high transposition rate. The result may be unexpected given that some mutations due to *copia* insertions (for example *w*^{a}) are very stable. It was also observed that the frequency of co-occupancy of a site by more than one type of transposable element was much higher than expected. This suggests either that insertion is not random and occurs after strand breakage or some similar event, or that the total number of occupable sites is restricted.

The P factor is a transposable element whose movement is responsible for a syndrome of germ-line aberrations in *D. melanogaster* known as hybrid dysgenesis. These aberrations are only found when wild males are crossed to females from long-established laboratory strains. Wild-type strains from the USA almost without exception carry this factor (P strains) while old-established laboratory strains do not (M strains). It had been thought that this loss was a consequence of inbreeding but new data on the relative frequency of such strains in collections from Europe and the Far East give a very different picture (M. Kidwell, Brown University). Here 'Q' strains, which are compatible with both P and M strains but contain many copies of the P element, are common, while M strains are of intermediate frequency and P strains are rare. In addition, some wild M strains are now known to contain some copies of the P element. The P element is known to be highly labile and it is not known whether any of the elements in these strains are functional. This complex pattern suggests that the element is itself undergoing rapid evolutionary change and possibly indicates an invasive rather than a symbiotic history.

Speculation that transposable elements may be involved in speciation has flourished following the discovery of their role in hybrid dysgenesis. If, however, the germ-line incompatibility is a consequence of a transient process of invasion, such involvement is much more difficult to envisage. It is hardly reasonable to propose a new invasion for each speciation event. Similarly, no clear pattern can yet be discerned on the general significance of insertional variation, which is apparently common in *Drosophila*, but is very rare in the human β-globin region. It seems more reasonable that the current difference between the mammalian and *Drosophila* data is due to the particular genes which have been studied in each organism to date [for example, the *dilute* coat colour mutation in the mouse is due to an insertion of retro-viral sequences (Jenkins, N. *et al. Nature* **293**, 370; 1981) and insertional polymorphism has also been found in man (Wyman & White, *PNAS* 77, 6754; 1980)].

These studies are beginning to reveal some of the processes which take place in the genome during evolution. It should be nevertheless recognized that the pursuit of detail is not a satisfactory end in itself. However much is learnt about a single gene, if the knowledge cannot be generalized we will not have discovered much about evolution. The greatest interest in the new developments stems from the fact that the whole genome has been rendered accessible by these techniques, and that is something that evolutionary biologists have waited a long time for. □

100 YEARS AGO

THE two Swedish gunboats which conveyed the circumpolar observation party to Spitzbergen, have just returned to Tromsö. Capt. Palander states that it was impossible to approach Mossel Bay, he having made two attempts, on account of heavy pack-ice, and that the party had therefore settled on Cape Thordsten as their residence, where observations commenced on the 15th inst. He further reports that all the Norwegian fishermen he met complained of the unfavourable season and the enormous quantity of ice this summer, no vessel having been able to get higher than Amsterdam Island, from where no opening could be seen by telescope in any direction.

The steamer *A.E. Nordenskjöld*, belonging to M. Sibiriakoff, left Tromsö on the 18th inst. for the Jenisei. The vessel has on board a cargo of English merchandise, two steam launches, and an engine for the Siberian gold works. The vessel will attempt to save some of the cargo lost in the *Oscar Dickson* in Gydaviken, and return next year with a full cargo of tea, which will be brought from China across the Baikal sea to Kureika on the Jenisei.

The death is announced of Count Lutke, well known in connection with Russian Arctic exploration, especially in the Novaya Zemlay region.

From *Nature* **26**, 447; August 31, 1882.

0028-0836/82/340794-01$01.00

Detectors in astronomy

Optical astronomy

from Alec Boksenberg

It is now more than a century since the invention of the gelatin photographic emulsion, but the photographic process still has many deficiencies, including nonlinear response, restricted dynamic range, reciprocity failure, adjacency effects, and a detection efficiency of only a few per cent. It does, however, have the advantage over all other detection media when a huge number of picture elements is required. However, for most detection and recording applications in astronomy it has been superseded by more efficient methods.

Direct interaction of photons with the recording medium occurs in photographic emulsion, electronically-scanned silicon devices such as the charge-coupled-device (CCD), and electron-beam-scanned television camera tubes of the simple vidicon type. In all other devices a photocathode is used to produce an intermediate electron image, which then is accelerated to relatively high energy to enable the signal to be enhanced by some gain process before recording.

Electronographic cameras

In 1934 Kiepenheuer proposed that an efficient detector could be made by accelerating and focusing electrons from a photocathode onto a photographic emulsion. This would give a considerable gain in sensitivity over a simple photographic emulsion because every high-energy electron entering the emulsion produces developable grains and there is no reciprocity failure. The overall efficiency should therefore depend mainly on the efficiency of the photocathode. Modifications to the technique, particularly by McGee, who in his 'Spectracon' used a mica barrier membrane to protect the photocathode and also allow the emulsion to be used in air (fine-grained nuclear emulsions are used in modern devices), and the later variant by McMullan, have resulted in more convenient operation.

Photocathodes are now fundamental in certain television camera tubes and in image intensifiers. The most commonly used photocathode in optical astronomy, trialkali, has an efficiency of about 20 per cent in the blue falling to about 1 per cent at 8,000 Å. Recently a new class of 'negative electron affinity' photoemitting materials, such as GaAs(Cs), have been discovered which have a high efficiency in the red and near infrared.

Integrating television camera tubes

Conventional television camera tubes can in principle be used to detect and record astronomical images, however, television broadcast cameras are severely limited by noise (from the video pre-amplifier) at low light levels. It is therefore important to use a camera tube with high internal gain and the capability to integrate a weak signal over a long period before readout. Two tubes having these properties are the SEC and SIT vidicons, both originally developed for the military market as night vision devices. A photocathode generates photoelectrons which are accelerated to a few keV in the image section and focused at the target. Electron multiplication takes place in the target and, at the end of the exposure, the amplified electron image is read by a scanning electron beam in the readout section. The SIT target has an electron amplification up to 2,000 but requires strong cooling (to –60°C) in order to reduce the dark current sufficiently to permit long integration times. The SEC target has lower gain (~100) but can integrate and store charge images indefinitely at room temperature without degradation, but it has the disadvantage of lower storage capacity and produces 'grainier' images. Notwithstanding, the SEC tube has been used successfully in several astronomy programmes, and is the prime detector on the International Ultraviolet Explorer observatory satellite where its operational simplicity is fully exploited.

Image intensifiers

Image intensifiers come in several forms, all using a photocathode for the initial conversion of photons into an electron image. They have arbitrary input and output spectral characteristics, for example a device may accept a UV image but convert it to an enhanced optical image. In the simplest case electrons from the photocathode are accelerated onto a phosphor screen to produce an enhanced optical image. A blue-light gain of 50 is typical for a simple device of this kind, but several such stages can be arranged in cascade to give a very high overall gain, a four-stage intensifier produced by EMI having a blue-light gain of about 10^7.

The microchannel plate (MCP) can also be employed as an image intensifier capable of extremely high gain. It consists of an array of fine, slightly conducting glass tubes having a secondary emission coefficient greater than unity. An accelerated electron entering one of the channels and striking the wall produces secondaries, which are accelerated by an internal electric field and in turn strike the wall, eventually producing an avalanche of electrons which emerges from the output of the channel.

The MCP can also be built into a very compact double proximity-focused structure using a conventional photocathode on its input window to give a 'wafer' intensifier with high gain and no distortion. Although the electron gain of a MCP with straight channels is limited by the onset of positive ion feedback, several techniques have now been introduced to suppress this, the most satisfactory being to curve the channels, which can give an electron gain greater than 10^7 without difficulty. Additionally, the output pulse sizes at such high gains are confined to a sharply peaked distribution which substantially decreases the added noise in the image compared to the low gain performance. Although the output of an image intensifier may be recorded photographically, this combination still suffers from non-linearity and small

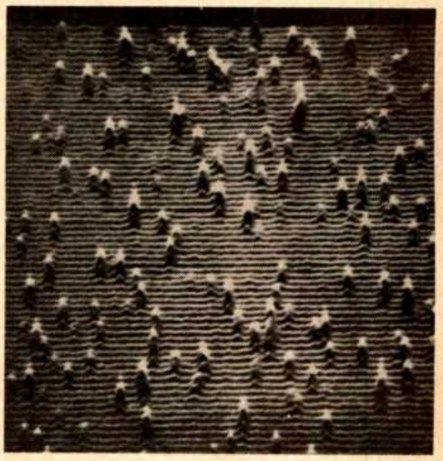

Fig. 1 Single photon events detected with a high gain image intensifier viewed by a television camera, as employed in the IPCS. This isometric display represents less than half of one per cent of the available television field.

Alec Boksenberg is Director of the Royal Greenwich Observatory, Herstmonceux Castle, Sussex.

0028-0836/82/340795-02$01.00

dynamic range. Coupling to a photoelectronic detector such as a television camera tube is far more satisfactory. This is exploited in the widely used technique of 'image photon counting' first developed by Boksenberg, who employed an EMI four-stage intensifier lens-coupled to a Philips 'Plumbicon' television camera tube.

Image photon counting systems (IPCS)

The basic idea of image photon counting is to amplify a faint image to a level where single photon events can be discerned above the readout noise of a television camera used to view the output screen of a high gain image intensifier (Fig. 1). The television camera acts as a spatially sensitive one-frame buffer store and passes the photon signals to a special pattern processor which records their central positions, and then passes these to the digital electronic memory of an on-line computer. Photon events registered in each television frame are then accumulated digitally. There is no limit to the length of exposure attainable because the system has no saturation capacity (unlike photographic emulsion or television camera targets). The technique shifts the emphasis from the detailed performance of the individual devices themselves to the real-time data processing of the fundamental signals delivered by the initial photon conversion layer in the system.

Recording only the central positions of each detected photon has two major advantages. Maximum efficiency is attained because each photon event is accorded equal statistical weighting, unlike the raw signals delivered by the television camera which are variously sized due to unequal gain processes associated with the coupled image intensifier. This would otherwise lead to uncertainty in the number of detected events. Second, a markedly sharper image is obtained because the image smearing inherent in the devices is removed in the processing of the photon events. Also, since all amplifier noise is rejected, there is no low-level threshold for very faint images, so images containing even a few photon events can be recorded accurately. Another major advantage of the system is the real-time display of the accummulating image on a monitor, which results in high operating efficiency in astronomy; considerable time may be saved by terminating exposures as soon as the required image signal-to-noise ratio has been achieved.

Two other systems also in routine use are the Robinson and Wampler image dissector scanner, and the intensified Reticon scanner developed by Shectman. These have more restricted channel capacity than a full IPCS but are excellent for many one-dimensional spectroscopic applications. Several more forms of image photon counting (or quasi-counting) detector are now being developed, employing various forms of intensification and readout, some resulting in very compact devices.

Solid state detectors

Various types of solid state imaging detectors based on silicon photodetectors have become available for astronomy in the past few years. Silicon is particularly efficient in the red and near-infrared compared to photoemissive surfaces, reaching about 80 per cent between 5,000 and 7,000 Å and extending beyond 11,000 Å. The various devices such as the Reticon and the charge-coupled device (CCD) are distinguished by the method of reading out the stored image. The detection efficiency is more or less limited by readout noise and build-up of charge background, and is highest for the CCD.

CCD devices all contain a two-dimensional array of sensitive elements (typically of dimension 15-30 μm), and arrays of up to 1,500 × 1,500 elements are under development. The device is essentially a silicon integrated circuit of MOS type and comprises an oxide covered silicon substrate upon which is formed an array of closely spaced electrodes. Each electrode is equivalent to the 'gate' of an MOS transistor. Signal information is carried in the form of an electric charge which is localized beneath the electrodes with the highest applied potentials. Charge accumulates in these potential wells and is released for conduction in the silicon by the action of the incident photons. 'Charge coupling' is the technique by which this signal charge can be transferred from beneath one electrode to the next. This is achieved by sequentially pulsing the voltages on the electrodes between high and low levels. Charge can therefore be made to pass down an array of many electrodes with hardly any loss and very little addition of noise. By this means the entire charge image can be shifted out bodily, and entered into a line readout section which delivers the now sequentially arranged signals to an on-chip video amplifier. The noise in this amplifier represents a limit to the minimum detectable signal, but in current devices can be as low as six electrons per image element. Cosmic ray events represent another limitation as silicon is an efficient detector of high-energy charged particles. For use in astronomy the devices must be cooled to avoid the build-up of thermally-induced charge, which would otherwise mask the signal. Exposures of several hours can then be achieved without excessive interference due to dark current.

Future improvements in image detection are likely to come at least as much from the application of new electronic processing and data reduction methods as from the development of better devices. The CCD is taking an increasing role in astronomy, and in future all detector devices may be of this type. Vast arrays might be built up of CCD configurations and internal gain might be achieved by avalanche processes already implemented in discrete diode structures. The technique of image photon counting, with its superior low light level performance, may then be achieved entirely in solid state. □

Infrared astronomy

from Erick T. Young

SINCE the first detection of infrared (IR) radiation from a celestial source by Sir William Herschel[1] in 1800, the sensitivity of IR detectors has improved by many orders of magnitude. However, the true revolution in IR astronomy came in the 1960s with the advent of cooled semiconductor detectors. With these devices, the barrier to detecting ever fainter sources became the natural backgrounds from the atmosphere and telescope rather than the detector itself.

The astronomical IR spans the wavelength range from just below 1μm to 1,000μm. Although groundbased observations are limited to a few atmospheric windows of below 30μm and at 350 and 450μm, observations from balloons, aeroplanes, and spacecraft have now opened the entire range to study. Detection techniques vary from optical methods at the shorter wavelengths to quasi-radio methods in the submillimetre range. The choice of detector for a system depends on cost, required sensitivity, wavelength coverage, backgrounds, cooling capabilities, and time resolution. The requirements of IR astronomy are quite distinct from most applications. Most importantly, astronomical sources are exceedingly faint, and consequently sensitivity is the most important detector parameter. To this end the detectors are usually operated cooled with restricted fields of view to keep the background noise to a minimum.

Sensitivity limits for detectors

The sensitivity of an IR detector is the ultimately limited by noise both in the detector and in the associated electronics. Thermal detectors are subject to phonon noise associated with the finite temperature of the sensing element. Photon detectors can have noise due to the random generation

---

Erick T. Young is at the Steward Observatory, University of Arizona, Tucson.

0028-0836/82/340796-03$01.00

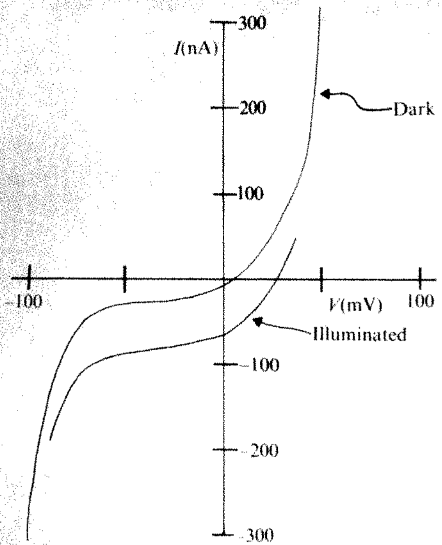

Fig.1 Current–voltage curves for an InSb photovoltaic detector operating at 77K. The two curves represent the case with background irradiation and the case without background irradiation.

and recombination of charge carriers, and all detectors suffer from Johnson noise due to the thermal motions of the charge carriers. Additionally, noise due to the fluctuations in the background photons seen by the detector can contribute significantly, and indeed are the most important source of noise with the current generation of IR detectors. The great promise of space experiments is the elimination of backgrounds due to the atmosphere and the telescope.

For an IR astronomer, the two most important parameters for detectors are the noise equivalent power (NEP) and the quantum efficiency η. The NEP gives the power incident on the detector which yields a unity signal-to-noise ratio in one second of integration time, and is therefore an indication of the required integration time for detecting an astronomical source at a given signal-to-noise ratio. The responsive quantum efficiency η is the ratio of electrons generated in the detector to incident photons. Of more use is the detective quantum efficiency η_D, first applied to IR detectors by Jones[2], $\eta_D = \mathrm{NEP}_{BL}^2/\mathrm{NEP}^2$, where NEP_{BL} is the noise equivalent power of a perfect detector, limited only by the background photon fluctuations, and NEP is the actual noise equivalent power for those conditions. η_D is therefore a measure of how closely a detector approaches the theoretical limit. The detective quantum efficiency is especially useful when the photon background fluctuations are the dominant noise source. In the absence of spurious noise, η_D has the same value as η.

Thermal detectors

Herschel's first IR detector was a thermal detector, a thermometer. Thermal detectors utilize the temperature dependence of some physical parameter for the detection of IR energy. The IR energy is converted into thermal energy of the lattice which is subsequently sensed. Currently, the most sensitive thermal detectors are liquid helium cooled germanium or silicon bolometers. With suitable doping, the impurity conductivity in silicon and germanium shows a very strong dependence on temperature[3]. By carefully mounting the semiconducting element so that the thermal conductance to the helium bath is small, minute amounts of IR energy will cause measurable changes in the conductivity of the device. Clearly the thermal fluctuations in the device can be a significant noise source, and it is highly advantageous to cool the detector. The gallium-doped germanium bolometer invented by Low[4] was the first device to approach the theoretical sensitivity limits at liquid helium tempertures. In the background conditions where the noise due to photon fluctuations is greater than the thermal fluctuation noise, the Ga-doped Ge bolometer is a virtually ideal detector with almost unity quantum efficiency. This detector is widely used in astronomical observations, and its application to photometry has been described in detail by Low and Rieke[5]. Typically these devices are cooled with superfluid helium to below 1.5 K, and NEPs as low as 7×10^{-15} W Hz$^{-1/2}$ have been realized. Because bolometers are thermal detectors, the wavelength limits to the response are set by the efficiency of coupling the radiative energy into the lattice. Using special absorbing materials, sensitive detectors into the millimetre wavelength range have been made. Current directions in research include developing bolometers for use at the much lower temperatures available with He III refrigerators and dilution refrigerators. NEPs better than 10^{-16} WHz$^{-1/2}$ appear to be realizable.

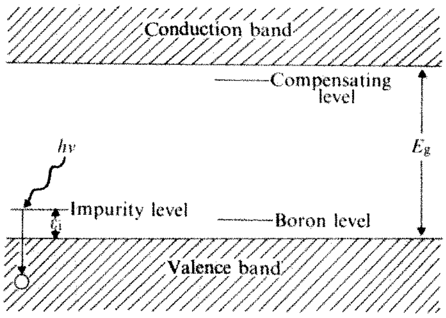

Fig.2 The band diagram of a typical extrinsic semiconductor with a shallow p-type dopant.

Photovoltaic detectors

At wavelengths below 5μm, the most commonly used IR detector is the InSb photodiode, which has generally replaced the older PbS detector in high performance applications. In groundbased observing conditions, the InSb detector offers excellent performance, with quantum efficiencies in excess of 60 per cent. In a photodiode, charge carriers are generated by photons in the depletion region and are swept out by the p–n junction voltage. Figure 1 shows the current–voltage curve for a high performance InSb photodiode. In the presence of photons, a current is generated across the junction that is proportional to the irradiance. These detectors became astronomically useful with the incorporation of the transimpedance amplifier (TIA)[6]. This amplifier acts as a current to voltage converter, and by maintaining a zero potential across the detector, noise contributions due to leakage currents are eliminated. The Johnson noise of the detector and noise in the associated electronics become the ultimate performance limitations. By cooling the detector to liquid helium temperatures and by using very low noise junction field effect transistors (J-FETs) in the amplifier, Rieke *et al.*[7] have attained background-limited performance at wavelengths as short as 2μm. NEPs of 7×10^{-17} W Hz$^{-1/2}$ have been reached, with operation limited to low frequencies.

Photoconductive detectors

When electron–hole pairs are created in a semiconductor by the absorption of photons, the conductivity of the material is temporarily increased until these charge carriers recombine. Application of a bias voltage allows the external detection of these carriers in an amplifier. Intrinsic photoconductivity can occur if the energy of the ionizing photon is greater than the bandgap of the material. As the intrinsic bandgaps of Si and Ge are 1.166 and 0.75 eV, respectively, these materials are not suitable for detection beyond 1.5 μm. Recent work has included the development of intrinsic materials such as HgCdTe with narrower bandgaps. To date, however, there has been little application of these materials in IR astronomy. Extrinsic photoconductivity utilizes energy levels due to impurities that lie within the forbidden gap. Figure 2 illustrates the energy bands of a typical semiconductor

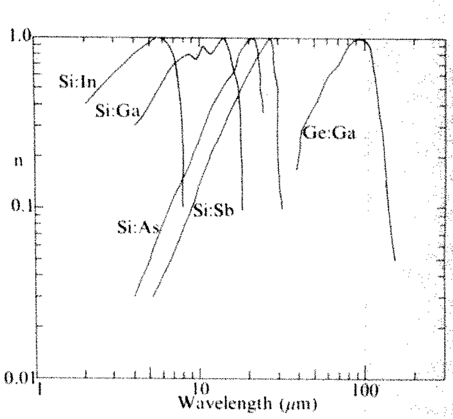

Fig.3 Normalized spectral response curves for some of the more important extrinsic detectors.

with a p-type dopant. In both silicon and germanium a wide variety of dopants with small ionization energies have been investigated[8], and spectral responses of some of the more important ones are illustrated in Fig. 3. By choosing a suitable dopant, the spectral response of the detector can be tailored to the specific requirements of the experiment. Since extrinsic photoconductors have a definite long wavelength cut-off, they are not subject to noise due to thermal fluctuations in the cooling bath. As long as the temperature is low enough to prevent thermally excited carriers, the only important noise source is the background.

Extrinsic photoconductors are currently the most sensitive detectors available for operation under reduced backgrounds. Consequently, they are the principal detectors in the current generation of low background space IR astronomy experiments, including the Infrared Astronomy Satellite (IRAS) and the Spacelab 2 Infrared Telescope[9] (SL-2 IRT). These space experiments will achieve greatly reduced background levels by cryogenically cooling the telescope. For example, the 12 μm band of IRAS will have $\sim 10^5$ times lower background power than with a comparable groundbased system. The better than 100-fold improvement in NEP translates to a 10^4-fold reduction in integration time.

Current extrinsic photoconductors have typical quantum efficiencies of 30 per cent, although values as high as 80 per cent have been reported[10]. Noise equivalent powers in the 10^{-17} to 10^{-16} W Hz$^{-1/2}$ range are attainable with TIA amplifiers and feedback resistors of $\sim 10^{10}\,\Omega$. These detector systems are adequate for the present generation of space experiments, where NEPs are limited by the thermal background from the interplanetary dust. Future IR astronomy experiments, such as the Shuttle Infrared Telescope Facility (SIRTF), possibly with diffraction-limited pixels and narrow bandwidths will require significant improvements in sensor technology to remain background-limited. In particular, amplification techniques will play a critical role in realizing the potential sensitivity.

A second exciting area of development is in large detector arrays. This technology has only recently become declassified, and much work remains to make arrays that are suitable for astronomical use. By the early 1990s, when SIRTF is hoped to be in operation, highly sensitive arrays of thousands of pixels should be available. ☐

---

1. Herschel, W. *Phil. Trans. R. Soc.* **90,** 284 (1800).
2. Jones, R.C. *Proc. Inst. Radio Engrs.* **47,** 1459 (1959).
3. Mott, N.F. & Twose, W.D. *Adv. Phys.* **10,** 107 (1961).
4. Low, F.J. *J. opt. Soc. Am.* **51,** 1300 (1961).
5. Low, F.J. & Rieke, G.H. in *Methods of Experimental Physics: Astrophysics* (ed Carleton, N.) **12,** Part A, 415 (Academic, New York, 1974).
6. Hall, D.N.B. *et al. Appl. Opt.* **14,** 450 (1975).
7. Rieke, G.H. *et al. Appl. Opt.* **20,** 814 (1981).
8. Bratt, P.R. in *Semiconductors and Semimetals* (eds Willardson, R.K. Beer, A.C.) **12,** 39 (Academic, New York, 1977).
9. Young, E.T. *et al. Proc. S.P.I.E.* **280,** 12 (1981).
10. Young, E.T. & Low, F.J. *Proc. S.P.I.E.* **172,** 184 (1979).

X-ray astronomy

from Brian Taylor

THE very rapid advance of X-ray astronomy through the 1970s has produced demands for new detector developments with emphasis on large energy bandwidth (within the total range from tens of eV to tens of keV) spectral resolution, background rejection and position sensing capability if the momentum of the 1970s is to be maintained through the last two decades of the century. In particular position resolution is crucial given the advent of grazing-incidence imaging optics capable of providing arc second image quality at low energies, and coded aperture masks providing arc minute image quality at the upper end of the energy range.

Proportional counters

The state-of-the-art in mechanically collimated gas-filled proportional counters, the traditional work-horse for X-ray astronomy above 1.5 keV, is probably best exemplified by the eight, multiwire detectors of the Medium Energy Experiment[1] to be flown later this year on the EXOSAT mission[2]. These detectors give an effective area of 1,600 cm^2, are collimated to 45 arc min full-width half maximum (FWHM) and cover the energy range up to 50 keV. Use of five-sided anticoincidence and risetime rejection techniques provide background rejection efficiencies >99 per cent in the range 1–6 keV, with an energy resolution of 22 per cent FWHM at 6 keV.

These collimated detectors, however, have a sensitivity limit of 0.3 millicrabs (10^{-11} erg cm^{-2} s^{-1}) due to source confusion in the field of view. For the study of the spectral and temporal characteristics of the bright X-ray sources (from the UHURU or Ariel 5 catalogues) this is not a draw-back, but for the determination of the high-energy spectral tails of weak sources detected by imaging telescopes better sensitivity is required. Conversely, the upper energy limit of current grazing-incidence optics (the Einstein observatory[3], EXOSAT[2], ROSAT[4]) is typically a few keV and collimated proportional counters are unsuitable for the spectral mapping of extended objects (SNRs, clusters of galaxies) or resolution of confused regions.

This has lead to the development of coded aperture mask telescopes for use with large area proportional counters with two-dimensional position sensing capability. Instruments to be flown[5] on Spacelab 2 in 1984 and those considered for the potential ESA mission[6] X-80 in 1988 are examples. In the case of Spacelab 2, the detector has a window area of 32 cm square, is filled with Xe-CH$_4$ to 1.5 atm and with multilayer, multiwire arrays a position resolution of ≤ 1 mm is achieved, using delay line readout from orthogonal cathode wire planes. The anode wires provide the energy signal; an overall resolution of ~ 25 per cent being achieved at 6 keV. With a mask/detector separation of 3 m, mask elements 2.5 mm square and a field-of-view of about 5°, an angular resolution of ~ 3 arc min is achieved for a telescope covering the energy range from 2.5 to 25 keV — well suited to the study of temperature variations, iron line emission (near 7 keV) and non-thermal emission over clusters of galaxies.

Brian Taylor is at the European Space Research and Technology Centre, Noordwijk, the Netherlands.

Proportional counters with position sensing in essentially one dimension may be used in conjunction with Bragg Crystal Spectrometers. Such instruments were flown on the Solar Maximum Mission[7] to study the solar X-ray spectrum, and Spherical Crystal Spectrometers[8] are specified for the X-80 mission[6] for the study of oxygen, silicon, sulphur and iron spectral features in cosmic x-ray sources. Resolutions $E/\Delta E$ of $\sim 10^3$ can be achieved, determined largely by crystal choice and geometry, and counters with a position resolution of ≤ 1 mm over a length of some 25 cm, achievable with the resistive wire anode, charge division technique are required. The spherical crystals allow the mapping of extended sources and position resolution in the plane orthogonal to the plane of dispersion is also required. The long, narrow counters require five-sided anticoincidence for good background rejection, given the relatively small crystal area contributing to a given energy and the long observation times of 10^4–10^5 s.

Proportional counters required to be sensitive above 1.5 keV normally employ thin (~ 50 μm) Be foil entrance windows. For observations below 1.5 keV thin plastic windows must be used. Polypropylene has been widely used, for example the position sensitive proportional counter[9] on EXOSAT has a 0.8 μm, 28 mm diameter window supported with a fine wire grid and withstands a pressure differential of 1.2 atm. However, to probe the XUV waveband at energies below 100 eV thinner windows are required and Lexan windows with thicknesses of ≤ 0.3 μm have been developed[10].

At these low energies imaging telescopes are used to provide a large X-ray collecting area, requiring relatively small detectors. However, the planned Advanced X-ray Astrophysics Facility (AXAF)[11] with its 10-m focal length and 1.2-m diameter outer mirror requires an imaging proportional counter with a window aperture of 18 cm diameter to cover its 1° field of view.

Numerous methods have been developed for determining the position of the photoelectric absorption of X rays in

0028-0836/82/340798-03$01.00

proportional counters in order to simplify the quantity of associated electronics. In the case of the Einstein IPC[12], the anode wire plane was sandwiched between two cathode planes, each comprising a resistive wire. A position resolution of 1.5 mm (FWHM) was achieved at 1.5 keV, corresponding to 1.5 arc min resolution through the optics. In the case of the EXOSAT PSD[9], the anode is a resistive disk with four orthogonal pick-offs at the circumference. Pre-launch calibration of the argon/20 per cent methane filled detector has shown an on-axis position resolution of 0.2 mm (FWHM) at 1.5 keV, with a gas gain of 6×10^4, equivalent to 40 arc s through the optics. The position resolution degrades off-axis with noticeable non-linearity, however, essentially distortion-free resistive anodes have been modelled[13] and are under development. The energy resolution in the EXOSAT PSD is ~35 per cent FWHM at 1.5 keV.

Position accuracy in a proportional counter is ultimately limited by lateral diffusion of the primary electron cloud in the absorption region, but noise and the configuration of the readout system play significant roles, however a figure of 100 μm FWHM at 1.1 keV has been achieved in a prototype XUV camera[14]. Such a detector performance coupled with a plate scale of the AXAF optics (50 μm/arc s) would yield a spectral mapping capability down to 2 arc s.

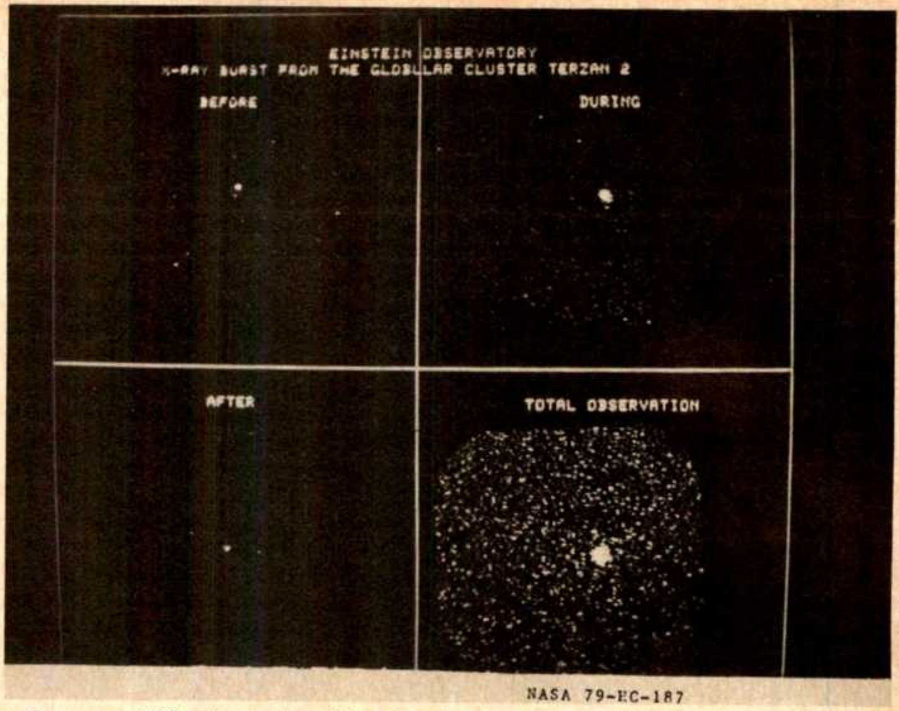

Sequence of 150-s observations of the X-ray burster in globular cluster Terzan 2 made with the Einstein Observatory IPC.

Gas scintillation proportional counters

The energy resolution of practical proportional counters is typically 20–25 per cent at 6 keV with a $E^{-0.5}$ energy dependence. The statistics of the photoabsorption process and electron multiplication at the anode wire contribute about equally to the resolution. The past few years has seen rapid development of the gas scintillation proportional counter (GSPC) as a practical detector for spectroscopy in X-ray astronomy. In this device, electron multiplication is avoided; the primary photoelectrons are accelerated by an electric field, typically 4 kV cm^{-1}, through pure xenon. Copious quantities of UV photons are released from molecules, and are de-exciting following collision of the accelerating electrons with the gas. These UV photons (1,600–1,900 Å) can be observed directly with UV sensitive photomultipliers.

An energy resolution of 7.5 per cent FWHM at 5.9 keV has been achieved with a small non-imaging detector[15] suitable for use with X-ray optics. The first flight of a 2×200 cm^2 effective area, spherical field GSPC took place in September 1980 with a 180 second rocket observation of the SNR Cas–A[16]. These detectors with 10 per cent FWHM were able to resolve the iron line emission feature at ~7 keV from the continuum in the raw data — amply demonstrating their potential as broad-band spectrometers. Generically similar detectors will be flown on EXOSAT[17], Spacelab 1 in 1983 (ref. 18) and the Japanese mission ASTRO-B[19] (1983). Background rejection within these first generation detectors relies exclusively on UV burst length discrimination, analogous to risetime discrimination in conventional proportional counters. On the basis of laboratory simulations and the results of a preliminary rocket flight, it is estimated that the EXOSAT GSPC will achieve 97 per cent background rejection efficiency in the range 2–10 keV (ref. 17).

A number of methods have been examined to provide position sensing in GSPCs, including the use of multiple photomultipliers[20,21], on the principle of the Anger camera[22], the coupling of a position sensitive photoionization detector (PID) using TMAE[23,24] (tetrakis [dimethylamine] ethylene with a photoionization potential of about 3.5 eV) and the coupling of a microchannel plate[25,26]. In the two former cases, the energy resolution performance of the GSPC is maintained while position resolutions of about 1 mm at 6 keV have been achieved. The first rocket flight of a GSPC/PID coupled to X-ray optics took place in 1981 yielding multicoloured images of the Cygnus loop from which the distribution of oxygen and temperatures across the shock-front could be determined[27]. Preliminary work with the coupled microchannel plate[26] and the use of coded TMAE as a liquid photocathode

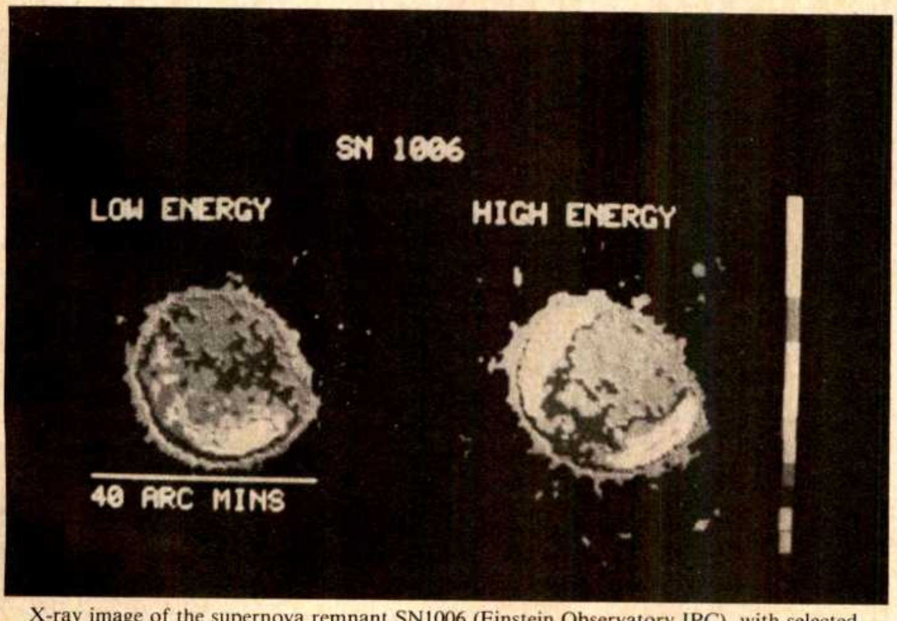

X-ray image of the supernova remnant SN1006 (Einstein Observatory IPC), with selected energy range 0.01–0.3 keV (left) and 1.2–4.0 keV (right). (X-ray Astronomy Group, University of Leicester/Harvard-Smithsonian Center for Astrophysics.)

in conjunction with a very low pressure proportional counter[28], indicates that 300–500 μm position resolution at 6 keV should be achievable. This apparently modest position resolution, however, has to be seen in the context of the off-axis performance of the associated optics. Indeed, the half energy width of the AXAF optics could be as much as 1 arc min at the edge of the field of view[11].

The problem of background contamination becomes very severe for observations above 20 keV where up to now the 'Phoswich' detector has been employed largely in balloon-borne instrumentation. Such an instrument was successful in discovering the spectral feature in Her X-1 at ~ 60 keV ascribed to cyclotron emission[29]. Alternatives to the phoswich are being developed including position sensitive proportional counters[30] and GSPCs[31] for use with coded aperture masks. These detectors are filled up to 5 atm of xenon to provide adequate stopping power and incorporate 'fluorescent gating', in which an event qualifies only if the initial photoabsorption is detected in conjunction with the detectors of a xenon k_α or k_β fluorescent photon. With fluorescence gating applied to a non-imaging GSPC a background rejection of between 99.3 and 99.8 per cent was achieved over the energy range 35–100 keV coupled with an energy resolution of 2.7 per cent FWHM at 60 keV (ref. 32).

Recently the intriguing possibility of combining the spatial resolution of proportional counters with the energy resolution of GSPCs has been investigated[33]. By employing a low drift field in a parallel plate proportional counter, the electron cloud is allowed to diffuse so that each individual electron produces its own independent avalanche, the light pulse from which can be detected and counted. As in the GSPC, energy resolution is determined by the statistics of the initial photoabsorption event and 19 per cent FWHM at 1.5 keV has been measured. Diffusion-limited position resolution has been achieved with an image intensifier.

Microchannel plates

The lower energy limit for gas-filled detectors is, of course, determined by the entrance window. Measurements into the EUV and XUV bands may be made using imaging optics in conjunction with the microchannel plate[34], an array of small (10–50 μm) channel electron multipliers. An energetic photon incident at the entrance to a channel liberates an electron which initiates an avalanche through secondary emission from a continuous dynode on the inside of a channel. By putting two or more plates in series and employing different bias angles (the angle of the channel to the plate surface) high charge gain (up to 10^8) can be achieved without ion feedback. Because the quantum efficiency of a microchannel plate is low it is customary to coat the surface of the front plate. In the case of the EXOSAT channel multiplier array (CMA) focal plane detector[9], a magnesium fluoride coating is used which provides 30 per cent efficiency at 0.05 keV falling to 10 per cent at 1 keV, much smaller than the position sensitive proportional counter.

Several methods have been developed for MCPs including charge division readout of crossed wire grids as in the case of the Einstein observatory's high resolution imager[35], the resistive disc readout method for the EXOSAT CMA[9] and various configurations of multi-anode readout arrays[36]. The position resolutions achieved with MCPs are independent of energy and are largely governed by the readout method. It is anticipated that 15 μm will be achieved in the case of the AXAF HRI (≡0.3 arc s) while 50 μm (≡ 10 arc s) is achieved by the EXOSAT CMA (plate diameter 50 mm, channel diameter 50 μm). Due to its saturated mode of operation, the microchannel plate has no intrinsic energy resolution, and offers the ultimate in 'black and white' imaging.

Focal plane detectors developed to date have been planar in section. However, the focal surface of grazing-incidence X-ray optics tends to be far from planar as one goes off-axis. The microchannel plate, by virtue of its construction, may be formed to adopt the contour of the focal surface. Such a development may be pursued for the wide-field, XUV camera of the ROSAT mission[37].

The detectors described above, the proportional counter, the gas scintillator and the microchannel plate are by no means the only ones employed or with potential in X-ray astronomy. Charge coupled devices (CCDs) have been adapted for the X-ray waveband[38], and with sizes of up to 25 mm square may achieve 15 μm position resolution and energy resolution comparable to the GSPC. A number of solid state detectors without position sensing properties and available in relatively small areas but with energy resolutions of 'a few per cent' cover the range from 1–100 keV, and include cooled Si(Li), intrinsic germanium[39], and mercuric iodide detectors[40], and finally there is the coded mask/sodium iodide crystal/Anger camera combination studied for the SIGMA mission[41].

Operation of the proportional counter

To be detected in a proportional counter an X-ray photon must pass through the window and be absorbed in the gas inside the device. All the photon's energy is used in producing electron–ion pairs and the number of electrons liberated is proportional to the energy of the incident photon. The negatively charged electrons drift towards the anode wires under the influence of the electric field. Anode wires with radii of 10–30 μm are used so that the electric field near the wires is large enough to cause the electrons to ionize the gas molecules further. This process causes an avalanche of electrons, and the number of electrons reaching the wire may be several thousand times the number produced in the initial ionization. This multiplication factor is independant of the original number of electrons and so the size of the pulse sensed by electronics connected to the anode wire is "proportional" to the energy of the incident photon. However, because of statistical variations in the initial ionization and avalanche, the response of a counter to X rays of a single energy is broadened, resulting in a finite energy resolution.

With a more complicated internal configuration and sophisticated electronics the location of the avalanche within the counter may be determined. By placing such a counter at the focus of an X-ray telescope it is therefore possible to obtain X-ray images. Unfortunately proportional counters are prone to many unwanted effects that may greatly degrade their performance. For this reason the choice of gas filling (usually based on an inert gas such as argon or xenon), and physical characteristics, are quite critical.

---

1. Turner, M.J.L. *et al. Space Sci. Rev.* **30,** 513 (1981).
2. Taylor, B.G. *et al. Space Sci. Rev.* **30,** 479 (1981).
3. Giacconi, R. *et al. Astrophys. J.* **230,** 540 (1979).
4. Aschenback, B. *et al. Space Sci. Rev.* **30,** 569 (1981).
5. Willmore, A.P. *et al. Space Sci. Rev.* **30,** 601 (1981).
6. Taylor, B.G. *et al. Proc. COSPAR Symp.*, Ottawa (1982).
7. Rapley, C.G. *et al. Rev. Sci. Instrum.* **48,** 1123 (1977).
8. Schnopper, H. *et al. Space Sci. Rev.* **30,** 607 (1981).
9. de Korte, P. *et al. Space Sci. Rev.* **30,** 495 (1981).
10. Huizenga, H. *et al. Rev. Sci. Insrum.* **52,** 673 (1981).
11. Zombeck, M.V. *Proc. COSPAR Symp.*, Ottawa (1982).
12. Gorenstein, P. *et al. IEEE Trans. nucl. Sci. NS-28*, No.1, 869 (1981).
13. Frazer, G.W. *et al. Nucl. Instrum. Meth.* **190,** 53 (1981).
14. Huizenga, H. thesis, Univ. Amsterdam (1980).
15. Peacock, A. *et al. Nucl. Instrum. Meth.* **169,** 613 (1980).
16. Andresen, R.D. *et al. Space Sci. Rev.* **30,** 243 (1981).
17. Peacock, A. *et al. Space Sci. Rev.* **30,** 525 (1981).
18. Andresen, R.D. *et al. Proc. COSPAR Symp.*, Ottawa (1982).
19. Inoue, H. *et al. Paper presented at 1981 INS int. Symp. on Nuclear Radiation Detectors*, Tokyo (1981).
20. Hoan, N. *Nucl. Instrum. Meth.* **154,** 597 (1978).
21. Davelaar, J. *et al. Space Sci. Rev.* **30,** 591 (1981).
22. Anger, H.O. *Rev. Sci. Instrum.* **29,** 27 (1958).
23. Anderson, D.F. *IEEE Trans. nucl. Sci. NS-28*, **1,** 842 (1981).
24. Ku, W.H.-M. & Hailey, C.J. *IEEE Trans. nucl. Sci. NS-28*, **1,** 830 (1981).
25. Hailey, C.J. *et al. Nucl. Instrum. Meth.* **184,** 543 (1981).
26. Taylor, B.G. *et al. Proc. COSPAR Symp.* Ottawa (1982).
27. Ku, W.H.-M. *et al. Proc. COSPAR Symp.* Ottawa (1982).
28. Anderson, D.F. *Phys. Lett.* (submitted).
29. Trümper, J. *et al. Ann. N.Y. Acad. Sci.* **302,** 538 (1977).
30. Barbareschi, L. *et al. Proc. COSPAR Symp.* Ottawa (1982).
31. Taylor, B.G. *et al. IEEE Trans. nucl. Sci. NS-28*, **1,** 861 (1981).
32. Sims, M.R. *et al. Nucl. Instrum. Meth.* (submitted).
33. Siegmund, O.H. *et al. Proc. COSPAR Symp.*, Ottawa (1982).
34. Timothy, J.G. & Lapson, L. *Appl. Opt.* **13,** 1417 (1974).
35. Kellogg, E. *et al. Rev. Sci. Instrum.* **47,** 282 (1976).
36. Timothy, J.G. *et al. IEEE Trans. nucl. Sci. NS-28*, **1,** 689 (1981).
37. Pounds, K.A. *SERC Bull.* **2,** 14 (1982).
38. Dardas, D. *et al. Rev. Sci. Instrum.* **49,** 1273 (1978).
39. Proctor, R. *et al. Nucl. Instrum. Meth.* (in the press).
40. Vallerga, J. *et al. IEEE Trans. nucl. Sci. NS-29*, (1982).
41. Debouzy, G. *Proc. COSPAR Symp.*, Ottawa (1982).

REVIEW ARTICLE

The inflationary Universe—birth, death and transfiguration

John D. Barrow
Astronomy Centre, University of Sussex, Brighton BN1 9QH, UK
Michael S. Turner
Astronomy and Astrophysics Center, University of Chicago, Chicago, Illinois 60637, USA

A number of exciting new experimental and theoretical developments have recently made a dramatic impact on the interdisciplinary study of cosmology and elementary particle physics. The Nuffield Foundation recently sponsored a 3-week workshop in Cambridge where theoreticians worked intensively on some of these problems. A brief review is given of the progress that was made as a result of the workshop, something of the background to the problems tackled, and the likely course of future developments.

FOR the past four years the Nuffield Foundation has sponsored a workshop devoted to related aspects of gravitation and particle physics. Last month's workshop, organized by Stephen Hawking and Gary Gibbons at Cambridge, focused on the theory of the very early Universe (events occurring during the first second of its expansion history). The spectrum of participants was international with five particle physicists and cosmologists from the Soviet Union and the remaining 25 from Europe and the United States. It transpired that the conference organizers could not have chosen a better topic for detailed collective scrutiny. During the past six months there have been a number of dramatic theoretical and experimental developments on the interface between particle physics and cosmology that threaten to revolutionize our thinking about the large-scale structure of the Universe and link together our studies of the very large and the very small more closely than ever before. Early this year Linde[1], in the Soviet Union, Albrecht and Steinhardt[2] in the United States and Hawking and Moss[3] in the UK proposed a model of the very early Universe (dubbed the 'new inflationary Universe') in which, through a phase transition soon after the big bang ($t \sim 10^{-35}$ s), a number of longstanding and outstanding cosmological problems seem to be simultaneously and naturally resolved. Then, last March, Cabrera of Stanford University, reported[4] experimental evidence consistent with the detection of a single magnetic monopole. If, and this has not yet been confirmed, he has indeed seen the magnetic monopole predicted to exist by new grand unified gauge theories[5] of elementary particle interactions at high energy (GUTs), then his result could provide a most dramatic and direct witness to the fact that the Universe was once at least as hot as 10^{27}K. Just to make things more interesting, it appears that Cabrera's monopole is inconsistent with the existence of the Galaxy's magnetic field; if these monopoles exist they should have discharged large-scale cosmic magnetic fields long ago[6–8]. In addition, monopoles would themselves provide microscopic 'laboratories' for the study of particle physics down at length scales $\sim 10^{-25}$ cm and a confirmation of the overall philosophy of grand unification. During the past year there has also emerged a growing interest in particle physics theories that not only unify the description of the three basic interactions (strong, weak and electromagnetic) but which are also supersymmetric (supersymmetry is a symmetry which relates the particles of integer spin (bosons) which do not obey the exclusion principle to those of half-integral spin (fermions) which do). The cosmological implications of such schemes are substantial but, so far, only partially explored. Almost all the work done and talks presented at the workshop involved aspects of one or more of these three exciting developments.

Symmetry breaking and unification

The study of the very early history of the Universe amalgamates two seemingly unrelated disciplines: cosmology and elementary particles. So far, gauge theories have been very successful in describing and predicting the behaviour of fundamental particle interactions: the strong (or colour) force controlling quarks is successfully described by an unbroken SU(3) symmetric gauge theory; the weak and electromagnetic forces are conjoined in an SU(2) × U(1) symmetric gauge theory (the Weinberg–Salam–Glashow model) which is spontaneously broken at an energy of about 10^3 GeV. The point of spontaneous symmetry breaking (SSB) is that although the laws of physics may be intrinsically symmetrical, that symmetry is not manifest below a certain temperature or energy level because the lowest energy state of the system (the vacuum, as it is called) is a particular solution of the equations that does not possess their symmetry. In spontaneously broken gauge theories the properties of the vacuum state are of vital importance and are described by the vacuum expectation value of a scalar field—the Higgs field[9]. The appearance of a non-zero vacuum expectation value signals SSB.

The mathematical elegance and experimental vindication of the SU(3) and SU(2) × U(1) models has led to their incorporation within proposals for the grand unification of the strong and electro-weak interactions. In such models a spontaneous breakdown of complete symmetry between the strength and properties of these three interactions occurs when the temperature falls to 10^{28} K, an energy of about 10^{15} GeV. Clearly, if we are going to check such ideas by experiment we need energies of $\sim 10^{15}$ GeV to probe the symmetric vacuum. Such energies are never likely to be attained by terrestrial accelerators; so far only energies up to 1,000 GeV have been attained. There are very few low-energy consequences of GUTs that we can test but there are two generic predictions which are both extraordinary and accessible to current technology. It is predicted that the proton will be unstable with a lifetime $\sim 10^{31\pm 2}$ yr and that stable, magnetic monopoles exist with a mass $\sim 10^{16}$ GeV (that is, about 10^{-8} g). At present about a dozen experiments are either operational or soon to be so and tuned to search for the characteristic proton decay events[10]. The Indian–Japanese collaboration, which is examining the stability of protons within about 140 tonnes of iron buried

0028-0836/82/340801—05$01.00

below the Earth's surface in the Kolar Gold Fields, has already reported six candidate events for proton decay[11,12] within the last two years, corresponding to a lifetime of about 10^{31} yr. Also, in the last month another claim to detect proton decay has been made by the CERN group experimenting inside Mt Blanc. They have detected a single candidate event.

The early Universe was not subject to the type of budgetary and technological limitations that we encounter today. According to the hot big bang model, temperatures corresponding to average particle energies as large as 10^{19} GeV should have been reached in the early Universe. So, it is clear that the early Universe provides an ideal 'theoretical laboratory' for the study of grand unification. By way of a corollary, grand unification can have remarkable consequences for the expansion and evolution of the Universe. Already, a key cosmological contribution has been made[13-19]: the same interactions that mediate proton decay today allow an initial universal state which is symmetric between matter and antimatter to evolve into one with an excess of matter which translates, after the antimatter annihilates, into one like our own that contains, on average, about 10^{10} photons for every nucleon of matter. Grand unified theories are able to explain both the origin of matter (rather than just radiation), the non-existence of antimatter in space, as well as the relative abundance of photons and nucleons—previously all unsolved puzzles.

Birth of the inflationary Universe

In 1981 Guth[20] proposed a new picture for the early stages of the hot big bang model which provided a 'natural' explanation for a collection of cosmological conundrums. The picture was christened the 'inflationary Universe'. Guth pointed out that if the Universe got 'caught' in the symmetric vacuum early on, when the temperature was below that at which the asymmetric vacuum was energetically more favourable (a lower energy state), then because of the large energy density associated with this state, the Universe would expand exponentially and 'supercool', erasing its previous history. (Such an exponential expansion was first discussed by de Sitter[21] for other, mathematical reasons.) When the transition to the asymmetric vacuum state does occur, an enormous 'latent' heat (the energy difference between the two vacuum states) is released, reheating the Universe so its subsequent evolution is that of the standard hot big bang model. As a result of this 'de Sitter' phase in its early evolution, the portion of the Universe that is observable today should be extremely uniform and expanding at a critical rate (that is, the ratio of the potential to the kinetic energy in the Universe, Ω, should be equal to 1). Without this de Sitter phase, in which the size of the Universe is greatly 'inflated' over what one would expect early on, the present uniformity of the Universe and the proximity of its expansion rate to the critical value remain a mystery. Our only 'explanation' would be to appeal to very special initial conditions which does not, of course, explain anything. Guth's inflationary Universe dispensed with the need for special initial conditions. Furthermore, it solved an embarrassing problem: the over-production of magnetic monopoles during the SSB phase transition of the GUT. In the earlier, more conventional models of the GUT phase transition so many monopoles were predicted to arise that they would contribute a density more than 10^{12} times larger than the maximum allowed by the observed deceleration of the Universe[22-23]. In the inflationary model, the period of accelerating expansion during the de Sitter phase dilutes the monopole density to a small and observationally permissible level. Unfortunately, as Guth and others realized, his original inflationary scenario possesses one fatal flaw: models in which the Universe gets trapped in the symmetric phase early on, end up with it caught there forever! If we are certain of nothing else, we can be sure that we do not live in a symmetric GUT vacuum—if we did then our protons would all decay in seconds.

Death and transfiguration

Six months ago Linde[1], Albrecht and Steinhardt[2] and Hawking and Moss[3] analysed a different class of GUTs (those which undergo SSB of a characteristic type first studied by Coleman and E. Weinberg[24]), and discovered that in these models the advantageous features of Guth's inflationary model could be retained whilst the difficulty of escaping from the symmetric vacuum of the de Sitter phase could be overcome. In their second generation model—the so-called 'new inflationary model'—the Universe never gets trapped in the symmetric vacuum state but instead simply takes a very long time to evolve from the symmetric to the asymmetric vacuum state, and while the Universe is evolving from the symmetric to the asymmetric state it expands exponentially due to the large energy density of the symmetric vacuum. In this new model the evolution to the true vacuum takes long enough for sufficient exponential expansion to occur to explain the uniformity, expansion rate and monopole-free composition of the present-day Universe.

Guth, Hawking, Linde, Moss and Steinhardt were all in attendance at the Nuffield Workshop and because of its potential explanatory power and topicality the 'new inflationary Universe' was the focal point of considerable critical scrutiny during the 3-week period. One exciting issue was actively investigated by four different research groups throughout the workshop (J. Bardeen, P. Steinhardt and M. Turner; A. Starobinskii; S. W. Hawking; A. Guth). They sought to calculate the form of the matter inhomogeneities that are spontaneously generated during the de Sitter phase and decide whether they explain the pattern of irregularity we see throughout the Universe today in the form of galaxies and clusters. In the new inflationary model the Universe emerges from the de Sitter phase too smooth to allow the subsequent development of objects like stars and galaxies. The four groups all considered the form of the density inhomogeneities that arise from spatial fluctuations in the scalar field that leads to the SSB of the GUT. Although by the second week of the workshop there was radical disagreement amongst the groups as to the magnitude of the final fluctuations—but complete agreement, both amongst themselves and with observation, as to the relative change in the magnitude from one length scale of the Universe to the next—by the end they were in agreement, and by very different methods had arrived at essentially the same result (testimony to the stimulating atmosphere of the programme). The result was bad news for the 'new inflationary Universe'—or at least for the simplest version studied so far: the resulting inhomogeneities were found to be far too big to lead to galaxies, rather everything would evolve to form superdense objects or black holes—not the type of Universe we live in. Linde[25] also reported that fluctuations in the scalar field might actually prevent the phase transition from occurring slowly enough to resolve the cosmological puzzles in the first place; again in the simplest model. The simplest model of new inflation was officially pronounced dead, just 6 months old.

However, the work done on this problem before and during the Cambridge meeting has been crucial. It has spelt out exactly what type of GUT is needed to have both a de Sitter phase and a resulting inhomogeneity spectrum in accord with present astronomical observations. By the end of the workshop Bardeen, Steinhardt and Turner had proposed a candidate supersymmetric model which satisfied these necessary criteria. At the moment, the basic idea of 'new inflation' still seems to possess attractive features. If an even 'newer' inflationary model can be constructed which is both a phenomenologically acceptable particle physics theory and without cosmological defect, then the marriage of GUTs and cosmology will have achieved a remarkable consummation. At a stroke a cluster of the most fundamental cosmological problems could be solved.

Lest anyone get carried away on the wave of euphoria surrounding inflation, the final summary talk of the workshop by Wilczek drew together several critical assessments that had been made earlier. The inflationary models 'predict' that today the density parameter Ω should be equal to unity to a very high degree of precision; certainly no measurements we can now make should be able to measure the difference from unity. But, as Rees and Efstathiou reminded the particle theorists, the best astronomical determinations of Ω all consistently suggest a much smaller value, less than 0.2. A possible way out of this conflict is if the Universe is dominated ($\Omega \sim 1$) by non-baryonic matter which coalesces only on very large scales so that the observations made to date would not have been sensitive to the presence of this matter. Candidates for the closure density of dark matter include massive neutrinos, or one of the zoo of new particles postulated in supersymmetric gauge theories. Earlier in the week, Sciama[50] had stressed the attractiveness of photinos (supersymmetric fermionic partners of the photon) for providing the closure density and dark matter in the galaxy.

In the inflationary models the only relic monopoles which are present in the Universe today should be those produced shortly after the de Sitter phase by particle collisions[26,51] and their abundance should be very small. This was one of the original virtues of the inflationary scenario. However, if Cabrera's observation of a monopole is correct and is representative of the typical flux in the Milky Way, then his observation appears to be in conflict with the inflationary model. Finally, Wilczek stressed that underlying the inflationary model is the value of the energy density associated with the vacuum. At present, particle physics calculations do not set the absolute scale of this energy density, only the difference in energy between the symmetric and asymmetric vacua. Our observations of the total mass density of the Universe show that, compared to this energy difference, the energy density of our asymmetric vacuum must be at least a factor 0 (10^{20}) smaller. If we define the energy density of the symmetric vacuum as the zero level then we can calculate the energy density of the asymmetric vacuum. Unfortunately, at present, we have no idea why the energy density of our vacuum should turn out to be so infinitesimal. An understanding of this 'fact' or a recasting of the problem ought to reveal a deep connection between particle physics and gravity—and that may even spring a few surprises of its own.

Monopoles

Ever since 1931, when Dirac[27] showed that the existence of magnetic monopoles requires the quantization of both electric and magnetic charge, physicists have continually searched for (and occassionally even claimed to have found) magnetic monopoles. The advent of GUTs has revived interest in monopole-hunting. These theories always predict the existence of magnetic monopoles with a mass close to the energy scale of grand unification[28,29]. Last March, Cabrera[4] reported experimental evidence consistent with the detection of a single monopole. He utilizes a SQUID to monitor the current in a superconducting loop surrounded by a superconducting magnetic shield which in turn enables him to detect magnetic charges. If a magnetic charge passes through the loop it induces a persistent current whose amplitude is proportional to the magnetic charge. Unfortunately, sources of noise and systematic error might also induce such flux jumps and only time will tell whether this event is a real monopole. Cabrera's event has the Dirac charge value and corresponds to a 'flux' (one event in 150 days) of about $10^{-9}\,\mathrm{cm}^{-2}\,\mathrm{sr}^{-1}\,\mathrm{s}^{-1}$. In his review of the 'monopole problem' at the workshop Preskill described several new types of experiment planned by Cabrera and others which will both increase the effective capture area of the detector and use independent cross-checks to eliminate many possible sources of systematic error. Within a year his 'observed flux' should be confirmed or disproved. Unfortunately, Cabrera's experiment (as well as all the other monopole searches planned or in operation) can give no indication of the monopole mass. To measure that, its path through a very strong magnetic field would have to be tracked very accurately as superheavy monopoles are not easily deflected from straight lines.

As mentioned above, if this measurement is really of a magnetic monopole, its implications for cosmology and particle physics are extremely significant. Astrophysically, Cabrera's flux contradicts everything we know about the magnetic field of the Galaxy. Monopoles should move along magnetic field lines in the Galaxy, thereby gaining kinetic energy at the expense of the magnetic field energy. A monopole flux in the Galaxy exceeding $\sim 10^{-15}\,\mathrm{cm}^{-2}\,\mathrm{sr}^{-1}\,\mathrm{s}^{-1}$ (the so-called Parker[6-8] limit) would rapidly dissipate the entire galactic field on a time scale shorter than that on which it can be regenerated. Our observation of an interstellar field of a few microgauss means that Cabrera's flux cannot be indicative of the average galactic flux of monopoles. However, we clearly occupy a special position in the Galaxy[30]—very close to a star, the Sun. Wilczek and Preskill discussed the possibility that the average galactic flux is close to, or less than $\sim 10^{-15}\,\mathrm{cm}^{-2}\,\mathrm{sr}^{-1}\,\mathrm{s}^{-1}$ but the Sun captures a cloud of monopoles by gravitational attraction leading to a flux in the solar neighbourhood that exceeds the average value in the Galaxy by a factor that can be as large as the required value $\sim 10^{6}$.

The GUT monopole is a remarkably interesting object. It has a size close to that of other elementary particles but an enormous mass (by microscopic standards), close to that of a bacterium. This means monopoles are not easily stopped and they pass through the Earth without significant energy loss. The monopole interior and outlying periphery has an onion-skin structure. Very close to its centre the vacuum is the GUT symmetric vacuum, a little farther out it is the $SU(2) \times U(1)$ symmetric vacuum. A single monopole thus provides a potential laboratory for studying grand unification and SSB.

The rich internal structure of a monopole also means that physics close by is likely to be extremely interesting. Callan[31], Rubakov[32] and Wilczek[33] have all pointed out that monopoles should catalyse proton decay, for example, via $M + p \rightarrow M + e^{+} + X$ where X = other particle debris. Callan and Rubakov argued that the cross-section for these exchanges should be large, comparable to a typical hadronic cross-section ($\sim m_{\pi}^{-2}$). At the workshop Ellis[34] discussed an interesting terrestrial consequence of this: terrestrial protons exposed to a Cabrera monopole flux should, on the average, decay with a lifetime of $\sim 10^{28}$ yr. The present experimental evidence on proton places a limit on the proton lifetime, $\geqslant 3 \times 10^{30}$ yr, which rules this out. Preskill and Wilczek also pointed out that if the Callan–Rubakov estimate is correct then neutron stars would present an even more serious problem[35,36]. Neutron stars are very effective at capturing monopoles because of their high densities and gravitational field strengths. Once captured by the neutron star, the monopoles would begin catalysing neutron decay and, unless the monopole flux were less than 10^{-8} of Parker's bound (and 10^{16} times smaller than Cabrera's flux) neutron stars would emit far more X-ray and UV radiation than is observed. This leads to an unfortunate conclusion: if the cross-section for this interesting process is large, then the flux of monoples must be undetectably small.

However, Preskill and Wilczek sharply disagree with the Callan–Rubakov estimates of the cross-section for monopole catalysis of proton decay. They presented convincing arguments that the cross-section should be a weak interaction cross-section, or something even smaller, and this means it is at least 10^{10} smaller than the estimates of Callan and Rubakov. The problem of computing this catalysis cross-section is a formidable mathematical task and its value must still be regarded as uncertain.

Monopoles are not the only esoteric structures that can emerge from the peculiar vacuum physics of GUTs. At the workshop Shafi and Vilenkin discussed the possibility that strings or walls of vacuum energy could be produced at phase transitions where SSB occurs and these structures could persist until the present[37-40]. (Strings, walls and monopoles are all topological structures associated with the direction in group space that the Higgs field responsible for SSB has in different regions of our physical space.) Unlike in the case of monopole production at the moment of SSB in GUTs there seems to be no problem in creating too many strings and walls. The possibility of wall structures appears to be ruled out by observation—the presence of one stretching across the observable Universe would create an anisotropy in the temperature distribution of the microwave background radiation much larger than is observed. Vilenkin argued that, by way of contrast, vacuum strings could have a very significant astrophysical role. A network of string-like structures might provide a natural explanation for the level of inhomogeneity necessary to create galaxies later on[52]. Also, the oscillation of strings that close upon themselves to form isolated loops could give rise to an observable flux of gravitational radiation. However, this conclusion seems to rest on an axiom of faith that the strings would dissipate their energy into gravitational waves rather than photons which would leave no trace if they were produced early enough in the history of the Universe. Finally, to give some feel for what a string is like, a vacuum string arising from the era of GUT would have a thickness of the order of the Compton wavelength of the Higgs scalars involved in the SSB ($\sim 10^{-27}$ cm) and a calculable mass per unit length such that a piece of vacuum string stretching 15 thousand million light years across the observable Universe would have a mass roughly equal to that of 10 million galaxies.

Supersymmetry

One of the most important unsolved problems of modern particle physics is the gauge heirarchy problem—the difficulty of constructing a theory that explains why SSB takes place on such widely separated energy scales, 10^3 GeV and 10^{15} GeV. One possible resolution which has been the focus of growing attention[41–44] is super-symmetric grand unification (SUSY). Supersymmetry requires the existence of a bosonic partner of identical mass for every known fermion and vice versa. As no such supersymmetric partners of the known quarks and leptons exist (they would have been seen), supersymmetry, like some of the gauge symmetries, must be a broken symmetry. Supersymmetry has its own intrinsic appeal for other reasons[26]: it is the only way to unify the description of particles with different spin statistics, and it is the only way to unify internal symmetries (that is, those associated with the gauge symmetries of particle physics) with the space-time symmetries of general relativity (and hence is a very good candidate for unifying gravity with the strong and electro-weak interactions). However, there appear to be a number of substantial cosmological hurdles in the path of supersymmetric GUTs. Ellis, Lazarides and Nanopoulos each discussed some of these difficulties and possible ways of overcoming them. In particular it seems to be difficult to arrange things so that our asymmetric vacuum is the lowest vacuum energy state, and even if this can be achieved, it is hard to guarantee that the Universe evolves into the asymmetric vacuum rather than the cul-de-sac of the symmetric state where it remains stuck forever. Furthermore, it is difficult to construct a grand unified SUSY model which generates the observed matter–antimatter asymmetry and specific entropy of the Universe because it is harder to get baryon non-conserving interactions out of equilibrium than in conventional GUTs. At present it is premature to accept or reject such models and SUSY remains an attractive idea for resolving the heirarchy problem and a possible pathway to a theory of quantum gravity since gravity can be incorporated when the supersymmetry is made a local rather than a global (as in SUSY GUTs) symmetry.

Gravitation

General relativity is a gauge theory although not a quantum theory but it has long been realized that quantum corrections to the classical equations of Einstein must arise at energies exceeding about 10^{19} GeV, or, in the cosmological problem at times, $t \lesssim 10^{-43}$ s. These energies exceed even those required for grand unification and as yet there has appeared no way of testing theories of quantum gravity by experiment. A full-blooded quantum theory of the gravitational field, including therefore the space–time geometry, is not yet on offer. A more modest programme is being undertaken to determine how quantum fields behave in a classical gravitational field[45,46] and progress in this area was reviewed in Cambridge by Hartle and Hu. As yet there is no 'standard' model in this work. To illustrate this, consider the problem of how quantum effects determine the evolution of the Universe before 10^{-43} s. In some models the singularity of infinite density at zero time remains, whilst in other, equally likely variants, it is removed and the Universe bounces; the pre-bounce state also admits a variety of possibilities and it is still premature to try and draw definite conclusions as to the first instants of the big bang.

Two topics of interest to quantum gravity pundits were presented at the workshop: the first, by Starobinskii[47], who showed how an inflationary phase of de Sitter expansion may have occurred at the Planck time, 10^{-43} s, rather than later at the time of grand unification. Of particular interest is the possibility that such an event might leave an observable imprint on the gravitational wave background in the Universe which we could one day detect. The other contribution by Novikov described how, close to the Planck epoch, the propagation of sound waves in the Universe may be described by a wave equation that is not conformally invariant. These sound waves can be amplified by interacting with the curvature potential created by the expansion of the Universe and give rise to a characteristic spectrum of irregularities today[48,49].

The fundamental cosmological puzzles—the expansion rate of the Universe, its isotropy, homogeneity, irregularity spectrum and specific entropy—all involve the very special *initial* conditions we seem to require at 10^{-43} s. It may be that these puzzles will be explained by events occurring at the Planck epoch rather than through inflation at the time of grand unification, and that a resolution of our quandaries must await the much sought synthesis of relativity and quantum field theories. What we have investigated so far is by no means the end but hopefully it is the beginning of a true story with a happy ending.

The consensus among the participants was that they had attended a significant and productive scientific gathering in which real scientific progress was made during its extent. The organizers and sponsors were largely responsible for this; without their efforts it would not have been possible for all the protagonists in the early Universe debate to meet and exchange ideas. The simplest 'new inflationary' Universe appears to be defunct; however, perhaps reports of its death 'have been greatly exaggerated' and a newer version will emerge to fulfil the criteria for success that were drawn up at the workshop. Important experimental and theoretical issues regarding the existence and behaviour of magnetic monopoles have emerged. Supersymmetric grand unification has been subject to significant scrutiny and has been pushed near the brink of viability. Many of these exciting developments have emerged only during the last year and no one has any doubt that this trend is going to continue for some considerable time.

We thank all the participants in the Nuffield Workshop for conversations and the Nuffield Foundation for support.

1. Linde, A. D. *Phys. Lett.* **108B**, 389–395 (1982).
2. Albrecht, A. & Steinhardt, P. J. *Phys. Rev. Lett.* **48,** 1220–1224 (1982).
3. Hawking, S. W. & Moss, I. G. *Phys. Lett.* **110B**, 35–38 (1982).
[illegible] Cabrera, B. *Phys. Rev. Lett.* **48,** 1378–1382 (1982).
5. Langacker, P. *Phys. Rep.* **72C**, 185–385 (1981).
6. Parker, E. N. *Astrophys. J.* **160,** 383–404 (1970).
7. Bludman, S. A. & Ruderman, M. A. *Phys. Rev. Lett.* **36,** 840–843 (1976).
8. Lazarides, G., Shafi, Q. & Walsh, T. F. *Phys. Lett.* **100B**, 21–24 (1981).
9. Abers, E. S. & Lee, B. *Phys. Rep.* **9C**, 1–141 (1973).
10. Weinberg, S. *Scient. Am.* **244**(6), 64–75 (1981).
11. Krishnaswamy, M. R. *et al. Phys. Lett.* **106B**, 339–346 (1981).
12. Goldhaber, M. & Sulak, L. R. *Comm. Nucl. Part. Phys.* **10,** 215–227 (1981).
13. Sakharov, A. D. *Soviet Phys. JETP Lett.* **5,** 24–27 (1967).
14. Yoshimura, M. *Phys. Rev. Lett.* **41,** 281–284 (1978).

15 Ignatiev, A. Y., Krasinokov, N., Kuzmin, V. & Tavkhelidze, A. *Phys. Lett.* **76**B,436–440 (1978).
16. Dimopoulos, S. & Susskind, L. *Phys. Rev.* D**18,** 4500–4509 (1978).
17. Toussaint, D., Treiman, S. B., Wilczek, F. & Zee, A. *Phys. Rev.* D**19,** 1036–1045 (1979).
18. Weinberg, S. *Phys. Rev. Lett.* **42,** 850 (1979).
19. Ellis, J., Gaillard, M. K. & Nanopoulos, D. V. *Phys. Lett.* **80**B, 360–364 (1978).
20. Guth, A. H. *Phys. Rev.* D**23,** 347–356 (1981).
21. de Sitter, W. *Mon. Not. Roy. astr. Soc.* **78,** 3–28 (1917).
22. Preskill, J. P. *Phys. Rev. Lett.* **43,** 1365–1368 (1979).
23. Zeldovich, Ya. B. & Khlopov, M. Yu. *Phys. Lett.* **79**B, 239–241 (1979).
24. Coleman, S. & Weinberg, E. *Phys. Rev.* D**7,** 1888–1910 (1973).
25. Linde, A. D. *Lebedev Phys. Inst. Preprint* (1982).
26. Turner, M. S. *Phys. Lett.* (in the press).
27. Dirac, P. A. M. *Proc. R. Soc.* A**133,** 160–172 (1931).
28. Polyakov, A. *Soviet Phys. JETP Lett.* **20,** 194–195 (1974).
29. t'Hooft, G. *Nucl. Phys.* **79**B, 276–284 (1974).
30. Dimopoulos, S., Glashow, S. L., Purcell, E. M. & Wilczek, F. *Nature* **298,** 824–825 (1982).
31. Callan, C. G. *Princeton Univ. Preprint* (1982).
32. Rubakov, V. S. *Soviet Phys. JETP Lett.* **33,** 644–646 (1981); *USSR Acad. Sci. Inst. Nucl. Res. Preprints* P-0204, P-0211 (1981).
33. Wilczek, F. *Phys. Rev. Lett.* **48,** 1146–1150 (1982).
34. Ellis, J., Nanopoulos, D. V. & Olive, K. A. *CERN Preprint* TH-3323 (1982).
35. Kolb, E. W., Colgate, S. A. & Harvey, J. A. *Phys. Rev. Lett.* (in the press).
36. Dimopoulos, S., Preskill, J. P. & Wilczek, F. (in preparation).
37. Kibble, T. W. B. *J. Phys.* **9**A, 1387–1398 (1976).
38. Zeldovich, Ya. B. *Mon. Not. R. astr. Soc.* **192,** 663–667 (1980).
39. Vilenkin, A. *Phys. Rev.* D**24,** 2082–2089 (1981).
40. Kibble, T. W. B., Lazarides, G. & Shafi, Q. *Phys. Lett.* **113**B, 237–239 (1982).
41. Dimopoulos, S. & Raby, S. *Nucl. Phys.* **192**B, 353–368 (1981).
42. Witten, E. *Nucl. Phys.* **188**B, 513–554 (1981).
43. Dine, M., Fishler, W. & Srednicki, M. *Nucl. Phys.* **189**B, 575–593 (1981).
44. Fayet, P. & Ferrara, S. *Phys. Rep.* **32**C, 249–334 (1977).
45. Birrell, N. & Davies, P. C. W. *Quantum Fields in Curved Space* (Cambridge University Press, 1982).
46. Isham, C., Penrose, R. & Sciama, D. W. *Quantum Gravity 2* (Oxford University Press, 1981).
47. Starobinskii, A. A. *Phys. Lett.* **91**B, 99–102 (1980).
48. Kompanyeets, D. A. & Lukash, V. N. *Soviet Astr.* **25,** 272–274 (1981).
49. Mukhanov, V. F. & Chibisov, G. V. *Soviet Phys. JETP Lett.* **33,** 532–535 (1981).
50. Sciama, D. W. *Phys. Lett.* **114**B, 19–22 (1982).
51. Preskill, J. P. *Harvard University Preprint* (1982).
52. Barrow, J. D. & Silk, J. *Astrophys. J.* **250,** 432–449 (1981).

ARTICLES

Phase transitions and dynamics of the Universe

Vahé Petrosian

Institute for Plasma Research and Department of Applied Physics, Stanford University, Stanford, California 94305, USA

The restoration of symmetry at grand unification in a closed contracting Robertson–Walker universe could slow down and halt the contraction, causing the universe to bounce and avoid the singular state or the big crunch. During subsequent expansion the symmetry is broken and the universe reverts back to its present (normal) state. A scenario is presented whereby the present entropy of the substance (resulting in $\sim 10^{90}$ photons) is created through a series of such bounces along with three possible initial states. The monopole, horizon and flatness difficulties faced in ordinary big bang models are also solved by the model presented.

DESPITE astronomical discoveries during the past half century, the basic and simple nineteenth century questions, such as age and size of the Universe, remain essentially unanswered. The open and flat models of the Robertson–Walker metric are unsatisfactory because of the need to extrapolate the local observations to infinity. The closed and finite (and therefore more appealing) model suffers from the fact that it will eventually collapse into a singular state. Although introduction of a positive and constant cosmological term will solve the collapse problem, there still remains (for all big bang models) the difficulty of dealing with the singular initial state which took place in a finite past. There is always the hope that quantum gravity will solve this problem around the Planck era (energies $\sim 10^{19}$ GeV). In this article, recent developments in microphysics are used to propose a possible scenario for the bounce of a collapsing closed universe occurring at the grand unification era (energies $\sim 10^{15}$ GeV) before it reaches the Planck era.

One of the intriguing results from the unification at high energies of various forces of nature is that as the expanding universe (or any system in thermal equilibrium) cools below some critical temperature the symmetry is spontaneously broken, the universe undergoes a first-order phase transition which induces a change in the vacuum energy density[1]. Without considering the details of the microphysics, most of which is still open to speculation, I take a phenomenological approach and investigate the modification of the dynamics of a Robertson–Walker universe due to a transition from a higher (or false) to lower (or true) vacuum state and vice versa.

Outline of the problem

It is well known[2,3] that a non-zero vacuum energy density E_v corresponds to a non-zero value of the cosmological constant $\Lambda = 8\pi G E_v/c^2$, whose effects on the dynamics of the universe can be taken into account by redefinition of energy density and pressure as $E = E_s + E_v$, $P = P_s + P_v = P_s - E_v$, where E_s and P_s are the energy density and pressure of substance (matter and radiation[4,5]). As proposed by Einstein, the cosmological term, or E_v, cannot be diverged. Variation in this term can be generated by a scalar field[6]. The possibility of a phase transition allows variation in the value of Λ or E_v. Then the conservation equations must be generalized to allow for the conversion of vacuum energy density into energy density of substance and vice versa[7]: $a(\mathrm{d}E_s + \mathrm{d}E_v) = -3(E_s + P_s)\mathrm{d}a$. Here a is the expansion parameter. We are interested in the early phase of the universe where E_s is dominated by radiation and relativistic pairs in thermal equilibrium. Then $P_s = E_s/3$ and $E_s = (1+g)E_r$ where g (which can vary across a phase transition) is the contribution of fermion and boson pairs, and $E_r \propto T^4$ is the energy density of radiation at temperature T.

In what follows, modified Planck units $8\pi G/3 = \hbar = c = 1$ are used. Normally $S^{4/3}E_s$ is a constant and in thermal equilibrium, $S = (1+g)^{3/4}0.15N_r$ (N_r is the total number of photons in the closed universe of volume $2\pi^2 a^3$), which is proportional to the total number of free particles in the universe, is also a constant or varies due to the changes in g. During a phase transition, however, because of presence of the $\mathrm{d}E_v$ term in the above conservation equation, this is no longer true and the differential equations governing the expansion parameter can be written as (overdot stands for derivative with respect to time t)

$$\begin{aligned}(\dot{a}a)^2 &= E_v a^4 - a^2 + S^{4/3} \\ \ddot{a}a^3 &= E_v a^4 - S^{4/3}\end{aligned} \qquad (1a)$$

from which (or from the conservation equations directly) we obtain a modified form for the conservation laws.

$$\mathrm{d}S^{4/3}/\mathrm{d}t = -a^4\dot{E}_v \qquad (1b)$$

0028-0836/82/340805—04$01.00

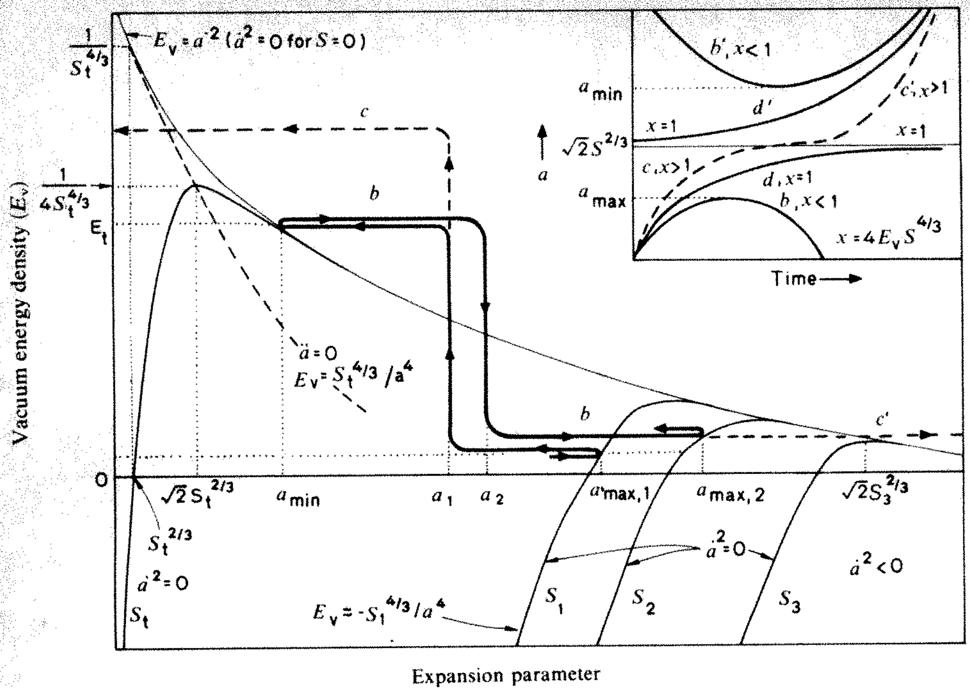

Fig. 1 Schematic variation of vacuum energy density with the expansion parameter for a radiation-dominated universe. Above the thin dashed line marked $\ddot a = 0$ expansion is accelerated. Thin solid lines represent $\dot a^2 = 0$. For higher values of S these curves shift to the right and decrease in amplitude. For each S the region below this line ($\dot a^2 < 0$) is forbidden. The heavy solid and dashed lines show various paths of evolution with phase transitions at a_1 during the contraction and at a_2 during the expansion. The letters b, b', c, c' refer to the type of models described in the inset, where $x = 1$ corresponds to the Einstein static model.

Conventional models

Let us first review briefly the relevant aspects of the usual closed models[8] with $\dot E_v = 0$. Figure 1 shows curves of E_v against a for $\ddot a = 0$ (thin dashed lines) and $\dot a = 0$ (thin solid lines) at various values of S. The schematic variation of the expansion parameter a with time is shown in the inset of Fig. 1 for $x = 4S^{4/3}E_v > 1$ (models c, c'), $0 < x < 1$ (models b, b') and $x < 1$ (models d, d' and the Einstein static model). Of particular interest are the models with $0 < x < 1$ where the universe has either a maximum or a minimum size:

$$\begin{aligned} a_{\max} &= (2E_v)^{-1}[1-(1-x)^{1/2}] \\ a_{\min} &= (2E_v)^{-1}[1+(1-x)^{1/2}] \end{aligned} \tag{2}$$

For a constant E_v (therefore a constant S) the expansion or contraction of the universe follows a horizontal path until it reaches an $\dot a = 0$ curve (for the appropriate value of S) after which it reverses its motion contracting to a singularity or expanding to infinity (see models b and b' in the inset to Fig. 1). For large values of $E_v (x > 1)$ $\dot a$ never becomes zero and expansion continues forever.

Models with variable cosmological terms

If $\dot E_v \neq 0$, then the evolution of the universe will not be constrained along a horizontal line and at different stages will be limited by the $\dot a = 0$ curves of different values of S. It is therefore clear that arbitrary variation of E_v (and the corresponding variation in S) could result in a complicated evolution of the universe. Here we examine the simple variation of E_v from a small value to a large value comparable with the energy density of substance at the time of the variation.

Let us assume that the universe is closed, $S = S_1$, and that the vacuum energy density $E_v = E_1 < (4S_1)^{-4/3}$ ($\sim 10^{-120}$ for our present universe[5,9]). The universe then will evolve as in model b (see inset to Fig. 1), expanding to a maximum size, $a_{\max}$, after which it begins to collapse, as shown by the heavy line directed to the left in Fig. 1. (Our present universe is matter dominated; therefore, it will reach a maximum value if $E_1 < M^{-2} \sim 10^{-122}$ where $M = 2\pi^2 a^3 \rho$ is the total mass of the non-relativistic particles in the universe. However, when it collapses to a size smaller than its present size by a factor of -10^3, it will become a radiation dominated universe and revert back to our idealized model. Note that the present observational limits on E_0 do not rule out ever-expanding models such as model c'.) As the universe collapses it will follow an E_v = constant track of a radiation dominated universe and the temperature will rise as

$$T = 1.11/(1+g)^{1/4} S^{1/3}/a \tag{3}$$

until it reaches the critical temperature T_0 of the phase transition above which the vacuum energy density will increase by $E_0 \sim T_0^4$ ($\sim 10^{-20}$ for grand unification phase transition = GUT). After the phase transition is completed the vacuum energy density is $E_v = E_t = E_1 + E_0$ and, according to equation (1b), the number of photons and pairs changes to S_t given by

$$S_t^{4/3} - S_1^{4/3} = -\int_{E_1}^{E_t} a^4 \, \mathrm{d}E_v \approx -a_1^4 E_0 \tag{4}$$

The last equality will be valid if the transition occurs at a_1 instantaneously, or on a time scale short compared with the Hubble time at that epoch which is about $E_v^{-1/2}$ ($\sim 10^{-10}$ for GUT). Otherwise, a_1^4 can be taken to be an average value of a^4 during the transition period. The fate of the universe after the transition depends on the value of S_t and E_t. Note that right after the transition the universe is still contracting

$$\dot a = -(E_t a^2 - 1 + S_t^{4/3}/a^2)^{1/2}, \qquad \ddot a = aE_t - S_t^{4/3}/a^3 > 0 \tag{5}$$

Initially the first terms in these equations are dominant and the contraction will be exponential; $a \propto \exp(-E_t t)$. However, as a decreases the other terms (due to curvature and substance) in these expressions become more important. Whether the universe will bounce or continue to contract will depend on which of these two terms in the expression for $\dot a$ becomes important first. If S_t is large, so that $x_t = 4S_t^{4/3}E_t > 1$, then the radiation term ($S_t^{4/3}/a^4$) will become important before the curvature term ($1/a^2$) and the universe will contract to a singularity as shown by the heavy dashed line (c) in Fig. 1. On the other hand, if S_t is small so that $x_t < 1$, then the curvature term becomes dominant first, and the universe will reach the minimum value of the expansion parameter given in equation (2) and then will expand with acceleration as in model b' of the inset and as shown by the heavy solid line directed to the right in Fig. 1. During this adiabatic contraction and expansion phase S_t remains constant and the energy density of the substance increases but never exceeds E_t. The evolution during the expansion phase may follow an inflationary scenario similar to Guth's and others[10–12] where the symmetry breaking is delayed, the universe supercools, but finally it undergoes the phase transition releasing the vacuum energy density which heats the universe back up to a temperature of the order of T_0. However, in the model proposed here the expansion does not begin with a high entropy state but instead is dominated by the curvature and vacuum energy density similar to the scenario proposed by Bludmann[13].

Suppose this transition occurs at $a = a_2$, then the final value of S is given by

$$S_2^{4/3} = S_t^{4/3} + a_2^4 E_0 = S_1^{4/3} + (a_2^4 - a_1^4)E_0 \qquad (6)$$

After the phase transition is completed the universe evolves as a radiation-dominated universe ($E_v = E_1 \ll E_s$, see model b in Fig. 1) and if $4E_1 S_2^{4/3} < 1$ it reaches a maximum expansion with $a_{\max,2} = S_2^{2/3}$. This cycle is then repeated if $4E_1 S_2^{4/3} < 1$ and $4E_t S_t^{4/3} < 1$. These results are summarized in Fig. 2 where we plot schematic variations of a, E_v, $S^{4/3}$ and the three terms in the expression for $(\dot{a}/a)^2$ versus time for a bounce.

Note that there may be more than one spontaneous symmetry breaking and corresponding numbers of phase transitions, so that S_1 and S_2 are not necessarily the final numbers of photons in the universe. Furthermore, the bounce would occur only for grand unification (or for a higher temperature) phase transition when the net baryon to photon number ratio $N_B/N_r \ll 1$. Otherwise, between t_1 and t_2 the universe never becomes curvature dominated and the net baryon term, N_B/a^3 (which, of course, cannot be eliminated during any phase transitions occurring at temperatures less than the grand unification temperature), remains more important than the curvature term, $1/a^2$. If N_B is not zero, then it can be shown that a bounce becomes possible if both $S_t < E_0^{-3/4}(\sim 10^{15}$ for GUT) and $N_B < E_0^{-1/2}/m_B(\sim 10^9$ for GUT). Here $m_B \sim 10^{-19}$ is the rest mass of the baryons. Similarly, our scenario requires that near the bounce the curvature term must also dominate terms due to anisotropies[14] or other sources.

Finally, if the process of symmetry restoration and breaking is not reversible, the two transitions may occur at different values of the expansion parameter. In particular, if $a_2 > a_1$, then $S_2 > S_1$ and entropy is generated during a bounce. This suggests that the 10^{90} photons we observe today may have been produced through many successive bounces of the universe (see Fig. 3). After each bounce the number of photons increases as $S_{i+1}^{4/3} = S_i^{4/3} + E_0(a_{2,i}^4 - a_{1,i}^4)$, and the $\dot{a}^2 = 0$ curve in Fig. 1 moves to the right and decreases in amplitude. If the residual vacuum energy density $E_{v,i+1}$ is not zero, eventually as S increases, one may reach the condition $S_i > (4E_{v,i})^{-3/4}$ which will give rise to an ever-expanding Lemaitre type model as shown by model c' and by the heavy dashed line directed to the right in Fig. 1. However, note that as the symmetry is restored before each bounce, there must be a fine tuning of the exact epoch of the transition a_1 so that S_t, the equivalent number of photons and pairs during the transition period, is not too large; $S_t^{4/3} < 1/(4E_0)$. Otherwise, as discussed above, a bounce will not occur.

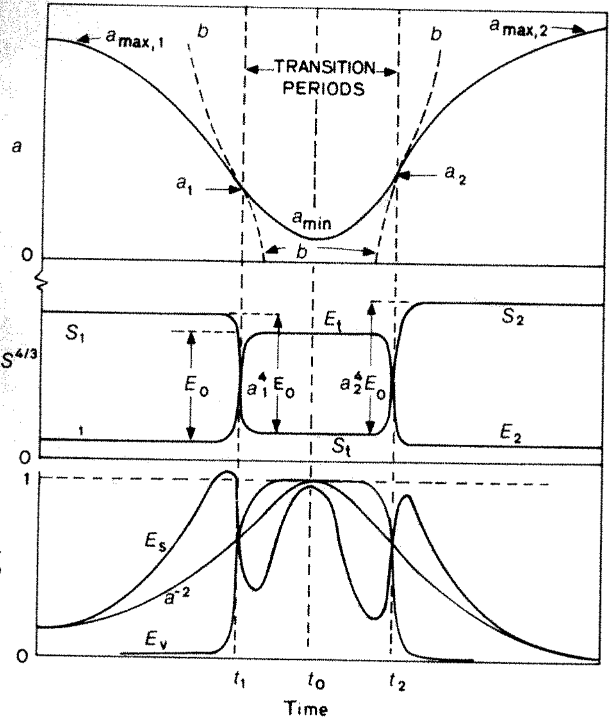

Fig. 2 Schematic variation with time of the expansion parameter (a), vacuum energy density (E_v), photon number (S), substance energy density (E_s), and the curvature term (a^{-2}), during a bounce. At t_1 and t_2 models b and b' (shown in Fig. 1) with two different values of S and with $a_{\min} < a_{\max}$ are joined smoothly. The minimum value of E_s at t_1 depends on the rate of the transition. The slower this rate the smaller the depth of the minimum. The minimum near t_2 depends on the degree of supercooling. Note that at $a_{\max}$, $E_s \approx a^{-2}$ and at $a_{\min}$, $E_v \approx a^{-2}$.

Discussion

Whether the above scenario will work in our Universe depends on the validity of the many assumptions involved. I now comment on these assumptions.

(1) The existence of the bounce requires an extremely small value for the total substance energy of the universe (more exactly the quantity $S_t^{4/3} = E_s a^4$) during the transition phase. We need $S_t < E_0^{-3/4}(\sim 10^{15}$ for GUT) as compared with $S_1 \sim 10^{90}$ for our Universe. This requires that, at the transition, E_s is very nearly equal to E_0 and that the transition occurs quickly so that the $P\mathrm{d}V$ work done by gravity during the transition is negligible. Such an extreme draining of energy from the substance clearly indicates that the two phases are not in thermal equilibrium or pressure balance. If equilibrium were maintained (say through a slow transition), then the substance energy would remain dominant (A. Guth, personal communication) and the entropy would be conserved, which, as shown by Sher[15], precludes any possibility of bounce.

(2) We have also assumed that the total energy density and pressure of the universe can be separated into two constituent parts, one for the radiation with $P_s = 1/3E_s$ and one for vacuum with $P_v = -E_v$. This clearly is true during times sufficiently far removed from the transition. Such a separation is also possible during the transition since, in general, given the total energy density E and pressure P with an arbitrary equation of state, we can always define $E_s = 3P_s = 3(E+P)/4$ and $E_v = -P_v = (E-3P)/4$, so that $E = E_s + E_v$ and $P = P_s + P_v$. However, the important requirement of the bounce is that during the transition E_v must increase monotonically from its initial value E_1 to the final value $E_1 + E_0$. If this variation is not monotonic, that is, if during some part of the transition $\dot{E}_v < 0$, then, according to equation (4), S_t will not be as small as required and it may even exceed S_1. Whether $\dot{E}_v$ remains positive throughout the transition depends on the details of the microphysics which determine the equation of state $P = P(E)$. We have shown that for the most commonly used (see, for example refs 1, 15) effective potential (or free energy) forms the vacuum part of the equation of state does, in fact, increase slowly and monotonically up to the temperature where the non-zero minimum of the potential disappears. As the temperature exceeds this value, the transition will probably occur very quickly. This will raise the vacuum energy density to its final value and, as demanded by energy conservation, will drain the substance of its energy.

Such a transition will destroy the thermal equilibrium of the substance and the normal relationship between entropy and energy density will no longer be valid. Thus, a decrease in the energy density E_s does not necessarily mean a decrease in entropy. The details of the variation of E_v and E_s and entropy will be discussed elsewhere.

(3) The most attractive feature of this scenario is that it allows for creation of substance through repeated bounces. This energy comes from the vacuum which, because of the nature of its equation state ($P_v = -E_v$), can be the source for creation of an unlimited amount of energy as the universe expands: $\mathrm{d}E = P_v\,\mathrm{d}V > 0$. However, our scenario cannot be extended to very small values of a number of particles. It will work as long as S·

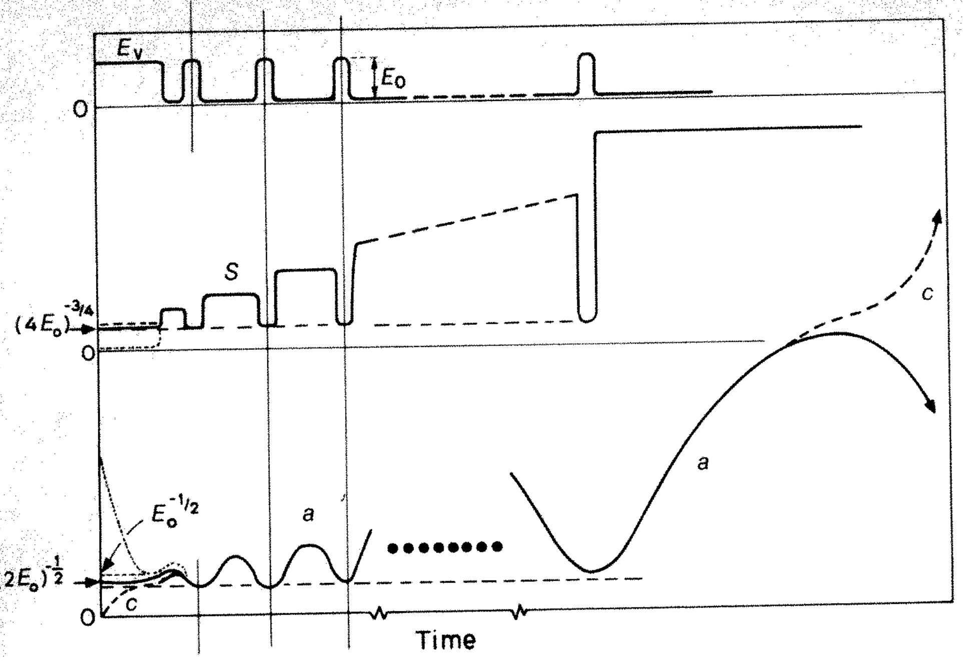

Fig. 3 Schematic variation of vacuum energy density (E_v), photon number (S) and expansion parameter (a) with time for repeated bounces. The oscillations stop if during the normal phase $4S_0^{4/3}E_0 < 1$); solid line for $x_0 = 1$ also Fig. 1.) Three possible initial conditions are shown. Dotted line is for initial $S_0 = 0$ (or $x_0 = 4S_0^{4/3}E_0 < 1$); solid line for $x_0 = 1$ has a static Einstein beginning; and the dashed line marked c (see also Fig. 1), with $x_0 > 1$, starts from a Planck era and undergoes a Lemaitre phase before the first phase transition.

in the symmetry broken (that is, normal) phase exceeds $(4E_0)^{-3/4}$ ($\sim 10^{15}$ for GUT). If S is less than this value, then $a_{\max} \sim S^{2/3}$ becomes less than $a_{\min} \sim E_0^{-1/2}$, indicating the breakdown of our analysis.

(4) There are various possible ways out of this dilemma with regard to the initial conditions. The universe may have started as a closed, vacuum-dominated deSitter universe, contracting from infinity to $a_{\min} = E_0^{-1/2}$ and then expanding with $a = +(E_0 a^2 - 1)^{1/2}$, as shown by the dotted lines in Fig. 3. If at $a = a_0$ the vacuum breaks down[1], then substance energy, with $S^{4/3} = E_0 a_0^4 > E_0^{-1}$ will be created. The expansion will continue at a new rate, $a = +(E_0 a_0^4/a^2 - 1)^{1/2}$, reaching a maximum expansion $a_{\max} = a_0^2/a_{\min}$. After this our previous scenario applies, the universe contracts, undergoes the usual symmetry restoring transition, rebounds at a new $a_{\min} > E_0^{-1/2}$, breaks the symmetry at a_2 and emerges with a higher value of S and so on. Another possibility is that the universe starts with $E_v = E_0$ and with some finite initial S_0. If $S_0 < (4E_0)^{-3/4}$, then the universe starts as described above with $a_{\min} < (E_0)^{-1/2}$ [or as an Einstein static universe with $a_{\min} = (2E_0)^{-1/2}$ if $S_0 = (4E_0)^{-3/4}$, solid line beginning in Fig. 3]. The result here will not be much different from that of the deSitter beginning described above. However, if $S_0 > (4E_0)^{-3/4}$ then the universe must begin from a Planck stage and undergo the first phase transition after it has cooled down below T_0 (dashed line marked c in Fig. 3).

Therefore, if the vacuum does not spontaneously break down to create $S_0 > E_0^{-3/4}$ pairs at once, then we must postulate a universe starting not only with $E_v = E_0$ but also containing $S_0 > (4E_0)^{-3/4}$ photons and pairs. We can relax this assumption if there exist other phase transitions at higher temperatures, with higher values of E_0 and, therefore, requiring lower values of S_0. In particular, phase transition near the Planck era ($E_0 = 1$ and $S_0 = 1$) will allow the universe to start with very little substance and create most of it through successive bounces.

(5) Finally let us consider the so-called monopole, horizon and flatness difficulties[16,17]. If the supercooling is extreme, the expected density of monopole would be acceptable as in Guth's[10] inflationary scenario. Furthermore, according to our scenario during the inflationary phase ($t_0 < t_2$) there are only S_1($\sim 10^{15}$ for GUT) photons and particles in the whole universe. Thus some of the restrictions imposed on the conventional models by the monopole problem will be alleviated. For example, if one bubble is nucleated per particle, then the total number of monopoles in the present universe would be $< 10^{15}$ and therefore insignificant.

It can also be shown that during the transition phase of each bounce ($t_1 < t < t_2$) signals moving with speed of light can circumnavigate the whole universe eliminating the horizon problem. The flatness problem is no longer a difficulty because during both reversals of each cycle the curvature term is important. During the in-between intervals ($t < t_1$ or $t > t_2$) the time duration for near flatness becomes longer and longer as the entropy increases through repeated bounces.

(6) A bounce will occur if the symmetry restoration process induces an increase in the vacuum energy density and a corresponding decrease in the energy of substance. These changes do not have to be equal to those expected from the reverse transition. However, if the two processes are not nearly symmetric, the occurrence of repeated bounces could not take place as simply as described here and the fine tuning process needed for continuation of the bounces would break down. This would cause the universe to expand indefinitely (or collapse and reach temperatures above the critical temperature T_0 of the phase transition) prematurely; that is before it has built up 10^{90} photons (and 10^{80} baryons). Such a model will not resemble our Universe and can be disregarded by appeal to the anthropic principle[18].

I thank Drs Lawrence Caroff and Robert Wagoner for critical readings of this manuscript and for valuable comments, also Drs Alan Guth, Marc Sher, Gary Steigman, Leonard Susskind and Michael Turner for interesting discussions. This work was supported in part by NASA–Ames Research Center grant NCA2-OR745-008.

Received 4 January; accepted 9 July 1982.

1. Linde, A. D. *Rep. Prog. Phys.* **42,** 390 (1979).
2. Lemaitre, G. E. in *Albert Einstein, Philosopher-Scientist* (ed. Schlepp, P. A.) 39 (Cambridge University Press, London, 1949).
3. Eddington, A. *Sci. Prog.* **34,** 225 (1939).
4. Zeldoric, Ya. B. *Soviet Phys. Usp.* **11** (1968).
5. Petrosian, V. in *Confrontation of Cosmological Theories with Observational Data* (ed. Longair, M. S.) 173 (Reidel, Dordrecht, 1974).
6. Wagoner, R. V. *Phys. Rev.* (1969).
7. Kazanos, D. *Astrophys. J. Lett.* **241,** L59 (1980).
8. Petrosian, V. & Salpeter, E. E. *Astrophys. J.* **151,** 411 (1968).
9. Gunn, J. E. & Tinsley, B. M. *Nature* **257** (1975).
10. Guth, A. *Phys. Rev.* D**23,** 347 (1981).
11. Linde, A. D. *Phys. Lett.* **108B**, 389 (1982).
12. Albrecht, A., Steinhardt, P. J., Turner, M. S. & Wilczeck, F. Preprint no. 82.09 (Enrico Fermi Institute, 1982).
13. Bludmann, S. *Pap. at Workshop at Institute for Theoretical Physics*, Santa Barbara (1981).
14. Barrow, J. D. & Turner, M. S. *Nature* **298,** 801–805 (1982).
15. Sher, M. A. *Phys. Rev.* D**22,** 2989 (1980).
16. Preskill, J. P. *Phys. Rev. Lett.* **43,** 1365 (1979).
17. Turner, M. S. *Proc. 2nd Workshop on Grand Unification*, Ann Arbor (1981).
18. Carter, B. *IAU Symp.* No. 63, 291 (1974).

Trace elements in orogenic lherzolites reveal the complex history of the upper mantle

Michel Loubet & Claude J. Allègre

Laboratoire de Géochimie-Cosmochimie, Institut de Physique du Globe et Département des Sciences de la Terre,
Université Pierre et Marie Curie, 4 Place Jussieu, 75230 Paris Cedex 05, France

Major and trace elements of several lherzolite-type bodies—at Lherz–Freychinède (French Pyrénées), Beni-Bouchera (Morocco), Lanzo (Italian Alps)—have been investigated. Quantitative model analysis of the element distributions shows that these bodies have undergone a rather complex series of events including successive partial meltings and subsequent differentiation of the melts produced. These events are related to the geodynamic evolution of these bodies within the upper mantle, and thus illustrate the multi-stage history of mantle material.

THE orogenic lherzolite type massifs[1], also called high-temperature peridotites[2] are thought to represent pieces of upper mantle material which were mechanically emplaced into the continental crust through large tectonic movements[3–5]. These massifs typically outcrop along major fault systems within chains where interactions between oceanic and crustal materials have occurred (for example, the Insubric line for the Alps massifs such as Lanzo and Baldissero and the North Pyrenean fault for the Pyrenean massifs such as Lherz and Freychinède).

These massifs are therefore unique and highly interesting because they occur as large bodies relative to the size of xenoliths embedded in highly reactive magmas, and are therefore exposed to possible contamination by their surroundings. Oxygen isotope studies show that the orogenic lherzolite type massifs are fresh representative samples of the upper mantle[6] and their analysis should provide important information on the composition, the structure and the evolution of the Earth's upper mantle.

Petrological and geochemical structure of the massifs

Many petrological and geochemical studies have already been performed on these massifs and, in particular, on Mt Albert (Canada)[7], Lizard (England)[8], Beni-Bouchera (Morocco)[9,10], Ronda (Spain)[10,11], Lherz (France)[12], Lanzo (Italian Alps)[13,14] and various Alps[15] massifs. Geochemical analyses were carried out at the Lizard (England)[16,17], Lherz and various Alps[18–24],

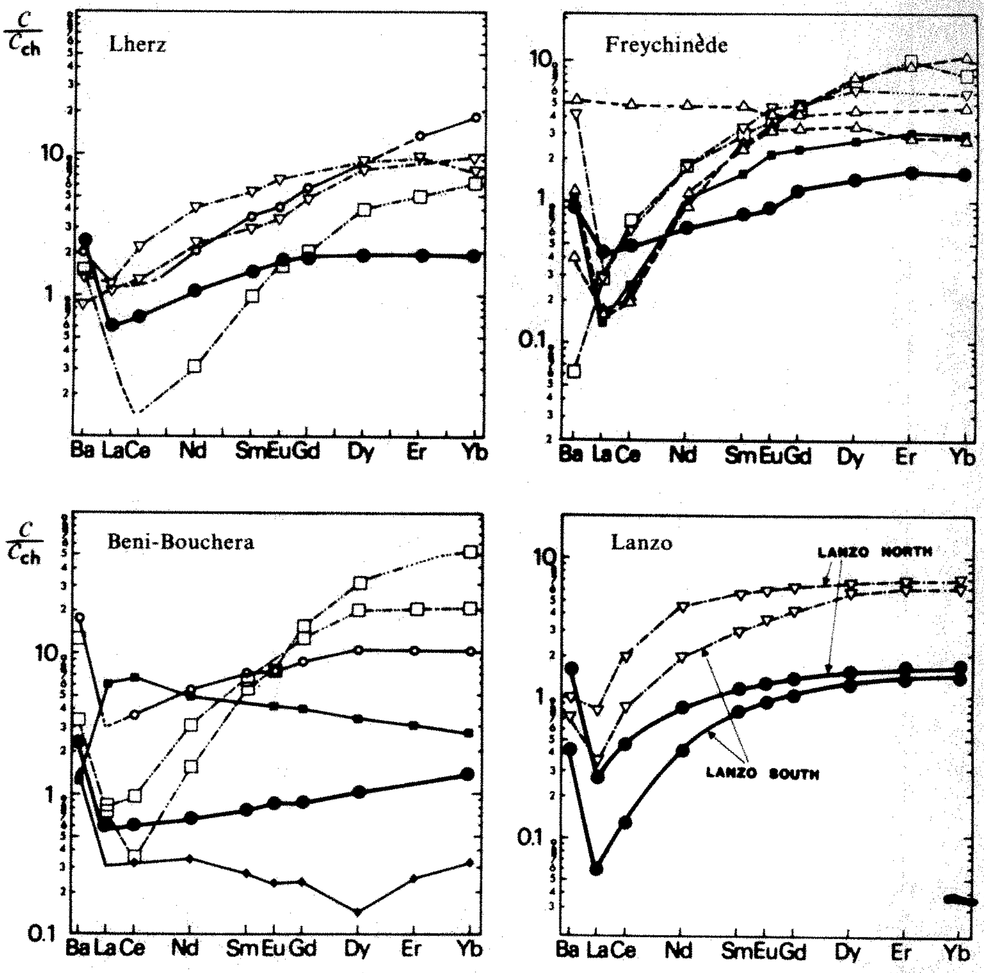

Fig. 1 Chondritic normalized representation of the REE + Ba content of some pyroxenite layers from the orogenic lherzolite bodies studied. Some 'common' lherzolites from these bodies have been plotted for reference. ●, Massive lherzolites; ■, olivine websterites; ◆, enstatites; ○, complex layer; △--△, garnet websterites; ▽-·-▽, garnet free websterites; □, garnet clinopyroxenites.

0028–0836/82/340809—06$01.00

Beni-Bouchera (Morocco)[23-26], Ronda (Spain)[27,28], Liguria (Italy)[29] bodies.

We have studied in detail the following lherzolite type orogenic bodies: Lherz and Freychinède, French Pyrénées (see ref. 12 for petrographic descriptions); Beni-Bouchera, Morocco (see refs 9, 10 for petrographic descriptions); Lanzo, Italian Alps (see refs 13, 14 for petrographic and structural descriptions). In other massifs from the Alps—Locana, Rivara, Baldissero and Alpe Arami[15]—only the lherzolites were looked for. We report here our results from the trace-element viewpoint and also present our main data. Detailed studies will be published elsewhere.

Orogenic lherzolite-type massifs are mainly formed of apparently rather homogeneous lherzolite which constitutes around 90–95% of the whole bodies. The remaining part is formed by mafic layers of various sizes apparently more or less parallel to one another. These layers are chemically basaltic but mineralogically variable, their modal composition extending from that of olivine websterite to that of garnet clinopyroxenite (pyroxenite layers). In some of the massifs late amphibole-bearing-type or gabbroic-type dykes cut across the mafic layers. Our data, presented in Tables 1 and 2 with details on the experimental procedure, include major element, rare-earth elements (REE) and transition element contents. The REE data

Table 1 Rare-earth element data from various peridotite bodies

	Ba	La	Ce	Nd	Sm	Eu	Gd	Dy	Er	Yb	Lu
Beni-Bouchera											
Peridotites											
M5-102	1.03	0.20	0.61	0.59	0.236	0.0985	0.386	0.537	0.342	0.337	
BB5	0.40	0.145	0.52	0.65	0.257	0.110	0.423	0.584	0.383	0.40	
M6–128	8.64	0.17	0.48	0.382	0.14	0.062	0.218	0.313		0.27	
Pyroxenites											
M6–79	45.5	0.22	0.29	1.24	1.03	0.55	3.89	9.41		10.0	
M7–58	63.3		2.90	3.20	1.31	0.534	2.23	3.20	1.89	1.93	
M5–367	12.1	0.24	0.75	1.78	1.26	0.641	3.35	6.09	3.78	3.99	
M7–701	1.11		0.30	0.35	0.12	0.056	0.178	0.21	0.148	0.16	0.03
M7–703	10.0	1.1	3.8	3.76	1.63	0.704	2.53	4.65		2.98	
M7–702	13.3	0.75	2.6	3.52	1.49	0.64	2.61	3.87	2.41		
M5–103	4.5	1.85	5.23	3.20		0.30	1.05	1.05	0.54	0.50	0.052
M6–78	5.2		0.25	0.20	0.050	0.016	0.061	0.43	0.45	0.60	0.12
Alps											
Peridotites											
Lanzo											
L705b	1.49	0.018	0.103	0.271	0.144	0.0656	0.271	0.398	0.270	0.29	
775	1.03	0.067	0.36	0.537	0.225	0.0954	0.375	0.492	0.309	0.327	
C50	0.323	0.0506	0.029	0.271	0.131	0.057	0.269	0.355	0.224	0.258	
Other Alps massifs											
Locana: L4	4.25	0.12	0.464	0.461	0.172	0.074	0.272	0.383	0.242	0.248	
Rivara: R1	1.72	0.027	0.124	0.278	0.144	0.067	0.326	0.407	0.263	0.285	
Baldissero: Ba	0.364	0.028	0.101	0.165	0.105	0.0484	0.216	0.345	0.240	0.266	
Alpe Arami: AA	1.02	0.167	0.623	0.563	0.230	0.100	0.433	0.698	0.460	0.484	
Pyroxenites											
Lanzo body											
779–b	3.6	0.24	1.66	2.61	0.96	0.38	1.53	2.03	1.23	1.26	
741–b	2.56	0.092	0.66	1.15	0.58	0.26	0.11	1.70	1.05		
Gabbro dykes and associated peridotites											
Lanzo											
751–3	20.8	0.48	0.90	0.51	0.124	0.246	0.17	0.17		0.0073	
C–55	5.52	0.46	0.87	0.62	0.17	0.236	0.24	0.284		0.13	
L684–d	12.7			1.66	0.82	0.58	1.41	1.77	1.02	0.87	
751–1G	7.3		0.03	0.014	0.0032	0.0097					
751–2G	0.61	0.028	0.093	0.112	0.052	0.024	0.090	0.122	0.073	0.082	
Freychinède–Lherz											
Freychinède peridotites											
71–335	3.3	0.12	0.376	0.40	0.15	0.0654	0.32	0.424	0.30	0.30	
Lherz peridotites											
70–367	8.6	0.16	0.54	0.66	0.265	0.11	0.48	0.55		0.34	
LZM1		0.16	0.50	0.483	0.322	0.116	0.39	0.483		0.322	
71–325	0.79	0.013	0.036	0.039	0.011	0.0049	0.019	0.020		0.011	
Freychinède pyroxenites											
74–57	17.7		4.03	2.8	0.98	0.30	1.35	1.37		0.9	
72–50	1.44	0.051	0.16	0.56	0.465	0.24	1.22	2.33	1.68	1.95	
70–357	4.29	0.045	0.168	0.64	0.45	0.234	1.22	2.33	1.68	1.95	
72–211	3.76	0.04	0.21	0.61	0.286	0.15	0.604	0.83	0.58	0.53	
72–49	14.7	0.084	0.51	1.00	0.60	0.33	1.21	1.84		1.05	
72–224	0.22	0.089	0.55	1.6	0.56	0.274	1.24	2.29	1.72	1.52	
Lherz pyroxenites											
70–379	7.2			1.22	0.66	0.30	1.05		2.47	3.4	0.55
70–291	5.6			0.18	0.180	0.117	0.51	1.23	0.91	1.14	
72–445	3.12	0.33	1.01	1.30	0.55	0.25	1.23	2.30		1.86	
69–356W	51.3	0.35	1.76	2.77	1.10	0.46		2.72	1.69	1.42	
69–356	8.3			0.84	0.33	0.136	0.524	0.71	0.45	0.47	0.075
73–78W	3.62	9.8	11.1	4.6	0.754	0.294	0.77	0.92	0.55	0.61	
[illegible]3–78	1.88	0.716	2.04	0.954	0.157	0.0636	0.179	0.200	0.140	0.152	
Minerals											
70–148 diopside	1.27	0.22	0.26	0.42	0.29	0.16	0.53	0.44		0.10	
70–367 diopside	501	0.88	2.66	3.35	1.38	0.56	2.21	3.10		2.14	

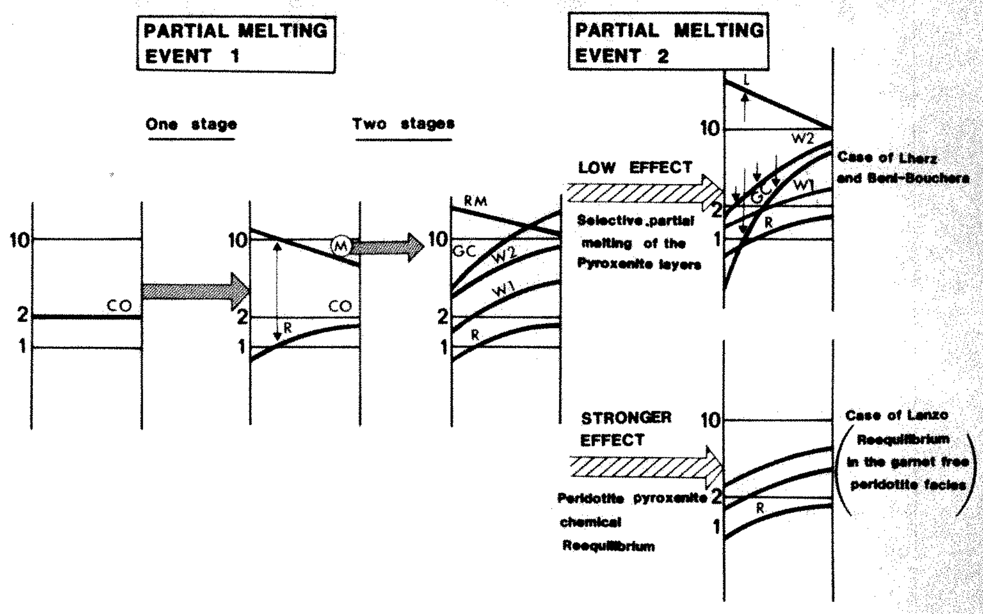
PARTIAL MELTING EVENT 1
One stage
Two stages
10
2
1
CO
R
M
RM
GC
W2
W1
PARTIAL MELTING EVENT 2
L
LOW EFFECT
Selective partial melting of the Pyroxenite layers
Case of Lherz and Beni-Bouchera
STRONGER EFFECT
Peridotite pyroxenite chemical Reequilibrium
Case of Lanzo
Reequilibrium in the garnet free peridotite facies

Fig. 2 Summary of the REE content evolution which, according to our analysis, has affected the various products found in the lherzolite-type bodies—in particular, the pyroxenite layers—during the various episodes of their history. The REE patterns are represented by the classical chondrite normalized diagram. Step 1: the pyroxenite layers are created through partial melting of a peridotitic upper mantle (CO), either undepleted (as in this figure) or depleted. This partial melting yields (one stage) residual peridotites (R) and melts (M) which can differentiate (two stages) through fractional crystallization into different cumulate types: websterites (types W_2 or W_1) or garnet pyroxenites (GC) and residual melts (RM). Step 2: a more recent partial melting event affects these pyroxenite layers. The effect of this last event may be rather small, affecting the pyroxenite layers only selectively—(thus we explain the Lherz–Freychinède and Beni-Bouchera features) or stronger and, then, affecting also the peridotites. In the latter case, a general reequilibration of the pyroxenite layers with the peridotites will occur (the Lanzo features are thus explained).

are shown in Fig. 1 according to the classical chondritic normalized diagram.

For data analysis we will consider in turn the common lherzolites, the pyroxenite layers and the late dykes. We have used quantitative models based on the concept of partition coefficient and on the formulation of partial melting and fractional crystallization processes for trace elements. For each case experimental data are compared with the results of computed models.

Lherzolites

Although apparently homogeneous, those peridotites that constitute the major part of the bodies exhibit significant variations in composition which can even exist in a single massif within several hundreds of metres of each other.

Major elements—some correlations are observed between CaO, Al_2O_3, Na_2O and TiO_2 as well as between MgO, NiO, Cr_2O_3 contents and the MgO/FeO ratio[9,10,18].

Trace elements—the distribution observed can be summarized as follows[20–27]: as far as we know, the elements characterized by high partition coefficients (highly compatible elements (Ni, Co and to a lesser extent Cr)) have a remarkably homogeneous content. Elements with intermediate partition coefficients such as Yb and Ti have content variations which do correlate with the CaO variations. Large variations are observed for the incompatible trace elements. In particular, the REE patterns of the lherzolites show remarkably similar characteristics. They are all light REE depeleted, the light REE contents varying within a rather wide range and the heavy REE contents in a rather narrow one[18–20]. Early results confirmed the preliminary study by Haskin *et al.*[30] and Frey[16,17] and were later supported by further data[27–29].

In agreement with Frey[16], we interpreted[18] these characteristics as those of a residual material which originated through partial melting of a rather homogeneous primitive peridotitic mantle. This primitive upper mantle may have been characterized by a REE chondrite normalized pattern parallel to the chondritic line of reference but with about double the chondritic value[18]. The most important conclusions reached from the quantitative models developed[18,19,26,27,28] are that the residual peridotites resulting from partial melting of an originally homogeneous lherzolitic upper mantle display a wide range of variations in light REE contents and a relatively small range of variations for the heavy REE—a feature effectively observed in the orogenic lherzolites.

The degree of partial melting which gave rise to these residual peridotites can be estimated from REE analysis to vary between 1 and 5% (ref. 18). The state of equilibrium of these peridotites during their partial melting is unclear due to uncertainty over the REE partition coefficients for clinopyroxene. This residual character also explains the small variation of Ni, Co, Cr and the covariation of CaO, Al_2O_3, Na_2O, TiO_2. Nd and Sr isotopic data corroborate the residual nature of this peridotitic upper mantle material[22–24]. Their Nd isotopic composition moves along the same Nd–Sr anticorrelation line as the one characteristic of the oceanic basalts, especially in the zone corresponding to high Nd isotopic values[24]. At the same time Nd isotopic data exclude alteration as a possible process for light REE depletion of these peridotites—as proposed elsewhere[29].

Thus, major elements, trace elements and isotope data agree with the idea that orogenic lherzolites are residues after extraction of a small amount of basaltic melt. This interpretation is supported by most authors who have studied these massifs[24,25,27–29], and agrees with the general idea, based on oceanic basalt trace elements[31–33] and isotope analysis[34–36], that the 'oceanic' upper mantle should be residual (extraction of small basaltic amount). At the same time this agreement suggests that the orogenic lherzolite massifs could effectively represent oceanic upper mantle material.

Pyroxenite layers

The chemical composition of these layers as a whole is basaltic. Thus, one could think of these layers as representing the peridotite complement, that is the part which was extracted during the partial melting of these rocks. However, the detailed mineralogical and chemical analysis of these layers implies that the process cannot be so simple. In particular it looks as though some differentiation processes should have occurred, as indicated by the symmetrical structure displayed by some complex pyroxenite layers formed by the superposition of several sublayers[9–12]. The models proposed for the origin of these layers should thus take this complexity into account.

REE contents of the pyroxenite layers

The REE patterns of the large set of pyroxenite layers is illustrated in Fig. 1 through the classical chondrite normalized representation. For the various lherzolite type bodies we studied, the main characteristics of these patterns are:

(1) In general the pyroxenite layers look more REE-enriched

Table 2 Major and transition elements in various peridotite bodies

	Beni-Bouchera					Freychinède					
	Peridotites		Pyroxenites			Peridotite	Pyroxenites				
	BB5	M5–102	M5–367	M6–79	M7–58	71–335	72–211	72–50	72–49	70–357	74–57
Major elements											
SiO_2	41.82	42.73	43.10	44.67	44.29	43.29	43.00	47.55	46.11	46.65	54.40
Al_2O_3	3.50	3.29	14.76	112.42	10.61	2.65	5.37	9.75	11.40	12.06	13.77
Fe_2O_3	9.06	9.19	17.35	13.96	10.65	9.16	11.20	8.51	8.24	8.18	8.39
MgO	37.99	38.90	11.20	13.87	17.50	40.32	0.12	0.18		0.18	
MnO					0.19	0.13	33.41	21.47	23.60	18.48	19.26
CaO	3.02	3.00	10.66	11.56	11.85	2.63	4.25	10.49	8.95	12.49	11.90
Na_2O				1.24	0.96	0.24	0.08	0.82	0.66	0.52	0.67
K_2O	0.014	0.015	0.02	0.02	0.026	0.018	0.018	0.013	0.03	0.009	0.01
TiO_2	0.14	0.14	1.01	0.50	0.55	0.14	0.232	0.32	0.46	0.405	0.38
P_2O_5	0.01	0.02	0.05	0.04	0.037	0.016	0.008	0.018	0.05	0.024	0.03
P at 110 °C	0.20	0.09		0.11	0.20	0.08	0.12	0.05	0.09	0.05	0.07
P at 1,050 °C	3.87	1.68		0.84	2.03	0.95	1.03	0.07	0.74	0.05	0.14
Total						99.498	98.383	99.241		99.098	
Transition elements											
Ti	840	840	6,060	3,000	3,300	634	1,392	1,920	2,760	2,430	2,280
V	42		381		305	58	92	252	162	232	205
Cr	1,340		600		1,120	2,210	1,940	1,370	2,200	1.080	875
Mn					1,470	1,000	930	1,390		1,390	
Fe					74,490	64,570	78.340	59.520		57.210	
Co	103		90		105	115	115	86	53	85	66
Ni	1,940		1,550		1,480	2,820	2,450	1,720	1,550	2,240	600
Cu	41		7		506	25	61	66	68	74	90
Zn	85		129		68	64	60	50	56	34	36

	Lherz						
	Pyroxenites					Amphibole-bearing dykes	
	71–325	73–78	70–379	70–291	72–445	68–110	70–242
Major elements							
SiO_2	41.44	41.94	44.88	45.95	44.54	42.67	40.12
Al_2O_3	0.65	2.07	12.33	12.92	12.04	12.71	13.36
Fe_2O_3	8.71	8.66	8.39	7.91	6.35	12.13	10.37
MgO	0.12	0.12	0.21	0.18	24.85	14.29	14.42
MnO	44.99	40.78	20.96	16.30	24.85	14.29	14.42
CaO	0.39	1.72	10.74	14.80	9.11	10.97	10.36
Na_2O	0.02	0.15	0.40	0.66	0.58	1.71	2.75
K_2O	0.014	0.015	0.022	0.013	0.01	0.56	1.40
TiO_2	0.015	0.058	0.194	0.100	0.29	2.74	5.06
P_2O_5	0.004	0.019	0.029	0.022	0.05	0.07	0.07
P at 110 °C	0.15	0.33	0.05	0.069	0.19	0.21	0.16
P at 1,050 °C	2.69	3.03	0.55	0.25	2.34	1.24	1.75
Total	99.193	98.892	98.665	99.073			
Transition elements							
Ti	90	348	1,164	600	1,740	16,440	30,360
V	25	50	350	257	189	540	198
Cr	1,940	2,580	1,460	1,720	2,420		
Mn	930	930	1,630	1,390			
Fe	60.920	60.570	58.680	54.620			
Co	115	113	80	95	113	158	25
Ni	2,840	2,880	2,250	2,700	1,600	1,500	500
Cu	10	25	49	6	45	142	24
Zn	58	64	52	46	87	128	32

	Lanzo								
	Peridotites					Pyroxenites		Peridotites associated with the gabbro dykes	
	RI	Ba	AA	705B	775	779b	741b	751–1G	751–2G
Major elements									
SiO_2	41.68	42.92	41.90	42.82	42.31	48.29	48.61	36.89	42.68
Al_2O_3	2.66	2.71	3.40	2.64	3.05	7.17	6.39	0.69	1.63
Fe_2O_3	8.68	9.73	9.48	9.11	9.01	6.37	6.40	10.29	9.26
MgO	38.42	41.34	39.62	40.42	38.80	0.12	0.12	0.12	0.12
MnO	0.13	0.13	0.14	0.12	0.12	26.27	24.80	46.76	41.20
CaO	2.90	2.64	3.21	2.84	3.02	8.87	11.46	0.14	2.32
Na_2O	2.90	2.64	3.21	0.03	0.20	0.58	0.58	0.010	0.016
K_2O	0.014	0.015	0.052	0.015	0.015	0.012	0.015	0.019	0.044
TiO_2	0.095	0.08	0.109	0.10	0.13	0.49	0.27	0.009	0.011
P_2O_5	0.012	0.012	0.017	0.008	0.015	0.020	0.025	0.23	0.08
P at 110 °C	0.27	0.04	0.11	0.12	0.13	0.16	0.12	4.33	1.31
P at 1,050 °C	3.91	0.38	1.07	0.31	2.37	0.69	0.68	99.538	98.861
Total	98.87	99.26	99.23	98.533	99.17	99.042	99.510	114	264
Transition elements									
Ti	570	480	654	600	780	2,940	1,620	114	264
V	55	58	55	58	58	140	145	21	52
Cr	2,440	2,480	2,930	2,820	2,680	3,280	3,030	3,680	3,920
Mn	1,000	1,000	1,080	930	930	930	930	930	930
Fe	60,710	68,050	66,300	63,718	63,020	44,550	44,760	71,970	64,770
Co	125	122	120	150	125	120	100	132	140
Ni	1,900	2,240	2,180	2,220	2,180	1,140	1,400	2,600	2,260
Cu	26	28	28	30	76	26	125	12	39
Zn	70	66	68	76	70	70	50	88	70

Major elements were analysed by X-ray fluorescence, transition elements by atomic absorption, rare earths by isotope dilution mass spectrometry with an accuracy of better than 2.5%. The experimental techniques have been described elsewhere[20].

than common peridotites. In particular the heavy REE content of some pyroxenite layers appears very high, for example, that of garnet clinopyroxenite layers (M5-367, M6-79 complex layers).

(2) They display a large variety of REE patterns characterized by a wide range of light REE fractionations relative to the heavy REE, some being light-REE enriched (74–57 in Freychinède, M5-103 in Beni-Bouchera), others light-REE depeleted.

(3) The light REE depleted pyroxenites are the most common with a tendency to be more light-REE depleted relative to the heavy REE than are the common lherzolites.

(4) No distinct Eu anomaly is observed in these patterns (with the exception of the websterite 73-78W from Lherz).

Quantitative models for estimating the REE contents that should represent the products resulting from partial melting of a lherzolitic upper mantle have been developed. The basic hypothesis is that the primitive upper mantle affected has a homogeneous and uniform composition.

In the single stage model we try to compute the composition of the various types of melts that are generated through a single partial melting. More complex models are needed to describe the composition of the various cumulates which may crystallize from these melts and the corresponding residual liquids after an evolution to these melts through fractional crystallization (two stage process). The most important conclusions of this quantitative modelling are: (1) the melts produced have a large diversity in their REE patterns, characterized by a wide range of fractionation of the light REE relative to the heavy REE. Taking into account the fractionated type partial melting process, these melts may indeed be light REE enriched or depleted relative to the heavy REE; (2) the cumulates which crystallize from these melts thus exhibit, as well as the melts, a wide range of REE patterns also characterized by a large variety of fractionations of the light REE relative to the heavy REE. This diversity in the REE patterns will be accentuated in the cumulates, given the variety of mineralogical assemblages which may crystallize; for example, the crystallization of garnet in the cumulates will yield a strong enrichment of such cumulates in heavy REE.

The large diversity of the REE patterns displayed by the pyroxenite layers conforms with what would be expected for products derived through partial melting of a peridotitic upper mantle, according to the models developed. However, we cannot decide from these REE data, whether most of the layers are cumulates or melts, because of the large range of contents these two types of products can display in such a model. To solve this problem, the use of elements with high partition coefficients appears adequate. Cumulates and melts should have very different properties for this kind of element.

Trace elements with high partition coefficients

Large variations are found in the literature for the partition coefficients of this kind of element so that the models obtained may be rather imprecise. A correct estimate may, however, be realized in a special case, that is for the cumulates supposed to correspond to the first per cent of crystallization of the primary melts. The phases of these first cumulates should have the same trace-element content as the phases of the common peridotites. So, taking values for peridotite phases from the literature, we estimated the content of several types of cumulates presenting different modal compositions, all supposed to have crystallized during the first per cent of crystallization of primary melts. This gives us some kind of upper limit for the content of the cumulates[26].

The pyroxenite layers seem to contain a rather large amount of such elements (Ni, Co, Cr), compared with our estimates. This convinces us that most of the pyroxenite layers should be cumulates representatives. Possible exceptions to this rule include some complex layers, the contents of which are close to melt estimates[26].

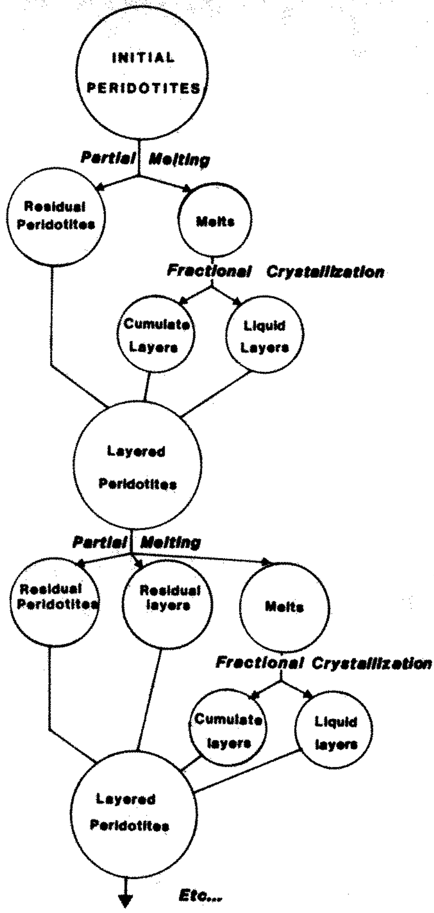

Fig. 3 Deduced model of evolution of the lherzolite type bodies. These peridotite bodies have been the object of successive melting events, each one producing melts possibly mobile and which differentiate through fractional crystallization. These derived products yield the pyroxenite layers. A later partial melting of this layered peridotite affects the various materials with variable intensities. Other types of products and layers will be generated through this new partial melting event.

Evidence for remelting

However, several observations suggest that most of the pyroxenite layers do not present primary structures and have been modified through a further process. More precisely we suspect that these pyroxenite layers have been affected after their formation by a further selective late partial melting event[19–22].

The main points supporting this hypothesis are first, in several bodies the rocks which have the lowest content of highly incompatible elements are the garnet clinopyroxenite layers. Such are the garnet clinopyroxenites 70-291 from Lherz, and M6-79 from Beni-Bouchera which have the lowest light REE content, even lower than the common lherzolites from these bodies. Such a low light REE content is surprising in these clinopyroxene-rich rocks which represent the latest stage of differentiation of the melts yielding the pyroxenite layers.

Second, in some peridotite bodies a peculiar evolution is observed[37]: a depletion in the content of the highly incompatible trace elements characterized by low partition coefficients when going from the slightly differentiated to the highly differentiated layers (from the olivine websterites to the garnet clinopyroxenites).

Third, some of the lherzolite type bodies that we studied effectively bear the mark of such a late partial melting event in the form of late dykes cutting the websteritic layering—in particular the amphibole bearing dykes—as in Lherz and Freychinède (French Pyrénées). The geochemical analysis of these dykes shows[20,37] that they may effectively represent products derived from the melts resulting from partial melting of these pyroxenite layers.

Sr isotope studies performed on these same rocks support this interpretation of a complex history of these layers[23] and were the basis for the Rb–Sr systematics given by Polve and Allègre[23].

The occurrence of such a late partial melting event has a direct consequence. As the primary trace element distribution of the pyroxenite layers has changed, a precise interpretation of the characteristics of the melts at the origin of these layers becomes difficult.

In the framework of our model for the origin of the pyroxenite layers from melts resulting from partial melting of the peridotitic mantle we would have liked to define precisely the nature of these melts. In Fig. 2, we retrace in the chondrite normalized representation, the various steps which according to our interpretation explain the actual REE content of these layers. They correspond to the different partial melting events suffered by these bodies.

Late dykes

In the Lherz massif late amphibole-bearing dykes do exist which cut across the pyroxenite layering[38]. The REE patterns of these dykes are characteristic—all being enriched in light REE relative to the heavy REE. From their trace-element distributions we interpret these dykes as representative of cumulates crystallized from melts highly enriched and fractionated in light REE relative to the heavy REE. We have already supported the idea that these melts may have been issued from the partial melting of the pyroxenite layers[20–37].

In the Lanzo body, the REE patterns displayed by the gabbroic-type dykes is characteristic of plagioclase bearing cumulates. In this massif there are some indications that the last partial melting event at the origin of these dykes also affected the peridotites[13,14].

Conclusions

The analysis of these orogenic lherzolites yields strong evidence that several magmatic events affected these bodies. One was at the origin of the formation of the pyroxenite layers. The last one affected the pyroxenite layers in a selective way in some massifs (Lherz and Freychinède–Beni-Bouchera) but also reached the peridotites in others (Lanzo). Other partial melting events may have previously affected these lherzolite bodies thereby giving their residual character to the peridotites. Each magmatic event is characterized by the formation of various melt types through partial melting, a possible mobility of the melts produced and further fractional crystallization of the melts.

Thus, the final image which emerges is that the actual state of the orogenic lherzolite bodies can be understood through a model in which these peridotite bodies suffered a complex history involving successive partial meltings and further differentiation of the melts so generated, the partial melting events giving rise each time to a diversity of products. The ^{87}Rb–^{87}Sr isotope systematics has also been interpreted in the light of a complex process[23]. Dickey *et al.*[28], through the study of the Ronda massif (Spain), also support a similar complex evolution for this body but without clear evidence for pyroxenite-layer remelting. Wilshire and Shervais[39] inferred that the upper mantle parts should have suffered a rather complex evolution through a petrological and structural analysis of ultramafic xenoliths from the western United States.

Such a complex history can be understood geodynamically as resulting from an evolution of these bodies in an upper mantle affected by convection processes and uprising movements to the surface through tectonic events. The partial melting events thus appear during the decompression stages[22,23,26].

Several characters displayed by these Alpine-type peridotite bodies can be explained in the light of such an evolution. First, the relatively uniform lherzolites characteristics found throughout these bodies would result from an evolution of these upper mantle bodies in active convection processes, implying large mixing and chemical reequilibration—favoured by the presence of melts and fluids generated through the partial melting events. Second, the specific characteristics of the pyroxenite layers in each body may be explained by the relative intensity of the last partial melting event (the one which selectively affected these layers) (Fig. 3). In some bodies (Lherz, Freychinède, Beni-Bouchera) this last event was of low intensity. It affected only the pyroxenite layers in a selective way. In others, such as Lanzo, this last event was more intense, also affecting the peridotites[13,14]. In this body the pyroxenite layers look perfectly equilibrated relative to the lherzolites.

This reequilibration should be a general phenomenon in the mantle—the temperatures being rather high, recrystallization occurring rather easily, the presence of melts or fluids permitting an efficient equilibration[40].

The apparent equilibrium of many websteritic layers with the surrounding peridotites in these bodies may result from such a further reequilibration process of ancient pyroxenite layers. In this case, these websteritic layers may be indicative of past partial melting events.

The oceanic mantle is composed of a mechanical mixture of an old subducted, elongated, sheared oceanic crust with a residual peridotite. Through several cycles of convection, including rising and melting at ridge crests, subduction with some rare melting events, origin of calcalkaline suites, and so on, we certainly have a quite complex petrological assemblage. Such a sequence of events, is in full agreement with petrological and isotopic data on orogenic lherzolite massifs[23,24]. If this were verified, the pyroxenite would represent the old oceanic crust, sometimes recycled, or melted in subduction zones and the peridotites, the residual mantle.

Received 16 February; accepted 19 May 1982.

1. Jackson, E. D. & Thayer, T. P. *24th Int. geol. Cong. Montréal*, Sect. 2, 289–296 (1972).
2. Green, D. H. *Ultramafic and Related Rocks* 212–221 (Wiley, New York, 1967).
3. MacKenzie, D. B. *Bull. Am. geol. Soc.* **71,** 303–318 (1960).
4. Ave Lallemant, H. G. *Leid. geol. Meded.* **42,** 1–57 (1967).
5. Nicolas, A., Bouchez, J. L. & Boudier, F. *Tectonophysics* **14,** 143–171 (1972).
6. Javoy, M. *Colloques int. Cent. natn. Rech. scient.* **272,** 279–287 (1980).
7. Smith, C. H. & MacGregor, I. D. *Bull. geol. Soc. Am.* **71,** 1978 (1960).
8. Green, D. H. *J. Petrol.* **5,** 134–188 (1964).
9. Kornprobst, J. *Contr. Miner. Petrol.* **23,** 283–322 (1969).
10. Dickey, J. S. *Miner. Soc. Am. Spec. Pap.* **3,** 33–49 (1970).
11. Obata, M. thesis, Massachusetts Inst. Technol. (1977).
12. Conquéré, F., *Bull. Soc. fr. Minér. Cristallogr.*, **100,** 42–80, 123–137 (1977).
13. Boudier, F. thesis, Univ. Nantes (1976).
14. Boudier, F., Nicolas, A. *Bull. suisse Miner. Petrol.* **52/1,** 39–58 (1972).
15. O'Hara, M. J. & Mercy, E. L. P. *Earth planet. Sci. Lett.* **1,** 295–300 (1966).
16. Frey, F. A. *Geochim. cosmochim. Acta* **33,** 1429–1447 (1969).
17. Frey, F. A. *Phys. Earth planet. Inter.* **3,** 323–330 (1970).
18. Loubet, M., Shimizu, N. & Allègre, C. J. *Contr. Miner. Petrol.* **53,** 1–12 (1975).
19. Loubet, M., Bougault, H., Shimizu, N. & Allègre, C. J. *EOS* **67,** 1025 (1976).
20. Loubet, M. thesis, Univ. Paris (1976).

[illegible] Loubet, M. & Allègre, C. J. *4th int. Conf. Geochronology Cosmochronology Isotope Geology*, 259–262 (1978).

22. Loubet, M., Polvé, M., Richard, P. & Allègre, C. J. *Colloques int. Cent. natn. Rech. scient.* **272,** 269–277 (1980).
23. Polvé, M. & Allègre, C. J. *Earth planet Sci. Lett.* **51,** 71–93 (1980).
24. Richard, P. & Allègre, C. J. *Earth planet. Sci. Lett.* **47,** 65–74 (1980).
25. Menzies, M., Blanchard, D., Brannon, J. & Korotev, R. *Contr. Miner. Petrol.* **64,** 53–74 (1977).
26. Loubet, M. & Allègre, C. J. *Geochem. J.* **13,** 69–75 (1979).
27. Suen, C. J. thesis, Massachusetts Inst. Technol. (1978).
28. Dickey, J. S., Obata, M. & Suen, C. J. *Bull. 96, Oregon Dept Geol. Min. Indust.* 79–89 (1977).
29. Ottonello, G., Piccardo, G. B. & Ernst, W. G. *Geochim. cosmochim. Acta* **43,** 1273–1284 (1979).
30. Haskin, L. A., Frey, F. A., Schmitt, R. A. & Smith, R. H. *Phys. Chem. Earth* **7,** 169–321 (1966).
31. Gast, P. W. *Geochim. cosmochim. Acta* **32,** 1057–1086 (1968).
32. Schilling, J. G. *Phil. Trans. R. Soc.* A**268,** 663–706 (1971).
33. Langmuir, C. H., Bender, J. F., Bence, A. E. & Hanson, G. N. *Earth planet. Sci. Lett.* **36,** 133–156 (1977).
34. De Paolo, D. J. & Wasserburg, G. J. *Geophys. Res. Lett.* **3,** 743–746 (1976).
35. O'Nions, R. K., Hamilton, P. J. & Evensen, N. M. *Earth planet. Sci. Lett.* **34,** 13 (1977).
36. Allègre, C. J., Ben Othman, D., Polvé, M. & Richard, P. *Phys. Earth planet. Inter.* **19,** 293–306 (1979).
37. Loubet, M. *J. Petrol.* (submitted).
38. Conquéré, F. *Contr. Miner. Petrol.* **33,** 32–61 (1971).
39. Wilshire, H. G. & Shervais, J. W. *Physics and Chemistry of the Earth* Vol. 9, 257–272 (Pergamon 1973).
40. Hofmann, A. W. & Hart, S. R. *Earth planet. Sci. Lett.* **38,** 44–62 (1978).

Reversion of a promoter deletion in yeast

Stewart Scherer*, Carl Mann & Ronald W. Davis

Department of Biochemistry, Stanford University School of Medicine, Stanford, California 94305, USA

Promoter function in yeast has been examined by obtaining revertants of a his3 *promoter deletion* in vivo. *Events which provide a new promoter for the* his3 *gene include insertion of the transposable element Ty*1, *rearrangements of the plasmid vector, and chromosomal mutations. A role for dicentric chromosomes as a source of the plasmid rearrangements is discussed.*

PROMOTER function was originally defined by mutations which reduced the fully induced level of expression of the lactose operon of *Escherichia coli*[1]. Since then, various selective methods have been developed to identify different types of altered promoter sequence. These include the isolation of mutations that increase gene expression and mutations which alter the regulation of specific genes[2]. Additional information about promoter function in prokaryotes has come from studies of the *in vitro* interactions of purified RNA polymerase with promoter sequences[3].

As most mutations that decrease gene expression, isolated *in vivo*, reside in coding sequences, genetic analysis of promoter function in eukaryotes has centred on systems where one can select for overproduction or altered regulation. An alternative approach to the study of promoter function is through the reversion of existing promoter mutations. Two eukaryotic promoter mutations have been examined in detail by this method: the *his4*-912 and *his4*-917 mutations of yeast[4]. In both cases, the pattern of revertants obtained by selection for restoration of *HIS4* function was influenced by the fact that the original mutations were due to the insertion of transposable elements.

Recombinant DNA techniques have made it possible to produce a series of deletions or base changes that modify promoter sequences. These altered promoters can then be returned to an appropriate host in order to examine their function *in vivo*[5–7].

Here we have studied the reversion of a promoter deletion of the yeast *HIS3* gene. The deletion was first constructed in *E. coli* and then introduced into yeast as a new chromosome: a plasmid containing a functional centromere, an *ARS* sequence, and additional selectable markers (see Figs 1, 3). The promoter mutant chosen, *his3*-Δ4, deletes to within a few nucleotides of the start point of *HIS3* transcription (41 ± 1 nucleotides from the start of translation) in wild-type strains and produces no detectable *HIS3* mRNA[7]. The deleted sequences are replaced with λ DNA (see Fig. 3) rightward from the *att* site to the *Bam*HI site at 0.577.

Revertants of this *his3* promoter deletion are extremely rare, less than 1 in 10^9 viable cells, but arise by a variety of mechanisms. Yeast cells require only low levels of *HIS3* transcription for growth; this provides for a wide range in the level of expression that can be detected in revertants. In this report we describe several types of revertants. Potential sources for certain classes of the revertants and mechanisms for the restoration of *HIS3* function are discussed.

Blocking recombination between a plasmid-encoded gene and a chromosomal copy

Previous attempts to examine the reversion of *his3* mutant genes introduced into yeast by DNA transformation have been hampered by recombination with the *his3* allele present at the normal location on chromosome 15 (ref. 8). One solution to this problem is to delete the homologous sequences at the normal *HIS3* locus. This approach has been used in the isolation of some of the revertants described below. In general, the removal of entire genes in yeast has been difficult. The intercistronic regions are frequently small and suspected silent regions may encode essential functions for which transcripts are not readily detected.

Another solution to the recombination problem is to block all homologous recombination. However, in yeast, one does not have a single mutation, analogous to the *rec*A mutants of *E. coli*, which effectively blocks most homologous recombination. The yeast *rad52* mutation[9] will block gene conversion but reciprocal recombination remains unaffected. This latter form of recombination was effectively blocked in the *rad52* strains used here by incorporation of a yeast centromere[10,11] into the plasmid. Cells containing the dicentric chromosomes which arise from reciprocal recombination of a centromere-containing plasmid into a normal yeast chromosome are not recovered in these strains.

The experiments which led to the above conclusion are summarized in Table 1. In each experiment, the host strain contained a *his3* gene with a small internal deletion and the plasmid contained the *his3*-Δ4 promoter deletion. In the situation where the host strain was $RAD52^+$ and the plasmid cen^-, both gene convertants and reciprocal recombinants were recovered. The cen^-, plasmids were unstable and in some cases where gene conversion events occurred, the other plasmid marker (and presumably the entire plasmid) had been lost. Cells that had integrated the plasmid by reciprocal recombination are at a selective advantage during the growth of the culture required to measure the recombination frequency. One would normally expect a rather higher ratio of gene conversion to reciprocal recombination than was observed[12]. When the *rad52* mutation was incorporated into strains containing the cen^- plasmids, only the reciprocal events were recovered (Table 1). In addition, a high background of apparent suppressors of *his3*-Δ4 was observed when using cen^- plasmids. This may be related to the poor control of copy number of the *his3* gene with these plasmids.

Table 1 Reversion to His^+ of strains carrying the *his3* promoter deletion on a plasmid

Strain	Plasmid	Reversion frequency	Fraction Ura^+
$RAD52^+$	cen^-	$\sim10^{-6}$	~40%
$RAD52^+$	CEN^+	$\sim10^{-7}$	~50%
$rad52^-$	cen^-	$\sim10^{-6}$	100%
$rad52^-$	CEN^+	$<10^{-9}$	100%

The background of apparent suppressors, which generally show poor growth in selective conditions, has been excluded (see text). The $RAD52^+$ strain was strain YNN36 (α *trp1*-289 *his3*-Δ1 *ura3*-52). The $rad52^-$ strain was YNN209 (α *trp1*-289 *his3*-Δ1 *ura3*-52 *ade2 rad52*). The cen^- plasmid was 2944 (YRp12 with the *Bam*HI fragment containing *his3*-Δ4) and the CEN^+ plasmid was 2961 (see Fig. 1) which contains a slightly smaller *his3*-Δ4 fragment. Reversion to His^+ of *his3*-Δ1 strains containing no plasmid was $<10^{-11}$.

---

* Present address: Division of Chemistry, California Institute of Technology, Pasadena, California 91125, USA.

0028-0836/82/340815—05$01.00

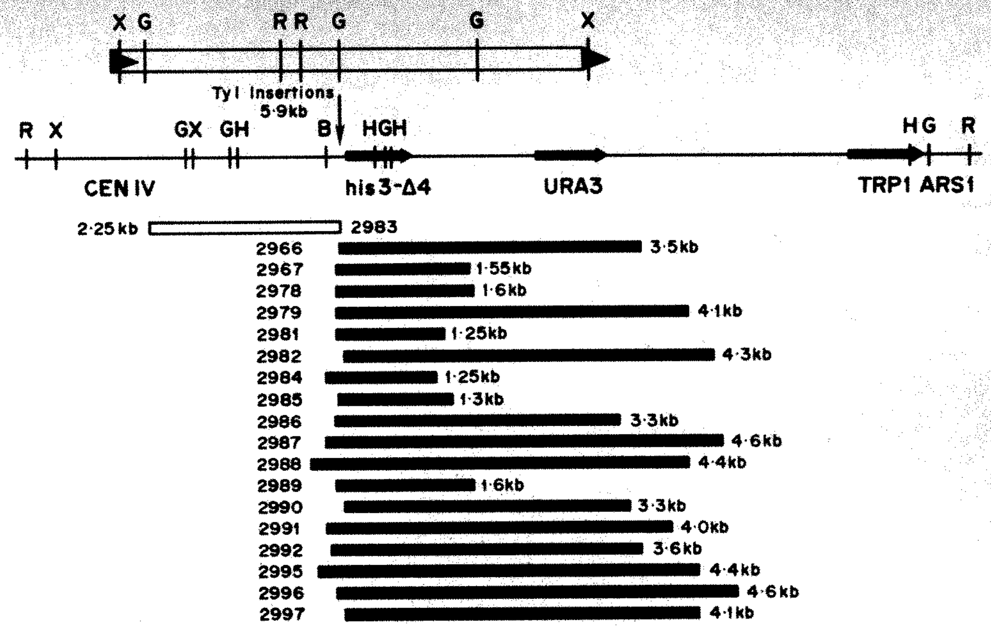

Fig. 1 Plasmid rearrangements associated with reversion of the *his3* promoter deletion. A linearized map of plasmid 2961 with the positions of certain restriction endonuclease cleavage sites is shown. The total length of the plasmid is 11.1 kb. The ColE1 origin and ampicillin resistance gene are located between the *URA3* and *TRP1* genes. R, *Eco*RI; B, *Bam*HI; H, *Hin*dIII; G, *Bgl*II; and X, *Xho*I. Above the map of the plasmid is a map of the prototype Ty*1* element[14]. The terminal repeats of Ty*1*, the δ sequences, are indicated as filled triangles. One of the Ty*1* elements which inserted into 2961 lacked the *Xho*I sites in the δ sequences. The Ty*1* elements all inserted into the vector in the orientation shown. Transcription of Ty*1* is from right to left as drawn. The single open box represents the deletion contained in one of the revertants. The solid bars indicate the regions duplicated in the other revertants. The sizes of the deletion and the tandem duplications are shown. The sizes are ±50 bp for the smaller rearrangements and ±100 bp for the largest ones.

CEN$^+$ plasmids in the *RAD52*$^+$ strain will also convert *his3* mutations on chromosome 15 to His$^+$. We did not determine whether plasmid integration by reciprocal recombination also occurred in this strain. Some of the His$^+$ recombinants no longer contained the plasmid as judged by the loss of the other plasmid markers, which may be due to the imperfect stability of the centromere plasmids. It has also been noted that gene conversion events near centromeres are frequently associated with chromosome loss[13]. Finally, when the *CEN*$^+$ plasmids were introduced into *rad52*$^-$ strains, the frequency of His$^+$ colonies fell dramatically. Among the His$^+$ revertants, no His$^+$ recombinants were detected (see below). In previous work[12], the block to gene conversion produced by *rad52* was not as complete as that observed here. However, in the experiments described here the regions of homology were quite small and one of the alleles contained an internal deletion. The frequency of viable recombinants in this situation is less than 1 in 10^{10} cells.

Revertants of the *his3-Δ4* promoter deletion

All the revertants obtained in our study were derived using the same plasmid vector, 2961 (Fig. 1). Two host strains were used: a *rad52* strain, YNN209, which contains the *his3-Δ1* allele[8] and strain YNN211, which contains a total deletion of the *his3* gene, *his3-Δ200* (M. Fasullo, unpublished strain). In both strains, the frequency of spontaneous His$^+$ revertants was <1 in 10^9 viable cells.

Spontaneous *His*$^+$ revertants of yeast strains YNN209 and YNN211 containing plasmid 2961 fall into three broad classes: insertions of the transposable element Ty*1*, rearrangements of the plasmid DNA, and apparent chromosomal mutations. The revertants were first characterized by isolation of the plasmid DNA from the revertant cells by transformation of *E. coli*. Certain revertants yielded plasmids that appeared identical to the starting plasmid. All of these yeast strains grew poorly on selective media and the plasmids obtained from them would not transform yeast *his3* mutants to His$^+$. These apparent chromosomal mutants have not been characterized further. The plasmid-encoded mutations are described below.

Reversion by insertion of the transposable element *Ty1*

Of 14 revertants isolated using the *rad52*/centromere-plasmid system described above, 6 were insertions of the transposable element Ty*1*, as determined by comparison with restriction site maps of other cloned Ty*1* elements[14] and confirmed by hybridization of ^{32}P-labelled Ty*1* sequences with the plasmid DNA recovered from the revertants (not shown). Restriction site mapping placed the insertion of the element near the 5′ end of the *his3* coding sequences. The orientation of the element, as shown in Fig. 1, was the same relative to the gene as observed at the cytochrome *c*[15] and alcohol dehydrogenase[16] loci. The Ty*1* elements inserted into at least four distinguishable sites. This was determined by digestion of heteroduplexes of revertant DNA and end-labelled parental DNA with S_1 nuclease and measurement of the distance from the labelled end to the novel joint in the revertant DNA (Fig. 2*a*). These results are summarized in Fig. 3.

All six plasmids containing Ty*1* insertions transformed *his3* mutants to His$^+$. The insertions which were closer to the start of the *HIS3* coding sequences expressed *HIS3* at a rather higher level as judged by growth in the presence of 10 mM 3-amino-1, 2, 4-triazole, an inhibitor of the *HIS3* gene product, imidazole glycerol phosphate dehydratase. Attempts to correlate the level of *HIS3* expression with insertion site were complicated by the fact that the Ty*1* elements that had inserted were not identical. Digestion with two restriction endonucleases, *Sal*I and *Xho*I, revealed that the presence of at least three different Ty*1* elements. Many polymorphisms of Ty*1* have been characterized[14,17] and it is possible that the six insertions were six different Ty*1* elements. These studies have demonstrated that Ty*1* elements can transpose to a non-promoter sequence (λ DNA) near a gene and activate that gene. Also, Ty*1* transposition can occur in a *rad52* strain.

Of 21 revertants of *his3-Δ4* obtained in a strain containing a total deletion of the chromosomal *his3* gene (YNN211); none were due to the insertion of Ty*1* elements. Thus, the frequency of transposition relative to the efficiency of other mechanisms available for reversion of the promoter deletion seems to be different for different strains. The source of the difference between these two strains is unknown.

Reversion by tandem duplication

Plasmids recovered from 15 revertants contained tandem duplications of a portion of the starting plasmid. Plasmids were screened for duplications by cleavage of the plasmid DNA with *Bgl*II endonuclease, which cleaves once in the *HIS3* gene and has no sites for ~6 kilobases (kb) downstream from this gene

(Fig. 1). As described below, all the duplications had one breakpoint near the 5′ end of *HIS3* and one well beyond 3′ of the gene in the vector sequences. These breakpoints produced a single novel junction near the 5′ end of the *HIS3* gene for each new plasmid.

Cleavage of the revertant DNA with *Bgl*II produced a pattern of fragments that contained all the fragments of the vector with an additional fragment, which corresponds to the size of the duplicated region. Several examples of this are shown in Fig. 4. Cleavage of the plasmid DNA from a revertant with any other enzyme which cleaves once in the duplicated segment will produce all the vector fragments normally observed for that enzyme and an additional fragment whose size is the same for all enzymes of this type.

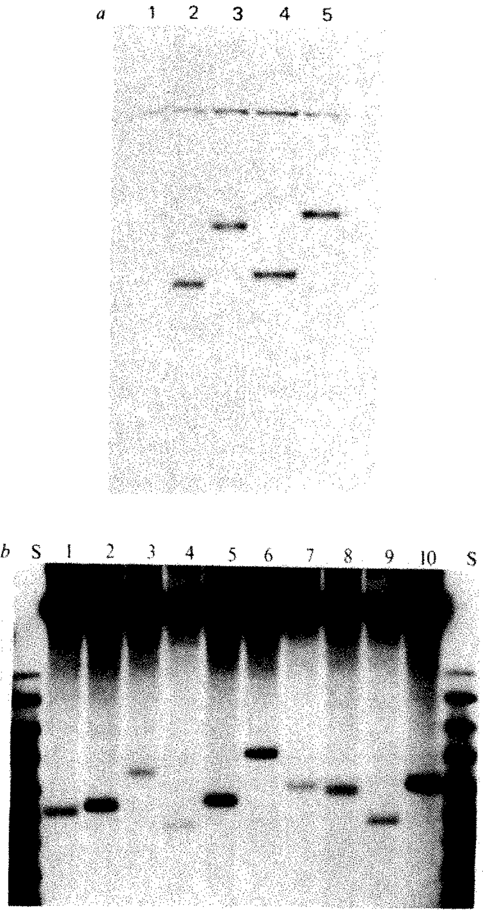

Fig. 2 Mapping of rearrangement breakpoints near *HIS3* with S_1 nuclease. ^{32}P-end-labelled DNA was prepared by treatment of *Hin*dIII-cleaved 2961 with calf intestine alkaline phosphatase followed by incubation with polynucleotide kinase and $[\gamma\text{-}^{32}\text{P}]$-ATP. In *b*, the fragment of interest was purified by gel electrophoresis; in *a* it was cleaved also with *Bam*HI endonuclease before separation. For each sample, the DNA was cleaved with *Bgl*II endonuclease in 20 µl of 10 mM Tris-HCl *p*H 7.5, 10 mM magnesium chloride, 1 mM dithiothreitol. In *a*, purified plasmid DNA was used; in *b*, DNA from rapid plasmid isolations was used. 3 µl of 0.1 M Na_3EDTA, 1 M NaOH and $\sim 10^4$ d.p.m. of probe fragment were added to each sample and incubated at room temperature for 15 min. The DNA was renatured by adding 3 µl of 2 M Tris-HCl and incubating at 65 °C for 3–5 min. The samples were diluted with 300 µl of 50 mM sodium acetate *p*H 4.4, 280 mM NaCl, 2 mM $ZnAc_2$ and digested with 1,000 units of S_1 nuclease at 37 °C for 30 min. After ethanol-precipitation, the samples were electrophoresed on a 5% polyacrylamide Tris–borate–7 M urea denaturing gel (*a*) or on a 2% agarose Tris–acetate–EDTA native gel (*b*). After electrophoresis, the gels were dried for autoradiography and exposed at −70 °C with an intensifying screen. The samples in *a* were: 1, no DNA; 2, 2970; 3, 2971; 4, 2973; and 5, 2976. The fragments were measured as 340–400 bp (standards not shown); the probe measures 575 bp. The samples in *b* were: 1, 2997; 2, 2996; 3, 2992; 4, 2990; 5, 2989; 6, 2987; 7, 2986; 8, 2985; 9, 2982; and 10, 2981. Standards, S, were *Bst*NI fragments of SV40 DNA.

The end point of the duplicated segment near the 5′ end of the *HIS3* gene was localized by an S_1 nuclease mapping procedure similar to that used for the Ty*1* insertions (see Fig. 2*b*); the results are shown in Fig. 3. The rearrangement breakpoints were spread over a wide region beginning near the start of the wild-type *HIS3* mRNA and extending back as far as 500 base pairs (bp) from that point.

Given the size of the duplication and one of its end points, the other end point was determined. The regions that were duplicated in each revertant are shown in Fig. 1. There are no obvious hotspots for the duplication breakpoints, nor is there any obvious correlation between the duplications that break in a given region of the vector DNA and a particular distance from the 5′ end of the *HIS3* gene for the other breakpoint. It is interesting that no duplications were found which fuse the *his3* gene to *URA3* sequences. The *URA3* gene is constitutively expressed and transcribed in the appropriate direction. About half of the revertants were selected in conditions where the *URA3* gene on the vector was also being selected. In these conditions, *URA3* is transcribed at a higher level[18].

Eight of the duplication-containing plasmids, including those with the closest and the two most distant breakpoints relative to the *HIS3* gene, were tested for the ability of the plasmid DNA to transform *his3* mutant strains to His$^+$. All transformants tested were His$^+$. All except those generated using 2988 DNA were resistant to 10 mM 2-amino-1, 2, 4-triazole and therefore must express *HIS3* at near wild-type levels. The duplications were responsible for the *HIS3* expression as removal of the duplication from two different plasmids by homologous recombination resulted in reversion of the His$^+$ phenotype to His$^-$.

Miscellaneous revertants

One revertant was a simple deletion of the starting plasmid; one breakpoint of the deletion was near the 5′ end of the *HIS3* gene (Fig. 3). The size of the deletion was ~2.25 kb, which placed the other breakpoint in a region of yeast DNA normally transcribed into poly(A)-containing RNA[11]. The deletion-containing plasmid retained at least partial *CEN4* function during mitotic growth.

Several revertants seemed to be duplications of most of the starting plasmid, excluding the *CEN4* region (not shown). The size of these duplications resulted in the production of a large number of coincidentally sized restriction fragments and made their characterization less certain.

Two plasmids were found to contain multiple rearrangements of the starting plasmid DNA. One was a triplication or two similar duplications; the other appeared to contain two different duplications (not shown).

Plasmids isolated from the revertants described in this section transformed *his3* mutants to His$^+$ and presumably represent the event in those cells that restored *HIS3* function.

Possible source of the plasmid rearrangements

Mutations associated with tandem duplications have been found in many systems. Some arise through recombination of repetitious DNA sequences and are generally sensitive to mutations affecting the general recombination systems of the organism. The large duplications of portions of the *Salmonella* chromosome are thought to arise by this type of mechanism[19]. In contrast, the frequency of spontaneous duplications of the phage λ chromosome is insensitive to such mutations[20].

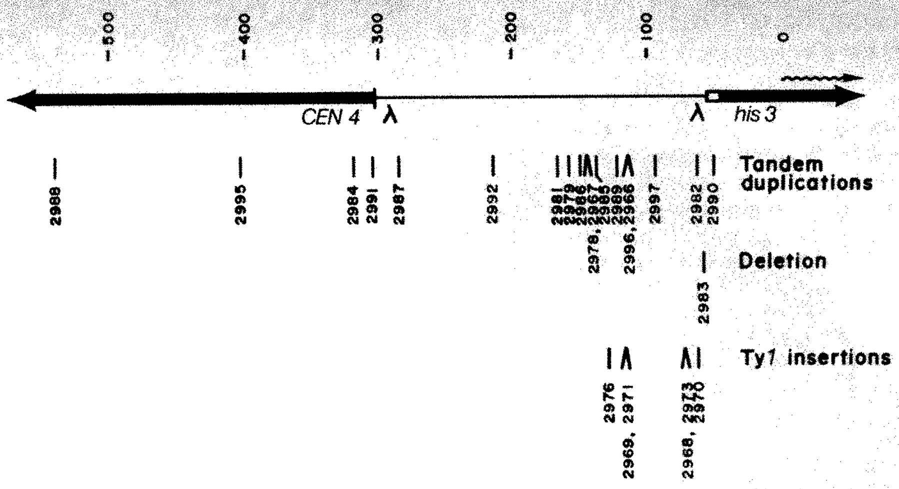

Fig. 3 Rearrangement breakpoints near *HIS3*. The position of the breakpoint for the tandem duplications, deletion, and Ty*1* insertions (mapped as described in Fig. 2 legend) are shown. The positions are ±10 bp for the closest breakpoints and ±20 bp for the more distant ones. Distances from the start of the *HIS3* coding sequences (ATG) are given in base pairs at the top. The yeast DNA sequences in 2961 (*his3*-Δ4 and *CEN4*) are indicated as thick lines. The *CEN4* function is associated with sequences 2 kb to the left of the λ DNA (see Fig. 1). The *HIS3* structural gene sequences are indicated by the wavy line. The small region of λ DNA, to the right of the *att* site, attached to *his3*-Δ4 is shown as a thin line. The λ *att* site, which has partial homology to the yeast DNA that it replaced, is represented by an open box. All revertants shown were independently isolated, except 2966, 2967, 2968 and 2969, which form one group. The strains containing the rearranged plasmids are: pNN163 (2966), pNN164 (2967), pNN165 (2967), pNN166 (2969), pNN167 (2970), pNN168 (2971), pNN169 (2973), pNN170 (2976), pNN171 (2978), pNN172 (2979), pNN173 (2981), pNN174 (2982), pNN175 (2983), pNN176 (2984), pNN177 (2985), pNN178 (2986), pNN179 (2987), pNN180 (2988), pNN181 (2989), pNN182 (2990), pNN183 (2991), pNN184 (2992), pNN186 (2995), pNN187 (2996), pNN207 (2997). pNN163 to pNN172 were selected in YNN209, and pNN173 to pNN207 were selected in YNN211.

DNA rearrangements are normally quite rare in yeast. Some are due to recombination of repeated DNA sequences: rearrangements of chromosome 3 through the mating type loci[21], recombination of Ty*1* sequences[8] and recombination of the partially homologous cytochrome coding sequences[22]. Duplications have been detected in several cases. The *SAD1* mutation[23] duplicates a portion of the right arm of chromosome 3; it appears to be an unequal cross-over between *MAT* and *HMR*[24]. Copper resistance is associated with tandemly repeated sequences (S. Fogel, personal communication). The results described here are unusual for yeast in that duplications seem to be the most abundant class of mutations.

We suggest that the formation of dimeric, dicentric plasmids may be an intermediate in the formation of the rearranged molecules found in the revertants described above. Asymmetric breakage of the dimer plasmids will be a source of deletions and tandem duplications (Fig. 5). The relative frequencies at which the revertants are recovered may reflect both the position of *his3* relative to the centromere in the starting plasmid and the locations of DNA sequences that can restore *HIS3* function.

With the isolation of centromeric DNA, it has become possible to construct dicentric chromosomes *in vitro*. In yeast, these molecules are rapidly rearranged, usually by deletion of one of the centromeres (C. M., unpublished results). Plasmids that do not contain centromeres will freely form multimeric molecules in yeast[25]; however, multimers of centromere plasmids are not readily detected[11].

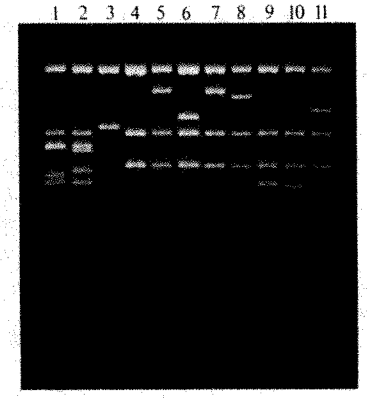

Fig. 4 Plasmid DNA from revertants. The samples were cleaved with *Bgl*II endonuclease and electrophoresed on a 0.8% agarose Tris–borate–EDTA gel. The samples in lanes 1 and 2 are 2976 and 2970, both Ty*1* insertions; lane 3, 2983, a deletion; lane 4, 2961, the parent plasmid; lanes 5–11, 2995, 2990, 2988, 2979, 2978, 2967, 2966 (all duplications). The sizes of the fragments of 2961 (lane 4) are: 6.15, 2.55, 1.90 and 0.55 kb (going from top to bottom).

Cyclization of the broken dimer plasmids leads directly to circular molecules containing simple duplications. Transformation of yeast with linear DNA molecules prepared from cloned circular DNA molecules has shown that these ends can be rapidly joined *in vivo* and that they appear to stimulate recombinational events involving the transforming DNA[26]. One would expect that the molecules containing linear duplications produced by the mechanism outlined above would rapidly convert to circular molecules and possibly catalyse more complicated rearrangements. Broken dicentric chromosomes in maize are known to precede multiple rearrangements that can be observed cytologically[27]. Consistent with this model is the observation that transformation of yeast with a dimer of plasmid 2961 yields >100 times the frequency of His$^+$ colonies as that for the monomer. We chose to isolate the His$^+$ revertants with the *HIS3* gene on a plasmid to facilitate rapid recovery of the functional *HIS3* DNA sequences. A different distribution of revertants would be predicted from the above model if the promoterless *HIS3* gene was located in a linear chromosome.

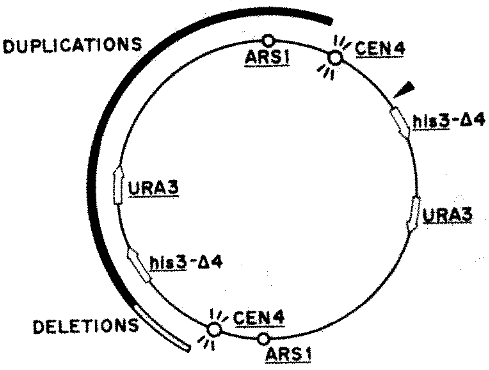

Fig. 5 A model for the origin of the duplications. A dimer of plasmid 2961 is shown. The various structural features of the plasmid are indicated. An arbitrary breakpoint near *his3* is marked by an arrowhead. The regions of the plasmid where a second break would yield a duplication (solid line) or a deletion (double line) are shown outside the plasmid.

Creation of promoters by genomic rearrangement

In almost all the *HIS3* revertants described above, a new promoter was created by a genomic rearrangement near the 5′ end of the gene. As can be seen with the tandem duplications, the distance from the start of the *HIS3* protein to the rearrangement breakpoint can be quite large, up to 500 bp.

The Ty*1* insertions are clustered more tightly than the duplications; however, the events that have been detected may reflect both the target specificity of the transposon, and the spectrum of sites from which it can activate a gene.

Activation of cryptic genes, or enhanced expression of wild-type functions by insertion of transposable elements, is found in many systems: for example, in *E. coli*, the major mechanism for activation of the genes for the metabolism of β-glucosides is the insertion of IS*1* and IS*5* (ref. 28). Similarly, the c-*myc* gene, the cellular homologue of the oncogene contained in the transforming virus MC29, is overproduced after nearby integration of a retrovirus[29].

Clearly, the orientation of the Ty*1* insertions is significant as all the insertions found here and all the insertions seen at cytochrome *c* (selecting for overproduction) and at alcohol dehydrogenase (selecting for altered regulation) are the same relative to the gene. This orientation is the reverse of that of transcription of the Ty*1* element itself[30]. One might imagine bidirectional positive control (promoter) sequences at one end of the element. Some portion of this information must reside outside the identical end repeat sequences of Ty*1*[8].

The duplications, which represent changes only in the arrangement of the plasmid DNA sequences, are more difficult to interpret. Most of the rearrangements involve only bacterial DNA sequences (λ and pBR322). Presumably several sequences which will pass for all or part of a promoter are to be found in the vector DNA; however, they do not function in their present positions. The one known functional promoter, *URA3*, has not been fused to *his3* in any of the duplications examined. This may indicate some specificity in the rearrangement breakpoints or an incompatability in the regulation of *URA3* with *HIS3* expression.

Duplication is an important mechanism in the evolution of chromosomes. It allows for new regulation of genes without loss of either the original copy of the gene or the source of the new regulation. One well-characterized example of this process is found in the mammalian globin genes. A series of related structural genes has evolved with different regulation for the various members of the family. Interspersed among these are several non-functional copies[31]. The new regulation developed after duplication need not be at the level of transcription. In the case of the immunoglobulin heavy chain constant region genes it appears to reside in additional genomic rearrangements[32].

Although the mechanism suggested above as the source of the duplications applies to circular chromosomes, duplications clearly occur in linear chromosomes. The ability to insert the promoterless *his3* derivative at almost any point in the yeast genome allows one to examine the mechanisms which may produce duplications or other rearrangements in the chromosomes.

The experiments described here indicate that genomic rearrangements can create new promoters at low but detectable frequencies. As studies on the various aspects of gene expression proceed it will become increasingly important to understand the mechanics of the chromosomes on which they reside.

We thank Robert Malone for providing strains containing the *rad*52 mutation. S.S. and C.M. were supported by NIH training grant funds. This work was supported by ACS grant no. NP-268B and NIH grant no. 21891.

Received 9 March; accepted 15 June 1982.

1. Scaife, J. & Beckwith, J. R. *Cold Spring Harb. Symp. quant. Biol.* **31,** 403–408 (1966).
2. Rosenberg, M. & Court, D. *A. Rev. Genet.* **13,** 319–353 (1979).
3. Losick, R. & Chamberlain, M. (eds) *RNA Polymerase* (Cold Spring Harbor Laboratory, New York, 1976).
4. Roeder, G. S., Farabaugh, P. J., Chaleff, D. T. & Fink, G. R. *Science* **209,** 1375–1380 (1980).
5. Benoist, C. & Chambon, P. *Nature* **290,** 304–310 (1981).
6. Fromm, M. & Berg, P. *Molec. cell. Biol.* (in the press).
7. Struhl, K. *Proc. natn. Acad. Sci. U.S.A.* **78,** 4461–4465 (1981).
8. Scherer, S. & Davis, R. W. *Science* **209,** 1380–1384 (1980).
9. Malone, R. & Esposito, R. *Proc. natn. Acad. Sci. U.S.A.* **77,** 503–507 (1980).
10. Clarke, L. & Carbon, J. *Nature* **287,** 504–509 (1980).
11. Stinchcomb, D. T., Mann, C. & Davis, R. W. *J. molec. Biol.* **158,** 157–179 (1982).
12. Jackson, J. A. & Fink, G. R. *Nature* **292,** 306–310 (1981).
13. Campbell, D. A. & Fogel, S. *Genetics* **85,** 573–585 (1977).
14. Cameron, J. R., Loh, E. Y. & Davis, R. W. *Cell* **16,** 739–751 (1979).
15. Errede, B., Cardillo, T. S. & Sherman, F. *Cell* **22,** 427–436 (1980).
16. Williamson, V. M. & Young, E. T. *Cell* **23,** 605–614 (1981).
17. Kingsman, A. J., Glimlich, R. L., Clarke, L., Chinnault, A. C. & Carbon, J. *J. molec. Biol.* **145,** 619–632 (1981).
18. Bach, M. L., Lacroute, F. & Botstein, D. *Proc. natn. Acad. Sci. U.S.A.* **76,** 386–390 (1979).
19. Anderson, P. & Roth, J. *Proc. natn. Acad. Sci. U.S.A.* **78,** 3113–3117 (1981).
20. Emmons, S. W., MacCosham, V. & Baldwin, R. L. *J. molec. Biol.* **91,** 133–146 (1975).
21. Strathern, J. N., Newlon, C. S., Herskowitz, I. & Hicks, J. B. *Cell* **18,** 309–319 (1979).
22. Ernst, J., Stewart, J. N. & Sherman, F. *Proc. natn. Acad. Sci. U.S.A.* **78,** 6334–6338 (1981).
23. Kassir, Y. & Herskowitz, I. *Molec. gen. Genet.* **180,** 315–322 (1980).
24. Nasmyth, K. A., Tatchell, K., Hall, B. D., Astell, C. & Smith, M. *Nature* **289,** 244–250 1981).
25. Stinchcomb, D. T., Struhl, K. & Davis, R. W. *Nature* **282,** 39–43 (1979).
26. Orr-Weaver, T., Szostak, J. W. & Rothstein, R. J. *Proc. natn. Acad. Sci. U.S.A.* **78,** 6354–6358 (1981).
27. McClintock, B. *Genetics* **26,** 234–282 (1941).
28. Reynolds, A. E., Felton, J. & Wright, A. *Nature* **293,** 625–629 (1981).
29. Hayward, W. S., Neel, B. G. & Astrin, S. M. *Nature* **290,** 475–480 (1981).
30. Elder, R. T., St John, T. P., Stinchcomb, D. T. & Davis, R. W. *Cold Spring Harb. Symp. quant. Biol.* **45,** 581–591 (1980).
31. Proudfoot, N. & Maniatis, T. *Cell* **21,** 537–545 (1980).
32. Sakano, H., Huppi, K., Heinrich, G. & Tonegawa, S. *Nature* **280,** 288–294 (1979).

Chemical evidence for the capsomeric structure of phage Qβ

Hisao Takamatsu & Koujiro Iso

Department of Chemistry, College of General Education, University of Tokyo, Komaba, Meguro, Tokyo 153, Japan

Novel capsomeric complexes, pentamers and hexamers were detected as chemical entities in phage Qβ. Both were composed of identical protein subunits and stabilized by intermolecular disulphide bonds. Their numbers per particle were about 12 for pentamers and about 20 for hexamers—consistent with theoretical expectation from the quasi-equivalent packing of 180 identical subunits in a coat protein shell.

SINCE Loeb and Zinder discovered RNA bacteriophages[1], several spherical RNA-containing coliphages have been isolated and classified into four groups according to serological and physicochemical properties[2,3]. Among them, groups I (for example, R17, f2 and MS2) and III (phage Qβ) have been extensively studied and have provided important insight into genetics and molecular biology.

A virus has a clearly defined and highly organized structure outside a cell, in contrast to the complexity of its form inside a cell. It was theoretically proposed that the protein

0028–0836/82/340819—06$01.00

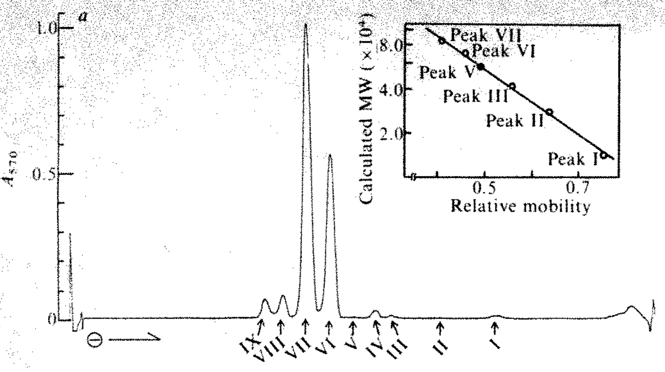

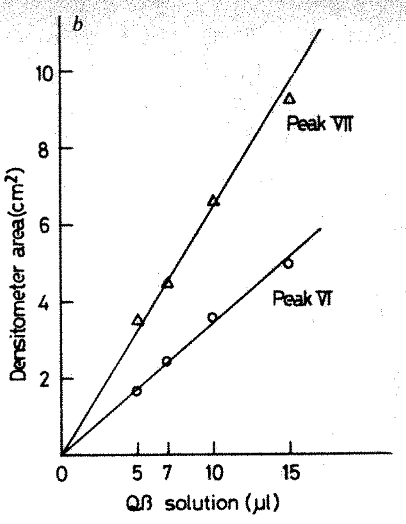

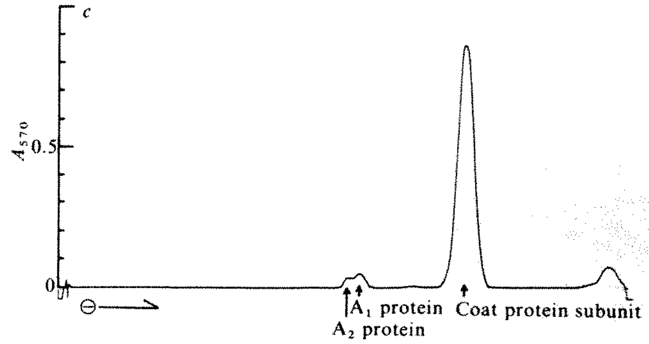

Fig. 1 SDS–polyacrylamide gel electrophoresis of phage Qβ protein. Purified phage Qβ were obtained by a published procedure[21]. Phage solution (0.05% in 0.01 M sodium phosphate, *p*H 7.2) was incubated with SDS (finally 3% w/v) at 90 °C for 30 min. Ten μl of solution were analysed by SDS–5% acrylamide gel electrophoresis according to the method of Weiner *et al.*[10]. For the first 30 min, electrophoresis was done at a constant current (2 mA per tube); it was then stopped to flush out the top of the gels with the tray buffer to remove RNA. The electrophoresis was re-started at 7 mA per tube until the marker dye had migrated 9 cm. Using this method, there was no need to separate protein and RNA before electrophoresis, and so we were able to analyse the entire protein. Gels were stained with Coomassie brilliant blue (0.25% w/v in 45% ethanol, 7% acetic acid) for 40 min and then were destained with 7% acetic acid. Gels were scanned at 570 nm with an Ozumor 82 microdensitometer. *a*, Protein peaks were designated I–IX from the peak having the highest mobility. Although peaks I–III and V were very small, they were observed when the gels were overloaded. Inset: peaks I–III, V–VII were tentatively assigned to be those of monomer, dimer, trimer, tetramer, pentamer and hexamer of coat protein subunits, as no other peaks except peak IV were observed in this region. Peak IV was later shown to be composed of A_2 protein. When their relative mobilities compared with the marker dye were plotted against their calculated MWs ($14{,}050 \times n$: n is an integer), a linear line was obtained. *b*, Various amounts (5–15 μl) of phage solution (0.05%) were electrophoresed. Each peak area of the traced patterns was measured with a planimeter. The measured areas were plotted against the applied quantities. Linearity was observed and the slope for peak VII was twice as steep as the slope for peak VI. Provided both peaks were composed of the same proteins, the weight ratio of peak VII to peak VI was 2.0. The same value was obtained after the gels were stained with Fast green which is also recommended for quantitative densitometry[22]. *c*, Phage solution was incubated with 2-ME (3% v/v) in the presence of SDS for 5 min at 90 °C. The reaction mixture was electrophoresed. The apparent MW was determined based on mobility relative to the marker proteins: ovalbumin (45,000), bovine serum albumin (67,000), chymotrypsinogen A (25,000) and myoglobin (17,800).

arrangement on the outer shell (capsid) of a virus could be predicted from a knowledge of the number of its constituent protein molecules[4]. For example, group I phage particles were estimated to contain about 180 molecules of coat protein, 1 molecule of maturation protein and 1 single-stranded RNA molecule[5]. The capsid structures were therefore considered to have a $T=3$ icosahedral symmetry[4], and, indeed, electron microscopic analysis has shown that the coat protein subunits of phages R17 and f2 are in dimer clusters based on the $T=3$ structure[6]. Phage Qβ is also predicted to have a $T=3$ icosahedral structure, as its protein composition is similar to that of group I phages, except for the presence of a few molecules of a third protein component[7] (discussed below).

Here we have approached the determination of the protein arrangement (including minor protein components) in phage Qβ, in two ways. First, by using a biochemical method, we have sought to characterize the constitutive intermediates during the assembly of protein subunits into the capsid. After the controlled dissociation of Qβ particle, we have found pentamer and hexamer complexes, presumably true constituents of a $T=3$ capsid, which are stabilized through intermolecular disulphide linkages. The capsid is estimated to consist of ~12 pentamers and ~20 hexamers. Second, using electron microscopy, we show that the Qβ capsid is composed of 32 morphological units (capsomeres) which we interpret to consist of 12 pentamers and 20 hexamers based on the quasi-equivalence theory[4]. The two approaches give consistent results.

This is the first report to describe the detection of a discrete substructure of a capsid, corresponding to a capsomere, as a chemical entity in a small spherical virus, and the verification of the quasi-equivalence theory by a chemical method. Detection of a substructure of a capsid may provide an important clue to the assembly process of a viral particle.

Specific dissociation of the phage Qβ particle

The capsid is known to be stabilized in part by hydrophobic forces between coat proteins[8], and the amino acid composition of coat protein is rich in hydrophobic residues[9]. We therefore reasoned that detergents or denaturing reagents might be useful for the disassembly of the capsid and the dissolution of the resulting products.

Phage Qβ particles were treated with SDS and the reaction mixture was subjected immediately to SDS gel electrophoresis[10]. Nine protein peaks (I–IX, in order of decreasing mobility) could be observed reproducibly (Fig. 1*a*). About 90% of the total area is comprised of peaks VI and VII, which are estimated by comparison with several marker proteins to have apparent molecular weights (MWs) of 65,000 and 78,000 respectively. As a linear relationship exists between the applied quantity of protein and peak area (Fig. 1*b*), we can estimate the weight ratio of peak VI to peak VII; the ratio is 0.5. As the phage capsid is mainly composed of coat protein subunits[5], the major peaks VI and VII probably consist of complexes of coat protein subunits.

Peaks I–III and V–VII are tentatively proposed to be monomer, dimer, trimer, tetramer, pentamer and hexamer of coat protein subunits respectively (peak IV is composed of A_2 protein, as described below). When the mobility of each peak is plotted against its calculated MW using the chemically determined MW (14,050)[11], a straight line is obtained (Fig. 1*a* inset). The pentamer of coat protein subunits (peak VI) and the hexamer (peak VII) are stable in SDS solution, so specific bonding must exist to keep these complexes intact; we suggest that it is disulphide bonding between protein subunits.

In addition to peaks VI and VII, there are seven small peaks in Fig. 1*a*. Peaks VIII and IX are particularly prominent and together comprise ~8% of the total area. Their apparent MWs are 98,000 and 110,000 respectively. The other peaks amount to only ~2% of the total area. They can be distinguished when excess amounts of phage protein are separated by electrophoresis and their apparent MWs are 52,000 (peak V), 44,000 (peak IV), 39,000 (peak III), 28,000 (peak II) and 17,000 (peak I).

Reduction of the coat protein complexes

To confirm the disulphide bonding, phage $Q\beta$ was treated with SDS in the presence of 2-mercaptoethanol (2-ME). As shown in Fig. 1*c*, three peaks can be observed, with mobilities corresponding to those of peaks I, III and IV. For convenience, the peaks have been designated peaks I, III and IV.

Peak I comprises ~94% of the total area, and peaks III and IV ~4% and ~2% respectively. The amount and relative mobility of each peak are consistent with published data[7,12,13] and we conclude that peaks I, III and IV consist of coat protein subunit, A_1 (or IIb)[7] protein and A_2 (IIa)[7] protein respectively. The apparent MW of the coat protein subunit is estimated to be higher in our system than the chemically determined MW; similar values[14,15] have been obtained by SDS-gel electrophoresis. These results show that our sample of phage $Q\beta$ is of sufficient purity and further confirm that the components of low mobilities (as shown in Fig. 1*a*) are held by intermolecular disulphide bonds.

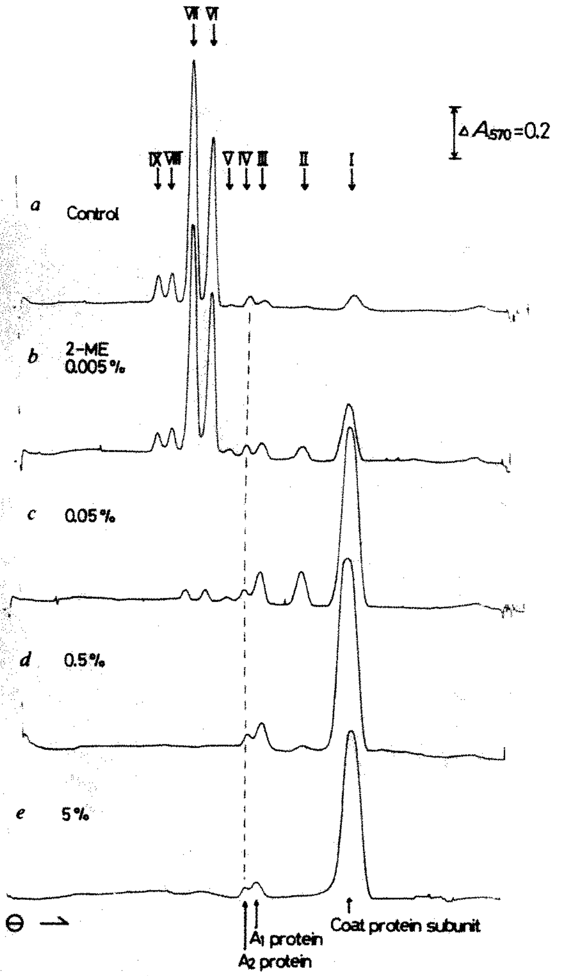

Fig. 2 Partial reduction of phage protein complexes. To the phage solution (0.05%, 10 μl) was added an equal amount of 0%, 0.01%, 0.1%, 1.0%, or 10% (v/v) 2-ME solution and the mixture was incubated for 20 min at room temperature. Immediately afterwards, reaction mixtures were electrophoresed. After treatment with 0.005% 2-ME, peaks I–III and V were increased compared with the non-treated sample. When the pattern of the 0.05% 2-ME treated sample was compared with that treated with 0.005% 2-ME it was clear that peaks VI–IX had decreased and peak I had increased. In the presence of 0.05–5% 2-ME, peak I still increased, while peaks II, V–IX disappeared. Peak III decreased, but remained as in Fig. 1*c*. Peak IV was not affected by these treatments.

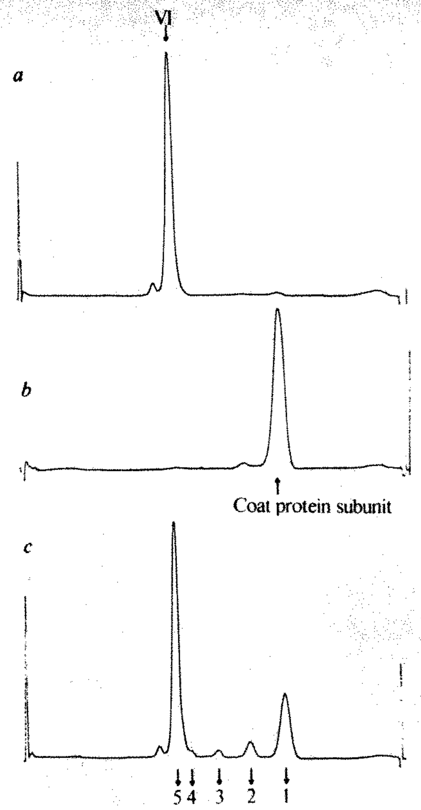

Fig. 3 Analysis of peak VI composition. Phage proteins were electrophoresed without treatment with 2-ME, as described in Fig. 1*a* legend. After electrophoresis, gels were frozen and sliced in 1-mm sections. Protein was then eluted from each slice into 0.2 ml of 0.1% SDS overnight at 37 °C with agitation. The protein solutions were divided into three parts: *a*, no further treatment and electrophoresed; *b*, treated with 5% 2-ME for 20 min at room temperature and then electrophoresed; *c*, treated with 0.005% 2-ME and immediately electrophoresed. As shown in *a*, the protein from peak VI was obtained. After treatment with 5% 2-ME, the peak of coat protein subunit was observed. In *c*, four new peaks can be seen, which have the same mobilities as peaks I–III and V in Fig. 1*a*. When the peaks were numbered as indicated by the arabic figures in *c*, peak VI was the fifth peak. No other peaks were detected in any other conditions. Peaks 1–5 had the same mobilities as peaks I–III, V and VI in Fig. 1*a* respectively.

We next tried to obtain an intermediate pattern between those of Fig. 1*a* and *c*. Phage $Q\beta$ was treated with various concentrations of 2-ME in the presence of SDS. Significant changes could be seen (Fig. 2): further reduction decreased peaks VI and VII, and increased peak I. Peaks VIII and IX decreased in the same manner as peaks VI and VII. At the intermediate degree of reduction, peaks II, III and V increased slightly, in a reproducible fashion. These peaks were further diminished at greater concentrations of 2-ME. After complete reduction, only three constituent proteins of phage $Q\beta$ could be observed. These results show that the complexes disassemble via intermediate products to the constituent protein subunits. These intermediates proved helpful in determining the structure of the complexes (see the following).

Structure of the specific complex

To determine the constitution of each peak, the gel was cut into slices and the protein eluted from each slice. The protein of peak VI was isolated, as shown in Fig. 3*a*. Reduction with 2-ME shifted the mobility of the protein peak to that corresponding to coat protein subunit (Fig. 3*b*). Thus peak VI was composed solely of coat protein subunits. The next question was how many coat protein subunits make up the complex of peak VI? As partial reduction of the complex led to the production of intermediates, in this case oligomers of coat protein subunits, it was possible to determine the polymerizing number of the original complex from the order of the intermediate oligomers. After mild reduction of the complex, four new peaks

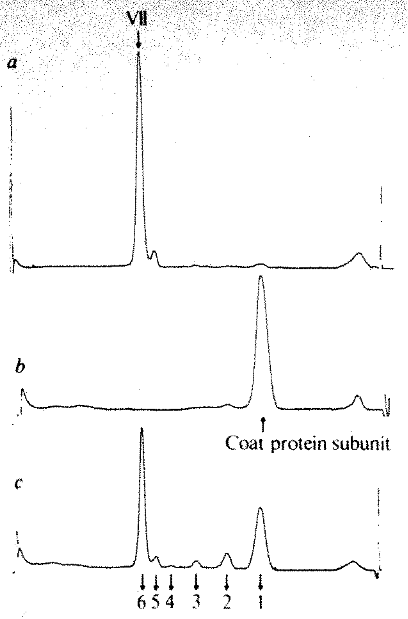

Fig. 4 Analysis of peak VII. The protein of peak VII was eluted from the sliced gel as described in Fig. 3 legend. The protein solution was treated with 0% (*a*), 5% (*b*) and 0.005% (*c*) 2-ME and then electrophoresed. After treatment with 5% 2-ME, only the peak corresponding to coat protein subunit was observed. Thus, peak VII was shown to consist of coat protein subunits. In *c*, six peaks were observed and no other peak could be detected in any other conditions. When the peaks were numbered as indicated by the arabic figures in *c*, peak VII was the sixth peak. Peaks 1–5 showed the same mobilities as corresponding peaks in Fig. 3*c*.

could be observed (Fig. 3*c*). No other peaks could be detected using different conditions, although greater reduction led to conversion of high molecular weight complexes to low molecular weight ones. Thus the four peaks are successive oligomers of coat proteins—monomer to tetramer. Therefore, the original complex (peak VI) must be a pentamer of coat protein subunits.

Peak VII (Fig. 4*a*) was analysed in the same way. Complete reduction leading to its full dissociation yielded only coat protein subunits, showing that peak VII consists of only coat protein subunits (Fig. 4*b*). With intermediate reduction, six peaks could be observed (Fig. 4*c*). No other peaks could be observed in different conditions, and the mobilities of the six peaks were the same as those of peaks I–III, V–VII in Fig. 1*a*. Thus peak VII consists of hexamers of coat protein subunits.

Next, peaks VIII and IX were examined. Because of their low mobilities, the separation distance between these peaks was relatively short compared with that between high-mobility peaks. Protein fractions eluted from the sliced gels therefore contained components of both peaks, in various ratios, depending on the position of the slices (peaks IX : VIII 10.1, 8.5, 3.0 and 0.7 in Fig. 5*a–d*). After treating each fraction with 2-ME, two peaks could be observed (Fig. 5*a–d*, lower patterns). The low-mobility peak corresponds to A_1 protein and the other to coat protein subunits. The molar ratios of coat protein subunit to A_1 protein are 4.6, 4.3, 4.1 and 4.9 in Fig. 5*a–d* respectively, assuming MWs of 39,000 for A_1 protein (electrophoretically determined) and 14,050 for coat protein subunit (ref. 11), and that the peak area is proportional to the applied quantity of protein, as shown in Fig. 1*c*. The high molar ratio for Fig. 5*d* is thought to be due to the contamination of peak VII (15%) which consists of coat protein subunits. On the basis of the molar ratios of A_1 protein to coat protein subunit, as well as the MWs of peaks VIII and IX, it is concluded that peak VIII consists of one A_1 protein molecule and four coat protein subunits, and peak IX consists of one A_1 protein molecule and five coat protein subunits. As the difference of the apparent MWs between peaks VIII and IX (12,000) equals that between peaks VI and VII (13,000), it is reasonable to conclude that the complex of peak IX is larger by one coat protein subunit than that of peak VIII.

Minor peaks I–III and V show the same mobilities as monomer, dimer, trimer and tetramer of coat protein subunits. It was observed, however, that the size of peak III increased with intermediate reduction and after full reduction it remained as an A_1 protein (Fig. 2). This suggested that peak III is a mixture of coat protein trimer and A_1 protein; this has been confirmed by a reduction experiment of the isolated components (not shown). Peak IV was not changed by treatment with various concentrations of 2-ME (Fig. 2), and after isolation, peak IV was shown to be composed of A_2 protein.

These results show that ~90% of the total phage protein is in the form of pentamers and hexamers, both of which are composed of only coat protein subunits. Accordingly, about 95% of all the coat protein subunits is calculated to be in the form of pentamers and hexamers since the fraction of the coat protein subunits in the whole phage protein is ~94%. The remaining coat protein subunits mostly form pentamers and hexamers with the A_1 protein molecules (peaks VIII and IX). Since the amount of A_1 protein is ~4% of the total phage protein and ~40% of peaks VIII and IX consists of A_1 protein, most of the A_1 protein molecules are in the form of pentamers and hexamers with coat protein subunits. A_2 protein does not form such a complex.

Capsid structure model

To formulate a model of the phage Qβ capsid, we had to determine the contribution from each component. The total weight of protein per particle is 2.7×10^6 daltons, using the reported MW of 4.2×10^6 for the the phage particle[16] and 1.5×10^6 for its RNA[17]. About 90% of all the protein is in the form of pentamers and hexamers which are made up of the

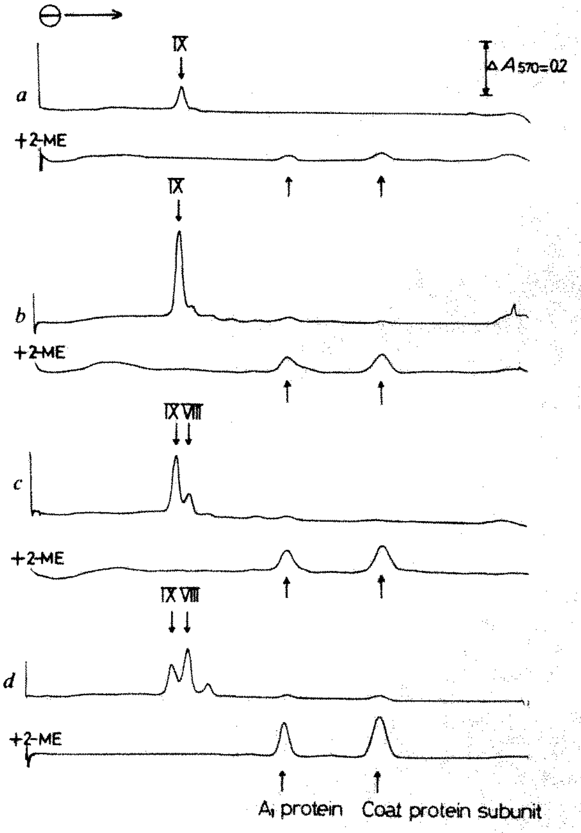

Fig. 5 Analysis of peaks VIII and IX. Protein was eluted from each sliced gel which contained the components of peaks VIII and IX. The ratio of components of peak IX to peak VIII were different in each slice: 10.1 (*a*), 8.5 (*b*), 3.0 (*c*) and 0.7 (*d*). There was a significant amount of peak VII (15%) (shown in *d*). The protein solutions were electrophoresed after treatment with 5% 2-ME (lower) or without treatment (upper). After treatment, two peaks were observed: the high-mobility one corresponds to coat protein subunit and the other to A_1 protein. The area ratios of coat protein subunit to A_1 protein were 1.64 (*a*), 1.54 (*b*), 1.49 (*c*) and 1.78 (*d*). The value for *d* was high due to the contamination of peak VII.

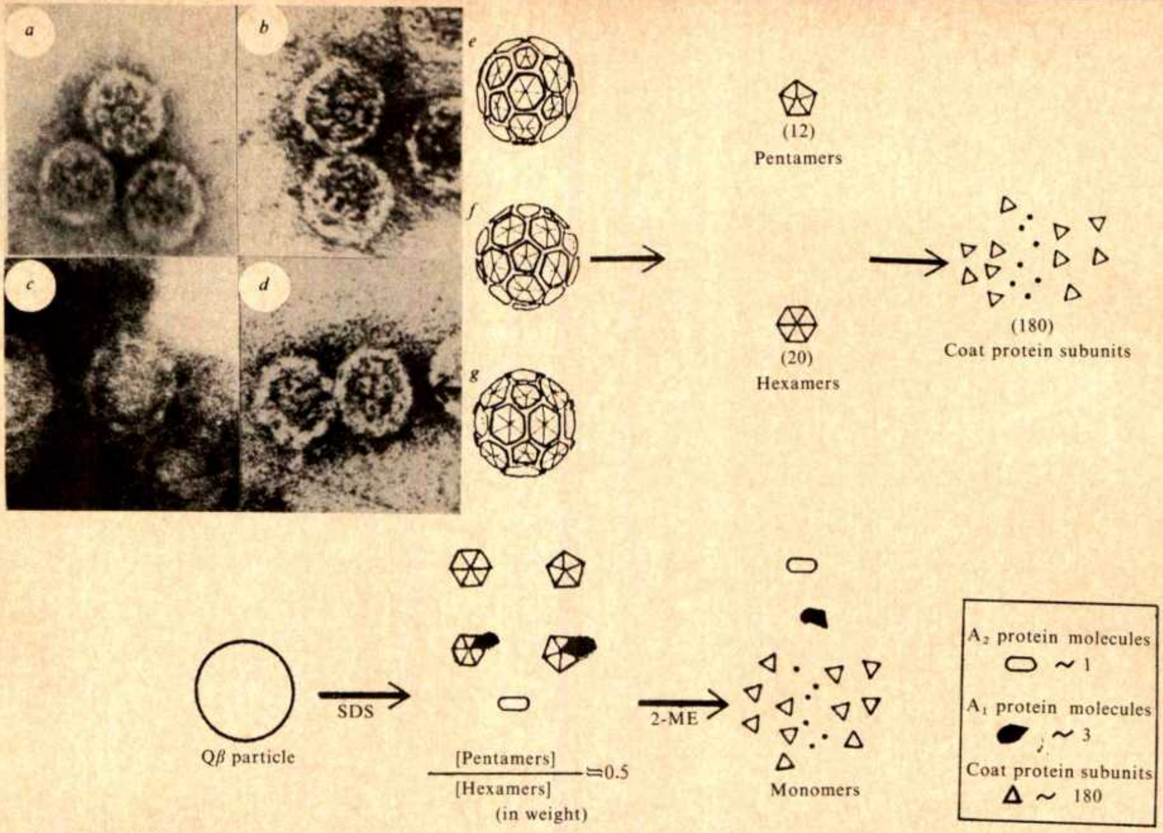

Fig. 6 Summary of electron microscopic (upper half) and chemical (lower half) observations. Phage Qβ particles were observed by electron microscopy as described previously[23] although they were stained with phosphotungstate. The phage Qβ was a spherical particle (mean diameter ~250 Å). On the particle surfaces, morphological units (capsomeres) were observed, which appeared as a hollow cylinder (~30 Å high and ~60 Å diameter with a ~25 Å diameter hole). Capsomeres were regularly arrayed on the particle in four ways: *a*, one capsomere surrounded by six capsomeres; *b*, one capsomere surrounded by five capsomeres; *c*, 10 capsomeres at the periphery of a partcle; *d*, four capsomeres arranged at the four corners of a lozenge respectively. Based on the electron microscopy observations, the particle model was constructed, in which capsomeres were located at each apex (12) and on each facet (20) of a icosahedral structure. The capsomeres at 3-fold axes were drawn as hexagons and those at 5-fold axes as pentagons. The model is illustrated, viewed along the 3-fold axes (*e*), along the 5-fold axes (*f*) and along the 2-fold axes (*g*). According to the quasi-equivalence theory[4], the capsomeres located at the 3-fold axes are hexamers and those at the 5-fold axes are pentamers. Then, the total number of subunits can be estimated to be $5\times12+6\times20=180$. Lower half: schematic drawings summarizing the chemical study. After phage Qβ particles were treated with SDS, pentamers and hexamers of coat protein subunits were produced in a weight ratio of 0.5:1. In addition, A_1 protein-containing pentamers and hexamers were detected as minor products. These pentamers and hexamers were dissociated to subunits after reduction with 2-ME. It was calculated that one particle contained as protein components ~180 coat protein subunits, ~3 A_1 protein molecules and ~1 A_2 protein molecule.

coat protein subunits, and the weight ratio of pentamer to hexamer is 0.5. The number of these complexes per particle, therefore, is calculated to be 11.5 for the pentamers and 19.2 for the hexamers, based on the chemically determined MW of the coat protein subunit (14,050). On the other hand, A_1 protein-containing pentamers and hexamers comprise ~8% of the total amount of protein and are present in an equal amount per particle. There are thought to be about one of each per particle, based on their MWs ($95{,}000=39{,}000+14{,}000\times4$ for the pentamer; $109{,}000=39{,}000+14{,}000\times5$ for the hexamer). Therefore, it is estimated that, on the average, one particle contains ~12 pentamers and ~20 hexamers. In addition, the particle contains A_2 protein as a minor component (~2% of total protein). As the MW of A_2 protein is 44,000, we estimate there is about one A_2 protein per particle; this is in good agreement with published data[9].

The presence of 12 pentamers and 20 hexamers is consistent with a structure based on the $T=3$ icosahedral surface lattice[4], but the symmetry cannot be exact since only some of the pentamers and hexamers contain A_1 protein, and we do not know the location of the one copy of A_2 protein per particle.

Electron microscopy

The relationship between the chemically obtained complexes and the morphologically expected units on the capsid was investigated by observing Qβ particles by electron microscopy. The Qβ particle appeared as a regular, spherical particle (~250 Å in diameter) with surface morphological units (capsomeres) consisting of hollow cylinders (~30 Å high and ~60 Å in diameter with a ~25 Å diameter hole) (Fig. 6). Capsomeres were regularly arrayed on the surface in one of four patterns: (1) one capsomere surrounded by the six nearest capsomeres (Fig. 6*a*); (2) one capsomere surrounded by the five nearest capsomeres (Fig. 6*b*); (3) ten capsomeres radially arranged at the periphery of a particle (Fig. 6*c*); (4) four capsomeres arranged at four corners of a lozenge respectively (Fig. 6*d*). These patterns would correspond to views of different sides of an icosahedral structure model as illustrated in Fig. 6, in which six capsomeres were arrayed around 3-fold axes (*e*), five capsomeres arrayed around 5-fold axes (*f*), 10 capsomeres located at the periphery (*f*) and four capsomeres arrayed in the 2-fold symmetrical position (*g*). From such consistency, it is concluded that the Qβ capsid is composed of 32 capsomeres, arranged in an icosahedral symmetry (details will be published elsewhere by H. T., H. Funakoshi and K. I.). These morphological observations are consistent with the chemical estimation of the number of pentamers and hexamers per particle.

Protein subunits and icosahedral capsid structure

We have demonstrated that the pentamers and hexamers are stabilized by intermolecular disulphide linkage. As the coat protein subunit (131 residues) has two cysteine residues at positions 73 and 79 (ref. 11), pentamers and hexamers of coat protein subunits can be held by successive disulphide bonds between subunits. Although we have no direct evidence of disulphide bonds in the particle, we believe this to be the case; even when Qβ particles were disassembled at the low pH (pH<4) or in the presence of an excess amount of iodoacetic acid[18] most of the coat protein subunits were in the form of pentamers and hexamers, in the ratio of 0.5 pentamers to 1.0 hexamer. Furthermore, spectrophotometric studies using 5, 5′-dithiobis(2-nitrobenzoic acid) in the presence of guanidine hydrochloride or SDS[19] showed most of SH groups were blocked (not shown). Pentamers and hexamers were clearly detected as chemical entities, although it remains to be determined whether the disulphide bonds are formed before or after virus assembly.

A_1 protein is known to be synthesized by the failure of termination of translation of coat protein cistron[12,13], but its role is unknown, though the protein was reported to be essential for the formation of infectious particles[20]. We have shown here that an A_1 protein molecule is substituted for a coat protein subunit in a pentamer and a hexamer. A_1 protein may bind coat protein subunits through the same contact between coat protein subunits since the N-terminus of A_1 protein molecule is identical to the entire stretch of coat protein subunit. A_1 protein may thus serve to modify the surface structure rather than to introduce a different intermolecular contact.

We particularly thank Professor Itaru Watanabe for giving us the opportunity to investigate phage Qβ and for stimulating advice, also Drs K. Furuse, T. Shiba, H. Akanuma, H. Funakoshi, M. Moroi and S. M. Jung for helpful suggestions and Professor M. Yamasaki for encouragement. This study is supported in part by Scientific Grants from the Ministry of Education, Science and Culture of Japan.

Received 23 October 1981; accepted 25 May 1982.

1. Loeb, T. & Zinder, N. D. *Proc. natn. Acad. Sci. U.S.A.* **47,** 282–289 (1961).
2. Watanabe, I., Nishihara, T., Kaneko, H., Sakurai, T. & Osawa, S. *Proc. Jap. Acad.* **43,** 210–213 (1967).
3. Miyake, T. *et al., Proc. natn. Acad. Sci. U.S.A.* **68,** 2022–2024 (1971).
4. Caspar, D. L. D. & Klug, A. *Cold Spring Harb. Symp. quant. Biol.* **27,** 1–24 (1962).
5. Hohn, T. & Hohn, B. *Adv. Virus Res.* **16,** 43–98 (1970).
6. Crowther, R. A., Amos, L. A. & Finch, J. T. *J. molec. Biol.* **98,** 631–635 (1975).
7. Horiuchi, K., Webster, R. E. & Matsuhashi, S. *Virology* **45,** 429–439 (1971).
8. Matthews, K. C. & Cole, R. D. *J. molec. Biol.* **65,** 1–15 (1972).
9. Weber, K. & Konigsberg, W. in *RNA Phages* (ed. Zinder, N. D.) 51–84 (Cold Spring Harbor Laboratory, New York, 1975).
10. Weiner, A. M., Platt, T. & Weber, K. *J. biol. Chem.* **247,** 3242–3251 (1972).
11. Konigsberg, W., Maita, T., Katze, J. & Weber, K. *Nature* **227,** 271–273 (1970).
12. Moore, C. H., Farron, F., Bohnert, C. & Weissmann, C. *Nature new Biol.* **234,** 204–206 (1971).
13. Weiner, A. M. & Weber, K. *Nature new Biol.* **234,** 206–209 (1971).
14. Strauss, E. G. & Kaesberg, P. *Virology* **42,** 437–452 (1970).
15. Furuse, K. *et al. Virology* **97,** 328–341 (1979).
16. Overby, L. R., Barlow, G. H., Doi, R. H., Jacob, M. & Spiegelman, S. *J. Bact.* **91,** 442–448 (1966).
17. Boedtker, H. & Gesteland, R. F. in *RNA Phages* (ed. Zinder, N. D.) 1–28 (Cold Spring Harbor Laboratory, New York, 1975).
18. Glazer, A. N. in *The Proteins* Vol. 2 (eds Neurath, H. & Hill, R. L.) 1–103 (Academic, New York, 1976).
19. Glazer, A. N., Delange, R. J. & Sigman, D. S. in *Chemical Modification of Proteins,* 113–114 (Elsevier, New York, 1975).
20. Hofstetter, H., Monstein, H.-J. & Weissmann, C. *Biochim. biophys. Acta* **374,** 238–251 (1974).
21. Watanabe, I., Miyake, T., Sakurai, T., Shiba, T. & Ohno, T. *Proc. Jap. Acad.* **43,** 204–209 (1967).
22. Gorovsky, M. A., Carlson, K. & Rosenbaum, J. L. *Analyt. Biochem.* **35,** 359–370 (1970).
23. Funakoshi, H. & Iso, K. *J. Biochem.* **70,** 201–204 (1971).

LETTERS TO NATURE

Is there a local source of magnetic monopoles?

S. Dimopoulos*, S. L. Glashow & E. M. Purcell

Lyman Laboratory of Physics, Harvard University, Cambridge,
Massachusetts 02138, USA

F. Wilczek

Institute for Theoretical Physics, University of California,
Santa Barbara, California 93106, USA

Cabrera[1] has reported the possible detection of a magnetic monopole in flight with magnetic charge g given by the Dirac condition[2] $2eg = \hbar c$. Here, we accept the Cabrera candidate as a t'Hooft–Polyakov[3,4] monopole of mass $M \sim 10^{16}$ GeV as expected[5] in SU(5) or other grand unified theories. The monopole flux on Earth, on the basis of the single candidate, is $f \sim (0.1)$ cm^{-2} yr^{-1} $(2\pi$sr$)^{-1}$, presumably consisting of roughly equal numbers of north and south monopoles. Galactic or intergalactic monopoles will have typical velocities of ~ 300 km s^{-1}. The Cabrera flux would correspond to a mass density $fM/v \sim 1$ GeV cm^{-3}. Because the mean mass density of the Universe cannot exceed 10^{-5} GeV cm^{-3}, the mean flux of monopoles in the Universe must be at least five orders of magnitude smaller than f (refs 6,7). This would not be a problem if the monopoles were concentrated in the Galaxy. However, Parker has shown[8] that the existence of galactic magnetic fields is inconsistent with a mean galactic monopole flux of 10^{-7} cm^{-2} yr^{-1}. It follows that f must be a local flux resulting from the special nature of the observation site. Three possibilities come to mind: the local monopole flux may be associated with the Earth, the Sun, or with the Solar System as a whole.

If the monopoles observed at the Earth's surface originate from the core, as does the local magnetic field, and if the flux is not time dependent, the Earth has emitted more than 10^{27} monopoles since its birth, implying an initial (or present) monopole density $n \sim 1$ cm^{-3}. However, the density of monopoles in the Earth's core is bounded by[8]

$$n < B/8\pi g v \tau \qquad (1)$$

where $\tau = 10^4$ yr is the characteristic growth time of the geomagnetic field, v is the monopole velocity within the core, and B is the magnetic field within the core. With a core field ~ 100 G, we expect $v \sim 3$ km s^{-1} on the basis of either magnetic or gravitational force arguments. This gives a limit $n < 10^{-9}$ cm^{-3}. Thus, the Cabrera flux cannot originate from the Earth.

Can the monopole flux seen on Earth originate from the Sun, in the fashion of radiant energy or solar wind? If so, the Sun has emitted (and presumably still contains) some 10^{36} monopoles. This implies a mean solar monopole density $n \sim 10^3$ monopoles cm^{-3}, with 10^{-5} of the solar mass made up of monopoles. If the monopoles are gravitationally bound to the Sun, they must have velocities ~ 400 km s^{-1} and kinetic energies $\sim 10^{10}$ GeV. They will lose energy in nuclear collisions, and by inducing currents in the highly conductive solar medium. The energy they dissipate by these losses must be compensated by magnetic acceleration. Thus, there must be a mean interior magnetic field in the Sun of $\sim 10^3$ G so that

$$g\langle B \rangle \sim \mathrm{d}E/\mathrm{d}x \sim 10 \text{ MeV cm}^{-1} \qquad (2)$$

The characteristic time of the solar interior field is assumed to be ~ 20 yr, the period of the sunspot cycle. With these values of B and τ, equation (1) yields an upper bound on the density of monopoles in the Sun, $n < 10^{-7}$ cm^{-3}. Moreover, the ohmic loss due to 10^{36} orbiting monopoles is $\sim 10^5 L_\odot$. For both these reasons, it is difficult to explain the observed monopole flux in terms of a direct solar flux. Of course, it could be that most of the solar monopoles are concentrated in the centre of the Sun, and are only rarely extricated by transient magnetic fields. Escape velocity for these monopoles is $\sim 1{,}400$ km s^{-1}, which would require magnetic fields $\sim 10^5$ G over distances $\sim R_\odot$.

Can the local monopole flux result from a diffuse cloud of monopoles which are in newtonian orbits about the Sun, rather

---

* Permanent address: Physics Department, Stanford University, Palo Alto, California 94305, USA.

0028-0836/82/340824-02$01.00

like meteorites and meteoritic dust? Their velocities about the Sun will then be $\sim 30\ \mathrm{km\ s^{-1}}$, while their arrival velocities at Earth will vary from 10 to $70\ \mathrm{km\ s^{-1}}$ as do the arrival velocities of meteorites. Their density must be $\sim 10^{-15}\ \mathrm{cm^{-3}}$ to explain the observed flux, corresponding to $\sim 10^{24}$ monopoles within the Earth's orbit. These monopoles are subject to a solar magnetic field $\sim 3\times 10^{-5}$ G, and a consequent magnetic force which is $\sim 10^{-4}$ of the solar gravitational force. Following Parker[9], we have estimated the time over which the magnetic perturbation significantly alters the energy of a monopole in solar orbit. We assume that the distant solar magnetic field fluctuates over a time scale of half a solar rotation period, $T = 10^6$s, and that its magnitude at 1 AU is 3×10^{-5} G. The residence time of a monopole in solar orbit is given by[9]

$$t = (v/c)^2 T^{-1} \omega^{-2} \tag{3}$$

where $\omega = gB/Mc \sim 2\times 10^{-15}$ Hz. We find $t \sim 100$ Myr. The eventual fate of the orbiting monopoles will be to fall into the Sun, or to escape the Solar System. In any case, to maintain the local monopole flux, a source of $\sim 10^9$ monopoles per second is required.

We must verify that the monopole flux on the Earth does not generate too great a monopole density within the Earth. The incident monopoles have kinetic energy $\sim 10^8$ GeV and lose $\sim 1\ \mathrm{MeV\ cm^{-3}}$ (hence $\leq 10^6$ GeV) as they traverse Earth. They pass through the Earth without stopping. Their density, $n \sim 10^{-15}\ \mathrm{cm^{-3}}$, is well within the bound set by equation (1).

The monopole cloud of the Solar System is maintained either by an external (cosmic) or internal (solar) flux. Cosmic monopoles traversing the Sun may lose enough energy by ohmic losses or magnetic deceleration to be captured into solar orbit. Indeed, $\sim 10^9$ monopoles per second pass through a hypothetical sphere of solar radius if the Parker bound on the flux of galactic monopoles is saturated. The actual number impacting the Sun is larger by the factor $[(1+(v_E/v)^2]$ where v is the monopole velocity and $v_E \sim 600\ \mathrm{km\ s^{-1}}$ is the escape velocity from the Sun. As $\langle v\rangle \sim 300\ \mathrm{km\ s^{-1}}$, the enhancement is considerable, particularly for slower monopoles. The Sun may well capture enough monopoles to sustain its cloud.

On the other hand, the cloud may be fed internally by a flux of $\sim 10^9$ monopoles per second which is extracted from the Sun by solar flares. Either mechanism implies a solar monopole number of $\sim 10^{26}$ and a density of $n \sim 10^{-7}\ \mathrm{cm^{-3}}$, corresponding to an acceptable ohmic dissipation of $10^{-5} L_\odot$. With kilogauss mean fields, equation (2) is satisfied. The limit on monopole density given by equation (1) is just saturated, a result whose significance we discuss below.

Simple considerations of magnetic diffusivity yield the expression $\tilde{T} = (4\pi\sigma/c^2)R^2$ for the characteristic time of the solar magnetic field. This is known to overestimate $\tilde{T}$ by six orders of magnitude[8]. In the presence of monopoles, $\tilde{T}$ is correctly determined to be ~ 20 yr by the magnetic dissipation time given in equation (1).

Monopoles within the Sun can have other significant effects. They can lead to a lower central temperature by promoting heat transfer from the solar interior, or by catalysing nuclear fusion or nucleon decay. This could ameliorate the solar neutrino problem.

It is suggested that magnetic monopoles may have a substantial cross-section σ to induce nucleon-number violating processes such as

$$\text{Monopole} + p \rightarrow \text{Monopole} + (e^+ \text{ or } \pi^+\bar{\nu}). \tag{4}$$

This process can be observed directly as monopoles pass through material on Earth; it can contribute to energy production in the Sun; and it can act as a source of high-energy solar antineutrinos which can be detected on Earth. Monopole-induced nucleon decay, seen in the laboratory, will not seem to conserve momentum because the recoiling monopole is not detected. A limit can be placed on σ from known limits on the nucleon lifetime: $f\sigma < \tau_p^{-1}$ where τ_p is the lower limit on the proton lifetime in experiments where momentum conservation is not imposed. Taking $\tau_p > 10^{29}$ yr, we obtain $\sigma < 10^{-28}\ \mathrm{cm^2}$. With this cross-section, catalytic nucleon decay within the Sun can account for no more than $10^{-6} L_\odot$. However, this process can also yield GeV electron antineutrinos, with a flux on Earth as high as $10^3\ \mathrm{cm^{-2}\ s^{-1}}$. A search for this kind of solar emanation is called for.

The net flux of monopoles from all stars in the Galaxy would amount to 10^{28} monopoles per year. These will be accelerated by galactic magnetic fields to an escape energy of 10^{10} GeV, requiring an energy source of $10^{38}\ \mathrm{GeV\ yr^{-1}}$. This is easily compatible with the estimated energy content of the galactic magnetic field $(B^2/8\pi)V \approx 10^{57}$ GeV and a restoration time of one galactic period, or 10^8 yr.

We conclude that the Cabrera flux of magnetic monopoles can be understood in terms of an orbiting cloud of monopoles in the Solar System, which is replenished by a small 'monopole wind' from the Sun or from the Galaxy. Monopoles may have an important role in solar energetics. Our hypothesis can be established if the monopole flux on Earth is shown to be similar (in velocity distribution, angular distribution, and its seasonal and diurnal variations) to the observed flux of meteorites, except for the fact that monopoles (but not meteorites) pass freely through the Earth.

We thank J. Preskill and R. Rosner for valuable discussions. This research is supported in part by the NSF under grant no. PHY77-22864.

Received 10 June; accepted 30 June 1982.

1. Cabrera, B. *Phys. Rev. Lett.* **48,** 1378–1381 (1982).
2. Dirac, P. A. M. *Proc. R. Soc.* **A133,** 60–72 (1931); *Phys. Rev.* **74,** 817–830 (1948).
3. t'Hooft, G. *Nucl. Phys.* B**79,** 276–284 (1974); B**105,** 538–547 (1976).
4. Polyakov, A. M. *Pis'ma Ekxp. Teor. Fiz.* **20,** 430–433 (1974); *JETP Lett.* **20,** 194–195 (1974).
5. Georgi, H. & Glashow, S. L. *Phys. Rev. Lett.* **32,** 438–441 (1974).
6. Preskill, J. *Phys. Rev. Lett.* **43,** 1365 (1979).
7. Lazarides, G., Shafi, Q. & Walsh, T. F. *Phys. Lett.* **100**B, 21–24 (1981).
8. Parker, E. N. *Astrophys. J.* **160,** 383–404 (1970).
9. Parker, E. N. *Astrophys. J.* **139,** 951–958 (1964).
10. Wilczek, F. *Phys. Rev. Lett.* **48,** 1146–1149 (1982).
11. Callan, C. *Dyon-Fermion Dynamics* (Princeton University Preprint, May 1982).

Interstellar scintillation and pulsar velocities

A. G. Lyne & F. G. Smith

University of Manchester, Nuffield Radio Astronomy Laboratories, Jodrell Bank, Macclesfield, Cheshire SK11 9DL, UK

Interstellar scintillation of the intensity of pulsar radio signals is known to be the effect of diffraction in random irregularities in electron density, with typical scales of 10^{13} cm and density fluctuations of typically $3\times 10^{-4}\ \mathrm{cm^{-3}}$. The observed fading pattern is believed to be due to the combined motion of the pulsar and the observer relative to an effectively stationary and quasi-static interstellar medium; this has, however, not been clearly demonstrated so far, and the possibility has remained open that the fluctuations are due at least partly to streaming or wave motions in the medium. Recent measurements of the proper motion of pulsars by radio interferometry[1] now allow a direct test. We present here new observations which show that the scintillation characteristics of pulsars are closely related to their velocities, as measured by their proper motions.

The basic theory of scintillation was presented by Scheuer[2], who analysed the effect of a thin screen of irregularities. An analytical solution for irregularities filling the whole path, and with a gaussian distribution of sizes, is due to Lerche[3], who extended previous work by Lee and Jokipii[4]. (For a review of theory and observations see ref. 5.)

0028-0836/82/340825—03$01.00

Table 1 Scintillation characteristics and velocities

PSR	Dispersion measure (cm^{-3} pc)	Distance D (kpc)	τ_{408} (s)	B_{408} (MHz)	V_s (km s^{-1})	V_t (km s^{-1})
0301+19	15.7	0.56	335	0.23	47	100±11
0329+54	26.8	2.3	270	0.10	78	229±11
0355+54	57	1.6	110	0.034*	92	62±23
0525+21	50.8	2.0	100*	(0.14)*	230	141±180
0809+74	5.7	0.17	1,100	2.0†	23	41±5
0823+26	19.4	0.71	200	0.9†	174	365±10
0834+06	12.9	0.43	480	2.0	84	104±6
0950+08	3.0	0.09	1,700	(20)	34	15±3
1133+16	4.8	0.15	360	(7)	124	264±2
1237+25	9.3	0.33	660	4.0†	76	178±6
1508+55	19.6	0.73	100	0.06*	91	346±10
1604−00	10.7	0.36	1,260	0.9	20	12±17
1642−03	35.7	0.16	132	0.14*	49	36±11
1929+10	3.2	0.08	600	3.0†	36	33±2
1944+17	16.3	0.43	540	0.3	29	19±8
1952+29	20	0.20	780	0.9	24	41±10
2016+28	14.2	1.3	630	0.18	33	15±18
2020+28	24.6	1.3	360	0.5	98	97±18
2021+51	22.6	0.68	430	0.28	44	56±13
2217+47	43.5	1.5	150	0.13*	128	230±43

$V_s = 4.36\times10^4\,(BD)^{1/2}\tau^{-1}$ V_t is the transverse velocity from ref. 1.
* Pulsars for which a separate series of observations was made at 930 MHz.
† Scintillation patterns exhibiting frequency drifting.

The velocity V of the pattern past the observer can be obtained from the characteristic time of fading τ provided that the scale S is known. Spaced receiver observations are of little use in determining S, as it is typically larger than the Earth's diameter. It is, however, closely related to the frequency structure of the pattern observed at a single site. This arises from the relation between multi-path propagation and θ, the angular spread of waves constituting the diffraction pattern. Lee and Jokipii[4] show that the scale S is related to θ by

$$S = V\tau = 0.113\,\lambda/\theta \tag{1}$$

and the correlation bandwidth Δf is related to θ by

$$\Delta f = \frac{c}{\pi D \theta^2} \tag{2}$$

where D is the distance of the pulsar. Hence at 408 MHz

$$V = 4.80\times10^4\,(D\Delta f)^{1/2}\tau^{-1}\ \mathrm{km\ s^{-1}} \tag{3}$$

where the units of D, Δf and τ are kpc, MHz and s.

In equation (1) we have chosen the relation for a Kolmogorov power law distribution of irregularities, in contrast to a gaussian distribution: the coefficient differs only by ~10%, but there is some evidence in favour of the power law even though there is as yet no complete analytical solution for diffraction in that case[6]. The bandwidth Δf in equation (2) is the frequency separation at which the correlation falls to 0.5.

We measured the characteristic fading time and correlation bandwidth at 408 MHz for 20 pulsars whose proper motions are known[1]. Observations were made with the Mark 1A radio telescope, with an integration time of 1 min and frequency resolutions of 0.5 MHz and 0.125 MHz, using eight adjacent frequency bands. A typical observation on one pulsar lasted 3 hours. The bandwidth and time scales were found by fitting gaussian autocorrelation functions: this is formally correct only for the time scales as the autocorrelation function in frequency, although not precisely known, probably resembles the more complex function given by Lerche for the restricted case of a gaussian distribution of irregularities. We tabulate vaues of τ and of bandwidth B both as values where the autocorrelation falls to $1/e$ and assumed that $B \approx 1.2\,\Delta f$.

In fitting gaussian functions we allowed both the height of the function and its zero level as degrees of freedom; this allows for broadband intrinsic variations in the pulsar signal both on short and long time scales, as discussed by Roberts and Ables[6].

For some pulsars for which the frequency structure was not resolved with these bandwidths, a separate series of observations was made at 930 MHz using a frequency resolution of 0.5 MHz in eight adjacent bands; the time scales and bandwidths were scaled to 408 MHz assuming that $\tau \propto \nu$ and $B \propto \nu^4$. These pulsars are indicated in Table 1.

The scintillation pattern for some pulsars shows organized frequency drifting. For these, marked in Table 1, we have taken the bandwidth as the maximum, following the slope of the frequency drift. We find that values of τ and B generally repeat within ~20–30% from day to day. Some doubtful values are enclosed in parentheses in Table 1.

Figure 1 shows the relation between the observed transverse speed of the pulsar (from proper motion) and the quantity $4.36\times10^4\,(DB)^{1/2}\tau^{-1}$ where D is the distance of the pulsar as used by Lyne *et al.*[1] in obtaining the proper motion. The theoretical relation is a line of slope unity through the origin.

Part of the correlation in Fig. 1 might arise artificially as a result of errors in the estimates of the distance D, as the ordinate contains a factor of D and the abcissa contains $D^{1/2}$. We therefore show in Fig. 2 the same results as an angular measure, that is as measured and expected proper motions. These quantities are entirely independent, and the correlation is seen to be at least as good as in Fig. 1.

The fact that there are roughly equal numbers of pulsars above and below the theoretical line in Fig. 2 is indicative of the success of the theory described earlier and of the model of the electron density distribution used to derive the distances[7]. The scatter in Fig. 2 is attributable to measurement errors of the proper motion, scintillation time scales and bandwidths as well as errors in the assumed distances. The small amount of scatter indicates that even in individual cases the distance estimates cannot be very much in error.

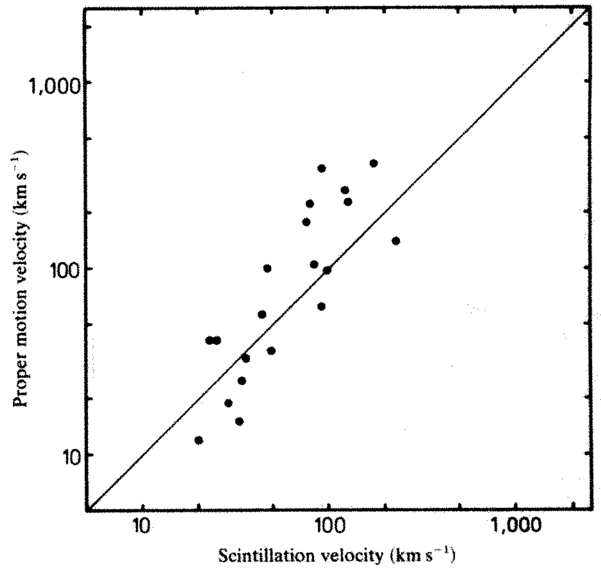

Fig. 1 The transverse speeds of 20 pulsars measured by their proper motions and compared with the speeds deduced from their scintillation characteristics.

We note that there is a good relation in Fig. 1 between observed and calculated speeds. The lower speeds obviously can be affected by the Earth's orbital velocity of 30 km s^{-1}: we suggest that this accounts for the larger than expected scintillation speeds for those pulsars having proper motions less than about 30 km s^{-1}. In contrast we note that most of the derived

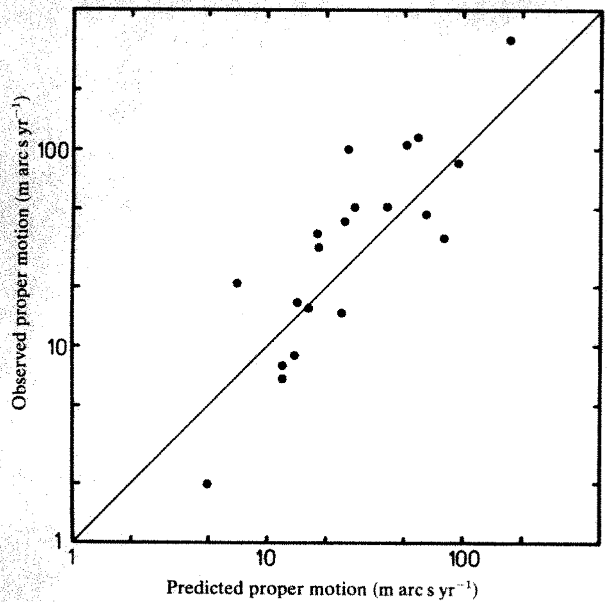

Fig. 2 The data of Fig. 1 expressed as angular motions: that is, a comparison between measured proper motions and angular speeds deduced from scintillation characteristics.

speeds of the faster moving pulsars are underestimates of the true values by a factor of about 2.

The agreement between theory and observation suggests that the irregularities are fairly evenly distributed between the pulsar and the observer. Most of the faster moving pulsars, for which the diffraction pattern is moving at about half the speed of the pulsar itself, are at large distances from the galactic plane: for these it is reasonable to suggest that the irregularities are concentrated within the half of the path closest to the observer. The main effect of such a concentration is a leverage which reduces the speed of the pattern by a factor of the order of 2.

These observations show that scintillation fading rates are directly related to the transverse velocities of the pulsars, with no appreciable contribution from velocities within the interstellar medium. This is in accordance with observations by Galt and Lyne[8] who used simultaneous reception at widely spaced sites to obtain correct values for the magnitude and direction of the velocity of PSR0329+54. Some other observations, by Rickett and Lang[9] and by Slee *et al.*[10], also using spaced receivers, gave a contrary indication, and found apparent reversals of velocity in the diffraction pattern: however, as Hewish[11] pointed out, these may have been the effect of frequency drifts in the pattern combined with small differences in receiver frequency.

We now suggest that the apparent speeds deduced from scintillation measurements alone may provide a useful indication of the magnitudes of the actual speeds of the pulsars, even at distances so large that proper motion itself cannot be directly observed.

Received 7 June; accepted 1 July 1982.

1. Lyne, A. G., Anderson, B. & Salter, M. J. *Mon. Not. R. astr. Soc.* (in the press).
2. Scheuer, P. A. G. *Nature* **218,** 920 (1968).
3. Lerche, I. *Mon. Not. R. astr. Soc.* **189,** 137 (1979).
4. Lee, L. C. & Jokipii, J. R. *Astrophys. J.* **206,** 735 (1976).
5. Rickett, B. J. *A. Rev. Astr. Astrophys.* **15,** 479 (1977).
6. Roberts, J. A. & Ables, J. G. *Mon. Not. R. astr. Soc.* (in the press).
7. Manchester, R. N. & Taylor, J. H. *Astr. J.* **86,** 1953 (1981).
8. Galt, J. A. & Lyne, A. G. *Mon. Not. R. astr. Soc.* **158,** 281 (1972).
9. Rickett, B. J. & Lang, K. R. *Astrophys. J.* **185,** 945 (1973).
10. Slee, O. B. *et al. Mon. Not. R. astr. Soc.* **167,** 31 (1974).
11. Hewish, A. *Mon. Not. R. astr. Soc.* **192,** 799 (1980).

Inclinations of the uranian rings

R. G. French*†, J. L. Elliot*‡ & D. A. Allen§

* Department of Earth and Planetary Sciences, Massachusetts Institute of Technology, Cambridge, Massachusetts 01239, USA
† Department of Astronomy, Wellesley College, Wellesley, Massachusetts 02181, USA
‡ Department of Physics, Massachusetts Institute of Technology, Cambridge, Massachusetts 02139, USA
§ Anglo-Australian Observatory, PO Box 296, Epping, New South Wales 2121, Australia

Rings formed with the birth of a planet are thought to arise after planetary condensation, from material remaining within the outer accretion limit—which has a radius of approximately two planetary radii, depending on the density of the material and the relative size of the particles[1,2]. Although the initial distribution of particles would be spherical, collisions would cause rapid evolution of the particle orbits into circular orbits in the equatorial plane of the planet[3]. Also, gaps might form at the position of strong resonances with the planet's satellites, in an otherwise broad ring. Observations of planetary rings at high spatial resolution have revealed a more complex situation. The nine confirmed uranian rings are narrow, not broad, and most have elliptical orbits, not circular. Furthermore, the Voyager observations have shown that Saturn's rings consist of a multitude of narrow ringlets, at least some of which have elliptical orbits. Here we report an additional feature that we have found for the uranian ring orbits, not predicted by current theoretical models: at least seven of the nine rings have orbits inclined to the equatorial plane of Uranus.

The kinematic models for the uranian ring orbits have become increasingly sophisticated as more occultation timings have expanded the data base over the past 5 yr. The first kinematic model[4] included only the α, β, γ and δ rings. It assumed their orbits to be circular, in a common plane that is coincident with the mean orbit plane of the five known uranian satellites. This would presumably be the equatorial plane of Uranus. The first improvement to the original model was made by Nicholson *et al.*[5], who demonstrated that the ϵ ring is elliptical and precesses under the influence of the first spherical harmonic in the uranian potential field. Following this, elliptical models were formulated for all the known rings, and six of the nine were found to have measurable ellipticities[6–9]. The most complete model[9] treats all nine rings as co-planar ellipses, precessing under the influence of the first two even harmonics of the uranian gravity potential; this model also includes the coordinates of the common orbit pole as free parameters. This model included 43 free parameters and was fitted by least squares to 105 occultation timings. The r.m.s. post-fit residual from this model is 0.31 s per degree of freedom, somewhat larger than the error of an occultation timing, which is <0.1 s in most cases. Hence, Elliot *et al.*[9] concluded that this discrepancy implied that modelling the ring orbits as co-planar ellipses is not adequate and the situation must be more complex.

Although not expected on the basis of traditional models of ring formation[3], the next step in a more complete kinematic model would include inclinations of the individual ring orbits to the equatorial plane of Uranus. For each of the nine rings we added two free parameters to our model: i, the inclination of the ring with respect to the uranian equatorial plane, and Ω_0, the angle between the line of nodes of the ring orbit and a common reference line in the equatorial plane.

An inclined, elliptical ring undergoes both precession in its orbit plane and regression of its orbital nodes. The rate of

0028-0836/82/340827—03$01.00

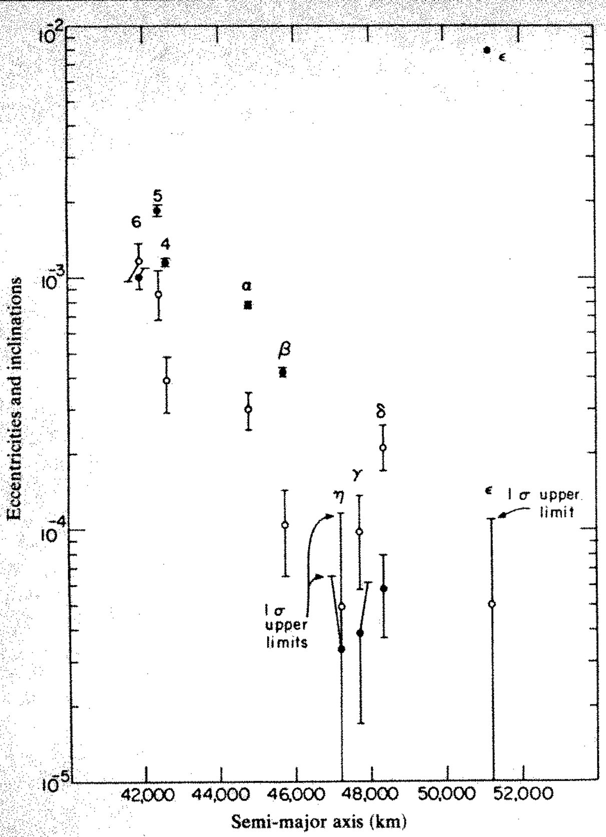

Fig. 1 Eccentricities (●) and inclinations (○) of the uranian rings. The eccentricity and inclination (in rad) for each of the nine presently known rings is plotted against the semi-major axis. Except for the eccentricity of the ε ring, the *e*s and *i*s show a decreasing trend with increasing semi-major axis. The eccentricities of the η and γ rings, as well as the inclinations of the η and ε rings, are not large enough to be statistically significant.

precession, $\dot{\varpi}$, is given to second order in i, e and J_2 by the expression

$$\dot{\varpi}=\left(\frac{GM}{a^3}\right)^{1/2}\left\{\frac{3}{2}J_2\left(\frac{R}{a}\right)^2(1+2e^2-2i^2)-\frac{15}{4}J_4\left(\frac{R}{a}\right)^4\right\} \quad (1)$$

where the terms have their usual definitions[9]. Similarly, the rate of nodal regression, $\dot{\Omega}$, is

$$\dot{\Omega}=-\left(\frac{GM}{a^3}\right)^{1/2}\left\{\frac{3}{2}J_2\left(\frac{R}{a}\right)^2(1+2e^2-i^2/2)-\frac{1}{4}\left(\frac{R}{a}\right)^4(15J_4+9J_2^2)\right\} \quad (2)$$

We fitted our expanded model to the available set of occultation timings, which included those used previously and a new set of 18 timings (see Table 1) from observation of the 26 April 1981 occultation by Uranus and its rings with the 3.9 m AAT[10]. The midtimes of the ring occultations were determined by methods used previously[6]. The results of the fit showed no substantial changes of the other parameters of the model[9], but seven of the nine rings showed statistically significant inclinations—the largest being $(1.15\pm0.21)\times10^{-3}$ rad for ring 6. The inclinations and eccentricities of the rings are plotted in Fig. 1. We note that the results for rings η and ε show no inclinations to the limit of our sensitivity. The r.m.s. post-fit residual per degree of freedom dropped from 0.31 to 0.14 s with inclinations included.

As a check on the consistency of our results, we also fitted the timing data with the precession and regression rates ($\dot{\varpi}$ and $\dot{\Omega}$) of the elliptical and inclined rings as free parameters (not calculated from J_2 and J_4 as given by equations (1) and (2)). The values for $\dot{\varpi}$ and $\dot{\Omega}$ obtained from this fit are plotted in Fig. 2, and can be compared with the solid line plot of the rates calculated from J_2 and J_4. The agreement is excellent.

Figure 1 shows that the inclinations generally decrease with increasing semi-major axis—a pattern noted earlier[9] for the eccentricities, which remains in our present model. The ε ring has an exceptionally large eccentricity compared with the other rings, but its inclination is consistent with zero. For all rings (except ε) the value of $ae\sim ai$ (within a factor of 4). Also, our results show that $e>i$ for rings 5, 4, α, β and ε. For rings 6, γ and δ we find $i<e$, but this result lies within the uncertainty imposed by statistical errors.

The widest eccentric rings—α, β and ε—have been shown to be in uniform precession[5,6], probably by the mechanism of self-gravity[11]. The uniform precession implies 'streamline' orbits, so that there is a gradient of *a*s and *e*s across the ring. Inclined rings in uniform precession would necessarily have inclination gradients within the ring. Such gradients would be more difficult to extract from the data than the eccentricity gradients, but we shall attempt to do so soon.

So far there has been little theoretical discussion about the significance of inclined rings. One way to form an inclined ring would be through the capture and tidal breakup of an incident, small body, which would almost certainly have an orbit inclined to the equatorial plane of Uranus[12,13]. This explanation is highly unlikely for the inclined uranian rings, because the inclinations are so small. The shepherd satellite model for narrow rings[14] can apparently account for orbital eccentricities[15], and according to Goldreich and Tremaine (personal communication), orbital inclinations could be produced if the shepherd satellites have inclined orbits. However, the ability of this model to account for orbital inclinations has not been examined in detail.

Even after inclinations have been included in our orbit model, we note that the r.m.s. residual per degree of freedom (0.14 s)

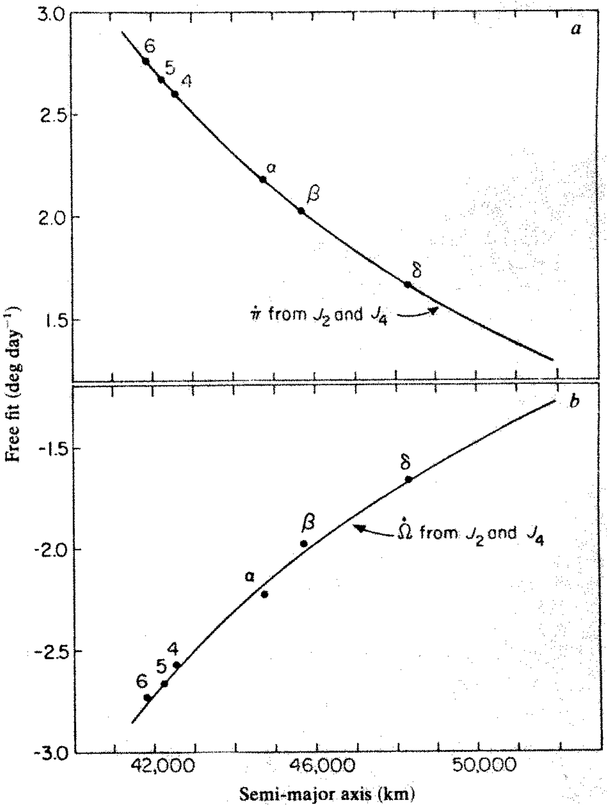

Fig. 2 Precession rates (*a*) and regression rates (*b*). The precession and regression rates for all rings having both a statistically significant inclination and eccentricity were fitted (not calculated from J_2 and J_4), simultaneously with all model parameters (except J_2 and J_4) allowed to vary in our previous fit (see Fig. 1). The results agree well with the rates calculated from equations (1) and (2), with fitted values for J_2 and J_4 (solid lines).

Table 1 Midtimes* of uranian ring occultations

Ring	Immersion	Emersion
6	19:18:56.56	20:17:50.43
5	19:18:31.03	20:18:11.02
4	19:18:19.24	20:18:27.74
α	19:16:30.51	20:20:18.76
β	19:15:42.38	20:21:05.74
η†	19:14:25.46	20:22:21.60
γ	19:14:02.63	20:22:44.16
δ	19:13:29.49	20:23:18.05
ε	19:11:10.02	20:25:28.10

* On 26 April 1981 UT.

† The occultation times for the η ring refer to the narrow core at its inner edge[9].

of our model is still significantly larger than the error in determining a ring occultation time. Hence, further improvements to our model should result in even more information about the Uranus system.

We thank A. Freedman, S. Tremaine and P. Goldreich for helpful discussions. This work was supported in part by NSF grant AST-8010699 and NASA grant NSG 7526.

Received 9 June; accepted 25 June 1982.

1. Smoluchowski, R. *Nature* **280,** 377–378 (1979).
2. Elliot, J. L. *et al. Nature* **294,** 526–529 (1981).
3. Burns, J. A. in *The New Solar System*, 129–142 (Sky Publishing, Cambridge, Massachusetts, 1981).
4. Elliot, J. L., Dunham, E., Wasserman, L. H., Millis, R. L. & Churms, J. *Astr. J.* **83,** 980–992 (1978).
5. Nicholson, P. D., Persson, S. E., Matthews, K., Goldreich, P. & Neugebauer, G. *Astr. J.* **83,** 1240–1248 (1978).
6. Elliot, J. L. *et al. Astr. J.* **86,** 127–134 (1981).
7. Nicholson, P. D., Matthews, K. & Goldreich, P. *Astr. J.* **86,** 596–606 (1981).
8. Nicholson, P. D., Matthews, K. & Goldreich, P. *Astr. J.* **87,** 433–447 (1982).
9. Elliot, J. L. *et al. Astr. J.* **86,** 444–445 (1981).
10. French, R. G. *et al. Icarus* (submitted).
11. Goldreich, P. & Tremaine, S. *Astr. J.* **84,** 1638–1641 (1979).
12. Smoluchowski, R. *Commun. Astrophys.* **8,** 69–78 (1979).
13. Aggarwal, H. R. & Obserbeck, V. R. *Astrophys. J.* **191,** 577–588 (1974).
14. Goldreich, P. & Tremaine, S. *Nature* **277,** 97–98 (1979).
15. Goldreich, P. & Tremaine, S. *Astrophys. J.* **243,** 1062–1075 (1981).

An example of induced centrifugal force in general relativity

Jeffrey M. Cohen*, William J. Sarill† & C. V. Vishveshwara‡

* Physics Department, University of Pennsylvania, Philadelphia, Pennsylvania 19104, USA
† Physics Department, Boston University, Boston, Massachusetts 02215, USA
‡ Raman Research Institute, Bangalore 560 080, India

Thirring's solution[1] for a rotating spherical mass is cited often as an example which exhibits induced Coriolis and centrifugal forces in general relativity[2,3]. Previously, it was pointed out[4] that the 'centrifugal terms' proportional to the square of the angular velocity actually represented quadrupole effects. These effects arose as a consequence of the latitude-dependent velocity distribution which generated an axially symmetric (non-spherical) mass distribution. This raises the question: Are there solutions to Einstein's equations which exhibit induced centrifugal force? If no such solutions exist, then the concept of induced rotation of inertial frames breaks down. Such a lack of connection between rotating masses and induced inertial frame rotation would in turn imply a breakdown of the Machian[5,6] idea that an inertial frame is a system of reference in which the stress-energy of the universe is at rest on the average[7]. Here we demonstrate that there are solutions to Einstein's equations which exhibit induced centrifugal force (other solutions may also be of interest in this connection[8]).

As pointed out elsewhere[2], velocity-dependent density distributions can give terms easily misinterpretable as centrifugal force—a difficulty which can be circumvented by treating a body for which the symmetry of the density distribution is velocity-independent; such a body is a rotating cylindrical shell. Other important advantages of this choice of source geometry are that it generates a simple geometry within the shell, that is, the flat space-time (ref. 9 and W.J.S., unpublished thesis), and the solution is exact. When written in the appropriate coordinates, flat space is well understood and easily interpreted. Furthermore, as the solution is exact, no ambiguities arise due to approximations.

A rotating cylindrical shell can be treated using a generalization of the Weyl–Levi-Civita[10,11] metric

$$ds^2 = -e^{+2\psi}\,dt^2 + e^{2(\gamma-\psi)}(dr^2 + dz^2) + r^2\,e^{-2\psi}(d\phi - \Omega\,dt)^2 \tag{1}$$

and the corresponding vacuum field equations

$$\begin{gathered}\nabla^2\psi = \tfrac{1}{2}r^2\,e^{-4\psi}\nabla\Omega\cdot\nabla\Omega\\ \nabla\cdot(r^2\,e^{-4\psi}\nabla\Omega) = 0\end{gathered} \tag{2}$$

derived by Ehlers[12] and later independently by the authors (ref. 13 and J.M.C. and W.J.S., unpublished). Here ∇ and ∇^2 are the usual flat space operators. The function γ is determined by quadrature from the equation

$$\gamma_r = r\psi_r^2 - \tfrac{1}{4}r^3\,e^{-4\psi}\Omega_r^2 \tag{3}$$

where the subscript denotes differentiation with respect to r and cylindrical symmetry has been assumed so that the derivatives with respect to z vanish. Inside the shell of uniform density, the only non-singular stationary exact solution is the flat space metric in rotating coordinates

$$ds^2 = -dt^2 + dr^2 + dz^2 + r^2(d\phi - \Omega dt)^2 \tag{4}$$

where Ω is a constant. This rotating form of the flat space-time is used to obtain an explicitly smooth match across the rotating shell; this form also facilitates an unambiguous identification of the Coriolis and centrifugal terms. The metric outside the shell can be obtained from the Weyl–Levi-Civita metric via the multivalued transformation $dt' = dt + K\,d\phi$ where K is a constant. The matching across the shell relates the constants Ω and K to the mass per unit length and angular velocity ω of the shell.

It is generally known that the geodesic equations corresponding to the flat space-time metric (3) contain Coriolis terms proportional to Ω and centrifugal terms proportional to Ω^2. The frame in which all these terms vanish simultaneously is defined as the inertial frame. When the angular velocity ω of the shell vanishes, Ω also vanishes. Thus, Ω can be interpreted as the induced angular velocity associated with the dragging of inertial frames. We conclude, therefore, that there are solutions of Einstein's equations which exhibit induced centrifugal as well as Coriolis forces in accordance with Machian ideas.

This work was supported in part by the NSF.

Received May 28; accepted 18 June 1982.

1. Thirring, H. *Phys. Z.* **19,** 33 (1918).
2. Pauli, W. *Theory of Relativity* (Pergamon, New York, 1958).
3. Einstein, A. *The Meaning of Relativity* (Princeton University Press, Princeton, 1950).
4. Cohen, J. M. & Sarill, W. J. *Nature* **228,** 849 (1970).
5. Brill, D. R. & Cohen, J. M. *Phys. Rev.* **143,** 1011 (1966).
6. Sciama, D. W. *Mon. Not. R. astr. Soc.* **113,** 34 (1953).
7. Dicke, R. H. *Scient. Am.* **47,** 25 (1959).
8. Cruz, V. de la & Israel, W. *Phys. Rev.* **170,** 1187 (1968).
9. Davies, H. & Caplan, T. A. *Proc. Camb. phil. Soc. math. phys. Sci.* **69,** 325 (1971).
10. Weyl, H. *Rc. Accad. Lincei* **54,** 117 (1917).
11. Levi-Civita, T. *Rc. Accad. Lincei* **26,** 381 (1917).
12. Ehlers, J. thesis, Univ. Hamburg (1958).
13. Vishveshwara, C. V. & Winicour, J. *J. Math. Phys.* **18,** 1280 (1977).

0028–0836/82/340829—01$01.00

Space shuttle ice nuclei

R. P. Turco*, O. B. Toon†, R. C. Whitten†
& R. J. Cicerone‡
* R & D Associates, Marina del Rey, California 90291, USA
† NASA Ames Research Center, Moffett Field,
California 94035, USA
‡ National Center for Atmospheric Research, Boulder,
Colorado 80307, USA

With the advent of the space shuttle era, increasing rocket activity is expected in the Earth's upper atmosphere. The space shuttle solid-fuelled booster rockets emit ~150 tonnes of alumina (Al_2O_3) particles per launch, much of which spreads throughout the upper troposphere and stratosphere[1]. Such particles can seed aerosols and clouds, and might therefore cause changes in the terrestrial radiation balance and climate[2]. Estimates are made here showing that average ice nuclei concentrations in the upper troposphere could increase by a factor of 2, and that an aluminium dust layer weighing up to 1,000 tonnes might eventually form in the lower stratosphere.

The morphology of alumina particles collected in high-altitude Titan exhaust trails may be summarized as follows[1,3]: typically smooth and spherical with occasional deeply-grooved surface structures; hexagonal α-Al_2O_3 or cubic γ-Al_2O_3 crystallography; heavy-element composition dominated by Al with smaller amounts of K, Na, Ti, Fe and Si; trace quantities of chlorine adsorbed on surfaces; and densities in the range of ~1.5 to ~3.5 g cm^{-3}, suggesting individual particles with a porous or hollow construction.

Previous theoretical investigations[4–6] focused on the role of Al_2O_3 particles as stratospheric condensation nuclei (CN, considered here as particles capable of nucleating supersaturated sulphuric acid vapour). However, space shuttle Al_2O_3 particles emitted in the stratosphere eventually filter downwards into the troposphere, after being widely dispersed over the hemisphere of injection. Inasmuch as alumina provides an excellent ice-forming epitaxy[7], they might contribute significantly to the population of background ice deposition nuclei (IN) at high altitude. IN produce ice crystals directly from the vapour phase at low temperatures (−5° to −25 °C) and supersaturations ($\geq$10%, or equivalently, relative humidities over ice ~100–110%). Cloud condensation nuclei (CCN), which can nucleate liquid water droplets at supersaturations $\leq$1%, are not subject to great influence by space shuttle emissions on a global scale.

Parungo and Allee[8,9] and Hindman and co-workers[10–13] studied IN concentrations in the stabilized ground clouds of solid-fuelled Titan rockets, which emit copious quantities of Al_2O_3 dust. They also discuss related laboratory data. Recognizing that the conditions in ground clouds are quite different from the conditions in high-altitude launch plumes, a consensus of the ground-cloud research nevertheless points to copious production of IN by rocket engines, perhaps as many as 10^{10} IN per gramme of fuel burned (active at −16° to −20 °C and 101% relative humidity over ice).

To estimate the accumulation of space shuttle IN (or SSIN) in the upper troposphere and lower stratosphere, a comprehensive one-dimensional model of multicomponent atmospheric aerosols was used[14,15]. The model segregates sulphate aerosols and unnucleated CN particles, and keeps track of the amounts of different CN materials incorporated into the aerosols by nucleation and coagulation. In this manner, the Al_2O_3 component of aerosols in the size range from 0.001 to 10 μm radius (subdivided into 40 distinct size bins) was calculated for the size- and height-dependent Al_2O_3 particle deposition rate associated with the space shuttle. The aerosol physics and chemistry treated in the model are discussed elsewhere[14]. In the present simulations, micrometeorites, which are the dominant natural stratospheric particles above ~1 μm radius, are neglected; their presence does not materially alter the results.

The adopted Al_2O_3 mass deposition profile corresponds to 52 space shuttle launches per year, with emissions averaged over the Northern Hemisphere and smoothed in time to yield a continuous injection rate[4]. All of the aluminium burned was assumed to condense as dust. Particle interactions in the rocket wake were ignored, as these interactions act mainly to reduce the particle population below ~0.01 μm radius (see below). Al_2O_3 particle injection above 8 km was included in the calculations, the total mass deposition amounting to ~5,000 tonnes yr^{-1}. The size distribution of the injected particles (the number injected per cm^3 of air per μm radius) was taken to be constant below 0.01 μm radius, and to vary as $r^{-\alpha}$ above 0.01 μm. The latter dependence, with α in the range 3.5–4.5, is suggested by direct sampling in Titan exhaust plumes[1,8,9]. The average particle density was assumed to be 1.7 g cm^{-3}, which emphasizes the number deposited.

The Al_2O_3 particle nucleation time in the stratosphere, τ_n, and the aerosol 'rainout and washout' lifetime in the troposphere, τ_r, were parameterized in a simple manner. For aluminium oxide dust, a fixed, relatively short nucleation time of 100 s was assumed as a base case[16]. Longer nucleation times up to 10^6 s were also tested. The simulated rainout loss rate decreases linearly from the ground-level value τ_r^{-1} to zero at the tropopause[14]. The baseline rainout rate of 10^{-6} s^{-1} at the ground translates into a rainout rate of ~10^{-7} s^{-1} near 10 km; ground-level rates as small as 10^{-7} s^{-1} were also considered.

To estimate the concentrations of SSIN in the upper troposphere and lower stratosphere using model predictions, three factors were taken into account: the composition of the particles, the extent of surface poisoning, and the size of the particles. The average composition of the sulphate aerosols in a given model size bin, i, is specified by the material volume fractions, $f_i(j)$, where j is a material index. Similarly, the volume fraction of material j in CN of size i is $f_i^{CN}(j)$. In the present work, the aerosol materials consist of three types: sulphuric acid aqueous solution, 'tropospheric' particulates, and aluminium oxide dust. The CN are composed of only the last

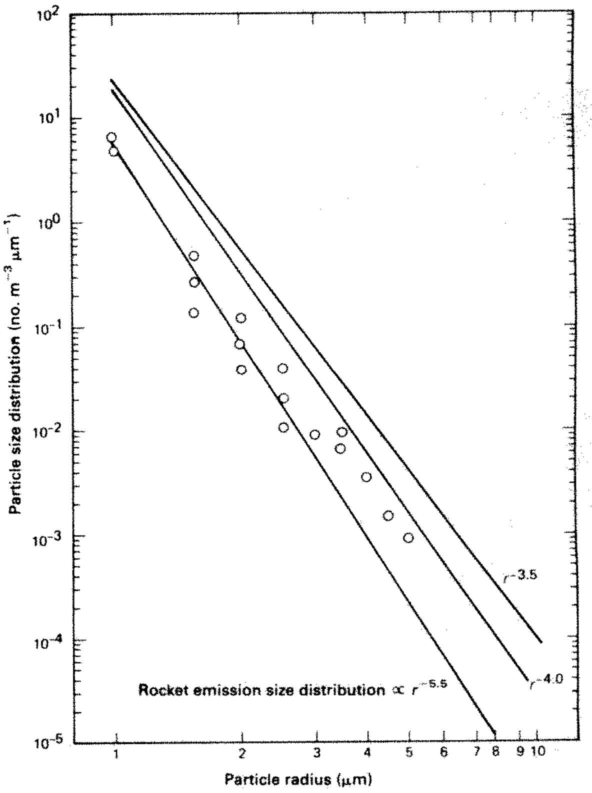

Fig. 1 Calculated stratospheric aerosol size distributions at 20 km with space shuttle particulate injection. 52 shuttle launches yr^{-1}, with emissions averaged over the Northern Hemisphere, were assumed. In each calculation, a nucleation time of 100 s was used (see text). Observations are compared: ○, data from ref. 3 for Al_2O_3 at 20 km, multiplied by 10.

0028–0836/82/340830—03$01.00

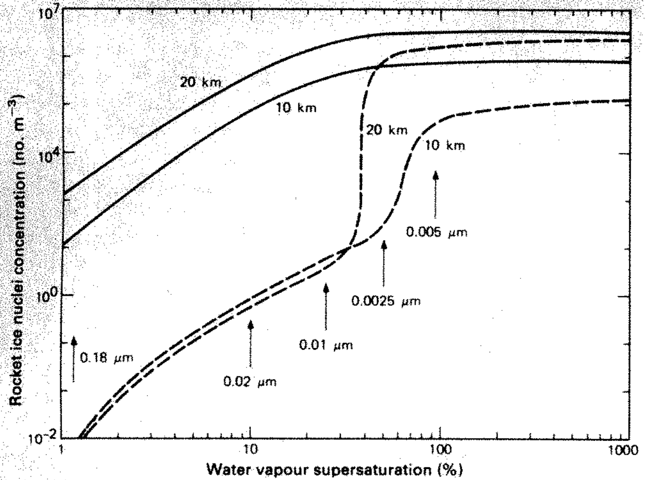

Fig. 2 Calculated space shuttle ice nuclei concentrations at 10 and 20 km altitude corresponding to different water vapour/ice supersaturations. The results were obtained for 52 shuttle launches per year with emissions averaged over the Northern Hemisphere, a dust emission size distribution of $r^{-4.5}$, and a nucleation time constant (τ_n) of 100 s. Estimates of the maximum (solid line) and average (dashed line) IN concentrations are given (see text). Also indicated are the minimum radii of spherical ice nuclei for several water vapour supersaturations at −30 °C.

two materials. The maximum number of CN identified as active SSIN in each model size bin was taken as the fraction, $f_i^{\mathrm{CN}}(\mathrm{Al})$, of the total number of CN in that size bin. Nucleated CN are classified as acid aerosols in the model, and are discussed below. Possible deactivation of Al_2O_3 CN by coagulation with background 'tropospheric' CN was neglected in the stratosphere, as the background CN concentrations are so low ($<10\ \mathrm{cm}^{-3}$).

For H_2SO_4 aerosols, two estimates of the SSIN concentration were made (and added to the CN SSIN concentrations derived above). They are a 'maximum' number and an 'average' number. Such an approach was called for because the precise extent of the poisoning of individual alumina particles cannot be predicted with the model. Rather, the average sulphate and Al_2O_3 composition fractions of all the aerosols in a given model size bin are predicted.

The maximum concentration of (nearly) pure Al_2O_3 particles identifiable among the total population of aerosols in size bin i was first estimated as

$$n_i(\mathrm{Al})_\mathrm{m} = n_i f_i(\mathrm{Al}) \qquad (1)$$

where n_i is the concentration of aerosols of size i (number cm^{-3}, excluding CN), and $f_i(\mathrm{Al})$ is the volume fraction of Al_2O_3 in aerosols of size i. However, the present model also provides information on the aerosol core size distribution in terms of the core volume moment fraction, h_i, which is a measure of the size dispersion of the cores in aerosols of size i, independent of core composition[14]. It can be shown that using h_i and f_i [where $f_i = \sum_j f_i(j)$], the maximum number of essentially-pure core aerosols may also be approximated as

$$n_i(\mathrm{core})_\mathrm{m} \doteq n_i[h_i^2 - f_i^2]/[1 + h_i^2 - 2f_i] \qquad (2)$$

Accordingly, the maximum concentration of aerosol SSIN of size i was taken as the lesser of $n_i(\mathrm{Al})_\mathrm{m}$ and $n_i(\mathrm{core})_\mathrm{m}$.

The 'average' number of aerosol SSIN was calculated by assuming that all of the aerosols of size i have an average coating, or film, of contaminating material (mainly liquid sulphuric acid). If, in any size bin, the contamination amounted to more than a uniform monolayer coating ≃4Å thick, all of the aerosols in that bin were considered to be poisoned.

The effect of particle size on the activity of rocket nuclei was estimated in two ways. In one case, the SSIN concentrations deduced above (including the contributions of CN and droplets) were truncated to exclude particles <0.01 μm radius; such particles generally require supersaturations exceeding ~10% to cause nucleation at ~−20° to −30 °C (refs 16, 17). In the second approach, the effect of particle size on the water vapour pressures of small ice spheres was calculated using the Kelvin relation[17]. At a temperature of −30 °C (adopted to estimate the critical size at each altitude) the minimum nuclei dimensions corresponding to water vapor supersaturations of 1, 10, 50, 100 and 900% are 0.19, 0.020, 0.0046, 0.0027 and 0.0008-μm radius, respectively.

Figure 1 shows projected aerosol size distributions at 20 km for several different Al_2O_3 emission size spectra, $r^{-\alpha}$. In the size range 1–10 μm, the aerosols are essentially pure alumina (>95% pure). The data of Brownlee *et al.*[3] are plotted for comparison. The close agreement between the observed size distribution and the computational results suggests that the present shuttle simulations are physically reasonable. Brownlee *et al.*[3] estimated the global stratospheric burden of Al_2O_3 in 1974–5 as ~100 tonnes. The stratospheric lifetime of particles in the size range 1–5 μm is ~1 month, implying an Al_2O_3 mass input rate of ~1,000 tonnes yr^{-1} worldwide. The space shuttle calculations in Fig. 1 yield ~10 times as many rocket alumina particles for a hemispherical input rate of ~5,000 tonnes yr^{-1}, in clear accord with the Brownlee *et al.* observations. The

Fig. 3 Predicted space shuttle ice nuclei (SSIN) concentrations in the lower stratosphere and upper troposphere. The cases shown are: *a*, $r^{-3.5}$, $\tau_n = 100$ s, $\tau_r = 10^6$ s; *b*, r^{-4}, $\tau_n = 100$ s, $\tau_r = 10^6$ s; *c*, $r^{-4.5}$, $\tau_n = 100$ s, $\tau_r = 10^6$ s; *d*, r^{-4}, $\tau_n = 10^6$ s, $\tau_r = 10^7$ s; *e*, r^{-4}, $\tau_n = 10^5$ s, $\tau_r = 10^6$ s (see the text for an explanation of these parameters). In cases *a*–*d*, 52 shuttle launches per year were assumed, with the effluent spread uniformly over the Northern Hemisphere. In case *e*, a 10-fold increase in the numbers of launches was assumed. A minimum nuclei radius of 0.01 μm was used to estimate the SSIN abundances. Maximum (solid line) and average (dashed line) numbers of Al_2O_3 nuclei are shown. △, Observed ice nuclei concentration in cirrus clouds at −30 °C. □, Maximum ice crystal concentration in cirrus clouds.

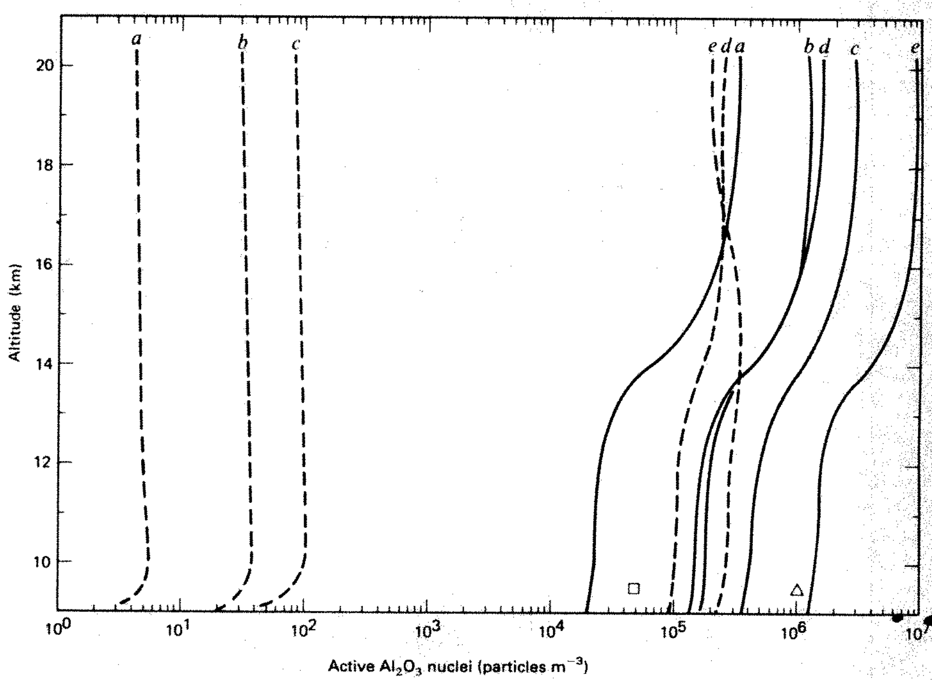

corresponding predicted global mass of the stratospheric alumina layer is ~1,000 tonnes.

The computed size distributions in Fig. 1 have a relatively simple explanation. If rocket particles are injected at all altitudes with the same size distribution ($r^{-\alpha}$), and if particle growth by condensation and coagulation can be neglected, then the resultant atmospheric aerosol size distribution depends on radius roughly as $r^{-\alpha-\beta}$, where β is the exponent of the radius dependence of the particle fall velocity; that is, $v(r) \propto r^{\beta}$. In the lower stratosphere, $1 < \beta < 2$ for particles with radii in the size range 1–10 μm. Thus, for Al_2O_3 rocket particles one expects $5 \leq (\alpha + \beta) \leq 6$, as is found in Fig. 1.

Figure 2 illustrates the influence of water vapour supersaturation on apparent SSIN concentrations. As expected, higher supersaturations yield larger IN abundances. The abrupt increase in the 'average' IN curves at S values of 40–80% is due to a substantial number of nearly-pure rocket dust particles at sizes below ~0.01 μm. For meteorologically significant supersaturations (<10%), the average number of IN in Fig. 2 is nearly four orders of magnitude smaller than the maximum number of IN. The difference represents, in one sense, the uncertainty in predictions of rocket IN abundances.

Predicted SSIN concentrations in the upper troposphere and lower stratosphere, for various physical parameter values, are given in Fig. 3. Several trends in the data are noteworthy. As in Fig. 2, with fast Al_2O_3 nucleation ($\tau_n = 100$ s), there is a difference of a factor of 10^4 between the 'average' and 'maximum' numbers of SSIN. Obviously, there is ample sulphate material present in the atmosphere to contaminate most of the injected dust grains. The maximum SSIN concentrations would apply if Al_2O_3 particle surfaces were not efficently nucleated and poisoned by H_2SO_4 vapour (see, for example, cases d and e in Fig. 3). Comparison of cases b, d and e suggests that the average SSIN concentration is roughly proportional to τ_n^{-1}. In other words, once nucleated, most Al_2O_3 grains accumulate enough sulphur vapour to be poisoned (in the model). Rainout has a much smaller influence on SSIN concentrations; the residence time of injected particles in the upper troposphere is controlled primarily by vertical diffusion (for the cases studied).

One might expect a short nucleation time ($\tau_n \sim 100$ s) to apply to Al_2O_3 dust released in the upper atmosphere. For one thing, the H_2SO_4 supersaturation ratio between 10 and 20 km altitude is quite large, ~10^4–10^5 (ref. 16). Hence, adsorption of H_2SO_4 on alumina surfaces should commence immediately on injection. Continuing growth of the dust particles larger than the critical (Kelvin) size would also be guaranteed. However, a factor which causes the effective nucleation time to be much longer is the time required to deposit a monolayer of acid molecules on the dust grain surfaces. The ambient quantity of H_2SO_4 vapour available in the neighbourhood of the launch plume is insufficient to coat more than a few per cent of the rocket particles. Nevertheless, it may be demonstrated that, within a day or so, individual launch plumes are dispersed widely enough for extensive acid adsorption to occur. This does not take into consideration the HCl vapour in the early launch plume, which acts to poison the dust surfaces at high concentrations[9–11], but appears to activate the surfaces at low concentrations[13]. Accordingly, an effective dust nucleation time $\leq 10^5$ s appears to be most appropriate for stratospheric conditions.

Many of the SSIN residing in the upper troposphere are injected between 8 and 12 km. At these altitudes, the transient space shuttle launch clouds should be considered. Case e in Fig. 3, which corresponds to a 10-fold enhancement in the average shuttle particle deposition rate, might crudely forecast the elevated IN concentrations to be expected in isolated launch plumes.

The maximum number of rocket IN that could be generated from 1 g of fuel, based on an r^{-4} Al_2O_3 dust size distribution and a minimum activation radius of 0.01 μm, is ~10^{15} IN g^{-1}. This number corresponds closely to the maximum number predicted by the model. By contrast, Hindman *et al.*[12] measured ~10^{10} IN g^{-1} in small shuttle propellant burns, while the present calculations yield estimates of average long-term shuttle IN yields ~10^{11} IN g^{-1}. Hence, the maximum SSIN profiles in Fig. 3 are very likely to represent upper-limit global-scale concentrations of artificial ice nuclei produced by space shuttles.

Typical IN concentrations measured at cirrus cloud heights are indicated in Fig. 3 (ref. 17). Maximum concentrations of ice crystals observed in cirrus clouds are also shown. Based on a comparison of measured and predicted IN concentrations, and the previous discussion, we conclude that planned space shuttle activity probably will not increase the global abundance of ice nuclei at cirrus cloud levels by more than a factor of 2, although larger transient increases might occur locally. Injected space shuttle alumina particles, on the other hand, could enhance the concentrations of stratospheric aerosols in the size range 1–10 μm radius by a factor of 10 or more, creating in the stratosphere an aluminium oxide layer exceeding 1,000 tonnes in weight.

Received 1 April; accepted 30 June 1982.

1. Potter, A. E. *Proc. Space Shuttle Environmental Assessment Workshop on Stratospheric Effects* (NASA TM X-58198, Houston, Texas, 1977).
2. Pollack, J. B. *et al. J. geophys. Res.* **81,** 1071–1083 (1976).
3. Brownlee, D. E., Ferry, G. V. & Tomandl, D. *Science* **191,** 1270–1271 (1976).
4. Hofmann, D. J., Carroll, D. E. & Rosen, J. M. *Geophys. Res. Lett.* **2,** 113–116 (1975).
5. Pollack, J. B., Toon, O. B., Summers, A., Van Camp, W. & Baldwin, B. *J. appl. Met.* **15,** 247–258 (1976).
6. Turco, R. P. *et al. J. appl. Met.* **19,** 78–89 (1980).
7. Hobbs, P. V. *Ice Physics* (Oxford University Press, 1974).
8. Parungo, F. P. & Allee, P. A. *J. appl. Met.* **17,** 1856–1863 (1978).
9. Parungo, F. P. & Allee, P. A. *J. appl. Met.* **19,** 128–130 (1980).
10. Hindman, E. E., II, & Lala, G. G. *J. appl. Met.* **19,** 122–128 (1980).
11. Hindman, E. E., Radke, L. F. & Eltgroth, M. W. *J. appl. Met.* (submitted).
12. Hindman, E. E. II, Garvey, D. M., Langer, G., Odencrantz, F. K. & Gregory, G. L. *J. appl. Met.* **19,** 175–184 (1980).
13. Hindman, E. E. & Finnegan, W. G. *Pap. 8th Conf. on Inadvertent and Planned Weather Modification*, Reno (1981).
14. Turco, R. P., Hamill, P., Toon, O. B., Whitten, R. C. & Kiang, C. S. *J. atmos. Sci.* **36,** 699–717 (1979); *The NASA-Ames Research Center Stratospheric Aerosol Model I. Physical Processes and Computational Analogs* (NASA TP 1362, 1979).
15. Turco, R. P., Toon, O. B., Hamill, P. & Whitten, R. C. *J. geophys. Res.* **86,** 1113–1128 (1981).
16. Hamill, P., Turco, R. P., Toon, O. B., Kiang, C. S. & Whitten, R. C. *J. Aerosol Sci.* (in the press).
17. Pruppacher, H. R. & Klett, J. D. *Microphysics of Clouds and Precipitation* Ch. 9 (Reidel, Dordrecht, 1978).

The Earth's early hydrosphere

A. Henderson-Sellers
Department of Geography, University of Liverpool, PO Box 147, Liverpool L69 3BX, UK

J. Graham Cogley
Department of Geography, Trent University, Peterborough, Ontario, Canada K9J 7B8

The date at which the Earth's hydrosphere came into existence is unknown. Although all current geological models for the very early Precambrian predict or suppose a hydrosphere[1–4], there are difficulties in reconciling this with geological and astronomical theories of planetary formation. Furthermore the effect of a substantial hydrosphere on the Precambrian climatic environment is difficult to determine. Recent developments make it possible to synthesize a picture of this environment during the 700 Myr preceding the deposition of the oldest known sediments[5]. We attempt such a synthesis here, drawing together work on the dynamics of accretion from the protoplanetary nebula[6,7] and of planetary differentiation[7], on the role of volatiles in impact cratering[8–10], and on the composition[11–22], isotope systematics[23–25] and radiation climatology[26–29] of the early hydrosphere. We can reconcile these diverse contributions if the hydrosphere—the inventory of excess volatiles[1]— is allowed to differentiate during accretion, with most of the H_2O and CO_2 going rapidly into oceans and sediments. Both gradual outgassing[30] and a massive CO_2 atmosphere[2] are unlikely, and a reduced mantle beneath a neutral hydrosphere is not paradoxical[1,3,17]. Results from both a one-dimensional radiative–convective (1D RC) model and a general circulation model suggest that self-regulating mechanisms are important in the climate of this early hydrosphere.

0028-0836/82/340832—04$01.00

The idea of early degassing[31] now seems more probable than slower degassing. The possible histories which cannot yet be excluded are very diverse, but the Earth probably grew over 10^7 yr or more [6] from a population of planetesimals, the largest having a mass not less than 1/500 that of the total accreted mass[7]. Not all of the impact heat is radiated away. Some of it is buried, and it sets up convection in the outer accreting layer and triggers formation of the core, perhaps as early as accreted mass $\sim 0.1 \times$ final mass. The energy released by core formation[7], and by subsequent steady settling of dense phases, establishes convection throughout the growing mantle, and volatiles differentiate upwards as iron phases segregate downwards. A growing planet tends to 'reject' icy impactors[8,9]. That is , the ratio r (ejecta mass escaping the planet/impactor mass) is large when the impactor density is small, and metals and silicates accrete much more readily than do ices; r depends also on impact velocity, however, and during growth the velocity needed for net erosion ($r > 1$) increases. In the late stages of growth only the most energetic impactors actually sputter the surface, and because the planet has depleted its source of planetesimals the latest arrivals are previously-rejected, volatile-rich bodies. This inhomogeneous accretion[32] yields an outer layer of more or less volatile-charged silicates, which separates efficiently into veneer and substrate under the influence of repeated impacts. Vapour volumes exceeding impactor volume are produced in a large proportion of impacts[8,10]. Hydrous and carbonate vapours disperse more widely, and precipitate less completely, than silicate vapours[10].

The earliest mantle, with volatiles strongly concentrated upwards, was thus overlain by an impact-processed protocrust, hydrated and carbonated but of uncertain thickness. Two points deserve emphasis:

First, geothermal energy sources were much larger during accretion than at any later time; models with outgassing due to radioactive warmup[30], or similar gradual processes, now seem mechanically and thermally improbable, and it is safest to conclude that the excess volatiles had a mass comparable with that of the present by the time accretion was completed.

Second, enrichment in ^{129}Xe of Earth-interior gases with respect to the present-day atmosphere and to Archaean shales[23,24] requires outgassing of the atmosphere within a few half-lives (17 Myr) of ^{129}I, with negligible net additions since 3,300 Myr ago[25]. The history described above explains this important observation well.

It is important to consider the oxidation state of the early hydrosphere. It seems to be accepted that H_2O and CO_2 were significant components even of the earliest atmosphere[11], but questions persist over the reduced species H_2, NH_3 and CH_4 (refs 2, 3, 12).

Modern volcanic gases have elemental bulk ratios similar to those of the excess volatiles[13], and have high-temperature low-pressure equilibria[14,15]; they seem to sample the modern hydrosphere, but not necessarily the juvenile source during accretion. The lower continental crust seems to be anhydrous[16], its volatiles dominated by CO_2. This is consistent with empirical thermodynamics[17], as is the observation that the upper mantle is strongly reduced[3,18,19]. The modern mantle seems to be closer to equilibrium with the core than with the hydrosphere. This pattern would evolve from our picture of accretion if (1) some of the H_2 in a reduced proto-mantle went to the core[20] and/or (2) the primitive outgassed volatiles were reduced. In case (2) we must explain how and when the hydrosphere lost its evolved reduced gases.

The primary control of atmospheric H_2 is escape from the top of the atmosphere[21], which for exospheric temperatures $T_x > 600$ K is controlled by hydrogen diffusion into the upper atmosphere. Most OH and H radicals, from photolysis of H_2O for example, will recombine, and only a fraction of the hydrogen arriving from below actually escapes (as H). Likely values[22] of T_x exceed 1,300 K, a temperature at which, if diffusion into the upper atmosphere were not restricted, the early Earth could evaporate an excess of hydrogen rather efficiently. In an early atmosphere without ozone, a very cold and nearly isothermal stratosphere[33] might indeed allow more H_2O vapour to diffuse upwards as the temperature inversion at the tropopause would be absent. A great excess of hydrogen, if produced by a large-body impact, would blow away very rapidly, possibly in a few minutes[21].

Other reduced constituents are also unlikely to persist. Ammonia is highly soluble in water and would be removed rapidly by rainout and by solution at the ocean surface. It would also be destroyed by photolysis[26]. It has been calculated that a mixing ratio of $<10^{-4}$ of NH_3 will convert irreversibly to N_2 in <40 yr (ref. 27). Methane photolyses at wavelengths <160 nm, where the incident solar flux is two orders of magnitude less than in the region important for the destruction of NH_3 ($\lambda <$ 230 nm), and where atmospheric water vapour will provide a substantial shield[28]. CH_4 is rapidly destroyed above 100 km (ref. 29), but at the surface it appears much more stable. However, photolysis of H_2O vapour forms large quantities of OH, an important intermediary in the methane oxidation chain. At an OH concentration of 10^5 cm^{-3} in the early troposphere[28], the life time of CH_4 at the surface is <50 yr.

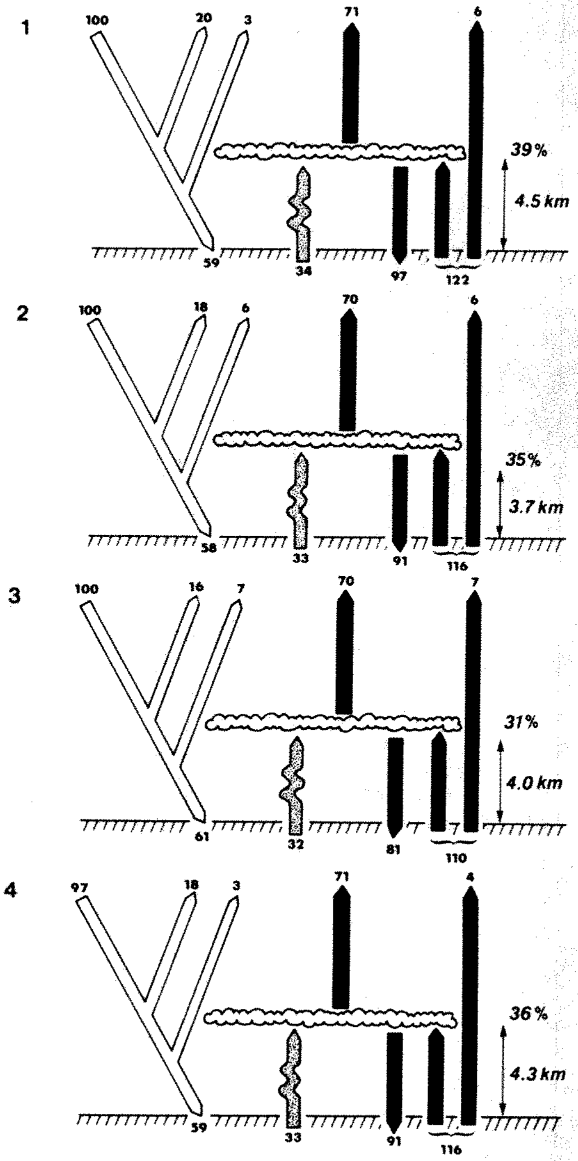

Fig. 1 Four likely configurations of the atmosphere/hydrosphere of the early Earth. The calculated fluxes have been normalized to the incident solar radiation of the standard case (1) (100 units $= \frac{1}{4}$ of 1,100 W m^{-2}). Solar fluxes (open arrows) are on the left of each sketch; upward arrows represent atmosphere (left) and surface (right) reflection. The wavy arrow represents convective heat flux from the surface, and infrared fluxes are on the right (solid arrows). Note the variations in mean cloud cover (per cent) and cloud height (km) at right.

Table 1 Radiative–convective model results

	Case 1	Case 2	Case 3	Case 4
Prescribed				
Incident solar radiation ($W m^{-2}$)	1,100	1,100	1,100	1,067
Surface albedo	0.05	0.10	0.10	0.05
CO_2 (p.p.m.v.)	1,650	1,650	330	1,650
Results				
T_s (K)	277.0	273.8	270.2	274.1
Cloud cover (%)	39.0	34.8	31.3	35.8
Mean cloud height (km)	4.48	3.71	3.99	4.32
Planetary albedo	0.23	0.24	0.23	0.22
Greenhouse ΔT (K)	29.7	27.7	22.9	28.3

The greenhouse temperature increment (present-day value ~33 K) is $T_s - [S(1-A)/4\sigma]^{1/4}$, where σ is the Stefan–Boltzmann constant, A is the planetary albedo and T_s is the mean surface temperature.

Hence in a water-vapour-dominated atmosphere neither NH_3 nor CH_4 can persist, H_2 escapes rapidly, and a reduced-gas greenhouse is at most transient, dissipating on time-scales shorter than that of accretion. Greenhouse warming was controlled by the amounts of CO_2 and H_2O vapour in the early atmosphere.

We assume that there is always enough greenhouse gas to avoid the very stable[34] 'deep freeze' predicted by some models of the present-day climate. Note, however, that little reliance can be placed on predictions made by EBMs[34] unless careful consideration is made of the changes in the horizontal advection term and the effect of clouds on the planetary albedo. We assume further that surface albedo was controlled by the presence of liquid water, as exposed land was probably less extensive (0–10% of total planetary surface) than during the Phanerozoic (20–30%)[35]. The earliest topography was probably unimodal, with a few kilometres of relief on a mechanically weak protocrust shaped by large impacts. The continental mass has increased in the course of time[36,37], and high-standing continents probably did not appear until after the end of accretion.

A massive CO_2 atmosphere, $P_{CO_2} \simeq 1,000$ mbar, is unlikely. It is not necessary in our model to invoke a passage of CO_2 from atmosphere to sediments on the long time scale of continental differentiation[5], because carbonates would form in the aftermath of large-body impacts. In any case, the P_{CO_2} of a surface mixed layer (say 50m deep and covering 70–100% of the planet) would equilibriate with the atmosphere in a few months or years. CO_2 downwelling, and reaction with the sea floor at geohydrological (a few times 10^4 yr)[38] and geological ($\simeq 10^6$–10^7 yr) rates, would increase with atmospheric CO_2. Massive quantities of both liquid water and gaseous CO_2 are thus not compatible for more than short times. We choose $CO_2 = 1,650$ p.p.m.v. ($5 \times$ PAL) in the work described below. Actual concentrations might have been much higher. However, our results (Table 1) suggest that if they were of the order of 300,000 p.p.m.v. (refs 2, 11) the Earth could have evolved into a runaway greenhouse. The hydrospheric feedbacks we describe give temperatures warmer than those of a non-interactive model both for reduced solar flux and for increased levels of greenhouse gases[33]. Some early, non-hydrothermal[39] sediments do suggest deposition from warm water[40], but there is no evidence for a runaway greenhouse in the geological or geochemical records.

Atmospheric water vapour concentration depends primarily on T_s. Cloud effects have generally been simulated crudely or neglected in studies of the early atmosphere[2,11,41] and this may[42] be a serious omission. We explore cloud effects with the GISS 1D RC model[43] due to Lacis, incorporating an interactive cloud prediction scheme[33] which makes the model much less sensitive: $\beta < \simeq 80$, down from $\beta \simeq 100$ as found in prescribed-cloud models[44]. ($\beta = S\Delta T/\Delta S$, where S is the present-day solar constant.) At each altitude, cloud cover depends on the water mixing ratio which is calculated from the mixing ratio at the previous time step by accounting for additions from condensation and removal by rainfall. In common with most 1D RC models a fixed lapse rate of 6.5 K km^{-1} and fixed relative humidity are assumed. Additionally the Bowen ratio linking latent heat flux to convective flux is a function of T_s but is assumed to be constant with height. When clouds are predicted at levels with $T < 246$ K they are assumed to be ice rather than water clouds and the effective particle radius and optical depth are adjusted accordingly. Since the cloud cover is predicted by the model, the feedbacks are internally consistent. In particular, an increase in high, optically-thin clouds tends to feed back positively on temperature[33].

Our standard state is shown as case (1) in Fig. 1 and Table 1. The solar flux is 1,100 W m^{-2} (80% of the present-day flux[45]), and the albedo and atmospheric CO_2 are consistent with our model for the close of accretion. T_s is 277 K, warm enough to support liquid water. The dark surface, and IR absorbers in the atmosphere, contribute to a greenhouse effect almost as large as it is at present. The albedo is rather low; if we increase it to represent a substantial emergence of land (case (2)), T_s drops to 274 K. If we next reduce CO_2 to its modern value (case (3)), perhaps representing consumption of CO_2 in silicate weathering, the greenhouse is weaker (23 K), although even now at $T_s = 270$ K the oceans will probably not freeze over. A largely ocean-covered Earth[36,37] is extremely difficult to glaciate. The pole–equator temperature gradient is likely to be smaller than today; but even with temperatures significantly <273 K at the poles, the absence of large land masses either to be the site of glaciers or to constrain oceanic circulation is likely to inhibit severely ice formation.

Note that the calculated temperatures (cases (1)–(3)) probably represent the lower limit to the evolutionary curve of T_s. This is because we have chosen to include the smallest likely CO_2 concentrations to focus attention on the feedback effects operating as a result of the existence of the hydrosphere. Despite this minimization of the CO_2 greenhouse effect, the lower limit temperature curve presented here is physically reasonable and is consistent with the geological data. This is because the sensitivity, β, of the interactive-cloud 1D RC model[33] is lower than that of any other climate model. If cases (1), (2) and (3) followed each other, as they well might have, then glaciation becomes more likely with time. More importantly, however, the interactive-cloud model continues to predict a stable climatic régime in the face of these radical climatic perturbations.

The most dramatic single perturbation of early climate is probably the large impact. Mass input rates were negligible in comparison, but such impacts certainly continued after the end of accretion; the lunar bombardment which formed Imbrium at 4,000–3,800 Myr may have obliterated evidence of still earlier bombardment[46]. The most significant atmospheric effects would probably be changes in the vertical distribution of water vapour and liquid water. The climatic perturbation due to a 10^{15} kg impactor depositing $\simeq 10^{16}$ kg of water in the upper atmosphere (only 0.2×10^{16} kg below 10 km) has recently been calculated using the GISS general circulation climate model[47,48]. Changes were transient (with a decay time <1 yr) and small (temperature increasing by a maximum of 0.5 K after 5 months). Long-term effects are seen only if perturbations to the lower atmosphere are strengthened by continual replenishment of species[49,50]; positive feedbacks internal to the climatic system do not seem likely.

Placement of the vapour and debris at a much higher level in the atmosphere, it has been suggested[51], may create a permanent near-worldwide layer of mesospheric ice clouds, cooling the surface through a reduction of planetary albedo by several per cent. We can simulate this albedo effect by reducing solar flux to 1,067 W m^{-2} (case (4) of Table 1 and Fig. 1). The result is a drop of only 3 K in T_s, to 274 K, within the range of cases (1)–(3) and unlikely to lead to a global freeze-over.

Comparable remarks hold for other perturbations. Even during accretion, interior convection can dissipate the input of impact and gravitational heat if lava lakes cover a fraction (10^{-3}–10^{-4}) of the surface[7]. Shallow heat radiates away rapidly from vapour clouds, ejecta and melt pools. Buried heat enhances[52] a geothermal flux due to radioactivity and energy of accretion, but even with extreme assumptions[53] this flux does not reach 1 W m^{-2}. Short-term changes with complex regional variability will follow large impacts, but we have no evidence that the climate cannot recover from these sporadic intervals of disturbance.

A substantial early hydrosphere, then, is both consistent with results from a variety of disciplines and, as our results show, powerful in solving the paradox of the faint young Sun[45]. The most plausible date for its origin is at the very beginning. Most of its properties, and especially its stability against large, irreversible changes of composition and climate, seem to follow if we identify the principal surface volatile as liquid water. There was thus a long expanse of pre-Isuan time during which the Earth could have sheltered and nurtured organisms or their precursors, and this expanse of time would surely repay closer attention.

We thank W. Rossow for helpful discussions in this work, which was begun while A. H.-S. was a NRC (US) visiting research fellow at the Goddard Institute for Space Studies. J. G. C. thanks NSERC (Canada) for support.

Received 8 February; accepted 23 June 1982.

1. Walker, J. C. G. *Evolution of the Atmosphere* (Macmillan, New York, 1977).
2. Owen, T., Cess, R. D. & Ramanathan, V. *Nature* **277,** 640–642 (1979).
3. Arculus, R. J. & Delano, J. W. *Nature* **288,** 72–74 (1980).
4. Henderson-Sellers, A., Benlow, A. & Meadows, A. J. *Q. Jl R. astr. Soc.* **21,** 74–81 (1980).
5. Moorbath, S. *Geol. Ass. Can. Spec. pap.* **20,** 89–115 (1981).
6. Safronov, V. S. *Icarus* **33,** 3–12 (1978); *Evolution of the Protoplanetary Cloud and Formation of the Earth and the Planets* (NASA Tech. Transl. TTF-677 Washington DC, 1972).
7. Kaula, W. M. *Geol. Ass. Can. Spec. pap.* **20,** 25–34 (1981); *J. geophys. Res.* **84,** 999–1008 (1979).
8. O'Keefe, J. D. & Ahrens, T. J. *J. geophys. Res.* (submitted); *Proc. 8th Lunar Sci. Conf.* 3357–3374 (1977).
9. Orphal, D. L., Roddy, D. J., Schultz, P. H., Borden, W. F. & Larson, S. A. *Pap. Conf. on Large Body Impacts and Terrestrial Evolution*, Snowbird, Utah, 41 (Lunar Planetary Institute, Houston, 1981).
10. Kieffer, S. W. & Simonds, C. H. *Rev. geophys. Space Phys.* **18,** 143–181 (1980).
11. Hart, M. H. *Icarus* **33,** 23–39 (1978).
12. Henderson-Sellers, A. & Schwartz, A. W. *Nature* **287,** 526–528 (1980).
13. Anderson, A. T. *Rev. geophys. Space Phys.* **13,** 37–55 (1975).
14. Fudali, R. F. *Geochim. cosmochim. Acta* **29,** 1063–1075 (1965).
15. Heald, E. F., Naughton, J. J. & Barnes, I. L. Jr *J. geophys. Res.* **68,** 545–557 (1963).
16. Newton, R. C., Smith, J. V. & Windley, B. F. *Nature* **288,** 45–50 (1980).
17. Perchuk, L. L. in *Energetics of Geological Processes* (eds Saxena, S. K. & Bhattacharji, S.) 285–352 (Springer, New York, 1977).
18. Melton, C. E. & Giardini, A. A. *Am. Miner.* **66,** 746–750 (1981).
19. Kramers, J. D., Smith, C. B., Lock, N. P., Harmon, R. S. & F. R. Boyd *Nature* **291,** 53–56 (1981).
20. Stevenson, D. J. *Nature* **268,** 130–131 (1977).
21. Hunten, D. M. *J. atmos. Sci.* **30,** 1481–1494 (1973).
22. Shimizu, M. *Precambr. Res.* **3,** 463–470 (1976).
23. Frick, U. & Chang, S. *Proc. 8th Lunar Sci. Conf.* 263–272 (1977).
24. Phinney, D. *Earth planet. Sci. Lett.* **16,** 413–420 (1972).
25. Thomsen, L. *J. geophys. Res.* **85,** 4374–4378 (1980).
26. Ferris, J. P. & Nicodem, D. E. *Nature* **238,** 268–269 (1972).
27. Kuhn, W. R. & Atreya, S. K. *Icarus* **37,** 207–213 (1979).
28. Levine, J. S. & Augustsson, T. R. in *Proc. College Park Colloquia on the Voyager Mission: Implications for Planetary Biology*, Oct. 4–6 (1981).
29. Lasaga, A. C., Holland, H. D. & Dwyer, H. D. *Science* **174,** 53–55 (1971).
30. Li, Y-H. *Am. J. Sci.* **272,** 119–137 (1972).
31. Fanale, F. P. *Chem. Geol.* **8,** 79–105 (1971).
32. Anders, E. & Owen, T. *Science* **198,** 453–465 (1977).
33. Rossow, W. B., Henderson-Sellers, A. & Weinreich, S. K. *Science* (in the press).
34. Ghil, M. *J. atmos. Sci.* **33,** 3–20 (1976).
35. Cogley, J. G. *Nature* **291,** 56–58 (1981).
36. McCulloch, M. T. & Wasserburg, G. J. *Science* **200,** 1003–1011 (1978).
37. Veizer, J. & Jansen, S. L. *J. Geol.* **87,** 341–370 (1979).
38. Gregory, R. T. & Taylor, H. P. Jr *J. geophys. Res.* **86,** 2737–2755 (1981).
39. Knauth, L. P. & Epstein, S. *Geochim. cosmochim. Acta* **40,** 1095–1108 (1976).
40. Costa, U. R., Fyfe, W. S., Nesbitt, H. W. & Kerrich, R. *EOS* **61,** 386 (1980).
41. Sagan, C. & Mullen, G. *Science* **177,** 52–56 (1972).
42. Wang, W-C., Rossow, W. B., Yao, M-S. & Wolfson, M. *J. atmos. Sci.* **38,** 1167–1178 (1981).
43. Hansen, J. E. *et al. Science* **213,** 957–966 (1981).
44. Wang, W-C. & Stone, P. H. *J. atmos. Sci.* **37,** 545–552 (1980).
45. Newman, M. J. & Rood, R. T. *Science* **198,** 1035–1037 (1977).
46. Wasserburg, G. J., Papanastassiou, D. A., Tera, F. & Huneke, J. C. *Phil. Trans. R. Soc.* **A285,** 7–22 (1977).
47. Kuhn, J. in *Proc. GISS Summer Inst. Planet. Climate*, 1981 (NASA, New York, 1981).
48. Hansen, J. E., Russell, G., Rind, D., Stone, P. H., Lacis, A., Lebedeff, S., Ruedy, R. & Travis, L. *Mon. Weath. Rev.* (submitted).
49. O'Keefe, J. D. & Ahrens, T. J. *Pap. Conf. on Large Body Impacts and Terrestrial Evolution*, Snowbird, Utah, 39 (Lunar Planetary Institute, Houston, 1981).
50. Toon, O. B. *et al. EOS* **62,** 886 (1981).
51. McKay, C. P. & Thomas, G. E. *Pap. Conf. on Large Body Impacts and Terrestrial Evolution*, Snowbird, Utah, 33 (Lunar Planetary Institute, Houston, 1981).
52. Onorato, P. I. K., Uhlmann, D. R. & Simonds, C. H. *J. geophys. Res.* **83,** 2789–2798 (1978).
53. Davies, G. F. *J. geophys. Res.* **85,** 2517–2530 (1980).

0028–0836/82/340835—04$01.00

Optimized anomalous dispersion in crystallography: a synchrotron X-ray polychromatic simultaneous profile method

U. W. Arndt*, T. J. Greenhough†, J. R. Helliwell†‡, J. A. K. Howard§, S. A. Rule† & A. W. Thompson‡

* MRC Laboratory of Molecular Biology, Hills Road, Cambridge CB2 2QH, UK
† Department of Physics, University of Keele, Keele, Staffordshire ST5 5BG, UK
‡ SERC, Daresbury Laboratory, Daresbury, Warrington WA4 4AD, UK
§ School of Chemistry, University of Bristol, Cantock's Close, Bristol BS8 1TS, UK

In principle, it is possible to phase the X-ray reflections from a macromolecular crystal which contains one heavy atom per molecule, without having recourse to the conventional method of multiple isomorphous replacement, by making use of anomalous dispersion effects alone[1]. To do this, it is necessary to measure each reflection over a narrow range of wavelengths centred on an absorption edge of the heavy atom, where f' and f'', the real and imaginary anomalous components of the scattering factor, are varying rapidly. The availability of powerful synchrotron radiation sources with a continuous energy spectrum has stimulated interest in such phasing methods, but previously experiments[1] have been limited to making measurements on only one reflection at a time and/or to measuring at only a few discrete wavelengths near the absorption edge. We are developing a method at the Daresbury Synchrotron Radiation Source (SRS) which produces an energy profile along an axis of each and every diffraction spot in a screenless oscillation photograph. We show here that the approach is feasible using a single crystal of heptahydrido *bis*(diisopropylphenyl)phosphine rhenium using the L_{III} absorption edge of rhenium at a wavelength of 1.1772 Å.

The white synchrotron radiation beam from a storage ring diverges from a small region at the tangent point of the beam line. A narrow wavelength band can be selected from this beam by reflection from a crystal monochromator; a cylindrically curved monochromator produces a converging X-ray beam. At the SRS protein crystallography station[2] the monochromator is a perfect crystal of either Si or Ge with the (111) planes cut at an angle α to the surface. The triangular crystal is clamped at its base and deflected at its tip: in this way[2–5] an accurately cylindrical curvature is achieved.

There is one curvature of the monochromator for a given Bragg angle (θ), angle of cut (α), image (p') and object (p) distances where all rays which are brought to a focus have been reflected at an equal angle so that they are all of the same wavelength. This 'achromatic condition' is usually referred to as the 'Guinier position' of the monochromator. However, for monochromator curvatures, R, other than that for the 'Guinier position', rays from a point source make different angles of incidence along the length, L, of the monochromator, over a range $\delta\theta_{\mathrm{corr}}$ where[2,4–6]

$$\delta\theta_{\mathrm{corr}} = \frac{L}{2}\left\{\frac{\sin(\theta-\alpha)}{p'} - \frac{\sin(\theta+\alpha)}{p}\right\}$$

$$\left|\left(\frac{\delta E}{E}\right)\right|_{\mathrm{corr}} = \left(\frac{\delta\lambda}{\lambda}\right)_{\mathrm{corr}} \approx \delta\theta_{\mathrm{corr}} \cot\theta$$

and

$$\frac{2}{R} = \frac{\sin(\theta-\alpha)}{p'} + \frac{\sin(\theta+\alpha)}{p}$$

(At the Guinier position $(\delta\lambda/\lambda)_{\mathrm{corr}} = 0 = \delta\theta_{\mathrm{corr}}$ and

$$\frac{1}{R} = \sin\frac{(\theta-\alpha)}{p'} = \sin\frac{(\theta+\alpha)}{p}.)$$

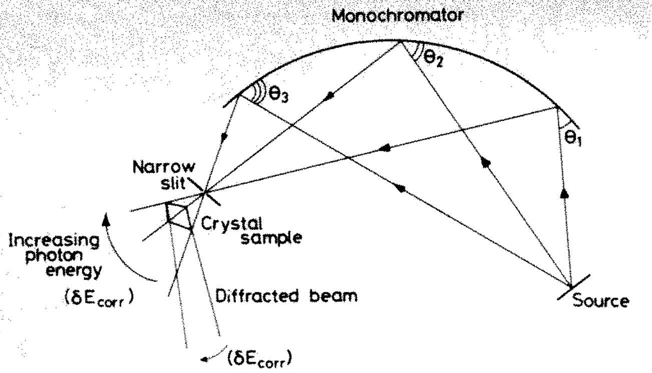

Fig. 1 When the monochromator curvature is not at the 'Guinier position' rays from a point on the source are incident at different angles to different points along the length of the monochromator and are reflected at different wavelengths (energies). At a point in the focus, defined by the narrow slit, the converging rays possess an exact correlation of photon energy with direction. The particular curvature of the monochromator that is needed is that for which $(\theta_3-\theta_1)=\delta\theta_{corr}$ gives a δE_{corr} adequate to straddle an absorption edge of interest (in this case rhenium L_{III}). We assume point-to-point focusing, $L \ll p, p'$.

The subscript 'corr' refers to the fact that there is a subsequent correlation of the direction of incidence of a ray towards the focus and its (photon) energy. Maier-Leibnitz[7] and later Thomas[8] first described the use of a focusing monochromator in this way in a 'modified Laue method' for neutrons.

By choosing appropriate angle of incidence and curvature of the monochromator the band-pass $(\delta\lambda/\lambda)_{corr}$ of the reflected X-rays can be made to straddle the absorption edge of a spectrum placed at or near the cross-over point. A cylindrical curvature does not exactly reproduce a point focus from a point source but instead a 'caustic'. However, for $L \ll p, p'$ this error is quite negligible[2]. Rays from different points of a finite source cross over at different points so that with such a source there is a finite focus width. However, an accurate correlation between direction and wavelength is maintained for all rays which pass through a sufficiently narrow slit placed at the foucs.

Matsushita[9] has used this property of the bent crystal monochromator for recording photographically the absorption spectrum of the K edge of a copper specimen placed at the cross-over point. The transmitted diverging X-beam produced a streak in which distance and wavelength were correlated.

We now suggest that, if a single crystal is placed near the cross-over point a diffraction pattern is produced in which each spot is drawn out into a streak in which the wavelength varies along the streak (Fig. 1). The theoretical basis for this has been established[10,11]. Every spot in the pattern then contains a complete energy profile across the absorption edge of one of the atoms in the specimen crystal. This method of producing the whole of all the streaks simultaneously makes much more efficient use of the synchrotron radiation spectrum than the rocking-monochromator streaks method proposed earlier[12] or the more usual appproach of measuring whole diffraction data sets at a few discrete wavelengths either with a double crystal monochromator[1] or the current monochromator at the 'Guinier position'[2].

In our preliminary experiments we used the SRS work-station with no modification other than that of placing a narrow adjustable slit at the 'front' end of a large diameter collimator (≈1 mm) mounted in the collimator bracket of an oscillation camera[13]. The X-ray beam was therefore effectively unrestricted in vertical height. In the horizontal plane the crystal sample was placed after the cross-over point so that the (now) diverging beam bathed most of the crystal, which also, therefore, accepted the full correlated energy bandwidth available (Fig. 1). The use of the narrow slit (Fig. 1) constrained the energy resolution within the diffraction spot profile to allow satisfactory sampling of the absorption edge fine structure[2,11].

We have tested our idea on a single crystal, in the form of a thin plate (0.1 × 1 mm approximately), of heptahydrido *bis*-diisopropylphenyl)phosphine rhenium, $(\mathrm{ReH_7(P^{i}_{r2}PhP)_2})$. This crystal structure has been solved[14] previously from low temperature X-ray data collected on a Nicolet P3/m 4-circle automated diffractometer with graphite monochromatized MoK_α X-ray irradiation.

The space group is $P2_1/n$ with refined cell parameters $a = 11.271$ Å, $b = 13.405$ Å, $c = 17.017$ Å, $\beta = 95.53°$. There is one rhenium aton , 2 phosphorus, 24 carbon and 45 hydrogen atoms in the asymmetric unit. Because the space group is

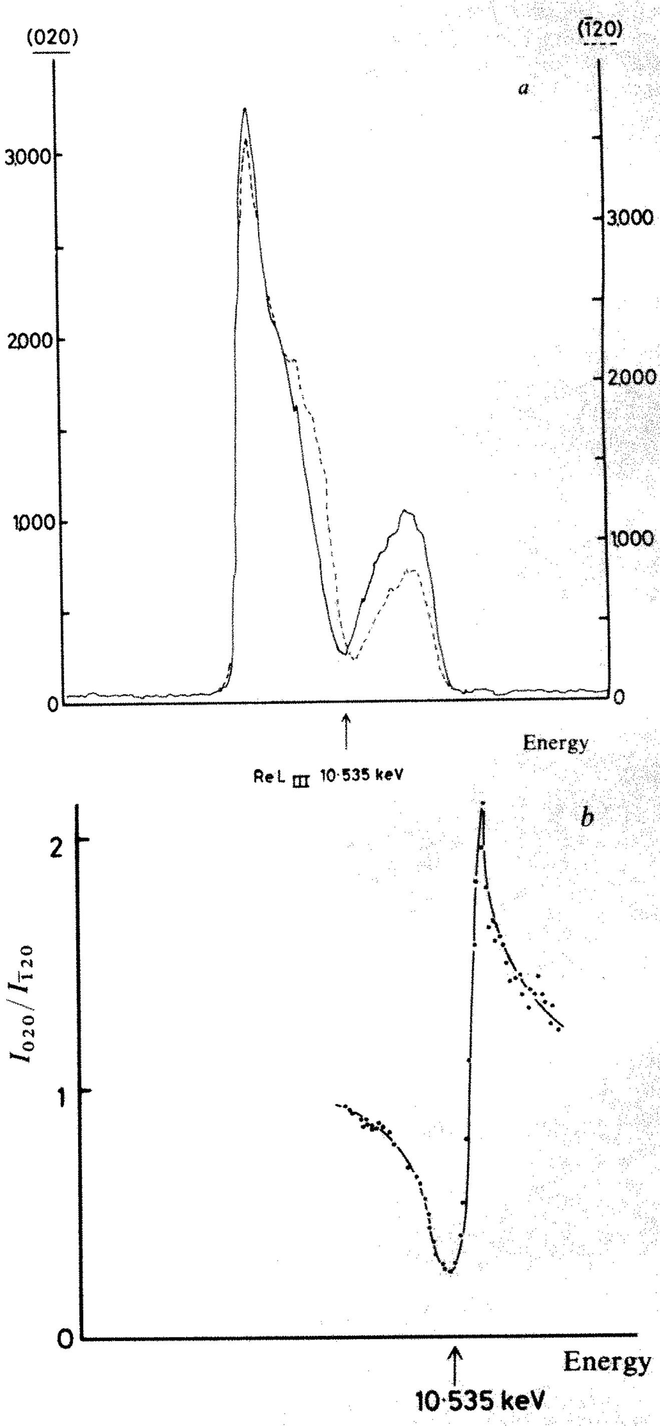

Fig. 2 *a*, Densitometer profiles of the two reflections with Miller indices $\bar{1}20$ and 020, for the 'on-edge' case. The ordinate scales have been selected to allow exact comparison of reflection widths and the position of the minima in the profiles. The 020 profile is shown as a solid line and $\bar{1}20$ as a broken line. *b*, The divided intensity profiles $(020/\bar{1}20)$, after removal of background, showing the effect of the expected dramatic variation due to f' 'on-edge'.

centrosymmetric, all phases are 0 or π and the variation in f'' has a negligible effect on the reflection intensity. At the SRS we aimed therefore to optimise the value of f' for the rhenium $L_{\rm III}$ edge ($\lambda = 1.772$ Å) across a diffraction spot energy profile with a total bandwidth of 67 eV. The monochromator was a triangular Si(111) monochromator 200 mm long (length in use 156 mm) with a measured oblique cut angle $\alpha = 6.73° \pm 0.05°$ (J.R.H., unpublished data) giving $\delta E_{\rm corr} = 67$ eV[10] for $p = 20.9$ m, $p' = 2.4$ m and $R = 45$ m. We recorded two oscillation photographs, one with the 67 eV centred on the point of inflection of the $L_{\rm III}$ absorption edge of the rhenium in the sample and the other with the 67 eV centred 200 eV below the edge. These two photographs can be compared in ref. 11. The wavelength was calibrated by step scanning the monochromator in 0.01° steps ($\delta E = 9$ eV) and measuring the intensity transmitted through a different but otherwise identical single crystal. At the two selected wavelengths about the rhenium edge the sequence of photographs produced was as follows; still 0°, still 85°, oscillation photograph 85–89.95, still 89.95. Exposure time for the 85–89.95° photographs was 5 seconds per degree with 10 oscillations. The crystal to film distance was 54.5 mm corresponding to an outer resolution limit on a flat plate cassette of 1.5 Å at this wavelength. The film used was low fog CEA Reflex 25 with three films in a data pack. The SRS was operating at 1.9 GeV with an injection current of ≈ 100 mA at the time of this experiment.

The diffraction patterns were indexed on the basis of a refined sample orientation (from the stills) taking account of the direction–energy correlation geometry[10] which introduces important changes compared with a conventional X-ray line source[15]. Because of the small unit cell, the same reflections are stimulated at both wavelengths though their positions on each film are slightly altered. In the on-edge photograph considerable fine structure is exhibited in the Bragg reflections. For a small heavy atom complex of this sort the absorption profile of the rhenium dominates the different intensities. This causes an apparent uniformity of fine structure between all reflections. The variations in spot-size and inclination for different reflections for this camera geometry is described elsewhere[10,11]. The on-edge photograph was recorded first; the fine structure recorded is not, therefore, due to a split crystal.

There is a considerable amount of information in these 'three-dimensional' rotation photographs (x, y, and energy). In this first report of the technique we have only analysed two reflections with the Miller indices 020 and $\bar{1}20$; both reflections are fully recorded. These reflections occur at a closely similar $\sin\theta$ value so that their absorption corrections as a function of λ across the edge are identical to within 1%, even at maximum absorption. However, in the $\bar{1}20$ reflection the rhenium atom happens not to dominate the structure amplitude. The reflection profile of the $\bar{1}20$ is therefore determined by the absorption profile. In the 020 reflection the rhenium does dominate the structure amplitude, hence the expected variation in f' across the edge (as well as absorption) will affect the 020 reflection intensity profile.

The reflections each at the two wavelengths were digitized using a Scandig flat bed densitometer with an aperture (raster) of 10 μm × 100 μm with a step size of 10 μm. The four central scans were averaged numerically making the sampling raster effectively 10 μm × 400 μm. The scan direction was along the variable energy direction which was here very close to horizontal[10,11] Figures 2*a* and 3*a* compare the profiles produced in each case. For the on-edge ($\bar{1}20$) profile the change in linear absorption coefficient is 28 mm^{-1}. Figures 2*b* and 3*b* show the reflection profile of the 020 divided by the $\bar{1}20$ profile at each wavelength; an average background was removed in each case. The relationship between wavelength and displacement along the streaks is linear within the 67 eV central position[10]. Neglecting the end effects the off-edge division shows a linear variation and the on-edge division does indeed reveal the expected dramatic variation of f' at the rhenium $L_{\rm III}$ edge.

Any estimate of f' from profile division should be based on a least squares refinement including many measured reflections, since small errors in alignment of the profiles may lead to large errors in f' estimates. This work is in progress, but the two reflections quoted here do provide useful evidence of the efficacy of the technique: they give f' estimates for Re which are in good agreement with those measured for Pr and Sm at SSRL[16]. From Fig. 2 we obtain estimates of $-27e^-$ at $f'_{\min}$ with an $f'_{\max}$ of $-1e^-$ and $-17e^-$ at the lower energy limit of our sampling. The energy width of the variation seen in f' from $f'_{\min}$ to $f'_{\max}$ is reasonable at 11 eV, although the position of the minimum f' value does not quite coincide with the point of

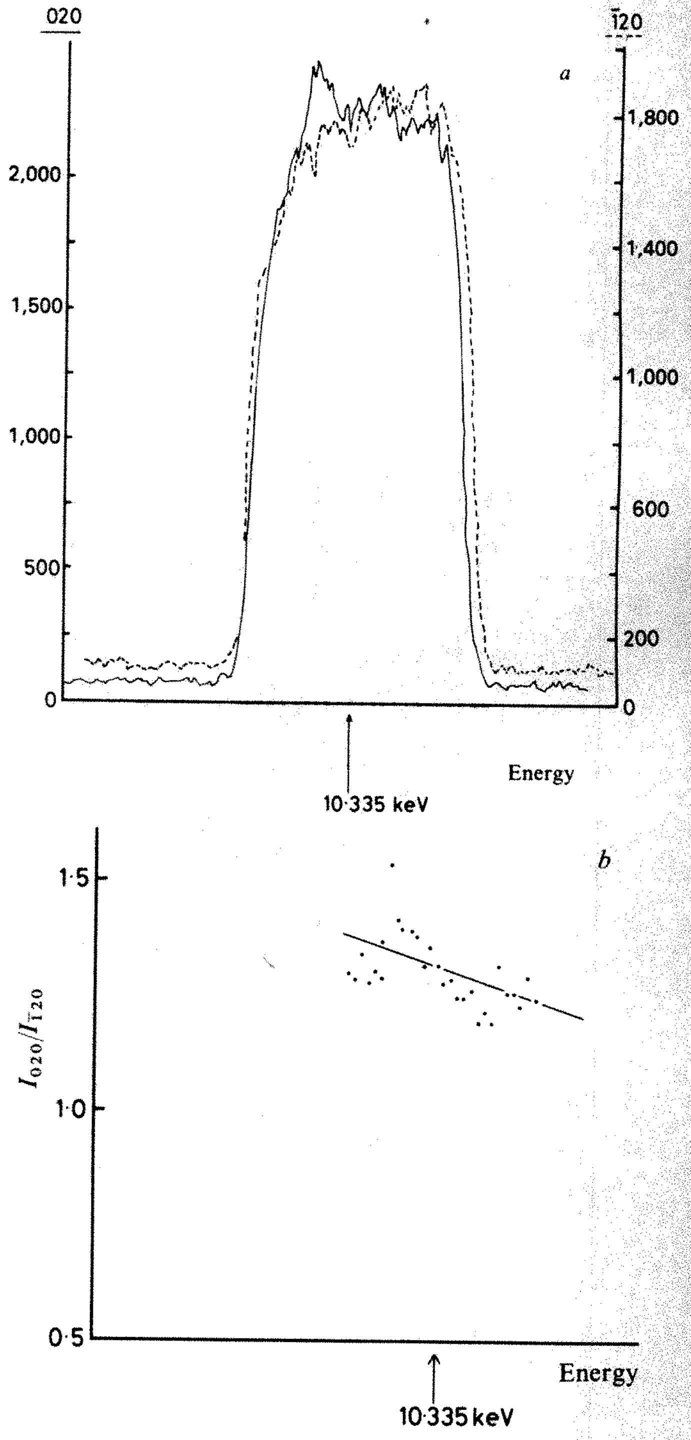

Fig. 3 *a*, Densitometered profiles of the two reflections $\bar{1}20$ and 020, for the 'off-edge' case. The 020 profile is shown as a solid line and the $\bar{1}20$ as a broken line. *b*, Divided intensity profiles (020/$\bar{1}20$), after removal of background, showing the effect of a slight linear variation due to f' 'off-edge'.

inflexion of the $\bar{1}20$ absorption profile which would have been expected. The energy resolution $\delta E/E$ at any point in the profiles, in this experiment, is of the order of 1×10^{-3}; this estimate makes allowance for monochromator rocking width, size of slit at focus, thickness of sample, sample mosaic spread, vertical sample size, beam cross-fire angles, correlated wavelength spread and slit–sample–film distances[11]. There are constraints on these quantities to preserve the energy resolution in a diffraction streak and their effects depend on the location of the spot on the film[11]. The necessary use of a thin sample also reduced absorption effects, but even so in general absorption corrections will be needed which will require the determination of a complete absorption surface for all energies in the pass-band. These can be determined by recording direct beam transmission streaks as a function of spindle angle ϕ and inclination angle μ of the rotation camera.

We believe that the method has the greatest potential for phasing the reflections from protein crystals containing only one anomalous scatterer per asymmetric unit: in such a case the mass-fraction of the heavy atom is very small (typically $\approx 1\%$); the change in the absorption of the sample at the edge is, therefore, much smaller than with our trial heavy atom complex. Although the heavy-atom contribution to protein structure amplitudes is very small, the atomic scattering factor, f_0, falls off rapidly with increasing $\sin\theta/\lambda$ whilst the values of f' and f'' of an anomalous scatterer do not; for high-angle reflections for a typical protein crystal the anomalous effect may be as great as 40% of the *average* structure amplitude (U.W.A., unpublished calculation.) The relative accuracy to which an intensity absorption correction would need to be determined for a protein metal atom derivative would be $\approx 5\%$.

It may be thought that order-to-order resolution for broad diffraction spots may be lost for a dense diffraction pattern from a protein crystal. The change in inclination of the reflection streaks around an oscillation photograph does in fact preserve order-to-order resolution parallel to the horizontal mounting axis outside the blind region (compare for example native protein crystal photographs at the Guinier position and off Guinier position in ref. 10). The overlap perpendicular to the mounting axis is controlled in any case by the size of the rotation angle. However, the use of a small raster step is an inconvenience and it would be necessary to reduce the volume of data produced with a flat-bed densitometer by resorting to an on-line pre-prediction control programme.

We thank MRC and SERC for support, and the SERC Daresbury Laboratory for providing synchrotron experimental beam time and facilities. We also thank Dr J. Spencer of the Department of Inorganic Chemistry, Bristol University for supplying suitable samples, Dr M. Elder of SERC Daresbury Laboratory for providing film densitometry facilities, and Drs S. Ealick of the University of Alabama and G. Taylor of Birkbeck College, London University for helpful discussions.

Received 30 March; accepted 20 June 1982.

1. Phillips, J. C. & Hodgson, K. O. in *Synchrotron Radiation Research* (eds Winick, H. & Doniach, S.) (Plenum, New York, 1980).
2. Helliwell, J. R. *et al. J. Phys.* E (in the press).
3. Underwood, J. H. & Turner, D. *Soc. Photoopt. Inst. Eng.* **106,** 125 (1977).
4. Lemonnier, M., Fourme, R., Rousseau, F. & Kahn, R. *Nucl. Inst. Meth.* **152,** 173–177 (1978).
5. Hendrix, J., Koch, M. J. & Bordas, J. *J. appl. Crystallogr.* **12,** 467–472 (1979).
6. Rosenbaum, G. & Holmes, K. C. in *Synchrotron Radiation Research* (eds Winick, H. & Doniach, S.) (Plenum, New York, 1980).
7. Maier-Leibnitz, H. *Ann. Acad. Sci. Fenn A* VI, p. 267 (1967).
8. Thomas, P. *J. appl. Crystallogr.* **5,** 83–88 (1972).
9. Matsushita, T. *Am. Inst. Phys. Conf. Rep.* **64,** 109 (1980).
10. Greenhough, T. J. & Helliwell, J. R. *J. appl. Crystallogr.* (in the press).
11. Greeenhough, T. J., Helliwell, J. R. & Rule, S. A. *J. appl. Cryst.* (submitted).
12. Arndt, U. W. *Nucl. Inst. Meth.* **152,** 307–311 (1978).
13. Arndt, U. W., Champness, J. N., Phizackerley, R. P. & Wonacott, A. J. *J. appl. Crystallogr.* **6,** 457–463 (1973).
14. Howard, J. A. K., Mead, K. A. & Spencer, J. L. *Acta crystallogr. B* (submitted).
15. Greenhough, T. J. & Helliwell, J. R. *J. appl. Crystallogr.* (in the press).
16. Templeton, L. K., Templeton, D. H. & Phizackerley, R. P. *J. Am. chem. Soc.* **102,** 1185–1186 (1980).

Australian seismic refraction results, isostasy and altitude anomalies

Peter Wellman

Bureau of Mineral Resources, PO Box 378, Canberra,
Australia 2601

Although there have been extensive seismic refraction measurements over areas of continental crust, the causes of variation in crustal thickness, and of variation in mean crustal seismic velocity, are poorly understood. If there is regional (3° × 3°) isostatic equilibrium of the crust, such as suggested by many studies of regional gravity, then crustal thickness variation should be caused largely by variation in surface altitude and crustal density. Seismic refraction results from Australia are used here to confirm that these crustal isostatic effects are a major (40%) cause of variation of crustal thickness even in a continent of little surface relief. However, there is an equally important regional variation in crustal thickness unrelated to crustal isostasy—this is thought to be due to density variation in the lower lithosphere[1].

It is initially assumed that the Earth's crust is in isostatic equilibrium relative to the uppermost mantle and, in addition, that the upper mantle density (σ_m) does not vary horizontally or vertically from where its upper surface under continents is shallow to where it is deep. Consider any crust of mean density σ, surface altitude h, and depth to the base of the crust below sea level H. A standard crust has a surface at sea level, base H_s below sea level, and mean density σ_s. For isostatic equilibrium[2]

$$H = \frac{H_s(\sigma_m - \sigma_s) + h\sigma}{\sigma_m - \sigma} \qquad (1)$$

Average densities of $\sigma_m = 3.3$ tonne m^{-3} and $\sigma_s = 2.9$ tonne m^{-3} can be assumed[2], so $\sigma/(\sigma_m - \sigma)$ averages ~7.25. In Australia h is generally <0.6 km, and σ varies from ~2.75 to 3.06 tonne m^{-3}, so the effect of h on H can be evaluated with an error of <2 km.

We define a depth of the base of the crust when corrected for surface altitude as H' ($H' = H - 7.25h$)

$$H' = \frac{H_s(\sigma_m - \sigma_s)}{\sigma_m - \sigma} \qquad (2)$$

The Nafe–Drake empirical correlation between rock density and seismic P-wave velocity[3] is almost linear in the velocity range 5.5–8 km s^{-1}. Assuming linearity, using velocity subscripts with the same meaning as for density, and inverting equation (2) gives

$$\frac{1}{H'} = \frac{V_m}{H_s(V_m - V_s)} - \frac{V}{H_s(V_m - V_s)} \qquad (3)$$

so there should be linear correlation between $1/H'$ and mean crustal velocity V.

Table 1 and Fig. 1 give those crustal seismic refraction results for Australian continental crust where both mean P-wave velocity of the crust and crustal thickness have been determined. Results from regions A, B, C and D are considered less accurate because only travel-times of critically refracted waves were used in the interpretation. Other results were derived using all available crustal and upper mantle seismic P phases. The locations given are those of the crustal thickness determinations, not the shot points.

A least-squares straight-line fit of mean crustal velocity with the inverse of the corrected depth of the base of the crust below sea level for all data is

$$1/H' = (0.123 \pm 0.019) - (0.015 \pm 0.003)V \qquad (4)$$

where the uncertainty is the coefficient of variation. The correlation coefficient ($r = 0.59$) is statistically significant at the 95%

confidence level. Errors in V are thought to be relatively small, and in equation (4) are assumed to be zero. If errors are partitioned equally between V and $1/H'$ this infers very large errors in the velocity measurements. For example, Pilbara mean crustal velocity would have a systematic error of 0.3 km s^{-1}; this is unacceptably high either as an error in the mean velocity, or as an error in the density–velocity relationship.

The following calculations suggest that equation (4) is consistent with the assumptions. For these calculations I have adopted the mean values of quantities in Table 1, but with coefficients of variation increased by a factor of 3 to allow for sampling bias

$$V_m = 8.07 \pm 0.08 \ \text{km s}^{-1}, \qquad V_s = 6.43 \pm 0.11 \ \text{km s}^{-1},$$
$$H_s = 37.8 \pm 3.6 \ \text{km}$$

When H' is infinite, then equation (4) gives an estimate of the mean uppermost-mantle velocity (P_n) of 8.3 ± 2 km s^{-1}; this is consistent with the mean of the measured uppermost-mantle velocities. (Note that mantle velocities were not used in equation (4).) The slope of equation (4) is consistent within experimental error with the value of 0.016 ± 0.002 found by evaluating $1/(H_s(V_m - V_s))$ using the means of the measured values given above. It is also consistent within experimental error with the value of 0.020 ± 0.003 found by evaluating equation (3) by using the Nafe–Drake empirical relationship between crustal density and crustal velocity, together with Woollard's[2] preferred range of values H_s between 33.2 and 34.5 km, and $\sigma_m - \sigma_s$ between 0.383 and 0.415 tonnes m^{-3}.

The least-squares correlation of mantle P_n velocity with depth of the base of the crust below sea level (H) is $V_m = (7.76 \pm 0.14) + (0.0078 \pm 0.0033)H$. Hence there is a systematic change in V_m from 7.99 km s^{-1} at 30 m depth to 8.15 km s^{-1} at 50 km depth; this is equivalent to an increase in mantle density of 0.04 tonnes m^{-3}. This small change would have an effect of less than <1 km on H' in equation (4). Regions B, C,

Table 1 Australian crustal seismic refraction results

Lat. (°S)	Long. (°E)	Altitude h (km)	Mean crustal velocity V (km s^{-1})	Crustal thickness $H + h$ (km)	Mantle velocity (km s^{-1})	Ref.
A Gawler craton						
31	133	0.04	6.4	42	8.00	14
30.5	130.5	0.16	6.3	37	8.16	14
B North-east orogens						
20.2	143.3	0.38	6.25	38.4	7.79	15
18.2	145.1	0.53	6.31	44.6	7.79	15
16.4	143.1	0.12	6.31	49.3	8.04	15
16.5	141.8	0.05	6.06	35.6	8.04	15
11.6	142.5	0.01	6.34	36.4	7.95	15
13.8	142.1	0.12	6.32	36.6	7.95	15
C Southern Yilgarn block						
31.4	120.2	0.41	6.50	35.5	8.34	16
31.7	117.0	0.28	7.05	43.0	8.34	16
35.0	118.0	0.00	6.43	34.0	8.06	16
D Central Tasman fold belt						
22.8	148.7	0.16	5.29	35.0	8.1	17
24.0	149.4	0.15	6.31	37.0	8.1	17
E Adelaide geosyncline						
31.0	138.5	0.38	6.19	38.5	7.97	18
33.2	138.0	0.10	6.30	38.5	7.97	18
32.5	138.7	0.43	6.25	34.0	7.97	18
F Southern Lachlan geosyncline						
35.9	148.4	1.37	6.61	50.5	8.02	19
35.3	149.5	0.78	6.70	50.5	8.02	19
35.8	147.4	0.43	6.65	42	8.05	20
35.8	147.7	0.54	6.62	44.5	8.04	20
36.7	148.6	0.62	6.65	50	8.03	20
33.2	150.8	0.26	6.64	43.5	8.05	21
34.2	150.4	0.31	6.68	41.5	8.12	21
34.8	149.3	0.67	6.52	43	7.95	21
G Pilbara block						
21	119.8	0.23	6.32	28	8.34	22
22.8	120	0.46	6.28	33	8.34	22
22	117	0.54	6.37	32	7.79	4
22.8	117.8	0.53	6.43	31	7.79	4
23.0	119.2	0.67	7.29	30	7.79	4
20.8	119.2	0.15	6.32	28	8.18	23
22.4	118.2	0.71	6.29	30	8.18	23
24	117.9	0.47	6.52	40	8.10	23
23.8	117.2	0.40	6.62	40	8.10	23
H Northern Yilgarn block						
25.9	118.9	0.55	6.51	52	8.3	22
26	118.2	0.46	6.60	55	8.10	23
I SE North Australian craton						
20.4	139	0.32	6.70	55	8.23	24
19.4	134.9	0.26	6.67	51	8.15	24
16.7	135.5	0.20	6.75	52	8.47	25
16.3	134	0.25	6.72	52	8.47	25
16.5	137	0.10	6.83	52	8.00	25
J North Northern Australian craton						
10.6	130.2	−0.04	6.01	31.4	7.91	26
10.4	130.7	−0.04	6.02	34.2	7.91	26
4.6	135.5	−0.03	5.91	26.6	7.63	26
10.5	130.5	−0.03	6.14	34	8.00	27

E, F, Q and J have mantle velocities measured from directions near right angles. Significant upper mantle anisotropy is suggested only by results from the Pilbara Block[4].

I conclude that the effect on crustal thickness of variations of surface altitude and mean crustal density can be adequately modelled using equation (3). This equation assumes regional isostatic equilibrium relative to the uppermost mantle, assumes that the mantle has constant density down to the level of the deepest crust, and assumes a linear correlation between P-wave velocity and density.

The relative magnitude of the components of crustal thickness variation are evaluated as follows. The total variance from the measured crustal thicknesses listed in Table 1 is $66.0\ \mathrm{km}^2$. Surface altitude variation and its associated crustal root variation is calculated from the difference in variance of H and H' to be 2% of this. The change in crustal thickness associated with change in mean crustal density is $\sim$38% of the variance ($r^2 = 0.38$ for equation (4)). The remaining variance (that causes deviation from equation (4)) can be split into within-region variance of $11.3\ \mathrm{km}^2$ (17% of total variance), and between-region variance causing the remaining 43%.

The within-region variance is caused both by errors in determination of relative crustal thickness and relative mean crustal velocity within each region, and by crustal strength being sufficiently high in western and central Australia that areas $<3° \times 3°$ are not in complete isostatic equilibrium[5]. The variance due to departures from isostatic equilibrium is unlikely to be $>$8% of total variance (one-half within-region variance) and so is much smaller than the variance due to the isostatic effects of topography and crustal density changes (40% of total variance). This reinforces the conclusion that isostatic equilibrium relative to the uppermost mantle is largely achieved.

Between-region variance is $\sim$43% of total variance, so its origin is important both in understanding and predicting crustal thickness. It is unlikely that errors in crustal thickness and crustal velocity contribute significantly to within-region or between-region variance, because the within-region variance is small both in the better studied regions (F, G and I) and in regions where independent investigators have made independent measurements (regions I and J). Between-region changes in mean atomic number could, in theory, cause regional changes in the velocity–density relationship[6,7]. There is no good evidence for significant differences in the chemistry of the surface rocks from the various regions so significant change in mean atomic number seems unlikely. The remaining possible causes of between-region variance—horizontal density variations in the lower lithosphere, and dynamic forces on the base of the lithosphere—are considered below by comparing mantle altitude anomalies under continents with those under oceans.

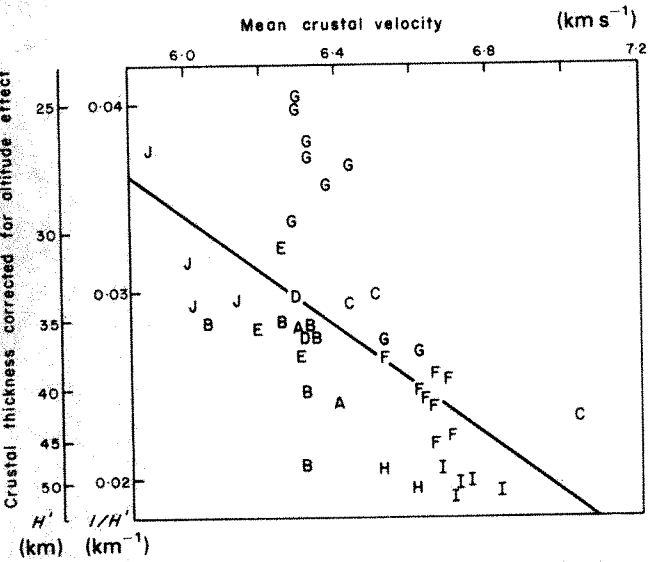

Fig. 1 Relation of inverse of corrected crustal thickness to mean crustal velocity. The letters refer to the regions of Table 1 and Fig. 2. The line gives the least-squares correlation.

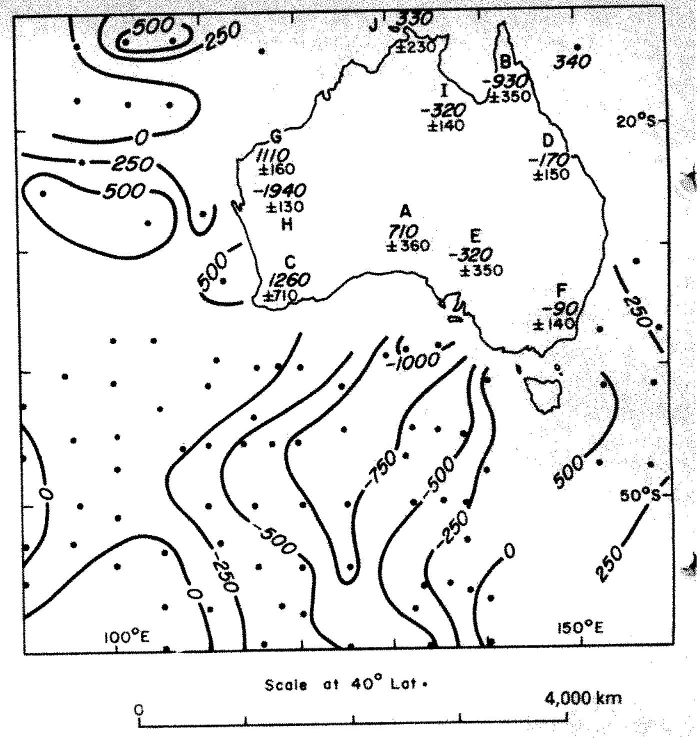

Fig. 2 Mean height anomalies in metres. Shallower areas have positive mean height anomalies. In oceanic areas dots show data points; contour interval, 250 m.

The between-region differences in H' residual are converted to equivalent differences in the upper level of mantle overlain by oceanic crust of assumed constant thickness and by seawater of density σ_w. A difference of p in the thickness of sea-level crust is equivalent to a difference of $p(\sigma_m - \sigma_s)/(\sigma_m - \sigma_w)$, or about $p/5.68$, in the upper level of oceanic mantle. For each region of Fig. 1, a mean altitude anomaly and its coefficient of variation has been calculated using H' residuals divided by 5.68.

In oceanic areas, altitude anomalies are calculated by subtracting from $1° \times 1°$ mean water depths, the expected water depth for that age crust, and correcting for the isostatic effect of sediment thickness[1]. The altitude anomalies used are the means of $5° \times 5°$ areas. Altitude anomalies derived for continental areas are assumed to have the same mean (zero) as those derived for areas of oceanic crust.

Figure 2 shows altitude anomalies derived from seismic refraction data in continental Australia, together with published altitude anomalies for the Indian and Southern Oceans[1]—these have been recontoured west of Australia. East of Australia in the Tasman and Coral Seas new rough estimates of altitude anomalies are given.

Altitude anomalies do not show a systematic trend across Australia, nor do they show a correlation with seismic P-wave residuals[8–10], heat flow variation[11], or long-wavelength gravity anomalies[1].

Continental and oceanic values do not show an overall pattern, as there seems to be a break between continental and oceanic values. The lack of systematic variation across the region indicates that altitude anomalies are unlikely to be due to dynamic asthenospheric forces on the base of the lithosphere as these would be continuous across lithosphere boundaries. The interpretation that altitude anomalies originate from horizontal density variation in the lower lithosphere[1] is therefore supported. Relative to oceanic altitude anomalies, those from the continent have a larger range and shorter wavelength; this supports models where the continental lithosphere has had a relatively long and diverse history[12]. An analysis of seismic refraction data from all continents would define the constants of equation (3) more precisely, and allow altitude anomalies to be mapped over the whole Earth.

I interpret variation in crustal thickness as being mainly due to two effects. (1) Because surface altitude and mean crustal density vary relatively rapidly on continents, the crust appears to be in isostatic equilibrium with an upper mantle of uniform density, so variation in surface altitude and mean crustal density show a strong correlation with variation in mean crustal thickness. (2) Isostatic equilibrium is actually between the whole lithosphere and the asthenosphere[13], so, to keep equal pressure on the asthenosphere and keep the continental crust near sea level, any regional variation in lower lithosphere density causes regional variation in continental crustal thickness.

This work is published with the permission of the Director, Bureau of Mineral Resources, Canberra.

Received 17 March; accepted 29 June 1982.

1. Cochran, J. R. & Talwani, M. *Geophys. J. R. astr. Soc.* **50,** 495–522 (1977).
2. Woollard, G. P. *Phys. Earth planet. Inter.* **3,** 484–498 (1970).
3. Talwani, M., Sutton, G. H. & Worzel, J. O. *J. geophys. Res.* **64,** 1545–1555 (1959).
4. Drummond, B. J., Smith, R. E. & Horwitz, R. C. *Geol. Soc. Aust. Spec. Publ.* **7,** 33–41 (1981).
5. Wellman, P. *BMR J. Aust. J. Geol. Geophys.* **1,** 297–302 (1976); **3,** 153–162 (1978); **4,** 373–382 (1979).
6. Manghnani, M. H., Ramananantoandro, R. & Clark, S. P. *J. geophys. Res.* **79,** 4527–5446 (1974).
7. Drummond, B. J. & Shelley, H. M. *BMR J. Aust. Geol. Geophys.* **6,** 137–143 (1981).
8. Cleary, J. *Bull. seis. Soc. Am.* **57,** 773–781 (1967).
9. Everingham, I. B. *Bur. Min. Resourc. Aust. Rec.* 1969/22 (1969).
10. Cleary, J. R., Simpson, D. W. & Muirhead, K. J. *Nature* **236,** 111–112 (1972).
11. Cull, J. P. *BMR J. Aust. Geol. Geophys.* **7,** 11–21 (1982).
12. Jordan, T. H. *Nature* **274,** 554–548 (1978).
13. Dooley, J. C. *BMR J. Aust. Geol. Geophys.* **2,** 1–5 (1977).
14. Cleary, J. R. *Tectonophysics* **20,** 241–248 (1973).
15. Finlayson, D. M. *J. geol. Soc. Aust.* **15,** 35–50 (1968).
16. Mathur, S. P. *Tectonophysics* **24,** 151–182 (1974).
17. Collins, C. D. N. *BMR J. Aust. Geol. Geophys.* **3,** 203–209 (1978).
18. Shackleford, P. R. J. & Sutton, D. J. *J. geol. Soc. Aust.* **28,** 491–500 (1981).
19. Finlayson, D. M., Collins, C. D. N. & Denham, D. *Phys. Earth planet. Inter.* **21,** 321–342 (1980).
20. Finlayson, D. M., Prodehl, C. & Collins, C. D. N. *BMR J. Aust. Geol. Geophys.* **4,** 243–252 (1979).
21. Finlayson, D. M. & McCracken, H. M. *J. geol. Soc. Aust.* **28,** 177–190 (1981).
22. Drummond, B. J. *BMR J. Aust. Geol. Geophys.* **4,** 171–180 (1979).
23. Drummond, B. J. *BMR J. Geol. Geophys.* **6,** 123–135 (1981).
24. Finlayson, D. M. *J. geophys. Res.* (in the press).
25. Collins, C. D. N. *BMR J. Aust. Geol. Geophys.* (in the press).
26. Jacobson, R. S., Shor, G. G., Kieckhefer, R. M. & Purdy, G. M. *Am. Ass. petrol. Geol. Mem.* **29,** 209–222 (1979).
27. Rynn, J. M. W. & Reid, I. D. *J. geol. Soc. Aust.* (in the press).

Vertical distribution and isotopic fractionation of living planktonic foraminifera from the Panama Basin

Richard G. Fairbanks*, Marc Sverdlove*,
Rosemary Free*, Peter H. Wiebe†
& Allan W. H. Bé*

* Lamont-Doherty Geological Observatory of Columbia University, Palisades, New York 10964, USA
† Woods Hole Oceanographic Institution, Woods Hole, Massachusetts 02543, USA

A model[1,2], which explains the vertical and seasonal distribution of planktonic foraminifera was developed using data from the western North Atlantic and is comprised of three tenets: (1) The conditions in the photic zone (upper 80–100 m) exclusively dictate planktonic foraminifera species composition and abundance throughout the water column. (2) Species are vertically stratified within the photic zone according to their temperature preference. Depth distribution according to temperature preference has been proposed by several authors[3] based on isotope analyses of sediments. Due to seasonal temperature variations, seasonal variations in the $\delta^{18}O$ composition of seawater, and species-specific isotope fractionation, rigorous proof of this hypothesis cannot be provided from sediment analyses alone. (3) The chlorophyll maximum is a major food source zone, which is preferentially exploited by foraminifera. Our data from the Panama Basin, which are presented here, are confirmation of this model. The Panama Basin in the eastern equatorial Pacific, which has a shallow and steep thermocline, was sampled for living planktonic foraminifera. A multiple opening–closing net and environmental sensing system (MOCNESS)[4] was used to collect 13 sets of eight vertically stratified oblique samples. We report here the quantitative distribution and stable isotopic composition of planktonic foraminifera from four MOCNESS tows taken over 5 days, during August 1979 (RV *Knorr* cruise 73) at 5°20′ N, 8°50′ W. Each tow consisted of eight samples which integrated ~12.5-m intervals from 0 to 100 m for MOC 126, 25-m intervals from 0 to 200 m for MOC 127, 100–150-m intervals from 0 to 1,000 m on MOC 128 and 250-m intervals from 0 to 2,000 m on MOC 131.

Oxygen and carbon isotope analyses were made on planktonic foraminifera from the MOCNESS tows and the surrounding seawater. Isotope determinations were made on a triple collector mass spectrometer (Micromass 903). The carbonate samples were vacuum roasted at 375 °C for 1 h and reacted with 100% phosphoric acid at 50 °C. The precision for carbonate is ±0.05‰ for oxygen and carbon. The $\delta^{18}O$ composition of seawater was determined with a rapid equilibration-extraction method described in ref. 5. The $\delta^{13}C$ composition of total dissolved CO_2 was predicted using the PO_4–$\delta^{13}C$ relationship given in ref. 6 and PO_4 data for a station occupied in between MOCNESS tows. The 0–100-m series provided an ideal test of the previous model[1,2] for several reasons. (1) Eight MOCNESS oblique tows at 12.5-m intervals (MOC 126) provide high resolution sampling. (2) There is a 15 °C temperature gradient in the upper 100 m, encompassing one of the steepest thermoclines (0.5 °C m^{-1}) in the world's oceans which occurs between 25 and 37.5 m. (3) The region is extremely productive, and foraminifera are abundant. (4) A sharp chlorophyll maximum is well developed in the thermocline[7]. (5) The water column was sampled for measurement of $\delta^{18}O$ of seawater.

Twenty-three species of planktonic foraminifera were identified in the Panama Basin tows. In the 0–100-m tow, MOC 126 (Fig. 1*a*), 16 species averaged more than 10 per 1,000 m^3. The dominant species, *Globoquadrina dutertrei*, showed a pronounced abundance peak between 25 and 50 m, precisely the interval corresponding to the steep thermocline, highest primary productivity and the associated deep chlorophyll maximum (DCM) (Fig. 1*a*)[7]. Nine out of 16 species or morphotypes showed pronounced maxima in the steep thermocline. Note that the abundance axis is logarithmic. *Globigerinoides sacculifer* and *Globigerinoides conglobatus* were numerically dominant at the chlorophyll maximum, but they showed comparable abundances in the surface mixed layer. *Globigerinoides ruber*, *Globigerinita glutinata*, *G. sacculifer* (without final sac chamber), and *G. conglobatus* were very abundant in the less productive surface mixed layer. Two species which secrete morphologically distinct terminal chambers, *Orbulina universa* and *G. sacculifer*, showed sharp maximum concentrations of these morphologies in the chlorophyll maximum zone between 25 and 37 m (Fig. 1*a*). *Globigerina calida* and *Globorotalia theyeri* had maxima below the steep thermocline. Of particular significance is the observation that the *G. theyeri* population descended from a maximum at 100 m on 4 August, MOC 127 (Fig. 1*b*) to between 250 and 375 m on 5 August, MOC 128 (Fig. 1*c*) to a maximum between 500 and 750 m on 8 August, MOC 131 (Fig. 1*d*). This averaged to a 170 m per day descent rate.

Oxygen isotope measurements of seawater (Fig. 2) and continuous temperature and conductivity measurements during the MOCNESS tows permit the construction of an accurate calcite

0028–0836/82/340841—04$01.00

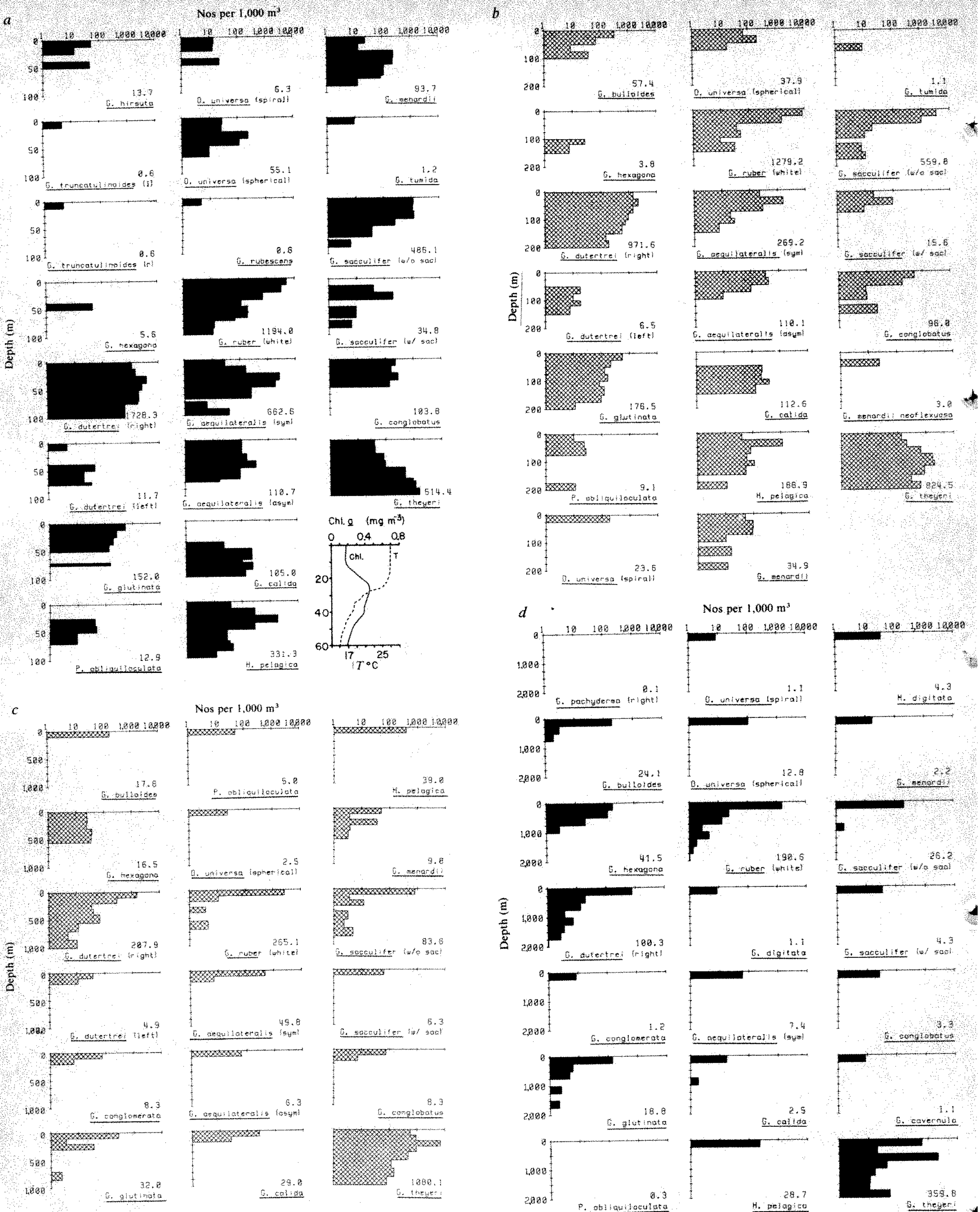

Fig. 1 *a*, Vertical profiles of living planktonic foraminifera caught in MOCNESS 126 oblique hauls in the Panama Basin between 0 and 100 m (3 August 1979; night). The number in the lower right corner of each histogram represents the average number per 1,000 m^3 over the interval towed, in this case 0–100 m. Temperature and chlorophyll profiles for this station are in the lower right corner. Chlorophyll data from Marra *et al.*[7]. *b*, Vertical profiles of living planktonic foraminifera caught in MOCNESS 127 oblique hauls in the Panama Basin between 0 and 200 m (4 August 1979; day). *c*, Vertical profiles of living planktonic foraminifera caught in MOCNESS 128 oblique hauls in the Panama Basin between 0 and 1,000 m (5 August 1979; day). *d*, Vertical profiles of living planktonic foraminifera caught in MOCNESS 131 oblique hauls in the Panama Basin between 0 and 2,000 m (8 August 1979; night).

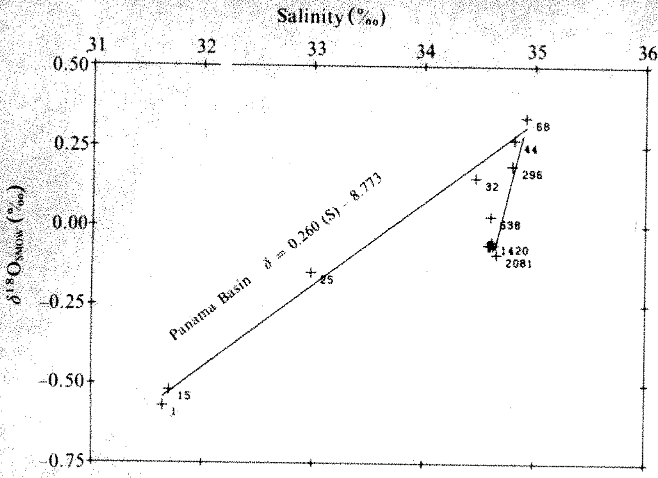

Fig. 2 Salinity versus $\delta^{18}O_{SMOW}$ for the Panama Basin. The numbers next to the symbols indicate water depth. The data indicate binary mixing between surface water and intermediate water, and deep water and intermediate water.

equilibrium profile (Fig. 3*a*) using the mollusc equation of Epstein *et al.*[8]. Oxygen isotope measurements of several different size fractions of nine foraminifera species or morphotypes show that shell growth is restricted to the upper 100 m, even though many species are found in abundance below 100 m. The oxygen isotope data indicate that specimens found below 100 m were simply descending through the water column while adding little or no additional calcite (Fig. 3*a*). It is also evident from the δ^{18}O versus depth plots (Fig. 3*a*) that most species generally grow within narrower depth intervals within the photic zone than their overall distribution would imply. For example, *G. ruber* is found in decreasing numbers between the surface and 100 m (Fig. 1*a*). Its δ^{18}O composition indicates that it is growing typically 0.5‰ lighter than equilibrium[1,2,9] in the surface mixed layer. Between 25 and 37.5 m *G. ruber* is adding some calcite, but below this level the data-point at 60 m indicates vertical descent from the mixed-layer.

G. dutertrei calcifies in oxygen isotope equilibrium[2] and the isotope data indicate growth in the thermocline, where *G. dutertrei* are found in maximum abundance (Fig. 1*a*). Between 37.5 and 100 m, *G. dutertrei* becomes only slightly enriched in δ^{18}O, and are far from equilibrium at these depths. This is evidence that they are descending from the steep thermocline (Fig. 3*a*). The slight δ^{18}O enrichment is probably due to shell thickening[2,3]. Scanning electron microscope observations are needed to confirm this hypothesis.

G. theyeri and *G. calida* appear to be in oxygen isotopic equilibrium between 50 and 100 m, where they are dominant in MOC 126 and MOC 127, but their isotopic values do not change when they are collected below the photic zone (approximately upper 100 m) even though they may be numerically dominant below 100 m. Again, vertical descent is obvious and, in these two examples, no additional calcite was added during descent, otherwise we would observe a shift towards the equilibrium line. Thus we feel confident that this sampling strategy adequately captures all adult stages of shell calcification and allows us to examine the entire calcification process.

There is a 2‰ decrease in the δ^{13}C of total dissolved CO_2 between the surface and 100 m at the site of MOC 126 (Fig. 3*b*). There is some evidence that the δ^{13}C compositions of *G. dutertrei* and *Globigerinella aequilateralis* are affected by this gradient. *G. dutertrei* decreases more than 1‰ δ^{13}C between the surface and 100 m (Fig. 3*b*). The largest drop in δ^{13}C for *G. dutertrei* is coincident with the 1.5‰ decrease in δ^{13}C of total dissolved CO_2 in the steep thermocline. *G. aequilateralis* show a less significant shift in δ^{13}C, but this species also parallels the seawater trend. The carbon isotope equilibrium line for inorganic calcite would fall to the right of the data, but parallel to the δ^{13}C of total dissolved CO_2 line (see ref. 9 for a discussion of calcite isotope equilibrium).

Note that *G. dutertrei* and *G. theyeri*, which calcify in oxygen isotope equilibrium, have the same carbon isotopic composition as ambient δ^{13}C of total dissolved CO_2 (Fig. 3*b*). As noted above, oxygen isotope measurements of *G. dutertrei* indicate equilibrium precipitation at ~30 m (Fig. 3*b*). Below 30 m *G. dutertrei* shows oxygen isotope enrichment, but the data are

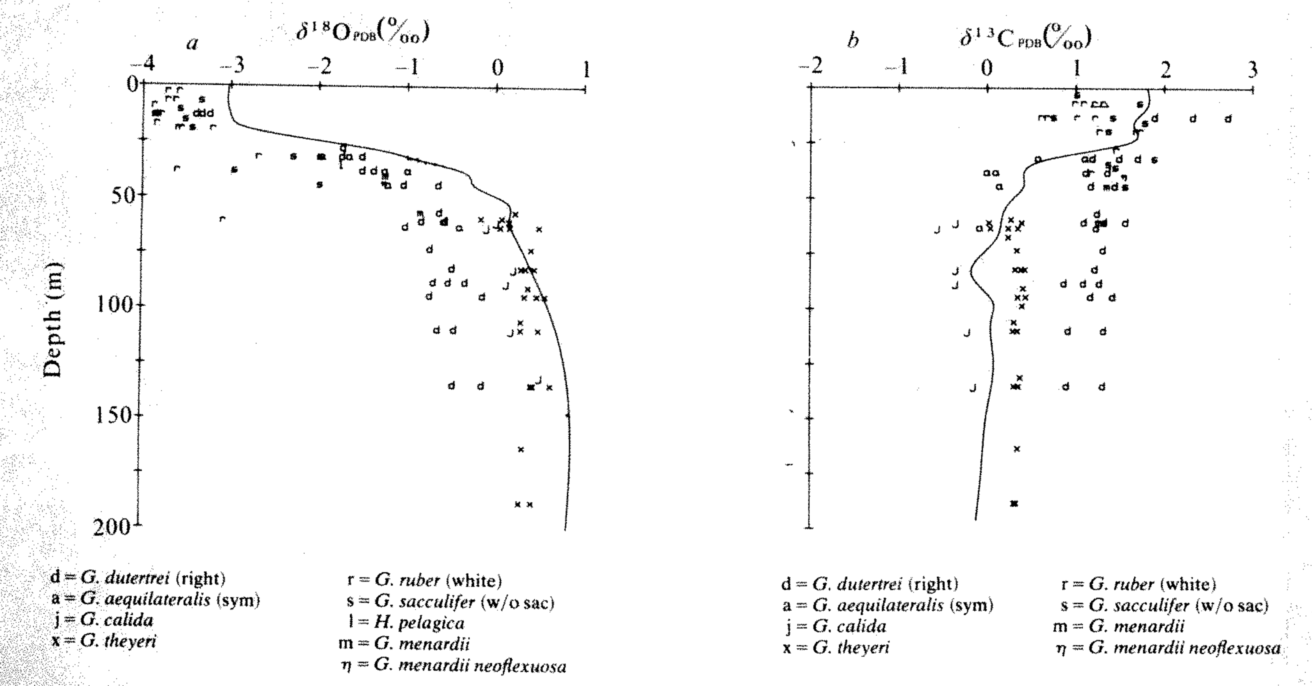

Fig. 3 *a*, Oxygen isotope composition of various size fractions of planktonic foraminifera as a function of depth in MOC 126, 0–100 m and MOC 127, 0–200 m. The solid line is the calculated equilibrium $CaCO_3$–δ^{18}O variation. All specimens plotted were protoplasm full. Corresponds to histograms in Fig. 1*a*, *b*. Carbon isotope composition of various size fractions of planktonic foraminifera as a function of depth in MOC 126, 0–100 m and MOC 127, 0–200 m. The solid line is the δ^{13}C of total dissolved CO_2.

significantly lighter than equilibrium, indicating vertical descent from 30 m. Similarly *G. dutertrei* calcite has the same $\delta^{13}C$ as the $\delta^{13}C$ of total CO_2 at 30 m and shows departure from the $\delta^{13}C$ of total CO_2 curve below 30 m, which is in agreement with the $\delta^{18}O$ data. *G. theyeri* is in oxygen isotope equilibrium between 50 and 75 m and also has the same $\delta^{13}C$ of carbonate as ambient $\delta^{13}C$ of total dissolved CO_2. *G. theyeri* differs from *G. dutertrei* by 1‰. The algal symbiont bearing species (such as *G. ruber*, *G. sacculifer*, *G. aequilateralis*) are generally depleted with respect to ^{13}C when compared with the ambient $\delta^{13}C$ of total dissolved CO_2.

We thank Greg Kolibas for stable isotope measurements, Ted Baker for computer programming and J. K. Bishop for providing PO_4 data. Contribution no. 3358 from Lamont-Doherty Geological Observatory of Columbia University and contribution no. 5139 from the Woods Hole Oceanographic Institution. This work was supported by NSF grant OCE 7725976 (R.G.F.) and ONR grants N00014-750210 and N00014-800098.

Received 25 March; accepted 24 May 1982.

1. Fairbanks, R. G. & Wiebe, P. H. *Science* **209,** 1524 (1980).
2. Fairbanks, R. G., Wiebe, P. H. & Bé, A. W. *Science* **207,** 61 (1980).
3. Emiliani, C. *Am. J. Sci.* **252,** 149 (1954).
4. Wiebe, P. H., Burt, K. H., Boyd, S. H. & Morton, A. W. *J. mar. Res.* **34,** 313 (1976).
5. Fairbanks, R. G. *J. geophys. Res.* **87,** 5796 (1982).
6. Broecker,, W. S. *Prog. Oceanog.* **11,** 151 (1982).
7. Marra, J. Wiebe, P. H., Stepien, J. C. & Bishop, J. K. (in preparation).
8. Epstein, S., Bucksbaum, R., Lowenstam, H. A. & Urey, H. C. *Bull. geol. Soc. Am.* **64,** 1315 (1953).
9. Williams, D. F., Bé, A. W. H. & Fairbanks, R. G. *Science* **206,** 447 (1979).
10. Turner, J. V. (in preparation).

Trans-sexually grafted antennae influence development of sexually dimorphic neurones in moth brain

Anne M. Schneiderman*‡, Steven G. Matsumoto* & John G. Hildebrand†

* Department of Neurobiology, Harvard Medical School, Boston, Massachusetts 02115, USA
† Department of Biological Sciences, Columbia University, New York, New York 10027, USA

Observations in insects reveal sexual differences in the central nervous system (CNS), associated with sexually dimorphic patterns of reproductive behaviour[1-9]. For example, in certain species of moths, including the sphinx moth *Manduca sexta*, only males fly towards a sexually receptive female or towards a source of the female sex pheromone[10,11]. In *Manduca*, specialized olfactory receptor cells found only on male antennae[12,13] respond sensitively and selectively to the female sex pheromone (unpublished experiments with K.-E. Kaissling and R. J. O'Connell). Their axons project into the macroglomerular complex (MGC), which is characteristic of male, but not female, antennal lobes (ALs; Fig. 1*b*, *d*)[1-3,5,8,9,14]. These afferents to the MGC presumably synapse with male-specific AL neurones[8,15] to begin the processing of phenomonal information. We have now devised a surgical procedure for producing antennal gynandromorphs of *Manduca* in which one of the two ALs receives sensory innervation from an antenna formed by a transplanted imaginal disk of the opposite sex. We report here that in these gynandromorphs, the physiological and morphological properties of certain AL neurones are influenced by the gender of the antennal sensory axons contacting them. In particular, neurones resembling the male-specific AL neurones appear in female ALs innervated by sensory axons from a grafted male antenna.

We produced 329 gynandromorphic larvae (Table 1, group 1), of which 78% metamorphosed and eclosed as adult moths. In 49% of these moths, the transplanted imaginal disk had everted and formed an antenna. All transplanted antennae exhibited structure characteristic of the donor's sex; none appeared to be modified by transplantation into a host of the opposite sex.

In 59% of the animals with everted grafts, the AL on the operated side was innervated by the nerve from the transplanted antenna. In these animals, the ingrowing sensory axons found their targets, the AL neurones, even though the pupal antennal nerve, comprising axons believed to provide contact guidance for antennal afferents[13,16], had been severed during surgery. We presume that the axons followed stumps of the 'guide fibres' still associated with the AL and suspect that the growing axons failed to do so in the remaining animals (41% of those with everted grafts). In the latter, the antennal nerve either ended abruptly as a mass of fibres near the base of the antenna or grew into the lateral protocerebrum, proboscis, or suboesophageal ganglion. In these animals, the operated AL was stunted, as in the deafferented AL in a deantennated moth[17,18]. No innervation of the contralateral AL by the graft was ever observed.

We examined histological sections from the brains of unoperated moths and antennal gynandromorphs (Fig. 1; Table 1,

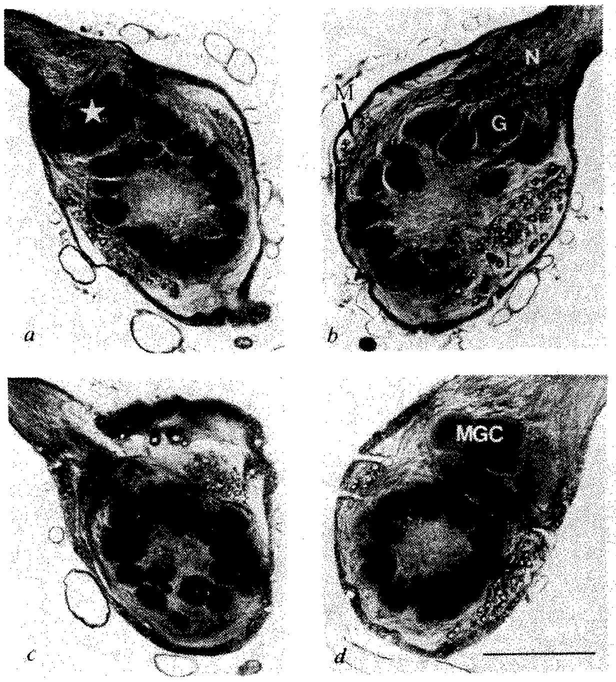

Fig. 1 Frontal sections through the operated (gynandromorphic) and control (normal) ALs of female (*a*, *b*) and male (*c*, *d*) moths, prepared from paraffin-embedded preparations and stained with Cresylecht violet and Luxol fast blue[18]. To produce antennal gynandromorphs of *Manduca*, antennal disks are transplanted unilaterally on the first or second day of the fifth (last) larval instar. Larvae are restrained in aluminium tubes and anaesthetized by chilling in a bath of ice-cold water. The antennal disk[14], which lies within the head capsule near the base of the larval antenna, is excised and replaced with the corresponding disk from a donor of the opposite sex. A mixture of phenylthiourea, streptomycin sulphate and penicillin (2 : 1 : 1)[19] is placed in the wound, which is then sealed by melted myristic acid (W. Harris, personal communication). In *b*, the antennal nerve (N) enters the normal female AL. The glomeruli (G) are arrayed around a central region of coarser neuropil. The cell bodies of the AL neurones are gathered in three cortical groups: a large lateral cluster (L), a smaller medial cluster (M) and a small group anterior to this plane of section. The normal male AL (*d*) characteristically exhibits the MGC, which lies near the entrance of the antennal nerve and is not present in the normal female AL (*b*). In the gynandromorphic female AL (*a*), a structure resembling the MGC (☆) lies near the entrance of the antennal nerve from the grafted male antenna. The gynandromorphic male AL (*c*) lacks a MGC. Scale bar, 200 μm.

---

‡ Present address: Department of Biological Sciences, 901 Fairchild, Columbia University, New York, New York 10027, USA.

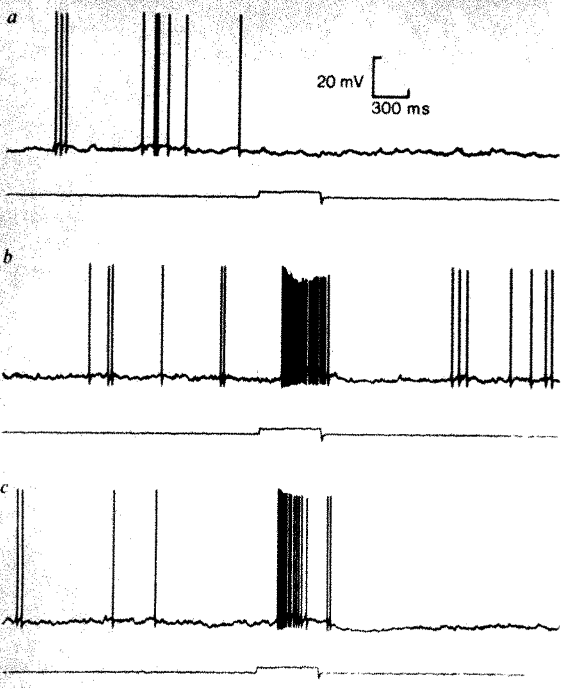

Fig. 2 Intracellular recording from a neurone in the operated AL of a female gynandromorph. Recordings were made with microelectrodes filled with a solution of 4% $CoCl_2$ in 0.75 M KCl and having impedances of 50–75 MΩ (ref. 8). This recording shows the postsynaptic responses elicited by directing pulses of air (*a*), *trans*-2-hexenal (*b*), or bombykal (*c*) on to the grafted male antenna. Odourants were delivered in carrier pulses (500–600 ms duration) of charcoal-filtered air. This cell was stimulated when the antenna was exposed to *trans*-2-hexenal or bombykal. AL neurones responsive to antennal stimulation with bombykal were not found in unoperated females or in the control AL of gynandromorphic females. Conversely, in gynandromorphic males, bombykal never elicited responses from neurones in the AL innervated by the grafted female antenna, although neurones in the control AL responded normally to pheromonal stimulation of the male's own antenna. Injection of cobaltous ions at the completion of recording was accomplished by passing 10 nA depolarizing current pulses of 200–300 ms duration for 15 min at 1 Hz.

group 1). In the brains of male gynandromorphs, the MGC was always missing from the AL innervated by the female graft (Fig. 1*c*). Conversely, the brains from female gynandromorphs invariably exhibited a structure resembling the MGC in the AL innervated by the male graft (Fig. 1*a*). In 100 control larvae, we transplanted a disk of the same sex into a host (Table 1, group 2) or re-implanted its own imaginal disk (Table 1, group 3). Of these animals, 86% survived; in 53% of the survivors, the graft formed an antenna; and in 72% of these the operated AL was innervated by the antennal nerve from the graft. Under the light microscope, the ALs of the latter animals were indistinguishable from those of unoperated animals: a male AL innervated by a male graft formed a MGC, but a female AL innervated by a female graft did not. We have observed that the degree of innervation of the AL by grafts ranges from none (where the antennal nerve does not reach the AL) to complete (where there is a full-size antennal nerve). Even in ALs innervated by reduced numbers of male antennal axons, a readily identifiable MGC-like structure developed.

Table 1 Summary of antennal disk-implantation experiments

Group	Type of disk grafted	Total animals* Female	Total animals* Male	Everted graft Female	Everted graft Male	Innervated AL† Female	Innervated AL† Male
1	Opposite sex	163 (122)	166 (135)	65	60	44 (12)	30 (13)
2	Same sex	13 (12)	34 (29)	8	14	6 (4)	10 (5)
3	Self	19 (18)	34 (27)	13	11	10 (7)	7 (4)

* Values in parentheses indicate number of animals that survived surgery.

† Values in parentheses indicate number of ALs sectioned for light-microscopic examination.

With the use of intracellular recording and staining[8], we characterized neurones in the ALs of gynandromorphic moths. In 14 of 16 females with ALs innvervated by male antennal grafts, male-like interneurones were present (21 out of 34 cells tested) that are never observed in normal females. Intracellular recordings from such cells (Fig. 2) showed that they responded postsynaptically when the transplanted antenna was stimulated with bombykal. Intracellular staining with cobalt sulphide revealed, moreover, that these cells sent dendritic processes into the MGC-like region of neuropil (Fig. 3). In four gynandromorphic males, whose operated ALs received sensory inputs from transplanted female antennae (lacking pheromone receptors), the characteristic male interneurones were not found. The MGC was missing in these ALs, and no interneurones were observed that either responded when the transplanted antenna was stimulated with bombykal (11 cells tested) or had neurites in the region of the AL where the MGC would normally form. We recorded intracellularly from AL neurones in four males with the same-sex grafts (from group 2 of Table 1) and one male whose own antennal disk had been re-implanted (from group 3 of Table 1). We observed AL neurones that were responsive to bombykal (5 out of 13 cells tested) and had arborizations in the MGC. Finally, normal females and males have AL neurones that respond when the antenna is stimulated with *trans*-2-hexenal ('leaf aldehyde') but not with bombykal, and these cells have arborizations in 'ordinary' glomeruli but not in the MGC[8]. We have observed analogous cells in female and male gynandromorphs. Thus, we note a positive correlation in AL neurones between physiological responsiveness on stimulation of the antenna with pheromone and possession of dendritic arborizations in the MGC.

These observations reveal a remarkable degree of plasticity in the development of sexually dimorphic neurones in the moth's AL. We find that the gender of afferent axons has a pronounced role in the differentiation of AL neurones. A MGC-like structure develops only in ALs, female or male, innervated by axons from a grafted male antenna. In female gynandromorphs, certain AL neurones show masculine patterns of arborization in the MGC-like structure. Moreover, these neurones establish functional connections with axons from the grafted male antenna and respond postsynaptically when the antenna is stimulated by the female pheromone. Whether the axons from the grafted antenna of one sex serve to sustain or suppress the development of gender-specific interneurones in the ALs of their host of the opposite sex, or to remodel or induce response properties and patterns of dendritic branching

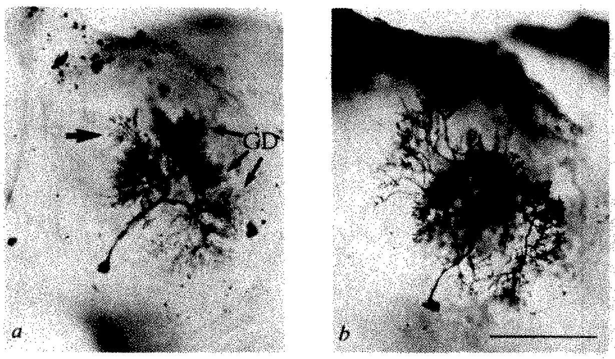

Fig. 3 *a*, Gynandromorphic female interneurone from which the intracellular recording in Fig. 2 was obtained. The cell was stained intracellularly with cobaltous sulphide, intensified with silver and viewed frontally in a whole-mount[8]. Like the normal male-specific, type-II local interneurone[8] shown in *b*, the cell in *a* lacks an obvious axon and has dendrites (GD) ramifying within the glomerular neuropil and within the MGC-like structure (arrow).● The cell body is located at the end of the primary neurite in the lateral cell cluster. Scale bar, 200 μm.

characteristic of the graft's gender, is an intriguing but unanswered question. Its answer will lead to a better understanding of the mechanisms underlying development of sexually dimorphic components in the CNS, and possibly those underlying developmental plasticity of neurones in general.

We thank Drs I. D. Harrow and L. P. Tolbert for critical reading of the manuscript; M. Imperato, R. Montague, A. Papier, P. Quartararo and J. Torrisi for assistance; Drs A. H. Baumhover, J. A. Svoboda and C. M. Williams for supplying *Manduca* eggs; and Dr K. H. Dahm for providing bombykal. This work was supported by USPHS research grants AI-16150 and AI-17711, NSF grants BNS-77-13281 and BNS-80-13511, USPHS training grant NS-07112-04 (A.M.S. and S.G.M.) and an NSF predoctoral fellowship (A.M.S.).

Received 27 April; accepted 16 June 1982.

1. Boeckh, J., Boeckh, V. & Kuhn, A. *Olfaction Taste, Paris* **6,** 315–321 (1977).
2. Boeckh, J. & Boeckh, V. *J. comp. Physiol.* **132,** 235–242 (1979).
3. Camazine, S. & Hildebrand, J. *Soc. Neurosci. Abstr.* **5,** 155 (1979).
4. Hausen, K. & Strausfeld, N. J. *Proc. R. Soc.* **B208,** 57–71 (1980).
5. Hildebrand, J. G. *et al.* in *Insect Neurobiology and Pesticide Action* (ed. Rickett, F. E.) 375–382 (Society for Chemical Industry, London, 1980).
6. Strausfeld, N. J. *Nature* **283,** 381–383 (1980).
7. Wohlers, D. & Bacon, J. *Cell Tissue Res.* **209,** 371–382 (1980).
8. Matsumoto, S. G. & Hildebrand, J. G. *Proc. R. Soc.* **B213,** 249–277 (1981).
9. Prillinger, L. *Cell Tissue Res.* **215,** 563–575 (1981).
10. Allen, N. & Hodge, C. R. *J. econ. Ent.* **48,** 526–528 (1955).
11. Allen, N., Kinard, W. S. & Jacobson, M. *J. econ. Ent.* **55,** 347–351 (1962).
12. Sanes, J. R. & Hildebrand, J. G. *Devl Biol.* **51,** 300–319 (1976).
13. Sanes, J. R. & Hildebrand, J. G. *Devl Biol.* **51,** 282–299 (1976).
14. Jawlowski, H. *Annls Univ. Mariae Curie, Sklodowska* **C8,** 403–434 (1954).
15. Tolbert, L. P. & Hildebrand, J. G. *Proc. R. Soc.* **B213,** 279–301 (1981).
16. Sanes, J. R. & Hildebrand, J. G. *Wilhelm Roux's Arch. devl Biol.* **178,** 71–78 (1975).
17. Sanes, J. R., Prescott, D. J. & Hildebrand, J. G. *Brain Res.* **119,** 389–402 (1977).
18. Hildebrand, J. G., Hall, L. M. & Osmond, B. C. *Proc. natn. Acad. Sci. U.S.A.* **76,** 499–503 (1979).
19. Schneiderman, H. A. in *Methods in Developmental Biology* (eds Wilt, F. H. & Wessels, N. K.) 753–766 (Crowell, New York, 1967).

Exaggerated salt appetite of spontaneously hypertensive rats is decreased by central angiotensin-converting enzyme blockade

R. DiNicolantonio, J. S. Hutchinson
& F. A. O. Mendelsohn

University of Melbourne, Department of Medicine, Austin Hospital,
Heidelberg, Victoria 3084, Australia

Injection of angiotensin II (AII) into the cerebral ventricles at doses as low as 1 pmol h^{-1} results in a marked stimulation of salt and water ingestion in the rat[1,2]. Evidence that AII is produced in the central nervous system independently of the circulating renin–angiotensin system (RAS)[3,4] raises the possibility that endogenous brain AII is involved in the physiological regulation of thirst[5]. The role of brain AII in salt appetite is still unclear[6]. Here we confirm that the spontaneously hypertensive rat (SHR), believed to have elevated levels of brain AII[7], possesses an exaggerated salt appetite compared with its normotensive controls. We also show that this exaggerated salt appetite is reduced by chronic central treatment with the angiotensin-converting enzyme inhibitor, captopril, while that of the normotensive controls is unaffected. Our study suggests that a central neuropeptide, probably AII, is involved in the maintenance of the exaggerated salt appetite in this model of hypertension.

Intracerebroventricular (i.c.v.) administration of AII receptor antagonists[8] or angiotensin-converting enzyme inhibitors[9] to the spontaneously hypertensive rat of the Okamoto strain, but not to the normotensive control Wistar Kyoto (WK) rat results in a marked, rapid, hypotensive response independent of the circulating RAS. Furthermore, an increased density of immunoreactive AII has been reported in hypothalamic neurones of the SHR[10]. As the circulating RAS in the SHR does not differ from that in the WK rat[11], these findings sugges an overactivity of the brain RAS in the SHR. The SHR have an exaggerated salt appetite compared with WK rats[12]. This given the evidence for overactivity of the brain RAS in the SHR, may be due to overproduction of central AII. To tes this hypothesis, we have monitored fluid intake in groups o SHR and WK animals offered a choice of water or saline before and after chronic infusion of captopril into the left latera cerebral ventricle in an attempt to block angiotensin II production.

Figures 1 and 2 show the fluid intakes of SHR and WK rats offered a choice of saline or water before and after infusion of either captopril, 80 μg h^{-1}, or vehicle. In the pretreatment control period, SHR drank 23.3 ± 1.0 ml per 100 g body weight per day (mean ± s.e.m. of 100 observations) of saline and 4.8 ± 0.3 ml per 100 g per day ($n = 100$) of water; this represents a saline preference of 83% of total fluid intake. In the same period, WK rats drank 7.1 ± 0.5 ml per 100 g per day ($n = 100$ of saline and 9.3 ± 0.3 ml per 100 g per day ($n = 100$) of water saline representing 43% of fluid intake. Therefore, SHR had nearly double the total fluid intake of the WK rats ($t = 8.3$ $P < 10^{-13}$) and also a significantly higher proportion of saline in this intake ($t = 12.7, P < 10^{-24}$). The effect of central captopril on the intake and choice of fluid of SHR is shown in Fig. 1 Vehicle-treated SHR showed no change in saline intake during the infusion period compared with the pre-implantation period ($F_{1,120} = 0.3, P > 0.6$). In contrast, captopril-infused rats showed a significant decrease (23%) in saline intake during the treatment period compared with either the pre-implantation period ($F_{1,108} = 20.3$, $P < 10^{-4}$) or vehicle-infused rats ($F_{1,112} = 9.2$ $P < 3 \times 10^{-3}$). Captopril-treated SHR also showed an increased (172%) water intake compared with the vehicle-infused SHR during the treatment period ($F_{1,112} = 33.9$, $P < 10^{-7}$), while no significant differences existed between the two groups during the pretreatment period ($F_{1,112} = 2.5, P > 0.12$). Whereas saline represented 83 ± 1% of total fluid intake of SHR before treatment, this fell to 77 ± 2% after captopril ($F_{1,112} = 6.4, P < 0.01$). Vehicle-treated SHR showed an increase of proportional saline intake from 84 ± 1% to 88 ± 1% ($F_{1,126} = 13.7$, $P < 3 \times 10^{-4}$). In contrast, as shown in Fig. 2, WK rats showed no changes in saline intake, water intake or proportional saline intake with either captopril or vehicle treatment.

The food intake of captopril-infused SHR did not differ from that of vehicle-infused SHR either before (68 versus 67 g per day, respectively; $F_{1,80} = 0.1, P > 0.8$) or during i.c.v. treatment (70 versus 68 g per day; $F_{1,80} = 0.9, P > 0.3$). Similarly, the food intake of captopril-infused WK rats was not different from that of vehicle-infused WK rats either before (66 versus 64 g per day, respectively; $F_{1,56} = 1.6, P > 0.2$) or during i.c.v. treatment (64 versus 61 g per day; $F_{1,70} = 1.4$, $P > 0.2$). The growth rate of captopril-infused SHR did not differ from that of vehicle-infused SHR either before (0.4 versus 0.01 g per day, respectively; $F_{1,80} = 0.1, P > 0.8$) or during i.c.v. treatment (2.0 versus 2.1 g per day; $F_{1,80} = 0.05, P > 0.8$). Similarly, the growth rates of captopril- or vehicle-infused WK rats were also similar before and during treatment (0.01 versus 0.5 g per day, respectively; $F_{1,56} = 0.6$, $P > 0.4$; and 0.4 versus 0.8 g per day, respectively; $F_{1,70} = 0.1$, $P > 0.8$). There was no significant difference in total fluid intake between either central captopril- or vehicle-infused SHR during the treatment period (24 versus 26 ml per 100 g per day, respectively; $F_{1,112} = 2.3$, $P > 0.1$).

It is possible that the fall in salt appetite during central captopril was secondary to renal sodium retention due to a fall in blood pressure. However, the animals showed no change in blood pressure during chronic infusion of captopril at this dose (pre-infusion: 187 ± 5 mmHg, post-infusion: 188 ± 4 mmHg; $F_{1,60} = 0.02$, $P > 0.5$). To examine this possibility further, five male SHR were treated with hydrallazine (5 mg per kg per day, orally) over a 4-day period. Blood pressure, measured by a tail cuff method, fell from a control value of 210 ± 10 mmHg to

149 ± 4 mmHg on day 4 of treatment. Saline consumption was significantly depressed on day 1 of treatment compared with the pretreatment period (14.1 versus 24.7 ml per 100 g per day, respectively; $F_{1,20} = 8.8$, $P < 0.01$), but this was not maintained and there was no difference in saline consumption on the following 3 days of treatment relative to the pretreatment period (22.3 versus 24.7 ml per 100 g per day; $F_{1,28} = 2.2$, $P > 0.1$), despite a maximal fall in blood pressure at this time.

To examine the potency of the effect of captopril on the salt appetite of the SHR, the experiments were repeated using a 10-fold lower dose of captopril (8 μg h^{-1}) infused into the lateral cerebral ventricle over a 7-day period in nine adult male SHR. This dose of captopril produced no change in blood pressure over the treatment period when compared with the 7-day control period (175 ± 4 versus 178 ± 4 mmHg, respectively; $F_{1,48} = 0.3$, $P > 0.5$). Mean saline consumption was 37.2 ± 2.2 ml per 100 g per day during the control period compared with 22.4 ± 1.0 ml per 100 g per day during the last 4 days of captopril infusion ($F_{1,88} = 22.3$, $P < 10^{-5}$). No change in saline intake occurred in nine vehicle-infused SHR during this period when compared with the pretreatment period (28.1 ± 2.0 versus 31.2 ± 2.0 ml per 100 g per day, respectively; $F_{1,88} = 1.1$, $P > 0.7$).

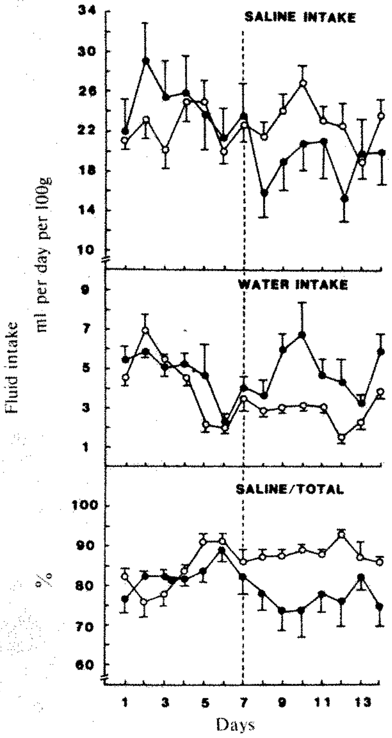

Fig. 1 Fluid intake of male SHR offered a choice of 0.9% saline or tap water. We used 20 male SHR and 20 male WK rats (weight range 320–410 g) housed in individual metabolic cages in conditions of 12-h light and 12-h dark (lights on 0700–1900 h), with room temperature maintained at 22 °C. Standard pelleted laboratory chow (Clarke King GR 2+, Melbourne) was available *ad libitum* and daily food intake was estimated by weighing uneaten and spilt food. A choice of tap water and 0.9% saline was available from individual bottles fitted with dripless stainless steel spouts (Gelman Clemco, Melbourne). Fluid intake was measured daily at 1700 h by weighing the bottles and the positions of saline and water bottles in individual cages were alternated daily. Following a 4-day acclimatization period, a further 7-day period was used to obtain control values of fluid and food intakes. Daily body weight was recorded at 1700 h and fresh saline prepared every second day. Following this control period, animals were lightly anaesthetized with ether and a 27-gauge stainless steel cannula was implanted into the left lateral cerebral ventricle at coordinates AP 1.0, L 1.5, H 4.0 using the bregma as reference. Cannulae were attached by PE 60 tubing to an Alzet osmotic minipump (Alza Corporation), with 10 SHR and 10 WK rats receiving captopril at 80 μg h^{-1} and 10 SHR and 10 WK animals receiving artificial cerebrospinal fluid as the vehicle. The minipump was inserted subcutaneously into the interscapular region. Following surgery, the animals were returned to their individual cages and the measurements continued for a further 7 days. At the end of this period, rats were decapitated and post-mortem examination of the brain performed to verify correct placement of the cannulae. The significance of changes in fluid intake was assessed by two-way analysis of variance. Fluid intakes were expressed per 100 g of body weight and the saline preference represents the percentage saline intake as a proportion of the total fluid intake. The dotted line indicates the start of the i.c.v. infusion of either captopril (●) or vehicle (○).

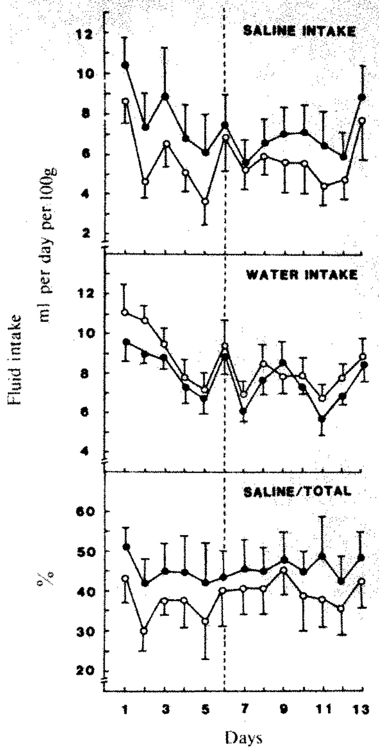

Fig. 2 Fluid intake of male WK rats offered a choice of 0.9% saline or tap water (see Fig. 1 legend). ●, Rats given i.c.v. captopril; ○, vehicle-treated rats.

The selective attenuation of the exaggerated salt appetite of the SHR by central captopril, as shown here, suggests that elevated central AII may contribute to this elevated salt appetite. The fact that central captopril had no effect on the food intake or growth rate of the SHR, and that central captopril was without any effect in the WK rat argues against a nonspecific effect of the drug. Furthermore, whereas a specific decrease in the proportional saline intake was seen in SHR treated centrally with captopril, total fluid intake remained unchanged, suggesting a specific action on sodium appetite.

The possibility that blockade of the circulating RAS, following leakage of captopril from central sites, contributed to the effects seen here may be excluded, as peripherally administered captopril not only lowers the threshold for salt detection but also increases saline ingestion in the rat[13].

As bradykinin[14,15] and the enkephalins[16] are substrates for angiotensin-converting enzyme, it is possible that the effects of captopril in our study are mediated by changes in these or other neuropeptides. However, the opioids seem to stimulate ingestive behaviour[17,18] and elevation of their central levels by captopril would not explain the results observed. According to one study, central administration of bradykinin failed to cause drinking[19], although a large dose of bradykinin has been reported to attenuate AII-induced drinking[20]; potentiation of this peptide might therefore contribute to the actions of central captopril in the SHR.

Centrally administered saralasin did not decrease thirst[21] or salt appetite[6] in previous reports. However, saralasin has agonist activity in most systems[22] and actually potentiated drinking in one study[23]. Furthermore, this peptide is of relatively high molecular weight and it has been suggested that captopril may have access to sites inaccessible to saralasin[24].

The cerebrospinal fluid of hypertensive humans has been reported to contain elevated levels of angiotensin I[25] and angiotensinogen[26]. It is intriguing to note, therefore, that hypertensives show a preference for sodium chloride and exhibit increased daily fluid intake[27], a pattern strikingly similar to that observed in the SHR. The present findings therefore raise the possibility that the brain RAS may be hyperactive in some forms of human essential hypertension.

This work was supported by the National Health and MRC and the National Heart Foundation of Australia.

Received 12 March; accepted 17 June 1982.

1. Bryant, R. W., Epstein, A. N., Fitzsimons, J. T. & Fluharty, S. J. *J. Physiol., Lond.* **301,** 365–382 (1980).
2. Avrith, D. B. & Fitzsimons, J. T. *J. Physiol., Lond.* **301,** 349–364 (1980).
3. Phillips, M. I. *Neuroendocrinology* **25,** 354–377 (1978).
4. Okamura, T., Clemens, D. L. & Inagami, T. *Proc. natn. Acad. Sci. U.S.A.* **78,** 6940–6943 (1981).
5. Ganten, D., Fuxe, K., Phillips, M. I., Mann, J. F. E. & Ganten, U. *Front. Neuroendocr.* **5,** 61–99 (1978).
6. Coghlan, J. P. *et al. Science* **214,** 195–197 (1981).
7. Phillips, M. I. in *Nervous System and Hypertension* (eds Meyer, P. & Schmitt, H.) 102–105 (Wiley, New York, 1979).
8. Phillips, M. I. *et al. Nature* **270,** 445–447 (1977).
9. Hutchinson, J. S., Mendelsohn, F. A. O. & Doyle, A. E. *Hypertension* **2,** 546–550 (1980).
10. Phillips, M. I., Weyhenmeyer, J. & Ganten, D. in *Proc. 4th int. Symp. Rats with Spontaneous Hypertension and Related Studies,* Heidelberg (Abstr.) 21 (1981).
11. Phillips, M. I. in *Enzymatic Release of Vasoactive Peptides* (eds Gross, F. & Vogel, G.) 335–363 (Raven, New York, 1980).
12. McConnell, S. D. & Henkin, R. I. *Am. J. Physiol.* **225,** 624–627 (1973).
13. Fregly, M. J. *Pharmac. exp. Ther.* **215,** 407–412 (1980).
14. Erdos, E. G. *Circulation Res.* **36,** 247–255 (1975).
15. Dorer, F. E., Kahn, J. R., Lentz, K. E., Levine, M. & Skeggs, L. T. *Circulation Res.* **34,** 824–827 (1974).
16. Erdos, E. G., Johnson, A. R. & Boyden, N. T. *Biochem. Pharmac.* **27,** 843–848 (1978).
17. McKay, L. D., Kenney, N. J., Edens, N. K., Williams, R. H. & Woods, S. C. *Life Sci.* **29,** 1429–1434 (1981).
18. Brown, D. R. & Holtzman, S. G. *Life Sci.* **28,** 1287–1294 (1981).
19. Fitzsimons, J. T. *J. Physiol., Lond.* **214,** 295–303 (1971).
20. Kenney, N. J. in *Neural Mechanisms of Goal Directed Behaviour and Learning* (eds Thompson, R. F., Hicks, L. H. & Shvyrkov, V. B.) 437–446 (Academic, New York, 1980).
21. Lee, M-C., Thrasher, T. N. & Ramsay, D. J. *Am. J. Physiol.* **240,** R75–R80 (1981).
22. Marshall, G. R. *Fedn Proc.* **35,** 2494–2501 (1976).
23. Malvin, R. L., Mouw, D. & Vander, A. J. *Science* **197,** 171–173 (1977).
24. Antonaccio, M. J. & Kerwin, L. *Hypertension* **3,** Suppl I, I54–I62 (1981).
25. Finkielman, S., Fischer-Ferraro, C., Diaz, A., Goldstein, D. J. & Nahmod, V. E. *Proc. natn. Acad. Sci. U.S.A.* **69,** 3341–3344 (1972).
26. Ito, T. *et al. Hypertension* **2,** 432–436 (1980).
27. Schechter, P. J., Horwitz, D. & Henkin, R. I. *J. Am. med. Ass.* **225,** 1311–1315 (1973).

Interphotoreceptor retinol-binding proteins: possible transport vehicles between compartments of the retina

Y. L. Lai*, B. Wiggert†, Y. P. Liu† & G. J. Chader†

* Bethesda Eye Institute, St Louis, Missouri 63110, USA
† National Eye Institute, National Institutes of Health, Bethesda, Maryland 20205, USA

In the eye, vitamin A (retinol) is mainly stored in the retinal pigment epithelium (RPE) although its primary function is in the visual process in the photoreceptor organelles of the neural retina (NR). It is well established that during light adaptation, the amount of retinol drops in the NR but rises in the RPE[1]. During dark adaptation, the converse occurs. This indicates a migration of retinoid between the two tissues, the direction of which is dictated by the state of light or dark adaptation of the photoreceptors. The mechanism by which this migration is effected is unknown. We now present evidence that at least one protein exists in the subretinal space or on the cell surfaces which demonstrates many of the unique characteristics one would expect of an interphotoreceptor retinol-binding protein and could function as a vitamin A transport vehicle between NR and RPE.

A technique in which sub-retinal fluid is collected by washing the inner photoreceptor space of the detached retina and by irrigating the apical surface of the RPE and the sub-choroidal space has made possible the study of biochemical parameters involved in the dynamic interaction of these tissues[2]. Previously, gel electrophoresis and scanning electron microscopy have given strong evidence that the tissues do, in fact, remain intact during the lavage procedure[2]. We have now measured ^{3}H-retinol binding in four retinal compartments in the rabbit eye: (1) supernatant of homogenized neural retina, (2) washes of the photoreceptor surface (retinal fraction of the sub-retinal fluid space (SRF/NR), (3) washes of the apical surface of the retinal pigment epithelium (RPE fraction of the sub-retinal space (SRF/RPE) and (4) supernatant of homogenized RPE-choroidal tissue. Eyes from young adult New Zealand albino rabbits were removed under light anaesthesia, NR and RPE gently separated and the surfaces washed with isotonic saline as previously described[2]. Animals were light- or dark-adapted overnight before experimentation. Manipulations involving dark-adapted samples were performed under dim red light. Preparation of the supernatant fraction of tissue homogenates and gradient analysis techniques have already been described[3].

We have previously shown that a 7S retinol-binding protein is present in the supernatant fraction of adult retina of several species as well as the more ubiquitous 2S cellular retinol-binding protein, CRBP[4,5]. Retinol is bound endogenously to the 7S species as well as to the 2S protein, as assessed by relative fluorescence intensity measurements[5]. The 7S species appears to be primarily associated with the photoreceptor outer segments since (1) it is not apparent before outer segments appear in the embryonic retina[6], (2) it is not present when outer segments are absent, as in the disease retinitis pigmentosa[7] and (3) its concentration is increased when outer segments are partially purified although it is lost on extensive purification[6]. Moreover, the 7S retinol-binding activity is greater in the soluble extract of light-adapted frog retina and outer segments than in those of the dark-adapted state[8]. In the present study with rabbit, we observed both 7S and 2S ^{3}H-retinol-binding proteins in the retinal supernatant fraction after sucrose gradient analysis (results not shown). Both binding proteins (7S at about fraction 13; 2S at about fraction 28) can also be observed in the washings of the photoreceptor surface of the retina, the subretinal fluid area (SRF/NR; Fig. 1*a*, *b*). 7S binding is appreciably greater (three times) in the light-adapted state than in the dark-adapted while the amount of 2S binding is virtually identical in the two samples (Table 1).

The specific activities of the 7S and 2S binding are much higher in the subretinal compartments than in the supernatant fraction of retinal homogenate (Table 1). In the light, this amounts to a 24-fold difference in 7S and a 65-fold difference in 2S binding when the SRF/NR wash is compared with the retinal supernatant. Examination of the washings of the pigment epithelial surface (SRF/RPE) reveals a similarly dramatic light/dark difference in 7S receptor binding, although there is a pronounced light effect on 2S binding as well which is not observed in the SRF/NR wash (Fig. 1*c*, *d*; Table 1). 7S binding is 6.6-fold higher in the light than the dark while 2S binding is 4.7-fold higher in the light. 2S ^{3}H-retinol binding is present in the supernatant fraction of RPE-choroidal tissue homogenate

Table 1 ^{3}H-retinol binding in retinal compartments

Compartment	pmol ^{3}H-retinol bound per mg protein 7S Light	Dark	2S Light	Dark
Retinal supernatant	3.4±0.5	2.1±0.4	1.5±0.3	2.6±0.5
SRF/NR wash	83.0±10	28.0±5	97.0±12	90.0±10
SRF/RPE wash	19.2±4	2.9±0.6	198.0±25	42.6±7
RPE choroidal supernatant	*	*	4.0±0.6	4.6±0.8

Conditions as given in Fig. 1 legend. Values given are averages±s.d. of duplicate gradients from three separate experiments.
* Below the limits of detection.

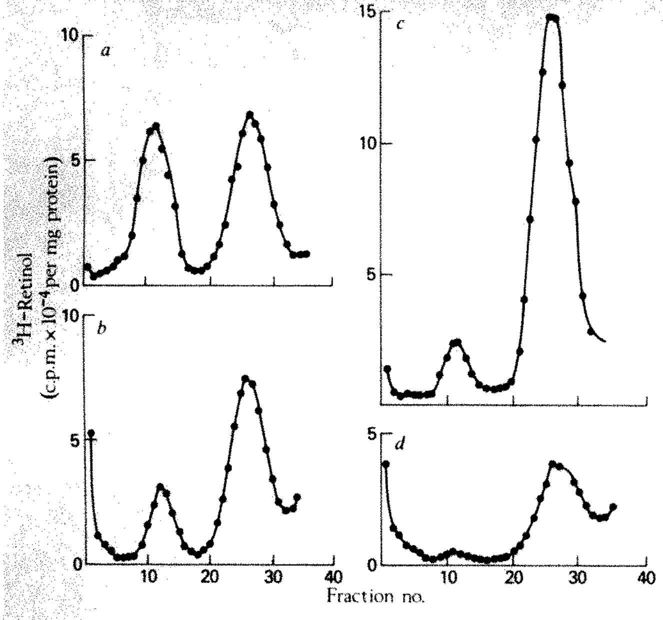

Fig. 1 Sucrose density gradient centrifugation patterns of ^{3}H-retinol binding to washings of *a*, *b*, the retinal photoreceptor surface (SRF/NR); *c*, *d*, the pigment epithelial surface (SRF/RPE). *a*, *c*, From light-adapted animals; *b*, *d*, from dark-adapted animals. The saline washes of the tissue surfaces were diluted 1:2 with Tris buffer (10 mM Tris, 10 mM KCl, 1 mM EDTA, 1 mM dithiothreitol) before gradient analysis and then incubated with 2.8×10^{-7} M all-*trans*, 1-^{3}H-retinol (5 Ci mmol^{-1}; NEN) for 2 h at 4°C in the dark. 250 µl aliquots were then layered on 4.6 ml continuous sucrose gradients (5–20% sucrose) in the Tris buffer and centrifuged for 16 h at 243,000 *g*. About 35 fractions were collected and their radioactivity determined. The top of the gradient is at higher fraction numbers. Protein concentration was determined by the method of Lowry *et al.*[15]. Binding specificity was checked by incubating parallel samples with a 500-fold molar excess of unlabelled retinol. The total amount of specific binding in each peak was determined by summing the total c.p.m. under the peak area and then subtracting the non-specific counts which lay below the peak nadirs. Patterns given are representative patterns from three separate experiments, each having duplicate analysis within the separate experiment.

but has a much lower specific activity than in either the SRF/NR or SRF/RPE fractions (Table 1). There is no detectable 7S binding in this compartment.

Kuhn[9,10] has shown that several proteins are differentially bound to photoreceptor membranes in light and dark. This offers the simplest explanation for our results—that the 7S and perhaps the 2S species are 'peripheral' proteins, loosely bound at the membrane surface. The enhancement in binding in the SRF washes compared with the tissue homogenates and the light/dark effect are both consistent with this postulate. As ^{3}H-retinoid binding studies do not measure the actual amount of binding protein, however, but rather the number of unoccupied binding sites, our results could be affected by several factors. For example, the decreased ^{3}H-retinol binding observed at 7S in the SRF/NR and SRF/RPE compartments and at 2S in the SRF/RPE compartment following dark adaptation could be due to an increase in endogenous unlabelled retinol in these compartments, a decrease in the actual amount of binding protein (turnover) or a change in the binding properties of the proteins. It will be of interest to investigate this in subsequent studies. Whether either of these proteins exhibits enzymatic activity is unclear but should also be investigated in light of the interesting finding that a defect in vitamin A metabolism may be involved in hereditary retinal degeneration in an animal model of retinitis pigmentosa[11]. LaVail *et al.*[12] have also established striking differences in inter-photoreceptor matrix mucosubstances between normal rats and those with inherited retinal dystrophy. What is clear from the present study is that the specific activities of the 7S protein and the 2S CRBP are extremely high in the extracellular subretinal space and that the apparent binding activities are markedly affected by light.

Since free retinol is labile and a potentially toxic substance which can alter cellular membranes[13], as exemplified by retinoid-evoked release of enzymes from NR and RPE lysosomes[14], some sort of carrier might be expected to be present at the various stages of retinoid transit into and through the cells. Moreover, retinoid, used in the visual cycle of the retina, is supplied through the PE cell from the choroidal blood supply, necessitating a generalized vectorial movement of retinoid as well as the more localized, light-evoked 'shuttle' movement between PE and retina during the visual cycle. It would seem likely, then, that the 7S binding protein and the 2S CRBP are both likely candidates for the role of retinoid transport vehicle between the sensory retina and the pigment epithelium. The 7S protein which we call interphotoreceptor retinol-binding protein seems to be a particularly interesting protein for further study due to its restricted presence in the retina, its localization and high concentration in the subretinal photoreceptor matrix and at the membrane surface and its apparent control of binding by light.

Received 23 March; accepted 24 June 1982.

1. Dowling, J. *Nature* **168,** 114–118 (1960).
2. Lai, Y.-L. *et al. Expl Eye Res.* **34,** 7–14 (1982).
3. Wiggert, B. & Chader, G. *Expl Eye Res.* **21,** 143–151 (1975).
4. Wiggert, B., Bergsma, D. & Chader, G. *Expl Eye Res.* **22,** 411–418 (1976).
5. Wiggert, B., Bergsma, D., Lewis, M. & Chader, G. *J. Neurochem.* **29,** 947–954 (1977).
6. Wiggert, B., Mizukawa, A., Kuwabara, T. & Chader, G. *J. Neurochem.* **30,** 653–659 (1978).
7. Bergsma, D., Wiggert, B., Funahashi, M., Kuwabara, T. & Chader, G. *Nature* **265,** 66–67 (1977).
8. Wiggert, B., Derr, J., Fitzpatrick, M. & Chader, G. *Biochim. biophys. Acta* **582,** 115–121 (1979).
9. Kuhn, H. *Biochemistry* **17,** 4389–4395 (1978).
10. Kuhn, H. *Nature* **238,** 587–589 (1980).
11. Berman, E., Segal, N., Photiou, S., Rathman, H. & Feeney-Burns, L. *Nature* **293,** 217–220 (1981).
12. LaVail, M., Pinto, L. & Yasumura, D. *Invest. Ophthalmol. Vis. Sci.* **21,** 658–668 (1981).
13. Meeks, R., Zaharevitz, D. & Chen, R. *Archs Biochem. Biophys.* **207,** 141–147 (1981).
14. Dewar, A., Barron, G. & Reading, H. *Expl. Eye Res.* **20,** 63–72 (1975).
15. Lowry, O., Rosebrough, N., Farr, A. & Randall, R. *J. biol. Chem.* **193,** 265–275 (1953).

Detection of K$^+$ and Cl$^-$ channels from calf cardiac sarcolemma in planar lipid bilayer membranes

Roberto Coronado & Ramon Latorre

Department of Physiology and Biophysics, Harvard Medical School,
Boston, Massachusetts 02115, USA

The ionic currents underlying the cardiac action potential are believed to be much more complex than those in nerve[1,2]. During the cardiac action potential, various membrane channels control the flow of K$^+$, Na$^+$, Ca^{2+} and Cl$^-$ across the sarcolemma of cardiac muscle cells[2–7]. Thus, it has become increasingly clear that a detailed knowledge of the mechanisms that activate (or inactivate) heart channels is required to understand cardiac excitability[8,9]. We report here the use of planar lipid bilayer techniques to detect and characterize K$^+$ and Cl$^-$ channels in purified heart sarcolemma membrane vesicles. We have identified four different types of channel on the basis of their selectivity, conductance and gating kinetics. We present in some detail the properties of a K$^+$ channel and a Cl$^-$ channel. We have tentatively identified the K$^+$ channel with the i_x type of current found in Purkinje[10], myocardial ventricular[11] and atrial[12] fibres. The chloride channel might be related to the transient chloride current found in Purkinje fibres[5,6,13].

We have used sarcolemmal membranes isolated from calf myocardium by a method similar to that described in ref. 14. This method is particularly suitable for our purposes because it minimizes contamination by sarcoplasmic reticulum. Ionic channels present in membrane vesicles purified from heart

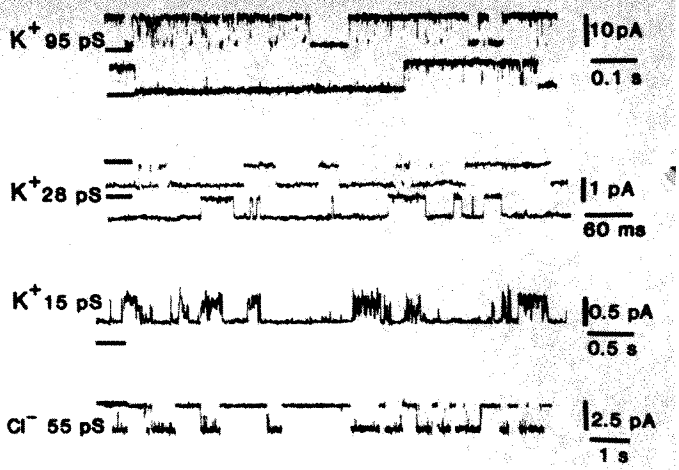

Fig. 1 Calf cardiac channels incorporated into planar lipid bilayers. Planar lipid bilayer membranes were formed from a mixture of bovine brain phosphatidylethanolamine (PE) and bovine brain phosphatidylserine (PS) at a PE/PS ratio of 1 : 1 in decane. This solution was made at a concentration of 50 mg ml^{-1}. Lipid bilayers were formed in Teflon partitions with apertures of 5×10^{-4} cm^2. The bilayer separated two aqueous chambers, each with a volume of ~100 µl. Electrical measurements were made with a two-electrode voltage clamp[17]. One of the chambers (*cis* side) was connected to a function generator to control membrane potential, while the second chamber (*trans* side) was connected to a current-to-voltage converter. Thus, the *trans* side is virtual ground. A positive current is defined as cation flow into the *trans* side. Ag/AgCl electrodes in series with 0.2 M KCl agar bridges served to connect the bilayer solutions to the electronics. Cardiac sarcolemma was prepared from calf ventricle using the procedure of Jones *et al.*[14]. Membranes were stored at −40 °C in 0.4 M sucrose, 10 mM HEPES-Tris, *p*H 7.4. The protocol used to incorporate single channels into the bilayer was as follows. Thawed vesicles were diluted to a final concentration of 50–100 µg protein per ml in 0.1 M KCl, 1 mM CaCl$_2$, 5 mM HEPES-Tris, *p*H 7.2. After forming the bilayer in symmetrical 0.1 M KCl, 5 mM HEPES-Tris, *p*H 7.2, the *cis* chamber was perfused with the vesicle-containing solution. Once the initial jump in conductance was observed, the *cis* chamber was extensively perfused with 0.1 M KCl, 5 mM HEPES-Tris, *p*H 7.2, to remove non-incorporated protein. All single-channel records were stored on FM tape for further analysis. By convention, in all records shown, the channel opening is an upward deflection (that is, 95 pS and 15 pS K$^+$ channels) if the applied voltage is positive, or a downward deflection if the applied potential is negative (that is, 28 pS K$^+$ channel and 55 pS Cl$^-$ channel). The conductance of the bare bilayer (≤5 pS in all cases) is indicated by the horizontal mark at the beginning of each single-channel trace. For the recordings shown, the applied potential was +100 mV for the 95 pS channel, −40 mV for the 28 pS channel, +30 mV for the 15 pS channel and −50 mV for the 55 pS channel. (K$^+$) or (Cl$^-$) indicates whether a given type of channel is Nernst selective for K$^+$ over Cl$^-$ (labelled K$^+$) or vice versa (labelled Cl$^-$). Experiments were performed at room temperature, 22 ± 2 °C.

sarcolemma can be transferred to planar membranes by a Ca^{2+}-induced fusion procedure[15,16]. Incorporation of channels proceeds very quickly, eliciting in a few minutes an increase in bilayer conductance of two or three orders of magnitude provided that two conditions are met: the presence of an osmotic gradient across the bilayer (the vesicle-containing side hyperosmotic), and the presence of Ca^{2+} in the vesicle-containing side. As described elsewhere, these conditions favour fusion of purified membrane vesicles[15–17] and liposomes[18] to planar bilayers. However, when the solutions bathing the membrane are kept symmetrical, and the Ca^{2+} concentration in the vesicle-containing compartment is low (1 mM), we usually observe the incorporation of single channels of one type. Figure 1 shows four types of single-channel current (which are also the most common) in the planar membrane. The first three records correspond to channels having reversal potential values typically observed when Cl$^-$ is completely excluded. The fourth record corresponds to a channel permeable to Cl$^-$ but not K$^+$. The 95 pS channel shown in Fig. 1 has a complicated gating kinetics consisting of one open and at least two closed states, is voltage independent and does not discriminate between K$^+$ and Na$^+$, or among other alkali cations. The 15 pS channel shows a 'noisy' open state and a permeability ratio, $P_{\mathrm{K}^+}/P_{\mathrm{Na}^+}$, of 3. None of the channels shown above is activated by Ca^{2+}, as they persist even if the Ca^{2+} concentration is 10^{-8} M. The kinetics of the 95 pS channel is, however, substantially modified

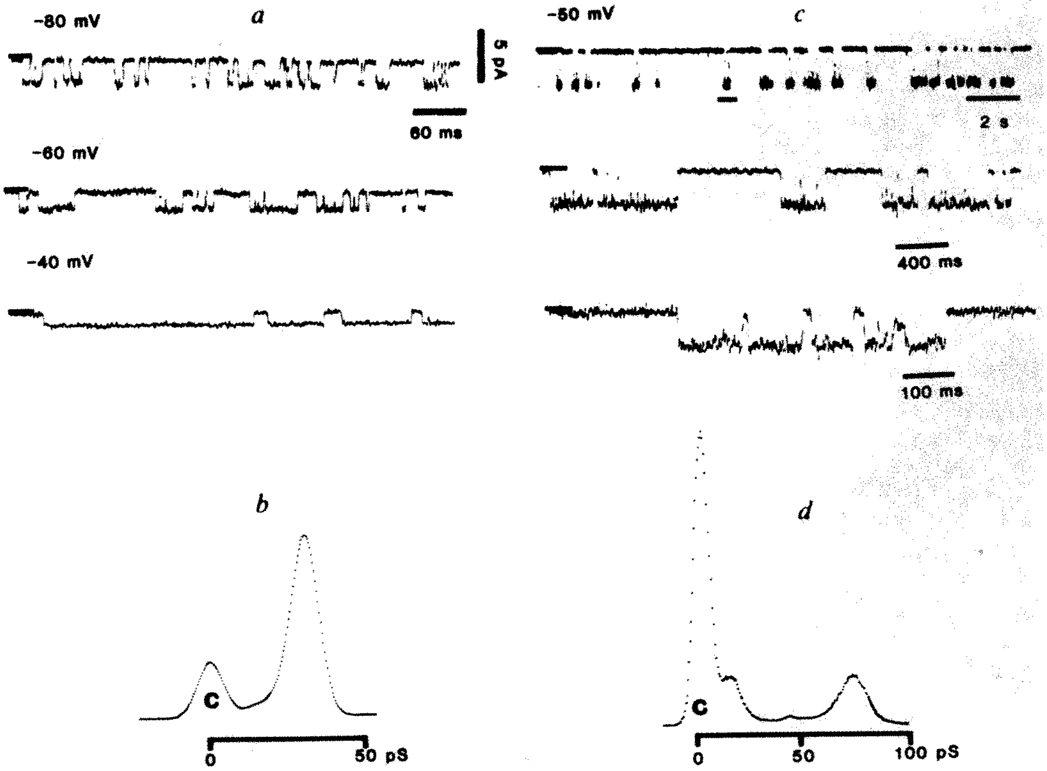

Fig. 2 Electrical characteristics of a K$^+$ and a Cl$^-$ channel. *a*, Recordings of the 28 pS K$^+$-conducting channel from the same membrane, at the voltages indicated. 1 KHz filtering. *b*, Histogram showing the relative occurrence of the two conductance levels of the 28 pS channel at −40 mV. It was obtained by feeding long records (>10 s) of current fluctuations, like those in *a*, into a pulse height analyser and sampling the current at a rate of 10^4 s^{-1}. The histogram is built by placing the sampled current in the bin corresponding to that particular current value. Thus, the peaks represent the most frequent values of conductance for a given record. The mean conductance value for the open state is 28 pS. *c*, Recordings of the 55 pS Cl$^-$-conducting channel at −50 mV. The bar underlying the single burst in the top trace is expanded in the bottom trace. The bar underlying the last three bursts is expanded in the middle trace. 1 KHz filtering. *d*, Histogram showing the relative occurrence of all current levels present in *c*. All measurements were done on symmetrical 0.1 M KCl, *p*H 7.2. C indicates the closed state peak.

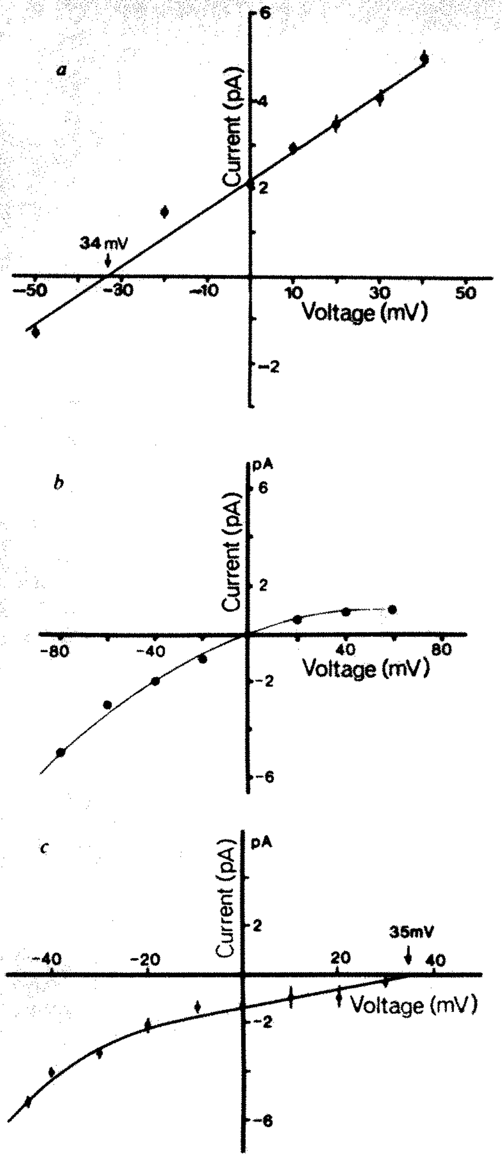

Fig. 3 Single-channel current–voltage curves for the 28 pS K^+ channel and 55 pS Cl^- channel. *a*, Mean single-channel currents obtained from histograms, such as that shown in Fig. 2*b* for the K^+ channel, were plotted for a membrane formed in 0.5 M KCl *cis* side, 0.1 M KCl *trans* side, 5 mM HEPES-Tris, *p*H 7.2, both sides. *b*, Single-channel current–voltage curve for the Cl^- channel in symmetrical 0.1 M KCl, 5 mM HEPES-Tris, *p*H 7.2. Time-average currents through the open states were measured by filtering bursts at 5–10 Hz and computing the mean current. *c*, Current–voltage curve for the same channel in 0.5 M KCl *cis* and 0.1 M KCl *trans*. Voltage indicated at the arrow corresponds to the extrapolated zero-current voltage.

by *cis* Ca^{2+}. As the *cis* Ca^{2+} is decreased below 1 mM, the long closing events (clearly seen at the bottom record of the 95 pS channel in Fig. 1) generally disappear. The properties of the 28 pS K^+ channel and the 55 pS Cl^- channel are described in more detail below.

The 28 pS K^+ channel shows well defined rectangular single-channel currents (Fig. 2*a*). The current step size is directly proportional to voltage; however, the time the channel remains in a given conductance state is voltage dependent. As the voltage is made more positive, the channel remains longer in the open configuration. For the records shown in Fig. 2*a*, the mean open time increases from 6 ms at −80 mV to 60 ms at −40 mV. The probability histogram (Fig. 2*b*) further corroborates the two-conductance-state nature of the channel, as only two peaks can be observed. The open state is, however, interrupted by fast closing events which are noticeable at high negative potentials. The mean closed time of these interruptions is 2–4 ms and may indicate the presence of a second kinetically distinguishable closed state. The electrical activity of the Cl^- channel is much more complicated (Fig. 2*c*). The channel may stay closed for several seconds, then it opens and begins to fluctuate rapidly between several conductance states (see bottom record of Fig. 2*c*). We interpret this type of record to represent the fluctuations of a single channel between several open conductance states and at least two closed states. The probability histogram in Fig. 1*d* shows clearly at least three open conductance states with conductances of 15, 39 and 61 pS.

For the K^+ channel shown in Fig. 2*a*, we also measured the current passing through a single channel in the presence of a fivefold KCl concentration gradient (Fig. 3*a*). The reversal potential for the current transported through a single channel is −34 mV, in agreement with that predicted by the Nernst equation for a K^+-selective channel. We have also measured the bi-ionic potential for 0.1 M KCl (vesicle-containing side)/0.1 M NaCl and found a reversal potential of −40 mV. This implies a permeability ratio $P_{K^+}/P_{Na^+} = 5$.

For Cl^- channels, because of the complexity of the records, we have plotted the average of the weighted mean current through the channel as a function of voltage. Figure 3*b* shows that the mean current through the single channel is a nonlinear function of potential. For negative potentials, current increases more than linearly. For positive potentials, however, the current reaches a limiting value. Analysis of histograms, such as that shown in Fig. 2*d*, indicates that the shape of the curve in Fig. 3*b* arises as a consequence of the voltage dependence of the number and distribution of the different conductance levels. Figure 3*c* shows the current passing through the channel in the presence of a fivefold KCl gradient. From Fig. 3*c*, we obtained a reversal potential of +35 mV. The diffusion potential expected when cations are completely excluded is +36 mV.

At this point, we would like to discuss the physiological role of K^+ channels in the heart. In Purkinje fibres, Noble and Tsien[10,19] described three time- and voltage-dependent outward currents in which the main current-carrying species was K^+. These currents are the pacemaker currents, i_{K_2} (but see ref. 20), and the repolarizing currents i_{x_1}, i_{x_2}. In addition, a fourth time-independent K^+ conductance showing inward-going rectification, i_{K_1}, is also present. More recently, Ca^{2+}-activated K^+ conductances have been shown to contribute to the early repolarization phase of Purkinje action potential[21] as well as to the steady-state K^+ conductance[22]. Many of these currents

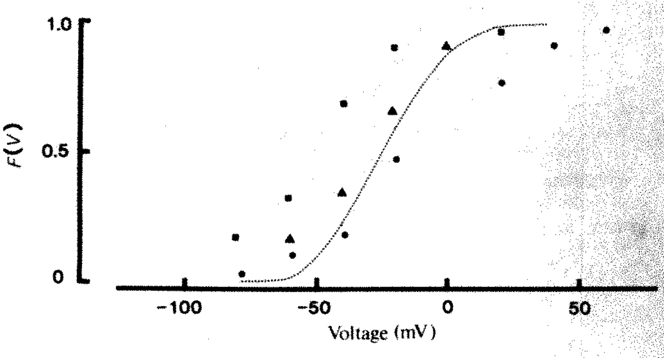

Fig. 4 Single-channel activation curves. The fraction of time in the open state [$F(V)$] of the 28 pS K^+ channel was obtained in three different membranes containing one channel in different ionic conditions. $F(V)$ was calculated from histograms such as that shown in Fig. 2*b*. ■, $F(V)$ in symmetrical 0.1 KCl, 5 mM HEPES-Tris, *p*H 7.2. ●, $F(V)$ in 1 M KCl, 5 mM HEPES-Tris, *p*H 7.2. ▲, $F(V)$ in 0.2 M KCl, 5 mM HEPES-Tris, *p*H 7.2 *cis*, 0.1 M KCl, 5 mM HEPES-Tris, *p*H 7.2 *trans*. Dashed line is the steady-state conductance voltage curve of the repolarizing current, i_{x_1}, and was taken as described in ref. 2.

are also present in ventricular and atrial fibres[11,12]. In agreement with the findings in cardiac muscle, we describe here several types of channel in which K^+ is the major current carrier. In particular, Fig. 4 shows that the voltage dependence of the 28 pS K^+ channel is comparable with that of the i_x currents (dashed line) described in ref. 2. Furthermore, a $P_{K^+}/P_{Na^+} = 5$ for this channel correlates well with the finding that i_x currents are not purely K^+ currents[10]. Although the assumption that i_x and the 28 pS channel activate with the same polarity of voltage is arbitrary, we are inclined to view the *cis* chamber as equivalent to the cytoplasmic side of the incorporated channel based on the following observations: (1) all 28 pS channels studied gate in the same direction, that is, the direction of Fig. 4; (2) inside-out cardiac sarcolemma vesicles fuse more readily than right-sided vesicles, which in the most simple model of fusion would leave the cytoplasmic face of the incorporated channels in the *cis* side[16]; and (3) the same incorporation procedure described here when applied to skeletal muscle membranes results in the incorporation of Ca^{2+}-activated K^+ channels with the Ca^{2+} site on the *cis* side[17]. Nevertheless, if the 28 pS channel were, in fact, to be activated in the cell by hyperpolarizing voltages, it would have the gating characteristics of the recently described inward pacemaker current, i_f (ref. 20). Thus, i_f is a time- and voltage-dependent inward current which activates by hyperpolarizing voltages and is a mixed K^+, Na^+ current[20]. Chloride ions, on the other hand, although clearly involved in the generation of the cardiac action potential, have not been unambiguously identified with a particular current component[5,6,13]. This makes it difficult to assign a physiological role to the Cl^- channel found in the present work, so that more experiments need to be performed in both cardiac cells and bilayers to make a complete identification of this channel. Finally, the channels from cardiac sarcolemma can be incorporated into bilayers made from monolayers (data not shown). This method has been recently used to reconstitute the acetylcholine channel[23-26]. In this type of membrane, we found that the electrical activity is quite complex and indicative of the presence of several types of channel. Using this method, we have been able to identify the 55 pS Cl^- channel and several of the K^+ channels described above. Our choice of the fusion method reported here to incorporate cardiac sarcolemma channels was based on the observation that membranes containing a single channel can be obtained easily. This enormously simplified the analysis of the data.

This work was supported by NIH grants GM-25277 and GM-28992 and by a postdoctoral fellowship to R.C. from the Muscular Dystrophy Association of America. We thank Marianita Sanchez for secretarial help.

Received 22 March; accepted 8 June 1982.

1. Noble, D. in *The Initiation of the Heartbeat* 2nd edn, 186 (Clarendon, Oxford, 1979).
2. McAllister, R. E., Noble, D. & Tsien, R. W. *J. physiol., Lond.* **251,** 1–59 (1975).
3. Rudel, J. & Rudel, R. *Pflügers Arch. ges. Physiol.* **315,** 136–158 (1970).
4. Lee, K. S., Weeks, T. A., Kao, R. L., Akaike, W. & Brown, A. M. *Nature* **278,** 269–271 (1979).
5. Carmeliet, E. *J. Physiol., Lond.* **156,** 375–388 (1961).
6. Fozzard, H. A. & Hiraoka, M. *J. Physiol., Lond.* **234,** 569–586 (1973).
7. Reuter, H. *A. Rev. Physiol.* **41,** 413–424 (1979).
8. Colquhoun, D., Neher, E., Reuter, H. & Stevens, C. F. *Nature* **294,** 752–754 (1981).
9. DeFelice, L. J. & Clapham, D. E. *Biophys. J.* **37,** 341a (1982).
10. Noble, D. & Tsien, R. W. *J. Physiol., Lond.* **200,** 205–231 (1969).
11. Beeler, G. W. & Reuter, H. *J. Physiol., Lond.* **268,** 177–210 (1977).
12. Brown, H. F., Clark, A. & Noble, S. *J. Physiol., Lond.* **258,** 547–577 (1976).
13. Kenyon, J. L., & Gibbons, W. R. *J. gen. Physiol.* **73,** 117–138 (1979).
14. Jones, G. R., Maddock, S. W. & Besch, H. R. *J. biol. Chem.* **255,** 9971–9980 (1980).
15. Miller, C. & Racker, E. *J. Membrane Biol.* **30,** 285–300 (1976).
16. Coronado, R. & Williams, A. *Biophys. J.* **37,** 343a (1982).
17. Latorre, R., Vergara, C. & Hidalgo, C. *Proc. natn. Acad. Sci. U.S.A.* **79,** 805–810 (1982).
18. Cohen, F. S., Zimmerberg, J. & Finkelstein, A. *J. gen. Physiol.* **75,** 251–270 (1980).
19. Noble, D. & Tsien, R. W. *J. Physiol., Lond.* **195,** 185–214 (1968).
20. DiFrancesco, D. *J. Physiol., Lond.* **314,** 377–393 (1981).
21. Siegelbaum, S. A., Tsien, R. W. & Kass, R. S. *Nature* **269,** 611–613 (1977).
22. Isenberg, G. *Pflugers Arch. ges. Physiol.* **371,** 71–76 (1977).
23. Schindler, H. & Quast, U. *Proc. natn. Acad. Sci. U.S.A.* **77,** 3052–3056 (1980).
24. Nelson, N., Anholt, R., Lindstrom, J. & Montal, M. *Proc. natn. Acad. Sci. U.S.A.* **77,** 3057–3061 (1980).
25. Boheim, G. *et al. Proc. natn. Acad. Sci. U.S.A.* **78,** 3586–3590 (1981).
26. Labarca, P., Lindstrom, J. & Montal, M. *Biophys. J.* **37,** 170a (1982).

Macrophage binding of *Staphylococcus albus* is blocked by anti I-region alloantibody

John Stewart, Elizabeth J. Glass & Donald M. Weir

Department of Bacteriology, University Medical School,
Teviot Place, Edinburgh EH8 9AG, UK

Cell surface interactions involving carbohydrate may be important in immune recognition. Previous work from this laboratory has demonstrated the presence of 'lectin-like' receptors on mouse peritoneal macrophages that bind bacteria by means of their cell wall sugars[1-4]. Others have shown that Ia molecules can bind antigen at specific sites which may be involved in presenting antigen to the immune system[5] and recent work has shown that these molecules can carry carbohydrate determinants[6-7]. It has also been found that human Ia molecules can bind to carbohydrates[8]. As cell surface carbohydrate recognition mechanisms have been implicated in other immune interactions[9-11] sugar-specific receptors may have a function in self—non-self recognition. We show here that the binding of the bacterium *Staphylococcus albus* to mouse peritoneal macrophages was inhibited by various conventional and monoclonal antibodies to Ia antigens suggesting that an I-region gene product may be associated with the binding of unopsonized bacteria.

The binding of *S. albus* to glass adherent mouse peritoneal macrophages was measured at 0°C in serum free buffer using a predetermined concentration (approximately 5×10^6 organisms per ml) that gave 25–50% binding to control macrophage preparations[4]. When macrophage monolayers from C3HfBu/Kam mice were pretreated with conventional alloantisera of defined specificity there was dose-dependent inhibition of binding (Fig. 1) as compared to untreated controls, with A.TH anti-A.TL at 1:100, 1:300 and 1:600 ($P < 0.05$) and WS9 at 1:100 ($P < 0.01$) and 1:333 and 1:1,000 ($P < 0.05$). However, A.TL anti-A.TH and WS4 were without effect at all dilutions of antibody used. At a dilution of 1/10 of WS4 (anti D^k) maximal fluorescence was obtained in a direct immunofluorescence test confirming that at the dilution used macrophages were maximally binding this antiserum. Both A.TH anti-A.TL and WS9 react with $H\text{–}2I^k$, as well as $H\text{–}2S^k$ and $H\text{–}2K^k$ respectively. A.TL anti-A.TH is directed against $H\text{–}2I^s$ and S^s while WS4 recognizes $H\text{–}2I\text{–}C^k$, S^k and D^k. These results suggest that an I-region determined product is involved

Table 1 Inhibition of binding of *S. albus* to macrophages by antibody H10–2.16 and anti-macrophage antibody

	Inhibition of binding (%)
a H10–2.16	
Unadsorbed	19.9±5.7
Adsorbed	32.6±7.9
b Anti-macrophage antibody	
Dilution	
$\frac{1}{2}$	2.6±11.2
$\frac{1}{4}$	1.9±5.9
$\frac{1}{8}$	−3.1±6.7

a, 1 ml of 1:10 dilution of H10–2.16 antibody incubated with 3×10^9 *S. albus* at 0 °C for 2 h. The bacteria were removed by centrifugation and antibody used at a final dilution of 1:50 as described in Fig. 1. Unabsorbed antibody was treated as above but without the addition of *S. albus*. Each figure represents the mean ±1.s.e. of four experiments. *b*, The monoclonal antibody specific for macrophages (rat IgG against mouse macrophages. Sera-lab, Sussex) was incubated with macrophage monolayers for 40 min at 0 °C before incubation with bacteria as described previously. Each figure represents the mean ±1.s.e. of three experiments.

in bacterial attachment to macrophages in the absence of opsonins.

In order to further investigate the H-2 region involved, the effect of two monoclonal antibodies on *S. albus* binding to C3HfBu/Kam peritoneal macrophages was determined (Fig. 1). Both antibodies which react with I-A products gave significant inhibition (H 8-109.13; 1:1,000 $P<0.001$; 1:10^4, 1:10^5 and 1:10^6 $P<0.01$: Antibody H 10-2.16; 1:20, 1:60, and 1:180 $P<0.05$), indicating a possible role for an I-A subregion product in bacterial binding. The possibility that the inhibition observed might be due to cross-reactivity of Ia antigens and the bacterial surface is excluded (1) by the extensive washing of the monolayers prior to the addition of bacteria and (2) by adsorption of the monoclonal antibody H 10-2.16 with *S. albus*. The latter treatment did not significantly alter the inhibitory capacity of the antibody (Table 2). Table 2 also shows that antibody directed against macrophage membrane determinants other than H-2 has no effect on bacterial binding. This indicates that the observed inhibition is a function of the alloantibody used.

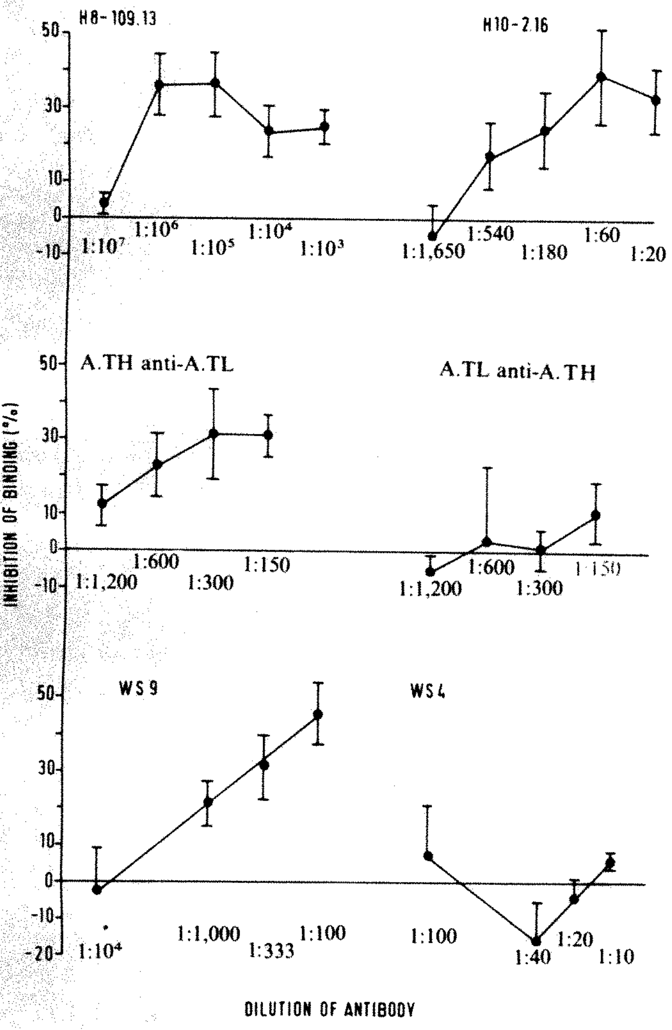

Fig. 1 The effect of various alloantisera on the binding of *S. albus* to C3HfBu/Kam peritoneal macrophages. Each point represents the mean ±1.s.e. of between 3 and 8 experiments. *S. albus* was grown in horse digest broth containing 2.5% glucose, cells were collected in log phase and killed by exposure to 0.5% formalin at 4 °C for 24 hours. Mouse peritoneal macrophages, obtained by lavage, were suspended in Eagles minimal essential medium (Wellcome Research Laboratories) without serum, buffered with HEPES and supplemented with penicillin streptomycin and glutamine, at a concentration of 2×10^5 macrophages per ml. One ml of the cell preparation was layered onto 13-mm diameter (No. 1) glass coverslips in 16-mm diameter tissue culture plates (Costar) and incubated for 1 h at 37 °C. Non-adherent cells were removed by washing with Dulbecco's phosphate-buffered saline containing Ca^{2+} and Mg^{2+} ions (D.PBS+B). Monolayers were incubated with 0.25 ml of appropriate dilution of alloantibody or diluent control (D.PBS+B) at 0 °C for 40 min and then washed twice with D.PBS+B. Coverslips were overlaid with 1 ml *S. albus* in D.PBS+B and incubated for 2 h at 0 °C. Cell viability was unaffected during incubations as judged by trypan blue exclusion and general morphology. Non-attached organisms were removed by repeated washing with D.PBS+B and the coverslips air dried, fixed in methanol and stained with May Grünwald/Giemsa. The degree of bacterial binding was estimated microscopically by determining the percentage of macrophage with organisms attached at two or more discrete points. Two hundred macrophages were counted on duplicate coverslips and % inhibition was calculated as the difference between control and test divided by the control × 100.

Table 2 The effect of antibody from cell line 8-109.13 on the binding of *S. albus* to macrophages

Dilution	Inhibition of binding (%) C57BL/6	BALB/c	C3H.OH
1:10^3	3.0±6.1	9.1±11.4	−6.1±5.0
1:10^4	−4.8±11.4	0.9±1.9	1.9±7.6
1:10^5	−2.7±3.1	10.1±5.6	−3.3±5.0
1:10^6	10.0±6.6	−10.1±9.2	6.9±2.2

C57BL/6 (b haplotype) and BALB/c (d haplotype) mice were from the Moredun Institute, Edinburgh, C3H.OH (o2 haplotype) were from Olec 76, Bicester and C3HfBu/Kam were from the departmental breeding colony. Each figure represents the mean ±1.s.e. of three experiments. Female mice age 6–8 weeks were used.

The monoclonal antibody from clone 8-109.13 is specific for a private determinant of I-A^k. Therefore this antibody should only inhibit bacterial binding to macrophages from a mouse with k haplotype. The effect of H8-109.13 on the binding of *S. albus* to peritoneal macrophages from various mouse strains, with different haplotypes is shown in Table 3. As described above binding to cells from C3HfBu/Kam mice (k haplotype) was blocked by this antibody (Fig. 1). However, the attachment was unaffected by pretreatment of macrophage monolayers prepared from mice with b, d or o2 haplotypes with this antibody. This observation further suggests that a product of the I-region is involved in unopsonised bacterial recognition and that the observed inhibition by the various alloantibodies was not due to crossreactivity with a general 'lectin-like' receptor showing similar antigenic determinants to a product of I-A^k.

The data do not necessarily imply the 'lectin-like' receptor for bacterial cell wall sugars and the Ia antigen on mouse peritoneal macrophages are identical and there are a number of possible explanations for the findings. For example, Ia antigens may bind bacteria, and possibly other antigens, directly or as postulated by Higgins *et al.*[7] protein-Ia acting as a glycosyl transferase could catalyse the attachment of bacteria to glycolipid Ia. The observed inhibition of bacterial binding by various alloantibodies could be due to blocking of these structures or inhibition of glycosyl transferase activity. The possibility has also not been excluded that the bacteria bind to a separate receptor which is in close proximity to the I-region determined structure and that the decrease in binding is due to steric hindrance.

Complete inhibition of bacterial binding was never obtained with any of the antibodies used. Similarly, in sugar inhibition studies with glucose or galactose, bacterial binding with *S. albus* to various phagocytes was only partially inhibited by the sugars[4]. These results indicate that the interactions of unopsonised bacteria with macrophages involve a number of recognition processes. These could include binding of bacteria by macrophage 'lectin-like' receptors[1] and attachment mediated by lectin molecules in the bacterial cell wall[12,13]. It has also been proposed that phagocytes can bind particles by nonspecific mechanisms[14] including hydrophobic interactions.

Results to date in which monolayers were treated with alloantibody and then with glucose or galactose showed no additional inhibition to that seen with alloantibody alone. This suggests that both reagents are reacting with the same site. Further work including cell membrane fractionation procedures is planned to determine the relationship between the macrophage 'lectin-like' receptor previously described by this laboratory and the I-A associated product responsible for the attachment described here.

The I-region of the murine MHC has a major role in regulating the immune system including cell–cell interactions and antigen presentation to lymphocytes. The data described above suggests that macrophages bearing an I-A gene product bind unopsonized bacteria. This interaction may lead to phagocytosis and initiation of the immune response in the non-immune animal.

This work was supported by a grant from the MRC. The monoclonal antibody from cell line 8–109.13, the WS9 and WS4 antisera were a gift from Professor H. Festenstein. The A.TH anti-A.TL and A.TL anti-A.TH were donated by Dr Jana McBride. The monoclonal antibody from cell line 10–2.16 was a gift from Dr E. Unanue.

Received 21 April; accepted 18 June 1982.

1. Ögmundsdottir, H. M. & Weir, D. M. *Clin. exp. Immun.* **26,** 334–339, (1976).
2. Freimer, N. B. *et al. Acta path. microbiol. scand. Sect. B.* **86,** 53–57 (1978).
3. Ögmundsdóttir, H. M., Weir, D. M. & Marmion, B. P. *Br. J. exp. Path.* **59,** 1–7 (1978).
4. Glass, E. J., Stewart, J. & Weir, D. M. *Immunology* **44,** 529–534 (1981).
5. Clark, R. B., Chiba, J., Zweig, S. E. & Shevach, E. M. *Nature* **295,** 412–414 (1982).
6. Parish, C. R., Higgins, T. J. & McKenzie, I. F. C. *Immunogenetics*, **6,** 343–354 (1978).
7. Higgins, T. J., Parish, C. R., Hogarth, P. M., McKenzie, I. F. C. & Hämmerling, G. J. *Immunogenetics* **11,** 467–482 (1980).
8. Mann, D. L. & Muchmore, A. *J. Immun.* **124,** 2218–2221 (1980).
9. Amsden, A., Evans, V., Yoshida, T. & Cohen, S. *J. Immun.* **120,** 542–549 (1978).
10. Fischer, A., Ballet, J. & Criscelli, C. *J. clin. Invest.* **62,** 1005–1013 (1978).
11. Muchmore, A. & Blaese, R. M. in *Proc. Brooke Lodge Symposium* 505–517 (Academic, New York, 1979).
12. Bagg, J., Paxton, I. R. & Weir, D. M. *J. clin. Lab. Immun.* **6,** 165–168 (1981).
13. Eshdat, Y., Ofek, I., Yahsour Gan, Y., Sharon, N. & Mirelman, D. *Biochem. biophys. Res. Commun.* **84,** 1551–1559 (1978).
14. Capo, C., Bongrand, P., Benoliel, A. M. & Depieds, R. *Immunology* **36,** 501–608 (1980).

A molecular basis for the two locus model of human complement component C4

M. H. Roos*, E. Mollenhauer†, P. Démant* & C. Rittner†

* Division of Genetics, Antoni van Leeuwenhoekhuis,
The Netherlands Cancer Institute, Amsterdam, The Netherlands
† Institute of Legal Medicine, University of Bonn,
D-5300 Bonn, FRG

The major histocompatibility complex(MHC)-linked fourth component of complement (C4) shows a high degree of polymorphism in several animal species[1-4]. In man C4 polymorphism was detected by distinct charge differences of the variants[5-7]. O'Neill *et al.*[8] showed that this C4 polymorphism was controlled by two closely linked genetic loci, *F* (*C4A*) and *S* (*C4B*) and these results were extended by Awdeh *et al.*[9] with an improved typing method. Biochemical analysis of human C4 has revealed that it consists of three polypeptide chains, α, β and γ[10]. In all reports so far on the molecular analysis of human C4[10-13], no molecular weight differences between the *A* and *B* locus-encoded molecules have been noticed. Here we demonstrate that the *C4A* and *C4B* locus-encoded α-chains have a molecular weight (MW) of 96,000 and 94,000, respectively, presenting for the first time a molecular basis for the difference between all C4A and C4B variants tested. Even rare variants that are difficult to allocate to the *A* or *B* locus on the basis of charge differences[14,15] could be identified as C4A or C4B variants in this way, thereby providing new insights into the relationships between the *C4A* and *C4B* loci.

Previous analysis of human C4 by SDS-polyacrylamide gel electrophoresis (SDS-PAGE) showed that the α-, β-, and γ-chains have a MW of about 95,000, 75,000 and 30,000 respectively for C4 from both loci[10-13]. By modifying the ratio of acrylamide to *N,N'*-methylene bisacrylamide (bis) in the gels, the separation properties of the gels are changed since both size and shape of the molecule determine the electrophoretic mobility in the gel. Thus, when C4 from several phenotypes, typed by agarose electrophoresis, was analysed by modified SDS-PAGE, a difference in MW between the α-chains encoded by the *A* and *B* loci became visible (Fig. 1). Plasma C4 phenotypes were determined by agarose electrophoresis according to the method of Awdeh *et al.*[9], designating the C4A variants A1, A2 and so on, the C4B variants B1, B2 and so on, and silent alleles *QO*. Figure 1*a* shows the SDS-PAGE analysis of the most common variants for each locus, A3 and B1, present in three phenotypes A3,3BQ0,Q0, A3,3B1,1,AQ0,Q0,B1,1 and as a negative control AQ0,Q0BQ0Q0 (lanes 1–4). The α-chain of the A3 variant has a MW of 96,000, while the α-chain of the B1 variant has a MW of 94,000. No difference in the β- and γ-chains was visible. As agarose typing of the C4 variants is usually carried out after removal of sialic acid with neuraminidase[9] we also analysed the same phenotypes after desialization (see Fig. 1*a*, lanes 5–7). A similar reduction of ~3,000 in the MW of both the C4A and C4B α-chains was visible. No change in MW of the β- and γ-chains was found.

To confirm the difference in MW between *A* and *B* locus-encoded α-chains, anti-Rodgers ($\mathrm{Rg^a}$) and anti-Chido ($\mathrm{Ch^a}$) sera, which have a known specificity for C4A and C4B molecules respectively[16-18] were used. C4, precipitated from neuraminidase-treated plasma of different haplotypes, was analysed by SDS-PAGE, followed by blotting of the proteins in the gel onto nitrocellulose sheets as described previously[19]. The sheets were then reacted with anti-$\mathrm{Ch^a}$, anti-C4 or anti-$\mathrm{Rg^a}$; the results are shown in Fig. 1*b*. The three C4 phenotypes reacted with anti-C4, revealing the C4 α-, β- and γ-chains (lanes 4–6), in addition to some background bands (lane 11). With anti-$\mathrm{Ch^a}$ only the C4B α-chains became visible (Fig. 1*b*, lanes 1–3), and with anti-$\mathrm{Rg^a}$ only the C4A α-chains were detected (lanes 7–9) over the background (lane 10). Samples which had not been treated with neuraminidase gave qualitatively similar results. Also, when unreduced C4 was analysed by SDS-PAGE in a 6% gel, a MW difference was found between native C4 from the *A* and *B* loci. After blotting and analysis of the variants A3 and B1 with anti-$\mathrm{Ch^a}$ and anti-$\mathrm{Rg^a}$ a reaction of the C4A molecule with anti-$\mathrm{Rg^a}$, and a reaction of the C4B molecule with anti-$\mathrm{Ch^a}$ was found (data not shown).

To establish whether the difference in α-chains between C4A and C4B variants applies also to other variants than the most common ones, we have analysed several different phenotypes, including some with rare and new C4 variants. The agarose electrophoresis patterns of 14 phenotypes are shown in Fig. 2*a*; as the pattern is highly complex a schematic presentation of the individual C4A and C4B variants is shown in Fig. 3. The C4A variants show generally a higher mobility than the C4B variants but some variants do overlap. This is especially the case for the B4, B5 and B5.1 variants which do overlap with most C4A variants and for the A1 variant which overlaps with most C4B variants. In this case C4A or C4B variants can only be identified by genetic studies and by analysing the functional activity with a lytic overlay (Fig. 2*b*), since the functional activity of the C4B variants is about 10-fold higher than C4A variants[9,14]. As can be seen from Fig. 2*a* and *b* the A1 variant (lane 5), like other C4A variants, does not show lytic activity, while the B4, B5 and B5.1 variants show a lytic activity similar to all other C4B variants. When the different phenotypes were analysed by SDS-PAGE (Fig. 4) all the C4A variants A1, A2, A3, A4, A5.1 and A6 (A5.1 not shown), showed an α-chain with a MW of 96,000 while all the C4B variants, B-2, B1, B1.1, B2, B4, B5 and B5.1 (B-2 and B4 not shown) showed α-chains with a MW of 94,000. Thus with this method even variants that overlap in the agarose gel electrophoresis can be identified structurally as C4A or C4B variants.

As some informative phenotypes were not available, however, our experiments do not exclude the possibility that the A4 and A5.1 variants contain an α-chain with a 94,000 MW in addition to the 96,000 α-chain; nor can it be excluded that the B-2, B1.1, B2, B4, B5 and B5.1 variants contain a 96,000 MW α-chain in addition to the 94,000 α-chain. This is, however, unlikely as the variants A1, A3, A6 and B1, which

0028-0836/82/340854—03$01.00

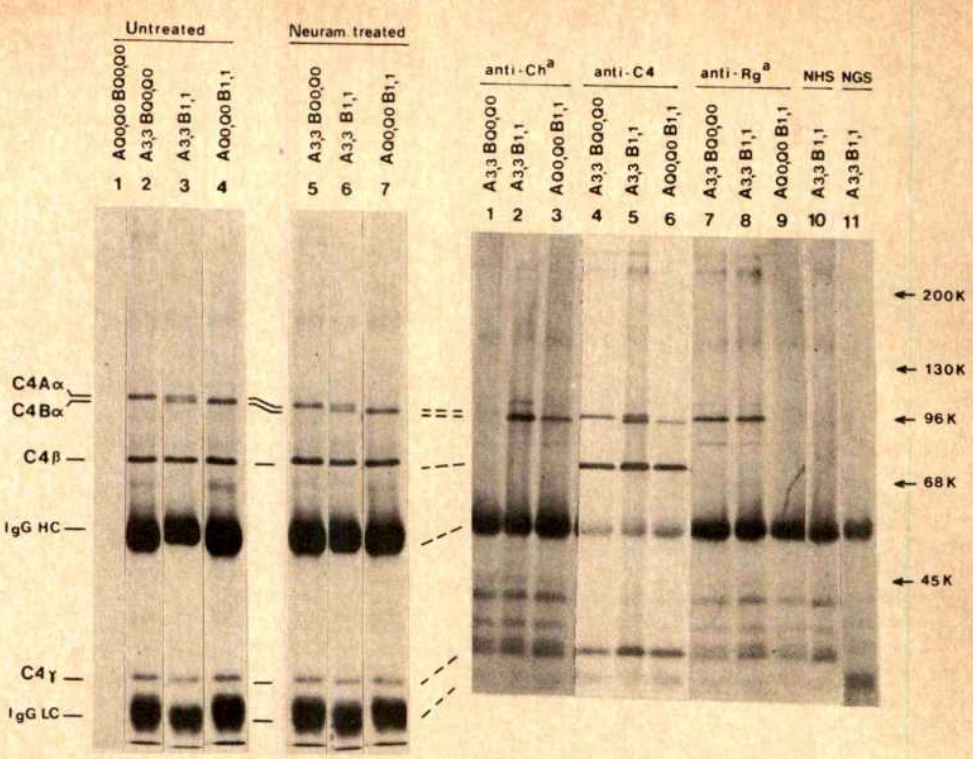

Fig. 1 Polymorphism of the C4 α-chains as detected by SDS-PAGE of human C4 and neuraminidase-treated human C4. *a*, C4 was immunoprecipitated from human EDTA–plasma with goat anti-human C4 (Atlantic Antibodies). The precipitates were washed, disintegrated and reduced as described previously[20], except that 10% 2-mercaptoethanol was used. SDS-PAGE was carried out according to a modification of the method of Laemmli *et al.*[28]; a 10% acrylamide gel was used with a ratio acrylamide: *N,N'*-methylene bisacrylamide (bis) of 1:0.006. For the separation of unreduced C4, a 6% acrylamide gel was used with an acrylamide : bis ratio of 6:0.0013. To prevent the gel from sticking to the glass plates, 0.3% agarose (Ultra Pure; Bio-Rad) was incorporated in the gel. *b*, After electrophoresis, proteins in the gel were blotted on to nitrocellulose sheets by compressing the gel for 1 h between two of these sheets and a 2-cm layer of tissues[19]. Thereafter, the gel was stained with Coomassie blue R250. The nitrocellulose sheets were incubated overnight with 15 ml blotting buffer (500 mM NaCl, 10 mM sodium phosphate (*p*H 7.3), 10 mM EDTA, 0.25% gelatin, 0.5% Triton X-100) supplemented with 50 µl anti-Ch^a serum, 20 µl anti-C4 serum or 50 µl anti-Rg^a serum. Then the sheets were washed for 1 h with 50 ml blotting buffer, incubated for 1 h with horseradish peroxidase-conjugated rabbit antiserum prepared against human IgG or goat IgG (DAKO). The sheets were washed for 1 h before a fresh solution containing 0.5 mg ml^{-1} phosphate-buffered saline (PBS) of the peroxidase substrate, 3-3'-diaminobenzidinetetrahydrochloride and 0.3% H_2O_2. The reaction was stopped after 10 min by washing with PBS. Neuraminidase treatment of human plasma was carried out according to Awdeh *et al.*[9]. *a*, SDS-PAGE: lanes 1–4, C4 precipitated from EDTA–plasma; lanes 5–7, C4 precipitated from neuraminidase-treated EDTA–plasma. *b*, Blots treated with: lanes 1–3, anti-Chido serum; lanes 4–6, anti-C4 serum; lanes 7–9, anti-Rodgers serum; 10, normal human serum (NHS); 11, normal goat serum (NGS).

were analysed in combination with 2 *QO* alleles present at the other locus, only showed one α-chain. In all cases where one or two C4A variants were present, an α-chain with a MW of 96,000 was found whereas an α-chain with a MW of 94,000 was always found when one or two C4B variants were present. Since the typing of the variants in agarose gels (Fig. 2) was carried out with neuraminidase-treated samples we analysed all the phenotypes described above by SDS-PAGE after neuraminidase treatment. This resulted, as shown in Fig. 1 for the A3 and B1 variants, in a decrease in the apparent MW of 3,000 for both the C4A and C4B α-chains; the difference between the α-chains of the C4A and C4B variants remained (data not shown). When comparing the concentration in the gel of the C4A α-chains with the C4B α-chains (Fig. 4)

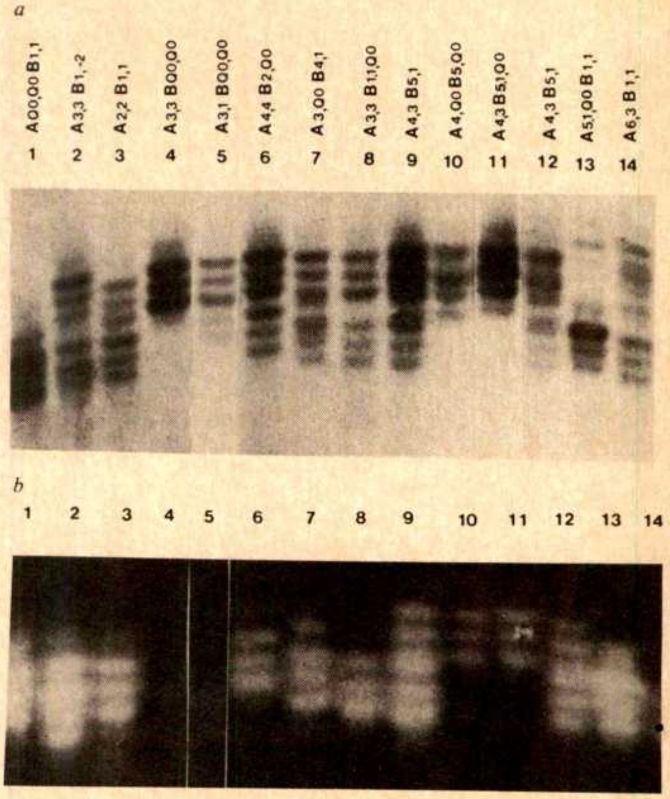

Fig. 2 Human C4 polymorphism as detected by agarose gel electrophoresis. EDTA–plasma samples were treated with neuraminidase (5 U per µl plasma; type VIII, Sigma) as described by Awdeh *et al.*[9]. Agarose gel electrophoresis was carried out according to the method of O'Neill *et al.*[8], on 20×20 cm glass plates covered with 2 mm 0.5% agarose (Litex HSA), for 5 h using a voltage gradient of 20 V cm^{-1} until the haemoglobin marker had migrated at least 10 cm from the origin (some variants may only be recognized in such extended runs); two plates were run in parallel. After completion, one plate was overlayed with goat anti-human C4 serum (Atlantic Antibodies) overnight, washed, dried and stained with Coomassie blue. The duplicate plate was covered with an agar overlay containing a haemolytic system with C4-deficient guinea pig serum as described previously[29]. The C4 variants were attributed to the *C4B* locus when they caused a lytic banding pattern in the functional overlay[9,14]. The individual *C4A* and *C4B* locus variants were identified by comparing the immunofixation banding patterns and lytic banding patterns with a reference set distributed by Dr G. Mauff to C4 typing laboratories in 1979 and the final designation of human C4A and B allotypes (A1, A2, ... B1, B2 ...) is in accordance with Awdeh *et al.*[9] and with a proposal of Drs G. Hauptmann, G. Mauff and C.R. (see also Fig. 3). The influence of silent alleles (*QO*) on the amount of C4A and C4B molecules present in the phenotypes was judged by comparing the relative strength of the *A* and *B* locus-encoded variants. In addition, in some cases, HLA-A, B, C, DR information (linkage disequilibrium) was also considered. Some variants could be followed in families by segregation[15]. *a*, Immunofixation banding pattern of 14 C4 phenotypes; *b*, haemolytic overlay banding pattern of the same samples.

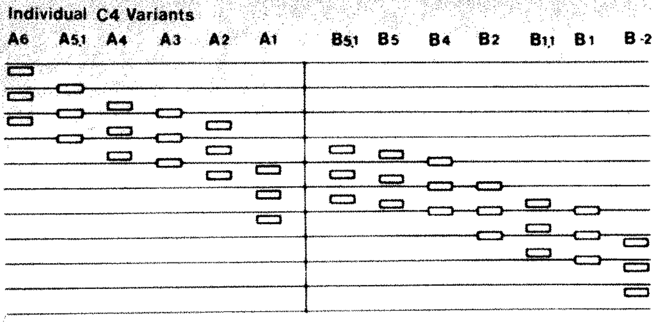

Fig. 3 Schematic representation of the C4 variants used in this study. These are all the variants that could be identified at present in the Bonn laboratory. Note the designation of the variants A5.1, B1.1, B5.1 and B-2.

sometimes a clear difference in the intensity of the α-chains was observed. Whether this represents the presence of a silent allele at the locus with the fainter band is under investigation[15].

Our results constitute the first evidence for a molecular difference between all C4A and C4B variants tested. All the C4A variants analysed contain an α-chain with an identical MW of 96,000 whereas all the analysed C4B variants contain an α-chain with an identical MW of 94,000. This indicates that the C4A and C4B variants differ structurally from each other even though some variants among both loci have very similar mobilities on agarose electrophoresis. The difference between C4A and C4B α-chains is another indication that the C4 structural genes are located in the *HLA* complex, and also provides a new analogy between human and mouse C4. In the mouse a different MW for the α-chains of C4 and the allotype Slp (sex limited protein) has been described[20,21] providing evidence that distinct structural *C4* and *Slp* loci are linked to the *S* region of the *H-2* complex. Another striking similarity between human and mouse C4 is the difference in functional activity between the products of the two loci. Human C4B variants possess a functional activity that is 10 times higher than that of the C4A variants[9,14]; in the mouse the *C4* locus produces a functionally active C4 molecule, while the *Slp* locus produces a molecule for which no functional C4 activity has been detected[21,22]. This could be a consequence of the structural difference between the α-chains of the two loci since the α-chains have been shown to be involved in the activation of C4[23].

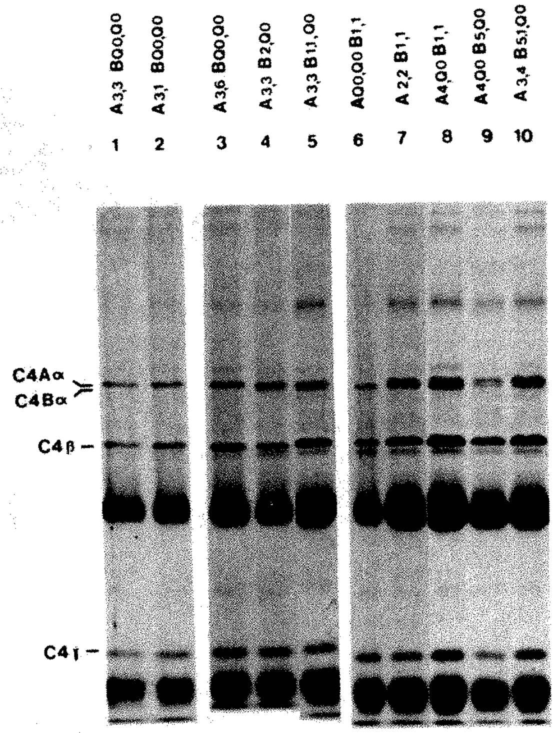

Fig. 4 Difference in MW of the *C4A* and *C4B* locus-encoded α-chains in 10 different phenotypes. Immunoprecipitation, SDS-PAGE and staining with Coommassie blue was performed as described in Fig. 1 legend. Lanes 1–10, analysis of 10 different phenotypes; lanes 3, 4, 5 are from a different gel. The total amount of C4 present in the samples in the gel is no indication of the level of C4 present in the plasma, as the C4 in the samples was adjusted to give clearly visible bands.

The antisera directed against the *HLA*-linked Chido and Rodgers blood group antigens[24,25] were shown previously to react specifically with the α-chains of the C4B and C4A variants, respectively, by the agglutination test and by inhibition of the antiglobulin test[17,18]. Our blotting method proved to be a new and sensitive way of analysing the reaction of the anti-Ch^{a} and anti-Rg^{a} sera with C4 α-chains of the A3 and B1 variants. Thus C4 variants, so far not found in a haplotype with a *QO* allele at the other *C4* locus and therefore considered to be Rodgers- or Chido-positive only by analogy or inference, can be analysed directly with our method for their reaction with anti-Rg^{a} or anti-Ch^{a} serum.

The removal of sialic acid from native C4 by neuraminidase affects the α-chains, as expected[12]. This result, together with the localization of both the Rg^{a} and Ch^{a} antigenic determinants[17,18] and the charge difference between the human C4 variants on the C4 α-chain[26], indicates that parts of the α-chain are exposed on the C4 molecule. However, the human C4 β- and γ-chains are not affected by neuraminidase, although the human C4 β-chain, in contrast to the murine C4 β-chain, also contained sialic acid[12,27] implying that at least the carbohydrate part of the β-chain is hidden inside the C4 molecule.

Our findings may open new ways for the biochemical characterization of the polymorphism of human C4 and of the genetic organization and structure of the human C4 genes. In addition, our results extend the homologies between *HLA* and *H-2* and may provide additional possibilities for investigation and understanding of the association of the early complement component genes with the MHC.

We thank Dr T. Meo for a gift of the C4-deficient serum and Drs C. Giles and R. Berger for the anti-Chido and anti-Rodgers sera and Mrs N. van Nuland-van Wijngaarde for secretarial assistance. This study was supported by the Queen Wilhelmina Foundation (Netherlands Cancer Foundation) and by the Deutsche Forschungsgemeinschaft (Ri 164-15-2).

Received 4 May; accepted 5 July 1982.

1. Rittner, C. *Hum. Genet.* **35,** 1–20 (1976).
2. Shreffler, D. C. *Transplantn Rev.* **32,** 140–167 (1976).
3. Shreffler, D. C., Atkinson, J. P., Brown, L. J., Parker, K. L. & Roos, M. H. in *7th International Convocation on Immunology* Niagara Falls, New York, 1980 (eds Zaleski, M., Abeyounis, C. J. & Kano, K.) 78–88 (Karger, Basel, 1981).
4. Alper, Ch.A. in *The Role of the Major Histocompatibility Complex in Immunobiology* (ed. Dorf, M. E.) 173–220 (Garland STPM, New York, 1981).
5. Teisberg, P., Åkeson, P., Olaisen, B., Geddedahl, T. Jr & Thorsby, E. *Nature* **264,** 253–254 (1976).
6. Mauff, G., Bender, K. & Fisher, B. *Vox Sang* **34,** 296–301 (1978).
7. Rittner, C. *et al. Immunobiology* **158,** 119–128 (1980).
8. O'Neill, G. J., Young Yang, S. & Dupont, B. *Proc. natn. Acad. Sci. U.S.A.* **75,** 5165–5169 (1978).
9. Awdeh, Z. H. & Alper, C. A. *Proc. natn. Acad. Sci. U.S.A.* **77,** 3567–3580 (1980).
10. Schreiber, R. D. & Müller-Eberhardt, H. J. *J. exp. Med.* **140,** 1324–1335 (1974).
11. Bolotin, C., Morris, S., Tack, B. & Prahl, J. *Biochemistry* **16,** 2008–2015 (1977).
12. Gigli, I., Von Zabern, I. & Porter, R. P. *Biochem. J.* **165,** 439–446 (1977).
13. Lundwall, A., Malmheden, I., Stalenheim, G. & Sjöquist, J. *Eur. J. Biochem.* **117,** 141–146 (1981).
14. Mauff, G. *Forensic Sci. Int.* **18,** 291 (1981).
15. Rittner, C. *et al.* (in preparation).
16. O'Neill, G. J., Yang, S. Y., Tegoli, J., Berger, R. & Dupont, B. *Nature* **273,** 668–679 (1978).
17. Tilley, C. A., Romans, D. G. & Crookston, M. C. *Nature* **276,** 713–715 (1978).
18. Chu, V. F. H., Marsh, W. L. & Gigli, I. *J. Immun.* **128,** 181–185 (1982).
19. Roos, M. H. & Démant, P. *Immunogenetics* **15,** 23–30 (1982).
20. Roos, M. H., Atkinson, J. P. & Shreffler, D. C. *J. Immun.* **121,** 1106–1115 (1978).
21. Ferreira, A., Nussenzweig, A. & Gigli, I. *J. exp. Med.* **148,** 1186–1197 (1978).
22. Carroll, M. C. & Capra, J. D. *Proc. natn. Acad. Sci. U.S.A.* **75,** 2424–2428 (1978).
23. Müller-Eberhardt, H. J. *A. Rev. Biochem.* **44,** 697–724 (1975).
24. Middelton, J. *et al. Tissue Antigens* **4,** 366–373 (1974).
25. Giles, C. M. *et al. Tissue Antigens* **8,** 143–149 (1976).
26. Merag, B., Olaisen, B. & Teisberg, P. *Scand. J. Immun.* **14,** 303–307 (1981).
27. Roos, M. H., Kornfeld, S. & Shreffler, D. C. *J. Immun.* **124,** 2860–2863 (1980).
28. Laemmli, U. K. *Nature* **227,** 680–682 (1970).
29. Rittner, C. & Mollenhauer, E. *Ärztl. Lab.* **27,** 232–238 (1981).

Nucleotide sequence of the rat skeletal muscle actin gene

R. Zakut, M. Shani, D. Givol*, S. Neuman, D. Yaffe & U. Nudel

Departments of Cell Biology and *Chemical Immunology,
The Weizmann Institute of Science, Rehovot 76100, Israel

The actins constitute a family of highly conserved proteins found in all eukaryotic cells. Their conservation through a very wide range of taxonomic groups and the existence of tissue-specific isoforms make the actin genes very interesting for the study of the evolution of genes and their controlling elements. On the basis of amino acid sequence data, at least six different mammalian actins have been identified (skeletal muscle, cardiac muscle, two smooth muscle actins and the cytoplasmic β- and γ-actins)[1–5]. Rat spleen DNA digested by the *Eco*RI restriction enzyme contains at least 12 different fragments with actin-like sequences but only one which hybridized, in very stringent conditions, with the skeletal muscle cloned cDNA probe[6]. Here we describe the sequence of the actin gene in that fragment. The nucleotide sequence codes for two amino acids, Met-Cys, preceding the known N-terminal Asp of the mature protein. There are five small introns in the coding region and a large intron in the 5′-untranslated region. Comparison of the structure of the rat skeletal muscle actin gene with the available data on actin genes from other organisms shows that while the sequenced actin genes from *Drosophila* and yeast have introns at different locations, introns located at codons specifying amino acids 41, 121, 204 and 267 have been preserved at least from the echinoderm to the vertebrates. A similar analysis has been done by Davidson[7]. An intron at codon 150 is common to a plant actin gene and the skeletal muscle acting gene.

Act15 is a recombinant bacteriophage containing the coding region of the rat skeletal muscle actin gene and 11 kilobases (kb) of its 5′-flanking region[6]. A 3.7-kb *Eco*RI DNA fragment was subcloned in pBR322 (pAct15-2); the restriction map of the subclone and the strategy used for sequencing are shown in Fig. 1. The sequence of the entire coding region and the 3′-untranslated region is given in Fig. 2*a*.

The coding sequence begins with codons for two amino acids, methionine and cysteine, which are absent from the mature protein. They are followed by the codon for Asp (GAC), the known N-terminal residue of actin. It is of interest that in all six *Drosophila* actin genes, the same two codons precede the codon specifying the N-terminal amino acids[8]. The translation initiator codon ATG was found in all eukaryotic genes. The preservation of the cysteine codon in actin genes of such remote organisms suggests a functional role for this sequence. The primary mRNA translation product probably contains the Met-Cys residues, which are then cleaved off the polypeptide chain. Note, however, that the Cys codon is absent from the rat β-actin gene (U.N. *et al.*, unpublished).

The amino acid sequence deduced from the nucleotide sequence is identical to that of rabbit skeletal muscle actin. (The sequence of rat skeletal muscle actin has not been determined.)

A recombinant cDNA plasmid (p106) containing the entire nucleotide sequence of the 3′-untranslated region of the rat muscle actin mRNA was isolated and sequenced[9,10]. Comparison of the 3′ region of the Act15 insert with p106 showed that the Act15 insert contains 75 base pairs (bp) of the 3′-untranslated region of the structural gene and lacks the last 165 bp of the 3′ end. The only differences in the overlapping region were two additional thymines in p106 and one A/T replacement. These differences may have arisen from mistakes in the sequence of p106 or from polymorphism in the sequence of the 3′-noncoding region of this gene. As the sequence of the terminal 165 nucleotides of the 3′-untranslated region was deduced from a cDNA clone, the existence of an intron in that region cannot be excluded.

The skeletal muscle actin gene contains five introns in the coding region (Fig. 1*c*). The sequences of the splice sites are in accordance with the consensus sequence for splice sites suggested by Breathnach and Chambon[11] (Fig. 2*a*). At the codon specifying amino acid 150, the intron sequence shows another potential splice site (CAG/GTA), which is present 32 bp downstream from the CG/GT splice site at codon 150 (Fig. 2*a*). The sequence between the two splice sites encodes 11 amino acids. Thus, if this site were involved in mRNA splicing, it could add an additional peptide (Gly-Glu-Cys-Ser-His-Thr-Ala-His-Ser-Gly-Pro) after Thr 149, without changing the reading frame downstream. This would produce a protein having the exact sequence of skeletal muscle actin, with an insert of 11 amino acids. The existence of such a protein has not been reported so far.

We have previously demonstrated by electron microscopy that the rat skeletal muscle actin gene has a large intron, ~750 bp long, at its 5′ end[6]. The sequencing data (Fig. 2*a*) do not reveal such a large intron in the coding region, therefore it should be localized in the 5′-untranslated region. The 5′ and 3′ borders of this intron were determined by S_1 endonuclease mapping[12], and were assigned to nucleotides 250/251 and nucleotides 1,206/1,207, respectively (that is, the intron is located 12 nucleotides upstream from the initiator ATG). The sequence of the two splice sites is in agreement with the consensus splice site sequences[11] (Fig. 2*b*). The sequence data indicate the existence of a potential Goldberg–Hogness box, TATAAA[13], starting at nucleotide 161, and a potential

Table 1 Positions of introns in actin genes

Source and type of actin gene			Intron location*										
Dictyostelium (several genes)[18]								None					
Yeast[19,20]			4	—	—	—	—	—	—	—	—	—	—
Drosophila[7]	*DmA* 6			—							307		
	DmA 4			13							—		
	DmA 2	5′-UT (−8)		—							—		
Sea urchin gene J†				—	—	41	121	—	203	267	—	—	—
Chicken skeletal muscle‡		5′-UT (−12)		—	—	41	—	150	204	267	—	327	—
Rat skeletal muscle		5′-UT (−12)		—	—	41	—	150	204	267	—	327	—
Rat β-cytoplasmic§		5′-UT (−6)		—	—	41	121	—	—	267	—	327	—
Soybean[16]				—	20	—	—	150	—	—	—	—	355

* The numbers indicate the codons at which introns are localized. Numbers in parentheses indicate the position of introns in the 5′-untranslated (5′-UT) region (the number of nucleotides upstream from the initiator ATG). No introns were found in the sites indicated by dashes.

† W. R. Crain and A. D. Cooper, personal communication.

‡ C. Ordahl, personal communication.

§ Ref. 6 and U.N. *et al.*, unpublished.

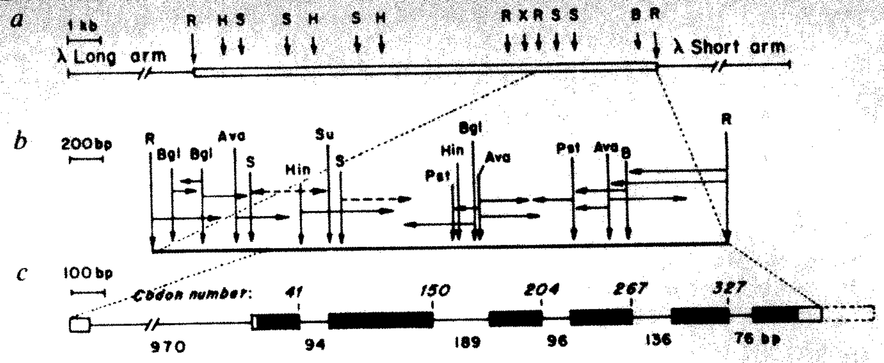
a
1 kb
λ Long arm
R H S S H S H R X R S S B R
λ Short arm
b
200 bp
R Bgl Bgl Ava S Su S Hin Bgl Hin Pst Ava Pst Ava B R
c
100 bp
Codon number: 41 150 204 267 327
970 94 189 96 136 76 bp

Fig. 1 The structure of the rat skeletal muscle actin gene. *a*, Restriction enzyme map of the rat DNA insert in the recombinant bacteriophage Act15. *b*, The strategy used to sequence the rat skeletal muscle actin gene. The 3.7-kb *Eco*RI DNA fragment was subcloned in pBR322 and the resulting recombinant plasmid pAC15.2 was sequenced using the restriction sites shown, in the directions indicated. Solid arrows indicate fragments sequenced by the method of Maxam and Gilbert[21]; broken arrows indicate fragments sequenced by the Sanger procedure[22]. The restriction enzymes used were: Ava, *Ava*I; B, *Bam* HI; Bgl, *Bgl*II; H, *Hin*dIII; Hin, *Hin*fI; Pst, *Pst*I; R, *Eco*RI; S, *Sac*I; Su, *Sau*3AI; X, *Xba*I. *c*, Structure of the rat skeletal muscle actin gene: the boxes represent exons and the solid lines introns. Open boxes, the 5′- and 3′-untranslated regions; solid boxes, the coding regions of the exons. The broken box represents the part of the gene which is absent from the genomic clone Act15 but present in the cDNA recombinant plasmid p106. The numbers above the exons indicate the location of the exon–intron junctions (numbered according to Vanderkerckhove and Weber[5]). The numbers beneath the introns indicate their sizes in bp.

transcription initiation site, ACAC[14], 30 nucleotides downstream from this box (Fig. 2*b*). The assignment of the transcription initiation site was verified by S_1 endonuclease mapping (data not shown).

Comparison of the sequences and location of introns in several gene families in the vertebrates (for example, genes for globin, ovalbumin and the immunoglobulins; for review see ref. 11) has indicated that whereas the nucleotide sequence of introns has changed rapidly during evolution, the location of introns in relation to the coding sequence has been highly conserved. On the other hand, the data on the actin genes offer a comparison of gene structure across a much greater evolutionary range, that is, from unicellular organisms to fungi, insects and vertebrates. From the available data, it is apparent that

a

```
                                                 10                                              20
 -2       1
Met Cys Asp Glu Asp Glu Thr Thr Ala Leu Val Cys Asp Asn Gly Ser Gly Leu Val Lys Ala Gly Phe
ATG TGT GAC GAG GAC GAG ACC ACC GCT CTT GTG TGT GAC AAC GGC TCT GGC CTG GTG AAA GCT GGC TTT
  Hpa II                            30                                          40
Ala Gly Asp Asp Ala Pro Arg Ala Val Phe Pro Ser Ile Val Gly Arg Pro Arg His Gln
GCC GGG GAT GAT GCC CCC AGG GCT GTG TTC CCA TCC ATC GTG GGT CGG CCC CGT CAC CAG/GTCAGGCTGCT

                                                                                       Gly Val
AGCAGAAGATAGGCTCTCCGAATACAGCCGGTGTTCTCCTGCCCCTGGCTGTAGTAACAAGTATCTGATGTCTCCATCTGCAG/GGT GTC
                            50                                          60
Met Val Gly Met Gly Gln Lys Asp Ser Tyr Val Gly Asp Glu Ala Gln Ser Lys Arg Gly Ile Leu Thr
ATG GTC GGT ATG GGT CAG AAG GAT TCC TAC GTG GGC GAC GAG GCC CAG AGC AAG CGA GGT ATC CTG ACC
                70                                          80
Leu Lys Tyr Pro Ile Glu His Gly Ile Ile Thr Asn Trp Asp Asp Met Glu Lys Ile Trp His His Thr
CTG AAG TAC CCC ATT GAA CAC GGC ATT ATC ACC AAC TGG GAC GAC ATG GAG AAG ATC TGG CAC CAC ACC
 90                                         100                                         110
Phe Tyr Asn Glu Leu Arg Val Ala Pro Glu Glu His Pro Thr Leu Leu Thr Glu Ala Pro Leu Asn Pro
TTC TAC AAT GAG CTG CGT GTG GCC CCC GAG GAG CAC CCG ACC CTG CTC ACT GAG GCC CCT TTG AAC CCC
                            120                                         130
Lys Ala Asn Arg Glu Lys Met Thr Gln Ile Met Phe Glu Thr Phe Asn Val Pro Ala Met Tyr Val Ala
AAA GCT AAC CGG GAG AAG ATG ACT CAA ATC ATG TTT GAG ACC TTC AAC GTG CCT GCT ATG TAT GTG GCT
                140
Ile Gln Ala Val Leu Ser Leu Tyr Ala Ser Gly Arg Thr Thr G
ATT CAG GCG GTG CTG TCT CTC TAT GCC TCC GGC CGA ACC ACC G/GTGAGTGCTCACACACGGCCCACTCTGGTCCAG

GTAGCGTCGCCCCAACATTCCAGCCCAGCTTTTGAATCCTCTGCCTCAGACCCTGCACCGTTCCCATTCAATCCCTGATGACCCCCAGTCC
                                                                                150
                                                                               ly Ile Val Leu Asp Ser
AGAACCACTGTCCCTGCTCTCTCTGCTGGTCCCCTCCACTCACACACTGCTCCTCCCCTGCACAG/GC ATC GTG TTG GAT TCT
                160                                         170
Gly Asp Gly Val Thr His Asn Val Pro Ile Tyr Glu Gly Tyr Ala Leu Pro His Ala Ile Met Arg Leu
GGG GAC GGT GTC ACC CAC AAC GTG CCC ATC TAT GAG GGT TAT GCC CTG CCA CAC GCC ATC ATG CGT CTG
    180                                     190                                         200
Asp Leu Ala Gly Arg Asp Leu Thr Asp Tyr Leu Met Lys Ile Leu Thr Glu Arg Gly Tyr Ser Phe Val
GAC CTC GCT GGT CGC GAC CTT ACT GAC TAC CTG ATG AAA ATC CTC ACC GAG CGT GGC TAT TCC TTC GTG


Thr Thr A
ACC ACA G/GTGCGTGCTCTCAACGCCCCGCTGAGGGTGGGCCGGCAGAGGGTGAGCACATGCCCCAGGCCTTGCTCTGAGGCCTCCCAC
                                            210                                         220
                       la Glu Arg Glu Ile Val Arg Asp Ile Lys Glu Lys Leu Cys Tyr Val Ala Leu
TGCTTCTGCTCCCTGCAG/CT GAA CGT GAG ATT GTG CGC GAC ATC AAA GAG AAG CTG TGC TAC GTG GCC CTG
                            230             234a                240
Asp Phe Glu Asn Glu Met Ala Thr Ala Ala Ser Ser Ser Ser Leu Glu Lys Ser Tyr Glu Leu Pro Asp
GAC TTC GAG AAT GAG ATG GCC ACC GCT GCC TCT TCC TCC TCC CTG GAA AAG AGC TAT GAG CTG CCT GAC
                            250                                         260
Gly Gln Val Ile Thr Ile Gly Asn Glu Arg Phe Arg Cys Pro Glu Thr Leu Phe Gln Pro Ser Phe Ile
GGG CAG GTC ATC ACC ATC GGC AAT GAG CGC TTC CGT TGC CCG GAG ACG CTC TTC CAG CCT TCC TTT ATC


G
G/GTGGCCTCCGGCTCCGCTGGTTTGCCGGAATCAATTTTCCCTCATCCCACGCCTCAGAGTACGGGGTCTCCTCCCGCCGGTGCCCTTAG
                                                                270
                                                   ly Met Glu Ser Ala Gly Ile His Glu Thr Thr Tyr
TCTGACTCTGGTTGCTCACACTGCCTCTCCCCCGGGCCACCAG/GT ATG GAG TCT GCG GGG ATC CAT GAG ACC ACC TAC
    280                                     290                                         300
Asn Ser Ile Met Lys Cys Asp Ile Asp Ile Arg Lys Asp Leu Tyr Ala Asn Asn Val Met Ser Gly Gly
AAC AGC ATC ATG AAG TGC GAC ATC GAC ATC AGG AAG GAC CTG TAC GCC AAC AAC GTC ATG TCA GGG GGC
                                310                                         320
Thr Thr Met Tyr Pro Gly Ile Ala Asp Arg Met Gln Lys Glu Ile Thr Ala Leu Ala Pro Ser Thr Met
ACT ACC ATG TAC CCC GGT ATC GCT GAC CGC ATG CAG AAG GAG ATC ACA GCT CTG GCT CCC AGC ACC ATG


Lys Ile Lys
AAG ATC AAG/GTGGATGACGCGCCTGGTACGGGCGGAGACCAGGGGCGGGGGAACTCGCAGGCACCTGACACTCTTGTCTTGCAG/
        330                                     340                                         350
Ile Ile Ala Pro Pro Glu Arg Lys Tyr Ser Val Trp Ile Gly Gly Ser Ile Leu Ala Ser Leu Ser Thr
ATC ATC GCC CCC CCT GAG CGC AAG TAC TCA GTG TGG ATC GGC GGC TCC ATC CTG GCC TCG CTG TCC ACC
                                        360                                         370
Phe Gln Gln Met Trp Ile Thr Lys Gln Glu Tyr Asp Glu Ala Gly Pro Ser Ile Val His Arg Lys Cys
TTC CAG CAG ATG TGG ATC ACC AAG CAG GAG TAC GAC GAG GCC GGC CCC TCC ATT GTG CAC CGC AAA TGC


Phe Ter               20                40                60 *     HaeIII 80
TTC TAG GCGCACCGCGTCTGTGTACGCGCTCTCTCTCCTCAGGACGACAATCGACCATCGTGCTATGGTTGCAGGGTGGCCCCATCCTC
            100               120               140               160
 CGCCGTGGCTCCATCGCCGCCACTGCAGCCGGCGCCTGTTTTTGACGTGTACATAGATTCGCTCGTTTTACCTCATTTTGTTATTTTTCAAA
   180               200               220
 CAAAGCCCTGTGGAAGGAAATGGAAAACTTGAAGCATTAAAGCCAGCCATTCTGTTTTGCTCC
```

b

```
                  20                    40                    60                    80
ACCTGGGCCAGGGCCAGTTCTCTCCTTCTTTGGTCAGTGCAGGAGACCCGGGCGGGACCCAGGCTGAGAAGCAGCCGAAG
                 100                   120                   140       SacI        160
GGACTCTAGTGCCCAACACCCAAATATGGCTTGGGAAGGGCAACAACATTCCTTCGGGCGGTGTGGAGAGCTCAGGACTA
                 180                   200                   220                 HinfI
TATAAAAACCTGAGGCTAGGGACAGGCGGTCACACGGACGTGAAGCCTCACTTCCTACCCTCGGCACCAGGGCCAGAGTC
                 260                   280                   300                   320
AGAGCAGCAG/GTAGGGTGGAGGTGGGGAGGGTGACCTGGAGACCCAGCAGAGAAACCTATTGAGCCTTGGGCCTGTATT
                 340                   360                   380                   400
TGTCACTGGGCTCTGGAAATTTCTCCAAACTCATATCCAGCCCATTTGGGATGCTGACTTTTTTGCTGGTGGGAGGGGTG
                 420                   440                   460                   480
TCTGACACCCATCCATTTCCACCCTCAGACTCTACCCTCCCCCCCCCCTTGCTGGGGACTAAATCCGAGTCCTCCTGCAA
                 500                   520                   540                   560
GTGAGCAAGCCAGTGTTTCCTACCGAGCCACACACCAGCCCCTGGTTGGTTGAGATTTCTCTCCCTGAATTAGTTTCCCC
                 580                   600                   620                   640
TCCTGCCTTTCATCCCTCTCTCCTCCCCACCCTCTTTCTCTGCTGGGATCAAATCTGGGCCCTTGTGATGCAAGAGGTGG
                 660                   680                   700                   720
GCTGGATCTCCCACAGAGCCAGCCCCTGGGAGACTGACTTGAAGATGAGTTTGGAGAGAGGCAAGCATTGTCTTAGCCTT
 SacI            740                   760                   780                   800
CTGAGCTCAAGGCTTTTCTAAAGCCCAAGCACCGTGCCAGGCTACTCTTCTCTGAAATAGGAGGCGGGTGGAAGGGTTCC
                 820                   840                   860                   880
TTCTGAGTTTGGATGCCGTGGGGCTTCAAACGGGCAATTCTTTCCAGAGTTGGGACAGTATTACCCTTCCTTGGGCAAAA
                 900                   920                   940                   960
TCCTTGCCGCTCTCATAAGACTGGCAGGTGGACCTTAATGCCTCCTTCACAGATTGAGATTGAGTAGAGAGGAATAGCGC
                 960                   980                  1000                  1020
GCGCTAGCTGTGACATGTGTGGCCAACAGCGAAGGCTGAGGATCTCAGGATGTCCTCTGCATGCCTACATGGAGGGATTA
                1040                  1060                  1080                  1100
AAGTGGCCAACAAACTGTTCCCATAGCAAAAAGCACAGCCTTGACCTGGGAGAGCATCCTCTGGCCCTGTGCAAGGAAGG
                1120                  1140                  1160                  1180
GGCTGGGGGAGAGGAGTGTGTGGATCTCCAAAGTGAAGATGGGTTAAGCAGAGCTTCACCTTAACCCCCATCACATACTC
                1200                           Met Cys Asp Glu Asp Glu Thr
ACAACGCTCAACACTTTCTCTTTGCAG/AAACTAGACACC ATG TGT GAC GAG GAC GAG ACC
```

Fig. 2 Nucleotide sequence of the rat skeletal muscle actin gene. *a*, The coding and 3′-untranslated regions of the skeletal muscle actin gene. The numbers in the coding region indicate the number of amino acids, as suggested by Vanderkerckhove and Weber[5]. The numbers in the 3′-untranslated region (italics) indicate the nucleotide number following the termination codon. The *Hae*III site at nucleotide 73 in the 3′-untranslated region is the end of the rat DNA insert in the bacteriophage Act15. (The recombinant bacteriophage Act15 was isolated from a *Hae*III partial digest rat gene library and thus ends at the *Hae*III site which is found in p106 at this position[6].) The sequence 3′ to the asterisk was deduced from the sequence of p106. *b*, Nucleotide sequence of the 5′-untranslated region of the skeletal muscle actin gene. Solid underlining indicates the splice sites. The nucleotide sequence of the intron is given in italics. The Goldberg–Hogness box (TATAAA) and the cap site (CACA) are underlined with broken lines. Restriction enzyme sites used for the S_1 nuclease mapping are indicated.

despite the great conservation of the amino acid sequence of actins, the number of introns and their positions vary greatly (Table 1).

Clearly, there is no similarity in the number and location of introns of actin genes between fungi, protostomes and the known actin genes of deuterostomes (except for the possible homology regarding the intron in the 5′-untranslated region of rat α- and β-actin genes and the *Drosophila* actin gene *DmA* 2)[8]. However, within the deuterostomes, all known intron positions in sea urchin actin genes (at codons 41, 121, 203 and 267) are found in the rat skeletal muscle actin gene or in the cytoplasmic actin gene, or in both. In addition, the vertebrate actin genes do contain introns which are not found in the known sea urchin actin genes (at codon 327 in α- and β-actin genes and at codon 150 in the α-actin gene). The locations of introns in the chicken muscle actin gene are identical to those in the rat muscle actin gene.

The great resemblances between the actins exclude the possibility of convergent evolution from different ancestral genes. It can be concluded, therefore, that the intron locations, although highly conserved when examined on a small evolutionary scale (that is, among the vertebrates), do change during evolution.

Despite the incomplete data, the homology of intron sites may be used as an indication of the evolutionary relatedness of actin genes. It seems that differences between intron locations in actin isogenes can be regarded as an indication of an ancient separation of these genes. Thus, the great differences in intron locations among the *Drosophila* actin genes suggest that these genes separated from one another very early in evolution. On the other hand, the available data (Table 1) on the intron locations in deuterostomes indicate that these actin genes evolved from a common ancestor more recently. Although all *Drosophila* actin genes apparently have been isolated and partially sequenced, it is of interest that the deduced amino acid sequence of all of them resembles that of the vertebrate cytoplasmic actins; no gene coding for amino acid sequences typical of vertebrate muscle actin has been found[8]. Thus, the known pattern of intron sites and the available amino acid data suggest that, despite their great similarity in specialization and function, the vertebrate muscle actin and the insect muscle actin genes evolved independently from non-muscle actin genes[15].

It has been suggested that split genes were assembled by rearrangement of several DNA regions containing coding sequences, into a new functional unit; noncoding flanking regions of these fragments formed the introns[16]. This would imply that the primordial actin gene was split in at least all those positions in which introns are found in the various actin genes, and that the variability in the location of introns was due to deletion of introns during evolution. However, without sufficient evidence, an alternative or additional mechanism should be considered also, namely that the variability in intron positions and numbers resulted from insertion and deletion of introns, possibly as transposable sequences. Studies on the structure of actin genes along the evolutionary track leading to the vertebrates may discriminate between these possibilities.

It was recently reported that a soybean actin gene contained introns at codons 20/21, 151 and 355/356 (ref. 17). When we aligned the codons of this gene with those of the rat skeletal muscle actin gene, we found that the plant actin gene intron at codon 151 and the rat skeletal muscle intron at codon 150 split the coding sequence at exactly the same position. Although we cannot exclude the possibility that the homology in intron sites in these two actin genes is coincidental, we consider this very unlikely. Thus, if these introns are evolutionarily related, the immediate conclusion is that the intron at codon 150 existed in the actin gene before the separation between the animal and plant kingdoms. Therefore, this intron cannot be considered a novel intron, specific to the skeletal muscle actin gene[7]; rather, the lack of an intron at this location in the known sea urchin actin genes and the rat β-actin gene is most probably due to a deletion. The data are compatible with the suggestion that a primordial actin gene common to plants and animals was split at all intron locations known in the actin genes and that the variability in intron sites was a result of deletion of introns.

We acknowledge the technical assistance of Ms Zehava Levy, and thank Drs L. L. Jagodzinsky, T. Sargent and J. Bonner for the rat gene libraries. This work was supported by NIH grant R01 GM 22767 and by grants awarded by the Muscular Dystrophy Association to D.Y. and U.N. U.N. holds an A. and E. Blum Career Development Chair in Cancer Research.

Received 1 April; accepted 11 June 1982.

1. Storti, R. V. & Rich, A. *Proc. natn. Acad. Sci. U.S.A.* **73,** 2346–2350 (1976).
2. Whalen, R. G., Butler-Browne, G. S. & Gros, F. *Proc. natn. Acad. Sci. U.S.A.* **73,** 2018–2022 (1976).
3. Garrels, J. & Gibson, W. *Cell* **9,** 793–805 (1976).
4. Elzinga, M. & Lu, R. in *Contractile Systems in Nonmuscle Tissues* (eds Perry, S. V., Margreth, A. & Adelstein, R.) 29 (North-Holland, Amsterdam, 1976).
5. Vanderkerchkove, J. & Weber, K. *Differentiation* **14,** 124–133 (1979).
6. Nudel, U. *et al. Proc. natn. Acad. Sci. U.S.A.* **79,** 2763–2767 (1982).
7. Davidson, E. H. in *Genome Evolution* (eds Dover, G. A. & Flavell, R. B.) (Academic, New York, 1982).
8. Fyrberg, E. A., Bond, B. J., Hershel, N. D., Mixter, K. S. & Davidson, N. *Cell* **24,** 107–116 (1981).
9. Katcoff, D. *et al. Proc. natn. Acad. Sci. U.S.A.* **77,** 960–964 (1980).
10. Shani, M. *et al. Nucleic Acids Res.* **9,** 579–989 (1981).
11. Breathnach, R. & Chambon, P. *A. Rev. Biochem.* **50,** 349–383 (1981).
12. Weaver, R. F. & Weissmann, C. *Nucleic Acids Res.* **6,** 1175–1193 (1979).
13. Goldberg, M. thesis, Stanford Univ. (1979).
14. Ziff, E. B. & Evans, R. M. *Cell* **15,** 1463–1475 (1978).
15. Yaffe, D. *et al.* in *Stability and Switching in Cell Differentiation* (eds Clayton, R. N. & Truman, D. E. S.) (Plenum, New York, in the press).
16. Gilbert, W. R. *Nature* **271,** 501 (1978).
17. Shah, D. M., Hightower, R. C. & Mengher, R. B. *Proc. natn. Acad. Sci. U.S.A.* **72,** 1022–1026 (1982).
18. Firtel, R. A., Timm, R., Kimmel, A. R. & McKeown, M. *Proc. natn. Acad. Sci. U.S.A.* **76,** 6206–6210 (1979).
19. Gallwitz, D. & Sures, I. *Proc. natn. Acad. Sci. U.S.A.* **77,** 2546–2550 (1980).
20. Ng, R. & Abelson, J. *Proc. natn. Acad. Sci. U.S.A.* **77,** 3912–3916 (1980).
21. Maxam, A. M. & Gilbert, W. R. *Proc. natn. Acad. Sci. U.S.A.* **74,** 560–564 (1977).
22. Sanger, F., Nicklen, S. & Coulson, A. R. *Proc. natn. Acad. Sci. U.S.A.* **74,** 5463–5468 (1977).

Structure of the human immune interferon gene

Patrick W. Gray & David V. Goeddel

Department of Molecular Biology, Genentech, Inc.,
460 Point San Bruno Boulevard, South San Francisco,
California 94080, USA

Sequence determination of cloned cDNAs and genes of the three classes of interferon (IFN-α, −β and −γ) has revealed more than a dozen members of the human IFN-α gene family[1–7] and a single gene for IFN-β[4,8–14]. These genes are found on chromosome 9 (ref. 15) and contain no introns[1,5–7,11–14]. We recently reported[16] that the 146-amino acid sequence of mature IFN-γ deduced from the nucleotide sequence of a cloned cDNA was quite unrelated to those of the other IFNs, and that the gene for IFN-γ contains at least one intron[16]. We now describe the isolation, characterization and DNA sequence of the human IFN-γ gene. It contains three introns, a repetitive DNA element, and is not highly polymorphic. All our evidence to date[16,17] and the present data suggest that this is the only gene for IFN-γ and that the resolution of IFN-γ into two components[18] is probably the result of post-translational processing of the protein.

A ^{32}P-labelled restriction fragment obtained from the IFN-γ cDNA clone p69 (ref. 16) was used as a hybridization probe to screen 10^6 plaques of a bacteriophage λ Charon 4A/human genomic library[19]. Six individual hybridizing plaques were isolated from the library, and DNA from each recombinant phage was isolated and mapped with five different restriction endonucleases (Fig. 1). The insert DNAs span a contiguous region of 33.5 kilobase pairs (kbp) of the human genome. Each phage DNA was analysed by Southern blotting[20] with the IFN-γ cDNA probe, after digestion with *Eco*RI, *Bam*HI, *Hin*cII and

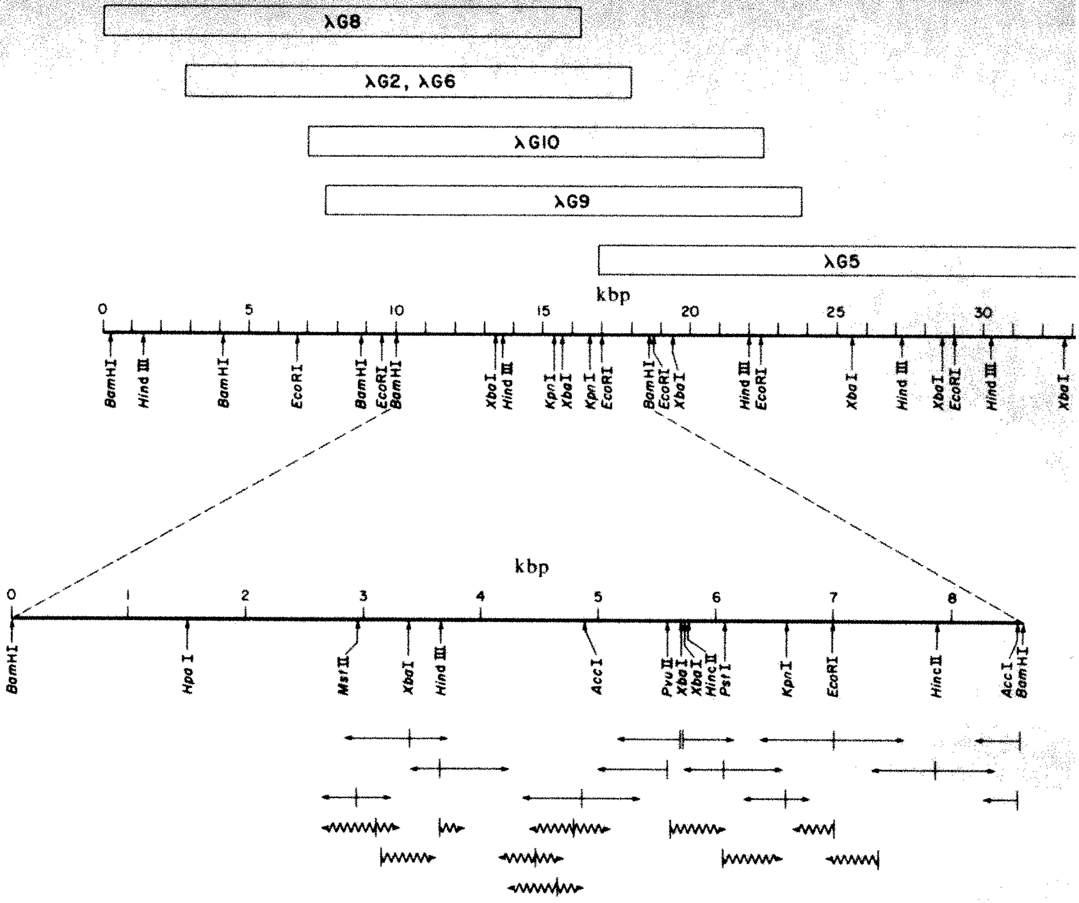

Fig. 1 Restriction endonuclease map of the IFN-γ gene region. The limits of each different phage DNA insert are shown at the top. Sites for *Eco*RI, *Bam*HI, *Hin*dIII, *Kpn*I and *Xba*I were determined by digestions of each individual phage DNA. Phage (10^6) from the recombinant human λ library described by Lawn *et al.*[19] were plated on to 10 15-cm plates and screened by the method of aniatis *et al.*[34] with 3 × 10^7 c.p.m. of ^{32}P-labelled[35] cDNA probe (887 bp *Sau*3A fragment, ref. 16). Plaques which hybridized positively with the probe were subjected to another round of plaque purification[34]. Individual hybridizing plaques were isolated and phage DNA was prepared[19,34] from 500-ml cultures. Each phage DNA was digested with *Eco*RI, *Bam*HI, *Hin*dIII, *Kpn*I and *Xba*I (either singly or in combination) and then electrophoresed on a 1% agarose gel. Gels were blotted on to nitrocellulose[20] and hybridized with the ^{32}P-labelled IFN-γ cDNA probe. The size of fragments was determined by comparison with *Hin*dIII λ molecular weight standards. The 8.6-kbp *Bam*HI fragment of λG9 was separated by electrophoresis through 1% agarose, electroeluted, and ligated into the *Bam*HI site of pBR322. One of the resultant recombinants, pB9KB-1, was extensively mapped with restriction endonucleases, and sequenced according to the strategy outlined below. Each sequence was determined from the marked positions and sequenced in the direction of the arrow; the length of each arrow corresponds to the length of sequence determined. Only those *Hin*cII sites which were used in sequencing are shown. Sequences determined by the Maxam–Gilbert method[36] are depicted with straight lines, while sequences determined by the dideoxy chain termination method[37] are represented by wavy lines. Synthetic single-stranded DNA primers, synthesized by the modified solid phase phosphotriester method[38], were used for dideoxy sequencing. The sequences of the primers were designed from the cDNA sequence[16]: dTCTCTCGGAAACG (found at nucleotides 97–109 of the cDNA), dGGTCATTCAGATG (229–241), dAATGCAGAGCCAA (309–321) and dCGAAAAGCTGACT (453–465). The reverse complements of the above primers were also used for sequencing in the 3′ to 5′ direction. In addition to the M13 *lac* primer[39], two other synthetic DNA primers were also used: dCTGCCAGGACCCA (174–186 of the cDNA) and dAAATATTGCAGGC (complementary to 620–632 of the cDNA). The templates for dideoxy sequencing were four restriction fragments (*Hpa*I–*Hin*dIII, *Hin*dIII–*Pvu*II, *Pvu*II–*Eco*RI and *Pst*I–*Hin*cII) which were subcloned in both orientations of the M13 vector mp7 (ref. 39).

*Pvu*II. Comparison of these hybridization patterns with those obtained earlier using human lymphocyte DNA[16] indicated that two phage DNAs (λG9 and λG10) appeared to contain the entire IFN-γ gene, as illustrated in Fig. 1. Clone λG9 was selected for further study. The region of λG9 hybridizing to the IFN-γ cDNA probe appeared to be contained entirely within an 8.6-kbp *Bam*HI fragment. This restriction fragment was subcloned into the *Bam*HI site of pBR322. The *Bam*HI insert from one of the resultant recombinants, pB9KB-1, was mapped with restriction endonucleases to allow DNA sequence analysis (Fig. 1).

Almost 6,000 contiguous base pairs (bp) of the IFN-γ gene region were determined by sequencing the majority of both strands (Fig. 1); these are shown in Fig. 2. The IFN-γ cDNA sequence previously determined[16] was aligned with the gene sequence as shown in Fig. 2. The two sequences matched completely except for a single base pair transition (4,712 of Fig. 2; position 588 of ref. 16) which changes the glutamine codon found at position 140 in the cDNA sequence to an arginine. However, we have subsequently sequenced five additional IFN-γ cDNAs which all contained arginine codons at this position[17].

There are three intervening sequences in the coding region of the gene. All three introns begin with a GT dinucleotide and end with an AG, sequences thought to be necessary for correct RNA splicing[21,22]. Intron 1 is 1,238 bp long; intron 2 is 95 bp, and intron 3 is 2,422 bp long. The four exons are less variable in length, coding for 38, 23, 61 and 44 amino acids, respectively. Each intron interrupts the reading frame precisely betwee codons.

Although there is no obvious overall amino acid homolog between IFN-γ and either IFN-α or IFN-β[16], a pattern c single amino acid homology between IFN-γ and IFN-α ha been reported[42], and the first exon of IFN-γ codes for tw groups of amino acids which have homology with IFN-α. Th four identical amino acids, Ser-Leu-Gly-Cys, are found at th junction between the signal peptide and mature interferon (where Cys is the first amino acid of the mature proteins)[4 Another homology with the first exon of IFN-γ is found neare the carboxy-terminus of IFN-α_2 (refs 2, 3):

	130	131	132	133					134	135	136
IFN-α	Tyr–	Leu–	Lys–	Glu–					Lys–	Lys–	Tyr
IFN-γ	Tyr–	Val–	Lys–	Glu–	Ala–	Glu–	Asn–	Leu–	Lys–	Lys–	Tyr
	7	8	9	10	11	12	13	14	15	16	17

If amino acids 11–14 of IFN-γ are neglected, six of seven amin acids are identical (17 of 21-nucleotide homology). Thi homology may be significant as the IFN-α sequence was foun to be highly conserved in this region when 11 different IFN- sequences were compared[4,5]. Furthermore, this region is pro posed to be highly α-helical[23]; the insertion of four amino acid would increase the length of the helix by one turn, but shoul not disturb the relative position of amino acids on the helix which is particularly important in a postulated helix of this typ with hydrophobic side chains on one side and hydrophilic side chains on the other.

The determination of the complete nucleotide sequence of the IFN-γ gene allows comparison of sequences thought to be important in gene regulation. One such sequence is the Goldberg–Hogness box[24,25], located ~30 bp upstream from the 5′ end of the site of RNA initiation. This sequence, 5′ $\mathrm{TATA}^{T}_{A}\mathrm{A}^{T}_{A}$ 3′, is thought to be important in determining the specificity of the initiation of RNA synthesis by RNA polymerase II[26–28]. Such a sequence, TATAAATA, is found in the IFN-γ gene 28 bp upstream from the 5′ end of the mRNA[17]. Interestingly, this same sequence is found in a comparable position in the IFN-β gene[13,14], although there is little further homology with IFN-β sequences in the 5′ extragenic region. However, seven different members of IFN-α contain the significantly different sequence, TATTTAA[6].

Another sequence which is relatively conserved at the 5′ end of many genes is the consensus sequence $\mathrm{GG}^{C}_{T}\mathrm{CAATCT}$[29], located ~80 bp upstream of the cap site. This sequence is thought to modulate transcription by RNA polymerase II[26] and has been shown to be necessary for efficient transcription of the rabbit β-globin gene *in vivo*[30]. A similar sequence, GTCACCATCT, found 89 bp upstream from the 5′ end of IFN-γ mRNA, is not detected in either the IFN-α genes or the IFN-β gene[6,13,14].

IFN-α and IFN-β have extensive homology in the 5′-flanking regions[13,14] which is not shared by IFN-γ. Perhaps it is not surprising that sequences potentially involved in the induction of IFN-γ gene transcription differ from those of IFN-α and IFN-β as the inducers and kinetics of induction of IFN-γ are quite distinct from those of the other interferons.

The coding region of the IFN-γ gene consists of unique, single-copy DNA, as shown by Southern[20] hybridization of a labelled cDNA probe to genomic human DNA[16]. To determine whether introns or flanking regions of the IFN-γ gene contained repetitive DNA sequences, probes from individual regions of the gene were prepared and hybridized with Southern blots of human genomic DNA. As shown in Fig. 3, all but one of the probes hybridized to unique human DNA fragments. The sizes of the hybridizing bands correspond to the lengths predicted from the map derived from the phage DNAs (Fig. 1). The first intron contains DNA which hybridizes to DNA throughout the blot, typical of repetitive sequences. We conclude therefore, that the IFN-γ gene consists of predominantly unique sequence DNA, but also contains a repetitive DNA element in the first intron.

The human genome contains more than 300,000 copies of a family of related sequences termed *Alu* sequences[31] which are ~300 bp long and for which no known function has been demonstrated. A computer comparison of the IFN-γ gene sequence (Fig. 2) with the *Alu* family repeat consensus sequence[32] failed to detect significant homology. Furthermore, an *Alu* family repeat probe (BLUR8; ref. 32) failed to hybridize with the first intron, but did hybridize with six different regions of the 33.5-kbp IFN-γ gene region, five of which are 'clustered' in 13 kbp upstream from the start of the IFN-γ gene (Fig. 4). Such a clustering of *Alu* family repeats has been observed in other human DNA regions[33] and in IFN-α genomic clones[6].

In six different IFN-γ cDNA clones, obtained using mRNA from four different individuals, only one nucleotide variation was observed[17], which suggests that the coding region of IFN-γ may be relatively consistent for all individuals. To determine if the IFN-γ gene sequence is conserved in a broader segment of the human population, we conducted a limited search for restriction fragment length polymorphisms. Genomic DNA isolated from lymphocytes of nine individuals of various ethnic backgrounds was cleaved with a series of restriction endonucleases (*Pvu*II, *Hin*cII, *Xba*I, *Pst*I, *Hin*fI, *Eco*RI and *Rsa*I) and analysed by Southern blotting using the IFN-γ cDNA probe. No detectable differences in mobility of hybridizing fragments were seen (data not shown), suggesting that the IFN-γ gene and surrounding DNA sequences are relatively conserved.

```
1    AGCAAATGATCAATGTGCTTTGTGAATGAAGAGTCAACATTTTACCAGGGCGAAGTGGGGAGGTACAAAAAAATTTCCAGTCCTTGAATGGTGTGAAGTA

101  AAAGTGCCTCAAAGAATCCCACCAGAATGGCACAGGTGGGCATAATGGGTCTGTCTCATCGTCAAAGGACCCAAGGAGTCTAAAGGAAACTCTAACTACA

201  ACACCCAAATGCCACAAAACCTTAGTTATTAATACAAACTATCATCCCTGCCTATCTGTCACCATCTCATCTTAAAAAACTTGTGAAAATACGTAATCCT
     MstII                                                          *
301  CAGGAGACTTCAATTAGGTATAAATACCAGCAGCCAGAGGAGGTGCAGCACATTGTTCTGATCATCTGAAGATCAGCTATTAGAAGAGAAAGATCAGTTA

                                                                                   Met Lys Tyr Thr Ser Tyr
401  AGTCCTTTGGACCTGATCAGCTTGATACAAGAACTACTGATTTCAACTTCTTTGGCTTAATTCTCTCGGAAACG   ATG AAA TAT ACA AGT TAT

     Ile Leu Ala Phe Gln Leu Cys Ile Val Leu Gly Ser Leu Gly Cys Tyr Cys Gln Asp Pro Tyr Val Lys Glu Ala
493  ATC TTG GCT TTT CAG CTC TGC ATC GTT TTG GGT TCT CTT GGC TGT TAC TGC CAG GAC CCA TAT GTA AAA GAA GCA

     Glu Asn Leu Lys Lys Tyr Phe
568  GAA AAC CTT AAG AAA TAT TTT  GTAAGTATGACTTTTTAATAGTACTTGTTTGTGGTTGAAAATGACTGAATATCGACTTGCTGTAGCATCTC
                                                                                             XbaI
660  TGATAGGCTGTCATCTCTTGTAGGCAGTCATTTTGAGATTTGGTGTTATTTTGTTAATTATTGACTAGATGAGTTCCTTGACTAAATAATCTAGATATTG

760  TTTTAACCTTCTGCTCAGTTTGTATAGAGACTTAAAAGGGATTTATGAATTTTCCAAAAGATGGGCATAATATGGGTATGAAGCATAATGATGTTAATAA

860  TTTTGTGGTGGGAACTCATTCAGTTGTGATAGTCAAGGAGTATGCAGATTGAAAAAAATGATTGGTTATTAGTTTTTGACTTCTCAGACTCTAAGGTCAA
                                                                   HindIII
960  GATTAGCATTAAAAAGGTAATAGGAAATGTTTACAAATTAAAGTCAAAAAGGTCCTTAAAGCTTTGGCTTAAAAAAATAACTGATAGGTGATTTTCTCCA
                                                          HpaII
1060 AAAAGTGATTTCAACATTCTGCTTCTCTATCTATATTACTTGTGAAGTATTCCGGAACTTCGTTGCTCACTGGGATTTTGGAAGAATTATGATTCTGGCT

1160 AAGGAATGTTTAAAAATTTTAAGTGAATTTTTTGAGTTTCTTTTAAAATTTTATTGATGGTTAATGAAAAGTTTTTACATTTTAAATATTTCATTATTTG

1260 TTTAAAACTTAGCTGTTATAATTATAGCTGTCATAATAATATTCAGACATTCACAATTGATTTTATTCTTACAACACAAAATCAAATCTCACACACACAC

1360 ACACACACACACACTCGCACATGTTTGGAACTATCTTTTAAAGCTCGTATAATAATACCCTACAGGAAGGCACAGTAGATGTAATAGAAACCTGTACCAT

1460 TGGGGGGCAGTATTTTATAGTGGGGTGGCTTTGCTGTTTTTTGTTTTTGTATTTTTTAGCCTAGCTTGAAAATACTTTCTTTAGCTTACTATAGTTTTTG
                                SacI
1560 GGACCTTTGGAGTATCAGCTTTGTTGAGCTCATTTGTGACATTGCAATTTAATGGTTATATTGGGAAATAAAAAAGCTAAAAGAACATAATAGTCTTTGT

1660 CTATATCTCACATAAGCCTTTTGGGAATACTTATTGTTAGAACTAAGCAGAAGAGTTGAAAAGGAAATCAGTGAATATTGTCACATCTGAGTTCAATGAA

                                                                             Asn Ala Gly His Ser Asp Val Ala
1760 ACTTGAAATATATTTTTAAGGCAATTTATGGGCTAATTGTAAACCAATTTTTTCTTTTTTTTTTTTAG AAT GCA GGT CAT TCA GAT GTA GCG

     Asp Asn Gly Thr Leu Phe Leu Gly Ile Leu Lys Asn Trp Lys Glu
1852 GAT AAT GGA ACT CTT TTC TTA GGC ATT TTG AAG AAT TGG AAA GAG  GTAAGCTGAATATTCCCATTTGGCTAATTTTCCTGTTGC

                                                                Glu Ser Asp Arg Lys Ile Met Gln Ser Gln Ile
1936 TTGCTTTCTGATGGATAAATTCACATCATCCTCTGTTTGTGCTCTTTCCTTCCAAG GAG AGT GAC AGA AAA ATA ATG CAG AGC CAA ATT

     Val Ser Phe Tyr Phe Lys Leu Phe Lys Asn Phe Lys Asp Asp Gln Ser Ile Gln Lys Ser Val Glu Thr Ile Lys
2025 GTC TCC TTT TAC TTC AAA CTT TTT AAA AAC TTT AAA GAT GAC CAG AGC ATC CAA AAG AGT GTG GAG ACC ATC AAG

2100 Glu Asp Met Asn Val Lys Phe Phe Asn Ser Asn Lys Lys Lys Arg Asp Asp Phe Glu Lys Leu Thr Asn Tyr Ser
     GAA GAC ATG AAT GTC AAG TTT TTC AAT AGC AAC AAA AAG AAA CGA GAT GAC TTC GAA AAG CTG ACT AAT TAT TCG
                                                                              AccI
2175 GTGAGGCTATTTAAATTCTTTCTTTGGTTTCATTGCCGAGGGTCTTGCAAAGCATTTATTCTCCAGAAAGTAGACATTAGCTATTTAACAGTTGCTAAAG

2275 CTATGAACTCAACTCATGGCTGAAACTCTACCTTACTATTTCCATTCGTGTTTGGGTGACTTTGCAAAGCCAGTAAGAGAATCGCTGAAGTATGTAATGT

2375 AGAGAAATGCTGGCATTGTAACTATTGCGTAAAGACAGGTGAGTTGACAAATTCCAGTGAAGAGGAAGTAGGTGAGGAAGAAGCAGGGAGTACTGAGAAG

2475 CAGTTCTCTCATTGTCCCTTGCTCATATGATGGAAATTCTCTTACTTTGAATGAGAGGCTGTCTGTCTTAATGGAAAGAGCAGTGGGAGGAGCTGAGAAG

2575 ATGTGTGTTCTCCTCCCAACTCAGCCACCAAGGAACTGTGATGAATCACATGGCTGGCTGGGCTCAGTTTCCTCATCTTAAAAGGAAACTGTTAGGTTCA
                                                                                                 KpnI
2675 CTGTATAAGTTTGATGACCTTCTTTGCTCCAAAACTCTACAATGCAAAGAATAGAAAATGAGAATGAGATAGAAGAAAGCTACAGTCTTTGAATAGGTAC

2775 CAGGGACACCCCACTGCAAGTCTCTAGCCAACCTATCAGATTGTACTGCCCAATTAGAAGCAAGAATGGTTGCTGTTTGTTTGTTTTTAGGGAAAAATAG

2875 ATAGAATTTATACCTTATGAAAAGATTGTTCTATCAACTCTCTATCAACTTTCAGAATATCTCAGCTGGAGAACTCCTTAGACTCCTAAGTCTTACCTCA
                                                                                              XbaI
2975 TGAACTTGTATCTTTAAGTTATGGCTTCTATAAACAGAAAGATAACGTTGAGGCATAAAGACAAATCATGTTTTTCAGAATGTTTCTAGAAGAGAAAGG
       XbaI               HincII
3075 CCTCTAGATTCCTTTGGGGTTGACTTTGATATAAATGGGCTCAAATGAGAGGGACCAGGGTCTTCAAGCTAGCATTTGTGTTCTTAGGATATGTGCTCAG

3175 CTTTCACTATTGCTGGGCCTGCCTCTCACTCCTCTCATGTAAGCCCCCAGAAACAGAAAGGAGAGACATGGCAACAGGTCTCCTTTGGTTATAAACTAGA

3275 CACTCAGCACTTGTTTCTAATCCAGTGGTGCCCCTGGCTTACTGTTCAGTCCTGGATAAGTCTCTTAGTTTCTTGGTGATGATTTGAACATTGGAAAGTA
                                                    PstI
3375 AAATCTGTCACTTGCAAACACACAGCTTGTCGAAAATTTTTTCTACTCTGCAGGAACTGGGCCTTAAAAAAATGAAAAAAAATCTGTGGTTTCTTCCTTC

3475 TGGAAGCTACAAACCTCCTGTTTCTTGATGGGCAATCTTGAGTGAGCTCTATTAATTATTATTCTCTTTGGCTCAGTTGCTAAGCTATTTTATGCATGTT

3575 ATGCCCTTTGACAATTAGTCTTTAGCTGTAATCCCCCAGCCATCCTCAGAAATGTGGTGAGGTAGCCATAGTGTTCCCAAGATTAGAAAAATGTAATGGC

3675 AGAGCCAAGAGGAAGGTAAATGGTCCACATCTTATGAAGCATCATCTAAATGGCCCTATTGGTTAGAGTGAGGAGATGCAAGTAGTTCAATTTGCTTGCC

3775 TAGAAGGCAGGGTACTGGAAAAGTTGTTGCAATTCTTAATTTTAAACTTTATATATCAGTAAGCCATATATAAATATGATTGGGGGTGTTTATTTTAAAA
                                                                                                 KpnI
3875 TCTATTATGGAAATTGAGAGACTGACCTAATCTGGGAGAAATTAAAAATTACAGTTTTCACTCGTTTTGGATTTGGTGTTTTCTAGGGTACCTAACCTAG

3975 ATCAGTGGTTCTCAAACTTAGGTGGATGTCAGAATCACCTGGGGAGCTTAGTGAATGCACAGGGCACAGTCCTTCCACTTCATGCACCTGGATCTCTGAG
                   HpaII
4075 GTCTTTGACAGGTTTCCGGATTAATCTGCTATGCACAACAGTGAGAATCATTGACCTATAGTTACTCATTTGATGCATACAGGAAAGACTGAAGTATAAA

4175 GTGATATAATTGGTAGATTGATGATAGAGAGGTCATAGAAACAGTCTCATCCTCCTTTAGATGAGAAAATAGAAGTTCAGAGAGGTTAAGTAGCTGGCTC
                                                                                                 EcoRI
4275 AAGGTCAGAATTATTGCATGCATGAGATTCAAACCCACCTTTTTATGCTGACTCCACAACCAGGAGTCTTTTCACTATATAATTTCAAGAATTCTATAGA

4375 AGTAGATTTAAAGATATGTGATGGACTCCACCACATTATAGCACAACTAGAAATGTAATTGTAATTTTTAGCTTCAACTGCTGAAGAAGTAAATATTGTA

4475 TATTAAGGTAATACGGTCCATTTTTTAAAGGAATACTTTTATTTTCACTGACCATCATGACATTAGCAGAATATCCTGATGGCTTATATGCCTGAAATTA

                                Val Thr Asp Leu Asn Val Gln Arg Lys Ala Ile His Glu Leu Ile Gln Val Met
4575 ATTTTGCTCTTTTCTTTCCCGATAG   GTA ACT GAC TTG AAT GTC CAA CGC AAA GCA ATA CAT GAA CTC ATC CAA GTG ATG

     Ala Glu Leu Ser Pro Ala Ala Lys Thr Gly Lys Arg Lys Arg Ser Gln Met Leu Phe Arg Gly Arg Arg Ala Ser
4654 GCT GAA CTG TCG CCA GCA GCT AAA ACA GGG AAG CGA AAA AGG AGT CAG ATG CTG TTT CGA GGT CGA AGA GCA TCC

     Gln OC
4729 CAG TAA  TGGTTGTCCTGCCTGCAATATTTGAATTTTAAATCTAAATCTATTTATTAATATTTAACATTATTTATATGGGGAATATATTTTTAGACTC

4826 ATCAATCAAATAAGTATTTATAATAGCAACTTTTGTGTAATGAAAATGAATATCTATTAATATATGTATTATTTATAATTCCTATATCCTGTGACTGTCT

4926 CACTTAATCCTTTGTTTTCTGACTAATTAGGCAAGGCTATGTGATTACAAGGCTTTATCTCAGGGGCCAACTAGGCAGCCAACCTAAGCAAGATCCCATG
                                                                                 HpaII
5026 GGTTGTGTGTTTATTTCACTTGATGATACAATGAACACTTATAAGTGAAGTGATACTATCCAGTTACTGCCGGTTTGAAAATATGCCTGCAATCTGAGCC

5126 AGTGCTTTAATGGCATGTCAGACAGAACTTGAATGTGTCAGGTGACCCTGATGAAAACATAGCATCTCAGGAGATTTCATGCCTGGTGCTTCCAAATATT
     HincII                                                                                         *
5226 GTTGACAACTGTGACTGTACCCAAATGGAAAGTAACTCATTTGTTAAAATTATCAATATCTAATATATATGAATAAAGTGTAAGTTCACAACTACTTATG

5326 CTGTGTTGGACTTTTTCTAAGTGAGACCTGGAGTGAAAGAACTACCTATTAATGAATTAGTAGGGAGGGGAGTCTTCTTAGCTGTGAAAATTTTAGAGTT

5426 GCATTTGGTTCCATTAAATGTGGTATTTCTTTCCACTAGCATTTTGTTGGCTTTCGCTTTTCCAGTTAGCAGCTCTTTGAATTATCTTTCTAAGATACAG

5526 ATTTAATTATGTCACTATTCAATTCAGAGGTTCTGCTATGGAATGTAGTTTAAACTGCTTAGCTTGGCACACAGAGATTTATTTCTAGCCCCTTCTCCAC

5626 CTTCCTATTTCCTCCTTCGTTTCAGAATCTTCCTCTCCCTCATCCAATGCTGGCAAACACCAGTGGGGGTGGAGTAGTGGGTGTAAGCTCTAGGGAGAAG

5726 GCTTGGATTGGAATCCAAGTTATTCCATTACAAGTAGTGTGACCTTTAATACATTATGTATATTGTCTAAGTTTCAGCTTTATTGTCTGAAAAAGAAAAA
                                                                                                AccI
5826 TAATTGTGTGTTCCTCATAATATTGTGGTACGAATTGATTCTTTCACTCAAGAAATATTTACTGGAGTACCTACTACATGCCTGGTGCTGTTGTAGACCT
                                  BamHI
5926 TGAGATACCTTACTCAAGCAAAACAGCCAAGGATCC(5961)
```

Fig. 2 Sequence of the human IFN-γ gene region. Only the sense strand is shown. The coding sequences of the exons have been translated. The CCAAT box[29], Goldberg–Hogness box[24,25] and polyadenylation site sequence (AATAAA)[40], have been underlined. The start of RNA transcription[20] is marked with a star, as is the position of polyadenylation. Restriction endonclease sites used in sequencing or Southern hybridizations are also shown.

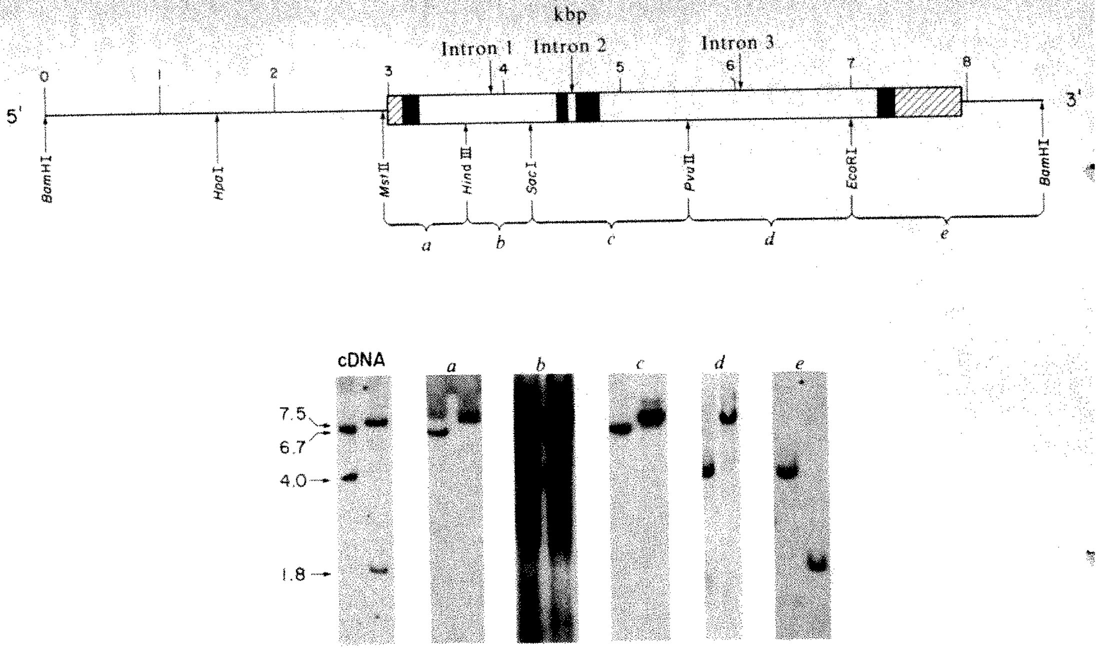

Fig. 3 The IFN-γ gene region contains a repetitive element. The cloned IFN-γ gene sequence was digested with the restriction endonucleases shown and the resulting fragments (*a–e*) were isolated on 5% polyacrylamide gels, electroeluted and used to synthesize ^{32}P-labelled probes by the calf thymus primer method[35]. The individual probes were hybridized with *Pvu*II (left) and *Eco*RI (right) digests of human genomic lymphocyte DNA (isolated by the method of Blin and Stafford[41]), separated on 1% agarose gels and transferred to nitrocellulose by the method of Southern[20]. Four of the probes (*a, c, d* and *e*) hybridized only to the single *Pvu*II or *Eco*RI fragments from which they were derived. Probe *b* hybridized throughout the genomic DNA. The 5'- and 3'-untranslated regions of the IFN-γ gene are shown as cross-hatched boxes and coding regions of exons are represented by solid boxes.

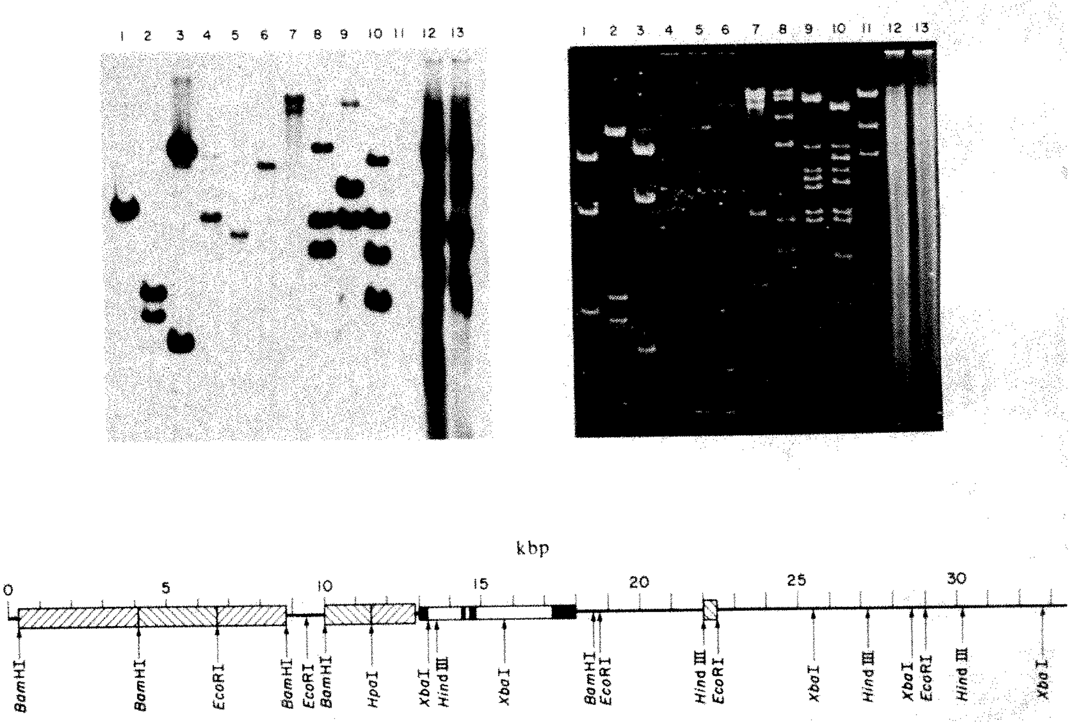

Fig. 4 Hybridization of the *Alu* family repeat probe to the IFN-γ gene region. The ^{32}P-labelled probe was prepared[35] from a 300-bp *Bam*HI fragment of pBLUR8 (provided by C. Houck and R. Lawn) which contains *Alu* family repeat DNA[32]. Electrophoresis in 1% agarose gel is shown on the right; lane 1, *Hin*dIII + *Sac*I digest of pB9KB-1; 2, *Hin*dIII + *Hpa*I digest of pB9KB-1; 3, *Bam*HI + *Hpa*I digest of pB9KB-1; 4, *Eco*RI digest of λ G5; 5, *Xba*I + *Hin*dIII digest of λ G5; 6, *Xba*I digest of λ G5; 7, *Xba*I digest of λ G9; 8, *Eco*RI digest of λ G6; 9, *Bam*HI digest of λ G8; 10, *Eco*RI + *Bam*HI digest of λ G8; 11, *Hin*dIII digest of λ DNA (size markers); 12, *Pvu*II digest of human genomic DNA; 13, *Eco*RI digest of human genomic DNA. The gel was transferred to nitrocellulose[20] and hybridized with 3×10^6 c.p.m. of probe (10^7 c.p.m. per μg DNA), shown on the left. Four different hybridizing signals are observed in λ G8 (lane 10). The signal in the subclone pB9KB-1 was shown to consist of two separate parts (lanes 2, 3). Only a single hybridizing signal was observed in the 3' region (λ G5, lanes 4–6). Mapping of these hybridizing regions (cross-hatched) is shown below on the map originally presented in Fig. 1. The IFN-γ gene region is represented by a smaller box with solid bars for exons and open bars for introns.

We thank Mark Vasser for deoxyoligonucleotide synthesis, Dr Ellson Chen for preparation of templates for dideoxy sequencing and Dr Richard Lawn for providing the human λ DNA library.

Received 10 May; accepted 14 June 1982.

1. Nagata, S., Mantei, N. & Weissmann, C. *Nature* **287,** 401–408 (1980).
2. Streuli, M., Nagata, S. & Weissmann, C. *Science* **209,** 1343–1347 (1980).
3. Goeddel, D. V. *et al. Nature* **287,** 411–416 (1980).
4. Goeddel, D. V. *et al. Nature* **290,** 20–26 (1981).
5. Lawn, R. M. *et al. Science* **212,** 1159–1162 (1981).
6. Lawn, R. M. *et al. Proc. natn. Acad. Sci. U.S.A.* **78,** 5435–5439 (1981).
7. Weissmann, C. *Interferon* **3,** 101–134 (1981).
8. Taniguchi, T., Ohno, S., Fujii-Kuriyama, Y. & Muramatsu, M. *Gene* **10,** 11–15 (1980).
9. Derynck, R. *et al. Nature* **285,** 542–547 (1980).
10. Goeddel, D. V. *et al. Nucleic Acids Res.* **8,** 4057–4073 (1980).
11. Lawn, R. M. *et al. Nucleic Acids Res.* **9,** 1045–1052 (1981).
12. Houghton, M. *et al. Nucleic Acids Res.* **9,** 247–266 (1981).
13. De Grave, W., Derynck, R., Tavernier, J., Haegeman, G. & Fiers, W. *Gene* **14,** 137–143 (1981).
14. Ohno, S. & Taniguchi, T. *Proc. natn. Acad. Sci. U.S.A.* **78,** 5305–5309 (1981).
15. Owerbach, D. *et al. Proc. natn. Acad. Sci. U.S.A.* **78,** 3123–3127 (1981).
16. Gray, P. W. *et al. Nature* **295,** 503–508 (1982).
17. Derynck, R., Leung, D., Gray, P. W. & Goeddel, D. V. *Nucleic Acids Res.* (in the press).
18. Yip, Y. K., Barrowclough, B. S., Urban, C. & Vilcek, J. *Proc. natn. Acad. Sci. U.S.A.* **79,** 1820–1824 (1982).

19. Lawn, R. M., Fritsch, E. F., Parker, R. C., Blake, G. & Maniatis, T. *Cell* **15,** 1157–1174 (1978).
20. Southern, E. M. *J. molec. Biol.* **98,** 503–517 (1975).
21. Breathnach, R., Benoist, C., O'Hare, K., Gannon, F. & Chambon, P. *Proc. natn. Acad. Sci. U.S.A.* **75,** 4853–4857 (1978).
22. Lerner, M. R. *et al. Nature* **283,** 220–224 (1980).
23. Wetzel, R. *et al.* in *Chemistry and Biology of Interferons: Relationship to Therapeutics* (eds Merigan, T. C., Friedman, R. M. & Fox, C. F.) (Academic, New York, in the press).
24. Goldberg, M. thesis, Stanford Univ. (1979).
25. Gannon, F. *et al. Nature* **278,** 428–434 (1979).
26. Grosschedl, R. & Birnstiel, M. L. *Proc. natn. Acad. Sci. U.S.A.* **77,** 1432–1436 (1980).
27. Wasylyk, B. *et al. Proc. natn. Acad. Sci. U.S.A.* **77,** 7024–7028 (1980).
28. Grosveld, G. C., Shewmaker, C. K., Jat, P. & Flavell, R. A. *Cell* **25,** 215–226 (1981).
29. Benoist, C., O'Hare, K., Breathnach, R. & Chambon, P. *Nucleic Acids Res.* **8,** 127–142 (1980).
30. Grosveld, G. C., de Boer, E., Shewmaker, C. K. & Flavell, R. A. *Nature* **295,** 120–126 (1982).
31. Houck, C. M., Rinehart, F. P. & Schmid, C. W. *J. molec. Biol.* **132,** 289–306 (1979).
32. Rubin, C. M., Houck, C. M., Deininger, P. L., Friedman, T. & Schmid, C. W. *Nature* **284,** 372–374 (1980).
33. Calabretta, B. *et al. Nature* **296,** 219–225 (1982).
34. Maniatis, T. *et al. Cell* **15,** 687–701 (1978).
35. Taylor, J. M., Illmensee, R. & Summers, S. *Biochim. biophys. Acta* **442,** 324–330 (1976).
36. Maxam, A. M. & Gilbert, W. *Meth. Enzym.* **65,** 499–560 (1980).
37. Smith, A. J. H. *Meth. Enzym.* **65,** 560–580 (1980).
38. Crea, R. & Horn, T. *Nucleic Acids Res.* **8,** 2331–2348 (1980).
39. Messing, J., Crea, R. & Seeburg, P. H. *Nucleic Acids Res.* **9,** 309–321 (1981).
40. Proudfoot, N. J. & Brownlee, G. G. *Nature* **263,** 211–214 (1976).
41. Blin, N. & Stafford, D. W. *Nucleic Acids Res.* **3,** 2303–2308 (1976).
42. Epstein, L. B. *Nature* **295,** 453–454 (1982).

DNA precursors in chemical mutagenesis: a novel application of DNA sequencing

Michael D. Topal*, Clyde A. Hutchison III† & Mary S. Baker*

Departments of *Pathology, †Bacteriology and Immunology, and the *Cancer Research Centre, University of North Carolina Medical School, Chapel Hill, North Carolina 27514, USA

Recently, we have shown that deoxyribonucleoside residues in the cellular DNA precursor pool are generally more susceptible to methylation than are residues within the DNA duplex[1]. The N-1 position of adenosine, for example, was found to be at least 13,000 times more susceptible to methylation by *N*-methyl-*N*-nitrosourea (MNU) than the same site in the DNA. These results suggest that potential sites for alkylation in the double-strand duplex are relatively inaccessible to direct alkylation *in vivo*. Many of these sites are probably protected from alkylation not only by their position in the interstices of the DNA helix[2,3], but also by further *in vivo* 'packaging' of the DNA in chromatin[4–8]. We have now used DNA sequencing to demonstrate the incorporation properties of products of the reaction of MNU with dATP and of deoxy-N^4-hydroxycytidine triphosphate during DNA replication *in vitro* by phage T4 DNA polymerase and the 'Klenow' fragment of *Escherichia coli* pol I. The results suggest that DNA precursor nucleotides due to their greater availability for alkylation, may offer routes for the introduction of alkylated residues into double-stranded DNA.

To investigate the ability of DNA polymerase to use products from the interaction of chemical mutagens with DNA precursors, we reacted MNU with dATP. The products were separated by chromatography on QAE-Sephadex. Chromatographic and enzymatic analyses (to be described elsewhere) revealed N-1 and N-3MedATP in an approximate ratio of 7:1, N-1/N-3MedATP, dADP with one methyl group associated with its terminal β-phosphate, mP$^{\beta}$-dADP, and dATP with one methyl group associated with its terminal γ-phosphate, mP$^{\gamma}$-dATP.

We investigated the incorporation of these products into DNA using a novel application of the 'plus and minus' DNA sequencing method[9]. A plus reaction with a modified dNTP, dN*TP, as substrate provides information about the incorporation properties of dN*TP when bands generated on an analysing gel by products of the reaction are compared with those generated on the same gel by products of control reactions from the same sequence (Fig. 1*a*). The incorporation properties of dN*TP can be determined also from minus reactions using dN*TP instead of the missing triphosphate. If dN*TP can substitute for the missing dNTP, then synthesis proceeds beyond those sites that are blocked in the control reaction because of the need for the missing dNTP. Incorporation of the methylated precursor eliminates bands in the gel (see Fig. 1*b*).

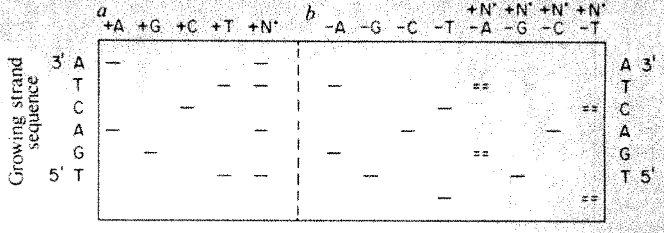

Fig. 1 Representation of a gel containing the products of: *a*, plus reactions; and *b*, minus reactions for the DNA sequence TGACTA. The gel bands indicated are the products of plus and minus reactions in the presence of a hypothetical modified triphosphate, dN*TP (N*), which incorporates as dATP and TTP (that is, against T and A template residues). Note the appearance of bands in the +N* slot that correspond to bands in the +A and +T but not the +G or +C slots. In minus reactions, bands in slots that analyse the products of −A and −T reactions with N* have decreased in intensity or are absent (indicated by pairs of dotted lines) compared with bands from −A and −T reactions without N*. No such effect was seen when the products of −G and −C reactions in the presence and absence of N* were compared.

N^4-hydroxy-dCTP (OH-dCTP; IUPAC numbering) was studied as a control in both plus and minus reactions (Fig. 2) because it may be able to act as both dCTP and TTP as suggested by studies of the incorporation of OH-rCTP into RNA[10,11]. As expected, OH-dCTP incorporated sometimes as dCTP and sometimes as TTP but never as dATP or dGTP. In a plus reaction, however, OH-dCTP incorporated opposite less than half of the available A and G sites (Fig. 2*a*) whereas in minus reactions containing OH-dCTP, almost all A and G template sites were used (Fig. 2*b*). This apparently different ability to incorporate in plus as opposed to minus reactions is probably related to the heavy dependence of plus reactions on the exonuclease and synthetic activities of the DNA polymerase. Once a residue (correct or incorrect) is incorporated during a minus reaction it may escape repeated scrutiny by the proofreading exonuclease through incorporation of the next residue. Analysis of OH-dCTP incorporation in plus reactions (Table 1) suggests

Table 1 Incorporation of OH-dCTP as T and C during plus reactions

a Four sites incorporate OH-dCTP at:			Two do not incorporate OH-dCTP at:	
Amount of incorporation	Site	ΦX174 coordinate	Site	ΦX174 coordinate
(m)	CT C GG	(4,683)	AG C AA	(4,677)
(s)	CC C TC	(4,685)	$_{5'}$GG C GT	(4,710)
(w)	GC C TT	(4,694)		
(w)	$_{5'}$TA C TG$_{3'}$	(4,724)		
***b* Two sites incorporate OH-dCTP at:**			**Five do not incorporate OH-dCTP at:**	
Amount of incorporation	Site	ΦX174 coordinate	Site	ΦX174 coordinate
(w)	CC T CG	(4,684)	CT T GC	(4,692)
(m)	$_{5'}$AC T GA$_{3'}$	(4,723)	AT T AG	(4,698)
			TG T GA	(4,706)
			CG T GT	(4,708)
			$_{5'}$GA T AG$_{3'}$	(4,720)

a, Six C sites and *b*, seven *T* sites tested for incorporation. The site of incorporation is indicated by the ΦX174 *am*3*cs*70 plus strand DNA sequence coordinate[18] shown next to each sequence. The minus (daughter) strand site of incorporation is indicated by the ΦX174 *am*3*cs*70 plus strand DNA sequence neighbours and next-nearest minus strand neighbours are also shown. A semi-quantitative measure of the ability of OH-dCTP to incorporate at the site indicated is represented by w, m or s (weak, moderate or strong), a measure of the effect on band intensity.

that the extent to which OH-dCTP can replace dCTP or TTP during DNA synthesis *in vitro* varies with sequence position; OH-dCTP apparently preferentially incorporates as dCTP when at least one of its nearest neighbours is T and as TTP when at least one of its nearest neighbours is C. The presence of purine residues on both sides of C or T sites inhibits OH-dCTP incorporation opposite those G or A template sites.

Analysis of the products of reaction of MNU with dATP by the plus reaction method (Fig. 3*a*) indicates that N-1/N-3MedATP, mP$^{\gamma}$-dATP and mP$^{\beta}$-dADP are incorporated into DNA by bacteriophage T4 DNA polymerase opposite T template residues but not opposite A, C or G template residues (not shown) at the concentration used. Incorporation of mP$^{\beta}$-dADP opposite T is suspect, however, for two reasons. First, it is believed that diphosphates cannot be incorporated by DNA polymerase. Second, this product chromatographs very closely to unreacted dATP, and so is possibly contaminated by dATP. All of the products were therefore re-purified until the diphosphate analogue no longer incorporated into DNA. Repurification did not alter the ability of products other than mP$^{\beta}$-dADP to pair as dATP. Use of repurified methylation products in minus reactions confirms that N-1/N-3MedATP and mP$^{\gamma}$-dATP preferentially incorporate opposite T template residues. Generally, mP$^{\beta}$-dADP at 10, 102 and 1,020 μM did not incorporate opposite any template residues (Fig. 3*b*); this result serves as a control against contamination by dATP. The slight incorporation at 1,020 μM suggests very low levels (< 4 nM) of dATP contamination. Yet lower levels of dATP contamination are expected for the other products as they chromatographed even further away from the unreacted dATP.

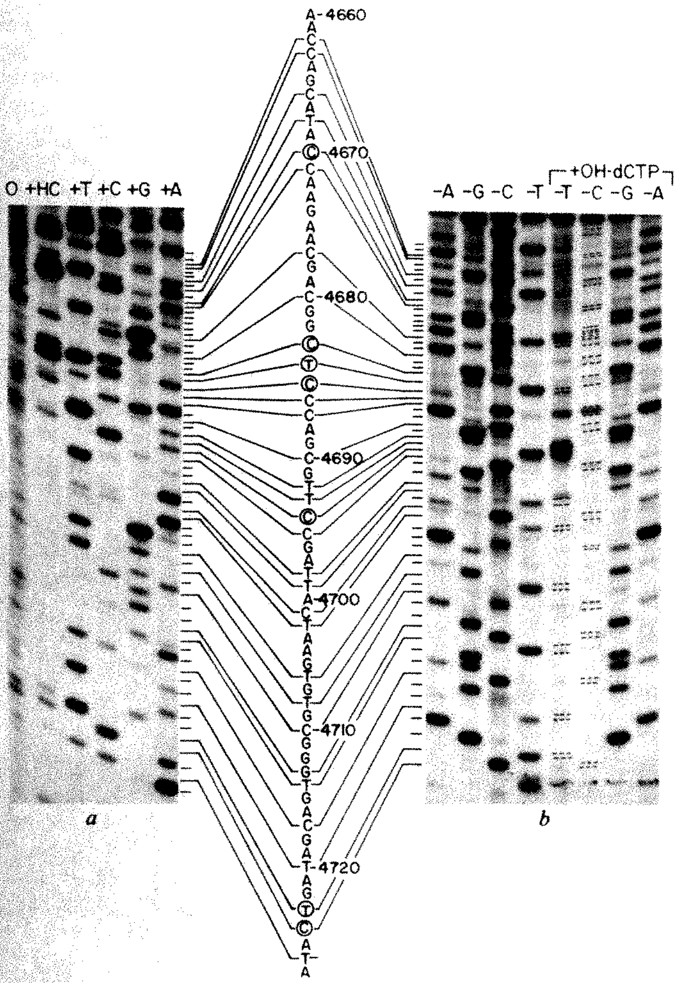

Fig. 2 Incorporation of OH-dCTP (HC) during: *a*, plus and *b*, minus sequencing reactions. OH-dCTP was synthesized according to published procedures[19], shown to be pure by HPLC, and identified by UV absorbance. Plus strand ΦX174 *am*3 *cs*70 DNA annealed with the *Hae*III restriction fragment Z9 (prepared as described elsewhere[20]) was incubated at 37 °C for 20 min with 0.4 μg of bacteriophage T4 DNA polymerase in the presence of 0.2 mM dNTP for plus reactions, or 10.0 μM dNTP for minus reactions. OH-dCTP (500 μM) was used where indicated. *a*, Products of normal plus reactions and products of a plus reaction in the presence of OH-dCTP are analysed on this gel. The sequence of the minus strand (growing strand) is shown. Sites at which OH-dCTP incorporated during plus reactions are indicated by circled bases in the sequence. Only those sites where incorporation was unambiguously assigned are indicated. Caution is required analysing this gel because the bands slant downwards as you proceed from left to right across the gel. *b*, Products of normal minus reactions and products of four extra minus reactions in the presence of OH-dCTP. Bands that have been diminished in intensity by the presence of OH-dCTP during minus reactions are indicated by pairs of dotted lines. The control slot, labelled O, contains the protein-free products of the asynchronous extension of template-primer (by Klenow pol I) in the absence of phage T4 DNA polymerase. All sequence sites are represented by radiolabelled primer extensions. These extended primers are either hydrolysed or elongated by DNA polymerase during plus and minus reactions, respectively.

N-1/N-3MedATP incorporates into DNA *in vitro* at T template sites (Fig. 3*b*) but not at A, G or C sites (not shown) at the concentrations used. Incorporation at some T template sites was noted at 10 μM and efficient incorporation was attained at 1,010 μM as demonstrated by the conversion of lower to higher molecular weight DNA fragments. In contrast, dATP incorporates at some sites at 4 nM and incorporates efficiently at 500 nM. This suggests that one N-1MedATP will incorporate for every 100–1,000 dATPs if both are present at equal concentrations during DNA replication. The use of chemically synthesized N-1MedATP in minus A reactions (unpublished results) indicates that it completely mimics the action of the N-1/N-3MedATP mix in a minus A reaction. Whether or not N-3MedATP can incorporate as dATP therefore remains unknown. mP$^{\gamma}$-dATP incorporates well opposite T (Fig. 3*b*) but not opposite A, G or C residues (not shown). Incorporation of mP$^{\gamma}$-dATP caused a shift of almost all the lower molecular weight DNA fragments, formed because of the absence of dATP during DNA synthesis, to higher molecular weight even at 10 μM—behaviour similar to that found with 10 μM dATP. Thus, the presence of a methyl adduct on the terminal phosphate of dATP does not interfere significantly with incorporation of this precursor.

In a preliminary report we suggested that some unpurified and unidentified products of the reaction of MNU with dATP incorporate as dGTP and dCTP as well as dATP at high concentrations[12]. The data presented here show that at much greater purity, those products that we have been able to isolate and clearly identify incorporate preferentially opposite T template residues.

Alkylation of DNA precursors may result in nucleotide pool imbalances, inhibition of nucleotide binding enzymes, and incorporation of modified residues into double-stranded DNA *in vivo*. The plus and minus DNA sequencing technique has proved a valuable tool in elucidating the third possibility. The technique requires only microgramme quantities of modified dNTP, does not require radiolabelling of the modified dNTP of interest, and allows us to locate specific sites where modified dNTPs are incorporated into DNA. By using this technique we have shown that N-1MedATP incorporates as dATP during replication of single-stranded DNA (ssDNA) *in vitro* by phage T4 DNA polymerase. Preliminary studies in our laboratory further indicate that the Klenow fragment of *Escherichia coli* pol I also incorporates N-1MedATP opposite T template residues. Similar *in vivo* conversion of N-1MedATP to N-1MedAMP template residues could be mutagenic as such template residues have been shown to cause misincorporation of C, G, U and A residues during 'transcription' of RNA with RNA polymerase[13]. Indeed, alkylation of unpaired DNA residues in the form of precursors and possibly single-strand

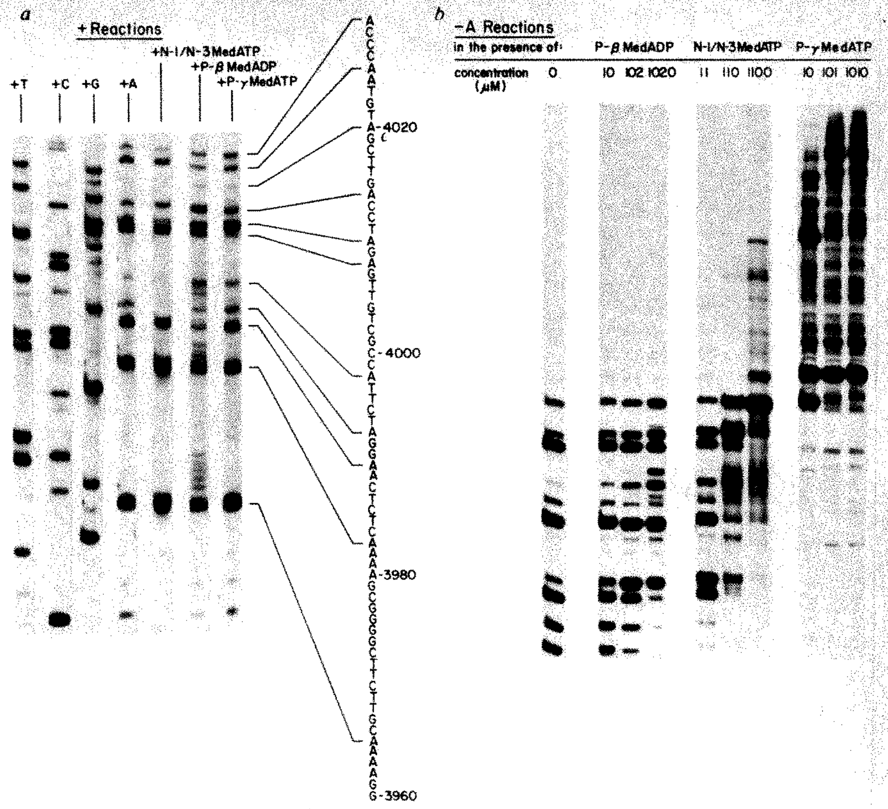

Fig. 3 Incorporation properties of products from the reaction of MNU with dATP during: *a*, plus and *b*, minus reactions. The template-primer is a synthetic oligodeoxyribonucleotide (P-L Biochemicals) complementary to positions 3,466 to 3,477 (pCAATAAACCAGC) of the pBR322 insert of R208, a pBR322/f1 chimaera[21], annealed to R208 ssDNA. The replicating daughter-strand sequence shown agrees with the published sequence for pBR322 (ref. 22). Reaction conditions are as described in Fig. 2 legend. *a*, Plus reactions: the concentrations of modified precursors were all 1.0 mM. All three products incorporated as dATP, as shown by the appearance of bands corresponding to A sites in the sequence (denoted by lines connecting bands with sequence sites). On further purification of the products, mP$^{\beta}$-dADP(P-βMedAP) lost its ability to incorporate. The other repurified products continued to incorporate as dATP, however, making the diphosphate analogue a good control against dATP contamination. These further purified products were used in minus reactions. *b*, The template-primer and reaction conditions were the same as for *a*. Note the increased shifting of bands to higher positions in the gels as you proceed from the control gel slot on the left to the highest concentration of mP$^{\gamma}$-dATP(P-γMedATP) at the extreme right. This shifting of bands indicates incorporation into DNA opposite T template residues.

residues at the replication fork, may offer a direct explanation for the S-phase dependence of both mutation[14] and neoplastic transformation[15] of cells in culture and of the chromosome replication point specificity of alkylating agents in bacteria[16,17].

This work was supported by USPHS grants to M.D.T. (GM 24798 and CA 28632), C.A.H. (GM 21313 and AI 08998) and M.S.B. (predoctoral training grant ES 07017).

Received 5 May; accepted 19 June 1982.

1. Topal, M. D. & Baker, M. S. *Proc. natn. Acad. Sci. U.S.A.* **79,** 2211–2215 (1982).
2. Shapiro, R., Braverman, B., Louis, J. B. & Servis, R. B. *J. biol. Chem.* **248,** 4060–4064 (1973).
3. Cramer, F. *Prog. Nucleic Acid Res. molec. Biol.* **11,** 391–421 (1973).
4. Kolchinsky, A. M., Mirzabekov, A. D., Gilbert, W. & Li, L. *Nucleic Acids Res.* **3,** 11–18 (1976).
5. Rajalakshmi, S., Rao, P. M. & Sarma, D. S. R. *Biochemistry* **17,** 4515–4518 (1978).
6. Moses, H. L., Webster, R. A., Martin, G. D. & Spelsberg, T. C. *Cancer Res.* **36,** 2905–2910 (1976).
7. Ramanathon, R., Rajalakshmi, S., Sarma, D. S. R. & Farber, E. *Cancer Res.* **36,** 2073–2079 (1976).
8. Bailey, G. S., Nixon, J. E., Hendricks, J. D., Sinnhuber, R. O. & Van Holde, K. E. *Biochemistry* **19,** 5836–5842 (1980).
9. Sanger, F. & Coulson, A. R. J. *J. molec. Biol.* **94,** 441–448 (1975).
10. Kochetkov, N. K. & Budowsky, E. I. *Prog. Nucleic. Acid. Res. molec. Biol.* **9,** 403–438 (1969).
11. Muller, W., Weber, H., Meyer, F. & Weissman, C. *J. molec. Biol.* **124,** 343–358 (1978).
12. Topal, M. D., Hutchinson, C. A. III, Baker, M. S. & Harris, C. *ICN-UCLA Symp. molec. cell. Biol.* **19,** 725–734 (1980).
13. Kroger, M. & Singer, B. *Biochemistry* **18,** 3493–3500 (1979).
14. Tong, C., Fazio, M. & Williams, G. M. *Proc. natn. Acad. Sci. U.S.A.* **77,** 7377–7379 (1980).
15. Grisham, J. W., Greenberg, D. S., Kaufman, D. G. & Smith, G. *Proc. natn. Acad. Sci. U.S.A.* **77,** 4813–4817 (1980).
16. Cerda-Olmeda, E., Hanawalt, P. C. & Guerola, N. *J. molec. Biol.* **33,** 705–719 (1968).
17. Hince, T. A. & Neale, S. *Mutat. Res.* **24,** 383–387 (1974).
18. Sanger, F. *et al. J. molec. Biol.* **125,** 225–246 (1978).
19. Budowsky, E. J., Shibaeva, R. P., Sverdlov, E. D. & Monastyrskaya, G. S. *Molec. Biol. USSR* **2,** 321–328 (1968).
20. Lautenberger, J. A. *et al. Proc. natn. Acad. Sci. U.S.A.* **75,** 2271–2275 (1978).
21. Boeke, J. D., Vovis, G. F. & Zinder, N. D. *Proc. natn. Acad. Sci. U.S.A.* **76,** 2699–2702 (1979).
22. Sutcliffe, J. G. *Cold Spring Harb. Symp. quant. Biol.* **43,** 77–90 (1979).

Antifreeze effect of thermal hysteresis agents protects highly supercooled insects

Karl Erik Zachariassen & Jon Arve Husby

Department of Zoology, University of Trondheim, 7055 Dragvoll, Norway

Insects that are cold-hardy but sensitive to freezing survive at low temperatures due to their capacity for supercooling—their supercooling points are below −25 °C. In addition to polyols, these insects produce proteinaceous thermal hysteresis antifreeze agents reported to prevent growth of ice crystals down to ~−10 °C, thus stabilizing the supercooled insects down to this temperature[1,2]. We report here that in the beetle *Rhagium inquisitor* the ability of thermal hysteresis agents to prevent growth of ice crystals increases substantially when the crystal size is diminished. Thus, supercooled insects may be protected against growth of embryo ice crystals over their whole supercooling range, that is, they may be protected against freezing even during prolonged exposures to temperatures as low as −30 °C. The present observations are in accord with the prevalent theories for the action of antifreeze agents.

Thermal hysteresis factors (THF) have been found in polar fish[3,4], molluscs[5] and insects[1,2]. They appear to act by causing a separation of melting point and freezing point (thermal hysteresis) of frozen samples of body fluid, so that ice crystals are prevented from growing on cooling until a temperature several degrees below the melting point is reached. At this temperature (the freezing point) a rapid growth of ice crystals is observed. Thermal hysteresis factors are present in cold-hardy freeze-sensitive beetles of many species, giving their body fluid freezing points down to ~−10 °C. However, all these beetles have supercooling points below −20 °C, suggesting that THF are of no protective value to the insects in the critical, highly supercooled state.

Preliminary experiments revealed that diminution of ice crystals was accompanied by a more pronounced thermal hysteresis effect. To investigate the exact relationship between ice crystal size and thermal hysteresis, experiments were done on haemolymph from cold-hardy freeze-sensitive cerambycid beetles, *R. inquisitor*. These beetles hibernate at the adult stage and incorporate accumulated glycerol and THF, thus depressing body fluid melting points to below −5 °C and supercooling points of intact animals to below −25 °C. Our experiments revealed (Fig. 1*a*) that there is a linear relationship between the freezing points and the logarithm of the ice crystal size over the whole range of the measurements, the freezing point corresponding to the smallest ice crystal tested being about −9 °C.

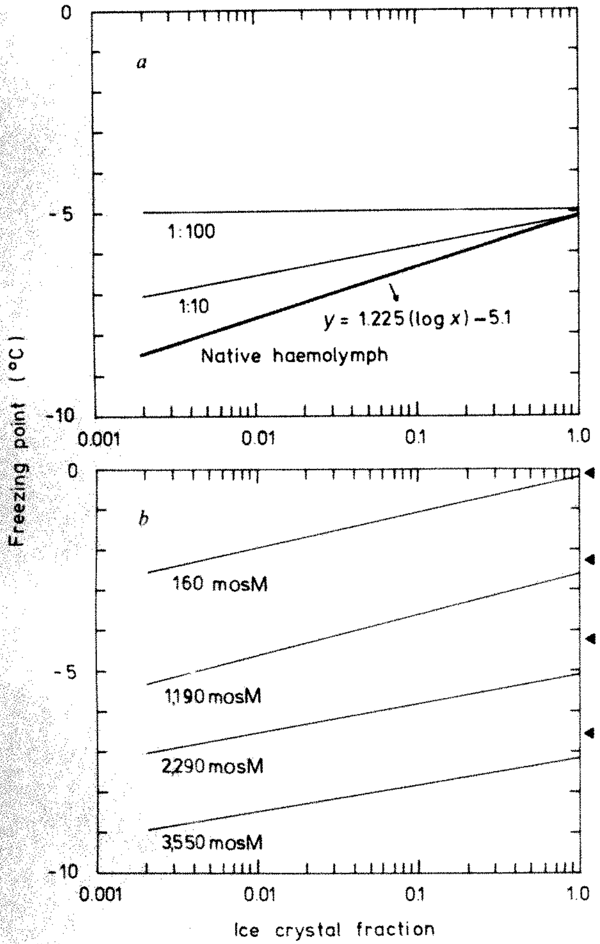

Fig. 1 *a*, Freezing point of native haemolymph of *R. inquisitor* beetles (thick line) and of haemolymph diluted 10-fold and 100-fold in isosmotic (2,290 mosM) glycerol solution (thin lines) as a function of ice crystal size. *b*, Freezing points of haemolymph of *R. inquisitor* beetles diluted 10-fold in four different concentrations of glycerol solution as a function of ice crystal size. The crystal size is expressed as the ice crystal fraction of the whole (2 nl) fluid sample. Assuming that the osmotic coefficients remain constant during freezing, the fraction of unfrozen water in a partly frozen sample is given by t_m/t_i, where t_m is the melting point of the fluid sample and t_i the temperature at which the ice crystal is stabilized. Thus, the ice crystal fraction has been calculated as $1 - t_m/t_i$. The linear regression lines were each calculated from ~75 individual points. The correlation coefficients range from 0.53 to 0.77, and the s.d. about the regression lines is about ±0.6 °C; the comparatively large s.d. may, at least in part, be due to the fact that the ice crystals were not ideal spheres. The experiments were carried out with a Clifton nanolitre osmometer, where 2 nl fluid samples could be observed through a microscope, while the temperature was regulated to within ±0.001 °C between 0 °C and −9.5 °C. The beetles were collected in the vicinity of Trondheim in January 1981. The dilutions were carried out with the haemolymph and glycerol solutions sandwiched between two layers of paraffin oil inside glass capillaries. Fluid was transferred between the capillaries and to the osmometer by means of a microsyringe.

Even the smallest ice crystal used in these experiments was large compared with the aggregates of water molecules present in the body fluid of a highly supercooled insect. Figure 1*a* indicates that the freezing points will continue to decrease with further diminution of the ice crystal. Hence, THF may be able to prevent ice crystal growth and thus stabilize supercooled insects at considerably lower temperatures than those tested experimentally. Unfortunately, the available techniques for temperature control do not allow stabilization of ice crystals at a smaller size. However, some information can be obtained by extrapolating the regression line representing pure haemolymph in Fig. 1 to smaller crystal sizes. The haemolymph used in the experiment was 2,290 mosM. *R. inquisitor* beetles with this haemolymph osmolality have supercooling points of ~−25 °C (ref. 6). Extrapolation of the regression line to this temperature reveals that the corresponding ice crystal fraction is $\sim -10^{-16}$, that is, an ice crystal radius of 3.6×10^{-17} mm (fluid sample volume = 2 nl). According to Chalmers[7], the critical crystal radius for nucleation by embryo ice crystals at −25 °C is 1.5×10^{-16} mm. The aggregations of water molecules in a supercooled insect are probably smaller than this critical size. The extrapolated regression line indicates that THF have the ability to prevent growth of embryo ice crystals of this size. Thus, THF seem to have considerably more efficient antifreeze effects at low temperatures than previously thought. They may in fact be able to stabilize supercooled insects over their whole supercooling range. Thus, the presence of THF probably explains why many hibernating insects can endure exposure to extreme cold for long periods without freezing.

The influence of varying concentrations of THF on the thermal hysteresis was investigated in another series of experiments, in which the concentration of THF was varied by diluting *R. inquisitor* haemolymph 10-fold and 100-fold in isosmotic (2,290 mosM) glycerol solution. These studies revealed (Fig. 1*a*) that even after 10-fold dilution there was still a pronounced thermal hysteresis effect, but this was absent following 100-fold dilution. Seasonal variations in the levels of THF may influence the freezing points in accordance with the varying slopes of the regression lines in Fig. 1*a*.

The fact that a pronounced thermal hysteresis was still present after 10-fold dilution of the haemolymph was used to investigate the relationship between glycerol concentration and thermal hysteresis (Fig. 1*b*). The results reveal that increasing glycerol concentrations cause a parallel displacement of the regression lines to lower freezing points, the freezing point depressions being greater than the corresponding melting point depressions. Thus, glycerol seems to act by extending the temperature range within which the THF performs its stabilizing antifreeze effect.

As THF appear to be unable to mask the effect of ice nucleating agents[8], their antifreeze function at very low temperatures is restricted to insects which have no nucleating agents in their body fluids[6,9,10].

The present results are in agreement with the model proposed by Raymond and DeVries[11,12] to describe the mechanism of the THF antifreeze effect. This model is based on the assumption that THF molecules are adsorbed to the ice crystal surface, thus confining ice growth to the spaces between adjacent THF molecules. The resulting increase in ice front curvature will displace ice growth to lower temperatures. When the ice crystal size is diminished as in the present experiments, more THF molecules may be adsorbed per unit ice surface area. The subsequent increase in ice front curvature will therefore cause a further decrease in the freezing points, as observed.

Received 8 April; accepted 1 July 1982.

1. Duman, J. G. *J. Insect Physiol.* **25,** 805–810 (1979).
2. Husby, J. A. & Zachariassen, K. E. *Experientia* **36,** 963–964 (1980).
3. DeVries, A. L. *Science* **172,** 1152–1155 (1971).
4. DeVries, A. L., Komatsu, S. K. & Feeney, R. E. *J. biol. Chem.* **245,** 2901–2908 (1970).
5. Theede, H., Schneppenheim, R. & Beress, L. *Mar. Biol.* **36,** 183–186 (1976).
6. Zachariassen, K. E. *J. comp. Physiol.* **140,** 227–234 (1980).
7. Chalmers, B. *Scient. Am.* **200** (2), 114–122 (1959).
8. Baust, J. G. & Zachariassen, K. E. *Cryo. Lett.* (submitted).
9. Zachariassen, K. E. & Hammel, H. T. *Nature* **262,** 285–287 (1976).
10. Sømme, L. & Conradi-Larsen, E. M. *Oikos* **29,** 118–126 (1977).
11. Raymond, J. A. & DeVries, A. L. *Proc. natn. Acad. Sci. U.S.A.* **74,** 2589–2693 (1977).
12. DeVries, A. L. in *Animals and Environmental Fitness* (ed. Gilles, R.) 583–607 (Pergamon, Oxford and New York, 1980).

E. coli F_1-ATPase interacts with a membrane protein component of a proton channel

John E. Walker, Matti Saraste & Nicholas J. Gay

Laboratory of Molecular Biology, MRC Centre, Hills Road,
Cambridge CB2 2QH, UK

The ATP synthases of bacteria, mitochondria and chloroplasts, which use the energy of a transmembrane proton gradient to power the synthesis of ATP, consist of an integral membrane component F_0—thought to contain a proton channel—and a catalytic component, F_1. To help investigate the way F_0 and F_1 are coupled, we have sequenced the b-subunit of the *Escherichia coli* F_0, which seems to be the counterpart of a thermophilic bacteria F_0 subunit thought to be essential for F_1 binding[1]. We report here that its sequence is remarkable, being hydrophobic around the N-terminus and highly charged in the remainder. We propose that the N-terminal segment lies in the membrane and the rest outside. The extramembranous section contains two adjacent stretches of 31 amino acids where the sequence is very similar: in the second of these stretches there is further internal homology. These duplicated stretches of the polypeptide probably fold into two α-helices which have many common features able to make contact with F_1 subunits. Thus protein b occupies a central position in the enzyme, where it may be involved in proton translocation. It is possibly also important in biosynthetic assembly.

The organization of the genes coding for ATP-synthase subunits in the *unc* operon is shown in Fig. 1. The three genes for F_0 polypeptides a, c and b are grouped together at the promoter-proximal end and are followed by the five F_1 genes. Gene b encodes a protein of molecular weight 17,212, which is not modified by post-translational processing[2]. The amino acid sequence of this product (Fig. 2) falls into two distinct parts. With the exception of single threonine and cysteine residues and one charged residue, Lys 23, residues 1–33 are hydrophobic. It is proposed that this section of the protein forms a single transmembrane α-helix (see below). Other transmembrane α-helices in bacteriorhodopsin also contain buried threonine residues[3]. The hydroxyl group can form a hydrogen bond with the main-chain polypeptide backbone, as can the thiol of cysteine. Buried charges are also proposed in bacteriorhodopsin but in protein b the side chain of Lys 23 could be near the membrane surface. In contrast, the rest of the sequence of protein b is highly polar, containing 26 basic and 26 acidic residues; this charged section of the protein has internal repeats (Fig. 3). Thus, residues 52–82 are homologous with residues 85–105 (Fig. 4). In addition, within the latter but not the former sequence, a shorter repeat is found, residues 85–99 being homologous to residues 100–115. It is of particular interest that the residues identical in the short repeat consist largely of those that are not conserved (10/14) in the long repeat (see Fig. 4). Thus it seems that part of the charged segment arose by duplication of a 31-amino acid stretch which itself was formed in an earlier event involving duplication of 15 amino acids.

Further information about the structure of protein b can be obtained from the secondary structure predicted from the amino acid sequence (Fig. 1). It is highly probable (probability >0.6) that the protein is almost entirely α-helical. Breaks in α-helices may occur at three points, around residues 27–28 (Pro–Pro), 83–86 (between the long repeats) and near residue 136. A weakening of α-helicity is also noted at residues 43–44. Thus the structure of the protein breaks down into two clear α-helical domains, the first of which (residues 1–20) is highly hydrophobic and could yield an α-helix spanning the membrane once. This helix presumably makes hydrophobic interactions with a and c, the two other constituents of F_0. It is hinged to the second highly charged region by residues 21–28, including the sequence Pro–Pro. The highly charged region appears to consist of at least two connected α-helices, with related sequences, and presumably presenting α-helical surfaces with many identical features able to interact with F_1 subunits. A clue to the nature of the interactions between the proposed α-helical structure of b and F_1 comes from a study of observed helix–helix interactions in proteins[4], which showed that Ala, Val, Leu, Ile and Phe constitute 50% of all residues involved in these interactions, and Asn, Gln, Glu, Asp, Lys and Arg a further 25%, in contrast to the residues involved in helix–α-sheet interactions[5]. The proposed extramembranous α-helical region of b consists mainly of Ala, Val, Leu and Ile (44%) and acidic and basic amino acids (39%). Thus, if the rules of protein–protein interactions are the same as found in proteins to date, it seems likely

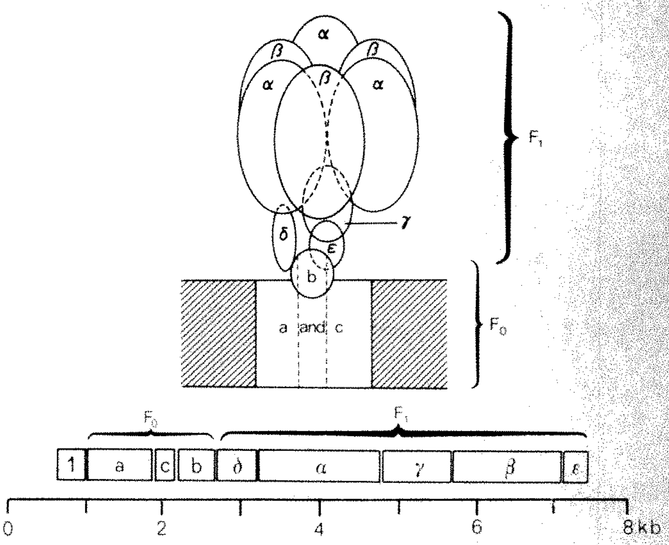

Fig. 1 Organization of polypeptides in the ATP-synthase complex and of their corresponding genes in the *unc* operon. The enzyme (upper panel) is bound to the inner membrane of *E. coli*. F_1 protrudes into the cytoplasm and is depicted with alternating α- and β-subunits although other arrangements have been proposed[13,18]. The hydrophobic F_0 subunits, a and c, are buried in the membrane. It is proposed here that a and c interact with the hydrophobic amino-terminal region of the third F_0 subunit, b. The rest of b is very polar and lies outside the lipid bilayer, making helix–helix contacts with the δ and ε subunits thus binding F_1 to the membrane. All three F_0 subunits are required to make a transmembrane proton channel (dotted line) linking the membrane proton potential to ATP synthesis in F_1. The genes encoding the ATP-synthase subunits are organized in the *unc* operon as shown in the lower panel. The order of genes was determined by DNA sequence analysis[16,19,20]. Gene a was identified by homology with mitochondrial ATPase-6 genes[21], c from total amino acid sequence[22]; b and δ from their molecular weight and charge[16] and N-terminal sequences[2]; α, γ, β and ε by sequence analysis of the *E. coli* proteins[23] and, in the case of α and β also from highly homologous beef proteins (M. J. Runswick, V. L. J. Tybulewicz and J.W., unpublished work). The presence of an active promoter preceding gene 1 and the transcription start point have been established by experiments *in vitro* (N.J.G., unpublished work). Parts of the sequence corresponding to genes a, c, b, δ and α have also been sequenced independently[2,24–26]. Gene 1 does not encode a structural protein of ATP-synthase, but may be involved in regulation of assembly[16].

that the interactions of b with F_1 proteins will be predominantly helix–helix.

The binding of F_1 to F_0 is mediated by δ and ε subunits[6–9]. In thermophile PS3 enzyme, which is very similar to the *E. coli* enzyme[10], both are required to bind the $\alpha\beta\gamma$ subcomplex to F_0 (ref. 7). Smith and Sternweis showed also that in *E. coli*, δ is involved in attachment of F_1 to F_0 (ref. 7). The δ protein in particular could make helix–helix interactions with b; it has a high α-helical content (65%) as estimated by circular dichroism spectroscopy of the PS3 protein[11]. In the same study ε and γ were estimated to contain 33% and 49% α-helix respectively, in general agreement with α-helix contents of 83%, 31% and 67% for δ, ε and γ, respectively, derived from secondary structures predicted from the *E. coli* protein sequences (J.W. and M.S., unpublished work).

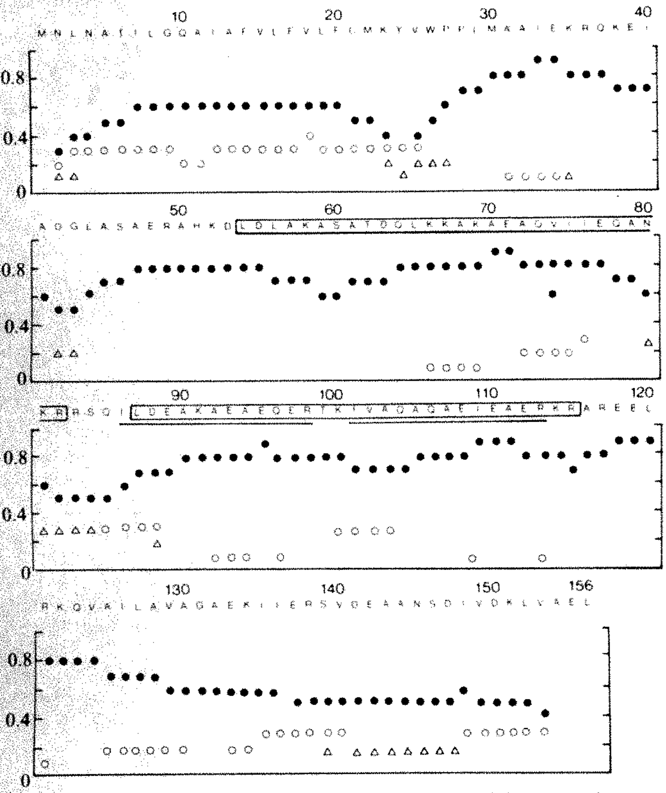

Fig. 2 Amino acid sequence of subunit b, and its secondary structure, predicted from the primary sequence using a program described by McLachlan[27]. The graphs beneath the sequence show probabilities (ordinate scale) of residues forming an α-helix (●), β-sheet (○) or β-bend (△). Boxed sequences represent related sequences (the long repeat); underlined segments are also related to each other (the short repeat, see Fig. 4).

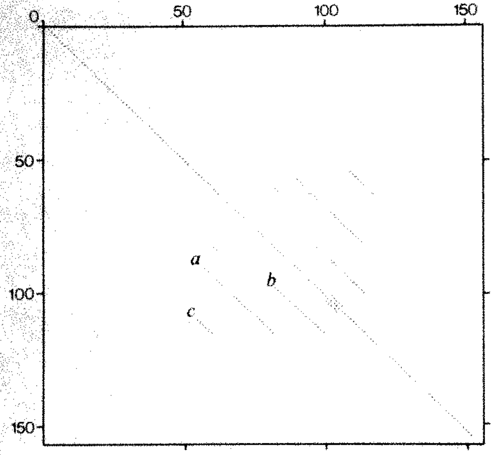

Fig. 3 Matrix of comparison of b with itself, performed with the interactive computer program DIAGON (R. Staden, unpublished work) adapted from earlier procedures[28]. Scoring is based on a mutation matrix calculated from observed changes in homologous proteins. The scoring level in the matrix shown corresponds to a double matching probability of 1.2×10^{-3}, that is, in a random sequence of the same composition only about one sequence in a thousand should reach this scoring level. The span used in the comparison was 25. Each point (midpoints of the span) has a score less than the 'cutting level'. The diagonal is b aligned with itself; *a* and *b* correspond to the long and short repeats, respectively (see Fig. 4), and *c* corresponds to alignment of residues 57–61 (A K A S A) with residues 103–107 (A Q A Q A), which is probably trivial.

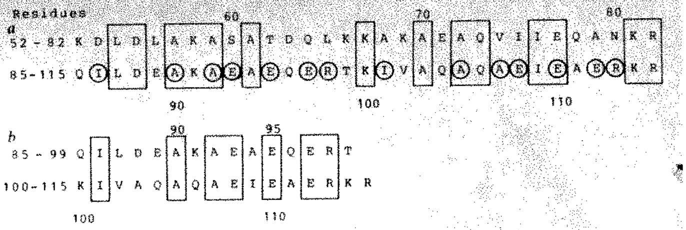
Residues
a
60
70
80
52 - 82 K D L D L A K A S A T D Q L K K A K A E A Q V I I E Q A N K R
85 - 115 Q I L D E A K A E A E Q E R T K I V A Q A Q A E I E A E R K R
90
100
110
b
90
95
85 - 99 Q I L D E A K A E A E Q E R T
100 - 115 K I V A Q A Q A E I E A E R K R
100
110

Fig. 4 Alignment of repeated sequences in protein b. *a*, The long repeats; *b*, the short repeats. Identities are boxed. In *a*, the 14 residues conserved in *b* are encircled; of these four residues are conserved in both *a* and *b*.

The stoichiometry of subunits in F_1 is $3\alpha:3\beta:1\gamma:1\delta:1\varepsilon$[12] with an estimated one or two copies of b per enzyme complex[13]. Thus it remains unclear whether two or four roughly equivalent α-helical segments in b are available in each F_0 to bind F_1, also how many complementary α-helices would be required in δ and ε.

As it occupies a central position providing an important structural link between the membrane and F_1, it seems likely that b will be involved directly in proton translocation with some of its charged residues contributing to the process. This is supported by the finding that mutants in b have drastically reduced proton translocation[1]. The γ-subunit has also been proposed to participate in this process by gating the proton channel[14]. Like protein b it appears to interact with δ and ε although not directly with F_0[9,14] and therefore not with b.

Biosynthetic assembly of ATP-synthase is poorly understood. It is clearly desirable to assemble the enzyme in a controlled manner to avoid open H^+ channels. Open H^+ channels would 'de-energize' the membrane leading to breakdown of several essential functions driven by the membrane proton potential[15]. The location of b in the enzyme complex, the *in vitro* assembly of F_1 from subunits and reassociation of F_1 and F_0 suggest that b will be important here also. In addition, the order of genes in the *unc* operon (Fig. 1) is striking: the genes for the hydrophobic components of F_0 (a and c) are followed by the gene for protein b, and then those for F_1, suggesting that insertion of F_0 polypeptides may occur early in assembly. This notion is not in accord with a study of *unc* mutants by Cox *et al.*[15], who proposed that α and β must bind to membranes containing a and c before b can enter the lipid bilayer to complete F_0 (although b was not shown to be present in the cytoplasm of these mutants). However, these studies did not take account of gene 1 (Fig. 1) which may encode a pilot protein to regulate the assembly process[16]. Indeed, identification of the role of this gene may be the key to understanding assembly of bacterial ATP-synthase.

Recently Hoppe *et al.*[17] have reported that *E. coli* protein b in F_1-depleted membranes is very sensitive to proteolytic degradation. Also F_1 protects b in these membranes from proteolysis. Additionally a photoactive hydrophobic phospholipid derivatives reacts with Cys-21. These experiments strongly support the structure of b proposed above.

We thank A. D. McLachlan and R. Staden for help with computer analyses and R. Hendersen and J. Deatherage for helpful comments. M.S. is supported by an EMBO fellowship and N.J.G. by an MRC studentship.

Received 29 March; accepted 22 June 1982.

1. Friedl, P., Bienhaus, G., Hoppe, J. & Schairer, H. U. *Proc. natn. Acad. Sci. U.S.A.* **78**, 6643–6646 (1981).

2. Nielsen, J., Hansen, F. G., Hoppe, J., Friedl, P. & Meyenberg, K. *Molec. gen. Genet.* **184,** 33–39 (1981).
3. Engleman, D. M., Hendersen, R., McLachlan, A. D. & Wallace, B. A. *Proc. natn. Acad. Sci. U.S.A.* **77,** 2023–2027 (1980).
4. Chothia, C., Levitt, M. & Richardson, D. *J. molec. Biol.* **145,** 215–250 (1981).
5. Janin, J. & Chothia, C. *J. molec. Biol.* **143,** 95–128 (1980).
6. Futai, M., Sternweis, P. C. & Heppel, L. A. *Proc. natn. Acad. Sci. U.S.A.* **71,** 2725–2729 (1974).
7. Smith, J. B. & Sternweis, P. C. *Biochemistry* **16,** 306–311 (1977).
8. Yoshida, M., Okamoto, H., Sone, N., Hirata, H. & Kagawa, Y. *Proc. natn. Acad. Sci. U.S.A.* **74,** 936–940 (1977).
9. Sternweis, P. C. *J. biol. Chem.* **253,** 3123–3128 (1978).
10. Takeda, K. *et al. J. Biochem., Tokyo* **91,** 695–701 (1982).
11. Yoshida, M., Sone, N., Hirata, H., Kagawa, Y. & Ui, N. *J. biol. Chem.* **254,** 9525–9533 (1979).
12. Bragg, P. D. & Hou, C. *Archs Biochem. Biophys.* **167,** 311–321 (1975).
13. Fillingame, R. H. *Curr. Topics Bioenerget.* **11,** 35–106 (1981).
14. Sone, N., Yoshida, M., Hirata, H. & Kagawa, Y. *Proc. natn. Acad. Sci. U.S.A.* **75,** 4219–4223 (1978).
15. Cox, G. B. *et al. J. Bact.* **148,** 30–42 (1981).
16. Gay, N. J. & Walker, J. E. *Nucleic Acids Res.* **9,** 3919–3926 (1981).
17. Hoppe, J. *et al. Eur. Bioenerget. Conf. Rep.* **2,** 85–86 (1982).
18. Futai, M. & Kanazawa, H. *Curr. Topics Bioenerget.* **10,** 181–215 (1980).
19. Gay, N. J. & Walker, J. E. *Nucleic Acids Res.* **9,** 2187–2194 (1981).
20. Saraste, M., Gay, N. J., Eberle, A., Runswick, M. J. & Walker, J. E. *Nucleic Acids Res.* **9,** 5287–5296 (1981).
21. Anderson, S. *et al. Nature* **290,** 457–465 (1981).
22. Hoppe, J., Schairer, H. U. & Sebald, W. *Eur. J. Biochem.* **112,** 17–24 (1980).
23. Walker, J. E. *et al. Eur. J. Biochem.* **123,** 253–260 (1982).
24. Kanazawa, H., Mabuchi, K., Kayano, T., Tamura, F. & Futai, M. *Biochem. biophys. Res. Commun.* **100,** 219–225 (1981).
25. Mabuchi, K., Kanazawa, H., Kayano, T. & Futai, M. *Biochem. biophys. Res. Commun.* **102,** 172–179 (1981).
26. Tamura, F., Kanazawa, H., Tsuchiya, T. & Futai, M. *FEBS Lett.* **127,** 48–52 (1981).
27. McLachlan, A. D. *Int. J. Quantum Chem.* **12,** Suppl. 1, 371–385 (1977).
28. McLachlan, A. D. *J. molec. Biol.* **61,** 409–524 (1971).

Evidence for hydrogen bonding of bound dioxygen to the distal histidine of oxycobalt myoglobin and haemoglobin

T. Kitagawa,* M. R. Ondrias† & D. L. Rousseau
Bell Laboratories, Murray Hill, New Jersey 07974, USA

M. Ikeda-Saito & T. Yonetani
Department of Biochemistry and Biophysics,
University of Pennsylvania School of Medicine,
Philadelphia, Pennsylvania 19104, USA

The origin of the differences in oxygen binding energy in various haemoglobins and myoglobins has long been debated. Perutz[1] proposed that the haem-coordinated histidine (proximal histidine) strains the haem iron in low affinity globins but relaxes it in high affinity globins. The existence of such tension in T-structure deoxyhaemoglobin (deoxyHb) was recently confirmed by electron paramagnetic resonance (EPR)[2,3], resonance Raman[4,5] and NMR[6] spectroscopy. Although its contribution to the free energy of cooperativity is insignificant in the deoxy state, the tension at the haem is considered to be ~1 kcal mol^{-1} for the ligated form in which the haem iron moves into the porphyrin plane[7]. The remaining free energy is probably stored in other parts of the molecule. Therefore, a study of the stabilization mechanisms of the oxygenated form became increasingly important. A hydrogen bond between the bound oxygen and the distal histidine has been proposed by Pauling[8]; this would be expected to stabilize the oxy form of the protein and could contribute to the regulation of the oxygen affinity through the oxygen dissociation rate. A series of EPR and functional studies on various cobalt-substituted monomeric haemoglobins and myoglobins suggested the presence of such hydrogen bonding[8–12] and it has recently been established in crystals of oxy iron myoglobin (oxyFeMb)[13] and in oxyhaemoglobin[14]. Here we present resonance Raman spectra of the oxy forms of cobalt–porphyrin-substituted myoglobin and haemoglobin (CoMb and CoHb) recorded in buffered H_2O and D_2O solutions at 406.7 nm excitation. Only the Raman lines corresponding to the O—O stretching mode of the bound oxygen[15], appearing near 1,130 cm^{-1}, are shifted (2–5 cm^{-1}) on replacement of H_2O by D_2O; no other vibrations, including the Co—O_2 stretching mode, exhibit any frequency shifts. This indicates that the bound oxygen in oxyCoMb and in both subunits of oxyCoHb interacts with the adjacent exchangeable proton, and confirms the formation of a hydrogen bond between the bound oxygen and the distal histidine[9].

The IR active vibrational frequencies of the bound dioxygen stretching modes in haemoglobin have been detected in the 1,100–1,160 cm^{-1} frequency range[16]. Resonance Raman spectroscopy probes the vibrational frequencies of the porphyrin chromophore and electronically associated ligands. Tsubaki and Yu[15] demonstrated by $^{16}O_2$–$^{18}O_2$ isotopic substitutions, that the dioxygen stretching mode of the bound oxygen of oxyCoMb and oxyCoHb, located near 1,130 cm^{-1}, was resonance-enhanced on excitation at 406.7 nm (ref. 15). In contrast, the spectra of oxyFeMb and oxyFeHb revealed no oxygen isotope-dependent frequencies in this region. Tsubaki and Yu[15] proposed that the dioxygen stretching mode is enhanced by coupling to a charge transfer transition in the cobalt-substituted haem that is absent from the iron haem. The O—O stretching frequency should be a sensitive probe of hydrogen bonding to the dioxygen molecule, therefore we investigated the frequency of the O—O stretching mode of oxyCoMb and oxyCoHb on deuterium substitution of the exchangeable protons.

CoMb, CoHb and iron–cobalt hybrid haemoglobins ($\alpha(Fe)_2\beta(Co)_2$ and $\alpha(Co)_2\beta(Fe)_2$) were prepared as described previously[2,17] and oxygenated in 50 mM Tris-HCl buffer *p*H (or *p*D) 9.0, except for the *p*H variation studies. The Raman spectra were recorded using the difference spectrometer described previously[18], the accuracy of the detected difference in the frequency was ~0.2 cm^{-1} and that of the absolute frequency ~ ±1 cm^{-1}.

Typical H_2O–D_2O difference spectra for oxyCoHb and oxyCoMb in the 1,000–1,250 cm^{-1} region are shown in Fig. 1*a*, *b*. The spectrum of oxyCoHb in H_2O (Fig. 1*b*) is in agreement with the reported spectrum in which Raman lines near 1,133 and 1,146 cm^{-1} were found to be $^{18}O_2$ isotope-sensitive[15]. These two lines show no frequency shift between *p*H 5.3 and 10.4. On replacing the H_2O by D_2O, however, the 1,133 cm^{-1} component exhibits a frequency shift of 5 cm^{-1} to 1,138 cm^{-1} (Fig. 1*b*). There may be a shift in the 1,146 cm^{-1} line also (see the difference spectrum) but its magnitude is obscured by the shift of the more intense line. In contrast to this behaviour in the cobalt haemoglobin, no frequency differences were detected on deuteration of iron haemoglobin. This was expected as the only Raman-active modes in the 1,050–1,150 cm^{-1} region of oxyFeHb, are porphyrin modes. Thus, the hydrogen bonding is probably present in the iron haems also but it is not spectroscopically detectable in our conditions. Figure 1*a* shows the spectra of oxyCoMb in which the H_2O–D_2O shift is from 1,134 to 1,136 cm^{-1}. In oxyCoMb the higher frequency component (~1,146 cm^{-1}) has been shown to be weaker than in oxyCoHb[15], thus obscuring any possible shift in frequency in this line.

The iron–cobalt hybrid haemoglobins were also examined. The absence of any H_2O–D_2O dependence in oxyFeHb allows determination of the relative contributions from the individual subunits in the hybrids as any shift must result from the cobalt subunit. The size of the shift and shape of the line on deuteration in the α- and β-subunits are depicted in Fig. 1*c*, *d*. The α-subunit gave a smaller shift (2 cm^{-1}) than the β-subunits (4 cm^{-1}). The magnitude of shift for each subunit was less than that of fully cobalt-substituted oxyHb. This is expected as the presence of Raman modes from the iron subunits of the hybrids that do not shift in this frequency region should dilute the contribution from the cobalt subunits. The frequency difference between the $\alpha(Fe)_2\beta(Co)_2$ and $\alpha(Co)_2\beta(Fe)_2$ oxyHbs, both in H_2O, is small. Therefore the frequency difference that we observe between the α- and β-subunits occurs in the deuterated form. A shape difference in this mode between the subunits is also noted in the deuterated form; the 1,136 cm^{-1} line of the

---

* Permanent address: Department of Molecular and Physiological Chemistry, Osaka University Medical School, 2-7 Daigakumachi, Osaka, Japan.

†Present address: Department of Chemistry, University of New Mexico, Albuquerque, New Mexico 87131.

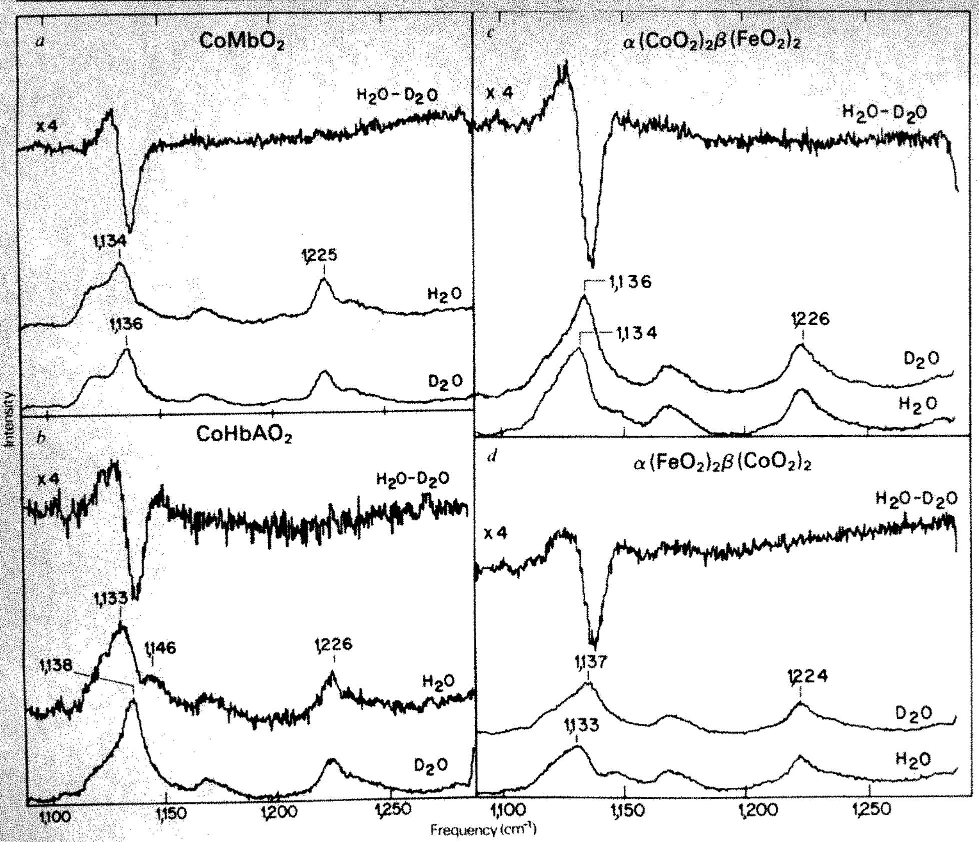

Fig. 1 Resonance Raman spectra of *a*, oxyCoMb; *b*, oxyCoHb; *c*, oxy $\alpha(Co)_2\beta(Fe)_2$; and *d*, oxy $\alpha(Fe)_2\beta(Co)_2$ in H_2O and D_2O. In each case the difference spectrum is plotted at the top with a sensitivity four times as high as the individual spectra. Excitation frequency 406.7 nm, laser power ~100 mW, spectral slit width ~4 cm^{-1}.

$\alpha(Co)_2\beta(Fe)_2$ oxygenated hybrid is narrower than that of the complementary hybrid.

Figure 2 shows the H_2O-D_2O difference spectrum of oxyCoMb in the Co—O_2 stretching region. The Raman line of oxyCoMb at 538 cm^{-1} was assigned previously to the Co—O_2 stretching mode[15]. Unexpectedly, this line did not show any frequency difference (<2 cm^{-1}) in the H_2O and D_2O solutions despite the clear shift of the O—O stretching mode.

Deuterium substitution of exchangeable protons of haemoglobin has been reported to stabilize the protein against thermal denaturation and auto-oxidation[19]. Thus, the hydrogen bonding in haemoglobin is presumably stronger in D_2O than in H_2O as expected on the basis of a lower zero point energy. Therefore, a resulting change of tertiary structure due to the deuterium substitution could alter a state of the Co—His (proximal) bond or a degree of charge delocalization between the haem and the bound dioxygen. This seems unlikely, however, because the Fe—His stretching mode of deoxyFeHb is not shifted by more than 1 cm^{-1} on deuterium substitution; nor is any frequency shift detected on deuteration for any of the porphyrin skeletal vibrations of oxyCoHb, and the Co—O_2 mode is unaffected by deuteration. In addition, Phillips and Shoenborn, using neutron diffraction[13], observed no significant difference between the tertiary structures of myoglobin in H_2O and D_2O. Therefore, the differences we have detected in the O—O stretching frequency in D_2O must result from a specific interaction between the oxygen and the apoprotein on the distal side of the haem.

Recently, Phillips and Schoenborn[13] made a direct observation of a hydrogen bond in crystals of oxyFeMb and reported that the N_ϵ—O^2 distance is 2.97 Å. According to a recent X-ray analysis[14] of crystalline oxyFeHb, the N_ϵ—O^2 distance is 2.7 Å and 3.4 Å for the α- and β-subunits, respectively. Furthermore, the N_ϵ—O^2 distance in crystals of oxyCoMb has also been shown to be compatible with hydrogen bonding[20]. The data reported here, obtained in solution, confirm the existence of hydrogen bonds in oxyCoMb and in both subunits of oxyCoHb. It is probable that the entire H_2O—D_2O shift of the O—O stretching frequency is caused by the change from the hydrogen—oxygen bond to the deuterium—oxygen bond. It is also possible, however, that a change in position of the distal histidine due to tertiary structural changes in the protein contributes to our observed frequency differences. The hydrogen bond to the distal histidine is (approximately) perpendicular to the O—O bond axis[13], therefore it seems reasonable that the Co—O_2 stretching frequency is less sensitive to the changes caused by deuteration than the O—O stretching frequency. More information is required to correlate the size and direction

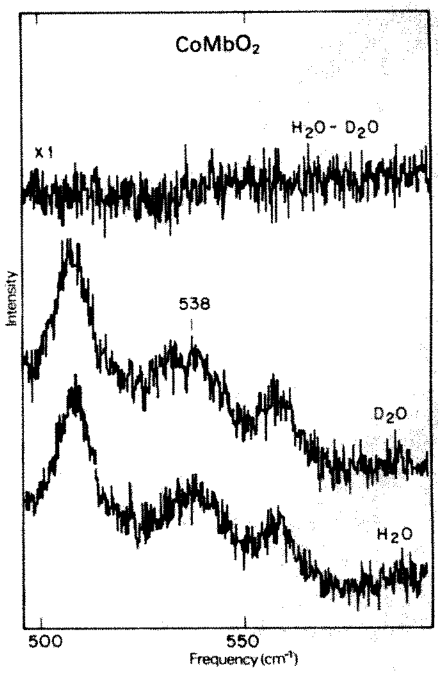

Fig. 2 Resonance Raman spectra of oxyCoMb in the region of the Co—O_2 stretching frequency (538 cm^{-1}). The absence of a significant shift on deuteration in this mode may be seen by examination of the difference spectrum plotted at the top. Excitation frequency 441.6 nm, laser power ~20 mW, spectral slit width ~4 cm^{-1}.

of the frequency shift with the strength of the hydrogen bond or with conformational changes. Analysis of the O—O stretching mode in oxyCoHbs in which a quaternary structure change can be induced should elucidate whether any free energy of cooperativity is localized in the hydrogen bonding interaction.

We thank M. F. Perutz for critically reading the manuscript. The portion of the work done at the University of Pennsylvania was supported by National Heart, Lung and Blood Institute grant HL-14508 and NSF grant PCM79-22841.

Received 31 March; accepted 24 June 1982.

1. Perutz, M. F. *Nature* **228,** 726–734 (1970).
2. Ikeda-Saito, M., Yamamoto, H. & Yonetani, T. *J. biol. Chem.* **252,** 8639–8644 (1977).
3. Inubushi, T., Ikeda-Saito, M. & Yonetani, T. in *Hemoglobin and Oxygen Binding* (ed. Ho, C.) 199–204 (Elsevier, New York, 1982).
4. Nagai, K. & Kitagawa, T. *Proc. natn. Acad. Sci. U.S.A.* **77,** 2033–2037 (1980).
5. Ondrias, M. R., Rousseau, D. L. & Simon, S. R. *Science* **213,** 657–659 (1981).
6. Nagai, K. & LaMar, G. N. *Biochemistry* (in the press).
7. Perutz, M. F. *et al. Biochemistry* **17,** 3640–3661 (1978).
8. Pauling, L. *Nature* **203,** 182–183 (1964).
9. Yonetani, T., Yamamoto, H. & Iizuka, T. *J. biol. Chem.* **249,** 2168–2174 (1974).
10. Ikeda-Saito, M., Iizuka, T., Yamamoto, H., Kayne, T. J. & Yonetani, T. *J. biol. Chem.* **252,** 4882–4887 (1977).
11. Ikeda-Saito, M., Brunori, M. & Yonetani, T. *Biochim. biophys. Acta* **533,** 173–180 (1978).
12. Ikeda-Saito, M., Hori, H., Inbushi, T. & Yonetani, T. *J. biol. Chem.* **256,** 10267–10271 (1981).
13. Phillips, S. V. E. & Schoenborn, B. P. *Nature* **292,** 81–82 (1981).
14. Schaanan, B. *Nature* **296,** 683–684 (1982).
15. Tsubaki, M. & Yu, N. T. *Proc. natn. Acad. Sci. U.S.A.* **78,** 3581–3585 (1981).
16. Barlow, C. H., Maxwell, J. C., Wallace, W. J. & Caughey, W. S. *Biochem. biophys. Res. Commun.* **55,** 91–95 (1973).
17. Yonetani, T., Yamamoto, H. & Woodrow, G. V. *J. biol. Chem.* **249,** 682–690 (1974).
18. Rousseau, D. L. *J. Raman Spectrosc.* **10,** 94–99 (1981).
19. Tomita, S. & Riggs, A. *J. biol. Chem.* **245,** 3104–3109 (1970).
20. Petsko, G. A., Rose, D., Tsernoglou, D., Ikeda-Saito, M. & Yonetani, T. in *Frontiers of Biological Energetics* (eds Dutton, P. L., Leigh, J. S. & Scarpa, A.) 1011–1016 (Academic, New York, 1978).

Myosin phosphorylation, agonist concentration and contraction of tracheal smooth muscle

Primal de Lanerolle, John R. Condit Jr, Mark Tanenbaum & Robert S. Adelstein

Laboratory of Molecular Cardiology, National Heart, Lung and Blood Institute, National Institutes of Health, Bethesda, Maryland 20205, USA

Myosin phosphorylation plays an important part in excitation–contraction coupling in smooth muscle. Phosphorylation by a Ca^{2+}, calmodulin-dependent kinase stimulates the actin-activated Mg^{2+}-ATPase activity of smooth muscle myosin[1–5], suggesting that myosin phosphorylation regulates smooth muscle contraction (see refs 5, 6 for discussions of alternative hypotheses). This hypothesis is supported by evidence that myosin is phosphorylated during contraction and dephosphorylated during relaxation of intact smooth muscles stimulated with a single agonist concentration[7–9]. However, there is little information regarding the response to stimulation with various agonist concentrations. As the dose–response relationships for phosphorylation and tension should be similar if myosin phosphorylation does, in fact, regulate smooth muscle contraction, we studied myosin phosphorylation in tracheal smooth muscle stimulated with a broad range of concentrations of the cholinergic agonist, methacholine. The results of these experiments are consistent with the hypothesis that myosin phosphorylation regulates smooth muscle contraction but they indicate a relatively complex relationship between myosin phosphorylation and the generation of isometric tension.

Canine tracheal smooth muscles were obtained and treated as previously described[8] except that: (1) muscles were maintained in the muscle baths as flat sheets in order to minimize non-uniform rates of agonist diffusion to receptor sites; (2) individual smooth muscle strips were maintained at a length of 2 cm, as defined by their *in vivo* length, from the time they were removed from the cartilaginous rings of the trachea until the end of the experiment; (3) muscle strips were kept in the muscle baths for 45 min before initiating contractile responses.

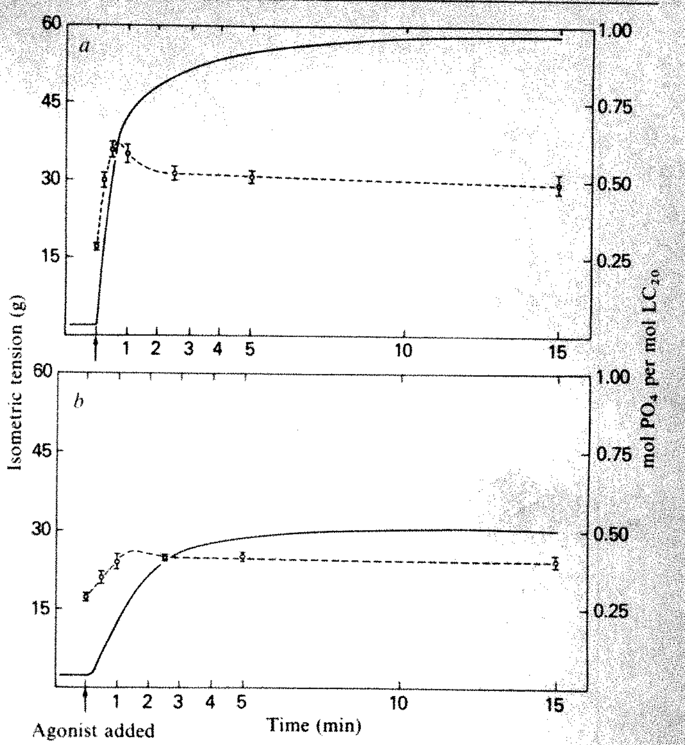

Fig. 1 Myosin phosphorylation and tension generated by tracheal smooth muscle contracted with 10^{-4} M (*a*) or 2×10^{-7} M (*b*) methacholine. Tracheal muscle from six consecutive tracheal rings was isolated and mounted in six myobaths. The data at 15 min in *a* were obtained from separate experiments. The solid lines represent tension generated by representative muscles contracted for 15 min; broken lines represent the phosphate content of muscles frozen at the times indicated. Error bars indicate the s.e.m. for phosphate determinations on at least five different pieces of tissue. Experiments on smooth muscles have demonstrated that a specific subunit of the myosin molecule, with a molecular weight of 20,000 (LC_{20}), is phosphorylated. A maximum of 1 mol PO_4 can be incorporated per mol LC_{20}. As there are 2 mol LC_{20} per mol myosin, the maximal level of myosin phosphorylation is 2 mol PO_4 per mol myosin. We have chosen to present the data as mol PO_4 per mol LC_{20} because this was the experimentally determined value.

The myosin phosphate content was quantitated using an immunoprecipitation–isoelectric focusing method as described previously[8].

Phosphate analyses on resting (unstimulated) tracheal muscle demonstrated 0.29 mol of phosphate incorporated per mol LC_{20}. (LC_{20} is a subunit of myosin—see Fig. 1 legend.) On stimulation with 10^{-4} M methacholine (Fig. 1*a*), the myosin phosphate content rose rapidly, reaching a peak of 0.62 mol PO_4 per mol LC_{20}, before the muscle generated maximal tension. The myosin phosphate content then decreased slightly, while the muscle was still contracting, to a stable level of 0.49 mol PO_4 per mol LC_{20}. Stimulation of tracheal muscle with 2×10^{-7} M methacholine (Fig. 1*b*), a concentration previously determined to produce half-maximal tension, contracted muscles more slowly than stimulation with 10^{-4} M methacholine (maximal rates of contraction were 31 and 129 g min^{-1}, respectively). Myosin was phosphorylated at a much slower rate, and the maximal and steady-state levels of phosphorylation were lower for muscles stimulated with 2×10^{-7} M methacholine (Fig. 1*b*) than for those stimulated with 10^{-4} M methacholine (Fig. 1*a*).

We have also determined the relationship between the steady-state level of myosin phosphorylation, tension and agonist concentration (Fig. 2). Muscles were stimulated with various concentrations of methacholine, then frozen 15 min after addition of the agonist and assayed to determine the myosin phosphate content. (Muscles were frozen at 15 min because the experiments in Fig. 1 indicated that tension and phosphorylation had reached a plateau by 10 min.) Myosin phosphorylation and active tension were expressed as a percentage of the

0028-0836/82/340871-03$01.00

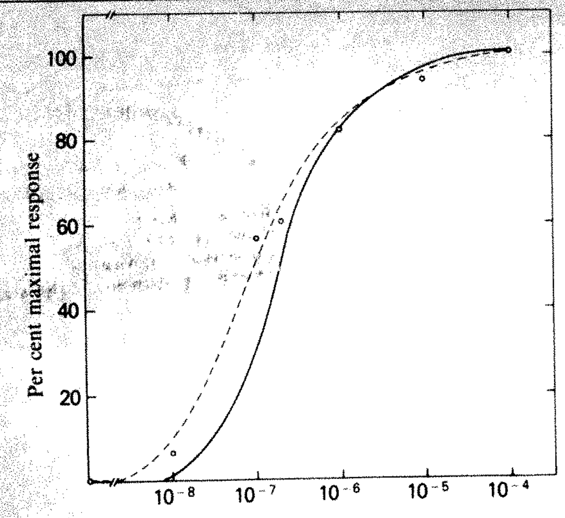

Fig. 2 The dose–response relationship for myosin phosphorylation and isometric tension in tracheal smooth muscle stimulated with methacholine. Myosin phosphorylation was determined on tracheal smooth muscle contracted for 15 min using the agonist concentration shown. The phosphorylation and tension data were expressed as per cent maximal increase using the equation $X - R/M - R$ where X = myosin phosphate content or tension at 15 min of muscles stimulated with various methacholine concentrations; R = the resting phosphate content (29%) or resting tension; and M = the myosin phosphate content (49%) or tension at 15 min of muscles stimulated with 10^{-4} M methacholine. The solid line represents the rise in tension after stimulation at each agonist concentration; the broken line represents the increase in myosin phosphorylation at each agonist concentration. Each point represents the mean from phosphate assays on at least five different pieces of tissue.

maximum (see Fig. 2 legend). These data, plotted as a function of log agonist concentration (Fig. 2), demonstrated similar agonist concentration–response relationships for both phosphorylation and tension. Analysis of variance indicated statistically significant differences ($P < 0.001$) between successive points on each dose–response curve. However, there were no statistically significant differences between the two curves at any given agonist concentration, indicating that the phosphorylation and tension data define superposable curves.

The data on myosin phosphorylation presented here argue against a simple relationship between the processes of myosin phosphorylation and tension generation by tracheal smooth muscle. Three major aspects of the phosphorylation data require comment—the resting myosin phosphate content, the overshoot in myosin phosphorylation and the steady-state level of myosin phosphorylation. Each of these may have a bearing on the manner in which tracheal muscle generates tension and will be discussed separately.

First, it should be noted that a substantial fraction of the myosin (29%) is phosphorylated in unstimulated tracheal smooth muscle. There is a low level of tension (2–5 g) in these muscles but this resting tension seems to be generated by passive elastic elements as a reduction in the myosin phosphate content does not decrease the resting tension[8]. It is possible that a high level of myosin phosphorylation is unique to tracheal smooth muscle because lower levels of myosin phosphorylation have been reported in resting[10,11] and pharmacologically relaxed[12] smooth muscles. Nevertheless, one explanation for this observation is that these represent monophosphorylated myosin molecules. Recent experiments[13] on the relationship between smooth muscle myosin phosphorylation and acto-myosin ATPase activity indicate the apparent requirement that both myosin heads be phosphorylated in order for the myosin to be activated by actin. Thus, it is possible that myosin molecules involved in generating tension in tracheal smooth muscle are monophosphorylated in resting conditions and do not begin to hydrolyse ATP and generate tension until the second head is phosphorylated.

Second, what is the significance of the overshoot in myosin phosphorylation seen in muscles maximally stimulated with methacholine (Fig. 1*a*)? Recent studies on intracellular calcium levels during contraction of smooth muscle cells[14,15] and stimulation of non-muscle cells[16] have demonstrated that intracellular calcium levels rise sharply, peak and then decay after stimulation of these cells. Furthermore, peak levels of intracellular calcium are reached before the smooth muscle cells generate maximal tension. As myosin kinase requires Ca^{2+}-calmodulin for activity[3], the activation of this enzyme probably follows the calcium transient. In fact, the overshoot in myosin phosphorylation may be a reflection of the redistribution of the intracellular calcium levels in response to stimulation of muscarinic receptors[17].

Finally, the most direct relationship between myosin phosphorylation and tension appears to be between the steady-state level of myosin phosphorylation and maximal isometric tension generated at a given agonist concentration. The data in Fig. 2 support this hypothesis as they demonstrate that both myosin phosphorylation and isometric tension are coupled to stimulation of muscarinic receptors. Uncoupling of either process, or a shift in the phosphorylation curve in relation to the tension curve, would have indicated a complex relationship between tension and steady-state myosin phosphorylation. The generation of superposable dose–response curves for phosphorylation and tension suggests that the active isometric tension maintained by tracheal smooth muscle is directly related to the steady-state level of myosin phosphorylation. The data also suggest that the myosin phosphorylation–dephosphorylation reaction can be regulated in tracheal smooth muscle so as to maintain defined levels of phosphorylation which, in turn, seem to determine the tension generated by the muscle.

In contrast to the data presented above, myosin phosphorylation does not remain elevated in hog carotid artery smooth muscle contracted with KCl[10]. In this case the myosin phosphate content decreased to a level slightly above the resting level after the carotid artery muscle had generated maximal tension, which suggested that smooth muscles can maintain tension through the formation of a special, non-cycling acto-myosin cross-bridge, termed a 'latch' bridge[10]. It is possible that latch bridges are formed only when carotid artery smooth muscles are stimulated by KCl, as the myosin phosphate content remains elevated in the same muscles contracted with histamine[11]. Although the presence of latch bridges in smooth muscles contracted with pharmacological agents cannot be discounted, the demonstration that the rise in both tension and myosin phosphorylation is related to the level of agonist stimulation (Fig. 2), and the observation that myosin phosphorylation remains elevated when smooth muscles are stimulated with pharmacological agonists (Fig. 1; and ref. 11), suggest that the steady-state level of myosin phosphorylation may be the major determinant of the tension maintained by a smooth muscle.

Thus, the data presented here support, but do not prove, the hypothesis that myosin phosphorylation regulates muscle contraction, and also demonstrate a relatively complex relationship between myosin phosphorylation and the process of tension generation by tracheal smooth muscle.

Received 13 April; accepted 18 June 1982.

1. Gorecka, A., Aksoy, M. O. & Hartshorne, D. J. *Biochem. biophys. Res. Commun.* **71,** 325–331 (1976).
2. Sobieszek, A. *Eur. J. Biochem.* **73,** 477–483 (1977).
3. Dabrowska, R., Sherry, J. M. F., Aromatorio, D. K. & Hartshorne, D. J. *Biochemistry* **17,** 253–258 (1978).
4. Sellers, J. R., Pato, M. D. & Adelstein, R. S. *J. biol. Chem.* **256,** 13137–13142 (1981).
5. Chacko, S. & Rosenfeld, A. *Proc. natn. Acad. Sci. U.S.A.* **79,** 292–286 (1982).
6. Ebashi, S. *Proc. R. Soc.* **B207,** 259–296 (1980).
7. Barron, J. T., Barany, M., Barany, K. & Storti, R. V. *J. biol. Chem.* **255,** 6238–6244 (1980).
8. de Lanerolle, P. & Stull, J. T. *J. biol. Chem.* **255,** 9993–10000 (1980).
9. Janis, R. A., Barany, K., Barany, M. & Sarmiento, J. G. *Molec. Physiol.* **1,** 3–11 (1981).
10. Dillon, P. F., Aksoy, M. O., Driska, S. P. & Murphy, R. A. *Science* **211,** 495–497 (1981).
11. Askoy, M. O., Murphy, R. A. & Kamm, K. E. *Am. J. Physiol.* **242,** C109–C116 (1982).
12. Somlyo, A. V., Butler, T. M., Bond, M. & Somlyo, A. P. *Nature* **294,** 567–569 (1981).
13. Persechini, A. & Hartshorne, D. J. *Science* **213,** 1383–1385 (1981).
14. Fay, F. S., Shlevin, H. H., Granger, W. C. Jr & Taylor, S. R. *Nature* **280,** 506–508 (1979).
15. Neering, I. R. & Morgan, K. G. *Nature* **288,** 585–587 (1980).
16. Tsien, R. Y., Pozzan, T. & Rink, T. J. *Nature* **295,** 68–71 (1982).
17. Bolton, T. B. *Physiol. Rev.* **59,** 606–718 (1979).

BOOK REVIEWS

University Colleges of Science & Technology
92, A.P.C. Rd., Cal.-9
LIBRARY COMPLEX
Departments of :
Chemical Engineering
Chemical Technology
Plastics & Rubber Technology

But is man a worm?

J. S. Jones

Darwin to DNA, Molecules to Humanity. By G. Ledyard Stebbins. Pp.491. Hbk ISBN 0-7167-1331-4; pbk ISBN 0-7167-1332-2. (W. H. Freeman: 1982.) Hbk $25, £21.80; pbk $12, £10.50.

THE most difficult thing in writing a book about evolution is to know what to leave out. Almost any biological observation can be discussed in Darwinian terms: indeed, the very universality of the theory of evolution is the main philosophical obstacle to subjecting it to scientific test. In the past few years we have had books dealing with, for example, evolutionary biochemistry, the evolution of animal behaviour and the mathematics of the evolutionary process, together with a mass of popular (or at least unscientific) works which purport to explain human behaviour and social organization in terms of evolutionary theory. In the rush to explain such complex matters in simple terms there has often been a danger of losing sight of the biological wood through the evolutionary trees. What interested Darwin was, of course, the diversity of living organisms. It is therefore surprising how small a part the variety of animals and plants plays in most of these volumes.

Here we have a book, aimed both at undergraduates and at a general audience, which sets out not only to describe the mechanisms and results of evolutionary change in a range of species from cycads to cephalopods but attempts also to apply such patterns to the evolution of human behaviour and the course of human history. Such attempts — and there are many of them — imply that man is indeed little more than a remarkably well-developed worm; the same rules which govern the evolution of amphibia from fish or of *Homo sapiens* from *Ramapithecus* have been responsible for the change from tribe to nation state or from feudalism to capitalism. How well does G. Ledyard Stebbins, an eminent plant evolutionist, succeed in establishing a seamless transition from the primordial slime to the Reagan administration?

It is immediately obvious that Stebbins is far better qualified to attempt this task than are most of his recent predecessors. Instead of the usual facile discussions of human society in terms of carefully selected anecdotes of animal behaviour, we have in the first two-thirds of the book a greatly compressed but remarkably complete account of modern evolutionary biology.

Courtesy *Punch*

The results of this compression are sometimes alarming; for example, Chapter 9 takes us "From Worms to Primates" in 31 pages of text. There is nevertheless much more insight into the process of evolution here than in many books claiming a far higher level of technical sophistication. Many of these insights are attractively phrased: thus Stebbins illustrates the inevitable incompleteness of the fossil record by pointing out that no one has seen the fossilized remnants of a passenger pigeon, although these birds flourished in millions in North America only a hundred years ago. There is even room for a few poetic touches, as when he talks of the oppressive silence of the Carboniferous forests before the evolution of animals capable of making sounds.

Stebbins illustrates the changes in the fortunes of Darwinism over the past century by recalling disparagingly that in his Harvard days in 1926 the theory outlined in the *Origin of Species* was described as having been long ago abandoned. The recent resurgence of anti-Darwinian models of speciation by "punctuated equilibrium" from the same institution shows how rapidly the pendulum of evolutionary fashion can swing. Stebbins himself considers that the pattern of change of animals and of societies does indeed show stability followed by relatively rapid change, although he is careful to point out that the enormous time scale of evolution in comparison to the brief generation interval of living organisms means that this can easily be accommodated in the Darwinian model.

Only three years after the publication of the *Origin*, Marx wrote to Engels:

> It is remarkable how Darwin recognizes among beasts and plants his English society with its division of labour, competition, opening up of new markets, inventions, and the Malthusian "struggle for existence".

Darwin was himself well aware of the possible application of his theory to human history but steadfastly refused to be drawn into discussion on the subject. Such restraint has scarcely been a characteristic of his successors. Indeed it is now almost an occupational hazard for elderly and distinguished biologists to produce biological overviews of human society. Stebbins is no exception, and it is in the last third of his book — "Human Evolution: Biological and Cultural" — that the clarity of his arguments begins to falter.

Although Stebbins criticizes some of the particularly inane statements of geneticists about history (such as Darlington's equation of the success of the Normans with their acquisition of genes both for horse-riding and for seamanship) he is not inhibited from discussing patterns of historical change — including such unjustifiably neglected episodes as the Revolt of the Red Eyebrows in first-century China — in genetic terms. This does provide occasional brilliant insights into human history. For example, the lack of speciation in the hominid line compared to that in other primates is ascribed to the development of tools, which themselves underwent adaptive radiation. However, for much of the time he is drawn onto the wilder shores of speculation as, for instance, when he discusses the presumed coincidence of nut-eating with the beginnings of intelligence, or of mental alertness with the idle ruminations of prehistoric night-watchmen by their newly-discovered fires and the favours bestowed on them by females as rewards for their wakefulness.

Stebbins is too good a scientist to draw simple lessons from the faulty and imperfect evidence of human history. As a result, he often reaches conclusions so broad as to be almost lacking in content:

> A safe generalization is that genetic templates transmit potentialities and capacities rather than adult behavioural traits . . . . In humans, cultural fitness, based to a large extent on a desire for approval by society, has both a genetic and a cultural basis. Is *Homo sapiens* just another species of animal that has evolved in the same way as have the various species of monkeys and apes? The answer to this question is a qualified 'no'.

In general, a large part of his answer to the question posed throughout — Can the evolution of man and society be explained in terms of the evolutionary rules affecting lower organisms? — is a similarly resounding "perhaps". The book therefore ends in a curiously flatfooted way: "Is the evolutionist better equipped than anyone else to recommend what is best for human society? Perhaps not". This conclusion is an honest one, but betrays the excellence of Stebbins's treatment of the evolutionary process. *Darwin to DNA* is fine; *Molecules to Humanity* could be considerably edited with little loss. □

J.S. Jones is in the Department of Genetics and Biometry at University College London.

Naked protoplasm and synchronous nuclei

Michael Carlile

Cell Biology of Physarum and Didymium. Vol. 1, *Organisms, Nucleus and Cell Cycle.* Edited by Henry C. Aldrich and John W. Daniel. Pp.444. ISBN 0-12-049601-1. (Academic: 1982.) $55, £36.40.

THE myxomycete plasmodium is a remarkable object. A mass of protoplasm not subdivided into cells it can, in the most intensively studied species *Physarum polycephalum,* attain the size of a dinner plate and contain hundreds of millions of nuclei which divide synchronously, at least twice a day in a well-nourished plasmodium.

A handful of enthusiasts for "naked protoplasm" have studied myxomycete plasmodia for over a century and since 1961, when workers at the McArdle Laboratory for Cancer Research at Madison grew plasmodia of *P. polycephalum* in pure culture on soluble media, many molecular, developmental and cell biologists have carried out work on this organism. A second species, *Didymium iridis,* has also been the subject of ultrastructural and genetical studies, but here biochemical investigation has been limited through failure to grow plasmodia in pure culture.

In spite of the wide interest in *Physarum* plasmodia, however, reviewing activity has been limited. Two recent works are now remedying this deficiency. In 1980 *Growth and Differentiation in* Physarum polycephalum, edited by W. F. Dove and H. P. Rusch, was published by Princeton University Press (for review see *Nature* **288,** 307; 1980). Now a different group of authors have contributed to the first of two volumes edited by Henry Aldrich, a leading student of myxomycete ultrastructure, and John Daniel, who with Howard Rusch was responsible for the crucial 1961 paper on pure culture.

The introductory section of the first volume consists of a chapter on the morphology and taxonomy of myxomycetes by Alexopoulos and one on *D. iridis* by Collins and Betterley, leading authorities on this organism. Subsequent pages are effectively confined to *P. polycephalum.* Tyson deals with periodic phenomena — not only synchronous nuclear division and other periodic events of the nuclear cycle, but also the control of the protoplasmic streaming that occurs in well-defined channels in the plasmodium at rates of up to a millimetre a second with reversals in the direction of flow taking place at approximately one minute intervals. The plasmodium is capable of rapid migration and among the sensory systems guiding migration is chemotaxis, which is being intensively studied in Japan and is reviewed here by Ueda and Kobatake. Protoplasmic streaming and its control is further considered by Kessler.

The difficult subject of *Physarum* genetics is dealt with ably by Jennifer Dee, the founder of the subject. Two chapters by Mohberg and Babcock then clarify in a succinct way the confusing topics of ploidy and of the genealogy of the strains of *P. polycephalum* in current use. The final four chapters of the first volume deal with nuclear organization (Lafontaine and Cadrin), chromosomal organization (Matthews and Bradbury), DNA (Evans) and RNA (Braun and Seebeck), the important topics of differentiation, metabolism and methodology being deferred to Vol. 2.

This first volume is lucidly written and admirably illustrated. I suspect — and hope — that the two-volume work will do much to promote work on myxomycetes and publicize the results among other biologists. □

Michael Carlile is Senior Lecturer in the Department of Pure and Applied Biology, Imperial College, University of London.

Putting the forams in order

John W. Murray

Foraminifera. By John R. Haynes. Pp.433. ISBN 0-333-28681-2. (Macmillan Press/Halsted: 1982.) £50, $79.95.

FORAMINIFERA are tiny animals that build themselves a test or shell. Their fossil remains occur in astronomical numbers from the Cambrian to the present day in sediments accumulating in estuaries, seas and oceans. These attributes, together with their great diversity, have made them of use to geologists both for correlating rocks of similar age (biostratigraphy) and for determining the environments of deposition of their enclosing sediment (palaeoecology). In addition, as foraminiferal tests survive the process of drilling boreholes, they are especially useful in the exploration for petroleum.

A sound taxonomic basis is an essential prerequisite for all such studies and Dr Haynes has taken this as the main theme of his book. In particular, his thorough account of how to write the description of a species and the compilation of a synonymy will prove invaluable to postgraduate students and researchers.

The main thrust of the volume is the introduction of a revised suprageneric classification. As the study of Foraminifera has progressed over the past 200 years, the importance of certain morphological features as criteria for grouping or dividing the species into genera, superfamilies and so on have varied. The revised classification follows previous ones in using the wall structure of the test as the primary means of grouping and subdivision but it takes into account the new information amassed from electron microscopy. Greater importance is attached to details of the aperture than is customarily the case.

Nine orders and thirty-two superfamilies are described. For each order there is discussion of the range of morphology observed, possible evolutionary relationships, an appraisal of their stratigraphic value, comments on their ecology and palaeoecology, and a summary of the classification. The latter includes diagnoses of the superfamilies and of the important genera.

The book is described in the preface as a general text which lays stress on the stratigraphical application of Foraminifera. This aim it achieves admirably with a synthesis of knowledge from more than 1,000 publications, but, in addition, it contains much original work. All those involved in the study of Foraminifera will find it both instructive and stimulating reading. □

J. W. Murray is Professor of Geology and Head of the Geology Department at the University of Exeter.

Extra genes, in and out of chromosomes

Joseph G. Gall

Gene Amplification. Edited by Robert T. Schimke. Pp.339. ISBN 0-87969-151-4. (Cold Spring Harbor Laboratory: 1982.) $35 (US), $42 (elsewhere).

WHEN mammalian tissue cultures are treated with gradually increasing concentrations of methotrexate (MTX), cell lines can be selected that are resistant to very high concentrations of the otherwise toxic drug. The basis of resistance may be decreased permeability of the cells to the drug or decreased binding between the drug and the target enzyme, dihydrofolate reductase (DHFR). In a significant number of lines, however, resistance is due to compensatory production of the enzyme, which itself is related to increased synthesis of the mRNA and ultimately to differential replication or amplification of the gene coding for DHFR.

These surprising facts were first reported four years ago in elegant experiments by Robert Schimke and his colleagues at Stanford University. Progress in the field has been rapid since then, and late last year Schimke organized a small symposium at Cold Spring Harbor to summarize that progress. This volume, *Gene Amplification*, contains 42 short papers based on presentations at the symposium.

Many of the papers are concerned with the chromosomal and molecular state of the amplified genes. It became evident early on that two unusual cytological phenomena could be associated with amplified cell lines: first, the presence of small acentric chromosomes, which, because they often occur in pairs, are called double minutes; and second the appearance of long chromosome segments with little evidence of G-banding, referred to as homogeneously staining regions. Amplified genes have now been demonstrated in both regions by *in situ* nucleic acid hybridization. There is a good but not perfect correlation between stability of the amplified condition (when MTX is removed) and the physical location of the amplified genes — homogeneously staining regions being characteristic of stable lines, double minutes of unstable ones. It is possible, therefore, that amplified gene copies appear first as small extrachromosomal elements that later become stably integrated into one or more chromosomes. The size of the amplified region has been measured by hybridizing DNA from amplified lines with genomic sequences that flank the DHFR gene. The amplified segment may be up to 100 kb in length, considerably longer than the coding region itself (31 kb counting its five introns).

Almost nothing is known about the initial molecular events of amplification in tissue cultures. A model discussed in the book by Botchan and by Spradling involves multiple rounds of replication at a single origin of replication, giving rise to an "onion-skin" configuration. An attractive feature of this model is the ease with which it can be applied to the chorion genes of *Drosophila*, whose amplification in the follicle cells of the oocyte has been analysed in detail by Spradling. In this case the chorion genes are more highly amplified than surrounding sequences, the level of amplification falling off progressively on both sides of the genes. This is just what one would expect if multiple replication forks move away from an origin of replication in or near the genes.

Several other specific amplifications have been induced in tissue cultures, of which the best characterized involve resistance to *N*-(phosphonacetyl)-L-aspartate or to the cadmium ion. These cases involve overproduction of the multifunctional protein "CAD" and of metallothionein-1 respectively. Several other likely cases are discussed in the book, and it seems probable that many genes can be amplified if a suitable inhibitor of enzyme activity is available. An interesting possibility is that random genomic fragments regularly detach from chromosomes and require only a selective force to undergo differential replication.

All 42 articles in the volume are short; indeed some are little more than expanded abstracts. The quality is variable, and since many are rather specialized the general reader will have to pick and choose to avoid getting bogged down in cytological and molecular detail. In addition, the title *Gene Amplification* is somewhat misleading. Schimke's major interest is drug-induced gene amplification in cultured cells, and that is what the book really covers. Gene amplification as a general biological phenomenon is touched upon, but readers unfamiliar with the field would not guess that naturally occurring gene amplification, particularly of rDNA, has been investigated extensively during the past 15 years in a variety of vertebrates, insects and protozoa. For a broader introduction to the topic one should begin with Adrian Bird's review article, "Gene reiteration and gene amplification", published in Vol.III of Prescott and Goldstein's *Cell Biology* (Academic, 1980).

Nevertheless this volume summarizes a large amount of work on an important topic. Like the much larger 1980 Cold Spring Harbor Symposium on movable genetic elements, it emphasizes the plasticity of the eukaryotic genome, a subject of great current interest. Because the book was published just six months after the meeting itself, the articles are timely and will prove useful to a wide audience. □

Joseph G. Gall is Professor of Biology, Molecular Biophysics and Biochemistry at Yale University.

Centrifugal Microfilters

Bioanalytical Systems introduces a centrifugal microfilter for membrane filtration of small volumes using the force of a conventional bench top centrifuge. Ideal for LC sample preparation, extraction of TLC spots, and many other applications.

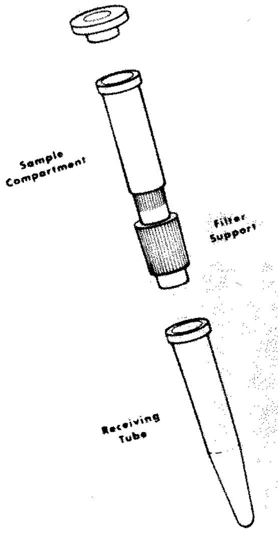

- minimize loss and contamination
- no vacuum or pressure required
- solvent resistant polyalomar
- filter many samples simultaneously
- a variety of filter materials are available
- reusable

Send for details...

BIOANALYTICAL SYSTEMS INC.

1205 Kent Avenue
West Lafayette, IN 47906
(317) 463-2505 telex 276141

Circle No.02 on Reader Service Card.

Meteoritics as petrography

John A. Wood

Meteorites: A Petrologic–Chemical Synthesis. By Robert T. Dodd. Pp.432. ISBN 0-521-22570-1. (Cambridge University Press: 1982.) £35, $69.50.

METEORITES are complex, ancient, enigmatic rock fragments from somewhere beyond Mars. They were formed at the same time as the Solar System, and they retain a cryptic record of the events of that time. In the 30 years since Harold Urey and Harrison Brown unleashed the techniques and concepts of post-War geochemistry on these objects, meteoritics has burgeoned into an important scientific subdiscipline. Many studies have been carried out and as many papers published; a number of important insights have been gained; and several riddles are still with us, more prickly and intractable than ever.

The field has always needed a good reference book, the more so as its literature has expanded to a scale greater than any one person can assimilate. Several books about meteorites have been written at a professional level in the past decade, but none can be said to fill the need. Robert Dodd's *Meteorites: A Petrologic–Chemical Synthesis* is the latest candidate. It is important to include the subtitle, because the emphasis of the book is very strongly on the petrology (or, to be more precise, the petrography) and chemistry of meteorites, Dodd's own speciality. (Petrography is the descriptive study of the microstructures and component mineralogies of rocks.)

Many good things can be said about the book. Dodd writes in a readable, straightforward style. His coverage of petrography and chemistry is comprehensive, scholarly and exhaustively referenced. Material is rationally organized, most of the chapters dealing with discrete subclasses of meteorites. (Two exceptions are a chapter on radiometric studies of meteorites, and one on the asteroid-sized parent bodies that they once resided in.) He strikes an appropriate balance between descriptions and interpretive discussions. In the latter, he is as objective as can reasonably be expected of a mortal in this contentious field. Each chapter is preceded by a précis that maps out for the reader the ground to be covered. There is an excellent index, and the illustrations are more than adequate in number and quality.

However, I fault the book for presenting a narrow view of meteoritics, that is, one largely limited to petrographic and geochemical studies. Perhaps it is unreasonable to expect Dodd, or anyone, to cover the whole marvellously diverse field of meteoritics as comprehensively as the author has treated meteoritic petrography and chemistry. The book would be twice as long and would cost Dodd far more than twice the labour, since he would have to venture beyond his field of experience.

But the book as it stands unfortunately presents the study of meteorites as an end in itself rather than as a means to a greater end: an understanding of the origin of the Solar System. The stage on which this drama occurred was the solar nebula, a giant accretion disk of gas and dust where the properties of the meteorites and, ultimately, the planets, were established. Dodd cannot avoid making repeated references to the nebula, the context in which everything happened; but he eschews any systematic discussion of astrophysical models of the nebula because they are "varied and changeable". Lacking such a framework, he cannot put the properties of meteorites to work in clarifying our view of the nebula.

"Nebula" does not appear in the index of the book; nor does "Solar System, origin"; nor does "FUN inclusions". The latter, the subject of intensive isotopic research which gives us a fascinating view of pre-Solar System events, are touched on only momentarily, and then not by the name "FUN". It is regrettable that the non-petrographic aspects of meteorites are given such short shrift: the most inspiring aspects of meteoritics are the grand vista it examines, and the close collaboration of researchers from many diverse disciplines in attacking the problem. *Meteorites: A Petrologic–Chemical Synthesis* exposes only a near-sighted and parochial view of the goals of this field. It is, however, a useful and excellent reference work within the unfortunately restrictive boundaries it has erected. ☐

John A. Wood is an Associate Director of the Harvard–Smithsonian Center for Astrophysics, Cambridge, Massachusetts.

Welcome to theoretical particle physics

P.V. Landshoff

Gauge Theories in Particle Physics: A Practical Introduction. By Ian J.R. Aitchison and Anthony J.G. Hey. Pp.341. Pbk ISBN 0-85274-534-6. (Adam Hilger/Heyden: 1982.) £14.50, $36.

THERE are still very few books on the topics that now excite the interest of particle theorists — the electroweak theory that brings together electromagnetism and the weak nuclear interaction, and quantum chromodynamics, the candidate theory of the strong nuclear interaction. So this book, which sets out to be a compact introduction to these subjects, will be warmly welcomed, especially for the attention it gives to the distinctive properties of the gauge symmetry underlying the new theories.

Quantum electrodynamics is the prototype gauge theory and is described by Aitchison and Hey as "the best theory we have". Its best test is the magnetic moment of the electron, whose calculated and measured values agree to within one part in 10^{10}. Electrodynamics is a gauge theory because its physical predictions are invariant under certain transformations of the electromagnetic potentials. Only this gauge invariance makes it possible to remove unphysical infinities from the quantized version of the theory (renormalization).

Quantum electrodynamics is based on Maxwell's equations, the first description of the electric and the magnetic force in the same set of equations. A century later, Glashow, Salam and Weinberg enlarged the theory so as to incorporate the weak interaction (responsible, for example, for neutron β-decay). Their unified electroweak gauge theory is steadily accumulating an impressive list of successes.

Another gauge theory, chromodynamics, seems to give a good description of the nuclear force. Attempts to unify this with the electroweak theory have led to the prediction that protons are unstable, with a lifetime of about 10^{31} years. Four candidate proton-decay events have recently been observed, but the data are not yet a sufficient test.

Quantum electrodynamics itself is far from easy, but the electroweak theory and chromodynamics are less accessible to most physicists because the groups of gauge transformations are not Abelian (which implies that the underlying gauge transformations do not necessarily commute with each other). This book sets out to make the theories as simple as possible. Everything is here, from the elements of relativistic quantum mechanics to a mention of proton decay in grand unified models, with renormalization and even a brief discussion of the quark–parton model on the way.

Inevitably in a short book of wide scope nothing is treated very fully. In places plausibility arguments replace proper derivations. But experimentalists especially will find it helpful in providing an understanding of the essential ideas behind what the theorists are talking about, while neophyte theorists will find it a valuable introduction to the more advanced texts. The second half of the book will be the most useful, for the painless insight that it gives into non-Abelian physics. ☐

Peter Landshoff is Reader in Mathematical Physics at the University of Cambridge.

nature

Author Index for Volume 298

July — August 1982

Issue no.	Issue date	Page nos
5869	1 July	1-106
5870	8 July	107-210
5871	15 July	211-312
5872	22 July	313-406
5873	29 July	407-500
5874	5 August	501-592
5875	12 August	593-694
5876	19 August	695-778
5877	26 August	779-876

Aaronson S. A. *see under* Santos E., **298,** 343

Abbott L. F. and Gavela M. B. Absence of thermal effects on photon mass measurements, *matters arising,* **298,** 873

Able P. K., Terrill S. B. and Cherry J. D. Not by mirrors, *correspondence,* **298,** 510

Abramowicz M. A. Twinkle, twinkle quasi star……, *news and views,* **298,** 789

Acuña M. H. *see under* Connerney J. E. P., **298,** 44

Adachi M. *see under* Sugisaki R., **298,** 644

Adams D. J. Dielectric constant of ice—Reply, *matters arising,* **298,** 401

Adefris T. *see under* Kalb J. E., **298,** 25

Adelstein R. S. *see under* de Lanerolle P., **298,** 871

Agsteribbe E. *see under* van den Boogaart P., **298,** 187

Ahrens T. J. *see under* O'Keefe J. D., **298,** 123

Aitchison I. J. R. and Hey A. J. G. Gauge Theories in Particle Physics: A Practical Introduction, *book review by* Landshoff P. V. **298,** 877

Aiuti F. *see under* D'Amelio R., **298,** 72

Akoyunoglou G. ***Editor***, Photosynthesis, *book review by* Evans M. C. W. **298,** 104

Alber S., Alpert J., Finkelstein E., Freiman G., Ioffe A., Irlin J., Lebonov A., Lerner A., Meiman N. and Reitman M. Help for refusniks, *correspondence,* **298,** 414

Aldrich Henry C. and Daniel J. W. ***Editors***, Cell Biology of *Physarum* and *Didymium* Vol. 1, Organisms, Nucleus and Cell Cycle, *book review by* Carlile M. **298,** 876

Alexander H. *see under* Bittle J. L., **298,** 30

Alexander P. *book review of* Cancer: A Comprehensive Treatise, Vol. 1, Etiology: Chemical and Physical Carcinogenesis, (Becker F. F. *editor*) **298,** 404

Allègre *see under* Loubet M., **298,** 809

Allen D. A. *see under* French R. G., **298,** 827

Alpert J. *see under* Alber S., **298,** 414

Altschuler R. A., Mosinger J. L., Harmison G. G., Parakkal M. H. and Wenthold R. J. Aspartate aminotransferase-like immunoreactivity as a marker for aspartate/glutamate in guinea pig photoreceptors, **298,** 657

Amara S. G., Jonas V., Rosenfeld M. G., Ong E. S. and Evans R. M. Alternative RNA processing in calcitonin gene expression generates mRNAs encoding different polypeptide products, **298,** 240

Ammerer G. *see under* Valenzuela P., **298,** 347

Anderson M. *see under* Ashby E., **298,** 207

Anderson W. F. *see under* Ohlendorf D. H., **298,** 718

Anderton B. *see under* Lane B., **298,** 706

Anderton B. H., Breinburg D., Downes M. J., Green P. J., Tomlinson B. E., Ulrich J., Wood J. N. and Kahn J. Monoclonal antibodies show that neurofibrillary tangles and neurofilaments share antigenic determinants, **298,** 84

Andrews J. N., Burgess W. G., Edmunds W. M., Kay R. L. F. and Lee D. J. The thermal springs of Bath, **298,** 339

Andrews J. N. and Kay R. L. F. Natural production of tritium in permeable rocks, **298,** 361

Ansell J. D. *see under* Burton D. I., **298,** 562

Antelman S. M. *see under* Chiodo L. A., **298,** 301

Antoniazzi G. *see under* D'Amelio R., **298,** 72

Antonovics J. *see under* Silander J. A., **298,** 557

Ardeshir F. *see under* Higgins C. F., **298,** 723

Arndt U. W., Greenhough T. J., Helliwell J. R., Howard J. A. K., Rule S. A. and Thompson A. W. Optimized anomalous dispersion crystallography: a synchrotron X-ray polychromatic simultaneous profile method, **298,** 835

Arp B., McMullen M. D. and Storb U. Sequences of immunoglobulin λ1 genes in a λ1 defective mouse strain, **298,** 184

Asai M. *see under* Kakidani H., **298,** 245

Ashby E. and Anderson M. The Politics of Clean Air, *book review by* Lincoln T. **298,** 207

Asofsky R. *see under* Glimcher L. H., **298,** 283

Atfield G. *see under* Mellor A. L., **298,** 529

Attenborough R. D. *book review of* Social Anthropology, (Leach E.) **298,** 403

Attimonelli M. *see under* Saccone C., **298,** 8

Aubin J. E. *see under* Turksen K., **298,** 763

Ausubel F. M. *see under* Long S. R., **298,** 485

Avery J. A. and Bowmaker J. K. Visual pigments in the four-eyed fish, *Anableps anableps*, **298,** 62

Axelson M., Sjövall J., Gustafsson B. E. and Setchell K. D. R. Origin of lignans in mammals and identification of a precursor from plants, **298,** 659

Babior B. M. and Parkinson D. W. The NK cell: a phagocyte in lymphocyte's clothing? *news and views,* **298,** 511

Badley R. A. *see under* Virtanen I., **298,** 660

Baekkeskov S., Neilsen J. H., Marner B., Bilde T., Ludvigsson J. and Lernmark A. Autoantibodies in newly diagnosed diabetic children immunoprecipitate human pancreatic islet cell proteins, **298,** 167

Baker J. B. *see under* Low D. A., **298,** 476

Baker J. R. The parasitic balance, *correspondence,* **298,** 510

Baker M. S. *see under* Topal M. D., **298,** 863

Baker V. R. The Channels of Mars, *book review by* Wilson L. **298,** 694

Baldwin C. T. *see under* Boulton G. S., **298,** 437

Baltimore D. *see under* Bothwell A. L. M., **298,** 380

Bancroft G. M. and Jean G. Gold deposition at low temperature on sulphide minerals, **298,** 730

Barbacid M. *see under* Santos E., **298,** 343

Barber J. *book review of* Techniques in Bioproductivity and Photosynthesis, (Coombs J. and Hall D. O., *editors*) **298,** 206

Barker P. Back-arc geodynamics, *news and views,* **298,** 119

Barnes W. M. *see under* Higgins C. F., **298,** 760

Barnstable C. J. Molecular heterogeneity and the nervous system, *news and views,* **298,** 708

Baross J. A., Lilley M. D. and Gordon L. I. Is the CH_4, H_2 and CO venting from submarine hydrothermal systems produced by thermophilic bacteria? **298,** 366

Barrow J. D. and Turner M. S. The inflationary Universe — birth, death and transfiguration, *review article,* **298,** 801

Barter G. Badgers still snared, *correspondence,* **298,** 702

Barthelme J. W. *see under* Owen R. B., **298,** 523

Barton J. R. Safe harbour, *correspondence,* **298,** 415

Bateson P. Centenary plea, *correspondence,* **298,** 414

Bé A. W. H. *see under* Fairbanks R. G., **298,** 841

Beale J. Synthetic peptides as the basis for future vaccines, *news and views,* **298,** 14

Beaumont T. J. *see under* Roder J. C., **298,** 569

Becker F. F. ***Editor***, Cancer: A Comprehensive Treatise, Vol. 1, Etiology: Chemical and Physical Carcinogenesis, *book review by* Alexander P. **298,** 404

Bell K., Blenkinsop J., Cole T. J. S. and Menagh D. P. Evidence from Sr isotopes for long-lived heterogeneities in the upper mantle **298,** 251

Belton M. J. S. and Butcher H. Limits on the nucleus of Halley's Comet, **298,** 249

Benjamin P., Strumph P., Kenny M. and Firshein W. DNA synthesis in purified DNA–membrane complexes extracted from a *Bacillus subtilis* pol A mutant, **298,** 769

Benson H. Body temperature changes during the practice of G Tum-mo yoga—Reply, *matters arising,* **298,** 402

Benson W. *see under* Römer D., **298,** 759

Berger R. *see under* Lenoir G. M., **298,** 474

Berger S. D. and Pennycook S. J. Detection of nitrogen at {100} platelets in diamond, **298,** 635

Bernheim A. *see under* Lenoir G. M., **298,** 474

Bernier I. *see under* Pauloin A., **298,** 574

Berry R. J. *book review of* Ecological Genetics, (Merrell D. J.) **298,** 205

Beverley P. C. L. *see under* Garson J. A., **298,** 375

Bhargava P. M. Whence high IQs? *correspondence,* **298,** 8

Bicknell R. J. and Leng G. Endogenous opiates regulate oxytocin but not vasopressin secretion from the neurohypophysis, **298,** 161

Bigazzi G. *see under* Obradovich J. D., **298,** 55

Bilde T. *see under* Baekkeskov S., **298,** 167

Birch P. Is the Universe rotating? **298,** 451

Bittle J. L., Houghten R. A., Alexander H., Shinnick T. M., Sutcliffe J. G., Lerner R. A., Rowlands D. J. and Brown F. Protection against foot-and-mouth disease by immunization with a chemically synthesized peptide predicted from the viral nucleotide sequence, **298,** 30

Björklund A., Stenevi U., Dunnett S. B. and Gage F. H. Cross-species neural grafting in a rat model of Parkinson's disease, **298,** 652

Blenkinsop J. *see under* Bell K., **298,** 251

Blithe D. L. *see under* Kasuga M., **298,** 667

Bookchin R. M. *see under* Lew V. L., **298,** 478

Borer P. N. *see under* Cruz P., **298,** 198

Borgia G. *see under* Charlesworth B., **298,** 494

Borst P. *see under* Grivell L. A., **298,** 703

Borthwick N. *see under* Fink G., **298,** 270

Boswell D. R. *see under* Carrell R. W., **298,** 329

Bothwell A. L. M., Paskind M., Reth M., Imanishi-Kari T., Rajewsky K. and Baltimore D. Somatic variants of murine immunoglobulin λ light chains, **298,** 380

Bouldin D. R. *see under* Duxbury J. M., **298,** 462

Boulton G. S., Baldwin C. T., Peacock J. D., McCabe A. M., Miller G., Jarvis J., Horsefield B., Worsley P., Eyles N., Chroston P. N., Day T. E., Gibbard P., Hare P. E. and von Brunn V. A glacio-isostatic facies model and amino acid stratigraphy for late Quaternary events in Spitsbergen and the Arctic, **298,** 437

Bowmaker J. K. *see under* Avery J. A., **298,** 62

Boyle E. *see under* Hester K., **298,** 260

Bradbury A. F., Finnie M. D. A. and Smyth D. G. Mechanism of C-terminal amide formation by pituitary enzymes, **298,** 686

Braddick O. Unscrambling amblyopia, *news and views,* **298,** 224

Brash D. E. and Haseltine W. A. UV-induced mutation hotspots occur at DNA damage hotspots, **298,** 189

Bredt W. *see under* Feldner J., **298,** 765

Bregman J. N. A corona around the Milky Way, *news and views,* **298,** 10

Breinburg D. *see under* Anderton B. H., **298,** 84

Brennan S. O. *see under* Carrell R. W., **298,** 329

Bridges B. and Lehmann A. Inducible responses to DNA damage, *news and views,* **298,** 118

Brimblecombe P. and Stedman D. H. Historical evidence for a dramatic increase in the nitrate component of acid rain, **298,** 460

Brock W. H. *et al.* ***Editors***, John Tyndall: Essays on a Natural Philosopher, *book review by* MacLeod R. **298,** 305

Brouet J.-C. *see under* Dellagi K., **298,** 284

Brown C. and Girdler R. W. Structure of the Red Sea at 20°N from gravity data and its implication for continental margins, **298,** 51

Brown F. *see under* Bittle J. L., **298,** 30

Brown K. W. *see under* Byrd P., **298,** 69

Brüggeller P. *see under* Mayer E., **298,** 715

Brum G. *see under* Osterrieder W., **298,** 576

Bryant S. V. *see under* Muneoka K., **298,** 369

Bubienko E. *see under* Cruz P., **298,** 198

Bugnon C., Fellmann D., Gouget A. and Cardot J. Ontogeny of the corticoliberin neuroglandular system in rat brain, **298,** 159

Buikema W. J. *see under* Long S. R., **298,** 485

Bull R. K. and Mold P. A search for evidence of superheavy-element fission in chondritic metal, **298,** 634

Bullman H. *see under* Mellor A. L., **298,** 529

Bunker J. P. and Fowles J. *book review of* Biomedical Innovation, (Roberts E. B. *et al. editors*) **298,** 405

Buonaguro F. M. *see under* Hill C. K., **298,** 67

Buongiorno-Nardelli M., Micheli G., Carrì M. T. and Marilley M. A relationship between replicon size and supercoiled loop domains in the eukaryotic genome, **298,** 100

Burbank D. W. and Johnson G. D. Intermontane-basin development in the past 4 Myr in the north-west Himalaya, **298,** 432

Burchard R. P. Evidence for contractile flexing of the gliding bacterium *Flexibacter* FS-1, **298,** 663

Burchfield R. W. ***Editor***, A Supplement to the Oxford English Dictionary Vol.III, O-Scz., *book review by* Maddox J. **298,** 309

Burgess W. G. *see under* Andrews J. N., **298,** 339

Burton D. I., Ansell J. D., Gray R. A. and Micklem H. S. A stem cell for stem cells in murine haematopoiesis, **298,** 562

Büscher H. H. *see under* Römer D., **298,** 759

Businco L. *see under* D'Amelio R., **298,** 72

Bustamante C. *see under* Maestre M. F., **298,** 773

Butcher E. C. *see under* Kraal G., **298,** 377

Butcher H. *see under* Belton M. J. S., **298,** 249

Butler J., O'Brien M., O'Malley K. and Kelly J. G. Relationship of β-adrenoreceptor density to fitness in athletes, **298,** 60

Bynum W. F. *book review of* Medical Thinking: A Historical Preface, (King L. S.) **298,** 105

Byrd P., Brown K. W. and Gallimore P. H. Malignant transformation of human embryo retinoblasts by cloned adenovirus 12 DNA, **298,** 69

Calvert P. D. Polymers for solar energy, *news and views,* **298,** 226

Cammack R. Iron–sulphur cluster interconversions and the activation of aconitase, *news and views,* **298,** 792

Campbell D. T. Do protons block Na+ channels by binding to a site outside the pore? **298,** 165

Campbell P. Atmospheric chemists *in flagrante? news and views,* **298,** 9

Campo M. S. Warts and all, *news and views,* **298,** 605

Camps R. A. *see under* Sinclair R., **298,** 127

Cann J. R. and Strens M. R. Black smokers fuelled by freezing magma, **298** 147
Cantor H. *see under* Galli S. J., **298,** 288
Cardot J. *see under* Bugnon C., **298,** 159
Carlile M. *book review of* Cell Biology of *Physarum* and *Didymium* Vol. 1, Organisms, Nucleus and Cell Cycle, (Aldrich Henry C. and Daniel J. W. *editors*) **298,** 876
Carlson E. A. Genes, Radiation, and Society: The Life and Work of H. J. Muller, *book review by* Pontecorvo G. **298,** 203
Carlsson A. and Olsson T. High rock stresses as a consequence of glaciation, **298,** 739
Carrell R. W., Jeppsson J.-O., Laurell C.-B., Brennan S. O., Owen M. C., Vaughan L. and Boswell D. R. Structure and variation of human α_1-antitrypsin, *review article,* **298,** 329
Carrì M. T. *see under* Buongiorno-Nardelli M., **298,** 100
Carter B. L. A. *see under* Piggott J. R., **298,** 391
Casella J. F. *see under* Masiello N. C., **298** 202
Catto C. J. D. *see under* Sinclair R., **298,** 127
Chader G. J. *see under* Lai Y. L., **298,** 848
Chakauya B. L. *see under* Thornton J. M., **298,** 296
Chambraud B. *see under* Panthier J.-J., **298,** 90
Chancellor G. More on Ovid, *correspondence,* **298,** 415
Chang P. W. *see under* Dawson G. J., **298,** 580
Chantler P. Retreats from the steric blocking of muscle contraction, *news and views,* **298,** 120
Charlesworth B., Toro M. A., Borgia G. and Wildish D. J. Female-biased sex ratios, *matters arising,* **298,** 494
Charlton H. M. *see under* Krieger D. T., **298,** 468
Chen K. K. *see under* Rice-Ficht A. C., **298,** 676
Cherchi A. and Montadert L. Oligo-Miocene rift of Sardinia and the early history of the Western Mediterranean Basin, **298,** 736
Cherry J. D. *see under* Able P. K., **298,** 510
Chervin R. M. *book review of* Monsoon Dynamics, (Lighthill J. and Pearce R. P. *editors*) **298,** 308
Chiodo L. A. and Antelman S. M. Do antidepressants induce dopamine autoreceptor subsensitivity?—Reply, *matters arising,* **298,** 301
Chroston P. N. *see under* Boulton G. S., **298,** 437
Chudomel V. *see under* Činátl J., **298,** 388
Cianfriglia M. *see under* Conzelmann A., **298,** 170
Cicerone R. J. *see under* Turco R. P., **298,** 830
Činátl J., Paluska E., Chudomel V., Malasková V. and Elleder M. Culture of macrophage cell lines from normal mouse bone marrow, **298,** 388
Clark S. *see under* Lichtler A. C., **298,** 195
Clement J. M. *see under* Higgins C. F., **298,** 760
Clutton-Brock T. H. Sons and daughters, *news and views,* **298,** 11 *Corrigendum* **298,** 328
Coakham H. B. *see under* Garson J. A., **298,** 375
Coe R. S. *see under* Vaughan P. J., **298,** 357
Cogley J. G. *see under* Henderson-Sellers A., **298,** 832
Cohen J. M., Sarill W. J. and Vishveshwara C. V. An example of induced centrifugal force in general relativity, **298,** 829
Cohen S. *see under* Lotan I., **298,** 572
Coimbra-Filho A. F. and Mittermeier R. A. ***Editors*****,** Ecology and Behavior of Neotropical Primates, Vol. I., *book review by* Dixson A. **298,** 308
Cole T. J. S. *see under* Bell K., **298,** 251
Coleman M. M. *see under* Painter P. C., **298,** 777
Collins D. M. Electron density images from imperfect data by iterative entropy maximization, **298,** 49
Collins S. and Groudine M. Amplification of endogenous *myc*-related DNA sequences in a human myeloid leukaemia cell line, **298,** 679
Colwell R. K. Female-biased sex ratios—Reply, *matters arising,* **298,** 494
Condit Jr J. R. *see under* de Lanerolle P., **298,** 871
Connerney J. E. P., Ness N. F. and Acuña M. H. Zonal harmonic model of Saturn's magnetic field from Voyager 1 and 2 observations, **298,** 44
Conroy G. C. *see under* Kalb J. E., **298,** 25
Conway Leovy *book review of* Weather and Climate on Planets, (Kondratyev K. Y. and Hunt G. E.) **298,** 208
Conzelmann A., Corthésy P., Cianfriglia M., Silva A. and Nabholz M. Hybrids between rat lymphoma and mouse T cells with inducible cytolytic activity, **298,** 170
Coombs J. and Hall D. O., ***Editors*****,** Techniques in Bioproductivity and Photosynthesis, *book review by* Barber J. **298,** 206
Cooper M. D. *see under* Marcu K. B., **298,** 327
Corliss B. H. Linkage of North Atlantic and Southern Ocean deep-water circulation during glacial intervals, **298,** 458
Coronado R. and Latorre R. Detection of K^+ and Cl^- channels from calf cardiac sarcolemma in planar lipid bilayer membranes, **298,** 849
Corthésy P. *see under* Conzelmann A., **298,** 170
Corvol P. *see under* Panthier J.-J., **298,** 90
Cotterill R. M. J. and Madsen J. U. Crystal instability and melting—Reply, *matters arising,* **298,** 874
Couchman P. R. Composition-dependent glass-transition temperatures and copolymers, **298,** 729
Coupar B. E. H. *see under* Cushley W., **298,** 77
Cousins F. W. Falklands story, *correspondence,* **298,** 8
Coveney J. and Woodland H. R. The DNase I sensitivity of *Xenopus laevis* genes transcribed by RNA polymerase III, **298,** 578
Cox B. *book review of* Mammal-Like Reptiles and the Origin of Mammals, (Kemp T. S.) **298,** 307
  New branches for old roots, *news and views,* **298,** 321
Cox B. M. Opioids at Cape Cod, *news and views,* **298,** 790
Coyle J. T. *see under* Ferkany J. W., **298,** 757
Cramer D. *see under* Kalb J. E., **298,** 25
Crawford M. and Schramm D. N. Spontaneous generation of density perturbations in the early Universe, **298,** 538
Crettaz M. *see under* Kasuga M., **298,** 667
Critchley C. Stimulation of photosynthetic electron transport in a salt-tolerant plant by high chloride concentrations, **298,** 483
Cronan D. S., Glasby G. P., Moorby S. A., Thomson J., Knedler K. E. and McDougall J. C. A submarine hydrothermal manganese deposit from the south-west Pacific island arc, **298,** 456
Cruise A. M. Hipparcos: space-age astrometry, *news and views,* **298,** 324
Cruz P., Bubienko E. and Borer P. N. A model for base overlap in RNA, **298,** 198
Cunningham D. D. *see under* Low D. A., **298,** 476
Cushley W., Coupar B. E. H., Mickelson C. A. and Williamson A. R. A common mechanism for the synthesis of membrane and secreted immunoglobulin α, γ and μ chains, **298,** 77
Czelusniak J., Goodman M., Hewett-Emmett D., Weiss M. L., Venta P. J. and Tashian R. E. Phylogenetic origins and adaptive evolution of avian and mammalian haemoglobin genes, **298,** 297
Daiger S. P., Wildin R. S. and Su T.-S. Sequences on the human Y chromosome homologous to the autosomal gene for argininosuccinate synthetase, **298,** 682
D'Amelio R., Seminara R., Galli E., Antoniazzi G., Businco L. and Aiuti F. Circulating immune complexes in infants fed on cow's milk, **298,** 72
Daniel J. W. *see under* Aldrich Henry C., **298,** 876
Das Gupta A., Lee M. C. and Klobuchar J. A. VHF Faraday polarization fluctuations and strong *L*-band amplitude scintillations near Appleton anomaly crests, **298,** 354
Dascal N. *see under* Lotan I., **298,** 572
Davies T. F. *see under* Krieger D. T., **298,** 468
Davis R. W. *see under* Scherer S., **298,** 815
Dawson G. J., Yates V. J., Chang P. W. and Oprandy J. J. Is avian adeno-associated virus an endogenous virus of chicken cells? **298,** 580
Day T. E. *see under* Boulton G. S., **298,** 437
de Jong A. F. M. and Mook W. G. An anomalous Suess effect above Europe, **298,** 641
de Lanerolle P., Condit Jr J. R., Tanenbaum M. and Adelstein R. S. Myosin phosphorylation, agonist concentration and contraction of tracheal smooth muscle, **298,** 871
Deaton L. E. *see under* Hilbish T. J., **298,** 688
Debanne M. T., Evans W. H., Flint N. and Regoeczi E. Receptor-rich intracellular membrane vesicles transporting asialotransferrin and insulin in liver, **298,** 398
Degens E. T. and Ittekkot V. *In situ* metal-staining of biological membranes in sediments, **298,** 262
Dellagi K. and Brouet J.-C. Redistribution of intermediate filaments during capping of lymphocyte surface molecules, **298,** 284
Démant P. *see under* Roos M. H., **298,** 854
Demong N. J. *see under* Hegner R. E., **298,** 264
DeNiro M. J. *see under* Krishnamurthy R. V., **298,** 640
Dennett D. C. *see under* Hofstadter D. R., **298,** 103
DePaolo D. J., Manton W. I., Grew E. S. And Halpern M. Sm–Nd, Rb–Sr and U–Th–Pb systematics of granulite facies rocks from Fyfe Hills, Enderby Land, Antarctica, **298,** 614
Der Simonian H. *see under* Galli S. J., **298,** 288
DeRosier D. J. *see under* Egelman E. H., **298,** 131
Destrade C. *see under* Malthête J., **298,** 46
Dexter T. M. Is the marrow stroma transplantable? *news and views,* **298,** 222
Diamond J. M. Big-bang reproduction and ageing in male marsupial mice, *news and views,* **298,** 115
  Man the exterminator, *news and views,* **298,** 787
  The biogeography of the Pacific Basin, *news and views,* **298,** 604
Dick H. *see under* Fink G., **298,** 270
Dick S. J. Plurality of Worlds: The Origins of the Extraterrestrial Life Debate from Democritus to Kant, *book review by* Hall A. R. **298,** 588
Dickler H. B. *see under* Lamers M. C., **298** 178
Dimopoulos S., Glashow S. L., Purcell E. M. and Wilczek F. Is there a local source of magnetic monopoles? **298,** 824
DiNicolantonio R., Hutchinson J. S. and Mendelsohn F. A. O. Exaggerated salt appetite of spontaneously hypertensive rats is decreased by central angiotensin-converting enzyme blockade, **298,** 846
Dixson A. *book review of* Ecology and Behavior of Neotropical Primates, Vol. I., (Coimbra-Filho A. F. and Mittermeier R. A. *editors*) **298,** 308
Dobbs M. *see under* Rosenmann E., **298,** 563
Dodd R. T. Meteorites: A Petrologic–Chemical Synthesis, *book review by* Wood J. A. **298,** 877
Donelson J. E. *see under* Rice-Ficht A. C., **298,** 676
Donovan J. J., Simon M. I. and Montal M. Insertion of diphtheria toxin into and across membranes: role of phosphoinositide asymmetry, **298,** 669
Doolittle R. F. *see under* Sauer R. T., **298,** 447
Douglas J. B. *see under* Trayhurn P., **298,** 59
Douglas M. and Wildavsky A. Risk and Culture: An Essay on the Selection of Technological and Environmental Dangers, *book review by* Nelkin D. **298,** 775
Dow R. C. *see under* Fink G., **298,** 270
Downes M. J. *see under* Anderton B. H., **298,** 84
Drew M. G. B. *book review of* Inorganic Stereochemistry, (Kepert D. L.) **298,** 106
Duchemin A. M. *see under* Quach T. T., **298,** 373
Dujardin G., Jacq C. and Slonimski P. P. Single base substitution in an intron of oxidase gene compensates splicing defects of the cytochrome *b* gene, **298,** 628
Dunnett S. B. *see under* Björklund A., **298,** 652
Duwe A. *see under* Roder J. C., **298,** 569
Duxbury J. M., Bouldin D. R., Terry R. E. and Tate R. L. III Emissions of nitrous oxide from soils, **298,** 462
Dvorak A. M. *see under* Galli S. J., **298,** 288
Dvorak H. F. *see under* Galli S. J., **298,** 288
Dyer T. A. Methylation of chloroplast DNA in *Chlamydomonas, news and views,* **298,** 422
Ebbesen T. W., Levey G. and Patterson L. K. Photoreduction of methyl viologen in aqueous neutral solution without additives, **298,** 545
Edén C. S., Freter R., Hagberg L., Hull R., Hull S., Leffler H. and Schoolnik G. Inhibition of experimental ascending urinary tract infection by an epithelial cell-surface receptor analogue, **298,** 560
Edmond J. M. *see under* Ming-hui H., **298,** 550
Edmunds W. M. *see under* Andrews J. N., **298,** 339
Egelman E. H., Francis N., and DeRosier D. J. F-actin is a helix with a random variable twist, **298,** 131
Ehrlich S. D. *see under* Goursot R., **298,** 488
Eigen M. and Winkler R. Laws of the Game: How the Principles of Nature Govern Chance, *book review by* Orgel L. **298,** 497
Eisenberg A. *see under* Yelon A., **298,** 415
Elde R. P. *see under* Vincent S. R., **298,** 65
Elkind M. M. *see under* Hill C. K., **298,** 67
Elleder M. *see under* Činátl J., **298,** 388
Elliot J. L. *see under* French R. G., **298,** 827
Emanuel W. R. *see under* Post W. M., **298,** 156
Emlen S. T. *see under* Hegner R. E., **298,** 264
Emson P. C. *see under* Goedert M., **298,** 163
Epstein C. J. *see under* Magnuson T., **298,** 750
Erasmus S. J. *see under* Sinclair R., **298,** 127
Ermler W. C. *see under* Mulliken R. S., **298,** 406
Evans M. C. W. *book review of* Photosynthesis, (Akoyunoglou G. *editor*) **298,** 104
Evans R. M. *see under* Amara S. G., **298,** 240
Evans W. H. *see under* Debanne M. T., **298,** 398
Eyles N. *see under* Boulton G. S., **298,** 437
Fairbanks R. G., Sverdlove M., Free R., Wiebe P. H. and Bé A. W. H. Vertical distribution and isotopic fractionation of living planktonic foraminifera from the Panama Basin, **298,** 841
Fairtlough G. H. Celltech and MRC, *correspondence,* **298,** 600
Falkner F. G. and Zachau H. G. Expression of mouse immunoglobulin genes in monkey cells, **298,** 286
Fallon S. *see under* Welch J., **298,** 301
Farmer G. *see under* Wigley T. M. L., **298,** 499
Feldner J., Göbel U. and Bredt W. *Mycoplasma pneumoniae* adhesin localized to tip structure by monoclonal antibody, **298,** 765
Fellmann D. *see under* Bugnon C., **298,** 159
Ferin M. *see under* Krieger D. T., **298,** 468
Ferkany J. W., Zaczek R. and Coyle J. T. Kainic acid stimulates excitatory amino acid neurotransmitter release at presynaptic receptors, **298,** 757
Feriuga J. *see under* Mellor A. L., **298,** 529
Ferro-Luzzi Ames G. *see under* Higgins C. F., **298,** 723
  see under Higgins C. F., **298,** 760
Festenstein H. *see under* Mellor A. L., **298,** 529
Fialkow P. J. *see under* Keating A., **298,** 280
Field D. and Starmer I. C. Graphite genesis in high-grade metamorphic rocks, *matters arising,* **298,** 303
Figueroa N. N. *see under* Marsh D., **298,** 220
Fink G., Sarkar D. K., Dow R. C., Dick H., Borthwick N., Malnick S. and Twine M. Sex difference in response to alphaxalone anaesthesia may be oestrogen dependent, **298,** 270
Finkelstein E. *see under* Alber S., **298,** 414
Finner E. *see under* Römer D., **298,** 759
Finnie M. D. A. *see under* Bradbury A. F., **298,** 686
Finter N. B., Woodroofe J. and Priestman T. J. Monkeys are insensitive to pyrogenic effects of human α-interferons, *matters arising,* **298,** 301
Firshein W. *see under* Benjamin P., **298,** 769
Fisher R. G. *see under* Ohlendorf D. H., **298,** 718
Fitch W. M. *see under* Müller U. R., **298,** 582
Flamm M. and Schachter D. Acanthocytosis and cholesterol enrichment decrease lipid fluidity of only the outer human erythrocyte membrane leaflet, **298,** 290
Flanagan M. D. *see under* Masiello N. C., **298** 202
Flavell R. A. *see under* Mellor A. L., **298,** 529
Fleischer R. C. and Johnston R. F. Natural selection on body size and proportions in house sparrows, **298,** 747
Fletcher J. M. Tree rings and archaeology: dating Roman oaks, *news and views,* **298,** 227
Flexon P. B. and Rodell C. F. Genetic recombination and directional selection for DDT resistance in *Drosophila melanogaster,* **298,** 672
Flint N. *see under* Debanne M. T., **298,** 398
Flockerzi V. *see under* Osterrieder W., **298,** 576
Flynn L. J. and Guo-qin Q. Age of the Lufeng, China, hominoid locality, **298,** 746
Fodor M. S. Nuclear dangers, *correspondence,* **298,** 320
Foote S. *see under* Panthier J.-J., **298,** 90
Ford M. J. The Changing Climate: Responses of the Natural Fauna and Flora, *book review by* Pigott C. D. **298,** 497
Fothergill J. From CoA to complement: thioesters as the spring in the molecular mouse trap, *news and views,* **298,** 705
Fowles J. *see under* Bunker J. P., **298,** 405
Fox R. F. Biological Energy Transduction: The Uroboros, *book review by* Macnab R. M. **298,** 693
Fox T. Do mitochondria share enzymes with the rest of the cell? *news and views,* **298,** 323
Foyer C., Leegood R. and Walker D. What limits photosynthesis? *news and views,* **298,** 326
Francis N. *see under* Egelman E. H., **298,** 131
Fredrickson D. S. *book review of* Puzzles, Problems and Enigmas: Occasional Pieces on the Human Aspects of Science, (Ziman J.) **298,** 305
Free R. *see under* Fairbanks R. G., **298,** 841
Freed C. R. *see under* Yamamoto B. K., **298,** 467
Freeman L. A. *see under* Sinclair R., **298,** 127
Freeman R. D. *see under* Ohzawa I., **298,** 266
Freiman G. *see under* Alber S., **298,** 414
French R. G., Elliot J. L. and Allen D. A. Inclinations of the uranian rings, **298,** 827
Freter R. *see under* Edén C. S., **298,** 560
Fricks C. *see under* Stanfield B. B., **298,** 371
Fuller C. A. *see under* Moore-Ede M. C., **298,** 589
Furutani Y. *see under* Kakidani H., **298,** 245
Gage F. H. *see under* Björklund A., **298,** 652
Gaillard M. K. Supersymmetry — fact or fiction? *news and views,* **298,** 420
Gaines G. L. Jr Langmuir–Blodgett films of long-chain amines, **298,** 544
Gall Joseph G. *book review of* Gene Amplification, (Schimke Robert T. *editor*) **298,** 876
Galli E. *see under* D'Amelio R., **298,** 72
Galli S. J., Dvorak A. M., Ishizaka T., Nabel G., Der Simonian H., Cantor H. and Dvorak H. F. A cloned cell with NK function resembles basophils by ultrastructure and expresses IgE receptors, **298,** 288
Gallimore P. H. *see under* Byrd P., **298,** 69
Garcia G. *see under* Higgins C. F., **298,** 723
Garcia M. C. *see under* Gonzalez-Serratos H., **298,** 292
Garg K. C. Index for patents, *correspondence,* **298,** 414
Garson J. A., Beverley P. C. L., Coakham H. B. and Harper E. I. Monoclonal antibodies against human T lymphocytes label Purkinje neurones of many species, **298,** 375
Gavela M. B. *see under* Abbott L. F., **298,** 873
Gay N. J. *see under* Walker J. E., **298,** 867
Gayton R. J. Mammalian neuronal actions of FMRFamide and the structurally related opioid Met-enkephalin-Arg^6-Phe^7, **298,** 275
Geisel T. Chaos, randomness and dimension, *news and views,* **298,** 322
Geisow M. Lysosome proton pump identified, *news and views,*

298, 515
Gibbard P. *see under* Boulton G. S., **298**, 437
Gibson M. J. *see under* Krieger D. T., **298**, 468
Gieringer D. H. Meltdown risks, *correspondence*, **298**, 510
Gilbert F. *see under* Masters G., **298**, 609
Gillan F. T. and Johns R. B. Oxic diagenetic products as indicators of past oceanic algal populations and diversity, **298**, 744
Gingerich O. *book review of* The Expanding Universe: Astronomy's 'Great Debate', (Smith R. W.) **298**, 776
Girdler R. W. *see under* Brown C., **298**, 51
see under Tamsett D.,
Givol D. *see under* Zakut R., **298**, 857
Glanzman D. L. A private matter, **298**, 414 *correspondence*,
Glasby G. P. *see under* Cronan D. S., **298**, 456
Glashow S. L. *see under* Dimopoulos S., **298**, 824
Glass E. J. *see under* Stewart J., **298**, 852
Glassley W. Graphite genesis in high-grade metamorphic rocks—Reply, *matters arising*, **298**, 303
Glimcher L. H., Hamano T., Asofsky R., Heber-Katz E., Hedrick S., Schwartz R. H. and Paul W. E. I region-restricted antigen presentation by B cell-B lymphoma hybridomas, **298**, 283
Göbel U. *see under* Feldner J., **298**, 765
Goebel W. *see under* Hofschneider P. H., **298**, 777
Goeddel D. V. *see under* Gray P. W., **298**, 859
Goedert M., Lightman S. L., Nagy J. I., Marley P. D. and Emson P. C. Neurotensin in the rat anterior pituitary gland, **298**, 163
Golde D. W. *see under* Lusis A. J., **298**, 75
Golden L. *see under* Mellor A. L., **298**, 529
Goldstein S. *see under* Zindler A., **298**, 519
Gonzalez-Serratos H., Valle-Aguilera R., Lathrop D. A. and Garcia M. C. Slow inward calcium currents have no obvious role in muscle excitation–contraction coupling, **298**, 292
Goodman M. *see under* Czelusniak J., **298**, 297
Gordon L. I. *see under* Baross J. A., **298**, 366
Gorza L. *see under* Sartore S., **298**, 294
Gouget A. *see under* Bugnon C., **298**, 159
Gough D. O. Evidence for an oblique magnetic solar rotator, **298**, 350
Internal rotation and gravitational quadrupole moment of the Sun, **298**, 334
Gough M. P. and Korth A. New light on the equatorial source of pulsating aurora, **298**, 253
Goursot R., Goze A., Niaudet B. and Ehrlich S. D. Plasmids from *Staphylococcus aureus* replicate in yeast *Saccharomyces cerevisiae*, **298**, 488
Govind C. K. and Kent K. S. Transformation of fast fibres to slow prevented by lack of activity in developing lobster muscle, **298**, 755
Gower M. *see under* Welch J., **298**, 301
Gowlett J. A. J. *book review of* The Palaeolithic Age, (Wymer J.) **298**, 204
Goze A. *see under* Goursot R., **298**, 488
Grafen A. How not to measure inclusive fitness, *news and views*, **298**, 425
Grau-Wagemans M. P. *see under* Moonen G., **298**, 753
Gray P. W. and Goeddel D. V. Structure of the human immune interferon gene, **298**, 859
Gray R. A. *see under* Burton D. I., **298**, 562
Green H. W. II *see under* Vaughan P. J., **298**, 357
Green P. J. *see under* Anderton B. H., **298**, 84
Greenhough T. J. *see under* Arndt U. W., **298**, 835
Greenwood J. J. D. Prions have feathers, *correspondence*, **298**, 510
Grew E. S. *see under* DePaolo D. J., **298**, 614
Grey Dimond E. Alternative to war, *correspondence*, **298**, 220
Grivell L. A. and Borst P. Mitochondrial mosaics — maturases on the move, *news and views*, **298**, 703
Groudine M. *see under* Collins S., **298**, 679
Guckenheimer J. Noise in chaotic systems, **298**, 358
Guo-qin Q. *see under* Flynn L. J., **298**, 746
Gustafsson B. E. *see under* Axelson M., **298**, 659
Haag P. D. *see under* Higgins C. F., **298**, 723
Hagberg L. *see under* Edén C. S., **298**, 560
Hall A. R. *book review of* Plurality of Worlds: The Origins of the Extraterrestrial Life Debate from Democritus to Kant, (Dick S. J.) **298**, 588
Hall B. Bone in the cartilaginous fishes, *news and views*, **298**, 324
Hall B. D. *see under* Valenzuela P., **298**, 347
Hall D. O. Plant biology at the Carnegie Institution, *news and views*, **298**, 226
see under Coombs J., **298**, 206
Hall T. C. *see under* Loesch-Fries L. S., **298**, 771
Halpern M. *see under* DePaolo D. J., **298**, 614
Hamada H. and Kakunaga T. Potential Z-DNA forming sequences are highly dispersed in the human genome, **298**, 396
Hamaguchi Y. *see under* Shimizu A., **298**, 82
Hamano T. *see under* Glimcher L. H., **298**, 283
Hamerton J. L. *see under* Rosenmann E., **298**, 563
Hamilton I. Koestler: A Biography, *book review by* Wade N. **298**, 587
Han A. *see under* Hill C. K., **298**, 67
Hanawalt P. C. *see under* Lewis R. J., **298**, 393
Hansen J. A. *see under* Torok-Storb B., **298**, 473
Harbers K. *see under* Jähner D., **298**, 623
Hare P. E. *see under* Boulton G. S., **298**, 437
Harlow E. *see under* Lane D., **298**, 517
Harmison G. G. *see under* Altschuler R. A., **298**, 657
Harper E. I. *see under* Garson J. A., **298**, 375
Harris J. R. *Editor*, Electron Microscopy of Proteins, *book review by* Wrigley N. G. **298**, 498
Harris L. J. *see under* Marcu K. B., **298**, 87
Harris R. and Paxman J. A Higher Form of Killing, *book review by* Hay A. **298**, 205
Harvey A. Burning question, *correspondence*, **298**, 8
Haseltine W. A. *see under* Brash D. E., **298**, 189
Hawkes P. W. *book review of* Image Analysis and Mathematical Morphology. (Serra J.) **298**, 498
Hay A. *book review of* A Higher Form of Killing, (Harris R. and Paxman J.) **298**, 205
Hayes T. L. *see under* Maestre M. F., **298**, 773
Haynes J. R. Foraminfera, *book review by* Murray J. W. **298**, 876
Heber-Katz E. *see under* Glimcher L. H., **298**, 283
Heckford S. E. *see under* Lamers M. C., **298** 178
Hedrick S. *see under* Glimcher L. H., **298**, 283
Hegner R. E., Emlen S. T. and Demong N. J. Spatial organization of the white-fronted bee-eater, **298**, 264
Helfand S. L. *see under* Roder J. C., **298**, 569
Heller A. H. *see under* White W. F., **298**, 655
Helliwell J. R. *see under* Arndt U. W., **298**, 835
Henderson-Sellers A. De-fogging cloud determination algorithms, *news and views*, **298**, 419
Henderson-Sellers A. and Cogley J. G. The Earth's early hydrosphere, **298**, 832
Hershkovitz P. Supposed squirrel monkey affinities of the late Oligocene *Dolichocebus gaimanensis*, *matters arising*, **298**, 201
Hescheler J. *see under* Osterrieder W., **298**, 576
Hester K. and Boyle E. Water chemistry control of cadmium content in Recent benthic foraminifera, **298**, 260
Hewett-Emmett D. *see under* Czelusniak J., **298**, 297 **Hey A. J. G.** *see under* Aitchison I. J. R., **298**, 877
Higgins C. F., Ferro-Luzzi Ames G., Barnes W. M., Clement J. M. and Hofnung M. A novel intercistronic regulatory element of prokaryotic operons, **298**, 760
Higgins C. F., Haag P. D., Nikaido K., Ardeshir F., Garcia G. and Ferro-Luzzi Ames G. Complete nucleotide sequence and identification of membrane components of the histidine transport operon of *S. typhimurium*, **298**, 723
Hilbish T. J., Deaton L. E. and Koehn R. K. Effect of an allozyme polymorphism on regulation of cell volume, **298**, 688
Hildebrand J. G. *see under* Schneiderman A. M., **298**, 844
Hill C. K., Buonaguro F. M., Myers C. P., Han A. and Elkind M. M. Fission-spectrum neutrons at reduced dose rates enhance neoplastic transformation, **298**, 67
Hill R. C. *see under* Römer D., **298**, 759
Hirose T. *see under* Kakidani H., **298**, 245
Hirshfeld A. and Sinnott R. W. *Editors*, Sky Catalogue 2000.0. Volume 1, Stars to Magnitude 8.0, *book review by* Hughes D. W. **298**, 588
Hodych J. P. Magnetostrictive control of coercive force in multidomain magnetite, **298**, 542
Hofmann F. *see under* Osterrieder W., **298**, 576
Hofnung M. *see under* Higgins C. F., **298**, 760
Hofschneider P. H. and Goebel W. *Editors*, Gene Cloning in Organisms Other than E coli. Vol.96 Current Topics in Microbiology and Immunology, *book review by* Murray N. **298**, 777
Hofstadter D. R. and Dennett D. C. The Mind's I: Fantasies and Reflections on Self and Soul, *book review by* Jahoda M. **298**, 103
Hökfelt T. *see under* Vincent S. R., **298**, 65
Honjo T. *see under* Shimizu A., **298**, 82
see under Taniguchi M., **298**, 172
Hoover E. A. *see under* Rojko J. L., **298**, 385
Horiuchi T. *see under* Oeda K., **298**, 98
Horsefield B. *see under* Boulton G. S., **298**, 437
Hostetter M. K., Thomas M. L., Rosen F. S. and Tack B. F. Binding of C3b proceeds by a transesterification reaction at the thiolester site, **298**, 72
Houck J. C. Cashing in, *correspondence*, **298**, 114
Houghten R. A. *see under* Bittle J. L., **298**, 30
Howard J. A. K. *see under* Arndt U. W., **298**, 835
Huang P. M. *see under* Shindo H., **298**, 363
Hughes D. W. Meteorite falls, *news and views*, **298**, 116
book review of Sky Atlas 2000.0, (Tirion W.) **298**, 588
book review of Sky Catalogue 2000.0. Volume 1, Stars to Magnitude 8.0, (Hirshfeld A. and Sinnott R. W. *editors*) **298**, 588
The beginnings of solar-terrestrial studies, *news and views*, **298**, 518
Hull R. *see under* Edén C. S., **298**, 560
Hull S. *see under* Edén C. S., **298**, 560
Hültner L. *see under* Staber F. G., **298**, 79
Hunt G. E. *see under* Kondratyev K. Y., **298**, 208
Hurst J. *see under* Mellor A. L., **298**, 529
Husby J. A. *see under* Zachariassen K. E., **298**, 865
Hussain A. A. .K. *see under* Thomas C. M., **298**, 674
Hutchinson J. S. *see under* DiNicolantonio R., **298**, 846
Hutchison III C. A. *see under* Topal M. D., **298**, 863
Ihara M. *see under* Kuchino Y., **298**, 684
Ikeda-Saito M. *see under* Kitagawa T., **298**, 869
Imanishi-Kari T. *see under* Bothwell A. L. M., **298**, 380
Inayama S. *see under* Kakidani H., **298**, 245
Ingram M. J. *see under* Wigley T. M. L., **298**, 499
International Study Group An inter-laboratory comparison of radiocarbon measurements in tree rings, **298**, 619
Ioffe A. *see under* Alber S., **298**, 414
Ip W.-H. *see under* Wallis M. K., **298**, 229
Irlin J. *see under* Alber S., **298**, 414
Ishizaka T. *see under* Galli S. J., **298**, 288
Iso K. *see under* Takamatsu H., **298**, 819
Isselbacher K. J. *see under* Shouval D., **298**, 567
Ittekkot V. *see under* Degens E. T., **298**, 262
Iversen S. *book review of* Handbook of the Hypothalamus Vol.3, Parts A and B, Behavioral Studies of the Hypothalamus, (Morgane P. J. and Panksepp J. *editors*) **298**, 306
Iwagami N. and Ogawa T. Thermospheric 63-μm emission of atomic oxygen in local thermodynamic equilibrium, **298**, 454
Izett G. A. *see under* Obradovich J. D., **298**, 55
Jacob M. *book review of* Basics of Electron–Positron Collisions, (Renard F. M.) **298**, 104
Jacobson A. J. *see under* Melchior M. T., **298**, 455
Jacoby G. C. and Ulan L. D. Reconstruction of past ice conditions in a Hudson Bay estuary using tree rings, **298**, 637
Jacq C. *see under* Dujardin G., **298**, 628
Jacques J. *see under* Malthête J., **298**, 46
Jaenisch R. *see under* Jähner D., **298**, 623
Jagoutz E. *see under* Zindler A., **298**, 519
Jähner D., Stuhlmann H., Stewart C. L., Harbers K., Löhler J., Simon I. and Jaenisch R. *De novo* methylation and expression of retroviral genomes during mouse embryogenesis, **298**, 623
Jahoda M. *book review of* The Mind's I: Fantasies and Reflections on Self and Soul, (Hofstadter D. R. and Dennett D. C.) **298**, 103
James R. F. L. *see under* Mellor A. L., **298**, 529
Jardetzky O. and Roberts G. C. K. NMR in Molecular Biology, *book review by* Redfield A. G. **298**, 692
Jarman R. H. *see under* Melchior M. T., **298**, 455
Jarvis J. *see under* Boulton G. S., **298**, 437
Jean G. *see under* Bancroft G. M., **298**, 730
Jeffrey A. *see under* Pabo C. O., **298**, 441
Jeppsson J.-O. *see under* Carrell R. W., **298**, 329
Johansson O. *see under* Vincent S. R., **298**, 65
Johns R. B. *see under* Gillan F. T., **298**, 744
Johnson G. D. *see under* Burbank D. W., **298**, 432
Johnson N. M. *see under* Zeitler P. K., **298**, 255
Johnston R. F. *see under* Fleischer R. C., **298**, 747
Jollès P. *see under* Pauloin A., **298**, 574
Jolly C. J. *see under* Kalb J. E., **298**, 25
Jonas V. *see under* Amara S. G., **298**, 240
Jones J. S. *book review of* Darwin to DNA: Molecules to Humanity, (Ledyard Stebbins G.) **298**, 875
Genetic differences in individual behaviour associated with shell polymorphism in the snail *Cepaea nemoralis*, **298**, 749
Jordan T. H. *see under* Masters G., **298**, 609
Kafatos M. and Michalitsianos A. G. The peculiar variable star R Aquarii and its jet, **298**, 540
Kahn C. R. *see under* Kasuga M., **298**, 667
Kahn J. *see under* Anderton B. H., **298**, 84
Kakidani H., Furutani Y., Takahashi H., Noda M., Morimoto Y., Hirose T., Asai M., Inayama S., Nakanishi S. and Numa S. Cloning sequence analysis of cDNA for porcine β-neo-endorphin/dynorphin precursor, **298**, 245
Kakunaga T. *see under* Hamada H., **298**, 396
Kalb J. E., Jolly C. J., Mebrate A., Tebedge S., Smart C., Oswald E. B., Cramer D., Whitehead P., Wood C. B., Conroy G. C., Adefris T., Sperling L. and Kana B. Fossil mammals and artefacts from the Middle Awash Valley, Ethiopia, **298**, 25
Kalb J. E., Oswald E. B., Tebedge S., Mebrate A., Tola E. and Peak D. Geology and stratigraphy of Neogene deposits, Middle Awash Valley, Ethiopia, **298**, 17
Kalnins V. I. *see under* Turksen K., **298**, 763
Kamen-Kaye M. Earth science in Ovid, *correspondence*, **298**, 114
Kana B. *see under* Kalb J. E., **298**, 25
Kanno M. *see under* Taniguchi M., **298**, 172
Kasuga M., Zick Y., Blithe D. L., Crettaz M. and Kahn C. R. Insulin stimulates tyrosine phosphorylation of the insulin receptor in a cell-free system, **298**, 667
Kawano S. *see under* Kuroiwa T., **298**, 481
Kay R. L. F. *see under* Andrews J. N., **298**, 339
see under Andrews J. N., **298**, 361
Keating A., Singer J. W., Killen P. D., Striker G. E., Salo A. C., Sanders J., Thomas E. D., Thorning D. and Fialkow P. J. Donor origin of the *in vitro* haematopoietic microenvironment after marrow transplantation in man, **298**, 280
Kelly J. G. *see under* Butler J., **298**, 60
Kemp J. D. *see under* Reinisch C. L., **298**, 176
Kemp T. S. Mammal-Like Reptiles and the Origin of Mammals, *book review by* Cox B. **298**, 307
Kenny M. *see under* Benjamin P., **298**, 769
Kent K. S. *see under* Govind C. K., **298**, 755
Kepert D. L. Inorganic Stereochemistry, *book review by* Drew M. G. B. **298**, 106
Kerr R. C. and Turner J. S. Layered convection and crystal layers in multicomponent systems, **298**, 731
Kidder T. The Soul of a New Machine, *book review by* Lavington S. **298**, 590
Killen P. D. *see under* Keating A., **298**, 280
Kim H. *see under* Welch J., **298**, 301
Kimmel J. *see under* Vincent S. R., **298**, 65
Kinching G. H. Nuclear risks, *correspondence*, **298**, 220
King L. S. Medical Thinking: A Historical Preface, *book review by* Bynum W. F. **298**, 105
Kitagawa T., Ondrias M. R., Rousseau D. L., Ikeda-Saito M. and Yonetani T. Evidence for hydrogen bonding of bound dioxygen to the distal histidine of oxycobalt myoglobin and haemoglobin, **298**, 869
Klein S. *see under* Levi D. M., **298**, 268
Klobuchar J. A. *see under* Das Gupta A., **298**, 354
Knedler K. E. *see under* Cronan D. S., **298**, 456
Knobler R. L., Lampert P. W. and Oldstone M. B. A. Virus persistence and recurring demyelination produced by a temperature-sensitive mutant of MHV-4, **298**, 279
Koehn R. K. *see under* Hilbish T. J., **298**, 688
Koenig J. L. *see under* Painter P. C., **298**, 777
Kondo K. *see under* Shimizu A., **298**, 82
Kondratyev K. Y. and Hunt G. E. Weather and Climate on Planets, *book review by* Conway Leovy **298**, 208
Koontz S. W. *see under* Starzyk R. M., **298**, 136
Korth A. *see under* Gough M. P., **298**, 253
Kozu T., Yagura T. and Seno T. *De novo* DNA synthesis by a novel mouse DNA polymerase associated with primase activity, **298**, 180
Kraal G., Weissman I. L. and Butcher E. C. Germinal centre B cells: antigen specificity and changes in heavy chain class expression, **298**, 377
Krammer P. H. *see under* Staber F. G., **298**, 79
Kranias E. G. and Solaro R. J. Phosphorylation of troponin I and phospholamban during catecholamine stimulation of rabbit heart, **298**, 182
Kreis C. *see under* Rosenmann E., **298**, 563
Krieger D. T., Perlow M. J., Gibson M. J., Davies T. F., Zimmerman E. A., Ferin M. and Charlton H. M. Brain grafts reverse hypogonadism of gonadotropin releasing hormone deficiency, **298**, 468
Krishnamurthy R. V., DeNiro M. J. and Pant R. K. Isotope evidence for Pleistocene climatic changes in Kashmir, India, **298**, 640
Krovatin W. *see under* Pabo C. O., **298**, 441
Kruger F. J. and Marsh J. S. Significance of $^{87}\mathrm{Sr}/^{86}\mathrm{Sr}$ ratios in the Merensky cyclic unit of the Bushveld Complex, **298**, 53
Kuchino Y., Ihara M., Yabusaki Y. and Nishimura S. Initiator tRNAs from archaebacteria show common unique sequence characteristics, **298**, 684
Kuhn H. and Waser J. Evolution of early mechanisms of translation of genetic information into polypeptides, **298**, 585
Kuroiwa T., Kawano S., Nishibayashi S. and Sato C. Epifluorescent microscopic evidence for maternal inheritance of chloroplast DNA, **298**, 481
Lai Y. L., Wiggert B., Liu Y. P. and Chader G. J. Interphotoreceptor retinol-binding proteins: possible transport vehicles between compartments of the retina, **298**, 848
Lambeck K. Where has that Moon been? *news and views*, **298**, 704
Lamers M. C., Heckford S. E. and Dickler H. B. Monoclonal anti-Fc IgG receptor antibodies trigger B lymphocyte

function, **298** 178
Lampert P. W. *see under* Knobler R. L., **298,** 279
Lanave C. *see under* Saccone C., **298,** 8
Landshoff P. V. *book review of* Gauge Theories in Particle Physics: A Practical Introduction, (Aitchison I. J. R. and Hey A. J. G.) **298,** 877
Lane B. and Anderton B. Focus on filaments: embryology to pathology, *news and views,* **298,** 706
Lane D. and Harlow E. Two different viral transforming proteins bind the same host tumour antigen, *news and views,* **298,** 517
Lang R. B. *see under* Marcu K. B., **298,** 87
Langway C. C. Jr *see under* Shoji H., **298,** 548
Lasky L. A. *see under* Lusis A. J., **298,** 75
Lass Y. *see under* Lotan I., **298,** 572
Lathrop D. A. *see under* Gonzalez-Serratos H., **298,** 292
Latorre R. *see under* Coronado R., **298,** 849
Laurell C.-B. *see under* Carrell R. W., **298,** 329
Lavington S. *book review of* The Soul of a New Machine, (Kidder T.) **298,** 590
Lawrence A. The outer regions of galaxies, *news and views,* **298,** 421
Leach E. Social Anthropology, *book review by* Attenborough R. D. **298,** 403
Leavitt S. W. and Long A. Evidence for $^{13}C/^{12}C$ fractionation between tree leaves and wood, **298,** 742
Leben L. *see under* Mellor A. L., **298,** 529
Lebonov A. *see under* Alber S., **298,** 414
Leder P. *see under* Talkington C. A., **298,** 192
Ledyard Stebbins G. Darwin to DNA: Molecules to Humanity, *book review by* Jones J. S. **298,** 875
Lee D. J. *see under* Andrews J. N., **298,** 339
Lee M. C. *see under* Das Gupta A., **298,** 354
Leegood R. *see under* Foyer C., **298,** 326
Leffler H. *see under* Edén C. S., **298,** 560
Lehmann A. *see under* Bridges B., **298,** 118
Lehto V.-P. *see under* Virtanen I., **298,** 660
Leigh Brown A. Evolution and molecular biology, *news and views,* **298,** 793
Leinwand L. A. *see under* Pease L. R., **298,** 382
Lemos J. R., Novak-Hofer I. and Levitan I. B. Serotonin alters the phosphorylation of specific proteins inside a single living nerve cell, **298, 64**
Leng G. *see under* Bicknell R. J., **298,** 161
Lenoir G. M., Preud'homme J. L., Bernheim A. and Berger R. Correlation between immunoglobulin light chain expression and variant translocation in Burkitt's lymphoma, **298,** 474
Lerner A. *see under* Alber S., **298,** 414
Lerner R. A. *see under* Bittle J. L., **298,** 30
Lernmark A. *see under* Baekkeskov S., **298,** 167
Levey G. *see under* Ebbesen T. W., **298,** 545
Levi D. M. and Klein S. Hyperacuity and amblyopia, **298,** 268
Levitan I. B. *see under* Lemos J. R., **298,** 64
Lew V. L., Tsien R. Y., Miner C. and Bookchin R. M. Physiological [Ca^{2+}]i level and pump-leak turnover in intact red cells measured using an incorporated Ca chelator, **298,** 478
Lewis M. *see under* Pabo C. O., **298,** 443
see under Sauer R. T., **298,** 447
Lewis R. J. and Hanawalt P. C. Ligation of oligonucleotides by pyrimidine dimers — a missing 'link' in the origin of life? **298,** 393
Lichtler A. C., Sierra F., Clark S., Wells J. R. E., Stein J. L. and Stein G. S. Multiple H4 histone mRNAs of HeLa cells are encoded in different genes, **298,** 195
Liebman J. *see under* Welch J., **298,** 301
Lighthill J. and Pearce R. P. ***Editors***, Monsoon Dynamics, *book review by* Chervin R. M. **298,** 308
Lightman S. L. *see under* Goedert M., **298,** 163
Lilley M. D. *see under* Baross J. A., **298,** 366
Lin S. *see under* Masiello N. C., **298** 202
Lincoln T. *book review of* The Politics of Clean Air, (Ashby E. and Anderson M.) **298,** 207
Lindahl T. Worthy of a detour, *news and views,* **298,** 424
Link C. D. and Reiner A. M. Inverted repeats surround the ribitol–arabitol genes of *E. coli* C, **298,** 94
Little J. W. *see under* Sancar A., **298,** 96
Liu Y. P. *see under* Lai Y. L., **298,** 848
Loesch-Fries L. S. and Hall T. C. *In vivo* aminoacylation of brome mosaic and barley stripe mosaic virus RNAs, **298,** 771
Löhler J. *see under* Jähner D., **298,** 623
Long A. 100 to 200 year solar periodicities, *news and views,* **298,** 223
see under Leavitt S. W., **298,** 742
Long S. R., Buikema W. J. and Ausubel F. M. Cloning of *Rhizobium meliloti* nodulation genes by direct complementation of Nod$^-$ mutants, **298,** 485
Lotan I., Dascal N., Cohen S. and Lass Y. Adenosine-induced slow ionic currents in the *Xenopus* oocyte, **298,** 572
Loubet M. and Allègre Trace elements in orogenic lherzolites reveal the complex history of the upper mantle, **298,** 809
Low D. A., Scott R. W., Baker J. B. and Cunningham D. D. Cells regulate their mitogenic response to thrombin through release of protease nexin, **298,** 476
Ludvigsson J. *see under* Baekkeskov S., **298,** 167
Lusis A. J., Golde D. W., Quon D. H. and Lasky L. A. Translation of mRNA for human granulocyte-macrophage colony-stimulating factor, **298,** 75
Lyne A. G. and Smith F. G. Interstellar scintillation and pulsar velocities, **298,** 825
Lyons L. What are quarks made of? *news and views,* **298,** 601
McCabe A. M. *see under* Boulton G. S., **298,** 437
McClintock P. Crossings and reconnections in superfluid helium-4, *news and views,* **298,** 225
McDougall J. C. *see under* Cronan D. S., **298,** 456
McGarry R. *see under* Roder J. C., **298,** 569
McGuckin M. M. *see under* Trayhurn P., **298,** 59
McIlwrath B. K. *see under* Stannard D., **298,** 140
MacLeod R. *book review of* John Tyndall: Essays on a Natural Philosopher, (Brock W. H. *et al. editors*) **298,** 305
McMullen M. D. *see under* Arp B., **298,** 184
McMurtry G. M. *see under* Malahoff A., **298,** 234
Macnab R. M. *book review of* Biological Energy Transduction: The Uroboros, (Fox R. F.) **298,** 693
MacNeil D. *see under* Welch J., **298,** 301
Maddox J. *book review of* A Supplement to the Oxford English Dictionary Vol.III. O-Scz., (Burchfield R. W. *editor*) **298,** 309
Madsen J. U. *see under* Cotterill R. M. J., **298,** 874
Maestre M. F., Bustamante C., Hayes T. L., Subirana J. A. and Tinoco Jr I. Differential scattering of circularly polarized light by the helical sperm head from the octopus *Eledone cirrhosa*, **298,** 773
Magnuson T., Epstein C. J., Silver L. M. and Martin G. R. Pluripotent embryonic stem cell lines can be derived from t^{w5}/t^{w5} blastocysts, **298,** 750
Malahoff A., McMurtry G. M., Wiltshire J. C. and Yeh H.-W. Geology and chemistry of hydrothermal deposits from active submarine volcano Loihi, Hawaii, **298,** 234
Malasková V. *see under* Činátl J., **298,** 388
Malnick S. *see under* Fink G., **298,** 270
Malthête J., Jacques J., Tinh N. H. and Destrade C. Macroscopic evidence of molecular chirality in columnar mesophases, **298,** 46
Maluski H., Proust F. and Xiao X. C. $^{39}Ar/^{40}Ar$ dating of the trans-Himalayan calc-alkaline magmatism of southern Tibet, **298,** 152
Mann C. *see under* Scherer S., **298,** 815
Manton W. I. *see under* DePaolo D. J., **298,** 614
Marcu K. B. and Cooper M. D. New views of the immunoglobulin heavy-chain switch, *news and views,* **298,** 327
Marcu K. B., Lang R. B., Stanton L. W. and Harris L. J. A model for the molecular requirements of immunoglobulin heavy chain class switching, **298,** 87
Marcucci F. *see under* Staber F. G., **298,** 79
Mariani A. P. Association amacrine cells could mediate directional selectivity in pigeon retina, **298,** 654
Marilley M. *see under* Buongiorno-Nardelli M., **298,** 100
Marley P. D. *see under* Goedert M., **298,** 163
Marner B. *see under* Baekkeskov S., **298,** 167
Marr D. Vision: A Computational Investigation into the Human Representation and Processing of Visual Information, *book review by* Sutherland S. **298,** 691
Marsh D. and Figueroa N. N. Access to journals, *correspondence,* **298,** 220
Marsh J. S. *see under* Kruger F. J., **298,** 53
Martin G. R. *see under* Magnuson T., **298,** 750
Marty J.-C. and Saliot A. Aerosols in equatorial Atlantic air: *n*-alkanes as a function of particle size, **298,** 144
Masiello N. C., Zucker M. B., Casella J. F., Flanagan M. D. and Lin S. Effect of cytochalasin D on thrombin-induced actin filaments in platelets, *matters arising,* **298** 202
Masters G., Jordan T. H., Silver P. G., and Gilbert F. Aspherical Earth structure from fundamental spheridal-mode data, **298,** 609
Masuda N., Nishimura M. and Torii T. Pathway and distribution of trace elements in Lake Vanda, Antarctica, **298,** 154
Matsumoto S. G. *see under* Schneiderman A. M., **298,** 844
Matthews B. W. *see under* Ohlendorf D. H., **298,** 718
Matthews D. H. BIRPS: deep seismic reflection profiling around the British Isles, *news and views,* **298,** 709
Maurer R. *see under* Römer D., **298,** 759
Mayer E. and Brüggeller P. Vitrification of pure liquid water by high pressure jet freezing, **298,** 715
Mebrate A. *see under* Kalb J. E., **298,** 17
see under Kalb J. E., **298,** 25
Medina A. *see under* Valenzuela P., **298,** 347
Mehrotra K. N. *see under* Sharma V. P., **298,** 210
Meiman N. *see under* Alber S., **298,** 414
Melchior M. T., Vaughan D. E. W., Jarman R. H. and Jacobson A. J. The characterization of Si–Al ordering in A-type zeolite (ZK4) by ^{29}Si NMR, **298,** 455
Mellor A. L., Golden L., Weiss E., Bullman H., Hurst J., Simpson E., James R. F. L., Townsend A. R. M., Taylor P. M., Schmidt W., Ferluga J., Leben L., Santamaria M., Atfield G., Festenstein H. and Flavell R. A. Expression of murine H–2K^b histocompatibility antigen in cells transformed with cloned *H–2* genes, **298,** 529
Menagh D. P. *see under* Bell K., **298,** 251
Mendelsohn F. A. O. *see under* DiNicolantonio R., **298,** 846
Mendelson R. X-ray scattering by myosin S-1: implications for the steric blocking model of muscle control, **298,** 655
Merrell D. J. Ecological Genetics, *book review by* Berry R. J. **298,** 205
Meyerson B. *see under* Vincent S. R., **298,** 65
Michalitsianos A. G. *see under* Kafatos M., **298,** 540
Micheli G. *see under* Buongiorno-Nardelli M., **298,** 100
Mickelson C. A. *see under* Cushley W., **298,** 77
Micklem H. S. *see under* Burton D. I., **298,** 562
Milburn O. Known quantity, *correspondence,* **298,** 114
Milkowski W. *see under* Römer D., **298,** 759
Miller G. *see under* Boulton G. S., **298,** 437
Miner C. *see under* Lew V. L., **298,** 478
Ming-hui H., Stallard R. F. and Edmond J. M. Major ion chemistry of some large Chinese rivers, **298,** 550
Mittermeier R. A. *see under* Coimbra-Filho A. F., **298,** 308
Mold P. *see under* Bull R. K., **298,** 634
Mollenhauer E. *see under* Roos M. H., **298,** 854
Montadert L. *see under* Cherchi A., **298,** 736
Montal M. *see under* Donovan J. J., **298,** 669
Montesano R. Drugs as carcinogens, *correspondence,* **298,** 600
Mook W. G. *see under* de Jong A. F. M., **298,** 641
Moonen G., Grau-Wagemans M. P. and Selak I. Plasminogen activator-plasmin system and neuronal migration, **298,** 753
Moorby S. A. *see under* Cronan D. S., **298,** 456
Moore P. D. Measuring competition in plant communities, *news and views,* **298,** 514
Moore-Ede M. C., Sulzman F. M. and Fuller C. A. The Clocks That Time Us: Physiology of the Circadian Timing System, *book review by* Winfree A. T. **298,** 589
Moreton R. B. *book review of* Membrane Physiology of Invertebrates, (Podesta R. B. *editor*) **298,** 106
Morgan P. *see under* Wendlandt R. F., **298,** 734
Morgane P. J. and Panksepp J. ***Editors***, Handbook of the Hypothalamus Vol.3, Parts A and B, Behavioral Studies of the Hypothalamus, *book review by* Iversen S. **298,** 306
Morimoto Y. *see under* Kakidani H., **298,** 245
Moriwaki K. *see under* Shimizu A., **298,** 82
Mosinger J. L. *see under* Altschuler R. A., **298,** 657
Mount D. W. *see under* Sancar A., **298,** 96
Müller U. R. and Fitch W. M. Evolutionary selection for perfect hairpin structures in viral DNAs, **298,** 582
Müller-Eberhard H. J. *see under* Tschopp J., **298,** 534
Mulliken R. S. and Ermler W. C. Polyatomic Molecules: Results of ab Initio Calculations, *book review by* Richards W. G. **298,** 406
Muneoka K. and Bryant S. V. Evidence that patterning mechanisms in developing and regenerating limbs are the same, **298,** 369
Muñoz E. *see under* Pestaña A., **298,** 608
Murray J. W. *book review of* Foraminfera, (Haynes J. R.) **298,** 876
Murray N. *book review of* Gene Cloning in Organisms Other than E coli. Vol.96 Current Topics in Microbiology and Immunology, (Hofschneider P. H. and Goebel W. *editors*) **298,** 777
Myers C. P. *see under* Hill C. K., **298,** 67
Nabel G. *see under* Galli S. J., **298,** 288
Nabholz M. *see under* Conzelmann A., **298,** 170
Naeser C. W. *see under* Obradovich J. D., **298,** 55
see under Zeitler P. K., **298,** 255
Nagle J. F. Dielectric constant of ice, *matters arising,* **298,** 401
Nagy J. I. *see under* Goedert M., **298,** 163
Nakanishi S. *see under* Kakidani H., **298,** 245
Narlikar J. V. Violent Phenomena in the Universe, *book review by* Press W. H. **298,** 103
Nathenson S. G. *see under* Pease L. R., **298,** 382
Needham M. *see under* Parker M., **298,** 92
Neilsen J. H. *see under* Baekkeskov S., **298,** 167
Nelkin D. *book review of* Risk and Culture: An Essay on the Selection of Technological and Environmental Dangers, (Douglas M. and Wildavsky A.) **298,** 775
Ness N. F. *see under* Connerney J. E. P., **298, 44**
Neuman S. *see under* Zakut R., **298,** 857
Niaudet B. *see under* Goursot R., **298,** 488
Nikaido K. *see under* Higgins C. F., **298,** 723
Nishibayashi S. *see under* Kuroiwa T., **298,** 481
Nishimura M. *see under* Masuda N., **298,** 154
Nishimura S. *see under* Kuchino Y., **298,** 684
Nixon W. C. *see under* Sinclair R., **298,** 127
Noda M. *see under* Kakidani H., **298,** 245
Novak-Hofer I. *see under* Lemos J. R., **298,** 64
Nudel U. *see under* Zakut R., **298,** 857
Numa S. *see under* Kakidani H., **298,** 245
Obradovich J. D., Naeser C. W., Izett G. A., Pasini G. and Bigazzi G. Age constraints on the proposed Plio–Pleistocene boundary stratotype of Vrica, Italy, **298,** 55
O'Brien M. *see under* Butler J., **298,** 60
Oeda K., Horiuchi T. and Sekiguchi M. The *uvrD* gene of *E. coli* encodes a DNA-dependent ATPase, **298,** 98
Ogawa T. *see under* Iwagami N., **298, 454**
Ohlendorf D. H., Anderson W. F., Fisher R. G., Takeda Y. and Matthews B. W. The molecular basis of DNA-protein recognition inferred from the structure of cro repressor, **298,** 718
Ohzawa I., Sclar G. and Freeman R. D. Contrast gain control in the cat visual cortex, **298,** 266
O'Keefe J. D. and Ahrens T. J. Impact mechanics of the Cretaceous–Tertiary extinction bolide, **298,** 123
Oldstone M. B. A. *see under* Knobler R. L., **298,** 279
O'Leary D. D. M. *see under* Stanfield B. B., **298,** 371
Olsen R. G. *see under* Rojko J. L., **298,** 385
Olsson T. *see under* Carlsson A., **298,** 739
O'Malley K. *see under* Butler J., **298,** 60
Ondrias M. R. *see under* Kitagawa T., **298,** 869
Ong E. S. *see under* Amara S. G., **298,** 240
Ooi B. S. *see under* Ooi Y. M., **298,** 389
Ooi Y. M. and Ooi B. S. Biosynthesis of membrane factor B by mouse peritoneal macrophages, **298,** 389
Oprandy J. J. *see under* Dawson G. J., **298,** 580
Orgel L. *book review of* Laws of the Game: How the Principles of Nature Govern Chance, (Eigen M. and Winkler R.) **298,** 497
Osterrieder W., Brum G., Hescheler J., Trautwein W., Flockerzi V. and Hofmann F. Injection of subunits of cyclic AMP-dependent protein kinase into cardiac myocytes modulates Ca^{2+} current, **298,** 576
Oswald E. B. *see under* Kalb J. E., **298,** 17
see under Kalb J. E., **298,** 25
Ottar B. Air pollution in the Arctic, *news and views,* **298,** 518
Owen M. C. *see under* Carrell R. W., **298,** 329
Owen R. B., Barthelme J. W., Renaut R. W. and Vincens A. Palaeolimnology and archaeology of Holocene deposits north-east of Lake Turkana, Kenya, **298,** 523
Pabo C. O. *see under* Sauer R. T., **298,** 447
Pabo C. O., Krovatin W., Jeffrey A. and Sauer R. T. The N-terminal arms of λ repressor wrap around the operator DNA, **298,** 441
Pabo C. O. and Lewis M. The operator-binding domain of λ repressor: structure and DNA recognition, **298, 443**
Pain R. Protein folding by numbers, *news and views,* **298,** 513
Painter P. C., Coleman M. M. and Koenig J. L. The Theory of Vibrational Spectroscopy and Its Application to Polymeric Materials, *book review by* Peticolas W. L. **298,** 777
Palmieri J. R. Be fair to parasites, *correspondence,* **298,** 220
Paluska E. *see under* Činátl J., **298,** 388
Panksepp J. *see under* Morgane P. J., **298,** 306
Pant R. K. *see under* Krishnamurthy R. V., **298,** 640
Panthier J.-J., Foote S., Chambraud B., Strosberg A. D., Corvol P. and Rougeon F. Complete amino acid sequence and maturation of the mouse submaxillary gland renin precursor, **298,** 90
Parakkal M. H. *see under* Altschuler R. A., **298,** 657
Parker M., Needham M. and White R. Prostatic steroid binding protein: gene duplication and steroid binding, **298,** 92
Parkinson D. W. *see under* Babior B. M., **298,** 511
Pasachoff J. M. and Strassburg M. A. Body temperature changes during the practice of G Tum-mo yoga, *matters arising,* **298,** 402
Pasini G. *see under* Obradovich J. D., **298,** 55
Paskind M. *see under* Bothwell A. L. M., **298,** 380
Patterson L. K. *see under* Ebbesen T. W., **298,** 545
Paul W. E. *see under* Glimcher L. H., **298,** 283
Pauloin A., Bernier I. and Jollès P. Presence of cyclic nucleotide–Ca^{2+} independent protein kinase in bovine brain coated vesicles, **298,** 574
Paxman J. *see under* Harris R., **298,** 205
Peacock J. D. *see under* Boulton G. S., **298,** 437
Peak D. *see under* Kalb J. E., **298,** 17
Pearce R. P. *see under* Lighthill J., **298,** 308
Pease L. R., Nathenson S. G. and Leinwand L. A. Mapping class I gene sequences in the major histocompatibility complex, **298,** 382
Pease R. S. *book review of* Fusion: Vol. 1, Magnetic Confinement, (Teller E. *editor*) **298,** 404
Pennycook S. J. *see under* Berger S. D., **298,** 635

Penston M. Remote operation of telescopes, *news and views*, **298**, 603
Perlow M. J. *see under* Krieger D. T., **298**, 468
Pestaña A. and Muñoz E. Anilides and the Spanish toxic oil syndrome, *news and views*, **298**, 608
Petcher T. J. *see under* Römer D., **298**, 759
Peticolas W. L. *book review of* The Theory of Vibrational Spectroscopy and Its Application to Polymeric Materials, (Painter P. C., Coleman M. M., Koenig J. L.) **298**, 777
Petrosian V. Phase transitions and dynamics of the Universe, **298**, 805
Pickles A. *see under* Visvanathan N., **298**, 41
Piggott J. R., Rai R. and Carter B. L. A. A bifunctional gene product involved in two phases of the yeast cell cycle, **298**, 391
Pigott C. D. *book review of* The Changing Climate: Responses of the Natural Fauna and Flora, (Ford M. J.) **298**, 497
Pippard B. Ball of fire? *correspondence*, **298**, 702
Podack E. R. *see under* Tschopp J., **298**, 534
Podesta R. B. *Editor*, Membrane Physiology of Invertebrates, *book review by* Moreton R. B. **298**, 106
Ponce F. A. *see under* Sinclair R., **298**, 127
Pontecorvo G. *book review of* Genes, Radiation, and Society: The Life and Work of H. J. Muller, (Carlson E. A.) **298**, 203
Post W. M., Emanuel W. R., Zinke P. J. and Stangenberger A. G. Soil carbon pools and world life zones, **298**, 156
Potter M. D. *see under* Richstone D. O., **298**, 728
Press W. H. *book review of* Violent Phenomena in the Universe, (Narlikar J. V.) **298**, 103
Preud'homme J. L. *see under* Lenoir G. M., **298**, 474
Priest E. R. *Editor*, Solar Flare Magnetohydrodynamics, *book review by* Rosner R. **298**, 693
Priestman T. J. *see under* Finter N. B., **298**, 301
Primack J. R. *see under* Sher M. A., **298**, 873
Proudfoot N. The end of the message, *news and views*, **298**, 516
Proust F. *see under* Maluski H., **298**, 152
Pulciani S. *see under* Santos E., **298**, 343
Purcell E. M. *see under* Dimopoulos S., **298**, 824
Quach T. T., Rose C., Duchemin A. M. and Schwartz J. C. Glycogenolysis induced by serotonin in brain: identification of a new class of receptor, **298**, 373
Quackenbush S. L. *see under* Rojko J. L., **298**, 385
Quon D. H. *see under* Lusis A. J., **298**, 75
Rabb T. K. *see under* Rotberg R. I., **298**, 499
Raff M. C. Do antigen-presenting cells distinguish self from non-self? *news and views*, **298**, 791
Rai R. *see under* Piggott J. R., **298**, 391
Rajewsky K. *see under* Bothwell A. L. M., **298**, 380
Redfield A. G. *book review of* NMR in Molecular Biology, (Jardetzky O. and Roberts G. C. K.) **298**, 692
Reed T. E. Living in the past? *correspondence*, **298**, 320
Regoeczi E. *see under* Debanne M. T., **298**, 398
Reiner A. M. *see under* Link C. D., **298**, 94
Reinisch C. L., Sing A. P., Waldron J. A. and Kemp J. D. Isolation of malignant and functional Ly1 + T-cell clones from B-cell lymphomas, **298**, 176
Reisfeld R. A. Monoclonal antibodies to human malignant melanoma, *news and views*, **298**, 325
Reitman M. *see under* Alber S., **298**, 414
Renard F. M. Basics of Electron–Positron Collisions, *book review by* Jacob M. **298**, 104
Renaut R. W. *see under* Owen R. B., **298**, 523
Reth M. *see under* Bothwell A. L. M., **298**, 380
Rice-Ficht A. C., Chen K. K. and Donelson J. E. Point mutations during generation of expression-linked extra copy of trypanosome surface glycoprotein gene, **298**, 676
Richards W. G. *book review of* Polyatomic Molecules: Results of ab Initio Calculations, (Mulliken R. S. and Ermler W. C.) **298**, 406
Richstone D. O. and Potter M. D. Character of 'prolate' galaxies, **298**, 728
Rigby P. W. J. *book review of* DNA Tumor Viruses, (Tooze J. *editor*) **298**, 406
Rittner C. *see under* Roos M. H., **298**, 854
Roberts E. B. *et al. Editors*, Biomedical Innovation, *book review by* Bunker J. P., Fowles J. **298**, 405
Roberts G. C. K. *see under* Jardetzky O., **298**, 692
Rodell C. F. *see under* Flexon P. B., **298**, 672
Roder J. C., Helfand S. L., Werkmeister J., McGarry R., Beaumont T. J. and Duwe A. Oxygen intermediates are triggered early in the cytolytic pathway of human NK cells, **298**, 569
Rojko J. L., Hoover E. A., Quackenbush S. L. and Olsen R. G. Reactivation of latent feline leukaemia virus infection, **298**, 385
Römer D., Büscher H. H., Hill R. C., Maurer R., Petcher T. J., Zeugner H., Benson W., Finner E., Milkowski W. and Thies P. W. An opioid benzodiazepine, **298**, 759
Roos M. H., Mollenhauer E., Démant P. and Rittner C. A molecular basis for the two locus model of human complement component C4, **298**, 854
Rose C. *see under* Quach T. T., **298**, 373
Rosen F. S. *see under* Hostetter M. K., **298**, 72
Rosenberger A. L. Supposed squirrel monkey affinities of the late Oligocene *Dolichocebus gaimanensis*—Reply, *matters arising*, **298**, 201
Rosenfeld M. G. *see under* Amara S. G., **298**, 240
Rosenmann E., Kreis C., Thompson R. G., Dobbs M., Hamerton J. L. and Wrogemann K. Analysis of fibroblast proteins from patients with Duchenne muscular dystrophy by two-dimensional gel electrophoresis, **298**, 563
Rosner R. *book review of* Solar Flare Magnetohydrodynamics, (Priest E. R. *editor*) **298**, 693
Rossi H. H. Complicating SI, *correspondence*, **298**, 320
Rossier J. Opioid peptides have found their roots, *news and views*, **298**, 221
Rotberg R. I. and Rabb T. K. *Editors*, Climate and History, *book review by* Schneider S. H. **298**, 499
Rougeon F. *see under* Panthier J.-J., **298**, 90
Rousseau D. L. *see under* Kitagawa T., **298**, 869
Rowan-Robinson M. *see under* Tarbet P. W., **298**, 711
Rowlands D. J. *see under* Bittle J. L., **298**, 30
Rule S. A. *see under* Arndt U. W., **298**, 835
Rupp W. D. *see under* Sancar A., **298**, 96
Rutter W. J. *see under* Valenzuela P., **298**, 347
Saccone C., Lanave C., Attimonelli M. and Simpson G. Sequence software, *correspondence*, **298**, 8
Sachs C. *see under* Vincent S. R., **298**, 65
Saliot A. *see under* Marty J.-C., **298**, 144
Salo A. C. *see under* Keating A., **298**, 280
Samallo J. *see under* van den Boogaart P., **298**, 187
Sancar A., Sancar G. B., Rupp W. D., Little J. W. and Mount D. W. LexA protein inhibits transcription of the *E. coli uvrA* gene *in vitro*, **298**, 96
Sancar G. B. *see under* Sancar A., **298**, 96
Sandbach F. Principles of Pollution Control, *book review by* White E. **298**, 778
Sanders J. *see under* Keating A., **298**, 280
Santamaria M. *see under* Mellor A. L., **298**, 529
Santos E., Tronick S. R., Aaronson S. A., Pulciani S. and Barbacid M. T24 human bladder carcinoma oncogene is an activated form of the normal human homologue of BALB- and Harvey-MSV transforming genes, **298**, 343
Saraste M. *see under* Walker J. E., **298**, 867
Sarill W. J. *see under* Cohen J. M., **298**, 829
Sarkar D. K. *see under* Fink G., **298**, 270
Sartore S., Gorza L. and Schiaffino S. Fetal myosin heavy chains in regenerating muscle, **298**, 294
Sato C. *see under* Kuroiwa T., **298**, 481
Sauer R. T. *see under* Pabo C. O., **298**, 441
Sauer R. T., Yocum R. R., Doolittle R. F., Lewis M. and Pabo C. O. Homology among DNA-binding proteins suggests use of a conserved super-secondary structure, **298**, 447
Schachter D. *see under* Flamm M., **298**, 290
Schellekens H. *see under* Weissman C., **298**, 301
Scherer S., Mann C. and Davis R. W. Reversion of a promoter deletion in yeast, **298**, 815
Schiaffino S. *see under* Sartore S., **298**, 294
Schimke Robert T. *Editor*, Gene Amplification, *book review by* Gall Joseph G. **298**, 876
Schimmel P. *see under* Starzyk R. M., **298**, 136
Schmidt W. *see under* Mellor A. L., **298**, 529
Schneider S. H. *book review of* Climate and History, (Rotberg R. I. and Rabb T. K. *editors*) **298**, 499
  book review of Climate and History: Studies in Past Climates and Their Impact on Man, (Wigley T. M. L., Ingram M. J., Farmer G. *editors*) **298**, 499
Schneiderman A. M., Matsumoto S. G. and Hildebrand J. G. Trans-sexually grafted antennae influence development of sexually dimorphic neurones in moth brain, **298**, 844
Schoolnik G. *see under* Edén C. S., **298**, 560
Schramm D. N. *see under* Crawford M., **298**, 538
Schwartz J. C. *see under* Quach T. T., **298**, 373
Schwartz R. H. *see under* Glimcher L. H., **298**, 283
Sclar G. *see under* Ohzawa I., **298**, 266
Scott C. No "remote viewing", *correspondence*, **298**, 414
Scott R. W. *see under* Low D. A., **298**, 476
Sekiguchi M. *see under* Oeda K., **298**, 98
Selak I. *see under* Moonen G., **298**, 753
Seminara R. *see under* D'Amelio R., **298**, 72
Seno T. *see under* Kozu T., **298**, 180
Serra J. Image Analysis and Mathematical Morphology, *book review by* Hawkes P. W. **298**, 498
Setchell K. D. R. *see under* Axelson M., **298**, 659
Shafritz D. A. *see under* Shouval D., **298**, 567
Shani M. *see under* Zakut R., **298**, 857
Sharma V. P. and Mehrotra K. N. Return of malaria, *correspondence*, **298**, 210
Shaw G. and Weber K. Differential expression of neurofilament triplet proteins in brain development, **298**, 277
Shaw S. *see under* van Leeuwen A., **298**, 565
Sher M. A. and Primack J. R. Absence of thermal effects on photon mass measurements—Reply, *matters arising*, **298**, 873
Shi Y. *see under* Wang C., **298**, 553
Shimizu A. *see under* Taniguchi M., **298**, 172
Shimizu A., Hamaguchi Y., Yaoita Y., Moriwaki K., Kondo K. and Honjo T. Japanese wild mouse, *Mus musculus molossinus*, has duplicated immunoglobulin γ2a genes, **298**, 82
Shindo H. and Huang P. M. Role of Mn (IV) oxide in abiotic formation of humic substances in the environment, **298**, 363
Shinnick T. M. *see under* Bittle J. L., **298**, 30
Shoji H. and Langway C. C. Jr Air hydrate inclusions in fresh ice core, **298**, 548
Shouval D., Shafritz D. A., Zurawski V. R. Jr, Isselbacher K. J. and Wands J. R. Immunotherapy in nude mice of human hepatoma using monoclonal antibodies against hepatitis B virus, **298**, 567
Sierra F. *see under* Lichtler A. C., **298**, 195
Silander J. A. and Antonovics J. Analysis of interspecific interactions in a coastal plant community — a perturbation approach, **298**, 557
Silva A. *see under* Conzelmann A., **298**, 170
Silver L. M. *see under* Magnuson T., **298**, 750
Silver P. G. *see under* Masters G., **298**, 609
Simon I. *see under* Jähner D., **298**, 623
Simon M. I. *see under* Donovan J. J., **298**, 669
Simon T. German universities, *correspondence*, **298**, 320
Simpson E. *see under* Mellor A. L., **298**, 529
Simpson G. *see under* Saccone C., **298**, 8
Sinclair R., Ponce F. A., Yamashita T., Smith D. J., Camps R. A., Freeman L. A., Erasmus S. J., Nixon W. C., Smith K. C. A. and Catto C. J. D. Dynamic observation of defect annealing in CdTe at lattice resolution, **298**, 127
Sing A. P. *see under* Reinisch C. L., **298**, 176
Singer J. W. *see under* Keating A., **298**, 280
Sinnott R. W. *see under* Hirshfeld A., **298**, 588
Sjövall J. *see under* Axelson M., **298**, 659
Skibinski D. O. F. and Ward R. D. Correlation between heterozygosity and evolutionary rate of proteins, **298**, 490
Slayter H. Clathrin locks up vesicle structure, *news and views*, **298**, 228
Slonimski P. P. *see under* Dujardin G., **298**, 628
Smart C. *see under* Kalb J. E., **298**, 25
Smith C. A. *see under* Thomas C. M., **298**, 674
Smith C. A. B. The numbers game, *correspondence*, **298**, 600
Smith D. J. *see under* Sinclair R., **298**, 127
Smith F. G. *see under* Lyne A. G., **298**, 825
Smith H. Light-piping by plant tissues, *news and views*, **298**, 423
Smith K. C. A. *see under* Sinclair R., **298**, 127
Smith P. J. Why honeycomb weathering? *news and views*, **298**, 121
Smith R. W. The Expanding Universe: Astronomy's 'Great Debate', *book review by* Gingerich O. **298**, 776
Smyth D. G. *see under* Bradbury A. F., **298**, 686
Snider M. D. Transport of sugars during glycoprotein synthesis, *news and views*, **298**, 117
Solaro R. J. *see under* Kranias E. G., **298**, 182
Solomon S. C. The internal evolution of Venus and the galilean satellites, *news and views*, **298**, 15
Sperling L. *see under* Kalb J. E., **298**, 25
Staber F. G., Hültner L., Marcucci F. and Krammer P. H. Production of colony-stimulating factors by murine T cells in limiting dilution and long-term cultures, **298**, 79
Stallard R. F. *see under* Ming-hui H., **298**, 550
Stanfield B. B., O'Leary D. D. M. and Fricks C. Selective collateral elimination in early postnatal development restricts cortical distribution of rat pyramidal tract neurones, **298**, 371
Stangenberger A. G. *see under* Post W. M., **298**, 156
Stannard D. and McIlwrath B. K. Extended radio structure of BL Lac type objects, **298**, 140
Stanton L. W. *see under* Marcu K. B., **298**, 87
Starmer I. C. *see under* Field D., **298**, 303
Starzyk R. M., Koontz S. W. and Schimmel P. A covalent adduct between the uracil ring and the active site of an aminoacyl tRNA synthetase, **298**, 136
Stedman D. H. *see under* Brimblecombe P., **298**, 460
Stein G. S. *see under* Lichtler A. C., **298**, 195
Stein J. L. *see under* Lichtler A. C., **298**, 195
Stenevi U. *see under* Björklund A., **298**, 652
Stevenson D. J. Volcanism and igneous processes in small icy satellites, **298**, 142
Stewart C. L. *see under* Jähner D., **298**, 623
Stewart J., Glass E. J. and Weir D. M. Macrophage binding of *Staphylococcus albus* is blocked by anti-I-region alloantibody, **298**, 852
Stewart P. J. Falklands alone? *correspondence*, **298**, 415
Storb U. *see under* Arp B., **298**, 184
Strassburg M. A. *see under* Pasachoff J. M., **298**, 402
Streeck R. E. A multicopy insertion sequence in the bovine genome with structural homology to the long terminal repeats of retroviruses, **298**, 767
Strens M. R. *see under* Cann J. R., **298** 147
Striker G. E. *see under* Keating A., **298**, 280
Strosberg A. D. *see under* Panthier J.-J., **298**, 90
Stroynowski I., van Cleemput M. and Yanofsky C. Superattenuation in the tryptophan operon of *Serratia marcescens*, **298**, 38
Stroynowski I. and Yanofsky C. Transcript secondary structures regulate transcription termination at the attenuator of *S. marcescens* tryptophan operon, **298**, 34
Struhl G. *Decapentaplegic* — hopes held out, *news and views*, **298**, 13
Strumph P. *see under* Benjamin P., **298**, 769
Stuhlmann H. *see under* Jähner D., **298**, 623
Su T.-S. *see under* Daiger S. P., **298**, 682
Subirana J. A. *see under* Maestre M. F., **298**, 773
Sugisaki R., Yamamoto K. and Adachi M. Traissic bedded cherts in central Japan are not pelagic, **298**, 644
Sulzman F. M. *see under* Moore-Ede M. C., **298**, 589
Supek I. Philosopher in gaol, *correspondence*, **298**, 510
Sutcliffe J. G. *see under* Bittle J. L., **298**, 30
Sutherland S. *book review of* Vision: A Computational Investigation into the Human Representation and Processing of Visual Information, (Marr D.) **298**, 691
Sverdlove M. *see under* Fairbanks R. G., **298**, 841
Sweeney J. F. Mid-Palaeozoic travels of Arctic-Alaska, **298**, 647
Tack B. F. *see under* Hostetter M. K., **298**, 72
Tahirkheli R. A. K. *see under* Zeitler P. K., **298**, 255
Takahashi H. *see under* Kakidani H., **298**, 245
Takamatsu H. and Iso K. Chemical evidence for the capsomeric structure of phage $Q\beta$, **298**, 819
Takeda Y. *see under* Ohlendorf D. H., **298**, 718
Talkington C. A. and Leder P. Rescuing the *in vitro* function of a globin pseudogene promoter, **298**, 192
Tallon J. L. Crystal instability and melting, *matters arising*, **298**, 874
Tamsett D. and Girdler R. W. Gulf of Aden axial magnetic anomaly and the Curie temperature isotherm, **298**, 149
Tanenbaum M. *see under* de Lanerolle P., **298**, 871
Taniguchi M. *see under* Tokuhisa T., **298**, 174
Taniguchi M., Tokuhisa T., Kanno M., Yaoita Y., Shimizu A. and Honjo T. Reconstitution of antigen-specific suppressor activity with translation products of mRNA, **298**, 172
Tarbet P. W. and Rowan-Robinson M. A pregalactic Population III: primordial helium and heavy elements and the microwave background, **298**, 711
Tashian R. E. *see under* Czelusniak J., **298**, 297
Tata J. R. Do steroid receptors recognize DNA sequences? **298**, 707
Tate R. L. III *see under* Duxbury J. M., **298**, 462
Taylor P. M. *see under* Mellor A. L., **298**, 529
Tebedge S. *see under* Kalb J. E., **298**, 17
  see under Kalb J. E., **298**, 25
Teller E. *Editor*, Fusion: Vol. 1, Magnetic Confinement, *book review by* Pease R. S. **298**, 404
Terenius L. *see under* Vincent S. R., **298**, 65
Termijtelen A. *see under* van Leeuwen A., **298**, 565
Terrill S. B. *see under* Able P. K., **298**, 510
Terry R. E. *see under* Duxbury J. M., **298**, 462
Thies P. W. *see under* Römer D., **298**, 759
Thomas C. M., Hussain A. A. .K. and Smith C. A. Maintenance of broad host range plasmid RK2 replicons in *Pseudomonas aeruginosa*, **298**, 674
Thomas D. Imperial echoes, *correspondence*, **298**, 510
Thomas E. D. *see under* Keating A., **298**, 280
Thomas J. B. and Wyman R. J. A mutation in *Drosophila* alters normal connectivity between two identified neurones, **298**, 650
Thomas M. L. *see under* Hostetter M. K., **298**, 72
Thompson A. W. *see under* Arndt U. W., **298**, 835
Thompson R. G. *see under* Rosenmann E., **298**, 563
Thomson A. J. Proteins containing nickel, *news and views*, **298**, 602
Thomson J. *see under* Cronan D. S., **298**, 456
Thorning D. *see under* Keating A., **298**, 280
Thornton J. M. and Chakauya B. L. Conformation of terminal regions in proteins, **298**, 296
Tinh N. H. *see under* Malthête J., **298**, 46
Tinoco Jr I. *see under* Maestre M. F., **298**, 773
Tirion W. Sky Atlas 2000.0, *book review by* Hughes D. W. **298**, 588
Tokuhisa T. *see under* Taniguchi M., **298**, 172

Tokuhisa T. and Taniguchi M. Constant region determinants on the antigen-binding chain of the suppressor T-cell factor, **298,** 174
Tola E. *see under* Kalb J. E., **298,** 17
Tomlinson B. E. *see under* Anderton B. H., **298,** 84
Toon O. B. *see under* Turco R. P., **298,** 830
Tooze J. ***Editor***, DNA Tumor Viruses, *book review by* Rigby P. W. J. **298,** 406
Topal M. D., Hutchison III C. A. and Baker M. S. DNA precursors in chemical mutagenesis: a novel application of DNA sequencing, **298,** 863
Torii T. *see under* Masuda N., **298,** 154
Toro M. A. *see under* Charlesworth B., **298,** 494
Torok-Storb B. and Hansen J. A. Modulation of *in vitro* BFU-E growth by normal Ia-positive T cells is restricted by HLA-DR, **298,** 473
Townsend A. R. M. *see under* Mellor A. L., **298,** 529
Trautmann A. Curare can open and block ionic channels associated with cholinergic receptors, **298,** 272
Trautwein W. *see under* Osterrieder W., **298,** 576
Trayburn P., Douglas J. B. and McGuckin M. M. Brown adipose tissue thermogenesis is 'suppressed' during lactation in mice, **298,** 59
Tronick S. R. *see under* Santos E., **298,** 343
Tschopp J., Müller-Eberhard H. J. and Podack E. R. Formation of transmembrane tubules by spontaneous polymerization of the hydrophilic complement protein C9, **298,** 534
Tsien R. Y. *see under* Lew V. L., **298,** 478
Turco R. P., Toon O. B., Whitten R. C. and Cicerone R. J. Space shuttle ice nuclei, **298,** 830
Turksen K., Aubin J. E. and Kalnins V. I. Identification of a centriole-associated protein by antibodies present in normal rabbit sera, **298,** 763
Turner J. S. *see under* Kerr R. C., **298,** 731
Turner M. Antigenic variation in the trypanosome, *news and views*, **298,** 606
Turner M. S. *see under* Barrow J. D., **298,** 801
Turner M. S. and Wilczek F. Is our vacuum metastable? **298,** 633
Twine M. *see under* Fink G., **298,** 270
Tytler D. QSO Lyman limit absorption, **298,** 427
Ulan L. D. *see under* Jacoby G. C., **298,** 637
Ulrich J. *see under* Anderton B. H., **298,** 84
Upton C. Too many drugs? *correspondence*, **298,** 114
Valenzuela P., Medina A., Rutter W. J., Ammerer G. and Hall B. D. Synthesis and assembly of hepatitis B virus surface antigen particles in yeast, **298,** 347
Valle-Aguilera R. *see under* Gonzalez-Serratos H., **298,** 292
van Cleemput M. *see under* Stroynowski I., **298,** 38
van den Boogaart P., Samallo J. and Agsteribbe E. Similar genes for a mitochondrial ATPase subunit in the nuclear and mitochondrial genomes of *Neurospora crassa*, **298,** 187
van Leeuwen A., Termijtelen A., Shaw S. and van Rood J. J. Recognition of a polymorphic monocyte antigen in HLA, **298,** 565
van Rood J. J. *see under* van Leeuwen A., **298,** 565
Van Valen L. M. Phylogenies in molecular evolution: *Prochloron*, **298,** 493 *matters arising*.
Vartio T. *see under* Virtanen I., **298,** 660
Vaughan D. E. W. *see under* Melchior M. T., **298,** 455
Vaughan L. *see under* Carrell R. W., **298,** 329
Vaughan P. J., Green H. W. II and Coe R. S. Is the olivine–spinel phase transformation martensitic? **298,** 357
Venta P. J. *see under* Czelusniak J., **298,** 297
Vincens A. *see under* Owen R. B., **298,** 523
Vincent S. R., Johansson O., Hökfelt T., Meyerson B., Sachs C., Elde R. P., Terenius L. and Kimmel J. Neuropeptide coexistence in human cortical neurones, **298,** 65
Virtanen I., Vartio T., Badley R. A. and Lehto V.-P. Fibronectin in adhesion, spreading and cytoskeletal organization of cultured fibroblasts, **298,** 660
Vishveshwara C. V. *see under* Cohen J. M., **298,** 829
Visvanathan N. and Pickles A. Optical identification of X-ray source H0139–68 with an AM Herculis-type system, **298,** 41
von Brunn V. *see under* Boulton G. S., **298,** 437
Waddell D. R. A predatory slime mould, **298,** 464
Wade B. Nuclear risks, *correspondence*, **298,** 702
Wade N. *book review of* Koestler: A Biography, (Hamilton I.) **298,** 587
Waldron J. A. *see under* Reinisch C. L., **298,** 176
Walford J. Oxygen treatment, *correspondence*, **298,** 702
Walker D. *see under* Foyer C., **298,** 326
Walker J. E., Saraste M. and Gay N. J. *E. coli* F_1-ATPase interacts with a membrane protein component of a proton channel, **298,** 867
Wallis M. K. and Ip W.-H. Atmospheric interactions of planetary bodies with the solar wind. *review article*, **298,** 229
Wands J. R. *see under* Shouval D., **298,** 567
Wang C., Shi Y. and Zhou W. Dynamic uplift of the Himalaya, **298,** 553
Ward R. D. *see under* Skibinski D. O. F., **298,** 490
Wark I. W. Social sciences, *correspondence*, **298,** 414
Waser J. *see under* Kuhn H., **298,** 585
Weber K. *see under* Shaw G., **298,** 277
Weir D. M. *see under* Stewart J., **298,** 852
Weiss E. *see under* Mellor A. L., **298,** 529
Weiss M. L. *see under* Czelusniak J., **298,** 297
Weissman C. and Schellekens H. Monkeys are insensitive to pyrogenic effects of human α-interferons—Reply, *matters arising*, **298,** 301
Weissman I. L. *see under* Kraal G., **298,** 377
Welch J., Kim H., Fallon S., Liebman J., MacNeil D. and Gower M. Do antidepressants induce dopamine autoreceptor subsensitivity? *matters arising*, **298,** 301
Wellman P. Australian seismic refraction results, isostasy and altitude anomalies, **298,** 838
Wells J. R. E. *see under* Lichtler A. C., **298,** 195
Wendlandt R. F. and Morgan P. Lithospheric thinning associated with rifting in East Africa, **298,** 734
Wenthold R. J. *see under* Altschuler R. A., **298,** 657
Werkmeister J. *see under* Roder J. C., **298,** 569
Westing A. H. Vietnam now, *correspondence*, **298,** 114
White E. *book review of* Principles of Pollution Control, (Sandbach F.) **298,** 778
White R. *see under* Parker M., **298,** 92
White W. F. and Heller A. H. Glycine receptor alteration in the mutant mouse *spastic*, **298,** 655
Whitehead P. *see under* Kalb J. E., **298,** 25
Whitten R. C. *see under* Turco R. P., **298,** 830
Wiebe P. H. *see under* Fairbanks R. G., **298,** 841
Wiggert B. *see under* Lai Y. L., **298,** 848
Wigley T. M. L., Ingram M. J. and Farmer G. ***Editors***, Climate and History: Studies in Past Climates and Their Impact on Man, *book review by* Schneider S. H. **298,** 499
Wilczek F. *see under* Dimopoulos S., **298,** 824
  see under Turner M. S., **298,** 633
Wildavsky A. *see under* Douglas M., **298,** 775
Wildin R. S. *see under* Daiger S. P., **298,** 682
Wildish D. J. *see under* Charlesworth B., **298,** 494
Williams P. W. Speleothem dates, Quaternary terraces and uplift rates in New Zealand, **298,** 257
Williamson A. R. *see under* Cushley W., **298,** 77
Williamson B. Gene therapy, *review article*, **298,** 416
Wilson L. *book review of* The Channels of Mars, (Baker V. R.) **298,** 694
Wilson M. C. Cut marks and early hominids: evidence for skinning, *matters arising*, **298,** 303
Wiltshire J. C. *see under* Malahoff A., **298,** 234
Winfree A. T. *book review of* The Clocks That Time Us: Physiology of the Circadian Timing System, (Moore-Ede M. C., Sulzman F. M., Fuller C. A.) **298,** 589
Winkler R. *see under* Eigen M., **298,** 497
Winter J. Shiverer peripheral myelin contains P_2, **298,** 471
Wood C. B. *see under* Kalb J. E., **298,** 25
Wood J. A. *book review of* Meteorites: A Petrologic–Chemical Synthesis, (Dodd R. T.) **298,** 877
Wood J. N. *see under* Anderton B. H., **298,** 84
Woodland H. R. *see under* Coveney J., **298,** 578
Woodroofe J. *see under* Finter N. B., **298,** 301
Worsley P. *see under* Boulton G. S., **298,** 437
Wrigley N. G. *book review of* Electron Microscopy of Proteins, (Harris J. R. *editor*) **298,** 498
Wrogemann K. *see under* Rosenmann E., **298,** 563
Wyman R. J. *see under* Thomas J. B., **298,** 650
Wymer J. The Palaeolithic Age, *book review by* Gowlett J. A. J. **298,** 204
Xiao X. C. *see under* Maluski H., **298,** 152
Yabusaki Y. *see under* Kuchino Y., **298,** 684
Yaffe D. *see under* Zakut R., **298,** 857
Yagura T. *see under* Kozu T., **298,** 180
Yamamoto B. K. and Freed C. R. The trained circling rat: a model for inducing unilateral caudate dopamine metabolism, **298,** 467
Yamamoto K. *see under* Sugisaki R., **298,** 644
Yamashita T. *see under* Sinclair R., **298,** 127
Yanofsky C. *see under* Stroynowski I., **298,** 34
  see under Stroynowski I., **298,** 38
Yaoita Y. *see under* Shimizu A., **298,** 82
  see under Taniguchi M., **298,** 172
Yates V. J. *see under* Dawson G. J., **298,** 580
Yeh H.-W. *see under* Malahoff A., **298,** 234
Yelon A. and Eisenberg A. Help for refusniks, *correspondence*, **298,** 415
Yocum R. R. *see under* Sauer R. T., **298,** 447
Yonetani T. *see under* Kitagawa T., **298,** 869
Zachariassen K. E. and Husby J. A. Antifreeze effect of thermal hysteresis agents protects highly supercooled insects, **298,** 865
Zachau H. G. *see under* Falkner F. G., **298,** 286
Zaczek R. *see under* Ferkany J. W., **298,** 757
Zakut R., Shani M., Givol D., Neuman S., Yaffe D. and Nudel U. Nucleotide sequence of the rat skeletal muscle actin gene, **298,** 857
Zeitler P. K., Johnson N. M., Naeser C. W. and Tahirkheli R. A. K. Fission-track evidence for Quaternary uplift of the Nanga Parbat region, Pakistan, **298,** 255
Zeugner H. *see under* Römer D., **298,** 759
Zhou W. *see under* Wang C., **298,** 553
Zick Y. *see under* Kasuga M., **298,** 667
Ziman J. Puzzles, Problems and Enigmas: Occasional Pieces on the Human Aspects of Science, *book review by* Fredrickson D. S. **298,** 305
Zimmerman E. A. *see under* Krieger D. T., **298,** 468
Zindler A., Jagoutz E. and Goldstein S. Nd, Sr and Pb isotopic systematics in a three-component mantle: a new perspective, **298,** 519
Zinke P. J. *see under* Post W. M., **298,** 156
Ziolkowski A. Coal in reserve, *correspondence*, **298,** 702
Zucker M. B. *see under* Masiello N. C., **298** 202
Zurawski V. R. Jr *see under* Shouval D., **298,** 567

4014

LAST REMINDER

Can Europe stay in the biotechnology race?

An international conference organised by The Economist at the Amstel Hotel, Amsterdam on 7-8 October 1982

e Economist, one of the first to recognise the ommercial potential of developments in otechnology, is now organising a conference discuss the present state and future of otechnology in Europe. The speakers are:

GER WHITTENBURY
fessor of Biological Sciences
niversity of Warwick, UK

BOB RABIN
Professor of Biochemistry
University College,
London, UK

ROB MARGETTS
General Manager, 'Pruteen'
ICI Agricultural Division, UK

ROBERT FILDES
President
Biogen Inc, USA

J SCHELL
Professor of Genetics
Laboratorium voor Genetica,
Belgium

VIVIAN MOSES
Professor of Microbiology
Queen Mary College, London,
UK

MICHAEL ROSE
Group Manager Biosciences
ICI Corporate Bioscience Group,
UK

R S CRESPI
Patents Controller
British Technology Group, UK

R E CAPE
Chairman
Cetus Corporation, USA

J D BU'LOCK
Wolfson Biomass Unit
University of Manchester, UK

PETER LAING
Manager
N M Rothschild
Asset Management
Limited, UK

GUNNAR WESSMAN
President
Fortia/Pharmacia, Sweden

SCOTT KING
Vice-President
Research Division
F Eberstadt & Co Inc, USA

B M RICHARDS
Vice-President
UK Preclinical Research & Development
G D Searle & Co Limited, UK

JOHN ASHWORTH
Vice-Chancellor
Salford University, UK

J A WOLHOFF
Board member of Dutch companies
Netherlands

If you are interested in the latest financial, commercial, legal or scientific developments in biotechnology, simply complete the coupon below now.

☐ Please send me further details.
☐ Please register me as delegate.
☐ Please send invoice (fee £275.00).

Please return to: The Economist Conference Unit, 25 St. James's Street, London SW1A 1HG. Telephone: 01-839 7000. Telex: 24344.

Circle No.20 on Reader Service Card.

NAME

COMPANY

ADDRESS

The Economist

Registered in London number 236383

BE4

A NEW QUARTERLY JOURNAL...

JOURNAL OF ATMOSPHERIC CHEMISTRY

Editors:
P.J. CRUTZEN, *Max-Planck-Institute for Atmospheric Chemistry, Mainz, F.R.G.*
D.H. EHHALT, *Institute for Atmospheric Chemistry, Kernforschungsanlage Jülich, F.R.G.*

The Journal will be devoted to the study of the chemistry of the Earth's atmosphere with emphasis on the region below about 100 km. Submission of original work on the following is welcome:
- composition and physico-chemical processes (excluding air pollution problems of only local importance);
- the role of the atmosphere in biogeochemical cycles;
- laboratory studies of transformation processes;
- novel instrumentation of direct importance for field measurements.

The first issue will appear in March 1983. Contributions should be submitted in triplicate to either of the above editors (for the first issue, by the end of September 1982). Further information can be obtained from the publisher.

Subscription rates:
Institutional: Dfl. 185,– / US $ 74.00. *Private:* Dfl. 85,– / US $ 34.00 (prices include postage and handling).

D. Reidel Publishing Company.
P.O. Box 17 3300 AA Dordrecht The Netherlands
RESERVE YOUR FREE SAMPLE COPY NOW.

Circle No.21 on Reader Service Card.

Located in a quiet downtown area, at a ten minute's walk from the Bahnhofstrasse. Direct tramline to the University.

60 rooms, all with bath, toilet, colour TV, radio, minibar and direct dial telephone.

Choice of two restaurants, offering attractive plateservice at reasonable prices and fine cuisine with local as well as classic international specialities. Wine list with more than 400 choices.

Big enough to offer all conveniences, small enough to take care of your individual needs.

WHILE IN ZURICH, WHY STAY ELSEWHERE?

ASCOT

Hotel, Jockey-Club-Restaurant und Turf Bar
Lavaterstrasse 15, 8027 Zürich, Switzerland
Tel.: 01/201 18 00, Telex: 52783

Circle No.14 on Reader Service Card.

"A unique guide to biological laboratory products."

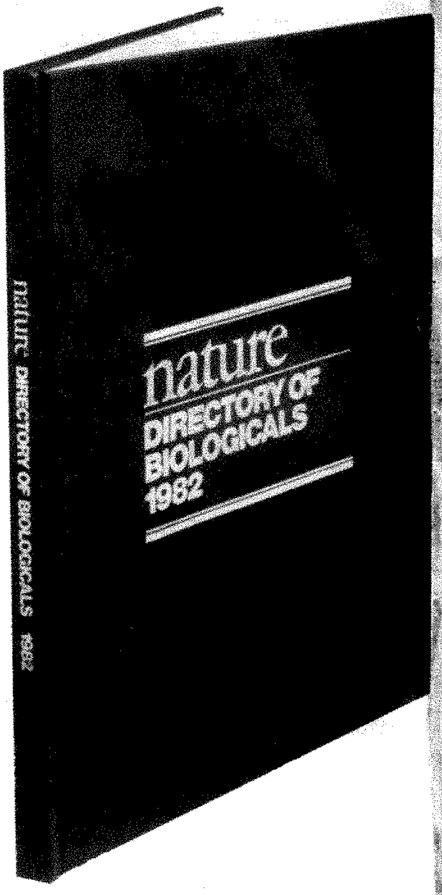

The Directory of Biologicals offers life scientists a comprehensive listing of what is on the market and where researchers can order these materials for their work. Designed to meet the day-to-day needs of active biologists searching for the right product to use in the laboratory, its simple alphabetical listings cover all of modern life science research. Clear and easy to use, it lists more than 2,000 products commercially available, with the names and addresses of companies throughout the world that offer them for sale. Telex and telephone numbers give users direct access to sales offices in your area. Company entries also briefly describe each supplier's specialization. A separate section lists products by trade name or registered trademark, keyed to the companies in the guide.

Helpful essays on how to use the directory, safety procedures, how to purchase biological materials, and the future of modern biology, make this the most useful directory ever published for biological research workers.

All subscribers to *Nature** automatically receive a handsome paperbound version of the directory. **But if you think you need a copy to stand up against constant use in your laboratory or your library, or if you are not a subscriber, you can purchase the deluxe hardcover edition.** (No paperback editions will be available after subscribers receive their free copy.) To order a hardcover edition, all you need do is fill out the form and mail it today.

297x210mm
232 pages
ISBN: 0 333 33233 4

U.S. and Canada: *Nature*, 15 East 26th Street, New York, NY 10010
U.K. and Rest of World: *Nature*, Canada Road, Byfleet, Surrey KT14 7JL, England.

☐ **Send me______copies of the deluxe, hardcover edition of the Directory of Biologicals @ $45/£22.50 each. (P&P free).** (Tax: N.Y. State Residents, please add sales tax.) (I understand that as a subscriber to *Nature* I will receive a free copy of the paperbound edition as part of my subscription.*)

Name________________________________
Address______________________________
____
City__________State__________Zip__________
Country______________________________
☐ I enclose $______/£______ ☐ I prefer to use my credit card account
Account No.____________ Expiry Date________
☐ Visa ☐ Access/Mastercard
☐ American Express Signature______________

In the U.S. you may make your order by telephone, using our toll-free number. Our operators are on duty 7 days a week, 24 hours a day.

Call toll-free now: (800) 824-7888. Ask for operator 130 (Dept. TNA)
In California: (800) 852-7777. Ask for operator 130 (Dept. TNA)

Please allow 6 weeks for delivery.

*If your subscription was in effect on November 30, 1981, you automatically receive a paperbound copy of the 1982 Directory of Biologicals. Those who entered subscriptions after that date will receive the 1983 Directory of Biologicals next spring.